PROCEEDINGS BOOK

Table of Contents

Topic 01. Smart farming - Precision agriculture

Expectations of machine-to-machine networking in dairy housing rise with experiences of farmers 17
Jernej Poteko, Jan Harms

Early detection of Esca disease in grapevines using in-field hyperspectral proximal sensing 22
Ainara López-Maestresalas, Jon Ruiz de Gauna, Carmen Jarén, Sara León-Ecay, Silvia Arazuri

On-site identification of Esca-affected vines using hyperspectral imaging 28
Sara León-Ecay, Jon Ruiz de Gauna, Ainara López-Maestresalas, Carmen Jarén, Silvia Arazuri

Site-specific yield recording in grassland and forage production using sensor technology on self-propelled forage harvesters 34
Maria Schneider, Juliana Mačuhová, Stefan Thurner

A variable-rate spraying system based on RGB-depth and object detection 41
Qi Gao, Alberto Carraro, Marco Sozzi, Francesco Marinello

Study of the individual information collection system for weaner pigs 49
Yi-Chich Chiu

Challenges and opportunities for remote sensing in agrivoltaic systems 55
Sergio Véleza, Shiva Gorjiana, Tamara Bretzel, Matthew F. Berwind, Mar Ariza-Sentís, Gonzalo Mier, João Valente, Max Trommsdorff

Prediction of nitrogen-fixing bacteria and phosphorus-solubilising bacteria in the soil using UAV multispectral images 63
David Mostaza-Colado, Alejandro Alonso-Conde, Elisa Gómez, Pedro Muñoz, José Marín, Pedro V. Mauri Ablanque

Finnish future farm - A physical and virtual co-creation platform for RDI, education and business acceleration in smart farming 68
Hannu Haapala, Annimari Lehtomäki, Jyrki Kataja

Micro-Near-Infrared (Micro-NIR) sensor for predicting organic carbon and clay contents in agricultural soil 76
Jiang Liu, Muhammad Abdul Munnaf, Abdul Mounem Mouazen

Smart control strategies for optimal environmental conditions and minimum energy requirements in livestock facilities 84
Stelios Kalogridis, Michael Moraitis, Athanasios Balafoutis, Bas Paris, Nikolas Ipiotis, Michail Savvakis, Dimitris Manolakos, Dimitrios Tyris

Data-driven solutions for farmer empowerment in smart agriculture: challenges and opportunities 94
Havva Uyar, Ioannis Karvelas, Clare Sullivan, Stamatia Rizou, Spyros Fountas

Advancing dairy farm management: leveraging data, neural networks, and interactive web design 103
Razieh Abdollahipour, Mostafa Sayeed, David Janke, Thomas Amon, Barbara Amon, Sebastian Opalinski, Joanna Frontczak, Sabrina Hempel

Influence of field, crop and climate variables on corn silage yield maps 108
Javier Bueno, Jorge Dafonte, José Miguel Edreira, Miguel Ángel Vilar

Classification model using cluster analysis with corn silage yield maps 115
Javier Bueno, Jorge Dafonte, José Miguel Edreira, Miguel Ángel Vilar

Optimization of mechanical and operating parameters for improving chisel plow performance in heavy clay soils 123
Abdul Salam J. Almoosawi, Majid H. Alheidary, Mortadha A. Alfaris

Agriculture digitalization: Development of a low-cost RGB camera system for soybean crop monitoring 131
Jordi Llop, Albert Aguasca, Antoni Broquetas, Aitor Meraver, Ramon Salcedo, Francisco Garcia, Emilio Gil

Estimating pomegranate fruit cracking through proximal and aerial remote sensing 136
Georgia Nikolakopoulou, Konstantinos-Elenos Grivakis, Evangelos Anastasiou, Manuela Zude-Sasse, Christian Regen, Nicolas Tapia Zapata, Victor Alchanatis, Avi Sadka, Idit Ginzberg, Meytal Laor, Spyros Fountas

Implementation of a proximal optical sensor for real-time characterization of extensive rainfed crops and targeted fertilizer applications 144
Sergio Artero, María Videgain, Alba Vigo-Morancho, Mariano Vidal, F. Javier García-Ramos

A UAV based model for obtaining high resolution cotton yield maps 152
Chris Cavalaris, Chris Karamoutis, Sofia Koukou, Evangelia Karakosta

AI-based in-field weeding quality assessment as a potential test standard 160
Oliver Schmittmann, Patrick Zimmer

Harnessing infrared thermometry and spectral indices for enhanced crop water stress monitoring in drip-irrigated rice cultivation with reclaimed wastewater 166
Gregorio Egea, Annkathrin Rosenbaum, María Muñoz, Manuel J. González-Ortega, Manuel Pérez-Ruiz

An economic analysis of bolus-sensor technology for precision dairy cattle management 174
Elias Maritan, Gundula Hoffmann, Friederike Schwierz, S. Mark Rutter, Andreas Meyer-Aurich, James Lowenberg-DeBoer, Karl Behrendt

Optimizing maize crop productivity: A variable rate approach from over-density trials with different inter-row spacing and sowing densities 183
Luís Alcino Conceição, Luís Silva, Tiago Silva Pinto, Susana Dias, Constantino Valero

Color image evaluation of fruits of grape in consideration of postharvest process 189
Yuki Iwase, Ken-ichiro Suehara, Kazuhiko Kawamura, Atsushi Hashimoto

Energy harvesting for a multi-sensor on dairy cattle 194
Susanne Demba, Annett Baudisch, Christopher Miersch, Danilo Zimmermann, Sarah Jahn, Doreen Nitsche, Steffen Pache, Kirsten Kouwert, Sandra Rose

Internet of livestock – A smart locatable multifunctional sensor device to enable interconnectivity between operators and actuators in dairy cattle farming 200
Susanne Demba, Sebastian Schäfer, Peter Schneider, Sarah Jahn, Doreen Nitsche, Steffen Pache, Kirsten Kouwert, Sandra Rose

Greenhouses energy audits – procedures and results 206
Catherine Baxevanou, Dimitrios Fidaros, Chryssoula Papaioannou, Nikolaos Katsoulas

Use of NIR regional scale calibrations to map soil characteristics for PA: A case study in 5 fields 215
Andrea Lazzari, Nicolò Pricca, Andrea Gasparini, Giovanni Cabassi

Detection of spectral signature and classification of Alternaria alternata and Alternaria solani diseases in tomato plant by analysis of hyperspectral images and support vector machine 223
Seyed Mohamad Javidan, Ahmad Banakar, Keyvan Asefpour Vakilian, Yiannis Ampatzidis, Kamran Rahnama

Assessing water and nitrogen stress in pepper plants (Capsicum annum L.) using hyperspectral data: A comparative analysis of machine learning and vegetation indices 229
Maria Bebie, Aris Kyparissis

Factors influencing the working time requirement and work rate of field robots when weeding organic sugar beet 237
Franz Handler, Michael Haider, Andreas Ettlinger

Temporal stability of soil electrical conductivity patterns: contact versus non-contact sensors 245
João Serrano, Shakib Shahidian, José Marques da Silva, Francisco Moral

Shaping the agricultural future: Engaging stakeholder feedback for the development of agricultural robotic solutions 253
Maria-Zoi Papantonatou, George Papadopoulos, Spyros Fountas, Havva Uyar, Frits Van Evert

Assessment of instance segmentation methods for amodal apple detection in challenging environments 262
Tito Arevalo-Ramirez, Juan Villacres, Michelle Viscaino, Francisco Yandún, Oswaldo Menéndez

Creation of an ISO11783-compliant prescription map for variable rate spraying in vineyards based on canopy 3D reconstruction 268
Björn Poss, Nikos Tsoulias, Galibjon M. Sharipov, Andreas Heiß, Dimitrios S. Paraforos

Orchard digital twin: A prototype for smart agricultural monitoring 274
Kyra Smith, Andrea Botta, Giovanni Colucci, Marco Piras, Giuseppe Quaglia, Elena Belcore

Can we leverage data sharing benefits to increase the adoption of smart farming technologies? 282
Clare S. Sullivan, Marilena Gemtou, Evangelos Anastasiou, Havva Uyar, Spyros Fountas

Detection of deficiency of iron, zinc and manganese in spinach plant under hydroponic cultivation conditions using digital image processing 292
Maryam Nadafzadeh, Ahmad Banakar, Saman Abdanan Mehdizadeh, Saeid Minaei, Mohammadreza Zare Bavani, Gerrit Hoogenboom, Abdul Mounem Mouazen

Topic 02. Automation, robotics and sensor technology
Adaptive nonlinear dynamic system identification for separation process of combine harvester 301
Tarek Kösters, Oliver Nelles

Operational limits for UAV livestock counting based on foundation models 308
Ricardo Ruiz Sánchez, Adrien Lebreton, João Valente

Stereo vision system guided variable rate sprayer with electric variable air assist system 316
Hongyoung Jeon, Heping Zhu, Carla Román, Javier Campos, Erdal Ozkan

Potential challenges encountered when adopting new technologies such as proximal sensing to realize VRA applications in cotton 323
Nikolaos Georgiadis, Konstantinos Papachristos, Vlasios Mangidis, Evangelia-Maria Giatsiou, Evangelos Adamopoulos, Christina Vogiatzi

A new mobile robot harvesting prototype for cotton production 328
Joe Mari Maja, Van Patiluna, Fazly Bin Mail, Gilbert Miller, Matthew Cutulle, Michael Marshall, Edward Barnes

A novel on-line dual-sensing system for soil property measurement and mapping 337
Rukayat Afolake Oladipupo, Muhammad Abdul Munnaf, Parsat Sanganta, Ajit Borundia, Abdul Mounem Mouazen

Automated needle-based trunk injection system for HLB-affected citrus trees 349
Yiannis Ampatzidis, Israel Ojo, Antonio de Oliveira Costa Neto, Ozgur Batuman

Automatic generation of shrub and tree crop datasets for use in deep learning detection algorithms on agricultural vehicles 355
Klaus Müller, Jan Kunze, Michael Möller, Klaus-Dieter Kuhnert

Monitoring environmental contaminants concentrations emitted from broilers in Greece: a real – time study 362
Alkmini Gavriil, Dimitris Giannopoulos, Vasileios Anestis, Thomas Bartzanas

Soil tillage quality measurement: a methodical approach 367
Marina Graf, Franz Fuchshumer, Marcus Geimer

Localization of metal piles in grapevine rows by means of LiDAR based 3D reconstruction 374
Andreas Heiß, Joseph Bleser, Nikos Tsoulias, Björn Poss, Dimitrios S. Paraforos

Study of physicochemical changes in loquat fruit during cold storage using non-destructive spectroscopy 382
M. Lopez-Chulia, S. Castillo-Girones, P. Talens, J. Blasco

Workspace partitioning and speed selection to improve harvesting speeds of multi-armed robotic harvesters 390
Natalie Pueyo Svoboda, Stavros Vougioukas

Development of a method for the real-time assessment of the risk from severe-hot microclimate in agricultural and forestry environments 398
Massimo Cecchini, Alfredo Mancini, Filippo Cossio, Carlo Macor

Evaluation of plant-response irrigation modellin in greenhouses 406
Angeliki Elvanidi, Ioannis Naounoulis, Nikolaos Katsoulas

Economics of retrofitted autonomous tractors for crop protection spraying: a case study from Greece 412
Tseganesh Wubale Tamirat, Søren Marcus Pedersen, Jens Erik Ørum

Topic 03. Artificial Intelligence, data processing and management

Establishing resilient AI applications in agriculture by redundancy and graceful degradation: Two use cases 423
Sebastian Bökle, Marcus Müller, Waldemar Keil, Hans W. Griepentrog, Anthony Stein

A neural network approach for real-time monitoring of cannabis sativa L. germination 428
Jose A. Brenes, Ana Codes, Carmen Rocamora, Javier Ferrández-Pastor

Advancements in coffee authenticity: A spectroscopic feature compression approach using eXplainable AI and vision transformer 436
Shanghua Liu, Majharulislam Babor, Leah Munyendo, Bernd Hitzmann, Barbara Sturm, Marina Höhne

Deliberate image chipping for free uncrewed aerial vehicles image deep learning generalization 443
Jurrian Doornbos, Louise Helary, Onder Babur, Joao Valente

Data-driven approach to classifying the nitrogen nutritional status of ryegrass-based forages 454
Luís Silva, Luís Alcino Conceição, Sofia Barbosa, Carla Barreto, Fernando Cebola Lidon, José Santos Silva

A deep-learning approach for automated phenological prediction in barley 461
Luis Sánchez-Fernández, Manuel Perez-Ruiz, Gregorio Egea

Computer vision-based early detection of Phytophthora spp. in orange grove 466
Diego Gallardo-Romero, Gregorio Egea, Manuel Pérez-Ruiz

Advancing precision livestock agriculture: Harnessing generative artificial intelligence for enhanced animal behaviour recognition 474
Regina Eckhardt, Reza Arablouei, Kieren McCosker, Heinz Bernhardt

Wheat grain yield predictions based on a Bayesian network approach fusing multi-source time specific data and experts' knowledge 481
Maria Karampoiki, Salar Mahmood, Lindsay Todman, Alistair Murdoch, John Hammond, Emanuele Ranieri, Hans W. Griepentrog, Dimitrios S. Paraforos

Application of artificial neural network to identify the closest variety to Ogbomoso mango fruit 491
Michael Mayokun Odewole, Toluwani Adedeji Adegbite

On the route optimisation for phytosanitary treatments in vineyards using electric-powered UAVs 495
Mar Ariza-Sentís, Gonzalo Mier, Sergio Vélez, João Valente

Agroview: enhance satellite imagery using super-resolution and generative AI for precision management in specialty crops 500
Christian Lacerda, Antonio de Oliveira Costa Neto, Yiannis Ampatzidis

Applications of artificial intelligence in the identification of objects for the analysis of waste in the Segura River 508
Ana María Codes Alcaraz, Carmen Rocamora Osorio, Herminia Puerto Molina

Artificial intelligence-based yield prediction in table grape production: A case study in the Vinalopó protected designation of origin 516
Ana María Codes Alcaraz, Carmen Rocamora Osorio, Herminia Puerto Molina

Comparative analysis of deep learning models for a dairy cow face recognition framework 522
Hao-Ping Chen, Chen-Yu Liao, Jih-Tay Hsu, Ta-Te Lin

Tracking and behavioural analysis of fattening pigs 530
Pieter-Jan De Temmerman, Jarissa Maselyne

Revolutionizing wine production: Innovative traceability solutions and metrology integration for enhanced transparency, efficiency, and sustainability 537
António Ferreira Dias, Ana Gonçalves, Pedro Moreira, Sérgio Carvalho, Tiago Santos, Vitor Sousa

Estimating air temperature using Modis LST aiming to feed daily evapotranspiration models - Case study for the plain of Arta Greece 547
Chris Koliopanos, Ioannis Tsirogiannis

Improving dairy cow feed intake monitoring: Insights from depth camera imaging 555
Marjaneh Taghavi, Tomas Izquierdo, István Fodor

A comprehensive dataset for monitoring germination of Cannabis sativa in greenhouse-controlled environments 562
José A. Brenes, Ana Codes, Javier Ferrández, Carmen Rocamora

AI-enhanced language support for advanced operation in controlled environment agriculture 570
Ramesh Arvind Naagarajan, Kiran Kumar Sathyanarayanan, Nadja Bauer, Philipp Sauerteig, Sebastian Bab, Stefan Streif

Evaluation of machine learning-driven sensor networks for observing separation processes in combine harvesters for estimating separation efficiency 578
Kevin Penner, Marvin Barther, Felix Wittenfeld, Michael Thies, Marc Hesse

Hyperspectral imaging based on AI algorithms for early detection of plant fungal diseases 586
Panagiotis Christakakis, Nikolaos Giakoumoglou, Christos Klaridopoulos, Eleni Kalogeropoulou, Dimitrios Tzovaras, Eleftheria-Maria Pechlivani

Artificial intelligence algorithms revolutionizing insect monitoring and detection challenges 595
Panagiotis Christakakis, Dimitrios Kapetas, Nikolaos Frangakis, Sofia Faliagka, Nikolaos Katsoulas, Dimitrios Tzovaras, Eleftheria-Maria Pechlivani

Performance assessment of RGB-D cameras in deep learning algorithms for obstacle avoidance systems in agriculture 604
Pierluigi Rossi, Leonardo Assettati, Riccardo Alemanno, Leonardo Vita, Davide Gattamelata, Leonardo Marrazzini, Martina Olivieri, Luca Landi, Luca Burattini, Danilo Monarca, Maurizio Cutini

Advanced UAV edge computing ML solutions for livestock management 612
Aristotelis C. Tagarakis, Costas Davarakis, Alexander Loos, Christian Weigel, Maria Theologou, Niki Rovatsou, Oliver Doll, Dimitrios Kateris, Dionysis Bochtis

An initial forest digitization approach using drone and quadruped robot 620
Charalampos-Rafail Medentzidis, Theocharis Tsenis, Vassilios Kappatos

Enhancing agriculture question-answering systems through re-ranking and in-memory computing 627
Nur Arifin Akbar

Topic 04. Soil, land and water engineering

Isotherms and desorption patterns of various natural zeolites during the removal of ammonium from wastewaters 635
Silvia Balzan, Giulio Galamini, Giacomo Ferretti, Barbara Faccini, Massimo Coltorti

Pesticide management: Modeling agricultural practices for sustainable soil and groundwater quality in Nabatyeh region – South Lebanon 641
Farah Kanj, Dany El-Obeid, Kadi Saleh, Hussein Yazbeck

CULTISENSOR: Testing a digitalized subsoiler capable of generating maps of soil resistance 652
Francisco Garcia-Ruiz, Ramón Salcedo, Francisco Fonseca, Emilio Gil

Hydraulic performance evaluation of low-cost gravity-fed drip irrigation systems under falling head conditions 658
Camille G. Martinez, Henry Mark Q. Binahon, Jeffrey A. Gonzales, Arthur L. Fajardo, Victor B. Ella

Topic 05. Integrated and sustainable farming systems

Understanding stakeholder perspectives on decision support tools for livestock farm emission management 667
Evangelos Alexandropoulos, Vasileios Anestis, Thomas Bartzanas

Development and deployment of a decision support tool for gas emissions at the dairy farm level: Analysis of two case studies for dairy farms 675
Evangelos Alexandropoulos, Vasileios Anestis, Thomas Bartzanas

D4AgEcol Platform: A web platform to promote the use of digital tools and technologies in agroecology 682
Evangelos Anastasiou, Panagiotis Stamatelopoulos, Pothitos Kotsiomitis, Spyros Fountas, Friederike Schwierz, Andreas Meyer-Aurich

LIFE AgrOassis - Regenerative approaches for building climate change resilience into EU agricultural regions prone to desertification 690
C. Cavalaris, P. Maletsika, G. Nanos, A. Kyparissis, C. Karamoutis, V. Giouvanis, P. Dalias, S. Stylianou, G. Theofanous, F. Filippou, A. Christodoulou, D. Sarris, A. Stelikou, A. Miliotou, I. N. Vogiatzakis, S. Zotos, P. Manolaki, E. Tzirkalli, Ch. Kalaitzidis, P. Champas, P. Paradisiotis, V. Perakis, A. Markinos, K. Kiourtsis, A. Yiordamli, K. Orountiotis

Harmonising agroecology and digitalisation for sustainable European agriculture 698
Andreas Meyer-Aurich, Friederike Schwierz, Alma Moroder, Jochen Kantelhardt, Karl Reimand, Søren Marcus Pedersen, Andrea Landi, Karl Behrendt, Elias Maritan, Andreas Gabriel, Spyros Fountas, Evangelos Anastasiou

Mechanical termination of cover crops - Corn cultivation for less erosion and less herbicide use 702
Markus Demmel, Hans Kirchmeier

Effect of solar panels on fruit quality for photovoltaic greenhouses 710
Pablo González-Planells, Coral Ortiz, Francisco Rovira-Más, Elena Chaveli-López, Carmina Reig, Víctor Añón

Technologies for monitoring pig and broiler welfare at the slaughterhouse – tracing back to farm, loading, transport and slaughter 719
Jarissa Maselyne, Slađana Blažević, Sandra Stojanović, Christian Manteuffel, Kristina Maschat, Konstantinos Perakis, Thomas Banhazi, Nicolas Galtier, Pol Llonch, Bas Rodenburg, Martijn Bouwknegt, Ronald Klont, Bart de Ruiter, Josep Reixach, Pauline Créach, Nemanja Kajari, Joanna Marchewka, Petra Thobe, Carsten Cruse, Jan Schulte-Landwehr, Christoph Bonk, Juliette Zamparini, Jorinde Mulder, Shanida Mullatahiri, Kenny van Langeveld, Noémie Van Noten, Anneleen Watteyn, Frank Tuyttens, Anneleen De Visscher

Interaction of agroecosystems and aquaculture through engineering: experiences with small-scale tilapia farms, aquaponics and agroecological systems in South Mexico 727
Francisco Javier Martínez-Cordero, Laura Patricia Silva-Ledezma

Bacillus Subtilis and Burkholderia Seminalis in promoting the growth of Solanum Lycopersicum L. 732
Henrique F. E. de Oliveira, Thiago Dias Silva, Priscila Jane Romano Goncalves Selari, Wesley Rangel de Melo, Jhon Lennon Bezerra da Silva, Marcio Mesquita, Marcus Vinicius da Silva

Indoor vertical greening for regulating building microclimate 740
Fabiana Convertino, Evelia Schettini, Giuliano Vox

Usage of artificial lighting to promote seed germination for microgreen production 747
Christos Vatistas, Dafni D. Avgoustaki, Thomas Bartzanas

Topic 06. Sustainable production in farm buildings

Effect of foliar application of silicon on the cultivation of mini watermelon cv. Sugar baby in mitigating the effects of water deficit 754
Marcio Mesquita, Viviane Correira dos Santos, Rafael Battisti, Rilner Alves Flores, Moemy Gomes de Moraes, Henrique Fonseca Elias de Oliveira

Effects of bedding material on performance, welfare and ammonia emissions of broiler chickens 759
Shutong Dong, Jan van Harn, Kris De Baere, Ine Kempen, Albert Winkel

Analysis of wall pressures and discharge rates in corrugated steel silos with centric and eccentric hoppers by discrete element models 768
Ana Grande-Gutiérrez, José-María Fuentes, Eutiquio Gallego, Francisco Ayuga

Optimization of poultry house ventilation system using computational fluid dynamics 775
Timothy Denen Akpenpuun, Sunday John Oluwaseun, Oyindamola Oluwadamilola Toye

Effect of installing organic photovoltaic panels on the environmental performance of greenhouse tomato in Greece 785
Andreas Giakoumatos, Vasileios Anestis, Thomas Bartzanas, Nikolaos Katsoulas

Wind loads on two insect-proof tunnel nethouses: Full-scale and CFD analysis 792
Anastasios Giannoulis, Antonis Mistriotis, Demetres Briassoulis

Microclimate conditions in two insect-proof tunnel nethouses with tomato cultivation: Full-scale and CFD analysis 800
Anastasios Giannoulis, Antonis Mistriotis, Demetres Briassoulis

Reducing ambient temperature to reduce NH3, N2O and CH4 emissions from a fattening piggery 808
Guingand Nadine, Rousselière Yvonnick, Thomas Johan

RES4LIVE – Progress on pilot systems for energy smart livestock farming towards zero fossil fuel consumption 814
Dimitrios Tyris, Thomas Amon, Lukas Wannasek, Christian Ammon, Stefano Benni, Francesco Tinti, Jarissa Maselyne, Manon Everaert, Petros Demissie Tegenaw, Steven Lecompte, Olivier Marchand, Thomas Bartzanas, Dimitrios Manolakos

Source segregation in dairy housing effectively separates organic matter and nutrients and facilitates acidification for ammonia emission reduction 824
J. El Mahdi, P. W. G. Groot Koerkamp, J. Deru, J. W. De Vries

Topic 07. New application technologies and mechanisation

Performance evaluation of different pumps and pumpsets for agricultural application 834
Arthur L. Fajardo, Charleen Grace V. Deniega, Fatima Joy J. Raytana-Aying, Marie Jehosa B. Reyes, Jerson Jose T. Menguito, Yaminah Mochica M. Pinca

Development of an inline injection and mixing system for sensor-guided variable-rate sprayers 842
Heping Zhu, Zhihong Zhang, Yue Shen, Hongyoung Jeon

Preliminary evaluation of a knapsack sprayer prototype that combines electrostatic technology and hydraulic spraying 849
Alba Vigo-Morancho, María Videgain, Mariano Vidal, Antonio Boné, F. Javier García-Ramos

Assessing the adaptive capability of an intelligent recycling tunnel sprayer system to vine canopy size 856
Ramón Salcedo, Nehad El Aissaoui, Bernat Martí, Bernat Salas, Jordi Biscamps, Jordi Llop, Francisco García-Ruiz, Emilio Gil

Evaluation of agrochemical aerial distribution from UAS on a vineyard 861
Alberto Sassu, Vasilis Psiroukis, Francesco Bettucci, Luca Ghiani, Spyros Fountas, Filippo Gambella

Insertion of carbon-rich exogenous materials with bio-stimulants into subsoil for promoting maize growth 871
Dewen Qiao, Ajit Borundia, Cristina Cruz, Abdul Mounem Mouazen

The bulbous bow shape adaptability for the soil ripper tool 880
Egidijus Katinas, Regita Bendikienė, Vytenis Jankauskas, Antanas Čiuplys

Development of a numerical rating system for the selection of agricultural and fisheries machinery in the Philippines 888
Rossana Marie C. Amongo, Ralph Kristoffer B. Gallegos, Adrian A. Borja, Arthur L. Fajardo, Arsenio N. Resurreccion, Adrian Daniel L. Pantano, Julius John Paul A. Cunan

Tracing pistachio nuts' origin and irrigation practices through hyperspectral imaging 902
Raquel Martínez-Peña, Salvador Castillo-Gironés, Sara Álvarez, Sergio Vélez

The aquaphotomic approach in the discrimination of the metabolic condition of dairy cows 910
Simone Giovinazzo, Laura Marinoni, Tiziana M. P. Cattaneo, Carlo Bisaglia, Massimo Brambilla

Multispectral Imaging (MSI) application for food safety and quality evaluation: A mini review 918
Marianna I. Kotzabasaki, Dimitris Giannopoulos, Chrysanthos Maraveas, Thomas Bartzanas

Strategies to reduce mechanical harvesting costs in traditional olive orchards 927
Arlindo Almeida, Anabela Fernandes-Silva

Comparing the impact of different work phases on operator and driver exposure to whole-body vibration during olive harvesting activities 934
Gianluca Coltrinari, Massimo Cecchini, Danilo Monarca

Automatic feed pushing in dairy barns: Considerations of TMR leftovers particle size 942
Andrea Lazzari, Simone Giovinazzo, Massimo Brambilla, Francesco Maria Tangorra, Aldo Calcante, Carlo Bisaglia

Harvesting date influence on multi-trunk traditional olive productivity in next years 948
Francisco J. Soto-Torres, Gregorio L. Blanco-Roldán, Sergio Peña-Valero, Francisco J. Castillo-Ruiz

Hitched two sides windrowing and chipping prototype development for olive pruning management in an only tractor wipe 956
Sergio Peña-Valero, Francisco J. Castillo-Ruiz, Francisco J. Soto-Torres, Gregorio L. Blanco-Roldán

Development of an oyster mushroom (Pleurotus spp.) substrate compactor-bagger 963
Jordan L. Abad, Helen F. Gavino, Romeo B. Gavino, Melba M. Denson

Terrain aware monoplotting for ortho UAV images 971
Ufuk Can Bicici, Peter Riegler-Nurscher

Topic 08. Circular economy

Investigation of production of grapevine seedlings inoculated with AMF and grown using organic compost with wine lees under water stress conditions 979
Pinelopi Baltzoi, Ioannis Tsirogiannis, Georgios Patakioutas, Olga Kostoula, Vasileios Papantzikos, Eleni Lampraki

Training needs analysis for intergrating bioeconomy approaches into the EU's agricultural sector 987
Dimitris Michas, Athanasios Balafoutis, Bas Paris, Ioannis Thermos, Duarte Pimentel, Carlota Silva

Advancing circular nitrient flows through the development of biofertilizers: P2GreeN project perspective 999
Athanasios Balafoutis, Bas Paris, Dimitris Michas, Michalis Moraitis, Ioannis Thermos

A critical review of the EU bioeconomy: Current status and the transition to a circular bioeconomy 1009
Bas Paris, Dimitris Michas, Athanasios T. Balafoutis, George Papadakis

Effects of assistance of high-frequency dielectric heating on vacuum freeze drying characteristics of all biomass wet-extruded plate 1020
Hana Tsuneoka, Ken-ichiro Suehara, Hiroshi Nonaka, Atsushi Hashimoto

Composting off-gas as alternative source of carbon dioxide for spirulina cultivation – a preliminary study 1026
Kelechi E. Anyaoha, Felix Krujatz, Isla Hodgkinson, Roman Maletz, Christina Dornack

Oenotrace – A data-driven approach to trace sustainable practices in wine-growing 1036
Marco Bignardi, Andreas Heiß, Nikos Tsoulias, Dimitrios Argyropoulos, Dimitrios T. Davarakis, Marco Moriondo, Davide Cammarano, Cristina Balaceanu, George Suciu, Dimitrios S. Paraforos

Evaluation of water and nutrients use efficiency in a cucumber-melon cascade hydroponic system 1044
Nikolaos Katsoulas, Ioannis Naounoulis, Sofia Faliagka, Efi Levizou

Assessing the liquid-phase from hydrothermal liquefaction (HTL) of distilled biomass of Lavandula x intermedia for novel herbicide development 1050
Gonzalo Ortiz de Elguea-Culebras, Jaime Carrasco, Tamara Ferrando-Beneyto, Enrique Melero-Bravo, Antti Haapala, Aitor Barbero-López

Topic 09. Energy and bioenergy

Energy management system for charging autonomous viticultural robotic vehicles with photovoltaic stations in a microgrid topology 1056
Vasilis Arapostathis, Christos-Spyridon Karavas, Athanasios T. Balafoutis, George Papadakis

Empirical determination of the compression behaviour of miscanthus round bales 1065
Bargen-Herzog Niklas, Knapp Johannes, Geimer Marcus

Thermal and electrical performance evaluation of a hybrid solar system for a livestock farm in Belgium 1073
Petros Demissie Tegenaw, Manon Everaert, Iván P. Acosta-Pazmiño, Alexander Loris, Steven Lecompte, Jarissa Maselyne

Assessing the environmental benefits of switching to renewable energy sources in cheese production: A case study from Western Macedonia, Greece 1081
S. Konstantinidi, A. Vatsanidou, V. Anestis

Compact Bio-CNG farm filling fuel production from anaerobic digestion: Hollow fibre permeation and hybrid compression for technically and economically feasible small scale biofuel production 1088
Lukas Wannasek, Dimitris Tyris, Josef Hoeckner, Detlef May, Christian Ammon, Barbara Amon, Olivier Marchand, Dimitris Manolakos, Thomas Amon

Modelling of energy usage on dairy farms using ANN - “Case study in Canterbury province, New Zealand” 1095
Majeed Safa, Hafiz Muhammad Abrar Ilyas

Fuel consumption prediction based on GNSS recordings of agricultural machinery 1103
Ying Chen, Liwei Pan, Xiaoqiang Zhang, Xiang Luo, Caicong Wu

A greenhouse plants’ heating system based on low temperature long wave radiation emission 1109
George Papadakis

Renewable sources and energy retrofitting solutions for microclimatic control in pig barns 1117
Stefano Benni, Carlos A. Perez Garcia, Marco Bovo, Alberto Barbaresi, Francesco Tinti, Patrizia Tassinari, Daniele Torreggiani

Wood vinegar: A renewable product for a sustainable agriculture 1124
Carolina Fabbri, Lorenzo Pezzola, Valerio Magalotti, Roberto Mussi

Energy management in agriculture - potential for farmers and the region 1131
Heinz Bernhardt, Jörn Stumpenhausen, Christoph Bader, Martin Höhendinger

Energy use and indoor climate in livestock buildings for pigs in North America and Europe - A literature review 1136
Therese Malm, Knut-Håkan Jeppsson, Dennis Johansson, Vahid M. Nik, Jenny Yngvesson, Marie-Claude Dubois

Topic 10. Post-harvest technologies and losses
Dragon fruit quality assessment using a grading machine prototype based on image analysis 1146
Pablo González-Planells, Coral Ortiz, Francisco Rovira-Más, Vicente Alegre

The effects of combined hot-air, microwave and infrared drying on color and β-carotene content of sweet potatoes 1152
Khuthadzo Mugodo, Tilahun Seyoum Workneh, Naushad Emmambux, Sunette Laurie

Authentication of cattle finishing diets (conventional vs. vegetable by-products) using near-infrared spectroscopy 1159
Sara León-Ecay, Ainara López-Maestresalas, Irantzu Goenaga, José Antonio Mendizabal, Kizkitza Insausti

Developing a plant for processing PGI 'Cipolla Rossa di Tropea Calabria' spring onions using compressed air 1164
Matteo Sbaglia, Lorenzo M. Abenavoli, Bruno Bernardi

Effect of maltogenic-amylase and tamarind paste mixture on the nutritional composition of bread 1170
Musliu Olushola Sunmonu, Mayowa Saheed Sanusi, AbdulKareem Bamidele Bello, Aishat Teni Ahman, Islamiyat Dolapo Jimoh, Omoniyi Akinnusi Friday

Topic 11. Education and rural development
Acceptance of cutting-edge technologies in viticulture: A students' perspective 1178
Tetiana Pavlenko, Eva Gößwein, Dimitrios S. Paraforos, Megan K. Bartlett, Spyros Fountas, Jacob Kambuta, Francesco Marinello, George Papadopoulos, Leo Pichon, Bruno Tisseyre, Magnus Liebherr

Growing together: Enhancing skill and cultivating sustainable winegrowing communities 1184
Manuel Pérez-Ruiz, Abdul Mouazen, Anastasios Michailidis, Daniele Sarri

Irrigation and population dynamics in depopulated rural environments: Causes, implications, and sustainable solutions 1190
M. T. Gómez-Villarino, D. Pereira, A. I. García, A. Sánchez de Medina, E. Ayuga-Téllez, M. Hidalgo, J. M. García-Asensio, F. Ayuga

Expectations of machine-to-machine networking in dairy housing rise with experiences of farmers

Jernej Poteko [a,*], Jan Harms [a]

[a] Bavarian State Research Center for Agriculture, Institute for Agricultural Engineering and Animal Husbandry, Prof.-Dürrwaechter-Platz 2, 85586 Poing, Germany

* Corresponding author. Email: jernej.poteko@LfL.bayern.de

Abstract

The integration of robotics in dairy housing systems has led to increased automation and autonomy in tasks such as milking, feeding, and manure removal. These machines enable a high level of autonomy. The intelligence of one machine enables the execution of tasks and work processes automatically, driven by data collected from sensors, mostly embedded within that particular machine. They are uninformed about tasks being carried out by other machines in the same dairy housing. Due to this the autonomy level of these machines must either be limited or manually switched off to avoid that the machines collide with other machines or work processes. Presently, farmers manually regulate various machines in the dairy housing when multiple machines are performing their tasks simultaneously because the data exchange between the devices is limited. However, to maximize the autonomy of all machines, they should not interfere with each other and should communicate the current task being executed and their own operational mode. To enable devices to coordinate operations based on exchanged data between them, effective Machine-to-Machine (M2M) networking is crucial. Especially, smaller automated machines (for example manure removal robot), which are often overlooked in the consideration of M2M communication, may clash with operations of larger devices if not synchronized. The detailed expectations and experiences of farmers regarding the connectivity of devices in the housing system are underexplored in the literature. The aim of this study was to capture farmers' expectations and experiences regarding machine networking in the dairy housing systems through online surveys. Insights from Bavarian dairy farmers (n=231) show varying expectations based on different housing systems and devices experience. Farmers with less experience with automated machines or robots anticipate lower benefits such as time savings and greater work flexibility through machine networking compared to those familiar with automated machines. Notably, the highest expectations for machine networking are seen among users of multiple machines in one dairy housing simultaneously. The integration of robotics in dairy housing offers significant potential, but effective M2M communication is essential for maximizing efficiency and realizing anticipated benefits.

Keywords: M2M, networking, robots, dairy housing technology, precision livestock farming.

1. Introduction

In dairy farming systems, robots are increasingly taking over everyday tasks such as milking, feeding, and manure removal with a high degree of automation and autonomy (Noack et al., 2023). Dairy farmers' interest in digital technology is evident and reflected in the increasing number of installed automatic milking systems (AMS) and the investment interest in expanding existing technology with digital systems such as feeding systems and herd management programs (HMP) (Egger-Danner et al., 2020; LKV Bayern, 2019).

This intelligent dairy housing technology allows for the adjustment of automated processes to current conditions within the dairy housing. Moreover, the devices in the dairy housing produce a variety of data in the course of their work. The increased availability of data forms the informational basis for making the right decisions at the right time (Schick, 2017). Although many decisions could be based on logical combinations of this information, the farmer cannot delegate the decision-making and its implementation to the system due to the lack of M2M networking (Tomic et al., 2014). This often eliminates the possibility of adjusting the dairy housing technology promptly and without the farmer's immediate intervention to better meet the needs of animals, the environment, and people (Poteko et al., 2022). The intelligence of these devices is primarily based on the data collected by their own sensors, enabling them to flexibly adapt their operations to the current needs in the dairy housing. However, the autonomy of the entire dairy housing system depends on the data flow between the devices or machines. Machine-to-machine (M2M) communication between the

devices would allow them to consider not only their own data but also the data from other devices when planning and executing rule-based operations.

Currently, the farmer regulates the devices in the dairy housing and makes manual settings, such as when and what to feed and where cleaning should take place. To fully exploit the autonomy of all devices in the dairy housing, M2M networking is fundamentally necessary. Smaller robots (e.g., manure removal robots) are often overlooked in M2M communication. However, if the autonomous devices independently change their operations, they can collide with the preset operations of these smaller devices. Currently, data exchange between the devices is also not possible (Poteko et al., 2022).

Personal conversations with farmers experienced with digital technologies have shown that they are linked to the number of automated or autonomous devices installed in their dairy housings (Poteko et al., 2023). Detailed expectations and experiences have not yet been thoroughly investigated in the scientific literature.

The online surveys are being used to capture the expectations and experiences of farmers regarding the networking and communication between devices in dairy housings. The goal is to investigate the expectations end users of the technology have from a labor management perspective and how they perceive the current situation regarding the connectivity of the devices in the dairy housing.

2. Materials and Methods

The data basis consists of an online survey conducted by the Bavarian State Research Center for Agriculture, Institute for Agricultural Engineering and Animal Husbandry, aiming to investigate the networking of digital technologies in dairy housings. This survey was carried out between November 2020 and February 2021 among individuals working on dairy farms. It gathers information on the dairy housing technology used on the farms as well as experiences and expectations with digital technologies.

The present results pertain to survey participants with dairy farms in Bavaria (n = 231), divided into six categories based on the degree of automation in the husbandry system. The survey included response options for various statements, allowing participants to indicate their level of agreement: "Applies," "Neutral," "Does not apply," and "I cannot judge." Two categories use mechanical technology (tied housing [M1], loose housing system with cubicles with a milking parlor [M2]). Automated farms use a loose housing with an automatic milking system [A1] and, in addition to A1, either a feed pushing robot [A2], a cleaning robot [A3], or both robots [A4]. The expectations and experiences with the networking of devices are presented using Likert scales.

3. Results and Discussion

The proportions of farmers who expect time savings (Figure 1) or increased work flexibility (Figure 2) through the networking of various dairy housing technologies depend on the degree of automation in their husbandry systems. It is clearly evident that farmers with less experience using automated devices (M1 and M2) have lower expectations of time savings and increased work flexibility compared to experienced users of automation (A1-4). The highest expectations were expressed by farmers who use the most automated technologies (A4).

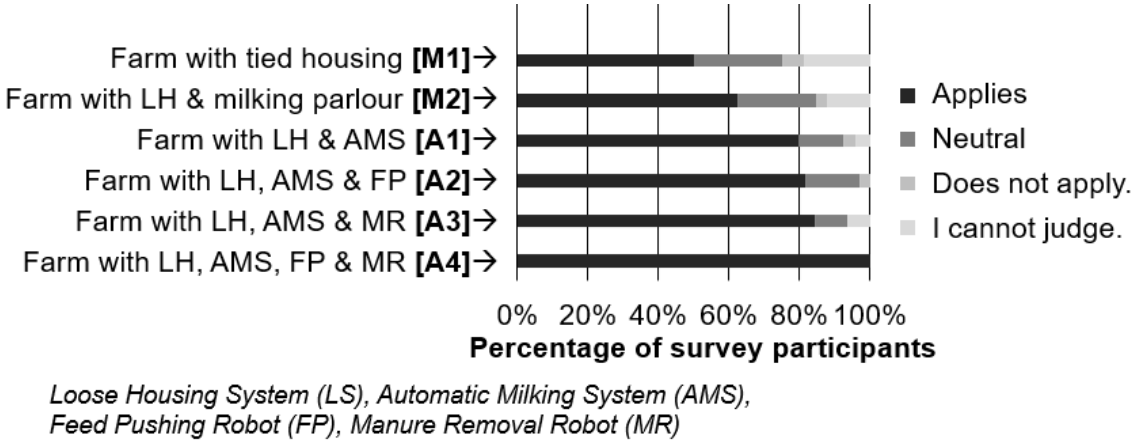

Figure 1: Percentage of survey participants anticipating time savings through machine networking in the dairy housing [n=231].

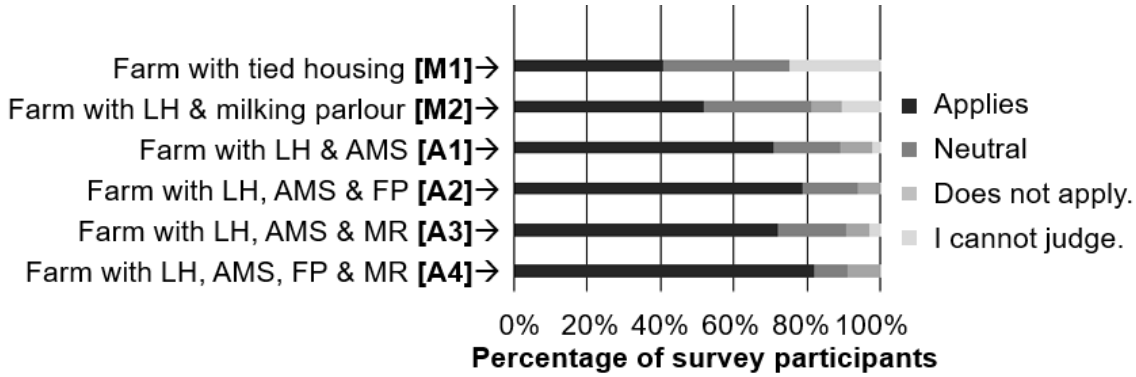

Figure 2: Percentage of survey participants anticipating greater work flexibility through machine networking in the dairy housing [n=231].

Prior experience is significant in relation to the need for device networking (Figure 3). While only about 10% of respondents from the [M1] group consider device networking inadequate, approximately 30% of experienced users of automated technology [A1-4] have already encountered a need for networking. Respondents [A4] assess that networking becomes a relevant issue as soon as multiple automated devices are installed in a dairy housing.

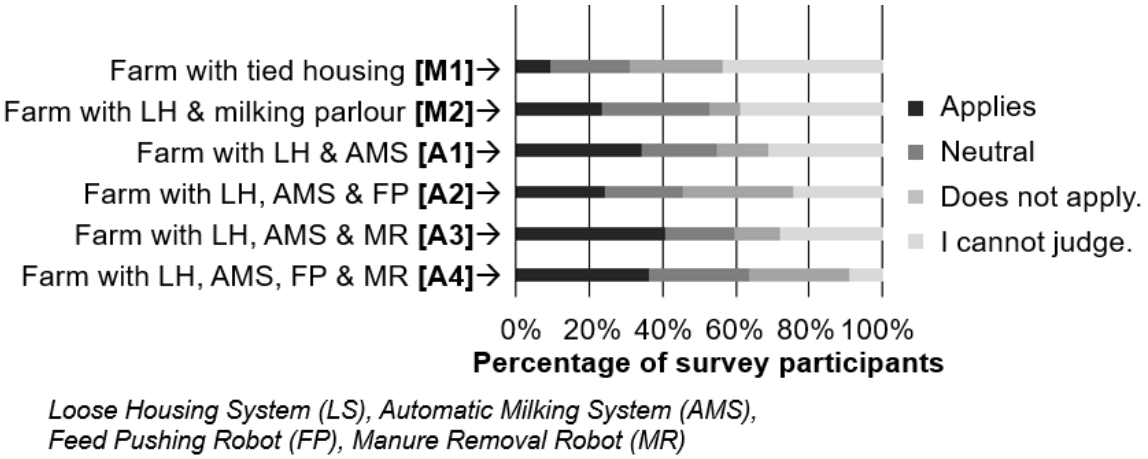

Figure 3: Percentage of survey participants who encountered insufficient machine networking in the dairy housing [n=231].

4. Conclusions

The integration of robotics in dairy housing offers significant potential, but effective M2M communication is essential for maximizing efficiency and realizing anticipated benefits. As long as autonomous devices are not informed about the activities of other devices, their decision-making capabilities often remain unused, and they cannot effectively support the end user. The need for M2M networking is particularly present when multiple autonomous devices are used in a dairy housing. The increasing number of intelligent devices in the future will amplify the importance and need for M2M networking. Further research and practical implementation are necessary to address current limitations and fully exploit the capabilities of intelligent dairy housing machines.

Acknowledgements

The project is funded by the Federal Ministry of Food and Agriculture (BMEL) based on a decision by the German Bundestag. The project is managed by the Federal Office for Agriculture and Food (BLE) within the framework of the Experimental Fields in Agriculture program. We extend our heartfelt thanks to the LKV Bayern, the University of Applied Sciences Weihenstephan-Triesdorf, and our industry partners for their support in distributing the online survey to agricultural enterprises.

References

Noack, P. O., Gerth, S., Hoffmann, C., Lorenzini, I., Poteko, J., Rothmund, M., Schlenz, F., Walther, H., 2023. Precision Farming – Smart Farming – Digital Farming. Grundlagen und Anwendungsfelder. VDE Verlag, Berlin. 224 S.

Poteko, J., Lübke, P., Harms, J., 2022. Vernetzung der Technik im Milchviehstall: Bedarf der Landwirte erkennen. In *15. Bau, Technik und Umwelt in der landwirtschaftlichen Nutztierhaltung 2022*, 13.-15. September 2022 in Soest.

Poteko, J., Harms, J., 2023. M2M networking of devices in the dairy barn. In: AgroVet-Strickhof Conference, Current and Future Research Projects, Lindau. S. 24.

Egger-Danner, C., Steininger, F., Suntinger, M., Mayerhofer, M., Koblmüller, M., Grandl, F., Duda, J., Linke, Auer, F.-J., Stegfellner, M., Drillich, M., Papst, F., Saukh, O., Fürst-Waltl, B., Klimek, P., Wittek, T., 2020. D4Dairy – Datenvernetzung im Kuhstall. In: Digitale Technologien am bäuerlichen Familienbetrieb. Gumpenstein, 22.-23.10.2020.

LKV Bayern, 2019. Milchleistungsprüfung in Bayern 2019, S. 55.

Schick, M., 2017. Digitale Tierhaltung. Interview, agri-bizz, Heft 1.

Tomic, D. K., Drenjanac, D., Lazendic, G., Hörmann, S., Handler, F., Wöber, W., Auer, W., 2014. agriOpenLink: Semantic Services for Adaptive Processes in Livestock Farming. In *Internat. Conf. of*

Agricultural Engineering, Zurich, 6.-10.7.2014.

Pfeiffer, J., Gabriel, A., Gandorfer, M., 2019. Gesellschaftliche Akzeptanz von Digitalisierung in der Landwirtschaft. In *39. GIL-Jahrestagung, Digitalisierung für landw. Betriebe in kleinstrukturierten Regionen-ein Widerspruch in sich?* S. 151–154.

Gabriel, A., Gandorfer, M., 2020. Landwirte-Befragung 2020, Digitale Landwirtschaft Bayern. LfL Bayern. Abgerufen am 15. 05. 2024 von https://www.lfl.bayern.de/mam/cms07/ilt/dateien/ilt6_praesentation_by_2390_27082020.pdf.

Early detection of Esca disease in grapevines using in-field hyperspectral proximal sensing

Ainara López-Maestresalas *, Jon Ruiz de Gauna, Carmen Jarén, Sara León-Ecay, Silvia Arazuri

Institute on Innovation and Sustainable Development in Food Chain (IS-FOOD), ETSIAB, Universidad Pública de Navarra, Campus de Arrosadia, 31006, Pamplona, Spain

* Corresponding author. Email: ainara.lopez@unavarra.es

Abstract

Esca is one of the most destructive vine diseases in the world. It causes significant economic losses, mainly due to reduced grape yield and quality. Currently, the approved methods of controlling esca include preventive methods such as the use of fungicides on plant wounds or the use of planting systems that do not require intensive pruning, among others. It is therefore advisable to monitor the crop to identify those vines that are susceptible to the disease. For this reason, in this study a proximal hyperspectral camera was used for early detection of esca presence in asymptomatic grapevine leaves. Images of 11 vines of the Tempranillo variety grown in Etxauri (Navarre, Spain) were analysed. Hyperspectral images were acquired using a Specim IQ snapshot camera, mounted on a tripod, working in the range of 400–1000 nm with a spectral resolution of 7 nm (204 bands), and an image resolution of 512 × 512 pixel including an RGB camera (5 Mpix). The images were taken under natural ambient light conditions on August 21, 2023. From the 11 vines selected, 9 showed visual symptoms of esca and the remaining 2 were asymptomatic to the naked eye. A total of 200 pixels were randomly selected from the dataset, 100 from asymptomatic leaves of asymptomatic vines (class 1) and 100 from asymptomatic leaves of symptomatic vines (class 2). Partial Least Square Discriminant Analysis (PLS-DA) was performed to classify the leaves into the two classes. Classification rates of 97% were achieved in the cross-validation dataset. Models were externally validated at pixel-level using one image of an asymptomatic vine and another of a symptomatic vine. The visualisation of the images confirmed the correct classification of the pixels into the two classes, indicating that by using proximal hyperspectral sensing an early identification of the disease is possible.

Keywords: trunk disease, PLS-DA, chemometrics, hyperspectral imaging, Vis-NIR

1. Introduction

Esca is a grapevine trunk disease that is considered one of the most destructive vine diseases in the world (Ouadi et al., 2019). Grapevine trunk diseases cause significant economic losses, mainly due to the reduction in grape yield and quality and the fact that they eventually lead to the death of the vine over a variable period of time (Fontaine et al., 2016). The global economic impact of replacing dead vines is estimated at $1.5 billion per year (Hofstetter et al., 2012). Furthermore, when analysing the economic impact at the national level, it can be seen that in a wine-producing country such as France, the annual loss in wine production reaches one billion euros (Ouadi et al., 2019).

Esca is not a single disease but a group of syndromes caused by a number of ascomycete and basidiomycete fungi. The main species involved are *Phaeomoniella chlamydospora* (Gams and Crous, 2000), and *Phaeoacremonium aleophilum* (Crous et al., 1996) in the ascomycetes, while *Fomitiporia mediterranea* is the main basidiomycetes pathogen (Fischer, 2002). These species infect the plant by means of spores, which can be transported by air or rain and enter the plant through wounds in the wood (caused by impact, mechanical work such as pruning, etc.) (Bertsch et al., 2013; Mugnai et al., 1999).

Prior to the appearance of visual symptoms on the leaves, there may be other earlier symptoms that can help in the early detection of the disease. These include a reduction in carotenoid content or a change in photosynthesis as a result of the defense mechanisms activated by the plant when it is under stress conditions (Altangerel et al., 2017; Baratto et al., 2022; Letousey et al., 2010; Magnin-Robert et al., 2011).

It should be noted that the chemical control of the disease is not possible as the use of sodium arsenite (the only known product capable of controlling the disease) was banned in 2003 (Fontaine et al., 2016). Currently, the approved methods of controlling this disease include preventive methods such as the use of fungicides on plant wounds, the use of planting systems that do not require intensive pruning, or the purchase of healthy plant material from nurseries (Fontaine et al., 2016; Mondello et al., 2018; Mugnai et al., 1999).

It is therefore advisable to monitor the crop to identify those vines that are susceptible to the disease. In this regard, optical sensors such as hyperspectral imaging (HSI) are presented as promising tools for the non-invasive evaluation of the physiological state of plants and for the diagnosis and detection of diseases (Mahlein, 2016; Zhang et al., 2019). Thus, HSI combined with a fine-scale chemometric approach can be very useful for disease detection and quantification (Bock et al., 2010), as it is able to provide a pixel-wise distribution of infection symptoms on the leaf surface.

For this reason, in this study a proximal hyperspectral camera was used for in-field early detection of esca disease in asymptomatic grapevine leaves of cultivar Tempranillo.

2. Materials and Methods

2.1. Plant material

Images of 11 vines of the Tempranillo variety grown on plots in Bodegas Otazu, in the town of Etxauri (Navarre, Spain) were used in this study (Figure 1). The vines are approximately 32 years old (planted in 1992) and all of them were selected from plots with a history of esca incidence and were; therefore, susceptible to the development of the disease. From the 11 vines selected, nine showed visual symptoms of esca (to a greater or lesser extent) and the remaining two were asymptomatic to the naked eye.

Figure 1. Picture of a vine taken in the field with the Spectralon plate (white reference).

2.2. Image acquisition and processing

Hyperspectral images were acquired by setting up an acquisition station, equipped with a Specim IQ snapshot camera (Specim Ltd., Oulu, Finland), mounted on a tripod, working in the range of 400–1000 nm with a spectral resolution of 7 nm (204 bands), and carrying a CMOS technology sensor with an image resolution of 512 × 512 pixel and an RGB camera (5 Mpix) (figure 2).

The images were captured in natural environmental light conditions in the field on August 21, 2023. The first step was the calibration of the equipment. The integration time was selected in automatic mode as the equipment optimizes the appropriate time for each acquisition. Both the focus and viewfinder camera views were manually aligned just before recording the image; while the white reference panel (a Spectralon plate) was placed to carry out a calibration scan. Reflectance was automatically calculated for each pixel, by the Specim IQ Studio camera software (Specim Ltd., Oulu, Finland). Once calibrated, camera acquired one image per vine, taking care to ensure that the entire front of the vine was captured in relation to the camera. Therefore, 11 individual images were obtained.

Figure 2. The imaging system used in this study capturing an image of a vine in the field.

Once the images were obtained, their processing consisted of several steps. First, the 3D image, or hypercube, had to be created. Second, the images were randomly divided into a calibration set, consisting of one image of an asymptomatic vine (class 1) and eight symptomatic vines (class 2), and a validation set, consisting one image from each class. The calibration and validation groups were processed differently. The images from the calibration group were used to randomly select pixels to form the calibration matrix, 100 pixels were selected from the Class 1 images and 100 from the Class 2 images. This was carried out with the HYPER-Tools 3.0 software, which works in the MATLAB R2023a environment (Figure 3). The result was a two-dimensional matrix with 200 rows and 204 columns corresponding to the wavelengths.

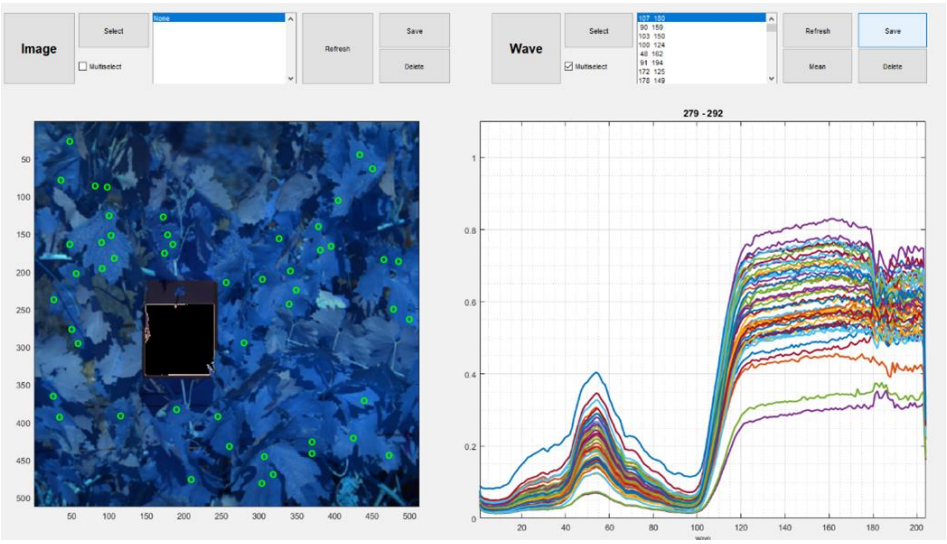

Figure 3. One of the selections with the selected pixels circled in green (a), and the spectra corresponding to the reflectance measured for each pixel at each of the 204 wavelengths recorded by the instrument (b).

On the other hand, the 2 images that formed the validation group were individually segmented to separate the region of interest (ROI) from the background. For this purpose, the k-means algorithm implemented in MATLAB was used. Next, unfolding was performed, which consists of transforming the information stored in the hypercube (3D) into a two-dimensional matrix (2D) containing the reflectance of each pixel at each wavelength. This resulted in two matrixes of 120,209 rows and 204 columns and of 122,348 rows and 204 columns.

2.3. Chemometric modelling

Partial Least Squares Discriminant Analysis (PLS-DA) was used to separate the two classes of leaves. PLS-DA is a pattern recognition technique that uses PLS regression to predict assignment classes or groups from the sample spectrum. To use this method, a binary matrix (Y) is created with the same number of rows as samples and the same number of columns as classes. In this way, PLS-DA performs a qualitative calibration. That is, instead of calibrating for a continuous variable, it calibrates for class membership (Shenk and Westerhaus, 1995).

In addition, different mathematical pre-treatments were applied to the spectra such as smoothing (SM), first (1st der) and second derivative (2nd der) of Savitzky Golay (SG) (2nd order polynomial and 15-window points), Standard Normal Variate (SNV) and Multiplicative Scatter Correction (MSC) either alone or in combination. The effect of no pre-treatment (None) was also analysed. A 10-fold Venetian blind cross-validation (CV) was used for internal validation.

To evaluate the effectiveness of the models, we mainly considered the percentage of correctly classified (%CC) samples (accuracy) in each class, as well as the sensitivity, specificity, and class error in Calibration and CV datasets. The best performing model was used for external prediction of the samples. Classification images were then displayed to visualise the spatial distribution pixels predicted as either Class 1 or 2 using in-house written codes.

The PLS_Toolbox software v. 9.3 (Eigenvector Research Inc., Wenatchee, WA, USA) under MATLAB R2023a (TheMathWorks, Inc., Natick, MA, USA) was used to apply the different pre-treatments and to build PLS-DA models.

3. Results and Discussion

Table 1 shows the results of the 8 PLS-DA models carried out using different pre-treatment combinations for the calibration and CV datasets. It shows the number of LV used; the percentage of variance explained; the percentage of correctly classified (%CC) samples of each class (asymptomatic and symptomatic) and the overall accuracy for each model. High accuracy rates (>90%) were obtained for all the models in CV. The highest accuracy among the models developed was obtained for the combination of SM+SNV with 97% of samples correctly classified in both calibration and CV. This model was built using 8 LV explaining 99.77% of variance.

Table 1.PLS-DA results of classification using different pre-treatment combinations.

			$\%CC_{Cal}$			$\%CC_{CV}$		
Pre-processing	LV	Variance (%)	Class 1	Class 2	Overall	Class 1	Class 2	Overall
None	5	99.97	99	88	93.5	98	88	93
SM	5	99.99	97	85	91	97	84	90.5
SNV	6	99.96	99	96	97.5	99	94	96.5
MSC	6	99.98	99	96	97.5	99	94	96.5
1st der	6	99.91	97	91	94	97	91	94
2nd der	4	99.64	97	88	92.5	96	87	91.5
SM+SNV	**8**	**99.77**	**99**	**95**	**97**	**99**	**95**	**97**
SM+MSC	6	100	98	92	95	98	92	95

LV, Latent variable; SM, smoothing; SNV, Standard Normal Variate; MSC, Mean Scatter Correction; 1st der, First derivative; 2nd der, Second derivative. Values in bold correspond to the best results obtained in terms of highest %CC in both Calibration and CV.

Table 2 shows the sensitivity, specificity and class error values for the best performing model. Regarding sensitivity and specificity values, asymptomatic pixels were slightly better classified into their class as they achieved a higher sensitivity value than symptomatic pixels.

Table 2. Sensitivity, specificity and error values of the best PLS-DA performing model.

		Cal			CV		
Pre-processing	Classes	Sensitivity	Specificity	Error	Sensitivity	Specificity	Error
SM+SNV	Class 1	0.99	0.95	0.03	0.98	0.95	0.035
	Class 2	0.95	0.99		0.95	0.98	

Figure 4 (b, d) shows the classification images obtained using the SM + SNV PLS-DA model with their corresponding RGB images (Figure 4 (a, c)). Slight foliar symptoms of esca can be observed in Figure 4c. In

class 1 (asymptomatic) a 94.46% of pixels were correctly classified as asymptomatic (Figure 4b pixels in blue), while a blind prediction was performed for the symptomatic pixels (Figure 4d). Figure 4b displays a few instances of false positives, indicated by orange pixels. These are observed at the upper end of the image, corresponding to the petioles of the leaves, and on the leaves themselves, corresponding to other symptoms that are not esca. Figure 4d illustrates that the majority of pixels classified as symptomatic (pixels in orange) were, in fact, symptomatic, as can be observed in Figure 4c. Nevertheless, it is also evident that some false positives can be observed mainly corresponding to the petioles of the leaves. The findings indicate that it is feasible to identify vines exhibiting symptoms of esca infection at an early stage, when the symptoms are barely perceptible. This information would allow a differentiated management of the vines identified as affected by esca, as well as facilitating the annual monitoring of the incidence of the disease in the vineyard.

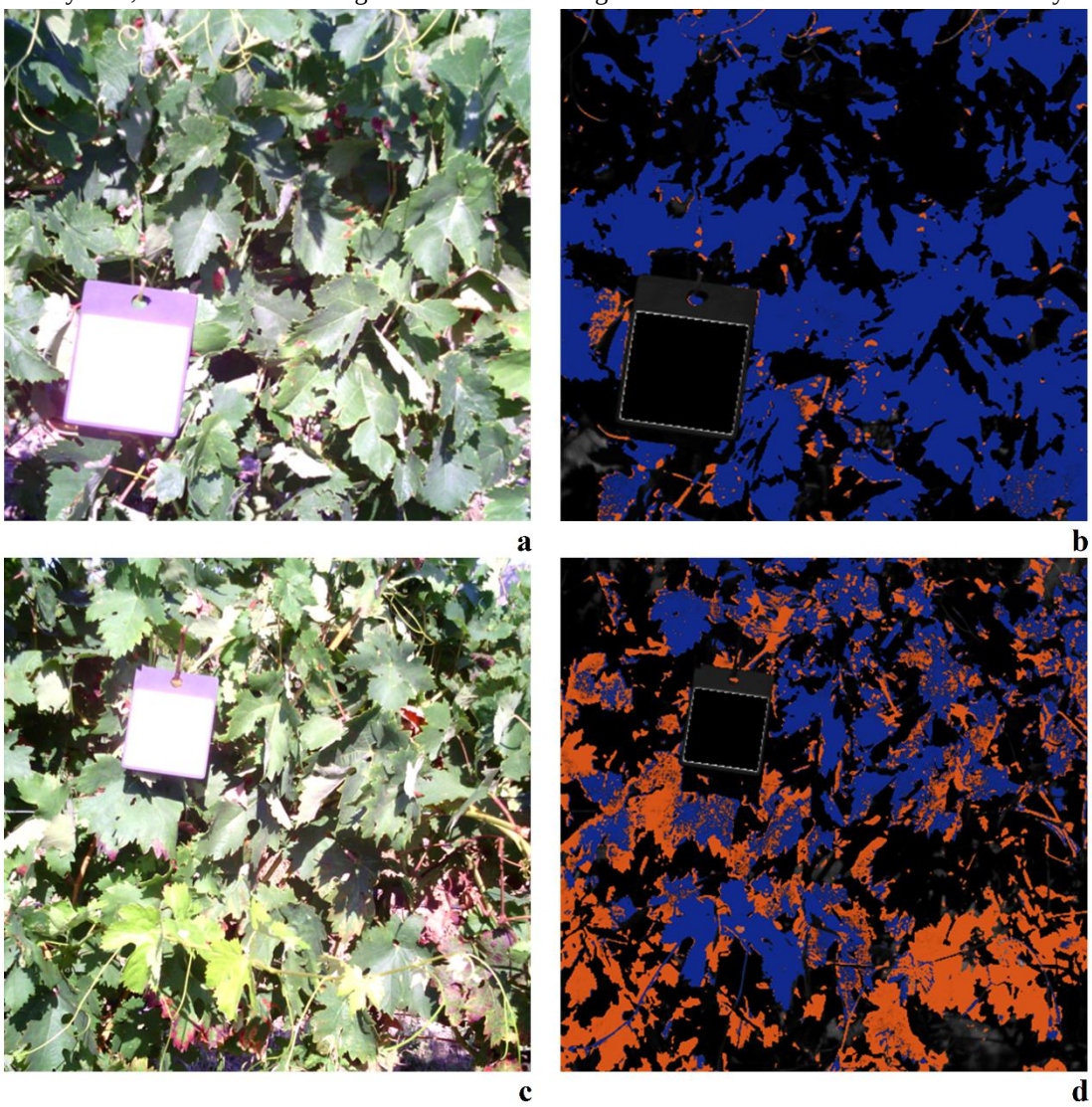

Figure 4. RGB images of the asymptomatic (a) and symptomatic (c) vines and classification images in the external validation. The blue pixels represent the true positives, that is, the asymptomatic pixels correctly classified (b) while the orange pixels represent the true negatives or the symptomatic pixels correctly classified in their class (d).

4. Conclusions

This study proposes that the combined use of an in-field hyperspectral imaging sensor with partial least squares-discriminant analysis enables the classification of vines according to the presence of esca at early stages of the disease. The PLS-DA model developed by applying the combination of smoothing followed by SNV pre-treatments obtained the best results, with a CV accuracy rate of 97%. Furthermore, the classification

images facilitated the visualization of the spatial distribution of asymptomatic and symptomatic pixels.

Despite the limitations of this study, including the relatively small number of samples used, among others, it can be concluded that HSI technology has significant potential for the detection of esca and possibly other grapevine trunk diseases in-field.

Acknowledgements

This research was supported by the Spanish Ministry of Science and Innovation and from the European Union Next-GenerationEU/PRTR (TED2021-130364B-I00).

References

Altangerel, N., Ariunbold, G. O., Gorman, C., Alkahtani, M. H., Borrego, E. J., Bohlmeyer, D., Hemmer, P., Kolomiets, M. V., Yuan, J. S., Scully, M. O., 2017. In vivo diagnostics of early abiotic plant stress response via Raman spectroscopy. Proceedings of the National Academy of Sciences, 114 (13), 3393-3396. https://doi.org/10.1073/pnas.1701328114

Baratto, C., Ambrosio, G., Faglia, G., Turina, M., 2022. Early Detection of Esca Disease in Asymptomatic Vines by Raman Spectroscopy. IEEE Sensors Journal, 22 (23), 23286-23292. https://doi.org/10.1109/JSEN.2022.3211616

Bertsch, C., Ramírez-Suero, M., Magnin-Robert, M., Larignon, P., Chong, J., Abou-Mansour, E., Spagnolo, A., Clément, C., Fontaine, F., 2013. Grapevine trunk diseases: Complex and still poorly understood. Plant Pathology, 62 (2), 243-265. https://doi.org/10.1111/j.1365-3059.2012.02674.x

Bock, C. H., Poole, G. H., Parker, P. E., Gottwald, T. R., 2010. Plant disease severity estimated visually, by digital photography and image analysis, and by hyperspectral imaging. Critical Reviews in Plant Sciences, 29 (2), 59-107. https://doi.org/10.1080/07352681003617285

Crous, P. W., Gams, W., Wingfield, M. J., van Wyk, P. S., 1996. Phaeoacremonium gen. Nov. Associated with wilt and decline diseases of woody hosts and human infections. Mycologia, 88 (5), 786-796. https://doi.org/10.1080/00275514.1996.12026716

Fischer, M., 2002. A new wood-decaying basidiomycete species associated with esca of grapevine: Fomitiporia mediterranea (Hymenochaetales). Mycological Progress, 1 (3), 315-324. https://doi.org/10.1007/s11557-006-0029-4

Fontaine, F., Gramaje, D., Armengol, J., Smart, R., Nagy, Z. A., Borgo, M., Rego, C., Corio-Costet, M.-F., 2016. *Grapevine trunk diseases. A review* (p. 24). OIV Publications.

Gams, W., & Crous, P. W. (2000). «Phaeomoniella chlamydospora» Gen. Et Comb. Nov., a Causal Organism of Petri Grapevine Decline and Esca. Phytopathologia Mediterranea, 39 (1), 112-118. https://doi.org/10.1400/57828

Hofstetter, V., Buyck, B., Croll, D., Viret, O., Couloux, A., Gindro, K., 2012. What if esca disease of grapevine were not a fungal disease? Fungal Diversity, 54 (1), 51-67. https://doi.org/10.1007/s13225-012-0171-z

Letousey, P., Baillieul, F., Perrot, G., Rabenoelina, F., Boulay, M., Vaillant-Gaveau, N., Clément, C., Fontaine, F., 2010. Early Events Prior to Visual Symptoms in the Apoplectic Form of Grapevine Esca Disease. Phytopathology®, 100 (5), 424-431. https://doi.org/10.1094/PHYTO-100-5-0424

Magnin-Robert, M., Letousey, P., Spagnolo, A., Rabenoelina, F., Jacquens, L., Mercier, L., Clément, C., Fontaine, F., 2011. Leaf stripe form of esca induces alteration of photosynthesis and defence reactions in presymptomatic leaves. Functional Plant Biology, 38 (11), 856-866. https://doi.org/10.1071/FP11083

Mahlein, A.-K., 2016. Plant disease detection by imaging sensors—Parallels and specific demands for precision agriculture and plant phenotyping. *Plant disease*, *100* (2), 241-251. https://doi.org/10.1094/PDIS-03-15-0340-FE

Mondello, V., Songy, A., Battiston, E., Pinto, C., Coppin, C., Trotel-Aziz, P., Clément, C., Mugnai, L., Fontaine, F., 2018. Grapevine trunk diseases: A review of fifteen years of trials for their control with chemicals and biocontrol agents. Plant Disease, 102 (7), 1189-1217. https://doi.org/10.1094/PDIS-08-17-1181-FE

Mugnai, L., Graniti, A., Surico, G., 1999. Esca (black measles) and brown wood-streaking: Two old and elusive diseases of grapevines. Plant Disease, 83 (5), 404-418. https://doi.org/10.1094/PDIS.1999.83.5.404

Ouadi, L., Bruez, E., Bastien, S., Vallance, J., Lecomte, P., Domec, J.-C., Rey, P., 2019. Ecophysiological impacts of Esca, a devastating grapevine trunk disease, on Vitis vinifera L. PLOS ONE, 14 (9), e0222586. https://doi.org/10.1371/journal.pone.0222586

Shenk, J. S., Westerhaus, M. O., 1995. Routine operation, calibration, development and network system management manual. *NIRSystems Inc., Silver Spring, MD, USA*.

Zhang, J., Huang, Y., Pu, R., Gonzalez-Moreno, P., Yuan, L., Wu, K., Huang, W., 2019. Monitoring plant diseases and pests through remote sensing technology: A review. Computers and Electronics in Agriculture, 165, 104943. https://doi.org/10.1016/j.compag.2019.104943

On-site identification of esca-affected vines using hyperspectral imaging

Sara León-Ecay, Jon Ruiz de Gauna, Ainara López-Maestresalas, Carmen Jarén, Silvia Arazuri

Institute on Innovation and Sustainable Development in Food Chain (IS-FOOD), ETSIAB, Universidad Pública de Navarra, Campus de Arrosadia, 31006, Pamplona, Spain

* Corresponding author. Email: sara.leon@unavarra.es

Abstract

Esca represents one of the greatest threats to modern viticulture as it causes large annual economic losses. At present, there is a lack of effective strategies for disease control, so a technique capable of detecting affected vines would allow annual monitoring of disease incidence in the vineyard leading to a better crop management and decision making. This study evaluates close-range hyperspectral imaging for the detection of esca naturally infected vines. Images of 11 vines of the Tempranillo variety grown on plots in Bodegas Otazu, in Etxauri (Navarre, Spain) were acquired. A Specim IQ snapshot hyperspectral camera was used to record the images on August, 21 2023 on the field under natural light conditions. The camera has a spectral resolution of 7 nm (204 wavelengths) and a spatial resolution of 512 x 512 in the 400 – 1000 nm spectral range (Vis-NIR). An individual image was acquired for each vine, of which 9 were symptomatic and 2 asymptomatic. Three classes were analysed: asymptomatic leaves of asymptomatic vines (Class 1), asymptomatic leaves of symptomatic vines (Class 2) and asymptomatic areas of symptomatic leaves of symptomatic vines (Class 3). A total of 300 pixels were randomly selected, 100 per class, for further analysis. Partial Least Square Discriminant Analysis (PLSDA) was used to classify the pixels into the three categories. An accuracy of 86% was achieved in the cross-validation dataset. Models were externally validated using an image of an asymptomatic vine and an image of a symptomatic vine. The visualisation of the images showed that the majority of the pixels of the asymptomatic vine image were classified as class 1, while most of the pixels of the symptomatic vine image were classified as either class 2 or class 3. Hence, this study demonstrated the potential of close-range HSI for the on-site detection of esca.

Keywords: trunk disease, accuracy, chemometrics, image, Vis-NIR

1. Introduction

Esca represents one of the greatest threats to modern viticulture as it causes large annual economic losses (Hofstetter et al., 2012; Ouadi et al., 2019). Esca is a disease complex caused by a few ascomycetes and basidiomycete fungi. The species mainly involved are *Phaeomoniella chlamydospora* (Gams and Crous, 2000) and *Phaeoacremonium aleophilum* (Crous et al., 1996) in the case of ascomycetes, while *Fomitiporia mediterranea* (Fischer, 2002) is the main agent in the case of basidiomycetes.

At present, there is a lack of effective strategies and means of disease control, so a technique capable of detecting affected vines would allow annual monitoring of disease incidence in the vineyard and therefore better crop management and decision making.

Therefore, the objective of this study is to evaluate the capability of a close-range hyperspectral imaging (HSI) system for the detection of naturally esca-infected vines.

2. Materials and Methods

2.1. Vegetal material

The plant material used corresponds to 11 vines of the Tempranillo variety grown on commercial plots in Bodegas Otazu, in the town of Etxauri located in Navarre, Spain. All the vines were selected from plots with a history of esca incidence. Of the 11 vines selected, nine exhibited visual symptoms of esca, while the remaining two were asymptomatic.

2.2. Hyperspectral image acquisition

Specim IQ snapshot portable camera (Specim Ltd., Oulu, Finland) was used to acquired hyperspectral images in field (Figure 1). This equipment is sensitive in the 400 – 1000 nm spectral range with a 7 nm bandwidth (resulting in 204 bands) and a spatial resolution of 512 × 512 pixels. The system also incorporates a 5 Mpix RGB camera. Images were taken under natural light conditions by placing the camera on a tripod on August 21, 2023.

The initial stage of the process involved the calibration of the equipment. The integration time was selected in an automated mode, whereby the equipment selects the optimal time for each acquisition. Prior to the acquisition of the image, the focus camera and viewfinder camera views were manually aligned with the camera. Additionally, a white reference panel (a Spectralon plate) was placed to facilitate a calibration scan. Then, the Specim IQ Studio camera software (Specim Ltd., Oulu, Finland) automatically calculated the reflectance for each pixel.

Afterwards, an image of each of the 11 vines was recorded (9 with visual symptoms of esca and 2 without visual symptoms).

a **b**

Figure 1. Specim IQ device front (a) and back (b) details.

2.2.1. Image processing

For image analysis, the software used for matrix formation and chemometric analysis was MATLAB version 2023b (TheMathWorks, Inc., Natick, MA, USA) with the Image Processing and Statistics Machine Learning products. This software was used in conjunction with HYPER-Tools version 3.0 (Amigo et al., 2015).

The individual images were assembled into 11 hypercubes, each with a size of 512 x 512 x 204. Subsequently, the images were randomly divided into two sets: a calibration set, comprising one image of an asymptomatic vine (Class 1) and eight symptomatic vines (Classes 2 and 3), and a validation set, comprising one image from each group. The calibration and validation datasets were processed in disparate ways. The images from the calibration group were employed to randomly select pixels to form the calibration matrix. A total of 100 pixels were selected from each of the three classes. This process was conducted using the HYPER-Tools 3.0 software, which operates within the MATLAB R2023a environment. The outcome was a two-dimensional matrix comprising 300 rows and 204 columns, corresponding to the wavelengths.

Conversely, the two images that constituted the validation group were individually segmented in order to separate the region of interest (ROI) from the background. In order to achieve this, the k-means algorithm, implemented in MATLAB R2023a, was employed. No further processing of the validation images was required.

2.3. Chemometric analysis

In order to differentiate between the three classes of pixels, a Partial Least Squares Discriminant Analysis (PLSDA) was conducted. PLSDA is a supervised classification technique based on PLS regression using to predict class membership of samples (Ballabio and Consonni, 2013). Classification models were constructed using the 300 x 204 matrix and subsequently validated externally using the two images comprising the validation dataset.

Furthermore, a variety of pre-processing algorithms alone or in combination were employed with the objective of reducing instrumental noise, scattering, and enhancing spectral peaks. Thus, denoising algorithms such as smoothing by the Savitzky-Golay method using a 15-point filter and light scattering

correction techniques as Standard Normal Variate (SNV) and Multiplicative Scatter Correction (MSC) were applied to the spectral data. Moreover, first (1st der) and second derivatives (2nd der) by the Savitzky Golay (SG) method using a second order polynomial and 15 window points were used in this study.

In order to assess the efficacy of the models, we primarily focused on the percentage of correctly classified samples (%CC) within each class, in addition to the sensitivity, specificity, and class error in the calibration and CV datasets. The most effective model was employed for the external prediction of the samples.

3. Results and Discussion

Table 1 presents the outcomes of the 8 PLSDA models, each utilising distinct pre-processing combinations for the calibration and cross-validation datasets. The number of LVs utilised, the overall accuracy for each model, and the percentage of unassigned samples is indicated in the table.

In terms of calibration, the accuracy rate ranges from 84% obtained for the model using smoothing pre-processing to 92% for the model using smoothing plus MSC. The proportion of unassigned samples varies from 20% for the model that utilises smoothing in conjunction with the first derivative of SG to 27% for the model that applies smoothing pre-processing in conjunction with SNV. With regard to cross-validation, the accuracy rate varies from 78% (for the model applying 2nd der) to 86% (the highest percentage model corresponds to that of the calibration.), while the percentage of unassigned samples ranges from 23% (in the model applying smoothing together with MSC) to 30% (in the model using the raw spectrum).

Table 1.PLSDA results of classification using different pre-processing combinations.

		Calibration		Cross-validation	
Pre-processing	LV	Accuracy (%)	Unassigned (%)	Accuracy (%)	Unassigned (%)
None	10	87	26	83	30
Smoothing	9	84	21	83	25
1st der	7	85	22	83	26
2nd der	9	85	22	78	27
Smoothing + 1st der	9	86	20	84	24
Smoothing + 2nd der	10	86	21	79	26
Smoothing + SNV	**6**	**89**	**27**	**85**	**23**
Smoothing + MSC	9	92	25	86	28

LV, Latent Variables; 1st der, First derivative; 2nd der, Second derivative; SNV, Standard Normal Variate; MSC, Mean Scatter Correction. Values in bold correspond to the best results obtained in terms of highest %accuracy and lowest % of unassigned samples in both Calibration and CV.

Regarding the overall accuracy, it is worth noting that the range of values obtained in the present analysis (between 80% and 90% approximately) is comparable to the value presented by Al-Saddik et al. (2018) for the classification of esca based on the spectrum (accuracy of 80.62%), as well as to the ranges reflected by Loggenberg et al. (2018) and Zovko et al. (2019) for modelling water stress in grapevines. Pérez-Roncal et al. (2022) achieved comparable results in terms of accuracy for esca-affected leaves using HSI at a laboratory scale.

On the other hand, when the results of the models are compared, it becomes evident that the pre-processing techniques do not significantly enhance the accuracy of the models. Indeed, only a marginal improvement is observed in the final two models (those that employ smoothing pre-processing in conjunction with SNV or MSC). Nevertheless, the majority of the models in which pre-processing algorithms are applied demonstrate an improvement in the non-assignment percentages, with these being reduced (Table 1). It is evident that the implementation of pre-processing methods enhances the efficacy of the models. This is logical, given that they are designed to eliminate superfluous information, such as noise, and to accentuate pertinent data.

It is important to note that of all the models generated, the one that uses the smoothing followed by SNV was considered to be the one with the best performance. Therefore, this model should be used for subsequent stages of the analysis, such as external validation. The rationale for this selection is that the model in question exhibits the second-highest accuracy in both calibration and cross-validation, while simultaneously using the lowest number of latent variables and a lower percentage of unassigned samples than the model with the highest accuracy (Table 1).

In order to gain further insight into the chosen model, it was deemed necessary to conduct an assessment of the model's sensitivity and specificity in each classification group. The aforementioned parameters are

presented in Table 2.

Table 2. Sensitivity and specificity values of the chosen model

		Calibration		Cross-validation	
Pre-processing	Classes	Sensitivity	Specificity	Sensitivity	Specificity
SM + SNV	Class 1	100	95	100	95
	Class 2	79	94	77	90
	Class 3	80	94	72	93

It can be observed that in Class 1, the sensitivity and specificity values for both calibration and cross-validation are 100% and 95%, respectively. For Class 2, the results of the cross-validation (CV) dataset indicate a sensitivity of 77% and a specificity of 90%. Finally, the sensitivity and specificity values for Class 3 in the cross-validation dataset are 72% and 93%, respectively (Table 2). It is evident that the values for Class 1 are considerably higher than those for Classes 2 and 3, particularly in terms of sensitivity. This indicates that the model is capable of effectively distinguishing between samples belonging to the first group (asymptomatic leaves from asymptomatic vines) and the other two groups, while the differentiation between samples corresponding to Class 2 and Class 3 (asymptomatic samples in symptomatic vines) is less straightforward.

Figure 2 illustrates the outcome of the validation process, conducted with the 3-group model and the smoothing pre-processing in conjunction with SNV, for the image containing the asymptomatic vine.

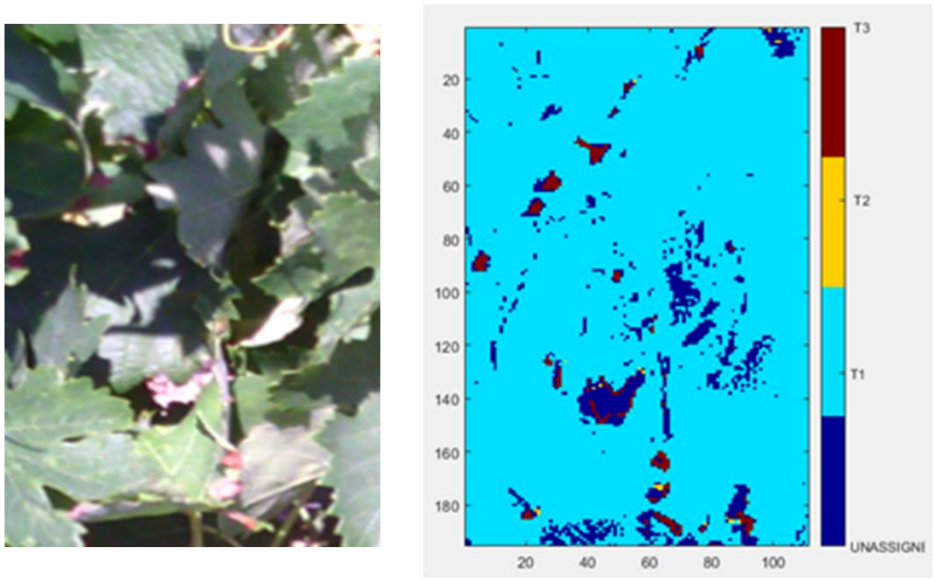

a **b**

Figure 2. RGB image of the asymptomatic vine (a) and classification image of the same vine in the external validation (b).

It can be seen that almost all pixels have been classified as Class 1, which is positive as this is the correct class as it is one of the asymptomatic vines. However, there are isolated areas with a predominance of pixels unassigned and/or assigned to classes other than Class 1 (Figure 2). The latter may be due to various causes, such as the error presented by the model itself or the existence of small areas that do not correspond to leaves. In any case, as the latter are very limited areas and, consequently, as there is a clear predominance of the correct classification, it could be said that the model works correctly in this case.

It can be observed how the majority of pixels have been classified as Class 1, which is a positive indication as this is the correct classification (asymptomatic vines). However, there are isolated areas where the majority of pixels are unassigned and/or assigned to classes other than Class 1 (Figure 2). The latter may be attributed to a number of potential causes, including the inherent limitations of the model, the presence of small areas that do not correspond to leaves, or the existence of areas damaged by factors other than esca, on the observed areas. In any case, as the latter are very limited zones and, consequently, there is a clear predominance of the correct classification, it could be said that the model functions correctly in this instance.

Figure 3 presents the results of the external validation, carried out with the 3-group model using the

smoothing pre-processing together with SNV, for the image containing the symptomatic vine.

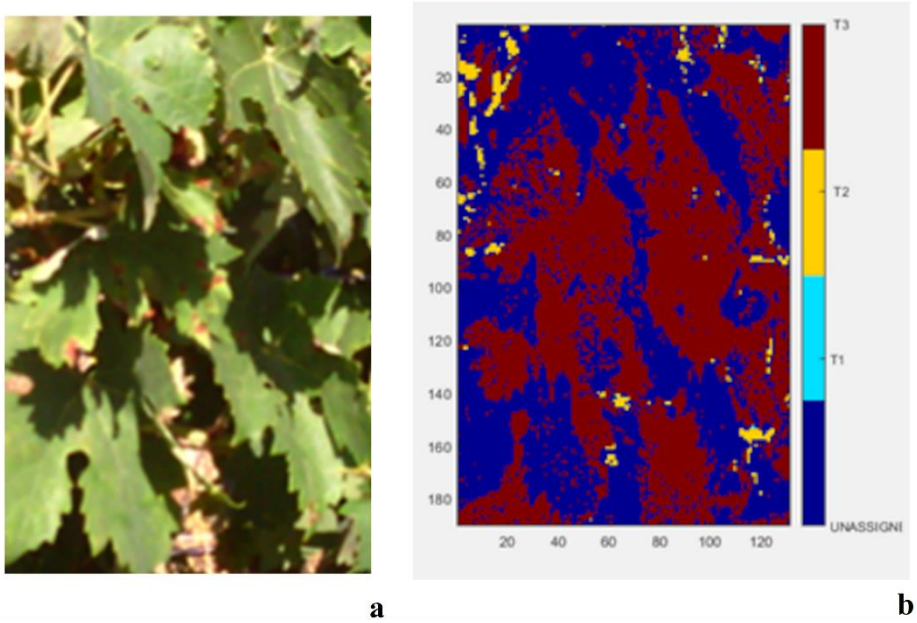

Figure 3. RGB image of the symptomatic vine (a) and classification image of the same vine in the external validation (b).

It can be observed that the majority of the pixels have been classified as Class 3 and few as Class 2. This is a positive finding, as both Class 2 and 3 are the correct classes for a symptomatic vine, and moreover, as the image is located in an area with clear visual symptoms. Nevertheless, it is evident that a considerable number of pixels remain unassigned (Figure 3). This further substantiates the assertion that the model is capable of discerning Class 1 with relative ease, while distinguishing between samples of Classes 2 and 3 is more challenging. The primary reason for this difficulty is believed to be that, despite the classification of three groups, there is a lack of understanding of the relationship between these groups and the stages of symptomatologic development. It is likely that such development is gradual, and therefore there are intermediate situations that are not taken into account during sampling. Given that the majority of classified pixels have been assigned to Class 3, it is reasonable to conclude that the majority of unassigned pixels are in an intermediate symptomatologic state between Class 2 and 3.

4. Conclusions

The results of the present study indicate that hyperspectral imaging technology can be employed to develop effective methods for the early detection of symptomatic vines with regard to esca. The models developed allow for a high degree of differentiation both in the calibration (calibration and cross-validation) and validation stages. However, for future studies, it would be advisable to improve the efficiency of the model in terms of differentiating between samples with early (Class 2) and more advanced (Class 3) symptoms.

Acknowledgements

This research was supported by the Spanish Ministry of Science and Innovation and from the European Union Next-Generation EU/PRTR (TED2021-130364B-I00).

References

Al-Saddik, H., Laybros, A., Billiot, B., Cointault, F. 2018. Using image texture and spectral reflectance analysis to detect yellowness and esca in grapevines at leaf-level. *Remote Sensing*, *10*(4), 618. https://doi.org/10.3390/rs10040618

Amigo, J. M., Babamoradi, H., Elcoroaristizabal, S. 2015. Hyperspectral image analysis. A tutorial. *Analytica Chimica Acta*, *896*, 34-51. https://doi.org/10.1016/j.aca.2015.09.030

Ballabio, D., Consonni, V. 2013. Classification tools in chemistry. Part 1: Linear models. PLS-DA. *Analytical Methods*, *5*(16), 3790-3798. https://doi.org/10.1039/C3AY40582F

Crous, P. W., Gams, W., Wingfield, M. J., van Wyk, P. S. 1996. Phaeoacremonium gen. Nov. Associated with wilt and decline diseases of woody hosts and human infections. *Mycologia*, *88*(5), 786-796. https://doi.org/10.1080/00275514.1996.12026716

Fischer, M. 2002. A new wood-decaying basidiomycete species associated with esca of grapevine: Fomitiporia mediterranea (Hymenochaetales). *Mycological Progress*, *1*(3), 315-324. https://doi.org/10.1007/s11557-006-0029-4

Gams, W., Crous, P. W. 2000. «Phaeomoniella chlamydospora» Gen. Et Comb. Nov., a Causal Organism of Petri Grapevine Decline and Esca. *Phytopathologia Mediterranea*, *39*(1), 112-118. https://doi.org/10.1400/57828

Hofstetter, V., Buyck, B., Croll, D., Viret, O., Couloux, A., Gindro, K. 2012. What if esca disease of grapevine were not a fungal disease? *Fungal Diversity*, *54*(1), 51-67. https://doi.org/10.1007/s13225-012-0171-z

Loggenberg, K., Strever, A., Greyling, B., & Poona, N. 2018. Modelling Water Stress in a Shiraz Vineyard Using Hyperspectral Imaging and Machine Learning. *Remote Sensing*, *10*(2). https://doi.org/10.3390/rs10020202

Ouadi, L., Bruez, E., Bastien, S., Vallance, J., Lecomte, P., Domec, J.-C., & Rey, P. 2019. Ecophysiological impacts of Esca, a devastating grapevine trunk disease, on Vitis vinifera L. *PLOS ONE*, *14*(9), e0222586. https://doi.org/10.1371/journal.pone.0222586

Pérez-Roncal, C., Arazuri, S., Lopez-Molina, C., Jarén, C., Santesteban, L. G., & López-Maestresalas, A. 2022. Exploring the potential of hyperspectral imaging to detect Esca disease complex in asymptomatic grapevine leaves. *Computers and Electronics in Agriculture*, *196*, 106863. https://doi.org/10.1016/j.compag.2022.106863

Zovko, M., Žibrat, U., Knapič, M., Kovačić, M. B., & Romić, D. 2019. Hyperspectral remote sensing of grapevine drought stress. *Precision agriculture*, *20*(2), 335-347. https://doi.org/10.1007/s11119-019-09640-2

Site-specific yield recording in grassland and forage production using sensor technology on self-propelled forage harvesters

Maria Schneider [a,*], Juliana Mačuhová [b], Stefan Thurner [b]

[a] Bavarian State Research Centre for Agriculture, Institute for Agricultural Engineering and Animal Husbandry, Poing-Grub, Germany

[b] Bavarian State Research Centre for Agriculture, Institute for Agricultural Engineering and Animal Husbandry, Freising, Germany

* Maria Schneider. Email: maria.schneider@lfl.bayern.de

Abstract

Sensor-based yield recording on self-propelled forage harvesters (SFH) were tested in the DigiMilch experimental field under practical conditions as a way of recording yield in grassland and silage maize throughout the year. The aim of the study was to test the accuracy, functionality and suitability of the sensor technology for use on commercial farms. The sensor technology on SFH from four different manufacturers was tested on ten Bavarian farms. The comparisons of the SFH data with the reference values for fresh mass yield recording via the sensors on the pre-compression rollers and the determination of the dry matter (DM) content via the near-infrared spectroscopy (NIRS) sensor showed very good compliance with high coefficients of determination of over 0.70 in both grassland and silage maize harvests. The very good concordance correlation coefficients (0.78 in grassland and 0.93 in silage maize), which resulted from the comparison of the site-specific DM yield (t ha^{-1}) from SFH data with that from reference data, confirmed the high accuracy of the sensors on the SFH. The nutrient components estimation via the NIRS sensor performed well, but a further optimisation of the calibration curves could improve the accuracy. The results of the study showed that if the crop is very wet or very dry or if the crop flow is low, yield recording will be less accurate. Site-specific yield recording can reveal the yield potential from the often very different sites on a (sub-) site-specific basis leading to possible management options for more efficiency. Improved roughage management can increase roughage quality and reduce operating costs. Due to the still unexploited potential for optimisation in data management, the sensor-based yield recording is not yet fully suitable for practical use.

Keywords: fresh mass, dry matter content, nutrient components, near infrared spectroscopy, data management

1. Introduction

Farmers are under increasing pressure from political and legal requirements as well as economic challenges and optimisation constraints. The optimisation of roughage management is one of the biggest factors in increasing the efficiency of a farm. The yield potential of individual grassland and fodder crop sites can be revealed by recording the farm's own site-specific yields throughout the year. With this knowledge, farmers can make targeted adjustments to management measures. Grassland sites are particularly heterogeneous in terms of yield potential, therefore they offer the greatest potential for optimisation (Worek and Thurner, 2021). With sensor-based yield recording on the self-propelled forage harvesters (SFH), dry matter (DM) yields can be determined on a (sub-) site-specific basis. In the DigiMilch experimental field this method was tested as a possibility for year-round yield recording under practical conditions during grassland and maize harvesting. The aim of the study was to test the accuracy and functionality of the sensor technology. The practical suitability of the method regarding the recording of site-specific yields was then tested. Particular attention was also paid to data processing and data management.

2. Materials and Methods

To test the accuracy of the sensors on the SFH, the technology of four different forage harvester manufacturers (Claas KGaA mbH, John Deere GmbH & Co. KG, Krone GmbH & Co. KG and CNH Industrial) were tested under practical conditions spread on ten farms located all over Bavaria. Sensors on the pre-compression rollers of the SFH determine the volume flow of the crop via their degree of deflection and speed, which correlates with the harvested fresh mass quantity. The DM content of the harvested crop can be determined using a near infrared spectroscopy (NIRS) sensor on the discharge spout of the SFH. The types of the NIRS sensors tested in the project and their measuring ranges are listed in Table 1. The DM yield in t ha^{-1} is obtained by multiplying the value for the fresh mass by the DM content and dividing the product

by the area size in ha. The yearly DM yield per ha is a key parameter for farmers. Therefore, the focus was also placed on checking the site-specific yield recording.

Table 1. Manufacturers of SFH models participating in the project, associated NIRS sensor models and their measurement ranges for dry matter (DM) (DLG, 2014a, 2014b, 2019a, 2019b, 2021)

SFH model	NIRS sensor model and manufacturer	Measurement range DM	NIRS sensor software version
John Deere 8300, 9700i	HarvestLab 3000 Carl Zeiss AG, Germany	26 – 37 %	V139, V142, V145
CNH Forage Cruiser FR550	NIRXact Dinamica Generale SpA, Italy	10 – 54 %	EST9.3.0.0-Update 3
Claas Jaguar 950, Jaguar 970	Claas NIR m-u-t GmbH, Germany	20.1 – 74.9 %	Silage grass V4.2 Silage maize V6.1
Krone BiG X 700-1, BiG X 780	Krone NIR Krone GmbH & Co. KG, Germany	21 – 40 %	1520200561-05
	AgriNIR Dinamica Generale SpA, Italy	10 – 54 %	unknown, sensor was only tested once and replaced with a new model
	KRONE NIR Control dual m-u-t GmbH Germany	26 – 43 %	1.75.29_APP 1.75.29_DAT

2.1. Verification of fresh mass recording and determination of DM content

The volumetric flow measurement was always calibrated with the net weight of one wagon load weighted on the farm on dynamic axle load scales or static cart scales at the start of harvesting and, optionally, when changing the field or the crop type. As a reference for checking the accuracy of the volume flow measurement, at least 20 loads per harvest date were weighed in grassland and silage maize using dynamic axle load scales (Intercomp, type LS630, accuracy 2 - 3 % at 6 km h-1) or static cart scales (on the Bavarian state farms (BaySG), accuracy +/- 10 kg) (Worek and Thurner, 2023). As a reference for comparison with the SFH values for DM content, the weighed loads were sampled after unloading in the silo (number of samples n = 50) (Thurner et al., 2011). The samples were well mixed and 2 subsamples were packed in bags (Crispac SM 305 x 600 mm, perforated (average hole size approx. 0.5 mm)) for the drying cabinet (Worek and Thurner, 2021). These were weighed on site to finally determine the DM content with the weight after complete drying. A total of 691 loads were weighed and sampled during grassland harvests at different cutting times and 450 loads during silage maize harvests between 2020 and 2023.

2.2. Checking the site-specific yield recording

Two different project farms (Farm A in the Upper Palatinate and Farm B in Upper Bavaria) were selected to test the site-specific yield recording in grassland and forage production. Between 2022 and 2023, the grassland and silage maize harvests from several sites and on different harvest dates were completely weighed and sampled. Each load was weighed using the types of scales mentioned in section 2.1. The net weights of the single loads were summed up to find the total area yield. Random samples (n = 50) were taken from each load in the silo, which were then mixed into one single sample per field. The reference for the DM content was determined in the laboratory. The reference weights per field and the reference DM content were combined as described above and divided by the field size (ha) to obtain a comparative value for the DM yield in t ha^{-1} determined by the SFH. The site-specific yield recording with the SFH was checked on a total of 29 sites and on ten different cutting dates in grassland and on a total of nine sites and on four different harvest dates for silage maize.

2.3. Determination of the nutrient components of the crop via the NIRS sensor

The NIRS sensor on the discharge spout of the SFH determines the nutrient components like crude protein (CP), crude fibre (CF), crude ash (CA), crude fat (CL), acid detergent fibre (ADF), neutral detergent fibre (NDF) and sugar (SU) in the harvested crop as well as starch (ST) in maize. To check the accuracy of the

nutrient content estimation, a sample (n = 50 random samples) per wagon load was packed airtight and a wet-chemical analysis was carried out in the laboratory using the *Weender* method. The samples were taken at different crop conditions (from very wet to very dry), from different crop types (grass from permanent grassland and the crops clover grass, alfalfa, silage maize), from different locations (eight test farms) and on different harvest dates to create a comparison that was as meaningful as possible. Between 2021 and 2023, a total of 157 samples of wilted grass and 125 samples of silage maize were tested in the laboratory.

3. Results and Discussion

In the following two sections, the results of four years (2020 to 2023) of tests in grassland and silage maize harvests are presented and discussed.

3.1. Accuracy of sensor technology at SFH

The comparison of the SFH data with the reference values per wagon load for the volume flow measurement showed very good compliance with a high coefficient of determination of $R^2 = 0.79$ in grassland and $R^2 = 0.90$ in silage maize (Figure 1). This indicates a high accuracy of the sensors on the pre-compression rollers of the SFH. The sensors are more accurate for silage maize harvesting than for grassland harvesting, as the maize crop was very homogeneous (Worek and Thurner, 2021). This is different in grassland, where the sensors reach their limits e.g. with small swath sizes due to low yields (Worek and Thurner, 2023). This is becoming increasingly common particularly in areas of Bavaria with low rainfall (e.g., Franconia or the Upper Palatinate) during midsummer harvests (usually the second or third cut, depending on the region).

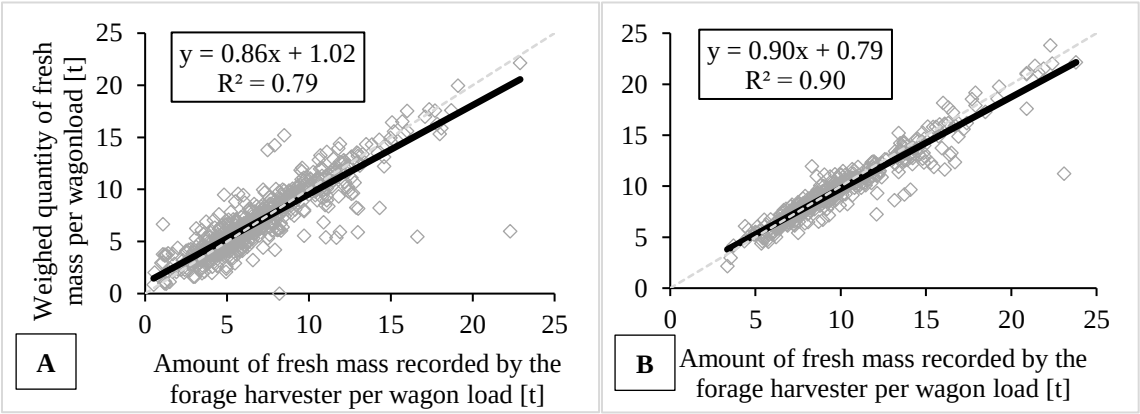

Figure 1. Comparison of the weighed quantity of fresh mass of wilted grass (A; n = 691) and silage maize (B; n = 450) with the fresh mass determined by the forage harvester per wagon load (different fields and harvest times, test years 2020 to 2023, ten Bavarian farms, four SFH manufacturers).

The comparison of the reference DM contents with the DM contents estimated by the NIRS sensor on the SFH also showed good compliance with a coefficient of determination of $R^2 = 0.71$ for wilted grass and $R^2 = 0.53$ for silage maize (Figure 2). When comparing the values for wilted grass (Figure 2, A), the strong deviations of the regression line from the zero line at very low DM contents (<27 %) and very high DM contents (>40 %) were obvious. On the one hand, the NIRS technology is an estimation method whose accuracy depends, for example, on the crop condition and the quantity of the crop flow. On the other hand, its measurement value range is limited due to the number of reference samples stored in the calibration, which no longer enables an accurate estimate outside the calibration which happens at very high and very low DM values (DLG, 2014a, 2014b, 2019a, 2019b). The comparison in silage maize showed a lower coefficient of determination than in wilted grass (Figure 2, B). Looking at the coefficients of determination for each sensor in Table 2, it can be concluded that the determination of DM content in silage maize performed very well. Only one sensor stood out with lower compliance, which therefore affects the overall result. A comparison of the calculated DM quantity per wagonload in t/DM from SFH data with that from reference data showed a good concordance correlation coefficient of 0.82 (confidence interval 0.79 to 0.84) in wilted grass and 0.90 (confidence interval 0.88 to 0.92) in silage maize. This proves the high accuracy of the sensor-based method in grassland and silage maize harvesting.

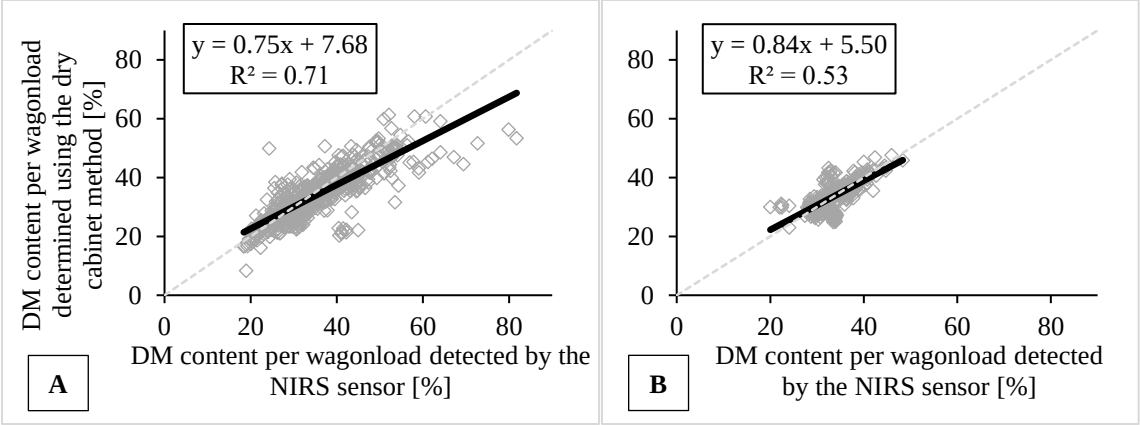

Figure 2. Comparison of the DM contents per wagon load determined by the drying oven method and those recorded by the NIRS sensor in wilted grass (A; n = 691) and silage maize (B; n = 450) (different fields and harvest times, test years 2020 to 2023, ten Bavarian farms, four NIRS sensor manufacturers with six NIRS sensor models).

Table 2. Coefficients of determination of the regression lines for the comparison between the reference DM contents with the DM contents recorded by the SFH, assigned to the sensor model (A-F, randomly assigned), test years 2020 - 2023

Sensor model	Coefficient of determination		Number of samples (n)	
	Grass	Silage maize	Grass	Silage maize
A	0.61	0.82	303	156
B	0.81	0.71	155	153
C	0.68	0.71	137	77
D	0.70	0.29	65	44
E	0.75	not tested	20	-
F	0.82	0.95	11	20

The comparison of the nutrient components in the harvested crop estimated by the NIRS sensor and the laboratory showed very different results between the individual parameters and between the crop types (Figure 3). It could be shown that CF (median: 2.68 % in wilted grass and 1.52 % in silage maize), NDF (median: 3.72 % in wilted grass and -15.75 % in silage maize) and ADF (median: 1.85 % in wilted grass and -7.40 % in silage maize) were the most accurately estimated parameters. Important parameters such as CP in grass (median: -8.36 %) and ST in maize (median: 6.29 %) could also be estimated relatively accurately, but there were often larger deviations (Figure 3). Because the crop has a high water content and the parameters are in very low concentrations in the DM, it is a challenge for the NIRS sensor to accurately estimate the nutrient content of the harvest material. In addition, the number of samples stored in the calibration curves is not yet optimal to ensure an accurate estimate.

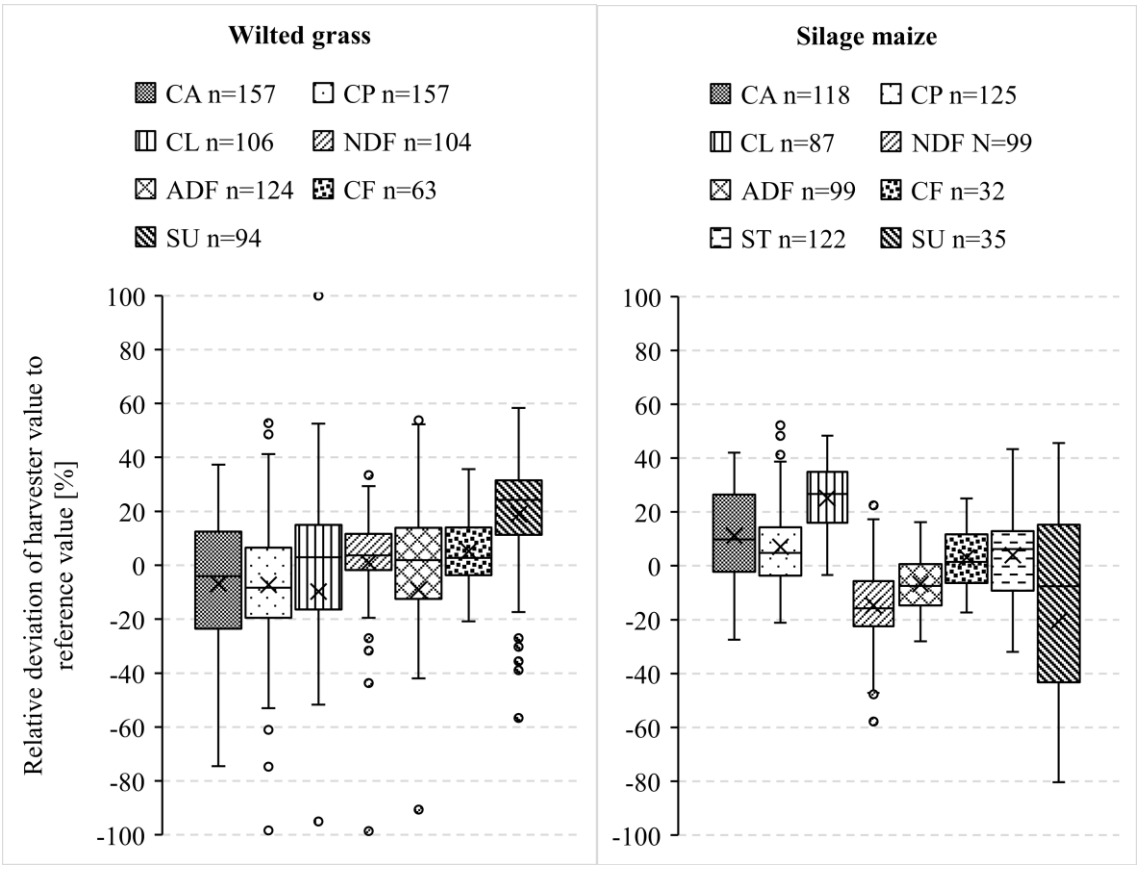

Figure 3. Relative deviation of the nutrient components in the harvested crop, recorded by the NIRS sensor, from the analysed nutrient components by the laboratory (crude protein (CP), crude ash (CA), crude fat (CL), crude fibre (CF), acid detergent fibre (ADF), neutral detergent fibre (NDF), sugar (SU), starch (ST)) (test years 2021 to 2023, eight test farms, three NIRS-sensor manufacturers and five sensor models).

3.2. Accuracy of site-specific yield recording

The comparison of the site-specific DM yield in t ha^{-1} from the SFH data with the reference values also showed a good correlation (Figure 4). A very good concordance correlation coefficient of 0.78 (confidence interval 0.66 to 0.86) in grassland and 0.93 (confidence interval 0.73 to 0.98) in silage maize confirms the high accuracy of the method. The difference between grass and silage maize was again clearly evident. As described above, the silage maize crop is very homogeneous. This means that there is always a constant crop flow during harvesting, which makes it easier for the sensors to record the yield (Worek and Thurner, 2021).

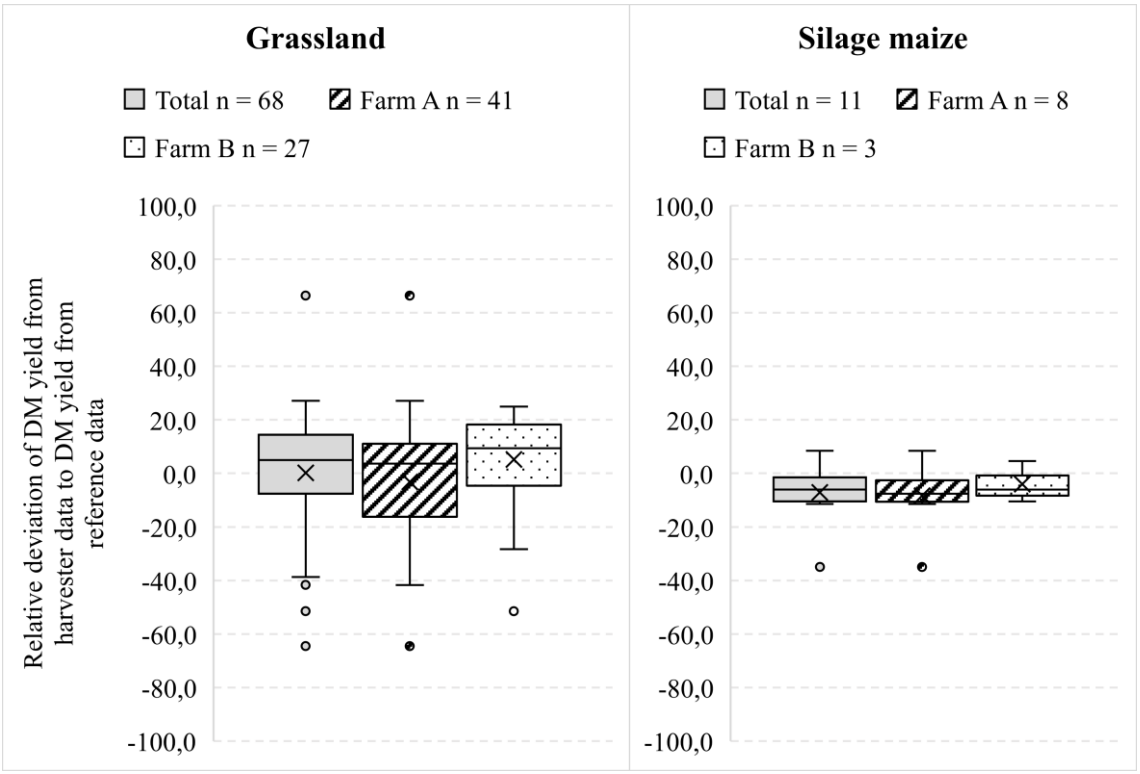

Figure 4. Relative deviation of the site-specific DM yield in t ha^{-1} calculated from SFH data from that based on reference data in grassland and silage maize (different sites and several harvests, different cuts in grassland, two SFH manufacturers, two Bavarian farms (farm A = Upper Palatinate, farm B = Upper Bavaria), years 2022 and 2023)

4. Conclusions

The test results between 2020 and 2023 showed that yields in grassland and silage maize can be very accurately recorded using sensor-based yield recording at the SFH. By recording yields throughout the year and over several years, the site-specific yield potential can be identified. The aim is always the annual DM yield in t ha^{-1}, which provides farmers with a decision-making basis for optimising site management. Measures such as fertilization and reseeding or overseeding can be adapted to the yield potential of (sub) sites and can therefore be made more efficient. Furthermore, the forage harvester terminal provides the farmer with information on harvest quality in real time. This can be used, for example, to precisely dose the silage additive or adjust the cutting length of the crop according to DM content (Worek and Thurner, 2023). Knowledge of the nutrient contents in the harvested crop can also provide farmers with information on the roughage quality during the harvest (via CP in the grass or ST in the maize) or the degree of contamination in the harvested crop (via CA). Farmers can then, for example, optimise silage management according to the quality or reconsider the adjustment of the harvesting machines. These advantages not only increase the quality of the roughage, but also save costs. For example the consumption of operating resources can be reduced by optimising the use of silage additive or roughage losses after the silage process can be avoided by optimising the silage management according to the crop quality. But there is still potential for optimisation in the expansion of the stored calibration curves of the NIRS sensors. Extreme harvesting conditions with very dry or very wet crops are no longer a rarity and should be considered by the manufacturers (Worek and Thurner, 2023). The same applies to the estimation of the nutrient components. Further potential for optimisation is given in data transfer and data management. There is a lack of interfaces for automatic data flow from the machine to a Farm Management Information System (FMIS) and recommendations for further utilisation of yield data. Most farmers are not yet fully exploiting the potential of sensor-based yield recording, which is more due to a lack of knowledge and possibilities than to a lack of willingness. If that optimisation potential is not implemented, the suitability of sensor-based yield recording for practical use cannot be fully established.

Acknowledgements

The project is funded by the Federal Ministry of Food and Agriculture (BMEL) on the basis of a resolution of the German Bundestag. The project is sponsored by the Federal Office for Agriculture and Food (BLE) as part of the promotion of digitization in agriculture with the funding code 28DE112A18.

References

DLG, 2019a: CLAAS NIR Sensor. Feuchtemessung in Gras (Dry matter measurement in grass). DLG test report 7020.

DLG, 2019b: New Holland NIR Sensor. Feuchtemessung in Mais. DLG test report 7032.

DLG, 2014a: CLAAS JAGUAR 960. Feuchtemessung in Mais mit einem NIR-Sensor am Auswurfkrümmer des Feldhäckslers (Moisture measurement in maize with an NIR sensor on the forage harvester's discharge spout). DLG test report 6168F.

DLG, 2014b: KRONE BiG X 700. Feuchtemessung in Mai smit einem NIR-Sensor am Auswurfbogen eines Feldhäckslers. DLG test report 6237F.

S. Thurner, A. Fröhner, B. Köhler and M. Demmel, 2011. Online measurement of yield and dry matter content of wilted grass with two forage harvesters - comparison with and verification of reference measurements. In: J. V. Stafford (ed.) *Precision Agriculture '11. 8th ECPA*. Prague, Czech Republic, Jul 19-22. Ed. J.V. Stafford 628-637

F. Worek and S. Thurner, 2023. Ertrags- und Qualitätsermittlung am Feldhäcksler im praktischen Einsatz. In *conference proceedings "Land.Technik für Profis 2023"*, Grieskirchen, Austria, Feb 14-15. 5 pages.

F. Worek and S. Thurner, 2021. Yield measurement of wilted forage and silage maize with forage harvesters. In *Precision Agriculture '21. 13th European Conference on Precision Agriculture (ECPA)*. Budapest, Hungary, Jul 19-22. Ed., J.V. Stafford 103-110.

A variable-rate spraying system based on RGB-depth and object detection

Qi Gao [a,*], Alberto Carraro [a], Marco Sozzi [a], Francesco Marinello [a]

[a] Department of Land, Environment, Agriculture and Forestry, University of Padova, Legnaro, Italy

* Corresponding author. Email: qi.gao@studenti.unipd.it

Abstract

Variable-rate spraying technology is designed to reduce the use of crop protection products and their negative impacts on the environment while ensuring spraying effectiveness compared to uniform-rate spraying applications. With the emergence of AI edge computing technology, combining RGB-depth (RGB-D) imaging with object detection can be considered a promising approach for variable-rate spraying applications. In this work, a variable-rate spraying system for vineyards has been developed. The system uses an RGB-D camera to capture both RGB images and depth information of grapevines. A low-cost and low-power AI edge computing platform, Jetson Nano, is utilized to process the RGB-D data. For the depth information, the system fully leverages the features of point clouds generated by the RGB-D camera and the parallel computing capability of Jetson Nano to construct mesh models of the grapevine canopies in real time. For the RGB images, an instance segmentation model based on YOLOv8 is applied for isolating the grapevine canopies within the mesh models. Subsequently, the system estimates the leaf area of the canopies and regulates the spraying volume with a pulse-width modulation (PWM) module. An experiment was conducted to evaluate the system, specifically to assess the accuracy of the leaf area calculated from the mesh models. The results demonstrate that the proposed variable-rate system offers considerable measurement accuracy and speed with the Jetson Nano. This technology shows great potential for improving the efficiency and sustainability of agricultural spraying practices.

Keywords: precision viticulture, edge computing, YOLOv8, mesh, pulse-width modulation

1. Introduction

Grapes, as a vital ingredient in winemaking, offer high economic benefits but also require stringent quality standards. To ensure both the yield and quality of vineyards, it is essential to apply plant protection products (PPPs) for pest and disease control. Typically, conventional vineyard spraying is applied at a uniform rate, often resulting in the over-application of PPPs on grapevines that either do not need treatment or require less. Such excessive application is recognised to have adverse environmental impacts, leading to widespread erosion of ecosystems and biodiversity. Variable-rate spraying was proposed in the United States in the 1970s to mitigate these environmental concerns. This technology adjusts spraying volumes to match real-time grapevine canopy data obtained from sensors and thus provides adequate spraying coverage with decreased applications of PPP (Z. Zhang et al., 2018). Several studies have shown that variable-rate spraying can save over 50% of PPPs (Li et al., 2017; Petrović et al., 2019). Due to its significant benefits, this technology has become a research focus in recent years.

A variable-rate spray system typically comprises a detection unit, a data processing system, and a variable control unit (Wei et al., 2022). The detection unit employs advanced sensors to detect the parameters of target plants. The data processing system, which includes both algorithms and hardware, translates these detected parameters into the desired flow rate or other operational parameters for variable-rate spraying. Control signals are then sent to the variable control unit, which adjusts the spray output accordingly.

Currently, variable-rate spraying based on infrared sensors, ultrasonic sensors, LiDAR (Light Detection and Ranging), and machine vision technology has been widely reported (Asaei et al., 2019; Cai et al., 2019; De Bortoli et al., 2022; Li et al., 2012; Palleja & Landers, 2017; Qiao et al., 2020; Xiao et al., 2017). Infrared and ultrasonic sensors are the oldest and simplest approaches, suitable for determining the average characteristics of the canopy and identifying large openings (Z. Zhang et al., 2018). Infrared sensors are scarcely influenced by temperature and humidity and provide measurements independent of atmospheric conditions; however, their detection distance is limited and influenced by plant characteristics or ambient light intensity (Z. Zhang et al., 2018). Ultrasonic sensors are robust, low-cost, and easy to implement, but their wide emission angle significantly limits measurement resolution and accuracy (Rosell & Sanz, 2012), and they suffer from interference when multiple sensors are used in close proximity (Narvaez et al., 2017). LiDAR is the most widely used non-destructive remote sensing technology for orchard spraying (Cheraïet et al., 2020). It could quickly and accurately measure target characteristics in varying ambient light, but it is sensitive to dust, fog and water (Narvaez et al., 2017). In addition, the LiDAR sensors are expensive compared to infrared or ultrasonic sensors and machine vision. Machine vision tries to mimic human perception to provide information based on processed image data. It can digitise the complex visual appearance of crops continuously at high resolution (Thorp & Tian, 2004) and offers better economic performance compared to LiDAR. Although unsatisfactory ambient illuminations could lead to uncertain quality of its outputs, and its applications require intensive computing capabilities, the potential of machine vision applied in various agricultural applications and extracting crop parameters has also been identified (Tian et al., 2020).

A machine vision application to digitise the visual appearance of the canopy requires stereo vision sensors, such as depth cameras and binocular cameras, which generally consist of two cameras at predetermined positions. After capturing

the images of the detected canopy, the processing algorithm identifies correspondences between two images to calculate the depth (distance) using a triangulation method (Jeon & Zhu, 2022). Subsequently, the depth data can be used to generate point cloud data, which contains the spatial coordinates of the canopy. Compared to LiDAR point clouds, the point clouds generated by stereo vision are more structured due to their alignment with the image's pixel grid. This grid-based structure makes the point cloud data more orderly and easier to integrate with other image processing techniques, as each point is associated with a specific location in the image and maintains a consistent spatial relationship with neighbouring points. Nevertheless, real-time processing of such structured point clouds remains a computationally intensive task.

To provide sufficient computational capacity for processing stereo vision data, some research employs x86-based computation platforms to build prototypes, such as laptops (Yan et al., 2021) or x86-based single-board computers (Jeon & Zhu, 2022). However, x86 systems are designed for personal computers rather than edge computing tasks. Some ARM-based single-board computers, such as the Raspberry Pi, can be used for edge computing tasks, but their computational capacity is insufficient to process the large amount of data generated by stereo vision sensors in real-time. In 2017, NVIDIA Corp. (Santa Clara, CA, USA) officially released the NVIDIA Jetson embedded computing platform. Compared to the Raspberry Pi, this ARM-based low-power embedded computer integrates NVIDIA CUDA (Compute Unified Device Architecture) cores, enabling it to provide powerful parallel computing capabilities and accelerate the processing of machine vision data, as well as support artificial intelligence (AI) edge computing tasks.

This work proposes a variable-rate spraying system, which fully utilises the structured point clouds generated by an RGB-Depth (RGB-D) camera and a Jetson platform's powerful parallel computing capability, and incorporates instance segmentation based on a YOLO (You Only Look Once) object detection algorithm. Thereby, it specifically captures the grapevine canopy and establishes its mesh model in real-time, based on which the system calculates the Leaf Area Index (LAI) and outputs Pulse-width Modulation (PWM) signals to achieve variable-rate spraying in vineyards.

2. Materials and Methods

2.1. Hardware Framework and Data Processing Workflow

The hardware framework of the proposed variable-rate spraying system is shown in Figure 1. First, the system uses an RGB-D camera to capture colour images and depth information of the grapevine canopies. Second, a Jetson computing device processes the data and outputs PWM signals with the assistance of a PWM driver module. Then, a PWM-controlled solenoid valve regulates the flow rate in the pipe, which is supported by a liquid tank and a water pump that provides a constant liquid pressure. Finally, the liquid flow is applied to the grapevine canopies via a spraying nozzle.

The data processing workflow of the system is illustrated in Figure 2. The RGB-D camera generates both colour frames and depth frames. Using the SDK (Software Development Kit) of the camera, point clouds are extracted from the depth frames. By leveraging the features of the structured point clouds, a global mesh model is constructed. A customised YOLOv8 instance segmentation model is applied to the colour frames to create masks of the grapevine canopies. The masks are then utilised to isolate the grapevine canopy mesh model from the global mesh model, from which LAI is calculated. Finally, the duty cycle of the PWM signals is determined based on the LAI.

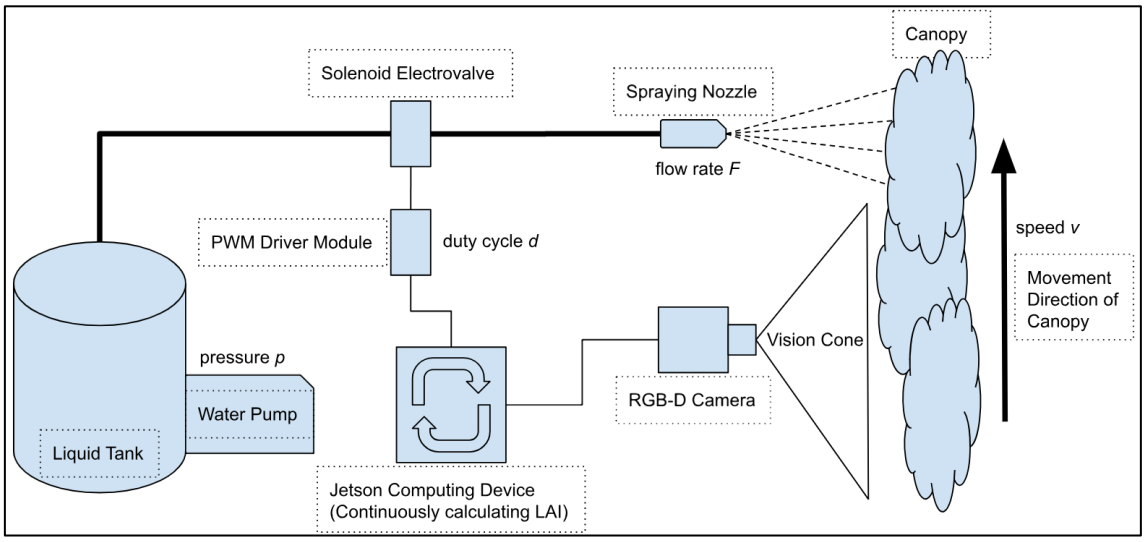

Figure 1. General overview of the variable-rate spraying system.

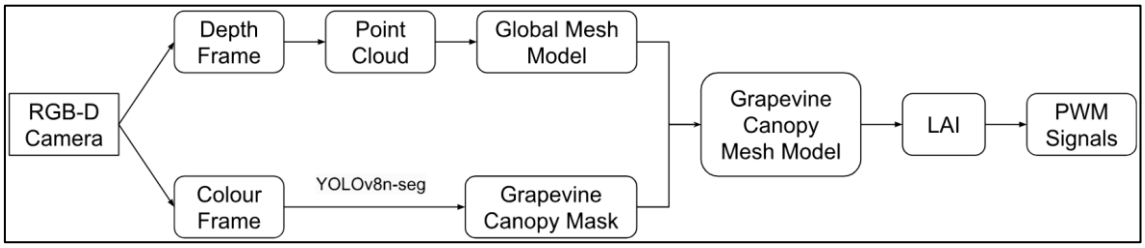

Figure 2. Data processing workflow.

2.2. Hardware Used

An RGB-D camera, RealSense D415 (Intel Corp., Santa Clara, CA, USA), is used to detect grapevine canopies. This camera is designed based on Active Infrared (IR) Stereo Vision Technology (Intel, 2024). It consists of one IR projector, two IR cameras and one RGB camera (Figure 3). The IR projector projects a non-visible static IR pattern to improve depth accuracy. The IR cameras capture depth information using the triangulation method while the RGB camera grabs colour images.

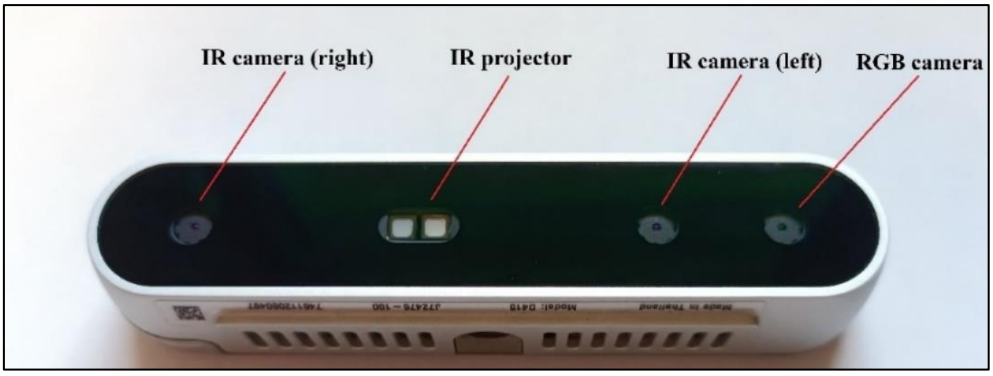

Figure 3. Key components of RealSense D415.

The detailed specifications of RealSense D415 are shown in Table 1.

Table 1. Technical specifications of Intel RealSense D415.

Parameter	Properties
Ideal Measuring Range	0.5 ~ 3 m
Baseline (Distance between two IR cameras)	55 mm
Focal Length	1.88 mm
IR Camera FOV (Field of View, 16:9)	Horizontal:65° / Vertical:40°
RGB Camera FOV	Horizontal:69° / Vertical:42°
Maximum Resolution	1280 × 720 pixels
Depth Accuracy	<2% at 2 m
Mechanical Dimensions & Weight	99 × 23 × 20 mm, 64g

An embedded computer, NVIDIA Jetson Nano, is used for data processing and computing. The NVIDIA Jetson family features a heterogeneous CPU–GPU architecture, small form factor, lightweight, and low power consumption, making it one of the most widely used edge device families (Assunção et al., 2022). Its built-in NVIDIA CUDA cores offer high parallel computing capabilities, which can accelerate graphics data processing and run machine learning inference tasks such as image classification, object detection, and segmentation. Table 2 shows the technical specifications of the Jetson Nano Developer Kit.

Table 2. Technical specifications of Jetson Nano Developer Kit.

Parameter	Properties
AI Performance	472 GFLOPS
GPU	128-core NVIDIA Maxwell architecture GPU
CPU	Quad-core ARM Cortex-A57 MPCore processor
Memory	4GB 64-bit LPDDR4
Storage	micro-SD card (64 GB)
Power	5W - 10W
Mechanical Dimensions	100 × 80 × 29 mm

The solenoid valve used in the variable-rate spraying system is a high-frequency solenoid valve (manufacturer unknown), capable of accepting PWM signals with frequencies from 1 to 10 Hz and duty cycles from 0% to 100%, with a maximum allowable pressure of 10 bar. The PWM-controlled solenoid valve can maintain a relatively constant pressure while adjusting the flow rate, resulting in consistent spray characteristics (Silva et al., 2018; Grella et al., 2022).

Additionally, it offers a quick response time and high accuracy. Due to the relatively low frequency, the Jetson Nano generates PWM singles by using custom Python code to directly control its GPIO (General-Purpose Input/Output) pins, toggling between high and low levels within a given cycle period. The high levels output by GPIO pins is 5V, while the solenoid valve requires a signal voltage of 12V. To address it, a PWM driver click (MikroElektronika, d.o.o., Belgrade, Serbia) is utilised, featuring a Si8711CC isolator (Silicon Laboratories, Inc., Austin, TX, USA). When connected to an external 12V power supply, this driver can convert the PWM single from 5V to 12V.

2.3. Instance Segmentation Model

YOLO, originally designed as a convolutional neural network solely for object detection, was expanded in January 2023 with the release of YOLOv8 (Ultralytics, Inc., Frederick, MD, USA). This version enables the algorithm to perform a variety of tasks, including object detection and tracking, instance segmentation, image classification, and pose estimation. Moreover, the lightweight version, YOLOv8n, offers substantial detection accuracy while significantly reducing computational resource demands, making it highly suitable for resource-constrained edge computing scenarios. With a manually labelled grapevine dataset, an instance segmentation model for grapevine canopies was trained based on the pre-trained weight (YOLOv8n-seg) given by Ultralytics.

The grapevine dataset was downloaded from an open-access dataset provided by the Washington State University Libraries (X. Zhang et al., 2020). The images were acquired in 2019 full stage (early-mid-harvest) at Washington State University Roza Experimental Site near Prosser, WA (USA) using a regular smartphone. A total of 218 images were selected for training the model, with 90 taken in the morning, 68 at noon, and 60 in the afternoon. The regions of interest (ROI) of grapevine canopies were manually labelled with the assistance of the Segment Anything Model (Kirillov et al., 2023). Proportionally from each time period, 70% of the images (153) were selected for the training set, 15% (33) for the validation set, and 15% (32) for the test set. Data augmentation was performed by scaling, flipping, and cropping, ultimately resulting in a training set of 3,060 images, a validation set of 660 images, and a test set of 640 images.

A desktop computer with an AMD Ryzen 7 5700X (Advanced Micro Devices, Inc., Santa Clara, CA, USA) CPU, an NVIDIA GeForce RTX 3060 12 GB GPU, 32 GB RAM, running Ubuntu 22.04 LTS, equipped with NVIDIA CUDA Toolkit 11.8 and PyTorch 2.3.0, was used for training the model. Following the tutorial provided by Ultralytics, the trained model was evaluated on the test set, achieving a segmentation accuracy of 99.5% for mAP50 and 91.9% for mAP50:95.

2.4. Grapevine Canopy Mesh Generation

Using the Intel RealSense SDK, point clouds can be easily generated from the depth frames. These point clouds are not randomly distributed but align with the pixel grid of the colour frames. By connecting any three adjacent points (within the pixel grid) in the point cloud, a global mesh can be constructed. The grapevine canopy mask, generated by the customised YOLOv8-seg instance segmentation model, is then applied to this global mesh to isolate the grapevine canopy mesh model. To illustrate this mesh model, assuming the 5×5 grid of points in Figure 4(a) represents a point cloud generated by the RGB-D camera, with green points indicating the grapevine canopy and black points indicating the background. The grapevine canopy mesh model mentioned above is depicted as the green area in Figure 4(b).

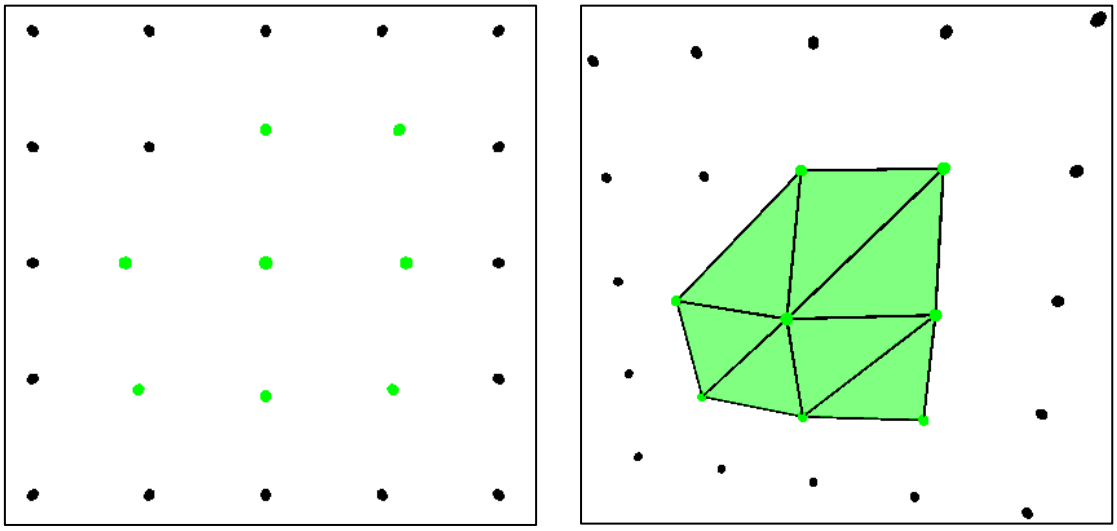

(a) (b)

Figure 4. An example of a grapevine canopy mesh model.

2.5. Usage of Mesh Model for Spraying Regulation

With the grapevine canopy mesh model, the surface area of grapevine canopy can be quickly measured. However, it remains to be experimentally determined whether this area accurately represents the actual leaf area. Additionally, although previous studies have established a formulaic relationship between LAI and the spraying flow rate (Planas et al., 2022), the relationship between the measured leaf area and the spraying flow rate is still uncertain. Therefore, this study conducted two experiments to address these issues.

Since the vineyard had not reached maturity at the time of this study, an artificial grapevine (Figure 5 (a), manufacturer unknown) was used for the LAI measurement experiment. The artificial grapevine consists of a main trunk, three large branches, and one small branch. The three large branches are exactly the same, and the leaves on each branch have similar shapes but differ in size. For this experiment, one large branch was selected for LAI measurement. First, a photo of a single leaf was taken (Figure 5 (b)), and the Segment Anything Model was used to calculate the ratio of the leaf area to its minimum bounding rectangle. Then, the dimensions of the minimum bounding rectangles for all other leaves were measured, and the total one-sided area of all leaves was calculated. Finally, the system was used to measure the surface area of the large branch, and the results were compared with manual measurements. To avoid the randomness of capturing from a single direction, images were taken from different directions.

(a) (b)

Figure 5. The artificial grapevine and its one leaf.

To determine the relationship between the flow rate and measured leaf area, an experimental platform was established to examine the relationship between the PWM duty cycle and flow rate. The platform was equipped with one standard valve, two solenoid valves as previously described, a liquid tank, and a water pump (Figure 6). During the test, only one solenoid valve was used. A manually adjustable 12V PWM signal generator was connected to the solenoid valve. The PWM signal frequency was fixed at 10 Hz, and the liquid flow pressure was maintained at 5 bar.

Figure 6. Experiment platform for valve and nozzle test.

3. Results and Discussion

First, the system was test with the entire artificial grapevine and it showed a test speed of 3.4 frames per second (FPS).

The visualized mask and mesh model are shown in Figure 7(a) and 7(b).

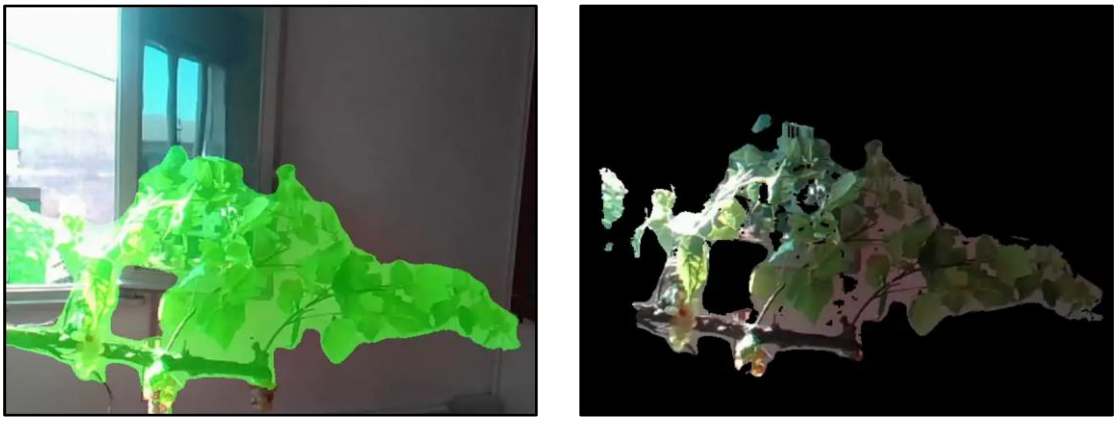

(a) (b)

Figure 7. The mask and the mesh model of the grapevine.

The results for the large branch indicate that the total area of the leaf shown in Figure 5(b) is 61.57% of its minimum bounding rectangle area. The large branch contains 30 artificial grape leaves, and the total one-sided area of all leaves was measured to be 0.207676 m² (Figure 8 (a)). The proposed system was used to measure the branch with directions from 0˚ to 315 ˚. The surface area measured by the system is presented in Figure 8 (b).

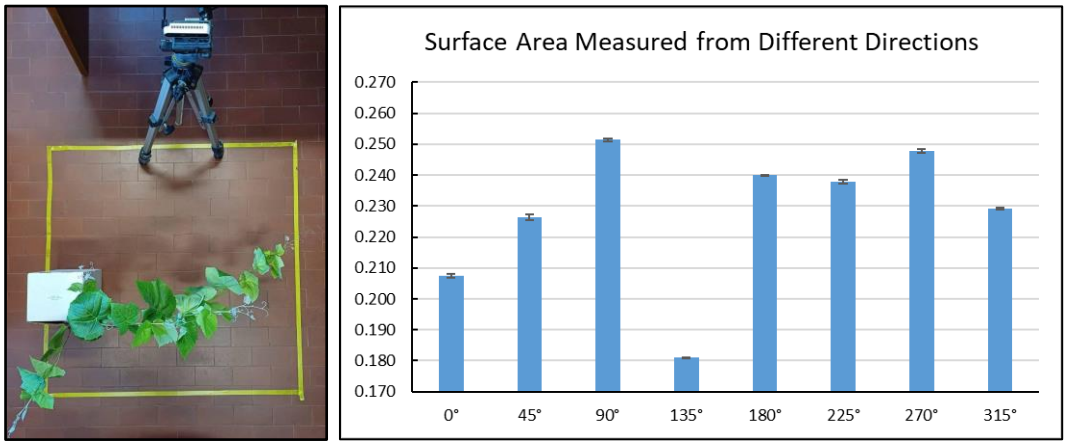

(a) (b)

Figure 8. Surface area measurements.

Although the measurements from the proposed system are generally higher than the manual measurements, this discrepancy is reasonable considering that the YOLOv8n-seg model includes grapevine branches in the mesh model, whereas the manual measurements only account for the leaf area. The significantly smaller measurement at direction 135˚ is attributed to a large leaf obscuring several smaller leaves behind it, as confirmed upon inspection. Since the experiment did not reveal any significant accuracy-compromising defects in the proposed system, and the existing accuracy can be improved by refining the instance segmentation model, we consider the experimental results to be satisfactory.

The results between the flow rate and the PWM duty cycle are presented in Figure 9. A simple interpolation suggests that the functional relationship between the duty cycle (d) and flow rate (F) is approximately as follows:

$$F = \begin{cases} 1106.1d + 231.1, & 0 < d \leq 0.82 \\ 1138.1, & 0.82 < d \leq 1 \end{cases} \quad (1)$$

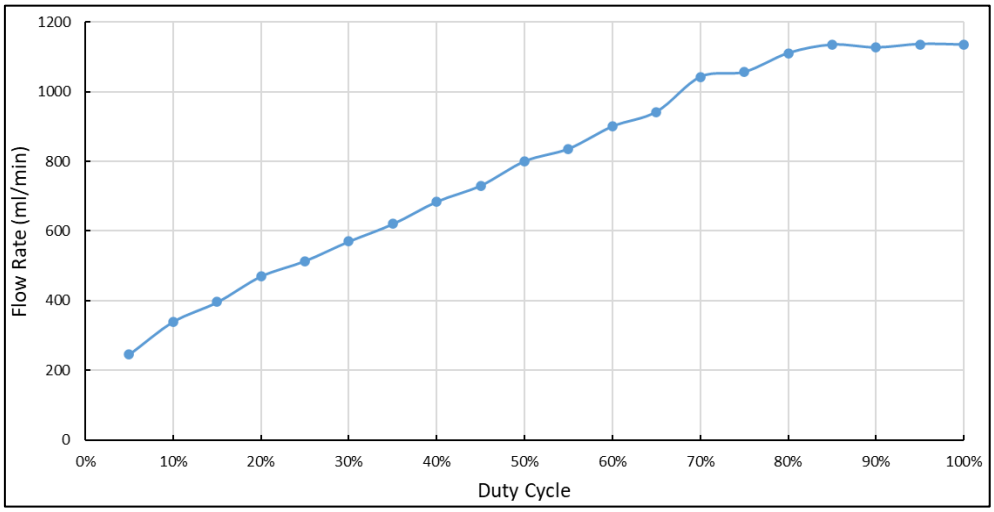

Figure 9. The effect of the duty cycle on the nozzle's flow rate at constant pressure and frequency.

According to the results, the solenoid valve used can accept a duty cycle only between 0% and 82%. This is likely because it is a high-frequency solenoid valve rather than a proportional solenoid valve. Flow variation in this type of valve is generated by the high-frequency opening and closing of the valve core. When the low-level signal duration within the cycle period is too short, the valve core does not have sufficient time to close. On the other hand, a proportional solenoid valve continuously adjusts the flow by precisely controlling the position of the valve core within the valve body. However, the downside is that it is significantly more expensive than a high-frequency solenoid valve. Nevertheless, the currently used solenoid valve is suitable for variable-rate spraying, as the flow output varies almost linearly between 0% and 82%.

4. Conclusions

The implementation of a variable-rate spraying system that utilizes deep learning to regulate a solenoid valve based on continuous recalculation of the Leaf Area Index (LAI) has demonstrated significant advancements in precision agriculture. By leveraging RGB-D data and the YOLOv8 algorithm, the system effectively captures real-time canopy characteristics, ensuring optimal spray application rates tailored to the specific needs of the vineyard. This innovative approach not only enhances resource efficiency by reducing chemical usage and environmental impact but also improves crop health and yield through precise targeting of the canopy. The integration of advanced machine learning techniques with agricultural practices paves the way for more sustainable and intelligent farming solutions, marking a substantial step forward in the automation and optimization of agricultural operations. Future work will focus on refining the system's accuracy and robustness, as well as exploring its applicability to other types of crops and environmental conditions.

References

Asaei, H., Jafari, A., & Loghavi, M. (2019). Site-specific orchard sprayer equipped with machine vision for chemical usage management. Computers and Electronics in Agriculture, 162, 431–439. https://doi.org/10.1016/j.compag.2019.04.040

Assunção, E., Gaspar, P. D., Mesquita, R., Simões, M. P., Alibabaei, K., Veiros, A., & Proença, H. (2022). Real-Time Weed Control Application Using a Jetson Nano Edge Device and a Spray Mechanism. Remote Sensing, 14(17), 4217. https://doi.org/10.3390/rs14174217

Cai, J., Wang, X., Gao, Y., Yang, S., & Zhao, C. (2019). Design and performance evaluation of a variable-rate orchard sprayer based on a laser-scanning sensor. International Journal of Agricultural and Biological Engineering, 12(6), 51–57. https://doi.org/10.25165/j.ijabe.20191206.4174

Cheraïet, A., Naud, O., Carra, M., Codis, S., Lebeau, F., & Taylor, J. (2020). An algorithm to automate the filtering and classifying of 2D LiDAR data for site-specific estimations of canopy height and width in vineyards. Biosystems Engineering, 200, 450–465. https://doi.org/10.1016/j.biosystemseng.2020.10.016

De Bortoli, L., Marsi, S., Marinello, F., Carrato, S., Ramponi, G., & Gallina, P. (2022). Structure from Linear Motion (SfLM): An On-the-Go Canopy Profiling System Based on Off-the-Shelf RGB Cameras for Effective Sprayers Control. Agronomy, 12(6), 1276. https://doi.org/10.3390/agronomy12061276

Grella, M., Gioelli, F., Marucco, P., Zwertvaegher, I., Mozzanini, E., Mylonas, N., Nuyttens, D., & Balsari, P. (2022). Field assessment of a pulse width modulation (PWM) spray system applying different spray volumes: Duty cycle and forward speed effects on vines spray coverage. Precision Agriculture, 23(1), 219–252. https://doi.org/10.1007/s11119-021-09835-6

Intel. (2024). Intel RealSense D400 Series Datasheet (Rev. 018). https://dev.intelrealsense.com/docs/intel-realsense-d400-series-product-family-datasheet

Jeon, H., & Zhu, H. (2022). Stereo Vision Controlled Variable Rate Sprayer for Specialty Crops: Part I. Controller Development. Journal of the ASABE, 65(6), 1397–1410. https://doi.org/10.13031/ja.15227

Kirillov, A., Mintun, E., Ravi, N., Mao, H., Rolland, C., Gustafson, L., Xiao, T., Whitehead, S., Berg, A. C., Lo, W.-Y., Dollár, P., & Girshick, R. (2023). Segment Anything (Version 1). arXiv. https://doi.org/10.48550/ARXIV.2304.02643

Li L., He X., Song J., Liu Y., Wang Z., Li J., Jia X., & Liu Z. (2017). Comparative experiment on profile variable rate spray and conventional air assisted spray in orchards. Transactions of the Chinese Society of Agricultural Engineering, 33(16), 56–63. https://doi.org/10.11975/j.issn.1002-6819.2017.16.008

Li L., Li H., He X., & H. A. (2012). Development and experiment of automatic detection device for infrared target. Transactions of the Chinese Society of Agricultural Engineering, 28(12), 159–163. https://doi.org/10.3969/j.issn.1002-6819.2012.12.026

Narvaez, F. Y., Reina, G., Torres-Torriti, M., Kantor, G., & Cheein, F. A. (2017). A Survey of Ranging and Imaging Techniques for Precision Agriculture Phenotyping. IEEE/ASME Transactions on Mechatronics, 22(6), 2428–2439. https://doi.org/10.1109/TMECH.2017.2760866

Palleja, T., & Landers, A. J. (2017). Real time canopy density validation using ultrasonic envelope signals and point quadrat analysis. Computers and Electronics in Agriculture, 134, 43–50. https://doi.org/10.1016/j.compag.2017.01.012

Petrović, D., Banaj, Đ., Banaj, A., Barač, Ž., Vidaković, I., & Tadić, V. (2019). The Impact of Conventional and Sensor Spraying on Drift and Deposit in Cherry Orchard. Tehnicki Vjesnik - Technical Gazette, 26(5), 1211–1217. https://doi.org/10.17559/TV-20171206133147

Planas, S., Román, C., Sanz, R., & Rosell-Polo, J. R. (2022). Bases for pesticide dose expression and adjustment in 3D crops and comparison of decision support systems. Science of The Total Environment, 806, 150357. https://doi.org/10.1016/j.scitotenv.2021.150357

Qiao B., He X., Wang Z., Han L., Liu W., Dong X., & Liang W. (2020). Development of variable-rate spraying system for high clearance wide boom sprayer based on LiDAR scanning. Transactions of the Chinese Society of Agricultural Engineering, 36(14), 89–95. https://doi.org/10.11975/j.issn.1002-6819.2020.14.011

Rosell, J. R., & Sanz, R. (2012). A review of methods and applications of the geometric characterization of tree crops in agricultural activities. Computers and Electronics in Agriculture, 81, 124–141. https://doi.org/10.1016/j.compag.2011.09.007

Silva, J. E., Zhu, H., & Cunha, J. P. A. R. (2018). Spray Outputs from a Variable-Rate Sprayer Manipulated with PWM Solenoid Valves. Applied Engineering in Agriculture, 34(3), 527–534. https://doi.org/10.13031/aea.12556

Thorp, K. R., & Tian, L. F. (2004). A Review on Remote Sensing of Weeds in Agriculture. Precision Agriculture, 5(5), 477–508. https://doi.org/10.1007/s11119-004-5321-1

Tian, H., Wang, T., Liu, Y., Qiao, X., & Li, Y. (2020). Computer vision technology in agricultural automation—A review. Information Processing in Agriculture, 7(1), 1–19. https://doi.org/10.1016/j.inpa.2019.09.006

Wei, Z., Xue, X., Salcedo, R., Zhang, Z., Gil, E., Sun, Y., Li, Q., Shen, J., He, Q., Dou, Q., & Zhang, Y. (2022). Key Technologies for an Orchard Variable-Rate Sprayer: Current Status and Future Prospects. Agronomy, 13(1), 59. https://doi.org/10.3390/agronomy13010059

Xiao, K., Ma, Y., & Gao, G. (2017). An intelligent precision orchard pesticide spray technique based on the depth-of-field extraction algorithm. Computers and Electronics in Agriculture, 133, 30–36. https://doi.org/10.1016/j.compag.2016.12.002

Yan C., Xu L., Yuan Q., Ma S., Niu C., & Zhao S. (2021). Design and experiments of vineyard variable spraying control system based on binocular vision. Transactions of the Chinese Society of Agricultural Engineering, 37(11), 13–22. https://doi.org/10.11975/j.issn.1002-6819.2021.11.002

Zhang, X., Lu, S., Karkee, M., & Zhang, Q. (2020). Full Stages of Wine Grape Canopy and Clusters [Application/zip]. Washington State University. https://doi.org/10.7273/000001846

Zhang, Z., Wang, X., Lai, Q., & Zhang, Z. (2018). Review of Variable-Rate Sprayer Applications Based on Real- Time Sensor Technologies. In S. Hussmann (Ed.), Automation in Agriculture—Securing Food Supplies for Future Generations. InTech. https://doi.org/10.5772/intechopen.73622

Study of the individual information collection system for weaner pigs

Yi-Chich Chiu [a,*]

[a] Department of Biomechatronic Engineering, National Ilan University, Yilan City, Yilan Country

* Corresponding author. Email: yichiu@niu.edu.tw

Abstract

The objective of this research is to develop an individual information collection system for weaner pigs, and integrate the Internet of Things technology for system construction. The weight change of weaner pigs during growth has a certain relationship with health. Therefore, it is very important to accurately measure the weight of pigs. However, it is difficult to measure the weight of weaner pigs by hand, which is easy to cause the pigs to be scared and urgent. Weaners are pigs that are between weaning and 56 days of age and weigh 6–20 kg. The system can give different feeds according to weight changes and nutritional needs during the growth of weaner pigs. Through the system, you can monitor the daily weight changes of each pig, track the growth status of individual pigs and mark them. When the abnormality is detected during the feeding process, it can be immediately improved to prevent more property loss and achieve maximum economic benefits. The system was divided into control unit, import and export unit, weighing unit and feeding unit. The system control was through the programming logical controller (PLC), including import and export gates, weight measurement and feed supply control. Use RFID to detect the number of each pig, and record the weight change, feed intake, etc., calculate the feed conversion rate and evaluate the growth rate of pigs by cloud system. In this study, the dynamic weighing test was carried out through three standard weights of 45, 50 and 55 kg. The optimal sampling time was 0.1 second, and the weighing system error rate was 1.2%. The test results showed that the individual information collection system of the weaner pigs was stability. Through the establishment of the individual information collection system for pigs, it can be reduced the burden on the on-site breeding staff, and obtained the pig weight growth curve instantly. Individual observations can be made during the breeding period, and pigs with poor growth status can be found early, in addition to improve pig breeding quality.

Keywords: Internet of Thing (IoT), weaner pigs, monitoring and control, wireless communication

1. Introduction

Pork is one of the meats favored by Han Chinese people. According to the annual report of Taiwan's Council of Agriculture (2018), the annual pork production in Taiwan in 2018 was valued at US$2.32 billion. In 2018, Taiwan had approximately 7,241 pig farms, which raised approximately 5.44 million pigs. In 2021, the number of pig farms was 6,308, the number of raised pigs was approximately 5.47 million, and the value of pork production was US$2.54 billion (COA 2023). Pork production accounts for 13.39%–14.31% of the total agricultural output in Taiwan, and the per capita consumption of pork in Taiwan is estimated to be approximately 40 kg. Therefore, the management of pig growth is crucial in Taiwan. Pigs are weighed and sold when they have grown to a weight of approximately 200 kg. In the pig market, pigs are numbered, weighed, stamped, and marked after a transaction; during this process, pigs are easily frightened by the loud noise of heavy gates and might become reluctant to move (Chen, 2016). Therefore, workers often use electric shock prods with a weak current of 30 V to make pigs move. Livestock experts have suggested that pigs can be easily made to move without the use of such devices; however, pigs can still be easily injured during auctions when markets are unable to respond suitably to the habits and behaviors of pigs. Substantial labor and resource investments are required to enable on-site managers to gain knowledge regarding the growth patterns of pigs, including their daily weight gains; feeding efficiencies; and survival rates during the nursing, growing, and finishing stages. Failure to grasp the production efficiency can increase operating costs. The accurate measurement of pig weight is crucial because this weight affects the price of the pig.

In 2011, Big Dutchman developed an electronic sow feeding system that earned a seal of approval for being humane. This system allows sows to roam freely and rest in large farms and has been praised for its animal-friendly nature. Under the aforementioned system, individual feeding is maintained during pregnancy, and the system can facilitate the management of groups of approximately 60 sows. Entrance and exit doors are pneumatically operated, and the side partitions are made of sturdy sound-absorbing materials to ensure that the sows can eat without external disturbance. Fancom also developed an intelligent pig feeding

and monitoring system. In addition, Big Dutchman developed an automatic weighing device for pigs ready for slaughter that can be used to group pigs according to weight. This device aids in preparing an accurate count and weight of the pigs to be slaughtered and assists in the planning of slaughter dates. Big Dutchman's system uses a single-channel, dual-door method; the entrance door opens when no pig is inside the weighing device and automatically closes when a change in weight is detected after a pig enters the device. At this point, only one pig is on the scale at a time, and only 2–3 s is required to obtain the weight. The system then calculates the weight category of the pig and finally opens the exit door to guide the pig out. The entrance and exit doors are pneumatically operated. Banhazi et al. (2012) argued that the livestock industry is moving toward the use of precision livestock farming technology. On pig farms, this technology is used for analysing live weight gain, feed intake, and environmental data. Banhazi et al. pre-processed images of pigs and conducted linear regression analysis on weight measurements to obtain daily weight gain data for the pigs. Their experiment involved capturing images of specific pigs by using a camera installed directly above and aimed at the center of the pigsty to acquire the visual appearance of the pigs for analysing their mean weight. A camera system was used with sensors for automatically quantifying the feed consumed by weaned piglets.

Currently, information on feed intake and growth weight is generally collected manually, which is not only time-consuming and labour-intensive but also might not provide the most accurate information. Therefore, Liu et al. (2017) used an ARM Cortex M3 STM32 microcontroller as a hardware platform and combined it with 4G communication technology, sensors, and RFID technology to develop a system that can track the feed intake and weight changes of breeding pigs. The data collected by this system are wirelessly transmitted to a remote server. Maselyne et al. (2014a, 2014b) developed a high-frequency RFID system that can be applied in an industrial environment to record pig feeding status and simulate the feeding patterns of growing and finishing pigs. This system has a sensing sensitivity of 88.58%, and its accuracy in distinguishing individual pigs is 98.34%. The system can be used with feeding status data to monitor pig health, welfare, and production status.

The present study aimed to develop a system for automatically determining the identification numbers and weights of pigs during feeding. The proposed system uses an Internet of Things architecture and a microcontroller connected to sensors for capturing weight and RFID data. This system calculates pig feed intake and pig feed efficiency, records data on individual pigs, and evaluates pig growth rate. Users can view these data on a webpage to monitor the growth of weaner pigs at any time. Through automated weighing, individual data collection, and automatic feeding, the labor cost of pig farms can be reduced. Automated weighing with the proposed system causes limited stress to the weighed pigs.

2. Materials and Methods

The developed individual data collection system for weaner pigs contains a programmable logic controller (PLC) as the control center. Data collected by sensors are transmitted according to the RS485 standard to a Linkit Smart 7688 Duo microcontroller, and the data are then uploaded to a cloud server through Wi-Fi. This section details each operation of the proposed system. Figure 1 shows a schematic of the proposed system, which includes an RFID reader, a feed motor, a solenoid valve for rear gate control, a motor-driven front gate, and a weighing platform. The overall dimensions of this system are 1,500 × 750 ×1,615 mm3 (l × w × h). The system is designed for weaner pigs with a weight of approximately 6–20 kg and a body length, width, and height of approximately 60–70, 25, and 35–40 cm, respectively.

2.1. Control design

The control unit of the designed system contains an FX3U PLC (Mitsubishi Electric Corporation) that is connected to a microcontroller. This PLC has matured industrial applications and can connect RS485 communication modules and use the Modbus communication protocol. It can also be connected with analog signal input modules to connect various sensors. The microcontroller unit (MCU) of the proposed system integrates a central processing unit, random-access memory, and various input/output serial ports in a single integrated circuit chip to achieve diversified applications. The use of this MCU in smart applications can not only decrease the development cost but also replace certain manual-labor tasks. In the proposed system, a serial peripheral interface pin is coupled with an RS485 to TTL module on a Linkit Smart 7688 Duo (MediaTek, Taiwan) controller board to receive RS485 differential signals and convert them according to the Modbus-RTU protocol.

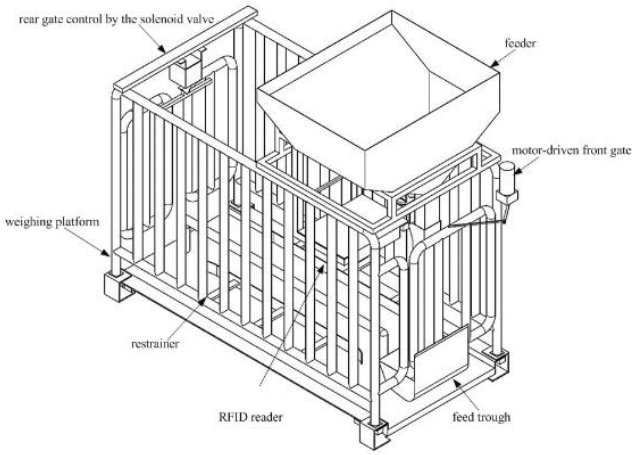

Figure 1. Schematic of the designed individual pig data collection system

2.2. Design of the data collection and analysis system

This system primarily collects data on individual pigs, such as the information obtained from the RFID reader, feed input quantity, and pig weight data, and uploads these data to a cloud server. In this system, an on-site PLC is paired with a Linkit Smart 7688 Duo microcontroller to conduct data collection and remote communication. The collected data are transmitted wirelessly through Wi-Fi to a cloud server and stored in a database. Pig weight data can be queried through a Web interface. The physiological status of a pig can be analysed by collecting data on its daily weight gain and daily feed quantity. Thus, statistics on the daily feed conversion rate can serve as a reference for farm administrators to evaluate the condition of a pig.

2.3. Test methods

2.3.1. Tests on the optimal weight measurement time

Weight measurements change when an animal moves on the weighing platform, and such motion results in inaccurate weight readings. Therefore, the stability of the designed weighing system was tested, and the optimal sampling time was calculated to minimize the error when weighing pigs. The testing of the optimal weight measurement time involved the weighing device detecting a weight exceeding 3 kg, a pause of 3 s, and the capturing of the weight detected on the scale. In this testing, set weights of 45, 50, and 55 kg were used, and weight measurements were performed at 0.1, 0.2, 0.3, 0.4, and 0.5 s to obtain 100 pieces of data for each group. Measurements were performed thrice for each sampling time in the dynamic weighing accuracy test. The MX SHEET communication software of the PLC was used to store the captured weight data directly in Excel. Weights measured using an electronic scale (SAMPO BF-L1501ML; precision of 0.1 kg) served as standard weights for comparison with the weights measured by the proposed system. Analysis of variance (ANOVA) was conducted to analyze the relationships between the three continuous weights, and Tukey's honest significance difference (HSD) test was performed for comparison. The optimal sampling time was determined by analysing the samples of each group.

2.3.2. Tests on dynamic weighing accuracy test

In addition to the optimal sampling time, the dynamic weighing accuracy was tested. When the proposed system detected a weight exceeding 3 kg, sampling was delayed for 3 s, following which continuous weight values were captured for 10 s to obtain 100 pieces of data. The measured weights were compared with the standard weights to determine the error between them. The weights of the test objects were set as 45, 50, and 55 kg, and the sampling times were the same as those in the testing of the optimal sampling time. Weight measurements were conducted thrice for each weight, and the mean measurement at a certain time was calculated. Moreover, the error rate was calculated using Equation (1), and the mean standard deviation per second was recorded to determine the optimal weight measurement time.

$$Error\ rate = \frac{Standard\ weight - measured\ weight}{Standard\ weight} \times 100\% \quad (1)$$

3. Results and Discussion

3.1. Results obtained on the individual data collection system

Figure 2 presents an image of the individual data collection system. This system has a rear gate as its entrance, a front gate as its exit, a weighing scale at its bottom, a restrainer in its middle part to limit the range of activity of the pig on the scale, and a motor below the feeder that dispenses feed.

Figure 2. Image of the individual data collection system for pigs

3.2. Results of the tests on the optimal sampling time

In the tests on the optimal sampling time, weights of 45, 50, and 55 kg were measured at sampling times of 0.1, 0.2, 0.3, 0.4, and 0.5 s; thus, 15 groups of data were obtained. A total of 100 pieces of data were collected for each group and tested three times. The standard deviation for each weight sampling changed with the sampling time. As displayed in Figure 3, the smallest standard deviation occurred when the sampling time was 0.1 s for all three weights, and the standard deviation increased with the sampling time. When the sampling time was 0.4 or 0.5 s, the largest standard deviation in dynamic weighing was observed for the weight of 55 kg (deviation of nearly 1 kg).

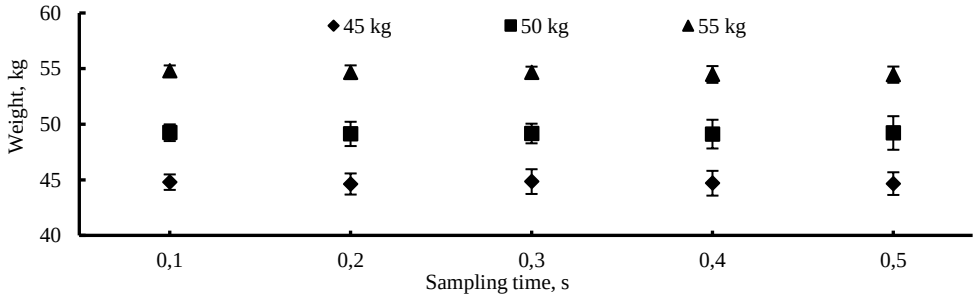

Figure 3. Weights measured at different sampling times

3.3. Results of the tests on dynamic weighing accuracy

The test on dynamic weighing accuracy was conducted thrice each for the standard weights of 45, 50, and 55 kg.

Figure 4 depicts the mean error graph for each weight, which indicates that the error rate for each weight

between 5 and 8 s was less than 1.2%. Therefore, the optimal weighing time was determined to be between 5 and 8 s, and the weight change during this period was considered the mean weight change.

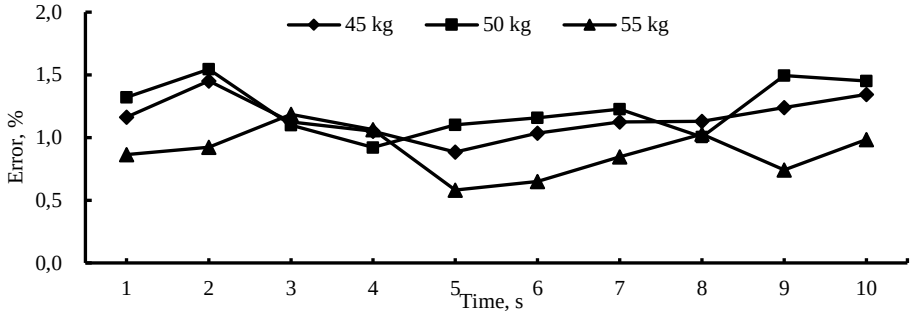

Figure 4. Mean errors for the three weights

4. Conclusions

This study designed and developed a system for collecting data on individual pigs. This system includes an RFID reader, a feed motor, a solenoid valve for rear gate control, a motor-driven front gate, and a weighing platform. The control unit of this system, which contains a PLC and microcontroller, can successfully transmit different types of data to a remote server through Wi-Fi and identify individual pigs on the basis of RFID data. The individual pig data collected by the proposed system include pig ID, pig weight, and feed quantity. Through cloud computing, the feed conversion rate of each pig can be calculated to enable farm administrators to understand the growth and health status of each pig. The proposed system, which contains hardware and software components, was used to perform tests on the optimal sampling time and dynamic weighing accuracy with standard weights of 45, 50, and 55 kg. The sampling times in the test on the optimal sampling time were set as 0.1, 0.2, 0.3, 0.4, and 0.5 s, and 100 pieces of data were collected for each data group. Moreover, three dynamic weighing tests were performed for each data group. The test results indicated that the optimal sampling time was 0.1 s. The mean measurements obtained with the proposed system for the standard weights of 45, 50, and 55 kg were 44.79 ± 0.70, 49.23 ± 0.75, and 54.79 ± 0.49 kg, respectively. The mean weight of each group closely approximated the standard weight, and a small standard deviation was observed. In the tests on the dynamic weighing accuracy, 0.1 s was used as the sampling time, and the testing duration was 10 s.

The developed data collection system for individual pigs has high site adaptability, mobility, and convenience; thus, this system makes it easy for farmers to collect individual pig data rapidly in the pigsty, to handle the collected data, and to use these data for monitoring the statuses of pigs. Data on the weight changes of pigs can be used for effectively analyzing their health statuses, and these data can be analysed to provide feedback to farm administrators as a reference for decision-making. Future studies can integrate the environmental parameters of a pig farm into the developed system and determine the optimal pigsty environment. Moreover, studies can conduct big data analysis on the growth information of pigs and other livestock to enable their efficient management on farms.

Acknowledgements

This study was supported by the National Science and Technology Council of Taiwan (MOST 107-2321-B-197-005). The authors are grateful to I-Yang Farm for providing access to the testing site and sharing their rearing experience and opinions on the environmental parameters.

References

Banhazi, T. M., L. Babinszky, V. Halas, M. Tscharke, 2012. Precision Livestock Farming: Precision feeding technologies and sustainable animal production. Int. J Agric. & Biol. Eng. 5(4), 1-8.

Big Dutchman, 2011. Electronic sow feeding system earns seal of approval. https://www.bigdutchman.com/en/pig-production/news/press-releases/detail/electronic-sow-feeding-system-earns-seal-of-approval/ Accessed February 6, 2018.

COA, 2018. Yearly report of Taiwan's Agriculture (2018). https://eng.coa.gov.tw/ws.php?id=2505553 Accessed February 5, 2018.

COA, 2023. Yearly report of Taiwan's Agriculture (2023). https://eng.coa.gov.tw/ws.php?id=2505553 Accessed February 14, 2023.

Chen, N., 2016. The last mile of pig. https://e-info.org.tw/node/117419 Accessed May 6 2019.

Fancom company, 2018. https://www.fancom.com/blog/smart-feeding Accessed February 6, 2018.

Liu, Y., S. P., Xu, Y. S. Wang, 2017. Remote Monitoring System for Breeding Pig Growth based on 4G Communication. Journal of Agricultural Science and Technology. 19(2), 59-64.

Maselyne, J., W. Saeys., B. D. Ketelaere., K. Mertens., J. Vangeyte., E. F. Hessel., S. Millet., A. V. Nuffel, 2014a. Validation of a high frequency radio frequency identification (HF RFID) system for registering feeding patterns of growing-finishing pigs. Computers and Electronics in Agriculture. 102,10-18.

Maselyne, J., A. V. Nuffel., B. D. Ketelaere., J. Vangeyte., E. F. Hessel., B. Sonck., W. Saeys, 2014b. Range measurements of a high frequency radio frequency identification (HF RFID) system for registering feeding patterns of growing-finishing pigs. Computers and Electronics in Agriculture. 108, 209-220.

Parsons, D. J., D. M. Green, C. P. Schofield, and C. T. Whittemore, 2007. Real-time control of pig growth through an integrated management system. Biosystem Engineering. 96(2), 257-266.

Challenges and opportunities for remote sensing in agrivoltaic systems

Sergio Vélez[a]*, Shiva Gorjian[a,b], Tamara Bretzel[a], Matthew F. Berwind[a], Mar Ariza-Sentís[c], Gonzalo Mier[d], João Valente[e] and Max Trommsdorff[a,f]

[a] Group Agrivoltaics, Fraunhofer Institute for Solar Energy Systems ISE, 79110 Freiburg, Germany

[b] Biosystems Engineering Department, Tarbiat Modares University (TMU), P.O. Box: 14115-111, Tehran, Iran

[c] Information Technology Group, Wageningen University & Research, 6708PB Wageningen, Netherlands Research, 6708 PB Wageningen, Netherlands.

[d] Laboratory of Geo-Information Science and Remote Sensing, Wageningen University & Research, 6708PB Wageningen, Netherlands

[e] Centre for Automation and Robotics (CAR), Spanish National Research Council (CSIC), 28006 Madrid, Spain

[f] Wilfried Guth Chair, Department of Economics, University of Freiburg, Wilhelmstr. 1b, 79085 Freiburg, Germany

*Corresponding author: sergio.velez@ise.fraunhofer.de

Abstract

Agrivoltaic systems integrate agricultural production with PV (photovoltaic) energy generation. They present unique challenges and opportunities for remote sensing technology that differ from those of individual systems. This study examines how current remote sensing methods, such as satellite imagery, UAV (unmanned aerial vehicle) surveys, and ground-based sensors, can be adapted to effectively monitor and manage these systems. Agrivoltaics makes remote sensing difficult due to structural elements that obstruct the sensors and the variable light conditions caused by the solar panels. Satellite imagery offers large-scale monitoring capabilities, but has problems with spatial resolution, image coverage and shadowing effects. UAVs offer high-resolution, flexible data collection and can fly closer to crops, making them suitable for detailed monitoring under solar panels. However, limitations include restricted flight times and potential difficulties in manoeuvring within agrivoltaics due to solar panel structures and regulatory constraints. UGVs (unmanned ground vehicles) can collect valuable soil, plant, and microclimate data, but have problems navigating within these systems. Ground-based sensors can help generate time series data and complement remote sensing observations, albeit limited to a fixed location. Integrating these technologies can provide a complete understanding of agrivoltaic systems, enabling better irrigation, fertilisation, and pest control decision-making. Furthermore, this study emphasises the importance of choosing the appropriate remote sensing technology based on the specific configuration of agrivoltaics. Considering the strengths of each technology and addressing its limitations, remote sensing can enhance the dual benefits of crop production and renewable energy generation. This approach can not only improve the management of solar panels and agriculture, but also support better farming practices, contributing to environmental sustainability and food security. Future advances in machine learning and artificial intelligence (AI), along with improved sensor technologies, will further expand the capabilities of remote sensing in agrivoltaic systems. This progress promises to drive innovation in sustainable agriculture and renewable energy production.

Keywords: Satellite; UAV; Remote sensing; Precision agriculture; Agrivoltaics

1. Introduction

Agrivoltaics combines agricultural production with photovoltaic (PV) energy production and involves complex interactions between plants and solar panels. Although integrating PV systems in agriculture can power new machinery, digital technologies, and automation systems, transforming agricultural activities (Gorjian et al., 2020), the presence of the structural elements of PV systems can interfere with agricultural operations, and the solar panels can create shadows and varying light conditions that create new problems and challenges for agriculture, although they also offer a range of opportunities depending on regional and climatic conditions (Weselek et al., 2019). Research on agrivoltaic systems is still in its infancy. However, some studies have already investigated methods to mitigate these challenges, such as using advanced algorithms for data correction and developing sensor systems that can work effectively under these conditions (Amaducci et al., 2018). These studies aim to develop models that can accurately predict crop yield and optimise the placement and orientation of solar panels to maximise both energy production and agricultural output (Malu et al., 2017). Other research efforts focus on integrating data from different types of sensors to gain a comprehensive understanding of the microclimate created by agrivoltaic systems (Dupraz et al., 2011)

Remote sensing technology has revolutionised the way we observe and interact with our environment. Using various platforms such as UAVs (unmanned aerial vehicles, also known as drones), satellites, UGVs (unmanned ground vehicles) and portable and fixed sensors, remote sensing enables the collection of detailed and timely data over large areas without direct contact and with minimal human intervention. This technology is critical in many areas, including environmental monitoring, urban planning and agriculture. The ability to collect high-resolution data on crop health, soil conditions and weather patterns facilitates informed decision-making and leads to increased productivity and sustainability (Anderson & Gaston, 2013)

On the one hand, remote sensing technologies in agriculture have significantly changed the agricultural landscape with advances in precision agriculture and sustainable farming practices. Technologies such as multispectral and hyperspectral imaging, LiDAR (Light Detection and Ranging) and thermal sensors provide insights that are difficult to obtain using traditional methods. The data collected can be processed and analysed to create detailed maps and 3D models (Buunk et al., 2023), that help optimise irrigation, fertilisation and pest control practices and reduce environmental impact by minimising the use of water, fertilisers and pesticides (Mulla, 2013). Remote sensing provides valuable insights into plant health by utilising a range of spectral bands, including visible, infrared and thermal. It facilitates the early detection of problems such as disease, stress or nutrient deficiencies, often before they are visible to the naked eye. This leads to higher crop yields and a reduced environmental impact from agricultural practices with unprecedented accuracy (Zhang & Kovacs, 2012).

On the other hand, remote sensing, combined with machine learning, is crucial for the efficient management of PV solar energy. It can detect and catalogue PV installations worldwide, addressing database gaps and identifying inequities in solar energy use to ensure equitable access to the benefits of solar energy. It can provide detailed, up-to-date information on the size and location of solar installations, helping researchers, policy makers and grid operators to plan and integrate solar energy (Kaack, 2021). In addition, remote sensing instruments are used to capture and process images to detect problems such as dirt accumulation, shading effects and physical damage, all of which affect the efficiency of solar modules. These events can lead to significant energy losses as they reduce the efficiency and power output of solar PV panels (Maghami et al., 2016), making it crucial to monitor and address these issues, emphasising the importance of regular cleaning and maintenance to ensure optimal performance and consistent energy production.

While remote sensing has practical and useful applications in both agricultural and PV monitoring, its techniques and tools may not be sufficient when applied to agrivoltaics. The combination of agriculture and photovoltaics brings new challenges that do not exist when each system is managed independently. Depending on the configuration, solar panels may interfere with monitoring crops from a nadir angle traditionally used in remote sensing. Moreover, when using UAVs or UGVs close to the plants, the structures supporting the solar panels and the panels themselves present complex obstacles that can be difficult to navigate. In addition, the panels cause varying degrees of shadowing and reflection, which can affect the accuracy of the data and the performance of the sensors. These unique conditions necessitate the development of advanced algorithms and sensor systems specifically designed to address these challenges.

This research investigates how current remote sensing techniques can be adapted to the unique configurations of agrivoltaic systems to address the challenges of integrating crop production and solar energy generation. A better understanding in this area will unlock the benefits of remote sensing for crop monitoring, improving efficiency and promoting more sustainable land use.

2. Opportunities of remote sensing in agrivoltaics

Current remote sensing methods such as satellite imagery, UAV surveys and ground-based sensors can significantly improve the management and monitoring of agrivoltaics. These techniques allow for better monitoring of both the solar panels and the plants, which are important components of the agrivoltaic system. Although the combination of these elements brings new challenges, remote sensing is already helping to identify problems with the solar panels while providing valuable data on the condition of the plants. Therefore, exploring current remote sensing techniques is a perfect first step.

Some studies have shown that remote sensing, especially thermal imaging, enables efficient inspection of solar panels and is a non-invasive and efficient method for maintenance and optimisation. Sriram and Sudhakar (Sriram & D. Sudhakar, 2023) highlighted the effectiveness of thermal image processing in identifying defects such as shading, dust and soiling, which can significantly affect the performance of solar panels. In studies conducted by Lee and Park in 2019, and Pruthviraj et al. in 2023, (Lee & Park, 2019;

Pruthviraj et al., 2023) a step was further taken by using UAVs equipped with thermal infrared sensors to conduct large-scale inspections, identifying defective cells and abnormal heat generation.

In agriculture, the use of remote sensing technologies to monitor crops varies in complexity depending on the type of crop and the platform chosen. Satellites, drones and UGVs are among the most important platforms. Their use differs mainly between vertical crops such as vineyards and espalier orchards and extensive crops such as cereals and legumes (Gautam & Pagay, 2020; Sishodia et al., 2020; Wu et al., 2023).

Satellites can face significant challenges when monitoring crops, especially woody crops, due to their limited spatial resolution and nadir viewing angle, which obstructs the view between rows and fails to capture the three-dimensional structure of the crop. Nevertheless, satellites have proven to be extremely effective for mapping large-scale crops (Tian et al., 2019). They enable efficient surveillance of huge areas by detecting large-scale variations in crop health. Satellite imagery combined with deep learning algorithms can even map tree crops with high accuracy, providing practical insights (Lin et al., 2021), and machine learning and deep learning models integrated with time-series satellite data have been shown to be effective in classifying multiple crop species in large regions, demonstrating high accuracy in crop area identification (Wang et al., 2022).

UAVs offer high-resolution, flexible, and targeted data collection capabilities. Although UAVs can provide similar information to satellites, such as tracking the crop cycle, the use of drones in agriculture shows that UAV high-resolution monitoring brings significant benefits compared to satellite platforms (De Lima et al., 2021). Flights can be precisely planned and are typically conducted at heights ranging from 20 m to 50 m or even up to 120 m, which is the legal limit in most European countries (Commission Implementing Regulation (EU) 2019/947 of 24 May 2019 on the Rules and Procedures for the Operation of Unmanned Aircraft, 2019). This flexibility enables thorough data collection from above (Vélez et al., 2022).

In addition, UAVs can also monitor vertically grown crops. They benefit from their ability to fly at low altitude and their flexible sensor angles, which provide even more useful high-resolution images. Their ability to capture images and video from oblique angles can improve detailed monitoring of plant health and identify disease or water stress, potentially alleviating the limitations of the nadir perspective (Buunk et al., 2023). Similarly, flight paths can be adapted to fly very close to plants and even within plant rows. In this way, even more detailed and specific data can be collected, providing a better insight into the condition of the plants and fruit (Ariza-Sentís et al., 2024). This feature could prove particularly useful when it comes to monitoring the condition of plants under solar panels, where satellite images may be obstructed.

Remote sensing data can also be collected from the ground with the help of UGVs. These are robotic systems that can perform precision agriculture and farm management tasks without human presence (Vasudevan et al., 2016). UGVs are invaluable for precision monitoring and soil sampling (Olmedo et al., 2020). They can include robotic arms to take soil or leaf samples for crop monitoring and work with other platforms, such as UAVs, to improve agricultural operations (Quaglia et al., 2019). Nevertheless, their operational range is somewhat limited compared to other platforms and although they are able to collect detailed ground-level data such as moisture and temperature, their efficiency is hampered by the difficulty of navigating uneven or densely planted terrain and the inability to collect data from the upper parts of plants or the structure of solar panels.

Finally, ground-based instruments such as soil moisture sensors and weather stations can provide continuous, real-time data that can complement remote sensing observations and help create time series data, albeit limited to a fixed location. Integrated with IoT networks, ground-based sensors can automate data collection and analysis, precisely monitor microclimatic conditions, soil health and crop growth, facilitate precision agricultural practices, and improve resource efficiency and crop yields, leading to improved modeling.

3. Challenges of remote sensing in agrivoltaics

Although remote sensing monitoring has proven useful in evaluating solar panels and crop health and offers potential for inclusion in precision agriculture, remote sensing in agrivoltaic systems presents numerous difficulties not encountered in the systems mentioned above. This is mainly due to the complicated interactions between the vegetation and the solar panels, as well as the effects of the solar panels and their structure, which completely change the agricultural environment (Weselek et al., 2019). The potential problems therefore depend on the configuration and location of the PV modules.

Agricultural use in the context of agrivoltaic systems can be roughly divided into two main groups (Figure

1): Category I, i.e. installations with sufficient clearance beneath the agrivoltaics setup for agriculture, and Category II, i.e. ground-level installations between the rows of the agrivoltaic system.

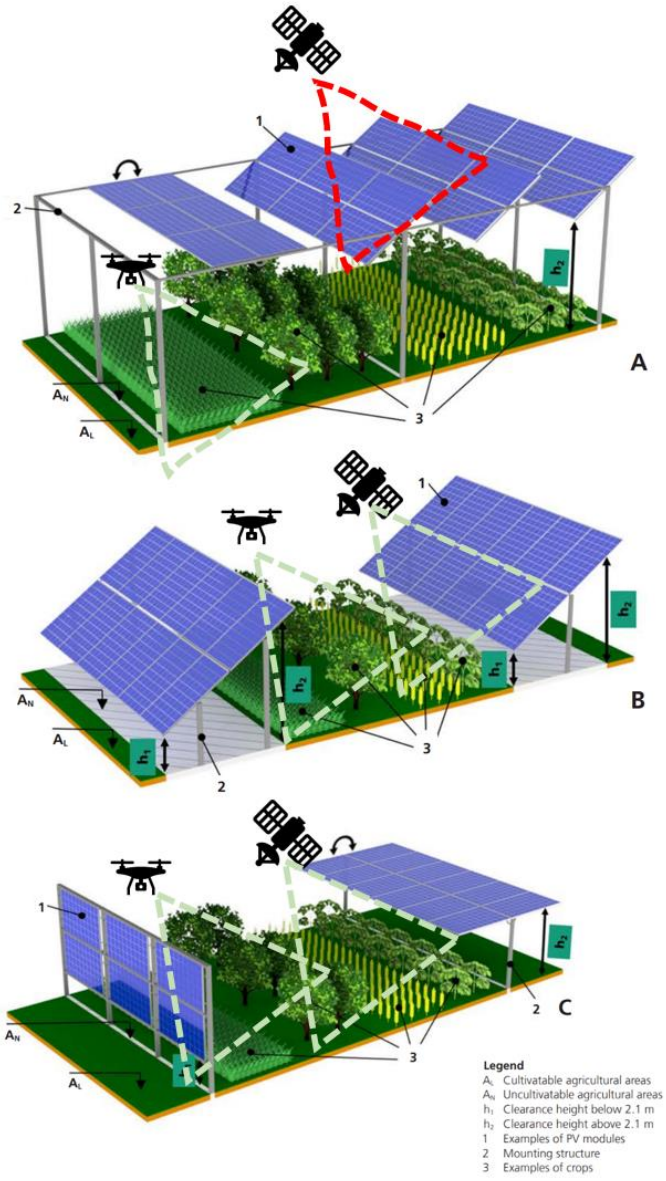

Figure 1. Interaction of remote sensing platforms with the different categories of land use as set out in DIN SPEC 91434, adapted from (Trommsdorff et al., 2022). A: Category I; B: Category II, variant 1; C: Category II, variants 1 and 2. Each diagram shows icons of UAVs and satellites, showing their unobstructed views towards the crop with green dashed lines and obstructed views with red dashed lines.

Category I lists four agricultural uses: 1A for permanent crops and perennial crops such as fruit, vines and hops; 1B for annual and biennial crops including field crops and fodder; 1C for permanent mobile grassland and 1D for permanent grazing grassland. Category II reflects these subdivisions, with 2A and 2B for permanent and annual crops respectively, and 2C and 2D for permanent mobile and grazing grassland respectively. These categories emphasise the adaptability and potential of agrivoltaic systems for a wide range of agricultural activities (DIN Deutsches Institut für Normung e. V., 2021).

Each configuration poses different challenges for remote sensing technologies. Figure 1 shows the views

of each platform indicated by cones, with unobstructed views indicated by cones in dashed green lines and obstructed views indicated by cones in dashed red lines, to assess the potential benefits and challenges of the different remote sensing platforms in monitoring vegetation according to the agrivoltaic configurations. For example, Figure 1A illustrates how high-mounted solar panels can obstruct the view of satellites. This is represented by a red cone indicating the challenges in monitoring, although UAVs could manoeuvre under the solar panels to collect data. Figure 1B shows that satellites and UAVs have a clear view between the lower mounted panels, which is ideal for crop monitoring. In Figure 1C, the vertical arrangement of the panels allows satellites and UAVs to observe both the plants and the undersides of the panels, although angled panels can make visibility difficult for satellites or UAVs flying with the sensor at nadir angle.

While some challenges are similar to those that already exist in agricultural facilities such as greenhouses, others are unique or more related to specific farm management techniques, such as crops growing under plastic film. (Farbo et al., 2024). For example, greenhouse roofs in greenhouses and overhead agrivoltaics can similarly interfere with remote sensing by satellites or high-altitude UAV remote sensing, but the problems with wind are different. The shape of agricultural installations changes wind and flow dynamics, altering airflow patterns, ventilation rates and temperature distributions. Greenhouse designs with walls, different roof shapes or ventilation configurations affect natural ventilation and internal microclimates, and obstructions such as plants or internal structures can create air resistance leading to pressure drop and heterogeneous climate conditions (Bournet & Rojano, 2022). While greenhouses are typically closed, vertical PV modules in agrivoltaics leave the top open, and overhead agrivoltaics have open sidewalls (Figure 2). Therefore, it is important to consider the unique challenges of different agrivoltaic configurations.

Figure 2. Left: Overhead agrivoltaic system with open sides, generating partial shade and solar electricity. Right: Greenhouse with semi-cylindrical roof and closed sides, with vents for climate control, adapted from (Akpenpuun et al., 2021).

In view of the above, these potential challenges include:

- Distinction between vegetation and solar panels: Remote sensing imagery must accurately distinguish between vegetation and solar panels. Accurate scene classification is essential to analyse the objects in the image, and the mixed signals in the images can make this difficult. This distinction is necessary to assess the health (Chang et al., 2020), and monitor the efficiency of solar panels, with effective image segmentation playing a crucial role in defect detection (Hong et al., 2022).
- Precise monitoring of crop condition in shaded areas: Agrivoltaic systems create shaded areas under the solar panels. These shaded areas can be more or less persistent depending on the configuration of the agrivoltaic system. Shade influences the growth, health and yield (Miller et al., 2015) but also the image and spectral information by obscuring the scene (Kushwaha et al., 2023). Remote sensing instruments must adapt to these variations in illumination to accurately capture crop conditions.
- Microclimate dynamics and wind patterns: Solar panels in agrivoltaic systems change the distribution of solar radiation, altering the microclimate (Weselek et al., 2021) and can generate wind currents that resemble wind tunnels and can change the flight stability of UAVs (Scicluna et al., 2019; Setlak & Kowalik, 2019) and even of robotic arms or handheld sensors used for monitoring.
- Complex environment to navigate: The structure and mount of the solar panels can create a complex and difficult environment to navigate. UAVs and robots must manoeuvre around the panels and their mounts, which can hinder efficient data collection and increase the risk of accidents.

– Obstruction of overhead PV modules: Overhead solar panels can obstruct images captured by satellites and UAVs with a nadir angle. This obstruction makes it difficult to monitor and manage agricultural activities through remote sensing technologies, as the panels can block the view of crops below.
– Develop specific models for agrivoltaics: New models must consider the unique interactions between solar panels, crops, and environmental factors to balance solar radiation for electricity generation and crop production because it is crucial to improving energy and agricultural outputs (Gorjian et al., 2022).

4. Future directions

The full potential of remote sensing in agrivoltaic systems can be exploited by combining different methods, provided they are compatible with the installed agrivoltaic configuration. Combining data from satellites, UAVs and ground-based sensors can provide a complete, multi-level understanding of the system. For example, satellite data can direct UAV surveys to areas showing signs of stress, while ground sensors can continuously monitor both the crops and the solar panels. Higher resolution data collected using UAVs and ground sensors allows for accurate monitoring of the condition of crops under the varying light conditions created by agrivoltaic systems. In addition, the incorporation of advanced UAV tools from other fields and the further development of UGVs with improved navigation capabilities can provide new opportunities for detailed micro-level monitoring that complement UAV and satellite observations.

At the same time, machine learning and AI advances can improve the analysis of remote sensing data and enable more accurate predictions and automated decision-making processes. Nevertheless, new, or existing algorithms should be trained with specific data sets. In addition, path planning should be developed that is tailored to the specifics of each individual agrivoltiac configuration, taking into account shadows and obstacles caused by solar panels. The continuous improvement of sensor technologies will increase the resolution, accuracy and diversity of the collected data and thus provide a better insight into the performance of agrivoltaic systems. Therefore, remote sensing will play an important role in optimising the management of agrivoltaic systems by enabling precise monitoring. This tool will increase the acceptance of agrivoltaics, promote sustainable agricultural practices and improve food security alongside renewable energy production.

5. Conclusions

The integration of current remote sensing methods offers enormous opportunities to improve the efficiency and sustainability of agrivoltaic systems. Satellite imagery, UAV and UGV surveys, and ground-based sensors can provide a complete and holistic view of these systems, allowing for better management and maximisation of crop production and renewable energy generation. These technologies can improve precision and accuracy by overcoming limitations such as distinguishing vegetation and solar panels, monitoring crops in shaded areas and navigating complex environments. Advanced path planning algorithms and artificial intelligence can help mitigate issues such as obstacles and lighting variations, while UAV flexibility and high-resolution sensors ensure detailed data collection even in challenging conditions. Remote sensing can address current challenges and support more sustainable and productive agrivoltaic practices.

Acknowledgements

This work has been supported by the Iberdrola Foundation and the European Commission under the Marie Skłodowska-Curie Actions (MSCA) - E4F, part of the Horizon 2020 program (Grant Agreement No 101034297, https://doi.org/10.3030/101034297).

References

Akpenpuun, T. D., Na, W.-H., Ogunlowo, Q. O., Rabiu, A., Adesanya, M. A., Addae, K. S., Kim, H.-T., & Lee, H.-W. (2021). Effect of Greenhouse Cladding Materials and Thermal Screen Configuration on Heating Energy and Strawberry (Fragaria ananassa var. “Seolhyang”) Yield in Winter. Agronomy, 11(12), 2498. https://doi.org/10.3390/agronomy11122498

Amaducci, S., Yin, X., & Colauzzi, M. (2018). Agrivoltaic systems to optimise land use for electric energy production. Applied Energy, 220, 545–561. https://doi.org/10.1016/j.apenergy.2018.03.081

Anderson, K., & Gaston, K. J. (2013). Lightweight unmanned aerial vehicles will revolutionise spatial ecology. Frontiers in Ecology and the Environment, 11(3), 138–146. https://doi.org/10.1890/120150

Ariza-Sentís, M., Vélez, S., Baja, H., Valenti, R. G., & Valente, J. (2024). An aerial framework for Multi-View grape bunch detection and route Optimisation using ACO. Computers and Electronics in Agriculture, 221, 108972. https://doi.org/10.1016/j.compag.2024.108972

Bournet, P.-E., & Rojano, F. (2022). Advances of Computational Fluid Dynamics (CFD) applications in agricultural building modelling: Research, applications and challenges. Computers and Electronics in Agriculture, 201, 107277. https://doi.org/10.1016/j.compag.2022.107277

Buunk, T., Vélez, S., Ariza-Sentís, M., & Valente, J. (2023). Comparing Nadir and Oblique Thermal Imagery in UAV-Based 3D Crop Water Stress Index Applications for Precision Viticulture with LiDAR Validation. Sensors, 23(20), 8625. https://doi.org/10.3390/s23208625

Chang, A., Yeom, J., Jung, J., & Landivar, J. (2020). Comparison of Canopy Shape and Vegetation Indices of Citrus Trees Derived from UAV Multispectral Images for Characterization of Citrus Greening Disease. Remote Sensing, 12(24), 4122. https://doi.org/10.3390/rs12244122

Commission Implementing Regulation (EU) 2019/947 of 24 May 2019 on the Rules and Procedures for the Operation of Unmanned Aircraft, 45 (2019). https://eur-lex.europa.eu/legal-content/EN/TXT/PDF/?uri=CELEX:32019R0947

De Lima, I. P., Jorge, R. G., & De Lima, J. L. M. P. (2021). Remote Sensing Monitoring of Rice Fields: Towards Assessing Water Saving Irrigation Management Practices. Frontiers in Remote Sensing, 2, 762093. https://doi.org/10.3389/frsen.2021.762093

DIN Deutsches Institut für Normung e. V. (2021). Agri-photovoltaic systems – Requirements for primary agricultural use ((DIN SPEC 91434:2021-05)). Beuth Verlag GmbH.

Dupraz, C., Marrou, H., Talbot, G., Dufour, L., Nogier, A., & Ferard, Y. (2011). Combining solar photovoltaic panels and food crops for optimising land use: Towards new agrivoltaic schemes. Renewable Energy, 36(10), 2725–2732. https://doi.org/10.1016/j.renene.2011.03.005

Farbo, A., Trombetta, N. G., De Palma, L., & Borgogno-Mondino, E. (2024). Estimation of Intercepted Solar Radiation and Stem Water Potential in a Table Grape Vineyard Covered by Plastic Film Using Sentinel-2 Data: A Comparison of OLS-, MLR-, and ML-Based Methods. Plants, 13(9), 1203. https://doi.org/10.3390/plants13091203

Gautam, D., & Pagay, V. (2020). A Review of Current and Potential Applications of Remote Sensing to Study the Water Status of Horticultural Crops. Agronomy, 10(1), 140. https://doi.org/10.3390/agronomy10010140

Gorjian, S., Bousi, E., Özdemir, Ö. E., Trommsdorff, M., Kumar, N. M., Anand, A., Kant, K., & Chopra, S. S. (2022). Progress and challenges of crop production and electricity generation in agrivoltaic systems using semi-transparent photovoltaic technology. Renewable and Sustainable Energy Reviews, 158, 112126. https://doi.org/10.1016/j.rser.2022.112126

Gorjian, S., Minaei, S., MalehMirchegini, L., Trommsdorff, M., & Shamshiri, R. R. (2020). Applications of solar PV systems in agricultural automation and robotics. In Photovoltaic Solar Energy Conversion (pp. 191–235). Elsevier. https://doi.org/10.1016/B978-0-12-819610-6.00007-7

Hong, F., Song, J., Meng, H., Wang, R., Fang, F., & Zhang, G. (2022). A novel framework on intelligent detection for module defects of PV plant combining the visible and infrared images. Solar Energy, 236, 406–416. https://doi.org/10.1016/j.solener.2022.03.018

Kaack, L. H. (2021). Machine learning enables global solar-panel detection. Nature, 598(7882), 567–568. https://doi.org/10.1038/d41586-021-02875-y

Kushwaha, S. K. P., Dali, A., Harshit, Singh, C. H., Rai, A., & Jain, K. (2023). Analysis of Shadow Interference on Chromatic Information in Unmanned Aerial Vehicle Optical Imagery. 2023 IEEE India Geoscience and Remote Sensing Symposium (InGARSS), 1–4. https://doi.org/10.1109/InGARSS59135.2023.10490379

Lee, D. H., & Park, J. H. (2019). Developing Inspection Methodology of Solar Energy Plants by Thermal Infrared Sensor on Board Unmanned Aerial Vehicles. Energies, 12(15), 2928. https://doi.org/10.3390/en12152928

Lin, C., Jin, Z., Mulla, D., Ghosh, R., Guan, K., Kumar, V., & Cai, Y. (2021). Toward Large-Scale Mapping of Tree Crops with High-Resolution Satellite Imagery and Deep Learning Algorithms: A Case Study of Olive Orchards in Morocco. Remote Sensing, 13(9), 1740. https://doi.org/10.3390/rs13091740

Maghami, M. R., Hizam, H., Gomes, C., Radzi, M. A., Rezadad, M. I., & Hajighorbani, S. (2016). Power loss due to soiling on solar panel: A review. Renewable and Sustainable Energy Reviews, 59, 1307–1316. https://doi.org/10.1016/j.rser.2016.01.044

Malu, P. R., Sharma, U. S., & Pearce, J. M. (2017). Agrivoltaic potential on grape farms in India. Sustainable Energy Technologies and Assessments, 23, 104–110. https://doi.org/10.1016/j.seta.2017.08.004

Miller, S. S., Hott, C., & Tworkoski, T. (2015). Shade effects on growth, flowering and fruit of apple. Journal of Applied Horticulture, 17(02), 101–105. https://doi.org/10.37855/jah.2015.v17i02.20

Mulla, D. J. (2013). Twenty five years of remote sensing in precision agriculture: Key advances and remaining knowledge gaps. Biosystems Engineering, 114(4), 358–371. https://doi.org/10.1016/j.biosystemseng.2012.08.009

Olmedo, N. A., Barczyk, M., Zhang, H., Wilson, W., & Lipsett, M. G. (2020). A UGV-based modular robotic manipulator for soil sampling and terramechanics investigations. Journal of Unmanned Vehicle Systems, 8(4), 364–381. https://doi.org/10.1139/juvs-2020-0003

Pruthviraj, U., Kashyap, Y., Baxevanaki, E., & Kosmopoulos, P. (2023). Solar Photovoltaic Hotspot Inspection Using Unmanned Aerial Vehicle Thermal Images at a Solar Field in South India. Remote Sensing, 15(7), 1914. https://doi.org/10.3390/rs15071914

Quaglia, G., Visconte, C., Scimmi, L. S., Melchiorre, M., Cavallone, P., & Pastorelli, S. (2019). Design of the positioning mechanism of an unmanned ground vehicle for precision agriculture. In T. Uhl (Ed.), Advances in Mechanism and Machine Science (Vol. 73, pp. 3531–3540). Springer International Publishing. https://doi.org/10.1007/978-3-030-20131-9_348

Scicluna, L., Sant, T., & Farrugia, R. N. (2019). Investigation of Wind Flow Conditions on the Flight Endurance of UAVs in Hovering Flight: A Preliminary Study. ASME 2019 2nd International Offshore Wind Technical Conference, V001T01A037. https://doi.org/10.1115/IOWTC2019-7514

Setlak, L., & Kowalik, R. (2019). Stability Evaluation of the Flight Trajectory of Unmanned Aerial Vehicle in the Presence of Strong Wind. WSEAS Transactions on Systems and Control, 14, 43–50.

Sishodia, R. P., Ray, R. L., & Singh, S. K. (2020). Applications of Remote Sensing in Precision Agriculture: A Review. Remote Sensing, 12(19), 3136. https://doi.org/10.3390/rs12193136

Sriram, A., & D. Sudhakar, T. (2023). Photovoltaic Cell Panels Soiling Inspection Using Principal Component Thermal Image Processing. Computer Systems Science and Engineering, 45(3), 2761–2772. https://doi.org/10.32604/csse.2023.028559

Tian, H., Huang, N., Niu, Z., Qin, Y., Pei, J., & Wang, J. (2019). Mapping Winter Crops in China with Multi-Source Satellite Imagery and Phenology-Based Algorithm. Remote Sensing, 11(7), 820. https://doi.org/10.3390/rs11070820

Trommsdorff, M., Gruber, S., Keinath, T., Hopf, M., Hermann, C., Schönberger, F., Högy, P., Zikeli, S., Ehmann, A., Weselek, A., Bodmer, U., Rösch, C., Ketzer, D., Weinberger, N., Schindele, S., & Vollprecht, J. (2022). Agrivoltaics: Opportunities for Agriculture and the Energy Transition. Fraunhofer Institute for Solar Energy Systems ISE.

Vasudevan, A., Kumar, D. A., & Bhuvaneswari, N. S. (2016). Precision farming using unmanned aerial and ground vehicles. 2016 IEEE Technological Innovations in ICT for Agriculture and Rural Development (TIAR), 146–150. https://doi.org/10.1109/TIAR.2016.7801229

Vélez, S., Vacas, R., Martín, H., Ruano-Rosa, D., & Álvarez, S. (2022). High-Resolution UAV RGB Imagery Dataset for Precision Agriculture and 3D Photogrammetric Reconstruction Captured over a Pistachio Orchard (Pistacia vera L.) in Spain. Data, 7(11), 157. https://doi.org/10.3390/data7110157

Wang, X., Zhang, J., Xun, L., Wang, J., Wu, Z., Henchiri, M., Zhang, S., Zhang, S., Bai, Y., Yang, S., Li, S., & Yu, X. (2022). Evaluating the Effectiveness of Machine Learning and Deep Learning Models Combined Time-Series Satellite Data for Multiple Crop Types Classification over a Large-Scale Region. Remote Sensing, 14(10), 2341. https://doi.org/10.3390/rs14102341

Weselek, A., Bauerle, A., Hartung, J., Zikeli, S., Lewandowski, I., & Högy, P. (2021). Agrivoltaic system impacts on microclimate and yield of different crops within an organic crop rotation in a temperate climate. Agronomy for Sustainable Development, 41(5), 59. https://doi.org/10.1007/s13593-021-00714-y

Weselek, A., Ehmann, A., Zikeli, S., Lewandowski, I., Schindele, S., & Högy, P. (2019). Agrophotovoltaic systems: Applications, challenges, and opportunities. A review. Agronomy for Sustainable Development, 39(4), 35. https://doi.org/10.1007/s13593-019-0581-3

Wu, B., Zhang, M., Zeng, H., Tian, F., Potgieter, A. B., Qin, X., Yan, N., Chang, S., Zhao, Y., Dong, Q., Boken, V., Plotnikov, D., Guo, H., Wu, F., Zhao, H., Deronde, B., Tits, L., & Loupian, E. (2023). Challenges and opportunities in remote sensing-based crop monitoring: A review. National Science Review, 10(4), nwac290. https://doi.org/10.1093/nsr/nwac290

Zhang, C., & Kovacs, J. M. (2012). The application of small unmanned aerial systems for precision agriculture: A review. Precision Agriculture, 13(6), 693–712. https://doi.org/10.1007/s11119-012-9274-5

Prediction of nitrogen-fixing bacteria and phosphorus-solubilising bacteria in the soil using UAV multispectral images

David Mostaza-Colado[a,*], Alejandro Alonso-Conde[a], Elisa Gómez[a], Pedro Muñoz[a], José Marín[b], Pedro V. Mauri Ablanque[a]

[a] Agro-environmental Research Department, IMIDRA (Madrid Institute for Research and Rural Development in Food and Agriculture), Alcalá de Henares, Spain.

[b] Area Verde MG Projects S.L., Madrid, Spain.

* Corresponding author. Email: david.mostaza@madrid.org

Abstract

Due to climate change, plants are impacted by drought and diseases, resulting in biochemical and physiological consequences for commercial crops. These effects influence parameters including germination, vitality, and yield, in addition to seed composition and nutrition. The use of plant biostimulants to improve the composition and structure of the soil is increasingly common, as it favors the development of the crop and improves its health and productivity. Nitrogen-fixing bacteria (NFB) and phosphorus-solubilising bacteria (PSB) are pivotal components of sustainable agricultural systems due to their capacity to enhance N and P availability to host plants; therefore, increasing the chances of adaptation of the crops. Furthermore, the use of new technologies such as UAV and multispectral images makes it easier to monitor the crop, treatments and assess whether they are being effective.

Within the framework of the SOCIAL-AGRI subproject, IMIDRA aims to evaluate the microbiological content of a nude soil, as an approach to remote sensing of the microbial biomass present in it. We will take soil samples to estimate the number of colonies forming units (CFU) for NFB and PSB bacteria in each plot, and correlate it with known indices (NDVI, eNDVI, MPRI, GNDVI and OSAVI) calculated from the multispectral images of nude soil gathered by drone. Expected results will show which plot has the highest number of CFU and if it can be correlated with some of the indices.

Future works aim to assess more soils along with known and new developed indices to estimate the microbial biomass of NFB and PSB.

Keywords: NFB, PSB, vegetation indexes.

1. Introduction

The utilisation of multispectral imagery to estimate soil microbial biomass represents an intriguing application of remote sensing in the fields of agriculture and soil science. Remote sensing is the process of acquiring information about an object, area or phenomenon through the analysis of data obtained by devices that are not in direct contact with the object under study (Hunt et al., 2010). Spectroscopy is a technique that allows the interaction between electromagnetic radiation and matter to be measured, thereby enabling the properties and composition of that matter to be determined. Multispectral images are those that capture information in different bands of the electromagnetic spectrum, beyond what is visible to the human eye. These images can be obtained from platforms such as satellites or drones and provide data on the reflectance of the Earth's surface at different wavelengths (red, blue, green, NIR, REDGE, etc.) (Pereira et al., 2022). Finally, soil microbial biomass refers to the quantity of living microorganisms present in the soil, including bacteria, fungi and other single-celled organisms. These microorganisms play a pivotal role in biogeochemical cycles and soil health (Basu et al., 2021; Dubey et al., 2019; Kumar and Verma, 2019; Malik et al., 2017; Shah et al., 2021; Smith et al., 2015).

The relationship between multispectral imaging and microbial biomass is based on the capacity of microorganisms to modify soil reflectance at specific wavelengths. For instance, certain microbial pigments may absorb or reflect light in disparate ways from other soil components, which can be discerned through multispectral image analysis (Lan et al., 2017; Polerecky et al., 2009; Schwieterman et al., 2015). To ascertain soil microbial biomass from multispectral images, analytical techniques that correlate reflectance in different bands with direct measurements of microbial biomass obtained in the laboratory are employed. These techniques may include the utilisation of statistical models or machine learning algorithms (Aji et al., 2021;

Biney et al., 2021; Solano-Alvarez et al., 2022).

The applications and benefits of this approach are as follows: The estimation of soil microbial biomass from multispectral imagery has the potential to be applied in several diverse contexts, including the monitoring of soil health, the assessment of soil quality in agricultural systems, and the planning of more sustainable soil management practices. Furthermore, it offers a non-invasive and efficient method for mapping the spatial distribution of microbial biomass at different scales (de Souza et al., 2022).

Within the framework of SOCIAL-AGRI subproject (participated by IMIDRA) we want to test the feasibility of estimating the content of N-fixing (NFB) and P-solubilizing (PSB) bacteria in the soil, so that we can have an approximation of the effects in the crop and the soil. SOCIAL-AGRI subproject belongs to AGRICULTURA 6.0 project, that aims to 1) integrate sensing technologies for monitoring the environmental and soil parameters to improve the competitiveness and efficiency of crops, 2) develop a computing continuum fog/edge/cloud-based architecture to compute/process, store data and make AI models for behaviour patterns and diseases early detection in plants, and 3) define a framework for the involved actors in a Woody Crop Observatory and evaluate the impact of Woody Crop Observatory for different sectors of society involved in the Living Lab; along with the other partners of the AGRICULTURA 6.0 project: Universitat Politècnica de València (UPV) subproject SOLUTION, and Universitat de València (UV) subproject 2CANDIS.

Therefore, the AGRICULTURA 6.0 project (http://agricultura6.es) can be considered as an interdisciplinary and multidisciplinary project because each group has its own research area that complements the other two. Additionally, each group is already composed by experts in different areas and some of those experts work on different complementary areas. AGRICULTURA 6.0 can be considered as a set of interrelated multidisciplinary activities of individual partners that makes essential the joining of experts from different fields (agronomy, environmental sciences, education, ICT, sensors, next generation of networks and artificial intelligence) that will work in a coordinated way.

2. Materials and Methods

The “El Encín” farm belongs to IMIDRA (public research organization of the Community of Madrid) and is located in the town of Alcalá de Henares, Spain. The farm has several experimental plots, one of them dedicated to the SOCIAL-AGRI subproject (https://agricultura6.es/socialagri-2/) with olive trees, vines and fruit trees (40.524148, -3.287676) (**Figure 1**). The SOCIAL-AGRI crops are long-term plantations that have been implemented for more than 10 years, as shown in **Table 1**.

Furthermore, the SOCIAL-AGRI subproject requires a series of data on soil temperature, humidity and conductivity that are captured by a series of sensors developed within the project and installed in the woody crop plots (A to C) (**Figure 1** and **Figure 2**). These data, in combination with those obtained through multispectral imaging by drone, and the soil samples taken to establish the colony forming unit (CFU) counts in diluvial sand (DS) per gram soil (dry weight) (CFU/g DS) of N-fixing and P-solubilizing bacteria, will feed the AI for decision making and scenario modelling.

On one hand, we will employ the Ashby culture media for the analysis of viable bacteria in the soil and to detect atmospheric NFB (Aquilanti et al., 2004). The components of the medium are briefly detailed as follows: glucose 2.0%, $CaCO_3$ 0.5%, K_2HPO_4 0.02%, $MgSO_4$ 0.02%, NaCl 0.02%, K_2SO_4 0.01%, and bacteriological agar 1.5%. The pH of the medium needs to be adjusted to 7.4. For the enumeration of PSB we will employ the National Botanical Research Institute’s Phosphate solid media (NBRIP). The phosphate solubilisation ability will be determined through plate assay: glucose 1.0%, $Ca_3(PO_4)^2$ 0.5%, $MgCl_2 \cdot 6H_2O$ 0.5%, $(NH_4)^2SO_4$ 0.01%, $MgSO_4 \cdot 7H_2O$ 0.025%, KCl 0.02%, and bacteriological agar 1.5% (Nautiyal, 1999). The pH of the medium should be adjusted to 7.0.

On the other hand, the Most Probable Number (MPN) technique will be employed to quantify soil bacteria (Woomer, 2018). To accomplish this, decimal dilutions will be prepared in a sterile saline solution of 0.9% (w/v). The initial dilution involves mixing 10.00 g of soil with 90 mL of sterile saline solution. Afterward, the mixture will be homogenised using an orbital shaker operating at 120 rpm while maintaining a temperature of (28.0 ± 0.5) ˚C for 60 min. A series of dilutions spanning from 103 to 105 will be established. For each decimal dilution, 5 sets of 5 µL each will be inoculated. Subsequently, these culture media will be subjected to incubation at (32.0 ± 1.0) ˚C for a period of 2 weeks.

The choice of these protocols is based on previous works of the IMIDRA research group, as they throw good results on the determination of CFU in this type of soils (Gómez et al., 2024). But, since the project is

still in the development phase (to be completed by the end of 2024), we are still working on the quantification of the microbiota in the soil and its correlation with the vegetation and soil indices obtained through drone flights and AI data analysis.

Regarding the process of capturing multispectral data, we are using a DJI Phantom 4 Pro RTK UAV (SZ DJI Technology Co., Ltd., Shenzhen, China) with one RGB camera and a 5-camera multispectral array covering the Blue (B), Green (G), Red (R), Red Edge (REDGE) and Near Infrared (NIR) bands, all with a 2 MP global shutter and a three-axis stabilizer. The flight altitude is 20 m and DJI GS Pro software is used for flight planning and execution. The processing of the images to create the orthomosaic is performed with OpenDroneMap's WedODM, and the analysis of the multispectral images is performed with ArcMap.

Figure 1. Location of SOCIAL-AGRI (A to C) fields.

Table 1. Crops cultivated in SOCIAL-AGRI project.

Project	Field	Crop
SOCIAL-AGRI	A	Olive trees
SOCIAL-AGRI	B	Vines
SOCIAL-AGRI	C	Fruit trees

a **b** **c**

Figure 2. a) sensor; b) gateway; c) digital twin (SOCIAL-AGRI's living lab).

3. Results and Discussion

The results of the trial are not yet conclusive since there is insufficient information available. The SOCIAL-AGRI sensors and flights started to be executed in mid-2023. The drone flights have made it possible to obtain digital models of the olive groves, vineyards and fruit orchards, so that they can serve as the basis for the digital twin (**Figure 3**). Once these models have been processed, the data obtained from the field sensors will be incorporated. Additionally, multispectral imaging data will be processed along with soil microbiological data for AI to determine if any correlation exists (**Figure 4**). This will provide information to predict possible problems in the crop or to determine the effect of the treatments and work done in the plots for their management.

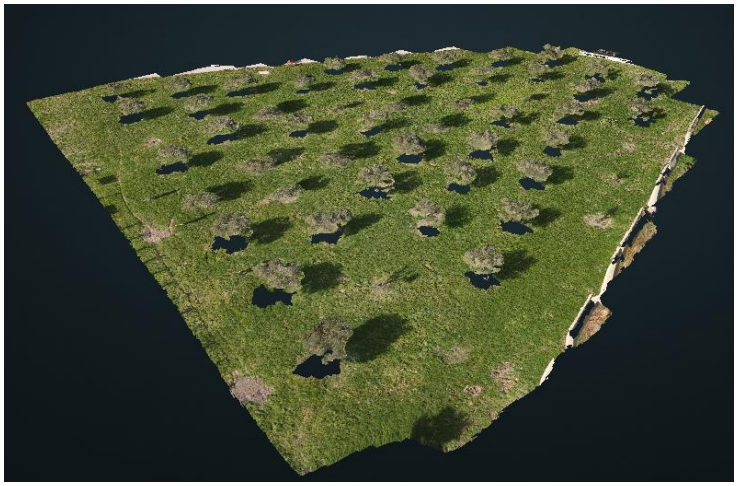

Figure 3. SOCIAL-AGRI 3D model of the olives orchard. Image captured February 2024.

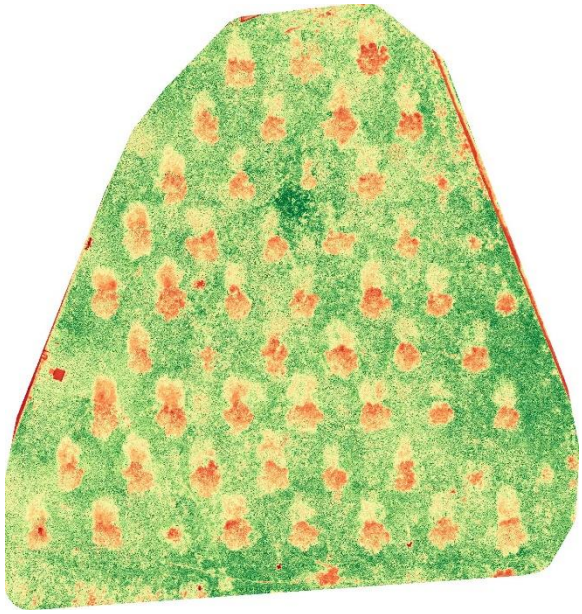

Figure 4. SOCIAL-AGRI olives orchard. Image captured February 2024.
eNDVI index used (range from 0 to 0.5).

4. Conclusions

AGRICULTURA 6.0 projects expects an important scientific and technical impact thanks to the introduction of new technologies and methods for smart agriculture to permit the digitalization of farming

systems and the creation of a Woody Crop Observatory to enhance the productivity and competitiveness. Additionally, the use of Next Generation-based architecture and intelligent tools for Smart Agriculture will allow the development of a demo tool for data visualization. Finally, the establishment of the Living Lab will permit the integration of citizens in the framework of AGRICULTURA 6.0 and the Woddy Crop Observatory.

Acknowledgements

SOCIAL-AGRI (AGRICULTURA 6.0) research project is funded by MCIN/AEI /10.13039/501100011033 and by the European Union Next Generation EU/ PRTR.

References

Aji, A., Iryanthony, S.B., Akhsin Budi Nur Sidiq, W., Trihatmoko, E., 2021. Relationship Between NDVI and the Microbial Content of Soil in Detecting Fertility Level at Semarang Regency, Jawa Tengah, Indonesia. Nature Environment and Pollution Technology 20, 425–432.

Aquilanti, L., Favilli, F., Clementi, F., 2004. Comparison of different strategies for isolation and preliminary identification of Azotobacter from soil samples. Soil Biol Biochem 36, 1475–1483.

Basu, S., Kumar, G., Chhabra, S., Prasad, R., 2021. Role of soil microbes in biogeochemical cycle for enhancing soil fertility. In: New and Future Developments in Microbial Biotechnology and Bioengineering. Elsevier, pp. 149–157.

Biney, J.K.M., Saberioon, M., Borůvka, L., Houška, J., Vašát, R., Chapman Agyeman, P., Coblinski, J.A., Klement, A., 2021. Exploring the Suitability of UAS-Based Multispectral Images for Estimating Soil Organic Carbon: Comparison with Proximal Soil Sensing and Spaceborne Imagery. Remote Sens (Basel) 13, 308.

de Souza, A.E.S., Barbosa Júnior, M.R., de Almeida Moreira, B.R., da Silva, R.P., Lemos, L.B., 2022. UAV Multispectral Data: A Reliable Approach for Managing Phosphate-Solubilizing Bacteria in Common Bean. Agronomy 12, 2284.

Dubey, A., Malla, M.A., Khan, F., Chowdhary, K., Yadav, S., Kumar, A., Sharma, S., Khare, P.K., Khan, M.L., 2019. Soil microbiome: a key player for conservation of soil health under changing climate. Biodivers Conserv 28, 2405–2429.

Gómez, E., Alonso, A., Sánchez, J., Muñoz, P., Marín, J., Mostaza-Colado, D., Mauri, P. V., 2024. Application of Biostimulant in Seeds and Soil on Three Chickpea Varieties: Impacts on Germination, Vegetative Development, and Bacterial Facilitation of Nitrogen and Phosphorus. Life 14, 148.

Hunt, E.R., Hively, W.D., Fujikawa, S., Linden, D., Daughtry, C.S.T., McCarty, G., 2010. Acquisition of NIR-Green-Blue Digital Photographs from Unmanned Aircraft for Crop Monitoring. Remote Sens (Basel) 2, 290–305.

Kumar, A., Verma, J.P., 2019. The Role of Microbes to Improve Crop Productivity and Soil Health. pp. 249–265.

Lan, S., Ouyang, H., Wu, L., Zhang, D., Hu, C., 2017. Biological soil crust community types differ in photosynthetic pigment composition, fluorescence and carbon fixation in Shapotou region of China. Applied Soil Ecology 111, 9–16.

Malik, Z., Ahmad, M., Abassi, G.H., Dawood, M., Hussain, A., Jamil, M., 2017. Agrochemicals and Soil Microbes: Interaction for Soil Health. pp. 139–152.

Nautiyal, C.S., 1999. An efficient microbiological growth medium for screening phosphate solubilizing microorganisms. FEMS Microbiol Lett 170, 265–270.

Pereira, F.V., Martins, G.D., Vieira, B.S., de Assis, G.A., Orlando, V.S.W., 2022. Multispectral images for monitoring the physiological parameters of coffee plants under different treatments against nematodes. Precis Agric 23, 2312–2344.

Polerecky, L., Bissett, A., Al-Najjar, M., Faerber, P., Osmers, H., Suci, P.A., Stoodley, P., de Beer, D., 2009. Modular Spectral Imaging System for Discrimination of Pigments in Cells and Microbial Communities. Appl Environ Microbiol 75, 758–771.

Schwieterman, E.W., Cockell, C.S., Meadows, V.S., 2015. Nonphotosynthetic Pigments as Potential Biosignatures. Astrobiology 15, 341–361.

Shah, K.K., Tripathi, S., Tiwari, I., Shrestha, J., Modi, B., Paudel, N., Das, B.D., 2021. Role of soil microbes in sustainable crop production and soil health: A review. Agricultural Science and Technology 13, 109–118.

Smith, P., Cotrufo, M.F., Rumpel, C., Paustian, K., Kuikman, P.J., Elliott, J.A., McDowell, R., Griffiths, R.I., Asakawa, S., Bustamante, M., House, J.I., Sobocká, J., Harper, R., Pan, G., West, P.C., Gerber, J.S., Clark, J.M., Adhya, T., Scholes, R.J., Scholes, M.C., 2015. Biogeochemical cycles and biodiversity as key drivers of ecosystem services provided by soils. SOIL 1, 665–685.

Solano-Alvarez, N., Valencia-Hernández, J.A., Vergara-Pineda, S., Millán-Almaraz, J.R., Torres-Pacheco, I., Guevara-González, R.G., 2022. Comparative Analysis of the NDVI and NGBVI as Indicators of the Protective Effect of Beneficial Bacteria in Conditions of Biotic Stress. Plants 11, 932.

Woomer, P.L., 2018. Most Probable Number Counts. pp. 59–79.

Finnish future farm - A physical and virtual co-creation platform for RDI, education and business acceleration in smart farming

Hannu Haapala[a,*], Annimari Lehtomäki[a], Jyrki Kataja[a]

[a] Jamk University of Applied Sciences, Department of Technology, Institute of Bioeconomy, Saarijärvi, Finland

* Corresponding author. Email: hannu.haapala@jamk.fi

Abstract

The Finnish Future Farm (FFF) project, running from 2023 to 2026, aims to develop a unique co-creation platform for RDI, education, and startup acceleration in Smart Farming technologies. Upon completion, FFF will offer a versatile testbed and Living Lab for User-Centered Design, integrating both a physical Smart Farm and a Digital Twin. The primary goal of FFF is to accelerate the adoption of Smart Farming technologies, contributing to the realization of the UN Sustainable Development Goals (SDGs). The Smart Farm, along with a network of partner farms, will analyze these technologies through a heavily instrumented setup. The Digital Twin will involve integrated use of GIS data and a metaverse environment.

A Multi-Actor Approach will be employed, engaging experts and users in collaborative use-cases to improve the acceptability of the solutions. The project focuses on technologies near market readiness (Technology Readiness Level 7+), developed in collaboration with leading companies like Valtra Inc., AgcoPower Inc., and Neste Inc., as well as innovative startups. These near-market solutions will be analyzed to identify adoption challenges, followed by the application of RDI and supporting actions. Tailored education for users, designers, and marketers will be provided as needed. Business development and acceleration services will be offered through the BioBoosters acceleration program, which includes investors and venture capital.

The FFF project's development route is reported, including the Smart Farm and the Smart Bioeconomy Testbed, a member of the Nordic Testbed Network since 2022. The Smart DIH (Digital Innovation Hub) service platform, developed under the Smart AgriHubs HEU project, is also detailed. Conclusions regarding the potential establishment of a future center of excellence are outlined. Located in Central Finland at the Bioeconomy Campus in Saarijärvi, FFF provides an excellent testing environment for technologies, including challenging soil variations, plant production, animal husbandry, fields, forests, and waters.

Key words: Smart Farming, Testbed, Digital Twin, Education, Business Accelerator

1. Introduction

Technologies related to sustainable development in agriculture have existed for a long time, but their practical application has been slow (Haapala 2013). For example, technologies necessary for precision farming have been available since the 1990s (Haapala 1995), but only a few have been widely adopted (Anand et al. 2023). Precision farming technologies such as field navigation and yield mapping are the most utilized, but site-specific control of production inputs is relatively underutilized (Talero Sarmiento, Parra-Sánchez & Lamos-Diaz, 2022). Smart farming, which utilizes precision farming technologies and intensive data processing, has gained attention in recent years. However, the adoption of smart farming also faces new obstacles, such as poor data availability and practical challenges of fair data economy.

Failure to use technologies that promote sustainability leads to unrealized potential and unmet Sustainable Development Goals (SDGs). Additionally, if there is a failure in the adoption phase, all the effort put into developing these technologies is virtually wasted. Thus, promoting adoption is desirable and economically viable.

Overcoming this challenge requires actions to eliminate obstacles to the adoption of smart technologies. These barriers exist in various areas related to the acceptability of solutions (Nielsen 1993), not solely economic, which is often cited as an explanation for poor adoption (Haapala, Pesonen & Nurkka, 2006; Haapala & Pasila, 2009). In agriculture, the end users of innovations are primarily farmers, who are often conservative and cautious adopters of new technologies. Fundamental reasons are related to lacking trust and low level of willingness to take risks (Wielinga et al., 2017). New technology itself induces fear and uncertainty, leading to reluctance in investment. Decision-making suffers from a lack of reliable and unbiased information regarding the effectiveness of alternative solutions.

Two projects were initiated. The goal of the development project for the Smart Farm at the Bioeconomy Campus (2021–2023) was to establish a unique hub for smart agriculture technology expertise in Tarvaala, Saarijärvi, in Central Finland. The resulting Smart Farm would provide an opportunity to test, develop, and demonstrate near-market (TRL 7-) technologies and services. The aim was to remove barriers to their adoption and accelerate innovation in the sector, significantly increasing the benefits for farmers and the related agricultural industry.

The Smart Farm project laid the groundwork for the Finnish Future Farm (FFF) project that commenced immediately after it. The FFF (2023-2026) involves a physical Smart Farm linked to a digital twin of the farm and extensive education and business acceleration sections. (Fig. 1)

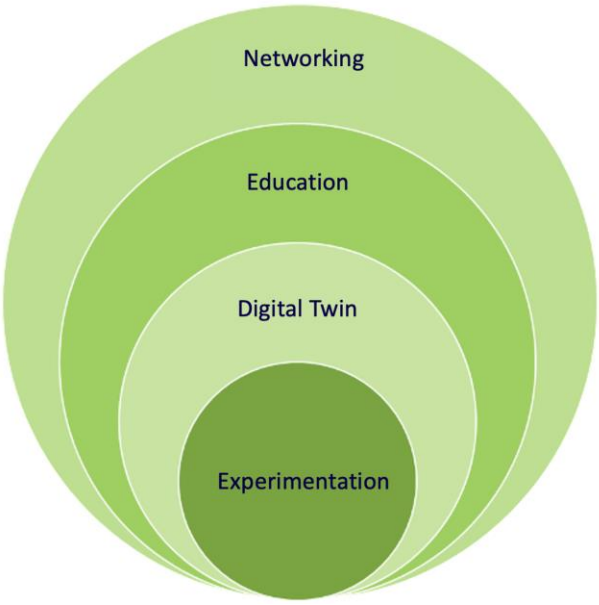

Figure 1. FFF project structure. The Smart Farm forms the foundation for experimentation upon which a virtual digital twin is created, along with an educational and networking component that utilizes them (Haapala et al. 2024).

The primary goal of FFF is to accelerate the adoption of Smart Farming technologies, contributing to the realization of the UN Sustainable Development Goals (SDGs). The Smart Farm, along with a network of partner farms, will analyze these technologies through a heavily instrumented setup. The Digital Twin will involve integrated use of GIS data and a metaverse environment.

The FFF project's development route is reported, including the Smart Farm and the Smart Bioeconomy Testbed, a member of the Nordic Testbed Network since 2022. Conclusions regarding the potential establishment of a future center of excellence are outlined.

2. Materials and Methods

The construction of the Smart Farm began in 2021 with a thorough needs definition. The starting point was the recognition of the necessity for abundant high-quality data, as Smart Farming fundamentally relies on the generation and utilization of big data (Wolfert et al., 2017). The objective was to fine-tune the functionalities required at the Smart Farm using various essential data types, laying the groundwork for future operations aimed at promoting broader adoption, in line with our vision.

Given that precision farming is crucial for achieving the Sustainable Development Goals (SDGs), we prioritized the collection of sensor data essential for its implementation, alongside data generated by tractors and machinery. Additionally, the performance of data transmission was measured, which will become increasingly critical with the future rise in automation.

During the growing seasons of 2022 and 2023, data was intensively collected from approximately 16 hectares of test plots where barley was cultivated. Barley was chosen as the test crop due to its prevalence as a typical cereal crop in the area. Regular measurements were taken from the soil, crops, and machinery equipped with ISOBUS technology.

Precision farming implementation was compared to traditional farming methods at the highly variable,

thus challenging, Huipuri test plot. Half of the plot was subjected to precision fertilization, while the other half was cultivated using a standard amount of fertilizer. The Maatalo plot was designated as an experimental area. (Figure 2)

Figure 2. Test Plots. On the left, a drainage map; on the right, the division of the Huipuri field for precision farming and traditional cultivation.

Various measurement instruments were employed in the test plots, including 20 wireless soil sensors (Figure 3), drone imaging equipped with RGB, multispectral, and thermal cameras, soil scanning equipment, satellite imagery, and tractor telematics data. Soil compaction was measured using positioned penetrometer measurements.

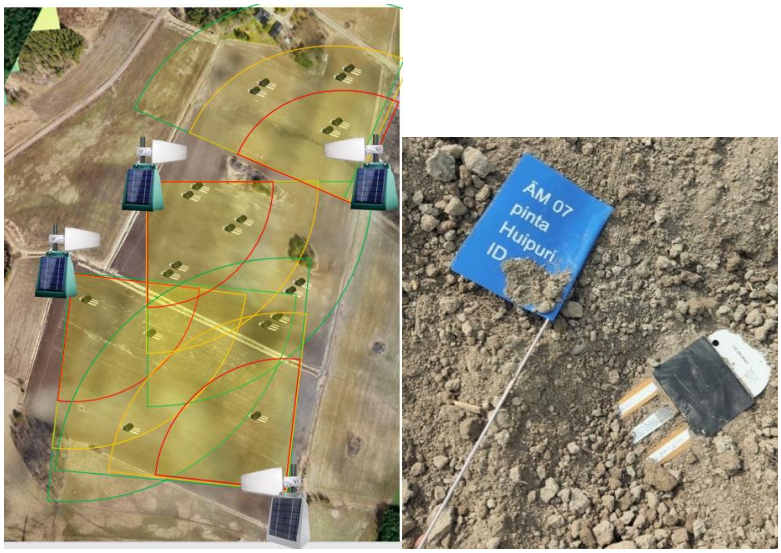

Figure 3. Placement of wireless soil sensors in the experimental plots (left). The sensor and its labeling (right).

3. Results and discussion

Automated field navigation with headland automation was compared to traditional manual driving methods (Figure 4). Using Geographic Information Systems (GIS) and data analysis, various maps, including profitability and energy consumption maps, were generated from the collected data.

Figure 4. Route map during the sowing process. Automatic steering on the left, manual steering on the right.

Precision fertilization was applied. Based on soil measurements (including soil sensors, soil scanning, soil sampling, and drone imaging), the selected fertilizer levels were selected (Figure 5).

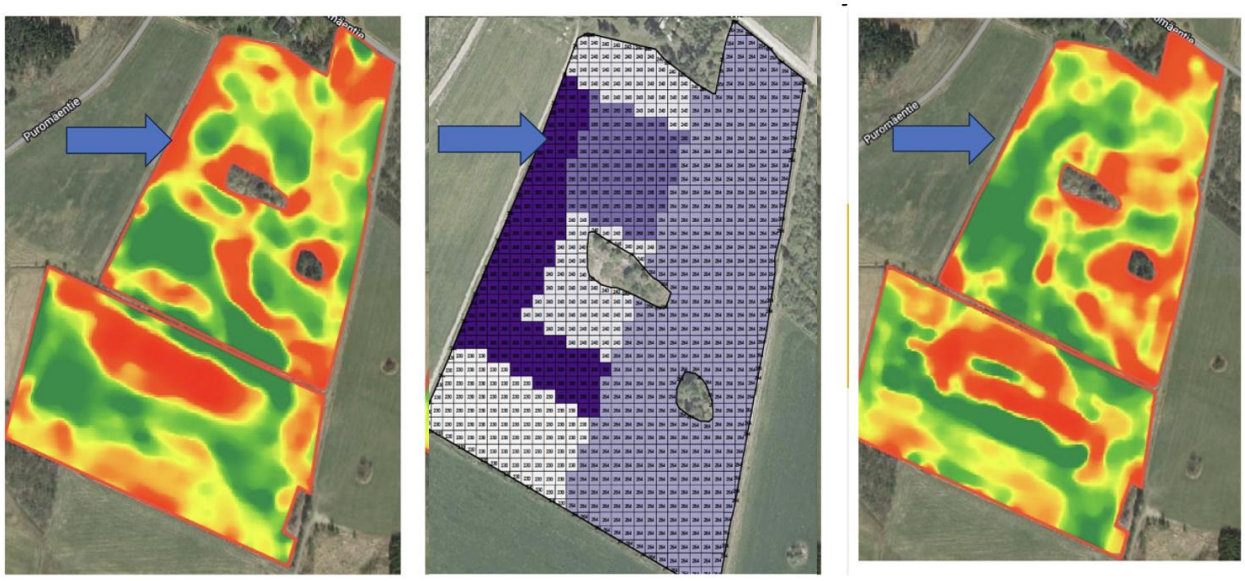

Figure 5. Precision farming in the experimental plots in 2022 and 2023. On the left, the yield map for 2022; in the middle, the fertilization map for 2023; on the right, the yield map for 2023.

In a data-driven smart agriculture system, data management is a key element. The farm's information system should be able to serve internal processes of the farm, e.g. FMIS, as well as external data users. To ensure that data is clearly in the farmer's possession and accessible to different users, it was decided to develop a specific Farmer's Data Warehouse, through which the farmer can license their data to the desired destination via a data intermediation service. The Farmer's Data Warehouse was implemented using example data from drone imaging and soil-sensor-produced soil data (Figure 6).

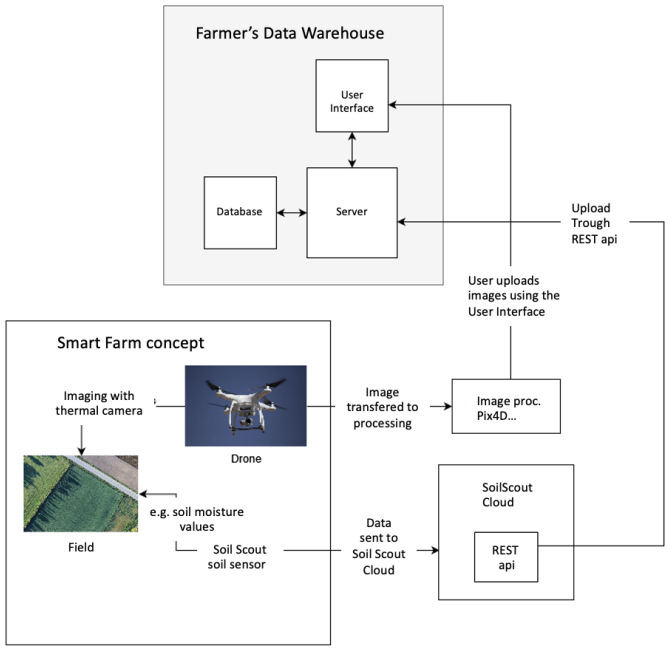

Figure 6. Farmer's Data Warehouse, featuring drone images and soil data produced by soil sensors.

To test the fluency of data transfer between the Farmer's Data Warehouse and auxiliary systems, the operation of a novel data intermediating system compliant with the new EU data regulations was demonstrated in collaboration with partner companies (Dataspace Europe, Soil Scout and Yield Systems).

Usability if 5G in machinery control was measured. In the 5G measurements, the signal coverage and usability were verified through field measurements and simulations. These measurements demonstrated that the tested measurement method, terminal devices, and measurement software were effective. Test setups validated the effects of buildings, forest canopy, and varying terrain elevations on the coverage of the 5G network signal (Figure 7).

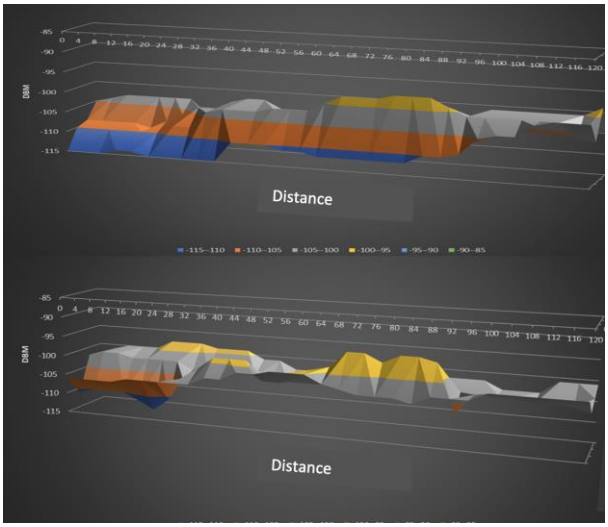

Figure 7. Field strength values (dBm) in terrain measurements at antenna heights of 2 and 3.5 meters. The yellow color indicates best values.

Various economics maps were generated from the data using GIS software. All costs and income were calculated for defined grids, e.g. 10x10 metres. The data also included the work time spent in each grid point since it was available from the telemetry data of the tractor. (Figures 8-9)

Figure 8. Economic maps. On the left: return map: on the right hourly wage map. Both on a 10x10 meter grid.

To fulfil the requirements set by the use cases, in FFF, a Multi-Actor Approach will be employed, engaging experts and users in collaborative use-cases to improve the acceptability of the solutions. The project focuses on technologies near market readiness (Technology Readiness Level 7+), developed in collaboration with leading companies like Valtra Inc., AgcoPower Inc., and Neste Inc., as well as innovative startups. These near-market solutions will be analyzed to identify adoption challenges, followed by the application of RDI and supporting actions. Tailored education for users, designers, and marketers will be provided as needed. Business development and acceleration services will be offered through the BioBoosters acceleration program, which includes investors and venture capital.

In the Finnish Future Farm (FFF) project, the development of the digital twin began with selecting the development environment. A metaverse was chosen, alongside related GIS software. These components are being integrated into a visually feasible solution with the help of gaming and data analytics experts. The resulting digital twin will encompass the smart farm outlined in the previous descriptions.

Example use cases are utilized to build the system incrementally, mirroring the step-by-step approach used for the physical farm. The solution incorporates open-source features from public sources such as the National Land Survey, the Finnish Meteorological Institute, and includes simulation models of plant growth and other biological systems. The heavily instrumented smart farm serves as a primary source of the necessary data, while a network of partner farms is also used to gather independent data. (Fig. 10)

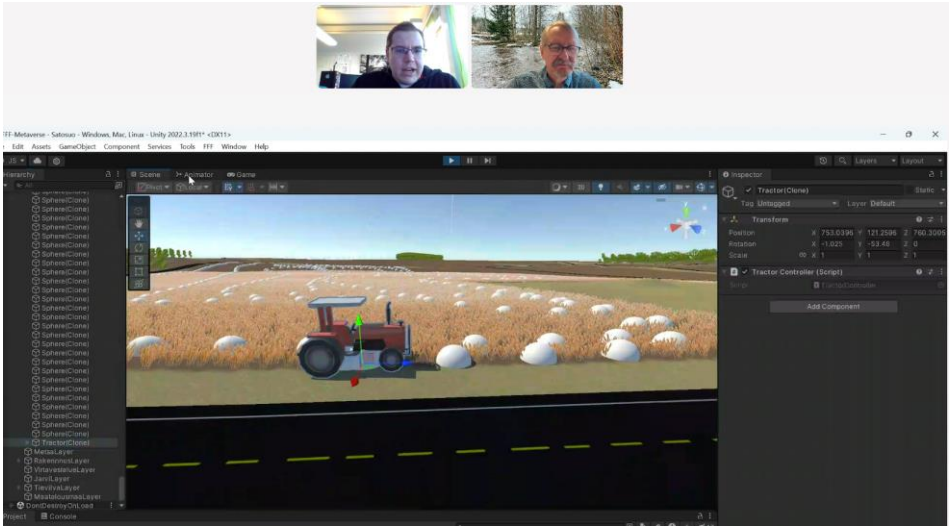

Figure 10. Developing the Digital Twin of the Tarvaala Smart Farm. GIS features are presented in a multiverse environment.

In the Finnish Future Farm (FFF) project, there are two work packages that build on the physical smart farm and the digital twin: the Education and Networking work packages (see Fig. 1).

The Education package develops simulation pedagogies that utilize the measured and simulated data to create use cases for profiled learners. The goal is to produce effective tools for different kinds of educational customers. To achieve this, four pilot groups will be run during the project.

The Networking package includes the further development and application of the existing BioBoosters business accelerator by Jamk. In addition to business acceleration cases with innovative startups and leading companies, bootcamps, hackathons, and other innovation events will be organized (Fig. 11).

Figure 11. Smart Bioeconomy Bootcamp in May 2024, with 22 participants from 14 nationalities.

The main goal of the projects was to establish a foundation for a Smart Farming competence hub that would accelerate the adoption of smart technologies on farms in alignment with the United Nations Sustainable Development Goals (SDGs). Achieving this required understanding the types of data collected on a farm and determining how the Smart Farm could handle it. This goal was successfully addressed using the example data available. Various data types, including sensor data, telemetry data, and drone imagery, were made accessible to the Smart Farm through the developed Farmer's Data Warehouse. Data transfer to external systems was achieved in various ways, incorporating principles of fair data economy according to forthcoming EU data regulations. This was demonstrated for the first time in Europe with an official data intermediation service (Tritom by Dataspace Europe Ltd). While 5G data transmission presented challenges, it was functional in some cases, aligning with current research (Heikkilä et al., 2022).

Through intelligent data analysis, various metrics were derived from the Smart Farm's data and could be presented in map format. These metrics can be used in the future to demonstrate and evaluate the benefits of SDG technologies. The economic maps of precision farming were the first reported in literature, emphasizing economic benefits as a powerful motivator for farmers to invest in smart farming technologies (Garcia et al., 2023).

The developed Smart Farm concept is international. The Nordic Testbed Network provides a valuable channel to connect with experts in smart agriculture and other related smart technology application fields. The concept is closely associated with R&D and education services, which will be offered in the form of a Digital Innovation Hub (DIH) in the future. DIH services were developed simultaneously with the EU-funded SAH project (SAH 2024), where Jamk laid the groundwork for defining the necessary services for various target groups.

4. Conclusions

The core of the established Smart Farm concept lies in the physical Smart Farm with continuous comprehensive measurements and monitoring, allowing it to be used extensively for testing and further development of Smart Farming technologies and practices. The partner farm network that is under construction enables real-life experimentation in a Living Lab style, providing insights into end-users' use-scenarios and requirements for new technologies. The collaborative network is an integral part of the Smart Farm concept. Through collaboration, the Smart Farm has already been involved in other networks promoting agricultural data economy, leading to collaborative projects where the connection between the Smart Farm and the agricultural data space is tested and developed concretely together.

The Finnish Future Farm (2023–2026) commenced based on the foundation of the physical smart farm, incorporating a digital twin of the farm. Both will be utilized for research, development, and innovation activities as well as education. Thus, the developed smart farm concept contributed to the formation of an expertise hub that significantly improves the profitability and environmental friendliness of farms in the future. The commitment of companies to continue the project indicates that the project has succeeded in its main objectives. The expanding startup network, together with leading companies, ensures the viability of the concept in the future.

Acknowledgments

We thank the project's main funder, the Regional Council of Central Finland, for the REACT and JTF funding we received, without which the projects would not have been realized. We also thank the projects' co-implementer, the Northern Central Finland Vocational College (POKE), whose fields and personnel made the experiments possible, and our partners, Valtra Ltd, Mtech Ltd, SoilScout Ltd, MTK Ry, AgcoPower, Neste, and the city of Saarijärvi, without whom the projects would not have succeeded.

References

Anand, J., Yusoff, N., Ab Ghani, H. & Thoti, K. 2023 Technological Applications in Smart Farming: A Bibliometric Analysis. Advanced and Sustainable Technologies (ASET) eISSN 2976-2294. Volume 2, No 2, December 2023. pp. 30-40.

Garcia, D., Cangirana, L., Queiroz, R. & Gimenes, R. 2023. Precision Farming technologies adoption: A state of the art survey. Boletim de conjuntura, 16(47), pp. 284–304.

Haapala 1995. Position Dependent Control (PDC) of Plant Production. Agric.Sci. in Finland 4: 239-350.

Haapala, H., Pesonen, L. & Nurkka, P. 2006. Usability as a Challenge in Precision Agriculture - case study: an ISOBUS VRT. Agricultural Engineering International: the CIGR Ejournal. 9 p.

Haapala, H. & Pasila. A. 2009. Agro Living Lab - an R&D platform- ensuring acceptability of new technology among farmers. 67th International Conference on Agricultural Engineering LAND.TECHNIK AgEng 2009. Hannover. Germany.

Haapala, H. 2013. Speeding up innovation in agricultural IT. Journal of Agricultural Engineering. Vol XLIV. p. 137-139.

Haapala, H., Kataja, J., Pirttiniemi, J., Sarvela, K., Ludwig, G., Appelgrén, I., Kalmari, J., Taavitsainen, M. & Vesiluoma, S. 2024. How and why we built our Smart Farm. In. Maataloustieteen päivät 2024. Suomen Maataloustieteellisen Seuran Tiedote 42. 8 p.

Heikkilä M, Suomalainen J, Saukko O, Kippola T, Lähetkangas K, Koskela P, Kalliovaara J, Haapala H, Pirttiniemi J, Yastrebova A, Posti H. Unmanned Agricultural Tractors in Private Mobile Networks. Network. 2022; 2(1):1-20. https://doi.org/10.3390/network2010001

Nielsen, J. 1993. Usability Engineering. Academic Press Inc. 362 p.

SAH 2024. Unleashing the innovation potential for the digital transformation of the European Agrifood Sector. https://www.smartagrihubs.eu/. Cited 29.2.2024.

Talero Sarmiento, L., Parra-Sánchez, D. & Lamos-Diaz, H. 2022 Opportunities and Barriers of Smart Farming Adoption by Farmers Based on a Systematic Literature Review. In: Int. conference on innovation, documentation and education. https://doi.org/10.4995/INN2022.2022.15746

Wielinga, E., Koutsouris, A., Knierim, A. & Guichaoua, A. 2017. Generating space for innovations in agriculture: the AgriSpin project. Studies in agricultural economics, 119 (1). pp. 26-33.

Wolfert, S., Ge, L., Verdouw, C. & Bogaardt, M-J. 2017. Big Data in Smart Farming – A review. Agricultural Systems 153. pp. 69-80.

Micro-Near-Infrared (Micro-NIR) sensor for predicting organic carbon and clay contents in agricultural soil

Jiang Liu [a], Muhammad Abdul Munnaf [a], Abdul Mounem Mouazen [a,*]

[a] Department of Environment, Ghent University, Ghent, Belgium

* Corresponding author. Email: Abdul.Mouazen@UGent.be

Abstract

Micro-near-infrared (Micro-NIR) spectroscopy has emerged as a promising technique for cost-effective estimation of key soil attributes when compared to the traditional wet chemistry methods and conventional NIR spectroscopy. Despite its potential, the full extent of its capabilities and applications remains unexplored. This study has evaluated the performance of a low-cost micro-NIR sensor for predicting soil organic carbon (SOC) and clay content. 92 samples (Randwijk, Netherlands) was scanned using a micro-NIR of 2000 ~ 2450 nm with 18 ~ 28 nm sampling resolution (NIRONE D2.5, Spectral Engine, Germany) in fresh and air-dried conditions. Partial least squares regression (PLSR) models were developed with and without feature selection by competitive adaptive reweighted sampling (CARS), successive projections algorithm (SPA), and slime mould algorithm (SMA). The best accuracy achieved for SOC prediction for the fresh samples (coefficient of determination in prediction (R_P^2) = 0.76; root mean square errors in prediction ($RMSE_P$) = 0.27 %) was improved for the dry samples (R_P^2 = 0.81; $RMSE_P$ = 0.27 %). The predictive performance for clay content was found relatively poor (R_P^2 = 0.48; $RMSE_P$ = 5.00 %). With the implementation of feature selection, SMA improved SOC prediction for fresh soil (R_P^2 = 0.79; $RMSE_P$ = 0.25 %) and CARS improved that of dry soil (R_P^2 = 0.84; $RMSE_P$ = 0.25 %). Using CARS also improved the results of clay prediction for dry soil (R_P^2 = 0.56; $RMSE_P$ = 4.62 %). Therefore, this study indicates that a micro-NIR sensor is a potential innovation that can accurately predict SOC, and clay content (to a smaller degree of accuracy) for a normally distributed dataset.

Keywords: micro-NIR spectroscopy, soil analyses, feature selection, organic carbon, clay.

1. Introduction

Soil plays a crucial role in agriculture, environment and climate change mitigation. The measurement of soil properties, including soil organic carbon (SOC) and clay content, is essential for comprehensively evaluating soil quality and capacity (Viscarra Rossel et al., 2006). SOC is a key indicator of soil health and fertility (Hong et al., 2022; Xie et al., 2022), while clay regulates soil physical, chemical, and biological processes (Tümsavaş et al., 2019). The accurate and timely measurement of SOC and clay content helps agricultural and environmental management decisions.

Near-infrared (NIR) spectroscopy has emerged as a widely accepted approach for measuring soil properties both at laboratory and field scales (Nawar and Mouazen, 2019). The interaction of near-infrared radiation with soil particles generates a unique spectral signature, which carries the characteristics information of soil properties to identify and quantify, making it a rapid and non-destructive soil measurement method (Stenberg et al., 2010). Despite proving its potential in a large number of studies (Soriano-Disla et al., 2014), NIR spectroscopy remains an expensive tool for soil analysis, particularly for the end users and practitioners. Therefore, affordably cheap but accurate NIR sensor development still remains a question to answer through research and development initiatives.

Advances in miniaturized technologies (e.g., Micro-Electro-Mechanical Systems) have led to the development of micro-NIR spectrometers (Malegori et al., 2017; Shen et al., 2022), which are cheaper than traditional NIR spectrophotometer (Sharififar et al., 2019). The term “micro-spectroscopy” refers to two distinct aspects i.e., its physical and optical size. Firstly, its compact size, the light source, photosensitive device, and processing unit are all integrated into a hand-sized shell. Secondly, the wavelength range of the sensor is typically narrower than the full NIR spectrum (i.e., 750 - 2500 nm). Micro-NIR sensor has gained most popularity in food industries for the analysis of fruits and tea (Li et al., 2021; Malegori et al., 2017; Ryckewaert et al., 2022; Teixeira Dos Santos et al., 2013). But its application in soil measurements remains limited to a few reports. The portable nature of the micro-NIR sensor renders it a suitable tool for in-situ soil measurements in field or forest settings, as it offers greater convenience than traditional laboratory-based

approaches. However, the feasibility of micro-NIR sensor in soil measurements remains a question yet to confirm.

The aim of this study was to evaluate the potential of a micro-NIR sensor with a narrow spectral range of 2000 ~ 2450 nm for predicting SOC and clay contents in agricultural soils under dry and fresh soil conditions. Performances of partial least squares regression (PLSR) models were compared for different feature selection methods.

2. Materials and Methods

2.1. Sample description

A total of 92 samples were gathered from the topsoil layer (0-20 cm) of an agricultural field (2.5 ha) in Randwijk, Netherlands (51.93758, 5.71425). The soil texture is sandy loam. Each soil sample was subsequently partitioned into three portions. One part was used for laboratory determination of SOC and clay content. The second portion was used for scanning at fresh soil condition, and the remaining portion was air-dried for a duration of two weeks, followed by grinding, sieving before spectral scanning. Dataset for fresh soil scanning was marked as F and for dry soil scanning was marked as D.

2.2. Sensor and scanning

This study used a micro-NIR sensor (NIRONE D2.5, Spectral Engine, Germany) to scan both fresh and dry soil samples. It is approximately 80 × 80 × 25 mm in size and weighs about 138 g. The sensor featured a sapphire window located at the centre of the bottom side, allowing for the transmission of both incident and reflected lights. Notably, this micro-NIR sensor has a very narrow wavelength range of 2000 ~ 2450 nm with a sampling resolution of 18 - 28 nm, which is narrower not only than the laboratory desktop spectrometers but also other miniaturized NIR sensors (Barthès et al., 2019; Sharififar et al., 2019). The distance between the sensor and sample was set at 2 mm to prevent direct harmful impact of the soil on the sapphire window, while ensuring a good signal-to-noise ratio. The 2 nm wavelength step ensured optimal measuring speed and minimized noise. Consequently, a total of 226 spectral bands were available between 2000 ~ 2450 nm.

Soil samples were scanned using a specialized hardware set-up, holding the micro-NIR sensor at a 2 mm distance from the soil sample (Figure 1). Soil samples were filled into Petri dishes whose surface was levelled to ensure homogenous diffuse reflectance. The micro-NIR sensor was placed on top of the holder facing downward, while the soil sample was placed underneath. The sensor was calibrated using a white reference in every 30 minutes. The spectral absorbance data of 5 scans per sample was logged onto a laptop through universal a serial bus communication and used for subsequent analysis.

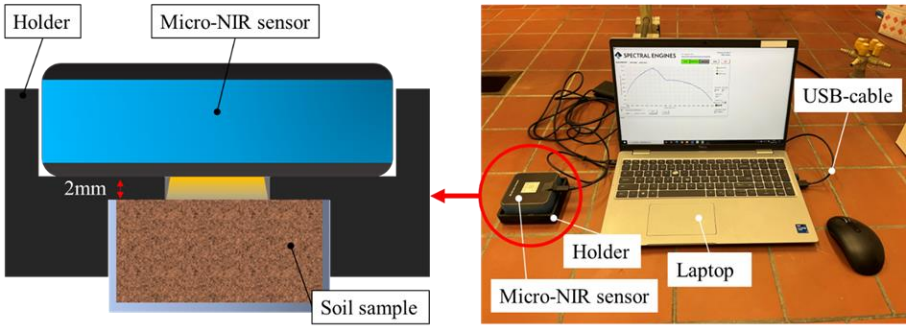

Figure 1. Micro-NIR sensor and laboratory set up for soil scanning.

2.3. Data analysis

2.3.1. Spectra pre-processing

The Monte-Carlo method was employed to identify and eliminate the spectral outliers (Li et al., 2018). Four data points that were far from the cluster were considered outliers. To reduce noises, the Savitzky-Golay (SG) filter was utilized with a window size of 21 points and a 3rd polynomial. To enhance the signal-to-noise

ratio and thus the predictive performance, the pre-processing method standard normal variate (SNV) was used. SNV is a common method of spectral pre-processing, reduces the effect of particle size (Reda et al., 2019).

2.3.2. Partial least squares regression (PLSR)

Each of the two datasets was divided into calibration and validation subsets using the Kennard Stone duplex algorithm (Li et al., 2018), where 75 % of the data was allocated to the calibration set and the remaining 25 % was assigned to the validation set. After the data split, PLSR was implemented on the calibration samples, and the resulting models were validated using samples of the validation sets. PLSR predicts a dependent variable (soil property) by extracting latent variables (LVs), which are orthogonal factors that provide maximum covariances between dependent and independent variables and thus ensure most accurate predictions (Li et al., 2018; Sharififar et al., 2019). PLSR models were trained using 10-fold cross-validation and the optimal number of LVs was selected based on the minimum root mean square error of cross-validation results. PLSR was conducted on each data set separately, using the full spectra as input or selected spectral features, using the feature selection algorithms described below.

2.3.3. Feature selection analyses

Feature selection analysis has been reported to select key wavelengths in the spectra that contribute most to the prediction (Yun et al., 2019). By this, feature selection reduces redundant spectral information and improves predictive accuracy or speeds up prediction time (Reda et al., 2019; Wu et al., 2022; Xie et al., 2022). Therefore, it may help in understanding the mechanism of how micro-NIR predicts SOC and clay content successfully. In this study, three feature selection methods i.e., competitive adaptive reweighted sampling (CARS), successive projections algorithm (SPA), and slime mould algorithm (SMA) were evaluated.

CARS is a variable selection technique that operates by repeatedly updating the weight of each variable based on the predefined criterion in each iteration and the feature variable with great competence can be eventually selected (Li et al., 2009; Wu et al., 2022; Yun et al., 2019). In this study, the root mean square error of PLSR in cross-validation was used as the evaluation standard (Li et al., 2009).

SPA utilizes simple projection operations in a vector space and a forward selection method to identify subsets of variables that exhibit minimal collinearity, and thus it is well-suited to NIR spectra modelling in particular (Cesar Ugulino Araujo et al., 2001; Yun et al., 2019). The minimum and maximum allowable variable numbers in SPA implementation were set to 5 and 20 (2 % ~ 8 % of wavelengths in the micro-NIR spectrum), respectively.

SMA is a swarm intelligence-based algorithm that is inspired by the intelligent foraging behaviour of slime moulds (Li et al., 2020). These organisms are known for their ability to locate the optimal food zone, and SMA replicates this behaviour. To achieve this, SMA requires a fitness function to be defined, which was set as the RMSE of PLSR in cross-validation.

2.3.4. Model evaluation

Performances of prediction models were evaluated based on the coefficient of determination in prediction (R_P^2) (Eq.1), the root mean square error in prediction ($RMSE_P$) (Eq.2), and the ratio of performance to interquartile range (RPIQ) (Eq.3). The higher R_P^2 and RPIQ and the lower the $RMSE_P$, the better is the prediction accuracies. R_P^2 measures the correlations and $RMSE_P$ indicates the residues between the observed and prediction quantities. RPIQ evaluates models' performance by taking into account both the prediction errors and the variability of measured values. The RPIQ criterion is considered more objective than the $RMSE_P$. Concerning RPIQ, spectral models can be ranked as excellent (RPIQ > 2.5), good (RPIQ = 1.7 – 2.5), fair (RPIQ = 1.4 – 1.7) and non-reliable (RPIQ < 1.4) (Nawar and Mouazen, 2017). The mathematical expressions of R_P^2, $RMSE_P$ and RPIQ are written below, respectively:

$$R_P{}^2 = 1 - \frac{\sum_{i=1}^{n}(y_{mea,i} - y_{pre,i})^2}{\sum_{i=1}^{n}(y_{mea,i} - \bar{y}_i)^2} \quad (1)$$

$$RMSE_P = \sqrt{\frac{\sum_{i=1}^{n}(y_{mea,i} - y_{pre,i})^2}{n}} \quad (2)$$

Where y_{mea} is the measured value, y_{pre} is the predicted value, $\bar{y}$ is the mean of the measured value, and n is the number of observation.

$$RPIQ = \frac{Q_3 - Q_1}{RMSE_P} \quad (3)$$

Where Q_1 and Q_3 are the first and third quartiles of the dataset, respectively.

3. Results and Discussion

3.1. Soil data

For the collected soil samples, SOC and clay contents varied between 0.3 and 2.7 % and 11 and 40 %, respectively (**Table 1**). Equal mean and median values were observed for both SOC and clay contents. The low skewness of 0.41 for SOC and 0.26 for clay indicated a normal distribution of the dataset. After the removal of 4 outliers, 66 samples of the 88 observations were assigned to the calibration dataset, while the remaining 22 samples were allocated to the validation dataset. The sample statistics of calibration and validation datasets were almost similar to each other (**Table 2**).

Table 1. Summary statistics of top (0-20 cm) soil organic carbon (SOC) and clay contents

Properties	Min	Max	Mean	Median	SD	Skewness
SOC, %	0.30	2.70	1.16	1.20	0.59	0.41
Clay content, %	11.00	40.00	23.69	23.00	6.18	0.26

Table 2. Summary statistics of top (0-20 cm) soil organic carbon (SOC) and clay contents of the calibration and validation datasets.

Soil properties	Datasets	Calibration (N=66)				Validation (N=22)			
		min	max	mean	SD	min	max	mean	SD
SOC, %	F	0.30	2.70	1.15	0.60	0.40	2.20	1.18	0.56
	D	0.30	2.70	1.11	0.55	0.50	2.30	1.25	0.64
Clay content, %	F	11.00	36.00	22.95	6.47	19.00	34.00	25.00	4.15
	D	11.00	36.00	23.20	5.66	11.00	35.00	24.00	7.12

3.2. Spectral analysis

The absorbance of both datasets F and D declined around 2000 ~ 2150 nm, which was more evident in the SNV based pre-processed spectra (

Figure 2). This decline corresponds to the absorbance peak at approximately 1950 nm, a well-known -OH absorption feature of soil spectra. NIR spectra usually exhibit three distinct and pronounced OH absorbance peaks at around 950 nm, 1450 nm, 1950 nm (Nawar et al., 2016; Stenberg et al., 2010; Viscarra Rossel and Behrens, 2010; Viscarra Rossel et al., 2006). A distinguished peak near 2200 nm was observed in the pre-processed spectra in both fresh and dry soil samples, with a distinct twist observed in the latter case. This peak is likely related to the absorption of Al-OH (Nawar et al., 2016; Viscarra Rossel and Behrens, 2010; Sharififar et al., 2019). Moreover, in the dry soil spectra, a minor peak was observed around 2350 nm. It may be related to C-H in methyls (Tekin et al., 2012) and illite or mixtures of smectite and illite in the soil (Viscarra Rossel and Behrens, 2010). The similarity between the spectra collected by the micro-NIR sensor and the spectra in previous works suggests that the configured measurement methods for micro-NIR sensor in this study is good to get the correct spectra.

3.3. Modelling results

Results of the F dataset in SOC prediction were deemed satisfactory (R_P^2 = 0.76, $RMSE_P$ = 0.27 %) (**Table 3**) by using SNV pre-processing method followed by PLSR modelling. Additionally, the model achieved an excellent level of reliability (RPIQ = 4.13). Predictive results for SOC of the D dataset were further improved thanks to the dry sample conditions, with R_P^2 = 0.80, indicating a high level of correlation,

and RPIQ = 4.26.

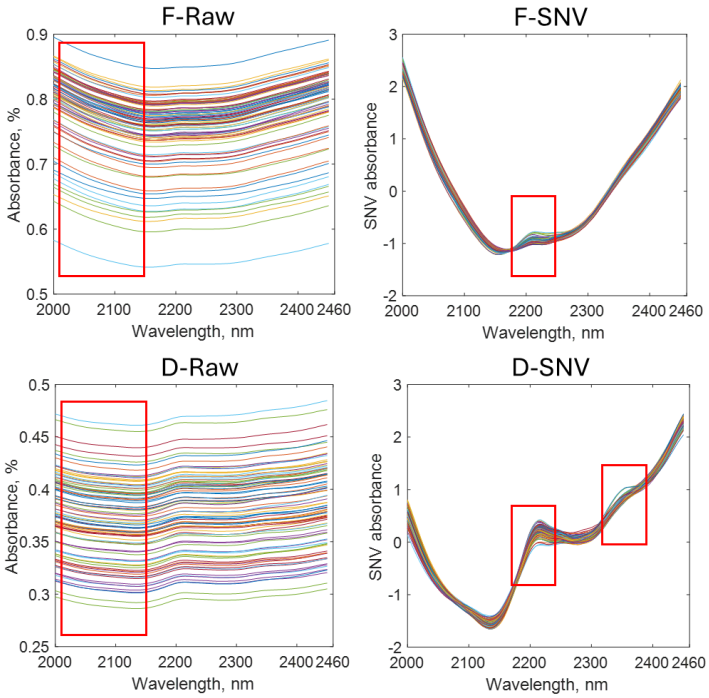

Figure 2. Raw and preprocess soil spectra by means of standard normal variation (SNV)

Table 3. Prediction accuracy of micro-NIR spectroscopy for top (0-20 cm) soil organic carbon (SOC) and clay contents using partial least squares regression (PLSR) analysis by means of standard normal variation (SNV).

Soil properties	Datasets	R_P^2	$RMSE_P$	RPIQ
SOC, %	F	0.76	0.27	4.13
	D	0.80	0.28	4.26
Clay content, %	F	0.34	3.29	1.52
	D	0.48	5.00	2.20

The predictive results for clay estimation of the F set using different pre-processing methods exhibited consistently poor performance. Although the results of the D set were slightly better than that of the F set, they were still rather of moderate accuracy (R_P^2 = 0.48). These could be viewed as relatively good models based on the RPIQ scores (RPIQ = 2.20).

3.4. Effect of spectral feature selection on model performance

The key spectral wavelengths selected by different feature selection methods were not the same. The most significant wavelengths of SOC were around 2160 nm, 2224 nm, 2260 ~2270 nm, 2350 nm, and 2450 nm, which were selected by almost all three methods for the F dataset. However, for the D dataset, the significant wavelengths were at 2056~2060 nm, 2160 nm, 2260 ~ 2270 nm, and 2450 nm. It was not hard to find that wavelengths centred around 2160 nm, 2260 ~ 2270 nm, and 2450 nm were selected for both the F and D datasets, which were consistent with or close to the reported wavebands associated with SOC prediction (e.g., 2160 nm [Hummel et al., 2001; Ng et al., 2019]; 2260 ~ 2270 nm [Hummel et al., 2001; Miloš et al., 2022; Tekin et al., 2012]; 2450 nm [Hummel et al., 2001; Liu et al., 2021; Miloš et al., 2022; Ng et al., 2019; Pinheiro et al., 2017]). Notably, wavebands around 2224 nm and 2350 nm were identified in models of the F dataset, but not in models of the D dataset. This suggests that the presence of soil moisture may influence the performance of micro-NIR for SOC prediction, since wavebands around 2224 nm and 2350 nm are influenced by the C-H band in functional groups of SOC (Hermansen et al., 2016; Tekin et al., 2012; Wu et al., 2022). Additionally, wavelengths around 2056~2060 nm were identified by all three feature selection methods in models with the dataset D, which is possible to be associated with the stretch combination of C-

N and C=O (Barthès et al., 2010).

The key featured wavebands of micro-NIR spectroscopy in clay prediction models were not found as distinct as those for SOC models. Wavebands centred around 2010 nm, 2200 nm, 2260 ~ 2270 nm, 2360 ~ 2370 nm, and 2430~2450 nm were consistently selected by three feature selection methods. Based on previous works, the absorption between 2100 and 2500 nm may be associated with clay minerals such as kaolinite, illite, and smectite (Jaconi et al., 2019).

The prediction accuracy of SOC for the F dataset was improved the most using selected bands after SMA (R_P^2 increased from 0.76 to 0.79 and RPIQ increased from 4.13 to 4.40; **Table 4**). All three feature selection methods improved the prediction accuracy of SOC for the D dataset, while CARS improved it the most (R_P^2 = 0.84; **Table 4**). However, the improvement achieved through feature selection was limited. The results of clay prediction were improved after spectral feature selection, for the two datasets (**Table 4**). Although improvement was observed in the prediction of clay content in the F dataset, the results did not meet the acceptable RPIQ threshold (RPIQ $\geqslant$ 1.4). Similarly, improvement was observed in the prediction of clay content in dry soil, despite the accuracy did not reach the next level (RPIQ > 2.5). Despite the relatively limited prediction accuracy for clay compared to that for SOC, the feature analysis approach was shown to enhance the accuracy of micro-NIR for SOC and clay content predictions.

Table 4. Prediction accuracy of micro-NIR spectroscopy for soil organic carbon (SOC) and clay contents for dataset of fresh samples (F) and dry samples (D) after feature selection.

Soil properties	Datasets	VS	R_P^2	$RMSE_P$	RPIQ
SOC, %	F	CRAS	0.78	0.26	4.28
		SPA	0.78	0.25	4.31
		SMA	0.79	0.25	4.40
	D	CRAS	0.84	0.25	4.84
		SPA	0.82	0.27	4.50
		SMA	0.83	0.26	4.67
Clay content,%	F	CRAS	0.36	3.24	1.54
		SPA	0.41	3.13	1.60
		SMA	0.31	3.38	1.48
	D	CRAS	0.56	4.62	2.38
		SPA	0.55	4.64	2.37
		SMA	0.51	4.85	2.27

VS: variable selection methods

4. Conclusions

The potential of a low-cost and short spectral range micro-NIR sensor coupled with PLSR has been evaluated for predicting the SOC and clay contents under fresh and dry soil sample conditions. Results showcased the potential of micro-NIR spectroscopy as a viable technique for measuring both SOC and clay contents. Micro-NIR sensor seemed to be accurate in predicting SOC in fresh soil and can provide improved accuracy for dry soils. However, the accuracy can be suboptimal for soil clay content predictions. Feature selection by the CARS method can enhance the accuracy of SOC (R_P^2 = 0.84 and RPIQ = 4.84) and clay contents (R_P^2 = 0.56 and RPIQ = 2.38) for dry soils, compared to the feature selection by SPA and SMA algorithms. Soil samples used in this research were collected from one field, further study is required to use samples with various soil texture and types in larger scales to evaluate the performance of the micro-NIR sensor.

Acknowledgements

This study was supported by the China Scholarship Council (CSC, Nr. 202206350031) for the first author stipend, and the financial support to run the project received by the Research Foundation - Flanders (FWO) for Odysseus I SiTeMan Project (Nr. G0F9216N), and FWO Grant for participation in a conference abroad covers the travel expenses for participating in the conference.

References

Barthès, B.G., Brunet, D., Brauman, A., Fromin, N., Lensi, R., Volant, A., Laclau, J.P., Blavet, D., Chapuis-Lardy, L., 2010. Determination of potential denitrification in a range of tropical topsoils using near infrared reflectance spectroscopy (NIRS). Applied. Soil. Ecology. 46, 81–89. https://doi.org/10.1016/j.apsoil.2010.06.009

Barthès, B.G., Kouakoua, E., Clairotte, M., Lallemand, J., Chapuis-Lardy, L., Rabenarivo, M., Roussel, S., 2019. Performance comparison between a miniaturized and a conventional near infrared reflectance (NIR) spectrometer for characterizing soil carbon and nitrogen. Geoderma 338, 422–429. https://doi.org/10.1016/j.geoderma.2018.12.031

Cesar Ugulino Araujo, M., Cristina Bezerra Saldanha, T., Kawakami Harrop Galvao, R., Yoneyama, T., Caldas Chame, H., Visani, V., Brazií, B., 2001. The successive projections algorithm for variable selection in spectroscopic multicomponent analysis. Chemom. Intell. Lab. Syst. 57(2), 65–73. https://doi.org/10.1016/S0169-7439(01)00119-8

Hermansen, C., Knadel, M., Moldrup, P., Greve, M.H., Gislum, R., de Jonge, L.W., 2016. Visible-Near-Infrared Spectroscopy Can Predict the Clay/Organic Carbon and Mineral Fines/Organic Carbon Ratios. Soil Sci. Soc. Am. J. 80, 1486–1495. https://doi.org/10.2136/sssaj2016.05.0159

Hong, Y., Chen, Y., Chen, S., Shen, R., Hu, B., Peng, J., Wang, N., Guo, L., Zhuo, Z., Yang, Y., Liu, Y., Mouazen, A.M., Shi, Z., 2022. Data mining of urban soil spectral library for estimating organic carbon. Geoderma 426. https://doi.org/10.1016/j.geoderma.2022.116102

Hummel, J.W., Sudduth, K.A., Hollinger, S.E., 2001. Soil moisture and organic matter prediction of surface and subsurface soils using an NIR soil sensor. Comput. Electron. Agric. 32(2), 149–165. https://doi.org/10.1016/S0168-1699(01)00163-6

Jaconi, A., Vos, C., Don, A., 2019. Near infrared spectroscopy as an easy and precise method to estimate soil texture. Geoderma 337, 906–913. https://doi.org/10.1016/j.geoderma.2018.10.038

Li, H., Liang, Y., Xu, Q., Cao, D., 2009. Key wavelengths screening using competitive adaptive reweighted sampling method for multivariate calibration. Anal. Chim. Acta. 648, 77–84. https://doi.org/10.1016/j.aca.2009.06.046

Li, H.D., Xu, Q.S., Liang, Y.Z., 2018. libPLS: An integrated library for partial least squares regression and linear discriminant analysis. Chemom. Intell. Lab. Syst. 176, 34–43. https://doi.org/10.1016/j.chemolab.2018.03.003

Li, L., Jin, S., Wang, Y., Liu, Y., Shen, S., Li, M., Ma, Z., Ning, J., Zhang, Z., 2021. Potential of smartphone-coupled micro NIR spectroscopy for quality control of green tea. Spectroc. Acta Pt. A-Molec. Biomolec. Spectr. 247. https://doi.org/10.1016/j.saa.2020.119096

Li, S., Chen, H., Wang, M., Heidari, A.A., Mirjalili, S., 2020. Slime mould algorithm: A new method for stochastic optimization. Futur. Gener. Comp. Syst. 111, 300–323. https://doi.org/10.1016/j.future.2020.03.055

Liu, J., Dong, Z., Xia, J., Wang, H., Meng, T., Zhang, R., Han, J., Wang, N., Xie, J., 2021. Estimation of soil organic matter content based on CARS algorithm coupled with random forest. Spectroc. Acta Pt. A-Molec. Biomolec. Spectr. 258. https://doi.org/10.1016/j.saa.2021.119823

Malegori, C., Nascimento Marques, E.J., de Freitas, S.T., Pimentel, M.F., Pasquini, C., Casiraghi, E., 2017. Comparing the analytical performances of Micro-NIR and FT-NIR spectrometers in the evaluation of acerola fruit quality, using PLS and SVM regression algorithms. Talanta 165, 112–116. https://doi.org/10.1016/j.talanta.2016.12.035

Miloš, B., Bensa, A., Japundžić-Palenkić, B., 2022. Evaluation of Vis-NIR preprocessing combined with PLS regression for estimation soil organic carbon, cation exchange capacity and clay from eastern Croatia. Geoderma Reg. 30. https://doi.org/10.1016/j.geodrs.2022.e00558

Mouazen, A.M., Karoui, R., De Baerdemaeker, J., Ramon, H., 2005. Classification of Soil Texture Classes by Using Soil Visual near Infrared Spectroscopy and Factorial Discriminant Analysis Techniques. J. Near Infrared Spectrosc. 13, 231–240. https://doi.org/10.1255/jnirs.541

Nawar, S., Buddenbaum, H., Hill, J., Kozak, J., Mouazen, A.M., 2016. Estimating the soil clay content and organic matter by means of different calibration methods of vis-NIR diffuse reflectance spectroscopy. Soil Tillage Res. 155, 510–522. https://doi.org/10.1016/j.still.2015.07.021

Nawar, S., Mouazen, A.M., 2017. Predictive performance of mobile vis-near infrared spectroscopy for key soil properties at different geographical scales by using spiking and data mining techniques. Catena. 151, 118-129. https://doi.org/10.1016/j.catena.2016.12.014

Nawar, S., Mouazen, A.M., 2019. On-line vis-NIR spectroscopy prediction of soil organic carbon using machine learning. Soil Tillage Res. 190, 120–127. https://doi.org/10.1016/j.still.2019.03.006

Ng, W., Minasny, B., Malone, B.P., Sarathjith, M.C., Das, B.S., 2019. Optimizing wavelength selection by using informative vectors for parsimonious infrared spectra modelling. Comput. Electron. Agric. 158, 201–210. https://doi.org/10.1016/j.compag.2019.02.003

Pinheiro, É.F.M., Ceddia, M.B., Clingensmith, C.M., Grunwald, S., Vasques, G.M., 2017. Prediction of soil physical and chemical properties by visible and near-infrared diffuse reflectance spectroscopy in the Central Amazon. Remote Sens. (Basel) 9. https://doi.org/10.3390/rs9040293

Reda, R., Saffaj, T., Ilham, B., Saidi, O., Issam, K., Brahim, L., El Hadrami, E.M., 2019. A comparative study between a new method and other machine learning algorithms for soil organic carbon and total nitrogen prediction using near infrared spectroscopy. Chemom. Intell. Lab. Syst. 195. https://doi.org/10.1016/j.chemolab.2019.103873

Rossel, R.A.V., Behrens, T., 2010. Using data mining to model and interpret soil diffuse reflectance spectra. Geoderma 158, 46–54. https://doi.org/10.1016/j.geoderma.2009.12.025

Ryckewaert, M., Chaix, G., Héran, D., Zgouz, A., Bendoula, R., 2022. Evaluation of a combination of NIR micro-spectrometers to predict chemical properties of sugarcane forage using a multi-block approach. Biosyst. Eng. 217, 18–25. https://doi.org/10.1016/j.biosystemseng.2022.02.019

Sharififar, A., Singh, K., Jones, E., Ginting, F.I., Minasny, B., 2019. Evaluating a low-cost portable NIR spectrometer for the prediction of soil organic and total carbon using different calibration models. Soil Use Manage. 35, 607–616. https://doi.org/10.1111/sum.12537

Shen, Z., D'Agui, H., Walden, L., Zhang, M., Yiu, T.M., Dixon, K., Nevill, P., Cross, A., Matangulu, M., Hu, Y., Viscarra Rossel, R.A., 2022. Miniaturised visible and near-infrared spectrometers for assessing soil health indicators in mine site rehabilitation. Soil 8, 467–486. https://doi.org/10.5194/soil-8-467-2022

Soriano-Disla, J.M., Janik, L.J., Viscarra Rossel, Macdonald, L.M., Macdonald, L.M., Mclaughlin, M.J., 2014. The performance of visible, near-, and mid-infrared reflectance spectroscopy for prediction of soil physical, chemical, and biological properties. Applied Spectroscopy Reviews 49 (2), 139–186. https://doi.org/10.1080/05704928.2013.811081.

Stenberg, B., Viscarra Rossel, R.A., Mouazen, A.M., Wetterlind, J., 2010. Visible and Near Infrared Spectroscopy in Soil Science, Adv. Agron. 107, 163–215. https://doi.org/10.1016/S0065-2113(10)07005-7

Teixeira Dos Santos, C.A., Lopo, M., Páscoa, R.N.M.J., Lopes, J.A., 2013. A review on the applications of portable near-infrared spectrometers in the agro-food industry. Appl. Spectrosc. 67 (11), 1215–1233 https://doi.org/10.1366/13-07228

Tekin, Y., Tumsavas, Z., Mouazen, A.M., 2012. Effect of Moisture Content on Prediction of Organic Carbon and pH Using Visible and Near Infrared Spectroscopy. Soil Sci. Soc. Am. J. 76, 188–198. https://doi.org/10.2136/sssaj

Tümsavaş, Z., Tekin, Y., Ulusoy, Y., Mouazen, A.M., 2019. Prediction and mapping of soil clay and sand contents using visible and near-infrared spectroscopy. Biosyst. Eng. 177, 90–100. https://doi.org/10.1016/j.biosystemseng.2018.06.008

Viscarra Rossel, R.A., Walvoort, D.J.J., McBratney, A.B., Janik, L.J., Skjemstad, J.O., 2006. Visible, near infrared, mid infrared or combined diffuse reflectance spectroscopy for simultaneous assessment of various soil properties. Geoderma 131, 59–75. https://doi.org/10.1016/j.geoderma.2005.03.007

Wu, J., Guo, D., Li, G., Guo, X., Zhong, L., Zhu, Q., Guo, J., Ye, Y., 2022. Multivariate methods with feature wavebands selection and stratified calibration for soil organic carbon content prediction by Vis-NIR spectroscopy. Soil Sci. Soc. Am. J. 86, 1153–1166. https://doi.org/10.1002/saj2.20449

Xie, S., Ding, F., Chen, S., Wang, X., Li, Y., Ma, K., 2022. Prediction of soil organic matter content based on characteristic band selection method. Spectroc. Acta Pt. A-Molec. Biomolec. Spectr. 273. https://doi.org/10.1016/j.saa.2022.120949

Yun, Y.H., Li, H.D., Deng, B.C., Cao, D.S., 2019. An overview of variable selection methods in multivariate analysis of near-infrared spectra. Trac-Trends Anal. Chem. 113, 102-115. https://doi.org/10.1016/j.trac.2019.01.018

Smart control strategies for optimal environmental conditions and minimum energy requirements in livestock facilities

Stelios Kalogridis [a,*], Michael Moraitis [b], Athanasios Balafoutis [b], Bas Paris [b,c], Nikolas Ipiotis [a], Michail Savvakis [a], Dimitris Manolakos [c], Dimitrios Tyris [c]

[a] Plegma Labs S.A., Athens, Greece

[b] Institute of Bio-Economy & Agri-Technology, Centre of Research & Technology Hellas, Volos, Greece

[c] Department of Natural Resources Development and Agricultural Engineering, Agricultural University of Athens, Athens, Greece

* Corresponding author. Email: stelios@pleg.ma

Abstract

In recent years the demand for animal products has increased considerably with a direct impact on increased energy consumption of livestock facilities. This problem can be managed by adopting energy efficient equipment and optimal planning of energy use picks but also by adopting Renewable Energy Sources (RES). By interconnecting these technologies using the Internet of Things (IoT) and controlling them with smart control systems based on artificial intelligence combined with the breeding and fattening cycles of the livestock, it is possible to optimize energy production and consumption and their respective emissions, with simultaneous improvement of the animals' well-being due to optimized microclimate. In this paper, we first reviewed the current state of the art of smart control technologies/practices and data analytics techniques for optimal indoor environmental conditions of the main livestock species (poultry, cattle and swine), combined with the main RES technologies for livestock facilities. Then, we showcase the research opportunities, technical and financial challenges as well as the knowledge gaps for precision environmental control of livestock buildings and finally a smart livestock building control system prototype is presented analysing its novel topology to enable: (i) remote monitoring of environmental parameters, (ii) optimal penetration of different RES units, and (iii) energy consumption reduction prospects aiming at optimum livestock performance in relation to the indoor environmental conditions and the energy consumed.

Keywords: livestock, indoor environmental smart control, energy consumption, renewable energy sources

1. Introduction

Several trends are driving transitions in the global livestock sector. On one hand, growing human population along with the rising income and modern lifestyle changes are driving increases in the demand for animal products and by-products (Michalk et al., 2019). On the other hand, the decreasing number of farmers, especially in developed countries, is leading the industry to focus production on larger farms in order to satisfy the market needs (Eurostat, 2022). In addition, there is a steady shift in consumer demand for livestock goods produced under well-being production strategies.

In this context, there is a need for the farming industry to adopt new practices towards healthier breeding conditions based on continuous monitoring of both animals' behaviour and the environmental parameters to gather data and implement smart control techniques that can optimise livestock living conditions (Jiang et al., 2023). To do so, already deployed technologies from other industries are adapted in livestock facilities, such as the IoT, which has experienced considerable development in recent years and can be applied to livestock farming utilizing different smart devices. IoT can allow smart processes during different stages of livestock rearing, such as management, feeding, energy efficiency, finances, safety, reliability, etc (Grogan, 2012). Each livestock type requires different environmental conditions in order to increase the output efficiency, but the main limiting factor for all types is optimal temperature control. In addition, other factors, including the relative humidity, the concentration of dangerous gases and the quantity and timing of feeding are also crucial (Hansen & Bjerg, 2018). Livestock housing systems that are able to control these major parameters along with others lesser ones, support the integration of Precision Livestock Farming (PLF) concept in existing and new livestock farms.

Additionally, increases in animal population and density in industrial farms in combination with the

high mechanisation of these facilities leads to increased energy consumption that reduce the profit margin and simultaneously add to the environmental impact of the livestock sector (Paris et al., 2022). These energy needs could be reduced by installing energy efficient equipment and the remaining energy consumption could be partly or in total covered by renewable energy systems, decreasing their environmental footprint and allowing for more sustainable animal husbandry. Furthermore, in the context of climatic change there is increasing recognition, which is reflected in policy and governance, that livestock practices need to become more sustainable and that "smart" technological systems play an important role in this transition.

Such a system, that supports effective precision indoor environmental control combined with RES integration in farm buildings regulated in accordance to the livestock facility energy needs, requires various systems to monitor a set of environmental and energy flow parameters that will allow the collected values to be stored and processed. This data can provide useful information towards overall animal comfort in real time, to allow the control of the different systems and ensure optimal living conditions for the animals, with low fossil energy consumption (Paris et al., 2022). Data processing techniques in such a system include a set of methods ranging from simple statistical analysis and a set of thresholds up to complex Machine Learning (ML) models. The output of this monitoring and analysis drives a set of automation and control methods that calibrate various parameters of the installed equipment for ventilation, heating, cooling, etc., thereby creating an optimal microclimate within the farm while also recording and projecting the energy needs provided by RES.

Relatively little previous research has been carried out on the smart control strategies for optimal environmental conditions and minimum energy requirements in livestock facilities. Farooq et al., (2020) conducted a systematic review of IoT technologies in agriculture and located only 67 relevant published articles between 2009 and 2019. This study aims to showcase a state of the art paradigm for smart control in livestock farms, aiming at combining optimal environmental conditions for animal livelihood with minimum energy requirements.

1.1. State of the art

1.1.1. Smart control systems

The main purpose of intelligent control systems is to allow integration of security, heating/cooling systems, air quality, energy monitoring, lightning, etc. by deploying smart devices, sensors and actuators to monitor and control different systems. Various smart control systems and techniques have been developed and introduced in recent years in order to ensure efficient environment control of the livestock building with extensive equipment used to measure different environmental values and vital livestock points. O'Grady and O'Hare (2017) provide an overview of various exemplar models for smart farming that effectively harnesses on farm information and communication technologies in livestock systems, including GRAZPLAN, EcoMod, NRC, Norfor, TDMI, Biopara-Milk, Karoline. Black & Banhazi (2013) have demonstrated the economic and social impact of the new technologies such as IoT and data analytics and the importance of proper data collection to optimize the livestock industry. Continuous sensing and adaptability of a smart control system is important and the ability for immediate response to optimize the environmental conditions increases the complexity of such systems.

In general, livestock facilities require different control and automation systems to handle a variety of factors for efficient indoor environment control. Ventilation is needed at all times to provide adequate fresh air to remove odours, minimize moisture and prevent airborne diseases. Natural ventilation in many cases is not adequate to mitigate these issues as it is affected by the environmental conditions such as temperature, wind blow rate fluctuations and other factors. Mechanical ventilation is required to ensure decent indoor conditions especially for small animals that are susceptible to low temperatures and sudden temperature changes (Jones et al., 2015). In recent years various studies have investigated the potential of "smart" mechanical ventilation systems including Fournel et al. (2017), who found that the general control strategies for thermal management of livestock buildings needs to be updated, while Shin et al. (2022) developed a smart system for demand-controlled ventilation.

Mechanistic approaches based on observations regarding the physiological and behavioural responses of animals to their physical microenvironment are primarily based on either the laws of physics and chemistry or on equations with known characteristics derived specifically to represent the perceived mechanisms of a system, supplemented with empirical values as needed. They offer a means of predicting

heat production under a broader range of conditions than empirical models do, by integrating, for instance, nutrition, genetics, and environment. Whereas dynamic data modeling recognizes that due to the dynamic changes of inputs (i.e. animal heat production and ventilation rate) and disturbing factors (outdoor climate), the calculated indoor conditions rapidly change over time (Banhazi et al., 2015).

Consequently, dynamic data-based models imply that the following statements are fulfilled: (i) animal responses to the microenvironment are measured continuously and the information is fed back to the controller, and (ii) a mathematical model of the system allows the process response to be predicted accurately under both steady-state and dynamic conditions.

1.1.2.IoT in the livestock industry

Continuous monitoring and the ability to mitigate in real-time changes of the indoor microclimate in relation to the livestock type, age and breed is highlighted above. In recent years, a range of technologies based around the IoT that provide smart devices capable to assist the continuous monitoring of critical factors, have been adopted by the livestock sector (Mateo-Fornés et al., 2021). This is important as IoT generally combines several "smart" technologies and focuses on creating efficiencies, scalability and interoperability between them.

Currently, most livestock farms are dependent on older and less efficient equipment. In these cases the procurement of a full system upgrade to up to date monitoring equipment and the upgrade of legacy systems is cost prohibitive. In these instances, IoT technology can be a solution as smart devices can be installed as standalone equipment, have the ability to retrofit legacy systems and can provide evidence and measurements to address the automatic control and monitoring of the farm. For instance, several studies suggest that using technologies such as wireless (Wi-Fi, ZigBee, LTE, LoraWAN, etc.) and wired communication sensing networks that transmit information to servers can be created. The data collected combined with expert knowledge and data processing techniques can realize critical actions towards precise farming and proactive actions to maintain an optimal environment for livestock (Symeonaki et al., 2021; Neethirajan & Kemp, 2021; Dos Reis et al., 2021; Zhang et al., 2016).

The ability to connect the IoT devices to the cloud allows remote monitoring, actuation and early warning. These can assist farmers make better decisions, while at the same time reducing their environmental footprint (Almalki et al., 2021). The IoT for agriculture is still in the early stages as most of the systems are in the development, prototype or research state (Farooq et al., 2020). Different stakeholders are trying to understand the ability of IoT in the agricultural sector and due to this, many studies focus on different aspects of IoT and adopt varying approaches, for instance, Ariza-Colpas et al. (2019) investigate the potential for geo-referencing livestock; Yadavalli et al. (2021) propose a monitoring and control mechanism for livestock agriculture that control a range of parameters through a smart algorithm; Paunova-Hubenova et al. (2021) investigate farm management information systems and their potential in dairy farming.

1.1.3.RES units and livestock farms

The current trends towards zero emission and carbon neutral farms combined with a focus on the circular economy and the current legislation towards minimization of energy consumption and the carbon footprint is pushing towards the wide adoption of RES technologies (Kumar et al., 2023). Popular RES technologies used on farms include: solar, wind, bioenergy, geothermal and heat pump systems. Their applicability, testing and adoption to the livestock sector have seen rapid increase in recent years driven by considerable technological improvements and cost reductions.

Microgrids combining different RES technologies including generation, storage and also proper dissipation of energy have been established. The technoeconomic aspect has been highlighted in various researches where different energy sources, including fossil fuels, have been evaluated (Ahmad et al., 2018). Various hybrid systems that combine energy from a variety of sources have been tested. Jahangir et al. (2022) investigates the potential of various hybrid RES systems for livestock farms finding that they can lead to considerable decreases in fossil dependency and Greenhouse Gasses (GHG) emissions. Elahi et al. (2019) optimises renewable and non-renewable energy inputs in livestock systems using an artificial neural network and Attard et al. (2017) investigates the RES potential of livestock wastes on Mediterranean islands.

Regarding specific RES sources, the role and potential of biogas production systems on livestock farms using manure as feedstock is well documented, though considerable potential in expanding these systems

remains (Scarlat et al., 2018; O'Connor et al., 2021). Similarly, in recent years the costs of solar power generation systems have fallen dramatically while efficiencies have increased in suggesting appropriate use to livestock systems. Various studies have commented on this (Paris et al., 2022). For instance, PVTs (Photovoltaic Thermal hybrid solar collectors) combine the features of standard PV (Photovoltaic) panels and solar thermal collectors, producing both heat and electricity and their energy yield per m^2 is about 40-50% higher than having separate PV and solar thermal collectors with the same total surface area, making them ideal for buildings with restricted rooftop surface (Sirin et al., 2023). Gad et al. (2020) compare poultry houses powered by PV and a flat-plate solar collector and Rudenko et al. (2019) provide technical recommendations for designing power supply systems for livestock based on solar and wind.

Following the rapid and successful development of heat pumps in the housing and construction sectors, efforts are being made to apply them to livestock facilities. Choi et al. (2012) observed that using a geothermal heat pump to heat broiler houses significantly reduces overall energy demand as compared to conventional systems and Islam et al. (2016) found that a geothermal heat pump in pig houses substantially reduces electricity use, carbon emissions and costs. Licharz et al. (2020) investigated the energy efficiency of heat pumps in two pig houses in Germany. These studies generally suggest that the adoption of heat pumps in livestock facilities are applicable to and will improve energy efficiencies of livestock systems. It is important to note that depending on the type of livestock sector and the local climate the heating and cooling requirements are very different. As such, different concepts of either passive or active cooling systems are necessary which in turn impact the load on the geothermal source and the cost-effectiveness of the system.

2. Materials and Methods

Based on technological developments, expert inputs and the research conducted in the framework of Horizon 2020 Project RES4LIVE, this study proposes an IoT system that provides effective remote monitoring and actuation by combining energy efficiency measures and the effective management of RES systems. The potential lies in combining smart systems, IoT and renewable production to move towards a sustainable and efficient livestock system. The proposed system that utilizes an IoT platform was applied to 4 pilot farms and its functionality is being tested. The system follows the IoT paradigm where IoT devices communicate through a local sensor network and monitor the indoor and outdoor microclimate conditions as well as any hazardous gasses and transmit the collected data to a cloud infrastructure. Then, data is analyzed and through the analysis, which includes various methods and techniques, a set of decisions and actions is proposed. The two pillars of the proposed IoT system are the: (a) monitoring and data collection and (b) smart control.

2.1. Monitoring and data collection

Monitoring equipment is crucial for IoT systems as in order to be able to perform effective data analysis and provide inputs for the smart control, different units and sensors are required. Each monitoring device may be used to measure one or more parameters, and the values are then transmitted to be stored, visualised and further processed. The system herein presented is used to: (a) collect data in real time and utilise it as input to the smart control system in order to optimise the microclimate in terms of indoor air quality and thermal environment and; (b) collect baseline data to compare the conditions before and after the installation of the smart control system and the integration of RES technologies in the pilot farms.

Various sensors and accompanying equipment were selected for the integrated system according to the specific needs of the 4 pilot farms and the available infrastructure. Indicatively, prerequisites such as buildings/barns of interest, internet availability, convenient sensor installation points, integration of legacy equipment, and many more were taken into account for the selection and installation of sensors aimed at indoor sensing, outdoor sensing, electricity consumption and fuel consumption. The sensors that were decided to be installed on site are divided into 3 separate categories:

- Environmental sensing
- Weather station
- Energy consumption

Each category required additional research in order to proceed by selecting the appropriate equipment suited for the harsh conditions of livestock monitoring and to be able to work within specific conditions and

the defined range. For each category, the research for the different requirements for each sensor included expert knowledge from the project partners according to the type of livestock, general research from academia and industry leaders and reports and findings from manufacturers. Factors such as availability, after sale support for calibration and maintenance, durability and expected lifetime, calibration intervals, and more, were taken into account.

2.1.1. Environmental sensing

The various sensors utilized for environmental sensing have been selected with respect to the sensing sensitivity required for the application and the longevity of the different sensors. The working principles of the sensors vary. For example, some sensors include transmitters that can communicate directly with the gateway, which is the preferred solution. On the other hand, in some other cases, an additional module is needed, which heavily increases the cost and sets some limitations. All sensors selected for ambient monitoring use widely available protocols and technologies; the 3 main technologies are listed below:

- Variable resistance load: These sensors include a variable resistance and measure the electric current or electric load to calculate the sensing value according to the ohmic value of the resistor, which changes according to the sensing value.
- Electrochemical: These sensors have the same working principles as the resistive load sensors described above, but the variable resistance is changing its ohmic value according to a chemical component that is very sensitive to the desired measured value.
- Optical: These sensors are based on converting the light rays into electronic signals. They measure the quantity of light and translate it into a readable form.

Different types of farms and different livestock led to a wide selection of sensors (Table 1). All environmental sensors were selected to be able to work with the Modbus TCP/RTU protocol, which is the industry standard.

Table 1. Environmental sensors' requirements.

Sensing value	Range	Accuracy	Sensor type
Temperature and Relative Humidity	0...100% RH -40...+85 ºC	0.1% RH 0.1 ºC	Digital
CO_2 (Carbon Dioxide)	0-10,000 ppm	1 ppm	Optical NDIR
NH_3 (Ammonia)	0-1000 ppm	1 ppm	Metal Oxide Semiconductor
H_2S (Hydrogen Sulphide)	0-100 ppm	0.1 ppm	Electrochemical
O_2 (Oxygen)	0-25%	0.01% vol	Electrochemical
VOC (Volatile Organic Compound)	0-1000 ppm	1 ppm	Metal Oxide Semiconductor

2.1.2. Weather station

A weather station is a collection of instruments that measure atmospheric conditions to help study the weather and climate of a specific location. Most weather stations measure temperature, humidity, barometric pressure, wind speed and direction, and rainfall. The selected weather stations utilise an external solar panel and a battery-powered central unit to avoid sudden power outages and be autonomous for up to 10 days. The weather stations were programmed to transmit wind speed and direction, solar radiation, air temperature, humidity and pressure, precipitation and rainfall level data every 15 minutes.

2.1.3. Energy consumption

In order to measure the various electrical loads in the 4 pilot farms, energy monitoring devices were required. The measurements are also being utilised for the comparison of the electricity needs before and after the interventions in the pilot farms to evaluate various installed technologies as well as the complete system through a thorough Life Cycle Assessment (LCA).

Between electromechanical type induction meters and electronic energy meters, the latter were selected to be used for the purposes of this study. Electronic energy meters are an accurate, precise and reliable type of measuring instrument when compared to electromechanical induction-type meters which are characterised by their proneness to tampering. Additionally, when connected to loads electronic energy meters consume less power and start measuring instantaneously.

The number of installed energy meters per farm varied, depending on the complexity of each facility and the number of consumers that were deemed necessary to be recorded. An example of the installed

meters can be seen on Figure 1 (Split core CTs – Current Transducers).

Figure 1. Installed energy consumption sensors in a pilot farm.

2.2. Smart control

Having installed the complete monitoring system, all data is sent to the cloud platform in order for the smart control operations to be carried out. The platform utilised (https://cloud.gr/) is a custom IoT cloud platform developed by PLEGMA S.A. that provides IoT management and efficiency services to commercial & residential buildings, smart cities & agriculture, and the energy & industrial sectors.

Within RES4LIVE, the smart control system (Figure 2) is able to offer multiple functionalities and targets maximizing the penetration of the energy produced by the RES units making use of the system components as described below, and finally reducing the energy consumption of the pilot farms. Moreover, the smart control system actuates the heat pumps, to achieve the optimal environmental conditions according to each farm type, and also controls the ventilation in some areas of the pilot farms, to make sure that certain thresholds of hazardous gases are not surpassed. The ventilation control may be performed either in a direct way, by controlling the fans/ventilators, or through notifications on mobile phones of the farm staff, in case actual remote control of ventilators/fans/windows is not possible.

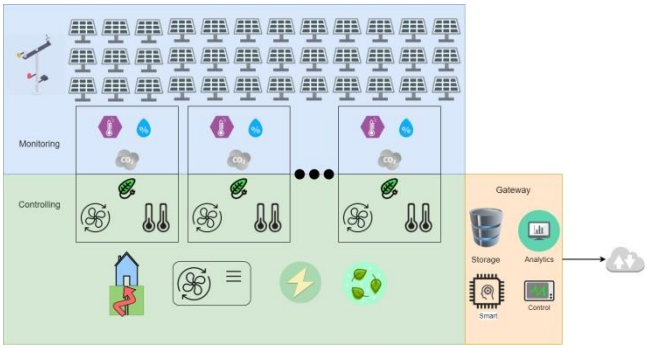

Figure 2. The proposed smart control system.

2.2.1. Smart control module

The Smart Control Module (SCM) is the key component of the gateway system that is used to maintain optimal conditions for animals. It gathers data from sensors or a local database and uses this information to make decisions about how to control the environment. The SCM uses an advanced rule engine and a smart control algorithm to determine the best actions to take to achieve the desired environment for the animals. It then prioritises and activates the necessary devices to maintain the desired conditions. Written in Node.js, the SCM is a reliable and efficient way to ensure that animals are living in a comfortable and healthy environment. The SCM has four main components: the rule engine, the smart control algorithm, the local actuator listener, and the cloud actuator listener. It runs the rules every time new sensor data arrives to ensure that the thresholds are strictly applied, and if it detects that values are below or above the threshold, it sends control commands to the heat pump and ventilation units to maintain temperature, humidity, and hazardous gas concentrations within the threshold levels.

It is important to note that the automation process described above can be overridden by manual actions from the farm administrator. In case the automation process is not working properly or maintenance of the farm is required, the administrator can turn off the module or override any actions taken by the system.

2.2.2. Rule engine

The rule engine is a solution that was customised and integrated into the platform to perform further analysis and apply meaningful rules that will be set and defined by heterogeneous sources and produce various outputs. It is triggered by the incoming or requested data in order to perform various actions and its main advantage is that it utilizes the suggestions received from the smart control algorithm, and it may apply additional rules on top of them. For example, override a command if a specific hazardous gas concentration exceeds a specific dangerous threshold, and prioritize the air quality by opening a ventilator, at the expense of energy consumption because of heat losses. Another important functionality is the ability to create notifications in case the data received from the sensor monitoring network, either the environmental sensors or the energy consumption sensors exceed specific thresholds set by the farm administration.

2.2.3. Demand forecasting

The prediction of electricity consumption is an important area of study for the efficient operation of power grids. Within the energy demand forecasting module, a Recurrent Neural Network (RNN) based approach which takes as input hourly energy demand data in kilowatt-hours (kWh) from the past week and forecasts the energy demand for the next hour is used. This module utilizes RNNs due to their superiority in solving problems with sequential data such as time series, according to the literature.

2.2.4. Solar forecasting

Forecasting the energy output of a solar power plant is crucial for the smart grid system, as it enables alignment of future supply and demand. This allows for scheduling high energy-consuming tasks during periods of high production to avoid wasting solar energy. In the context of this study, weather forecasts are provided through third-party services and/or the weather stations that are installed in the pilot farms.

2.2.5. Energy-intensive task scheduler

This module is developed to provide energy-intensive task scheduling recommendations to the farm managers based on the forecasted energy generation of the solar panels. This asset is supposed to assist them in better organizing and scheduling energy-intensive tasks (e.g. EV charging, heating, cleaning with hot water, etc.) to save energy and/or costs according to the different consumption tariffs. The input of the component is the schedule of the user, along with the prediction of the hourly generation of the PV panels in kWh with the relevant timestamps.

3. Results and Discussion

The proposed smart control system results in the control of the selected farm equipment either automatically or through suggestions of actions to be taken manually by the farms' staff as follows:

3.1. Automatically controlled equipment

The equipment that is controlled through the smart control system are all the heat pumps that are installed in the pilot farms, as well as the complete ventilation system in two pilot farms, and part of the ventilation system in the third farm.

The heat pumps are controlled through the smart control mechanism, which employs the Modbus protocol to manage its various functions. This allows the heat pump to be controlled remotely from expert personnel or automatically, and makes it possible to integrate the heat pump into a variety of different systems and environments.

A ventilation control system is a set of devices that work together to regulate the amount of fresh air that enters each barn. The Smart Control system monitors factors like temperature and humidity and concentrations of various hazardous gases (e.g., CO_2, VOC, NH_3, O_2, H_2S) and adjusts ventilation accordingly to keep indoor air quality within safe levels.

An indicative example of a control strategy at the poultry pilot farm made possible by the smart control systems is the operation of a heat pump, when the barn houses both pullets and laying hens, each requiring different thermal conditions. In the farm, the system user first specifies on the cloud platform that both rooms are occupied and sets the required temperature for each. Since pullets need higher temperatures and

are more sensitive to temperature fluctuations, the heat pump prioritizes maintaining the pullets' room at its set point before attending to the laying hens' room.

Depending on the weather conditions, if the laying hens' room needs heating, the heat pump also provides heating to the pullets' room. If the laying hens' room requires cooling while the pullets' room needs heating, thermal lamps supply the necessary heat for the pullets. When the heat pump operates in cooling mode, the fans supplying air to the pullets' room are either deactivated or run at low speed to maintain a higher temperature.

3.2. Manual control through suggested actions

It was deemed necessary for the system to be able to suggest specific actions, besides the directly controlled equipment. Current implementation supports suggestions to open windows or doors within a specific room in order to increase the airflow and to facilitate temperature control and the various hazardous gases concentration control. Thus, if the smart control algorithm outputs decide that a specific door or window within a barn should change its state (either open or close), it alerts through an email notification the assigned persons, so that they can go to that location and manually perform the suggested action. The system supports any kind of relevant action suggestions, which allows the system to be expandable and scalable in case additional requirements arise.

4. Conclusions

Agriculture 4.0 is the new approach towards farm management and precision agriculture. The ability to harness the technology advancements from other industries such as computer science allowed, agricultural sector to evaluate and adopt them to achieve energy efficiency and optimal indoor conditions for the livestock. Agriculture 4.0 is combining low-cost sensors and actuators, with cloud computing and Artificial Intelligence to achieve its goals and help farmers make better decisions, while at the same time reducing their environmental footprint.

Utilizing farmer-defined scenarios that consider specific livestock requirements, the areas occupancy and other characteristics, the IoT system is enabling smart control towards heating, cooling and ventilation and optimize the microclimate, in terms of indoor air quality and thermal environment.

To allow the smart control system to operate automatically, farms utilize smart sensors to monitor the different environmental parameters, such as temperature, relative humidity, wind speed and direction, hazardous gases, as well as energy consumption data. Moreover, the system collects baseline data to evaluate, assess and compare “before” and “after” conditions.

Precise indoor environmental and energy smart control are integral parts of the RES4LIVE Project implementation. Data is available in real time through the cloud platform, which: (a) allows remote monitoring, (b) provides useful analytics, and (c) performs actual control of the connected devices. The above-mentioned features will assist in both everyday operations and long-term farm management.

It is expected that the Project will finalise its findings by Q3 2024. Detailed information about the system installations as well as the ongoing technical, economic, environmental and social assessments can be requested by the RES4LIVE Project Consortium through the dedicated contact form at https://res4live.eu/contacts/.

Acknowledgements

The work above has been carried out in the context of the Horizon 2020 IA Project RES4LIVE: Energy Smart Livestock Farming towards Zero Fossil Fuel Consumption, which has received funding from the European Union’s Horizon 2020 Research and Innovation Programme under Grant Agreement No. 101000785.

References

Ahmad J., M. Imran, A. Khalid, W. Iqbal, S.R. Ashraf, M. Adnan, S.F. Ali, K.S. Khokhar, 2018. Techno economic analysis of a wind-photovoltaic-biomass hybrid renewable energy system for rural electrification: A case study of Kallar Kahar., Energy. doi: 10.1016/j.energy.2018.01.133.

Almalki, F.A., B.O. Soufiene, S.H. Alsamhi, H. Sakli, 2021. A Low-Cost Platform for Environmental Smart Farming Monitoring System Based on IoT and UAVs. Sustainability, 13, 5908. https://doi.org/10.3390/su13115908.

Ariza-Colpas, P., R. Morales-Ortega, M. A. Pineres-Melo, F. Melendez-Pertuz, G. Serrano-Torne, G. Hernandez-Sanchez, H. Martinez-Osorio, 2019. Teleagro: IOT Applications for the Georeferencing and Detection of Zeal in Cattle. In: Saeed, K., Chaki, R., Janev, V. (eds) Computer Information Systems and Industrial Management. CISIM. Lecture Notes in Computer Science(), vol 11703. Springer, Cham. https://doi.org/10.1007/978-3-030-28957-7_19

Attard, G., A. Comparetti, P. Febo, C. Greco, M.M. Mammano, S. Orlando, 2017. Case study of potential production of Renewable Energy Sources (RES) from livestock wastes in Mediterranean islands. Chem. Eng. Trans. 58, 553–558, doi:10.3303/CET1758093.

Banhazi, T., A. Aarnink, H. Thuy, S. Pedersen, J. Hartung, H. Payne, B. Mullan, D. Berckmans, 2015. Review of the Consequences and Control of High Air Temperatures in Intensive Livestock Buildings. 7, 63–78, doi:10.1080/14488388.2009.11464800.

Black, J.L., Banhazi T.M., 2013. Economic and social advantages of precision livestock farming in the pig industry. In Proceedings of the 6th European conference on precision livestock farming. Berckmans, D., Vandermeulen, J., Eds., p. 199.

Choi, H.C., H.M. Salim, N. Akter, J.C. Na, H.K. Kang, M.J. Kim, D.W. Kim, H.T. Bang, H.S. Chae, O.S. Suh, 2012. Effect of heating system using a geothermal heat pump on the production performance and housing environment of broiler chickens. Poult. Sci., 91, 275–281, doi:10.3382/PS.2011-01666.

Dos Reis, B.R., Z. Easton, R.R. White, D. Fuka, 2021. A LoRa sensor network for monitoring pastured livestock location and activity. Transl. Anim. Sci., 5, 1–9, doi:10.1093/TAS/TXAB010.

Elahi, E., C. Weijun, S.K. Jha, H. Zhang, 2019. Estimation of realistic renewable and non-renewable energy use targets for livestock production systems utilising an artificial neural network method: A step towards livestock sustainability. Energy, 183, 191–204, doi:10.1016/J.ENERGY.2019.06.084.

Eurostat Farms and farmland in the European Union - statistics - Statistics Explained, 2022. Available online: https://ec.europa.eu/eurostat/statistics-explained/index.php/Farms_and_farmland_in_the_European_Union_-_statistics.

Farooq, M.S., S. Riaz, A. Abid, T. Umer, Y. B. Zikria, 2020. Role of IoT Technology in Agriculture: A Systematic Literature Review. Electron. Vol. 9, Page 319 2020, 9, 319, doi:10.3390/ELECTRONICS9020319.

Fournel, S., B. Laberge, A.N. Rousseau, 2017. Rethinking environment control strategy of confined animal housing systems through precision livestock farming. Biosyst. Eng., 155, 96–123, doi:10.1016/J.BIOSYSTEMSENG.2016.12.005.

Jiang, B., W. Tang, L. Cui, X. Deng, 2023. Precision Livestock Farming Research: A Global Scientometric Review. Animals, 13, 2096. https://doi.org/10.3390/ani13132096.

Gad, S., M.A. El-Shazly, K.I. Wasfy, A. Awny, 2020. Utilization of solar energy and climate control systems for enhancing poultry houses productivity. Renew. Energy, 154, 278–289, doi:10.1016/J.RENENE.2020.02.088.

Grogan, A., 2012. Smart Special - Smart Farming | E&T Magazine, Available online: https://eandt.theiet.org/content/articles/2012/06/smart-special-smart-farming/.

Hansen, R.K., B.S. Bjerg, 2018. Optimal Ambient Temperature with Regard to Feed Efficiency and Daily Gain of Finisher pigs. In the Proceedings of the European Conference on Agricultural Engineering AgEng2018. Wageningen University and Research, Ed., Wageningen, pp. 785–790.

Islam, M.M., H.S. Mun, A.B.M.R. Bostami, S.T. Ahmed, K.J. Park, C.J. Yang, 2016. Evaluation of a ground source geothermal heat pump to save energy and reduce CO2 and noxious gas emissions in a pig house. Energy Build, 111, 446–454, doi:10.1016/J.ENBUILD.2015.11.057.

Jahangir, M.H., M. Montazeri, S.A. Mousavi, A. Kargarzadeh, 2022. Reducing carbon emissions of industrial large livestock farms using hybrid renewable energy systems. Renew. Energy, 189, 52–65, doi:10.1016/J.RENENE.2022.02.022.

Jones, D., W.H. Friday, S. DeForest, 2015. Environmental Control for Confinement Livestock Housing.

Kumar, S., A. Darshna, D. Ranjan, 2023. A review of literature on the integration of green energy and circular economy, Heliyon, Volume 9, Issue 11, e21091, ISSN 2405-8440, https://doi.org/10.1016/j.heliyon.2023.e21091.

Licharz, H., P. Rösmann, M.S. Krommweh, E. Mostafa, W. Büscher, 2020. Energy Efficiency of a Heat Pump System: Case Study in Two Pig Houses. Energies, Vol. 13, Page 662 2020, 13, 662, doi:10.3390/EN13030662.

Mateo-Fornés, J., A. Pagès-Bernaus, L.M. Plà-Aragonés, J.P. Castells-Gasia, D. Babot-Gaspa, 2021. An Internet of Things Platform Based on Microservices and Cloud Paradigms for Livestock. Sensors, Vol. 21, Page 5949 2021, 21, 5949, doi:10.3390/S21175949.

Michalk, D.L., D.R. Kemp, W.B. Badgery, J. Wu, Y. Zhang, P.J. Thomassin, 2019. Sustainability and future food security-A global perspective for livestock production. L. Degrad. Dev., 30, 561–573, doi:10.1002/LDR.3217.

Neethirajan, S., B. Kemp, 2021. Digital Livestock Farming. Sens. Bio-Sensing Res., 32, 100408, doi:10.1016/J.SBSR.2021.100408.

O'Connor, S., E. Ehimen, S.C. Pillai, A. Black, D. Tormey, J. Bartlett, 2021. Biogas production from small-scale anaerobic digestion plants on European farms. Renew. Sustain. Energy Rev., 139, 110580, doi:10.1016/J.RSER.2020.110580.

O'Grady, M.J., G.M.P. O'Hare, 2017. Modelling the smart farm. Inf. Process. Agric., 4, 179–187, doi:10.1016/J.INPA.2017.05.001.

Paris, B., F. Vandorou, D. Tyris, A.T. Balafoutis, K. Vaiopoulos, G. Kyriakarakos, D. Manolakos, G. Papadakis, 2022. Energy Use in the EU Livestock Sector: A Review Recommending Energy Efficiency Measures and Renewable Energy Sources Adoption. Appl. Sci., Vol. 12, Page 2142 2022, 12, 2142, doi:10.3390/APP12042142.

Paunova-Hubenova, E., E. Trichkova-Kashamova, 2021. Smart Solutions for Control and Management in Livestock Farms. Big Data, Knowl. Control Syst. Eng. - Proc. 7th Int. Conf. BdKCSE, doi:10.1109/BDKCSE53180.2021.9627269.

Rudenko, N., V. Ershov, D. Trints, 2019. Increasing power supply efficiency of livestock complexes at small farms using renewable energy sources. IOP Conf. Ser. Earth Environ. Sci., 403, 012123, doi:10.1088/1755-1315/403/1/012123.

Scarlat, N., F. Fahl, J,.F. Dallemand, F. Monforti, V. Motola, 2018. A spatial analysis of biogas potential from manure in Europe. Renew. Sustain. Energy Rev., 94, 915–930, doi:10.1016/j.rser.2018.06.035.

Shin, H., Y. Kwak, S.K. Jo, S.H. Kim, J.H. Huh, 2022. Applicability evaluation of a demand-controlled ventilation system in livestock. Comput. Electron. Agric., 196, 106907, doi:10.1016/J.COMPAG.2022.106907.

Sirin, C., J. Goggins, M. Hajdukiewicz, 2023. A review on building-integrated photovoltaic/thermal systems for green buildings, Applied Thermal Engineering, Volume 229, 120607, ISSN 1359-4311, https://doi.org/10.1016/j.applthermaleng.2023.120607.

Symeonaki, E., K.G. Arvanitis, D. Loukatos, D. Piromalis, 2021. Enabling IoT Wireless Technologies in Sustainable Livestock Farming Toward Agriculture 4.0. Lect. Notes Data Eng. Commun. Technol., 67, 213–232, doi:10.1007/978-3-030-71172-6_9.

Yadavalli, P.K., A.K. Mutyala, V.K. Palla, A. Pappu, N. Prathipati, 2021. Smart IOT System for Monitoring and Controlling Livestock Parameters. SSRN Electron. J., doi:10.2139/SSRN.3621946.

Zhang, Y., Q. Chen, G. Liu, W. Shen, G. Wang, 2016. Environment Parameters Control Based on Wireless Sensor Network in Livestock Buildings. doi:10.1155/2016/9079748.

Data-driven solutions for farmer empowerment in smart agriculture: challenges and opportunities

Havva Uyar [a,b*], Ioannis Karvelas [a], Clare Sullivan [b], Stamatia Rizou [a], Spyros Fountas[b]

[a] Research and Development Department, SingularLogic, Athens, Greece

[b] Department of Natural Resources Development and Agricultural Engineering, Agricultural University of Athens, Athens, Greece

* Corresponding author. Email: huyar@singularlogic.eu

Abstract

The adoption of digital technologies in agriculture offers significant potential to enhance productivity, sustainability, and resilience. This paper presents initial insights derived from an ongoing study aimed at evaluating the challenges and opportunities for farmers in adopting data-driven solutions. During the initial phases, the study utilised an online workshop with 46 participants from various agri-stakeholder groups to conduct a comprehensive PESTLE analysis, exploring the political, economic, social, technological, legal, and environmental factors influencing the adoption of data-driven solutions in agriculture.

Key findings indicate that cohesive governmental policies, innovative business models, and targeted educational initiatives are essential for fostering digital transformation in agriculture. Political and regulatory challenges such as aligning cross-border data sharing frameworks and ensuring consistent policy implementation must be addressed. High costs and technical knowledge requirements are substantial economic barriers, particularly for smallholder farmers, necessitating tailored financial support and cooperative business models. Socially, the digital divide and trust issues in data security highlight the need for equitable infrastructure distribution and trust-building measures. Technological advancements like IoT and blockchain offer opportunities but require robust data governance and cybersecurity frameworks. From a legal perspective, simplifying regulatory compliance and clarifying data ownership are crucial for facilitating adoption. While digital agriculture practices support sustainability goals, environmental risks such as electronic waste and increased carbon footprint need careful management.

The insights gathered from diverse agri-stakeholders provide an understanding of the factors impacting digital transformation in agriculture. This research contributes to understanding the specific barriers faced by farmers in adopting data-driven solutions and offers actionable recommendations for creating inclusive and effective data-driven agricultural initiatives.

Keywords: smart farming, digitisation, smallholder farmers, technology adoption, climate resilience.

1. Introduction

Smart agriculture is revolutionising traditional farming practices by leveraging advanced technologies to optimise agricultural processes. The integration of various technologies such as cloud computing, remote sensing, big data analytics, and the Internet of Things (IoT) can potentially enable data-driven decision-making, enhance crop yields, and improve the quality of food products (Wolfert et al., 2017). The essence of smart agriculture lies in its data-driven approach, where data management and smart analytics play pivotal roles in supporting critical decision-making processes (Wolfert et al., 2017). The utilisation of Artificial Intelligence (AI) and Machine Learning (ML) algorithms further enhances the monitoring and efficiency of agricultural operations, contributing to improved ecological outcomes (Gupta et al., 2023). Despite the significant potential benefits, the adoption of smart farming technologies is not without challenges. Farmers, especially smallholders, face numerous obstacles, including climate change, low commodity prices, environmental degradation, and limited access to resources (Jiménez et al., 2019). Moreover, the acceptance and trust of farmers in these technologies are crucial for their successful implementation (Schukat & Heise, 2021).

Understanding the unique challenges and opportunities specific to farmers is vital in the context of smart agriculture. Most smart farming research focuses on technological advancements and their potential impacts on agricultural productivity, often overlooking the complexities involved in the adoption process from the farmers' perspective. This gap is particularly pronounced for smallholder farmers, who constitute a significant portion of the global farming community (FAO, 2021).

This study aims to address this gap by conducting a thorough exploration of the challenges and opportunities based on insights gathered from an online workshop involving diverse agri-stakeholders, including agricultural professionals, researchers, data scientists, policymakers, farmers, educators, agribusiness representatives, and students. Utilising a PESTLE (Political, Economic, Social, Technological, Legal, and Environmental) analysis, this research examines the external factors influencing digital transformation in agriculture. The insights gained from this analysis provide valuable guidance for policymakers, industry leaders, and other stakeholders in crafting strategies to support the digital transformation of agriculture.

2. Methodology

2.1. Participants and Stakeholders

The online workshop was held, with a total of 46 participants joining out of 60 registered individuals. The participants represented a diverse array of agri-stakeholders, including agricultural professionals, researchers, data scientists, policymakers, farmers, educators, agribusiness representatives, and students. The diversity of the cohort allowed for obtaining a comprehensive perspective on the adoption of data technologies in agriculture. Participants registered by providing their names, email addresses, institutional affiliations, and occupation statuses.

2.2. Workshop Design, Data Collection and Data Analysis

The workshop was conducted using Microsoft Teams, with a Miro Board integrated to facilitate interactive activities and collect real-time feedback. The agenda was designed to ensure maximum engagement and effective data collection. The core of the workshop consisted of a brainstorming session focused on the PESTLE analysis. Participants added their own suggestions of challenges and opportunities related to each factor. The session concluded with discussions on future steps and closing remarks. The Miro Board captured all participant inputs during the brainstorming and discussion sessions. The data collected from the Miro Board was subjected to thematic analysis (Braun & Clarke, 2012). Each frame's content was reviewed to identify common themes and significant factors within each PESTLE category. This qualitative approach ensured that the analysis captured the depth and breadth of the participants' insights. Key themes were synthesised to provide a coherent PESTLE analysis.

3. Results and Discussion

3.1. Political Factors

The digital transformation in agriculture is inherently political, demanding a critical approach that incorporates local contexts and broader political economy perspectives (Benegiamo et al., 2023). Participants identified a significant need for a common contractual framework for cross-border data sharing, emphasising the importance of aligning member states within the European Union (EU) and subsequently expanding this framework globally. Such a framework would facilitate smoother and more secure data exchanges between countries, enhancing the effectiveness of digital technologies in agriculture. This need is supported by literature that underscores the necessity for robust governmental frameworks and enhanced data exchange among stakeholders (Nehrey et al., 2023).

Participants also highlighted that state-protected policies and activities can enhance trust among farmers towards these technologies, which is vital for their widespread adoption. Creating policies that focus on the needs and perspectives of farmers ensures they are practical and beneficial, further facilitating adoption. Literature supports this argument, noting the pressing need for comprehensive laws, regulatory frameworks, and public-private cooperation to foster trust and market structure (Kosior, 2020). Existing voluntary codes of conduct, like the EU Code of Conduct on agri-data sharing, offer guidance but highlight the need for modernised regulations to address data privacy and security issues (Kaur & Dara, 2023).

Participants identified the importance of partnerships with governmental agencies and policymakers in advancing digital transformation in agriculture. Participants indicated that many incentives provided by governments have the power to encourage farmers to adopt digital technologies. Subsidies and grants can reduce the financial burden of investing in new technologies, addressing one of the main reasons farmers hold back. Additionally, it was mentioned that some governments have introduced digital notebooks to track

crop data, which help maintain records of crop activities and data, facilitating better decision-making and compliance with agricultural standards.

Despite these potentials, key policy challenges involve issues of data ownership, control, access to technology, and data security. Addressing these requires reshaping the political and economic landscape to ensure equitable agricultural practices, particularly in the context of tensions between digital agri-tech developments and agroecological approaches (Rotz et al., 2019). Moreover, the limitations of digital infrastructure, such as high-speed internet and mobile coverage pose barriers, emphasising the role of policy and investment in overcoming these technical challenges (Knierim et al., 2019).

3.2. Economic Factors

Economic constraints were a major focus of the workshop discussion. High costs and the required technical knowledge associated with digital tools were referenced as significant obstacles for many farmers. Participants noted that high costs and long amortisation processes often mean that by the time technology costs are recovered, the technology might already be obsolete. Literature supports this, highlighting that the high cost associated with adopting robotic technologies and smart farming systems remains a significant drawback, particularly for smallholder farmers (Yépez-Ponce et al., 2023). Farmers are particularly concerned about the return on investment (ROI) when implementing new technologies, as the scarcity of relevant on-farm examples and intangible benefits, such as simplifying farming tasks or increasing enjoyment, complicates ROI calculations (Yépez-Ponce et al., 2023). This uncertainty can reduce lenders' willingness to finance large technology investments due to the perceived high risk for early adopters, leading to inhibited or delayed financing (Eastwood et al., 2023).

Participants also mentioned that cooperation in sharing technologies can reduce costs, and aggregated data can provide better decision support, leading to efficiencies and risk management (Jakku et al., 2019; Regan, 2019). However, in case of cooperation, the literature indicates that farmers fear that competitors might use their data to outbid them in markets for land and other resources, that agribusinesses could target marketing efforts more effectively, and that governments might impose stricter regulations (Rozenstein et al., 2024). Even if issues of data ownership, privacy, and standardisation are resolved, economic and social constraints such as the lack of demonstrated value, mistrust of data aggregation organisations, and the cost of adopting new technologies will persist (Rozenstein et al., 2024). While anonymisation has facilitated data sharing in other sectors, anonymising farm field data is challenging due to the unique field signatures provided by soil type, yield maps, and other spatial information. Thus, anonymisation by a trusted organisation is essential, but financial or other incentives are necessary to motivate data collection (Rozenstein et al., 2024).

Participants raised concerns about the economic viability of products from startups, highlighting the challenges new entrants face in establishing financially sustainable operations. Literature shows that while there are inspiring examples of startup companies providing digital technologies to smallholder farmers in developing countries, such as the "Uber for Tractors" initiative, there is widespread concern that digital agriculture may enhance the market power of large agribusiness enterprises (Birner et al., 2021). Non-governmental organisations have expressed concerns that access to extensive data from numerous farmers could reinforce existing trends of concentration in the input industries, enabling manufacturers to optimise machinery costs and gain competitive advantages (Birner et al., 2021). Additionally, these manufacturers might exploit this information for pricing strategies, increasing their profit margins at the expense of farmers.Additionally, participants highlighted the importance of utilising market analytics to help farmers make informed decisions and gain monetary benefits. It was stated that the current business models do not generate sufficient income to justify the high costs of digital technologies, making them particularly prohibitive for smallholder farmers. Innovative business models, such as technology cooperatives or subscription-based services, could mitigate these issues by spreading costs and risks among multiple users.

Participants discussed the potential economic value of data. The economic value of information technologies hinges on the decisions altered by access to new information, which can be challenging to quantify as it requires comparing decisions made with and without the new information. The availability of economic incentives and financial support mechanisms was seen as essential to promoting the adoption of digital technologies. Financial support for research and development (R&D) and the availability of grants for tool implementation and training opportunities were also highlighted as crucial incentives that could drive adoption. These incentives should be designed to be more accessible and targeted towards the unique needs

of all scales of farmers.

3.3. Social Factors

The social environment plays a crucial role in the adoption of digital technologies in agriculture, encompassing cultural attitudes, social norms, and equity issues. Participants in the workshop highlighted that cultural attitudes and social norms significantly impact the acceptance and integration of digital technologies. Educating local farmers and communities about the benefits of sustainable farming was seen as essential to enhancing this acceptance. However, there is a prevailing uncertainty and resistance among farmers regarding the trustworthiness of digital advice compared to traditional 'in the field' decisions. Literature supports this, noting that farmers often value traditional practices and peer recommendations over external directives, showing greater trust in data generated on their own farms (Eastwood et al., 2023; Jiménez et al., 2019).

A major barrier identified is the low level of trust in data security, with many farmers fearing that digital technologies might compromise their privacy. This is corroborated by studies indicating widespread discomfort among farmers with data sharing and concerns over the lack of transparency and control over their data (Wiseman et al., 2019; Falcão et al., 2023). Additionally, the unequal distribution of digital infrastructure and resources in rural areas exacerbates the digital divide. The World Bank's 2021 report highlights the critical need for rural broadband expansion to support digital agriculture. This divide is further deepened by generational differences, with younger farmers being more open to new technologies than older generations, and by gender inequities, which worsen existing disparities in agriculture (Kaur & Dara, 2023; Birner et al., 2021).

There are also concerns about the potential impact of digital agriculture on job roles and the overall number of jobs in the agricultural sector. Automation could shift farm work from hands-on activities to more management-focused tasks, potentially altering the sector's job landscape (van der Burg et al., 2019; Eastwood et al., 2023; Regan, 2019). Moreover, the increasing market power of large agribusinesses through digital agriculture could exacerbate the divide between different types of farms and regions. Nonetheless, public initiatives and the involvement of new actors could help mitigate these threats and promote equitable access to digital technologies (Birner et al., 2021).

For smallholder farmers, trust issues with agri-tech providers and a lack of clearly defined roles for data intermediaries pose significant barriers. However, fostering an open-minded mentality and self-awareness among farmers regarding new digital solutions can drive adoption.

Addressing these social barriers requires innovative approaches that consider ethical dimensions and ensure technology development and governance systems are inclusive and reflective of all stakeholders' needs, particularly small-scale farmers in developing regions (Eastwood et al., 2023). By fostering trust, transparency, and equitable access, the digital transformation in agriculture can be directed towards more inclusive and socially just outcomes.

3.4. Technological Factors

Participants identified technological innovations as offering unique advantages for improving agricultural productivity and efficiency. The potential for enhanced efficiency and improved quality of agricultural production through digital technology has been widely recognised in the literature, leading to increased awareness among farmers about the benefits of integrating computer and IT networks into their production processes (Yao & Sun, 2023).

Robust modelling based on weather and soil data, mentioned by the participants, can improve farm sustainability by optimising input usage and managing risks. Providing precise data to farmers through advanced data analytics and modelling techniques enhances decision-making, ensuring more sustainable agricultural practices (Fielke et al., 2019; Jakku et al., 2019). For instance, integrating weather station data was highlighted as a significant enhancement of agricultural productivity by providing farmers with precise information for critical decision-making. Participants also noted that IoT sensors are a vital innovation, allowing for the monitoring of various agricultural parameters such as soil moisture, crop health, and environmental conditions. Blockchain technology emerged as a valuable tool for ensuring transparency in agricultural processes, from farm to table, according to the participants. Automated technologies that require minimal maintenance, labour, or technical knowledge were discussed as ways to streamline agricultural

operations, making them more efficient and less dependent on human intervention. However, significant disparities exist among agricultural producers in terms of their technological development, financial capabilities, and resource quality, creating substantial constraints on the widespread adoption of digital technologies in the sector (Kurnosova et al., 2021). Farmers may also struggle to access up-to-date and reliable technology performance reviews, further hindering the adoption of new technologies (Ingram et al., 2022).

Participants pointed out a lack of interoperability between agriculture and other industries. They stressed the importance of developing interoperable systems that enable communication and data exchange between different agricultural technologies and platforms to create a cohesive agricultural ecosystem. Inadequate data infrastructure, particularly in regions with fragmented smallholder farms, where public policy and access to digital infrastructure are insufficient, is a key barrier (Kaur & Dara, 2023). Participants also identified a low level of trust in data security and interoperability obstacles between on-farm machinery and data transfer between providers as major issues. Insufficient standards on data governance highlight the need for robust ethical frameworks for data exchange, ensuring data integrity and security. This is supported by literature, which notes that technical issues related to data quality, transfer, privacy, and ownership pose significant challenges at multiple scales, impacting the seamless integration and utilisation of digital technologies (Ingram et al., 2022; Eastwood et al., 2023). Developing new models of data ownership and governance that are transparent and inspire trust is vital. This includes the use of interoperable standards, publicly funded development of analytic tools, and responsible innovation approaches that incorporate ethical considerations (Eastwood et al., 2023).

Concerns about how collected data are stored and who has access to them were paramount among the participants. They noted that agricultural data might reveal sensitive personal information, such as farmers' financial situations, leading to privacy risks. To address these concerns, participants suggested the need for mediators between technological solutions and end-users, ensuring that privacy and security issues are adequately managed. Technical limitations and compatibility issues can hinder the seamless integration of digital tools across different farming systems. Literature suggests that this digital divide is exacerbated by differences in digital knowledge and expertise between agri-tech providers and farmers. Ag-tech providers, possessing advanced skills in collecting, aggregating, and analysing farm data, can dominate the establishment of processes and protocols, leading to power imbalances (Kaur & Dara, 2023). The performance and design of digital technologies must be robust enough to withstand on-farm conditions and align with farming practices (Eastwood et al., 2023). Cybersecurity vulnerabilities and data privacy concerns were also mentioned as significant risks to the integrity and reliability of digital agriculture systems. Participants, especially smallholder farmers, highlighted the significant risks from cyber-attacks, which can compromise farms' data and operations. Compliance with technical standards was identified as another barrier, as many small farmers find it difficult to understand and follow these standards. Participants stressed that technologies need to be both economically viable and easy to use, ensuring that smallholder farmers can see a tangible economic payback.

Developing a trust framework that is easy to understand and implement is essential to foster confidence among smallholder farmers in adopting digital technologies. Finally, poor internet connectivity in rural areas was noted by participants as a challenge that further exacerbates these issues. Literature supports this argument, noting that the lack of reliable rural internet access remains a critical challenge, as most data-driven agricultural technologies depend on robust internet connectivity, which is often sporadic or non-existent in many rural areas (Rozenstein et al., 2024).

3.5. Legal Factors

During the workshop, participants discussed various legal factors, highlighting the importance of regulatory frameworks, intellectual property rights, and data governance in enabling digital transformation in agriculture. They emphasised that ensuring regulatory compliance is not just about adherence but also about fostering an environment that encourages ongoing innovation in the agricultural sector. Adherence to local, national, and EU regulations, particularly in data handling and agricultural practices, is essential for protecting the innovation and adoption of digital technologies in agriculture. Compliance with these regulations ensures that digital practices are legally sound and can be safely integrated into existing agricultural systems. Literature further emphasises this, noting that the legal dimension of digital transformation in agriculture encompasses several challenges, primarily revolving around the protection and

management of agricultural data. A significant hurdle is the absence of comprehensive regulatory frameworks for safeguarding farm data, often leading to terms of use being established through complex and potentially biased data license agreements (Kaur & Dara, 2023; Wiseman et al., 2019).

Participants highlighted those differences in data privacy regulations between Europe and other continents further complicate compliance, leading to challenges in managing data across borders. Literature supports this by pointing out that legislation often lacks clarity, particularly in distinguishing between data production and intellectual property rights related to information systems derived from that data (Ellixson & Griffin, 2017). Participants stressed the importance of clarifying data ownership—whether it belongs to the farmers or the agri-tech companies—to mitigate legal risks and ensure compliance. The ongoing nature of data streams complicates the establishment of ownership and usage rights, making it challenging to contract and manage these resources effectively. Data ownership disputes further complicate the landscape, with various sectors and stakeholders claiming ownership while having differing needs and interests (Rozenstein et al., 2024). The intertwining of private and commercial data, especially in family-run farms, adds another layer of complexity, as personal financial records and business data often overlap, raising privacy concerns (Brown et al., 2023). This ambiguity can hinder the buying, selling, sharing, and management of agri-data.

Workshop participants noted that complex regulatory requirements and a lack of clear guidance act as significant barriers, making it difficult for farmers to navigate the legal landscape. Simplifying these regulations and providing clear, accessible information can help farmers embrace digital technologies more readily. There is a pressing need for standardised, ready-to-use data sharing contract templates that farmers can utilise to protect their rights and facilitate smooth transactions. These templates can reduce the complexity of legal agreements and provide clear guidelines for data usage and sharing. Such frameworks, participants noted, facilitate international collaboration and data exchange, enhancing the global applicability of digital agricultural technologies. Literature supports this argument, highlighting the development and enforcement of legal frameworks that govern the collection, sharing, and usage of farm data as crucial to encouraging the adoption of smart farming technologies among farmers (Wiseman et al., 2019). Another issue discussed in the workshop is the context-dependent value of data. Data that might seem insignificant to one actor could be invaluable to another, creating obstacles in persuading stakeholders to share their data without clear compensation mechanisms (Kenney et al., 2020). The value of agri-data is complex and yet not clearly defined or measurable in literature. Additionally, the spatial component of agricultural data, essential for adding value through geolocation, can inadvertently disclose sensitive information about individual farms, posing additional privacy risks.

Participants also mentioned that establishing specific data standards and protocols could ensure compliance with regulations and facilitate data sharing and product traceability within the food chain, which is vital for maintaining the integrity and trustworthiness of digital agricultural practices. Positive incentives for data sharing, coupled with advanced legislation, could enable the utilisation of accumulated agricultural data for the public good (Rozenstein et al., 2024). Therefore, a trust-reinforcing regulatory framework is imperative for effective farm data gathering, sharing, and analysis.

3.6. Environmental Factors

Participants discussed both the potential benefits for sustainability and the environmental risks and challenges that digital technologies might entail. Precision agriculture, involving the use of digital tools to minimise inputs such as water, fertilisers, and pesticides, was cited as a method to significantly reduce the overall environmental footprint of farming activities and maintain biodiversity. They also pointed out that monitoring and optimising energy consumption can lead to more sustainable farming operations. Efficient use of resources like water and fertilisers not only conserves these vital inputs but also supports more sustainable farming practices. Additionally, digital tools can help farmers adapt to changing climatic conditions by providing timely information and forecasts, enhancing their resilience to climate change. Preventing desertification was highlighted as another significant benefit, with digital technologies able to monitor soil health and manage land use more effectively.Karunathilake et al. (2023) supports the argument by stating that precision agriculture demonstrates the potential of using technology to manage spatial and temporal variability in agricultural fields, enhancing performance and environmental quality. Site-specific management practices enable more accurate decision-making per unit area and time, which conserves agricultural inputs, reduces costs, and mitigates environmental impacts. Digital agriculture is often perceived as innovative and modern, with societal recognition of its potential to improve environmental stewardship

(Fielke et al., 2022; Eastwood et al., 2023). Enhanced food system traceability methods also facilitate the certification of goods based on their environmental performance or the sustainability of their production practices. The benefits of digital transformation extend beyond individual farms, creating broader environmental advantages that justify public policy support. The reduction in monitoring costs and ensuring that environmentally beneficial practices are applied have expanded the range of agri-environmental policy options (Weersink et al, 2018). Public policies play a crucial role in maximising these external benefits, ensuring that digital agriculture contributes positively to environmental sustainability while addressing the concerns and challenges faced by farmers.

Despite these benefits, participants acknowledged that the widespread use of digital technologies in farming can also pose environmental risks and lead to unintended consequences. One primary concern is the increase in electronic waste resulting from the higher usage of digital devices. The production and disposal of these devices contribute to the carbon footprint, and the energy consumption required for digital infrastructure can have an unintended environmental impact. Changes in the farming landscape, such as the encouragement of larger, more uniform fields, might result from the implementation of digital technologies. Participants also expressed concerns that over-reliance on digital solutions may lead to the loss of unique local farming knowledge, which is valuable for maintaining diverse and resilient agricultural practices. There were also concerns among farm groups about the potential misuse of data by environmental groups or regulatory agencies to penalise farms for non-compliance with regulations, particularly in nutrient management. However, data can also help farms demonstrate compliance with sustainability certifications more accurately, thereby reducing litigation risks (Coble et al., 2016). Environmental threats and climate-related challenges can disrupt agricultural production systems and undermine the effectiveness of digital interventions. Extreme weather conditions, such as floods, droughts, and storms, can damage digital infrastructure and limit the effectiveness of digital tools. Climatic suitability is crucial, as some digital devices may not function effectively in extreme conditions, limiting their usefulness. These climate extremes pose a direct threat to the reliability and functionality of digital agricultural technologies.

4. Conclusions

This study utilised an online workshop with 46 participants from various agri-stakeholder groups to conduct a comprehensive PESTLE analysis of the factors influencing the adoption of digital technologies in agriculture. The analysis revealed multifaceted challenges and opportunities across political, economic, social, technological, legal, and environmental dimensions. The workshop highlighted the necessity for cohesive and farmer-centric policies, innovative and accessible business models, and targeted education and support to bridge the digital divide. The importance of robust data governance, clear regulatory frameworks, and sustainable practices was also emphasised.

Key takeaways from the workshop include the need for governments to harmonise cross-border data sharing frameworks and develop cohesive policies that involve stakeholders at all levels in the decision-making process. Providing targeted incentives, such as subsidies and tax breaks, can encourage technology adoption across various farm sizes. Innovative business models, like cooperative cost-sharing schemes and subscription-based services, can make digital technologies more accessible and financially viable. Investing in rural broadband infrastructure and offering targeted education and training programmes to build digital literacy and trust in data security is essential to bridge the digital divide. Establishing robust data governance frameworks and developing privacy-preserving technologies will ensure data privacy and security, fostering a trustworthy digital ecosystem. Promoting the use of open data can empower farmers with access to valuable climate and market information, enhancing their decision-making capabilities and integration into the emerging data economy.

For smallholder farmers, these measures are particularly critical. Tailored business models, affordable technology solutions, and specific financial support mechanisms can help overcome the unique barriers they face. Additionally, supporting the environmental sustainability of digital agriculture by ensuring proper disposal of electronic waste, minimizing the carbon footprint of digital devices, and preserving local farming knowledge alongside digital innovations is crucial.

In conclusion, addressing these identified challenges holistically will be crucial for fostering a more productive, sustainable, and resilient agricultural sector. The insights gained from this workshop provide a valuable foundation for policymakers, industry leaders, and stakeholders to drive forward the digital transformation of agriculture, ensuring that all farmers, particularly smallholders, can benefit from these

advancements.

Acknowledgements

This research was funded by the EnTrust project (MSCA-DN-101073381) within the Horizon Europe Marie Skłodowska-Curie Actions and by the AgriDataValue project (Grant Agreement No. 101086461) from the EU Horizon Europe research and innovation programme.

References

Benegiamo, M., Corrado, A., & Fama, M. (2023). Agricultural digitalisation and just transition: a framework for the analysis. *Italian Review of Agricultural Economics*, *78*(2), 5-17.

Birner, R., Daum, T., & Pray, C. (2021). Who drives the digital revolution in agriculture? A review of supply-side trends, players and challenges. *Applied economic perspectives and policy*, *43*(4), 1260-1285.

Braun, V., & Clarke, V. (2012). Thematic analysis. *American Psychological Association.*

Brown, C., Regan, Á., & Van Der Burg, S. (2023). Farming futures: Perspectives of Irish agricultural stakeholders on data sharing and data governance. *Agriculture and Human Values*, *40*(2), 565-580.

Coble, K., Griffin, T., Ahearn, M., Ferrell, S., McFadden, J., Sonka, S., & Fulton, J. (2016). Advancing US agricultural competitiveness with big data and agricultural economic market information, analysis, and research.

Eastwood, C., Turner, J. A., Romera, A., Selbie, D., Henwood, R., Espig, M., & Wever, M. (2023). A review of multi-scale barriers to transitioning from digital agriculture to a digital bioeconomy. *CABI Reviews*, (2023).

Ellixson, A., & Griffin, T. (2016). Farm data: Ownership and protections. *Available at SSRN 2839811*.

Falcão, R., Matar, R., Rauch, B., Elberzhager, F., & Koch, M. (2023). A Reference Architecture for Enabling Interoperability and Data Sovereignty in the Agricultural Data Space. *Information*, *14*(3), 197.

FAO Report (2021) Small family farmers produce a third of the world's food. https://www.fao.org/newsroom/detail/Small-family-farmers-produce-a-third-of-the-world-s-food/en

Fielke, S. J., Garrard, R., Jakku, E., Fleming, A., Wiseman, L., & Taylor, B. M. (2019). Conceptualising the DAIS: Implications of the 'Digitalisation of Agricultural Innovation Systems' on technology and policy at multiple levels. *NJAS: Wageningen Journal of Life Sciences*, *90*(1), 1-11.

Ingram, J., Maye, D., Bailye, C., Barnes, A., Bear, C., Bell, M., ... & Wilson, L. (2022). What are the priority research questions for digital agriculture?. *Land Use Policy*, *114*, 105962.

Jakku, E., Taylor, B., Fleming, A., Mason, C., Fielke, S., Sounness, C., & Thorburn, P. (2019). "If they don't tell us what they do with it, why would we trust them?" Trust, transparency and benefit-sharing in Smart Farming. *NJAS-Wageningen Journal of Life Sciences*, *90*, 100285.

Jiménez, D., Delerce, S., Dorado, H., Cock, J., Muñoz, L. A., Agamez, A., & Jarvis, A. (2019). A scalable scheme to implement data-driven agriculture for small-scale farmers. *Global Food Security*, *23*, 256-266.

Kaur, J., & Dara, R. (2023). Analysis of Farm Data License Agreements: Do Data Agreements Adequately Reflect on Farm Data Practices and Farmers' Data Rights?. *Agriculture*, *13*(11), 2170.

Karunathilake, E. M. B. M., Le, A. T., Heo, S., Chung, Y. S., & Mansoor, S. (2023). The path to smart farming: Innovations and opportunities in precision agriculture. *Agriculture*, *13*(8), 1593.

Kenney, M., Serhan, H., & Trystram, G. (2020). Digitization and platforms in agriculture: organizations, power asymmetry, and collective action solutions. *Power Asymmetry, and Collective Action Solutions (June 20, 2020)*.

Knierim, A., Kernecker, M., Erdle, K., Kraus, T., Borges, F., & Wurbs, A. (2019). Smart farming technology innovations–Insights and reflections from the German Smart-AKIS hub. *NJAS-Wageningen Journal of Life Sciences*, *90*, 100314.

Kosior, K. (2020). Economic, ethical and legal aspects of digitalization in the agri-food sector. *Zagadnienia Ekonomiki Rolnej/Problems of Agricultural Economics*.

Kurnosova, N. S., Kurnosov, S. A., & Ulez'ko, A. V. (2021, June). About models of agriculture digital transformation. In *IOP Conference Series: Earth and Environmental Science* (Vol. 786, No. 1, p. 012011). IOP Publishing.

Nehrey, M., Klymenko, N., & Kostenko, I. (2023, March). Formal and Non-formal Education of Ukraine: Analysis of the Current State and the Role of Digitalization. In *International Conference on Computer Science, Engineering and Education Applications* (pp. 1085-1098). Cham: Springer Nature Switzerland.

Regan, Á. (2019). 'Smart farming'in Ireland: A risk perception study with key governance actors. *NJAS-Wageningen journal of life sciences*, *90*, 100292.

Rotz, S., Duncan, E., Small, M., Botschner, J., Dara, R., Mosby, I., ... & Fraser, E. D. (2019). The politics of digital agricultural technologies: a preliminary review. *Sociologia ruralis*, *59*(2), 203-229.

Rozenstein, O., Cohen, Y., Alchanatis, V., Behrendt, K., Bonfil, D. J., Eshel, G., ... & Lowenberg-DeBoer, J. (2024). Data-driven agriculture and sustainable farming: friends or foes?. *Precision Agriculture*, *25*(1), 520-531.

Schukat, S., & Heise, H. (2021). Smart Products in Livestock Farming—An Empirical Study on the Attitudes of German Farmers. *Animals*, *11*(4), 1055.

Van der Burg, S., Bogaardt, M. J., & Wolfert, S. (2019). Ethics of smart farming: Current questions and directions for responsible innovation towards the future. *NJAS-Wageningen Journal of Life Sciences*, *90*, 100289.

Weersink, A., Fraser, E., Pannell, D., Duncan, E., & Rotz, S. (2018). Opportunities and challenges for big data in agricultural and environmental analysis. *Annual Review of Resource Economics*, *10*, 19-37.

Wiseman, L., Sanderson, J., Zhang, A., & Jakku, E. (2019). Farmers and their data: An examination of farmers' reluctance to share their data through the lens of the laws impacting smart farming. *NJAS-Wageningen Journal of Life Sciences*, *90*, 100301.

Wolfert, S., Ge, L., Verdouw, C., & Bogaardt, M. J. (2017). Big data in smart farming–a review. *Agricultural systems*, *153*, 69-80.

Yao, W., & Sun, Z. (2023). The impact of the digital economy on high-quality development of agriculture: A China case study. *Sustainability*, *15*(7), 5745.

Yépez-Ponce, D. F., Salcedo, J. V., Rosero-Montalvo, P. D., & Sanchis, J. (2023). Mobile robotics in smart farming: current trends and applications. *Frontiers in Artificial Intelligence*, *6*.

Advancing dairy farm management: leveraging data, neural networks, and interactive web design

Razieh Abdollahipour [a,*], Mostafa Sayeed [a], David Janke [a], Thomas Amon [a, b], Barbara Amon [c, d], Sebastian Opalinski [e], Joanna Frontczak [f], Sabrina Hempel [a]

[a] Department of Sensors and Modelling, Leibniz Institute of Agricultural Engineering and Bioeconomy, Potsdam, Germany

[b] Department of Veterinary Medicine, Institute of Animal Hygiene and Environmental Health, Free University Berlin, Berlin, Germany

[c] Department of Technology Assessment, Leibniz Institute of Agricultural Engineering and Bioeconomy, Potsdam, Germany

[d] University of Zielona Gora, Faculty of Civil Engineering, Architecture and Environmental Engineering, Zielona Góra, Poland

[e] Department of Environment Hygiene and Animal Welfare, Wroclaw University of Environmental and Life Sciences, Wrocław, Poland

[f] University of Zielona Góra, Institute of Sociology, Zielona Góra, Poland

* Corresponding author. Email: rabdollahipour@atb-potsdam.de

Abstract

Within the framework of the ET4D project, we introduce a data management system (DMS) designed to transform dairy farm management. This system builds on findings from a social diagnosis of attitudes along the dairy production chain and a detailed analysis of on-farm communication ecosystems. It utilizes cutting-edge technology, including deep neural networks, for in-depth data analysis and predictive insights. Additionally, it features an interactive and user-friendly web application designed to improve operational transparency and sustainability. The transdisciplinary ET4D initiative is spearheaded by the Leibniz Institute for Agricultural Engineering and Bioeconomy (ATB) in Germany alongside partners from seven countries representing academia and industry. It provides a data space and uses data analysis and machine learning to process and interpret farm data. This approach enables the modeling of farm dynamics, yielding predictions and insights. Key focus areas include enhancing animal welfare, optimizing productivity, and minimizing environmental impact. At the heart of this project is a user-centered dynamic web application, characterized by its interactive and engaging design. Users from various segments of the dairy industry, including farmers, stakeholders, and consumers, are equipped with tailored tools and dashboards. Users can access relevant, up-to-date information, facilitating informed decision-making and strategic planning. In conclusion, this segment of the ET4D project is setting new standards in dairy farm management. By blending cutting-edge artificial intelligence technology with a focus on interactive web design, we aim to usher in a new era of data-driven decision-making. This project not only enhances farm productivity and sustainability but also reshapes the interaction between technology and agriculture, driving the industry toward a more informed, responsible, and collaborative future.

Keywords: Data Management System, Dairy Farming, Machine Learning, Software development, Sustainability.

1. Introduction

The increasing demand for sustainability and transparency in dairy farming necessitates innovative technological solutions. Precision Livestock Farming, a concept driven by data analytics, sensor technologies, and machine learning, promises significant improvements in farm management and environmental sustainability. However, the complexity of dairy farm management necessitates innovative approaches. Within this context, the ET4D project ("Development of a practical data management system with embedded sensors for improved environmental management and transparency of dairy farming") aims to develop and implement a comprehensive Data Management System (DMS) that leverages sensor data, empirical modeling, and machine learning to improve dairy farm management.

Multi-criteria assessment (MCA) frameworks have been widely used to evaluate and improve farm management practices. Oliveira et al. (2021) explored the circular economy in dairy production by employing integrated environmental assessments to promote efficient resource use and waste management. Zucali et al.

(2016) proposed a comprehensive scoring system to assess dairy farms based on animal welfare, environmental impact, and production efficiency, while Herva and Roca (2013) reviewed combined MCA approaches for corporate environmental evaluation. Moreover, Hajkowicz and Wheeler (2008) used MCA to evaluate dairy effluent management options, illustrating the need to consider both economic and environmental factors. Van Calker et al. (2006) developed a multi-attribute sustainability function specifically for Dutch dairy farms, balancing economic, environmental, and social criteria. More recently, Wilfart et al. (2023) introduced DEXi-Dairy, an ex-post MCA tool to assess dairy production systems across Europe. These studies underscore the value of holistic assessment frameworks in improving transparency and decision-making in dairy farming.

Empirical modeling is essential for predictive analysis and decision support in dairy farming. Machine learning algorithms, particularly supervised learning models, have shown promise in predicting various aspects of farm management. Yeo et al. (2023) applied regression models to estimate internal air temperature and CO_2 concentrations in pig houses, while El Alaoui et al. (2023) evaluated machine learning methods for predicting greenhouse microclimate parameters. Bovo et al. (2021) used Random Forest models to predict milk yield under heat stress, and Arulmozhi et al. (2021) developed machine learning-based models to forecast indoor temperature and humidity in swine buildings. In dairy farming, Hempel et al. (2020) demonstrated the potential of supervised machine learning for estimating methane emissions in naturally ventilated dairy barns.

Overall, these empirical models and machine learning algorithms provide a strong foundation for data-driven decision support systems in dairy farming. The ET4D project builds upon these methodologies, integrating embedded sensors with a comprehensive Data Management System (DMS) to improve environmental management and transparency in dairy farming.

The ET4D project focuses on achieving the following primary objectives:

- Improve Dairy Farm Communication Infrastructure: Develop dependable wireless connectivity for seamless data transfer within the farm and towards the cloud.
- Create an Advanced DMS Platform: Integrate embedded sensors with machine learning algorithms to provide valuable predictive insights.
- Enable Evidence-Based Decision Making: Offer dairy farmers tailored reports and data visualizations via an intuitive web application to support their operational strategies.
- Promote Sustainable Practices: Utilize data insights to enhance animal welfare, optimize productivity, and minimize environmental impact.

More information can be found at the ET4D homepage: https://et4d.eu/.

2. Materials and Methods

The ET4D project adopts a comprehensive, transdisciplinary approach to develop a Data Management System (DMS) designed to improve environmental management and transparency in dairy farming. The DMS integrates embedded sensors, multi-criteria assessment, empirical modeling, and web-based decision support systems. The project comprises six work packages, of which four are depicted in Figure 2. Work packages 5 and 6 focus on 'Dissemination, Exploitation and Communication,' and 'Project Coordination and Facilitation,' respectively. Currently, the project is in the first half of its progression.

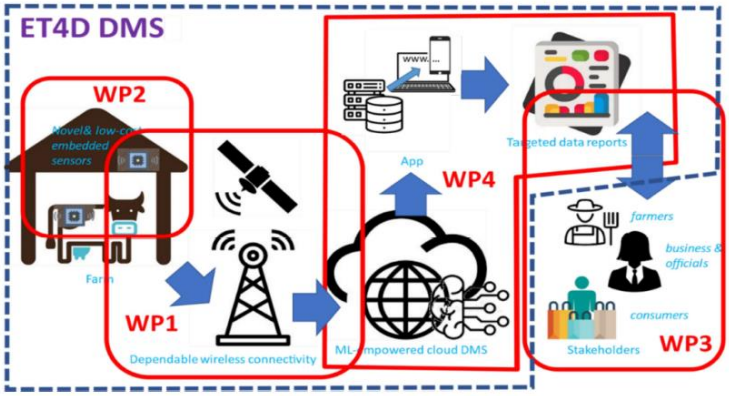

Figure 1. Four of the basic work packages involved in the ET4D data management system.

2.1. Embedded Sensors and Communication Infrastructure

Work Package 1 of the ET4D project currently focuses on analyzing and modeling existing communication infrastructures in selected regions for our on-farm case studies. Enhancement measures for connectivity are still under discussion and have not yet been implemented. In Work Package 2, we have selected case study farms, reviewed existing sensors, and started integrating additional project-specific sensors.

This sensor network will monitor environmental parameters, animal welfare indicators, and production efficiency metrics. The data collected will eventually be transferred to a cloud-based repository through a wireless connectivity.

2.2. Social Diagnosis and Multi-Criteria Assessment

A social diagnosis involving surveys and in-depth interviews is designed to understand the information requirements of different stakeholders along the dairy production chain. Based on these insights, a multi-criteria assessment framework is developed, incorporating criteria such as animal welfare, environmental compatibility, human health, production costs, disease management, and regulatory compliance.

Each criterion will be weighted appropriately, leading to a comprehensive scoring system that classifies and aggregates data into Key Performance Indicators. These indicators provide insights into animal welfare, environmental impact, production efficiency, and overall farm sustainability.

We have started with a small pilot study on consumer attitudes in May 2024, which will be followed by a larger study in autumn 2024 and a study with farmers in winter 2024. The results shall be the basis for refining the design of the demo web app.

2.3. Data Aggregation, Management, and Empirical Modeling

Data collected from embedded sensors and the social diagnosis will be aggregated into the DMS. Some empirical models are developed using machine learning algorithms such as LSTM, ARIMA, and SARIMA. These models provide predictive insights into the future values of certain features. To ensure accuracy and reliability, the models are evaluated using metrics such as Root Mean Square Error (RMSE) and Mean Absolute Error (MAE). Predictions may include methane (CH_4), ammonia (NH_3), and carbon dioxide (CO_2) emissions, depending on the needed criteria. The functionality of these models will then be compared to determine the most effective one.

2.4. Web App Design

We are developing a web application using the Django framework, providing an intuitive user interface tailored to different user groups (farmers, stakeholders, consumers). The application features a dynamic dashboard where users can log in and access data, based on their specific needs.

The data in the DMS will be updated automatically and frequently. Users can visualize time series data collected from farms and view predictive insights from machine learning models. They can interact with the dashboard to explore how changes in one parameter affect other controllable parameters, providing valuable decision support for strategic planning and operational optimization. Figure 2 illustrates a demo of the dashboard.

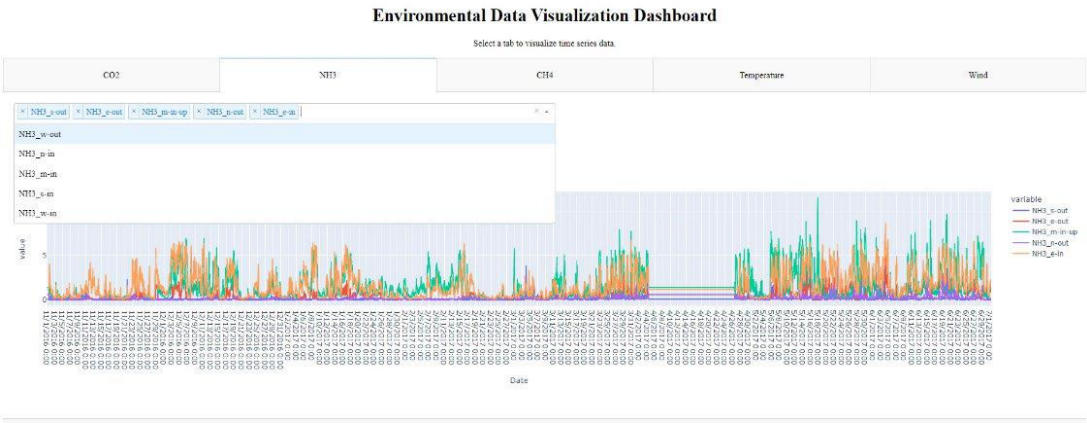

Figure 2. A part of the Environmental Data Visualization Dashboard

This interactive dashboard provides tailored insights, enhancing transparency and evidence-based decision-making in dairy farm management.

3. Conclusions

The ET4D project aims to develop a comprehensive data management system to improve environmental management and transparency in dairy farming. By integrating data from embedded sensors with multi-criteria assessment and machine learning models, the project seeks to provide valuable insights into farm productivity, greenhouse gas emissions, and animal welfare. The web application will offer tailored dashboards and predictive tools, enabling farmers, stakeholders, and regulators to visualize data and understand some parameters affect other factors. This approach supports informed decision-making and strategic planning, working towards enhancing transparency and sustainability in dairy farming.

Sensor implementation began in Poland in April 2024, focusing on measuring humidity, temperature, dust, and gas concentration. Initial data collection from the sensor network on one farm in Poland is successfully completed and preliminary analysis is started. The basic structure of the web app design is in progress. The next steps include installing sensors in other partner farms, investigating different predictive models to find a suitable model for our data, and continued integration of sensor data for environmental management and farm productivity. We anticipate that the final outcome of this project will be a useful and effective DMS that enhances currently available farming tools and that makes livestock farming conditions more transparent for regulating bodies and the broader public.

Acknowledgements

ET4D is part of the ERA-NET Cofund ICT-AGRI-FOOD, with funding provided by national sources and co-funding by the European Union's Horizon 2020 research and innovation program, Grant Agreement number 862665.

The work leading to this manuscript was financially supported by the German Federal Ministry of Food and Agriculture (BMEL) through the Federal Office for Agriculture and Food (BLE), grant number 2823ERA20H, and co-financed by the National Center for Research and Development in Poland.

We would like to further thank all our international partners for their invaluable contributions to the ET4D project: University of Zielona Góra, Tokat Gaziosmanpasa University, AgHiTech Ltd., MIGAL Galilee Research Institute, Estonian University of Life Sciences, Wroclaw University of Environmental and Life Sciences, Aarhus University, AKI Agrárközgazdasági, Centre for Wireless Communications – Networks and Systems, and Innvite ApS. We further acknowledge the national funding bodies of our international partners supporting the ET4D project.

References

Arulmozhi, E., Basak, J. K., Sihalath, T., Park, J., Kim, H. T., & Moon, B. E. 2021. Machine learning-based microclimate model for indoor air temperature and relative humidity prediction in a swine building. *Animals*, 11(1), 222.

Bovo, M., Agrusti, M., Benni, S., Torreggiani, D., & Tassinari, P. 2021. Random forest modelling of milk yield of dairy cows under heat stress conditions. *Animals*, 11(5), 1305.

El Alaoui, M., Chahidi, L. O., Rougui, M., Mechaqrane, A., & Allal, S. 2023. Evaluation of CFD and machine learning methods on predicting greenhouse microclimate parameters with the assessment of seasonality impact on machine learning performance. *Scientific African*, 19, e01578.

Hajkowicz, S., & Wheeler, S. 2008. Evaluation of dairy effluent management options using multiple criteria analysis. *Environmental Management*, 42(4), 609-623. http://dx.doi.org/10.1007/s00267-007-9060-8

Hempel, S., Adolphs, J., Landwehr, N., Janke, D., & Amon, T. 2020. How the selection of training data and modeling approach affects the estimation of ammonia emissions from a naturally ventilated dairy barn - classical statistics versus machine learning. *Sustainability*, 12, 1030.

Hempel, S., Adolphs, J., Landwehr, N., Willink, D., Janke, D., & Amon, T. 2020. Supervised machine learning to assess methane emissions of a dairy building with natural ventilation. *Applied Sciences*, 10(19), 6938.

Herva, M., & Roca, E. 2013. Review of combined approaches and multi-criteria analysis for corporate environmental evaluation. *Journal of Cleaner Production*, 39, 355-371.

Oliveira, A. I., Coelho, P., Barros, A. T., & Domingos, T. 2021. Circular economy in the agro-industry: Integrated environmental assessment of dairy products. *Renewable and Sustainable Energy Reviews*, 151, 111524. http://dx.doi.org/10.1016/j.rser.2021.111524

Van Calker, K. J., Berentsen, P. B. M., Giesen, G. W. J., & Huirne, R. B. M. 2006. Development and application of a multi-attribute sustainability function for Dutch dairy farming systems. *Ecological Economics*, 57(3), 640-658. http://dx.doi.org/10.1016/j.ecolecon.2005.05.016

Wilfart, A., Dupraz, P., Cappelli, G., & Teissier, D. 2023. DEXi-Dairy: An ex post multicriteria tool to assess the sustainability of dairy production systems in various European regions. *Agronomy for Sustainable Development*, 43(3). http://dx.doi.org/10.1007/s13593-023-00935-3

Yeo, U. H., Jo, S. K., Kim, S. H., Park, D. H., Jeong, D. Y., Park, S. J., Shin, H., & Kim, R. W. 2023. Applicability of machine-learned regression models to estimate internal air temperature and CO_2 concentration of a pig house. *Agronomy*, 13(2), 328.

Influence of field, crop and climate variables on corn silage yield maps

Javier Bueno [a,*], Jorge Dafonte [a], José Miguel Edreira [a], Miguel Ángel Vilar [b]

[a] Department of Agroforestry Engineering, University of Santiago de Compostela, Lugo, Spain

[b] Department of Applied Mathematics, University of Santiago de Compostela, Lugo, Spain

* Corresponding author. Email: javier.bueno@usc.es

Abstract

Precision Agriculture with silage corn (*Zea mays* L.) can reduce annual agricultural operating costs by optimizing resources such as seeds, fertilizers, and pesticides. Self-Propelled (SP) Forage Harvesters equipped with yield monitor systems record yield data files that can be used to obtain yield maps. In this study, we have worked with 201 silage corn yield files recorded by an agricultural contractor company in northwest Spain during four harvest seasons (2019-2022). Yield data files were obtained in 68 fields and cleaned with SMS Advanced software (Spatial Management System - Ag Leader Technology) to remove errors.

The study's main objective was to analyse the spatial and temporal variability of the corn silage dry yield data gathered by the SP Forage Harvesters. Dry matter yield, fresh matter yield, crop moisture, FAO maturity group, precipitation, thermal integral, field area, average field slope, average field topographic wetness index (TWI), and corn seeding rate were used as variables. To estimate the precipitation data, data from Meteogalicia (Galician regional meteorological agency) and AEMET (Spain state meteorological agency) were used. An estimation of the precipitation was carried out using regression kriging with secondary variables (latitude, longitude, and elevation) using a script in R computing software.

A Principal Component Analysis (PCA) of all the variables studied has been carried out. When the individual data were analysed, two populations were observed, one corresponding to the year 2019 and another population to the years 2020, 2021 and 2022. This feature probably was caused because the year 2019 recorded the lowest rainfall in the summer. When analysing only the data from the years 2020, 2021 and 2022, the first component that is associated with the yield parameters is also closely related to topographic factors such as TWI, slope and elevation of the plot

Keywords: Precision Agriculture, Yield Maps, Variability, Corn Silage**,** Principal Components.

1. Introduction

Corn silage is a major crop in northwest Spain, where the Galicia region is ranked first in dairy production in the whole country. In 2022 71,257 ha were planted in this region, which represents 82% of the total crop area in Spain (MAPA, 2023). The self-propelled forage harvesters used for corn silage harvesting have sensors that measure forage production and moisture content, so georeferencing this data with the positions calculated by a GNSS receiver located above the cabin, allows yield maps to be obtained (Bueno et al., 2023). Yield maps allow to visualize yield variability and to manage it with precision agriculture tools. But variability in crop yield occurs spatially and temporally, and only with several years' worth a geospatially explicit yield data can these be fully understood (Adhikari et al., 2023).

Properties of the field such as topographic parameters (elevation, slope) have an important role on the temperature and humidity regimes, which are related to yield (Heil et al., 2018). Also, properties of the crop as seeding rate and maturity group or climate variables as rainfall or degree-days, affect spatial and temporal variability. Even there are other factors (e.g. fertility level, plant management, and insect, disease, and weed pressures, etc.) that can affect the production of maize, there is no doubt that precipitation is one of the most important factors controlling maize yield both for grain and silage (Maitah et al., 2021). Early maturing hybrids within location yield less than later types (Guyader et al., 2018) because longer-season hybrids tend to produce higher silage yield. Different weather conditions in different seasons can recommend changing the hybrid maturity group for adapting the crop to a sooner or later planting date.

The main objective of this work was to develop a model to predict the spatial and temporal variability of the corn silage dry yield using field, crop and climate variables.

2. Materials and Methods

2.1. Yield datasets and yield data cleaning

Yield monitor data were collected from 68 fields located in northwest Spain (Galicia and Asturias regions) with planting and harvesting data during the seasons of 2019, 2020, 2021 and 2022. In total, 201 yield files have been managed. AgFiniti cloud-based platform (Ag Leader Technology) was used as a gateway to download these files from the John Deere Operations Center (JDOC) to the SMS software (Ag Leader Technology). Raw data files were cleaned with the SMS software where two filters were applied. We have first eliminated data points of corn silage with a moisture content of less than 46% following the protocol of Kharel et al. (2018). Then the data with yields whose values deviate by +/- 1 standard deviations (STD) from the mean have been deleted, thus disappearing anomalous values with very high or very low yields.

2.2. Field, crop and climate variables

For each field and year, the average wet and dry yield data and moisture content of corn silage were calculated automatically by taking the clean yield files for each field and year. In turn, the climatological data of daily precipitation and average daily temperature were interpolated in a 200 m cell from the Meteogalicia and AEMET data, using a script in R, through regression kriging-RK (using the X, Y coordinates and elevation as secondary variables for estimation). If it was not possible to apply regression kriging due to problems in fitting a semivariogram model, the ordinary kriging (OK) method was used to estimate the mean temperature and daily precipitation data in the centre of each field for each field and year.

In geostatistical predictions, the use of secondary variables can help improve estimates, which is known as a multivariable model. The simplest way to consider two or more variables is the Additive Model, which assumes that the variables act linearly and independently (Rossiter, 2017). In the case of this work, the use of the elevation of the terrain can be used to improve the quality of the prediction. In the estimation by KR, the additive method is carried out using the commands of the GSIF package of R, while for the KO it was carried out using the commands of the gstat package. To increase the speed of the calculation process for regression kriging, parallel programming was used, dividing the tasks to be performed between the different cores of the processor, reducing the process time by approximately half.

With the daily average temperature data, 8ºC was used as a base temperature to calculate degree days. The mean data of elevation, slope, aspect and topographic wetness index (Beven and Kirby, 1979) were also calculated for each plot. These topographic parameters were calculated from the IGN MDTs of 2 m resolution.

Soil moisture affects key environmental processes and controls the growth, distribution and development of plant communities (Fan et al., 2019; Kemppinen et al., 2019; le Roux et al., 2013). To indirectly estimate the different soil moisture areas of the field, soil moisture indicators derived from digital elevation models (DEM) are used. Without a doubt, the most popular is the Topographic Wetness Index (Beven and Kirkby, 1979). The Topographic Wetness Index (TWI) integrates water supply from the uphill catchment area and downhill water drainage for each cell in a DEM. TWI is calculated as a natural logarithm of the quotient between the upstream drainage area divided by the width of the cell, and the slope (Beven and Kirkby, 1979). SAGA-GIS has been used to calculate TWI. The spatial pattern of TWI depicts areas that show local water accumulation and therefore high soil water saturation.

2.3. Principal component analysis

An analysis of main components was carried out. Principals can be assumed as a comprehensive method of Factor Analysis. The goal of principal component analysis (PCA) is to construct new variables, known as principal components, from a set of existing original variables. New variables are created by linearly combining the current variables. The PCA reduces an extensive dataset of variables into a few elements known as the principal components, which can then be analyzed to show the underlying data structure. One of the characteristics of the primary components is that they are not correlated or orthogonal to each other. When a dataset has significant variance, the first major component absorbs and represents as much variance as possible. The second component absorbs the remaining variation as possible, and so on. The maximum number of principal components or major components is equal to the total number of variables in a model

unless otherwise is specified. Principal component analysis is recommended to reduce the dimensionality of multivariate data and to work with highly correlated data. The work of Reyes et al (2019) used PCA to delineate two types of cluster analysis were applied to delineate management zones. This analysis was performed using the R package factoextra (Kassambara and Mundt, 2020) and FactoMineR (Le et al., 2008). Hierarchical cluster analysis (HCA) was applied to studied parameters to group sites with similar characteristics. Cluster analysis identifies relatively homogeneous groups of objects based on their similarities/dissimilarities.

3. Results and Discussion

3.1. PCA analysis

After performing PCA, the first three components were retained; These components explain 63% of the total variance. The factor loadings for the variables and the three retained components are shown in Table 1 and Figure 1a. Figure 2a presents the factor loadings of the first three components. The factor loadings most associated with the first component, which explains 27% of the total variance, were dry and wet matter yield, elevation, TWI, and slope. The dry and wet matter yield, precipitation and seeding rate explained 20% of the total variance. In the third component, which represents 17% of the total variance, the greatest contributions came from the FAO maturity group and degree days. In Figure 1a, it is observed that in component 1 there is a positive correlation between the yield variables and TWI and an inverse correlation with elevation and slope, results that are logical.

Table 1. Factor loadings of each variable for the first three principal components. In parentheses are the percentages of explained variance for each component of the data for the years 2019, 2020, 2021 and 2022.

	Dim.1 (26.5%)	Dim.2 (19.9%)	Dim.3 (16.8%)
Dry yield tonne ha^{-1}	0.49	0.72	-0.39
Moisture %	0.46	0.11	0.16
Wet yield tonne ha^{-1}	0.60	0.70	-0.31
FAO Maturity group	0.22	0.16	0.84
Area planted ha	0.04	0.11	0.27
Seed rate_seeds ha^{-1}	-0.10	-0.51	-0.05
Elevation m	-0.80	0.37	-0.10
TWI	0.83	-0.22	-0.20
Slope %	-0.79	0.36	-0.10
Degrees-day	0.19	0.17	0.83
Precipitation mm	-0.24	0.73	0.24

It can be seen in Figure 3 that there is a clearly differentiated population in 2019, with different values of component 2, associated with production. The data of accumulated precipitation and average air temperature from May to September are showed in Figure 4, where 2019 was the year with the lowest precipitation in summer. Another issue related with the different behaviour of 2019 data could be the fact that it was the first year that the contractor company obtained yield maps with the SP Forage Harvesters. The lack of experience of operators in the use of the yield monitor could have affected the quality of data. Due to this reason, the analysis of principal components was done again without considering the data of the year 2019.

After performing this second PCA analysis, the first three components explain 65% of the total variance. The factor loadings for the variables and the three principal components are shown in Table 2 and Figure 1b. Figure 2b presents the factor loadings of the components. The factor loadings most associated with the first component, which explains 29% of the total variance, this component is closely linked to the yield parameters, and is also highly correlated with TWI. The FAO maturity group, degree days and precipitation explained 19% of the total variance. In the third component, which represents 17% of the total variance, the greatest contributions came from the yield parameters and the seeding rate. In Figure 1a, it is observed that in component 1 there is a positive correlation between the yield variables and TWI and an inverse correlation with elevation and slope, results that are logical, in the analysis excluding the data from 2019 it is possible to exclude the effect of precipitation on the main components is linked to production.

Table 2. Factor loadings of each variable for the first three principal components. In parentheses are the percentages of explained variance for each component of the data for the years 2020, 2021 and 2022.

	Dim.1	Dim.2	Dim.3
Dry yield tonne ha^{-1}	0.66	0.05	0.57
Moisture %	0.55	0.19	0.38
Wet yield tonne ha^{-1}	0.76	0.10	0.59
FAO Maturity group	0.45	0.72	-0.27
Area planted ha	0.07	0.29	0.17
Seed rate_seeds ha^{-1}	-0.08	-0.34	0.55
Elevation m	-0.72	0.31	0.41
TWI	0.75	-0.43	-0.17
Slope %	-0.71	0.24	0.45
Degrees-day	0.32	0.70	-0.39
Precipitation mm	-0.14	0.73	0.19

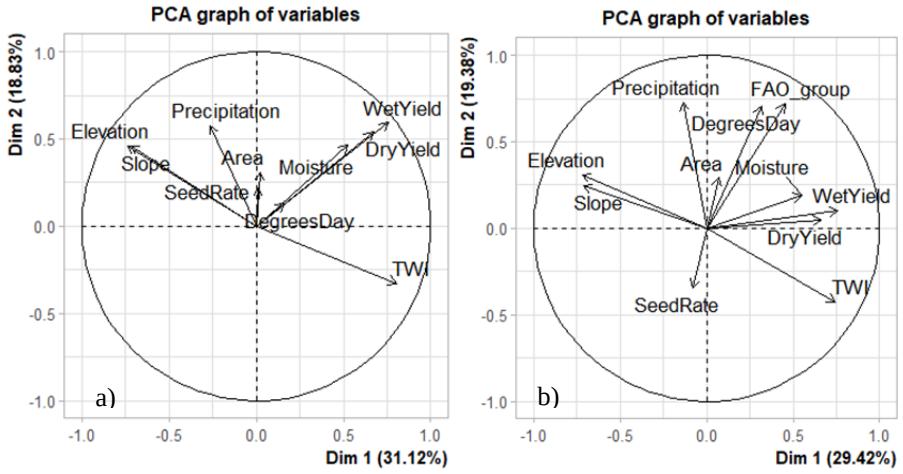

Figure 1. a) Grouping of the variables in two principal components for years 2019, 2020, 2021 and 2022. b) Grouping of the variables in two principal components for years 2020, 2021 and 2022.

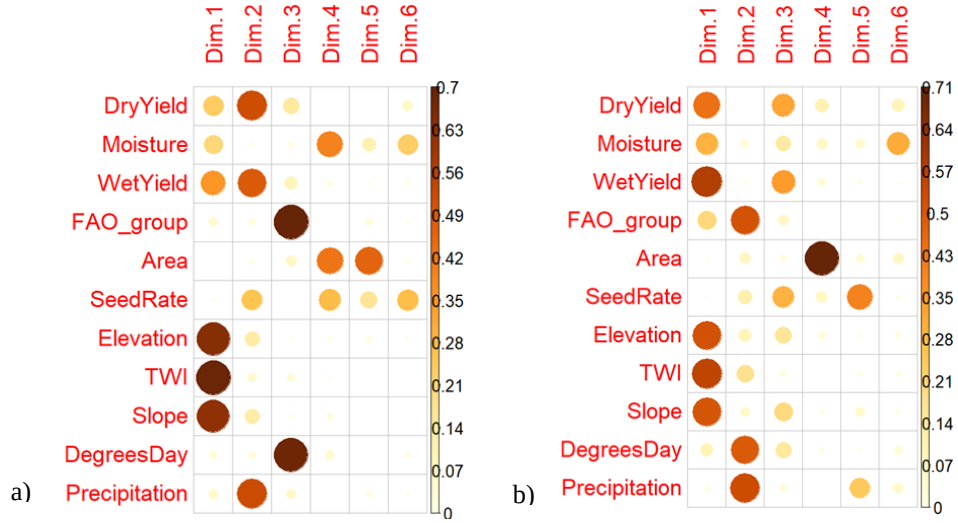

Figure 2. a) Square cosine or squared coordinates of variables for each dimension for years 2019 to 2022. b) Square cosine or squared coordinates of variables for each dimension for years 2020 to 2022.

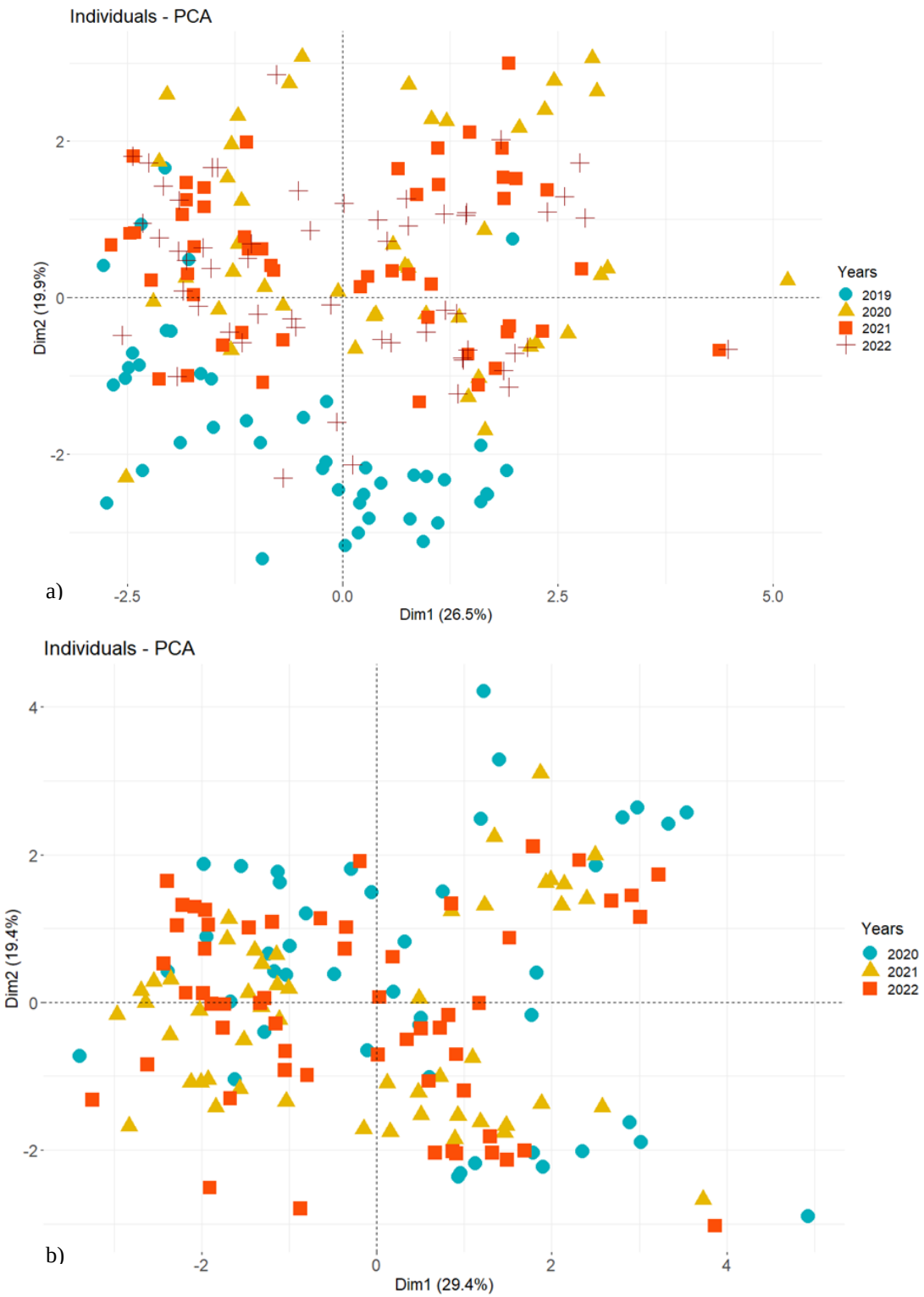

Figure 3. a) PCA biplot for two principal components for years 2019, 2020, 2021 and 2022. b) PCA biplot for two principal components for years 2020, 2021 and 2022.

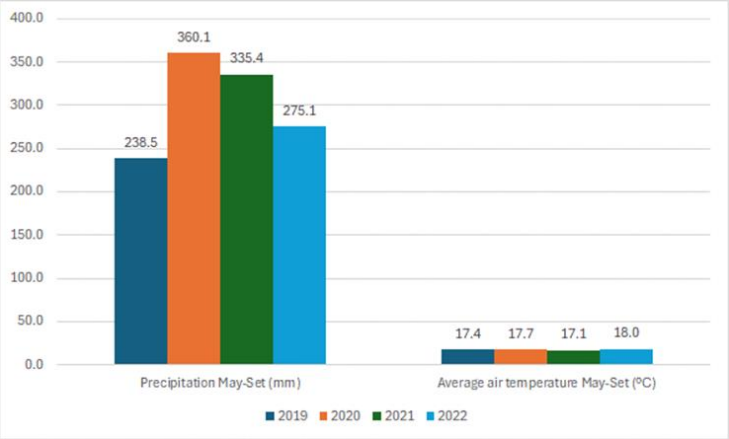

Figure 4. Accumulated precipitation and average air temperature from May to September

4. Conclusions

The principal component analysis made it possible to distinguish the different behaviour of the variables studied in 2019, probably due to the lower rainfall in the summer of that year. When performing the principal component analysis with the rest of the years, it was found that the first main component that is related to the yield parameters is closely related to the topographic parameters TWI, slope and elevation. Therefore, TWI is an important parameter related to the water content of the land, and the analysis of principal components allowed us to discriminate the factors most related to the yield parameters.

Acknowledgements

This work is part of the project "GO MilloPreciso - Precision Agriculture with Corn Silage in Galicia", a project financed by the aid for the execution of projects of the operational groups of the Agricultural European Innovation Partnership (EIP-AGRI), co-financed by 75% with the European Agricultural Fund for Rural Development (EAFRD) within the framework of the Rural Development Program (RDP) of Galicia 2014-2020 with own funds of the Xunta de Galicia by 22.5% and with funds from the Ministry of Agriculture, Fisheries and Food by 2.5%. The Consellería do Medio Rural is the body of the Galician Administration that is responsible for proposing and executing the general guidelines in rural areas, and encompasses the competences in agriculture, livestock, rural development and regional planning, rural structures, agri-food and forestry industries, forests, prevention and defense of forest fires.

The collaborative project of the Campus Terra "AgriPreMaF – Precision Agriculture with Corn Silage", funded within the framework of the Collaboration Agreement between the USC and the Department of Culture, Education and University of the Xunta de Galicia, has also contributed to this study. Finally, thanks to the contractor companies Agropres S.L. and Marcos Otero S.L. for their collaboration in these two projects.

References

Adhikari, K., DR Smith, C Hajda, TP Kharel, 2023. Within-field yield stability and gross margin variations across corn fields and implications for precision conservation. Precision Agriculture (2023) 24:1401–1416. https://doi.org/10.1007/s11119-023-09995-7

Beven, K.J., MJ Kirkby, 1979. A physically based, variable contributing area model of basin hydrology. Hydrological Science Bulletin. 24 (1): 43–69. doi:10.1080/02626667909491834.

Bueno, J., MA Vilar, JM Pereira, 2023. Processing Corn Silage Yield Data from Forage Harvesters. Proceedings of the XL CIOSTA & CIGR Section V International Conference. September 10–13, 2023, Évora, Portugal. 122-128.

Fan, Y., M Clark, DM Lawrence, S Swenson, LE Band, SL Brantley, PD Brooks, WE Dietrich, A Flores, G Grant, JW Kirchner, DS Mackay, JJ McDonnell, PCD Milly, PL Sullivan, C Tague, H Ajami, N Chaney, A Hartmann, P Hazenberg, J McNamara, J Pelletier, J Perket, E Rouholahnejad-Freund, T Wagener, X Zeng, E Beighley, J Buzan, M Huang, B Livneh, BP Mohanty, B Nijssen, M Safeeq, C Shen, W Verseveld, J Volk, D

Yamazaki, 2019. Hillslope hydrology in global change research and earth system modelling. Water Resour. Res., 55 (2019), pp. 1737-1772, 10.1029/2018WR023903.

Guyader, J., VS Baron, KA Beauchemin, 2018. Corn Forage Yield and Quality for Silage in Short Growing Season Areas of the Canadian Prairies. Agronomy 2018, 8, 164; doi:10.3390/agronomy8090164.

Heil, K., P Heinemann, U Schmidhalter, 2018. Modeling the Effects of Soil Variability, Topography, and Management on the Yield of Barley. Front. Environ. Sci. 6:146. doi: 10.3389/fenvs.2018.00146.

Kharel, T., SN Swink, C Youngerman, A Maresma, KJ Czymmek, QM Ketterings, P Kyveryga, J Lory, TA Musket, V Hubbard, 2018. Processing/Cleaning Corn Silage and Grain Yield Monitor Data for Standardized Yield Maps across Farms, Fields, and Years. Cornell University, Nutrient Management Spear Program, Department of Animal Science, Ithaca NY.

Kassambara, A., F Mundt, 2020. Factoextra: Extract and Visualize the Results of Multivariate Data Analyzes. R Package Version 1.0.7. https://CRAN.R-project.org/package=factoextra

Kemppinen, J., P Niittynen, J Aalto, PC le Roux, M Luoto, 2019. Water as a resource, stress and disturbance shaping tundra vegetation. Oikos, 128 (2019), pp. 811-822, 10.1111/oik.05764.

Lê, S., J Josse, F Husson, 2008. FactoMineR: An R Package for Multivariate Analysis. Journal of Statistical Software, 25(1), 1–18. https://doi.org/10.18637/jss.v025.i01

le Roux, P.C., J Aalto, M Luoto, 2013. Soil moisture's underestimated role in climate change impact modeling in low-energy systems. Glob. Chang. Biol., 19 (2013), pp. 2965-2975, 10.1111/gcb.12286.

Maitah, M., K Malec, K Maitah, 2021. Influence of precipitation and temperature on maize production in the Czech Republic from 2002 to 2019. Nature, Scientific Reports (2021) 11:10467. https://doi.org/10.1038/s41598-021-89962-2.

MAPA, 2023. Anuario de Estadística (Yearly Statistics). Ministry of Agriculture, Fisheries and food. Spanish Government.

Reyes, J., O Wendroth, C Matocha, J Zhu, 2019. Delineating Site-Specific Management Zones and Evaluating Soil Water Temporal Dynamics in a Farmer's Field in Kentucky. Vadose Zone Journal. 18. 10.2136/vzj2018.07.0143.

Rossiter, D.J., 2017. An introduction to geostatistics with R.
https://www.css.cornell.edu/faculty/dgr2/_static/files/R_PDF/gs_intro_20Mar2019.pdf

Classification model using cluster analysis with corn silage yield maps

Javier Bueno [a,*], Jorge Dafonte [a], José Miguel Edreira [a], Miguel Ángel Vilar [b]

[a] Department of Agroforestry Engineering, University of Santiago de Compostela, Lugo, Spain

[b] Department of Applied Mathematics, University of Santiago de Compostela, Lugo, Spain

* Corresponding author. Email: javier.bueno@usc.es

Abstract

The analysis of clusters with the K-means method and the Pam method, using the Silhouette width criterion, gives us the optimal number of 2 clusters. The K-means method is considered ideal, since it allows us to discriminate the two populations according to the first principal component that is linked to the yield parameters. This classification model was tested with 35 fields for which yield data for the years 2020, 2021 and 2022 were available. The model classified 32 fields in the same cluster for the 3 years, indicating stability in production.

The Random Forest (RF) model was used for estimating dry matter yield. This model explained a 50% percentage variance and a correlation coefficient of 0.7 when we used data from year 2019 to 2022. The most important variables in the model were year, geographic longitude, and topographic wetness index (TWI). The RF model also was performed without considering the data from the year 2019, and the model in this case has a less explained variance of the order of 20%. The TWI index of the field had a great importance in the model.

Keywords: Precision Agriculture, Yield Maps, Cluster Analysis, Corn Silage.

1. Introduction

Precision Agriculture (PA) is a farming management concept based on observing, measuring and responding to inter and intra-field variability in crops. In northwest Spain, agricultural contractor companies that work with self-propelled (SP) forage harvesters equipped with yield mapping systems, usually harvest lots of small fields in every season. For example, the contractor company that has obtained the yield files used in this work harvests around 700 fields each season, of which 50% have an area of less than 1 ha. In this scenario, working with between-field variability may be more advisable for optimizing the management of each field (seeding rate, corn variety, fertilizer rate…). Between-field variability implies the variability among fields, where each field can be considered as a unit.

In this work we test a classification model using cluster analysis in order to have a tool for a better management of great number of small fields in corn silage production.

2. Materials and Methods

2.1. Yield datasets and yield data cleaning

Yield monitor data were collected from 68 fields located in northwest Spain (Galicia and Asturias regions) with planting and harvesting data during the seasons of 2019, 2020, 2021 and 2022. In total, 201 yield files have been managed. AgFiniti cloud-based platform (Ag Leader Technology) was used as a gateway to download these files from the John Deere Operations Center (JDOC) to the SMS software (Ag Leader Technology). Raw data files were cleaned with the SMS software where two filters were applied. We have first eliminated data points of corn silage with a moisture content of less than 46% following the protocol of Kharel et al. (2018). Then the data with yields whose values deviate by +/- 1 standard deviations (STD) from the mean have been deleted, thus disappearing anomalous values with very high or very low yields.

2.2. Field, crop and climate variables

For each field and year, the average wet and dry yield data and moisture content of corn silage were calculated automatically by taking the clean yield files for each field and year. In turn, the climatological data of daily precipitation and average daily temperature were interpolated in a 200 m cell from the Meteogalicia

and AEMET data, using a script in R, through regression kriging-RK (using the X, Y coordinates and elevation as secondary variables for estimation). If it was not possible to apply regression kriging due to problems in fitting a semivariogram model, the ordinary kriging (OK) method was used to estimate the mean temperature and daily precipitation data in the centre of each field for each field and year.

With the average daily temperature data, to calculate degree days, 8ºC was used as a base temperature. The mean data of elevation, slope, aspect and topographic wetness index (Beven and Kirby, 1979) were also calculated for each plot. These topographic parameters were calculated from the IGN MDTs of 2 m resolution.

2.3. Cluster analysis

The principal components analysis (PCA) is detailed in Bueno et al. (2024). Cluster analysis was carried out on the principal component data of the crop parameters, climatic parameters of the years 2020, 2021 and 2022, and topographic parameters. After dimension reduction, clustering of the features obtained by PCA analysis will be done. One of the most popular methods of clustering es the K- means algorithm. The method requires to choose optimal metric and number of clusters.

Firstly, proper number of clusters was established by Silhouette statistics graph, The Silhouette width ranges between -1 and 1 and well clustered observations have a value close to 1 (Rousseeuw, 1987). Two clustering methods were used: K- Means, that it's one of the most popular methods of clustering algorithms (MacQueen, 1967; Hartigan and Wong, 1979) and PAM - Partitioning Around Medoids (Kaufman and Rousseeuw, 1990). The second method of clustering is PAM algorithm, which is a more robust version of K- means and less sensitive to outliers. This cluster analysis was tested with the 35 of the 68 fields for which yield data for the years 2020, 2021 and 2022 were available.

2.4. Random Forest

For the estimation of dry and wet production parameters of forage corn, random forest classification and regression models were constructed using the 'Random Forest' package (Liaw and Wiener, 2002) in the free statistical software R (R Core Team, 2021). Random forest regression models were constructed using 500 trees derived from 500 bootstrap data sets. The random forest algorithm can rank the relative importance of each predictor variable. The importance of the variable is based on the regression prediction error of the out-of-bag portion of the data, also called OOB (Breiman, 2001; Liaw and Wiener, 2002; Rossiter, 2019; Everingham et al., 2016). For classification models, the prediction error is calculated as the classification error rate, while for regression, the root mean square error is calculated. In the 'Random Forest' package, the importance of the predictor variable is reported as a mean percentage decrease in the classification rate for the classification model or a mean increase in the mean squared error for the regression model if that variable was removed of the analysis (Everingham et al., 2016). Additionally, for each tree we can use observations that were not used to build it for true validation (OOB validation), in this case the method averages the OOB cross-validations calculated during forest construction (Rossiter, 2019).

To apply the random forest model to predict the dry matter yield of corn silage, we used continuous and qualitative parameters as predictors: year, latitude, longitude, FAO maturity group, precipitation, degree days, slope and mean elevation of the field, aspect, TWI and corn seeding rate.

3. Results and Discussion

Figure 1 show the biplot graph of the two components of the years 2020 to 2022. In Figure 2 can be seen that component 1 is very linked to yield and topographic parameters. A Silhouette analysis was performed to determine the optimal number of clusters for both K-means method (Figure 3a) as for the PAM method (Figure 3b). Average Silhouette is equal to 0.6 for both the K-means method as for PAM method which means that clustering quality is between reasonable and strong. The reason of that could also be low intra-cluster variability in relation to total variability.

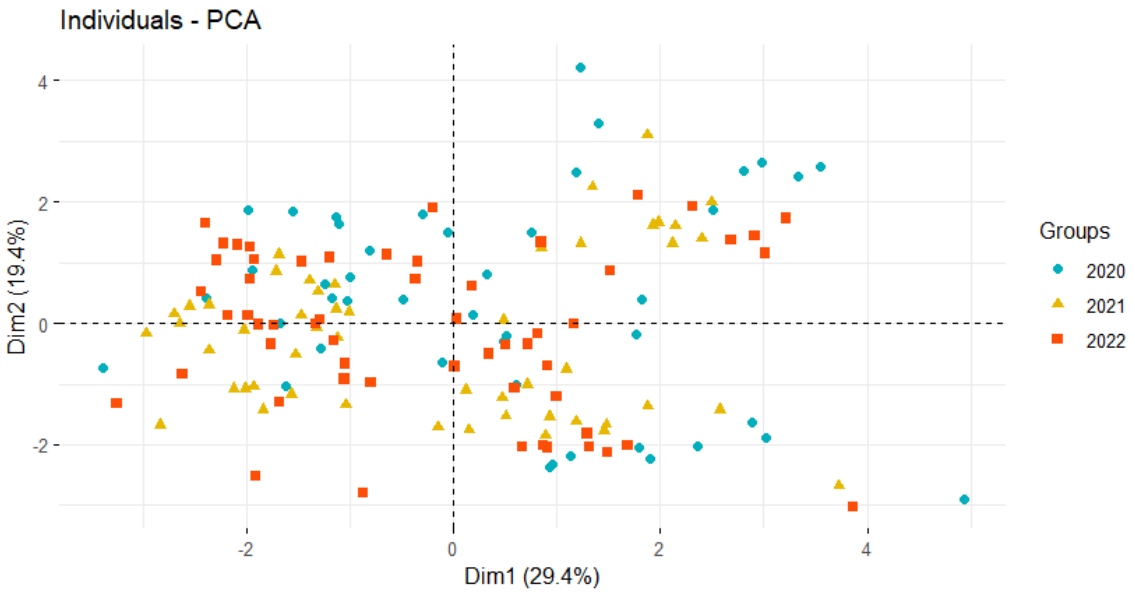

Figure 1. Biplot graph of the first two components main for each plot and year.

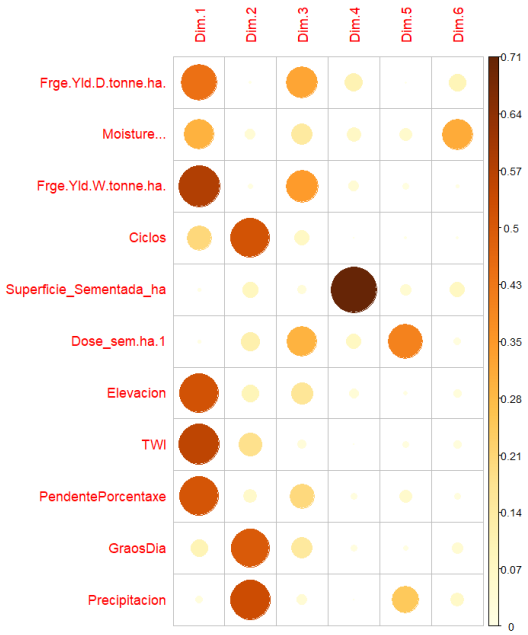

Figure 2. Parameter participation in each main component.

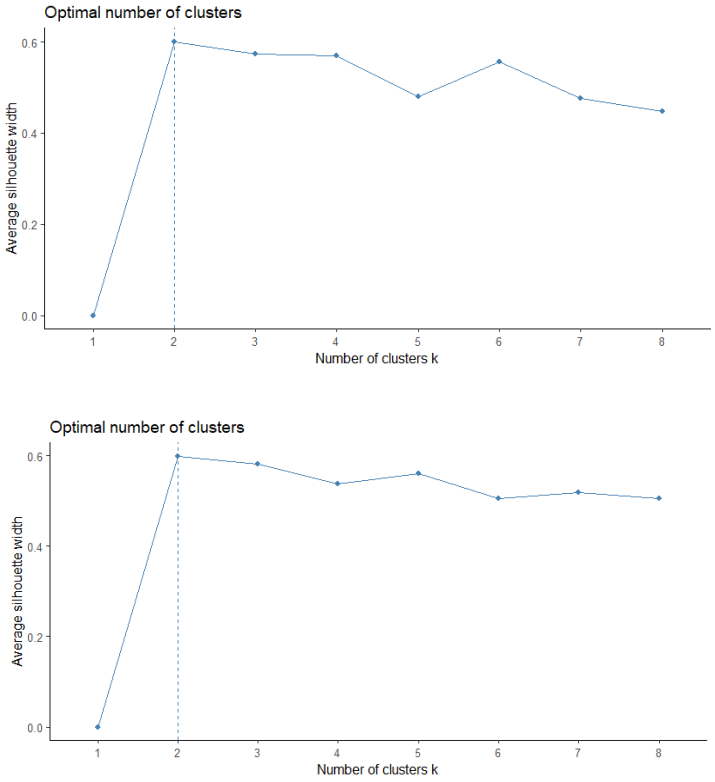

Figure 3. (a) Silhouette mean width of the number of clusters for the k-means method.
(b) Silhouette half width of the number of clusters for the PAM method

Figure 4 show the plot with the clusters wearing the K-means method and in Figure 5 the grouping is found in clusters wearing the PAM method, choose the K-means method, since it groups the data in function mainly from the value of component 1, which is the most linked to the factors of crop yield.

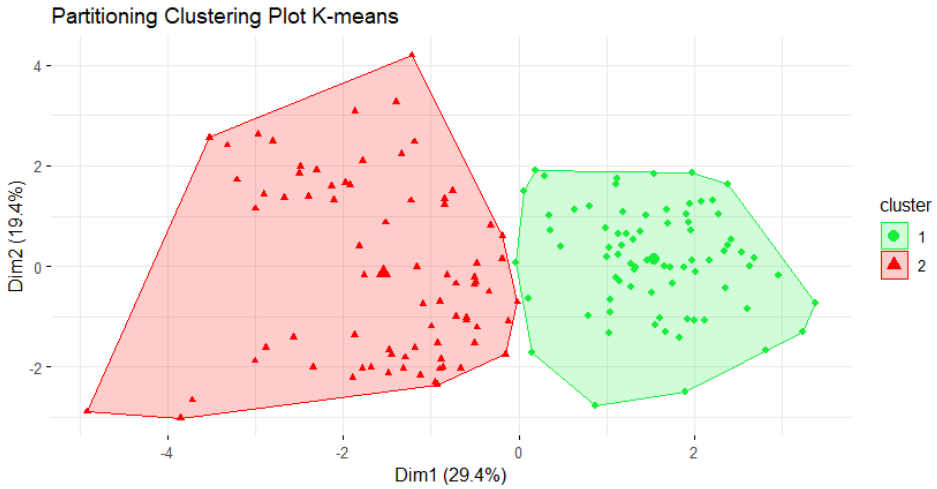

Figure 4. Clusters for K-means method.

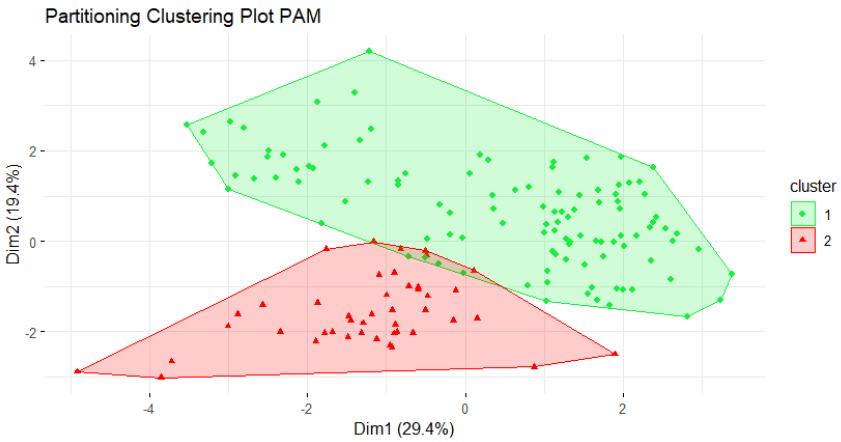

Figure 5. Clusters for PAM method.

To analyse the stability of the plots in regarding the production parameters, it has been used the cluster analysis using K-means method, using only the data from the 35 fields where were available yield data for the years 2020, 2021 and 2022. 32 fields of the 35 were classified in the same cluster for all years, of which 13 plots were in cluster 1 (linked to higher crop yield) and 19 plots in cluster 2.

Random forest regression model combines multiple decision trees to create a single model. Each tree in the forest builds from a different subset of the data and makes its own independent prediction. The final prediction for input is based on the average or weighted average of all the individual trees' predictions. It was decided to apply this method to data wearing as a dependent variable of production the dry matter yield.

First, the 4 years of data (2019-2022) were used, using all parameters, in a single simulation obtained the data shown in Table 1.

Table 1. Random Forest model parameters for dry matter yield for the years 2019, 2020, 2021 and 2022.

	% IncMSE	IncNodePurity
Year	54.66	990.25
Latitude	11.37	172.17
Longitude	21.99	295.36
FAO maturity group	9.43	41.95
Planted area	3.16	104.88
Seeding rate	11.29	129.50
Elevation	15.82	128.81
TWI	22.24	237.02
Slope	7.30	82.95
Aspect	3.72	111.69
Degree-days	8.21	152.90
Precipitation	8.90	79.72
N_days	6.90	79.51

% IncMSE es the most robust and informative measure. % IncMSE is simply the average increase in squared residuals of the test set when variables are randomly permuted (little importance = little change in model when variable is removed or added) and IncNodePurity is the increase in homogeneity in the data partitions. Data in Table 1 shown that the most important parameter is the year, followed by the TWI and the geographical longitude. In this case is obtained a variance explained by the model of 55%, a mean square error of 2.6 and a correlation coefficient between observed and estimated by model 0.74, you can see In Figure 6 the relationship existing among the results observed and estimated by the model.

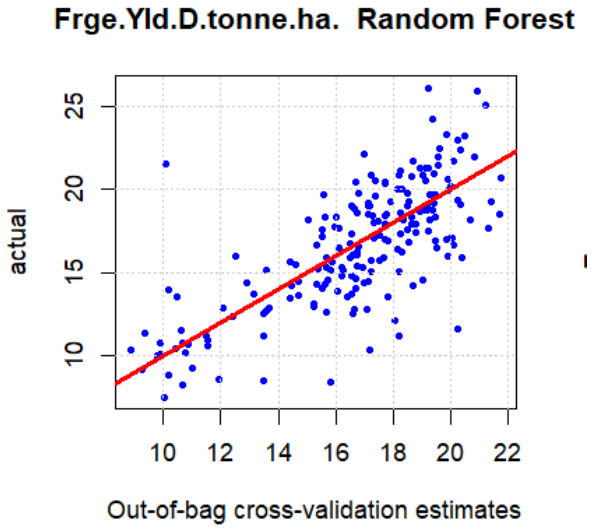

Figure 6. RF Model Results vs. Data measured for the years 2019, 2020, 2021 and 2022.

As has been discussed previously in the paper by Bueno et al. (2024), the data corresponding to the year 2019 have a different behaviour, which is why the analysis with random forest method was repeated excluding the data from the year 2019, obtaining the results shown in Table 2 and in Figure 7.

Table 2. Random Forest model parameters for dry matter yield for the years 2020, 2021 and 2022.

	% IncMSE	IncNodePurity
Year	3.55	33.75
Latitude	10.03	146.98
Longitude	14.58	158.35
FAO maturity group	9.10	40.73
Planted area	5.47	96.45
Seeding rate	8.96	125.42
Elevation	15.07	112.11
TWI	19.82	215.70
Slope	6.17	82.36
Aspect	5.96	53.99
Degree-days	3.39	94.99
Precipitation	8.23	77.81
N_days	3.76	77.04

Data of Table 2 shown that the most important parameter is the TWI, elevation, and geographical longitude, and the year has no longer importance as an explanatory variable. In this case is obtained a variance explained by the model of 28%, a mean square error of 2.6 and a correlation coefficient between observed and estimated by the model of 0.54. Figure 7 show the relationship among the results observed and estimated by the model.

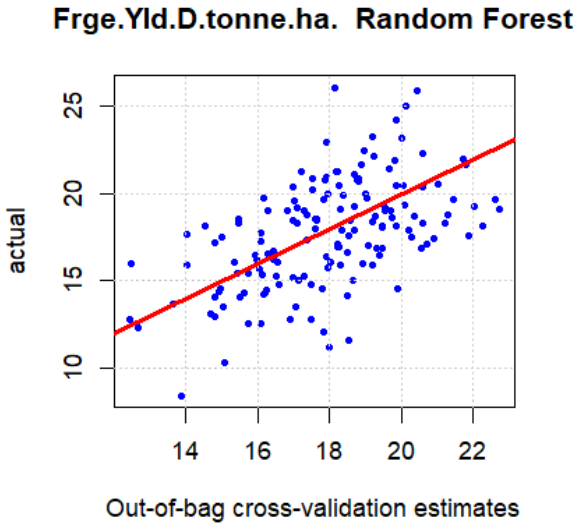

Figure 7. RF Model Results vs. Data measured for the years 2020, 2021 and 2022.

As a conclusion, it can be said that excluding the variable “year” that has a great influence in the model when considering the data for the year 2019, it is of great importance in the model the TWI index of the field, since this parameter provides information on the degree of soil wetness in a particular area based on the topography of the land. TWI is calculated using the slope and flow accumulation of the terrain and can be used to identify areas of the landscape with high or low soil moisture content.

The low variance value explained in the RF model with data from the years 2020, 2021 and 2022, can be seen as a negative result. Explained variance is a measure of how well out-of-bag predictions explain the target variance of the training set. Unexplained variance would be due to true random behaviour or lack of fit.

4. Conclusions

Cluster analysis using the K-means method allows us to discriminate two populations based on the first component, which is related to crop yield parameters. It also should be highlighted that the cluster analysis indicates the stability in terms of the classification of clusters of the three years studied, since 32 of the 35 plots are classified in the same cluster for all three years.

The random forest model allows us to consider the influence of the year on the dry matter yield, with an explained variance of more than 50%. If the data are analyzed without considering the data for the year 2019, the explained variance is greatly reduced and the most important factor in the dry matter yield model is TWI. This topographical index is a parameter closely related to the moisture content of the soil and easily estimated from a digital elevation model of the terrain.

Acknowledgements

This work is part of the project "GO MilloPreciso - Precision Agriculture with Corn Silage in Galicia", a project financed by the aid for the execution of projects of the operational groups of the Agricultural European Innovation Partnership (EIP-AGRI), co-financed by 75% with the European Agricultural Fund for Rural Development (EAFRD) within the framework of the Rural Development Program (RDP) of Galicia 2014-2020 with own funds of the Xunta de Galicia by 22.5% and with funds from the Ministry of Agriculture, Fisheries and Food by 2.5%. The Consellería do Medio Rural is the body of the Galician Administration that is responsible for proposing and executing the general guidelines in rural areas, and encompasses the competences in agriculture, livestock, rural development and regional planning, rural structures, agri-food

and forestry industries, forests, prevention and defense of forest fires.

The collaborative project of the Campus Terra "AgriPreMaF – Precision Agriculture with Corn Silage", funded within the framework of the Collaboration Agreement between the USC and the Department of Culture, Education and University of the Xunta de Galicia, has also contributed to this study. Finally, thanks to the contractor companies Agropres S.L. and Marcos Otero S.L. for their collaboration in these two projects.

References

Breiman, L., 2001. Random forests. Mach. Learn. 45 (1), 5–32.

Bueno, J., J Dafonte, JM Edreira, MA Vilar, 2024. Influence of Field, Crop and Climate Variables on Corn Silage Yield Maps. AgEng 2024. Athens.

Everingham, Y., J Sexton, D Skocaj, G Inman-Bamber, 2016. Accurate prediction of sugarcane yield using a random forest algorithm. Agron. Sustain. Dev. 36 (2), 1–9.

Hartigan, J.A.. MA Wong, 1979. Algorithm AS 136: A K-Means Clustering Algorithm. Journal of the Royal Statistical Society. Series C (Applied Statistics), 28, 100–108. https://www.jstor.org/stable/2346830.

Kaufman, L., PJ Rousseeuw, 1990. Finding groups in data; an introduction to cluster analysis. J. Wiley., Chichester (UK).

Liaw, A., M Wiener, 2002. Classification and Regression by random Forest. R News 2(3), 18--22.

MacQueen, J., 1967. Some methods for classification and analysis of multivariate observations, Proceedings of the Fifth Berkeley Symposium on Mathematical Statistics and Probability, 1, 281—-297, https://doi.org/10.2307/2346830, https:// www.jstor.org/stable/2346830.

R Core Team, 2021. R: A language and environment for statistical computing. R Foundation for Statistical Computing, Vienna, Austria. URL https://www.R-project.org/.

Rossiter, D.J., 2017 An introduction to geostatistics with R.

https://www.css.cornell.edu/faculty/dgr2/_static/files/R_PDF/gs_intro_20Mar2019.pdf

Rousseeuw, P.J., 1987. Silhouettes: A graphical aid to the interpretation and validation of cluster analysis. Journal of Computational and Applied Mathematics, 20, 53–65, https://doi.org/10.1016/0377-0427(87)90125-7 , https://linkinghub.elsevier.com/retrieve/pii/0377042787901257,545 1987.

Optimization of mechanical and operating parameters for improving chisel plow performance in heavy clay soils

Abdul Salam J. Almoosawi, Majid H. Alheidary*, Mortadha A. Alfaris

Department of Agricultural Machines & Equipment, College of Agriculture, University of Basrah, Basrah, Iraq

***Corresponding author: Majid Alheidary (majid.reshaq@uobasrah.edu.iq)**

Abstract

A chisel plow is considered an effective implement in different agricultural soils, especially in heavy soils requiring improvement of their physical properties. The effectiveness of this plow may differ depending on various parameters as soil type, tillage depth, operating work conditions, power required, and chisel tines shape. So, the main goal of this study is to ameliorate the performance of chisel plow in heavy soils using different mechanical and operating parameters. Three main factors were studied four sweep chisel widths (pointed-15cm, pointed-20cm, severed-15cm, and served-20 cm), three tillage depths (15, 25, and 35cm), and two tillage speeds (1.87, and 2.74km.hr^{-1}). A complete randomized block design in split-split plot was used to analyze data. The findings illustrated that the chisel pointed shape-20 cm using a tillage depth of 15 cm and tillage speed of 2.74 kmh^{-1} significantly influenced in comparison to the other chisel shapes in recording the lowest draft force of 12.91 kN.m^{-2}, the lowest slippage percentage of 31.37%, and the lowest fuel consumption rate (4.78 lha^{-1}). Although the severed chisel with a width of 20 cm was superior in increasing the percentage of pulverized soil and reducing the percentage of resistance to the soil penetration, it recorded the highest percentage of slippage, 44.4%. The interaction between the tillage speed (2.74 km.h^{-1}) and the chisel-pointed shape at 20 cm width recorded the highest value in the efficiency of energy (38.35 Mj.m^{-3}) using the tillage depth 15cm. it is recommended by using a chisel-pointed shape, a maximum tillage speed, and the lowest depth as result to ameliorate the performance of the chisel plow under heavy soil conditions.

Keywords: Tillage depth, forward speed, tines shape, soil characteristics, energy

1. Introduction

Obtaining acceptable soil properties largely depends on the quality of the soil tillage which enhances the effectiveness of all subsequent agricultural processes (Upadhyaya et. al., 2001; Muhsin, 2017). Tillage equipment using agricultural machinery is considered one of the main solutions and key to the improvement of soil quality and minimizing power consumption. So, soil tillage is a major concept in the process of crop production, which consumes nearly 30 to 35% of the total energy requirements of crop production (Osman et al., 2014). Chisel tillage refers to soil conservation technologies, and chisel tools provide low power. In addition, preservation and rational use of soil moisture that is relevant in arid climates. Using a chisel plow in heavy soils compared to conventional tillage systems was investigated in various studies to improve their performance (Aday and Muhsin, 2019). The best benefit of a chisel plow in the field is to leave more crop residue on the ground surface and fuel consumption is significantly lower. As well as, the weeds and large amounts of straw may also cause considerable practical difficulties and require adequately dimensioned chisel plows. Sowing equipment that can cope with surface residue is required (El-Iraqi et al., 2009). The chisel was able to penetrate down to the bottom of a compacted layer at 12–20 cm depth except for the duck-foot type. The plow works in comparison with the other primary tillage equipment except the subsoiler plows provides more depth of soil (0.38 m when 0.15 m real tillage and 0.2 m in the control variant) at comparable energy consumption.

During operating conditions, different factors affect the performance chisel plow as the tine shape on the plow frame, the forward speed and the working depth (Kirisci , 1993; Grisso et al., 1996; Chandon et al., 2002). The draft force of the plow is affected by the tillage depth, especially in the heavy soil. The increases in the draft force were significant with an increase in depth due to the change in moisture content, soil cohesion, and the volume of soil accumulated in front of the plow (Moinfar and Shahgholi, 2018). Various researchers carried out many modifications to the chisel plow, aiming to increase the efficiency and performance of the plow, which often contributes to an increase in the draft force necessary by adding the shallow tines on the sides of the plow (Jebur et al., 2016). As a result, the increase in depth will cause the tractor to carry an additional load, then increasing the engine load and increasing the rate of fuel consumption. This matter requires additional fuel and a lot of energy spent from the engine to overcome the load located behind the tractor (Ghali, 2019). So, the main objective of this work is to evaluate and optimize the performance of the developed chisel plow in heavy clay soils using different tine shapes, depths tillage, and tillage speeds.

2. Materials and methods

2.1. Chisel plow structure

The chisel plow at a total working width (7 tines) is placed in two rows. The distance between two adjacent tines in one row is 50 cm, and between one row and another is 80 cm. The plow tines are placed interchangeably so that the distance between the plow tines is approximately 25 cm, the penetration angle of the plow tines was 30º. Two different types of chisel plow were used in the current study as shown in Figure 1.

Figure 1: Main features and construction of chisel plows used (a) traditional plow (b) developed plow

2.2. Measurement of soil penetration resistance:

A digital Cone Pene Trometer device was used to measure soil penetration resistance. To use this device, by applying pressure of the device handle perpendicular the soil surface to push the cone into the soil surface. Measuring the pressure necessary to push the cone to the required depth using the pressure gauge supplied with it.

2.3. Measuring soil moisture content and bulk density:

The soil moisture content and soil density were determined by taking depth samples from the trail field. Then, the samples were dried in the oven using Core at a temperature of (105 °C) for 10 hours. The oven percentage was calculated for moisture based on dry weight. The bulk density of soil was calculated from Equation (1) according to the method described in (Black et al., 1993), and the results are shown in a Table (1)

$$pb = \frac{M_s}{V_t} \dots\dots\dots\dots\dots (1)$$

Where P_b is the bulk density ($Mg.m^{-3}$); M_s is the mass of dry particles (g); V_t is the total of soil volume (m^{-3}).

Table 1: Some of physical soil characteristics in the experimental field

Depth tillage (m)	Penetration resistance ($kN.m^{-2}$)	Bulk density ($Mg.m^{-3}$)	Moisture content (%)
0-15	2200	1.20	16
15-25	3100	1.22	16.65
25-35	5600	1.25	22.44

2.4. Soil texture

Soil separations were estimated using the absorbent method mentioned in (Black et al., 1993), to determine the texture, and the results are shown in Table (2).

Table 2: Soil texture in the experimental field

Clay ($gm.kg^{-1}$)	sand ($gm.kg^{-1}$)	loam ($gm.kg^{-1}$)	Soil texture
527.74	261.05	211.21	Clay

2.5. General procedure

After determining the main factors to perform the experiments, two types of agricultural tractors (Massey-Ferguson) were used in this study. The first one (driver tractor) was used for pulling. The second type (driven tractor) was utilized for mounting the chisel plow. The main characteristics of the tractors are shown in Table 3.

Table 3: Main description of tractors used in this study

Characteristic	**Type of Tractor**	
	Massey-Ferguson 440 extra (driver tractor)	Massey-Ferguson 285s (driven tractor)
Total weight (kg)	33.64	31.5
Nb of cylinders	4	4
Total cylinder size (cm^3)	4400	1552
Total volumetric engine size (liter)	4.4	4.06
Maximum engine speed (rpm)	2200	2200
Total energy (kw)	60.1	56.60
Wheel drive type	2WD	2WD
Type of engine	Diesel	Diesel
Manufacture year	2011s	1995s

2.6. Draft force measurement

To calculate the draft force for the chisel plow using a load cell device, the load cell was used on the drawbar of the driver tractor (Figure 2). The driven tractor and the chisel plow were pulled using a flexible wire, while the tractor was being driven, the gearbox remained in the neutral position when working, traction force readings were separately recorded via a laptop for each depth, tine shape, and forward speed through the Load cell connector connected to the load cell.

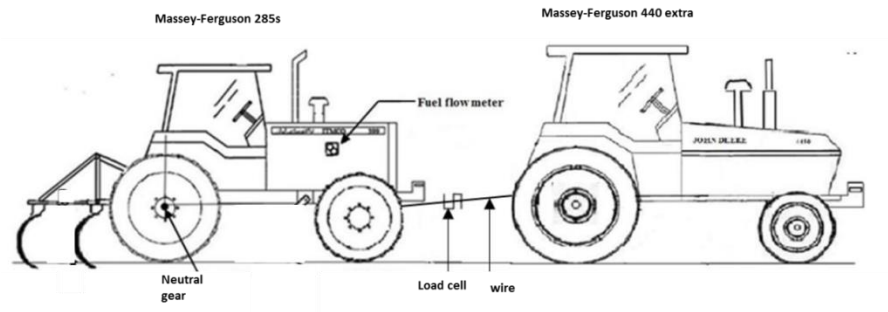

Figure 2: Draft force measurement using the load cell

2.7. Specific resistance

The specific resistance of chisel plow was calculated using the equation 2 by dividing the plow draft force on the total pulverized area of soil.

$$SR = \frac{F}{A} \dots\dots\dots\dots\dots\dots (2)$$

Where SR, is the specific resistance ($kN.m^{-2}$); F is the draft force (kN); A is the pulverized area (m^2).

2.8. The requirement of the draft energy

The draft energy was calculated according to the following equation (3)

$$Dp = F * V_a \dots\dots\dots\dots\dots\dots (3)$$

Where D_p, is the draft energy (kw); F, is the draft force (kN); Va, is the actual forward speed ($m.sec^{-1}$).

2.9. Determination of mean weighted diameter

Soil samples were randomly collected from the field in three replications for each treatment, and then manually sifted using different diameters sizes of sieves (02, 10., 30, 50, 90, 120, 250, 350, 450) mm. Each soil sample on the sieve was weighed and then after calculating the total weight for the sample by summing the weights of the soil collected on each sieve. The percentage of each weight on the sieve was calculated according to the method mentioned in (Hille, 1980) by the following equation (4)

$$MWD = \frac{m.w_i}{\sum w} \dots\dots\dots\dots\dots\dots (4)$$

Where, MWD, is the mean weight diameter; wi, is the weight of soil collected on the sieve (kg); m, is the mean sieve diameter (mm); w, is the total sample weight (kg)

The power lost by slipping the wheels of a tractor was calculated from the equation that proposed by Macmillan (2002).

$$power\ lost\ (kw) = \frac{draft\ force\ (therotical\ speed - actual\ speed)}{3.6} \dots\dots\dots (5)$$

The actual field productivity and soil volume were calculated according to the method of Roth et al. (1977) and Bukhari et al., (1988)

3. Results and discussion

3.1. Effect of chisel tine shape, tillage depth, and forward speed on draft force

The results in Figure 3 showed a highly significant effect of the tine plow shape used on the draft force compared to the traditional chisel plow. The traditional chisel plow recorded the highest draft force of 19,421 kN. Meanwhile, the developed plow type (severed-15cm) had the lowest draft force (11,712 kN), this may be attributed to the large area of soil contact with the traditional type in comparison to the developed plow shape in their small area of contact with the soil. In addition to, the developed plow contains two types of shape. These results are agreed with Al Nuaimi and Al Rijabo (2020). The results in Figure (3) also showed an increase in the draft force with increasing of the plowing depth. The depth of (35 cm) recorded the highest draft force of 15.768 kN.m^{-2}. This increase may be attributed to increased soil volume with an increasing of plowing depth. Results also illustrated that the draft force increases due to forward speed increases.

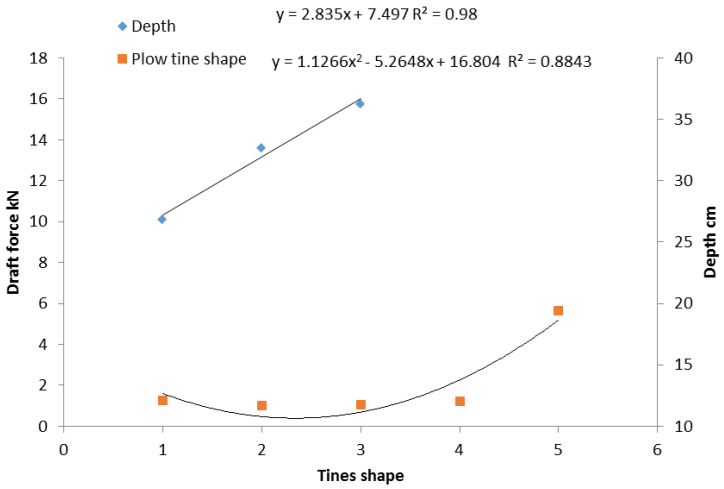

Figure 3: Draft force values according to plow tines shape and depth

The forward speed of 2.74 kmh^{-1}, recorded the highest draft force of 13.891 kN.m^{-2}. These results agreed with the results of Alrijabo and Al-TAI (2013) and Bashir et al., (2015). For the interaction between the depth and the shape of the plow (Figure 3), the pointed shape at (20 cm) width with a depth of 15 cm recorded the lowest draft force (8.019 kNm^{-2}). This decrease may be due to the space required for the plow to be pulverized at a depth of 15 cm. This contributed to the plow for penetrating the soil and reducing the draft force. This result agreed with Al Nuaimi and Al Rijabo (2020).

3.2. Effect of chisel tine shape and plowing depth on the fuel consumption rate

Results as shown in Figure (4) showed a highly significant difference between the types of tines used on the developed chisel plow. The use of the pointed shape (20 cm width) contributed to a clear decrease in the rate of fuel consumption (5.726 lha^{-1}). Meanwhile, the traditional chisel plow recorded the highest fuel consumption rate (9.386 lha^{-1}). This reduction may be due to the design of the tine shape and their arrangement in two rows in the developed plow. As well as, the second row contains two types of tines that contribute to facilitating the penetrating into the soil. These results are agreed with the findings of Al Nuaimi and Al Rijabo (2020). The findings also illustrated a significant difference between the plowing depth and forward speed on the fuel consumption rate (Figure 4). The depth of 35 cm and the speed of 2.74 kmh^{-1} recorded the highest fuel consumption rate of 8.081 lha^{-1}. This increase may be attributed to increased load engine, especially when the plowing depth increases as a result of a larger volume of soil. This result is agreed with the findings of Jebur et al., (2016); and

Ghali (2019). The interaction between the plowing depth and the shape of plow on the fuel consumption rate, the pointed type at 20cm performed the lowest fuel consumption rate (4.782 lha^{-1}). This reduction may be attributed to the developed plow better penetrating the soil than the traditional plow, which contributes to reducing the draft force and then reduces the fuel consumption rate.

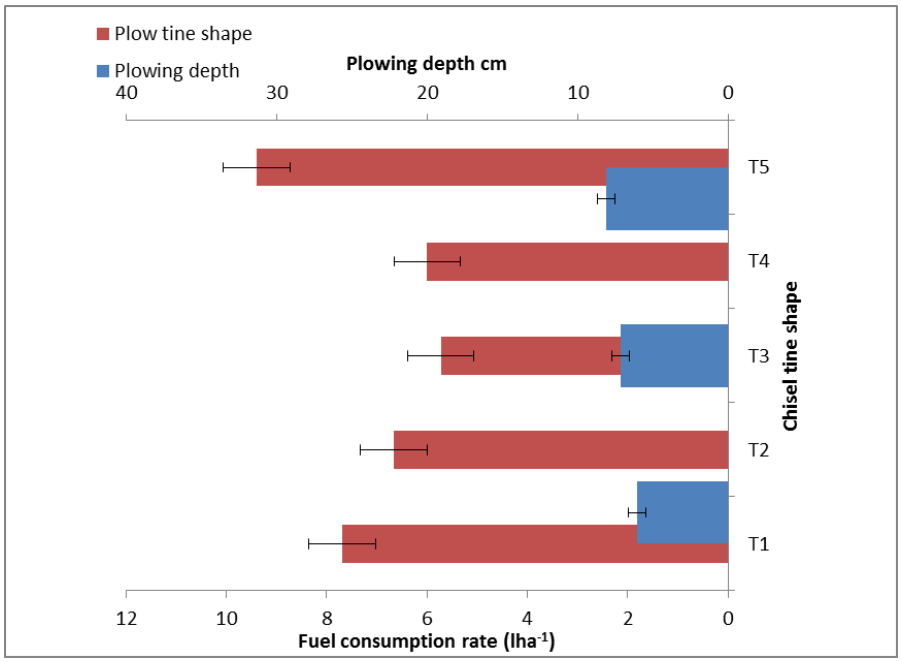

Figure 4: Fuel consumption rate according to plow tines shape and the plowing depth

3.3. Effect of chisel tine shape and plowing depth on the power loss

Figure (5) showed highly significant differences in the power lost for chisel tine shape compared to the traditional chisel plow. The lowest rate of power lost due to slippage wheel of the tractor (3.15 kW) (T3). Whereas, the traditional chisel plow (T5) recorded the highest percentage of power lost due to slippage (7.61 kW). The findings also revealed a significant effect of plowing depth on the power lost due to slippage. The plowing depth (30 cm) recorded the highest rate of power lost due to slippage wheel (5.87 kW). While, the plowing depth (15 cm) recorded the lowest of power lost (3.39 kW). This increase can be attributed to the increase in the volume of soil, which increased the density of the soil with plowing depth. This result is agreed with the findings of Aday et al., (2010); Al Nuaimi and Al Rijabo (2020).

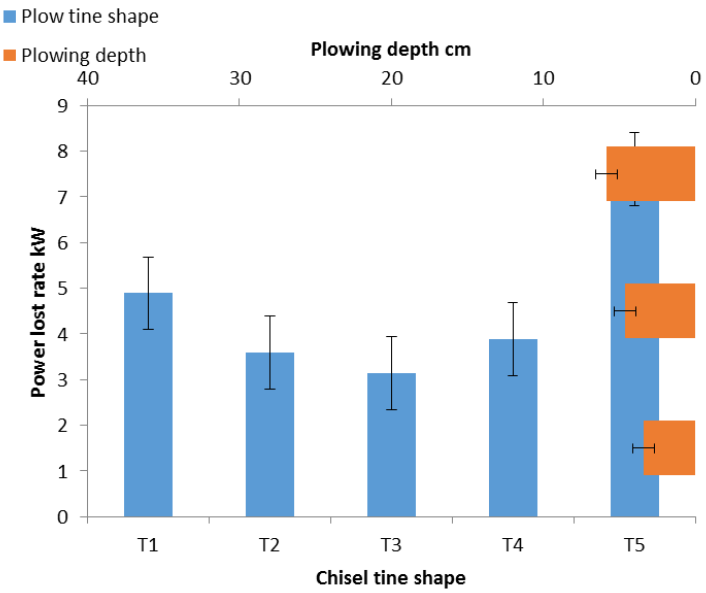

Figure 5: Statement of power loss rate according to tine shape and working depth

4. Conclusions

It can be concluded that the developed chisel plow is significantly superior to the traditional plow by recording less draft force, fuel consumption rate, slip percentage, and power reduction loss. The interaction between the plowing depth of 15 cm and the pointed shape type (T3) revealed the least draft force, the best fuel consumption rate, and the lowest slip percentage. Also, adding an upper tine to the back row of the developed chisel plow contributed to the movement of some soil at the top, reducing penetration resistance and increasing soil fragmentation. This development in a chisel plow improved both mechanical and operating parameters especially in the clay soils.

References

Aday, S. H.; and S. J . Muhsin, 2019. Effect of the Operating Depth and the Lateral Inclination Angle on the Draft Force Requirements and the Lateral Force of the Vertical and Laterally Inclined Mole Plows in Silt Clay Soil. International Journal of Engineering Research & Technology, 8: 567-575.

Aday, Sh. H., H., El-edan and J C., Al-maliky, 2010. Further development of a modified chisel plow and studying: (A) The draft force and power requirements and the ability of soil pulverization (MWD) (part1). Basrah Journal of Agricultural Sciences, 23 (1): 1-19.

Al Nuaimi, B., S., Al Rijabo, 2020. Design and Manufacture of Chisel Plow Shares and Their Effect on Some Field Prformance Indicators. Tikrit Journal for Agricultural Sciences, *20*(1), 10-19.

Alrijabo, S. A., M. E. A., Al-Tai, 2013. Effect of tillage depths and blade shapes for chisel plow on tractor performance and some physical properties of soil. Kirkuk Journal of Agricultural Sciences, 4 (2): 65-80. doi: 10.58928/KU13.04207

Bashir, M.A., M.I., Dawelbeit, M.O. Eltom, H., Tanakamaru, 2015. Performance Of Different Tillage Implements And Their Effects On Sorghum And Maize Grown In Gezira Vertisols, Sudan. International Journal of Scientific and Technology Research, 4 (4): 237-242.

Black, C.A., D.D., Evans, J., L., white, J.E., Ensminger, F.E., Clark,1993. Methods of soil analysis 6ed, Am. SOC. Agron. Madison, Wisconsin, U.S.A.

Bukhari, Sh., M. A. Bhutto, J. M. B., Mirani, 1988. Performance of selected tillage implements. Agricultural Mechanization in Asia, Africa and Latin America 19(4)9-14.

Chandon, K, R. L. Kushwaha, 2002. Soil forces on deep tillage tools, The AIC 2002 Meeting CSAE/SCGR program Saskatoon, Saskatchewan,Canada July 14-17: 1-12.

El-Iraqi, M. E., S. A., Marey, A. M., Drees, 2009. A modified shape chisel plow 9evaluation and performance test). Misr journal of Agricultural Engineering 26(2): 644-666.

Ghali, A.A., 2019. Effect of soil Moisture and Tillage Depth on some Mechanical Properties for Tillage Machines Type (Moldboard Plow). Journal of University of Babylon for Pure and Applied Sciences, 27(2) 195-207.

Grisso, R. D., M. Yasin, M. F. Kocher, 1996. Tillage implement force operating in silty clay loam. *Trans. of the ASAE*,39:1977-1983.

Hillel. D., 1980. Application of soil physics. Academic press New York.
http://pakinsight.com/?ic=journal&journal=63

Jebur, H. A. , A.,Yasir, A., Alsayyah, 2016. The effect of soil moisture content on the energy requirement and fuel consumption of the machinery unit. International Journal of soil. Engineering Sciences & Research Technology, 5(10), 261-266.

Kirisci,V. A., 1993. A field method for predicting the draught forces of tillage implements.PhD Thesis, Silsoe College of Cranfield University, Silsoe, Bedford.

Macmillan, R. H., 2002. The mechanics of tractor-implement performance. *A textbook for students and engineers, International Development Technologies Centre, University of Melbourne*.

Moinfar, A. M. ; G. Shahgholi., 2018. Dimensional Analysis of the Tractor Tractive Efficiency Parameters. Acta Technologica Agriculturae. 21(3): 94-99.

Muhsin, S.J., 2017. Performance Study of Moldboard Plow with Two Types of Disc Harrows and Their Effect on Some Soil Properties Under Different Operating Conditions. Basrah Journal of Agricultural Sciences, 30(2): 1-15. https://doi.org/10.37077/25200860.2017.37

Osman, T., M .B., Zaied, A M., El Naim, 2014. Field performance of a modified chisel plow. International Journal of Natural Sciences Research, 2(6): 85-96.

Roth, L.O, F.R.Grow, G.W.A.Mahony, 1977. An Introduction to Agricultural Engineering, AVI Publishing Company, INC. Oklahoma State University.

Upadhyaya, S. K., K. P.Lancas, A. G., Santos-Filho, N. S., Raghuwanshi, 2001. Evaluation of one-pass tillage equipment versus conventional tillage system. University of california, Davis, CA

Agriculture digitalization: Development of a low-cost RGB camera system for soybean crop monitoring

Jordi Llop[a], Albert Aguasca[b], Antoni Broquetas[b], Aitor Meraver[a], Ramon Salcedo[a,*], Francisco Garcia[a], Emilio Gil[a]

[a] Department of Agrifood and Biotechnology Engineering, Universitat Politecnica de Catalunya, Castelldefels, Spain
[a] Department of Theory and Communication Signal, Universitat Politecnica de Catalunya, Castelldefels, Spain
* Corresponding author. Email: ramon.salcedo@upc.edu

Abstract

Technology and the digital transition appear as a fundamental solution to improve the efficiency of companies on the agrifood sector and respond to the current problems. One aspect in which technology can improve the efficiency of farmers is in crop monitoring, since it is a valuable tool to optimize agricultural production, study the evolution of the crop, identify problematic areas within the field, etc. This project aims to improve the acquisition and analysis of data on vegetative parameters of a crop using a low-cost RGB camera (camera acquisition cost was 35€) and image processing software with which valuable vegetation indexes of interest could be extracted. A low-cost RGB mounted on a dedicated 2m high frame was used to monitor a soybean crop (*Glycine maz (L.) Merril*) seeded on April 2023. This camera was operated and images were acquired by mobile App. Image analysis was carried out using ImageJ free software obtaining Excess Green Index (ExGI) and the ground canopy cover (GCC). ExGI and GCC were compared with main crop parameters obtained by destructive methodologies (plant biomass, plant water content and leaf area index) and manual non-destructive methodologies (phenological stage and height of plant). The ExGI showed a strong correlation with the water content of plants and with plant biomass (R^2 =0.9) indicating this technic as a prominent tool to reduce efforts on field for crop monitoring. In addition, ground canopy coverage expressed as a ratio of the ground and ground covered by leaves, was related with leaf area index (R^2 = 0.84) with maximum values of LAI of 0.84. The low-cost RGB camera arises as a fast and cheap solution for intense crop monitoring both for research purpose and for farmer. Data obtained is correlated with main indicators of health of the crop (water content, biomass and leaf area index) that are used for crop management inputs such us crop protection, fertilization and irrigation needs.

Key words (max. 5): Low-cost image, ExGI, Soybean, digitalization, crop monitoring

1. Introduction

Crop monitoring is a valuable tool for optimizing agricultural production, studying crop development, identifying problem areas within the field, improving managing decision for resource efficiency, distinguishing diseases, deficiencies, or other threats to the harvest, and assisting in complex issues related to food security. In this sense, several studies had demonstrated the effectiveness of the RGB cameras (Lu et al., 2019, Wang et al., 2023, Barbosa et al., 2019) as a tool to obtain data from crops.

Among many RGB image data indicators, two well-studied indices can be used to analyse and evaluate vegetation: the Excess Green Index (ExGI) and the percentage of vegetation cover. Studies that have used these two indices, even when using simple image acquisition devices, show good results in both open-field and controlled greenhouse cultivation, although, in the case of ExGI, a greater effectiveness was observed on greenhouse crops. As other authors have noticed, using these indices instead of traditional methodologies to study crop development can result in a considerable reduction in time spent on these tasks (Xiong et al., 2019, Meyer & Neto, 2008).

The main objective presented in this research work was present a simple and easy way to use RGB camera based to characterize and monitor a soybean crop during a complete season measuring vegetative parameters. For this purpose, a low-cost system to obtain images was developed. Vegetative parameters were assessed as height of the crop, % of ground surface covered by crop, biomass expressed as water content, foliar area and EXGI parameter.

2. Materials and Methods

2.1. Field plot

Field experiments were carried out at Barcelona School of Agricultural and Biosystems Engineering from the Universitat Politècnica de Catalunya, (Castelldefels, Spain) at coordinates 41º16'36''N 1º59'11''E. A dedicated parcel of 21m width and 45m long was used to seed a soybean crop to be monitored during a complete season (from 06/01/2023 until 09/29/2023). For this purpose, soybean variety Avril inoculated with Rhizobium (*Bradyrhizobium japonicum*) was seed at a plant density of 356000 plants ha^{-1} corresponding to a plant pattern of 3.75 x 75 cm (distance between seeds by distance between lines). Seeds were planted at a depth of 3 to 5 cm. The crop was irrigated to supply the plants water need. To improve the efficiency of the irrigation and reduce the water loses, dripping system underneath the crop at 10cm depth was deployed. With the underneath system, two objectives were accomplished: first, avoid mechanical breaking of the system due the monitoring process; second: avoid the effect of the dripping line on the obtention of RGB images.

The parcel was divided into 6 different zones with the same size to obtain biomass, crop height and leaf area surface, into 9 zones with same size for RGB image gathering.

2.2. Low-cost camera photo acquisition system

The RGB camera used during the campaign was a LILYGO model TTGO T-Camera ESP32 WROVER with a resolution of 1200 x1600 pixels. It operates powered by an external 5V battery and it is operated through a Wi-Fi connection hosted by the camera device by a mobile phone. The camera was mounted on a dedicated 2 m high plastic frame, where the camera was holded zenithally at a distance of 1m from the vertical frame. The total cost of the image acquisition device was 36.2 € (in Spain on 1^{rst} semester of 2023) divided into: 17.79 €/camera, 5.45 €/plastic frame, 12 € external battery, 0.96€/cable USB connection.

The operation of the camera was carried out through mobile telephone, where the configuration was adjusted according the height and focus of the camera. All images were recorded on the mobile telephone data storage system.

2.3. Data acquisition

Samples and measurements of the soybean plants were taken starting on 06/12/2023, 2 weeks after sowing, until 09/29/2023, when the crop was considered to have reached full maturity. During the last 3 weeks, the field showed no changes, so the crop was considered finished. Biomass, leaf area surface and RGB image were monitored once a week, and the height of the crop that was measured twice a week. Height of the plants were measured from the ground level to the most extended leaf. 20 measurements were carried out in each zone of the parcel, resulting into 120 measurement per parcel and date of measuring.

Biomass data of the plant was obtained through a destructive methodology. This process involves cutting the plants at ground level, quickly placing them into a sealed paper bags (without handles) to avoid dry matter losses, loading them onto heat-resistant plastic trays, and stored into the laboratory. The freshly cut plants are weighed to obtain the fresh weight, then placed back in the paper bags. The bags are then placed in a convection oven for at least 48 hours at 60°C. After the 48 hours of drying, the dehydrated samples are removed and weighed, providing the dry weight of the plant. A total of 2 plant per zone were selected resulting into 12 samples per date of sampling. From the biomass, data Water Content (PWC) expressed as fresh height content was obtained.

Leaf area surface of the crop was expressed as Leaf Area Index (LAI) that is an indicator of the photosynthetic capacity of the plants and helps us understand the relationship between biomass accumulation and crop yield. The same plants used to obtain the plant biomass were used to determine leaf area. All leaves from each individual plant selected were scanned (without considering stems of the plant). A post processed analysis of the leaves scanned was carried out using ImageJ free software. LAI was expressed as a ratio of total leaf area surface of a plant and proportion of the ground associated to this plant.

As mentioned previously, from RGB images two parameters were obtained: Excess Green Index (ExGI) and vegetation cover (%VC) (Figure 1). ExGI is an indicator obtained by contrasting the green channel (or the green band) of the visible spectrum with the blue and red channels to discern vegetation from soil. This index provides information about the intensity of green in the plants, primarily the leaves. Since the shades

of green in the leaves indicate photosynthetic efficiency and activity, this index gives us a general idea of the state of the plants. The ExGI is expressed as two times green channel minus red and blue channel (Woebbecke et. al., 1995). To obtain ExGI, RGB images were processed using a modified version of an original macro developed by Mathew et. al. (2021) obtained from "Image.sc" developed for ImageJ.

The vegetation cover (%VC) is an indicator that express the coverture of the ground produced by the leaves. Obtaining the percentage of vegetation cover allows us to monitor and study crop growth, the area occupied by the plants, and the time it takes for them to completely cover the soil. RGB images were processed to calculate the percentage of pixels in an RGB image that correspond to the vegetation cover relative to the total number of pixels, assuming that the total number of pixels are composed by pixels related to crop cover and pixels with no crop cover (Xiong et. al., 2019).

To obtain these values, the RGB images obtained during soybean season were processed with the program ImageJ. The developed program was an adaptation of a code developed by Xiong et. al. (2019).

Figure 1. Example of the RGB image taken with the low-cost device measuring ExGI and VC.

3. Results and Discussion

Different relations were observed among different measures carried out during the soybean season. The most relevant and interesting for crop monitoring are expressed on Table 1. As it is observed, the global Coefficient of correlation that estimates the relation between Vegetative cover and LAI I close to 0.85, indicating a very good correlation. During dry period of the crop, the leaf area index has been reduced dramatically in comparison to VC (Figure 2). In contrast, the correlation at vegetative period of the Plant water content and ExGE is very low, indicating that the assessment of the green index is very bad during the first 30 days after transplanting (Figure 3). After that, the ExGI is a good estimator of the plant water content.

Table 1. Coefficient of correlation between VC and LAI and PWC and ExGI for the average values obtained during the complete season separated by crop period

	VC vs LAI	PWC vs ExGI
Vegetative period	0.95	0.28
Reproductive and maturity period	0.9	0.97
Dry period	0.83	0.98
Global	0.84	0.9

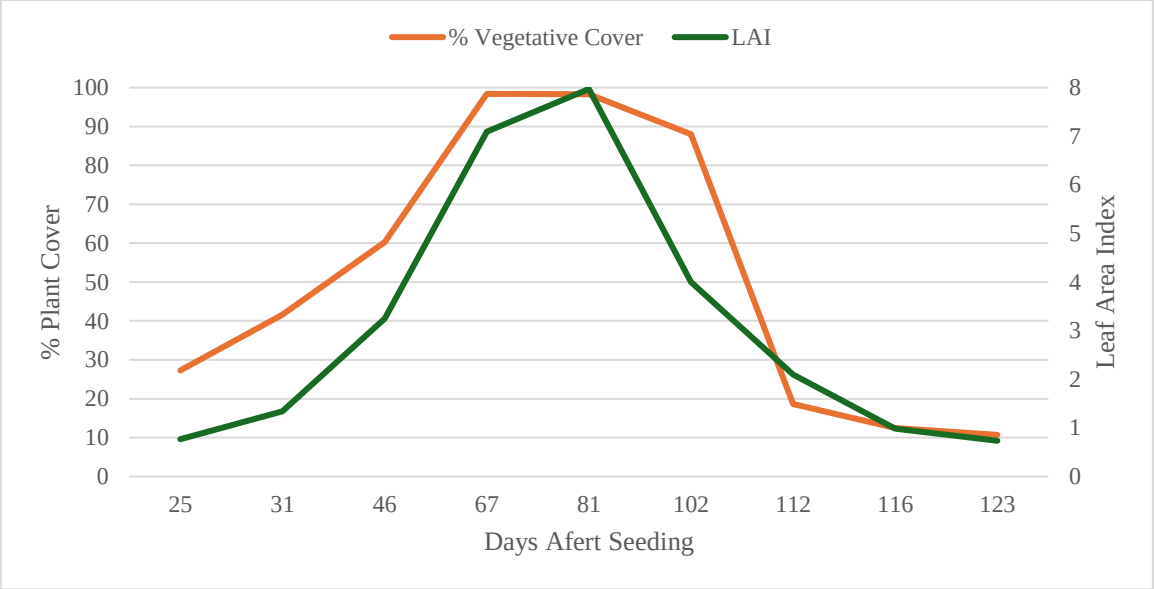

Figure 2. Evolution of the % of Plant Cover and Leaf Area Index during the soybean crop period expressed as days afters seeding.

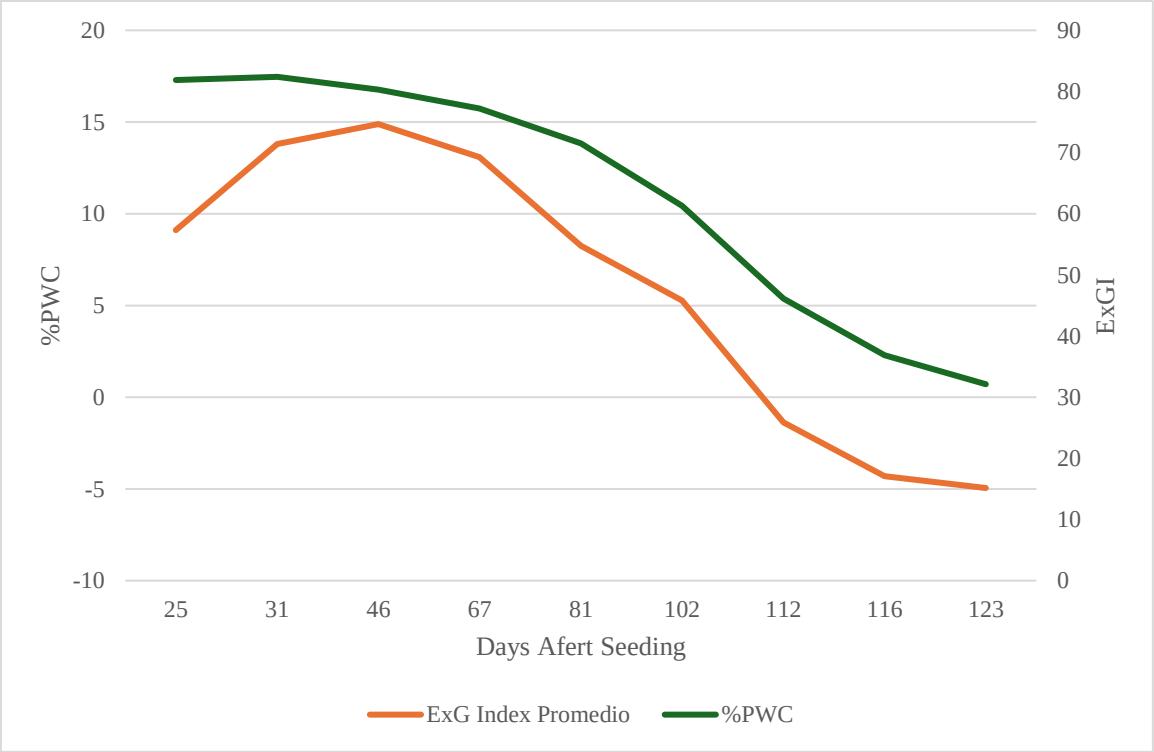

Figure 3. Evolution of the % of Plant Water Content and the Excess Green Index during the soybean period expressed as days after seeding.

4. Conclusions

The results of this campaign demonstrate that it is possible to develop a system for obtaining useful RGB images in crop monitoring without large. Image processing has been possible using free public code for open source ImageJ software.

Both indices (ExGI and VC) complement each other showing significant correlations with various vegetative parameters and providing with information on both the crop's health status and the evolution of its biomass.

In the case of ExGI, it shows a strong correlation with plant water content (PWC), with an almost perfect Pearson correlation coefficient "R" of 0.97 and R^2 coefficient of 0.9; providing the idea of the crop's water demand at that moment. On the other hand, the analysis of vegetation cover shows a strong correlation with leaf area index (LAI), with a Pearson correlation coefficient "R" of 0.9 and an R^2 coefficient of 0.84, with 14.33 being the highest LAI value observed during the campaign, belonging to a plant with a leaf area of 4020.5 cm^2. The analysis of vegetation cover (VC) also presents a strong correlation with biomass and a slightly lower correlation with crop height evolution.

Although determining crop vegetative parameters through manual destructive and non-destructive methods provides empirical and reliable results, obtaining such data is a lengthy and tedious process. The incorporation of a system for obtaining useful RGB images in crop monitoring can lead to a reduction in both economic costs and time spent monitoring a crop, at least in a small field.

Acknowledgements

This research study has been possible in the framework of the Hydrosoil project (Aguasca et al 2021). HydroSoil is a measurement campaign, funded by the European Space Agency (ESA)

References

Aguasca, A.; Broquetas, A.; Fabregas, F.; Mallorqui, J.J.; Vilalvilla, P.; Biscamps, J.; Llop, J.; Gallart, M.; Gil, E.; Gras, A, 2021. Hydrosoil, soil moisture and vegetation parameters retrieval with a C-Band GB-SAR: Campaign implementation and first results. IGARSS 2021, 2021 IEEE International Geoscience and Remote Sensing Symposium: 12-16 July, 2021, virtual symposium, Brussels, Belgium: proceedings

Barbosa, B.D.Si, Ferraz, GAS, Gonçalves, L.M, Marin, D.M., Maciel, D.T., Ferraz, P.F.P, Rossi, G., 2019. RGB vegetation indices applied to grass monitoring: a qualitative analysis. Agronomy Research. 17. 349-357. https://doi.org/10.15159/AR.19.119

Mathew (October 2021), Vegetation indices calculed by Fiji, Image.sc, de: https://forum.image.sc/t/vegetation-indices-calculed-by-fiji/23804

Meyer, G.E., Neto, J.C., 2008. Verification of color vegetation indices for automated crop imaging applications. Computer and electronics in agriculture. 63 (2) 282-293. https://doi.org/10.1016/j.compag.2008.03.009

Lu, N., Zhou, J., Han, Z.et al., 2019. Improved estimation of aboveground biomass in wheat from RGB imagery and point cloud data acquired with a low-cost unmanned aerial vehicle system. Plant Methods 15, 17 https://doi.org/10.1186/s13007-019-0402-3

Wang, Y., Yang, Z., Kootstra, G., and Khan, H.A, 2023. The impact of variable illumination on vegetation indices and evaluation of illumination correction methods on chlorophyll content estimation using UAV imagery. Plant Methods 19, 512023). https://doi.org/10.1186/s13007-023-01028-8

Woebbecke, D.M., Meyer, G.E., Bargen, K.V., Mortensen, D.A., 1995. Color indices for weed identification under various soil, residue, and lighting conditions. Transactions of the ASAE 38, 259-269. https://doi.org/10.13031/2013.27838

Xiong, Y., West, C.P., Brown, C.P., Green, P.E., 2019. Digital image analysis of old world bluestem cover to estimate canopy development. Agronomy Journal, 111: 1247-1253. https://doi.org/10.2134/agronj2018.08.0502

Estimating pomegranate fruit cracking through proximal and aerial remote sensing

Georgia Nikolakopoulou [a,*], Konstantinos-Elenos Grivakis[a], Evangelos Anastasiou[a], Manuela Zude-Sasse[b], Christian Regen[b], Nicolas Tapia Zapata[b], Victor Alchanatis[c], Avi Sadka[c], Idit Ginzberg[c], Meytal Laor[c], Spyros Fountas[a]

[a] Department of Natural Resources Management & Agricultural Engineering, Agricultural University of Athens, Iera Odos 75, 11855 Athens, Greece

[b] The Volcani Institute - Agricultural Research Organization (ARO), Derech HaMaccabim 68, Rishon LeTsiyon, Israel

* Corresponding author. Email: gnikolakopoulou@aua.gr

Abstract

Fruit cracking, a major concern causing significant yield loss, is influenced by a complex interplay of plant traits, environmental conditions, and management practices such as irrigation and nutrient application. This study investigates the effectiveness of remote sensing techniques and analyzes the integration of proximal and remote sensing data to observe and understand fruit cracking in pomegranate (*Punica granatum*) crops. Conducted in Argos, central-east Peloponnese in Greece, the study aims to evaluate the correlation between vegetation indices (NDVI and EVI) and the incidence of fruit cracking under different irrigation treatments. The experiments involved intensive data collection using proximal methods alongside unmanned aerial vehicles (UAVs). Ground-based data collection was undertaken using a thermal camera, complemented by LiDAR sensor, and manually measuring on-tree fruit weight, stem water potential, and the total number of cracked fruit per plot for each treatment. The UAVs were equipped with multispectral and thermal cameras, which generated valuable data on various vegetation indices and captured unique spectral signatures emitted by the crops. The methodology enabled the creation of detailed 3D point clouds under varying orchard conditions, providing essential geometric information about the crop canopy and segmented fruit. The results revealed that NDVI values for red fruit (0.654 ± 0.109) were significantly higher than for harvest-dark red development stage (0.382 ± 0.03) with a p-value of 0.0014, indicating significant variation in vegetation density between these two stages. Other parameters, such as EVI, SWP, on-tree fruit weight, and canopy temperature, remained relatively stable across different developmental stages and irrigation treatments.

Keywords: Punica granatum, fruit cracking, remote sensing, proximal sensing, Unmanned Aerial Vehicle

1. Introduction

The fleshy fruit of pomegranates, like other fruits such as citrus and apples, is protected by a peel (skin or rind) comprising a thick, spongy inner tissue and a smooth outer layer. This structure must endure growth stresses and protect against pests, pathogens, and harsh environmental conditions (Joshi *et al.*, 2021). Fruit cracking, a prevalent disorder affecting fruit marketability by reducing quality and yield, begins with surface cracks that penetrate deep into the fruit, compromising its appearance, promoting moisture loss, and facilitating pathogen invasion (Knoche & Lang, 2017). Environmental factors such as climate and orchard management practices, including irrigation and nutrition, significantly influence the likelihood of cracking (Khadivi-Khub, 2015). Research has shown that extreme climate conditions and improper irrigation during key growth phases can weaken the fruit's skin, increasing cracking susceptibility. Despite the observed correlation between high water content and cracking, optimal irrigation strategies tailored to local conditions are still under development. Efforts to enhance skin resilience through the application of growth regulators and minerals like calcium have shown promise, though their cost and applicability vary across different crops.

In crops, proximal and remote sensing technologies may offer crucial insights into various fruit parameters, including cracking. Proximal sensing tools, such as non-contact infrared thermal measurements and advanced RGB sensing technologies, help monitor temperature variations and structural characteristics of fruit and canopies. These tools facilitate the characterization of light and water interception, moisture distribution, and fruit ripening. Remote sensing provides vital data for agricultural management by capturing information on plant health and environmental conditions from a distance and provide information for automated harvesting process (Ranjan *et al.*, 2022) or irrigation management. Techniques like fluorescence-, RGB-, laser-scanning, thermal imaging, and near-infrared spectroscopy (NIRS) assess water status. These

remote technologies, integrated with machine learning, are proving invaluable in enhancing the precision of crop management and the mitigation of risks like fruit cracking (Whatley *et al.*, 2023).

The aim of this study is to investigate the effectiveness of integrating proximal and aerial remote sensing techniques in monitoring and understanding the factors contributing to fruit cracking in pomegranate crops. Specifically, the study seeks to evaluate the correlation between vegetation indices (NDVI and EVI) and the incidence of fruit cracking under different irrigation treatments, and to determine the role of these indices and irrigation practices in managing and mitigating fruit cracking.

2. Materials and Methods

2.1. Field site and irrigation plan

The study area is located in Argos, near Corinth, Greece (Fig. 1), situated in the central-eastern part of the Peloponnese peninsula. The geographic coordinates are 37°38'59.8"N latitude and 22°47'22.0"E longitude, based on imagery from Google Earth (Google Earth, 2023). The area encompasses a 0.35 ha plot, which is organized into 9 rows. The terrain is generally flat and exhibits a regular topography. Soil samples were collected on October 11, 2023, from depths of 0-30 cm and 30-60 cm in the experimental pomegranate orchard. The soil is predominantly clayey, with 34.7 % sand, 18.6 % silt, and 46.7 % clay. Key findings indicate high pH and salinity levels, highlighting the need for organic matter maintenance, strategic nitrogen application, and sodium drainage. Elevated Total $CaCO_3$ levels also suggest micronutrient challenges that require attention.

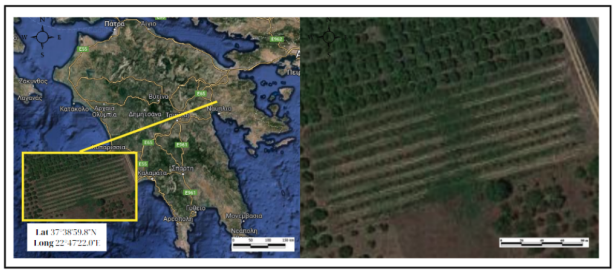

Figure 1. Experimental site location on a scale of 1:1,200,000 and the study area (Google Earth, 2023).

Based on this analysis, irrigation was carried out from March to October, consisting of 20 irrigation events. Each event lasted 3 hours, with an irrigation dose of 40 m³ per hour. The irrigation experimental design involved three distinct protocols for pomegranate trees: the standard method with eight drippers per tree, a high water amount (HWA) protocol which increased water supply by 20 % above the standard by adding two additional drippers, and a low water amount (LWA) protocol which reduced water supply by approximately 30 %, utilizing only five drippers per tree (Fig. 2). These variations aimed to assess the impact of different water availability levels on fruit cracking and overall crop performance.

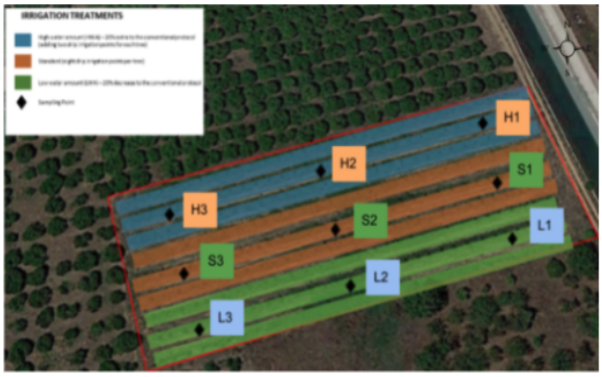

Figure 2. Experimental design for pomegranate irrigation treatments in the pomegranate orchard. Plots labeled with 'H' represent the high water amount treatment, 'S' denotes the standard commercial water amount application, and 'L' indicates the low water amount treatment (Google Earth, 2023).

The study was conducted during the 2023 season in a pomegranate orchard, featuring the 'Wonderful'

cultivar of *Punica granatum* on both scion and rootstock, which was established in 2020. Therefore, it was in its third year of growth at the time of the study. The plants were arranged in a layout of 2.8 m by 4.1 m, resulting in a density of 180 trees per hectare.

2.2. Climate data

Daily and hourly climatic information is gathered from an on-site meteorological station. This data includes Daily Leaf Temperature (°C) and Precipitation (mm), which are critical for understanding the environmental conditions affecting the pomegranate crops.

Figure 3. Select and use the built-in styles in this template.

Daily Leaf Temperature provides insights into the thermal stress experienced by the plants, while precipitation data helps in assessing the water availability and its impact on fruit cracking (Fig. 3).

2.3. Data Collection

2.3.1. Aerial remote sensing measurements

For this study, two types of unmanned aerial vehicles (UAVs) were utilized: one equipped with a multispectral camera and the other with a thermal camera sensor. The DJI Mavic 3 Thermal, equipped with a high-resolution thermal imaging camera and a 12 MP zoom camera, was used for crop health analysis and irrigation planning. It features synchronization of the drone, camera, and RTK with ground control points, flying at a 50 m altitude. Additionally, the DJI Mavic 3 Multispectral was employed, which combines a RGB camera and a multispectral camera (4 × 5 MP, G/R/RE/NIR), providing centimeter-level RTK positioning and microsecond-level time synchronization, also flying at 50 m.

2.3.2. Isolating and analyzing trees of interest using NDVI and EVI indices

Crop vigour at 2 different critical developmental stages of the pomegranate, namely, the red fruit and harvest-dark red, was assessed by measuring the Normalized Difference Vegetation Index (NDVI) and the Enhanced Vegetation Index (EVI) (Table 1). These developmental stages were selected for cracking observation because high temperatures and irrigation practices during critical growth stages significantly impact fruit integrity.

Table 1. The spectral vegetation indices that were used in this study.

Spectral Vegetation Index	Equation	Bibliography
Normalized Difference Vegetation Index	$NDVI=\frac{NIR-RED}{NIR+RED}$	Rouse *et al.*, 1973
Enhanced Vegetation Index	$EVI=G\frac{N-R}{N+C1R-C2B+L}$	Jiang *et al.*, 2008

To isolate only the trees of interest, a Shapefile mask was initially created. This mask was later used to clip the data within its boundaries to calculate statistical data for each tree. Using the Raster Calculator in ArcGIS, the spectral index NDVI was calculated. NDVI values indicate soil, water, or vegetation, and it was observed that values greater than 0.20 primarily correspond to vegetation. Therefore, pixel values less than 0.20 were disregarded as they would affect the statistical results. To eliminate pixels with values less than 0.20, the Reclassify command was used to assign values below 0.20 as 0 and values above 0.20 as 1. After calculating the NDVI and EVI spectral indices, these indices were multiplied by the corresponding Reclassify channel, ensuring zero values for non-vegetation pixels. To remove zero values, they were declared as No Data Values during export. The "Extract by Mask" command was then used to limit the data to the boundaries of the trees

of interest. Finally, from the properties of the channels created with the "Extract by Mask" command for each tree, statistical data for each index and for all dates, including maximum, minimum, and average values and standard deviation, were obtained.

2.3.3. Proximal sensing measurements

Stem water potential (SWP) was monitored monthly using a pressure chamber (Pump-Up Pressure Chamber, PMS Instrument Company, Albany, USA), limited to 20 bar, to assess the water status of the trees. The higher the value is read in the pressure cell, the higher the stress is (more pressure is needed to apply in order to get the water drop). SWP values need to be converted into negative values to reflect the value in the plant. To ensure accurate measurement of the stem water potential and not the leaf water potential, the leaves were covered for 2 hours with aluminum bags before measurement. Also, on tree-fruit weight was recorded to determine the effects of irrigation treatments on yield. Specifically, two fruits were randomly collected from each tree, and the average weight was calculated for analysis. Additionally, meteorological data were collected from a nearby meteorological station, providing information on temperature, humidity, wind speed, and precipitation to correlate with physiological data and environmental conditions.

Geometric and thermal information of pomegranate canopies were obtained using a terrestrial orchard monitoring system (TOMMY) (Fig. 4). This multisensory platform includes a 2D mobile LiDAR sensor (LRS-4000, Sick AG, Germany) and a thermal camera (A655sc, FLIR Systems Inc., USA) with a 6.5 mm focal length lens. The sensors, mounted on a tooth belt linear conveyor, recorded canopies at 10 mm/s constant speed. Temperature-annotated 4D point clouds were created by calibrating the LiDAR and thermal camera using a method by Tsoulias, Jörissen, and Nüchter (2022). The pomegranates were then manually segmented from the canopy using CloudCompare (2.10, GPL software, Paris, France), and all fruit point clouds were exported as comma-separated files (.csv).

Figure 4. Terrestrial orchard multisensor monitoring yaw (TOMMY).

1.1. Fruit cracking rate

For the assessment of fruit cracking, the total number of fruit and the number of cracked fruit in each plot were recorded. The fruit cracking rate was calculated using the formula (Kaur et al., 2023):

$$Fruit\ cracking\ rate\ (\%) = \frac{total\ number\ of\ cracked\ fruit}{total\ number\ of\ fruit} \times 100$$

This method provided a quantitative measure of the extent of fruit cracking, allowing for a comparison across different irrigation treatments and conditions. The percentage of cracked fruits was determined by dividing the number of cracked fruits by the total number of fruits and multiplying by 100.

2.4. Map construction and statistical analysis

The maps for vegetation indices of the study were produced using ArcGIS 10.2 software (ESRI Inc., Redlands, CA, USA). Statistical analyses were performed using STATGRAPHICS Centurion XVI.I and Microsoft Office Excel 2013. Analysis of variance (ANOVA) at a 5% significance level and Pearson's correlation were conducted to evaluate the relationships between different variables and to identify significant differences among the treatments and developmental stages. These analyses help determine the impact of various irrigation treatments on key parameters such as NDVI, EVI, SWP, on-tree fruit weight, and canopy temperature, as well as the incidence of fruit cracking. By understanding these relationships, the study aims to develop more effective irrigation strategies and improve overall crop management practices.

3. Results and Discussion

3.1. Fruit cracking (%)

No fruit cracking was observed in any plots on any dates before harvest, as expected. Additionally, none of the commercially-standard irrigated plots exhibited cracking at all. However, at the harvest stage, significant differences were noted. The highest irrigation application exhibited 8.667 ± 21.229 cracked fruits, whereas the lowest irrigation application showed only 0.667 ± 1.634 cracked fruits (Table 4). Also, no early micro-cracks, which are typically lignified, were observed; only late cracks leading to fruit splitting were present.

Figure 5. Cracked pomegranate fruit from HWA Treatment.

The proceedings book requires that all figures be formatted consistently and highly legible. Please read the following suggestions to create high quality printing of your figures.

- Design or resize your figures so that the text in the figure will appear approximately 10 pt font size, which is the size of Body Text in the paper.
- Format the Layout of figures using "In line with Text." Do not have floating figures.
- Colour will be shown in the e-version only, but not in the printed book. Please test your colour figures by printing in black and white paper and make sure that they are legible.
- Figures will not be reduced in printing. Limit their maximum width to 15 cm.
- Figures should be high quality (1200 dpi for line art, 600 dpi for grayscale and 300 dpi for colour, at the correct size).

1.1. Vegetation index maps

To analyze vegetation health, NDVI and EVI maps were generated by isolating the nine trees of interest, excluding other trees and soil from the dataset. This method ensured precise and focused analysis on the selected plots. The resulting maps, presented in the accompanying figure (Fig.6), illustrate the vegetation indices, offering a detailed assessment of crop health and vigor for the nine targeted trees.

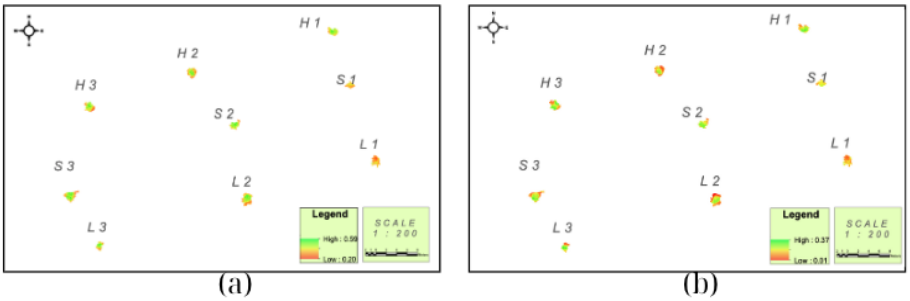

Figure 6. Maps of NDVI and EVI during the harvest-dark red development stage for the plots of interest are presented. The first image (a) shows the NDVI values, and (b) displays the EVI values.

3.2. Stem water potential (SWP) and on-tree fruit weight

The on-tree fruit weight is an important parameter as it directly relates to the overall yield and marketability of the pomegranate crops. It helps in assessing the effects of different irrigation treatments and developmental stages on fruit growth and quality. The average values of SWP and on-tree fruit weight are presented in Table 3 for the developmental stages and Table 4 for the different irrigation treatments.

1.1. Canopy temperature of fruit analyzed by TOMMY system

The mean fruit temperatures of segmented pomegranate fruits for each scanned canopy are shown in Table 4, while Figure 7 presents histograms and density plots of temperature distributions for canopies with cracked fruits, illustrating the Gaussian distribution of the recorded temperatures.

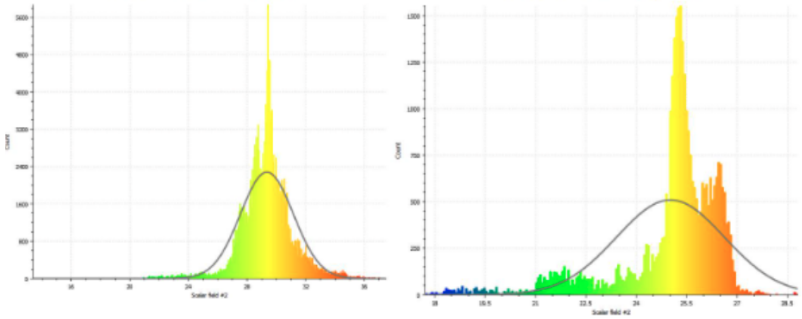

Figure 7. Histogram and density plot of all segmented pomegranate trees for canopy with cracked fruits, according to gaussian distribution.

The errors in the temperature estimation may be due to wind and resulting moving branches, disabling to register precise canopy point clouds. The thermal data provided a sum of the moving plant parts and various backgrounds appearing during the scan, resulting in high standard deviation and bias according to the background temperatures.

3.3. Comparative analysis of developmental stages and irrigation treatments

The analysis of average values and standard deviations of NDVI, EVI, SWP, on-tree fruit weight, on-site tree canopy temperature collected from the TOMMY system, and the percentage of fruit cracking between the developmental stages red fruit and harvest-dark red revealed notable findings (table 2). Among these parameters, NDVI displayed statistically significant differences with a p-value of 0.0014, indicating significant variation in vegetation density between these two stages. Specifically, the NDVI values for red fruit (0.654 ± 0.109) were significantly higher than for harvest-dark red (0.382 ± 0.03). This suggests NDVI is a reliable indicator of changes in vegetation health that correlate with the incidence of fruit cracking..

In contrast, no statistically significant differences were observed for EVI, SWP, on-tree fruit weight, on-site tree canopy temperature, or the percentage of fruit cracking between the red fruit and harvest-dark red stages. For example, the EVI values were 0.159 ± 0.117 for red fruit and 0.183 ± 0.007 for harvest-dark red. Additionally, the percentage of fruit cracking was 0% for red fruit and 6.222 ± 17.2176% for harvest-dark red. These findings suggest that while NDVI significantly varies and can be a key variable in monitoring and managing fruit cracking in pomegranate crops, the other parameters remain relatively stable between these two critical developmental stages.

Table 2. Average values and standard deviation of all parameters at red fruit and harvest-dark red stages.

Development stage	NDVI	EVI	Cracked fruits (%)	On-tree weight (g)	SWP (bar)	Canopy temperature (°C)
Red fruit	$0.654^{a} \pm 0.109$	$0.159^{a} \pm 0.117$	0^{a}	$258.667^{a} \pm 365.032$	$-10.833^{a} \pm 1.118$	$28.18^{a} \pm 2.856$
Harvest-dark red	$0.382^{b} \pm 0.03$	$0.183^{a} \pm 0.007$	$6.222^{a} \pm 17.2176$	$264.889^{a} \pm 366.875$	$-10.556^{a} \pm 1.261$	$26.914^{a} \pm 1.273$

Note: Means sharing different letters differ significantly at P≤0.05.

Table 3 presents the average values and standard deviations for NDVI, EVI, percentage of cracked fruits, on-tree weight, SWP, and canopy temperature for the three irrigation treatments: high water amount (HWA), standard (S), and low water amount (LWA). The only parameter showing a statistically significant difference, with a p-value of 0.0001, is the stem water potential (SWP). Specifically, the SWP for the LWA treatment (-9.333 ± 0.931 bar) is significantly higher compared to both the HWA (-11.417 ± 0.492 bar) and S (-11.333 ± 0.408 bar) treatments, as indicated by different letters (a, b) in the table. This significant difference in SWP

suggests that the LWA treatment induces less water stress in the trees compared to the higher water treatments. In contrast, the NDVI, EVI, percentage of cracked fruits, on-tree weight, and canopy temperature did not show statistically significant differences among the treatments, indicating that these parameters remain relatively stable across different irrigation levels. This stability implies that while SWP is sensitive to irrigation variation, the other measured factors are more resilient or less directly affected by the changes in water amount.

Table 3. Average values and standard deviation of all parameters for the 3 different treatments.

Development stage	NDVI	EVI	Cracked fruits (%)	On-tree weight (g)	SWP (bar)	Canopy temperature (°C)
HWA	0.483[a]± 0.113	0.123[a]± 0.073	8.667[a]± 21.229	539.0[a]± 535.578	-11.417[a]± 0.492	27.475[a]± 2.127
S	0.54[a]± 0.190	0.205[a]± 0.0929	0[a]	149.167[a]± 34.307	-11.333[a]± 0.408	27.825[a]± 1.556
LWA	0.531[a]± 0.160	0.185[a]± 0.064	0.667[a]± 1.634	97.167[a]± 24.71	-9.333[b]± 0.931	27.025[a]± 2.886

Note: Means sharing different letters differ significantly at P≤0.05.

3.4. Pearson product-moment correlations between each pair of variables

Table 4 shows Pearson product-moment correlations between each pair of variables, measuring the strength of their linear relationships. P-values below 0.05 indicate statistically significant correlations at the 95.0% confidence level.

Among the parameters analyzed, no pairs of variables exhibited statistically significant correlations, as all p-values were above 0.05. Despite this, some notable relationships were observed:

- EVI and on-tree weight: Moderate negative correlation (-0.274, p = 0.272).
- EVI and NDVI: Moderate positive correlation (0.264, p = 0.289).
- On-tree weight and SWP: Notable negative correlation (-0.459, p = 0.055).
- NDVI and canopy temperature: Moderate positive correlation (0.351, p = 0.263).
- SWP and EVI: Moderate positive correlation (0.307, p = 0.215).
- Percentage of cracked fruit and NDVI: Weak negative correlation (-0.185, p = 0.463).

These findings indicate that while some parameters exhibit moderate correlations, none were statistically significant, implying that the linear relationships between the parameters are not robust enough to draw definitive conclusions from this dataset.

	EVI	On-tree weight	NDVI	Percentage of cracked fruits	SWP	Canopy temperature
EVI		-0.274 (0.272)	0.264 (0.289)	0.063 (0.805)	0.307 (0.215)	0.233 (0.466)
On-tree weight	-0.277 (0.272)		-0.179 (0.476)	-0.101 (0.69)	-0.459 (0.055)	-0.268 (0.401)
NDVI	0.264 (0.289)	-0179 (0.476)		-0.184 (0.463)	0.022 (0.932)	0.351 (0.263)
Percentage of cracked fruits	0.063 (0.805)	-0.101 (0.690)	-0.185 (0.463)		-0.029 (0.908)	-0.219 (0.493)
SWP	0.307 (0.215)	0.021 (0.932)	0.022 (0.932)	-0.0229 (0.901)		-0.189 (0.557)
Canopy temperature	0.233 (0.467)	-0.267 (0.401)	0.351 (0.263)	-0.219 (0.493)	-0.189 (0.557)	

4. Conclusions

The results of this study indicate that NDVI is a reliable indicator for monitoring changes in vegetation health that correlate with fruit cracking in pomegranate crops. Specifically, the significant variation in NDVI between the red fruit and harvest-dark red stages underscores its potential as a key variable in precision agriculture. The NDVI values were 0.654 ± 0.109 for red fruit and 0.382 ± 0.03 for harvest-dark red, with a p-value of 0.0014, highlighting the significant difference between these stages. Additionally, the percentage of cracked fruits was 0% for red fruit and 6.222 ± 17.2176% for harvest-dark red, indicating an increase in fruit cracking at later stages.

In contrast, no statistically significant differences were found for EVI, SWP, on-tree fruit weight, or canopy temperature between the red fruit and harvest-dark red stages, suggesting these parameters are more stable and less influenced by developmental changes. Furthermore, the irrigation treatments revealed that SWP was significantly higher in the LWA treatment (-9.333 ± 0.931 bar) compared to the HWA (-11.417 ± 0.492 bar) and S (-11.333 ± 0.408 bar) treatments, with a p-value of 0.0001, indicating reduced water stress under lower water conditions.

One critical reason for not having many cracked fruits is that during September, the temperature and rainfall were optimal, which likely contributed to the reduced incidence of fruit cracking. Due to the limited data collected in this initial year of study, these results should be considered preliminary. The study will continue for two more years, during which additional data will be collected and analyzed to validate these findings and provide a more comprehensive understanding of the factors influencing fruit cracking. The extended duration of the study will help refine irrigation strategies and enhance the effectiveness of remote sensing technologies in mitigating fruit cracking, ultimately contributing to improved yield and quality of pomegranate crops.

Acknowledgements

This study was funded by The European Commission, Horizon2020 Project number 101086300 (CrackSense). We would like to thank Pegasus COOP for their collaboration in conducting our field experiments in their field.

References

Joshi, M., Schmilovitch, Z. E., & Ginzberg, I. (2021). Pomegranate fruit growth and skin characteristics in hot and dry climate. Frontiers in Plant Science, 12, 725479.

Knoche, M., & Lang, A. (2017). Ongoing growth challenges fruit skin integrity. Critical Reviews in Plant Sciences, 36(3), 190-215.

Khadivi-Khub, A. (2015). Physiological and genetic factors influencing fruit cracking. Acta Physiologiae Plantarum, 37(1), 1718.

Ranjan, R., Sinha, R., Khot, L. R., & Whiting, M. (2022). Thermal-RGB imagery and in-field weather sensing derived sweet cherry wetness prediction model. Scientia Horticulturae, 294, 110782.

Whatley, C. R., Wijewardane, N. K., Bheemanahalli, R., Reddy, K. R., & Lu, Y. (2023). Effects of fine grinding on mid-infrared spectroscopic analysis of plant leaf nutrient content. Scientific Reports, 13(1), 6314.

Rouse, J.W., Haas, R.H., Schell, J.A., Deering, D.W., 1973. Monitoring vegetation systems
in the Great plains with ERTS. Third ERTS Symposium 309–317 NASA SP-351 I.

Jiang, Z., Huete, A. R., Didan, K., & Miura, T. (2008). Development of a two-band enhanced vegetation index without a blue band. Remote sensing of Environment, 112(10), 3833-3845.

Kaur, G., Kaur, N., Gill, P. P. S., & Gupta, N. (2023). Assessing relationship between fruit cracking, metabolic and ultrastructural changes in the peel of pomegranate varieties during fruit development. Acta Physiologiae Plantarum, 45(10), 118.

Tsoulias Nikos, Sven Jörissen, and Andreas Nüchter. 2022. An approach for monitoring temperature on fruit surface by means of thermal point cloud, MethodsX, 9: 101712.

Implementation of a proximal optical sensor for real-time characterization of extensive rainfed crops and targeted fertilizer applications

Sergio Artero[a], María Videgain[a,b,*], Alba Vigo-Morancho[a], Mariano Vidal[a], F. Javier García-Ramos[a,b]

[a] Escuela Politécnica Superior, University of Zaragoza, Ctra. Cuarte s/n, 22071 Huesca, Spain.

[b] Instituto Agroalimentario de Aragón – IA2 (CITA-University of Zaragoza), EPS, University of Zaragoza, Ctra. Cuarte s/n, 22071 Huesca, Spain.

* Corresponding author email: mvidegain@unizar.es

Abstract

Many modern agricultural machines incorporate Precision Agriculture (PA) technologies, such as variable rate application of inputs. To implement variable rate dosing, an initial assessment of within-field variability is often conducted, followed by the creation of a prescription map that is uploaded to the machine prior to application. However, this process is streamlined in the context of topdressing fertilization through the integration of proximity optical sensors on the machinery. These sensors detect field variability in real-time, and using specific software, translate this information into an appropriate application rate, commanding the fertilizer spreader to adjust accordingly within milliseconds. This approach eliminates the need for the labour-intensive and costly creation of prescription maps.

This study aims to analyze the readings obtained from proximity optical sensors and compare them with crop variability indicators. Specifically, soil apparent electrical conductivity (ECa) was measured, and satellite imagery was captured concurrently with the sensor readings to calculate the Normalized Difference Vegetation Index (NDVI). The analysis focused on evaluating the correlation between sensor readings, NDVI, and ECa. Results indicated a strong correlation between the proximity optical sensor readings and NDVI, whereas the correlation with ECa was notably lower. These findings suggest that the real-time application rate adjustments made by the sensors would closely mirror those derived from a prescription map based on the field's NDVI, thus validating the efficacy of using proximity optical sensors for real-time variable rate fertilization.

Keywords: precision agriculture, satellite images, apparent electrical conductivity, variable rate application, cereal management.

1. Introduction

The heterogeneity within plots, often influenced by field leveling due to land consolidation or similar activities, results in variable crop performance within the same plot (Valero, 2020). This phenomenon is known as intra-plot variability. Understanding and managing this variability is crucial for maintaining productivity (Martínez-Casasnovas et al., 2022). Data collection and subsequent analysis enable the identification of zones within a plot that exhibit variability, facilitating decision-making to enhance efficiency and reduce costs. Additionally, the integration of sensors and actuators in agricultural machinery (Moreno, 2020) can improve, simplify, and automate operations, allowing for differential treatment of each zone (Uribeetxebarria et al., 2018).

Current agriculture demands precise nitrogen fertilization management due to rising costs and environmental restrictions (Cartelat et al., 2005). Precision Agriculture employs advanced technology and machinery (Pina, 2023), leveraging the convergence of physical, digital, and biological realms to achieve extraordinary technological advancements (Moreno, 2020). The common factor is data-driven decision-making and execution (Ibarra, 2022).

PA technologies can be categorized into information technologies and action technologies. Information technologies include all devices that capture data and convert it into georeferenced maps, such as mobile soil sensors (measuring electrical conductivity, organic matter, moisture), vegetation sensors (optically measuring crop vigor), fixed crop sensors (measuring soil moisture, rainfall, temperature), remote sensing (satellite or drone imagery), external databases (weather, irrigation, market data), production sensors on harvesters (quantifying yield per square meter), machinery sensors for operational monitoring, and satellite positioning (Valero, 2020). Action technologies encompass systems that enable differential input application in the field,

including auto-guidance, variable rate technology (VRT) machinery (fertilizers, seeds, water, pesticides), and autonomous agricultural robots (Valero, 2020).

Within-field variability can be spatial, due to fertility, organic matter percentage, texture, or topography; or temporal, due to rainfall, nitrogen fertilization, moisture, crop type and variety, or rotation (Ramos del Viejo, 2017). Crop performance is usually interpreted as a good indicator of within-field variability. Understanding this variability requires knowledge of both physical and chemical soil properties, which can enhance productivity and product quality. However, farmers often perceive this information as expensive and fail to see the short, medium, and long-term benefits (Best et al., 2014). Moreover, this information is only useful if utilized for crop management.

Nitrogen is the nutrient most directly influencing plant production and grain crop protein content (Aranguren, 2021). Excessive fertilizer application is common to ensure potential yield is achieved annually (Aranguren et al., 2019). However, excessive nitrogen fertilization is costly and results in nitrogen losses through volatilization, denitrification (conversion of nitrate to nitrous oxide), contributing to global warming (Aranguren et al., 2019), and nitrate leaching into groundwater, causing eutrophication (Gaju et al., 2016), and negatively impacting the environment (Argento et al., 2021). Conversely, insufficient fertilization results in suboptimal yields and lower product quality (Argento et al., 2021). Studies show that variable rate fertilization can reduce fertilizer use by 20% compared to conventional application and improve harvest efficiency by 30% (Morimoto et al., 2017). Nitrogen content in plants is generally determined through laboratory chemical analyses, though alternatives like sap nitrate testing or chlorophyll measurement as an indirect indicator of plant nitrogen content exist (Gómez, 2016).

PA variable rate technology (VRT) includes two approaches: on/off application with 100% or 0% rates and continuously variable rate application. The latter involves either prescription map-based application or real-time sensor-based application. Prescription map-based application involves several stages: analyzing current or historical data to detect within-field variability and delineate management zones, implementing the map in the field, obtaining an application map that should closely match the prescription map, and generating new production data for future management (Escolà et al., 2018; Valero et al., 2010). Real-time (TR) sensor-based application involves mobile sensors that continuously read soil fertility or, more commonly, crop vigor (Valero, 2010). These readings are used to calculate vegetative indices, which feed into algorithms that determine and implement the appropriate fertilizer rate in real-time (Escolà et al., 2018).

Various proximal optical sensors measure crop nitrogen status, classified into fluorometers, chlorophyll meters (transmittance), and reflectance sensors or radiometers (Padilla, 2016). These sensors measure specific spectral regions (Gómez, 2016), capture crop variability, and translate it into nitrogen requirements, automatically adjusting the fertilizer spreader. Good correlations between yield and plant spectral response have been found, making these sensors widely used (Best et al., 2014).

2. Materials and Methods

The experimental trial was conducted on several rainfed agricultural plots located in the towns of Valsalada and Tardienta, in the province of Huesca, NE Spain. The study area consists of seven irregular plots, covering a total area of approximately 56 ha. The plots are numbered as V1, V2, and V3 for the three plots situated in Valsalada and T1, T2, T3, and T4 for the plots situated in Tardienta. These soils are typical of semi-arid regions with a high presence of limestone. The annual precipitation is below 451 mm, with significant temperature fluctuations, a pronounced water deficit, and irregular rainfall distribution. Due to these climatic characteristics, the area is classified as semi-arid rainfed land in the Ebro Valley. During the cropping season in which the trial was conducted, all plots were sown with winter cereals: durum wheat (*Triticum durum* L.) and barley (*Hordeum vulgare* L.).

For intra-plot characterization, the Topcon CropSpec proximity optical sensor was implemented in a tractor John Deere 6155 R. This active sensor measures crop reflectance using near-infrared (as an indicator of biomass) and red-edge (highly sensitive to nitrogen deficiency stress even at later growth stages), calculating a vegetation index known as S1. The CropSpec system employs a dual-sensor configuration, with an oblique viewing angle (15° relative to the horizontal) and sensors mounted on top of the tractor cab. Installation required a base platform (1.67 m x 0.18 m) mounted transversely on the cab roof, with brackets that secure each sensor, allowing for easy mounting, dismounting, and position adjustment through simple screw adjustments. The sensors were directly connected to the Topcon console through its own Isobus line,

independent of the tractor's Isobus line. The sensors were also linked to the compact GNSS AGM1 receiver (placed on the same platform as the sensors), enabling geolocation of the data obtained (scalable accuracy: Autonomous and Egnos). The X25 Isobus console was connected to both sensors and the Isobus spreader, sending real-time variable rate data. Simultaneously, the tractor operated with its own independent receiver and guidance system. To set the sensor measurement area, specific measurements were taken and entered into the console's configuration system. The sensors covered a width of 3.81 m on each side of the tractor, and the sensor position was crucial to sweep the desired width and avoid the tractor tracks. The measurements were carried out in March, during the late tillering stage of the cereal. The data obtained from the sensor were downloaded from the commercial platform from Top Con into a vector file in shapefile format and geostatistically interpolated using local kriging with the VESPER (Variogram Estimation and Spatial Prediction Plus Error) software to generate a raster image containing the collected information.

To compare the intra-plot variability detected by the CropSpec sensor and correlate it to soil properties, an ECa map was generated using the Veris 3100 sensor (Veris Technologies, Salina, KS, US), a contact (or galvanic) apparent electrical conductivity meter. The sensor reports ECa values from the topsoil layer (0—30 cm) and deeper layers (0—90 cm). These data were used to generate an interpolation grid with 2 x 2 m pixels, where ECa values were estimated using local kriging with the VESPER and QGIS V 3.16.4 software. Additionally, for analyzing satellite images obtained from the PlanetScope constellation, QGIS was employed. Using the raster calculator in this program, the Normalized Difference Vegetation Index (NDVI) for the same date was calculated from the images. The pixel size of the satellite images is 3 x 3 m. To compare NDVI with the data read by the CropSpec sensor, satellite images taken on the same day as the sensor readings were used.

Using the *Point Sampling Tool* in QGIS, data from all measurements were collected into a single layer of random points. To ensure the absence of autocorrelation, distances between points were established to be greater than the stabilization distances of the semivariograms developed during the interpolation process. From these data, a matrix containing all analyzed variables was created. The correlations between the variables were then studied using Spearman's test in SPSS V 26 software.

3. Results and Discussion

Figures 1 and 2 depict the NDVI maps, CropSpec S1 values, and ECa maps for the Valsalada plots (V1, V2, and V3) and the Tardienta plots (T1, T2, T3, and T4), respectively.

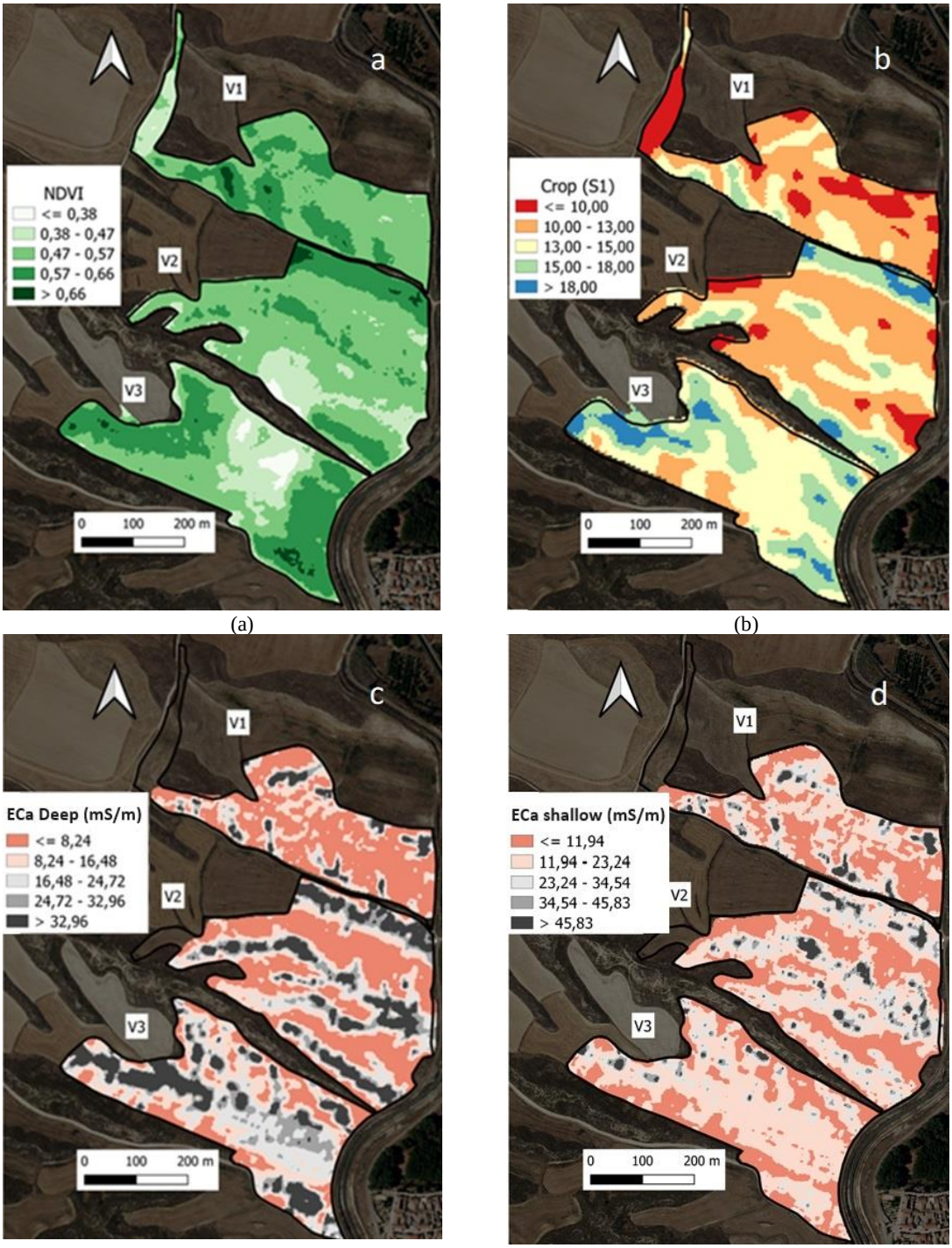

Figure 1. (a) NDVI map; (b) S1 value map read by the CropSpec sensor; (c) ECa map - depth; (d) ECa map – shallow; for the V1, V2 and V3 plots.

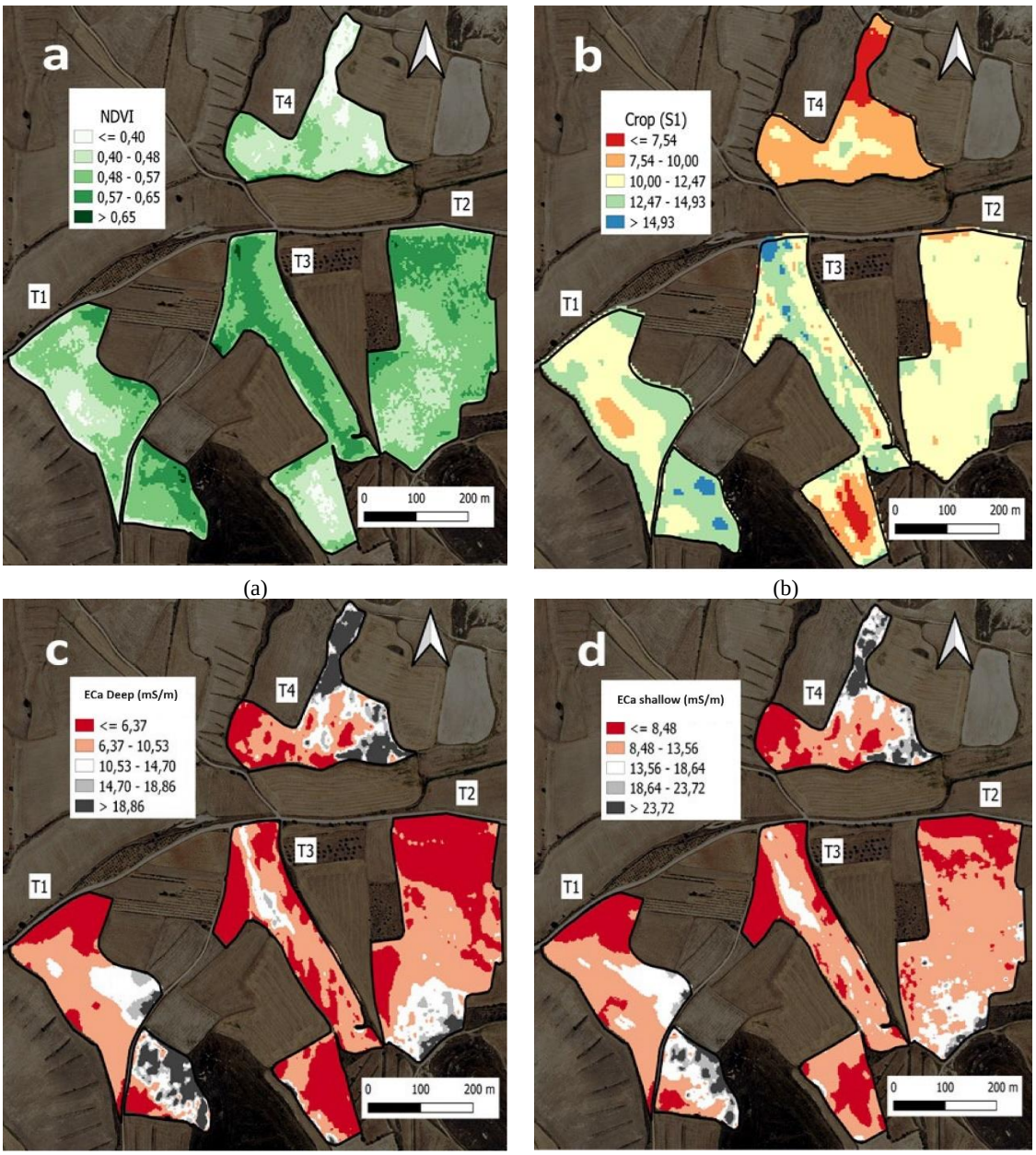

Figure 2. (a) NDVI map; (b) S1 value map read by the CropSpec sensor; (c) ECa map - depth; (d) ECa map – shallow; for the T1, T2, T3 and T4 plots.

The figures show that in both locations, all plots exhibited a strong visual similarity among the three analyzed parameters. Previous studies had already demonstrated a high correlation between NDVI and ECa (Minuesa, 2021). Furthermore, a strong correlation between ECa shallow and ECa depth was detected.
Table 1 summarizes all the correlations obtained across the analyzed plots.

Table 1. Spearman correlation coefficients between NDVI, ECa shallow, ECa depth, and CropSpec S1 measurements (p-valor < 0.0001 for all the correlations).

Parcela	Variables	NDVI	CropSpec	CEa Shallow	CEa Deep
V1	NDVI	1	0.667	0.285	0.408
	CropSpec		1	0.484	0.549
	ECa Shallow			1	0.841
	ECa Deep				1
V2	NDVI	1	0.627	0.530	0.577
	CropSpec		1	0.637	0.719
	ECa Shallow			1	0.843
	ECa Deep				1
V3	NDVI	1	0.687	0.431	0.455
	CropSpec		1	0.454	0.411
	ECa Shallow			1	0.771
	ECa Deep				1
T1	NDVI	1	0.735	0.504	0.485
	CropSpec		1	0.513	0.487
	ECa Shallow			1	0.958
	ECa Deep				1
T2	NDVI	1	0.510	-0.443	-0.551
	CropSpec		1	0.142	0.103
	ECa Shallow			1	0.902
	ECa Deep				1
T3	NDVI	1	0.711	0.359	0.329
	CropSpec		1	0.514	0.466
	ECa Shallow			1	0.880
	ECa Deep				1
T4	NDVI	1	0.644	-0.519	-0.553
	CropSpec		1	-0.524	-0.529
	ECa Shallow			1	0.956
	ECa Deep				1

The correlation analysis revealed a significant relationship between the variability observed in the NDVI and CropSpec mpas. This similarity, though slightly less pronounced, was also evident when comparing the NDVI or CropSpec values with the ECa maps. Notably, there was a high degree of similarity between shallow and depth ECa values, as indicated by the correlations observed across all analyzed plots.

Previous studies by Minuesa et al. (2021) demonstrated that areas with high ECa levels are typically associated with loamy textures, while areas with low ECa levels tend to have clay-loam textures. Moreover, higher levels of macronutrients were observed in high ECa areas compared to low ECa areas. Additionally, areas with high ECa exhibited greater water retention capacity and cation exchange capacity, correlating with higher vigor observed in both NDVI and CropSpec readings.

It is noteworthy that, contrary to the majority of analyzed plots, high ECa values were associated with higher vegetation indices and CropSpec S1 values. However, in plots T2 and T4, negative correlations were observed between NDVI and ECa, suggesting that higher ECa values corresponded to lower vegetation indices and reduced crop vigor. This phenomenon may be attributed to differences in soil texture or the type of crops cultivated in these plots.

4. Conclusions

The CropSpec optical proximity sensors from Topcon have proven to be an effective tool for real-time variable fertilizer application, offering a viable alternative to prescription maps. However, it is important to note that the variability observed between different plots, influenced by factors such as planting date, crop variety, and the inherent heterogeneity of the terrain, requires prior plot readings to properly calibrate fertilization limits and variable application levels. Otherwise, significant discrepancies may arise between the entered parameters and the actual fertilizer application.

Despite these considerations, CropSpec sensors can be highly beneficial by streamlining part of the prescription map generation process, thereby facilitating the rapid implementation of PA, particularly regarding variable fertilization among farmers.

The correlation results with NDVI and soil ECa, both depth and shallow, indicate that the measurements from the CropSpec sensors are well correlated with NDVI, suggesting they can accurately measure crop variability. This positions them as a valid tool for real-time variable fertilization, yielding results similar to fertilization based on prescription maps generated from NDVI.

Acknowledgements

This work is part of the cooperation actions of agents of the agricultural sector of the Rural Development Program for Aragon 2023-2027, co-financed by the Government of Aragon and the European Agricultural Fund for Rural Development (FEADER). GCP-2023000300.

References

Aranguren, M., 2021. Diagnóstico nutricional nitrogenado en trigo mediante sensores y aporte de subproductos orgánicos (Doctoral dissertation, Universidad del País Vasco-Euskal Herriko Unibertsitatea).

Aranguren, M.; Castillón, A.; and Aizourua, A., 2019. Herramientas para ajustar la dosis de fertilizante mineral en cobertera de cereal. Vida rural (468), 40-44.

Argento, F., Anken, T., Abt, F., Vogelsanger, E., Walter, A., and Liebisch, F., 2021. Site-specific nitrogen management in winter wheat supported by low-altitude remote sensing and soil data. *Precision Agriculture*, *22*(2), 364–386. https://doi.org/10.1007/s11119-020-09733-3

Escolà, A., Arnó-Satorra, J., and Martínez-Casanovas, J., 2018. Operación en el campo: gestión en terrenos específicos utilizando tecnologías de aplicación variable. New Ag International, Oct/Nov 2018, 18-22.

Gaju, O., DeSilva, J., Carvalho, P., Hawkesford, M. J., Griffiths, S., Greenland, A., and Foulkes, M. J., 2016. Leaf photosynthesis and associations with grain yield, biomass and nitrogen-use efficiency in landraces, synthetic-derived lines and cultivars in wheat. Field Crops Research, 193, 1-15.

Gómez, L. R., 2016. Evaluación de medidas de nitrógeno en planta para su uso como sistema de recomendación de abonado nitrogenado en el cultivo de coliflor (Doctoral dissertation, Universidad de La Rioja).

Ibarra, G., 2022. Agricultura de Precisión: La integración de las TIC en la producción Agrícola. Computer and Electronic Sciences: Theory and Applications, 3(1), 34-38.

Martínez-Casasnovas, J. A., Arnó-Satorra, and J., Escolà, A., 2022. Sensores de conductividad eléctrica aparente para el análisis de la variabilidad del suelo en Agricultura de Precisión. Tecnología Hortícola Mediterránea. Evolución y futuro: viveros, frutales, hortalizas y ornamentales. Biblioteca de Horticultura, 1077, 765-845.

Minuesa, C., Videgain, M., Arnó, J., García-Ramos, F., Vidal, M., and Martinez-Casasnovas, J., 2021. Dosificación Variable de Insumos con Técnicas de Agricultura de Precisión en Cultivos Extensivos de Secano de la Provincia de Huesca. XI Congreso Ibérico de Agroingeniería, online.

Moreno Párrizas, H. A. (2020). Optical sensors for crop monitoring–From 2D to 3D reconstruction (Doctoral dissertation, Agronomica).

Morimoto, E., Fuji, H., Yoshida, T., Shu, S., Kamijima N., and Hasegawa, Y., 2017. Development of smart 2nd fertilizer application system by using canopy sensor. In 7th Asian-Australasian conference on precision agriculture.

Morimoto, E., 2017. Design of big data acquisition for professional grower based on smart agricultural machinery systems. 7th Asia-australian Conference on Precision Agriculture.

Pina Herce, L. E., 2023. Agricultura de precisión. Optimización del uso de herbicidas mediante visión artificial. Trabajo Final master dissertation. UNED. Available at: http://62.204.194.43/fez/eserv/bibliuned:master-ETSInformatica-ICD-Lepina/Pina_Herce_Luis_Enrique_TFM.pdf

Uribeetxebarria, A., Arnó, J., Escolà, A., and Martínez-Casasnovas, J. A., 2018. Apparent electrical conductivity and multivariate analysis of soil properties to assess soil constraints in orchards affected by

previous parcelling. *Geoderma*, *319*(January), 185–193. https://doi.org/10.1016/j.geoderma.2018.01.008

Valero, C., 2020. La revolución inevitable de las agriculturas de precisión y digital. Tecnología Hortícola, 229.

Valero, C., Navas, L. M., González, F., Gómez, J., Ruiz, G., Barreiro, P., and Garrido Izard, M. (2010). Ahorro y eficiencia energética en la Agricultura de Precisión.

A UAV based model for obtaining high resolution cotton yield maps

Chris Cavalaris, Chris Karamoutis, Sofia Koukou and Evangelia Karakosta

University of Thessaly, Department of Agriculture, Crop Production and Rural Environment,
Fytokou str. Volos 38446 Greece

* Corresponding author. Email: chkaval@uth.gr

Abstract

Unmanned aerial vehicles – UAVs is a novel technology introduced recently in agriculture for remote sensing purposes and field task operations. Their ability to carry small sensors, able to capture high resolution images has made them a unique tool for monitoring several crop attributes including yield. In the case of cotton, yield is associated with the intensity of the fiber when the crop is about to harvest. The presence of fiber can be easily recognized from a simple, high-resolution RGB image captured from a UAV platform. The present study capitalizes on that fact and examines different image resolutions and flight altitudes for choosing the most appropriate for accurate yield prediction. An UAV with a 4K RGB camera was used to monitor the field from alternative altitudes (15m, 30m, 45m and 60m) that provided different ground resolutions. The RGB images were converted to binary fiber, non-fiber rasters using a semi-automatic image classifier tool. Consequently, an index describing the fiber density named Cotton Fiber Index – CFI, was estimated. Ground truth, boll fiber samples were collected afterwards manually from a selected spot in the field. A fractional handpicking procedure was followed with successive harvesting and imaging events over the same spot. The gradual harvesting along with UAV images captured right after, allowed to build an accurate, CFI based model to address the cotton yield. The model was validated by additional samples obtained randomly in the field. Five pilot fields representing variable cultivation conditions were totally monitored that way in central and northern Greece during the 2022-23 period. The overall data was used to establish a universal linear regression model with a high accuracy (R^2 = 0.870, RMSE = 0.501 t ha^{-1}) in yield prediction. The experience gained from the present study was condensed on a protocol with well-defined steps for performing UAV-based, cotton yield surveys for research or commercial purposes.

Keywords: Drones, UAS, remote sensing, smart farming

1. Introduction

Yield maps are an essential asset for quantifying crop performance, farm inputs and cultivation practices efficiency, spatial variability of field productivity and for planning precision farming operations. Cotton is a crop with an advantage that allows a visual assessment of the expected yield prior harvesting by judging of the density of the fiber. Farmers, traders, and other stakeholders usually capitalize on this trait and make farm visits to get some primary yield assessments. Their judgment however is empirical and strongly restricted by their close to the ground field of view. The assessments are usually based on field border observations or on field scouting that still dismiss the “big picture” of a yield map. Today, yield maps can be obtained primarly from special sensors integrated on the cotton harvesting equipment. These sensors however are usually rare, they provide a low spatial resolution, and the information is obtained after harvesting. Another opportunity is the use of remote sensing. Some early attempts made by researchers like Huang et al. (2013) using aircraft platforms provided however poor outcomes.

The introduction of UAV remote sensing into the agricultural sector recently, revealed new perspectives for obtaining cotton yield maps, prior harvesting. Their ability to fly safety at low altitudes allow the capturing of low cost, high-resolution images. Therefore, researchers are making several attempts to predict cotton yield from UAV imagery. Shi et al. (2022) for instance found that the difference between open cotton bolls and other targets in the blue and green bands is larger than that in the red band. They defined an index that normalizes the near-infrared band by the sum of blue, green, and red bands, which exhibited a high performance in highlighting information on open cotton bolls. Huang et al., (2016) utilized Laplacian image processing for segmenting cotton bolls from the background of digital images obtained just prior to harvest and defined an index called Cotton Unit Coverage (CUC), addressing the number of cotton boll pixels in a plot to the total number of pixels in the plot area. The index showed a good correlation with yield but the authors stress out that it is too difficult to directly segment cotton bolls in an RGB image using a global threshold value due to the light variation. To overcome this burden, Feng et al (2020), defined a similar index

called Cotton Fiber Index (CFI) that focused on cotton fiber instead of cotton bolls because cotton fiber was more easily discriminated from the soil and leaves background. They utilized also Laplacian filtering for increasing the contrast and sharpness of the original images and discriminated the fiber with a normalization process. They found that plant height during the flowering stage and CFI close to harvest had the best performance in yield prediction. Ma et al. (2022) combined vegetation indices from visible bands with textural features based on Gray-Scale Co-occurrence matrix obtained from a UAV with an RGB camera flying at an altitude of 10 m that allowed ultra-high-resolution images. They found out that the combination of these features were highly correlated with the cotton yield. They also found that the non-linear regression models presented a higher accuracy. Xu et al. (2020) used fully convolutional networks to recognize the opening cotton bolls in high resolution RGB images obtained from a UAV and implemented a back propagation neural networks model to predict the single boll weight. The same author, on a later work (Xu et al., 2021) used a U-Net semantic segmentation network to extract the boll opening pixels and associate an index called Boll Opening Pixel percentage (BOP) with cotton yield. Rodriguez-Sanchez et al., (2022) used also machine learning and trained a Support Vector Machine (SVM) classifier with four selected features to recognize the cotton pixels achieving an accuracy of 89%.

Undoubtfully, the current efforts provide promising results that pave the way for further investigations in order to establish a simplified procedure that can be broadly implemented and produce accurate estimations of cotton yield. The present study expands the positive findings of our preliminary work (Cavalaris et al., 2023) by incorporating additional data from extra fields to capture alternative cotton growing conditions. It aims to introduce an alternative and transparent method with a clear monitoring and processing protocol for obtaining accurate, high resolution and low-cost cotton yield maps with the help of a small UAV equipped with a simple RGB sensor.

2. Materials and Methods

2.1. Field survey

University of Thessaly established five cotton field trials in central (Magnesia, Trikala) and northern (Rodopi) Greece, in 2022 and 2023. The main objective of the trials was to compare conservation agriculture (CA) and traditional agriculture (TA) practices in cotton production. For that scope, each field was split into two plots, one conservational and one traditional. The fields were either irrigated or dryland, contained different cotton varieties planted at different densities and treated with a defoliant or not, according to the pre-harvest conditions. Therefore, they represent a wide variety of crop conditions that resulted in a high variance of cotton yields among the fields and between the treatments, as depicted in Table 1.

Table 1. Experimental field characteristics. The ranges indicate the average values for CA and TA plots.

Field code	Year	Region	Watering	Variety	Area CA+TA (ha)	Final population (1000pl. ha^{-1})	Open bolls m^{-2}	Yield (t ha^{-1})	Defoliant
F1	2022	Magnesia	Irrigated	Elsa	1.8+3.8	155-190	50.8-78.6	2.67-3.07	Yes
F2	2022	Trikala	Irrigated	Elsa	1.4+1.7	265-279	76.5-91.2	4.49-4.52	Yes
F3	2022	Rodopi	Dryland	Olivia	0.6+0.7	123-128	38.4-42.6	1.22-1.31	No
F4	2023	Rodopi	Dryland	Olivia	0.6+0.7	90-96	27.8-30.5	0.76-0.78	No
F5	2023	Rodopi	Irrigated	Olivia	1.1+1	169-173	57.4-84.6	3.10-3.85	No

A field survey was conducted on each field, one day prior the mechanical harvesting. A small orthogonal spot comprising of four adjacent rows, 4m each (4 x 0.95m x 4m = 15.20m^2) was selected randomly for building the yield prediction model. The border plants outside the “model spot” were removed to provide a clear region of interest and the four corners of the region were marked with Ground Control Points (GCPs) to help align exactly all the successive images. The area was photographed with a DJI Phantom 4 Pro UAV using its on board 4K RGB camera set at a 20MP resolution and a nadir position. Successive images were captured from four heights, 15m, 30m, 45m and 60m providing respective ground resolutions of 0.40, 0.80, 1.10 and 1.50cm. After the first set of images, a cluster of randomly selected open bolls from each of the four rows were picked up manually and the fiber seed was separated and weighted on a portable balance. One third of these bolls were selected from the top part of the plants, one third from the middle part and one third

from the lower part. Consequently, a second set of vertical UAV images were obtained from the same heights and the procedure continued until all the open bolls were harvested. Three to six sets of images were totally obtained from each "model spot" until all the plants were stripped (Figure 1a). The successive weights of fiber seed were utilized to estimate the "yield fractions" that is the yield remaining in the "model spot" after each consequent handpicking.

After accomplishing the "model spot" surveys, the whole fields were also monitored successively from the same four heights (15, 30, 45 and 60m). Prior this, GCPs were placed on the edges of each field as well as at particular number of "validation spots" (8-18) within the fields (Figure 4). The "validation spots" had double GCPs at both sides of two adjacent rows marking a clear distance of 2m on each. These spots were used later for model validation. The field survey was performed using the Pix4D Capture mobile app to schedule the flight missions for the DJI Phantom 4 Pro over the area. Nadir position images were captured with an 80% frontal and side overlap. The images were later processed with the Pix4D Mapper software (https:// pix4d.com) using its Ag RGB template to obtain four RGB orthomosaics from each field, for the four different heights. After completing the UAV surveys, the open boll fiber from the "validation spots" were harvested manually and weighted. The following day, the whole plots (CA and TA) were harvested mechanically and their weight was also registered.

2.2. Image processing

The RGB field orthomosaics as well as all the sets of single images obtained over the "model spots" were imported into the QGIS 3.36 open-source suite (QGIS Association. http://www.qgis.org) and georeferenced using the corresponding GCPs. An orthogonal vector polygon of the same dimensions with the "model spot" (3.8 by 4m) was designed to surround the plants inside the spot.

The RGB images obtained from the "model spot" were grouped into four sets of the same pixel resolution (0.40, 0.80, 1.10 and 1.50cm). The images were classified into two major classes (fiber and non-fiber) using the open source QGIS Semi-Automatic Classification plugin (SCP v.7.10.5), (Congedo, 2021). A training input file was created for each set of images. The training file consisted of five macro-classes (cotton, bright vegetation, shadowed vegetation, bright soil, shadowed soil) while each macro-class was obtained from 5-15 manually drawn regions of interest (ROIs). An empirical, stepwise process was followed using the classification preview option of the tool to test the performance and new ROIs were added or removed accordingly, until a satisfactory result was obtained. A separate final "training input" file was created for each field and each set of images on which the fiber pixels were assigned a value of "1" while all the non-fiber pixels were assigned to "0". The outcome of this process were binary rasters of the same dimensions with "1" representing fiber and "0" no fiber (Figure 1b). Consequently, the average value of each binary raster at a particular area was calculated. This area was either the whole "model spot" or its four separate, 4x0.95 m rows when they were clear distinct. The average value of the same resolution binary rasters was actually, the Cotton Fiber Index (CFI) defined by Feng et al (2020).

$$CFI = \frac{number\ of\ pixels\ classified\ as\ cotton\ fiber}{total\ number\ of\ pixels\ in\ the\ area} \quad (1)$$

3. Results and Discussion

3.1. Model calibration.

Figure 1 shows two sets of successive images obtained from a height of 60m above ground with a ground resolution of 1.5 cm. The images are cropped to the ROI defined by the "model spot" vector (3.8 x 4m). The first set (a) comprises of 4K, 20MP RGB images and the second set (b), of corresponding, binary classified fiber – non fiber images. Each successive image was obtained after handpicking a fraction of open bolls. A CFI was estimated for each classified image.

The CFI values obtained from each set of same resolution images were plotted against the corresponding "yield fractions" of the successive harvests. As shown in Table 2, the coefficient of determination between CFI and yield were very high ($R^2 > 0.930$ for single fields and $R^2 > 0.907$ for all the fields) for all the ground resolutions.

Since the lower resolution 1.50 cm images (obtained from a 60 m flight altitude) were considered sufficient accurate in providing a fiber – non fiber segmentation (Table 2) that is well associated with yield, we decided to continue our further analysis only with the above dataset. The opportunity to fly a UAV at a higher altitude during a field survey allows greater speeds and eliminate the density of the successive passages, providing though the chance to survey a bigger area during a single mission.

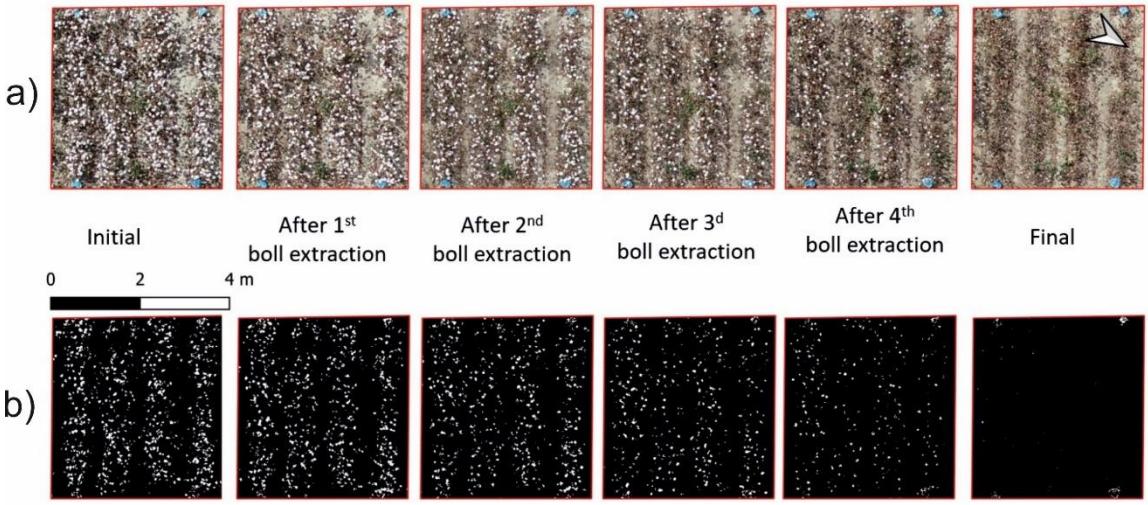

Figure 1. Model calibration at the "model spot" (4x3.8 m) area at field F1 with successive handpicking and photographing events. (a) 4K RGB images captured vertically from a height of 60m. (b) the corresponding classified images (white colour depict cotton fiber, black colour everything else).

Table 2. Coefficients of determination (R^2) for cotton yield and CFI obtained from RGB images captured from alternative heights on the "model spots" of five alternative fields.

Mission height	Pixel resolutiion	R^2, (CFI - Yield)					
		F1	F2	F3	F4	F5	All
60 m	1.50 cm	0.973	0.974	0.982	0.957	0.970	0.929
45 m	1.10 cm	0.975	0.990	0.989	0.989	0.978	0.927
30 m	0.80 cm	0.983	0.974	0.989	0.934	0.972	0.907
15 m	0.40 cm	0.962	0.968	0.947	0.928	0.966	0.928

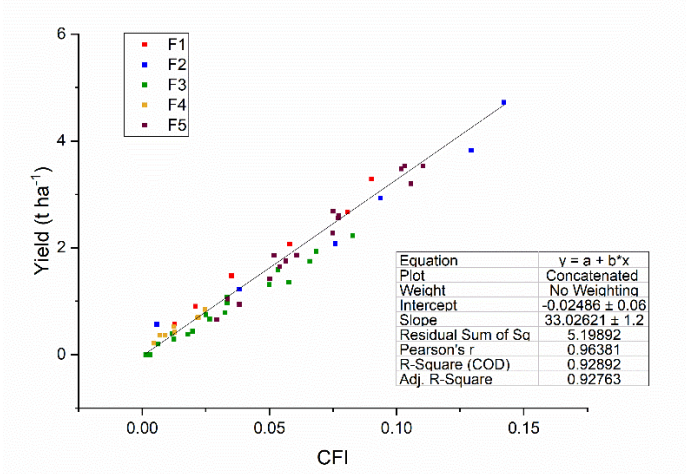

Figure 2. Correlations of CFI with cotton yield for RGB images captured on the "model spots" from an 60m height providing a ground resolution of 1.5cm (F1-F5 = pilot field code).

Figure 2 shows the linear regression of yield and CFI obtained from the 1.5 cm resolution (60m altitude)) RGB images captured at the "model spots" of the different fields. A universal equation using a linear fitting model is derived as follows (equation 2)

$$Y = 33.03 \cdot CFI - 0.02 \quad (2)$$

were Y = cotton yield (t ha^{-1}) and CFI = the Cotton Fiber Index (dimensionless). The accuracy of the prediction model is high with a coefficient of determination $R^2 = 0.929$.

3.2. Model validation.

Having decided to utilize the 60m flight dataset, the corresponding 1.50 cm resolution orthomosaics obtained from the whole field surveys were initially georeferenced in QGIS and accordingly converted to a binary "fiber – non fiber" classified raster using the associated SCP QGIS training input file. The GCPs placed on the "validation spots" (Figure 5c) were utilized to draw vector polygons of 2 x 1.90 m encapsuling the two adjacent cotton rows. Accordingly, CFI was calculated for the "validation spots" and the universal equation 2 was used to estimate the cotton yield from the corresponding CFI values. The results were plotted against the handpicked obtained yield (Figure 3a). The validation reveal a high performance of the model. The R^2 was 0.87, the RMSE 0.501 t/ha and the correlation line was close to the intersection 1:1 line. It is a sufficient result with fewer parameters compared to Feng et al (2020) who suggested the combination of CFI with plant height traits to predict cotton yield with an $R^2 = 0.90$. The Cotton Unit Coverage (CUC) defined by Huang et al., (2016) had an $R^2 = 0.83$ for predicting yield from segmented cotton bolls.

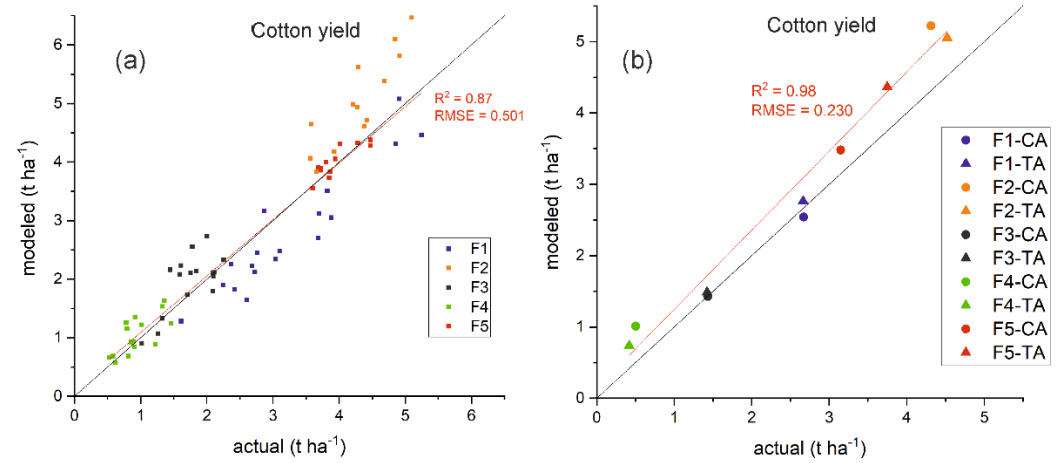

Figure 3. Validation of the remote sensing prediction model against actual yield data obtained from ground truth handpicked samples (a) and from cotton picker average plot yield (b). (F1-F5 = pilot field code, CA = Conservation Agriculture plot, TA= Traditional Agriculture plot)

3.3. Yield maps

A 0.95x0.95m vector grid was laid over the binary, fiber – non fiber whole field rasters defining small rectangular polygons. The 0.95x0.95m size was selected to guarantee that each grid cell contains one cotton row regardless its orientation. A CFI was estimated for each polygon. Figure 4 presents a close view of the process over a small area of field F1. Figures 5a and 5b present the RGB orthomosaic and the resulting CFI map for the whole F1 field. Since the model validation revealed a high accuracy in yield prediction, the yield map in Figure 5c may be considered an accurate estimate of the actual yield and its variation in the field. Furthermore, Figure 3b depicts a plotting of the cotton picker estimated yield against the model yield. As mentioned on the beginning, the pilot fields were established to compare conservation agriculture (CA) and traditional agricultural (TA) practices. Each plot was harvested separately. The coefficient of determination is high ($R^2 = 0.98$) but the fit line lies above the intersection line. This is reasonable as the mechanical harvesting induce yield losses which are overcounted with the remote sensing approach. Therefore, the suggested approach is proved more accurate for comparing field trial plots.

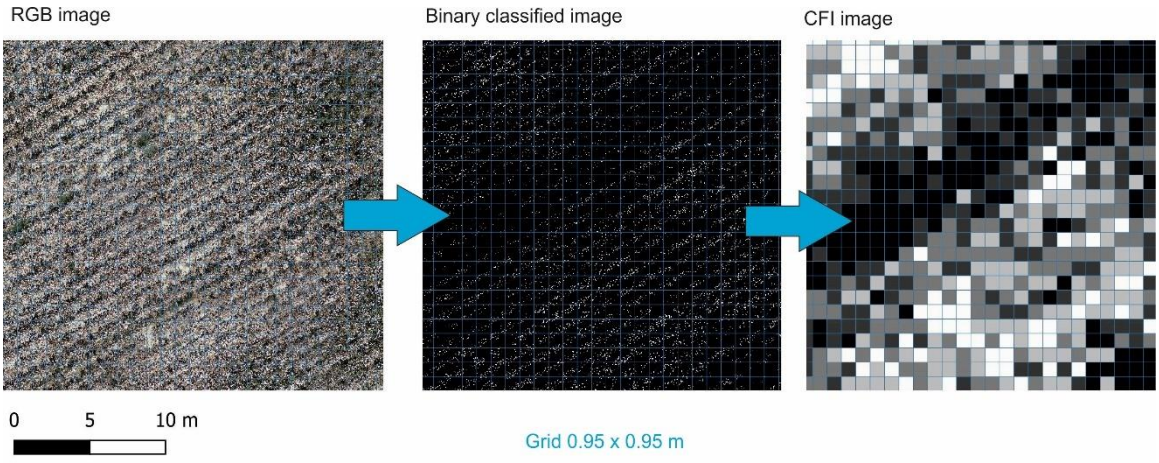

Figure 4. Conversion of an RGB part of an orthomosaic (left) to a binary classified image (center) with white pixels representing cotton fiber and black pixels non-fiber material. The right image shows a Cotton Fiber Index (CFI) image part at a resolution of 0.95x0.95m.

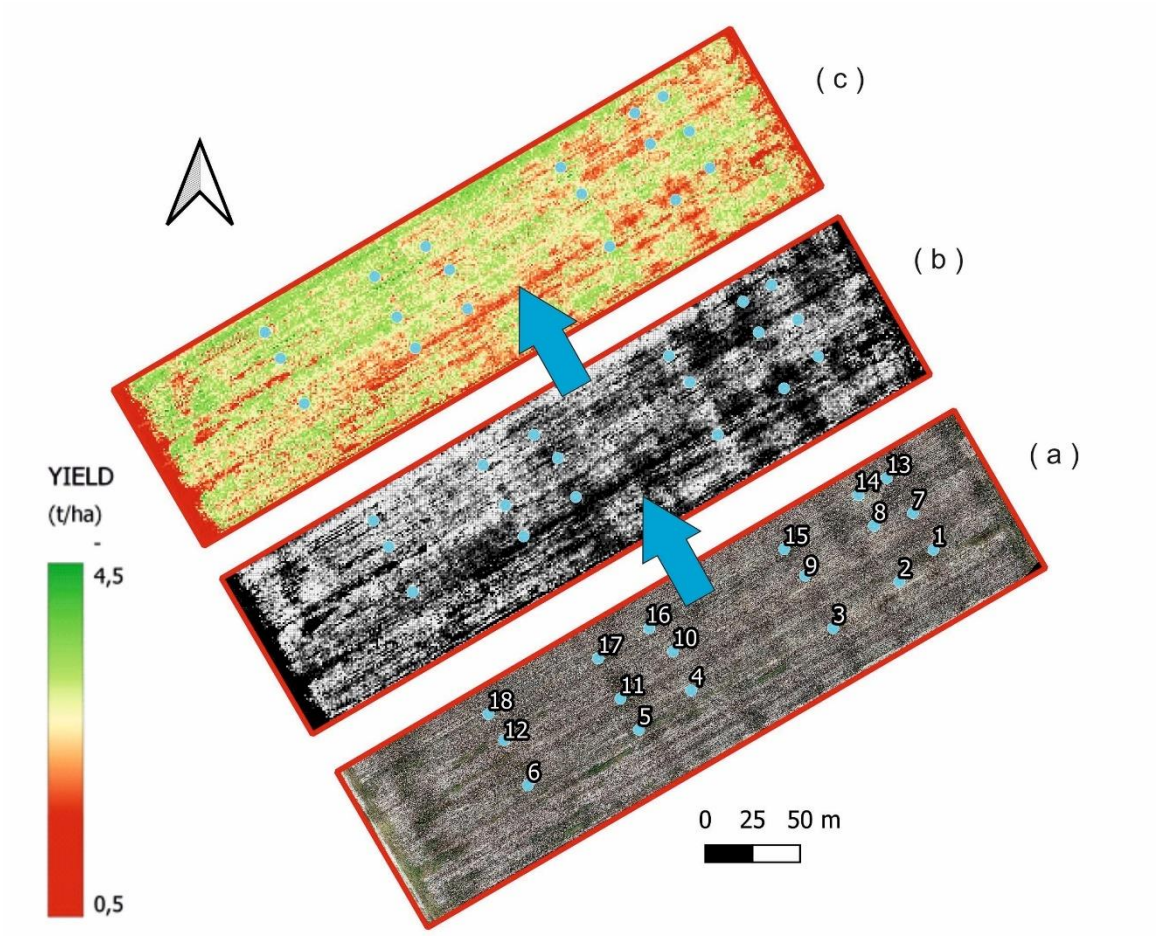

Figure 5. Pilot field F1 overview. Estimation of yield map (c) from a model based on a CFI map (b) that was obtained from an RGB image with a 1.50 cm ground resolution (a) after a fiber / non-fiber classification. Numbered points indicate spots of ground truth measurements for model validation.

3.4. Yield mapping protocol

Based on the experience gathered through the present study, a cotton yield mapping protocol with simplified steps is established in Figure 6. Two levels of field surveillance are defined:

- The grey and the blue frames summarize the whole procedure followed in the current study.
- The blue frames by their own, provide a brief standalone guideline that capitalize on the present findings, for creating valuable cotton yield maps.

The novel, fractional harvesting – successive imaging approach suggested here. allow the artificial creation of high variable yield potentials, at the same field, that help build a safe and site-specific accurate yield prediction model. This is quite useful because researchers often have to establish their own, time and resources consuming field trials to introduce a natural yield variation in the alternative plots or search for other available such trials.

The main weakness of the present approach is the subjective nature of the semi-automatic classification followed to segment the fiber from the background. It was true that in some of the examined fields (eg F4 and F5) it was quite difficult and required a lot of effort until a satisfactory segmentation result was achieved. A potential case of an investigator failing to address effectively all the visible fiber on the images may probably lead to an underestimation of the actual yield. More robust, and independent methods should be implemented on this step, and this is a potential objective of some future research that will compare the alternative methods proposed by other authors (eg. Xu et al., 2021, Shi et al., 2022, Rodriguez-Sanchez et al., 2022 etc) along with the testing of some polar filters on the RGB cameras during the field surveys in order to augment the presence of the fiber on the images.

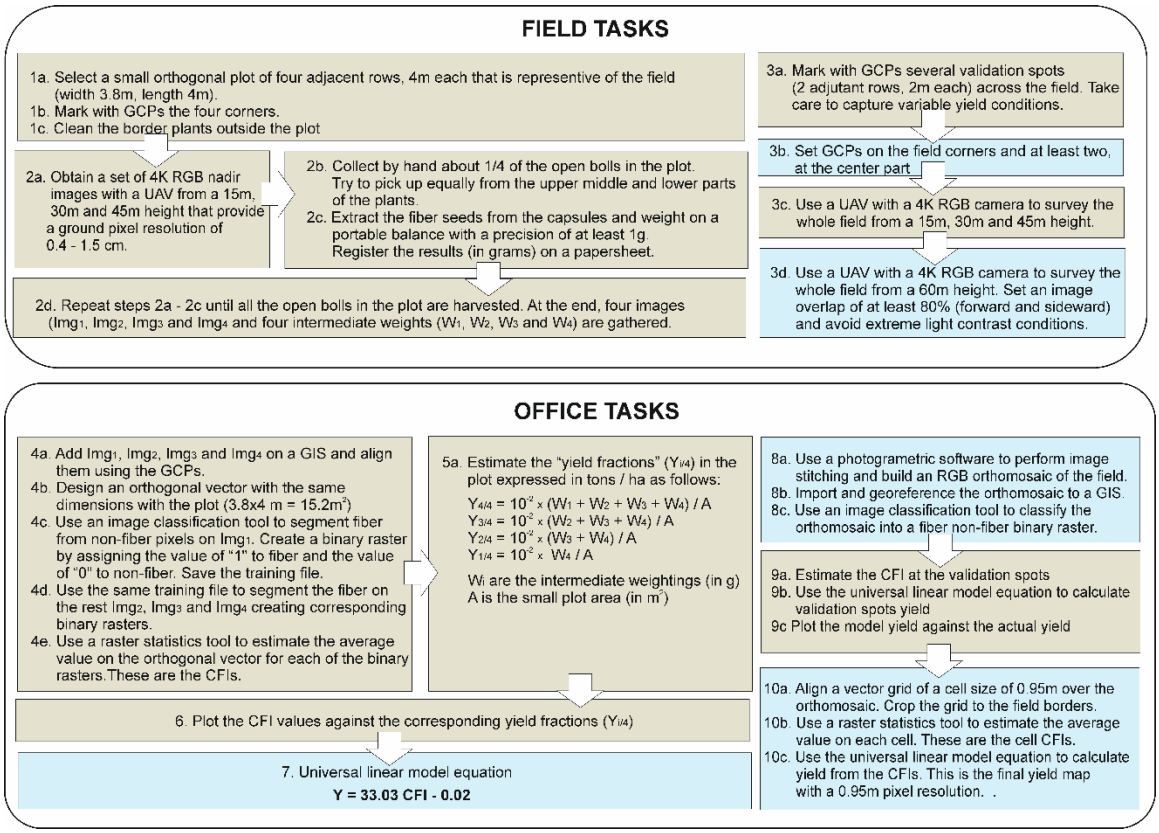

Figure 6. Yield mapping protocol.

1. Conclusions

- Efficient, low-cost cotton yield mapping is feasible thanks to the opportunity of using small and cheap UAVs carrying a simple RGB camera to survey large areas.
- The cotton yield maps are of high resolution containing much more detail compared to maps obtained from cotton picker onboard sensors.
- A universal, linear regression model was estimated that fits well to variable crop conditions (variety, plant density, plant vigour etc).
- The validation of the model provided a high (R^2 = 0.870, RMSE = 0.501 t/ha) prediction accuracy.
- A novel method with a clear monitoring and processing protocol is introduced on the present study for obtaining high accuracy cotton yield maps little before the mechanical harvesting.
- The suggested, UAV based cotton yield mapping approach may be used effectively to build cotton yield maps as also to make yield comparison on cotton field trials.

Acknowledgements

The scientific team would like to acknowledge BASF Hellas for providing the opportunity to establish regenerative cotton trials in Greece that were utilized also for the current study..

References

Cavalaris C., Chris Karamoutis, Vasilis Giouvanis and Sofia Koukou (2023). A novel UAV based method for mapping cotton yield. Proceedings of the 13th National Conference of Agricultural Mechanization, Athens 2023, http://www.egme.gr

Congedo, L. (2021). Semi-Automatic Classification Plugin: A Python tool for the download and processing of remote sensing images in QGIS. J. Open Source Softw. 2021, 6, 3172, doi:10.21105/joss.03172.

Feng, A., Sudduth, K., Vories, E., & Zhou, J. 2019. Evaluation of cotton stand count using UAV-based hyperspectral imagery. In Paper presented at the 2019 ASABE annual international meeting. Boston, Massachusetts, ASABE Paper No. 1900807 doi:10.13031/aim.201900807

Feng, A.; Zhou, J.; Vories, E.D.; Sudduth, K.A.; Zhang, M. 2020. Yield estimation in cotton using UAV-based multi-sensor imagery. Biosyst. Eng. 2020, 193, 101–114, doi:10.1016/j.biosystemseng.2020.02.014.

Huang, Y.B.; Sui, R.X.; Thomson, S.J.; Fisher, D.K. 2013. Estimation of cotton yield with varied irrigation and nitrogen treatments using aerial multispectral imagery. Int. J. Agric. Biol. Eng. 2013, 6, 37–41, doi:10.3965/j.ijabe.20130602.00?

Huang, Y.; Brand, H.J.; Sui, R.; Thomson, S.J.; Furukawa, T.; Ebelhar, M.W. 2016. Cotton yield estimation using very high-resolution digital images acquired with a low-cost small unmanned aerial vehicle. Trans. ASABE 2016, 59, 1563–1574, doi:10.13031/trans.59.11831.

Ma Y, Ma L, Zhang Q, Huang C, Yi X, Chen X, Hou T, Lv X, Zhang Z. 2022. Cotton Yield Estimation Based on Vegetation Indices and Texture Features Derived From RGB Image. Front Plant Sci. 15;13:925986. doi: 10.3389/fpls.2022.925986.

Rodriguez-Sanchez J, Li C, Paterson AH. Cotton Yield Estimation From Aerial Imagery Using Machine Learning Approaches. Front Plant Sci. 2022 Apr 26;13:870181. doi: 10.3389/fpls.2022.870181.

Shi, Guanwei, Xin Du, Mingwei Du, Qiangzi Li, Xiaoli Tian, Yiting Ren, Yuan Zhang, and Hongyan Wang. 2022. "Cotton Yield Estimation Using the Remotely Sensed Cotton Boll Index from UAV Images" Drones 6, no. 9: 254. https://doi.org/10.3390/drones6090254

Xu, W.; Yang, W.; Chen, S.; Wu, C.; Chen, P.; Lan, Y. 2020. Establishing a model to predict the single boll weight of cotton in northern Xinjiang by using high resolution UAV remote sensing data. Comput. Electron. Agric. 2020, 179, 105762, doi:10.1016/j.compag.2020.105762.

Xu, W.; Chen, P.; Zhan, Y.; Chen, S.; Zhang, L. 2021. Cotton yield estimation model based on machine learning using time series UAV remote sensing data. Int. J. Appl. Earth Obs. Geoinf. 2021, 104. doi:10.1016/j.jag.2021.102511

AI-based in-field weeding quality assessment as a potential test standard

Oliver Schmittmann *, **Patrick Zimmer**

Institute of Agricultural Engineering University of Bonn, Nussallee 5, 53115 Bonn, Germany

* Corresponding author. Email: o.schmittmann@uni-bonn.de

Abstract

Suitable test standards for plant protection technologies exist but are not adapted to modern sensor-based or autonomous systems. Evaluations of the working success are lacking, partly due to the time-consuming data collection and low comparability.

This gap was addressed in WeedAI and objective potential test methods were proposed. To test the guidance accuracy sugar beet – as an example – should be sown by use of generated AB-sinus-lines. Each weeding treatment is tracked by RTK. All waypoints can be compared and used for analyses of row-following precision.

Hit-rate is proposed to determine the percentage of covered weeds by herbicides and the ratio of spot and plant size can be used to estimate potential herbicide savings.

A prediction model for plant species was developed by use of instance-based segmentation and a mask2former framework. Drone observations provide the field images. The benefits of automated plant recognition were presented based on a field trial. Its estimation accuracy for recognizing sugar beet is about 98%, and 90% for recognizing weeds.

The model is currently being further developed at the Institute of Agricultural Engineering for a far-reaching agronomic interpretation. Tests on guidance accuracy and hit accuracy are currently underway.

All in all, the methods presented will be able to close the gap in machine testing.

Keywords: AI weed detection, spot-sprayer, sensor hoes, drone observation

1. Introduction

Technological advances are having a huge impact on modern agriculture. For example, sensor-based weed detection can help to reduce the use of herbicides and thereby environmental impact [BmELF, 2013] as well as costs to the farmers. While such systems (figure 1) are being extensively researched and are becoming commercially available, they typically directly aim at the production level. However, there also is a demand for weed identification in agricultural trials, which typically require labor-intensive screening, which is inefficient as it typically implies manual plant counting or weed coverage estimation.

- Lack of standardized methods to test systems like sensor hoes, spot sprayers, robots, …
- Hard to interpret their effectiveness; lack of objectiveness

So far, the test standard in place asks for (1) technology classification; (2) objective general description; (3) special features/characteristics; (4) general assessment; (5) tests and evaluation of function, operation, interface, among others; (6) field tests; (7) individual laboratory and field tests; (8) summary; as well as (9) commentary from the manufacturer.

The aim is to extend this test norm by standardized tests regarding:

- The accuracy of row guidance control or hit-rate of tools or nozzles as a technology assessment
- Vegetation mapping (crops and weeds) before and after treatment events for assessment of effect
- Detection, identification, counting, and measuring size and properties of crops and weeds
- Calculation and evaluation of agronomically relevant metrics, including environmental performance

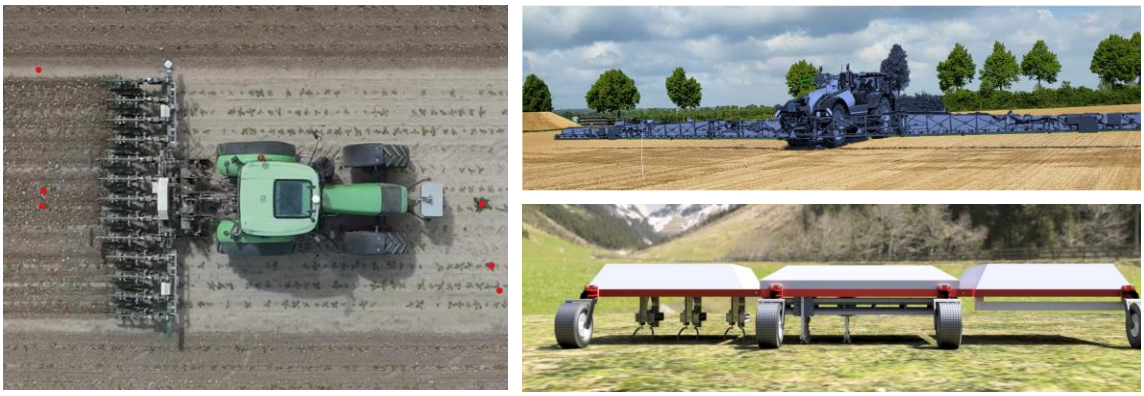

Figure 1. Modern weeding technology: Sensor hoe (Garford), spot-sprayer (Prototype) and weeding robot (Dynamobot)

In this paper, the proposed methods and workflows are described in general. For drone observation and plant recognition results are shown and discussed as an example for our testing method.

2. Materials and Methods

2.1. Test the guidance accuracy: Row following – detection and stearing

Guidance accuracy is important for mechanical weeding. Precise guidance increases the affected area by tools and hereby the weeding success. As a standard, a 100 m test lane is proposed. One-third straight, one with two moderate lateral deflections right and left, and the last with two longer deflections. This so-called AB-sinus line is generated between two given coordinates by an own software application.

The lane will be sown out by use of an RTK-guidance system. On top of the precise seeder, an additional Leica GS 18 T GNSS-RTK-Rover (20 Hz sampling rate) is mounted to track the seeding path.

For each machine test, the same RTK-tracking system is mounted on an equivalent position to track the lane.

All logged tracks will be compared and analyzed for further use.

2.2. Test of hit-rate

The hit-rate determination targets the quality of weed coverage by herbicides. By using colored water, two results are of interest:

- Percentage how often a weed is covered by an herbicide
- Ratio between spot size and weed size to estimate herbicide savings

All those parameters are measured by use of a drone and the ILT-WeedAI prediction.

2.3. Automated plant scouting

For this study, we captured a diverse set of RGB drone image data from sugar beet fields over the course of two consecutive years, with special emphasis on weed treatment assessment. In 2022, we recorded data from 11 different fields, each at multiple dates to cover weeding events as well as various relevant growth stages and environmental conditions. Further, those fields were distributed over a larger area within the Rhineland and Niederrhein regions in western Germany to increase diversity in soil types and weed species. In 2023, we collected data from a specifically designed trial field (see. Section …), in a similar timely manner to cover both before and after weeding scenarios. The diverse dataset from the first year was used to train the WeedAI- models, while the analysis in this study is run on unseen data from the second year. The evaluation of the models is carried out by use of the orthomosaics with the predictions on screen by persons.

2.3.1. Sensor

All data were captured using a DJI Matrice 300 RTK drone and a 45 Megapixel DJI Zenmuse P1 camera, equipped with either a 35 mm lens in 2022 or 50 mm in 2023, resulting in ground sampling distances (GSD) of 1.5 mm/px or 1.1 mm/px, respectively. For our AI model, we downsampled the higher resolution test data to match the settings of those used for training.

2.3.2. Data Processing

Agisoft Metashape [Agisoft, 2022] was used with default settings to obtain 3D representations and georeferenced orthomosaics of the fields. Further, we selected a diverse set of 124 crops from the original images sized 1024x1024 px for model development. All plants were hand-labeled individually in a pixel-perfect manner to enable high-precision instance segmentation tasks. We use 95 of those images to finetune a Mask2Former model [Bowen, 2022] with Swin-large backbone which was verified on the remaining 29 images. For inference on the 2023 trial data, we use overlapping tiles of the same size as the training images. Leveraging information contained in the Metashape model, we project the center points of detected masks onto the orthomosaic to obtain their georeferenced locations. Using distance-based clustering, we are able to filter out redundant detections resulting from large overlaps in either the individual drone images or the tiling step at inference time. In the same step, we further use this redundancy to identify falsely occurring detections and classifications, thereby maximizing the precision of our predictions.

Visualization, processing, and archiving of each dataset are managed by the use of QGIS [QGIS, 2024; Schmittmann, 2024].

2.4. Agronomical Evaluation

Weed mapping can be used to assess both the efficiency of plant protection measures and their harmful effects. In the first step, it is the percentage of weed coverage [Wilbos, 2004], in the second the population densities and harmful effects of certain weed species that lead to an agronomic assessment. Environmental performance can also be taken into account.

2.5. Test design

The field trials with 3 repetitions were arranged on the experimental farm Campus Klein-Altendorf next to Bonn. This is a high-yielding site with loess soil. Each plot size was about 2000 m². Sugar beets are cultivated by use of good business practice with row distances of 50 cm and 20 cm spacing. Tree herbicide applications were done as usual.

The technology was a precise seeder by Kleine synchro-drive (12 rows) [Ziegler, 2012], a sensor-guides hoe by Garford InRow (12 rows), and a spot-sprayer prototype (33 m boom width).

3. Results and Discussion

By use of a drone and the ILT-WeedAI prediction plants on the test site could be detected, located, and allocated into weeds and crops (figure 2). Also, the stem position is detected with high precision. The quality of differentiating between sugar beet was over 98 % and for weeds about 90 %.

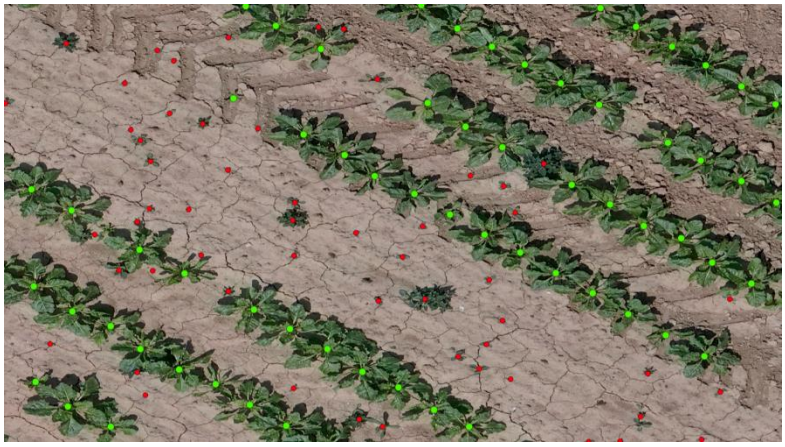

Figure 1. Excerpt of an orthomosaic of the field trial. Centre point of sugar beets marked with green, crops with red dots.

As shown in figure 3, the relevant plots with the predictions can be selected individually. Maps can be created.

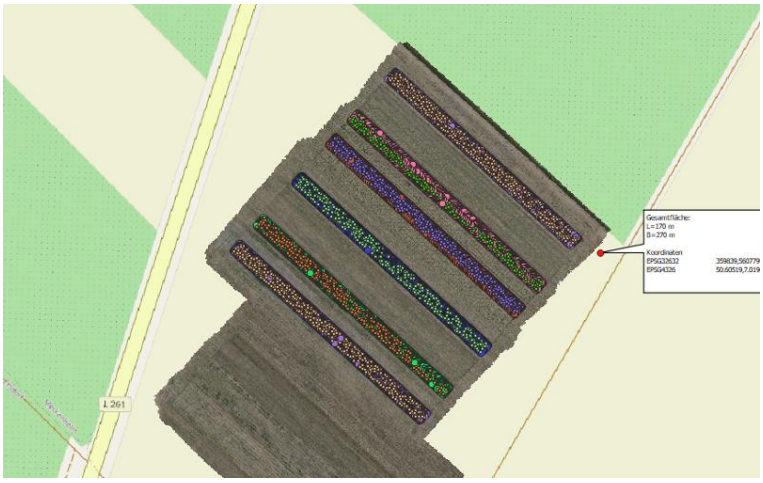

Figure 3. Selection of relevant plots for further use.

The output of all data are files in CSV-format for use in Excel or other applications to calculate the efficiency of the weeding treatment and the corresponding values. Agronomical interpretation including threshold of damage and ecological effects can be derived.

Plant data can be assigned to different treatments and used to evaluate different technologies or setups. (figure 4). The variants can be compared and assessed in terms of their plant density, taking into account the aforementioned estimation accuracy.

The degree of coverage of weeds as a further evaluation factor and the individual plant size are also determined. Based on this result data and its statistical evaluation, differences in technologies and spraying strategies can be determined in a scientifically correct manner. A comparison of different technologies such as hoes, sprayers, spot sprayers, hoeing automates or robots can also be carried out using meaningful parameters.

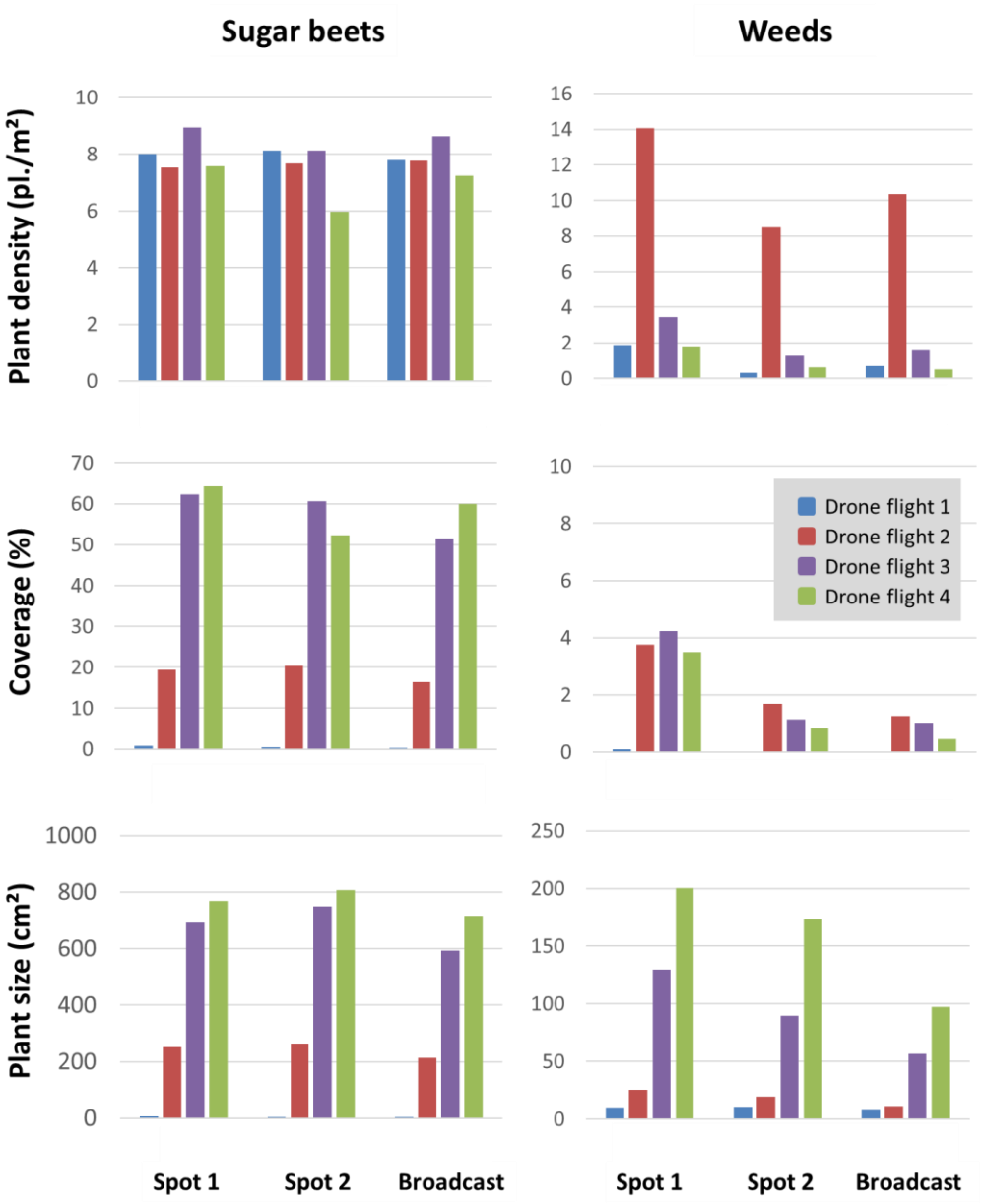

Figure 4. Plant number, size, and plant coverage of two spot-sprayer settings and a broadcast sprayer before and after three applications resp. four growing stages.

4. Conclusions

Suitable test standards for plant protection technologies exist but are not adapted to modern sensor-based or autonomous systems. Evaluations of the working success are lacking, partly due to the time-consuming data collection and low comparability.

This gap was addressed in WeedAI and objective potential test methods were proposed. The use and benefits of automated plant recognition were presented based on a field trial. Its estimation accuracy for recognizing sugar beet is about 98%, and 90% for recognizing weeds.

The model is currently being further developed at the Institute of Agricultural Engineering for a far-reaching agronomic interpretation. Tests on guidance accuracy and hit accuracy are currently underway.

All in all, the methods presented will be able to close the gap in machine testing.

Acknowledgements

Manny thanks to Chris McCool, head of our *Agrobotics* group, and colleges for scientific exchange about plant detection with instance-based segmentation. Also, manny thanks for the support to the team of our experimental farm Campus Klein-Altendorf which are indispensable for successful field trials.

References

Agisoft Metashape, (2022). Version 1.8.5, Agisoft LLC, St. Petersburg, Russia.

BmELF, (2013). Nationaler Aktionsplan zur nachhaltigen Anwendung von Pflanzenschutzmitteln

Bowen, C., Misra, I., Schwing, A. G., Kirillov, A., Girdhar,.R. (2022). Masked-attention Mask Transformer for Universal Image Segmentation. IEEE/CVF Conference on Computer Vision and Pattern Recognition (CVPR) (2021): 1280-1289.

Halstead, M., Ahmadi, A., Smitt, C., Schmittmann, O., McCool, C. (2021). Crop Agnostic Monitoring Driven by Deep Learning, Frontiers in Plant Science

QGIS, (2024) free open-source geographic information system, QGIS Development Team 3.36.3

Schmittmann, O., Zimmer, P., McCool, C. (2024). Development of a method for testing weeding-technologies in field – quality determination of spot-sprayer. Book of Abstracts, 79th IIRB Congress in Brussels, 27th-28th February 2024

Wilbois, K.-P.; Schwab, A.; Fischer, H., Bachinger, J., Palme, S., Peters, H., Dongus, S. (2004). Leitfaden für Praxisversuche; BÖL-Bericht-ID 2830, Online: http://forschung.oekolandbau.de

Ziegler, K. Göbel, E., Schmittmann O. und P. Schulze Lammers (2012). Precision seed drill tests in Germany/Franconia. International Sugar Journal, Vol 114, 8-15

Harnessing infrared thermometry and spectral indices for enhanced crop water stress monitoring in drip-irrigated rice cultivation with reclaimed wastewater

Gregorio Egea [a,*], Annkathrin Rosenbaum [a], María Muñoz [b], Manuel J. González-Ortega [a], Manuel Pérez-Ruiz [a]

[a] School of Agricultural Engineering, University of Seville, Seville, Spain

[b] TEPRO Consultores Agrícolas S.L., Seville, Spain

* Corresponding author. Email: gegea@us.es

Abstract

Efficient water management in rice cultivation is imperative for sustainable agriculture, especially in water-scarce regions like southern Spain. This study explores the effectiveness of infrared thermometry and spectral indices in monitoring crop water stress in rice cultivation using reclaimed wastewater under varying soil water conditions. The field experiment spanned the 2022 and 2023 growing seasons at the Technological Center for New Water Technologies (Carrión de los Céspedes, Seville), utilizing an experimental wastewater treatment plant's effluent for irrigation. Two irrigation treatments were implemented: (T1) rice irrigated at 100% of crop water requirements (ETc); (T2) rice irrigated at 90% ETc. Each treatment comprised 100 m2 plots with three replications, and water requirements were determined following FAO-56 methodology. Infrared thermometers and spectral reflectance sensors were deployed to continuously measure crop canopy temperature and vegetation indices (NDVI). Stomatal conductance was also monitored throughout the growing season in both treatments. Crop temperature and climatic data were used to establish reference non-water-stress baselines for calculating the Crop Water Stress Index (CWSI) under aerobic conditions. The derived reference baselines remained stable between 12-17h and across growth cycles. The CWSI, calculated using these baselines, effectively captured variations in crop water status induced by the irrigation treatments, correlating with stomatal conductance dynamics. In the initial growth stages, when CWSI accuracy was compromised due to the fraction of bared soil seen by the thermal sensor, NDVI provided complementary insights for interpretation. This study underscores the viability of infrared thermometry and spectral indices for real-time crop water stress assessment, offering a valuable tool for precision agriculture and informed water management decisions in rice cultivation.

Keywords: deficit irrigation, *Oryza sativa*, thermal sensing, water stress

1. Introduction

Rice is the world's third most produced cereal, followed by corn and wheat, which rank first and second. Spain has a cultivated rice area close to 100,000 hectares (ESYRCE, 2023), making it, along with Italy, the main rice-producing countries in the European Union. Andalusia, located in the marshlands of the Guadalquivir River, accounts for nearly 40% of the cultivated rice area in Spain. The rice fields in this region are entirely irrigated under flooding.

Unlike the major rice-producing areas in Asia, rice cultivation in Spain heavily relies on irrigation water. The rice growing cycle in the Guadalquivir marshlands coincides with months of high evapotranspiration demand and low rainfall, making rice production highly dependent on freshwater inputs. The primary source of freshwater for rice irrigation is the Guadalquivir River, pumped by irrigation communities and distributed through a network of canals to the fields.

Due to the proximity of the rice-growing area to the river mouth, the zone where the water is pumped is influenced by ocean tides, resulting in high salinity levels unsuitable for rice cultivation. Therefore, significant releases of freshwater by authorities are required to push the saline wedge towards the estuary, allowing for water intake with a tolerable salinity level for rice cultivation.

The primary challenges of this water management system involve the substantial volumes of freshwater needed for release into the river and the resulting reduction in cultivated rice areas due to drought-induced water shortages. As a result, alternative management strategies are necessary to reduce the vulnerability of the rice sector to increasingly frequent drought periods and high competition for available water resources. Two alternatives that can help mitigate the impact of drought on rice cultivation are the use of unconventional water sources, such as reclaimed wastewater, and implementing localized irrigation systems.

Reclaimed wastewater offers several advantages for agricultural irrigation, including reducing pressure on freshwater resources and providing nutrients that can reduce the use of mineral fertilizers. However, the salinity of some regenerated waters or the presence of pathogens can negatively impact crops and human health (Intriago et al., 2018). Likewise, although less commonly associated with rice cultivation, drip irrigation has shown promising results in optimizing water usage in this crop species (Bozkurt Çolak, 2021; Parthasarathi et al., 2018).

Under aerobic conditions, such as drip irrigation, where the water supply to the crop is not constant, crop monitoring tools could enhance irrigation management. Given rice's high sensitivity to water deficit (Yang et al., 2019), developing indices for crop water status monitoring using remote or proximal sensing tools can be valuable for optimizing irrigation management. Thermal sensors are among the remote sensors that have provided more promising results for monitoring crop water status, owing to the existing relationship between canopy temperature and crop transpiration rate (Egea et al., 2017). However, one drawback of this technique is that the relationship between crop temperature and stress level is not univocal, as it is influenced by other climatic variables such as solar radiation, air temperature, or wind speed (Maes and Steppe, 2012).

Various normalization methods for crop temperature have been proposed to address this issue, including thermal indices. One of the most renowned indices is the Crop Water Stress Index (CWSI), which can be empirically determined using the following expression (Idso et al., 1981):

$$CWSI = \frac{(T_c - T_a) - (T_c - T_a)_{LL}}{(T_c - T_a)_{UL} - (T_c - T_a)_{LL}} \quad (1)$$

where T_c and T_a represent crop and air temperatures, respectively, and LL and UL subscripts represent, respectively, the differences T_c-T_a for non-limiting soil water conditions and for a crop with maximum stress level and therefore not transpiring at all.

Both reference values must be determined from reference lines that can be empirically obtained using the following expressions:

$$(T_c - T_a)_{LL} = a + b \cdot VPD \quad (2)$$

$$(T_c - T_a)_{UL} = a + b[e_s(T_a) - e_s(T_a + a)] \quad (3)$$

where a and b are empirical coefficients, VPD is the vapor pressure deficit, and e_s represents the saturated vapor pressure.

In recent years, there has been increasing interest in using infrared thermometry to monitor water stress in rice cultivation. This interest stems from the desire to optimize water usage in rice cultivation by transitioning to aerobic production systems or implementing management techniques that may induce water stress, such as Alternate Wetting and Drying (AWD) in paddy farms. However, while its effectiveness has been studied in various contexts, such as traditional rice cultivation, its evaluation in drip irrigation systems and under Mediterranean climate conditions remains unexplored. Therefore, this study aims to assess the efficacy of infrared thermometry in these specific conditions and establish reference lines for Crop Water Stress Index (CWSI) determination in drip irrigated rice.

2. Materials and Methods

2.1. Experimental site

The experiment was conducted at the Technological Center for New Water Technologies (Carrión de los Céspedes, Seville, Spain) during the 2022 and 2023 growing seasons. This center has been developed on an urban wastewater treatment plant, whose reclaimed water has been used for drip irrigation of rice plots. The growth cycle 2022 took place outside the usual growth cycle in the region, which usually occurs between June and September. In 2022, the rice seeding and harvesting dates were August 2nd and January 17th, respectively. In 2023, the seeding and harvesting dates were June 6th and November 8th, respectively. The climate in the area is Mediterranean, with variable rainfall, dry and very hot summers, and mild and often

rainy winters that concentrate more than half of the annual rainfall. The soil is characterized to be sandy-loamy with low salinity, low organic matter content, and low - normal nitrogen content. The plots were fertilized with NPK 4-4-12 four days before sowing. Plots were seeded with the ssp. Indica cultivar 'Hispalong'. Seeding was conducted with a precision seeder using a seeding density of 170 kg/ha at a depth of 3 cm and a row spacing of 17 cm. Three days after seeding, the drip irrigation system was installed in the subplots and connected to the tanks of reclaimed wastewater. The drip irrigation system comprises PE 16 driplines spaced 0.5 m apart, with drippers (1.7 L/h) also spaced 0.5 m apart. These driplines were connected to PE 50 submains, with each subplot equipped with a flow meter.

2.2. Experimental design and irrigation treatments

Two irrigation treatments were established with three replications per treatment in a randomized block design. Each replication consisted of a 100 m² rice subplot. Treatment T1 was an irrigation treatment without water limitation, receiving 100% of the crop's water requirements (ETc). Treatment T2 was a mild water stress treatment, receiving 90% of the ETc throughout the growing cycle. The ETc was determined following the FAO-56 methodology (Allen et al., 1998), using daily reference evapotranspiration values from an agro-climatic station belonging to the Junta de Andalucía, located near the experimental plot.

2.3. Real-time measurements

Four infrared thermal sensors (model IR120, Campbell Scientific Ltd., Shepshed, UK) equipped with IR-SS Solar Shields (Campbell Scientific Ltd., Shepshed, UK) were installed in two of three plots in T1 and T2 irrigation treatments. The sensors were positioned facing the crop at an inclination angle of approximately 45º from the vertical (Figure 1). Crop temperatures of T1 were used to determine the reference baselines (Eqns. 2, 3) needed for CWSI (Eqn. 1) determination. Only sunny and non-rainy days were used to determine the reference baselines. Additionally, an air temperature and humidity sensor (model ATMOS 14, METER Group, München, Germany) were installed to determine the vapor pressure deficit (VPD) values as follows:

$$VPD\ (kPa) = e_s(kPa) - e_a(kPa) \quad (4)$$

where e_s and e_a denote the saturated and actual water pressures. Additionally, five spectral reflectance sensors (SRS-NDVI) (Meter Group, Inc. Pullman, WA, USA), each equipped with two photodiodes with peak sensitivities at 650 and 810 nm, were installed in two out of three plots in T1 and T2 irrigation treatments. Of the five SRS-NDVI sensors, four were NDVI-field stop sensors with a field of view restricted to 36º, designed to point downward to measure canopy reflected radiation (Nr). The NDVI-field stop sensors were installed on masts at an inclination angle of approximately 45º from the vertical (Figure 1). The remaining SRS-NDVI sensor was a hemispherical sensor constructed with Teflon diffusers to perform hemispherical (180º field of view) cosine-corrected measurements, primarily designed for upward incident radiation (Ni) measurements. The reflectance values (Nr/Ni) calculated for each waveband were used to calculate the Normalize Difference Vegetation Index (NDVI) as follows:

$$NDVI = \frac{(Nr/Ni)810nm - (Nr/Ni)650nm}{(Nr/Ni)810nm + (Nr/Ni)650nm} \quad (5)$$

where $(Nr/Ni)\ 810nm$ and $(Nr/Ni)\ 650nm$ represent the canopy reflectance at 810 nm and 650 nm, respectively. All sensors were connected to a CR1000 datalogger (Campbell Scientific Ltd., Shepshed, UK) powered by a solar panel, which took readings every minute and stored the 30-minute averages.

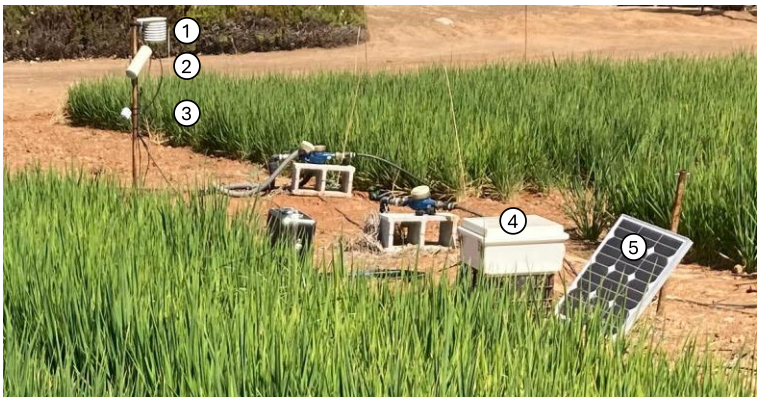

Figure 1. Image of the experimental plot. 1: ATMOS 14 sensor, 2: IR120 sensor, 3: SRS-NDVI field stop sensor, 4: CR1000 data logger protective box, 5: solar panel.

2.4. Gas exchange

Stomatal conductance measurements were taken at midday in five fully expanded leaves per sub-plot (15 per treatment) throughout the 2023 growing cycle in both irrigation treatments. A leaf porometer model SC-1 (METER Group, München, Germany) was used.

3. Results and Discussion

Rice is susceptible to soil water deficit (Peng et al., 2006; Yang et al., 2019). Under aerobic conditions (e.g., drip irrigation), inappropriate water management can lead to significant yield losses. This study highlights that a mild reduction (10%) in the water required to meet the crop's needs negatively impacts both the crop's water status and vegetative development. Figure 2a illustrates the dynamics of the temperature difference between the crop and the air (ΔT; a well-known indicator of water stress), showing higher crop temperatures in the T2 treatment. These differences were more evident up to approximately 80 days after seeding, decreasing after that due to the onset of leaf senescence. Regarding vegetative development, the NDVI index also showed differences between the two irrigation treatments (Figure 2b).

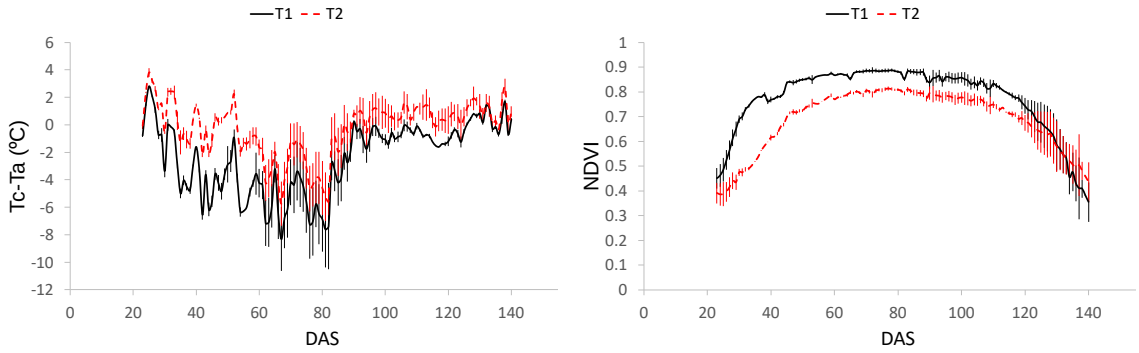

(a) (b)

Figure 2. (a) Temperature differences between canopy (Tc) and air (Ta) for T1 and T2 irrigation treatments throughout the 2023 growing season; (b) Seasonal dynamic of NDVI for T1 and T2 throughout the 2023 growing season. Vertical bars denote ± SD. DAS: days after seeding.

Despite the sensitivity of ΔT to water stress, it must be normalized to be used as a crop water status indicator (Equation 1). This normalization requires the establishment of reference baselines (Equations 2 and 3) calibrated for local conditions. Figure 3 shows the strong relationship obtained (R^2=0.90) between ΔT and VPD for the T1 treatment (absence of water stress), confirming the stability of the relationship for the period

from 12 to 17 hours (local time). Using average ΔT values for the 12 to 17h period, it was confirmed that the relationship obtained during an autumn growing cycle matched that obtained during the summer growing cycle, despite the marked differences in VPD observed between the two periods (Figure 4). This relationship showed a slope similar to that obtained by Ramos-Fernández et al. (2024) on the northern coast of Peru for flood-irrigated rice. However, the intercept differed significantly (negative value in their case). Under humid climate conditions and flood irrigation, the relationship obtained by Godson-Amamoo et al. (2022) differed substantially from that obtained in this study, both in slope and intercept. These results underscore the need to determine reference baselines for the local conditions of each region.

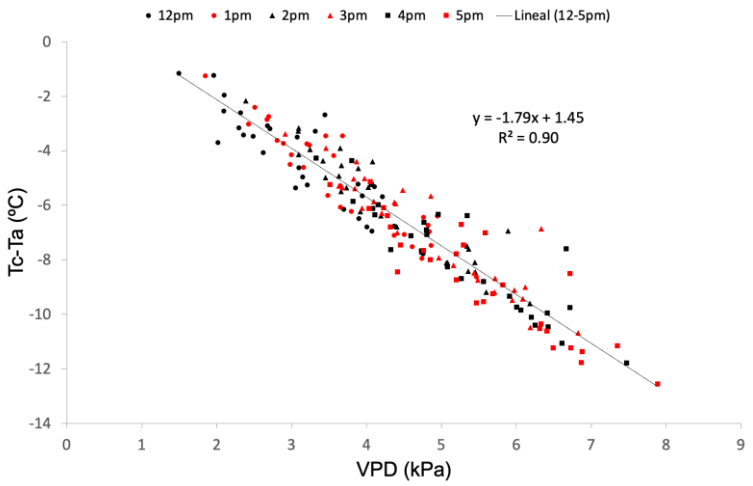

Figure 3. Relationship between canopy-to-air temperature difference and vapour pressure deficit (VPD) for well-watered drip-irrigated rice (T1) during the diurnal period 12-17h (local time). The plotted data pertain to the 2023 growth season, from 56 to 86 days after sowing (August). This period was selected because the crop cover fraction had already reached its maximum (see Fig. 2b), minimizing the background (soil) effect. Of the two thermal sensors installed in T1, only the data from the plot that recorded the lowest temperatures were used to obtain this relationship, ensuring that the relationship corresponds to non-limiting water conditions. Only sunny days are plotted.

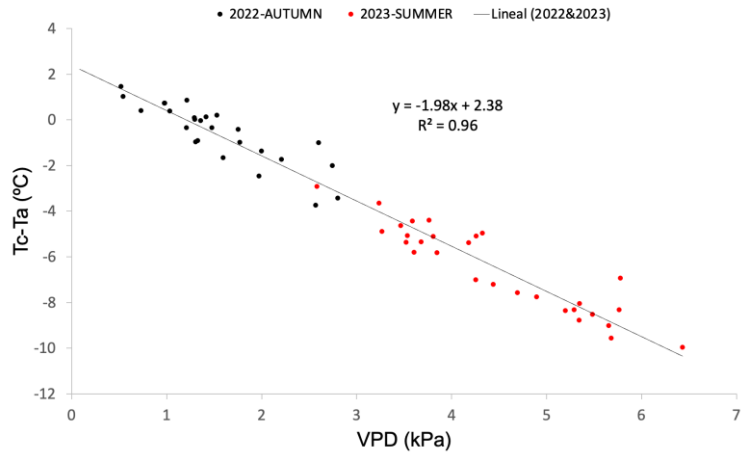

Figure 4. Relationship between canopy-to-air temperature difference and vapour pressure deficit (VPD) for well-watered drip-irrigated rice (T1) during the diurnal period 12-17h (local time) and over two growing seasons (2022 and 2023). The 2022 data pertain to 74 to 126 days after sowing (October-November). Only sunny days are plotted. The mean canopy temperatures between 12:00 PM and 5:00 PM are displayed for each sampling day.

The reference baselines obtained in this study (Equations 2 and 3; Figure 4) were used to determine the CWSI index in T1 and T2 (Figure 5). This figure shows (1) that T2 maintained higher values than T1 for most of the growth cycle, (2) that until DAS 40, coinciding with NDVI values equal to or greater than 0.8, the CWSI of T1 did not reach the near-zero values typical of a well-watered crop, and (3) that from approximately DAS 90, the CWSI values of T1 and T2 increased again due to the onset of leaf senescence. To validate the sensitivity of CWSI to water stress, Figure 6 shows the dynamics of stomatal conductance (g_s) in both treatments, with lower g_s observed in T2 for almost the entire crop cycle.

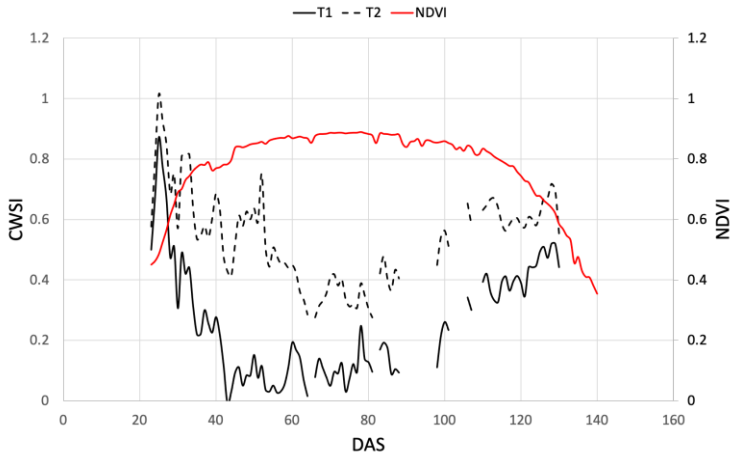

Figure 5. Seasonal time-course of crop water stress index (CWSI) in T1 and T2 treatments and normalized difference vegetation index (NDVI) in T1. CWSI has been determined using equations 1-3 and the empirical relationship obtained in Figure 4. Only sunny days are plotted. The mean canopy temperatures between 12:00 PM and 5:00 PM were used for CWSI computation. The data correspond to the 2023 growth cycle. DAS: days after seeding.

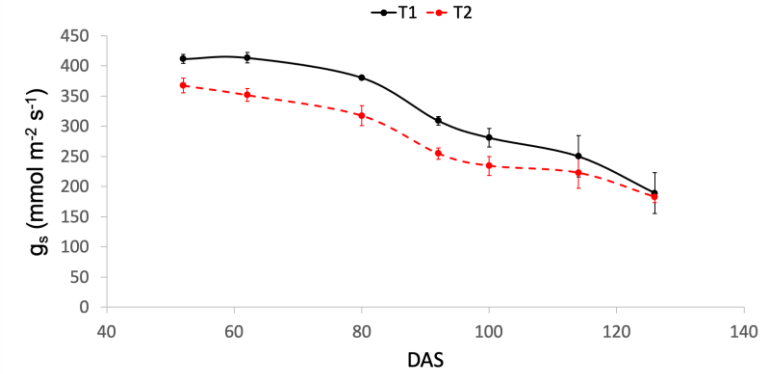

Figure 6. Seasonal time-course of stomatal conductance (g_s) in T1 and T2 irrigation treatments. The data correspond to the 2023 growth cycle. The error bars represent the standard error of the mean (n=3).

The high CWSI values observed in T1 during the onset of the rapid vegetative growth phase are due to the fraction of soil seen by the sensor, whose temperature is higher than that of the crop canopy. The relationship obtained between CWSI of well-watered rice plants and NDVI during the vegetative growth period (Figure 7) could be useful for interpreting CWSI values during the crop's vegetative growth phase. In this sense, when the crop presents an NDVI lower than 0.8, the measured CWSI should be compared with that obtained from the relationship shown in Figure 6 to elucidate whether or not the crop is water stressed. However, further experimental data are still needed to validate this hypothesis.

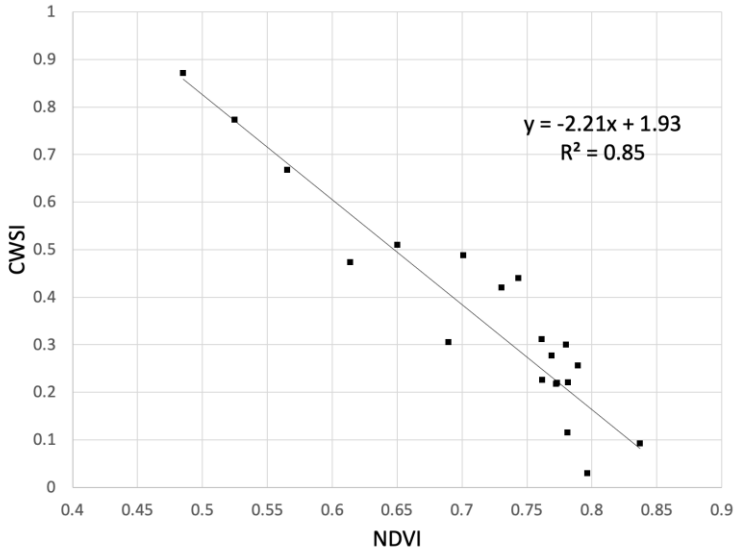

Figure 7. Relationship between CWSI and NDVI for well-watered drip irrigated rice plots (T1). The data correspond to the period 25 to 45 DAS (2023), coinciding with NDVI values within the range of 0.45 to 0.85 (incomplete vegetative development). DAS: days after seeding.

4. Conclusions

Mild soil water deficit caused reductions in vegetative development and the water status of drip-irrigated rice. The CWSI index has proven to be a good indicator of the crop's water status. During phenological stages where the vegetative cover is still incomplete, the NDVI index can be useful for interpreting the CWSI values recorded during that period. The derived reference baselines for CWSI computation remained stable between 12-17h and across growth cycles, which implies that mean values of canopy temperature in the 12-17h period can be used to determine robust CWSI values.

Acknowledgements

The experiments were carried out as part of the SOS-AGUA-XXI project (EXP-00146288/MIG-20211026) funded by the Next Generation EU funds through the Missions Science and Innovation program of the CDTI (Spanish Ministry of Science, Innovation and Universities).

References

Allen, R.G., Pereira, L.S., Raes, D., Smith, M., 1998. Crop Evapotranspiration. FAO Irrigation and Drainage paper Nº 56. FAO, Rome.

Bozkurt Çolak, Y., 2021. Comparison of aerobic rice cultivation using drip systems with conventional flooding. Journal of Agricultural Science 159, 544–556. https://doi.org/10.1017/S0021859621000824

Egea, G., Padilla-Díaz, C.M., Martinez-Guanter, J., Fernández, J.E., Pérez-Ruiz, M., 2017. Assessing a crop water stress index derived from aerial thermal imaging and infrared thermometry in super-high density olive orchards. Agric Water Manag 187, 210–221. https://doi.org/10.1016/j.agwat.2017.03.030

ESYRCE, 2023. Encuesta sobre Superficies y Rendimientos de Cultivos. Análisis de los Regadíos en España, Ministerio de Agricultura, Pesca y Alimentación.

Godson-Amamoo, S., Kato, T., Katsura, K., 2022. Empirical Setting of the Water Stressed Baseline Increases the Uncertainty of the Crop Water Stress Index in a Humid Temperate Climate in Different Water Regimes. Water (Switzerland) 14. https://doi.org/10.3390/w14121833

Idso, S.B., Jackson, R.D., Pinter, P.J., Reginato, R.J., Hatfield, J.L., 1981. Normalizing the stress-degree-day parameter for environmental variability. Agricultural Meteorology 24, 45–55. https://doi.org/10.1016/0002-1571(81)90032-7

Intriago, J.C., López-Gálvez, F., Allende, A., Vivaldi, G.A., Camposeo, S., Nicolás Nicolás, E., Alarcón, J.J., Pedrero Salcedo, F., 2018. Agricultural reuse of municipal wastewater through an integral water reclamation management. J Environ Manage 213, 135–141. https://doi.org/10.1016/j.jenvman.2018.02.011

Maes, W.H., Steppe, K., 2012. Estimating evapotranspiration and drought stress with ground-based thermal remote sensing in agriculture: a review. J Exp Bot 63, 4671–4712. https://doi.org/10.1093/jxb/ers165

Parthasarathi, T., Vanitha, K., Mohandass, S., Vered, E., 2018. Evaluation of drip irrigation system for water productivity and yield of rice. Agron J 110, 2378–2389. https://doi.org/10.2134/agronj2018.01.0002

Peng, S., Bouman, B., Visperas, R.M., Castañeda, A., Nie, L., Park, H.K., 2006. Comparison between aerobic and flooded rice in the tropics: Agronomic performance in an eight-season experiment. Field Crops Res 96, 252–259. https://doi.org/10.1016/j.fcr.2005.07.007

Ramos-Fernández, L., Gonzales-Quiquia, M., Huanuqueño-Murillo, J., Tito-Quispe, D., Heros-Aguilar, E., Flores del Pino, L., Torres-Rua, A., 2024. Water Stress Index and Stomatal Conductance under Different Irrigation Regimes with Thermal Sensors in Rice Fields on the Northern Coast of Peru. Remote Sens (Basel) 16. https://doi.org/10.3390/rs16050796

Yang, X., Wang, B., Chen, L., Li, P., Cao, C., 2019. The different influences of drought stress at the flowering stage on rice physiological traits, grain yield, and quality. Sci Rep 9, 1–12. https://doi.org/10.1038/s41598-019-40161-0

An economic analysis of bolus-sensor technology for precision dairy cattle management

Elias Maritan [a*], Gundula Hoffmann [b], Friederike Schwierz [c], S. Mark Rutter [d], Andreas Meyer-Aurich [c], James Lowenberg-DeBoer [a], Karl Behrendt [a]

[a] Food, Land & Agribusiness Management Department, Harper Adams University, Newport, United Kingdom
[b] Sensor and Modelling Department, Leibniz Institute of Agricultural Engineering and Bioeconomy, Potsdam, Germany
[c] Technology Assessment Department, Leibniz Institute of Agricultural Engineering and Bioeconomy, Potsdam, Germany
[d] Animal Health, Behaviour and Welfare Department, Harper Adams University, Newport, United Kingdom
[*] Corresponding author. Email: emaritan@harper-adams.ac.uk

Abstract

Bolus-sensors are a precision livestock farming tool measuring physiological, behavioural, and production indicators of individual animals to improve herd productivity. Bolus-sensors collect data such as animal activity, rumination, and body temperature. On dairy farms, these data may be used to assess general cattle health, detect oestrus, and monitor presence of disease.

This study focuses on oestrus detection and clinical mastitis (CM) monitoring via bolus-sensors on two dairy farms in northeastern Germany. The two farms use an automatic (AMS) and a conventional milking system (CMS), respectively. A Monte Carlo partial budgeting analysis is performed to quantify the probability of positive net economic outcomes after bolus-sensor adoption. Following previous economic research, the bolus-sensor is assumed to affect milk production and herd growth rates. Annual net economic outcomes are calculated for the two target functions and combined to assess the overall outcome when the bolus-sensor is utilised as a multi-functional tool.

Analysis results show that economic outcomes differ across farm types and functions considered. For CM monitoring, the probability of bolus-sensor adoption leading to increased profits is 58% on AMS farms and 99% on CMS farms. Conversely, the probabilities for oestrus detection on AMS and CMS farms are 80% and 59%, respectively. When the two functions are combined, the likelihood of increased profit is 75% on AMS farms and 93% on CMS farms. Annual economic benefits span from €26,470 to €110,301 on the AMS farm, and from €27,420 to €197,763 on the CMS farm. The mean economic advantage for both target applications is €126,257 year^{-1} on the AMS farm and €214,670 year^{-1} on the CMS farm. However, these outcomes are highly variable and more data on the effects of bolus-sensors on herd productivity are required. Additionally, further research is needed to identify potential trade-offs among economic benefits, animal welfare, and other non-economic aspects.

Keywords: partial budgeting, Monte Carlo simulation, mastitis monitoring, oestrus detection, precision livestock farming

1. Introduction

Precision livestock farming (PLF) is a management system relying on continuous, real-time, and automatic collection of data related to individual animal behaviour, health, welfare, production, reproduction, and possibly environmental impact (Mayo *et al*., 2019; Herlin *et al.*, 2021). PLF technologies are adopted to optimise livestock system efficiency (Mayo *et al.*, 2019). Since the advent of milking robots in the 1990s, sensor technologies capable of measuring physiological, behavioural, and production indicators of individual animals have gained increased attention in PLF (Steeneveld *et al*., 2015; Herlin *et al*., 2021). These tools may replace or even enhance human inspection, thus leading to substantial labour savings, while also enabling more intensive livestock management by markedly increasing the amount of collected data (Herlin *et al*., 2021). Frequent, precise, and systematic data collection may also improve farmers' ability to abide with animal welfare standards, which are increasingly being imposed via regulation globally (Herlin *et al.*, 2021).

Sensors can be categorised as animal- and non-animal-based (Herlin *et al.*, 2021). Animal-based sensors may be fixed to ear tags, worn as collars or leg straps, or administered to the animal in the form of boluses (Herlin *et al*., 2021). Non-animal-based sensors are usually developed for indoor systems and installed in the animals' vicinity (e.g., heat stress detection cameras) (Herlin *et al.*, 2021). On dairy cattle farms, sensor systems are increasingly being used on a large scale to optimise farmers' decision-making processes (Steeneveld *et al.*, 2015). These sensors may provide information on feed and water intake, oestrus, calving, and presence of disease (Herlin *et al.*, 2021). Certain diseases may even be detected before the manifestation of clinical signs, thus helping reduce milk losses and antimicrobials use (Kim *et al*., 2019; Herlin *et al.*, 2021). Because most research efforts have concentrated on single-use sensors (Benaissa *et al*., 2020), this analysis focuses on two target applications in dairy cattle systems to understand the economic performance of multi-functional sensor technology. The type of sensor studied is an animal-based sensor-bolus placed in the cattle reticulorumen.

The first target application of the selected technology is the monitoring of clinical mastitis (CM). CM has been the first focus of sensor development in the dairy sector (Hogeeven *et al.*, 2010). It usually occurs during lactation, thus severely impairing milk quantity and quality parameters on dairy farms (Kim *et al*., 2019). Early CM detection may reduce negative economic and animal welfare impacts (Kim *et al.*, 2019). Using temperature data for CM detection is a reliable approach (e.g., Kim *et al.*, 2019). This is especially true when data are gathered by sensor-boluses which, unlike external sensors, have no temperature interference from the surrounding ambient (Kim *et al.*, 2019; Herlin *et al.*, 2021). When compared to other diseases, CM leads to short-lived internal body temperature increases (Kim *et al.*, 2019). Temperature data are usually augmented by other data types (e.g., cattle activity parameters) to improve CM detection accuracy. CM is conventionally monitored via visual inspection of pre-milk (Hogeeven *et al*., 2010; Kim *et al*., 2019). This makes it impossible to detect mastitis at the subclinical stage because clinical symptoms must first manifest (Kim *et al.*, 2019). On dairy farms using automatic milking systems (AMS), CM monitoring via visual observation is even more challenging (Hogeeven *et al.*, 2010). Alternative approaches to identifying CM cases include milk colour and homogeneity tests, measurement of milk electrical conductivity (EC), and quantification of L-Lactate dehydrogenase (LDH) or somatic cell counts (SCC) in milk (Hogeeven *et al*., 2010). Of these, EC, LDH and SCC are the most reliable (Hogeeven *et al*., 2010), but LDH and SCC usually require third-party laboratory tests whose cost hinders farmers' motivation to diligently manage this disease (Boker *et al*., 2023). Thus, when visual observation of pre-milk is infeasible or impractical (e.g., on AMS farms), EC readings are frequently used to monitor CM and identify milk samples requiring laboratory testing (Steeneveld *et al*., 2015). Since the EC of milk can also be affected by factors other than CM presence, temperature and other data collected by sensors may further improve the efficiency of EC monitoring systems (Hogeeven *et al.*, 2010).

The second target application of the studied technology is oestrus detection. The reproduction efficiency of cattle significantly affects profitability on dairy farms (Benaissa *et al.*, 2020). The most common approach to oestrus detection is visual observation of animals manifesting sexually receptive behaviours that are associated with reproductive readiness (Mayo *et al*., 2019; Lodkaew *et al*., 2023). Because this method is labour-intensive, costly, and prone to errors (Mayo *et al*., 2019; Lodkaew *et al*., 2023), sensor technologies are increasingly being used to monitor such behaviours automatically and continuously on dairy farms (Mayo *et al.*, 2019; Benaissa *et al.*, 2020; Lodkaew *et al.*, 2023). If oestrus is not promptly detected, farmers may fail to artificially inseminate cattle at the optimal time before ovulation and must wait for another reproductive cycle (Lodkaew *et al*., 2023). Breeding failure results in fewer calf births and consequently in lower herd growth rates (Lodkaew *et al.*, 2023). Previous research indicates that economic losses amount to US$ 360 per missed oestrus (Mayo *et al.*, 2019). Sensor systems have been shown to detect 80-85% of oestrus events, compared to approximately 55% when these are identified via visual methods (Steeneveld *et al.*, 2015). Improving oestrus detection by adopting sensor technologies may reduce calving intervals, which is a known contributor to increased milk production on dairy farms (Steeneveld *et al.*, 2015).

The sensor-bolus selected for the present economic analysis is commercialised by smaXtec Animal Care GmbH (Graz, Austria). The smaXtec® sensor-bolus continuously collects body temperature, rumination, water intake, rumen pH, and activity data (smaXtec, 2024). It is currently commercialised in the US, New Zealand, and several European countries (smaXtec, 2024). Upon sensor-bolus administration and activation, data are wirelessly transmitted to the smaXtec Cloud TruD™ and processed by artificial intelligence (AI) (smaXtec, 2024). Subsequently, the user receives processed data on a mobile phone application as well as recommendations for action (smaXtec, 2024). It is here hypothesised that the multi-purpose smaXtec® sensor-bolus could improve the economic performance of dairy farms. Economic effects of its use for CM monitoring and oestrus detection are assumed to be variations in milk production and herd growth rates. A Monte Carlo (MC) simulation is performed to quantify these effects on two dairy farms located in Germany. The two farms are an AMS farm and a conventional milking system (CMS) farm. Results are generated to answer the three following research questions (RQ): (i) what is the probability that smaXtec® provides a positive economic net outcome compared to conventional CM monitoring approaches? (RQ1); (ii) what is the probability that smaXtec® provides a positive economic net outcome compared to oestrus detection via visual observation? (RQ2); and (iii) what is the probability that smaXtec® provides a positive economic net outcome when simultaneously considering CM monitoring and oestrus detection applications? (RQ3). Interpretation of results is conducted from an agroecological perspective by discussing some implications of sensor-bolus adoption that go beyond economic considerations.

2. Materials and Methods

2.1. Description of the modelled farms

The two fictitious farms modelled in this study are located in the State of Brandeburg in northeastern Germany. On the AMS farm, conventional CM monitoring and oestrus detection methods are assumed to be EC readings and visual observation of cattle behaviour, respectively. The EC readers are installed on the AMS. AMSs may be sold with an optional SCC sensor (e.g., GEA Group, 2024), but these sensors often rely on California Mastitis Test protocols, which have been questioned for their low specificity rate (e.g., Lam *et al*., 2009; Kim *et al*., 2019). Besides, a farm survey of 414 dairy farms conducted by Steeneveld *et al.* (2015) in the Netherlands found that EC sensors were the most widely used sensor types on AMS farms. Thus, this analysis assumes that the AMS is not equipped with SCC sensors and that the farm manager sends milk samples identified via EC readings to a laboratory for diagnosing CM via more reliable tests such as the Porta SCC (Lam *et al.*, 2009). The adoption rates of AMSs are difficult to quantify because equipment retailers do not make their data publicly available (Eastwood and Renwick, 2020). A recent estimate reported that 15% of German dairy farms used AMSs as of 2018 (Eastwood and Renwick, 2020). Thus, a second CMS farm was included in this study because CMSs are still widely used in Germany. On the modelled CMS farm, conventional CM monitoring is conducted via visual observation of pre-milk (Lam *et al*., 2009; Boker *et al*., 2023), while conventional oestrus detection follows the same method of the AMS farm. Labour times for conventional CM monitoring and oestrus detection are based on authors' experience. It is assumed that it takes 15 minutes to monitor the EC sensors at each milking event for the entire herd on the AMS farm, and 15 seconds per cow at each milking event to visually assess pre-milk on the CMS farm. Average milkings per day are assumed to be 2.7 and 2.2 on the AMS and CMS farms, respectively. For oestrus detection, visual observation of cattle behaviour requires 50 minutes per day for the entire herd. The farm labour hourly rate is assumed to be € 21.00 per hour (Achilles *et al.*, 2020). The herd size is 227 milking cows, coinciding with the mean herd size in Brandeburg (Tergast *et al.*, 2023).

Both the AMS and CMS farms adopt the smaXtec® bolus-sensor system and move away from conventional CM monitoring and oestrus detection practices. Milk production and herd growth rate variations pre- and post-adoption of the bolus-sensor system are obtained from Steeneveld *et al.* (2015). Milk production is simulated via 10,000 MC iterations using mean, standard deviation, and correlation parameters provided in Steeneveld *et al.* (2015). The assumed milk price is the weighted average price in Germany in 2023 (CLAL, 2024). Herd growth rate increases are 2.50% and 2.20% on the AMS and CMS farms, respectively (Steeneveld *et al.*, 2015). Calf value is € 136.65 $head^{-1}$ (Saxon State Ministry for Energy, Climate Protection, Environment and Agriculture, 2024). This value is for bull calves, which are assumed to be sold after four weeks following common practice in the study area (Tergast *et al.*, 2023). On the other hand, heifer calves are usually kept on farm as replacement cattle (Tergast *et al*., 2023). Calf management costs are assumed at € 69.81 per bull calf from birth to sale (Redman, 2023). The latter include direct labour and variable costs such as milk substitute, concentrate, and bedding (Redman, 2023).

2.2. Description of the adopted bolus-sensor system

The smaXtec® bolus-sensor has a size of 105 x 35 mm (**Figure 1**) (smaXtec, 2024). It is administered orally using conventional bolus applicators (smaXtec, 2024). It has a data measurement frequency of 10 minutes and an internal memory capacity of 6 days (smaXtec, 2024). The smaXtec® classic bolus collects the following data types: (i) inner body temperature (accuracy of ± 0.01°C), (ii) water intake, (iii) rumination, and (iv) animal activity (smaXtec, 2024). The adoption of the smaXtec® system involves three cost components. The upfront cost per sensor-bolus in Germany is € 29.99 (smaXtec, 2024. Pers. Comm.). The sensor-boluses have an average useful life of 5 years (smaXtec, 2024. Pers. Comm.). Subscription costs depend on the herd size, but these are on average € 2.99 per sensor per month (smaXtec, 2024. Pers. Comm.). Subscription costs cover data processing, internet connection, customer support and sensor replacement charges in case of technical failure (smaXtec, 2024. Pers. Comm.). Based on these figures, the per-cow annual cost of the smaXtec® technology is estimated at € 41.88. Additionally, the smaXtec® system requires the installation of a base station costed at € 6,500, including infrastructure, installation labour, and farmer training fees (smaXtec, 2024. Pers. Comm.). The base station is where the data continuously collected by the sensor-boluses are processed. It is equipped with a common subscriber identity module card, an antenna, a bolus applicator and climate sensors collecting ambient temperature, air pressure, and humidity data (smaXtec, 2024. Pers. Comm.). The base station communicates with the smaXtec Cloud TruD™ and provides the user with processed data, alerts, and recommendations for action via a mobile application (smaXtec, 2024. Pers. Comm.). With an assumed useful life of 10 years, base station costs are estimated at € 1007.50 $year^{-1}$ $herd^{-1}$. This figure includes annual insurance (assumed at € 65.00 $year^{-1}$, i.e. 1% of the base station cost) and opportunity cost of capital (€ 292.50 $year^{-1}$ based on the most recent European Central Bank fixed rate of 4.50%).

Figure 1. The classic smaXtec® bolus-sensor (smaXtec, 2024)

Following personal communication with smaXtec Animal Care GmbH, it is assumed that it requires approximately 15 minutes per day to supervise the mobile application alerts received by the system for the entire herd. For the herd size considered in this study, this is equivalent to 0.40 hours per cow per year for either CM monitoring or oestrus detection. The smaXtec® system exploits AI algorithms to provide farmers with CM case probabilities for individual animals based on body temperature, rumination, and activity data (smaXtec, 2024. Pers. Comm.). CM can be confidently detected after a second alert but, depending on the specific CM pathogen, certain CM cases may be detected at the first alert (e.g., *E. coli* CM) (smaXtec, 2024. Pers. Comm.). This may enable substantial savings in antimicrobial use and laboratory testing even on AMS farms where the EC sensors cannot detect EC changes in milk up to 48 hours after the first smaXtec® system alert (smaXtec, 2024. Pers. Comm.). For oestrus detection, the smaXtec® AI algorithms rely on rumination activity and animal movement patterns (smaXtec, 2024. Pers. Comm.). System alerts are triggered when an animal behaves in a substantially different manner compared to the rest of the group (smaXtec, 2024. Pers. Comm.).

Although sensitivity and specificity percentages of the smaXtec® sensor are not available, this preliminary analysis assumes that this system has a reasonably accurate performance for the two tested functions. Ingestible sensors are an effective tool for CM monitoring, especially when body temperature data are correlated with additional biometric data (Hogeveen *et al*., 2010; Kim *et al.*, 2019). According to Hogeveen *et al.* (2010), the minimum specificity and sensitivity of a CM detection system should be 80% and 99%, respectively. It is here assumed that the smaXtec® system meets these requirements. Likewise, sensor-supported activity monitoring is regarded as the most successful tool for oestrus detection (Benaissa *et al.*, 2020). Thus, for oestrus detection, the smaXtec® sensor is assumed to at least match the previously reported 80-85% oestrus detection rate (Steeneveld *et al.*, 2015). These assumptions will be revised in future research as more data become available.

2.3. Description of the partial budgeting model

The partial budgeting model used in the present economic analysis relies on the approach by Davies *et al.* (2022). Davies *et al.* (2022) conducted a MC simulation with 10,000 iterations to explore the net economic outcomes of transthoracic ultrasonography testing in subclinical cases of pulmonary adenocarcinoma in live sheep. This methodology is applied to the use of the smaXtec® system for CM monitoring and oestrus detection in dairy cattle over one year to quantify the probability of increased profit after the adoption of smaXtec®. The economic factors considered include a higher milk production and an increased herd growth rate (Steeneveld *et al.*, 2015). The latter is a result of potentially shorter calving intervals. The net economic outcomes for CM monitoring (Scenario 1) and oestrus detection (Scenario 2) are separately calculated and subsequently combined to estimate an overall net outcome when smaXtec® is used as a multi-purpose technology (Scenario 3) (**Table 1**). The relative influence of individual model parameters is explored via sensitivity analyses. The model was developed in Microsoft® Excel® (Microsoft Corporation, 2024).

Table 1. Scenarios tested in the Monte Carlo partial budgeting model

Net economic outcome	AMS farm	CMS farm
Clinical mastitis monitoring	Scenario 1a	Scenario 1b
Oestrus detection	Scenario 2a	Scenario 2b
Overall net economic outcome	Scenario 3a	Scenario 3b

Net economic outcomes in Scenarios 1 and 2 are calculated via **Eq.1**. The individual components of **Eq.1** are estimated using **Eq.2**, **Eq.3**, and **Eq.4** for Scenario 1 and **Eq.5**, **Eq.6**, and **Eq.7** for Scenario 2. Overall net outcomes (i.e., Scenario 3) are calculated via **Eq.8**.

$$\text{Net outcome} = [\text{Effect on revenue (a)}] - [\text{Increased costs (b)}] + [\text{Saved costs (c)}] \quad (1)$$

$$a^{CM} = \Delta\alpha * HS * p \quad (2)$$

where a^{CM} is the effect on revenue of using smaXtec® for CM monitoring (€ year^{-1}); $\Delta\alpha$ is a stochastic variable accounting for the effect on milk production after adoption of the smaXtec® system (l cow^{-1}); *HS* is the herd size of the modelled farm; and *p* is the average weighted milk price in Germany in 2023 (€ kg^{-1}).

$$b^{CM} = \left(\beta_1^{CM} * lab + \gamma_1\right) * HS + \gamma_2 \quad (3)$$

where b^{CM} is the cost increase incurred after adopting smaXtec® for CM monitoring (€ year^{-1}); β_1^{CM} is the labour time requirement to monitor the CM alerts on the smaXtec® application (h year^{-1} cow^{-1}); *lab* is the hourly labour rate in Germany (€ h^{-1}); γ_1 is the yearly adoption cost per cow of the smaXtec® system excluding infrastructure costs (€ year^{-1} cow^{-1}); γ_2 is the yearly adoption cost per herd for the infrastructure costs of the smaXtec® system (€ year^{-1} herd^{-1}); and *HS* is described in **Eq. 2**.

$$c^{CM} = \beta_0^{CM} * lab * mpd * 365 * HS \quad (4)$$

where c^{CM} are the costs saved thanks to the adoption of the smaXtec® system for CM monitoring (€ year^{-1}); β_0^{CM} is the labour time requirement to monitor CM via visual observation of pre-milk (h milking^{-1}); *mpd* are average milkings per day; and *HS* and *lab* are described in **Eq.2** and **Eq.3**, respectively.

$$a^{OD} = (\Delta\alpha * HS * p) + (\Delta HS * HS * cv) \quad (5)$$

where a^{OD} is the effect on revenue of using smaXtec® for oestrus detection (€ year^{-1}); ΔHS is the herd growth rate increase after adoption of smaXtec® (%); *cv* is bull calf value in Germany as of April 2024 (€ head^{-1}); and $\Delta\alpha$, *HS* and *p* are described in **Eq.2**.

$$b^{OD} = (\beta_1^{OD} * lab + \gamma_1) * HS + \gamma_2 + \Delta HS * HS * cmc \quad (6)$$

where b^{OD} is the cost increase incurred after adopting smaXtec® for oestrus detection (€ year^{-1}); β_1^{OD} is the labour time requirement to monitor the oestrus detection alerts on the smaXtec® application (h year^{-1} cow^{-1}); *cmc* is the bull calf management cost until its sale (€ head^{-1}); *lab*, γ_1, *HS*, and γ_2 are described in **Eq.3**; and ΔHS is described in **Eq.5**.

$$c^{OD} = \beta_0^{OD} * lab * HS \quad (7)$$

where c^{OD} are the costs saved thanks to the adoption of the smaXtec® system for oestrus detection (€ year^{-1}); β_0^{CM} is the labour time requirement to detect oestrus via visual observation of cattle behaviour (h year^{-1} cow^{-1}); and *HS* and *lab* are described in **Eq.2** and **Eq.3**, respectively.

$$\text{Overall net outcome} = a^{CM} + a^{OD} - b^{CM} - b^{OD} + c^{CM} + c^{OD} - \gamma_1 * HS - \gamma_2 \quad (8)$$

where a^{CM}, b^{CM}, c^{CM}, a^{OD}, b^{OD} and c^{OD} are the outputs of the previous six equations; *HS* is described in **Eq.2**; and γ_1, γ_2 are described in **Eq.3**. The latter are subtracted from the overall net outcome to avoid double counting of the smaXtec® system adoption costs.

3. Results

The probability that smaXtec® provides a positive net economic outcome compared to conventional CM monitoring approaches was 58% on the AMS farm and 99% on the CMS farm (RQ1). Annual mean net economic outcomes for Scenarios 1a and 1b are shown in **Table 2**.

Table 2. Mean net economic outcomes of clinical mastitis (CM) monitoring via smaXtec®. Standard deviation values are provided in parentheses.

	AMS farm (Scenario 1a)	**CMS farm (Scenario 1b)**
Effect on revenue (a^{CM})	€ 33,671 (± € 138,444)	€ 194,234 (± € 86,930)
Increased costs (b^{CM})	€ 12,421 (± € 0)	€ 12,421 (± € 0)
Saved costs (c^{CM})	€ 5,220 (± € 0)	€ 15,950 (± € 0)
Mean net economic outcome	**€ 26,470**	**€ 197,763**

The probability that smaXtec® provides a positive net economic outcome compared to oestrus detection via visual observation was 80% on the AMS farm and 59% on the CMS farm (RQ2). Annual mean net economic outcomes for Scenarios 2a and 2b are shown in **Table 3**.

Table 3. Mean net economic outcomes of oestrus detection via smaXtec®. Standard deviation values are provided in parentheses.

	AMS farm (Scenario 2a)	**CMS farm (Scenario 2b)**
Effect on revenue (a^{OD})	€ 116,990 (± € 132,843)	€ 34,044 (± € 112,344)
Increased costs (b^{OD})	€ 13,077 (± € 0)	€ 13,012 (± € 0)
Saved costs (c^{OD})	€ 6,388 (± € 0)	€ 6,388 (± € 0)
Mean net economic outcome	**€ 110,301**	**€ 27,420**

The overall economic outcome of smaXtec® adoption was calculated by combining the mean net economic outcomes shown in **Table 2** and **Table 3**. The probability of overall increased profits was 75% on the AMS farm and 93% on the CMS farm (RQ3). Cumulative distribution functions and descriptive statistics of overall net economic outcomes for the two farms are provided in **Figure 2**. The cumulative distribution function of the CMS farm was found to stochastically dominate its AMS counterpart in the first-degree sense. The expected shortfall at 10% level on the AMS farm was substantially larger than that on the CMS farm indicating that adopting the smaXtec® system was a greater investment risk for the former farm type.

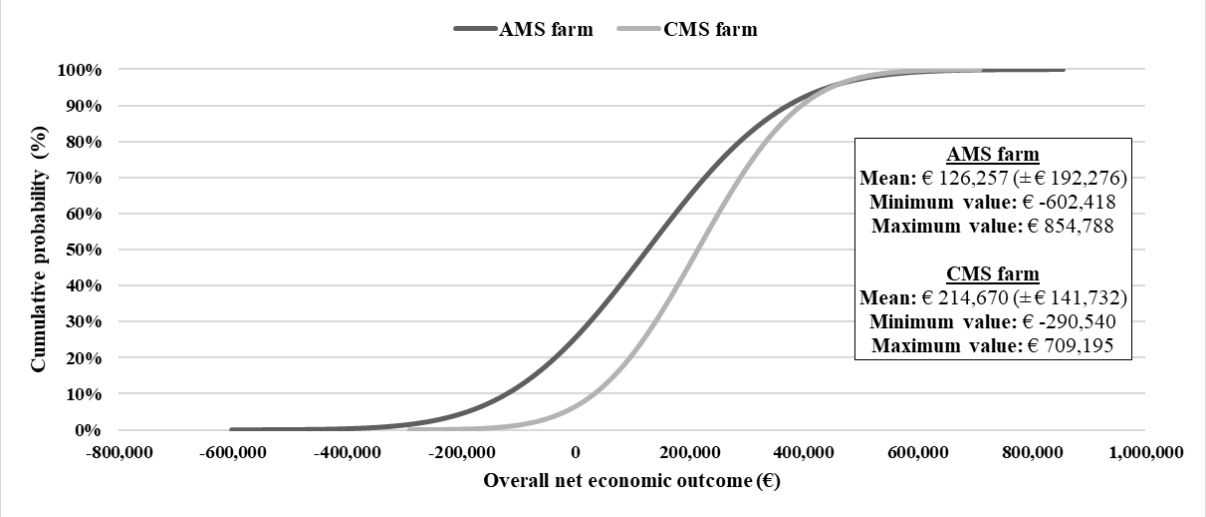

Figure 2. Cumulative distribution functions and descriptive statistics of overall net economic outcomes for the AMS and CMS farms when smaXtec® is used as a multi-purpose technology (Scenarios 3a and 3b)

Finally, sensitivity analyses were conducted to quantify the influence of the input data on the estimated net economic outcome probabilities. Parameter sensitivities were tested between 50% and 150% of the correspondent baseline value with a 25% step. Probability variations of up to 1% were considered negligible and were therefore not reported in this paper. Positive net outcome probabilities were found to be slightly sensitive (-2%) to a 50% milk price reduction on the AMS farm for CM monitoring (Scenario 1a) and on the CMS farm for oestrus detection (Scenario 2b). In the latter scenario, the probability of a positive economic outcome was also sensitive to a 50% smaller herd size (+2%), and a 50% reduction (+2%) or increase (-2%) in the per-cow costs of the smaXtec® system (i.e., the γ_1 parameter).

4. Discussion

The mean net economic outcomes shown in **Table 2** and **Table 3** are always positive on both the AMS and the CMS farms. However, their magnitude depends on the milking system type considered. The AMS farm had a higher probability of obtaining a positive economic outcome when smaXtec® was used for detecting oestrus, whereas the CMS farm was more likely to achieve economic benefits when this technology was used for CM monitoring. Indeed, it is known that farms equipped with different milking systems tend to adopt sensors for distinct target applications (Steeneveld *et al.*, 2015). When the AMS farm used smaXtec® for CM monitoring besides oestrus detection, the probability of achieving a positive economic outcome decreased from 80% to 75% (-5%). Similarly, on the CMS farm, utilising smaXtec® as a multi-functional sensor resulted in a 6% reduction of

positive economic outcome probability from 99% to 93%. Thus, both farms were more likely to benefit from the smaXtec® system when this was used as a single-purpose technology targeting the most economically beneficial function i.e., oestrus detection on the AMS farm and CM monitoring on the CMS farm.

The high standard deviation values in Scenarios 1 and 2 indicate that effects on revenue, and consequently economic outcomes, were extremely variable. This was particularly the case on the AMS farm, where the expected shortfall at 10% level in overall net economic outcomes (Scenario 3a) spanned from € -602,418 to € -114,842. The high variability is also reflected in the remarkably wide range between minimum and maximum overall profits for both farm types (**Figure 2**), though the first-degree stochastic dominance of the CMS curve indicated that smaXtec® adoption was a less risky investment in Scenario 3b. This high variability is due to the uncertain effects of sensor adoption on milk production. In the scientific literature, data on these effects are rarely available or do not possess sufficient detail to correlate productivity parameters with specific sensor types. For example, in the study by Steeneveld *et al.* (2015), the effects on milk production after adopting a CM monitoring sensor were aggregated for colour, EC, SCC, LDH, or other sensors despite distinct approaches achieving substantially different levels of accuracy. More field studies are required to fill this data gap.

To further explore the uncertain effects of sensor adoption on farm economic outcomes, sensitivity tests were performed on all deterministic parameters. Depending on the milking system type and target sensor function, positive net outcome probabilities were found to be only slightly sensitive to milk price, herd size and cost of the smaXtec® bolus-sensors and monthly subscription costs. On the AMS farm, a 50% milk price reduction resulted in a 2% decrease of the positive net outcome probability when monitoring CM (Scenario 1a). A comparable decrease was found on the CMS farm when smaXtec® was used to detect oestrus (Scenario 2b). However, such a milk price has not occurred since June 2016 (CLAL, 2024). The lowest annual average milk price after 2016 was encountered in 2020, corresponding to a 28% reduction in 2023 prices (CLAL, 2024). A 25% milk price reduction reduced the probability of increased profits by 1%. Herd size and per-cow smaXtec® costs affected net economic outcome probabilities in Scenario 2b. A 50% smaller herd size led to an increased probability of positive economic outcomes by 2%. Considering the lack of influence of parameters such as herd growth rate, calf maintenance costs, personnel costs and labour requirements, this was likely due to savings in the per-cow cost of the smaXtec® system. Indeed, γ_1 was ten times the base station cost per cow (i.e., γ_2/HS) with a herd size of 223 and still about five times the base station cost per cow when herd size was 50% smaller. A 50% reduction and increase in personnel costs and labour requirements led to a 2% increase and a 2% decrease in positive net outcome probabilities, respectively. The relatively low influence of the tested parameters seems to corroborate that the milk production effect of sensor adoption is the most important variable.

The cost increases across scenarios mainly resulted from the investment required to adopt the smaXtec® technology. These were always greater than the saved costs except for Scenario 1b. Nevertheless, the initial investment in the smaXtec® system appeared to be economically viable in all scenarios because of positive effects on revenue resulting from higher milk production and/or herd growth rates. The largest cost savings (€ 15,950) were achieved in Scenario 1b. Substituting visual observation of pre-milk for smaXtec® CM monitoring led to a large reduction in labour requirements, which was an important contributor to the high probability of achieving economic benefits after its adoption on the CMS farm. Labour savings are often regarded as a major driver for adoption of sensors and automatic milking systems on conventional dairy farms (Steeneveld *et al.*, 2015; Eastwood and Redwick, 2020). A strong motivation for adopting sensor systems for CM monitoring on AMS farms might be antimicrobial use and laboratory test savings when mastitis is treated at the sub-clinical stage. However, these savings could not be quantified in this analysis in the absence of accurate data.

A lower reliance on antimicrobial use and lower laboratory testing requirements, but also an increased work flexibility and a reduction in repetitive physical work are some of the potential non-economic and more agroecologically based benefits of smaXtec® adoption. Assigning a monetary value to improved working conditions is difficult. However, besides labour cost savings, reduction in drudgery and an improved work-life balance are among the major drivers for farmers' adoption of AMSs (Eastwood and Redwich, 2020) and animal sensors (Steeneveld *et al.*, 2015) across the world. The smaXtec® technology seems to be technically capable of enabling these benefits while maintaining economic feasibility. Besides, continuous, unbiased and reliable data collection from individual animals through sensors may facilitate abiding with animal welfare standards (Stygar *et al.*, 2021). Compliance with such standards is gaining a growing attention from European consumers, who are willing to pay a 31% premium for milk produced on dairy farms proactively managing animal health and welfare (Stygar *et al.*, 2021). Due to this increased attention by consumers, animal welfare standards are increasingly being mandated by regulation.

In Germany, the Animal Welfare Act of 1972 and subsequent amendments requires livestock managers to regularly supervise animal health (Bundesministerium der Justiz, 1972). When animal health is monitored with the aid of technology, the Act imposes the implementation of precautionary measures in case of technical

malfunctions (Bundesministerium der Justiz, 1972). The smaXtec® system has a failure rate of 3% (smaXtec, 2024. Pers. Comm.). When data transmission from a sensor-bolus stops, the system sends an error message to the user via the dedicated mobile application. After a second error message, the user receives an automated email. The farmer has 6 days to replace a faulty sensor without losing animal data, which keep being collected even when they are not wirelessly transmitted to the base station. Other issues may occur if cattle walk too far from the base station, if the base station goes offline, or if the bolus-sensor battery runs out (smaXtec, 2024. Pers. Comm.). In all these cases, alerts will be triggered so that the farm manager may promptly act to solve the issue and implement precautionary measures if needed. However, more studies are required to validate sensor-based welfare assessment, especially on commercial farms (Herlin *et al.*, 2021; Stygar *et al.*, 2021). Animal welfare is a multidimensional concept which is unlikely to be captured by a single technology and potential trade-offs should be taken into consideration (van Erp-van der Kooij and Rutter, 2020). For example, replacing human contact with sensors for monitoring CM and oestrus may lead to increased stress when animals are manually handled for other tasks (Herlin *et al.*, 2021). Stygar *et al.* (2021) investigated into the commercial validation rate of available PLF sensor technologies for animal welfare assessment. They found that only 14% of the 129 identified technologies had been validated, with sensor-boluses representing the least validated category (7%).

5. Conclusions

The present analysis focused on the economic performance of the smaXtec® bolus-sensor system implemented for CM monitoring and oestrus detection on fictitious AMS and CMS dairy farms in Germany. Probabilities of positive net economic outcomes were estimated using a partial budgeting approach and a Monte Carlo simulation of the effect of bolus-sensor adoption on milk production and herd growth rates. The probability of achieving increased profits on the AMS farm for CM monitoring and oestrus detection were 58% and 80%, respectively. On the CMS farm, the probabilities were 99% for CM monitoring and 59% for oestrus detection. When smaXtec® was used as a multi-purpose tool targeting both functions, positive net outcome probabilities were 75% on the AMS farm and 93% on the CMS farm.

Depending on the target application, the mean annual net economic outcomes of smaXtec® adoption ranged from € 26,470 to € 110,301 on the AMS farm, and from € 27,420 to € 197,763 on the CMS farm. When the two target applications were simultaneously considered, the mean overall net economic outcome was € 126,257 year^{-1} on the AMS farm and € 214,670 year^{-1} on the CMS farm. The higher profits were mostly due to the increased milk production, higher herd growth rates and labour savings achieved after adopting the studied technology. However, the economic performance of the smaXtec® system was found to be highly variable and consequently these results should be interpreted with care.

Agroecologically based benefits of bolus-sensor adoption on dairy farms may include an increased work flexibility, a reduction in repetitive physical work and an improved compliance with animal welfare standards and regulation. However, these aspects are not well documented in the scientific literature, especially as far as animal welfare is concerned. Further research is required to identify potential economic, social, and environmental trade-offs of sensor-bolus use on dairy farms in Germany and globally.

Acknowledgments

This study was co-funded by UK Research and Innovation (UKRI Reference No.10037994) and by the EU's Horizon Europe research and innovation programme (Grant Agreement No.101060759) as part of the "Digitalisation for Agroecology" project (D4AgEcol | https://d4agecol.eu/). The authors wish to thank Dr. ir. Wilma Steeneveld at Utrecht University and the UK SmaXtec Animal Care team for their kind support in providing some of the data used in the present analysis.

References

Achilles, W., Eckel, H., Eurich-Menden, B., Frisch, J., Fritzsche, S., Funk, M., Gaio, C., Grebe, S., Grimm, E., Grube, J., Hartmann, W., Horlacher, D., Kloepfer, F., Kron, K., Meyer, B., Sand, I., Schroers, J.O., Schultheiss, U. and Wulf, S. 2020. *Betriebsplanung Landwirtschaft 2020/21*. Germany: Kuratorium für Technik und Bauwesen in der Landwirtschaft

Benaissa, S., Tuyttens, F.A.M., Plets, D., Trogh, J., Martens, L., Vandaele, L., Joseph, W. and Sonck, B. 2020. Calving and estrus detection in dairy cattle using a combination of indoor localization and accelerometer sensors. *Computers and Electronics in Agriculture*, 168, 105153

Boker, A.R., Bartel, A., Duc, P.D., Hentzsch, A., Reichmann, F., Merle, R., Arndt, H., Dachrodt, L., Woudstra, S. and Hoedemaker, M. 2023. Status of udder health performance indicators and implementation of on farm monitoring on German dairy cow farms: results from a large scale cross-sectional study. *Frontiers in Veterinary Science*, 10:1193301

Bundesministerium der Justiz. 1972. *Animal Welfare Act*. [Online]. Germany Federal Government. Available from: https://www.gesetze-im-internet.de/tierschg/BJNR012770972.html [Accessed 13 January 2024]

CLAL srl. 2024. *Farm-gate milk prices, Germany*. [Online]. CLAL srl. Available from: https://www.clal.it/en/index.php?section=latte_germania [Accessed on 30 April 2024]

Davies, P., Strugnell, B., Thomas, L., Lovatt, F. and Willison, I. 2022. To scan or not to scan? The economics of transthoracic ultrasonography for 'whole-flock' ovine pulmonary adenocarcinoma screening in UK sheep flocks. *Veterinary Record*, e1980, pp.1-8

Eastwood, C.R. and Renwick, A. 2020. Innovation Uncertainty Impacts the Adoption of Smarter Farming Approaches. *Frontiers in Sustainable Food Systems*, 4(24) https://doi.org/10.3389/fsufs.2020.00024

GEA Group. 2024. *GEA DairyRobot R9500 Robotic Milking System*. [Online]. GEA Group Aktiengesellschaft. Available from: https://www.gea.com/en/products/milking-farming-barn/dairyrobot-automated-milking/dairyrobot-r9500-robotic-milking-system/ [Accessed on 29 April 2024]

Herlin, A., Brunberg, E., Hultgren, J., Hogberg, N., Rydberg, A. and Skarin, A. 2021. Animal welfare implications of digital tools for monitoring and management of cattle and sheep on pasture. *Animals*, 11(829)

Hogeveen, H., Kamphuis, C., Steeneveld, W. and Mollenhorst, H. 2010. Sensors and Clinical Mastitis – The Quest for the Perfect Alert. *Sensors*, 10, pp.7991-8009

Kim, H., Min, Y. and Choi, B. 2019. Real-time temperature monitoring for the early detection of mastitis in dairy cattle: Methods and case researches. *Computers and Electronics in Agriculture*, 162, pp.119-125

Lam, T.J.G.M., Olde Riekerink, R.G.M., Sampimon, O.C. and Smith, H. 2009. Mastitis diagnostics and performance monitoring: a practical approach. *Irish Veterinary Journal*, 62, pp.34-39

Lodkaew, T., Pasupa, K. and Loo, C.K. 2023. CowXNet: An automated cow estrus detection system. *Expert Systems with Applications*, 211, 118550

Mayo, L.M., Silvia, W.J., Ray, D.L., Jones, B.W., Stone, A.E., Tsai, I.C., Clark, J.D., Bewley, J.M. and Heersche Jr., G. 2019. Automated estrous detection using multiple commercial precision dairy monitoring technologies in synchronized dairy cows. *Journal of Dairy Science*, 102(3), pp.2645-2656

Microsoft Corporation. 2024. Microsoft® Excel®: Version 2403. Redmond, WA, USA: Microsoft Corporation

Redman, G. ed. 2023. John Nix Pocketbook for Farm Management for 2024. 54th Edition. UK: The Pocketbook

Saxon State Ministry for Energy, Climate Protection, Environment and Agriculture. 2024. *Livestock prices for calves in Central Germany and East Germany.* [Online]. Government of Germany. Available from: https://www.landwirtschaft.sachsen.de/nutztierpreise-kaelber-mitteldeutschland-und-ostdeutschland-54528.asp [Accessed 16 January 2024]

SmaXtec. 2024. *THE SMAXTEC HEALTH SYSTEM*. [Online]. SmaXtec Animal Care GmbH. Available from: https://smaxtec.com/ [Accessed 15 January 2024]

Steeneveld, W., Vernooij, J.C.M. and Hogeveen, H. Effect of sensor systems for cow management on milk production, somatic cell count, and reproduction. *Journal of Dairy Science*, 98, pp.3896-3905

Stygar, A.H., Gomez, Y., Berteselli, G.V., Dalla Costa, E., Canali, E., Niemi, J.K., Llonch, P. and Pastell, M. 2021. A systematic review on commercially available and validated sensor technologies for welfare assessment of dairy cattle. *Frontiers in Veterinary Science*, 8:634338

Tergast, H., Hansen, H. and Weber, E.C. 2023. *Steckbriefe zur Tierhaltung in Deutschland: Milchkühe.* [Online]. Thünen-Institut für Betriebswirtschaft. Available from: https://www.thuenen.de/media/ti-themenfelder/Nutztierhaltung_und_Aquakultur/Haltungsverfahren_in_Deutschland/Milchviehhaltung/Steckbrief_Milchku__he_2023.pdf [Accessed 16 January 2024]

van Erp-van der Kooij, E. and Rutter, S.M. 2020. Using precision farming to improve animal welfare. *CAB Reviews*, 15, 051

Optimizing maize crop productivity: A variable rate approach from over-density trials with different inter-row spacing and sowing densities

Luís Alcino Conceição[1,2,3], Luís Silva[1,2,4], Tiago Silva Pinto[5], Susana Dias[1,2], Constantino Valero[6]

[1]Polytechnic Institute of Portalegre, 7300-110 Portalegre, Portugal

[2]VALORIZA - Research Center for Endogenous Resource Valorization, Polytechnic Institute of Portalegre, 7300-110 Portalegre, Portugal

[3]InovTechAgro—National Skills Center for Technological Innovation in the Agroforestry Sector, 7300-110 Portalegre, Portugal

[4]Earth Sciences Department, NOVA School of Science & Technology, Campus of Caparica, NOVA University Lisbon, 2829-516 Caparica, Portugal

[5]INOVMILHO—National Skills Center for Maize and Shorgum, António Teixeira Experimental Station, 2100-127 Coruche, Portugal

[6]LPF-TAGRALIA, School of Agricultural, Food and Biosystems Engineering (ETSIAAB), Technical University of Madrid, Avenida Puerta de Hierro 2-4, 28040 Madrid, Spain

* Corresponding author. Email: luis_conceicao@ipportalegre.pt

Abstract

The implementation of two maize crops with a 0.75 cm inter-row spacing faces recurring challenges, particularly regarding the optimal emergence of sown maize. To address this, an experimental trial was conducted on a 1.3-hectare plot, assessing the impact of widening inter-row distances while adjusting sowing doses and plant populations per hectare. By increasing row spacing to 1.50 meters, an over-density of plants within the rows was created, especially when augmenting the sowing dose. The primary objective of the experiment was to measure the emergence rate of over-density trials with a row spacing of 1.50 meters and sowing densities of 80000 and 16000 plants per hectare. A comparison was made with traditional row spacing of 0.75 meters and a density of 80000 plants per hectare. The results showed that the 80000-plant trial achieved a yield of 14.7 t ha^{-1}, and the 160000-plant trial yielded 15.3 t ha^{-1}, suggesting that widening inter-row spacing does not directly impact yield compared to traditional spacing and that maize variety is a factor influencing productivity, prompting the research of other varieties under this system in future research.

Keywords: *Zea mays* L., crop management, economic return, grain yield.

1. Introduction

Maize, one of the world's most crucial cereal crops, plays a pivotal role in global food security and agricultural economics. Its cultivation practices significantly influence yield, resource efficiency, and sustainability. Farmers need to consider the specific hybrid's characteristics and the local growing conditions when deciding on plant densities. Modern hybrids allow for higher densities without significant yield penalties, but the exact density should be optimized based on factors like soil fertility, moisture availability, and risk of disease (Sangoi et al., 2002; Coulter at al., 2010; Green et al., 2019). Recent advances in precision agriculture have led to the exploration of variable rate (VRT) sowing as a potential strategy to optimize maize crop productivity (Ficher et al., 2018; Ramirez et al., 2020). This approach adjusts sowing densities and inter-row spacings based on localized field conditions, aiming to maximize yield while minimizing resource waste.

By combining the precise delivery of water and nutrients via drip irrigation with the benefits of larger inter-row spacing, maize growers can significantly improve the efficiency and productivity of their farming operations. This method aligns well with sustainable agriculture practices by optimizing resource use and minimizing environmental impact. Using large inter-row spacing combined with drip irrigation in maize crops enhances crop management, water efficiency, and overall yield. Drip irrigation, by delivering water directly to the root zone, minimizes water loss due to evaporation or runoff. Larger inter-row spacing can help reduce weed growth as it discourages weed germination between rows by targeting water more precisely where it's needed and not moistening the entire soil surface. This setup also allows for better air circulation, which can decrease humidity around the plants and lower the risk of fungal diseases. The increased space makes field operations such as planting and harvesting easier and allows machinery to navigate without harming the plants.

Moreover, with more room available, maize plants' roots can expand more effectively without

competition, leading to stronger, healthier plants and potentially higher yields. The extra space can also be utilized for inter-cropping, improving field biodiversity, enhancing soil health, and providing an additional source of income. This method is not only efficient in optimizing resource use but also aligns with sustainable agricultural practices by preserving soil structure and reducing environmental impact.

The concept of VRT is rooted in the understanding that spatial variability within fields affects crop performance. Traditional uniform sowing practices may not address the diverse environmental conditions present within a single agricultural plot, such as soil fertility, moisture levels, and microclimatic variations (Lobell et al., 2009; Zhang & Kovacs, 2012; Bernardes et al., 2021). Consequently, there is a growing interest in adapting planting strategies to better suit local conditions, potentially enhancing crop output and efficiency. In essence, VRT addresses the variability within fields by adjusting input applications in real-time according to the conditions detected, which is particularly beneficial in scenarios where precision is critical, such as with narrow inter-row spacing in maize crops. This not only helps in solving immediate issues related to irrigation and crop emergence but also enhances the overall sustainability and profitability of the farming operation.

In this context, our study titled "Optimizing maize crop productivity: a variable rate approach from over-density trials with different inter-row spacing and sowing densities" aims to assess whether such variations could lead to an optimization of emergence rates, growth patterns, and ultimately, crop yield.

2. Materials and Methods

The trial took place in Coruche, Portugal (geographical coordinates 38.941844, -8.512472) between May and September 2023 on a 1.3ha plot in a CSa Mediterranean climate region. According to Portugal's soil chart, the predominant soil types are Vt (litholic, non-humic, slightly unsaturated normal soils, with coarse sandstones) and Ppt (podzolised soils - non-hydromorphic podzols, with surraipa, with an incipient A2 horizon, in or on sandstones). These soils are characterised by their low organic matter content and poor water retention capacity.

The technical itinerary followed a minimum tillage model, with drip irrigation, and the sowing operation was carried out using an air-assisted, mechanically operated, seeder with seed distribution regulation in the row and inter rows. A control and two varieties of maize were sown under two different inter row width and two sowing rates, as shown in Table 1 and Figure 1.

Table I. Variables per installed test

Trial	Maize varieties	Inter-row width (m)	Sowing density (nº seeds/ha)
Control	DKC 6092	0.75	75 000
1	DKC 6092	1.50	80 000
2	DKC 6092	1.50	160 000
3	Ixabele	1.50	80 000
4	Ixabele	1.50	160 000

Figure 1. Trial with 1.50m inter row spacing of the variety DKC 6092 with hiper density, and tester "Wile 200" used to measure the moisture content, test weight and temperature of grain.

Samples for yield assessment were collected in 3 representative points, by marking 5 linear metres in the crop row, where the following parameters were observed: number of plants; number of corncobs; total weight of grain harvested; moisture content and specific weight of the grain. Yield and adjusted yield were determined following equations 1) and 2).

$$\text{Yield (kg/ha)} = 1000 \text{ Kernel Weight} \text{Number of Ears per Hectare} \times \text{Average Kernel Weight per Ear} \times 100 \quad \text{eq.1)}$$

$$\text{Adjusted Yield} = \text{Measured Yield} \times (\text{Standard Moisture Content}/\text{Standard Moisture}) \quad \text{eq.2)}$$

The data was subjected to descriptive statistical analysis and a mean comparison test.

3. Results and Discussion

Figures 1 to 5 show the average value of the samples to the number of plants and number of ears per variety and per sowing density, percentage of plants per variety and sowing density, specific weight of harvested grain by variety and sowing density, moisture content of harvested grain by variety and sowing density and estimated total yield and at 14% moisture by variety and sowing density, respectively.

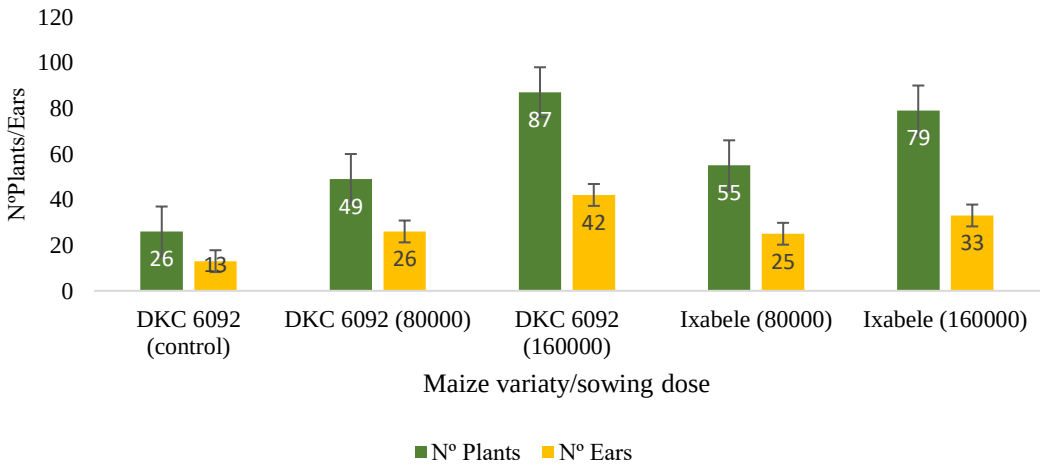

Figure 1. Number of plants and number of ears per variety and per sowing density.

The trials with a 1.50 metre row had higher plant numbers than the control, as would be expected given the higher sowing densities. However, it is the control trial that has the highest success rate of plants emerging (or reaching the end of the cycle), and only trial 3 comes close with a figure of 91.7 per cent. All the other trials have a lower emergence rate than the control trial (Figure 2).

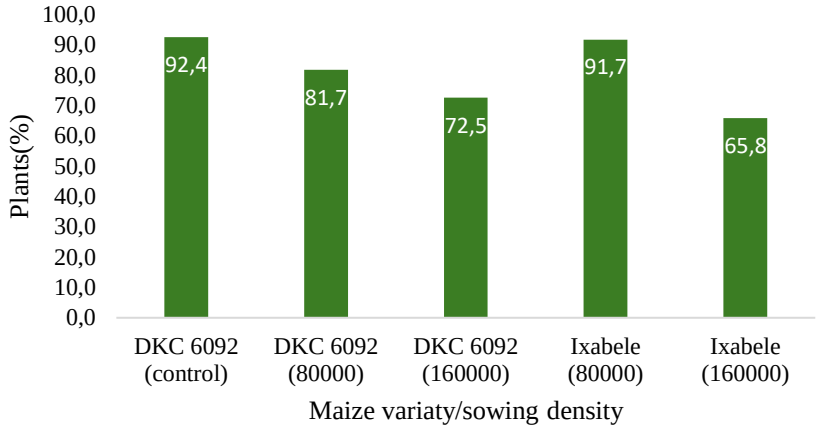

Figure 2. Percentage of plants per variety and sowing density.

The trial with the highest specific weight was the control trial (75.8), followed by the trials with a sowing density of 160000 plants. The trials with a planting density of 80000 plants, regardless of variety, had the lowest specific weight values (Figure 3).

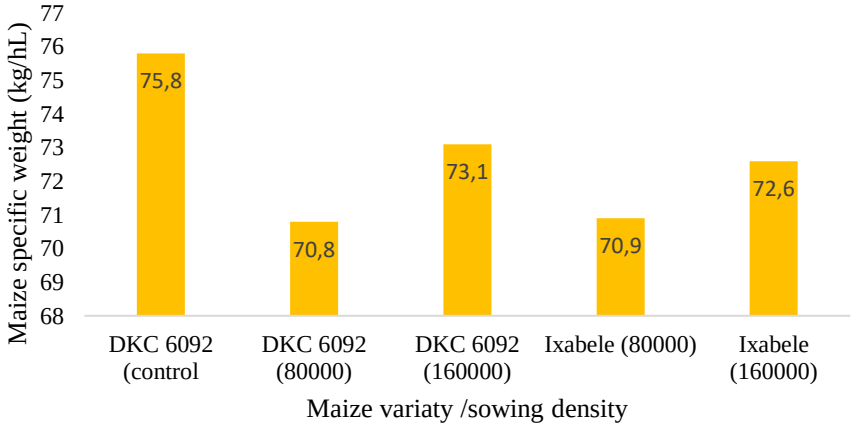

Figure 1. Specific weight of harvested grain by variety and sowing density.

In respect to the moisture content, the DKC 6092 variety had a similar moisture content in all three trials, between 18.8 and 20 per cent. The trials with the Ixabele variety had higher grain moisture content values (Figure 4).

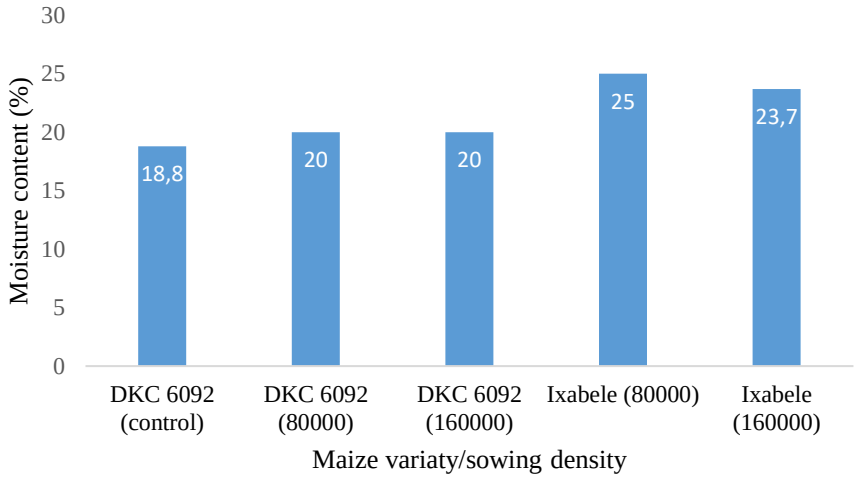

Figure 4. Moisture content of harvested grain by variety and sowing density.

The yield of the control trial was 14163.6 kg of grain maize per hectare at 14% moisture. The hyper density trials with the same variety were very close to the control trial, with the 80000-plant density trial achieving a yield of 14746.1 kg/ha and the 160000-plant trial achieving a yield of 15294.2 kg/ha. The trials with the Ixabele variety yielded around 12000 kg/ha. These results are shown in Figure 5.

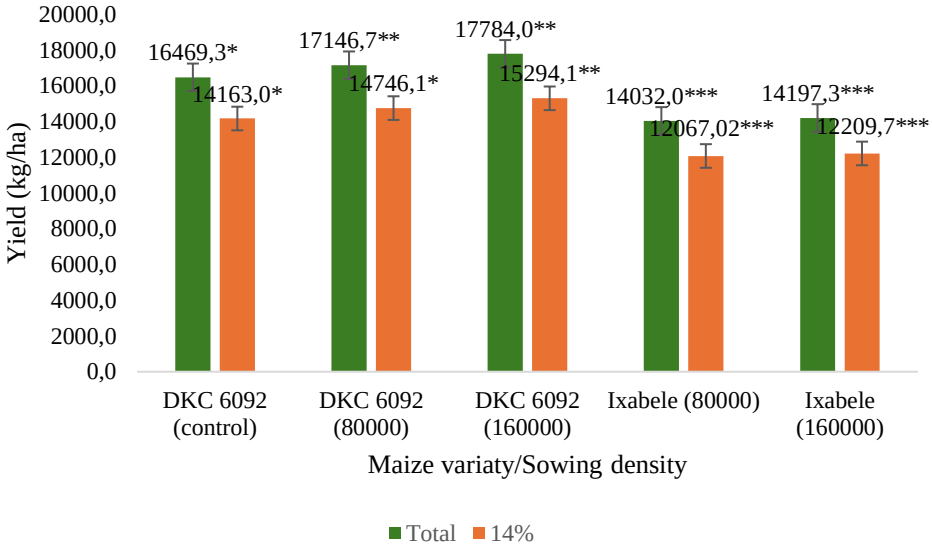

Significance using Student's t test: *significative (P<0.05); **very significative (P<0.01); ***highly significative (P<0.001)

Figure 5. Differences of the estimated total yield and adjusted yield to 14% moisture content by variety and sowing density.

Considering that one of the main objectives of the trial was to measure the emergence rate of the hyper density trials with a 1.50 metre row spacing and compare them with a traditional 0.75 metre row spacing, it can be concluded that this method showed lower values than the control.

However, the trials with a planting density of 80000 plants were close to the control, with deviations that appear to be of little significance. The trials with a density of 160000 plants were a little further away from

the control, so it might be interesting to investigate intermediate densities to see how this factor influences the rate of plant emergence and the number of plants that can fulfil the crop cycle by producing. Production remained the same from the control trial to the trials with a 1.50 row spacing, which means that this method of cultivation can be installed without directly altering production compared to the traditional row spacing.

Regarding the second main objective of the trials, which is to analyse the influence of the 1.50 m row spacing on crop yields, we can see that the DKC 6092 variety achieved yields in the hyperdensity regime that were very similar to the yields in the control trial. However, the Ixabele variety yielded less than the control variety, but remained consistent with each other, with no major difference from one sowing density to the next. These results may indicate that the DKC 6092 variety is better suited to being sown with a 1.50 metre row spacing than the Ixabele variety. With this case study, it seems that the variety is a factor that can influence productivity, so it would be interesting to evaluate the performance of other varieties in this system.

4. Conclusions

This study opening strategies to the use of variable rate adoptions highlighting the importance of the maize variety and sowing density on productivity. It suggests exploring other varieties and densities to optimise the desired results by further research to better understand their impact on plant emergence and the number of plants that manage to complete crop cycle.

Acknowledgements

The authors wish to express their gratitude to the VALORIZA and GeoBioTec research centres as well as to INOVMILHO in Coruche – Portugal for providing the fields and trial crops.

References

Bernardes, T. G., & Morais, P. P. (2021). Enhancing maize production through precision agriculture: A case study from southern Brazil. Agricultural Systems, 188, 102983.

Coulter, J. A., Sheaffer, C. C., & Wyse, D. L. (2010). Divergent selection for establishment vigour in maize inbreds: Yield responses and agronomic characteristics. Journal of Agronomy and Crop Science, 196(5), 345-353.

Fischer, M. A., & Smith, L. W. (2018). Technological advancements in maize cultivation: An overview of variable rate seeding. Journal of Crop Improvement, 32(2), 161-178.

Green, J. M., & Bradley, K. R. (2019). Optimizing plant population and spatial configurations in maize under various water availability conditions. Agricultural Water Management, 222, 213-224.

Lobell, D. B., Cassman, K. G., & Field, C. B. (2009). Crop yield gaps: Their importance, magnitudes, and causes. Annual Review of Environment and Resources, 34, 179-204.

Ramirez, D. A., & Wang, E. (2020). Spatial variability management in maize: The role of soil sensors and variable rate technology. Precision Agriculture, 21(6), 1120-1134.

Sangoi, L., Gracietti, M. A., Rampazzo, C., & Bianchetti, P. (2002). Response of Brazilian maize hybrids from different eras to changes in plant density. Field Crops Research, 79(1), 39-51.

Zhang, N., & Kovacs, J. M. (2012). The application of small unmanned aerial systems for precision agriculture: A review. Precision Agriculture, 13(6), 693-712.

Color image evaluation of fruits of grape in consideration of postharvest process

Yuki Iwase [a], Ken-ichiro Suehara [a], Kazuhiko Kawamura [b], Atsushi Hashimoto [a*]

[a] Graduate School of Bioresources, Mie University, Tsu, Japan

[b] Advanced Research & Innovation Center, Chubu Electric Power Co., Inc., Nagoya, Japan

* Corresponding author. Email: hasimoto@bio.mie-u.ac.jp

Abstract

We developed a simple, easy, rapid, and non-chemical method to evaluate grape characteristics in the field. Grapes (Vitis vinifera 'Shine Muscat') grown in Makinohara City, Japan, in 2022 and 2023 were used as samples. An exemplary farmer visually inspected the bunches at different ripeness levels and categorized them into four groups: A (unripe) to D (overripe). After harvesting, the grape bunches were stored in a constant temperature chamber set at 25˚C (ambient temperature). Color images of the fruits and infrared spectra of the squeezed juices were acquired. At harvesting, the surface color parameters of the fruits differed among the ripeness levels, with significant differences observed in the *H* (Hue) values. The sweetness values of the juices were calculated based on infrared spectral analysis, which predicted the glucose, fructose, and sucrose content. These values increased as the fruits ripened, and the relationship between them showed good linearity for the grapes cultivated in 2022 and 2023. This experimentally demonstrates that the sweetness of the fruits at harvesting could be quantitatively determined by evaluating the *H* values of the surface color. Additionally, the sweetness values increased over time during storage and were well-fitted by a logistic function. These results suggest that it is possible to non-destructively predict the sweetness of the fruits based on the information taken at harvesting, considering the postharvest stage.

Keywords: color image analysis, infrared spectroscopy, storage. sweetness, cultivation management

1. Introduction

Data-driven agriculture, a subsystem of the smart food system aiming to sustainably produce high-quality agricultural products, requires the development of simple, easy, rapid, and non-chemical measurement methods for acquiring biological information in the field. These methods are desirable as they can be applied to pre- and post-harvest processes, where the quality of agricultural products typically changes. Focusing on grapes, which are widely used for raw consumption and processed foods such as wines, we studied the relationship between their surface color and internal quality, as surface color information is readily obtainable. For internal quality evaluation, we applied infrared spectroscopy to understand the formation of constitutive components rather than relying on macro indices like Brix%. We selected Shine Muscat grapes, known for their deliciousness and high cost, as the sample.

2. Materials and Methods

2.1. Materials

Grapes (*Vitis vinifera* 'Shine Muscat') cultivated in Makinohara City, Shizuoka Prefecture, in 2022 and 2023 were used. An exemplary farmer visually sampled bunches of grapes at different ripeness levels, along with the leaves directly above the bunches. The ripeness of the grapes was classified into four groups: A (unripe) to D (overripe), where group C indicated optimal ripeness. Samples were brought to Mie University immediately after harvesting using a private vehicle. The surface color images of the fruits were acquired, and the infrared spectra of the squeezed fruit juices were collected. Additionally, the bunches were stored at a constant temperature of 25°C (room temperature).

2.2. Methods

2.2.1. Storage

The sampled bunches were stored in a thermostatic chamber (FSL-2KPH, ESPEC Corp., Osaka, Japan)

maintained at 25°C (room temperature). Surface color image acquisition and infrared spectral measurement of the squeezed fruit juice were conducted periodically throughout the storage period to observe changes over time.

2.2.2. Color image acquisition

The standard imaging acquisition system developed in our laboratory (Motonaga et al., 2004; Tsukahara et al., 2020) was used to take color images of the fruit surface. Two light sources (Vitalight, 5500 K color temperature, CIE daylight, spiral bulb type) were placed outside a cylindrical white Kent paper, and the illumination was adjusted to 140 lx. A digital single-lens reflex camera (EOS Kiss7, Canon Inc., Tokyo, Japan) was used to acquire the images. A black felt-wrapped board was placed behind the grapes to create a black background, preventing reflected light and facilitating extraction of the fruit images. Five grapes were placed inside the imaging system and photographed from a single side. As the images were saved in RAW format, they were converted to TIFF files using Photoshop (Adobe Inc., San Jose, CA). *RGB* values for each pixel in the image were then obtained using the ColorImageAnalysis software (Hashimoto et al., 2015). Additionally, *HSL* values were calculated from the RGB values at each pixel, and the average values were obtained.

2.2.3. Infrared spectroscopic measurement

Five grapes per bunch, free of blemishes or discoloration, were sampled. The fruites were washed with pure water and cut horizontally. A drop of squeezed juice was placed onto a diamond IRE (Internal Reflection Element). Infrared spectra of the fruit juice were obtained using a compact FTIR (Fourier Transform Infrared) spectrometer (ALPHA, Bruker Optics Inc., Billerica, MA) equipped with an ATR (Attenuated Total Reflectance) accessory. The measured spectra were analyzed using the OPUS software (Bruker Optics Inc., Billerica, MA).

3. Results and Discussion

3.1. Optical sensing information at harvesting

Figure 1 presents examples of infrared spectra in the fingerprint region (1200 to 900 cm^{-1}) for grape juice components harvested in 2023. These spectra have been corrected by subtracting the water spectrum from the juice spectra. Variations in absorbance intensity and slight spectral patterns were observed among the different ripeness levels. These slight spectral differences could be attributed to variations in the composition of the juice at different ripeness stages. Similar results were also observed for the grapes cultivated in 2022.

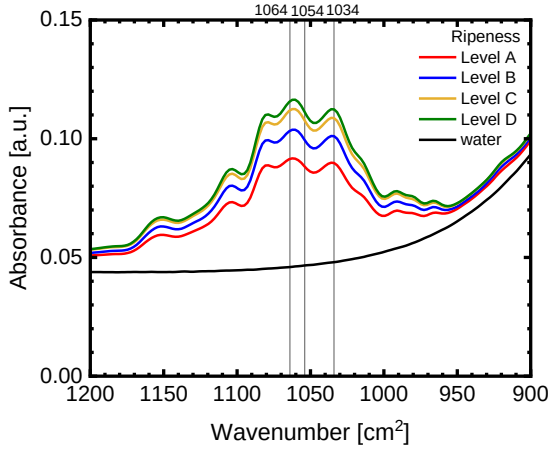

Figure 1. Examples of infrared spectra of squeezed juice components in the fingerprint region.

Figure 2 illustrates the influence of ripeness levels on the fructose, glucose, and sucrose content in grape juice. The content of each sugar was calculated simultaneously using spectral information at 1064, 1054, and 1034 cm^{-1}, corresponding to the characteristic absorption peaks for fructose, glucose, and sucrose,

respectively. This calculation was performed under the assumption of spectral additivity for the saccharides (Kameoka et al., 1998; Kanou et al., 2005). The content of all sugars increased with increasing ripeness levels, but the trends differed among the sugars. These findings suggest that the sweetness of the grapes increased, and the sugar composition changed as the ripeness level progressed.

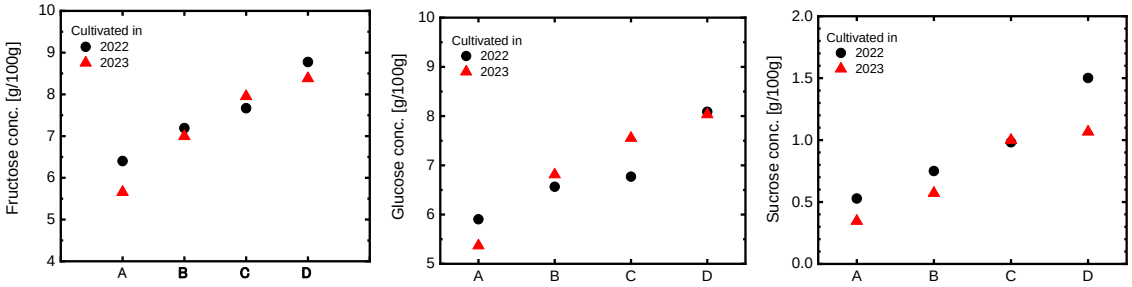

Figure 2. Sugar concentration in squeezed fruit juice by ripeness level at harvesting. (a) fructose, (b) glucose and (c) sucrose.

The surface color of the grapes was also influenced by the ripeness levels at harvest. Figure 3 depicts the relationship between the sweetness of the fruit juice and the average hue (*H*) value of the fruit's surface color. Sweetness was calculated based on individual sugar content, and it is influenced by the ratios and concentrations of these sugars (Maebashi, 2011). As shown in Figure 3, a very good linear relationship exists between sweetness and *H* values, regardless of the year of cultivation. These results suggest that sweetness at harvest can be quantitatively estimated by analyzing the surface color. Furthermore, infrared spectroscopic information, which can provide the concentration of each constituent sugar, is considered a valuable tool for evaluating fruit quality. Additionally, previous studies have demonstrated the ability to quantitatively evaluate surface color using a commercial digital camera under various lighting conditions in agricultural fields (Hashimoto et al., 2015; Hashimoto et al., 2017). In other words, it is possible to estimate the sweetness of grapes simply by capturing an image at harvest.

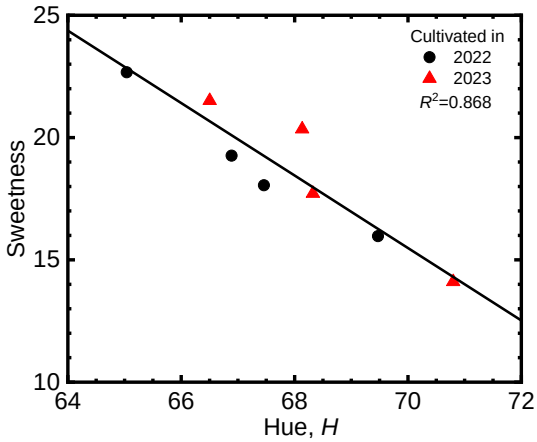

Figure 3. Relationship between sweetness of squeezed fruit juice and hue values of surface color of fruit at harvesting.

3.2. Quality change during storage

This section studies the relationship between changes in the sweetness of the squeezed fruit juice and the surface color of the fruits during storage. Figure 4 presents the time courses of the sweetness of the juice during storage. The sweetness increased exponentially during the storage period in this study. Additionally, the sweetness values for group D were the highest, while those for group A were the lowest. As illustrated in Figure 4, it is evident that the sweetness curves were influenced by the initial sweetness.

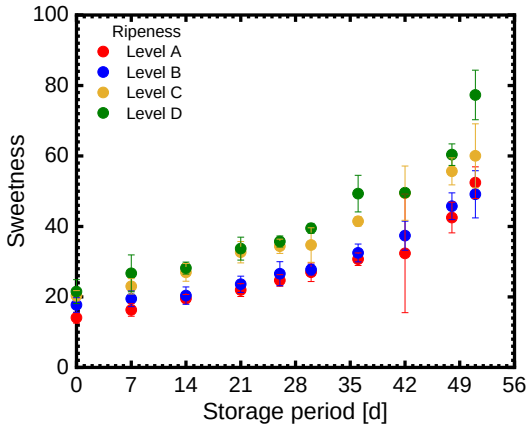

Figure 4. Time courses sweetness of squeezed fruit juice during storage.

The time axis of the sweetness changes shown in Figure 4 was shifted parallel to the initial glucose concentration at the lowest ripeness level. The modified time courses are presented in Figure 5. As shown in Figure 5, all time course data exhibited one curve-like trend. We then performed curve fitting using a logistic function, with an upper limit set based on the fructose concentration, which contributes most to sweetness. The storage periods were shifted by -20, -18, and -5 days for grapes of Levels A, B, and C, respectively, at 25°C. The data was well fitted with a determination coefficient of 0.96. These results, shown in Figures 3 and 5, suggest that sweetness in the post-harvest process can be estimated solely by capturing an image at harvest.

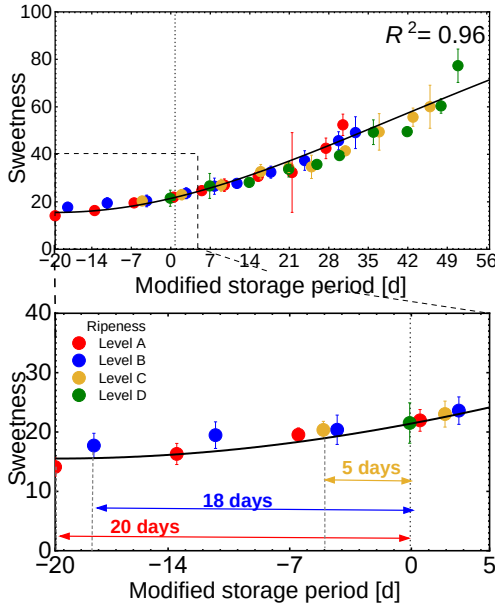

Figure 5. Changes of sweetness of squeezed fruit juice in modified time during storage.

4. Conclusions

The sweetness values of the fruit juices were calculated based on the predicted glucose, fructose, and sucrose contents derived from the infrared spectral information. Sweetness at harvest could be quantitatively determined by evaluating the *H* values of the fruit's surface color. Additionally, the sweetness values increased over time during storage, and were well-fitted by a logistic function. Consequently, these results suggest that it is possible to non-destructively predict the sweetness of the fruits based on information acquired at harvest, considering the post-harvest process.

References

Hashimoto, A., K. Suehara, T. Kameoka, 2015. Quantitative surface color measurement of tomato fruit using illuminating spectral information of natural lighting. Chemical Engineering Transactions, 44, 163-168. https://doi.org/10.3303/CET1544028.

Hashimoto, A., T. Muramatsu, K. Suehara, S. Kameoka, T. Kameoka, 2017. Color evaluation of images acquired using open platform camera and mini-spectrometer under natural lighting conditions. Food Packaging and Shelf Life, 14, 26-33. https://doi.org/10.1016/j.fpsl.2017.08.008.

Kameoka, T., T. Okuda, A. Hashimoto, A. Noro, Y. Shiinoki, K. Ito, 1998. A rapid FT-IR/ATR method for sugar content determination in food. Nippon Shokuhin Kagaku Kogaku Kaishi. 45(3), 199-204. https://doi.org/10.3136/nskkk.45.199.

Kanou, M., K. Nakanishi, A. Hashimoto, T. Kameoka, 2005. Influences of monosaccharides and its glycosidic linkage on infrared spectral characteristics of disaccharides in aqueous solutions. Applied Spectroscopy. 59(7), 885-892. https://doi.org/10.1366/0003702054411760.

Maebashi, K. 2011. A basic knowledge of sweetness, Journal of the Brewing Society of Japan, 106(12), 818-825. https://doi.org/10.6013/jbrewsocjapan.106.818.

Motonaga, Y., H. Kondou, A. Hashimoto, T. Kameoka, 2004. A method of making digital fruit color charts for cultivation management and quality control. International Journal of Food, Agriculture and Environment, 2(3&4), 160-166. https://doi.org/10.1234/4.2004.275.

Tsukahara, A., S. Kameoka, R. Ito, A. Hashimoto, T. Kameoka, 2020. Evaluation of freshness of lettuce using multi-spectroscopic sensing and machine learning, Journal of Applied Botany and Food Quality, 93, 136 – 148. https://doi.org/10.5073/JABFQ.2020.093.018.

Energy harvesting for a multi-sensor on dairy cattle

Susanne Demba [a], Annett Baudisch[b], Christopher Miersch[b], Danilo Zimmermann[b], Sarah Jahn[c], Doreen Nitsche[d], Steffen Pache[d], Kirsten Kouwert[d], Sandra Rose[a*]

[a] Department of Agricultural Machinery, Hochschule Neubrandenburg, University of Applied Sciences, Neubrandenburg, Germany

[b] nubix Software-Design GmbH, Dresden, Germany

[c] Institute of Epidemiology, Friedrich-Loeffler-Institut, Greifswald, Germany

[d] Department 74: Animal Husbandry, Saxon State Office for Environment, Agriculture and Geology, Köllitsch, Germany

* Corresponding author. Email: rose@hs-nb.de

Abstract

The world is now positioned in the first stages of the Fourth Industrial Revolution, complete with the Internet of Things (IoT) connected devices and non-IoT connected devices numbering in the billions. According to Statista, there will be just over 10 billion non-IoT active devices by 2025. Installing, maintaining, and replacing billions of batteries is a big logistical issue. In addition, improperly discarded lithium-ion (Li-Ion) batteries leak into the soil at landfills and cause air contamination. A special focus in the "Internet of Livestock" project is pointed on the topic of energy harvesting at the sensor level, since long-term life cycles must be assumed for practical acceptance, especially in the case of sensors on animals. A number of approaches within the project "Internet of Livestock" to self-power a Multi-Sensor NECKTAG® to measure animal behavior and climate conditions directly at the individual animal have been investigated. It was also determined whether there is enough light available in the barn for energy generation via a solar cell even in darker periods such as autumn and winter. The solar cell output increases linearly with increasing illuminance and have problems to generate enough energy in different barn areas. The energy yield due to the Seebeck effect was surprising. By means of a Peltier element, the cow's body heat can be used to generate a flow of electricity. Especially in the cold and dark season, this effect can support energy production very well. The results of the present study indicated that a combination of a solar cell and a Peltier element would be ideal to supply energy to a Multi-Sensor. Due to the opposite conditions, the highest energy yield for the solar cell in the bright season and for the Peltier element in the cold season, this combination makes it possible to provide energy for the Multi-Sensor all year around.

Keywords: Bluetooth 5.1, Multi-Sensor, animal tracking, energy harvesting, power supply

1. Introduction

Today's livestock industry faces many challenges in order to stay competitive. Increase the production to respond the global growing food demand, while preserving natural resources, the environment (Carillo and Abeni, 2020) and animal welfare as well as working cost efficient, while compensating the lack of skilled labor seem to be the main challenges in the livestock production. One opportunity to address these challenges is the increasing use of sensors and sensor networks in animal husbandry.

In livestock husbandry, sensors can be used to monitor physiological and behavioral parameters of livestock animals. This allows farmers to evaluate the health and welfare status of the animals (Neethirajan, 2017). Helwatkar et al. (2014) defined a sensor used in dairy husbandry as a device that measures a physiological or behavioral parameter of an individual cow and enables automated, on-farm determination of changes in this condition. Usually, this is related to a health or welfare issue and requires action of the farmer (Ahmann et al., 2024). Thereby, the monitoring will be done by two types of sensors: body sensors which monitor the vital parameters of the animals and environmental sensors to monitor the environmental conditions of the animals such as the barn climate (Bhavsar and Arolkar, 2012). Helwatkar et al. (2014) divide the sensors used for animal health monitoring in non-invasive and invasive sensors. Non-invasive sensors can be immobile sensors located in the barn (e.g. cameras, sensors to detect the barn climate) or mobile sensor boxes attached to the animal (e.g. pedometers, positioning sensors, ruminating sensor in a neck collar etc.). In contrast, invasive sensors are mobile sensor boxes swallowed or implanted to the animal (e.g. rumen bolus).

Livestock industry has developed a lot of sensors to monitor more animals without increased contact time

and number of labor, and to provide reliable measures of animal health and welfare (Helwatkar et al., 2014, Neethirajan, 2017). Many of these systems are able to automatically record animal-related data of individual animals as well as group of animals in real-time to support health and welfare monitoring (Stachowicz and Umstätter, 2020). The long-term energy supply is a major challenge for these sensors.

One possibility to face this challenge is the use of energy harvesting. Energy harvesting is defined as the production of a small amount of energy from environment sources like solar, thermal, wind or vibration (Anisi et al., 2017). Besides using energy from the environment, other sources such as body heat, foot strike or finger strokes could be converted to electrical energy as well (Sudevalayam and Kulkarni, 2011). According to Akhtar and Rehmani (2015), these sources can be used to prolong sensors battery life.

In previous studies some energy harvesting methods were tested regarding their application in dairy farming. Machts et al. (2015) developed and tested thermoelectric generators using the temperature difference between the sensor probe and the ruminal fluid during water intake to provide a rumen bolus with energy. With this method a maximum electric power of 32 µW could be generated. Minnaert et al. (2018) investigated the possibility to use a wireless, inductive power transfer to charge on-body sensor networks for cattle wile cows are eating. It was possible to transfer on average 96 J per meal (average eating time: 160 s) using this method. Kong et al. (2022) and Blažević et al. (2022) successfully used the movements of the cows to convert kinetic into electrical energy. Dang et al. (2024) developed a self-powered cow monitoring system using 915 MHz radio-frequency for sensor charging. With this system it is possible to charge the sensor tag within 5 min and to use the tag over 90 min without the need for recharging.

Since the most frequently used energy sources for sensors used in livestock husbandry are lithium-ion batteries which still have short battery lives, alternatives have to be investigated. Therefore, the aim of the present study was to investigate different energy harvesting methods to supply energy to a Multi-Sensor for dairy cattle.

2. Materials and Methods

A solar cell and a Peltier element were tested as energy harvesting methods to supply a Multi-Sensor with energy. The Multi-Sensor was developed to measure animal behaviour by use of the animals location as well as the climate conditions directly at the individual animal.

2.1. Experiment 1 – Solar cell

In a first step, measurements regarding the lighting conditions in different areas of the experimental barn were performed to find the most suitable solar cell. Based on these measurements, solar cells that are suitable especially for diffuse light and with a wideband light spectrum were investigated for their use as an energy harvesting method for a Multi-Sensor attached on dairy cows. Thus, a total of four solar cells were tested under laboratory conditions.

Therefore, the solar cells to be tested were illuminated with a light source at different illuminance levels (50 lux; 100 lux; 200 lux; 300 lux). The generated current and voltage were measured using multimeters (Figure 1).

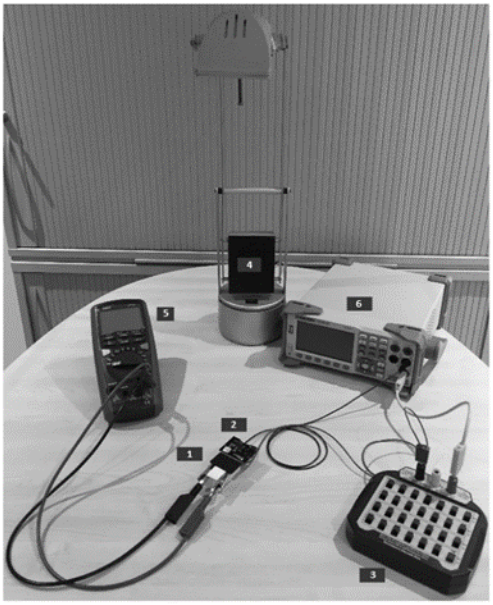

Figure 1: Experimental setup to test different solar cells regarding their suitability as an energy harvesting method for a Multi-Sensor attached on dairy cows.

2.2. Experiment 2 – Peltier element

With this experiment, it was investigated whether energy can be obtained from temperature differences between the cow and its environment using the Seebeck effect. This effect is utilized by a Peltier element so that a current flow is generated when there is a temperature difference at this element. Therefore, the Peltier element to be tested was thermally connected to a cold plate, the temperature of which is monitored directly under this Peltier element using the multimeter (Figure 2). There was a second Peltier element on this one to be tested, which acts as a heat source (temperature difference generates a current flow ↔ current flow generates temperature difference). The temperature on the top of the Peltier element to be tested was measured using a thermal camera. The harvester board was used as a load and charges a capacitor (470 mF). The capacitor was deliberately oversized in terms of capacity so that the harvester could not charge it up to the end-of-charge voltage during the test period, which would have made a correct evaluation impossible.

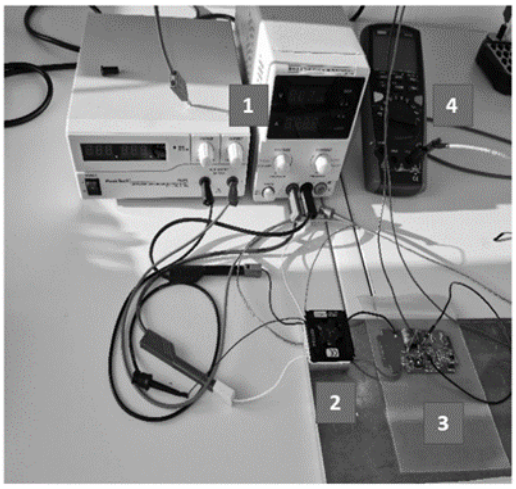

Figure 2: Experimental setup to test a Peltier element regarding the suitability as an energy harvesting method for a Multi-Sensor attached on dairy cows.

Tests were carried out with two temperature differences (5 K and 10 K) with a duration of 30 min for each temperature difference. The voltage of the capacitor is measured at the beginning and end of the test.

3. Results and Discussion

3.1. Solar cell

Measurements of the lighting conditions in the different barn areas show average values of 150 to 250 lux during the day. For comparison, outside the barn in the open air, values between 10000 lux (cloudy) and > 50000 lux (sunny, value exceeded the possible measuring range) were possible. As expected, the solar cell output increases linearly with increasing illuminance (Figure 3).

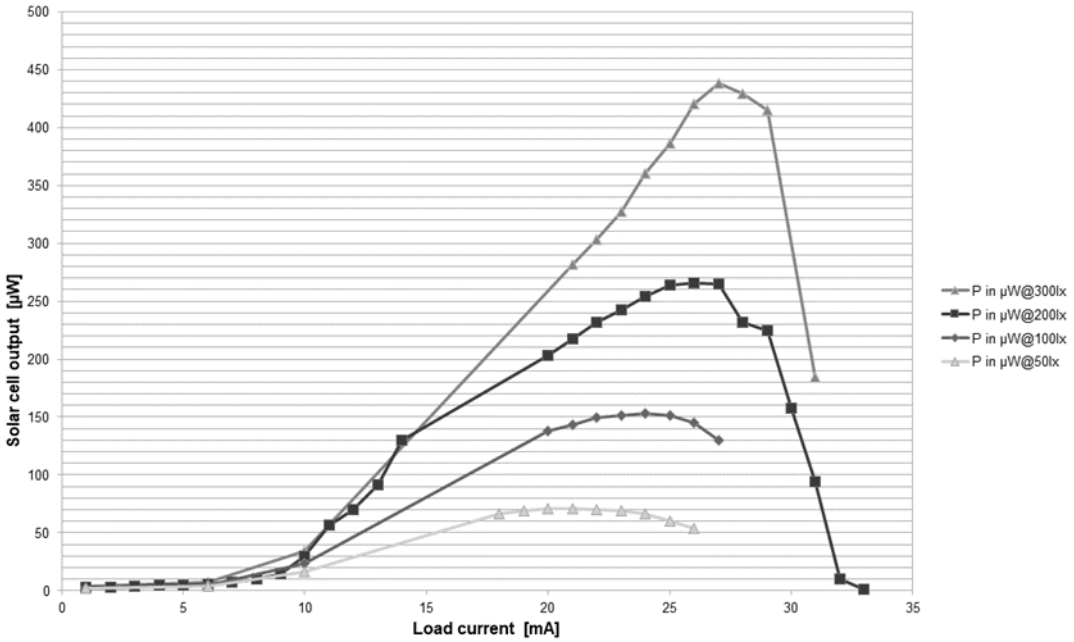

Figure 3: Measured solar cell output detected with different illuminance level.

However, it was already clear at this stage of development that the energy supply from the solar cell alone would not be sufficient. Akhtar and Rehmani (2015) confirm these results as they say that enough amount of light has to be available for optimal function of a solar cell. According to the authors, solar power is not steadily available since it is highly time and seasonal dependent. To efficiently use solar cells indoor, the source of indoor light is an important factor as the diverse sources have different types of irradiance spectra and outdoor solar cells are not suitable for indoor use (Biswas and Kim, 2020).

3.2. Peltier element

Under laboratory condition, energy could be generated using a Peltier element (Table 1).

Table 1: Generated energy by using two temperature differences with the help of a Peltier element

	5 K	**10 K**
Voltage at the beginning of the test	0,08 V	0,146 V
Voltage at the end of the test	2,01 V	2,695 V
Generated energy	0,948 Ws	1,702 Ws
Average power value	527 µW	945 µW

These results could be confirmed by the findings of other investigations. Earlier studies have shown that the Seebeck and the Peltier effect could be used to generate voltage (Sharma et al., 2017, Qasim et al., 2022). Zhou et al. (2021) found a high energy output using the Seebeck effect as well. Yuan et al. (2023) found out that thermoelectric generator systems based on the Seebeck effect are able to convert the heat energy in a road into electricity. Due to the measuring principle of the Peltier element, it will produce more energy in autumn and winter season because its efficiency depends on the temperature differences between the cows and the environment. The energy yield is higher, the colder it is in the barn.

4. Conclusions

Despite the poor lighting conditions in the barn and milking parlour, a significant energy yield can be achieved with the solar cell. However, a second, alternative energy source is needed to ensure the energy supply at night as well. Based on the measurement results, the decision was made in favour of the Peltier element. Under certain conditions, this energy source can generate a significant amount of energy. The Peltier element will tend to dominate energy generation in the cooler and darker seasons, as its efficiency depends on the ambient temperature. The colder it is in the barn, the higher the energy yield. The opposite is the case with solar cells, where efficiency increases on bright, sunny days. These opposite conditions make it possible to provide energy for the system all year round.

Acknowledgements

This work was financially funded by the German Federal Ministry of Food and Agriculture (BMEL) based on a decision of the Parliament of the Federal Republic of Germany, granted by the Federal Office for Agriculture and Food (BLE; grant number: 281C208C19)

References

Ahmann, J., K. Höse, A. Schmidt, K. Thiemann, H. Neeland, W. Büscher, S. Pache, and C. Umstätter. 2024. Agricultural assistance systems for decision support in livestock farming. agricultural engineering.eu 79(2).

Akhtar, F. and M. H. Rehmani. 2015. Energy replenishment using renewable and traditional energy resources for sustainable wireless sensor networks: A review. Renewable and Sustainable Energy Reviews 45:769-784.

Anisi, M. H., G. Abdul-Salaam, M. Y. I. Idris, A. W. A. Wahab, and I. Ahmedy. 2017. Energy harvesting and battery power based routing in wireless sensor networks. Wireless Networks 23(1):249-266.

Bhavsar, A. R. and H. A. Arolkar. 2012. Wireless sensor networks: a possible solution for animal health issues in rural area of Gujarat. International Journal of Enterprise Computing and Business Systems 2(2).

Biswas, S. and H. Kim. 2020. Solar Cells for Indoor Applications: Progress and Development. Polymers 12(6):1338.

Blažević, D., S. Philipp, J. Ruuskanen, J. Dizdarević, R. Niiranen, P. Rasilo, and A. Jukan. 2022. A farm animal kinetic energy harvesting device for IoT applications. Vol. 12090. SPIE Defense + Commercial Sensing. SPIE.

Carillo, F. and F. Abeni. 2020. An Estimate of the Effects from Precision Livestock Farming on a Productivity Index at Farm Level. Some Evidences from a Dairy Farms' Sample of Lombardy. Animals 10(10):1781.

Dang, T. H., L. Nkenyereye, V. T. Tran, and W. Y. Chung. 2024. Self-Powered Cattle Behavior Monitoring System Using 915 MHz Radio Frequency Energy Harvesting. IEEE Access 12:33779-33791.

Helwatkar, A., D. Riordan, and J. Walsh. 2014. Sensor Technology For Animal Health Monitoring. International Journal on Smart Sensing and Intelligent Systems 7(5):1-6.

Kong, L., M. Tang, Z. Zhang, Y. Pan, H. Cao, X. Wang, and A. Ahmed. 2022. A near-zero energy system based on a kinetic energy harvester for smart ranch. iScience 25(12):105448.

Machts, R., T. Reuter, P. V. Prokop, O. Schewtschenko, M. Stubenrauch, C. Schilling, and H. Witte. 2015. Energy harvesting for active implants: powering a ruminal pH-monitoring system. Current Directions in Biomedical Engineering 1(1):18-21.

Minnaert, B., B. Thoen, D. Plets, W. Joseph, and N. Stevens. 2018. Wireless energy transfer by means of inductive coupling for dairy cow health monitoring. Computers and Electronics in Agriculture 152:101-108.

Neethirajan, S. 2017. Recent advances in wearable sensors for animal health management. Sensing and Bio-Sensing Research 12:15-29.

Qasim, M. A., V. I. Velkin, and A. K. Hassan. 2022. Seebeck Generators and Their Performance in Generating Electricity. Journal of Operation and Automation in Power Engineering 10(3):200-205.

Sharma, A., H. Lee Jun, H. Kim Kyung, and P. Jung Jae. 2017. Recent Advances in Thermoelectric Power Generation Technology. 마이크로전자및패키징학회지 24(1):9-16.

Stachowicz, J. and C. Umstätter. 2020. Übersicht über kommerziell verfügbare digitale Systeme in der Nutztierhaltung. Agroscope Transfer 294(20):2-26.

Sudevalayam, S. and P. Kulkarni. 2011. Energy Harvesting Sensor Nodes: Survey and Implications. IEEE Communications Surveys & Tutorials 13(3):443-461.

Yuan, D., W. Jiang, A. Sha, J. Xiao, W. Wu, and T. Wang. 2023. Technology method and functional characteristics of road thermoelectric generator system based on Seebeck effect. Applied Energy 331:120459.

Zhou, W., K. Yamamoto, A. Miura, R. Iguchi, Y. Miura, K.-i. Uchida, and Y. Sakuraba. 2021. Seebeck-driven transverse thermoelectric generation. Nature Materials 20(4):463-467.

Internet of livestock – A smart locatable multifunctional sensor device to enable interconnectivity between operators and actuators in dairy cattle farming

Susanne Demba [a], Sebastian Schäfer [b], Peter Schneider[b], Sarah Jahn[c], Doreen Nitsche[d], Steffen Pache[d], Kirsten Kouwert[d], Sandra Rose [a,*]

[a] Department of Agricultural Machinery, Hochschule Neubrandenburg, University of Applied Sciences, Neubrandenburg, Germany

[b] Schneider Elektronik GmbH & Co. KG, Großharthau, Germany

[c] Institute of Epidemiology, Friedrich-Loeffler-Institut, Greifswald, Germany

[d] Department 74: Animal Husbandry, Saxon State Office for Environment, Agriculture and Geology, Köllitsch, Germany

* Corresponding author. Email: rose@hs-nb.de

Abstract

The objective of the project "Internet of Livestock" (IoL) was the development of a multifunctional sensor to record health-related data from dairy cows and to directly connect these data with operators, e.g. barn climate control operators.

The sensor was developed for attachment to the cow's collar located on the back of the neck. The Multi-Sensor is designed according to a modular principle and contains of different sensors for data recording.

With the developed sensor it is possible to measure the environmental traits illuminance (lux), relative humidity (%), air pressure (hPa), temperature (°C), as well as the air quality directly on the animal. The selected traits are suitable for detecting and describing deviations in behaviour and animal welfare from the biological normal state. With the new sensor system, a localization of the cows in the barn is possible as well. Therefore, an antenna system for networking the sensors as well as the connection to the host computer based on BLE_5.1 including 3D real-time localization was set up.

Data were transmitted using energy-saving Bluetooth 5.1 technology to the host computer, in order to create a standardized information provision for farm management and information systems at the farmer. Furthermore, the BLE_5.1 technology makes it possible for the first time to develop bidirectional communication for controlling actuators on the animal, on machines/devices or at the operator. The location data achieves sufficient measurement accuracy and reproducibility (within ±1m) to create animal-specific tracking routes and derive animal behaviour characteristics.

By means of the developed application-open host computer software interface, the platform-independent data exchange and the networking option to higher-level farm management and information systems (Internet, cloud or farm network) as well as the feedback of control functions to the above-mentioned sensor technology were realized.

Keywords: Bluetooth 5.1, Multi-Sensor, animal welfare, animal behaviour, dairy cattle tracking

1. Introduction

The automation and digitalization of various production and management processes have found their way into modern dairy farming. The use of innovative sensor technologies enables automatic and sensor-based data collection in almost all areas of the barn. Nowadays, there are virtually no limits to data collection. The continuous digital recording of data on the animal and its environment should enable conclusions to be drawn about animal welfare and increased productivity in dairy farming.

Stachowicz and Umstätter (2020) already describe a large number of digital assistance systems, particularly for the dairy cattle sector. The sensor offerings in the agricultural sector are diverse but are only isolated solutions. The interfaces to the farm management systems are not compatible, which is why it is not yet possible to connect the sensors. The collected raw data is not transferred, but only aggregated. Therefore, livestock farmers are concerned about data ownership in their barns (Fadul-Pacheco et al., 2022) and they can only use the sensors to a limited extent. The integration of human, animal and technique in the development and use of digital assistance systems plays an important role as well (Ahmann et al., 2024).

While sensors for recording health parameters such as activity, feeding time and rumination have become established in practice, the combination with environmental parameters plays a minor role. According to Leliveld et al. (2024), there are currently no systems available that integrate barn environment conditions in the detection of the animal welfare status. This led to the conclusion that curtains, ridge openings, fans and light are controlled by measuring the climate conditions outside the barn and not depending on the animal's welfare status. Hempel et al. (2018) concluded that measurements to assess the barn climate should be taken in a height of about 3 m–3.5 m, because this height could represent the conditions in the animal occupied zone. According to the current state of knowledge, there is no evaluated sensor that takes measurements of the microclimate on the cow and derives

automated measures to improve the barn climate.

Furthermore, there may be interference with sensors in the same frequency range. For this reason, most of the sensors established on the market for localization and health monitoring cannot be used in parallel in a barn.

The use of the Bluetooth 5.1 (BLE_5.1) radio protocol standard provides options for bidirectional, low-energy data transmission and theoretically decimetre-accurate real-time localization (Unold et al., 2020). According to Makario and Maina (2021) the use of BLE_5.1 wireless communication protocol can help to improve farm management. Based on this standard, it is therefore possible to aggregate sensor and actuator information and control the status of the actuators via bidirectional transmission, in addition to real-time localization.

The objective of the present study was to develop and test a smart locatable multifunctional sensor device for dairy cows to enable interconnectivity between operators and actuators by using Bluetooth Low Energy and energy harvesting.

2. Materials and Methods

2.1. Sensor device

The sensor device consists of a sensor tag that measures animal related data, an antenna array that transfer the measured data and a host computer for data analysis.

The tag is attached to the cow via collar and it is located on the back of the neck (Figure 1). The Multi-Sensor is designed according to a modular principle and contains of different sensors for data recording. The sensor is able to measure the environmental traits illuminance (lux), relative humidity (%), air pressure (hPa), temperature (°C), as well as the air quality directly on the animal. A localization of the cows in the barn is possible as well.

Figure 1: Sensor on the collar of a cow.

The tag uses BLE_5.1 for data transmission to the host computer and is supplied with energy via energy harvesting.

Antenna arrays were developed to transfer the data measured by the sensor tag (Figure 2). These arrays use BLE_5.1 as well. With the help of the arrays a 3D real-time localization via 3D positioning of the sensors, which could be used for animals, machines and facilities, is possible. Due to a Power-Over-Ethernet connection, the antenna arrays communicate with the host computer and were supplied with energy. They have a water- and dustproof housing that make them suitable for indoor and outdoor use.

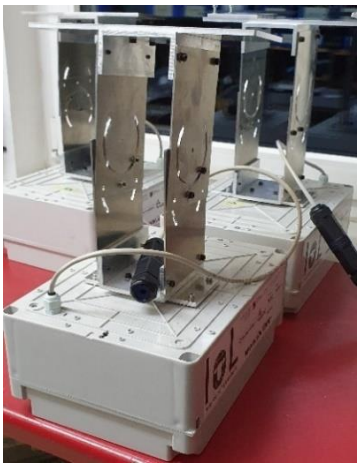

Figure 2: Antenna array with housing and external mounting for installation in the barn.

The HOST-PC is used as the data and software centre. The developed software (Figure 3) was used for sensor data aggregation of the sensor as well as for antenna array control, data exchange and calculation of the 3D real-time localization data and storage of the data in the database. It was also used to provide an interface for platform-independent data exchange with higher-level third-party systems.

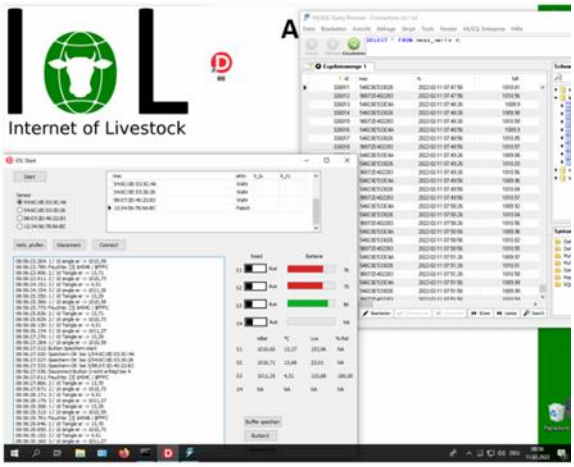

Figure 3: Desktop view of the developed software on the host computer.

2.2. Accuracy test of the localization system in a cubicle barn

All accuracy tests of the developed localization system were performed in the dairy barn of the Saxon State Office for Environment, Agriculture and Geology in Köllitsch, Germany.

This is a cubicle barn built in 1998 with a slatted floor for 120 dairy cows, which are divided into four performance groups and one wellness group. The cubicles are fitted with rubber mats, cleaned daily and overspread with a mixture of sawdust and lime. The slurry channel is located directly under the slatted floor, into which the animals' excrement is pushed several times a day by a slatted robot. The sides of the barn are open and can be opened or closed with curtains, depending on the weather conditions. The gable ends are fitted with wooden spaceboards at roof truss height. The gaps are designed to be 28 mm to allow light and air through.

2.2.1.Static accuracy test

The localization accuracy was tested at 14 measuring points uniformly distributed over the complete barn area (Figure 4).

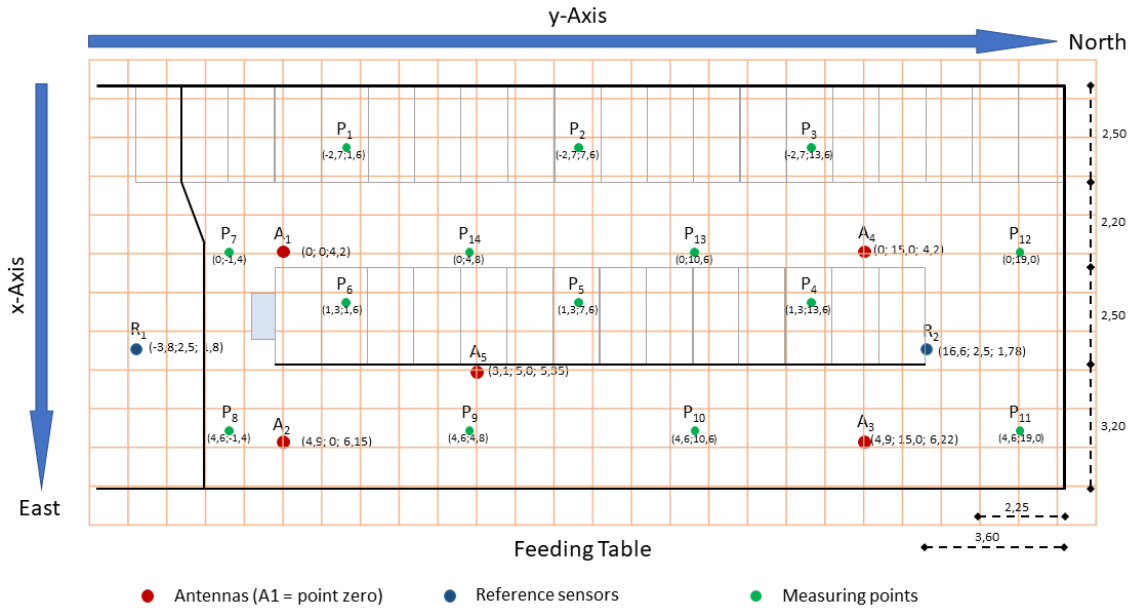

Figure 4: Arrangement of the antennas (red), the reference sensors (blue) and the measuring points (green) in the barn compartment.

At each measurement point, each of the two transmitters 80:66 and 6D:C9 was positioned at heights of 1.45 and 0.45 m for three minutes to compare its true position with the positions determined by the antenna array via BLE 5.1.

2.2.2.Dynamic animal localization test including animal observation

To determine the accuracy of animal location measurements, the locations measured by the sensor tags were compared with direct observations. Therefore, four lactating cows were equipped with a sensor tag with the help of a collar. Direct observations were performed on six days for 2 hours from (7.30-09.30 a.m.) and on one day for 4 hours (07.30-11.30 a.m.) by one observer. The locations of the animals (row/column of the barn grid) as well as the position (standing or lying) were recorded every two minutes. This means that 480 observation values were assessed for the four experimental animals. The tags recorded values every 30 seconds.

3. Results and Discussion

3.1.1.Static accuracy test

When determining the position of the tags every 5 seconds, a positioning accuracy of 1 m was maintained. The tag C6:D9 deviated more strongly from the current position than the tag 80:66 and had some failures in the position determination. Tag 80:66, on the other hand, showed the actual position well at a radial distance of less than one meter. The technical error in tag C6:D9 was corrected after the examinations.

The results of the static accuracy test show that the accuracy of the tested smart locatable multifunctional sensor device was not as good as that of commercially available systems. Ipema et al. (2013) found an average accuracy of 30.5 cm (± 25 cm) during a static accuracy test of a positioning system using Ultra-High-Frequency. A positioning system based on Ultra Wide Band radio signals measured the location of the tags in a static test with an accuracy of 17 ± 17 cm (Frondelius et al., 2014).

3.1.2. Dynamic animal localization test including animal observation

In figure 5, the observations show that cow number 42 (green), cow number 117 (yellow) and cow number 41 (red) moved around during this observation period. Cow number 21 (blue) was lying down in cubicle 4, but was located in cubicle. During the dynamic animal localization test, an accuracy of 0.5-1.0 m could be achieved.

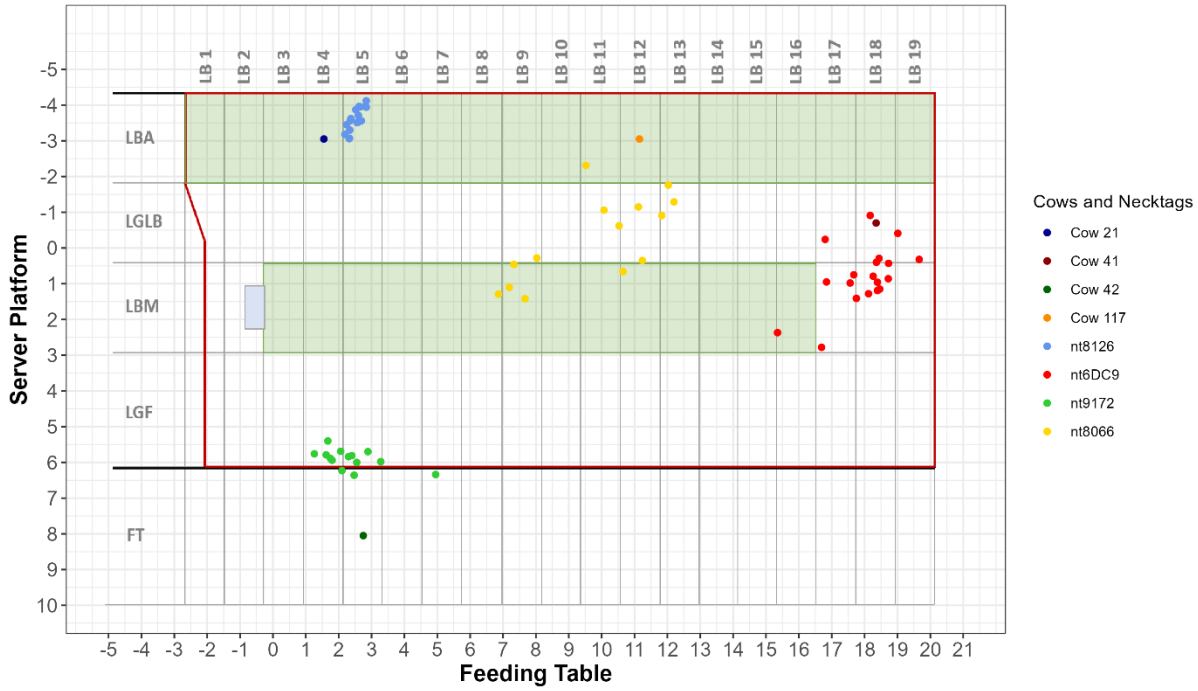

Figure 5: Results of the dynamic accuracy test with animal position determined by direct observations (dark coloured dots) and animal position detected by the sensor system (light coloured dots).

The mentioned accuracy detected with the developed sensor system was also not as precise in the dynamic tests as those of other systems. Frondelius et al. (2014) found an accuracy of 0.17±0.17 m using Ultra Wide Band radio signals to detect the cow position. However, they did not mount their tags on moving cows, but on a wooden plank which was moved back and forth on eight specific measuring lines. Tullo et al. (2016) used a localization system using Ultra-High-Frequency and found correlations of 0.82, 1.00, 0.98 and 0.88 for the locations alley, cubicles, trough and at the drinker, respectively.

4. Conclusions

It could be concluded that a cow localization system using BLE_5.1 could be used to find dairy cows in the barn. Since this data transfer method is energy-saving compared with Ultra-High-Frequency or Ultra Wide Band, it could help to extend the lifetime of the sensor tags. Nevertheless, further developments and investigations are necessary to improve the accuracy of the localization system.

Acknowledgements

This work was financially funded by the German Federal Ministry of Food and Agriculture (BMEL) based on a decision of the Parliament of the Federal Republic of Germany, granted by the Federal Office for Agriculture and Food (BLE; grant number: 281C208C19).

References

Ahmann, J., K. Höse, A. Schmidt, K. Thiemann, H. Neeland, W. Büscher, S. Pache, and C. Umstätter. 2024. Agricultural assistance systems for decision support in livestock farming. agricultural engineering.eu 79(2). https://www.agricultural-engineering.eu/landtechnik/article/view/3305

Fadul-Pacheco, L., S. R. Wangen, T. E. da Silva, and V. E. Cabrera. 2022. Addressing Data Bottlenecks in the Dairy Farm Industry. Animals 12(6):721. https://doi.org/10.3390/ani12060721

Frondelius, L., M. Pastell, and J. Mononen. 2014. Validation of the TrackLab positioning system in a cow barn environment. Pages 125-128 in Proc. Proceedings of Measuring Behavior, Wageningen, The Netherlands. http://www.measuringbehavior.org/mb2014/proceedings

Hempel, S., König, M., Menz, C., Janke, D., Amon, B., Banhazi, T.M., Estellés, F., and Amon, T. 2018. Uncertainty in the measurement of indoor temperature and humidity in naturally ventilated dairy buildings as influenced by measurement technique and data variability. Biosystems Engineering 166:58-75. https://doi.org/10.1016/j.biosystemseng.2017.11.004

Ipema, A., T. Van De Ven, and P. Hogewerf. 2013. Validation and application of an indoor localization system for animals. Pages 135-144 in Proc. 6th European Conference on Precision Livestock Farming, Leuven, Belgium.

Leliveld, L. M. C., C. Brandolese, M. Grotto, A. Marinucci, N. Fossati, D. Lovarelli, E. Riva, and G. Provolo. 2024. Real-time automatic integrated monitoring of barn environment and dairy cattle behaviour: Technical implementation and evaluation on three commercial farms. Computers and Electronics in Agriculture 216:108499. https://doi.org/10.1016/j.compag.2023.108499

Makario, J. and C. w. Maina. 2021. A Bluetooth Low Energy (BLE) Based System for Livestock Tracking and Localization. Pages 1-7 in Proc. 2021 IST-Africa Conference (IST-Africa). http://repository.dkut.ac.ke:8080/xmlui/handle/123456789/4862

Stachowicz, J. and C. Umstätter. 2020. Übersicht über kommerziell verfügbare digitale Systeme in der Nutztierhaltung. Agroscope Transfer 294(20):2-26.

Tullo, E., I. Fontana, D. Gottardo, K. H. Sloth, and M. Guarino. 2016. Technical note: Validation of a commercial system for the continuous and automated monitoring of dairy cow activity. Journal of Dairy Science 99(9):7489-7494. https://doi.org/10.3168/jds.2016-11014

Unold, O., M. Nikodem, M. Piasecki, K. Szyc, H. Maciejewski, M. Bawiec, P. Dobrowolski, and M. Zdunek. 2020. IoT-Based Cow Health Monitoring System. Computational Science – ICCS 202020th International Conference, Amsterdam, The Netherlands, June 3–5, 2020, Proceedings, Part V 12141:344-356. https://doi.org/10.1007/978-3-030-50426-7_26

Greenhouses energy audits – procedures and results

Catherine Baxevanou [a], Dimitrios Fidaros [b], Chryssoula Papaioannou[a], Nikolaos Katsoulas[b],*

[a] Department of Agrotechnology, University of Thessaly, Gaiopolis, 41500 Larisa, Greece

[b] Laboratory of Agricultural Constructions and Environmental Control,
Department of Agriculture Crop Production and Rural Environment, University of Thessaly,
Fytokou Street, 38446 Volos, Greece

* Corresponding author. Email: nkatsoul@uth.gr

Abstract

Modern greenhouses are energy consumers in order to control appropriately the internal microclimate and to serve the requirements of the crop growth. For the design of energy-efficient greenhouses with the possibility of utilizing locally available renewable energy sources, it is necessary to know not only the total annual energy consumption but also additional data such as: a) The time distribution of energy consumption (daily and yearly variation), b) The type of consumed energy (thermal or electrical) and, c) its distribution among the various production and environment control procedures. For the collection of the above information a procedure of energy audit is required. In the present text a procedure for the first steps of operational rating review is presented and applied to various greenhouses in Greece.

The energy audits results are presented in terms of (i) power and energy distribution pies by energy type and procedure, (ii) SANKEY diagrams, and (iii) energy indices per greenhouses area and per production unit. To date, in the existing relevant bibliography it is customary to calculate the energy consumption in greenhouses with reference to the greenhouse unit area resulting to a wide dispersion of prices even for greenhouses located in the same climatic conditions and with the same cultivation since greenhouses mechanization level is ignored. Thus, low-tech greenhouses may appear better than high-tech greenhouses in terms of energy consumption, leading to a distorted picture since it ignores the greater productivity of high-tech greenhouses. In this work both energy indicators are calculated, energy consumption per greenhouse uit area in order to compare with the literature, and energy consumption per production unit. The energy audit results can guide the greenhouse manager to decision about operational strategy, used type of energy, equipment characteristics and local energy sources exploitation.

Keywords: greenhouse, energy audit, energy performance, energy indices

1. Introduction

Modern greenhouses are energy consumers in order to control appropriately the internal microclimate and to serve the requirements of the crop growth. For the design of energy-efficient greenhouses with the possibility of utilizing locally available renewable energy sources, it is necessary to know not only the total annual energy consumption but also additional data such as: a) The time distribution of energy consumption (daily and yearly variation), b) The type of consumed energy (thermal or electrical) and, c) its distribution among the various production and environment control procedures. This information will allow the choice of adequate energy type, energy sources and equipment characteristics that would ensure reduced energy consumption and reduced environmental footprint.

For the collection of the above information a procedure of energy audit is required. The concept of energy audit has been initially developed in USA and adopted in many applications in Europe almost 20 years ago. For the energy audits conduction (for industry and buildings) was developed methodologies according to relative European Union Directives (from 93/76/EC to 2018/844/EU) (EC 1993, 2010, 2018, EC/EP 2002, 2012). Especially for the energy audits of conventional buildings this methodology was specified according to 2002/91/EC (Paris, Vandorou *et al.*, 2022) directive supported by a number of European and International Norms. The case of industry energy audits has been addressed through European research and development projects like FP7 or Intelligent Energy and more recently Horizon2020, without to lead yet in specific Directive other that the 93/76/EC (EC 1993).

Energy audit is a systematic process that aims to: a) form a comprehensive view on the energy consumption profile of a building or system by identifying the factors that affect it, b) consider energy saving

options taking into account the total cost of the product, c) provide a comprehensive proposal to the unit manager regarding the energy saving measures he can implement (Baxevanou, Fidaros *et al.,* 2021).

In the present text a procedure for the first steps of operational rating review is presented and applied to various greenhouses in Greece. In this procedure various parameters affecting the energy consumption are accounted like: a) the local external climatic conditions, b) the cultivation characteristics, c) the greenhouse construction, d) the greenhouse operation strategy, e) the installed equipment for production and environmental control. The energy audits results are presented in terms of (i) energy distribution pies by energy type and procedure, (ii) SANKEY diagrams, (iii) greenhouse gases emissions and (iii) energy indices per greenhouses area and per production unit.

2. Materials and Methods

2.1. Energy audit procedure

An energy audit is consisted of two discrete phases. The first phase is an operational rating approach which means that the energy consumption is calculated directly using the data of energy bills and of the production data. From the first phase auditor acquire a general perspective about the greenhouse energy performance but an analysis is required in order to be able to: a) distribute the consumed energy among the different procedures inside a greenhouse, b) allocate the most energy consuming activities, c) assess the efficiency of various procedures and finally d) suggest energy performance improvement measures. This analysis is realized in the second phase which is an asset rating approach (Baxevanou *et al.,* 2021). The present work focuses in the first phase of the energy audit and extend in part of the second phase eg until distribution of the consumed energy among different procedures inside the greenhouse.

In the first step (site visit) auditor: (i) records the installed equipment which consumes energy, (ii) record the construction characteristics, (iii) records the basic characteristics of the surrounding area, (iv) interview the unit manage (Baxevanou *et al.,* 2021).

In the second step auditor should collect data that cannot be recorded by greenhouse inspection. Most of them are collected and delivered by the owner/manager after the interview or during it. These data include: (i) Construction plans of the chambers and plans of the area, (ii) Manuals and technical characteristics specifications of the equipment, (iii) Existing energy consumption measurements, (iv) Energy consumption invoices (v) Production data in annual base for the last three years, (vi) Local climatic data. Energy consumption invoices can have covered the financial data (Baxevanou *et al.,* 2021).

The data analysis phase is constituted by following steps: (a) elaboration of the collected data, (b) Calculation of energy indices, (c) identifying energy-intensive processes and low performing equipment. The last will be analyzed in section 2.3

2.2. Examined case studies

The above-described energy audit procedure was implemented in 4 greenhouses in Central Greece. The basic characteristics of the 4 examined greenhouses where the procedure of energy audit were implemented are summarized in the following Table

Table 1. Examined greenhouses characteristics

Greenhouse number	1-Commercial	2–Commercial	3–Commercial	4–Experimental
Greenhouse type	Hydroponic, Gothic, multispan	Arched, multispan	Arched roof, multispan	Gothic, multispan
Greenhouse crop	Cucumber	Potted flowers	Tomato	tomato
When was it constructed	2010	2010	2011	2018
When was it renovated	2018, new (hanging) grow gutters	2023, a new 1000 m^2	No	No
Greenhouse location	N 39^o 54’ 43’’ E 22^o 37’ 21’’	N 39^o 14’ 14.56’’ E 22^o 43’ 48.51’’	N 39^o 15’ 16.3’’ E 22^o 44’ 19.18’’	N 39^o 23’ 41.14’’ E 22^o 45’ 29.16’’

Altitude of greenhouse location	65 [m]	70 [m]	81 [m]	85 [m]
Greenhouse ground area	5040 [m^2]	8000 [m^2]	5000 [m^2]	800 [m^2]
Mean greenhouse heigh	Gutter 5 [m], top 7.35 [m]	Gutter 4 [m], top 6.2 [m]	Gutter 3.5 [m] top 6.1 [m]	Gutter 5 [m], top 7.35 [m]

2.3. Data analysis

The data analysis is the most interesting part and requires combination of recording, gathered information (from the manager interview), calculations and literature data. The elaboration of collected data in order to calculate the total installed power, the total consumed energy, the distribution of installed power to different procedures, the calculation of power indices and the calculation of general energy consumption indices is straight forward. However, for the distribution of consumed energy it is required calculations and use of the energy consumption invoices time series in monthly base with the concept of base load. This procedure will be shortly described here with two examples of realized for the project energy audit.

After elaboration of three years data the basic yearly pattern is determined. This pattern along with analytical calculations about the theoretical energy consumption is used for the determination of operation hours of each individual device, with the assumption that each device operates at full load continually. As already said the electrical energy consumption can be distinguished to the following procedures: (i) heating, (ii) cooling, (iii) ventilation, (iv) irrigation, (v) lighting, (vi) refrigeration, (vii) fertigation, (viii) transport system, (ix) other.

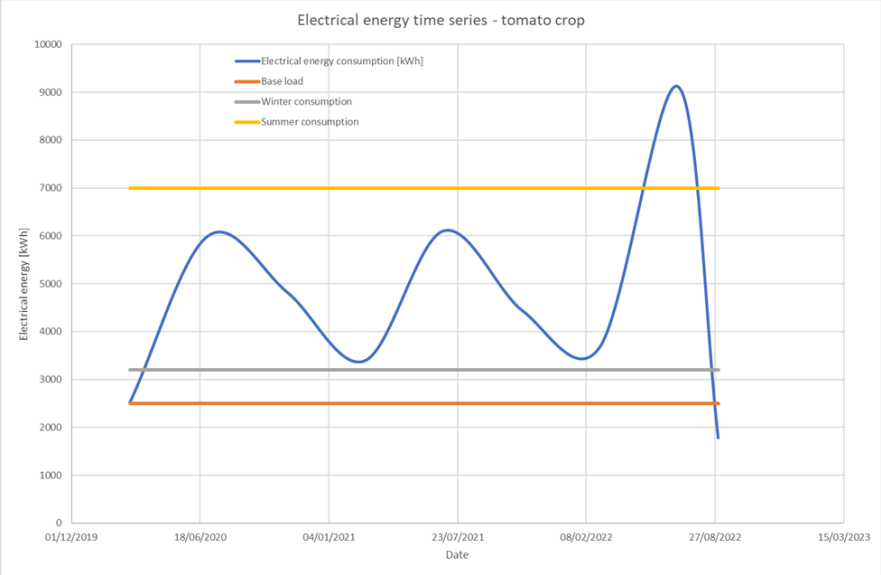

Figure 1. Electrical energy time series in a Tomato crop greenhouse in Greece

Usually from the manager interview information about the operation conditions of transport systems, refrigeration and other machines operation which however according to the literature are not the main power consumption points are gathered. Furthermore, with theoretical calculation of heating demand and the known power of heating production equipment the hours of operation of heating equipment can be calculated. Finally, the energy consumption for irrigation can be calculated theoretically by the water consumption (Kittas, Katsoulas *et al.*, 2014) and from there the irrigation system operation time. It can also be considered that the operation time of fertigation system is the same with the operation time of irrigation system. Then the unknown operation hours concern the cooling system, the ventilation system and the lighting system. From the time series a base load (the lowest energy consumption usually achieved in autumn or spring months) can be determined that correspond to consumption independent of climatic conditions. The summer maximum corresponds to base load plus the cooling load and the winter maximum correspond to base load plus the lighting load. Thus, a system with three equations and three unknowns is produced that allow the

operation time of equipment for cooling, ventilation and lighting. Of course, the above procedure each time is adapted to the characteristics of each examined greenhouse, the type of the crop and the information given by the manager. The heating needs are calculated in monthly base using the concept of representing day (according to ISO13790 (ISO 2008)) with quite accuracy, while the calculation of cooling needs would require more hideous calculations in hourly base and are not considered adequate for the purposes of an energy audit. In Figure 1 an example of the application of this method is presented. In the Figure 1 the electrical consumption time series of a tomato cultivation greenhouse in Central Greece is presented constructed from four months' invoices. In the specific greenhouse energy is consumed for heating, cooling, ventilation and irrigation and fertigation. It should also account that the crop schedule is from January to September or October. In this case the base load corresponds to fertigation and irrigation, the winter load corresponds to base load + heating and the summer load corresponds to base load + ventilation+ cooling.

3. Results and Discussion

As stated earlier the energy audits results will be presented in terms of power and energy distributions, energy balance flow charts and energy intensity indices.

3.1 Power and energy distributions

In the Table 2 the distribution of total installed power among thermal and electrical is presented for the four examined greenhouses. From the total power distribution, it clearly comes out that thermal power accounts for the bigger part of the total installed power with merits that range between 4 to 13 %. In the Figure 2 the distribution of thermal energy to various procedures is presented. In the tomato greenhouses all the thermal installed power is used for heating, while in the other two greenhouses thermal power is also used for electricity production with generator pairs. This represents the 4% of the thermal power for the cucumber greenhouse and the 8% of the thermal power for the potted flower greenhouse.

Table 2. Distribution of total installed power

Greenhouse	Total thermal power [%]	Total electrical power [%]
Cucumber commercial	94	6
Potted flower commercial	96	4
Tomato commercial	87	13
Tomato experimental	91	7

In the Figure 2 the electrical power distribution among various procedures is presented. In all the commercial greenhouses the fertigation represents the 10 – 12 % of the installed electrical power. The installed power for lighting is negligible except for the case of potted flowers greenhouse where it represents the 25% of the total installed electrical power. As far it concerns heating and cooling the vegetable production greenhouses have similar behaviour while the potted flower greenhouse has no installed power for cooling but important installed power for heating. Installed power for ventilation ranges from 6 to 15%. While the installed power for irrigation is high enough in almost all the cases. It should be noted that usually this is due to drilling pumps which, however may serve other purposes too in the farm where the greenhouse is installed.

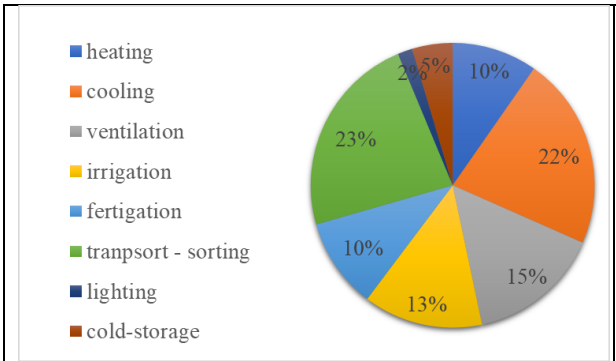

Cucumber Commercial

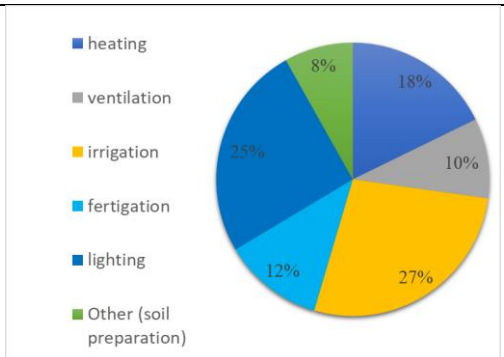

Potted flowers

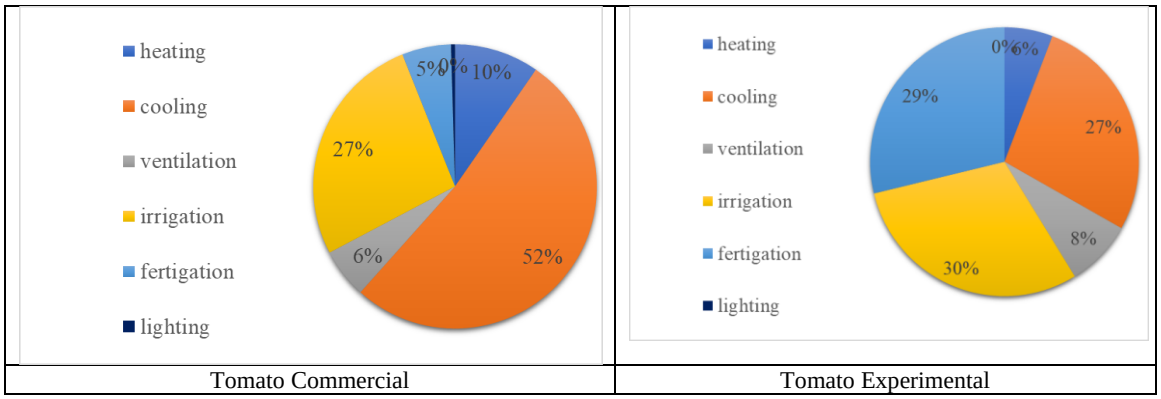

Tomato Commercial | Tomato Experimental

Figure 2. Distribution of installed electrical power

From the above it comes out that an important energy consumption procedure is the greenhouses heating. In the following Table 3 the efficiency of heating systems in each greenhouse is summarized. In the cases of biomass burners very low efficiency heating systems are observed.

Table 3. Heating systems efficiency and fuel

Audited greenhouse	Heating system total efficiency	Fuel
Cucumber	26%	Biomass
Potted flower	42%	Biomass
Tomato commercial	65%	Diezel
Tomato experimental	89%	Diezel

For the commercial greenhouses data for real energy consumption are available. Since it is obvious that heating is the main thermal energy consumption it is good to account for the efficiency of heating systems used in each greenhouse and to adapt the real energy consumption for heating to the one that would arise if a heating efficiency degree of 75% would have been achieved. In this case the distribution between thermal and electrical energy consumption in terms of primary energy is presented in the Table 4.

Table 4. Primary energy distribution

Audited greenhouse	Thermal energy [%]	Electrical energy [%]
Cucumber	65	35
Potted flower	66	34
Tomato commercial	69	31

From Table 4 it arises the important contribution of electrical energy in the final energy consumption in greenhouses. For that reason, in the next Figure 3 the distribution of electrical energy consumption among various procedures is studied for two of the commercial greenhouses.

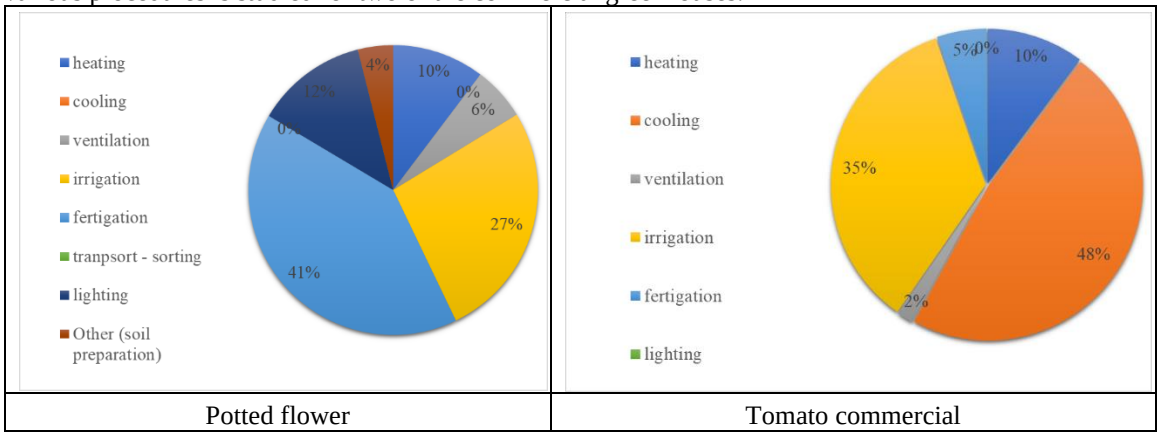

Potted flower | Tomato commercial

Figure 3. Electrical energy distribution

In both greenhouses the electrical energy consumed for heating is the 10%. In the tomato greenhouse cooling with 48% is the major power consumption process while in the potted flower greenhouse there is no such consumption and the need for cooling is covered by ventilation (representing the 6% of the consumption). In both irrigation accounts for the 1/3 of the total energy consumption. Fertigation system and

lighting complete the energy consumption for the potted flower greenhouse while in the tomato greenhouse the fertigation accounts for the 5% of the total consumption and the consumption for lighting is negligible. From the Table 5, where the distribution of final energy consumption of various procedures is presented along with literature values, it occurs that the observed values fall within the internationally expected range.

Table 5. Comparative presentation of procedures participation in final energy consumption in Greenhouses

s/n	Procedure	Energy audits	Literature (Paris *et al.*, 2022)
1	Heating	78 – 93%	0 – 99%
2	Cooling	0 – 11%	
3	Ventilation	0.5%	
4	Irrigation	2 – 8%	1 – 19%
5	Fertigation	1 – 3%	1 – 27%
6	Pesticide		0 – 6%
7	Lighting	0 – 1%	1%
8	Other	0 - 0.5%	-

3.2 Energy indices

In order to be able to assess the energy efficiency, the energy indices should be calculated. The international practice is to calculate the energy consumption reduced to the area of the greenhouse. Table 6 shows the energy indices of the examined greenhouses as well as values derived from the international literature. The table shows a wide distribution of values of this energy index even for the same crops in areas with similar climatic conditions. This is due to different degrees of mechanization of the examined greenhouses. But in this way the energy indicator becomes unreliable because a different degree of mechanization means a different production per unit of greenhouse surface. For this reason, the energy consumption reduced to the production unit of the greenhouse is proposed as an energy indicator.

Table 6. Comparative presentation of energy index kWh/m^2

Case	Energy consumption per area [kWh/m^2]
Tomato energy audit	8.79
Cucumber energy audit	488.9
Potted Flower energy audit	78.17
Spain high energy intensity tomato (Baptista, Silva *et al.*, 2012)	386
Spain low energy intensity tomato (Alonso and Guzmán 2010)	5.58
Spain low energy intensity lettuce (Alonso and Guzmán 2010)	4.03
Spain low energy intensity peppers (Alonso and Guzmán 2010)	5.56
Spain low energy intensity beans (Alonso and Guzmán 2010)	4.31
Greece high energy intensity tomato (Kittas, Elvanidi *et al.*, 2016)	237
Greece high energy intensity lettuce (Trypanagnostopoulos, Kavga *et al.*, 2017)	200
Greece high energy intensity flowers (Vourdoubas 2015)	318
Greece low energy intensity tomato (de Visser, de Buisonje *et al.*, 2012)	7.14
Greece low energy intensity cucumber (de Visser *et al.*, 2012)	6.9
Italy low energy consumption tomato (Campiglia, Colla *et al.*, 2007)	3.49
Italy low energy consumption lettuce (Campiglia *et al.*, 2007)	1.75
Netherlands tomato (de Visser *et al.*, 2012, Stanghellini, Baptista *et al.*, 2016) (av.)	368
Netherlands cucumber (de Visser *et al.*, 2012)	398
Netherlands sweet pepper (de Visser *et al.*, 2012, Stanghellini *et al.*, 2016) (av.)	376
Germany tomato (de Visser *et al.*, 2012)	351
Germany cucumber (de Visser *et al.*, 2012)	362

In the Table 7 the energy intensity is given in terms of produced volume and produced pieces for the potted flower greenhouse and in terms of produced mass for the tomato greenhouse.

Table 7. Energy consumption indices per greenhouse production

Energy consumption	Potted flower [kWh/piece]	Potted flower [kWh/lt]	Tomato [kWh/kg]
Thermal	5.212	3.148	8.792
Electrical	0.400	0.242	0.935
Total Primary	6.371	3.848	11.504
Thermal Heating	5.191	3.136	8.792
Power generation	0.020	0.012	0.000
Electrical heating	0.041	0.025	0.095
Electrical cooling	0.000	0.000	0.447
Electrical ventilation	0.024	0.014	0.016
Electricla irrigation	0.106	0.064	0.328
Electrical fertigation	0.163	0.098	0.049
Electrical tranpsort - sorting	0.000	0.000	0.000
Electrical lighting	0.050	0.030	0.000
Electrical cold-storage	0.016	0.010	0.000

3.3 Energy flows

In addition to energy indicators, an efficient way of representing the energy efficiency of a production facility is the visualization of energy flows through SANKEY diagrams. In the Figure 4 the SANKEY diagram of the energy flows for the potted flower greenhouse is presented in terms of final energy consumption as an example.

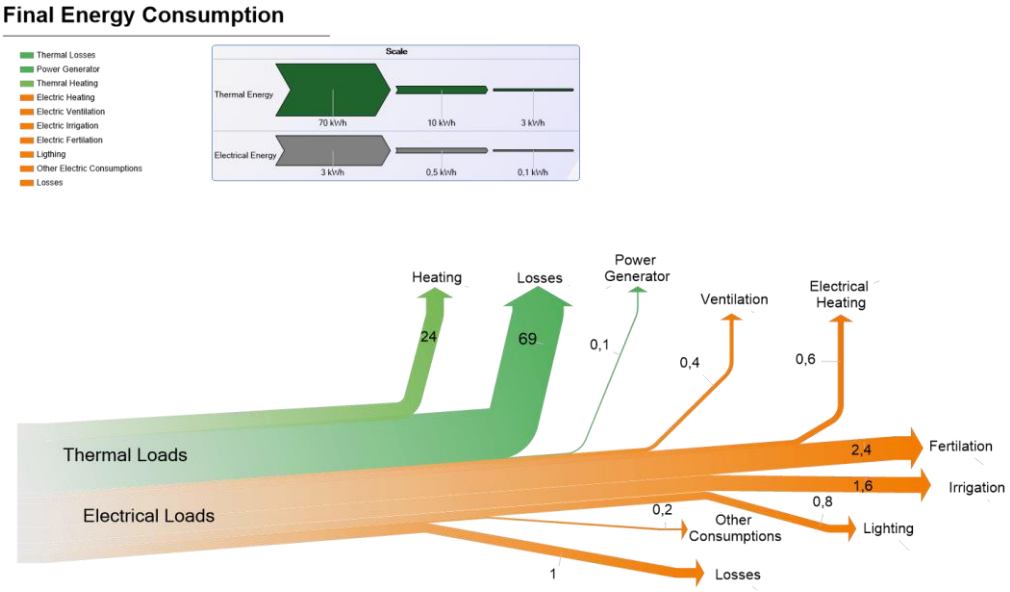

Figure.4 SANKEY diagram of energy flows for potted flower greenhouse

4. Conclusions

This paper presents the process of the first stages of an energy audit of greenhouses, the operational rating phase. This process was applied in four greenhouses in central Greece with different crops and different technologies. From the produced results produced, it comes out that even the application of only the first steps of an energy audit can provide valuable information on the energy efficiency of the greenhouse and to enable the identification of energy-intensive and energy-inefficient processes. In the operational rating approach, no model was used for the prediction of greenhouse energy consumption, beyond the calculation model for the energy demand for heating. However, an energy audit to be considered completed require not only the identification of the energy-inefficient processes but also the proposal of measures accounting for their cost and their energy performance improvement.

In agreement with the international literature, it appears that the main energy consumption concerns

heating. From the implemented energy audits, it comes out that biomass heating systems are often characterized by low efficiency which is not only due to the fuel but also due to the lack of standardization and automation. However, in terms of primary energy consumption electricity represents the 1/3 of the total primary energy consumption, and this draws attention not only to the improvement of electrical systems but also to the necessity of developing local energy production systems from renewable sources making photovoltaics the preferred option. This necessity becomes more pronounced when considering that electrical consumption will increase as greenhouses become mechanized in a move towards precision agriculture.

Finally, the use f energy indices referred to production unit prove to be more adequate than energy indices referred to greenhouse area in order to assess the greenhouse energy performance. Furthermore, the use of SANKEY diagrams can also be used in this production process, as it is already done in all industrial processes, offering visualization of energy flows (however they can also be used for material flows) which easily leads to the identification of energy-intensive processes.

Acknowledgements

This project has received funding from the European Commission's Horizon Europe Coordination and Support Actions programme under grant agreement No 101096056 (project acronym: REGACE). The European Commission is not responsible for any use that may be made of the information it contains

References

Alonso, A. M. , G. J. Guzmán, (2010). Comparison of the Efficiency and Use of Energy in Organic and Conventional Farming in Spanish Agricultural Systems. Journal of Sustainable Agriculture **34**(3): 312-338.DOI: 10.1080/10440041003613362.

Baptista, F. J., A. T. Silva, L. M. Navas, A. C. Guimarães , J. F. Meneses, (2012). Greenhouse energy consumption for tomato production in the Iberian peninsula countries, International Society for Horticultural Science (ISHS), Leuven, Belgium.

Baxevanou, C., D. Fidaros, I. Giannenas, E. Bonos , I. Skoufos, (2021). Reduction of Energy Intensity in Broiler Facilities: Methodology and Strategies. Frontiers in Veterinary Science **8**.DOI: 10.3389/fvets.2021.671183.

Campiglia, E., G. Colla, R. Mancinelli, Y. Rouphael , A. Marucci, (2007). Energy balance of intensive vegetable cropping systems in central Italy, International Society for Horticultural Science (ISHS), Leuven, Belgium.

de Visser, C. L. M., F. E. de Buisonje, H. H. Ellen, C. Stanghellini , M. P. J. van der Voort, (2012). State of the Art on Energy Efficiency in Agriculture, Country data on energy consumption in different agroproduction sectors in the European countries, agrEE.

EC, (1993). Council Directive 93/76/EEC to limit carbon dioxide emissions by improving energy efficiency. EEC. Brussels, Belgium

EC, (2010). Directive 2010/31/EU of the European Parliament and of the Council on the energy performance of buildings. 2010/31/EU. European Council Brussels, Belgium

EC, (2018). Directive 2018/844 of the European Parliament and of the Council amending Directive 2010/31/EU on the energy performance of buildings and Directive 2012/27/EU on energy efficiency. 2018/844/EP. European Parliament. Brussels, Belgium

EC/EP, (2002). Directive 2002/91/EC of the European Parliament and of the Council on the energy performance of buildings. EC. Brussels, Belgium

EC/EP, (2012). Directive 2012/27/EU of the European Parliament and of the Council on energy efficiency. EU. Brussels, Belgium

ISO (2008). EN ISO 13790 - Energy performance of buildings - Calculation of energy use for space heating and cooling. Geneva, Switzerland.

Kittas, C., A. Elvanidi, N. Katsoulas, K. P. Ferentinos , T. Bartzanas, (2016). Reflectance indices for the detection of water stress in greenhouse tomato (Solanum lycopersicum), International Society for Horticultural Science (ISHS), Leuven, Belgium.

Kittas, C., N. Katsoulas , T. Bartzanas, (2014). Energy needs and energy saving in mediterranean greenhouses, International Society for Horticultural Science (ISHS), Leuven, Belgium.

Paris, B., F. Vandorou, A. T. Balafoutis, K. Vaiopoulos, G. Kyriakarakos, D. Manolakos , G. Papadakis, (2022). Energy Use in Greenhouses in the EU: A Review Recommending Energy Efficiency Measures and Renewable Energy Sources Adoption. Applied Sciences **12**(10): 5150.

Stanghellini, C., F. Baptista, E. Eriksson, C. Gilli, F. Giuffrida, F. L. K. Kempkes, P. Munoz, A. Stepowska , J. I. Montero, (2016). Sensible use of primary energy in organic greenhouse production. [Netherlands], BioGreenhouse.

Trypanagnostopoulos, G., A. Kavga, M. Souliotis , Y. Tripanagnostopoulos, (2017). Greenhouse performance results for roof installed photovoltaics. Renewable Energy **111**: 724-731.DOI: https://doi.org/10.1016/j.renene.2017.04.066.

Vourdoubas, J., (2015). Overview of Heating Greenhouses with Renewable Energy Sources a Case Study in Crete-Greece.

Use of NIR regional scale calibrations to map soil characteristics for PA: A case study in 5 fields

Andrea Lazzari [a,*], Nicolò Pricca [a], Andrea Gasparini [a], Giovanni Cabassi [a]

[a]CREA - Research Centre Animal Production and Aquaculture, Via Antonio Lombardo, 11, 26900 Lodi (LO), Italy.

* Corresponding author. Email: andrea.lazzari@crea.gov.it

Abstract

In Italy, the adoption of precision agriculture is escalating. Near-infrared spectroscopy (NIR) is an established low-cost technique used for soil analysis. This research presents the result of the application of NIR at a sub-field scale for PA mapping purposes. The selected trial fields exhibit varied soil types and have undergone different tillage and fertilisation practices, which could affect soil attributes. Soil samples were collected according to a 50-meter regular grid at a depth of 30 cm. These samples were both analysed by an external laboratory employing standard wet reference methods and analysed utilizing a FOSS NIRSystem 5000 spectrometer. The NIR analysis, conducted on spectra obtained in diffuse reflectance within the 1100-2500 nm range, employed the LOCAL calibration technique (US Patent # 5,798,526). The NIR-based estimations for clay, clay+silt, and organic carbon content were evaluated using Root Mean Square Error (RMSE), Mean Absolute Error (MAE), and bias metrics. Specifically, the analysis focused on bias and the coefficient of determination (R^2) correlating the actual, laboratory-measured values with the NIR-predicted values (0.70, 0.62, 0.68 respectively). The bias evaluation identified a low value for the soil components under analysis in all the fields, except for one in clay+silt (bias > ±100) and two in organic carbon (bias > ± 0.4). Results showed good skill of the NIR calibrations to estimate field averages of the parameters under analysis. The Range/MAE allowed the identification of in-field variation gradients. For clay the ratio ranged from 2.4 to 9.9, for clay+silt from 1.4 to 8.4; for organic carbon from 3.4 to 5.9, depending on the variability of the field. The findings indicate that, after adjusting for bias, NIR LOCAL calibration data can be used not only for mean field values determination but also for effectively identifying trends in soil texture variation and organic carbon gradients.

Keywords: Precision agriculture, NIR spectroscopy, soil characterisation, soil mapping.

1. Introduction

Precision Agriculture (PA), in Italy, has been growing fast in the last decade and the 10% target set is being achieved (Italy Ministerial Decree 33671, 2017).

The adoption of PA techniques depends on rapid, cheap and non-destructive analysis for soil mapping, crop management and variable rate fertilisation (Kodaira and Shibusawa, 2012). Knowing the spatial and temporal characteristics of soil is very important to applying PA and allows farmers to make the best choice for the fields (Virgawati et al., 2018).

Soil texture is, together with Organic Carbon (OC), one of the most important parameters of soil; it affects structure, aggregation, water infiltration, nutrient availability and compaction. Estimating soil texture is time-consuming and expensive and concerns the sieving and sedimentation of suspended soil in solution (Jaconi et al., 2019).

Spectroscopy is a valid alternative and low-cost OC and soil texture analysis technique. Specifically, the clay fraction is important for many physical and chemical processes (Jury and Horton, 2004); the clay+silt fraction protects the OC from microbic degradation (Hassink, 1997) and OC gives, with its mineralisation, a part of the nutrient necessary for plant growth (Bhupinderpal-Singh and Zed, 2007).

The bibliography provides different studies on spectroscopy analysis with different instruments and different elaborations of soil spectra. Coblinski et al. (2020) use two different regions of spectra, Visible (VIS) - Near Infra-Red (NIR) – Shortwave Infrared (SWIR) and Mid Infra-Red (MIR), to estimate sand and clay in different soil samples; the cubistic model is applied to manage soil spectra acquired. The results confirm a good soil texture prediction for both spectra regions: MIR is more robust than VIS-NIR-SWIR with the highest R^2 (0.94 for clay and 0.88 for sand) and lower RMSE (3.7 for clay and 5.1 for sand). The combination of this two different regions of spectra doesn't improve the prediction value.

Another study by Viscarra Rossel et al. (2006) compares three different regions of spectra (VIS, NIR and

MIR) for predicting soil attributes. The results show that the VIS region had lower R^2 and less accuracy; MIR spectra are the best choice with more accurate results and major R^2. However, the advantage taken by the accuracy of MIR instead of VIS or NIR spectra may not be significant because of the higher cost of MIR instruments, especially for the in-field variability.

With portable instruments, this low-cost technique has the opportunity to be installed on agriculture machinery for "on-the-go" mapping. Several studies have been conducted to compare laboratory spectra with on-the-go spectra. On-the-go sensors have minor predictive accuracy compared to laboratory instruments and do not describe the accuracy of the in-field variability. A valid solution is to use a sensor installed on machinery to take the variations of the field, and then recalibrate the results with laboratory instruments to correct the value of the predictive attribute of soil (Bricklemyer and Brown, 2010).

This paper aims to use a NIR system to evaluate details of soil attributes (clay, clay+silt and OC) at a sub-field scale for PA purposes in five different locations in upper Po Valley with varied soil types, tillage and fertilizations that could affect soil properties. The study evaluates the prediction ability of NIR and applies a script to estimate the systematic error of the component (BIAS) to improve the accuracy of predictions using only a few samples analysed with laboratory reference methods, with the target of reducing the operational costs of PA.

2. Materials and Methods

2.1. Field location and description

The five fields are located in different zones of Po Valley (San Giuliano Milanese, Northern Italy, 45.389282N 9.247408E; Basiglio, Northern Italy, 45.343367N 9.156350E; Orzinuovi, Northern Italy, 45.383283N 9.889133E; Sant'Angelo Lodigiano, Northern Italy, 45.227808N 9.427056E; San Giorgio di Lomellina, Northern Italy, 45.155391N 8.763586E). The total amount of experimental fields is 40 hectares.

The history of soil and cultivation is very diverse: San Giuliano Milanese, Basiglio and Oriznuovi fields are characterized by long-term manure history and were continuously cultivated with maize for silage and, possibly, with the introduction of Italian ryegrass in winter months; San Giorgio di Lomellina field was cultivated with a single mono-succession of maize for grain and fertilized by civil wastewater sewage sludge; finally, the Sant'Angelo Lodigiano fields don't have a yearly contribution of OC with manure, the principal nutrient for maize for grain cultivation comes from inorganic fertilizers.

2.2. Soil sample and analysis

Topsoil (0.0m – 0.3m) samples were collected at 186 (all fields) georeferenced points on a regular mesh grid of 50 meters (Figure 1), using a gouge auger (Eijkelkamp, 40-mm diameter) after maize harvest. 6 Kg for each sample were air-dried and sieved (Filtra Vibracion S.L., 2mm mesh) for correct skeleton estimation. The soil <2mm was analysed for physical and chemical properties with the reference methods (Table 1) and NIR spectroscopy; a portion of the samples was sieved to 0.5 mm for C:N.

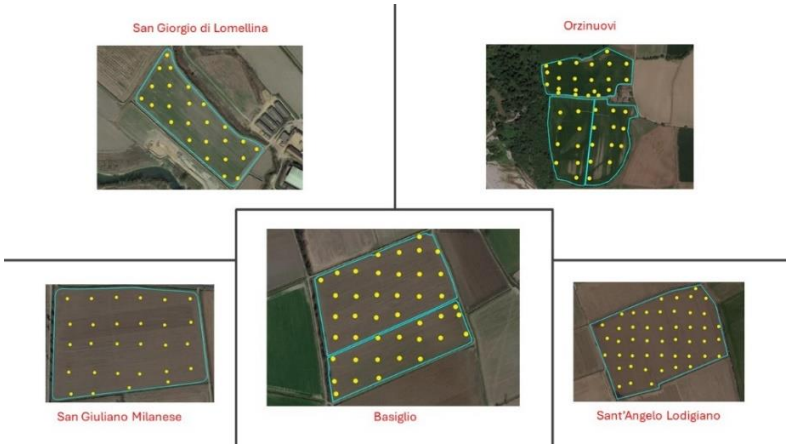

Figure 1. Experimental design of 186 samples of soil collected. (Google Satellite, modified by CREA)

Table 1. Analytical reference method of soil analysis (Ministero delle Politiche Agricole e Forestali, 2000)

Attribute	Method	Method number
Sand content (g kg^{-1})	Dispersion by $(NaPO_3)_6$ and determination with pipette method	II.5
Silt content (g kg^{-1})	Dispersion by $(NaPO_3)_6$ and determination with pipette method	II.5
Clay content (g kg^{-1})	Dispersion by $(NaPO_3)_6$ and determination with pipette method	II.5
Carbonate (g kg^{-1})	Decomposition by HCl and volumetric determination of the evolved CO2 with a calcimeter	V.1
OC (g kg^{-1})	Total carbon measured by dry combustion with an elemental analyser. OC is calculated by subtracting inorganic Carbonate	VII.1
Total N (g kg^{-1})	Dry combustion with an elemental analyser.	VII.1

Soil NIR spectra of 186 samples were collected in diffuse reflectance (range 1,100-2,500 nm) using a NIR system 5000 spectrometer equipped with a sample transport device (FOSS, Denmark). Texture and OC were predicted using a locally weighted regression calibration model (LOCAL, patent number US5798526A) developed for Northen Italy soils (Cabassi et al, 2005). This calibration is based on selecting a small calibration data set customised to the unknown sample from a big library of soil characteristics (0-30 cm) to obtain a specific calibration equation. LOCAL is a well-weighted mean of Partial Least Squares (PLS) models.

2.3. Data processing

Data were collected and elaborated using Microsoft Excel® with .csv and .xls extension.

Clay, clay+silt and OC content estimation with NIR were evaluated with Root Mean Square Error (RMSE – Eq. 1), Mean Absolute Error (MAE – Eq. 2) and BIAS metric (Eq. 3), the systematic error of the component.

$$RMSE = \sqrt{\frac{1}{n}\sum_{i=1}^{n}\left(\gamma_i - \widehat{\gamma_i}\right)^2} \quad (1)$$

where γ_i are observed values (laboratory measured); $\widehat{\gamma_i}$ are predicted values (NIR); n is a total amount of observations.

$$MAE = \frac{1}{n}\sum_{i=1}^{n}\left|\gamma_i - \widehat{\gamma_i}\right| \quad (2)$$

where γ_i are observed values (laboratory measured); $\widehat{\gamma_i}$ are predicted values (NIR); n is a total amount of observations.

$$BIAS = \left(\frac{\sum_{i=1}^{n}\gamma_i}{n}\right) - \left(\frac{\sum_{i=1}^{n}\widehat{\gamma_i}}{n}\right) \quad (3)$$

where γ_i are observed values (laboratory measured); $\widehat{\gamma_i}$ are predicted values (NIR); n is a total amount of observations.

Finally, the coefficient of determination (R^2 – Eq. 4) was determined for each soil component under analysis in comparison with laboratory-measured values.

$$R^2 = \frac{\sum_{i=1}^{n}\left(\widehat{\gamma_i} - \overline{\gamma_i}\right)^2}{\sum_{i=1}^{n}\left(\gamma_i - \overline{\gamma_i}\right)^2} \quad (4)$$

where γ_i are observed values (laboratory measured); $\widehat{\gamma_i}$ are predicted values (NIR); $\overline{\gamma_i}$ is the mean observed value; n is a total amount of observations.

2.4. Script-writing

MATLAB R2023b (© 1994-2024 The MathWorks, Inc.) was used to create a script for calculating the optimal number of samples to be analysed with the reference method for the correction of NIR prediction.

A random sampling approach was used to simulate the estimate of the BIAS using all of possible combinations of 3,4,5,6 samples to correct NIR prediction. Finally, the normalized histogram of the BIAS estimates distribution was plotted for 13 classes and every soil attribute and combination created.

3. Results and Discussion

The results obtained in the paper concern: i) the ability of calibration to predict soil attributes with NIR and ii) the estimation of BIAS of NIR predictions using a subset of few reference data from analysed with reference methods.

3.1. Quality of prediction

The prediction value was calculated by the use of NIR with LOCAL calibration. The value obtained with NIR is compared to data with the referenced method (Table 2).

Table 2. Descriptive statistics of soil data (n=186) where pH pH in KCl, OC organic carbon, Ntot total nitrogen

			Measured Variable						
Field	Analysis		pH	OC (g kg^{-1})	Ntot (g kg^{-1})	C:N	Sand (g kg^{-1})	Silt (g kg^{-1})	Clay (g kg^{-1})
San Giuliano Milanese	NIR	Mean	6.1	14.4	1.4	10.7	562.0	322.7	115.3
		SD	0.1	2.7	0.3	1.5	51.6	43.2	19.3
		CV	1.6	18.8	21.4	14.0	9.2	13.4	16.7
	Reference method	Mean	5.7	14.6	1.5	9.7	432.6	426.7	140.7
		SD	0.3	2.1	0.2	0.4	80.1	57.9	26.6
		CV	5.3	14.4	13.5	3.9	18.5	13.6	18.9
Basiglio	NIR	Mean	6.4	17.4	1.7	10.5	571.8	281.6	146.6
		SD	0.2	2.2	0.3	1.2	56.6	38.6	33.3
		CV	3.1	12.6	17.6	11.4	9.9	13.7	22.7
	Reference method	Mean	6.1	15.9	1.7	9.4	480.0	342.5	177.5
		SD	0.3	2.5	0.3	0.5	48.7	41.9	25.7
		CV	4.9	15.7	15.3	5.0	10.1	12.2	14.5
Orzinuovi	NIR	Mean	7.0	19.6	2.0	10.0	479.1	339.4	181.4
		SD	0.2	2.1	0.2	0.7	73.7	51.6	27.1
		CV	2.9	10.7	10.0	7.0	15.4	15.2	14.9
	Reference method	Mean	7.3	15.5	1.7	8.9	492.0	334.0	174.0
		SD	0.1	2.7	0.3	0.6	119.8	90.3	35.4
		CV	1.4	17.4	17.2	6.6	24.3	27.0	20.3
Sant'Angelo Lodigiano	NIR	Mean	6.3	11.6	1.5	8.0	454.4	405.3	140.2
		SD	0.1	1.1	0.2	0.6	48.9	38.8	15.1
		CV	1.6	9.6	10.7	7.9	10.8	9.6	10.8
	Reference method	Mean	6.2	9.7	1.1	8.8	356.7	486.4	157.0
		SD	0.1	1.2	0.2	0.5	59.6	54.2	16.5
		CV	2.3	12.1	13.8	5.5	16.7	11.1	10.5
San Giorgio di Lomellina	NIR	Mean	6.7	19.0	2.0	9.7	650.3	290.5	59.2
		SD	0.1	1.7	0.2	1.0	67.3	49.3	28.1
		CV	1.5	8.9	10.2	10.3	10.3	17.0	47.4
	Reference	Mean	7.0	22.9	2.3	10.1	577.4	357.9	64.8

	method	SD	0.1	2.4	0.2	0.5	63.6	61.7	10.2
		CV	1.4	10.5	10.6	5.0	11.0	17.2	15.8

SD and CV are the standard deviation and the coefficient of variation, respectively

OC, was considered equal to total C according to the pH values and preliminary screening of samples with higher pH

First of all, the soil parameters clay, claysilt and OC of the five fields are plotted to calculate R^2: 0.70, 0.62 and 0.68 respectively (Figure 2).

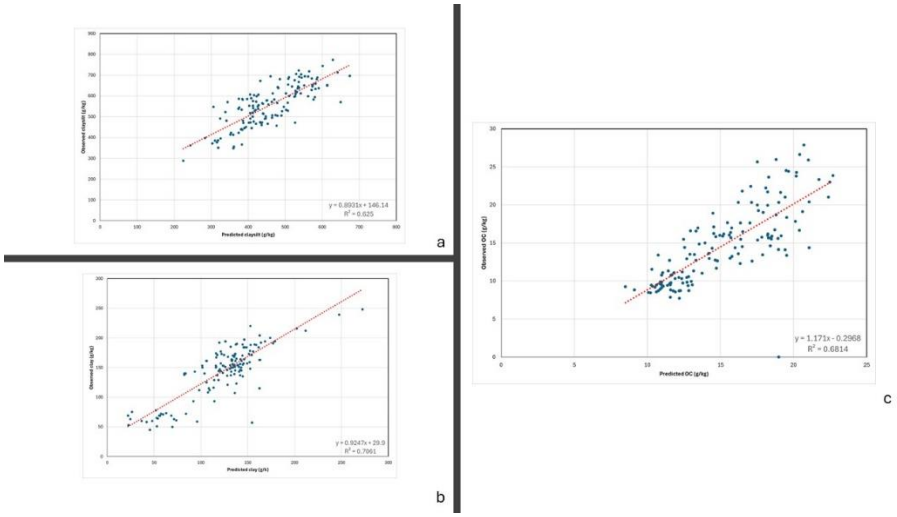

Figure 2. Scatterplots and R2 of the model validation results for clay content (a), claysilt (b) and soil organic carbon (c)

The coefficient of determination obtained by the 5 fields' data was quite similar for all the soil attributes in the literature. For clay parameters, the bibliography has a range of 0.62 to 0.93; high values were obtained by Tiruneh et al. (2022) in a study carried out in Ethiopia; values quite similar to those under study like 0.70 (Camargo et al., 2015), and 0.66 (Silva et al., 2021).

The attribute OC have a good R^2 comparable to several studies in the literature: ranging from 0.57 to 0.93 (Yang et al., 2012; Leone et al., 2012).

Two different formulas were applied to measure the error in the prediction value of the five fields under analysis. Table 3 resumes the data obtained.

Table 3. BIAS and evaluation of prediction error in the five fields for the three soil parameters under analysis.

Field	Attribute	BIAS	RMSE	MAE	Range/RMSE	Range/MAE
San Giuliano Milanese	Clay	25.36	41.48	38.02	3.06	3.34
	Claysilt	-129.39	157.71	149.36	3.57	3.91
	OC	0.01	0.22	0.19	3.47	4.01
Basiglio	Clay	30.91	37.70	32.48	5.69	7.12
	Claysilt	91.81	109.90	96.43	4.17	5.45
	OC	-0.14	0.28	0.23	4.97	5.90
Orzinuovi	Clay	-7.31	27.10	20.32	5.32	7.24
	Claysilt	-12.71	83.77	62.67	6.20	8.44
	OC	-0.41	0.48	0.42	4.56	5.52
Sant'Angelo Lodigiano	Clay	16.74	19.71	17.55	7.77	9.91
	Claysilt	97.76	109.39	97.76	5.52	6.50
	OC	0.19	0.22	0.20	3.13	4.11
San Giorgio di Lomellina	Clay	5.52	29.13	20.67	1.68	4.47
	Claysilt	72.89	90.32	75.80	4.61	6.18
	OC	0.38	0.58	0.45	1.74	3.36

Range is calculated by the difference between maximum and minimum of the samples in each field. Range/RMSE and Range/MAE are calculated with the BIAS correction.

The prediction data in the fields comparable with results reported in other studies. The results in literature ranged from 2.21 to 5.40 for clay (Tiruneh et al., 2022; Vasava et al., 2019) and from 0.27 to 0.78 for OC (Tiruneh et al, 2002; Kuang et al. 2012).

The data collected with NIR in comparison with wet reference method have proven to be a valid solution to show the field trend of soil texture and OC. Additionally, the calculated indices Range/RMSE and Range/MAE demonstrated the capacity of NIR to identify the intra-field variation of soil attributes, necessary for PA purposes and for a qualitative identification of different management zones.

3.2. Quantity of prediction

To achieve the true value of the samples with the use of NIR models in order to have accurate estimated of the parameters it was necessary to correct the prediction with BIAS, the systematic error of the component arising from instrumental drift and from mall variations in the sample preparation method over time.

As an example, the estimation of BIAS on the Sant'Angelo Lodigiano field is shown using reference data of 3,4,5 or 6 samples randomly selected from the sample population. The procedure is the same for the remaining fields.

MatLab software was used to create all the combinations in the 48 points of the field with three, four, five and six samples for BIAS calculation. The normalized distribution of the soil attribute means under analysis is shown in Figure 3.

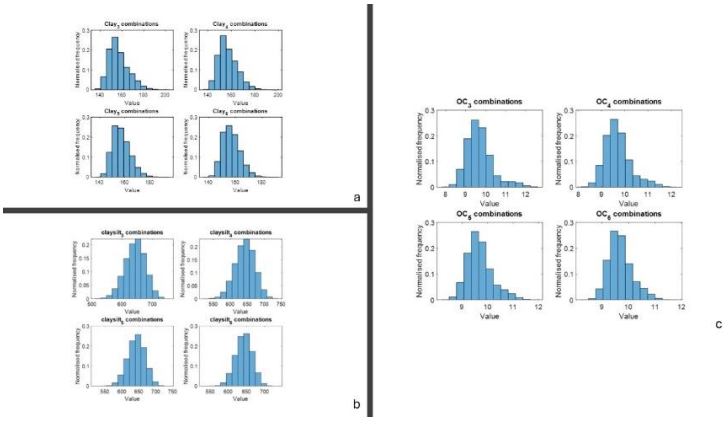

Figure 3. Normalised histogram of the mean distribution in all combinations calculated for clay (a), claysilt (b) and OC (c).

The value in Figure 4 shows that the number of samples to be subjected to referenced analysis for BIAS calculation increases the accuracy of BIAS estimation.

The distributions of the estimated sample means have shown, in accordance with the Central Limit Theorem, a progressively more Gaussian and less skewed behavior as the sample subset size increases. (Pelosi et al., 2009). This type of trend is more noticeable in the soil texture parameters (clay and claysilt); in contrast, the OC data show less intensely the increase in accuracy as the number of analysed samples increases.

Finally, we calculated median BIAS estimations with the results of the different combinations, associated with each standard deviation.. The results show the reduction of SD, hence a more accurate estimation the greater the number of samples taken into account for laboratory analysis. SD are resumes in Table 4.

Table 4. SD of the soil attributes under analysis with the different number of combinations sub-dataset.

Attribute	Number of combinations	BIAS estimated	SD
Clay content (g kg^{-1})	3	-15.29	9.30
	4	-15.70	7.95
	5	-15.95	7.03
	6	-16.29	6.34
Claysilt (g kg^{-1})	3	-98.98	33.45
	4	-98.56	28.63
	5	-98.31	25.31
	6	-98.14	22.83
OC (g kg^{-1})	3	1.97	0.66
	4	1.96	0.56
	5	1.96	0.49
	6	1.95	0.44

BIAS estimated is calculated as the difference between the mean of the NIR value and the median of the observed value in each combination.

4. Conclusions

NIR analysis is a quick and cheap excellent solution for the estimation of primary soil parameters (texture and OC), allowing the study of the in-field variations and highlighting different intra-field zones for careful management of fertilisation, sowing, etc. following the dictates of precision agriculture.

The analysis of a reduced number of samples by laboratory reference methods in combination with NIR analyses, which are more expeditious and economical, can be a valid solution for estimating the quantitative value of clay, claysilt and OC. As noted, the greater the number of samples analysed, the greater the accuracy of our data. However, it is not possible to define the optimal number of samples, this will be a trade-off between costs and the size of the field and the degree of accuracy we wish to achieve.

Further studies in this regard may use other expeditious technologies in association with NIR, e.g. geo-electrical soil resistivity analysis, to help the farmer in the choice of soil points to be analysed by laboratory methods, reducing the error in the final accuracy of the estimate.

Acknowledgements

The authors acknowledge Regione Lombardia, Italy, for funding the research within the EIP-AGRI Operational Group project of the European Agricultural Fund for Rural Development (2014-2020).

Acknowledgements are also extended to the Department of Economics, Engineering, Society and Business Organization (DEIM) in cooperation with the Department of Agriculture and Forestry Sciences (DAFNE) of the University of Tuscia for this work carried out as part of the PhD in “Engineering for Energy and Environment – Biosystems and Environment”.

References

Bhupinderpal, S., Z. Rengel, 2007. The Role of Crop Residues in Improving Soil Fertility. In: Marschner, P., Rengel, Z. (eds) Nutrient Cycling in Terrestrial Ecosystems. Soil Biology, vol 10. Springer, Berlin, Heidelberg. https://doi.org/10.1007/978-3-540-68027-7_7

Bricklemyer R.S., D.J. Brown, 2010. On-the-go VisNIR: Potential and limitations for mapping soil clay and organic carbon. Computers and Electronics in Agriculture. 70, 209-216. https://doi.org/10.1016/j.compag.2009.10.006

Cabassi, G., P. Marino Gallina, M. Piombino, D. Orfeo, G. Maffioli, 2005. Estimation of the properties of heterogeneous soils on a multi regional scale in Italy using near infrared spectroscopy and LOCAL calibration procedures. In 12th International Conference of Near Infrared Spectroscopy. Auckland, New Zealand, April 9-15. New Zealand Near Infrared Spectroscopy Society, Hamilton, N.Z. 341-350.

Camargo L. A., J.M. junior, V. Barron, L.R.F. Alleoni, R.S. Barbosa, G.T. Pereira, 2015. Mapping of

clay, iron oxide and adsorbed phosphate in Oxisols using diffuse reflectance spectroscopy. Geoderma. 251-252, 124-132. https://doi.org/10.1371/journal.pone.0270629

Coblinski, J. A., E. Giasson, J. A. M. Demattê, A. Carnieletto Dotto, J. J. Ferreira Costa, R. Vašát, 2020. Prediction of soil texture classes through different wavelength regions of reflectance spectroscopy at various soil depths. Catena. 189, 104485. https://doi.org/10.1016/j.catena.2020.104485

Hassink, J., 1997. The capacity of soils to preserve organic C and N by their association with clay and silt particles. Plant and Soil. 191, 77-87. https://doi.org/10.1023/A:1004213929699

Italy Ministerial Decree n. 33671 of 22/12/2017. https://www.politicheagricole.it/flex/cm/pages/ServeBLOB.php/L/IT/IDPagina/12069

Jaconi, A., C. Vos, A. Don, 2019. Near infrared spectroscopy as an easy and precise method to estimate soil texture. Geoderma. 337, 906-913. https://doi.org/10.1016/j.geoderma.2018.10.038

Jury, W. A., R. Horton, 2004. Soil Physics. 6th ed. New Jersey, USA: John Wiley & Sons, Inc.

Kodaira, M., S. Shibusawa, 2013. Using a mobile real-time soil visible-near infrared sensor for high resolution soil property mapping. Geoderma. 199, 64-79. https://doi.org/10.1016/j.geoderma.2012.09.007

Kuang, B., A.M. Mouazen, 2012. Influence of the number of samples on prediction error of visible and near infrared spectroscopy of selected soil properties at the farm scale. European journal of soil science. 63(3), 421-429. https://doi.org/10.1111/j.1365-2389.2012.01456.x

Leone, A.P., R.A. Viscarra-Rossel, P. Armenta, A. Buondonno, 2012. Prediction of Soil Properties with PLSR and vis-NIR Spectroscopy: Application to Mediterranean Soils from Southern Italy. Current Analytical Chemistry. 8(12), 283-299. https://doi.org/10.2174/157341112800392571

Pelosi, M.K., T.M. Sandifer, P. Cerchiello, P. Giudici, 2009. Introduzione alla statistica. The McGraw-Hill Companies, S.r.l. 487 p.

Silva, I.M., D.J. Romero, C.C. Barbosa Guimaraes, M.R. Alves, L. Prado Osco, A. Barros e Souza, A. Pires da Silva, J.A.M Demattê, 2021. Readily dispersible clay in soils from different Brazilian regions by visible, near, and mid-infrared spectral data. International Journal of Remote Sensing. 42(18), 6943-6960. https://doi.org/10.1080/01431161.2021.1948625

Tiruneh, G.A., D.T. Meshesha, E. Adgo., A. Tsunekawa, N. Haregeweyn, A.A. Fenta, A. W. Belay, N. Tadesse, G. Gekadu, J.M. Reichert, 2022. Use of soil spectral reflectance to estimate texture and fertility affected by land management practices in Ethiopian tropical highland. Plos ONE. 17(7), 1-20. https://doi.org/10.1371/journal.pone.0270629

Vasava, H.B., A. Gupta, R. Arora, B.S. Das, 2019. Assessment of soil texture from spectral reflectance data of bulk soil samples and their dry-sieved aggregate size fractions. Geoderma. 337, 914-926. https://doi.org/10.1016/j.geoderma.2018.11.004

Virgawati, S., M. Mawardi, L. Sutiarso, S. Shibusawa, H. Segah, M. Kodaira, 2018. Mapping the Variability of Soil Texture Based on VIS-NIR Proximal Sensing. Journal of applied geospatial information. 2 (1), 108-116. ISSN Online: 2579-3608

Viscarra Rossel, R.A., D.J.J. Walvoort, A.B. McBratney, L.J. Janik, J.O. Skjemstad, 2006. Visible, near infrared, mid infrared or combined diffuse reflectance spectroscopy for simultaneous assessment of various soil properties. Geoderma. 131, 59-75. https://doi.org/10.1016/j.geoderma.2005.03.007

Yang, H., B. Kuang, M. Mouazen, 2012. Quantitative analysis of soil nitrogen and carbon at a farm scale using visible and near infrared spectroscopy coupled with wavelength reduction. European journal of soil science. 63(13), 410-420. https://doi.org/10.1111/j.1365-2389.2012.01443.x

Detection of spectral signature and classification of *Alternaria alternata* and *Alternaria solani* diseases in tomato plant by analysis of hyperspectral images and support vector machine

Seyed Mohamad Javidan[a], Ahmad Banakar[a]*, Keyvan Asefpour Vakilian[b], Yiannis Ampatzidis[c], Kamran Rahnama[d]

[a] Department of Biosystems Engineering, Tarbiat Modares University, Tehran, Iran*

[b] Department of Biosystems Engineering, Gorgan University of Agricultural Sciences and Natural Resources, Gorgan, Iran

[c] Agricultural and Biological Engineering Department, Southwest Florida Research and Education Center, University of Florida, 2685 FL-29, Immokalee, FL 34142, USA

[d] Department of Plant Protection, Faculty of Plant Production, Gorgan University of Agricultural Sciences and Natural Resources, Gorgan, Iran

* Corresponding author. Email: ah_banakar@modares.ac.ir

Abstract

Monitoring plant health during the growth period is essential for ensuring product quality and reducing production costs. Therefore, early diagnosis of plant diseases is crucial. Hyperspectral imaging and artificial intelligence have enabled the diagnosis of plant diseases in their early stages and provide a distinct spectral signature for each disease. In this study, two tomato diseases, *Alternaria alternata* and *Alternaria solani*, were investigated using spectral reflectance analysis in the span of 400-950 nm. To this end, a dataset of images was recorded on days 1 to 7 (every other day) after disease transmission, and color, texture, and shape features were extracted in each band. Finally, two groups of diseased leaves and one group of healthy leaves were classified by the support vector machine algorithm. The classification results for days 1, 3, 5, and 7 were 89, 91, 93 and 96%, respectively. Spectral reflectance in the imaging band range of 400 to 950 nm shows the spectral differentiation between the two diseases, indicating their unique spectral signatures compared to healthy leaves. Also, the Relief feature selection algorithm showed that texture features such as energy in bands 550 and 841, entropy in band 600, correlation in band 746, and standard deviation in band 905 are superior to other features. This study demonstrated the potential of hyperspectral imaging and artificial intelligence for early detection and management of plant diseases.

Keywords: Artificial Intelligence, Early Diagnosis, Monitoring Plant Health, Spectral Reflectance, Tomato Diseases.

1. Introduction

Plant leaves' spectral characteristics change due to alterations in plant biochemistry and cell composition. However, it is also essential to note that the spectral properties of leaves are not static, but rather change over time with various factors such as plant growth, aging, senescence, decay, and disease development (Javidan et al., 2023a). Despite the potential of hyperspectral imaging (HI) for plant disease diagnosis, the complex nature of the hyperspectral data and the need for efficient processing methods are significant challenges to maximizing its capabilities for identifying and managing plant diseases (Javidan et al., 2023b).

In recent years, the demand for artificial intelligence (AI) enabled spectral sensing systems to identify plant diseases has increased. Consequently, the number of studies on AI-driven systems has also increased (Barbosa Júnior et al., 2024). These systems often rely on machine learning models for processing the hyperspectral data, with the goal of maximizing the accuracy of disease identification (da Cunha et al., 2023; Hariharan et al., 2023; Javidan et al., 2022). However, the complexity of these models and the need for efficient processing methodologies to produce accurate and interpretable results are significant challenges to unlocking the full potential of HS for improved plant disease diagnosis and management.

Fernández et al. (2021) studied powdery mildew in cucumber leaves using hyperspectral imaging in the range of 400-900 nm. They used principal component analysis to determine sensitive wavelengths in disease diagnosis. Two spectral variables, the red-well point and the red-edge inflection point, were extracted, and the support vector machine (SVM) with linear kernel was used to classify diseased and healthy leaves. The algorithm had an accuracy of 89% on day 6 after disease transmission. Zhang et al. (2022) used hyperspectral imaging in the range of 400-1000 nm to study rice blast disease. They used SVM for classification, which

had an accuracy of 92.92%. Last, Wu et al. (2023) identified gray mold disease in strawberries using hyperspectral images at 400-1000 nm. They used texture and vegetation characteristics from 24-hour infected leaves and healthy leaves. The classification models, namely, extreme learning machine (ELM), SVM, and k-Nearest Neighbor (k-NN), showed accuracies of 93.33, 93.33, and 96.67%, respectively.

Image data acquisition with high precision and resolution allows the sensor to capture detailed information from the electromagnetic spectrum (Mohamadzamani et al., 2020). However, the large number of variables (i.e., features, wavelengths) measured leads to high-dimensional data that increases the complexity of processing to produce relevant information (Mohammad Zamani et al., 2023). In addition, the spectral data assessed in near-contiguous variables likely exhibits similar or overlapping information, leading to potential data redundancy and increased complexity in the analysis interpretation and the chance of overfitting occurrence. As a result, feature selection methods have been developed to identify and extract the most relevant and distinctive spectral features without sacrificing important information (Khakrangin et al., 2021). In this study, to evaluate the potential of hyperspectral imaging in the detection of two widespread fungal diseases affecting tomato leaves, analysis was performed on days 1 to 7 after disease transmission. Also, the detection performance of hyperspectral images and AI in the early, middle, and late stages of disease development was evaluated. The spectral signature of each disease was determined and the most optimal and effective features extracted from the images were identified as the most essential features for the diagnosis of fungal diseases.

2. Materials and Methods

The research is divided into 3 main parts: 1. Sampling, purification, and transfer of the disease to the plant, 2. Hyperspectral image capturing, and 3. Diagnosis and classification of the disease. This research was conducted on two tomato diseases, *Alternaria alternata* and *Alternaria solani*, which are among the most common and destructive fungal diseases in greenhouse and field crops. Figure 1 shows the different steps in this research.

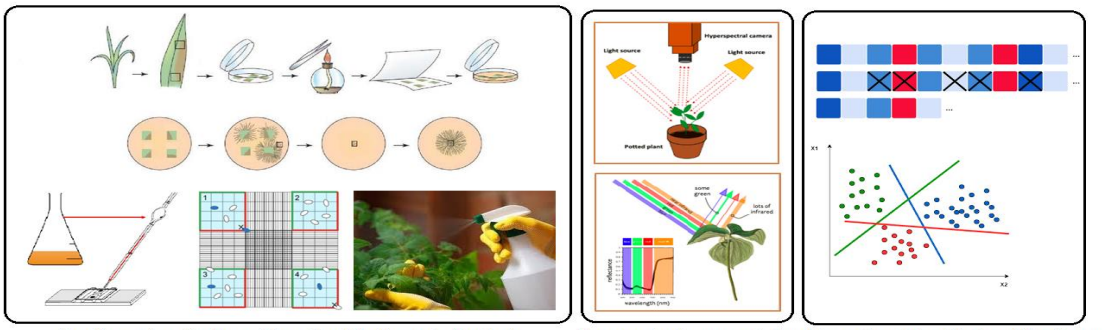

Figure 1. Three steps in diagnosing tomato diseases by hyperspectral images

2.1. Sampling, purification, and transfer of the disease to the plant

In order to prepare and isolate the disease agent, samples were taken from tomato fields. The samples were placed separately in paper envelopes and kept at a temperature of 4°C after being transferred to the laboratory. Using a sterile scalpel, small pieces of 1 cm size were cut from the infected tissues. The cut pieces were surface disinfected in 10% sodium hypochlorite solution for 10 minutes and immediately washed twice with water. After dewatering with filter paper, the samples were cultured on nutrient medium (potato dextrose agar) PDA. Then, the plates were incubated for 3 to 5 days at 25°C. From the grown colonies that had the characteristics of the disease considered in this study, they were purified by removing single spore or spore chain. 5 mm pieces of growing colonies were removed and cultured on PDA. To stimulate the sporulation pattern, the plates were incubated at 24°C with a light cycle of 8 hours of light and 16 hours of darkness for 5 to 7 days. The isolates were identified using the general patterns of sporulation, including the arrangement of spores on the spore carrier, the number of spores in each chain, and the branching pattern of the chains, and the pathogenicity test of the isolates was proved. After 10 days of purification, the surface of petri dish was washed with sterile distilled water. 10 microliters of the solution obtained from disease spores was taken by a sampler and the number of disease spores was counted and their concentration was determined by counting under a light microscope with a hemocytometer slide. In counting the spores, it is important that the spores attached to the square lines of the slide at the top and right side can be counted, and the spores at the

bottom and left cannot be counted. The number of spores allowed at the time of disease transmission was $5x10^6$ for each disease.

2.2. Hyperspectral image capturing

The Spectral images of healthy and infected leaves were captured daily under laboratory conditions using a spectroscopic camera (Hyspim HSI-Vis_Nir-15fps, Sweden) with a spectral range of 400-950 nm in 1, 3, 5, and 7 days after the disease transfer to the plants. The halogen light was vertically from above the leaf, and a dark background was used to place the leaf on the device scanner. To avoid the interference of natural light, the camera and the halogen lamps were placed in a chamber for image acquisition. The distance of the cameras from the leaves was 25 cm. Finally, for each disease and healthy leaf, 100 hyperspectral images were taken. Therefore, 300 images per sampling day and 1,200 images in total were obtained.

2.3 Diagnosis and classification of the disease

After the image was taken, in order to access all the information of an image, the features of texture (contrast, correlation, energy, homogeneity, mean, standard deviation, entropy, RMS, variance, smoothness, kurtosis, and skewness), color (mean, maximum, standard deviation, and median), and shape (area, perimeter, number of objects, major and minor axis length of the spots, eccentricity index, form, circular index, and compression index) were extracted from each band of the image (Javidan et al., 2024a,b). After that, images were classified by the support vector machine classifier. Then, the Relief feature selection (Javidan et al., 2023a) algorithm was used to identify the best and most important influencing features.

Also, the spectral signatures (reflectance spectra) of two common fungal diseases of tomato leaves were evaluated, and the ability of these spectral features to differentiate between the diseases was analysed. The spectral range of the measurements was selected to encompass the region of interest, including the visible and near-infrared regions, between 400 to 950 nm. The spectral signatures of the two fungal diseases were found to be unique and characteristic, and their distinguishing features were analysed in detail. This study has demonstrated the effectiveness of hyperspectral imaging in the diagnosis of plant diseases and the identification of specific spectral signatures associated with different diseases.

2.3.1 Performance evaluation of the support vector machine classifier

A classification algorithm's performance is determined by its classification accuracy, which is calculated by maximizing TP and TN while minimizing FP and FN in a two-class problem, as represented in Eq 1.

$$Accuracy = \frac{(TP + TN)}{(TP + TN + FP + FN)} \quad (1)$$

3. Results and Discussion

3.1 Disease classification

After extracting the features of texture, color, and shape from hyperspectral images and forming the feature matrix, the classification was done with the support vector machine, and the disease classification accuracy for each day of imaging (i.e. days 1, 3, 5, and 7) was obtained. Based on this, the classification accuracy for days 1, 3, 5, and 7 was 89, 91, 93, and 96%, respectively. Table 1 shows the results of the support vector machine classification. The obtained results showed that the algorithm was able to diagnose and classify the two diseases in early disease development stages, even when symptoms of both diseases looked similar visually, with high accuracy. Also, to compare the classification results of the SVM, other machine learning models such as k-nearest neighbor, decision tree, and random forest were trained and evaluated (Table 1). In previous studies using hyperspectral images for crop disease monitoring, spectral and textural features were used simultaneously to develop a disease detection model that performed well (Kuncheva & Faithfull, 2014; Xiao et al., 2021; Khan et al., 2021; Guo et al., 2021; Chen et al., 2022; Nguyen et al., 2023).

Table 1. Classification results of machine learning models on different days.

Classifier	Day 1	Day3	Day 5	Day 7
k-Nearest Neighbor	60	63	71	86
Decision Tree	63	70	75	88
Random Forest	75	79	83	91

Support Vector Machine	89	91	93	96

3.2 Feature selection

It is very critical to identify the most important features that play a major role in the diagnosis of diseases. This can help researchers in future research to develop low-cost multi-spectral cameras to target these selected features for early disease detection. In this research, the relief feature selection algorithm was used to rank the features and determine the most important and influential ones. The most important features and bands for hyperspectral images are shown in Table 2. Among the top ten selected features, texture features had the most impact, followed by statistical features and descriptive shape. As can be seen in the images of disease symptoms, texture and descriptive statistical features are clearly effective in diagnosing diseases.

Table 2. Features and bands effective in identifying and classifying diseases in Hyperspectral images.

Rank	Features Type	Feature Selected	Band (nm)
1	Texture	Energy	550
2	Texture	Entropy	600
3	color	Max	480
4	color	mean	663
5	Texture	Correlation	746
6	Texture	Standard Deviation	886
7	color	Median	850
8	color	Median	460
9	Texture	Energy	841
10	Texture	Standard Deviation	905

3.3 Spectral signatures of the *Alternaria alternata* and *Alternaria solani* diseases

As can be seen in Figure 2, the spectral identification symptoms for two tomato leaf diseases in the range of bands 500 to 550 and 740 to 950 have more distinction for identifying and diagnosing the disease in the early stages. Also, the average changes of the disease spectrum compared to the healthy spectrum in the leaf area are shown in Figure 2 A, B, and C respectively for the target area of *Alternaria alternaria*, *Alternaria solani*, and healthy leaf. According to Figure 2A, the light reflectance recorded in the *Alternaria alternata* disease in the spectral range of 550 to 950 nm was lower than the spectral reflectance in the healthy area, and it showed a sign of the disease symptoms in this area, which is the spectral sign of this disease. As mentioned before, slight changes in the healthy area were due to the slight heterogeneity of the leaf tissue, the surface structure of the tomato leaf, and its interaction with radiation. As Figure 4B shows, in the case of *Alternaria solani* disease, the reflection of the spectrum in the diseased area in the range of 550 to 950 nm showed less symptoms than the *Alternaria alternata* disease (due to the later showing of symptoms in this type). The light is reduced in this area compared to the healthy area of Figure 4C, and it can be used as a basis for diagnosing and identifying the disease of *Solani* species. Different substances, such as chlorophyll, display distinct absorption and reflectance values in specific wavebands, creating unique spectral characteristics (Nevalainen et al., 2017). The reflectance peaks near 550 nm and 700 nm correspond to the strong reflection region of chlorophyll, and the red edge phenomenon results from the low red reflectance and high internal leaf scattering of chlorophyll (Heim et al., 2015). Moisture absorption troughs near 1470 nm and 1940 nm and low reflectance in the range of 1300–2500 nm are related to plant moisture content and CO2 emissions (Mutanga et al., 2009; Lai el al., 2021). Hyperspectral imaging of the biological processes during plant–pathogen interactions allows for the detection of plant diseases using hyperspectral imaging technology (Roth et al., 2015; Pu et al., 2019).

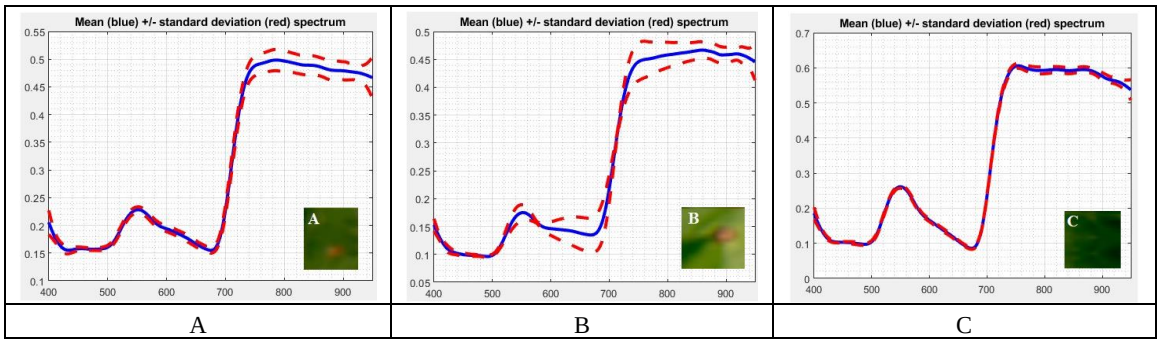

Figure 2. Spectral signatures for: a. *Alternaria alternata* b. *Alternaria solani* and C. healthy leaf

4. Conclusions

The early diagnosis of plant diseases is necessary for effective disease management. Hyperspectral imaging and artificial intelligence have enabled the diagnosis of plant diseases in their early stages by analysing the images and providing a distinct spectral signature for each disease. In this study, two tomato diseases, *Alternaria alternata* and *Alternaria solani*, were investigated using spectral reflectance analysis in the span of 400-950 nm. The results showed a high level of accuracy in the classification of diseased leaves with accuracy rates of 89%, 91%, 93%, and 96% for days 1, 3, 5, and 7, respectively. The classification accuracy indicates the potential of hyperspectral imaging for early disease detection. The spectral reflectance in the imaging band range of 400 to 950 nm demonstrates the spectral differentiation between the two diseases, indicating their unique spectral signatures. Also, the results suggest that texture features such as energy in bands 550 and 841, entropy in band 600, correlation in band 746, and standard deviation in band 905 are superior to other features for disease identification. The Relief feature selection algorithm provided insights into the effectiveness of different features, demonstrating that texture features are more precise for disease identification. Moreover, the study suggested the potential for a low-cost portable or UAV-based device, equipped with several light-emitting diodes/photodiodes in the range of visible 500-550 nm and near-infrared 740 to 950 nm, for the detection of major tomato fungal diseases. These devices can be used instead of expensive laboratory equipment, providing the necessary data to classify diseases in a cost-effective and efficient manner.

References

Barbosa Júnior M.D., Moreira B.R.A., Carreira V.S., Brito Filho A.L., Trentin C., Souza F.L.P., Tedesco D., Setiyono T., Flores J.P., Ampatzidis Y., Silva R.P., Shiratsuchi L.S., 2024. Precision Agriculture in the United States: A comprehensive meta-review inspiring further research, innovation, and adoption. Computers and Electronics in Agriculture, 221, 108993, https://doi.org/10.1016/j.compag.2024.108993.

Cen, Y., Huang, Y., Hu, S., Zhang, L., & Zhang, J, 2022. Early Detection of Bacterial Wilt in Tomato with Portable Hyperspectral Spectrometer. *In Remote Sensing* (Vol. 14, Issue 12, p. 2882). MDPI AG. https://doi.org/10.3390/rs14122882

da Cunha V.G., A. Hariharan J., Ampatzidis Y., Roberts P., 2023. Early detection of tomato bacterial spot disease in transplant tomato seedlings utilizing remote sensing and artificial intelligence. Biosystems Engineering, 234, 172-186, https://doi.org/10.1016/j.biosystemseng.2023.09.002.

Fernández, C. I., Leblon, B., Wang, J., Haddadi, A., & Wang, K, 2022. Cucumber powdery mildew detection using hyperspectral data. In B. Beres (Ed.), *Canadian Journal of Plant Science* (Vol. 102, Issue 1, pp. 20–32). Canadian Science Publishing. https://doi.org/10.1139/cjps-2021-0148

Hariharan J., Ampatzidis Y., Abdulridha J., Batuman O., 2023. An AI-based spectral data analysis process for recognizing unique plant biomarkers and disease features. Computers and Electronics in Agriculture, 204, 107574, https://doi.org/10.1016/j.compag.2022.107574

Heim, R., Jürgens, N., Große-Stoltenberg, A., & Oldeland, J, 2015. The Effect of Epidermal Structures on Leaf Spectral Signatures of Ice Plants (Aizoaceae). In Remote Sensing (Vol. 7, Issue 12, pp. 16901–16914). MDPI AG. https://doi.org/10.3390/rs71215862

Javidan, S. M., Ampatzidis, Y., Vakilian, K. A., & Mohammadzamani, D, 2024a. A Novel Approach for Automated Strawberry Fruit Varieties Classification Using Image Processing and Machine Learning. In 2024 10th International Conference on Artificial Intelligence and Robotics (QICAR). 2024 10th International Conference on Artificial Intelligence and Robotics (QICAR). IEEE. https://doi.org/10.1109/qicar61538.2024.10496652

Javidan, S. M., Banakar, A., Asefpour Vakilian, K., & Ampatzidis, Y, 2023a. Diagnosis of grape leaf diseases using automatic K-means clustering and machine learning. In Smart Agricultural Technology (Vol. 3, p. 100081). Elsevier BV. https://doi.org/10.1016/j.atech.2022.100081

Javidan, S. M., Banakar, A., Asefpour Vakilian, K., & Ampatzidis, Y, 2023b. Tomato leaf diseases classification using image processing and weighted ensemble learning. In Agronomy Journal (In Press). Wiley. https://doi.org/10.1002/agj2.21293

Javidan, S. M., Banakar, A., Asefpour Vakilian, K., & Ampatzidis, Y, 2022. A feature selection method using slime mould optimization algorithm in order to diagnose plant leaf diseases. In 2022 8th Iranian Conference on Signal Processing and Intelligent Systems (ICSPIS) (pp. 1-5). IEEE. https://doi.org/10.1109/ICSPIS56952.2022.10043928

Javidan, S. M., Banakar, A., Vakilian, K. A., Ampatzidis, Y., & Rahnama, K, 2024b. Diagnosing the spores of tomato fungal diseases using microscopic image processing and machine learning. In Multimedia Tools and Applications. Springer Science and Business Media LLC. https://doi.org/10.1007/s11042-024-18214-y

Khakrangin, R., MohamadZamani, D., & Javidan, S. M, 2021. Recognition of Fill and Empty Walnuts Using Acoustic Analysis and Fuzzy Logic. Journal of Nuts, 12(1). https://doi.org/10.22034/jon.2021.1918546.1103

Kuncheva, L. I., & Faithfull, W. J, 2014. PCA Feature Extraction for Change Detection in Multidimensional Unlabeled Data. *In IEEE Transactions on Neural Networks and Learning Systems* (Vol. 25, Issue 1, pp. 69–80). Institute of Electrical and Electronics Engineers (IEEE). https://doi.org/10.1109/tnnls.2013.2248094

Lai, Y., Zhang, J., Song, Y., & Gong, Z, 2021. Retrieval and Evaluation of Chlorophyll-a Concentration in Reservoirs with Main Water Supply Function in Beijing, China, Based on Landsat Satellite Images. In International Journal of Environmental Research and Public Health (Vol. 18, Issue 9, p. 4419). MDPI AG. https://doi.org/10.3390/ijerph18094419

Mohamadzamani, D., sajadian, S., & javidan, S. M, 2020. DDetection of Callosobruchus maculatus F. with image processing and artificial neural network. *Applied Entomology and Phytopathology*, *88*(1), 103-112. doi: 10.22092/jaep.2020.341684.1324

Mohammad Zamani, D., Javidan, S. M., Zand, M., & Rasouli, M, 2023. Detection of Cucumber Fruit on Plant Image Using Artificial Neural Network. *Journal of Agricultural Machinery*, *13*(1), 27-39. doi: 10.22067/jam.2022.73827.1077

Mutanga, O., Van Aardt, J., & Kumar, L, 2009. Imaging spectroscopy (hyperspectral remote sensing) in southern Africa: an overview. South African Journal of Science, 105(5), 193-198. Google Scholer

Nevalainen, O., Honkavaara, E., Tuominen, S., Viljanen, N., Hakala, T., Yu, X., Hyyppä, J., Saari, H., Pölönen, I., Imai, N., & Tommaselli, A, 2017. Individual Tree Detection and Classification with UAV-Based Photogrammetric Point Clouds and Hyperspectral Imaging. In Remote Sensing (Vol. 9, Issue 3, p. 185). MDPI AG. https://doi.org/10.3390/rs9030185

Pu, H., Lin, L., & Sun, D, 2019. Principles of Hyperspectral Microscope Imaging Techniques and Their Applications in Food Quality and Safety Detection: A Review. In Comprehensive Reviews in Food Science and Food Safety (Vol. 18, Issue 4, pp. 853–866). Wiley. https://doi.org/10.1111/1541-4337.12432

Roth, G. A., Tahiliani, S., Neu-Baker, N. M., & Brenner, S. A, 2015. Hyperspectral microscopy as an analytical tool for nanomaterials. In WIREs Nanomedicine and Nanobiotechnology (Vol. 7, Issue 4, pp. 565–579). Wiley. https://doi.org/10.1002/wnan.1330

Vakilian, K. A., Moreau, M., & Javidan, S. M, 2024. An IoT-based smart biosensor for the measurement of nitrate concentration in liquid samples. In 2024 20th CSI International Symposium on Artificial Intelligence and Signal Processing (AISP). 2024 20th CSI International Symposium on Artificial Intelligence and Signal Processing (AISP). IEEE. https://doi.org/10.1109/aisp61396.2024.10475236

Wu, G., Fang, Y., Jiang, Q., Cui, M., Li, N., Ou, Y., Diao, Z., & Zhang, B, 2023. Early identification of strawberry leaves disease utilizing hyperspectral imaging combing with spectral features, multiple vegetation indices and textural features. *In Computers and Electronics in Agriculture* (Vol. 204, p. 107553). Elsevier BV. https://doi.org/10.1016/j.compag.2022.107553

Xiao, Y., Dong, Y., Huang, W., Liu, L., & Ma, H, 2021. Wheat Fusarium Head Blight Detection Using UAV-Based Spectral and Texture Features in Optimal Window Size. *In Remote Sensing* (Vol. 13, Issue 13, p. 2437). MDPI AG. https://doi.org/10.3390/rs13132437

Zhang, G., Xu, T., & Tian, Y, 2022. Hyperspectral imaging-based classification of rice leaf blast severity over multiple growth stages. *Research Square Platform LLC*. https://doi.org/10.21203/rs.3.rs-1756611/v1

Assessing water and nitrogen stress in pepper plants (*Capsicum annum L.*) using hyperspectral data: A comparative analysis of machine learning and vegetation indices

Maria Bebie [a,*], Aris Kyparissis [a]

[a] Department of Agriculture, Crop Production and Rural Environment, University of Thessaly, Volos, Greece

* Corresponding author. Email: mbempi@uth.gr

Abstract

Early detection of plant stress is crucial for optimizing crop yield and quality in precision agriculture. Reflectance data analysis from remote sensing technologies has significantly advanced the identification and quantification of physiological responses in stressed crops. Machine learning (ML) algorithms can analyse complex datasets and identify subtle patterns missed by traditional methods. This study presents two modeling approaches to assess water and nitrogen stress in pepper (*Capsicum annuum* L.) plants using hyperspectral data. A controlled experiment with a 3 x 3 factorial design evaluated three water stress levels and three nitrogen fertilizer levels across nine treatment groups. Hyperspectral data were collected using a spectroradiometer. The ecophysiological parameters measured include chlorophyll content (a & b), carotenoid levels, leaf specific mass and relative water content. Both modeling approaches compared reflectance data with each ecophysiological parameter individually. The first approach used linear regression models based on vegetation indices (NDVI, PRI, GNDVI, NDRE, NIRv). The second approach used the reflectance data as inputs for four ML algorithms: Random Forest, K-Nearest Neighbors, Support Vector Machines and Regularized Linear Regression. Results showed that the ML-based approach generally outperformed the VI-based approach. All four ML algorithms demonstrated high performance with most ecophysiological parameters (chlorophylls: $R^2 > 0.83$, RMSE < 0.42; carotenoids: $R^2 > 0.84$, RMSE < 0.39; LSM: $R^2 > 0.65$, RMSE < 0.61). Among VI-based models, NDRE and GNDVI performed best (chlorophylls: $R^2 > 0.8$, RMSE < 0.42; carotenoids: $R^2 > 0.75$, RMSE < 0.45), while the other indices showed moderate to low performance (chlorophylls: $R^2 < 0.52$, RMSE > 0.7; carotenoids: $R^2 < 0.45$, RMSE > 0.71; LSM: $R^2 < 0.5$, RMSE > 0.7). These findings indicate the potential of ML algorithms to surpass conventional VI-based methods for early detection and monitoring of plant stress using hyperspectral data in precision agriculture.

Keywords: pepper, hyperspectral data, machine learning, vegetation indices, abiotic stress

1. Introduction

Water and nitrogen (N) are critical factors in agricultural production. Water, essential for normal growth and development, becomes a major limiting factor when mismanaged (Shao et al., 2009). Similarly, nitrogen is a vital nutrient for plants. Plants absorb nitrogen from the soil in the form of nitrate (NO^{3-}) or ammonium (NH^{4+}) ions. Nitrogen is then utilized in various metabolic processes, including protein synthesis, nucleic acid synthesis, and energy production (Von Wirén et al., 1997). It is responsible for plant development, as it is essential for the structure of chlorophyll, the function of photosynthetic proteins and enzymes, and maintaining photosynthetic capacity (Mu & Chen, 2021). Effective management of these resources is imperative for crop productivity and environmental sustainability, as inadequate practices often result in agricultural pollution and economic losses. Accurate assessment of crop needs and timely application of water and nitrogen are essential to address these challenges. However, to achieve optimal management, accurate and early detection of plant stress is needed.

Remote sensing technologies offer a promising solution for non-destructive and efficient monitoring of plant stress in agriculture. Among these, hyperspectral imaging stands out for its ability to capture detailed information across hundreds of narrow spectral bands, providing insights into various plant traits and stressors (Behmann et al., 2014; Maki et al., 2023). While multispectral sensors, whether airborne or ground-based, have traditionally detected stressors such as N deficiency or water stress (Eitel et al., 2008), accurate differentiation remains challenging. Multiple stress factors often coexist, leading to similar outcomes such as chlorophyll decrease. Thus, a key objective is to distinguish between different factors. (Wang et al., 2011). Vegetation indices (VIs) derived from spectral data have been widely used to assess plant stress, offering insights into variables like biomass, chlorophyll content, and N concentration (Xue & Su, 2017). However, interpreting these indices is complicated by stress interactions and environmental factors, posing challenges in accurately quantifying individual stressors (Barnes et al., 2000).

To address these limitations, machine learning (ML) techniques have emerged as valuable tools for analyzing hyperspectral data and extracting meaningful information related to plant stress. Fundamentally, machine

learning employs data-driven learning to detect patterns that may be overlooked using traditional analytical methods (Zhang & Ma, 2012). ML can utilize the entire range of the primary spectral information instead of a set of few spectral bands used in VIs. In agriculture, they can detect patterns using simultaneous combinations of multiple factors instead of examining traits individually (Fu et al., 2019). This can be proven really useful considering the high complexity of the environment surrounding plants.

This study aims to investigate the potential of ML algorithms for accurately assessing water and nitrogen stress by leveraging hyperspectral reflectance data. The performance of ML models is compared to conventional vegetation index-based approaches, utilizing a variety of commonly used VIs in agriculture.

2. Materials and Methods

2.1. Experimental Design

Pepper plants (*Capsicum annuum* L., cultivar "Shelby") were cultivated in 7-liter white plastic pots. The soil, sourced from the University Farm in Velestino, Thessaly, Greece, was mixed with perlite in a 3:1 ratio to enhance aeration and promote optimal growth conditions. The mixture filled the pots to approximately 5.5 litres each. The pepper plants were transplanted on May 9th, 2023, and the experiment ran for 63 days, concluding on July 10th, 2023. A 3 x 3 factorial design was employed, evaluating three nitrogen fertilization levels in combination with three irrigation levels. This resulted in a total of nine treatment combinations. No additional fertilizers, herbicides, or pesticides were applied throughout the experiment. Each treatment was replicated ten times, bringing the total number of pots to 90.

2.1.1. Nitrogen Fertilization

A total of 20 units of nitrogen (N) per plant was designated as the optimal dosage for the experiment's duration. The three N fertilization levels consisted of a negative control (N_1: 0 N), a half-optimal dose (N_2: 10 units N), and the optimal dose (N_3: 20 units N). Ammonium nitrate fertilizer (34.5% N) was used, divided into four equal applications administered every 13-15 days. The first application occurred eight days post-transplantation (May 16th, 2023), with the final dose applied on June 30th, 2023.

2.1.2. Irrigation

The initial irrigation levels were set at 200 ml (H_1), 400 ml (H_2), and 600 ml (H_3) per application. However, due to rising temperatures, these levels were subsequently adjusted to 300 ml, 450 ml, and 600 ml, respectively. All 90 pots were irrigated simultaneously during each watering event. Plants were watered every 3 to 4 days. During the second month of the experiment, as temperatures rose, the watering frequency was increased to every 1 to 2 days. Over the experiment, the low, medium, and high irrigation treatments received a total of 10.1 L, 14.8 L, and 19.5 L of water, respectively.

2.2. Measurements and Analyses

2.2.1. Physiological Measurements

Physiological measurements focused on plant water status and photosynthetic pigments and were performed in a weekly basis. Relative Water Content (RWC) and Leaf Specific Mass (LSM) were determined to evaluate plant water stress. RWC was calculated using the equation:

$$\text{Relative Water Content, RWC} = \frac{\text{FW - DW}}{\text{TW - DW}}$$

where FW is fresh weight, TW is turgid weight, and DW is dry weight. Leaf discs were cut and weighed to obtain fresh weight. Turgid weight was determined after putting the discs in distilled water for 24 hours. Finally, dry weight was obtained after oven drying at 80°C for 24 hours. LSM was calculated using the equation:

$$\text{Leaf Specific Mass, LSM} = \frac{\text{DW}}{\text{A}}$$

where DW is dry weight (g) and A is leaf area (dm^2). Chlorophyll a and b content, along with carotenoid content, were measured to assess photosynthetic activity. Pigments were extracted using 80% acetone followed by

centrifugation at 4000 rpm for 10 minutes. The absorbance of the supernatant was measured at specific wavelengths (720, 663, 646, and 470 nm) using a dual-beam spectrophotometer (SHIMATZU, UV-1900). Concentrations of chlorophyll a, b, and carotenoids were calculated using the equations established by Lichtenthaler and Wellburn (Lichtenthaler & Wellburn, 1983).

The parameters derived from pigment extraction included the total concentration of chlorophylls and carotenoids per leaf surface area (μg cm^{-2}) and leaf dry weight (μg g^{-2}), and ratios chlorophyll a to b ratio and chlorophyll to carotenoid. These ratios are important indicators of stress response. For instance, the chlorophyll a to b ratio, typically around 3:1 in healthy plants, decreases under stress conditions, signifying degradation of chlorophyll b. Similarly, the chlorophyll to carotenoid ratio changes during stress, with chlorophylls tending to decline more rapidly than carotenoids (Merzlyak et al., 1999). Overall, eight physiological parameters used as dependent variables in both modelling approaches.

2.2.2. Hyperspectral Reflectance Data

Hyperspectral data, consisting of reflectance measurements from plant leaves, were collected non-invasively using a spectroradiometer (JAZ Spectrometer, Ocean Optics) on a weekly basis. The device captured reflectance, absorbance, and transmittance data from 340 nm to 1025 nm, encompassing the near-ultraviolet, visible, and near-infrared light regions. It offered a spectral resolution of approximately 0.3 nm. Importantly, the same leaf from each pot was used for each weekly measurement of all parameters (physiological and hyperspectral). Spectral data were collected first, followed by leaf collection for laboratory analyses of physiological parameters.

2.3. Modeling

Both modeling approaches that were developed to assess nitrogen and water stress in pepper plants, compared the reflectance data with each ecophysiological parameter individually. The first modeling approach comprised linear regression models based on vegetation indices (NDVI, PRI, GNDVI, NDRE, NIRv). In the second approach, the reflectance data from the spectroradiometer were used as input parameters in four machine learning model algorithms, i.e., Random Forest (RF), K-Nearest Neighbors (KNN), Support Vector Machines (SVM) and Regularized Linear Regression (RLR).

2.3.1. Vegetation Index – Based Approach

In this modeling approach, hyperspectral data derived from the spectroradiometer were used to construct vegetation indices. The indices used in the experiment included NDVI, PRI, GNDVI, NDRE, NIRv, and REP. The indices were calculated using the following equations:

$$\text{Normalized Difference Vegetation Index, NDVI} = \frac{R_{845} - R_{665}}{R_{845} + R_{665}}$$

$$\text{Photochemical Reflectance Index, PRI} = \frac{R_{531} - R_{570}}{R_{531} + R_{570}}$$

$$\text{Green Normalized Difference Vegetation Index, GNDVI} = \frac{R_{845} - R_{560}}{R_{845} + R_{560}}$$

$$\text{Normalized Difference Red Edge, NDRE} = \frac{R_{845} - R_{715}}{R_{845} + R_{715}}$$

$$\text{Near-infrared Reflectance of Vegetation , } NIR_V = R_{845} \times \text{NDVI}$$

$$\text{Red Edge Position , REP}$$

where Rx represents the reflectance at wavelength x, calculated as the average reflectance over a 10 nm range centred around x. For instance, instead of using a single value at 845 nm, the average reflectance from 840 nm to 850 nm was used. This approach was adopted to prevent small fluctuations between measurements from affecting the final value of each index. The Red Edge Position (REP) corresponds to the wavelength between 680 nm and 760 nm at which the first derivative of reflectance reaches its maximum value.

Vegetation indices (VIs) are used in precision agriculture to assess plant stress. NDVI assesses plant health and growth (Huang et al., 2021). PRI, sensitive to carotenoid pigments, evaluates photosynthetic efficiency and stress (Thenot et al., 2002). GNDVI, using the green band, correlates with Leaf Area Index and biomass, being

more sensitive to chlorophyll than NDVI (Candiago et al., 2015). NDRE detects nitrogen stress more accurately than NDVI (Li et al., 2014). NIRv, a newer VI, improves accuracy in estimating plant productivity and photosynthesis (Badgley et al., 2017). REP is sensitive to chlorophyll content and stress, shifting towards shorter wavelengths under stress (Velichkova & Krezhova, 2019).

Each vegetation index was calculated for all nine treatments across four dates, ranging from May 30 to June 22, 2023. This resulted in a sample size of 36. These variables were then used to construct the linear regression models. Each VI was used as a single predictor and was correlated with each individual physiological parameter, resulting in 48 simple linear regression models (6 VIs × 8 parameters).

2.3.2. Machine Learning – Based Approach

In this approach, the hyperspectral data derived from the spectroradiometer were used as independent variables in four commonly used ML algorithms, i.e., random forests (RF), k-nearest neighbors (KNN), support vector machines (SVM) and regularized linear regression (RLR).

Random Forest constructs multiple decision trees for regression, averaging predictions to reduce overfitting and enhance accuracy (Cutler et al., 2012). It is widely used in plant stress detection for its accuracy, robustness, and simplicity (Chemura et al., 2017; Vitrack-Tamam et al., 2020). K-Nearest Neighbors (KNN) predicts values by averaging the k nearest neighbors, handling classification and regression tasks effectively (Aha et al., 1991). Support Vector Machines (SVM) identify the optimal hyperplane for classification and use kernel functions for non-linear data, effective in high-dimensional spaces and robust against overfitting (Kecman, 2005), performing well in plant stress detection (Karimi et al., 2006; Moshou et al., 2014). Regularized Linear Regression (RLR) adds penalties to prevent overfitting, with Ridge (L2) and Lasso (L1) being common forms, robust and interpretable for multi-dimensional data (Pillonetto et al., 2022).

The raw hyperspectral data, obtained directly from the spectroradiometer, span a wavelength range from 340 nm to 1025 nm, with a spectral resolution of approximately 0.3 nm. The process of constructing the ML models involved data cleaning to remove noise and averaging approximately 15 consecutive values, resulting in a reduced spectral resolution of 5 nm. This process aimed to reduce the total number of independent variables utilized for training, testing, and validation. Ultimately, the final dataset comprised 90 independent variables, ranging from 500 nm to 1000 nm. In all modeling approaches, data were randomly split into a training set (80% of data) and a validation set (20% of data) to assess performance efficiency. The same data splitting method was applied consistently across all models.

2.4. Statistics

The simple linear regressions between the predictors and the dependent variables for the first modeling approach and the machine learning for the second, were performed with JASP software version 0.18.3 (JASP, 2024). Models' performance was evaluated by the coefficient of determination (R^2), root mean square error (RMSE, z-score standardized) and the slope of the best-fit line between measured and modeled values.

3. Results

3.1. Nitrogen and water stress

Figure 1 presents the total chlorophyll content (per leaf area) (1a) and RWC (1b) for all nine treatments throughout the experiment. In 1a, clear differentiation is observed between N_1, N_2, and N_3 treatments, with chlorophyll content increasing with higher N doses. Additionally, chlorophylls increase within each treatment as the experiment progresses. Regarding RWC (1b), it tends to be higher with increased irrigation levels, with the most apparent difference occurring on 14/06/2023. Conversely, within the same irrigation level, higher N levels correspond to lower RWC values. This is expected due to increased biomass (Table 1), resulting in higher water requirements.

Table 1. Total average dry weight (g) per treatment. Each value corresponds to the average dry weight for each treatment at the end of the experiment.

Treatment	H_1N_1	H_1N_2	H_1N_3	H_2N_1	H_2N_2	H_2N_3	H_3N_1	H_3N_2	H_3N_3
Dry Weight (g)	12.77	17.48	20.21	15.38	25.57	30.77	18.09	31.69	40.50

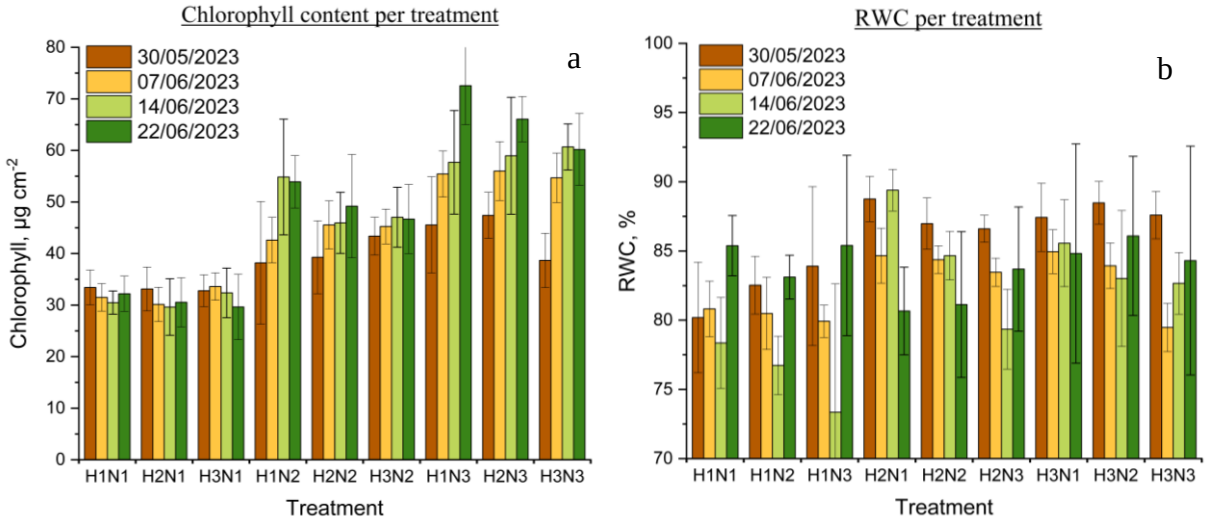

Figure 1. Chlorophyll content (a) and RWC (b) per treatment. Each color represents a different measurement at dates indicated in the graphs. H_1, H_2, H_3 and N_1, N_2, N_3 indicate low, mid and high levels of water and nitrogen, respectively.

3.2. Vegetation Index – Based Approach

The results of the simple linear regression models demonstrate extensive variability in the performance across different physiological parameters and vegetation indices (Table 2). It is observed that several physiological parameters exhibit relatively high performance when correlated with certain vegetation indices. Overall, the best performing LR models feature NDRE as the independent variable, with an $R^2 > 0.79$ and an RMSE < 0.47 for total chlorophylls (Figure 2a) and carotenoids per leaf area, and the chlorophyll to carotenoids ratio. The second-best performing results were demonstrated when using GNDVI as an independent variable, with an $R^2 > 0.73$ and an RMSE < 0.53 for the same three physiological parameters. Figure 2b presents GNDVI's performance whit total chlorophylls per leaf area as the dependent variable. It is also important to note that GNDVI achieves the highest performance with chlorophyll content per dry weight ($R^2 > 0.71$ and an RMSE < 0.49). Conversely, NDVI, PRI, NIRv, and REP generally exhibit moderate to poor performance across most physiological parameters, with $R^2 < 0.6$ and RMSE > 0.63 for all eight physiological parameters. An interesting observation is that NDVI, despite its widespread usage in plant stress detection, ranks among the least effective indices in this experiment. Regarding the physiological parameters used individually as dependent variables in the LR models, most of them exhibit consistent patterns in their correlation with the VIs. For example, most indices demonstrate poor performance in predicting RWC and LSM, with extremely low R^2 (< 0.1) and high RMSE (> 1.2). An exception is observed in the NIRv – LSM linear regression model, which shows moderate performance with R^2 = 0.56 and RMSE = 0.68.

Table 2. Performance comparison of the vegetation index – based, simple linear regression models (VI – LR). All eight parameters were used individually as dependent variables in combination with all six VIs. VIs were constructed by using hyperspectral reflectance data from 400 nm to 1025 nm. R^2, coefficient of determination and RMSE, root mean square error (standardized, unitless) between measured and modeled values. The sample size used in the experiment is 36.

Parameters	VI - Linear Regression Models											
	NDVI		PRI		GNDVI		NDRE		NIRv		REP	
	R^2	RMSE	R^2	RMSE	R^2	RMSE	R^2	RMSE	R^2	RMSE	R^2	RMSE
RWC	0.001	1.299	0.041	1.350	0.087	1.340	**0.169**	**1.429**	0.064	1.411	0.149	1.509
LSM	0.057	1.577	0.020	1.214	0.000	1.395	0.063	1.236	**0.567**	**0.677**	0.030	1.360
Chl (µg cm⁻²)	0.263	0.855	0.522	0.695	0.800	0.424	**0.933**	**0.276**	0.200	1.014	0.611	0.632
Car (µg cm⁻²)	0.279	0.809	0.450	0.717	0.758	0.448	**0.897**	**0.330**	0.210	0.975	0.572	0.657
Chl (µg g⁻²)	0.374	0.734	0.459	0.733	**0.818**	**0.407**	0.740	0.487	0.014	1.228	0.522	0.701
Car (µg g⁻²)	0.432	0.670	0.312	0.815	**0.713**	**0.491**	0.545	0.631	0.005	1.301	0.382	0.797
Chl/Car	0.234	0.961	0.521	0.779	0.738	0.533	**0.792**	**0.473**	0.104	1.195	0.562	0.708
Chla/Chlb	0.000	1.157	0.214	1.441	0.123	1.219	0.300	1.351	**0.405**	**1.564**	0.142	1.366

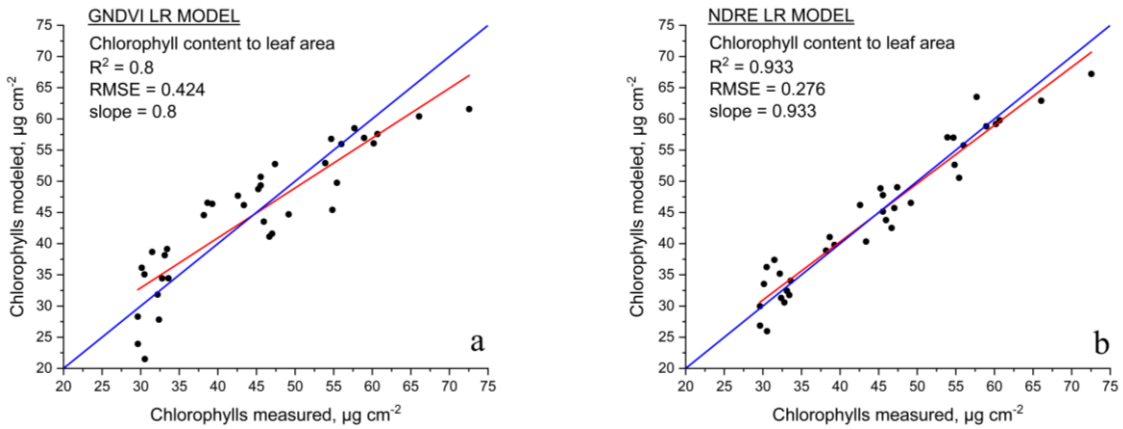

Figure 2. Relationships between measured and modeled values based on the VI-LR approach, when using GNDVI (a) and NDRE (b) as predictors, with chlorophyll content to leaf surface area as a dependent variable. The coefficient of determination (R^2), the root mean square error (RMSE) and the slope of the best-fit line are shown in the inserts. Blue line corresponds to the 1:1 line and red line to the best-fit line.

3.3. Machine Learning – Based Approach

In this approach, all hyperspectral data were used as independent variables in combination with each physiological parameter. All machine learning models outperformed the simple linear regression models (Table 3). Additionally, all algorithms demonstrate comparable performances. No single algorithm stands out as superior. The best performing models are once again those concerning chlorophylls and carotenoids per leaf surface area ($R^2 > 0.83$ and RMSE < 0.42 and $R^2 > 0.84$ and RMSE < 0.39, respectively). Another improvement over the first modeling approach is the relatively high performance of all algorithms in predicting LSM, with $R^2 > 0.65$ and RMSE < 0.61. Lastly, RWC remains the only parameter that no algorithm can accurately predict ($R^2 < 0.3$ and RMSE > 0.93). In Figure 3, four of the best performing ML models are depicted.

Table 1. Performance comparison of the ML – based models. All eight parameters were used individually as dependent variables and all hyperspectral reflectance data (500 nm to 1000 nm) were used as independent variables. R^2, coefficient of determination and RMSE, root mean square error (standardized, unitless) between measured and modeled values. Sample size is 36.

Parameters	Algorithms							
	RF		KNN		SVM		RLR	
	R^2	RMSE	R^2	RMSE	R^2	RMSE	R^2	RMSE
RWC	0.304	0.934	0.139	1.104	0.065	1.204	**0.308**	**0.930**
LSM	0.732	0.530	0.654	0.610	0.708	0.555	**0.805**	**0.447**
Chl (μg cm^{-2})	0.826	0.421	**0.937**	**0.249**	0.872	0.358	0.908	0.303
Car (μg cm^{-2})	0.875	0.354	0.844	0.397	**0.924**	**0.275**	0.897	0.320
Chl (μg g^{-2})	0.691	0.573	0.715	0.548	**0.824**	**0.423**	0.731	0.531
Car (μg g^{-2})	0.695	0.569	0.665	0.599	0.680	0.583	**0.698**	**0.566**
Chl/Car	0.814	0.436	0.725	0.537	**0.88**	**0.347**	0.854	0.385
Chla/Chlb	**0.483**	**0.770**	0.472	0.780	0.480	0.773	0.470	0.782

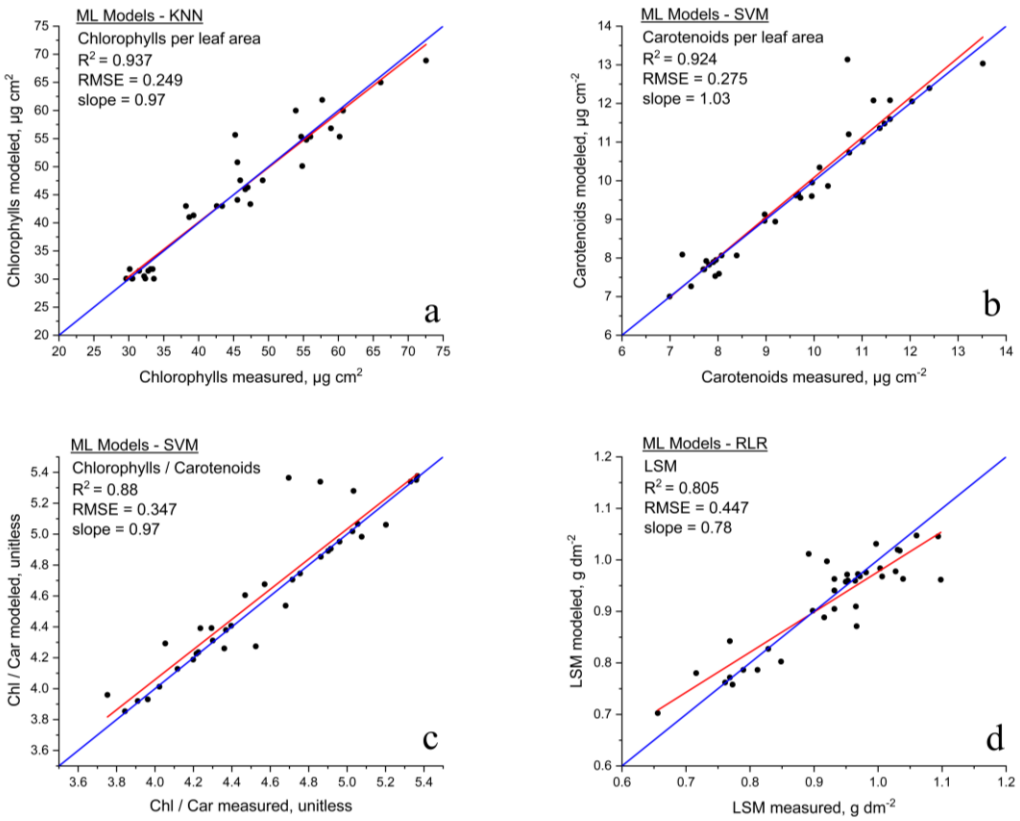

Figure 3. Relationships between measured and modeled values based on the ML approach, when using chlorophyll content (a), carotenoid content (b), chlorophyll to carotenoid ratio (c) and LSM (d) as dependent variables. The type of regression, the coefficient of determination (R^2), the root mean square error (RMSE) and the slope of the best-fit line are shown in the inserts. Blue line corresponds to the 1:1 line and red line to the best-fit line.

4. Discussion

In this study, the nine treatments created correspond to different combinations of water and nitrogen stress, as assessed by the different parameters (e.g. chlorophyll and carotenoid content, RWC, LSM) between treatments. The study findings highlight the differences between VI-based and ML-based approaches for assessing plant stress by utilizing hyperspectral data. In the former, specific indices, such as NDRE and GNDVI, display superior performance with certain physiological parameters, while others like NDVI and PRI show relatively inferior performance across most parameters. In the ML-based approach, all algorithms surpass the simple linear regression models. Notably, models correlating with chlorophylls and carotenoids as dependent variables consistently outperform others, indicating their importance in stress assessment. However, the performance of models for RWC remains subpar across both approaches. These results underscore the potential of ML algorithms in effectively analysing hyperspectral data for plant stress detection. Nonetheless, challenges persist, particularly in accurately quantifying specific physiological parameters like RWC. Further research is needed to examine various plant species and their distinct characteristics. Additionally, expanding the range of physiological parameters, such as fluorescence, and testing and refining different computational techniques is essential. Furthermore, incorporating a wider array of abiotic and biotic stresses into the models is recommended for enhancing their effectiveness.

References

Aha, D. W., Kibler, D., Albert, M. K., & Quinian, J. R. (1991). Instance-Based Learning Algorithms. In Machine Learning (Vol. 6, pp. 37–66). Springer. https://doi.org/https://doi.org/10.1007/BF00153759

Badgley, G., Field, C. B., & Berry, J. A. (2017). Canopy near-infrared reflectance and terrestrial photosynthesis. Science Advances, 3(3). https://doi.org/10.1126/SCIADV.1602244/SUPPL_FILE/1602244_SM.PDF

Barnes, E., Colaizzi, P., Haberland, J., & Waller, P. (2000). Coincident detection of crop water stress, nitrogen status, and canopy density using ground based multispectral data. Fifth International Conference on Precision Agriculture. https://www.researchgate.net/publication/43256762

Behmann, J., Steinrücken, J., & Plümer, L. (2014). Detection of early plant stress responses in hyperspectral images. ISPRS Journal of Photogrammetry and Remote Sensing, 93, 98–111. https://doi.org/10.1016/J.ISPRSJPRS.2014.03.016

Candiago, S., Remondino, F., De Giglio, M., Dubbini, M., & Gattelli, M. (2015). Evaluating multispectral images and vegetation indices for precision farming applications from UAV images. Remote Sensing, 7(4), 4026–4047. https://doi.org/10.3390/rs70404026

Chemura, A., Mutanga, O., & Dube, T. (2017). Remote sensing leaf water stress in coffee (Coffea arabica) using secondary effects of water absorption and random forests. Physics and Chemistry of the Earth, 100, 317–324. https://doi.org/10.1016/j.pce.2017.02.011

Cutler, A., Cutler, R. D., & Stevens, J. R. (2012). Random Forests. In Ensemble Machine Learning (pp. 157–177). Springer New York. https://doi.org/10.1007/978-1-4419-9326-7

Eitel, J. U. H., Long, D. S., Gessler, P. E., & Hunt, E. R. (2008). Combined Spectral Index to Improve Ground-Based Estimates of Nitrogen Status in Dryland Wheat. Agronomy Journal, 100(6), 1694–1702. https://doi.org/10.2134/AGRONJ2007.0362

Fu, P., Meacham-Hensold, K., Guan, K., & Bernacchi, C. J. (2019). Hyperspectral leaf reflectance as proxy for photosynthetic capacities: An ensemble approach based on multiple machine learning algorithms. Frontiers in Plant Science, 10. https://doi.org/10.3389/FPLS.2019.00730

JASP—A Fresh Way to Do Statistics le. Available online: https://jasp-stats.org (accessed on 31 May 2024)

Huang, S., Tang, L., Hupy, J. P., Wang, Y., & Shao, G. (2021). A commentary review on the use of normalized difference vegetation index (NDVI) in the era of popular remote sensing. Journal of Forestry Research, 32(1), 1–6. https://doi.org/10.1007/S11676-020-01155-1/FIGURES/2

Karimi, Y., Prasher, S. O., Patel, R. M., & Kim, S. H. (2006). Application of support vector machine technology for weed and nitrogen stress detection in corn. Computers and Electronics in Agriculture, 51(1–2), 99–109. https://doi.org/10.1016/J.COMPAG.2005.12.001

Kecman, V. (2005). Support Vector Machines - An Introduction. In Support Vector Machines: Theory and Applications (pp. 1–47). Springer. https://doi.org/https://doi.org/10.1007/10984697_1

Li, F., Miao, Y., Feng, G., Yuan, F., Yue, S., Gao, X., Liu, Y., Liu, B., Ustin, S. L., & Chen, X. (2014). Improving estimation of summer maize nitrogen status with red edge-based spectral vegetation indices. Field Crops Research, 157, 111–123. https://doi.org/10.1016/J.FCR.2013.12.018

Lichtenthaler, H. K., & Wellburn, A. R. (1983). Determinations of total carotenoids and chlorophylls a and b of leaf extracts in different solvents. Biochemical Society Transactions. https://doi.org/https://doi.org/10.1042/bst0110591

Maki, H., Lynch, V., Ma, D., Tuinstra, M. R., Yamasaki, M., & Jin, J. (2023). Comparison of Various Nitrogen and Water Dual Stress Effects for Predicting Relative Water Content and Nitrogen Content in Maize Plants through Hyperspectral Imaging. AI 2023, Vol. 4, Pages 692-705, 4(3), 692–705. https://doi.org/10.3390/AI4030036

Merzlyak, M. N., Gitelson, A. A., Chivkunova, O. B., & Rakitin, V. Y. (1999). Non-destructive optical detection of pigment changes during leaf senescence and fruit ripening. Physiologia Plantarum, 135–141.

Moshou, D., Pantazi, X. E., Kateris, D., & Gravalos, I. (2014). Water stress detection based on optical multisensor fusion with a least squares support vector machine classifier. Biosystems Engineering, 117(1), 15–22. https://doi.org/10.1016/J.BIOSYSTEMSENG.2013.07.008

Mu, X., & Chen, Y. (2021). The physiological response of photosynthesis to nitrogen deficiency. Plant Physiology and Biochemistry : PPB, 158, 76–82. https://doi.org/10.1016/J.PLAPHY.2020.11.019

Pillonetto, G., Chen, T., Chiuso, A., De Nicolao, G., & Ljung, L. (2022). Regularization of Linear Regression Models. In Regularized System Identification: Learning Dynamic Models from Data (pp. 33–93). Springer. https://doi.org/https://doi.org/10.1007/978-3-030-95860-2_3

Shao, H. B., Chu, L. Y., Jaleel, C. A., Manivannan, P., Panneerselvam, R., & Shao, M. A. (2009). Understanding water deficit stress-induced changes in the basic metabolism of higher plants – biotechnologically and sustainably improving agriculture and the ecoenvironment in arid regions of the globe. Critical Reviews in Biotechnology, 29(2), 131–151. https://doi.org/10.1080/07388550902869792

Thenot, F., Méthy, M., & Winkel, T. (2002). The Photochemical Reflectance Index (PRI) as a water-stress index. International Journal of Remote Sensing, 23(23), 5135–5139. https://doi.org/10.1080/01431160210163100

Velichkova, K., & Krezhova, D. (2019). Extraction of the red edge position from hyperspectral reflectance data for plant stress monitoring. AIP Conference Proceedings, 2075. https://doi.org/10.1063/1.5091303

Vitrack-Tamam, S., Holtzman, L., Dagan, R., Levi, S., Tadmor, Y., Azizi, T., Rabinovitz, O., Naor, A., & Liran, O. (2020). Random forest algorithm improves detection of physiological activity embedded within reflectance spectra using stomatal conductance as a test case. Remote Sensing, 12(14). https://doi.org/10.3390/rs12142213

Von Wirén, N., Gazzarrini, S., & Frommer, W. B. (1997). Regulation of mineral nitrogen uptake in plants. In Plant and Soil (Vol. 196, Issue 2, pp. 191–199). Springer. https://doi.org/10.1023/A:1004241722172/METRICS

Wang, T. C., Ma, B. L., Xiong, Y. C., Saleem, M. F., & Li, F. M. (2011). Optical sensing estimation of leaf nitrogen concentration in maize across a range of water-stress levels. Crop and Pasture Science, 62(6), 474–480. https://doi.org/10.1071/CP10374

Xue, J., & Su, B. (2017). Significant remote sensing vegetation indices: A review of developments and applications. Journal of Sensors, 2017. https://doi.org/10.1155/2017/1353691

Zhang, C., & Ma, Y. (2012). Ensemble Machine Learning. Springer.

Factors influencing the working time requirement and work rate of field robots when weeding organic sugar beet

Franz Handler [a,*], Michael Haider [a], Andreas Ettlinger [a]

[a] HBLFA Francisco Josephinum, Wieselburg, Austria

* Corresponding author. franz.handler@josephinum.at

Abstract

Based on process analyses and working time studies when using two different robots for in-row weeding of organic sugar beets, the time requirements of the robots and the operators are modelled. If the time requirement is based on the hectare of area worked, it can be seen that on fields smaller than 3 ha, both the time requirement of the robot and the operator increases significantly. When the field size increases beyond 10 ha, the time required by the robot hardly decreases. That of the operator even begins to increase slightly. Furthermore, the working speed, turning time, working width and number of faults have a significant influence on the time required by the robot. The operator's working time requirement is strongly influenced by the time required for teaching in the field, the frequency of malfunctions and necessary checks, and the field-yard distance.

Keywords: in-row hoeing, field efficiency, fault time, execution time, operation time

1. Introduction

Weed control is very time-consuming when growing sugar beets organically. Fishkis et al. (2024) report an annual working time requirement of 164 - 172 h ha^{-1} for hand hoeing sugar beets. In Austria, farmers indicate in surveys that the working time required for hand hoeing is up to 200 h ha^{-1} (Jungwirth and Handler, 2022). Numerous authors (van der Weide et al., 2008; Kunz, 2017; Lampridi et al., 2019; Vasconez et al.; 2019; Bručienė et al., 2021; Vahdanjoo et al., 2023) show that precisely controlled hoeing devices, in-row hoeing devices and robots can make a significant contribution to reducing the working time required for hand hoeing sugar beets in organic farming. In order to exploit this potential, robots with in-row hoeing devices have been used in Austria since 2021. Although the robots can sow and hoe autonomously, they require an operator to transport from field to field, teach-in the field boundaries, adjust and monitor the quality of work and resolve faults. Based on work analysis and time studies, this study uses model calculations to examine the factors influencing the robots' work rate and the operator's working time requirements.

2. Materials and Methods

Two robots were used to collect data. The robots differed significantly from each other in terms of design. Robot I worked in six rows and had RTK-GNSS controlled in-row hoeing device. It could only be used on fields sown by it, as it recorded the exact position of the plants when sowing to control the hoeing tools. Before the first use on a field, the field boundaries and obstacles had to be digitized. To do this, the corner points of the field and the obstacles (e.g. wells) had to be approached with the robot mounted on the tractor's three-point linkage or with an RTK measuring rod and their position saved. Robot II also navigated via RTK-GNSS. The inter-row hoeing tools were guided along the row using camera controls. The in-row hoeing tools were controlled via camera systems with AI-based individual plant recognition. The field boundaries were taught-in here by remote-controlled hoeing of the first working width in the partial areas of the field (headland, main area).

Before the working time studies began, in a first step, analyses of the work process in relation to the robot and the operator were carried out on both robots when sowing or hoeing sugar beets. Based on this, the work process was divided into sections and work elements and the factors influencing their working time requirement were assigned. The developed structure formed the basis for the working time studies in the field. The procedure is based on Frisch et al., 2022. The data collected for the sections of the work process and the work elements was analysed using Analysis of Variance and General Linear Models in Statgraphics.

Based on the results of the analysis of the work process and working time studies (Haider and Handler, 2023, Jungwirth and Handler, 2022), model calculations (Handler and Blumauer, 2022) were carried out.

These were used to systematically examine the size of the influence of various factors such as field size, field shape, working width, working speed, time required per turn and frequency of robot malfunctions on the time requirement and the work rate of the robot and the working time requirement of the operator.

To display the results of the model calculations, the total time is divided into operation time, fault time and non-productive time (Frisch et al., 2022). The operation time includes the working time necessary for the scheduled completion of the work task. It includes the time types execution time in narrower sense, turning time, loading time (e.g. refilling seeds), as well as time for adjustment and checking. The actual purpose of the work is carried out during the execution time in narrower sense. Fault time includes unplanned interruptions to work that delay the achievement of the work purpose and can be divided into functional and technical fault time, organizational fault time and weather-related fault time. The non-productive time describes planned activities that are necessary to establish and maintain the work system and to restore the initial state. It includes supply time (e.g. refuelling), job preparation and job closing time (e.g. set-up, operation briefing) as well as transit time between fields or between the field and the yard). The proportion of execution time in narrower sense in the total time of the robot corresponds to the field efficiency.

$$E = \frac{t111 * 100}{tG} \qquad (1)$$

where *E* is field efficiency (%); t111 is execution time in narrower sense (h) and tG is total time (h).

3. Results and Discussion

Surveys on practical farms show that, in addition to sowing, the robot must be used for five to six hoeing passes (Jungwirth and Handler, 2022) in order to achieve sufficient weed reduction in sugar beet. Figure 1 shows the total time required by the six-row robot - Robot I - (top) and the operator (bottom) for sowing and hoeing depending on the field size. For this purpose, a rectangular field with a length-to-width ratio of 3:1, a working speed of the robot of 750 m h^{-1}, 45 cm distance between the rows and a field-to-yard distance of 2 km are assumed. Six hoeing passes are taken into account in the model calculation. The time required per hectare for Robot I decreases significantly as the field size increases. The decrease between the one-ha field and the three-ha field is particularly clear at 24%. After that, the degression decreases significantly. The operation time is reduced primarily by reducing the proportion of turning time and the time required for adjustment (setting the field boundaries, the sowing elements and hoeing tools). The time required per hectare for hoeing (execution time in narrower sense) and refilling with seeds, on the other hand, changes relatively little depending on the field size. The non-productive time includes robot transport to and from the field as well as conversion from hoeing to sowing and vice versa. Since the duration of these process sections does not depend on the field size, there is a significant decrease in non-productive time per hectare. The fault times can be caused by blockages in the seeding elements, coulters and hoeing shares as well as by the detection of an obstacle or the onset of precipitation. The frequency of occurrence of faults varies greatly in practice and depends largely on factors such as soil conditions (unevenness, soil crusting, fluctuations in reconsolidation, soil moisture or soil type), stones, crop residues, slope and homogeneity of the crop. In the model calculation on which Figure 1 is based, it is assumed that a fault occurs on average every three hours (execution time in narrower sense) due to residues from the previous crop and root weeds on the headland. As the proportion of headlands decreases with increasing field size, the number of faults (see Table 1) and time required per hectare for faults decreases. It ranges between 4 and 2% of the total time required by the robot. If the working conditions are unfavourable and the operator's reaction time is longer, the duration of the faults can increase significantly.

Figure 2 is based on the data from Figure 1 and shows the work rate and field efficiency of the robot when hoeing sugar beet depending on the field size. The work rate in relation to the execution time in narrower

Table 1. Number of faults and work rate of the robot.

		Field size [ha]					
		1	2	3	5	10	20
Figure 1	Mean number of faults per hectare	1.21	0.87	0.72	0.56	0.40	0.28
	Work rate when hoeing based on total time [ha h^{-1}]	0.12	0.14	0.15	0.16	0.17	0.18
Figure 3	Mean number of faults per hectare	2.00	2.00	2.00	2.00	2.00	2.00
	Work rate when hoeing based on total time [ha h^{-1}]	0.11	0.13	0.14	0.15	0.16	0.16

sense changes little with increasing field size, since the execution time in narrower sense in Figure 1 also hardly changes with increasing field size. Since the proportion of other operation time, fault time, and non-productive time of the robot decrease with increasing field size (see Figure 1), field efficiency increases from 64 to 93%.

When using tractor-drawn hoeing machine for mechanical weed control, the working time required of the operator is higher than the operating time of the machines used due to the set-up time taken into account (Agroscope, 2024). When using a robot, the operator spends significantly less time overseeing the robot than the robot spends working on the field. In Figure 1 (bottom), the operator's total working time requirement for

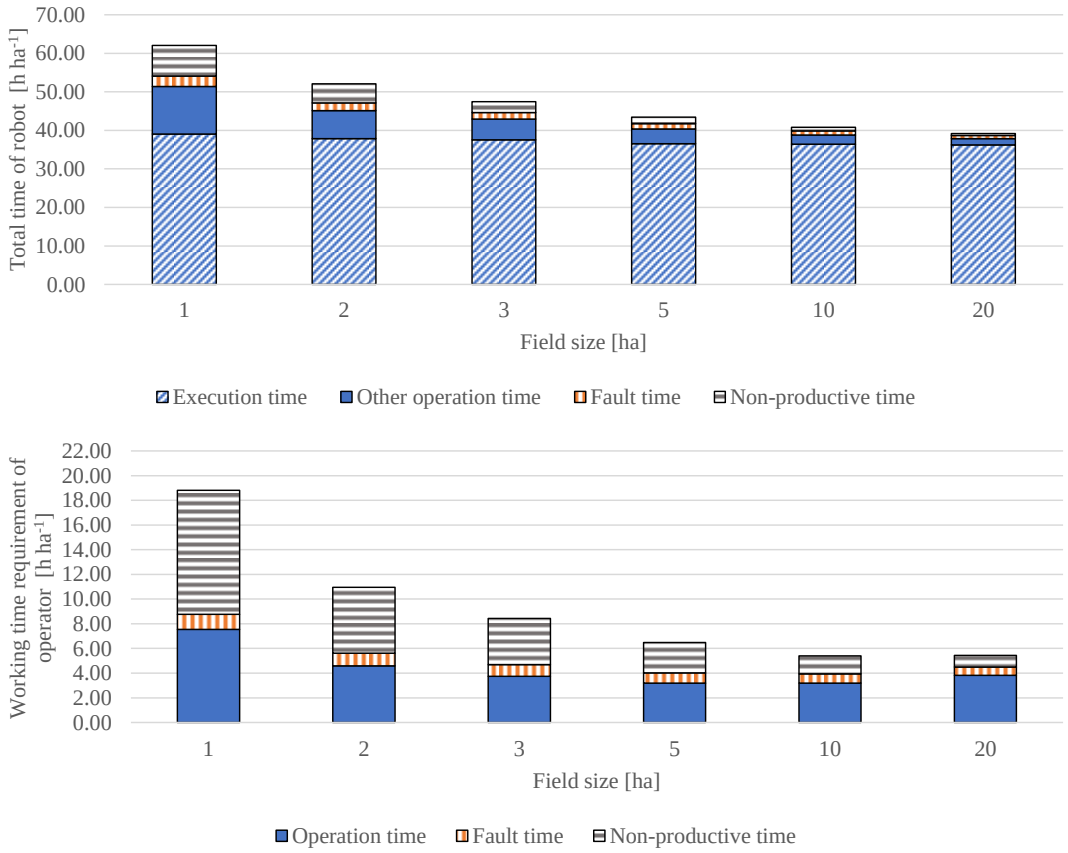

Figure 1. Total time required by the six-row robot - Robot I - (top) and the operator (bottom) for sowing and hoeing organic sugar beet six times, depending on the field size (rectangular field with length-width ratio of 3:1, robot working speed 750 m h^{-1}, 45 cm row spacing, field-yard distance 2 km).

a field size of 1 ha accounts for 30% of the robot's time requirement. This value drops significantly up to a field size of 3 ha (18%). After that, the ratio changes little and is between 13 and 15%. The smaller the field, the more the operator's work is dominated by non-productive time, such as robot transport to and from the field and conversion from hoeing to sowing and vice versa, which occur regardless of the field size. It decreases per hectare as the field size increases. The operation time includes checking the quality of work when sowing and hoeing, refilling the seeds, recording the field boundaries, defining the field on the control terminal and adjusting the sowing and hoeing tools. Work sections such as recording the field boundaries, defining the field on the control terminal and adjusting the sowing and hoeing tools, which essentially only occur once at the beginning of the field processing, lead to a decrease in the operator's working time required per hectare as the field size increases. The frequency of checking required can vary greatly as it depends on the likelihood of faults that the robot does not detect and the changing operating conditions and the operator's willingness to take risks. In the present model calculation, it is assumed that an inspection tour to check the robot takes place every eight hours. The working time required per inspection tour increases with the size of

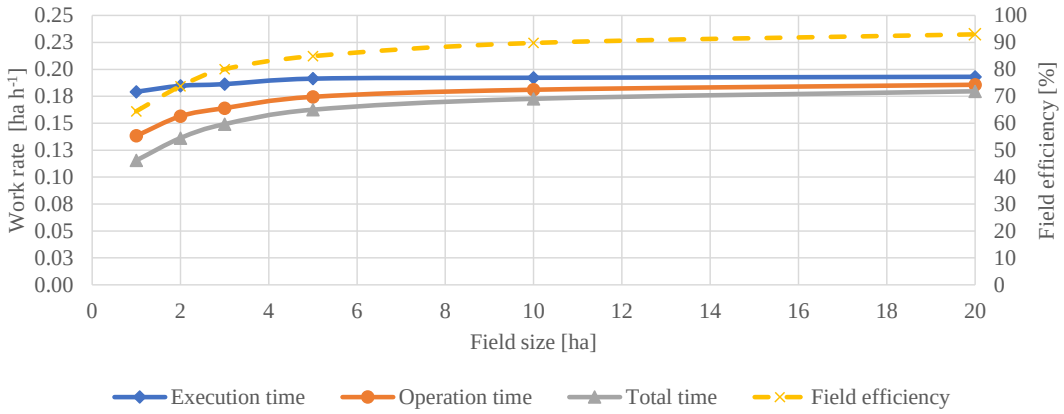

Figure 2. Mean work rate and field efficiency of a six-row robot - Robot I - for hoeing organic sugar beet depending on the field size (rectangular field with length-width ratio of 3:1, robot working speed 750 m h^{-1}, 45 cm row spacing, field-yard distance 2 km).

the field, as longer distances have to be covered on foot in the field. The same applies to refilling seeds. This means that the operation time of the operator begins to increase again for field sizes over 5 ha, so that the total working time requirement per hectare is also higher for a field size of 20 ha than for a field size of 10 ha. Due to the decrease in the proportion of headlands as the field size increases and assuming that faults due to unfavourable working conditions only occur on the headland, the operator's working time requirement per hectare to resolve faults also decreases. It ranges between 6 and 9% of the total working time requirement.

Compared to Figure 1, in Figure 3 the frequency of faults is increased to two faults (e.g. blockages on the coulters or hoeing shares) per hectare (see Table 1). As the size of the field increases, this causes the work rate of the robot to decrease by 3 to 11% based on the total time of the robot. The working time requirement of the operator to resolve faults increases with the size of the field, as longer distances have to be covered on

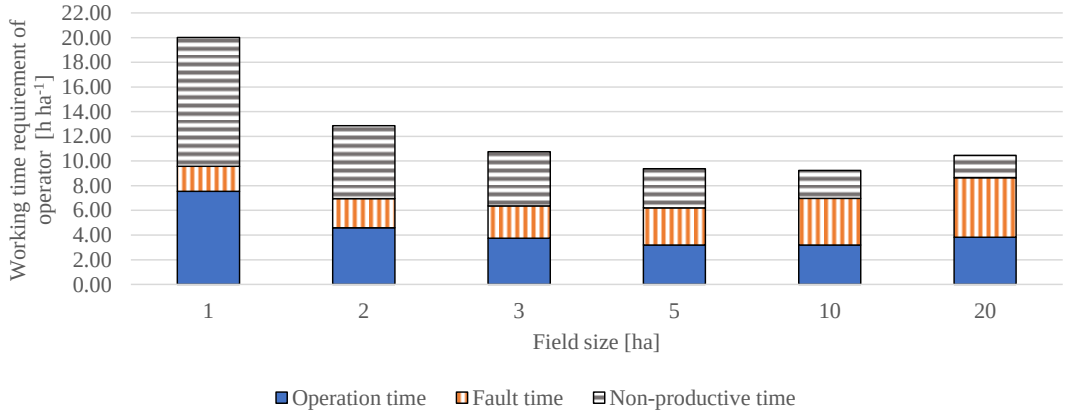

Figure 3. Working time requirement of the operator of a six-row robot - Robot I - for hoeing organic sugar beet depending on the field size (rectangular field with length-width ratio of 3:1, robot working speed 750 m h^{-1}, 45 cm row spacing, field-yard distance 2 km).

foot in the field. There is also a significant increase in the proportion of fault time to 10 to 46% of the operator's total working time requirement. At the same time, the operator's non-productive times also increase, as the transit times between the field and the farm caused by the faults are counted as non-productive time. Compared to Figure 1 in Figure 3, this increases the operator's total working time requirement between 6 and 92%.

Figure 4 shows the work rate of a three-row robot for hoeing organic sugar beet fields three times. For each hectare of field size, two faults due to blockages in the hoeing shares and one inspection tour to the

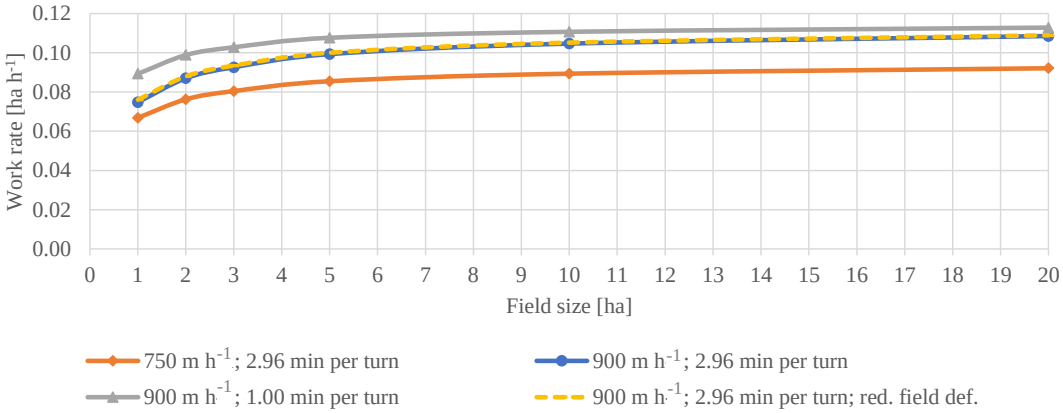

Figure 4. Mean work rate based on the total time for hoeing organic sugar beet by a three-row robot - Robot II - at different working speeds, turning times and reduced time required for recording and defining the field (rectangular field with length-width ratio of 3:1, 45 cm row spacing, field-yard distance 2 km).

robot every eight hours are taken into account on average. The possible working speed when hoeing depends largely on the robot design, the hoeing tools, the soil conditions and the growth stage of the crop and weeds. If the working speed when hoeing can be increased from 750 to 900 m h^{-1}, the work rate of the robot increases between 11 and 15% under the assumptions made in the model calculation. The raise increases with increasing field size (compare line "900 m h^{-1}; 2.96 min per turn" with line "750 m h^{-1}; 2.96 min per turn"). The higher working speed results in a shorter execution time in narrower sense, which decreases field efficiency. For example, it decreases from 74 to 70% for a field size of 2 ha and from 88 to 86% for a field size of 10 ha (see Table 2). The corresponding working time requirement of the operator in Figure 5 for three chopping passes decreases by 0.14 to 0.49 h ha^{-1} (2 to 11%) due to the higher working speed. The reason for this is the assumption made in the model that inspection tours are carried out every eight hours of the robot's operation time. Surveys on farms by Haider and Handler (2023) show that three hoeing passes are necessary to reduce the weed population sufficiently.

The proportion of turning time in the total working time of the robot decreases with increasing field size. Therefore a reduction in turning time from 2.96 min per turn to 1.00 min per turn with decreasing field size leads to a higher increase in the work rate of the robot (compare line "900 m h^{-1}; 2.96 min per turn" with "line 900 m h^{-1}; 1.00 min per turn"). The increase in Figure 4 ranges between 19% for a field size of 1 ha and 4% for a field size of 20 ha. At the same time, field efficiency increases from 60 to 71% for a field size of

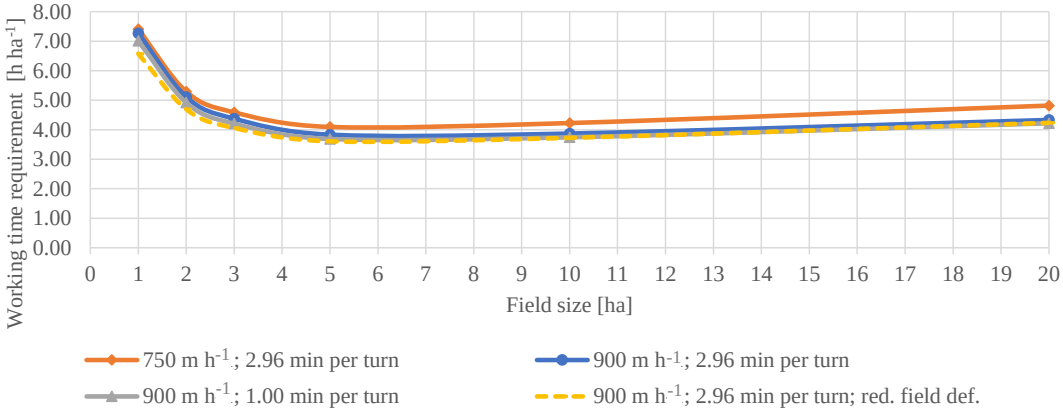

Figure 5. Working time requirement of the operator for hoeing organic sugar beet by a three-row robot - Robot II - at different working speeds, turning times and reduced time required for recording and defining the field (rectangular field with length-width ratio of 3:1, 45 cm row spacing, field-yard distance 2 km).

1 ha and from 89 to 92% for a field size of 20 ha (see Table 2). The operator's working time requirement decreases between 4 and 2% or between 0.26 and 0.11 h ha^{-1} as the field size increases (see Figure 5). The reason for this is the assumption made in the model that inspection tours are carried out every eight hours of the robot's operation time.

Table 2. Mean field efficiency of a three- or four-row robot - Robot II – when hoeing sugar beet with reference to Figures 4 and 6.

Conditions	Field size [ha]					
	1	2	3	5	10	20
900 m h^{-1}; 2.96 min per turn and 3:1; 3-rows; 2 km	60%	70%	75%	81%	86%	89%
750 m h^{-1}; 2.96 min per turn	64%	74%	79%	83%	88%	91%
900 m h^{-1}; 1.00 min per turn	71%	80%	84%	87%	91%	92%
900 m h^{-1}; 2.96 min per turn; red. field def.	61%	71%	76%	81%	86%	89%
3:1; 4-rows; 2 km	55%	66%	72%	78%	83%	87%
2:1; 3-rows; 2 km	58%	68%	74%	79%	84%	88%
3:1; 3 rows; 10 km	57%	69%	74%	80%	85%	88%

The time for field definition is part of the adjustment time and, for Robot II, includes recording the field boundaries and defining the field on the operating terminal. When working on the field for the first time, for example for a 2-ha field, it requires 60 minutes for the robot and operator and increases to 80 minutes for a 5-ha field. Reducing the time required for field definition to 20% of the initial value causes an increase of the robot´s work rate by around 1% (compare line “900 m h^{-1}; 2.96 min per turn” with line “900 m h^{-1}; 2.96 min per turn; red. field def.” in Figure 4). Field efficiency increases by around one percentage point. For the operator, it leads to a reduction in the total working time requirement in the range of 3% (0.10 h ha^{-1}) for 20-ha fields to 10% (0.69 h ha^{-1}) for 1-ha fields (see Figure 5).

Figure 6 shows the influence of field shape, working width and field-yard distance on the work rate of the robot. Line “900 m h^{-1}; 2.96 min per turn” in Figures 4 and 5 corresponds to the line “3:1; 3-rows; 2 km” in Figures 6 and 7. Under the chosen general conditions, the change in the ratio of field length to field width from 3:1 to 2:1 leads to a decrease in work rate between 4 and 1% (compare line “3:1; 3-rows ; 2 km” with “line 2:1; 3 rows; 2 km”). The difference decreases as the field size increases. Field efficiency drops by 1 to 2 percentage points (see Table 2). The operator's working time requirement also decreases due to the shorter distances to be covered during inspection tours. With a field size of 2 ha it is reduced by 1% (0.01 h ha^{-1}), with a field size of 20 ha the reduction is 6% (0.27 h ha^{-1}).

Increasing the working width from three to four rows brings a significant increase in work rate of 23 to 31%, although this is higher on large fields (compare line “3:1; 3-rows; 2 km” with line “3:1; 4-rows; 2 km” in Figure 6). Due to the decrease in execution time in narrower sense, increasing the working width reduces field efficiency by 2 to 4 percentage points. The difference decreases as the field size increases. The operator's

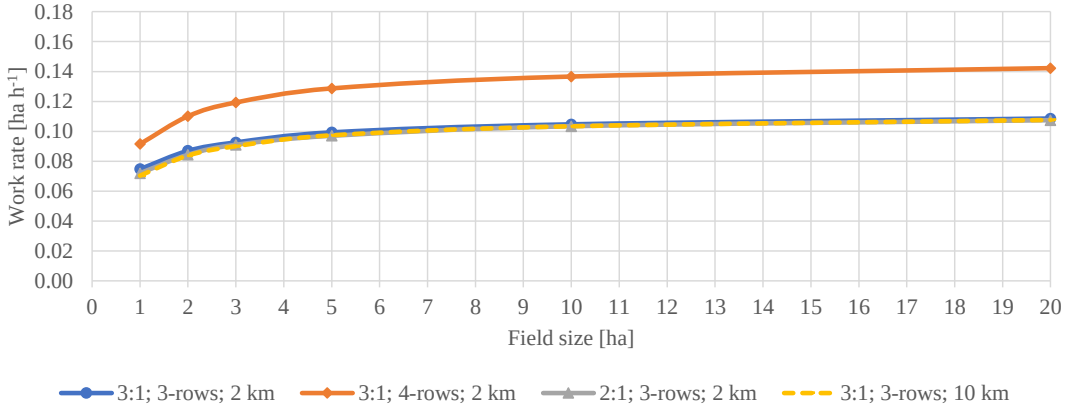

Figure 6. Mean work rate based on the total time for hoeing organic sugar beet by a three- or four-row robot - Robot II - at different field shapes and field-yard distances (rectangular field, 45 cm row spacing, working speed 900 m h^{-1}, 2.96 min per turn).

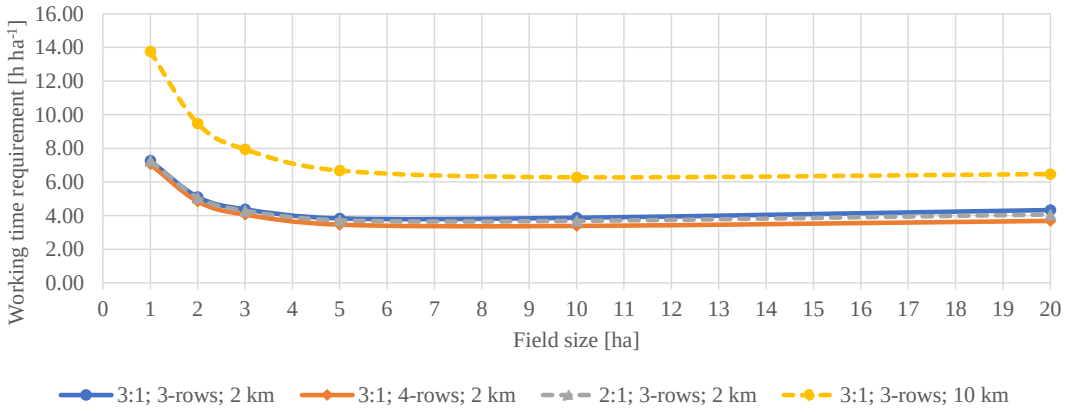

Figure 7. Working time requirement of the operator for hoeing organic sugar beet by a three- or four-row robot - Robot II - at different field shapes and field-yard distances (rectangular field, 45 cm row spacing, working speed 900 m h^{-1}, 2.96 min per turn).

working time requirement decreases by 3 to 15% by increasing the working width (compare line "3:1; 3-rows; 2 km" with line "3:1; 4-rows; 2 km" in Figure 7). The reason for this is the decreasing operation time of the robot, which, according to the assumptions made in the model, reduces the number of inspection tours.

By increasing the field-yard distance from 2 to 10 km, the work rate drops between 1 and 5% (compare line "3:1; 3-rows; 2 km" with line "3:1; 3-rows; 10 km" in Figure 6). At the same time, field efficiency also drops between 1 and 3 percentage points. In contrast, there is a significant increase in the working time requirement of the operator because he has to travel between the field and the yard more often than the robot. For example, for a field size of 2 ha the increase amounts 85% (4.37 h ha^{-1}) or for a field size of 10 ha it amounts 62% (2.41 h ha^{-1}) (compare line "3:1; 3-rows; 2 km" with line "3:1; 3-rows; 10 km" in Figure 7). The average driving speed assumed in the model is 60 km h^{-1} for trips for resolve faults, checks and refuelling and 20 km h^{-1} for robot transport.

Table 3. Relationship between working time requirement of the operator and the robot.

Conditions	Field size [ha]					
	1	2	3	5	10	20
900 m h^{-1}; 2.96 min per turn and 3:1; 3-rows; 2 km	18%	15%	13%	13%	13%	16%
750 m h^{-1}; 2.96 min per turn	16%	13%	12%	12%	13%	15%
900 m h^{-1}; 1.00 min per turn	21%	16%	14%	13%	14%	16%
900 m h^{-1}; 2.96 min per turn; red. field def.	17%	14%	13%	12%	13%	15%
3:1; 4-rows; 2 km	22%	18%	16%	15%	15%	17%
2:1; 3-rows; 2 km	17%	14%	13%	12%	13%	15%
3:1; 3 rows; 10 km	32%	26%	24%	22%	22%	23%

Table 3 shows the relationships between the working time requirements of the robot and the robot operator with reference to Figures 5 and 7. The numbers given indicate how many percent the working time requirement of the operator represents in relation to the time requirement of the robot. With regard to the time required by the robot, the operator spends the least amount of working time looking after the robot under the general conditions of the model calculations with an average field size of 5 ha. The values for a field size of 10 ha are also at a similar level. The values for a field size of 20 ha are somewhat higher. This is because, as the field size increases, longer distances have to be covered on foot in the field during checks, faults and refuelling. The increase in fields with one or two hectares is primarily caused by work sub-processes such as defining the field boundaries or transporting the robot to and from the field. Increasing the distance between the field and the yard also caused a significant increase in the working time required by the operator in relation to the time required by the robot. However, reducing the time required by the robot by increasing the working width to four rows also worsened the relationship, as the time required by the robot fell more than that of the operator. The same applies to reducing the turning time.

4. Conclusions

The work rate of the robot depends largely on the size of the field. Due to the decreasing field efficiency, the work rate decreases relatively sharply, especially on fields smaller than 3 ha. At the same time, the working time required by the operator per hectare increases significantly. Even on areas larger than 10 hectares, the operator's working time requirement per hectare begins to increase, as the distances covered on foot in the field for checks and troubleshooting increases as the size of the field increases. Depending on the general conditions, the working time required by the operator accounts for between 12 and 32% of the time required by the robot. Faults on the robot that have to be resolved by the operator, in combination with large field-yard distances, significantly increase the operator's working time requirement. One-off work sections in the field, such as recording the field boundaries or transporting the robot, has a negative impact on the operator's working time per hectare, especially in small fields. Increasing the working width and working speed as well as reducing the turning time are measures to improve the robot's work rate.

Acknowledgements

This article was created as part of the Innovation Farm (www.innovationfarm.at), which is supported by the federal government, the federal provinces and the European Union within the Austrian Rural Development Programme 2014 - 2020.

References

Agroscope, 2024. Online-Plattform für die Arbeitsplanung auf dem Bauernhof. Online https://www.arbeitsvoranschlag.ch, accessed on May 13th, 2024.

Bručienė, I., D. Aleliūnas and E. Šarauskis, 2021. Time and costs analysis of different non-chemical weed control methods in sugar beet. In Actual Tasks on Agricultural Engineering, Proceedings of the 48th International Symposium, Zagreb, Croatia, 2 - 4 March, 371 - 380.

Fishkis, O., J. Weller, J. Lehmhus, F. Pöllinger, J. Strassemeyer and H. Koch, 2024. Ecological and economic evaluation of conventional and new weed control techniques in row crops. Agriculture, Ecosystems & Environment, Volume 360, 108786, ISSN 0167-8809, https://doi.org/10.1016/j.agee.2023.108786.

Frisch, J., M. Funk, B. Haidn, J. Mačuhová, E. Quendler, St. Reith, M. Schick, J. Sonnen, T. Steckel, Ch, Umstätter and B. Winkler, 2022. Arbeitswirtschaft in der Landwirtschaft – Einführung, Arbeitszeitanalyse, Zeitbedarfskalkulation. Darmstadt: Kuratorium für Technik und Bauwesen in der Landwirtschaft e.V., 172 p.

Haider, M. and F. Handler, 2023. Arbeitsablauf, Zeitbedarf und Maschinenkosten autonomer Roboter zur Unkrautbekämpfung. Endbericht zum Projekt im Rahmen des KTBL – Arbeitsprogramms Kalkulationsunterlagen 2023, HBLFA Francisco Josephinum, Wieselburg, Austria.

Handler, F. and E. Blumauer, 2022. Working time requirement of operators and process-related idle time of semiautonomous field robots. In Conference Proceedings of Sima Agritech Day 5th Edition, Paris, France, November 5th, Axema Promotion & Services, ISBN: 978-2-491070-03-8. 63 - 72.

Jungwirth M. and F. Handler, 2022. Arbeitswirtschaftliche Aspekte am Beispiel eines teilautonomen Feldroboters beim Säen und Hacken von Biozuckerrüben. In Lecture Notes in Informatics, Volume P317, Gesellschaft für Informatik, Bonn, Germany, ISBN 978-3-88579-711-1. 147 - 152.

Kunz, Ch., 2017. Integrated weed control in sugar beet (Beta vulgaris), using precision farming technologies and cover cropping. Dissertation, Institute of Phytomedicine, Faculty of Agricultural Sciences, University of Hohenheim, Stuttgart, Germany.

Lampridi, M. G., D. Kateris, G. Vasileiadis, V. Marinoudi, S. Pearson, C. G. Sørensen and D. Bochtis, 2019. A case-based economic assessment of robotics employment in precision arable farming. Agronomy, 9(4), 175.

Vahdanjoo, M., R. Gislum and C.A.G. Sørensen, 2023. Operational, Economic, and Environmental Assessment of an Agricultural Robot in Seeding and Weeding Operations. AgriEngineering, 5, 299 - 324. https://doi.org/10.3390/agriengineering5010020.

Vasconez, J. P., G.A. Kantor and F.A.A. Cheein, 2019. Human-robot interaction in agriculture: A survey and current challenges. Biosystems engineering, 179, 35 - 48.

van der Weide, R. Y., P.O. Bleeker, V. T. J. M. Achten, L. A. P. Lotz, B. Melander and F. Fogelberg, 2008. Innovation in mechanical weed control in crop rows. Weed Research, 48 (3), 215 - 224. https://doi.org/10.1111/j.1365-3180.2008.00629.x.

Temporal stability of soil electrical conductivity patterns: contact versus non-contact sensors

João Serrano [a], Shakib Shahidian [a], José Marques da Silva [a,*], Francisco Moral [b]

[a] MED—Mediterranean Institute for Agriculture, Environment and Development and CHANGE—Global Change and Sustainability Institute, Universidade de Évora, Pólo da Mitra, Ap. 94, 7006-554 Évora, Portugal

[b] University of Extremadura, Escuela de Ingenierías Agrarias, Departamento de Expresión Gráfica, Avenida de Elvas s/n, 06006 Badajoz, Spain

* Corresponding author. Email: jmsilva@uevora.pt

Abstract

Previous research has shown that the amount of soil spatial variability across a farm and within an agricultural field is of key importance to determine the potential benefits of adopting effective management strategies. Precision agriculture (PA) intends to validate technological tools that capture soil and crop spatial variability, which constitute the basis for the establishment of differentiated management zones (MZs). Soil apparent electrical conductivity (ECa) sensors are commonly used to survey soil spatial variability. It is essential for surveys to have temporal stability to ensure correct medium- and long-term decisions. The aim of this study was to assess the temporal stability of MZ patterns using different types of ECa sensors, namely an ECa contact-type sensor (Veris 2000 XA) and an electromagnetic induction sensor (EM-38). These sensors were used in four fields of dryland pastures in the Alentejo region of Portugal. The first survey was carried out in October 2018, and the second was carried out in September 2020. Data processing involved synchronizing the geographic coordinates obtained using the two types of sensors in each location and establishing MZs based on a geostatistical analysis of elevation and ECa data. The ECa measurements showed statistically significant correlations in all experimental fields (correlation coefficients between 0.449 and 0.618), which were reflected in the spatially stable patterns of the MZ maps (averaging 52% of the total area across the four experimental fields). This is a good indicator of potential for the use of ECa in medium and long-term management decisions. These results provide perspectives for future developments, which will need to occur in the creation of algorithms that allow the spatial variability and temporal stability of ECa to be validated through smart soil sampling and analysis to generate recommendations for sustained soil amendment or fertilization.

Keywords: pastures, spatial variability, management zones.

1. Introduction

Previous research has shown that the amount of soil spatial variability across a farm and within a field is of key importance to determine the potential benefits of adopting effective management strategies (King et al., 2005). Understanding this spatial variability is the first step for site-specific crop management (Peralta et al., 2015). On the other hand, spatial variability and temporal stability are two essential conditions for the adoption of differential management strategies and are the bases for variable rate technology (VRT) implementation. However, relatively little is known about the degree of within-field spatial variation in soils used for livestock production, which leads to the common practice of uniform field management (Serrano et al., 2017). Site-specific crop management aims to increase profitability and reduce the negative environmental impact of modern farming (Mat Su and Adamchuk, 2023).

Numerous studies use data from sensors to map soil physical and chemical properties to divide the field into smaller, more homogeneous areas (management zones, MZs) (Adamchuk et al., 2004). Surveying soil spatial variability is the basis for identifying within-field areas of soil similarity, defining MZs, and supporting decision making, for example, to decide on the locations of direct soil sampling (smart soil sampling) or for variable rate application (VRA) of agricultural inputs (McCutcheon et al., 2006; Medeiros et al., 2016; Serrano et al., 2017). These subfield regions constitute areas that have similar permanent characteristics, such as topography and nutrient levels (Moral et al., 2010). Typically, soil sampling of a field comprises a grid-sampling approach as well as laboratory work (Peralta et al., 2015). This is impractical at

the farming scale because it requires many soil samples in order to achieve a good representation of the soil spatial patterns, and it is labor intensive, time consuming, and expensive (King et al., 2005; Peralta et al., 2015). Therefore, it is desirable to find other more rapid and low-cost means of obtaining information for detailed soil mapping (King et al., 2005).

The use of geospatial measurements of apparent soil electrical conductivity (EC_a), combined with global navigation satellite systems (GNSSs) and geographical information systems (GISs), has become instrumental in characterizing the spatial patterns of soil properties within fields (Moral et al., 2010; Peralta et al., 2015). There are two types of electrical conductivity sensors that are currently on the market: (i) contact sensors, such as the Veris 2000 XA (Veris Technologies, Salina, KS, USA) sensor, which use electrodes, in the shape of coulters, that make contact with the soil to measure the electrical resistivity (the inverse of electrical conductivity); and (ii) non-contact sensors, such as the Dualem 1S (Dualem, Inc., Milton, ON, Canada) or the EM-38 (Geonics Ltd., Mississauga, ON, Canada) sensors, which are based on the principle of electromagnetic induction (Moral et al., 2010). It is generally recognized that both types of sensors represent practical tools to delineate soil-based MZs (McCutcheon et al., 2006).

Soil electrical conductivity has been frequently used in the establishment of soil MZs and in the inference of several edaphic physicochemical properties and their respective spatial variations (Peralta et al., 2015). Many studies carried out on agricultural soils have reported the relationship of EC_a with other soil attributes, including salinity, texture, depth, pH, moisture, organic matter, and cation exchange capacity (Peralta et al., 2015; Medeiros et al., 2016). According to Farahani and Buchleiter (2004), although the magnitudes of the absolute values of EC_a may change in response to modifications in the soil dynamic properties, it is expected that the pattern of EC_a spatial variability will not change significantly over time (Medeiros et al., 2016). It is therefore essential that EC_a measurements portray the soil's spatial variability pattern, expressed in terms of delineation of MZ, but to also do so in a stable way over time [13], guaranteeing the sustainability of management decisions in the medium and long term (Serrano et al., 2017). Considering that an MZ is often used for several years, the variables should be temporally stable (Schenatto et al., 2017).

Several previous studies have evaluated and reported the temporal stability of EC_a. Some have reported weak temporal associations [11], and others have shown that EC_a has temporal stability (Martini et al., 2017; Serrano et al., 2017); however, there are no known studies evaluating the temporal stability of MZ, especially when obtained from measurements using sensors with different principles.

The aim of this study was to assess the temporal stability of MZ patterns using two different types of EC_a sensors, namely a contact-type (Veris 2000 XA) and an electromagnetic induction type (EM-38), after approximately 2 years in four fields of dryland pastures in the Alentejo region of Portugal.

2. Materials and Methods

2.1. Description of Experimental Fields

The experimental work was carried out at four fields, namely two in the "Mitra" experimental farm ("ECO", 38°53.10'N and 8°01.10' W; area = 4.3 ha; and "MIT" 38°32.17'N and 7°59.83' W, area = 20.2 ha; both with loamy sand soil), one in the "Murteiras" farm ("MUR", 38°23.4'N and 7°52.5' W; area = 29.6 ha; sandy loam soil), and another in the "Padres" farm ("PAD", 38°36.4'N and 8°8.7' W; area = 32.2 ha; sandy loam soil), which are all permanent and biodiverse dryland pastures of the Montado ecosystem, located in Alentejo, in the district of Évora, in southern Portugal.

In this mixed ecosystem, the predominant trees are Holm oak trees, and the main animal species are cows and sheep in extensive grazing. The soil type is Cambisol, originating from granite [(FAO, 2006). The location of these fields is representative of the temperate climatic conditions of Portugal (classified as 'Csa': hot summer Mediterranean climate according to the Köppen–Geiger climate classification).

2.2. Topographic and Soil Electrical Conductivity surveys

A topographic survey of the four experimental fields was carried out using a Real-Time Kinematic (RTK) GNSS instrument (Trimble RTK/PP-4700 GNSS, Trimble Navigation Limited, Sunnyvale, CA, USA). The elevation data were sampled in the field with the GNSS antenna assembled on a tractor. For each field, the digital elevation model (DEM) was generated using the triangulated irregular network (TIN) interpolation

tool from ArcGIS 9.3. The TIN algorithm uses sample points to create a surface formed by triangles based on nearest neighbor point information. This vector information was converted into a grid surface with a 1 m resolution using the "Spatial Analyst" tool.

The EC_a in the four fields was measured using a Veris 2000 XA contact-type sensor (Veris Technologies, Salina, KS, USA) in October 2018. This sensor was mounted on a chassis supported by two wheels, and its active components consisted of two pairs of coulter-electrodes—adjustable rotating discs. The adjustment of the discs generates a set of topsoil data (from 0 to 0.30 m in depth). The sensor, equipped with a GNSS antenna, was towed by a tractor at an average speed of 2.0 m s^{-1}, and successive passes spaced 10 m apart were made across the field. The EC_a measurements were recorded every second, resulting in a spatial resolution of a 2 m by 10 m grid.

The EC_a was also measured using an EM38 non-contact sensor (Geonics Ltd., Mississauga, ON, Canada). It was employed in the horizontal dipole orientation to perform EC_a surveys in each pasture field in September 2020. The two receiver coils were positioned 0.5 m away from the transmitter. Although this sensor provided data from depth ranges of 0.75 m and 0.375 m, only the topsoil data in the range of 0–0.375 m were utilized in this study. The device was towed by an all-terrain vehicle equipped with a GNSS antenna. The vehicle maintained an average speed of 2.5 m s^{-1}, making successive passes across the fields and recording the EC_a measurements every second. From these EC_a data, Kriged EC_a maps were generated for each pasture field using the collected EC_a data. The EC_a values at each sample location were then extracted from these EC_a maps.

The estimation of EC_a at unsampled locations was performed using the ordinary point kriging algorithm, which integrates the spatial correlation structure described with the variograms. The resulting kriged maps show the spatial distribution of EC_a in the experimental field. Finally, the kriged EC_a maps were generated using the ArcMap module of ArcGIS.

2.3. Soil Sampling and Analysis

On both dates and in each experimental field, following the EC_a measurements, eight georeferenced composite soil samples were collected at depths ranging from 0 to 0.30 m using a gouge auger and a hammer. Each composite sample resulted from the combination of five sub-samples collected within an approximately 10 m × 10 m area: one from the center of the sampling area and the other four from the respective quadrant. Soil samples were transported to the laboratory in metallic boxes, weighed, and then dried at 105 °C until a constant weight was achieved. Once cooled, they were weighed to establish the mean soil moisture content (SMC). Subsequently, the fine components of the soil (fraction with a diameter < 2 mm) underwent chemical analyses of pH, organic matter (OM), phosphorous (P_2O_5), potassium (K_2O) and cation exchange capacity (CEC) using standard reference laboratory methods (AOAC, 2005). On date 2 (September 2020), soil samples were also processed for particle size distribution.

2.4. Statistical Analysis and Data Processing

The data of EC_a obtained by a Veris sensor in October 2018 and by EM-38 in September 2020 were synchronized using the geographic coordinates of each point to evaluate the temporal stability of the EC_a measurements.

A combined dataset was created for each date: each Veris data point obtained was paired with the nearest data point obtained by EM-38 based on GNSS coordinates. If a match in spatial coordinates was not found within a 5 m radius, that point was removed from the dataset. The sets of data, that is, points with common geographic coordinates in both surveys (date 1 and date 2) in each experimental field underwent linear correlation analysis, which was conducted using the IBM SPSS statistical package (version 25, IBM Corp, Armonk, NY, USA), to obtain the Pearson correlation coefficients (r) using the method of least squares ($p < 0.05$).

The EC_a results obtained on each date, combined with elevation data (survey conducted on the first date), served as the input for the geostatistical analyses, enabling the delineation of management zones (MZ) for each date and experimental field. These homogeneous subfields were determined using a fuzzy cluster algorithm Höppner et al. (1999), and the MZ Analyst (MZA) software (Microsoft Corp., Redmond, WA, USA) was employed in this study. The procedures for delineating and evaluating the number of MZs used in this software were described by Fridgen et al. (2004). From a practical standpoint, three MZs with different

productive potential (less, intermediate, and more potential) were considered in each experimental field.

In order to analyze the temporal stability of the MZ defined in each field, a comparison was carried out between each pixel of the MZ maps based on the EC_a measurements made with both sensors. Thus, for each field, a reclassification process was performed on the two MZ maps, assigning the value 0 to the pixels of the MZ with higher potential, 1 to those with intermediate potential, and 2 to those with low potential. Subsequently, using map algebra, both MZ maps were overlaid, producing a new map distinguishing three possible zones: one where pixels have a value of 0, meaning that the MZ coincides on both maps; another where pixels have a value of 1, meaning that there is a difference of 1 between the values of the pixel on the two maps; and a third zone with pixels whose value is 2, meaning that the pixel of the two maps have a difference of 2 between them. In this new map, the zone containing pixels with a value of 0 is denominated "stable", the zone with pixels having a value of 1 is called "unstable", and the zone containing pixels with a value of 2 is called "very unstable".

3. Results and Discussion

3.1. Correlation between Soil Apparent Electrical Conductivity Measurements

The correlation between the EC_a measurements in each date, after coordinate synchronization, for each experimental field is shown in Figure 1: ECO (a), MIT (b), MUR (c), and PAD (d). All correlations were statistically significant ($p < 0.01$), with very interesting correlation coefficients, between 0.449 (MIT field) and 0.618 (MUR field).

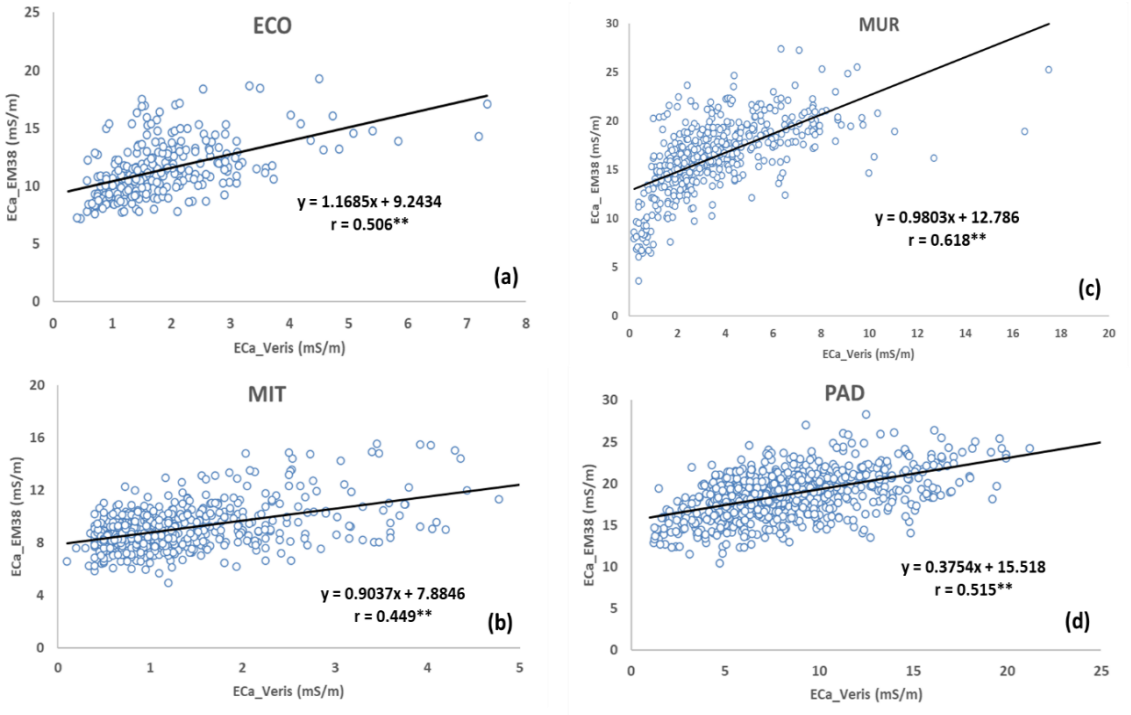

Figure 1. Correlation between soil apparent electrical conductivity (EC_a) measured using Veris 2000 XA and EM-38 sensors in each experimental field: "ECO" (a), "MIT" (b), "MUR" (c), and "PAD" (d). ** Statistically significant at 99% confidence level ($p < 0.01$).

The spatial regressions and paired t-tests applied by McCutcheon et al. (2006) to investigate differences between the EC_a values from different measurement dates (temporal persistence) with a contact sensor (Veris) provided correlation coefficients with a white range of variation (between 0.10 and 0.76). Martini et al. (2017) compared repeated EMI measurements with high-resolution soil moisture and temperature data and reported that the spatial patterns of EC_a differed from those of the soil water content and that the relation between both variables was changing over time. Various correction or standardization methods have been

proposed, and it has been recommended that measurements be made under similar conditions; however, this is often not feasible in practice in fields where conditions change on small spatial scales. By using an EMI device four times (Dualem 1S), Serrano et al. (2017) found temporally stable spatial EC_a patterns in a Mediterranean pasture over a period of 7 years despite changing environmental and management conditions. Various studies have demonstrated the possibilities for significant changes in the measured EC_a over time, nevertheless, with relatively stable spatial structure representations (Mat Su and Adamchuk, 2023).

In this study, the smallest number of points obtained by coordinate synchronization was found in the ECO field, which is a small field compared to the others (only 4 ha, while the rest have areas of 20 to 30 ha). The MUR field also has a smaller number of points, since in the southwestern area, the Veris sensor faced some measurement problems, which can be associated with the presence of stones on the surface, which interrupt the contact between the electrodes and the ground and reinforces the aforementioned difficulty of contact sensors in stony soils. It is important to note that the surveys were carried out by independent service providers. The results would have certainly improved if the sensor transects in the second survey had followed the paths of the first survey in each field, which would have allowed a much greater number of points as a result of synchronization and thus would have strengthened the correlation.

3.2. Temporal Stability of Management Zones

The application of geostatistical algorithms based on elevation and EC_a data allowed for the MZs and the correspondent maps in each date to de defined and in each experimental field.

Table 1 shows the area of each MZ (low, intermediate, and high potential) in each date, in percentage of the total area of each field.

Table 1. Area of each management zone (MZ) in each date, shown in percentage of the total area of each field.

Field	ECO	ECO	MIT	MIT	MUR	MUR	PAD	PAD
Date	1	2	1	2	1	2	1	2
MZ (%)								
Low Potential	45.7	76.9	28.7	28.5	49.9	27.4	14.3	0.9
Intermediate Potential	41.5	17.2	31.6	37.2	34.9	32.3	60.1	42.3
High Potential	12.8	5.9	39.7	34.3	15.2	40.3	25.6	56.8

In this study, the temporal stability of an MZ was evaluated by an overlap reclassification process of MZ maps, allowing for the definition of three new zones, namely stable, unstable, and very unstable, expressed as percentages of the total area of each field (Table 2; Figure 2). In average, 52% of the area presented temporal stability (in the same MZ category in both EC_a surveys, with a minimum value of 37.6% in the MIT field and a maximum of 71.2% in the MUR field), 42% of the area presented temporal instability (in the next or previous category in both EC_a surveys), and only 6% presented very temporal instability (two categories above or below in both EC_a surveys). This information, presented spatially through temporal stability maps (Figure 2), provides good prospects for the use of EC_a in the medium- and long-term definition of MZ. If a spatial pattern is temporally stable within a field, then it is reasonable to suppose that it should be a reasonably good predictor of the spatial patterns in the following years. This assumes that the prevailing conditions and limiting factors are consistent over the years (Blackmore, 2000).

Table 2. Temporal stability of management zones (MZ) between dates of evaluation, in percentage of total area of each field.

Field	ECO	MIT	MUR	PAD
Stable	52.5	37.6	71.2	48.1
Unstable	41.8	48.8	27.5	49.5
Very unstable	5.7	13.6	1.3	2.4

The results of this study, especially those relating to the temporal stability of the MZ patterns obtained by different sensors, are very encouraging. However, various authors have shown inconsistent relationships

between the EC_a and soil characteristics, probably since the EC_a is influenced by various complex interactions between site-dependent soil properties (Moral et al., 2010).

Despite the temporal stability of the EC_a patterns, in relative terms, reflected in the temporal stability of the patterns of the MZ maps, it will be interesting, in future works, to extend the findings to other types of soils (in particular, with finer textures) and conditions (namely different SMCs) to identify the source of the discrepancy in absolute terms in the measurement of the EC_a using different sensors (contact versus non-contact), with systematically higher values obtained using the EMI sensor (EM-38 in this case) compared to the contact sensor (Veris 2000 XA in this case).

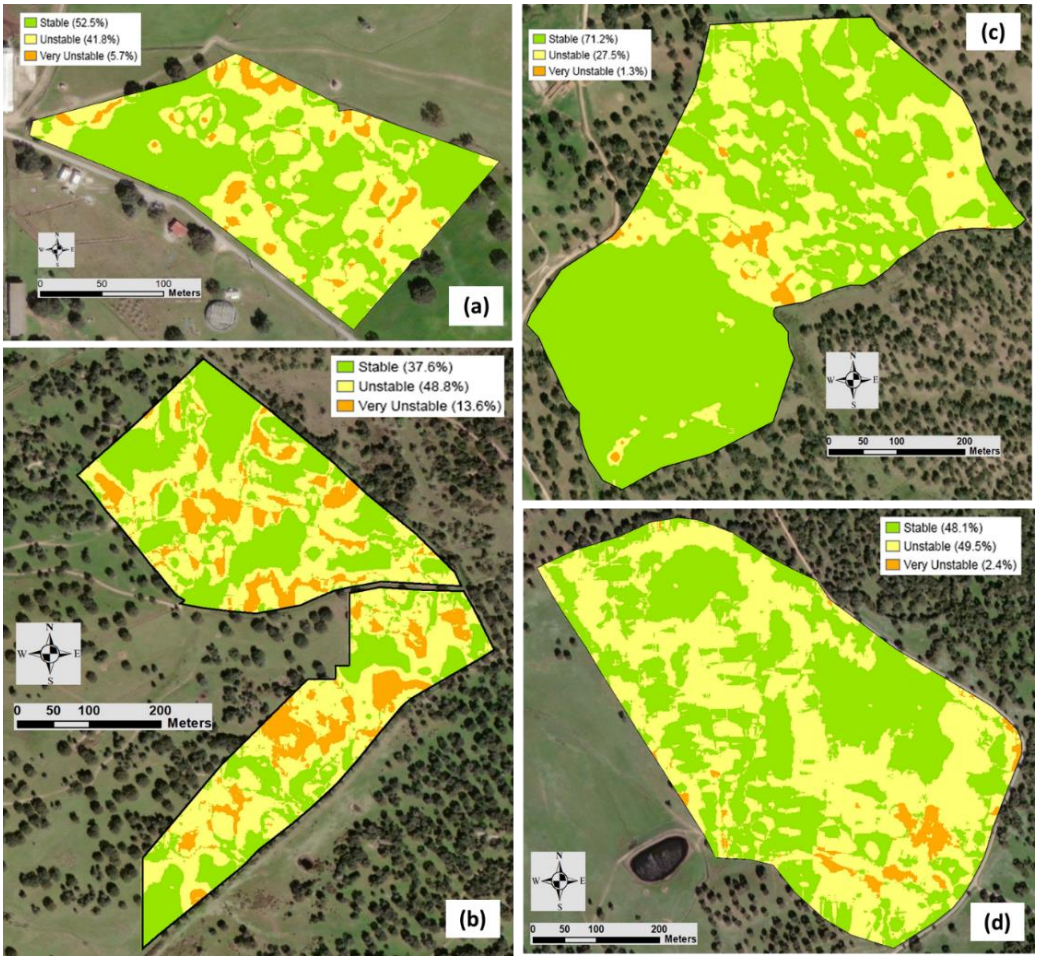

Figure 2. Maps of temporal stability of management zones (MZ) of each experimental field: "ECO" (a), "MIT" (b), "MUR" (c), and "PAD" (d). Stable, unstable, and very unstable areas are indicated as percentages of total area.

These results also suggest a next step in the logic of validating the MZ obtained by each of the sensors, either through soil smart sampling carried out in each MZ (Moral et al., 2010) or through the evaluation of vegetation indices, or VIs (namely the NDVI), which is an approach that has been followed in several research works (Georgi et al., 2018). Through a soil analysis, it will be possible to find the relationship between EC_a measurements and soil parameters with potential for site-specific management in dryland pastures, for example, in terms of the differentiated application of lime or phosphorus amendments. To transpose these MZ maps to amendment or fertilization prescription maps, it is fundamental to develop algorithms to evaluate the agronomic significance of this classification (MZ) and establish more general methods of mapping and quantifying variable input prescriptions, for example, lime amendment and nitrogen or phosphorous fertilizer application (Bönecke et al. 2021). On the other hand, there is a growing interest in rapid MZ validation methodologies, such as those based on VIs obtained from remote sensing, by recovering

the time-series of the NDVI (for example) throughout the vegetative cycle, which is related with pasture productivity and quality, and complementing and improving the rigor of the validation obtained from smart soil sampling (Georgi et al., 2018).

Given that this is an exploratory study that was carried out in a relatively restricted soil type under specific coarse-textured soils, further studies using different soil types should be conducted.

4. Conclusions

The results obtained in this study show significant correlation between soil apparent electrical conductivity measurements (different dates and sensors) after coordinate synchronization in all experimental fields (with correlation coefficients between 0.449 and 0.618).

Based on a geostatistical analysis of the soil electrical conductivity and topographic surveys, three management zones were defined (with high, intermediate, and low potential). The soil electrical conductivity measurements with different sensors (contact and non-contact), carried out almost two years apart, revealed spatial patterns in management zones with remarkable temporal stability (averaging 52% of the total area across four fields), which is a good indicator of potential for the use of soil electrical conductivity in medium- and long-term management decisions.

These results suggest that future developments should focus on creating algorithms to validate the spatial variability and temporal stability of soil electrical conductivity through smart soil sampling, extending the database and thereby enhancing the process of recommendations for sustained soil amendment or fertilization.

Acknowledgements

This research was funded by national funds through the FCT (Foundation for Science and Technology) under Project UIDB/05183/2020.

References

Adamchuk, V.I., J.W., Hummel, M.T., Morgan, S.K., Upadhyaya, 2004. On-the-go soil sensors for precision agriculture. Computers and Electronics in Agriculture. 44, 71-9.

AOAC. 2005. Official Methods of Analysis of AOAC International, 18th ed., AOAC International: Arlington, VA, USA.

Blackmore, S. 2000. The importance of trends from multiple yield maps. Computers and Electronics in Agriculture. 26, 37-51.

Bönecke, E., S., Meyer, S., Vogel, I., Schröter, R., Gebbers, C., Kling, E., Kramer, K., Lück, A., Nagel, A., G., Philipp. 2021. Guidelines for precise lime management based on high resolution soil pH, texture and SOM maps generated from proximal soil sensing data. Precision Agriculture. 22, 493-523.

FAO. 2006. IUSS Working Group WRB. World reference base for soil resources. In *World Soil Resources Reports No. 103*, FAO: Rome, Italy.

Farahani, H.J., G.W., Buchleiter. 2004. Temporal stability of soil electrical conductivity in irrigated sandy fields in Colorado. Transactions of the ASAE. 47, 79-90.

Fridgen, J.J., N.R., Kitchen, N.R., K.A., Sudduth, S.T., Drummond, W.J., Wiebold, C.W., Fraisse 2004. Management zone analyst (MZA): software for subfield management zone delineation. Agronomy Journal. 96, 100-108.

Georgi, C., D., Spengler, S., Itzerott, B., Kleinschmit. 2018. Automatic delineation algorithm for site-specific management zones based on satellite remote sensing data. Precision Agriculture. 19, 684-707.

Höppner, F., F., Klawonn, R., Kruse, T.A., Runkler. 1999. *Fuzzy Cluster Analysis*, Wiley: Chichester, UK.

King, J., P., Dampney, R., Lark, H., Wheeler, R., Bradley, T., Mayr, T. 2005. Mapping potential crop management zones within fields: Use of yield-map series and patterns of soil physical properties identified by electromagnetic induction sensing. Precision Agriculture. 6, 167-181.

Martini, E., U., Werban, S., Zacharias, M., Pohle, P., Dietrich, U., Wollschläger, U. 2017. Repeated electromagnetic induction measurements for mapping soil moisture at the field scale: Validation with data from a wireless soil moisture monitoring network. Hydrology and Earth System Science. 21, 495-513.

Mat Su, A.S., V.I., Adamchuk. 2023. Temporal and operation-induced instability of apparent soil electrical conductivity measurements. Frontiers in Soil Science. 3, 1137731.

McCutcheon, M.C., H.J., Farahani, J.D., Stednick, G.W., Buchleiter, T.R., Green. 2006. Effect of soil water on apparent soil electrical conductivity and texture relationships in a dryland field. Biosystem Engineering. 94, 19-32.

Medeiros, W.N., D.M., de Queiroz, D.S.M., Valente, F., de Pinto, C., Melo. 2016. The temporal stability of the variability in apparent soil electrical conductivity. Bioscience Journal. 32, 150-159.

Moral, F., J., Terrón, J.M., da Silva 2010. Delineation of management zones using mobile measurements of soil apparent electrical conductivity and multivariate geostatistical techniques. Soil and Tillage Research. 106, 335–343.

Peralta, N.R., P.L., Cicore, P.L., M.A., Marino, M.A., J.R., Marques da Silva, J.L., Costa. 2015. Use of geophysical survey as a predictor of the edaphic properties variability in soils used for livestock production. Spanish Journal of Agricultural Research. 13, e1103, 1-8.

Schenatto, K., E.G., de Souza, C.L., Bazzi, A., Gavioli, N.M., Betzek, H.M., Beneduzzi. 2017. Normalization of data for delineating management zones. Computers and Electronics in Agriculture. 143, 238-248.

Serrano, J., S., Shahidian, J., Marques da Silva. 2017. Spatial variability and temporal stability of apparent soil electrical conductivity in a Mediterranean pasture. Precision Agriculture. 18, 245-263.

Shaping the agricultural future: Engaging stakeholder feedback for the development of agricultural robotic solutions

Maria-Zoi Papantonatou[1,2], George Papadopoulos[1,2], Spyros Fountas[1], Havva Uyar[3,1], Frits Van Evert[4]

[1]Department of Natural Resources Management and Agricultural Engineering, Agricultural University of Athens, [2]Faculty of Crop Science, Agricultural University of Athens, [3] Singular Logic, [4]Agrosystems Research, Wageningen University & Research,

* Maria-Zoi Papantonatou. Email: m.papantonatou@aua.gr

Abstract

Smart farming technologies and robotic solutions may enable farming to move towards a more environmentally friendly agriculture landscape. These solutions, whether already commercially available or still under development, represent the future of agriculture and will play a crucial role in supporting farmers in crop production. The involvement and opinions of farmers, advisors, and agriculture students are vital in ensuring the adoption and smooth transition from traditional to smart, robotic, and data-driven methods. Field demonstrations are an important method to familiarise these stakeholders with the new technologies. Autonomous robotic solutions were presented for weeding and spraying applications developed within the EU-funded project Robs4Crops in Greece. Feedback was collected from farmers, advisors and students who attended the demonstration. The survey aimed to engage them by documenting their opinions and beliefs during these demonstrations. The aim of the study was to present and analyse their feedback on the effectiveness of such demonstrations, the level of understanding of the presented robotic solutions, and insights into challenges and potential solutions for market adoption. The main results of the survey showed a very positive reaction towards the new innovative agricultural robotic solutions. The demonstrations significantly improved the participants' understanding of robotic technologies, with an impressive 100% expressing full agreement and approval of the presented solutions. In addition, 96% reported that their perception of the potential benefits of robotic agriculture was positively altered by the demonstrations, highlighting a transformative effect on their views. This collective agreement of opinion among farmers, advisors, and agricultural students illustrates the effectiveness of the demonstrations in providing valuable information and promoting a more informed perspective on the potential and benefits of robotic agriculture technologies. The findings suggest that such demonstrations could play a key role in accelerating the adoption of smart agriculture technologies, paving the way for a more efficient and sustainable agricultural sector.

Keywords: Robotic solutions, Smart Agricultural Technologies, Farmers' perception, Students' perception, questionnaire survey

1. Introduction

Smart farming technologies, including robotic solutions and precision agriculture technologies are considered as key components to achieve the transition towards a more environmentally sustainable future (Papadopoulos et al., 2024). To ensure a smooth transition from traditional practices to smart, data-driven agriculture, it requires not only innovative technological enhancements but also a comprehensive adoption process through effective strategies and engagement of key stakeholders such as farmers, students, and agricultural advisors (Kanesh et al., 2022). These stakeholders play a crucial role not only as a knowledge base but also as influential decision-makers within the agricultural sector. Their perspectives and involvement are crucial for the adoption and incorporation of smart farming technologies into the current agricultural practices.

Studying the smart farming technologies adoption process and impact is important for an effective transition to a new agricultural framework and thus many studies have been carried out world-wide to identify it. In their study, Kanesh et al. (2022) explored the perceptions and attitudes of farmers towards adopting smart farming technologies in the Batticaloa district of Sri Lanka. They gathered primary data through a questionnaire survey conducted with randomly selected farmers from February to April 2020. To analyse this data, they employed the Technology Acceptance Model to assess how farmers adopt and use precision agricultural techniques. Further analysis using Structural Equation Modelling, preceded by

Confirmatory Factor Analysis, helped them identify significant relationships between various factors. The findings revealed a generally positive perception among farmers regarding the adoption of precision agricultural techniques.

Furthermore, Vrchota et al. (2022) investigated the adoption of precision agriculture technologies among Czech agricultural enterprises. They conducted a questionnaire survey involving 131 farms and employed a Chi-squared test to analyse the data. The survey revealed that 58% of enterprises used intelligent weather stations, 89% utilized unmanned vehicles, and 62% employed navigation and optimisation systems for journey optimisation. These findings underscore a robust willingness among agricultural enterprises to embrace new technologies. They also provide valuable insights for policymakers on the implementation of these technologies and suggest directions for targeted funding towards grants and projects. This study, along with the survey by Kanesh et al., highlights the critical role of farmer engagement in integrating smart farming technologies into daily routines.

Within the EU-funded Robs4Crops project, which aims to develop robotic solutions for spraying applications, demonstrations were conducted in Greece showcasing to farmers, advisors, and students two innovative technologies: a) the autonomous spraying capabilities of a retrofitted tractor, and b) the practical applications and benefits of a Farming Controller (FC) through the use of Digital Twins (DT). These demonstrations were intended to engage directly with participants and enhance their understanding of these agricultural technologies, setting the stage for future improvements. Following the demonstrations, a survey was conducted to gather feedback and assess participants' perspectives on smart agricultural technologies and robotic solutions.

The aim of this study was to present and analyse the results obtained from this survey, assessing the impact of demonstration activities on stakeholders' understanding, perception, and readiness to adopt smart farming technologies. Through structured demonstrations and subsequent surveys among farmers, agricultural advisors, and students, the study sought to identify key drivers of engagement, the educational effectiveness of the demonstrations, and the challenges and barriers to market adoption of robotic farming technologies. Additionally, the study aimed to gather actionable insights to inform future strategies for technology implementation and educational efforts, facilitating smoother integration of innovative agricultural technologies into mainstream farming practices.

2. Materials & Methods

2.1. Online questionnaires survey

To facilitate the survey process, participants were categorised into two distinct groups: a) farmers and agricultural advisors, and b) students. Data collection was carried out through separate online questionnaires using Google forms, each comprising a structured format with a diverse range of questions grouped into specific categories. The breakdown of the survey questions categories used for each group are described below:

Farmers, agricultural advisors: Eleven survey questions were formulated, each tailored to address the following categories: 'Participant Background and Affiliation', 'Evaluation of Demonstration Activities'. 'Factors Influencing Attendance', 'Familiarity and Understanding of Robotic Farming', 'Quality of Information and Perception Change', 'Challenges and Solutions in Market Adoption', and 'Suggestions for Improvement'.

The section 'Participant Background and Affiliation' aimed to categorise the participants based on their professional background and affiliation, helping to understand the diversity of attendees. Subsequently, the questions under 'Evaluation of Demonstration Activities' focused on quality and impact assessment of the demonstrations. Attendance feedback and ratings provided quantifiable measures for satisfaction and perceived effectiveness. The questions under 'Factors Influencing Attendance', explored the motivations for attending the demonstrations providing insights into what drew participants to the event. Following this, the section 'Familiarity and Understanding of Robotic Farming', aimed to understand the participants' knowledge baseline regarding robotics and evaluate how effectively the demonstrations enhanced their understanding as well as the educational impact of the demonstrations. The questions under the 'Quality of Information and Perception' provided feedback to evaluate the quality of information provided and whether the demonstrations influenced attendees' perceptions about the benefits of robotic farming. Lastly, the segment on 'Quality of Information and Perception Change' endeavoured

to evaluate the quality of information provided and whether the demonstrations influenced attendees' perceptions about the benefits of robotic farming.

Student engagement: Ten survey questions were formulated, each tailored to address the following categories: 'Familiarity and Understanding of Technologies', 'Demonstration Impact and Perception', 'Interactive Experience and Further Interest', 'Enthusiasm and User-Friendliness', 'Benefits, Challenges, and Enhancements'.

The section 'Familiarity and Understanding of Technologies' aimed to assess participants' initial familiarity with the technologies, thereby providing a context for their level of understanding. Subsequently, the questions under 'Demonstration Impact and Perception' focused on evaluating how the demonstration influenced participants' understanding and perception of the technologies' importance, as well as their opinions on the potential future impact of these technologies. The questions under 'Interactive Experience and Further Interest', delved into participants' interest in hands-on experiences and further educational opportunities related to the technologies showcased. Following this, the section 'Enthusiasm and User-Friendliness', aimed to evaluate participants' enthusiasm for adopting the technologies and assess their perceived ease of use. Lastly, the segment on 'Benefits, Challenges, and Enhancements' endeavoured to identify perceived benefits and potential advantages of the technologies, as well as the obstacles that might encounter when adopting them. Additionally, it gathered students' suggestions on how demonstrations could be enhanced to be more engaging and beneficial.

2.2 Agricultural stakeholders' outreach and Scale-up demonstrations

The demonstrations were conducted in Greece, showcasing the application of autonomous spraying with a retrofitted tractor in a vineyard, alongside the use of a FC enhanced by DT. In total, four demonstrations were held: one for farmers and agricultural advisors in the Kiato region of Peloponnese and three for students at the Agricultural University of Athens.

During these events, detailed presentations were given on the robotic solutions developed under the Robs4Crops project while for the student sessions a focus was given on the features of the FC and integrated DT for educational purposes. At the Kiato event, farmers and agricultural advisors were given the opportunity to witness a live demonstration of autonomous spraying with a retrofitted tractor, showcasing the technology in action. In contrast, at the Agricultural University of Athens, students were engaged through video presentations that not only demonstrated the FC and integrated DT but also included footage of the autonomous spraying technology being applied in vineyards. At the end of the demonstrations a discussion was followed up and then all attendees were invited to complete the online survey.

2.3. Data collection & statistical analysis

This study involved primary data collection from a total of 46 farmers and agricultural advisors, alongside 63 students from the Agricultural University of Athens. Data was obtained using the two online questionnaires and the responses were extracted from Google survey directly into an Excel file for feedback analysis.

For the statistical analysis, descriptive statistical methods were employed to summarize and interpret the participants' responses based on the predefined categories. Data were presented using frequency distributions, percentages, and graphical representations such as bar charts and pie charts to illustrate key findings.

3. Results

3.1. Farmers' Perspective

3.1.1. Participant Background and Affiliation

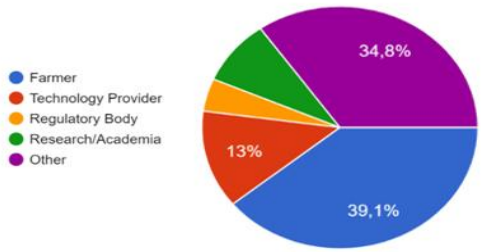

Figure 1: Distribution of Participant Background and Affiliation - Pie Chart

The results of the survey indicated a diverse representation of respondents in terms of their professional roles or affiliations (Figure 1). Farmers constitute the largest percentage, representing 39.13% of the participants, highlighting a significant presence of individuals directly involved in agricultural practices. Technology providers comprise 23.91% of respondents, showing significant interest from those offering agricultural tech solutions. Research/academia professionals account for 19.57%, representing individuals involved in agricultural research and education. Regulatory bodies account for 4.35% of the participants, showcasing a smaller presence. The remaining 13.04% falls into the "Other" category, which implies a variety of roles not explicitly mentioned in the provided options. Overall, the data underscores a diverse and engaged group of participants, encompassing a range of stakeholders from farmers and technology providers to researchers and regulatory bodies.

3.1.2 Evaluation of Demonstration Activities

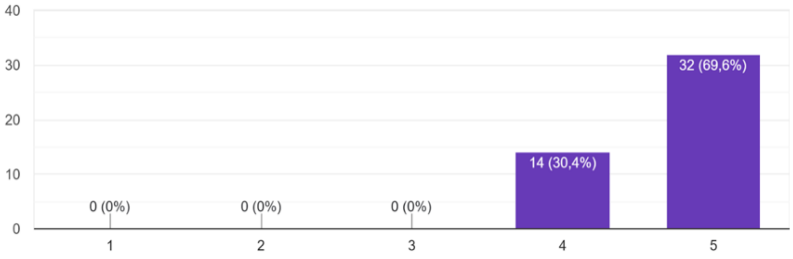

Figure 2: Feedback for the evaluation of demonstration - Bar Chart

Through the feedback collection for the evaluation of the demonstration activities, it has been identified through the answers, that a 69.6% of participants rated the activities as excellent (5/5), while 30.4% gave a very positive rating of 4/5 (Figure 2). The high percentage of top ratings reflects a strong endorsement and suggests that the participants found the demonstrations to be not only satisfactory but also of a particularly high standard.

3.1.3. Factors Influencing Attendance

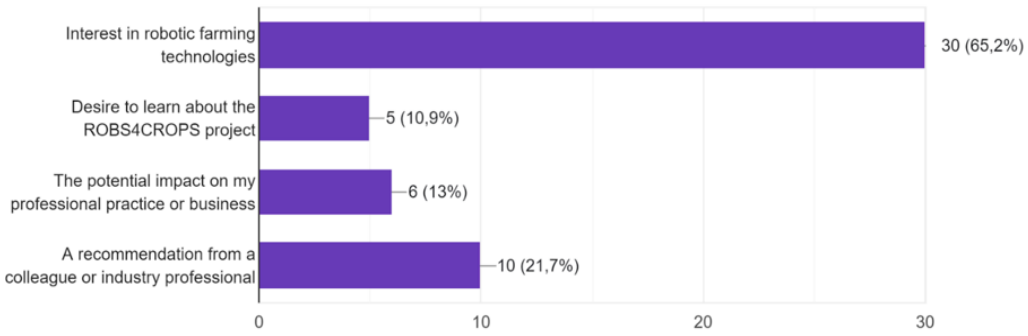

Figure 3: Feedback for the factors affecting attendance - Bar Chart

The survey was designed to capture the multi-faceted reasons for participants' participation and allowed for multiple factor choices. A total of 51 responses were collected, providing insight into the factors influencing participation in the demonstration activities of this demonstration (Figure 3).

A notable 65.2% of the participants stated a high interest in robotic farming technologies as the primary motivator for their participation. This was followed by 13.0% who highlighted the potential impact on their professional practice or business, while 10.9% expressed a specific interest in learning about the ROBS4CROPS project. Notably, recommendations from colleagues or industry professionals significantly influenced the decision of 21.7% of participants.

3.1.4. Familiarity and Understanding of Robotic Farming

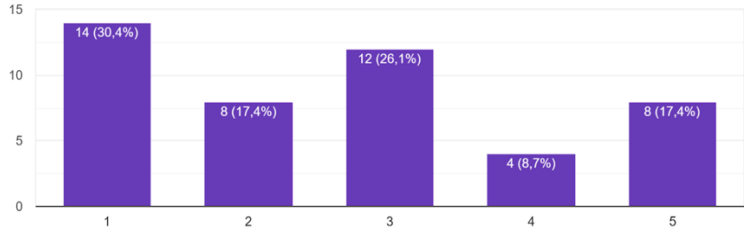

Figure 4: Feedback for Familiarity and Understanding of Robotic Farming - Bar Chart

Participants' responses to the questions regarding their familiarity with robotic farming before attending the demonstrations represent a diverse knowledge landscape (Figure 4). About 30.4% stated limited prior knowledge (rating 1/5), while 17.4% expressed advanced familiarity (rating 5/5). The middle ground (ratings 2/5, 3/5, and 4/5) accounts for 52.17%, illustrating a spectrum of moderate familiarity.

In addition, a subsequent question on whether the demonstrations had improved understanding of the participants received positive feedback of 100% 'yes', indicating the success of the programme in achieving its educational objectives. This collective agreement suggests that the demonstrations effectively provided valuable insights, fostering a more informed perspective on robotic farming technologies among all participants.

3.1.5. Quality of Information and Perception Change

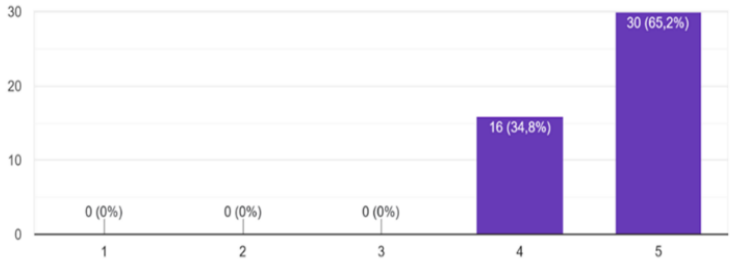

Figure 5: Feedback for Quality of Information and Perception Change - Bar Chart

Participants' feedback on the quality of information and knowledge disseminated during the demonstration activities reflects a highly satisfactory experience, with 65.2% giving the highest rating of 5 and an additional 34.8% rating it a 4 (Figure 5). The combined 100% approval underscores widespread satisfaction with the information presented, suggesting its high value. Moreover, when asked if the demonstrations altered their perception of the potential benefits of robotic farming, a significant 95.7% responded affirmatively. This indicates a transformative effect on their views, emphasizing the program's success in influencing perspectives and fostering a greater appreciation for the advantages of robotic farming.

3.1.6 Challenges and Solutions in Market Adoption

The survey responses reveal a range of challenges anticipated in the market adoption of robotic farming technologies. A recurring concern is the high cost associated with these farming technology innovations, creating financial barriers for farmers. Funding emerges as a potential solution to alleviate this challenge, suggesting a need for financial support mechanisms. Additionally, the insufficient education among farmers, particularly regarding the acceptance and understanding of robotic technologies is also considered as a challenge. The proposed solution involves intensifying educational efforts through seminars and demonstrations to enhance operator knowledge. Other identified obstacles include the high cost of specific products, lack of expertise, and resistance from older generations. To overcome these challenges, strategies such as reducing product costs, providing economical alternatives, and facilitating farmer education are suggested. The survey reveals the importance of addressing constraints and promoting comprehensive initiatives to foster the successful integration of robotic farming technologies into the agricultural landscape.

3.1.7 Suggestions for Improvement

There is a strong agreement among the survey respondents regarding the need for enhanced educational initiatives in future demonstration events or activities related to robotic farming technologies. The suggestions emphasize more active involvement of farmers, revealing the importance of real-life examples showcasing the successful implementation of these technologies in the fields. The desire for easy

access to seminars, more free education opportunities, and constant updates reveals the importance of ongoing learning. Additionally, recommendations were made for better presentations, including more tractors and technologies, involving farmers who have first-hand experience with the equipment.

3.2. Students' Perspective

3.2.1. Familiarity and Understanding of Technologies

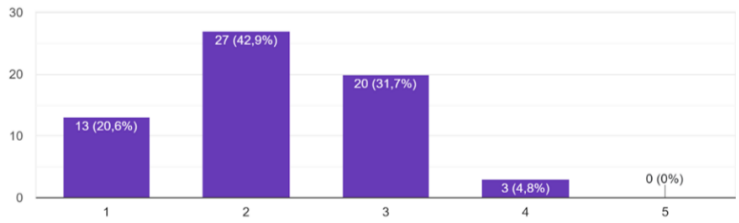

Figure 6: Familiarity and Understanding - Bar Chart

Responses from students regarding their familiarity with robotic farming before the demonstration reflect a varied knowledge landscape (Figure 6). A total of 20.63% reported a lack of familiarity, assigning a rating of 1/5. Limited knowledge (rating 2/5) was indicated by 42.9% of participants. The middle ground, representing moderate familiarity (rating 3/5), accounted for 31.7% of responses. High familiarity (rating 4/5) was expressed by 4.8% of the respondents. Notably, none of the participants claimed to be "Very familiar" with the tools, highlighting a lack of highest-level familiarity with the technologies.

3.2.2. Demonstration Impact and Perception

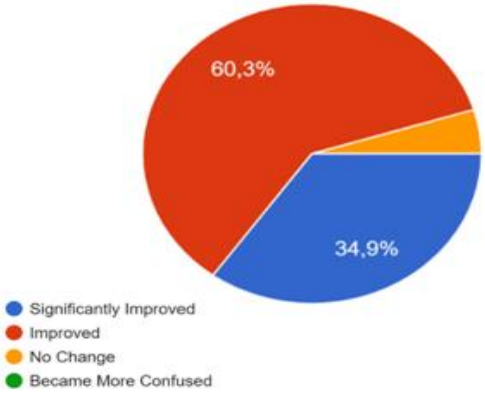

The responses to the question assessing the impact of the demonstration on students' understanding of the FT combined with DT indicate a substantial positive effect. A significant 60.3% of respondents reported an "Improved" understanding, while 34.9% noted a "Significantly Improved" comprehension. Notably, only 4.8% stated that there was "No Change" in their understanding. This distribution highlights the effectiveness of the demonstration in improving participants' understanding of the FC and DT integration (Figure 7).

Figure 7: Feedback for Demonstration Impact and Perception- Pie Chart.

Furthermore, the responses strongly indicate a positive perception of the integration in shaping the future of agriculture. A significant 63.5% of students rated these tools a "crucial role" in the future of agriculture (rating 5/5), with an additional 30.2% expressing a belief in their significance but with slightly less intensity (rating 4/5). 6.3% of the respondents stated mid-range rating with 3/5. Importantly, no respondents rated lower than 3/5, indicating a strong agreement on the significant role of these technologies in shaping agriculture (Figure 8).

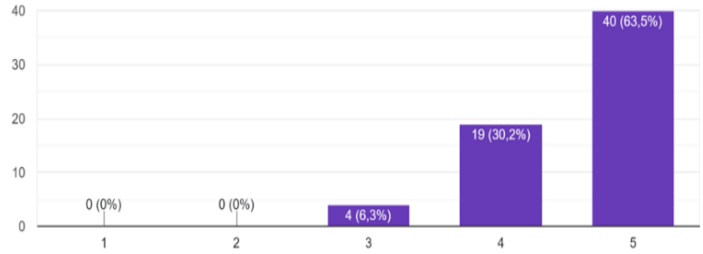

Figure 8: Feedback for Demonstration Impact and Perception- Bar Chart

3.2.3. Interactive Experience and Further Interest

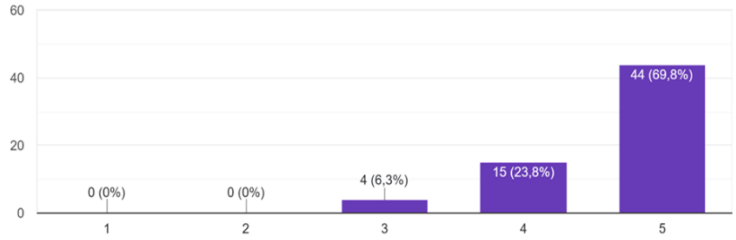

Figure 9: Feedback regarding the Interactive Experience and Further Interest -Bar Chart

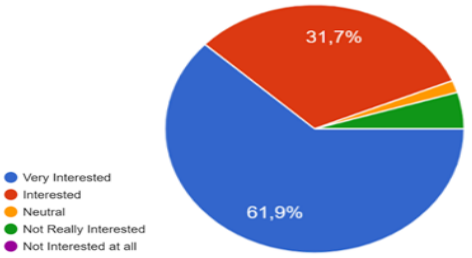

Figure 10: Feedback regarding the Interactive Experience and Further Interest -Pie Chart

Participants' feedback regarding their willingness for an interactive experience with the FC combined with DT indicates a strong positive inclination. A significant 69.8% of respondents rated their interest at 5/5, expressing high enthusiasm for interactive experiences. Additionally, 23.8% rated it 4/5, showing a positive attitude, while only 6.35% gave a mid-range rating of 3/5. (Figure 9) Notably, no participants rated below 3/5. This high percentage of positive responses underscores the potential appeal of incorporating interactive elements into demonstrations.

Similarly, students' responses indicate strong interest in more in-depth training on the FC combined with DT. Notably, 61.9% of respondents were "Very Interested," and 31.7% were "Interested," while only 6.4% were neutral or less enthusiastic (Figure 10). With 93.6% expressing interest, there is a strong desire for comprehensive educational resources and training opportunities related to these technologies.

3.2.4. Enthusiasm and User-Friendliness

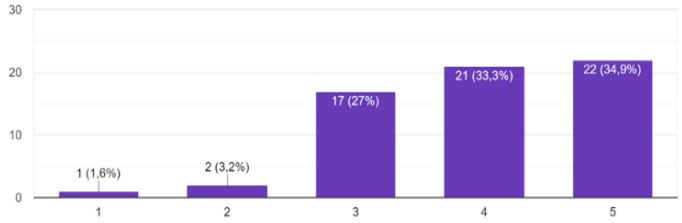

Figure 11: Feedback for Enthusiasm and User-Friendliness - Bar Chart

The students' responses regarding their enthusiasm for engaging with technologies in their future agricultural careers are overall positive. A significant 68.2% of students rated their excitement at 4/5 or 5/5, indicating substantial enthusiasm. Additionally, 27% gave a moderate rating of 3/5, rated it 2/5, and only 1.6% a negative response (Figure 11).

Overall, participants showed a positive outlook on adopting agricultural technologies in their future careers, with many expressing high anticipation for these opportunities. Regarding user-friendliness of the FT and DT the responses suggest a generally positive perception. About 9.5% of students rated it 5/5, and 49.2% rated it 4/5, indicating high satisfaction (Figure 12). Meanwhile, 39.7% gave a moderate rating of 3/5, and only 1.6% rated it 2/5, indicating a less positive view.

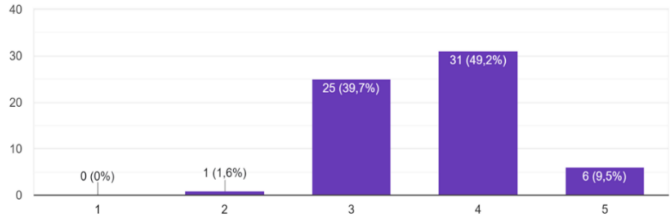

Figure 12: Feedback for Enthusiasm and User-Friendliness - Bar Chart

3.2.5. Benefits, Challenges, and Enhancements

Benefits: Participants' feedback on integrating the FC with DT in modern farming reveals optimistic views on its benefits. Students emphasised reduced input costs, increased efficiency, and environmental sustainability, while highlighting precision agriculture's potential for automation and field management optimization.

Challenges & Proposed Solutions: Survey responses highlight also challenges in adopting these technologies. Common barriers include high costs, financial constraints, limited farmer education, resistance to change, and difficulties in understanding new technologies. Additionally, factors like insufficient land availability and technological illiteracy pose also challenges. Proposed solutions include

expanding technology use through funding, implementing eco-schemes, developing user-friendly environments, promoting machinery rental, and organizing practical training sessions. Other suggestions involve government or EU funding, industry cooperation, and continuous education programs. These insights offer valuable strategies to overcome adoption barriers and enhance technology integration in agriculture.

Enhancements: The feedback from students indicates a strong desire for more engaging and beneficial demonstrations of technologies like the FC combined with DT. They expressed the need for more interactive experiences including workshops with practical engagement and real-time exercises in the field while also suggested incorporating educational elements such as seminars and lessons. They seek more interactive, practical, and first-hand experiences to deepen their understanding and engagement with these advanced agricultural technologies.

4. Discussion

This survey indicated a significant shift in participants' views on smart farming technologies and robotic solutions, with 95.7% of them reporting that the demonstrations positively influenced their perceptions. This strong interest mirrors the findings from Jabbari et al. (2023), who reported a 90.91% engagement rate among 550 farmers in Jizan, Saudi Arabia, showing a similar interest in IoT technologies for crop monitoring. Their study linked farmers' awareness of IoT technologies to perceived benefits and willingness to adopt them. Additionally, students identified reduced input costs, increased efficiency, and environmental sustainability as notable benefits aligning with Tey and Brindal (2012) findings, who noted profitability as a major factor for using precision agriculture tools. As supported by Yarashynskaya et al. (2022), younger farmers, in particular, are showing a faster adoption rate due to their higher interest in new technologies. Students' responses strongly indicated a positive perception of the integration in shaping the future of agriculture. A significant 63.5% rated these tools as playing a "crucial role" in the future of agriculture (rating 5/5), while a significant overall 93.6% (69.8% rated their interest at 5/5, 23.8% rated it 4/5) expressed high enthusiasm for interactive experiences, confirming the younger generation's high interest in smart farming technologies.

Despite the high enthusiasm, the survey identified several barriers to adoption, with financial challenges at the forefront. The substantial costs associated with these technologies pose significant hurdles, as also highlighted by Yarashynskaya et al. (2022), who pointed to limited credit availability as a major obstacle due to high initial investments. Therefore, the findings of this study suggest that robust financial support mechanisms are essential to facilitate the adoption of these technologies. Furthermore, the study revealed that education level had a strong impact on technology adoption. The insufficient education among farmers, particularly regarding the acceptance and understanding of robotic technologies, was identified as a significant barrier. Therefore, as also suggested by the participants, intensifying educational efforts through seminars and demonstrations could enhance knowledge and acceptance of new technologies. These findings align with Bai et al. (2022) and Tamirat et al. (2018), whose studies highlighted the importance of socio-economic factors in the adoption of technologies.

5. Conclusion

The survey results highlighted a substantial interest in smart farming technologies, with 65.2% of participants citing it as their main motivator for attending, underscoring their enthusiasm for innovative agricultural practices. The demonstrations significantly improved participants' understanding of robotic technologies, with 100% expressing full agreement and approval of the presented solutions. Additionally, 96% reported a positive change in their perception of the potential benefits of robotic solutions, underscoring the transformative impact of the demonstrations. The evaluation of the demonstration activities also revealed a high level of satisfaction, with 97% of participants rating the activities as excellent (5/5) or very positive (4/5), indicating the successful introduction of new agricultural technologies to stakeholders.

Unlike other surveys, the inclusion of students' opinions, who represent the future of agriculture, proved to be essential revealing a strong interest in integrating these tools into agricultural practices. Furthermore, the vast majority of them (93.6%) expressed the desire for further educational and training opportunities related to these technologies. This high level of interest highlights the importance of engaging the next generation in discussions and initiatives related to modern farming technologies.

Nevertheless, the survey also identified challenges in market adoption, such as high costs and insufficient education, suggesting the need for financial support and intensified educational efforts. Benefits noted by participants included reduced input costs, increased efficiency, and environmental sustainability. Addressing these constraints and promoting comprehensive initiatives are essential for successfully integrating robotic farming technologies into modern agriculture. These insights are invaluable for guiding future research and enhancements, ensuring that the adoption of robotic farming technologies can be effectively supported and expanded.

References

Anastasiou, E., Fountas, S., Koutsiaras, M., Voulgaraki, M., Vatsanidou, A., Barreiro-Hurle, J., ... & Gómez-Barbero, M. (2023). Precision farming technologies on crop protection: A stakeholders survey. Smart Agricultural Technology, 5, 100293.

Papadopoulos, G., Arduini, S., Uyar, H., Psiroukis, V., Kasimati, A., & Fountas, S. (2024). Economic and Environmental Benefits of Digital Agricultural Technologies in Crop Production: A review. Smart Agricultural Technology, 8, 100441. https://doi.org/10.1016/j.atech.2024.100441

Suresh, K., Narmilan, A., Ahmadh Rifai Kariapper, R. K., & Sabraz Nawaz, S. (2022). Farmers' Perception on Precision Farming Technologies: A Novel Approach. *Indian Journal of Agricultural Economics, 77(2), 264-276*

Vrchota, J., Pech, M., & Švepešová, I. (2022). Precision Agriculture Technologies for Crop and Livestock Production in the Czech Republic. *Agriculture, 12(8), 1080.*

Balafoutis, A., Beck, B., Fountas, S., Tsiropoulos, Z., Vangeyte, J., van der Wal, T., Soto, I., Gómez-Barbero, M., & Pedersen, S. M. (2017). Smart Farming Technologies – Description, Taxonomy and Economic Impact.

Van Evert, F., Gaitán Cremaschi, D., Fountas, S., & Kempenaar, C. (2017). Can Precision Agriculture Increase the Profitability and Sustainability of the Production of Potatoes and Olives?. *Sustainability, 9, 1863.*

Jabbari, A., Humayed, A., Reegu, F. A., Uddin, M., Gulzar, Y., & Majid, M. (2023). Smart Farming Revolution: Farmer's Perception and Adoption of Smart IoT Technologies for Crop Health Monitoring and Yield Prediction in Jizan, Saudi Arabia. *Sustainability, 15(19), 14541*.

Bai, A., Kovách, I., Czibere, I., Megyesi, B., Balogh, P. 2022. Examining the Adoption of Drones and Categorisation of Precision Elements among Hungarian Precision Farmers Using a Trans-Theoretical Model. Drones. 6(8):20

Yarashynskaya, A., & Prus, P. (2022). Precision Agriculture Implementation factors and adoption potential: The Case Study of Polish Agriculture. Agronomy, 12(9), 2226. https://doi.org/10.3390/agronomy12092226

Tamirat, T.W.; Pedersen, S.M.; Lind, K.M. Farm and operator characteristics affecting adoption of precision agriculture in Denmark and Germany. Acta Agric. Scand. Sect. B—Soil Plant Sci. 2018, 68, 349–357.

Tey, Y.S., & Brindal, M. (2012). Factors influencing the adoption of precision agricultural tech-nologies: A review for policy implications. Precision Agriculture, 13, 713-730.

Assessment of instance segmentation methods for amodal apple detection in challenging environments

Tito Arevalo-Ramirez [a,*], Juan Villacres[b] , Michelle Viscaino[c] , Francisco Yandún[d] , Oswaldo Menéndez[e]

[a] Faculty of Engineering, Pontificia Universidad Católica de Chile -- Campus San Joaquín, Santiago, Chile

[b] Department of Biological and Agricultural Engineering, University of California, Davis, USA

[c] Department of Radiology, School of Medicine & DataLab: Data Science and Informatics, University of California, Davis California, USA

[d] Robotics Institute, Carnegie Mellon University, Pittsburgh, Pittsburgh Pensilvania, USA

[e] Departamento de Ingeniería de Sistemas y Computación, Universidad Católica del Norte, Antofagasta, Chile

* Corresponding author. Email: tito.arevalo@uc.cl

Abstract

Recent advancements in sensor technologies and deep learning algorithms have significantly contributed to continuously monitoring crops and vegetation in agricultural fields. Notably, researchers have extensively explored the identification and characterization of fruits on farms, as the physical attributes of fruits can offer valuable insights into the status of orchards. Visual sensors have been utilized to estimate fruit health and quality parameters. At the same time, robotic systems have been used to automate picking and harvesting tasks based on the location of fruits. Despite existing work on detecting and segmenting fruits in images, developing a robust application in real-world conditions remains a challenge. To address this, researchers have focused on leveraging different sensing modalities and deep learning techniques, particularly emphasizing the issue of fruit occlusion through semantic amodal segmentation approaches. Thus, the current study evaluates three state-of-the-art instance segmentation algorithms—cascade-RCNN, mask-RCNN, and rf-RCNN—for the amodal semantic segmentation of apples in challenging scenarios. The study encompassed 2304, 814, and 807 images from a Fuji apple orchard for training, validation, and testing. The results demonstrated a mAP@75 value of approximately 0.71, 0.71, and 0.67 for cascade-RCNN, mask-RCNN, and rf-RCNN, respectively. Furthermore, qualitative assessments revealed that the evaluated networks exhibited potential for detecting occluded apples, with cascade-RCNN and Mask-RCNN showing the best outcomes. The insights revealed in the current work motivate the development of more sophisticated architectures to enhance the performance further and facilitate the deployment of the sensing systems in real-world agricultural settings.

Keywords: amodal segmentation, instance segmentation, apple occlusion, deep learning.

1. Introduction

Currently, the apple industry in the United States is facing several challenges, including inflation and labor shortages. The last one is especially defiant since labor conditions, low wages, urbanization, and short-term contracts have made workers switch to other industries. Given that manual labor is the main means to execute tasks like pruning and harvesting, in many cases, automation has become not just an option but a necessity. Using automated machinery or robots has the potential to revolutionize agricultural practices, optimize operations, reduce labor costs, and minimize food waste.

A first step towards automation is the development of robust fruit detection systems, which can estimate the location of the fruit location within the canopy. While there is a vast amount of research work in this matter Koirala et al., 2019; Fu et al., 2020, robustness to changing illumination and occlusions has proven to be especially challenging in practical applications. For example, Tian et al., 2019 used known machine learning models to detect apples at different stages of growth. However, results showed a significant decrease in the performance of the detectors when the fruits were occluded by the canopy or by overlapping. To address occlusion, Li et al., 2022 used RGB images and a 3D point cloud to detect apples and estimate the location of their center. While the overall results outperformed the baseline, in most cases with occlusions, partial detection of the fruits resulted in a failure of the subsequent 3D reconstruction process. To solve this issue, Gené-Mola et al., 2023 presented a methodology to detect Fuji apples, "complete" the fruit shape

(including visible and occluded regions), and measure their size. The mean absolute error (MAE) recorded was 4.5mm, with heavily occluded samples significantly contributing to the overall error.

While the results for detecting occluded apples using specific deep-learning algorithms have been promising, there is still a gap in the research. To the best of our knowledge, no benchmark models provide insights into the types of architectures that are most effective for amodal detection of apples. Precisely, this work aims to evaluate the suitability of three state-of-the-art instance segmentation algorithms for this task, namely cascade-RCNN, mask-RCNN, and rf-RCNN. We employed a public dataset previously published by Gené-Mola et al., 2024, which contains images of Fuji apples with different occlusion levels and illumination conditions.

This work is organized as follows: Section 2 presents the Apple dataset for amodal segmentation and the deep learning methodologies for performing instance segmentation. Section 3 shows the assessment of instance segmentation models and discusses the overall results of this study. Section 4 describes some concluding remarks on the applicability of these architectures for the recognition of apples in challenging scenarios.

2. Materials and Methods

This work focuses on evaluating advanced instance segmentation algorithms. Specifically, three state-of-the-art algorithms—Cascade-RCNN, Mask-RCNN, and RF-RCNN—have been selected given their performance on large instance segmentation datasets (e.g., COCO dataset Lin et al., 2014). The general scheme of the methodology followed in this work is shown in Fig. 1. The process begins with training and validating these models using an amodal dataset that includes images of apple trees with corresponding annotations, accounting for occluded and non-occluded apples. The trained models are then tested on separate images to identify and segment apples in real-world scenarios. The advanced instance segmentation algorithms were implemented and trained using the deep learning framework mmDetection Chen et al., 2019.

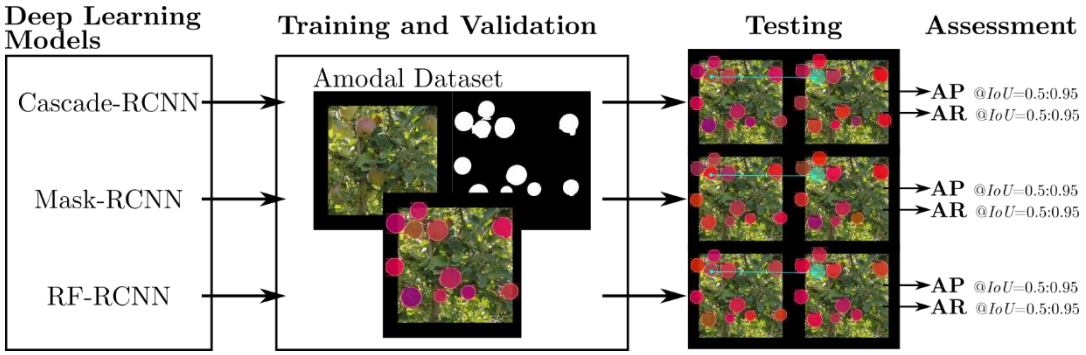

Figure 1. General scheme of the implemented methodology. The cyan arrows show no apples detected within the image. The AP and AR acronyms refer to Average Precision and Average Recall.

2.1. Dataset

The dataset used for this study was published by Gené-Mola et al., 2024. It contains 3925 and 2731 RGB-D images for the Fuji and Elstar apples, respectively. This dataset includes both modal and amodal segmentation masks; modal masks cover only visible apple portions, while amodal masks also include occluded areas. Amodal masks were explicitly created by considering the spherical shape of apples and converting this into pixel dimensions through the pinhole camera model; see details Gené-Mola et al., 2024. Annotations were made with the VIA annotator software, ensuring detailed and accurate data. The dataset is available at https://doi.org/10.34810/data916. The Fig. 2 shows samples from this subset.

In the current work, we evaluated instance segmentation algorithms with the amodal masks from the Fuji apple dataset. In particular, it has more than fifteen thousand apple samples in challenging scenarios, as shown in Fig. 2. The challenges to be faced in this dataset include but are not limited to self-occlusion, slice occlusion, and partial occlusion, among others. The Fuji apple images are grouped randomly into 2304, 814, and 807 training, validation, and testing sets.

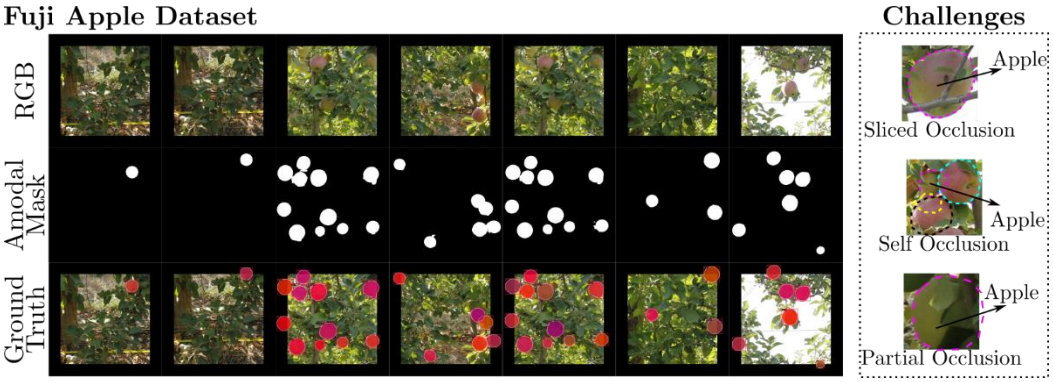

Figure 2. Fuji apple instances from the amodal segmentation dataset. The second row shows black and white amodal masks, and the third row overlays the masks on the RGB images.

2.2. Instance segmentation models

The amodal segmentation of apples was carried out using state-of-the-art instance segmentation models. The implementation is based on the project Open-MMlab, particularly mmDetection Chen et al., 2019. In particular, the models selected for this comprehensive study are Cascade-RCNN (Cai & Vasconcelos, 2018), Mask-RCNN (He et al., 2020), and RF-RCNN (Gao et al., 2022).

2.2.1. Cascade-RCNN

This architecture has been proposed for addressing low-quality detection and bad detection performance due to the common fixation of Intersection over union (IoU) threshold (Cai & Vasconcelos, 2018). To this aim, the authors build a sequence of detector layers trained with an increasing IoU threshold. Specifically, a progressive resampling approach is implemented by using the output of a detector as a training set for the next.

2.2.2. Mask-RCNN

The Mask-RCNN can be seen as an extension of Faster RCNN that includes a branch for determining object masks while, in parallel, predicting a recognition bounding box (He et al., 2020). This network is one of the state-of-the-art models that won the COCO 2016 challenge. One of its main features is adding a small overhead to the Faster RCNN, running at five frames per second; core details can be found in He et al., 2020.

2.2.3. RF-RCNN

The RF-RCNN model is based on temporal/spatial receptive fields, yet instead of deriving a hand-designed receptive field, the authors propose a global-to-local search scheme (Gao et al., 2022). The proposed scheme allows for determining an effective receptive field. Note that coarse combination can be found by the global search, while the local search helps on infering refined combination of receptive fields.

3. Results and Discussion

The experiments were carried out using a 12 GB NVIDIA GeForce RTX 4070 Ti, Intel Core i7-14700KF, and 32 GB RAM. The instance segmentation models were trained using a batch size of two, 12 epochs, and a validation interval of three. The optimizer was a Stochastic Gradient Descent with a weight decay of 0.0001, learning rate of 0.0025, and momentum of 0.9. Once the models were trained and validated, they were tested and evaluated using the mean Average Precision (mAP) metric and qualitative outcomes. The mAP values were computed by evaluation routines from the mmDetection framework using different *IoU* values.

The performance of each instance segmentation network is shown in Tables 1 and 2. Specifically, the former shows segmentation outcomes, and the latter depicts detection results. Detection results refer to the computation of mAP and mAR using solely bounding boxes rather than segmentation masks. Tables 1 and 2 show that instance segmentation models have similar performance when comparing the mAP@0.5; the maximum difference between them is about 0.041 and 0.034 for segmentation and detection experiments, respectively. Note that these values are computed considering all Apple instance sizes. However, the instance

segmentation metric values significantly decrease for IoU values ranging from 0.50 to 0.95. The behavior leads to the idea that Apple segmentation and detection might need to be more robust so that the predicted mask correctly aligns with the actual masks.

Regarding the evaluation metrics for apples that occupy different area sizes within the image, it can be noted that the worst metric values are for the small areas. This outcome could be explained because the available images from the dataset were cropped to enhance the ratio between apple size (in pixels) and image size; see Gené-Mola et al., 2024. In this sense, it is inferred that most of the apples on the image occupy small and medium areas, the latter easier to identify, according to the mapped metric.

Figure 3 shows that the models report similar performance in terms of AP. Although the three models show similar outcomes, one should be aware that images that yield an AP are equal to zero. However, these AP values take place on images with no apples. Thus, such images might be discarded in future works when performing training, validation, and testing procedures. In the current articles, those images were kept for comparing the current outcomes with the ones reported by Gené-Mola et al., 2023. Specifically, the work presented by Gené-Mola et al., 2023 shows that one can achieve an average precision between 0.44 to 0.51 in terms of amodal detection when using a custom deep learning network based on Mask-RCNN and ResNet architectures. Although the outcomes reported in the current work surpass the ones shown by Gené-Mola et al., 2023, the latter work focused on estimating apple diameters rather than improving amodal segmentation outcomes.

Qualitative outcomes are shown in Fig. 4. However, only the worst instance segmentation outcomes for the Cascade-RCNN model are depicted because of space limitations. In general, the instance segmentation networks fail to detect apples when a representative area of the apples is partially and self-occluded. In the former scenario, the deep learning models confuse the apple with the background. Conversely, in the self-occlusion case, the model tends to segment as a single apple a group of apple instances; see Fig. 4. The still non-solved drawbacks open the opportunity for developing robust algorithms to recognize apples in complex scenarios. In particular, future work is envisioned to evaluate the performance recognition models at different occlusion levels.

Table 1. Summary of instance segmentation outcomes for each deep learning model. The small, medium and large areas refer to $< 32 \times 32$, $32 \times 32 \leqslant \leqslant 96 \times 96$, and $> 96 \times 96$ image pixels areas.

	mean Average Precision					
	All			Area		
				Small	Medium	Large
IoU @	0.5:0.95	0.5	0.75	0.5:0.95	0.5:0.95	0.5:0.95
Cascade-RCNN	0.623	0.861	0.715	0.659	0.705	0.000
Mask-RCNN	0.595	0.902	0.710	0.638	0.667	0.002
RF-RCNN	0.599	0.886	0.669	0.637	0.680	0.001

Table 2. Summary of instance segmentation outcomes for each deep learning model. The small, medium and large areas refer to $< 32 \times 32$, $32 \times 32 \leqslant \leqslant 96 \times 96$, and $> 96 \times 96$ image pixels areas.

	mean Average Precision					
	All			Area		
				Small	Medium	Large
IoU @	0.5:0.95	0.5	0.75	0.5:0.95	0.5:0.95	0.5:0.95
Cascade-RCNN	0.627	0.870	0.727	0.663	0.719	0.001
Mask-RCNN	0.646	0.904	0.741	0.687	0.727	0.003
RF-RCNN	0.596	0.887	0.675	0.639	0.686	0.001

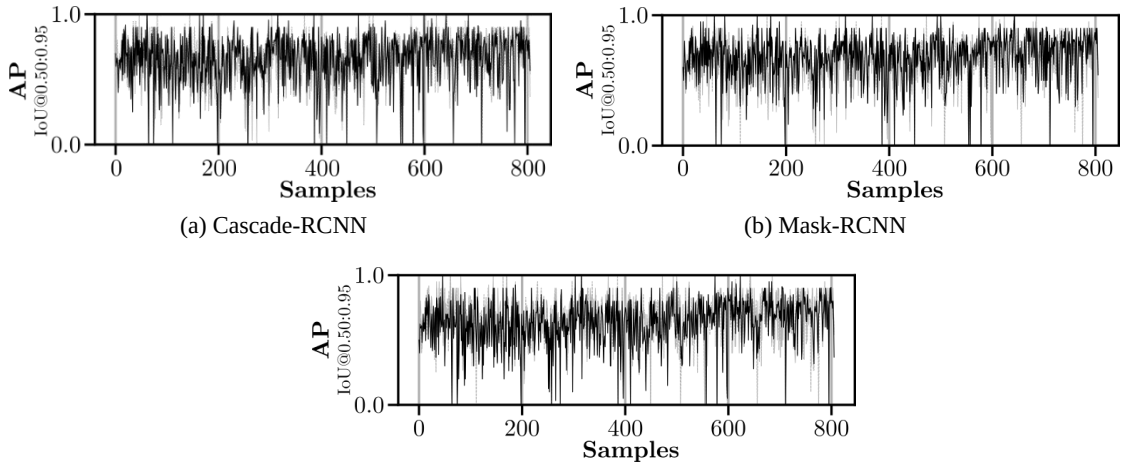

(a) Cascade-RCNN (b) Mask-RCNN

(c) RF-RCNN

Figure 3. Average precision for each instance segmentation models at IoU=0.50:0.95 per each sample. The solid black line represents the AP of the current model, the gray lines, behind black line, represent the performance of the other instance segmentation methods.

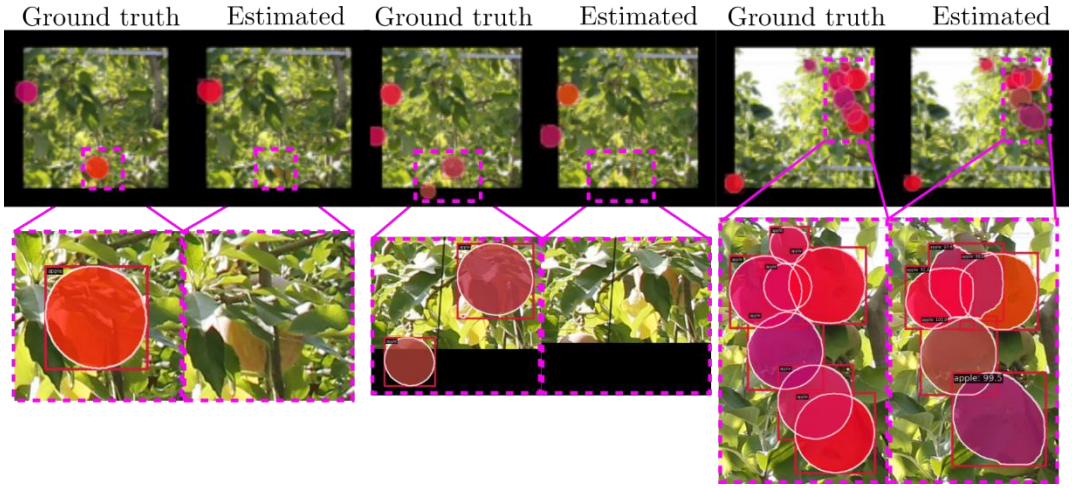

Figure 4. The worst qualitative instance segmentation outcomes for the Cascade-RCNN model. The problematic areas are zoomed in.

4. Conclusions

We presented the assessment of three state-of-the-art instance segmentation models for the amodal segmentation of apples. Cascade-RCNN and Mask-RCNN presented the best mAP@75 metric values. In this sense, both networks are suitable for recognizing apples in challenging scenarios. Moreover, the evaluated deep learning models outperform the detection metric of previous research supporting the application of instance segmentation strategies for amodal segmentation. However, challenges remain and need to be addressed in future works. Specifically, one can be aware that the evaluated models have not completely solved partial and self-occlusion issues. The performance of implemented models tends to worsen in scenarios with apples partially or self-occluded. In this sense, future works are encouraged to leverage the insights of the current works and explore the effects of different occlusion levels for improving the identification of apples in real environments.

Acknowledgements

TAR appreciates the support from the Pontificia Universidad Católica de Chile by the PIA-2023-VRA-

PUC.

References

Cai, Z., & Vasconcelos, N. (2018). Cascade R-CNN: Delving Into High Quality Object Detection. *2018 IEEE/CVF Conference on Computer Vision and Pattern Recognition*, 6154–6162. https://doi.org/10.1109/CVPR.2018.00644

Chen, K., Wang, J., Pang, J., Cao, Y., Xiong, Y., Li, X., Sun, S., Feng, W., Liu, Z., Xu, J., Zhang, Z., Cheng, D., Zhu, C., Cheng, T., Zhao, Q., Li, B., Lu, X., Zhu, R., Wu, Y., … Lin, D. (2019). *MMDetection: Open MMLab Detection Toolbox and Benchmark*. https://doi.org/10.48550/ARXIV.1906.07155

Fu, L., Gao, F., Wu, J., Li, R., Karkee, M., & Zhang, Q. (2020). Application of consumer RGB-D cameras for fruit detection and localization in field: A critical review. *Computers and Electronics in Agriculture*, *177*, 105687. https://doi.org/10.1016/j.compag.2020.105687

Gao, S., Li, Z.-Y., Han, Q., Cheng, M.-M., & Wang, L. (2022). RF-Next: Efficient Receptive Field Search for Convolutional Neural Networks. *IEEE Transactions on Pattern Analysis and Machine Intelligence*, 1–19. https://doi.org/10.1109/TPAMI.2022.3183829

Gené-Mola, J., Ferrer-Ferrer, M., Gregorio, E., Blok, P. M., Hemming, J., Morros, J.-R., Rosell-Polo, J. R., Vilaplana, V., & Ruiz-Hidalgo, J. (2023). Looking behind occlusions: A study on amodal segmentation for robust on-tree apple fruit size estimation. *Computers and Electronics in Agriculture*, *209*, 107854. https://doi.org/10.1016/j.compag.2023.107854

Gené-Mola, J., Ferrer-Ferrer, M., Hemming, J., Van Dalfsen, P., De Hoog, D., Sanz-Cortiella, R., Rosell-Polo, J. R., Morros, J.-R., Vilaplana, V., Ruiz-Hidalgo, J., & Gregorio, E. (2024). AmodalAppleSize_RGB-D dataset: RGB-D images of apple trees annotated with modal and amodal segmentation masks for fruit detection, visibility and size estimation. *Data in Brief*, *52*, 110000. https://doi.org/10.1016/j.dib.2023.110000

He, K., Gkioxari, G., Dollar, P., & Girshick, R. (2020). Mask R-CNN. *IEEE Transactions on Pattern Analysis and Machine Intelligence*, *42*(2), 386–397. https://doi.org/10.1109/TPAMI.2018.2844175

Koirala, A., Walsh, K. B., Wang, Z., & McCarthy, C. (2019). Deep learning – Method overview and review of use for fruit detection and yield estimation. *Computers and Electronics in Agriculture*, *162*, 219–234. https://doi.org/10.1016/j.compag.2019.04.017

Li, T., Feng, Q., Qiu, Q., Xie, F., & Zhao, C. (2022). Occluded Apple Fruit Detection and Localization with a Frustum-Based Point-Cloud-Processing Approach for Robotic Harvesting. *Remote Sensing*, *14*(3), 482. https://doi.org/10.3390/rs14030482

Lin, T.-Y., Maire, M., Belongie, S. J., Bourdev, L. D., Girshick, R. B., Hays, J., Perona, P., Ramanan, D., Dollár, P., & Zitnick, C. L. (2014). Microsoft COCO: Common Objects in Context. *CoRR*, *abs/1405.0312*. http://arxiv.org/abs/1405.0312

Tian, Y., Yang, G., Wang, Z., Wang, H., Li, E., & Liang, Z. (2019). Apple detection during different growth stages in orchards using the improved YOLO-V3 model. *Computers and Electronics in Agriculture*, *157*, 417–426. https://doi.org/10.1016/j.compag.2019.01.012

Creation of an ISO11783-compliant prescription map for variable rate spraying in vineyards based on canopy 3D reconstruction

Björn Poss [a,*], Nikos Tsoulias [a], Galibjon M. Sharipov [a,b], Andreas Heiß [a], Dimitrios S. Paraforos [a]

[a] Department of Agricultural Engineering, Hochschule Geisenheim University, Geisenheim, Germany

[b] Department of Agricultural Engineering, University of Hohenheim, Stuttgart, Germany

* Corresponding author. Email: bjoern.poss@hs-gm.de

Abstract

The adoption of ISO11783-compliant (commonly designated as ISOBUS) sprayers in viticulture lags behind their use in arable farming. Recent advancements in tractor technology, notably the integration of ISOBUS connectivity in narrow-tracked tractors, present an opportunity to enhance vineyard management, particularly in the area of crop protection. This technological development opens the door to more efficient and precise agricultural practices. Precision application of pesticides, driven by economic and environmental considerations, is becoming increasingly important. By optimizing pesticide usage, growers can significantly reduce costs and minimize environmental impact, ensuring a more sustainable approach to viticulture.

This paper proposes a methodology to develop ISOBUS-compliant prescription maps for variable rate application (VRA) tailored to the specific needs of grapevine rows. Implementing this approach involves creating detailed prescription maps that reflect the heterogeneity of vineyard canopies, ensuring that each vine receives the appropriate amount of treatment based on the leaf area. To achieve this, 3D point cloud data were collected in the vineyard with a light detection and range (LiDAR) sensor and correlated with manual leaf area measurements. The resulting leaf areas from the vine rows were then used for the prescibed dose rates for individual sections in the prescription map.

The results show a high correlation with $R^2 = 0.92$ between the manual measured leaf areas and the number of points from the generated point cloud. This served as the basis for calculating a dose rate and creating a grid-based prescription map in ISO-XML format, which can be used with ISOBUS-compliant VRA sprayers. The map created allows the dose rate to be varied for one meter of leaf wall and for the left and right sides of the sprayer simultaneously.

Keywords: Vineyard, LiDAR, Precision Viticulture, ISOBUS, VRA

1. Introduction

Recent years have seen significant benefits in precision agriculture, particularly in arable farming, with the rise of ISO11783-compliant technologies facilitating standardized communication between tractor and implement. This standardization ensures compatibility and improves operational efficiency by allowing seamless control of multiple devices from a single terminal. Additionally, ISOBUS enhances data management and Precision Farming by facilitating the transfer of operational data and enabling precise control over application rates and equipment operation.

While the utilization of this technology in agriculture has steadily expanded in recent years, ISOBUS-compliant implements remain relatively uncommon in viticulture (Sharipov et al., 2023). Only in the last few years tractor manufacturers started to offer ISOBUS connectivity for narrow-tracked tractors. This opens up new opportunities for the integration of vineyard management equipment, particularly for plant protection. Developing prescription maps for variable rate application (VRA) and utilizing ISOBUS-enabled sprayers can significantly enhance precision in pesticide usage, offering economic benefits and promoting environmental protection by adapting application rates to the heterogeneity of the vines, thus allowing for on-demand crop protection delivery.

In the field of detecting canopy parameters in vineyards, several publications have been published over the last few decades. There is already a wide range of sensors available for detection, such as mobile laser scanners (Sanz et al., 2013), camera systems (López-Granados et al., 2020), multispectral (Campos et al., 2021) or ultrasonic sensors (Llorens et al., 2011). LiDAR systems, which benefit from high resolution and point density when analysing leaf walls, are particularly promising (Escolà et al., 2023). The data obtained was correlated with leaf area, volume or density and used to determine canopy characteristics. The resulting data can then be processed into dose rates for prescription maps and used for VRA sprayers (Gil et al., 2014).

The development and use of prescription maps in ISO-XML format in arable farming is already widespread (Sharipov et al., 2020). In the meantime, polygon-based maps were also used in spatial cultivation, including in viticulture (Campos et al., 2020, Garcia-Ruiz et al., 2023). However, these maps are often based on manufacturer's proprietary formats, not standards like ISOBUS. Additionally, due to the high heterogeneity in vineyards, high-resolution prescription maps are required in comparison to arable farming. To achieve that, this work aims to develop a methodology to create an ISOBUS compliant prescription map for vineyards based on the leaf area derived from a 3D point cloud of grapevine rows by means of light detection and range (LiDAR) systems.

2. Materials and Methods

2.1. Leaf area estimation

During the growing season from 39 to 109 days after bud break (DABB) in 2023, a phenotyping platform with a LiDAR (Puck Lite VLP-16, Velodyne, San José, CA, USA), an inertial measurement unit (IMU, VN-100, VectorNav, Dallas, TX, USA) and an RTK-GNSS (R10, Trimble, Sunnyvale CA, USA) was mounted on a tractor to acquire georeferenced 3D point clouds of vines (Figure 1). The trials took place in a vineyard at Geisenheim University (49.9945 N, 7.9747 E, Geisenheim, Hesse, Germany) planted to Vitis vinifera L. ´Riesling´ grafted to ´Börner´ rootstock. The tractor was driven at 0.5 km h^{-1} along the rows, while the LiDAR mounted parallel to the vines. The 360° field of view of the LiDAR allowed to simultaneously acquire both sides of the vine in one row. The data acquisition of the individual sensors was done with a C# software. Sensor data fusion and point cloud reconstruction were then carried out in Matlab software (R2023a, MathWorks, Natick, MA, USA) (Figure 2).

The points were extracted from soil, steel stakes, metal wires, trunks and branches using various segmentation methods. The first step was to filter only the points from 0.3 to 2 m in height and up to 1 m in depth to eliminate the soil and points that belong to other rows. The second part was the calibration of the reflectance. Board targets, coated with white barium sulphate (BaSO4, ODP97, Tuerkenfeld, Germany) for maximum and blackened topcoat (90FH, NEXTEL Suede Coating 3101, Mankiewicz Gebr. & Co., Hamburg, Germany) for minimum referencing were applied to calibrate the backscattered intensity of the LiDAR, obtaining the reflectance at 903 nm for each point in the 3D point cloud. This was used to calibrate the backscattered reflectance, in the range between 0 and 100 %. To eliminate the steel stakes and metal wires, only the points above the threshold of 15 % of the calibrated reflectance were used for further processing. The last filtering step was the calculation of point cloud density at a radius of 0.2 m using the Matlab function "findNeighborsInRadius" and the segmentation of the sections with a number of points higher than 1500.

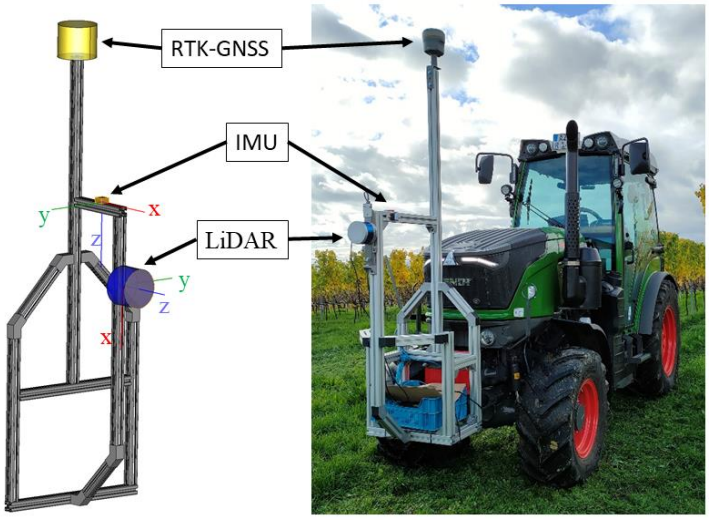

Figure 1. Sensor frame for the data acquisition in vineyards

In addition to the LiDAR recordings, manual measurements were carried out by means of defoliation of two vines over the growing stages (n = 19). A leaf area scanner (LI-3100C, LI-COR, Bad Homburg, Germany) was used to estimate the entire leaf area per 2 vines. The total number of points (NoP) on both vines was determined from the LiDAR data after the filtering process described above. Thus, a linear regression model was built to express the relationship between manually obtained leaf area data and remaining NoP, separately for each growth stage. The resulting regression equation can then be used to calculate the leaf areas and the associated dose rates for creating the prescription map.

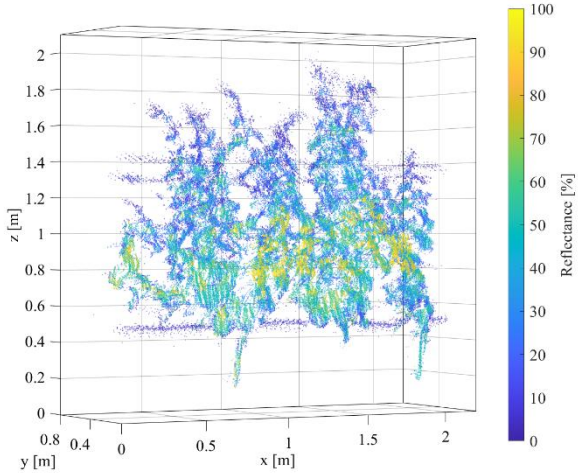

Figure 2. Generated point cloud of two vines with the calibrated reflection

2.2. Prescription map

The creation of a prescription map with a dose rate adapted to the leaf area was divided into two parts. In the first part, a grid-based map was created as a shape file using the QGIS software (3.36.0, QGIS.ORG, Grüt, Gossau, Switzerland). In the second step, the shape file was imported into the SMS farming software (Spatial Management System Basic 24.00, Ag Leader Technology, Ames, Iowa, USA) and exported to an ISO-XML file by considering the necessary parameter selections according to the ISO11783 standard.

Creating a map as a shapefile involved several steps. Initially, a shape layer was generated as a line along the rows of vines, which was then divided into parallel lines with the specific row width. Subsequently, points were generated along these lines at a defined interval of 1 m, and rectangles with a length of 1 x 2 m were created from the centre of these points. The size of the rectangles was based on the row width of 2 m and, in relation to the length of 1 m, on an estimate of the delay between the set and the actual dose rate at a tractor speed of 6 km/h. These rectangles were then rotated to adjust their orientation to the vines and their corner points have been extracted. The result was exported as a csv file and utilized in Matlab for dose rate calculation. For each rectangle, the corresponding georeferenced leaf-filtered point cloud was extracted by using the Matlab function “inpolygon” with the coordinates of the corner points. Subsequently the leaf area was calculated based on the number of points using the established correlation from manual leaf area measurements.

A dose rate per rectangle was calculated from the leaf area per rectangle and a ratio of the average leaf area per row and the application rate recommended by the regional authorities according to growth stage. Thus, the rate along the rows varies by the dose rate used in practice with traditional spraying methods. Finally, the table with rectangles and dose rates were imported into QGIS again and saved as a Shapefile in WGS84 coordinate system.

The final shapefile was then loaded into the SMS software and a spraying prescription map was created. A field boundary was also defined and individual parameters such as farm, field and year were specified. The developed map was then converted to the ISO-XML task file that is readable and recommended format for the ISOBUS-compliant virtual terminals (VT).

3. Results and Discussion

3.1. Leaf area estimation

The field measurements with the sensor frame provided georeferenced point clouds throughout the growth period. The applied filtering steps resulted in an almost pure leaf-based point cloud without steel or woody parts, albeit with longer computation times (Figure 3Figure 2). It should be mentioned that there are already a large number of other filtering algorithms that could possibly improve the extraction and make the extracted point cloud more precise (Garrido et al., 2015). The extracted number of points were then used for calculations of the prescribed dose rates.

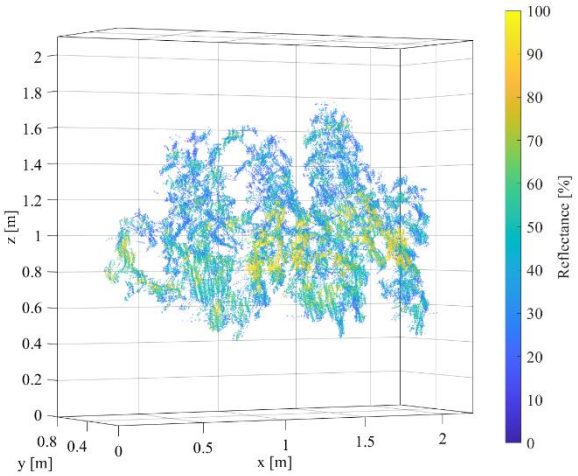

Figure 3. Leaf extracted point cloud of two vines with the calibrated reflection

The correlation between leaf area (*LA*) and the number of points (*NoP*) from filtered point cloud is shown in Figure 4 with a scatter plot and the corresponding regression line. The high coefficient of determination (R^2) of 0.92 indicates a strong linear relationship between the measured leaf areas and the number of points in the point cloud. This suggests that the method for estimating leaf area using point clouds is promising. However, it should be noted that the number of measurements (n=19) is limited. Therefore, further measurements are needed for more reliable conclusions. The resulting regression equation was used to calculate the prescribed dose rate per rectangle and is given by:

$$LA = 5 \times 10^{-5} \times NoP - 0.5353 \quad (1)$$

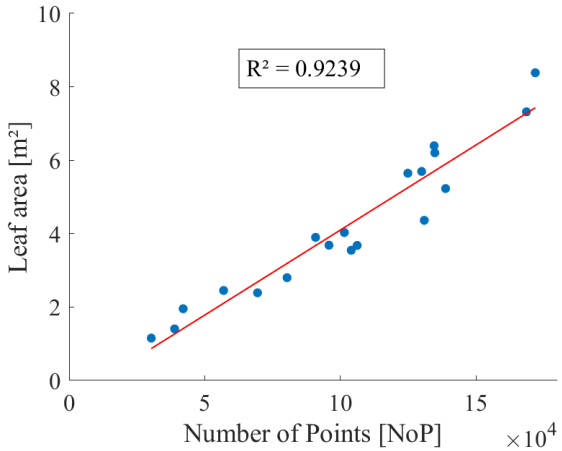

Figure 4. Linear regression between the number of points and the measured leaf area (n = 19).

3.2. Prescription map

The generated map in shape format illustrates the spatial distribution of rectangles along the vine rows (Figure 5). A single rectangle with a width of one metre extends centrally over a vine and ends in the middle of the row. This ensures that an individual dosing rate is specified for both the right and left side when travelling with the sprayer. The calculation of dose rate was based on a ratio of the average leaf area per row and the prescribed dose rate according to growth stage and professional practice. This representation allows for a more precise adjustment of dosage based on leaf area variation along the vine rows.

After exporting the prescription map in ISO-XML format, the task file can be transferred to any ISOSBUS-capable terminal. The prerequisite for applicability is the AEF ISOBUS functionalities “Task Controller Geo” and “Section Control” with the addition of subsections to differentiate between the right and left sides. Secondly, the sprayer must be able to process the dosing rates received individually for both sides.

Figure 5. Prescription map with 1 x 2 m grids and leaf area adapted dose rates

4. Conclusions

The data obtained from the vineyard using the phenotyping platform provided a leaf segmented point cloud by applying several filtering steps. The manual leaf area measurements showed a 0.92 coefficient of determination with the number of points from the plants. Based on these results, the dose rates to be applied were determined and a VRA ISO-XML prescription map was created successfully. This allows a dosage recommendation for both sides of the sprayer adapted to the characteristics of the vines with a resolution of one meter in relation to the length of the leaf wall along the row.

Future work includes the validation of the actual dose rates compared to the prescribed ones by using a prototype ISOBUS sprayer for vineyards, on the test facilities of Geisenheim University that are utilized for commercial spraying machine certification. Another point to investigate is the delay between the set and the actual dose rate at the nozzles including the possibility of smaller grids and higher resolution, respectively. Further development of the prescription map to address vertical heterogeneity and individual nozzle control is also planned for future research. In addition, the degree of automation of the entire workflow could be improved and the possibility of direct export to ISO-XML, without additional software such as SMS, could be investigated in more detail.

Acknowledgements

The work is supported by funds from the Federal Ministry of Food and Agriculture (BMEL) based on a decision of the Parliament of the Federal Republic of Germany. The Federal Office for Agriculture and Food (BLE) provides coordinating support for digitalisation in agriculture as funding organisation, grant number 28DE105A22.

References

Campos, J., Gallart, M., Llop, J., Ortega, P., Salcedo, R., Gil, E., 2020. On-Farm Evaluation of Prescription Map-Based Variable Rate Application of Pesticides in Vineyards. Agronomy, 10(1), 102. https://doi.org/10.3390/agronomy10010102

Campos, J., García-Ruíz, F., Gil, E., 2021. Assessment of vineyard canopy characteristics from vigour maps obtained using uav and satellite imagery. Sensors, 21(7). https://doi.org/10.3390/s21072363

Escolà, A., Peña, J. M., López-Granados, F., Rosell-Polo, J. R., de Castro, A. I., Gregorio, E., Jiménez-Brenes, F. M., Sanz, R., Sebé, F., Llorens, J., Torres-Sánchez, J., 2023. Mobile terrestrial laser scanner vs. UAV photogrammetry to estimate woody crop canopy parameters – Part 1: Methodology and comparison in vineyards. Computers and Electronics in Agriculture, 212. https://doi.org/10.1016/j.compag.2023.108109

Garcia-Ruiz, F., Campos, J., Llop-Casamada, J., Gil, E., 2023. Assessment of map based variable rate strategies for copper reduction in hedge vineyards. Computers and Electronics in Agriculture, 207. https://doi.org/10.1016/j.compag.2023.107753

Garrido, M., Paraforos, D. S., Reiser, D., Arellano, M. V., Griepentrog, H. W., & Valero, C., 2015. 3D maize plant reconstruction based on georeferenced overlapping lidar point clouds. Remote Sensing, 7(12), 17077–17096. https://doi.org/10.3390/rs71215870

Gil, E., Arnó, J., Llorens, J., Sanz, R., Llop, J., Rosell-Polo, J. R., Gallart, M., Escolà, A., 2014. Advanced technologies for the improvement of spray application techniques in Spanish viticulture: An overview. In *Sensors.* Switzerland, Vol. 14, Issue 1, pp. 691–708. https://doi.org/10.3390/s140100691

Llorens, J., Gil, E., Llop, J., Escolà, A., 2011. Ultrasonic and LIDAR sensors for electronic canopy characterization in vineyards: Advances to improve pesticide application methods. Sensors, 11(2), 2177–2194. https://doi.org/10.3390/s110202177

López-Granados, F., Torres-Sánchez, J., Jiménez-Brenes, F. M., Oneka, O., Marín, D., Loidi, M., Castro, A. I. de, Santesteban, L. G., 2020. Monitoring vineyard canopy management operations using UAV-acquired photogrammetric point clouds. Remote Sensing, 12(14). https://doi.org/10.3390/rs12142331

Sanz, R., Rosell, J. R., Llorens, J., Gil, E., Planas, S., 2013. Relationship between tree row LIDAR-volume and leaf area density for fruit orchards and vineyards obtained with a LIDAR 3D Dynamic Measurement System. Agricultural and Forest Meteorology, 171–172, 153–162. https://doi.org/10.1016/j.agrformet.2012.11.013

Sharipov, G. M., Heib, A., Griepentrog, H. W., Paraforos, D. S., 2020. Evaluation of centrifugal spreader response to variable rate application by using task file data. IFAC-PapersOnLine, 53(2), 15804–15809. https://doi.org/10.1016/j.ifacol.2020.12.213

Sharipov, G. M., Heiß, A., Bresilla, T., Nieuwenhuizen, A. T., Hemming, J., van Evert, F. K., Baron, S., Benrais, A., Avgoustakis, I., Mylonas, N., Fountas, S., Vasilaros, P., Karagiannis, P., Vidal, J., Paraforos, D. S., 2023. Smart implements by leveraging ISOBUS: Development and evaluation of field applications. Smart Agricultural Technology, 6. https://doi.org/10.1016/j.atech.2023.100341

Orchard digital twin: A prototype for smart agricultural monitoring

Kyra Smith[a*], Andrea Botta[b], Giovanni Colucci[b], Marco Piras[a], Giuseppe Quaglia[b], Elena Belcore[a]

[a] Department of Environment, Land and Infrastructure Engineering, Politecnico di Torino, 10129 Torino, Italy

[b] Department of Mechanical and Aerospace Engineering, Politecnico di Torino, 10129 Torino, Italy

* Corresponding author. Emails: name.surname@polito.it

Abstract

This study presents a method for creating detailed digital twins (DT) of apple orchards using an unmanned ground vehicle (UGV) and a combination of sensors, including a handheld laser scanner (HLS), a low-cost depth camera, and a Global Navigation Satellite Systems (GNSS) receiver. We aim to provide an updatable 3D geospatial database to automate agricultural processes, such as apple monitoring and collection. The workflow was tested in a portion of an apple orchard in northwest Italy and is comprised of four phases. Phase 1 involves sensor-integration on the vehicle and data acquisition. Phase 2 defines and stores the orchard's geometries in a georeferenced 3D model; this phase also includes the segmentation of individual trees within each row. Phase 3 detects and segments apples using an artificial intelligence (AI) algorithm applied to RGB images captured by the depth camera; segmented apples are then projected onto the 3D model. Our work demonstrates how unmanned ground vehicles (UGVs) integrated with sensors can be applied to create a detailed, updatable orchard DT, a tool which can inform and automate agricultural tasks, ultimately increasing efficiency and reducing waste.

Keywords: smart farming, agricultural digital twin, mobile robotics, artificial intelligence, crop monitoring

1. Introduction

The optimisation of agricultural systems is vital as they face growing demands and pressures. One widespread approach to achieving this is precision agriculture (PA). PA uses spatiotemporal data from agricultural systems to guide management decisions and improve productivity, sustainability, and resource-use efficiency (ISPA, 2024). In the 1990s, PA was hailed as “an information technology revolution”. Today, agriculture is experiencing another revolution, called “Agriculture 4.0”, which includes the rise of smart farming (Javaid et al., 2022). Smart farming goes a step further than PA, utilising information and communications technologies (ICT), such as artificial intelligence (AI) and Internet of Things (IoT), to automate and optimise not only agricultural operations but overall farm management, leading to even greater efficiency and productivity (Kamilaris et al., 2016; Moysiadis et al., 2021).

The employment of unmanned ground vehicles (UGVs) in agriculture is on the rise thanks to its synergy with the smart farming paradigm, which depends heavily on extensive and repetitive data collection to perform informed, precise agricultural tasks. In this context, a UGV can assist farmers by effortlessly performing repetitive tasks without losing accuracy throughout the day.

Besides a limited number of robotic UGVs developed to autonomously perform agricultural tasks such as weeding, pruning, spraying, and harvesting (Visentin et al., 2023), most agricultural UGVs are entirely dedicated to sensing and monitoring of the crop or the soil. In this sense, UGVs navigate through the field as mobile sensor carriers to collect data such as soil structure and composition, water content, plant and fruits condition, presence of pests or diseases, crop yield, and more (Vulpi et al., 2022). Different combinations of sensors can be mounted on the UGV at different times to collect all relevant data, making modular robotic platforms very flexible and effective (Tiozzo Fasiolo et al., 2023). This ability to carry multiple sensors or robotic components gives UGVs an advantage over unmanned aerial vehicles (UAVs), which are more mobile but limited by the weight of their payload (Tardaguila et al., 2021; Apeinans et al., 2023).

The synergy between smart farming and robotics enables the collection of vast amounts of crop data, which must be organised, processed, and stored. When the collected information describes the system exhaustively, it can be organised and stored in a Digital Twin (DT).

A DT is comprised of three parts: (1) the physical component, (2) the virtual component, and (3) the flow of information that connects them (Grieves, 2015). The European Commission’s Destination Earth program (Destination Earth, 2024) aims to expand the use of DTs to describe the processes of our planet and the related human activities, including agricultural systems. Agricultural DTs are accurate digital

replicas of real agricultural systems, continuously updated by smart farming techniques and sensors. They have been proposed to simulate machinery performance (Tsolakis et al., 2019), provide a decision support system for aquaponics (Ghandar et al., 2021), and to improve water efficiency by automating irrigation systems (Alves et al., 2023), among other applications.

Nonetheless, adoption of DTs in agriculture has been found to be lagging behind other sectors, with most agricultural DTs still in the prototype stage (Pylianidis et al., 2021). Furthermore, most of the agricultural DTs reviewed were of non-living systems (such as machinery or structures) rather than living systems, likely due to their complexity (Pylianidis et al., 2021). For the few DTs of living systems, the reported benefits included early detection of disease and other threats, lower costs, and higher product quality (Pylianidis et al., 2021).

Orchards are an ideal agricultural setting for testing methods of generating DTs of living systems, as the objects of interest (principally trees) are sessile, can be differentiated from one another, and are often organised in recognisable patterns. These qualities allow for repeatable data collection and data storage at the tree-level. Potential applications of orchard DTs include yield estimation, monitoring fruit development, detecting pests or diseases, autonomous harvesting, and more. To date, there are few examples of orchard DTs and, to the knowledge of these authors, none that propose an exhaustive workflow combining UGV technology and sensors to build a georeferenced DT of an apple orchard.

This work seeks to develop a workflow for the creation of a high-quality DT of an apple orchard. This requires the achievement of several sub-objectives, which are: (1) to test the performance of the UGV 'Agri.Q' in an orchard environment and the arrangement of sensors on Agri.Q; (2) to create a 3D model of the orchard and segment individual trees in order to increase our resolution from a row- to tree-level; (3) to train a deep learning model to segment apples.

2. Materials and Methods

This work was carried out in three phases that correspond to our sub-objectives.

Phase 1: Data acquisition

Data acquisition was carried out on October 10, 2023, in an apple orchard belonging to the Research Centre for Fruit Cultivation (Centro Ricerche per la Frutticoltura) of Fondazione Agrion, located in Manta, Piedmont, Italy (Fig.1(a)). The study area was comprised of flat, grassy terrain with three parallel rows of mature apple trees, each row about 90m long and 4m apart (Fig.1(b)). At the time of acquisition, the trees were fruit-bearing. Several apple varieties were represented. 16 black and white geometric markers were placed at varying heights throughout the rows to be used as references during point cloud construction.

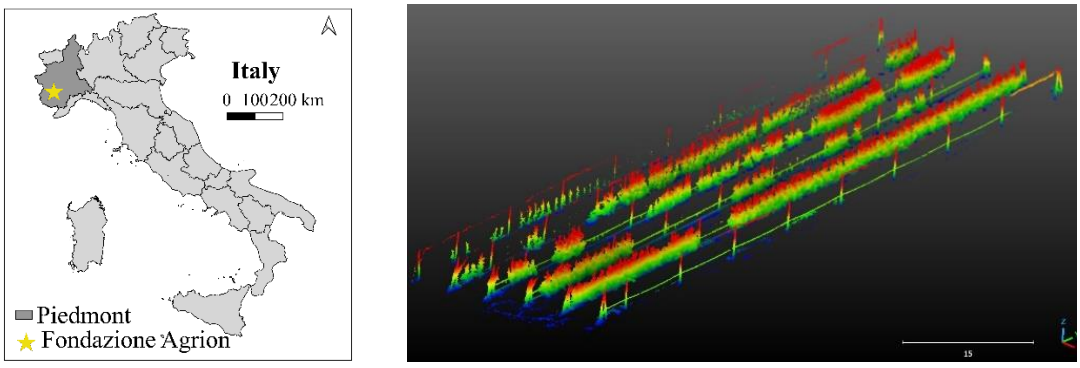

(a) (b)

Figure 1. (a) The location of Fondazione Agrion in Piedmont, Italy and (b) orchard HLS point cloud.

Agri.Q represents an innovative UGV specifically engineered for PA applications within vineyards and orchards. This UGV demonstrates adaptability to unstructured environments and uneven terrain thanks to its unique architecture. As depicted in Fig. 2, the UGV consists of two skid-steering modules, each equipped with two locomotion units that drive two tires each via a chain drive system. This architectural design ensures efficiency comparable to traditional wheeled systems while effectively

distributing pressure on the ground, akin to tracked vehicles. Consequently, this design feature, coupled with the UGV's relatively modest weight of approximately 110kg, reduces the tires sinkage and mitigates soil degradation in comparison to conventional agricultural machinery.

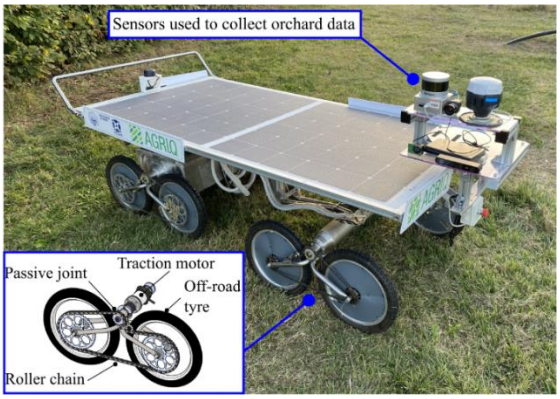

Figure 2. The Agri.Q UGV has four skid-steer modules, each characterised by a single drive motor that transmits power to two off-road wheels via a chain transmission. The passive joint allows Agri.Q to adapt to uneven and complex terrain.

Agri.Q can be equipped with an array of instruments and sensors tailored to specific tasks such as field mapping and crop monitoring. Notably, it can feature a redundant 7 degrees of freedom (DOF) collaborative robot arm, facilitating interactions with the environment, including soil, leaf, and fruit sample collection (Quaglia et al., 2024). Moreover, it incorporates a 2 DOF photovoltaic (PV) panel capable of self-orientation to optimise solar energy collection for battery recharge, but, also, to provide an always level landing platform for drones to seamlessly collaborate with UAVs when required (Visconte et al., 2021; Botta and Cavallone, 2022). Additionally, the robotic arm and the sensor unit are mounted on the frame of the orientable platform, enabling dynamic adaptation of the robot's manipulation workspace (or the sensors' field of view) to various tasks and scenarios (Colucci et al., 2023), as showed in Fig. 3. Regarding the specific application in apple orchards, Agri.Q has been equipped with a sensor support plate positioned on the rear module of the UGV so that its pitch adjustment mechanism can raise the sensors from a height of 700 mm to 1600 mm. It's worth noting that a hinge joint has been incorporated to keep the plate parallel to the ground, even when the Agri.Q panel is tilted.

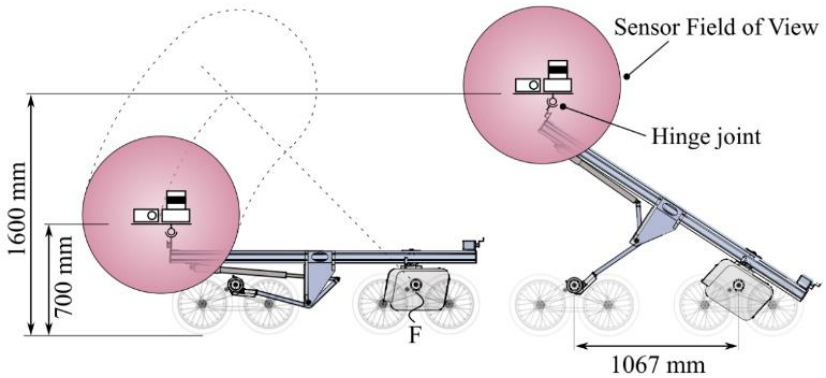

Figure 3. The sensors carried on the rear plate can be raised by means of the pitch mechanism adjustment, which imposes to the Agri.Q panel a rigid rotation around point F. The hinge joint between the plate and the panel allows to keep the plate parallel to the ground.

Three optical sensors were used, in addition to a dual frequency GNSS receiver used to georeference the DT (Table 1). The Kaarta Stencil 2 is a HLS that uses Velodyne LiDAR and advanced simultaneous localisation and mapping (SLAM) algorithms that integrate visual odometry (Velodyne Lidar, 2023). The Stencil 2 was integrated with an Emlid Reach 2 GNSS receiver in Network Real Time Kinematic (NRTK) acquisition to georeference the trajectory estimated by Stencil 2. The ZED 2 is a stereo camera produced by StereoLabs. It collected images with a resolution of 1920 x 1080 at a rate of 30 frames per second (fps). The Mapir 3N collects images in the red (R), green (G) and near-infrared (NIR) bands with 1 Hz frequency and it has a field of view of 41°.

Sensor Name	Sensor Type	Data Collected	Information	CRS
Kaarta Stencil 2	Handheld Laser Scanner (HLS)	Point cloud of orchard Point cloud of HLS trajectory	X, Y, Z Intensity values Time Confidence value (trajectory only)	Local
Emlid Reach 2	GNSS Receiver	HLS position	East, North, elevation above the Ellipsoid Root Mean Squared Errors	Global, EPSG: 32632
ZED 2	Stereo Camera	RGB images Depth images Colourised point cloud of orchard	Left RGB (stereo pairs) Right RGB (stereo pairs) Depth images	Local
Mapir 3N	Multispectral Camera	Multispectral images (R, G, NIR)	3-bands images: Near Infrared 850nm, Red 660nm, and Green 550nm	Local

Table 1. Sensors used to collect orchard data. CRS= Coordinate Reference System

All sensors were affixed to Agri.Q's sensor support plate using screws. The HLS, stereo camera, and multispectral camera were oriented such that the image plane was parallel to the row of trees (Fig. 4). Horizontal and vertical offsets between the centres of the sensors were recorded. The GNSS receiver was connected to the HLS via USB. All sensors were activated before the UGV began to move and they collected data continuously throughout the acquisition. During the test, the UGV was commanded to navigate between three rows at a constant speed ($0.2 m \cdot s^{-1}$).

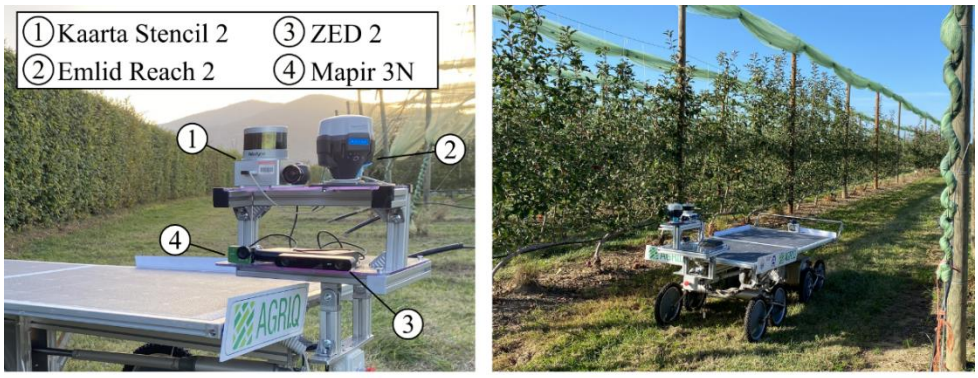

(a) (b)

Figure 4. (a) The arrangement of the sensors on Agri.Q platform. (b) Agri.Q while navigating the apple orchard.

Phase 2: Data processing and information extraction

The HLS was initially optimized using the Adaptive Data Replay tool provided by Stencil 2, which allows for the re-processing of the point cloud by adjusting parameters that control feature matching (Di Pietra et al., 2020) and the Loop Closure algorithm. The communication between the SLAM and GNSS systems enabled the time synchronization of the data acquisition, allowing for the association of SLAM and GNSS trajectories; the offsets between their centres of phase were considered when roto-translating the SLAM cloud in the global projected reference system (EPSG: 32632). The point cloud was then filtered and clipped to the area of interest.

The HLS point cloud was used to generate the 3D geometric model for data visualization and storage. We decided to use the single tree as the reference unit for our DT and associate measurements to each one. A local maxima individual tree detection (ITD) technique was used to identify individual trees. This approach was chosen because height and treetop-based models have proven effective so far, given the structure of the orchard, where all the plants have a distinct treetop and small heights that fall into Kaarta HLS range capabilities. Using the Cloth Simulation Filter (CSF) algorithm implemented in Cloud Compare software, the Digital Terrain Model (DTM) was extracted (Zhang et al., 2016), which was then

used to calculate the normalized DTM (nDTM), as the difference between the Digital Surface Model (DSM) and the DTM. To reduce the computation time of the algorithm, the CHM was scaled to 25cm/pixel. The stems were detected using "local minima and maxima" algorithm in SAGA; outliers were removed successively according to maxima distribution. Finally, Voronoi polygons were computed upon the treetops to define the canopy geometry and then projected on the point cloud. The goodness of the ITD method was assessed by comparing the treetop detection with the ones manually identified and computing precision, recall, F1-score and accuracy metrics (Belcore et al., 2021).

The data gathered by the ZED 2 stereo camera was stored in StereoLabs' proprietary .svo format. Point clouds were extracted in .ply format using the ZEDFu software. 35,122 image pairs were captured by the stereo camera and used to automatically generate depth maps. 32,196 RGB image and depth map pairs were exported .png format with a resolution of 1920 x 1080. Only RGB images taken by the left camera were exported.

To examine the quality of the stereo camera point clouds and to test their correspondence with the HLS data, point cloud registration was performed on a test section of the orchard. This section was located at the end of the second row, contained 12 trees, and had a length of 33m and an area of 341m^2. This test section was selected based on the presence of red, highly visible apples on the trees. This allowed for easier visual assessment of apple representation in the stereo camera point cloud, using the corresponding RGB images as a reference.

Point cloud registration was carried out using Cloud Compare software. The HLS point cloud was used as the reference cloud. The HLS point cloud was clipped to the area of interest, and the stereo camera cloud was registered first manually, then using the ICP algorithm (Theoretical overlap = 70%) before being merged. The root of the mean square (RMS) error was calculated to assess the quality of the ICP registration.

Phase 3: Apple detection and segmentation

An Ultralytics YOLOv8 (Jocher et al., 2023) segmentation model was trained to detect and segment apples. A training dataset was prepared using the RGB images previously exported from the stereo camera. Images were subsampled and filtered to include only images of apple-bearing trees with minimal overlap, resulting in 65 images. To supplement the dataset, 670 images from the MinneApple dataset (Häni et al., 2020) were added. All images were sliced into smaller images of the optimal YOLOv8 input size (640 x 640), labelled, then split into training (1963), validation (379), and testing (405) datasets.

Training was conducted using a medium pre-weighted segmentation model (YOLOv8m-seg.pt) with default parameters (epochs = 100, batch size = 16, image size = 640, data augmentation = enabled) and validation was automatically conducted. At the conclusion of training, the best model was saved.

3. Results

Phase 1: Data acquisition

Agri.Q travelled a total of 580m in 30 minutes. All sensors remained securely fixed to the platform and gathered data for the duration of the journey.

Phase 2: Data processing and information extraction

The raw HLS point cloud consisted of 30,000,000 points and covered an area of approximately 6,000 m^2. The final cloud had 20,749,929 points and the RTK acquisition had an error of 4 centimetres.

The local maxima algorithm detected 243 treetops. Through the analysis if the heights distribution, the outlier threshold was selected (inflection point). 40 points were identified filtered out as outliers.

The goodness of the detection was then validated through comparison with the Voronoi polygons built on the treetop identified through visual interpretation. This resulted in 113 matched elements (the treetop falls within the reference polygon, true positive), 24 missed (no treetop within the reference polygon, false negative), 31 oversampled (more than one treetop within the reference polygon, false positive), and 35 (treetop outside the reference polygons, false positive).

The calculated precision, recall, F1 score, and accuracy metrics are listed in Table 3.

Metric	Precision	Recall	F1	Accuracy
Value	0.63	0.85	0.72	0.69

Table 3. Treetop detection accuracy metrics.

The stereo camera point cloud representing the registration test section consisted of 1,971,919 points while the HLS cloud clipped on the test rows consisted of 2,011,972 points. The RMS error of the ICP

alignment was 0.064 m.

Phase 3: Apple detection and segmentation

The trained segmentation model was able to detect and segment apples in our images with high accuracy (F_1 = 0.89), detecting nearly all the apples (recall = 0.91) with a high degree of precision (0.87) (Fig. 5).

(a) (b)

Figure 5. (a) The original image and (b) the same image with YOLOv8-generated segmentation masks (red)

4. Discussion

Agri.Q proved to be a suitable UGV for orchard use. It easily navigated the terrain and the sensor-mounting platform allowed for the simple, secure installation of four sensors and auxiliary tools, including a battery and a laptop. While Agri.Q is currently controlled remotely by an onsite operator, automation would increase its utility, allowing farmers to concentrate on other tasks while Agri.Q performs data collection missions independently.

The HLS and GNSS receiver performed as expected and provided a high-quality, georeferenced point cloud. The ZED 2 stereo camera did not perform as well as expected, generating sparse, low-quality point clouds. Other studies using ZED and ZED 2 stereo cameras in orchards have encountered similar problems (Wang et al., 2017; Chen et al., 2021; Neupane et al., 2021). Still, stereo cameras have the advantage of (a) being significantly less expensive than LiDAR sensors and (b) integrating RGB data directly with depth data. Further testing of the ZED 2 under different lighting conditions and orientations, as well as comparisons with other available RGB-D sensors, is advisable. While images from the Mapir 3N were ultimately not included in our workflow, they could eventually be integrated to add information about photosynthetic activity and plant health.

The ITD method tends to overestimate the number of trees. This can be attributed to the tendency of lateral branches to grow upwards. The result is acceptable and consistent with the performance of automated treetop extraction algorithms from LiDAR (Ozdarici-ok and Ok, 2023). The advantage lies in the speed of the method, with the total processing time being 26 seconds to extract the maxima and 1 second to generate the Voronoi polygons, significantly faster than point cloud segmentation methods.

Upon visual inspection of the stereo camera point clouds, apples were identifiable by colour, however the sparseness of the point cloud resulted in somewhat undefined shapes and difficulty distinguishing individual apples where several were growing in close proximity. Tree branches and leaves were also often indistinct, while tree trunks were slightly better. Vertical wooden posts installed along the rows at roughly 9m intervals were often the most recognizable features. Due to their sparseness and lack of structural details, the stereo camera point clouds would not be suitable for the construction of a DT if used independently.

Therefore, it was necessary to register the stereo camera point cloud with the HLS point cloud. The accuracy of the alignment was poorer than expected, with an RMS error of 6.4cm and several persistent visual artifacts. Given that one of the potential uses of the DT is fruit-picking, which requires precise and accurate measurements, this is not acceptable.

Apple detection and segmentation was highly satisfactory, with excellent recall and precision. Visual analysis of results showed that the model was successful at detecting all or nearly all apples in clear, well-lit images, but struggled to detect all apples in blurry, poorly lit images, resulting in some false negatives. The abundance of high-quality, accurately labelled images from the MinneApple benchmark dataset (Häni et al., 2020) likely helped to compensate for the relatively small size of our own dataset. The variety of trees, apples, colours, and lighting conditions represented in the MinneApple dataset served to prevent overfitting and make the model more generalisable.

The final goal of this workflow is to generate a 3D model of the orchard structure using the LiDAR system so that the information collected by the YOLO algorithm can be associated with each tree and georeferenced. By knowing the depth camera pose coordinates and their relation to the depth camera point cloud, it is possible to transform them into the global reference system. The YOLO model can be uploaded to the depth camera and run during the acquisition, enabling instantaneous detection.

In our case study, we did not load the detection model into the camera because it was developed after the acquisitions. The depth camera's point cloud was aligned with that of the HLS, also thanks to the markers on the poles. This procedure can be further automated if the markers are encoded.

The major limitations and difficulties encountered in the work are related to the data acquisition methods. While the terrestrial laser scanner, being an active sensor, did not encounter particular problems, the depth camera was mainly affected by light exposure and camera orientation. The rows oriented north were in the shade, and the images taken were underexposed. We believe this limiting factor can be overcome with better scheduling of the surveys avoiding hours when the sun is low on the horizon.

The second limiting aspect was the difficulty of reconstructing the depth camera's point cloud. The repetitive geometries and the serpentine trajectory caused inaccuracies in the visual odometry algorithm, resulting in the data only being exportable and processable in different segments. To reduce these errors, we intend to orient the camera not perpendicular to the row but rotated by about 10° so that the entire row is visible and more points are available for the visual odometry algorithm. We are currently researching these aspects to improve and automate the prototype further. Having successfully prepared the 3D and 2D components of a DT, the next steps will focus on their unification via the projection of the 2D colour data and apple detections onto the segmented 3D model. Then, fruit-count data and other metrics can be assigned to each tree, and the full DT will be stored in a queryable webGIS.

5. Conclusions

Here we present a comprehensive workflow for the creation of a DT of an apple orchard. We demonstrate the suitability of an agricultural UGV, Agri.Q, as a mobile sensor carrier in an apple orchard. We also obtained a detailed 3D model and successfully performed ITD, allowing for the eventual association of crop measurements to individual trees. While we did not gather measurements such as fruit count and size, these can be derived from the results of apple detection and segmentation. Using a refined AI model, we performed apple detection and segmentation on RGB images with excellent results. The next phase of this work will focus on the automatization of the data collection and the projection of the 2D detections and RGB data onto the 3D model in order to realize the final georeferenced, segmented, colourised DT.

As the Agriculture 4.0 revolution ushers in the age of smart farming, agricultural DTs will move rapidly from the conceptual to the real world. To facilitate this transition and ensure the readiness of the technology, the development and testing of DT generation methods must begin now. Our proposed methodology represents one of the first start-to-finish workflows for the creation of a DT of an apple orchard and provides a foundation on which future DTs of complex, living agricultural systems can be built.

Acknowledgements

The authors acknowledge the Agrion research center for providing their experimental orchards for these tests.

This study was carried out within the Agritech National Research Center and received funding from the European Union Next-GenerationEU (PIANO NAZIONALE DI RIPRESA E RESILIENZA (PNRR) – MISSIONE 4 COMPONENTE 2, INVESTIMENTO 1.4 – D.D. 1032 17/06/2022, CN00000022). This manuscript reflects only the authors' views and opinions, neither the European Union nor the European Commission can be considered responsible for them.

References

Alves, R. G., R. F. Maia, and F. Lima. 2023. Development of a Digital Twin for smart farming: Irrigation management system for water saving. Journal of Cleaner Production. 388, 135920. https://doi.org/10.1016/j.jclepro.2023.135920.

Apeinans, I., L. Litavniece, S. Kodors, I. Zarembo, G. Lacis, and J. Deksne. 2023. Smart Fruit Growing Through Digital Twin Paradigm: Systematic Review and Technology Gap Analysis. Engineering Management in Production and Services. 15 (4), 128–143.

Belcore, E., M. Pittarello, A. M. Lingua, and M. Lonati. 2021. Mapping Riparian Habitats of Natura 2000 Network (91E0*, 3240) at Individual Tree Level Using UAV Multi-Temporal and Multi-Spectral Data. Remote Sensing. 13 (9), 1756. https://doi.org/10.3390/rs13091756.

Botta, A., and P. Cavallone. 2022. Robotics Applied to Precision Agriculture: The Sustainable Agri.q Rover Case Study. *Proceedings of I4SDG Workshop 2021*. 41–50. https://doi.org/10.1007/978-3-030-87383-7_5.

Chen, M., Y. Tang, X. Zou, Z. Huang, H. Zhou, and S. Chen. 2021. 3D global mapping of large-scale unstructured orchard integrating eye-in-hand stereo vision and SLAM. Computers and Electronics in Agriculture. 187, 106237. https://doi.org/10.1016/j.compag.2021.106237.

Colucci, G., L. Tagliavini, A. Botta, L. Baglieri, and G. Quaglia. 2023. Decoupled motion planning of a mobile manipulator for precision agriculture. Robotica. 41 (6), 1872–1887. https://doi.org/10.1017/S0263574723000243.

Destination Earth, 2024. Destination Earth. https://destination-earth.eu/

Di Pietra, V., N. Grasso, M. Piras, and P. Dabove. 2020. Characterization of a mobile mapping system for seamless navigation. The International Archives of the Photogrammetry, Remote Sensing and Spatial Information Sciences. XLIII-B1-2020, 227–234. https://doi.org/10.5194/isprs-archives-XLIII-B1-2020-227-2020.

Ghandar, A., A. Ahmed, S. Zulfiqar, Z. Hua, M. Hanai, and G. Theodoropoulos. A decision support system for urban agriculture using digital twin: A case study with aquaponics. IEEE Access. 9, 35691-35708. https://doi.org/10.1109/ACCESS.2021.3061722.

Grieves, M. 2015. Digital Twin: Manufacturing excellence through virtual factory replication. White paper. Digital Twin Institute.

Häni, N., P. Roy, and V. Isler. 2020. MinneApple: A Benchmark Dataset for Apple Detection and Segmentation. IEEE Robotics and Automation Letters. 5 (2), 852–858. https://doi.org/10.1109/LRA.2020.2965061.

ISPA, 2024. International Society of Precision Agriculture: Precision Ag Definition. https://www.ispag.org/about/definition.

Javaid, M., A. Haleem, R. P. Singh, and R. Suman. 2022. Enhancing smart farming through the applications of Agriculture 4.0 technologies. International Journal of Intelligent Networks. 3, 150–164. https://doi.org/10.1016/j.ijin.2022.09.004.

Jocher, G., A. Chaurasia, and Q. Jing. 2023. Ultralytics YOLO (Version 8.0.0) [Computer software]. https://github.com/ultralytics/ultralytics

Kamilaris, A., F. Gao, F. X. Prenafeta-Boldu, and M. I. Ali. 2016. Agri-IoT: A semantic framework for Internet of Things-enabled smart farming applications. *2016 IEEE 3rd World Forum on Internet of Things (WF-IoT)*. 442–447. https://doi.org/10.1109/WF-IoT.2016.7845467.

Moysiadis, V., P. Sarigiannidis, V. Vitsas, and A. Khelifi. 2021. Smart Farming in Europe. Computer Science Review. 39, 100345. https://doi.org/10.1016/j.cosrev.2020.100345.

Neupane, C., A. Koirala, Z. Wang, and K. B. Walsh. 2021. Evaluation of Depth Cameras for Use in Fruit Localization and Sizing: Finding a Successor to Kinect v2. Agronomy. 11 (9), 1780. https://doi.org/10.3390/agronomy11091780.

Ozdarici-ok, A., and A. O. Ok. 2023. Using remote sensing to identify individual tree species in orchards: A review. Scientia Horticulturae. 321, 112333. https://doi.org/10.1016/j.scienta.2023.112333.

Pylianidis, C., S. Osinga, and I. N. Athanasiadis. 2021. Introducing digital twins to agriculture. Computers and Electronics in Agriculture. 184, 105942. https://doi.org/10.1016/j.compag.2020.105942.

Quaglia, G., L. Samperi, L. Baglieri, G. Colucci, L. Tagliavini, and A. Botta. 2024. Design of an Under-Actuated Mechanism for Collecting and Cutting Crop Samples in Precision Agriculture. Advances in Service and Industrial Robotics. 533–541. https://doi.org/10.1007/978-3-031-59257-7_53.

Tardaguila, J., M. Stoll, S. Gutiérrez, T. Proffitt, and M. P. Diago. 2021. Smart applications and digital technologies in viticulture: A review. Smart Agricultural Technology. 1, 100005. https://doi.org/10.1016/j.atech.2021.100005.

Tiozzo Fasiolo, D., A. Pichierri, P. Sivilotti, and L. Scalera. 2023. An analysis of the effects of water regime on grapevine canopy status using a UAV and a mobile robot. Smart Agricultural Technology. 6, 100344. https://doi.org/10.1016/j.atech.2023.100344.

Tsolakis, N., D. Bechtsis, and D. Bochtis. 2019. AgROS: A Robot Operating System Based Emulation Tool for Agricultural Robotics. Agronomy. 9 (7), 403. https://doi.org/10.3390/agronomy9070403.

Velodyne Lidar, 2023. Velodyne Lidar, Inc.: Automated with Velodyne. https://velodynelidar.com/automated-with-velodyne/kaarta/.

Visconte, C., P. Cavallone, L. Carbonari, A. Botta, and G. Quaglia. 2021. Design of a Mechanism with Embedded Suspension to Reconfigure the Agri_q Locomotion Layout. Robotics. 10 (1), 15. https://doi.org/10.3390/robotics10010015.

Visentin, F., S. Cremasco, M. Sozzi, L. Signorini, M. Signorini, F. Marinello, and R. Muradore. 2023. A mixed-autonomous robotic platform for intra-row and inter-row weed removal for precision agriculture. Computers and Electronics in Agriculture. 214, 108270. https://doi.org/10.1016/j.compag.2023.108270.

Vulpi, F., R. Marani, A. Petitti, G. Reina, and A. Milella. 2022. An RGB-D multi-view perspective for autonomous agricultural robots. Computers and Electronics in Agriculture. 202, 107419. https://doi.org/10.1016/j.compag.2022.107419.

Wang, Z., K. B. Walsh, and B. Verma. 2017. On-Tree Mango Fruit Size Estimation Using RGB-D Images. Sensors. 17 (12), 2738. https://doi.org/10.3390/s17122738.

Zhang, W., J. Qi, P. Wan, H. Wang, D. Xie, X. Wang, and G. Yan. 2016. An Easy-to-Use Airborne LiDAR Data Filtering Method Based on Cloth Simulation. Remote Sensing. 8 (6), 501. https://doi.org/10.3390/rs8060501.

Can we leverage data sharing benefits to increase the adoption of smart farming technologies?

Clare S. Sullivan [a,*], Marilena Gemtou [a], Evangelos Anastasiou [a], Havva Uyar [a,b], Spyros Fountas [a]

[a] Department of Natural Resources Development and Agricultural Engineering, Agricultural University of Athens, Athens, Greece

[b] Research and Development Department, SingularLogic, Athens, Greece

* Corresponding author. Email: c.sullivan@aua.gr

Abstract

Smart farming practices provide decision-making support for farmers facing economic, social, and environmental challenges. However, the adoption of smart farming remains low in many areas due to the perceived costs, required skills, and hesitancies about sharing agricultural data. While many studies have examined the factors influencing smart farming adoption in different agricultural contexts, none have specifically reviewed the motivators and obstacles of agri-data sharing within smart farming. This research aimed to identify and classify the primary drivers and barriers for agri-data sharing among stakeholders by examining existing literature. A Systematic Literature Review was conducted using the PRISMA 2020 methodology, initially identifying 491 papers from Scopus and Web of Science and narrowing down to 34 empirical and 25 non-empirical papers for final assessment. This paper presents the main findings from the 34 empirical studies. Factors affecting the willingness and ability to engage in agricultural data sharing were categorized into socio-economic, systemic, technical, and legal categories. The most prominent drivers for agri-data sharing were socio-economic and systemic, mentioned in 65% and 59% of the empirical papers, respectively. Technical factors were the most common barriers, discussed in 68% of the literature. Key enablers for data sharing included perceived knowledge gain for better decision-making, trust and collaboration across the agri-value chain, practical usage, and clear data sovereignty. Major concerns included a lack of understanding of the purpose and benefits of data sharing, mistrust about who benefits from the data, data privacy and security issues, and unclear data ownership and right of uses. The findings from this study will inform research efforts across the EU to promote the benefits of agri-data sharing and increase the adoption of smart farming technologies.

Keywords: agri-data sharing, smart farming, drivers, barriers, trust

1. Introduction

Farmers worldwide are in a challenging situation: to produce enough for a growing population, decrease their environmental impact, meet consumer and political demands for responsible practices, navigate increasingly adverse and volatile weather, and ensure the survival of their farming operations. Despite these overwhelming challenges, new technologies providing high-quality information can assist farmers in making critical decisions and increasing efficiencies. Over the past three decades, smart farming practices have been developed to address many economic, social, and environmental challenges in agriculture (Fragomeli et al., 2024). Smart farming practices can help reduce inputs and maximise outputs (Wolfert et al., 2017), streamline on-farm processes and redistribute labour needs (Jerhamre et al., 2022), and use resources more sustainably, such as through precision irrigation and targeted pesticide application (Jakku et al., 2019; van Evert et al., 2017).

Data are central to all smart farming processes and management decisions. These data are collected from farms via sensors, machines, drones, or satellites, and from the value chain tracking consumption, prices, input supplies, and energy use (Klerkx et al., 2019). By processing and interpreting these data, farmers can make better decisions at both the farm and value-chain levels (van der Burg et al., 2020). To fully realise the benefits of optimized production, enhanced sustainability, and risk mitigation, these data must be shared. This involves farmers sharing their data with stakeholders such as farm advisory services, ag-tech companies, research institutions, and government agencies. However, data sharing is a complex socio-technical process that is hampered by stakeholder concerns over data privacy, interoperability, unclear governance, and mistrust about who benefits from the shared data (Wiseman et al., 2019).

Whereas trust in smart farming adoption studies is centred on trust in the technology, such as whether the equipment gathers accurate data, trust is discussed very differently in agri-data sharing research. Issues with

trust in data sharing stem from stakeholders' (primarily farmers') perceptions of what will happen to their data once shared, including who will use it for what purpose, and potential repercussions. Some believe trust can be ensured through policies, codes of conduct, and regulation; however, van der Burg et al. (2021) argue that such measures can only help maintain trust previously built through relationships. This review highlights that socio-economic, systemic, technical, and legal factors intersect to influence trust in data sharing.

Numerous studies have identified agri-data sharing as a factor affecting smart farming adoption (Drewry et al., 2019; Jerhamre et al., 2022), but few have focused on it specifically. Previous reviews have examined the technical or privacy aspects of big data in agriculture (Amiri-Zarandi et al., 2022; Kamilaris et al., 2017), only the barriers to data sharing in digital agriculture (Eastwood et al., 2023; Šestak & Copot, 2023), or specific technologies like blockchain (Akella et al., 2023). However, to the best of our knowledge, no reviews have comprehensively explored the motivations and obstacles of agri-data sharing. This research aims to identify and classify the key drivers and barriers for agri-data sharing across stakeholders by reviewing existing literature. Our paper fills the gap with a review of the most prominent factors influencing data sharing in the agri-value chain identified in 34 empirical studies.

2. Materials and Methods

This article forms part of a comprehensive Systematic Literature Review (SLR) recently conducted by Sullivan et al. (2024) using the PRISMA 2020 methodology. This review presents the main findings from the empirical papers identified in the original systematic review. Empirical studies gather and analyse data as evidence, and include both qualitative (e.g., interview) and quantitative (e.g., survey) measurements.

2.1. Identification criteria and screening process

The original search was conducted on February 15, 2024, and utilised Scopus and Web of Science. The search query employed a combination of keywords and their synonyms based on previous reviews (Da Silveira et al., 2021; Gemtou et al., 2024) and was selected after testing several combinations of search terms. The final query used was:

("smart farm*" OR "smart agricult*" OR "precision agricult*" OR "precision farm*" OR "digital agricult*" OR "digital farm*" OR "data-driven agricult*" OR "agriculture 4.0") AND ("data shar*" OR "agri-data" OR "agricult* data" OR "farm* data" OR "sharing data" OR "data exchange" OR "data access" OR "data governance" OR "data privacy" OR "data ownership" OR "data sovereignty" OR trust OR "information sharing") AND (factor* OR barrier* OR deter* OR obstacle* OR limit* OR prevent* OR discourag* OR driver OR motivat* OR encourag* OR attitud* OR perspective OR adopt*)

The keywords were searched within titles, abstracts, and keyword lists. The search was limited to journal articles and conference papers written in English. The search resulted in 491 studies eligible for screening. After removing duplicates, the number of articles was reduced from 489 to 353. The initial screening was conducted by reading titles and abstracts of the 353 papers to make sure the papers fell within the scope of the review. This step removed 227 records. The remaining 126 papers were then screened by reading the full text to determine if they met the following inclusion criteria: (i) Original research (not a review paper); (ii) Study related to digital agriculture; (iii) Discussed a driver or barrier for agricultural data sharing; and (iv) Available for download as full text. This second screening resulted in 32 empirical and 24 non-empirical papers. Two additional empirical papers were added from outside of the query because they were commonly referenced. This resulted in a final number of 34 empirical studies to be analysed for this review.

2.2. Data extraction and analysis

Driver and barrier categories were established based on existing literature (Gemtou et al., 2024; Rozenstein et al., 2024) to analyse results and identify the most prominent factors affecting agricultural data sharing. The four main categories used were: (i) socio-economic factors; (ii) systemic factors; (iii) technical factors; and (iv) legal factors. Data were extracted manually and recorded in a spreadsheet after reading each article. When discussed in the main body of a paper, details of the driver or barrier were recorded in the appropriate category. In this way, the number of papers that addressed the four main drivers or barriers was calculated. Factors discussed were further analysed by assigning them into four or five sub-categories per main category. The frequency of a sub-category was determined by summing the number of times the sub-category was marked across the set of papers. This review presents the two most prominent drivers and barriers per category, while all the sub-categories recorded are discussed in Sullivan et al. (2024).

3. Results and Discussion

3.1. General overview of selected articles

A total of 34 empirical studies published from 2011 to 2024 were analysed for this review. Data sharing is a recent area of research, with 90% of the articles published since 2019. Other reviews have noted a recent surge in social and behavioural science studies related to smart farming, particularly from 2018 onwards (Klerkx et al., 2019; McGrath et al., 2023). The high number of publications in 2019 is attributed to a special issue of *Wageningen Journal of Life Sciences* focused on social science within smart farming. Agri-data sharing was found to be only a component of the research or discussion in many of the papers (e.g., data sharing as a factor influencing the adoption of smart farming). However, twelve of the papers (35%) focused specifically on agri-data sharing and in this review are referred to as "the main data sharing studies".

The published studies included: 10 papers from North America; 9 from Europe; 8 from Oceania; 3 from Africa; 2 from Asia; 1 from South America, and 1 conducted world-wide. Australia and the Unites States of America were the countries with the largest number of articles (24% and 21% of articles, respectively). Five of the twelve main data sharing studies (42%) examined perspectives on agricultural data sharing in Australia. Nearly 90% of the papers were journal articles, with only four conference papers included.

The studies included the perspective of farmers (~80% of studies), agronomists, technology providers, government, and researchers. All the main data sharing studies included the perspective of farmers. The two most common methodologies used for gathering stakeholder insights were interviews (32% of studies) and surveys (29%). The main data sharing studies centred on farmers' perspectives of the benefits and risks of data sharing, data governance, and willingness to engage in data sharing.

3.2. Overview of factors affecting agricultural data sharing

Factors influencing the willingness and ability to participate in agricultural data sharing were identified across socio-economic, systemic, technical, and legal categories. Socio-economic factors encompass the social and economic realities that influence stakeholders' decisions to engage in activities (Chisenga, 2015). Systemic factors, operating at the agri-chain level, create feedback loops that impact stakeholders' decisions (Gemtou et al., 2024). Technical factors are related to technological challenges or solutions, and legal factors are shaped by regulations and policies. The most prominent drivers for agri-data sharing discussed were the socio-economic (65% of papers) and systemic factors (59% of papers; Figure 1). This result was emphasised in the main data sharing papers: 100% of the twelve papers discussed socio-economic enablers and 67% discussed systemic ones. Technical factors were the most frequently referenced barriers to data sharing, discussed in 68% of the studies (Figure 1). In the subset of main data sharing studies, systemic and legal barriers were the most prevalent, both in 75% of the studies.

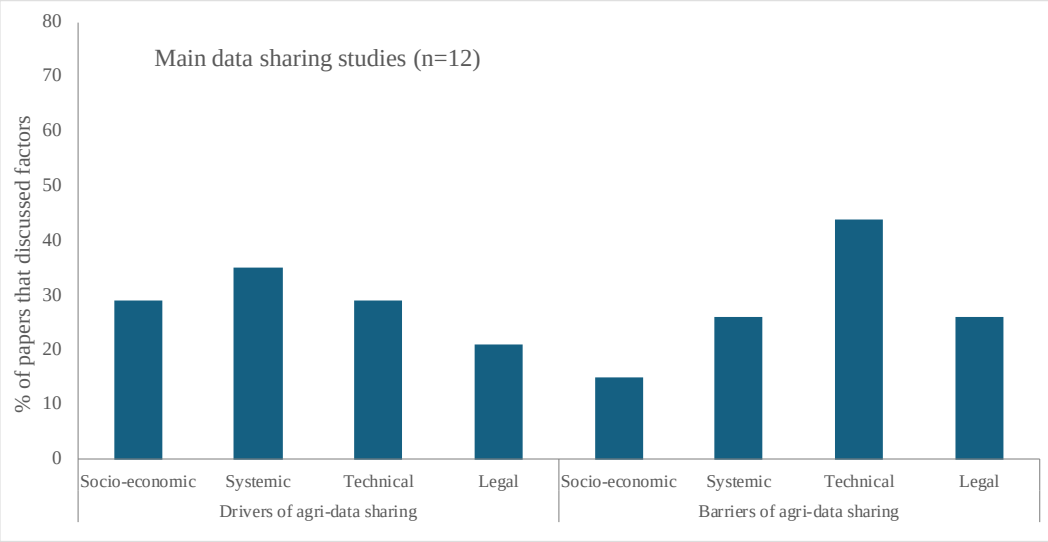

Figure 1. Prominence of factors identified as influencing agri-data sharing. Light blue denotes main data sharing studies.

3.3. Sub-categorisation of factors

Within the four main categories, sub-categories were created based on findings from the literature. Table 1 includes the two most prominent sub-categories identified under each main category and examples found in the literature. Data governance is a complex and overarching topic, and its different aspects were allocated to the technical and legal categories. Discussions around data privacy and security were recorded within technical; while discussions of data ownership and rights of use were grouped as 'data sovereignty' and included in the legal category. The papers were not restricted to only one categorisation, as they could include references to multiple main and sub-categories. The percentage of papers in which the sub-category was discussed are included in Table 1 in brackets.

Table 1. Examples of the most prominent drivers and barriers of agri-data sharing identified in each category. The number in brackets is the percentage of articles (n=34) in which the factor was discussed.

Driver category & sub-category examples	**Barrier category & sub-category examples**
Socio-economic drivers	*Socio-economic barriers*
Knowledge gain (38%) Informed decision-making; risk management; improved farm production	**Lack of knowledge about data sharing (26%)** Unclear about data benefits, data use, value of data, return on investment
Awareness of data sharing (26%) Clear understanding of value proposition	**Required investment (12%)** Time, money, and training needed
Systemic drivers	*Systemic barriers*
Trust and relationship building (29%) Use of existing trusting relationships	**Lack of trust between stakeholders (35%)** Unknown fate of data and who will benefit; exposure to competition
Collaboration across agri-value chain (29%) Sharing knowledge for the common good; supply chain efficiencies; enhanced marketability	**Power imbalance and data misuse (29%)** Fear of data used to influence market; farmers at mercy of technology providers
Technical drivers	*Technical barriers*
Practical usage (21%) Ease-of-use of interface; data collection linked to farm realities; data storage & access	**Privacy and security (53%)** Lack of privacy and cybersecurity protection; complexity of personal/non-personal data
Improved technologies (15%) New technologies; improved data analysis and modeling	**Interoperability (24%)** Incompatibilities; restricted data exchange; lack of transferability; data 'lock-in'
Legal drivers	*Legal barriers*
Data sovereignty (26%) Clarity and/or policy of data ownership and rights of use; transparency about data sharing licenses	**Lack of data sovereignty (41%)** Lack of clarity for data ownership and rights of data use; lack of transparency in policies
Beneficial policies and incentives (21%) Government incentives; CAP alignment; ease of administrative burden	**Harmful policies and regulations (15%)** Compliance and regulations for data sharing; restrictive policies on data sharing

3.4. Drivers of agri-data sharing

Identification of the most prominent drivers found in research studies can help inform future strategies aimed at promoting the benefits of agri-data sharing. While socio-economic factors emerged as the most prominent overall category of drivers, we also identified specific drivers discussed in the literature.

3.4.1. Socio-economic drivers

The perceived knowledge gain when sharing agricultural data was the most prominent driver identified across all papers (Table 3). Benefits related to knowledge gain, such as improved decision-making and risk management (Jakku et al., 2019; Newton et al., 2020; Regan, 2019), were discussed in 38% of all papers and

50% of the main data sharing papers, highlighting its importance from the farmer perspective. Discussions highlighted how farmers valued access to individual and pooled data for better opportunities and risk mitigation. Aggregated data could help address climate and market uncertainties, reduce inputs, improve crop quality, and increase efficiency and economic gain (McCarthy et al., 2023; Thompson et al., 2021; Wang et al., 2024). Other agri-data sharing research projects have identified optimised production and risk management, tailored farming recommendations, and increased quality and quantity of products as key drivers for sharing data (van der Burg et al., 2020; Giesbers & Adema, 2021).

For these perceived benefits to drive interest in data sharing, farmers must understand the value proposition of agri-data sharing. The second most frequent enabler was individual awareness of the risks and benefits of sharing agricultural data (Table 3). This clear understanding was highlighted in seven of the twelve main data sharing studies as a prerequisite for agri-data sharing (Brown et al., 2023; Charvát et al., 2021; Wiseman et al., 2019; Zhang et al., 2021).

3.4.2. Systemic drivers

Building trust in relationships and collaboration across the agri-value chain work hand-in-hand and were the two most frequently discussed systemic drivers for sharing agricultural data (Table 1). Aggregate data was viewed as beneficial for industry decision-making to optimise supply chain logistics and improve market projecions (Jakku et al., 2019). Stakeholders saw the potential of using larger datasets for the common good of the industry, either by exchanging knowledge and sharing insights, or enhancing marketability of a sector (Boisier et al., 2021; Charvát et al., 2021; Eastwood et al., 2012; McCarthy et al., 2023). Stakeholders in Australia envisioned product traceability creating niche markets to meet consumer demands (Jakku et al., 2019), and data sharing in Ireland was viewed as a means of presenting a positive public image of the agricultural sector (Brown et al., 2023).

For the collaborative benefits of data sharing to be realised, trust and relationship building is required. The importance of involving stakeholder groups in the data sharing process that were already trusted partners of farmers was emphasised in the research. Farmers were most willing to share their data with researchers or other farmers, and least likely to share with the government (McCarthy et al., 2023; Turland & Slade, 2020; Zhang et al., 2021). As found in the wider literature, farmers' willingness to share data is influenced by who the data will be shared with, who they will be working with, and how much they trust this stakeholder group (Amiri-Zarandi et al., 2022; Eastwood et al., 2023).

3.4.3. Technical drivers

The technical drivers discussed most frequently in the papers were factors that improved the practicalities of data sharing, such as ease of use and increased data storage (Table 1). User-friendly interfaces were a significant enabler for data collection based on farmer surveys (Jerhamre et al., 2022; Wang et al., 2024). Incorporating data collection into farmers' normal activities further enhanced their willingness, such as linking data collection to a regular farm activity (Eastwood et al., 2012) or using a data platform that was integrated into an existing farm management software (Schambow et al., 2022).

The second most prominent technical driver were new technologies that spur innovation across the agri-sector (Table 1). Examples included higher-quality weather and crop models coupled with data analysis (Newton et al., 2020) and the possibilities from new technologies like artificial intelligence (Alexander et al., 2024). This optimistic outlook of innovative technologies is supported by other literature reviews related to big data and smart farming (Abbasi et al., 2022; Akella et al., 2023).

3.4.4. Legal drivers

In the legal category, it was widely reported that clarification of data ownership and transparent data use licenses were a critical incentive for agri-data sharing (Brown et al., 2023; Charvát et al., 2021; Idowu et al., 2023; McCarthy et al., 2023; van der Burg et al., 2021; Zhang et al., 2021). This is supported by discussions in the wider literature of legal frameworks that tackle accountability and responsibility within the data-sharing chain (Amiri-Zarandi et al., 2022; Eastwood et al., 2023). While codes of conduct have been developed to help protect farmers' rights and make data sharing more transparent, these codes of conduct are voluntary, including the European Union Code of Conduct on Agricultural Data Sharing by Contractual Agreement (van der Burg et al., 2021).

Beneficial governmental policies and incentives were discussed as encouragements of data sharing (Jerhamre et al., 2022), especially if data aggregation and analysis support was provided (Newton et al.,

2020). Sharing data digitally was also viewed as a way to decrease the administrative burden for demonstrating compliance with regulations or in applying for government subsidies (Kutter et al., 2011; Reissig et al., 2022).

3.5. Barriers of agri-data sharing

The main barriers af agricultural data sharing identified in the papers were often the "lack" of the associated driver (Table 1). As a main category, technical factors were discussed in 68% of all papers and were the most prominent barriers to agri-data sharing.

3.5.1. Socio-economic barriers

Lack of knowledge about the benefits or use of shared data was by far the most significant socio-economic obstacle for sharing farm data (Table 1). Almost 60% of the main data sharing papers referenced lack of clarity about the value, applicability, or benefit of data to farmers as a serious deterrent for sharing agri-data (Jakku et al., 2019; Marshall et al., 2022). Although much less prevalent, the required investment of time and money to adopt a technology and learn new skills was referenced in 17% of the papers. When the benefits of data sharing are not clear, farmers are less likely to invest in a new practice. In these instances, the farmer may lose interest in data-gathering technologies that are not required because the risks outweigh the unclear benefits (Brown et al., 2023; Regan, 2019). In contrast to reviews on the adoption of smart farming practices (Fragomeli et al., 2024; Gemtou et al., 2024), farm and farmer characteristics such as farm size, age, and education were not identified as prominent barriers to agri-data sharing in our review.

3.5.2. Systemic barriers

Lack of trust between stakeholders was the most prominent systemic barrier, identified in 35% of the papers (Table 1). Uncertainty and fear about the fate of data generated once it left the farm was reported by farmers, resulting in mistrust towards data aggregators. The sense of mistrust was ascribed to not knowing how data would be used, who would benefit from their data, and the repercussions with competitors (Alexander et al., 2024; Brown et al., 2023; Charvát et al., 2021; Zhang et al., 2021). These concerns were further exacerbated by the complex power imbalance that exists across the agri-value chain and fear of data being misused.

Trust in data sharing and fear of misuse was dependent on who the data was shared with. For example, growers were found to be least willing to share data with government for fear of selective data being used to misrepresent an industry or in the creation of unjust policies (Brown et al., 2023; Wiseman et al., 2019; Zhang et al., 2021). Farmers were also concerned that agriculture companies could adjust prices based on aggregated farm input or output data (Brown et al., 2023). The imbalance in operation size, bargaining power, data knowledge, and technology access between individual farmers and agricultural technology providers has left farmers at the mercy of large technology providers.(Boisier et al., 2021; Charvát et al., 2021). Unbalanced power relationships and lack of trust are barriers that have been identified in wider research related to data-driven agriculture (Abbasi et al., 2022; Atik, 2023; Kamilaris et al., 2017; Klerkx et al., 2019). In exploring the creation of shared data spaces, Eastwood et al. (2023) and Šestak and Copot (2023) identified mistrust in the data-sharing process as a serious and complex obstacle.

3.5.3. Technical barriers

The challenge surrounding data privacy and cybersecurity was the most prominent barrier identified in the study, referenced in 53% of all papers and 58% of the main data sharing studies (Table 1). From the farmers' perspective, there was a lack of confidence and trust that their privacy and cybersecurity would be maintained across the data-sharing chain (e.g., Bach et al., 2020; Drewry et al., 2019; Ibrahim et al., 2020; Jakku et al., 2019). The difficulty in separating 'personal' from 'non-personal' data within farm production data exacerbated this concern (Brown et al., 2023). The prominence of security and data privacy as challenges is supported in technical reviews on the use of big data in agriculture and data sharing obstacles (Amiri-Zarandi et al., 2022; Kamilaris et al., 2017; Wolfert et al., 2017).

The second most prominent technical challenge was data interoperability, although it was discussed less frequently in the main data sharing studies (17%). Because agricultural data is collected and stored in different formats, it is very difficult to integrate datasets. Farmers referred to both the incompatibility between systems on-farm (machinery) and between different service providers or databases as significant technical obstacles for sharing data (Bach et al., 2020; Jakku et al., 2019; Jerhamre et al., 2022; Wang et al., 2024).

The inability to transfer datasets between providers or equipment manufacturers is discussed in the wider literature as resulting in restricted data exchange and farmers being 'locked-in' with the first technology provider they sign on with (Atik, 2023; Kosior, 2020).

3.5.4. Legal barriers

The lack of clarity and assurance on data ownership, data use, and transfer rights (together termed 'data sovereignty') was the most significant legal barrier for engaging in data sharing (Table 1). Studies discussed farmers' desires for data ownership rights and transparency in data use agreements but highlighted the complexity of 'data ownership' vs 'data use' (Atik, 2023; van der Burg et al., 2021). It is possible for farmers to own their data, but have very little control over its use, since data use is part of the license agreement that farmers need to sign to use smart farming technologies (Wiseman et al., 2019). The research indicates that farmers are often unaware of, or do not understand the contracts they sign and have limited trust in protection guidelines (Gabriel, 2023; Wiseman et al., 2019). Other studies from the wider literature highlight that the primary challenge in agri-data sharing is the lack of protection or regulations regarding data sovereignty (Giesbers & Adema, 2021; McGrath et al., 2023).

Potential regulatory repercussions were discussed in 12% of the studies as a reason to now share data. These included concerns of harmful policies based on selective data (Brown et al., 2023) or restrictive data-driven regulations (McCarthy et al., 2023; Regan, 2019; Schambow et al., 2022).

3.6. Intersection of drivers and barriers

The socio-technical complexity of data sharing makes it difficult to separate the factors impacting data-sharing willingness (Eastwood et al., 2023). Promoting data sharing by highlighting knowledge benefits (socio-economic driver) requires trusted relationships and clear communication of risks and benefits (systemic drivers), privacy assurance (technical driver), and clarity on data usage rights (legal driver). Data privacy, a technical barrier, is tied to socio-economic concerns about data misuse (systemic barrier) and harmful regulations (legal barrier). Farmers worry about data privacy but often lack understanding of service agreements due to poor communication and policy transparency (systemic and legal barriers).

3.7. Future work

To enhance data sharing in agriculture, trust needs to be addressed from various perspectives. Literature suggests that clarifying data sharing benefits across stakeholder groups, leveraging existing trusted relationships, involving farmers in technology research and data governance, and transparent data sharing policies can foster trust (Raturi et al., 2022; van der Burg et al., 2021). However, concrete strategies to achieve these goals are lacking. Given that only twelve studies in this review specifically addressed agri-data sharing, there is a clear need for more stakeholder-centred research. The next step is to link the review's findings with practical research in Europe that is context-specific. The aim should be to develop a framework and strategy that leverages the prominent data-sharing enablers to overcome significant barriers. The benefits of agri-data sharing must be promoted in a way that encourages the adoption of data-gathering technologies as a means of enhancing farm viability.

4. Conclusions

The factors influencing stakeholders' motivation and capability to share agri-data into socio-economic, systemic, technical, and legal categories. Key enablers included perceived knowledge gain (socio-economic), collaborative benefits and building trust (systemic), clarity surrounding data sovereignty (legal), and improving the practicalities of data sharing (technical). The most significant barrier was the concern of maintaining data privacy and cybersecurity (technical), followed by unclear data ownership and rights of use (legal), trust issues (systemic), and a lack of understanding data sharing benefits and risks (socio-economic). This review stresses the complexity and interconnected nature of these factors and emphasises the need for balanced policies that encourage innovation while protecting farmers' interests. The classification of factors conducted in this review will help guide future research in promoting feasible data-sharing practices.

Acknowledgements

This research is funded by the European Commission under the Doctoral Networks Programme (MSCA-DN-101073381–EnTrust) within the Horizon Europe (HORIZON) Marie Skłodowska-Curie Actions.

References

Abbasi, R., Martinez, P., & Ahmad, R. (2022). The digitization of agricultural industry – a systematic literature review on agriculture 4.0. Smart Agricultural Technology, 2, 100042. https://doi.org/10.1016/j.atech.2022.100042

Akella, G. K., Wibowo, S., Grandhi, S., & Mubarak, S. (2023). A Systematic Review of Blockchain Technology Adoption Barriers and Enablers for Smart and Sustainable Agriculture. Big Data and Cognitive Computing, 7(2), 86. https://doi.org/10.3390/bdcc7020086

Alexander, C. S., Yarborough, M., & Smith, A. (2024). Who is responsible for 'responsible AI'?: Navigating challenges to build trust in AI agriculture and food system technology. Precision Agriculture. Scopus. https://doi.org/10.1007/s11119-023-10063-3

Amiri-Zarandi, M., Dara, R. A., Duncan, E., & Fraser, E. D. G. (2022). Big Data Privacy in Smart Farming: A Review. Sustainability, 14(15), 9120. https://doi.org/10.3390/su14159120

Atik, C. (2023). Horizontal intervention, sectoral challenges: Evaluating the data act's impact on agricultural data access puzzle in the emerging digital agriculture sector. Computer Law & Security Review, 51. https://doi.org/10.1016/j.clsr.2023.105861

Bach, D., Khmelevsky, Y., Lembke, S., & Cartier, L. (2020). BC tree fruit system-of-systems information architecture (initial design and review). In *SYSCON 2020 - 14th Annual IEEE International Systems Conference, Proceedings.* Scopus. https://doi.org/10.1109/SysCon47679.2020.9275921

Boisier, G., Hahn, K., Geldes, C., & Klerkx, L. (2021). Unpacking the Precision Technologies for Adaptation of the Chilean Dairy Sector. A Structural-functional Innovation System Analysis. Journal of Technology Management and Innovation. Scopus. https://doi.org/10.4067/S0718-27242021000400056

Brown, C., Regan, Á., & van der Burg, S. (2023). Farming futures: Perspectives of Irish agricultural stakeholders on data sharing and data governance. Agriculture and Human Values, 40(2), 565–580. Scopus. https://doi.org/10.1007/s10460-022-10357-8

Charvát, K., Obot, A., Kalyesubula, S., Zampati, F., Löytty, T., Kubíčková, H., Uhlíř, P., & Zadražil, F. (2021). INSPIRE Hackathons and SmartAfriHub—Roadmap for Addressing the Agriculture Data Challenges in Africa. Agris On-Line Papers in Economics and Informatics. Scopus. https://doi.org/10.7160/AOL.2021.130404

Chisenga, C. M. (2015). Socio-economic factors associated with the adoption of conservation agriculture among women farmers in Balaka District, Malawi. Open Acccess Theses, 542. https://docs.lib.purdue.edu/open_access_theses/542

Da Silveira, F., Lermen, F. H., & Amaral, F. G. (2021). An overview of agriculture 4.0 development: Systematic review of descriptions, technologies, barriers, advantages, and disadvantages. Computers and Electronics in Agriculture, 189, 106405. https://doi.org/10.1016/j.compag.2021.106405

Drewry, J. L., Shutske, J. M., Trechter, D., Luck, B. D., & Pitman, L. (2019). Assessment of digital technology adoption and access barriers among crop, dairy and livestock producers in Wisconsin. Computers and Electronics in Agriculture, 165, 104960. https://doi.org/10.1016/j.compag.2019.104960

Eastwood, C., Chapman, D., & Paine, M. (2012). Networks of practice for co-construction of agricultural decision support systems: Case studies of precision dairy farms in Australia. Agricultural Systems, 108, 10–18. https://doi.org/10.1016/j.agsy.2011.12.005

Eastwood, C., Turner, J. A., Romera, A., Selbie, D., Henwood, R., Espig, M., & Wever, M. (2023). A review of multi-scale barriers to transitioning from digital agriculture to a digital bioeconomy. CABI Reviews, cabireviews.2023.0002. https://doi.org/10.1079/cabireviews.2023.0002

Fragomeli, R., Annunziata, A., & Punzo, G. (2024). Promoting the Transition towards Agriculture 4.0: A Systematic Literature Review on Drivers and Barriers. Sustainability, 16(6), 2425. https://doi.org/10.3390/su16062425

Gabriel, A. (2023). Farmers' attitudes towards data security in agriculture when using digital technologies. Lecture Notes in Informatics (LNI), Proceedings - Series of the Gesellschaft fur Informatik (GI). Scopus. https://www.scopus.com/inward/record.uri?eid=2-s2.0-85176380096&partnerID=40&md5=df823827a4e16b46e14246d4f6a440e1

Gemtou, M., Kakkavou, K., Anastasiou, E., Fountas, S., Pedersen, S. M., Isakhanyan, G., Erekalo, K. T., & Pazos-Vidal, S. (2024). Farmers' Transition to Climate-Smart Agriculture: A Systematic Review of the

Decision-Making Factors Affecting Adoption. Sustainability, 16(7), 2828. https://doi.org/10.3390/su16072828

Giesbers, E., & Adema, H. (2021). Toward broader sharing of farm data: Recommendations from the use case coordinators. https://edepot.wur.nl/586530

Ibrahim, R. E., Elramly, A., & Hassan, H. M. (2020). Open systems science: Digital transformation and developing business model toward smart farms' platform. International Journal of Circuits, Systems and Signal Processing. Scopus. https://doi.org/10.46300/9106.2020.14.134

Idowu, A. R., Wachenheim, C., Hanson, E., & Sickler, A. (2023). The disposition of data from precision agricultural technologies: What do young agriculturalists think? Technology in Society, 75, 102389. https://doi.org/10.1016/j.techsoc.2023.102389

Jakku, E., Taylor, B., Fleming, A., Mason, C., Fielke, S., Sounness, C., & Thorburn, P. (2019). "If they don't tell us what they do with it, why would we trust them?" Trust, transparency and benefit-sharing in Smart Farming. NJAS - Wageningen Journal of Life Sciences, 90–91, 100285. https://doi.org/10.1016/j.njas.2018.11.002

Jerhamre, E., Carlberg, C. J. C., & Van Zoest, V. (2022). Exploring the susceptibility of smart farming: Identified opportunities and challenges. Smart Agricultural Technology, 2, 100026. https://doi.org/10.1016/j.atech.2021.100026

Kamilaris, A., Kartakoullis, A., & Prenafeta-Boldú, F. X. (2017). A review on the practice of big data analysis in agriculture. Computers and Electronics in Agriculture, 143, 23–37. https://doi.org/10.1016/j.compag.2017.09.037

Klerkx, L., Jakku, E., & Labarthe, P. (2019). A review of social science on digital agriculture, smart farming and agriculture 4.0: New contributions and a future research agenda. NJAS - Wageningen Journal of Life Sciences, 90–91, 100315. https://doi.org/10.1016/j.njas.2019.100315

Kosior, K. (2020). Economic, ethical and legal aspects of digitalization in the agri-food sector. Zagadnienia Ekonomiki Rolnej, 363(2), 53–72. https://doi.org/10.30858/zer/120456

Kutter, T., Tiemann, S., Siebert, R., & Fountas, S. (2011). The role of communication and co-operation in the adoption of precision farming. Precision Agriculture, 12(1), 2–17. https://doi.org/10.1007/s11119-009-9150-0

Marshall, A., Turner, K., Richards, C., Foth, M., & Dezuanni, M. (2022). Critical factors of digital AgTech adoption on Australian farms: From digital to data divide. Information Communication & Society, 25(6), 868–886. https://doi.org/10.1080/1369118X.2022.2056712

McCarthy, C., Nyoni, Y., Kachamba, D., Banda, L., Moyo, B., Chisambi, C., Banfill, J., & Hoshino, B. (2023). Can Drones Help Smallholder Farmers Improve Agriculture Efficiencies and Reduce Food Insecurity in Sub-Saharan Africa? Local Perceptions from Malawi. Agriculture-Basel, 13(5). https://doi.org/10.3390/agriculture13051075

McGrath, K., Brown, C., Regan, Á., & Russell, T. (2023). Investigating narratives and trends in digital agriculture: A scoping study of social and behavioural science studies. Agricultural Systems, 207, 103616. https://doi.org/10.1016/j.agsy.2023.103616

Newton, J., Nettle, R., & Pryce, J. (2020). Farming smarter with big data: Insights from the case of Australia's national dairy herd milk recording scheme. Agricultural Systems, 181. https://doi.org/10.1016/j.agsy.2020.102811

Raturi, A., Thompson, J. J., Ackroyd, V., Chase, C. A., Davis, B. W., Myers, R., Poncet, A., Ramos-Giraldo, P., Reberg-Horton, C., Rejesus, R., Robertson, A., Ruark, M. D., Seehaver-Eagen, S., & Mirsky, S. (2022). Cultivating trust in technology-mediated sustainable agricultural research. Agronomy Journal, 114(5), 2669–2680. https://doi.org/10.1002/agj2.20974

Regan, Á. (2019). 'Smart farming' in Ireland: A risk perception study with key governance actors. NJAS: Wageningen Journal of Life Sciences, 90–91(1), 1–10. https://doi.org/10.1016/j.njas.2019.02.003

Reissig, L., Stoinescu, A., & Mack, G. (2022). Why farmers perceive the use of e-government services as an administrative burden: A conceptual framework on influencing factors. Journal Of Rural Studies, 89, 387–396. https://doi.org/10.1016/j.jrurstud.2022.01.002

Rozenstein, O., Cohen, Y., Alchanatis, V., Behrendt, K., Bonfil, D. J., Eshel, G., Harari, A., Harris, W. E., Klapp, I., Laor, Y., Linker, R., Paz-Kagan, T., Peets, S., Rutter, S. M., Salzer, Y., & Lowenberg-DeBoer, J.

(2024). Data-driven agriculture and sustainable farming: Friends or foes? Precision Agriculture, 25(1), 520–531. https://doi.org/10.1007/s11119-023-10061-5

Schambow, R., Colin, Y., Dave, W., Schettino, D. N., & Perez, A. M. (2022). Enhancing passive surveillance for African swine fever detection on U.S. swine farms. Frontiers in Veterinary Science. Scopus. https://doi.org/10.3389/fvets.2022.1080150

Šestak, M., & Copot, D. (2023). Towards Trusted Data Sharing and Exchange in Agro-Food Supply Chains: Design Principles for Agricultural Data Spaces. Sustainability (Switzerland), 15(18). Scopus. https://doi.org/10.3390/su151813746

Sullivan, C. S., Gemtou, M., Anastasiou, E., & Fountas, S. (2024). Building Trust: A Systematic Review of the Drivers and Barriers of Agricultural Data Sharing. Smart Agricultural Technology, 100477. https://doi.org/10.1016/j.atech.2024.100477

Thompson, N. M., DeLay, N. D., & Mintert, J. R. (2021). Understanding the farm data lifecycle: Collection, use, and impact of farm data on U.S. commercial corn and soybean farms. Precision Agriculture. Scopus. https://doi.org/10.1007/s11119-021-09807-w

Turland, M., & Slade, P. (2020). Farmers' willingness to participate in a big data platform. Agribusiness, 36(1), 20–36. https://doi.org/10.1002/agr.21627

van der Burg, S., Oosterkamp, E., Marc-Jeroen Bogaardt, Regan, A., Popa, E. O., Tabeau, E., Brunori, G., Favelli, E., & Wattel, C. (2020). Futures of farm data sharing practices; perspectives of European farmers, researchers and agri-tech businesses (Report IOF2020). https://doi.org/10.13140/RG.2.2.21562.41924

van der Burg, S., Wiseman, L., & Krkeljas, J. (2021). Trust in farm data sharing: Reflections on the EU code of conduct for agricultural data sharing. Ethics and Information Technology, 23(3), 185–198. https://doi.org/10.1007/s10676-020-09543-1

van Evert, F. K., Fountas, S., Jakovetic, D., Crnojevic, V., Travlos, I., & Kempenaar, C. (2017). Big Data for weed control and crop protection. Weed Research, 57(4), 218–233. https://doi.org/10.1111/wre.12255

Wang, Y.-J., Wang, N., Li, M., Li, H., & Huang, G. Q. (2024). End-users' acceptance of intelligent decision-making: A case study in digital agriculture. Advanced Engineering Informatics, 60, 102387. https://doi.org/10.1016/j.aei.2024.102387

Wiseman, L., Sanderson, J., Zhang, A., & Jakku, E. (2019). Farmers and their data: An examination of farmers' reluctance to share their data through the lens of the laws impacting smart farming. NJAS - Wageningen Journal of Life Sciences, 90–91, 100301. https://doi.org/10.1016/j.njas.2019.04.007

Wolfert, S., Ge, L., Verdouw, C., & Bogaardt, M.-J. (2017). Big Data in Smart Farming – A review. Agricultural Systems, 153, 69–80. https://doi.org/10.1016/j.agsy.2017.01.023

Zhang, A., Heath, R., McRobert, K., Llewellyn, R., Sanderson, J., Wiseman, L., & Rainbow, R. (2021). Who will benefit from big data? Farmers' perspective on willingness to share farm data. Journal of Rural Studies, 88, 346–353. https://doi.org/10.1016/j.jrurstud.2021.08.006

Detection of deficiency of iron, zinc and manganese in spinach plant under hydroponic cultivation conditions using digital image processing

Maryam Nadafzadeh [a], Ahmad Banakar [a,*], Saman Abdanan Mehdizadeh [b], Saeid Minaei [a], Mohammadreza Zare Bavani [c], Gerrit Hoogenboom [d], Abdul Mounem Mouazen [e]

[a] Department of Mechanical Engineering of Biosystems, Faculty of Agricultural, Tarbiat Modares University (TMU), Tehran, Iran

[b] Department of Mechanical Engineering of Biosystems, Faculty of Agricultural and Rural Development, Agricultural Sciences and Natural Resources University of Khuzestan, Ahvaz, Khuzestan, Iran

[c] Department of Horticultural Science, Faculty of Agricultural , Agricultural Sciences and Natural Resources University of Khuzestan, Ahvaz, Khuzestan, Iran

[d] Department of Agricultural and Biological Engineering, University of Florida, Gainesville, Florida, USA

[e] Department of Environment, Faculty of Bioscience Engineering, Ghent University, Ghent, Belgium

*Correspond Author. Email: ah_banakar@modares.ac.ir; ah_banakar@yahoo.com

Abstract

Controlling the amount of nutrients needed in the spinach can reduce the consumption of chemical fertilizers, and also increase the production rate of this crop and preserve its quality. In fact, monitoring the growing conditions of products manually and traditionally has high costs and takes time, and sometimes lack of experience causes damage and quality reduction in products. Therefore, it is very important to provide a suitable and practical solution based on new and non-destructive technologies such as image processing that has the ability to recognize the needs of plants (including the need for different nutrients). These technologies have facilitated the monitoring of plant nutrient requirements, reducing reliance on human judgment and enhancing intuitive decision-making. The objective is to investigate deficiencies in three key nutrients - iron, zinc, and manganese - at five different levels of application of nutrients (ranging from none to 100% of the recommended amount). To achieve this, a comprehensive analysis was conducted, involving the extraction of color features (such as RGB, rgb, Lab, HSV, XYZ, I1I2I3, h*, and Chroma), morphological features (specifically Area), and various texture features obtained through the GLCM (Gray Level Co-occurrence Matrix) method (including Contrast, Energy, Entropy, Homogeneity, Correlation, and Prominence). After imaging of samples by a digital camera and data extraction, feature selection operation was carried out using five different algorithms (SFS (Sequential Forward Search), SBS (Sequential Backward Search), SFFS (Sequential Floating Forward Search), SFBS (Sequential Floating Backward Search), and ReliefF), with the SFBS method demonstrating superior performance. Subsequently, five classification methods (ANN (Artificial Neural Network), Naive Bayes, KNN (K-Nearest Neighbors), SVM (Support Vector Machine), and Random Forest) were evaluated using the selected features as input in a predetermined order based on the SFBS results. The classification accuracy rates were determined for varying numbers of input features through multiple iterations. In order to accurately compare the performance of these classification methods, several output classes including different levels of each of the nutrients iron, zinc and manganese were investigated. The study revealed that the classification methods achieved the highest average detection accuracy when operating with two output classes (0.813). Acceptable accuracy rates were also observed for three output classes (0.609), while performance significantly declined when handling four or five output classes. Notably, the performance decreased substantially to less than 20% when considering all levels of iron, zinc, and manganese nutrient deficiencies as outputs. In conclusion, the artificial neural network algorithm was recognized as the most suitable classification method in order to identify micronutrient deficiencies such as iron, manganese and zinc.

Keywords: Micronutrients, Image processing, Spinach, Sequential feature selection, Classification

1. Introduction

Measuring nutrients in plants through destructive methods in the laboratory is usually time-consuming and expensive. Therefore, a non-destructive and low-cost method is needed to scrupulously monitor the condition of plants (Polder et al., 2024). Based on this, researchers, knowing the advantages of plant monitoring systems, have paved the way for the commercialization of intelligent systems in greenhouse conditions. Also, the high demand

for producing more products per unit area, and the need to save costs and energy, have made the use of new technologies in agriculture inevitable.

High amounts of nitrogen fertilizers are usually used in the production of leafy vegetables, especially spinach. This is while excessive use of nitrogen fertilizers causes environmental problems, and decreases the amount of some nutrients such as iron and manganese in spinach (Dhillon et al., 1987). In addition, the unbalanced amount of elements in the soil, high pH of the soil and its calcareousness, excessive irrigation and eroded soil, low soil temperature, as well as weak air flow in the soil are among the factors that cause the lack of some nutrients, especially iron, manganese and zinc in plants (Guo et al., 2016).

Recently, various researches have been conducted in the field of stress detection in plants by using color, morphological and texture features (Nadafzadeh et al., 2024; Rahadiyan et al., 2022; Nadafzadeh and Abdanan Mehdizadeh, 2019; Igathinathane et al., 2006).

In a study, a set of color, texture and shape parameters were used to detect the deficiencies of phosphorus, potassium and nitrogen nutrients in rice plants. According to the results of this study, samples lacking these three nutrients were identified by the learning vector quantization (LVQ) method with an accuracy of 87.5% (Sulastri et al., 2021). Another group of researchers used deep convolutional neural networks to monitor the status of several nutrients (potassium, phosphorus and nitrogen) in lettuce. The performance of this method was evaluated using KNN, SVM, K-means, decision tree and simple thresholding algorithms. Finally, the highest accuracy rate of the proposed model was 96.5% to separate four groups of lettuce plants under the stress of potassium deficiency, phosphorus deficiency, nitrogen deficiency, and also a group of plants with full nutrition from each other (Taha et al., 2022).

Story et al. (2010) with the aim of detecting calcium deficiency in lettuce plants under greenhouse conditions, investigated a set of parameters of energy, entropy and uniformity as the most important features extracted from the images of the plant canopy. In this research, a method based on regression analysis was used to distinguish between stressed and controlled samples. The results showed that the designed machine vision system is able to identify calcium deficient lettuce plants with an R^2 equal to 97%. In one research, Espejo-Garcia et al. (2022) scrutinized the symptoms caused by the deficiency of some macro and micro nutrients using RGB imaging. For this purpose, a set of images of sugar beet plants were considered to detect the lack of nitrogen, phosphorus and potassium nutrients, and a set of orange tree images were prepared to detect the lack of iron, potassium, magnesium and manganese nutrients. In order to identify the lack of nutrients in these two data sets, the accuracy of the algorithm based on deep neural networks was reported as 98.65% and 98.52%, respectively.

By monitoring the growth process of crops, it is possible to take timely action to meet the needs of plants. In this study, a set of color, morphological and texture features were extracted from the images of the spinach samples that were under stress (deficiency of iron, zinc and manganese nutrients). These features were used as input data for several different classifiers (ANN, Naive Bayes, KNN, Random Forest, and SVM), and then, the performance of these classifiers was evaluated in terms of accuracy in separating the output classes, which were different levels of nutrient deficiency.

2. Materials and methods

2.1. Preparation of samples

To investigate the independent effects of five different levels of iron, zinc and manganese nutrients on spinach plant (0%, 25%, 50%, 75% and 100% of the recommended amount), 78 samples of Baby spinach variety were grown under hydroponic cultivation conditions for 6 weeks (Figure 1). The imaging operation of the samples started when the true leaves of the plant were fully developed.

Hoagland's formula was used to make the nutrient solution, which is a common solution for growing vegetables in the hydroponic system (Levine and Mattson, 2021). It should be noted that all experiments were conducted in the research greenhouse of the Agriculture and Natural Resources University of Khuzestan (Iran).

Figure 1. Cultivation of spinach plants under hydroponic conditions in the greenhouse.

2.2. Image analysis

In order to take pictures of spinach plants, a CASIO digital camera (model Exilim EX-ZR700, made in Japan) was placed above the canopy of the plants at a fixed distance of 75 cm from the samples. After transferring the images to the computer, the image processing operations was performed using Matlab 2018b software.

In this study, image processing included three stages of preprocessing, segmentation, and feature extraction. First in the preprocessing part, the captured images were improved in terms of color by applying the histogram uniformity method, and then the noises were removed using the area opening method. By implementing the segmentation process, the images were divided into regions consisting of pixels with similar characteristics. In the last step, a set of color features (RGB, rgb, Lab, HSV, XYZ, I1I2I3 and h* and Chroma), morphological (Area) and several texture features obtained from the GLCM method (Contrast, Energy, Entropy, Homogeneity, Correlation and Prominence) were calculated through the final image (Nadafzadeh and Abdanan Mehdizadeh, 2019).

2.3. Feature selection and classification

In this research, the feature selection operation was performed according to the study of Mallikarjuna and Guru (2022) by using the ReliefF algorithm, and the Sequential feature selection algorithm which had four different modes ((SFS) Sequential Forward Selection, (SBS) Sequential Backward Selection, (SFFS) Sequential Floating Forward Selection and (SFBS) Sequential Floating Backward Selection).

Subsequently, a set of statistical and intelligent classification methods including ANN, Naive Bayes, KNN, Random Forest and SVM were used according to the studies of Nadafzadeh et al. (2024), Chou et al. (2007), Sohail et al. (2021), Ansori et al. (2024), and Yang et al. (2023) respectively, in order to determine the highest level of accuracy in detecting iron, zinc and manganese deficiency levels. The number of different classes of four levels of deficiency of each of the nutrients iron, zinc, and manganese were investigated by these classification methods (Table 1).

Table 1. Output classes in classification operations.

Number of output classes	Description of the classes
Two	Comparison of the controlled group with each level of 0, 25%, 50% and 75% of iron, manganese and zinc elements
Three	✓ Comparison of the controlled group with two iron and manganese groups at zero level ✓ Comparison of the controlled group with two groups of iron and zinc at zero level ✓ Comparison of the controlled group with two groups of manganese and zinc at zero level
Four	Comparison of the controlled group with three groups of iron, zinc and manganese elements at zero level
Five	✓ Comparison of controlled group with four levels of iron deficiency ✓ Comparison of the controlled group with four levels of manganese deficiency ✓ Comparison of controlled group with four levels of zinc deficiency
Thirteen	Comparison of the controlled group with three nutrients iron, zinc and manganese at four different levels

3. Results and discussion

3.1. The results of the feature selection

The performance of the feature selection methods is shown in Table 2. According to Table 2, the SFBS method had the highest correct classification rate compared to other methods in the field of classification of output classes. After that, the order of superiority of feature selection algorithms was obtained as follows: SFFS, SFS, SBS and ReliefF. Therefore, in the following, the results of the SFBS method were used in the classification algorithms.

Table 2. Results of feature selection using SFS, SBS, SFFS, SFBS and ReliefF algorithms.

Method of feature selection	Correct classification rate
SFS	0.506 ± 0.005
SFFS	0.543 ± 0.003
SBS	0.501 ± 0.003
SFBS	0.556 ± 0.002
ReliefF	0.397 ± 0.006

Figure 2 shows the number of occurrences of each feature after implementing the SFBS algorithm during 25 iterations. These features were used as the input data of the classifiers according to the order seen in the diagram of Figure 2.

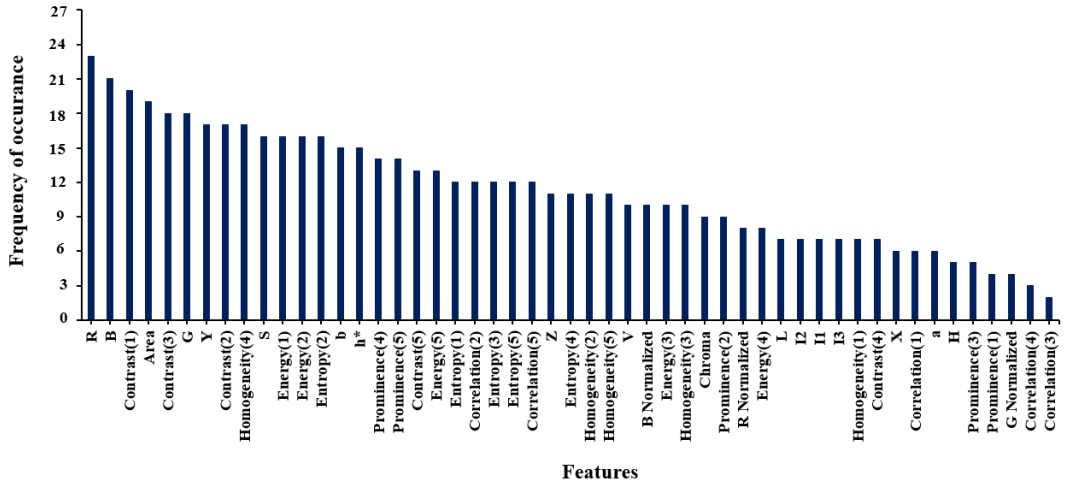

Figure 2. The diagram resulting from the implementation of SFBS feature selection algorithm.

3.2. Investigation of the classification results

3.2.1. Classification with two output classes

The comparison results of the controlled group with each of the four different levels of iron deficiency (0, 25, 50 and 75%) can be seen in Figure 3. Pursuant to Figure 3, compared to other classification methods, the ANN method had the highest level of accuracy in detecting the controlled group with each of the four levels of iron deficiency, and the number of the most suitable input features in this algorithm for each of the levels of 0, 25, 50 and 75% were obtained as 6, 10, 6 and 18 features, respectively. After the ANN algorithm, the best classifiers in detecting iron deficiency at zero level compared to the controlled group were: KNN, SVM, Naive Bayes and Random Forest, respectively. The priority order of the classifiers for separating the control group and the plants under iron stress of 25% was also similar to the iron group of 0%, but with the difference that the Naive Bayes method was in the third place and the SVM method was in the fourth place. When the iron levels were 50% and 75% of one of the two classification groups, the SVM method had the highest classification accuracy after the ANN method. Then, the best classification methods for detecting the level of 50% iron element were Naive Bayes, KNN and Random Forest methods respectively, but in the case of 75% iron level, the Random Forest method was in the third place and the Naive Bayes was in the last place. As can be seen in Figure 3, the best methods in detecting each of the four different levels of iron deficiency (0, 25, 50 and 75%) compared to the controlled group are ANN (0.927), SVM (0.862), KNN (0.840), Naive Bayes (0.805) and Random Forest (0.801).

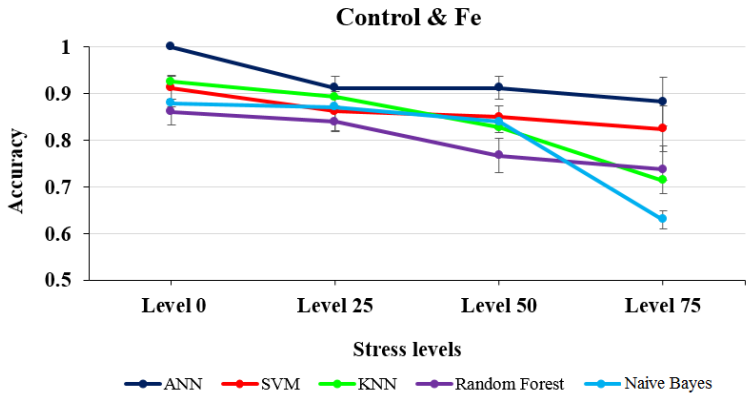

Figure 3. Comparison of the performance of several different algorithms for classifying the controlled group and each of the four different levels of iron deficiency

According to the diagram shown in Figure 4, the priority order of the classification methods for each stress level of manganese deficiency are: ANN, Random Forest, KNN, Naive Bayes and SVM at the 0% level; ANN, Random Forest, Naive Bayes, SVM and KNN at the 25% level; ANN, Random Forest, KNN, SVM and Naive Bayes at 50% level; and ANN, Random Forest, SVM, KNN and Naive Bayes at the 75% level. As shown in Figure 4, the ANN algorithm is also highly accurate in detecting each of the four levels of manganese nutrient deficiency compared to the controlled group, and the number of input features of this method for each level of 0, 25, 50 and 75% was 13, 11, 6 and 3, respectively.

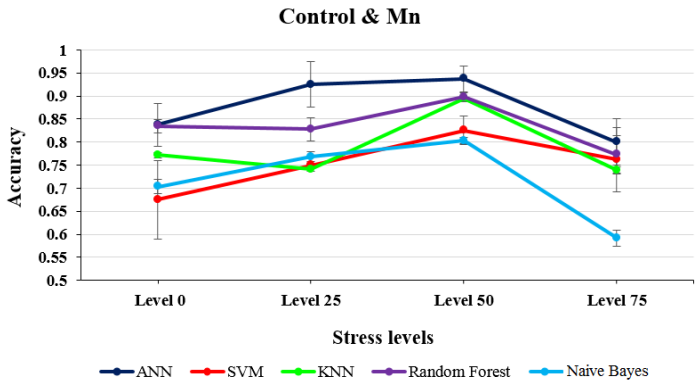

Figure 4. Comparison of the performance of several different algorithms for the classification of the controlled group and each of the four different levels of manganese deficiency

It can be seen in Figure 4 that the Random Forest method has the highest detection accuracy (0.833) after ANN, then KNN (0.786), SVM (0.753) and Naive Bayes (0.716) algorithms were the best classification methods, respectively.

According to Figure 5 and considering the average values of recognition accuracy of the desired classifiers, ANN (0.883), KNN (0.827), SVM (0.784), Random Forest (0.781) and Naive Bayes (0.733) were reported as the most suitable classification methods in identifying each of the four levels of 0, 25, 50 and 75% of zinc nutrient deficiency compared to the controlled group. It is necessary to explain that the number of input features in the ANN algorithm for each of the 0, 25, 50 and 75% levels was equal to 6, 5, 6 and 10 features respectively. In addition, the order of preference of classification methods for each stress level of zinc deficiency are: ANN, SVM, KNN, Random Forest and Naive Bayes at 0% level; ANN, KNN, Naive Bayes SVM and Random Forest at 25% level; ANN, SVM, KNN, Random Forest and Naive Bayes at the 50% level; and ANN, KNN, Random Forest, SVM and Naive Bayes at the 75% level (Figure 5).

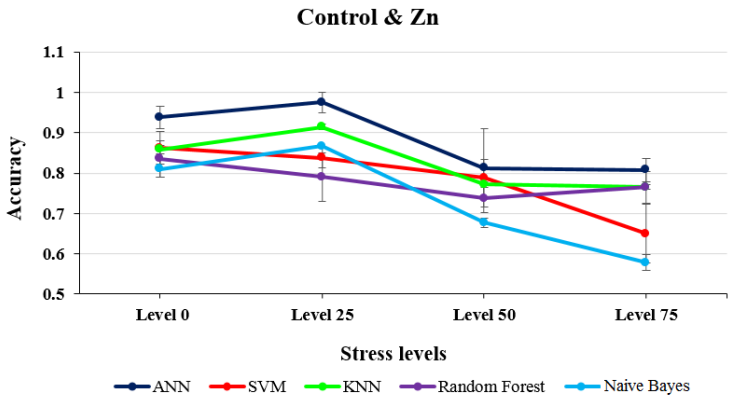

Figure 5. Comparison of the performance of several different algorithms for the classification of the controlled group and each of the four different levels of zinc deficiency

In total, based on the results of comparing five different classification methods, it was determined that ANN (0.895), KNN (0.818), Random Forest (0.804), SVM (0.800) and Naive Bayes (0.751) methods are respectively the best classification methods with the number of two output classes (controlled group and each stress level of deficiency of three nutrients iron, zinc and manganese).

3.2.2. Classification with the number of three and four output classes

As seen in Figure 6, ANN with 13 input features and detection accuracy of 0.700 was recognized as the most appropriate method to separate plants under iron and manganese stress of 0% from the controlled samples, and then KNN (0.663), Naive Bayes (0.630), SVM (0.626) and Random Forest (0.561) were placed. When the output classes of the ANN algorithm were the controlled group and the samples under the stress of iron and zinc nutrient deficiencies at level 0%, it again had the highest recognition accuracy (0.712), but this time with 11 input features. After this, KNN (0.663), SVM (0.607), Random Forest (0.538) and Naive Bayes (0.533) methods had the best performance. To detect manganese and zinc elements at the level of 0% compared to the controlled group, the KNN with 2 input features and with an accuracy of 0.666 was recognized as the best method, and after that, ANN with an accuracy of 0.637 and SVM with an accuracy of 0.580 were in the second and third places, respectively. Then Naive Bayes was in the fourth place with an accuracy of 0.517 and Random Forest was in the last place with an accuracy of 0.504. Generally, it can be said that the order of preference of these classification methods with the number of three output classes is: ANN (0.683), KNN (0.664), SVM (0.604), Naive Bayes (0.560) and Random Forest (0.534).

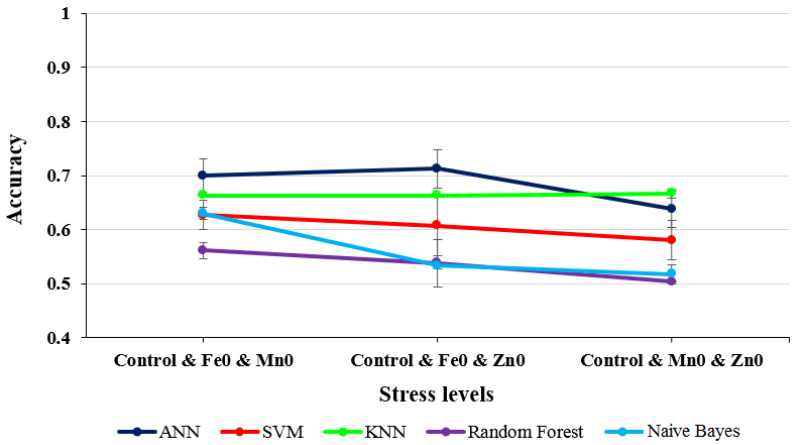

Figure 6. The results of several different classification methods with three output classes

In classification with the output number of four classes (controlled group and groups under stress of iron, manganese and zinc elements at zero level), ANN with 24 input features and recognition accuracy of 0.611 was considered as the most suitable classification method, and then there were KNN (0.521), Naive Bayes (0.426), SVM (0.417) and Random Forest (0.400), respectively (Figure 7).

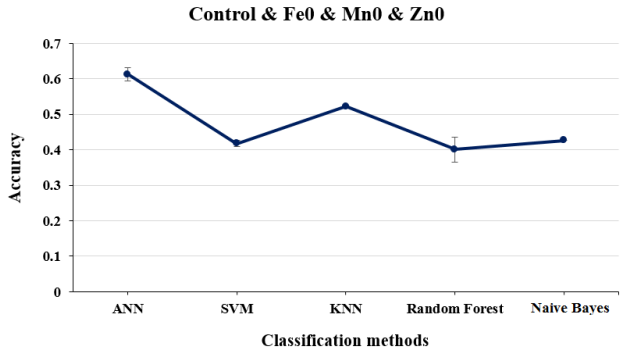

Figure 7. The results of several different classification methods with four output classes

3.2.3. Classification with five output classes

Figure 8 shows the results of several different classification methods with five output classes (controlled group and four levels of deficiency of a nutrient element) for three groups of iron, zinc and manganese elements. As can be seen in Figure 8, in all these groups, the best classification method is the ANN algorithm with an average detection accuracy of 0.478. The number of input features of this classifier in the groups under the stress of iron, manganese and zinc deficiency was 7, 24 and 28, respectively. After this method, the ranking of classification methods was: KNN (0.401), Random Forest (0.304), Naive Bayes (0.300) and SVM (0.293).

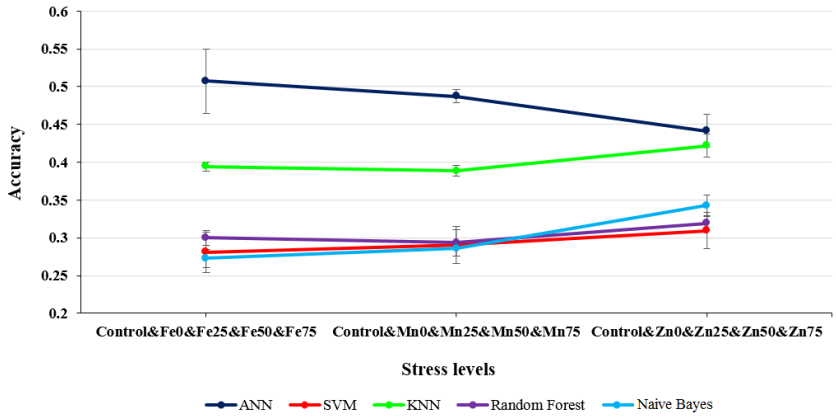

Figure 8. The results of several different classification methods with five output classes

3.2.4. Classification with thirteen output classes

After examining the desired classification methods with the number of thirteen output classes (controlled group and all levels of iron, zinc and manganese nutrient deficiencies), it was found that the ANN with the recognition accuracy of 0.170 and the number of 8 input features has the highest performance in the classification operation, and then there were KNN (0.160), Random Forest (0.114), SVM (0.112) and Naive Bayes (0.110) (Figure 9).

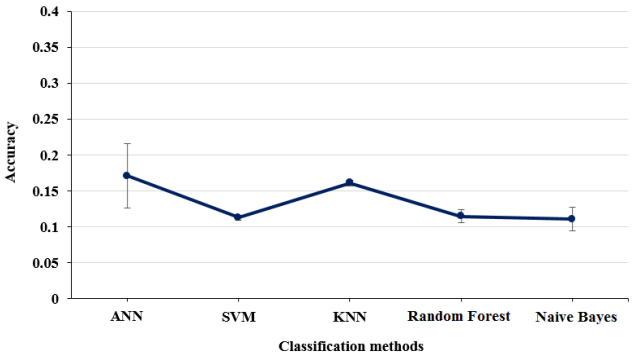

Figure 9. The results of several different classification methods with thirteen output classes

Based on the obtained results, it can be generally said that the order of superiority of the desired methods in carrying out classification operations of different levels under the stress of nutrients iron, zinc and manganese are: ANN (0.567), KNN (0.513), SVM (0.445), Random Forest (0.431) and Naive Bayes (0.429).

It is worth mentioning that these five different classification algorithms showed the highest performance (the average detection accuracy = 0.813) when the number of their output classes was equal to two. Also, the classification operation by the desired methods with three output classes had an acceptable accuracy (0.609). The performance of all these methods in correctly detecting the status of samples with four classes and five output classes reached less than 50%, so that the average detection accuracy for these two modes was 0.475 and 0.355, respectively. When all the levels of iron, zinc and manganese nutrients were considered as the output of these classifiers, the performance of all methods significantly decreased to less than 20% (0.133).

In another study, in order to classify the six conditions of the plant (healthy, lacking elements of calcium, magnesium, sulfur, magnesium-sulfur, as well as multiple deficiencies), artificial neural network algorithms with Multilayer Perceptron (MLP) architecture, Random forest, SVM, Naive Bayes and Convolutional Neural Network (CNN) were compared with each other. The most suitable algorithms in this field were CNN, SVM and MLP algorithms with accuracy of 97.76, 90.55 and 89.70% respectively (Rahadiyan et al., 2023). In a research with the aim of monitoring plant nutrients in the greenhouse, the task of diagnosing and providing iron nutrient deficiency in spinach plants was studied. The most suitable features (G, Area, Energy, Entropy, R and L) were selected from the set of parameters extracted from the images of the samples. Further, the detection of iron deficiency in plants was conducted with an accuracy of 96% by artificial neural network (Nadafzadeh et al., 2024). Kavitha (2024) also used digital image processing technique to identify nitrogen, phosphorus and potassium nutrient deficiencies in rice plants. According to the results, the accuracy of detecting the deficiency of three nutrients nitrogen, phosphorus and potassium by random forest was 94.66, 89.63 and 89.71% respectively. Meanwhile, the Naive Bayes algorithm had relatively weaker performance to identify the nitrogen deficiency (87.83%), phosphorus deficiency (78.58%) and potassium deficiency (79.45%).

4. Conclusion

In this study, identifying the deficiency of three nutrients iron, zinc and manganese in spinach plant was considered. To reach this goal, a set of statistical and intelligent classification methods were examined and compared. Based on the obtained results, it can be said that the order of superiority of the desired methods in the classification of different levels of iron, zinc and manganese nutrient deficiencies are: ANN, KNN, SVM, Random Forest, and Naive Bayes.

Acknowledgments

The authors express appreciation for the financial support provided by Tarbiat Modares University.

References

Ansori, N., A. Rachmad, E.M.S. Rochman, H.B. Fauzan, Y.P. Asmara, 2024. Corn stalk disease classification using random forest combination of extraction features. Commun. Math. Biol. Neurosci., 2024, pp. Article-ID.

Chou, J. J., C.P. Chen, J.T. Yeh, 2007. Crop identification with wavelet packet analysis and weighted Bayesian distance. Computers and electronics in agriculture. 57 (1), 88-98.

Dhillon, K.S., S.K. Dhillon, B. Singh, B.D. Kansal, 1987. Effect of different levels of nitrogen on yield and chemical composition of spinach (Spinacea oleracea L.). J. Research, Punja Agril. Univ. 24 (1), 31-36.

Espejo-Garcia, B., I. Malounas, N. Mylonas, A. Kasimati, S. Fountas, 2022. Using EfficientNet and transfer learning for image-based diagnosis of nutrient deficiencies. Computers and Electronics in Agriculture. 196, p. 106868.

Guo, W.L., H. Nazim, Z.S. Liang, D.F. Yang, 2016. Magnesium deficiency in plants: an urgent problem. The Crop Journal. 4, 83–91.

Igathinathane, C., V.S.S. Prakash, U. Padma, G. Ravi Babu, A.R. Womac, 2006. Interactive computer software development for leaf area measurement. Computers and Electronics in Agriculture. 51 (1), 1-16.

Kavitha, S., 2024. Identification of Nutrient Deficiency Based on Leaf Image Data Using Machine Learning. In 2024 International Conference on Emerging Smart Computing and Informatics (ESCI). March. pp. 1-5. IEEE.

Levine, C.P., N.S. Mattson, 2021. Potassium-deficient nutrient solution affects the yield, morphology, and tissue mineral elements for hydroponic baby leaf spinach (Spinacia oleracea L.). Horticulturae. 7(8), p. 213.

Mallikarjuna, P.B., D.S. Guru, 2022. Selective Harvesting of Tobacco Leaves: An Approach Based on Texture Features. Stat. Appl. 20, 33-49.

Nadafzadeh, M., A. Banakar, S.A. Mehdizadeh, M.Z. Bavani, S. Minaei, G. Hoogenboom, 2024. Design, fabrication and evaluation of a robot for plant nutrient monitoring in greenhouse (case study: Iron nutrient in spinach). Computers and Electronics in Agriculture. 217, p. 108579.

Nadafzadeh, M., S. Abdanan Mehdizadeh, 2019. Design and fabrication of an intelligent control system for determination of watering time for turfgrass plant using computer vision system and artificial neural network. Precision Agriculture. 20 (5), 857-879.

Polder, G., J.A. Dieleman, S. Hageraats, E. Meinen, 2024. Imaging spectroscopy for monitoring the crop status of tomato plants. Computers and Electronics in Agriculture. 216, p. 108504.

Rahadiyan, D., S. Hartati, A.P. Nugroho, 2022. Design of an Intelligent Hydroponics System to Identify Macronutrient Deficiencies in Chili. International Journal of Advanced Computer Science and Applications. 13 (1).

Rahadiyan, D., S. Hartati, A.P. Nugroho, 2023. Feature aggregation for nutrient deficiency identification in chili based on machine learning. Artificial Intelligence in Agriculture. 8, pp. 77-90.

Sohail, R., Q. Nawaz, I. Hamid, S.M.M. Gilani, I. Mumtaz, A. Mateen, J.N. Chauhdary, 2021. An analysis on machine vision and image processing techniques for weed detection in agricultural crops. Pak. J. Agri. Sci. 58 (1), pp. 187-204.

Story, D., M. Kacira, C. Kubota, A. Akoglu, L. An, 2010. Lettuce calcium deficiency detection with machine vision computed plant features in controlled environments. Computers and electronics in agriculture. 74 (2), 238-243.

Sulastri, M.J., D.R. Sulistyaningrum, and H. Nurhadi, 2021. Detection of Nutrient Deficiency in Rice Plants Based on Leaf Image. In 2021 International Conference on Advanced Mechatronics, Intelligent Manufacture and Industrial Automation (ICAMIMIA). December. pp. 143-148. IEEE.

Taha, M.F., A. Abdalla, G. ElMasry, M. Gouda, L. Zhou, N. Zhao, N. Liang, Z. Niu, A. Hassanein, S. Al-Rejaie, Y. He, 2022. Using deep convolutional neural network for image-based diagnosis of nutrient deficiencies in plants grown in aquaponics. Chemosensors. 10 (2), p. 45.

Yang, R., Z. Wu, W. Fang, H. Zhang, W. Wang, L. Fu, Y. Majeed, R. Li, Y. Cui, 2023. Detection of abnormal hydroponic lettuce leaves based on image processing and machine learning. Information Processing in Agriculture. 10 (1), pp. 1-10.

Adaptive nonlinear dynamic system identification for separation process of combine harvester

Tarek Kösters [a,*], Oliver Nelles [a]

[a] Automatic Control – Mechatronics, University of Siegen, Siegen, Germany

* Corresponding author. Email: tarek.koesters@uni-siegen.de

Abstract

In this paper, we introduce a novel method for online identification of the nonlinear dynamic input/output behavior of a combine harvester's separation process. This nonlinear dynamic process is highly influenced by crop properties of the harvested fruit. Current model approaches, based on previously gathered data, can only partially capture the actual process behavior. As consequence of changes in the crop properties, the models fail to approximate the process. This necessitates adaptive modelling techniques to incorporate the current conditions. We address this by using an initial dynamic nonlinear model, based on the local-model-network (LMN) architecture, trained with data from a previous wheat harvest. For adaptation we propose to employ the recursive least squares (RLS) algorithm for computational efficient model updates. Our approach also considers the variability in crop types across different fields, by introducing a variable forgetting factor. Hence, the model adaptation is responsive to these variations through situation-dependent adjustments in the adaptation algorithm. This ensures robust and rapid model updates. Field trials have validated the effectiveness of our adaptation algorithm across various fields and crops. Focused on the threshing and separation section, we demonstrated the ability of the model adaptation to accurately predict separation efficiency in wheat. Decreasing error rates on test data indicate both the adaptation speed and robustness. Therefore, this novel approach using dynamic nonlinear model adaptation significantly increases the resulting process information in comparison to state-of-the-art methods. In summary, a fast and robust adaptation to incorporate the current harvesting conditions into a dynamic nonlinear model is developed.

Keywords: Online-Identification, Nonlinear Dynamic Model, Combine Harvester, Machine-Learning

1. Introduction

The combine harvester is a crucial part of modern crop harvest. It can seamlessly integrate various tasks. These tasks range from cutting and collecting the crop from the field as well as the separation of the crop into its valuable parts, e.g. grains, and non-valuable parts. The most important task is the separation that takes place inside the machine. Historically, the main development enhanced the throughput capacity while ensuring high quality harvest results. Exemplary investigations can be found in the work by Nguyen (2008) or Schwarz (2018) and the references in there.

Over the last two decades research and development have also encountered the field of automation and operator support (Böttinger, 2023). This is a result of the wide application field a combine harvester is deployed to. On the one hand, different crop types are harvested. On the other hand, the harvest takes place under environmental conditions that can change dramatically, caused by weather, time of harvest or field conditions. To enable the combine harvester to react on these various conditions, the separation process is equipped with several adjustment options. Up to ten possible adjustments can be performed by the operator strongly influencing the process in an interconnecting manner. Consequently, precise alignments of the process to the current conditions can be made. However, finding the optimal adjustment setup, results in a complex task for the operator. Hence, methods to automatically find the best adjustments aligned with the current conditions have been developed to support the operator in this demanding task (Eggerl, 2017; Hermann, 2018; Vöcking et al., 2017).

A major part of all automation systems is played by process models. In general, the process comprises a nonlinear dynamic behavior, e.g. (Hermann et al. 2016; Maertens et al., 2001). Different approaches have been employed to derive models of the process. This ranges from physical-based models, e.g. (Miu and Kutzbach, 2000) to data-driven models, e.g. (Craessaerts et al., 2007; Kösters and Nelles, 2023). However, these models are not suited for general application. This is caused due to very specific conditions, e.g., how data were collected or due to models only describing general process properties which are too inaccurate for automation purpose.

To tackle this problem Neu et al. (2012) and Maertens et al. (2004) propose adaptive model approaches. They incorporate information of the current process operation into the models to keep up with the present conditions. However, none of these approaches can incorporate both the nonlinearity and the dynamics of the process into their adaptive models. Consequently, in this contribution we propose a method able to fill this research gap.

Adaptive modeling utilized in automation methods requires low computational demand to be able to be incorporated into embedded hardware. One methodology capable of modeling nonlinear dynamic processes and ensure low computational demand during adaptation are local model networks (LMNs), e.g. (Skrjanc et al., 2019). Additionally, Kösters and Nelles (2023) showed their suitability for modeling the combine harvester separation processes. Hence, in this contribution we propose an adaptation algorithm based on this model structure.

This contribution is structured as follows. First, Sect. 2 introduces the combine harvester separation process in detail. Additionally, the LMN framework and its corresponding adaptation algorithm is presented. With these methods harvest experiments are conducted and the results are discussed in Sect. 3. Finally, the work is concluded in Sect. 4.

2. Materials and Methods

The following section is divided into two parts. First, we introduce the combine harvester process under investigation. Second, the adaptive LMN framework is presented. Additionally, novel extensions made to this framework aligned with the specific combine excitation are introduced.

2.1. Combine Harvester Separation Process

In this contribution, a hybrid combine harvester is investigated. Furthermore, the investigation is focused on the threshing and secondary separation section of the combine. In Fig.1 this part of the combine harvester separation process is shown.

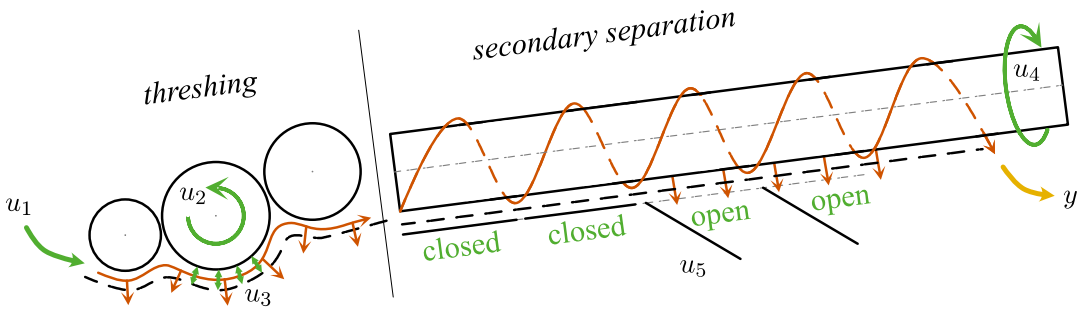

Figure 1. Combine harvester separation process and adjustment options.

The harvested crop first enters the threshing section. Its amount (u_1) is measured right before entering the threshing section. It is well known that the amount of crop processed inside the combine harvester is one of the most influencing factors of the whole process. Consequently, it is considered as the first input to the process model, which is used for the adaptation. Inside the threshing section, two adjustment options are available. The first option is the rotational speed (u_2) of the threshing drum. Together with the concave clearance (u_3) it influences the threshing aggressiveness. This in turn has influence on the composition and distribution of the material flows leaving the threshing section. The more aggressive the threshing is performed the better the grains are separated. Thus, these options are also utilized as inputs to the model.

Two departing material flows are produced by the threshing section. The first material flow exits the threshing section through the concave. The second material flow is conveyed to the secondary separation. For this study only the second material flow is of importance. It is further processed in the secondary separation. Here, the rotational speed of the rotor (u_4) can be set. On the one hand, it influences the grain separation of the remaining grains in the secondary separation. On the other hand, also the separation of short straw and chaff is influenced. To avoid unnecessary separation of materials other than grain (MOG), rotor flaps (u_5) can be closed to cover the rotor concave. This stops material form leaving the secondary separation

on this way. Finally, the grain losses (y) are measured at the end of the secondary separation. It is the number of grains in the material flow leaving the rotor to the field.

2.2. Local Model Network – LMN

Local Model Networks (LMNs) are structured by dividing the model space into subspaces, each defined by one function linearly dependent on its parameters. This division is achieved through the activation functions Φ_i, which determine the local activity based on the position within the model space. The combined local model outputs and activation functions produce the output value of the approximator, calculated as

$$\hat{y} = \sum_{i=1}^{n_{\mathrm{LM}}} \mathrm{LM}_i(\underline{x}, \underline{\theta}_i)\Phi_i(\underline{z}, \underline{c}_i, \underline{\sigma}_i) \quad (1)$$

The inputs to the local models $\underline{x}$, and activation functions $\underline{z}$, are selected based on the required features. Two parameter groups can be distinguished. Each local model is defined by its local parameters $\underline{\theta}_i$. The partitioning of the model space is realized through activation functions. Here, normalized Gaussians are deployed, where each Gaussian $\mu_i(\underline{z})$ is defined by its mean $\underline{c}_i$ and standard deviation $\underline{\sigma}_i$ as shown in the following formulas:

$$\mu_i(\underline{z}) = \exp\left(-\frac{1}{2}(\underline{z} - \underline{c}_i)^T \mathrm{diag}(\underline{\sigma}_i)^{-1}(\underline{z} - \underline{c}_i)\right) \quad (2)$$

$$\Phi_i(\underline{z}) = \frac{\mu_i(\underline{z})}{\sum_{j=1}^{n_{\mathrm{LM}}} \mu_j(\underline{z})} \quad (3)$$

The normalization ensures partition of unity across the input space, meaning the sum of all activation functions equals one at every point in the input space $\underline{z}$.

Training of the LMN involves two aspects. On the one hand, the model structure has to be defined through the parameters $\underline{c}_i$ and $\underline{\sigma}_i$. Various methods from heuristic-based to data-driven approaches exist (Nelles, 2020). In this study, we deploy the data-driven local-linear-model-tree (LOLIMOT) algorithm, to establish the LMN structure (Nelles, 2020). On the other hand, the local model parameters $\underline{\theta}_i$ must be identified. The utilized structure allows to deploy the least squares (LS) algorithm for their identification. To incorporate the locally different activity of each local model, the weighted LS algorithm is used. Hence, the local model parameters can be identified by

$$\underline{\hat{\theta}}_i = \left(\underline{X}^T \underline{Q}_i \underline{X}\right)^{-1} \underline{X}^T \underline{Q}_i \underline{y} \quad (4)$$

Here, $\underline{X}$ is defined as regressor matrix and $\underline{Q}_i = \mathrm{diag}\left(\left[\Phi_i\left(\underline{z}(1)\right) \quad \cdots \quad \Phi_i\left(\underline{z}(N)\right)\right]\right)$ is used to realize the local weighting for each local model.

With this framework a combine separation model is build. It is trained from data collected during field tests, see (Kösters and Nelles, 2023). For the adaptation algorithm it serves as initial model that is updated to fit the current conditions.

2.3. Adaptation Algorithm

Similar to the training of the LMN explained in the previous section, the adaptation can be performed in two ways. The first update possibility involves the structure of the LMN ($\underline{c}_i, \underline{\sigma}_i$). The other option is to update the local model parameters ($\underline{\theta}_i$). Both possibilities have been investigated with the result of different algorithms (Skrjanc et al., 2019). Additionally, it is stated that a structure update is much more complex than updating the local model parameters. Hence, structure updates are only advisable if the underlying process nonlinearity changes significantly or no data are available to train an initial model to start the adaptation from (Lughofer, 2011; Nelles 2020).

For the combine separation model, we assume that significant changes in the underlying nonlinearity are not to be expected. Furthermore, data are available to start the adaptation with a good initial model. Consequently, in this contribution we propose to only update the local model parameters ($\underline{\theta}_i$).

Similar to the initial training, the structure of the LMN allows to utilize the computationally effective recursive least squares (RLS) algorithm to update these parameters. To incorporate the local activity introduced through the LMN, the weighted RLS is utilized here (Lughofer, 2011). It allows for a recursive update rule, which is given by

$$\underline{\hat{\theta}}_i(k) = \underline{\hat{\theta}}_i(k-1) + \underline{\gamma}_i(k)\left(y(k) - \underline{x}^T(k)\underline{\hat{\theta}}_i(k-1)\right), \quad (5)$$

$$\underline{\gamma}_i(k) = \frac{1}{\rho(k)/\Phi_i\left(\underline{z}(k)\right)+\underline{x}(k)^T\underline{P}_i(k-1)\underline{x}(k)}\underline{P}_i(k-1)\underline{x}(k), \quad (6)$$

$$\underline{P}_i(k) = \frac{1}{\rho}\left(\underline{I}-\underline{\gamma}_i(k)\underline{x}^T(k)\right)\underline{P}_i(k-1). \quad (7)$$

This adaptation rule is applied separately for each local model. This allows to only update regions of the model that have been excited during the adaptation. Furthermore, it prevents the model from unlearning the initial model behavior in unexcited regions. This property is advantageous for the combine separation model, since during standard operation, usually no complete excitation of the operating region is performed.

To be able to keep up with time variant processes a forgetting factor ($\rho(k)$) is utilized. It allows to place more importance on recently collected data in comparison to data collected a long time ago. Keeping the forgetting factor constant would result in the same forgetting in every situation. However, when the process operates under well excited conditions, e.g. dynamical changes in the process inputs, the resulting data are more informative than in situation with low excitation. To avoid information loss in low excitation situations and allow greater changes in well excited situations, a time variant forgetting factor is proposed. It is based on the method proposed by Fortesque et al. (1981). With the incorporation of the local model activity the algorithm is defined by

$$\rho(k) = 1 - \left(1 - \underline{x}(k)^T\underline{\gamma}_i(k)\right)\Phi_i(k)e(k)^2/\Sigma_0, \quad (8)$$

with $e(k)^2$ being the squared model error and Σ_0 being a tuning factor to adjust the adaptation speed. Low values for Σ_0 result in faster adaptation, whereas high values for Σ_0 reduce the adaptation speed.

2.4. Experimental Setup

To test the stated adaptation algorithm, we developed an experimental setup which was conducted during several harvest periods. The experiment is subdivided into two parts. The first phase is called adaptation phase. Here, data are collected that are used for adaptation of the combine harvester separation model. The second phase comprises the collection of test data that are utilized to test the model during the adaptation phase. Figure 2 shows the path at which the combine is operated on an exemplary field.

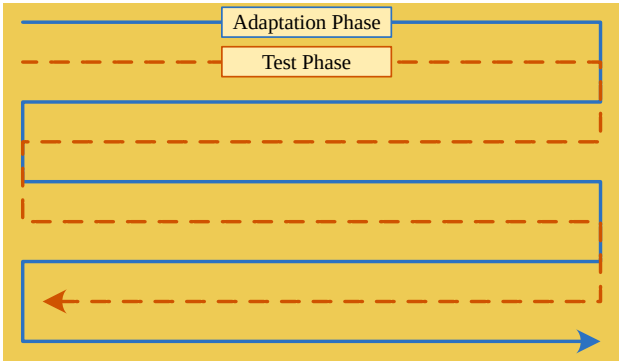

Figure 2. Experimental setup for harvest test.

To reduce the effect of crop changes that arise only locally on the field, both phases operate at every second row during harvest. Because of that, the maximum similarity for both phases can be ensured. Beside the path of operation also the excitation of the inputs to the process must be chosen.

For the test phase, an OMNIPUS (Kösters et al. 2022) excitation is chosen. Its design is desired to excite the dynamics of the process on the one hand. On the other hand, it comprises an equally distributed excitation of the input amplitudes. Due to these properties, it ensures that the model can be tested for the whole operating range of the process.

For the adaptation phase an excitation signal is derived from typical combine operation. It is much less informative, since typically once a well performing operating point is found, the combine settings are only marginally changed.

To evaluate the model performance, the updated model is saved at several time instances during the adaptation phase. These saved models are than tested on the collected data from the test phase. Hence the progress of the model quality can be investigated. The root-mean-squared error

$$\mathrm{RMSE} = \sqrt{\frac{1}{N}\sum_{i=1}^{N}\left(y(i) - \hat{y}(i)\right)^2} \tag{9}$$

is utilized as quality criteria.

3. Results and Discussion

This section shows and discusses the results of the experiment introduced in Section 2.4. Three different investigations are conducted. First, the estimated output of the updated model is compared to the measured process output. The second investigation shows the progress of the model error on test data. Finally, the model prediction on test data is presented.

3.1. Prediction during Adaptation Phase

Figure 3 shows the comparison of the predicted model output and the measured grain losses during the beginning of the adaptation.

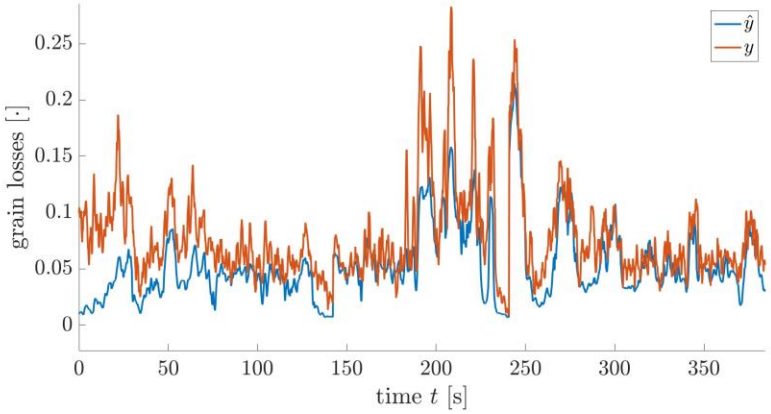

Figure 3. Comparison of predicted and measured grain losses during adaptation phase.

At the very beginning, it can be seen, that the estimated output and the measured output deviate from each other. From here onwards, the approximation starts approaches to the measured grain losses. After approximately 150 seconds of operation, the prediction accurately follows the measured value. This behavior can also be seen for the following operation. Therefore, it can be reasoned that after an initialization phase the adapted model is able to accurately predict the nonlinear dynamic process behavior. However, the prediction only allows to reason about the prediction of the model at the current operating point.

3.2. Model Performance during Adaptation Phase

To evaluate the model performance not only for the current operating point, but for the whole input space of the process, the second investigation evaluates the updated model during the adaption phase on the data from the test phase. This is done several times during the adaptation to gather information on the progress of the model performance. Figure 4 shows this progress for different choices on the tuning-parameter Σ_0.

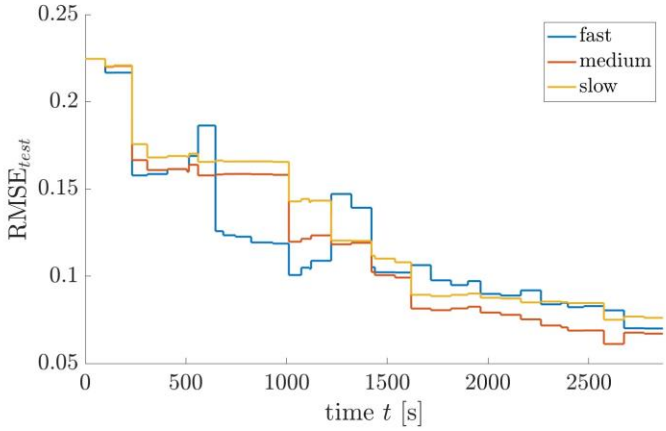

Figure 4. Model performance during adaptation on test data for different Σ_0.

In general, all choices on the adaptation speed Σ_0 result in a decreasing progress of the model error. Hence, the adaptation fulfills its desired goal to incorporate the current conditions into the updated model. The different choices of the adaptation speed result in different behavior of the model error. The progress of the fast adaptation speed drops the fastest in comparison to the other adaptation speed choices. However, especially in the time period $t = [500\,\text{s} \ldots 1400\,\text{s}]$ the model error does not increase monotonically but increases and decreases several times. This behavior shows that this choice on the adaptation speed reduces the robustness of the algorithm.

The model errors for the medium and slow choice behave very similar. However, the medium adaptation speed algorithm outperforms the slow adaptation speed throughout the whole experiment. Additionally, at the end of the adaptation phase the medium adaptation speed shows the best model performance. In consequence, the medium adaptation speed is chosen as robust and well performing parameterization for the adaptation algorithm.

Figure 5 shows the prediction of the updated model at the end of the adaptation phase for the medium adaptation speed choice.

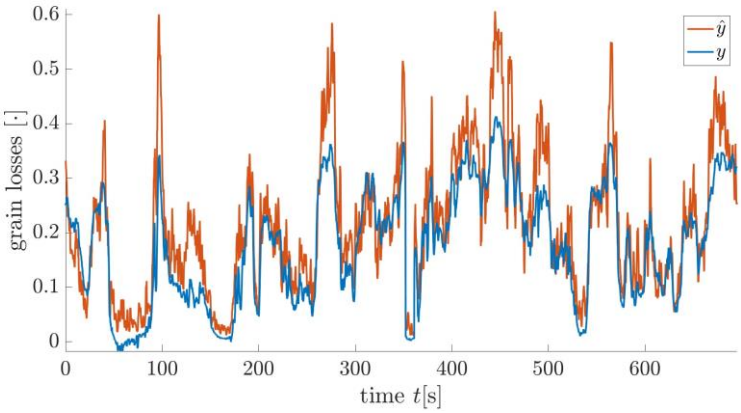

Figure 5. Prediction of updated model at the end of the adaptation phase on test data.

In comparison to the measured grain losses, the updated model accurately predicts the process behavior. The model adaptation thus enables the model to accurately predict the process even if the conditions are unknown in advance.

4. Conclusions

In this contribution we propose a novel adaptation algorithm to update a nonlinear dynamic model for the combine harvester separation process. The investigations conducted show, that the proposed adaptation algorithm is able to incorporate the current conditions into the model. The proposed algorithm can also cope

with different excitation situations that could be present during the combine operation. Additionally, the parameter study on the adaptation speed reveals a robust and well performing parameterization for the adaptation algorithm. This choice comprises a compromise between speed of adaptation and adaptation robustness. The model performance achieved with this choice is considered as satisfactory. Thus, the model adaptation enables the model to accurately predict the process even if the conditions are unknown in advance. The accurate nonlinear dynamic model therefore delivers process information that are not available with the state-of-the-art methodology.

Consequently, in future work the model adaptation is utilized as basis to optimize the combine settings. Based on the continuously updated model, it is intended to develop an optimization algorithm that automatically finds to optimal operating point for the combine harvester under the present conditions.

References

Böttinger, S., 2023. Mähdrescher. Jahrbuch Agrartechnik 2022, vol. 34.

Craessaerts, G., Saeys, W., Missotten, B., De Baerdemaeker, J., 2007. A genetic input selection methodology for identification of the cleaning process on a combine harvester, part ii: Selection of relevant input variables for identification of material other than grain (mog) content in the grain bin. Biosystems Engineering 98, 297–303.

Eggerl, A., 2017. Optimization of combine processes using expert knowledge and methods of artificial intelligence. Ph.D. thesis, Technische Universität Dresden, Dresden, Germany.

Fortescue, T., Kershenbaum, L., Ydstie, B., 1981. Implementation of self-tuning regulators with variable forgetting factors. Automatica 17, 831–835. https://doi.org/10.1016/0005-1098(81)90070-4.

Hermann, D., Bilde, M.L., Andersen, N.A., Ravn, O., 2016. A framework for semi-automated generation of a virtual combine harvester. IFAC-PapersOnLine 49, 55–60. 5th IFAC Conference on Sensing, Control and Automation Technologies for Agriculture.

Hermann, D., 2018. Optimisation of combine harvesters using modelbased control. Ph.D. thesis, Technical University of Denmark, DTU Elektro, Lyngby, Denmark.

Kösters, T., Heinz, T.O., Nelles, O., 2022. Optimization based excitation signal design tailored to application specific requirements. IFAC-PapersOnLine 55, 451–456. 2nd Modeling, Estimation and Control Conference MECC 2022

Kösters, T., Nelles, O., 2023. Nonlinear dynamic system identification of separation unit for raw materials. In *2023 IEEE Conference on Control Technology and Applications (CCTA)*, pp. 992–997.

Lughofer, E., 2011. *Evolving Fuzzy Systems - Methodologies, Advanced Concepts and Applications*. Springer Berlin, Heidelberg.

Maertens, K., De Baerdemaeker, J., Ramon, H., De Keyser, R., 2001. An analytical grain flow model for a combine harvester, part i: Design of the model. Journal of Agricultural Engineering Research 79, 55–63. https://doi.org/10.1006/jaer.2000.0679.

Maertens, K., Ramon, H., De Baerdemaeker, J., 2004. An on-the-go monitoring algorithm for separation processes in combine harvesters. Computers and Electronics in Agriculture 43, 197–207. https://doi.org/10.1016/j.compag.2004.01.004.

Miu, P., Kutzbach, H., 2000. Simulation of threshing and separation processes in threshing units. Agrartechnische Forschung Sonderheft 6, 1–7.

Nelles, O., 2020. *Nonlinear System Identification*. Springer International Publishing.

Neu, S., Vöcking, H., Wilken, A., 2012. Online modellbildung verfahrenstechnischer prozesse. VDI-Berichte Nr 2173.

Nguyen, X.T., 2008. Grundlagenuntersuchungen zur Kombination von zwei Tangentialdreschwerken mit tangentialer Gutzuführung. Ph.D. thesis, Technische Universität Dresden, Dresden, Germany.

Schwarz, M., 2018. Grundlagenuntersuchungen am Mähdrescher-Vorbereitungsboden mit pneumatischer Unterstützung. Ph.D. thesis, University of Hohenheim, Hohenheim, Germany.

Skrjanc, I., Iglesias, J.A., Sanchis, A., Leite, D., Lughofer, E., Gomide, F., 2019. Evolving fuzzy and neuro-fuzzy approaches in clustering, regression, identification, and classification: A survey. Inf. Sci. (Ny) 490, 344–368.

Vöcking, H., Heitmann, C., Wilken, A., 2017. Automatic adjustments of combine harvesters. In *Land.Technik AgEng 2017*, VDI Verlag, pp. 99–104.

Operational limits for UAV livestock counting based on foundation models

Ricardo Ruiz Sánchez[a], Adrien Lebreton[b], João Valente[c,*]

[a] University of Utrecht, Utrecht, The Netherlands

[b] L'Institute d'Elevage Idele, Digne-les-bains, France

[c] Spanish National Research Council (CSIC), Madrid, Spain

* Corresponding author. Email: joao.valente@csic.es

Abstract

In the face of scarce resources and an increasingly challenging environment, resource-efficient management strategies driven by drone services can shape a more resilient society by implementing precision livestock farming. Livestock causes different pressures with different effects on the ecosystem depending on its numbers. Excessive numbers lead to overgrazing, resulting in a reported decline in biodiversity. A better counting livestock method contributes to a stronger monitoring system to ensure long-term sustainability in ecosystem services. In this paper, two foundation models are compared across different livestock imagery taken by UAV to determine what factors lead to a better counting performance. GroundingDINO and T-Rex were the two state-of-the-art detection-based models. These pre-trained models do not require any supervised training with annotated images. The dataset tested included heterogeneous scenarios at different altitudes of cattle and goat species. Its metadata defines the different operation conditions. Previous works evaluated the performance and limitations of foundation models on different objects, from small items to dense or camouflaged entities. However, this paper aims to identify operational limits that facilitate safe counting accuracy for cattle farmers when current limitations and risks of these foundation models apply. UAV imagery taken between 15 meters of sparse herd scored the best performance using the foundation models T-Rex and Grounding-DINO by offering the lowest Normalised Absolute Error (NAE). However, as the complexity of the scenarios increased with smaller sizes of animals observed from an altitude of 50m, only T-Rex was able to count small livestock such as goats to some extent. Defining operational limits for aerial footage reduces the limitations of emerging foundation models' predictions, facilitating its immediate application in real-world scenarios.

Keywords: Livestock management, UAV imagery, Object counting, Computer vision, Foundation models

1. Introduction

In the face of scarce resources and an increasingly challenging environment, drone services can shape a more resilient society by providing resource-efficient management strategies. In fact, remote sensing information obtained by UAV (Unmanned Aerial Vehicle) technology is becoming more relevant (Aquilani et al., 2022), where radio frequency tags along with global positioning systems, and accelerometers were frequently used in pasture-based systems. Too much livestock generates high-sheep grazing pressure on pasture systems such as the Scottish Highlands, reducing the biodiversity, a phenomena known as "wet desert". (Marrs et al., 2020). For example, in the domain of computer vision, images obtained by UAV and processed by artificial intelligence have been used to count livestock, reducing labour costs and significant errors (Bárbulo Barrios et al., 2024; Sarwar et al., 2018) .

However, the rapid development of these machine learning technologies is not only attributed to new-state-of-the-art algorithms and architectures (such as YOLOv8), but also to the availability of big data for training the model. The cost of these large, annotated datasets is high, as supervised learning requires manual feature labelling that increases labor costs and generalisation errors (Pu et al., 2022). To face this problem, new foundation models based on self-supervised learning do not require any human annotators as input (Xu et al., 2020). In this study, two pre-trained models regarded as foundation models are considered: Grounding DINO and T-Rex.

GroundingDINO is a generic object detector with Referring Expression Comprehension (REC) that allows the user to add attributes to better describe the target object (Liu et al., 2023). GroundingDINO detects the object as an image and its class as a text, returning a pair of object boxes and noun phrases. T-Rex is a detection-based counting model that detects all objects with similar patterns given an initial detection drawn by the user (Jiang et al., 2023). Unlike other models limited by categories, T-Rex perspective focuses on providing an open-set counting system that does not require any categories. Additionally, it is interactive,

making it possible to correct errors, such as those caused when a model generalises across heterogeneous scenarios. This is achieved through intuitive visual feedback that facilitates the user's interpretation and by using a visual promptable system. This foundation model can be used as an object counter or automatic-annotation tool in domains such as livestock, but also transportation or biology, among others.

Although previous works evaluate the performance and limitations of other foundation models such as Segment Anything Model (SAM) on camouflaged objects (Tang et al., 2023) or small and dense objects (Ma et al., 2023), this paper aims to identify operational limits that facilitate a safe counting accuracy for livestock farmers when these limitations and risks of foundation models applies. To achieve this goal, the following research questions arise:

- What metadata contained in the images describes the operational envelope of UAV footage?
- How do the foundation models T-Rex and Grounding DINO count performance vary across a range of heterogenous operational parameters?
- Which instructions could avoid the limitations of these foundation models to be applied in livestock management?

2. Materials and Methods

This section comprises four sub-sections. The study area indicated where the UAV aerial images were captured. The data section described what types of livestock, cattle, and goats, were included in this study. The ground truth section showed how to obtain the ground truth values required to test the foundation model's count performance. Lastly, the section evaluation metrics explains how to quantify this counting performance.

2.1. Study area

The subset of the dataset used in this study included 108 aerial pictures of cattle and goats taken in two different locations. On the one hand, the cattle footage is taken at the Experimental Farm of Derval, located in France with the collaboration of L'Institute d'Elevage. This farm specializing in dairy herd management includes 80 Prim'Holstein dairy cows and 100 hectares of terrain[1]. On the other hand, the goat's footage is taken in the Axarquía region (Spain) with the collaboration of a local goatherd, anonymized as "C." The goat herd breeds are Malagueña, Florida, and Murciano Granadina[2]. Figure 1 shows both locations and their sampling locations.

[1] https://formation-pays-de-la-loire.chambres-agriculture.fr/efea/localiser-les-sites-de-formation/etablissements-en-loire-atlantique-44/ferme-experimentale-de-derval/

[2] https://www.mapa.gob.es/es/ganaderia/temas/zootecnia/razas-ganaderas/razas/catalogo-razas/

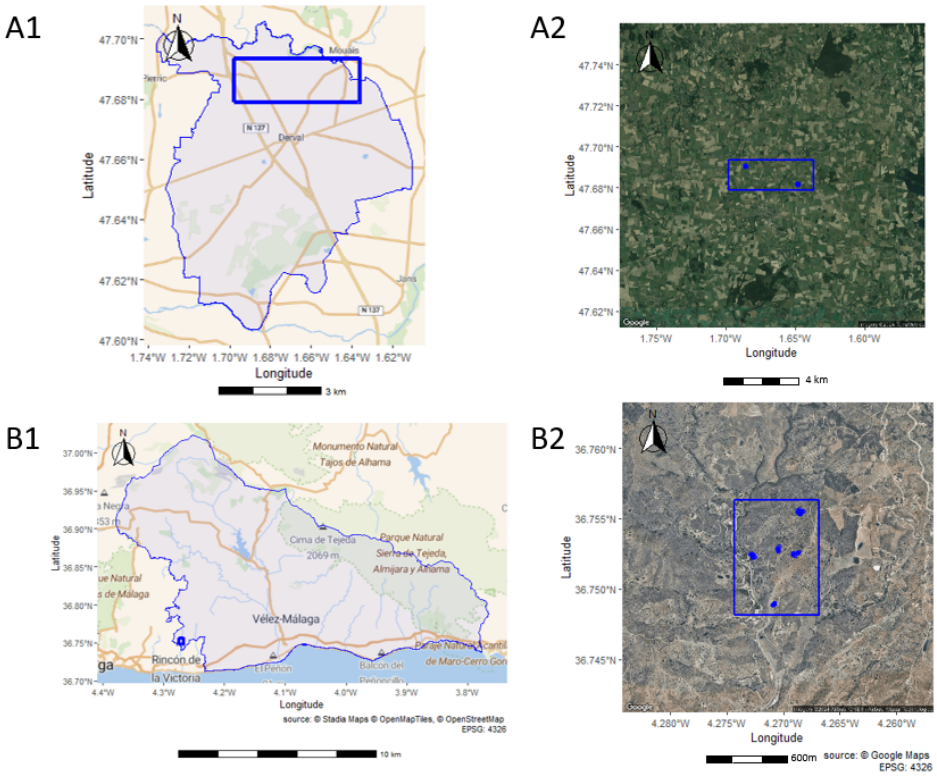

Figure 1. The Experimental Farm of Derval (A1) in France, and the Axarquía region (B1) in Spain. The blue bounding boxes revealed the sampling area, while the blue points showed the location of each aerial image.

2.2. Data

The relative heights of 15m, 30m and 50m defined the data collection establishing three groups. Each of these groups contained 18 UAV images for each type of livestock. The total amount was 54 pictures per specie. The image dimension for the goat herd was 4608x2592 (Potensic Atom), while the cattle's footage was 4032x2268 (DJI Mini 3 Pro). Since previous studies used 80m to reduce disturbance to livestock (Sarwar et al., 2020), the drone's takeoff and landing area was far from the herd. Additionally, the drone was operated at a minimal speed at all times and descending from 50m to 30m and 15m slowly. Finally, to test the foundation models' performance and to detect possible limitations, the pictures captured different sizes of herd and various degrees of clustering.

2.3. Ground Truth

The comparison between the foundation model T-Rex and Grounding DINO across heterogeneous operational parameters required the number of livestock in the scene to measure its model counting performance. The reason is that counting evaluation metrics needed the ground truth values to be computed. For this purpose, a grid of 1000x1000 px created different areas for counting the livestock with the purpose of reducing systematic errors. This idea was based on grid-based sampling methods, which are used in fields such as Ecology to assess species richness (Mueller et al., 2021).

Additionally, the foundation model T-Rex also required a bounding box of the target object, in this case, a goat or cattle. To improve the reproducibility of the experiment, the bounding box used as an input for T-Rex is manually measured and stored. This first bounding box was the detected object with the highest accuracy level using Grounding DINO, if possible. This was not always the case, since on occasions the detected object did not correspond with the target object, even achieving the highest detection accuracy level.

2.4. Evaluation metrics

The Mean Absolute Error (MAE) and the normalised relative error (NAE) assessed the counting performance of the models. Where (n), is the total number of images, and (y) and ($\hat{y}$) are respectively the real (ground-truth) and predicted counts. These metrics were applied individually and grouped by the three altitudes and clustering degree. As MAE increased, the counting performance decreased. On the contrary, a decrease in the NAE increased the counting performance. The Eq (1) and Eq (2) show both metrics used to evaluate counting performance.

$$MAE = \frac{1}{n}\sum_{i=1}^{n}|y_i - \hat{y}_i| \quad (1)$$

$$NAE = \frac{1}{n}\sum_{i=1}^{n}\frac{|y_i - \hat{y}_i|}{y_i} \quad (2)$$

Previous studies included these evaluation metrics in the field of object counting, and applied them to specialised datasets for this task, such as FSC147 and CARPK (Shi et al., 2023).

2.5 Methods

The software used to collect the metadata from the UAV footage was the Exiftool software using the R library Exiftoolr (O'Brien, 2024). One of the metadata used to define the operational envelope for the drone model DJI Mini3 Pro was the "RelativeAltitude", creating the heights categories 15m, 30m and 50m to test the foundation counting performance. For the Potensic Atom drone model, only the "GPS Altitude" was available. The GPS Latitude and Longitude revealed where the flight operation was conducted. Lastly, the date of the image's capture allowed us to add auxiliary information such as hourly weather conditions.

The Open-meteo API[3] in R used the date to retrieve their weather conditions with the library Openmeteo (Pisel, 2023). The metadata provided the data required to query the weather history, offering a location and a point in time. The cloud coverage was selected as a relevant variable, since previous studies on counting livestock created different training datasets based on the cloud coverage highlighting its effect on detection performance (Sarwar et al., 2018).

After gathering all the metadata and auxiliary information, the foundation models T-Rex and Grounding DINO assessed their counting performance by detecting the goats or cattle of this study-s dataset. For Grounding DINO, the category names "goat", and "cattle" or "cow" with an accuracy threshold set at 0.25 generated the detections without any need to train the model. The bounding box from the detection with the highest accuracy level from the Grounding DINO detection, or manually measured, provided the only input required by T-Rex, the first target object. For T-Rex, the API kindly facilitated by the International Digital Economy Academy (IDEA) team generated two outputs. The masks of all the detected objects and the object detections. These results contained the bounding box, score, and mask for each detection. The centroids calculated from these objects allowed to quantify the clustering degree of the UAV images.

An analysis of the spatial patterns of these centroids used the Clark-Evans test to detect how sparse or clustered the herd was. This was in line with studies that employed similar strategies (Ramage et al., 2013). The R package "spatstat" (Baddeley et al., 2016) performed the Clark-Evans test.

3. Results

The location and weather conditions of a subset of UAV images shown in Table 1 defined the operational envelop based on the metadata. The cloud coverage during the month of May was higher in the Cattle UAV dataset than the goat UAV footage located in southern latitudes. In both cases, both footage contained images taken at the altitudes of 15m, 30m and 50 min.

[3] https://open-meteo.com/en/docs/historical-weather-api

Table 1. UAV Information obtained from the metadata to define operational envelope.

UAV imagery	Location			Weather Conditions	
	lat	lon	Altitude (m)	Date (yyyy-mm-dd hh:mm:ss)	Cloud Coverage
Cattle					
DJI_0274.JPG	47.682	-1.648	50	2024-05-07 10:02:38	33
DJI_0321.JPG	47.690	-1.686	30	2024-05-07 11:11:4	48
DJI_0302.JPG	47.682	-1.648	15	2024-05-07 10:10:06	33
Goat					
SING0033.JPG	36.749	-4.270	15	2024-04-24 12:35:02	4
SING0170.JPG	36.752	-4.269	50	2024-05-25 20:36:52	19
SING0062.JPG	36.752	-4.272	30	2024-05-25 12:42:25	0

The counting performance of T-Rex and Grounding DINO across these relative altitudes varied based on the specific type of livestock.

For the goat herd (A), as the altitude increased, the number of errors also grew (please, refer to Table 2). When comparing both foundation models, Grounding DINO effectiveness was limited to 15 meters, having a sudden increase in errors at 30m. Conversely, T-Rex was more stable, suffering less variation in the counting performance across the range of altitudes. In general, both models' performance was similar at 15m of altitude. However, at 15m only T-Rex was able to count livestock to some extent.

For the cattle herd (B), the increase in altitude did not lead to an increment in errors (please, refer to Table 2). In fact, Grounding DINO scored better counting performance at 30m altitude than at 15 m. Regarding T-Rex, the variance in the NAE and MAE metrics across the altitude was less, offering a more stable counting performance. However, in overall, the NAE values were higher than Grounding DINO indicating a worse counting performance.

Apart from the type of livestock, its number and background context greatly differed between both datasets. The number of goats ranged from 18 to 226, while the number of cattle varied from 7 to 19. In terms of background, the cattle dataset took place in green pastures, while the goat dataset displayed a more challenging scenario with livestock hidden in bushes and trees.

Table 2. The foundation model Grounding DINO and T-Rex counting performance applied to two types of livestock across different relative altitudes.

	Counting model performance			
	NAE		MAE	
UAV imagery	T-Rex	Grounding DINO	T-Rex	Grounding DINO
Cow				
15m	0.0556	0.126	0.667	1.89
30m	0.0944	0.089	1.39	1.33
50m	0.0694	0.25	1.06	3.89
Goat				
15m	0.188	0.178	9.56	11
30m	0.449	0.737	61.3	105
50m	0.586	0.974	103	164

Despite these differences, both datasets contained aerial images of livestock that had different clustering patterns. As the Clark Evans-test index increased, indicating a sparse distribution of the herd, the NAE values decreased, obtaining a better counting performance. On the opposite hand, clustered herds offered a more challenging task for both foundation models, increasing their errors. This poor performance was consistent with previous studies on dense objects aggregated in clusters that used models based on supervised learning (X. Wang et al., 2023). The degree of clustering especially limited the counting performance on the goat dataset, obtaining a higher difference in the NAE mean for both foundation models as shown in Table 3.

Table 3. Avoiding clustered herds reduces the limitation of the counting model performance of the foundation models Grounding DINO and T-Rex.

	Model performance			
	NAE		MAE	
UAV imagery	T-Rex	Grounding DINO	T-Rex	Grounding DINO
Cow				
Clustered	0.106	0.222	1.590	3.31
Intermediate	0.063	0.163	0.778	2.56
Sparse	0.0194	0.029	0.188	0.56
Goat				
Clustered	0.699	0.963	124	167
Intermediate	0.441	0.724	65.3	112
Sparse	0.228	0.326	18.1	30.5

Additionally, A qualitative analysis of a selection of the dataset shown in the Figure 4 revealed strengths and weakness of the foundation models T-Rex and Grounding DINO.

Figure 2. The first row shows the strength of these foundation models by showing an outstanding counting performance. The second row indicates some of the weaknesses. In the bottom left corner, the Grounding DINO detection with the highest accuracy level groups the whole cattle herd in only one detection. In the bottom right corner, T-Rex mistakenly identified the goatherd "C." generating a false positive.

False positives, where other objects were mistakenly identified as target object, were frequent for both models. Although those false positive detections had a low accuracy level on many occasions, this was not always the case. It was possible to find the detection with the highest accuracy level by identifying the herd as a single animal, which the second row of the Grounding DINO column shown in Figure 4 shown. Even so, some predictions were a perfect match of the ground truth, mostly in sparse herds, for both models,

Regarding the count performance across a range of heterogeneous parameters, an intermediate relative altitude of 30m improves the counting performance of Grounding DINO for the cattle dataset. After analysing some images at a closer elevation of 15m, it was observed how false positives were more frequent than at intermediate or high altitudes for the cattle herd. For the goat herd, 50m altitudes were shown to be away from the operational envelope when using Grounding DINO. However, T-Rex was able to count livestock to some degree at those heights. One downside between the comparison of both herds is the vast difference in the number of livestock in the two types of herds, as well as the different number of livestock for the same species across all the UAV images of the dataset.

4. Discussion

The metadata contained in the aerial images describes one of the limitations for safe counting accuracy, the altitude of the drone. Counting small objects from high altitude is one of the most challenging computer vision tasks, with a specific detection framework specifically designed for this task (Koyun et al., 2022; G. Wang & Jin, 2023). Additionally, metadata such as the date and location of the image allows us to obtain auxiliary information such as the weather conditions, that affects the object detection and counting performance (Sarwar et al., 2018). One limitation of this study was using drones that provide the altitude from different metadata, while the DJI Mini 3 Pro distinguishes between absolute and relative altitude using the variables "GPSAltitude" and "RelativeAltitude", the Potensic Atom dron only showed the "GPSAltitude".

Another important aspect that plays a key role in the counting performance for the foundation models T-Rex and Grounding DINO in this study is the degree of clustering. In fact, dense objects are claimed as the main challenge to detecting objects in aerial images (X. Wang et al., 2023). Similarly, the supervised algorithm TPH-YOLOv5 is built to address dense scenarios such as those seen in sheep barns (Pu et al., 2022). The findings of this study, sparse herds obtaining lower NAE values, also support this limitation for the foundation models tested. Nevertheless, a disadvantage of the method used in this study was relying on the centroids obtained from T-Rex to quantify the degree of clustering rather than the centroids from the ground truth.

In all cases, one limitation of these foundation models applied in livestock management are the generation of false positives. Objects in the background such as humans, trees, bushes, or stores are considered target objects for the model. This is not exclusive for foundation models. For example, it is claimed that one-stage detectors such as SSD or YOLO give more false positive detections than two-stage detectors (Sarwar et al., 2020).

5. Conclusions

The importance of this study is to bring awareness of the importance of setting operational limits to use foundation models in real-world scenarios. In these conditions, T-Rex and Grounding DINO can be used to detect and count scarce and valuable resources, not only in the field of precision livestock farming, but also in a broad range of fields. Counting and monitoring these resources could allow us to better respond to challenging environments by detecting an increase in the population or adjusting allotted grazing rights depending on the ecosystem service's status.

Further studies could address the problem of generating false positives by processing the detections or setting different accuracy thresholds. Similarly, pre/processing activities such as removing the background could reduce these false positives and facilitate more detections. Applying the operational limits, obtaining aerial images between 15m-30m and on scenarios such as pasture, where the livestock tend to be more sparse than in barns, could be used to test the capacity of these foundation models to count different objects, from livestock to flora, helping to create drone services that offer a better resource-efficient management by monitoring different ecosystem resources with more accurate inventories. .

References

Aquilani, C., Confessore, A., Bozzi, R., Sirtori, F., & Pugliese, C. (2022). Review: Precision Livestock Farming technologies in pasture-based livestock systems. *Animal*, *16*(1), 100429. https://doi.org/10.1016/j.animal.2021.100429

Baddeley, A., Rubak, E., & Turner, R. (2016). *Spatial point patterns: Methodology and applications with R*. CRC Press, Taylor & Francis Group.

Bárbulo Barrios, D., Valente, J., & Van Langevelde, F. (2024). Monitoring mammalian herbivores via convolutional neural networks implemented on thermal UAV imagery. *Computers and Electronics in Agriculture*, *218*, 108713. https://doi.org/10.1016/j.compag.2024.108713

Jiang, Q., Li, F., Ren, T., Liu, S., Zeng, Z., Yu, K., & Zhang, L. (2023). *T-Rex: Counting by Visual Prompting* (arXiv:2311.13596). arXiv. http://arxiv.org/abs/2311.13596

Koyun, O. C., Keser, R. K., Akkaya, İ. B., & Töreyin, B. U. (2022). Focus-and-Detect: A small object detection framework for aerial images. *Signal Processing: Image Communication*, *104*, 116675. https://doi.org/10.1016/j.image.2022.116675

Liu, S., Zeng, Z., Ren, T., Li, F., Zhang, H., Yang, J., Li, C., Yang, J., Su, H., Zhu, J., & Zhang, L. (2023). *Grounding DINO: Marrying DINO with Grounded Pre-Training for Open-Set Object Detection* (arXiv:2303.05499). arXiv. http://arxiv.org/abs/2303.05499

Ma, Z., Hong, X., & Shangguan, Q. (2023). *Can SAM Count Anything? An Empirical Study on SAM Counting* (arXiv:2304.10817). arXiv. http://arxiv.org/abs/2304.10817

Marrs, R. H., Lee, H., Blackbird, S., Connor, L., Girdwood, S. E., O'Connor, M., Smart, S. M., Rose, R. J., O'Reilly, J., & Chiverrell, R. C. (2020). Release from sheep-grazing appears to put some heart back into upland vegetation: A comparison of nutritional properties of plant species in long-term grazing experiments. *Annals of Applied Biology*, *177*(1), 152–162. https://doi.org/10.1111/aab.12591

Mueller, L., Eulenstein, F., Mirschel, W., Schindler, U., Sychev, V. G., Rukhovich, O. V., Sheudzhen, A. K., Romanenkov, V., Lukin, S. M., McKenzie, B. M., Jones, M., Dannowski, R., Blum, W. E. H., Salnjikov, E., Saparov, A., Pachikin, K., Hennings, V., Scherber, C., Hoffmann, J., … Dronin, N. M. (2021). Optimizing Agricultural Landscapes: Measures Towards Prosperity and Sustainability. In L. Mueller, V. G. Sychev, N. M. Dronin, & F. Eulenstein (Eds.), *Exploring and Optimizing Agricultural Landscapes* (pp. 91–130). Springer International Publishing. https://doi.org/10.1007/978-3-030-67448-9_3

O'Brien, J. (2024). *exiftoolr: ExifTool Functionality from R* (0.2.4) [Computer software]. https://cran.r-project.org/web/packages/exiftoolr/index.html

Pisel, T. (2023). *openmeteo: Retrieve Weather Data from the Open-Meteo API* (0.2.4) [Computer software]. https://cran.r-project.org/web/packages/openmeteo/index.html

Pu, J., Yu, C., Chen, X., Zhang, Y., Yang, X., & Li, J. (2022). Research on Chengdu Ma Goat Recognition Based on Computer Vison. *Animals*, *12*(14), 1746. https://doi.org/10.3390/ani12141746

Ramage, B. S., Marshalek, E. C., Kitzes, J., & Potts, M. D. (2013). Conserving tropical biodiversity via strategic spatiotemporal harvest planning. *Journal of Applied Ecology*, *50*(6), 1301–1310. https://doi.org/10.1111/1365-2664.12149

Sarwar, F., Griffin, A., Periasamy, P., Portas, K., & Law, J. (2018). Detecting and Counting Sheep with a Convolutional Neural Network. *2018 15th IEEE International Conference on Advanced Video and Signal Based Surveillance (AVSS)*, 1–6. https://doi.org/10.1109/AVSS.2018.8639306

Sarwar, F., Griffin, A., Rehman, S. U., & Pasang, T. (2020). *Towards Detection of Sheep Onboard a UAV* (arXiv:2004.02758). arXiv. http://arxiv.org/abs/2004.02758

Shi, Z., Sun, Y., & Zhang, M. (2023). *Training-free Object Counting with Prompts*. https://doi.org/10.48550/ARXIV.2307.00038

Tang, L., Xiao, H., & Li, B. (2023). *Can SAM Segment Anything? When SAM Meets Camouflaged Object Detection* (arXiv:2304.04709). arXiv. http://arxiv.org/abs/2304.04709

Wang, G., & Jin, P. (2023). Research on UAV Small Target Detection Algorithm Based on Improved YOLOv5s. *2023 19th International Conference on Natural Computation, Fuzzy Systems and Knowledge Discovery (ICNC-FSKD)*, 1–6. https://doi.org/10.1109/ICNC-FSKD59587.2023.10280829

Wang, X., Yan, Y., Sun, H., & Zhu, D. (2023). Dense-and-Similar Object detection in aerial images. *Pattern Recognition Letters*, *176*, 153–159. https://doi.org/10.1016/j.patrec.2023.10.028

Xu, B., Wang, W., Falzon, G., Kwan, P., Guo, L., Chen, G., Tait, A., & Schneider, D. (2020). Automated cattle counting using Mask R-CNN in quadcopter vision system. *Computers and Electronics in Agriculture*, *171*, 105300. https://doi.org/10.1016/j.compag.2020.105300

Stereo vision system guided variable rate sprayer with electric variable air assist system

Hongyoung Jeon[a,*], Heping Zhu[a], Carla Román[b], Javier Campos[b], Erdal Ozkan[b]

[a] USDA-ARS Application Technology Research Unit, Wooster, Ohio, USA.

[b] The Ohio State University, Department of Food, Agriculture and Biological Engineering, Wooster, Ohio, USA.

* Corresponding author. Email: hongyoung.jeon@usda.gov

Abstract

Pesticide applications are economical and effective ways to protect tree crops from pests and diseases for preserving crop quality and quantity although they accompany with the potential risks of environmental contamination and unintended exposure. Common approaches to minimize the risks have been variable rate pesticide applications which characterize crop canopies by various advanced sensing technologies and apply tailored pesticide volume. Although these approaches are effective in reducing pesticide uses substantially, their focus is to modulate spray outputs to match targeted crop canopy characteristics without adjusting other application parameters such as air to assist droplet penetration. Since air assist systems of conventional sprayers are mainly designed to discharge vigorous air assistance for matured tree crops, they tend to create large amount of spray drift. Therefore, variable-rate sprayers could reduce the amount of pesticide use but the adverse effects of pesticide applications such as spray drifts still exist, which are similar to conventional sprayers when they discharge sprays without adjusting intensities of air assist. An electric variable air assist system (EVAAS) was developed to address such issues by applying variable air assist along with spray applications while enhancing penetration and deposition of tree crop spray applications. The EVAAS was built with an air channel, a battery, pulse width modulated controller, and a microcontroller which were integrated to variable rate sprayer guided by a stereo vision system to control air assist outputs based on the presence of the tree crop canopy. The performance of variable rate sprayer with EVAAS was evaluated in an apple orchard for its performance in spray deposition and coverage compared to a conventional sprayer. The results showed that variable rate sprayer with EVAAS had more spray deposition by 50.2% and coverages by 2.6% compared to the conventional sprayer. In addition, variable rate sprayer with EVAAS had more than 64.2% reduction in spray drift compared to the conventional sprayer. The variable rate sprayer with EVAAS provides an effective solution to improve spray penetration, deposition and coverage while minimizing spray drift.

Keywords: Variable rate application, Computer vision, Variable air assist, Automation, Precision agriculture

1. Introduction

Pesticide contamination is one of consumer's main concerns when they buy produces and fruits. Although they are concerned about the contamination, they understand pesticide applications are necessary. They are more likely to accept the applications when the applications are made with targeted manner (Croplife America, 2022). Automated variable rate sprayers that apply sprays on crops or weeds only have been researched a quite while with various sensors e.g., ultrasonic sensors, lidar, stereo vision system and other sensors (Gil et al., 2007; Jeon and Zhu, 2012; Shen et al., 2017; Román et al., 2023). Research on these technologies has been made substantial progress and are capable of substantially reducing pesticide uses compared to conventional applications (Jeon and Zhu, 2012; Chen et al., 2013; Shen et al., 2017; Román et al., 2023). General approaches for these systems have been retrofitted variable rate systems on conventional sprayers to simple and wide adaptability. However, there is still a problem associated with spray drift caused by droplets passing through target plants despite the sprayers do not spray empty space between target plants or above the plants. This is particularly concerned for specialty crop applications that typically use vigorous air assist with spray to penetrate spray into crop canopies.

Typically, air assist for specialty crop applications is provided by an axial fan mechanically driven by power takeoff of a tractor which generates exit air velocity as high as 46 m s^{-1} (Salcedo et al., 2021). Since there is a wide variability of air assist systems, most research efforts to improve the system have been focused on changing airflow of conventional air assist systems by changing inlets (Gu et al., 2014; Mahmud et al., 2021) or outlets (Khot et al., 2012) of air assist systems. However, most developments were retrofitted systems that used conventional air assist systems which potentially generate too much airflow. Lately, Jeon and Zhu (2024a) developed an electronic air assist system (EAAS) for tower sprayers. Their system consisted of a 2.1-m high vertical duct with five electric fans coupled with motor drivers, a 400-Ah battery and a microcontroller. The maximum air velocity of the system was approximately 18.8%–24.5% of a conventional air assisted sprayer (Salcedo et al., 2021, Gu et al., 2014), and airflow outputs of their system can be controlled with a pulse width modulation (PWM) driver, and a microcontroller. Their system was integrated with a conventional sprayer in apple orchard for its impacts on spray depositions and coverages of conventional spray applications with 0, 30, 50 and 100% airflow of the system (Jeon and Zhu, 2024b). Their results showed that spray application with the 100% airflow from EAAS actually decreased spray deposition on apple tree canopies, and increased spray

depositions on off-target trees. In terms of spray canopy deposition on tree canopies, spray application would not need more than 50% airflow from the system for the apple trees in the orchard they tested.

However, current EAAS provided as a constant air assist regardless of absence or presence of tree canopies although they could electrically modulate its outputs to reduce spray droplets drifting beyond tree canopies to minimize spray drift. Therefore, the objectives of this research were to integrate electric variable air assist system to stereo vision guided variable-rate sprayer and evaluate its on- and off-target tree canopy deposits in apple orchard.

2. Materials and Methods

2.1. Stereo vision guided variable rate sprayer

Details of the controller and stereo vision guide variable rate sprayer are well described in Jeon and Zhu (2022) and Román et al. (2023). A brief description of the sprayer is given here as informative purpose. Stereo vision guided variable rate sprayer (fig. 1) was equipped with a custom-made vertical boom with five flat fan nozzles (XR8006, TeeJet Technologies, Glendale Heights, IL, USA) to apply sprays to trees. The lowest nozzle was approximately 55 cm above the ground, and the space between nozzles were 0.41 m. A solenoid valve (115880-1-12, Teejet Technologies, Glendale Heights, IL, USA) was attached to each nozzle to turn on and off its outputs. The controls of on and off the valves were possible with solid state relays, a microcontroller, and duty cycle (DC) modulation of PWM cycles. A gas engine driven diaphragm pump generated water flow to nozzles, and a pressure regulator adjusted its flow to achieve a pressure of 276 kPa when they were discharging their spray. Most components for spraying system were in a steel frame with a 3 point hitch while all electrical components were in an enclosure. A narrow tractor (John Deere 5100GN, Deere and Co., Moline, IL, USA) carried the sprayer by its 3-point hitch to travel the field. Detecting tree canopies was possible with a stereo vision system (D455, Intel Co., Santa Clara, CA, USA) which has horizontal and vertical viewing angles of 87° and 58°, respectively. The system was streamed its RGB (Red-Green-Blue), infrared (IR) and depth images to the host computer, and streamed data were processed by algorithms embedded in a graphical user interface (GUI) developed with Visual Studio Professional 2017 (Microsoft Co., Redmond, Washington, USA) and RealSense™ software development kit (Intel Co. Ltd, Santa Clara, CA, USA). The stereo vision system was ahead of the nozzles by 0.9 m for ample image processing time.

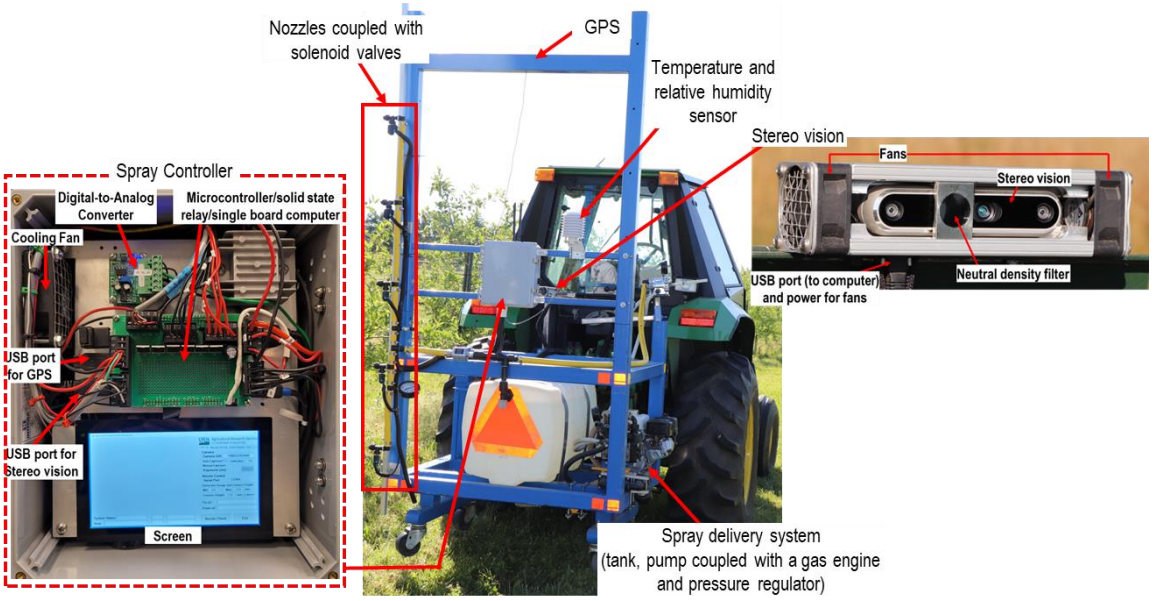

Figure 1. Stereo vision guided variable rate sprayer

2.2. Stereo vision guided variable rate sprayer with electric variable air assist system

Details of electric variable air assist system (EVAAS) is given in Jeon and Zhu (2024a) (fig. 2). Therefore, a brief description of EVAAS is provided herein. Five fans (VA18-AP71/LL-59A, Spal Automotive Srl, Correggio, Italy) were mounted on the opposite end of the opening of a 2.1-m high custom designed air ducts. Each fan generated the maximum airflow of 0.95 m^3 s^{-1}. The opening width of the duct was approximately 152 mm. The

EVAAS discharged the maximum air approximately 13.3 m s^{-1} at the opening. A microcontroller modulated DCs of PWM signal cycles, and these signals were fed to stepper motor drivers to control speeds of the fans. The power for EVAAS was supplied by a LiFePO4 Battery (Redodo LiFePO4 Battery, 400 Ah, Shenzhen Maicheng Technology Innovation Co., Ltd, Shenzhen, China).

EVAAS was integrated to stereo vision guided variable rate sprayer. However, increasing airflow of EVAAS for variable air assist applications to above 30% of the maximum from a complete stop was not feasible due to the time that it requires to obtain the speeds, and short distance between the stereo vision system and EVAAS (0.9 m). To overcome these limitations, EVAAS was automatically started at 30% DC (an approximate exit air speed of 4 m s^{-1}), and increased its airflow as needed (less than 70% of the maximum) to enable automatic variable air assist since achieving higher canopy deposition with air assist of EVAAS with DCs less 50% (Jeon and Zhu, 2024b). As variable air assists were achieved by changing DCs, GUI for the sprayer was undated to include a multivariable linear model to determine DCs based on leaf area index and canopy pass through spray coverage to modulate airflows of EVAAS based on tree canopy presence. A C++ program to direct the operation of EVAAS and communicate with the host computer was developed and flashed to the microcontroller. More details of EVAAS performance to the sprayer are given in Jeon and Zhu (2024b).

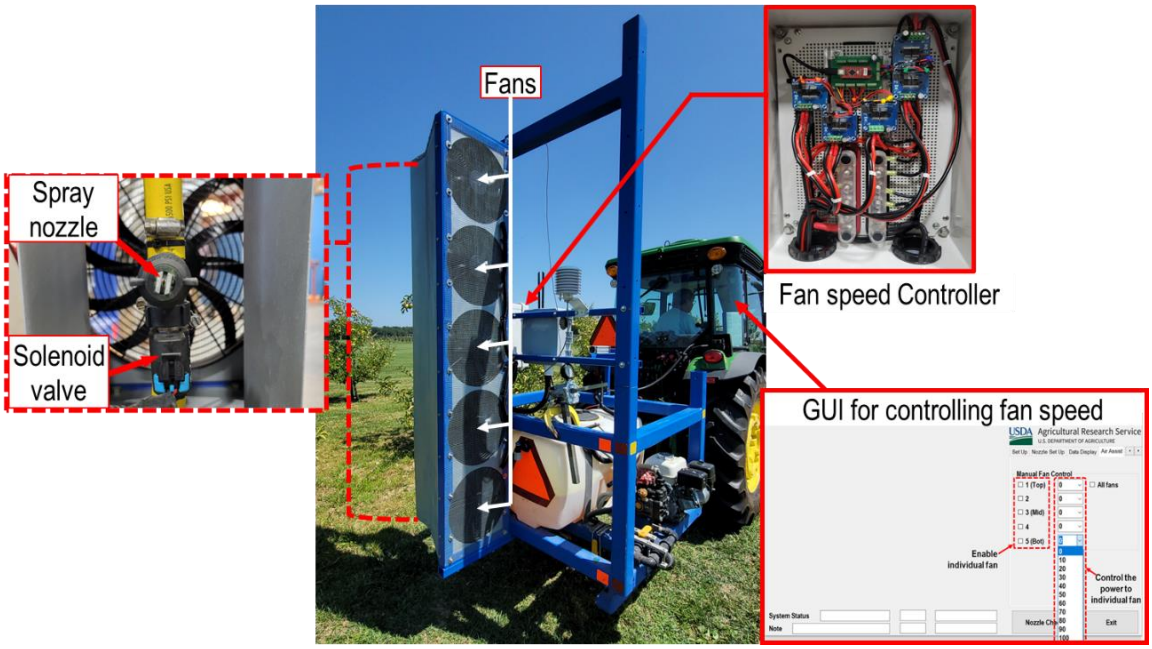

Figure 2. Stereo vision guided variable rate sprayer equipped with electric variable air assist system

2.3. Performance of the sprayer in depositing spray on- and off-target tree canopies

The sprayer was tested for its performance in spray depositions on and off target apple tree canopies in Horticultural Research Unit 2 of The Ohio State University in Franklin township, Wayne County, OH. Two application conditions were tested: conventional application with constant air assist at the maximum EVAAS fan speed (treatment 1) and variable rate spray application with variable air assist (treatment 2). The tractor with the sprayer was travelled at 3.2 km h-1 while applying the tank mix of BSF (Brilliant Sulfaflavine, MP Biochemicals Inc., Aurora, OH, USA, Concentration: 1.6 g L^{-1}) at the pressure of 275 kPa. For the conventional application, spray nozzles were continuously modulated with a DC of 50% to deliver the spray volume of approximately 385 L ha^{-1}. Functions of variable rate spray and variable air assist were enabled for the other treatment. For variable rate spray application, the sprayer applied a spray volume of 80 ml for every 1 m^3 of apple tree canopy. Airflow intensities of variable air assist system, controlled by the fan's power DCs, were determined by the embedded multivariable linear model with leaf area index of 2.2 and canopy pass through spray coverage of 5%. For both treatments, the sprayer centre was approximately 2.7 m away from the trunk of the trees.

Before the treatments, three representative sizes of apple trees, considering each tree as a replication, were selected to have 7 spray targets, 60-mesh stainless steel disks (SSD) and water sensitive papers (WSP), in the row being sprayed. Four SSDs and WSPs were on leading and following edges, and top and bottom of the canopy. The other three targets were outer edge, middle and inner edge of the canopies on approximately vertical and horizontal centre. In addition, additional three trees, aligned with trees with SSDs and WSPs in the spray direction, were selected from the row next to the one being sprayed to have five SSDs and WSPs to capture spray being drifted approximately 5.5 m away from the application site. After the application of each treatment, SSDs and WSPs were dried and collected in glass bottles and letter paper templates for processing in the lab to obtain BSF deposition in µL cm^{-2} and coverage percentage. Detailed sample processing procedures and other were described in Jeon and Zhu (2024b). In addition, the sprayer stored DC data for spray nozzles and fans, RGB, IR and depth images, and other data in local hard drive of the computer to analyze data for its air assist changes, spray outputs, canopy detection and spray volume.

During the tests, weather conditions were monitored by local weather station which reported average wind speed of 1.26 m s^{-1} (0.4 to 2.5 m s^{-1}) from south-southeast (159°) to south-southwest (202°). The temperatures and relative humidities during the tests were 18.9–29.4 °C and 50.0%–80.0%, respectively, during the tests.

3. Results and Discussion

3.1 Spray deposit on- and off-target tree canopy

Fig. 3 shows spray and air assist outputs for three apple trees from the conventional sprayer (treatment 1) and the variable rate sprayer with EVAAS (treatment 2). The sprayer with EVAAS detected canopy volumes of 2.9, 2.0 and 3.4 m^3 for apple tree 1, 2 and 3, respectively. The general trend was that the conventional sprayer applied a constant volume of spray and air assist to trees regardless of their canopy sizes. However, the variable rate sprayer with EVAAS started increasing its spray and air assist outputs when it started detecting tree canopies (tree canopy started at the tree width of 0 m). The sprayer with EVAAS occasionally discharged more spray volume than the conventional sprayer did to compensate for the large volume of the canopy section detected. The sprayer with EVAAS started to reduce its spray and air assist outputs when the sprayer passed the biggest canopy section of each tree. Also, the spray volume became to zero and airflow reached its initial flow when the sprayer did not the tree canopies (fig. 3).

For those three trees, the variable rate sprayer with EVAAS applied 223.9, 155.0 and 269.5 ml of BSF solution for tree 1, 2 and 3, respectively while the conventional sprayer applied 331.2, 283.9 and 388.0 ml of BSF solution to tree 1, 2 and 3, respectively. In addition, treatment 2 applied air assist volume approximately 35.7 % of air assist volume of treatment 1 while increasing its airflow with presence of the trees.

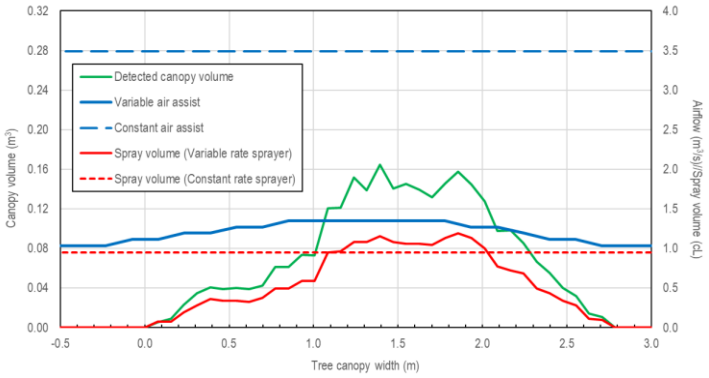

(a) Tree 1

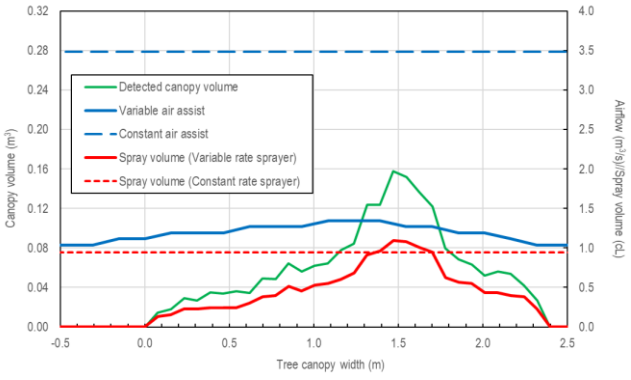

,

(b) Tree 2

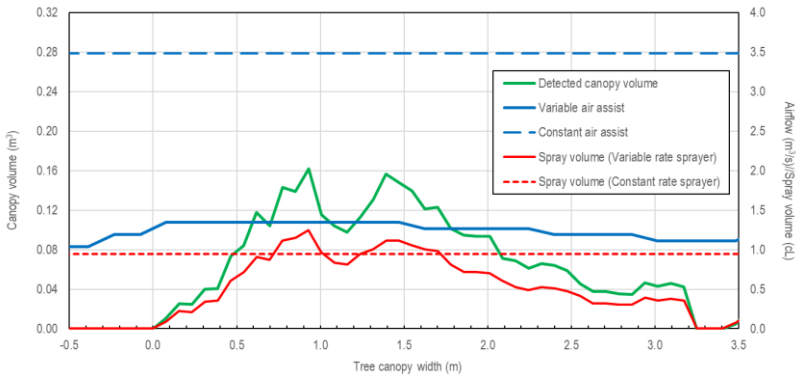

(c) Tree 3

Figure 3. Outputs of sprays and air assists for three apple trees from the conventional sprayer and the variable rate sprayer with EVAAS

Table 1 shows the spray depositions and coverages of treatment 1 and 2 on targeted apple tree canopies. The conventional sprayer (treatment 1) and the variable rate sprayer with EVAAS (treatment 2) delivered average spray depositions of 4.5–5.7 µL cm^{-2} and 7.3–8.2 µL cm^{-2}, respectively, to three trees. Treatment 2 consistently had 44.0%-61.6% more depositions on each tree compared to treatment 1, and treatment 2 deposited approximately 50.2% more spray depositions compared to treatment 1 in overall deposition averages. The spray coverages had a similar trend as well although the coverage differences between two treatments for each tree were much smaller (11.1% to 21.3%). The difference of overall coverage averages between of two treatments was 2.6%. This shows encouraging preliminary spray deposition and coverage data, and the results suggest that variable rate sprayer with EVAAS (treatment 2) was more effective to deliver more spray depositions on targeted trees compared to the conventional sprayer. This also suggests that vigorous air assist from conventional sprayers might have negative influences in spray depositions although further in-depth studies must carry out to acquire more data to confirm the differences.

Table 1. Average spray depositions and coverages of treatment 1 and 2 on on-target apple tree canopies

	Treatment 1		Treatment 2	
	Avg. spray deposition (μL cm^{-2})	Avg. spray coverage (%)	Avg. spray deposition (μL cm^{-2})	Avg. spray coverage (%)
Tree 1	5.7 (46.7)*	50.9 (57.5)	8.2 (66.8)	53.0 (51.1)
Tree 2	4.5 (73.3)	45.5 (54.9)	7.3 (74.8)	50.9 (65.5)
Tree 3	5.1 (45.4)	43.0 (48.7)	7.4 (56.7)	41.0 (41.0)
Overall Avg.	5.1 (52.9)	47.0 (52.5)	7.7 (63.4)	48.3 (57.0)

*Coefficient of variation (%) of the data.

Fig. 4 shows spray depositions and coverages on off-target apple canopies which were approximately 5.5 m away from the application sites. Treatment 1 and 2 had average spray depositions of 2.9 and 1.0 μL cm^{-2}, respectively, which suggest that the conventional sprayer drifted its spray approximately 3 times more than the variable rate sprayer with EVAAS under this test conditions. In addition, the spray coverage average of treatment 1 (16.2%) was approximately 20.5 times higher than the coverage average of treatment 2 (0.8%). These substantially less spray coverage and deposition averages from treatment 2 were likely because the sprayer with EVAAS only provided spray with increased air assist when the tree canopies were presence. Therefore, sprays from treatment 2 were only discharged to the tree canopies with increased air assist to penetrate to targeted tree canopies. In addition, even if some droplets were undeposited, their fate would be driven by gravity or ambient wind instead of being drifted a far distance by vigorous air assist from a conventional sprayer. Thus, spray deposition and coverage from off-target apple trees show that variable rate sprayer with EVAAS could be a potential solution to substantially minimize spray drift although further tests are necessary to have more comprehensive understanding of EVAAS.

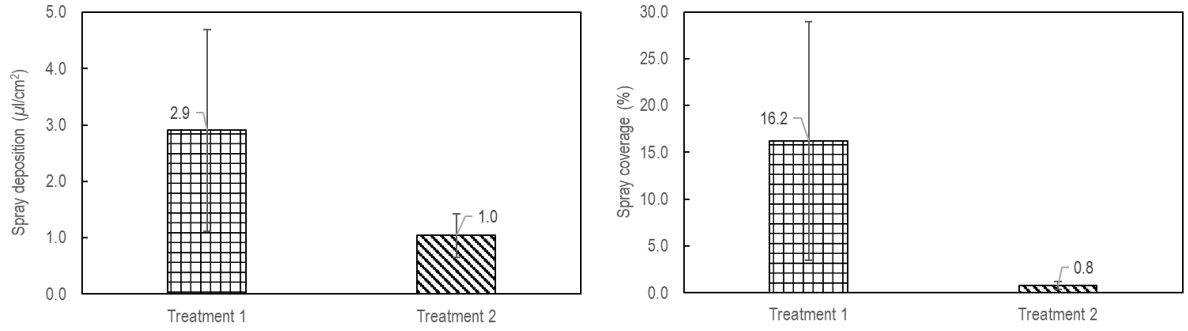

(a) Spray depositions on off-target tree canopies (b) Spray coverages on off-target tree canopies

Figure 4. Spray depositions and coverages of treatment 1 and 2 on off- target apple tree canopy

4. Conclusions

EVAAS was integrated to variable rate sprayer to adjust it airflows for the outputs of the sprayer, and the GUI to harmonize the operations of the sprayer and EVAAS was developed. The performance of the variable rate sprayer with EVAAS was evaluated against the conventional sprayer. The test data show that the variable rate sprayer with EVAAS applied 54.6% to 60.5% of spray volumes compared to the conventional sprayer. However, the variable rate sprayer with EVAAS had 44.0%-61.6% more depositions on each tree compared to the conventional sprayer. Furthermore, the variable rate sprayer with EVAAS had approximately 35.8% of spray drifts, considerably less spray drift, compared to the conventional sprayer.

Although the variable rate sprayer with EVAAS showed great potential of increasing spray deposition on targeted tree canopies and reducing spray drift on off-target tree canopies, further experiments should be carried out to validate the outcomes from this study. Furthermore, EVAAS should also be tested with different crops with more dense canopies particularly to broaden its use with various crops. The design of the fan can be optimized as well for spray applications.

Acknowledgements

Mention of company or trade names is for description only and does not imply endorsement by the USDA. The USDA is an equal opportunity provider and employer. The authors acknowledge Adam Clark and Andy Doklovic for their technical assistance and Bob Filbrun, Ken Scaife, and their crews from Agricultural Operations of the Ohio State University Wooster Campus for maintaining the apple orchard. This research was supported by USDA-ARS in-house project 5082-21620-001-00D.

References

Chen, Y., H.E. Ozkan, H. Zhu, R.C. Derksen, C.R. Krause, 2013. Spray deposition inside tree canopies from a newly developed variable-rate air-assisted sprayer. Transactions of the ASABE. 56(6), 1263-1272.

CropLife America, 2022. Public opinion toward pesticides https://croplifeamerica.morningconsultintelligence.com/ Accessed on May 20, 2024.

Gil, E., A. Escolà, J. R. Rosell, S. Planas, L. Val, 2007. Variable rate application of plant protection products in vineyard using ultrasonic sensors. Crop Protection. 26(8), 1287-1297. https://doi.org/10.1016/j.cropro.2006.11.003.

Gu, J., H. Zhu, W. Ding, X. Wang, 2014. Characterization of air profiles impeded by plant canopies for a variable rate air assisted sprayer. Transactions of ASABE. 57(5), 1307 – 1315. https://doi.org/10.13031/trans.57.10646.

Jeon, H., H. Zhu, 2012. Development of a variable-rate sprayer for nursery liner applications. Transactions of ASABE. 55 (1), 303 – 312. https://doi.org/10.13031/2013.41240.

Jeon, H., H. Zhu, 2024a. Development of an electric variable air assist system for apple orchard sprayer. Journal of ASABE, Accepted as publication.

Jeon, H., H. Zhu, 2024b. Performance of a tree crop sprayer with an electric variable air assist system. Journal of ASABE, Submit for review.

Khot, L., R. Ehsani, G. Albrigo, P. Larbi, A. Landers, J. Campoy, C. Wellington, 2012. Air-assisted sprayer adapted for precision horticulture: Spray patterns and deposition assessments in small-sized citrus canopies. Biosystems Engineering. 113(1), 76–85. https://doi.org/10.1016/j.biosystemseng.2012.06.008

Mahmud, M. S., A. Zahid, L. He, H. Zhu, D. Choi, G. Krawczyk, P. Heinemann, 2021. Development of an automatic airflow control system for precision sprayers based on tree density. Journal of ASABE. 65(6), 1225–1240. https://doi.org/10.13031/ja.14972

Román, C., H. Jeon, H. Zhu, J. Campos, E. Ozkan, 2023. Stereo vision controlled variable rate sprayer for specialty crops: Part II. Sprayer development and performance evaluation. Journal of ASABE, 66(5): 1005–1017, https://doi.org/10.13031/ja.15578.

Salcedo, R., H. Zhu, E. Ozkan, D. Falchieri, Z. Zhang, Z. Wei, 2021. Reducing ground and airborne drift losses in young apple orchards with PWM-controlled spray systems. Computers and Electronics in Agriculture, 189, 106389. https://doi.org/10.1016/j.compag.2021.106389.

Shen, Y., H. Zhu, H. Liu, Y. Chen, E. Ozkan, 2017. Development of a laser-guided, embedded-computer-controlled, air-assisted precision sprayer. Transactions of the ASABE. 60(6), 1827-1838. https://doi.org/10.13031/trans.12455

Potential challenges encountered when adopting new technologies such as proximal sensing to realize VRA applications in cotton

Nikolaos Georgiadis [a], Konstantinos Papachristos [a], Vlasios Mangidis [a], Evangelia-Maria Giatsiou [a], Evangelos Adamopoulos [a], Christina Vogiatzi [a,*]

[a] CNH Industrial, Athens, Greece

* Corresponding author. Email: christina.vogiatzi@external.cnhind.com

Abstract

Increased public awareness along with the rising new technologies are key driving forces towards sustainable productivity. Precision agriculture -based on data-driven decisions- is a valuable asset, the utilization of which might contribute to achieving this goal. The scope of this study was to evaluate the efficiency of Variable Rate Applications (VRA) in cotton when utilizing proximal sensing technologies compared to conventional farming techniques. Large scale pilots have been set up, where split-plot applications have been performed. The different treatments include VRA's of inputs typically applied in-season including insecticides, plant growth regulators and harvest aids, along with the respective flat rate applications per agrochemical. The VRA treatments were realised using a multispectral, camera-based system (Augmenta ™). This system gathers data regarding the field's condition and generates a Vegetation Index (NDVI based) upon which proprietary, agronomic algorithms are utilized enabling VRAs in real-time without further need for additional calibration. For the evaluation of the VRA's efficiency the yield of each plot was determined gravimetrically. In VRA treatments an average of 3% and 7.2% of savings were realized in PGR and HA respectively. Despite the positive outcome, several challenging points are to be considered, if high adoption of such an approach is to be expected including the farm size and the subsequent time for the Return On Investment (ROI), the farmers' demographic profile, the existing farming techniques, and machinery along with the available infrastructure. Plug and Play solutions are to be considered as an affordable solution towards that end.

Keywords: precision agriculture, variable rate applications, proximal sensing, vegetation indices

1. Introduction

Global trends and regulations appoint sustainable productivity as an inevitable one-way (Heyl et al., 2022), where optimized input applications will mitigate unsolicited environmental ramifications without imposing compromises in farmers' income. Precision Agriculture, as a farming management approach, can positively contribute towards that end utilizing rising technologies such as high precision GPS's and remote sensing to ensure that the crops receive exactly what they need (Shafi et al., 2019). Implementations of these technologies enable a wide range improved cultivations techniques such as Variable Rate Applications (VRA) of seeds, fertilizers and other agrochemicals, variable irrigation and others (Nowak, 2021).

The scope of this study was to determine the impact of Variable Rate Applications of multiple inputs including fertilizers, plant growth regulators and harvests aids on sustainable productivity of cotton, using a commercial proximal sensing system (Augmenta ™) as a plug and play solution. During the setting up and the execution of the pilots several factors that might impose a challenge were identified and accounted for to ensure -to the extent possible- a wide adoption rate of the solution offered.

2. Materials and Methods

2.1. Pilot setup

A pilot with split applications has been set in three cotton fields in the Prefecture of Thessaly (Greece) covering a total area of 15,7ha. Each field was split into two equivalent parts in terms of soil properties and productivity potential (Fig 1.). The inputs tested during this years' pilot were insecticides for preventative applications, Plant Growth regulators and Boll openers as Harvest Aids. The outline of the pilot setup is shown on Table 1. In both parts of the field the standard cultivating techniques were performed to ensure

the unimpeded productivity. In one part of the field, the input of interest was added at a Fixed-Rate recommended by the collaborating agronomist. On the other half, the same recommended rate of input was applied at a Variable Rate utilizing a proximal sensing, passive, multispectral camera system (Augmenta ™) mounted on top of a tractor at 3.15m height.

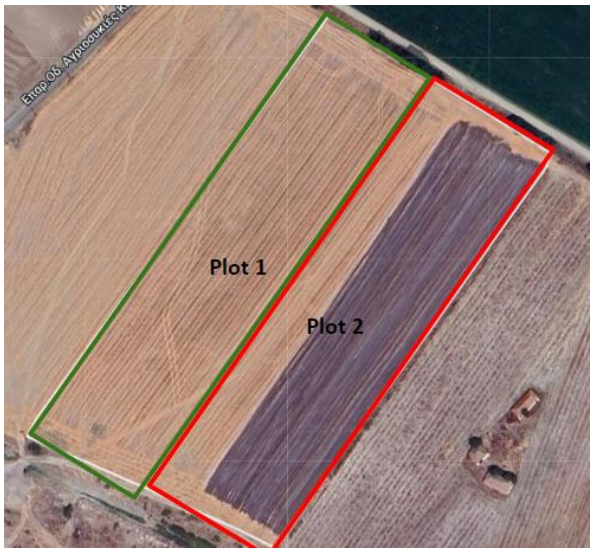

Figure 1. Design of Experiment in a cotton field in Thessaly Prefecture, Greece (2022). Plot 1 is the Control Plot treated with Fixed Rate applications, while in Plot 2 all treatments were VRA.

2.2. Data gathering and analysis

During all operations the proximal sensing, multispectral camera system logs data regarding the Vegetation Index and the inputs' consumption (15 fps) covering a Field of View of 16m and the full working width. The Vegetation Index is a proprietary NDVI-based index [0.1, where lower values correspond to low vegetation while higher values correspond to dense vegetation. For the evaluation of the impact of the VRA treatments, data gathered during the applications (Vegetation Index maps, Application maps, etc.) have been compared to yield data gravimetrically gathered at the end of the growing season (Figure 2).

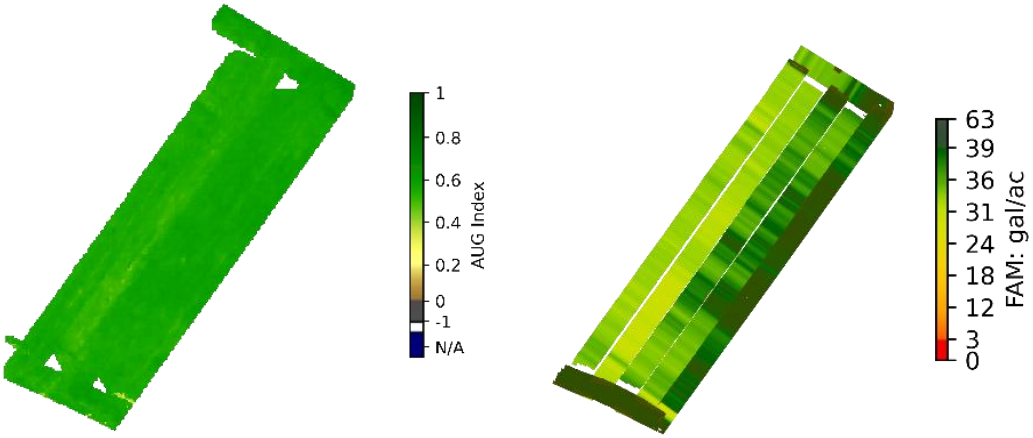

(a) (b)

Figure 2. (a) Vegetation Index (AUG index) map and Field Application Map (FAM) of Harvest Aid VRA in a cotton field in Magnesia Prefecture, Greece (2022).

3. Results and Discussion

The key principle of the proprietary algorithms utilized is that savings can be realized in certain regions of the field which are proportional to the overall condition of the field and the variability encountered. For example, reduced volume of PGR compared to the recommended rate is required when lower biomass is detected. The reduction of the rate is proportional to the reduction of biomass detected. Likewise, the volume of Harvest aids applied might be reduced in parts of the field where senescence has started. The average savings per hectare of PGR realized were 3% and of Harvest Aids were 7,2%. Despite the savings imposed –or possibly because of them- a yield increase was achieved averaging 4.1%. The reduction of the dose in PGR allowed smaller plants to develop further and generate more production units or possibly allowed them to reach the minimum desirable height for harvesting as suggested in other studies carried out in Brazil (Trevisan et al., 2018; Baio et al., 2018) and in the States (Vaz et al.,2023).

Table 1. Pilot setup along with savings (%) achieved during the VRA operations per treatment, the respective yields achieved and the respective yield increased observed between the VRA and the respective Fixed rate treatments, Magnesia Prefecture (GR), 2022.

Field	Operation	Treatment	Area (ha)	Savings (%)	Yield (kg/ha)	Yield Increase (%)
Field 1	Insecticide	VRA	2,7	9,6%	6168	0,28%
		Fixed Rate	2,9	-	6151	
Field 2	PGR + HA (Ball Opener)	PGR VRA	2,9	4,1%	3415	3,6%
		HA VRA		6,2%		
		Fixed Rate	3,0	-	3296	
Field 3	PGR + HA (Ball Opener)	PGR VRA	2,3	1,6%	2377	4,7%
		HA VRA		8,4%		
		Fixed Rate	2,0	-	2271	
		Total	**15,7**		**Average**	**4,1%**

Significant savings (9,6%) were realised in the field where VRA of insecticides were performed preventatively. Despite the reduction of the tested input imposed the yield of the respective part of the field remained unaffected. Similar results were obtained in a study carried out in vineyards (D'Ambrosio, 2023).

The tested approach is considered a plug and play solution that will automatically decide, adjust and apply each input, in accordance with the dose recommended by the collaborating agronomist, making agricultural technology accessible to the majority of farmers.

The profile of the end-user is a detrimental factor upon which the adoption rate is highly dependent. Previous research (Daskalopoulou and Petrou, 2002) carried out in 14 prefectures in Greece has shown that approximately 17% of the local farms have a size <1ha and consequently the mechanisation level for these farms is low. More than two thirds of the farms have a farm size <20 ha, and only 6,6% of the farms have a size of >2ha that will allow a return of investment within a year. Daskalopoulou and Petrou (2002) are of the opinion that average-sized farms are more prone to consciously adjust their production practices since it will enable their sustainability. On the other hand, according to Barlas et al. (2000) larger agroholdings are more likely to have the resources that will allow them to pursue strategies that will decrease their production cost and/or improve their productivity. This suggestion is concise with the findings of Damianos and Giannakopoulos (2002), who also suggested that age and educational level seem to have a positive influence towards the adoption of new practices that will result in sustainable productivity. However, since agricultural technologies and management practices become mainstream it is likely that this correlation will eventually become less significant (O'Donoghue and Heanue, 2018).

The Greek agricultural sector was mechanised during the second half of the previous century. Socioeconomic factors such as the austerity measures and the adjustment policy in the process of the EMU of the EU that were imposed from the early 2000s and on resulted in reduces investment in agricultural machinery (Papageorgiou, 2015). Consequently, the existing equipment is mostly outdated and any solutions suggested should be able to retrofit and adjust to the existing infrastructure.

The use of fog computing and Wi-Fi-based long-distance network in Internet of Things might improve efficiency of farm management provided that specific requirements met that will ensure that any solution proposed is scalable (Ahmed et al., 2018) and applicable given rural areas in Greece are often under-served Micholia et al., 2018).

4. Conclusions

Rising technologies are the upcoming driving force in the agricultural sector. Preliminary results suggest that precision Agriculture tools such as proximal sensing might enable effective production management via reducing inputs whenever possible without compromising productivity. However, if such solutions are to become widely available, they need to comply with the existing infrastructure and the limitations it might impose including the outdated machinery, the lack of Wi-Fi coverage in rural areas etc. Likewise, any solution recommended should comply with the existing agricultural practices given the profile of the end users.

Acknowledgements

The pilots were carried out as part of the Quantifarm Project, co-funded under the Horizon Europe by the European Union. Views and opinions expressed are however those of the author(s) only and do not necessarily reflect those of the European Union. Neither the European Union nor the granting authority can be held responsible for them.

References

Ahmed, N., D. De, I. Hussain, 2018. Internet of Things (IoT) for smart precision agriculture and farming in rural areas. IEEE Internet of Things Journal, 5(6), 4890-4899.

Baio, F.H.R., D.C. Neves, H.B. Souza, A.J.F. Leal, R.C. Leite, J.P. Molin, S.P. Silva, 2018. Variable rate spraying application on cotton using an electronic flow controller. Precision Agricriculture, 19, 912-928.

Barlas, Y., D. Damianos, E. Dimara, C. Kasimis, D. Skuras, 2001. Factors Influencing the Integration of Alternative Farm Enterprises Into the Agro-Food System. Rural Sociology, 66 (3), 342-358. https://doi.org/10.1111/j.1549-0831.2001.tb00071.x

D'Ambrosio, R., M. Furiosi, T. Caffi, F. Graziosi, T. Frioni, S. Poni, M. Gatti, 2023. Testing crop protection performances in a vineyard subjected to real-time volume adjustment through an adapted conventional sprayer. In Precision agriculture'23 (115-122). Wageningen Academic.

Damianos, D., N. Giannakopoulos, 2002. Farmers' participation in agri-environmental schemes in Greece. British Food Journal, 104 (3/4/5), 261-273.

Daskalopoulou, I., A. Petrou, 2002. Utilising a farm typology to identify potential adopters of alternative farming activities in Greek agriculture. Journal of rural studies, 18 (1), 95-103.

Heyl, K., F. Ekardt, L. Sund, P. Roos, 2022. Potentials and limitations of subsidies in sustainability governance: the example of agriculture. Sustainability, 14 (23), 15859. https://doi.org/10.3390/su142315859.

Micholia, P., M. Karaliopoulos, I. Koutsopoulos, L. Navarro, R.B. Vias, D. Boucas, ... P. Antoniadis, 2018. Community networks and sustainability: a survey of perceptions, practices, and proposed solutions. IEEE Communications Surveys & Tutorials, 20(4), 3581-3606.

Nowak, B., 2021. Precision agriculture: Where do we stand? A review of the adoption of precision agriculture technologies on field crops farms in developed countries. Agricultural Research, 10(4), 515-522.

O'Donoghue, C., K. Heanue, 2018. The impact of formal agricultural education on farm level innovation and management practices. The Journal of Technology Transfer, 43, 844-863. https://doi.org/10.1016/S0743-0167(01)00027-4

Papageorgiou, A. (2015). Agricultural equipment in Greece: Farm machinery management in the era of economic crisis. Agriculture and Agricultural Science Procedia, 7, 198-202.

Shafi, U., R. Mumtaz, J. García-Nieto, S.A. Hassan, S. A. R. Zaidi, N. Iqbal, 2019. Precision agriculture techniques and practices: From considerations to applications. Sensors, 19 (17), 3796. https://doi.org/10.3390/s19173796.

Trevisan, R. G., N.S. Vilanova Junior, M. T. Eitelwein, J. P. Molin, 2018. Management of plant growth regulators in cotton using active crop canopy sensors. Agriculture, 8(7), 101. https://doi.org/10.3390/agriculture8070101

Vaz, C. M., J. C. Franchini, E. A. Speranza, R. Y. Inamasu, L. A. D. C. Jorge, L. M. Rabello, ... & J. Schepers, 2023. Zonal Application of Plant Growth Regulator in Cotton to Reduce Variability and Increase Yield in a Highly Variable Field. The Journal of Cotton Science 27:60–73.

A new mobile robot harvesting prototype for cotton production

Joe Mari Maja [a,*], Van Patiluna [a,b], Fazly Bin Mail [c], Gilbert Miller [c], Matthew Cutulle [d], Michael Marshall [d], Edward Barnes [e]

[a] Center of Applied Artificial Intelligence for Sustainable Agriculture, 1890 Research and Extension, PSA, South Carolina State University, 300 College Avenue, Orangeburg, South Carolina 29117, USA

[b] Department of Computer Engineering, University of San Carlos, Cebu City 6000, Philippines

[c] Edisto Research and Education Center, Clemson University, 64 Research Road, Blackville, South Carolina 29817, USA

[d] Department of Plant and Environmental Sciences, Clemson University, 171 Poole Agricultural Center, Clemson, South Carolina 29634, USA

[e] Cotton Incorporated, 6399 Weston Parkway, Cary, North Carolina 27513, USA

* Corresponding author. Email: jmaja@scsu.edu

Abstract

The economic impact of cotton extends far beyond its production and cultivation. As a crucial natural fiber and oil crop, it is widely grown in the US, China, and India. The global cotton industry generates over $600 billion and employs over 4 billion people. However, cotton faces significant challenges, such as increased pest resistance, labor shortages, high labor costs, and the labor-intensive nature of its harvesting. While some farmers use mechanical harvesting machines, many still rely on manual harvesting, particularly in China and India. These mechanical harvesters are large, expensive to operate and maintain and contribute to soil compaction issues. Additionally, they can only be used for 2-3 months each year. This study focuses on developing a proof-of-concept cotton harvester that addresses cost and soil compaction concerns. A finger roller concept harvester was designed to pull and extract cotton bolls. The harvesting module was mounted on a mobile platform with adjustable width and height. Two eductors and blowers were used to transport the harvested cotton bolls to storage bins on both sides, and a secondary finger roller at the back provided the final detachment of the bolls. The platform was tested for four days in 2023 (October 30, November 4, 8, and 9) in a field with rows spaced 96.5 cm apart and plants spaced 10 cm apart within rows. The field experiment used a completely randomized block design with three replicates, adjusting the front roller's rotation at three different duty cycles: 25%, 50%, and 100%. Nine initial subplots measuring 3 m long with a 1 m buffer zone on each side were selected to mitigate the bolls collected from adjacent rows. After modifying the front mechanism, 10 additional subplots were added to test the rotation direction of the front roller (forward and backward). Results showed that the backward rotation (with a duty cycle higher than 25%) of the front roller had influenced the amount of harvested cotton bolls in the bin compared to the forward rotation. Meanwhile, the forward rotation influences the number of bolls on the ground, the header, and the amount of trash regardless of the duty cycle used. Although the efficiency results in pulling cotton from the plants were high, calculating efficiency via the bin was very small. This could be attributed to many factors, e.g., clogging at the educator entrance or the speed of the second finger roll. Based on the lessons learned, a discussion on the new design addressing this problem is presented.

Keywords: cotton industry, labor shortage, mechanical harvesting, mobile platform

1. Introduction

The cotton industry in the United States is a significant economic driver, with cotton being one of the country's most crucial cash crops (Chen & Burke, 2015). Cotton production contributes substantially to the agricultural sector and plays a vital role in the economy due to its widespread applications in textiles and various industries. The sustainability and growth of the cotton industry depend on improved cotton varieties, efficient management of soil and water resources, and effective control of pests, diseases, and weeds (Dadd-Daigle et al., 2021). These aspects are essential for ensuring the continued success and profitability of cotton farming in the US.

Historically, the US cotton industry has undergone significant transformations, particularly in labor practices and harvesting methods. Following World War II, there was a notable shift in labor dynamics, with millions of cotton workers, particularly African Americans, leaving the fields permanently as farmers began to mechanize the cotton harvest (Grove & Heinicke, 2003). This transition from manual labor to

mechanization revolutionized the industry and profoundly impacted the workforce and agricultural practices.

Mechanization in the cotton industry brought both benefits and challenges. It increased efficiency and productivity by reducing reliance on manual labor and improving overall output. However, it also raised concerns about labor displacement and the impact on traditional harvesting practices (Peterson & Kislev, 1986). The adoption of machine harvesting was driven by increased nonfarm wages and the decreased cost of mechanized harvesting, highlighting the complex interplay between economic incentives and technological advancements (Peterson & Kislev, 1986). This shift led to a restructuring of the labor market in cotton-producing regions, with many traditional cotton pickers moving into other sectors, such as manufacturing (Jung, 2018).

Moreover, mechanization has improved efficiency but also raised environmental and sustainability concerns. Cotton cultivation exerts significant pressure on natural resources such as land and water, leading to environmental issues and the overuse of pesticides (Natálio & Maria, 2018). The extensive use of pesticides, insecticides, and irrigation with fresh water poses environmental risks and contributes to ecological imbalances, necessitating sustainable practices and resource management in cotton farming (Tausif et al., 2018).

The economic impact of the cotton industry extends beyond the agricultural sector, influencing various aspects of the economy and society. Cotton cultivation and processing support millions globally, including farmers, production workers, and individuals in the textile and garment industries (Witjaksono et al., 2014). The industry's economic significance is underscored by its estimated global impact of around US$500 billion annually, emphasizing its substantial contribution to the world economy (Makhmadjanov et al., 2023).

The US cotton industry is prominent in the agricultural and economic landscape, with its production and processing activities influencing various sectors and livelihoods. While the industry's economic significance is undeniable, challenges related to sustainability, environmental impact, and labor practices underscore the need for continuous innovation, responsible resource management, and equitable labor practices to ensure the industry's long-term viability and contribution to the economy.

Integrating advanced robotics into cotton farming can revolutionize various aspects of the cultivation and harvesting processes. Autonomous robots equipped with precision agriculture technologies can perform tasks such as planting, weeding, and pest control more accurately and efficiently than traditional methods. These robots can use sensors and machine learning algorithms to monitor soil health, detect pests, and apply the appropriate treatments, reducing the need for chemical inputs and enhancing sustainability. Robotic systems can improve the harvesting process, which is traditionally labor-intensive and costly. Robots designed for cotton picking can operate continuously and with precision, reducing the reliance on seasonal labor and minimizing the physical strain on workers. These robots can be programmed to selectively harvest only mature bolls, ensuring higher quality yields and reducing waste. Additionally, robotics can help address the issue of soil compaction by using lightweight, agile machines that cause less disruption to the soil structure than heavy machinery.

Adopting robotic systems in cotton production presents numerous opportunities to enhance efficiency, reduce costs, and promote sustainable farming practices. As technology advances, the potential for robotics to transform the cotton industry and address its longstanding challenges will only grow, offering a promising future for cotton farmers worldwide.

The overall objective of this work is to develop multiple cotton production operations using robotics. The specific objectives of the study were to design and test the Finger Roller Harvester to pull and extract cotton bolls efficiently, attach to a mobile platform with adjustable dimensions, and evaluate the developed harvester's efficiency through field experiments focusing on different rotation duty cycles and rotation directions.

2. Materials and Methods

The study is focused on developing and testing a proof-of-concept cotton harvester (Figure 1a) designed to address cost and soil compaction issues. The primary component of the harvester was a mobile platform, a 4 x 4 electric skid steer vehicle (Amiga, Farm-NG, Watsonville, CA, USA) and a harvesting module with a finger roller system engineered to pull and extract cotton bolls efficiently (Figure 1b). This harvesting module was integrated into a mobile platform with adjustable width and height to accommodate various field conditions. An eductor (Figure 1c) and blower system were installed to facilitate the transport of harvested cotton bolls to storage bins on either side of the platform. A secondary finger roller at the back of the platform

was included to ensure the final detachment of the bolls for transport to the bins.

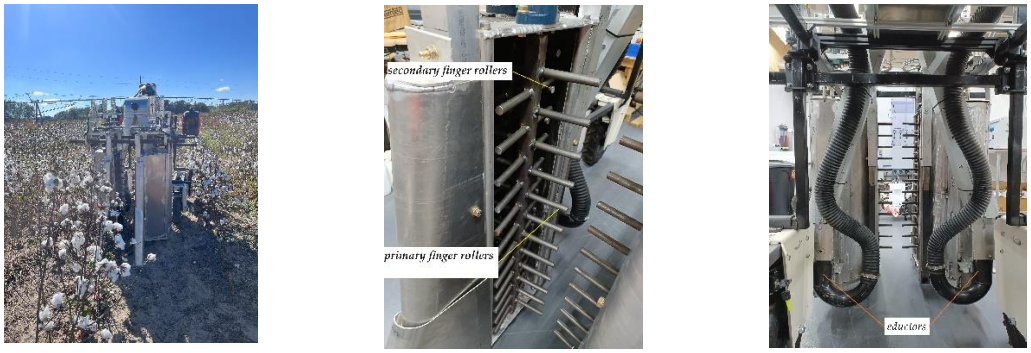

(a) (b) (c)

Figure 1. (a) The mobile platform used for this work, (b) the finger rollers used to pull the cotton bolls, and (c) the eductors for moving the harvested bolls to the bin.

Field testing was conducted at Edisto Research and Education Center's Cotton Plot (33.346009, -81.315102) on four days: October 30, November 4, 8, and 9, 2023. in a field with rows spaced 96.5 cm apart and plants spaced 10 cm apart within rows. A total of 19 small rows were selected for this field test. The field was planted with Deltapine 2038B3XF and managed according to South Carolina Cotton growers' guidelines. The experimental design followed a completely randomized block format with three replicates. The front roller's rotation varied at three different duty cycles: 25%, 50%, and 100%, and the direction of the rotation. Initial testing involved nine subplots, each measuring 3 m long with a 1 m buffer zone on each side to mitigate the collection of bolls from adjacent rows.

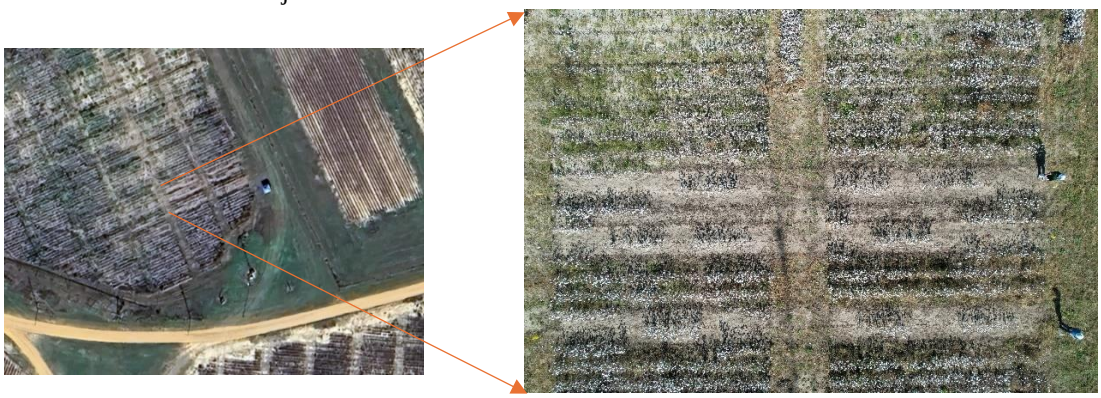

Figure 2. Plot location for the field test.

Subsequent modifications to the front mechanism to direct the plant stem (Figure 3) in the middle led to adding 10 more subplots to evaluate the impact of the front roller's rotation direction (forward and backward).

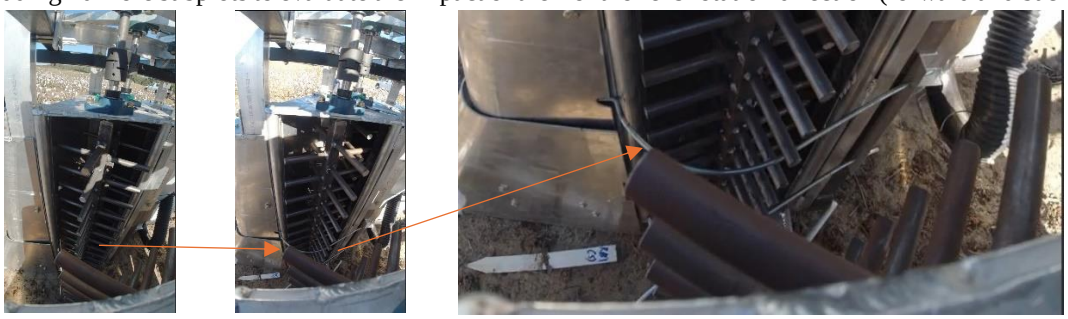

(a) (b) (c)

Figure 3. (a) The previous design on the front roller, (b) additional guide rails to direct plants to move in the middle, and (c) these guide rails were installed in the front rollers.

The forward rotation of the front roller means the right roller rotates counterclockwise while the left roller rotates clockwise. Conversely, the right roller rotates clockwise for backward rotation, and the left rotates counterclockwise, as shown in Figure 4.

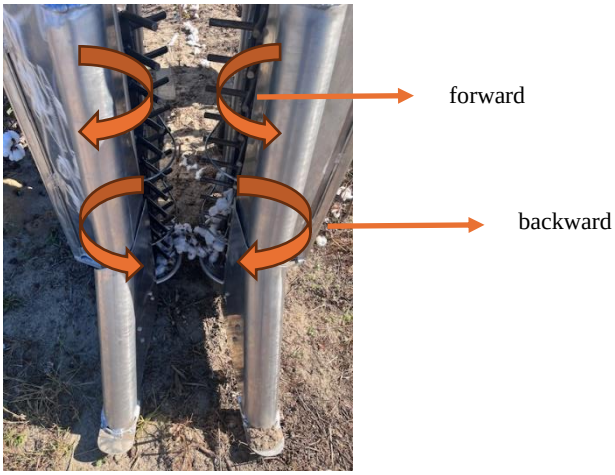

Figure 4. The rotation of the front roller under study.

The efficiency of the harvester, as shown in Eqn (1), was measured by calculating the number of bolls collected in the storage bins. Cotton bolls were counted before and after harvesting for each of the 19 small rows. Data collection included recording the number of bolls, weighing the collected bolls in the collecting bin, weighing trash limbs in the header and bolls on the ground, and other relevant operational metrics that will be used for further analysis related to yield and quality. Multivariate analysis (MVA) was also used to determine which of the rotations and duty cycles had more influence on the cotton bolls on the bin, the ground, and the trash in the header. The variables used for the MVA were bolls left on the plants, bolls on the ground after harvest, bolls on the header, trash in the header, and bolls on the bin. Similarly, the same data on weights for bolls on the plants, ground, and header were included, although they showed similar results.

$$Efficiency = \frac{Output}{Input} x100\% \quad (1)$$

where Output is the bolls collected at the harvest bin, and Input is the number of bolls on the plants before the harvest.

3. Results and Discussion

Field tests revealed that the backward rotation direction of the front roller, when operated at 50% and 100% duty cycles, achieved the highest efficiency in harvesting cotton bolls at 15% and 27%, respectively. This configuration resulted in lower losses and minimal trash in the header, indicating a better effective extraction and collection process than forward direction with all three duty cycles. However, despite these promising results, the total number of bolls collected in the storage bins remained relatively low due to clogging issues at the bottom of the eductor system.

The randomized block design employed in the field experiments provided robust data, highlighting the impact of varying duty cycles and rotation directions on harvesting performance. The initial nine subplots indicated a significant improvement in boll collection efficiency with higher duty cycles. In comparison, the subsequent 10 subplots confirmed that the backward rotation direction was more effective than the forward direction. These findings suggest that optimizing the rotation speed and direction of the finger roller is crucial for maximizing harvesting efficiency.

The results for the MVA showed that the backward rotation has a more positive influence on the amount of harvested cotton bolls in the bin and the number of remaining cotton bolls on the plants, as shown on the scores and correlation loading plots in Figures 5a and 5b.

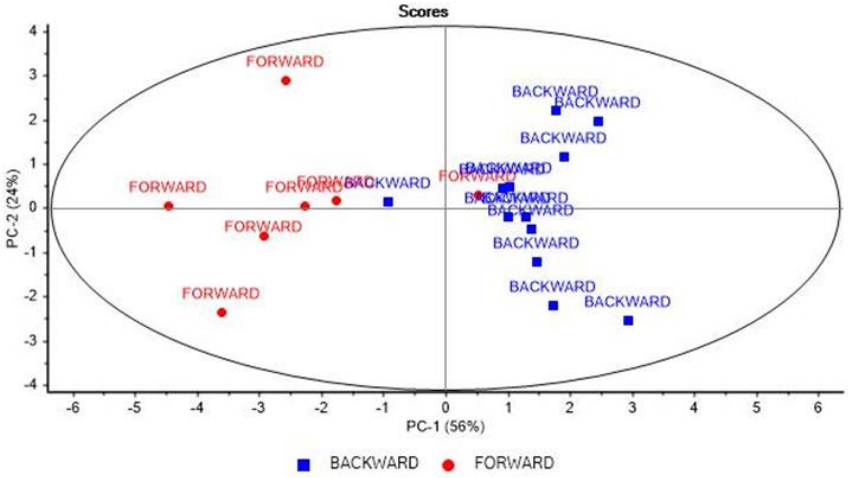

(a)

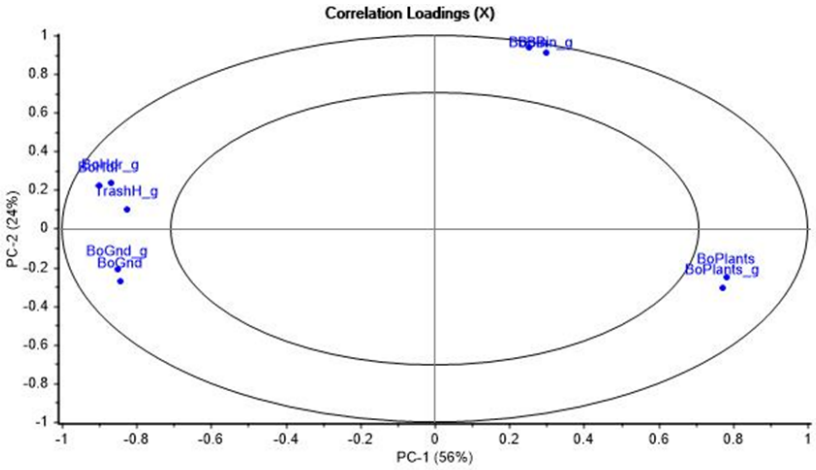

(b)

Figure 5. (a) Score plot for the direction of the front rollers, and (b) Correlation Loading plot for the variables used for this field test.

For the duty cycles, both 50% and 100% on the backward rotation positively influenced the number of cotton bolls in the bin, as shown on the score plot in Figure 6.

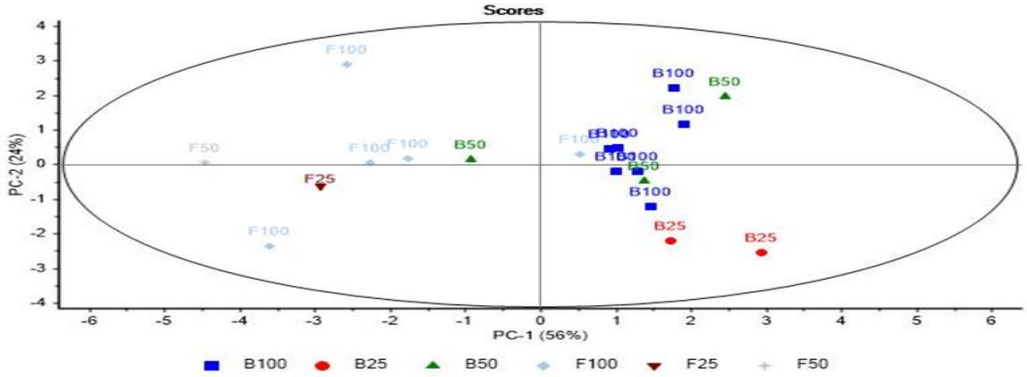

Figure 6. The score plot using direction and duty cycles (B50 means, backward with 50% duty cycle).

The results of this study demonstrated that the developed proof-of-concept cotton harvester showed promising potential in addressing the issues of cost and soil compaction associated with traditional mechanical harvesters.

Despite the overall success in improving efficiency and reducing trash, the study identified a critical area for further development: the clogging of bolls at the bottom of the eductor. This issue limited the amount of cotton that could be effectively transported to the storage bins, thus impacting the overall yield. Addressing this challenge will be essential for the practical implementation of the harvester.

3.1. Field Test Observations

The trial proceeded well, with several bolls collected in the harvesting bin. However, an issue was identified at the end of the sub-row trial when some trees were uprooted due to their stems tangled in the rear roller shafts. This created resistance to the rollers' rotation. In the subsequent sub-row, the same problem caused the motor to rotate on its mount due to the enormous resistance on the shaft, stretching and eventually fraying the wires. Replacing the motor temporarily resolved this issue. In the following sub-rows, tangled cotton stems caused the internal fuse of one motor driver on the first motor controller board to blow. Eventually, the field trials were terminated when the other motor controller shut down and would not turn on, also due to blown internal fuses caused by the increased load from the resistance to the roller shaft. Additionally, this problem resulted in debris being caught inside the header chamber.

Initial observations suggested that branches entered directly into the rear roller, caught on the fingers, and wound around the shaft. The force of the rotating shaft uprooted entire cotton plants, and the tangled stems and branches prevented the shaft from rotating. On the electrical side, the load surge damaged only the motor controller, preventing a catastrophic failure of the control system. The electronic complications were primarily caused by stems getting caught in the rear rollers and stopping their rotation.

To solve this problem, modifications were made to the header to prevent branches or stems from entering the rear rollers directly. A bottom plate was added to each header to force the branches upright. A curved stainless-steel rod was mounted over the header opening to prevent stems or branches from entering the rear rollers directly. To protect the motor controller from damage, a fuse was added to the positive side of the power supply. Despite these modifications, some branches with cotton bolls were prevented from reaching the rear rollers. The smooth surface of the fingers in the rollers allowed the branches with cotton bolls to glide freely and bypass the rollers. The cotton bolls flicked by the rear rollers should be sucked into the bin by the negative pressure generated by the eductor. However, due to the inherent property of cotton, it tends to stick to rough surfaces, causing a buildup near the entry to the eductor.

Another prevailing issue with the robot's construction was the weight distribution. The heaviest parts of the harvester assembly are the two headers located at the front, causing a weight imbalance that contributes to structural and mechanical stress on the chassis and front wheels. The robot struggles with grip at the rear due to the differential nature of its wheels. Although both generators and 94 lbs of counterweight are placed at the rear, this does not solve the balance issue and adds more load. The robot's gross weight far exceeded the rated load of the mobile platform. Consequently, the fuses of the Amiga platform's batteries blew due to spikes in motor load, particularly on the front wheels. The motor also frequently overheated and required significant cooldown time, further delaying the field trials.

Based on observations from all field trials, the problems can be summarized as follows:

1. The front rollers were inadequate at directing the branches to the rear rollers, which was exacerbated by the modifications.

2. The inlet to the eductors caused a buildup of cotton bolls and debris, blocking the suction.

3. Uneven weight distribution led to mobility problems, especially on uneven farm grounds with loose soil.

4. The motors overheated due to overloading the Amiga platform, compounded by its uneven weight distribution.

3.2. Addressing the issues

Revising the cotton harvester robot aims to increase harvesting efficiency by addressing the identified problems. The strategy is to focus first on the most critical part: the header assembly and the harvesting

mechanism. Once these are improved, the rest of the design will evolve around them.

Based on the analysis of the harvester's mechanical action from both animated simulations and actual field trials, the following revisions or additions are needed:

1. Adjust the position of the front and rear rollers relative to each other to capture more cotton bolls from the branches.

2. Optimize the proximity of the headers to each other to maximize branch exposure to the front rollers.

3. Redesign the fingers in the rollers to better grab the branches and effectively feed them to the rear rollers.

4. Add an additional blower to clear the inlet of the eductor, ensuring a smooth flow of cotton bolls through the system.

Figure 7 compares the header assembly design between the original design (left) and the updated version (right). The first major change in the design is the elimination of pulleys and belts to drive the finger rollers (A). These have been replaced with a 90-degree angled gearbox featuring 1:1 and 1:2 gear ratios for the front and rear rollers. The system retains the same planetary gear motors, but the rear roller now uses a 320-rpm motor. This allows the rear roller to achieve a maximum rotation speed of 620 rpm, three times higher. With the gearbox, an additional motor for the rear roller is no longer needed. The second significant modification involves the front finger rollers (B). The new design features an angled finger at approximately 15 degrees, constructed from cut aluminum instead of a steel tube. This angled finger can grab branches more effectively than the previous straight, round design. The rear roller has a 3/4” round steel tube shaft, which maintains the original design but uses a round steel tube instead of a square one.

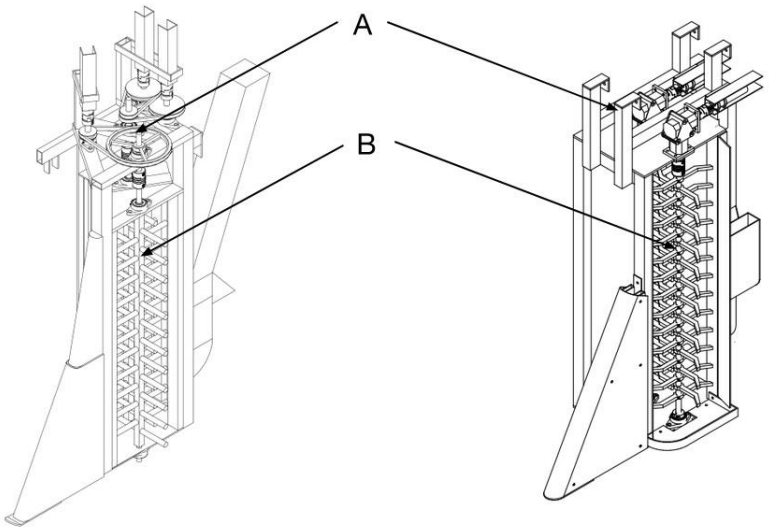

Figure 7. The front roller original (left) and updated (right) design.

Another major change is the positioning of the rollers relative to each other. Figure 8 illustrates this difference. In the original design, the front and rear rollers were offset at an angle of about 54 degrees (Figure 8a). In the revised design, the rollers are aligned side-by-side (Figure 8b). The offset in the original design aimed to narrow the header but reduced the rear roller's effectiveness, as it only hit cotton bolls pulled deep enough by the front roller. By aligning the rollers side-by-side, even cotton bolls that are not pulled deeply can still be reached by the fingers on the rear roller. With the faster rotation of the rear roller, cotton bolls, whether pulled shallow or deep, have a greater chance of being picked. Additionally, an air blower has been installed inside the eductor to reduce the buildup of cotton bolls and debris at the inlet. This blower is powered by a third blower that provides a constant air stream.

(a) (b)

Figure 8. Finger roller positions: (a) original and (b) updated version.

Most of the robot's weight is concentrated at the front, causing balance issues even with counterweights and placing tremendous stress on the support structure. To address these problems, several considerations must be made in revising the chassis:

1. Relocate the header to improve support and minimize balance issues.
2. Enable on-field adjustment of the header's ground clearance.
3. Allow for load adjustments to improve overall balance and weight distribution.
4. Weld the chassis structure instead of using tube clamps.

Figure 9 shows the entire cotton harvester robot assembly. The header, bin, blowers, and generators are mounted on a ladder frame (B). This frame can be moved forward or backward to adjust balance and weight distribution and is not welded to the chassis. A sub-frame on the ladder frame holds the header assemblies (C), allowing the header height to be adjusted by jacking up the sub-frame and inserting 10 mm spacers until the correct height is achieved. The Amiga chassis, where the ladder frame will be mounted (D), will be welded rather than using tube clamps. Welding eliminates the need for tube clamps, allowing the ladder frame to be mounted lower. By addressing the balance issue, the robot no longer requires a counterbalance, resulting in less weight and reduced stress on the platform.

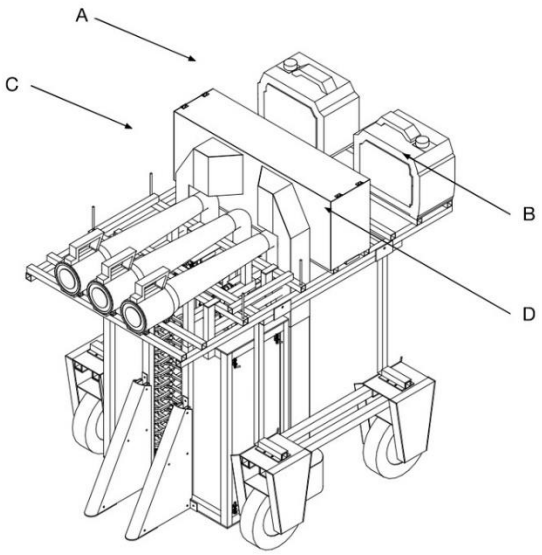

Figure 9. Cotton Harvester v2.0 Full Assembly.

4. Conclusions

In conclusion, this project successfully developed and tested a proof-of-concept cotton harvester robot to increase harvesting efficiency and address critical issues related to weight distribution, mechanical stress, and cotton boll collection. The revisions, including eliminating pulleys and belts in favor of a 90-degree angled gearbox, realignment of front and rear rollers, and adding an air blower in the educator, significantly improved the harvester's performance. These changes enhanced the harvester's ability to capture cotton bolls

more effectively while reducing debris buildup and minimizing the strain on the support structure.

The adjustments to the chassis, such as relocating the header for better support, enabling on-field ground clearance adjustments, and welding the chassis structure, further contributed to a balanced and robust design. These modifications improved the overall balance and weight distribution and reduced the need for counterweights, thereby decreasing the stress on the Amiga platform.

Despite encountering challenges during the field trials, such as motor overheating and structural imbalances, the iterative improvements made throughout the project demonstrated the potential for a viable, efficient, and sustainable cotton harvesting solution.

Future work will focus on refining these design elements, addressing any remaining mechanical and electronic issues, and optimizing the autonomous navigation capabilities of the robot. Additional efforts will include improving the robustness of the harvesting mechanism to prevent clogging and enhancing the durability of the motor and electronic systems to withstand field conditions. Furthermore, integrating advanced sensors and machine learning algorithms for better decision-making and precision harvesting will be explored. These enhancements aim to transition the proof-of-concept harvester into a commercially viable product, ultimately benefiting the cotton industry by increasing efficiency, reducing labor costs, and promoting sustainability.

This project lays a solid foundation for developing advanced agricultural robotics, promising significant benefits for the cotton industry through increased efficiency, reduced labor costs, and improved sustainability.

Acknowledgments

This project was supported by funding from Cotton Incorporated under Project No. 17-029. We also gratefully acknowledge the travel funding provided by Dr. Lamin Drammeh, Associate Vice President and Director of Strategic Initiatives, Evaluation, and Engagement at South Carolina State University 1890 Research and Extension, Public Service and Agriculture. Their financial support and encouragement were invaluable to successfully completing this research.

References

Chen, J. and Burke, J. 2015. Developing fiber specific promoter-reporter transgenic lines to study the effect of abiotic stresses on fiber development in cotton. Plos One, 10(6), e0129870. https://doi.org/10.1371/journal.pone.0129870

Dadd-Daigle, P., Kirkby, K., Chowdhury, P., Labbate, M., & Chapman, T. 2021. The verticillium wilt problem in australian cotton. Australasian Plant Pathology, 50(2), 129-135. https://doi.org/10.1007/s13313-020-00756-y

Grove, W. and Heinicke, C. 2003. Better opportunities or worse? the demise of cotton harvest labor, 1949–1964. The Journal of Economic History, 63(03). https://doi.org/10.1017/s0022050703541973

Heinicke, C. and Grove, W. 2005. Labor markets, regional diversity, and cotton harvest mechanization in the post-world war ii united states. Social Science History, 29(2), 269-297. https://doi.org/10.1017/s0145553200012955

Jung, Y. 2018. The legacy of king cotton: agricultural patterns and the quality of structural change.. https://doi.org/10.31235/osf.io/trjfz

Makhmadjanov, S., Tokhetova, L., Daurenbek, N., Tagaev, A., Kostakov, A. 2023. Cotton advanced lines assessment in the southern region of kazakhstan. Sabrao Journal of Breeding and Genetics, 52(2), 279-290. https://doi.org/10.54910/sabrao2023.55.2.1

Natálio, F. and Maria, R. 2018. Structural evolution of gossypium hirsutum fibers grown under greenhouse and hydroponic conditions. Fibers, 6(1), 11. https://doi.org/10.3390/fib6010011

Peterson, W. and Kislev, Y. 1986. The cotton harvester in retrospect: labor displacement or replacement? The Journal of Economic History, 46(1), 199-216. https://doi.org/10.1017/s0022050700045587

Tausif, M., Jabbar, A., Naeem, M., Basit, A., Ahmad, F., & Cassidy, T. 2018. Cotton in the new millennium: advances, economics, perceptions and problems. Textile Progress, 50(1), 1-66. https://doi.org/10.1080/00405167.2018.1528095

Witjaksono, J., Wei, X., Mao, S., Gong, W., Li, Y., & Yuan, Y. 2014. Yield and economic performance of the use of gm cotton worldwide over time. China Agricultural Economic Review, 6(4), 616-643. https://doi.org/10.1108/caer-02-2013-0028

A novel on-line dual-sensing system for soil property measurement and mapping

Rukayat Afolake Oladipupo[a], Muhammad Abdul Munnaf[b], Parsat Sanganta[c], Ajit Borundia[d] and Abdul Mounem Mouazen[e]*

Department of Environment, Ghent University, Gent, Belgium

* Corresponding author. Email: abdul.mouazen@ugent.be

Abstract

Real-time assessment of within-field soil fertility variation is crucial for making informed and sustainable decisions, like crop nitrogen (N) fertilisation. Two commonly used soil sensors i.e., visible-near-infrared (vis-NIR) spectroscopy and ion-selective electrodes (ISE) have been reported to successfully estimate various soil macronutrients and nitrate-N, respectively, however, their integrated use for mapping a full-scale soil fertility variation has not been taken into consideration to date. The aim of this study is to use an integrated on-line dual-sensor system of vis-NIRS and ISE to estimate and map within-field variation in soil pH, organic carbon (OC), extractable- phosphorus (P), potassium (K), calcium (Ca) and moisture content (MC) and nitrate-N. The sensing system was mounted to the three-point linkage of a tractor and surveyed two arable fields in Belgium. Partial least squares regression models for vis-NIRS sensor were calibrated and validated, while a linear regression model was established to validate the ISE sensor. Geostatistical surface maps for on-line measured soil attributes were generated using the inverse distance weighting and ordinary kriging methods for ISE data and vis NIR, respectively. The linear correlation confirms a very high similarity between ISE-measured nitrate-N and laboratory-analysed nitrate-N (coefficient of determination (R2) = 0.93). Besides, the vis-NIRS demonstrates very good prediction accuracies for all the fertility attributes with R2 = 0.70-0.78, root mean square error (RMSE) =0.52-2.46 %, residual of prediction deviation (RPD) = 1.89 – 2.13 and the ratio of the performance to interquartile distance (RPIQ) = 1.72 – 6.56. Validation between laboratory and on-line measured soil maps also shows quite comparable spatial distribution patterns. Therefore, the proposed dual on-line sensor system has a high potential to estimate and map within-field spatial fertility distributions including nitrate-N, offering a basis for sustainable management decisions for precision soil and crop production.

Keywords: Near-infrared spectroscopy, Ion selective electrodes, Soil fertility, On-line sensing.

1. Introduction

Over the years, on-line soil nutrient mapping has gained significant attention as a valuable procedure for precision agriculture and sustainable soil management. This approach allows for real-time monitoring of soil nutrient levels, enabling farmers to make informed decisions regarding fertiliser application and crop management. Among the various sensing technologies employed, electrochemical sensors (Adamchuk et al., 2005) specifically the ion-selective electrode (ISE) and visible and near-infrared spectroscopy (vis-NIRS) (Gurrero et al., 2021, Kuang et al., 2012, Mouazen et al., 2011) have emerged as promising methods for on-site and non-destructive soil nutrient analysis. The vis-NIRS has shown promising results in predicting various soil properties, including organic matter (OM), phosphorus (P), total nitrogen (TN), potassium (K), clay content, moisture content (MC), cation exchange capacity (CEC) (Mouazen et al., 2007, Nawar and Mouazen, 2017, Gurrero et al., 2021). Apart from those properties, vis-NIRS was earlier reported as an efficient sensor for mineral N estimation (Ehsani et al., 1999), however, only a very limited number of studies was found in the literature to substantiate the claim. Therefore, it can be inferred that vis-NIRS demonstrates limited success in predicting mineral nitrogen levels, a conclusion supported by existing literature (Guererro et al., 2021, Kuang et al., 2012).

The ISE has been reported to measure soil nitrate-N although most have focused on measurements in laboratory modes (Adamchuk et al., 2002, Kim et al., 2007, Sibley et al., 2009, Shaw et al., 2013) and in-situ (Li et al., 2019, Sibley et al., 2010, Bendikov et al., 2005). However, these two measurement modes do not effectively capture in-field variabilities as the on-line mode, hence, not meeting the requirement of high-resolution data to reveal the spatial variability for accurate and robust precision management decisions (Guerrero et al., 2021). Only a limited number of studies on the on-line measurement of soil nitrate-N can be

found in the literature, which can be mostly attributed to the sampling complexities (Li et al., 2019, Adamchuk et al., 2005, Adsett et al., 1999, Sibley et al., 2009). Over the years, efforts have been made to optimise ISE on-line measuring systems (Adamchuk et al., 2002, 2004, 2005, Adamchuk and Rossel, 2010, Sethuramasamyraja et al., 2008) yet, no robust system has found its way into practice or research.

Examining the literature about these two sensors indicates that each has the potential to complement the other for assessing and mapping within-field fertility variation accurately. The fusion of both sensor technologies will enable the on-line measurement of macro soil fertility attributes and soil nitrate N. However, this has not been reported so far, although many studies have proposed the use of multi-sensors data fusion approach for mapping soil nutrients (Adamchuk et al., 2004, Sethuramasamyraja et al., 2008, Adamchuk et al., 2011, Gurrero et al 2021). To the best of our knowledge, there is no previous study focusing on the integrated use of ISE and vis-NIRS sensors for rapid on-line soil fertility mapping. Therefore, the aim of this study was to evaluate the performance of the proposed dual-sensor system consisting of ISE and vis-NIRS sensors for on-line estimation and mapping of soil nitrate-N along with key soil macronutrients i.e., P, K, OC, MC, pH, and Ca, respectively. This study hypothesises that the ISE estimated nitrate-N can add additional values to the vis-NIRS spectra-based information of K, P, OC, MC, pH, and Ca thus, an integration of these two sensors is assumed to provide a holistic understanding of within-field variability in soil fertility. This dual-sensor approach is expected to provide rapid and valuable soil information immediately before the design of soil and crop management decisions, like seeding and fertilisation.

2. Materials and Methods

The research work followed four methodological steps which began with field scanning using the dual sensor system. While the vis-NIRS sensor recorded soil spectra in the 350-1750 nm spectral range, the ISE sensor measured nitrate-N directly based on a previously developed calibration function. At the same time, soil samples were collected and used for laboratory measurements of key soil properties i.e., K, P, MC, Ph, OC and Ca. The partial least squares regression (PLSR) analysis was employed to develop calibration models for the vis-NIRS sensor to predict the listed properties using the on-line collected spectra. Geo-statistical interpolation was used to map and compare all soil properties. The following subsections will discuss these steps in detail.

2.1. Dual on-line sensing system

The dual-sensing system used in this study integrates both an ISE and a vis-NIRS sensor installed on a versatile mobile platform. This platform also has provision to mount an electronic control box, a water tank, a differential global positioning system (DGPS) receiver, a semi-rugged laptop, and a subsoiler. This platform is a single unit, easily attachable to a tractor through a three-point linkage. The ISE sensing system consists of three units of mechanisms, namely, sampling unit, measurement unit and control unit. The sampling unit comprises a conveyor and a sampling auger designated to pick soil samples, convey, and deliver them to the measurement unit. The sampler is a 50 cm^3 metal cup attached to a conveyor chain powered by a hydraulic motor. The conveyor consists of a 12.5 mm pitch roller chain and 2 sprockets. As the conveyor rotates, the sampler collects soil samples as it approaches the soil surface. As the conveyor proceeds in its movement, the soil sampler dispenses its contents into a measuring cup situated along its path just above the input sprocket. The measuring cup is a component within the measurement unit which encompasses a sensor housing, a mixing mechanism, a filter and a stirrer. In the cup, a soil solution is prepared by adding water from the water tank in which an ISE sensor (SENTEK_Nitrate 3021 combination ISE) measures nitrate-N concentration. Once the measurement is completed, the cups will be cleaned, to be ready for the next measurement cycle. An electronic control unit uses a C++ computer program language to automate the entire system for soil sampling, conveying, measuring, and restoring the system in iterative patterns while the data is recorded using dedicated LabVIEW software.

Besides, the on-line vis-NIRS sensing system designed and developed by Mouazen (2006), consists of a subsoiler, which makes trenches in the soil, the bottom of which is smoothened by the subsoiler due to downward vertical forces. An optical probe hosted in a mild steel lens holder is appended to the back of the subsoiler chisel to measure soil spectra in diffuse reflectance mode from the smoothed bottom of the trench. A fibre-type, vis–NIRS sensor (CompactSpec from Tec5 Technology, Germany), with a measurement range of 305–1750 nm and spectral resolution of 1 nm is mounted on the platform to collect soil reflectance spectra.

2.2. In-field soil sensing and sampling

Two arable fields in the Flanders region of Belgium (Figure 3) (Field 1 = 1.3 ha and Field 2 = 0.7 ha) were chosen for this study. Both fields have a similar texture of sandy loam as determined by Robinson-Kohn pipette method (ISO 11277).

For the field measurement, the on-line dual-sensing system was driven across the field by a tractor at a speed of 2.3 km/hr. The sampling unit of the ISE sensor collected soil samples through a sampler and auguring mechanism, and samples were subsequently conveyed to the mixing cup where the soil was mixed with deionised water to extract the nitrate ions. A water pump was utilised to facilitate the infusion of water into the measuring cup, thereby enabling the creation of a soil solution (soil: water, 1: 5). Subsequently, the stirrer was activated ensuring a homogeneous soil solution. The soil nitrate-N concentration was then measured using the ISE sensor, which is positioned in the mixing cup and connected to a computer through a universal serial bus cable, where the measurements were stored once every second until an equilibrium measurement was achieved after about 10 seconds. Afterward, the measuring cup discharged its material contents and a cleaning cycle was promptly initiated to prepare it for the subsequent sample. This operational process enabled the continuous acquisition of data, with the measuring cup ready to receive a new sample after each cleaning cycle.

Similarly, the vis-NIRS sensor utilized an optical probe, for the collection of soil spectra within the trench created by the subsoiler. A PTFE disc, serving as a 99.99% white reference, was routinely scanned at 30-minute intervals to calibrate the vis-NIRS sensor to standardise measurement intensity. The spectra were equally recorded in a computer connected to the sensor via an ethernet local area network cable. A differential global positioning system (DGPS) (Trimble AG., Trimble Navigation Ltd., Sunnyvale, Canada) recorded the position of each measurement. Soil spectra and nitrate-N values together with GPS location data were logged at a frequency of 1 Hz by a custom-made LabVIEW software using a semi-rugged laptop computer (Toughbook, Panasonic UK Ltd., Bracknell, UK).

Field measurements were conducted on well-harrowed and ploughed soil, which was beneficial for smooth and effectively collecting the right amount of grounded soil necessary for homogenous soil solution making for ISE measurement, although not essential for vis-NIRS measurement. During the on-line field survey, a total of 18 soil samples (10 from field 1 and 8 from field 2) were collected randomly from the bottom of trenches created by the subsoiler. These were required for subsequent laboratory analysis for calibrating the vis-NIRS sensor and validating the ISE measurements. Additionally, a second batch of 20 soil samples was randomly collected for additional validation and calibration of the ISE sensor. The intention was to investigate how long the ISE-measured nitrate-N can be valid for management decisions.

2.3. Laboratory chemical and optical measurements

A day after the field sensing, each of the collected 18 soil samples was divided into three sub-samples. The first part was sent to the Soil services of Belgium (BDB, Heverlee, Belgium) for the analyses of nitrate-N, available P, K, Ca, OC and pH using standard laboratory methodologies. The second portion was used for moisture content (MC) determination using the oven method after 24 hr drying at 105 0C. The third portion was passed for both vis-NIRS scanning as well as ISE measurement. These laboratory ISE measurements were used to validate the ISE on-line measurements and the vis-NIRS measurements were added to the vis-NIRS model calibration dataset to enhance the prediction accuracy.

Similar to the ISE field measurement, the same calibration standard solutions were used to calibrate the ISE sensor for the same soil-to-water ratio (1:5). 50g of each sample was measured and placed in a beaker to which 250 ml of distilled water was added. This was mixed thoroughly 10seconds and filtered using a 10-micron filter paper. The sensor was immersed into the filtered solution and the potentiometric values were logged in millivolts (mV) at 1-second intervals through the LabVIEW software. After 10 seconds of measurement, the logged Mv values were averaged to a single value.

For laboratory vis-NIRS scanning, about 150 g of each sample from the third portion was used to prepare three Petri dishes, each measuring 4 cm in diameter and 1 cm in depth. To optimize the signal-to-noise ratio, the soil surface was compacted using a spatula. Spectral measurements were conducted under dark chambers to eliminate the influences of external lights. Each Petri dish underwent ten consecutive scans (resulting in a total of 30 soil spectra per sample), which were then averaged to derive a single spectrum. Like the field measurement, vis-NIRS sensor was calibrated using the same PTFE standard reflectance once every 30

minutes.

Furthermore, the second batch of 20 samples were passed for the in-lab ISE sensing and in-lab nitrate-N measurements using the same procedure i.e., ISE sensor and continuous flow method, respectively, as the method used by BDB for the first batch of samples. This time, nitrate-N was measured using the same continuous flow auto-analyser but in the soil fertility laboratory of Ghent University. This step was intended to check the error due to a time gap of 15 days between the first laboratory and ISE measurements, which could introduce biases. This gap occurred as a result of logistical delays in transporting and processing of samples.

2.4. Sensors data analysis and modelling

The in-field observations of potentiometric readings of the ISE sensor were transformed from millivolts (mV) to Parts Per Million (ppm) using a calibration model. This model was developed by correlating the mV values from the sensor with known concentrations of five standard nitrate solutions (ranging from 0.25 to 40 ppm). The sensor was placed in each solution, logging mV readings at 1 Hz, and the data were fitted to a semi-log scale to create the calibration curve. The potentiometric readings obtained in field measurement were subsequently projected to ppm using this fitted curve. These measured ppm values were compared with standard laboratory measurements to validate the sensor and to confirm its reliability for on-line measurement.

Besides, modelling vis-NIRS spectra for predicting on-line collected spectra requires a multivariable calibration method. The collected 18 soil samples were merged with additional samples from a locally available spectral library hence, a total of 154 soil samples were used to develop the models for both fields. Firstly, soil spectra were cleaned by removing the non-soil and noisy spectra, followed by jump corrections at 1045 nm where the two detectors of the vis-NIR spectrometer joined each other. Subsequently, a Savitzky-Golay filter was applied to smoothen the spectra, and the noisy regions were trimmed, resulting in spectral ranges of 400 to 1680 nm. The standard normal variate (SNV) technique was employed as it is a suggested technique for effectively normalising spectra and minimising variations (Syvilay, et al., 2015) After spectra pre-processing, PLSR analysis was chosen to establish the calibration models, given its suitability over other linear regression algorithms in dealing with multicollinearity, which usually exists in the spectral dataset. The dataset was divided into train and test sets at 70 over 30 %, respectively, splits using the Kennard-Stone algorithm (Kennard & Stone 1969). The PLSR modelling involved iterating training over up to 10 components using the training set, using leave-one-out cross-validation. Models were then validated using the independent test dataset. The prediction performance was assessed relying on root mean square error (RMSE), ratio of prediction deviation (RPD), ratio of the performance to interquartile distance (RPIQ) and coefficient of determination (R2). The modelling process was executed in Python 3.3 using libraries such as NumPy and Pandas for data manipulation, Matplotlib for visualisation, and Scipy's savgol_filter for signal smoothing. Ultimately, the final models were used to predict the target variables (pH, OC, P, K, Ca and MC) using the large on-line collected spectral set over the entire field area.

2.5. Mapping

Maps of various soil properties (measured and predicted), including nitrate-N, K, MC, P, pH, OC, and Ca, were generated for laboratory observations and on-line predictions. The inverse distance weighting (IDW) interpolation with a power of 2 was utilised for the laboratory data and on-line ISE data, given the relatively smaller sample sizes of 10 and 8 (laboratory samples) and 56 and 32 (on-line ISE data points) for the fields 1 and 2, respectively. On the other hand, ordinary kriging with a stable semi-variogram model was employed for the predicted soil data, being a large dataset with over 1588 and 722 (vis-NIRS) data points for fields 1 and 2, respectively. Both maps were categorised into five classes to ensure a meaningful visual comparison between the laboratory-measured and predicted property maps using the Kappa value.

3. Results and Discussion

3.1. Evaluation of ISE sensor

3.1.1. Measurement accuracy

Figure 1 presents the similarity plot of nitrate data obtained from the ISE sensor under (a) on-line ($ISE_{\_On\text{-}line}$), lab measurements ($ISE_{\_lAB}$), and standard laboratory measurement (SLM) conducted by BDB ($SLM_{\_BDB}$) (b) Laboratory measurement ($ISE_{\_lAB2}$) and Standard laboratory measurement conducted at Ghent ($SLM_{\_UGENT}$) revealing a striking convergence between ISE-Online and $ISE_{\_lAB}$ with substantial overlap. This signifies a notably high degree of correlation between the on-line ISE measurements obtained in the field and those conducted within the laboratory setting with R^2 of 0.99 for field 1 and 0.98 for field 2. However, there was an evident disparity between the $SLM_{\_BDB}$ and ISE values, despite the high R^2 of 0.84 with $ISE_{\_LAB}$ and 0.78 with $ISE_{\_On\text{-}line}$ (Figure 2(a) and (b)).

These observations align with prior studies by Adamchuk et al. (2005) and Li et al. (2019), who reported disparities between ISE measurements and SLM measurements. These observed deviations can be attributed to potential biases introduced through soil mineralisation processes, likely occurring during the time laps (15 days) between ISE measurements and $SLM_{\_BDB}$. $SLM_{\_BDB}$ observed mostly higher nitrate concentration than ISE measurements except for an observation, where the $SLM_{\_BDB}$ showed slightly lower concentration than $ISE_{\_LAB}$ and $ISE_{\_On\text{-}line}$. This is in agreement with Bailey et al. (2021), who observed an increase in soil nitrate levels immediately after sampling, with a continuation of this increase during storage at refrigeration. Despite the observed disparities, the ISE measured nitrate quite satisfactorily.

A comparison of ISE Laboratory measurement ($ISE_{\_LAB2}$) with the SLM conducted at a second laboratory at Ghent ($SLM_{\_UGENT}$) for the second batch of samples (i.e. 20 samples), employing the same methodology as BDB, revealed a strong coefficient of determination (R^2) (Figure 2(c)). This confirms the effect of time laps on measurement accuracy due to soil N mineralisation, which was observed for the first batch of samples left in the refrigerator at -4 ^{0}C for 15 days before being measured in the laboratory. When the second batch of samples was immediately analysed after soil sampling at the UGent laboratory, the correlation between the $SLM_{\_UGENT}$ and $ISE_{\_LAB2}$ was high ($R^2 = 0.93$), proving the ISE sensor used in this study provided accurate readings for nitrate both under laboratory and on-line measurement conditions. The similarity plot in Figure (1(b)) further shows the similarity between the $SLM_{\_UGENT}$ and $ISE_{\_LAB2}$ with over 70% of the points closely located. This observation further confirms the accuracy and reliability of the ISE measurements. With this observation, it is evident that the time-lap induced a discrepancy between $ISE_{\_On\text{-}line}$ and $SLM_{\_BDB}$ and later it was possible to neutralise such discrepancy by fitting a linear function ($ISE = 1.2636\ ISE_{\_On\text{-}line} - 0.4607$) before producing the on-line soil nitrate maps.

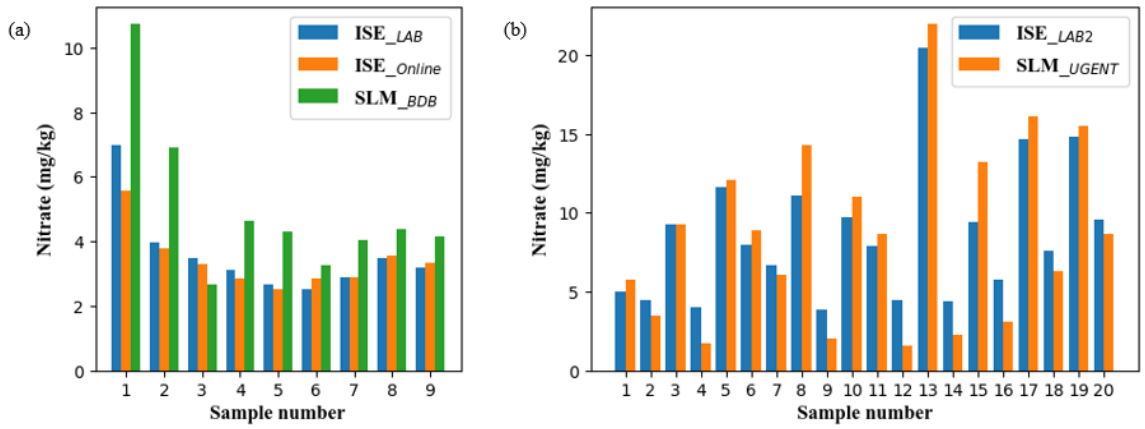

Figure 1: Similarity plots comparing: (a) measurement with ion selective electrode in the laboratory ($ISE_{\_LAB}$), ISE on-line ($ISE_{\_On\text{-}line}$) and standard laboratory measurement by the soil service of Belgium ($SLM_{\_BDB}$) and (b) measurements of the second batch of samples done with ion selective electrode in the laboratory ($ISE_{\_LAB2}$) and standard laboratory measurement conducted at Ghent ($SLM_{\_UGENT}$)

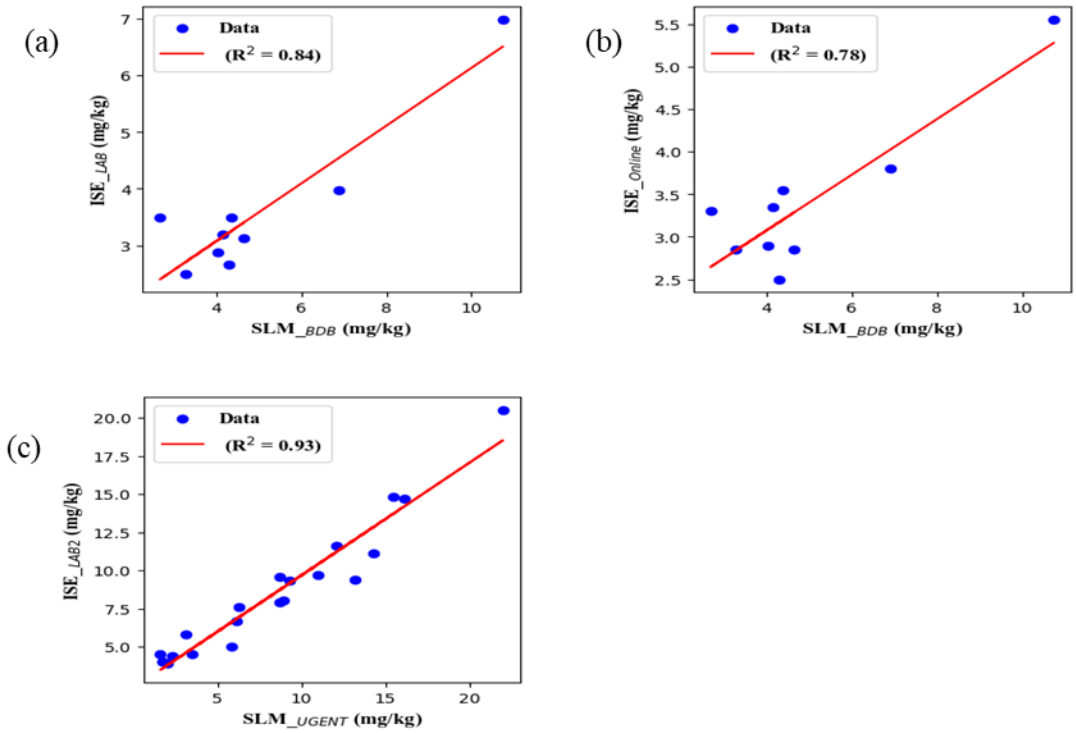

Figure 2. Scatter plots between (a) ion selective electrode (ISE) laboratory measurement ($ISE_{\_LAB}$) and standard laboratory measurement conducted by the soil service of Belgium (BDB) ($SLM_{\_BDB}$), (b) on-line ISE measurement ($ISE_{\_On\text{-}line}$) and standard laboratory measurement conducted by BDB ($SLM_{\text{-}BDB}$) and (c) ISE laboratory measurement for the second batch of samples ($ISE_{\_LAB2}$) and standard laboratory measurement conducted at Ghent University ($SLM_{\_UGENT}$).

3.2. Assessment of on-line vis-NIRS sensor

3.2.1 Accuracy of vis-NIRS prediction models

The vis-NIRS models demonstrate favourable performance in both the training and testing sets for MC, K, pH, and P (R2= 0.70 to 0.78, RMSE = 0.52 to 2.46%)). These indicate that the models can effectively explain a substantial portion of the variability in the respective soil properties with relatively small errors compared to the observed values, signifying reasonable accuracy. However, the model performance for OC and Ca were relatively low (R2 0.63 and 0.68), suggesting a moderate level of explained variability. This might be attributed to the low range of OC and high range of prediction for Ca compared to other properties. This is in agreement with the findings of Kuang and Mouazen (2011) who noted that a small range of sample concentration might result in poor model calibration. Moreover, the RMSE values for Ca are noticeably high, at 17.85% in the test set and 16.59% in the training set. This implies that the model predictions for Ca may have larger errors compared to the actual values. In addition, the RPD from all models remained within the range of 1.64 to 2.13. Categorizing the RPD values based on the criteria proposed by Rossel et al., (2006), the model can be considered as very good for K, good for P, pH and MC, while fair for Ca and OC. Additionally, evaluating the model performance using the criteria proposed by Nawar and Mouazen (2017) using the RPIQ, as defined by Bellon-Maurel et al. (2010) as;

$$RPIQ = IQ/RMSE \quad (1)$$

where IQ is the difference between the third and first quartiles (IQR = Q3 − Q1) and RMSE is the root mean square error, MC, K, P and Ca models performed excellently while the pH model was very good and OC can

be classified as a good model.

Table 1. Result of soil property prediction performance for the visible and near-infrared spectroscopy (vis-NIRS) sensor on training and test sets.

	Training set		Test set				
Soil property	R^2	RMSE	R^2	RMSE	LV	RPD	RPIQ
MC (%)	0.75	1.69	0.74	1.69	9	2.00	4.68
K (mg/100g)	0.78	2.34	0.77	2.46	10	2.13	2.87
PH	0.74	0.61	0.7	0.67	10	1.96	2.24
P (mg/100g)	0.72	2.35	0.71	2.36	9	1.89	6.56
OC (%)	0.63	0.52	0.61	0.54	8	1.64	1.72
Ca (mg/100g)	0.68	16.59	0.65	17.85	8	1.77	5.8

R2: coefficient of determination, RMSE: root mean square error, LV: latent variable, RPD: residual prediction deviation, RPIQ: ratio of the performance to interquartile distance, MC: moisture content, K: potassium, P: phosphorus, OC: organic carbon, and Ca: calcium.

3.2.2. Maps of Soil Fertility Attributes

The vis-NIRS-based spatial distribution maps (Figure 3) for all properties emerge with a consistent pattern for those measured in the laboratory condition while the on-line predicted values emerged with maps with moderate similarities with the reference laboratory distribution maps. Field 1 shows higher nutrient constituents along the north-east edge of the field which was consistent across all the properties. The peak fertility in Field 2 was observed mostly around the west edges of the field. Particularly, the on-line-measured OC exhibits a moderate level of congruence with the reference laboratory measurements across the study area, with pronounced agreement observed around the peak regions for both fields with considerable variation of OC (Field 1 : 1.2-2.5%, Field 2 : 1.2-2.8%) observed over the entire area of the field irrespective of the size of the field (0.7 and 1.3 ha). In general, such high organic carbon (OC) content usually enhances the soil quality, structure and physical stability (Munnaf and Mouazen, 2021). Furthermore, comparative range of OC measurements obtained through these two methods demonstrates a considerable level of agreement with the laboratory measurement mostly in field 2 with a kappa value of 0.56 while a moderate level of congruencies is observed in field 1 with kappa value of 0.44.

Similar to OC, the spatial distribution of on-line measured MC shows a moderate level of agreement with the laboratory measurement for both fields, with kappa values of 0.59 and 0.56 for field 1 and field 2 respectively. The utility of the vis-NIRS sensor for MC assessment has been well-documented in previous studies by Mouazen et al. (2007), and the modest average mean errors of 0.24% for field 1 and 0.15% for field 2 further validates its dependability for MC measurements. The MC peaks were concentrated along the edges of field 1, which can be attributed to the presence of trees in these regions, thereby limiting evaporation around these areas. As expected, high OC content was also observed in these regions since OC is usually positively associated with soil water holding capacity, and hence soil MC.

The soil pH maps reveal a conspicuous similarity between the on-line and laboratory measurement approaches for both Fields despite relatively narrow measurement ranges of 5.3-6.8 and 6.0-7.4 and the relatively low kappa values of 0.3 and 0.4 observed in field 1 and field 2, respectively. The peak pH values were found mostly around the corners of the field which are equally the regions with observed high moisture content. According to Zhang and Wienhold (2002), an increase in pH values is likely to occur at high moisture content due to the anaerobic condition resulting from water-filled pore spaces. Soil P presents a moderate level of consistency for both on-line and reference laboratory measurements, with average values of 42mg/100g for field 1 for both on-line and laboratory and 40 and 42mg/100g for field 2 for on-line and laboratory measurements, respectively. This indicates a high P content in both soils according to the soil nutrient criteria of BDB analysis. A relatively moderate kappa value of 0.58 is observed in field 1 and 0.67 in field 2 confirming the high similarity between the maps. The high P values may be attributed to the application of organic manure, which was a regular practice in the fields used in this study.

The variability of K maps for both on-line and laboratory-measured values exhibit a noteworthy degree

of resemblance, with the peak K value observed around the Northeastern edges of field 1 for both maps. For field 2, the peak K values were mostly concentrated on the northwest corner, while the lower values converged around the far southeastern part of the field. The values of K for both fields can be classified as average to high according to BDB with values ranging between 19.6 and 53.8mg/100g. Both fields exhibit moderate similarity between laboratory and on-line maps with kappa value of 0.58. Ca reveals a substantial degree of congruence between the reference laboratory method and the on-line approach with the peak values converging around the same regions for both maps. The high kappa values of 0.71 and 0.63 computed for field 1 and field 2, respectively, further showed the high degree of similarity between the maps.

Based on fertility ratings, pH of soils was acidic with field 1 slightly more acidic than field 2 but mostly within the range suitable for optimum availability of other soil macronutrients and uptake of P and K (Munnaf and Mouazen 2021, Jensen and Thomas, 2010). OC and P contents were high for both fields while Ca and K were high in field 2 but within the normal range for crop growth as suggested by BDB. Overall, soil maps indicate that the soil fertility attributes in field 2 were slightly better predicted and mapped than those in field 1 with clear and distinctly similar regions between on-line and laboratory-measured maps. Nonetheless, the maps of both fields adequately captured the distinct variation across the field. Notably, both laboratory-measured and on-line predicted maps had their peak and low values located at similar positions for all properties measured within both fields thereby adequately classifying the field into different fertility classes.

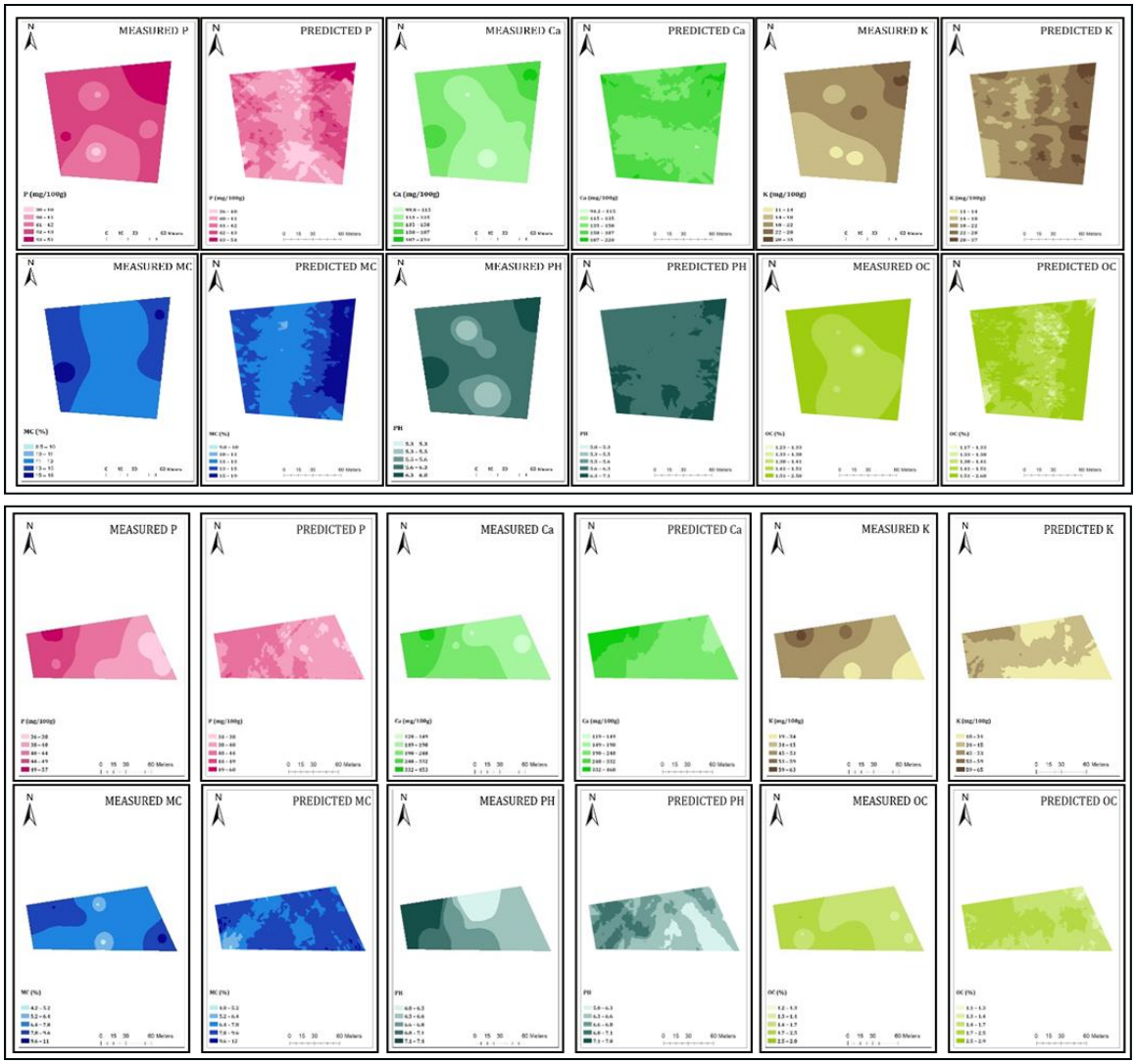

Figure 3. Maps for laboratory-measured and on-line visible and near infrared spectroscopy (vis-NIRS) spectra predicted soil pH, organic carbon (OC), moisture content (MC), extractable phosphorous (P), potassium (K), and calcium (Ca).

3.3. Spatial association between on-line vis-NIRS and ISE measurements

Figure 4 shows maps of nitrate-N obtained from on-line ISE and other fertility attributed measured with vis-NIRS for field 1 and field 2. The distribution pattern of the nitrate-N exhibited striking similarity with other soil properties, with similar peaks and valleys observed for all properties except MC, which exhibited a slightly different pattern in field 2. This resemblance is attributed to established correlations among these properties, as reported in prior research. For example, Wibowo and Kasno (2021) showed a strong positive correlation (0.8 to 0.9) between soil nitrate levels and OC content. Similarly, Kuśmierz et al. (2023) observed a driving contribution of OC to the availability of mineral N. Carbon and nitrogen mineralisation have been reported to increase with an increase in soil organic matter (Marzi et al., 2020), hence, a positive correlation exists between OC and nitrate N. Conversely, the correlation of nitrate-N with pH level has been reported to be relatively weak (0.3%), (Wibowo and Kasno, 2021). Some studies have reported a negative correlation between pH with nitrate content for highly alkaline soil (pH>7.5) with most of the soil macronutrients tending to be available within a pH range of 6.0 to 7.5 (Jensen and Thomas, 2010), which aligned with pH levels observed in this study. Furthermore, the similar distribution of nitrate-N and K aligned with findings reported by Ramazanoglu (2019) with a strong positive correlation (0.78). Additionally, Franzen et al. (1996) reported a strong positive correlation between soil P and nitrate levels. Likewise, soil MC exhibits a strong positive correlation with soil nitrate which gradually declines as the soil becomes oversaturated (Zhang and Wienhold, 2002). It is important to note that due to leaching, higher concentrations of soil nitrate are typically found in the lower soil layer (Gao et al., 2013) Therefore, it is challenging to establish a direct relationship between soil nitrate and MC given that this study was conducted on well-drained soils and at 30 cm depth layer. Low nitrate concentrations can be observed in relatively dry soil (Ramazanoglu, 2019), explaining the low nitrate values observed in the present study.

Evidently, the maps demonstrate distinct variations in different sections of the fields. The similarity between the nitrate-N map and on-line predicted soil properties predominantly aligned around the peak fertile areas. The low fertility regions did not exhibit a distinct pattern on the maps. Consequently, these could only effectively delineate a management zone into low and high fertility classes, thereby lacking the granularity required for an efficient variable rate application. Therefore, the fusion of data from both ISE sensor and vis-NIRS would provide a better insight into the field fertility classes thereby offering crucial requirements for delineating the management zone, which would be more efficient for variable rate fertilization application than the current practice (Guerrero et., 2021) that lacks information about soil nitrate.

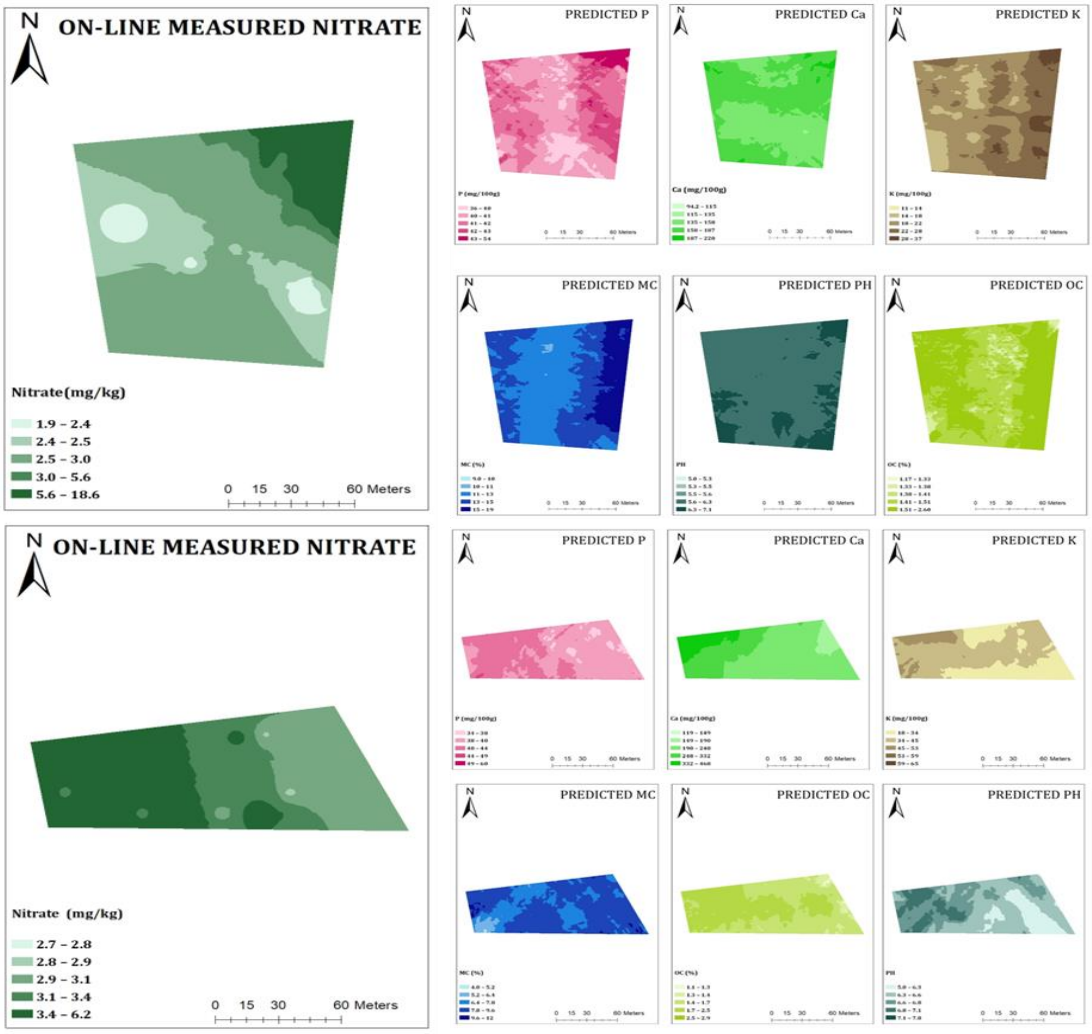

Figure 4. Comparison between maps of nitrate-N with maps of corresponding soil properties measured with on-line visible and near-infrared spectroscopy (vis-NIRS) spectra predicted phosphorus (P), calcium (Ca), potassium (K), moisture content (MC), organic carbon (OC), and pH for field 1 and field 2.

4. Conclusions

A novel dual-sensor platform combining the ion-selective electrode (ISE) and visible and near-infrared spectroscopy (vis-NIRS) techniques was used for soil nitrate-N and extractable K, P, Ca, total OC, MC and pH. The combination of both sensors offered a comprehensive understanding of spatial variability in soil fertility and soil nutrient dynamics, addressing the limitations faced by each technique separately. The validation showed a strong correlation of 0.93 between on-line ISE and laboratory measurements. Notably, the spatial distribution of nitrate-N measured on-line with ISE exhibited profound similarities with laboratory ISE measurements. However, the time lag between measurement conditions may affect nitrate assessment.

The use of the vis-NIR spectroscopy in the dual-sensor setup showed favourable results for predicting several soil properties of interest with a reasonable RPD ranging from 1.64 to 2.13 and RPIQ between 1.72 and 6.56. Strong spatial similarities were also observed between the laboratory-measured and on-line-predicted properties, enhancing our understanding of within-field soil nutrient levels.

The synergy between ISE and vis-NIR techniques thus offers a powerful and comprehensive approach for on-line soil nutrient prediction and mapping. By combining the real-time measurements of nitrate-N with the extensive spectral information obtained from vis-NIR spectroscopy, farmers and agronomists can make informed fertilisation decisions. Future research can explore and refine this approach to maximise its benefits and applicability in diverse agricultural contexts.

Acknowledgements

Authors acknowledge the financial support to run the project received by the Research Foundation - Flanders (FWO) for Odysseus I SiTeMan Project (Nr. G0F9216N). The Tertiary Education Trust Fund (TETFund), Nigeria is acknowledged for the PhD scholarship support.

References

Adamchuk, V. I., & Rossel, R. A. V., 2010. Development of On-the-Go Proximal Soil Sensor Systems. Proximal Soil Sensing, 15–28. https://doi.org/10.1007/978-90-481-8859-8_2.

Adamchuk, V. I., Dobermann, A., Morgan, M. T., & Brouder, S. M., 2002. Feasibility of on-the-go mapping of soil nitrate and potassium using ion-selective electrodes. ASAE Annual Meeting.

Adamchuk, V. I., Hummel, J. W., Morgan, M. T., & Upadhyaya, S. K., 2004. On-the-go soil sensors for precision agriculture. Computers and Electronics in Agriculture, 44(1), 71–91. https://doi.org/10.1016/j.compag.2004.03.002

Adamchuk, V. I., Lund, E. D., Sethuramasamyraja, B., Morgan, M. T., Dobermann, A., & Marx, D. B., 2005. Direct measurement of soil chemical properties on-the-go using ion-selective electrodes. Computers and Electronics in Agriculture, 48(3), 272–294. https://doi.org/10.1016/j.compag.2005.05.001

Adamchuk, V. I., Rossel, R. V., Sudduth, K. A., & Lammers, P. S., 2011. Sensor fusion for precision agriculture. Sensor fusion-foundation and applications, 27-40.

Adsett, J. F., Thottan, J. A., & Sibley, K. J., 1999. Development of an automated on-the-go soil nitrate monitoring system. Applied Engineering in Agriculture, 15(4), 351.

Bailey, T., Robinson, N., Farrell, M., Macdonald, B., Weaver, T., Antille, D. L., ... & Abiven, S., 2021. Storage of soil samples leads to over-representation of the contribution of nitrate to plant-available nitrogen. Soil Research, 60(1), 22-32.

Bellon-Maurel, V., Fernandez-Ahumada, E., Palagos, B., Roger, J. M., & McBratney, A., 2010. Critical review of chemometric indicators commonly used for assessing the quality of the prediction of soil attributes by NIR spectroscopy. TrAC Trends in Analytical Chemistry, 29(9), 1073-1081.

Bendikov, T. A., Kim, J., & Harmon, T. C., 2005. Development and environmental application of a N selective microsensor based on doped polypyrrole films. Sensors and Actuators, B: Chemical, 106(2), 512–517. https://doi.org/10.1016/j.snb.2004.07.018

Ehsani, M. R., Upadhyaya, S. K., Slaughter, D., Shafii, S., & Pelletier, M., 1999. A NIR technique for rapid determination of soil mineral nitrogen. Precision agriculture, 1, 219-236.

Franzen, D. W., Cihacek, L. J., & Hofman, V. L., 1996. Variability of soil nitrate and phosphate under different landscapes. In Proceedings of the Third International Conference on Precision Agriculture (pp. 521-529). Madison, WI, USA: American Society of Agronomy, Crop Science Society of America, Soil Science Society of America.

Gao, H. Y., Yang, L. H., Li, T., & Guo, Z. P., 2013. The Effect of Human Activity on the Distribution of Soil Nitrate Nitrogen in Unsaturated Zone. Advanced Materials Research, 790, 202-205.

Guerrero, A., de Neve, S., & Mouazen, A. M., 2021. Current sensor technologies for in situ and on-line measurement of soil nitrogen for variable rate fertilization: A review. Advances in Agronomy, 168, 1–38. https://doi.org/10.1016/BS.AGRON.2021.02.001.

Jensen, T. L., & Thomas, L. (2010). Soil pH and the availability of plant nutrients. IPNI Plant Nutrition Today, 2.

Kennard, R. W., & Stone, L. A., 1969. Computer aided design of experiments. Technometrics, 11(1), 137-148.

Kim, H.-J., Hummel, J. W., Sudduth, K. A., & Motavalli, P. P., 2007. Simultaneous Analysis of Soil Macronutrients Using Ion-Selective Electrodes. Soil Science Society of America Journal, 71(6), 1867–1877. https://doi.org/10.2136/sssaj2007.0002

Kuang, B., Mahmood, H. S., Quraishi, M. Z., Hoogmoed, W. B., Mouazen, A. M., & van Henten, E. J., 2012. Sensing Soil Properties in the Laboratory, In Situ, and On-Line: A Review. Advances in Agronomy, 114, 155–223. https://doi.org/10.1016/B978-0-12-394275-3.00003-1

Kuśmierz, S., Skowrońska, M., Tkaczyk, P., Lipiński, W., & Mielniczuk, J., 2023. Soil Organic Carbon and Mineral Nitrogen Contents in Soils as Affected by Their pH, Texture and Fertilization. Agronomy, 13(1), 267.

Li, Y., Yang, Q., Chen, M., Wang, M., & Zhang, M., 2019. An ISE-based On-Site Soil Nitrate Nitrogen Detection System. Sensors 2019, Vol. 19, Page 4669, 19(21), 4669. https://doi.org/10.3390/S19214669

Marzi, M., Shahbazi, K., Kharazi, N., & Rezaei, M. (2020). The influence of organic amendment source on carbon and nitrogen mineralization in different soils. Journal of Soil Science and Plant Nutrition, 20, 177-191.

Mouazen, A. M., Kuang, B., & Quraishi, M. Z., 2011. A system for on-line measurement of key soil properties. GRASPA WORKING PAPERS, 1-4.

Mouazen, A. M., Maleki, M. R., de Baerdemaeker, J., & Ramon, H., 2007. On-line measurement of some selected soil properties using a VIS–NIR sensor. Soil and Tillage Research, 93(1), 13–27. https://doi.org/10.1016/J.STILL.2006.03.009

Mouazen, A.M., 2006. Soil Survey Device. International publication published under the patent cooperation treaty (PCT). World Intellectual Property Organization, International Bureau. International Publication Number: WO2006/015463, PCT/BE2005/000129, IPC: G01N21/00, G01N21/00.

Munnaf, M. A., & Mouazen, A. M., 2021. Development of a soil fertility index using on-line Vis-NIR spectroscopy. Computers and Electronics in Agriculture, 188, 106341. https://doi.org/10.1016/J.COMPAG.2021.106341

Nawar, S., & Mouazen, A. M., 2017. Predictive performance of mobile vis-near infrared spectroscopy for key soil properties at different geographical scales by using spiking and data mining techniques. Catena, 151, 118-129. https://doi.org/10.1016/J.CATENA.2016.12.014.

Ramazanoglu, E., & Campus, O., 2019. Determination and mapping of the relationship between potassium and Ammonium of Calcareous Soils with Different Moisture Content. International Journal of Scientific and Technological Research, 5(7), 17-26.

Rossel, R. V., Walvoort, D. J. J., McBratney, A. B., Janik, L. J., & Skjemstad, J. O., 2006. Visible, near infrared, mid infrared or combined diffuse reflectance spectroscopy for simultaneous assessment of various soil properties. Geoderma, 131(1-2), 59-75.

Sethuramasamyraja, B., Adamchuk, V. I., Dobermann, A., Marx, D. B., Jones, D. D., & Meyer, G. E., 2008. Agitated soil measurement method for integrated on-the-go mapping of soil pH, potassium and nitrate contents. Computers and Electronics in Agriculture, 60(2), 212–225. https://doi.org/10.1016/J.COMPAG.2007.08.003.

Shaw, R., Williams, A. P., Miller, A., & Jones, D. L., 2013. Assessing the potential for ion selective electrodes and dual wavelength UV spectroscopy as a rapid on-farm measurement of soil nitrate concentration. Agriculture, 3(3), 327-341.

Sibley, K. J., Astatkie, T., Brewster, G., Struik, P. C., Adsett, J. F., & Pruski, K., 2009. Field-scale validation of an automated soil N extraction and measurement system. Precision Agriculture, 10(2), 162–174. https://doi.org/10.1007/s11119-008-9081-1

Sibley, K. J., Brewster, G. R., Astatkie, T., Adsett, J. F., & Struik, P. C., 2010. In-field measurement of soil nitrate using an ion-selective electrode 1 X In-field measurement of soil nitrate using an ion-selective electrode. In Advances in measurement systems.

Syvilay, D., Wilkie-Chancellier, N., Trichereau, B., Texier, A., Martinez, L., Serfaty, S., & Detalle, V., 2015. Evaluation of the standard normal variate method for Laser-Induced Breakdown Spectroscopy data treatment applied to the discrimination of painting layers. Spectrochimica Acta Part B: Atomic Spectroscopy, 114, 38-45.

Wibowo, H., & Kasno, A., 2021. Soil organic carbon and total nitrogen dynamics in paddy soils on the Java Island, Indonesia. In IOP Conference Series: Earth and Environmental Science (Vol. 648, No. 1, p. 012192). IOP Publishing.

Zhang, R., & Wienhold, B. J., 2002. The effect of soil moisture on mineral nitrogen, soil electrical conductivity, and pH. Nutrient cycling in Agroecosystems, 63, 251-254.

Automated needle-based trunk injection system for HLB-affected citrus trees

Yiannis Ampatzidis[a,*], Israel Ojo[a], Antonio de Oliveira Costa Neto[a], Ozgur Batuman[b]

[a] Agricultural and Biological Engineering Department, Southwest Florida Research and Education Center, University of Florida, 2685 FL-29, Immokalee, FL 34142, USA

[b] Plant Pathology Department, Southwest Florida Research and Education Center, University of Florida, 2685 FL-29, Immokalee, FL 34142, USA

* Corresponding author. Email: i.ampatzidis@ufl.edu

Abstract

Citrus Huanglongbing (HLB) is the most significant threat to the citrus industry worldwide, resulting in substantial economic losses in global citrus production. Currently, no cure exists for HLB-affected trees. The fastidious HLB-causing bacteria (CLas) resides in the phloem of the plant tissue. Although several control methods have been applied, the most effective method currently to control CLas is the trunk injection of oxytetracycline (OTC), which has shown remarkable success in improving tree health, yield, and fruit quality. However, existing trunk injection methods are labor-intensive and time-consuming and, hence, have a high application cost, posing implementation challenges. For example, the most commonly used devices for the injection of OTC in citrus trees in Florida are drill-based and pressurized. OTC injection via these devices is very labor-intensive and requires that the device remain attached to the tree for a prolonged period (from 20 min to 24 hours). Another major concern with these drill-based systems is the possibility of tree injury because they make relatively large holes, which serve as entry points for pathogens or insects. The estimated cost for OTC injection using these devices is $1.34 to $2.70 per tree, not including labor and injection devices. The cost of each device is ~$17, and growers in Florida usually buy 2,000 to 3,000 devices each. In response, we have developed a drill-free, non-passive, automated trunk injection device that can be mounted on existing farm vehicles to control HLB and potentially other tree diseases. In field experiments, it was found that 100 ml OTC can be applied by the automated trunk injection system in less than 1 minute. To the best of our knowledge, this is the first automated trunk injection system developed for tree crops.

Keywords: Automated needle-based injection, Huanglongbing, Oxytetracycline, Plant diseases.

1. Introduction

Citrus production has been declining since the Huanglongbing (HLB) disease was discovered. Florida's orange production is expected to be 3.4 million tons, which is comparable to harvest records from before World War II (USDA citrus April prediction, 2022). A phloem-limiting bacterium carried by the Asian citrus psyllid is the source of the deadly HLB disease. According to Wang et al. (2016), infection by the fungus that causes HLB impairs vascular mobility weakens the tree root system, rapidly deteriorates tree health, and eventually lowers production.

Due to foliar spray off-target losses, on-target evaporation or degradation of active ingredients, and inadequate penetration into the tree vasculature where the bacteria resides, attempts to increase the yield of citrus trees affected by HLB have failed (Hu et al., 2018; McCollum and Baldwin, 2016). In addition to being ineffective against HLB disease, soil drenching has demonstrated better results than foliar spray for citrus canker (Francis et al., 2009). This is because the bactericide binds easily to soil particles, potentially harming the soil ecosystem and raising the risk of runoff and groundwater pollution. HLB-affected trees have also been treated with thermotherapy techniques; however, this method primarily addresses the tree canopy rather than the roots (Ghatrehsamani et al., 2021; Ghatrehsamani et al., 2019a; Ghatrehsamani et al., 2019b).

A currently confirmed successful strategy for controlling HLB is chemotherapy by trunk injection of antibacterial chemicals or plant defense activators (Berger and Laurent, 2019; Wang et al., 2016). By delivering medications directly to the target area, trunk injection essentially boosts treatment efficacy by removing both on-target and off-target losses. Trunk injection's lower danger of environmental pollution makes it possible to use it in cities (Ferracini and Alma, 2008). There are three types of trunk injection techniques: drill-based, needle-based, and cut-based. Because numerous drill bit sizes are available, drill-based injection offers a wide range of hole sizes; nevertheless, the shearing action of drilling might damage the xylem vessels and limit injectate uptake (Montecchio, 2013; Ojo et al., 2022; Ojo et al., 2024a).

Drill-free methods reduce tree wounding and promote quicker recovery but rely on natural sap flow for solution uptake, which is time-consuming and infeasible for commercial orchard systems. However, existing trunk injection methods are labor-intensive, time-consuming, and hence, have a high application cost, making trunk injection impractical for commercial citrus production (Li and Nangong, 2022; Wang et al., 2016). Additionally, an irregular distribution of the injectate within the tree upon injection has also been observed (Roach, 1939) Although a uniform spatial distribution of injected compounds can be obtained via a multi-puncture approach, this would only increase labor, time, and cost of application and hence the need to automate the process of chemotherapy by trunk injection. For these reasons, an automated drill-free trunk injection system was developed and evaluated to treat HLB-affected citrus trees. To the best of our knowledge, this is the first automated trunk injection system developed for tree crops.

2. Materials and Methods

2.1. Automated injection system

The automated trunk injection system (Figures 1 and 2) features (i) an end effector consisting of the injection needles, (ii) a positioning arm mountable to a utility-type vehicle (UTV), and (iii) a flow system (Ojo et al., 2024b). The 3D modeling and finite element package in Solid Edge (Siemens PLM Software, Plano, TX) was used to create a computer-aided design (CAD) model of the trunk injection device (Figure 1) and perform structural analysis of the needle, end effector, and positioning arm using the Von Mises Stress test and total translation displacement test. The automated trunk injection system is mounted on UTV via the positioning arm. The extension and retraction of the frame to position the end effector such that the opposite-facing needles are positioned radially across the stem are manually controlled. Needle penetration is achieved by the end effector clamp mechanism driven by a hydraulic actuator (maximum push and pull forces; 7.8 kN and 5.34 kN, respectively). The needles are inserted radially to a depth of 25.4 mm. The injectate is then forced into the stem by a metering pump selected to supply injected fluid at a flow rate of 3.6 ml/s and a pressure of 6 Mpa.

The flat-tip needles (Figure 1C), 25.4 mm in length and 3.937 mm in diameter, had four outlet holes placed radially along the circumference of the needle, each 1.27 mm in diameter and was radially inserted on opposite sides of the tree to dispense the solution. The end effector consists of two needles, an injection manifold, and a gripper mechanism (Figure 1A). The end effector is powered by a hydraulic actuator (Midway, DA SERIES, KS, USA) connected to a battery-powered hydraulic pump (Vevor 15QDAMHP, CA, USA). The trunk injection system was designed to operate attached to a utility-type vehicle (UTV) via a positioning arm (Figure. 1C) consisting mainly of three telescoping tubes (1.52 m long) and 127-mm-threaded rods. The design considered an extension length of 3.7 m to be covered by the telescoping tubes away from the UTV. The positioning arm provides for the extension and retraction of the end effector and supports its weight (~30 kg.) at a maximum distance (center of the bed to tree; 1.13 m) without bending and retracting to a compact structure behind the UTV.

Preliminary experiments informed the selection of a metering pump (Neptune 525-E-N3-CORD-PUMP, CA, USA). The pump supplies the injected material from a receptacle via flexible hoses and fittings. Two check valves (Stratflo 3695RB-038, IN, USA) attached to each side of the end effector were used to ensure unidirectional flow, while a flow meter (Vision Turbine Meter BV1000TRN025B WI, USA) attached to a datalogger (OM-CP-PULSE101A, CT, USA) and a pressure gauge (Monarch Instrument, 2000 PSIG, NH, USA) records the flow and pressure respectively.

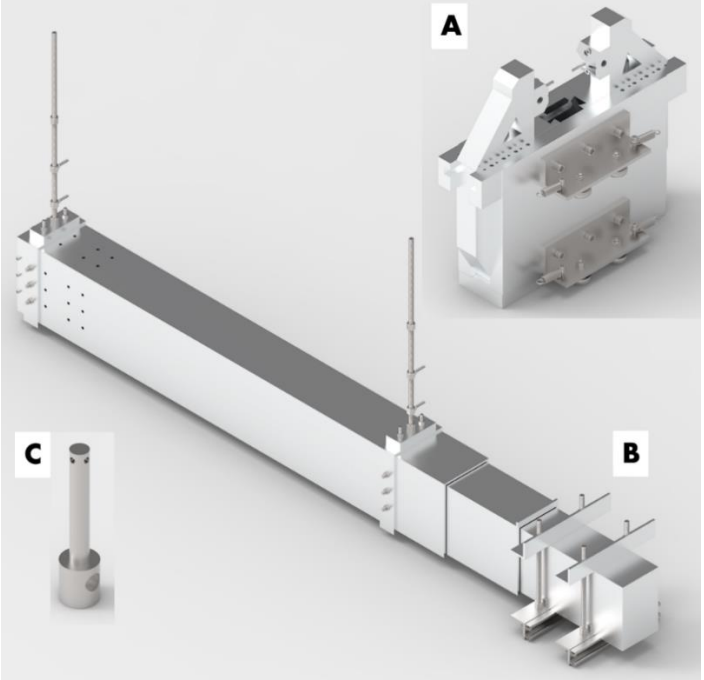

Figure 1. CAD model for the (**A).** End effector showing injection manifold, needle and track rollers, and extension springs. (**B).** Positioning arm showing telescoping tubes, UTV, and end effector mounts. (**C).** Flat tip needle showing radially positioned holes at the tip and lock screw hole at the base to connect with the end effector jaw.

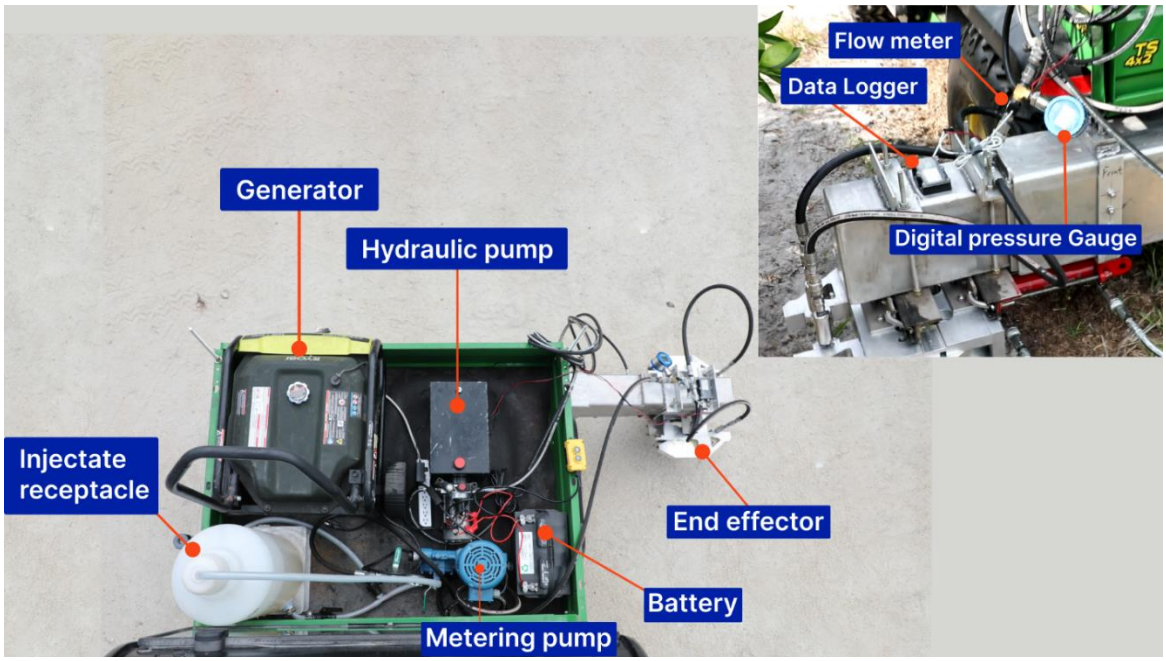

Figure 2. Top and proximate views of the automated injection system.

3. Results

In the Fall of 2023, water injection experiments were conducted on 24 Valencia orange trees in a commercial citrus grove, with varying trunk diameters, to assess flow and pressure rates on trees at different times of the day. Measurements were taken between 9:45 am and 4:12 pm, with pressure and flow rate

recorded every second during injection at a fixed height of 0.2 m above the ground. Before injection, the flow system was primed with water, and injection was performed.

Furthermore, in the Spring of 2024, HLB-affected Navel orange trees were injected using the automated trunk injection system with deionized water, and 11,000 ppm oxytetracycline (OTC) within 7 hours of mixing the solution.

3.1. Fall injection with water

Water injections were performed for each tree until the flow stopped while recording the injection flow rate and pressure. The minimum volume of water injected was 53.9 mL, and the maximum was 243.6 mL at a duration of 44 s and 68 s, respectively. Injection duration ranged from 30 s to 72 s for all trees. The total volume injected for morning injections was not statistically different from afternoon injections, with an average total volume of 103.8 mL and 106.3 mL in the morning and afternoon, respectively. The volume per time decreased for the afternoon injection compared to the morning injection (Figure 3). The average total volume injected was 101.6 mL, 94.7 mL, 95 mL, and 129 mL for group mean trunk diameter of 73.96 mm, 83.7 mm, 87.79 mm, and 94.79 mm, respectively.

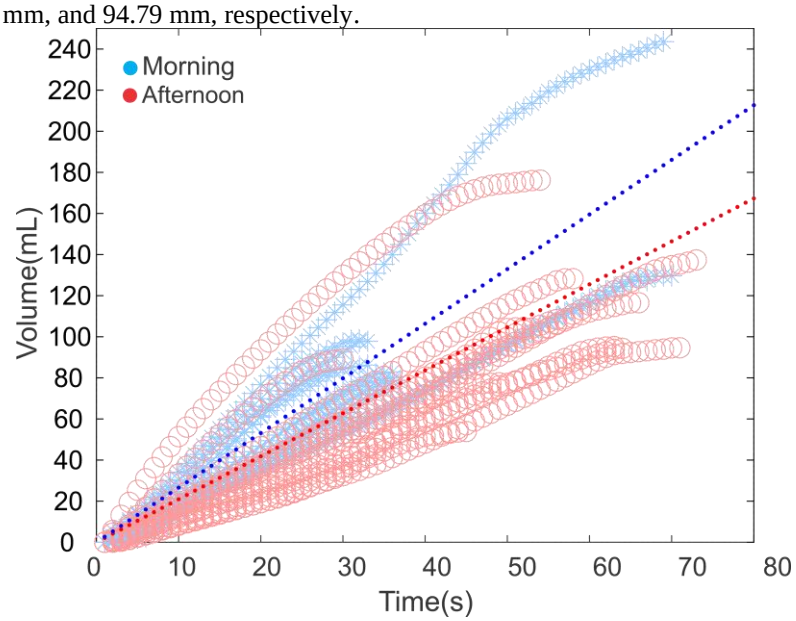

Figure 3. Cumulative volume as a function of time. Solid dotted lines are the average linear function of data from each tree injected in the morning (blue) and afternoon (red).

3.2. Comparison of spring injection with water and OTC

In the spring of 2024, a comparison between injection with water and OTC was made based on a fixed injected volume of 100 ml. By using the automated injection system, the minimum and maximum injection duration, recorded when the injected volume was 100 ml, was 9 s and 42 s, 12 s and 40 s, for 11,000 ppm OTC and water injection, respectively. The average injection duration was not statistically different ($p<0.05$) between morning and afternoon injections and between 11,000 ppm OTC and water injections. On average, injection duration was 17.8 s and 23.1 s for 11,000 ppm OTC and water injection, respectively (Figure 4).

Variability in total volume injected and injection time was observed, similar to findings from Himelick (1972). The cumulative volume injected was notably influenced by soil moisture, increasing by 55.2% during irrigation. Although sap flow was not measured, studies suggest a positive correlation between soil moisture and sap flow. Daily irrigation significantly enhances sap flow in citrus trees, potentially accelerating the translocation of the injected solution. Contrary to expectations, morning injection did not exhibit a substantial increase in total volume, suggesting that injection time may have a less significant impact on material intake.

Water injection showed a higher injection duration compared to OTC, likely due to the lower pH of the OTC solution. Research on xenobiotic mobility indicates that a lower pH accelerates the movement and dispersion of a compound throughout a tree and into the canopy (Archer and Albrecht, 2023) since the

translocation of xenobiotics heavily relies on factors such as pKa, charge, and molecular characteristics.

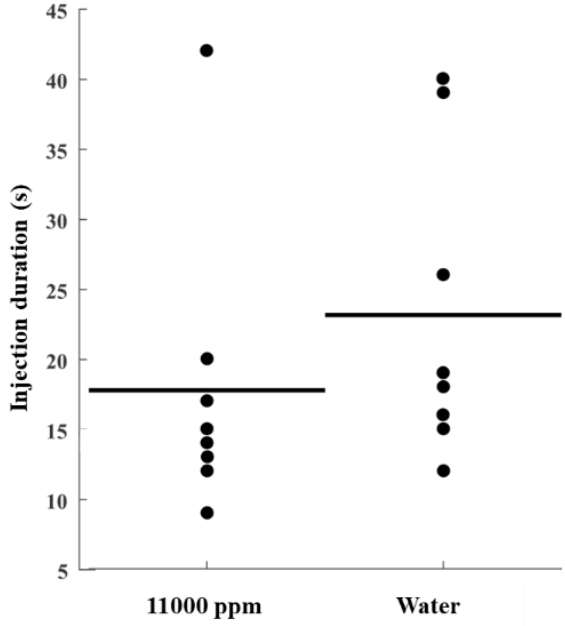

Figure 4. Injection duration for 11,000 ppm OTC, and water injection.

4. Conclusions

Tree trunk injection of therapeutic compounds is an environmentally responsible method of tree chemotherapy that is especially effective for treating HLB disease. Conventional (and manual) trunk injection, however, has its drawbacks. It is labor-intensive and time-consuming and has a high application cost, making it impractical for commercial citrus production. This highlights the need to develop an automated system that is optimized for commercial orchard production. Our results showed that the automated injection system successfully injected trees both with water and OTC and was much faster than manual injection systems which typically are left attached to the tree for up to 24 hours. Further investigation comparing the duration of injection, pressure, and flow rate of manual trunk injection systems and the employed injection system is required based on the findings from this study. Finally, artificial intelligence enabled sensing systems could be used to estimate in real-time tree canopy volume (Ampatzidis et al., 2020; Partel et al., 2020) and trunk diameter in order to select the optimal amount of therapeutic materials for individual trees.

Acknowledgments

This material was made possible, in part, by a Cooperative Agreement from the US Department of Agriculture's SCRI CDRE through grant 2019-70016-29096. Its contents are solely the responsibility of the authors and do not necessarily represent the official views of the USDA.

References

Ampatzidis, Y., V. Partel, and L. Costa, 2020. Agroview: Cloud-based application to process, analyze and visualize UAV-collected data for precision agriculture applications utilizing artificial intelligence. *Computers and Electronics in Agriculture*, 174, 105157. https://doi.org/10.1016/j.compag.2020.105457

Archer, L., and U. Albrecht, 2023. Evaluation of trunk injection techniques for systemic delivery of huanglongbing therapies in citrus. *HortScience*, *58*(7), 768–778. https://doi.org/10.21273/hortsci17172-23

Berger, C., and F. Laurent, 2019. Trunk injection of plant protection products to protect trees from pests and diseases. *Crop Protection*, *124*. https://doi.org/10.1016/j.cropro.2019.05.025

Ferracini, C., and A. Alma, 2008. How to preserve horse chestnut trees from Cameraria ohridella in the urban

environment. *Crop Protection*, *27*(9), 1251–1255. https://doi.org/10.1016/j.cropro.2008.03.009

Francis, M. I., A. Redondo, J.K. Burns, and J.H. Graham, 2009. Soil application of imidacloprid and related SAR-inducing compounds produces effective and persistent control of citrus canker. *European Journal of Plant Pathology*, *124*(2), 283–292. https://doi.org/10.1007/s10658-008-9415-x

Ghatrehsamani, S., J. Abdulridha, A. Balafoutis, X. Zhang, R. Ehsani, R., &and Y. Ampatzidis, 2019a. Development and evaluation of a mobile thermotherapy technology for in-field treatment of Huanglongbing (HLB) affected trees. *Biosystems Engineering*, *182*, 1–15. https://doi.org/10.1016/j.biosystemseng.2019.03.011

Ghatrehsamani, S., E. Czarnecka, F.L. Verner, W.B. Gurley, R. Ehsani, and Y. Ampatzidis, 2019b. Evaluation of mobile heat treatment system for treating in-field HLB-affected trees by analyzing survival rate of surrogate bacteria. *Agronomy*, *9*(9). https://doi.org/10.3390/agronomy9090540

Ghatrehsamani, S., Y. Ampatzidis, J.K. Schueller, and R. Ehsani, 2021. Simulation and evaluation of heat transfer inside a diseased citrus tree during heat treatment. *AgriEngineering*, *3*(1), 19–28. https://doi.org/10.3390/agriengineering3010002

Himelick, E. B., 1972. High pressure injection of chemicals into trees. *Arborist's News*, *37*(9), 97–103.

Hu, J., J. Jiang, and N. Wang, 2018. Control of citrus huanglongbing via trunk injection of plant defense activators and antibiotics. *Phytopathology*, *108*(2), 186–195. https://doi.org/10.1094/PHYTO-05-17-0175-R

Li, M., and Z. Nangong, 2022. Precision trunk injection technology for treatment of huanglongbing (HLB)-affected citrus trees -A review. *Journal of Plant Diseases and Protection*, *129*, 15–34. https://doi.org/10.1007/s41348-021-00510-6

McCollum, G., and E. Baldwin, 2016. Huanglongbing: devastating disease of citrus. *Horticultural Reviews*, *44*, 315–361. https://doi.org/10.1002/9781119281269.ch7

Montecchio, L. (2013). A venturi effect can help cure our trees. *Journal of Visualized Experiments*, *80*, 1–8. https://doi.org/10.3791/51199

Ojo, I., Y. Ampatzidis, A.O.C. Neto, and H.K. Bayabil, 2024a. The development and evolution of trunk Injection mechanisms -A review. *Biosystems Engineering*, *240*, 123–141. https://doi.org/10.1016/j.biosystemseng.2024.03.002

Ojo, I., Y. Ampatzidis, A.O.C. Neto, and O. Batuman, 2024b. Development of an automated needle-based trunk injection system for HLB-affected citrus trees. *Biosystems Engineering*, *240*, 90–99. https://doi.org/10.1016/j.biosystemseng.2024.03.003

Ojo, I., V. Vijayakumar, Y. Ampatzidis, O. Batuman, S. Kunwar, U. Albrecht, L. Archer, A. Fernando, B. Haimanote, and J.K. Schueller, J. K. 2022. Prototype development of an automated needle-based delivery system to treat HLB affected citrus trees. *ASABE Annual International Meeting*. https://doi.org/10.13031/aim.202200615

Partel, V., L. Costa, and Y. Ampatzidis, 2021. Smart tree crop sprayer utilizing sensor fusion and artificial intelligence. *Computers and Electronics in Agriculture*, 191, 106556, https://doi.org/10.1016/j.compag.2021.106556

Roach, W.A., 1939. Plant injection as a physiological method. Annals of Botany, 3(9), 155–226. https://www.jstor.org/stable/42906705

Wang, N.N., D.W. Sun, Y.C. Yang, H. Pu, and Z. Zhu, 2016. Recent Advances in the Application of Hyperspectral Imaging for Evaluating Fruit Quality. Food Analytical Methods, 9(1), 178–191. https://doi.org/10.1007/s12161-015-0153-3

Automatic generation of shrub and tree crop datasets for use in deep learning detection algorithms on agricultural vehicles

Klaus Müller [a,b,*], Jan Kunze [b], Michael Möller [a], Klaus-Dieter Kuhnert [b]

[a] Computer Vision Group, University of Siegen, Siegen, Germany

[b] Institute for Realtime Learning Systems, University of Siegen, Siegen, Germany

* Corresponding author. Email: klaus.mueller@uni-siegen.de

Abstract

Deep learning-based object detection algorithms are increasingly finding their way into agricultural technology. These promise high recognition rates under real-time conditions. However, a large data set is required to train the appropriate model. This is no problem for everyday objects, where large datasets are available. The situation is different in agriculture and, in particular, in special crops. Datasets are rare here and manual generation is very time-consuming and therefore costly. In this paper we present a system for the automatic annotation of tree and shrub crops in RGBD data recorded by vehicle-mounted cameras.

Based on the depth data, the plants are localized and segmented using classical computer vision methods. The 3D bounding box of each detected plant are then projected into the RGB image and the congruent pixels are assigned to a plant label. The image including the plant labels is added to the dataset.

We tested the system on plantations for Christmas trees. The data was recorded with Intel's Realsense D455 and D435i cameras. Over 50.000 trees were automatically annotated on a total of 7.000 images.

For testing, a pre-trained model (YOLOV8) was trained with the dataset. While training YOLOV8 on the generated dataset saturates with a Mean Average Precision (mAP) of 0.69, qualitative results suggest that the resulting model outperforms the noisy model-based process for generating training data. The model was able to deliver significantly better results than the detection system used to generate the training data, particularly at the edge of the field.

Compared to manual annotation, our system makes work much more efficient while at the same time offering a high recognition rate. It can be used to quickly generate a recognition model even for less common special crops.

Keywords: plant detection, automated data labeling

1. Introduction

In precision farming, the focus of cultivation is increasingly shifting to the individual plant. Individual plant cultivation is often based on GNSS systems. The position of the plant is known and can be easily localized during processing. It is more difficult if no position data of the plant is available or if localization using GNSS systems is not possible due to a lack of signal. In this case, systems are used that detect and localize the plant based on sensor data and then provide position and plant information for the subsequent processing step.

Figure 1. Trees from a vehicle perspective (left) and from a bird's eye view (right).

In today's systems, deep-learning-based convolutional neural networks are often used to detect plants in image data. To train the system, large amounts of labeled data are required, which are hardly available, especially for special crops. Researchers are often forced to label large amounts of images manually (Ramcharan et al., 2017, Ozguven and Adem, 2019).
In their survey Lu and Young (2020) presented different datasets for precision agriculture. They come to the conclusion that there are still too few public datasets in this field of research which hinders the advancement of neural network-based systems. This problem was also pointed out in the surveys of Wu et al. (2021) and Attri et al. (2023). In Attri et al. (2023) survey about the use of deep learning techniques in agriculture, it was necessary in many of the reviewed research papers to create a dataset due to the lack of public data.
To deal with lack of public data sets and the high effort for manually labeling data, different approaches have been proposed. Li and Yang (2021) see the problem of small datasets as a few-shot classification problem. They identify the three main solutions for this problem, which are data augmentation, transfer learning and meta-learning. Ragu and Teo (2023) list in their review about few shot learning in agriculture multiple studies, that used this method with success. They come to the conclusion that few shot learning can greatly improve the detection performance on small datasets. Lu and Young (2020) recommend Data Augmentation to increase the size of small labeled datasets. Transfer Learning was used by Bosilj et al. (2020) to improve the training time a semantic segmentation of crops and weed by 80% with fully labeled data. They also show that with transfer learning you can take a pretrained crop segmentation classifier to train a new CNN classifier for a different crop type using only partially labeled data.
In order to reduce the workload and speed up the labeling process Desmond et al. (2021) used AI assisted pre-labeling of datasets to reduce the decision space for human annotation.
(Wu et al., 2021) see semi- and unsupervised learning as one of the major development trends in weed detection for the future because of the lack of public datasets and to avoid the manual labeling of large amounts of data. Bah et al. (2018) presented a new method for Weed Detection with unsupervised Data Labeling. They created lines for crops (bean and spinach) growing in lines from UAV images. They used these lines to detect inter-row weeds and thus created an unsupervised training set for a neural network which could perform close to the same neural network trained with supervised data.
This paper presents a system for the automatic generation of datasets for agricultural tree and shrub crops. Similar to Bah et al. (2018), the structure of the plantation is used to segment trees and shrubs within point clouds and use this information to annotate RGB images. Unlike Bah et al. no aerial images are used here, but images from a vehicle-guided camera are processed. This has the advantage that the trained model can later be used directly on field machines. However, this also has disadvantages: the plants in a row occlude each other, which makes labeling more difficult (see Figure 1).

2. Materials and Methods

The method used here is based on the fact that the objects to be labeled are geometrically separated from each other and only one type of plant grows on the plantation. In addition, there should be no other objects on the plantation that are geometrically similar to the plant being searched for.

2.1. Image acquisition

The system is based on the assumption that a depth image exists for every RGB image, in which geometric shapes, in this case bushes and trees, can be found using traditional methods of point cloud analysis. In principle, any type of 3D data is suitable for processing, whereby the depth data must be referenced with the RGB data. This condition is fulfilled by RGBD cameras, which generate depth data based on stereography or time-of-flight and combine it with the RGB data both temporally and spatially, usually without additional calibration. These sensors are also more cost-effective than lidar systems and are now also available as water and dust-protected versions that can be mounted on agricultural vehicles.
In the case described here, two different RGBD cameras (Intel Realsense D455 and D435) were used, which have an RGB resolution of 1280x800 (D455) or 1920x1080 (D435) pixels and a depth resolution of 1280x720 pixels. The depth sensor has a range of 6 m. The cameras were mounted on the front of a tracked vehicle in the direction of travel at a height of 80 cm or 130 cm (see Figure 2). The cameras are connected to the vehicle computer. The vehicle computer is also used to control the vehicle and uses the robotics middleware ROS (Quigley et al., 2009). The RGBD video stream from the cameras is stored on the computer's hard disk during the crossing at a frame rate of 30 frames per second (fps). The ROS component

rosbag, which stores the RGB data and the depth data (as a point cloud) time-stamped, is used for this purpose.
The vehicle was used on various Caucasian fir *(Abies nordmanniana)* plantations. The trees had an age of four to seven years and a height of 50 cm to 150 cm. The vehicle was navigated through the rows by both remote control and GNSS navigation. Recording began as soon as the vehicle started driving across the plantation and ended when the last row was completed. The speed of the vehicle was 5 km/h.

Figure 2. Robot equipped with various sensors, including two RGBD (red frame) cameras.

2.2. Plant detection in point cloud

Once the recordings have been completed, the saved data stream is analyzed frame by frame in the following steps. To detect the tree, the depth data is processed in the form of a point cloud as follows. For the calculation the open source library *Point Cloud Library* was used. (Point Cloud Library, 2024). The result is shown in Figure 3.

1. *Crop point cloud*
   The point cloud is cropped to the area in front of the vehicle (4m x 6m [width x length]). Data outside this area is undefined or inaccurate due to the limited range of the camera.
2. *Filtering outliers*
   Outliers are recognized and eliminated with the help of a statistical analysis. Points that are significantly outside their neighborhood are removed (see Rusu, 2008).
3. *Search for local maxima*
   The local maxima are searched for in the point cloud. These represent the tips of the trees or bushes. A radius is defined in which a maximum of one local maximum may occur. In this way, false detections (e.g. double peaks) can be reduced and the structure of the plantation can be taken into account. The radius can be manually adapted to the conditions.
4. *Cluster the point cloud of each tree*
   To cluster the point cloud, a min-cut algorithm (see Golovinskiy, 2009) is used, which divides point clouds into different areas based on the theory of graph cuts. In this case, the tree cluster is separated from the subsurface. Since the point of the tip of the potential tree cluster has already been found by determining the local maximum, this is defined as the foreground point and used as the starting point.
5. *Cluster validation and discarding based on size criteria*
   After successful clustering, the cluster is validated based on its size. If these are not within the expected value (width and height), the cluster is discarded.

Figure 3: On the left you can see the point cloud clusters found in different colors from a bird's eye view. The image on the right shows the bounding boxes resulting from the clusters from a vehicle perspective.

2.3. Dataset creation

The previously determined clusters serve as a starting point for labeling the trees in the RGB space. In the work presented here, the trees are labeled using a bounding box. The first step is to calculate the bounding box of the tree cluster in 3D space. This is then projected into the 2D RGB image. The projection matrices required for this are attached to the images as metadata in the case of the Realsense cameras. The result is one 2D bounding box per recognized 3D point cloud cluster. The RGB image is saved together with the pixel coordinates of the bounding boxes.

2.4. Test setup

To test the overall system, a total of 7,000 images were recorded and analyzed in several passes over different crops. A total of 50,000 trees were detected on these images. The data set was divided into training data, validation data and test data in a ratio of 70% - 20% - 10%.
The CNN-based object recognition algorithm Yolov8 (You only look Once, see Terven, 2023) was used for testing. To improve the performance of the model, we used a pre-trained model (Yolov8s) which was trained on the Coco dataset (COCO Consortium, 2023). This provides a solid basis and is real-time capable on edge-devices, which would allow later use on agricultural machinery. The model was trained with a batch size of 8 in 50 epochs. The training took place on an Ubuntu 20.04 computer with an Intel i9-9900 CPU and an Nvidia Quadro RTX3000 (6 GB memory) GPU.

3. Results and Discussion

3.1. Dataset creation

For validation, 100 randomly selected images from the test dataset were annotated manually using the *anylabeling* tool (The Anylabeling Project, 2024). It became apparent that the row structure and the resulting occlusion made manual annotation very difficult. Trees further away were particularly difficult to distinguish from neighboring trees. For this reason, the label was limited to the first three rows in front of the camera. Nevertheless, the time required for labeling was high.
In the automatically annotated data set, an average of 8.0 trees per frame (minimum 3, maximum 15) were found. In the manual annotated comparison group, an average of 7.4 trees (minimum 3, maximum 13) were found. On average, 71% of the manually annotated boxes were found (e. g. Figure 4).
In addition, a random qualitative analysis of the data set was carried out. The following points stood out:

- Due to the camera-related range restriction of 6 meters, only trees within this radius were added to the data set.
- As a result of the row-related shading, trees in the back rows are partially provided with cut-off bounding boxes.

- As the point cloud analysis only uses the geometric properties of the tree, plants and objects with similar proportions to the trees were incorrectly detected, especially in the peripheral areas.

Figure 4: The manually (green) and automatically (red) generated labels in comparison.

Tree detection using point cloud analysis took approx. 40 ms per frame on the system mentioned in 2.4.

3.2. Training with Yolov8

As described in 2.4, a YOLOV8 model was trained on the basis of the automatically generated data set. The training takes 2.16 hours on the hardware mentioned. An mAP50 (mean average precision) of 0.69 was achieved.

A visual analysis of the results showed that the trained model significantly outperformed the original training dataset in some critical areas. This was particularly evident in the edge areas of the plantation, where the point cloud analysis sometimes recognized incorrect objects (e.g. bushes at the edge of the field) as trees (see Figure 5 - bottom-left). This could be due to the fact that only a very small amount of data in the training dataset contains these false detections and is therefore not very relevant during training. However, this should be investigated in more detail in future research. Furthermore, on average more trees were found with the trained CNN-model than with the point cloud analysis, which is probably due to the limited range of the 3D camera on which the point cloud analysis is based.

The inference per image took an average of 10 ms, which is four times faster than the point cloud analysis.

4. Conclusions

The system presented was used to quickly generate training data for recognizing Christmas trees from the vehicle's perspective. For this purpose, an algorithm was developed that detects trees in RGBD-data and label the trees in the corresponding RGB image. In a test, the method was able to find 71% of the ground truth bounding boxes fully automated. The time-consuming labeling process can thus be reduced to a minimum.

The data set created in this way was then used to train a CNN model (YOLOV8). Despite inaccuracies of the dataset (30% of the ground truth bounding boxes were not found by the algorithm), the Yolo model converged quickly during training and was convincing in the test.

The resulting model was even able to outperform the method used to create the data set: it detected more trees and was able to reduce false detections in the peripheral areas. In addition, only a quarter of runtime was needed per frame.

Thus, the presented method offers a good possibility to quickly create a labeled data set of tree and shrub crops, which can be successfully used to train a CNN model.

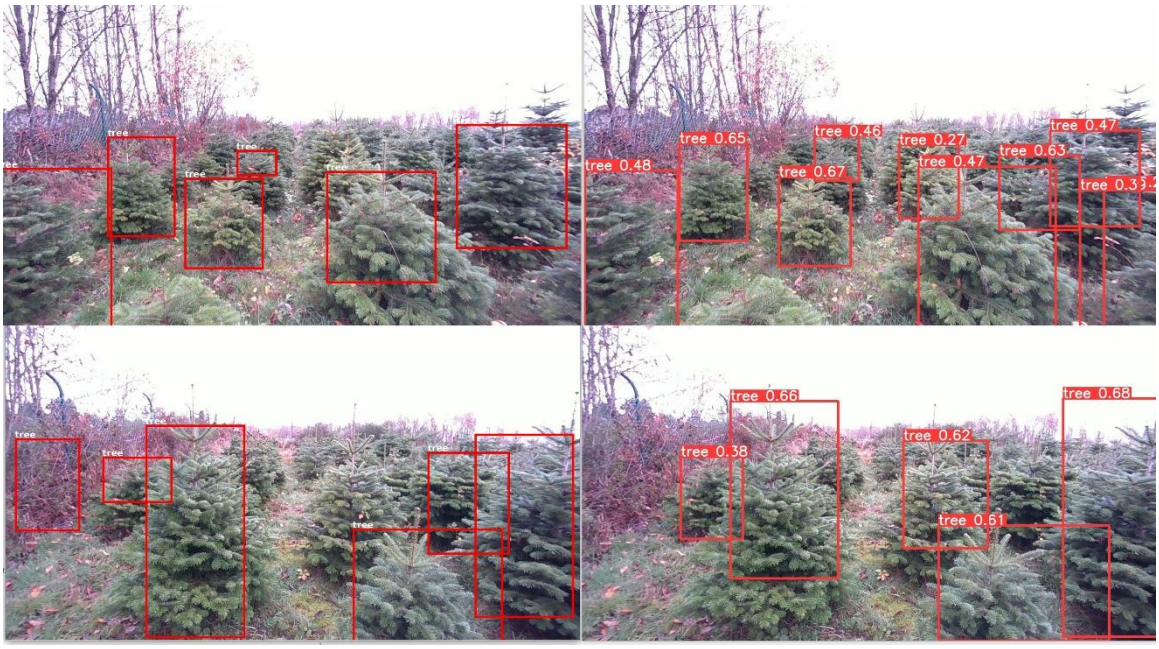

Figure 5. Automatic generated labels (left) and by Yolo-model predicted trees (right).

Acknowledgements

The project is supported by funds of the Federal Ministry of Food and Agriculture (BMEL) based on a decision of the Parliament of the Federal Republic of Germany via the Federal Office for Agriculture and Food (BLE) under the innovation support programme.

References

Attri, I., Awasthi, L. K., Sharma, T. P., & Rathee, P. (2023). A review of deep learning techniques used in agriculture. *Ecological Informatics*, 102217.

Bah, M. D., Hafiane, A., & Canals, R. (2018). Deep learning with unsupervised data labeling for weed detection in line crops in UAV images. *Remote sensing*, 10(11), 1690.

Bosilj, P., Aptoula, E., Duckett, T., & Cielniak, G. (2020). Transfer learning between crop types for semantic segmentation of crops versus weeds in precision agriculture. *Journal of Field Robotics*, 37(1), 7-19.

COCO Consortium. (2023). Common Objects in context. COCO. *https://cocodataset.org/*

Desmond, M., Muller, M., Ashktorab, Z., Dugan, C., Duesterwald, E., Brimijoin, K., ... & Pan, Q. (2021, April). Increasing the speed and accuracy of data labeling through an ai assisted interface. In *26th International Conference on Intelligent User Interfaces* (pp. 392-401).

Golovinskiy, A., & Funkhouser, T. (2009, September). Min-cut based segmentation of point clouds. In *2009 IEEE 12th International Conference on Computer Vision Workshops, ICCV* Workshops (pp. 39-46). IEEE.

Li, Y., & Yang, J. (2021). Meta-learning baselines and database for few-shot classification in agriculture. *Computers and Electronics in Agriculture*, 182, 106055.

Lu, Y., & Young, S. (2020). A survey of public datasets for computer vision tasks in precision agriculture. *Computers and Electronics in Agriculture*, 178, 105760.

Ozguven, M. M., & Adem, K. (2019). Automatic detection and classification of leaf spot disease in sugar beet using deep learning algorithms. *Physica A: statistical mechanics and its applications*, 535, 122537

Point Cloud Library. 2024. The Point Cloud Library (PCL) is a standalone, large scale, open project for 2D/3D image and point cloud processing. *https://pointclouds.org/*

Quigley, M., Conley, K., Gerkey, B., Faust, J., Foote, T., Leibs, J., ... & Ng, A. Y. (2009, May). ROS: an open-source Robot Operating System. *In ICRA workshop on open source software* (Vol. 3, No. 3.2, p. 5).

Ragu, N., & Teo, J. (2023). Object detection and classification using few-shot learning in smart agriculture: A scoping mini review. *Frontiers in Sustainable Food Systems*, 6, 1039299.

Ramcharan, A., Baranowski, K., McCloskey, P., Ahmed, B., Legg, J., & Hughes, D. P. (2017). Deep learning for image-based cassava disease detection. *Frontiers in plant science*, 8, 1852.

Rusu, R. B., Marton, Z. C., Blodow, N., Dolha, M., & Beetz, M. (2008). Towards 3D point cloud based object maps for household environments. *Robotics and Autonomous Systems*, 56(11), 927-941.

Terven, J., & Cordova-Esparza, D. (2023). A comprehensive review of YOLO: From YOLOv1 to YOLOv8 and beyond. *arXiv preprint* arXiv:2304.00501.

The AnyLabeling Project. (2023). AnyLabeling – Smart Image Labeling Tool. https://anylabeling.nrl.ai

Wu, Z., Chen, Y., Zhao, B., Kang, X., & Ding, Y. (2021). Review of weed detection methods based on computer vision. *Sensors*, 21(11), 3647.

Monitoring environmental contaminants concentrations emitted from broilers in Greece: a real – time study

Alkmini Gavriil [a], Dimitris Giannopoulos [a], Vasileios Anestis [a]*, Thomas Bartzanas[a]
Laboratory of Farm Structures, Department of Natural Resources Development and Agricultural Engineering, Agricultural University of Athens, Athens, Greece
* Corresponding author. Email: vanestis@aua.gr

Abstract

The impact of livestock in the emission of environmental (aerial) contaminants is increasingly gaining scientific attention, especially the last decades where intensive livestock is more prevalent. This study aimed to monitor in real-time the environmental and climate conditions of a large-scale poultry facility and to identify potential correlations among the recorded variables. Two different sensor systems, uradmonitorA3 and Cynomys, were placed in-house a large-scale (~ 17.000 broilers), closed-type, forced-ventilated poultry house in Greece. Sensor installation was performed at a representative spot of the facility, approximately 30 – 40 cm above the ground. Monitoring was performed during the broilers' growing period, from March to May 2022 (54 days). Monitored parameters included air temperature and humidity, carbon dioxide (CO_2), volatile organic compounds (VOCs), particulate matter of 1.0, 2.5 and 10 μm ($PM_{1.0}$, $PM_{2.5}$, PM_{10}), noise levels, ammonia and luminosity. The measurements were recorded every 5 (CO_2, VOCs, $PM_{1.0}$, $PM_{2.5}$, PM_{10}, noise levels) or 15 minutes (ammonia, luminosity), based on the technical characteristics of each sensor. Air temperature and humidity were recorded in both sensor systems. Data were remotely collected from the cloud platforms and were used to calculate the daily mean values of each variable. The correlation between the variables was determined using the Pearson linear correlation coefficient. A gradual increase ($p < 0.05$) in the ammonia daily mean concentration levels from 0.1 up to ~ 3.0 – 3.5 ppm was observed during the first 30 – 31 days of growth. This increase was followed by an approximately 2 units reduction ($p < 0.0.5$) until the end of growth period. The final ammonia concentrations were between 1.2 – 1.5 ppm. On the contrary, the daily VOCs and CO_2 concentrations fluctuated during the first 30 -31 days of growth, followed by a gradual increase ($p< 0.05$) and decrease ($p < 0.05$), respectively, to their final levels. Pearson statistical analysis showed a strong positive correlation between CO_2 and temperature, whereas VOCs levels had a strong negative correlation with both temperature and CO_2. Particulate matters ($PM_{1.0}$, $PM_{2.5}$, PM_{10}) were strongly correlated to each other. In conclusion, during intensive livestock farming, air quality is changing as a result of animal – related emitted compounds. Given the multiple adverse effects of these aerial contaminants both on animal health and the environment, monitoring their concentration levels is essential for establishing farm-specific control and mitigation practices.
Keywords: environmental contaminants, sensors, real – time monitoring, broiler's house

1. Introduction

The last decades have seen an increasing demand of food followed by a dramatic growth population. This has put great pressure on both the livestock as well as the agricultural sector, which struggle to meet the current demands in a world severely affected by the climate change. Indeed, the earth temperature is rising. Temperature rise is an ongoing crisis and one of the major challenges of the 21st century. This increase in the Earth's average surface temperature, widely known as the global warming effect, can be attributed to the increase in the greenhouse gases (GHG) emissions (main GHG are water vapor, carbon dioxide, methane, nitrous oxide and ozone) (Jose et al., 2016; Seijan et al., 2016). Although the global warming effect is generally considered to be necessary for the living organisms, the continuously growing accumulation of the greenhouse gas emissions in the atmosphere due to the intensification of man-made activities over the last decades has resulted in the magnification of the greenhouse effect. The industrial and agricultural sectors are main emitters of GHG (Seijan et al., 2016).

The livestock sector is the leading source of greenhouse gas (GHG) emissions for the broad agricultural sector, contributing directly and indirectly to their production, e.g. through animal physiology, animal housing, manure storage, manure treatments, and land application of manure and chemical fertilizers (Rojas-Downing et al., 2017). In addition to the GHG emissions that highly impact the Earth's climate, concentrated animal feeding operations can also emit other polluting compounds, such as ammonia, volatile compounds and particulate matter of different sizes ($PM_{1.0}$, $PM_{2.5}$ and P_{10}). The emission of these compounds although not contributing to the GHG effect, can drastically alter the air quality of the farm facilities. This effect

severely compromises human and animal health due to the serious side effects they have. Thus, livestock-related air pollutants can adversely affect the climate and the ecosystem in multiple ways: they contribute to climate change, contaminate the environment, threaten the safety of animals and farmers, ultimately rendering food safety questionable.

Appropriate monitoring of livestock-related air pollutant concentrations is challenging and requires a lot of effort. Generally, classical analytical techniques are used for measuring the in-house air pollutants concentrations. Analysis based on this approach includes air sampling from specific spots of the housing facility, with air samples being subsequently analysed. These techniques, however, although considered to be more precise and accurate, have several limitations. They are time consuming, labour intensive, require skilled personnel and provide retrospective, off-site information (Khizar et al., 2022). Due to these limitations, analytical techniques allow only for a small number of samples to be analysed. On the other hand, monitoring with appropriate sensors provides an overall and more representative overview of the air concentration dynamics, allowing to continuously control the air quality conditions in the animal housing facility in real time and with lower price in comparison to classical, analytical methods (Khizar et al., 2022). This is especially valuable for the large-scale facilities, that need to provide an appropriate and healthy environment for animal's rearing. Regarding the requirements of the Green Deal for a sustainable *farm-to-fork* continuum, the need for controlling the air conditions within the farms is becoming even more urgent.

Despite the interest of the last decades regarding these pollutants and their key role in the air quality of farm facilities, there is still little progress in Greece. Therefore, the aim of this study was to imprint the dynamic conditions that prevailed in a large – scale, forced ventilated closed type broilers house in Greece and to identify possible interactions among the monitored variables.

2. Materials and Methods

Two real time sensor systems, uRADMonitorA3 (Magnasci SRL, Timisoara, Romania) and cynomys (Cynomys S.r.l., Genova, Italy) (**Figure 1**) were installed in a large-scale, closed-type poultry house located in Evoia, Greece. The building was 125 m in length and 10 m in width (**Figure 2)** and was forced-ventilated using a tunnel ventilation system that consisted of 12 fans equally split in one side of the building. The batch consisted of approximately 17.000 broilers.

The uRADMonitorA3 system was used to measure carbon dioxide (CO_2), volatile organic compounds (VOCs), particulate matter of 1.0, 2.5 and 10 μm ($PM_{1.0}$, $PM_{2.5}$, PM_{10}) and noise levels, whereas ammonia and luminosity levels were monitored using the cynomys system. Air temperature and humidity were measured in both systems. Measurements were taken every 5 minutes or 15- 20 minutes for the uRADMonitorA3 and cynomys sensors, respectively.

Figure 1. uRADMonitorA3 (right) and cynomys sensor systems (left) placed in the broiler house.

The sensors were placed in a representative spot of the facility (30 x 5m), approximately 30 – 40 cm above the ground (**Figure 1**). Since the room inside the building was gradually released based on the broilers age, the sensors were installed in a spot where broilers were present throughout their growth period.

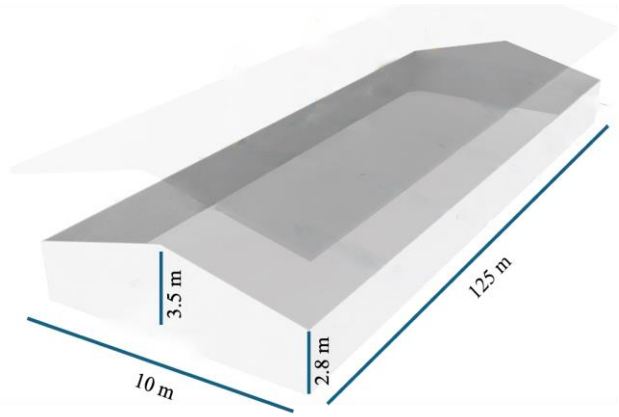

Figure 2. Overview of the poultry facility where the sensors were installed.

Following installation, data collection was performed continuously during the entire broilers' growth period (1-day-old chicks to 54 days-old, finished broilers), from March to May 2022. Data were collected remotely from the corresponding cloud platform in *csv* files. In the case of uradmonitorA3, data were transformed into measurements using the equation provided by the sensor supplier (uRADMonitor, 2024).

Mean daily values were calculated and statistically compared using Pearson linear corelation to identify possible correlations between the collected variables. Comparisons were performed for each pair of monitored variables. All the combinations between the measured variables were taken into consideration. Results were assessed as follows: variables were thought to have a strong correlation for *r* values above 0.7 or below -0.7, whereas for *r* values between 0.5 to 0.7 or -0.5 to-0.7 the variables were thought to have a moderate correlation. For *r* values below 0.5 or -0.5, variables were considered to have a weak correlation, whereas for *r* values below 0.3 or -0.3, variables were not correlated at all. Where necessary, *t-test* statistical analysis was performed using the collected (raw) data of each variable measured in different time intervals (days) to identify significant differences between the mean daily concentrations of the targeted air pollutants in different days of the broilers' growth period.

3. Results and Discussion

The daily mean levels of the air quality pollutants throughout the broilers' growth period are presented in **Figure 3.** Among the collected variables, ammonia was identified as the one with the highest changes. Indeed, ammonia concentrations showed a gradual increase ($p < 0.05$), from 0.1 ppm to approximately ~ 3.0 – 3.5 ppm during the first 30 – 31 days of growth. This increase was followed by a reduction to the final levels at the end of the growth period (1.2 – 1.5 ppm). Ammonia in livestock is formed due to the biological and chemical breakdown of manure protein, uric acid and urea during manure storage and decomposition. As degradation begins due to microbial activity, ammonia is released and volatilized in the atmosphere, making manure and urine a primary source of ammonia. According to the Pearson statistical analysis, ammonia had moderate positive and negative correlations with temperature and humidity, respectively (**Table 1**).

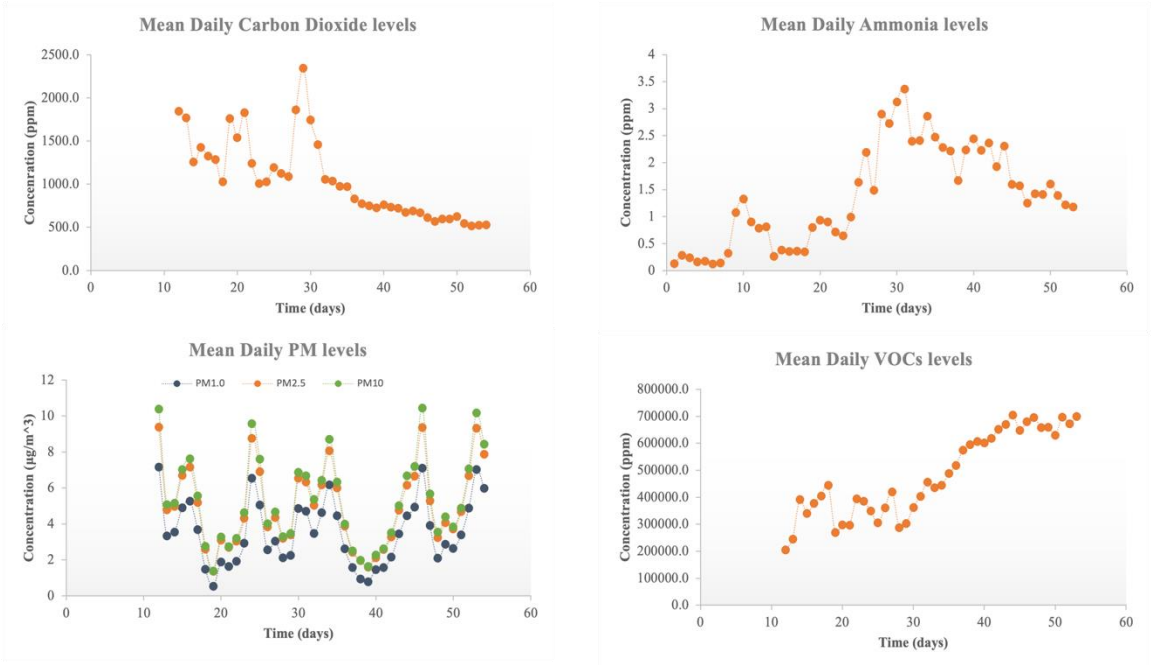

Figure 3. Mean daily concentration dynamics of the targeted air pollutants during the broilers' growing period (54 days).

On the contrary, the daily VOCs and CO_2 concentrations fluctuated during the first 30-31 days of growth, followed by a gradual increase ($p < 0.05$) and decrease ($p < 0.05$), respectively, to their levels at day 54. The final concentration levels of VOCs and CO_2 were 699955.3 and 527.6 ppm, respectively. The production of livestock -VOCs is attributed to multiple sources, such as feces, urine and feed (Aizawa et al., 2010).

Among the climate parameters, temperature was identified as the one with the highest impact on the concentrations of the pollutants, affecting both the levels of VOCs and CO_2, though in different ways. Pearson statistical analysis showed a strong positive correlation between CO_2 and temperature, whereas VOCs levels had a strong negative correlation with both temperature and CO_2. Particulate matters ($PM_{1.0}$, $PM_{2.5}$, PM_{10}) were strongly correlated to each other, with Pearson values being above 0.9 in all cases (**Table 1**).

Table 1. Pearson linear correlation results. Red and yellow cells indicate values with moderate and strong negative correlation, respectively; green and blue cells indicate values with moderate and strong positive correlation, respectively.

	Temperature	**Humidity**	**Carbon dioxide**	**VOCs**	**$PM_{1.0}$**	**$PM_{2.5}$**	**PM_{10}**	**Noise**	**Ammonia**
Humidity	-0.2382								
Carbon dioxide	0.8371	0.0411							
VOCs	-0.9163	0.0019	-0.8911						
$PM_{1.0}$	-0.1222	0.4528	-0.0985	0.0003					
$PM_{2.5}$	-0.1023	0.4480	-0.0876	-0.0149	0.9990				
PM_{10}	-0.1055	0.4503	-0.0954	-0.0084	0.9977	0.9990			
Noise	-0.5472	-0.0765	-0.6030	0.6683	-0.2059	-0.2145	-0.1986		
Ammonia	-0.5389	0.5800	-0.0973	0.1971	0.0229	0.0026	-0.0074	0.1078	
Luminosity	-0.5944	0.1320	-0.5741	0.7439	0.0212	0.0010	0.0035	0.5597	0.2605

4. Conclusions

In intensive poultry farms, air quality is subjected to changes mostly due to animal – related emitted compounds. Given the multiple adverse effects of these aerial contaminants both on animal health and the environment, monitoring their concentration levels is essential for establishing farm-specific control and mitigation practices.

Acknowledgements

This study was funded from the European Union's Horizon 2020 research and innovation program with the acronym DiTECT under Grant Agreement No 861915.

References

Aizawa, A., A. Miyazaki and N. Tanaka. 2022. Emissions of Volatile Organic Compounds from dairy cattle manure in a cattle shed in Japan. Asian Journal of Atmospheric Environment 16, 2022024, 122 – 134. https://doi.org/10.5572/ajae.2022.024

Jose, V.S, V. Sejian, M. Bagath, A. P. Ratnakaran, A. M. Lees, Y. A. S. Al-Hosni, M. Sullivan, R. Bhatta and J. B. Gaughan. 2016. Modeling of Greenhouse Gas Emission from livestock. Frontiers in Environmental Science 4, 10.3389/fenvs.2016.00027.

Khizar, S., Zine, N., Jaffrezic-Renault, N., Elaissari, A., & Errachid, A. 2022. Prospective analytical role of sensors for environmental screening and monitoring. TrAC Trends in Analytical Chemistry, 157, 116751. https://doi.org/10.1016/J.TRAC.2022.116751

Rojas-Downing, M. M., A. P. Nejadhashemi, T. Harrigan and S. A. Woznickin. 2017. Climate change and livestock: Impacts, adaptation, and mitigation. Climate risk management 16, 145-163. https://doi.org/10.1016/j.crm.2017.02.001

Sejian, V., R. Bhatta, P. K. Malik, B. Madiajagan, Y. A. S. Al-Hosni, M. Sullivan and J. B. Gaughan. 2016. Livestock as Sources of Greenhouse Gases and Its Significance to Climate Change. In GreenHouse Gases. London, United Kingdom: IntechOpen. p. 243 – 259.

uRADMonitor. 2024. Dashboard. Available at: https://www.uradmonitor.com/dashboard/ (Accessed: May 2024)

Soil tillage quality measurement: a methodical approach

Marina Graf [a,b*], Franz Fuchshumer [a], Marcus Geimer [b]

[a] Research & Advanced Engineering, AGCO GmbH, Marktoberdorf, Germany

[b] Institute of Mobile Machines, Karlsruhe Institute of Technology, Karlsruhe, Germany

* Corresponding author. Email: marina.graf@agcocorp.com

Abstract

This paper presents a methodical approach for measuring the process quality of the agricultural task soil tillage. This is a crucial step towards the development of automation in the context of autonomous agricultural field work. Therefore, the relevant parameters that define the process quality for autonomous tillage must be identified. These parameters depend on the agricultural task, such as primary tillage, stubble cultivation, or seedbed preparation, and are based on the farmer's expertise and focus. The quality parameters are the identified set of parameters for each task that indicate the quality of the process. For each individual parameter, the proposed measurement method can be applied. The method involves three basic steps. (1) Different algorithms are implemented to characterize the quality parameter based on, e.g., 3D point cloud data or image data. The algorithms are verified in a deterministic environment, such as a simulation environment or a test bench. (2) Afterwards, the Spearman correlation coefficient of the various parameter metrics is analyzed to cluster the metrics into groups with similar physical properties. Based on the clustering, parameters can be chosen considering defined criteria (low resource-intensive, sensor-setup specific, etc.). (3) Finally, the selection of the parameter metric is validated by testing the implementation infield, considering challenging cases, anomalies, and influencing factors such as working speed or soil dependencies. The measurement method for the quality parameter could be used to derive a model that describes the variation of the parameters concerning the degrees of freedom of the agricultural task, e.g. the working speed or working depth for the tillage process.

Keywords: Tillage, Agricultural Process Quality, Measurement Method, Process Sensor Technology

1. Introduction

Soil tillage in agriculture aims to create an optimal soil structure for the crop, including the processes of germination and growth. Tillage tasks vary throughout the year, depending on the crop rotation. Farmers perform primary tillage before seedbed preparation and sowing to mix and loosen the soil. This is typically accomplished using implements such as plows or heavy cultivators. During seedbed preparation, the uppermost layer of soil is loosened, finely crumbled, and reconsolidated, typically with implements like a seedbed combination or rotary harrow. Stubble cultivation after harvest in summer and the incorporation of cover crops in spring are carried out only as deep as necessary to break the soil's capillarity and protect the water content in the soil. A fine cultivator or disk harrow can be used here.

Despite the diversity of the tasks, objectives, and implements, tillage is often a research focus regarding automation in agriculture. A potential explanation is its greater tolerance to error than other tasks, such as sowing. The interest in tillage automation is also underlined by the scarcity of skilled labor in agriculture, especially for tasks with low area performance (ha/h). In addition to these benefits, there are also sustainability aspects in the automation of tillage. Automation of the tillage process can improve energy efficiency or help protect the soil through minimized soil intervention, enhancing biological activity and forming a more resilient soil structure with higher resistance to erosion.

Features such as guidance systems and telemetry solutions are already established in the market. Streitberger et al. (2018) state that these features are classified within automation levels 1 and 2. Moving on to automation level 3, the automated vehicles must monitor the process and environment. Verband Deutscher Maschinen- und Anlagenbau (VDMA) Landtechnik & Bayerischer Bauernverband (2020) specifies autonomy level 2 concerning soil tillage as manual adjustment and guidance of the implement with an assistance system. In contrast, level 3 describes the automatic control and documentation of subtasks according to the farmer's specifications. A measurement system is required to assist during the process and assess and document the process's output, which is here defined as process quality.

Surface roughness, crop residue cover, and aggregate size distribution are potential process quality parameters that could be considered for measurement in the context of tillage. Most metrics and algorithms for the description of surface roughness are based on height profiles. These height profiles can be derived from contact-measurement devices like relief meters (Kuipers, 1957) or non-contact-measurement devices like laser scanners or stereo vision systems (Boysen et al., 2023; Martinez-Agirre et al., 2016; Riegler-Nurscher et al., 2017; Taconet & Ciarletti, 2007; Thomsen et al., 2015). The evaluated

metrics range exemplary from the prediction of the surface storage capacity (Hansen et al., 1999) over to the standard deviation of individual elevation points, respectively, the index of Currence and Lovely (1970) to the Peak Frequency (Römkens & Wang, 1986).

Sieve analysis is widely applied to determine the aggregate size distribution. However, it can be influenced by changes in aggregate structure resulting from frictional effects caused by transport, filling the sieve, and oscillation motion of the sieve (Anisch et al., 2016). Sensor-based evaluations may be based on 3D data, as exemplified by the method presented by Steinhaus and Frerichs (2020), or on the evaluation of image data. The various image-based algorithms can be classified into computer vision (e.g. Bosilj et al., 2020; Itoh et al., 2008) or machine learning approaches (e.g. Ajdadi et al., 2016; Alirezazadeh et al., 2021; Azizi et al., 2020). The aggregate size distribution can be described over the working width or summarized as the mean weighted diameter. Furthermore, it is possible to describe aggregates' spatial distribution.

There are several methods for determining crop residue cover. The so-called meter stick or line method determines the degree of cover based on the overlap of organic material with a placed stick. Another method is to compare images indicating a specified crop residue cover level. Measurement methods can also be based on image data (e.g. Pforte, 2010; Riegler-Nurscher et al., 2018; Schmidt, 2022). Potential metrics for describing the parameter include crop residue cover based on individual detected pixels/grid points, the area with a defined percentage of crop residue cover, or the distribution of the crop residue cover. In addition, it could be possible to determine the orientation of the crop in 3D data and verify if the organic matter has been effectively pulled out/separated from the soil.

Measurement methods based on non-contact measurement devices like laser scanners or camera systems provide higher accuracy for these exemplary process quality parameters. However, they need manually labeled data as a reference. Regarding crop residue cover, Riegler-Nurscher et al. (2018) demonstrated that these human-labeled data also underlay uncertainty. They examined the standard deviation of ten evaluators and showed that the deviations for soil, living biomass, and remains in the classes to be labeled were 5.5 %, 4.2 %, and 3.5 %, respectively. Analyses of aggregates are similarly subject to uncertainty. The intricate fracture patterns observed in soil mechanics can impede the clear identification of aggregate boundaries.

Despite the large variety of potential metrics and algorithms for the various process quality parameters, there is still no commonly applied framework for comparing measured and evaluated parameters in the field. Therefore, this paper presents a methodical approach to identify the most relevant metric to describe the individual process quality parameter to monitor and measure the quality of the tillage process. The method ensures that the measured parameters are verified in controlled, reproducible conditions to derive reference values. The validation is then conducted by field trials.

2. Methodical Approach for Tillage Process Quality Measurement

Before the measurement, it is necessary to identify the process quality parameters to be measured. The process quality parameters are selected after literature research and interviews with experts (farmers, agronomists, etc.). This parameter identification step, exemplary for the tillage process with a cultivator, is visualized in the bottom line in **Figure 1**. For the tillage process with a plow, process quality parameters candidates are crop residue cover (target value 0...5 % (Bernacki et al., 1972)), furrow width, depth, and evenness or shape of cut soil bar.

After identifying the process quality parameters, the measurement method for each parameter itself can be applied. The first step involves the implementation of various metrics to characterize process quality parameters related to the tillage process. Different metrics can evaluate varying data fundamentals, such as 3D point clouds for spatial metrics and 2D images for texture analysis. Testing the algorithms for the different parameter metrics under various conditions in a deterministic environment is necessary to verify the algorithms. In this verification step, it is possible to ascertain whether the metric accurately reflects the intended process quality parameter and its behavior, as well as to derive reference values from simulations. Simulation techniques or controlled experiments conducted in laboratory settings (e.g., soil bin) can be utilized for this purpose. The validation of the simulation or the test bench setup is not part of the proposed measurement method.

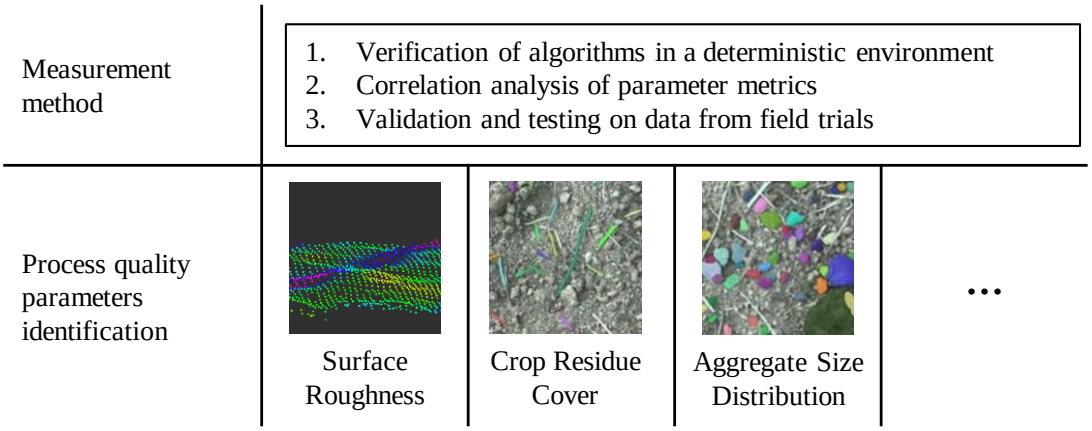

Figure 1. Proposed Methodical Approach to measure process quality in tillage processes.

In the second step, the evaluated metrics undergo statistical evaluation using Spearman's rank correlation coefficient. Spearman rank correlation coefficient is relatively robust against outliers and therefore preferred to the Pearson correlation coefficient (Bortz & Schuster, 2010). The reason for this is the use of the ranks of the analyzed values instead of their actual value. The Spearman's rank correlation coefficient r_S is calculated

$$r_S = \rho_{R(X),R(Y)} = \frac{\mathrm{cov}(R(X), R(Y))}{\sigma_{R(X)}\sigma_{R(Y)}} \quad (1)$$

where $\rho_{R(X),R(Y)}$ is the Pearson correlation coefficient of the ranked variables $R(X), R(Y)$, $\mathrm{cov}(R(X), R(Y))$ is the covariance matrix, and $\sigma_{R(X)}, \sigma_{R(Y)}$ are the standard deviations of the ranked variables $R(X), R(Y)$ (Bortz & Schuster, 2010). This analysis enables the identification of parameter metrics that share similar physical properties. The correlation of metrics with r_S values close to 1 or -1 suggest similar physical properties. By identifying clusters among the parameters, we can efficiently select those from the cluster that describe a process quality parameter, for example, with minimal computation time or the best fit with the existing sensor setup. Parameters that do not fit into any cluster require special consideration as they could indicate a distinct property or be suited only for specific circumstances.

In the third step, the chosen process quality parameter metrics must be validated using data from field trials. The investigations under determinate environmental conditions ensured the metrics' correctness. So, for infield data, the process quality parameter values classified on an ordinal scale must correspond to the subjective classifications of a sample of farmers and agronomists. Anomaly cases should be considered. In addition, Spearman correlation coefficients can again be calculated. In addition to the parameters' sensitivity to e.g. anomaly cases, the agreement of the results with those of the deterministic environment should also be analyzed. Any unexpected differences must then be investigated in more detail.

The following chapter outlines the methodological approach for the tillage task with a cultivator as an example. The cultivator, characterized by its limited adjustment options and wide range of applications, facilitates data generation across various scenarios with differing quality requirements and long operating times throughout the year. This design supports a focus on data collection rather than attachment settings, thereby focusing on the methodological approach.

3. Methodical Process Quality Measurement of the Cultivator

In textbooks by authors such as Köller (1981), Köller and Hensel (2019), Soucek & Pippig (1990), or Estler & Knittel (1996), the primary objectives of tillage are to maintain or enhance the soil's characteristics to create favorable germination and growth conditions for crops and to minimize the growth of undesirable vegetation. Surface roughness, residue crop cover, and aggregate size distribution are possible parameters to determine the quality of tillage using a cultivator. The optimal parameter values and their relative importance vary from case to case and are, therefore, at the process planner's discretion, namely the farmer.

To extract suitable metrics to describe the process quality parameters, the method presented in Chapter 2 is used. A simulation environment represents the deterministic environment. Since the widely used sieve analysis, for instance, only measures static diameters, modeling the soil aggregates with hemispheres is proposed in the initial step. Based on this, deformed spheres (modified in size and shape) can

also be used. These spheres are distributed on a ground plate based on the Rosin-Rammler-Sperling-Bennett distribution (Hillig, 1986; Soucek, 1986). The ground plate can imitate the landscape with heights and depths and thus, for example, represent an uneven terrain. In addition to the soil aggregates, organic material can be simulated in various distribution densities on the ground. It is recognized that the simulation approach offers the potential to investigate a range of sensors and their suitability efficiently. Nevertheless, it is crucial to acknowledge that this simplified simulation approach does not fully reflect the complexities of reality. As an alternative to the simulation, a test bench scenario, such as a soil bin, also provides a deterministic environment.

The Spearman correlation coefficient is then calculated for the various metrics described in Chapter 2 and analyzed in correlation matrices. Correlating parameters form a cluster. Metrics are selected based on the clusters and the decision criteria, e.g., low resource-intensive, sensor-setup specific.

The selection of the parameter metrics must then be validated. An experimental setup is suitable for this purpose. **Figure 2** shows three field sections (peat soil). Section 1 is not processed, while sections 2 and 3 are processed at different working speeds with the same cultivator and cage roller. If, for example, the selected roughness metric is to be validated, the metric for section 2 should give the smallest values. Larger values should result for section 3 and 1. An alternative value system that is entirely at odds with the aforementioned one would also be acceptable.

Figure 2. Soil surface after the tillage process with a cultivator with cage roller.

4. Discussion

This paper's measurement method could help identify suitable metrics for measuring the tillage process quality. Such a measurement system would be necessary for the next tillage autonomy level 2 and 3, as outlined by VDMA Landtechnik & Bayerischer Bauernverband (2020). The assistance system (level 2) and the automatic control and documentation of subtasks according to the farmer's specifications (level 3) require a control loop, as exemplified in **Figure 3**. The farmer is still responsible for the process planning and specifying the agronomical boundary conditions and process parameters (working depth, implement, objectives, …). Furthermore, the farmer defines the process quality parameters as reference variables for the automated system. The proposed measurement method supports the selection of the measured input values for the controller. Influences on the soil fracture behavior, like non-homogeneous soil type, moisture, or density, must be considered in the modeling (Bögel, 2022; Elijah, D. L. & Weber, 1971). The control idea can be expanded by the efficiency aspect, as suggested by Kazenwadel et al. (2023), so that it results in a multicriterial optimization problem. It should be considered that it is not easy to model all the influences cleanly, as the implement itself (roller, type of tines/blades) also strongly impacts the process quality. Therefore, modeling will probably first run out for separate implement configurations. By adopting this modeling approach, the necessity for continuous measurement in the control loop could eventually be significantly reduced.

The methodology primarily focused on process quality parameters, assuming optimal implementation functionality. However, process parameter monitoring is imperative for the automated system. This includes, for example, the material flow in the implement (detection of blockages) or the condition of the tines or blades.

Additionally, the proposed method omits the validation of the simulation itself, noting that the simulation environment serves as a means to an end. Nonetheless, given the method's requirement for validation on real data for each parameter, the authors find this approach acceptable.

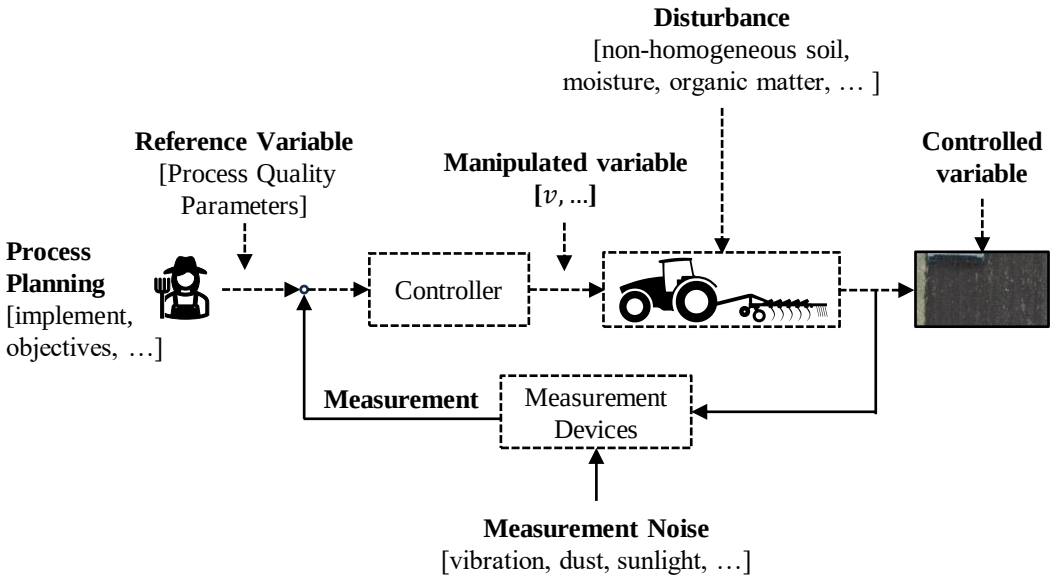

Figure 3. Exemplary Closed Control Loop of an automated tillage process.

5. Conclusion

The literature introduces various parameters with many metrics to describe the quality of the tillage process. This paper presented a methodological approach to evaluate the different metrics to find the most relevant ones. Therefore, the method consists of three steps: In the first step verifying the parameter's metric in a deterministic environment (simulation, test bench) is done. In the second step, the available metrics are clustered based on similar physical properties identified using the Spearman correlation coefficient. In the last step, the most significant metrics are validated on infield data. The idea of modeling the parameters over the possible degrees of freedom (manipulated variable and disturbances) needs further investigation but could be one possible use case for the method.

References

Ajdadi, F. R., Gilandeh, Y. A., Mollazade, K., & Hasanzadeh, R. P. (2016). Application of machine vision for classification of soil aggregate size. *Soil and Tillage Research*, *162*, 8–17. https://doi.org/10.1016/j.still.2016.04.012

Alirezazadeh, P., Rahimi-Ajdadi, F., Abbaspour-Gilandeh, Y., Landwehr, N., & Tavakoli, H. (2021). Improved digital image-based assessment of soil aggregate size by applying convolutional neural networks. *Computers and Electronics in Agriculture*, *191*, 106499. https://doi.org/10.1016/j.compag.2021.106499

Anisch, S., Grosa, A., Bögel, T., & Herlitzius, T. (2016). Zum Stand der Bewertung des Zerkleinerungsergebnisses bei der Saatbettbereitung. *Agricultural Engineering.Eu*, *71*(3), 90–97. https://doi.org/10.15150/lt.2016.3125

Azizi, A., Abbaspour-Gilandeh, Y., Vannier, E., Dusséaux, R., Mseri-Gundoshmian, T., & Moghaddam, H. A. (2020). Semantic segmentation: A modern approach for identifying soil clods in precision farming. *Biosystems Engineering*, *196*, 172–182. https://doi.org/10.1016/j.biosystemseng.2020.05.022

Bernacki, H., Haman, J., & Bernacki, H. (1972). *Grundlagen der Bodenbearbeitung und Pflugbau*. Verlag Technik, VEB.

Bögel, T. (2022). *Identifikation von Form- und Einstellparametern passiver, keilförmiger Arbeitsorgane zur Optimierung der Wechselwirkung von Arbeitsfunktion und Zugkraftbedarf*. Springer Vieweg.

Bortz, J., & Schuster, C. (2010). *Statistik für Human- und Sozialwissenschaftler* (7th ed.). Springer.

Bosilj, P., Gould, I., Duckett, T., & Cielniak, G. (2020). Estimating soil aggregate size distribution from images using pattern spectra. *Biosystems Engineering*, *198*, 63–77. https://doi.org/10.1016/j.biosystemseng.2020.07.012

Boysen, J., Zender, L., & Stein, A. (2023). Modeling the soil-machine response of secondary tillage: A deep learning approach. *Smart Agricultural Technology*, *6*, 100363. https://doi.org/10.1016/j.atech.2023.100363

Currence, David H., & Lovely, W. G. (1970). The Analysis of Soil Surface Roughness. *Transactions of the ASAE*, *13*(6), 0710–0714. https://doi.org/10.13031/2013.38702

Elijah, D. L., & Weber, J. A. (1971). Soil Failure and Pressure Patterns tor Flat Cutting Blades. *Transactions of the ASAE*, *14*(4), 0781–0785. https://doi.org/10.13031/2013.38389

Estler, M., & Knittel, H. (1996). *Praktische Bodenbearbeitung: Grundlagen, Gerätetechnik, Verfahren, Bewertung* (2nd ed.). DLG-Verl. [u.a.].

Hansen, B., Schjønning, P., & Sibbesen, E. (1999). Roughness indices for estimation of depression storage capacity of tilled soil surfaces. *Soil and Tillage Research*, *52*(1–2), 103–111. https://doi.org/10.1016/S0167-1987(99)00061-6

Hillig, U. (1986). *Ermittlung der Gesetzmäßigkeit des Zerkleinerungsergebnisses durch ausgewählte Bodenbearbeitungswerkzeuge auf unterschiedlichen Standorten* [Ph.D. dissertation]. TU Dresden.

Itoh, H., Matsuo, K., Oida, A., Nakashima, H., Miyasaka, J., & Izumi, T. (2008). Aggregate size measurement by machine vision. *Journal of Terramechanics*, *45*(4), 137–145. https://doi.org/10.1016/j.jterra.2008.09.001

Kazenwadel, B., Becker, S., Graf, M., & Geimer, M. (2023). Aligning process quality and efficiency in agricultural soil tillage. *At - Automatisierungstechnik*, *71*(11), 979–986. https://doi.org/10.1515/auto-2023-0042

Köller, K. (1981). *Bodenbearbeitung ohne Pflug Ergebnisse mehrjähriger Vergleichsuntersuchungen verschiedener Geräte und Verfahren auf vier Standorten*. Ulmer.

Köller, K., & Hensel, O. (Eds.). (2019). *Verfahrenstechnik in der Pflanzenproduktion*. Verlag Eugen Ulmer.

Kuipers, H. (1957). A reliefmeter for soil cultivation studies. *Netherlands Journal of Agricultural Science*, *5*(4), Article 4. https://doi.org/10.18174/njas.v5i4.17727

Martinez-Agirre, A., Álvarez-Mozos, J., & Giménez, R. (2016). Evaluation of surface roughness parameters in agricultural soils with different tillage conditions using a laser profile meter. *Soil and Tillage Research*, *161*, 19–30. https://doi.org/10.1016/j.still.2016.02.013

Pforte, F. (2010). *Entwicklung eines Online-Messverfahrens zur Bestimmung des Bodenbedeckungsgrades bei der Stoppelbearbeitung zu Mulchsaatverfahren* [Ph.D. dissertation]. Universität Kassel.

Riegler-Nurscher, P., Karner, J., Huber, J., Moitzi, G., Wagentristl, H., Hofinger, M., & Prankl, H. (2017). A system for online control of a rotary harrow using soil roughness detection based on stereo vision. In *Land.Technik AgEng 2017* (pp. 559–566). VDI Verlag. https://doi.org/10.51202/9783181023006-559

Riegler-Nurscher, P., Prankl, J., Bauer, T., Strauss, P., & Prankl, H. (2018). A machine learning approach for pixel wise classification of residue and vegetation cover under field conditions. *Biosystems Engineering*, *169*, 188–198. https://doi.org/10.1016/j.biosystemseng.2018.02.011

Römkens, M. J. M., & Wang, J. Y. (1986). Effect of Tillage on Surface Roughness. *Transactions of the ASAE*, *29*(2), 0429–0433. https://doi.org/10.13031/2013.30167

Schmidt, M. (2022). AI-Based Tillage Job Quality Assessment for Advanced Machine Automation in Agriculture. In VDI Wissensforum GmbH (Ed.), *AgEng-LAND.TECHNIK 2022: International Conference on Agricultural Engineering: Vol. Bd. 2406* (pp. 567–572).

Soucek, R. (1986). *Beiträge der Grundlagen- und angewandten Forschung zur Entwicklung von Bodenbearbeitungsgeräten und -maschinen* [Ph.D. dissertation]. TU Dresden.

Soucek, R., & Pippig, G. (1990). *Maschinen und Geräte für Bodenbearbeitung, Düngung und Aussaat* (1st ed.). Verl. Technik.

Steinhaus, S., & Frerichs, L. (2020). A novel approach to determine the soil aggregate size distribution from high-resolution 3D point clouds. In *LAND.TECHNIK 2020: The Forum for Agricultural Engineering Innovations* (1. Auflage, Vol. 2374, pp. 361–368). VDI Verlag. https://doi.org/10.51202/9783181023747-361

Streitberger, N., Balbach, F., & Eberhard Nacke. (2018). Vom manuellen Fahren zur vollen Autonomie: Ein Ansatz zur systematischen Definition verschiedener Stufen der Automation in der Landtechnik. In *LAND.TECHNIK*

2018 Conference: Agricultural Engineering—Conference: Agricultural Engineering: Leinfelden-Echterdingen, 20. Und 21. November 2018 Tagung Land.Technik (pp. 293–300). VDI Verlag.

Taconet, O., & Ciarletti, V. (2007). Estimating soil roughness indices on a ridge-and-furrow surface using stereo photogrammetry. *Soil and Tillage Research*, *93*(1), 64–76. https://doi.org/10.1016/j.still.2006.03.018

Thomsen, L. M., Baartman, J. E. M., Barneveld, R. J., Starkloff, T., & Stolte, J. (2015). Soil surface roughness: Comparing old and new measuring methods and application in a soil erosion model. *SOIL*, *1*(1), 399–410. https://doi.org/10.5194/soil-1-399-2015

Verein Deutscher Maschinen und Anlagen (VDMA) Landtechink & Bayerischer Bauernverband. (2020). *Digital erfolgreich werden: Betriebs-Check und Planungshilfe für Praktiker*. https://www.vdma.org/documents/34570/040eb2e2-8921-89c0-ef75-2e887509ce5f

Localization of metal piles in grapevine rows by means of LiDAR based 3D reconstruction

Andreas Heiß [a,*], Joseph Bleser [a], Nikos Tsoulias [a], Björn Poss [a], Dimitrios S. Paraforos [a]

[a] Department of Agricultural Engineering, Geisenheim University, Geisenheim, Germany

* Corresponding author. Email: andreas.heiss@hs-gm.de

Abstract

Pruning is one of the most important and at the same time most labour-intensive processes in viticulture. With mechanical pre-pruners, this task can be significantly facilitated. Operating these machines, however, is still challenging and tiring. Systems for automated avoidance of piles in the supporting material are commercially available but have different limitations based on the used sensor technology. Light detection and ranging (LiDAR) sensors are a robust technology that has proven its suitability for digital reconstructions of vineyards. Therefore, this work aimed at developing and validating an algorithm for automated detection of metal piles by means of LiDAR based 3D reconstruction.

A multi-sensor setup including a LiDAR, an inertial measurement unit (IMU), as well as RTK-GNSS was employed to make scans in an experimental vineyard during dormancy. The simultaneously recorded data were fused in order to generate a georeferenced 3D reconstruction. A novel algorithm was developed to segment the point cloud, detect the metal piles based on reflectivity values from the LiDAR and reconstruct the piles. The validation comprised further independent datasets, as well as ground-truth positions measured manually with RTK-GNSS.

The validation results have shown a high reliability of the developed algorithm with 100% true-true detections among the grapevine canopy datasets comprising 163 metal piles. Further, the statistical analysis has shown a high absolute and relative accuracy in the prediction of the piles' upper and lower ends, with root mean square (RMS) values in the range of approx. 5 cm, as well as mean absolute errors (MAE) and mean bias errors (MBE) below 5 cm for the x-y plane. This was considered sufficient for use in systems for automated pile avoidance. Further, the results have implied also a high potential of the method not only for detection of piles but also trunk inventory.

Keywords: viticulture, pruning, pre-pruner, LiDAR, 3D reconstruction.

1. Introduction

Due to the lack of personnel and growing economic pressure, mechanisation alternatives for particularly labour-intensive tasks in viticulture are becoming relevant for more and more practitioners. Pruning is of great importance for grapevine growing but at the same time one of the most time-consuming tasks (Fernandes et al., 2021). Especially in regions, where grapevines are grown in trellis training with supporting wire frames, digging up the pruned vine wood is physically demanding and accounts for the majority of the time required. With pre-pruners, the upper part of vines can be removed mechanically by cutting and mulching it. These machines make the subsequent lifting process much easier and are also considered as an important component to facilitate autonomous pruning in the future (Silwal et al., 2022). Their operation, however, is relatively complex and requires operators to continuously check and readjust the various setting parameters, which leads to fatigue over time and an increased safety risk. Specifically, the bypassing of piles in the wire frame requires a high level of attention to avoid damage. There are commercial systems using optical, inductive or mechanical sensors to detect the piles and automatically open and close the cutting tools accordingly (e.g. Rinieri Sensing-CPL, ERO AOS 2.0, Pellenc Visio). However, these systems are only suitable for certain pile materials and diameters, or have only limited reliability and precision, respectively. Recent camera-based systems (e.g. ERO VITIassist, Clemens C.VISION) still need to prove their functionality in practice, especially under varying environmental conditions.

There has been significant technical progress in sensor systems based on the 'light detection and ranging' (LiDAR) principle in recent years and such sensors have been successfully used in various studies for the 3D reconstruction of fruit trees (Tsoulias et al., 2020) and to quantify different phenotypic variables in viticulture (Arnó et al., 2012; Siebers et al., 2018). They are a promising approach for recognising different structures in the vine rows, even in dormancy. Main advantages of this sensor technology are a high resolution and

accuracy combined with a low susceptibility by environmental influences. For the present paper, a project was set up to develop a methodology to identify metal piles in vineyard rows from georeferenced 3D reconstructions. Main objectives to achieve this aim were the fusion of LiDAR data with RTK-GNSS and inertial measurement unit (IMU) data, as well as the development of a pile detection algorithm including its validation with data acquired in a vineyard.

2. Materials and Methods

2.1. Instrumentation

For data acquisition, a sensor frame was designed and attached to a standard narrow-width tractor for vineyards. A VLP-16 Puck Lite LiDAR (Velodyne Lidar Inc., San Jose, CA, USA), a VN-100 inertial measurement unit (IMU) (VectorNav, Dallas, TX, USA), as well as an R10 RTK-GNSS receiver (Trimble, Sunnyvale, CA, USA) were mounted on the frame as illustrated in Figure *1*a. In Figure *1*b, the orientation of the LiDAR's and IMU's coordinate systems are shown, where the IMU coordinate system corresponds to the body frame. The spatial offsets x_{off} and z_{off} between LiDAR and GNSS equalled to 0.272 m and 1.09 m, respectively (Figure *1*c). The LiDAR acquired distance values in 16 layers of 360° around the z_L-axis, where the layers were arranged in a field of view from -15° to 15°. It worked with a laser firing frequency of 18.08 kHz in single return mode, where the firings alternated continuously between the 16 layers. The rotation speed around the z_L-axis was set to 300 rpm and the range accuracy was indicated with ± 3 cm by the manufacturer. Further, the LiDAR outputted reflectivity values between 0 and 100, indicating the percentage of light reflected by diffuse reflector surfaces. The IMU's static accuracy was indicated with 2° RMS for the magnetic heading and 0.5° RMS for roll and pitch. The RTK-GNSS's horizontal accuracy was given as ± 8 mm + 1 ppm RMS and its vertical accuracy with ± 15 mm + 1 ppm RMS. To acquire the different sensor streams simultaneously, a C# software with a multi-thread architecture was used (Paraforos et al., 2016).

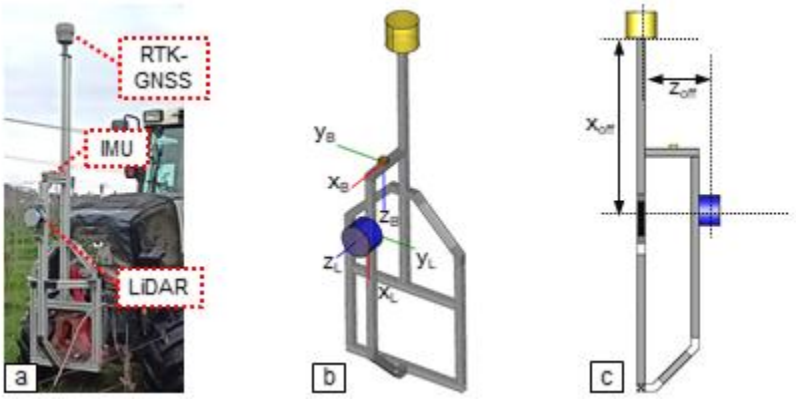

Figure 1. (a) Sensor frame with (b) indications of coordinate systems and (c) spatial offsets.

2.2. Field experiments

Measurements were carried out on 29th March 2023 prior to pruning in a vineyard of Geisenheim University (49.986 N, 7.948 E Geisenheim, Hesse, Germany). The training system was a flat cane guyot with an average canopy height of approx. 2 m. Row width and distance between the plants were approx. 2 m and 0.5 m, respectively, while the overall length of the rows was approx. 100 m. All rows were planted with different varieties of *Vitis berlandieri* with very similar phenotypes. The greening had been mulched in autumn. Hence, there were no weeds longer than approx. 15 cm on the ground. Data were collected from four rows, i.e. five canopies at a speed of 0.5 km h^{-1}. Figure *2* gives an overview of the experimental vineyard with Figure *2*a showing an aerial photo and the measured rows indicated in white, Figure *2*b showing a view into an exemplary row and Figure *2*c showing schematically the setup of the measured rows. Each pass collected data from two canopies, left and right of the tractor. Rows 1 and 3 were taken together as a dataset for the southbound direction, and rows 2 and 4 were taken together for the northbound direction. The first two piles in rows 2, 3 and 4 were removed due to incomplete data acquisitions at the beginning. Consequently, there were 83 and 80 piles examined in rows 1&3 and rows 2&4, respectively. The data set with rows 1&3

was used to develop the algorithm for pile detection, while rows 2&4 were used to validate, if the algorithm worked without adjustment. For the assessment of the developed algorithm, ground truth data were taken manually on 13th November and 13th December 2023 as point data from the bottom and top of the piles using the R10 RTK-GNSS with a survey rod. Further, pile heights were measured manually from the ground to the top for later determination of the optimum search radius for the pile reconstruction.

Figure 2. (a) Vineyard for field experiments with measured rows indicated in white, (b) view into an exemplary row and (c) setup of measured rows (aerial image source: Google LLC).

2.3. Pile detection algorithm development

Data processing was mainly conducted in Python programming language. The development of the pile detection algorithm followed a sequence, which is illustrated schematically in Figure *3*. In a first step, the LiDAR raw data, which were recorded in polar coordinates and associated reflectivity values, were transformed to cartesian point coordinates ($P_{cart,i}$) within the LiDAR coordinate system indicated in Figure 1b. Further, points were filtered according to the measured distance, where all points with a distance of more than two meters to the LiDAR were excluded from the further analysis because they were considered as not belonging to adjacent canopies within a row. As the GNSS and IMU data streams had a much lower frequency, the recorded data were interpolated linearly to the LiDAR timestamps.

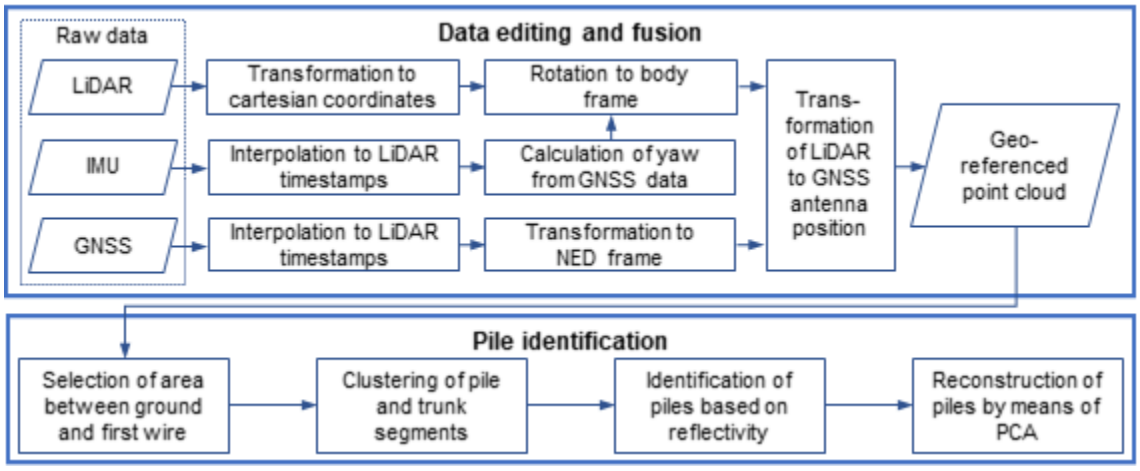

Figure 3. Schematic flow of the single processing steps for the pile detection algorithm.

The first necessary step to generate a georeferenced LiDAR point cloud was the transformation of the GNSS data, which had been recorded as WGS84 coordinates in latitude, longitude and altitude. Using the

Python library pyproj, they were first transformed to the Earth-Centered-Earth-Fixed (ECEF) frame. Then, the ECEF coordinates were transformed to a local cartesian North-East-Down (NED) frame in three subsequent steps, where the ECEF position of the reference point ($P_{reference}$) was first subtracted from each recorded position P_i in ECEF frame. The resulting $P_{antenna,i}$ was used to calculate the final NED position $P_{ned,i}$ as follows:

$$P_{ned,i} = P_{antenna,i} \times R_{ned} \tag{1}$$

where R_{ned} was defined according to:

$$R_{ned} = \begin{pmatrix} -\sin(\varphi) \times \cos(\lambda) & -\sin(\varphi) \times \sin(\lambda) & \cos(\varphi) \\ -\sin(\lambda) & \cos(\lambda) & 0 \\ -\cos(\varphi) \times \cos(\lambda) & -\cos(\varphi) \times \sin(\lambda) & -\sin(\varphi) \end{pmatrix} \tag{2}$$

with φ and λ representing the latitude and longitude, respectively, of the reference point. The reference point was a nearby position close to the examined rows and it was used for all of them. As the IMU was not capable of outputting an accurate heading relative to true north, a heading ψ_i was derived from GNSS data for each point recorded by the LiDAR. For this, a vector was constructed from the GNSS position of 800.000 detections prior to the point of interest. This corresponded to approx. 3 s time difference and a distance of approx. 5.4 m. The heading ψ_i was then derived with basic trigonometric calculations.

In order to rotate the LiDAR to the body frame, hence aligning it with the IMU's coordinate frame, and consider the orientation of the body frame in terms of roll, pitch and yaw relative to the NED frame, the following procedure was conducted:

$$P_{cartrot,i} = P_{cart,i} \times R_{yaw}(180°) \times R_{roll}(90°) \times R_{yaw}(\psi_i) \times R_{pitch}(\chi_i) \times R_{roll}(\omega_i) \tag{3}$$

where $P_{cartrot,i}$ corresponds to the cartesian LiDAR point coordinates after rotations, and χ_i, ω_i and ψ_i designate the interpolated pitch and roll angles as recorded by the IMU, as well as the heading derived from GNSS coordinates, respectively. The rotation matrices $R_{yaw(\psi)}$, $R_{pitch(\chi)}$ and $R_{roll(\omega)}$ were defined as follows:

$$R_{yaw}(\psi) = \begin{pmatrix} \cos(\psi) & \sin(\psi) & 0 \\ -\sin(\psi) & \cos(\psi) & 0 \\ 0 & 0 & 1 \end{pmatrix} \tag{4}$$

$$R_{pitch}(\chi) = \begin{pmatrix} \cos(\chi) & 0 & -\sin(\chi) \\ 0 & 1 & 0 \\ \sin(\chi) & 0 & \cos(\chi) \end{pmatrix} \tag{5}$$

$$R_{roll}(\omega) = \begin{pmatrix} 1 & 0 & 0 \\ 0 & \cos(\omega) & \sin(\omega) \\ 0 & -\sin(\omega) & \cos(\omega) \end{pmatrix} \tag{6}$$

In order to eventually transform the $P_{cartrot,i}$ to NED coordinates, they were added to the individual NED coordinates of the GNSS antenna $P_{ned,i}$ ($x_{ned,i}$, $y_{ned,i}$, $z_{ned,i}$) and the spatial offsets x_{off} and z_{off} between GNSS antenna and LiDAR as indicated in Figure 1c were compensated. Both was done by applying the following formula:

$$P_{pc,i} = P_{cartrot,i} \times T_x(x_{off}) \times T_z(z_{off}) \times T_x(x_{ned,i}) \times T_y(y_{ned,i}) \times T_z(z_{ned,i}) \tag{7}$$

where $P_{pc,i}$ are the final points of the georeferenced point cloud in NED coordinates and the translation matrices $T_x(x)$, $T_y(y)$ and $T_z(z)$ are defined as:

$$T_x(x) = \begin{pmatrix} 1 & 0 & 0 & x \\ 0 & 1 & 0 & 0 \\ 0 & 0 & 1 & 0 \\ 0 & 0 & 0 & 1 \end{pmatrix} \tag{8}$$

$$T_y(y) = \begin{pmatrix} 1 & 0 & 0 & 0 \\ 0 & 1 & 0 & y \\ 0 & 0 & 1 & 0 \\ 0 & 0 & 0 & 1 \end{pmatrix} \tag{9}$$

$$T_z(z) = \begin{pmatrix} 1 & 0 & 0 & 0 \\ 0 & 1 & 0 & 0 \\ 0 & 0 & 1 & z \\ 0 & 0 & 0 & 1 \end{pmatrix} \quad (10)$$

The point cloud data were differentiated into left and right canopy for each measured row. As a first step for the pile identification, for each canopy row, the lower part between ground and first wire was selected. For this, the initial cartesian point coordinates of every streamed package, which contained data from one full rotation of the LiDAR, were filtered for this lower area of the canopy. This was done by assuming the centreline of the canopy 1 m left and right of the LiDAR and considering the lowest detections above ground. By doing so, virtual tube with a height of 0.55 m above ground and a width of 0.4 m in the canopy's centreline was generated, where there were then mainly grapevine trunks and lower parts of the piles. By looking up the corresponding georeferenced points $P_{pc,i}$ in this area, the lower part of each canopy was selected under consideration of the topographical course of each examined row.

In order to discriminate the pile and trunk sections within this lower canopy area as individual objects, a novel clustering method was developed because preliminary examinations with existing techniques like k-means and DBSCAN had not resulted in a satisfactory performance. The lower canopy area was virtually sliced into segments of 0.01 m length all along the direction of travel. The points inside these segments were counted and any segment with a point density below a set threshold was discarded. Due to a lower point density, this threshold was set to 100 points for the first and last 1.5 m of each canopy. For the rest, the threshold was set at 130 points per segment. Since most materials have a specific reflectivity, this was used as a criterion to further differentiate between the wooden trunks and metal piles. Manual histogram analyses have revealed that metal piles had mostly low reflectivity values. Eventually, all segments containing less than 200 points with a reflectivity below 18 were discarded. As final step to cluster the pile segments, the maximum distance between two segments was calculated and all segments with a maximum distance of 0.7 m were combined. Clusters that contained less than three segments were dropped.

In order to reconstruct the entire piles from their segmented lower parts between ground and first wire, a trendline was constructed through each pile segment by calculating its first eigenvector via Principal Component Analysis, which corresponds to the general orientation of the cluster. After the trendline was constructed, all points $P_{pc,i}$ of the initial georeferenced point cloud within a radius of 0.02 m around the trendline were added to the pile segment. This search radius had been determined manually in an iterative process, where the resulting height of the reconstructed pile was compared to the manually measured height and eventually a radius with a low discrepancy in terms of the root mean squared error (RMSE) was chosen. Its calculation followed the following formula:

$$RMSE = \sqrt{\frac{\sum_{i=1}^{n}(e_i - p_i)^2}{n}} \quad (111)$$

where e_i and p_i are the estimated and measured value, respectively, an n corresponds to the total number of considered observations. Beyond that, a diameter of 0.04 m matches well with the diameter of a real metal pile. After that, every selected structure with less than 1000 points was discarded to remove any other remaining structures such as e.g. grape stems that fell off the grid of this analysis step.

1.1. Pile detection algorithm validation

The ground truth data for the validation of the absolute positioning of the piles were taken at the centre of the piles' upper and lower end. Therefore, the highest and lowest point of each segmented pile point cloud were projected onto the trendline and chosen as the points to be validated. As neighbouring rows share a common canopy, the predicted piles of row 1 and 3, and row 2 and 4, respectively, were combined for evaluation. Upper and lower points were assessed separately. For each point the differences between predictions and ground truth values were calculated in terms of easting, northing, height and the x-y plane defined by easting and northing. To evaluate the average deviation, the RMSE was calculated following equation (11). For evaluating the absolute accuracy of the estimated (e_i) and measured values (p_i), the mean absolute error (MAE) and mean bias error (MBE) were calculated as follows:

$$MAE = \frac{1}{n}\sum_{i=1}^{n}\sqrt{(e_i - p_i)^2} \quad (12)$$

$$MBE = \frac{1}{n}\sum_{i=1}^{n}(e_i - p_i) \quad (23)$$

To assess the distribution of absolute differences d_i, they were used together with their mean value d_{mean} in

order to calculate the standard deviation σ as follows:

$$\sigma = \sqrt{\frac{\sum_{i=1}^{n}(d_i - d_{mean})^2}{n-1}} \quad (34)$$

Finally, the distance RMSE (dRMSE) was calculated to evaluate the combined relative accuracy in the x-y plane of distances between measured and predicted point ($d_{pe,i}$), where $x_{p,i}$ and $x_{e,i}$ correspond to the predicted and measured easing values, and $y_{p,i}$ and $y_{e,i}$ correspond to the predicted and measured northing values:

$$d_{pe,i} = \sqrt{\left(x_{p,i} - x_{e,i}\right)^2 + \left(y_{p,i} - y_{e,i}\right)^2} \quad (45)$$

$$dRMSE = \sqrt{\frac{\sum_{i=1}^{n}\left(d_{pe,i}\right)^2}{n}} \quad (56)$$

2. Results and Discussion

The results of the main steps during the development of the pile detection algorithm are presented in visually in Figure 4 for an exemplary section of the examined row 1. The aggregated, georeferenced point cloud is illustrated in Figure 4a, where the grapevine canopies and the different structures within are clearly differentiated. Figure 4b shows the same row, filtered for the lower canopy parts from the ground to the first supporting wire. The clustering has resulted in a removal of ground, wires and thin canes in the upper part of the canopy, whereas single grapevine trunks and sections of metal piles are clearly distinguishable. Beyond that, it is striking that trunk and pile sections clearly differ in their reflectivity values. Figure 4c shows the remaining metal piles, after any trunk parts within the point cloud had been removed and the piles had been fully reconstructed with the aid of the generated trendline. These results already allow a qualitative assessment of the developed algorithm's functionality.

The quantitative analysis of the developed algorithms validity has revealed in a first step that for both, the identification dataset with row 1&3, as well as the validation dataset with row 2&4, a 100% true-true detection of real piles was achieved. So, no real pile was missed and no pile was recognized mistakenly. This indicates already that the developed LiDAR-based method is capable of detecting metal piles in a vineyard row and to differentiate these piles from other structures such as grapevines. Concerning the accuracy of the detections, the upper and lower end points of the piles were of interest. The spatial discrepancy between the ground-truth positions and the ones estimated by the pile detection algorithm was examined by means of various statistical parameters and the numerical results are presented in Table 1, where the MAE is a measure for the mean absolute deviation, the MBE indicates the average bias, the standard deviation σ allows an assessment of the variance within the deviations and the dRMSE indicates the 2-dimensional relative accuracy.

Table 1. Numerical results of the pile detection algorithm's validation.

		MAE	MAB	σ	dRMSE
northing	row 1&3 lower	0.028	0.002	0.040	
	row 1&3 upper	0.048	-0.038	0.052	
easting	row 1&3 lower	0.023	-0.016	0.029	
	row 1&3 upper	0.037	0.030	0.076	
height	row 1&3 lower	0.163	0.159	0.172	
	row 1&3 upper	0.215	0.214	0.263	
x-y plane	row 1&3 lower				0.049
	row 1&3 upper				0.078
northing	row 2&4 lower	0.028	0.016	0.035	
	row 2&4 upper	0.035	0.024	0.036	
easting	row 2&4 lower	0.019	0.002	0.027	
	row 2&4 upper	0.029	-0.025	0.055	
height	row 2&4 lower	0.019	0.002	0.027	
	row 2&4 upper	0.029	-0.025	0.055	
x-y plane	row 2&4 lower				0.045
	row 2&4 upper				0.060

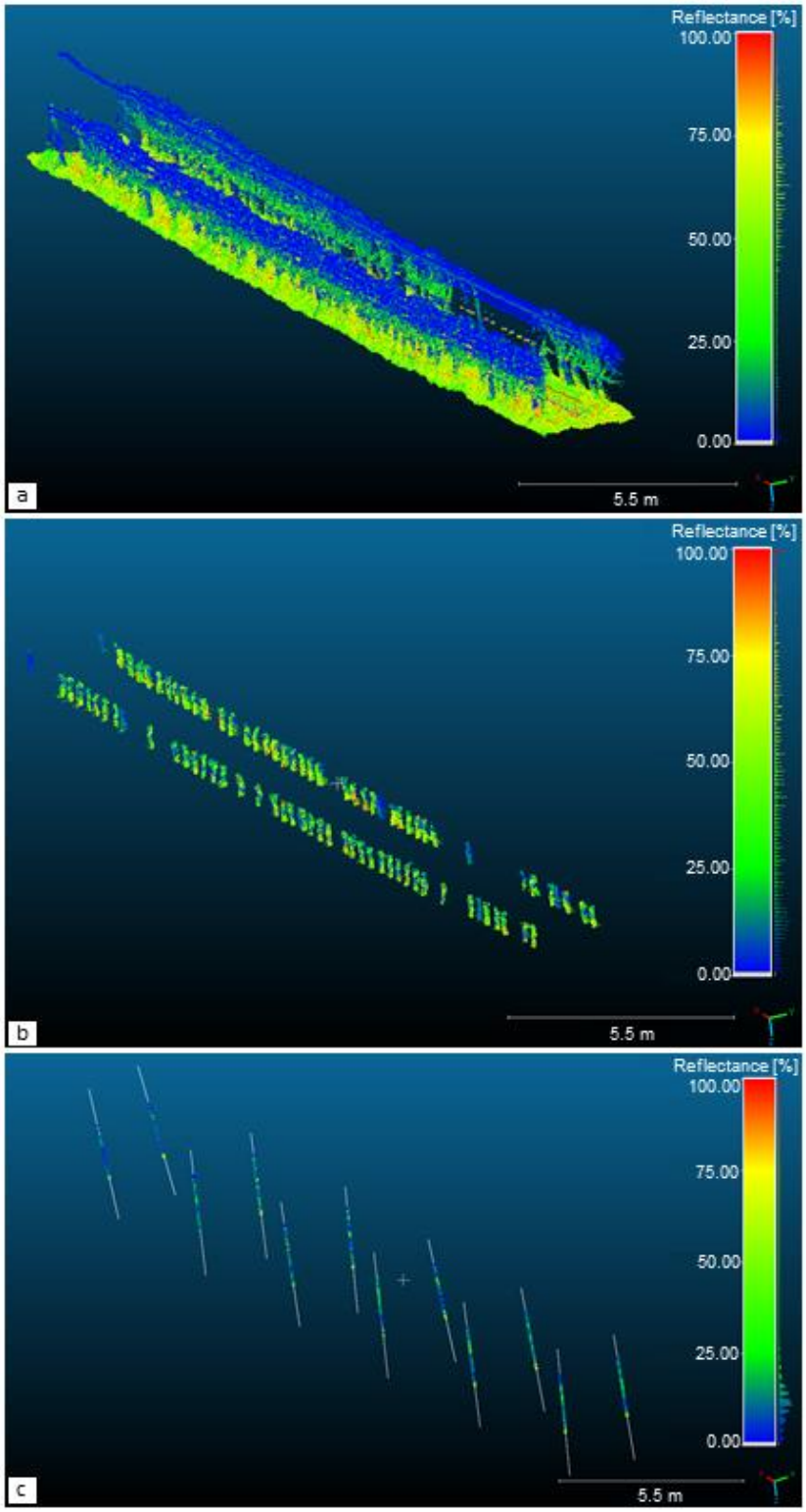

Figure 4. Point cloud of a section of row 1 (a), segmented lower part (b) and reconstructed piles (c).

Concerning northing and easting, as well as the x-y plane, all statistical parameters were in a comparable range for the identification, as well as the validation dataset. Further, the results for the lower points were slightly better, which can be explained by the fact that the trendline for the pile reconstruction was based on their lower section until the first wire. In general, with the statistical parameters ranging largely below 5 cm,

a high relative and absolute accuracy was achieved, which can be considered sufficient for the pre-pruning process. For the latter's control, even larger safety distances for pile avoidance would presumably be necessary to compensate technical latencies within the machine.

When it comes about the assessment of the accuracy in terms of the height, it is noticeable that there are significant discrepancies in the accuracy between the identification dataset row 1&3 and the validation dataset row 2&4, respectively. While, for row 2&4 they have values that are comparable to the ones for northing, easting and the x-y plane, the σ values for the height in row 1&3 indicate a high variation in the height differences and a low relative accuracy. Also, the values for the absolute accuracy, i.e. MAE and MAB were in similar ranges. The most obvious reason for the lower accuracy in row 1&3 are two extra end piles at the beginning of row 1. Because of the attached anchor wires in the lower part of the outer piles, the selected clusters were slightly distorted, which lead to tilts in the trendline affecting the position of the higher and the lower end point. Nevertheless, again, the accuracy can be regarded as sufficient because for pre-pruning, mainly the accuracy in the x-y plane is of interest, when it comes about the avoidance of piles.

3. Conclusion

With the developed methodology, a fusion of LiDAR data with data from inertial and GNSS sensor was successfully performed to achieve a valid 3D reconstruction of vineyard rows. With the aid of a newly developed pile detection algorithm including a novel clustering approach, metal piles were reliably detected and successfully reconstructed. The relative accuracy in the prediction of the upper and lower pile ends can be considered high because the calculated RMS values were in the range of approx. 5 cm for the x-y plane in terms of northing and easting. This was also confirmed by the MAE and MBE values, which were below 5 cm for this dimension, hence implying a high absolute accuracy and sufficiency for pre-pruning. The entire approach was validated by examining different datasets for identification and validation of the algorithm. The results show also a high potential not only for detection of piles but also trunk inventory.
Further research needs to be done to test the method for piles of different materials such as wood, plastic, or concrete due to their presumably differing reflectivity values. Beyond that, the methodology should be developed further to real-time capability to make its application for pre-pruning more realistic.

Acknowledgements

The project is supported by funds of the German Board of Trustees for Technology and Construction in Agriculture (KTBL e.V.).

References

Arnó, J., Del Moral, I., Escolà, A., Company, J., Masip, J., Sanz, R., Rosell, J.R., Martínez-Casasnovas, J.A., 2012. Mapping the Leaf Area Index in vineyards using a ground-based LiDAR scanner. In *11th International Conference on Precision Agriculture*. Indianapolis, USA, July 15-18.

Fernandes, M., Scaldaferri, A., Guadagna, P., Fiameni, G., Teng, T., Gatti, M., Poni, S., Semini, C., Caldwell, D., Chen, F., 2021. Towards Precise Pruning Points Detection using Semantic-Instance-Aware Plant Models for Grapevine Winter Pruning Automation (preprint). https://doi.org/10.48550/arXiv.2109.07247

Paraforos, D.S., Griepentrog, H.W., Vougioukas, S.G., 2016. Methodology for designing accelerated structural durability tests on agricultural machinery. Biosyst. Eng. 149, 24–37. https://doi.org/10.1016/j.biosystemseng.2016.06.004

Siebers, M.H., Edwards, E.J., Jimenez-Berni, J.A., Thomas, M.R., Salim, M., Walker, R.R., 2018. Fast phenomics in vineyards: Development of grover, the grapevine rover, and LiDAR for assessing grapevine traits in the field. Sensors 18. https://doi.org/10.3390/s18092924

Silwal, A., Yandun, F., Nellithimaru, A., Bates, T., Kantor, G., 2022. Bumblebee: A Path Towards Fully Autonomous Robotic Vine Pruning. F. Robot. 2, 1661–1696. https://doi.org/10.55417/fr.2022051

Tsoulias, N., Paraforos, D.S., Xanthopoulos, G., Zude-Sasse, M., 2020. Apple shape detection based on geometric and radiometric features using a LiDAR laser scanner. Remote Sens. 12. https://doi.org/10.3390/RS12152481

Study of physicochemical changes in loquat fruit during cold storage using non-destructive spectroscopy

M. Lopez-Chulia [a], S. Castillo-Girones [a], P. Talens [b], J. Blasco [a]*

[a] Centro de Agroingeniería, Instituto Valenciano de Investigaciones Agrarias (IVIA), Valencia, Spain

[b] Instituto Universitario de Ingeniería de Alimentos – FoodUPV, Universitat Politècnica de València (UPV), Valencia, Spain

* Corresponding author. Email: blasco_josiva@gva.es

Abstract

Non-destructive monitoring of physicochemical changes in fruits during cold storage is one of the most significant challenges in postharvest technology. Spectral sensors are a promising technology that can enhance and automate the monitoring operations. This study assessed the potential of Vis/NIR spectroscopy for monitoring physicochemical changes in loquats during cold storage. A total of 1080 loquats from two cultivars (‘Algerie’ and ‘Xirlero’) were harvested at commercial maturity. Initial characterisation of 120 fruits (60 per cultivar) was conducted upon arrival at the laboratory. The remaining fruit was equally stored at 1 °C and 3 °C. Each week for four weeks, 60 fruits of each cultivar were taken from the cold chamber. 30 fruits were immediately analysed, and the remaining 30 were analysed after five days at 20 °C, simulating commercial conditions. The analyses consisted of the non-destructive measurement reflectance spectra of each fruit, acquired by a multi-channel spectrometer covering the visible and near-infrared range (450-1700 nm). Destructive analyses were later performed to obtain soluble solid content (SSC) and titratable acidity (TA) used as reference values. Predictive models were developed using partial least squares (PLSR) to set correlations between the measured spectra and the reference values. Spectral pre-processing was performed using standard normal variate (SNV) and first derivative (1D). Storage at 1 °C resulted in lower acidity loss compared to storage at 3 °C in ‘Algerie’. For ‘Xirlero’ no differences were observed under cold storage, but after 5 days at 20 °C, more acidity loss was observed in the fruit stored at 3 °C. These results show the importance of monitoring changes during the evolution of loquats under cold and commercialisation storage conditions. Preliminary results for predictive models showed correlations between NIR spectra for both cultivars in predicting SSC and TA. This work points out the potential of this technology as a tool for monitoring the postharvest quality of the loquat during storage, offering a non-destructive alternative to conventional analyses.

Keywords: Chemometrics, Near-infrared (NIR) spectroscopy, Postharvest, Storage temperatures

1. Introduction

Non-destructive monitoring of physicochemical changes in fruits during cold storage is a major challenge in postharvest technology. Loquat fruit (*Eriobotrya japonica* Lindl.), is highly susceptible to mechanical damage during harvesting and handling, leading to browning spots on the surface and in the pulp (Lin et al., 1999). This research focuses particularly 'Algerie' and 'Xirlero' varieties, which present specific storage challenges. 'Algerie' is known for its high sugar content and balanced acidity, while 'Xirlero' is valued for its firm texture and storage stability (Gil et al., 2018). Precise monitoring is essential to optimize postharvest conditions and preserve the quality of loquat, as improper storage can lead to significant losses in weight, acidity, and sugar content (Munera et al., 2021). Visible and Near-infrared (Vis-NIR) spectroscopy has emerged as a promising non-destructive tool to enhance and automate internal quality in fruit (Walsh et al., 2020). This technology has been successfully used in predicting quality parameters like soluble solids content and firmness, offers detailed chemical composition insights non-destructively (Arana et al., 2005; Morales et al., 2013; Shimizu et al., 2011). This study aims to explore the application of Vis/NIR spectroscopy in monitoring physicochemical changes in loquats during postharvest handling.

2. Materials and Methods

2.1. Plant material and experimental design

Loquat fruit cultivars 'Algerie' and 'Xirlero' at commercial maturity stage were selected, as they are two commonly cultivated varieties in the Mediterranean region. A total of 1080 loquats (540 samples per cultivar) were analysed. Fruits 120 fruits (60 per cultivar) were initially characterised upon arrival at the laboratory.

The remaining fruit was split and equally stored at 1 °C and 3 °C. Weekly evaluations were conducted for four weeks, with 60 fruits of each cultivar taken from cold storage each week. 30 fruits were analysed immediately, while the other 30 were evaluated after 5 days at 20 °C to simulate commercial conditions. Fruit was individually numbered, and spectra collection and reference analysis were performed on the same day.

2.2. Spectral data acquisition

The spectral data was collected in reflectance mode using a UV-Vis spectrometer (AvaSpec-ULS2048L-USB2 StarLine) and a multi-channel platform (AVS-DESKTOP-USB2, Avantes BV, The Netherlands) equipped with a VNIR spectrometer (AvaSpec-ULS2048 StarLine, Avantes BV, The Netherlands) and a NIR spectrometer (AvaSpec-NIR256-1.7 NIRLine, Avantes BV, The Netherlands). The UV-Vis spectrometer covered a range of 200-750 nm with a 0.7 nm resolution, the VNIR covered 600-1100 nm with a 1.2 nm resolution, and the NIR covered 900-1750 nm with a 12 nm resolution. Lighting was provided by a stabilized 10 W tungsten halogen light source (AvaLight-HAL-S, Avantes BV, The Netherlands).

A reflectance fiber-optic probe with a 45º angle tip minimized specular reflectance and bifurcated optical fibers carry the signal to each detector. Calibration involved dark and white reference spectra using a 99 % reflective reference tile. Measurements were acquired at four equatorial locations on each loquat, and mean spectra were used for analysis. The mean reflectance of each sample was converted to relative reflectance using dark and white references.

2.3. Reference parameters

Standard destructive quality measurements were conducted after the acquisition of spectral data to determine quality properties for use as reference values. Juice was manually extracted from each sample with a cloth to estimate the Soluble Solid Content (SSC) and titratable acidity (TA). SSC were determined with a digital refractometer (Atago PR1, Tokyo, Japan) and results were expressed as ºBrix. TA was determined by titration with sodium hydroxide 0,1 M with an automatic titrator (model T50, Mettler-Toledo, Switzerland) to equivalent point and was expressed as equivalent of malic acid/100 mL of juice (% malic acid).

2.4. Data processing and analysis

2.4.1. Spectral pre-processing

The spectral pre-processing was performed using Python (Rossum & Drake, 2009). Three separate spectral windows identified as VIS (450-750 nm), VNIR (600-960 nm) and NIR (980-1695 nm), were analysed. Techniques used were Standard Normal Variate (SNV) transformation for correcting multiplicative scatter and particle size interferences (Barnes et al., 1989) and the first derivative (1D) of the spectral data was computed using the Savitzky-Golay filter, which smooths the data and reduces noise while retaining important spectral features (Savitzky & Golay, 1964). Python libraries used for these preprocessing steps included NumPy for numerical operations, pandas for data manipulation, SciPy for applying the Savitzky-Golay filter, and scikit-learn for additional preprocessing functions.

2.4.2. Chemometric data treatment

Chemometric data treatment involved conducting a one-way analysis of variance (ANOVA) and developing regression models to analyse the physicochemical properties of the loquats. Python was used for this purpose. A one-way ANOVA was performed to determine significant differences in the physicochemical properties among the different storage conditions. For predictive modelling, Partial Least Squares Regression (PLSR) models were developed for each analysed compound and variety. Each dataset was divided into training and cross-validation (80 %) and external validation (20 %). Python libraries such as NumPy, pandas, SciPy, and scikit-learn were employed to perform these analyses. The performance of the PLSR models was assessed using the Root Mean Square Error (RMSE), the Residual Predictive Deviation (RPD), and the coefficient of determination (R^2). RMSE indicates the average prediction error, RPD evaluates the predictive quality relative to the standard deviation of the reference data while R^2 measures the proportion of variance explained by the model.

3. Results and Discussion

3.1. Evolution of TA and SSC during storage

The study investigated the effects of storage temperatures (1 °C and 3 °C) on the changes in SSC and TA in loquat fruits harvested at commercial maturity. Fruits were cold stored for up to four weeks and after each week, they were analysed after cold storage and commercial conditions. Figure 1 illustrates the evolution of TA in both conditions at both temperatures for each variety.

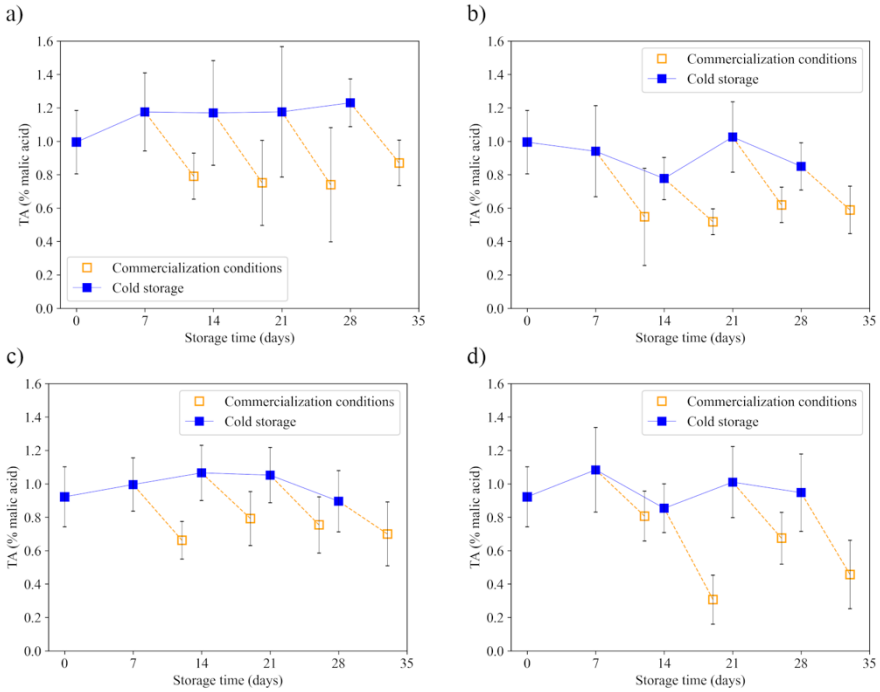

Figure 1. Evolution of TA during cold storage (close box) and after commercialization simulation (open box). a) Algerie at 1 ºC; b) Algerie at 3 ºC; c) Xirlero at 1 ºC; d) Xirlero at 3 ºC.

A significant decrease in fruit acidity was observed, particularly during the commercialization simulation, for both cultivars and at the two studied temperatures. Fruit stored at 1 ºC exhibited less acidity loss (Figure 1a and 1c) compared to those stored at 3 °C (Figure 1b and 1d). Storage at 1 ºC keep fruit acidity better that 3 ºC for this period. Commercialization conditions produced a more marked reduction in TA, decreasing in some cases from 0.8 % to 0.3 % of malic acid content. Moreover, difference between varieties were found after 1 month of cold storage and 5 days at 20 ºC. 'Xirlero', after 28 days in cold storage and 5 days at commercial conditions, showed a higher loss of acidity at both temperatures (0.7 and 0.5 %) than 'Algerie' (0.9 and 0.6 %), with a greater loss when it was stored at 3 ºC. As Besada et al. (2013) reported, acidity is an important parameter of loquat sensorial quality, due to that the right ratio between sweetness and acidity is greatly appreciated by loquat consumers. Special care is needed during long-term storage, as decreased acidity affects general perception of loquat fruit (González et al. 2003).

Results of SSC during storage can be seen in Figure 2. In contrast with acidity, SSC did not suffer significant changes under both temperatures of cold storage and shelf-life condition. SSC ranged between 10 and 12 ºBrix during the four weeks of storage. González et al. (2003) obtained the same results when studying 'Algerie' cold storage and shelf-life conditions for 10 weeks.

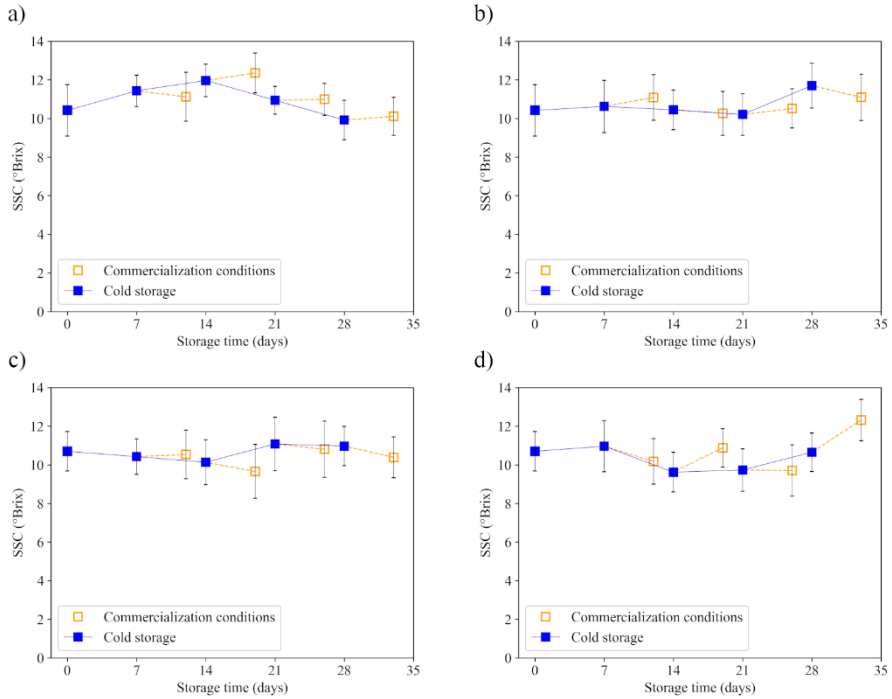

Figure 2. Evolution of SSC during cold storage (close box) and after commercialization simulation (open box). a) Algerie at 1 ºC; b) Algerie at 3 ºC; c) Xirlero at 1 ºC; d) Xirlero at 3 ºC.

3.2. Reference values and spectra

Destructive analyses obtained a mean SSC of 10.9 ± 1.3 ºBrix and TA of 1.0 ± 0.3 % of malic acid for 'Algerie' and a mean SSC of 10.9 ± 1.2 ºBrix and TA of 0.7 ± 0.3 % of malic acid for 'Xirlero'. The statistical values of the SSC and TA in the datasets for both varieties are shown in Table 1.

Table 1. Statistical values of SSC (ºBrix) and TA (% malic acid) of the studied loquats per cultivar.

Dataset	SCC (ºBrix)				TA (% malic acid)			
	Min	Max	Mean	STD	Min	Max	Mean	STD
'Algerie'	8.0	14.8	10.9	1.3	0.3	2.0	1.0	0.3
'Xirlero'	7.9	14.3	10.9	1.2	0.1	1.3	0.7	0.3

Preprocessing steps were performed: SNV and SNV with first derivative (SNV+1D). In addition, raw data was also analysed (Figure 3). The optimal number of factors for the PLSR models was determined using a criterion used by Davey et al. (2009), selecting the minimum number of factors corresponding to the first lowest value of the RMSE.

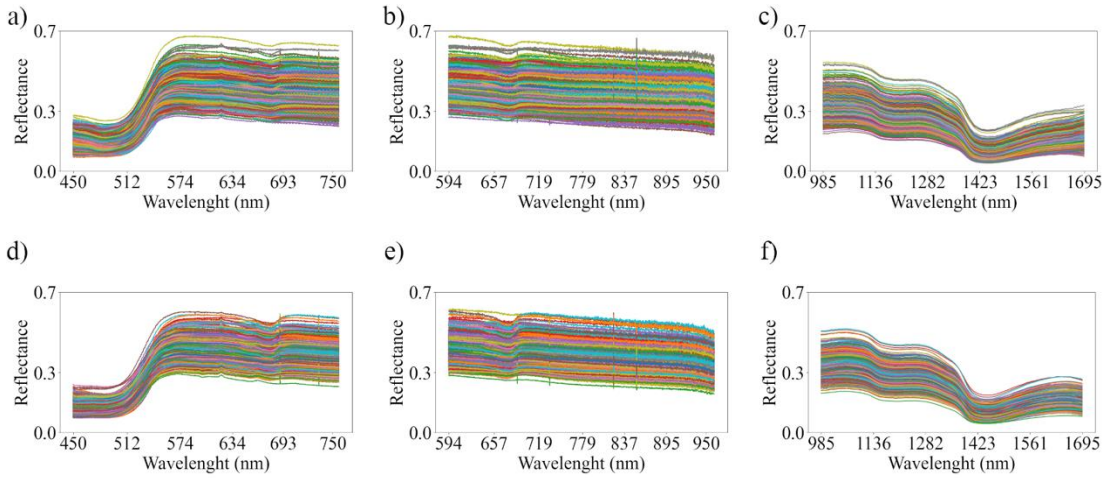

Figure 3. Raw reflectance spectra of loquat fruit dataset of both varieties.
a) 'Algerie' for the Vis region; b) 'Algerie' for the VNIR region; c) 'Algerie' for the NIR region;
d) 'Xirlero' for the Vis region; e) 'Xirlero' for the VNIR region; f) 'Xirlero' for the NIR region

3.3. SSC predictions

Figure 4 presents the results for the calibration and prediction models for SSC.

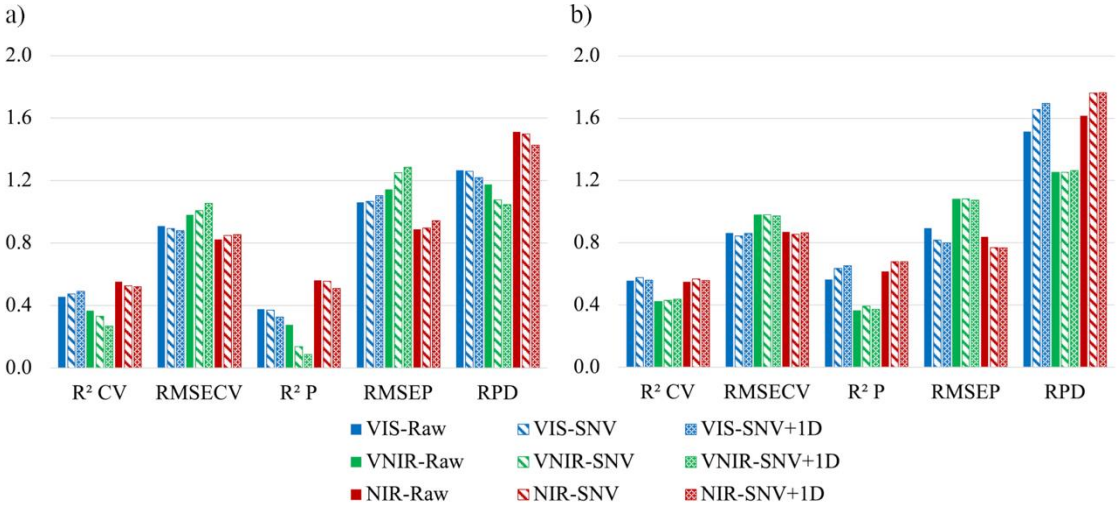

Figure 4. Results of the PLSR for the prediction of SSC (ºBrix) for a) 'Algerie' and b) 'Xirlero'.

The models showed noticeable differences for the different spectral regions. Specifically, models constructed with the visible (450-750 nm) and VNIR (590-960 nm) ranges exhibited inferior results. This trend was particularly evident for 'Algerie' (Figure 4a), where lower R^2, higher RMSE, and lower RPD values were observed in these regions. In case of 'Xirlero' (Figure 4b), models developed with the Vis and NIR regions yielded similar results, with RPD values of 1.7 and 1.8, respectively, when using SNV+1D pretreatments.

Regarding RMSE for the cross-validation (RMSECV) and prediction (RMSEP), Fu et al. (2009) obtained similar, or even higher, values in their study of four Chinese varieties of loquat fruit with FT-NIR. By creating models with the full wavelength range (800-2500 nm), RMSE values obtained vary between 0.9 and 1.2 for both cross-validation and prediction. In this study, working with NIR range (980-1695 nm) resulted in lower values, 0.9 for 'Algerie' and 0.8 for 'Xirlero'.

Magwaza et al. (2014) observed comparable results when predicting sugar content in mandarins,

obtaining higher regression coefficients using the NIR range. This was attributed to the fact that NIR region corresponds to the second overtone of the H-O-H stretching overtone of water (980 nm), the second overtone of C–H and C–H_2 stretching related to sugar molecules (1200 nm), as well as the first overtone of O-H stretching (1450 nm) vibrations of water hydrogen bonds with sugar molecules (Kawano et al., 1993). For all cases studied, better results were obtained for 'Xirlero' compared to 'Algerie'. For 'Algerie', the models built using the raw data resulted in a better RPD of 1.5. However, for 'Xirlero', using spectra pretreated with SNV+1D, an RPD = 1.8 was achieved.

3.4. Acidity predictions

Figure 5 presents the results for the calibration and prediction models for TA. In this case, no differences were found between models developed for the different spectral regions. In the case of 'Algerie' (Figure 5a) similar results for all regions were achieves without differences between pretreatments. Best performance was obtained for the spectra from the visible region with SNV pretreatment, achieving an RMSEP of 1.2 and an RPD of 1.4. For 'Xirlero' (Figure 5b), best model was obtained using raw spectra from the visible region (RMSEP = 0.2 and RPD = 1.9). Comparing models developed for SSC (Figure 4) and for TA (Figure 5), for both cultivars, R^2 and RMSECV and RMSEP where higher and lower respectively for prediction of TA. Meanwhile, RPD was similar for both cultivars. The opposite case was observed by Fu et al. (2009) in their study with four Chinese loquat varieties to predict TA, where the results for acidity prediction were worse than those for SSC.

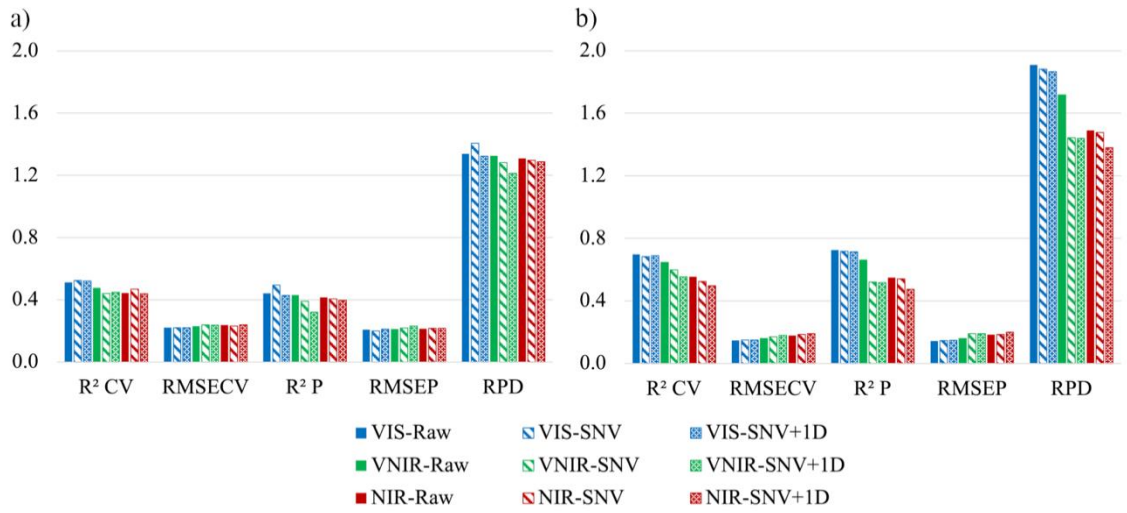

Figure 5. Results of the PLSR for the prediction of TA (% malic acid) for a) 'Algerie' and b) 'Xirlero'.

A model is considered commonly poor-performing when the RPD is below 1.5, whereas an RPD ranging from 1.5 to 2 indicates moderate performance. An RPD between 2 and 2.5 suggests good performance, while an RPD exceeding 2.5 indicates excellent performance (Askari et al., 2015). Using this categorization, best models developed in this study indicate moderate performance. Fan et al. (2020) reported similar predictions when evaluating SSC of apples using a portable Vis/NIR device. In their work, they highlighted that the high variability in the physical and chemical properties of fruits affected the optical properties and their interaction with light, thus lowering the performance of prediction models.

Figure 6 shows measured versus predicted data for the best PLSR models obtained for 'Xirlero' variety for both parameters as an example of data obtained.

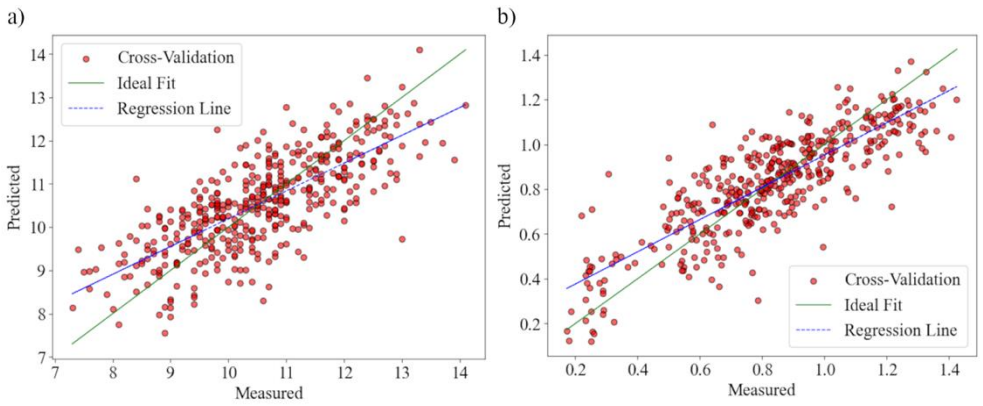

Figure 6. Best performance PLSR cross-validation results for a) SSC and b) TA for 'Xirlero'.

de Santana et al (2021) reported, in a comparative study of PLSR and SVM models for soil organic matter using vis-NIR spectral libraries, that PLSR usually offers the advantage of dealing with irrelevant and noisy variable issues. However, the predictive capacity of PLSR can be lower in situations where the number of samples is far smaller than the number of variables, as in the case of spectral data. Moreover, relationship between NIR spectra and targeted constituents to be modelled is not always linear. In this case, as can be seen in Figure 6, for SSC and TA there could be appreciated some tendence in data, but it cannot be described as linear. Low values of measured SSC were predicted as high. On the contrary, the high SSC values measured were predicted to be lower. The same applies to TA measurements and predictions. As Munawar et al (2022) pointed out in their study comparing regression approaches, the source of nonlinearity may vary widely, and is difficult to identify. This means that classical linear regression like PLSR methods cannot always be the most suitable option. The intrinsic non-linearity in NIR spectral data and chemical components cannot be corrected by using only spectral pre-treatments and require the use of specialised nonlinear adjustment approaches.

4. Conclusions

Based on the results achieved, the feasibility of employing Vis/NIR technology for postharvest quality control in loquats is evident, offering a non-destructive method ideally suited to loquat's characteristics and sensitivity to physical damage. Correlations between measured and predicted TA values were observed using NIR spectroscopy, particularly when employing PLSR models within the NIR range (980-1695 nm). Additionally, good correlations were noted between spectral information and SSC analysed using PLSR models. Spectral pre-treatments are promising in enhancing model parameters, depending on the desired range and parameter to be determined. Moving forward, further studies employing non-linear approaches are warranted to develop more robust models for predicting SSC and TA in loquats. These findings highlight the potential of NIR spectroscopy for rapid, non-destructive assessments of fruit quality, offering a practical tool for monitoring physicochemical changes in loquats during cold storage.

Acknowledgements

This work was partially funded by ERDF funds of the GVA 2021-2027 and projects GVA-IVIA 52204B and GVA-PROMETEO CIPROM/2021/014.

References

Arana, I., Jarén, C., Arazuri, S., & Diago, M. P., 2005. Principal Components-Artificial Neural Networks for predicting SSC and Firmness of Fruits based on Near Infrared Spectroscopy. Biosystems Engineering. 91 (2), 166-173. https://doi.org/10.1016/j.biosystemseng.2005.02.003.

Askari, M. S., Cui, J., O'Rourke, S. M., & Holden, N. M., 2015. Evaluation of soil structural quality using VIS–NIR spectra. Soil and Tillage Research. 146, 108-117. https://doi.org/10.1016/j.still.2014.09.009.

Barnes, R. J., Dhanoa, M. S., & Lister, S. J., 1989. Standard normal variate transformation and detrending of near-infrared diffuse reflectance spectra. Applied Spectroscopy. 43 (5), 772-777. https://doi.org/10.1366/0003702894202201.

Besada, C., Salvador, A., Sdiri, S., Gil, R., & Granell, A. (2013). A combination of physiological and chemometrics analyses reveals the main associations between quality and ripening traits and volatiles in two

loquat cultivars. Metabolomics, 9(2), 324-336. https://doi.org/10.1007/s11306-012-0447-z

de Santana, F. B., Otani, S. K., de Souza, A. M., & Poppi, R. J., 2021. Comparison of PLSR and SVM models for soil organic matter and particle size using vis-NIR spectral libraries. Geoderma Regional. 27, e00436. https://doi.org/10.1016/j.geodrs.2021.e00436.

Davey, M. W., Saeys, W., Hof, E., Ramon, H., Swennen, R. L., & Keulemans, J. (2009). Application of visible and near-infrared reflectance spectroscopy (Vis/NIRS) to determine carotenoid contents in banana (Musa spp.) fruit pulp. Journal of agricultural and food chemistry, 57(5), 1742-1751. https://doi.org/10.1021/jf803137d

Fan, S., Wang, Q., Tian, X., Yang, G., Xia, Y., Li, J., & Huang, W., 2020. Non-destructive evaluation of soluble solids content of apples using a developed portable Vis/NIR device. Biosystems Engineering. 193, 138-148. https://doi.org/10.1016/j.biosystemseng.2020.02.008.

Fu, X. P., Li, J. P., Zhou, Y., Ying, Y. B., Xie, L. J., Niu, X. Y., ... & Yu, H. Y. (2009). Determination of soluble solid content and acidity of loquats based on FT-NIR spectroscopy. Journal of Zhejiang University Science B, 10(2), 120-125. 10.1631/jzus.B0820097

Gil, R., Salvador, A., Bermejo, A., Navarro, P., & Besada, C., 2018. Evolution of sugars and acids during the maturation of two mutations of 'Algerí' loquat. In F. Artés-Hernández et al. (Eds.), Acta Horticulturae. 1194, Proc. VIII International Postharvest Symposium: Enhancing Supply Chain and Consumer Benefits – Ethical and Technological Issues (pp. 895-902). ISHS. DOI: 10.17660/ActaHortic.2018.1194.137.

González, E. M., Grau, A., Miquel, B., Reig, C., & Iglesias, D. J., 2003. Maturation of loquat fruit (Eriobotrya japonica Lindl.) under Spanish growing conditions and its postharvest performance. Scientia Horticulturae. 98 (4), 239-246. https://doi.org/10.1016/S0304-4238(03)00010-0.

Kawano, S., Fujiwara, T., & Iwamoto, M., 1993. Nondestructive determination of sugar content in satsuma mandarin using near infrared (NIR) transmittance. Journal of the Japanese Society for Horticultural Science. 62 (2), 465-470. https://doi.org/10.2503/jjshs.62.465.

Lin, S., Sharpe, R.H., & Janick, J., 1999. Loquat: Botany and horticulture. Hort. Rev. 23, 233-276. https://doi.org/10.1002/9780470650851.ch8.

Magwaza, L. S., Landahl, S., Cronje, P. J., Nieuwoudt, H. H., Mouazen, A. M., Nicolaï, B. M., ... & Opara, U. L. (2014). The use of Vis/NIRS and chemometric analysis to predict fruit defects and postharvest behaviour of 'Nules Clementine' mandarin fruit. Food chemistry, 163, 267-274. https://doi.org/10.1016/j.foodchem.2014.04.085

Morales, R., Serra, N., Casals, M., & Rosselló, C., 2013. A combination of physiological and chemometrics analyses reveals the main associations between quality and ripening traits and volatiles in two loquat cultivars. Journal of Food Quality. 36 (3), 185-192. https://doi.org/10.1111/jfq.12028.

Munawar, A. A., Meilina, H., & Pawelzik, E., 2022. Near infrared spectroscopy as a fast and non-destructive technique for total acidity prediction of intact mango: Comparison among regression approaches. Computers and Electronics in Agriculture. 193, 106657.https://doi.org/10.1016/j.compag.2021.106657.

Munera, M., Gómez-Sanchis, J., Aleixos, N., Vila-Francés, J., Colelli, G., Cubero, S., Soler, E., Blasco, J., 2021. Discrimination of common defects in loquat fruit cv. 'Algerie' using hyperspectral imaging and machine learning techniques. Postharvest Biology and Technology, 171, 111356. https://doi.org/j.postharvbio.2020.111356.

Rossum, G.V. & Drake, F.L. (2009) Python 3: Reference manual. United States: SohoBooks.

Savitzky, A., & Golay, M. J. E., 1964. Smoothing and differentiation of data by simplified least squares procedures. Analytical Chemistry. 36 (8), 1627-1639. https://doi.org/10.1021/ac60214a047.

Shimizu, Y., Nagasaka, S., & Ueda, T., 2011. Postharvest physiology and technology of loquat (*Eriobotrya japonica* Lindl.) fruit. Acta Horticulturae. 887, 337-344. https://doi.org/10.17660/ActaHortic.2011.887.45.

Rossum, G.V. & Drake, F.L. (2009) *Python 3: Reference manual*. United States: SohoBooks.

Walsh, K., Blasco, J., Zude-Sasse, M., & Sun, X., 2020. Visible-NIR 'point' spectroscopy in postharvest fruit and vegetable assessment. Postharvest Biology and Technology, 168, 111246. https://doi.org/10.1016/j.postharvbio.2020.111246.

Workspace partitioning and speed selection to improve harvesting speeds of multi-armed robotic harvesters

Natalie Pueyo Svoboda, Stavros Vougioukas *

Department of Biological Systems Engineering, University of California Davis, Davis, USA

* Corresponding author. Email: svougioukas@ucdavis.edu

Abstract

Orchard growers are moving towards mechanization due to ongoing labor shortages, leading to a resurgence of research into mechanized fruit harvesting. Our research focuses on increasing fruit picking throughput (FPT, the average number of fruits picked per unit of time) using harvesters with many linear arms while achieving a high fruit picking efficiency (FPE, the percent of harvestable fruits harvested). This paper studied two strategies to improve the combined FPT and FPE of multi-arm harvesters, which travel at a constant speed as they harvest. The first strategy tested the effects of partitioning arms in rows of equal height versus rows containing the same number of fruits. The second strategy compared using fixed travel speeds versus computing a speed that maximizes FPT while achieving a minimum FPE. All schedules were computed using a First-Come-First-Served policy on 3.5 m segments of digitized, real fruit distributions. Both partitioning methods achieved a user-defined minimum required FPE of 95%; however, partitioning by fruit allowed the harvester to move faster, leading to higher FPT. As the number of arms increased, the difference in FPT between the partitioning methods increased; for the same number of arms, results were better when the arms were divided into more rows rather than more columns. For the second strategy, low fixed speeds resulted in high FPE but low FPT, whereas fast fixed speeds had the opposite effect. Choosing the best speed resulted in the best combined FPE and FPT. It led to high FPT, only lower than the two highest FPT values while keeping FPE at or above 95%. The insights gained in this paper provide two simple strategies that could be implemented on multi-armed harvesters to improve the combined FPE and FPT.

Keywords: apples, orchards, precision agriculture, multi-armed robots.

1. Introduction

Fresh fruit harvesting is a labour-intensive operation, and growers are challenged by increasing farm labour cost and shortages (Christiaensen et al., 2021). Harvesting robots are a promising technology that could significantly reduce the labour needed to harvest. Robot prototypes have been built over the years by academic groups and start-up companies with varying levels of success (Bac et al., 2014; Koostra et al., 2021). Cost-effective robots that can be commercialized must aim to maximize two major performance metrics (Harrell, 1987): Fruit Picking Efficiency (FPE) and Fruit Picking Throughput (FPT). The first, FPE, measures the percent of harvestable fruits the system harvests. The second metric, FPT, measures the harvest speed in fruits per second.

One way to increase FPT is to harvest with several robot arms coordinated in some fashion (Zion et al., 2014; Mann et al., 2016; Williams et al., 2019; Li et al., 2023). One challenge when considering multi-armed harvesters is selecting the machine's travel speed as it harvests and the arm-fruit assignments and pick schedules that maximize performance. Some researchers consider static harvesting, where the machine stands still, harvests the fruits in the segment of the row inside its workspace, and then proceeds to its next position. Since fruit distributions in tree canopies are typically non-uniform (Arikapudi et al., 2016), such an approach will typically result in some arms being idle (no fruits in their workspace) while other arms are still harvesting. Also, the time to move from one position to the next is non-productive, as the machine travels along the harvested segment; hence, FPT will be negatively impacted. The other approach is continuous harvesting, where the machine moves along the orchard row while it harvests (the arms compensate for this motion). This approach can result in increased FPT if the speed is selected properly (Edan et al., 1993). A high travel speed results in shorter time windows when fruits can be picked, hence lower FPE. A low speed allows enough time to pick but increases the time to finish the row, reducing the overall FPT. So, FPT and FPE are conflicting metrics when selecting the travel speed, which must be selected carefully. Furthermore, harvest scheduling depends on the travel speed because the available time window for each arm to pick a fruit depends on the speed.

This paper considers a multi-arm harvester design that consists of *C* rectangular frames (also referred to as work cells, cells, or columns) placed side-by-side, and *R* low-cost linear arms inside each column (Fig. 1). We study two strategies to improve the combined FPT and FPE of the multi-arm harvester, which travels at a constant speed as it harvests. The first strategy tests the effects of partitioning arms in rows of equal height versus rows containing the same number of fruits. The second strategy compares fixed travel speeds versus a speed that maximizes FPT while achieving a minimum FPE.

2. Materials and Methods

2.1. Harvest Modelling

The harvester design under study (Fig. 1) features arms that are are identical, with three linear axes that move independently based on trapezoidal velocity profiles. The vertical positioning of an arm inside a column is physically constrained only by the arm(s) above or below it or the frame. The flexibility in vertical motion is advantageous in the presence of non-uniform fruit distributions (Arikapudi & Vougioukas, 2023) because it results in potentially better load balancing (for example, arms in a cell can 'cluster' to harvest regions of the canopy with high fruit density). However, workspace sharing introduces the possibility of collisions and requires solving simultaneously the arm-fruit assignment and scheduling and the arm motion planning.

To simplify the problem, we restrict the arms across columns to move vertically within virtual rows. Each row is defined – in software - by the lower and upper *z* coordinates inside which the arms in all columns are allowed to move. This approach guarantees collision avoidance but may result in sub-optimal performance.

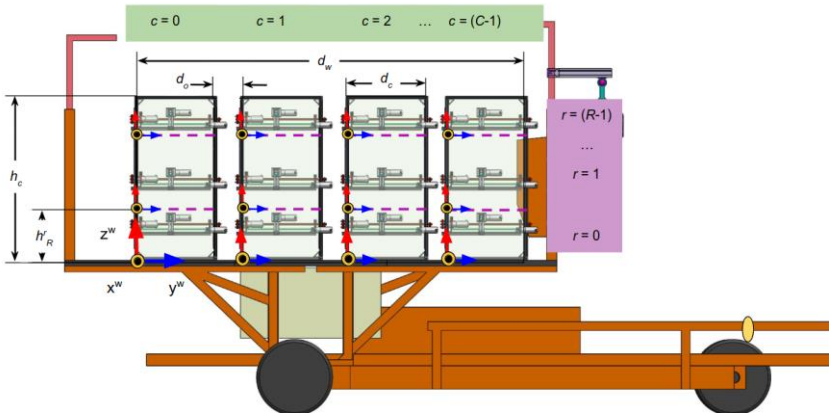

Figure 1. The CAD rendition of the robotic harvester comprises four work cells and three arms per cell. Each column has its frame of reference centered at its bottom left corner. The *x*-axis points to the tree canopies, the *y*-axis points along the orchard row in the direction of travel, and the *z*-axis points upwards.

We consider a scenario where the machine harvests fruits inside a segment of length *D* of the orchard row, moving at a constant travel speed, *V*. For scheduling purposes, all fruit locations inside the segment are assumed to be known (estimated via a computer vision system) and static. An arm starts at a retracted position (the gripper is away from the canopy) and takes the following steps to harvest a fruit:

• "approach": the arm moves inside the column frame ($Y-Z$ plane) from its current position to the target fruit location (T_{yz} seconds)

• "extension": the arm extends out from the $Y-Z$ plane to the target fruit location (T_x seconds)

• "detachment": the arm grasps and detaches the fruit (T_g seconds – assumed constant)

• "retraction": the arm retracts to the column frame, mirroring the extension step (T_x seconds).

After retracting, the arm does not need to travel to another location to deposit the fruit into a conveyance system. Hence, the single-arm pick cycle to harvest a fruit is

$$T_p = T_{yz} + 2T_x + T_g \qquad (1)$$

Next, a harvesting schedule must be generated for each arm. We assign a unique index, *i*, to each fruit in the segment. If fruit *i* is the *k*th fruit to be harvested by the arm in row *r* and column *c*, let $\sigma(k) = [i, t_i, c, r]$, where t_i is the time the arm must reach fruit *i*. The picking schedule for arm *r*, *c* that is assigned to harvest $F^{c,r}$ fruits is $\Sigma^{c,r} = \{\sigma(1), \sigma(2), \ldots, \sigma(F^{c,r})\}$. The set of the individual arm picking sequences $\Sigma^{c,r}$ is the multi-arm harvester picking sequence Σ.

First Come First Served (FCFS) is the scheduling algorithm that computes Σ. Fruits are sorted by their *y*-coordinate, and the time window available to reach each fruit is calculated based on the travel speed, *V*, the work cell geometries and configuration, pick cycle, T_p, and the locations and states ('idle' or 'busy') of the arms. An arm that is "idle," i.e., not already assigned to a fruit, is assigned to the first (closest) fruit within the arm's row and has not been harvested nor assigned to another arm in the same row. Once an arm is assigned to a fruit, it is set as "busy" until it has finished harvesting it and retracted. For scheduling purposes, we assume that every fruit assigned to an arm will be harvested.

For a given travel speed and a harvest schedule, the total number of harvested fruits is calculated as the sum of fruits harvested by each arm. This number is a function of the harvest schedule and the travel speed.

$$P(\Sigma, V) = \sum_{c=0}^{C-1} \sum_{r=0}^{R-1} P^{c,r} \qquad (2)$$

The FPE for *P* harvested fruits in a segment with *N* fruits is, by definition

$$FPE = P/N \qquad (3)$$

FPT is calculated by dividing the number of picked fruits by the overall travel time, *T*, to traverse the segment ($T = D/V$)

$$FPT = P/T \qquad (4)$$

The computed harvest schedule, Σ, depends on the travel speed, *V*, because the speed determines the time window available to pick each fruit. A high travel speed results in shorter time windows, fewer picked fruits (smaller *P*), and hence lower FPE. A low speed allows enough time to pick but increases the time to traverse the segment (larger *T*), reducing the overall FPT. Since FPT and FPE are conflicting metrics with respect to the travel speed, we define the "best" speed as the one that maximizes FPT but results in an FPE value higher than a grower/user-defined minimum acceptable threshold, which in our case is set to 95%. The best speed is computed using Exhaustive Speed Search (ESS), a grid-search algorithm that loops through discrete speed values in ascending order, calculates Σ and terminates when FPE drops below 95% (it stores the previous solution). This strategy works because as the harvester's speed increases, FPE is a monotonically non-increasing function, and FPT is a monotonically non-decreasing function (Fei & Vougioukas, 2024).

3. Experimental Design

Two sets of simulation experiments were performed using real, digitized fruit coordinates from a V-trellised Pink Lady apple orchard in Lodi, CA, USA (38.075018, -121.182455) on October 14, 2022. A total of 111 segments were used, each 3.5 m long. Each work cell was 1 m long and 3.5 m tall, with 0.15 m of space between cells. Each arm's linear DOF - the corresponding motor - was characterized by a maximum acceleration, velocity, and deceleration. For the *x*-axis, $v_{max} = 4$ m/s, and $a_{max} = 2$ m/s^2, for the *y*-axis $v_{max} = 2.8$ m/s, and $a_{max} = 1.4$ m/s^2, and for the *z*-axis, $v_{max} = 2.8$ m/s, and $a_{max} = 1.4$ m/s^2. The maximum motor acceleration and deceleration were always equal in magnitude.

3.1. Workspace partitioning

The first set of experiments compared two methods that partition the cells into rows. The first method divides the workspace so all rows are equal in height (partitioned "by height"). The second method divides

the workspace so that all rows contain an equal number of fruits (partitioned “by fruits”) and, thus, more equal workloads across rows. Because fruit distributions are non-uniform, partitioning the columns of arms by height and by fruits would intuitively produce different results. Partitioning by fruits should react to the non-uniformity while by height does not. Thus, we hypothesize that partition by fruit will produce better FPT results for configurations with multiple rows of arms. FPE should be similar for both partition methods because ESS chooses speeds that lead to schedules that harvest at least 95% of fruits in a segment. We test these methods on nine harvester configurations ranging from one arm in one column to nine total arms in three columns.

To evaluate if there is a difference between partitioning the columns based on fruits and partitioning based on height, we tested the changes to FPE and FPT of the two methods and different harvester configurations. We use Welch’s t-test to compare the mean FPE and FPT obtained in each experiment, with the null hypothesis being that the mean of both partitioning methods does not differ for any one harvester configuration. A 95% confidence level is used for all t-tests. To determine the direction of possible differences in mean, the spread of the FPE and FPT are plotted in a box plot and analyzed visually.

3.2. Harvester travel speed

The second set of experiments compared the harvest performance when each segment is harvested using the ‘best’ speed calculated by ESS versus traversing all segments with the same fixed speed. Six fixed speeds, V = 1, 5, 10, 15, 20, 100 cm/s, were used as baseline speeds, while the discrete speed values were $V_{ESS} \in \{1, 2, 3, ..., 100\}$ cm/s. Once a speed is chosen, that value is constant throughout the segment. The five baseline and best speeds are tested on the same nine $C/R/C * R$ configurations. All runs have the arm workspaces partitioned by fruits. The mean FPE and mean FPT of each harvester speed and configuration are plotted to help visualize the effects of the speeds on the means.

4. Simulation results and discussion

4.1. Workspace partitioning

As the number of arms increased, we saw that the mean FPT generally rose while the mean FPE remained stable above 95%. For all configurations with more than one row of arms, the means of the two partition methods were likely not the same (confidence level of 95%). Visually, both plots in Fig. 2 show that partition by fruit obtained a higher mean FPT. The largest difference was for configuration 3/3/9, where partition by fruit achieved a mean FPT of 1.374 fruits/s while partition by height achieved 1.049 fruits/s. Compared to the FPT obtained by both partition methods for configuration 1/1/1, at 0.247 fruits/s, partition by fruit has a gain of 0.618 fruits/s per arm, while partition by height gets a gain of 0.472 fruits/s per arm. For configurations with the same number of arms, more rows performed better than more columns, as shown by dips in the mean FPT in Fig. 2a. The columns are 3.5 m high, and it takes the arms a long time to move up and down that length. Furthermore, the left-to-right movement of the arms within the column is aided by the harvester’s forward speed.

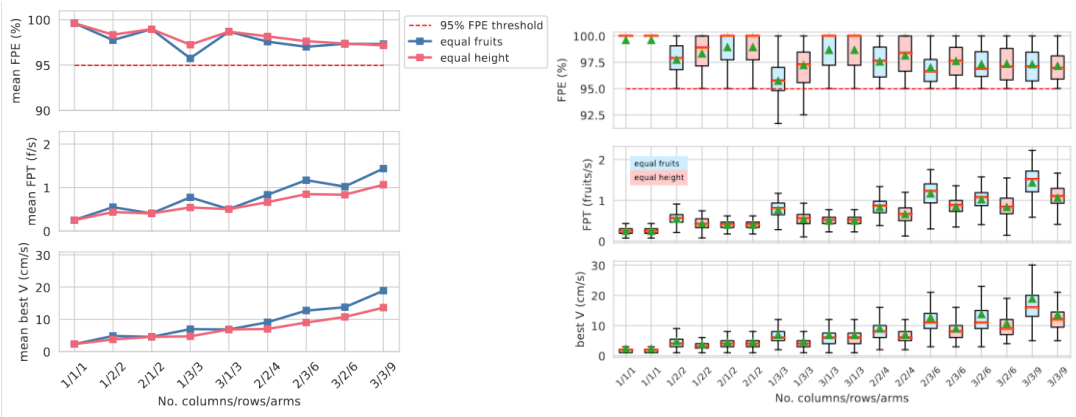

Figure 2. Plots compare the results of partitioning workspaces by fruit vs. by height for 111, 3.5 m segments of digitized apples. The plots show the FPE, FPT, and the chosen 'best 'harvester speed for nine harvester column and row configurations. In the box plots, the means are indicated by green triangles.

For the 1/2/2 and 1/3/3 harvester configurations, a small drop in FPE can be observed. The reason is that these are single-column harvester configurations, and fruits whose height is inside a zone centered at the row line and equal to the height of the arm's height cannot be harvested. On the other hand, harvester configurations 2/1/2 and 3/1/3 saw a drop in FPT. As single-row configurations, the arms had to harvest fruits along the whole column, potentially moving 3.5 m up and down between fruits. This led to schedules with slower harvester speeds to ensure the 95% FPE threshold was met.

The relationships between the number of fruits in each segment and the FPT and harvester speed, when the workspaces are partitioned by fruits, can be visualized in Fig. 3. These plots showed that the harvester speeds trended down. At the same time, FPT trended up as the number of fruits increased until reaching a steady state when there are too many fruits for the arms to handle. The harvester speed's maximum value was limited by its relationship to the number of arms, the distance traveled, the number of fruits, and the handling time of fruits defined by the following equation

$$V_{\overline{T_h}} = \frac{D*C*R}{N*\overline{T_p}} \quad (5)$$

where the bound for the harvesters 'speed is computed based on the mean fruit handling time, $\overline{T_p}$, the distance traveled, the number of arms, and the number of available fruits. In the plots in Fig. 3, these were constant parameters, except for the number of fruits. Because of this, the harvester speed followed a curve related to $1/N$ as N increased. This affected FPT, which has a relationship with FPE defined by the equation

$$FPT = \frac{N*V*FPE}{D} \quad (6)$$

The limits on the speed meant that FPT remained low when there were few fruits. As the number of fruits increased, FPT increased, though very slowly, as described in the equation

$$FPT_{max} = \frac{C*R}{T_{p,min}} \quad (7)$$

which describes a maximum theoretical FPT, given the number of arms and the minimum observed handling time $T_{h,min}$. This indicated that FPT followed a logarithmic curve with the form $A * ln(N) + B$. Using the Index of Agreement error metric (Willmott, 1981), we saw that the fit for the logarithmic curve was a bit low, perhaps due to the discrete nature of the number of fruits and the harvester speeds. The curve for the harvester speed was found by setting Equation 7 equal to FPT's logarithmic equation and solving for the harvester speed. Thus,

$$V = D\frac{Eln(N)+F}{N} \quad (8)$$

where $E = (D * A)/FPE$ and $F = (D * B)/FPE$. It is important to note that the fruit localization data was obtained after the first harvest had already taken place. This means the tests are based on lower densities than the harvester would be expected to work on.

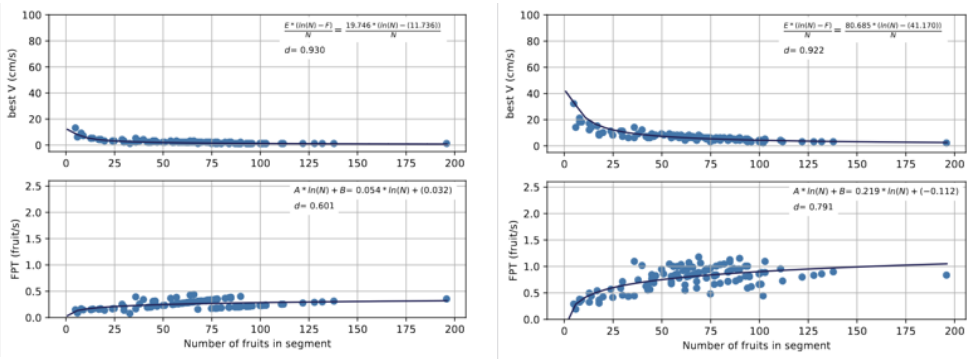

(a) $C/R/C*R = 1/1/1$ (b) $C/R/C*R = 1/3/3$

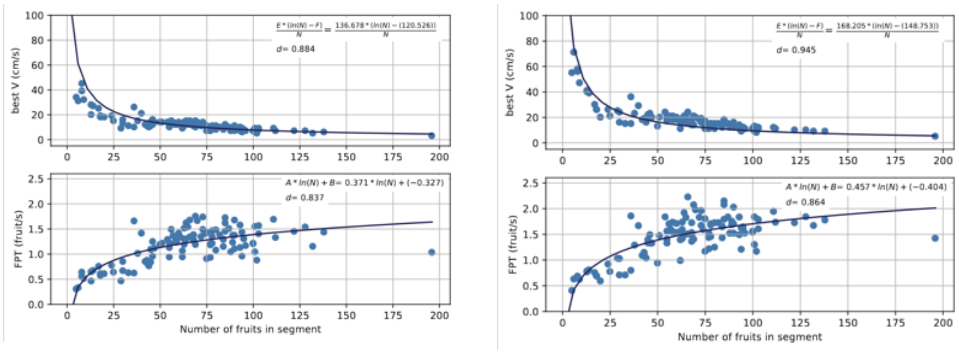

(c) $C/R/C*R = 2/3/6$ (d) $C/R/C*R = 3/3/9$

Figure 3. The scatter plots show the relationship between the number of fruits in a segment and the best harvester speed and FPT when the rows are partitioned by fruits. Each point represents the results from running the scheduler on 111 segments, each 3.5 m long. Harvester speed is chosen with ESS to maximize FPT while achieving a minimum FPE of 95%.

4.2. Harvester travel speed

Fig. 4 shows that low baseline speeds had high mean FPE and low mean FPT. Higher speeds had the opposite effect. The highest fixed speed, 100 cm/s, had the lowest FPE and a lower FPT than the best speed, as well as 5, 10, and 20 cm/s. This indicated that at speeds higher than a threshold, the harvester picked too few fruits to cancel out the gains in FPT because the speed was too high. In contrast, choosing the best speed led to a mean FPE above 95%, while the mean FPT remained high. The best speed matched or exceeded the mean FPT of the following fixed speeds: 1, 5, 10, and 100 cm/s. This meant that, although finding the best speed never resulted in the highest FPE or FPT, it led to the best combined FPE and FPT.

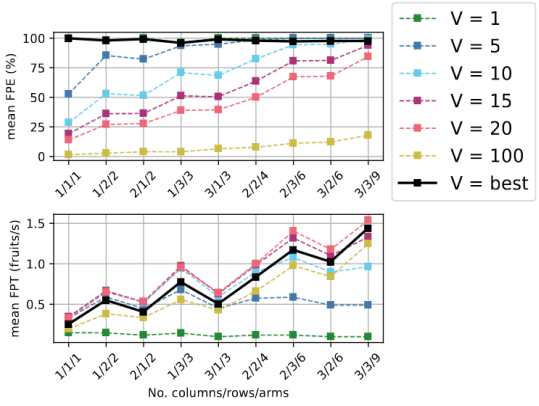

Figure 4. The plot compares the mean FPE and mean FPT using fixed speeds vs. the best speed for each segment. Scheduling is performed with FCFS with ESS. Results are shown for five baseline speeds, V = 1, 5, 10, 15, 20, 100 cm/s, and the best speed for all nine harvester configurations.

5. Conclusion

In the first experiment, two-row partitioning strategies were compared, dividing the columns so rows had equal heights or an equal number of fruits. The best speed was found for each segment. Both partitioning methods achieved the minimum 95% FPE; however, partitioning by fruit allowed the harvester to move faster, leading to higher FPT. As the number of arms increased, the difference in FPT between the partitioning methods increased. With that said, results were better for the same number of arms when more arms were configured in more rows rather than more columns. This was because there was a maximum horizontal distance of 1 m compared to a maximum vertical distance of 3.5 m. The more arms in a column, the less they would have to move up and down to harvest all fruits while the horizontal travel stayed the same.

Results also showed that FPT followed a logarithmic curve with respect to the number of fruits in a segment. Few fruits limited the speed such that FPT remained low. FPT increased as the number of fruits increased, though the rate of increase became slower. On the other hand, speed followed a curve related to ln (N)/N with respect to the number of fruits. Few fruits in a segment allow the system to choose faster speeds. As the number of fruits in a segment increased, a slower speed would be chosen to reach the required 95% FPE. This shows that the number of arms greatly affects the chosen speed and resulting FPT. More arms allow for faster speeds and, thus, faster FPT.

In the second experiment, we compared scheduling 3.5 m segments with six fixed speeds versus choosing the best speed for each segment for both partitioning methods. Low fixed speeds resulted in high FPE but low FPT, while fast fixed speeds had the opposite effect. Choosing the best speed resulted in the best combined FPE and FPT. It led to high FPT values while keeping FPE at or above 95%, unlike the fixed speeds, which traded one for the other. This indicates that speed selection is very important when maximizing FPE and FPT simultaneously. FCFS with ESS could be made faster by switching ESS to binomial search, speeding up results. Although FCFS's speed is not a bottleneck, per se, Binomial Search could be useful if the number of speeds is increased by adding fractional values, such as having the step between speeds be 0.25 cm/s. However, more informed optimization algorithms can lead to better combined FPT and FPE. For example, minimizing makespan would provide near-optimal schedule and speed combinations, though its generally slow computation times need to be assessed.

Acknowledgements

This work was funded by USDA-NIFA Grant 2020-67021-30759 under the NSF National Robotics Initiative.

References

Arikapudi, R., S.G., Vougioukas, F., Jiménez- Jiménez, F. Khosro Anjom, 2016. Estimation of Fruit Locations in Orchard Tree Canopies Using Radio Signal Ranging and Trilateration. Computers and Electronics in Agriculture (125): 160-172.

Arikapudi, R., and S. G. Vougioukas, 2023. Robotic tree-fruit harvesting with arrays of cartesian arms: A study of fruit pick cycle times. *Computers and Electronics in Agriculture*, *211*, 108023.

Bac, C. W., E. J. van Henten, J., Hemming, & Y., Edan, 2014. Harvesting robots for high-value crops: State-of the-art review and challenges ahead. *Journal of Field Robotics*, *31*(6), 888–911.

Christiaensen, L., Z. Rutledge, and J. E. Taylor, 2021. The future of work in agri-food, Food Policy 99, 101963.

Edan, Y., B. Engel, and G. E. Miles, (1993). Intelligent control system simulation of an agricultural robot. *Journal of intelligent and Robotic Systems*, *8*(2), 267–284.

Fei, Z., S.G. Vougioukas, 2024. A robotic orchard platform increases harvest throughput by controlling worker vertical positioning and platform speed. Computers and Electronics in Agriculture, 218, 108735.

Harrell, R., 1987. Economic analysis of robotic citrus harvesting in Florida. Transactions of the ASAE. 30 (2), 298–304

Koostra, G., X. Wang, P. Blok, M. Hemming, and E. van Henten, 2021. Selective harvesting robotics: Current research, trends, and future directions. *Current Robotics Reports*, *2*(1), 95–104.

Li, T., F., Xie, Z., Zhao, H., Zhao, X., Guo, Q., Feng, 2023. A multi-arm robot system for efficient apple harvesting: Perception, task plan and control. Computers and Electronics in Agriculture, 211, 107979.

Mann, M. P., B., Zion, I., Shmulevich, D., Rubinstein, R., Linker, 2016. Combinatorial Optimization and Performance Analysis of a Multi-arm Cartesian Robotic Fruit Harvester—Extensions of Graph Coloring. J Intell Robot Syst, 82 (3-4), 399–411.

Williams, H. A., M. H., Jones, M., Nejati, M. J., Seabright, J., Bell, N. D., Penhall, J. J., Barnett, M. D., Duke, A. J., Scarfe, H. S., Ahn, 2019. Robotic kiwifruit harvesting using machine vision, convolutional neural networks, and robotic arms. Biosystems Engineering, 181, 140–156.

Willmott, C. J., 1981. On the validation of models. *Physical geography*, *2*(2), 184–194.

Zion, B., M., Mann, D., Levin, A., Shilo, D., Rubinstein, I., Shmulevich, 2014. Harvest-order planning for a multiarm robotic harvester. Computers and Electronics in Agriculture, 103, 75–81.

Development of a method for the real-time assessment of the risk from severe-hot microclimate in agricultural and forestry environments

Massimo Cecchini [a*], Alfredo Mancini [a], Filippo Cossio [a], Carlo Macor [a]

[a] Department of Agriculture and Forest Sciences, University of Tuscia, Viterbo, Italy

* Corresponding author. Email: cecchini@unitus.it

Abstract

Agricultural workers, operating both in open fields and in greenhouses, are exposed to several risks, including exposure to severe hot microclimates. The study, carried out in an open field and in a greenhouse in central Italy, allowed the detection of the main microclimatic parameters to be used for risk assessment according to the technical standard EN ISO 7933 (Predict Heat Strain model). The aim of this work was to identify, by implementing the P.H.S. model, any achievement of the critical threshold of rectal temperature (t_{re}) and the maximum sweat rate (Sw_{max}), which, if exceeded, would compromise the worker's safety. This study is the basis for the development of a tool to provide, in real time and with the use of modern technologies (e.g. smartphone or smartwatch), a warning signal to the worker before he or she reaches the critical threshold of heat exposure and is subject to immediate safety risks.

Keywords: work safety, prevention, hot environment, P.H.S., real time risk assessment.

1. Introduction

"Microclimate" refers to the physical parameters characterizing living and working environments that influence thermal comfort and worker productivity. Key factors include temperature, relative humidity, ventilation, mean radiant temperature, and air quality. Extreme climatic events like heat waves also play a crucial role. Maintaining an optimal microclimate is essential for worker safety and productivity (Schulte and Chun, 2009).

Microclimatic conditions in work environments vary based on several elements: production cycle requirements; environmental characteristics (e.g., underground or high-altitude work); structural characteristics of workplaces (construction materials and thermal properties); equipment used to control climatic conditions (fans, air conditioners, etc.).

Microclimatic environments are classified as "moderate" or "severe." Moderate environments offer thermal comfort, while severe environments (hot or cold) can strain the body's thermoregulation, compromising health. Extreme conditions often arise from production needs or outdoor climatic conditions.

In severe hot environments, heavy work stresses the cardiovascular system, risking heatstroke. Factors such as direct sun exposure, water loss, heavy physical work, insufficient recovery periods, and protective clothing contribute to health risks. Common heat-related illnesses include heat cramps, sweat dermatitis, hydromineral imbalances, heat syncope, heat exhaustion, and heatstroke.

The growing interest in climate change has highlighted its impact on workplace safety. Studies show a link between extreme temperatures and increased workplace accidents (Gariazzo et al., 2023). High-risk sectors include agriculture, construction, utilities, and transportation (Bonafede et al., 2016). Common accidents due to high temperatures involve transportation incidents, slips, falls, and contact with objects or equipment (Adam-Poupart et al., 2015).

Di Blasi et al. (2023) confirmed that heat impacts workplace injuries, correlating accidents in the Italian agricultural sector with daily average air temperatures. The study estimated 2,050 heat-attributable accidents from 2014 to 2018. The World Health Organization predicts that climate change could cause up to 250,000 deaths per year between 2030 and 2050. Vulnerable groups, including outdoor workers, face significant health risks (Gariazzo et al., 2023; Binazzi et al., 2019). Binazzi et al. (2019) identified males and younger workers as high-risk categories due to their occupations and physical demands.

Currently, no methodology quantifies accidents due to high-temperature exposure in agriculture, as the mechanisms increasing injury risk are complex. Interventions include regulations, training, and developing heat stress prediction systems, such as the "Worklimate" project (INAIL, 2022).

Factors influencing susceptibility to temperature-related occupational risks include age, mass, physical fitness, acclimatization, metabolism, substance use, health status, and clothing. Heat-induced occupational

diseases and injuries occur when total heat load exceeds the body's capacity to maintain normal functions without excessive strain (Schulte and Chun, 2009).

This work aims to detect key microclimatic parameters (ambient temperature, relative humidity, air velocity, mean radiant temperature) indoors and outdoors, monitor their daily trends, and identify critical threshold exceedances that compromise worker health and safety. Following a measurement campaign in greenhouses (indoor) and open fields (outdoor), specific software (GidasTEA - LSI-LASTEM) will process microclimatic indices to verify limit value exceedances. This study will help develop a tool for real-time worker alerts, preventing immediate safety risks like dehydration or heatstroke.

2. Materials and Methods

The measurement campaign was conducted in an open field and a greenhouse at the Didactic-Experimental Agricultural Farm "Nello Lupori" of the University of Tuscia, Viterbo, Italy, from July to September 2023, with measurements taken between 9:00 AM and 4:30 PM. Probes were positioned approximately 1 m above the ground to simulate worker exposure.

The LSI-LASTEM sensors used (complying with ISO 7726 standards) include: hot-wire anemometer ESV306 (resolution: 0.01 m/s); dry bulb thermometer BSU102 PT100 (resolution: 0.01°C); wet bulb thermometer BSU102 PT100 (resolution: 0.01°C); natural ventilation wet bulb thermometer BSU121 PT100 (resolution: 0.01°C); globe thermometer BST131 (resolution: 0.01°C). The data were recorded using the M-Log (ELO009) data logger.

2.1. Greenhouse description

The greenhouse is oriented northeast with a gable roof, covered with 3 mm thick glass, and measures 30 m x 14 m with a ridge height of 5.5 m and a side height of 2.75 m.

2.2. P.H.S. model

The Predicted Heat Strain (P.H.S.) model (EN ISO 7933) evaluates heat stress based on laboratory studies of physiological responses. It accounts for the time dependence of physiological variables, movement effects on clothing insulation, and metabolic energy effects on core temperature. The energy balance equation of the human body used in the model is:

$$E_{req} = M - W - C_{res} - E_{res} - C - R - dS_{eq} \quad (1)$$

where:

E_{req}: required evaporative heat loss through sweating to maintain thermal neutrality (Wm^{-2});

M: metabolic rate (ISO 8996) (Wm^{-2});

W: effective mechanical power (Wm^{-2});

C_{res}: respiratory convective heat flow (Wm^{-2});

E_{res}: respiratory evaporative heat flow (Wm^{-2});

C: convective heat flow (Wm^{-2});

R: radiative heat flow (Wm^{-2});

dS_{eq}: body heat storage rate for increase of core temperature associated with the metabolic rate (Wm^{-2}).

The P.H.S. model calculates parameters such as:

- w_p: predicted skin wettedness (dimensionless);
- SW_{tot}: total water loss rate per minute (Wm^{-2});
- human body temperatures: t_{sk}: mean skin temperature (°C); t_{cr}: core temperature (°C); t_{re}: rectal temperature (°C).

Going through the calculation of intermediate parameters (respiratory convective heat flow, respiratory evaporative heat flow, convective heat flow at the skin surface, radiative heat flow at the skin surface, skin temperature) the P.H.S. model allows you to determine the parameters that describe the expected heat strain:

- t_{re}: rectal temperature (°C): represents the worker's internal temperature;
- D_{max}: maximum water loss to maintain normal physiological parameters for the given work (g);

- D_{max50}: maximum water loss to protect a mean subject (g);
- D_{max95}: maximum water loss to protect 95% of the working population (g);
- $D_{limloss50}$: maximum allowable exposure time for water loss to protect a mean subject (minutes);
- $D_{limloss95}$: maximum allowable exposure time for water loss to protect 95% of the working population (minutes);
- $D_{lim\ tre}$: maximum allowable exposure time for heat storage (minutes).

The limit values of the stress indices Sw_{max} and w_{max} are calculated as shown in table 1, and those for total water loss (D_{max}) as shown in table 2.

Table 1. Limit values of the stress indices Sw_{max} and w_{max}.

	Non-acclimatized subject	Acclimatized subject
Sw_{max}	$2{,}6 \times (M - 32) \times A_{Du}$ (2)	$3{,}25 \times (M - 32) \times A_{Du}$ (3)
w_{max}	0,85	1

where:

$$A_{Du} = 0.007184 \times Height^{0.725} \times Mass^{0.425} \quad (4)$$

Table 2. Limit values for total water loss.

	Subject free to drink	Subject not free to drink
D_{max50}	7% of body mass	3% of body mass
D_{max95}	5% of body mass	3% of body mass

The P.H.S. model inputs include the metabolic rate (M) and the thermal insulation of clothing (I_{cl}) (estimated respectively according to EN ISO 8996 and EN ISO 9920 standards), activity duration, worker's mass and height, water replacement ability, acclimatization, air temperature (t_a), mean radiant temperature (t_r), air velocity (v_a), and water vapor partial pressure (p_a). Metabolic activity is measured in met (1 met = 58.2 Wm^{-2}), while clothing insulation is measured in clo (1 clo = 0.155 m^2KW^{-1}). The model helps evaluate the probability of thermal collapse for workers in severe hot environments, emphasizing the importance of accurate parameter estimation and timely measurements, especially in environments with variable conditions (Diano et al., 2015).

2.3. Data analysis

The collected data was processed using the "GidasTEA LSI" software. This software requires inputting specific parameters such as the type of work (for assigning a met value), the clothing worn (for assigning a clo value), and the worker's position. These inputs are then associated with the microclimatic parameters of the workday. The software calculates the P.H.S. and checks whether the operator's exposure limit value has been exceeded.

2.4. Implementation of a dynamic model for calculating the Predicted Heat Strain

The standard computation method for the P.H.S. model in EN ISO 7933 assumes constant environmental conditions, which does not account for daily temperature variations and thermal accumulation. To address this, a dynamic model was developed to consider the integral of the environmental parameters recorded over time. This approach provides a more accurate assessment of the thermal accumulation experienced by the operator.

A specialized software was developed, similar to "GidasTEA LSI", but with dynamic modeling capabilities. It requires inputting worker parameters such as mass, height, clo, met, and initial rectal temperature (t_{re}). Additionally, it inputs ambient temperature (t_a), globe thermometer temperature (t_g), vapor pressure (p_a), and air velocity (v_a) for each minute.

The model considers the worker's posture, with "standing" being the appropriate choice for greenhouse work. Wind speed was deemed negligible in the greenhouse setting.

Key inputs for the model include:

- metabolic rate (M): for greenhouse work, a value of 150 W/m² was chosen.
- clothing thermal insulation (I_{cl}): a value of 0.5 clo was selected for the clothing worn.
- static moisture permeability index (i_{mst}): an average value of 0.38 was used.
- body surface fraction covered by reflective clothing (A_p): set at 54% based on EN ISO 7933.
- emissivity of clothing: set at 0.97, unless special materials are used.
- operator's mass and height (75 kg and 180 cm respectively).

The software outputs rectal temperature (t_{re}) and sweat rate (Sw_{max}) for each minute. The rectal temperature over a specific interval is compared with the maximum tolerable rectal temperature of 38°C, as per EN ISO 7933. This allows predicting the remaining work time before the operator could suffer from heat stress.

This dynamic model improves the accuracy of thermal load predictions by accounting for cumulative thermal exposure. By integrating environmental parameters over the sampling period, the model provides a comprehensive assessment of thermal conditions and their impact on the operator. This enhances the management and mitigation of heat stress risks in severe hot environments, ensuring worker safety and compliance with relevant standards.

3. Results and Discussion

For the analytical processing, the day with the highest climatic values was considered, which was recorded on 01/08/2023. The data related to the situation involving the highest thermal load for workers (greenhouse work) were taken into consideration. The data downloaded from the data logger had values acquired approximately every 3 seconds. Therefore, considering a typical seven-hour workday, about 8500 measurements were collected throughout the day for each measured parameter.

To streamline the data load and achieve a better graphical representation, it was decided to reduce the data to approximately 420 measurements. Instead of reporting 20 measurements per minute (as provided by the data logger), only one data point per minute was considered. This operation was done with a specific criterion: the average of the twenty values recorded within a minute was calculated to obtain a single, most representative value for that time interval. Subsequently, each measured parameter was individually processed and graphically represented to show the trend throughout the entire workday. This graphical representation helps in understanding the fluctuations and patterns in the environmental conditions over time, providing a clearer picture of the thermal load and its impact on the workers.

By reducing the data and using averages, the analysis becomes more manageable and the visual representation more comprehensible, allowing for more accurate assessments and decision-making regarding worker safety and thermal stress management.

3.1. Temperature and humidity

The ambient temperature (t_a) throughout the workday, shown in Fig. 1, peaked at 35°C at 12:15 PM and remained above 34°C until 2:54 PM. A comparison was made between the recorded t_a and the simple moving average (sma) of these values to smooth out fluctuations and provide a consistent temperature trend, calculated as follows:

$$sma = \frac{\text{sum of temperatures over n periods}}{n} \quad (5)$$

The sma trend shows a gradual increase throughout the day and a peak of 32.35°C at 3:30 PM.

Comparing t_a with wet-bulb temperature (t_w) and globe thermometer temperature (t_g), the trends of the three curves are nearly identical, though the specific temperatures differ (Fig. 1). t_w, crucial for assessing temperature and humidity, ranged from 22°C in the morning to 27°C at 2:43 PM. Recent research indicates critical t_w thresholds are 25-28°C in hot-dry environments and 30-31°C in hot-humid environments, such as greenhouses. Exceeding these values impairs the body's cooling ability through sweating.

t_g considers radiant heat, air temperature, and wind speed, showing higher values than t_a, up to 44°C in our case. This is vital in greenhouses as it significantly affects heat sensation (Oliveira et al., 2019).

Fig. 1 also shows the relative humidity (W_a) trend, remaining within the safe range of 40-60%, with a peak of 57% in the early morning. W_a is crucial for thermal comfort, representing the water vapor in the air, which increases with temperature, affecting perceived heat sensation.

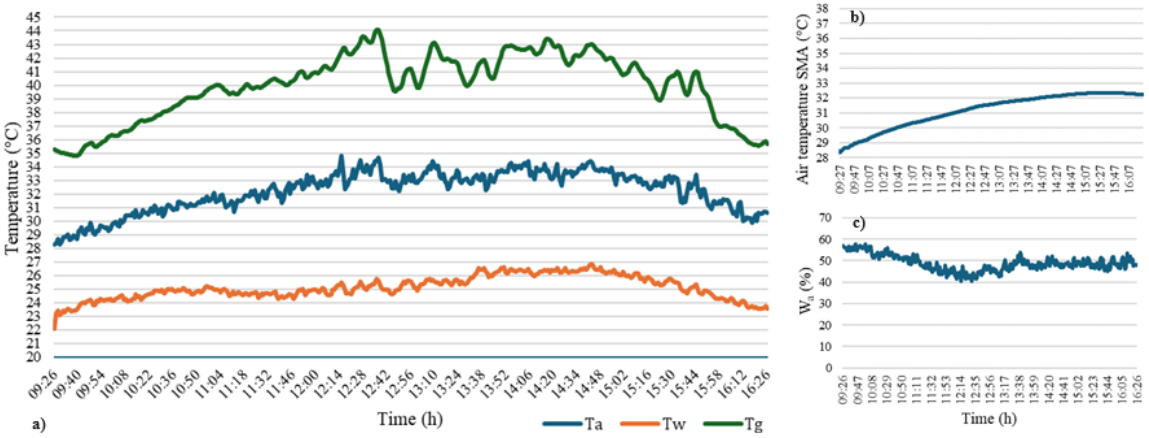

Figure 1. Trends of: a) ambient temperature (t_a), wet-bulb temperature (t_w), and globe thermometer temperature (t_g); b) ambient temperature simple moving average (t_a *sma*); c) relative humidity (W_a) (01/08/2023).

3.2. Rectal temperature (t_{re}) and water loss (Sw_{max})

Using the software with the P.H.S. model, rectal temperature (t_{re}) and fluid loss (Sw_{max}) trends were analyzed for 01/08/2023 (K_0).

Fig. 2a shows an exponential increase in t_{re} during the first hour, stabilizing around 37.4-37.5°C throughout the day, and decreasing in the last hour. t_{re} never reached the 38°C risk threshold set by EN ISO 7933. Fig. 2b, using the simple moving average for ambient temperature, confirms a similar t_{re} trend and maximum temperature.

Fig. 3a illustrates fluid loss trends for a standard operator (75 kg, 180 cm) as per EN ISO 7933, with a metabolic rate (M) of 150 Wm^{-2} (moderate activity).

Fluid loss gradually increases, with non-acclimatized subjects reaching the critical threshold around 16:00; acclimatized subjects do not reach this threshold. Acclimatization enhances heat tolerance and reduces hyperthermia risks (Chong et al., 2020; Maughan, 1997).

Fig. 3b, applying the moving average temperature, shows that threshold values for Sw_{max} are not reached for either subject group.

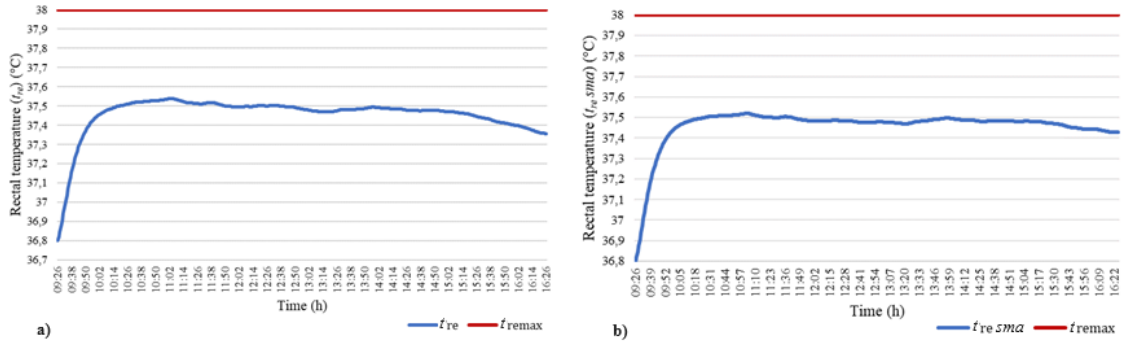

Figure 2. Trend of: a) t_{re}; b) t_{re}*sma* (simple moving average) (01/08/2023).

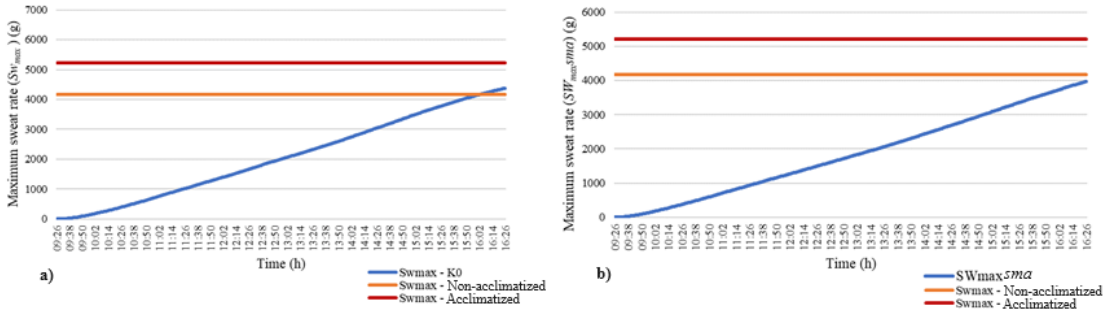

Figure 3. Trend of: a) SW_{max}; b) $SW_{max}sma$ (simple moving average) (01/08/2023).

3.3. Simulations of rectal temperature (t_{re}) and water loss (Sw_{max}) varying t_a

Climate change, marked by a 1°C rise in global temperatures in recent decades, poses significant health risks (Kenny et al., 2020). Evaluating its health impacts is crucial (Cecchini et al., 2010; Abdel-Ghany et al., 2013). On 01/08/2023, P.H.S. calculations showed no critical t_{re} or Sw_{max} values, as temperatures did not reflect typical August conditions (Fig. 2 and 3).

Simulations were conducted by adding 1°C increments to the ambient temperature (t_a). The P.H.S. calculations for t_{re} and Sw_{max} trends are shown in Fig. 4.

The graph indicates that t_{re} rises faster with each 1°C increase. Starting from K_0 (maximum 35°C), the critical 38°C threshold is not reached. However, by K_4 (maximum 39°C), t_{re} approaches 37.8°C. At K_5 (maximum 40°C), t_{re} reaches the critical threshold around 15:00. From K_6 to K_9 (41-44°C), the critical threshold is reached before midday, sometimes after just 90 minutes of work.

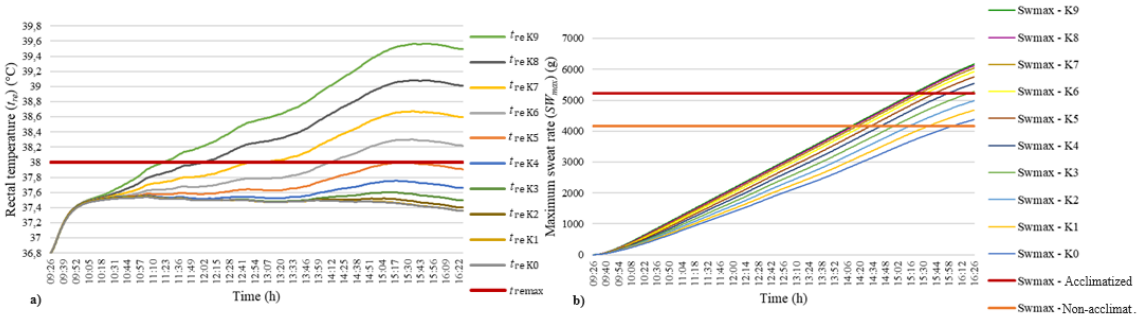

Figure 4. Trend of: a) t_{re}; b) Sw_{max}, with respective simulations (01/08/2023).

Fig. 4b shows that fluid loss increases with starting of the activity, reaching critical levels faster as temperature increases. For K_0, non-acclimatized subjects exceed the critical threshold by the end of the day. For K_4, it occurs around 15:00, and for K_9, it occurs before 14:00. Acclimatized subjects exceed the threshold only from K_4 at the end of the day, and for K_9, by 15:00. Acclimatization delays reaching critical thresholds, enhancing worker safety.

3.4. Simulations of rectal temperature (t_{re}) and water loss (Sw_{max}) varying worker's mass

Simulations were conducted for two body types: robust (120 kg) and small (60 kg), keeping height constant (Fig. 5). Differences in A_{Du} values and sweating thresholds were calculated.

For t_{re}, no significant differences were observed. For Sw_{max}, robust subjects reached the critical threshold for non-acclimatized individuals about an hour earlier than standard-mass subjects. Small size individuals reached the threshold almost identically to standard-mass subjects.

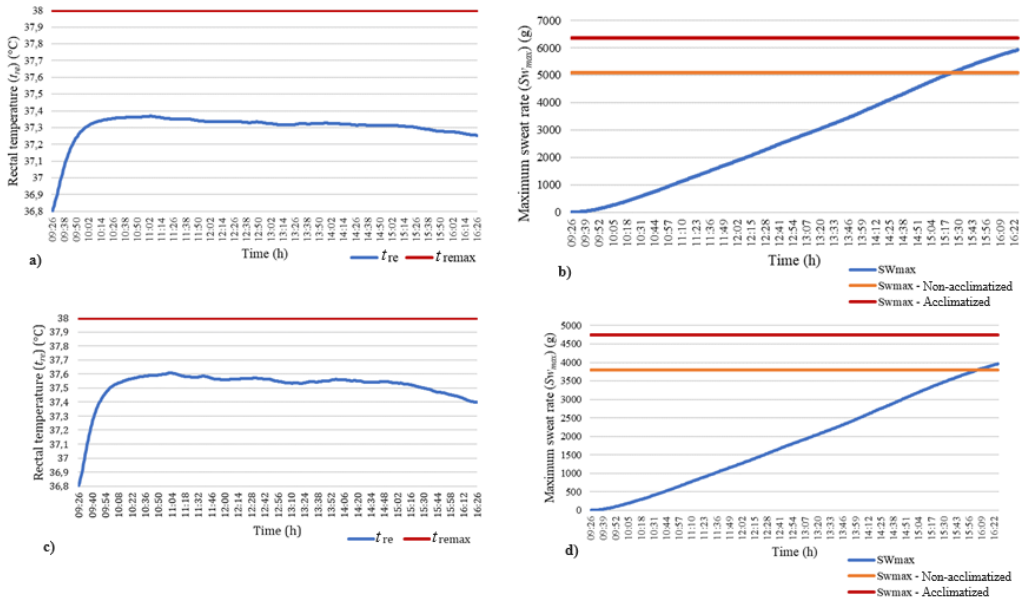

Figure 5. Trend of: a) t_{re} ; b) Sw_{max} (over size subject); c) t_{re} ; d) Sw_{max} (small size subject) (01/08/2023).

4. Conclusions

Despite the increasing frequency and intensity of heatwaves due to climate change, there are no dedicated heat monitoring and alert systems for the occupational sector in Europe or globally. Existing alert systems rely on weather and climate data from ground meteorological stations, which provide risk levels based on observed conditions or simulations and require interpretation by qualified personnel.

The P.H.S. model, as described in Annex E of ISO 7933, has limitations due to its reliance on constant input of environmental parameters. This does not account for variations typical in agricultural work environments. The complex calculations and precise measurements required by the P.H.S. model make it unsuitable for a heat alert system. Additionally, most international alert systems do not provide forecasts beyond five days, except for the "Heat-Shield" platform (www.heat-shield.eu). Temperature and other environmental parameters constantly change during the workday. The developed software considers these continuous changes to provide a real-time prediction of the critical threshold based on collected data.

An effective predictive system balances input data characteristics from the microclimate model with detailed heat risk information. Wearable sensors, common in sports and medicine, can provide real-time data on physiological parameters and climatic conditions to prevent heat-related risks. These sensors monitor heart rate and derive core temperature using algorithms like Buller's. In the U.S., a next-generation arm sensor for workplace heat stress prevention measures heart rate, body and ambient temperature, and relative humidity, and includes an accelerometer. This device alerts workers via an app during heat stress conditions but is not available in the E.U. due to safety requirements. Testing in the E.U. is needed for integration into the heat risk prevention system.

Developing a smartwatch app to alert workers when approaching the critical core temperature threshold could enhance safety. Monitoring liquid loss by weighing workers is complex and does not offer real-time information.

This study explored a real-time heat stress monitoring system for severe hot environments using the Predicted Heat Strain (ISO 7933) method. Results support further development of real-time data processing software for worker alerts, with validation essential before commercial or community use.

Acknowledgements

This study was carried out within the Agritech National Research Center and received funding from the European Union Next-GenerationEU (PIANO NAZIONALE DI RIPRESA E RESILIENZA (PNRR) – MISSIONE 4 COMPONENTE 2, INVESTIMENTO 1.4 – D.D. 1032 17/06/2022, CN00000022). This

manuscript reflects only the authors' views and opinions, neither the European Union nor the European Commission can be considered responsible for them.

References

Abdel-Ghany, A.M., I.M. Al-Helal, M.R. Shady, 2013. Effect of the evaporative cooling on the human thermal comfort and heat stress in a greenhouse under arid conditions. Advances in Meteorology, 2013. doi: 10.1155/2013/361471.

Adam-Poupart, A., A. Smargiassi, M.A. Busque, P. Duguay, M. Fournier, J. Zayed, F. Labrèche, 2015. Effect of summer outdoor temperatures on work-related injuries in Quebec (Canada). Occup Environ Med, 72 (5), 338-345. doi: 10.1136/oemed-2014-102428.

Ashley-Smith ,J., A. Burmester, M. Eibl, 2010. Climate for collections - Standards and uncertainties. Archetype Publications.

Binazzi, A., M. Levi, M. Bonafede, M. Bugani, A. Messeri, M. Morabito, A. Marinaccio, A. Baldasseroni, 2019. Evaluation of the impact of heat stress on the occurrence of occupational injuries: Meta-analysis of observational studies. Am J Ind Med. 62 (3), 233-243. doi: 10.1002/ajim.22946.

Bonafede M., A. Marinaccio, F. Asta, P. Schifano, P. Michelozzi, S. Vecchi, 2016. The association between extreme weather conditions and work-related injuries and diseases. A systematic review of epidemiological studies. Annali dell'Istituto Superiore di Sanità, 52 (3), 357-367. doi: 10.4415/ANN_16_03_07.

Cecchini, M., A. Colantoni, R. Massantini, D. Monarca, 2010. Estimation of the Risks of Thermal Stress Due to the Microclimate for Manual Fruit and Vegetable Harvesters in Central Italy. J Agric Saf Health, 16 (3), 141-159. doi: 10.13031/2013.32040.

Chong, D., N. Zhu, W. Luo, Z. Zhang, X. Pan, 2020. Effects of heat acclimation on individual safety performance in hyperthermal indoor environments. Build Environ, 168. doi: 10.1016/j.buildenv.2019.106537.

Di Blasi, C., A. Marinaccio, C. Gariazzo, L. Taiano, M. Bonafede, A. Leva, M. Morabito, P. Michelozzi, F.K. de' Donato, 2023. Effects of Temperatures and Heatwaves on Occupational Injuries in the Agricultural Sector in Italy. Int J Environ Res Public Health, 20 (4). doi: 10.3390/ijerph20042781.

Diano, M., M. Valentini, I. Di Gesu, P. Samele, 2015. Lo stress termico dei lavoratori impegnati nelle lavorazioni in serra: studio della variabilità del rischio in funzione delle condizioni di lavoro" Available: https://www.researchgate.net/publication/277870786

EN ISO 7726:2001. Ergonomics of the thermal environment - Instruments for measuring physical quantities.

EN ISO 7933:2023. Ergonomics of the thermal environment - Analytical determination and interpretation of heat stress using calculation of the predicted heat strain.

EN ISO 8996:2021. Ergonomics of the thermal environment - Determination of metabolic rate.

EN ISO 9920:2009. Ergonomics of the thermal environment - Estimation of thermal insulation and water vapour resistance of a clothing ensemble.

Gariazzo, C., L. Taiano, M. Bonafede, A. Leva, M. Morabito, F. de' Donato, A. Marinaccio, 2023. Association between extreme temperature exposure and occupational injuries among construction workers in Italy: an analysis of risk factors. Environ Int, 171, doi: 10.1016/j.envint.2022.107677.

INAIL, 2022. Esposizione a temperature estreme ed impatti sulla salute e sicurezza sul lavoro. Il progetto Worklimate e la piattaforma previsionale di allerta.

Kenny, G.P., S.R. Notley, A.D. Flouris, A. Grundstein, 2020. Climate Change and Heat Exposure: Impact on Health in Occupational and General Populations. Exertional Heat Illness, Springer, pp. 225–261. doi: 10.1007/978-3-030-27805-2_12.

Maughan, R. 1997. Heat acclimatisation and rehydration strategy. Br J Sports Med, 31 (7), 77. doi: 10.1136/bjsm.31.1.77

Oliveira, A.V.M., A.M. Raimundo, A.R. Gaspar, D.A. Quintela, 2019. Globe Temperature and Its Measurement: Requirements and Limitations. Ann Work Expo Health, 63 (7), 743-758. doi: 10.1093/annweh/wxz042.

Schulte, P. A., H.K. Chun, 2009. Climate change and occupational safety and health: Establishing a preliminary framework. J Occup Environ Hyg, 6 (9), 542-554. doi: 10.1080/15459620903066008.

Evaluation of plant-response irrigation modellin in greenhouses

Angeliki Elvanidi, Ioannis Naounoulis, Nikolaos Katsoulas [a,*]

Lab of Agricultural Constructions and Environmental Constrol, Department of Agriculture Crop Production and Rural Environment, University of Thessaly, Fytokou Str, 38446, Volos, Greece.

* Corresponding author. Email: nkatsoul@uth.gr

Abstract

Determining the timing and quantity of irrigation in hydroponics is crucial for effective greenhouse management. Traditionally, for automated irrigation management in greenhouses, most farmers have used a timer to regularly drive irrigation or measure the substrate water content and air humidity neglecting to consider the plant physiological status. The development of Decision Support Systems (DSSs) that combine environmental and crop data can assist growers in making more precise and consistent decisions in irrigation management. In the current research, a model that evaluates stomatal conductance (g_{ws}) and photosynthesis rate (Ps) as the plant-response key in the decision making process was developed. The innovation of the current model lies in the integration of Ps values estimated by means of remote sensing using a photochemical reflectance index (PRI). Logarithmic regression was employed using independent variables like temperature (Tair), vapor pressure deficit (VPD), and leaf-air temperature difference, to predict g_{sw} status. Next, the correlation between g_{sw} and Ps was initially established to fit a logarithmic curve. The mean response of Ps at maximum g_{sw} was considered as Ps_{max}. Then the regression model was utilized to inversely predict g_{sw} values corresponding to these percentages of Ps_{max}, resulting in the determination of different g_{sw} cutoff points. Statistical performance of the model was evaluated. The results indicate that the system achieved a significantly small error.

Keywords: Decision support system, photosynthesis, photochemical reflectance index, stomatal conductance, calibration

1. Introduction

Hydroponic greenhouse systems have become increasingly popular in recent years as a method for growing crops with high yields and reduced land and water usage compared to traditional soil-based agriculture. According to the Markets and Markets (2025) report, the global commercial smart greenhouse market size is expected to grow from USD 29.6 billion in 2020 to USD 50.6 billion in 2025, expanding at a compound annual growth rate of 11.3% during the forecast period (Fang et al., 2022). Consequently, facility greenhouse has become an essential method of agricultural production globally. To further increase productivity within the existing greenhouse-covered areas, it is necessary to redesign operational control systems and establish more demonstrative greenhouses.

A key limitation of many hydroponic greenhouses is their reliance on outdated or inefficient irrigation control systems. These systems often use timer-based watering schedules that fail to adequately account for changing plant needs, environmental conditions, or resource availability (Elvanidi and Katsoulas, 2022 (a)). This can lead to over-watering, waste of valuable water and nutrients, and suboptimal plant growth. Furthermore, the lack of real-time monitoring and automated adjustments in these systems undermines the potential efficiency benefits of hydroponics.

Other systems utilize climate data to help growers make more precise and consistent decisions regarding irrigation management (Lu et al., 2015). Recent research has highlighted the effectiveness of vapor pressure deficit (VPD) control technology in tomato greenhouses, showing promising results (Zhang et al., 2017). While greenhouse controls based on atmospheric or root conditions can enhance plant growth and boost crop yields (Li et al., 2021), controlling greenhouses based on plant responses is more accurate and appropriate. This approach is preferable because plant physiological responses result from the interaction between the atmosphere, root, and the plant itself.

Until recently, real-time monitoring of crop physiological parameters without physical contact or destructive sampling has been challenging. However, advancements in computational intelligence have enabled the development of hyperspectral optical systems that can provide insights into crop physiology and morphology. These systems leverage a series of reflectance indices, such as the Photochemical Reflectance Index (PRI), which have been shown to correlate strongly with crop green biomass and photosynthesis rates

(Garbulsky et al., 2011). The PRI, in particular, was originally interpreted as a reflectance parameter capable of detecting the spectral signature of xanthophyll cycle pigments involved in the dissipation of excess light through non-photochemical quenching (Kováč et al., 2018).

Optical systems that measure canopy reflectance offer advantages over the traditional approach of using integrating spheres to measure leaf-scale reflectance factors (Lukeš et al., 2017). However, these high-cost sensors can be difficult to handle and lack the flexibility for deployment in multi-sensor platforms. The recent development of remote soft-sensors, which are mathematical models utilizing real-time sensor data, allows for the integration of plant-based indices and indicators (Elvanidi and Katsoulas, 2023 (b)). This more robust and user-friendly methodology enables the study of hourly variations in photosynthesis under different climatic and fertigation conditions, not just for a few days, but over an entire cultivation season.

In the current research, remotely measured data on photosynthesis were used to define the crop physiology cutoff points, which were subsequently integrated into a decision support system (DSS). This DSS aims to combine both environmental and crop physiology parameters. The data were collected from a tomato crop grown under extreme irrigation and environmental conditions. Initially, a logarithmic curve was fitted to establish the correlation between g_{sw} and photosynthesis (Ps). The mean response of Ps at maximum g_{sw} was considered as the maximum photosynthesis rate (Ps_{max}). Control standards were then defined as 70% of the Ps_{max}. Using the regression model, the researchers inversely predicted the corresponding g_{sw} values for these percentages of Ps_{max}. This allowed them to determine different g_{sw} cutoff points that could be used as thresholds in the DSS.

2. Materials and Methods

The measurements were carried out from May to December of 2019 in one of the five compartments of a multi-tunnel greenhouse with a total ground area of 1500 m^2 (250 m^2 each compartment). The establishments were located at the facilities of the University of Thessaly, Velestino, Volos (latitude 39° 22, longitude 22° 44′ , and altitude 85 m) in the continental area of eastern Greece.

The tomato plants (*Solanum lycopersicum* cv. Elpida) were cultivated in slabs filled with perlite slabs (ISOCON Perloflor Hydro 1, ISOCON S.A., Athens, Greece). The plants were fertigated with a fresh nutrient solution with set points of electrical conductivity (EC) around 2 dS m^{-1} and pH 5.8. The nutrient solution supplied to the crop was a standard nutrient solution for tomatoes grown in open hydroponic systems adapted to Mediterranean climatic conditions. The nutrient solution was supplied via a drip system and con-trolled by a time program irrigation controller (8 irrigation events per day).

In order to define the different g_{sw} cutoff points, records of different physiological responses of the plants to their surrounding microclimate under extreme conditions were gathered. These conditions included low (LTS) and high air temperatures (HTS), low nitrogen concentration (LNS), and low water concentration in the root zone (LWS). Additionally, measurements of no stressed (NoS treatment) plants were recorded.

The data were gathered by a multisensory tower consisting of an air temperature sensor (Thygro SDI-12, Symmetron, Gerakas, Greece), relative humidity sensor (Thygro SDI-12, Symmetron, Gerakas, Greece), solar radiation sensor (SP-SS, Apogee Instruments, Logan, UT, USA), leaf temperature sensor (Thermocouples, type T), and PRI sensor (type SRS-PRI, Meter group, Pullman, WA, USA). The multisensory tower was placed within the greenhouse, parallel to the vertical axis of the tomato's main stem. The measurements started 10 days after each treatment was applied and lasted for 25 days.

Totally, air temperature (Ta, °C), relative humidity (RH, %), solar radiation (SR, W m^{-2}), leaf temperature (TL, °C) and photochemical reflectance index (PRI) were recorded.

2.1. Calibration and statistics

The Based on PRI values, the photosynthesis rate (Ps, μmol m^{-2} s^{-1}) under extreme conditions were calculated:

$$Ps = 324.37*PRI + 8.92 \quad (1)$$

The calibration procedure of the remote PRI sensor and the Ps calculation was presented in Elvanidi & Katsoulas (2021).

Additionally, based on environment and photosynthesis data, g_{ws} was calculated based on Penman-Monteith equation (Katsoulas and Stanghelini, 2019):

$$g_{ws} = k*(1 - (RH\%/100))*VPD \quad (2)$$

where k is a constant equal to 0.69 and VPD is vapor pressure deficiency calculated according to methodology described in Katsoulas and Kittas (2008).

Then is to correlated g_{sw} status model with Ps values as the most direct physiological indicator of crop production. Initially, the g_{sw} is related to *Ps* by using g_{sw} as the independent variable (*X*) and *Ps* as the dependent variable (*Y*) to fit a logarithmic curve (Equation (1)).

$$Y = \beta_0 + \beta_1 \ln(X) + \varepsilon_i \quad (3)$$

where β_0 and β_1 are the model parameters and ε_i is the error term.

After the relationships between *Ps* and g_{sw} were established, the mean response of *Ps* corresponding to the maximum g_{sw} in the data was considered the upper bound of *Ps* (Ps_{max}). Considering the practical seedling cultivation, the values of maintained 70% of Ps_{max} were used as the control standards. The regression model of g_{sw} on Ps was used to inversely predict g_{sw} values corresponding to 70% of Ps_{max} and then to obtain the g_{sw} cutoff points.

3. Results and Discussion

The physiological data of tomato under extreme conditions, were used to fit a logarithmic curve with g_{sw} and Ps as the independent and dependent variables, respectively. In Figure 1 is illustrated the fitted logarithmic curve in LTS and HTS plants correlated with the values occurred in healthy plants (NS). The logarithmic curve is presented as Equation (4), (5) and (6) for NS, LTS and HTS respectively with $R^2 = 0.91$, $R^2 = 0.91$ and $R^2 = 0.90$.

$$NS: Ps = 6.30In*(g_{ws}) + 24.61 \quad (4)$$

$$LTS: Ps = 10.97*In(g_{ws}) + 33.4 \quad (5)$$

$$HTS: Ps = 7.65*In(g_{ws}) + 15.09 \quad (6)$$

Similar, in Figure 2 is illustrated the fitted logarithmic curve in LNS and LWS plants correlated with the values occurred in healthy plants (NS). The logarithmic curve of LNS and LWS is presented as Equation (7) and (8) with $R^2 = 0.91$, $R^2 = 0.90$ and $R^2 = 0.91$, respectively.

$$LTS: Ps = 10.97*In(g_{ws}) + 33.4 \quad (8)$$

$$HTS: Ps = 7.65*In(g_{ws}) + 15.09 \quad (9)$$

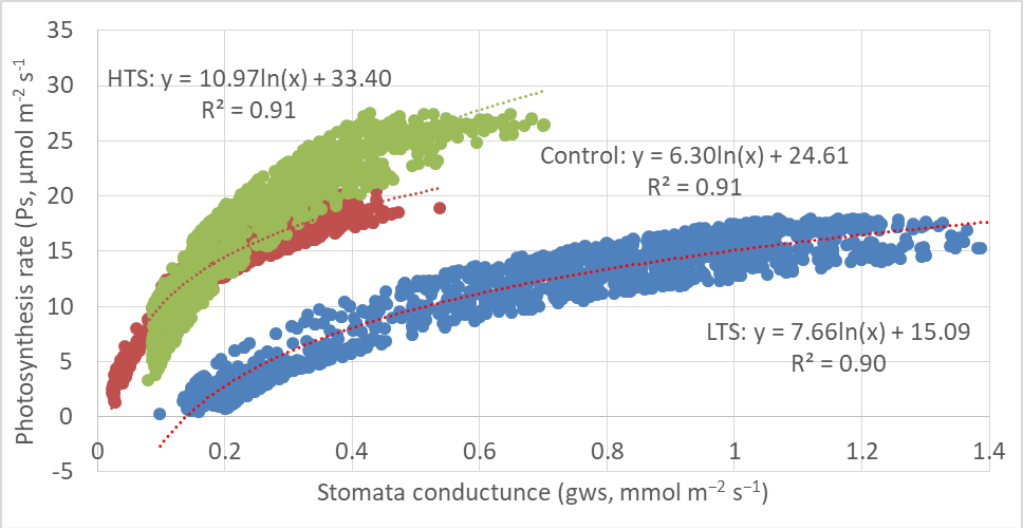

Figure 1. Logarithmic curve between the photosynthesis rate (Ps, µmol m^{-2} s^{-1}) and stomatal conductance (g_{ws}, mmol H_2O m^{-2} s^{-1}) values performed in plants growth in low temperature stress (LTS) and high temperature stress (HTS) compared to the no stressed (NS) plants.

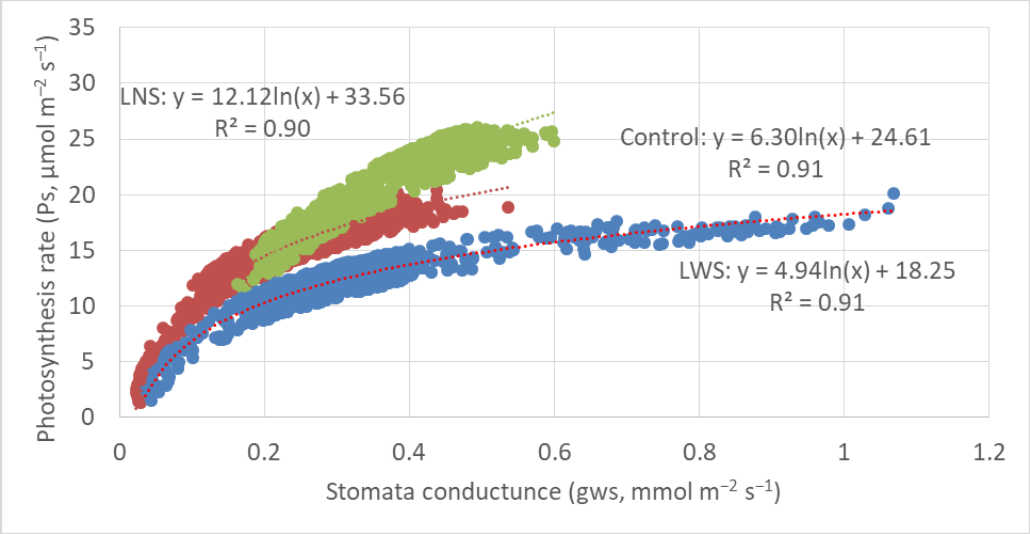

Figure 2. Logarithmic curve between the photosynthesis rate (Ps, µmol m^{-2} s^{-1}) and stomatal conductance (g_{ws}, mmol H_2O m^{-2} s^{-1}) values performed in plants growth in low nitrogen stress (LNS) and low water stress (LWS) compared to the no stressed (NS) plants.

The relationship between Ps and g_{ws} under different environmental conditions is crucial for understanding how plants respond to stress. According to the results, in no stress conditions, the photosynthesis rate increases moderately with an increase in stomatal conductance. The constant a = 6.30 indicates the sensitivity of Ps to changes in g_{ws}, and b = 24.61 represents the baseline Ps when ln(g_{ws}) is zero. This relationship suggests that under optimal conditions, plants maintain a relatively high baseline photosynthesis rate, with moderate increases as g_{ws} increase. Under low temperature stress, the photosynthesis rate shows a higher sensitivity to changes in stomatal conductance compared to no stress conditions, as indicated by the larger constant a = 10.97. The baseline photosynthesis rate is also higher (b = 33.4), suggesting that plants under low-temperature stress might increase their photosynthetic activity more sharply with increases in g_{ws} to compensate for the stress conditions. For high-temperature stress, the Ps is less sensitive to changes in g_{ws} compared to low temperature stress but more sensitive than in no stress conditions, with a = 7.65. The baseline photosynthesis rate is lower (b = 15.09), indicating that high temperatures might suppress the overall photosynthetic capacity of the plants. In summary, the baseline Ps is highest under low temperature stress, indicating an elevated photosynthetic capacity as a response to cold stress. In contrast, plants under high

temperature stress show a lower baseline photosynthesis rate, reflecting the suppressive effects of high temperatures on photosynthesis. The no stress condition maintains a moderate baseline photosynthesis rate and sensitivity, representing optimal growing conditions. Under low water stress, the baseline photosynthesis rate is lower than that of no stress conditions. This reduction reflects the significant impact of insufficient water availability on the plant's photosynthetic capacity. According to Fang et al. (2022), in plants under drought stress, g_{sw} is reduced and the heat loss through leaf transpiration is also hindered, thereby increasing plant temperature. Similar findings were reported by Zhang et al. (2013). These fobservations highlight the importance of tailored greenhouse management practices to mitigate the effects of temperature stress and optimize plant growth and productivity.

Understanding these relationships is essential for optimizing irrigation and climate control in greenhouses. When the logarithmic curves of g_{sw} and Ps were obtained, the maximum g_{sw} value of 1.00 mol H_2O m^{-2} s^{-1} was incorporated into Equations (4-9) to achieve the corresponding value of Ps, which was different according to the treatment. Taking this value as the Ps_{max} of tomato crop, the maintenance of 70% of Ps_{max} was defined as the control standards of the system for each stress. In the Table 1 is presented the average and maximum Ps_{max} value of the 70% Psmax sample. Additionally, the number of values (%) corresponding to each 70% Ps_{max} of the logarithmic curve is also shown.

The table provides a clear comparison of how different stress conditions affect the photosynthesis rate of tomato crops. HTS results in the highest average Ps_{max}, suggesting that tomato plants may exhibit increased photosynthetic activity under such conditions, although the percentage of values corresponding to 70% of Ps_{max} is the lowest at 30%. In contrast, LWS shows a lower average Ps_{max} and the lowest percentage of values at 14%, indicating a more significant adverse effect on photosynthesis. The results highlight the importance of managing environmental and nutritional conditions to optimize the photosynthetic efficiency and overall health of tomato crops in greenhouse settings.

Table 1. Average, maximum and value count in % of the 70% Ps_{max} sample.

Type stress in tomato crop	Aver. 70% Ps_{max} (μmol m^{-2} s^{-1})	Max. 7 70% Ps_{max} (μmol m^{-2} s^{-1})	Value count in %, 70% Ps_{max} (μmol m^{-2} s^{-1})
No stress	17.34	20.4	50
Low temperature Stress	15.23	17.97	49
High temperature stress	27.48	27.48	30
Low nitrogen stress	23.48	26.05	64
Low water stress	16.83	20.08	14

These values serve as critical cutoff points for defining the physiological status of the crop under different stress conditions. By establishing these thresholds and enabling climate data, a conceptual plant-response-based strategy for a DSS it is performed to accurately the irrigation frequency and dosage of tomato crops cultivated under greenhouse conditions.

4. Conclusions

This research highlights the critical importance of integrating crop physiology data in the new strategies for optimizing irrigation management in greenhouse settings. By utilizing remotely measured photosynthesis data, precise crop physiology cutoff points were established and incorporated into a decision support system (DSS). hese cutoff points are pivotal in defining the irrigation strategy system. This innovative approach enables a more accurate and responsive irrigation strategy, tailored to the actual needs of the plants.

References

Markets and Markets. Commercial Greenhouse Market by Product Type (Fruits, Vegetables, Flowers & Ornamentals, Nursery Crops), Type (Glass Greenhouse, Plastic Greenhouse), Equipment (Heating Systems, Cooling Systems), and Region—Global Forecast to 2025. Available online: **https://www.marketsandmarkets.com/Market-Reports/commercial-greenhouse-market-221045451.html** (accessed on 8 February 2022).

Elvanidi A, Katsoulas N. Machine Learning-Based Crop Stress Detection in Greenhouses. *Plants*. 2023; 12(1):52. https://doi.org/10.3390/plants12010052 (a)

Elvanidi A, Katsoulas N. Performance of Gradient Boosting Learning Algorithm for Crop Stress Identification in Greenhouse Cultivation. *Biology and Life Sciences Forum*. 2022; 16(1):25. https://doi.org/10.3390/IECHo2022-12508 (b)

Elvanidi, A., Katsoulas, N. (2021, May). Calibration Methodology of a Remote PRI Sensor for Photosynthesis Rate Assessment in Greenhouses. In *Biology and Life Sciences Forum* (Vol. 3, No. 1, p. 60). MDPI

Fang S-L, Chang T-J, Tu Y-K, Chen H-W, Yao M-H, Kuo B-J. Plant-Response-Based Control Strategy for Irrigation and Environmental Controls for Greenhouse Tomato Seedling Cultivation. *Agriculture*. 2022; 12(5):633. https://doi.org/10.3390/agriculture12050633

Garbulsky, M. F., Peñuelas, J., Gamon, J., Inoue, Y., & Filella, I. (2011). The photochemical reflectance index (PRI) and the remote sensing of leaf, canopy and ecosystem radiation use efficiencies: A review and meta-analysis. *Remote sensing of environment*, *115*(2), 281-297. https://doi.org/10.1016/j.rse.2010.08.023

Katsoulas, N., & Kittas, C. (2008). Impact of greenhouse microclimate on plant growth and development with special reference to the Solanaceae. *Eur. J. Plant Sci. Biotechnol*, *2*(1), 31-44.

Katsoulas N, Stanghellini C. Modelling Crop Transpiration in Greenhouses: Different Models for Different Applications. *Agronomy*. 2019; 9(7):392. https://doi.org/10.3390/agronomy9070392

Kováč, D., Veselovská, P., Klem, K., Večeřová, K., Ač, A., Peñuelas, J., & Urban, O. (2018). Potential of photochemical reflectance index for indicating photochemistry and light use efficiency in leaves of European beech and Norway spruce trees. *Remote Sensing*, *10*(8), 1202. https://doi.org/10.3390/rs10081202

Li, H., Guo, Y., Zhao, H., Wang, Y., & Chow, D. (2021). Towards automated greenhouse: A state of the art review on greenhouse monitoring methods and technologies based on internet of things. *Computers and Electronics in Agriculture*, *191*, 106558. https://doi.org/10.1016/j.compag.2021.106558

Lu, N., Nukaya, T., Kamimura, T., Zhang, D., Kurimoto, I., Takagaki, M., ... & Yamori, W. (2015). Control of vapor pressure deficit (VPD) in greenhouse enhanced tomato growth and productivity during the winter season. *Scientia Horticulturae*, *197*, 17-23. https://doi.org/10.1016/j.scienta.2015.11.001

Lukeš, P., Homolová, L., Navrátil, M., & Hanuš, J. (2017). Assessing the consistency of optical properties measured in four integrating spheres. *International journal of remote sensing*, *38*(13), 3817-3830. https://doi.org/10.1080/01431161.2017.1306144

Markets and Markets. Commercial Greenhouse Market by Product Type (Fruits, Vegetables, Flowers & Ornamentals, Nursery Crops), Type (Glass Greenhouse, Plastic Greenhouse), Equipment (Heating Systems, Cooling Systems), and Region—Global Forecast to 2025. https://www.marketsandmarkets.com/Market-Reports/commercial-greenhouse-market-221045451.html

Zhang, D., Du, Q., Zhang, Z., Jiao, X., Song, X., & Li, J. (2017). Vapour pressure deficit control in relation to water transport and water productivity in greenhouse tomato production during summer. *Scientific Reports*, *7*(1), 43461. https://doi.org/10.1038/srep43461

Zhang, S.Y., Zhang, G.C., Liu, X. *et al.* The responses of photosynthetic rate and stomatal conductance of *Fraxinus rhynchophylla* to differences in CO_2 concentration and soil moisture. *Photosynthetica* 51, 359–369 (2013. https://doi.org/10.1007/s11099-013-0033-2

Economics of retrofitted autonomous tractors for crop protection spraying: a case study from Greece

Tseganesh Wubale Tamirat[a*], Søren Marcus Pedersen[a] , and Jens Erik Ørum[a]
[a] Department of Food and Resource Economics, University of Copenhagen, 1958 Frederiksberg C., Denmark
* Corresponding author. Email: twt@ifro.ku.dk

Abstract

High reliance on labour and soil compaction are among the top challenges for European crop farmers. Given the high seasonality nature of field crop farming, the consequences of lack of access to affordable labour when needed would be devastating as was manifested during the COVID pandemic. The issue is alarming in view of aging of the farming population. Moreover, repetitive field crop operations such as spraying of crop protection chemicals expose farm workers to chemicals detrimental to their health and the environment. Autonomous systems may help tackle the labour challenge while providing opportunities to improve efficiency, curb emission, reduce soil compaction and improve biodiversity. However, autonomous systems involve high upfront investment cost and uncertainty regarding expected benefits, calling for context-relevant cost-benefit-analysis (CBA) studies. Retrofitting machinery which farmers are familiar with presents interesting aspects (e.g., possibility to function both as an autonomous and conventional platform, relatively known retrofitting cost compared to purpose-built robots). This study aims to provide farm level cost benefit analyses of autonomous systems being developed by a European project called ROBS4CROPS which combines smart implements, autonomous vehicles and high-level planning and scheduling software. This paper focuses on autonomous spraying using retrofitted tractors drawing on a case study of table grapes spraying in Corinth, Greece.

Data for the CBA was gathered through interviews with project site managers, field visits, field experiment data, price quotes from technology providers, literature, and expert opinion. Cost of other operations, crop yield and quality are assumed the same between conventional and autonomous systems. Alternative scenarios were defined considering farm characteristics, market price of machinery and inputs, agronomic constraints and robotic system reliability and regulation. In the analysis, reference farm size of 10 ha and average field size of 4 ha was used. The costs and benefits of the robotic retrofitted system were evaluated against existing practices using conventional tractors. Results show that the retrofit system is moderately cheaper than conventional system in many of the scenarios considered. Considerable labour saving appears to be feasible (32%). However, as pesticide costs account for the major share of total private cost of spraying, the robotic system does not pay off without sizable reduction in pesticide use.

Keywords: Autonomous spraying, table grape, Greece.

1. Introduction

Critical challenges in contemporary European mechanized farming are soil compaction induced by heavy machinery (Lamandé et al., 2018; Piccoli et al., 2022; Tamirat et al., 2022), and scarcity and high cost of labour (van Evert et al., 2024; Ørum et al., 2023). A survey of farmers from four European countries shows that farmers' top challenges associated with conventional machinery are high reliance on labour and soil compaction (Pedersen et al., 2023).

Given the high seasonality (sensitivity to timing) nature of field crop farming, the consequences of lack of access to affordable labour when needed would be devastating. This was clearly manifested during the COVID pandemic which restricted the flow of workforce because of which many crops perished in the field. The situation is alarming in view of aging of the farming population where the young generation is getting away from farming as a way of life and/or engaging in farming tasks that involve dirt and inconvenience (e.g., weeding).

An equally pressing challenge is that repetitive field crop operations such as spraying of crop protection chemicals expose farm workers to chemicals detrimental to their health (let alone the environment). This is not to forget that climate change is already challenging European agriculture calling for management

practices and technological solutions to curb emission of greenhouse gases.

Autonomous systems may help tackle the labour challenge while also providing opportunities to improve input use efficiency (Gonzalez-de-Santos et al., 2017; Gonzalez-de-Soto et al., 2015) and curb Green-House-Gas emission (Ghalazman et al., 2022; Gorjian et al., 2020). Owing to their smaller size, robots also present opportunities to reduce soil compaction (Duckett et al., 2018; King, 2017).

Practical adoption of commercial agricultural robots is low (Gil et al., 2022) partly because the costs and benefits associated with their use are not yet clear. Limited access to information about field robots and supplementary services are also important limiting factors (Pedersen et al., 2023). Earlier attempts to assess economic feasibility studies were done by Pedersen et al. (2006), Pedersen et al. (2017) and Shockley et al. (2019). Pradel et al. (2022) presented comparative life cycle assessment of intra-row and inter-row weeding practices using autonomous robot systems in French vineyards.

Literature on the economics of autonomous robots in field crop farming is still sparse. This is partly because most of the parameters to calculate costs and benefits associated with such technologies are not yet known. A guiding framework to estimate the costs associated with robotic systems is provided by (Lampridi et al., 2019). Following this framework, Vahdanjoo et al. (2023) assess the operational, economic and environmental performance of robotic seeding and weeding operations in arable farming context using Robotti of AgroIntelli. The study concluded that the robotic system provides considerable operational and economic performance benefits even though it takes longer time to complete operation of a given farm area.

Lowenberg-DeBoer et al. (2021) documented promising technical and economic feasibility of arable crop production with autonomous equipment which allows medium size farms to approach minimum per unit production cost levels. According to Lowenberg-DeBour (2020), investment for conventional and robotics machinery are comparable for smaller farms but larger farm sizes have comparative advantage in terms of substantial saving in farm equipment through intensive use of robotic components. Possibilities to retrofit existing machinery appear to partly limit this divide. An added value of retrofitting is that most of the cost components are known compared to that of purpose-built robotic systems (Lowenberg-DeBour, 2020).

There have been developments in techniques to retrofit conventional tractors for autonomous capability (Celenta and De Simone, 2020). Backman et al. (2022) provided an example of how to build a robot tractor integrating commercially available components and widely used standards. Baillie et al. (2017) provides and overview of developments in autonomous tractors. An integral component of agricultural automation is navigation. (Xu and Rai, 2024) presented an example for autonomous tractors operating in peach orchards which use vision-based autonomous navigation stack. As Shutske (2023) highlighted, safety and risk assessment should be at the forefront while designing agricultural automation and choosing the extent of machine autonomy.

Costs and benefits of robotic solutions for field crop operations are not yet clear. Hence, there is a clear need for context-relevant estimates on costs and benefits associated with the technology. This paper contributes to this by presenting a cost-benefit analysis of autonomous spraying of crop protection chemicals using retrofitted tractors drawing on a case study in table grapes in Corinth, Greece.

2. Materials and Methods

2.1. Study context

This study is a part of an European project called ROBS4CROPS which aims to develop reliable and fully autonomous robotic solutions for repetitive, labour demanding and tedious field operations primarily focusing on weeding and spraying of crop protection chemicals. To achieve this, the project combines smart implements, autonomous vehicles and high-level planning and scheduling software (referred to as 'farming controller') which orchestrates the planning and execution of the agricultural operations using digital twin technology (Paraforos et al., 2022; Van Evert et al., 2023). Testing and further development of the robotic solutions undertakes on real farm conditions in Large Scale Pilots (LSPs) situated in Greece, France, Spain and the Netherlands. This study focuses on spraying of table grapes in Greece using (semi)autonomous retrofitted tractor. The pilot farm in Greece is run by PEGASUS–a cooperative of farmers producing table grapes on 200 ha of land as of 2023. Operating under the brand name 7grapes, PEGASUS exports 95% of its fresh table grape production to several countries with Great Britain, Germany and Netherlands being the major destinations.

2.2. Overview of conventional practice

Table grapes in Corinth, Greece receive many spray treatments of foliar nutrients, crop protection agents, and crop growth regulators (Anastasiou et al., 2023). Per season, about 11 spraying passes are needed but could be more depending on variety (by maturity), disease infestation and weather conditions (a brief summary of when operation starts and ends is provided in Table 1). To minimize health risks from chemical residues on fruits, spraying must stop two weeks before harvest.

Table 1: Operation calendar for table grape spraying in Corinth, Greece

Variety group	Example varieties	Spray start	Spray end	Operations per season
Early season	Thompson seedless	2nd week of March	1st week of July	10
Mid-season	Crimson	2nd week of April	1st week of August	10
Late season	Pristine	Last week of April	End of September*	13

* In North Greece (e.g., valley of Stimaga), spraying lasts until November (harvest until December) depending on weather condition.

Grape farmers in Corinth are increasingly being challenged by unfavourable weather conditions limiting water availability. An unfavorable weather condition (rain, heatwave) just a week before harvest can destroy fruits of hard work thereby leaving farmers devastated (Mr. Thanos Dritsopoulos, Pegasus, 20 October 2023). The vehicle used as a reference is a 52 kW (=70 hp) conventional tractor from John Deere served by a sprayer of 600 L capacity (see Figure 1).

Figure 1 Reference tractor for conventional practice
Source: Photo taken during field visit on 15 June 2023.

2.3. The retrofitted robotic system

During 2023 season, the Robs4crops experiment was conducted on a small plot of 0.6 ha situated 3 km away from PEGASUS' pack house. For the experiments, the retrofitted tractor was used with an ASM sprayer of 200 L capacity (

Figure 2). Detailed description of autonomous capabilities the robotic systems being developed under the project is provided in Roure and Rascón (2021).

Adjusting perception unit for field test

Filling sprayer tank with water in the village

Retrofit system during field experiment

Figure 2 Robs4crops retrofit system
Source: Photos taken during a field visit on 15 June 2023.

2.4. Data collection and validation process

Data inputs needed for the economic analyses were identified through a combination of approaches including preparation of protocol for data collection, insights from farmer surveys in case study areas conducted in 2022/23 (as input to Pedersen et al. (2023)), case specific needs identified in consultation with LSP managers, review of literature, and expert opinion. The study involved an iterative process of data collection, scenario development, data validation, setting up economic model, evaluating relevance and adequacy of economic model in close collaboration with Robs4crops LSP managers.

Most of the data used in this study was accessed through the LSP managers who gathered the data consulting relevant sources blending with their experiences as agronomists/advisors/dealers. Following consultation meetings, the UCPH team would share templates for the LSP managers to fill data in. In most cases, data updates were done interactively during discussion meetings. When doubts arise during discussions, the LSP managers would make a call to farmers and agronomists to verify/clarify those issues on the spot when possible. When the data inputs were believed to be completed, review sessions followed to check if results of the economic model reflect realities on the ground. Efforts have been made to incorporate the views of other partner partners. There were many instances which led to revision of assumptions, data inputs and estimation of intermediary parameters.

2.5. Key concepts and terminology

Key concepts and terminology are defined as below:

Operation window: an agronomically reasonable duration (number of days) during which a spraying operation needs to be done to avoid crop damage. This surely depends on phenological stage, disease infestation and/or weather conditions. There are differences in acuteness depending on the type of disease targeted. A 7-day operation window was chosen for the BASE scenarios.

Workable hours per day: number of hours during which a target operation can be performed with potentially beneficial effect. This is conditioned by an interplay of soil/weather conditions, plant conditions, machinery capacity and labour availability. In the case study area (Corinth, Greece), table grape spraying is normally done early in the morning or late in the afternoon for best possible effect considering temperature, humidity and wind speed. After 11am, wind from the sea is often a challenge which sometimes subsides at about 6pm. Even when weather conditions allow spraying all night, absorption can be limited after 9pm in the evening by closure of plat stomata. In March and April, the temperature may allow spraying around noon but during June and July it would simply mean burning the leaves. Bringing the human factor into the equation, late evening spraying may entail high labour cost. However, in the case study area, as many of the farmers use own labour, this is not often considered binding constraint. As such, five hours is optimal workable hours per day but in practice farmers do extend the working hours.

Effective field capacity: farm area that can be worked per unit of time which depends on working speed, working width and field efficiency (the later assumed to be 70% following Vahdanjoo et al. (2023)).

Scaling farm size: farm area that can be served by one vehicle unit during operation window and beyond which investing in extra unit of machinery is needed.

Extra machinery capacity: the difference between total available machinery hours per year (technically possible and adjusted by use norms in the case study area) and the total number of hours needed to complete spraying of the reference farm size for the respective cases. This extra capacity is assumed to be fully utilized during a year by use of machinery for other operations, other crops and/or sharing it out with other farmers. Irrespective of the mode of use, we applied a per hour contractual rate which was determined in consultation with the respective pilot case leaders for the respective use cases.

Extra cost to society: an indicator for undesirable (negative) externalities to society because of actions of farmers. This is approximated by the sum of CO_2 emission tax and pesticide tax. As no such regulations are in action in the case study area, these cost estimates are not included in cost estimates for farmers. Cost estimates presented in section **Error! Reference source not found.** can be regarded as private cost to f armers. In the case of such regulations in future and if farmers are required to pay, then these extra costs should be incorporated into farm-level costs as well.

2.6. Scenario definition

BASE scenario for the robotic and conventional systems is defined by the parameter inputs presented in section **Error! Reference source not found.**. An effort has been made to use parameter values that reflect t he situation in the respective case study areas. However, even farmers in the same area growing the same crops often have different circumstances. Moreover, parameters of the model involve uncertainties especially those associated with the robotic system due to early stage of development (e.g., investment cost, supervision time, work capacity). To partly consider these concerns, relevant alternative scenarios have been set up and evaluated considering changes in values of input parameters related to:

- Farm structure (farm size, field size, field-to-field and field-to-barn distance),
- Market price (labour price, fuel price, machinery and implement price),
- Agronomic constraints (window of operation, workable hours per day), and
- Robotic system reliability and regulation (working speed, economic life, degree of human operation).

Table 2: Scenario definition

Scenario name	Definition	Parameter change applicable to
Costly labour	Labour price up by 35%	Conventional & Robotic system
Costly fuel	Fuel price up by 25%	
Big farm with big fields	Farm size up by 300% and Field size up by 60%. [Farm size= 30 ha; Field size= 6.4 ha]	
Big farm with average-sized fields	Farm size up by 300% [Farm size= 30 ha]	
Adjacent fields	F2F & F2B down by 99%	
Scattered fields	F2F & F2B up by 50%	
Flexible operation	Operation window=14	
Acute operation	Operation window=4	
Cheap robot	Vehicle and implement price down by 25%	Robotic system only
Workaholic robot	Workable hours up by 25%	
Fast robot	Working speed up by 10%	
Short-life robot	Economic life down by 25%	
Low autonomy robot	Degree of human operation up by 50%	
High autonomy robot	Degree of human operation down by 50%	

Performance indicators chosen to compare robotic system against conventional system under additional scenarios (defined in Table 2) are: labour time, fuel consumption, cost of other (non-machinery) inputs, machinery cost and total private cost (under full utilization of machinery capacity).

2.7. Data for Base scenario

Table 3 presents data about farm characteristics, agronomic constraints, operational parameters, and investment cost under BASE scenario.

For farmers having table grapes as their main crop, below 8 ha is not economically justifiable (interview with Markos and Thanos, 14 June 2023). Hence, the reference farm size for the analysis was chosen considering this threshold.

Table 3: Farm, operation, and investment data for BASE scenario

Feature	Unit	Conventional tractor (52 kW)	Retrofitted (55 kW)
Farm size	ha	10	10
Field size	ha	4	4
Field to field distance	km	3	3
Field to barn distance	km	2	2
Fuel use operation	L/ha	5.5	5
Fuel use transport	L/h	10	10
Transport speed	km/h	25	40
Working speed	km/h	5	4
Working width	m	2.7	2.7
Workable hours per day	H	7	9
Number of operations per season	-	11	11
Vehicle investment	€	50000	85000
Sprayer	€	10000	10000
Sensors*	€	-	11000
Labour price	€/h	20	20
Fuel price	€/L	1.5	1.5
Water price	€/100L	0.15	0.15
Rent-out fee per hour of machinery	€/h	15	15

* Includes speed sensor, work-quality sensor, and perception unit.

Labour time includes time to test and inspect equipment, fill spray tank, fill fuel tank, mount implements for operation, disassemble for transport, transport (from barn to field and between fields) and direct human operation of machinery. Labour time components specific to robotic systems are time to load robot on trailer and unload, start-up operation, intervention to restart and/or fix equipment malfunction during operation, and supervision. Given the current state of technology, some degree of direct human operation of the robotic/retrofit systems is required. For base scenario, 65% autonomous operation is used. During autonomous operation, the robotic system is under supervision (be it from within the field or remotely). 'Effective' time used for supervision is calculated under the assumption that the supervisor could use 75% of the supervision 'duration' to perform some other tasks alongside (e.g., field monitoring, planning, etc.). Human intervention to resume if robot operation gets interrupted is assumed to be 5% of field operation time. During transport, the retrofit system can be driven by tractor drivers the same way as conventional tractor.

Due to difficulties in getting precise data on amount of pesticide and price by product type, it was decided to directly use pesticide cost (as it was relatively easier for LSP managers to provide). In Corinth area of Greece, pesticide cost for table grapes spraying is approximately €2150/ha with fungicides and insecticides accounting for the major share. As the project experiment was at an early stage, it was not possible to find reliable data on the amount of pesticide saving through improved precision using the robotic system. Average water use for conventional spraying was 800L/ha per operation. As per LSP managers' expectations, a 15% reduction of pesticide and water (compared to conventional practice) was used for the base scenario.

Cost items are grouped into machinery cost and other input (non-machinery cost). Machinery cost includes investment as well as repair and maintenance cost for both vehicle and implements, and insurance for vehicle. In the case of contracting extra capacity, reported machinery cost is net of income from contracting. Input (non-machinery) cost includes cost of labour, fuel, transport (fuel and labour time included in labour cost), water, pesticide (herbicide, fertilizer[1], growth regulator, fungicide, insecticide, etc.). In the case of the robotic system, this also includes annual subscription fee for enabling features for automated operation (precision navigation, internet network, planning and scheduling software referred to as 'Farming

[1] Cost of fertilizers included in the CBA is for only those crop nutrients applied to leaves and fruit through spraying (i.e., basic fertilization to the crop root is excluded).

Controller').

2.8. Working assumptions

The following working assumptions were made for the basic scenario:

1. No change in other management practices apart from the target operation in each use case. Hence, there is no systematic change in the cost of other operations.
2. Same yield level and quality under robotic and conventional practices:
3. Extra capacity beyond what is needed for the spraying operation on the reference farm is assumed to be fully utilized during a year by use of machinery for other operations, other crops and/or renting out to other farmers. In this paper, all these possible ways of machinery utilization are referred to as 'rent-out'. In situations where sharing and/or renting-out is not an option as such, bigger size farms (and/or farms growing a mix of crops possibly with differing operation calendars) would have comparative advantages through intensive use of machinery and robotic components. Machinery and total cost estimates are calculated for both cases (with and without rent-out).
4. Mixed mode of acquisition: Farmer owns tractor, robot and implements whereas enabling features for the robotic system (Precision guidance, network, scheduling & planning software) are accessed through annual subscription.

Given assumptions #1 and #2, the difference in economic performance between the robotic and conventional systems comes from differences in the cost of spraying.

3. Results and Discussion

3.1. Results under BASE scenario

Per hour of operation, it is possible to spray 0.76 ha with the retrofit system whereas the conventional system can cover nearly a hectare (Table 4). Due to longer workable hours for the robotic system, daily area capacity of the two systems is comparable. In total, the spraying operations for the reference farm size of 10 hectares use only 145 hours leaving 845 hours of extra machinery capacity.

Table 4 Machinery utilization and use of labour and fuel

Parameter	Unit	Conventional	Retrofit
Effective field	ha/H	0.95	0.76
Farm area per day	ha/day	6.62	6.80
Scaling farm size	ha	46	48
Operation hours	H/ha/year	11.64	14.55
Extra machinery	H/year/farm	883.6	854.5
Labour time	H/ha/year	12.69	8.68
Fuel consumption	L/ha/year	69	76

Given the small size of the reference farm, there is a wide difference between costs with and with-out rent-out.

Table 5 Cost estimates under BASE scenario

Parameter	Unit	Trac_C	Retrofit
Total investment	€	60000	108750
Lifetime insurance cost	€	9712	12512
Lifetime R&M cost	€	12626	17149
Present value of income from renting-out machinery extra capacity	€	128726	157229
Input (non-machinery) cost	€/ha/year	2520	2146

Machinery cost with rent-out	€	-478	-256
Machinery cost without rent-out	€/ha/year	848	1881
Total private cost with rent-out	€/ha/year	2042	1890
Total private cost without rent-out	€/ha/year	3368	4026

The negative average machinery cost estimates in Table 5 reflect that when renting out extra machinery capacity is a possibility, small holder farmers could potentially more than offset initial investment cost.

3.2. Results under alternative scenarios

Results under alternative scenarios (as defined in Table 2) are presented in Table 6. For the Greece case, when evaluated in terms of per hectare cost of spraying, the robotic (retrofitted) system is moderately cheaper than conventional system in many of the scenarios considered except in the case of 'Flexible operation' scenario and 'Shortlife robot' scenario.

Table 6: Scenario analysis for table grape spraying (ratio of robotic to conventional)

Scenario	Labour	Fuel	Average	Input	Total
BASE	0.68	1.1	0.54	0.85	0.93
Costly labour	0.68	1.1	0.54	0.85	0.92
Cheap robot	0.68	1.1	1.5	0.85	0.7
Big farm with big fields	0.68	1.11	18.09	0.85	0.93
Big farm with average sized fields	0.68	1.1	18.09	0.85	0.93
Adjacent fields	0.69	1.14	0.54	0.85	0.93
Scattered fields	0.68	1.09	0.54	0.85	0.92
Flexible operation	0.68	1.1	8.27	0.85	1.09
Acute operation	0.68	1.1	0.75	0.85	0.88
Workaholic robot	0.63	1.1	0.54	0.85	0.92
Fast robot	0.62	1	0.6	0.84	0.9
Shortlife robot	0.68	1.1	-0.23	0.85	1.1
Low autonomy robot	0.83	1.1	0.54	0.87	0.94
High autonomy robot	0.53	1.1	0.54	0.84	0.91

In Greece where suitable daytime work hours are very limited by weather (e.g., hot summer days), ability to work longer outside of those hours (e.g., work long late afternoon and at night) would mean a lot. As most farmers in Corinth area use own (family) labour for spraying operations, labour cost is likely not a strong motivator to use autonomous systems. Rather, the potentials for pesticide saving and minimal human exposure to chemicals could be priority considerations. Given that farm sizes are very small in Corinth, farmer-acquisition of robotic solutions may not be economical unless full utilization of machinery capacity is possible. Table grape farmers in the area also grow other crops such as olive, orange and apricot for which the robotic system could potentially be used. If the robotic system brings tangible results for early adopters, strong social capital of Greece farmers could be capitalized on to promote adoption.

Indirect effects such as soil compaction and health risk could not be included in the current results due to lack of estimates. To partly reflect undesirable societal costs, estimates have been included for CO_2 emission and pesticide using 'regulation through tax' approach. But these costs are not included in the cost estimates for farmers because no such regulations are in effect in the case study areas. In future, if such regulations come into play and farmers must pay those taxes, they potentially respond by changing their pesticide and fuel consumption thereby changing the entire cost-revenue structure as well as management practices. For example, reduced use of pesticide may compromise crop yield and quality. The intention in this study is to indicate that possible reduction in amount of pesticide and fuel consumption would bring about direct cost savings for farmers while at the same time minimizing unintended extra costs to society.

4. Conclusion

Given the data and assumptions, a considerable reduction in labour hours is possible. Though the cost differentials are not so pronounced, estimates show moderate cost advantage with the robotic system. Admittedly, there are uncertainties on some parameters and/or estimated results given that some aspects of the robotic system are yet under development. Given the possibilities, we believe that the economic model has set a solid foundation which can be updated as we learn more in the remaining period of the project and beyond. Moreover, the reported results shed important light into understanding key features that influence relative economic performance of the envisioned robotic system.

Further advances in sensor technologies, communication platforms, better internet connectivity on farms, etc., would create conducive environments for robotic solutions and bring about rewarding benefits for farmers and stakeholders. Long-term success of robotic systems of course depends on accessibility of complimentary services (such as robot servicing, data analytics), clear regulations and compliance regarding data ownership, context-relevant market models, etc., all calling for quality collaboration among stakeholders.

Future research about economics of robotic applications in field crop farming should consieder socio-environmental impacts such as health risk, pesticide pollution, soil compaction; full-farm modelling considering multi-cropping and multiple operations; and data from several seasons and use cases substantiated with narratives learnt through direct engagement with farmers, robot service providers, etc.

Implications for technology design, implementation and market models include a need for further work in ensuring ‘safe and reliable autonomy’ of robotic systems such that labour time can be kept to minimum. Given high investment cost added to the general observation that operation time with robotic systems is longer, they are least likely to pay off if need for human involvement is not minimal. With more established and reliable robotic systems and accompanying decision support platforms, one person would potentially monitor several robots at a time there by reducing monitoring cost. Considering that not all operations currently performed using a conventional tractor and a driver are achievable with a robot, the possibility of ‘full utilization of machinery capacity’ may rather be limited. In the face of high investment cost, farmers will not reap the promised benefit of robotic system if they invest in it at all. One important implication is modular design of robots to enable versatile functionality. Especially in the case of small farm sizes, market models embracing the principles of ‘shared economy’ (e.g., ‘shared ownership’, accessible rental/leasing/contracting services, etc.) need to be explored. Existing communal schemes such as farming cooperatives could potentially play a critical role in facilitating sharing-based acquisition models which may otherwise be impractical due to challenges in coordination, issues of trust and high transaction cost, among others. Regulatory authorities could play a crucial role in moderating the technology transition by creating a level playground among actors through clear regulations and reliable enforcement as well as providing incentives. This study puts forward the below to be considered as integral parts of policy toolbox:

- Financial incentives: tax deductions during defined trial periods, and ‘shared acquisition’ subsidies (e.g., subsidy to a cooperative which buys robots to offer affordable services to its members);
- Conducive institutional environment that supports ‘sharing economy’ arrangements;
- Socio-environmental stewardships based on credibly documented improvements (e.g., if a user considerably reduces pesticide use and human exposure to harmful chemicals from using smart robots); and
- Monitoring and governance mechanisms to combat green washing and unfulfilled promises.

References

Anastasiou, E., Templalexis, C., Lentzou, D., Biniari, K., Xanthopoulos, G., and Fountas, S. J. S. A. T. (2023). Do soil and climatic parameters affect yield and quality on table grapes? *Smart Agricultural Technology* **3**, 100088.

Backman, J., Linkolehto, R., Lemsalu, M., and Kaivosoja, J. (2022). Building a Robot Tractor Using Commercial Components and Widely Used Standards. *IFAC-PapersOnLine* **55**, 6-11.

Baillie, C., McCarthy, D., Thomasson, Z., and Sukkarieh, S. (2017). Developments in autonomous tractors. *In* "Grains Research Update", pp. 30.

Celenta, G., and De Simone, M. C. (2020). Retrofitting techniques for agricultural machines. *In* "New Technologies, Development and Application III" (I. Karabegović, ed.), pp. 388-396. Springer International Publishing.

Duckett, T., Pearson, S., Blackmore, S., and Grieve, B. (2018). "Agricultural Robotics: The Future of Robotic Agriculture. UK-RAS White Paper Series." UK-RAS.

Ghalazman, A., Das, G. P., Gould, I., Zarafshan, P., S., V. R., Heselden, J., Badiee, A., Wright, I., and Pearson, S. (2022). Chapter 10 - Applications of robotic and solar energy in precision agriculture and smart farming. *In* "Solar Energy Advancements in Agriculture and Food Production Systems" (S. G. a. P. E. Campana, ed.), pp. 351-390. Academic Press.

Gil, G., Casagrande, D., Cortés, L. P., and Verschae, R. (2022). Why the low adoption of robotics in the farms? Challenges for the establishment of commercial agricultural robots. *Smart Agricultural Technology* **3C**.

Gonzalez-de-Santos, P., Ribeiro, A., Fernandez-Quintanilla, C., Lopez-Granados, F., Brandstoetter, M., Tomic, S., Pedrazzi, S., Peruzzi, A., Pajares, G., and Kaplanis, G. J. P. A. (2017). Fleets of robots for environmentally-safe pest control in agriculture. *Precision Agriculture* **18**, 574-614.

Gonzalez-de-Soto, M., Emmi, L., Garcia, I., and Gonzalez-de-Santos, P. (2015). Reducing fuel consumption in weed and pest control using robotic tractors. *Computers and Electronics in Agriculture* **114**, 96–113.

Gorjian, S., Minaei, S., MalehMirchegini, L., Trommsdorff, M., and Shamshiri, R. R. (2020). Applications of solar PV systems in agricultural automation and robotics. *In* "Photovoltaic Solar Energy Conversion" (S. Gorjian and A. Shukla, eds.), pp. 191-235. Academic Press.

King, A. J. N. (2017). Technology: The future of agriculture. *Nature* **544**, S21-S23.

Lamandé, M., Greve, M., and Schjønning, P. J. C. (2018). Risk assessment of soil compaction in Europe–Rubber tracks or wheels on machinery. *Catena* **167**, 353-362.

Lampridi, M. G., Kateris, D., Pearson, S., Sørensen, C. G., Vasileiadis, G., Marinoudi, V., Balafoutis, A., and Bochtis, D. (2019). A Case-Based Economic Assessment of Robotics Employment in Precision Arable Farming. *Agronomy* **9**.

Lowenberg-DeBoer, J., Franklin, K., Behrendt, K., and Godwin, R. J. P. a. (2021). Economics of autonomous equipment for arable farms. *Precision Agriculture* **22**, 1992-2006.

Lowenberg-DeBour, J. (2020). Being a farmer in the age of robotics and artificial intelligence. Ted talk on 18 May 2020 https://www.youtube.com/watch?v=lhQosWrq0vo . Last accesed on 26 January 2024.

Paraforos, D. S., Aubé, C., Athanasakos, L., Avgoustakis, I., Baron, S., Bresilla, T., Fountas, S., Hemming, J., Karagiannis, P., and Mylonas, N. J. I.-P. (2022). Connecting agricultural robots and smart implements by using ISO 11783 communication. *IFAC-PapersOnLine* **55**, 200-205.

Pedersen, S., Tamirat, T. W., and Ørum, J. (2023). "D7.1. Report on social impact." Robs4crops.

Pedersen, S. M., Fountas, S., Have, H., and Blackmore, B. J. P. a. (2006). Agricultural robots—system analysis and economic feasibility. *Precision Agriculture* **7**, 295-308.

Pedersen, S. M., Fountas, S., Sørensen, C. G., Van Evert, F. K., and Blackmore, B. S. J. P. A. T. E. P. (2017). Robotic seeding: Economic perspectives. *Precision Agriculture: Technology Economic Perspectives*, 167-179.

Piccoli, I., Seehusen, T., Bussell, J., Vizitu, O., Calciu, I., Berti, A., Börjesson, G., Kirchmann, H., Kätterer, T., and Sartori, F. J. L. (2022). Opportunities for mitigating soil compaction in Europe—Case studies from the soilcare project using soil-improving cropping systems. *Land* **11**, 223.

Pradel, M., de Fays, M., and Seguineau, C. J. S. o. T. T. E. (2022). Comparative Life Cycle Assessment of intra-row and inter-row weeding practices using autonomous robot systems in French vineyards. *Science of The Total Environment* **838**, 156441.

Roure, F., and Rascón, J. F. (2021). "Robs4crops D3.1. Autonomous capabilities definition." Robs4crops project.

Shockley, J. M., Dillon, C. R., and Shearer, S. A. (2019). An economic feasibility assessment of autonomous field machinery in grain crop production. *Precision Agriculture* **20**, 1068–1085.

Shutske, J. M. (2023). Agricultural automation & autonomy: Safety and risk assessment must be at the forefront. *Journal of Agromedicine* **28**, 5-10.

Tamirat, T. W., Pedersen, S. M., Farquharson, R. J., de Bruin, S., Forristal, P. D., Sørensen, C. G., Nuyttens, D., Pedersen, H. H., Thomsen, M. N. J. S., and Research, T. (2022). Controlled traffic farming and field traffic management: Perceptions of farmers groups from Northern and Western European countries. *Soil Tillage Research* **217**, 105288.

Vahdanjoo, M., Gislum, R., and Sørensen, C. A. G. (2023). Operational, Economic, and Environmental Assessment of an Agricultural Robot in Seeding and Weeding Operations. *Agricutltural Engineering* **5**, 299-324.

Van Evert, F. K., Avgoustakis, G., Baron, S., Bresilla, T., Dritsopoulos, T., Fountas, S., Hemming, J., Hilbrands, H., Hommes, K. J., Karagiannis, P., Koutsiaras, M., Legas, M., Makris, S., Michalos, G., Mylonas, N., Nieuwenhuizen, A., Paraforos, D., Pedersen, S. M., Pinel, B., Radisic, M., Rascón, J. F., Rizzo, C., Sanchez, R., Scovill, A., Serra, O., Sharipov, G., Veldhuisen, B., Vidal, J., and Wolters, J. (2023). Implementing a digital twin for flexible operation of agricultural robotics

van Evert, F. K., Bresilla, T., Nieuwenhuizen, A., Veldhuisen, B., Hemming, J., Avgoustakis, G., Fountas, S., Koutsiaras, M., Mylonas, N., and Baron, S. (2024). Implementing a digital twin for flexible operation of agricultural robotics. *In* "Advances in agri-food robotics" (E. v. Henten and Y. Edan, eds.), pp. 185-222. Burleigh Dodds Science Publishing.

Xu, S., and Rai, R. (2024). Vision-based autonomous navigation stack for tractors operating in peach orchards. *Computers and Electronics in Agriculture* **217**, 108558.

Ørum, J. E., Tamirat, T. W., Pedersen, S. M., Stratton, A. D. H., Veldhuisen, B., and Hilbrands, H. J. S. A. T. (2023). Optimal use of an agricultural robot in an arable crop rotation: a case study from the Netherlands. *Smart Agricultural Technology*, 100261.

Establishing resilient AI applications in agriculture by redundancy and graceful degradation: Two use cases

Sebastian Bökle[a]*, Marcus Müller[b], Waldemar Keil[c], Hans W. Griepentrog[a], Anthony Stein[d]

[a]Department of Agricultural Engineering, Technology in Crop Production, University of Hohenheim, Stuttgart, Germany

[b]Smart Site Solutions GmbH, Unterensingen, Germany

[c]EXA Computing GmbH, Hamm, Germany

[d]Department of Agricultural Engineering, Artificial Intelligence in Agricultural Engineering, University of Hohenheim, Stuttgart, Germany

* Corresponding author. Email: sebastian.boekle@uni-hohenheim.de

Abstract

Digital agriculture encompasses the development of AI-supported machines and processes. The resulting intelligent agricultural technologies have the potential to increase process and resource efficiency and to simplify farmers' workflow of crosschecking the validity of machinery adjustments. In this paper, the benefits of a digitised and AI-assisted sowing process of cereals are presented. This case study focuses on (i) the prediction of the remaining working time and (ii) the prediction and order placement of in-time delivery of seed refill. As farming processes are subject to variable weather conditions, the time windows for their application are narrow, which holds for the seeding process in particular. On the other hand, the integration of AI for digital support of the seeding process may lead to possible constraints due to vulnerable networks and unreliable internet connectivity. This raises the necessity of a high level of technical resilience for the investigated use case of AI-supported seeding. To counteract this connectivity issue, redundant fall-back options for scenarios (i) and (ii) have been developed. More precisely, for (i), we follow a graceful degradation approach. While not maintaining the predictive accuracy level of the cloud-based prediction using the full amount of telemetry data, it still enables a seamless process continuation based on cached data of the most recent calculations. For scenario (ii) another redundant fall-back solution was developed, where the prediction is computed on a farm server proactively caching a permanent status report, traced from the former cloud-based predictions. Thus, the principle behind is not a parallel calculation but a permanently occurring poll, sent to the corresponding digital service, assuring permanent access to the required data for on-edge computations during fieldwork. Within the context of food production as critical infrastructure, we consider the thoughtful incorporation of technical resilience in AI-enhanced agriculture as paramount to ensure a fail-safe food production system.

Keywords: Seeding, AI, process prediction, graceful degradation, resilience

1. Introduction

The quality of the seeding process is decisive for the maximum germination rate and the final yield response (Li and Li, 2022; Pinheiro et al., 2018). Also, the adaption to spatial variability of soil quality has a positive effect on several yield parameters (Egidijus et al., 2023). (Romaneckas et al., 2022) verified several coherences between soil parameters and sowing depths, also highlighting the correlation between seedbed roughness, sowing depth, and consequently germination rate. Therefore, seedbed preparation plays a decisive role in the seeding process for a successful yielding crop. This shows, that the sowing process is a complex combination of interacting conditions, which normally farmers have to operate and control by themselves. While trying to find the best solution or compromise for the parameter combination, often constant and thus suboptimal adjustments are chosen. This situation offers a high potential for the implementation of artificial intelligence to find an optimal combination of all factors, constantly adapting to soil and other conditions reaching out for high-level efficiency and maximum yield.

In regions dominated by small and middle scaled farms, like in the south of Germany, new (digital) technologies are in most cases hardly affordable for farmers (Rohleder et al., 2020; Schleicher and Gandorfer, 2018). Therefore contractors, machinery rings, or local farmer groups cooperate to share expensive investments. As time windows for several field works are narrow, due to the dependency on good weather conditions, an optimized organization of the shared machinery is necessary, for all participants getting their work done in time. These management tasks consist on the one hand of calculations of the remaining sowing process within the currently worked field and the just-in-time

organisation of seed refill. On the other hand of the overall calculation of the farmers who use the machinery in a row, where a seamless handover is targeted and inevitable for the collaboration of farmers in sowing, as one of the most important and time-critical processes of farming.

Taking into account that agriculture and ultimately food production are part of the critical infrastructures of a society resilience and reliability must be considered and at least to a certain degree be guaranteed (Kuntke et al., 2022). That means for relevant processes backup solutions are needed, which can bridge possible supply gaps in connectivity or computing performance. For the investigated case study the calculation of the remaining working time in the field and the order of seedrefill is focused.

The aim of this work is to demonstrate the integration of AI in processes of practical agriculture for increased efficiency under the consideration of resilience aspects due to the responsibility before the background of the critical infrastructure of food production. The first objective is to establish resilience for the calculation of the remaining working time in the field, ensuring the planning of the schedule of a working day with a fictitious number of farmers. This backup version is the approach of graceful degradation in case of missing connectivity as levelled system redundancy (Blackmore et al., 2001). The second objective is to order seed refill in time and to demonstrate the backup version based on a constant pol to the farm server as a redundant backup solution.

2. Materials and Methods

In (Bökle et al., 2022) resilience was scaled into levels from Level 1, with no measures to convey resilience for digital infrastructure on a farm, up to Level 5, which corresponds to complete redundancy of all digital applications and devices. The two developed round trips in this work cover Level 4 (Graceful Degradation) and Level 5.

2.1 Graceful degradation

The actual remaining working time within the current cultivated field, during undisturbed network conditions, is constantly predicted with actual machine data, sent via telemetry, by the connected cloud. Thus, the following users of the machinery always have actual schedule information of the ordered machinery. In this calculation, the latest results are sent to the farm server and cached. On the farm server known data about the machinery, algorithms and the following clients are additionally available and are the basis for the continuation of the prediction procedure for the remaining working time in case of lost connectivity to the cloud. Graceful degradation doesn’t cover the cloud-based calculation redundantly but continues the calculation and maintains planning security for the responsible person of the machinery and the next customer in the schedule. which compares to resilience level 4.

2.2 Redundancy

During sowing, seeds need to be refilled regularly. For maximized efficiency, the refill order comes just in time and needs to be reliable for a continuous sowing process. For task allocation and task monitoring, we rely on cloud technology as it provides a high level of redundancy in itself already, e.g. redundant power supply, redundant network access, and multiple redundant service instances that are running in parallel. All layers of the architecture are operated redundantly as well. Upstream load balancer ensures that the request load is routed to the system parts that are still running in case some system parts fail. The container virtualization used, including container automation with corresponding automated infrastructure and system monitoring, ensures additional reliability and resilience. In the unlikely event that the cloud is anyway unavailable, a decentral methodology is chosen in which predictions calculated in the cloud next to relevant data of the sowing process are copied to the farm server in a defined frequent poll. Thus, the farm server is sniffing the cloud predictions and in case no signal is received in a certain time, because of system failures, the farm server continues the predictions and executes orders. All necessary algorithms and data for this are available on the farm server. If a connection is back, the farm server hands over again predictions to the cloud. Here the farm server is an additional knot in the system, it is running the AI algorithms for task allocation and monitoring and therefore compares to Level 5 of resilience.

3. Results

3.1 AI-assisted sowing

The sowing process includes in this case study the seedbed preparation with a power harrow combined with the seeder. As seedbed quality is very important for optimal germination conditions this process is optimized by methods of AI. (Boysen et al., 2023) presented a promising approach to model the environment of the tractor-seeder combination in the field, predicting a soil-machine response for a constantly optimized combination of seedbed quality, fuel consumption, and area output. With further developments such methods bring significant relief to farmers in the operation of a complex machine. At the same time efficiency of tractor or seeder combination regulated adjustments and the use of operating materials such as fuel and seeds, increase. With AI-adjusted settings, farmers are enabled to focus mainly on the performance of the constantly AI-regulated settings of tractor-seeder combination.

3.2 Graceful degradation

The constantly calculated time for the remaining work (Figure 1 grey arrows) in the cultivated field is cached by the farm server. Moreover, all field data and data of the next customers are available on the farm server. In the event that the internet connection or cloud computing is interrupted, the farm server calculates the remaining working time based on the last average data and the available data. The accuracy of this fallback methodology is lower because the changes in the actual working speed can't be updated. But it still allows the timely ordering of seed refill and the approximate arrival at the field of the next customer. The precise description of the software round trip is still in progress.

Figure 1: The grey symbols represent the regular way of communication and prediction by AI. In case of interrupted communication, the farm server continues automatically the same prediction procedure with the latest machine data. (Translation of picture descriptions: Weed seeding; working time: 2h 6min, area output: 1.88 ha/h, field efficiency: 86%, fuel consumption: 12,25 l/ha)

3.3 Redundancy of task allocation and monitoring

An efficient sowing process requires an efficient supply of raw materials and supplies, such as seeds and fuel. The supply chains can be organized on an inter-company basis. This makes the coordination of various legally and economically independent entities particularly important. The supply process must

be efficiently coordinated with the sowing process across company boundaries.

In the developed solution is determined who must have started or completed which task at what time so that the overall process can run without friction. If there are disruptions or delays at one farm affecting the overall process all entities involved get informed and coordination is carried out again.

The invented procedure for the (inter-company) allocation of tasks takes resources into account that are used by several companies (shared resources). Once tasks are initially allocated to resources (task allocation), the execution, start, and completion of the tasks are monitored automatically. This is based on movement patterns that are determined using GNSS sensors. Every start, end, and task execution has its learnable movement pattern.

If the algorithm detects deviations from the initial schedule, e.g. a delayed start of a task, the effects on the overall process are calculated and, if necessary, rescheduled, possibly with a new task allocation. The hereby achieved increase of efficiency in the AI-assisted inter-company applicated sowing process is assured by fallback methods (Figure 2 and Chapter 2.2.) to guarantee resilience as necessary for critical infrastructures.

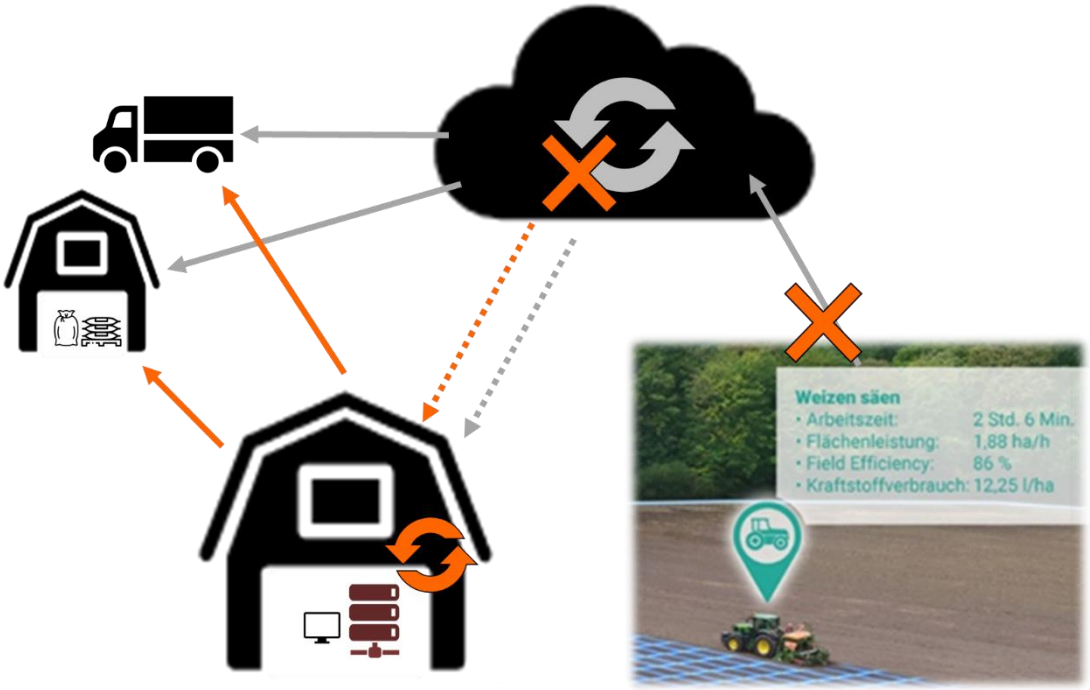

Figure 2: The regular procedures in grey are replaced by red arrowed communication ways in case of interruption of internet communication or cloud computations. (Translation of picture descriptions see Figure 1)

4. Discussion

From the perspective of small and middle-scaled farmers with an average farm size of 30ha like in southwest Germany, the presented approach of just-in-time delivery of seeds and fuel might appear exaggerated. The needed amounts of seeds often suffice for several fields and fuel possibly for a few days. Also, the purchase of seeds is often done in advance and bought in stock. This is also the case if the machinery is driven or provided by a contractor. However, as the contractor gets seed from each farm separately it is very efficient for farmers to be always updated about the schedule of the contractor knowing when their field gets sown. The described system assures timely information for all participants helping them to plan other tasks efficiently around the sowing.

Also the volatile situation in international markets for agricultural products and operating materials (Landesanstalt für Landwirtschaft, Ernährung und Ländlichen Raum (LEL), 2024) in the last years illustrates the importance of the right time for purchasing seeds or fertilizer. Thus, the situation might occur that a short-term purchase of seeds, fertilizer, or fuel might bring significant financial savings, which benefits the described system for knowing the exact time when delivery of seeds or fuel is needed.

For time-critical planting of vegetable seedlings for example this applies even more also for small-scale farms as the condition of the seedling at planting date is decisive for its survival and yield performance also considering if irrigation is needed. The higher the input in general the more likely this approach proves itself as relevant.

With the implementation of the resilient bypasses (Figures 1 and 2) over the farm servers, the effort for additional service and maintenance must be considered. For farmers in most cases, this is hardly to accomplish which makes it necessary to have an external service provider or a cooperative like Machinery Rings which can hire someone for this task.

Acknowledgments

The project is supported by funds from the Federal Ministry of Food and Agriculture (BMEL) based on a decision of the Parliament of the Federal Republic of Germany. The Federal Office for Agriculture and Food (BLE) provides coordinating support for artificial intelligence (AI) in agriculture as funding organization, grant number 28DK109A20.

References

Blackmore, S., Have, H., Fountas, S., 2001. A specification of behavioural requirements for an autonomous tractor, in: Automation Technology for Off-Road Equipment. Presented at the International Symposium on Fruit, Nut and Vegetable Production Engineering, Qin Zhang, Potsdam, pp. 25–36.

Bökle, S., Paraforos, D.S., Reiser, D., Griepentrog, H.W., 2022. Conceptual framework of a decentral digital farming system for resilient and safe data management. Smart Agricultural Technology 2, 100039. https://doi.org/10.1016/j.atech.2022.100039

Boysen, J., Zender, L., Stein, A., 2023. Modeling the soil-machine response of secondary tillage: A deep learning approach. Smart Agricultural Technology 6, 100363. https://doi.org/10.1016/j.atech.2023.100363

Egidijus, Š., Marius, K., Indrė, B., Vilma, N., Kęstutis, R., Sidona, B., Dainius, S., Mouazen, A.M., 2023. Impact of soil electrical conductivity-based site-specific seeding and uniform rate seeding methods on winter wheat yield parameters and economic benefits. Precision Agric 24, 2438–2455. https://doi.org/10.1007/s11119-023-10047-3

Kuntke, F., Linsner, S., Steinbrink, E., Franken, J., Reuter, C., 2022. Resilience in Agriculture: Communication and Energy Infrastructure Dependencies of German Farmers. Int J Disaster Risk Sci 13, 214–229. https://doi.org/10.1007/s13753-022-00404-7

Landesanstalt für Landwirtschaft, Ernährung und Ländlichen Raum (LEL), 2024. Agrarmärkte [WWW Document]. URL https://www.lfl.bayern.de/iem/agrarmarkt/171066/index.php (accessed 5.23.24).

Li, B., Li, J., 2022. Optimized Deep Neural Network and Its Application in Fine Sowing of Crops. Computational Intelligence and Neuroscience 2022, 1–10. https://doi.org/10.1155/2022/3650702

Pinheiro, M.G., Souza, C.A., Carneiro Jr, J., Elijanara Raissa Silva, E., Vieira Stefen, D., 2018. Initial development of wheat and triticale under different sowing depth. Am. Eurasian J. Agric. Environ. Sci 18, 206–215.

Rohleder, D.B., Krüsken, B., Reinhardt, D.H., 2020. Digitalisierung in der Landwirtschaft 2020.

Romaneckas, K., Steponavičius, D., Jasinskas, A., Kazlauskas, M., Naujokienė, V., Bručienė, I., Švereikaitė, A., Šarauskis, E., 2022. How to Analyze, Detect and Adjust Variable Seedbed Depth in Site-Specific Sowing Systems: A Case Study. Agronomy 12, 1092. https://doi.org/10.3390/agronomy12051092

Schleicher, S., Gandorfer, M., 2018. Digitalisierung in der Landwirtschaft: Eine Analyse der Akzeptanzhemmnisse, in: Meyer-Aurich et al., A. (Ed.), Informatik in der Land-, Forst- und Ernährungswirtschaft. Presented at the Referate der 38. GIL-Jahrestagung, Kiel, Gesellschaft für Informatik e.V. (GI), Kiel, pp. 203–206.

Icons Figure 1 and 2:
https://www.flaticon.comdekostenlose-iconssack title=sack IconsSack Icons erstellt von Freepik – Flaticona
https://www.flaticon.comdekostenlose-iconssack title=sack IconsSack Icons erstellt von Smashicons - Flaticona

A neural network approach for real-time monitoring of cannabis sativa L. germination

Jose A. Brenes [a, *], Ana Codes [b], Carmen Rocamora [b], Javier Ferrández-Pastor [c]

[a] CITIC-ECCI-PPCI, University of Costa Rica, San José, Costa Rica

[b] CIAGRO, University Miguel Hernández, Orihuela, Spain

[c] I2RC, University of Alicante, Alicante, Spain

* Corresponding author. Email: joseantonio.brenes@ucr.ac.cr

Abstract

One of the primary challenges in detecting crop germination in seedbeds using computer vision is the difficulty of accurately analysing cases of overlapping seedlings. This study investigates the effectiveness of Convolutional Neural Network (CNN) models and Long Short-Term Memory (LSTM) models in addressing this issue. Utilizing a substantial dataset comprising over 80,000 labelled images of Cannabis Sativa plants, our research aims to compare the performance of standalone CNN models with hybrid architectures (CSS+LSTM model). A noteworthy aspect of our experimental methodology is the deliberate omission of data augmentation techniques during dataset preparation. This decision enables us to evaluate the inherent quality and utility of our curated dataset without introducing artificial modifications. Furthermore, recognizing the significance of incorporating a temporal component in germination detection, we conduct a specific assessment of the hybrid model (CNN+LSTM) against the standalone CNN model. Through comprehensive experimentation and analysis, we evaluate the relative effectiveness of each model in accurately classifying germination status across different levels of seedling overlap. Preliminary results reflect a better performance of the hybrid model compared to the standalone CNN model. However, it is crucial to consider the computational resources, time, and effort required for training and testing the model. Thus, our study provides valuable insights into the intricate interplay among model architecture, dataset characteristics, and the complexity of the germination detection task. Moreover, this research contributes to the advancement of practical applications of deep learning methodologies in agricultural monitoring, emphasizing the necessity of tailored model designs to overcome the unique challenges encountered in greenhouse environments.

Keywords: CNN, LSTM, Computer vision, Germination detection, *Cannabis sativa*.

1. Introduction

In contemporary agriculture, a thorough monitoring of germination processes holds critical significance, representing a crucial stage in crop cultivation that directly impacts subsequent growth and yield outcomes. Among the myriad challenges faced by farmers, the accurate detection of germination, particularly amidst the complexities of overlapping seedlings, emerges as an obstacle. The proliferation of dense vegetation within seedbeds presents a challenging scenario, where traditional manual inspection methods prove laborious, time-consuming, and prone to inaccuracies. Consequently, the adoption of advanced technological solutions becomes imperative to streamline this essential agricultural task.

Real-time monitoring of germination processes heralds a paradigm shift in agricultural practices, offering unparalleled insights into crop development dynamics and enabling proactive interventions to optimize cultivation outcomes. The arrival of neural network approaches, particularly Convolutional Neural Networks (CNNs), Long Short-term Memory Networks (LSTMs), and their hybrid architectures, has revolutionized image analysis tasks, empowering researchers, and practitioners with sophisticated tools for pattern recognition and decision-making.

CNNs excel at extracting complex spatial features from visual data, making them well-suited for tasks such as object detection and classification. LSTMs, on the other hand, are adept at modelling sequential data and capturing temporal dependencies, thus proving invaluable in analysing time-series information. The fusion of these two architectures in hybrid models combines the strengths of both approaches, offering enhanced capabilities for analysing complex spatio-temporal patterns in image datasets.

Against this backdrop, our research endeavours to address the pressing need for effective germination detection in seedbeds, with a specific focus on supporting farmers in their cultivation practices. Our goal is

to analyse if a hybrid model of CNN and LSTM neural networks is able to detect effective germination, including scenarios with overlapping seedlings, against single models like CNN neural networks. By harnessing the power of neural network methodologies, we aim to develop a robust framework capable of accurately identifying germination events amidst the challenges posed by overlapping seedlings. Through experimentation and analysis, our objectives encompass not only the refinement of model architectures but also the validation of real-time monitoring capabilities to empower farmers with timely insights into crop development stages.

Furthermore, our contribution addresses cannabis sativa cultivation concerns, where overlapping seedlings pose unique challenges due to the strict regulations on the number of plants allowed for cultivation. In this context, enabling real-time germination monitoring is essential for farmers. Thus, by focusing on cannabis sativa, we aim to provide tailored insights and solutions that meet the unique needs of cannabis growers, thereby advancing the practical applications of deep learning methodologies in agricultural monitoring.

In the next section, we review several studies that focus on automatic germination detection using artificial intelligence techniques.

2. Background

In this section, we present an overview of the existing literature on the automatic detection of plant germination employing Artificial Intelligence (AI) techniques. To ensure a thorough and wide-ranging analysis, we conducted a literature review across three digital libraries: Scopus, IEEE Xplore, and Springer. Our objective was to identify and analyse studies that have employed AI for automatic germination detection. We performed a general query *("detection" AND "germination" AND "agriculture"*) on the databases' search tools to find relevant studies. We then filtered the results to include only those studies that specifically addressed automatic germination detection using AI techniques. The following analysis provides a concise summary of the principal findings and methodologies from the reviewed studies.

Most of the found studies in literature are related to seed germination detecting the radicle in early stages of germination. Kim et al. (2010) introduced a detailed process for extracting seed characteristics crucial for germination detection through image processing techniques. The proposed methodology involves circle detection, noise filtering, image segmentation, thresholding, morphological operations, and object labelling, all tailored to optimize system performance. The proposed procedure automates seed analysis by detecting Petri dishes, segregating background from seeds, and computing essential seed parameters for subsequent analysis.

Nguyen et al. (2018) presented a system for automating the evaluation of rice seed germination rates using computer vision and machine learning. The proposed method employed U-Net model for seed segmentation, followed by distance transform and thresholding for seed detection, and ResNet model for seed classification. Results demonstrated the superiority of Convolutional Neural Networks over traditional methods, with F1-scores of 93.38% and 95.66% for segmentation and classification tasks, respectively.

Shadrin at al. (2019) integrated AI into a low-power sensing system for seed germination detection. By implementing a custom CNN model, researchers achieved significant accuracy, with an average Intersection over Union (IoU) score of 83% on the test dataset and 97% seed recognition accuracy on the validation dataset. The researchers demonstrated the potential benefit of seed germination automatic detection at industrial facilities thought Internet of Things (IoT) applications.

Chaivivatrakul (2020) explored automated methods for determining seed germination rates using the top of paper germination method. This study encompassed four-time repetitions of chili and guinea seeds germination with two sets of germination groups, totalling 400 seeds each. Besides, two detection methods were proposed and compared: binary thresholding and maximum likelihood based on color analysis. Results indicated both methods achieved accuracy rates exceeding 93%, with binary thresholding being lightweight and suitable for resource-limited environments, while maximum likelihood demonstrated flexibility to varying light conditions.

In addition, Grant et al. (2023) developed an AI system using CNNs and image processing techniques to detect corn seed germination. This study used a dataset of 400 images of corn seeds at various germination stages and used the CIELAB color model for radicle and seed segmentation detection. The employed AI technique was k-fold cross-validation, and the model achieved a detection accuracy of 98.14%.

Regarding the use of mobiles, Ahmad et al. (2023) employed smartphone cameras in combination to image processing to detect fungal infections in chickpea seeds. In this study, images of 15 seeds were collected every 24 hours for three days. Two spectral indexes combining different colour bands were used for detection. Combining both indexes achieved an average accuracy of 96.66% and precision of 93.33%, significantly outperforming individual indexes. In this case, the selected artificial intelligence technique was Discriminant Analysis. This method shows promise for early fungal infection detection and could be implemented as a mobile application for practical use.

In another study, Donapati et al. (2023) introduced a novel fusion model for seed detection and germination analysis in precision agriculture. By combining U-Net for seed segmentation and CNN for classification, the model achieves effective seed germination analysis. The model was implemented on the NVIDIA Jetson Nano embedded GPU platform. Results showed notable performance metrics, including 0.91 pixel accuracy, 0.84 intersection over union (IoU), and 0.90 precision, outperforming ResNet50, Inception, and LeNet. The implemented model also exhibited low latency of 0.26 ms, demonstrating its suitability for real-time applications in precision agriculture.

In a more recent study, Chen et al. (2024) presented a novel techniques and methodology for seed vigor detection in maize cultivation. Advanced algorithms like HSI and 3DCNN were utilized, alongside RGB imaging, to develop robust models for classifying corn seed vitality. Also, researchers presented a new dataset comprising pictures of corn seeds taken under six contrasting conditions. This dataset enabled accurate prediction and grading of seed germination and vigor, enhancing the validity of non-destructive seed vigor identification in smart agriculture.

Regarding the detection of leaves and plants, Ma et al. (2022) presented a rapid and accurate method for detecting peanut seed germination in large fields. The researchers combined deep learning-based object detection (OD) with unmanned aerial systems (UAS) to identify early germination. For the analysis, Faster RCNN and SSD object detection models were used to compare multispectral imagery from a MicaSense Rededge camera. The results showed Faster RCNN achieved higher accuracy, although with longer computation times. Notably, RGB-based detection performed comparably to multispectral imagery, indicating cost-effective alternatives. Resnet-34 was identified as the optimal backbone for Faster RCNN.

As evidenced by numerous studies found in the literature, artificial intelligence techniques have been increasingly utilized to automate the detection of germination. However, most of these studies have primarily concentrated on radicle detection and have been conducted within laboratory settings. While only one study has ventured into field-based detection, it relied on costly UAV systems for image capture. In contrast, our study focuses on the detection of germinated plants, specifically targeting the identification of cotyledon and leaves within the seedbed. This approach aims to alleviate the burden on farmers by reducing manual effort. Additionally, we conducted our study within a greenhouse environment, offering a more accessible and controlled growing environment for farmers.

Next, we outline the prerequisites and methodology employed in our proposal.

3. Materials and Methods

This section provides an overview of the image dataset employed in our study, the selected deep learning models considered in the analysis, and the entire methodology we followed to conduct the research. Frist, we present some details regarding the image dataset.

3.1. Image dataset of Cannabis Sativa L. plants germination

To conduct a comprehensive comparative analysis of neural network models for detecting *Cannabis sativa* germination in seedbeds, we curated an extensive dataset comprising over 80,000 images of seedbed cells. This dataset was meticulously assembled to capture various stages of germination, ensuring a robust input for training, and evaluating our models.

The dataset was created in a controlled experimental setup established within a greenhouse to simulate typical growing conditions of Cannabis Sativa L. plants. The setup included a high-resolution camera in a zenithally position over the seedbeds. The camera was connected to an embedded system (Raspberry Pi). This configuration enabled automated image capture, ensuring consistent imaging conditions throughout the experiment.

Germination experiments were conducted over various periods of 14 days each one. During each period,

the camera system captured images every hour to document the progression of germination. Since each image consisted of an entire seedbed, it was necessary to cut them into individual cells for detailed analysis. This process yielded a dataset that encompassed images with a diverse range of germination stages, including instances of overlapping seedlings from neighbouring cells. Figure 1 depicts a sample image captured by the camera, along with examples of extracted cell images.

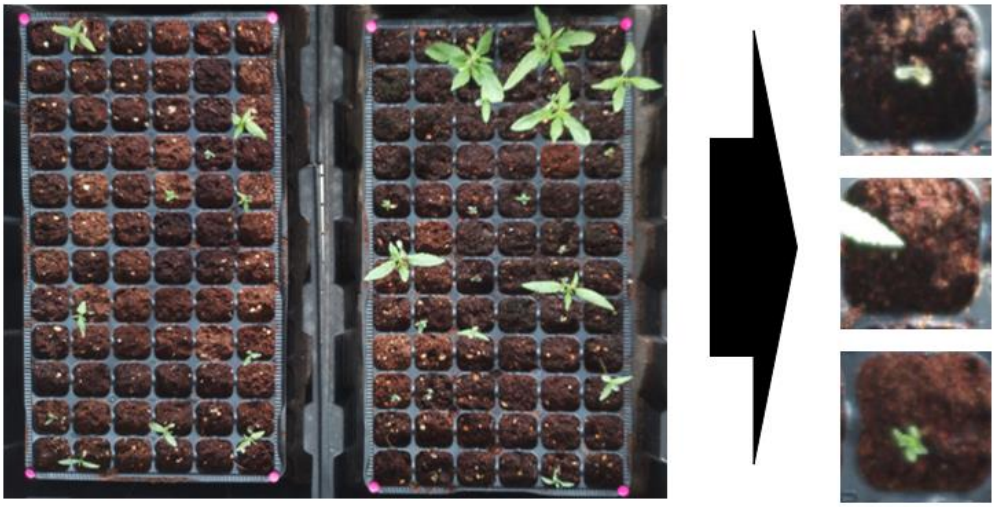

Figure 1. Seedbed image and samples of cells extracted from the seedbed image.

Each seedbed image was processed to extract individual cells, resulting in a collection of cell-level images. Then, the images were carefully labelled based on their content in the following categories:

- Germinated Plant: Cells containing a germinated Cannabis Sativa L. plant.
- Overlapping Plant: Cells where the plant is overlapped with seedlings from neighbouring cells.
- Non-germinated Cell: Cells without any visible germination.

This labelling process was critical to ensure the accuracy of our dataset and to facilitate the training and evaluation of the selected neural network models.

3.2. Models' architectures

We developed two distinct neural network models for the classification task:

- Convolutional Neural Network (CNN): The CNN architecture was designed to extract spatial features from the cell images. It consisted of multiple convolutional layers followed by pooling layers, culminating in fully connected layers for classification. Figure 2 shows the architecture of the CNN model. The primary focus of this model was to identify germination and overlapping plants based on spatial patterns within the images.

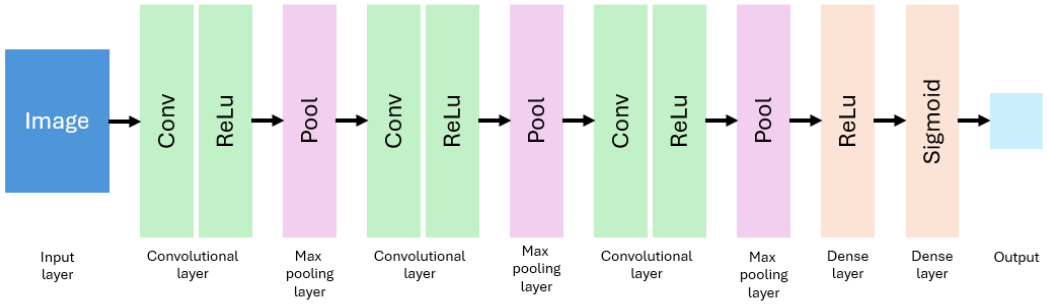

Figure 2. CNN model's architecture.

- Hybrid Model (CNN+LSTM): We created an hybrid model combining the spatial feature extraction capabilities of CNN with the temporal analysis capabilities of Long Short-Term Memory (LSTM) networks. The CNN component, identical to the standalone model, was responsible for extracting features from the images. These features were then fed into an LSTM layer, which captured temporal dependencies across the sequence of images. This architecture was designed to enhance the model's ability to detect germination events by considering the temporal progression of the germination process. Figure 3 shows the architecture of the CNN model.

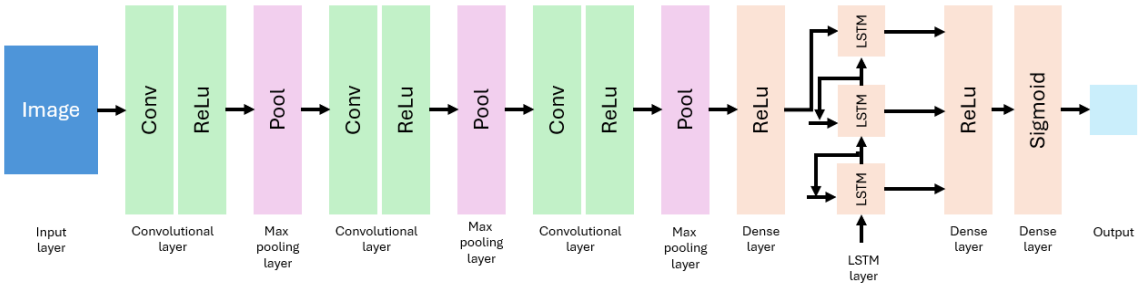

Figure 3. Hybrid model's architecture

Next, we outlined the experimental configuration employed to train, test, and validate the selected network models.

3.3. Experimental setup

Both models were trained using the created image dataset. The dataset was split into training, validation, and test sets to ensure a rigorous evaluation. The training process involved using standard backpropagation techniques with appropriate loss functions and optimisation algorithms. During training, key performance metrics such as accuracy, precision, recall, and F1 score were monitored to evaluate the models' effectiveness.

Upon completion of the training phase, the performance of the two models was compared based on their ability to accurately classify germination status in the seedbed images. The evaluation was conducted using the test set, and the results were analysed to assess:

- Accuracy: the overall correctness of the model's predictions. This metric is calculated based on the Equation 1.

$$\text{Accuracy} = \text{Number of correct predictions} / \text{Total number of predictions} \quad (1)$$

- Precision: it can be defined as the ratio of correctly predicted positive observations to the total predicted positives. The precision reflects models' ability to correctly identify germinated and overlapping plants. Precision is calculated based on Equation 2.

$$\text{Precision} = TP / (TP + FP) \quad (2)$$

Where TP is True Positive

FP is a False Positive

- Recall: also known as sensitivity or true positive rate. Recall measures the ability of a classification model to identify all relevant instances within a dataset. It is calculated based on Equation 3.

$$\text{Recall} = TP / (TP + FN) \quad (3)$$

Where TP is True Positive

FN is a False Negative

- F1 Score: is a metric used to evaluate the performance of a classification model, balancing both precision and recall. It is the harmonic mean of precision and recall, providing a single measure that captures both aspects of model performance. F1 score is calculated based on Equation 4.

$$F1\ \text{Score} = 2 \times (\text{Precision} + \text{Recall}) / (\text{Precision} \times \text{Recall}) \quad (4)$$

Additionally, the computational resources, time, and effort required for training and testing each model were analysed to understand their practical feasibility for real-time monitoring applications.

The training and testing of the models was conducted on a high-performance workstation equipped with the following hardware specifications:

- Graphics Processing Unit (GPU): The training utilized CUDA for accelerated computation, specifically leveraging a Nvidia Quadro T2000 GPU with 4GB of dedicated GPU RAM. This setup facilitated efficient parallel processing and significant reductions in training time.
- Central Processing Unit (CPU): An Intel Xeon W-10855M processor, operating at 2.8 GHz with 6 cores, was used for general computation tasks. This processor ensured reliable performance and supported the GPU in tasks that required CPU intervention.
- System Memory: The system was equipped with 32 GB of RAM, providing ample memory for handling large datasets and ensuring smooth operation during the training process.

Besides, the training, testing and validation were conducted during 35 epochs with a batch size of 48.

Our research specifically focuses on the challenges posed by overlapping seedlings in *Cannabis sativa* L. cultivation. Regarding cultivation regulations for this crop, we aim to provide custom-made insights and solutions that cater to the unique needs of cannabis growers. The detailed analysis and comparative evaluation of CNN and hybrid models seek to contribute to the advancement of deep learning methodologies in agricultural monitoring, highlighting the importance of model design in overcoming the specific challenges encountered in greenhouse environments.

In the next section, we present the obtained results for this research.

4. Results

After conducting training, test and validation of the two analysed models, Figure 4 shows the performance comparison between the Convolutional Neural Network (CNN) model and the hybrid model over a span of 35 epochs. These charts highlight the improvements achieved by the hybrid model in terms of validation accuracy and validation loss.

Regarding the models' accuracy, section left of Figure 4 depicts the results for both the CNN and hybrid models across epochs. The blue line with circle markers indicates the validation accuracy of the CNN model, while the green line with circle markers represents the validation accuracy of the hybrid model. It can be seen from the chart that the hybrid model achieves higher accuracy at almost every epoch, demonstrating its better capability in correctly identifying the classes. Notably, the validation accuracy of the hybrid model remains above 0.97 throughout the training period, while the CNN model shows slightly lower performance, especially in the initial epochs.

By other hand, the right section of Figure 4 presents the validation loss for both the CNN and hybrid models over the same epochs. As mentioned, validation loss measures the discrepancy between the predicted and actual class labels, with lower values indicating better model performance. The red line with circle markers represents the validation loss of the CNN model, and the magenta line with circle markers represents the validation loss of the hybrid model.

The hybrid model achieved lower validation loss compared to the CNN model. This trend indicates that the hybrid model not only makes more accurate predictions but also has a better fit to the validation data. The reduction in validation loss is particularly significant in the early epochs, where the hybrid model quickly converges to lower loss values. This suggests that the hybrid model is more effective in learning from the training data and generalising to unseen samples.

In terms of overall performance, the Figure 4 shows that the hybrid model, which integrates both Convolutional Neural Networks (CNN) and Recurrent Neural Networks (LSTM), provides substantial improvements over the CNN model alone. The hybrid model achieves higher validation accuracy and lower validation loss, indicating better performance in classifying samples as germinated or non-germinated. These results underscore the enhanced capability of the hybrid model to leverage both spatial and temporal features, leading to more accurate and reliable classification outcomes.

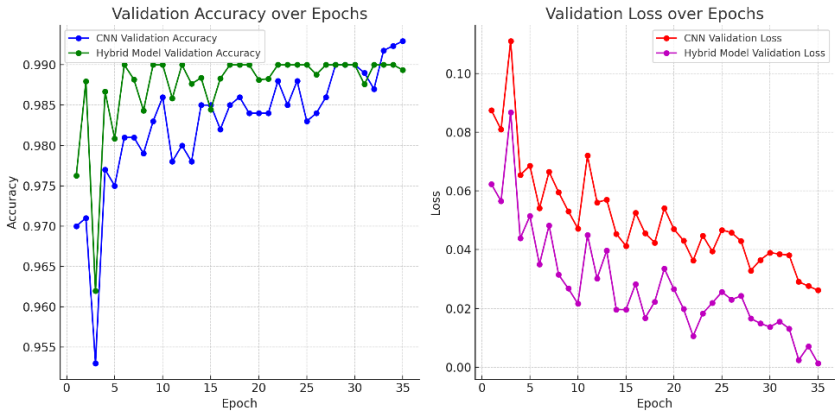

Figure 4. Accuracy and loss results for CNN and Hybrid model.

Regarding resource and time consumption, it is important to note that the hybrid model incurs higher costs to achieve its enhanced performance. Its complex architecture, especially the recurrent layers, requires extensive computations, resulting in significantly longer training times. Moreover, the hybrid model demands more computational resources. For example, the CNN model took 5 hours, 38 minutes, and 23 seconds to complete training, testing, and validation over 35 epochs. In contrast, the hybrid model required 9 hours, 22 minutes, and 45 seconds for the same process, highlighting the additional time and resource investment needed for the hybrid model.

Optimizing the hybrid model also requires more effort and expertise. Extensive hyperparameter tuning and a deeper understanding of both CNN and LSTM functionalities are essential for effective optimization. During validation and testing, the hybrid model consumes more time as each sample undergoes both convolutional and sequential processing, affecting overall evaluation efficiency. While the hybrid model achieves better classification performance, these improvements must be weighed against the higher costs in time, computational resources, and optimization effort. These trade-offs are important considerations for implementing hybrid models in practical applications.

5. Conclusions

The results of this study show a better performance of the hybrid model in classifying the samples into germinated (G) and non-germinated (NG) classes compared to the CNN model. The validation accuracy of the hybrid model exceeded that of the CNN model across all epochs. This finding indicates the hybrid model's enhanced ability to correctly identify germinated and non-germinated samples, reflecting its robustness and effectiveness in handling the classification task. Nevertheless, hybrid model consumes more time and effort than the CNN model to achieve that performance.

Furthermore, the validation loss for the hybrid model was significantly lower than that of the CNN model. Lower validation loss indicates that the hybrid model made fewer errors in its predictions, further confirming the usefulness of having series of images in the training dataset and memory capability in the model. The incorporation of temporal features such as the day and hour of image capture enabled the hybrid model to utilise additional context, leading to more informed and accurate predictions. This integration of temporal data proved to be a critical factor in enhancing the model's classification capacity. By leveraging both spatial and temporal features through the combination of convolutional neural networks (CNN) and recurrent neural networks (LSTM), the hybrid model was able to achieve superior classification results.

Overall, the hybrid model's ability to integrate CNNs with LSTM networks to leverage both spatial and temporal features represents a significant advancement. The superior classification results achieved by the hybrid model underscore its potential for practical applications in seed germination analysis and similar domains requiring precise classification of time-sequenced visual data. These findings pave the way for further exploration and optimization of hybrid models, promising even greater improvements in performance and applicability across various fields of machine learning and artificial intelligence.

For future work, we plan to compare the hybrid model with other alternative models and techniques to validate its utility in detecting effective germination of *Cannabis sativa* L. plants. This comparative analysis will help determine the robustness and generalizability of the hybrid model, ensuring its effectiveness and

reliability in practical applications. Additionally, exploring various optimization strategies and model enhancements will be crucial in further improving its performance and efficiency.

Acknowledgements

This study is part of the AGROALNEXT program (AGROALNEXT/2022/048) and has been supported by MCIN with funding from the European Union NextGenerationEU (PRTR-C17.I1) and the Generalitat Valenciana. C. Rocamora has been funded by the Ministry of Universities and by the European Union-Next Generation EU within the framework of Grants for the Requalification of the Spanish University System, in the University teaching staff modality. This study was also partially supported by the Research Centre for Communication and Information Technologies (CITIC), Research Project No. 834-B9-189. J.A. Brenes has been funded by the Office of International Affairs and External Cooperation OAICE (Short-Term Scholarship) and the Postgraduate Studies System SEP (Restricted Fund 082) of the University of Costa Rica.

References

Ahmad, A., Diaz, F. J., Parra, L., Sendra, S. and Lloret, J. (2023). Turning Smartphone Camera into a Fungal Infection Detector for Chickpea Seed Germination. In 2023 International Conference on Multimedia Computing, Networking and Applications (MCNA), Valencia, Spain, 2023, pp. 27-32, doi: http://doi.org/10.1109/MCNA59361.2023.10185850

Chaivivatrakul, S. (2020). Automatic Assessment of Seed Germination Percentage. In Engineering Journal (Vol. 24, Issue 4, pp. 85–96). Faculty of Engineering, Chulalongkorn University. https://doi.org/10.4186/ej.2020.24.4.85

Chen, C., Bai, M., Wang, T., Zhang, W., Yu, H., Pang, T., Wu, J., Li, Z., & Wang, X. (2024). An RGB image dataset for seed germination prediction and vigor detection - maize. In Frontiers in Plant Science (Vol. 15). Frontiers Media SA. https://doi.org/10.3389/fpls.2024.1341335

Donapati, R. R., Cheruku, R., & Kodali, P. (2023). Real-Time Seed Detection and Germination Analysis in Precision Agriculture: A Fusion Model With U-Net and CNN on Jetson Nano. In IEEE Transactions on AgriFood Electronics (Vol. 1, Issue 2, pp. 145–155). Institute of Electrical and Electronics Engineers (IEEE). https://doi.org/10.1109/tafe.2023.3332495

Grant, S., Castaneda, J., Samouei, H., Tabei, F., Parker, D., & Askarian, B. (2023). Novel Machine Learning and Image Processing Method for Detecting Seed Germination. In 2023 Omaha, Nebraska July 9-12, 2023. 2023 Omaha, Nebraska July 9-12, 2023. American Society of Agricultural and Biological Engineers. https://doi.org/10.13031/aim.202300869

Kim, C. L., Li, C., Raheja, A., & Still, D. W. (2010). Automated Extraction of Seed Characteristics for Germination Detection. In Signal and Image Processing. Signal and Image Processing. ACTAPRESS. https://doi.org/10.2316/p.2010.710-012

Ma, S., Zhou, Y., Flynn, K. C., & Aakur, S. N. (2022). Peanut Seed Germination Detection from Aerial Images. In 2022 IEEE Applied Imagery Pattern Recognition Workshop (AIPR). 2022 IEEE Applied Imagery Pattern Recognition Workshop (AIPR). IEEE. https://doi.org/10.1109/aipr57179.2022.10092219

Nguyen, T. T., Hoang, V.-N., Le, T.-L., Tran, T.-H., & Vu, H. (2018). A Vision Based Method for Automatic Evaluation of Germination Rate of Rice Seeds. In 2018 1st International Conference on Multimedia Analysis and Pattern Recognition (MAPR). 2018 1st International Conference on Multimedia Analysis and Pattern Recognition (MAPR). IEEE. https://doi.org/10.1109/mapr.2018.8337511

Shadrin, D., Menshchikov, A., Ermilov, D., & Somov, A. (2019). Designing Future Precision Agriculture: Detection of Seeds Germination Using Artificial Intelligence on a Low-Power Embedded System. In IEEE Sensors Journal (Vol. 19, Issue 23, pp. 11573–11582). Institute of Electrical and Electronics Engineers (IEEE). https://doi.org/10.1109/jsen.2019.2935812

Advancements in coffee authenticity: A spectroscopic feature compression approach using eXplainable AI and vision transformer

Shanghua Liu [a,*], Majharulislam Babor [a], Leah Munyendo [b], Bernd Hitzmann[b], Barbara Sturm [a,c], Marina Höhne [a,d]

[a] Leibniz Institute for Agricultural Engineering and Bioeconomy, Max Eyth Allee 100, Potsdam, 14469, Germany

[b] University of Hohenheim, Garbenstr. 23, Stuttgart, 70599, Germany

[c] Humboldt University of Berlin, Hinter der Reinhardtstr. 6–8, Berlin, 10115, Germany

[d] University of Potsdam, An der Bahn 2, Potsdam, 14476, Germany

* Corresponding author. Email: SLiu@atb-potsdam.de

Abstract

Verifying the authenticity of food and its ingredients is crucial in food supply chains (FSC), particularly for those facilitating fair trade. Roasted Arabica coffee, being one of the most extensively traded tropical commodities, demands stringent measures to trace its origin and prevent fraudulence. The variations in cup quality, aroma, and economic value tied to geographical origin pose challenges intensified by diverse species and roasting degrees. Using spectroscopic techniques with machine learning approaches can promote fair trade and ensure the reliability of these methods in real-world scenarios. In this scope, a gap remains in understanding how these models interpret redundant information within spectra. Employing only relevant spectral data via portable spectroscopy can reduce expenses, enhancing the practicality and adoption of these methods. In this study, we used near-infrared (NIR) spectra to identify the geographical origin of Arabica coffee from South America, Central America, and Africa, across varying roasting levels: light, medium, and dark. Beyond traditional machine learning methods such as Support Vector Machine (SVM) and Linear Discriminant Analysis (LDA), we integrated the eXplainable AI (XAI) approach with the cutting-edge Vision Transformer (ViT) architecture to discern relevant spectral features crucial for authenticating origin. Our method yields an outstanding accuracy of 99.8 % in our geographical origin determination dataset. The robustness of our method was demonstrated through standard dataset partitioning and 10-fold cross-validation using 1823 coffee spectral samples. Moreover, the application of XAI method GradCAM++ provided insights into the decision-making process of the models, facilitating the elimination of less relevant features, thus enabling feature compression and pruning. Remarkably, reducing the feature space to 1.1 % (53 wavelengths) led to a varied performance among models, with ViT exhibiting the least drop in accuracy (86.4 %) compared to SVM (32.8 %) and LDA (65.7 %). Our study highlights the potential of advanced deep learning techniques and explainable AI in precise coffee authenticity determination, thereby ensuring fair value. Moreover, by illuminating feature redundancy within spectra, the findings offer practical solutions for real-time monitoring of coffee authenticity.

Keywords: coffee authenticity determination, explainable AI, spectroscopic feature compression, transformer

1. Introduction

Ensuring food authenticity is essential for maintaining integrity within food supply chains (FSC), especially those committed to fair trade practices. It guarantees that food products are genuine and accurately labeled, which helps maintain consumer trust (Wu et al. 2021; Corallo et al. 2021). Adulteration and mislabeling can lead to fraud and deceive consumers, who rely on labeled information to make informed dietary choices (Kemsawasd et al. 2023). Geographically authentic food products often command higher prices and can therefore be targeted by fraudsters (Katerinopoulou et al. 2020; Cardin et al. 2022; Pamukcu et al. 2021). Disruptions within the FSC can affect the economic interests of both producers and consumers.

Identifying the authenticity of food products is crucial to avoid counterfeiting and ensure that legitimate producers are fairly compensated, providing consumers with value for their money. Moreover, many food products are closely tied to specific regions and cultural identities. Authenticating these products helps preserve traditional methods and regional specialties, supporting local economies and cultural heritage Cvijanovic et al. 2020). However, maintaining such quality within FSC poses significant challenges. Differentiating the origin of food and its ingredients is complex, especially as fraudsters become increasingly

clever at blending cheaper alternatives for financial gain. This makes the authenticity detection process even more challenging. Traditional methods involve taking samples from food lots and conducting laboratory experiments, which is time-consuming and impractical for many batches of products from different regions (Hong et al. 2017; Hassoun et al. 2020).

A more efficient approach is to implement real-time monitoring processes that can identify authenticity using sensor signals. This method leverages advanced technology to continuously monitor food products throughout the FSC, ensuring that any anomalies are detected rapidly. Real-time monitoring can significantly reduce the time and labor involved in authenticity testing, providing a more practical and scalable solution (Sharma et al. 2022). Additionally, integrating AI models with sensor data can enhance the accuracy and reliability of authenticity detection, ensuring that consumers receive genuine products and that producers are protected from economic losses due to fraud (Othman et al. 2023).

Ensuring coffee authenticity through advanced spectroscopic techniques integrated with machine learning can promote fair trade and prevent fraud (Dharmawan et al. 2023; Deng et al. 2024; Yang et al. 2021). Despite significant advancements, a gap exists in effectively interpreting redundant information within spectral data. This gap highlights the need for methodologies that not only accurately verify coffee authenticity but also optimize spectral data usage to reduce costs and improve practical application in real-world scenarios. Efficient data processing techniques can filter out irrelevant information, focusing on important spectral features that are indicative of authenticity. Additionally, developing human understandable approaches for these advanced technologies can facilitate widespread adoption by stakeholders across the FSC, from producers to retailers. The implementation of such technologies can support the coffee industry by ensuring that products labeled as premium or origin-specific truly meet these standards, thereby preserving the economic value associated with authentic products. Furthermore, it reinforces consumer confidence and supports fair compensation for producers who adhere to quality and authenticity standards.

Near-Infrared (NIR) spectroscopy, known for its non-destructive and rapid analysis capabilities, has been studied for coffee authentication (de Carvalho Couto et al. 2022; Correia et al. 2018; de Arau´jo et al. 2021). When combined with machine learning techniques such as Principal Component Analysis (PCA) and Linear Discriminant Analysis (LDA), NIR spectroscopy has shown promise in differentiating coffee varieties and detecting adulterants (Quan et al. 2023; Baqueta et al. 2023; Mutz et al. 2023). Despite these advancements, a challenge remains in refining these models to focus solely on the most relevant spectral features, thereby enhancing their efficiency and reliability. Current NIR spectroscopy models often process a vast amount of data, much of which may be redundant or irrelevant to the specific authentication task. This not only increases computational complexity but also poses significant challenges for developing portable monitoring devices, which are in high demand in FSC. These portable devices are crucial for ensuring on-the-spot verification at the point of inspection, eliminating the need to transport samples to centralized verification stations.

In this study, we address these challenges by employing a novel approach that integrates eXplainable AI (XAI) with the Vision Transformer (ViT) architecture proposed by Dosovitskiy et al. (2020). Originally designed for 2D image analysis, ViT has been adapted to handle the unique characteristics of 1D NIR spectra, aiming to improve the accuracy of geographical origin determination of Arabica coffee. To compare the performance of ViT, we implemented classical machine learning methods including Support Vector Machine (SVM) and Linear Discriminant Analysis (LDA). By utilizing GradCAM++ by Chattopadhyay et al. (2017) within the XAI framework, we gain insights into the decision-making processes of the models, enabling the compression and pruning of spectral features. Our approach not only achieves remarkable accuracy in coffee authenticity determination but also demonstrates the potential for significant cost reductions. By reducing the feature space to only the most relevant wavelengths, we enhance the practical applicability of these models for real-time monitoring of coffee authenticity. This advancement holds promise for ensuring fair value distribution within the coffee trade, safeguarding both consumers and producers against fraudulent practices.

2. Materials and Methods

2.1. NIR Measurements

In this paper, we utilized the NIR spectra acquired by Munyendo et al. (2023). The Arabica coffee beans were purchased from Buxtrade GmbH, An den Geestbergen 1, 21614 Buxtehude, Germany, including varieties from Kenya, Guatemala, and Colombia. All samples were subjected to three different roasting

levels: light, medium and dark. The roasting process was conducted using a Gene Cafe CBR-101 coffee roaster at 240°C for 10, 15, and 20 minutes, respectively. Finally, all the samples were ground to fine powder using an electric grinder (Melitta Calibra EU 1027–01 Mill 160 W, Germany). The spectra of Arabica coffee samples were obtained using a Fourier Transform NIR spectrometer (Bruker, Germany) equipped with OPUS software (Version 7, Bruker, Germany). Spectra were collected in diffuse reflectance mode within the spectral range of 12 500 cm-1 to 3600 cm-1, with a resolution of 4 cm-1, resulting in 4615 channels.

2.2. Evaluation Metrics

For assessing the performance of the classification models employed in this study, we used accuracy evaluation metrics, which is the proportion of correctly classified instances over the total number of instances, and can be calculated as follows:

$$Accuracy\ [\%] = \frac{\text{Number of correct predictions}}{\text{Total number of predictions}} \times 100$$

2.3. Feature Compression based on XAI

In this study, we adapt the Vision Transformer (ViT) architecture, originally designed for 2D image analysis, to handle 1D spectral data for the classification of coffee origin. The ViT model is chosen for its ability to effectively capture long-range dependencies and complex patterns in the input data, which is critical for accurate classification in high-dimensional spectra. We use GradCAM++ to explain the decision-making process of ViT model in coffee authenticity determination by highlighting the important wavelengths.

3. Results and Discussion

Table 1 presents the distribution of samples categorized by geographical origins—Africa, Central America, and South America—and roasting levels: light, medium, and dark. **Figure 1** provides examples of spectra corresponding to lightly roasted Arabica coffee cultivated in three different global regions. The dataset contains 1823 coffee samples, which we randomly split into training, validation, and test sets using the common practice ratio of 6:2:2.

Table 1. Number of samples from which the spectra were acquired for the studied dataset

Geographical regions	Roasting levels			Total Samples
	Light	Medium	Dark	
Kenya (Africa)	202	202	206	610
Guatemala (Central America)	203	202	202	607
Colombia (South America)	202	202	202	606

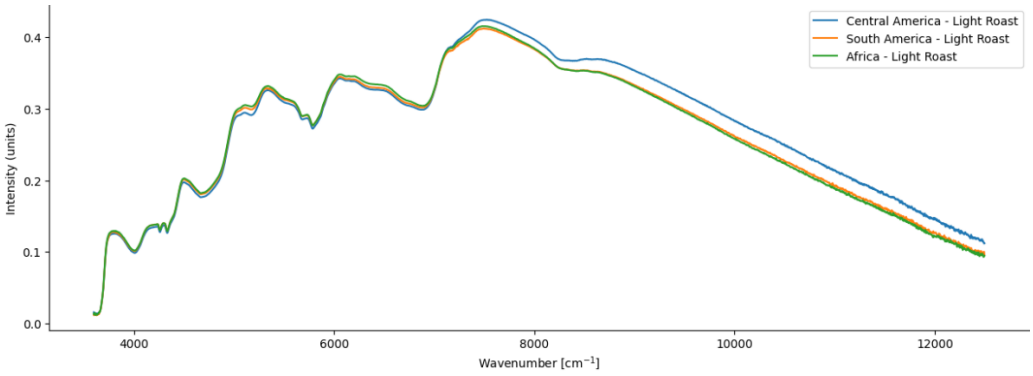

Figure 1. Spectra examples of light roasted Arabica coffee from three geographical origins.

The applied 1D-ViT model achieved an accuracy of 99.8 % in classifying the origin of coffee, while LDA and SVM achieved accuracy of 100 % and 91.2 %, respectively, as shown in **Table 2**. By using the full NIR

spectrum, SVM performed poorly compared to LDA and ViT. **Figure 2** provides a visual example, where the colors on the spectral data represent the extent to which each region contributes to the model's predictions. Specifically, regions with an importance score higher than 0.5 are highlighted with vertical lines.

Table 2. Model performance comparison using all wavelengths of NIR spectra

Model	SVM	LDA	ViT
Accuracy	91.2 %	100 %	99.8 %

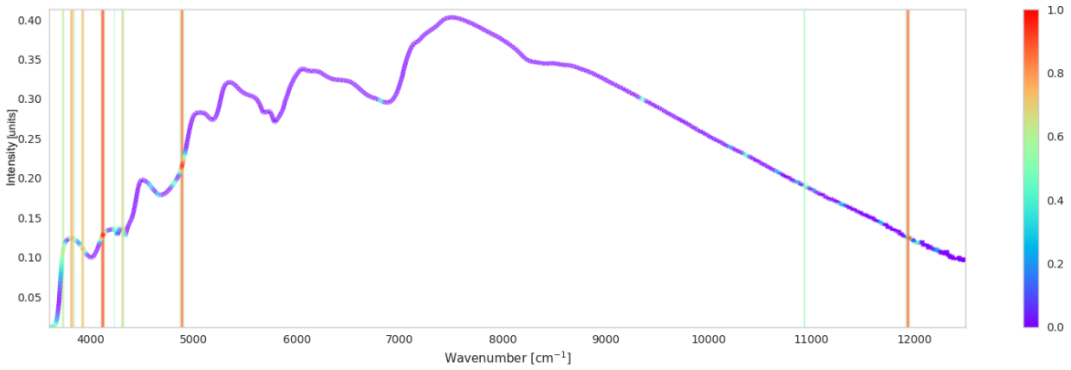

Figure 2. Example spectrum highlighting important regions of spectrum with vertical lines for ViT model prediction. Here, different colors indicate varying importance scores identified by GradCAM++ with red being the most important wave numbers in identifying the geographical authenticity of the Arabica coffee from Africa.

For feature compression, we first identified regions with importance scores higher than 0.5 and record the occurrence of each wave number. **Figure 3** shows the occurrence of the wavelengths deemed important during ViT model's prediction of all the test samples. A higher occurrence for a wavelength indicates greater importance for the model decision-making in the test phase. We set various occurrence thresholds θ = [0, 40, 50, 60, 70, 80, 90], where θ = 0 represents selecting all wavelengths found important for at least one test sample, and θ = 90 represents selecting only those wavelengths that were highly important for more than 90 test samples. The findings revealed that only 1 % of the total wavelengths were important for more than 90 test samples.

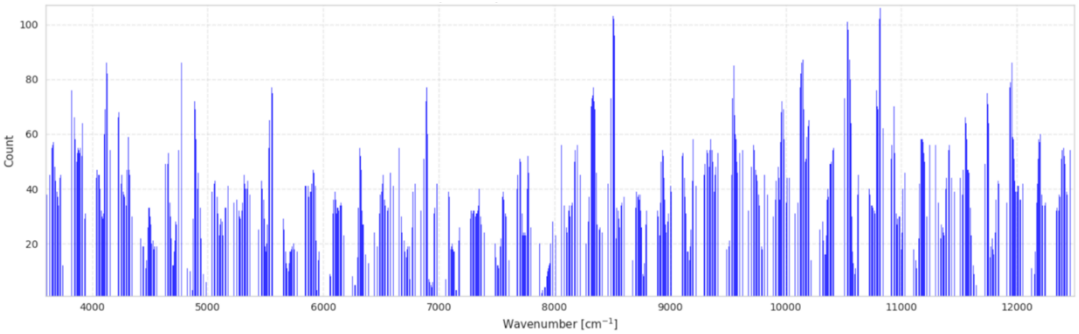

Figure 3. Distribution of occurrences indicating how often each wavelength was deemed important during sample testing. Higher counts correspond to greater importance in the test samples.

We evaluated the performance of the ViT, SVM and LDA to investigate the trade-off between accuracy and the number of selected wavelengths. The results of the experiments are presented in **Figure 4**. The figure indicates that as compression increases, SVM performance declines sharply, whereas LDA and ViT maintain consistent accuracy in identifying coffee authenticity. With 95 % wavelength compression, LDA achieved 100 % accuracy but dropped to 65.7 % with the smallest wavelengths space (1 % of total wavelengths). In contrast, ViT exhibited minimal performance decline with higher compression rates, maintaining an accuracy

of 86 %.

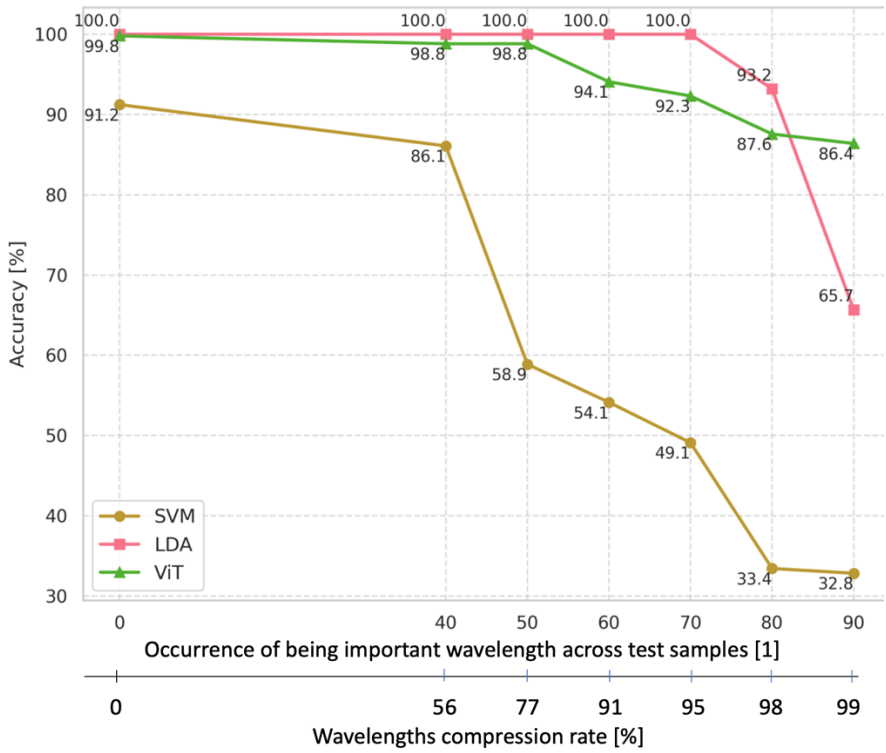

Figure 4. Comparison of model performance in identifying the geographical authenticity of Arabica coffee using varying sizes of NIR wavelengths as input. The input wavelengths were compressed from 0 % to 99 %, where 0 % indicates the use of the original spectra and 99 % indicates that only 1 % of the total wavelengths were used. The compression was based on GradCAM++ attribution values, retaining the most important wavelengths at the final stage of compression.

4. Conclusions

In this study, we adapted the Vision Transformer (ViT) architecture, originally designed for 2D image analysis, to handle 1D near-infrared (NIR) spectral data for identifying the geographical authenticity of Arabica coffee, achieving an accuracy of 99.8 %. By utilizing GradCAM++, an explainable AI tool, we significantly reduced the feature space, using only 1 % of the total wavelengths while maintaining an accuracy of 86.39 %. Our method demonstrates the potential of combining advanced deep learning techniques with explainable AI to ensure food authenticity, support fair trade practices, and protect against fraudulent activities in the coffee industry.

References

Baqueta, M.R., Alves, E.A., Valderrama, P., Pallone, J.A.L., 2023. Brazilian canephora coffee evaluation using nir spectroscopy and discriminant chemo- metric techniques. Journal of Food Composition and Analysis 116, 105065. doi:10.1016/j.jfca.2022.105065.

Cardin, M., Cardazzo, B., Mounier, J., Novelli, E., Coton, M., Coton, E., 2022. Authenticity and typicity of traditional cheeses: A review on geographical origin authentication methods. Foods 11. URL: https://www.mdpi.com/ 2304-8158/11/21/3379, doi:10.3390/foods11213379.

de Carvalho Couto, C., Freitas-Silva, O., Morais Oliveira, E.M., Sousa, C., Casal, S., 2022. Near-infrared spectroscopy applied to the detection of multiple adulterants in roasted and ground arabica coffee. Foods 11. URL: https: //www.mdpi.com/2304-8158/11/1/61, doi:10.3390/foods11010061.

Chattopadhyay, A., Sarkar, A., Howlader, P., Balasubramanian, V.N., 2017. Gradcam++: Generalized gradient-based visual explanations for deep convolutional networks. CoRR abs/1710.11063. URL: http://arxiv.org/abs/1710. 11063, arXiv:1710.11063.

Corallo, A., Latino, M.E., Menegoli, M., Pizzi, R., 2021. Assuring effectiveness in consumer-oriented traceability; suggestions for food label design. Agronomy 11. URL: https://www.mdpi.com/2073-4395/11/4/613, doi:10.3390/ agronomy11040613.

Correia, R.M., Tosato, F., Domingos, E., Rodrigues, R.R., Aquino, L.F.M., Filgueiras, P.R., Lacerda, V., Roma˜o, W., 2018. Portable near infrared spectroscopy applied to quality control of brazilian coffee. Talanta 176, 59–68. URL: https://www.sciencedirect.com/science/article/pii/ S0039914017308287, doi:https://doi.org/10.1016/j.talanta.2017. 08.009.

Cvijanovic´, D., Ignjatijevic´, S., Vapa Tankosic´, J., Cvijanovic´, V., 2020. Do local food products contribute to sustainable economic development? Sustainability 12. URL: https://www.mdpi.com/2071-1050/12/7/2847, doi:10.3390/ su12072847.

de Arau´jo, T.K.L., No´brega, R.O., de Sousa Fernandes, D.D., de Arau´jo, M.C.U., Diniz, P.H.G.D., da Silva, E.C., 2021. Non-destructive authentication of gourmet ground roasted coffees using nir spectroscopy and digital images. Food Chemistry 364, 130452. URL: https://www.sciencedirect.com/science/article/pii/S0308814621014588, doi:https://doi.org/ 10.1016/j.foodchem.2021.130452.

Deng, Z., Wang, T., Zheng, Y., Zhang, W., Yun, Y.H., 2024. Deep learning in food authenticity: Recent advances and future trends. Trends in Food Science & Technology 144, 104344. URL: https://www.sciencedirect.com/science/article/pii/S0924224424000207, doi:https://doi.org/10.1016/j.tifs.2024.104344.

Dharmawan, A., Masithoh, R.E., Amanah, H.Z., 2023. Development of pca-mlp model based on visible and shortwave near infrared spectroscopy for authenticating arabica coffee origins. Foods 12. doi:10.3390/foods12112112.

Dosovitskiy, A., Beyer, L., Kolesnikov, A., Weissenborn, D., Zhai, X., Unterthiner, T., Dehghani, M., Minderer, M., Heigold, G., Gelly, S., Uszkoreit, J., Houlsby, N., 2020. An image is worth 16x16 words: Transformers for image recognition at scale. CoRR abs/2010.11929. URL: https: //arxiv.org/abs/2010.11929, arXiv:2010.11929.

Hassoun, A., Måge, I., Schmidt, W.F., Temiz, H.T., Li, L., Kim, H.Y., Nilsen, H., Biancolillo, A., A¨ıt-Kaddour, A., Sikorski, M., Sikorska, E., Grassi, S., Cozzolino, D., 2020. Fraud in animal origin food products: Advances in emerging spectroscopic detection methods over the past five years. Foods 9. URL: https://www.mdpi.com/2304-8158/9/8/1069, doi:10.3390/ foods9081069.

Hong, E., Lee, S.Y., Jeong, J.Y., Park, J.M., Kim, B.H., Kwon, K., Chun, H.S., 2017. Modern analytical methods for the detection of food fraud and adulteration by food category. Journal of the science of food and agriculture 97, 3877—3896. URL: https://doi.org/10.1002/jsfa.8364, doi:10.1002/ jsfa.8364.

Katerinopoulou, K., Kontogeorgos, A., Salmas, C.E., Patakas, A., Ladavos, A., 2020. Geographical origin authentication of agri-food products: A review. Foods 9. URL: https://www.mdpi.com/2304-8158/9/4/489, doi:10.3390/foods9040489.

Kemsawasd, V., Jayasena, V., Karnpanit, W., 2023. Incidents and potential adverse health effects of serious food fraud cases originated in asia. Foods 12. URL: https://www.mdpi.com/2304-8158/12/19/3522, doi:10.3390/ foods12193522.

Munyendo, L., Njoroge, D., Zhang, Y., Hitzmann, B., 2023. Novel method for the detection of adulterants in coffee and the determination of a coffee's geographical origin using near infrared spectroscopy

complemented by an autoencoder. International Journal of Food Science & Technology 58, 1284–1298. doi:10.1111/ijfs.16283.

Mutz, Y.S., do Rosario, D., Galvan, D., Schwan, R.F., Bernardes, P.C., ConteJunior, C.A., 2023. Feasibility of nir spectroscopy coupled with chemometrics for classification of brazilian specialty coffee. Food Control 149, 109696. doi:10.1016/j.foodcont.2023.109696.

Othman, S., Mavani, N.R., Hussain, M., Rahman, N.A., Mohd Ali, J., 2023. Artificial intelligence-based techniques for adulteration and defect detections in food and agricultural industry: A review. Journal of Agriculture and Food Research 12, 100590. URL: https://www.sciencedirect.com/science/article/pii/S2666154323000972, doi:https://doi.org/ 10.1016/j.jafr.2023.100590.

Pamukc ̧u, H., Sarac ̧ o., Aytug ̆ar, S., Sandıkc ̧ı, M., 2021. The effects of local food and local products with geographical indication on the development of tourism gastronomy. Sustainability 13. URL: https://www.mdpi.com/2071-1050/ 13/12/6692, doi:10.3390/su13126692.

Quan, N.M., Phung, H.M., Uyen, L., Dat, L.Q., Ngoc, L.G., Hoang, N.M., Tu, T.K.M., Dung, N.H., Ai, C.T.D., Trinh, D.N.T., 2023. Species and geographical origin authenticity of green coffee beans using uv–vis spectroscopy and pls–da prediction model. Food Chemistry Advances 2, 100281. doi:10.1016/j.focha.2023.100281.

Sharma, A., Sharma, V., Jaiswal, M., Wang, H.C., Jayakody, D.N.K., Basnayaka, C.M.W., Muthanna, A., 2022. Recent trends in ai-based intelligent sensing. Electronics 11. URL: https://www.mdpi.com/2079-9292/11/10/1661, doi:10.3390/electronics11101661.

Wu, W.P., Zhang, A., van Klinken, R.D., Schrobback, P., Muller, J., 2021. Consumer trust in food and the food system: A critical review. Foods 10. URL: https://api.semanticscholar.org/CorpusID:239372121.

Yang, S., Li, C., Mei, Y., Liu, W., Liu, R., Chen, W., Han, D., Xu, K., 2021. Determination of the geographical origin of coffee beans using terahertz spectroscopy combined with machine learning methods. Frontiers in Nutrition 8. doi:10.3389/fnut.2021.680627.

Deliberate image chipping for free uncrewed aerial vehicles image deep learning generalization

Jurrian Doornbos [a,*], Louise Helary [b], Onder Babur [a, c], Joao Valente [d],

[a] Information Technology Group, Wageningen University, Wageningen, The Netherlands

[b] Institut de l'Élevage, Paris, France

[c] Department of Mathematics and Computer Science, Technical University of Eindhoven, Eindhoven, The Netherlands

[d] Centre for Automation and Robotics, Spanish Research Council, Madrid, Spain

* Corresponding author. Email: jurrian.doornbos@wur.nl

Abstract

In UAV applications, leveraging image-focused Deep Learning (DL) approaches can significantly enhance farm management capabilities. Integrating UAV-captured images with DL models enables a fully autonomous sensing platform, providing critical insights into cattle location, health, and headcounts. These models must generalize across various cattle breeds and environments. Although DL models, such as DALL-E, exhibit broad generalization capabilities, their applicability in UAV agriculture is limited by the scope and diversity of training datasets. Creating comprehensive datasets involves extensive efforts, including multiple UAV flights across different seasons, locations, and cattle breeds, and manually annotating ground-truth data.

To address these challenges, this study explores five training-set augmentation techniques aimed at improving model accuracy and generalization: overlapping, rotating, and zooming training chips, styling chips using the Segment Anything Model, and pseudolabel distillation through the DINO model. Findings indicate that augmentations like overlap and rotation significantly enhance model performance and robustness. However, the effectiveness of these augmentations is contingent on the breed variety within the training set.

Moreover, leveraging transformer networks like DINO, which excel in generalization due to self-supervised attention mechanisms and large dataset pretraining, shows promise in feature extraction for agricultural applications. These sophisticated feature-extractors require domain adaptation for specific UAV and precision agriculture (PA) tasks. Thus, sharing best practices for adapting large pretrained networks to PA tasks is crucial, potentially involving classifiers or thresholds applied to feature maps. This study underscores the importance of dataset diversity and advanced augmentation techniques in developing robust DL models for UAV-assisted cattle detection.

Keywords: drones, deep learning, cattle detection, generalization, augmentation

1. Introduction

Uncrewed Aerial Vehicles (UAVs) pose an ideal solution to farm manager activities in cattle farming. Regular check-ins with the cattle when outdoors, to localize and count the cattle herd is deemed as a labor-intensive task, a task ideally situated to be supported from the aerial perspective (Shao et al., 2019). Especially for areas with difficult to access terrain, the UAV offers a distinct advantage with its flexibility of deployment (Doornbos et al., 2024).

This is also in line with the paradigm of Agriculture 5.0, with its increased reliance on technologies such as Artificial Intelligence (Ryan et al., 2023) to support sustainability goals whilst increasing yield to feed a growing population. Even though the environmental context is getting more difficult, with productive soil decreasing, water scarcity and fertilizers getting more expensive (Fraser & Campbell, 2019).

For UAV applications, it is the image-focused Deep Learning approaches from Artificial Intelligence that can open doors to farm management beyond an eye-in-the-sky. A combination of UAV images, fed through a image-based Deep Learning model that could enable a fully autonomous sensing platform to provide insights about the location, health and headcounts of the cattle (Shao et al., 2019; Rivas et al., 2020).

The requirements for such a image-based Deep Learning model is the ability to detect all varieties of cattle, in any environment. Deep Learning has the capacity of such generalizations within a single

model, as seen with image generation models, such as Dall-E being able to generate an image of almost anything imaginable (Radford et al., 2021). Whilst the architecture and design of such models enables wide generalization, it is the training data that limits its UAV-agricultural applicability (Udandarao et al., 2024). The LAION dataset that such generalized image-generation models are trained on ranged between 100 million and 5 billion images (Schuhmann et al., 2022). Which is largely out of the scope for any agricultural-UAV application. Finally, on top of the size, it is the variety within these datasets that enable generalization (Barbedo, 2018).

Rather obvious, a Deep Learning model such as Dall-E, exclusively trained on varieties of grass, will not be able to generate a tree. Translated to the cattle detection case, a Deep Learning model needs to have seen the complete variety of breeds, during various times of day, image angles, and environments, before it can have a chance at detection the subject (somebody) in a robust and generalizing manner (Safonova et al., 2023).

However, such varying datasets require much effort to create. Often through multiple UAV flights, in multiple seasons, in multiple areas and with various breeds of cattle. On top of these efforts is the resource-intensive task of creating ground-truth labels. Ground-truth is information related to the task you want the Deep Learning model to perform. This can be a bounding box of the cattle, the class (cow), perhaps breeds (Holstein), or even more difficult estimations like weight, health or age. Such data is always manually linked to the object in the image.

Cattle detection is not the only field grappling with the ‘requires large data’ problem. Many tricks have been developed to pose a solution to require ground truth in the dataset. Such tricks can be approached at two levels, the model and the dataset. Tricks at the model-level aim to alter the architecture of Deep Learning networks to require less data to acquire good accuracies, examples include multi-task learning or few-shot learning (Safonova et al., 2023). At the data-level, the data-input is altered before it is seen by a model, examples include rotating the image, adjusting the HSV values, and style-transfer (Xiong et al., 2021).

Finally, models, data and training approaches are combined and mixed for the best possible results, and the final model can perhaps best be seen as a snapshot of ‘best efforts at the time’. A Deep Learning model like ChatGPT has gone through an ongoing, iterative process of training, dataset adjustment and finetuning (Kauffmann et al., 2023). Weakly-supervised models for example are both trained on labelled and unlabeled instances simultaneously, usually through some unsupervised learning mechanism that aims to increase similarity between known samples and unknown samples. Similarly, in active learning, the model itself identifies where the unknowns in unlabeled data are, so a human can act to correctly label them.

The gap of knowledge for these methods is applying them to real-world, data-scarce areas (Udandarao et al., 2024). As presented earlier, acquiring all possible permutations of environment and breeds in the training data is unachievable. Even though it is of high importance to achieve generalization in cattle-detection to achieve meaningful support from the aerial perspective to the farm-manager. This results in an ideal testbed to explore various approaches to improve generalization in cattle-detection.

Therefore, this study both explores the dataset and model-level as an opportunity for attaining higher model accuracy and improve out-of-sample generalization by providing five distinct, but compatible techniques for training-set augmentation.

The five techniques are as follows: 1. Overlapping training chips, 2. Rotating training chips, 3. Zooming the training chips, 4. Styling the training chips using the Segment Anything Model, and 5. Pseudolabel distillation through the DINO model.

2. Materials and Methods

There are three parts to the methods: 1. the cattle dataset, 2. the dataset augmentations and 3. the detection model. The cattle dataset is an open-source dataset developed in the ICAERUS project for cattle detection in France, section 2.1. will focus especially on how this dataset will evaluate generalization. The dataset augmentations are four techniques on dataset style adjustments, and also include the process of pseudolabel distillation, all presented in section 2.2. The chosen Deep Learning detection model is YOLOv8-nano, which is further explained in section 2.3.

2.1. Dataset: ICAERUS Grazing cows

The base dataset used in this study is an open grazing-cows UAV-image dataset developed by Institut de

l'Élevage (IDELE) for the ICAERUS project[1]. In this dataset, multiple UAV flights covering sites in France, with four breeds. The UAV was a DJI Mavic 3 Enterprise. The three areas are Jalogny, Derval and Mauron. With breeds covering Holstein/Normande (black, black-white), Charolais (white), Holstein-crossbreed (brown-white) and Salers (brown). All the cows in the images were annotated using CVAT[2] with their respective bounding-boxes (see figure 1 for a few examples of the dataset).

Table 1. Cow detection dataset splits overview. Train is the base training set on which augmentations were performed.

Location	Breeds	Subset	No. UAV raw images
Jalogny	Charolais (white)	Train	113
		Validation	25
Derval	Holstein/Normande (black-white), Holstein (black)	Test	41
Mauron	Holstein/Normande (black-white), Charolais (white), Salers (brown)	Test	62

The main focus for this study is exploring generalization of Deep Learning methods for cattle detection. To evaluate generalization, it was chosen to only train on Charolais (white) cattle, whilst evaluating on both Charolais and all other breeds (see table 1 for the overview). On the one hand to show that Deep Learning overfits on the training set, which is highly limiting to many UAV and agricultural applications. Whilst simultaneously exploring methods to overcome these overfitting tendencies. Additionally, the large-sized UAV images were chipped in 512x512 resolution to fit the input dimensions of the YOLOv8-nano model.

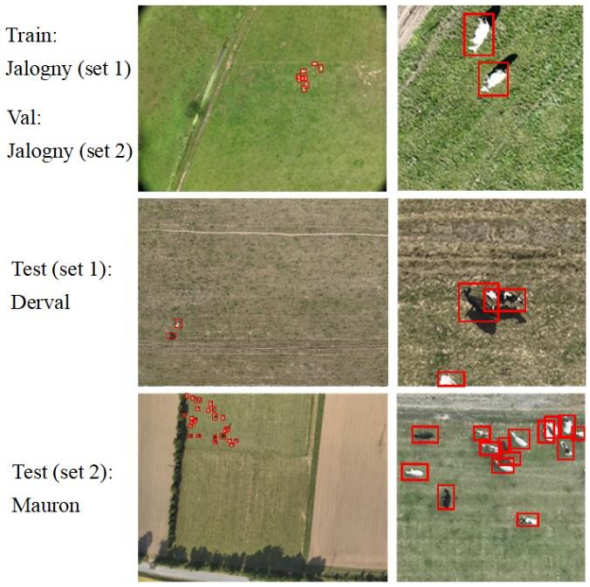

Figure 2. Sample images and ground truth labels from the three datasets. Left: an original image (4000x3000 pixels resolution) as taken by the UAV with bounding-box annotations. Right: an example chip of 512x512 pixels resolution with bounding-box annotations. Note the variety of cow-colours not seen in the training data.

2.2. Dataset augmentations

The core contribution of this paper is in exploring dataset augmentation for generalization. Five augmentations are presented: overlap, rotate, multi-scale, SAM-augment and DINO-Pseudo. The augmentations are used on the training dataset, to create additional labelled samples, without requiring any

[1] https://zenodo.org/records/10245396
[2] https://www.cvat.ai

additional labelling. The baseline method is to cut the large UAV input image (4000x3000 pixels) in 512x512 chips, without any overlap. When a cow is inbetween two images, and is cut in half, the detection is only kept when it is larger than 20pixels. This is roughly the smallest object a Deep Learning model based around Darknet, such as the YOLO family of detectors, can detect. Examples of all augmentations are presented in the appendix.

Overlap is a simple augmentation, where the large UAV input is cut with 50% overlap between the chips. This results in overlapping images, when a cow detection is cut in half in one chip, it will be fully visible in the next image. This results in much more images than the baseline dataset.

Rotate is another simple augmentation, where the input chip is randomly rotated around its' axis. This method results in the same amount of data as the baseline set, just with an even higher variance of images, as they are rotated.

Multi-scale is a method where the imagery is upscaled or downscaled. During image-chipping, both a 1024x1024 or 256x256 resolution chip is cut out of the larger resolution image, which is then up or downscaled to 512x512 resolution. This results in smaller and larger sizes of objects to be included in the dataset. As a cow-detection in a 1024x1024 chips is smaller in size than in 512x512 and vice-versa.

SAM-augment is a newly proposed method, which alters the input object with colour, hsv-shifting, contrast and noise. These methods are shown to increase generalization for deep learning (Khan et al., 2020). SAM-augment uses the Fast Segment Anything model (Zhao et al., 2023) to only apply these augmentations on the object in the image (a cow), whilst ignoring things such as the background. The bounding-boxes of the cows and the images are fed through a pretrained FastSAM to acquire a mask of the object. The image is now randomly augmented in one or two methods of HSV-shifting, contrast increase, added gaussian noise, and/or band-mixing.

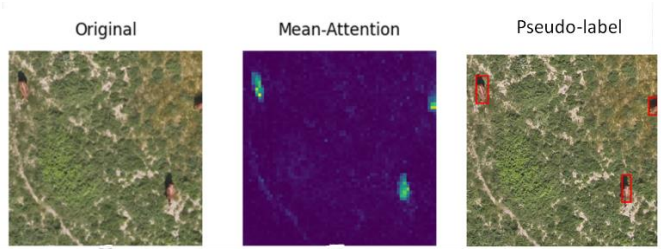

Figure 2. Using DINO attention map to acquire pseudo-labels. Left is the input-image, middle is the DINO attention map, and right is the output pseudo-label box in red from thresholding the sizes for a reasonable bounding box.

DINO-Pseudo is another proposed method of creating pseudo-labels for unseen data. DINO is pretrained Deep Learning model which is highly useful as an unsupervised feature-extractor (Caron et al., 2023). The model creates a set of attention maps, which show where DINO is focussing attention on. In the cattle images, these attention maps correspond very closely to the cows in the image. Therefore, a bounding box is drawn around the areas with high attention across all the attention-maps. The bounding box is kept when the size of this bounding box falls between a minimum and maximum threshold of the size of a cow in the image of the training data. This results in a pseudo-label, as the output label of this method is not checked again. This method is used to generate labels on the test-dataset, these pseudo-labels are then learned by the YOLOv8-nano model.

For an overview of the number of images in the training data, and its corresponding training duration, refer to table 2 below.

2.3. YOLOv8-nano detection model

The YOLO family of Deep Learning detections models, as originally presented in Redmon et al. (2015), attempts to detect both the class and the bounding box of the objects in the image in a single evaluation. Furthermore, the YOLO models come with a variety of preprocessing steps, such as mosaicking and random cropping of the image to increase robustness. YOLOv8 has the same architecture, although builds upon YOLOv5 by replacing the non-maximum suppression of overlapping bounding boxes by SoftNMS, which better deals with overlapping boxes, YOLOv8 also uses anchor-free bounding box suggestions and

only a single detection head, instead of three (Reis et al., 2023). Finally, YOLO comes in various sizes, these sizes indicates the number of parameters in the network, and therefore complexity and ability to capture more and more complexity in the dataset. Larger networks often result in higher accuracies, but does not linearly scale, so there is a trade-off between compute required and accuracy. As we are dealing with a single class (cow) which have similar features, the 'nano' model is chosen, as it offers the fastest training and inference. It is assumed that the experiments can be translated to any Deep Learning detection network and size.

The YOLOv8-nano model was instantiated with random weights from a set seed. Then it was trained on the training dataset, as presented in table 2, for 200 epochs with linear learning-rate decay and a batch-size of 16. All the YOLOv8 augmentations such as rotating, mosaicking and translating were turned off. The best performing model during training was selected for evaluation. This resulted in a baseline model and a model for every training-dataset augmentation. Given the various sizes of pretraining datasets, different training durations are also indicated in table 2. With all above augments, all the possible permutations of augmentations were included, and was therefore much longer to train.

Four accuracy measures were evaluated on unseen data during training: Box Recall, Box Precision, mAP50, mAP50-95. Precision represents the accuracy of detected objects, indicating the proportion of correct detections. Recall reflects the model's ability to identify all instances of objects within images. mAP50: Mean Average Precision calculated at an IoU (Intersection over Union) threshold of 0.50, providing a measure of model accuracy for "easy" detections. mAP50-95: Average of Mean Average Precision calculated across IoU thresholds from 0.50 to 0.95, offering a comprehensive assessment of model performance across varying detection difficulty levels (Reis et al., 2023). These test-scores were measured on the validation set, to show an ideal case, where only white cows are present, as well as test scores on images from Mauron and Derval.

Table 2. Training dataset augmentation variations.

Training Dataset	No. Training Images	Training duration (s)
Baseline	418	1908
Overlap	1572	7175
Rotate	418	1908
Multi-scale	1401	6394
SAM augment	418	1908
All above augments	8430	38479
DINO-Pseudo	912	4162
DINO-Pseudo + SAM augment	912	4162

3. Results and Discussion

The main focus of this research is to explore data augmentation techniques for increasing generalization. This is tested by training YOLOv8 exclusively on the Jalogny training dataset, which only contains white cows, whilst evaluating in two different areas. Only the training data augmentation technique is altered between each evaluation. In this section, accuracies in the Jalogny validation set, Derval test and Mauron test are presented. A perfect model would score 1 on all measurements. This model would create identically shaped and sized bounding boxes, at the same location in the image. Whilst a poor model would score 0, with non-overlapping bounding boxes, and missing bounding boxes altogether. Furthermore, it can be argued that recall is the most important variable in this study, as this tests for all detections by the model that are also in the ground-truth, therefore the ability of the model to generalize into the testing set on unseen cows.

Table 3 shows the accuracy of the model on the Jalogny validation set. This set has similar features to the training set, with white grazing cows in a bright green pasture. The overlap method indicates a better model over the baseline. It is therefore no surprise that it shows high accuracy in the baseline as well as

augmentations. The SAM-augments and DINO methods are lower in accuracy, compared to the baseline. The additional labels and variety in data has therefore also caused more confusion for the YOLOv8 model.

Table 3. YOLOv8n accuracies on the Jalogny validation dataset when trained on different training datasets. Bold indicates the highest value in the accuracy metric. Italics indicate a score lower than the baseline.

Training Dataset	Box Precision	Box Recall	mAP50	mAP50-95
Baseline	0.947	0.905	0.948	0.755
Overlap	0.957	**0.931**	**0.961**	**0.796**
Rotate	0.963	*0.883*	0.952	0.758
Multi-scale	**0.966**	0.909	0.955	0.772
SAM augment	*0.944*	*0.896*	0.951	0.761
All above augments	0.952	*0.897*	*0.946*	0.785
DINO-Pseudo	*0.904*	*0.826*	*0.901*	*0.641*
DINO-Pseudo + SAM	*0.932*	*0.799*	*0.898*	*0.641*

Table 4 shows the accuracies of the model on the Derval test set. This test-set is significantly different in terms of background, which are pastures with a wider variety of cows colours: black, white and and mixes are present. The accuracy is low across all augmentation training datasets, especially the much important Recall shows that the YOLOv8-nano model is not able to generalize across different breeds of cattle it has not seen during training. However, the DINO pseudo-labels and the SAM augmentations are a significant large improvement over the baseline (between 80% and 110% increase in the accuracy measurements) and outperform all the simpler augmentations. However, the accuracy is still not as high as would be deemed usable in terms of precision agricultural application.

Table 4. YOLOv8n accuracies on the Derval test dataset when trained on different training datasets. Bold indicates the highest value in the accuracy metric. Italics indicate a score lower than the baseline.

Training Dataset	Box Precision	Box Recall	mAP50	mAP50-95
Baseline	0.301	0.176	0.206	0.0898
Overlap	0.414	*0.169*	0.272	0.125
Rotate	0.402	0.232	0.271	0.121
Multi-scale	*0.192*	*0.106*	*0.12*	*0.042*
SAM augment	*0.235*	*0.169*	*0.171*	*0.0696*
All above augments	0.408	0.204	0.273	0.128
DINO-Pseudo	0.535	0.324	0.421	0.155
DINO-Pseudo + SAM	**0.571**	**0.366**	**0.465**	**0.181**

For the Mauron test dataset in table 5, the results are somewhat similar as the Derval test set. The largest difference is that in Mauron there are more white Holstein cattle. As previously mentioned, the simpler augmentations are highly accurate at detection these, showing the high precision. The DINO pseudo-labels show that the Precision is much lower than the other methods, whilst Recall is much higher. This indicates that it is difficult for the YOLOv8-nano model to both capture the pseudo labels of the differently coloured cattle, whilst maintaining a high accuracy for the white coloured cattle.

Table 5. YOLOv8n accuracies on the Mauron test dataset when trained on different training datasets. Bold indicates the highest value in the accuracy metric. Italics indicates a score lower than the baseline.

Training Dataset	Box Precision	Box Recall	mAP50	mAP50-95
Baseline	0.803	0.259	0.542	0.383
Overlap	**0.884**	*0.239*	0.568	**0.438**
Rotate	0.853	0.291	**0.581**	0.424
Multi-scale	0.863	*0.241*	0.558	0.404
SAM augment	0.811	*0.258*	*0.539*	*0.38*
All above augments	0.882	*0.251*	0.575	0.432
DINO-Pseudo	*0.516*	**0.549**	0.435	*0.196*
DINO-Pseudo + SAM	*0.541*	0.504	0.419	*0.198*

Finally, for a visual overview of what detections the various models succeed and struggles with is shown in figure 3. The left-side Jalogny images have identical detections, although the all-augments and DINO augmentations show a lower confidence score. Furthermore, in the Mauron and Derval imagery, many of the non-white cows are not detected in the baseline, with a small increase in cow detections for the all-augments model. DINO-SAM pseudo labels and augments has increased the number of true positives significantly. Important is that sometimes the white spots on a Holstein (black-white) cow are detected as an subject.

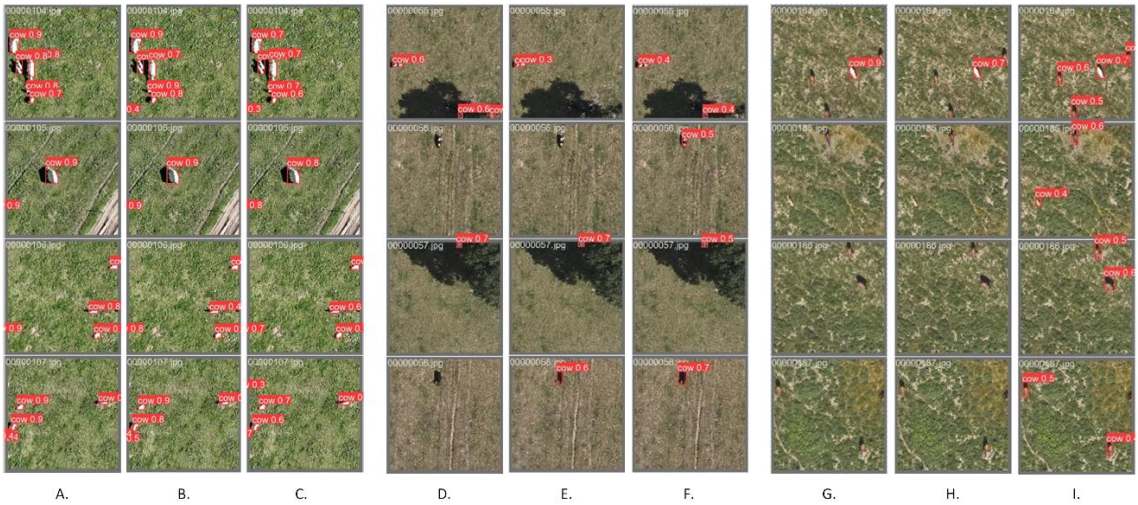

Figure 3. Examples of detections across three areas. From left to right: A, B, C are from the Jalogny validation set, D, E, F are from the Derval test set, G, H, I are from the Mauron test set. A, D, G are detections from the baseline model, B, E, H are detections from the all-augments model, C, F, I are detections from the DINO-SAM pseudo-augment model. The proposed DINO-SAM detects a larger variety of cows, when trained on pseudo-labels.

4. Conclusions

The aim of this research was to explore 'free' data augmentation techniques, in which no new labels are required to increase accuracy in unseen variations. The YOLOv8-nano model was chosen as a state-f-the-art Deep Learning detection model for fully supervised training methods. This model was trained on various augmented versions of the training set. Afterwards, the models were evaluated on three test-sets with a wider variety of cows present. The accuracies of the baseline and data augmentation models are high in the Jalogny evaluation set (a set with only Charolais cows, like the training data). However, as these models have not seen a different variety of cattle, it fails to detect these other breeds. The Pseudo-label methods increase the accuracy of unseen varieties significantly, the Recall on these datasets is much higher than the baseline and even augmentation models.

As a rule of thumb, if the baseline of breeds variety in the training set is not good, the simple data augmentation techniques will only minimally increase or decrease the accuracy for an increase to

robustness to perturbations (such as rotation, subject-sizes and gaussian noise over the image). Interestingly, the all-augments model did not perform better than other data augmentation techniques, and due to the large increase in training time is not recommended as a preprocessing augmentation technique. Furthermore, a small but significant increase in accuracy was measured with the overlap and rotate method across most evaluations over baseline. As this is essentially a 'free' method, it is recommended to be a standard procedure for dataset preprocessing. The rotation is already implemented within the YOLO framework, but the overlap ought to be a standard procedure.

Finally, it is the variation of breeds in the training dataset that really matters. Therefore, pseudolabeling through the DINO model was also introduced. The self-supervised attention mechanism and large dataset pretraining, the transformer network such as DINO are often very good at generalization into unseen data. The backbone of these models are often much better at feature extraction, in comparison to complete training from scratch. Therefore, these models can be used as highly sophisticated feature-extractors.

In agriculture, the feature outputs of the new generation transformer networks are good for any task-specific activity (Radford et al., 2021). However, they are not directly useable and require domain-adaptation with the specific knowledge and tasks within the agriculture or UAV domains. Additional focus should therefore be made on sharing best practices of how these large pretrained networks are adapted for the PA tasks. These adaptations can range from placing a kNN classifier or even a threshold on the feature or maps.

Whilst transformer models might be too complex and large to run in real-time, they are still accurate and can serve as a teacher model for smaller, more specific fully supervised networks such as YOLO. An adapted transformer can work as a pseudo-labeller, or even ground truth labeller if a user would check the results.

Finally, there are many preprocessing steps before training a detector for cattle in UAV imagery as well as next steps in the pipeline after an accurate detection model has been achieved. For adoption of all these methods, processes and approaches, clear documentation, sharing of data and availability of code is a key requirement. Furthermore, collaboration with end-users will always be a necessity if AI is really to be used, trusted, and serve its proposed purpose on the farm to achieve sustainable end-goals.

Acknowledgements

This work has been carried out in the scope of the Horizon Europe Innovation and Capacity building in Agricultural Environmental for Rural Uav Services (ICAERUS) project, which has been funded by the European Commission in the scope of its Horizon Europe program (contract number 101060643, https://icaerus.eu/). The authors acknowledge valuable help and contributions from all partners of the project.

References

Barbedo, J. G. A. (2018). Impact of dataset size and variety on the effectiveness of deep learning and transfer learning for plant disease classification. *Computers and Electronics in Agriculture*, *153*, 46–53. https://doi.org/10.1016/J.COMPAG.2018.08.013

Caron, M., Touvron, H., Misra, I., Jegou, H., Mairal, J., Bojanowski, P., & Joulin, A. (2021). Emerging Properties in Self-Supervised Vision Transformers. *Proceedings of the IEEE International Conference on Computer Vision*, 9630–9640. https://doi.org/10.1109/ICCV48922.2021.00951

Doornbos, J., Bennin, K. E., Babur, Ö., & Valente, J. (2024). Drone Technologies: A Tertiary Systematic Literature Review on a Decade of Improvements. *IEEE Access*, *12*, 23220–23240. https://doi.org/10.1109/ACCESS.2024.3364676

Fraser, E. D. G., & Campbell, M. (2019). One Earth Commentary Agriculture 5.0: Reconciling Production with Planetary Health. *One Earth*, *1*, 278–280. https://doi.org/10.1016/j.oneear.2019.10.022

Kaufmann, T., Weng, P., Kunshan, D., Bengs, V., & Hüllermeier, E. (2023). *A Survey of Reinforcement Learning from Human Feedback*. https://arxiv.org/abs/2312.14925v2

Khan, A., Atzori, M., Otálora, S., Andrearczyk, V., & Müller, H. (2020). Generalizing convolution neural networks on stain color heterogeneous data for computational pathology. *Https://Doi.Org/10.1117/12.2549718*, *11320*, 173–186. https://doi.org/10.1117/12.2549718

Radford, A., Kim, J. W., Hallacy, C., Ramesh, A., Goh, G., Agarwal, S., Sastry, G., Askell, A., Mishkin, P., Clark, J., Krueger, G., & Sutskever, I. (2021). Learning Transferable Visual Models From Natural Language Supervision. *Proceedings of Machine Learning Research*, *139*, 8748–8763. https://arxiv.org/abs/2103.00020v1

Reis, D., Kupec, J., Hong, J., & Daoudi, A. (2023). *Real-Time Flying Object Detection with YOLOv8*. https://arxiv.org/abs/2305.09972v1

Ryan, M., Isakhanyan, G., & Tekinerdogan, B. (2023). An interdisciplinary approach to artificial intelligence in agriculture. *NJAS: Impact in Agricultural and Life Sciences*, *95*(1), 1–32. https://doi.org/10.1080/27685241.2023.2168568

Safonova, A., Ghazaryan, G., Stiller, S., Main-Knorn, M., Nendel, C., & Ryo, M. (2023). Ten deep learning techniques to address small data problems with remote sensing. *International Journal of Applied Earth Observation and Geoinformation*, 125, 103569. https://doi.org/10.1016/J.JAG.2023.103569

Schuhmann, C., Beaumont, R., Vencu, R., Gordon, C., Wightman, R., Cherti, M., Coombes, T., Katta, A., Mullis, C., Wortsman, M., Schramowski, P., Kundurthy, S., Crowson, K., Schmidt, L., Kaczmarczyk, R., Jitsev, J., Berkeley, U., Data, G., & Darmstadt, T. (2022). LAION-5B: An open large-scale dataset for training next generation image-text models. *Advances in Neural Information Processing Systems*, *35*, 25278–25294. https://laion.ai/laion-5b-a-new-era-of-open-large-scale-multi-modal-datasets/

Shao, W., Kawakami, R., Yoshihashi, R., You, S., Kawase, H., & Naemura, T. (2020). Cattle detection and counting in UAV images based on convolutional neural networks. *International Journal of Remote Sensing*, 41(1), 31–52. https://doi.org/10.1080/01431161.2019.1624858

Udandarao, V., Prabhu, A., Ghosh, A., Sharma, Y., Torr, P. H. S., Bibi, A., Albanie, S., & Bethge, M. (2024). No "Zero-Shot" Without Exponential Data: Pretraining Concept Frequency Determines Multimodal Model Performance. *ArXiv*. https://arxiv.org/abs/2404.04125v2

Xiong, L., Ye, M., Zhang, D., Gan, Y., Li, X., & Zhu, Y. (2021). Source data-free domain adaptation of object detector through domain-specific perturbation. *International Journal of Intelligent Systems*, *36*(8), 3746–3766. https://doi.org/10.1002/INT.22434

Zhao, X., Ding, W., An, Y., Du, Y., Yu, T., Li, M., Tang, M., & Wang, J. (2023). *Fast Segment Anything*. https://arxiv.org/abs/2306.12156v1

Appendix

A. Baseline images example:

B. Overlap images example:

C. Multi-scale images example:

256 x 256

512 x 512

1024 x 1024

D. SAM augment images example:

Data-driven approach to classifying the nitrogen nutritional status of ryegrass-based forages

Luís Silva[a,b,c]*, Luís Alcino Conceição[b,c,d], Sofia Barbosa[a], Carla Barreto[b,c], Fernando Cebola Lidon[a], José Santos Silva[e]

[a] Earth Sciences Department, NOVA School of Science & Technology, Campus of Caparica, NOVA University Lisbon, 2829-516 Caparica, Portugal

[b] Polytechnic Institute of Portalegre, 7300-110 Portalegre, Portugal

[c] VALORIZA - Research Center for Endogenous Resource Valorization, Polytechnic Institute of Portalegre, 7300-110 Portalegre, Portugal

[d] InovTechAgro—National Skills Center for Technological Innovation in the Agroforestry Sector, 7300-110 Portalegre, Portugal

[e] INIAV—National Institute of Agricultural and Veterinary Research, I.P., 2005-424 Vale de Santarém, Portugal

* Corresponding author: Luís Silva. Email: lmr.silva@campus.fct.unl.pt

Abstract

Critical N dilution curves (CNDC) are very useful for identifying the optimal N concentration (%Nc) and managing nitrogen (N) fertilization. A Bayesian model, superior to sequential models, offers a single-step estimation of critical N parameters. This research highlights the need for sophisticated models to improve N fertilization accuracy and concentrates on N dilution in plant tissues during the growth of crops. The primary objective is to analyze the implementation of a hierarchical model using a relatively small dataset of Plant Dry Matter (PDM) and Plant Nitrogen Content (PNC) from ryegrass-based fodder crops, to estimate CNDC parameters and assess their uncertainty. The study conducted experimental trials during the 2022-2023 season at the INIAV - Elvas Innovation Centre, Portugal (38°53'38.52"N; 7°3'19.01"W). The experimental design addresses a randomized block split-plot model with variations in N topdressing doses and water management scenarios (rainfed and irrigated). PDM and PNC data were collected at two critical crop stages—ryegrass tillering (t1) and stem elongation (t2). PDM ranges from 0.34 to 1.99 t ha^{-1} at t1 and 0.98 to 5.02 t ha^{-1} at t2. Meanwhile, PNC varies between 1.21-2.70% and 1.15-2.29% at the respective sampling moments. To estimate CNDC parameters, the study employs a Bayesian hierarchical model. The resulting CNDC under no-till management and semiarid conditions indicates an average A1 value of 3.33 [confidence interval (%CI)=(3.23;3.43)] and A2 equal to 0.66 [%CI=(0.63;0.69)]. The N Nutritional Index (NNI) reveals variations between 0.48 and 1.45. The paper showcases the potential of open-source software for data processing and the application of a hierarchical model, serving as a foundation for ongoing crop nutritional monitoring, and tailored N site-specific fertilization plans. This approach makes it possible to mitigate the risks of over-fertilization and improve the sustainability of agricultural systems.

Keywords: Critical N, Grassland, Soil nutrients, Remote Sensing.

1. Introduction

The dilution of nitrogen (N) in plant tissues during crop growth has been widely discussed by various authors and different mathematical models have been applied to describe it. Initially, Lemaire and Salette (Lemaire et al., 1984) established the concept of the critical N dilution curve (CNDC). This allometric approach describes the decline in optimum N concentration ($\%N_c$) as the accumulation of dry matter (PDM;t ha^{-1}) of forage according to $\%N_c = A1*PDM^{-A2}$, where $\%N_c$ is the total concentration of N in the forage (which produces an amount of plant dry matter (PDM; t ha^{-1}), expressed in g N kg^{-1} of forage PDM; A1 is the coefficient that represents the $\%N_c$ of the forage at 1 t PDM ha^{-1}; and A2 is the coefficient that characterises the pattern of decrease in $\%N_c$ during crop growth (Lemaire & Gastal, 1997). N concentrations below $\%N_c$ impair plant growth, and CNDCs help predict the N nutritional index (NNI). The NNI for a given amount of plant PDM can be estimated by comparing the current N concentration (PNC; %) with the $\%N_c$ calculated by the dilution curve (Lemaire & Meynard, 1997). An NNI value equal to or close to 1 means the crop is at the optimum value to achieve maximum yield. This value can be used as a yield and quality reference to correct gaps in crop management (Hoogmoed et al., 2018). It should be noted that the NNI can only diagnose the N status of the crop but cannot quantify the dose of N to be applied in top dressing, especially when the NNI is <1. It is necessary to clarify the relationship between the N status of the crop and the dose to be applied

depending on the crop's development stage, and to achieve a process to be applied in real-time (Li et al., 2022).

Following the Lemaire and Salette (1984) CNDC validated for fescue, Greenwood *et al.* (1990) proposed simplifying by creating a general curve for C3 crops and another for C4 crops. However, other authors have created and validated CNDCs specifically for forage crops such as rainfed annual ryegrass (Marino et al., 2004), Timothy grass (Bélanger & Ziadi, 2008), perennial ryegrass (Gislum & Boelt, 2009), irrigated annual ryegrass (Agnusdei et al., 2010), oats and again for fescue (Agnusdei et al., 2010), and hybrid annual ryegrass (Sandaña et al., 2019). These curves differ, and the value of A1 varies between 3.2 and 6.3, and the value of A2 is between -0.71 and -0.26 (Table 1). These variations prove the consensus presented by most authors that these curves vary depending on the year (climatic conditions), the crop, the variety and the crop management practised.

Table 1. Information of Prior CDNCs for fodder crops.

Crop/Species	A1	A2	Ref.
Festuca arundinacea Schreb. and Dactylis glomerata L.	4.8	0.32	(Lemaire et al., 1984)
C3 crops	5.7	0.50	(GREENWOOD et al., 1990)
Lolium multiflorum L. 1	4.1	0.38	(Marino et al., 2004)
Pheleum pratense L.	3.7	0.35	(Bélanger & Ziadi, 2008)
Lolium perenne L.	6.3	0.71	(Gislum & Boelt, 2009)
Lolium multiflorum L. 2	3.5	0.36	(Agnusdei et al., 2010)
Festuca arundinacea Schreb.	4.7	0.55	(Agnusdei et al., 2010)
Avena sativa L.	3.2	0.26	(Agnusdei et al., 2010)
min	3.2	0.71	
max	6.3	0.26	

Makowski *et al.* (2020) were concerned that these curves (sequential method) did not have the level of uncertainty with which they predict the $\%N_c$ and recommended the Bayesian model (hierarchical method) to estimate the parameters of the CNDC from experimental data in a single step. The model can estimate the A1 and -A2 parameters directly from the PDM-$\%N_c$ pair of observations using freely available software. Lacasa *et al.* (2023) compared both statistical methods and evaluated their performance, considering different observation times throughout the crop cycle, different fertiliser doses and different levels of measurement accuracy. They showed that the sequential models result in poor statistical properties of the estimated parameters and overestimate the $\%N_c$ values. The estimates of N requirements to reach N sufficiency levels exceeded the values estimated by the hierarchical model by around 30 to 100 kg N ha^{-1}. Lacasa *et al.* (2023) corroborate the model presented by Makowski *et al.* (2020) indicating that its use reduces the risk of over-fertilization. Fernandez *et al.*, (2022) re-analysed the PDM and $\%N_c$ dataset from 14 fescue studies, also using the Bayesian model. They suggested that the original curve ($\%N_c = 4.79*PDM^{-0.32}$) by Lemaire and Salette (1984) was overestimated and obtained a curve ($\%N_c = 3.93*PDM^{-0.42}$) established by grouping the data sets according to a wide range of Crop x Environment x Management conditions. They emphasise that the use of an inappropriate experimental design reduces the reliability of CNDCs, especially in the case of a limited number of data collected under non-limiting N conditions or in the case of a limited range of PDM values (Fernandez et al., 2022).

The potential of methods for estimating the site-specific crop N nutritional status are challenged by various factors. In this paper, we will find the CNDC that most closely matches our short database in annual ryegrass-based forage crops, using the Bayesian method, and estimate the NNI.

2. Materials and Methods

2.1. Field trial conditions and design

The experimental trials were conducted in Caia, Elvas, Portugal (38°53'38.52‘N and 7°3'19.01’W) during the 2022-2023 autumn/winter agricultural season. The trial design followed a split-plot randomised block model (ORAL, 2018; Perez et al., 1996). The main block had 3 doses of N topdressing (0, 120 and 200 kg ha^{-1} of fertiliser with 27% N), while the sub-blocks had two different forage crops, and the sub-sub-blocks had two water management scenarios (rainfed and irrigated). The plots in the blocks had a total size of 2 x 8 metres (Figure 1). Each plot was replicated 4 times, totalling 48 plots. They were set up in a location with no relief, so as not to influence possible run-off, either of water or the nutrients themselves.

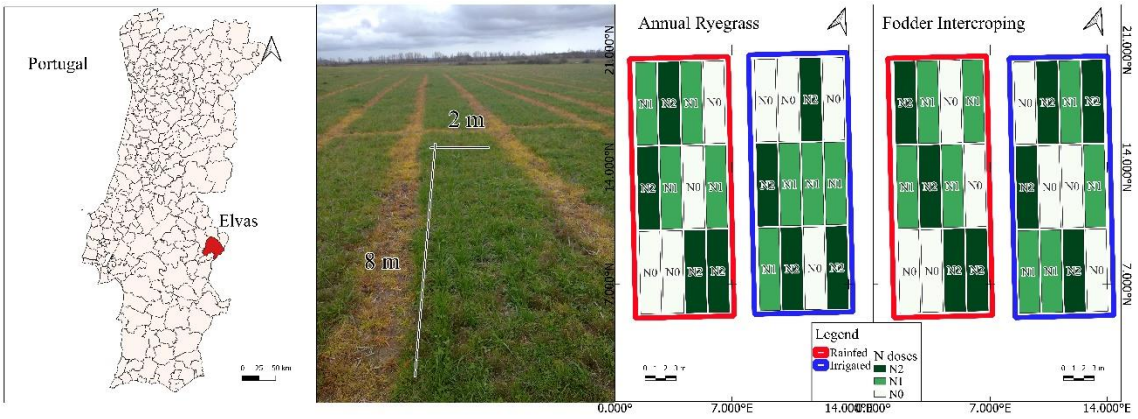

Figure 1. Location and design of trial blocks.

The crops of i) annual ryegrass and ii) fodder intercropping based on annual ryegrass and clovers (Table 2), were sown separately with an inter-row of 0.18 m and a depth of 0.01 m. The sowing doses were 1,400 seeds m^{-2} for annual ryegrass and 4,070 seeds m^{-2} for intercropping (Ryan-Salter & Black, 2012). Before sowing, sufficient doses of phosphorus (16.1 kg ha^{-1} P2O5) and potassium (13.8 kg ha^{-1} K2O) were applied, along with a dose of N (27.6 kg ha^{-1} N) distributed evenly across all the plots to ensure correct crop emergence. Irrigation was also applied evenly at this time. Weeds and diseases were controlled, where necessary, following good experimental practice.

Table 2. Characteristics and dates of crop establishment operations.

Crop	Ryegrass (Crop 1)	Legume-ryegrass mix (Crop 2)			
Species and varieties (%)	*Lolium multiflorum L.* cv Diamond T	*Lolium multiflorum L.* cv Hellen	*Trifolium vesiculosum cv* Comm	*Trifolium resupinatum cv* Lightning	*Trifolium michellianum cv* Balansa Paradana
	100	67	10	17	6
Seeds m^{-2}	1,400	1,531		2,539	
Basal fertilization	28/10/2022				
Seeding	07/11/2022				
Sampling dates	t1 – tillering stage; t2 – elongation stem stage				

The predominant soil at the test site, according to the FAO classification, is a Luvisol which corresponds to a type of Mediterranean soil Pag and Sr (Cardoso, 1974), and the climate, according to Köppen-Geiger is Csa (Köppen, 1900).

2.2. Fit CNDC and NNI

The R code created by Makowski *et al.* (2020) was used to adjust the CNDC, in which the PDM-PNC data pairs from each experiment plot were entered. Since the model for calculating the CNDC should not incorporate data pairs with PDM of less than 1 t ha^{-1}, of the 96 initial pairs, only 58 were considered for adjusting the N curve. The $\%N_c$ was calculated based on the PNC of annual ryegrass and intercropping together, because, given the similarities in the crops, other authors have already proven that the values of the CNDC parameters do not change from one crop to another (Louarn et al., 2021; Soussana & Arregui, n.d.). The curves achieved by other authors in fodder crops, already described in the introduction and specified in Table 1, were considered.

With this adjustment, the values of the A1 and A2 parameters of the CNDC ($\%N_c = A1 * PDM^{-A2}$) were estimated, using the most appropriate curve for estimating the $\%N_c$ of these crops, installed by no-till in sandy soil, in this particular year. Knowing the value of PNC and $\%N_c$, it was possible to calculate the NNI using the ratio between these two parameters:

$$NNI = PNC/\%\mathrm{Nc} \quad (1)$$

where PNC is the actual concentration of the sample and %Nc is the optimum concentration of N in the plant.

2.3. Statistical analysis

To begin analysing the general data, a statistical analysis was carried out, analysing the coefficient of variation, standard deviation and interquartile analysis to eliminate outliers. This was done using the R 4.3.2 software. The data was then grouped by crop, parameter (PDM and PNC), time of sampling, N treatment and water management.

In a second analysis, only data pairs with PDM greater than 1 t ha^{-1} were used. An interquartile analysis was carried out to eliminate outliers. With the data pairs resulting from this filtering, the NNI and N utilisation parameters were calculated.

3. Results and Discussion

3.1. Variations of forage production and N utilisation

3.1.1. Variations of crops PDM and PNC

From a total set of 95 lines of data, 3 outliers were eliminated, leaving a set of 92 lines of data. Looking at the total data set, the average value of the parameters increased from the 1st to the 2nd sampling time, except for the PNC of intercropping. In all parameters, fodder intercropping showed higher values than annual ryegrass (Figure 2).

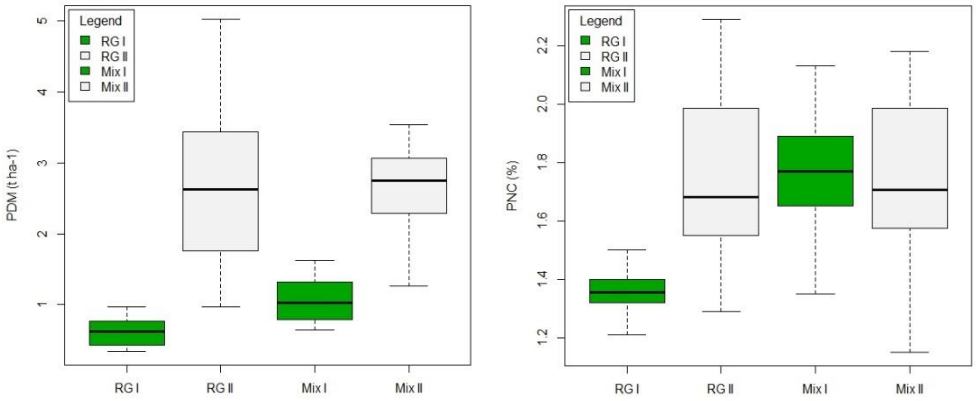

Figure 2. PDM and PNC variations for each crop, by sampling time and water management.

Looking at the 2nd sampling time (in which we can see the influence of the different N doses applied at the 1st time), notice that in irrigated areas the parameters values increase with the increase in the N dose (Figure 3). However, in rainfed areas, the higher N dose does not always represent the highest value of PDM or PNC. In both intercropping and ryegrass, the PNC increases, but PDM production decreases. This relationship allows the nutritional status of intercropped plants to increase, but it is not enough to increase that of ryegrass plants.

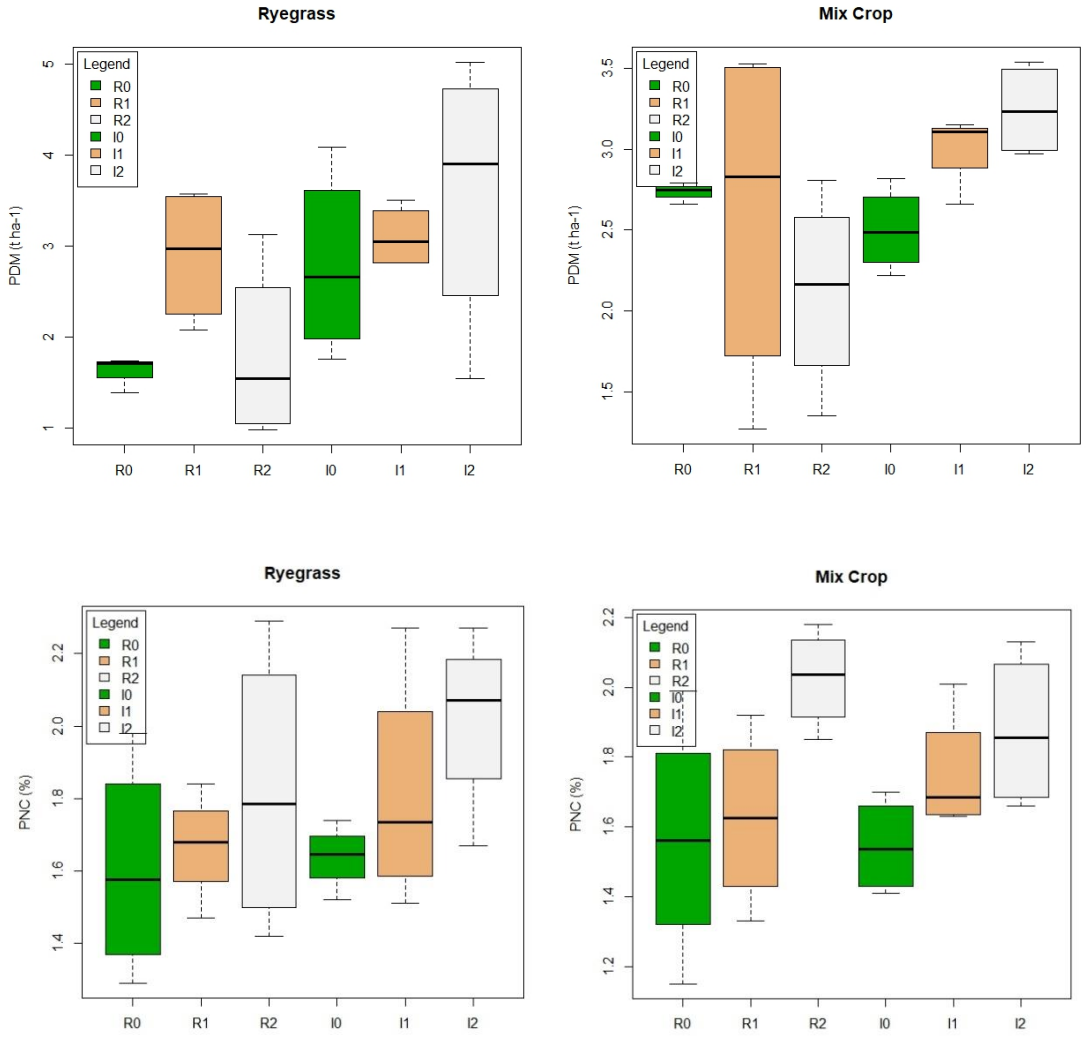

Figure 3. PDM and PNC variations by N doses.

3.1.2.CNDC and variations in NNI patterns

The CNDC of the crops under study was established using the Bayesian statistical model, according to Makowski *et al.* (2020), as well as the confidence interval (CI) associated with all the data (PDM and PNC) recorded. Samples with PDM of less than 1 t ha^{-1} were not included in the curve fitting. The A1 and A2 parameters range from 3.22 to 3.44 and 0.63 to 0.69, respectively. Finally, the CNDC that was determined is $\%N_c = 3.33 * PDM^{-0.66}$ (Table 3).

Table 3. Coefficient values and their calculated errors.

	A1	A2
Mean	3.3319	0.6643
SD	0.1060	0.0320
Naive SE	0.0009	0.0003
Time-Series	0.0030	0.0009

With this adjusted curve, it was possible to calculate the NNI value for each plot under study. The descriptive statistics of the calculated results are shown in Table 4. The average NNI value is 0.89.

Table 4. Descriptive statistics of the parameters and NNI of the study blocks.

	PDM	PNC	%Nc	NNI
Nº of samples	58	58	58	58
Min	1.03	1.15	1.31	0.48
Max	4.09	2.27	3.27	1.45
Mean	2.33	1.72	2.07	0.89
Median	2.30	1.70	1.92	0.86
DP	0.84	0.24	0.55	0.25
CV	36.25	13.96	26.69	28.20

NNI is related to PDM, since the better the plants were nourished with N, the more PDM they had. It is also related to the PNC since plants with a higher NNI have a higher PNC. NNI is closely related to N absorption by the plants, since the higher the NNI, the greater the amount of N absorbed.

4. Conclusions

The paper showcases the potential of open-source software for data processing and the application of a hierarchical model, serving as a foundation for ongoing crop nutritional monitoring, and tailored N site-specific fertilization plans. This approach makes it possible to mitigate the risks of over-fertilization and improve the sustainability of agricultural systems. Further studies could analyse the possibility of measuring the PDM and PNC parameters using remote sensing. This advance would make it possible to remotely calculate the parameters, or even the NNI itself directly, measuring the N nutritional status of crops more quickly and relatively economically.

Acknowledgements

The authors wish to express their gratitude to the VALORIZA and GeoBioTec research centres as well as to INIAV, I.P. – Elvas Innovation Centre, Portugal for providing the fields and trial crops.

References

Agnusdei, M. G., Assuero, S. G., Lattanzi, F. A., & Marino, M. A. (2010). Critical N concentration can vary with growth conditions in forage grasses: implications for plant N status assessment and N deficiency diagnosis. *Nutrient Cycling in Agroecosystems*, *88*(2), 215–230. https://doi.org/10.1007/s10705-010-9348-6

Bélanger, G., & Ziadi, N. (2008). Phosphorus and Nitrogen Relationships during Spring Growth of an Aging Timothy Sward. *Agronomy Journal*, *100*(6), 1757–1762. https://doi.org/10.2134/agronj2008.0132

Fernandez, J. A., van Versendaal, E., Lacasa, J., Makowski, D., Lemaire, G., & Ciampitti, I. A. (2022). Dataset characteristics for the determination of critical nitrogen dilution curves: From past to new guidelines. *European Journal of Agronomy*, *139*, 126568. https://doi.org/10.1016/j.eja.2022.126568

Gislum, R., & Boelt, B. (2009). Validity of accessible critical nitrogen dilution curves in perennial ryegrass for seed production. *Field Crops Research*, *111*(1–2), 152–156. https://doi.org/10.1016/j.fcr.2008.11.009

GREENWOOD, D. J., LEMAIRE, G., GOSSE, G., CRUZ, P., DRAYCOTT, A., & NEETESON, J. J. (1990). Decline in Percentage N of C3 and C4 Crops with Increasing Plant Mass. *Annals of Botany*, *66*(4), 425–436. https://doi.org/10.1093/oxfordjournals.aob.a088044

Hoogmoed, M., Neuhaus, A., Noack, S., & Sadras, V. O. (2018). Benchmarking wheat yield against crop nitrogen status. *Field Crops Research*, *222*, 153–163. https://doi.org/10.1016/j.fcr.2018.03.013

Lacasa, J., Makowski, D., Hefley, T., Fernandez, J., van Versendaal, E., Lemaire, G., & Ciampitti, I. (2023). Comparison of statistical methods to fit critical nitrogen dilution curves. *European Journal of Agronomy*, *145*, 126770. https://doi.org/10.1016/j.eja.2023.126770

Lemaire, G., & Gastal, F. (1997). N Uptake and Distribution in Plant Canopies. In *Diagnosis of the Nitrogen Status in Crops* (pp. 3–43). Springer Berlin Heidelberg. https://doi.org/10.1007/978-3-642-60684-7_1

Lemaire, G., & Meynard, J. M. (1997). Use of the Nitrogen Nutrition Index for the Analysis of Agronomical Data. In *Diagnosis of the Nitrogen Status in Crops* (pp. 45–55). Springer Berlin Heidelberg. https://doi.org/10.1007/978-3-642-60684-7_2

Lemaire, G., Salette, J., Sigogne, M., Terrasson, J.-P., & LEMAIRE Jean SALETTE Monique SIGOGNE Jean-Pierre TERRASSON LNRA, G. (1984). *Relation entre dynamique de croissance et dynamique de prélèvement d'azote pour un peuplement de graminées fourragères. I.-Etude de l'effet du milieu Relation entre dynamique de croissance et dynamique de prélèvement d'azote pour un peuplement de graminées fourragères. I. — Etude de l'effet du milieu* (Vol. 4, Issue 5). https://hal.science/hal-00884655

Li, X., Ata-UI-Karim, S. T., Li, Y., Yuan, F., Miao, Y., Yoichiro, K., Cheng, T., Tang, L., Tian, X., Liu, X., Tian, Y., Zhu, Y., Cao, W., & Cao, Q. (2022). Advances in the estimations and applications of critical nitrogen dilution curve and nitrogen nutrition index of major cereal crops. A review. *Computers and Electronics in Agriculture*, *197*, 106998. https://doi.org/10.1016/j.compag.2022.106998

Louarn, G., Bedoussac, L., Gaudio, N., Journet, E.-P., Moreau, D., Steen Jensen, E., & Justes, E. (2021). Plant nitrogen nutrition status in intercrops– a review of concepts and methods. *European Journal of Agronomy*, *124*, 126229. https://doi.org/10.1016/j.eja.2021.126229

Makowski, D., Zhao, B., Ata-Ul-Karim, S. T., & Lemaire, G. (2020). Analyzing uncertainty in critical nitrogen dilution curves. *European Journal of Agronomy*, *118*, 126076. https://doi.org/10.1016/j.eja.2020.126076

Marino, M. A., Mazzanti, A., Assuero, S. G., Gastal, F., Echeverría, H. E., & Andrade, F. (2004). Nitrogen Dilution Curves and Nitrogen Use Efficiency During Winter–Spring Growth of Annual Ryegrass. *Agronomy Journal*, *96*(3), 601–607. https://doi.org/10.2134/agronj2004.0601

ORAL, E. (2018). EFFECT OF NITROGEN FERTILIZATION LEVELS ON GRAIN YIELD AND YIELD COMPONENTS IN TRITICALE BASED ON AMMI AND GGE BIPLOT ANALYSIS. *Applied Ecology and Environmental Research*, *16*(4), 4865–4878. https://doi.org/10.15666/aeer/1604_48654878

Perez, C. M., Juliano, B. 0, Liboon, S. P., Alcantara, J. M., & Cassman, K. G. (1996). *Effects of Late Nitrogen Fertilizer Application on Head Rice Yield, Protein Content, and Grain Quality of Rice*.

Ryan-Salter, T. P., & Black, A. D. (2012). Yield of Italian ryegrass mixed with red clover and balansa clover. *Proceedings of the New Zealand Grassland Association*, 201–207. https://doi.org/10.33584/jnzg.2012.74.2862

Sandaña, P., Lobos, I. A., Pavez, P. B., & Moscoso, C. J. (2019). Validation of a critical nitrogen dilution curve for hybrid ryegrasses. *Grass and Forage Science*, *74*(3), 370–380. https://doi.org/10.1111/gfs.12405

Soussana, J., & Arregui, M. (n.d.). *Impact de l'association sur le niveau de nutrition azotée et la croissance du ray-grass anglais et du trèfle blanc*. https://hal.science/hal-00885673

A deep-learning approach for automated phenological prediction in barley

Luis Sánchez-Fernández [a,*], Manuel Perez-Ruiz [a], Gregorio Egea [a]

[a] Department of Ingeniería Aeroespacial y Mecánica de Fluidos, University of Seville, Seville, Spain

* Corresponding author. Email: lsanchez1@us.es

Abstract

Current and anticipated climate changes are set to profoundly impact crop cultivation, leading to reduced harvests, increased costs, and the need for significant deviations from traditional farming methods. To address the challenge of feeding a growing population in the context of an expanding economy, yields must be increased by 70% over the next 30 years. A critical strategy in meeting this challenge is the development of new crop cultivars that are more resilient and adaptable to evolving climate conditions. Obtaining new cultivars in cereals is labor-intensive and relies on manual measurements of height, vigor, disease resistance, or water use efficiency. Many of these parameters are manually collected by trained technicians, and subjective variables like vigor introduce a level of uncertainty, diminishing the reliability and efficiency of the breeding process. Global efforts are being made to automate the collection of objective data useful for breeders. This research presents a novel deep-learning model designed and trained to accurately predict the BBCH scale of barley based on RGB images, environmental factors, and structural parameters that can be automatically obtained. We gathered BBCH, temperature, crop height and RGB data during 2022-2023 crop cycle on the University of Seville campus farm. Additionally, we captured and labelled 1162 RGB images that we used to train a convolutional neural network (CNN). These images were randomly split into training (80%), validation (15%), and testing (5%) sets. Our model demonstrated an accuracy of $r^2 = 0.97$ in predicting the BBCH scale of the studied barley crop after 24 epochs with a batch size of 32.

Keywords: Deep-learning model, Phenotyping, Phenology, BBCH, Barley

1. Introduction

Current and anticipated climate changes are set to profoundly impact crop cultivation, leading to reduced harvests, increased costs, and the need for significant deviations from traditional farming methods. To address the challenge of feeding a growing population in a context of expanding economy (United Nations, 2022), yields must be increased by 70% over the next 30 years (Searchinger et al., 2018). A critical strategy in meeting this challenge is the development of new crop cultivars that are more resilient and adaptable to evolving climate conditions. However, the annual genetic gain of cereal crops hovers around 0.5-1% (del Pozo et al., 2022; Masuka et al., 2017), falling significantly short of meeting the predicted demands. Moreover, improvements in yield resulting from increased harvest index are becoming increasingly more complex to achieve as we approach the biological limits in our major cereal crops. Future yield improvements must come from more efficient biomass accumulation and, in many cases, under water-stress conditions. Obtaining new cultivars in cereals is labor-intensive and relies on manual measurements of height, vigor, disease resistance, or water use efficiency. Many of these parameters are manually collected by trained technicians, and subjective variables like vigor introduce a level of uncertainty, diminishing the reliability and efficiency of the breeding process.

Global efforts are increasingly focused on automating the collection of objective data to aid breeders in surpassing current limitations that only allow the phenotyping of a few cultivars during each growing season. One of the technologies currently being developed and beginning to be used by breeders is phenotyping platforms. Until recently, the introduction of this technology in the agricultural sector was limited by the high prices of sensors and the limited processing capacity and automatization in the field. However, the recent widespread adoption of remote sensing technology and the development of new, more affordable sensors have facilitated the introduction of these innovative tools into the breeding sector. Equipped with remote sensing capabilities, phenotyping platforms are emerging as a pivotal tool with the potential to accelerate the breeding process. These platforms enable the phenotypic characterization of multiple cultivars in response to

specific environments and at distinct phenological stages, increasing the scalability of breeding programs worldwide.

A key aspect of the breeding process is using the BBCH scale, a widely adopted system for categorizing plant growth stages. This scale is crucial for optimizing agricultural management practices and enhancing the plant breeding process. Traditionally, determining BBCH in breeding experimental fields is a labor-intensive process that relies on manual observations by trained technicians. An automatic crop phenology classification method is essential to bring the potential capabilities of autonomous phenotyping platforms to the breeding sector. Such a method would allow us to automatically link the measured phenotypes to the corresponding phenological stages of crops, thereby significantly accelerating the breeding process.

Our research aimed to develop a deep-learning model capable of predicting the BBCH scale of barley that would be deployable on a phenotyping platform. Our model demonstrated an accuracy of $r^2 = 0.97$. This work presents a novel deep-learning model designed and trained to accurately predict the BBCH scale of barley based on RGB images, days after sowing, crop height, and accumulated Growing Degree-Days (GDD).

2. Materials and Methods

2.1. Experimental design and dataset obtention

The dataset was generated during 2022-2023 crop cycle on the University of Seville campus farm. The experimental site had 6 plots of barley, *Hordeum vulgare L. var. nutans* "Traveler", each plot measured 6 x 1.5 m. The seeding date was the 30 of December 2022, fifteen days later, we carried out nitrogen fertilization by applying 50 $Tn \cdot ha^{-1}$ of N. BBCH, height and RGB data were taken regularly, twice, or thrice a week during the crop cycle. RGB data obtention was performed using a Canon EOS 250D camera with a Canon EFS18-15mm lens attached and with a Samsung Galaxy A54 64 MP cellphone camera. Images were resized to a 512 x 512 resolution using a Python script. After resizing, we randomly split the 1156 RGB images the data set obtained in a proportion of 80% for training, 15% for testing and 5% for validation. The labels and non-image features associated with each image were stored in a .csv file for each set. The inputs for the created model were the RGB images, days after sowing, crop height and growing degree days (GDD). GDD was calculated by applying Eq.1. Weather data was collected on-site using a weather station (Raincrop, Sencrop, Lile, FR).

$$GDD = \sum_{n}^{0} (T_{avg} - T_b) \tag{1}$$

where GDD represents the accumulated growing degree-days in Celsius; n is the days after sowing of each sampling day; T_{avg} is the daily average temperature; and T_b is the base temperature. For this study, we used a T_b of 4.5°C based on the work by Rubio et al., 2017.

2.2. Deep-learning model

The deep learning model proposed is based on a Convolutional Neural Network (CNN) for the RGB image processing and concatenation layers to combine the image processing part of the model with the non-image input features, combining them into a single layer. The model was built using the TensorFlow Python library and comprises 4 2D convolutional layers of 32, 64, 128 and 256 filters or kernels, respectively. Each layer has a filter size of 3x3 and a Rectified Linear Unit (ReLU) activation function. After each 2D convolutional layer, a max pooling layer was added to reduce each spatial dimension by half. A Flattening layer was added to flatten the 3D output of the last convolutional layer into a 1D vector, which could be fed into dense, fully connected layers. A final layer of 512 kernels and ReLU activation function was added to the model, followed by a dropout layer with a dropout rate of 0.5 to prevent overfitting. Non-image features were called from a .csv file associated with each image. These features fed the model through a concatenated layer that combines the output of the processing part of the model with the non-image input features,

combining them into a single layer. Finally, an additional dense layer of 128 kernels activated by a ReLU function and a dropout layer with a dropout rate of 0.25 was added. Given the regression nature of the BBCH prediction model, a final output layer was added using a linear activation function. The model was compiled with the Adam (Adaptive Moment Estimation) optimizer, mean squared error loss function, and mean absolute error as a metric. Optimal training was found at 24 epochs with a batch size of 32.

3. Results and Discussion

Our results show a good fit between our testing data and the predictions given by our model, $r^2 = 0.97$ (Figure 1). Our model's Mean Absolute Error (MAE) and Mean Squared Error (MSE) were 2.82 and 14.12 respectively. This high correlation was expected and aligns with previous research indicating a strong correlation between the BBCH of crop development and accumulated degree-days, as well as the robustness of the accumulated degree-days models (Juskiw et al., 2001; Wang & Engel, 1998). The proposed deep-learning model shows promise in scenarios where weather data, sowing date and crop height are available. The acquisition of inputs for this model can be automated using appropriate sensors capable of providing crop height measurements, such as LiDAR sensors, RGB-h cameras, or ultrasound sensors.

Our model shows a higher error between BBCH stages 50 to 60, which might be explained by the visual similarities between both phenological stages, variability in the development within the plants in the same plot and a reduced number of samples during crop the 60 – 90 BBCH stages. Given the differences in GDD, crop height, and the different lengths in the crop cycle of each cultivar, our model may require some adjustments to maintain accuracy in other cultivars.

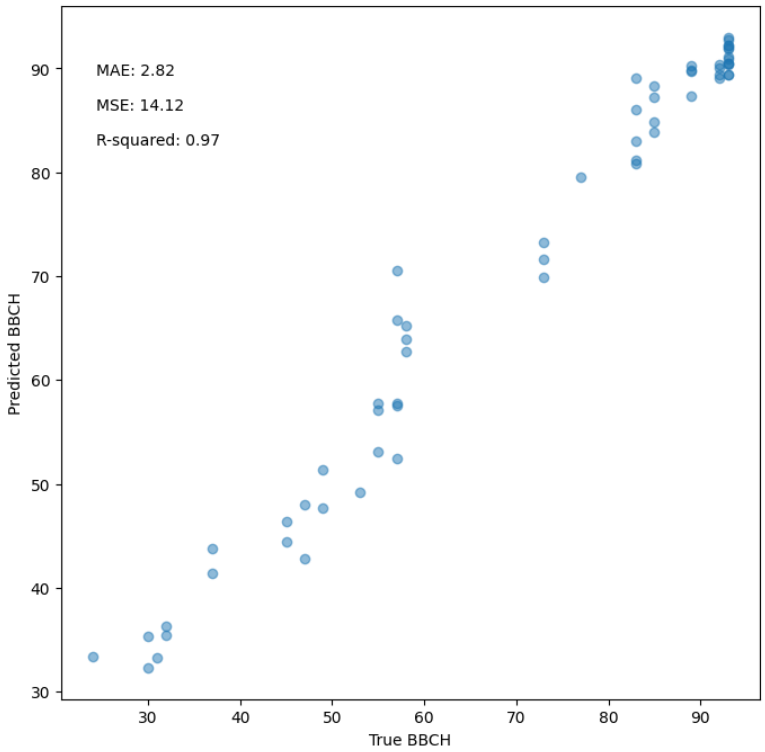

Figure 1. True vs predicted BBCH results were obtained by our deep learning model using RGB and non-image features with mean absolute error (MAE) and mean squared error (MSE) values.

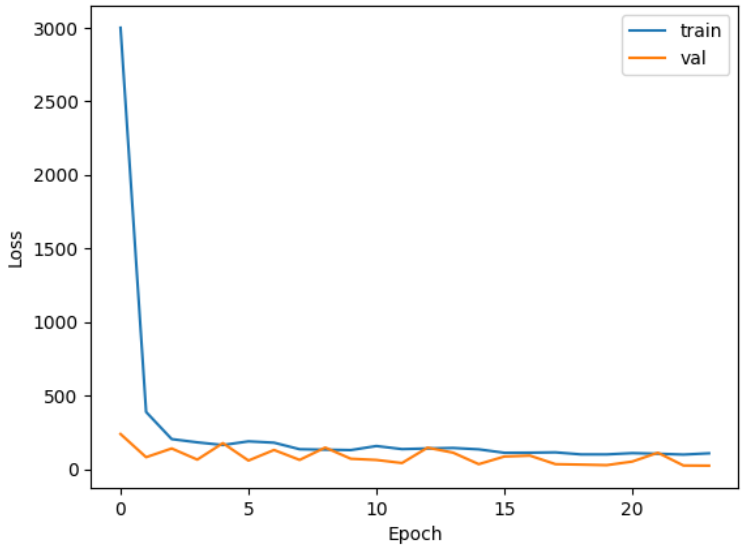

Figure 2. Training and validation loss of our model.

4. Conclusions

This work presents a deep-learning model based on RGB images and non-image features such as crop height, days after sowing and accumulated degree days. This model achieved an accuracy of $r^2 = 0.97$ and could be implemented on a phenotyping platform capable of collecting RGB images, crop height and weather data. Implementing deep learning models in phenotyping platforms for BBCH prediction will increase the scalability of breeding programs, contributing to the obtention of new cultivars and accelerating the breeding process. However, validating this model in different scenarios is pivotal, given the other parameters characteristic of each phenotype and the environmental variables that can affect the crop cycle length.

Acknowledgements

The authors acknowledge the Spanish Ministry of Science and Innovation funding through the program "National Plan 2021-2023 - Targeted Research Projects" (project reference PID2021-125080OB-I00) to conduct the experiments.

References

del Pozo, A., Jobet, C., Matus, I., Méndez-Espinoza, A. M., Garriga, M., Castillo, D., & Elazab, A. (2022). Genetic Yield Gains and Changes in Morphophysiological-Related Traits of Winter Wheat in Southern Chilean High-Yielding Environments. *Frontiers in Plant Science*, *12*. https://doi.org/10.3389/fpls.2021.732988

Juskiw, P. E., Jame, Y. W., & Kryzanowski, L. (2001). Phenological development of spring barley in a short-season growing area. *Agronomy Journal*, *93*(2), 370–379. https://doi.org/10.2134/agronj2001.932370x

Masuka, B., Atlin, G. N., Olsen, M., Magorokosho, C., Labuschagne, M., Crossa, J., Bänziger, M., Pixley, K. V., Vivek, B. S., Von Biljon, A., Macrobert, J., Alvarado, G., Prasanna, B. M., Makumbi, D., Tarekegne, A., Das, B., Zaman-Allah, M., & Cairns, J. E. (2017). Gains in maize genetic improvement in eastern and southern Africa: I. CIMMYT hybrid breeding pipeline. *Crop Science*, *57*(1), 168–179. https://doi.org/10.2135/cropsci2016.05.0343

Rubio, V., Garcia, A., Pereira, S., 2017. Impacto de la variabilidad climática en el cultivo de trigo. Revista INIA 49. pp. 13-16. http://www.ainfo.inia.uy/digital/bitstream/item/6994/1/revista-INIA-49.p.13-16.pdf

Searchinger, T. D., Wirsenius, S., Beringer, T., & Dumas, P. (2018). Assessing the efficiency of changes in land use for mitigating climate change. *Nature*, *564*(7735), 249–253. https://doi.org/10.1038/s41586-018-0757-z

United Nations. (2022). *World Population Prospects 2022: Summary of Results*.

Wang, E., & Engel, T. (1998). Simulation of Phenological Development of Wheat Crops. In *Agricultural Systems* (Vol. 58, Issue 1).

Computer vision-based early detection of *Phytophthora spp*. in orange grove

Diego Gallardo-Romero*, Gregorio Egea , Manuel Pérez-Ruiz

Department of Aerospace Engineering and Fluid Mechanical, University of Sevilla, Sevilla, Spain
* Corresponding author. Email: dgallardo@us.es

Abstract

In an agricultural sector that faces significant challenges and is committed to food security, spreading pathogens represents a severe threat. In this context, the need arises to implement new methodologies and tools capable of mitigating or alleviating existing problems. In Spain, this concern is aggravated in crops of great interest and economic impact, such as citrus fruits, especially oranges, since more than 150,000 hectares are dedicated to their production, representing a fundamental part of the country's agricultural economy. The orange tree crop suffers from a series of pathologies that affect its development and production, causing significant economic losses. To address this situation, this study applies cutting-edge technology such as computer vision and multispectral sensors carried on UAVs. Experimental results show the capacity of the YOLOv8-seg model to identify trees affected by *Phytophthora spp*. at early stages of infection when symptoms are not visible. With accuracy values of 94.3%, recall of 87.1% and mAP50 of 68.6% for segmentation and classification. These results represent a crucial step forward in developing an early identification system for *Phytophthora spp.* in young orange groves and highlight the potential of advanced technologies in the agri-food sector.

Keywords: Plant pathology, unmanned aerial vehicles, multispectral images, deep learning, segmentation models.

1. Introduction

In a changing world marked by resource scarcity, population growth or climate change, long-term sustainability and food security have become a concern, and the conservation of crops has become a priority (Pereira, 2017; Hídricos, 2020). This concern is significant for orange cultivation in Spain since, according to the Ministry of Agriculture, Fisheries and Food (MAPA, 2022), around 150,000 hectares are cultivated, representing 10.7% of the orange groves in the European Union and 35.2% of the total orange production in the EU, which highlights the economic and cultural importance of the crop in the country. It is vital to protect the crop against pathogens that threaten production. *Phytophthora spp.*, a fungus that causes collar or root rot in orange trees, is one of the most problematic pathogens. This fungal disease damages the roots and stem base of the trees, making it difficult for them to absorb nutrients and water. Most worryingly, the symptoms of infection are difficult to detect in the early stages, which facilitates the silent spread of the disease and causes significant damage before it is detected (Sáenz Pérez et al., 2019). In the face of pathogens such as these, early detection is crucial in mitigating food safety risks and minimising production costs.

Since the beginning of agriculture, the detection of pathogens in crops has been based on observation and the experience and knowledge of professionals or producers. Although it has been, and still is today, a widely used methodology, it has severe limitations in the current context of changing agriculture. Aspects such as the shortage of qualified personnel or the physical and temporal requirements may limit the capacity to respond to unforeseen situations, with consequent economic and yield losses. Due to these limitations, exploring and researching the development and adoption of new technologies that can complement traditional pathogen detection methods is imperative. Many research projects have been carried out over the last decades to obtain and offer innovative solutions to this challenge. A clear example of disruptive and innovative technology is drones, also known as unmanned aerial vehicles (UAVs), due to their great capacity to collect data quickly and efficiently (Nex and Remondino, 2014). Specialised sensors and cameras allow drones to monitor large areas of crops in a relatively short time. They can also access hard-to-reach areas where visual detection would be virtually impossible (Khan et al., 2022). Multispectral cameras are another technology with great potential, as they simultaneously capture information in several bands of the electromagnetic spectrum, such as the red edge or near-infrared (NIR). Such cameras are popularly used in drones and

satellites, as they provide information that is not visible to the human eye. They allow detailed information on the vegetative state of crops or the soil, facilitating the optimisation of resources and supporting decision-making.

The concept of artificial intelligence (AI) emerged in the 1950s (McCarthy, 2007), a term coined at the Dartmouth conference. But it was not until the 2000s that this technology became a true revolution, thanks to advances and improvements in computer science (Kaul et al., 2020). ML (El Naqa and Murphy, 2015) and DL (LeCun, 2015) models offer the ability to learn complex patterns and extract relevant features from large volumes of data and images, making AI a key element in the day-to-day life of most industries (Hamet and Tremblay, 2017; Bannerjee et al., 2018; Chen et al., 2020). The study's main objective was to develop an identification system for early detection of the presence of *Phytophthora spp*. in young orange plantations using multispectral images captured with a UAV and a DL model. This new methodology has great potential to improve food security and increase the economic profitability of farmers.

2. Materials and Methods

This study uses multispectral images taken with UAV to segment and classify healthy trees and trees affected by *Phytophthora spp*. The fulfilment of this main objective involves a series of steps: I) acquisition of field images; II) data processing and creation of the training-validation-testing dataset; III) implementation of a DL model; IV) tree segmentation and classification; V) calculation of evaluation metrics and analysis of the results obtained. Figure 1 shows the study workflow diagram.

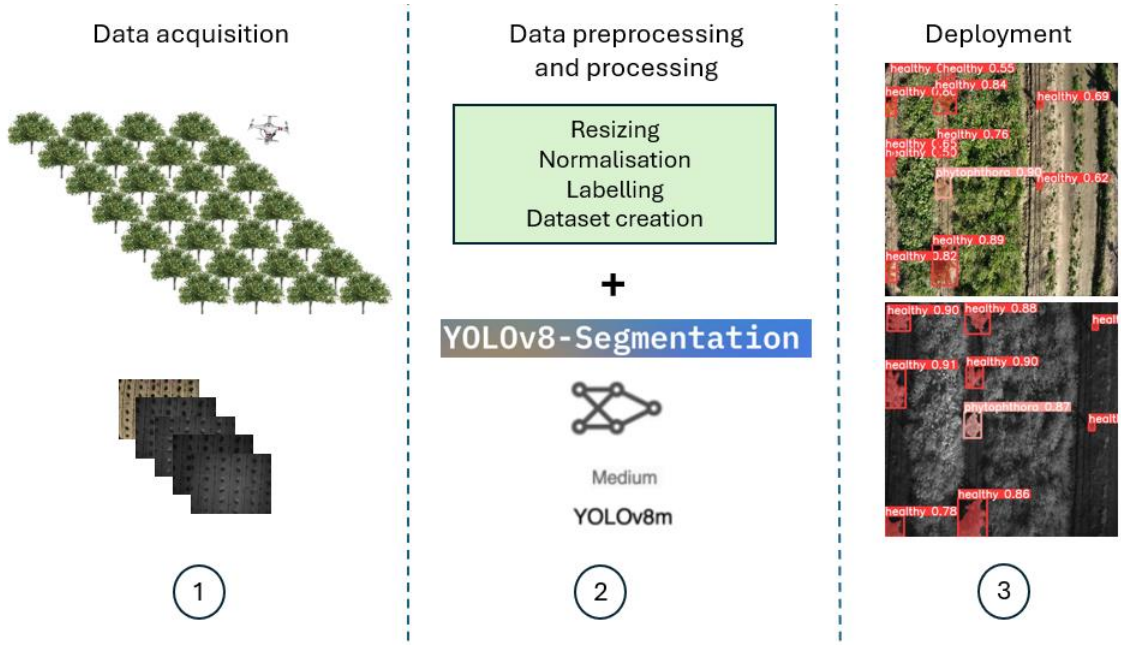

Figure 1. Workflow diagram for developing an early detection system for *Phytophthora spp.* in orange grove. Own source.

2.1. Study Area

The experiment was carried out during the 2023 campaign in a plot of orange trees located in Brenes, Seville, Spain (Latitude: 37.554419º N, Longitude: -5.895260º W). The plot was selected by technical experts in the field who identified trees infected with *Phytophthora spp*. The orchard is plantated with 2-year-old Navelina orange tree seedlings, which occupies a total area of 4105 m^2. The trees are grown on ridges at a tree spacing of 5.5 x 3.5 m^2 and are drip irrigated using two polyethilene pipelines per tree row and cover crop in the alleys.

2.2. Identification of healthy and diseased trees as ground-truth data

The early detection of trees infected with Phytophtora spp. requires the use of diseased trees without visible syptoms as ground truth. To select these trees in the field, an experienced technician identified diseased trees (through incipient stem collar damage) that were marked with eva-rubber targets designed and placed next to each of the identified trees (Figure 2). Black and white targets were used to be easily identifiable in the images taken by the UAV. Healthy trees were considered all those that were not identified as diseased trees.

Figure 2. Identification of the tree affected by *Phytophthora spp.*. Own source.

2.3. Drone-based Multispectral Imagery

The DJI Mavic 3 Multispectral UAV was used to collect ground data. This compact UAV features an omnidirectional anti-collision system, i.e. it has a series of sensors that detect obstacles in all directions to avoid collisions and RTK positioning at the centimetre level. In addition, it integrates an imaging system based on a 20 MP RGB camera and four 5 MP multispectral cameras (green, red, red edge and near-infrared or NIR). This UAV also integrates a light sensor that captures solar radiation, which allows light compensation in the images, providing greater consistency in the data collected over time.

2.4. Image acquisition

On January 11th 2024, between 12:00 and 14:00 hours, a flight was conducted to collect ground data. The day was selected based on a previous analysis performed by the field technician. Data collection required an initial identification of healthy and pathogen-affected trees. Healthy and pathogen-affected trees served as 'field data', and targets were placed next to the affected trees. Subsequently, it was decided to carry out a first automatic flight at 40 metres to obtain the images necessary to reconstruct the plot by creating the orthomosaic in Pix4D. A second flight was then carried out. In this case, a flight at a height of 12 metres in static and manual mode facilitates the data's labelling. This allowed us to copy the labels generated in one of the bands and paste them into the rest of the bands, reducing the labelling time. Four hundred forty-four images were obtained in the Green, Red, Red Edge, NIR and RGB bands from 74 sampling zones.

2.5. Image pre-processing

Image pre-processing is a vitally important step before image processing by an ML model. Tasks such as cropping, rotating, normalising, or resizing allow the image data to be transformed for further processing. The specific steps used during pre-processing are detailed below.

The project was developed using an HP laptop with an Intel Core (TM) i7-7700HQ CPU @ 2.80GHz 2.81 GHz, 8 GB RAM, and a 64-bit operating system. The implementation of the DL model, YOLOv8-seg.

was carried out using Google Colab, a cloud-based platform that offers an open-source development environment based on Jupyter Notebook, allowing for the free execution of Python projects. It also provides access to computational resources such as CPU, GPU, and TPU, making it particularly suitable for ML and DL tasks (Bisong, 2019).

2.5.1. Normalisation

Normalisation is a scaling or mapping technique to manipulate data, mainly to fit values to a common scale (Patro and Sahu, 2015). Different normalisation techniques exist such as histogram normalisation, min-max normalisation, z-score normalisation, fixed-range normalisation, etc. In this study, a fixed-rank normalisation [0-1] was used, as it is a simple but effective technique widely used in data pre-processing for DL models.

2.5.2. Resizing

Resizing the images is another key step in the pre-processing stage, where the dimensions of the images are modified. After analysing the format and size of the images, it was found that the dimensions of the RGB images were 5280 x 3956 pixels, while those of the multispectral images were 2592 x 1944 pixels. The RGB images were first resized to convert their dimensions to those offered by the multispectral images. This facilitated and reduced the labelling time.

Once the images were labelled, a second resizing was carried out. This aimed to adapt the size of the images to the size used for training the DL model, i.e. 640 x 640 pixels. In this resizing, the dimensions of the .txt files generated for each image in the labelling process were simultaneously modified.

2.5.3. Labelling and dataset creation

Labelling or annotating data is an essential preprocessing step before the application and/or data processing by a machine learning system. Through it, descriptive information is added to the dataset in labels, facilitating machine learning models' understanding of the data. Although there are different types of data labelling, depending on the task (detection, classification, and segmentation), polygon-based labelling was decided to be used, as it is the most suitable for identifying healthy and diseased trees.

Using the open-source tool LabelMe, 335 images were labelled, for which two classes or labels were defined: ‘healthy’ and ‘phytophthora’. Note that in Figure 3, the labelling process is on an RGB image. See the yellow polygons forming the canopy of trees affected by *Phytophthora spp*. and the violet polygons corresponding to the canopy of healthy trees.

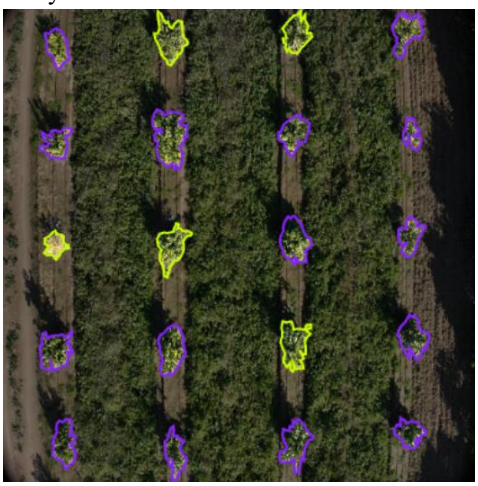

Figure 3. RGB image labelled with LabelMe.

After the labelling process, the image dataset was divided into a training set representing 80% of the data, a validation set comprising 15% and a test set comprising 5%.

2.6. Deep learning (DL) models

You Only Look Once (YOLO) is a popular network model used in object detection tasks (Redmon et al., 2015). Unlike other DL algorithms, this model and its later versions are based on single-stage detection, allowing faster and more efficient detection. Over the years, different YOLO models have been developed (Figure 4).

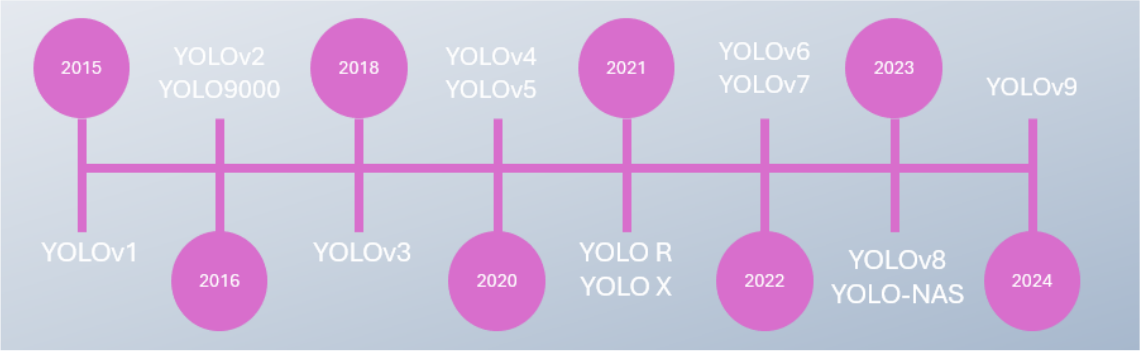

Figure 4. Developed YOLO models. Source: Ultralytics.

YOLOv8, developed and launched by Ultralytics in 2023, offers, like the previous models, five versions: YOLOv8n (nano), YOLOv8s (small), YOLOv8m (medium), YOLOv8l (large) and YOLOv8x (extra-large) (Jocher et al., 2023). YOLOv8 is very different from its predecessors, as it supports a variety of vision tasks, such as object detection, segmentation, pose estimation, tracking and classification. This model employs a backbone called C2f similar to that of YOLOv5, which allows combining high-level features with contextual information to improve accuracy in the detection process. In addition, YOLOv8 uses an anchorless model with a decoupled head, allowing each branch to focus on its task. YOLOv8 employs CIoU and DFL loss functions for bounding box loss and binary cross-entropy for classification loss (Li et al., 2023). As mentioned at the beginning of this section, YOLOv8 provides a semantic segmentation model called YOLOv8-seg. The architecture of this model is almost the same as that of the YOLOv8 model for detection. Still, it includes an additional output module in the head that generates the mask coefficients and FCN layers called Proto module that produces the masks. In this study, YOLOv8-seg uses the default hyperparameters provided by Ultralytics to ensure consistency with its original implementation and is trained for 30 epochs. On the other hand, the model output was adjusted to save the relative coordinates of the vertices of the masks generated in each tree in .txt format.

2.7. Evaluation metrics

The development and implementation of AD models require the application of evaluation metrics to measure their performance and effectiveness on a specific task (Li et al., 2018). In this study, metrics such as precision (P), recall (R) or Mean Average Precision (mAP) were used. P measures the accuracy of the model's predictions and is defined as the percentage of true positives (TP) to total predictions (Tharwat, 2020), as shown in equation (1). On the other hand, R (Eqn. 2) measures the ratio of true positives to the total number of true positives (Grandini et al., 2020). mAP (Eqn. 4) is calculated by considering the average precision values (AP) of each defined object category. In addition, it uses the intersection over union (IoU) to evaluate the quality of the expected bounding boxes. IoU is the ratio between the intersection and union areas of the expected bounding box and the actual bounding box (see equation 3) (Yang and Yu, 2021).

$$P = \frac{TP}{TP+FP} \quad (1)$$

$$R = \frac{TP}{TP+FN} \quad (2)$$

$$IoU = \frac{Area\ of\ Intersection}{Area\ of\ Union} \quad (3)$$

$$mAP = \sum_{q=1}^{Q} \frac{AveP\ (q)}{Q} \quad (4)$$

where *FP* are the false positive, and *FN is* the false negative. In equation (4), *q* is the number of queries, *Q* is the total number of classes, and *AveP (q)* is the average precision for the query in question.

3. Results and Discussion

In this study, a system capable of early detection of orange trees affected by *Phytophthora spp*. was developed. The results obtained demonstrate the high accuracy and efficiency of the model in classification and segmentation tasks, underlining its potential. The model used achieved accuracy values of 0.943 for classification and 0.941 for segmentation. Equally high values were obtained for recall, 0.871 and 0.869, respectively. In the case of mAP50 and Map50-95, the values for classification were 0.96 and 0.686, while for segmentation, they were 0.957 and 0.597. These values show the model's excellent performance for the target task, making it a powerful tool.

Figure 5a shows the model's accuracy evolution during the segmentation and classification training process in 30 epochs whereas Figure 5b shows the evolution of the loss in the 30 defined epochs. In terms of accuracy, both for classification accuracy, cls_P, hereafter, and segmentation accuracy (seg_P), Figure 5a shows the similarity of the values obtained and an increasing trend in the first 15 epochs to reach steady conditions later on. Regarding the loss, which represents the error made by the model when predicting the segmentation and object classes, a remarkable difference is observed between segmentation loss (seg_loss) and classification loss (cls_loss) lines. This is because the segmentation task is more complex than the classification task. Even with this difference, a decrease in loss is observed in both cases, indicating that the model continues to learn over epochs.

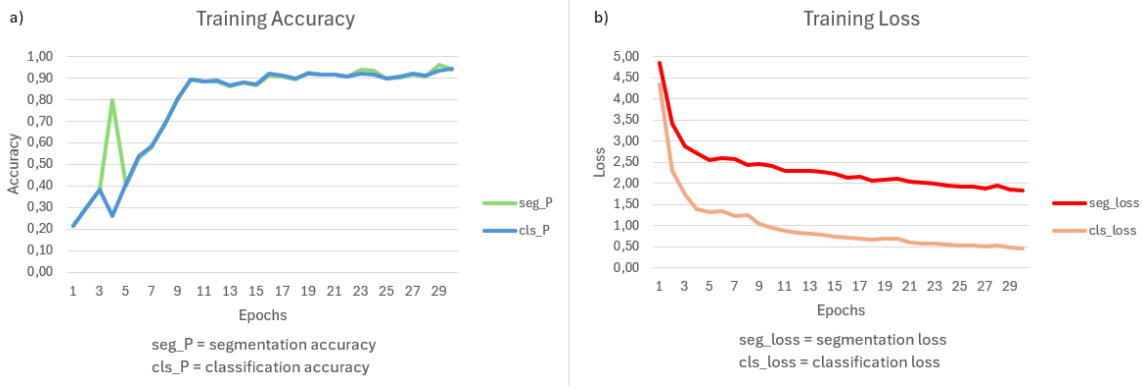

Figure 5. Evaluation metrics during the training process of the YOLOv8-seg.

The result of the developed system is the visual representation of the segmentation and classification of the trees, the count with the number of trees belonging to each class, and a file in .txt format that collects the relative coordinates of each mask originated. Figure 6 shows, as an example, the results obtained by the YOLOv8-seg model for the segmentation and classification of healthy and *Phytophthora spp*. affected trees. Figure 6a shows the results obtained by the model for a test image in the RGB bands; while Figure 6b shows the results for the same test image in the NIR band.

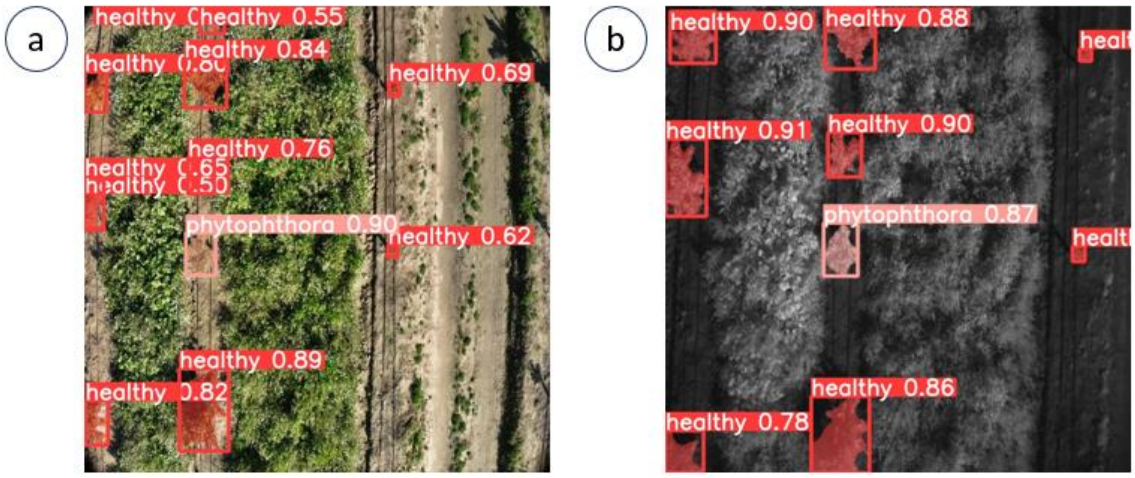

Figure 6. Result of the segmentation and classification of trees in an RGB image (a) and another in the NIR band (b).

This figure represents the ability of YOLOv8-seg to segment and classify trees in RGB images and images taken in other spectral bands. This is due to the model's ability to learn from any image data type. Images in other spectral bands provide additional information on tree health and vegetative state not available in RGB images, which makes it easier for the model to identify patterns in the data.

4. Conclusions

Early detection of pathogens in crops is vital to reducing production costs, guaranteeing production quality, and ensuring food safety. Technologies such as airborne multispectral cameras or AI algorithms offer innovative, accurate and efficient solutions to this challenge, potentially transforming the way crops are monitored. In this study, the YOLOv8-seg. DL model and its ability to segment and classify healthy trees and those affected by *Phytophthora spp*. This new model of the YOLO family has significant advantages over its predecessors, the most notable being the incorporation of an additional output module in the head and FCN layers to, in addition to classifying objects, perform object segmentation.

Furthermore, this study has shown that it is possible to train a DL model developed from RGB images with images in other spectral bands from UAVs. In the context of improvement, future work is proposed to capture multispectral images of orange trees affected by different pathogens. In this way, it will be investigated whether a DL model can identify this pathology early.

Acknowledgements

The authors would like to express their gratitude to the research group "AGR-278; Smart Biosystems Lab" for their constant support throughout the development of this study. They would also like to thank the project GOPG-SE-20-0007, co-financed by the European Union through the FEADER fund and the Junta de Andalucía.

References

Pereira, L. S., 2017. Water, agriculture and food: challenges and issues. *Water Resources Management*, *31*(10), 2985-2999.

Hídricos, R., 2020. Agua y Cambio climático.

Ministerio de agricultura pesca y alimentación (MAPA). 2022. Superficie y producciones anuales de cultivos. Retrieved from:

https://www.mapa.gob.es/es/estadistica/temas/estadisticas-agrarias/agricultura/superficies-producciones-anuales-cultivos/.

Sáenz Pérez, C. A., Hernández, E. O., Estrada Drouaillet, B., Poot Poot, W. A., Delgado Martínez, R., & Herrera, R. R., 2019. Principales enfermedades en cítricos. *Revista mexicana de ciencias agrícolas*, *10*(7), 1653-1665.

Nex, F., & Remondino, F., 2014. UAV for 3D mapping applications: a review. *Applied geomatics*, *6*, 1-15.

Khan, M. A., Menouar, H., Eldeeb, A., Abu-Dayya, A., & Salim, F. D., 2022. On the detection of unauthorized drones—Techniques and future perspectives: A review. *IEEE Sensors Journal*, *22*(12), 11439-11455.

McCarthy, J. (2007). What is artificial intelligence.

El Naqa, I., & Murphy, M. J., 2015. *What is machine learning?* (pp. 3-11). Springer International Publishing.

LeCun, Y., Bengio, Y., & Hinton, G., 2015. Deep learning. *nature*, *521*(7553), 436-444.

Hamet, P., & Tremblay, J. (2017). Artificial intelligence in medicine. *Metabolism*, *69*, S36-S40.

Bannerjee, G., Sarkar, U., Das, S., & Ghosh, I., 2018. Artificial intelligence in agriculture: A literature survey. *international Journal of Scientific Research in computer Science applications and Management Studies*, *7*(3), 1-6.

Chen, L., Chen, P., & Lin, Z., 2020. Artificial intelligence in education: A review. *Ieee Access*, *8*, 75264-75278.

Kaul, V., Enslin, S., & Gross, S. A., 2020. History of artificial intelligence in medicine. *Gastrointestinal endoscopy*, *92*(4), 807-812.

Bisong, E. (2019). *Building machine learning and deep learning models on Google cloud platform* (pp. 59-64). Berkeley, CA: Apress.

Patro, S. G. O. P. A. L., & Sahu, K. K., 2015. Normalization: A preprocessing stage. *arXiv preprint arXiv:1503.06462*.

Redmon, J., Divvala, S., Girshick, R., & Farhadi, A., 2016. You only look once: Unified, real-time object detection. In *Proceedings of the IEEE conference on computer vision and pattern recognition* (pp. 779-788).

Jocher, G.; Chaurasia, A.; Qiu, J. YOLO by Ultralytics. 2023. Available online: https://github.com/ultralytics/ultralytics (accessed on 13 May 2024).

Li, Y., Fan, Q., Huang, H., Han, Z., & Gu, Q., 2023. A modified YOLOv8 detection network for UAV aerial image recognition. *Drones*, *7*(5), 304.

Liu, Y., Chen, X., Wang, Z., Wang, Z. J., Ward, R. K., & Wang, X., 2018. Deep learning for pixel-level image fusion: Recent advances and future prospects. *Information fusion*, *42*, 158-173.

Tharwat, A., 2020. Classification assessment methods. *Applied computing and informatics*, *17*(1), 168-192.

Grandini, M., Bagli, E., & Visani, G., 2020. Metrics for multi-class classification: an overview. *arXiv preprint arXiv:2008.05756*.

Yang, R., & Yu, Y., 2021. Artificial convolutional neural network in object detection and semantic segmentation for medical imaging analysis. *Frontiers in oncology*, *11*, 638182.

Advancing precision livestock agriculture: Harnessing generative artificial intelligence for enhanced animal behaviour recognition

Regina Eckhardt [a,*], Reza Arablouei [b], Kieren McCosker [c], Heinz Bernhardt [a]

[a] Department of Agricultural Systems Engineering, Technical University of Munich, Freising, Germany

[b] CSIRO's Data61, Pullenvale QLD, Australia

[b] Queensland Alliance for Agriculture and Food Innovation, University of Queensland, St Lucia QLD, Australia

* Corresponding author. Email: regina.eckhardt@tum.de

Abstract

In precision livestock agriculture, the acquisition of sensor data is crucial for understanding animal behaviour and welfare. As farms and herds expand, managing this data becomes increasingly complex. Existing datasets often lack diversity, limiting their applicability for advanced analysis, particularly when employing artificial intelligence (AI) models. In this work, we propose a novel approach employing generative AI (genAI) to overcome these limitations by synthesizing extensive sensor datasets. Our approach involves two main steps: Firstly, we employ genAI, specifically the Autoformer model based on the Transformer architecture, to generate synthetic accelerometer sensor data. This approach demonstrates promising results, enabling accurate animal behaviour prediction across diverse scenarios. Secondly, we outline an AI model designed to predict cattle behaviour using datasets augmented via synthesised sensor data. Our study underscores genAI's critical role in augmenting data resources for effective livestock management, enhancing predictive models tailored for livestock management and developing sustainable strategies. This approach represents a significant advancement in precision agriculture, expanding the utility of AI in agricultural systems engineering and providing farmers with tools to adapt to evolving environmental and managerial conditions.

Keywords: accelerometer data, cattle behaviour, climate change, generative AI, precision agriculture

1. Introduction

The future of agriculture faces considerable uncertainty, not only from the direct effects of climate change but also from necessary adaptations such as dietary shifts aimed at reducing emissions and coping with environmental variations. Climate change directly impacts livestock agriculture, making it a focal point in discussions on emissions reduction. Thus, a reliable baseline is crucial to effectively manage the related challenges while ensuring that strategies for livestock welfare are aligned with broader environmental and economic considerations. Despite the widespread exploration of generative artificial intelligence (genAI) in various domains, its application in association with livestock sensor data remains largely unexplored.

Our research seeks to fill this gap by harnessing genAI to generate synthetic accelerometer data that accurately reflects cattle movements. This synthetic data will enable the simulation of scenarios such as climatic impacts, dietary adjustments, and changes in husbandry practices, where empirical data may be lacking. We delve into the architecture and functionalities of Transformer-based models, adapting them for use with sensor data, and outline the necessary model adjustments required for this adaptation. Through rigorous evaluation, we assess the efficacy of these models in enabling accurate prediction of cattle behaviour across diverse conditions. In addition, we examine potential interpretations of these model's outcomes and how they can provide insights into cattle welfare. This discussion aims to set the stage for future research in this field, where the actual application of the model can be further pursued.

The importance of data in agriculture, particularly within precision livestock farming (PLF), cannot be overstated. The potential of genAI to produce realistic synthetic data holds promise, especially given livestock agriculture's significant contribution to global emissions, with cattle playing a substantial role. As such, projecting and evaluating possible future scenarios is crucial for preparing for climate-related impacts on agriculture and global food supply.

Synthetic data generation is motivated by the practical challenges associated with physically testing every potential future scenario, as well as the substantial resource demands involved. Our work with genAI aims to address these challenges by providing realistic synthetic data for future analysis, enabling proactive assessment of various scenarios without the need for real-world experimentation, which may be complicated or even unethical.

In this paper, we explore the development of a Transformer-based model adapted for sensor data and describe an AI model intended to analyse newly generated data to simulate cattle behaviour. By facilitating the creation of realistic data for crucial scenarios, genAI has the potential to enhance our ability to strategically manage and mitigate future challenges

in agriculture.

2. Materials and Methods

Our objective is to generate synthetic data, enriching training datasets for various AI models and simulating data for future scenarios or complex conditions that are challenging to capture through traditional data collection methods. This necessitates a robust model capable of crafting precise synthetic data.

In the subsequent sections, we initially delineate the data utilised in this study. Subsequently, we delve into the architecture and functionality of Transformer-based models, specifically focusing on the Autoformer model. We provide justification for our selection of these models for processing accelerometer data, elucidating the unique attributes of the Transformer and Autoformer models. Following this, we highlight the necessary adaptations to customise these models for sensor data applications. Finally, we describe the animal behaviour recognition model employed to analyse the synthetically generated data.

2.1. Data and Preprocessing

In this work, we utilise data sourced from an experiment conducted at the University of Queensland's Darbalara Farm. The data was obtained using a 3-axis accelerometer on a smart collar tag called eGrazor, which has specifically been designed for monitoring livestock, particularly cattle. A group of 23 cattle were fitted with eGrazor collar tags, capturing 50 measurements per second across the x, y, and z axes over a span of 30 days. The measurements were accompanied by corresponding accurate timestamps acquired via an onboard global navigation satellite system (GNSS) receiver.

Upon initial analysis, it was evident that the data from the first two days consistently exhibited constant and hence implausible values, which were consequently excluded from further examination. Given the extensive data and the complexity of the considered models, we selected a one-hour segment comprising around 180,000 triaxial accelerometer measurements for analysis. We partitioned this segment into 70% for training, 10% for validation, and 20% for testing, while preserving the chronological order of the data.

We derived additional auxiliary variables from the timestamps, including minutes within each hour, thereby augmenting the dataset. These auxiliary variables can aid the model in identifying temporal patterns. Throughout the analysis, we maintained the chronological order of the data to uphold the integrity of the time series. The modelling efforts primarily centred on the accelerometer measurements along the x, y, and z axes, serving as the primary target variables.

2.2. Transformer and Autoformer

Accelerometer data, characterised by substantial fluctuations and seasonal variations, serves as a rich source of information reflecting diverse behaviours in cattle. A sophisticated architecture to understand and provide tailored output for sequential data was proposed as the Transformer model by Vaswani et al. (2017). While there exist several Transformer-based models designed for time series data, very few like Luptáková et al. (2022) are suitable for accelerometer data.

The Autoformer model, proposed by Wu et al. (2021), excels in handling time-series data characterised by significant seasonality, thus standing out as a particularly promising model. While Luptáková et al. (2022) have shown that Transformer models can effectively interpret human activity from wearable sensors, applying these models to cattle accelerometer data requires additional considerations. Cattle behaviour shows unique patterns and complexities such as pronounced seasonal and daily rhythms which may not be present in human activity data. The Autoformer is specifically designed to handle time series data with significant seasonality and trend components, potentially making it more suitable for agricultural settings where these patterns are common.

We intend to customise the Autoformer model to suit the intricacies of accelerometer data. However, to fully utilise Autoformer's capabilities, it is imperative to first understand the strengths and limitations of the Transformer model, upon which Autoformer is built. Thus, we begin by exploring the architecture of Transformer, followed by a detailed examination of Autoformer's specialised features.

Transformer, structured with an encoder-decoder architecture, excel in transforming one sequence into another by leveraging two pivotal components: the encoder and the decoder. Central to Transformer’s effectiveness is the attention mechanism, which enables the model to capture non-local dependencies and interactions in the input data. Unlike conventional models processing data sequentially, the attention module in Transformer is amenable to parallel

processing. This module generates variables dubbed as queries, keys, and values from the input data, essential elements in the attention mechanism.

Each query is matched against all keys to compute the attention scores, indicating the relevance of each input data component. These scores determine the weighting of values, representing the input data content. This mechanism enables the model to focus on pertinent input sections for any given task, enhancing efficiency and facilitating the handling of long-range dependencies in data.

Within an attention module, one or multiple attention heads operate independently, each calculating its attention scores. This allows the model to simultaneously explore various features of the data. The outputs from all attention heads are combined to form the output of the attention module.

Moreover, Transformer-based models are particularly adept at tasks necessitating context from past and future, rendering them well-suited for complex sequence transformation tasks often encountered in natural language processing (NLP) and, increasingly, in other domains such as time-series analysis of accelerometer sensor data.

While Transformer is originally devised for NLP tasks, its adeptness in handling sequential data makes it fitting for time series data analysis. However, since time series data can significantly differ from textual data, specialised Transformer-based models have been developed for time series forecasting. These specialised models leverage the Transformer architecture but include additional features, such as temporal attention mechanisms, enhancing their capability to capture time-related dependencies and seasonality.

The Autoformer model refines the basic Transformer model by adopting an encoder-decoder structure with unique decomposition blocks. These blocks aim at separating long-term trends from seasonal variations, addressing challenges conventional Transformer-based models may encounter with time series data. Moreover, Autoformer introduces auto-correlation functions, replacing traditional self-attention mechanisms. These functions identify and consolidate similarities across sub-series based on their periodicity, enhancing the model's ability to recognise patterns in data with prominent seasonality.

In Autoformer, the encoder primarily focuses on modelling seasonal variations, while the decoder synthesises these insights into coherent predictions. This structure makes Autoformer particularly suitable for handling intricate seasonality inherent in accelerometer data captured from livestock, providing a robust foundation for predicting cattle behaviour across varying conditions.

2.3. Model Adjustments

Initially designed for NLP applications, the Transformer model requires several adaptations to effectively process accelerometer data. Primarily, data preprocessing involves normalization and feature engineering to capture the inherent temporal patterns within accelerometer readings. These features must seamlessly integrate into the dataset to enhance model comprehension.

Defining features specifically tailored for the Transformer architecture is imperative to ensure optimal utilization. Given that Transformer operates on fixed-length sequences, selecting an appropriate input sequence length is crucial for efficient training and accurate temporal pattern recognition. Additionally, the number of attention heads needs careful consideration. Given the three-axis nature of accelerometer data, multiple attention heads can help the model focus on interrelated movements and behaviours concurrently.

Beyond these Transformer-specific adjustments, other important considerations are listed in Table 1.

Table 1. Model specifications to be taken into account in adjustments.

Model specification	Goal of adjustment
Number of Layers	Capture complex patterns in accelerometer data
Positional Encoding	Accurately represent temporal positioning of data points within sequences
Learning Rate and Optimization	Effective model training, ensuring fast converge with high accuracy without overfitting
Regularization	Prevent overfitting, enhancing the model's generalizability and performance

We configure the input sequence length to 256 time steps, a setting validated for analysing sensor data according to (Arablouei et al., 2021). We initially adhere to the settings prescribed by the original Autoformer paper (Wu et al., 2021). The only adjustment we make is to the length of the predicted sequence, set to ten time steps. This shorter length helps

manage the inherent fluctuation and high granularity of sensor data, facilitating more accurate predictions.

The specific values for the model settings outlined in Table 1 are based on the recommendations from the Autoformer paper, showcasing promising results in time-series analysis. We employ the root mean square error (RMSE) and median absolute error (MedAE) measures for model evaluation. While RMSE provides an intuitive measure of the error magnitude, MedAE offers a more realistic assessment due to its robustness to outliers, aligning with the characteristics of our data.

2.4. Modelling Cattle Behaviour

In our exploration of modelling cattle behaviour via sensor data, we turned to Scopus for its comprehensive coverage across disciplines. Our literature search concentrated on sensor technologies, cattle behaviour studies, and behavioural analysis methodologies, using keywords aligned with our research focus on cattle welfare and behaviour and the prominent use of accelerometer sensors.

Table 1. Keywords for the literature review on modelling cattle behaviour using accelerometer sensor data.

	Aspects		
Synonyms	"accelerometer sensor*"	Cattle	Behavio*r
	accelerometry	Cow	

This search yielded 98 relevant studies, highlighting the effectiveness of machine learning (ML) techniques across a broad spectrum of applications. These studies employed a diverse range of ML models, including Support Vector Machines (SVMs), as introduced by Martiskainen et al. (2009), and Random Forests, applied in multiple studies, including Cabezas et al. (2022), Foldager et al. (2020) and Gou et al. (2019). Advanced Deep Learning (DL) models were showcased by Arablouei et al. (2023), Bloch et al. (2023), and Pavlovic et al. (2021). Additionally, comprehensive analyses by Balasso et al. (2023), Busch et al. (2018), and Wang et al. (2023) compared the performance of a wide range of algorithms, considering multiple model types to enhance the robustness of their findings.

Our review underscored DL as notably effective, surpassing other models in detailed behavioural analysis, as documented by (Chapman et al., 2023; El Moutaouakil & Falih, 2024; Nogoy et al., 2022). Drawing from these findings, we advocate employing DL models to predict cattle behaviour based on accelerometer data. Despite their considerable computational demands, the superior accuracy of DL models in both real-time and non-real-time applications establishes them as the preferred choice for attaining our research objectives.

3. Results and Discussion

An initial application of the Autoformer model to accelerometer data demonstrates promising results in generating realistic sequences. As illustrated in Figures 1, 2, and 3, the predicted values (orange) generally align with the trends of the actual values (blue), indicating Autoformer's effectiveness in capturing underlying patterns within the accelerometer data. However, the match between predicted and actual values varies across the figures. While there are intervals where predictions closely mirror the actual data, denoting high accuracy, discrepancies emerge, especially at peaks, where predicted values diverge notably from actual values, hinting at challenges in handling abrupt changes or extremes in the data.

The model exhibits sensitivity to data fluctuations, accurately predicting smaller peaks and troughs in accordance with the data. However, its performance wanes with larger spikes, a crucial consideration if these spikes represent significant behavioral events such as specific movements or actions. The observed variability in prediction error is noteworthy, indicating the extent to which predicted values deviate from actual values, which amplifies with the magnitude of the data points. This trend indicates potential reliability concerns in scenarios with higher magnitudes, potentially stemming from model constraints or intrinsic data characteristics.

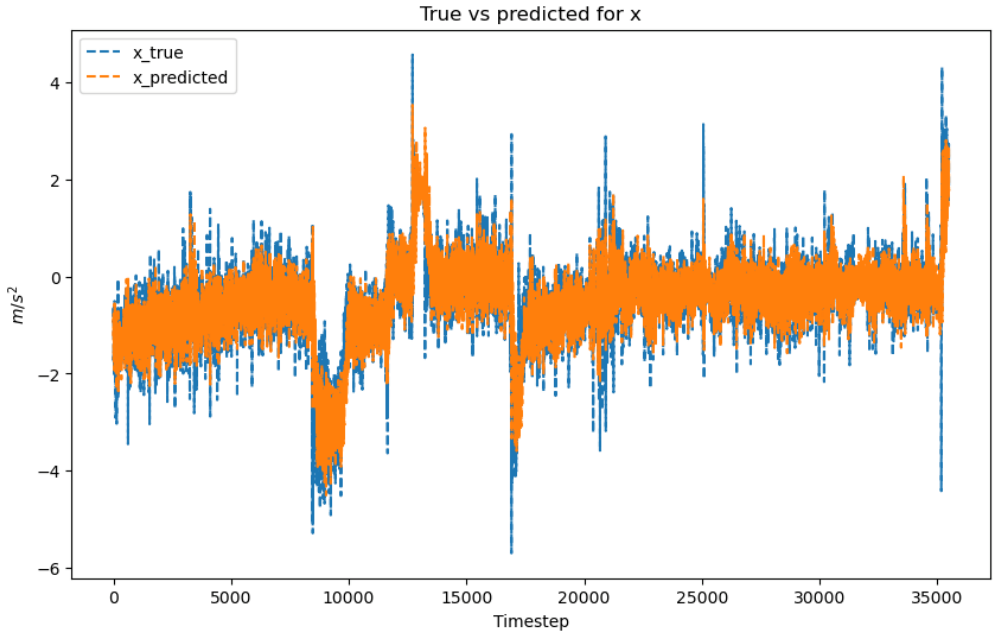

Figure 1. Results for the x-axis when applying the Autoformer model to one hour of the dataset.

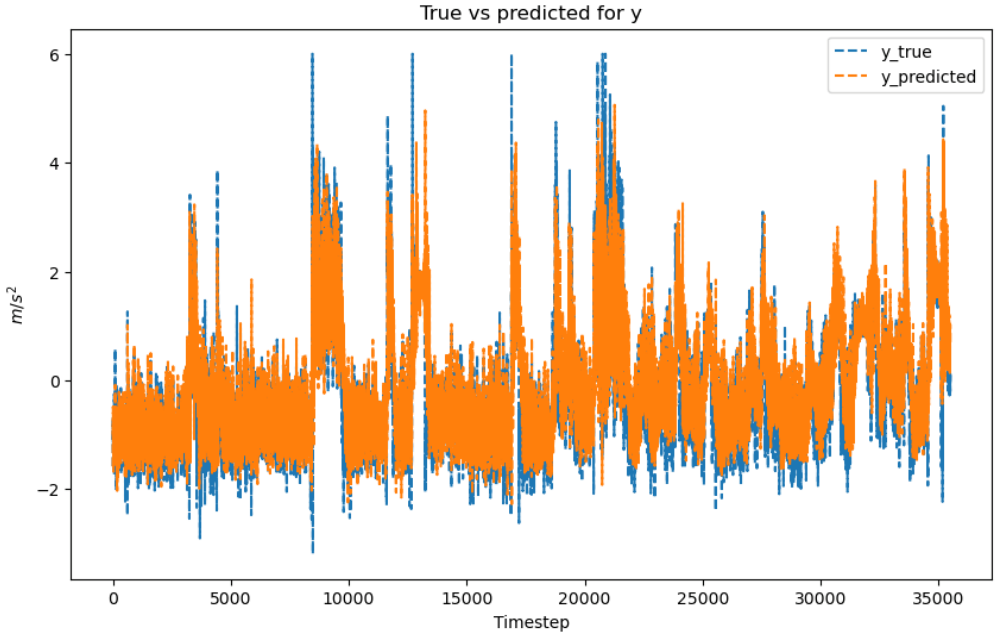

Figure 2. Results for the y-axis when applying the Autoformer model to one hour of the dataset.

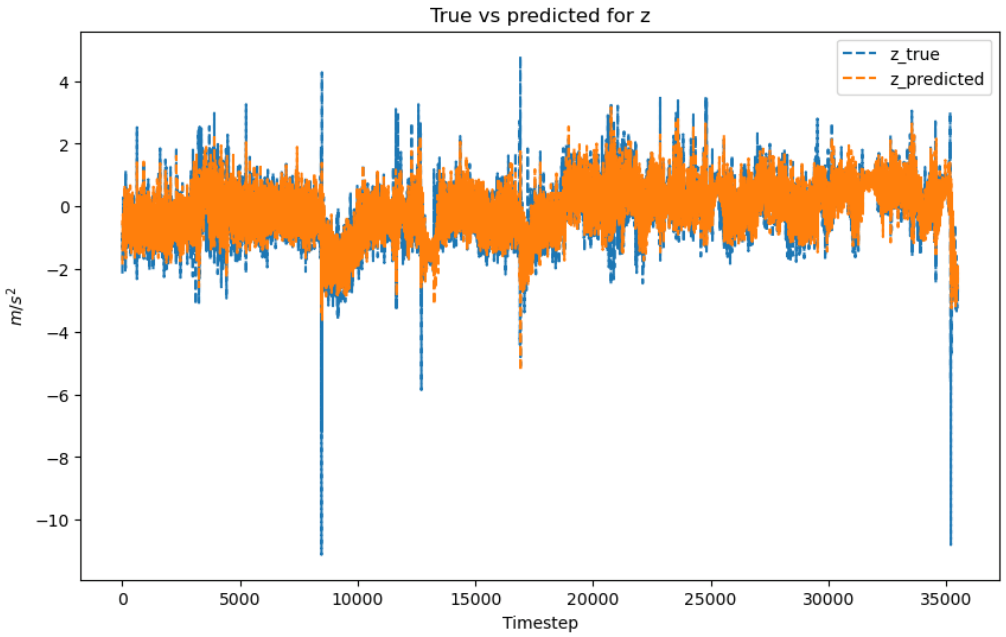

Figure 3. Results for the z-axis when applying the Autoformer model to one hour of the dataset.

Applying the Autoformer model to accelerometer data yielded promising results, with an RMSE of 0.503 and a MedAE of 0.239. Each training iteration of the model required approximately 0.5 seconds. Given that the data range was 17.1 m/s^2 and the standard deviation was 0.9 m/s^2, both the RMSE and MedAE are significantly small, highlighting the effectiveness of the model. These favourable performance measure values align with the visual trends observed in the figures.

We selected a small subset of the available accelerometer data to train our generative model given the high computational demands of Transformer-based models like Autoformer. Training Autoformer on this subset, which comprises one hour of data or approximately 180,000 data points, took around six hours on an Intel Xeon CPU. While one hour of accelerometer data contains a substantial number of data points, it only encompasses a limited range of behaviours. This duration does not adequately capture the full diversity of cattle behaviours required for effective behaviour classification. Therefore, while we can evaluate Autoformer's performance using this subset, it does not allow us to directly correlate synthetic data with specific cattle behaviours. This avenue remains a focus of our future research.

4. Conclusions

Initial findings from utilizing the Autoformer model for data generation show promise, albeit based on a limited dataset. The model encounters difficulties in accurately predicting extreme values, particularly at higher data values, indicating areas for refinement. To enhance performance in capturing rapid changes and high-magnitude values, we suggest adjustments to the model architecture, fine-tuning hyperparameters, or incorporating a more diverse training dataset.

Expanding the dataset to cover longer time periods, spanning several hours or days, can offer deeper insights and enhance training outcomes, considering the predictable seasonal patterns and routine behaviors in cattle. This expansion is crucial for broader applications of behaviour models and facilitates modelling environmental impacts due to climate or dietary changes. It is essential to develop and integrate additional features at the same granularity level as accelerometer data, with adjustments to model settings to effectively incorporate these new features.

A significant concern lies in the substantial computational resources required for training the Autoformer model, with up to six hours needed for processing just one hour of data. Future research ought to explore alternative solutions to alleviate computational costs and enable more efficient training of larger datasets over extended periods.

In summary, while the initial applications of Autoformer demonstrate potential in transforming livestock management through enhanced data generation, ongoing improvements and adaptations are essential to fully exploit its capabilities and address challenges such as computational efficiency and data complexity in future research endeavours.

References

Arablouei, R., Currie, L., Kusy, B., Ingham, A., Greenwood, P. L., & Bishop-Hurley, G. (2021). In-situ classification of cattle behavior using accelerometry data [Article]. *Computers and Electronics in Agriculture*, *183*, Article 106045. https://doi.org/10.1016/j.compag.2021.106045

Arablouei, R., Wang, L., Currie, L., Yates, J., Alvarenga, F. A. P., & Bishop-Hurley, G. J. (2023). Animal behavior classification via deep learning on embedded systems. *Computers and Electronics in Agriculture*, *207*, Article 107707. https://doi.org/10.1016/j.compag.2023.107707

Balasso, P., Taccioli, C., Serva, L., Magrin, L., Andrighetto, I., & Marchesini, G. (2023). Uncovering Patterns in Dairy Cow Behaviour: A Deep Learning Approach with Tri-Axial Accelerometer Data. *Animals*, *13*(11), Article 1886. https://doi.org/10.3390/ani13111886

Bloch, V., Frondelius, L., Arcidiacono, C., Mancino, M., & Pastell, M. (2023). Development and Analysis of a CNN- and Transfer-Learning-Based Classification Model for Automated Dairy Cow Feeding Behavior Recognition from Accelerometer Data. *Sensors*, *23*(5), Article 2611. https://doi.org/10.3390/s23052611

Busch, P., Stupmann, F., & Ewald, H. (2018). Determination of cattle standing-time with decscion trees and neural nets by using only acceleration data from collar. Proceedings - 2018 2nd European Conference on Electrical Engineering and Computer Science, EECS 2018,

Cabezas, J., Yubero, R., Visitación, B., Navarro-García, J., Algar, M. J., Cano, E. L., & Ortega, F. (2022). Analysis of accelerometer and GPS data for cattle behaviour identification and anomalous events detection. *Entropy*, *24*(3), Article 336. https://doi.org/10.3390/e24030336

Chapman, N. H., Chlingaryan, A., Thomson, P. C., Lomax, S., Islam, M. A., Doughty, A. K., & Clark, C. E. F. (2023). A deep learning model to forecast cattle heat stress. *Computers and Electronics in Agriculture*, *211*, 107932. https://doi.org/https://doi.org/10.1016/j.compag.2023.107932

El Moutaouakil, K., & Falih, N. (2024). Deep learning-based classification of cattle behavior using accelerometer sensors. *IAES International Journal of Artificial Intelligence*, *13*(1), 524-532. https://doi.org/10.11591/ijai.v13.i1.pp524-532

Foldager, L., Trénel, P., Munksgaard, L., & Thomsen, P. T. (2020). Technical note: Random forests prediction of daily eating time of dairy cows from 3-dimensional accelerometer and radiofrequency identification. *Journal of Dairy Science*, *103*(7), 6271-6275. https://doi.org/10.3168/jds.2019-17613

Gou, X., Tsunekawa, A., Peng, F., Zhao, X., Li, Y., & Lian, J. (2019). Method for classifying behavior of livestock on fenced temperate Rangeland in Northern China. *Sensors (Switzerland)*, *19*(23), Article 5334. https://doi.org/10.3390/s19235334

Luptáková, I. D., Kubovčík, M., & Pospíchal, J. (2022). Wearable Sensor-Based Human Activity Recognition with Transformer Model. *Sensors*, *22*(5), Article 1911. https://doi.org/10.3390/s22051911

Martiskainen, P., Järvinen, M., Skön, J. P., Tiirikainen, J., Kolehmainen, M., & Mononen, J. (2009). Cow behaviour pattern recognition using a three-dimensional accelerometer and support vector machines. *Applied Animal Behaviour Science*, *119*(1-2), 32-38. https://doi.org/10.1016/j.applanim.2009.03.005

Nogoy, K. M. C., Chon, S. I., Park, J. H., Sivamani, S., Lee, D. H., & Choi, S. H. (2022). High precision classification of resting and eating behaviors of cattle by using a collar-fitted triaxial accelerometer sensor. *Sensors*, *22*(16), Article 5961. https://doi.org/10.3390/s22165961

Pavlovic, D., Davison, C., Hamilton, A., Marko, O., Atkinson, R., Michie, C., Crnojević, V., Andonovic, I., Bellekens, X., & Tachtatzis, C. (2021). Classification of cattle behaviours using neck-mounted accelerometer-equipped collars and convolutional neural networks. *Sensors*, *21*(12), Article 4050. https://doi.org/10.3390/s21124050

Vaswani, A., Shazeer, N., Parmar, N., Uszkoreit, J., Jones, L., Gomez, A. N., Kaiser, Ł., & Polosukhin, I. (2017). Attention is all you need. Advances in Neural Information Processing Systems,

Wang, L., Arablouei, R., Alvarenga, F. A. P., & Bishop-Hurley, G. J. (2023). Classifying animal behavior from accelerometry data via recurrent neural networks. *Computers and Electronics in Agriculture*, *206*, Article 107647. https://doi.org/10.1016/j.compag.2023.107647

Wu, H., Xu, J., Wang, J., & Long, M. (2021). Autoformer: Decomposition Transformers with auto-correlation for long-term series forecasting. Advances in Neural Information Processing Systems,

Wheat grain yield predictions based on a Bayesian network approach fusing multi-source time specific data and experts' knowledge

Maria Karampoiki[a,*], Salar Mahmood[b], Lindsay Todman[b], Alistair Murdoch[b], John Hammond[b], Emanuele Ranieri[c], Hans W. Griepentrog[a], Dimitrios S. Paraforos[a,d]

[a] Institute of Agricultural Engineering, Technology in Crop Production, University of Hohenheim, Stuttgart, Germany

[b] School of Agriculture, Policy and Development, University of Reading, Reading, United Kingdom

[c] Agricolus SRL, Perugia, Italy

[d] Department of Agricultural Engineering, Hochschule Geisenheim University, Geisenheim, Germany

[*] maria.karampoiki@uni-hohenheim.de

Abstract

Wheat (*Triticum aestivum* L.) is a globally important crop, and accurate prediction of its grain yield plays a crucial role in optimising agricultural practices. Although numerous models have been developed and evaluated, reliable yield prediction remains one of the most challenging problems in precision agriculture to date. Predicting crop yield depends on a variety of interdependent variables such as weather, soil type, crop genotype, and management techniques. So to solve this problem, data from multiple sources is required and must be carefully integrated.

This study introduces a machine learning approach using Bayesian Networks (BN) to predict winter wheat yield in Germany by integrating data from various sources and expert knowledge. Data collected includes electrical conductivity (EC) from the Veris iScan sensor, combine harvester yield data, and Sentinel 2 (S2) images from 15 fields for the 2020-2022 crop seasons. The topographic wetness index (TWI) was calculated using ArcGIS 10.6 and yield data. S2 images were processed to compute monthly normalised difference vegetation index (NDVI) values. A weather model was developed, incorporating expert knowledge of extreme events. The grain yield model combined the inherent potential index (IP), NDVI, temporal average yield, and normalised grain yield, and was trained using expectation maximisation (EM) on data from the 2020, 2021, and 2022 seasons.

The results showed that the model achieved an accuracy of 73 % based on the statistical indices, showcasing its ability to make accurate predictions. The correlation analysis (R^2) between actual and predicted yield with 50 % probability ranging from 0.68 to 0.78. Additionally, similar patterns of spatial variation were observed in the actual and predicted maps with a 50 % probability. This shows a robust and consistent predictive ability over a wide range of scenarios by showing a strong correlation between the model's predictions and the observed results.

Keywords: Bayesian Network, inherent potential, yield predictions.

1. Introduction

Winter wheat (*Triticum aestivum* L.) is one of the most important crops globally, and reliable crop yield estimation can help in developing efficient crop management strategies, mitigating crop failure risks, and optimizing resource allocation to improve crop productivity. Therefore, the improving crop yield predictions' accuracy has received increasing attention (Schauberger et al., 2022). As reviewed by Jin et al. (2022), even though the predicted results of these studies are sufficient, their predictive periods (i.e., from the forecast date to harvest date) are typically too short to allow farmers sufficient time to respond and make decisions. For instance, German winter wheat has a growing season lasting 180-250 days, although yield forecasts are usually not available until 1-3 months prior to harvest (Karampoiki et al., 2022). Certain field interventions by farmers may be limited at this point because the crop is approaching the end of its growth (Helman et al., 2019). Thus, long-term yield forecasts at an earlier stage, also known as early-season yield forecasts, are required to better manage future yield uncertainty and resource use efficiency (Khaki et al., 2020; Ziliani et al., 2022).

In terms of methodology, three main yield estimation methods (i.e., survey-based methods, simulation-based methods, and machine learning (ML)-based methods) have been employed in existing yield prediction research, among which machine learning techniques are emerging as the most popular due to their ability to accurately quantify the impact of climate (e.g., temperature, rainfall) on crop yields (Li et al., 2021a).

However, insufficient data make it almost impossible for machine learning models to learn complex relationships between climate and crop yields and thus they often fail to provide accurate yield forecasts (Chen and Tao., 2022; Feng et al., 2020b). This limitation has not yet been properly addressed and needs further investigation (Mitchell et al., 2022). Therefore, when employing ML algorithms, high prediction accuracy, quick computation, and outcome consistency must be given priority. As an example, Wang et al. (2021) utilised and contrasted six ML models: (i) Ordinary Least square (OLS); (ii) Least Absolute Shrinkage, and Selection Operator (LASSO); (iii) Support vector machine (SVM); (iv) Random forest (RF); (v) AdaBoost; and (vi) Deep Neural Network (DNN), to forecast the winter wheat yield at the county level in the United States during the growing season. AdaBoost was found to be the most effective algorithm (R^2 = 0.86, RMSE = 0.51 t ha^{-1}). Furthermore, Cao et al. (2021) compared the three Deep Learning (DL) methods with Random Forest (RF), the conventional ML method, i.e., Deep Neural Network (DNN), 1 Dimension Convolutional Neural Network (1D-CNN), and long short-term memory networks (LSTM), to forecast winter wheat yields in China, and found that each of the approaches under test worked well for this purpose (RMSE ranging from 0.56 to 0.96 t ha^{-1}).

This study aims to co-create with farmers a time-series grain yield prediction model based on a Bayesian Network (BN). The key contribution of this method lies in the integration of inherent potential index (IP) and a weather algorithm. Specifically, our objectives are: (1) to predict spatial variation of yield within winter wheat fields in a time-series, using novel algorithms by fusing multi-source data; (2) to assess model accuracy and precision; (3) to validate grain yield predictions with 50 % probability against ground truthing observations; and (4) to integrate the model into a software platform (Agricolus) to which farmers can subscribe.

2. Materials and Methods

2.1. Study area

The study area is located in Füge and Landfried Farm, near Gauersheim, Rhineland-Palatinate, Germany, as illustrated in Figure 1. This area lies between lat. 49° 40' 38.39" N and long. 8° 03' 22.93" E.

Farmers' knowledge of known spatial variability in soil type and topography, the availability of historical data (such as yield maps of past crops, soil types, and soil electrical conductivity), and farmers' access to precision agricultural technology, specifically yield mapping, were the main criteria used to select the 15 fields.

Figure 1. Google Earth image showing the location of the German winter wheat fields in Füge and Landfried Farm based in Gauersheim, Rhineland-Palatinate, Germany.

2.2. Topographic and soil data

Topographic wetness index (TWI) is used as a measure of soil moisture in the fields where there are variations in elevation. TWI was computed using ArcGIS 10.6 and the digital elevation model (DEM) using the following formula (Kopecký et al., 2021):

$$\text{TWI} = ln\ \frac{a}{\tan b} \quad (1)$$

where: a = upslope contributing area (m^2), b = slope in radians.

Soil electrical conductivity (EC) was measured using a Veris iScan-sensor (Veris Technologies Inc., Salina, KS, USA).

2.3. Remote sensing data

A total of 75 cloud-free Sentinel-2 (A and B) (S2) images from March 2020 to July 2022 were downloaded from the European Space Agency (ESA) website (https://scihub.copernicus.eu/dhus/#/home). S2 offers 13 spectral bands (443-2190 nm), with a variable spatial resolution of 10, 20, 60 m pixel size and with a revisit time of 5 days. The data were used to calculate the normalised difference vegetation index (NDVI) with a spatial resolution of 10 m for different times during the growing season. The NDVI was calculated using the following formula:

$$\text{NDVI} = \frac{R842 - R665}{R842 + R665} \quad (2)$$

2.4. Yield data

Yield data for winter wheat and previous crops were provided using a John Deere combine harvester (Deere & Company, Moline, Illinois, USA) at 2 m intervals with a 9 m swath. In the 2020, 2021 and 2022 harvest seasons, thousands of observations per field were collected, 97,263 in total, providing a clear picture of spatial variability. The number of observations varied from field to field depending on the area.

2.5. Data cleaning, processing and integration

Numerous outliers, which can impact the map's reliability, are typically present in the yield data supplied by the combine harvester. These anomalies are caused by a variety of harvesting-related errors. For that reason, these outliers were categorised using an automated data cleaning protocol that has been suggested (Natale et al. 2020).

Since numerous sources of data were used to gather the information, including satellite data, soil electrical conductivity, TWI, and sensors on the combine, there was variation in the spatial distribution and density of the measurement points within the field. In order to create a regular grid of data points in which all data sources were interpolated or extrapolated onto a common grid, ArcMap 10.6 (ArcGIS Desktop: Release 10. Redlands, CA: Environmental Systems Research Institute). was used. A 6 x 6 m grid size was selected to align with farming machinery having a 6 m working width. For every variable, interpolation maps were made. A 6 × 6 m grid was superimposed on the interpolation maps to create a raster map, from which the value at each point was extracted. The raster map of each satellite band was covered with a 6 × 6 m grid for NDVI purposes, and each pixel's value was assigned to all points within it.

2.6. Model development

To build an effective yield forecast model and climate forecast processes, a BN machine learning algorithm was used. It has been widely applied for agriculture-related forecasting and generally exhibits satisfactory performances (Chawla et al., 2016).

In a BN, the 'nodes' of the network represent each variable and links between nodes represent the interactions between variables. The resulting structure can be used for probabilistic inference, that is the probability that a yield at a specified grid point will equal or exceed a given value. It also allows the conditional dependence of variables to be represented so that variables are not considered to contribute

additive effects, but rather a BN can combine the information from correlated variables. For example, to infer that in situations when a particular location in a field repeatedly provides high relative yields over two or more years there is likely to be higher 'Inherent Potential' than a location that has a more variable yield in different years.

An MLA is used to estimate the Prior Inherent Potential (PIP) and Inherent Potential (IP) of each grid point in a field. These are considered latent variables that cannot be directly measured or observed. Factors such as soil properties and nutrient availability influence the crop's potential to develop, with high PIP often leading to higher IP and ultimately to higher yield. Improvements in estimating the IP can be made by observing soil properties like texture and carbon content, which impact water storage and nutrient availability for the crop. IP also considers other factors such as weed growth. In this study, the BN used in combination with the MLA aims to categorise each node within each field from high to low PIP based on the data available for a given field. Thus, the PIP was characterised by electrical conductivity (EC) and the topographic wetness index (TWI) (Figure 2 left), and the IP was characterised by crop type, observed yields, and PIP, ranging from very low to very high (Figure 2 right). To facilitate comparisons between yields of different crops in different fields in different years, the yield data for a given field was normalised as percentages of the mean yield for that field.

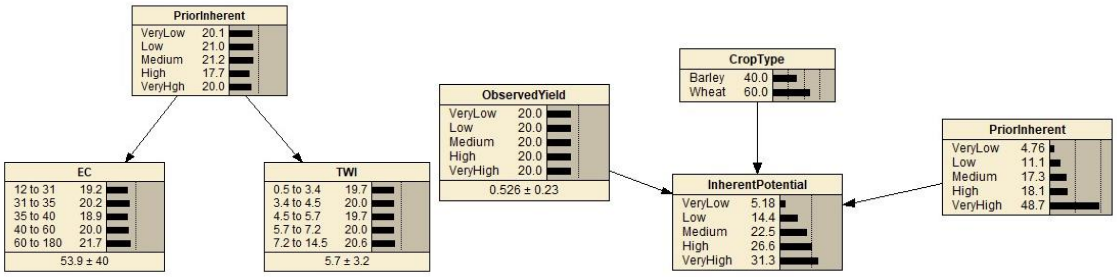

Figure 2. Diagrams for the MLA of 'Prior Inherent Potential' (left) and 'Inherent Potential' (right). The probability distribution across states is shown as a %-probability and visualised with black horizontal bars. At the bottom of the Electrical conductivity (EC), Topographic Wetness Index (TWI) and ObservedYield as a % of the mean yield, the numbers show the mean and the SD of the values for each node.

Since significant season to season variation in winter wheat yields is also caused by the variability in weather conditions, in particular rainfall and mean temperature (Addy et al., 2020). To represent this (Figure 3), the Reference Yield node was used that described the expected average yield due to the weather conditions throughout the season (Mahmood et al., 2023). Here, we interview experts, including farmers, to build a Bayesian Network (BN) model that incorporates their years of experience into a quantitative model. These specialists determined that the time frame from the start of anthesis to the end of the grain filling stage was crucial, and that precipitation, mean temperature, and maximum temperature were important meteorological factors that should be included in the BN. The conditional probability table for the BN was created based on the experts' expected influence on the mean yield of various weather conditions in order to keep the time input from them manageable.

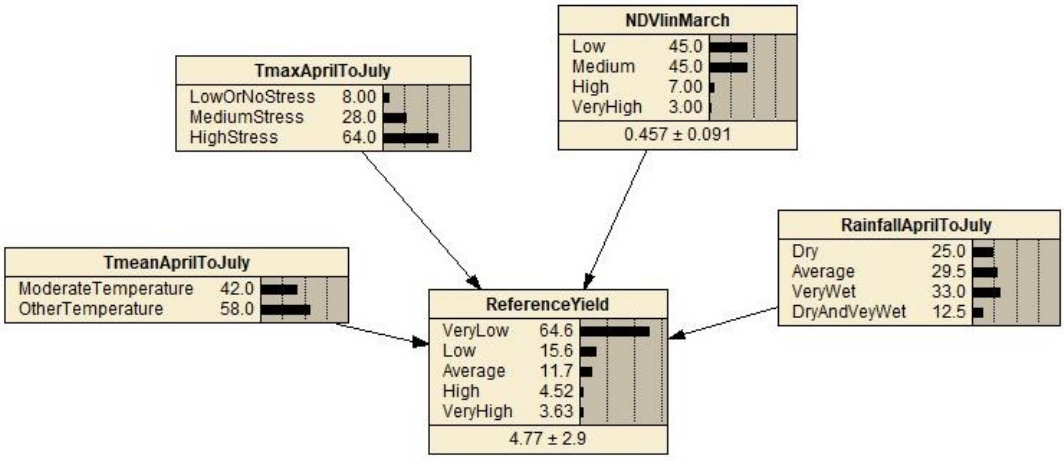

Figure 3. Model structure showing the categories of crop biomass (NDVI) in March and weather variables from beginning of anthesis to the end of grain filling stage and categories of simulated wheat yield. The probability distribution across states is shown as a %-probability and visualised with black horizontal bars. At the bottom of the TmaxAprilToJuly, NDVIinMarch, RainfallAprilToJuly and ReferenceYield (t ha^{-1}) nodes, the numbers show the mean and the SD of the values for each node (Mahmood et al., 2023).

The output of the IP and the weather algorithm were combined with in-season crop biomass data (based on NDVI from March to June) to forecast grain yield. The model structure outlined how variables were connected to predict winter yield for German fields (Figure 4). The model was tested at a farm level, with 10 fields used for training and five for testing. The fields were randomly split using Matlab R2020a software. The relationships between variables were determined using 75 % of the data with expectation maximisation in Netica software, then validated with the remaining 25 %. Yields were normalized at the farm level. Probabilities for each grid point were obtained from Netica, and the output was processed in Matlab to calculate predicted values with 50 % probability. The predicted grain yields were mapped for each field and compared to actual yields.

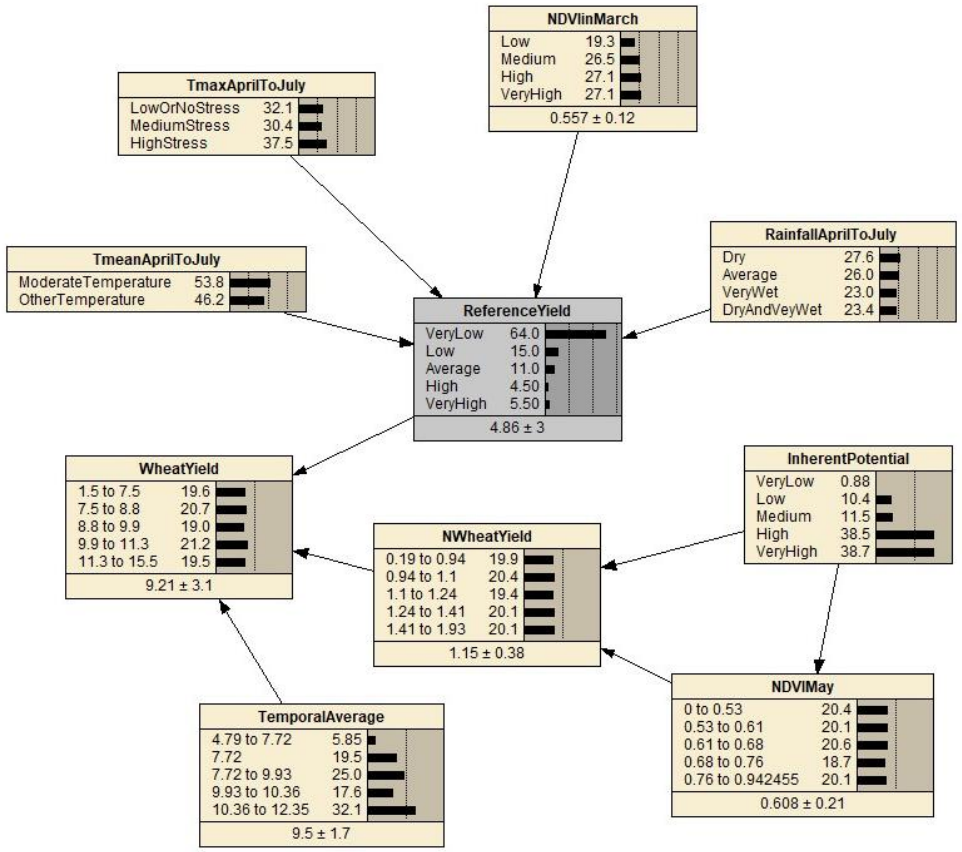

Figure 4. Example of diagram for MLA learning model for predicting wheat yield based on Inherent Potential, NDVI in May, and the weather algorithm. The model was applied on a farm basis. The probability distribution across states is shown as a %-probability and visualized with black horizontal bars. At the bottom of the nodes, the numbers show the mean and the SD of the values for each node.

2.7. Model performance and evaluation

In this study, confusion matrix metrics i.e. accuracy, precision (P), recall (R), F1-score for multi-label classification were used to assess the quality of predictions. The formulas are expressed as follows:

$$\text{Accuracy} = \frac{TP+TN}{TP+TN+FP+FN}, \text{Precision} = \frac{TP}{TP+FP}, \text{Recall} = \frac{TP}{TP+FN}, \text{F1-score} = \frac{2 \times Precision \times Recall}{Precision + Recall} \quad (3)$$

where TP = true positive, TN = true negative, FP = false positive, FN = false negative.

To further measure the performance of the model, R^2 and RMSE (Cheng et al., 2022; Li et al., 2021b), were applied

$$R^2 = 1 - \frac{SSE}{SST} \quad (4)$$

where SSE is the sum of squared error, SST is the sum of squared total.

$$RMSE = \sqrt{\frac{\sum_{i=1}^{N}(Predicted_i - Actual_i)^2}{N}} \quad (5)$$

where N is the total number of observations, Predicted is the predicted value for the ith observation, Actual is the observed (actual) value for the ith observation.

3. Results and discussion

3.1. Model accuracy and evaluation

A Confusion matrix is a square matrix used to assess the performance of a classification model. It compares the actual target values with the predictions made by the machine learning model. By analysing this matrix, we can evaluate how well our model is performing and the types of errors it is making. The confusion matrix, shown in Table 1, showcases the accuracy of the model in predicting each class in the data set. It helps us evaluate the quality of predictions by looking at the actual and predicted values which grouped into five classes representing normalised yields. The diagonal elements are the correctly predicted samples in April. A total of 24,534 samples were correctly predicted out of the 26,807 samples. Thus, the overall accuracy in April is 92%. The value equals to 38 implies that the model does not confuse samples originally belonging to class 1.30 to 1.92 with class 1.12 to 1.22. It turned out to be a good classifier for our dataset, considering how well our values classified.

Table 1. Example of confusion matrix results regarding to testing data set corresponding to yield predictions in April.

Actual values \ Predicted values	0.19	0.98	1.12	1.22	1.30 to	Total
0.19 to 0.98	6,000	0	0	0	0	6,000
0.98 to 1.12	420	3,600	550	0	0	4,797
1.12 to 1.22	10	150	7,050	0	38	7,050
1.22 to 1.30	0	67	38	2,762	1,000	2,800
1.30 to 1.92	0	0	0	0	5,122	6,160
Total	6,430	3,817	7,638	2,762	6,160	26,807

In Table 2, the accuracy, precision, recall and F1-score were calculated using the equations mentioned in 2.7 when forecasting winter wheat yield in different months of the growing season. Comparing the results, the highest accuracy, precision, recall and F1-score were observed in April with a value of 92%, 82%, 91% and 91% respectively. The lowest accuracy observed in March at the tillering stage, with a value of 72%.

Table 2. The outcome of the confusion matrix metrics to access model performance.

Month	Accuracy	Precision	Recall	F1-score
March	0.72	0.63	0.71	0.70
April	0.92	0.82	0.91	0.91
May	0.80	0.79	0.80	0.79
June	0.79	0.68	0.78	0.79

3.2. Validation of time-series predictions against ground truthing observations

The algorithm predicts the grain yield for each (6×6 m) grid node within a given field. We used two crop seasons to train the model and one crop season to test the model. The yield predictions in the fields used to test the model were good, reaching an accuracy of 92%. For example, using one field (Horn, 3.12 ha), the kriged maps of predicted yield with 50 % probability and observed yield showed similar patterns of spatial variation (Figure 5). The ground-truth yield and predicted yield values with 50 % probability from March till June were plotted (Figure 6) to see how close the prediction results are to the ground-truth values. The deviation of the data points from the 1:1 line shows the distribution of residuals. In April, the predicted and ground-truth values had a higher correlation compared to the other months (March, May and June), with R^2 equals to 0.78, 0.68, 0.76, 0.75 respectively. Similar results with R^2 equals to 0.68, 0.70 have been presented by Zhang et al. (2023) developing a Bayesian optimised CatBoost regression model. The RMSE varied ranged from 14 to 15. The fitted 1:1 line shows that the model overestimated the yield in low yielding areas of the field and underestimated the yield in high yielding areas of the fields. Potential sources of inaccuracy in predictions could be explained by weed infestations, diseases or the model being overfitted.

There are limited studies that incorporate climate, soil, topographic, and historic yield data for winter wheat yield predictions in cooperation with the farmers, therefore, there are still uncertainties in the yield predictions, primarily due to data sources. One of the main limitations is the poor quality of data, such as the low resolution of remote sensing, meteorological, and soil datasets. This can reduce the effectiveness of machine learning in predicting yields and lead to potentially uncertain results (Jin et al., 2017). The launch of higher-resolution remote sensing satellites, such as sentinel-2 (with the maximum resolution of 10×10 m) offers new opportunities to provide more accurate yield prediction (Vergara-Díaz et al., 2016). It is noteworthy that the current study only includes three years' worth of winter wheat yield data, which results in a relatively small sample size. Expanding the sample size will therefore be the main goal of future research in order to improve the model's accuracy and robustness. Nitrogen data can also be added to the model to increase its robustness and boost yield prediction accuracy and precision.

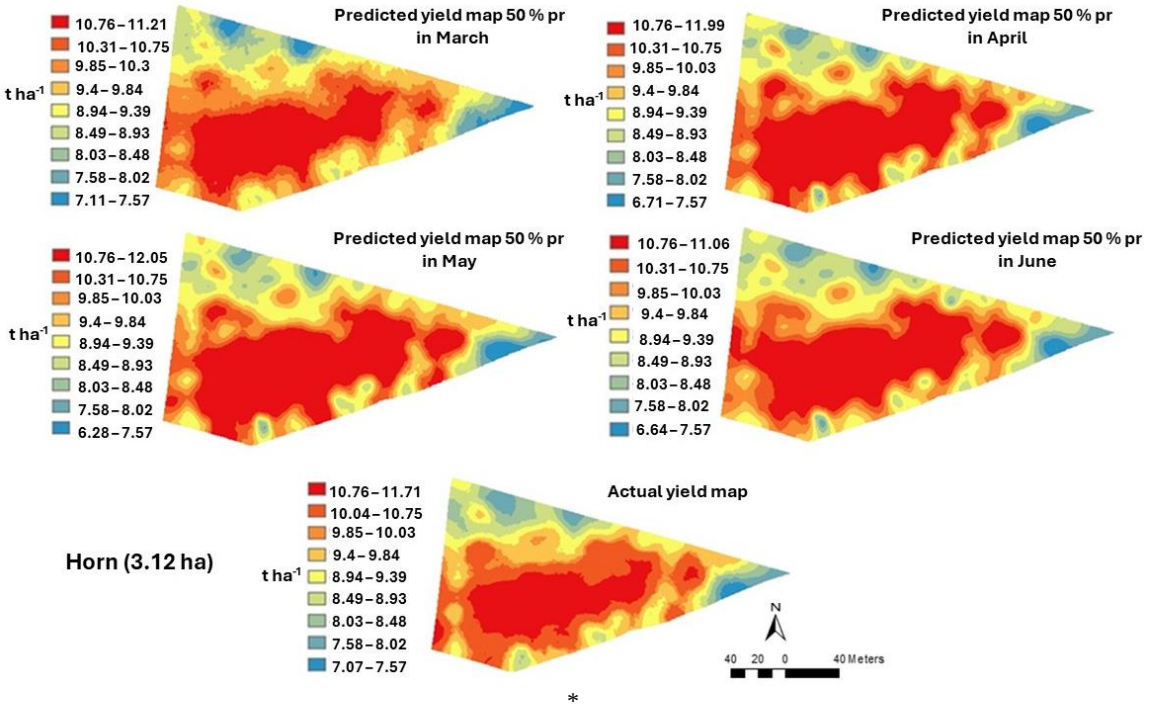

Figure 5. Maps of predicted wheat yield (t ha^{-1}) based on data from March, April, May and June and the actual yield in Horn field (3.12 ha), which was used to test the model. The predicted maps are based on 50 % probability. The values on the colour ramp cover slightly different ranges.

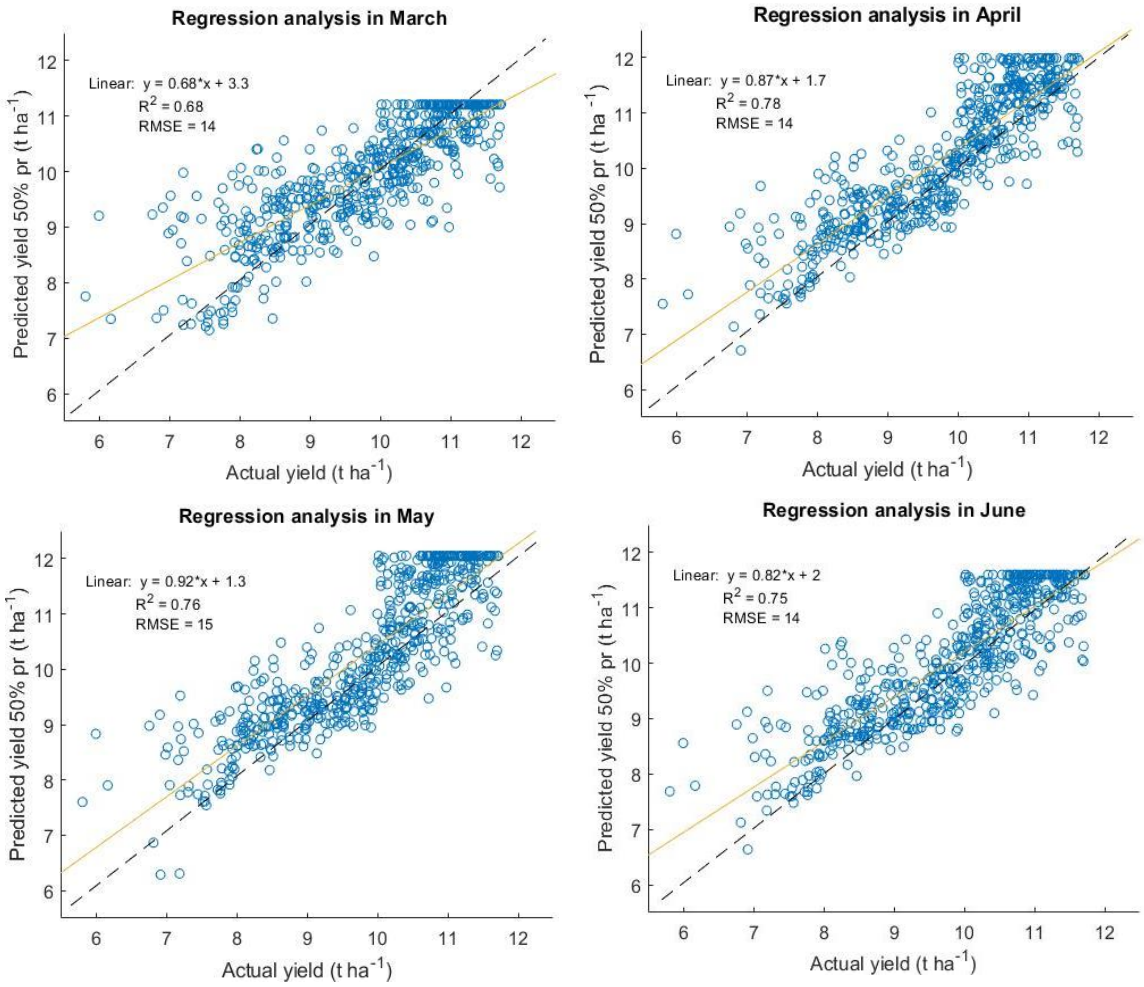

Figure 6. Predicted yields 50 % probability versus recorded yields from March to June. The solid line indicates that predicted yields are equal to recorded yields, and the dotted line indicates the 1:1 relationship.

4. Conclusion

The main task of this study was to predict winter wheat yield based on time-specific data across a time-series, at the farm level using BN based on climate (precipitation and temperature), NDVI, soil, topographic and recorded yield data embedding expert's opinion. The introduction of IP was an indicator of the representation of different spatial locations to support wheat growth based on PIP and historical yield data. The results showed that the model accomplished a 72 % accuracy rate in March, demonstrating its predictive capacity earlier in the season compared to other models. The correlation analysis between actual and predicted yield with 50 % probability ranging from 0.68 to 0.78. Additionally, similar patterns of spatial variation were observed in the actual and predicted maps with a 50 % probability chance of achieving. Future work is needed to improve the model accuracy including more data as well as nitrogen data.

Acknowledgements

The project received co-funding from EIT Food, part of the European Institute of Innovation and

Technology, a body of the European Union, under Horizon 2020 and Horizon Europe, the EU Framework Programmes for Research and Innovation. While the authors are grateful for this support, this paper does not necessarily reflect the views of the European Union. They also thank the many farmers and other rural stakeholders for taking part in the research.

References

Journal articles:

Addy, J.W., Ellis, R.H., Macdonald, A.J., Semenov, M.A. & Mead, A. (2020). Investigating the effects of inter-annual weather variation (1968–2016) on the functional response of cereal grain yield to applied nitrogen, using data from the Rothamsted Long-Term experiments. Agricultural and Forest Meteorology 284: article 107898.

Cao J, Zhang Z, Tao F, et al. (2021b). Integrating multi-source data for rice yield prediction across China using machine learning and deep learning approaches. Agricultural and Forest Meteorology 297: 108275.

Cao, J., Zhang, Z., Luo, Y., Zhang, L., Zhang, J., Li, Z., & Tao, F. (2021a). Wheat yield predictions at a county and field scale with deep learning, machine learning, and google earth engine. European Journal of Agronomy, 123, 126204.

Cheng, M., Penuelas, J., McCabe, M. F., Atzberger, C., Jiao, X., Wu, W., & Jin, X. (2022). Combining multi-indicators with machine-learning algorithms for maize yield early prediction at the county-level in China. Agricultural and Forest Meteorology, 323, 109057.

Feng, P., Wang, B., Liu, D. L., Waters, C., Xiao, D., Shi, L., & Yu, Q. (2020). Dynamic wheat yield forecasts are improved by a hybrid approach using a biophysical model and machine learning technique. Agricultural and Forest Meteorology, 285–286, 107922. doi:10.1016/j.agrformet.2020.107922

Helman, D., Lensky, I. M., & Bonfil, D. J. (2019). Early prediction of wheat grain yield production from root-zone soil water content at heading using Crop RS-Met. Field Crops Research, 232, 11-23.

Jin, H., Li, M., Hopwood, G., Hochman, Z., & Bakar, K. S. (2022). Improving early-season wheat yield forecasts driven by probabilistic seasonal climate forecasts. Agricultural and Forest Meteorology, 315, 108832.

Khaki, S., Pham, H., & Wang, L. (2021). Simultaneous corn and soybean yield prediction from remote sensing data using deep transfer learning. Scientific Reports, 11(1), 11132.

Kopecký, M., Macek, M., & Wild, J. (2021). Topographic Wetness Index calculation guidelines based on measured soil moisture and plant species composition. The Science of the Total Environment, 757(143785), 143785. doi:10.1016/j.s citotenv.2020.143785.

Li, L., Wang, B., Feng, P., Wang, H., He, Q., Wang, Y., ... & Yu, Q. (2021). Crop yield forecasting and associated optimum lead time analysis based on multi-source environmental data across China. Agricultural and Forest Meteorology, 308, 108558.

Mahmood S.A., Karampoiki M., Hammond J.P., Paraforos D.S., Murdoch A.J., Todman L. (2023): Embedding expert opinion in a Bayesian network model to predict wheat yield from spring-summer weather. Smart Agricultural Technology 4. doi: 10.1016/j.atech.2023.100224

Mitchell, P. J., Waldner, F., Horan, H., Brown, J. N., & Hochman, Z. (2022). Data fusion using climatology and seasonal climate forecasts improves estimates of Australian national wheat yields. Agricultural and Forest Meteorology, 320, 108932.

Schauberger, B., Jägermeyr, J., & Gornott, C. (2020). A systematic review of local to regional yield forecasting approaches and frequently used data resources. European Journal of Agronomy, 120, 126153.

Vergara-Díaz, O.; Zaman-Allah, M.A.; Masuka, B.; Hornero, A.; Zarco-Tejada, P.; Prasanna, B.M.; Cairns, J.E.; Araus, J.L. (2016). A novel remote sensing approach for prediction of maize yield under different conditions of nitrogen fertilization. Frontiers in Plant Science, 7, 666. doi:10.3389/fpls.2016.00666

Wang, Y., Li, R., Hu, J., Fu, Y., Duan, J., & Cheng, Y. (2021). Daily estimation of gross primary production under all sky using a light use efficiency model coupled with satellite passive microwave measurements. Remote Sensing of Environment, 267, 112721.

Zhang, H., Zhang, Y., Liu, K., Lan, S., Gao, T., & Li, M. (2023). Winter wheat yield prediction using integrated Landsat 8 and Sentinel-2 vegetation index time-series data and machine learning algorithms. Computers and Electronics in Agriculture, 213, 108250. doi:10.1016/j.compag.2023.108250.

Ziliani, M. G., Altaf, M. U., Aragon, B., Houborg, R., Franz, T. E., Lu, Y., ... & McCabe, M. F. (2022). Early season prediction of within-field crop yield variability by assimilating CubeSat data into a crop model. Agricultural and forest meteorology, 313, 108736.

Conference proceedings papers and book sections:

Karampoiki, M., Todman, L., Mahmood, S., Murdoch, A., Hammond, J., Ranieri, E., & Paraforos, D. (2022). A Bayesian Network for wheat yield prediction using topographic, soil and historical data. In Proceedings of the 15th International Conference on Precision Agriculture (unpaginated, online). Monticello, IL

Natale, A., Antognelli, S., Ranieri, E., Cruciani, A., Boggia, A. (2020). A novel cleaning method for yield data collected by sencors: A case study on winter cereals. 20th International Conference, Cagliari, Italy, July 1–4, 2020, Proceedings, Part V.

Theses and dissertations:

Chawla, V., Naik, H. S., Akintayo, A., Hayes, D., Schnable, P., Ganapathysubramanian, B., Sarkar, S. (2016). A Bayesian Network approach to County-Level Corn Yield Prediction using historical data and expert knowledge. Retrieved from http://arxiv.org/abs/1608.05127

Application of artificial neural network to identify the closest variety to *Ogbomoso* mango fruit

Michael Mayokun Odewole[a,*], **Toluwani Adedeji Adegbite**[b]
[a]Department of Food Engineering, University of Ilorin, Ilorin, Nigeria
[b]Department of Agricultural and Biosystems Engineering, University of Ilorin, Ilorin, Nigeria
* Corresponding Author. Email: odewole.mm@unilorin.edu.ng

Abstract

Several varieties of mango fruits have different physical properties, differentiating them from one another. Some of these physical properties may be similar, but not the same. This situation may lead to wrong produce identification by unsuspecting potential end users. Therefore, the objective of this study was to use existing selected physical properties (major, minor, intermediate, geometric mean diameters, surface area and sphericity) of four (4) varieties of mangoes (Julie, *Ogbomoso*, Saigon, and John Bull) with the aid of Artificial Neural Network (ANN) to identify the closest variety of mango to *Ogbomoso* mango fruit. The aforementioned physical properties of fifty (50) samples of each variety of mango were subjected to four (4) ANN models. The ANN software was tasked to specifically identify *Ogbomoso* mango among the four (4) varieties. The model had six (6) inputs, one (1) hidden layer and four (4) outputs. Six (6) data of *Ogbomoso* (sample, major, minor and intermediate diameters, geometric mean diameter and surface area) were used as input while sphericity of all the four (4) varieties were used as an output. The ANN analysis was done using four (4) transfer functions, TanhAxon, SigmoidAxon, BiasAxon and Axon. Results showed that TanhAxon predicted (identified) best out of the four (4) transfer functions used, with 87.5% for *Ogbomoso* mango, 80% for Saigon, 0% for Julie and 40% for John Bull, with mean square error of 0.02374. Also, from the results, Saigon had the closest prediction value of 80% (most similar) to *Ogbomoso* mango (87.5%). This implied that, Saigon is the variety usually misidentified as *Ogbomoso* mango by unsuspecting potential end users. The outcome of this study can be used to develop efficient and effective mango sorting systems.

Keywords: ANN, Mango, Physical Properties, *Ogbomoso*

1. Introduction

Artificial Neural Network (ANN) is a computational model that works similarly to the working of biological neural networks. In ANN, signals are processed and either stored or forwarded to the next neighboring neurons in the network (Kumar and Garg, 2018). Three (3) concepts are necessary in the ANNs characterization, they are; *neuron*, which is the basic computational unit in a network; *architecture*, the topological structure of how the neurons are connected; and *learning*, the process that adapts the network in order to compute a desired function or perform an assignment (Zhang and Zimba, 2017). ANN is an interconnection of artificial neurons. Every neuron in the layer is connected to all the neurons of previous and next layers. Each neuron receives input which is the output of neurons of the previous layer. ANN structure comprises of input layer (s), hidden layer (s) and an output layer (s) of neurons. ANN is a data processing system based on the structure of the biological neural system. Prediction via ANN is not like conventional modeling and simulation, but by learning from data generated experimentally or using validated models.

Mangoes are popular nutritional tropical fruit, which are one of the most important fruits crops in the tropical and the subtropical areas of the world. They originated from India over 4000 to 6000 years ago (Yadav and Singh 2017). Beginning in the16th Century, mangoes were gradually distributed from India to other tropical countries in Asia, such as the Philippines, Indonesia, China and Thailand (Rashid *et al.*, 2019; Kabeel *et al.*, 2021).

Ogbomoso mango is a peculiar local variety in Nigeria. This variety is named after *Ogbomoso* (8.1227° N, 4.2436° E), a town in Oyo state, South West region of Nigeria. *Ogbomoso* is widely accepted to be the location where this variety of mango naturally thrives in abundance in Nigeria. *Ogbomoso* mango is one the most popular varieties of mango fruits in Nigeria, and its demand is high due to itsndue to its unique taste. It has sweet fruit pulp, fibrous, rich in a variety of phytochemicals, high in prebiotic fibres, vitamin C, polyphenol and pro-vitamin A carotenoids as reported by (Ezekiel and Olukuewu, 2013). However, many

unsuspecting potential end users of the mango usually misidentify and wrongly select a closely similar mango variety instead of the *Ogbomoso* variety. Therefore, the objective of this study was to use existing selected physical properties (major, minor, intermediate, geometric mean diameters, surface area and sphericity) of four (4) varieties of mangoes (Julie, *Ogbomoso*, Saigon, and John Bull) with the aid of Artificial Neural Network (ANN) to identify the closest variety of mango to *Ogbomoso* mango fruit.

2. Materials and Methods

In this study, six (6) existing physical properties (major, minor, intermediate, geometric mean diameters, surface area and sphericity) of four (4) varieties of mango fruits (*Ogbomoso*, Saigon, Julie and John bull) were converted comma-separated values (CSV) format file using Excel spreadsheet. This was done to make the data compatible to the ANN software (NeuroSolutions version 6.0) used for analysis.

The ANN software was tasked to identify *Ogbomoso* variety among *Ogbomoso*, Saigon, Julie and John Bull varieties. The primary data used for this model was *Ogbomoso*. The model had six (6) inputs, one (1) hidden layer and four (4) outputs. Six (6) data of *Ogbomoso* (sample, major, minor and intermediate diameters, geometric mean diameter and surface area) were used as input while sphericity of all the four (4) varieties were used as the output. Sphericity was chosen to be the desired output since it has relationship with size of an object. In the process of neural building, 70% of the data was used for training, 15% was used for testing and 15% was used for cross validation. The ANN analysis was done using four (4) transfer functions (TanhAxon, SigmoidAxon, BiasAxon and Axon). The existing data of fifty (50) samples of each variety of mango were subjected to the four (4) ANN models.

3. Results and Discussion

3.1. ANN Models

Table 1 shows the results of ANN models for *Ogbomoso*, Saigon, Julie and John Bull mangoes, using four (4) transfer functions. From the table, TanhAxon function correctly predicted (identified) *Ogbomoso* mango with 87.5% accuracy, but wrongly identified Saigon and John Bull as *Ogbomoso* with 80% and 40% indices respectively. However, Julie (0%) was correctly identified as Julie, it was not in any way wrongly identified as *Ogbomoso*. These results agreed with the determined physical parameters of the mangos in such that, both *Ogbomoso* and Saigon had similar shapes and sizes, with minor differences. Also, TanhAxon function had mean square error of 0.02374. Huang *et al.*, (2021) predicted the key fruit quality of loquat using artificial neural network. Two transfer functions, Log-sigmoid and Tangent-sigmoid were used for the prediction. It was observed that Log-sigmoid for fruit weight had the lowest MSE prediction of 0.01511 and highest of 0.03699 while Tangent-sigmoid had the lowest MSE of 0.02363 and highest of 0.03712. The prediction is in agreement with 0.02374 which TanhAxon predicted for *Ogbomoso* Mango. Mean squared error (MSE) measures the amount of error in statistical models. It assesses the average squared difference between the observed and predicted values. When a model has no error, the MSE equals zero. The mean squared error is also known as the mean squared deviation (MSD) (Collier *et al.*, 2018). Mean squared error (MSE) is ideal as an objective measure of model performance, but it gives insight into what aspects of model performance are “good” or “bad” (Hodson *et al.*, 2021).

Furthermore, SigmoidAxon function correctly predicted (identified) *Ogbomoso* with 62.5% accuracy, but wrongly identified Saigon as *Ogbomoso* with 86.67% index. Conversely, Julie and John Bull were correctly identified as Julie and John Bull respectively, with 0% index for both. SigmoidAxon had the lowest mean square error of 0.0148 of all the four (4) functions. This is in line with the prediction of Log-sigmoid for loquat fruit weight, having the lowest MSE of 0.01511 (Huang *et al.*, 2021). Also, Cevher and Yıldırım (2022) recorded lowest MSE of 0.018 for the prediction of pear fruit.

BiasAxon function wrongly identified Saigon and John Bull as *Ogbomoso* with 93.3% and 30% indices respectively. Also, it correctly identified *Ogbomoso* with 75% accuracy, and all Julie mangoes as Julie, with no occurence of wrong identification (0%) as another variety of mango. BiasAxon activation function had MSE of 0.0357 which was high compared to what TanhAxon and SigmoidAxon functions. It was also similar to what was obtained in the prediction of weight of loquat fruit using Log-sigmoid which had the highest MSE of 0.03699 (Huang *et al.,* 2021).

In addition, Axon function correctly identified *Ogbomoso* mango with 87.5% accuracy. It wrongly identified Saigon and John Bull with 80% and 20% indices respectively. However, all Julie mangoes were identified as Julie, as indicated with 0% index. This trend is almost the same with TanhAxon, except for John Bull which has 20% (against 40% for TanhAxon).

Finally, according to Table 1, it can be observed that TanhAxon and Axon activation functions correctly identified the *Ogbomoso* mango variety with the same accuracy index (87.5%). However, TahnAxon is a better identifier due to its lower MSE of 0.0237, as compared to MSE of 0.0371 for Axon. The lower the MSE, the better a prediction (Du *et al*., 2020). This observation for TanhAxon is in-line with 0.02363 obtained for loquat fruit with Tangent-sigmoid ANN function (Huang *et al.,* 2021).

Table 1. ANN Predictions (Identifications)

Transfer Functions	TanhAxon	Sigmoid Axon	BiasAxon	Axon
Ogbomoso	87.50%	62.50%	75.00%	87.50%
Saigon	80.00%	86.67%	93.30%	80.00%
Julie	0.00%	0.00%	0.00%	0.00%
John Bull	40.00%	0.00%	30.00%	20.00%
MSE	0.0237	0.0148	0.0357	0.0371

4. Conclusions

The TanhAxon function under ANN correctly predicted (identified) *Ogbomoso* mango with 87.5% accuracy, but wrongly identified Saigon as *Ogbomoso* mango with 80% index. The closeness in the physical properties of both varieties was responsible for higher indices of wrong identification in all the four (4) ANN functions used. This could lead to mix-up in the identification/selection between the two (2) varieties. Therefore, the closest variety to *Ogbomoso* mango is the Saigon variety. This implied that, Saigon is the variety usually identified wrongly in most cases as the *Ogbomoso* mango by many unsuspecting potential end users.

Acknowledgements

Federal Government of Nigeria (FGN) through University of Ilorin, Ilorin, Nigeria, for the full sponsorship of the conference attendance from the Tertiary Education Trust Fund (TETFund) grant.

References

Cevher, E.Y. and Yıldırım, D. (2022). Using Artificial Neural Network Application in Modeling the Mechanical Properties of Loading Position and Storage Duration of Pear Fruit. Processes, 10, 2245. https://doi.org/10.3390/pr10112245

Collier, N., Hoffman, F. M., Lawrence, D. M., Keppel-Aleks, G., Koven, C. D., Riley, W. J. Randerson, J. T. (2018). The International Land Model Benchmarking (ILAMB) system: Design, theory, and implementation. *Journal of Advances in Modeling Earth Systems*, 10(11), 2731–2754. https://doi.org/10.1029/2018ms001354

Du X., Chen Z., Meng Q. and Song Y. (2020). Experimental analysis and ANN prediction on performances of finned oval-tube heat exchanger under different air inlet angles with limited experimental data. Open Physics, 18: 968–980. https://doi.org/10.1515/phys-2020-0212

Ezekiel, 0.0.and Olukuewu, M.T. (2013). Chemical. Microbiological and Sensory Characteristics of Leather Blends Produced from Mango *(Mangifera indica* 'Ogbomoso') and Carrot *(Daucus carota). Acta Hort.* 1007, 471-477

Hodson, T. O., Over, T. M., & Foks, S. S. (2021). Mean squared error, deconstructed. *Journal of Advances in Modeling Earth Systems*, *13*, e2021MS002681. https://doi.org/10.1029/2021MS002681

Huang, X., Wang, H., Qu S., Luo, W. and Gao, Z. (2021). Using artificial neural network in predicting the key fruit quality of loquat. Food science & Nutrition,1074. DOI:10.1002/fsn3.2166

Kabeel, E. H., Khater, E. G., Bahnasawy, A. H. and Atawia, A. A.R. (2021). Some Physical and Chemical Properties of Mango Fruits. Annals of Agric. Sci., Moshtohor, Vol. 59(3), 679 – 688. ISSN 1110-0419 https://assjm.journals.ekb.eg.

Kumar, V. and Garg, M.L. (2018). Predictive Analytics: A Review of Trends and Techniques. *International Journal of Computer Applications,* 182(1): 0975 – 8887.

Rashid, M.M., Khatun, H., Rayhan, M.F., Plabon, M.E.A., Hossain, M.U., Mozid, M.A., Kamal, M.M., Hasan, M.K., El Sabagh, A. and Islam, M.S. (2019). Comparative Study on Physicochemical Properties of Selected MANGO (*Mangifera Indica* L.) Varieties in Northern Bangladesh. Cercetări Agronomice în Moldova. 1 (177): 54-65

Yadav, D. and Singh, S. P. (2017). Mango: History origin and distribution. Journal of Pharmacognosy and Phytochemistry, 6(6): 1257-1262.

Zhang, H. and Zimba, P. V. (2017). "Analyzing the effects of estuarine freshwater fluxes on fish abundance using artificial neural network ensembles," *Ecological Modelling*, no. Supplement C, (359):103–116.

On the route optimisation for phytosanitary treatments in vineyards using electric-powered UAVs

Mar Ariza-Sentís[a]*, Gonzalo Mier[b], Sergio Vélez[a,c], and João Valente[a,d]

[a] Information Technology Group, Wageningen University & Research, 6708 PB Wageningen, Netherlands
[b] Laboratory of Geo-Information Science and Remote Sensing, Wageningen University & Research, 6708 PB Wageningen, Netherlands.
[c] Group Agrivoltaics, Fraunhofer Institute for Solar Energy Systems ISE, 79110 Freiburg, Germany
[d] Centre for Automation and Robotics (CAR), Spanish National Research Council (CSIC), 28006 Madrid, Spain

Abstract

Phytosanitary has a significant impact on the environment and biodiversity of agricultural fields. It is therefore important to adopt sustainable farming practices that reduce generalised pesticide usage while targeting its application only to infested plants or weak plants prone to develop diseases. UAVs offer a promising solution to optimise chemical usage. By determining flight paths, UAVs can effectively spray all the infested plants and maximise the effectiveness of pest management strategies. Nevertheless, UAVs have a short battery life. This paper aims to propose a two-step approach for enhanced disease spraying. A first flight is executed with a multispectral camera to acquire data about the current field conditions, including terrain and canopy information. The knowledge gained is used to compute a heatmap of the areas which have a higher risk of developing a disease. Afterwards, the heatmap is divided into cells, where each vine is embodied in two, one for each lateral of the canopy. Two campaigns are studied (2021 and 2023) with different percentages of infection. The Vehicle Routing Problem is modelled to spray the plants with a higher probability of developing the disease considering the battery limitation and having a big penalisation for each non-sprayed cell with high risk. For the 2021 campaign (38.1% of infested plants) the UAV required 42.1% more spraying time and 30.7% more travelled distance than for the 2023 campaign, with only 21.6% of infection. Compared to Coverage Path Planning, the proposed algorithm travels up to 38.0% less distance. Further, since many canopy sides with high risk might not be sprayed due to the battery constraint, multiple spraying sessions are considered to spray all the potentially diseased cells. For 2021, 6 spraying sessions were required, whereas 2023 needed 3 sessions. The proposed approach fosters a more sustainable method through decreased energy expenditure and battery utilisation.

Keywords: Pesticide Reduction, Vineyards Management, Precision Spraying, Disease Control, UAV.

1. Introduction

Disease detection in agriculture is constrained by time limitations as extensive areas need to be surveyed within specific timeframes by field operators (Tang et al., 2010), often resulting in delayed responses. Recent advancements in Machine Learning and Deep Learning algorithms have introduced a paradigm shift by enabling early disease detection through pattern recognition (Burr, 2008), primarily focusing on visible symptoms. However, there are certain diseases, for instance in vineyards, that start being developed inside the grape bunch and remain undetectable until advanced stages, emphasising the need for alternative detection methods (AL-Saddik et al., 2017; Kumar et al., 2016). A novel approach involves assessing disease probability based on biophysical field conditions, avoiding the reliance on symptom manifestation and predicting areas with the highest disease development probability. Utilising Unmanned Aerial Vehicles (UAVs) equipped with multispectral imagery, researchers have achieved high accuracy in disease presence assessment, notably correlated with ground truth data (Vélez et al., 2023).

Despite the promising applications of UAVs in pesticide spraying, challenges such as limited battery life hinder their efficacy, necessitating resource optimisation for larger coverage (Cavalaris, 2023). While UAV path planning has been implemented in agriculture, there is a need to shift focus towards targeted applications on infested plants instead of performing Coverage Path Planning (CPP) (Guo et al., 2021; Li et al., 2023). This is specifically relevant in vertical trellis systems like vineyards, where both sides of the canopy should be considered. Furthermore, a significant advantage of UAVs compared to other spraying platforms such as tractors and ground robots, is their capability to perform interrow manoeuvres, changing the canopy side by

flying over it (Figure 1). This capacity demonstrates the potential to minimise both the time and distance covered by the UAV in contrast to other spraying machines.

The objective of this research is to evaluate the feasibility of utilising UAVs for spraying operations, contributing to the advancement of precision agriculture techniques in viticulture. Additionally, the research aims to address the constraint posed by limited battery life in UAVs, which can impact their spraying efficiency. Furthermore, the study incorporates the capability of UAVs to change canopy sides in the middle of the row.

Figure 1. UAV for aerial spraying across the vineyard. When two infested cells are within the same row, the straight green arrow is followed. Conversely, when the infested cells are in different rows, the UAV highlights its ability to change row side (curved green arrow).

2. Materials and Methods

The disease assessment begins with capturing raw multispectral imagery using a UAV. This data undergoes processing to create multiple maps, which are then employed to train a Random Forest algorithm for predicting the probability of disease occurrence. Subsequently, the trained algorithm is utilised to generate a disease risk map based on the existing biophysical conditions of the vineyard, as outlined by (Vélez, Ariza-Sentís, & Valente, 2023b). This heatmap serves as the basis for devising spraying routes, determined by the threshold at which pesticides should be applied.

The risk map illustrates the likelihood of disease development, partitioned into smaller cells using a grid system. Each plant is represented by two cells, situated on either side of the canopy. To optimise the spraying task, the UAV requires an efficient route, a problem that can be conceptualised as the Vehicle Routing Problem (VRP) (Dantzig & Ramser, 1959; Toth & Vigo, 2002). The VRP seeks to minimise the cost function while visiting each node exactly once and returning to the starting point with a single vehicle.

$$\min \sum_{i \in V} \sum_{j \in V} c_{ij} x_{ij} \tag{1}$$

where c_{ij} represents the distance and time cost from the node i to j, x_{ij} is a binary variable determining if the vehicle moves from i to j, and Vdenotes the list of nodes, ensuring each node is visited once.

Given the finite battery capacity of UAVs, route planning must account for this constraint to avoid incomplete spraying. This necessitates modelling the time required for the UAV to spray each plant, with penalties imposed for unsprayed cells. However, due to battery limitations, many cells with a high disease probability may remain untreated, necessitating multiple UAV sessions to cover different areas. To address this, the problem is reformulated as the multiple Vehicle Routing Problem (mVRP), where each vehicle represents a pesticide application session.

$$\sum_{i,j} t_{ij} * x_{ij} < B \quad (2)$$

Here, t_{ij} denotes the time for the UAV to travel from cell i to j and spray cell j, with B representing the battery life.

In order to validate the proposed algorithm, it is compared with a baseline CPP algorithm that travels the total length of each row of the field.

3. Results and Discussion

Two experiments were conducted in a 0.1-ha vineyard during the 2021 and 2023 campaigns. In 2021, there were 38.1% risk areas, while in 2023, the percentage decreased to 21.6%. For the proposed algorithm, it is assumed that UAVs require 5 seconds to treat each risk area since they must stop flying to apply the chemical. It is also considered that the UAV speed is assumed to be 4 m/s (Qin et al., 2016; Xue et al., 2016) and 12 minutes of battery life according to the DJI Agras T40 (DJI Sciences and Technologies Ltd., Shenzhen, Guangdong, China). When considering the CPP algorithm, the UAVs travel the whole length of the rows, which is approximately 110 meters each. Six rows are inspected, and both sides of the canopy should be considered. Therefore, the travelled distance is 110 x 6 x 2 meters, a total of 1,320 meters, regardless of the percentage of infection.

Figure 2 illustrates the optimised aerial paths for the 2021 and 2023 campaigns. It can be observed that in the case of 2021, since there is a higher percentage of infested plants, the spraying time and the travelled distance are higher than for 2023. Moreover, more spraying sessions are required to cover the infested area. Furthermore, the travelled distance is lower in both campaigns than 1,320 meters, meaning that the UAVs employ less distance and hence time when considering the proposed algorithm.

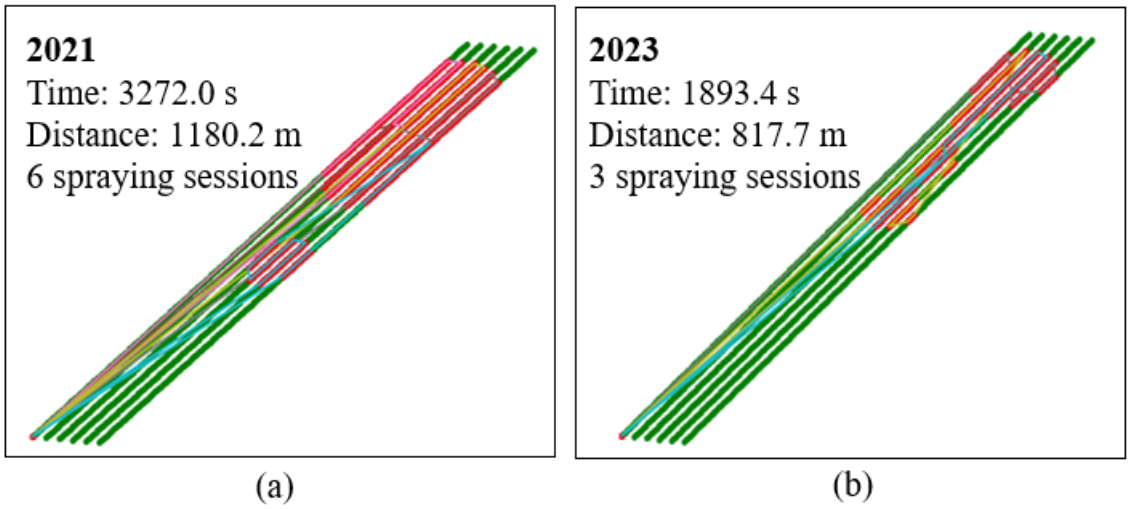

Figure 2. Optimised UAV spraying paths (coloured lines) along with the spraying time, the distance travelled and the number of spraying sessions required for the (a) 2021 campaign, and (b) 2023 campaign. The red dots represent the sprayed cells, whereas the green ones indicate the non-diseased and hence non-sprayed cells.

This study introduces a methodology that offers significant environmental advantages in vineyard management. By employing UAVs equipped with multispectral cameras for disease assessment and chemical tanks for spraying, the approach accurately maps the biophysical characteristics of the vineyard, facilitating precise chemical application tailored to the crop's development stage. Additionally, by dividing the task into two phases—mapping disease risk and actual spraying—battery life usage is optimised, addressing a previously identified limitation (Hafeez et al., 2023). Previous research has explored UAV path planning for precise spraying (Li et al., 2023; Nanavati et al., 2023; Xu et al., 2023). However, these studies often overlook biophysical field parameters and battery constraints. Moreover, the capability of UAVs to fly over canopies

and change sides/rows (Figure 1) presents a distinct advantage in vertical trellis systems, focusing this study on vineyards rather than continuous crops like wheat or maize.

Figure 2 indicates the optimal UAV routes for precise spraying only to infested plants for two campaigns, with a different percentage of infection. Moreover, it also includes the time required to spray all infested areas and the travelled distance, along with the number of spraying sessions, considering the battery life, that is required to spray the whole infested area. It can be observed that, for the 2021 campaign, with a larger affected area than in the 2023 campaign, the algorithm travelled 363 more meters (30.7% more distance) and needed 1379 seconds (almost 23 more minutes) than in 2023. This can be attributed to the fact that, even if the increase in infested areas is only 16.5%, it needed 3 more spraying sessions to cover all those areas. Moreover, the travelled distance is 10.6% and 38.0% lower for the 2021 and 2023 campaigns, respectively, compared to a baseline algorithm (CPP). The fact that UAVs have a limited battery life can be a drawback in scenarios where there is a widespread outbreak of diseases. Those cases should be further studied to validate whether UAVs are a good alternative or whether other spraying platforms would provide optimal solutions.

The application of phytosanitary measures differs when applied via UAV compared to tractor sprayers, as they have different tank capacities, potentially necessitating research into appropriate concentrations for low-capacity sprayers to avoid leaf damage. However, this study did not include tank capacity as a constraint since battery limitations were deemed more restrictive, with UAVs returning home to recharge batteries and also refilling their tanks.

4. Conclusions

The two-phase strategy of first mapping disease risk and then conducting spraying operations not only optimises battery life but also ensures resource efficiency, representing a significant advancement in mitigating the environmental impact of intensive phytosanitary practices in vineyards. Moreover, the study includes battery constraints, which is translated to an increased number of spraying sessions to cover the field. The proposed methodology travels up to 38.0% less distance than baseline algorithms such as Coverage Path Planning since it only sprays infested plants. Future research should focus on refining spraying concentrations, further enhancing operational efficiency while minimising chemical usage.

Acknowledgements

This work has been carried out in the scope of the H2020 FlexiGroBots project, which has been funded by the European Commission in the scope of its H2020 programme (contract number 101017111, https://flexigrobots-h2020.eu/). The authors acknowledge valuable help and contributions from 'Bodegas Terras Gauda, S.A.' and all partners of the project. This publication is part of the project "Fields2Cover: Robust and efficient coverage paths for autonomous agricultural vehicles" (with project number ENPPS.LIFT.019.019 of the research programme Science PPP Fund for the top sectors which is (partly) financed by the Dutch Research Council (NWO). Dr Sergio Vélez contract has been supported partially by the Iberdrola Foundation and the European Commission under the Marie Skłodowska-Curie Actions (MSCA) - E4F, part of the Horizon 2020 program (Grant Agreement No 101034297, https://doi.org/10.3030/101034297). The authors would like to extend their sincere appreciation to Sytze de Bruin for his assistance and insightful feedback.

References

AL-Saddik, H., Simon, J.-C., & Cointault, F. (2017). Development of Spectral Disease Indices for 'Flavescence Dorée' Grapevine Disease Identification. Sensors, 17(12), Article 12. https://doi.org/10.3390/s17122772

Burr, T. (2008). Pattern Recognition and Machine Learning. Journal of the American Statistical Association, 103(482), 886–887. https://doi.org/10.1198/jasa.2008.s236

Cavalaris, C. (2023). Chapter 10—Energy efficiency for in-farm unmanned aerial system applications. In D. Bochtis, A. C. Tagarakis, & D. Kateris (Eds.), Unmanned Aerial Systems in Agriculture (pp. 231–244). Academic Press. https://doi.org/10.1016/B978-0-323-91940-1.00010-4

Dantzig, G. B., & Ramser, J. H. (1959). The Truck Dispatching Problem. Management Science, 6(1), 80–91. https://doi.org/10.1287/mnsc.6.1.80

Guo, Y., Liu, C., & Coombes, M. (2021). Spraying Coverage Path Planning for Agriculture Unmanned Aerial Vehicles. 2021 26th International Conference on Automation and Computing (ICAC), 1–6. https://doi.org/10.23919/ICAC50006.2021.9594271

Hafeez, A., Husain, M. A., Singh, S. P., Chauhan, A., Khan, Mohd. T., Kumar, N., Chauhan, A., & Soni, S. K. (2023). Implementation of drone technology for farm monitoring & pesticide spraying: A review. Information Processing in Agriculture, 10(2), 192–203. https://doi.org/10.1016/j.inpa.2022.02.002

Kumar, S., Röder, M. S., Singh, R. P., Kumar, S., Chand, R., Joshi, A. K., & Kumar, U. (2016). Mapping of spot blotch disease resistance using NDVI as a substitute to visual observation in wheat (Triticum aestivum L.). Molecular Breeding, 36(7), 95. https://doi.org/10.1007/s11032-016-0515-6

Li, J., Sheng, H., Zhang, J., & Zhang, H. (2023). Coverage Path Planning Method for Agricultural Spraying UAV in Arbitrary Polygon Area. Aerospace, 10(9), Article 9. https://doi.org/10.3390/aerospace10090755

Nanavati, R. V., Meng, Y., Coombes, M., & Liu, C. (2023). Generalized data-driven optimal path planning framework for uniform coverage missions using crop spraying UAVs. Precision Agriculture, 24(4), 1497–1525. https://doi.org/10.1007/s11119-023-09999-3

Qin, W.-C., Qiu, B.-J., Xue, X.-Y., Chen, C., Xu, Z.-F., & Zhou, Q.-Q. (2016). Droplet deposition and control effect of insecticides sprayed with an unmanned aerial vehicle against plant hoppers. Crop Protection, 85, 79–88. https://doi.org/10.1016/j.cropro.2016.03.018

Tang, S., Tang, G., & Cheke, R. A. (2010). Optimum timing for integrated pest management: Modelling rates of pesticide application and natural enemy releases. Journal of Theoretical Biology, 264(2), 623–638. https://doi.org/10.1016/j.jtbi.2010.02.034

Toth, P., & Vigo, D. (Eds.). (2002). The Vehicle Routing Problem. Society for Industrial and Applied Mathematics. https://doi.org/10.1137/1.9780898718515

Vélez, S., Ariza-Sentís, M., & Valente, J. (2023). Mapping the spatial variability of Botrytis bunch rot risk in vineyards using UAV multispectral imagery. European Journal of Agronomy, 142, 126691. https://doi.org/10.1016/j.eja.2022.126691

Xu, Y., Han, Y., Sun, Z., Gu, W., Jin, Y., Xue, X., & Lan, Y. (2023). Path Planning Optimization With Multiple Pesticide and Power Loading Bases Using Several Unmanned Aerial Systems on Segmented Agricultural Fields. IEEE Transactions on Systems, Man, and Cybernetics: Systems, 53(3), 1882–1894. https://doi.org/10.1109/TSMC.2022.3205695

Xue, X., Lan, Y., Sun, Z., Chang, C., & Hoffmann, W. C. (2016). Develop an unmanned aerial vehicle based automatic aerial spraying system. Computers and Electronics in Agriculture, 128, 58–66. https://doi.org/10.1016/j.compag.2016.07.022

Agroview: enhance satellite imagery using super-resolution and generative AI for precision management in specialty crops

Christian Lacerda , Antonio de Oliveira Costa Neto, Yiannis Ampatzidis *

Agricultural and Biological Engineering Department, University of Florida, Immokalee, USA

Southwest Florida Research and Education Center, Immokalee, USA

* Corresponding author. Email: i.ampatzidis@ufl.edu

Abstract

Unmanned aerial vehicles (UAVs) and satellites are popular technologies for data acquisition in precision agriculture. However, both technologies have advantages and disadvantages. UAVs offer higher resolution but have a limited collection range, resulting in higher costs per acre. Satellite imaging is a cost-effective solution but has limitations of lower spatial resolution (> 0.5-10 m), which is not suitable for crop assessment in specialty crops. For example, our award-winning, cloud- and artificial intelligence (AI) based platform, Agroview, requires high-resolution images (~10 cm resolution) as inputs for accurate data analytics (aka., creation of plant inventory and fertility maps, plant canopy volume measurements, yield prediction, etc.). However, most available satellite images have much lower resolution (from 1-2 m up to 10 m). Several specialty crop growers and other stakeholders (e.g., crop insurance companies, crop consulting companies, etc.) expressed the need for developing a more cost-effective and less time-consuming data collection technology for precision crop management. The ideal solution would have near-UAV resolution levels with the cost and data collection advantage of satellites. In this study, generative AI models, particularly generative adversarial networks (GANs), were used to address atmospheric interference and sensor limitations to upscale satellite images. These models were trained on large datasets of low (e.g., satellite images) and high (UAV images) resolution images, learning to predict and recreate high-resolution details. The process of training a GAN to enhance satellite image resolution was conducted in a stepwise manner. This approach aimed to detect the points at which the GAN may encounter limitations in achieving the desired resolution of the original UAV ground truth images. This step-by-step analysis was essential for identifying specific stages in the training process where the GAN's performance may deteriorate, requiring adjustments or additional training to effectively enhance satellite image resolution.

Keywords: Crop monitoring, Image processing, Satellite imagery, Tree identification.

1. Introduction

Satellite images have proven useful for a wide range of tasks, including environmental and climate monitoring, urban planning, and land management, among many others. Within precision agriculture, farmers use satellite images to monitor and obtain crop data, but the collection of these images, although effective in various analyses, is still very expensive and not widely used in specialty crop production (Barbosa Júnior et al., 2024; Ghatrehsamani et al., 2018). Super resolution methods have been developed to enhance satellite images (and other low-resolution images, e.g., airplane images) and are turning into a breakthrough in several fields, from urban planning and precision farming to environmental monitoring. For example, interpolation, which includes bilinear and bicubic approaches, is essentially a prediction technique that fills in missing pixels based on the values of nearby pixels. Chang et al. (2006) and Neetha and Kantipudi (2022) demonstrated significant enhancements in image clarity through locally adaptive wavelet-based methods and adaptive edge-based bilinear interpolation, respectively. Since interpolation just estimates the image's existing information rather than adding new information, it can produce images that appear smoothed out and lack sharp detail.

Image-based reconstruction methods (Kala et al., 2018; Kawulok et al., 2019; Bätz et al., 2016) require multiple images of the same object with slight deviations. However, this is not always feasible or practicable, especially in remote sensing scenarios or when the required number of raw images is limited. Furthermore, such methods may require more calculations and be less successful at replicating high-frequency details. Deconvolution (Krishnan and Fergus, 2009; Levin et al., 2009) can bring details back into blurred images, assuming that the blur is known and can be modeled, which is not always the practice case. It can also amplify noise when trying to correct blurring, resulting in unwanted effects.

Generative artificial intelligence (AI) models such as generative adversarial networks (GANs) were also used to convert low-resolution images into high-quality data. GANs are a class of AI algorithms composed of two interacting neural networks, a discriminator network that determines whether the images generated by the generator network are real or manufactured. Through an iterative process of competition amongst the networks, the quality of the images generated is improved, leading to a resolution that is not achievable with previous methods. In recent years, significant progress has been achieved in the super-resolution field, particularly with the use of deep learning methods (Bashir et al., 2021; Zhang et al., 2020; Wang et al., 2022).

Traditional methods based on machine learning (Dong et al., 2014; Yang et al., 2010), may not capture the complexity and variety of the data in the same way as GANs, resulting in super-resolutions that often look less natural or fail to reintroduce realistic detail. Patch-based super-resolution (Bevilacqua et al., 2012; Freeman et al., 2002) may be limited by the quality and diversity of the high-resolution patch database. If the available patches do not adequately cover all the possible variations found in new images, the quality of the resulting image may be poor. GANs, however, are capable of generating entirely new and realistic details that may not have been present in the original training set.

Due to this feature, super-resolution by GANs is becoming essential for extracting detailed and accurate information from images that initially had resolution limitations (He et al., 2021; Karwowska and Wierzbicki, 2022; Wang et al., 2020), allowing for a clearer and more detailed view in essential applications such as climate change monitoring, natural resource management and optimization of agricultural practices, where fine details can be crucial for effective analysis and intervention. In Wang et al. (2020), a significant advance is made in terms of computational techniques for super-resolution. High computational complexity was achieved by restructuring the residual blocks to avoid problems such as vanishing gradient and loss of information propagation. The work of Karwowska and Wierzbicki (2022) focuses on a more general approach to improving the spatial resolution of satellite images, but without being used in a field of application.

Agroview is an award-winning, AI-enabled, and cloud-based application for crop monitoring and analysis, which uses high-resolution images captured by UAVs to provide detailed and effective information for precision crop management (Ampatzidis and Partel, 2019; Ampatzidis et al., 2020; Costa et al., 2022). Ampatzidis et al (2019) utilized Agroview to evaluate citrus rootstock varieties in commercial fields and reduce data collection time and cost. However, Agroview, requires high-resolution images (1024x1024 pixels and ~10 cm resolution) as inputs for the development of accurate data analytics (aka., creation of plant inventory). Since UAVs have a limited collection range and high costs per acre, the use of AI-enhanced satellite images could provide another alternative with a lower data collection cost and a high temporal resolution (compared to UAVs). Hence, the enhancement of low-resolution satellite images using GANs could be a decisive improvement in reducing costs, as well as improving performance and speed in the delivery of field evaluations. This study aims to improve the resolution of images taken by satellites and airplanes using super-resolution techniques and overcome the limitations of previously developed AI-enabled models. The effective use of these enhanced images on Agroview is evaluated too.

2. Materials and Methods

He et al. (2021) developed a GAN model able to produce images with a resolution of 256x256 pixels. However, this resolution proved to be insufficient for the effective performance of the Agroview AI detection models, which were trained using images collected by UAVs with a resolution of at least 1024x1024 pixels (around 10 cm resolution per pixel). To overcome this challenge, a new GAN model was developed able to convert low resolution images (e.g., satellite images of 200x126 pixel resolution; ~2 m resolution per pixel) to higher resolution (e.g., 600x600 pixels, ~40 cm per pixel).

The first step was to generate low-resolution images to be used with their corresponding high-resolution image through the training process following the same pattern as He et al. (2021). To achieve this, an algorithm was created to remove pixels from the high-resolution UAV images decreasing its resolution. The final resolution of the low-resolution images generated was between 200x126 and 219x140 pixels (~2 m resolution).

Then, a model was developed to create 512x512 pixel resolution (~45 cm per pixel) images. The total size of the model reached about 32 GB, which made it difficult to fit in only one GPU. This problem was solved by running the model on a server, which has 4 L40s Ada Lovelace architecture GPUs, each with 48 GB of memory (model # SYS-741GE-TNRT, Supermicro Computer Inc., San Jose, California, USA). Model

parallelism was used for this purpose, which is defined as a strategy for partitioning different parts of the GAN model into different processors. Pytorch provides specific features to run the layers of the model on different GPUs without creating a gap in the backtracking process. The objective of this step was to continue the process of increasing the output image size to 600x600 pixels (~40 cm resolution per pixel).

After setting a layer distribution strategy, we could control the metrics and the model converged as a consequence. The developed code was composed of the Generator (G), the Discriminator (D), and the Exponential Moving Average (EMA) version of the Generator (G-EMA). This one uses the same architecture defined for the Generator differing only in how its parameters are updated. Therefore, G and G-EMA were the neural networks demanding more memory.

The final and stable GAN model is represented in Figure 1. The dashed lines emphasize the synchronization between the layers of the G and G-EMA. The accumulate function shown by Equation 1 is one part of the training process strongly affected by a wrong layer's distribution strategy.

$$Param_{(EMA)} = \beta \cdot Param_{(EMA)} + (1 - \beta) \cdot Param_{(EMA)} \quad (1)$$

where, β is a decay factor (typically close to 1, e.g., 0.999) that controls the update rate. Without the proper distribution, the corresponding layers would have their parameter values in different GPUs creating the necessity of sending all values to the same processing device before calculating the equation value for every training iteration. The final model size for 600x600 output configurations was 18 GB – GPU 0, 36 GB – GPU 1, and 15 GB – GPU 2, with the training session batch size of 2 images. To train the GAN model, 20,000 images, collected by UAVs, were used. Figure 2 shows an example of the low-resolution and high-resolution of the same image.

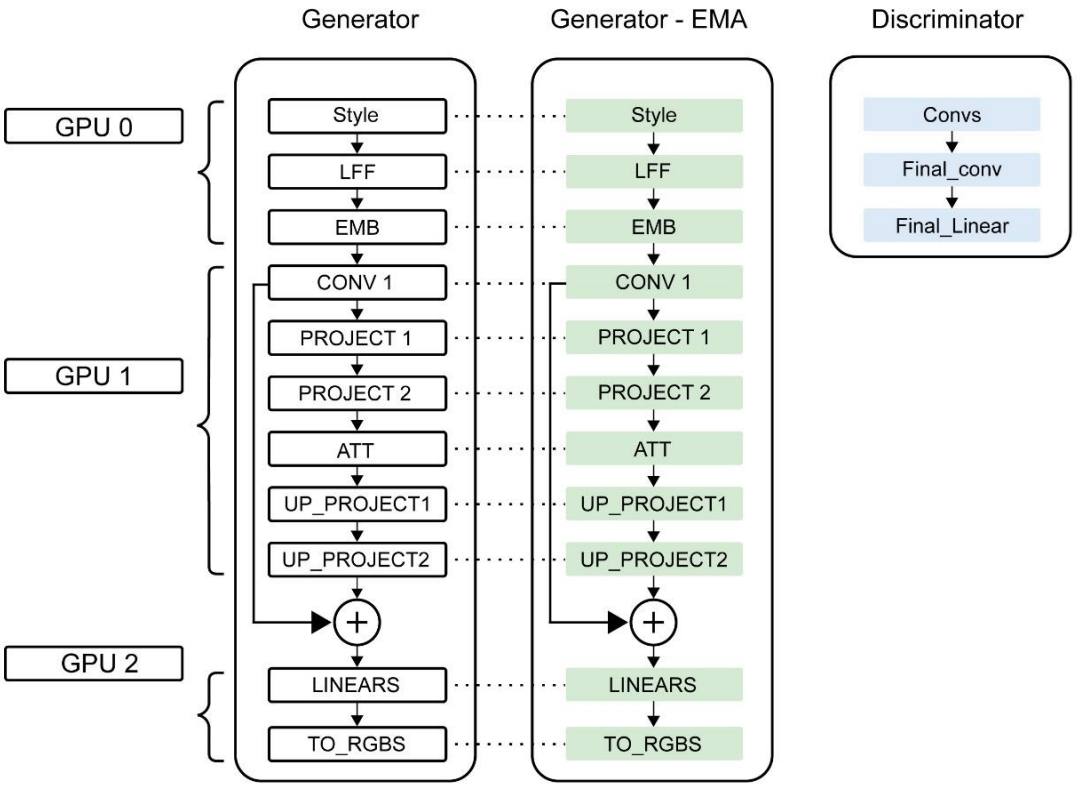

Figure 1. Workflow of the multi-GPU GAN model.

(a) (b)

Figure 2. Examples of images used to train the proposed GAN model: (a) Low resolution image, and (b) High resolution image (taken by UAVs).

3. Results

The current Agroview process pipeline starts with the upload of the collected images from the orchards, then an engine stitches the images to an orthomosaic map, and then the orthomosaic is sent to the detection AI-enabled algorithm. In this context, the first milestone was creating images with a minimum resolution that the stitching engine (Pix4D, https://www.pix4d.com) would be able to use and create the orthomosaic map.

First, the model was trained to produce 256x256 pixels resolution images. At this resolution, the stitching engine generated errors related to a lack of information to stitch the images. There was not enough resolution for the Pix4D software to find the matching points and create the orthomosaic. The next step was training the model to output 512x512 pixels images. This was the first resolution that Pix4D could find the correlation among the images and stitch them. Figure 3 shows the 512x512 pixels image output from the GAN model, and Figure 4 shows the first orthomosaic map created from generated images.

Figure 3. Example of a 512x512 pixels (~45 cm per pixel) resolution image generated by the GAN model.

Figure 4. Orthomosaic map generated by Pix4D using GAN generated images.

After successfully stitching the generated images, Agroview's performance in creating tree inventories was evaluated (Figure 5). The total number of trees in Figure 5 was 167 (ground truth) and the number of trees detected by Agroview was 105. Therefore, there is an error of 37.12% for an orthomosaic created from images about half the size of the images on which the Agroview detection algorithm was trained.

Then, the 600x600 pixels resolution images (Figure 6) were used to create an orthomosaic map. Setting the image output to this size increased the GAN model to more than 300 million parameters. The images were stitched and uploaded to Agroview in the same way as the 512x512 images. Figure 7 shows the Agroview detection results; the total number of trees detected by Agroview was 127 with an error of 29.95%. Another important parameter, obtained after increasing the output size from 512x512 to 600x600, was the increase in image quality.

Figure 5. Agroview tree detection on the orthomosaic created from 512x512 GAN generated images (dot colors represent different tree height categories).

Figure 6. Example of a 600x600 pixels (~40 cm per pixel) resolution image generated by the GAN model.

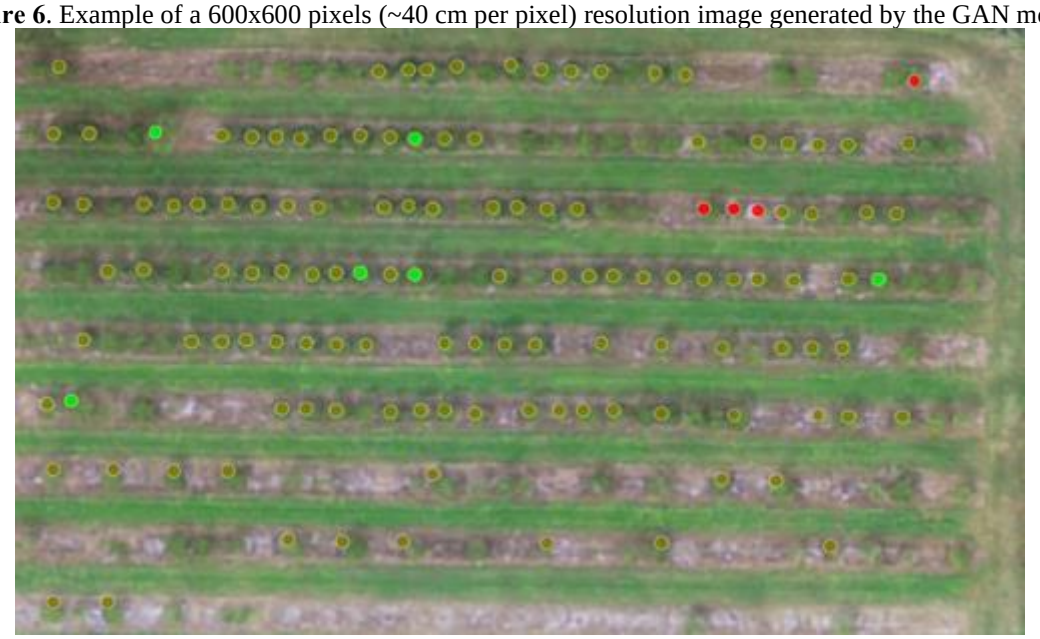

Figure 7. Agroview tree detection on the orthomosaic created from 600x600 GAN generated images (dot colors represent different tree height categories).

4. Discussion

First, the GAN model was tested at different resolutions to analyze how Agroview's detection AI model would perform. The process using 256x256 pixel images proved ineffective in creating an orthomosaic map. The results obtained by increasing the resolutions showed a clear improvement in Agroview's tree detection process starting with the 512x512 pixel resolution, where an error of 37.12% was obtained. The 600x600 pixel resolution achieved an even lower error of 29.95%, indicating a marked increase in accuracy with the same dataset. A resolution increase greater than this is still being analyzed, which may indicate an even greater improvement in accuracy but at a higher computational cost.

5. Conclusions

The study showed that even with increased resolutions of 512x512 and 600x600 pixels, there are still challenges in achieving high tree detection accuracy comparable to the original high-resolution images used to train Agroview. However, the results indicate that even with a relatively high error in tree detection with 37.12% for 512x512 pixels and 29.95% for 600x600 pixels images, increasing the resolution as well as different GAN strategies and models adopted can considerably increase the accuracy of tree detection by Agroview. This study represents an important step toward improving the applicability of super-resolution images in the field of precision agriculture. The proposed AI-enabled technology could be used as a digital twin of an agricultural field and as a climate-smart technology to help farmers rapidly calculate losses and better communicate recovery needs to ensure business viability and minimize interruption to the U.S. produce supply chain due to unexpected weather and climatic events.

Acknowledgments

We would like to thank Supermicro Computer Inc. and NVIDIA for providing a server with 4 L40s Ada Lovelace architecture GPUs (model # SYS-741GE-TNRT) for developing and training the GAN models.

References

Ampatzidis Y. and V. Partel, 2019. UAV-based high throughput phenotyping in citrus utilizing multispectral imaging and artificial intelligence. Remote Sensing, 11(4), 410, doi: 10.3390/rs11040410.

Ampatzidis, Y., V. Partel, B. Meyering, and U. Albrecht, 2019. Citrus rootstock evaluation utilizing UAV-based remote sensing and artificial intelligence. Computers and Electronics in Agriculture, 164, 104900, doi.org/10.1016/j.compag.2019.104900.

Ampatzidis, Y., V. Partel, and L. Costa, 2020. Agroview: Cloud-based application to process, analyze and visualize UAV-collected data for precision agriculture applications utilizing artificial intelligence. Computers and Electronics in Agriculture, Volume 174, 105457, ISSN 0168-1699. https://doi.org/10.1016/j.compag.2020.105457

Barbosa Júnior M.D., B.R.A. Moreira, V.S. Carreira, A.L. Brito Filho, C. Trentin, F.L.P., Souza, D. Tedesco, T. Setiyono, J.P. Flores, Y. Ampatzidis, R.P. Silva, L.S. Shiratsuchi, 2024. Precision Agriculture in the United States: A comprehensive meta-review inspiring further research, innovation, and adoption. Computers and Electronics in Agriculture, 221, 108993, https://doi.org/10.1016/j.compag.2024.108993.

Bashir, S.M.A., Y. Wang, M. Khan, and Y. Niu, 2021. A comprehensive review of deep learning-based single image super-resolution. PeerJ. Computer science, 7, e621. https://doi.org/10.7717/peerj-cs.621

Bätz, M., J. Koloda, A. Eichenseer, and A. Kaup, 2016. Multi-image super-resolution using a locally adaptive denoising-based refinement. In Proceedings of the 2016 IEEE 18th International Workshop on Multimedia Signal Processing (MMSP), Montreal, QC, Canada, pp. 1-6. https://doi.org/10.1109/MMSP.2016.7813343

Bevilacqua, M., A. Roumy, C.M. Guillemot, and M-L Alberi-Morel, 2012. Low-Complexity Single-Image Super-Resolution based on Nonnegative Neighbor Embedding. In British Machine Vision Conference.

Chang, S.G., Z. Cvetković, and M. Vetterli, 2006. Locally Adaptive Wavelet-Based Image Interpolation. IEEE Transactions on Image Processing, 15(6), 1471-1485. https://doi.org/10.1109/TIP.2006.871162

Costa, L., S. Kunwar, Y. Ampatzidis, and U. Albrecht, 2022. Determining leaf nutrient concentrations in citrus trees using UAV imagery and machine learning. Precision Agriculture, 23(3), 854-875, https://doi.org/10.1007/s11119-021-09864-1.

Dong, C., C.C. Loy, K. He, and X. Tang, 2014. Learning a Deep Convolutional Network for Image Super-Resolution. Proceedings of the European Conference on Computer Vision (ECCV) 2014. https://doi.org/10.48550/arXiv.1501.00092

Freeman, W.T., T.R. Jones, and E.C. Pasztor, 2002. Example-based super-resolution. IEEE Computer Graphics and Applications. 22 (2): 56-65. http://dx.doi.org/10.1109/38.988747

Ghatrehsamani S., T. Wade T., and Y. Ampatzidis, 2018. The adoption of precision agriculture technologies by Florida growers: a comparison of 2005 and 2018 survey data. XXX International Horticultural Congress, II International Symposium on Mechanization, Precision Horticulture, and Robotics, 12-16 August, 2018, Istanbul Turkey.

He, Y., D. Wang, N. Lai, W. Zhang, C. Meng, M. Burke, ... and S. Ermon, 2021. Spatial-temporal super-resolution of satellite imagery via conditional pixel synthesis. Advances in Neural Information Processing Systems, Volume 34, ISSN 27903-27915. https://doi.org/10.48550/arXiv.2106.11485

Kala, S., S. Nalesh, B.R. Jose, and J. Mathew, 2018. Image Reconstruction Using Novel Two-Dimensional Fourier Transform. In: Hassanien, A., Oliva, D. (eds) Advances in Soft Computing and Machine Learning in Image Processing. Studies in Computational Intelligence, vol 730. Springer, Cham. https://doi.org/10.1007/978-3-319-63754-9_31

Karwowska, K., and D. Wierzbicki, 2022. "Improving Spatial Resolution of Satellite Imagery Using Generative Adversarial Networks and Window Functions." Remote Sens. 14: 6285.https://doi.org/10.3390/rs14246285

Kawulok, M., P. Benecki, S. Piechaczek, K. Hrynczenko, D. Kostrzewa, and J. Nalepa, 2019. Deep Learning for Multiple-Image Super-Resolution. IEEE Geoscience and Remote Sensing Letters. https://doi.org/10.48550/arXiv.1903.00440

Krishnan, D., and R. Fergus, 2009. Fast image deconvolution using hyper-Laplacian priors. Proceedings of the 22nd International Conference on Neural Information Processing Systems, 1033-1041.

Levin, A., Weiss, Y., Durand, F., & Freeman, W. T. (2009). Understanding and evaluating blind deconvolution algorithms. In Proceedings of the 2009 IEEE Conference on Computer Vision and Pattern Recognition (CVPR), Miami, FL, USA, pp. 1964-1971. https://doi.org/10.1109/CVPR.2009.5206815

Neetha, C.H., and M.P. Kantipudi, 2022. Adaptive edge-based bilinear interpolation for smart healthcare. 6th Smart Cities Symposium (SCS 2022), Hybrid Conference, Bahrain, 2022, pp. 7-13, https://doi.org/10.1049/icp.2023.0312

Wang, X., J. Yi, J. Guo, Y. Song, J. Lyu, J. Xu, W. Yan, J. Zhao, Q. Cai, and H. Min, 2022. A Review of Image Super-Resolution Approaches Based on Deep Learning and Applications in Remote Sensing. Remote Sens. 14: 5423. https://doi.org/10.3390/rs14215423.

Wang, Z., K. Jiang, P. Yi, Z. Han, and Z. He, 2020. Ultra-dense GAN for satellite imagery super-resolution. Neurocomputing. 398: 328-337. ISSN 0925-2312.https://doi.org/10.1016/j.neucom.2019.03.106

Yang, J., J. Wright, T.S. Huang, and Y. Ma, 2010. Image Super-Resolution Via Sparse Representation. IEEE Transactions on Image Processing, 19(11), 2861-2873. https://doi.org/10.1109/TIP.2010.2050625

Zhang, C., A. Marzougui, and S. Sankaran, 2020. High-resolution satellite imagery applications in crop phenotyping: An overview. Computers and Electronics in Agriculture. 175: 105584. ISSN 0168-1699. https://doi.org/10.1016/j.compag.2020.105584

Applications of artificial intelligence in the identification of objects for the analysis of waste in the Segura River

Ana María Codes Alcaraz [a,*], Carmen Rocamora Osorio [a, b], Herminia Puerto Molina [a, b]

[a] Centre for Agri-Food and Agro-Environmental Research and Innovation CIAGRO, Orihuela, Spain

[b] Engineering Department, University Miguel Hernandez, Orihuela, Spain

* Email: acodes@umh.es

Abstract

Plastic pollution in marine ecosystems presents a significant contemporary challenge due to its pervasive presence in rivers and oceans and its enduring persistence. This research specifically targets the river and traditional irrigation system of Vega Baja del Segura, situated in south-eastern Spain, where substantial accumulations of floating waste hinder efficient water distribution in irrigation ditches and drainage channels. The primary objective of this study is to develop an algorithm capable of automatically identifying and quantifying various types of debris through image analysis using aerial photographs captured by drones at multiple locations along the river and canals. The YOLOv5 algorithm was employed for training, with mean Average Precision (mAP) serving as the benchmark for evaluation. A mAP of 0.5 yielded an accuracy of 97%, while accuracy ranged at 79% for mAP values between 0.5 and 0.95. This methodology promises to mitigate subjectivity in debris quantification and facilitate swift and secure identification of their sources within the river ecosystem.

Keywords: YOLOv5, Python, Plastic, Waste, Rivers.

1. Introduction

Plastic waste in the marine ecosystem nowadays is a great concern due to its large amount in rivers and oceans (Hafeez et al., 2019) and its persistence in them (van Emmerik & Schwarz, 2020). Several studies have long established that the main source of marine plastic pollution is land-based and due to littering, plastic bag usage and solid waste disposal (Derraik, 2002). Rivers transport plastic to the oceans (Jambeck et al., 2015; Lebreton et al., 2017). This waste reaches the sea and ends up generating microplastics that are incorporated into the trophic chain and affect the quality of fishing (Cole et al., 2013; Thompson et al., 2004). Since there is evidence that not all the plastic that enters a river is released into the ocean (van Emmerik et al., 2022), there is a growing interest in characterizing the flow of macroplastic residues in rivers in order to identify and design measures to reduce global plastic pollution (Hurley et al., 2023).

In the river and in the traditional surface irrigation system of Vega Baja del Segura, located in the southeast of Spain, a large amount of floating waste accumulates at certain points, causing problems in the distribution of irrigation in ditches and drainage channels (Rocamora et al., 2021).

In this area, the traditional surface irrigation system dating from the 13th century is still in use. The crops are supplied with the water diverted from the Segura River by means of dams, and it is distributed throughout the farmland through a set of irrigation canals or ditches that make up the so-called "living waters network". Due to the low filtering capacity of the land (silt-clay), it became necessary to build a network of drainage aqueducts or *azarbes*, called the "dead water network". The presence of this floating waste on many occasions hinders the flow of water through some sections of the syphons and prevents the normal operation of the gates and therefore the management of irrigation water.

In addition, floating waste causes economic damage to the irrigators. The irrigation communities are responsible for the maintenance of their infrastructures and the water that arrives is poured back into public channels. The river authority has the power to impose sanctions on the irrigation communities if they do not keep their channels clean and allow the discharge of floating material into the river. Farmers must face the cost of removal of floating waste, or the fines imposed by the river authority (Rocamora et al. 2021). The

floating debris that is found in the river and irrigation network has varied origins, predominantly plant waste from the river itself, such as reeds, as well as waste from domestic, agricultural and industrial activities, among which plastic waste predominates (Rocamora et al., 2021).

To eliminate this problem, it is necessary to characterize the floating waste to know their origin and thus be able to act at the source. Several studies have developed different methodologies to quantify and characterize floating debris, such as the development of software to quantify large amounts of waste in the oceans (de Vries et al., 2021), a deep-learning based methodology to detect floating macroplastics on water surface images (van Lieshout et al., 2020) and an algorithm based on convolutional neural networks (CNN) to classify litter items in different classes (Wolf et al., 2020).

The objective of this work is to propose a standardized and quick methodology to characterize the floating waste found in the irrigation system to detect changes in its composition and origin. This objective will be attained by training a YOLO algorithm to automatically detect the different residues for their classification and quantification through image analysis, and by taking overhead photographs with a drone at various strategic points of the river and channels along time. This methodology will enable to monitor the status of the sampling points reducing the subjective component of the manual quantification and characterization of floating waste in the system of the Segura River and irrigation channels in the Vega Baja.

The determination of the composition of the floating debris can assist the evaluation of actions taken by local authorities aimed at reducing plastic pollution from land origin.

2. Materials and Methods

The study was carried out in the system formed by the Segura River in its last section, in Vega Baja, and the irrigation and drainage channels of the traditional irrigation area. The acquisition of images was carried out in certain points of accumulation of floating waste in the river, ditches and drainage channels (Figure 1).

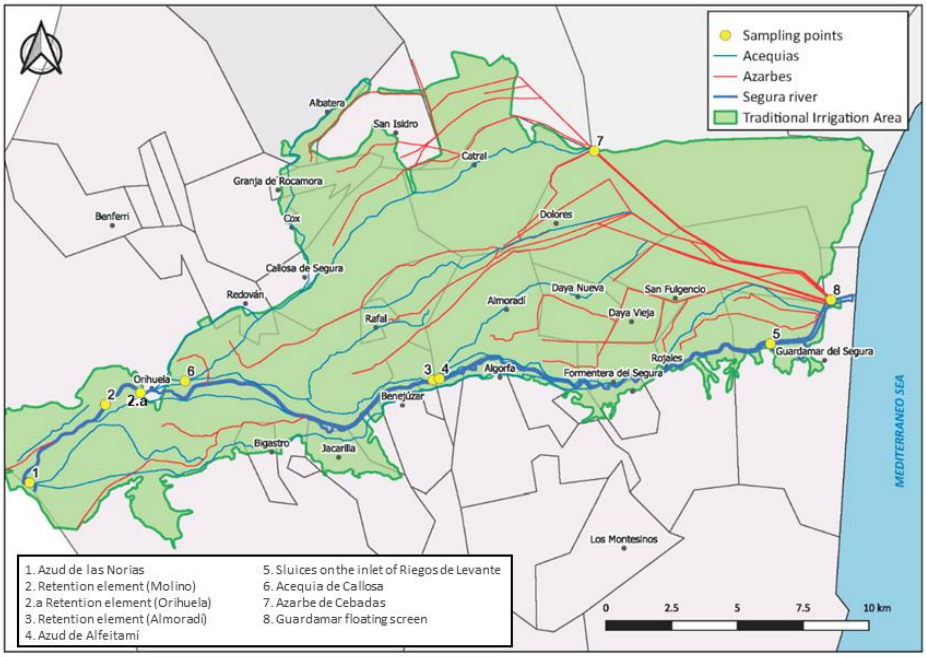

Figure 1. Location of sampling sites.

2.1. Image acquisition

The images obtained were with an unmanned aerial vehicle (UAV), the Autel EVO 2 model drone, a quadrotor. The drone specifications are as follows: weight: 1127 grams, wheelbase: 397mm, removable 7100 mAh 11.55V batteries, maximum flight time: 40 minutes, maximum horizontal flight speed: 20m/s,

maximum flight distance: 25 km. Camera specifications: effective pixels: 48MP, field of view: 79º and lens dimensions: 25.6 mm.

The flight planning was programmed for each of the different sampling points. In this study, a total of 3 flights were carried out at each of the different selected points of the river on July the 28th, September the 8th, and October the 31st of year 2022. These flights were made at different heights: 5 meters, 10 meters and 20 meters. The drone's camera captured aerial images from a zenithal view, with the number of photos at each point varying between one and nine, depending on the extent of waste found in the river. A total of 61 images were analysed, including all sampling dates and points.

2.2. Types of waste

The most abundant residues were known from a previous study (Rocamora et al., 2021). In that study, the largest class of waste was made up of bottles of bottled water, which represented 74.2% of the total number of items counted. The number of containers of domestic origin (food containers, personal hygiene, and cleaning products) represented 14.9% and finally, the number of agricultural wastes, that is, bottles and cans of phytosanitary products, represented only 3.8 %. Based on this information, we trained the algorithm to identify the following types of waste: a) Different size plastic water bottles, b) Bleach bottles, c) Detergent bottles, d) Drums of chemical products from agricultural activity, e) Game balls.

2.3. Software

Makesense is a free online photo tagging tool that does not require any installation. We used Makesense to add all the labels of the different identified waste to a total of 477 images. Once the labelling was finished, these images were downloaded in YOLO format.

YOLO (You Only Look Once) is an object detection algorithm that divides images into a grid system. Each grid cell is responsible for detecting objects within itself. Besides, it is one of the most famous object detection algorithms due to its speed and accuracy (Redmon et al., 2016). YOLO series algorithms have developed rapidly in recent years. In 2020, two versions of YOLO v4 and YOLO v5 appeared successively. YOLO v5 is the most advanced detection network of the YOLO object detection algorithm. Based on YOLO v3 and YOLO v4 algorithms, where arithmetic ensemble innovation was carried out to improve detection speed. In 2020 Glenn Jocher released YOLO v5 (Zhang et al., 2022).

We used Colaboratory, a product of Google Research which allows any user to write and execute arbitrary Python code in the browser. Python is a programming language created by Guido van Rossum in 1991 (Van Rossum et al., 2009). It is characterized by being high-level and interpreted, with special emphasis on code readability. It uses dynamic types and is a multi-paradigm language, which means that it supports object-oriented, structured, functional, etc. It can be expandable, that is, it consists of a core to which modules and libraries can be added as required.

2.4. Training

The entire process was carried out with an ASUS computer with Intel CORE i5 and Windows 8. The first step was to label our images with the Makesense software, where we used the following labels: Water bottle, Detergent bottle, Bleach bottle, Agricultural drum, and Ball. 430 images were labelled for training and 47 for model validation. This dataset presented images from the 2019 study (Rocamora et al., 2021), images of the objects to be identified, and aerial images taken with an UAV in 2022.

Once these images were labelled, they were divided into two folders: one called "*train*" where the images in this folder are the ones that will be used to train the algorithm and the next one called "*val*" which will be used to validate the algorithm's training. Once the labelling is finished, we proceed to extract these images in YOLO format, where we will use them in Google Colab using YOLOv5. The number of classes, class names, and the locations of our *train* and *val* folders were specified in a Sublime Text file.

Finally, the image size, 1024 pixels, and the number of epochs, 126, were written in a new cell. The image size refers to the number of times an image is divided when being analysed, if we increase this number the image is analysed more accurately. The number of epochs is a hyperparameter that defines the number of

times the learning algorithm will work on the entire training data set. An epoch means that each sample in the training data set has had a chance to update the parameters of the internal model. The number of epochs is traditionally large, often hundreds or thousands, allowing the learning algorithm to run until the model error has been sufficiently minimized (Brownlee 2022). In this case there were 126 epochs since from that number the training did not improve. In the precision graph (Figure 2) an asymptote is observed where it has already reached its training maximum. The batch size used was 2 because it provided good results, and choosing a larger batch size would consume more computing time.

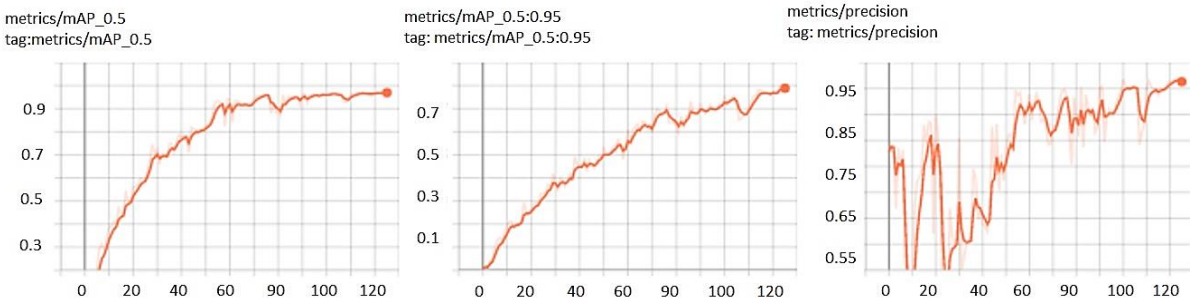

Figure 2. Precision graphs.

Once the training cell was executed, a folder was created with a validation and prediction of the results, as well as a folder with the graphs analysing the effectiveness of our trained algorithm. Finally, once the algorithm training was validated, the 61 images taken in the riverbeds and channels in 2022 were analysed.

3. Results

The results cell gave us all the images analysed with the characterization and identification of each one of the residues by means of bounding boxes (Figure 3).

Figure 3. Automatic characterization of waste at sampling point ID6, 22/10/31.

To verify the efficiency of the model, indicators such as precision, recall, mAP (mean Average Precision), detection speed and F1 score were used for evaluation in this study.

Precision Eq. (1) is the proportion of true positive samples among all positive samples predicted by the model.

$$P = \frac{TP}{TP + FP} 100(\%) \quad (1)$$

where TP is the number of true positive cases, and FP is the number of false positive cases.

Recall in Eq (2) indicates the proportion of true positive samples predicted by the model out of all true positive samples.

$$R = \frac{TP}{TP + FN} 100(\%) \quad (2)$$

where TP and FN are as in Eq (1), and FN is the number of false negative cases.

Typically, there is a negative correlation between accuracy and recall, where one increases and the other decreases. From the precision and recall values, a PR chart (Figure 4) is plotted to observe their distribution. To balance the effects of precision and recall and evaluate a model more comprehensively, AP (Average Precision) can be entered as a comprehensive evaluation index.

The value of AP in Eq (3) is the area under the PR curve, and a higher value means better model performance.

$$AP = \int_0^1 P(R)dR \quad (3)$$

The F1 score in Eq (4) is the reconciled mean of precision and recall, taking into account both the precision in Eq (1) and recall in Eq (2) of the classification model.

$$F1 \quad score = \frac{2 \cdot P \cdot R}{P + R} \quad (4)$$

Model performance can be represented by average precision, precision, recall, test time, and F1 score. In this experiment, a confidence threshold of 0.5 is set, and precision, recall, and F1 score are derived on this basis. The results obtained for this model were: a training time of 3h 7 min; a precision of 92.04%; a Recall of 97.07%; a mAP of 96.90% and a F1 score of 94.48%.

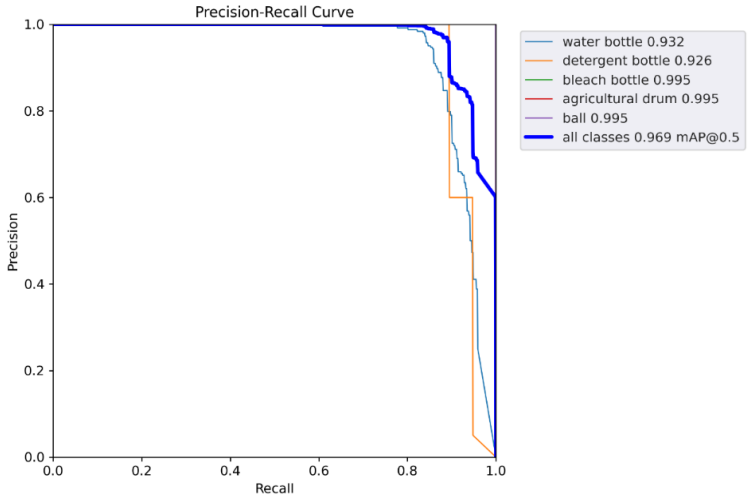

Figure 4. Precision – Recall curve.

The objective of this work is to identify the different residues quickly and accurately, for which the mAP values (96.90%) and the detection speed, 81.7 ms to detect an image, were used as the main evaluation metrics, where the higher the mAP value, the better the detection result.

Once the algorithm was validated, it was applied to the images captured throughout 2022 on the sampling points defined. A total of 61 images were analysed in the results cell, leading to the automatic counting of each one of them.

To assess the reliability of this training, a statistical study of automatic counting through AI and manual counting using the ImageJ application was also carried out (Table1).

Table 1. Comparison of the count of objects detected with the algorithm and with the manual count.

		Automatic counting with algorithm					Manual counting with ImageJ				
Date	ID	Water bottles	Agricultural drum	Detergent bottles	Bleach bottles	Balls	Water bottles	Agricultural drum	Detergent bottles	Bleach bottles	Balls
28/07/22	1	0					0				
	2	69		2		4	88				
	2.a*	0					0				
	3	3					4				
	4	17					20				
	5	0					6				
	6	4					4				
	7	40	5	4	3		58	2	2	1	
	8	2		1	1		2				
08/09/22	1	21					29		3		
	2	121		1	1		128	1	1	1	
	2.a*	233	1	2	2	1	243	2	10	6	2
	3	154	2	5	2	1	173	3	5	6	2
	4	10		1	1		19			2	
	5	0					9				
	6	59				1	63		2		1
	7	37	2	5	2		49	4	2		
	8	90	1	3			96		2		
	8.a	236	1		2	1	329			5	3
	8.b	55					74		1		
	8.c	130		3			130	1	9		
	8.d	141	1	4	2		141	0	5	2	
	8.e	37					46	1	4		
31/10/22	1	62	1	2	1		81	1		1	
	2	5	1	1	1	2	20				
	2.a*	118	1			14	166	1			
	3			1	2	2	236		1	2	
		209									2
	4	0					0				
	5	199	6	8	4	1	218	4	9	4	1
	6	167	2	5	1		170	1	6	1	
	8	185		2	3		204		2	3	
	8.a	400	1	1	6		524	1	1	6	
	8.e	153		2	8		174		2	8	
	8.d	58			1		72			1	

According to the study of Rocamora *et al*. (2021), in this research we can also see how the most common objects are plastic bottles with a proportion of 91.05% of the total. These bottles are the most difficult to characterize as they are found in large numbers and can be seen stacked together, making the bottle look in different shapes. On the contrary, bleach bottles and drums are easier to identify since they have a characteristic shape and colour, and they are not found in large quantities.

For water bottles, detergent bottles and bleach bottles, the model tends to count less objects than the manual count (positive bias). On the contrary, the model tends to count more agricultural drums and balls than the manual count. In the case of water bottles, the bias seems to change with count number, becoming higher when the count number is higher, probably due to the stacking of the bottles that can be appreciated in the manual count but not in the automatic one.

3.1. Discussion

Due to the shortage of convolutional neural technology (CNN) for the detection of plastic waste in the aquatic environment via drone images, we introduced this dataset to improve and facilitate the task of identification and characterization of plastic waste to expedite cleaning tasks and to be able to apply measures for a faster way to solve this problem. The results of this study show excellent performance in computing time and waste identification. The model works well for both isolated residues and grouped residues, accurately detecting them. However, our model suffers from false detections in the background of the images identifying them as plastic bottles.

To compare the results of the algorithm with those of the manual count, it is essential to highlight the time investment inherent in both methodologies. Manual counting of 61 images using the Image J application required 7 hours and 34 minutes. In contrast, the automatic counting of the same 61 images took a mere 42 seconds. Consequently, a pronounced reduction in analysis time is evident. Moreover, it is noteworthy that automatic counting circumvents issues such as subjective biases or fatigue that may arise during manual counting.

The data obtained enables the continuous monitoring of floating waste presence across all surveyed points throughout the study period. Consequently, this methodology facilitates near real-time results, with drone flights for image capture being the sole limiting factor.

The algorithm developed by Wolf et al. (2020) can classify anthropogenic waste into different classes such as water bottles, Styrofoam, canisters, cartons, bowls, shoes, polystyrene packaging, cups, textile and carry bags small or large. The algorithm developed in this work can classify different types of plastic bottles: water bottles, bottles of hygiene and cleaning products, and cans of chemical products used in agriculture. This distinction represents an enhancement over the algorithm of Wolf et al. (2020) since the type of bottle reveals its origin, which allows awareness campaigns or other measures to be addressed to the suitable population target.

The algorithm shows a good agreement with the manual count except for the case of counting playing balls that are found in very reduced numbers. For water, detergent and bleach bottles, as well as for agricultural drums, the algorithm shows a good agreement with the manual count by a trained observer.

4. Conclusions

The results show that there are no significant differences between both counts, demonstrating the effectiveness of the algorithm in accurately detecting waste residues, as evidenced by its mAP score of 97%.

While the developed detection algorithm performs admirably in identifying isolated objects, its efficacy diminishes when confronted with stacked objects, such as those accumulated in booms and other retention structures.

We can conclude that this method can eliminate human biases inherent in manual counting processes. Moreover, the automatic count reduced dramatically the analysis time, providing expedited and reliable insights into the origins of riverborne waste. This procedure will enable targeted interventions tailored to various sectors of the population, contingent upon the diverse origins of waste types.

The reduction of floating waste is the responsibility of the whole society but specially of the local and regional authorities tasked with legislating against plastic waste dumping and enforcing regulatory compliance. The image acquisition and automatic counting methodology that we propose in this work is a tool that can be useful, due to its speed and objectivity, in evaluating public policies aimed at curbing plastic contamination in the traditional irrigation network.

References

Brownlee, Jason (2022) https://machinelearningmastery.com/difference-between-a-batch-and-an-epoch/ Accessed December 2022

Cole, M., Lindeque, P., Fileman, E., Halsband, C., Goodhead, R., Moger, J., & Galloway, T. S. (2013). Microplastic ingestion by zooplankton. Environmental Science and Technology, 47(12). https://doi.org/10.1021/es400663f

de Vries, R., Egger, M., Mani, T., & Lebreton, L. (2021). Quantifying floating plastic debris at sea using vessel-based optical data and artificial intelligence. Remote Sensing, 13(17). https://doi.org/10.3390/rs13173401

Derraik, José G.B. 2002. "The Pollution of the Marine Environment by Plastic Debris: A Review." Marine Pollution Bulletin 44 (9): 842–52. https://doi.org/10.1016/S0025-326X(02)00220-5.

Hafeez, S., Sing Wong, M., Abbas, S., Y. T. Kwok, C., Nichol, J., Ho Lee, K., Tang, D., & Pun, L. (2019). Detection and Monitoring of Marine Pollution Using Remote Sensing Technologies. In Monitoring of Marine Pollution. https://doi.org/10.5772/intechopen.81657

Hurley, Rachel, Hans Fredrik Veiteberg Braaten, Luca Nizzetto, Eirik Hovland Steindal, Yan Lin, François Clayer, Tim van Emmerik, et al. 2023. "Measuring Riverine Macroplastic: Methods, Harmonisation, and Quality Control." Water Research 235 (May): 119902. https://doi.org/10.1016/J.WATRES.2023.119902.

Jambeck, J. R., Geyer, R., Wilcox, C., Siegler, T. R., Perryman, M., Andrady, A., Narayan, R., & Law, K. L. (2015). Plastic waste inputs from land into the ocean. Science, 347(6223). https://doi.org/10.1126/science.1260352

Lebreton, L. C. M., Van Der Zwet, J., Damsteeg, J. W., Slat, B., Andrady, A., & Reisser, J. (2017). River plastic emissions to the world's oceans. Nature Communications, 8. https://doi.org/10.1038/ncomms15611

Redmon, J., Divvala, S., Girshick, R., & Farhadi, A. (2016). You only look once: Unified, real-time object detection. Proceedings of the IEEE Computer Society Conference on Computer Vision and Pattern Recognition, 2016-December. https://doi.org/10.1109/CVPR.2016.91

Rocamora, C., Puerto, H., Abadía, R., Brugarolas, M., Martínez-Carrasco, L., & Cordero, J. (2021). Floating debris in the low Segura river basin (Spain): Avoiding litter through the irrigation network. Water (Switzerland), 13(8). https://doi.org/10.3390/w13081074

Thompson, R. C., Olson, Y., Mitchell, R. P., Davis, A., Rowland, S. J., John, A. W. G., McGonigle, D., & Russell, A. E. (2004). Lost at Sea: Where Is All the Plastic? Science, 304(5672). https://doi.org/10.1126/science.1094559

van Emmerik, T., & Schwarz, A. (2020). Plastic debris in rivers. Wiley Interdisciplinary Reviews: Water, 7(1). https://doi.org/10.1002/wat2.1398

van Emmerik, Tim, Yvette Mellink, Rahel Hauk, Kryss Waldschläger, and Louise Schreyers. 2022. "Rivers as Plastic Reservoirs." Frontiers in Water 3 (January). https://doi.org/10.3389/frwa.2021.786936.

van Lieshout, C., van Oeveren, K., van Emmerik, T., & Postma, E. (2020). Automated River Plastic Monitoring Using Deep Learning and Cameras. Earth and Space Science, 7(8). https://doi.org/10.1029/2019EA000960

Van Rossum, G., Drake, F. L., Harris, C. R., Millman, K. J., van der Walt, S. J., Gommers, R., Virtanen, P., Cournapeau, D., Wieser, E., Taylor, J., Berg, S., Smith, N. J., Kern, R., Picus, M., Hoyer, S., van Kerkwijk, M. H., Brett, M., Haldane, A., Del Río, J. F., … Oliphant, T. E. (2009). Python 3 Reference Manual. In Nature (Vol. 585, Issue 7825).

Wolf, M., Van Den Berg, K., Garaba, S. P., Gnann, N., Sattler, K., Stahl, F., & Zielinski, O. (2020). Machine learning for aquatic plastic litter detection, classification and quantification (APLASTIC-Q). Environmental Research Letters, 15(11). https://doi.org/10.1088/1748-9326/abbd01

Zhang, Y., Guo, Z., Wu, J., Tian, Y., Tang, H., & Guo, X. (2022). Real-Time Vehicle Detection Based on Improved YOLO v5. Sustainability (Switzerland), 14(19). https://doi.org/10.3390/su141912274

Artificial intelligence-based yield prediction in table grape production: A case study in the Vinalopó protected designation of origin

Ana María Codes Alcaraz [a,b], Carmen Rocamora Osorio [a,b], Herminia Puerto Molina [a,b]

[a] Centre for Agri-Food and Agro-Environmental Research and Innovation CIAGRO, Orihuela, Spain and [b] Engineering Department, University Miguel Hernandez, Orihuela, Spain

* Email: acodes@umh.es

Abstract

Accurate yield prediction is crucial for effective harvest planning and manufacturing optimization in table grape production, especially given the labour-intensive nature of the process. This study introduces the outcomes of training a detection model Yolov5 to predict the yield of a table grape plot within the Protected Designation of Origin "Uva de mesa embolsada del Vinalopó" in Alicante (Spain). The main objective was to develop a fast and efficient methodology for cluster bag counting and grape production estimation. An unmanned aerial vehicle conducted a single flight over a commercial plot, capturing images parallel to the trellis rows at a height of 10 meters and a 35º angle. A dataset comprising 55 labelled images, each containing an average of 150 cluster bags, was utilized for model training. Of these, 50 images were dedicated to training, while 5 were reserved for model validation. The results of the model training revealed a swift detection speed of 78.5 milliseconds, with a Precision of 80.38%, Recall of 85.63%, mean Average Precision of 86.40%, and an F1 rate of 83.13%. When applied to a different set of images, the artificial intelligence (AI) model accurately counted 20,520 cluster bags. Notably, the production estimation using this methodology exhibited a mere 6.2% underestimation in comparison to the farmer's estimate, which experienced a considerably higher underestimation of 37.67%. While these results showcase the potential of the proposed AI based methodology for yield prediction, it is acknowledged that further refinement and updating the detection model to the new version of Yolov7 are essential. Expanding the dataset to include more plots or multiple campaigns will enhance the robustness of the methodology. This research signifies a substantial stride towards leveraging AI technologies in viticulture, promising improved accuracy and efficiency in the crucial task of yield prediction and allowing the analysis of spatial and temporal variability, ultimately contributing to the sustainable advancement of table grape production practices.

Keywords: Table Grape Production, Artificial Intelligence (AI), Yield Prediction, Unmanned Aerial Vehicle (UAV), Precision Agriculture.

1. Introduction

The use of artificial intelligence (AI) in agriculture is becoming more widespread and has great potential for practical applications. There are studies where AI has been used to predict crop yields, either from an algorithm trained on soil properties or by counting flowers (Papageorgiou et al., 2013; Robson et al., 2017; Sola-Guirado et al., 2017; Wu et al., 2020).

Estimating the production of a farm is an important piece of information for the proper management of a farm, but it involves laborious work that requires time and labour with experience or specific training, which is why many studies have focused on the estimation of production by detecting fruits on the tree. There are examples for apples, cherry, grape, avocado, mango, passion fruit, and several types of fruit at once. This type of prediction of a farm's production can be done with a detection of the trees using aerial images taken from a drone and the subsequent counting of these trees or a detection of the fruit by images taken from the ground (Robson et al., 2017; Häni et al., 2020; Shi et al., 2020; Tu et al., 2020; Wan & Goudos, 2020; Affair et al., 2021; Osco et al., 2021; Yijing et al., 2021; Jintasuttisak et al., 2022; Wiggers et al., 2022).

In the particular case of the grape, there are studies that successfully identify and detect grape bunches by training an algorithm with images taken from the ground, this has the disadvantage that it requires a high time consumption to obtain the images, but it has the advantage of being able to take images in areas with flight restrictions (Sozzi et al., 2022; Wang et al., 2021).

In the province of Alicante, there are emblematic crops of high economic value, such as the Vinalopó bagged table grape with Protected Designation of Origin (PDO). Bagged table grapes are exclusive to the province of Alicante and are distinguished by their unique ripening process: the bagging technique protects the grapes and imparts qualities such as sweetness, thin skin, and natural preservation, allowing for later harvest dates. The economic value of Vinalopó's bagged table grape production amounted to 26 million euros in the 2022 campaign. Accurate harvest prediction for these grapes is crucial, as it can significantly enhance yield management, market planning, and economic returns, further solidifying the crop's importance to the region.

The objective of this work is to obtain an effective and fast methodology to estimate grape production in plots belonging to the Vinalopó bagged table grape PDO. For that, an algorithm for the detection of objects using images in the visible spectrum taken from a drone was trained and compared with the estimate made by the owner of the plot to have a first indication of the goodness of the automated estimate.

2. Materials and Methods

2.1. Description of the experimental site

The plot where the measurements were made is located in the municipality of Monforte del Cid (Alicante) and has an area of 11,230 m^2 The plantation, of the Italia variety, was made in 2008 and is conducted on trellises, with a width of 2.70 m and separation between vines of 1.50 m within the row. The height of the trellis from the ground to the top wire was 1.50 m. All the bunches of grapes were bagged in white paper bags, according to usual practice and complying with the requirements of the PDO of Vinalopó Table Grapes.

2.2. Description of Imaging

The aerial images were taken on July 5, 2022 with an Autel EVO 2 pro model drone (UUC Technology Co., Ltd., Hong Kong), equipped with a visible camera with a 1" CMOS sensor (Sony Group Corporation, Tokyo), adjustable F2.8-F11 aperture capable of 20 MP resolution and video recording in 4K/30 FPS. The flight was made at a height of 10 m automatically, which is the minimum height at which the drone can fly, for greater accuracy in the images. During the flight, the camera was tilted at a 35º angle as it provided a good view of the bags and allowed the largest number of bags to be captured per image, and the drone's flight remained parallel to the crop lines. The flight time of the drone needed to obtain images of the entire plot was 20 minutes, the overlap of these images was 10% and the total images of the plot were 140 images with dimensions of 3840 x 2160 pixels.

2.3. Model Training

The entire process of training the algorithm and labelling images was done with an ASUS computer with Intel CORE i5. The following are the main characteristics of the programs used in image processing and model training.

Makesense is a free cloud-based photo tagging tool that doesn't require any installation. Here some of the images obtained from the bagged grapes that were not going to be used in the final count were added, and each bag was manually labelled with the name "grape". Once the labelling was completed, these images were downloaded in YOLO format, which is the algorithm that was later used to finally perform the object detection. (https://www.makesense.ai/).

YOLO (*You Only Look Once*) is an object detection algorithm that divides images into a grid system. Each cell in the grid is responsible for detecting objects within itself. It is also one of the most famous object detection algorithms due to its speed and accuracy. The algorithms of the YOLO series have developed rapidly in recent years. In 2020, two versions of YOLO appeared successively, YOLO v4 and YOLO v5. At the time of the start of this work, YOLO v5, released in 2020 by Glenn Jocher, was the most advanced object

detection algorithm, based on the YOLO v3 and YOLO v4 algorithms, where the arithmetic set was perfected to improve the detection speed (Redmond et al., 2016; Gai et al., 2021; Zhang et al., 2022).

The first step was to obtain the images from the drone in order to create a database. Once the images were obtained, they were labelled using the *Makesense* application, where each of the bags where the grapes were found was labelled by means of rectangles. A total of 55 images taken at a height of 10 m were labelled, of which 50 images were used for training and 5 images for model validation. The extraction of these images was done in YOLO format.

Once the database was created with our tagged images, two folders were created, one called "*train*" and the other "*val*", these folders were copied to our *Google Colaboratory page*, a Google Research cloud product which allows any user to write and execute arbitrary Python code in the browser, where YOLO v5 was installed.

Finally, in a cell of Google colaboratory, the size of our image was specified as 1024. In an initial test, images were resized to 608, but the results were not as good as with 1024. The number of epochs, that refers to the iterations of algorithm training, was set to a minimum of 135 in this study, as this was the point where the algorithm produced the best results and the cell stopped training the algorithm.

In the precision graphs (Figure 1) it can be seen that for 135 epochs the training has reached its maximum.

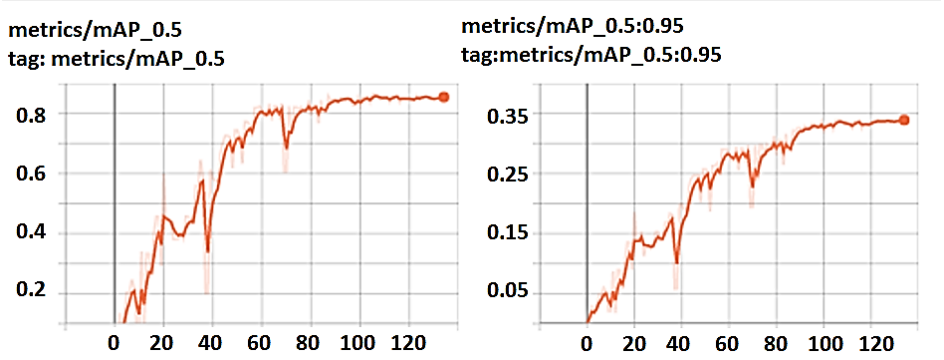

Figure 1. Precision Charts

Once this cell was executed, a series of graphs were obtained where the result of the training was represented and finally a folder was also created with the validation and prediction of the results, giving rise to the trained algorithm ready to be used.

This algorithm was used on the photos of bagged grapes from the commercial plot. The result of the execution of the algorithm was the automatic identification and counting of bags that appeared in each image.

3. Results and Discussion

3.1. Model training Results

To verify the effectiveness of the model, indicators such as accuracy, recall, mAP (mean Average Precision), detection speed, and F1 score were used for evaluation in this study (Yijing et al., 2021).

Precision (Eq. 1) is the ratio of true positive samples among all positive samples predicted by the model. Retrieval (Eq. 2) indicates the proportion of true positive samples predicted by the model to all true positive samples. There is usually a negative correlation between accuracy and recovery, where one increases and the other decreases. From the accuracy and recall values, a PR (Precision-Recall) graph (Figure 2) can be plotted to observe their distribution. To balance the effects of accuracy and retrieval and evaluate a model more holistically, AP (Average Precision) can be entered as a comprehensive evaluation index. The AP value (Eq. 3) is the area under the PR curve, and a higher value means better model performance. The F1 score (Eq. 4) is the reconciled mean of accuracy and recall, taking into account both the accuracy and recall of the classification model.

$$P = \frac{TP}{TP + FP} 100(\%) \quad (1)$$

$$R = \frac{TP}{TP + FN} 100(\%) \quad (2)$$

$$AP = \int_0^1 P(R)dR \quad (3)$$

$$F1 - score = \frac{2 \cdot P \cdot R}{P + R} \quad (4)$$

where TP, FP, and FN are the numbers of true positive cases, false positive cases, and false negative cases respectively (Yijing et al., 2021).

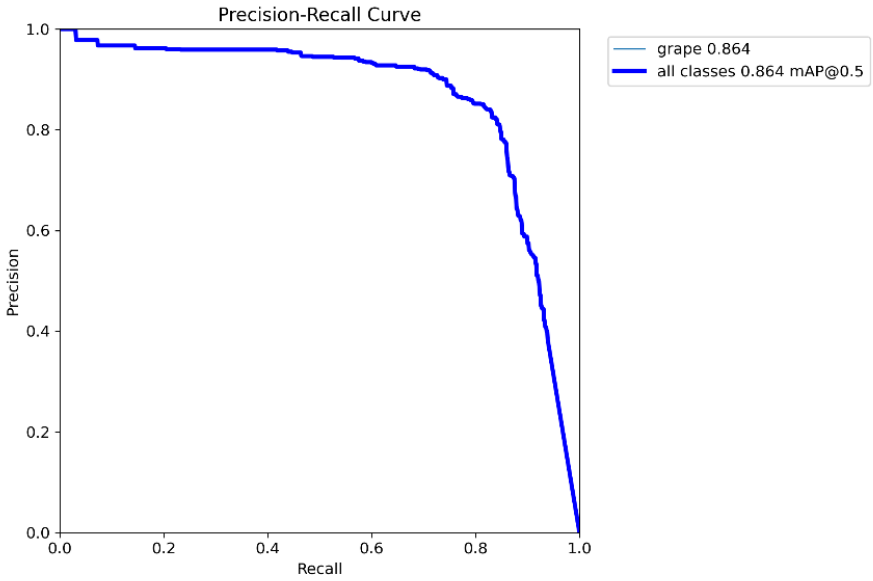

Figure 2. PR Curve

Table 1. Model performance

Detection speed	Precision	Recall	mean Average Precision	F1 score
78,5 ms	80,38%	85,63%	86,40%	83,13%

In this experiment, a confidence threshold of 0.5 is set, and on this basis accuracy, recall, and F1 score are obtained. The test time is represented by the average value of the model's test time in the 55 images analyzed.

The objective of the present work is to quickly and accurately identify the grape bags, so the mAP values (86.63%) and the detection speed (78.5 ms) were used as the main evaluation metrics where, the higher the mAP value, the better the detection result. Finally, high values of accuracy (80.38%), recall (85.63%) and F1 (83.13%) (Table 1) indicate that the model works effectively, giving a high proportion of true positive samples predicted by the model (Wan & Goudos, 2020).

It can be seen that the model achieves very good detection results even when the grape bags overlap each other (Figure 3).

Figure 3. Image taken from 10 meters

3.1.2. Results of bag counting in the test plot.

Prior to counting with the model, the images were cropped crosswise, to avoid overlaps, and longitudinally, so that each trellis row was seen in only one of the images analysed. Table 2 show the results of the automatic count. To estimate the production, the number of bags obtained was multiplied by the average weight per bunch, 1.1 kg/bunch, provided by the DO cooperative of the bagged grapes of Vinalopó. The actual production of the plot was provided by the cooperative itself.

Table 2. Model estimation

Plot	Bag Counting	Harvest Prediction	Farmer's Estimate	Actual production
1	20,520	22,572 kg	15,000 kg	24,064 kg

4. Conclusions

The AI model was able to count the cluster bags in the images taken from the commercial plot within a moderate amount of time. The estimation of the production using the proposed methodology underestimated the actual production of the plot by 6.2%. This underestimation by the model may be due to the non-detection of existing clusters in the images. However, it was much more accurate than the farmer's estimate, which underestimated the harvest by 37.67%. To generalize this methodology, it is necessary to expand the sample to include more plots and conduct additional observation campaigns in order to better assess the model's accuracy.

There are other aspects to consider. To develop a fast and practical method, it is necessary to automate the cropping of images during post-processing. Also, increasing the drone's flight altitude can reduce flight time and expand the dataset for training the model, thereby improving its detection accuracy.

References

Gai, R., Chen, N. & Yuan, H. (2021). A detection algorithm for cherry fruits based on the improved YOLO-v4 model. *Neural Computing and Applications*. https://doi.org/10.1007/s00521-021-06029-z

Häni, N., Roy, P. & Isler, V. (2020). A comparative study of fruit detection and counting methods for yield mapping in apple orchards. *Journal of Field Robotics*, *37*(2). https://doi.org/10.1002/rob.21902

Jintasuttisak, T., Edirisinghe, E. & Elbattay, A. (2022). Deep neural network based date palm tree detection in drone imagery. *Computers and Electronics in Agriculture*, *192*, 106560. https://doi.org/10.1016/J.COMPAG.2021.106560

Osco, L. P., dos Santos de Arruda, M., Gonçalves, D. N., Dias, A., Batistoti, J., de Souza, M., Gomes, F. D. G., Ramos, A. P. M., de Castro Jorge, L. A., Liesenberg, V., Li, J., Ma, L., Marcato, J. & Gonçalves, W. N. (2021). A CNN approach to simultaneously count plants and detect plantation-rows from UAV imagery. *ISPRS Journal of Photogrammetry and Remote Sensing*, *174*, 1–17. https://doi.org/10.1016/j.isprsjprs.2021.01.024

Papageorgiou, E. I., Aggelopoulou, K. D., Gemtos, T. A. & Nanos, G. D. (2013). Yield prediction in apples using Fuzzy Cognitive Map learning approach. *Computers and Electronics in Agriculture*, *91*. https://doi.org/10.1016/j.compag.2012.11.008

Redmon, J., Divvala, S., Girshick, R. & Farhadi, A. (2016). You only look once: Unified, real-time object detection. *Proceedings of the IEEE Computer Society Conference on Computer Vision and Pattern Recognition*, *2016-December*. https://doi.org/10.1109/CVPR.2016.91

Robson, A., Rahman, M. M. & Muir, J. (2017). Using worldview satellite imagery to map yield in avocado (Persea americana): A case study in Bundaberg, Australia. *Remote Sensing*, *9*(12). https://doi.org/10.3390/rs9121223

Shi, R., Li, T. & Yamaguchi, Y. (2020). An attribution-based pruning method for real-time mango detection with YOLO network. *Computers and Electronics in Agriculture*, *169*. https://doi.org/10.1016/j.compag.2020.105214

Sola-Guirado, R., Castillo-Ruiz, F., Jiménez-Jiménez, F., Blanco-Roldan, G., Castro-Garcia, S. & Gil-Ribes, J. (2017). Olive Actual "on Year" Yield Forecast Tool Based on the Tree Canopy Geometry Using UAS Imagery. *Sensors*, *17*(8), 1743. https://doi.org/10.3390/s17081743

Sozzi, M., Cantalamessa, S., Cogato, A., Kayad, A. & Marinello, F. (2022). Automatic Bunch Detection in White Grape Varieties Using YOLOv3, YOLOv4, and YOLOv5 Deep Learning Algorithms. *Agronomy*, *12*(2), 319. https://doi.org/10.3390/agronomy12020319

Tu, S., Pang, J., Liu, H., Zhuang, N., Chen, Y., Zheng, C., Wan, H. & Xue, Y. (2020). Passion fruit detection and counting based on multiple scale faster R-CNN using RGB-D images. *Precision Agriculture*, *21*(5). https://doi.org/10.1007/s11119-020-09709-3

Wan, S. & Goudos, S. (2020). Faster R-CNN for multi-class fruit detection using a robotic vision system. *Computer Networks*, *168*, 107036. https://doi.org/10.1016/j.comnet.2019.107036

Wang, J., Zhang, Z., Luo, L., Zhu, W., Chen, J. & Wang, W. (2021). SwinGD: A Robust Grape Bunch Detection Model Based on Swin Transformer in Complex Vineyard Environment. *Horticulturae*, *7*(11), 492. https://doi.org/10.3390/horticulturae7110492

Wiggers, K. L., Pohlod, C. D., Orlovski, R., Ferreira, R. & Santos, T. A. (2022). Detection and counting of plants via deep learning using images collected by RPA. *Revista Brasileirade Ciencias Agrarias*, *17*(2). https://doi.org/10.5039/AGRARIA.V17I2A1353

Wu, D., Lv, S., Jiang, M. & Song, H. (2020). Using channel pruning-based YOLO v4 deep learning algorithm for the real-time and accurate detection of apple flowers in natural environments. *Computers and Electronics in Agriculture*, *178*, 105742. https://doi.org/10.1016/j.compag.2020.105742

Yijing, W., Yi, Y., Xue-Fen, W., Jian, C. & Xinyun, L. (2021). Fig fruit recognition method based on YOLO v4 deep learning. *ECTI-CON 2021 - 2021 18th International Conference on Electrical Engineering/Electronics, Computer, Telecommunications and Information Technology: Smart Electrical System and Technology, Proceedings*, 303–306. https://doi.org/10.1109/ECTI-CON51831.2021.9454904

Zhang, Y., Guo, Z., Wu, J., Tian, Y., Tang, H. & Guo, X. (2022). Real-Time Vehicle Detection Based on Improved YOLO v5. *Sustainability (Switzerland)*, *14*(19). https://doi.org/10.3390/su141912274

Comparative analysis of deep learning models for a dairy cow face recognition framework

Hao-Ping Chen [a,*], Chen-Yu Liao [a] , Jih-Tay Hsu [b], Ta-Te Lin [a]

[a] Department of Biomechatronics Engineering, National Taiwan University, Taipei, Taiwan, ROC

[b] Department of Animal Science and Technology, National Taiwan University, Taipei, Taiwan, ROC

* Corresponding author. Email: haopingchen1999@gmail.com

Abstract

In dairy farming, cow face recognition stands as a crucial technology, particularly for individualized health monitoring. This approach allows farms to effectively track individual cows' health conditions, such as body temperature and nutritional intake, which directly influence milk production and overall farm efficiency. This study aims to assess and enhance the accuracy and reliability of deep learning models in identifying individual dairy cows. Large-scale cow face images were collected from two dairy farms, comprising 405 unique cows. We built deep learning models utilizing different backbone architectures (Vision Transformer and ResNet) and loss functions (Arcface and Softmax Loss) based on the collected image datasets. Additionally, these models were trained on datasets with varying numbers of dairy cow IDs. This setup allows us to thoroughly investigate how these key factors affect model performance. Our findings indicate that models using ArcFace loss achieved over 99% accuracy in closed-set testing and demonstrated superior performance in open-set testing compared to those using Softmax loss. We compared critical factors such as model backbone architecture and loss functions, observing that these factors significantly influenced model performance. Notably, the choice between Arcface and Softmax loss functions played a crucial role in the precision and effectiveness of dairy cow identification. Overall, our study sheds light on the potential of deep learning models for enhancing the accuracy and reliability of cow face recognition systems in dairy farming, with implications for improved individualized health monitoring and farm management.

Keywords: Cow Face Recognition, Deep Learning, Arcface, Precision Livestock Farming

1. Introduction

In dairy farming, individualized health monitoring is critical for optimizing production efficiency and ensuring animal health condition. Accurate cow identification allows for effective tracking of each cow's health, location, and nutritional intake, directly influencing milk production and overall farm performance. Traditional identification methods like ear tags and RFID have limitations in practice, as they are susceptible to physical damage and require intensive human labor to set up (Awad, 2016). Nowadays, the advent of sophisticated biometric identification techniques has leveraged deep learning to overcome these limitations. The idea that individual cattle have unique facial features that can distinguish them from others in a herd has led to the use of cow faces for identification purposes (Xu et al., 2022; Yao et al., 2019).

The objective of this research is to assess and enhance the accuracy of deep learning models for dairy cow face recognition. We focus on evaluating two prominent backbone architectures, ResNet (He et al., 2016) and Vision Transformer (Dosovitskiy et al., 2020), along with two types of loss functions: Softmax and Additive Angular Margin Loss (ArcFace) (Deng et al., 2019). ArcFace is particularly notable for its capacity to enhance discriminative power by increasing the compactness within classes and the differentiation between classes. Additionally, we investigate how varying the size of the training dataset impacts model's performance.

To thoroughly evaluate the models, we conduct both closed-set and open-set testing. Closed-set testing assesses the model's performance on the same cow IDs used during training, measuring recognition accuracy for known identities. Open-set testing evaluates the model's ability to generalize by using a separate set of cow IDs not seen during training, testing its capacity to recognize new identities. By systematically comparing these configurations, we aim to optimize model selection for practical deployments in dairy farming, ultimately contributing to improved individualized health monitoring and farm management.

2. Materials and Methods

2.1. Dataset Collection and Setup

The dataset comprised face images of lactating Holstein cows, captured via security cameras from two distinct environments in Taiwan. 45 unique cow identities (IDs) were recorded at the National Taiwan University (NTU) Experimental Farm, and the other 360 cow IDs are from a commercial dairy farm, forming a dataset with 405 unique cow IDs. These images are taken in various angles and lighting conditions under natural farm conditions. Each image was then manually labeled with the corresponding cow's ID.

In our dataset of 405 unique cow IDs, we randomly split it into two groups: “train_324” where contains 324 IDs for training models and an additional 81 IDs (unseen_81) reserved exclusively for open-set testing. For each cow, 200 images were utilized for training purposes, while a separate collection of 50 images was used for testing.

2.2. Model Training Experimental Design

2.2.1.Model Architecture and Loss Function

To systematically evaluate and compare the effectiveness of different backbone architectures and loss functions in the context of dairy cow face recognition, we selected two prominent backbone architecture: ResNet50 and Vision Transformer (ViT_b), each configured to produce 512-dimensional embedding feature. These architectures are further trained with two different loss functions: ArcFace loss, known for enhancing the discriminability of features for face recognition tasks, and the traditional Softmax loss, typically used for general classification problems. The training framework is shown below in Figure 1.

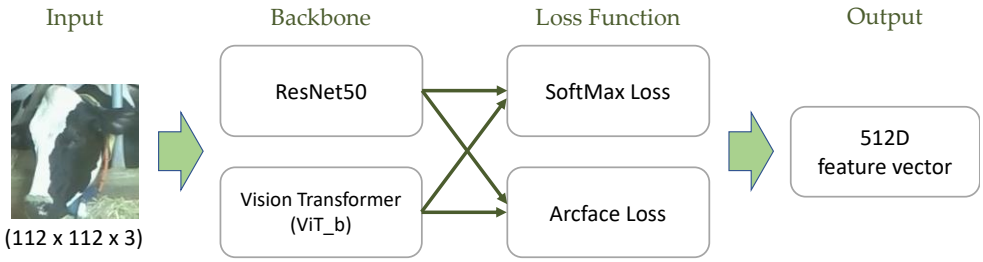

Figure 1. The proposed framework for training cow face recognition models

The comparative analysis encompasses four distinct models resulting from the combination of the mentioned architectures and loss functions. These are:

1. **ResNet50 with ArcFace Loss**
2. **ViT_b with ArcFace Loss**
3. **ResNet50 with Softmax Loss**
4. **ViT_b with Softmax Loss**

All cow face images are resized to112x112 pixels for training and testing, and the models were trained with a batch size of 128 and an initial learning rate of 0.01. The computational setup included two NVIDIA Titan RTX graphics cards with 24 GB memory each, and two NVIDIA RTX A6000 cards with 48 GB memory each.

2.2.2.Training Data Variability

In the open-set scenario, we reduce the number of training cow IDs to explore the influence of training set size on model. This examination helps us understand how variations in the training set affect models’ capability to adapt to entirely new identities. Initially, models trained with 324 cow IDs (train_324) are evaluated against “unseen_81” which was not seen during the training phase. Subsequently, the number of cow IDs used for model training is reduced to 162 (train_162) and then to 81 (train_81), with each configuration tested on the same "unseen_81". This experiment allows us to evaluate how the size of the training dataset (Table 1.) impacts the model's performance in recognizing new individuals.

Table 1. Composition of datasets used in cow face recognition framework

Dataset	Cow IDs	Training images per ID	Testing images per ID
train_324	324	200	50
train_162	162	200	50
train_81	81	200	50
unseen_81	81	-	50

2.3. Identification Strategy and Performance Evaluation

For each testing image, the model extracts a 512-dimensional feature vector. We then calculate an average feature vector for each cow ID, which serves as a representative for that ID. To identify the ID of a new image, we compute the Euclidean distance between its feature vector and the average vectors of all IDs. The ID with the closest average vector is assigned to the image. This straightforward approach uses the minimum distance to determine the most similar ID.

To assess and compare the effectiveness of the models, we utilize accuracy, precision, recall, and F1-score as key performance metrics. Accuracy shows the proportion of total correct predictions. Precision and Recall assess the accuracy of positive predictions and the ability to capture all positive instances, respectively. F1-score combines precision and recall to serve as an overall indicator. Precision, recall, and F1-score are calculated in their weighted versions, meaning they are averaged across all IDs while taking into account the frequency of each ID in the dataset, ensuring a balanced evaluation across all IDs.

Additionally, we use t-SNE to project these 512-dimensional feature vectors onto a 2D plane. This visualization is used to assess how effectively the model can separate different cow IDs, providing insights into the discriminative power of the model.

3. Results and Discussion

3.1. Model Performance Analysis

3.1.1. Closed-set Testing

In this study, four distinct models were trained using the same dataset, which included 324 unique cow IDs: ResNet and Vision Transformer (ViT) each combined with either ArcFace or Softmax loss functions. These models were then evaluated in a closed-set testing scenario, where the model was tested against the same 324 cow IDs used during training. The performance of these models is summarized in Table 2. We can observe that models employing ArcFace loss, regardless of the backbone architecture (ResNet or ViT), consistently achieved accuracies exceeding 99.5%. While models using Softmax loss showed slightly inferior performance.

Table 2. Evaluation index for different model architectures under closed-set scenario.

Models	Accuracy	Precision	Recall	F1-score
ResNet with ArcFace Loss	0.996	0.996	0.996	0.996
ViT with ArcFace Loss	0.995	0.995	0.995	0.995
ResNet with Softmax Loss	0.974	0.978	0.974	0.974
ViT with Softmax Loss	0.992	0.992	0.992	0.992

Furthermore, all testing images are processed through the models to extract 512-dimensional feature vectors, then reduced to 2D using t-SNE. Images from the same cow are plotted in the same color and the t-SNE visualization is shown in Table 3. Each cluster represents feature vectors from multiple testing images of a single cow, illustrating the discriminative capability of the models. We can see that all models generally identify cows effectively. However, the model trained on ResNet combined with Softmax loss showed considerable overlap among some cow IDs. This indicates its limited effectiveness in differentiating cow IDs.

Table 3. t-SNE visualization of 324 cows face feature extracted by different models

Backbone \ Loss	Arcface	Softmax
ResNet	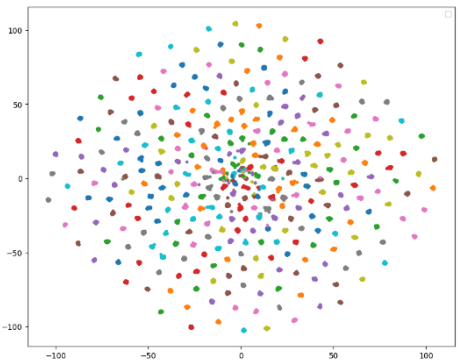	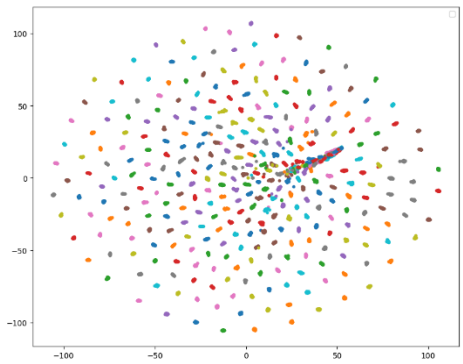
ViT	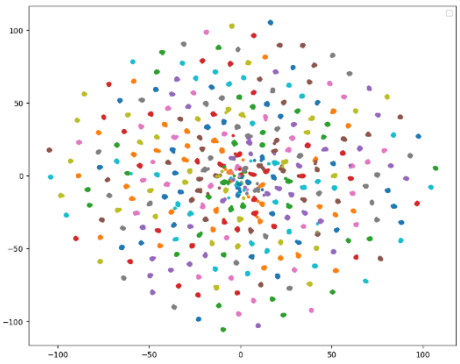	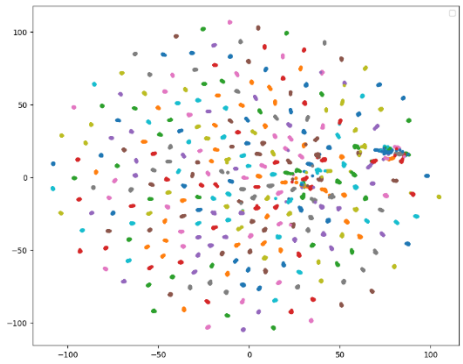

3.1.2. Open-set Testing

In the open-set testing scenario, we focused on assessing the generalization ability of the trained models to recognize cow IDs that were not included in the training dataset. This tests the models' robustness when faced with completely new data, a common challenge in practical applications where dairy cow IDs often change. For this test, the models trained on a dataset of 324 cow IDs were evaluated against an unseen dataset comprising 81 cow IDs ("unseen_81"). The results are shown below in Table 4.

Table 4. Performance for models trained on 324 cows and tested on 81 unseen cow face dataset.

Model	Accuracy	Precision	Recall	F1-score
ResNet with ArcFace Loss	0.969	0.973	0.969	0.970
ViT with ArcFace Loss	0.961	0.962	0.961	0.961
ResNet with Softmax Loss	0.920	0.936	0.920	0.924
ViT with Softmax Loss	0.939	0.946	0.939	0.943

The performance under open-set scenario was slightly lower compared to closed-set testing as expected. The results indicated a clear distinction in performance between the models utilizing ArcFace loss and those using Softmax loss. ArcFace models show better accuracy and consistency in recognizing new cow IDs. This reinforces the effectiveness of ArcFace loss in enhancing model reliability under open-set conditions.

3.2. Training Set Size Impact

In this section, we investigate how varying the size of the training set impacts the performance of our models. We trained models on three different training set sizes (324, 162, and 81 cow IDs) and evaluated their accuracy under open-set conditions(unseen_81). The accuracy of models with different training configuration are shown below in Table 5.

Table 5. Accuracy of models trained with various training size under open-set testing

(a) ResNet

Train set	Arcface	Softmax
train_324	0.969	0.920
train_162	0.956	0.516
train_81	0.931	0.369

(b) ViT

Train set	Arcface	Softmax
train_324	0.961	0.939
train_162	0.947	0.863
train_81	0.926	0.627

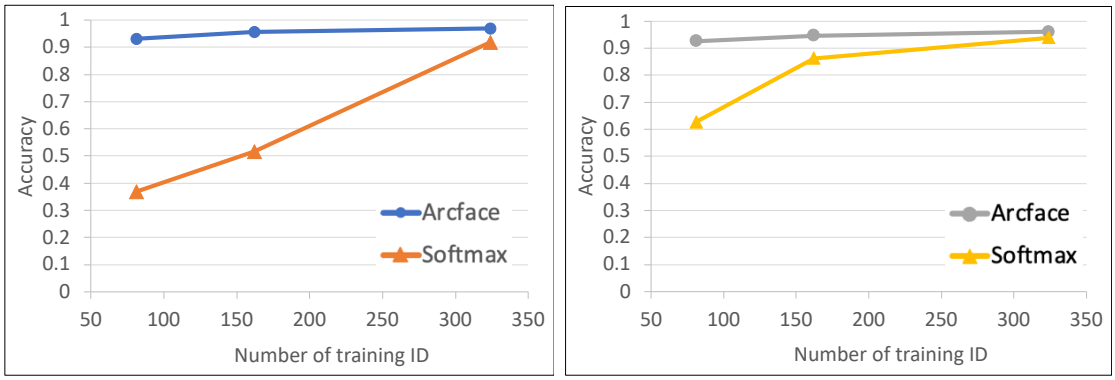

(a) (b)

Figure 2. Accuracy of models trained on different amount of cow IDs (a) ResNet (b)ViT

The results in Figure 2. show a clear trend: as the training set size increases, the accuracy of all models improves, especially those using Softmax loss. This indicates that a larger training set provides more diverse and comprehensive information, allowing the models to better generalize to unseen data. With ArcFace loss, both ResNet and ViT models can achieve a decent accuracy of over 90% even with a quarter or half of the 324 IDs training set. However, models using Softmax loss perform poorly with a training set of only 81 IDs. ResNet with Softmax achieves an insufficient accuracy of 36.9%, making it barely usable in an open-set scenario.

ArcFace loss consistently yields higher accuracy across all training set sizes compared to Softmax loss. In Table 6, it is obvious that Arcface loss has a stronger discriminative power to identify different cows' features. However, there are many overlapping clusters for models utilizing Softmax loss, indicating that Softmax loss function can not effectively differentiate cow individuals especially when the training set size decrease. This suggests that while Softmax loss benefits significantly from larger training sets, ArcFace loss provides robust performance even with smaller datasets.

In conclusion, models utilizing ArcFace loss normally outperform those using Softmax loss, particularly when the training set size is small. This highlights the importance of selecting appropriate loss functions and ensuring adequate training data to achieve reliable and accurate cow face recognition. These findings are critical for optimizing model configurations in practical deployments, where the availability of training data may vary due to the diverse conditions of farm environments.

Table 6. t-SNE visualization of 81 unseen cows' features extracted by ResNet models trained with various amount of cow IDs.

Train size \ Loss	Arcface	Softmax
324 cow IDs	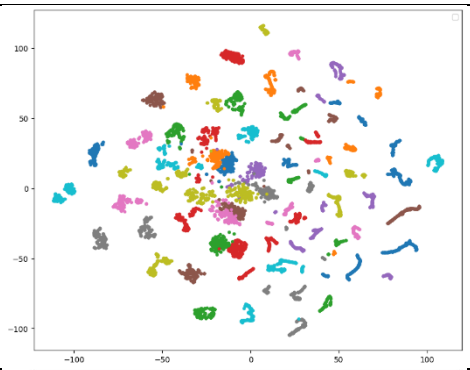	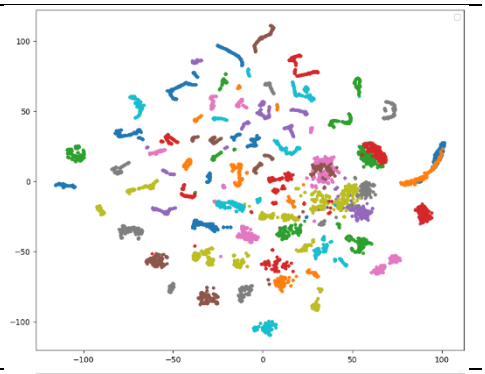
162 cow IDs	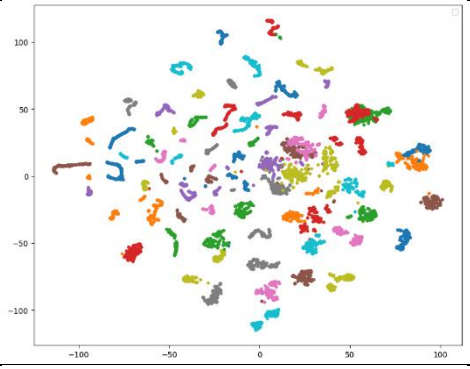	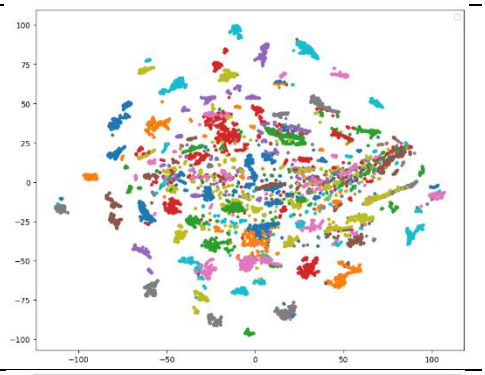
81 cow IDs	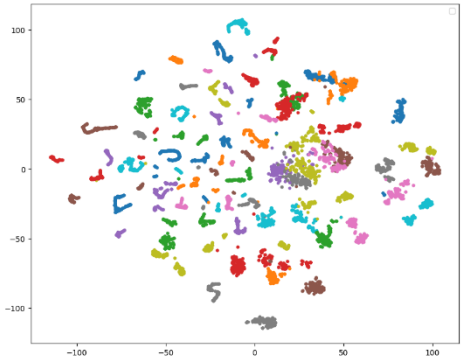	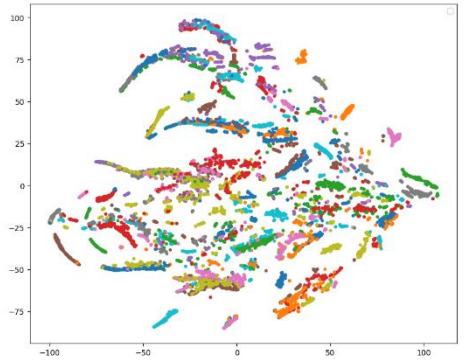

3.3. Error Analysis

We identified common misclassified cow on both ViT and ResNet models with either arcface or softmax loss, trained on train_324 and tested on unseen_81. Table 7 highlights four pairs of cow faces that look very similar and are often confused by models using Softmax loss. In contrast, models using ArcFace loss can separate these pairs more effectively.

Table 7. Sample pairs of cow ID easily misclassified by model using Softmax loss

		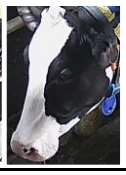	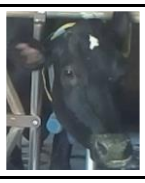					
ID	10906	10813	05	10	15	16	3269	2468

When we evaluated these models, we found several factors contributing to wrong identification. First, cows with similar facial features can confuse the model, especially with Softmax loss. Second, manual labelling which is labor-intensive task, sometimes leads to errors where different cows are mistakenly grouped in the same folder. Lastly, the lack of diverse angles and orientations in the training dataset can lead to incorrect predictions. For instance, a model primarily trained on frontal images may struggle to accurately recognize side views during testing. Additionally, if a cow ID includes both right and left face images in the testing set but they don't appear similar, the model might misidentify them as two different cows.

To address these issues, improving data pre-processing to ensure clean and accurate labels is essential. Expanding the training dataset to include various angles and orientations will enhance the model's ability to recognize cows from different perspectives. Also, proper facial alignment of cow face images could also help mitigate these issues by ensuring that the features are consistent and comparable across different images. Addressing these common errors will lead to more robust and reliable cow face recognition models, advancing precision livestock farming.

4. Conclusions

The study reveals that models utilizing ArcFace loss achieve exceptionally high accuracy, with both ResNet and Vision Transformer (ViT) surpassing 99% accuracy in closed-set testing. ArcFace loss demonstrates better robustness in open-set testing with an accuracy of 96%, outperforming models that use Softmax loss. In addition, the training set size significantly impacts model performance. Models with ArcFace loss maintain competitive accuracy even with smaller training sets. These findings suggest that selecting appropriate loss functions and ensuring sufficient training data are crucial for optimizing model configurations in practical dairy farming deployments. Enhanced cow face recognition systems can significantly benefit individualized health monitoring and farm management. In the future, we recommend improving data pre-processing for accurate labelling, expanding the training dataset to include more cow IDs with various angles to enhance model performance.

Acknowledgements

The data collection process was performed at NTU Experimental Farm and Home Love Farm. We thank many colleagues for their help at farms, in particular the owner of Home Love Farm, Mr. Huang. Without his corporation we can not acquire such a dataset with more than 400 cows. Also Mr. Kao's assistance in NTU Experimental Farm, he is always glad to help us perform different experiments at farm.

References

Andrew, W., Gao, J., Mullan, S., Campbell, N., Dowsey, A. W., & Burghardt, T. (2021). Visual identification of individual Holstein-Friesian cattle via deep metric learning. Computers and Electronics in Agriculture, 185, 106133.

Awad, A. I. (2016). From classical methods to animal biometrics: A review on cattle identification and tracking. Computers and Electronics in Agriculture, 123, 423-435.

Deng, J., Guo, J., Xue, N., & Zafeiriou, S. (2019). Arcface: Additive angular margin loss for deep face recognition. In Proceedings of the IEEE/CVF conference on computer vision and pattern recognition (pp. 4690-4699).

Dosovitskiy, A., Beyer, L., Kolesnikov, A., Weissenborn, D., Zhai, X., Unterthiner, T., ... & Houlsby, N. (2020). An image is worth 16x16 words: Transformers for image recognition at scale. https://doi.org/10.48550/arXiv.2010.11929.

Hossain, M. E., Kabir, M. A., Zheng, L., Swain, D. L., McGrath, S., & Medway, J. (2022). A systematic review of machine learning techniques for cattle identification: Datasets, methods and future directions. Artificial Intelligence in Agriculture, 6, 138-155.

He, K., Zhang, X., Ren, S., & Sun, J. (2016). Deep residual learning for image recognition. In Proceedings of the IEEE conference on computer vision and pattern recognition (pp. 770-778). https://doi.org/10.48550/arXiv.1512.03385.

Xu, B., Wang, W., Guo, L., Chen, G., Li, Y., Cao, Z., & Wu, S. (2022). CattleFaceNet: A cattle face identification approach based on RetinaFace and ArcFace loss. Computers and Electronics in Agriculture, 193, 106675.

Yao, L., Hu, Z., Liu, C., Liu, H., Kuang, Y., & Gao, Y. (2019, May). Cow face detection and recognition based on automatic feature extraction algorithm. In Proceedings of the ACM turing celebration conference-china (pp. 1-5).

Tracking and behavioural analysis of fattening pigs

Pieter-Jan De Temmerman, Jarissa Maselyne*

Technology and Food Science Unit, ILVO (Flanders Research Institute for Agriculture, Fisheries and Food), Merelbeke, Belgium

* Corresponding author. Email: jarissa.maselyne@ilvo.vlaanderen.be

Abstract

Pig behavioural analysis can reveal upcoming and present disease, welfare and productivity problems. For group-housed pigs, individual monitoring of behaviour by applying cameras is challenging due to (1) low farm ceilings, sometimes leading to multiple cameras needed to cover one pen, (2) bad image quality and (3) pigs being (partly) occluded. To tackle these challenges an approach is presented to monitor fattening pig behaviour by processing camera images, detecting and classifying objects, tracking pigs and identifying pigs in tracks using HF (High Frequency) RFID (Radio Frequency Identification) readers on the feeder and drinkers. During one fattening round, 35 fattening pigs were housed in a 4.3m by 9m pen equipped with 3 cameras placed on the ceiling at 2m45 above the floor. Videos were collected for 83 days and frames with sufficient lighting were labelled and used for detection and tracking. From each of the 1475 videos, the first frame was selected, and pigs were labelled using the "segment anything" approach with behaviours: eating, drinking, lying on the side, lying on the belly, sitting with front legs up and standing on four legs. The Yolov8 segmentation model was trained on a 4 to 1 split training and validation dataset keeping the first 33 days as test dataset. Pig identification was performed with HF RFID antennas around the feeder and two drinkers. The segmentation model obtained a detection accuracy of 81.5% and 75.0171% and a classification accuracy of 76% and 72.7% for the validation and test dataset respectively. Yolov8 tracking resulted in raw tracks with an average duration of 51±10 seconds which was increased with post-processing to 1.5±1.1 hours on average for each identified pig on each day. These results demonstrate the feasibility of long-term individual pig tracking using multiple cameras which can be applied to monitor pig health and wellbeing.

Keywords: Multi-object tracking, HF RFID identification, Pig Tracking, Multi camera, Pig Behaviour

1 Introduction

Applications of cameras and computer vision become more common in precision pig farming and are used for pig identification, behaviour analysis and early disease detections (Arulmozhi et al., 2021). Research applications of computer vision are often based on single top view cameras to visualise a complete pen and the analysed datasets are generally small (less than 20 000 frames) due to limitations of processing power and time (Zhou et al., 2023, Zhang et al., 2019, Cowton et al., 2019). Zhou et al. (2023), Zhang et al. (2019) and Cowton et al. (2023) have shown promising results for computer vision applications, with Multi-Object Tracking accuracy of more than 70%. Besides object identification and tracking, Tu et al. (2024) and Lou et al. (2021) have automatically classified the behaviours standing, lying, eating and other of pigs using convolution neural networks and obtained an accuracy of about 90%. Liu et al. (2020) used computer vision for recognition of tail-biting behaviour. Finally, for tracking individual pigs, progress has been made mainly focussing on comparing different detection and tracking models and methods to match track snippets (Zhou et al., 2023, Zhang et al., 2019, Cowton et al., 2019). Van der Zande et al. (2021) reported tracking of individual pigs with top view cameras for almost one hour on average using Yolov3 and SORT for long video sequences of 7h. Melfsen et al. (2023) reported average track lengths of 18 minutes for 5 observation days with video sequences of 12h. In these studies, computer vision models are applied to track about 10 pigs per pen, or up to 20 pigs in 2 pens visualised with a top view camera (Parmiggiani et al., 2023, Liu et al. 2023). Automated identification of individual pigs was reported by several authors (Van der Zande et al., 2021, Kashiha et al., 2013) using external markings on the pigs and using numbered ear tags (Psota et al., 2020). However, manually applying external markings to identify pigs on a regular basis is a time-consuming work, fade over time and numbered ear tags may become illegible.

The aim of the present study is to broaden applicability of camera monitoring of pigs by investigating and providing solutions for four challenges: (1) identifying single pigs, in videos of low (576p) resolution (2) using 3 cameras to allow visualising larger pig pens, (3) tracking 35 pigs in one pen simultaneously, (4) tracking identified pigs for up to 83 consecutive days.

2 Materials and Methods

2.1 Experimental design

The study was based on video material collected by Maselyne et al. (2018) where one pen out of 4 identical pens was visualised with three cameras at variable angles on the ceiling at 2m45 above the floor. The pigs were housed in an automatically ventilated barn at the experimental farm of ILVO (Melle, Belgium). The pen measured 4.3m by 9m with

approximately 40% slatted concrete floor and 60% solid concrete lying area. The two drinkers and one feeder in the pen were equipped with HF RFID antennas (more information in Maselyne et al., 2014, 2016 and 2018). In addition to natural light, artificial lighting was provided from 7:00 to 21:00. For 83 days between 13/1/2015 and 5/4/2015 video material was available. Each pig was given a number which was linked to the two HF RFID tags it carried (one in each ear).

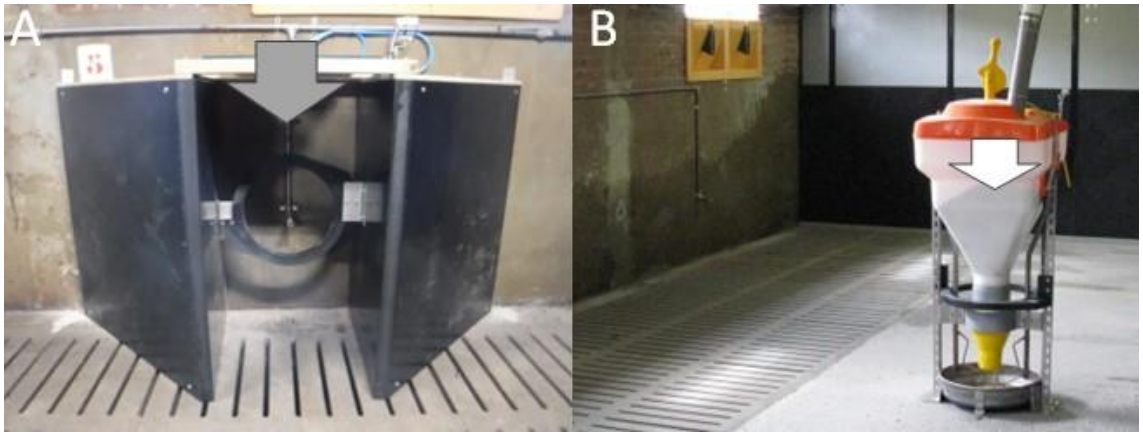

Figure 1: The HF RFID drinker and feeding systems. A: Drinker with HF RFID antenna attached to triangular side walls used for the attachment of the antenna and as separator limiting the registration of pigs that are not drinking. B: Round feeder with an HF RFID antenna to identify eating pigs.

2.2 Image labelling

Video material was available in 3-hour sub-videos recorded at 25 frames per second (fps) and image size of 704 by 576 pixels (576p video). From each of the 1475 videos, the first frame was selected and labelled using the "segment anything" approach available in Labelbox (Labelbox Inc., USA). Pigs were labelled in frames with sufficient lighting resulting in 1145 labelled images and 330 images not labelled (included in the dataset as background images). The labelling of 1145 images resulted in 17417 ground truth annotations with behaviours: eating (1855 instances), drinking (200 instances), lying on the side (7706 instances), lying on the belly (4425 instances), sitting with front legs up (394 instances) and standing on four legs (2837 instances) as illustrated in Figure 2 and 3. The first 33 days were used as test dataset, the 50 remaining days were split into a training (80%) and validation (20%) dataset. The Yolov8 nano segmentation model was trained on a desktop with two A5000 (24gb VRAM) and one RTX 3090 (24GB VRAM) with AMD Ryzen Threadripper PRO 5955WX 16-Cores, 130 GB RAM running Ubuntu 22.04.

Figure 2: Examples of the pig behaviours showing drinking (A), eating (B), lying on the side (C) or belly (D), sitting (E) and standing (F)

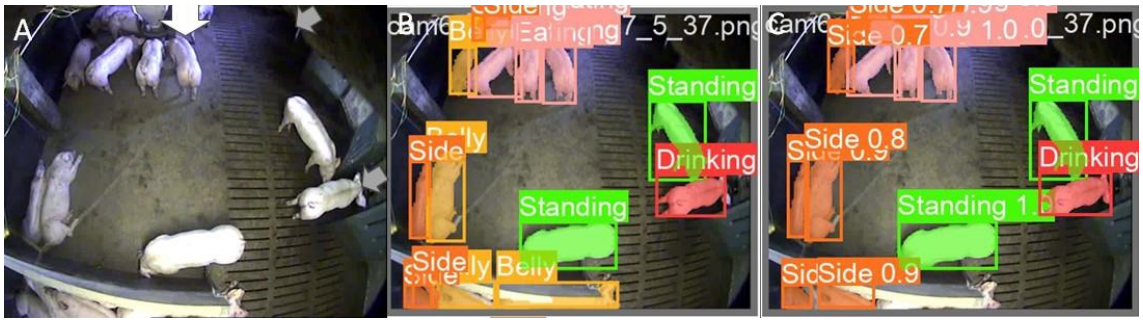

Figure 3: Example of ground truth labelling (B) of the original image (A), with the different labelled behaviours, and predictions by the model (C). Values shown in (C) illustrate the confidence of the segmentation model. Arrows indicates the feeder (white) and two drinkers (grey) in image (A).

2.3 Model inference

On each day five 3-hour videos were concatted in a single 15h video per day while reducing the framespeed to 5 fps. The Yolov8 model was applied to all videos using "yolo track" standard settings (BOTSORT tracker) using 6 parallel sessions split over 3 GPUs in a terminal multiplexer tmux (version 3.2). The predictions of each frame were saved in individual TXT files, zipped, converted in a Pandas dataframe and stored as Feather file format using Jupyter-notebook (Project Jupyter, USA) python (version 3.10.12). Since not all videos started on the same moment and sometimes the camera stopped recording, a timestamp was calculated for each frame in each video using the timestamp in the title of each 3-hour video and the number of frames in each subvideo.

2.4 Linking tracks to each other

To increase the individual track lengths, matching of track snippets was performed. This was obtained by defining 2 regions in each camera view as illustrated in Figure 4 by numbers in grey or white circles. When the track was broken in the main field of view (area 1, 3 or 5), it was assumed that the pig was still visible for the same camera but that the track was lost or the pig was temporarily occluded. When the pig was in region 2 or 4 when its track had stopped or started, this assumption was not made since the pig could have been exiting/entering the area that one camera visualized (see 2.5). Track snippets that started or ended in area 1, 3 or 5 and that have a length of minimum 60 frames were relinked by first determining the last detection (lost track) and first detection (new track) timestamp and ordering lost and new tracks by their timestamp. Tracks were coupled for every lost track followed by a new track; all other tracks were not linked.

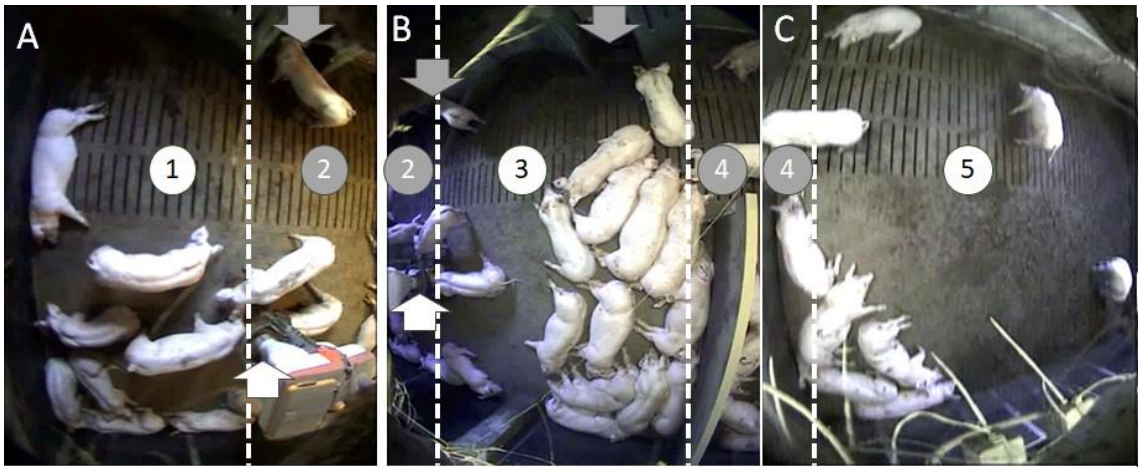

Figure 4: Overview of the camera set-up showing the field of view of the 3 cameras (A, B and C) that cover one pen. Images were rotated to show the overlapping areas side by side. Arrows indicate the feeder (white) and two drinkers (grey) in the pen. Areas 1, 3 and 5 show the area where track snippets are relinked when they are lost and re-occur. Identifications of pigs in area 4 are used to link the pig identifications of feeders and drinkers by camera (B) to pigs tracked with camera (C).

2.5 Multicamera tracking

Cameras (A) and (B) shown in Figure 4 allowed HF RFID identifications of pigs on the feeder and drinkers. Matching of pigs moving from camera (A) to (B) and back was not performed and relied on matching HF RFID identification of tracks. For camera (C) there was no HF RFID antenna, so pigs identified on camera (B) had to be linked to tracks on camera (C) when pigs moved in the area 4 indicated on Figure 4. Matching was performed based on centre of the pig located in area 4, timestamp and "standing" behaviour. Detections in other regions and other behaviour were ignored.

3 Results

3.1 Model inference

The segmentation model achieved a detection accuracy of 81.5% and 75.0% and a classification accuracy of 75.7% and 72.7% on validation and test dataset respectively. The F1 score for the validation and test dataset was 90.5% and

85.7% for drinking and 85.4% and 85.9% for eating respectively as calculated from the confusion matrix (Table 1). The drinking and eating classes were used to link tracks containing eating and/or drinking behaviour with HF RFID identifications with antennas on the drinkers and feeder.

Table 1: Confusion matrix of the trained model on the validation dataset (2389 labels) and test dataset (8899 labels). Showing the ground truth labels (columns) and predictions (rows) for classes drinking (drink), eating (eat), lying on the side or belly, sitting (sit) standing (stand) and background (backg)

		Validation dataset								Test dataset						
		drink	eat	side	belly	sit	stand	backg		drink	eat	side	belly	sit	stand	backg
Predictions	drink	19	0	0	1	0	1	2	drink	81	0	0	4	0	11	6
	eat	0	184	13	5	1	22	20	eat	0	711	42	37	7	67	106
	side	0	5	713	150	11	14	184	side	1	21	2203	559	28	73	743
	belly	1	4	114	314	13	33	112	belly	3	18	480	909	61	159	363
	sit	0	0	4	8	7	3	16	sit	2	0	12	18	20	14	51
	stand	1	13	7	33	16	236	46	stand	6	42	51	85	22	923	156
	backg	0	3	31	18	2	9		backg	0	28	533	171	9	63	

3.2 Identifying pigs in tracks

In total, 780.3 million pig detections and behaviour classifications were recorded during the 83 days with 3 cameras (Figure 5) with an average (± stdev) track length of 51±10 seconds. During the first 30 days pigs stayed together in the area visualised by cameras (A) and (B) occasionally standing in area (C) as illustrated in Figure 5. After 30 days less pigs were observed by camera (A) while more pigs were observed lying down by camera (C). Before linking tracks, 129 million detections (16.6%) were part of tracks containing feeding or drinking that could be coupled with HF RFID identifications. This resulted in on average (± stdev) 1.35 ± 0.55 hours of tracks for each identified pig on each camera (A and B) per day. Four pigs were not tracked until the end of the recording since they were removed from the pen on 9/2, 28/2, 16/3 and 17/3. Performance of the cameras varied, where Camera (B) was the most reliable and each day all frames were recorded. In respect to the frames collected by Camera (B), Camera (C) was offline for on average 12.3% of the frames. Camera (A) was offline for on average 23.6% of the collected frames mainly occurring in month 3 as illustrated in Figure 5.

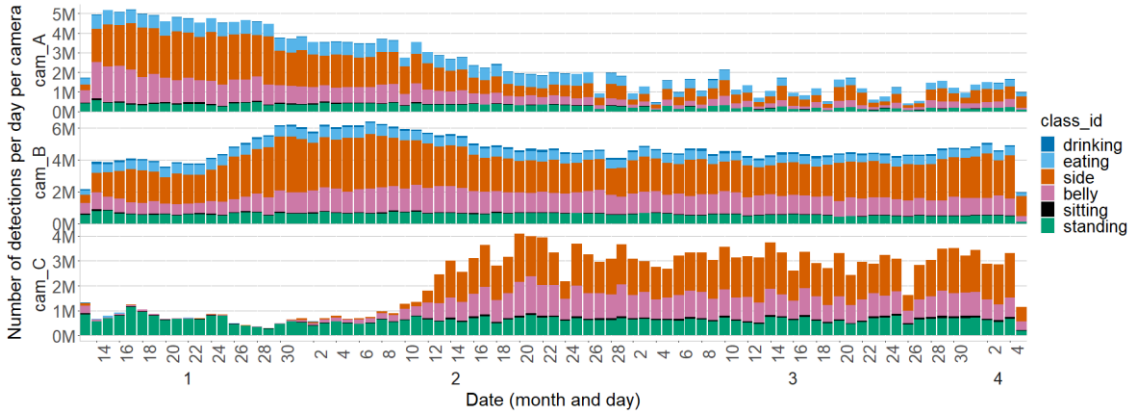

Figure 5: Illustration of the total number of segmentations (in million, M) classified in behaviours drinking, eating, lying on the side and belly, sitting and standing per camera (A, B and C) recorded for 35 pigs for 83 days.

3.3 Linking tracks to each other & multi camera tracking

By coupling tracks lost in areas 1, 3 and 5 (Figure 4) the average rack length of 51±10 seconds increased, and 203.4 million detections (26.0%) were part of tracks containing eating and/or drinking behaviour that were coupled with HF RFID identification on the feeder and drinker. This resulted in on average (± stdev) 2.12 ± 0.84 hours of tracks for each identified pig on each camera (A and B) per day and no tracks for camera (C). Coupling tracks of camera (B) with tracks on camera (C) allowed pig identification in areas without HF RFID antenna and 213.6 million detections (27.3%) were part of tracks containing HF RFID coupled eating and drinking behaviour. This resulted in on average (± stdev) 25 ± 11 minutes of tracks for each identified pig on camera (C) per day (average 1.6 ± 1.1 hours for the three cameras). The maximum number of days tracks were linked to specific pigs was 81 days obtained for 23 pigs. Gaps in the HF RFID and

video recordings (see 3.2) resulted in an average of 67 days of linked tracks for each pig out of the 83 days. The height of these values can be explained by: (1) HF RFID and video recording gaps, (2) including only tracks with a length of at least 60 frames, hereby ignoring more than 50% of the track snippets and (3) when there were multiple pigs on the feeder one HF RFID could have been linked to multiple tracks, while other HF RFID may not have been linked to any track.

The identification of each pig on each day, matching track snippets and matching pigs moving from one area to another allowed visualizing behaviour of single pigs over the 83 days as illustrated in Figure 6 for pig number 109. Figure 7 illustrates the results for pig number 109 on 8/3/2015 moving on 18h33 out of the area visualised by camera (C) area into the area visualised by camera (B) where it was identified on the drinker and feeder. Manual verification of these results is illustrated in Figure 8. First the frame at the timestamp that pig 109 was drinking was determined (Figure 8C), then the pig was manually tracked back and forward in frames to select the frames where the pig was at the feeder (Figure 8D) and moving from Camera (C) to (B) (Figure 8 A, B).

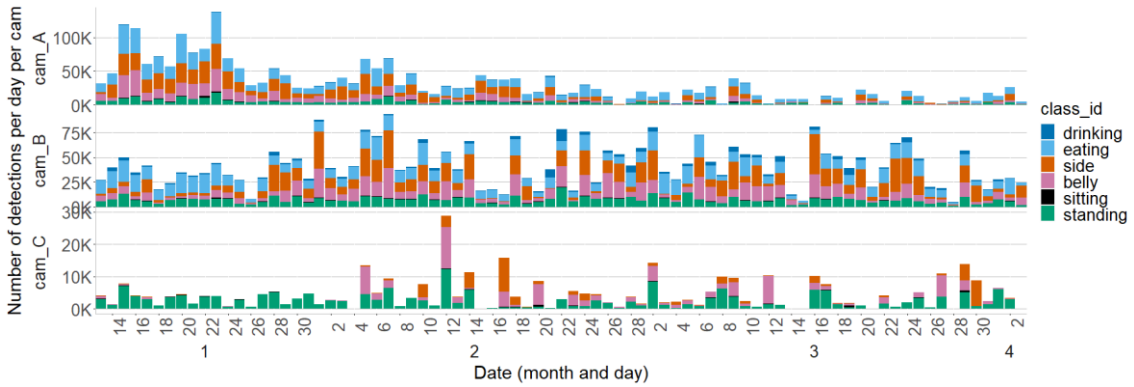

Figure 6: Illustration of the total number of segmentations (in thousands, K) classified in behaviours drinking, eating, lying on the side and belly, sitting and standing per camera (A, B and C) recorded for pig number 109 for 83 days.

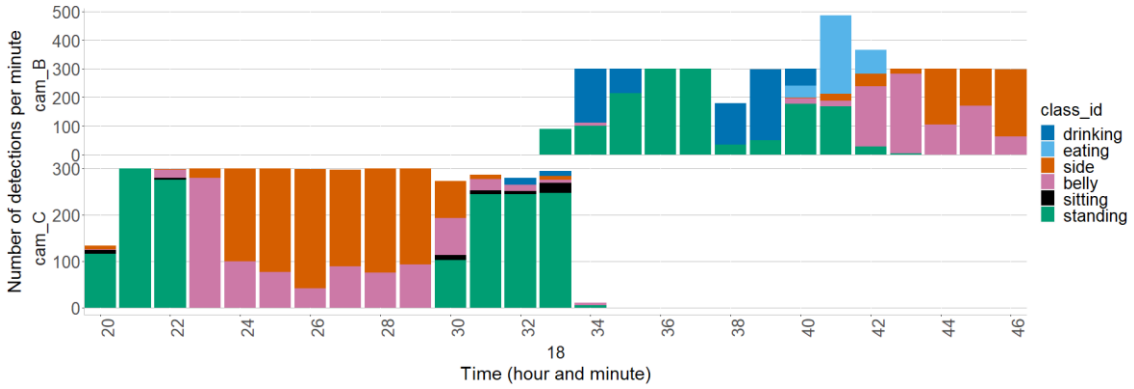

Figure 7: Illustration of the total number of segmentations classified in behaviours drinking, eating, lying on the side and belly, sitting and standing per camera (B and C) recorded between 18h20 and 18h46 on 8/3/2015 for pig number 109 moving from the area visualised by camera (C) to the area visualised by camera (B).

Figure 8: Screenshots illustrating manual verification of the track of pig 109 on 8/3/2015 showing the pig (A, black and white arrow) on camera (cam_C, A) moving into the area visualized by camera (cam_B, B) identified when drinking (C) and identified while eating (D). Images show the drinkers (grey arrows) and feeding station (white arrows) where HF RFID identification can be performed in the area visualised by cam6.

4 Discussion

This paper shows an approach that uses computer vision combined with HF RFID identification to detect, segment, track and classify the behaviour of 35 pigs in a pen. Track snippets were linked within a camera view and between 3 cameras. This way, 27.3% of the segmented objects were classified as drinking, eating, lying on the side and belly, sitting and standing and linked with HF RFID to a specific pig for 83 days.

Tracking the behaviour of pigs for 83 days for on average 2 hours per day is higher than previously reported research showed linking track snippets obtaining tracking of pigs from a couple of minutes to up to 10 hours (Zhang et al., 2019, Zhou et al., 2023, Jaoukaew et al., 2024, Cowton et al., 2019, Van der Zande et al., 2021). Identifying pigs during multiple days was obtained by HF RFID identification with antennas on the feeder and drinker. However more than one track could have been linked to the same pig while no tracks were coupled to other pigs. As reported by Maselyne et al. (2016) multiple simultaneous detections on the drinker can be resolved by blocking access to the drinker for more than one pig.

Segmentation labelling with segment anything in Labelbox allowed segmenting pigs that were close to each other by drawing a rectangle around the object and visually verifying the suggested segment. The “segment anything” approach lowers the labour intensiveness and expensiveness of instance segmentation as indicated by Liu et al. (2023) who suggested oriented bounding boxes as alternative.

Classification of behaviour of each segmented object provided additional filtering possibilities before linking tracks with HF RFID identification and within and between camera field of view connection of track snippets. Matching eating, drinking or standing pigs with each other is faster than techniques that link all detected pigs on each frame as suggested by Jaoukaew et al. (2024) and Parmiggiani et al. (2023). Finally linking lost tracks with new tracks was reduced to its most simple form by filtering objects that are located in a specific area and only keeping one lost track in memory until a new track occurred in the same area.

The video recordings of 576p resolution was low enough to allow yolov8 nano segmentation model training and model inference of videos at native resolution. More recent publications report similarly applied resolutions (Jaoukaew et al., 2024, Zhou et al., 2023), lower resolutions (Van der Zande et al., 2021) or higher resolution recorded videos (1080p), followed by downscaling (Melfsen et al, 2023, Cowton et al., 2019, Zhang et al. 2019). When increasing image size, larger yolov8 models may be necessary to process more inputs, both increasing hardware requirements while slowing inference speed.

By combining videos of 3 cameras, up to 35 pigs could be simultaneously tracked. Which is more than the up to 10 pigs reported by other authors (Cowton et al., 2019, Jaoukaew et al., 2024, Van der Zande et al., 2021, Zhang et al., 2019, Zhou et al., 2023). The camera synchronization by recalculating each frame to the timestamp and using the same computer to collect all data allowed a precision at the second level where all 5 frames recorded during that second were linked to the start of that second. Shifts in synchronization between cameras and HF RFID measurements in the (sub)second level was however not corrected for. Furthermore, to synchronize multiple cameras and HF RFID detections at the (sub)second level a physical process to record the frames at the same time on all cameras may be necessary (Chen et al., 2020).

Future research can focus on using better cameras with infrared recording during the night, longer recording covering the full fattening period, improved tracking and matching algorithms and more complex pig behavioural analysis. The approach is not limited to pigs in a pen, but can be applied to other situations where animals can move from one area to another or situations where additional cameras need to be used to reduce occlusion of animals by walls and other pen infrastructure

5 Conclusions

This paper shows the application of an approach identifying 35 pigs in one pen using HF RFID and track their behaviour for 83 days using three cameras. The results demonstrate that 23 pigs out of 35 could be identified and tracked on 81 out of the 83 days for on average 2 hours out of 15 hours recorded per camera per day. Monitoring changes in behaviour, pig health and wellbeing of individually identified pigs may become possible by expanding the monitoring period to the full fattening duration of pigs.

Acknowledgements

This work has received co-funding from the European Union's Digital Europe Programme under grant agreement Nº 101100622 (project “Testing and Experimentation Facility for Agri-Food - agrifoodTEF”). Views and opinions expressed are however those of the author(s) only and do not necessarily reflect those of the European Union. Neither the European Union nor the granting authority can be held responsible for them.. Special thanks to the technical staff and animal caretakers of ILVO for the work, technical support provided and daily care of the pigs.

References

Arulmozhi, E., Bhujel, A., Moon, B.E., Kim, H.T., 2021. The application of cameras in precision pig farming: An overview for swine-keeping professionals. Animals 11, 2343. https://doi.org/10.3390/ani11082343

Chen, X., Wu, X., Gao, S., Xie, X., Huang, Y., 2020. Synchronization and calibration of a stereo vision system, IEEE. pp. 1–6. https://doi.org/10.1109/IEEECONF38699.2020.9389422

Cowton, J., Kyriazakis, I., Bacardit, J., 2019. Automated individual pig localisation, tracking and behaviour metric extraction using deep learning. IEEE Access 7, 108049–108060. https://doi.org/10.1109/ACCESS.2019.2933060

Jaoukaew, A., Suwansantisuk, W., Kumhom, P., 2024. Robust individual pig tracking. International Journal of Electrical and Computer Engineering (IJECE) 14, 279–293. https://doi.org/10.11591/ijece.v14i1.pp279-293

Kashiha, M., Bahr, C., Ott, S., Moons, C.P.H., Niewold, T.A., Odberg, F.O., Berckmans, D., 2013. Automatic identification of marked pigs in a pen using image pattern recognition. Computers and electronics in agriculture 93, 111–120. https://doi.org/10.1016/j.compag.2013.01.013

Liu, D., Oczak, M., Maschat, K., Baumgartner, J., Pletzer, B., He, D., Norton, T., 2020. A computer vision-based method for spatial-temporal action recognition of tail-biting behaviour in group-housed pigs. Biosystems Engineering, 195, 27-41. https://doi.org/10.1016/j.biosystemseng.2020.04.007

Liu, D., Parmiggiani, A., Psota, E., Fitzgerald, R., Norton, T., 2023. Where's your head at? Detecting the orientation and position of pigs with rotated bounding boxes. Computers and Electronics in Agriculture, 212, 108099. https://doi.org/10.1016/j.compag.2023.108099

Luo, Y., Zeng, Z., Lu, H., Lv, E., 2021. Posture detection of individual pigs based on lightweight convolution neural networks and efficient channel-wise attention. Sensors, 21(24), 8369. https://doi.org/10.3390/s21248369

Maselyne, J., Saeys, W., De Ketelaere, B., Mertens, K., Vangeyte, J., Hessel, E. F., et al., 2014. Validation of a High Frequency Radio Frequency Identification (HF RFID) system for registering feeding patterns of growing-finishing pigs. Computers and Electronics in Agriculture, 102. https://doi.org/10.1016/j.compag.2013.12.015

Maselyne, J., Adriaens, I., Huybrechts, T., De Ketelaere, B., Millet, S., Vangeyte, J., Van Nuffel, A., Saeys, W., 2016. Measuring the drinking behaviour of individual pigs housed in group using radio frequency identification (rfid). Animal 10, 1557–1566. https://doi.org/10.1017/S1751731115000774

Maselyne, J., Van Nuffel, A., Briene, P., Vangeyte, J., De Ketelaere, B., Millet, S., Van den Hof, J., Maes, D., Saeys, W., 2018. Online warning systems for individual fattening pigs based on their feeding pattern. Biosystems engineering 173, 143–156. https://doi.org/10.1016/j.biosystemseng.2017.08.006

Melfsen, A., Lepsien, A., Bosselmann, J., Koschmider, A., Hartung, E., 2023. Describing behavior sequences of fattening pigs using process mining on video data and automated pig behavior recognition. Agriculture 13, 1639. https://doi.org/10.3390/agriculture13081639

Parmiggiani, A., Liu, D., Psota, E., Fitzgerald, R., Norton, T., 2023. Don’t get lost in the crowd: graph convolutional network for online animal tracking in dense groups. Computers and Electronics in Agriculture, 212, 108038. https://doi.org/10.1016/j.compag.2023.108038

Psota, T. E., Schmidt, T., Mote, B., C. Pérez, L., 2020. Long-term tracking of group-housed livestock using keypoint detection and map estimation for individual animal identification. Sensors, 20(13), 3670. https://doi.org/10.3390/s20133670

Tu, S., Cai, Y., Liang, Y., Lei, H., Huang, Y., Liu, H., Xiao, D., 2024. Tracking and monitoring of individual pig behavior based on YOLOv5-Byte. Computers and Electronics in Agriculture, 221, 108997. https://doi.org/10.1016/j.compag.2024.108997

Van der Zande, L.E., Guzhva, O., Rodenburg, T.B., 2021. Individual detection and tracking of group housed pigs in their home pen using computer vision. Frontiers in animal science 2, 669312. https://doi.org/10.3389/fanim.2021.669312

Zhang, L., Gray, H., Ye, X., Collins, L., Allinson, N., 2019. Automatic individual pig detection and tracking in pig farms. Sensors 19, 1188. https://doi.org/10.3390/s19051188

Zhou, H., Chung, S., Kakar, J.K., Kim, S.C., Kim, H., 2023. Pig movement estimation by integrating optical flow with a multi-object tracking model. Sensors 23, 9499. https://doi.org/10.3390/s23239499

Revolutionizing wine production: Innovative traceability solutions and metrology integration for enhanced transparency, efficiency, and sustainability

António Ferreira Dias[1]; Ana Gonçalves[1]; Pedro Moreira[1]; Sérgio Carvalho[1]; Tiago Santos[1]; Vitor Sousa[1]

[a] L.C.S.D - Associação Data CoLAB, Laboratório Colaborativo de Serviços de Inovação Orientados Para Os Dados, Viana do Castelo, Portugal

Email : ana.goncalves@datacolab.pt ; antonio.dias@datacolab.pt; pedro.moreira@datacolab.pt; sergio.carvalho@datacolab.pt; tiago.santos@datacolab.pt; vitor.sousa@datacolab.pt

Abstract

In contemporary markets, wineries face increasing pressure to adopt sustainable and transparent practices to remain competitive and comply with regulatory standards. Regardless, the industry resists generating, using and sharing data.

To address this issue, we developed and proposed a solution to achieve precise data acquisition at critical stages of the winemaking value chain, while enhancing stakeholder value and data transparency. Our technological solution included a mobile application, IoT devices equipped with GPS, humidity, and temperature sensors, and a B2B platform and was implemented as proof-of-concept in the Galicia Wine Region (Spain) during the harvest season of 2023. During harvest, each grape harvesting box was equipped with a unique QR code and a custom-built hardware device. To ensure data accessibility for grape producers, winemakers, and cellar operators, the QR codes allowed box scanning at various stages of the process to collect critical information regarding identifying parameters such as field location, trajectory of transfers, transport conditions and timestamps for winery entry and processing. Additionally, the hardware device guaranteed processes and data legitimacy and reliability. In the post-harvest period, the solution included relevant data, such as total harvest quantities per vineyard, transportation history, grape quantities delivered to each wine cellar, and the alcoholic grade of each delivery in a user-friendly display, assisting stakeholders to improve processes and field management. Such critical data was then automatically transmitted to the regulatory entity to ensure compliance with regulatory standards. Limitations in field implementation included poor network coverage areas, which were addressed through app and hardware adjustments.

Nevertheless, the developed solution has proven effective in the acquisition of the intended data and the value of data-driven operations for all stakeholders in the proof-of-concept stage. Despite the recurrent use and acceptance of these technologies, technological literacy campaigns among end-users in the field are necessary.

Keywords: Traceability, Sustainability, Transparency, Data Collection, Wine Industry

1. Introduction

1.1. State of the art

In contemporary agriculture, traceability serves as the cornerstone for ensuring food safety, maintaining product quality, and fostering transparency across the entire supply chain. A diverse array of technologies and strategies has emerged to fortify traceability, extending from the early stages of production to the hands of the discerning consumer. This meticulous tracking of data throughout the supply chain lays the foundation for informed decision-making and strategic planning. Embracing a data-driven approach empowers producers' adaptability to changing conditions, mitigate risks, and drive innovation in agriculture, ultimately contributing to the resilience and prosperity of the sector. As highlighted by Ouafiq *et al* (2022), effective data management strategies are essential for maximizing the value of agricultural data and leveraging its potential to inform decision-making and drive sustainable practices.

Furthermore, the Internet of Things (IoT) has triggered a shift in the agricultural paradigm by enabling real-time monitoring and data collection, which often provides accurate and reliable insights that are crucial for crop management and to assure compliance with standards and best practices. Najmul Mowla *et al* (2023) aligned with that vision, highlighting the IoT transformative role in enhancing traceability and management across various agricultural domains. Such technologies can optimize processes, reduce waste and enhance traceability of agricultural practices. In parallel, Lu Wang. *et al* (2021) investigated the efficacy of quick response (QR) codes in augmenting traceability within the agricultural supply chain. Their meticulous study elucidated the utility of QR codes in streamlining traceability processes and bolstering efficiency. Scanning a QR code can reveal detailed information about associated processes, such as planting details, farm data, enterprise qualifications, and other relevant information. These features demonstrate how QR codes can be used as a simple and comprehensive traceability solution for all stakeholders involved. Additionally, a recent study by Nino Adamashvili *et al* (2024) explored the fusion of IoT and traceability solutions such as blockchain technologies, specifically for wine traceability, showcasing the transformative potential of these innovations in enhancing reliability and accountability in wine production processes. Collectively, these studies offer a comprehensive panorama of the

technologies and methodologies harnessed in traceability and underscore the pivotal role of technological innovation, regulatory standards, and collaborative efforts between research and industry in safeguarding the safety, quality, and sustainability of agricultural products.
Despite the advancements and potential benefits of data and technology in the wine value chain, there are significant challenges in the widespread adoption of technologies such as IoT for traceability in agriculture, particularly in vineyards. Even though several advantages come from using the previously mentioned technologies and methodologies, grape producers often face difficulties in adapting to technological change, integrating new devices into existing workflows, and overcoming barriers related to technological literacy, as noted by Tardaguila, J. *et al* (2021). Additionally, the initial investment and maintenance costs of these systems may pose financial challenges for smaller wine producers. Overcoming these limitations is a primary goal of the present project. To achieve this, several technologies have been designed and tested to ensure higher implementation acceptance, enhance decision-making support, and provide the authenticity and transparency demanded by markets and regulators.

2. Methods

2.1. Preliminary requirements elicitation

To fulfill the objective of increased transparency, acceptance and data-driven management for the wine sector, a pilot project on traceability, from field to bottle, was initiated in collaboration with an Origin Control regulatory Council from Galicia, along with its wineries and grape producers. The Regulatory Council identified the harvest as a critical stage in the winemaking process, raising significant concerns about the authenticity and conditions of grapes, particularly for wines with a controlled designation of origin. Being the stage with the greatest impact on all stakeholders in the value chain, a proof of concept (POC) specific for the harvest was conducted in August 2023.
The implementation of the detailed solutions was conducted in partnership with three Galician wineries: one cooperative, one medium size, and one family owned. The selection of wineries and grape producers was based on a survey aimed at identifying the most representative entities in the sector, encompassing a spectrum of digital literacy levels and process complexities. The goal was to ensure that the solution was applicable and operational for all participants with diverse digital skill sets.
To ensure a proper POC evaluation, it was essential to understand the main steps in the preparation and execution of a harvest, as well as the critical data that needed to be acquired. A working group consisting of grape producers, winemakers, and regulators was established to define the data flow and data governance model. This model specified when and how data should be collected, establishes data ownership, and distinguishes which data should be shared directly with regulators and which should remain restricted for decision support. With these models established, technological solutions were developed and implemented to ensure accurate data acquisition and management. The solutions implemented during this stage are described in the subsequent chapter.

2.2. System architecture

The developed traceability solution integrated a mobile application (app) and various field, transport, and winery IoT solutions, all connected to a business to business (B2B) platform linked to a blockchain network. These technologies collectively focus on acquiring data throughout the entire process, from field to bottle, providing a comprehensive and accurate overview of the entities, equipment, products, and processes involved in producing a specific wine. In particular, the harvest phase employs a dedicated module of the B2B platform, alongside the mobile app and IoT technologies for transport in order to gather, integrate, and transmit detailed data on grape harvesting and delivering activities. These capabilities ensure (i) the traceability of grape origin for authenticity, (ii) monitor field and transport conditions and (iii) manage the specific information on the reception and integration phases at the winery. With this data, wineries and grape producers can enhance the overall process by optimizing resource management and minimizing the time spent on various bureaucratic procedures. Ultimately, these technologies provide a comprehensive and transparent framework for sharing accurate, reliable, and verifiable data, ensuring compliance with key guidelines on grape collection and processing. Figure 1 displays the overall concept of the system architecture.

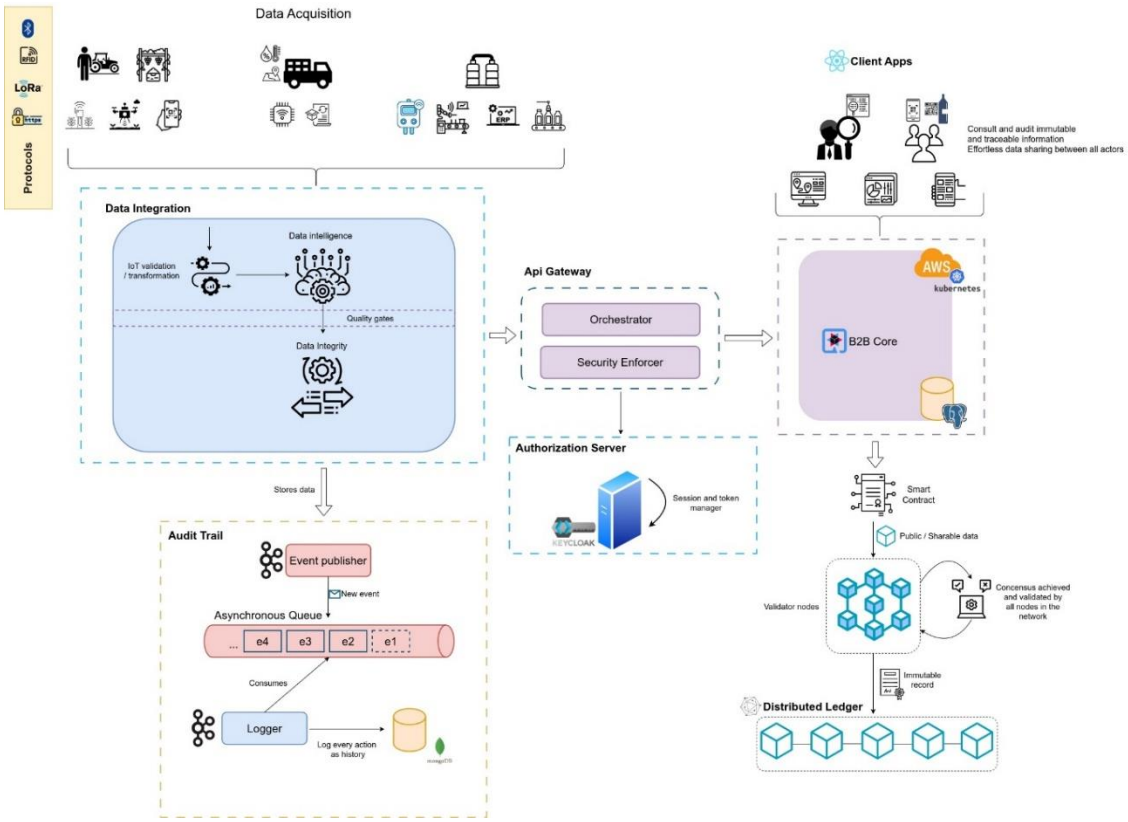

Figure 1 – Main System Architecture for the overall traceability process.

2.2.1.Harvest Modules

2.2.1.1. Data Acquisition Module

The development of specific data acquisition solutions considered two relevant factors: the data to be acquired and the conditions of acquisition and integration. During the harvest season, stakeholders identified critical moments for collecting relevant data on grape picking, transport, reception, and integration. It was vital to document the location and time of grape collection, the estimated weight, and the humidity and temperature conditions to which the grapes were exposed post-harvest. Additionally, tracking the entire transport route and conditions, the time of entry into the winery, the time of integration into the press, the actual weight at entry, and the alcohol content of the grapes delivered was also essential.

The Regulatory Council defines limits for grape producers producing grapes with controlled origins, establishing the *cupo* concept, which signifies the maximum allowable production in kilograms per hectare of registered land. Recognizing this concept was crucial, since the main goal of the POC was to mitigate fraud concerning grapes of uncertain origins.

Moreover, given the harvest's fast-paced and often hectic nature, additional features necessary for the solution had to comprise (i) robustness, (ii) integration of automatic detection functionalities whenever possible and (iii) elementary, user-friendly interfaces or those demanding minimal interaction to reduce the likelihood of failure or fraudulent activities. Consequently, three distinct solutions were conceived for data acquisition from the field to grape processing.

a) Vine DataTracker Mobile app & Webapp

The mobile app acted as a tool for grape producers to manage various aspects of their vineyards registered under the specific denomination of origin. It allowed monitorization of the *cupo* allocation for each vineyard and the cumulative *cupo* for all registered vineyards, as well as registration of grape boxes in the field, which were previously marked with unique QR codes, and tracked the transportation of grapes to the winery. Producers only have access to their own digital area after an individual registration and login.

Developed using React Native for both iOS and Android platforms, the application facilitates the transfer of acquired data to a web-based version managed by the winery, where all app-connected grape producers are managed as a group. This feature enabled the winery to accurately monitor the progress of the grape producer's harvest and oversee its subsequent intake. Furthermore, the Regulatory Council can verify the data to ensure compliance with established guidelines. As mentioned earlier, this solution operated within an ecosystem that

fosters RGPD compliant data sharing among all three stakeholders under the predefined data governance model. Figure 2 display represents the app mobile main interface. This Figure has been changed to protect personal and confidential data.

Figure 2 – Main interfaces of the mobile App used by grapes producers.

As presented in Figure 2, the application provided a straightforward interface, offering grape producers two primary data flows to manage:

1. Grape producers had the option to select the vineyard from a list and choose a work mode between the options "harvest," "transport," or "arrival at winery." If the grape producer selected the harvest mode, the camera for QR code scanning was automatically activated. This mode incorporated several features designed to prevent double scanning and assisted the grape producer in ensuring the operation's accuracy. Furthermore, if the grape producer changed the selected mode to “transport”, the mobile app would automatically initiate more frequent data collection on global positioning system (GPS) coordinates, temperature, and humidity until arrival to the winery.
2. Grape producers could overview previous harvests and trips, along with their associated conditions. This information is listed and can be filtered by date or vineyard for easy access and analysis.

The application additionally stored data, allowing grape producers to view the weight collected from each vineyard and control the achievement of its *cupo*. This data could be correlated to information gathered at the winery, such as the actual delivered weight and the grapes' specific alcoholic grade.

b) Tracking solution for grape transport:

Optionally, the mobile phone App could be linked to a tracking solution by Bluetooth, necessary to provide the Regulatory Council with more precise GPS coordinates for grape collection and transportation, as well as accurate temperature and humidity information. The hardware architecture of the harvest tracking and monitoring solution was based on an Arduino platform, using a combination of sensors and modules for environmental data collection and geolocation. The DHT22 sensor measured temperature and humidity, crucial for ensuring ideal conditions during the transport of grapes. Geographical coordinates were precisely captured by the TinyGPS++ GPS module. Interactions with the system were facilitated by an OLED display controlled by the U8g2lib library, offering a clear and legible interface. Additionally, the solution allowed grape producers to connect via Bluetooth but prevented any other activities from being carried out since access to the producer was blocked and only with their login the work mode could be changed. This ensured the system could only be connected or disconnected by each grape producer, without risk of disruption. Figure 3 displays the described hardware solution.

Figure 3- Tracking device for grape transportation.

For wireless communication, the ArduinoBLE module enabled Bluetooth Low energy (BLE) transmission, essential for transmission of data to the mobile device or B2B platform in real time. The system also included a memory module that allowed data to be stored locally, ensuring the integrity and availability of information even without immediate network connectivity.
The software integrated into the Arduino was programmed to initialize and manage the different sensors and communication modules, as well as handle the algorithms for switching between the different operating modes, from "harvest" to "transport" and "arrival at the winery". As the hardware gathered information from each scanned box of grapes, it saved data connecting location data and environmental conditions to the specific load. As data was recorded and stored in the hardware, in case network conditions were not favorable, it was also possible to continue. This system not only enhanced traceability and ensured compliance with the regulatory council, but also supported future decisions when combined with fertilization data and the application of phytopharmaceuticals. Once assembled the entire production in the field and known where more grapes were produced in the previous year, it would be possible to manage and improve such parameters in the future.
In the context of transportation for this proof of concept, all data was recorded at one-minute intervals. This interval met the project's requirements since most trips ranged from five minutes between small plots of smaller producers to longer journeys of twenty or thirty minutes. It was important to track every trip, shortest or longest, to ensure comprehensive monitoring and among other concerns to mitigate any possibility of fraud during transit. Furthermore, six tracking solutions were employed in the field for each grape grower in order to evaluate the precision of the data and the quality of the implementation.

c) Data acquisition solution in the winery for automatic detection of QR marked boxes.

The final stage of the process involved the utilization of reading equipment for data acquisition and occurred when the grape harvesting boxes arrived at the winery, where their receipt was recorded. Automatic readers were integrated into the reception and washing lines to register the entry of grapes into the winery and press, operating independently without human assistance. The automated scanning of received boxes at the winery was conducted using the Vuquest 3320g Hands-Free Scanner, designed for industrial use due to its resilience to humid environments and susceptibility to impacts. Capable of rapid reading without disrupting the normal operation of grape reception lines, this equipment was connected to a computer to directly transmit the scanned ID, along with the timestamp. This data was subsequently forwarded to the B2B Backend running on AWS cloud infrastructure through a JavaScript configuration and a REST API, where the weight and quality grade of each scanned basket were processed and appended. Both weight and grade units were already under automatic digital control by the winery, requiring only integration into our system. Figure 4 illustrates the implemented schema.

Figure 4 - Automated box scanner employed during the grape reception phase at wineries.

2.2.1.2. Data Integration & Management Module

Data integrity entails accuracy, consistency, and validity of data collected from various sources thorough validation and transformation. Meanwhile, Data intelligence processes focus on extracting valuable insights and patterns from integrated data, including analyzing historical data, business rules, trends, and anomalies. When data enters the system, it undergoes various standardization and transformation processes in backend components to ensure accurate analysis, for example the creation of a unique integration identifier for each event made of both a unique database generated Id and the physical Id scanned from the QR code on each box. Algorithms were employed to provide context to events, ordering and relating them to previously received ones, and assess or filter out duplicate data using key attributes like timestamps and unique identifiers. Gaps in the data were also addressed (e.g., if the unloading event is received before the loading event, the system updated the unloading event to relate to the newly created loading event). Subsequently, the data was verified against industry-specific business rules and the totals for the producer were adjusted accordingly.
The system also incorporated an Audit Trail Module, which recorded all events within the system, regardless of data validation, to support auditing and debugging efforts. These processes occurred in real-time, ensuring that whenever winegrowers initiated any activities, the winery was promptly informed and could use this information to manage its resources and plan receptions accordingly.
All the backend components mentioned in this topic were developed using the Java framework *Quarkus* and deployed using a cloud-native approach via Kubernetes on the AWS Cloud.
The relationship between the entities and the modules explained in 2.2.1.1 and 2.2.1.2 are described in Figure 5.

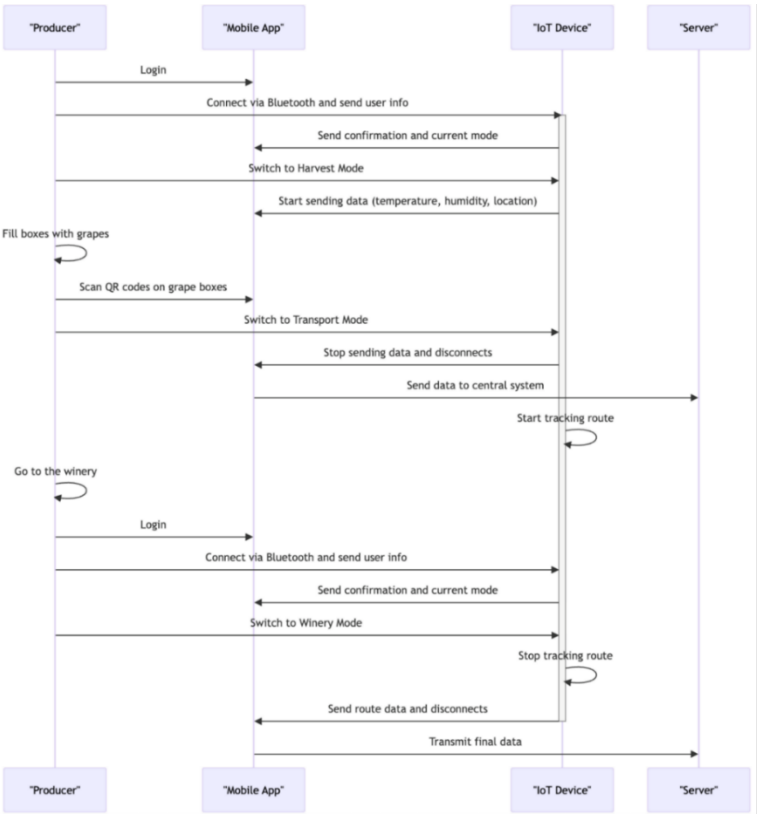

Figure 5 - Process Flow representing the relationships between entities and solution modules.

2.2.1.3. Data Visualization Module

Once the data generated through the solutions has been processed, validated, and integrated, the data and reports were synchronized in the B2B platform and associated client apps, which were part of the full traceability architecture. In addition to the data collected during the harvest, this module of the platform incorporated other pertinent data that would help stakeholders in decision making. It is noteworthy to highlight that should any of the entities edit or delete data, this information remained accessible on the platform, thereby ensuring the integrity of the entire process.

3. Results and Discussion

The field implementation of the solution was well-received by the stakeholders, but it revealed the importance of adjusting several processes. It became clear that grape producers were filling and storing boxes randomly until transportation as well as grouping boxes from different locations in only one vineyard for the transportation to the winery. Those actions created misconceptions in the traceability process but were addressed in the field in the early phases of the harvest. Ensuring grape producers' alignment on the importance of scanning boxes at the exact harvest location by a single responsible person simplified and enhanced the process and guaranteed the acquisition of accurate data. The mobile application's feature of a fixed *cupo* limit for each vineyard also pushed producers to act according to the guidelines of tracing grapes in their origin vineyard. Figure 6 illustrates the enhanced process with the implemented solutions in the harvest and transportation.

Figure 6 – Grape harvesting boxes during grape collection and transportation.

At the end of the harvest, all data acquisition solutions successfully facilitated the scanning and monitoring of each grape-filled box. Specifically, 16 vineyards were harvested, resulting in the tracing of 57,567 kg of grapes within 2,964 marked boxes, over 18 transportations. Figure 7 illustrates an example of a transportation of the traced grapes, providing all stakeholders with a comprehensive traceability report for a delivery to the winery. Sharing this information within the ecosystem in real-time, in accordance with the established data governance model, enhanced confidence in data authenticity for the regulator, reduced bureaucracy, and improved resource management for both the winery and the grape growers. This Figure has been changed to protect personal and confidential data.

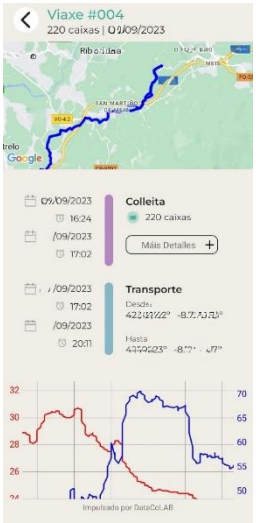

Figure 7 – Example of the obtained traceability for a harvest and transportation.

Given that the mobile app and the built hardware shared common functionalities such as GPS, temperature, and humidity control, the degree of error between the data obtained by the two solutions was investigated. It was found that the GPS error of the hardware tracking solution was only 3 meters and the one from the mobile phone could go up from a few meters to tens of meters when medium network conditions were found. Moreover, the hardware tracking solution provided higher reliability. Still, for this particular use case, both solutions provided consistent results since most grape producers were harvesting under normal 4G network conditions.

Regarding temperature and humidity control, the error of the mobile app was significantly higher as the collected data came from a meteorological API named Open-Meteo. Thus, priority was given to using the hardware alongside the mobile app to obtain more accurate data on grape conditions, particularly when the regulatory council aimed to audit processes.

When delivering grapes to the winery, it was confirmed that only one tracking device was needed instead of multiple sensors on each box. Most of the measurements from several tracking solutions were consistent across all controlled transports in enclosed transportation. This was particularly beneficial for all stakeholders, as installing sensors in each box was not economically or practically feasible.

Additionally, the best position for the tracking hardware was assessed. As shown in Figure 8, by positioning two separate hardware devices in several consignments of 200 boxes – one in the top middle of the boxes and one on the trailer's wall – it was possible to confirm a small but noticed influence of wind and sun on the temperature readings from the hardware positioned on the wall (graph on the left, hardware 1 line, in orange). In contrast, the

humidity during transportation increased when the hardware was positioned in the box at the top middle (graph on the right, hardware 2 line, in green). Both devices were later placed inside grape boxes at the winery after transportation (after 16:08 h) while awaiting reception.

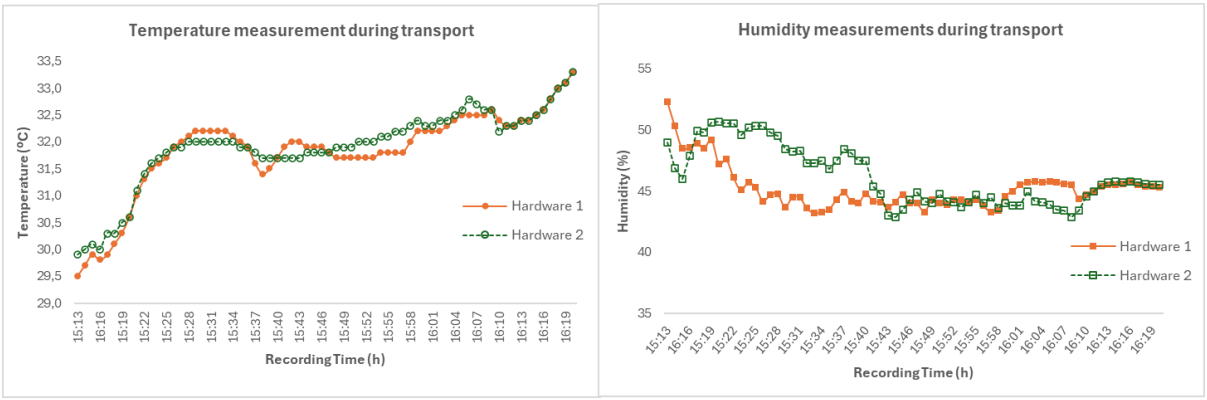

Figure 8- Temperature (left) and humidity (right) readings from two tracking devices during a transportation event.

The preferred tracking hardware position was the top middle in these conditions, since it described the best suited conditions to evaluate compliance with the main guidelines. On the other hand, as anticipated, when tractors were utilized for transportation, the top box exhibited the most significant fluctuations in temperature and humidity conditions due to exposure to the elements. Hence, even in those circumstances, only one tracking device was employed, with priority given to the top boxes for assessment.

The receptions at the winery also proceeded positively, with the QR reader successfully scanning all the boxes entering the reception lines. However, the reader positioned on the cleaning lines encountered more difficulties, due to the large amount of water involved in the process, which created a film over the reader's protective cover, reducing its scanning efficiency. Additionally, the sensor's placement relative to the light had to be considered, as excessive light presence diminished the sensor's detection capability. Nonetheless, good results were achieved with minor adjustments to the sensor's placement.

Once the grape harvest was completed, it was possible to automatically provide a descriptive analysis of the activity. The grape producers who managed to mark the boxes at the exact location of the harvest were able to obtain information about the weight, distribution and alcohol content of the grapes collected. An example of the analysis conducted for a plot of one of the pilot wineries can be found in the Figure 9.

Figure 9- Descriptive analysis on grape production and alcoholic grade per vineyard.

By analysing this dashboard, grape producers can discern areas of higher and lower production, as well as identify extremes in alcohol content. This facilitates an evaluation of vineyard activity, offering valuable insights for optimizing harvest practices and future vineyard management strategies. However, some field errors may be seen in the Figure 9, caused by malpractices in the scanning process. In that case, some baskets were manually moved to the location of the transport, resulting in a cloud of boxes outside of the declared vineyard. For the regulatory

entity, this traceability is still acceptable but under ideal conditions, it would be crucial to collect data precisely where the grapes were harvested to guarantee that the collected insights reflect the reality in place.

3.1. Limitations and opportunities for improvement

One of the faced limitations was the battery life of all devices involved in data acquisition in the field. To address this issue, several strategies were implemented such as (i) optimizing the main program loop to reduce processing time, (ii) implementing sleep techniques to put the device in a low-power state when inactive, (iii) implementing efficient algorithms, and (iv) creating a customized power profile for the device. These measures extended the device's lifespan throughout the entire harvest period and reduced the mobile app's consumption. However, further field tests are necessary to determine its full capacity and understand its potential across different use cases.

Additionally, some efficiently problems were also found while sending environmental data files via BLE to an embedded device with limited resources, such as Arduino. The solution involved developing an efficient file transmission algorithm that divided the file into small data chunks and sent them sequentially through the BLE connection. Additionally, memory and processing optimization techniques were implemented to ensure the device operated efficiently and prevented data loss during file transfers, which proved effective for correct data acquisition. However, more field tests are needed to confirm the solution's scalability.

Finally, the population's literacy level poses an additional challenge to the adoption of such technologies. Although the traceability solution incorporated user-friendly features for the various stakeholders, all activities required initial guidance followed by tailored adjustments to the harvest process. Moreover, stakeholders are unlikely to embrace a technical solution that necessitates changing processes and workflows without fully understanding the potential benefits. Therefore, future data literacy and agriculture 4.0 training initiatives are essential for stakeholders to grasp the value and become more engaged in these types of ecosystems.

4. Conclusion

This project showcased the potential of IoT technologies to enhance traceability and transparency in wine production. By collaborating with wineries and grape producers in Galicia and focusing on critical stages like the harvest, a robust traceability solution was developed that included mobile applications, B2B platforms, Bluetooth-enabled tracking devices, and automated QR code scanners to collect and manage data, ensuring regulatory compliance and better decision-making.

The pilot implementation revealed several key findings. The Bluetooth-enabled tracker provided accurate real-time data on grape harvesting, transport, and reception at the winery. The mobile app solutions for acquiring data, despite higher error rates in poor network areas, effectively collected field data for the harvest activities. Both solutions offered reliable and accurate data, demonstrating to the Regulatory Council the origin of the harvested grapes and the compliance to the key guidelines.

Challenges for broader adoption includes high initial costs and maintenance, as well as varying levels of technological literacy among stakeholders. The provided solutions took these factors into account and reduced the investment burden for all involved parties. However, achieving full adoption will implicate instructions from regulatory bodies, as well as further data literacy initiatives to disclose the full potential of data-driven and transparent organizations.

In conclusion, this project has established a strong foundation for comprehensive traceability in the wine industry, enhancing transparency, resource management, and product authenticity. Continuous refinement of technologies and methodologies, along with stakeholder education and support, will be essential to fully realize the benefits.

References

Ouafiq, E. M., Saadane, R., & Chehri, A. (2022). Data Management and Integration of Low Power Consumption Embedded Devices IoT for Transforming Smart Agriculture into Actionable Knowledge. Agriculture, 12(3), 329. https://doi.org/10.3390/agriculture12030329

Mowla, M. N., Mowla, N., Shah, A. F. M. S., Rabie, K. M., & Shongwe, T. (2023). Internet of Things and Wireless Sensor Networks for Smart Agriculture Applications: A Survey. IEEE Access, 10.1109/ACCESS.2023.3346299

Wang, L., Xu, L., Zheng, Z., Liu, S., Li, X., Cao, L., Li, J., & Sun, C. (2021). Smart Contract-Based Agricultural Food Supply Chain Traceability. *IEEE*

Adamashvili, N., Zhizhilashvili, N., & Tricase, C. (2024). The Integration of the Internet of Things, Artificial Intelligence, and Blockchain Technology for Advancing the Wine Supply Chain. Computers, 13(3), 72. https://doi.org/10.3390/computers13030072

Tardaguila, J., Stoll, M., Gutiérrez, S., Proffitt, T., & Diago, M. P. (2021). Smart applications and digital technologies in viticulture: A review. Smart Agricultural Technology, 1, 100005. https://doi.org/10.1016/j.atech.2021.100005

Estimating air temperature using Modis LST aiming to feed daily evapotranspiration models - Case study for the plain of Arta Greece

Chris Koliopanos [a,*], Ioannis Tsirogiannis [a]

[a] Department of Agriculture, University of Ioannina, Arta, Greece

* Corresponding author. Email: ch.koliopanos@uoi.gr

Abstract

Accurate, site specific, air temperature data is essential for effective agricultural management activities including decisions regarding irrigation water management. Traditional methods rely on dense networks of agro-meteorological stations, which can provide precise measurements but can be costly to install and maintain and may not detect micro-climatic variations adequately. Alternatively, satellite data constitute a promising solution as they offer Land Surface Temperature (LST) measurements at high spatial resolutions. However, challenges such as intermittent availability due to orbital dynamics and cloud coverage hinder its widespread application. In this study, we explore the utilization of satellite derived LST data from the MODIS instrument onboard TERRA and AQUA satellites to estimate air temperature for the plain of Arta, Greece. Historical timeseries from local ground stations are also used and two distinct methodologies, namely empirical estimation and machine learning approach are employed. The empirical method establishes linear regression relationships between satellite-derived LST and ground-based air temperature data, providing foundational equations for conversion. In contrast, the machine learning method utilizes Random Forest Regression (RFR) algorithms, leveraging auxiliary data to predict air temperature parameters such as maximum, minimum, and mean temperatures. By integrating satellite data with ground measurements, this study contributes to enhancement of spatial and temporal coverage of air temperature data, which could provide improved relevant timeseries.

Keywords: agrometeorological stations, reference evapotranspiration, Hargreaves – Samani, irrigation management

1. Introduction

Air temperature (T_{air}) near the Earth's surface is a crucial parameter for numerous research areas and engineering applications. Daily mean air temperature, when combined with humidity, wind speed, and solar radiation, can be used to estimate evapotranspiration (Allen et al., 1998). T_{air} is typically measured directly at weather stations with temperature sensors mounted in shelters located 2 meters above ground (FAO. Doorenbos, 1977). Achieving a high-resolution spatial representation of T_{air} requires a dense meteorological network, as interpolation methods that are used to improve resolution can introduce significant errors and unrepresentative spatial patterns (Willmott et al., 1995). The accuracy of these interpolations is highly dependent on station network density and the scale of spatial and temporal variability (Vogt et al., 1997), (Herrera et al., 2018).

Satellite remote sensing technology offers an attractive means to obtain high-resolution data, though T_{air} is not directly measured by satellites. Several researchers have proposed methods to estimate T_{air} using remote sensing data. Satellite sensors capture signals composed of energy emitted from the Earth's surface, absorbed and re-emitted by the atmosphere, primarily from the contained water vapor. At the surface level, this energy is a mixture of temperatures from vegetation, sunlit and shadowed soil, and artificial objects (Cresswell et al., 1999). The quality of Land Surface Temperature (LST) retrievals is influenced by sensor characteristics, atmospheric conditions, variations in spectral emissivity, surface type heterogeneity, soil moisture, viewing geometry, and assumptions related to the split-window method. Although LST and T_{air} are strongly correlated, differences arise due to factors such as high background temperatures in regions with mixed vegetation and bare soil. LST also depends on the evapotranspiration rate and environmental factors like incoming solar radiation and wind speed. Common methods for estimating T_{air} from LST include:

i) Statistical approaches based on regression techniques, from simple to advanced methods (Viau et al., 1997; Stathopoulou et al., 2006).

ii) Machine learning techniques that account for the non-linearity between predictors and LST, incorporating many explanatory variables in the physical-deterministic modeling. These

techniques include Bayesian-based modeling, support vector regression, Artificial Neural Networks (ANN), and Random Forests (RF) (Kamoutsis et al., 2013; Ovando et al., 2022).

iii) The temperature–vegetation index which is based on the assumption that the top-of-canopy temperature equals the within-canopy temperature for an infinitely thick canopy (Goward et al., 1985).

iv) Physically based energy-balance approaches, which require extensive information (Goward et al., 2002).

This study aims to estimate T_{air} through both statistical analysis and machine learning algorithms, utilizing remote sensing data for LST and ground-measured temperature data from a network of agrometeorological stations. The statistical method employed linear regression, while the machine learning one, used various algorithms, ultimately selecting the Random Forest Regressor. Mayer et al. (2016) and Lezama et al. (2021) highlighted the validation of auxiliary data for evaluating LST and emphasized methods in training, evaluation, and prediction techniques to mitigate overfitting in machine learning models.

2. Materials and Methods

MODIS LST was successfully used to estimate T_{air} for various regions of the world using a variety of methods (Mostovoy et al., 2006; Colombi et al., 2007; Vancutsem et al., 2010; Benali et al., 2012; Zhu et al., 2013; Sohrabinia et al., 2014). In this study, T_{air} within the region of interest was estimated utilizing LST data derived from the thermal bands of the MODIS instrument onboard the TERRA and AQUA satellites. Additionally, a network comprising of six agrometeorological stations served as ground reference. We employed two distinct methods to estimate T_{air}. The first method, termed as “empirical estimation method", relies on establishing a linear regression relationship between satellite-derived and ground-based data. This approach yields a foundational equation for converting LST satellite data into T_{air} values. The second method, known as the “machine learning method”, utilizes regression algorithms within a machine learning framework to develop models that use satellite data to predict T_{air} values, as well as other air temperature parameters such as maximum temperature (T_{max}), minimum temperature (T_{min}), and mean temperature (T_{mean}).

2.1. Study area, data and data preparation.

The plain of Arta (Figure 1) is situated in western Greece within the region of Epirus and spans approximately 450 km^2 (45,000 hectares). The elevation of the area ranges from 2 to 10 m above sea level. Predominant crops include citrus fruits and kiwifruit, with the latter increasingly occupying a larger share of cultivated land. The region features a Mediterranean climate characterized by rainy winters and hot summers. Annual rainfall exceeds 1,000 mm, while two rivers and a rich underground aquifer provide abundant water resources to the plain (Fotia et al., 2021).

The observational dataset for T_{air} was sourced from six weather stations (WS), part of the University of Ioannina agrometeorological network at the region of Epirus (Figure 1, Table 1). These stations consistently record data at 10-minute intervals, spanning from April 2015 to December 2023. All stations measure T_{air} at 2 m height from the ground following WMO provisions for agricultural meteorology (WMO, 2012). Prior analysis, data preparation procedures were executed on the T_{air} dataset from each station. Using the Python Pandas library, missing values were systematically eliminated to ensure data integrity. Furthermore, a comprehensive examination of T_{air} measurements was conducted, involving pair-wise comparisons between stations to identify and subsequently eradicate corrupted values.

MODIS (Moderate Resolution Imaging Spectroradiometer) is a satellite-based sensor mounted on both TERRA and AQUA satellites, capable of capturing data across 36 spectral bands. Notably, MODIS sensors are sensitive to Thermal InfraRed (TIR) radiation, with specific channels, 31 (10.78–11.28 μm) and 32 (11.77–12.27 μm), utilized for LST and cloud temperature measurements. The spatial resolution of MODIS LST data is 1 km. To mitigate atmospheric effects, the split-window algorithm is employed, leveraging the differential absorption of radiation in the atmosphere. In this study, version 6 products (MOD11A1/MYD11A1) from both TERRA and AQUA satellites were utilized, covering the same temporal period as the weather station observations (April 2015 to December 2023). Due to the orbital characteristics of the satellites, LST TERRA and LST AQUA data are available during both day and nighttime,

approximately between 10:00–13:00 and around 21:00–2:00 local time. From the MODIS LST dataset, only values with a "GOOD" quality flag were retained for analysis. Consequently, the final satellite data comprised the day and time of observation, land surface temperature, and satellite view angle, exclusively for measurements with a high-quality confidence rating.

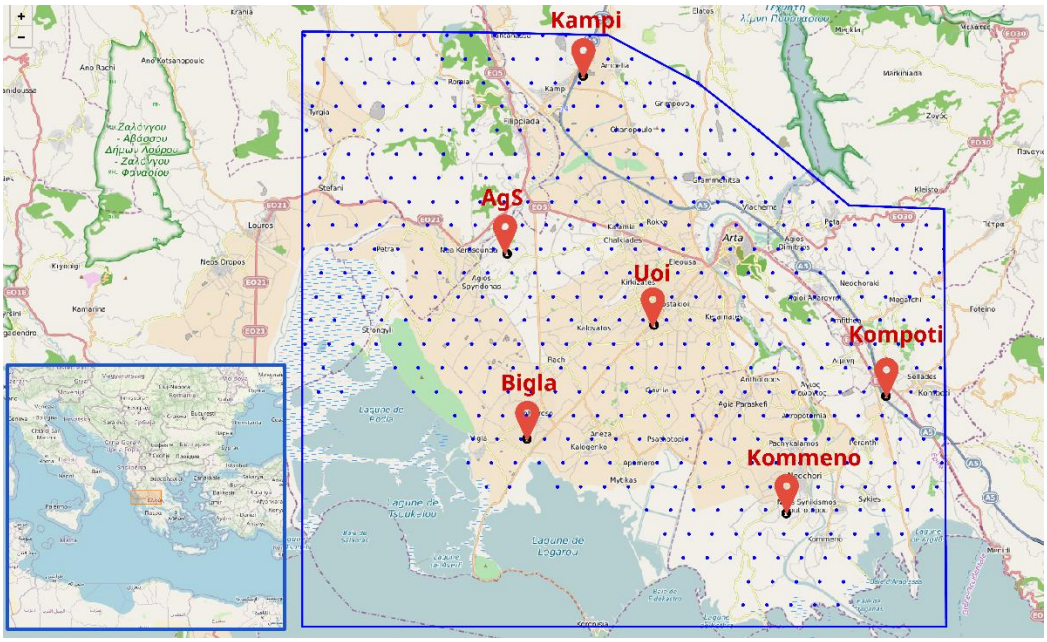

Figure 1. Study area. Plain of Arta with locations of the ground agrometeorological stations.

Table 1. Information (coordinates in WGS84) of agrometeorological weather stations at the plain of Arta, Greece

WS name	WS web page link (Mamasis et al,. 2021)	Longitude	Latitude
UoI	https://system.openhi.net/stations/1402/	39.12208	20.94755
Bigla	https://system.openhi.net/stations/1405/	39.07888	20.88525
AgS	https://system.openhi.net/stations/1403/	39.14904	20.87591
Kampi	https://system.openhi.net/stations/1404/	39.21634	20.91295
Kompoti	https://system.openhi.net/stations/1407/	39.09518	21.06071
Kommeno	https://system.openhi.net/stations/1406/	39.05061	21.01207

The study area was divided into grids of 1 km resolution and covers temporal the period from 2015 to 2023. All MODIS LST data was acquired using Google Earth Engine. Agrometeorological stations served as reference points, and LST values were aggregated within a 1.5 km radius around each station. Additionally, local weather station measurements were collected concurrently with the LST data for comparison purposes.

2.2. Estimation of Air Temperature Using MODIS LST Data and Simple Linear Regression

The first method aims to develop an empirical methodology for estimating air temperature (T_{air}) by utilizing MODIS Land Surface Temperature (LST) data through simple linear regression techniques. Researchers found that corelation between LST and T_{air} for day and night measurements differs. Benali et al. (2012) noted that the integration of MODIS TERRA and AQUA data has great potential for air temperature estimation. Tomlinson et al. (2012) compared the nighttime LST from MODIS with ground-measured air temperature across a conurbation and found that the measured air temperature was always greater than the MODIS-derived LST. Hachem et al. (2012) found that the mean daily LST was more strongly correlated with near-surface air temperature in an area with continuous permafrost when the TERRA/AQUA MODIS

data were combined than when these values were considered separately (TERRA or AQUA, daytime or nighttime). In this study LST data from MODIS was separated into day and nighttime blocks and examined separately.

Simple linear regression analyses were conducted for each agrometeorological station, with LST as the independent variable and T_{air} from ground stations as the dependent variable. This analysis yielded the coefficients 'a' and 'b' of the equation $Y = a \times X + b$, as well as the R^2 value, indicating the goodness of fit of the regression model. A very strong relationship ($0.89 < R^2 < 0.95$) between T_{air} and T_{LST} was observed across all weather stations and for all years. Utilizing the 'a' and 'b' coefficients derived from the regression analysis, a new linear equation was calculated as the mean of all weather stations for all years, termed as "Total MEAN" for both daytime and nighttime.

2.3. T_{air} estimation using MODIS LST and machine learning

Researchers, after considering various algorithms, found that Random Forest Regressor (RFR) algorithm performed very successfully in predicting air temperature (T_{air}) from LST data (Noi et al., 2017). NASA publication refers in using RFR for downscaling land surface temperatures at regional scales (Hutengs and Vohland, 2016). Random Forest is a type of ensemble learning algorithm that works by building multiple decision trees during training and outputting the average prediction of the individual trees. It is an extension of the Random Forest algorithm, which is widely used for both classification and regression tasks. In RFR, multiple decision trees are trained on random subsets of the training data, and predictions are made by aggregating the predictions of all the individual trees. This ensemble approach helps to reduce overfitting and improve the generalization performance of the model. Compared to classical linear regression, RFR can capture more complex relationships between LST and T_{air}. It does not rely on the assumption of linearity and can handle non-linear relationships and interactions between variables more effectively. Additionally, Random Forest models tend to be more robust to outliers and noise in the data.

Utilizing the Random Forest Regressor enables the calculation of air temperature (T_{air}) in various instances, T_{ins} (instant Temp), T_{max}, T_{min}, and T_{mean}. Here's how each instance is typically defined:

1. T_{ins} refers to the instantaneous prediction of air temperature at a specific moment in time based on the corresponding Land Surface Temperature (LST) data.
2. T_{max} represents the maximum predicted air temperature within a given period, such as a day, based on the maximum LST values observed during that day.
3. T_{min} denotes the minimum predicted air temperature within a specific day, derived from the minimum LST values recorded during that day.
4. T_{mean} calculates the average predicted air temperature within a specific day, utilizing the average LST values over the same day.

The data set of each calculation was split in the following way. For the total dataset a random 10% was kept hidden from model. The rest 90% was divided to 70% for train and 30% for testing each model. After the model construction the previous hidden 10% of the data was used to validate the model.

The independent variables (also named as features in ML) are the measured LST values from MODIS instrument, for each location and time of area of interest. Compared with the closed spatial and temporal T_{air} values of all weather stations was feed each model to train it. Auxiliary data, also known as supplementary data or side information, refers to additional information that is not directly part of the primary dataset but can be useful for improving the performance of a machine learning model or providing context for the analysis. Not all Auxiliary data have a considerable importance for a ML model (Meyer et al, 2016; Lezama et al, 2021). In this study we have calculated and tried a various auxiliary data as:

1. The MODIS satellite name (Terra – Aqua)
2. The day of the year (value 1-365)
3. The month of the measurement. (value 1-12)
4. The time of measurements (value AM or PM)
5. The time difference from each day solar noon and solar midnight (values in min).
6. Max MODIS Temp of the day.
7. Min MODIS Temp of the day.
8. Mean MODIS Temp of the day.
9. Distance from coast.

3. Results and Discussion

According to the methodology that was followed, two separated types of products was performed. The first based on the "empirical estimation method" as also a "machine learning method" with the following results.

3.1 Empirical method

Both daytime and nighttime R^2 calculations shown a strong relationship between LST and T_{air} measurements from weather stations. Separate analysis for day and nighttime confirmed that a better correlation at nighttime exists, as shown at Table 2, and mentioned previously at literature. Figure 2 shows a representative example of linear regression (AgS weather station for the year 2023), for both day and nighttime. In Figure 2 it can be observed that at nighttime colour distribution is evenly above and under the regression line in addition to daytime plot where some months are located more at one side. This observation can be further examined at future studies. Other weather stations plots are similar to Figure 2 and a complete set for all years can be found at this GITHUB link as open-source material.

Table 2. R^2 for linear regression analysis and final a, b coefficients.

WS name	R^2 day	R^2 night	Total Mean regression daytime	Total Mean regression nighttime
AgS	0.90 to 0.92	0.90 to 0.97		
Bigla	0.89 to 0.93	0.94 to 0.96		
Kampi	0.92 to 0.94	0.92 to 0.95	a = 0.87 b = 3.67	a = 0.98 b = 1.30
Kommeno	0.90 to 0.95	0.95 to 0.97		
Kompoti	0.91 to 0.93	0.94 to 0.97		
UoI	0.89 to 0.92	0.97 to 0.98		

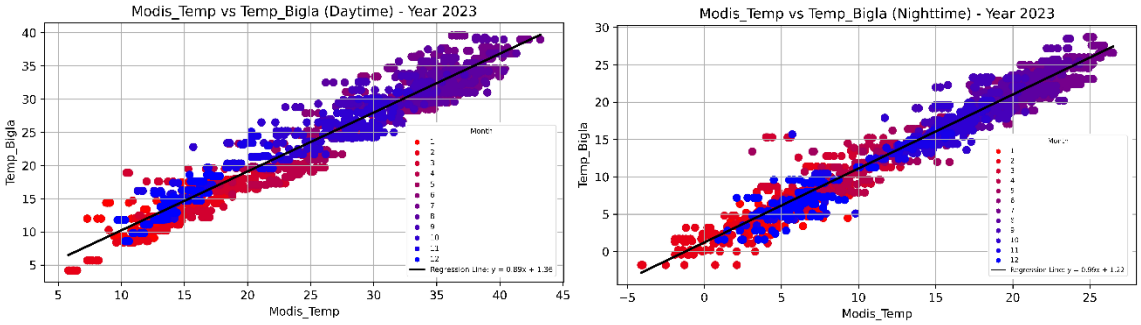

Figure 2. T_{air} to LST regression for daytime – nighttime MODIS data (AgS weather station for the year 2023). Coloured dots, from red to blue, indicates the month of the year.

Utilizing a and b coefficients a mean daytime and mean nighttime linear equations (1 and 2) can be calculated as:

Daytime: $y = 0.87x + 3.67$ (1)

Nighttime: $y = 0.98x + 1.30$ (2)

Both equations can be used as empirical tools representing air temperature distribution in the area of interest and can be compared with interpolation methods in future work.

3.2 Machine learning method

Results from "machine learning method" realises models for T_{ins}, T_{max}, T_{min} and T_{mean} directly from satellite LST data. All models were performed with high R^2 value as Table 3 shows, with the Mean Absolute Error (MAE) to be around to 1-1.5 ^{0}C. Training dataset, except LST data, was also included auxiliary data.

Performing a variety of different training dataset combinations, we concluded to specific auxiliary data that perform better for each model training. For T_{inst} model training, data with the best importance were Modis_Temp (78%) and number of the month (22%). For T_{max}, T_{min} and T_{mean} model training, best importance set were Max_Modis_temp, Min_Modis_temp and Mean_Modis_temp. Number of the month as auxiliary data had a low importance for T_{max}, T_{min} and T_{mean} models. Data importance was found as the following.

1. T_{max} Mean MODIS_Temp (48%), Max MODIS_Temp (28%), Min_MODIS_Temp (22%), month (2%)
2. T_{min} Mean MODIS_Temp (33%), Max MODIS_Temp (18%), Min MODIS_Temp (47%), month (2%)
3. T_{mean} Mean MODIS_Temp (47%), Max MODIS_Temp (21%), Min MODIS_Temp (31%), month (1%)

Finally, auxiliary data of MODIS satellite name (TERRA – AQUA), day of the year, time of measurements, solar noon and solar midnight as distance from coast had no considerable importance to models training.

Table 3. Machine learning models results.

WS name	Tinst	Tmax	Tmin	Tmean
AgS	R^2= 0.9656 RMSE = 1.7348 MAE = 1.2914	R^2= 0.9345 RMSE = 1.8873 MAE = 1.4218	R^2= 0.9447 RMSE = 1.6478 MAE = 1.2216	R^2= 0.9696 RMSE = 1.2899 MAE = 1.0147
Bigla	R^2= 0.9604 RMSE = 1.7209 MAE = 1.2955	R^2= 0.9307 RMSE = 1.8896 MAE = 1.4230	R^2= 0.9516 RMSE = 1.4598 MAE = 1.0995	R^2= 0.9667 RMSE = 1.2971 MAE = 0.9607
Kampi	R^2= 0.9699 RMSE = 1.5561 MAE = 1.1299	R^2= 0.9449 RMSE = 1.8753 MAE = 1.3716	R^2= 0.9375 RMSE = 1.7532 MAE = 1.3084	R^2= 0.9707 RMSE = 1.2939 MAE = 1.0212
Kommeno	R^2= 0.9697 RMSE = 1.6137 MAE = 1.1575	R^2= 0.9270 RMSE = 1.8394 MAE = 1.4634	R^2= 0.9513 RMSE = 1.5798 MAE = 1.1908	R^2= 0.9638 RMSE = 1.3558 MAE = 1.0217
Kompoti	R^2= 0.9681 RMSE = 1.7558 MAE = 1.2836	R^2= 0.9288 RMSE = 2.0226 MAE = 1.5702	R^2= 0.9513 RMSE = 1.5773 MAE = 1.1930	R^2= 0.9648 RMSE = 1.4227 MAE = 1.1005
UoI	R^2= 0.9699 RMSE = 1.5561 MAE = 1.1299	R^2= 0.9360 RMSE = 1.8133 MAE = 1.3610	R^2= 0.9142 RMSE = 1.8227 MAE = 1.9403	R^2= 0.9600 RMSE = 1.4033 MAE = 1.0766

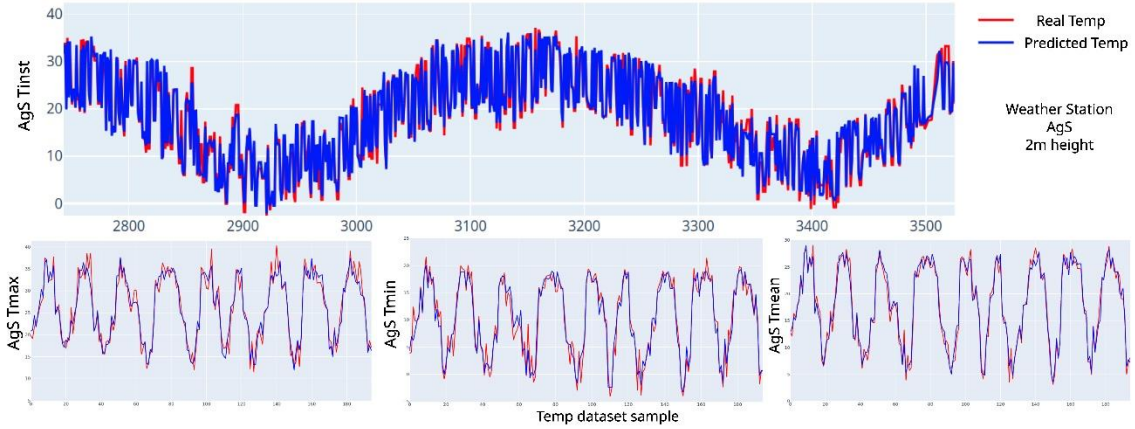

Figure 3. Real and predicted Temp for AgS weather station using ML.

All other weather stations models are similar to Figure 3 and a complete set for all years can be found at this GITHUB link as open-source material.

4. Conclusions

The goal of the presented research was to provide models based on statistical analysis and machine learning algorithms and fed with free remote sensing data for the estimation of T_{air}. To develop these models, data from ground agrometeorological stations were used. For the statistical method linear regression, and for the machine learning one, the Random Forest Regressor were employed respectively. The results from both methods were good and promising for both models. The machine learning approach proved capable of providing various temperature products (T_{ins}, T_{min}, T_{mean} and T_{max}). Several practical uses could arise from this outcome. For example, they could be used to detect problems in ground weather stations measurements, to provide temperature timeseries for any location within an area of interest, and to feed calculations of complex agricultural management parameters, for example the calculation of reference evapotranspiration (ET_o). The latest can be based only in temperature measurements by applying the Hargreaves – Samani approach (Mamasis et al,. 2021) and provide precious information for irrigation water balance models.

References

Allen, R.G., Pereira, L.S., Raes, D., and Smith, M. (1998). Crop Evapotranspiration - Guidelines for Computing Crop Water Requirements. FAO Irrigation and Drainage Paper 56, Rome, Italy

Benali, A., Carvalho, A., Nunes, J., Carvalhais, N., Santos, A. Estimating air surface temperature in Portugal using MODIS LST data. Remote Sens. Environ. 124, 108–121

Colombi, A., De Michele, C., Pepe, M., Rampini, A., 2007. Estimation of daily mean air temperature from MODIS LST in alpine areas. EARSeL eProced, 6, 38–46

Cresswell, M. P., Morse, A. P., Thomson, M. C., & Connor, S. J., 1999. Estimating surface air temperatures, from Meteosat land surface temperatures, using an empirical solar zenith angle model. International Journal of Remote Sensing, 20(6), 1125–1132

Doorenbos, J. 1977 (revised: 1992). Crop Water Requirements. FAO Irrigation and Drainage Paper No 24

Fotia, K., Mehmeti, A., Tsirogiannis, I., Nanos, G., Mamolos, A.P., Malamos, N., Barouchas, P., Todorovic, M., 2021. LCA-Based Environmental Performance of Olive Cultivation in Northwestern Greece: From Rainfed to Irrigated through Conventional and Smart Crop Management Practices. Water 13, no. 14: 1954. https://doi.org/10.3390/w13141954

Goward, S.N., Yongkang Xue, Czajkowski, K.P., 2002. Evaluating land surface moisture conditions from the remotely sensed temperature/vegetation index measurements: An exploration with the simplified simple biosphere model, Remote Sensing of Environment, 79 (2–3), 225-242

Hachem, S., Duguay, C. R., and Allard, M., 2012. Comparison of MODIS-derived land surface temperatures with ground surface and air temperature measurements in continuous permafrost terrain, The Cryosphere, 6, 51–69, https://doi.org/10.5194/tc-6-51-2012

Herrera, S., Kotlarski, S., Soares, P.M., Cardoso, R.M., Jaczewski, A., Gutiérrez, J.M., Maraun, D., 2018. Uncertainty in gridded precipitation products: Influence of station density, interpolation method and grid resolution. 04 October 2018 https://doi.org/10.1002/joc.5878

Hutengs, C, Vohland, M., (2016). Downscaling land surface temperatures at regional scales with random forest regression. Remote Sensing of Environment, 178, 127-141

Kamoutsis, A. P., Matsoukis, A. S., Chronopoulos, K. I., 2013. Air Temperature Estimation by Using Artificial Neural Network Models in the Greater Athens Area, Greece", International Scholarly Research Notices, vol. 2013, Article ID 489350, https://doi.org/10.1155/2013/489350

Lezama Valdes, M., Katurji, M., Meyer, H., 2021.A Machine Learning Based Downscaling Approach to Produce High Spatio-Temporal Resolution Land Surface Temperature of the Antarctic Dry Valleys from MODIS Data.' Remote Sensing 13, No. 22

Mamassis, N., Mazi, K., Dimitriou, E., Kalogeras, D., Malamos, N., Lykoudis, S., Koukouvinos, A, Tsirogiannis, I., Papageorgaki, I., Papadopoulos, A., 2021. OpenHi.net: A Synergistically Built, National-Scale Infrastructure for Monitoring the Surface Waters of Greece. Water 13(19):2779. https://doi.org/10.3390/w13192779

Meyer, H., Katurji, M.; Appelhans, T.; Müller, MU., Nauss, T., Roudier, P., Zawar-Reza, P., 2016. Mapping Daily Air Temperature for Antarctica Based on MODIS LST. Remote Sensing 8 (9)

Mostovoy, G.V., King, R.L., Reddy, K.R., Kakani, V.G., Filippova, M.G., 2006. Statistical estimation of daily maximum and minimum air temperatures from MODIS LST data over the state of Mississippi. GISci. Remote Sens., 43, 78–110

Noi, P.T.; Degener, J.; Kappas, M. Comparison of Multiple Linear Regression, Cubist, 2017. Regression, and Random Forest Algorithms to Estimate Daily Air Surface Temperature from Dynamic Combinations of MODIS LST Data. Remote Sens. 2017, 9, 398. https://doi.org/10.3390/rs9050398

Ovando, G., Sayago, S., Bocco, M., 2022. Developing machine learning models for air temperature estimation using MODIS data. AgriScientia. 39. 15-28. 10.31047/1668.298x.v39.n1.33225

Samuel. N., Goward, G., Cruickshanks, D., Hope, A.S., 1985. Observed relation between thermal emission and reflected spectral radiance of a complex vegetated landscape, Remote Sensing of Environment, 18 (2) 137-146

Sohrabinia, M., Zawar-Reza, P.; Rack, W., 2015. Spatio-temporal analysis of the relationship between LST from MODIS and air temperature in New Zealand. Theor. Appl. Climatol. 2014, 119, 567–583

Stathopoulou, M., Cartalis, C., Chrysoulakis, N., 2006. Using midday surface temperature to estimate cooling degree-days from NOAA-AVHRR thermal infrared data: An application for Athens, Greece, Solar Energy, Volume 80, Issue 4, 414-422

Tomlinson, C.J.; Chapman, L.; Thornes, J.E.; Baker, C.J.; Prieto-Lopez, T., 2012. Comparing night-time satellite land surface temperature from MODIS and ground measured air temperature across a conurbation. Remote Sens. Lett. 2012, 3, 657–666

Vancutsem, C., Ceccato, P.; Dinku, T.; Connor, S.J., 2010. Evaluation of MODIS land surface temperature data to estimate air temperature in different ecosystems over Africa. Remote Sens. Environ., 114, 449–465.

Viau, A., Paquet, F., 1997. Mapping Regional Air Temperature Fields Using Satellite Derived Surface Skin Temperatures. Int. Journal of Climatology 17, 1559-1579.

Vogt, J.; Viau, A.A.; Paquet, F., 1997 Mapping regional air temperature fields using satellite maximum, minimum and mean air temp. Int. J. Clim. 1997, 17, 1559–1579

Willmott, Cort, J., Robeson S.M., 1995. "CLIMATOLOGICALLY AIDED INTERPOLATION (CAI) OF TERRESTRIAL AIR TEMPERATURE." International Journal of Climatology 15: 221-229.

WMO, World Meteorological Organisation, 2012. Guide to Agricultural Meteorological Practices No. 134 https://library.wmo.int/records/item/35689-guide-to-agricultural-meteorological-practices

Zhu, W., Lü, A., Jia, S., 2013. Estimation of daily maximum and minimum air temperature using MODIS land surface temperature products. Remote Sens. Environ. 130, 62–73

Improving dairy cow feed intake monitoring: Insights from depth camera imaging

Marjaneh Taghavi *, Tomas Izquierdo, István Fodor
Wageningen University & Research, P.O. Box 338, 6700 AH Wageningen, the Netherlands
* Marjaneh.taghavi@wur.nl

Abstract

Monitoring individual dairy cow feed intake is crucial for optimizing feed efficiency and detecting health events. In this study, we investigated the effects of camera-to-feed distance and time of day on the relationship between estimated feed volume and measured feed weight. An Intel® RealSense D455 camera was positioned above a heap of feed (Total Mixed Ration) and was paired with a digital scale to measure feed weight. RGB-depth images of the feed were taken across a range of 0.5-20 kg, with increments of 0.5 kg, at two different heights (1 m and 2.6 m), and under varying light conditions (morning and afternoon). Each setup captured five different shapes for every feed weight, resulting in a total collection of 800 RGB-depth images. The Segment Anything deep learning model was used to segment the feed on each RGB image and applied the resulting masks to the depth images. After generating a point cloud of the segmented feed, a Delaunay 2.5D algorithm was used to create a mesh, and feed volume was calculated by summing up the triangle volumes within the mesh. We used a linear model to study the relationship of estimated feed volume with feed weight, accounting for camera-to-feed distance and light conditions. We observed an interaction between the light condition and weight ($P=0.003$), with estimated feed volume increasing by 8.4% and 6.7% with every 10% increase in feed weight in the morning and afternoon, respectively. Camera-to-feed distance was also significantly related to estimated feed volume ($P<0.001$). The linear model explained 66.5% of volume variance at 1 m distance, and only 38.1% at 2.6 m. Therefore, models predicting feed intake of individual cows using RGB-depth recordings as input should take into account distance from the camera and light conditions. These models would mark an important step towards more sustainable dairy farming.

Keywords: Feed intake, Computer vision, Precision dairy farming

1. Introduction

Individual dairy cow feed intake is closely related to the feed efficiency, feeding behaviour and health status of cows. Changes in feeding behaviour are one of the key indicators to predict disease (i.e. mastitis, ketosis, and lameness) in dairy cows (González et al., 2008), with diseased cows generally eating less than healthy cows. In addition, individual feed efficiency, which is an important trait for more sustainable dairy farming, can be estimated based on the feed consumption, together with milk production and composition data (Johansen et al., 2018). Therefore, developing an automated system to monitor individual feed intake in dairy cows would reduce the amount of feed needed to produce a unit of milk, which would reduce land use and improve dairy herd health management at the same time. Moreover, individual feed intake information could also support decision-making on the dairy farms, as feed costs represent the main operating cost for dairy farmers (Buza et al., 2014).

Several approaches and tools have been developed to monitor feed intake and feeding behaviour. For example, using the Ultra-Wide Band (UWB) system the time spent in the feeder zone can be estimated, however, it cannot specify when the animal is eating (Shane et al. 2016). Pressure sensors can also be used to monitor chewing movement by attaching them to dairy cows (Ruuska et al., 2016). These sensors give a good monitoring performance, but they are only suitable for research due to high cost. A roughage intake control bin is a common method for measuring the feed quantity provided and feed intake of individual cows in research (Bach et al., 2004; Chapinal et al., 2007; DeVries et al., 2003; Ferris et al., 2006; Krawczel et al., 2012). However, these bins are not applicable on commercial farms due to their high investment costs and the frequent cleaning required.

A more affordable option to monitor feed intake in practice would be to use a computer vision-based approach to measure feed intake. Some computer vision-based systems determine a linear correlation between the image features, e.g. the volume of a feed pile, and the pile's actual weight. The weight of the feed pile can be calculated by using depth cameras by calculating the volume of point clouds received directly from the camera (Borchersen et al., 2018; Lassen et al., 2018; Shelley et al., 2016).

A Time-of-Flight (ToF) camera measures the distance from the camera to an object by emitting and

sensing infrared light. The camera only obtains useful images when shielded from sunlight, as sunlight naturally contains infrared light. Studies have found it difficult to achieve reliable results due to sunlight interference with the cameras' infrared sensors (Borchersen et al., 2018). These methods can be impractical on a commercial farm mainly because of their sensitivity to sunlight. A computer vision approach based on deep learning algorithms has been studied and investigated in recent years. The deep learning model learns different features and representations of image data. (Bezen et al., 2020) investigated the use of RGB and depth images with the use of computer vision and with light variation conditions. They propose that using the differences between two feed pile images, subtracting the image of the pile after the meal from the image of it before the meal can decrease the final error prediction; however, the proposed method was developed for short distances, which is not practical in a barn.

In this study, we investigated the effects of camera-to-feed distance and light conditions on the relationship of estimated feed volume with feed weight, using RGB-depth images. More information on these effects can facilitate the development of accurate feed intake prediction models on dairy farms, using computer vision.

2. Materials and Methods

2.1. Data collection and workflow

An Intel® RealSenseTM D455 depth camera was installed at the Dairy Campus research facility of Wageningen University and Research (Leeuwarden, the Netherlands). The camera was placed on a frame above a pile of feed (Total Mixed Ration), and the feed weight was measured using a digital scale with 0.1 kg accuracy. RGB-depth images of the feed were captured within a 0.5-20 kg range (with 0.5 kg increments) at two different vertical distances from the camera (1 m and 2.6 m), under two light conditions (morning and afternoon light) in the barn. Five different shapes were captured for each feed weight in each setup. In total, 800 RGB-depth images were collected. An example of one weight (i.e. 6kg) with five different shapes is shown in Figure 1.

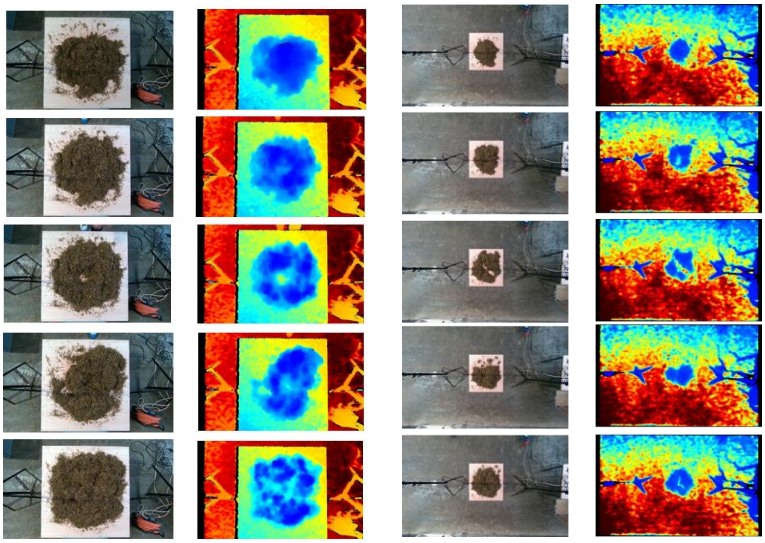

(a) (b)

Figure 1. RGB and depth images of five distinct shapes within a 6 kg feed pile captured at (a) a distance of 1 meter and (b) a distance of 2.6 meters.

2.2. Image pre-processing and segmentation

The orientation of the wooden frame placed below the feed pile was detected for each setup and applied automatically to all images within the set to crop the RGB and depth images. An open-source deep learning algorithm for image segmentation, "Segment Anything", was used to segment the feed pile within the RGB image (Kirillov et al. 2023). Two points on the feed were randomly selected in the image for each distance

(1m, 2.6m) and used as input with the RGB image to the Segment Anything model. Image pre-processing and segmentation is shown in Figure 2.

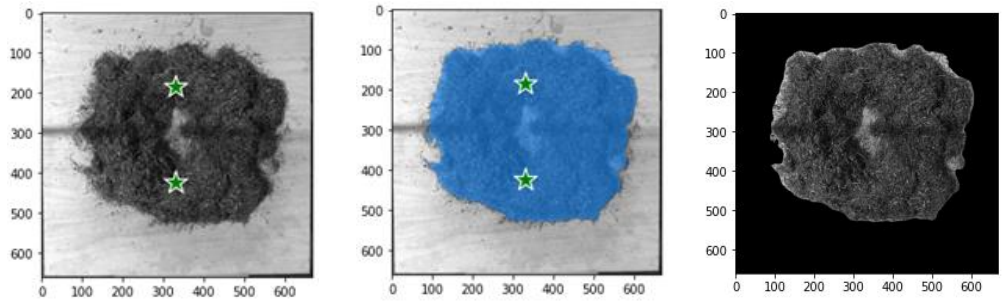

(a) (b) (c)

Figure 2. Feed segmentation. (a) Cropped RGB image with two points as inputs of segmentation model (b) Segmented mask output from the segmentation model, (c) Segmented feed

2.3. Point cloud and Mesh creation

The RGB and depth images were used to create a point cloud with Open3D, a Python library for 3D data processing (Zhou et al., 2018). To compute the volume from the point cloud, a mesh is needed. To transition from the point cloud to the mesh, a surface reconstruction algorithm called Delaunay 2.5D was used (Bobach et al., 2007). In a point cloud, each point has associated 3D coordinates (x, y, z), obtained from the depth sensor. However, the points themselves do not inherently represent a surface; they are merely scattered points in space. The Delaunay 2.5D surface reconstruction method involved several steps: first, the point cloud data was projected onto the XY plane by removing the Z-coordinate, creating a set of 2D points. Next, the Delaunay triangulation algorithm was applied to these 2D points to generate a set of triangles covering the 2D surface. Then, each triangle's 2D vertices were replaced with their corresponding 3D vertices from the original point cloud, extending the triangulation into 3D space while preserving connectivity. Finally, the resulting set of triangles with 3D vertices represented the surface reconstruction of the original point cloud, achieving a Delaunay 2.5D approach for surface reconstruction. Figure 3 shows an example of a point cloud and the reconstructed mesh.

(a) (b)

Figure 3. An example of (a) point cloud and (b) mesh creation for 3 kilogram feed, captured from 1 m at morning light.

2.4 Statistical analysis

To test the relationship of the estimated feed volume with camera-to-feed distance and light conditions, a linear model was fitted to the data with log-transformed feed volume as the dependent variable, and log-transformed feed weight, camera-to-feed distance (1 m vs. 2.6 m), light condition (morning vs. afternoon), and all two-way interactions as explanatory variables. Observations with standardized residuals greater than 2 in absolute value were removed as outliers. After removing the non-significant interactions ($P>0.05$), the final model included log-transformed feed weight, camera-to-feed distance, light condition, and the interaction between log-transformed feed weight and light as explanatory variables. Statistical analyses were

performed in R version 4.3.1 (R Core Team, 2023). The level of significance was set to P≤0.05.

3. Results and Discussion

3.1. Feed volume estimation

The estimated feed volumes from different camera-to-feed distances and light conditions are shown in Figure 4. We observed more variation in the volumes within weight estimated from 2.6 meters, as expected, because of the lower accuracy of the depth images and the incomplete point clouds as a result.

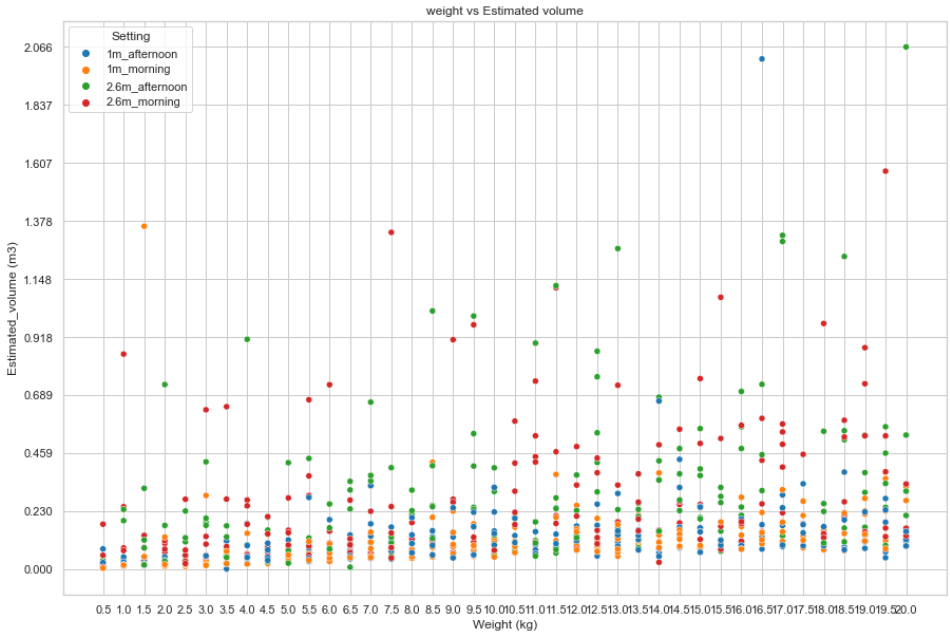

Figure 4. Feed volumes estimated at different light conditions (morning and afternoon) and camera-to-feed distances (1 m and 2.6 m)

3.2. Relationship of feed weight and feed volume at different distance and light setups

Log-transformed weight (P<0.001), camera-to-feed distance (P<0.001), and light conditions (P<0.001) were related to the estimated volume, moreover, the interaction of log-transformed feed weight and light was also significant (P=0.003). Every 10% increase in feed weight increased estimated feed volume by 6.7% in the afternoon. On the other hand, the same increase in feed weight increased the estimated volume by 8.4% in the morning (Figure 5.). Camera-to-feed distance also influenced the estimated volumes, as feed volumes recorded from 2.6 m were larger than those recorded from 1 m for the same weight (Figure 5). When fitted separately by distance, the model explained 66.5% of volume variance at 1 m distance, but only 38.1% at 2.6 m, probably reflecting the noisier measurements from the higher distance.

Therefore, camera-to-feed distance plays an important role in estimating the volume of the feed and should be considered when predicting feed weight from the estimated feed volume. In practice, cameras should not be placed close to cow level because of the risk of damage. One option would be to choose a high-quality camera that can capture accurate depth images even from larger distances. Light condition also plays an important role, and its effect should be minimized when building prediction models to phenotype feed intake of individual cows using depth images as inputs in practice.

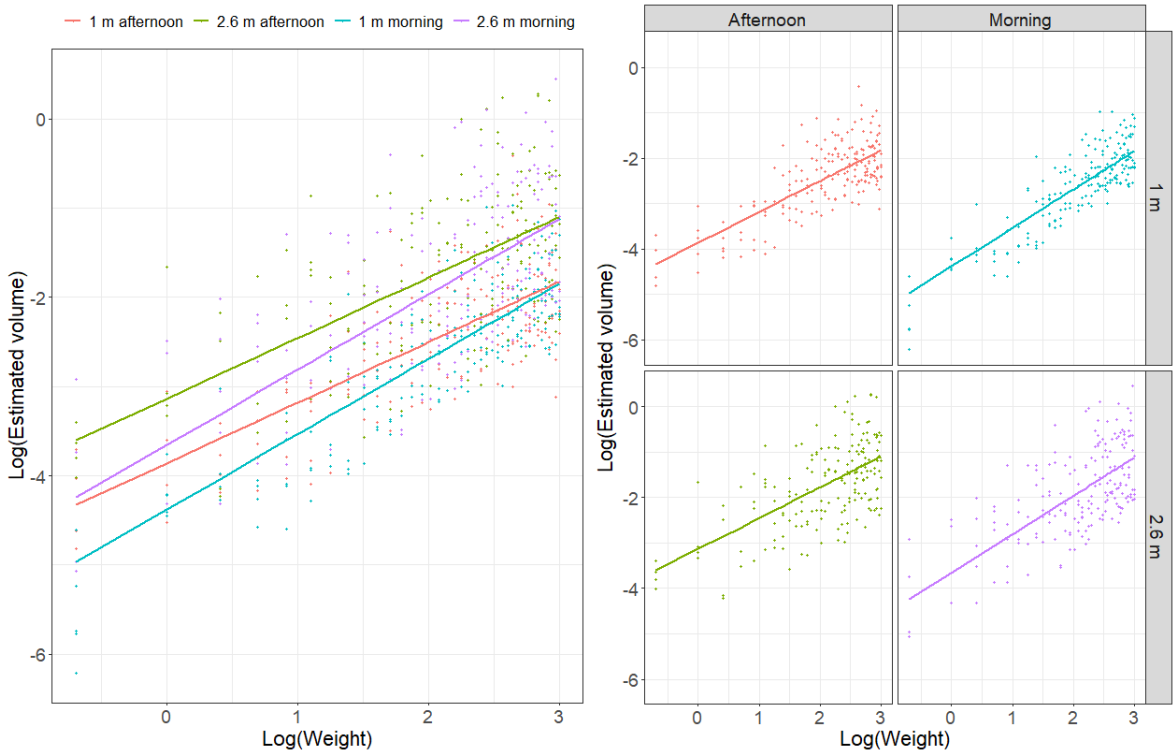

Figure 5. The relationship of log-transformed feed weight with log-transformed feed volume at different camera-to-feed distances and light conditions

4. Conclusion

The vision-based approach to estimate the feed volume and related feed weight can be a good approach as it is scalable, non-invasive, and cost-effective. However, the effects of distance and light should be taken into account for further model development.

Acknowledgements

The study was supported by the TKI Agri & Food project LWV19143 and the partners Melkveefonds and imec-OnePlanet.

References

Bach, A., Iglesias, C., & Busto, I. (2004). Technical note: a computerized system for monitoring feeding behavior and individual feed intake of dairy cattle. *Journal of Dairy Science*, *87*(12), 4207–4209.

Bezen, R., Edan, Y., & Halachmi, I. (2020). Computer vision system for measuring individual cow feed intake using RGB-D camera and deep learning algorithms. *Computers and Electronics in Agriculture*, *172*, 105345.

Bobach, T., Farin, G., Hansford, D., & Umlauf, G. (2007). Discrete harmonic functions from local coordinates. In *Mathematics of Surfaces XII* (pp. 93–103). Springer Berlin Heidelberg.

Borchersen, S., Hansen, N. W., & Borggaard, C. (2018). System for determining feed consumption of at least one animal (USPTO Patent No. 9861081). In *US Patent* (No. 9861081). https://patentimages.storage.googleapis.com/d6/ea/fd/512c7c9353a3a3/US9861081.pdf

Buza, M. H., Holden, L. A., White, R. A., & Ishler, V. A. (2014). Evaluating the effect of ration composition on income over feed cost and milk yield. *Journal of Dairy Science*, *97*(5), 3073–3080.

Chapinal, N., Veira, D. M., Weary, D. M., & von Keyserlingk, M. A. G. (2007). Technical Note: Validation of a System for Monitoring Individual Feeding and Drinking Behavior and Intake in Group-Housed Cattle. *Journal of Dairy Science*, *90*(12), 5732–5736.

DeVries, T. J., Von Keyserlingk, M. A. G., Weary, D. M., & Beauchemin, K. A. (2003). Validation of a system for monitoring feeding behavior of dairy cows. *Journal of Dairy Science*, *86*(11), 3571–3574.

Ferris, C. P., Keady, T. W. J., Gordon, F. J., & Kilpatrick, D. J. (2006). Comparison of a Calan Gate and a Conventional Feed Barrier System for Dairy Cows: Feed Intake and Cow Behaviour. *Irish Journal of Agricultural and Food Research*, *45*(2), 149–156.

González, L. A., Tolkamp, B. J., Coffey, M. P., Ferret, A., & Kyriazakis, I. (2008). Changes in feeding behavior as possible indicators for the automatic monitoring of health disorders in dairy cows. *Journal of Dairy Science*, *91*(3), 1017–1028.

Johansen, M., Lund, P., & Weisbjerg, M. R. (2018). Feed intake and milk production in dairy cows fed different grass and legume species: a meta-analysis. *Animal: An International Journal of Animal Bioscience*, *12*(1), 66–75.

Krawczel, P. D., Klaiber, L. M., Thibeau, S. S., & Dann, H. M. (2012). Technical note: Data loggers are a valid method for assessing the feeding behavior of dairy cows using the Calan Broadbent Feeding System. *Journal of Dairy Science*, 95(8), 4452–4456.

. Lassen, J.R. Thomasen, R.H. Hansen, G.G.B. Nielsen, E. Olsen, P.R.B. Stentebjerg, N.W. Hansen, S. Borchersen. Individual measure of feed intake on in-house commercial dairy cattle using 3D camera system

Proc. 11th World Congr. Genetics Appl. Livest. Prod, Al Rae Center for Genetics and Breeding, Massey University (2018), pp. 635-640.

R Core Team. 2023. R: A Language and Environment for Statistical Computing. R Foundation for Statistical Computing, Vienna, Austria. https://www.R-project.org/.

Ruuska, S., Kajava, S., Mughal, M., Zehner, N., & Mononen, J. (2016). Validation of a pressure sensor-based system for measuring eating, rumination and drinking behaviour of dairy cattle. *Applied Animal Behaviour Science*, *174*, 19–23.

Shelley, A. N., Lau, D. L., Stone, A. E., & Bewley, J. M. (2016). Short communication: Measuring feed volume and weight by machine vision. In *Journal of Dairy Science* (Vol. 99, Issue 1, pp. 386–391). https://doi.org/10.3168/jds.2014-8964

Zhou, Q.-Y., Park, J., & Koltun, V. (2018). Open3D: A Modern Library for 3D Data Processing. In *arXiv [cs.CV]*. arXiv. http://arxiv.org/abs/1801.09847

A comprehensive dataset for monitoring germination of *Cannabis sativa* in greenhouse-controlled environments

José A. Brenes [a], Ana Codes [b], Javier Ferrández [c], Carmen Rocamora [b, *]

[a] CITIC-ECCI-PPCI, University of Costa Rica, San José, Costa Rica

[b] CIAGRO, Miguel Hernández University, Orihuela, Spain

[c] I2RC, University of Alicante, Alicante, Spain

* Corresponding author. Email: rocamora@umh.es

Abstract

Germination monitoring in crucial: it aids in planning and maximizing crop yields, contributing to sustainable agriculture practices. Furthermore, in the cultivation of *Cannabis sativa* L., precise control over the number of plants during the germination process is critical due to legal and regulatory restrictions. To assist growers in tracking germination progress, we planned to developed a classifier that informs them precisely when a plant has successfully germinated in the seedbed. A well-curated dataset is essential for teaching the algorithm to recognize different features. The dataset should encompass a diverse range of examples to ensure that the classifier can accurately identify and categorize instances it encounters during its operation. The quality and diversity of the dataset play a pivotal role in the performance and reliability of the developed classifier. Due to the limited information available on cannabis crops, we undertook the task of constructing an image dataset from the ground up. This dataset was meticulously crafted through a rigorous process. To build the dataset, we sow two varieties of cannabis, Finola and Kompolti, in separate seed trays, each containing 72 cells, in a greenhouse. A camera fixed above the seedbeds took one image every hour throughout the germination experiment. Four iterations were carried out: two without controlling climatic conditions, and two with controlled conditions and photoperiod. Then, we cropped the images and applied a homography process to correct perspective. The resulting images of each cell for each date and hour were labelled using six categories. first, the images were labelled considering the categories germination, non-germination, only cotyledon, and true leaves, then, they were labelled again using the categories invasion and non-invasion. The result was a comprehensive dataset comprising 80,640 images of seedbed cells showcasing plants at various growth stages. This paper outlines the step-by-step process employed in creating this image dataset.

Keywords: Cannabis sativa, germination, artificial vision.

1. Introduction

Seed is the most important input in agriculture, thus the need to ensure viability (Basu, 1995) and vigour (Dornbos, 1995). Seed vigour refers to both the ability and strength of a seed to germinate successfully and establish a normal seedling. Germination and seedling development monitoring is very time consuming and requires well trained technicians, resulting in very high personnel costs. Besides, classification process is not uniform and depends on skills and personal circumstances, which justifies the attempts to automate these tasks (Ureña et al., 2001).

Systems for monitoring seed germination based on artificial vision have been developed. Some of these systems are based on images of the seeds germinated in an incubator or in Petri dishes, recorded with a fixed frequency, in which seed evolution was analysed. Ducournau et al. (2004) designed a machine vision system to count the number of emergent radicle tips in seed lots under controlled lighting, temperature, and hygrometric conditions, performing continuous recording of sunflower seed germination at a frequency of one shot per hour. Dell'Aquila (2005) used a CCD camera to study broccoli and radish germination, monitoring the extent of imbibition phases through the assessment of seed area increase and timing of radicle emergence detected in individual seeds. Li et al. (2015) used image analysis to calculate the changes in seed length. Changes in seed area and length towards radicle emergence over time were used to identify the onset of germination.

Ureña et al. (2001) developed an automatic system for monitoring lettuce, cauliflower and tomato seeds germination based on the automatic measurement of leaf area, followed by classification of these measurements within a fuzzy logic-based framework. A mobile high resolution colour CCD camera captured

the image and the trays were placed manually. After image acquisition and pre-processing, automatic calculation of the leaf area of cotyledons and leaves was performed by using image processing algorithms: segmentation to obtain separate seedlings and description using leaf area. Seedling detection was based on the colour difference between the seedlings (green) and the trays' rooting media. A pixel was considered to be a green one if its proportion of green component was greater than that of its red and blue components. Fuzzy logic and expert knowledge was used to classify the degree of development of the seedlings. Since they had to work in realistic conditions, they captured images around solar midday trying to minimize the influence of light on the shadows and the colour of the images.

With the development of transplanting robots, machine vision systems to detect seedlings have been developed, based on leaf area. Artificial vision is used to identify and locate empty positions in the seedling tray. Ryu et al. (2001) developed a robotic transplanter that used a vision system to detect empty cells in high-density plug trays by counting and comparing the number of white pixels representing the seedling leaves with a predefined value. The vision system was also used to determine the leaf direction of the seedlings to minimise damage to them.

More recently, a vision system was used to measure the leaf area in each cell to distinguish "bad" and "good" plugs, achieving relative identification accuracies of seedling quality of 98.6%, 96.4%, 98.6% and 95.2% for tomato, cucumber, aubergine and pepper, respectively (Tong et al., 2013). An algorithm was developed that could segment overlapping leaves from neighbouring cells; additionally, an algorithm was developed to calculate the leaf area including intruding leaves.

Jin et al. (2022) proposed a low-damage transplanting method for leafy vegetable seedlings based on machine vision. Image processing based on Python-OpenCV was performed to obtain the seedlings' height and extreme edge points. The pixel coordinates in the RGB image were then obtained, and the depth image was aligned with the RGB image to acquire the depth information of the corresponding extreme points.

Cannabis cultivation is restricted around the world by governments. According to European Monitoring Centre for Drugs and Drug Addiction (2018), in the European Union, it is legal to cultivate and supply cannabis plants for hemp fibre if they have low levels of THC, the psychoactive substance present in cannabis plants. Additionally, medicinal cannabis can be produced if the farmers obtain a license from the Office of Medicinal Cannabis (OMC), the organisation in charge of controlling the production and supplying to pharmacies. Controlling the number of plants produced during the germination process could be beneficial for farmers to comply with license restrictions.

We propose implementing an integrated architecture to support farmers in the cultivation of cannabis for medicinal and industrial purposes. In this architecture, we take advantage of advances from emergent technologies like the Internet of Things (IoT), Wireless Sensor Networks, and Artificial Intelligence to provide a solution to support the germination process of cannabis plants. Our goal is that farmers can follow up on the germination of plants more easily, knowing when the germination occurs, the number of germinated plants, and other relevant information from the cultivation environment.

In order to assist farmers in monitoring germination, our aim is to develop a classifier that enables them to determine the number of plants that have germinated in the seedbed. Training the classifier requires a collection of labelled images.

Several datasets of cannabis images have been published for various purposes. Eranga et al. (2022) published a dataset containing different climate, soil, and yield data related to cannabis cultivation. Chumchu and Kailas (2023) released a dataset of cannabis seed images for machine learning applications. The same authors (Kailas and Chumchu, 2024) published a dataset for botanical exploration, including images of entire plants. However, none of these datasets include images of the plant's germination process.

Due to the limited information available on hemp cultivation, we have created a dataset. In this paper, we outline the rigorous process undertaken to capture, clean, label and organise the images to ultimately generate the dataset necessary for training the classification algorithm.

2. Materials and Methods

We work in a greenhouse where we deploy sensors to monitor ambient conditions. The greenhouse's size is approximately 56 square meters (9.75 m x 5.83 m), distributed in six crop tables, one of which was used for the germination experiment. The greenhouse can automatically control environmental conditions like temperature, humidity, and lightning. We have deployed a web platform to monitor and control the distinct

parameters in the greenhouse. We can access the sensors using the web platform and query the data gathered. We have also configured notification services to get alerts when a parameter is out of range or a sensor is disconnected. In Fig. 1, we show the distinct subsystems deployed in the greenhouse.

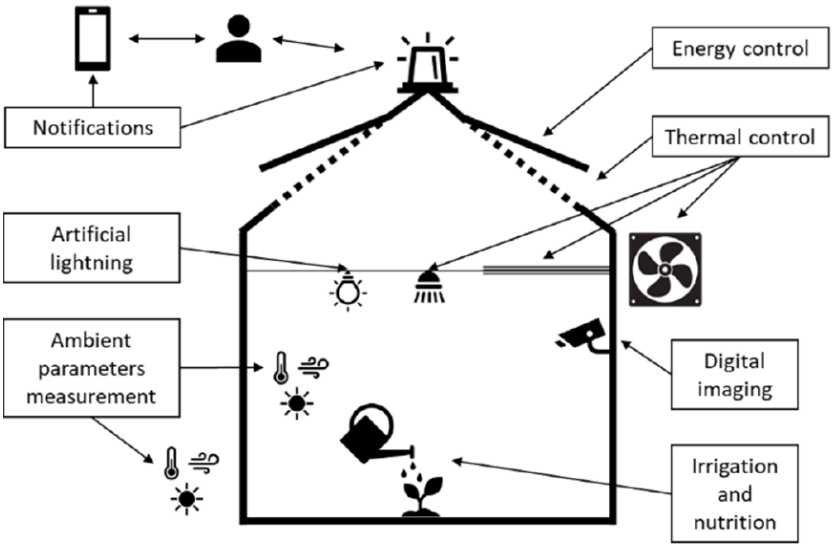

Figure 1. Greenhouse components

2.1. Germination experimental setup

Seeds of two varieties of *Cannabis sativa* L. were sown: Finola and Kompolti. The research group has a license from the Spanish Agency of Medicines and Medical Devices (AEMPS) to cultivate these hemp varieties. Finola is an oilseed hemp variety and was admitted to the European Union's list of subsidized crops in February of 2003. Kompolti is cultivated industrially and used for cosmetics, oils and even flours.

Each variety was sown in a 72-cell seedbed. The substrate was a mixture of blonde peat (65%), coconut fibre (20%), perlite (10%), and black peat (5%). During the germination tests, the substrate moisture was maintained by manually spraying the seedbeds with osmotised water with a pH of 6.2 and an electrical conductivity of 1.2 $mS \cdot cm^{-1}$.

We conducted four iterations each lasting 14 days since seeding. Two iterations were carried out without environmental control and two iterations were conducted under controlled conditions: the ambient temperature of the greenhouse was maintained between 18 and 26 ºC, the relative humidity between 55 and 80 %, and a photoperiod of 18 hours.

We put a camera above the seedbeds and connected it to a Raspberry Pi 4B. We created a python script to control the camera and take pictures. During each iteration, a photo was taken every hour. In Table 1, we detail the camera's specifications used in the experiment. Only the camera's focus was adjusted for the initial setup to avoid blur in the result images.

Table 1. Camera specification.

Camera model	Arducam 64 MP Auto-focus Camera
Optical size	Type 1/1.7” 9.25 mm Diagonal (7.4x5-55 mm)
Focus type	Manual/Auto
Sensor resolution	9152x6944
Color filter	Quad Bayer Coding (QBC)
Focus	8cm
Focal ratio (F-stop)	F1.8
Focal length	5.1 mm
View Angle	84 degrees (diagonal)

2.2. Images captured from overhead camera

Figure 2 shows an example of the image captured by the camera. We put drawing pins in the corners of the seedbeds for later processing of the photos. After completing each iteration, we collected the images and prepared the next iteration. Then, we created a python script to process the images. At the beginning of the process, we applied filters to clean the image and reduce the noise. Then, by using the drawing pins and Hough Circle Transform (Yuen et al., 1989), we detected the four corners of the seedbeds. After that, we used the coordinates of each corner and applied a Homography process (Hartley and Zisserman, 2004) to correct and align the image. At the end of the process, we cut the resultant image to get each cell of the seedbed. The whole process is detailed in Figure 3.

Figure 2. Example of an image captured by the camera. Left: Finola hemp variety samples. Right: Kompolti hemp variety samples.

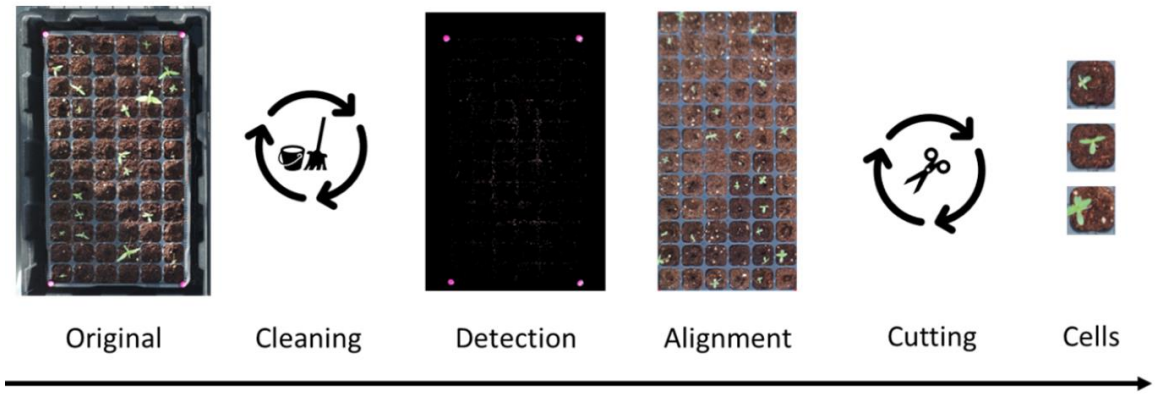

Figure 3. Images pre-processing steps.

To finish this process, we saved the images of cells. An automated labelling process was employed, wherein each image from the seedbed was cropped and assigned a name indicating the variety, iteration, day, time, and position within the seedbed. The cells were renamed as follows:

Variety_iteration_day_hour_cell-Row_cell-Column.jpg

For example: Finola_1_1_10_3_5.jpg.

Table 2 shows the possible values of the automatic labelling. Each iteration lasted 14 days. Every day 10 pictures were cropped, starting from 8 to 17 or from 9 to 18, according with the sun hours. Experiments were conducted during November 2022 to January 2023.

Table 2. Automatic labelling.

Label	Possible values
Variety	Finola / Kompolti
Iteration	1/2/3/4
Day	1/2/3/4/5/6/7/8/9/10/11/12/13/14
Hour	1/2/3/4/5/6/7/8/9/10
Row	1/2/3/4/5/6/7/8/9/10/11/12
Column	1/2/3/4/5/6

2.3. Pre-processed images

Figure 4 shows an example of the images pre-processed for a seedbed cell at days 6, 10, and 14. The pictures of Figure 4 correspond to a Finola hemp variety sample. Therefore, these images are easy to classify.

Figure 4. Example of images for the same cell at day 6 (left), 10 (center), and 14 (right).

Figure 5 shows examples of cells that are more difficult to classify. They correspond to different scenarios such as the presence of a plant sprouted in an adjacent cell, whether there is germination in the cell or not, or a plant whose leaves are not visible in the picture. This often occurs when the stems grow and bend.

Figure 5. Examples of scenarios where a plant is present, not always indicating germination in the cell. Left: plant leaves are missing, yet a germinated plant is present. Centre: neighbouring plant leaves alongside a germinated plant in the cell. Right: presence of a neighbouring plant, but no germinated plant within the cell.

Once we got images representing cells at different times, we labelled each one. To do that, we conducted two labelling phases and used six categories. The categories and stages are detailed in Table 2.

Table 2. Labelling phases and categories.

First labelling phase		Second labelling phase	
- Non-germination	NG		
- Germination	G	- Invasion	I
+ Cotyledon Only	CO	- Non-invasion	NI
+ Cotyledon and True Leaves	TL		

By combining two labels, we can support the correct classification of cells in germination.

For example: in general, a cell with the label Germination and Invasion means the presence of a plant. On the other hand, Non germination and Non Invasion correspond to not presence of a plant inside the cell. Meanwhile, there are another two cases in which a plant can be presented in a cell, when it is labelled as Germination and Non Invasion, and when it is labelled as Non germination and Invasion.

3. Results and discussion

A dataset has been created consisting in 80,640 images.

The images underwent thorough cleaning and organization processes, followed by the assignment of appropriate names and labelling. The dataset was meticulously curated to ensure consistency and accuracy in its contents.

The first automated labelling ensured efficient organisation and categorisation of the dataset, laying the groundwork for subsequent manual labelling and analysis. The systematic naming convention adopted facilitated easy retrieval and referencing of individual images during the dataset creation process, contributing to the overall coherence and accessibility of the dataset for research purposes.

Following the automated labelling process, manual labelling was conducted to further categorise the images based on several criteria. Each image was manually classified according to the presence of germinated plants, distinguishing between images depicting seedlings with only cotyledons and those exhibiting true leaves. Additionally, images were annotated to identify instances of plant invasion from adjacent cells. This meticulous manual labelling process enabled the creation of a richly annotated dataset, providing valuable insights into the progression of seedling development and interactions within the seedbed environment.

The combination of automated and manual labelling strategies ensured the accuracy and granularity of the dataset, enhancing its utility for a wide range of research applications in plant biology and agriculture.

Table 4. Example of a doubly labelled image from the dataset.

Image	Variety	Iteration	Day	Hour	Row	Column	Classes
Finola_it1_6_1_3_2.jpg	Finola	1	6	1	3	2	I/CO

The dataset provides researchers with a valuable resource for studying seedling development and related phenomena.

Having a dataset of seed germination images is of paramount importance for future research worldwide. These datasets serve as invaluable resources for scientists and researchers across various fields, providing a rich source of data to study the intricate processes involved in seed germination.

By collecting and curating such datasets, researchers can gain insights into the factors influencing germination rates, timing, and success, thereby advancing our understanding of plant biology and agricultural practices.

This dataset enables the development and validation of machine learning algorithms and computer vision techniques for automated seed germination detection and analysis, paving the way for innovative solutions in precision agriculture and crop management.

This dataset can be further enhanced by incorporating images of germinated cannabis plants exhibiting various stress conditions such as nutrient deficiencies, water stress, pest infestations, and diseases. It can also be supplemented by incorporating images of hemp plants in later stages of development.

By augmenting the dataset with these additional images, it will be possible to train more sophisticated algorithms capable of accurately detecting and diagnosing a range of pathophysiological conditions.

Having a dataset with images of cannabis plants at more advanced stages of development may allow to

determine the sex of the plants at an earlier stage, which is particularly important for cannabis cultivation, where the identification of male plants is crucial to prevent them from pollinating female plants. It would be also possible to perform a detailed analysis of the growth patterns and morphological changes over time and to predict the potential yield of the crop.

4. Conclusion

In this work, we have presented the creation of a dataset comprising images of cannabis seed germination for the Kompolti and Finola varieties. This dataset has been meticulously and rigorously developed, encompassing the entire process from image capture, pre-processing, and cropping of individual seedbed cells, to the systematic naming and labelling of the resulting images. Each cell was labelled to indicate the presence or absence of germination, whether the seedling exhibited only cotyledons or true leaves as well, and whether invasion from an adjacent cell was observed.

This dataset will enable the training of an algorithm for the automatic classification of seedbed images. It represents the first systematic dataset published with images of *Cannabis sativa* germination. The publication of this dataset will provide a valuable resource for researchers needing high-quality images to train their algorithms.

Moreover, the dataset can be further enhanced by incorporating images of plants affected by pests and diseases or images of plants at more advanced stages of development. This would facilitate the training of more sophisticated algorithms capable of detecting a broader range of conditions and traits, thereby expanding the utility and impact of this resource.

By making this dataset available, we aim to support the scientific community in advancing research in cannabis cultivation, ultimately contributing to improved agricultural practices and plant health monitoring.

Acknowledgements

This study is part of the AGROALNEXT program (AGROALNEXT/2022/048) and has been supported by MCIN with funding from the European Union NextGenerationEU (PRTR-C17.I1) and the Generalitat Valenciana. C. Rocamora has been funded by the Ministry of Universities and by the European Union-Next Generation EU within the framework of Grants for the Requalification of the Spanish University System, in the University teaching staff modality.

This study was partially supported by the Research Center for Communication and Information Technologies (CITIC), Research Project No. 834-B9-189. J.A. Brenes has been funded by the Office of International Affairs and External Cooperation OAICE (Short-Term Scholarship) and the Postgraduate Studies System SEP (Restricted Fund 082) of the University of Costa Rica.

References

Basu R. N. 1995. Seed viability. In *Seed Quality. Basic Mechanism and Agricultural Implications*, Food Products Press, The Haworth Press, Inc. New York, Ed. A.S. Basra, pp 1-44.

Chumchu P., K. Patil, 2023. Dataset of cannabis seeds for machine learning applications, Data in Brief, 47, 2023, 108954. https://doi.org/10.1016/j.dib.2023.108954.

Dell'Aquila, A, 2005. The use of image analysis to monitor the germination of seeds of broccoli (*Brassica oleracea*) and radish (*Raphanus sativus*). Annals of Applied Biology 146, 545–550. https://doi.org/10.1111/j.1744-7348.2005.040153.x.

Dornbos D. L. 1995. Seed Vigor. In *Seed Quality. Basic Mechanism and Agricultural Implications*, Food Products Press, The Haworth Press, Inc. New York, Ed. A.S. Basra, pp 45-80.

Ducournau, S., A. Feutry, P. Plainchault, P. Revollon, B. Vigouroux, M. Wagner, 2004. An image acquisition system for automated monitoring of the germination rate of sunflower seeds. Computers and Electronics in Agriculture 44, 189–202. https://doi.org/10.1016/j.compag.2004.04.005.

European Monitoring Centre for Drugs and Drug Addiction, Hughes, B., 2018. Cannabis legislation in Europe – An overview, Publications Office of the European Union, https://data.europa.eu/doi/10.2810/566650

Hartley, R.; A. Zisserman, 2004. Multiple View Geometry in Computer Vision; Cambridge University Press, 2004. https://doi.org/10.1017/cbo9780511811685.

Jin, X.; R. Li, Q. Tang, J. Wu, L. Jiang, C. Wu, 2022. Low-damage transplanting method for leafy vegetable seedlings based on machine vision. Biosystems Engineering 220, 159–171. https://doi.org/10.1016/j.biosystemseng.2022.05.017.

Li, C., A. Raheja, D. Still, 2015. Application of Computer Vision for Lettuce Seeds Germination Detection. In *WORLDCOMP'15-The 2015 World Congress in Computer Science, Computer Engineering, and Applied Computing*. WORLDCOMP, Las Vegas, NV, USA, pp.1-5.

Patil K., P. Chumchu, 2024. A comprehensive dataset of eight Thai cannabis classes for botanical exploration, Data in Brief, 54, 110292. https://doi.org/10.1016/j.dib.2024.110292.

Ryu, K.; G. Kim, J. Han, 2001. AE—Automation and Emerging Technologies: Development of a Robotic Transplanter for Bedding Plants. Journal of Agricultural Engineering Research 78, 141–146. https://doi.org/10.1006/jaer.2000.0656.

Tong, J.H., J.B. Li, H.Y. Jiang, 2013. Machine vision techniques for the evaluation of seedling quality based on leaf area. Biosystems Engineering 115, 369–379. https://doi.org/10.1016/j.biosystemseng.2013.02.006.

Ureña, R., F. Rodrıguez, M. Berenguel, 2001. A machine vision system for seeds quality evaluation using fuzzy logic. Computers and Electronics in Agriculture 2001, 32, 1–20. https://doi.org/https://doi.org/10.1016/S0168-1699(01)00150-8.

Wimalasiri E.M., E. Jahanshiri, T.A. Syaherah, N. Kuruppuarachchi, V.G.P. Chimonyo, S.N. Azam-Ali, P.J. Gregory, 2022. Datasets for the development of hemp (*Cannabis sativa* L.) as a crop for the future in tropical environments (Malaysia). Data in Brief, 40, 107807. https://doi.org/10.1016/j.dib.2022.107807.

Yuen, H.K., J. Princen, J. Dlingworth, J. A. Kittler, 1989. Comparative Study of Hough Transform Methods for Circle Finding. In *Proceedings of the Alvey Vision Conference*. Alvey Vision Club, Reading, U.K., September 1989. Ed K. D. Baker. https://doi.org/10.5244/c.3.29.

AI-enhanced language support for advanced operation in controlled environment agriculture

Ramesh Arvind Naagarajan [a], Kiran Kumar Sathyanarayanan [b,*], Nadja Bauer [a], Philipp Sauerteig [b], Sebastian Bab [a], and Stefan Streif [b,c]

[a] Department of Computer Science, University of Applied Sciences and Arts, Dortmund, Germany

[b] Automatic Control and System Dynamics Lab, Chemnitz University of Technology, Chemnitz, Germany

[c] Department of Bioresources, Fraunhofer Institute for Molecular Biology and Applied Ecology

* Corresponding author. Email: kiran.sathyanarayanan@etit.tu-chemnitz.de

Abstract

Optimization-based control of greenhouses and indoor farms has gained popularity due to the growing demand for energy-efficient and sustainable crop production. Model Predictive Control (MPC) is an advanced optimization-based control strategy that regulates the greenhouse climate based on a mathematical model and weather forecast data. Despite gaining popularity among researchers, the acceptance of this method among suppliers of greenhouse climate control systems and growers remains limited. The primary reasons are the lack of transparency and the understandability of the control algorithms. Additionally, there is difficulty in quickly comprehending the output generated by the control algorithm for various goals and grower-defined bounds. In this paper, we introduce a language-based support system designed to offer a comprehensive summary of the greenhouse's single-day climate trajectories. The language-based support system as a first step, dynamically segments the generated time-series reference data to identify the significant slope change. Secondly, the Natural Language Generation (NLG) method is employed to generate meaningful and coherent long texts of the generated non-linguistical data. The detailed long texts are finally condensed into user-friendly information using a pre-trained Large Language Model (LLM) by formulating an output-focused prompt. The proposed support system aims to act as a bridge between proven advanced control and real-time implementation of optimal control in Controlled Environment Agriculture (CEA) farms.

Keywords: Natural language generation, model predictive control, time-series to text, large language models

1. Introduction

The projected increase in the global population from 7 billion in 2010 to an estimated 9.8 billion by 2050 is predicted to lead to a significant 50% rise in food demand (Searchinger et al., 2019). However, the necessity to boost food production encounters significant obstacles, as the expansion of agricultural land is limited by rapid urbanization and the adverse effects of climate change. Thus, the adoption of sustainable techniques is becoming more and more crucial in the field of agriculture. Controlled Environment Agriculture (CEA) farms like greenhouses, vertical farms, and indoor farms have gained popularity due to their capability to maintain the climate and produce high yields in limited space. However, the efficient and sustainable operation of CEA farms relies on the automatic control of climate to influence crop growth.

In greenhouses, classical control methods like on/off and Proportional-Integral-Derivative (PID) control are employed to regulate temperature and humidity (Iddio et al., 2020). Apart from these methods, Model Predictive control (MPC) has demonstrated its ability to achieve energy-efficient operations economically (Van Beveren et al., 2015; Padmanabha et al., 2020). Employing a hierarchical control scheme based on timescale decomposition facilitates the implementation of MPC by mitigating its intricacy and computational load in complex systems such as greenhouses (Van Henten et al., 2009). Additionally, it contributes to heuristic performance evaluation, encompassing factors like energy consumption, irrigation water use efficiency, and maximum yield (Ramírez-Arias et al., 2020).

The current state of computerized control in greenhouse farming poses challenges due to the lack of understanding and the complexity of the control algorithm in generating the programmable trajectories. Modifications to these trajectories can significantly impact energy consumption, resource utilization, and crop growth, yet the exact effects remain largely unknown to growers (Van Straten et al., 2010). As a first step towards understanding the control algorithm, this paper proposes providing textual descriptions of refer-

ence trajectories generated within a hierarchical control framework using a Natural Language Generation (NLG) method.

NLG is a branch of artificial intelligence and computational linguistics focused on developing computer systems capable of generating understandable texts in human languages, like English, from non-linguistic representations of information. NLG finds diverse applications, including generating reports for soccer matches, weather forecasts, financial reports, and clinical summaries (Gatt et al., 2018).

In this paper, our goal is to develop a data-to-text generation method to summarize reference trajectories, explaining the planned climate conditions of a greenhouse. Sharma et al. (2021) propose T^3 - a domain-agnostic neural approach for time-series narration, leveraging transfer learning from a pretrained Large Language Model (LLM). The universal nature of T^3 may limit accuracy for specific fields like greenhouses or vertical farms. Furthermore, the absence of a training dataset for greenhouse climate and its description, necessitates an alternative approach.

Therefore, we propose using a rule-based modular NLG approach for generating the summary. Initially, the data undergoes analysis, and significant change points are detected using temporal analysis techniques. These change points serve as input to the NLG algorithm. The NLG output comprises a detailed report, which is then summarized using an LLM to generate a concise report based on a predefined prompt. This language-based support system aims to empower growers with insights into the anticipated outcomes for the next day's operations and lays the groundwork for future iterations of the control algorithm.

2. Hierarchical Model Predictive Control of the Greenhouse

MPC is a control scheme where a dynamic mathematical model is employed to predict the system's future behaviour over a finite horizon. Based on these predictions and the previously measured state of the system, optimal control inputs are generated on solving a constrained dynamic optimization problem with a user-defined objective (Rawlings et al., 2017). An economic objective function to maximize the yield and minimize the growing costs is of special interest to the greenhouse system.

2.1 Greenhouse System Description

We consider a Venlo-type semi-closed greenhouse growing tomato crop. The greenhouse climate is defined in terms of temperature (T), CO_2 concentration (C), and relative humidity (H) of the air inside the greenhouse. The crop growth is defined as the fresh weight biomass (B), estimated using an observer. The variables $x = (T,C,H,B)$ describing the current status of the greenhouse are called the states of the greenhouse system. These variables are influenced by various control inputs, including ventilation, CO_2 injection, heating, and cooling, collectively termed control inputs (u) of the system. Additionally, external variables such as outdoor temperature, CO_2 levels, relative humidity, and solar radiation known as disturbances (d) of the system affect the greenhouse climate. For the mathematical model equations describing the greenhouse climate dynamics and crop growth, refer to Sathyanarayanan et al. (2024). The dynamic system is summarized as

$$\dot{x} = f(x,u,d). \tag{1}$$

The greenhouse climate has a direct effect on crop growth and health, and it is essential to maintain them within defined bounds, see e.g. Sanchez-Guerrero et al. (2005), Zarnescu et al. (2019).

2.2 Hierarchical Control Strategy

The complexity and the computational burden of the MPC problem increase with increasing prediction horizon (e.g. one day or one week). The hierarchical control strategy decreases the complexity by decomposing the problem into smaller subproblems and arranging it in a hierarchical tree. A two-level hierarchical framework of greenhouse control shown in Figure 1 is considered, and for further details see Sathyanarayanan et al. (2024). The control framework consists of an open-loop optimization problem in the upper level and a reference tracking MPC in the lower level. With an objective to maximize yield and minimize growing costs, the upper level generates the input and state reference trajectories $x^{\mathrm{ref}}, u^{\mathrm{ref}}$ for a single day using forecast data of d. Then, the lower-level controller tracks these generated references in real time.

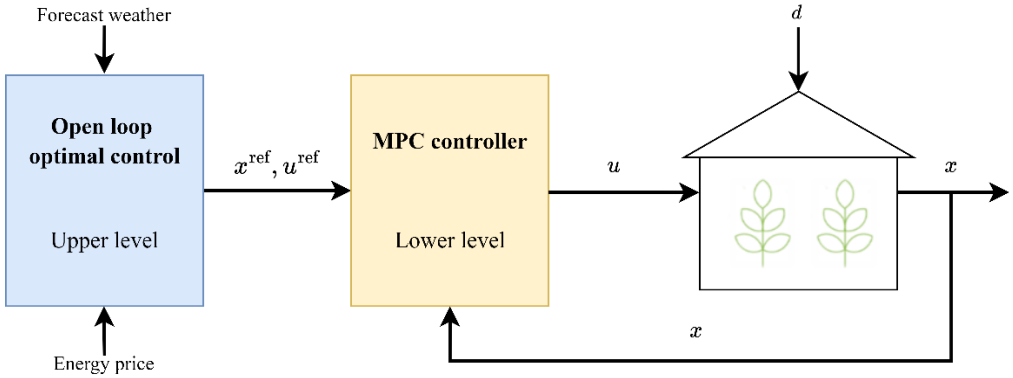

Figure 1. Hierarchical control of the greenhouse

3. Language Support System (LSS) Architecture

The time series data (reference trajectories) generated from the upper level of the hierarchical control is the foundation of our architecture. The architecture as shown in Figure 2 is developed using the insights from Section 2, and these reference trajectories are the input to the LSS. These trajectories are instrumental in extracting meaningful insights from the dataset, which includes measurements of key state variables. Each observation in the dataset is recorded at a frequency of 5-minute intervals, covering the entire duration of a single day, from 00:00 to 23:55.

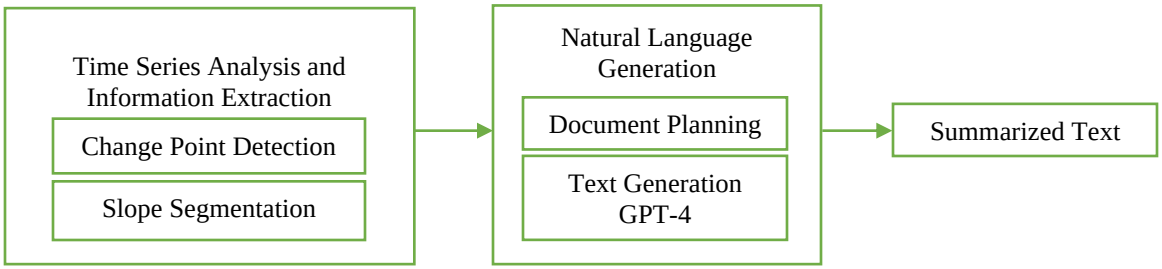

Figure 2 AI-enhanced language support system architecture

3.1 Temporal Analysis Techniques

Temporal analysis involves observing data over a period to perceive its behaviour, with a primary emphasis on identifying patterns, trends, and alterations that occur over time. The focus is on comprehending the dataset's temporal evolution by constructing trajectories and investigating change point identification techniques to detect notable shifts or transitions within the dataset.

3.1.1 Change Point Detection

The process of detecting change points in time series data is a complex task that involves identifying abrupt variations, which may signify transitions between different timestamps (Kawahara and Sukiyama, 2012). A key aspect of this process is the minimization equation, which is crucial for selecting the optimal segmentation S and is formally defined as a model selection problem. Over the last few decades, researchers have developed numerous methods for identifying change points. A comprehensive analysis of the most common methods can be found in Aminikhanghahi and Cook (2017). Based on the dynamic changes of the state variable, we used an unknown change point detection method (Troung et al., 2019). Three different approaches are used: Pruned Exact Linear Time (PELT) (Killick et al., 2012), Cumulative Summation (CUMSUM) (Wei and Xei, 2023), and Exponentially Weighted Moving Average (EWMA) (Raza et al., 2015). After evaluating their performances in Section 4.1, we select the best approach that suits our dataset.

3.1.2 Slope Segmentation

In the previous section, we introduced various change point detection methods and their significance in analysing our greenhouse dataset. To analyse the data further, we employed slope segmentation. This technique involves fitting linear regression models to relevant data segments to determine each segment's slope. By comparing these slope values between adjacent segments, we can detect abrupt shifts indicative of potential future changes (Sharma et al., 2023). Using slope segmentation, we applied customized criteria tailored to the unique features of our greenhouse dataset. Such criteria allow us to classify segments based on their temporal properties, providing a deeper understanding of the dataset's dynamics. This customized strategy improves the level of detail in our analysis, enabling us to extract deeper insights from the dataset.

3.2 Natural Language Generation and Prompt Engineering

NLG is a branch of Artificial Intelligence (AI), plays a significant role in the interpretation of data. It automatically generates natural language text from structured data or other input forms. NLG systems, utilizing various techniques, convert data into a coherent and contextually appropriate language, mirroring human communication.

3.2.1 Document Planning

Data-driven NLG approaches leverage machine learning algorithms and statistical models to analyse and understand text. These methods learn patterns and associations directly from data, such as extensive collections of text corpora, without relying on predefined rules or linguistic knowledge. By learning from data, these approaches can capture complex patterns and nuances in natural language, leading to more accurate and robust NLG systems. In NLG document planning, it acts as a critical intermediary, converting time series data into a human-readable format. It is the link between raw data interpretation and the final text generation. We created comprehensive documents tailored to temperature, humidity, and CO_2 levels.

3.2.2 Prompt Engineering

Prompt engineering involves systematically designing and optimizing input prompts to guide the responses of LLM, ensuring accuracy, relevance, and coherence in the generated output. This process is essential for unlocking the full potential of these models, making them more accessible and applicable across diverse domains. Contemporary prompt engineering includes a range of techniques, from foundational approaches like role-prompting (Shanahan et al., 2023) to more advanced methods such as "chain of thought" prompting (Wei et al., 2022).

Researchers have observed that a Generative Pre-trained Transformer (GPT-4) (OpenAI et al., 2023) produces overly general output when provided with basic instructions without explanation (Luo et al., 2019). This instruction technique, sometimes called re-reading, utilizes human reading strategy heuristics (Xu et al., 2023). The model faces a wide range of alternatives when given basic instructions, which result in a comprehensive outcome (Yang et al., 2019).

Most LLM systems employ a wide range of textual data, a compilation of concepts from many authors. When given broad or ambiguous prompts, the model usually produces general output suitable for various scenarios but may not be optimal for a particular case. Conversely, a clear and detailed prompt allows the model to produce data that almost matches the unique requirements of the given case. These recommendations reduce the uncertainty and drive towards more accurate responses (Chen et al., 2023).

4. Evaluation and Result

We evaluated the time series data, i.e. the reference trajectories generated by the upper level of hierarchical control. From this simulated data, we randomly selected 20 days for evaluation. This dataset comprises simulated observations of state variables. These simulated observations are recorded at regular intervals, reflecting the dynamic nature of the greenhouse environment over the specified time frame. The above-mentioned change point detection methods are implemented and evaluated based on three key metrics: the coefficient of determination (R^2), F1 Score and Jaccard Similarity. These metrics provide comprehensive insights into the performance and effectiveness of the change point detection method

concerning the available greenhouse dataset.

4.1 Evaluation of Change Point Algorithms

In Table 1, we identified change points for each of the algorithms. Then, a piecewise linear regression is placed to estimate the relationship between these points this correspond to $\bar{y}$ estimates. This allows us to compare the R^2 values generated by different algorithms across various state variables, providing insight into the goodness of fit between segments. The formula for calculating R^2 is:

$$R^2 = 1 - \frac{\sum_{i=1}^{n}(y_i - \bar{y})^2}{\sum_{i=1}^{n}(y_i - \hat{y}_i)^2} \quad (2)$$

In the context of our analysis, y_i represents the actual observed values of the dependent variable (e.g. state variables) at each data point i obtained directly from the dataset. On the other hand, $\hat{y}_i$ represents the predicted values of the dependent variable at each data point i as estimated by the piecewise linear regression model fitted to the data.

Table 1: Comparison of R^2 values for different state variables and algorithms

Parameter	Algorithm		
	PELT	CUMSUM	EWMA
T	0.7491	0.8839	0.8826
C	0.7117	0.012	0.2010
H	0.3995	0.2178	0.1461

From the Table 1, we can see that the PELT algorithm performed better than the others in most cases, showing that it is good at predicting changes in the greenhouse environment. The F1 score is a harmonic mean of precision and recall, offering a single metric that balances both precision and recall, with higher values signifying better performance in binary classification tasks (Nancy, 1992). To establish change points for the F1 score, we manually labelled potential change points for all randomly selected 20 dates and each state variable. These potential change points were determined by visual inspection of the data. Subsequently, we utilized the PELT algorithm to identify change points automatically. By comparing the manually labelled change points with those identified by the PELT algorithm, we computed the F1 score for each algorithm in Table 2, the average F1 score (AvgF1) can be calculated using the formula:

$$AvgF1 = \frac{1}{n}\sum_{i=1}^{n} F1_i \quad (3)$$

where n represent the total number of samples, i is the index representing individual sample and $F1_i$ is the sample of F1 score for i^{th} sample. The Jaccard similarity quantifies the similarity between two sets by comparing their intersection to their union. It is beneficial for evaluating the overlap or agreement between two state variables, as shown in Table 2, where a higher Jaccard Similarity score indicates a greater degree of similarity or overlap, while a lower score suggests more divergence or dissimilarity (Levandowsky and Winter, 1971). Weight F1 and Weight Jaccard weights are chosen based on the relative importance of precision (captured by F1 score) and similarity (captured by Jaccard score) in the context of the application. As both F1 and Jaccard scores lie between 0 and 1 and need to be maximized, we assign equal weights to reflect their relative significance in the combined score calculation.

The combined score (Combined Score) for an algorithm can be calculated as

$$CombinedScore = \left(WeightF1 \cdot AvgF1\right) + \left(WeightJaccard \cdot AvgJaccard\right) \quad (4)$$

Table 2: Comparison of F1 score, Jaccard similarity and combined metrics for different algorithms

Algorithm	F1 Score			Avg_F1	Jaccard Similarity			Combined Score
	T	*C*	*H*		*T*	*C*	*H*	
PELT	0.0909	0.3636	0.2857	0.2464	0.0476	0.2222	0.1667	0.1961
CUMSUM	0.1667	0.0	0.2	0.0889	0.0909	0.0	0.111	0.0949
EWMA	0.0	0.1053	0.2	0.0351	0.0	0.0556	0.111	0.0787

Therefore, based on the analysis of Table 1 and Table 2, our evaluation, mainly through the combined score, which considers both the F1 score and Jaccard similarity across all state variables (*T*, *C*, *H*), provides a comprehensive understanding of each algorithm's performance. Among the algorithms assessed, the PELT algorithm performs better than others in detecting change points within the dataset. PELT's efficiency lies in its computational approach, employing an exact linear time segmentation method that proves highly effective for large datasets. This iterative process carefully considers all potential change points, selecting the most optimal ones at each step (Killick et al., 2012).

Despite PELT's initial effectiveness, we recognized the need for further refinement to optimize its performance. This led us to fine-tune crucial parameters, such as penalty and jump values, to balance detecting change points and ensuring segment fit. The penalty value regulates the number of change points detected, while the jump value influences the algorithm's sensitivity to small changes in the data. Through evaluation of various parameter combinations, we identified that a penalty value of 10 and a jump value of 6 yielded the best fit. This optimization, supported by visual examination and goodness of fit evaluation, ensures PELT's optimal performance in accurately detecting change points within our greenhouse dataset.

4.2 Slope Segmentation Analysis

A slope calculation approach is employed to identify trends between two dataset segments. The slope calculation function assigns descriptive labels to the calculated slopes based on their magnitude, which is customized to this research and can be adjusted for different systems. (i.e., Mild: Slope values between -0.03 and 0.03, Decrease: Slope values between -0.1 and -0.03, Sharp Decrease: Slope values between -0.5 and -0.1, Exponential Decrease: Slope values less than -0.5, Increase: Slope values between 0.03 and 0.1, Sharp Increase: Slope values between 0.1 and 0.5, Exponential Increase: Slope values greater than 0.5.) This mapping allowed us to identify the trend direction and magnitude, as exemplified by the temperature trend illustrated in Figure 3, providing valuable insights into the dataset's behaviour.

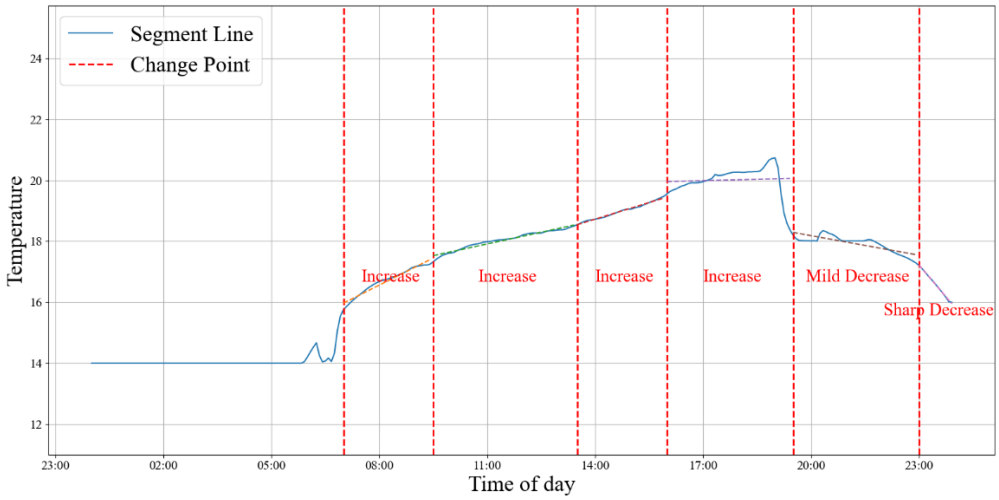

Figure 3: Change point detection and slope segmentation for temperature reference trajectory

4.3 Document Generation Approaches

The first approach is creating templates containing critical information extracted from the time series data. These templates are structured to include relevant details such as daily fluctuations, trends, and significant occurrences within the data. For example, in the case of temperature data, the template may include sections highlighting daily temperature ranges and significant temperature spikes or drops. Similarly, templates for humidity and CO_2 levels would focus on capturing fluctuations using *mapped_ feature_name* as shown below. The second approach entails adding annotated slope values to the document as *description* in the document planning, as shown below.

For example, the illustration about the document planning process is shown below:

1. At the beginning of the day, the *{mapped_feature_name}* was *{start_value:.2f} {unit}*.
2. From *{start_hour:02d}:{start_minute:02d}* to {*last_merged_end_hour:02d}: {last_merged_end_minute:02d}*, the *{mapped_feature_name}* experiences *{description}* from *{previous_value:.2f} {unit}* to *{actual_y:.2f} {unit}*.

By systematically analysing each feature and segmenting the data, we provide a comprehensive overview of greenhouse conditions, facilitating better understanding and decision-making. Due to space constraints, our detailed report focuses on a single state, *T*. However, we have provided a comprehensive report in Section 4.4, accommodating all features for summarization results.

Detailed Generated Report

On June 02, 2011, let us explore how the greenhouse conditions changed throughout the day. At the beginning of the day, the *Temperature* was *14.0* °C. From *07:00* to *09:30*, the *Temperature* experiences an *Increase* from *15.7* °C to *17.3* °C. From *09:30* to *13:30*, the *Temperature* experiences an *Increase* from *17.3* °C to *18.5* °C. From *13:30* to *16:00*, the *Temperature* experiences an *Increase* from *18.5* °C to *19.5* °C. From *16:00* to *19:30*, the *Temperature* experiences an *Increase* from *19.5* °C to *20.1* °C. From *19:30* to *23:00*, there was a sudden drop and the *Temperature* experiences a *Mild Decrease* from *18.2* °C to *17.2* °C. From 23:00 to 23:55, the *Temperature* experiences a *Sharp Decrease* from *17.2* °C. to *16.0* °C. By the end of the day at *23:55*, the *Temperature* will be *16:0* °C, reflecting the last observed value
For the above climate growth conditions, we can see a biomass growth from *17.1* kg/m^2 to *17.5* kg/m^2.

4.4 Summarization

The GPT-4 model is utilized in the summarization process to incorporate sophisticated natural language processing techniques. With its ability to comprehend and summarize language, this model is exceptional in producing clear and concise abstract paragraphs from transcriptions. It uses the GPT-4 and prompting function to summarize the main conclusions from the document planning process. The function summarizes the greenhouse conditions at each time of day, as shown below. This summary highlights significant trends and variations in temperature, humidity, biomass levels, and CO_2 concentration.

Summarized result in GPT-4

On June 2, 2011, the greenhouse conditions varied throughout the day. The temperature steadily increased from 14.0 °C to 19.5 °C before slightly decreasing to 16.0 °C by the end of the day. CO_2 levels experienced fluctuations, initially decreasing from 859.6 ppm to 954.76 ppm, then increasing to 965.1 ppm, and finally decreasing to 865.8 ppm at the end of the day. Relative humidity saw drastic changes, starting at 89.9%, dropping to 48.1%, then increasing to 89.9%, and further fluctuating until it reached 96.2% by the end of the day. These changes in climate growth conditions led to biomass growth from 17.1 kg/m^2 to 17.5 kg/m^2.

5. Conclusions

This paper presents a language support system architecture utilizing NLG techniques, transforming complex numerical data of planned CEA climate trajectory into readable text. We proposed change point detection algorithms to find shifts in the data and used slope segmentation to identify trends. Additionally, NLG's document planning approach is used to create detailed reports. Finally, concise summaries are generated using GPT-4 with pre-defined prompts. Thus, leveraging advanced natural language processing techniques to make informed CEA farm management decisions enhances productivity and efficiency.

Future research will focus on optimizing the change point detection method in generating more robust and accurate results Additionally, exploring advanced visualization techniques aims to present data insights more understandably for practical use.

Acknowledgments

This work has been developed within the framework of the project SensCEA - Sensor-based efficiency increase in Controlled Environment Agriculture, funded by the ESF Plus - MINT skilled worker program in the Free State of Saxony (InnoTeam), reference number - E6563D8EN.

References

Aminikhanghahi, S. and Cook, D.J., 2017. A survey of methods for time series change point detection. *Knowledge and information systems*, 51(2), pp.339-367.

Chen, B., Zhang, Z., Langrené, N. and Zhu, S., 2023. Unleashing the potential of prompt engineering in large language models: a comprehensive review. *arXiv preprint arXiv*:2310.14735.

Gatt, A. and Krahmer, E., 2018. Survey of the state of the art in natural language generation: Core tasks, applications and evaluation. *Journal of Artificial Intelligence Research*, 61, pp.65-170.

Iddio, E., Wang, L., Thomas, Y., McMorrow, G. and Denzer, A., 2020. Energy efficient operation and modeling for greenhouses: A literature review. *Renewable and Sustainable Energy Reviews*, 117, p.109480.

Kawahara, Y. and Sugiyama, M., 2012. Sequential change-point detection based on direct density-ratio estimation. *Statistical Analysis and Data Mining: The ASA Data Science Journal*, 5(2), pp. 114–127.

Killick, R., Fearnhead, P. and Eckley, I.A., 2012. Optimal detection of changepoints with a linear computational cost. *Journal of the American Statistical Association, 107*(500), pp.1590-1598.

Levandowsky, M. and Winter, D., 1971. Distance between sets. *Nature, 234*(5323), pp.34-35.

Luo L., Ao X., Song Y., Li J., Yang X., He Q., & Yu D., 2019, Unsupervised Neural Aspect Extraction with Sememes, in *Proceedings of the Twenty-Eighth International Joint Conference on Artificial Intelligence, IJCAI-19*, pp:5123-5129.

Nancy C., 1992, MUC-4 Evaluation Metrics. In *Fourth Message Understanding Conference (MUC-4)*: Proceedings of a Conference Held in McLean, Virginia, June 16-18.

OpenAI, 2023, GPT-4 Technical Report.

Padmanabha, M., Beckenbach, L. and Streif, S., 2020. Model predictive control of a food production unit: a case study for lettuce production. *IFAC-PapersOnLine*, 53(2), pp.15771-15776.

Ramírez-Arias, A., Rodríguez, F., Guzmán, J.L. and Berenguel, M., 2012. Multiobjective hierarchical control architecture for greenhouse crop growth. *Automatica, 48*(3), pp.490-498.

Rawlings, J.B., Mayne, D.Q. and Diehl, M., 2017. *Model predictive control: theory, computation, and design* (Vol. 2). Madison, WI: Nob Hill Publishing.

Raza, H., Prasad, G. and Li, Y., 2015. EWMA model based shift-detection methods for detecting covariate shifts in non-stationary environments. *Pattern Recognition, 48*(3), pp.659-669.

Sathyanarayanan, K., Sauerteig P., Streif S., 2024. Deep neural network based optimal, control of greenhouses, accepted for presentation at *European Control Conference* (ECC).

Searchinger, T., Waite, R., Hanson, C., Ranganathan, J., Dumas, P., Matthews, E. and Klirs, C., 2019. Creating a sustainable food future: A menu of solutions to feed nearly 10 billion people by 2050. Final report.

Shanahan, M., McDonell, K. and Reynolds, L., 2023. Role play with large language models. *Nature, 623*(7987), pp.493-498.

Sharma, M., Brownstein, J.S. and Ramakrishnan, N., 2021, December. T 3: Domain-agnostic neural time-series narration. In *2021 IEEE International Conference on Data Mining (ICDM)* (pp. 1324-1329). IEEE.

Truong, C., Oudre, L. and Vayatis, N., 2020. Selective review of offline change point detection methods. *Signal Processing, 167*, p.107299.

Van Beveren, P.J.M., Bontsema, J., Van Straten, G. and Van Henten, E.J., 2015. Minimal heating and cooling in a modern rose greenhouse. *Applied energy, 137*, pp.97-109.

Van Henten, E.J. and Bontsema, J., 2009. Time-scale decomposition of an optimal control problem in greenhouse climate management. *Control Engineering Practice, 17*(1), pp.88-96.

Van Straten, G., van Willigenburg, G., van Henten, E. and van Ooteghem, R., 2010. *Optimal control of greenhouse cultivation*. CRC press.

Wei, J., Wang, X., Schuurmans, D., Bosma, M., Xia, F., Chi, E., Le, Q.V. and Zhou, D., 2022. Chain-of-thought prompting elicits reasoning in large language models. *Advances in neural information processing systems, 35*, pp.24824-24837.

Wei, S. and Xie, Y., 2022. Online kernel CUSUM for change-point detection. *arXiv preprint arXiv*:2211.15070.

Xu, X., Tao, C., Shen, T., Xu, C., Xu, H., Long, G. and Lou, J.G., 2023. Re-reading improves reasoning in language models. *arXiv preprint arXiv*:2309.06275.

Yang M., Qu Q., Tu W., Shen Y., Zhao Z., & Chen X., 2019, Exploring Human-Like Reading Strategy for Abstractive Text Summarization. In *Proceedings of the AAAI Conference on Artificial Intelligence*, vol. 33(01), pp:7362-7369.

Evaluation of machine learning-driven sensor networks for observing separation processes in combine harvesters for estimating separation efficiency

Kevin Penner [a,*], Marvin Barther [a,], Felix Wittenfeld [a], Michael Thies [a], Marc Hesse [a]**

[a] Cognitronics & Sensor Systems, Bielefeld University, Bielefeld, Germany

* Email: kpenner@techfak.uni-bielefeld.de

** Email: m.barther@uni-bielefeld.de

Abstract

Accurate measurement of combine harvester separation process efficiency - the amount of grain separated from straw and material other than grain (MOG) - is crucial to process automation and economic efficiency in agriculture. Traditional methods rely on structure-borne noise sensors for grain counting. In most combines of leading harvester manufactures there is a single sensor line at the end of the separation unit to measure the amount of grain within the straw fraction, some manufactures are already using multiple sensors. The signal processing underlies disturbance variables like varying grain, field, and weather conditions, which interferes with predictions for the separation process.

This study introduces a novel approach utilizing a large grid aligned sensor network within the combine harvester's separation unit, in conjunction with a suite of machine learning regression models. The models used to predict the separation efficiency are k-nearest neighbours (k-NN), support vector regression (SVR), decision trees (DT), fully connected neural networks (FCNN), convolutional neural networks (CNN), and recurrent neural networks (RNN). Through the analysis of sensor and combine setting data represented in one-, two-, and three-dimensional spatial tensor formats, we demonstrate that FCNNs and CNNs, especially with three-dimensional data representations, yield the highest prediction accuracy, while CNNs are the best models when just sensor data is considered.

Most models achieved validation accuracy, evidenced by an average R^2 score of up to 90 % with k-fold cross-validation on the limited recorded data, thereby proving their reliability across varying conditions. Machine learning models like k-NN or DT with an R^2 score of up to 79 % could not achieve such validation results. A major difference between CNNs and most other machine learning models is the inherent focus on location-dependent data due to the convolutional calculations, which indicates to be the main benefit in analysing separation processes.

Keywords: separation process, separation efficiency, sensor network, machine learning, neural networks

1. Introduction

Grain harvest is a seasonal process within a short period of time. The separation efficiency, which is the amount of grain separated from straw and material other than grain (MOG), must be as high as possible to minimize grain losses. The separation efficiency is crucial to process automation and economic efficiency of combine harvesters (P. Miu, 2015).

Using single sensors and polynomial functions (S. Nath et. al., 1982) was the first approach to predict grain losses. Structure-borne noise sensors were used for impulse measurements as grain counting signals. Soon after, the polynomial models and the sensor systems were developed further and the models were fit on multiple sensors, which were installed under the separation unit (A. Bjork, 1990; C. Liu, 1990; C. Liu and J. Leonard, 1993). For grain counting, the piezoelectric sensors (S. Meyer zu Hoberge and U. Hilleringmann, 2011) and acoustic sensor systems (J. N. Gelinske et. al., 2015) have become common. The manufacture AGCO protected by patent using multiple sensors at specific positions (J. Koch et. al., 2019).

While grain loss monitors can directly be used as input value for machine optimization algorithms based on machine learning models like neural networks (NN) (T. M. Gundoshmia et. al., 2020; T. Kösters and O. Nelles, 2023), machine learning models can be designed as virtual grain loss sensors, which are based just on combine settings (M. Isa Bomoi et. al., 2023). The manufacture John Deere protected by patent a specific

model of virtual grain loss sensors based on NNs as reference for the physical grain loss sensors (W. Yu et. al., 2020).

The utilisation of deep learning methodologies for extracting higher-level abstractions from sparsely distributed data points has found application across diverse domains. For instance, C. Bilgera et. al. (2018) used a distributed sensor network comprising gas sensors employs a convolutional neural network with long short-term memory units (CNN-LSTM) architecture to process sparse data and infer spatio-temporal patterns. Similarly, O. Costilla-Reyes et. al. (2018) demonstrates the effectiveness of capturing spatio-temporal characteristics by examination of human gait pattern classification using plastic optical fibre sensors arranged on a mat, employing a CNN 3D architecture. These investigations illustrate the versatility of machine learning methodologies, particularly within image-based data modalities, for analysing spatial-temporal data structures and deriving actionable insights.

In this study, utilizing a large grid aligned sensor network within the separation unit of the combine harvester, we introduce different machine learning regression models for separation efficiency prediction. Due to the required ability to run on combine harvesters during the harvest process, we focus on adapting the model size and type to ensure compatibility with resource-limited hardware. Additionally, the models undergo testing on consumer hardware CPUs and GPUs, as well as with a TinyML framework on a resource-constrained microcontroller platform (µC).

2. Materials and Methods

In this section, we describe the experimental setup of the sensor network, the recordings of the reference data and give an overview of the considered machine learning models for regression. At last, we dive into the datasets and their representations and the model evaluation methodology.

2.1. Experimental Setup

A grid aligned sensor network with almost 100 structure-borne noise sensors has been installed under the separation unit of the combine harvester. The sensor signals have been optimized for measuring grain. The sensor network output is defined as a two-dimensional (2D) array with grain counting values. However, individual positions within the sensor array may remain unoccupied, either due to non-essential symmetry in sensor placement or variations in sensor-to-sensor spacing.

The data has been recorded during grain harvest seasons with focus on wheat in Central Europe in different years, which presented contrasting grain, field, and weather conditions. The sensor network has been lined up in multiple combine harvesters. The tests contain different combine settings and throughputs, with repetitions in years and on different fields. The test runs include initialization periods to reach a steady state operation, test periods within the steady state operation, and a shut-down period. The sensor network has been recorded continuously at a sampling rate of 1 Hz, along with combine settings like revolution speeds or sieve openings and material characteristics like throughput or moisture.

As reference, the grain loss mass flow of the separation unit Q_{out} (Figure 1) has been collected selectively during the test periods within steady state operations. Grain has been separated from MOG with a semi-automated cleaning process and the separation efficiency has been calculated. Time stamps for selective material collection have been generated with automatic trigger for precise reference with the sensor network.

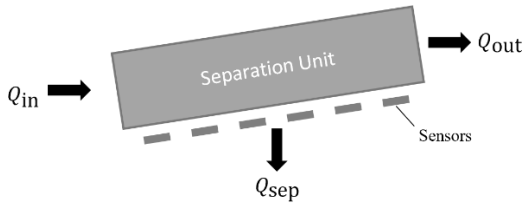

Figure 1. Grain mass flow diagram of a combine harvester's separation unit with Q_{in} as the combine input grain mass flow, Q_{sep} as the separated grain mass flow, and Q_{out} as the grain loss mass flow.

The separation efficiency W is defined as the relation between the separated grain mass flow Q_{sep} and the input grain mass flow Q_{in} as shown in Figure 1 (P. Miu 2015). The separated grain mass flow can be

calculated by the difference between the input grain mass flow Q_{in} and grain loss mass flow Q_{out} (Equation 1). The mass flows are measured in $t \cdot h^{-1}$.

$$W = \frac{Q_{\text{sep}}}{Q_{\text{in}}} = \frac{Q_{\text{in}} - Q_{\text{out}}}{Q_{\text{in}}} \quad (1)$$

2.2. Overview of Machine Learning Models for Regression

In this section, we look at the machine learning methods used in this study, explaining the comprehensive range of algorithms used for regression analysis. These include traditional models (T. Hastie et. al., 2009) such as k-nearest neighbours (k-NN), support vector regression (SVR) and various decision trees (DT), as well as advanced NN architectures (C. C. Aggarwal, 2018) such as fully connected neural networks (FCNN), convolutional neural networks (CNN), and recurrent neural networks (RNN). The algorithm selection process is based on a comparative analysis to identify the most suitable method for our regression problem. The aim is to identify the most effective algorithm that meets the specific requirements of our data and optimizes performance for our target regression results.

The **k-NN** algorithm is a non-parametric method used for regression. It analyses the k most similar instances (neighbours) in the training data to predict the output variable for a new sample. As a non-parametric method, it does not make strong assumptions about the form of the mapping function from inputs to outputs. This allows it to adapt to various data distributions. The prediction is often the mean of the target values of the nearest neighbours. The effectiveness of k-NN in regression problems depends on the choice of k and the distance metric used to identify the nearest neighbours.

SVR adapts the support vector machine framework for regression tasks by implementing a margin of tolerance (ε), which defines an error-insensitive zone around the regression line. This mechanism allows SVR to fit the data within a specified margin while minimizing deviations and enhancing model robustness. SVR is particularly adept at handling high-dimensional data, as it implicitly maps inputs into a higher-dimensional space to accommodate complex data structures and non-linear relationships. SVR's versatility is further enhanced through various kernel options, allowing customisation to different data types. The model's performance and complexity can be fine-tuned using parameters such as the regularisation parameter C and ε, which balance between training accuracy and generalisation.

DTs, including CART and ExtraTrees, are flexible algorithms for classification and regression tasks. CART uses features and thresholds for maximum information gain at each node, while ExtraTrees builds multiple trees and averages to increase accuracy and minimize overfitting. DTs are valued for their interpretability because they provide a clear insight into how decisions are derived from data features. However, they tend to overfit, especially when the trees are deep.

FCNNs, also known as dense neural networks, consist of multiple layers of interconnected neurons. In regression tasks, FCNNs show an exceptional ability to model complex non-linear relationships by adjusting weights and biases. Key parameters that affect performance include the depth, width, and activation functions of the network. However, their "black box" nature can affect the understanding of their decision-making processes. In contrast to the traditional DT, SVR and k-NN methods, FCNNs can handle larger and more complex datasets, but require more computational resources and are less interpretable.

CNNs are particularly adept at image processing and are also well suited to regression tasks involving spatial or temporal data, even image-like sensor grid data. Using convolutional layers, CNNs learn spatial feature hierarchies so that they are capable to recognize underlying patterns in datasets with spatial relationships. While CNNs are valued for their ability to process large amounts of data and their efficiency in feature extraction, they require significant computational resources and have longer training times than FCNNs. However, the pattern recognition capability of CNNs comes at a higher price in terms of complexity and lower interpretability compared to simpler models such as DTs.

RNNs are designed to process sequential data and are therefore well suited to time series regression tasks. They contain feedback loops that allow information to persist and influence future outputs, capturing the temporal dynamics and dependencies within the data. Advanced variants such as Long Short Memory (LSTM) and Gated Recurrent Unit (GRU) further enhance this capability. A regression part, usually consisting of FCNN layers, is typically attached to translate temporal features into precise continuous outputs. To reduce the number of parameters for the LSTM layers and to give rise to neighbourhood dependency processing, structures of RNN with preceding FCNN (NN-RNN) or CNN (CNN-RNN) are considered.

2.3. Strategies for Model Evaluation, Representation, and Optimization

This section outlines our approach to assessing and refining machine learning models for regression tasks by detailing our dataset and the used data representations, by presenting our use of k-fold cross-validation to partition our dataset, and by describing our approach to measuring inference runtime on diverse hardware to test the practicality of our models for real-world scenarios.

2.3.1. Datasets and Model Configuration

The sensor network has been recorded continuously. For training and validation, only data from the test periods have been considered. The data has been latency corrected. After selecting for viable data, there are more than 8,000 data points with known separation efficiency.

The data can be represented in different structures: The simplest way is the vector representation. The sensor values, combine settings, and material characteristics are stored in specific order in a vector (Figure 2 (a)). This data representation can be used for most machine learning algorithms like k-NN, SVR, DT, FCNN, RNN, and NN-RNN. To support neighbourhood dependencies, the sensor values can be represented by a 2D array (Figure 2 (b)) for CNN and CNN-RNN models. The combine settings and material characteristics are stored in a data vector, which is a parallel input next to the convolutional layers. To support additional data dependencies of the sensor values, the sensor network can be represented by a three-dimensional (3D) array (Figure 2 (c)). The sensor values are stored in one array layer. Other layers can contain sensor-specific data such as sensor positions or sizes, as well as combine settings or material characteristics specific to certain positions. Sensor unspecific data is stored in the data vector as before.

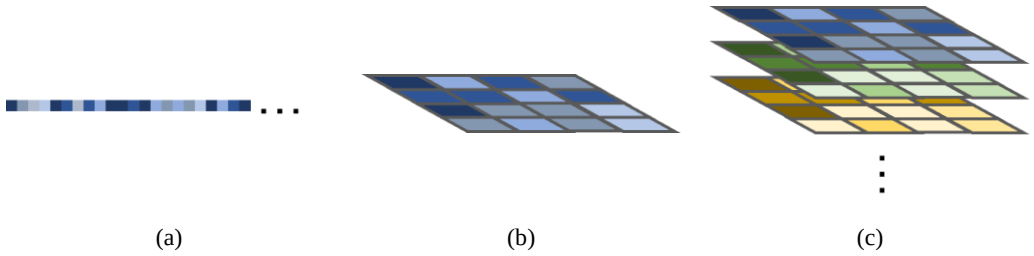

(a) (b) (c)

Figure 2. Data representations for NNs: The vector representation in (a), the 2D representation for sensor values in (b) and the 3D representation for sensor values and sensor specific meta data in (c).

All data has been normalized. The sensor values are normalized to the maximum sensor value of the current time stamp. The combine settings and material characteristics have been normalized to the interval of expected values.

To research combine setting and material characteristic dependencies, the models are trained with different input types: The smallest input data amount is using just sensor values, the highest is using the sensor values with all additional data containing combine settings and material characteristics. For CNNs, sensor meta information like sensor positions can be included and sensor specific combine settings and material characteristics can be coded in array layers. In Table 1 there is an overview of all input types and their signs in the model names.

Table 1. Description of the different input types for all models and their signs in model names.

Sign	Models	Description
(V)	all	Just sensor values.
(A)	all	All data.
(DS)	CNNs	Sensor values and sensor meta information.
(DA)	CNNs	Sensor values, sensor meta information, and sensor specific coded combine settings and material characteristics.

The model sizes and for NNs the layer designs are crucial for the results. We carefully designed all considered models to have a reasonable parameter count with respect to the training data point count. The

biggest model is the NN-RNN (A) with 7,841 parameters. For each considered NN model FCNN, CNN, RNN, NN-RNN, and CNN-RNN we designed different models varying in layer depth, sequence, and type. Only the best model is considered in this study.

2.3.2. Cross-Validation Strategy and Evaluation Metrics

The k-fold cross-validation is well-established for ensuring robust model generalisability on small amounts of data. Eight k-folds have been identified for validation data, containing for example a mixture of tests of different years and tests of just a single year or tests with a uniform mixture of combine settings and tests with only combine boundary settings. The train-validation-split is done test-wise. The amount of validation data points is varying between 19 % and 25 %. Due to machine symmetry the data has been augmented by mirroring along the machine length, giving rise to more than 16,000 data points in total.

The models have been optimized and trained on the root mean squared error (RMSE, J. M. Wooldridge, 2015). For comparison, both RMSE and the coefficient of determination R^2 (J. M. Wooldridge, 2015) are considered.

2.3.3. Hardware Platform Performance Assessment

By investigating the runtime inference performance of our models on different hardware platforms, we aim to ensure their practical utility in diverse environments, including resource-constrained settings. Understanding how our models perform on various hardware configurations enables us to optimize them for deployment on edge devices, which may include those integrated within the combine harvester. This assessment provides crucial insights into the computational efficiency of our models, guiding us in tailoring them to meet the specific requirements of edge hardware. CPUs and GPUs run the models in a Python environment on Ubuntu 22, while the µC utilizes TensorFlow Lite Micro (R. David et. al., 2020) on Mbed OS. Our focus is on assessing model performance without quantization or pruning, using float32 parameters, to understand their raw computational efficiency on diverse hardware configuration.

3. Results

In Figure 3, the k-fold cross validation average results of RMSE and R^2 of all models with combine settings and material characteristics as input are listed. The FCNN is the best model with a RMSE of 0.60 % and an R^2 of 90.58 %, directly followed by the CNN with considered sensor specific values, combine settings, and material characteristics (A). All recurrent models and k-NN are worse than FCNN and CNN, with the best RMSE of 0.87 % and R^2 of 82.19 %. DTs and SVR are the worst models, considering the RMSE. While DTs have the worst R^2, the SVR models with an R^2 to up to 83.24 % seem to be as good as FCNN and CNN, but the RMSE is much higher.

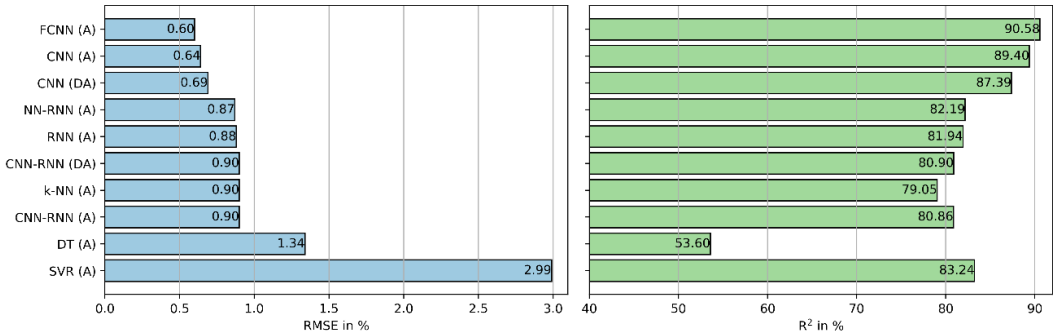

(a) (b)

Figure 3. Average RMSE in (a) and average R^2 in (b) of the k-fold cross validation results of all models with combine settings and material characteristics (input types A and DA).

In Figure 4, the k-fold cross validation average results of RMSE and R^2 of all models without combine

settings and material characteristics as input are listed. The CNN is the best model for both input types (DS, V) with a RMSE of 0.75 % and an R^2 of 84.76 %. The FCNN is directly following. Again, recurrent models and k-NN are worse than CNN and FCNN, while k-NN is slightly leading this group. DTs still do not get good results as the NNs and the SVR with an R^2 of 85.41 % being better than CNN still has the worst RMSE.

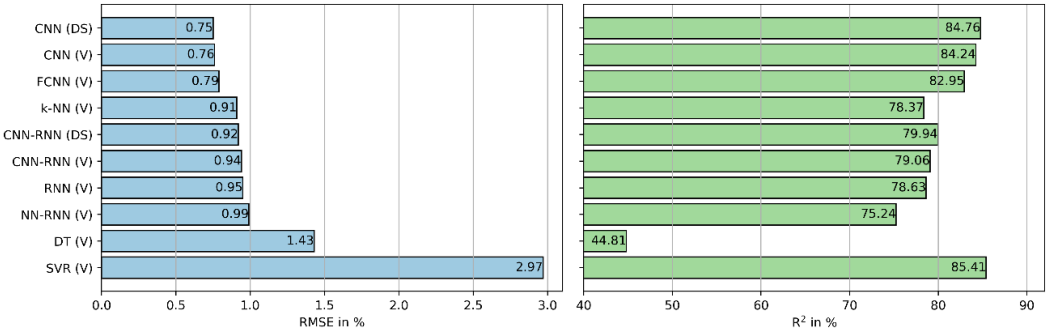

(a) (b)

Figure 4. Average RMSE in (a) and average R^2 in (b) of the k-fold cross validation results of all models with only sensor values or sensor values and sensor meta information (input types V and DS).

The evaluation of advanced CNN and FCNN models across various computational platforms, including CPUs, GPUs, and a µC, has demonstrated considerable performance capabilities (Figure 5). For CPUs, the AMD Ryzen 9 5950X, with a 3.4 GHz clock speed and 16 cores, achieved the best inference time at approximately 22 milliseconds. This showcases its suitability for high-throughput tasks, although standard consumer CPUs also performed robustly, confirming their adequacy for complex model computations. The performance variance among the CNN and FCNN models on these CPUs was notably small.

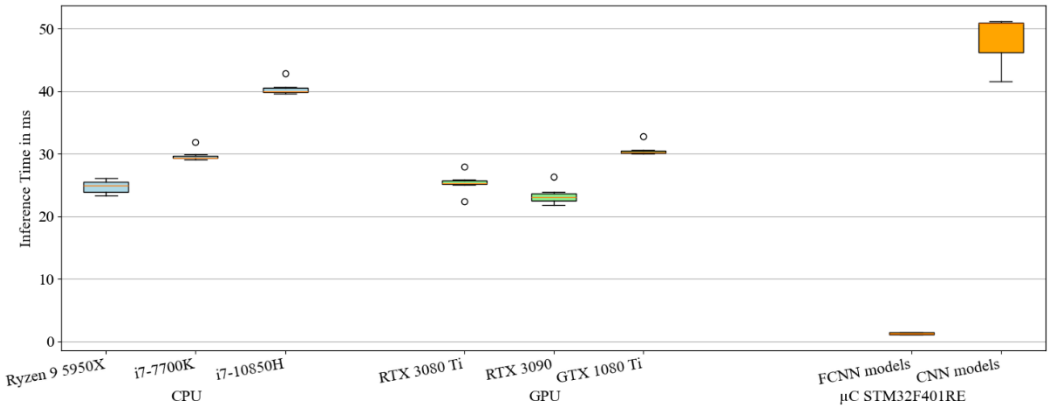

Figure 5. The boxplots display inference times for top-performing CNNs and FCNNs on CPUs (AMD Ryzen 9 5950X, Intel i7-7700K, Intel i7-10850H) and GPUs (NVIDIA RTX 3080 Ti, RTX 3090, GTX 1080 Ti), each based on the average of 100 runs. For the STM32F401RE µC, inference times for FCNNs and CNNs are plotted separately to highlight performance differences for this resource-constrained hardware.

GPU performance was also strong, with inference times spanning from 22 to 30 milliseconds, indicating that these devices are well-equipped to handle NN tasks efficiently. In contrast, the µC STM32F401RE with an 80Mhz clock speed showed a greater disparity in performance times: FCNNs were exceptionally fast, clocking in at around 1 millisecond, while CNNs lagged significantly, requiring over 51 milliseconds. This discrepancy can be attributed to the different requirements of the two network types and their execution on µCs. CNNs, which require extensive matrix multiplications and multiple filters, inherently require more operations between layers, which further increases their computational load. Despite the increased

requirements, the performance of both types of networks on µCs is very close to that of more robust CPUs and GPUs. This unexpectedly high efficiency is due to the lower overhead of µCs, simpler threading and the use of C programming, which reduces overhead and optimizes performance in resource-constrained environments.

Given that sensor data is sampled at 1 Hz, all tested hardware configurations comfortably met the operational requirement of sub-second execution times. This performance underscores the feasibility of deploying these models on even the most resource-constrained devices such as µCs that operate in the milliwatt power range, broadening the scope for applying deep learning technologies in environments where power efficiency and space are critical constraints.

4. Discussion

The models FCNN and CNN are the most effective at predicting separation efficiency. The inclusion of additional information leads to improved RMSE and R^2. However, when using only sensor values or values combined with sensor-specific information, the CNN is more resilient due to its focus on location-dependent calculations. This suggests that sensor neighbourhood information is crucial for the prediction of separation efficiency with only sensor values.

Surprisingly, recurrent models are the worst NN models. But the data sets contain just data from regular steady state harvest operations. These models could have an advantage over non-recurrent models if initializing harvesting periods, combine setting changes, or harvest condition changes were included. The regression models k-NN, DT and SVR are the worst of all considered models, even though the R^2 of the SVR models were at the same scale as the FCNN and CNN.

The inference time measurements demonstrate that both FCNNs and CNNs are suitable for real-time applications, particularly given the 1 Hz sensor measurement rate in sensor acquisition systems. All tested platforms, including the resource-constrained STM32F401RE µC, delivered inference times well below the one-second threshold required for real-time decision-making. The use of µCs, which typically have less overhead and a simpler threading architecture than CPUs and GPUs, enhances real-time capabilities, making them particularly effective for tasks like on-the-fly grain separation efficiency predictions. This ensures that regardless of the hardware's computational power, the deployment of these models remains feasible for real-time applications.

5. Conclusion

In this study, we validated different machine learning models for grain separation efficiency prediction. Taking all data into account, including combine settings and material characteristics, the FCNN is the most precise model. But processing just on sensor values, the CNN models are recommended. The main advantage of CNN models is the inherent focus on location-dependent data due to the convolutional calculations.

Having very different results depending on the input type for each considered model, the expert knowledge about model design and input shapes still has an important impact on model results. Additionally, data pre-processing including data collection, data reference, data latency correction, and data sorting is still fundamental for machine learning.

For this study, just a data amount of more than 8,000 samples of regular steady state harvesting operations was available from Central Europe. To give rise to more data variability in grain, field, and weather conditions, more data should be collected in several harvest seasons and in different countries. Even though operating combine harvesters in steady states is recommended, the non-steady state operations should also be analysed for advantages of recurrent models. Additionally, these models should also be tested with other grain than wheat, but with similar harvesting conditions like barley, rye, triticale, canola, or maize.

Finally, the sensor network still contains many sensors. There are investigations needed to reduce the number of sensors. Respectively, it is recommended to research sensor anomalies and to analyse sensor network reduction conditionally on sensor anomaly influence on grain separation efficiency prediction.

Acknowledgements

This research and development project was funded by the Ministry of Economic Affairs, Industry, Climate Action and Energy of the State of North Rhine-Westphalia (MWIKE), Germany, in the context of

the Leading-Edge Cluster “Intelligent Technical Systems OstWestfalenLippe (it‘s OWL)” and supervised by Project Management Jülich (PtJ). The responsibility for the content of this publication lies with the authors.

The authors would like to thank Bielefeld University and CLAAS for their cooperation and contributions to this work.

References

J. Adebayo, G. J., M. Muelly, I. Goodfellow, M. Hardt, and K. B, 2018. Sanity Checks for Saliency Maps. In *Advances in Neuronal Information Processing Systems*. Volume 31, https://doi.org/10.48550/arXiv.1810.03292.

C. C. Aggarwal, 2018. Neural Networks and Deep Learning. Springer, Cham, Switzerland, ISBN 978-3-319-94462-3, https://doi.org/10.1007/978-3-319-94463-0.

C. Bilgera, A. Yamamoto, M. Sawano, H. Matsukura, H. Ishida, 2018. Application of Convolutional Long Short-Term Memory Neural Networks to Signals Collected from a Sensor Network for Autonomous Gas Source Localization in Outdoor Environments. In *Sensors*, https://doi.org/10.3390/s18124484.

A. Bjork, 1990: A three-dimensional arithmetic model to calculate grain separation and losses for a rotary combine. In *Canadian Agricultural Engineering*. Nacka, Sweden, November 26.

M. I. Bomoi, N. M. Nawi, S. A. Aziz, and M. S. M. Kassim, 2023: Application of Artificial Neural Networks and Genetic Algorithm for the Prediction of Grain Loss from a Medium-sized Combine Harvester. In *XL CIOSTA & CIGR Section V International Conference*, Évora, Portugal. September 10-13, https://doi.org/10.2478/jaiscr-2014-0017.

O. Costilla-Reyes, P. Scully and K. B. Ozanyan, 2018. Deep Neural Networks for Learning Spatio-Temporal Features From Tomography Sensors. In *IEEE Transactions on Industrial Electronics*, vol. 65, https://doi.org/10.1109/tie.2017.2716907.

R. David, J. Duke, A. Jain, V. Janapa Reddi, N. Jeffries, J. Li, N. Kreeger, I. Nappier, M. Natraj, S. Regev, R. Rhodes, T. Wang, and P. Warden, 2020. TensorFlow Lite Micro: Embedded Machine Learning on TinyML Systems, https://doi.org/10.48550/arXiv.2010.08678.

J. N. Gelinske, B. D. Batcheller, P. A. Nystuen, A. A. Reich, B. R. Thurow, and B. K. Schleusner, 2015 US9631964, 2015. Acoustic Material Flow Sensor. United States Patent, No. US 9,631,964.

T. M. Gundoshmian, S. Ardabili, A. Mosavi, and A. R. Várkonyi-Kóczy, 2020. Prediction of Combine Harvester Performance Using Hybrid Machine Learning Modeling and Response Surface Methodology. In *INTER-ACADEMIA 2019*. Switzerland, Springer Nature Switzerland, pages 345-360, https://doi.org/10.20944/preprints201908.0202.v1.

T. Hastie, R. Tibshirani and J.H. Friedman, 2009. The elements of statistical learning: data mining, inference, and prediction, Vol. 2, by Springer, New York, USA, https://doi.org/10.1007/b94608.

J. Koch, J. Leininger, G. R. Johnson, 2019. Harvesting Machine with Visualization System. World Intellectual Property Organization, International Patent Application, No. WO 2019/171246.

T. Kösters and O. Nelles, 2023: Nonlinear Dynamic System Identification of Separation Uni for Raw Materials. In *2023 IEEE Conference on Control Technology and Applications (CCTA)*. Bridgetown, Barbados, August 16-18, https://doi.org/10.1109/ccta54093.2023.10253214.

C. Liu, 1990: Microprocessor Based Real-Time Grain Loss Monitoring and Prediction System for an Axial-Flow Combine. Department of Agricultural Engineering, University of Alberta, Edmonton, Alberta, Canada, https://doi.org/10.1016/0168-1699(93)90041-X.

C. Liu and J. Leonard, 1993. Monitoring actual grain loss from an axial flow combine in real time. In *Computers and Electronics in Agriculture*. Amsterdam, Netherlands, May 19, pages 231-242, https://doi.org/10.1016/0168-1699(93)90041-X.

S. M. Lundberg and S.-I. Lee, 2017. A Unified Approach to Interpreting Model Predictions. In *Advances in Neuronal Information Processing Systems*, Volume 30, https://doi.org/10.48550/arXiv.1705.07874.

S. Meyer zu Hoberge and U. Hilleringmann, 2011: Piezoelectric Sensor Array with Evaluation Electronic for Counting Grains in Seed Drills. In *IEEE Africon 2011 - The Falls Resort and Conference Centre*. Livingstone, Zambia, September 13-15, https://doi.org/10.1109/AFRCON.2011.6072063.

P. Miu, 2015. Combine Harvesters. Theory, Modeling, and Design. USA, July 16. Boca Raton, Florida: CRC Press, Taylor & Francis Group, https://doi.org/10.1201/b18852.

S. Nath, W. H. Johnson, and G. A. Milliken, 1982. Combine Loss Model and Optimization of the Machine System. In *American Society of Agricultural Engineers 0001-2351*. January 1982, https://doi.org/10.13031/2013.33526.

S. Wachter, B. Mittelstadt, and C. Russel, 2017. Counterfactual Explanations without Opening the Black Box: Automated Decisions and the GDPR. In *Harv. JL & Tech*. Volume 31, page 841, https://doi.org/10.2139/ssrn.3063289.

J. M. Wooldridge, 2015. Introductory econometrics: A modern approach. Mason, USA, South-Western, 5th edition, pages 38, 659, https://doi.org/10.1002/jae.665.

W. Yu, V. Fuchs, and W. Todd, 2020. Virtual Sensor for Grain Loss in Combine Harvester. European Patent Application, No. EP 3 744 167.

Hyperspectral Imaging Based on AI Algorithms for Early Detection of Plant Fungal Diseases

Panagiotis Christakakis [a], Nikolaos Giakoumoglou [a], Christos Klaridopoulos [b], Eleni Kalogeropoulou [c], Dimitrios Tzovaras [a], Eleftheria-Maria Pechlivani [a,*]

[a] Information Technologies Institute, Centre for Research and Technology Hellas, 57001 Thessaloniki, Greece

[b] iKnowHow S.A., 15451 Athens, Greece

[c] Benaki Phytopathological Institute, 14561 Athens, Greece

* Corresponding author. Email: riapechl@iti.gr

Abstract

In agriculture, timely intervention of crop pathogens is crucial, as fungal pathogens worldwide cause significant crop losses worth $100-$200 billion annually. To mitigate such substantial economic losses, Artificial Intelligence (AI) plays a vital role in early detection process. Currently, potential infections are visually detected and confirmed through laborious laboratory analyses. Early detection is crucial not only for the rapid disease control strategies but also to minimize impacts on crop production and the environment. This study aims to detect grey mould caused by *Botrytis cinerea* on cucumber plants, early by integrating Deep Learning (DL) techniques and multispectral imaging. Cucumber leaves were artificially inoculated with *B. cinerea* and employing multispectral imaging in the initial days post-inoculation, a dataset was created for diverse DL models. Both classification and object detection techniques were employed, demonstrating remarkable accuracy. The best-performing classification model achieved 0.93 accuracy and 0.89 F1-score, while the object detection model reached 0.88 mAP_{50} (mean Average Precision), providing valuable insights into informative wavelengths. Further research focused on the more challenging DL task of semantic segmentation, creating a comprehensive dataset featuring healthy and infected plants subjected to two different inoculation methods. DL models were developed to segment specific leaf regions. The dataset contained photographs of the cucumber plants captured with a multispectral camera during the experiment, focusing on the early days, to test whether it is possible to detect early symptoms that are invisible to the naked eye. The resulting model exhibited impressive accuracy of 0.90 and a Dice Coefficient of 0.67. The model effectively detected early symptoms from the second to the sixth day, providing a crucial window for timely intervention. These implementations showcase AI's potential for early pathogen detection in agriculture. Applying these models to autonomously navigated agro-robots and mobile apps can enhance real-time monitoring, enabling efficient and timely proactive disease management strategies.

Keywords: artificial intelligence, deep learning, hyperspectral imaging, early detection, smart agriculture

1. Introduction

Botrytis cinerea is a destructive fungus that affects over 500 different types of plants, leading to significant economic losses in agriculture (Williamson *et al.*, 2007) [1]. Each year, it causes damage exceeding $10 billion globally due to reduced crop production (Weiberg *et al.*, 2013) [2]. It is ranked as the second most significant plant pathogen because of these factors (Dean *et al.*, 2012) [3].

Cucumber (*Cucumis sativus*) is a widely cultivated plant, revered for its nutritional and economic value globally (Mallick, 2022) [4]. As a significant component of the agricultural sector, cucumber serves not just as a staple in dietary consumption but also plays a role in various industrial applications (Mallick, 2022) [4]. However, like many crops, cucumber plants are susceptible to a range of diseases, with *B. cinerea* being one of the most devastating (Ben-Shalom *et al.*, 2003) [5].

The significant economic impact of B. *cinerea* is a concern for farmers, economists, and policymakers. Its ability to quickly infect a wide range of hosts, particularly in greenhouse settings, underscores the need for innovative detection methods. Traditionally, B. *cinerea* management relies on fungicides once symptoms appear. Early detection is crucial for preserving crop yield and quality and controlling pathogen spread. However, current diagnostic methods like ELISA and PCR are complex, expensive, and time-consuming (Weßling and Panstruga, 2012) [6]. Thus, there's a pressing need for advanced, rapid, and precise detection technologies to mitigate economic losses by detecting and managing the disease early.

Spectral imaging has emerged as a tool for non-invasive crop assessment, improving plant disease

detection (Terentev *et al.*, 2022) [7]. By capturing images across different spectral bands, multi-spectral imaging offers high-resolution insights, especially for vegetables (Pechlivani *et al.*, 2023) [8]. The Near-Infrared (NIR) spectrum is notable in plant pathology for its ability to identify infected leaf areas with precision (Fahrentrapp *et al.*, 2019) [9], potentially revealing disease-related physiological changes before visible symptoms manifest.

Recent advancements in Deep Learning (DL) have revolutionized computer vision, offering new avenues for early pest and disease detection in crops (Singh *et al.*, 2016) [10]. Convolutional Neural Networks (CNN) and Vision Transformers (ViTs) have demonstrated potential in improving the efficiency and accuracy of detection, particularly in the initial stages. Additionally, integrating CNNs with multi-spectral imaging enhances the comprehensiveness and detail of analysis, significantly improving disease diagnosis accuracy and precision (Piao *et al.*, 2019) [11].

This paper aims to highlight earlier research from our team already published that prompted us to conduct further study on the early detection of B. *cinerea* in Cucurbitaceae crops before symptoms responses become visible to the human eye. Our past study presented here (Giakoumoglou *et al.* (2023) [12]), investigates the effectiveness of multi-spectral imaging combined with DL models for B. *cinerea* detection in cucumber plants. The paper contributes by establishing a multi-spectral image dataset, conducting experiments for detection and classification, and exploring the usefulness of the NIR spectrum for identification. Building upon this foundation, our new approach (Giakoumoglou *et al.* (2024) [13]) proposes a novel methodology for early B. *cinerea* detection at all disease stages in Cucurbitaceae crops. Robust DL segmentation models are developed and tested using a specially created imagery dataset based on artificially inoculated plants. These models utilize multi-spectral imaging to capture various disease stages within the first week of growth, providing detailed insights from barely visible symptoms to late-stage disease signs. This dataset serves as a valuable resource for developing DL models to detect B. *cinerea*.

2. Materials and Methods

2.1. Classification and detection of *Botrytis cinerea* cucumber plants using multi-spectral imaging

Giakoumoglou *et al.* (2023) [12] explored the use of multi-spectral imaging to detect B. *cinerea* in cucumber plants with DL models. This study had three main goals: i) create a multi-spectral image dataset for detecting and classifying B. *cinerea*-infected and healthy plants, ii) experiment with detection and classification methods to find the best approach, and iii) assess the usefulness of the NIR spectrum for identifying B. *cinerea* and determine the most important spectral band.

2.1.1. Dataset

Healthy cucumber plants (Cucumis sativa variety MURAT F1) were artificially inoculated with B. *cinerea* for data collection. Spores from 3-week-old cultures grown on Potato Dextrose Agar were suspended in glucose water, filtered, and adjusted to 1×10^5 spores/ml. Four inoculated cucumber plants and four control plants were used. Lesions were created on leaves, and inoculum droplets were applied. The inoculated plants were covered to maintain moisture. Multi-spectral images were captured using a Qcell MUSES9-MS camera at six wavelengths (460, 540, 640, 700, 775, and 875 nm) over five days, starting immediately after inoculation. Images were taken daily at 12:00 under both artificial and natural light to capture early fungal symptoms not visible to the naked eye (Figure 1).

The dataset contains 121 annotated images (98 symptomatic, 23 healthy), with bounding boxes around infected and healthy leaves. A custom leaf detector, based on YOLOv5 (Jocher *et al.*, 2022) [14] and trained on the PlantDoc dataset (Singh *et al.*, 2020) [15], was used to annotate the images, with adjustments by an agronomist. This resulted in 580 annotated leaves (138 infected, 442 healthy).

Two datasets were created: *Botrytis-detection* (bounding box annotations) and *Botrytis-classification* (cropped images of each bounding box). Both datasets were split into training and testing sets, with all images of one specific infected plant reserved for testing to ensure unbiased model training. The image counts for each dataset are detailed in “Table 1” of Giakoumoglou *et al.* (2023) [12].

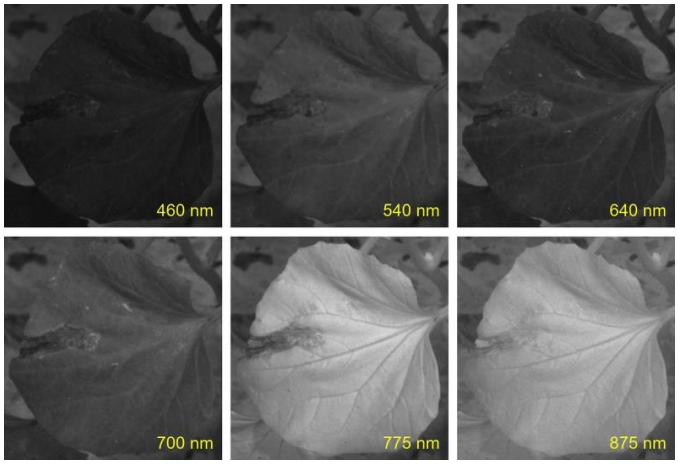

Figure 1. The six different spectral bands (460, 540, 640, 700, 775, 875) of a cucumber leaf infected with B. *cinerea*, captured 4 days post inoculation, from the *Botrytis-classification* dataset [12].

2.1.2. Experiments and evaluation metrics

The Botrytis datasets were evaluated through two main tasks: classification using CNNs on the *Botrytis-classification* dataset, and object detection on the *Botrytis-detection* dataset with bounding box annotations. The goal was to identify the most informative wavelengths for detection by leveraging classification results.

For classification, the F1-score was the primary metric, with accuracy, recall, and precision also reported. Accuracy indicates overall model performance, precision measures relevance of identified objects, and recall assesses the model's ability to find all relevant cases. For object detection, COCO detection metrics (Lin *et al.*, 2015) [16] were used, including mean average precision (mAP) across 10 IoU thresholds (0.5 to 0.95) and mAP at IoU = 0.5 (mAP_{50}). Precision and recall were also measured.

Data augmentation techniques were employed to improve model generalization due to the limited dataset size. For the *Botrytis-classification* dataset, techniques included horizontal flipping, scaling, and translation. For the *Botrytis-detection* dataset, mosaic augmentation (Bochkovskit *et al.*, 2020) [17] was used to address occlusion and translation issues. These techniques were applied only during training, not evaluation.

2.2. Early detection and segmentation of *Botrytis cinerea* cucumber plants

Building on the promising findings from our previous research, we expanded our efforts by curating a novel dataset and refining DL segmentation models (Giakoumoglou *et al.* (2024) [13]). Our goal was to precisely segment leaves affected by B. *cinerea*, with a primary focus on early detection.

2.2.1. In planta assays and disease assessment

This study used cucumber (Cucumis sativus L.) cv. Hasan from the Green Baboo variety. Seedlings with fully expanded first true leaves were transplanted into 24 cm diameter, 24 cm high plastic pots with sterile compost and grown in controlled environment chambers. Conditions were 21 ± 1°C, 16 hours of light at 352.81 µmol/sec, and 85%-90% relative humidity. Plants were irrigated twice weekly and kept under these conditions for about two months, mimicking greenhouse environments.

Botrytis *cinerea* was isolated from naturally infected cucumbers showing grey mould symptoms. The isolate was stored at −20°C in a conidial suspension (10^6 conidia/mL) in 20% aqueous glycerol (Decognet *et al.*, 2009) [18]. Before use, it was cultured on Potato Dextrose Agar (PDA) in Petri dishes and incubated at 21°C for seven days.

The bioassays at Benaki Phytopathological Institute (BPI) used two controlled environment growth chambers with identical conditions (21 ± 1°C, 16 h light/8 h dark, 85%–90% humidity) for B. *cinerea*-inoculated and mock-inoculated (water-treated) plants. Plants at the four-leaf stage were inoculated using two methods: (*i*) spraying leaves with conidial suspension until runoff (De Meyer *et al.*, 1998) [19] (method "A"), and (*ii*) placing mycelial plugs on leaves (method "B"). Mock inoculations followed the same procedure without the pathogen. Each group had 10 plants per inoculation method, with 29 mock-inoculated plants. After inoculation, plants were kept in the dark for 24 hours to promote conidia germination.

Each plant and leaf were numbered, and disease severity was assessed twice a week for 37 days post-inoculation (dpi). Disease severity, expressed as the percentage of infected leaf area, was transformed using the logit function (Eq. 1 in the research paper) to linearize the data (Campbell and Madden, 1990) [20]. Linear regression in SPSS was used to estimate the slope and intercept of disease progression for each leaf. The results provided stable and interpretable summaries, with slopes indicating constant infection rates. These models helped estimate the time of infection onset (y=0.001) for each leaf.

2.2.2. Image acquisition, annotation and dataset creation

For crops like vegetables, imaging in the visible (400-700 nm) and NIR (700-1300 nm) spectrums is particularly useful (Peñuelas and Filella, 1998) [21]. A customized Qcell Phenocheck camera, capturing wavelengths at 460, 540, 640, 775, and 875 nm, was used to collect multi-spectral images at 3096×2080 pixels resolution. Images were taken daily for the first five days post-inoculation and then weekly until 37 dpi, resulting in 1061 images: 418 from method A, 210 from method B, 355 from mock-inoculated method A, and 78 from mock-inoculated method B. An example of some individual spectra of a *B. cinerea*-inoculated plant can be seen in Figure 2.

(a) (b) (c)

Figure 2. Multi-spectral imaging of B. *cinerea*-inoculated plant. This figure showcases the individual spectra captured at different wavelengths: (a) 540 nm, (b) 640 nm, (c) 775 nm [13].

Images were annotated using Roboflow to classify leaves based on disease symptoms: "control", "healthy", "invisible", "visible", and "unaffected". A total of 373 leaves were labeled as "control", 2049 as "healthy", 269 as "invisible", 794 as "visible", and 283 as "unaffected". Images were then reclassified into three categories: "healthy", "invisible", and "visible". For training, B. *cinerea*-inoculated plants numbered 2, 3, 6-10, 12, 13, 15-20 were used, while 1, 5, 11, and 14 were for validation. Control plants 4-6, 8-10, 12-17, 19-29 were for training, and 1-3, 7, and 18 for validation. Detailed statistics are provided in Table 1.

Table 1. Dataset's class distribution statistics [13].

Proportion	Proportion	Proportion	Proportion
0-healthy	Train	1998	71.15%
	Valid	707	73.65%
1-invisible	Train	195	6.94%
	Valid	74	7.70%
2-visible	Train	615	21.90%
	Valid	179	18.65%

2.2.3. Deep learning segmentation training and evaluation metrics

The dataset, with three classes, was used to train DL models, resizing images to 1024×1024 pixels. Three architectures were employed: U-Net++, DeepLabV3, and DeepLabV3+. U-Net++ is an advanced U-Net for biomedical image segmentation, featuring a deeply-supervised encoder-decoder network with nested skip pathways for detailed feature extraction. DeepLabV3 uses atrous convolutions and spatial pyramid pooling for handling object scale and detail. DeepLabV3+ enhances this with an encoder-decoder structure for better segmentation precision. Encoders used included ResNet-34, ResNet-50, and MobileViT-S. ResNet-34 and ResNet-50 offer a balance of performance and efficiency, while MobileViT-S combines CNN and ViT strengths. Models were adapted to handle five spectral channels, fully utilizing the multi-spectral data for image segmentation. To adapt to the unique dataset comprising multi-spectral images, the input channels of these models were adjusted to process five distinct spectral channels.

The DL segmentation models were trained with specific hyperparameters. Each backbone was initially

randomized. U-Net++ used Dice loss combined with Binary Cross Entropy (BCE) loss, while DeepLabV3 and DeepLabV3+ employed Cross-Entropy (CE). To manage class imbalance, loss functions were weighted based on class frequencies, adjusted to range from 1.0 to 0.1. Optimizers varied: Adam and AdamW for U-Net++, Adam for DeepLabV3, and Nesterov momentum and AdamW for DeepLabV3+. Learning rates were set at $5 \cdot 10^{-4}$ for U-Net++, $5 \cdot 10^{-3}$ for DeepLabV3, and $2 \cdot 10^{-3}$ for DeepLabV3+. A 5-epoch warm-up phase used a learning rate ten times the base rate, followed by a cosine scheduler reducing the rate over 100 epochs. Weight decay was 10^{-4} for models with ResNet encoders and 10^{-2} for ViT encoders. Batch sizes ranged from 2 to 8 based on computational resources. For DeepLabV3+ with Nesterov momentum, the momentum coefficient was 0.9.

The DL segmentation models were evaluated using several metrics to assess accuracy, reliability, and effectiveness in identifying botrytis infection stages. Pixel accuracy measured the proportion of correctly classified pixels. Intersection over Union (IoU) assessed the overlap between predicted and actual labels, indicating the model's class differentiation ability. Recall evaluated sensitivity, and precision assessed specificity. The Dice Coefficient (DC) provided a comprehensive view of segmentation performance by combining precision and recall insights.

3. Results and Discussion

3.1. B. *cinerea* leaf classification and detection results

For the classification task, various state-of-the-art DL models were used, including AlexNet, DenseNet-121, EfficientNet B0 and B1, GoogLeNet, MobileNet v3 small, ResNet-18, ResNet-34, ResNet-50, and VGG-11 with and without Batch Normalization (BN). The aim was to find the best architecture for each wavelength combination.

All models were pre-trained on ImageNet and fine-tuned on the *Botrytis-classification* dataset. Only the last fully connected layer was modified from 1000 to 2 classes. Each model was fine-tuned using Stochastic Gradient Descent with a batch size of 16 for 100 epochs, a learning rate of 0.001 decaying every 30 epochs by a factor of 0.1, and weight decay and momentum parameters set to 0.0001 and 0.9, respectively. Input image size was 224×224. Experiments were implemented using PyTorch (Paszke *et al.*, 2019) [22].

Table 2 presents the classification performance metrics for models using triplet wavelength combinations. Tests with various vegetation indices (Calderón Madrid *et al.*, 2015) [23], all six wavelengths, and PCA-transformed wavelengths yielded poor results. The RGB and NIR wavelengths performed similarly across all metrics. However, the combination of 875 nm with 460 nm and 640 nm achieved the highest F1-score of 0.888 and the highest Recall, crucial for detecting B. *cinerea*. The top models also included the 875 nm wavelength, which boosted Recall. The VGG-11 with BN architecture showed high generalization ability, performing well regardless of input.

Table 2. Botrytis classification results [12].

Wavelength	Architecture	Acc.	F1	Rec.	Prec.
460, 540, 640	**ResNet-50**	**0.925**	**0.870**	**0.822**	**0.925**
460, 540, 700	DenseNet-121	0.850	0.822	0.881	0.951
460, 540, 775	Resnet-50	0.891	0.818	0.800	0.837
460, 540, 875	VGG-11 (BN)	0.911	0.853	0.844	0.863
460, 640, 700	VGG-11 (BN)	0.911	0.843	0.777	0.921
460, 640, 775	VGG-11 (BN)	0.911	0.853	0.844	0.863
460, 640, 875	**VGG-11 (BN)**	**0.932**	**0.888**	**0.888**	**0.888**
460, 700, 775	VGG-11 (BN)	0.918	0.857	0.800	0.923
460, 700, 875	VGG-11 (BN)	0.898	0.814	0.733	0.916
460, 775, 875	**Efficient Net B0**	**0.925**	**0.870**	**0.822**	**0.925**
540, 640, 700	ResNet-34	0.925	0.864	0.777	0.972
540, 640, 775	VGG-11	0.918	0.853	0.777	0.945
540, 640, 875	VGG-11 (BN)	0.918	0.866	0.866	0.866
540, 700, 775	VGG-11 (BN)	0.918	0.857	0.800	0.923
540, 700, 875	VGG-11 (BN)	0.918	0.869	0.888	0.851
540, 775, 875	**VGG-11 (BN)**	**0.925**	**0.876**	**0.866**	**0.886**
640, 700, 775	VGG-11 (BN)	0.925	0.867	0.800	0.947

640, 700, 875	VGG-11 (BN)	0.904	0.837	0.800	0.878
640, 775, 875	ResNet-50	0.918	0.853	0.777	0.945
700, 775, 875	**VGG-11 (BN)**	**0.925**	**0.870**	**0.822**	**0.925**

* The rows in **bold** indicate the trials with the highest F1-score.

For object detection, state-of-the-art DL models YOLOv5 and YOLOv7 (Wang *et al.*, 2022) [24] were evaluated on the *Botrytis-detection* dataset. YOLOv5 used CSP-Darknet53 as the backbone, while YOLOv7 used E-ELAN. Both models were trained with Stochastic Gradient Descent, a batch size of 8, a learning rate of 0.001, weight decay of 0.0001, and momentum of 0.937. Input image size was 1024×1024. Detection experiments were conducted using PyTorch.

Table 3 shows the detection results. YOLOv5m performed best among YOLOv5 variants, and YOLOv7-E6E excelled in the YOLOv7 category. The key metrics were *m*AP$_{50}$ and recall, which reflect the model's ability to detect Botrytis-infected leaves. The combination of 460, 640, and 875 nm achieved the highest *m*AP$_{50}$. However, for a better balance between *m*AP$_{50}$ and recall, the combination of 460, 775, and 875 nm was optimal, with a recall of 0.857, significantly higher than the best mAP50 model. Combining RGB and NIR bands improved performance, with the 875 nm wavelength being crucial for high accuracy in detecting Botrytis.

Table 3. Botrytis detection results [12].

Model	Wavelength	*m*AP$_{50}$	*m*AP	Prec.	Rec.
YOLOv5	460, 540, 640	0.866	0.738	0.877	0.768
YOLOv5	460, 640, 875	0.838	0.718	0.721	0.857
YOLOv5	460, 775, 875	0.789	0.658	0.707	0.821
YOLOv5	540, 775, 875	0.810	0.695	0.754	0.821
YOLOv5	700, 775, 875	0.766	0.634	0.767	0.768
YOLOv7	460, 540, 640	0.859	0.733	0.823	0.750
YOLOv7	**460, 640, 875**	**0.882**	**0.716**	**0.872**	**0.732**
YOLOv7	**460, 775, 875**	**0.873**	**0.739**	**0.787**	**0.857**
YOLOv7	540, 775, 875	0.834	0.714	0.867	0.696
YOLOv7	700, 775, 875	0.834	0.705	0.857	0.749

* The rows in **bold** indicate the trials with the highest *m*AP$_{50}$ score.

3.2. Segmentation and early detection results for B. *cinerea* cucumber bioassays

3.2.1. Disease severity

Disease severity was assessed per leaf and plant by calculating the percentage of leaf area with grey mould symptoms. This assessment occurred every 3 to 5 days for 37 days post-inoculation (dpi). The progression of grey mould was tracked on leaves across ten cucumber plants inoculated with B. *cinerea* using two methods. Leaves inoculated artificially showed rapid initial disease progression, while non-inoculated leaves displayed symptoms later, typically between 9 and 23 dpi. Factors such as leaf age, position, nutrient content, and secondary disease cycles influenced disease progress. B. *cinerea* infection routes vary based on plant species and tissue type, with conidia playing a major role in spread through air currents or mechanical forces. Greenhouse crops, especially vegetables, are vulnerable due to labor-intensive practices that create numerous infection sites and facilitate spore transfer.

3.2.2. Deep learning performance evaluation

The evaluation of DL segmentation models for B. *cinerea* severity classification, shown in Table 4, highlights the effectiveness of different architectures and encoders. U-Net++ with MobileViT-S outperformed others with a Dice Coefficient (DC) of 0.677, IoU of 0.656, and recall of 0.807 at epoch 80, benefiting from its efficient design with fewer parameters. In contrast, ResNet-50's higher complexity sometimes led to overfitting. Comparing U-Net++ to DeepLabV3 with the same encoder, U-Net++ was superior with a DC of 0.475 for DeepLabV3 and 0.633 for DeepLabV3+. ResNet-34 showed consistent performance across models, while ResNet-50 performed better with DeepLabV3 architectures but less effectively with U-Net++.

Table 4. Overall performance of deep learning segmentation models (best-performing model highlighted in bold) [13].

Architecture	Encoder	Accuracy	DC	IoU	Recall
U-Net++	ResNet-34	0.843	0.570	0.534	0.701
U-Net++	ResNet-50	0.765	0.421	0.479	0.595
U-Net++	**MobileViT-S**	**0.901**	**0.677**	**0.656**	**0.807**
DeepLabV3	ResNet-34	0.843	0.630	0.522	0.762
DeepLabV3	ResNet-50	0.849	0.590	0.565	0.770
DeepLabV3	MobileViT-S	0.745	0.475	0.431	0.614
DeepLabV3+	ResNet-34	0.863	0.646	0.543	0.754
DeepLabV3+	ResNet-50	0.851	0.624	0.520	0.722
DeepLabV3+	MobileViT-S	0.868	0.633	0.598	0.768

3.2.3. Early-stage evaluation

On dpi 0, 10 plants underwent inoculation with method A, while another 10 were subjected to method B. To gauge early detection capabilities, the model's performance was assessed using IoU metrics from dpi 1 to dpi 6, capturing the initial week post-inoculation. The model demonstrated adeptness in identifying the invisible B. *cinerea* class early on for both inoculation methods, as shown in Figure 3. Initial detection at dpi 1 yielded an IoU of 0.230, progressively intensifying to 0.375 on dpi 2 and 0.403 on dpi 3. This incremental trend suggests a growing sensitivity to evolving pathogen presence, showcasing the model's ability to tentatively spot early infection signs. As the infection advanced, the model's performance improved, reaching an IoU of 0.430 on dpi 5, indicating enhanced capability in detecting pathogen manifestation. A significant milestone was reached on dpi 6, with a peak performance IoU of 0.437, underscoring the model's robust early detection capability. Despite initial challenges in detecting the visible class, a notable increase was observed from dpi 3 to dpi 5. Lower IoU values early on were attributed to misidentifying the visible class when B. *cinerea* was predominantly invisible. Continued improvement from dpi 5 to dpi 6 solidifies successful B. *cinerea* detection, indicating the model's proficiency in spotting advanced disease stages. Combining results from invisible and visible classes alongside known infection status reinforces early-stage detection confirmation from dpi 2, with accuracy peaking at dpi 6. This capability is pivotal, preceding obvious symptom appearance, providing a critical window for timely agricultural intervention and management strategies by dpi 2.

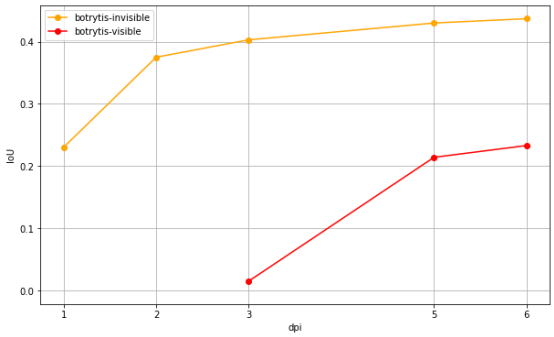

Figure 3. Mean IoU for B. *cinerea* invisible and visible classes at dpi 1-6 for both inoculation methods. Specifically, the model achieved an IoU of 0.230 on dpi 1, 0.375 on dpi 2, 0.403 on day 3, 0.430 on dpi 5, and 0.437 on dpi 6 for the B. *cinerea* invisible class. For the visible symptoms of B. *cinerea*, the model achieved an IoU of 0.154 on dpi 3, 0.214 on dpi 5, and 0.233 on dpi 6 [13].

3.2.4. Qualitative results

Accurate identification and segmentation of grey mould severity on cucumber plants is vital for effective plant pathology. This entails detecting subtle differences in disease progression, from early, invisible symptoms to more obvious signs. This section presents qualitative results from the top-performing model, focusing on its ability to identify and segment varying severity levels of B. *cinerea* infection in cucumber plants. The assessment reveals the model's strengths and limitations. Figure 4 (a)-(c) depict original images with true masks, while Figure 4 (d)-(f) show predicted masks by the model. Figure 4 (d) aligns well with its true label (Figure 4 (a)), showcasing accuracy in delineating infected areas. However, Figure 4 (e) erroneously classifies parts of healthy leaves as affected by invisible B. *cinerea*, inconsistent with its true label (Figure 4 (b)). Similarly, Figure 4 (f) misinterprets healthy regions as infected and segments areas

without annotations, indicating misidentification, partly due to the dataset including leaves with unknown disease status.

Figure 4. Qualitative assessment of segmentation performance: (a)-(c) present the original images resized to 1024×1024 overlaid with the true masks; (d)-(f) depict the images, resized to 1024×1024 overlaid with the predicted masks from the best-performing model [13].

4. Conclusions

Combining the insights from both studies, our research showcases the efficacy of DL techniques in the classification and early detection of B. *cinerea* infection in *Cucurbitaceae* crops. Leveraging multispectral imaging and advanced DL segmentation models, we observed significant improvements in detecting infected leaves. Specifically, integrating NIR spectra with RGB channels yielded superior results, emphasizing the importance of spectral contrast for accurate detection. Moreover, our experiments demonstrated the potential of DL models to achieve high classification accuracy and detection rates, with F1-scores of 0.89 and mAP_{50} of 0.88, respectively. Furthermore, the disease severity of *B*. *cinerea* was addressed using DL segmentation models for the early and late detection of grey mould disease in cucumber plants grown under controlled conditions that were similar to those prevailing in a greenhouse. The evaluation of the U-Net++ model with ViT encoder resulted in a DC of 0.677, an IoU of 0.656, a recall rate of 0.807, with a total accuracy of 90.1%, while it managed to detect early stages of *B. cinerea* at dpi 2 with an IoU of 0.375.

The success of this approach in early disease detection highlights the potential of advanced DL techniques in precision agriculture and proactive disease management in greenhouse environments. This approach, combined with multi-spectral imaging, provides a powerful solution for fast, on-site, early disease detection in crops, allowing farmers to make quick, informed decisions and manage crop health more efficiently. This advancement has the potential to optimize resource usage, decrease chemical inputs, and improve yield and food security. Integrating these models into daily farming practices will benefit the agricultural sector, ushering in a new era of smart agriculture.

Acknowledgements

This work is supported by the EU Green Deal project PestNu, which has received funding from the European Union's Horizon 2020 research and innovation programme under Grant Agreement no. 101037128.

References

[1] B. Williamson, B. Tudzynski, P. Tudzynski, and J. A. L. Van Kan, "*Botrytis cinerea* : the cause of grey mould disease," *Molecular Plant Pathology*, vol. 8, no. 5, pp. 561–580, Sep. 2007, doi: 10.1111/j.1364-3703.2007.00417.x.

[2] A. Weiberg *et al.*, "Fungal Small RNAs Suppress Plant Immunity by Hijacking Host RNA Interference Pathways," *Science*, vol. 342, no. 6154, pp. 118–123, Oct. 2013, doi: 10.1126/science.1239705.

[3] R. Dean *et al.*, "The Top 10 fungal pathogens in molecular plant pathology," *Molecular Plant Pathology*, vol. 13, no. 4, pp. 414–430, May 2012, doi: 10.1111/j.1364-3703.2011.00783.x.

[4] P. K. Mallick, "Evaluating Potential Importance of Cucumber (Cucumis sativus L. -Cucurbitaceae): A Brief Review," *Int J Appl Sci Biotechnol*, vol. 10, no. 1, pp. 12–15, Mar. 2022, doi: 10.3126/ijasbt.v10i1.44152.

[5] N. Ben-Shalom, R. Ardi, R. Pinto, C. Aki, and E. Fallik, "Controlling gray mould caused by Botrytis cinerea in cucumber plants by means of chitosan," *Crop Protection*, vol. 22, no. 2, pp. 285–290, Mar. 2003, doi: 10.1016/S0261-2194(02)00149-7.

[6] R. Weßling and R. Panstruga, "Rapid quantification of plant-powdery mildew interactions by qPCR and conidiospore counts," *Plant Methods*, vol. 8, no. 1, p. 35, 2012, doi: 10.1186/1746-4811-8-35.

[7] A. Terentev, V. Dolzhenko, A. Fedotov, and D. Eremenko, "Current State of Hyperspectral Remote Sensing for Early Plant Disease Detection: A Review," *Sensors*, vol. 22, no. 3, p. 757, Jan. 2022, doi: 10.3390/s22030757.

[8] E. M. Pechlivani, A. Papadimitriou, S. Pemas, N. Giakoumoglou, and D. Tzovaras, "Low-Cost Hyperspectral Imaging Device for Portable Remote Sensing," *Instruments*, vol. 7, no. 4, p. 32, Oct. 2023, doi: 10.3390/instruments7040032.

[9] J. Fahrentrapp, F. Ria, M. Geilhausen, and B. Panassiti, "Detection of Gray Mold Leaf Infections Prior to Visual Symptom Appearance Using a Five-Band Multispectral Sensor," *Front. Plant Sci.*, vol. 10, p. 628, May 2019, doi: 10.3389/fpls.2019.00628.

[10] A. Singh, B. Ganapathysubramanian, A. K. Singh, and S. Sarkar, "Machine Learning for High-Throughput Stress Phenotyping in Plants," *Trends in Plant Science*, vol. 21, no. 2, Art. no. 2, Feb. 2016, doi: 10.1016/j.tplants.2015.10.015.

[11] J. Piao, Y. Chen, and H. Shin, "A New Deep Learning Based Multi-Spectral Image Fusion Method," *Entropy*, vol. 21, no. 6, p. 570, Jun. 2019, doi: 10.3390/e21060570.

[12] N. Giakoumoglou, E. M. Pechlivani, A. Sakelliou, C. Klaridopoulos, N. Frangakis, and D. Tzovaras, "Deep learning-based multi-spectral identification of grey mould," *Smart Agricultural Technology*, vol. 4, p. 100174, Aug. 2023, doi: 10.1016/j.atech.2023.100174.

[13] N. Giakoumoglou *et al.*, "Early detection of Botrytis cinerea symptoms using deep learning multi-spectral image segmentation," *Smart Agricultural Technology*, p. 100481, Jun. 2024, doi: 10.1016/j.atech.2024.100481.

[14] G. Jocher *et al.*, "ultralytics/yolov5: v6.1 - TensorRT, TensorFlow Edge TPU and OpenVINO Export and Inference." Zenodo, Oct. 22, 2022. doi: 10.5281/zenodo.6222936.

[15] D. Singh, N. Jain, P. Jain, P. Kayal, S. Kumawat, and N. Batra, "PlantDoc: A Dataset for Visual Plant Disease Detection," in *Proceedings of the 7th ACM IKDD CoDS and 25th COMAD*, in CoDS COMAD 2020. New York, NY, USA: Association for Computing Machinery, Jan. 2020, pp. 249–253. doi: 10.1145/3371158.3371196.

[16] T.-Y. Lin *et al.*, "Microsoft COCO: Common Objects in Context." arXiv, Feb. 20, 2015. doi: 10.48550/arXiv.1405.0312.

[17] A. Bochkovskiy, C.-Y. Wang, and H.-Y. M. Liao, "YOLOv4: Optimal Speed and Accuracy of Object Detection." arXiv, Apr. 22, 2020. doi: 10.48550/arXiv.2004.10934.

[18] V. Decognet, M. Bardin, Y. Trottin-Caudal, and P. C. Nicot, "Rapid Change in the Genetic Diversity of *Botrytis cinerea* Populations After the Introduction of Strains in a Tomato Glasshouse," *Phytopathology®*, vol. 99, no. 2, pp. 185–193, Feb. 2009, doi: 10.1094/PHYTO-99-2-0185.

[19] G. De Meyer, J. Bigirimana, Y. Elad, and M. Höfte, "Induced systemic resistance in Trichoderma harzianum T39 biocontrol of Botrytis cinerea," *European Journal of Plant Pathology*, vol. 104, no. 3, pp. 279–286, 1998, doi: 10.1023/A:1008628806616.

[20] C. Lee Campbell and Laurence V. Madden, *Introduction to Plant Disease Epidemiology*, 1st edition. New York: Wiley-Interscience, 1990.

[21] J. Peñuelas and I. Filella, "Visible and near-infrared reflectance techniques for diagnosing plant physiological status," *Trends in Plant Science*, vol. 3, no. 4, pp. 151–156, Apr. 1998, doi: 10.1016/S1360-1385(98)01213-8.

[22] A. Paszke *et al.*, "PyTorch: An Imperative Style, High-Performance Deep Learning Library." arXiv, Dec. 03, 2019. doi: 10.48550/arXiv.1912.01703.

[23] R. Calderón Madrid, J. Navas Cortés, and P. Zarco-Tejada, "Early Detection and Quantification of Verticillium Wilt in Olive Using Hyperspectral and Thermal Imagery over Large Areas," *Remote Sensing*, vol. 7, pp. 5584–5610, May 2015, doi: 10.3390/rs70505584.

[24] C.-Y. Wang, A. Bochkovskiy, and H.-Y. M. Liao, "YOLOv7: Trainable bag-of-freebies sets new state-of-the-art for real-time object detectors." arXiv, Jul. 06, 2022. doi: 10.48550/arXiv.2207.02696.

Artificial intelligence algorithms revolutionizing insect monitoring and detection challenges

Panagiotis Christakakis [a], Dimitrios Kapetas [a], Nikolaos Frangakis [c], Sofia Faliagka [b], Nikolaos Katsoulas [b], Dimitrios Tzovaras [a], Eleftheria-Maria Pechlivani [a,*]

[a] Information Technologies Institute, Centre for Research and Technology Hellas, 57001 Thessaloniki, Greece

[b] Department of Agriculture Crop Production and Rural Environment, University of Thessaly, 38446 Volos, Greece

[c] iKnowHow S.A., 15451 Athens, Greece

* Corresponding author. Email: riapechl@iti.gr

Abstract

Insect crop attacks present a significant challenge that Artificial Intelligence (AI) can help address. Early insect detection and insect population growth prediction can bolster yield in both open fields and greenhouse cultivations. Olive trees, vulnerable to the olive fruit fly, Bactrocera oleae (BO), and vegetables like tomatoes and cucumbers, often attacked by pests like Tuta absoluta, aphids, and whiteflies, underscore the significance of AI in agricultural applications. This study, aims to provide Deep Learning (DL) models for crop monitoring and early detection of these insects and their plant symptoms, aligning with the Green Deal 2030 principles of agricultural sustainability and reduced reliance on chemical pesticides. This study utilizes available RGB images from libraries in combination with synthetic datasets and datasets created with insect traps. In particular, four implementations were developed. a) For detecting infestations of Tuta absoluta, DL was combined with ensemble techniques, by merging outputs from multiple models, enhancing detection metrics by 20% and elevating the mAP_{50} (mean Average Precision) from 0.58 to 0.70. b) To overcome insufficient data of small insects (1 and 4 mm), adhesive traps were employed to capture images of prevalent insects in vegetable crops, including whiteflies and black aphids and the DL models reached 0.75 mAP_{50} for the detection of these miniscule insects. c) To tackle whiteflies data scarcity, a synthetic dataset was generated, reaching 0.66 mAP_{50}, coupled with a high accuracy of 0.76. d) For the detection of BO, a threat to the olive industry, a DL technique for creating lightweight models was used, reaching 0.81 mAP_{50}, enabling real-time detection in-situ. These high-performing results apply to a range of digital tools (mobile apps, argo-robots, AI-based robotic traps). Real-time monitoring, insect population growth prediction, and integration with Decision Support Systems is achieved, providing essential data for informed decision-making in crop protection while also enabling timely intervention.

Keywords: artificial intelligence, smart agriculture, deep learning, insect detection, smart farming

1. Introduction

The tomato plant (Solanum lycopersicum L.) plays a vital role in global agriculture, being a significant contributor to food systems worldwide. A substantial threat comes from the tomato leaf miner, Tuta absoluta (Meyrick) (Zekeua *et al.*, 2017) [1], which has expanded beyond its native South America, causing considerable damage globally since its identification in Europe in 2006 (Urbaneja *et al.*, 2007) [2]. Despite efforts involving various pest management methods, such as pesticides and resistant tomato varieties, effectively controlling T. absoluta remains challenging. Consequently, there's a demand for digital-based technologies that leverage deep learning to achieve fast, accurate, and non-invasive detection.

Farmers often resort to using chemical insecticides to combat insect threats, leading to environmental and health consequences (Aktar *et al.*, 2009) [3]. The challenge lies in timely and accurate pest diagnosis, which can enable the implementation of appropriate preventive measures and pest management strategies. Traditionally, insect and crop disease detection relied on visual inspection, a time-consuming process (Banga *et al.*, 2018) [4]. Computer vision offers a more efficient alternative, requiring clear and high-resolution images. Adhesive traps, baited with pheromones, are used to capture insects and provide clear images for analysis.

A costly and tedious part of the machine learning process in agriculture is the data annotation. Creating synthetic datasets can alleviate this problem (Zhang *et al.*, 2020) [5]. Transfer learning with synthetic data can improve algorithm performance by accounting for environmental variations (Yang *et al.*, 2022) [6]. Additionally, synthetic data can address challenges when real data collection is limited or expensive (Prakash *et al.*, 2019) [7]. Traditional methods for generating synthetic datasets involve 3D rendering, but recent advancements include generative models like GANs and VAEs (Goodfellow *et al.*, 2014), (Kingma and

Welling *et al.*, 2022) [8], [9]. Diffusion probabilistic models have emerged as effective tools for image generation (Song and Ermon *et al.*, 2020) [10].

Another under threat plant that holds great culinary and economic significance (Galili *et al.*, 1997) [11] is the Olive tree (Olea europaea), with over 11 million hectares cultivated globally, primarily in the Mediterranean region which produces about 98% of the world's olives. However, the invasive pest Bactrocera oleae (BO) poses a severe threat to olive crops, potentially causing losses up to 80% in oil value and 100% in table olive cultivars in some areas (Nardi *et al.*, 2005) [12]. Traditionally, farmers have relied on visual identification using traps for insect detection, a method that is labor-intensive, error-prone, and unreliable (Khan *et al.*, 2022) [13]. Recently, convolutional neural networks (CNNs) within deep learning models have shown promise in pest and disease detection in agriculture (Singh *et al.*, 2016) [14], enabling efficient early detection of BO infestations (Sarker, 2021) [15].

Finally, an important step towards effective insect management in agriculture besides the ability to detect the active insect population count, is the ability to also forecast its development so that mitigation actions can be taken accordingly. To that end, algorithmic approaches of machine learning and time series analysis can be applied and be effective (Khanna and Kaur, 2022), (Chiu *et al.*, 2019) [16], [17].

This paper aims to highlight earlier research from our team already published, focused on real-time early detection of Tuta absoluta (Giakoumoglou *et al.*, 2023 [18]), black aphids and whiteflies (Giakoumoglou *et al.*, 2022 [19], Giakoumoglou *et al.*, 2022 [20]) and Bactrocera oleae (Giakoumoglou *et al.*, 2023) in crops of importance. These papers collectively demonstrate how DL techniques can be used for accurate insect detection, facilitating applications in robotic systems such as agro-robots, AI-based robotic traps, and mobile apps. Furthermore, we provide an approach of how AI predictions about insect populations can be integrated into such systems, enhancing the functionality of robotic traps. Additionally, these studies explore solutions for dataset insufficiencies. These studies align with the overarching goals of the Green Deal 2030 for pesticide reduction in farming and better crop monitoring.

2. Materials and Methods

2.1. Lightweight deep learning models for *Tuta absoluta* infestation detection

In this research, Giakoumoglou et al. (2023) [18] assessed the effectiveness of four ensemble techniques in improving the detection of T. absoluta infestations on tomato plants using deep learning object detection models. The use of real-life data from open fields and greenhouses presents unique challenges for detection, necessitating optimization of the models to operate on a mobile platform integrated into a fully autonomous robot. The collected data undergoes processing within a robust decision support system, ensuring precise detection and evaluation of infestations.

2.1.1. Dataset

An RGB dataset captured under real-life conditions in fields and greenhouses is utilized in this study, illustrating damage inflicted by *T. absoluta* on tomato plants. The dataset consists of 659 images. Expert agronomists annotated each image with bounding boxes around areas of damage. These images and annotations were sourced from the EDEN Library (https://edenlibrary.ai). Sample images demonstrating characteristic damage caused by *T. absoluta* on tomato leaves are depicted in Figure 1.

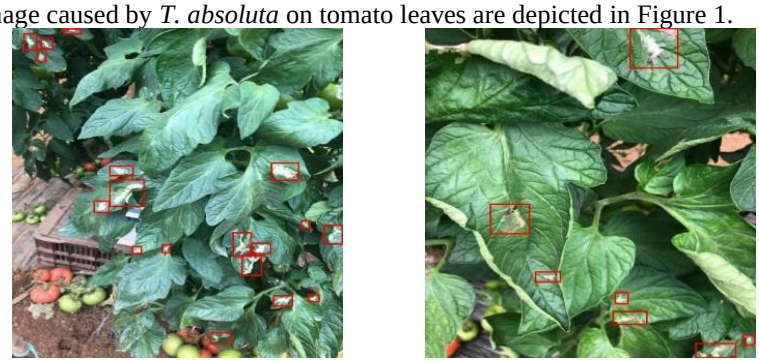

(**a**) (**b**)

Figure 1. Samples from the dataset: (**a**)-(**b**) images resized to 1024×1024 pixels, with bounding box annotations in red highlighting *T. absoluta* damage on tomato leaves [18].

2.1.2. Object Detection Models and Ensemble Techniques

This study utilizes two popular object detection models, Faster R-CNN and RetinaNet, to detect T. absoluta damage in tomato crops. For Faster R-CNN models, configurations include Feature Pyramid Network (FPN) heads with ResNet-50 and ResNet-101 backbones, incorporating Convolutional Layer 4 (C4) and Dilated Convolutional Layer 5 (DC5) heads. RetinaNet configurations employ ResNet-50 and ResNet-101 backbones, both complemented with FPN heads.

The ensemble techniques employed in this study to combine predictions from multiple object detection models, were Non-Maximum Suppression (NMS), Soft Non-Maximum Suppression (Soft NMS), Non-Maximum Weighted (NMW), and Weighted Boxes Fusion (WBF). The process commences by inputting an image into multiple object detection models, each autonomously identifying and locating T. absoluta infestations, resulting in annotated images with bounding boxes around detected damage instances. These outputs are amalgamated using ensemble techniques, leveraging the strengths of each model to enhance accuracy and reliability, thus ensuring a more comprehensive representation of T. absoluta damage instances within the input image. NMS eliminates duplicate detections by retaining only the bounding box with the highest confidence score, while Soft NMS reduces the confidence scores of overlapping detections based on the degree of overlap. NMW employs a weighted combination of overlapping detections to form a more accurate bounding box, and WBF generates a weighted box based on detection scores, yielding a fused result reflecting all detection outcomes according to the score.

All ensemble techniques were applied post-training of the models, obviating the necessity for further training. This approach conserves computational resources and enhances the robustness and accuracy of the detection process, rendering it suitable for real-world agricultural applications.

2.1.3. Training and Evaluation Metrics

The object detection models underwent training with specific hyperparameters. Training was conducted on images sized 1024 x 1024 employing the Stochastic Gradient Descent (SGD) optimization algorithm. Data augmentation techniques were utilized, including vertical and horizontal flipping, rotation, and Contrast Limited Adaptive Histogram Equalization (CLAHE). Evaluation involved the use of COCO detection metrics with the main metric of interest being mAP_{50}, at an Intersection over Union (IoU) threshold of 0.5 across all classes.

2.2. Dataset creation and detection of whiteflies and black aphids

In this study, Giakoumoglou *et al.* (2022) [19] contributed by: i) establishing an image dataset of black aphids and whiteflies, addressing a gap in existing datasets, ii) presenting statistics on image and insect instances within this dataset, iii) conducting benchmark experiments on insect localization and classification, evaluating the accuracy and inference latency trade-off for different object detectors.

2.2.1. Yellow Glue Paper Traps

The Yellow Glue Paper Traps dataset comprises images of targeted insects captured on adhesive traps placed in open fields with vegetable crops (tomato) in Volos, Greece. Color images were taken using a digital camera with a resolution of 3840 × 2160. A total of 225 images were captured while Figure 2 shows an example of an acquired image with bounding boxes enclosing the insects, while Figure 3 shows a closer look at the target insects.

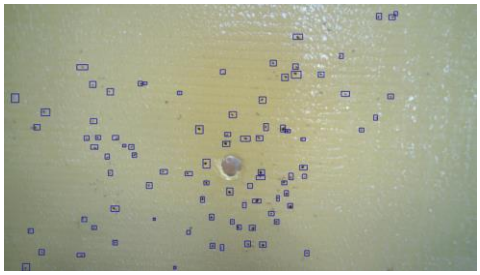

Figure 2. Example of an acquired image from the trap with bounding boxes enclosing the insects [19].

Expert agronomists from the University of Thessaly (UTH) performed data annotation using Roboflow, labeling the location and class of insects. In total, 5904 insect instances were labeled, with 2431 whiteflies and 3473 black aphids, averaging 26.24 annotations per image across both classes. To validate the dataset, the images were split into training and validation subsets, with 180 images for training and 45 for validation,

maintaining an 80-20% proportion. The split ensured a similar ratio and distribution of classes between the training and validation subsets. The insect counts in each subset are detailed in “Table 1” of Giakoumoglou *et al.* (2022) [19].

Figure 3. Two examples of whitefly (left) and black aphid (right) [19].

2.2.2. Training and Evaluation Metrics

To evaluate the Yellow Glue Paper Traps Dataset comprehensively, the utilized learning architectures included RetinaNet, YOLOv3, YOLOv5, Faster R-CNNs and Mask R-CNNs. For backbone architectures, we selected ResNet-50, ResNet-101, and ResNeXt-101 with Feature Pyramid Networks (FPN) for Faster R-CNNs and Mask R-CNNs, and ResNet-50 and ResNet-101 for RetinaNet.

Data augmentation techniques such as horizontal flipping, vertical flipping, and rotation were employed to expand the dataset artificially. We utilized Detectron2 for RetinaNet, Faster R-CNN, and Mask R-CNN, and PyTorch for YOLOv3 and YOLOv5 implementations.

For model validation, detection metrics included the *m*AP calculated across various Intersection over Union (IoU) thresholds and the at mAP_{50}. Additionally, the detection speed in milliseconds (ms) was captured to evaluate the accuracy versus inference speed trade-off.

2.3. Synthetic dataset creation and detection of tiny insects

In this study, Giakoumoglou *et al.* (2023) [20] aimed to create a realistic synthetic dataset using the *Generate-Paste-Blend-Detect* methodology for detecting insects in agriculture, specifically focusing on whiteflies. The contributions include proposing a methodology for generating and adding object instances to background datasets and conducting experiments to detect these objects using deep learning models.

2.3.1. Dataset

The methodology employs two datasets: D_{bg} as a background scene dataset for model training, and D_{obj} to train a model for generating objects from random noise, akin to "Cut, Paste and Learn". Denoising Diffusion Probabilistic Models (DDPM) were preferred over GANs or VAEs due to data annotation limitations and training complexities. DDPM adds noise to images for a set number of timesteps. Generated objects are placed on backgrounds manually or automatically using annotated datasets, with augmentation techniques like rotation and flipping ensuring diverse coverage. Poisson image blending is used for seamless integration, improving aesthetic appeal without requiring a foreground mask.

As this study aims at detecting whiteflies insects contained in multiple leaves with different types of background conditions with varying lighting conditions. For that reason, the PlantDoc dataset was selected as the background dataset denoted ($\mathcal{D}_{bg}$) which will be used to add the insects on leaves. By leveraging 762 PlantDoc images, 644 were augmented with whiteflies. However, the scarcity of insect image datasets remains a significant challenge in agriculture. To confront this limitation, manual cropping was employed to create an object dataset ($\mathcal{D}_{obj}$) comprising 113 whitefly images. This analytical approach underscores the careful consideration of dataset characteristics and the proactive steps taken to address data scarcity in the agricultural domain.

DDPM was configured with $T = 1000$, with variances increasing from $\beta 1 = 10^{-4}$ to $\beta T = 0.02$. Reverse processing employed a U-Net backbone with group normalization and self-attention, enduring 1300 epochs with a batch size of 4 and 64×64 image dimensions. Employing the AdamW optimizer and cosine annealing scheduler, satisfactory results emerged post-epoch 1000, exhibiting near-realistic images. Foreground masks were predicted via U-Net architecture (Ronneberger *et al.*, 2015) [21], as attempts with GANs and VAEs proved futile due to fluctuating model parameters, necessitating DDPM. The results of the generative model for every 100 epochs is shown in “Fig. 2” of Giakoumoglou *et al.* (2023) [20].

Subsequently, 500 whitefly instances were generated with DDPM and applied to 649 images from the PlantDoc dataset. Objects were inserted into the Dbg dataset with a pixel size of 10 ± 10%, maintaining aspect ratios, and subjected to random rotations and flips. Each image underwent three variations: unblended, Gaussian blurred, and Poisson blended, ensuring fair comparison. The resultant dataset boasted 53,401

annotations, averaging 82.9 annotations per image, with object counts ranging from 1 to 421.

2.3.2. Training and Evaluation Metrics

The synthetic dataset underwent assessment using all YOLOv8 models. Training was done with input image dimensions of 1024×1024 and the applied data augmentation encompassed hue, saturation, and value augmentation, along with rotation, translation, scaling, shearing, and horizontal and vertical flipping, as well as copy-paste techniques (Ghiasi *et al.*, 2021) [22].

Evaluation included the *m*AP across IoU thresholds from 0.05 to 0.95 (stride 0.05) denoted as mAP, and *m*AP at IoU = 0.5 denoted as mAP_{50}. Precision and recall metrics complemented the evaluation process.

2.4. Lightweight deep learning models for Bactrocera oleae detection

The study of Giakoumoglou *et al.* (2023) named "Deep Learning-based Lightweight Models for Bactrocera Oleae Detection" focused on deploying deep learning techniques on resource-limited devices to detect BO infestations. The goal was to develop lightweight architectures suitable for embedded devices such as IoT-based traps, mobile phones, and tablets, ensuring effective operation within constrained environments.

2.4.1. Dataset

The DIRT Dataset (Kalamatianos *et al.*, 2018) [23] was utilized in this study, which includes 841 annotated trap images with BO classifications. Using Roboflow, preprocessing adjustments ensured bounding boxes did not exceed image boundaries. The final dataset included 6,623 annotated BO insects, averaging 7.9 insects per image. The dataset was divided into training and testing sets with an 80:20 split.

2.4.2. Object Detection Models

This study explored various object detection models, including Faster R-CNN and SSD with different backbones: EfficientNet B0, MobileNet v3, ResNet-18, and ResNet-50. Each backbone was randomly initialized. For Faster R-CNN, the backbones (MobileNet v3, ResNet-18, ResNet-50) were integrated with a Feature Pyramid Network (FPN) and used a Fast R-CNN predictor for two classes. EfficientNet B0 within Faster R-CNN utilized an RPN anchor generator. The SSD Lite model with a 320x320 input size and MobileNet v3 backbone was used. EfficientNet-B0 with SSD included anchor boxes with specified aspect ratios and scales. SSD models with ResNet-18 and ResNet-50 backbones used default anchor box settings with specified aspect ratios and scales.

2.4.3. Training and Evaluation Metrics

For consistent comparison, all models were trained using the ADAM optimizer with learning rates from 10^{-2} to 10^{-6}, the epochs set to 1000 and a batch size of 4. Early stopping was set with patience of 10 epochs based on validation loss. Images were resized to 416x416 pixels. Data augmentation included flipping, random rotation, and blurring. Performance was evaluated focusing on *m*AP at an IoU threshold of 0.5 (mAP_{50}), with mAP and mAP_{50} used interchangeably. Additionally, the number of model parameters and inference time per image (in milliseconds) were captured.

2.5. AI pest prediction of population growth

2.5.1. Dataset and pest detection

For this experiment, images were collected using a smartphone camera by UTH, capturing daily photos of yellow sticky traps placed in greenhouses throughout the crop cycle (Figure 4a). Environmental data such as temperature and humidity were also automatically collected via on-site sensors.

The images were annotated with Roboflow. Initially, the dataset was small, with only 223 RGB images of black aphids. To expand this dataset, augmentation techniques like 90° rotation, brightness, and blurring adjustments increased were applied bringing the dataset size to 548 images. Each image was pre-processed and resized to ensure compatibility with the neural network. For the detection, a YOLOv8 model was trained for 100 epochs. Training parameters included a batch size of 2 and an image size of 960×960 pixels..

2.5.2. Environmental data manipulation and pest population prediction

The 223 images spanned a 44-day period, despite being taken over 28 days. Environmental data were collected daily for these 44 days, including non-working days (weekends and holidays), which resulted in gaps in the photo data. To even out the data distribution for better prediction, insect counts on return days were spread across the missing days. This created a dataset with temperature, humidity, and insect count over 44 days.

Using this dataset, machine learning models were developed to predict black aphid populations over a 7-day periods, leveraging weather forecast data from the open-meteo API (https://open-meteo.com/). Given the limited data, a plethora of machine learning and time series forecasting models were employed. The machine learning models included Random Forest Regressor, Gradient Boosting Regressor and LSTM. For time series forecasting, ARIMA, ARIMAX, and SARIMAX models were used. The dataset was split 80/20 for training and testing.

3. Results and Discussion

3.1. Tuta absoluta infestation detection and ensemble results

The initial performance evaluation, highlighted varying effectiveness among object detection models, considering both accuracy and inference time, summarized in "Table 1" of Giakoumoglou et al. (2023) [18].

Table 1 presents ensemble results, demonstrating the impact of different configurations on *m*AP$_{50}$ scores and associated inference times. An illustration of the superiority of ensemble models in *m*AP$_{50}$ scores compared to individual models, despite increased inference times can be found at Figure 4 of Giakoumoglou et al. (2023) [18].

Initial evaluations of Faster R-CNN and RetinaNet models suggested a need for a refined strategy to enhance performance. Ensemble techniques, effectively improved detection predictions, leading to enhanced *m*AP$_{50}$ scores. Particularly, WBF increased the mAP score by 20%, from 0.58 to 0.70, demonstrating the potential of ensemble methods.

Table 1. Ensemble results (*m*AP$_{50}$) using different configurations of models and ensemble techniques [18].

Ensemble Configuration	WBF	NMW	Soft NMS	NMS
All models	0.70	0.66	0.63	0.61
All Faster R-CNN	0.69	0.66	0.63	0.61
All RetinaNet	0.64	0.63	0.60	0.59
All Faster R-CNN ResNet-101	0.64	0.62	0.60	0.59
All Faster R-CNN ResNet-50	0.67	0.64	0.61	0.60
All Faster R-CNN C4	0.63	0.61	0.60	0.59
All Faster R-CNN DC5	0.63	0.62	0.60	0.60
All Faster R-CNN FPN	0.61	0.60	0.58	0.56

3.2. Whiteflies and black aphids dataset detection results

Table 2 displays the detection results and inference speed of the methods mentioned at a resolution of 1024×1024. Despite sub-optimal resizing from the initial 3840×2160 images, we focused on inference speed for timely detection. Each model was pretrained at specific dimensions: the Faster RCNN and Mask R-CNN were pretrained at 1024×1024, the YOLOv3, YOLOv5n, and YOLOv5s were pretrained at 640×640, and the YOLOv5m, YOLOv5l, and YOLOv5x were pretrained at 1280×1280.

Table 2. Detection Results [19].

Model	Backbone	*m*AP$_{50}$	*m*AP	speed	Model	Backbone	*m*AP$_{50}$	*m*AP	speed
YOLOv3	DarkNet53	0.48	0.11	35.3	Faster R-CNN	ResNet-101	0.67	0.45	104.4
YOLOv5n	CSP-Darknet53	**0.75**	**0.46**	**3.3**	Faster R-CNN	ResNetX-101	0.68	0.48	213.1
YOLOv5s	CSP-Darknet53	0.71	0.33	7.2	RetinaNet	ResNet-50	0.68	0.47	74.71
YOLOv5m	CSP-Darknet53	0.62	0.21	17.7	RetinaNet	ResNet-101	0.69	0.49	101.0
YOLOv5l	CSP-Darknet53	0.60	0.20	32.4	Mask R-CNN	ResNet-50	0.74	0.51	104.7
YOLOv5x	CSP-Darknet53	0.60	0.21	54.5	Mask R-CNN	ResNet-101	0.73	0.50	128.9
Faster R-CNN	ResNet-50	0.70	0.51	79.3	Mask R-CNN	ResNetX-101	0.72	0.52	238.7

Error! Reference source not found. The performance summary of the Yellow Glue Paper Traps Dataset, with YOLOv5n and CSP-Darknet53 outperforming other detectors in both accuracy and speed can be found in Giakoumoglou et al. (2022) [19] with the tag "Figure 5". In terms of inference latency, YOLO series had lower latency than RetinaNet (one-stage models), followed by Faster R-CNN (two-stage models), and Mask R-CNN (three-stage models). Mask R-CNN performed slightly better than Faster R-CNN and similarly to YOLOv5n and YOLOv5s.

The experimental results highlight YOLOv5n's superiority with an *m*AP$_{50}$ of 0.75 and *m*AP of 0.46, while Mask R-CNN achieved similar results with an *m*AP$_{50}$ of 0.74 and *m*AP of 0.51, showcasing the potential of

this work in insect pest management.

3.3. Synthetic dataset of tiny insect detection results

According to (Dwibedi *et al.*, 2017) [24], Gaussian blurring and Poisson blending were employed to evaluate the detection model, contrasting with scenarios where no blending was applied. Table 3 showcases detection outcomes across all three cases. The YOLOv8m model with Gaussian blurring achieved the highest accuracy (mAP_{50} = 0.661, *m*AP = 0.316). Despite high precision, all models exhibit lower recall, indicative of missed relevant objects, given an average of 82.9 small-sized objects per image.

Table 3. Object detection results [20].

Model	mAP_{50}	*m*AP	Precision	Recall
No blending				
YOLOv8n	0.594	0.245	0.735	0.530
YOLOv8s	0.627	0.262	0.725	0.567
YOLOv8m	0.627	0.262	0.752	0.549
YOLOv8l	0.624	0.268	0.744	0.551
YOLOv8x	0.618	0.253	0.736	0.546
Gaussian Blurring				
YOLOv8n	0.605	0.256	0.735	0.542
YOLOv8s	0.642	0.298	0.748	0.567
YOLOv8m	**0.661**	**0.316**	0.762	**0.573**
YOLOv8l	0.647	0.306	**0.770**	0.565
YOLOv8x	0.632	0.285	0.757	0.563
Poisson Blending				
YOLOv8n	0.623	0.275	0.740	0.561
YOLOv8s	0.642	0.300	0.746	0.575
YOLOv8m	**0.654**	**0.309**	**0.759**	**0.577**
YOLOv8l	0.652	0.307	0.757	0.567
YOLOv8x	0.642	0.293	0.759	0.567

* The rows in **bold** indicate the models with the highest metric.

3.4. Bactrocera oleae detection results

Table 4 summarizes the detection results in terms of *m*AP, number of parameters, and inference time for different models. The Faster R-CNN with ResNet-18 is the preferred choice due to its balance of performance, lower latency, and fewer parameters.

Table 4. Number of parameters in million (M), *m*AP, and inference time in milliseconds (ms).

Object Detection	Backbone	Parameters (M)	mAP_{50}	Inference time (ms)
Faster R-CNN	MobileNet v3	18.9	0.7154	26.49
Faster R-CNN	ResNet-18	**28.3**	0.8016	**38.63**
Faster R-CNN	ResNet-50	43.3	**0.8134**	63.99
Faster R-CNN	EfficientNet B0	84.1	0.7046	39.01
SSD	MobileNet v3	**3.4**	0.1869	39.57
SSD	ResNet-18	24.7	0.6821	**21.26**
SSD	ResNet-50	28.4	**0.7171**	26.27
SSD	EfficientNet B0	4.3	0.1865	22.19

3.5. AI pest prediction of population growth results

The models' results were 61.3% mAP50 for the YOLOv8x model with the SGD optimizer, 40.4% mAP50 for the YOLOv8x model with the Adam optimizer, and 60.1% mAP50 for the YOLOv8l model with the SGD optimizer. Figure 4b displays YOLOv8x model predictions, with red bounding boxes highlighting black aphids and their detection confidence scores.

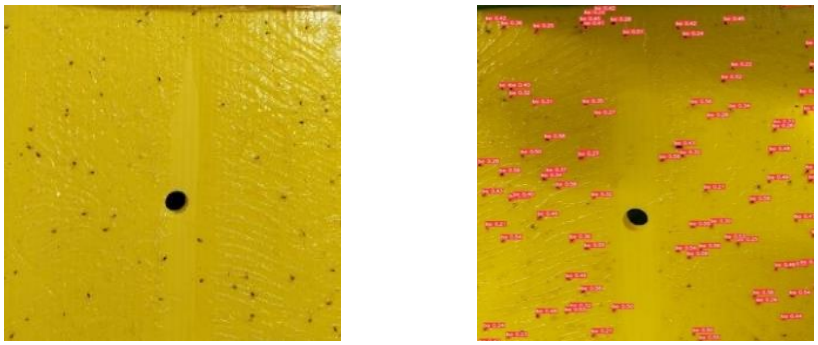

(**a**) (**b**)

Figure 4. Images from the dataset used: (a) image collected manually for insect annotation and modelling; (b) YOLOv8x Black-Aphids detection.

The Mean Squared Error (MSE) proved that the Time Series models outperformed the typical machine learning models. ARIMA had 102.45 MSE, SARIMAX had 90.49 MSE and ARIMAX had 75.61 MSE. In conclusion, ARIMA yielded good results with dates and insect counts, while ARIMAX improved performance by almost 27% by including temperature and humidity. SARIMAX, incorporating seasonality, didn't outperform ARIMAX but may improve with more data from future crop cycles. The prediction model needs a 30-day initial data gathering period to adapt to new greenhouses [17]. This adaptation ensures robust predictions across different environments. If ARIMAX predicts a significant rise in aphid populations, farmers can proactively implement pest management strategies, safeguarding their crops.

4. Conclusions

The aforementioned studies, underscore the potential of DL techniques in enhancing and automating agricultural processes. With focus on early pest detection and monitoring across various crops and leveraging advanced DL models, highlighted become the enhanced detection capabilities of such models in a variety of pests including Tuta Absoluta, Black Aphids and Whiteflies. The detections, achieved by either singular models or ensemble techniques, achieved impressive real-time results with mAP_{50} ranging from 0.7 to 0.81 for all pests combined. The synthetic dataset created for whiteflies also proved an important approach and shined a light in the potential of artificially enhancing datasets to overcome data insufficiencies. Finally, the population prediction techniques, especially with Time Series analysis models proved appropriate to enable timely intervention on crop infestations. These technologies and their integration with digital tools and robotic systems offers a promising pathway towards improved crop yields and reduced environmental impacts leading the way for advanced technological solutions in modern agriculture.

Acknowledgements

This work is supported by the EU Green Deal project PestNu, which has received funding from the European Union's Horizon 2020 research and innovation programme under Grant Agreement no. 101037128. We would like to thank Nikolaos Giakoumoglou from the Centre for Research and Technology Hellas (CERTH) for his contributions to our study.

References

[1] N. Zekeya, M. Chacha, P. A. Ndakidemi, C. Materu, M. Chidege, and E. R. Mbega, "Tomato Leafminer (Tuta absoluta Meyrick 1917): A Threat to Tomato Production in Africa," *Journal of Agriculture and Ecology Research International*, pp. 1–10, 2017, doi: 10.9734/JAERI/2017/28886.

[2] A. Urbaneja, R. Vercher, V. Navarro-Llopis, F. Marí, and J. Porcuna, "La polilla del tomate, Tuta absoluta- The tomato leafminer, Tuta absoluta (in Spanish)," *Phytoma España*, pp. 16–23, Jan. 2007.

[3] Md. W. Aktar, D. Sengupta, and A. Chowdhury, "Impact of pesticides use in agriculture: their benefits and hazards," *Interdiscip Toxicol*, vol. 2, no. 1, pp. 1–12, Mar. 2009, doi: 10.2478/v10102-009-0001-7.

[4] K. S. Banga, N. Kotwaliwale, D. Mohapatra, and S. K. Giri, "Techniques for insect detection in stored food grains: An overview," *Food Control*, vol. 94, pp. 167–176, Dec. 2018, doi: 10.1016/j.foodcont.2018.07.008.

[5] Q. Zhang, Y. Liu, C. Gong, Y. Chen, and H. Yu, "Applications of Deep Learning for Dense Scenes Analysis in Agriculture: A Review," *Sensors*, vol. 20, no. 5, Art. no. 5, Jan. 2020, doi: 10.3390/s20051520.

[6] S. Yang, L. Zheng, X. Chen, L. Zabawa, M. Zhang, and M. Wang, "Transfer Learning from Synthetic In-vitro Soybean Pods Dataset for In-situ Segmentation of On-branch Soybean Pod." arXiv, Apr. 22, 2022. doi: 10.48550/arXiv.2204.10902.

[7] A. Prakash *et al.*, "Structured Domain Randomization: Bridging the Reality Gap by Context-Aware Synthetic Data," in *2019 International Conference on Robotics and Automation (ICRA)*, Feb. 2019, pp. 7249–7255. doi: 10.1109/ICRA.2019.8794443.

[8] I. J. Goodfellow *et al.*, "Generative Adversarial Networks." arXiv, Jun. 10, 2014. doi: 10.48550/arXiv.1406.2661.

[9] D. P. Kingma and M. Welling, "Auto-Encoding Variational Bayes." arXiv, Dec. 10, 2022. doi: 10.48550/arXiv.1312.6114.

[10] Y. Song and S. Ermon, "Improved Techniques for Training Score-Based Generative Models." arXiv, Oct. 23, 2020. doi: 10.48550/arXiv.2006.09011.

[11] E. Galili, D. J. Stanley, J. Sharvit, and M. Weinstein-Evron, "Evidence for Earliest Olive-Oil Production in Submerged Settlements off the Carmel Coast, Israel," *Journal of Archaeological Science*, vol. 24, no. 12, pp. 1141–1150, Dec. 1997, doi: 10.1006/jasc.1997.0193.

[12] F. Nardi, A. Carapelli, R. Dallai, G. K. Roderick, and F. Frati, "Population structure and colonization history of the olive fly, Bactrocera oleae (Diptera, Tephritidae)," *Molecular Ecology*, vol. 14, no. 9, pp. 2729–2738, 2005, doi: 10.1111/j.1365-294X.2005.02610.x.

[13] A. Khan, A. D. Vibhute, S. Mali, and C. H. Patil, "A systematic review on hyperspectral imaging technology with a machine and deep learning methodology for agricultural applications," *Ecological Informatics*, vol. 69, p. 101678, Jul. 2022, doi: 10.1016/j.ecoinf.2022.101678.

[14] A. Singh, B. Ganapathysubramanian, A. K. Singh, and S. Sarkar, "Machine Learning for High-Throughput Stress Phenotyping in Plants," *Trends in Plant Science*, vol. 21, no. 2, Art. no. 2, Feb. 2016, doi: 10.1016/j.tplants.2015.10.015.

[15] I. H. Sarker, "Deep Learning: A Comprehensive Overview on Techniques, Taxonomy, Applications and Research Directions," *SN COMPUT. SCI.*, vol. 2, no. 6, p. 420, Aug. 2021, doi: 10.1007/s42979-021-00815-1.

[16] A. Khanna and S. Kaur, *Time Series Analysis of Environmental Data by using ARIMA and LSTM models for Precision Agriculture*. 2022. doi: 10.21203/rs.3.rs-2157455/v1.

[17] L.-Y. Chiu, D. J. Arcega Rustia, C.-Y. Lu, and T.-T. Lin, "Modelling and Forecasting of Greenhouse Whitefly Incidence Using Time-Series and ARIMAX Analysis," *IFAC-PapersOnLine*, vol. 52, no. 30, pp. 196–201, Jan. 2019, doi: 10.1016/j.ifacol.2019.12.521.

[18] N. Giakoumoglou, E.-M. Pechlivani, N. Frangakis, and D. Tzovaras, "Enhancing Tuta absoluta Detection on Tomato Plants: Ensemble Techniques and Deep Learning," *AI*, vol. 4, no. 4, Art. no. 4, Dec. 2023, doi: 10.3390/ai4040050.

[19] N. Giakoumoglou, E. M. Pechlivani, N. Katsoulas, and D. Tzovaras, "White Flies and Black Aphids Detection in Field Vegetable Crops using Deep Learning," in *2022 IEEE 5th International Conference on Image Processing Applications and Systems (IPAS)*, Genova, Italy: IEEE, Dec. 2022, pp. 1–6. doi: 10.1109/IPAS55744.2022.10052855.

[20] N. Giakoumoglou, E. M. Pechlivani, and D. Tzovaras, "Generate-Paste-Blend-Detect: Synthetic dataset for object detection in the agriculture domain," *Smart Agricultural Technology*, vol. 5, p. 100258, Oct. 2023, doi: 10.1016/j.atech.2023.100258.

[21] O. Ronneberger, P. Fischer, and T. Brox, "U-Net: Convolutional Networks for Biomedical Image Segmentation," 2015, doi: 10.48550/ARXIV.1505.04597.

[22] G. Ghiasi *et al.*, "Simple Copy-Paste is a Strong Data Augmentation Method for Instance Segmentation." arXiv, Jun. 23, 2021. doi: 10.48550/arXiv.2012.07177.

[23] R. Kalamatianos, I. Karydis, D. Doukakis, and M. Avlonitis, "DIRT: The Dacus Image Recognition Toolkit," *Journal of Imaging*, vol. 4, no. 11, Art. no. 11, Nov. 2018, doi: 10.3390/jimaging4110129.

[24] D. Dwibedi, I. Misra, and M. Hebert, "Cut, Paste and Learn: Surprisingly Easy Synthesis for Instance Detection." arXiv, Aug. 04, 2017. doi: 10.48550/arXiv.1708.01642.

Performance assessment of RGB-D cameras in deep learning algorithms for obstacle avoidance systems in agriculture

Pierluigi Rossi [a, *], Leonardo Assettati [a], Riccardo Alemanno [a], Leonardo Vita [b], Davide Gattamelata [b], Leonardo Marrazzini [c], Martina Olivieri [c], Luca Landi [d], Luca Burattini [d], Danilo Monarca [a], Maurizio Cutini [e]

[a] Department of Agriculture and Forest Sciences - University of Tuscia - Via San Camillo de Lellis, snc – 01100, Viterbo, ITALY.

[b] Department of technological innovations and safety of plants, products and anthropic settlements - Italian National Institute for Insurance against Accidents at Work (INAIL) - Via Roberto Ferruzzi 38/40, 00143 Rome, ITALY.

[c] Department of Civil and Industrial Engineering, University of Pisa, Largo Lucio Lazzarino 2, 56126 Pisa, ITALY

[d] Department of Engineering, University of Perugia - Via G. Duranti 93, 06125 Perugia, ITALY

[e] CREA Consiglio per la Ricerca in Agricoltura e L'analisi Dell'economia Agraria (Research Centre for Engineering and Agro-Food Processing), Via Milano 43, Treviglio, 24047, ITALY

* Corresponding author. Email: pierluigi.rossi@unitus.it

Abstract

Run-over accidents represent one of the most common occupational hazards related to agricultural machinery and obstacle detection systems can represent a major step forward in workers' safety. In this field of research, the use of colour (RGB) and depth cameras (D) is a possible solution to support both driving assistance technologies for tractor drivers and computer vision for autonomous vehicles. The object of this study, funded by the Italian National Institute for Insurance against Accidents at Work (INAIL), is therefore to evaluate the performance of RGB-D cameras in agricultural contexts for detection tasks at various ranges. To do so, a real-time pipeline of images has been captured by an RGB-D camera that provides both RGB and depth frames at the same pixel resolution and rate. Colour frames have been analysed through a deep-learning algorithm using a TensorFlow-lite object classification model, which has been run on a Raspberry Pi 4 coupled with a Google Coral AI accelerator. The distance of detected obstacles on the three axes have then been estimated from the corresponding depth frames to get both frontal and lateral distances this way. Tests have been run with clear illumination conditions and detection data has finally been compared to the georeferenced data of obstacles obtained with satellite navigation technology provided by Real Time Kinematics (RTK). Despite the assessed depth distances showed an absolute error of 0.84 m within 10 metres and 0f 6 m for obstacles beyond 16 metres, the lateral distance from the camera proved to be quite reliable an all ranges, with a minimum absolute error of 0.04 m and a maximum of 1.42 m at far ranges. Results showed that RGB-D cameras in agricultural environments can be particularly effective in estimating the risk of collision with obstacles in the vehicle's trajectory.

Keywords: Farming automation, Sensors, ADAS, safety, obstacle detection.

1. Introduction

Agricultural environments represent one of the most challenging scenarios for health and safety at work (Dogan et al., 2010; Türkoğlu et al., 2017) given the wide range of hazards that might be present and particular socio-technical constraints that often make risks unavoidable or severe (Pickett et al., 2005; Swanton et al., 2015)

In this context, agricultural vehicles are naturally exposed to hazards that involve obstacles (Kröyer, 2015), infrastructures along their path and nearby persons or animals that might be on their trajectory(Nour et al., 2021): whether they are pedestrians like in road traffic or workers on foot, run-over accidents represent a consistent part of fatal accidents in many sectors. Risk mitigations strategies often include signal standardisation, traffic lights, acoustic alerts and on-board sensors that can provide significant improvements in the safety management and a reduction of accidents in many sectors. Agriculture, although, presents additional challenges like harsh weather, dust, particular terrain conditions and lack of standardisations or

limited communication ways between drivers and bystanders. The ability to avoid impacts against obstacles is also affected by such environmental and socio-technical factors, increasing both the likelihood of accidents and incidents to happen.

Nowadays, computer vision (CV) is a useful technological advance that is practically paramount to achieve safe use of robots, autonomous vehicles and remote-controlled machinery (Ali et al., 2022; Chen et al., 2020; Mohammed et al., 2017). It can provide important information by analysing colour patterns, by segmenting objects and by detecting human gestures; plus, depth imaging can also help drawing contours in images and generate 3D models of reality through point clouds. Despite a fast evolution of CV techniques in road traffic, agricultural environments have critical features that are still hard to overcome and this is utterly influenced by a generalised lack of data: common Artificial Intelligence (AI) algorithms are, in fact, based on training material in the form of datasets made of thousands images for every labelled subject contained by them and presented in common situations like rooms, public places or roads and with various light conditions (Kragh et al., 2017; Tian et al., 2020). Agriculture is therefore quite demanding in terms of training data(Kragh et al., 2017), which also requires particular attention to let algorithms detect partially hidden obstacles (i.e. worker dressed in green partially covered by vegetation, or obstacles in shaded areas) and avoid overfitting in doing so.

The possibility of including such tools in driving systems results in many different approaches in which the use of AI spans from little support in helping drivers perform an action to the deployment of automatic systems such as emergency breaks. This aspect is often enhanced by several types of sensors that increase the chances of detecting obstacles: lidars, cameras and ultrasounds are just an example of the solutions that have been explored so far. Regarding cameras, an interesting possibility is represented by depth cameras, that altogether with RGB cameras (RGB-D) can provide a significant amount of useful information for obstacle detection (Mayrhofer et al., 2014). The evolution of sensors for these field applications was also improved through the development of specific software libraries that helped with 3D data analysis (Rusu and Cousins, 2011) and increased the domain of possible usage. This can also lead to safety applications, such as anomaly detection in the background (Christiansen et al., 2016), collision avoidance safety systems (Gunturu et al., 2022) and their use on agricultural robots (Skoczeń et al., 2021).

This research focused on determining the feasibility of using RGB-D cameras in agricultural contexts to detect obstacles at various ranges. To do so, tests have been run to estimate the measurement errors of such devices in all the axes and even outside of their working range: results of the research would therefore show the degree in which such technology could be suitable for a driving assistance system on board of tractors.

2. Materials and Methods

In order to fulfil the aim of this research, several aspects have been covered to provide a valid research protocol for field tests. Given the specific working conditions and outputs that authors wanted to investigate, information must be provided on all the tools that have been tailored to the case, more specifically:

- Hardware configuration;
- Software configuration;
- Performance assessment methodology.

The elements that have been just pointed out have been deeply described in the following sections, together with useful details that are necessary to achieve the expected results.

2.1. Hardware configuration

The hardware utilised during the test comprised an Intel RealSense D455 depth camera *Figure 1-a)*, which has already been evaluated for agricultural environments in a range of 0.1 m to 10 metres (Condotta et al., 2020), mounted on a Raspberry Pi 4 running Raspbian Bullseye as operating system. To enhance the system's inference capability, the Raspberry Pi was equipped with a Google Coral USB accelerator.

During the field test, the system was powered by a portable power source with a voltage of 5 Volts and an energy capacity of 20 Ah. The entire system was mounted on a base constructed from aluminium profiles, which provided a solid and stable footing on the ground. The height above ground of the depth camera, once mounted on the support, is 1 meter which is consistent with the possible positioning of a similar device on a

vehicle.

The camera was operated by a Python script which was based on its own SDK package, while data has been monitored and collected through the 10 inches touch display visible behind the camera (figure 1b) together with the Raspberry Pi board.

To determine the position of the camera and of the obstacles a DGNSS Real Time Kinematics (RTK) system was used by using Ublox Zed-F9P board (figure 1c) as GNSS receiver connected to the NTRIP server of Lazio Region, hence receiving corrections every second from a base station positioned within 3 km at the Civil Engineering Department of Viterbo.

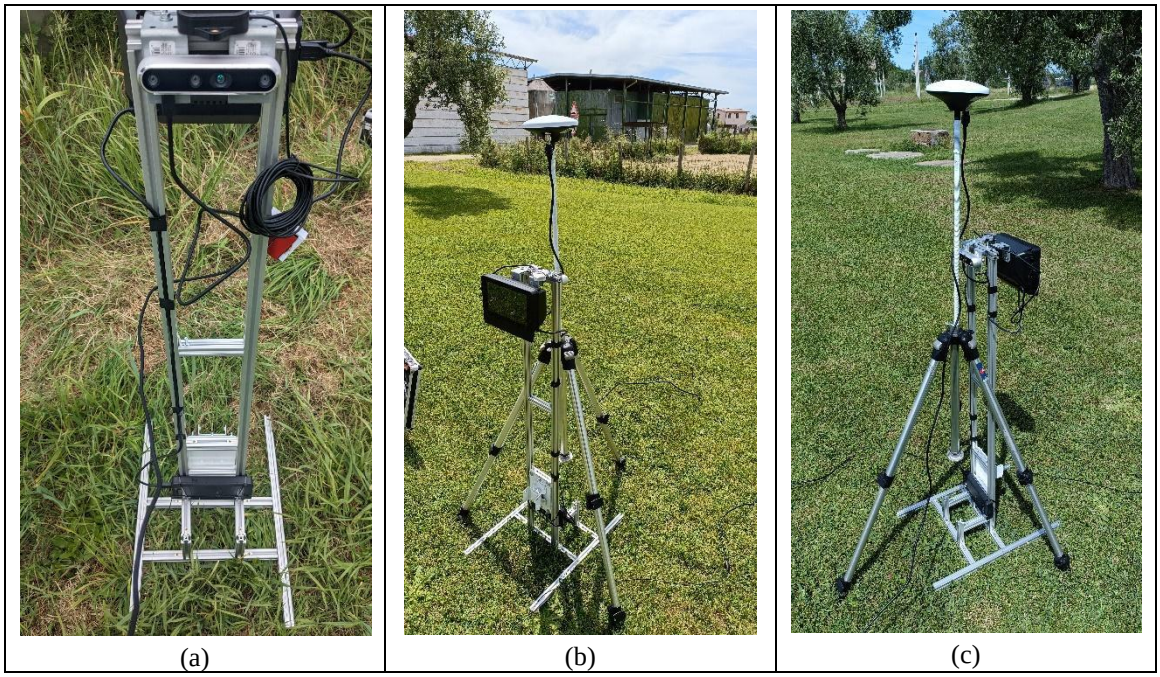

(a) (b) (c)

Figure 1. Design of the hardware configuration used in field tests. In image a), RGB-D camera and support structure are visible; in image b), the touch display that contains the Raspberry Pi 4 board operating the camera is visible just behind it; in image c), the RTK antenna plugged to the U-blox ZED-F9P module is positioned over the camera for georeferencing purposes.

2.2. Software configuration

Data from the RealSense Camera has been collected using its SDK (written in C language) through Python wrappers specifically compiled for version 3.6 in order to avoid compatibility issues with the rest of the system. In fact, also Google Coral USB Accelerator which was required to process the image streams provided Python wheels that work in Python 3.6 only. Moreover, newer versions of Raspberry OS do not support that version anymore, so the Bullseye 64-bit OS edition has been used.

The code was able to handle both the colour frame stream and the depth frame stream at 30 frames per second with various resolutions that, however, must be the same for both of them: this will allow the possibility of knowing the depth of each pixel in the RGB frame.

Colour frames have then been processed to be passed to the Google Coral AI USB accelerator and provide object detection through a neural network. To facilitate this step, a frozen MobileNet (Howard et al., 2017) neural network pretrained on COCO dataset (Lin et al., 2014). The model has been processed with TensorFlow Lite and loaded in the Raspberry Pi with its labels.

The script, as shown in *Figure 2*, was able to provide the bounding box around detected persons in the field: using this information gathered from the neural network, data has been further augmented with data from the depth frame to estimate the distance of the center of the box from the camera, its frontal distance

and lateral offset from it.

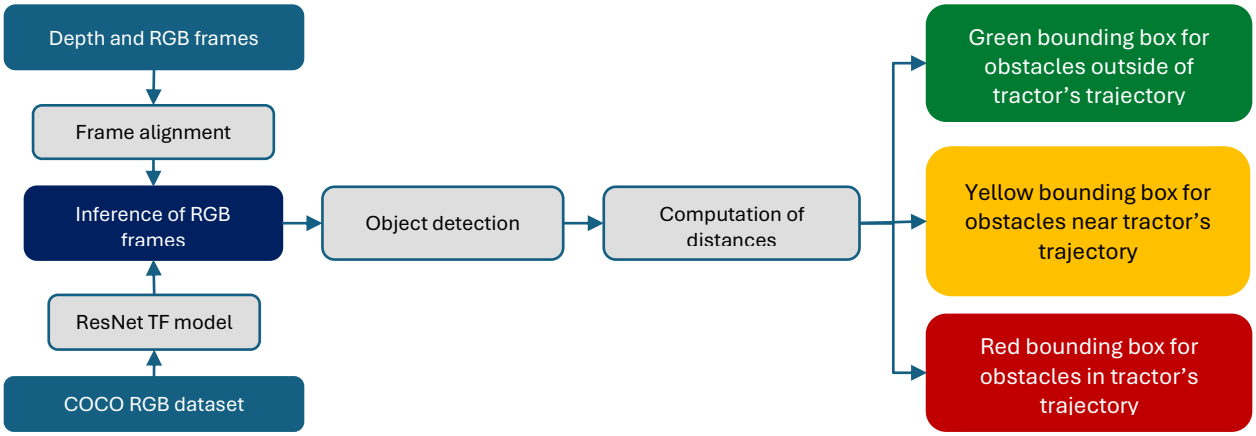

Figure 2. Flowchart of the algorithm

2.3. Performance assessment methodology

The depth camera is designed to work in a range of 6-10 m, but errors may vary according to the distances in three dimensions. To verify its performances, four points have been tested in front of the camera and another set of four points have been tested on the limits of its field of view. Tests have been run at several distances, both inside the optimal working range and outside its range.

a b

Figure 3. Layout of field tests. Obstacles are indicated with white placemarks in figure a), ground truth data collection is shown in figure b).

An overview of the testing field is provided in *Figure 3*. Points of obstacles have been established with the goal of estimating the feasibility of using such devices even beyond the optimal range of use for specific applications, such as determining the possibility of impact according to trajectories rather than just exact distances as other motion planning systems for autonomous navigations do (Aghi et al., 2020; Xiong et al., 2023). Given the aim of the research, distances on x, y and z axis will be calculated to verify the measurement errors in all directions. An additional point at 20 m in front of the camera has been used as reference point

to determine the frontal distance of obstacles and their offset from the camera, as shown in *Figure 4*.

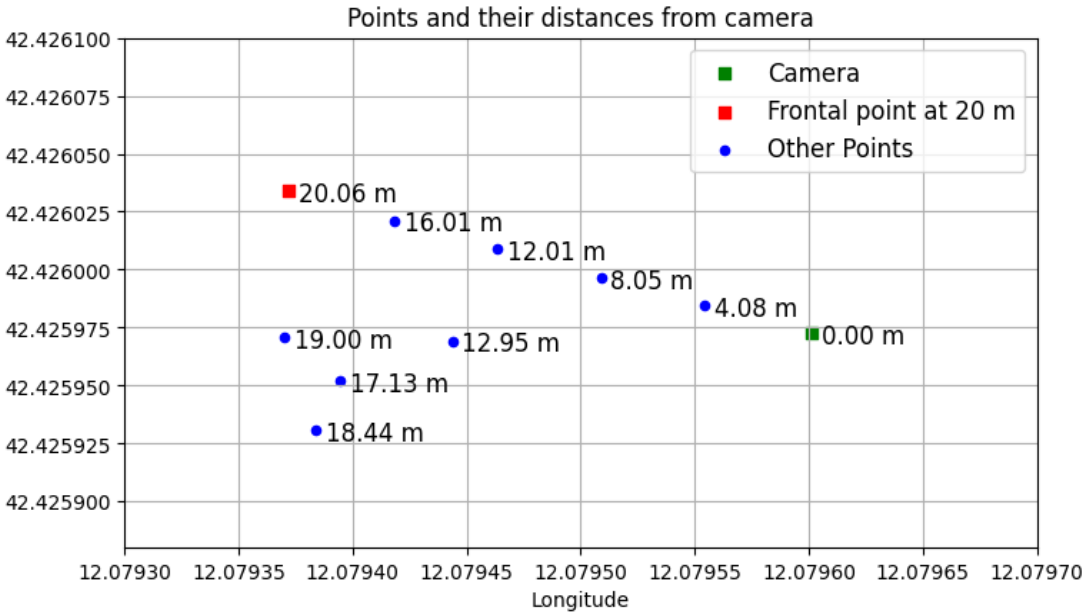

Figure 4. Ground truth obstacle georeferencing

3. Results

The results of the field test are represented in *Figure 5*, in that the red square symbols indicate the position of the camera and obstacles according to RTK georeferencing, while cross symbols indicate the position of the obstacles measured by the depth camera: same colours indicate the same obstacle, so that ground truth from RTK and estimated positions can be compared for each one of them.

The image

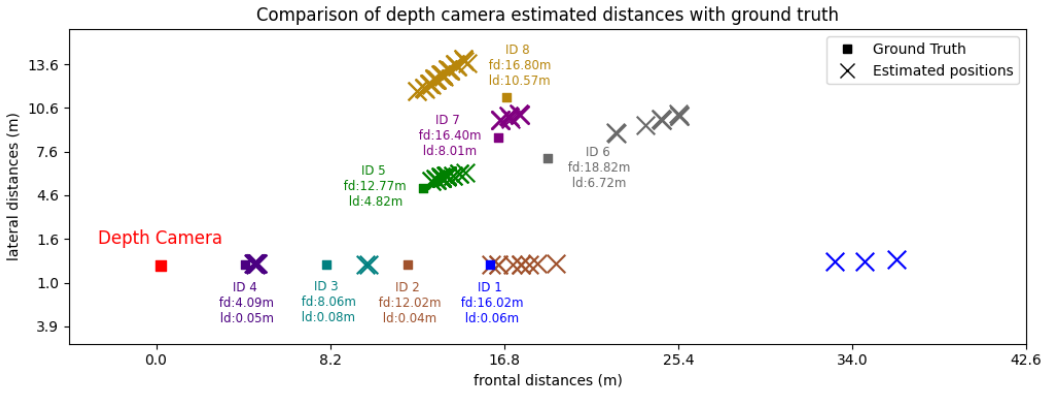

Figure 5. Depth distance measurements and its comparison with ground truth data. Same color indicates the same obstacle.

Statistical analysis of the results is also reported in the ***Table 1***. Test data include the depth of the obstacles from the camera, the frontal distance of the object from the camera, the lateral distance of the object from the camera (offset) and ground truth data for each one of them. After comparing ground truth with test data, absolute errors and relative errors have been computed.

Table 1. Depth measurement for test obstacles and comparison with ground truth data

	ID 1	ID 2	ID 3	ID 4	ID 5	ID 6	ID 7	ID 8
Average Depth distance	32.38 m	16.43 m	9.48 m	4.34 m	14.15 m	24.71 m	18.58 m	17.68 m
Ground truth distance	16.01 m	12.01 m	8.05 m	4.09 m	12.95 m	19 m	17.13 m	18.44 m
Absolute error depth	16.37 m	4.42 m	1.43 m	0.25 m	1.2 m	5.71 m	1.45 m	0.76 m
Relative error depth	102%	37%	18%	6%	9%	30%	8%	4%
Average depth frontal distance	32.33 m	16.39 m	9.45 m	4.33 m	12.96 m	22.89 m	15.98 m	12.88 m
Ground truth frontal distance	16.01 m	12 m	8.05 m	4.09 m	12.77 m	18.81 m	16.4 m	16.8 m
Absolute error frontal	16.32 m	4.39 m	1.4 m	0.24 m	0.19 m	4.08 m	0.42 m	3.92 m
Relative error frontal	102%	37%	17%	6%	1%	22%	3%	23%
Average depth lateral distance	0.29 m	0.01 m	0.03 m	0.09 m	5.6 m	9.22 m	9.43 m	12.1 m
Ground truth lateral distance	0.06 m	0.04 m	0.07 m	0.05 m	4.82 m	6.72 m	8.01 m	10.57 m
Absolute error lateral	0.23 m	0.03 m	0.04 m	0.04 m	0.78 m	2.5 m	1.42 m	1.53 m
Relative error lateral	383%	75%	57%	80%	16%	37%	18%	14%

Absolute errors are greater as the distance increases, especially outside the standard working range of the depth camera. Especially at small angles of inclination from the depth sensors, which happen when obstacles are right in front of the camera, distances that are widely beyond the operational limits of the instrument are assessed with greater errors as happened for obstacle ID1 at approximately 16 metres of distance. Despite relative error are greater for obstacles at closer range, it must be noted that such values show instead a small absolute error. Another important aspect should be noted regarding lateral distances, where the errors are minimal even when differences among ground truth distances and measure depths are high: this means that, even outside of the camera's working range, the estimated lateral distance of objects seem to be precise. Moreover, the obstacles that are positioned near the limits of the field of view have shown better depth measurements compared to obstacles in front of the camera. Further data analysis reported in ***Table 2*** shows a comparison regarding distances by dividing data in three ranges which are 0-10 m (suggested camera working range), 10-16 m (limit range) and 16+ m of distance (way outside of the range, but with still some detection capabilities).

Table 2. Benchmark of measurement errors at different ranges

	0 m - 10 m	10 m - 16 m	16+ m
Number of observations	43	56	118
Average absolute depth error	0.84	2.807	6.071
Average absolute frontal error	0.82 m	2.29 m	6.19 m
Average absolute lateral error	0.04 m	0.41 m	1.42 m

Data in ***Table 2*** shows a different increase of error among ranges and different axes, with unreliable measurements beyond 16 m but still better results for lateral errors. A significant increase in the error for

depth measurements is already visible outside of the standard working range of 10 m, while it is smaller than 1 metre for measurements within that range.

4. Discussion

Results show that RGB-D data provides fairly good precision in the working range suggested by the manufacturer, with an error that starts increasing as the frontal distance from the camera increases. Data analysis in far ranges showed that over 16 m depth measurements become hardly usable for an obstacle avoidance system, while obstacles within the range 10-16 m can be useful in contexts where such distances are covered in a significant amount of time.

An interesting result is related to the assessment of lateral position (offset) of the obstacles, which proved to be reliable even at great distances and that was always smaller than 0.5 m even in tests performed in ranges between 10 m and 16 m.

The detection was also influenced by shapes of the obstacles since the centre of every one of them has been used as reference point and can be therefore considered as the median point of the bounding boxes calculated by the algorithm rather than the average distance of the whole shape of the obstacle. It is also important to note that background data should always be removed or processed before calculating the distances because hollow obstacles might return background distance data instead of the distance of the obstacles themselves.

5. Conclusions

Field tests showed that RGB-D cameras in agricultural environments can be a useful tool to reduce the risk of collision and run-over hazards to workers on foot: in particular, they are not just useful for distance assessment in all the axes, but they are rather useful to understand their offset compared to the trajectory of the vehicle. This would already be useful as a driving assistance system since the classification of obstacles could not be necessary and tractor drivers already know the path of the vehicle in the field and the algorithm already considers the shape of the tractor to assess the risk accordingly.

Future tests could be run in different working conditions and agricultural contexts, while further enhancements on the algorithms could focus on image segmentation by computer vision thresholds to separate the obstacles from the background and therefore avoiding the use of AI pre-trained models for object detection and classification.

Acknowledgements

The research is part of the project called *"Obstacle detection and tracking system for fixed and moving obstacles in agriculture"* (BRiC 2022 ID04 SIRTRAck), funded by the Italian National Institute for Insurance against Accidents at Work (INAIL).

References

Aghi, D., Mazzia, V., Chiaberge, M., 2020. Local motion planner for autonomous navigation in vineyards with a RGB-D camera-based algorithm and deep learning synergy. Machines 8. https://doi.org/10.3390/MACHINES8020027

Ali, M., Wu, B., Wheeler, C., Wang, D., Tao, Y., 2022. Active-Laser Scanning and Intelligent Picking for Automated Loading of Agricultural Commodities to Processing Machines, in: 2022 ASABE Annual International Meeting. https://doi.org/10.13031/aim.202200459

Chen, Y., Zhang, B., Zhou, J., Wang, K., 2020. Real-time 3D unstructured environment reconstruction utilizing VR and Kinect-based immersive teleoperation for agricultural field robots. Comput. Electron. Agric. 175. https://doi.org/10.1016/j.compag.2020.105579

Christiansen, P., Nielsen, L.N., Steen, K.A., Jørgensen, R.N., Karstoft, H., 2016. DeepAnomaly: Combining background subtraction and deep learning for detecting obstacles and anomalies in an agricultural field. Sensors (Switzerland) 16. https://doi.org/10.3390/s16111904

Condotta, I.C.F.S., Brown-Brandl, T.M., Pitla, S.K., Stinn, J.P., Silva-Miranda, K.O., 2020. Evaluation of low-cost depth cameras for agricultural applications. Comput. Electron. Agric. 173. https://doi.org/10.1016/j.compag.2020.105394

Dogan, K.H., Demirci, S., Sunam, G.S., Deniz, I., Gunaydin, G., 2010. Evaluation of farm tractor-related fatalities. Am. J. Forensic Med. Pathol. 31, 64–68. https://doi.org/10.1097/PAF.0b013e3181c21bf0

Gunturu, S., Munir, A., Ullah, H., Welch, S., Flippo, D., 2022. A Spatial AI-Based Agricultural Robotic Platform for Wheat Detection and Collision Avoidance. AI 3, 719–738. https://doi.org/10.3390/ai3030042

Howard, A.G., Zhu, M., Chen, B., Kalenichenko, D., Wang, W., Weyand, T., Andreetto, M., Adam, H., 2017. MobileNets: Efficient Convolutional Neural Networks for Mobile Vision Applications.

Kragh, M.F., Christiansen, P., Laursen, M.S., Larsen, M., Steen, K.A., Green, O., Karstoft, H., Jørgensen, R.N., 2017. FieldSAFE: Dataset for obstacle detection in agriculture. Sensors (Switzerland) 17. https://doi.org/10.3390/s17112579

Kröyer, H.R.G., 2015. Is 30km/h a "safe" speed? Injury severity of pedestrians struck by a vehicle and the relation to travel speed and age. IATSS Res. 39, 42–50. https://doi.org/10.1016/j.iatssr.2014.08.001

Lin, T.-Y., Maire, M., Belongie, S., Hays, J., Perona, P., Ramanan, D., Dollár, P., Zitnick, C.L., 2014. LNCS 8693 - Microsoft COCO: Common Objects in Context. Comput. Vision–ECCV 2014 13th Eur. Conf. Zurich, Switz. 740–755.

Mayrhofer, H., Quendler, E., Boxberger, J., 2014. Prevention aspects for avoiding run-over incidents in agriculture together for tractors, Self-propelled harvesting machinery and material handling machinery. Agric. Eng. Int. CIGR J. 16, 148–156.

Mohammed, A., Schmidt, B., Wang, L., 2017. Active collision avoidance for human–robot collaboration driven by vision sensors. Int. J. Comput. Integr. Manuf. 30, 970–980. https://doi.org/10.1080/0951192X.2016.1268269

Nour, M.M., Field, W.E., Ni, J.Q., Cheng, Y.H., 2021. Farm-Related Injuries and Fatalities Involving Children, Youth, and Young Workers during Manure Storage, Handling, and Transport. J. Agromedicine 26, 323–333. https://doi.org/10.1080/1059924X.2020.1795034

Pickett, W., Brison, R.J., Berg, R.L., Zentner, J., Linneman, J., Marlenga, B., 2005. Pediatric farm injuries involving non-working children injured by a farm work hazard: Five priorities for primary prevention. Inj. Prev. 11, 6–11. https://doi.org/10.1136/ip.2004.005769

Rusu, R.B., Cousins, S., 2011. 3D is here: Point Cloud Library (PCL). Proc. - IEEE Int. Conf. Robot. Autom. 1–4. https://doi.org/10.1109/ICRA.2011.5980567

Skoczeń, M., Ochman, M., Spyra, K., Nikodem, M., Krata, D., Panek, M., Pawłowski, A., 2021. Obstacle detection system for agricultural mobile robot application using rgb-d cameras. Sensors 21. https://doi.org/10.3390/s21165292

Swanton, A.R., Young, T.L., Leinenkugel, K., Torner, J.C., Peek-Asa, C., 2015. Nonfatal tractor-related injuries presenting to a state trauma system. J. Safety Res. 53, 97–102. https://doi.org/10.1016/j.jsr.2015.03.002

Tian, H., Wang, T., Liu, Y., Qiao, X., Li, Y., 2020. Computer vision technology in agricultural automation —A review. Inf. Process. Agric. https://doi.org/10.1016/j.inpa.2019.09.006

Türkoğlu, A., Sehlikoğlu, K., Tokdemir, M., 2017. Analysis of Tractor-Associated Fatalities. Am. J. Forensic Med. Pathol. 38, 306–311. https://doi.org/10.1097/PAF.0000000000000344

Xiong, J., Liang, J., Zhuang, Y., Hong, D., Zheng, Z., Liao, S., Hu, W., Yang, Z., 2023. Real-time localization and 3D semantic map reconstruction for unstructured citrus orchards. Comput. Electron. Agric. 213. https://doi.org/10.1016/j.compag.2023.108217

European Committee for Electrotechnical Standardization, 2019. EN TS 62998: Safety of machinery – Positioning of safeguards with respect to the approach speeds of parts of the human body. Brussels: CENELEC.

Advanced UAV edge computing ML solutions for livestock management

Aristotelis C. Tagarakis[1], Costas Davarakis[2], Alexander Loos[3], Christian Weigel[3], Maria Theologou[2], Niki Rovatsou[2], Oliver Doll[3], Dimitrios Kateris[1], and Dionysis Bochtis[1]

1 Institute for Bio-Economy and Agri-Technology (IBO), Centre of Research and Technology-Hellas (CERTH), 6th km Charilaou-Thermi Rd, GR 57001 Thessaloniki, Greece
2 Nydor System Technologies, Kondilaki 7, Psychico, Greece
3 Fraunhofer Institute for Digital Media Technology (IDMT), Ilmenau, Germany

Abstract

The role of Unmanned Aerial Systems (UAS) in different application areas in the agricultural sector is increasing rapidly. Following the current trends, the focus of SPADE EU Project (HE 101060778) is to investigate the potential benefits of UAS contributing to multiple field operations and processes and promote sustainable digital services in the sectors of agriculture, forestry, and livestock. Part of the developments within the SPADE ecosystem involves deployment of UAV formations (single UAV, collaborating UAVs, UAV swarms) equipped with edge-computing devices (AI/ML) for direct applications in livestock management such as detecting focused risks. These developments are being evaluated in real field conditions through the dedicated pilot activities.

The current work presents the preliminary results of SPADE livestock use cases undergone two trials to evaluate the performance of UAS-enabled edge-computing AI tools, for ML modelling & data assimilation. The scope is to enable the flying systems for real time monitoring of sheep in open field grazing environments. Within this framework, the SPADE Livestock setup utilized state-of-the-art object detectors and edge computing devices. The Models being investigated included Faster R-CNN, YOLO, and SSD as backbone object detection in aerial images captured by the UAS. The acquired dataset was used to train selected Tiny Object Detection algorithms.

The trials included flights at varying altitudes for capturing objects at different scales and evaluate the motion blur due to high-speed at low-altitude flights. The analysis proposed the utilization of TPH-YOLOv5 model, an enhanced version of YOLOv5, where an additional prediction head is introduced to detect objects at different scales. Furthermore, the original prediction heads are replaced with Transformer Prediction Heads (TPH), which leverage a self-attention mechanism to enhance object detection capabilities. Moreover, the convolutional block attention model (CBAM) was integrated into the model to identify attention regions in scenarios with dense objects. The results showed that TPH-YOLOv5 exhibits excellent performance when applied to drone-captured scenarios and thus outperformed competing methods. Specifically, on the DET-test-challenge dataset, TPH-YOLOv5 achieved an average precision (AP) of 39.18%, surpassing the previous state-of-the-art method by 1.81%. Plans for future work include the implementation of further in-situ pilot trials, to evaluate the real-time response of the system.

Keywords: Digital Agriculture, Unmanned Aerial Systems, Edge-computing, Machine learning, Livestock management

1. Introduction

Some of the key applications of UAVs in livestock health care include Aerial Surveillance, Environmental Monitoring, Grazing Management, Predator Management, Herd Management and Mustering, Data Collection and Analysis, Remote Access, and Monitoring. This work addresses the utilisation of UAVs with edge computing capabilities as tools for more efficient Livestock management. This concept is enhanced by combining direct sensing on the physical livestock assets (i.e. animals) with remote sensing using UAV edge computing ML tools aiming at implementing digital twin(s) modelling. The latter enables augmenting the traditional role of UAVs, in supporting livestock health care and farming operations, by providing knowledge-full aerial surveillance, grazing management, environmental and healthcare monitoring. Moreover, our ecosystem determines interoperability between two independent DTs that are addressing two independent dataspaces corresponding to the same physical phenomenon (livestock). Thus, we are achieving the implementation of a cognitive continuum among independent dataspaces defined by direct sensing (DT1)

and UAV-based remote sensing (DT2).

In the literature there are object detection and tracking algorithms that can be utilised in UAV footage, to be implemented on edge devices. Such modern deep learning technologies can help farmers to optimize livestock management. In this work, a state of the art overview was done based on which such algorithms can be categorised in the following categories based on their applications:

a) General Object Detection
b) Object Tracking
c) Edge Computing
d) Tiny Object Detection on UAVs

a) General Object Detection: Automatic object detection is one of the most well studied fields of research in the computer vision domain. Especially with the rise of deep learning and publicly available large annotated datasets, automatic detection and classification of objects gained huge popularity. One of the first attempts to utilize CNNs for object detection called Regions with CNN features (R-CNN) was published by Girshick et al. (2014). Several improvements of this basic algorithm such as Fast R-CNN (Girshick, 2015) and Faster R-CNN (Ren et al., 2015) were developed afterwards. As an alternative, a one-stage object detector called YOLO (You Only Look Once) was introduced by Redmon et al (2015). Compared to previous deep-learning frameworks for object detection, YOLO is extremely fast. Since then, several improvements of the original implementation of YOLO were made over the years which results in a whole family of object detection architectures and models pretrained on the COCO dataset. Another one-stage detector that eliminated the need for region proposals called SSD (Single-Shot-Detector) was presented in Liu et al. (2015). More recently, the authors of Tan et al. (2020) presented what is known as EfficientDet, a family of object detectors that focuses on achieving a balance between accuracy and efficiency. It utilizes EfficientNet (Tan et al., 2019) as backbone, a high-performance CNN which has fewer parameters and thus requires less computational resources. Another family of anchorless one-stage object detectors is CenterNet (Duan et al., 2019). Unlike other object detectors that focus on predicting bounding box coordinates or keypoints, CenterNet aims to simplify the detection by focusing on detecting object centers and relative bounding box dimensions rather than bounding box coordinates directly. Another advantage of CenterNet is that it replaces the need for Non-Maximum-Suppression (NMS) as post processing step with a more efficient algorithm which can directly be integrated into the CNN. Consequently, removing NMS as post-processing step enables much faster inference than competing methods.

b) Object Tracking: Furthermore, real-time object tracking is a vital component of UAV-based applications. Traditional tracking algorithms such as Kalman Filters and Particle Filters as well as more advanced deep learning-based trackers such as DeepSORT (Wojke et al., 2017), StrongSORT (Du et al., 2023), ByteTrack (Zhang et al., 2022), and CenterTrack (Zhou et al., 2020), enable UAVs to continuously track and follow objects of interest in real-time, even in complex and dynamic environments. Continuous multi-object tracking and object association in consecutive frames builds the basis for subsequent tasks such as motion analysis for instance. By tracking objects over time, computer vision systems can analyse their motion patterns, speed, direction, and trajectories. This information is valuable for tasks such as activity recognition, behaviour analysis, and anomaly detection.

c) Edge Computing: With the proliferation of edge computing and onboard processing capabilities in modern UAV systems, there is a growing demand on performing object detection and analysis directly on the UAV itself. Edge computing offers several advantages for deep learning applications: Firstly, edge computing reduces the latency and response time by performing computations directly on edge devices or embedded systems. This enables real-time decision-making which makes it well-suited for time-sensitive applications like real-time surveillance of livestock for instance. Secondly, edge computing minimizes the reliance on cloud connectivity, ensuring that deep learning models can operate even in remote or disconnected environments which is particularly beneficial in scenarios where reliable network connectivity may be limited. Thirdly, edge computing reduces the bandwidth and storage requirements by processing data locally. Deep learning models can be deployed directly on edge devices, eliminating the need to send large amounts of raw data to the cloud for processing. This results in significant cost savings and optimized resource utilization, as only relevant information needs to be transmitted.

In recent years, several edge devices for deep learning applications have been developed by the industry. The NVIDIA Jetson family, such as the Jetson Nano, Jetson Xavier, or Jetson TX2, for instance, is one of the most popular edge computing platforms designed specifically for accelerating deep learning applications

on the edge. An alternative to this is Google's Coral which is a platform of hardware components equipped with Google's Edge TPU (Tensor Processing Unit) and software tools for deep learning inference on the edge.

d) Tiny Object Detection on UAVs: With the astonishing capabilities of state-of-the-art object detectors and the rise of edge computing devices, also automatic object detection and tracking in UAVs has seen significant advancements in recent years. Models like Faster R-CNN, YOLO, and SSD have emerged as the backbone of object detection in aerial images, but since UAVs usually fly in high altitudes, a variety of adjustments and advancements had to be invented to accurately detect oriented tiny objects with high accuracy. A comprehensive overview of state-of-the-art object detectors especially designed for small objects and object localization in UAV images were presented by Chen et al. (2023) and Wu et al. (2022). One interesting approach to cope with objects being captured at different scales due to varying altitudes at which drones navigate as well as motion blur due to high-speed and low-altitude flight of drones was presented in Zhu et al. (2021).

In the following chapters we describe the ecosystem developed within the framework of SPADE EU project focusing on the enhanced management of Livestock utilising DTs that are based on wearable technologies and ML algorithms for UAVs with edge computing capabilities.

2. Concept and Methodology

The SPADE Project Livestock Pilot

Addressing the needs of the Livestock sector and its community, SPADE's (https://spade-horizon.eu/) efforts focused on the Digital Twin (DT) concept that is being standardized (ISO/IEC JTC 1/SC 41) and especially in a DT System of Systems (SoS) Virtual to Physical ecosystem (Figure 1).

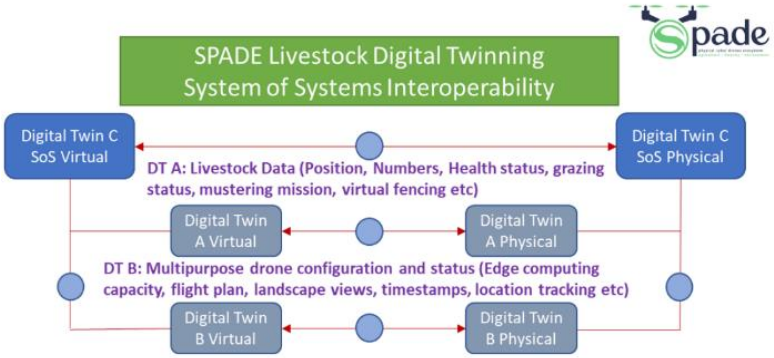

Figure 1. Digital Twinning of SPADE Livestock platform in line with ISO 2022 ISO/IEC JTC1/SC 27

In this approach Livestock animal-based sensing and Livestock UAV-based monitoring are being simulated by two DT interoperability cases. The DT A represents the Physical to Virtual space monitoring of Livestock data using wearable devices. The DT B represents the Physical to Virtual space monitoring of Livestock data using UAV based equipment. In DT A, physical conditions such as herd position, mobility, and deduced activity can be extracted to the virtual space, while in DT B the physical conditions of the UAV and its flight mission as well as Livestock physical conditions such as herd-flock and animal tracking, grazing landscape status monitoring, environmental and predator risk assessment, can be extracted to the virtual space.

***Objectives, piloting, and ecosystem prototype**:* This work develops a prototype platform to pilot sheep breeding and healthcare monitoring (Madesis et al., 2019), which is an essential economic activity offering hundreds of jobs. It also helps to shape the ecosystem and adds significantly to the agricultural, cultural, and gastronomic history of regions. The system evaluation is performed on the Greek island of Lesvos, where sheep breed consists of 350,000 purebred animals distributed in approximately 2.000 flocks. Almost 80% of the animals are kept in the north-western part of the island. The average milk yield is 223±70 kg in a milking period of 163±34 days. The breed's prolificacy is 1.10 - 1.25 lambs/ewe. Therefore, this work presents a

scenario case where a multipurpose drone is used for enabling livestock grazing and healthcare monitoring, in line to assisting the overall livestock management. The overall objective of this work is the optimization of both animal grazing and healthcare management, to improve milk yield, safeguard the sector's sustainability and contribute to the authentication, tracing, monitoring and conservation of traditional production systems and sheep rearing. Moreover, the proposed technology aspires to improve the working conditions and income of farmers and entice young farmers to engage in traditional sheep rearing by offering a platform capable of providing evidence-based decision support and minimize the effort required for everyday tasks.

3. Results and discussion

3.1. Physical and health-care conditions in the grazing process (DT A), usage of wireless animal wearable sensors

Motivation: For DT A we use animal wearable sensors to trace animal location and correlate animal movements (via x,y,z accelerometers) with activity/grazing and/or health status. This solution attempts to have a first level of automated tracking and detection of activity and potential healthcare issues. Focusing on grazing, we realized that eating habits may imply a first level animal healthcare status. Therefore, DT A implements a digital mapping of the physical situation as per monitoring a number of animals (the optimum would be all) via wearables. The expected outcome, based only on DT A, would be detecting fluctuations in eating patterns (e.g. lower grazing times) and thus identifying whether animals might be unhealthy, lame, or unwell.

During the first SPADE project stage lightweight wearable devices were used comprising of a multi-sensor cellular IoT prototyping platform (Nordic Thingy:91) using LTE-M and GNSS. The cellular communication combined with the GNSS positioning systems and the multitude of sensors for motion and impact are making this solution ideal for grazing and healthcare monitoring. As depicted in Figure 2, a lightweighted device (Thingy:91) attached to sheep collars is used as a 'wearable'. The device is a dedicated, battery-operated microcontroller equipped with low-power inertial sensors (accelerometer and gps) and wireless communication. Furthermore, the device is built around the nRF9160 System-in-Package (SiP), it is certified for a broad range of LTE bands globally and it supports LTE-M, NB-IoT and GNSS, and a nRF52840 board controller, with Bluetooth Low Energy and NFC. The position of the animal is detected with the GNSS integrated in the nRF9160 SiP while the accelerometers provide the measurements to perform animal motion analysis. The device samples regular accelerometer and tracking measurements at the frequency of 20 Hz. The SPADE Livestock platform is currently under development utilizing the OpenRemote open-source platform (OpenRemote IoT Platform). The prototype version has been customized by NST (http://www.nydorsystem.com/) for position tracking and activity status monitoring. The direct sensing part of the experiment **resulted in a successful real time feed** of the SPADE Livestock platform from the direct animal sensing collars. The system showed high potential for real time tracking of animals' status as well as detection of specific animal behaviour patterns (grazing, limping, moving in cycles). Communication issues have been clarified and timestamping has been satisfactorily employed as the main reference element to establish coherence between DTA and DTB datasets. Further development is planned to enhance the combined DTA – DTB system via augmenting the timestamping reference element with animal IDs and location tracking.

Preliminary results on using monitoring technologies for direct livestock healthcare and grazing management*:* SPADE decided to exploit a direct sensing link (DT A) using wearables directly on animals and UAVs as well as a remote sensing link (DT B) utilising remote sensing provided by UAVs with edge computing capabilities. Field trials have been conducted for testing the system in real field conditions and these will be continued throughout the next 24 months. Hitherto, monitoring real time grazing has been evaluated in conjunction with parts of DT B, where remote sensing via UAV flight sensing missions tests advanced computer vision algorithms for animal detection/tracking/identification/counting towards behavioural patterns recognition.

Figure 2. The physical to digital context of SPADE Livestock in DT A: wearable device attached to animal collar (left); the digital representation on the OpenRemote cloud platform, showing both position in the herd and activity based on a three-axis acceleration (right).

3.2. Computer Vision on Edge Devices for Livestock Monitoring (DT B), usage of UAVs and ML edge computing tools

Motivation: Unmanned aerial vehicles (UAVs) equipped with automated animal detection systems implemented on edge devices have emerged as promising tools for wildlife monitoring, conservation, and livestock farming. Advanced computer vision algorithms, integrated into aerial platforms, for animal detection and tracking in footage from UAVs provides researchers, conservationists, and farmers with a non-intrusive, cost-effective, and efficient way to monitor livestock, increasing animal welfare and optimising livestock management.

Preliminary results on selecting a tiny objects detection ML model and training with Livestock footage acquired in SPADE: The authors propose TPH-YOLOv5, an enhanced version of YOLOv5, where an additional prediction head was introduced to detect object at different scales. Furthermore, the original prediction heads are replaced with Transformer Prediction Heads (TPH), which leverage a self-attention mechanism to enhance object detection capabilities. To identify attention regions in scenarios with dense objects the convolutional block attention model (CBAM) was integrated into the model. The authors showed that TPH-YOLOv5 exhibits excellent performance when applied to drone-captured scenarios and thus outperformed competing methods. Specifically, on the DET-test-challenge dataset, TPH-YOLOv5 achieves an average precision (AP) of 39.18%, surpassing the previous state-of-the-art method by 1.81%.

Using State of The Art on Animal Detection in UAV images: Large, annotated datasets are a prerequisite to properly train and evaluate object detectors for animal detection in UAV images. To compare different approaches and their ability to detect sheep in UAV images, two datasets are considered: The first dataset we currently investigate is SheepCounter which consists of 1731 images containing only white sheep mainly on meadows (Nolan G., 2021). The second, more challenging dataset, is called Sheep Detection from Above with 2018 images (it3915masterpreparatoryproject, 2022). Compared to Nolan G. (2021), this dataset not only contains white sheep but also brown, black, and grey sheep, which makes the dataset more diverse. Additionally, terrain and illumination are more challenging.

Due to the lack of available video datasets and to be able to benchmark different types of object detectors and tracking paradigms, we recorded a dataset of videos from drones showing herds of sheep on the University Farm of Aristotle University of Thessaloniki (A.U.Th.). The dataset currently contains 17 videos of different lengths, ranging from 30 seconds to over 4 minutes. We are currently annotating the dataset using the open-source Computer Vision Annotation Tool (CVAT) , an open-source web-based tool specifically designed for annotating images and videos to create training datasets for computer vision algorithms.

Although, general object detection is getting not only more accurate but also more efficient, detecting animals in UAV images is still a challenging problem. Especially in precision livestock farming or monitoring of endangered species, high accuracy is demanded while smaller and more energy efficient models are needed due to implementation on mini-computers and edge devices. In relevant work (de Lima et al., 2023), the authors compared YOLOv4 and YOLOv5 models to count bovine cattle in images taken at altitudes of 20, 40, 80 and 100 m. All variants of YOLOv5 exceed a precision of 92% with the smallest model reaching a precision of 96% and the largest model 98%. In Wang et al. (2023) the newer YOLOX nano model was used and improved the detection performance for small objects. The obtained mean average precision (mAP) for cattle, sheep and horses is 86.47% at a height of 300m. In case of common cranes, it was shown in Chen et al., (2023) that the use of automatic approaches to count individuals in UAV images can be more

accurate than manual counting of field observers, who underestimated the population. The applied YOLOv3 model reached a precision of 99.91% and a recall of 94.59% for RGB images at daylight.

Within SPADE we already trained and compared several state-of-the-art object detectors, achieving promising results on the SheepCounter dataset mentioned above. Figure 4 shows the performance of the SSD object detector with MobileNetV2 backbone on a test image of the SheepCounter dataset.

Figure 2. Detection results of SSD with MobileNetV2 backbone on an image of the SheepCounter dataset. The green boxes represent the detected bounding boxes.

4. Conclusions

This work produced a first set of tangible results in line with the EU Horizon (HE) project SPADE. On the Tiny Object Detection on UAVs tasks, satisfying results were achieved especially on a self-created hyperspectral image dataset with a F1-score of 0.836. Although the achieved results are promising, the proposed model architecture is relatively complex which makes implementation on edge devices infeasible. Another interesting approach was presented by Fan and Lu (2021). The authors used a simplified AlexNet CNN architecture for landscape classification but introduced a spatial and spectral feature fusion paradigm to improve crop classification robustness, raising the accuracy for their dataset from 86.07% to 92.76%.

On the process of modelling Livestock assets via Digital Twinning our first results proved several benefits for Livestock Farming: Animal Health and Welfare: Digital twinning can contribute to monitoring and improving animal health and welfare by creating virtual representations of livestock and integrating data from wearable sensors. In addition, to support the UAV flight mission, the wearables introduced in the architecture of the Livestock platform to provide to the UAV pilot the exact GPS position of the herd. Based on the conclusions from the Livestock trial, the wearables can be used to achieve a) tracking and reporting, in real time, the exact position of the animals by tracking the bell animals of the herd, b) if equipped with extra sensors like accelerometer and thermometer, the wearables can be used for the data collection aiming to train and validate AI models to detect animal's activity (such as normal non-grazing activity, normal grazing activity, abnormal activity (i.e., illness, kneeling, moving in cycles, fever, etc.), c) testing the virtual fencing of the pasture area as well as to validate the UAV's calculations of animals trespassing.

Overall, this work presented findings from the SPADE Livestock pilot trials on the automatic detection of sheep from aerial images. This work is being improved by comparing different state-of-the-art object detectors. Although first results are promising, we further need to investigate advantages and shortcomings as well as their feasibility to be implemented on edge devices.

Moreover, we plan to combine object detection with tracking algorithms, to derive semantically higher information from videos such as animal counting or behaviour analysis. Another research direction we plan to investigate is to automatically classify grassing regions which enable farmers to strategically allocate grazing areas for their livestock.

Acknowledgements

This work has been supported by the SPADE project, funded by the European Union's Horizon Europe Research and Innovation programme within HORIZON-CL6-2021-GOVERNANCE-01 under Grant Agreement no. 101060778.

References

Nordic Thingy:91 Cellular IoT prototyping platform, [Online]. Available: https://www.nordicsemi.com/-/media/Software-and-other-downloads/Product-Briefs/Nordic-Thingy-91-PB.pdf. [Accessed June 2023].

OpenRemote IoT Platform, [Online]. Available: https://www.openremote.io/.

Chen A., Jacob M., Shoshani G. and Charter M., Using Computer Vision, Image Analysis and UAVs for the Automatic Recognition and Counting of Common Cranes (Grus grus), Journal of Environmental Management, vol. 328, 2023.

Chen C., Zheng Z., Xu T., Guo S., Feng S., Yao W.and Lan Y., YOLO-Based UAV Technology: A Review of the Research and Its Applications, Drones, vol. 7, no. 3, 2023.

CVAT, Open Data Annotation Platform, cvat.ai, [Online]. Available: https://www.cvat.ai/. [Accessed 7 June 2023].

de Lima Weber F., de Moraes Weber V. A., de Moraes P. H., Matsubara E. T., Paiva D. M. B., de Nadai Bonin Gomes M., de Oliveira L. O. F., de Medeiros S. R. and Cagnin M. I., Counting Cattle in UAV Images Using Convolutional Neural Network, Remote Sensing Applications: Society and Environment, vol. 29, pp. 2352-9385, 2023.

Du Y., Zhao Z., Song Y., Zhao Y., Su F., Gong T. and Meng H., StrongSORT: Make DeepSORT Great Again, IEEE Transactions on Multimedia, 2023.

Duan K., Bai S., Xie L., Qi H., Huang Q. and Tian Q., CenterNet: Keypoint Triplets for Object Detection, in IEEE/CVF International Conference on Computer Vision (ICCV), 2019.

Fan C. and Lu R., UAV image crop classification based on deep learning with spatial and spectral features, IOP Conference Series: Earth and Environmental Science, vol. 783, 2021.

Girschick, R., Fast-RCNN, Proceedings of the International Conference on Computer Vision (ICCV), 2015.

Girshick, R., Rich Feature Hierarchies for Accurate Object Detection and Semantic Segmentation, Proceedings of the IEEE Conference on Computer Vision and Pattern Recognition (CVPR), 2014.

ISO/IEC JTC 1/SC 41, Internet of Things and Digital Twin, 2021. [Online]. Available: https://www.iec.ch/dyn/www/f?p=103:7:601537151799192::::FSP_ORG_ID,FSP_LANG_ID:20486,25.

it3915masterpreparatoryproject, Roboflow, 2022. [Online]. Available: https://universe.roboflow.com/it3915masterpreparatoryproject/sheep-detection-from-above/browse?queryText=&pageSize=50&startingIndex=0&browseQuery=true. [Accessed 7 June 2023].

Liu W., Anguelov D., Erhan D., Szegedy C., Reed S. E. and Fu C.-Y., SSD: Single Shot MultiBox Detector, CoRR, abs/1512.02325, 2015.

Manessis G, Gelasakis AI and Bossis I., The Challenge of Introducing Point of Care Diagnostics in Farm Animal Health Management, Biomedical Journal of Scientific & Technical Research, p. 4, 2019.

Nolan G., Sheepcounter Dataset, 2021. [Online]. Available: https://universe.roboflow.com/riisprivate/sheepcounter. [Accessed 7 June 2023].

Redmon J., You Only Look Once: Unified, Real-Time Object Detection, CoRR abs/1506.02640, no. http://arxiv.org/abs/1506.02640, 2015.

Ren, S. He, K., Girshick R. B., and Sun J., Faster R-CNN: Towards Real-Time Oject Detection with Region Proposal Networks, CoRR, abs/1506.01497, 2015.

Tan M., Pang R.and Le Q. v., EfficientDet: Scalable and Efficient Object Detection, in Computer Vision and Pattern Recognition (CVPR) , 2020.

Tan M.and Le Q. V., EfficientNet: Rethinking Model Scaling for Convolutional Neural Networks, in International Conference on Machine Learning (ICML), 2019.

Wang Y., Ma L., Wang Q., Wang N. and Wang D., A Lightweight and High Accuracy Deep Learning Method for Frassland Grazing Livestock Detection Using UAV Imagery, Remote Sensing, vol. 15, no. 6, 2023.

Wojke N., Bewley A. and Paulus D., Simple online and realtime tracking with a deep association metric, in IEEE International Conference on Image Processing (ICIP), 2017.

Wu X., Li W., Hong D., Tao R. and Du Q., Deep Learning for Unmanned Aerial Vehicle-Based Object Detection and Tracking: A survey, IEEE Geoscience and Remote Sensing Magazine, vol. 10, no. 1, pp. 91-124, 2022.

Zhang Y., Sun P., Joang Y., Yu D., Weng F., Yuan Z., Luo W.and Wang X., ByteTrack: Multi-object Tracking by Associating Every Detection Box, in European Conference on Computer Vision (ECCV), 2022.

Zhou X., Koltun V. and Krähenbühl P., Tracking Objects as Points, in European Conference on Computer Vision (ECCV), 2020.

Zhu X., Lyu S., Wang X. and Zhao Q., TPH-YOLOv5: Improved YOLOv5 Based on Transformer Prediction Head for Object Detection on Drone-captured Scenarios, in IEEE/CVF International Conference on Computer Vision Workshops (ICCVW), 2021.

An initial forest digitization approach using drone and quadruped robot

Charalampos-Rafail Medentzidis [a,*], Theocharis Tsenis [a], Vassilios Kappatos[a]

[a] Hellenic Institute of Transport, Centre for Research and Technology Hellas, Thessaloniki, Greece

* Corresponding author. Email: charmede@certh.gr

Abstract

In the endeavor to safeguard Mediterranean forests amidst evolving environmental and societal shifts, leveraging cutting-edge technologies becomes imperative. This paper introduces an initial approach to forest digitization, harnessing the capabilities of both drone and quadruped robot. Through the integration of machine learning algorithms, crucial parameters such as soil moisture, tree crowns, and tree species were estimated. The findings underscore a remarkable precision and recall, 0.983 and 0.982, in soil moisture, with notable advancements in tree crowns and tree species. This synergistic fusion of aerial and terrestrial technologies heralds a promising frontier in advancing forest management practices.

Keywords: Forest digitization, Drone, Quadruped Robot, Machine Learning, Sustainable Forest Management.

1. Introduction

The Mediterranean (MED) region, which encompasses over 25 million hectares of forests and approximately 50 million hectares of other wooded lands, is at a critical juncture. The potential repercussions of climatic and socio-economic changes in the region could lead to the loss of vital ecosystem services and could trigger a host of economic, social, and environmental issues. Forest managers and industries in the region face significant challenges, primarily due to limited or missing access to current and emerging digital technologies. These technologies often appear outdated in key areas or fail to address some of the most pressing difficulties that the industry is expected to confront in the coming decades. Compounding these challenges, traditional methods of data collection often fall short in providing comprehensive and accurate information about forest health. This combination of technological limitations and inadequate data collection methods presents a formidable obstacle to effective forest management [1].

Drones have become an essential tool in modern forestry, providing comprehensive and detailed multispectral images that are instrumental in monitoring the bio-structural health of forest trees. These images, particularly those captured in the infrared band, enable the detection of water content in plant tissues and chlorophyll content in leaves, aiding in the timely diagnosis of dehydration or malnutrition in trees. In addition to health monitoring, multispectral imagery significantly contributes to forest inventory management by facilitating a better understanding of vegetation types, species composition, and distribution in forests, thereby promoting sustainable resource management. The imagery's ability to capture leaf's colour and spectral reflectance of plants allows for the detection of changes in different vegetation types and densities. Furthermore, multispectral imagery plays a crucial role in harvesting and regeneration processes by detecting tree age and growth, thereby determining which trees are suitable for harvesting or preservation. This information enables foresters to plan specific harvesting or renewal programs, maximizing the use of existing resources and increasing the success of forest plantations [2].

A notable study by Qu et al. (2024) [3], provides an exhaustive analysis of how drone multispectral technology can be harnessed for real-time monitoring and analysis of soil moisture across extensive agricultural lands. The study introduces a rapid inversion model for deep soil moisture (0–200 cm) in dryland agriculture, utilizing data from drone-based multispectral remote sensing. The crops under study were maize, millet, sorghum, and potatoes, with multispectral data, canopy leaf, and soil moisture content at various depths collected at intervals of 3 to 6 days. Vegetation indices exhibiting a high correlation with crop canopy leaf moisture content ($p < 0.01$) were identified using Pearson correlation analysis. This led to the development of linear and nonlinear regression models for predicting moisture content in canopy leaves and soil. The results demonstrated a significant linear correlation between the predicted and actual canopy leaf moisture levels for the four crops, according to the chosen vegetation indices. The use of canopy leaf moisture content to predict surface soil moisture (0–20 cm) exhibited enhanced accuracy. The models designed for the top 20 cm of soil moisture successfully estimated deep soil moisture levels (up to 200 cm) for all four crops. The study concludes that using drone-based multispectral technology, leaf water content can be forecasted

via vegetation index analysis, facilitating swift and effective soil moisture inversion. This research introduces a novel method for monitoring and managing agricultural water resources, providing a scientific basis for precision farming and moisture variation monitoring in dryland areas.

In a study conducted by Greifeneder et al. (2021) [4], a machine learning (ML) based approach was introduced for high spatial resolution (50 m) mapping of soil moisture. The methodology integrated Landsat-8 optical and thermal images, Copernicus Sentinel-1 C-Band SAR images, and modelled data, executable in the Google Earth Engine. The novelty of this approach lies in applying an entirely data-driven ML concept for global estimation of the surface soil moisture content. Globally distributed in situ data from the International Soil Moisture Network acted as an input for model training. Based on the independent validation dataset, the resulting overall estimation accuracy, in terms of Root-Mean-Squared-Error and R^2, was 0.04 $m^3 \cdot m^{-3}$ and 0.81, respectively. This study demonstrates the potential of ML in providing accurate and high-resolution soil moisture estimations, thereby contributing significantly to the fields of meteorology, hydrology, and agriculture.

Ball et al. (2023) [5], developed a method based on the Mask R-CNN computer vision framework for delineating tree crowns in tropical forests from aerial RGB imagery. Their approach, named Detectree2, is capable of recognizing the irregular edges of individual tree crowns. The study highlighted the potential of Detectree2 for effective forest monitoring and understanding of forest response to global change. It emphasized that Detectree2 can be rapidly trained to perform well in new types of forest and other ecosystems. Moreover, Detectree2 has demonstrated its effectiveness in a real-world scenario. It was independently tested in a temperate deciduous forest in Japan, where it outperformed DeepForest, achieving an F1 score of 0.57.

Gan et al. (2023) [6], conducted a comprehensive study on tree crowns detection and delineation in a temperate deciduous forest using two deep learning approaches: DeepForest and Detectree2. They used drone-acquired RGB imagery to detect tree crowns in an alpine, temperate deciduous forest with a complicated species composition. The study involved 499 digitized crowns, including four dominant species, with corresponding, accurate inventory data in a 1.5 ha study plot. The results showed that the spatial resolution had a significant effect on the estimation accuracy of tree crowns detection, especially when the resolution was greater than 0.1 m. Furthermore, Detectree2 could estimate tree crowns areas accurately, highlighting its potential and robustness for tree detection and delineation.

In a systematic review by Zhao et al. (2023) [7], explored the use of convolutional neural networks (CNNs) for individual tree crowns detection and delineation from remotely sensed data. They found that CNN models, when applied to high-resolution RGB images, showed significant improvements in accuracy over traditional methods. One study highlighted in the review reported an increase in detection accuracy of over 11%, while two studies noted increases in F1-score of over 16%. The review concluded that future research could benefit from exploring data fusion approaches, improving data efficiency with customized sampling and synthetic samples, and evaluating the impacts of pre-training and parameter tunings.

Quadruped robots, with their advanced manoeuvrability and adaptability, are increasingly being recognized as valuable tools in forestry and environmental monitoring. These robots can navigate difficult terrains and dense forest areas that are often inaccessible to humans or wheeled vehicles, making them ideal for ground-level data collection. Equipped with various sensors and cameras, quadruped robots can gather detailed environmental data and monitor the health of individual trees and plant communities.

In a study conducted by Tsenis et al. (2024) [8], a robust NDE quadruped robotic platform were utilized to perform monitoring and inspection in energy producing infrastructures. This platform addressed the challenges associated with conducting inspections in diverse and complex environments, offering flexibility, accuracy, and safety. The results highlighted the effectiveness of employing quadruped robots to access hazardous areas and perform comprehensive evaluations, ultimately contributing to the overall sustainability and performance of energy infrastructure systems.

A study conducted by Idrissi et al. (2022) [9], evaluated the forest ecosystem through a semi-autonomous quadruped robot and a hexacopter drone. The study aimed to improve the resilience of forests for economic growth and climate regulation. The quadruped robot was equipped with an integrated camera and an external sensing platform with light and infrared cameras, computing, communication, and power modules. The robot was used to observe forest health indicators from the ground, such as burrows and deadwood, which are inaccessible from the air. The study concluded that the use of quadruped robot and drone can significantly reduce the time required for forest monitoring by reducing computation and conserving energy.

Another study by Cheng et al. (2024) [10], focused on the traversal of 3D complex environments by quadruped robots with limited perception. The study proposed an end-to-end learning-based quadruped robot motion controller that relies solely on proprioceptive sensing. This controller can accurately detect, localize, and agilely respond to collisions in unknown and complex 3D environments, thereby improving the robot's traversability in complex environments. The study concluded that methods based on collision detection can enhance a robot's perception of environmental obstacles, enabling quadruped robots to successfully traverse challenging obstacles in various complex environments.

This paper introduces an initial forest digitization approach, leveraging drone and quadruped robot. Its aim is to address limitations in traditional data collection methods and enhance accuracy in capturing vital forest ecosystem data. By integrating advanced sensor technologies and machine learning algorithms, the study focuses on assessing key parameters such as soil moisture, tree crowns and tree species. Through detailed methodology descriptions and performance evaluations, it emphasizes the potential of this integrated approach to transform forest monitoring.

The remainder of the paper is organized as follows: Section (2) provides the background theory of vegetation indices, laying the theoretical groundwork for understanding the key vegetation indices used in forest monitoring. Section (3) elaborates on our methodology, outlining the data gathering, processing, and describes our drone and robot models. Section (4) presents the results and discussion, regarding the drone and robot models, including performance evaluations. Finally, section (5) presents conclusions and future work, summarizing the key findings and further research to enhance the methodologies and technologies discussed in the paper.

2. Background Theory of Vegetation Indices

Vegetation indices are mathematical combinations of spectral bands designed to highlight specific characteristics of vegetation, such as biomass, chlorophyll concentration, or stress levels. These indices are typically derived from remote sensing data collected by satellites, drones, or other aerial platforms. By comparing the reflectance of light in different spectral bands, vegetation indices provide insights into the health and vigor of plant communities. This paper focuses on three commonly used vegetation indices: the Normalized Difference Vegetation Index (NDVI), the Normalized Difference Red Edge Index (NDRE), and the Green Normalized Difference Vegetation Index (GNDVI).

NDVI is one of the most widely used vegetation indices, particularly effective at assessing vegetation health and density. The NDVI is calculated using the following formula:

$$NDVI = \frac{NIR-Red}{NIR+Red}$$

where NIR represents the reflectance in the near-infrared band (approximately 700-1100 nm) and R represents the reflectance in the red band (approximately 600-700 nm). Healthy vegetation absorbs most of the visible light (particularly red) and reflects a large portion of the near-infrared light, whereas unhealthy or sparse vegetation reflects more visible light and less near-infrared light. By comparing the difference and sum of the near-infrared and red reflectance, NDVI effectively measures the density and health of vegetation. NDVI values range from -1 to 1, with higher values indicating healthier and denser vegetation.

Tucker et al. (1979) [11], introduced the NDVI, describing its formulation and its utility in monitoring vegetation health and density using remote sensing data. The study demonstrated how NDVI could be used to assess vegetation cover and provided the theoretical foundation for its widespread use in ecological and agricultural applications.

NDRE is similar to NDVI but uses the red-edge portion of the spectrum instead of the red band. It is particularly useful for detecting stress in vegetation earlier than NDVI. The NDRE is calculated using the following formula:

$$NDRE = \frac{NIR-RE}{NIR+RE}$$

where NIR represents the reflectance in the near-infrared band and RE represents the reflectance in the red-edge band (approximately 700-750 nm). The red-edge band is located at the transition zone between the

red and near-infrared bands, where there is a sharp change in the reflectance of chlorophyll. This makes NDRE more sensitive to changes in chlorophyll content and, consequently, better at detecting early signs of stress or changes in plant health. NDRE is especially valuable in precision agriculture for monitoring crop conditions and optimizing inputs like water and nutrients.

In a study conducted by Gitelson et al. (1994) [12], explored the spectral characteristics of leaves during senescence and highlighted the importance of the red-edge region for chlorophyll estimation. This research laid the groundwork for the development of indices like NDRE, which leverage the red-edge band to detect early signs of plant stress and changes in chlorophyll content.

GNDVI focuses on the green portion of the spectrum, making it sensitive to the amount of chlorophyll present in vegetation. The GNDVI is calculated using the following formula:

$$GNDVI = \frac{NIR-G}{NIR+G}$$

where NIR represents the reflectance in the near-infrared band and G represents the reflectance in the green band (approximately 540-570 nm). The green band corresponds to the peak reflectance of healthy chlorophyll, making GNDVI particularly effective at assessing chlorophyll content and photosynthetic activity. Like NDVI, GNDVI values range from -1 to 1, with higher values indicating greater chlorophyll content and healthier vegetation. GNDVI is useful for monitoring crop health, estimating yield potential, and managing agricultural practices.

In a study Gitelson et al. (1996) [13], discussed the potential of using the green band for vegetation monitoring and proposed the GNDVI as an alternative to NDVI. The study demonstrated that GNDVI is particularly sensitive to variations in chlorophyll concentration, making it a useful tool for assessing vegetation health and photosynthetic activity.

In summary, NDVI, NDRE, and GNDVI are essential tools in remote sensing, providing critical insights into vegetation health, stress, and chlorophyll content. By utilizing different spectral bands, these indices enable early stress detection and effective monitoring, enhancing sustainability practices and ecological assessments.

3. Our Methodology

The employed methodology involves data collection, data processing and data storage. The data collection is conducted via drone and robot. The drone autonomously executes pre-programmed flight paths to gather high-resolution RGB and multispectral imagery across various spectral bands—Green, Near Infrared, Red, and Red Edge. Concurrently, the quadruped robot traverses designated forest trails, capturing RGB images from the ground, leveraging its semi-autonomous navigation system. The data harvested by the drone and robot are analyzed through machine learning algorithms. These algorithms are adept at deducing critical parameters like soil moisture from multispectral images and tree crowns/species from RGB images.

3.1 Our Developed Drone Model

The study utilized drone equipped with multispectral and RGB cameras. Flight parameters were fine-tuned to optimize data collection efficiency. Maintaining an altitude of 25 meters allowed for close-up views of the forest area. A flight speed of 4 m/s struck a balance between detailed image capture and efficient area coverage. Front and side overlaps were carefully configured at 70%. The gimbal was positioned towards the ground. Continuous image capture at 1.5-second intervals ensured uninterrupted data acquisition throughout the flight duration.

The process of soil moisture detection, as depicted in

Figure 1, begins with the implementation of histogram equalization to counteract the effects of diverse lighting conditions. Subsequently, vegetation indices are computed to transform the band images into valuable insights about the vegetation of the forest area. The gathered images are then converted into 25x25 square meter tiles and resized to pixel dimensions using the field of view and relative altitude from the ground, with the aid of trigonometry. The link between the measurements and image tiles was established by cross-referencing the GPS coordinates. For each tile, statistical features such as mean, standard deviation, and kurtosis were extracted. The tiles that correspond to the measurements were then used for training,

validation, and testing.

The model is trained with a distribution ratio of 70:20:10 for the training, validation, and test sets, respectively. The training phase spans 100 epochs, with a batch size of 64 and a learning rate of 0.0001. The model architecture includes three fully connected layers, consisting of 512, 256, and 128 neurons respectively, and concludes with a softmax activation layer at the output. After training, the model's performance is evaluated using metrics like precision and recall.

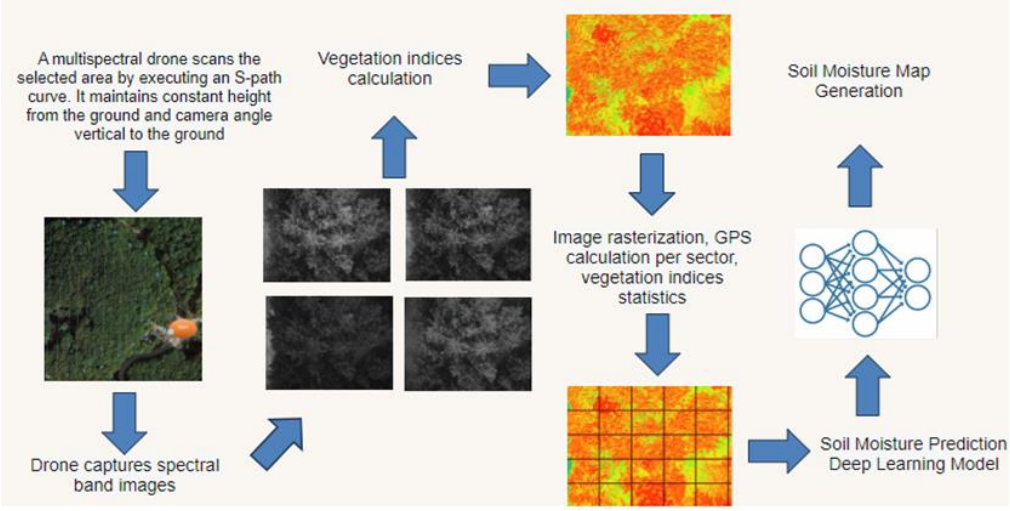

Figure 1: Soil Moisture Detection Process

The procedure of tree crowns/species detection, as illustrated in Figure 2, commences with the preprocessing of collected RGB images. To ensure consistency across the dataset, each image is resized to a dimension of 640x640 pixels. Histogram equalization was applied to images, to counteract variations in lighting conditions. After preprocessing, the dataset is augmented to increase variability and enhance model robustness. Techniques such as horizontal and vertical flips were used to create mirrored images, thereby diversifying the dataset. Random rotations, within a range of -15° to +15°, were employed to simulate various viewing angles and orientations of trees. Furthermore, horizontal and vertical shears, ranging from -10° to +10°, were implemented to account for perspective distortions.

A pretrained model, specifically the YOLO (You Only Look Once) model, were then utilized and fine-tuned on the preprocessed and augmented dataset. This fine-tuning process enables the model to accurately detect regions of tree crowns in images. The effectiveness of the predicted crowns was evaluated through metrics such as precision and recall.

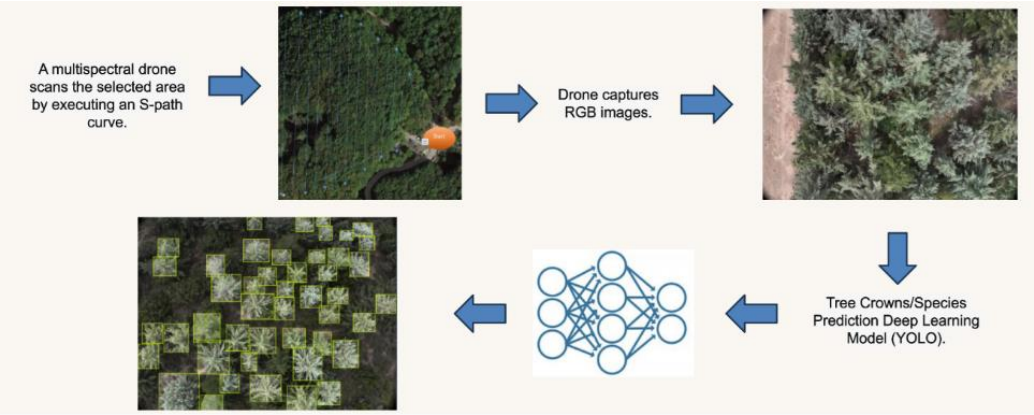

Figure 2: Tree Crowns Detection Process

3.2 Our Developed Quadruped Robot Model

The robot's data collection process, as illustrated in Figure 3, employs a quadruped robot to gather data from the ground. The robot navigates in pre-defined trails operating in a semi-autonomous manner, using markers named fiducials that contain information about localization and mapping. Before each mission, the path was recorded and stored. The robot uses a walk-stop technique to capture RGB images while moving. It stops approximately 20 meters from trees, to optimize the angle of view, and captures images with its front camera.

The collected images were processed using the YOLO model to estimate tree species based on leaf volume. The procedure for detecting tree species was similar to that of tree crowns, with the added step of estimating species based on leaf volume. As a result, additional labels were added to the annotations, indicating the tree species as determined by the volume of their leaves.

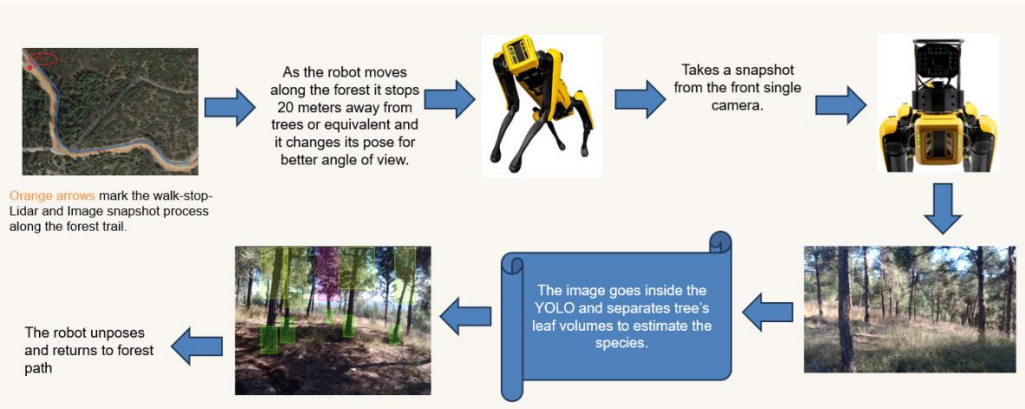

Figure 3: Robot's Data Collection Process

4 Results and Discussion

This section presents the outcomes of the study, focusing on the performance evaluation of the developed models utilizing drone and quadruped robot technology for forest digitization. The soil moisture prediction model achieved high precision and recall scores of 0.983 and 0.982, respectively, on the test set. These scores indicate the robustness and accuracy of the model in predicting soil moisture levels across different classes, which include low, medium, and high moisture content. The precision and recall scores for tree crowns detection were 0.724 and 0.580, respectively. For tree species detection, the model achieved a precision score of 0.686 and recall of 0.528. Table 1 summarizes the evaluation for each model on the test set.

Overall, the results indicate promising outcomes in soil moisture detection, showcasing the effectiveness of drone imagery coupled with machine learning algorithms. Accurate soil moisture assessments are pivotal for comprehending forest health and managing water resources efficiently. However, the performance of tree crowns and species detection underscores the complexity of these tasks, particularly concerning the diverse nature of forest ecosystems in terms of crowns structures and species diversity. This study emphasizes the need for developing more robust models tailored to address the intricacies of forest diversity.

Table 1: Soil Moisture and Tree Crowns/Species Models Performance - Evaluation on Test Set

	Precision	Recall
Soil Moisture	0.983	0.982
Tree Crowns	0.724	0.580
Tree Species	0.686	0.528

5 Conclusions - Future Work

This study has effectively showcased the potential of initially integrating drone and quadruped robot technology with advanced machine learning algorithms for forest digitization and monitoring. The soil moisture prediction model, with its impressive precision and recall scores, emerges as a robust tool for assessing forest health. While the tree crowns and species detection models did not attain the same level of accuracy, outlined the complexity of capturing information on tree crowns and species in diverse forest ecosystems.

Future work will focus on enriching data and refining methodologies. Expanding the data collection process to encompass diverse forest ecosystems and seasonal variations will provide a solid foundation for developing robust models capable of generalizing across various forest conditions. Methodologically, efforts will concentrate on implementing image processing algorithms, and optimizing machine learning models. These enhancements aim to enhance the precision of forest monitoring tools, ensuring adaptability and accuracy in addressing environmental variability and the intricate dynamics of forest ecosystems.

Acknowledgements

The aforementioned work effort in this paper is conducted under the framework of the DigiMedFor project, funded by the European Union under grant agreement No. 101081928.

6 References

[1] 24 5 2024. [Online]. Available: https://digimedfor.eu/.

[2] [Online]. Available: https://www.autelpilot.com/blogs/news/drones-in-forestry-applications-of-multispectral-imagery. [Accessed 24 5 2024].

[3] T. a. L. Y. a. Z. Q. a. Y. Y. a. W. Y. a. L. F. a. Z. W. Qu, "Drone-Based Multispectral Remote Sensing Inversion for Typical Crop Soil Moisture under Dry Farming Conditions," *Agriculture*, vol. 14, p. 484, 2024.

[4] F. a. N. C. a. W. W. Greifeneder, "A machine learning-based approach for surface soil moisture estimations with google earth engine," *Remote Sensing*, vol. 13, p. 2099, 2021.

[5] J. G. a. H. S. H. a. J. T. D. a. K. X. J. a. H. J. a. J. W. a. A. M. a. A.-K. M. a. V. G. a. C. D. A. Ball, "Accurate delineation of individual tree crowns in tropical forests from aerial RGB imagery using Mask R-CNN," *Remote Sensing in Ecology and Conservation*, vol. 9, pp. 641--655, 2023.

[6] Y. a. W. Q. a. I. A. Gan, "ree crown detection and delineation in a temperate deciduous forest from UAV RGB imagery using deep learning approaches: Effects of spatial resolution and species characteristics," *Remote Sensing*, vol. 15, p. 778, 2023.

[7] H. a. M. J. a. P. G. a. S. J. Zhao, "A systematic review of individual tree crown detection and delineation with convolutional neural networks (CNN)," *Current Forestry Reports*, vol. 9, pp. 149--170, 2023.

[8] T. a. T. A. a. K. V. Tsenis, "NDE Using Quadruped Robotic Platform for Renewable Energy Producing Infrastructures," in *2024 IEEE 8th Energy Conference (ENERGYCON)*, Qatar, IEEE, 2024, pp. 1--6.

[9] M. a. H. A. a. B. B. a. O. A. a. A. R. a. A. A. a. A. T. Idrissi, "Evaluating the forest ecosystem through a semi-autonomous quadruped robot and a hexacopter uav," *Sensors*, vol. 22, p. 5497, 2022.

[10] Y. a. L. H. a. P. G. a. Y. L. a. L. H. a. L. B. Cheng, "Quadruped robot traversing 3D complex environments with limited perception," *arXiv preprint arXiv:2404.18225*, 2024.

[11] C. J. Tucker, "Red and photographic infrared linear combinations for monitoring vegetation," *Remote sensing of Environment*, vol. 8, pp. 127--150, 1979.

[12] A. a. M. M. N. Gitelson, "Spectral reflectance changes associated with autumn senescence of Aesculus hippocastanum L. and Acer platanoides L. leaves. Spectral features and relation to chlorophyll estimation," *Journal of plant physiology*, vol. 143, pp. 286--292, 1994.

[13] A. A. a. K. Y. J. a. M. M. N. Gitelson, "Use of a green channel in remote sensing of global vegetation from EOS-MODIS," *Remote sensing of Environment*, vol. 58, pp. 289--298, 1996.

Enhancing agriculture question-answering systems through re-ranking and in-memory computing

Nur Arifin Akbar [a,*],

[a] Dipartimento Mathematica e Informatica, Universita degli Studi di Palermo, Palermo, Italy

* Corresponding author. Email: nurarifin.akbar@unipa.it

Abstract

The agriculture sector has more complicated information demands, needing retrieval-augmented generation (RAG) models that are advanced enough to offer precise and contextually fitting answers. This study puts forward a fresh method for enhancing RAG models in the field of agriculture by combining re-ranking tactics along with in-memory computing. The strategy aims to better the importance of brought back documents and lessen response delay which assists real-time precise answering for varied inquiries related to agriculture. The research commences with a summary about RAG architectures and talks of why there is drive to create domain-specific optimizations for agriculture. The method suggested here uses top-level components like Sentence Transformer model for embedding generation, FAISS for vector search that's fast and a pre-trained language model to make high-quality responses. This system gets trained on an extensive agriculture QA dataset so it can handle various questions about managing crops, controlling pests, soil health and other relevant topics. For the study, to make sure the documents that are found stay relevant, they use re-ranking methods based on zero-shot classification. In simple terms, re-ranking means giving a score to each document and then rearranging them according to how closely they match with the query. The effectiveness of this re-ranking process is tested in many experiments which show better accuracy compared to basic methods. Additionally, the study uses in-memory computing with the help of FAISS to cut down retrieval delay and support instantaneous functioning. The procedure of memory indexing for question embeddings results in considerable speed enhancements compared to usual retrieval methods based on disks. The benchmarks show effectiveness improvements attained by using in-memory calculation, making it good for big-scale applications and real-time answering of questions about agriculture.

Keywords: Agri-Data, Retrieval Augmented Generation, QA Systems, LLM, RAG

1. Introduction

1.1 Background on agriculture information needs and retrieval-augmented generation (RAG) models

In the sector of agriculture, there is a rising need for precise and prompt information to help in decision-making. Farmers, experts in agriculture, and those who make policies require access to knowledge that is relevant for tackling different difficulties like managing crops, controlling pests or ensuring soil's good health. The usual systems used for finding information have difficulty giving answers with appropriate context when asked complicated questions about farming matters. Models known as Retrieval-augmented generation (RAG), that make use of both retrieval and generation methods, show potential in dealing with this task. RAG models use a big collection of agricultural knowledge for getting back useful papers according to a query given, and then creating responses that make sense within the context. These models could change how we do things with agriculture question-answering systems by giving correct and complete answers to many different types of queries. Nevertheless, because agriculture sector is special in various ways like having diverse information needs or needing quick performance, more improvements on RAG models are needed for their full potential.

1.2 Motivation for enhancing RAG models in the agriculture domain

In general question-answering tasks, RAG models have shown good performance. However, when we use them for agriculture domain it is not straightforward because there are some challenges unique to this field. Queries related to agriculture may contain intricate ideas, terminology specific to the area and a broad array of subtopics like types of crops, methods for controlling pests and soil nutrient needs. To handle these

queries well with RAG models in the agriculture field, we must optimize them accordingly. Furthermore, the sector of agriculture requires quick action. For instance, a farmer may need instant responses to decide on certain things. In RAG models, the processes of getting back and creating should be speedy to give fast answers for user questions. Also, these models must be easy to scale up as more and more queries are made with the increasing use of digital technology in agriculture.

1.3 Research Objective and Contributions

This research has a main goal to have better RAG models for agriculture area. It also include re-ranking plans and in-memory computing, with the aim of making documents that are found more relevant and cutting down on response time delay. The key contributions of this research are as follows:

a. A new method is suggested to enhance RAG models for the agriculture field by using re-ranking strategies and in-memory computing.
b. Testing performance of our improved RAG model on the Agriculture QA dataset, showing marked enhancements in accuracy and retrieval speed compared to basic methods.
c. Understand about the efficiency of re-ranking tactics and in-memory computing to improve RAG models for agriculture QA data.
d. Advancement in the progress of RAG architectures and their use in the field of agriculture, making it possible for farm data easily processed within generative AI systems

Our research aims to bridge the gap between the information needs of farmers and the available knowledge resources. The enhanced RAG models developed in this study have the potential to revolutionize agriculture question-answering systems and support data-driven decision-making in agriculture.

1.4 Related Works

1.4.1 Retrieval Augmented Generations

Models with retrieval augmentation are being used in different areas. For example, they can assist in task-oriented dialog systems where responses get produced from chosen snippets using Retrieval Augmented Generation (Thulke, 2021). These models merge pre-trained parametric and non-parametric memory with deep learning methods for language production (Lewis, 2020). When we add the strategy of retrieval, it helps neural generative models to perform better (Li et al., 2018). A particular method, Generation-Augmented Retrieval (GAR), is meant to handle open-domain queries by producing related contexts lacking external supervision (Mao et al., 2021). These ways are about increasing the chance of getting results that match a query and retrieved contexts at the same time (Tian et al., 2019). Furthermore, retrieval augmentation allows for the addition of data beyond parametric models which can improve general performance (Sonsbeek et al., 2023). Also, the use of models with retrieval augmentation has shown promise in improving Out-of-Distribution (OOD) robustness. This suggests their ability to enhance model performance (Zhang & Zhou, 2014). Several studies have also explored the use of retrieval methods in various tasks, like generating common sense and understanding semantics. This shows how versatile approaches with retrieval are (Wang et al., 2021; Pasupat et al., 2021). These models can control generative processes by manipulating retrieval indices and constructing queries. There have been suggestions to distill knowledge from big generative models into models that retrieve information. The aim is to improve effectiveness in open-domain conversations (Kim et al., 2021).

1.4.2 Reranking Strategies

Re-ranking strategies are very important for improving the performance of information retrieval systems. Different methods have been suggested to enhance document rankings after the first retrieval process. For instance, (Ji et al., 2009; dealt with document re-ranking to boost the ranking of pertinent documents post-initial retrieval (Ji et al., 2009;. In the work of (Yang et al., 2006), a fresh re-ranking method is presented that uses label propagation-based semi-supervised learning algorithms. This technique takes advantage of the internal structure existing within big document datasets (Yang et al., 2006; . For document ranking

refinement, there are two main approaches: indirect re-ranking with Query Expansion (QE) strategies and direct re-ranking on initially retrieved documents discussed by Villatoro et al., 2012. In Addition, strategies for re-ranking have been studied in various situations. For example, there is visual re-ranking for multi-aspect information retrieval (Klouche et al., 2017). A method of re-ranking was introduced that uses information from relevance feedback to improve rankings (Villatoro-Tello et al., 2009). Also, Teng et al. Teng et al. (2009) emphasized the significance of entropy-based clustering in enhancing document re-ranking, placing it as a step between initial retrieval and query expansion within information retrieval systems. Additionally, studies have shown that re-ranking algorithms are helpful in many areas. This includes re-sequencing of web data based on knowledge domains (Zhao & Zhang, 2019), and Ren et al. (2021) have demonstrated Passage Language Model (PLM)-based rerankers that use cross-encoder architecture for passage re-ranking which resulted in substantial improvement over traditional methods. The work of Ren et al. (2021) pointed out the effectivity of using document-passage graphs to re-rank search results (Bendersky & Kurland, 2008).

1.4.3 Existing Agri-Data QA systems

The work of Li (2023) shows a Q&A system for agricultural planting technology, using text matching algorithms and crop planting knowledge maps to improve precision in answering farming-related questions. Jain et al. (2019) present AgriBot that is an agriculture-focused question-answering system made especially for responding to farmer's queries. Additionally, in 2019 there was a project that concentrated on making an Agriculture Chatbot with the help of machine learning methods. Particularly, RNN deep learning algorithms were used to offer exact answers related to agriculture area.

2 Material and Methods

2.1 Overview of Proposed Approach

The method intends to improve Retrieval-Augmented Generation (RAG) models in the agriculture field by combining re-ranking strategies and in-memory computing. It is developed for making the documents found more relevant, reducing response delay as well as delivering precise answers in real time for agriculture-based questions.

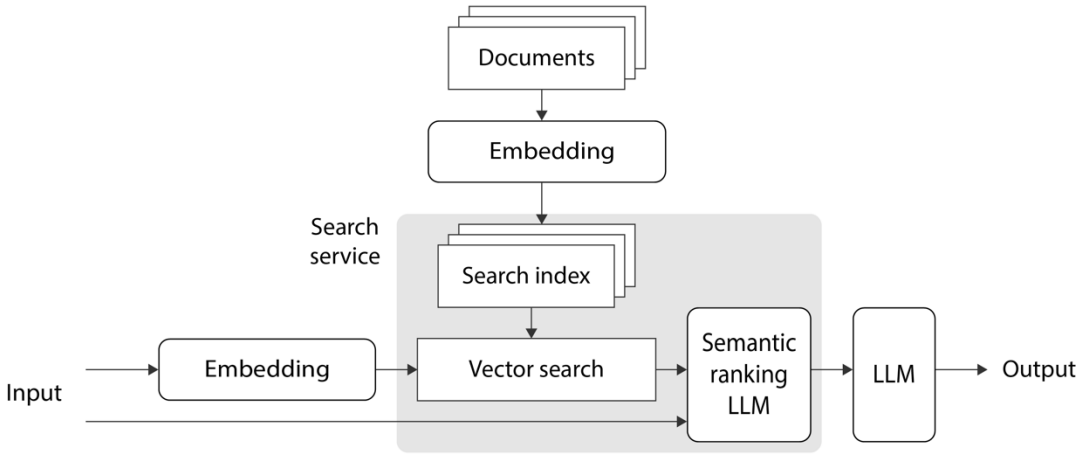

Figure 1. Proposed Model

2.2 Dataset and Preprocessing

This study uses the dataset Agriculture QA English version from KisanVaan dataset. The data is a well-rounded compilation of questions and their corresponding answers on subjects related to agriculture. The dataset offers various topics, like managing crops, controlling pests, and maintaining soil health making it perfect for training and assessing the improved RAG model. We got the dataset via HuggingFace datasets library which assures easy merging with other data as well as preprocessing convenience. To make the dataset ready for training, we began by using the SentenceTransformer model "all-mpnet-base-v2" to create embeddings for each question. We followed these steps in preprocessing: first load dataset with help from datasets library, then use SentenceTransformer model on GPU for generating embeddings towards questions and save them to be used later during retrieval processes. Moreover, documents were broken into manageable pieces through RecursiveCharacterTextSplitter so that they can be retrieved at their best performance level.

For each question in the embedding model, while Q represent set of question and fe is sentence transformer given that :

- Q is the set of questions in the Agriculture QA dataset.
- f_e is the SentenceTransformer model "all-mpnet-base-v2" used for generating embeddings.

For each question q_i in Q, the embedding e_i is generated as follows:

$$e_i = f_e(q_i) \quad (1)$$

The structure of RAG model has two main parts, which are the retriever and the generator. The role of the retriever part is to find important documents from a big collection using input query. In this method, we used FAISS (Facebook AI Similarity Search), an effective vector search library for quick and expandable retrieval tasks that can manage large amounts of agricultural information. The generator part makes a fitting and contextually correct answer using the documents that have been found by the retriever. In this implementation, we used an already trained language model called Meta-Llama-3-8B which can generate good quality responses by taking advantage of context from retrieved documents. This component guarantees that the answers are not only pertinent but also linguistically smooth and enlightening.

Re-ranking strategies were used to enhance the accuracy of documents found. The process of re-ranking involves giving scores to these documents that have been retrieved, according to how relevant they are with the query. After scoring, we reorder them to put higher importance on those which are considered more related in content and context. Zero-shot classification was used for relevance scoring by applying the pre-trained model "facebook/bart-large-mnli". It has ability to evaluate each document's significance in relation with given query without any specific training needed for this task or function. This approach allows for flexible and accurate relevance assessment across diverse queries.

The re-ranking algorithm was implemented in three steps. First, a set of candidate documents got from FAISS. Second, each document in the list was given a score by the zero-shot classification model. Finally, we rearranged all these documents based on their scores starting with most relevant ones to less relevant ones. This process of re-ranking guarantees that only those documents which are very related to the conversation will be utilized for producing final response that will improves precision and appropriateness of answers.

To lessen the delay in retrieving answers and improve real-time activity, we utilized in-memory computing with FAISS. We made an index of the query embeddings through FAISS, which permits swift vector searching. Storing these embeddings in memory has greatly cut down on time needed for finding related documents. The accuracy explained as follows :

- R is the set of generated responses by the RAG model.
- A is the set of ground truth answers from the Agriculture QA dataset.

- I is the indicator function, which returns 1 if its argument is true and 0 otherwise.

The accuracy ACC is calculated as follows:

$$\text{ACC} = \frac{1}{|R|}\sum_{i=1}^{|R|} I(r_i = a_i) \quad (2)$$

where r_i belongs to R and a_i belongs to A. Here, $|R|$ equals $|A|$, representing the number of generated responses and ground truth answers. In order to assess improvements in performance due to using in-memory computing, a set of benchmarking tests was performed. These compared FAISS's in-memory retrieval with the traditional way of retrieving from disk. The benchmarking process measured how long it took for each method to retrieve data, using an identical group of questions taken from the Agriculture QA Dataset. The retrieval time improvement factor F is calculated as follow :

- T_d is the average retrieval time for disk-based retrieval.
- T_m is the average retrieval time for in-memory retrieval using FAISS.

$$F = \frac{T_d}{T_m} \quad (3)$$

3 Results and Discussion

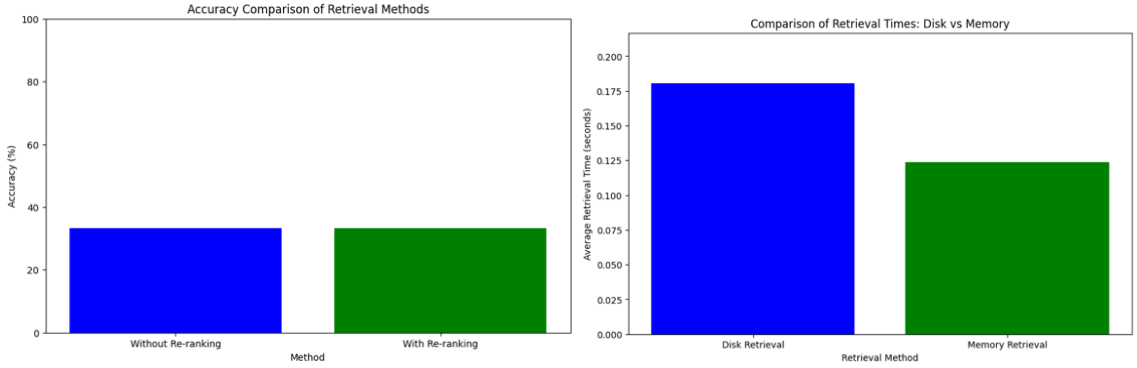

Figure 2. Comparison Results

RAG model accuracy was measured in two different approaches: with re-ranking methods and without them. The model, which had been trained on the agriculture QA dataset from Kisan Vaani, was tested using a subset of that same dataset. For scoring the accuracy, we compared responses generated by our model to ground truth answers from this test set.

The tests we did showed that the base RAG model, when re-ranking is not used, got an accuracy of 33.33%. This matches with the other result where we added re-ranking strategy to RAG model. The inclusion of re-ranking methods for fine-tuning did not deliver substantial benefits in terms of precision compared against our starting point. This indicates that the process of re-ranking utilized in this analysis had only a restricted effect on fostering precision within the model's response generation ability towards queries centered around agriculture subjects.

Also, this study did not completely investigate how well re-ranking strategies can bring out improvements. The assessment only happened on a small part of the dataset, so more tests with different questions and bigger sample sizes might give extra understanding into how good these strategies are. Looking

into other re-ranking algorithms or adjusting the re-ranking model to fit better for agriculture field might possibly produce better outcomes (Villatoro-Tello et al., 2009; Zhao & Zhang, 2019).

For assessing the time needed to retrieve results, we compared two methods: one based on disk storage and another that uses in-memory retrieval with FAISS. In the process using disk, a file containing question embeddings was read to mimic getting data from storage and doing similarity search (Sun et al., 2019; Ling et al., 2023). Then we compared this approach with in-memory retrieval where FAISS is employed for indexing question embeddings and executing fast similarity searches.

The tests to compare show how long it takes to get back a set group of questions, during many repeats. For the retrieval on disk, they found an average time of 0.180653 seconds needed for each go. On the other hand, in-memory retrieval using FAISS showed a much lower average time needed for every single go through.

The contrast of in-memory retrieval with FAISS and disk-based retrieval makes clear the quicker speed in-memory approach offers for real-time retrieval. This reduced time for retrieving answers is very important to improve user experience, as it enables systems dealing with agriculture topics to give instant replies when users ask questions (Thenmozhi & Srimathi, 2017). The better efficiency also helps handle more queries at one time, making this system expandable for big deployments (Chakraborty & Bhunia, 2021).

4 Conclusions

4.1 Experiment Result Summary

From the experiment's results, it was found that adding re-ranking did not significantly increase accuracy when compared to the basic RAG model without re-ranking. The starting point and again-ranked RAG models both achieved an accuracy of 33.33% on a part of agriculture QA dataset from Kisan Vaani. This shows that for this study's method of using re-ranking, there isn't much difference in how well it helps with making accurate responses for agriculture-related questions. Nevertheless, the experiments for benchmarking showed how superior in-memory retrieval using FAISS is for reducing retrieval latency. The average time required by in-memory retrieval was considerably less than that of disk-based retrieval. This shows big efficiency improvements achieved from combining in-memory computing with FAISS to quickly find similarities.

4.2 Implications for Agriculture Question-Answering Systems

The results found in this study give us useful understanding for creating agriculture question-answering systems. Although the re-ranking methods did not bring about big accuracy enhancements with the present model, a noticeable reduction in retrieval latency by using FAISS for in-memory computing has significant consequences on real-time performance. Using FAISS for in-memory retrieval can quickly reduce the time it takes to get information, which is a key factor that affects the user experience of agriculture question-answering systems. By responding fast to queries from users, these systems become more helpful in supporting timely decision-making and daily operations for farmers. The speedy ability of retrieval also helps handle more queries at the same time, making it good for big scale use. Also, the combination of in-memory computing and RAG models gives a fresh chance for instant memory-based knowledge retrieval and question-answering in agriculture. By using the huge amount of agricultural data that exists, these systems can offer farmers immediate access to suitable information, expert suggestions, and customized advice. This empowers them to take knowledgeable decisions for their farming methods.

4.3 Future Research Directions

This study gives useful understanding about how re-ranking methods and in-memory computing are used in agriculture question-answering systems. However, there are many possible research paths to make these systems are more effective and easy for people to use. Firstly, trying out different re-ranking algorithms or adjusting the re-ranking model may provide better accuracy results. It is possible that including knowledge and features specific to agriculture could enhance this process. In order to evaluate the proposed approach, it would be beneficial to perform experiments on various query types and larger subsets of the agriculture QA dataset. This is important for understanding if the results can be widely applied, and to see if there are any shortcomings or areas needing enhancement. Utilizing user ratings, comments, or suggestions could assist in the growth of the agriculture question-answering system by allowing it to learn from real-world interactions. This way, the system can keep on improving and adapting itself to better suit.

To sum it up, this study shows how much in-memory computing through FAISS can boost the effectiveness and real-time abilities of agriculture question-answering systems. Although our re-ranking methods did not produce notable accuracy enhancements in the present setup, later studies might concentrate on improving the re-ranking method itself, carrying out broader evaluations and investigating additional techniques to enhance these systems' precision and usefulness. By enhancing agriculture question-answering technology's cutting-edge state, we seek to offer farmers prompt and precise information that contributes towards sustainable expansion in farming.

Acknowledgements

This project has received funding from the European Union's Horizon 2021 research and innovation programme under the Marie Skłodowska-Curie grant agreement No 101073381

References

Akturk, I., & Karpuzcu, U. (2017). Recomputation enabled efficient checkpointing. https://doi.org/10.48550/arxiv.1710.04685

Bendersky, M., & Kurland, O. (2008). Re-ranking search results using document-passage graphs. https://doi.org/10.1145/1390334.1390539

Chakraborty, P., & Bhunia, S. (2021). Neural storage: a new paradigm of elastic memory. https://doi.org/10.48550/arxiv.2101.02729

Jain, N., Jain, P., Kayal, P., Sahit, J., Pachpande, S., Choudhari, J., … & Singh, M. (2019). Agribot: agriculture-specific question answer system. https://doi.org/10.35543/osf.io/3qp98

Ji, D., Zhao, S., & Xiao, G. (2009). Chinese document re-ranking based on automatically acquired term resource. Language Resources and Evaluation, 43(4), 385-406. https://doi.org/10.1007/s10579-009-9106-z

Karunaratne, G., Schmuck, M., Gallo, M., Cherubini, G., Benini, L., Sebastian, A., … & Rahimi, A. (2021). Robust high-dimensional memory-augmented neural networks. Nature Communications, 12(1). https://doi.org/10.1038/s41467-021-22364-0

Kim, B., Seo, S., Han, S., Erdenee, E., & Chang, B. (2021). Distilling the knowledge of large-scale generative models into retrieval models for efficient open-domain conversation. https://doi.org/10.48550/arxiv.2108.12582

Klouche, K., Ruotsalo, T., Micallef, L., & Andolina, S. (2017). Visual re-ranking for multi-aspect information retrieval. https://doi.org/10.1145/3020165.3020174

Lewis, P. (2020). Retrieval-augmented generation for knowledge-intensive nlp tasks. https://doi.org/10.48550/arxiv.2005.11401

Li, J., Jia, R., He, H., & Liang, P. (2018). Delete, retrieve, generate: a simple approach to sentiment and style transfer. https://doi.org/10.18653/v1/n18-1169

Li, Y. (2023). A knowledge graph-based q and a system for agricultural planting technology. https://doi.org/10.1117/12.2671231

Ling, Y., Huang, X., Li, Y., Zhou, H., Yu, Y., Bao, H., … & Miao, X. (2023). self-selective memristor-enabled in-memory search for highly efficient data mining. Infomat, 5(5). https://doi.org/10.1002/inf2.12416

Mao, Y., He, P., Liu, X., Shen, Y., Gao, J., & Chen, W. (2021). Generation-augmented retrieval for open-domain question answering. https://doi.org/10.18653/v1/2021.acl-long.316

Nunn, J., Reim, K., Lee, K., Lorenz, V., Sussman, B., & Jaksch, D. (2008). Multimode memories in atomic ensembles. Physical Review Letters, 101(26). https://doi.org/10.1103/physrevlett.101.260502

Pasupat, P., Zhang, Y., & Guu, K. (2021). Controllable semantic parsing via retrieval augmentation. https://doi.org/10.18653/v1/2021.emnlp-main.607

Ren, R., Qu, Y., Liu, J., Zhao, W., She, Q., Wu, H., … & Wen, J. (2021). Rocketqav2: a joint training method for dense passage retrieval and passage re-ranking. https://doi.org/10.18653/v1/2021.emnlp-main.224

Sonsbeek, T., Zhen, X., Mahapatra, D., & Worring, M. (2023). Probabilistic integration of object level annotations in chest x-ray classification. https://doi.org/10.1109/wacv56688.2023.00362

Sun, Z., Pedretti, G., Ambrosi, E., Bricalli, A., Wang, W., & Ielmini, D. (2019). Solving matrix equations in one step with cross-point resistive arrays. Proceedings of the National Academy of Sciences, 116(10), 4123-4128. https://doi.org/10.1073/pnas.1815682116

Sun, Z., Pedretti, G., Bricalli, A., & Ielmini, D. (2020). One-step regression and classification with cross-point resistive memory arrays. Science Advances, 6(5). https://doi.org/10.1126/sciadv.aay2378

Teng, C., He, Y., Ji, D., Zhou, C., Geng, Y., & Chen, S. (2009). Entropy-based clustering for improving document re-ranking. https://doi.org/10.1109/icicisys.2009.5358089
Thenmozhi, M., & Srimathi, H. (2017). An analysis on the performance of hash table-based dictionary implementations with different data usage models. International Journal of High Performance Computing and Networking, 10(1/2), 78. https://doi.org/10.1504/ijhpcn.2017.083203
Thulke, D. (2021). Efficient retrieval augmented generation from unstructured knowledge for task-oriented dialog. https://doi.org/10.48550/arxiv.2102.04643
Tian, Z., Bi, W., Li, X., & Zhang, N. (2019). Learning to abstract for memory-augmented conversational response generation. https://doi.org/10.18653/v1/p19-1371
Vernaz-Gris, P., Tranter, A., Everett, J., Leung, A., Paul, K., Campbell, G., … & Buchler, B. (2018). High-performance raman memory with spatio-temporal reversal. Optics Express, 26(10), 12424. https://doi.org/10.1364/oe.26.012424
Villatoro, E., Juárez, A., Montes, M., Villaseñor, L., & Sucar, L. (2012). Document ranking refinement using a markov random field model. Natural Language Engineering, 18(2), 155-185. https://doi.org/10.1017/s1351324912000010
Villatoro-Tello, E., Villaseñor-Pineda, L., & Montes-y-Gómez, M. (2009). Ranking refinement via relevance feedback in geographic information retrieval., 165-176. https://doi.org/10.1007/978-3-642-05258-3_15
Wang, H., Liu, Y., Zhu, C., Shou, L., Gong, M., Xu, Y., … & Zeng, M. (2021). Retrieval enhanced model for common sense generation. https://doi.org/10.18653/v1/2021.findings-acl.269
Yang, L., Ji, D., Zhou, G., Nie, Y., & Xiao, G. (2006). Document re-ranking using cluster validation and label propagation. https://doi.org/10.1145/1183614.1183713
Zhang, L., & Zhou, Q. (2014). Crispr/cas technology: a revolutionary approach for genome engineering. Science China Life Sciences, 57(6), 639-640. https://doi.org/10.1007/s11427-014-4670-x
Zhao, G., & Zhang, X. (2019). Re-ranking web data per knowledge domain. International Journal of Service and Knowledge Management, 3(1), 66-84. https://doi.org/10.52731/ijskm.v3.i1.274.

Isotherms and desorption patterns of various natural zeolites during the removal of ammonium from wastewaters

Silvia Balzan[1]*; Giulio Galamini[2]; Giacomo Ferretti[1]; Barbara Faccini[3]; Massimo Coltorti[3]

[1] Department of Chemical, Pharmaceutical and Agricultural Sciences, University of Ferrara, Luigi Borsari 46, 44121 Ferrara, Italy

[2] Department of Chemical and Geological Sciences, University of Modena and Reggio Emilia, Giuseppe Campi 103, 41125 Modena, Italy

[3] Department of Environmental and Prevention Sciences, University of Ferrara, 44121 Ferrara, Italy

*Corresponding author. silvia.balzan@unife.it

Keywords: zeolite -rich tuff, ammonium adsorption, desorption of ions

Abstract

Animal manure management and field application significantly contribute to nitrogen (N) loss, leading to environmental impacts such as soil acidification, eutrophication, and greenhouse gas (GHG) emissions. Technologies to reduce these losses and impacts have been developed. The adsorption of ammonium (NH_4^+) using zeolite-rich tuff is a promising technology for the treatment of livestock effluents among the many methods available. Due to their high cation-exchange capacity and molecular sieve properties, zeolite-rich tuff are strategic materials both for recovering N from livestock effluents and for improving the fertility of soils. Nevertheless, among the numerous species available on the market, it is crucial to select the natural zeolites most suitable for the process, taking into consideration not only their intrinsic exchange capacities, but also their distinct exchangeable ions.

The aim of the study is to evaluate the potential application in the recovery of N from livestock effluents of three zeolite-rich tuff selected from different geographical locations: clinoptilolite from Romania (CLP_RU), clinoptilolite from Turkey (CLP_TR), and chabasite from Italy (CHA_IT). For each sample, two particle size were studied namely coarse- and micro-sized zeolites.

Thus, the sorption and desorption behaviour of the of zeolite-rich tuff have been investigated at 25°C by performing adsorption experimental batches with an NH_4Cl solution under equilibrium conditions. The initial and equilibrium concentrations of NH_4^+ in solution were measured with a Kjeldahl apparatus while major exchangeable cations were determined by Inductively Coupled Plasma Mass Spectrometry. Isotherm fitting was performed with the software R and PUPAIM package.

Among the tested models, the Langmuir Non-Linear Model showed the best fit with experimental data, with R^2 ranging from 0.907 to 0.998 and p-values always < 0.05. For each zeolite, an inverse relationship was observed between grain size and the maximum adsorption capacity (Q_{max}). Q_{max} accounted for 0.019 and 0.015 g g^{-1} for CLP_RU μ and g, 0.027 and 0.019 g g^{-1} for CHA_It μ and g, and 0.028 to 0.016 g g^{-1} for CLP_RU μ and g, representing increases of 24%, 28%, and up to 40%, respectively. While all the zeolites showed satisfactory NH_4^+ removal efficiencies, the desorption study highlighted high Na^+ levels were released by CLP_RU, making this zeolite potentially unsuitable for livestock effluents treatment as elevated quantities of Na^+ can be toxic to crops if discharged into the environment. This work provides valuable insights into the potential use of various types of zeolite-rich tuff for nitrogen (N) removal, highlighting the importance of considering the specific properties of these materials to achieve effective circularity in livestock effluent treatment technologies.

Introduction

Livestock effluents (LE) are a valuable resource due to their nutrient content, which is essential for crop production. However, after field application, these nutrients undergo transformative processes that lead to significant losses and environmental impacts (De Vries et al., 2015). Among these, nitrogen (N) is converted to nitrate (NO_3^-), which can leach and run off into ground and surface waters. Consequently, the spreading of LE is regulated by the 'Nitrates Directive' (91/676/EC).

When the available land for the spreading is insufficient compared to the volume of the LE accumulated and its nutrient content, treating LE to reduce the concentration of N, mainly in the form of ammonium (NH_4^+) is mandatory to meet the requirements of the 'Nitrates Directive'. Therefore, LE are perceived primarily as a financial constraint rather than a resource. While it is imperative to improve existing treatment technologies and develop new ones, it is equally important to face the prevailing skepticism by emphasizing the significant opportunities presented by nutrient recovery from animal production system (Case et al., 2017). A wide range of treatment strategies based on different processes are available, and those that imply adsorption or ion exchange are particularly relevant for this purpose (De Gisi et al., 2016). The zeolite-rich tuff used as adsorbent material can play a crucial role in enhancing the recycling of N while increasing social acceptance due to its effectiveness, absence of both chemicals and significant technical challenges (Faccini et al., 2015). A zeolite is a crystalline substance with a structure characterized by cavities in the form of channels and cages occupied by H_2O molecules and extra-framework cations (Coombs et al. 1997). Thanks to this structure zeolite-rich tuff is capable of adsorbing positively charged ions or molecules (as NH_4^+) from a solution by replacing the extra-framework cations present into the channels and cages. In agricultural context, NH_4^+ enriched zeolite-rich tuff can be used as slow-release amendments reducing the high N losses that normally occurs after LE application and increasing thus fertilization efficiency (Faccini et al., 2018).

Many quarries of natural zeolites are present in numerous regions of the world, with affordable costs compared to other adsorbents however, among the over 60 families of zeolites, is required to identify those suitable for the recovery of N from LE. In zeolites, adsorption is a selective process, meaning that to achieve high performance, it could be necessary to select materials with a good affinity to the adsorbate (in this case NH_4^+) (Ferretti et al., 2020) (Galamini et al., 2020). At the same time, it is crucial to consider the amount and nature of the exchangeable cations, which are released into the treated LE by ion exchange as these can be unsuitable for the further reuse of the wastewater, once the treatment is complete. Na-zeolites in this sector is discouraged because excessive amounts of Na^+ in the treated LE could be toxic for many crops. Choosing instead materials that release beneficial nutrients for plants, such as zeolites naturally rich in exchangeable K^+ or Ca^{2+}, is preferable.

Therefore, the aim of this study is to investigate the interaction of three zeolites with NH_4^+ and evaluate their potential application and feasibility in treating LE. These materials were collected from different geographical location, namely Romania, Turkey and Italy, and they had a similar selling price. For all of them, the effect of different particle sizes was evaluated as well. Since this research marks the preliminary phase of a broader applied project, we aim to focus on the interaction between zeolites and NH_4^+ neglecting any potential phenomena of ionic competition. For this reason, we opted to establish ideal conditions and conduct the experiments using a synthetic solution of NH_4Cl. Analyzing adsorption isotherms is crucial for assessing adsorption capacity under various conditions, determining whether the adsorbent material is suitable for a specific application and establishing optimal adsorbent dosages.

Materials and Methods

The zeolites tested were a Romanian clinoptilolite (CLP_RU), Turkish clinoptilolite (CLP_TR), and Italian chabasite (CHA_IT). Their mineralogical composition was determined by X-ray powder diffraction (XRPD) and Rietveld refinement. For each zeolite a micro-sized (< 50 μm) and coarse-sized (0.3 – 3.5 mm) particle fractions were studied, selected by sieving. They are indicated in the text with μ and *g* prior to the acronym.

Prior to laboratory activity, all the zeolites were dried at 105 °C for 24 h to eliminate the most of water in the extra-framework spaces.

In order to establish ideal conditions and neglect any ionic competition, a synthetic solution of NH_4Cl was used, with $[NH_4^+]$ of 1.50 ± 0.08 g L^{-1}, which is plausible for many LE.

Following Galamini et al., 2020, equilibrium batches with temperature set at 25 °C were performed to characterize isotherm models for the specific combination of zeolites and grain sizes. 50 ml of NH_4Cl l solution were mixed with distinct amounts of zeolites (g) to achieve the following dose percent (w:v): 3.5, 6, 8, 10, 13, 18, 20 and 21 %. Mixing was conducted using an orbital shaker (711/CT) at approximately 250 rpm for 24 hours, assumed as a sufficient time to reach equilibrium conditions. Then, samples were centrifuged at 4000 rpm for 4 minutes to separate the solid phase from the supernatant. To consider the potential effect of air stripping, and/or the adsorption onto plastic components, a blank was investigated as well, containing only NH_4Cl which undergone the same mixing process (CRT). Major exchangeable cations (Ca^{2+}, Na^+, Mg^{2+}, K^+) released in the supernatant during ion exchange with NH_4^+ were measured by ICP-MS (iCAP TQ, Thermo Fisher Scientific, Waltham, USA).

The initial (C_0) and equilibrium (C_e) concentration of NH^+_4 in solution into each supernatant were determine with a Kjeldahl apparatus (Kjelflex K-360, Buchi, Switzerland, Europe) coupled with an automated titration unit (Metrohm Titrino plus 877, Buchi).

The NH^+_4 equilibrium adsorption capacity (Q_e, g g^{-1}) was derived with Eq. 1:

$$Q_e = \frac{(C_0 - C_e) \times V}{m}$$

where C_0 and C_e are respectively the initial and equilibrium [NH^+_4] (g L^{-1}), V (L) is the volume of the NH_4Cl synthetic solution, and *m* (g) is the mass of zeolite.

Isotherm fitting was performed with the open-source software R and the PUPAIM package.

Results and Discussions

In Table 1 is shown the mineralogical composition of the geomaterials. The analysis reveals more than 50% by weight of zeolite minerals in all the zeolite-rich tuff.

Table 1. Mineralogical characterization of the zeolite-rich tuffs used in this study obtained by X-Ray Diffraction (XRPD) analysis and Rietveld refinement method; the characterization is expressed as weight percentages. "*" indicates the zeolite minerals.

	CLP_RU	CLP_TR	CHA_IT
plagioclase	12.5 ± 2	5.4 ± 2	1.3 ± 2
K-feldspar		7.7 ± 2	11.6 ± 3
mica	9.2 ± 5	1.8 ± 1	1.6 ± 2
tridymite/ cristobalite	9.0 ± 8	12.9 ± 1.1	
quartz	3.4 ± 1	9.6 ± 1	0.9 ± 1
calcite	1.1 ± 1	0.5 ± 1	
clinoptilolite*	56.0 ± 3	51.4 ± 4	
chabazite*			63.3 ± 9
volcanic glass	8.8 ± 1.1	10.7 ± 1.2	21.3 ± 1

Air stripping and/or adsorption onto plastic falcon during the experiment can be considered negligible because CRT and blank show the same [NH^+_4]. By applying Eq. 1, the Q_e values were estimated, and the best fit between the experimental data and the non-linear adsorption models contained in PUPAIM was investigated.

Among the tested models, Harkins-Jura, Freundlich, and Langmuir shows the highest R^2 value as reported in Table 2, indicating a good correlation with the experimental data. The Harkins-Jura isotherm model was initially formulated for gas- solid systems and assumes the possibility of multilayer adsorption on the surface of adsorbents having a heterogeneous pore distribution. The parameters of the model are characteristics for the adsorption behaviour of the adsorbent, as α indicates the amount of adsorbate particles accommodated on the surface and β relates with adsorption energy and the heterogeneity of the adsorption sites (Dada et al, 2021). The Freundlich isotherm stands as one of the earliest formulations for non-ideal and reversible adsorption. It is an empirical model based on multilayer adsorption and non-uniform distribution, which exhibit varying sorption energies, resulting in the occupation of sites with stronger energy first (Foo & Hameed, 2010). K_F Freundlich indicates the adsorption capacity while *n* shows the intensity and favourability of the adsorption process (Dada et al, 2021). Langmuir isotherm is a physical model developed to describe the adsorption between gas molecules and solid adsorbents. It assumes only monolayer adsorption - meaning that adsorption happens only close to the surface, in a fixed number of identical sites with equal affinity for the adsorbate - and that the adsorption sites are homogeneous in terms of spatial distribution and that are equipotential. The Langmuir model therefore implies the existence of a maximum adsorption capacity (Q_{max}; g g^{-1}) that cannot be overcome (Foo & Hameed, 2010). K_L is the Langmuir isotherm constant (L g^{-1}) which also relates to the energy involved in adsorption. The mathematical expressions of the three models described above and the statistical parameters characterizing the experimental adsorption isotherms are reported in Table 2.

The Langmuir model is considered the most suitable because it shows R^2 values always greater than 0.90, ranging from 0.907 to 0.998, which implies a monolayer adsorption for all the zeolite-rich tuff tested. Micronized zeolites exhibit

higher adsorption capacities compared to the coarse samples, the Q_{max} accounted for 0.019 and 0.015 g g^{-1} for CLP_RU μ and g, 0.027 and 0.019 g g^{-1} for CHA_IT μ and g, and 0.028 to 0.016 g g^{-1} for CLP_RU μ and g, representing increases of 24%, 28%, and up to 40%, respectively. This evidence is likely linked to the increased specific surface of the micronized zeolites.

Figure 1 reports the experimental data and the characteristic isotherm curve according to the Langmuir Model. The conditions of solid-liquid ratios that allow the maximum NH_4^+ uptake by the zeolite is always below 6%.

Table 2. Mathematical expressions of Harkins-Jura, Freundlich, and Langmuir isotherm models. The parameters of each experimental isotherm according to the model are reported below. The investigated zeolites are CLP_RU, CLP_TR and CHA_IT, both in coarse (*g*) and micro (μ) size. The equilibrium experiment was conduct at temperature of 25°C with a NH_4Cl solution with [NH^+_4] of 1.50 ± 0.08 g L^{-1}.

	Harkins-Jura			Freundlich			Langmuir		
Non-Linear Equation	$Q_e = \left(\frac{\alpha}{\beta - \log C_e}\right)^{\frac{1}{2}}$			$Q_e = K_F \cdot C^{1/n}$			$Q_e = \frac{Q_{max} K_L C_e}{1 + K_L C_e}$		
	R^2	α	*B*	R^2	K_F	*n*	R^2	K_L	Q_{max}
*g*_CLP_RU	0.779	0.031	1.789	0.868	0.009	1.700	0.907	1.461	0.015
*μ*_CLP_RU	0.943	0.052	1.572	0.986	0.016	2.326	0.976	3.798	0.019
*g*_CHA_IT	0.974	0.035	0.846	0.963	0.017	1.977	0.929	3.334	0.019
μ _CHA_IT	0.990	0.022	0.846	0.998	0.012	1.420	0.991	0.780	0.027
*g*_CLP_TR	0.994	0.028	1.365	0.992	0.010	1.890	0.980	1.565	0.016
μ _CLP_TR	0.970	0.020	0.898	0.958	0.011	1.372	0.998	0.594	0.028

Figure 1. Equilibrium adsorption capacity Q_e (g g^{-1}) against equilibrium concentration C_e (g L^{-1}). The circles show the experimental data obtained by mixing a solution of NH_4Cl for 24 hours at 25°C with CLP_RU, CHA_IT, and CLP_TR. The experimental data refers to the following solid – liquid ratio: 3.50, 6, 8, 10, 13, 18, 20, 21 %. The dashed line shows the Langmuir isotherm with the R^2 value.

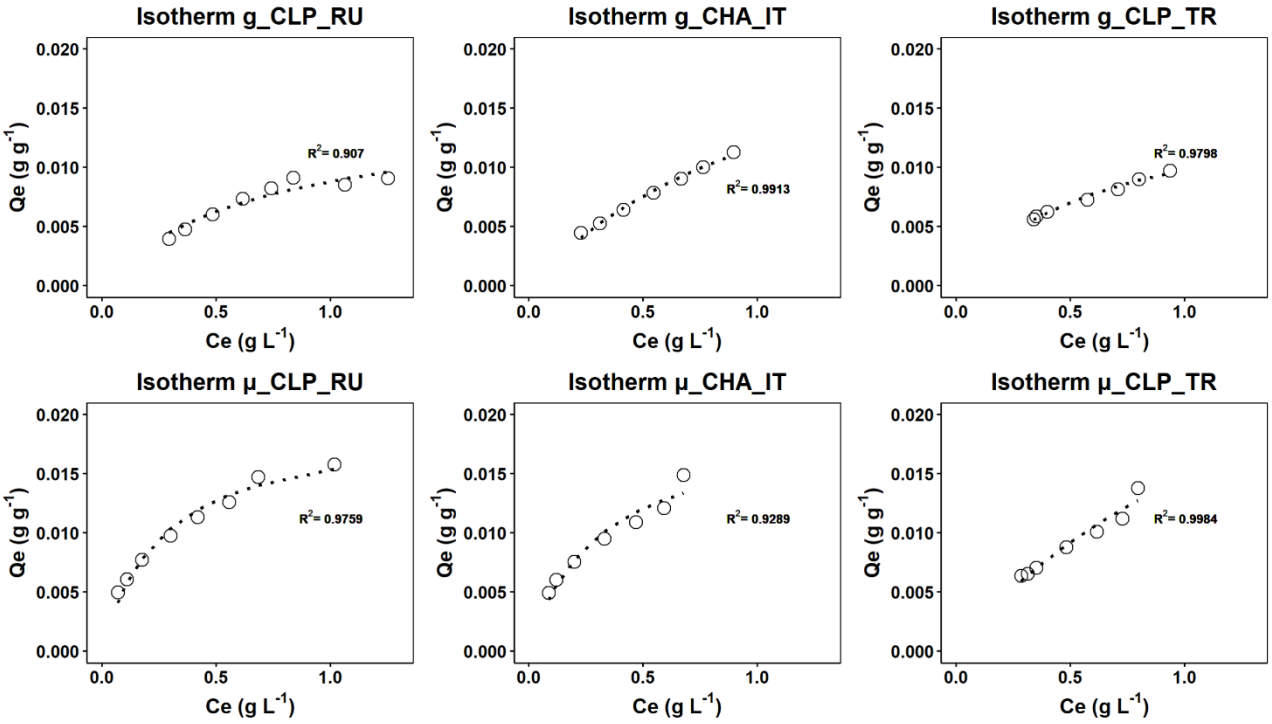

Micronized zeolite showed higher removal efficiency compared to coarse materials, but handling micronized substances is more complex and leads to greater engineering challenges. Due to these operational complexities, which could make the application of micronized zeolites more demanding, the release of ionic species in response to the ion exchange process was analysed only for the coarse material.

Figure 2 reports the concentrations values (mg L^{-1}) of the major cations (Ca^{2+}, K^+, Mg^{2+}, Na^+) released by the coarse zeolites at 3.5% and 21%. Even though all the investigated zeolite-rich tuff showed comparable NH_4^+ removal efficiencies, the desorption study revealed that *g*_CLP_RU released high concentration of Na^+ in the supernatant, making this material unsuitable for LE treatment, as elevated quantities of sodium, if discharged into the environment, can be toxic to crops. In contrast, *g*_CLP_TR and *g*_CHA_IT showed lower Na^+ releases in favour of nutrients such as Ca^{2+} and K^+.

Figure 2. Concentration values (mg L^{-1}) of the major cations (Ca^{2+}, K^+, Mg^{2+}, Na^+) released by the coarse zeolites at 3.5% and 21%.

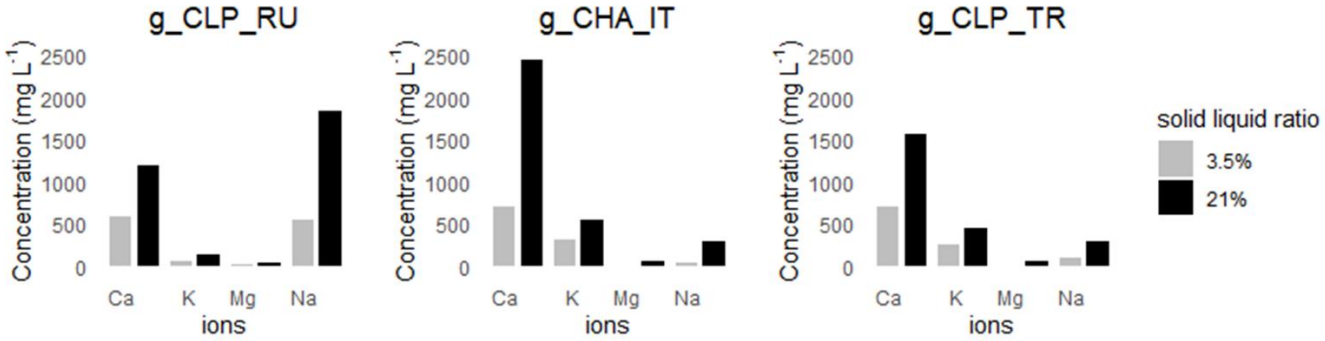

Conclusion

Isotherm studies regarding the interaction between three zeolite-rich tuff and NH_4^+ were carried out coupled with an analysis of the desorption process.

It was found that the optimal adsorbent dosages are less than 6%. The adsorption model that best describes the behaviours of the samples is the Non-Linear Langmuir Model. For the same particle size, all the investigated zeolites show comparable NH_4^+ removal efficiencies, while the micronized sizes exhibit higher adsorption capacities compared to the granular. However, despite all the zeolites appears to be suitable for LE treatment, further investigations taking into account the desorption process reveal that CLU_RU is associated with significant Na^+ release, which makes this material unsuitable for the purpose.Further studies need to be conducted to test the materials with real LE, thus also considering ion competition, and varying the operating conditions.

References

1. Case, S.D.C., Oelofse, M., Hou, Y., Oenema, O., Jensen, , L.S., 2017. Farmer perceptions and use of organic waste products as fertilisers – A survey study of potential benefits and barriers. Agricultural Systems. 151, 84-95. https://doi.org/10.1016/j.agsy.2016.11.012

2. Coombs, D., Alberti, A., Armbruster, T., Artioli, G., Colella, C., Galli, E., Grice, J.D., Liebau, F., Mandarino, J.A., Minato, H., Nickel, E., H., Passaglia, E., Peacor, D.R., Quartieri, S., Rinaldi, R., Ross, M., Sheppard,

3. R.A., Tillmanns, E., Vezzalini, G., 1997. Recommended nomenclature for zeolite minerals: report of the subcommittee on zeolites of the international mineralogical association, Commission on New Minerals and Mineral Names. Can. Mineral. 35, 1571-1606.

4. Dada, A.O., Adekola, F.A., Odebunmi, E.O., Ogunlaja, A.S., Bello, O.S., 2021. Two–three parameters isotherm modeling, kinetics with statistical validity, desorption and thermodynamic studies of adsorption of Cu(II) ions onto zerovalent iron nanoparticles. 11, 16454. https://doi.org/10.1038/s41598-021-95090-8

5. De Gisi, S., Lofrano, G., Grassi, M., Notarnicola, M., 2016. Characteristics and adsorption capacities of low-cost sorbents for wastewater treatment: A review. Sustainable Materials and Technologies. 9, 10-40. https://doi.org/10.1016/j.susmat.2016.06.002.

6. De Vries, J.W. , Hoogmoed, W.B., Groenestein, C.M., Schröder, J.J., Sukkel, W., De Boer, I.J.M., Groot Koerkamp P.W.G., 2015. Integrated manure management to reduce environmental impact: I. Structured design of strategies. Agricultural Systems. 139, 29–37. http://dx.doi.org/10.1016/j.agsy.2015.05.010

7. Faccini, B., Di Giuseppe, D., Malferrari, D., Coltorti, M., Abbondanzi, F., Campisi, T., Laurora A., Passaglia, E., 2015. Periodico di Mineralogia. 84, 2, 303-321. DOI: 10.2451/2015PM0015

8. Faccini, B., Di Giuseppe, D., Ferretti, G., Coltorti, M., Colombani, N., Mastrocicco, M., 2018. Nutrient Cycling in Agroecosystems. 110 (2), 1385-1314. https://doi.org/10.1007/s10705-017-9904-4)

9. Foo K.Y, Hameed B.H., 2010. Insights into the modeling of adsorption isotherm systems. Chemical Engineering Journal. 156 (1) 2–10.

10. Ferretti, G., Galamini, G., Medoro, V., Coltorti, M., Di Giuseppe, D., Faccini, B., 2020. Impact of Sequential Treatments with Natural and Na-Exchanged Chabazite Zeolite-Rich Tuff on Pig-Slurry Chemical Composition. Water. 12, 310; doi:10.3390/w12020310

11. Galamini, G., Ferretti, G, Medoro, V., Tescaro, N., Faccini, B., Coltorti, M., 2020. Isotherms, Kinetics, and Thermodynamics of NH_4^+ Adsorption in Raw Liquid Manure by Using Natural Chabazite Zeolite-Rich Tuff. Water. 12(10):2944. https://doi.org/10.3390/w12102944

Pesticide management: Modeling agricultural practices for sustainable soil and groundwater quality in Nabatyeh region – South Lebanon

Farah Kanj[a,b*], Dany El-Obeid[a,b], Kadi Saleh[a], Hussein Yazbeck[a]

[a] Lebanese University, Faculty of Agriculture Engineering and Veterinary Sciences, Lebanon

[b] Lebanese University, Faculty of Sciences, Lebanon.

* Corresponding author: farh.kanj@ul.edu.lb

Pollution of groundwater by leaching of pesticide active ingredients has become a relevant issue worldwide. The Lebanese agriculture has experienced excessive use of pesticide and chemical fertilizers for decades. From there, the pollution of groundwater by the leaching of these active ingredients has experienced an extension and is progressively causing worrying effects.

Studies dealing with these issues of pesticide pollution are very rare in Lebanon. In this study, the impact of pesticide use on soil and groundwater contamination in Al Nabatieh Govenorate (South Lebanon) was assessed. This region is characterized by diverse production systems and agricultural practices. PEARL model and Geographic Information System were used by the study to acquire new understanding and to visualize the spatial distribution of vulnerable areas by introducing the treatment frequency indicator. The validation of this model was performed by comparing the concentration of an active material (in our case Nitrate) in four groundwater samples analyzed in the laboratory and the values predicted by the model.

The results of the analysis allowed us to identify areas of high phytosanitary pressure and the most used substances in the study area (alfa cypermethrin, mancozeb, emamectin benzoate, methomyl and chlorpyrifos-ethyl). Results also allowed for the evaluation of the quality of groundwater based on the predictions of the concentrations of active ingredients leached at the level of the study area.

Four active ingredients were identified as the most leached to groundwater: methomyl, chlorpyrifos-ethyl, mancozeb, and alfa cypermethrin. Our results of forecasting the concentrations of these pesticides annually allowed us to identify vulnerable zones in terms of a risk of contamination. The areas cultivated with citrus and eggplant on sandy and sandy clay soils were found to be sensitive to the active ingredient ethyl-chlorpyrifos (> 0.1µg / l) and alfa-cypermethrin (> 1µg / l). Areas cultivated with lettuce on sandy and sandy clay soils were found to be sensitive to the active ingredient methomyl (> 1µg / l); and finally, area cultivated with cucumber on sandy soils were found to be sensitive to the active ingredient mancozeb with a concentration ranging between 0.1 and 1 µg / l.

Keywords: pesticides, active material, modeling, PEARL model, soil, groundwater, agricultural practices.

I- INTRODUCTION

Diffuse pollution of agricultural origin is one of the main causes of soil degradation and groundwater quality whose preservation requires a better understanding of the interaction between agricultural pressures and the natural environment. Several studies conducted in Lebanon have addressed the issue of diffuse pollution excluding those from agricultural origin and more specifically the impact of pesticides. However, studies around the question of diffuse pollution from agricultural origins remain very rare. For decades, the Lebanese agriculture has experienced periods of excessive use of pesticides and chemical fertilizers making Lebanon at the forefront of pesticide consumers in Arab countries with 5.5 kg / ha (Rifai, 2013). At the level of Mediterranean countries, Lebanon is equally a very large user of chemical fertilizers in terms of hectare (ha) per production. Even at the international level, Lebanon is ranked among the highest consuming countries of the world using more than twice the average amount of fertilizer (FAO, 2013).

According to a study by Jean-Claude Mantigaud in 2004, 40% of fruits and vegetables in Lebanon contain pesticide residues exceeding the authorized standards. Another study conducted by the Lebanese University in 2009 also revealed the presence of pesticide residues sometimes exceeding 25 folds the international standard in some fruits and vegetables (Rozelier, 2011). According to Youssef *et al*. 2012, the existence of banned pesticides, mainly organochlorines such as aldrin, heptachlor epoxide and DDT (Dichlorodiphenyltrichloroethane), persists in the aquatic environment of southern Litani River. The same study states that DDE (Dichlorodiphenyldichloro-ethylene) and HCB (Hexachlorobenzene) were the most frequently detected pesticides in surface water (93.3%) and groundwater (100%). Similarly in 2016, a study by Chbib *et al*. showed a highly significant water contamination by organochlorine pesticides including DDT and HCH (Hexachlorocyclohexane) which have been internationally banned for decades.

Thousands of tons of fertilizers and pesticides are usually used on an annual basis by farmers. Some public institutions and local communities (municipalities) also use chemical fertilizers and pesticides for maintenance of green spaces. A number of these pesticides and fertilizers are responsible for the contamination of soil-groundwater system especially due to massive quantities and successive uses, knowing that pesticide residues could remain in the soil and water for periods ranging from several months to several years.

Between 1985 and 1992, a national pesticide survey was conducted in Lebanon by the EPA (Environmental Protection Agency), Pesticides and Toxic Substances Office and water establishments to identify the number of drinking water wells that contain pesticides and nitrates on the one hand and analyze the concentration of these substances on the other.

The survey, which included samples from more than 1,300 rural domestic water utilities, found that about 3.6% of wells contained nitrate concentrations above the federal contamination level, while more than the half contained nitrates above the minimum required "reporting maximum limit for nitrates (50 mg / L)" (Groundwater protection directive, EU, 2006).

Investigations also revealed that around 0.8% of tested wells contained pesticides above the maximum level of contaminants. Only 10% of the wells classified as rural were actually located on farms. After careful analysis, the EPA estimated that, for wells that contain pesticides, a significant percentage likely contains chemical concentrations that exceed the federally authorized health limits. About 14.6% of the tested wells contained levels of one or more pesticides above the minimum reporting limit set in the survey (EPA, 1991) with the intensification of agricultural production in Lebanon, a new assess of the state of at concerning pesticide contamination of groundwater is highly needed.

Given the above, the risk assessment of pesticides and their impact on public health and environment is seen as extremely necessary to assess the sustainability of the Lebanese agriculture. From the notion of pesticide transfer at the base of this work, the transfer of pesticides and their dissipation in the different compartments of the natural environment generate negative effects on the quality of soil and groundwater and can affect food safety. As a result, local actors and public decision makers are becoming increasingly aware of the problems related to the diffuse pollution due to the use of pesticides. A question is therefore raised. Which indicator should be developed as a decision support tool for the assessment and management of risks related to diffuse pollution? To answer this question, we have developed mechanisms for the management of pesticides use and the reduction of diffuse pollution using modeling, with diffuse pollution as a spatial and temporal problem.

II- METHODOLGY

2.1. Model Choice

Several models have been evaluated over time in order to simulate the fate of contaminants in the environment. These models make it possible to first evaluate the state of a system and, secondly, to perform a predictive evaluation of the effect of certain modifications in the parameters or the input data for the output variables.

According to literature (Villeneuve et al., 1998; Rousseau et al., 2000; Gustafson, 1990), the simplest approach to modeling the outcome of pesticides in the environment is an undistributed empirical approach. Over the years, 68 models have been created: 36 for the watershed-scale models and 32 for parcel-scale models. As far as risk assessment models for soil-related environmental pollution, several studies (Tiktak et al., 1994; Jarvis, 1994; Jarvis et al., 2000 et Devillers, 2005 …) have shown that soil plays a major role in the transformation of active substances in the environment. However, our review of literature has shown that only a few models were developed for the evaluation of pesticides in soil relating to agronomy.

In the late 1980s, the PESTLA model was first developed and used to assess pesticide leaching in groundwater (Van den Berg *et al.,* 1999, Boesten and Gottesburen 2000). In the Netherlands, the PESTRAS model appeared in 1994 aiming to provide a simultaneous estimate of groundwater leaching and accumulation in the upper soil layer (Tiktak *et al.,* 1994). The MACRO model was next used in Sweden and is a one-dimensional model which simulates the transfer of water and pesticides to the first layers of soil (Jarvis *et al*., 1994; Jarvis, 2000). In the United States, the Pesticide Root Zone Model (PRZM) was used to estimate the probability of pesticide dispersal below the crop area at the level of roots (Trevisan *et al.,* 1992; Trevisan *et al.,* 2000). This PRZM model was later modified into the Pesticide Leaching Model (PALMO) version and used in Germany. Both PRZM and PALMO models are widely used in the assessment of leaching, runoff and erosion losses. With these models however, there yet existed a limit where the prediction of pesticides concentration profiles in the soil remained rather risky (Klein *et al.,* 2000). This is when the Pesticide Leaching at Regional and Local scale (PEARL) model was built in the Netherlands in 2002. PEARL is a one-dimensional model that aims to assess the risk of pesticides at the level of the environment, especially in the soil and at the plot scale.

The PEARL model is one of the models which goes beyond the simple mathematical modelling and is considered as a real decision support tool for assessing the effect of management practices on soil and water quality. PEARL, using the Richards equation, conducts a more detailed description of hydrological data (Tiktak *et al.*, 2002) and has already been validated for both water and soil components as well as for the transfer of active ingredients beyond the root zone. An advantage also lies in the ability to apply the model to different scales from small parcels up to larger catchment or regional levels. Additionally, the model predicts the risk of soil pollution by pesticides and thus provides an opportunity to guide farmers in selecting better farming practices. It should be noted that the PEARL model accounts, on one hand, for all physical factors of a studied territory such as climatic data, soil type, irrigation, treatment date and others as well as, on the other hand, for the methods in which pesticides are applied by farmers such as surface spraying, incorporation or injection into the soil. Yet, PEARL also considers the effects of moisture content and soil depth on the fate of pesticides. In particular, this model predicts the lost quantities of an active ingredient in the environment and especially at soil and groundwater levels.

2.2. The Study Area

Nabatiyeh governorate is 1,052 km2, divided into four districts that are largest in South Lebanon: Bent Jbeil, Hasbaya, Marjaayoun and Nabatiyeh. The governorate is in the far south of Lebanon, bordered from the north by Mount of Rihan and Jezzine whereas as by Litany River valley from the east and south (fig. 1).

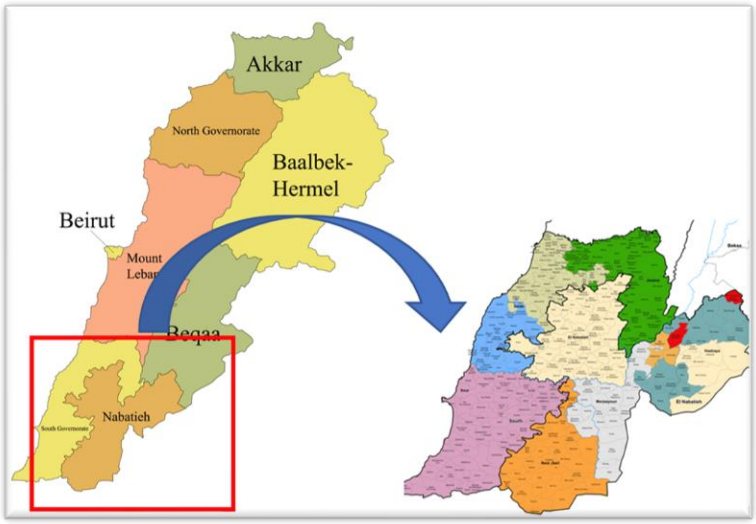

Figure 1: Location of the study area - Nabatiyeh governorate in South Lebanon (source: CNRS database, 2019, realized by: F. Kanj, 2024).

This territory is marked by a strong interaction between diversified socio-economic activities (agricultural, trade ...) and is characterized by agricultural, environmental and socio-economic issues as well.

2.3. The Soil

According to the 2004 agriculture atlas and at the level of the study area, we note that:

- The soil texture is the variable which plays a determining role in the leaching of active ingredients in groundwater.
- Nabatyeh region is composed of ten soil types each of which is composed of 3 horizons. The maximum depth reaches 155 cm (based on data collected from national remote sensing center) and the pH varies between 6.5 and 7.2 depending on the soil type.

2.4. The Climate

The average annual temperature in Nabatiyeh region is around 18.7°C. The average annual rainfall is 852 mm and the variation in the annual temperature is around 14.4°C. The driest month is July, with almost no rainfall, August is considered the warmest month of the year with an average temperature of almost 25.7°C. January is the coldest, the precipitation reaches its peak with an average 215mm, having an average temperature of 11.3°C. ("Nabatiyeh Topography and Agriculture Cdr).

The variation of temperature and precipitation is very clear between 2017 and 2021. The yearly temperature change in Nabatiyeh region where the mean temperature in 2017 was 17.4°C to increase in 2020 and 2021 to achieve 18.1°C.

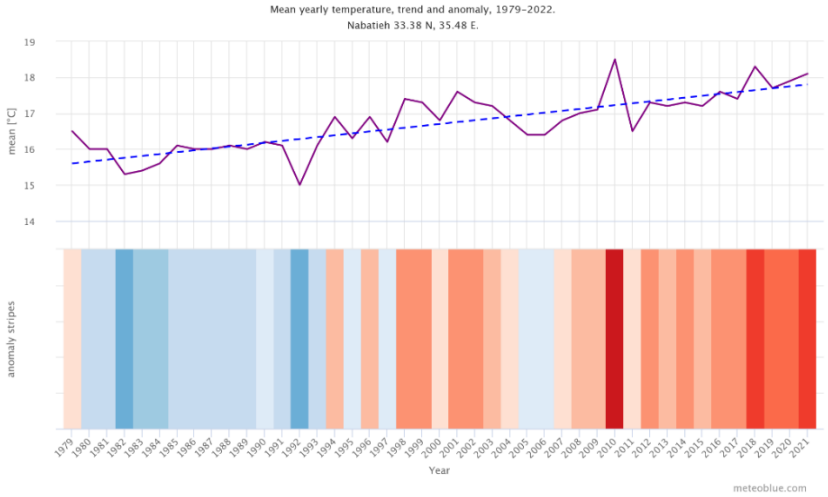

Figure 2: Yearly temperature between 1979 and 2020.

As for the precipitation, the observed peaks of mean precipitation also decreased from 906 mm in 2003 to 630 mm in 2021.

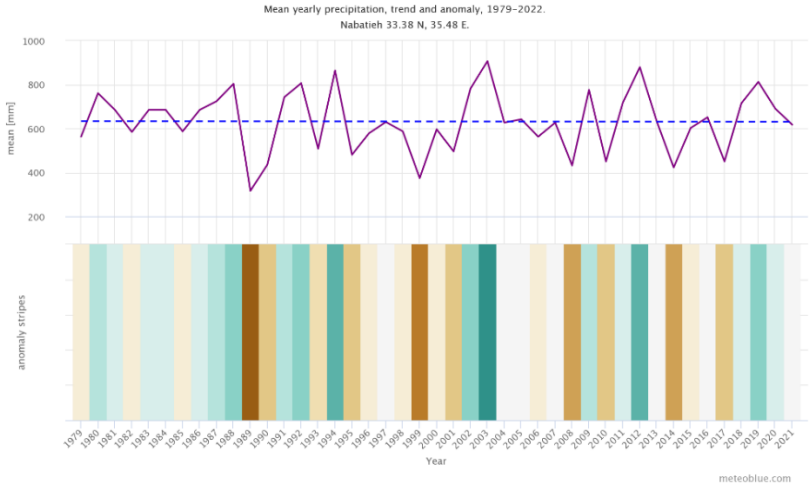

Figure 3: Yearly precipitation between 1979 and 2022.

2.5. Cultivations and Land Use

Crops in the study area are distributed as 68% permanent and 32% seasonal. Land use is mainly characterized by the predominance of olive trees (49.49%), followed by cereals (18.18%), industrial crops (12.12%), fruit trees (9.9%), vegetable crops (7.7%) and fodder crops (1%) (fig. 3).

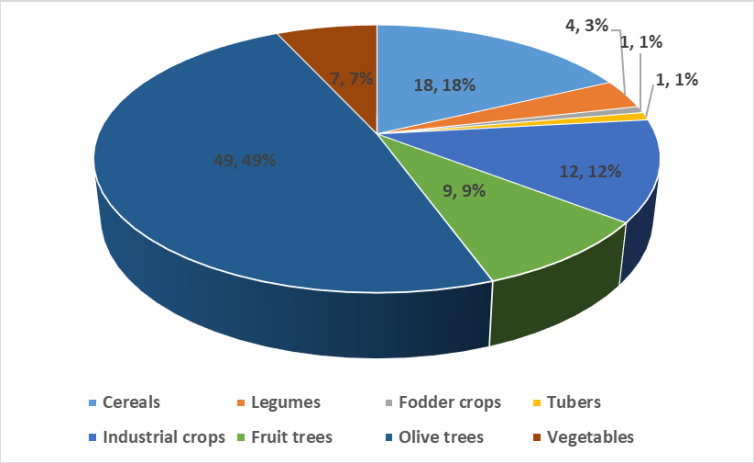

Figure 4: Land use in the study area. (Source: Census report, MoA, 2010).

Based on the above, it becomes evident how the study area is characterized by diverse production systems, soil, climate and land use. The strong concentration of the abovementioned crops inevitably leads to the question of agricultural practices being implemented by farmers in the region and especially to the methods in which fertilizers and pesticide products are being used.

2.6. Expression of the Used Indicator: Treatment Frequency Indicator (TFI)

The TFI indicator allows the evaluation of the pressure exerted by pesticides on each plot (Champeaux *et al.*, 2006). It is expressed as the number of registered doses per ha applied to a certain plot during a cropping season. For each realized treatment per plot, the normalized quantity is obtained by dividing the actual dose applied per ha, issued from the survey, by the approved dose per ha of that product for the concerned crop:

$$TFI\ product/ha = \frac{\text{Applied dose/ha}}{\text{Approved dose}/ha}$$

$$TFI\ treatment = \sum TFI\ product\ \times proportion\ of\ the\ treated\ field$$

$$TFI\ field = \sum TFI\ treatment$$

2.7. Used Data

Table 1 summarizes the needed material and data used to develop this study.

Table 1: Used Material

Used information	Software
1- Soil data: texture, soil type, conductivity, infiltration rate, horizon, organic matter content, pH (CNRS, National Center for Remote Sensing). 2- Agricultural Atlas (MOA, 2014). 3- Climate data: 20-year rainfall, solar energy, evapotranspiration, wind speed, humidity, minimum and maximum temperature (Nabatyeh topography and Agriculture Cdr, 2022). 4- Diagnostic data collected from 150 farmers in 2023 regarding farmers' practices, inputs: active ingredient, registered dose, number of treatments, target. 5- TFI calculations allowed the identification of the highest **pesticide** consuming cultures and the most used active ingredients.	1- PEARL model.

2.8. Applied Methodology

The methodology used is based on the prediction of leached active ingredients mostly used in the study area and their impact on the quality of groundwater while accounting for the types of crops and soils, using the PEARL model.
The database was established based on bibliographic research of agricultural activities characterizing the study area, previous studies conducted on that same area (Khoury et al., 1975), interviews with experts and local stakeholders (agricultural engineers, agricultural advisers, head of the agricultural center, etc.) and direct surveys of farmers (Figure 5). Data analysis was conducted following the classification of agricultural holdings through a structural typology according to the stratified production system and spatial distribution. After the selection of holdings, areas with high phytosanitary pressure were identified by calculating the Treatment Frequency Indicator (TFI) per crop and per ha at the territorial level. Accordingly, high pesticide-consuming crops were identified based on calculations of TFIs quartiles per ha and per territory, as well as the mostly used pesticides which in turn reflect the applied active ingredients per crop and therefore those most consuming pesticides in our territory.

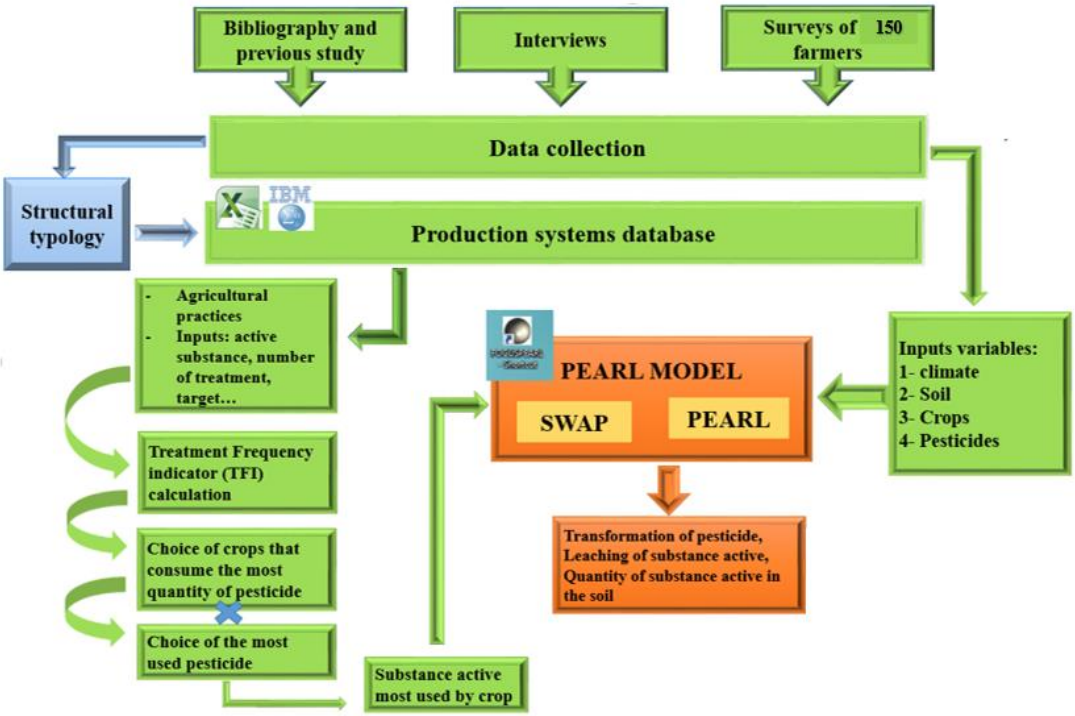

Figure 5: Conceptual diagram of the methodology (Kanj F., 2023)

After identifying active ingredients, data was collected for the most pesticide-consuming crops and frequently applied active substances so that to feed the PEARL model. The latter was therefore used to investigate the impact of these pesticides while accounting for physical factors of the territory on different components of the environment and specifically on groundwater pollution. Noted PEARL model take into consideration the first meter depth of soil.
These results can be mapped in GIS and analyzed at the scale of the Nabatyeh region but in our stage we will limited to identified the crops with high risk of active ingredients leaching and which require emergency intervention.
To consider that our results are valid, it was necessary to validate the model with an active material that is easy to analyze in the laboratory. This active ingredient is Nitrate. We have taken four samples of well water located in Bekaa area to assess the quality of this water and whether the water is contaminated or not. Likewise, we entered the model input data for the region of these samples in order to compare the results of predicted and the laboratory results. The table below describes the results of two analyses:

Table 2: Comparison between Nitrate concentration in groundwater based on laboratory results and Nitrate concentration predicted by PEARL model.

Sites	Nitrate concentration in water (laboratory analysis) (mg/l)	Nitrate concentration predicted by PEARL Model (mg/l)
Zahle Berdawni 1	7.63	8.0115
Zahle Berdawni 2	11.18	11.962
Moualka 1	60.5	63.525
Moualaka 2	9.26	9.630

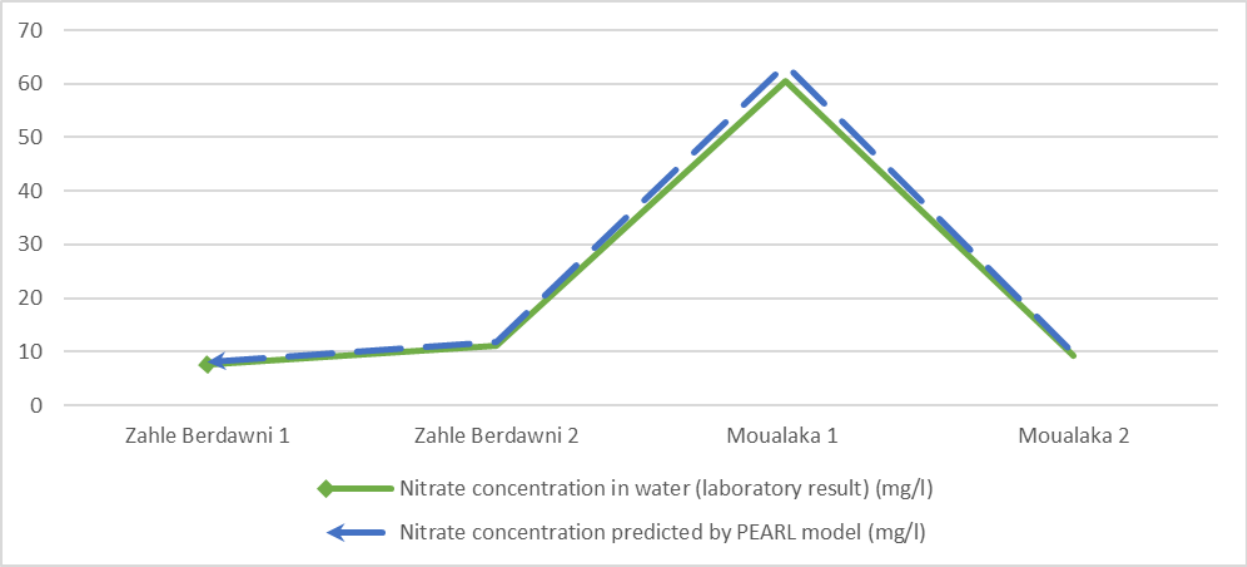

Figure 6: Representation of Nitrate concentration in groundwater based on laboratory results and Nitrate concentration predicted by PEARL model.

Based on the results in figure 6 and table 2, we can note the model prediction was considered reasonably accurate for most model results and the model prediction error was considered acceptable (4 - 6%).

III- RESULTS

The obtained results and analyzed elements corresponding to the different spatial zones of the study area highlighted the diversity of farms that characterize agriculture in that territory. Different strategies and tactics have been adapted to the structure of cultivation, soil and climate conditions, and thus the hydro-agricultural development.

3.1. Leached active ingredients at groundwater level

Leaching of active substances was studied so that to analyze the diffusion of pesticides in the water section of soil and its subsequent possibility of contaminating groundwater. Several factors can affect the vertical transfer of pesticides into the soil such as surface preparation, structure, water content, solubility of each substance and important external factors as application time and rain.

This is why we had to study the leaching of each active ingredient per soil type and per culture since their behavior differs from one culture to another. Once the active ingredients with a high percentage of dissipation by leaching were identified along with their treated cultures, the simulation of these active ingredients were repeated by soil type and by culture followed by the retrieval of leached quantities (µg/l) of each ingredient per soil type.

The characteristics of active substances with a high percentage of dissipation are represented in table 2 below:

Table 2: Characteristics of the active ingredients (Source: FOOTPRINT database)

Actives substances	K_{oc}[1]	Log K_{oc}[2]	DT_{50}[3]	Interpretation
Methomyl	25.2	1.4	7	Mobile and easily degradable
Mancozeb	997.5	1.33	1358	Mobile and slightly degradable

Chlorpyrifos ethyl	395	2.59	385	Fairly mobile and slightly degradable
Alfa cypermethrin	889	2.9	91	Fairly mobile and fairly degradable
Dimethoate	30.1	1.47	3	Mobile and easily degradable
Proquinazid	12850	4.1	60	Barely mobile and slightly degradable
Glyphosate	1424	3.1	32	Slightly mobile and fairly degradable

1: Soil organic carbon sorption coefficient of the pesticide, 2: Soil sorption coefficient, 3: Pesticide half-life.

According to the characteristics of the active ingredients, the soils are thus more susceptible to their leaching (transfer to groundwater). For example, methomyl and mancozeb are much less sensitive than proquinazid and glyphosate. Indeed, when the retention coefficient of organic matter is very low (case of methomyl with a K_{om} of 3.36 $dm^3.kg^{-1}$) or when the half-life is relatively high (case of flutriafol with a DT50 of 1350 days), the active ingredient is more rapidly leached because it is less retained by the organic matter of the soil (as the case of methomyl) or degrades less quickly and therefore remains available in the soil to be possibly leached during precipitation or during irrigation. When the retention coefficient of an active ingredient over soil organic matter is very high and when coupled with a low half-life, as the case for glyphosate, then the pesticide concentration becomes more or less low (1633 $dm^3. kg^{-1}$ and DT50 of 32 days), whereby the concentration of the leached pesticide is similarly low (<0.01 $\mu g.l^{-1}$). The pesticide in this case is strongly retained by organic matter in the soil (since its Log K_{oc} is elevated) and is more rapidly degraded (DT50 of 32 days). In addition, only methomyl, mancozeb, chlorpyrifos-ethyl and alfa cypermethrin allow to distinguish between the relatively contrasted regions from the perspective of soil sensitivity to the leaching of pesticides. This is why it would be interesting to develop the work based on these four active ingredients. The combination of the PEARL model results and soil type in the study area allowed the representation of leaching of each active ingredient (Figure 6). This results therefore helps in identifying specific areas at risk of contamination with each of the active ingredients. According to the European directive n°80/778/EEC, the groundwater contamination threshold for a single substance is around 0.5 $\mu g.l^{-1}$. However, for organophosphorus, which is the case of Chlorpyrifos-etyl, that threshold is of the order of 0.1 $\mu g.l^{-1}$. Amounts leached at levels higher than 1 $\mu g.l^{-1}$ after one year of application were identified in areas cultivated with lettuce for methomyl in addition to areas cultivated with citrus and eggplants for alfa-cypermethrin. This rate indicates that groundwater quality is contaminated. Leached amounts between 0.1 and 1 $\mu g.l^{-1}$ after one year of application were identified in most areas cultivated by cucumber for the mancozeb. This rate indicates that groundwater quality is poor but not contaminated. However, it is important to note that our analysis did not consider previous years since farmers have no traceability and do not record the application of used pesticides.

3.2. Discussions

Based on the above findings, the strong spatial contrast observed in the study region in terms of leached active ingredients (methomyl, mancozeb, chlorpyrifos-ethyl and alfa-cypermethrin) shows a positive correlation with the sand content and negative correlation with the clay content on one hand, and with the hydraulic conductivity on the other.

In fact, for methomyl for example, an increase in leached concentrations with the increase in soil sand content (1.362 $\mu g.l^{-1}$ for sandy soil) is observed. In addition, with the variation of water balance (mm/year) from one zone to another in the study area, the concentrations of leached pesticides is noticed to decrease with the increase in the soil organic matter content which, together with the clay proportion of the soil, play an adsorbent (retention) role for pesticides.

Nevertheless, the residual pesticides (methomyl and mancozeb) after the onset of agricultural activities in the Nabatyeh region (spring) is notably sensitive to the amount of water (irrigation or precipitation) and soil type, during which PEARL predicts higher levels of leached pesticides than others. This confirms that the fraction of pesticides which percolates deep is extremely sensitive to the amount of water due to irrigation especially in the period immediately following the application of the product. Significant irrigation practices events that directly follow pesticide applications are particularly involved in the transfer of pesticides to groundwater, especially with a coarse texture such as sandy soil.

It should also be noted that the soil pH is an important factor in determining the fate of certain pesticides. Certain pesticides exhibit sorption behaviors directly dependent on soil pH, with acidic pH (<5) leading to low retention of leachate whereas pH greater 5 leads to a higher retention. The soil pH in our study area is between 6.5 and 7.2, that it can be noted the pH has no influence on our results.

Moreover, it is important to emphasize that the results of leached pesticide concentrations that have been realized in the study represent the sensitivity of only the first meter depth of soil. Hence, these are not global risk related to the use of pesticides. At the level of the Nabatyeh region, and to consider that the representation of the concentration of the active ingredients (methomyl, mancozeb, chlorpyrifos-ethyl and alfa cypermethrin) as results with the purpose of an overall decision-making tool, it is relevant to consider a probability threshold which covers a large part of the risk.

This probability threshold may encompass the 80th spatial percentile of leached pesticide concentrations, which accordingly means that 80% of the spatial variability is covered (FOCUS 2000, FOCUS 2009). This 80th percentile value is considered as the reference value in the decision-making process. In our case, and in the context of protecting groundwater vis-à-vis the contamination with pesticides, i.e. to consider water as potable, the concentration of a single pesticide must not exceed 0.1 µg.l^{-1}. If the 80th percentile of a leached pesticide concentration is above this target value of 0.1 µg.l^{-1}, then one can assume that the soil is susceptible to leaching of that pesticide in question. In concrete terms, we therefore look at whether 80% of these variabilities have a leached pesticide concentration below the 0.1 µg.l^{-1} limit concentration for groundwater. We thus tolerate that 20% cases exceed this limit. For the soil types spread in the study area, we estimated the concentrations of the studied pesticides that are leached, while considering the 80% of the variables predicted by PEARL for each type of soil (Table 3).

Table 3: 80th percentile of pesticide concentrations leached in the soil type (source: developed by Kanj F., 2016-2017).

Active substance	80th percentile - Sandy (µg/l)	80th percentile – Silty-clay (µg/l)	80th percentile- Sandy clay-loam (µg/l)	80th percentile Sandy-clay (µg/l)	80th percentile Clay (µg/l)
Alfa cypermethrin	0.70816	0.71096	0.71424	0.71952	0.70752
Chlorpyrifos-ethyl	0.254	0.069992	0.15856	0.000023936	0.02712
Mancozeb	0.32472	0.013128	0.08488	1.26E-09	1.184
Methomyl	0.9984	0.8288	0.9144	0.3996	0.7496

These results show that the leached concentration of Alfa cypermethrin and methomyl in any type of soil is much greater than 0.1 µg.l^{-1} which reflects a high risk of groundwater contamination. Considering their physico-chemical characteristics and since alfa cypermethrin is quite mobile and fairly degradable while methomyl is mobile and easily degradable (Table 1), then, over time, groundwater contamination risks will be higher with alfa cypermethrin than with methomyl.

While the leached concentration of chlorpyrifos ethyl and mancozeb differs from one soil to another and is in direct relation to their physico-chemical characteristics, then:

- Leached Chlorpyrifos-ethyl concentration in silty clay, sandy clay and clay is <0.1 µg.l^{-1} which shows that the risk of contamination is lower than in sandy and sandy clay soil where the concentration is> 0.1 µg.l^{-1}
- While that of flutriafol in silty clay, sandy clay loam and sand clay soil is < µg.l^{-1} which reflects a lower risk of contamination than in sandy and clay soil.

Conclusion

The aim of this work is to identify the least and most vulnerable zones in terms of the leaching of active pesticides ingredients and to demonstrate the application of a unidimensional risk assessment model for pesticides, the PEARL model. The crosscutting of various factors as agricultural practices, pedological, agronomic and climatic data used in the model for the predicting of quantities of active material leached show that soils, at the level of the study area, are sensitive to the transfer of methomyl substances, mancozeb, chlorpyrifos-ethyl and alfa cypermethrin to groundwater.

The results indicate that areas cultivated with citrus and eggplant on sandy and sandy clay soils are particularly sensitive to the active ingredients ethyl-chlorpyrifos (concentrations > 0.1 µg/l) and alpha-cypermethrin (concentrations > 1 µg/l). Additionally, areas cultivated with lettuce on sandy and sandy clay soils are sensitive to the active ingredient methomyl (concentrations > 1 µg/l). Lastly, areas cultivated with cucumber on sandy soils are sensitive to the active ingredient mancozeb, with concentrations ranging between 0.1 and 1 µg/l.

These results will therefore enable decision-makers to better implement actions based on the acquired understanding of polluted areas, the products involved and the estimated risk rate by the concentration levels.

In addition, the tools used in this study could help in building a collective project thanks to the introduced understanding provided by the representations. These could thereby benefit users and stakeholders working in the management and use of ecosystem in utilizing its dynamics and interactions between regulated use and behavior of local actors.

It should be finally noted that this work consists of the first attempt performed at the level of the Lebanese territory in terms of risk assessment modeling of the transfer of pesticides at the levels of the soil and groundwater.

Limits of the model include having a simulation sensitivity at only 1-meter-deep from the ground level and covering only one year in duration. This is why more improvements can be introduced to enrich the scientific contribution of this work and to develop the tool into a more reliable and more generic form. These could include:

- Validating predicted results by collecting onsite soil and groundwater samples from areas identified with concentrations above the limit threshold.
- Extending the duration of the study over several years to assess the state of soil and groundwater quality at the territorial level, as affected by the as usual business and the sustainable practices.
- Running the simulation with other active ingredients and assessing the risks of these substances on various compartments of the environment, including food safety.

REFERENCES

Agriculture Atlas of Lebanon, 2004, Ministry of Agriculture.

BOESTEN J.J.T.I. et GOTTESBUREN B., 2000, "Testing PESTLA using two models for bentazone and ethoprophos in a sandy soil", Agricultural Water Management, 44(1-3): 283-305.

CHAMPEAUX C., 2006, « Recours à l'utilisation de pesticides en grandes cultures, évolution de l'indicateur de fréquence de traitement à travers d'enquêtes : « pratiques culturales » du SCEES entre 1994 et 2001, In : INRA, rapport d'étude commandité par MAP (DGFAR).

CHAZA, C., SOPHEAK, N., MARIAM, H. *et al.* Assessment of pesticide contamination in Akkar groundwater, northern Lebanon. *Environ Sci Pollut Res* **25,** 14302–14312 (2018). https://doi.org/10.1007/s11356-017-8568-6

CHBIB C. et al., 2016, « Evaluation de la contamination des eaux souterraines par les pesticides Organochlorés dans la zone d'Akkar – Nord du Liban » (46éme congrès du groupe français des pesticides, Bordeaux, France)

CNRS (National Council for Scientific Research), 2007, « Final Report of the project on: Towards an Ecosystem Approach to the Sustainable Management of the Litani Watershed.", I RC, CNRS, SA, LRA.

Union Européen, 2010, "la directive "nitrate" de l'UE ». https://ec.europa.eu/environment/pubs/pdf/factsheets/nitrates/fr.pdf

DEVILLERS J., 2005, "Indicateurs pour evaluer les risques liee a l'utilisation des pesticides », Tec and Doc, Lavoisier (in French), Paris, France.

FAOSTAT, 2013, http://www.fao.org/faostat/en/#data;

FOCUS, 2000, "FOCUS Groundwater Scenarios in the EU review of active substances". Report of the FOCUS Groundwater Scenarios Workgroup, EC Document Reference SANCO/321/2000- rev.2. 202 pp, as updated by the Generic Guidance for FOCUS groundwater scenarios, version 1.1 dated April 2002.

FOCUS, 2009, "Assessing Potential for Movement of Active Substances and their Metabolites to Ground Water in the EU". Report of the FOCUS Workgroup, EC Document Reference SANCO/13144/2010-version.1. 604 pp, as outlined in Generic Guidance for Tier 1 FOCUS groundwater Assessment, version 2.0 dated January 2011.

Groundwater protection directives, EU, 2006.

GUSTAFSON D.L, 1990, "Field calibration of SURFACE: a model of agricultural chemicals in surface waters", Journal of Environmental Science and Health - B, 25(5): 665-687.

JARVIS N.J., *et al.*, 1994, "Simulation of dichlorprop and bentazon leaching in soils of contrasting texture using the MACRO model", *Journal of Environmental Science and Health. Part A: Environmental Science and Engineering and Toxicology*, 29(6), 1255–1277.

JARVIS N., 2000, "Sources of error in model predictions of pesticide leaching: a case study using the MACRO model", Agricultural Water Management, 44(1-3): 247-262.

JAVIS N., 2000, "CRACK-NP: a pesticide leaching model for cracking clay soil", Agricultural water management, 44 (1-3): 183-199.

KANJ F., 2018, « Outils et méthodes pour une politique territoriale de gestion raisonnée des pratiques agricoles : cas d'application dans la région de la Béqaa au Liban ». Thèse (Dr d'Université en Géographie et Aménagement de l'Espace) : Université Paul Valéry, Montpellier (France). 376 p. École doctorale ED 60 : TTSD - Territoires, Temps, Sociétés et Développement. UMR Gred. Plateforme doctorale du CIHEAM-IAMM.

KHOURY Y. *et al*., 1975, « Méthode de préparation de la carte scolaire : la caza de zahlé- Liban », un projet de recherche de l'IIPE dirigé par jacques Hallak, Paris : Institut international de planification de l'éducation.

KLEIN M. et al., 2000, « Comparing pesticide leaching models: results for the Tor Mancina data set (Italy)", Agriculture water management 44: 135-151.

LARI, 2016, « Lebanese Agricultural Research Institut », Tall Amara – Bekaa, Liban.

MANTIGAUD J-C., 2004, "Les filières fruits et légumes frais au Liban : structures, fonctionnement et perspectives », FAO.

MULLEN, A.J, *et al*., 1992, "Effects of freezing and storage on the phenolics, ellagitannins, flavonoids and antioxidant capacity of red raspberries", Journal of Agricultural and Food Chemistry, 50 (18): p. 5197–5201

RIFAI A., 2013, « Étude de la dégradation par photolyse directe de pesticides - Caractérisation structurale et toxicité potentielle des photoproduits », Thèse de doctorat, Ecole Polytechnique ParisTech.

ROUSSEAU A.N. *et al.*, 2000a, "GIBSI - An integrated modelling system prototype for river basin management", Hydrobiologia, 422/423: 465-475.

ROZELIER M., 2011, «L'envolée du bio», Commerce de Levant, mars 2011.

TIKTAK A. *et al*., 1994, "PESTRAS: A one dimensional model for assessing leaching and accumulation of pesticides in soil", RIVM, Bilthoven, the Netherlands.

TIKTAK A. et al., 2000, "Manual of focus PEARL version 1", RIVM report 711401008 alterra report 28, National institute of public health and environment.

TIKTAK A., 2002, "Modelling the leaching and drainage of pesticides in the Netherlands: the GeoPEARL model", Agronomie, 22: 373-387.

TREVISAN M. *et al.,* 2000, « Pesticide leaching potentiel in the Trasimeno lake area – Assessment of uncertainty associated with the simulation process.", in A. Walker (ed) 2001, BCPC symposium Proc.

VAN DEN BERF F. and BOESTEN J.J.T.I., 1998, "Pesticide leaching and accumulation model (PESTLA)", version description and user's guide, SC-DLO technical document 43, Wageningen, The Netherlands, pp. 150.

VAN DEN BERG F. *et al*. 1999, « Emission of pesticides into the air. », Water Air Soil Pollution 115:195–218

VILLENEUVE J.P. *et al.,* 1998, « Rapport Final du Pro/et GIBSI : Gestion de l'Eau des Bassins Versants à l'Aide d'un Système Informatisé », Mars 1998: Tome 1. R-462. INRS - Eau, SainteFoy

YOUSSEF L. et al., 2012, "Occurrence and levels of pesticides in South Lebanon water", Chemical speciation and bioavailability, 27 (2), 62 -70.

CULTISENSOR: Testing a digitalized subsoiler capable of generating maps of soil resistance

Francisco Garcia-Ruiz [a,*], Ramón Salcedo [a], Francisco Fonseca [b], Emilio Gil [a]

[a] Department of Agri-Food Engineering and Biotechnology, Universitat Politècnica de Catalunya, Spain

[b] AKIS International S.L., Lleida, Spain

* Corresponding author. Email: fco.jose.garcia@upc.edu

Abstract

Precision agriculture relies on data that is translated into management prescriptions. Soil mapping allows fields to be divided into homogeneous management zones and then site-specific inputs and labour can be allocated. Soil compaction is an important factor to consider, as it affects several soil and crop processes, including water infiltration rates, root development and water availability to crops. In this study, a new prototype of a fully digitised commercial subsoiler (Jympa, Castellserà, Spain) has been developed in the framework of the CULTISENSOR project. The machine was equipped with a GNSS system and oil pressure sensors, as well as an ultrasonic sensor to monitor the working height. A control unit developed by Waatic (Abrera, Spain) is capable of storing the data read at each point of the plot, allowing the oil pressure of the whole system to be traced in real time and digital maps of soil resistance (MPa) to be generated. In this context, an evaluation of the system's performance was carried out on a commercial plot. On the one hand, the data provided by the prototype was evaluated concerning the spatial structure of the data. On the other hand, the prototype was compared with satellite based canopy maps and the EM38-MK2 electromagnetic soil sensor (Geonics, Canada) was also used to produce maps of apparent electrical conductivity (ECa). These maps were used to assess the spatial variability of the soil and to compare its distribution with that generated by the prototype subsoiler. The results showed that the prototype is capable of delivering geospatially structured data, and soil maps match in high degree the canopy maps generated using satellite imagery. It was not observed a good matching with the EM38-MK2 sensor maps. This study has served to carry out a first validation of the prototype developed in the CULTISENSOR project and to propose new adjustments to be conducted to improve the validity and reliability of the soil maps.

Keywords: Soil mapping, Machinery, Telemetry, Soil Compaction, Precision Agriculture.

1. Introduction

Crop yield variability within a field depends, among others, on soil properties and environmental conditions. Soil heterogeneity within a plot is linked to the type of soil, topography and in-field management strategies (Khan et al. 2023). In order to implement crop and soil management strategies based on precision agriculture concepts, a sufficient amount of reliable data is required to determine the spatial variability at field level. The traditional method of exploring field soil variation is through grid sampling, which is time-consuming, labour-intensive, and costly (Oliver and Webster, 2014). New technological advancements and developments in digital soil mapping have allowed real-time measurement of soil properties with proximal sensors.

Soil compaction is one of the most important physical properties affecting the health of the soil in agriculture. It has impact on seed emergence, root development, water infiltration and soil water holding capacity, among others. Soil compaction is related to soil mechanical resistance, and its estimation with field sensors has been broadly studied to assess its variability in agricultural fields (Rockström et al., 1999; Gaston et al., 2001; Raper et al., 2005; Chung et al., 2006; Topakci et al., 2010). Kostic et al. (2016) used a soil tillage resistance sensor (Kostic et al. 2014) and compared the variability maps against different soil parameters sampled in the field. They concluded that the strongest correlation was found between soil resistance and cone penetration resistance, indicator of soil compaction. Understanding and mapping soil compaction open the possibility of variable depth soil management (Hanquet et al., 2004), impacting on different factors such as the reduced soil perturbation, improved crop yield, and increasing soil management sustainability from the environmental and economic point of view.

The use of existing machinery, fitted with sensors to monitor soil condition is one objectives of the

national project CULTISENSOR (AEI-010500-2023-242). The idea behind the project lays on being able to determine and map the spatial variability of soil resistance while the traditional soil preparation activities are carried out in field crops. After being achieved the first milestone of the project, consisting on the implementation of an oil pressure sensor and a control unit on a commercial subsoiler, this study aims at assessing the possibilities of this new prototype, and to validate the spatial structure and the data coherence captured.

2. Materials and Methods

2.1. Test site

The experiment was conducted on a 0.89 ha commercial field located in Castellserà (Lleida, Spain, 41.756740º N, 0.993165º E). The soil type is Calcaric Regosol (WRB, 2014) and the topography of the plot can be considered completely flat with a slope of less than 1% (Figure 1). This soil type is characterized by a good drainage, with medium to fine textures, absence of coarse elements and presence of calcium carbonate nodes. In this plot, different irrigated crop rotations of cereal and alfalfa have been cultivated during the last years, with preceding crop of corn in 2023, and the experiment was carried out in January 2024 when there was not crop cultivated in the field. Prior to any cultivation, the deep layers of soil are broken using a subsoiler, and chisel plowing is used to prepare the seed bed.

Figure 1. Commercial plot used for the experiment

2.2. Field measurements

Three different measurements were conducted in the trial plot. On the one hand, the soil resistance sensor developed in the CULTISENSOR, second, the canopy vigour was extracted using satellite imagery from the study area and, finally, the apparent soil electrical conductivity was determined with an electromagnetic sensor.

2.2.1. Real-time soil resistance measurement system

A commercial subsoiler model POLARIS-7 (Jympa 1971, Lleida, Spain) was used as the basis for the development of the real-time soil resistance measurement prototype (Figure 2). This implement is used for decompressing and breaking the subsoil to oxygenate it, to favour the filtration of the water and the development of the roots. The subsoiler was fitted with a set of sensors to capture the working data in real-time, a Global Navigation Satellite System (GNSS) to establish the coordinates of each data point recorded, and a commercial controlling unit (WAATIC, Abrera, Spain) that was storing the data and providing live visualization of the telemetry. The system was designed to monitor the oil pressure (MPa) of the whole hydraulic system managing all the arms of the subsoiler. For this, a pressure sensor was installed in the hydraulic circuit of the machine, as well as a temperature sensor to monitor the temperature of the oil in the circuit, and an ultrasonic sensor was used to measure the working height of the machine with respect to the

ground. The experimental field work was done using a 200 horse power tractor driving at 5 km h^{-1} with the subsoiler working at constant depth defined as 0.5 m, and the information provided by the sensors were recorded at a frequency of 1 Hz along with the GNSS coordinates. Once the field work was finalized, a GeoJSON file was generated containing the date and time of the recorded point, the latitude and longitude (decimal degrees), the oil pressure (MPa) and the real working speed recorded by the GNSS (km h^{-1}). The output data was interpolated block kriging using local semivariograms with search radius of 25 m and a raster map for the oil pressure was generated (considered as soil resistance to traction). The central co-ordinates of the satellite image pixels covering the study area were used as the grid points for variable interpolation.

Figure 2. Detail of the soil resistance monitoring prototype developed, the control unit and the user interface

2.2.2. Satellite based imagery

Satellite imagery was used to determine de canopy vigour in the field and assess the spatial variability of the crop response to soil characteristics and agricultural management practices. Given the small size of the plot, high spatial resolution Super Dove nano-satellite (Planet Labs Inc.) was used. Super Dove nano-satellites offer nearly daily imagery in monitoring mode at 3 m $pixel^{-1}$ and with eight spectral bands in the range of VIS-NIR. An image was collected at the end of March 2023 coinciding with the maximum vegetation growth of the previous crop before the subsoiling process with the prototype was conducted. With the multispectral image, the Normalized Differential Vegetation Index (NDVI) was calculated combining the bands in the red and near infrared regions of the spectrum. The NDVI pixels were classified into two classes, class 1 for low vigour and 2 for high vigour, using the K-means clustering function in the QGIS plugin Attribute Based Clustering.

2.2.3. Apparent soil electrical conductivity

Apparent soil electrical conductivity (EC_a) has been widely used for estimating soil properties such as salinity, water content and texture. The electromagnetic induction sensor used for sampling EC_a in this trial was the Geonics EM38-MK2 (Geonics Ltd., Mississauga, Ontario, Canada). The EM38-MK2 has two receiver coils spaced at 0.5 m and 1 m from the transmitter coil. The transmitter coil is powered by an alternating current, creating a magnetic field that changes over time within the earth. This magnetic field induces current to flow through the soil, producing a secondary magnetic field. The intensity of this secondary electromagnetic field is directly linked to the electrical conductivity of the soil. The sensors was passed throughout the entire plot at different transects separated approximately 10 m between them. The resulting file obtained contained the latitude and longitude of each reading and the measured EC_a at 0.5 and

1 m deep. For mapping EC_a, a similar process than the methodology used to generate the oil pressure maps was implemented interpolating by block kriging to the central co-ordinates of the satellite image pixels covering the study area.

2.3. Data analysis

The database used to compare the different sensing techniques consisted on a grid file containing the information from each of the technologies used to sample the variability of the field, meaning the soil resistance sampling prototype (oil pressure in MPa), the NDVI, and the EC_a at 0.5 and 1 m depth. The grid was established based on the pixel size and location of the satellite image, and every cell contained the data for each of the four parameters sampled.

Two different assessments were made. First, an analysis of the spatial structure of the data acquired by the soil resistance sampling prototype was conducted by studying the local variability reflected by the global semivariogram (Oliver, 2010). Furthermore, the Cambardella Index (CI) was used to determine the spatial dependency of the data (Cambardella et al., 1994). The CI was calculated from the nugget and sill averages of the local semivariogram after the local kriging interpolations of the oil pressure data.

A second assessment consisted on comparing the interpolated maps of each of the measurement sources used. For this, a k-means classification into two clusters (given the size of the plot) was made, and the clustered maps were compared against each other using the software Map Comparison Kit (MCK version 3.2.3 http://mck.riks.nl/). To compare the map pairs, two statistics were employed: the FC and the KI. The FC (fraction correct), which represents the percentage of agreement, is calculated by dividing the number of equal cells in both maps by the total number of cells in the map. The Kappa index of agreement, on the other hand, is based on a contingency table that summarizes the cross-distribution of categories across the two maps.

3. Results and Discussion

3.1. Spatial structure of soil resistance data

Results showed that the data obtained by the prototype developed in the CULTISENSOR project is able to determine the soil resistance linked to the pressure of the hydraulic circuit in the subsoiler. The first question raised was whether the data would be randomly distributed, not showing the soil variability inherent trends, or if the soil resistance would show some kind of geospatial trend. According to the global semivariogram calculated, it was seen that there existed a spatial dependency (autocorrelation) between the data generated using the soil resistance prototype sensor (Figure 3). The nugget value of the semivariogram revealed that there exists and certain variability in the data in close distances, something that has also been reported by other authors when working with agricultural data (Sandonís-Pozo et al., 2022).

The Cambardella Index resulted in 29.7% being considered a moderate-high spatial autocorrelation of the soil resistance prototype data. This indicates that the spatial structure of the sampled points is consistent and not randomly distributed in the field.

The interpolated map depicts the subsoil physical properties with very high detail while representing the spatial trends, and offers a fast and easy to use estimation of soil condition along the plot.

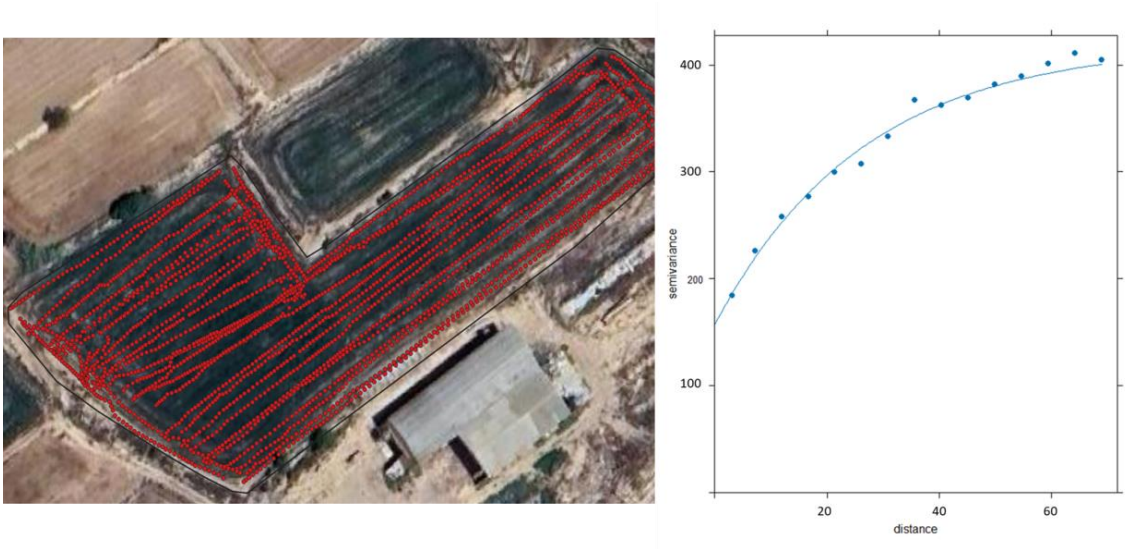

Figure 3. Data points measured by the soil resistance prototype sensor (left) and global semivariogram with an exponential fitting model (right)

3.2. Comparison with other sensors

3.2.1.NDVI

When comparing the soil resistance clustered map generated using the sensing prototype with the clustered NDVI canopy map, it was found that the FC value of 0.82 while the KI parameter was significantly lower (0.63). FC is a method which only considers the percentage of change of pixels; on the contrary, the KI is based on a contingency table that summarizes the cross-distribution of categories over the two maps. The KI tends to be more restrictive than FC (Visser & De Nijs, 2006). The map comparison yielded a moderate-to-high concordance between the prototype based map and the satellite based NDVI map, providing evidences that the prototype is able to measure the soil resistance with a reliable spatial distribution of the data.

3.2.2.EM38

The map comparison of the interpolated soil resistance versus the EC_a at 0.5 and 1 m respectively, did not show significant concordance between them. For EC_a at 0.5 m deep, the FC was 0.48 while the KI was negative (-0.01). Similar results were seen for EC_a measeured at the depth of 1 m, with slightly lower FC (0.38) and KI (-0.28). The initial hypothesis was that the value of EC_a would correlate in some degree with soil porosity and to some extent to the compaction of the soil, but the data obtained revealed that EC_a is being dominated by other parameters in the soil (e.g. salinity, water availability, etc.).

4. Conclusions

This study showed that a commercial subsoiler can be digitalized using different sensors and electronics to provide on-the-go mapping of soil resistance in field crops. The results showed that the data recorded keeps a certain degree of autocorrelation which provides confidence about the reliability of the information registered. Furthermore, the soil resistance maps generated were observed to match in high degree the spatial patterns estimated in the canopy by means of satellite based NDVI maps. Combination of NDVI and soil resistance maps (surface and subsurface layers of the soil-plant continuum) make possible site specific soil amendments and actions such as application of organic matter, drainage systems, etc. Future work will be focused on collecting soil samples with a digital penetrometer in specific areas of the field and relating the measures with the oil pressure of the subsoiler to establish relationships between the two measures.

Acknowledgements

The CULTISENSOR project (AEI-010500-2023-242) was funded by the Spanish Ministry of Science and Universities.

References

Cambardella, C., T. Moorman, J. Novak, T.B. Parkin, D. Karlen, R. Turco, et al., 1994. Field-scale variability of soil properties in central Iowa soils. Soil Science Society of America Journal, 58(5), 1501–1511. https://doi.org/10.2136/sssaj1994.03615995005800050033x

Chung, S.O., K.A. Sudduth, L.W. Hummel, 2006. Design and validation of an on-thego soil strength profile sensor. Transactions of the ASABE 49 (1), 5–14.

Gaston, L.A., M.A. Locke, R.M. Zablotowicz, K.N. Reddy, 2001. Spatial variability of soil properties and weed populations in the Mississippi delta. Soil Science Society of America Journal 65, 449–459.

Hanquet, B., D. Sirjacobs, M.F. Destain, 2004. Analysis of soil variability measured with a soil strength sensor. Precision Agriculture 5, 227–246.

Khan, H., T. Esau, A. Farooque, Q. Zaman, F. Abbas, A. Schumann, 2023. Chapter 2 - Soil spatial variability and its management with precision agricultura. Precision Agriculture, Evolution, Insights and Emerging Trends, 19-36.

Kostic´, M., D. Rakic´, H. Licˇen, N. Malinovic´, 2014. Design and construction of three point hitch device for measuring draft of tillage implement. Data acquisition and post processing analysis. Journal of Food Agriculture and Environment 12 (2), 1300–1307

Kostic´, M., D. Rakic´, L. Savic, N. Dedovic´, M. Simikic´, 2016. Application of an original soil tillage resistance sensor in spatial prediction of selected soil properties. Computers and Electronics in Agriculture, 127, 615-624. http://dx.doi.org/10.1016/j.compag.2016.07.027

Oliver, M.A., 2010. Geostatistical applications for precision agriculture. Springer.

Oliver, M.A., R. Webster, 2014. A tutorial guide to geostatistics: computing and modeling variograms and kriging. Catena 113 (2014), 56–69.

Raper, R.L., E.B. Schwab, S.M. Dabney, 2005. Measurement and variation of sitespecific hardpans for silty upland soils in the Southeastern United States. Soil Till. Res. 84, 7–17.

Rockström, J., J. Barron, J. Brouwer, S. Galle, A. de Rouw, 1999. On-farm spatial and temporal variability of soil and water in pearl millet cultivation. Soil Science Society of America Journal 63, 1308–1319.

Topakci, M., I. Unal, M. Canakci, Kursat, H. Celik, D. Karayel, 2010. Design of a horizontal penetrometer for measuring on-the-go soil resistance. Sensors 10, 9337–9348.

Visser, H., T. De Nijs, 2006. The map comparison kit. Environmental Modelling and Software, 21(3), 346–358. https://doi.org/10.1016/j.envsoft.2004.11.013

Hydraulic performance evaluation of low-cost gravity-fed drip irrigation systems under falling head conditions

Camille G. Martinez[a], Henry Mark Q. Binahon[b], Jeffrey A. Gonzales[b], Arthur L. Fajardo[c,*], Victor B. Ella[b]

[a] Department of Engineering Science, University of the Philippines Los Baños, Los Baños, Philippines

[b] Land and Water Resources Engineering Division, University of the Philippines Los Baños, Los Baños, Philippines

[c] Agribiosystems Machinery and Power Engineering Division, University of the Philippines Los Baños, Los Baños, Philippines

* Corresponding author. Email: alfajardo@up.edu.ph

Abstract

To ensure optimal water use efficiency in drip irrigation, it is imperative to assess the hydraulic performance of the system. Hence, this study evaluated and compared the hydraulic performance of two locally available low-cost drip irrigation kits in the Philippines (denoted as Drip Kit A and Drip Kit B) under falling head conditions, simulating actual field conditions in which the water level in the tank decreases during operation. Built upon a previous study by Martinez et al. (2022) that focused on the hydraulic performance of low-cost gravity-fed drip irrigation kits under constant head conditions, this study employed the same drip kit components but under falling head conditions of 4.3 m to 4.1 m, 4.1 m to 3.9 m, and 3.9 m to 3.7 m. Results revealed a decrease in emitter discharge rates as the operating head falls. For both drip kits, Christiansen's coefficient of uniformity (CU), emission uniformity (EU), and coefficient of variation (CV) varied from 91.89 to 96.02, 84.13 to 92.19, and 0.08 to 0.15, respectively. Also, statistical analysis indicated that varying the operating heads did not significantly affect (α=5%) the CU, EU, and CV of both drip kits. Moreover, Drip Kit A (0.53 to 0.57 lph) demonstrated higher emitter discharges compared to Drip Kit B (0.52 to 0.54 lph), establishing Drip Kit A's superior performance. The CU and EU during the falling head test did not deviate far from the constant head test. In terms of design and operation, the factors to be considered in relation to emitter discharge are irrigation period, water supply, and wetting area.

Keywords: drip irrigation, hydraulic performance evaluation, falling head

1. Introduction

Drip irrigation is the most efficient water and nutrient delivery system for growing crops. It delivers water and nutrients directly to the plant's root zone in the right amount at the right time, so each plant gets exactly what it needs when it needs it, to grow optimally. Farmers can increase yields while using less water, fertilizer, energy, and even crop protection products by using drip irrigation. Water and nutrients are delivered across the field in pipes called 'dripperlines' featuring smaller units known as 'drippers'. Each dripper emits drops containing water and fertilizers, resulting in the uniform application of water and nutrients directly to each plant's root zone, across an entire field (Netafim, 2024).

Drip irrigation technology has undergone significant advancements, resulting in the development of sub-membrane drip irrigation, subsurface drip irrigation, aerated drip irrigation, and other irrigation technologies. Overall, drip irrigation technologies have played an essential role in enhancing crop yield and quality and promoting efficient water resource management (Yang et al., 2023).

One of the major drawbacks of drip irrigation is its high investment costs; thus, it is mainly used in high-value commercial crop production. However, its water use efficiency is very high compared to other irrigation methods (Brouwer et al., 1985). Emitter discharge variation and water distribution uniformity are the commonly used parameters in evaluating the performance of a drip irrigation system. Water distribution uniformity, in particular, uses the emitter discharge value to compute the uniformity indices. There have been several studies that assessed a drip irrigation system's performance based on its water distribution uniformity and variation (Zellman, 2016; Yavuz et al., 2010; Zhang et al., 2017) taking into account the occurrence of emitter clogging (Barragan et al., 2006; Bralts et al., 1981; Almajeed and Alabas, 2013), manufacturing variations (Ganda, 2005), pressure losses (Balenzon, 2006), gravity-fed drip irrigation system in crop production (Dela Cruz, 2004), and performance evaluation as affected by water heads and length of laterals (Mashandudze et al., 2015).

This study was a continuation of the research of Martinez et al. (2022) on the hydraulic performance evaluation of low-cost gravity-fed drip irrigation systems. In this study, the hydraulic performance of two locally available low-cost gravity-fed drip irrigation systems was evaluated under falling head conditions. The falling head condition simulates the actual field drip system operation wherein the water level inside the tank descends, without refilling, during the irrigation operation.

2. Materials and Methods

2.1. Drip Irrigation Experimental Layout and Setup

The experiment was conducted using the same locally available low-cost gravity-fed drip irrigation kits used in the study of Martinez et al. (2022). Similarly, the two (2) kits were referred to in this study as Drip Kit A and Drip Kit B. Both kits were designed to irrigate a 200 m^2 plot and each kit was composed of a 1000-L intermediate bulk container (IBC) tank, 14×20-m lateral lines equally spaced at 0.75 m, and a 10-m submain line. Table 1 shows the list of components and specifications of both drip irrigation kits.

Table 1. Specifications of the drip irrigation kits used in the study (Martinez et al., 2022).

Components	Drip Kit A	Drip Kit B
Main and submain line	LLDPE hose, 32-mm outer diameter, 2-mm wall thickness	LLDPE hose, 25-mm outer diameter, 2.5-mm wall thickness
Lateral line and emitter	Non-pressure compensating thin-walled drip line with cascade labyrinth emitter, 30-cm spacing, 17-mm nominal diameter, 1.0 lph	Non-pressure compensating thin-walled drip line with cascade labyrinth emitter, 30-cm spacing, 17-mm nominal diameter, 1.0 lph
Valve	32-mm PVC ball valve, female/female	25-mm PVC ball valve, female/female
Screen filter	130 microns	125 microns
Main-submain line fittings	32-mm compression fittings: 1 pc equal tee 1 pc female adapter 1 pc male adapter 2 pcs equal elbow 2 pcs end cap	25-mm compression fittings: 1 pc equal tee 1 pc female adapter 1 pc male adapter 2 pcs equal elbow 2 pcs end cap
Lateral line fittings	16-mm PE: 14 pcs start connector 14 pcs end line	16-mm PE: 14 pcs start connector 14 pcs end line
Package Price[a]	$200.00	$140.00

[a] The drip kits contain additional parts but the approximate price will not significantly vary. The package does not include the IBC tank and tank stand.

Each drip irrigation kit was installed using the end-feed layout as shown in Figure 1. With an end-feed layout, the IBC tank supplies water to only one end of the lateral lines through the submain line. The main line divides the submain line, at the center, into two (2) equal parts and it connects the IBC tank to the submain line. After laying out, the submain and lateral lines were leveled with respect to the junction of the main and submain lines. This was done to eliminate the effect of slope in testing the drip irrigation kits. As presented in Figure 2, the IBC tank was installed in the manner that the top of the tank is at 4.5 m above the main and submain line junction levels. The tank was also marked at 3.7 m, 3.9 m, 4.1 m, and 4.3 m for the three (3) falling head setups to be tested – (1) 4.3 m to 4.1 m, (2) 4.1 m to 3.9 m, and (3) 3.9 m to 3.7 m.

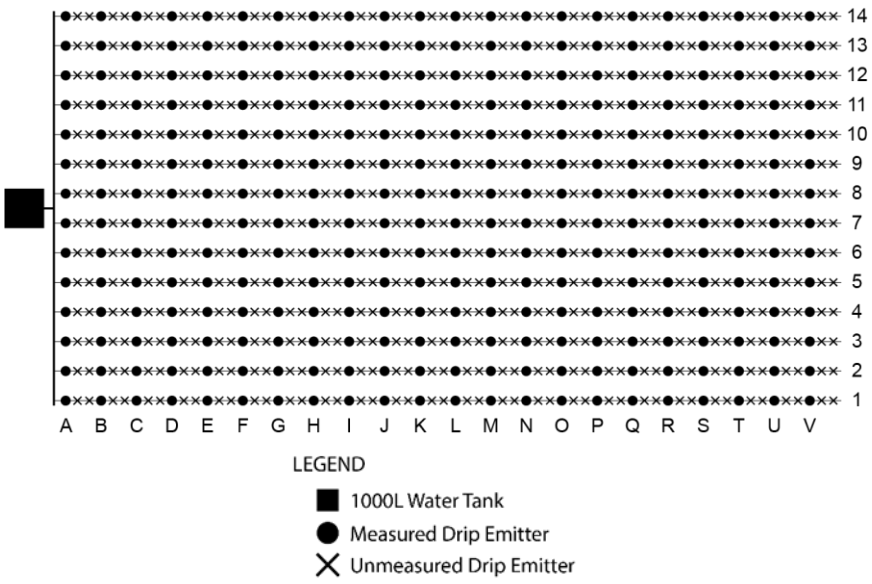

Figure 1. Drip irrigation layout showing the selected sampling emitters in the performance testing (Martinez et al., 2022).

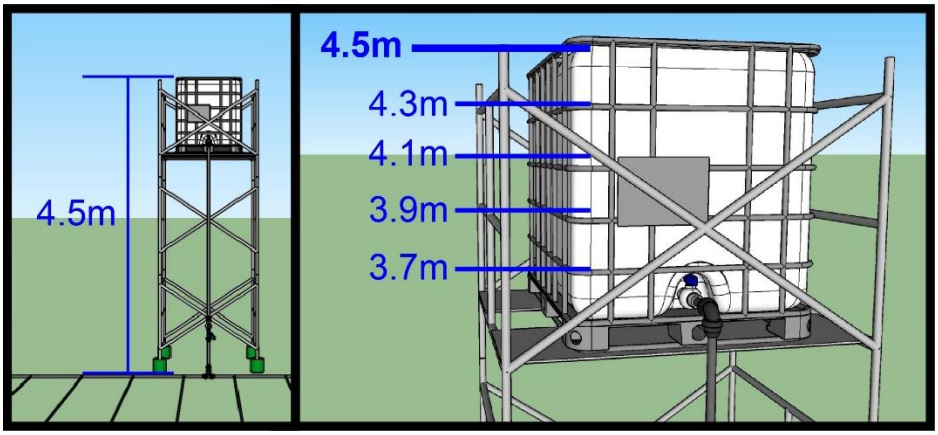

Figure 2. Falling hydraulic head setup used in the study.

2.2. Data Collection and Emitter Discharge Rate Calculation

For the sampling, 308 emitters out of a total of 926 emitters in the setup were selected. For each falling operating head setup, three (3) trials of emitter discharge measurements were conducted. The location of each sampling emitter was identified according to its lateral line and position in the lateral line. The lateral lines are labeled with numbers 1 to 14 whereas the positions of the sampling emitters on the lateral lines are labeled with letters A to V as shown in Figure 1.

Given the considerable number of data to be gathered, the gravimetric method was employed to determine the discharge rate of each sampling emitter. Collecting the water discharge during the trials was done using pre-weighed 300 mL melamine cups. The total time for the water to descend in the IBC tank according to the falling operating head setup being tested was also recorded. After each trial, the mass of each cup containing the collected water from the sampling emitter was measured using a digital weighing scale. Assuming that the density of water is 1.0 g/cm^3, the emitter discharge rate was computed using Eq (1):

$$q = \frac{3}{50}\frac{m_t - m_c}{t} \quad (1)$$

where q is the individual sampling emitter discharge in lph; m_t is the total mass of the cup and collected water discharge in g; m_c is the total mass of the cup in g; and t is time in minutes.

The resulting emitter discharge rate values were then analyzed and used to generate mathematical models to describe the relationship of the falling operating head to the average emitter discharge rate for Drip Kit A and Drip Kit B. Additionally, the emitter discharge rate variation along the lateral line for both drip irrigation kits was also examined.

2.3. Water Distribution Uniformity

The water distribution uniformity of the systems/kits was computed using the following performance metrics:

2.3.1. Coefficient of Uniformity, CU (Christiansen, 1942)

$$CU = \left(1 - \frac{\sum_{i=1}^{n}|q_i - M|}{\sum_{i=1}^{n} q}\right) \times 100 \quad (2)$$

where CU is the coefficient of uniformity in %; n is the number of observed emitter discharge rate values; q_i is the individual emitter discharge rate in lph; and M is the average of emitter discharge rate values computed as $\frac{1}{n}\sum_{i=1}^{n} q_i$ in lph.

Table 2. Drip irrigation system uniformity classification based on uniformity coefficient.

Uniformity coefficient, CU (%)	Classification
>90	Excellent
90-80	Good
80-70	Fair
70-60	Poor
<60	Unacceptable

Source: ASAE Standards EP458 (1996)

2.3.2. Emission Uniformity, EU (Keller and Bliesner, 1990)

$$EU = \left(\frac{q_{LQ}}{M}\right) \times 100 \quad (3)$$

where EU is the emission uniformity in %; q_{LQ} is the average of the lowest quarter of the emitter discharge rate values in lph; and M is the average of the emitter discharge rate values in lph.

Table 3. Drip irrigation system uniformity classification based on emission uniformity.

Emission Uniformity, EU (%)	Classification
94 - 100	Excellent
81 - 87	Good
65 - 75	Fair
56 - 62	Poor
< 50	Unacceptable

Source: ASAE Standards EP458 (1996)

Note: The discontinuities in the EU scale cater to the 95% confidence limits of the measures and these tend to be high for low uniformities.

2.3.3. Coefficient of Variation, CV (Al-Amoud, 1995)

$$CV = \frac{\sigma}{M} \times 100 \quad (4)$$

where *CV* is the coefficient of variation; σ is the standard deviation of the emitter discharge rates in lph; and *M* is the average of the emitter discharge rate values in lph.

Table 4. Drip irrigation system classification based on the coefficient of variation.

Coefficient of Variation, CV	Classification
<0.1	Excellent
0.1 – 0.2	Very Good
0.2 – 0.3	Acceptable
0.3 – 0.4	Low
>0.4	Unacceptable

3. Results and Discussion

3.1. Effect of Operating Head on Emitter Discharge

For all head settings, the emitter discharge of Drip Kit A is relatively higher compared to Drip Kit B (Table 5). The highest average emitter discharge was 0.57 lph at 4.3 to 4.1 m head from Drip Kit A, while the lowest average emitter discharge was 0.52 lph at 3.9 to 3.7 m head from Drip Kit B. The emitter discharge values were within the values obtained during the constant head test conducted by Martinez et al. (2022). In the constant head test, the average emitter discharge of Drip Kit A was 0.56 lph at 3.5 m head, 0.58 lph at 4.0 m head, and 0.59 lph at 4.5 m head. Moreover, the average emitter discharge of Drip Kit B was 0.52 lph at 3.5 m head, 0.56 lph at 4.0 m head. and 0.59 lph at 4.5 m head (Martinez et al., 2022). In general, the emitter discharge decreases with decreasing operating head (Figure 3).

Table 5. Minimum, average, and maximum emitter discharge values of the drip kits under falling operating heads.

Head, m	Average Emitter Discharge, lph					
	Drip Kit A			Drip Kit B		
	Minimum	Average	Maximum	Minimum	Average	Maximum
4.3 to 4.1	0.43	0.57	0.62	0.04	0.54	0.59
4.1 to 3.9	0.34	0.55	0.60	0.06	0.53	0.58
3.9 to 3.7	0.36	0.53	0.59	0.07	0.52	0.58

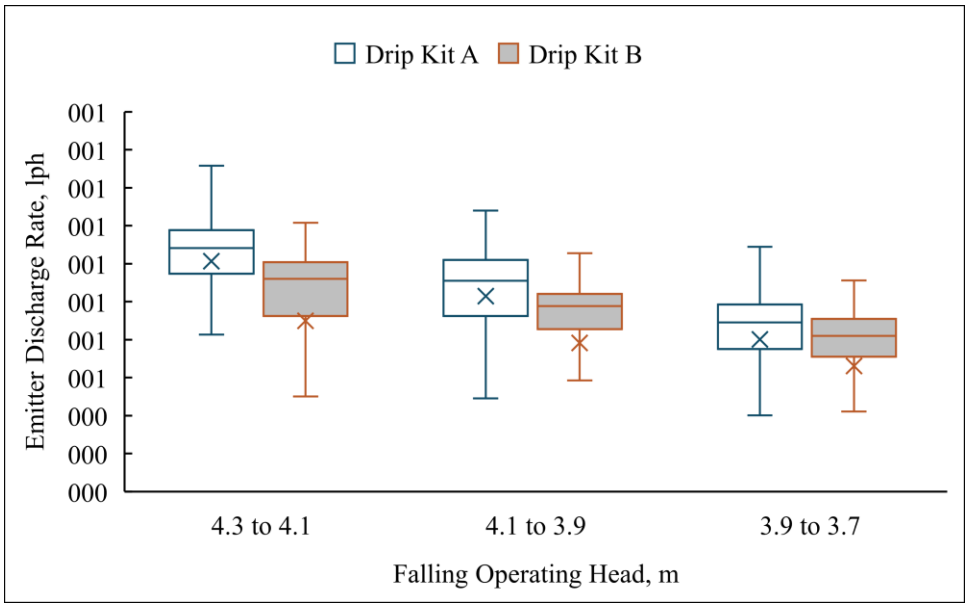

Figure 3. Box plot of emitter discharge (lph) at different falling operating heads (m).

Regression analysis was performed to express the relationship of the average emitter discharge to the operating heads for each drip kit using Equation 1 (Figure 4). Results showed a strong relationship between the average emitter discharge and operating pressure head for both drip kits, as shown in Table 6.

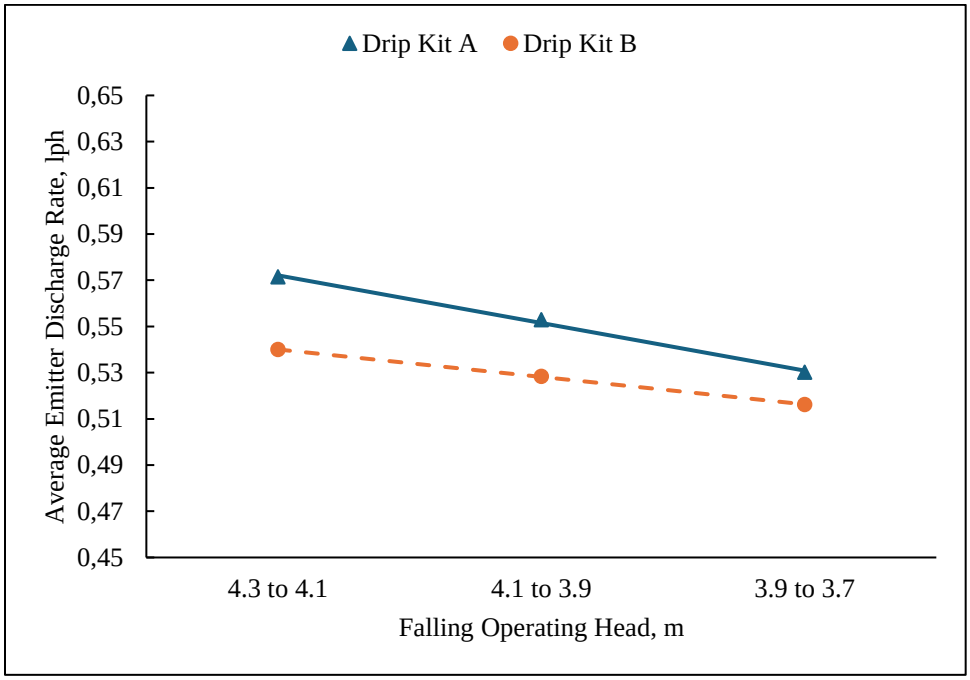

Figure 4. Relationship between average emitter discharge and falling operating head for the drip kits.

Table 6. Linear regression models for average emitter discharge as a function of falling operating head.

Drip Kit	Linear Regression Model	R^2
A	q = -0.0206H+0.5927	0.99
B	q = -0.0119H+0.5519	0.99

Note: *q* is the average emitter discharge in lph and *H* is the falling operating pressure head in m.

3.2. Effect of Emitter Distance Along the Lateral on Emitter Discharge

It is also important to examine the variability of the emitter discharge along the laterals to check the water distribution. The average emitter discharge along the laterals was plotted against its distance for each operating head for the two drip kits as presented in Figure 5. It could be observed that emitter discharge along the lateral varies widely in relation to the drip kit and operating head. The result of the constant head test of Martinez et al. (2022) showed a relatively defined trend for emitter discharge. It could be observed that the emitter discharge of Drip Kit A showed a significant trend as presented in the results of the regression analysis of the emitter discharge with its distance in Table 7. The R^2 values obtained from the varying head test (Table 7) were way below the values obtained from the constant head test (Martinez et al., 2022). For Drip Kit A, the emitter discharge along the lateral increases at 4.3 to 4.1 m head while emitter discharge decreases at 4.1 to 3.9 m and 3.9 to 3.7 m heads.

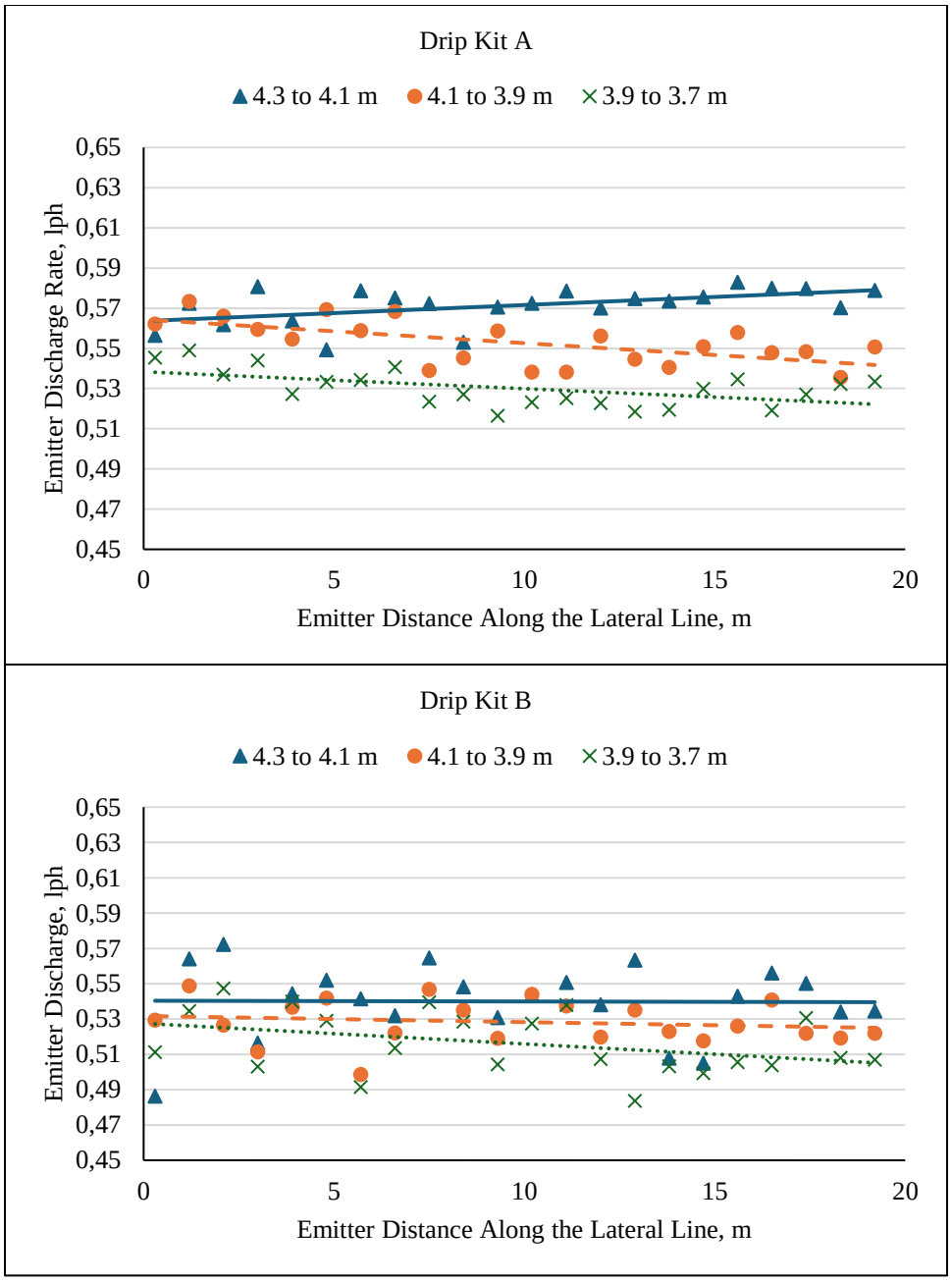

Figure 5. Emitter discharge variation along the lateral at different operating heads.

Table 7. Linear regression models for the average emitter discharge along the lateral line at different falling operating heads.

Head, m	Drip Kit A		Drip Kit B	
	Linear Regression	R^2	Linear Regression	R^2
4.3 to 4.1	$Y = 8.02\times10^{-4} X + 0.56$	0.26	$Y = -4.22\times10^{-5} X + 0.54$	0.00
4.1 to 3.9	$Y = -1.18\times10^{-4} X + 0.56$	0.38	$Y = -3.49\times10^{-4} X + 0.53$	0.03
3.9 to 3.7	$Y = -8.43\times10^{-4} X + 0.54$	0.29	$Y = -1.20\times10^{-3} X + 0.53$	0.15

Note: *Y* is the individual emitter discharge rate in lph and *X* is the distance of the emitter along the lateral line from the submain line in m.

3.3. Analysis of Water Distribution Uniformity

Table 8 shows the computed CU, EU, and CV of the two locally available drip kits used in the study. Generally, the EU has lower values compared to the CU. Drip Kit A yielded better water distribution uniformity (CU: 96.02% to 94.56%; EU: 89.53% to 89.67%; CV: 0.08 to 0.09). On the other hand, Drip Kit B yielded better water distribution uniformity during the constant head test (Martinez et al., 2022). Based on the classifications shown in Tables 2 and 3, both drip kits exhibited excellent overall performance in terms of CU. Drip Kit A exhibited excellent performance in terms of EU while Drip Kit B showed good performance.

Table 8. Coefficient of uniformity, emission uniformity, and coefficient of variation of Drip Kits A and B at different falling operating heads.

Head, m	Drip Kit A			Drip Kit B		
	CU, %	EU, %	CV	CU, %	EU, %	CV
4.3 to 4.1	94.56	89.67	0.09	91.89	84.13	0.15
4.1 to 3.9	96.02	92.19	0.08	92.47	85.58	0.15
3.9 to 3.7	94.98	89.53	0.09	93.23	86.71	0.14

Using the Shapiro-Wilk test of normality, it was found that the data gathered for both drip kits did not follow the normal distribution. Hence, to validate whether the CU, EU, and CV values significantly differ on operating heads, the Kruskal-Wallis H test was employed with a 95% confidence level. The statistical test showed that CU ($H(2) = 3.47$, $p = 0.18$), EU ($H(2) = 2.76$, $p = 0.25$), and CV ($H(2) = 1.42$, $p = 0$ .49) of Drip Kit A are not significantly different for the operating falling heads, i.e., changing the operating heads will not influence the CU, EU, and CV values for Drip Kit A. Likewise, the CU ($H(2) = 1.69$, $p = 0.43$), EU ($H(2) = 1.07$, $p = 0.59$), and CV ($H(2) = 2.49$, $p = 0.29$) of Drip Kit B also showed similar results.

4. Summary and Conclusion

The CU and EU obtained during the falling head test did not deviate far from those measured during the constant head test. For all head settings, the emitter discharge of Drip Kit A is relatively higher compared to Drip Kit B. Emitter discharge along the lateral varies widely in relation to the drip kit and the operating head. For this study, both drip kits exhibited excellent overall performance in terms of CU. Drip Kit A exhibited excellent performance in terms of EU and good performance for Drip Kit B. In terms of design and operation, the factors to be considered in relation to emitter discharge are irrigation period, water supply, and wetting area.

Acknowledgements

This study was supported by the Commission on Higher Education – Philippine-California Advanced Research Institutes (CHED-PCARI) through the PCARI WiSEIr project entitled “Development of Wireless Sensor Network-based Water Information System for Efficient Irrigation Water Management in the Philippines”.

References

Al-Amoud, A.I. 1995. Significance of Energy Losses Due to Emitter Connections in Trickle Irrigation Lines. J. Agric. Engng. Res. (1995) 60, 1-5. https://doi.org/10.1006/jaer.1995.1090

Almajeed, A., M. Alabas. 2013. Evaluation of the hydraulic performance of drip irrigation system with multi cases. Glob. J. Eng. Res. 13(2-J).

[ASAE] American Society of Agricultural Engineers. 1996. EP458. Field evaluation of microirrigation systems. ASAE Standards, 43rd Edition, ASAE, St. Joseph, 756-761.

Balenzon, W.D. 2006. Evaluation of gravity-type drip irrigation system in tomato production. Unpublished Undergraduate Thesis. Mariano Marcos State University. Philippines.

Barragan, J., V. Bralts, I.P. Wu. 2006. Assessment of emission uniformity for micro-irrigation design. Biosystems Eng. 93(1) 89–97. https://doi.org/10.1016/j.biosystemseng.2005.09.010

Bralts, V.F., I.P. Wu, H.M. Gitlin. 1981. Manufacturing variation and drip irrigation uniformity. Trans. ASAE 24(1) 113–19. https://doi.org/10.13031/2013.34209

Brouwer, C., K. Prins, M. Kay, M. Heibloem. 1985. Irrigation Water Management: Training Manual No. 5: Irrigation methods. FAO Land and Water Development Division. Rome, Italy.

Christiansen, J.E. 1942. Irrigation by sprinkling. Calif. Agric. Exp. Stn. Bull. 670 Univ. 385 Calif. Berkeley Calif.

Dela Cruz, S.G. 2004. Performance evaluation of a gravity-type drip irrigation system as affected by varying water heads and length of laterals. Unpublished Undergraduate Thesis. Mariano Marcos State University. Philippines.

Ganda, M. 2005. Evaluation of gravity-type drip irrigation system for lettuce. Unpublished Undergraduate Thesis. Mariano Marcos State University. Philippines.

Keller, J., R.D. Bliesner. 1990. Sprinkler and trickle irrigation. Van Nostrand Reinhold, New York.

Martinez, C.G., C.L.R Wu, A.L. Fajardo, V.B. Ella. 2022. Hydraulic Performance Evaluation of Low-Cost Gravity-Fed Drip Irrigation Systems Under Constant Head Conditions. IOP Conf. Ser.: Earth Environ. Sci. 1038 012005, 13pp.

Mashandudze, W., N.L. Mufute, J. Masaka. 2015. A performance evaluation of a one-hectare gravity fed drip irrigation system under varying vertical head. Midlands State University. J. Sci. Agric. Technol. 93–111.

Netafim. 2024. What is Drip Irrigation? https://www.netafim.asia/Drip-irrigation/#:~:text=Drip%20irrigation%20is%20known%20to,are%2060%2D70%25%20efficient.

Yang, P., L. Wu, M. Cheng, J. Fan, S. Li, H. Wang, L. Qian. 2023. Review on Drip Irrigation: Impact on Crop Yield, Quality, and Water Productivity in China. Water. 15(9), 1733. https://doi.org/10.3390/w15091733

Yavuz, M., K. Demarel, O. Erken, E. Bahar, M. Devecaler. 2010. Emitter clogging and effects on drip irrigation systems performances. Afr. J. Agric. Res. 5(7) 532–38.

Zellman, P. 2016. Drip Irrigation System Evaluations: How to Measure & Use Distribution Uniformity Tests

Zhang, L., P. Wu, D. Zhu, C. Zheng. 2017. Effect of pulsating pressure on labyrinth emitter clogging. Irrig. Sci. 35(4) 267–74. https://doi.org/10.1007/s00271-017-0532-1

Understanding stakeholder perspectives on decision support tools for livestock farm emission management

Evangelos Alexandropoulos [a,*], Vasileios Anestis [a], Thomas Bartzanas [a]

[a] Department of Natural Resources Development and Agricultural Engineering, Agricultural University of Athens, Athens, Greece

* Corresponding author. Email: vagalexandr1991@aua.gr

Abstract

To assess the expected needs for Decision Support Systems (DSS) related to Greenhouse Gas (GHG) emissions in global livestock production at the farm level, the perspectives of stakeholders were sought. Direct communication with stakeholder parties in various countries was established to explore their experiences with existing GHG-based DSS at the farm scale. Collecting this information was crucial to understanding the current demand for integrating GHG and ammonia emissions estimation into the decision-making process at the farm scale across different countries. Additionally, it aimed to evaluate and present the potential for utilizing these DSS at the farm scale in the near future. Understanding the requirements of potential users can offer valuable insights to developers of emissions-based decision support tools, enabling them to improve existing tools and align them better with users' needs. The majority of respondents were livestock farmers' advisors (73 out of 109), followed by livestock farmers (23 respondents), inventory compilers (9 respondents), and authority officials/policymakers (4 respondents). The survey respondents represented various countries, including Greece, Poland, Germany, France, and Chile. While most stakeholders who responded were aware of software-based DS tools, less than half of them actually used such tools. Furthermore, even fewer respondents reported using software-based DS tools that estimate GHG and ammonia emissions at the livestock farm level to incorporate emission reduction in decision-making. Although the adoption of farm-scale emission-based DSS in livestock farming is limited, it is clear that farmers who embrace technological developments are aware of the potential environmental impact of their farms. In fact, 87% of respondents expressed interest in being informed about software-based DS tools that estimate and utilize GHG and ammonia emissions in decision-making. Around 60% of stakeholders expressed a willingness to participate in a future consultation process for developing software-based DS tools that estimate and incorporate GHG and ammonia emissions in decision-making. This highlights the need for continued development and promotion of such tools across all participating countries

Keywords: Greenhouse Gas Emissions, Ammonia Emissions, Stakeholders' Opinion, Decision Support Systems, Livestock Farming

1. Introduction

Software-based farm-scale Decision Support Systems (DSSs) centered on greenhouse gas (GHG) emissions, become increasingly important due to the need of the farming systems to reduce their GHG emissions (e.g. Alexandropoulos et al., 2023). Usability, design, and credibility are key factors in maintaining the ongoing use of such DSSs. Recent efforts focused on bridging the gap between farmers' experience and DSS utilization, by developing stakeholder-oriented systems (Lundström & Lindblom, 2018; Krzywoszynska, 2016; Mackrell et al., 2009). Recognizing and leveraging farmers' experience is essential for enhancing agricultural practices towards sustainability (Lundström & Lindblom; Mackrell et al. 2009). Successful farming requires diverse skills encompassing crop production knowledge, financial planning, organizational proficiency, and compliance with compliance with regulations(Mackrell et al. 2009). While cutting-edge agricultural technology offers benefits, there are growing concerns towards science-based intervention principles, known as the 'transfer-of-technology' push, particularly among potential DSS end-users (Mackrell et al. 2009; Kuhlmann and Brodersen, 2001; Lynch and Gregor, 2004).

The active engagement of stakeholders in the evaluation and development phases of agricultural Decision Support Systems (DSSs) has been examined by various studies in the last 20 years (Carberry et al., 2002; Nelson et al., 2002; Van Meensel et al., 2012; Reiter et al., 2019). The participation of farmers (e.g. the use, the development of DSSs etc) and stakeholders was suggested to significantly enhance research outcomes, ensuring that they effectively align with the participants' expectations (Carberry et al., 2002). Adopting a participatory approach aims to overcome the challenges related to the unique cases of decision-makers

(Nelson et al., 2002). Additionally, the involvement of stakeholders in a DSS development process via knowledge exchange between participants and developers, is expected to make this process more efficient (Reed, 2008). A key parameter of the success of the stakeholders' participation is to include suitable stakeholders (e.g. expertise, public accepted, respected) from diverse groups (Voinov and Gaddis, 2008).

Thus, comprehension of the potential users' needs would further be of assistance to the developers of emissions-based decision support tools in order to further improve the existing tools and better meet these needs. This paper aspires to address this objective by using questionnaires tailor-made for various interested parties from the livestock production sector across various European countries and Chile. In this work, the questionnaires and the responses from a quantitative and qualitative point of view will be reported, both at the individual country level and at the cumulative level of all participating partner countries. The results from the responses are collected and briefly discussed and useful conclusions are drawn regarding the willingness of the stakeholders to participate in the process of the improvement of existing emission-based decision support tools.

2. Materials and Methods

The aim of the questionnaires was to collect insights from stakeholders involved in the livestock production sector about the DSSs they currently utilize. We primarily focused on on the use of GHG and ammonia emissions estimation on the decision-making process but also on the needs of the various stakeholder groups to know the size of the GHG and ammonia emissions at the farm level.

Forming simple online questionnaires from the emission-based DSS developer point of view, was considered a comfortable way of extracting information from the stakeholders of interest, as these could be easily translated to different languages and distributed to stakeholders either electronically (via emails) or via short-duration interviews.

The relevant stakeholder groups surveyed included:

- Livestock farmers
- Advisors to livestock farmers
- Authorities / Policy makers
- National Inventory Compilers

The basic principles followed when developing the tailor-made questionnaires were the following:

- Completion of the questionnaire in a short amount of time and development of questionnaires to be answered in maximum 10 minutes to avoid receiving incomplete questionnaires or no questionnaires answered.
- Use of easily comprehensive and direct language, targeting all educational levels (especially when referring to livestock farmers) and avoiding misunderstanding of questions.
- Considering the time limitation, the questions need to perfectly fit the research objectives.
- Using questions which also include other types of farm-scale computer-based DS tools for livestock farm management to differentiate between these tools and the emission-based DS tools of interest.
- Preparation of the relevant questions' list for each stakeholder group.

To develop the questionnaires, previous work found in the scientific literature and targeting stakeholders' behaviour when using decision support systems was used (e.g. Cheung et al., 2016; Howitt & McManus, 2012; Lundström & Lindblom, 2018; Mackrell et al., 2009; N. Georgantzis, 2019; Reiter et al., 2019). Additionally, two tools were employed for visualizing and finalizing the questionnaires:

- Building a questionnaire tree using XMind, a software specifically aiming at the development of decision trees. This facilitated visualizing different answer options and the subsequent questions linked to the respondents' answers.
- Finalizing and testing the questionnaires using Google Forms' templates, which allowed for easy distribution and management of the received responses.

3. Results

3.1. Livestock Farmers

The country with the highest representation of livestock farmers was Greece, accounting for 15 out of 23 responses. The livestock farmers approached and those who responded to the questionnaire appear to belong to a relatively young demographic, mostly 50 years old or younger (Figure 1), with a high level of education. While software-based decision support (DS) tools are familiar to these farmers (Figure 2), only a minority of them actually utilize them, with 6 respondents indicating positive usage (Figure 3). Among those who reported using such tools, half are new users. The most common applications cited for these tools include animal and farm management.

The majority of livestock farmers who use these tools learned about them through other farmers or cooperatives they are associated with, suggesting a level of trust among peers. This reliance on peer endorsement indicates that farmers are unlikely to adopt such tools without first witnessing their benefits demonstrated by colleagues. Improved animal and farm management, particularly for farms with larger livestock populations, emerged as the primary motivation for utilizing DS tools.

Accessibility through devices, PCs, and the internet is the preferred method of accessing these DS tools among respondents. A combination of graphical and textual data presentation is considered most convenient by farmers for receiving and interpreting information output from these tools. The frequency of usage varies depending on the application. Most of the farmers who responded use DS tools on a daily basis.

Interestingly, all farmers using DS tools were aware of the greenhouse gas (GHG) and ammonia emissions from their farms, yet none reported using these tools to estimate such emissions. The lack of emission estimation features in DS tools, despite their technological advancement, is not surprising and seems to be common among respondents from all countries. However, the majority of respondents expressed interest in learning about and actively participating in the development of software-based DS tools that can estimate GHG and ammonia emissions at the farm level, if properly informed and invited (Figure 4).

Furthermore, reasons for not adopting software-based DS tools include cost constraints, perceived lack of benefits, and the elevated time requirements associated with their use.

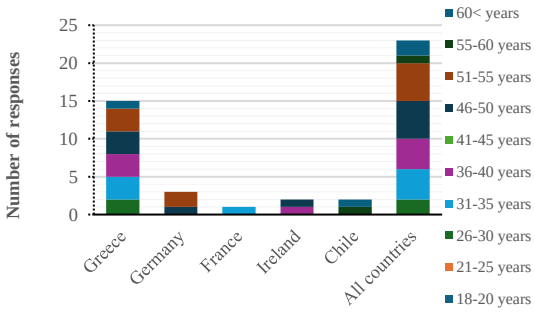

Figure 1. Groups of ages of the livestock farmers that responded to the questionnaire.

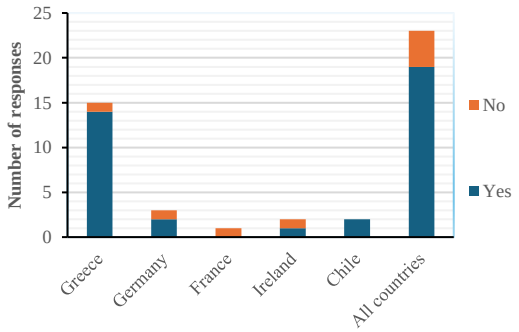

Figure 2. Awareness of the livestock farmers on software-based decision support tools for more efficient farm management.

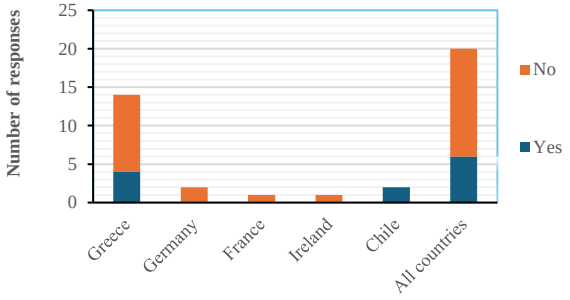

Figure 3. Use of software-based decision support tools for farm management by the livestock farmers.

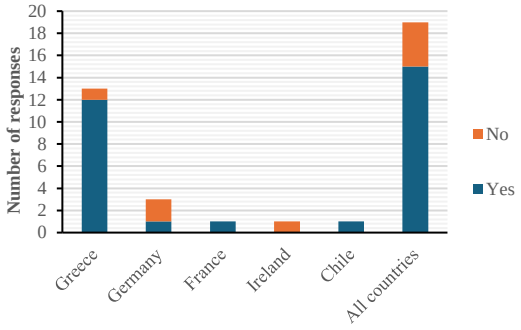

Figure 4. Interest of the livestock farmers in getting actively involved in the consultation process during the development of a software-based DS tool that estimates GHG and ammonia emissions at the farm level.

3.2. Farmer's Advisors

Livestock farmers' advisors constitute the largest group of respondents in the surveys conducted for this deliverable. Polish advisors participated the most, accounting for 58 out of 72 responses. The majority of respondents were aged over 26 (Figure 5) and possessed a high level of education, which not surprising given the required skills for this profession. Most advisors (68 out of 72 responses) were aware of software-based Decision Support (DS) tools for enhancing livestock farm management efficiency (Figure 6). However, less than half of them (27 out of 68) currently utilize such tools for providing advice (Figure 7), indicating a prevalent lack of trust among advisors regarding the DS tools' usefulness and efficiency.

Additionally, it was observed that 40% of respondents offer advice across diverse farming systems, including variations in size, livestock numbers, and production methods (conventional vs. organic). Furthermore, the majority of DS tool users have employed them for advising farmers for five years or less, suggesting recent widespread adoption of marketing and promotion efforts targeting livestock farmers' advisors.

The most common applications of software-based DS tools among respondents were financial management, nutrient management and fertilization, farm management, and animal management. Conversely, tools for emission and sustainability assessment were utilized by only a small fraction of respondents.

The decision to adopt DS tools was primarily motivated by factors such as work facilitation, necessity, and enhanced data recording. Improving environmental performance emerged as a key focus area for advisors, although only a minority use tools specifically designed for emission and sustainability assessment. Nevertheless, more than half of DS tool users provide advice on greenhouse gas and ammonia emissions to livestock farmers.

The majority of livestock farmers' advisors use DS tools infrequently, preferably receiving information output in a combination of text and graphical formats. They express interest in accessing such tools via the internet and personal computers. Additionally, nearly 85% of respondents are keen to learn more about DS tools estimating GHG and ammonia emissions at the farm level.

Around half of the advisors expressed interest in actively participating in the development of DS tools for estimating GHG and ammonia emissions, particularly if informed and invited (Figure 8). However, reasons for not participating include lack of time and expertise.

Finally, reasons for not using DS tools related to GHG and ammonia emissions include lack of awareness about their existence or the emissions from livestock farming, as well as the perception that such tools are not beneficial.

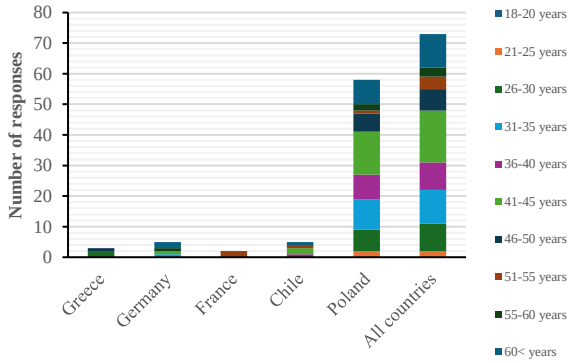

Figure 5. Groups of ages of the livestock farmers' advisors that responded to the questionnaire.

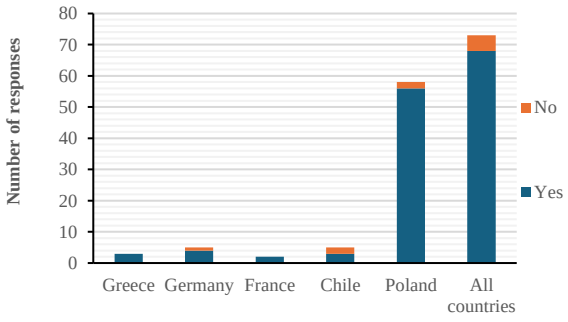

Figure 6. Awareness of the farmers' advisors on software-based decision support tools for more efficient farm management.

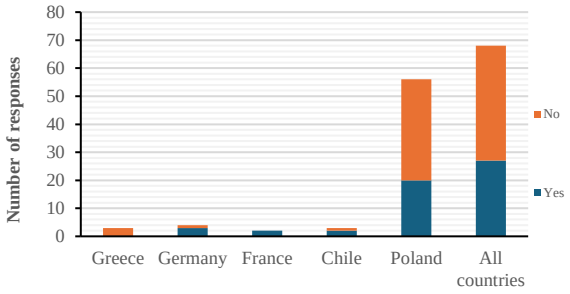

Figure 7. Use of software-based decision support tools for farm management by the livestock farmers' advisors.

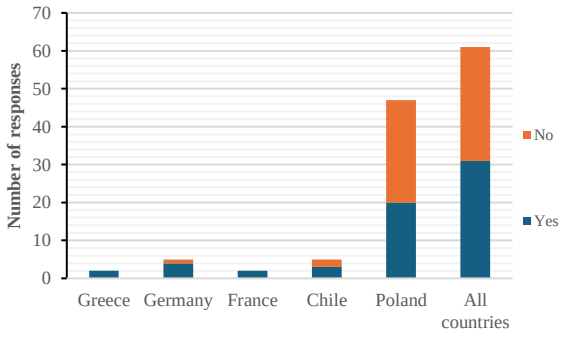

Figure 8. Interest of the livestock farmers' advisors in getting actively involved in the consultation process during the development of a software-based DS tool that estimates GHG and ammonia emissions at the farm level.

3.3. Inventory compilers

The second lowest response number was recorded from national inventory compilers, totalling 9 responses overall. Germany and Austria emerged as the most represented countries with 5 respondents each. The vast majority of these compilers (8 out of 9) expressed unawareness of software-based DS tools designed to enhance inventory compilation efficiency (Figure 9). This indicates a current lack of popularity for such tools among the responding inventory compilers. Even among those aware of these tools, none utilized them for compiling livestock farm emissions inventories. However, all respondents expressed interest in learning about software-based DS tools estimating GHG and ammonia emissions at the farm level.

Presently, the majority of inventory compilers (7 responses) are primarily engaged in compiling GHG emission inventories, while work on ammonia, nitrogen oxides, particulate matter, and NMVOCs inventories is deemed of lower priority. It follows logically that none of the respondents use software-based decision support tools for estimating greenhouse gas and ammonia emissions from livestock farming. Most respondents believe that livestock farmers are uninformed about the GHG and ammonia emissions from their farms. However, an equal number (6 responses) also stated that livestock farmers receive national-scale advice on reducing GHG emissions from their farms (Figure 10).

Approximately half of the respondents indicated the existence of national-scale regulations forcing livestock farmers to reduce farm-scale greenhouse gas and ammonia emissions, with all these respondents originating from European Union member states (Figure 11). Likewise, the same number reported the presence of national-level incentives for livestock farmers to reduce their farm-scale greenhouse gas and ammonia emissions, all from EU member states.

Moreover, the majority of inventory compilers (6 out of 9) expressed interest in participating in further research projects focused on country-specific emission factor development for the broader Agricultural Sector. They also indicated willingness to be actively involved in a consultation process during the

development of software-based DS tools estimating GHG and ammonia emissions at the farm level (Figure 12). However, a smaller proportion would be available to participate in such a consultation process, especially if it commenced in 2022, primarily due to time constraints.

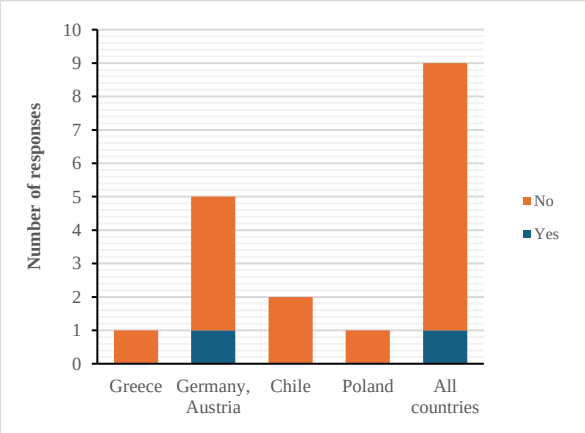

Figure 9. Awareness of national inventory compilers on software-based decision support tools for more efficient farm management.

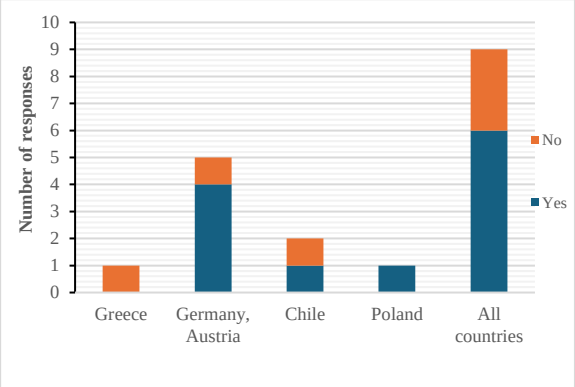

Figure 10. Responses of national inventory compilers regarding their opinions on whether livestock farmers are provided advice at the national scale for the reduction of greenhouse gas emissions from their farms.

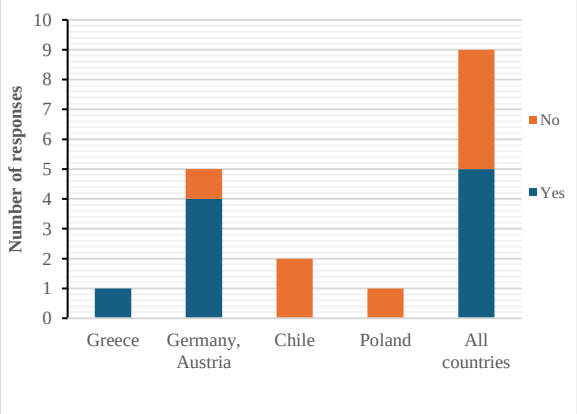

Figure 11. Responses of national inventory compilers regarding the existing regulations at the national scale forcing livestock farmers to reduce greenhouse gas emissions from their farms.

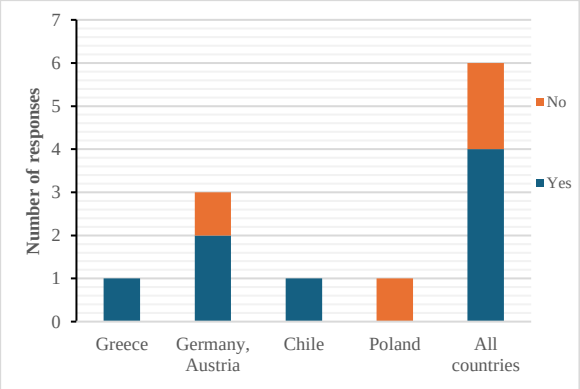

Figure 12. Availability of national inventory compilers for participating in a consultation process for the development of a DS tool which considers GHG and ammonia emissions at the farm-level in the decision-making.

3.4. Authorities / Policy makers

The lowest number of responses was received by the wider group of authority officials and policy makers (4 responses in total). Most of the responses came from Chile (3 out of 4). None of the respondents was aware of existing software-based DS tools for more efficient management of livestock farms. However, all of them would be interested in getting informed about software-based DS tools that estimate GHG and ammonia emissions at the livestock farm level and all of them would further be interested in getting actively involved in the consultation process during the development of a software-based decision support tool (livestock farm scale) which estimates GHG emissions. Finally, all of them would be willing to participate in such consultation initiatives in case they are informed and invited.

4. Discussion

Livestock farmers' advisors constituted the largest respondent group (73 out of 109 responses), followed by livestock farmers (23 respondents), inventory compilers (9 respondents), and authority officials/policy makers (4 respondents). Notably, nearly half of the respondents (58 out of 105) were livestock farmers'

advisors from Poland, reflecting a significant representation of Polish advisors' perspectives in the collected data. Greek livestock farmers predominated within the livestock farmers' stakeholder group (15 out of 23 responses), while national inventory compilers from Germany and Austria were prominent within their category (5 out of 9 responses), and policy makers/authority officials from Chile represented their respective group (3 out of 4 responses).

It's worth noting that the directly involved stakeholder groups, particularly livestock farmers and advisors, tend to have higher levels of education. This suggests an increased likelihood of interest in exploring and testing emerging technologies such as software-based decision support tools for enhancing farm management practices.

A majority of respondents (88 out of 109) were aware of software-based decision support tools. However, the actual users of such tools comprised less than half of those aware of their existence (33 out of 88 responses). Even fewer respondents reported using software-based tools specifically for estimating GHG and ammonia emissions at the farm level for integration into decision-making processes (5 out of 33 responses, all from livestock farmers' advisors in various participating countries). Nonetheless, livestock farmers' advisors, who play a crucial role in advising on emission reduction strategies, expressed a high level of concern regarding improving the environmental performance of livestock farms, despite not being able to precisely estimate emissions.

Regarding awareness of emissions among stakeholders, most livestock farmers' advisors believed that livestock farmers are aware of GHG and ammonia emissions from their farms, whereas most inventory compilers reported the opposite. However, it can be inferred that farmers already using decision support tools are more likely aware of their farms' environmental impact.

Most national inventory compilers from EU member states reported the existence of national-scale regulations mandating livestock farmers to reduce greenhouse gas and ammonia emissions, along with incentives and advice provided at the national level for this purpose.

Importantly, around 87% of responding stakeholders expressed interest in being informed about software-based decision support tools that estimate and utilize GHG and ammonia emissions in decision-making processes. Moreover, approximately 60% of these stakeholders expressed willingness to actively participate in the consultation process during the development of such tools, provided they are informed and invited.

5. Conclusions

This work aimed to understand the views and needs of potential users regarding software tools for estimating and reducing greenhouse gas (GHG) and ammonia emissions in their decision-making processes. Specifically, four stakeholder groups were targeted: livestock farmers, livestock farmers' advisors, national inventory compilers, and authority officials/policy makers. Each group received a tailored questionnaire.

The findings highlighted the need for further development and promotion of software-based decision support tools that estimate and utilize GHG and ammonia emissions in decision-making processes across all participating countries in the survey. Such efforts would be particularly beneficial for all stakeholder groups involved.

References

Alexandropoulos E, Anestis V, Dragoni F, Hansen A, Cummins S, O'Brien D, Amon B, Bartzanas T. Decision Support Systems Based on Gaseous Emissions and Their Impact on the Sustainability Assessment at the Livestock Farm Level: An Evaluation from the User's Side. *Sustainability*. 2023; 15(17):13041. https://doi.org/10.3390/su151713041

Carberry, P.S.; Hochman, Z.; Mccown, R.L.; Dalgliesh, N.P.; Foale, M.A.; Poulton, P.L.; Hargreaves, J.N.G.; Hargreaves, D.M.G.; Cawthray, S.; Hillcoat, N.; et al, 2002 The FARMSCAPE Approach to Decision Support: Farmers', Advisers', Researchers' Monitoring, Simulation, Communication and Performance Evaluation;; Vol. 74. https://doi.org/10.1016/S0308-521X(02)00025-2

Cheung, K. L., Evers, S. M. A. A., Hiligsmann, M., Vokó, Z., Pokhrel, S., Jones, T., Muñoz, C., Wolfenstetter, S. B., Józwiak-Hagymásy, J., & de Vries, H. , 2016. Understanding the stakeholders' intention to use economic decision-support tools: A cross-sectional study with the tobacco return on investment tool. Health Policy, 120(1), 46–54. https://doi.org/10.1016/j.healthpol.2015.11.004

Georgantzis, N., Tisserand, JC and Akaka, J.. , 2019. Stakeholders behavior regarding the use of Decision Support Systems. A preliminary picture from WP5 data and WP6 workshops on IPM Decisions. Horizon 2020.

Howitt, M., & McManus, J., 2012. Stakeholder Management: An instrument for decision making. Management Services, 56(3), 29–34.

Krzywoszynska, A., 2016. What Farmers Know: Experiential Knowledge and Care in Vine Growing. Sociol Ruralis. 56, 289–310, doi:10.1111/soru.12084

Kuhlmann, F.; Brodersen, C., 2001. Information Technology and Farm Management: Developments and Perspectives; Vol. 30.

Lundström, C., Lindblom, J., 2018. Considering Farmers' Situated Knowledge of Using Agricultural Decision Support Systems (AgriDSS) to Foster Farming Practices: The Case of CropSAT. Agric Syst, 159, 9–20, https://doi.org/10.1016/j.agsy.2017.10.004

Lynch, T., Gregor, S., 2004. User Participation in Decision Support Systems Development: Influencing System Outcomes. European Journal of Information Systems, 13, 286–301. https://doi.org/10.1057/palgrave.ejis.3000512

Mackrell, D., Kerr, D., & von Hellens, L. 2009. A qualitative case study of the adoption and use of an agricultural decision support system in the Australian cotton industry: The socio-technical view. Decision Support Systems, 47(2), 143–153. https://doi.org/10.1016/j.dss.2009.02.004

Nelson, R.A.; Holzworth, D.P., Hammer, G.L., Hayman, P.T., 2002. Infusing the Use of Seasonal Climate Forecasting into Crop Management Practice in North East Australia Using Discussion Support SoftwareVol. 74. https://doi.org/10.1016/S0308-521X(02)00047-1

Get rights and content.

Reed, M.S., 2008. Stakeholder Participation for Environmental Management: A Literature Review. Biol Conserv, 141, 2417–2431. https://doi.org/10.1016/j.biocon.2008.07.014

Reiter, D., Meyer, W., & Parrott, L., 2019. Stakeholder engagement with environmental decision support systems: The perspective of end users. Canadian Geographer. https://doi.org/10.1111/cag.12555

Van Meensel, J., Lauwers, L., Kempen, I., Dessein, J., Van Huylenbroeck, G., 2012. Effect of a Participatory Approach on the Successful Development of Agricultural Decision Support Systems: The Case of Pigs2win. Decis Support Syst, 54, 164–172. https://doi.org/10.1016/j.dss.2012.05.002

Voinov, A., Gaddis, E.J.B., 2008. Lessons for Successful Participatory Watershed Modeling: A Perspective from Modeling Practitioners. Ecol Modell, 216, 197–207. https://doi.org/10.1016/j.ecolmodel.2008.03.010

Development and deployment of a decision support tool for gas emissions at the dairy farm level: Analysis of two case studies for dairy farms

Evangelos Alexandropoulos [a,*], Vasileios Anestis [a], Thomas Bartzanas [a]

[a] Department of Natural Resources Development and Agricultural Engineering, Agricultural University of Athens, Athens, Greece

* Corresponding author. Email: vagalexandr1991@aua.gr

Abstract

To meet national and global air quality and climate change policies, it is essential to equip the agricultural sector with farm-level decision support tools for gaseous emissions. Developing these tools presents a significant challenge, as their reliability must be ensured through the incorporation of the latest methodologies and calibration using precise case study data. To address this issue, the authors modified and updated a previous version of a tool designed to estimate greenhouse gas emissions, and ammonia emissions. This resulted in the development of a Prototype Livestock Farm-scale Gas Emission-based Decision Support Tool (PDST). The tool's modification includes the integration of the most up-to-date estimation methodologies, such as IPCC, EMEP/EEA, UNECE, and ASAE. To assess its efficacy, both the PDST and the older version were used for one commercial farm in Greece and in Poland. Both case studies refer to intensive systems, with deep litter housing and dunghill manure storage. To demonstrate the differences between the PDST and the older version, two scenarios were defined for each case study. The first scenario includes the older version with the already embedded agroecological zone data, while the second scenario uses the PDST with specific climate data from Greece and Poland. The use of the PDST resulted in a reduction in annual emissions per kg of raw milk produced. This was due to the modifications made to gas emission estimation methodologies, such as the estimation of volatile solids, various emission factor (EF) values (e.g. ammonia EF for housing and ammonia and nitrous oxide EF for external manure storage), the methane conversion factor, as well as other parameter values, such as feedstuff, livestock breeds, and external manure storage types. The PDST shows promising potential for providing gas emission estimates from dairy farms in Greece and Poland, according to the latest emission inventory methodologies.

Keywords: Greenhouse Gas Emissions, Ammonia emissions, Farm-scale, Prototype Tool Development, Dairy Cattle Farming

1. Introduction

The livestock sector is a major contributor to global greenhouse gas (GHG) emissions (Hörtenhuber et al., 2022). These emissions include the direct release of carbon dioxide (CO_2), methane (CH_4), and nitrous oxide (N_2O), as well as the indirect N_2O emissions after the conversion of ammonia (NH_3) and different nitrogen (N) compounds (Rotz et al., 2018). Several production activities on a farm have the potential to generate greenhouse gas emissions. Feeding practices and feed digestion as well as animal housing, manure handling (removal, storage and field application) and soil management practices all drive these emissions (Rotz et al., 2018).

Assessment and reduction of the GHG emissions from livestock farming is crucial for addressing global climate change (Kipling et al., 2021). Quantification of GHG emissions is facilitated through the use of computer-based decision support (DS) tools (Rotz et al., 2018), which must yield dependable results for effective action. The effectiveness of these tools hinges on incorporating the latest emission estimation methodologies and relevant parameter values to ensure reliable emission estimates (Rose, 2018).

A Prototype Decision Support Tool (PDST), based on the FarmAC v.1.8 model (FarmAC, 2024), was launched to address the need for a comprehensive farm-level DSS that incorporates cutting-edge methodologies for compiling gas emission inventories. The PDST improves upon its predecessor by offering refined estimates of GHG and other nitrogenous emissions, such as NH_3 and nitrogen oxides (NO_x), at the farm level.

The objective of this paper is to present the validation procedure of the PDST, by employing data collected from two commercial, intensive dairy cattle farming systems (one located in Greece and one in Poland) and comparing the PDST's direct and indirect GHG emission outputs for these systems with the corresponding

outputs of its predecessor but also with findings from the existing literature for similar dairy cattle production systems.

2. Materials and Methods

2.1. Modifications to the code

The PDST builds upon the C# code of FarmAC v1.8 model (FarmAC, 2024), incorporating adjustments tailored to dairy cattle farming systems. These enhancements are related to the integration of the most recent guidelines for inventory compilation, as established by the Intergovernmental Panel on Climate Change (IPCC) (IPCC, 2019) and the European Monitoring and Evaluation Programme (EMEP) of the European Environment Agency (EEA) (EMEP/EEA, 2023), as well as information from guidance documents (UNECE, 2015) and other standards (ASAE, 2005).

Revisions in the FarmAC algorithmic architecture include:

- Tailoring of existing agroecological zones to also reflect the Hellenic and Polish climatic conditions. The climate data related to Greece and Poland were retrieved from the CEDA archive Database (CEDA, 2023), following the recommendations of IPCC (2019).
- Adjusting the empirical models and underlying algorithms used for refined emission estimation.
- Integration of additional parameters, such as feed types and livestock breeds.

Advancements in the PDST's coding framework were executed in two stages:

- A thorough audit of the default systemic values and parameters encoded within the FarmAC framework.
- Modification of empirical models and computational algorithms for emission estimation regarding volatile solids and enteric methane emissions from cattle.

2.2. Integration of case studies

Data were collected from two commercial, intensive dairy cattle systems, one in Greece and one in Poland, using templates for environmental impact assessment via Life Cycle Analysis (LCA). Only livestock-related inputs were necessary to run the tools for the Greek case study, while both livestock and crop-related inputs were necessary for the Polish case study. The Greek case study involves data collected in December 2021, while the Polish case study in November 2021. Additionally, projects such as Feedipedia (Feedipedia, 2023) and Feed Tables (Feed Tables, 2023) were consulted to determine the dry matter content per feed component. Furthermore, in the Polish case study, the daily nitrogen excretion per animal (ASAE, 2005) was utilized to estimate the amount of nitrogen in the cattle manure applied per hectare as organic fertilizer, after having subtracted the nitrogen emission flows at the cattle housing and manure storage stages. The total nitrogen application per hectare was estimated after having considered the synthetic fertilizer's NPK content.

To apply the PDST to these cattle production systems, a two-step approach was employed for utilizing the collected data:

- Initially, baseline estimates for GHG and NH_3 emissions were derived using the FarmAC model and the data collected.
- Subsequently, to refine the PDST output, additional agroecological zones were developed to integrate climate data for Greece and Poland, as well as refined emission factors and other parameters.

Additionally, to compute energy-corrected milk (ECM) and fat/protein-corrected milk (FPCM) (Mc Geough et al., 2012; Gislon et al, 2020), Eq. (1) and (2) were utilized:

$$ECM = (0.25 \times Total\ Milk\ Production) + (12.2 \times Total\ Milk\ Fat\ Production) + (7.7 \times Total\ Milk\ Protein\ Production) \quad (1)$$

$$FPCM = Total\ Milk\ Production \times ((0.1266 \times Total\ Milk\ Fat\ Production) + (0.0776 \times Total\ Milk\ Protein\ Production) + 0.2534) \quad (2)$$

ECM and FPCM were computed to compare the emission results of the present study with relevant scientific literature results.

An allocation factor was applied to distribute the emissions to milk production, as the dairy cattle farms produced both raw milk and cattle live-weight, according to Eq. (3) (IDF, 2015).

$$Milk\ Allocation\ Factor = 1 - 6.04 * (total\ kg\ of\ live\ weight\ sold\ per\ year / total\ kg\ of\ FCPM\ produced\ per\ year) \quad (3)$$

3. Results and Discussion

3.1. Inputs

The inputs utilized for scenario definition in both FarmAC and the PDST can be categorized as:

- Livestock-related: number of animals, breed (e.g., Holstein, Jersey), growth stage (e.g., calves, heifers, dairy cows, young bulls), feed types and dry matter content of ration (kg), housing type, and manure storage type.
- Climate-related: selection of the agroecological zone corresponding to the country of interest.
- Crop-related: soil type, start and end date of crop production, area surface (ha), irrigation development (yes/no), and yield of each cultivated crop (kg).
- Fertilizers: type and amount (kg) of fertilizer, nitrogen applied per hectare (kg), application method.

3.1.1. Polish case study

In Tables 1 and 2, the livestock-related and crop-related inputs of the Polish dairy farm are shown, respectively. The total farm size is 90ha. It covers 80ha of utilized agricultural land, along with an additional hectare designated as woodland. 38% of this agricultural land is used for fodder production. Various crops are also cultivated such as maize, rye, oats, barley, meadows, and alfalfa. The herd size is based on the average daily number of animals (Holstein dairy cattle). In 2021, the farm produced a total of 432,000 litres of milk (8,640 litres per cow on average). The cattle live-weight production is minimal, as the young bulls (n=20) are sold at a low average weight (50 kg), while the cull cows (n=5) at 650kg. The allocation factor to raw milk was estimated to be 0.94.

Table 1. Livestock-related inputs (dairy cows) in the Polish case study.

Cattle sub-category / Size (heads)	Diet component / Dry matter (kg / day)	Housing type	External manure storage type
Dairy cows (lactating) / 50	Maize silage / 9.74 Grass silage / 5.39 DDGS (wheat and corn) / 1.35 Molasses/ 0.26 Vitamins / 0.35	Deep litter	Dunghill, no cover
Heifers and dairy cows (dry) / 4	Maize silage / 2.19 DDGS (wheat and corn) / 0.45 Sugar pulp / 0.44 Grass hay / 0.91	Deep litter	Dunghill, no cover

Table 2. Crop-related inputs for the Polish case study.

Crop	Duration of cultivation (days)	Soil type	Area (ha)	Irrigation	Fertilizer type	Applied N (kg/ha)	Application method	Yield (kg)
Maize	161	Clay Loam	65	No	Solid manure	3298.37	Spreading	65000
					Urine	5497.28	Spraying	
					Urea	207	Spreading	
Rye	91	Clay Loam	4	Yes	Ammonium nitrate	67	Spreading	6000
					Urea	92	Spreading	
Winter Barley	71	Clay Loam	6	No	-	-	-	4000

Oats	184	Clay Loam	6	No	-	-	-	4000
Grass - alfalfa	Permanent cultivation	Clay Loam	12	No	Superphosphate	0	Spreading	19000
Grass	Permanent cultivation	Clay Loam	47.5	No	Solid manure	1649.19	Spreading	22500

3.1.2. Greek case study

Table 3 includes information about the livestock-related inputs of the Greek case study. The dairy enterprise occupies 0.6ha of the total farm area. As in the Polish case study, the herd size reflects the average number of cattle present daily. In 2021, the farm achieved a milk yield of 3,094,000 litres, averaging 8,840 litres per cow. In addition, the farm sold an important quantity of cattle live-weight, including 60 cull cows (650kg each), 7 bulls in mature weight (850kg each), 75 young bulls (450kg each) and 20 male calves (50kg each). The allocation factor to raw milk was estimated to be 0.86.

Table 3. Livestock-related inputs (dairy cows) in the Greek case study.

Cattle sub-category / Size (heads)	Diet component / Dry matter (kg / day)	Housing type	External manure storage type
Dairy cows (lactating) / 350	Maize grain, dried, conventional / 5.67 Soybean meal 48, transformed in Europe / 3.39 Regulator, balancer / 0.29 Sodium chloride / 0.11 Calcium carbonate (<63µm) / 0.11 Alfalfa hay, conventional / 0.89 Oat hay / 0.89 Maize silage, conventional / 3.25	Deep litter	Dunghill, no cover
Dairy cows (dry) (2 months)) / 10	Maize grain, dried, conventional / 1.55 Soybean meal 48, transformed in Europe / 0.53 Regulator, balancer / 0.21 Sodium chloride / 0,03 Calcium carbonate (<63µm) / 0.03 Alfalfa hay, conventional / 0.89 Oat hay / 0.89 Maize silage, conventional / 3.25	Deep litter	Dunghill, no cover

3.2. Product and emission outputs

In Table 4, the annual milk production (kg) as well as the estimated annual ECM (kg) and FPCM (kg) for the Polish and Greek dairy cattle farms (PDCF and GDCF) are shown.

Table 4. Annual milk production (kg) of the two dairy cattle farms (Greek and Polish).

Dairy cattle farming system	Milk production	Energy corrected milk (ECM)	Fat and Protein corrected milk (FPCM)
PDCF	432,000	439,269.83	446,446.08
GDCF	3,094,000	3,332,374.53	3,387,001.8

Table 5 shows a reduction in all direct and indirect GHG emissions from the various sources when comparing the PDST with its predecessor and for both the PDCF and the GDCF, except for the direct CH_4 emissions from the PDCF where the PDCF showed a higher value. Total on-farm GHG emissions encompass combined direct and indirect emissions from both livestock and crop production. However, to facilitate the comparison between the emissions from the PDCF and the GDCF and the literature, livestock-related emissions (including direct enteric CH_4, direct CH_4 from manure, direct N_2O from manure, indirect N_2O due

to NH_3 from housing and indirect N_2O due to NH_3 from manure) were separately presented.

Table 5. Product and emission outputs of the two dairy cattle farms (Greek and Polish) as provided by the PDST and its predecessor.

Annual product (kg) and GHG emissions (tn CO_2eq)	**PDCF - CAEZ[1]**	**PDCF - PAEZ[2]**	**GDCF - MAEZ[3]**	**GDCF - GAEZ[4]**
Direct enteric CH_4	193.23	198.12	1191.68	1158.66
Direct CH_4 from manure (housing and storage)	34.9	71.6	619.44	500.26
Direct N_2O from manure (housing and storage)	142.31	102.57	3282.82	957.15
Direct N_2O from field application of synthetic fertilizers and manure	1066.6	710.41		
Direct CO_2 from crop fields	18.03	18.03		
Change in C stored in soil	-480.1	-304.35		
Total direct GHG emissions	974.91	796.38	5093.93	2616.07
Indirect N_2O, due to NH_3 from housing	33.79	13.71	852.71	133.8
Indirect N_2O, due to NH_3 from manure storage	135.28	25.1	3411.99	244.29
Indirect N_2O, due to NH_3 from field application of manure	18.06	12.93		
Indirect N_2O, due to NH_3 from field application of synthetic fertilizers	12.11	5.7		
Indirect N_2O, due to N leaching	425.72	405.47		
Total indirect GHG emissions	624.95	462.9	4264.69	378.09
Total farm-level GHG emissions (direct + indirect) allocated to raw milk	1535.87	1183.72	8048.42	2574.98
Total livestock-related GHG emissions (direct + indirect) allocated to raw milk	507.14	386.3	8048.42	2574.98
Farm-level GHG emissions (kg CO_2eq/kg raw milk (ECM; FPCM))	3.5; 3.44	2.7; 2.6	2.42; 2.38	0.77; 0.76
Livestock-related GHG emissions (kg CO_2eq/kg raw milk (ECM; FPCM))	1.16; 1.14	0.88; 0.8	2.42; 2.38	0.77; 0.76

[1]Polish Dairy Cattle Farm – Continental Agroecological Zone, as implemented in the FarmAC v.1.8 model; [2]Polish Dairy Cattle Farm – Polish Agroecological Zone, as implemented in the PDST; [3]Greek Dairy Cattle Farm – Mediterranean Agroecological Zone, as implemented in the FarmAC v.1.8 model; [4]Greek Dairy Cattle Farm – Greek Agroecological Zone, as implemented in the PDST.

The effects on the estimated GHG emissions noticed in Table 5 were based on the implemented modifications:

- CH_4 from enteric fermentation: It was estimated using the IPCC Tier 2 methodology, with the predecessor tool considering a global warming potential (GWP100) for biogenic CH_4 equal to 37.3 kg CO_2eq/kg, while the PDST equal to 27.2 kg CO_2eq/kg (Foster et al., 2021).
- CH_4 from manure (housing and storage): The use of the PDST shows lower emissions in the GDCF and higher emissions in the PDCF due to changes in carbon flows' estimation methods. Additionally, the methane conversion factor (MCF) was increased from 0.02 to 0.21 (deep bedding >1 month) and from 0.04 to 0.225 (deep bedding >1 month and solid storage, for similar duration) for the Polish and Greek case studies, respectively, since the climate parameters in the PDST were updated considering both in-house and external manure storage for both PDCF and GDCF.
- Direct N_2O from manure (housing and storage): It was lower in the PDST even if the emission factor of N_2O doubled (0.005 to 0.01 kg N_2O-N / kg Nitrogen excreted), and the GWP100 of N_2O decreased (from 416.4 to 273 kg CO_2eq/kg).
- Direct N_2O from field application: Discrepancies arise from different climate data in the two tool versions and the modification in the GWP100 of N_2O.
- Indirect N_2O due to NH_3 from housing: The differences between the tool versions, can be explained by the increased housing emission factor for NH_3 (from 0.12 to 0.16 kg NH_3-N/kg ammonium in housing) and the decrease in the GWP100 of N_2O.
- Indirect N_2O due to NH_3 from manure storage: The lower value in the PDST is attributed to a decrease in the emission factor value for manure storage (from 0.544 to 0.32 kg NH_3-N/kg ammonium in storage) and the decrease in the GWP100 of N_2O.

- Indirect N_2O after field application of fertilizers: This variation results from the change in the emission factor of leached NO_3-N (from 0.0075 to 0.0112 kg N_2O-N emitted/kg NH_3-N emitted) and the decrease in the GWP100 of N_2O.

It is important to note that in the PDST the estimation of CH_4 emissions from manure management conforms to the updated IPCC guidelines (e.g. MCF integration for the existing manure management systems, revised emission factors for both direct and indirect GHG emissions), whereas its predecessor calculated manure carbon flows, based on degradable, non-degradable and humic carbon. Moreover, in the previous version of the tool, carbon degradation and organic nitrogen degradation of manure were interconnected.

3.3. Use of literature findings to confirm the PDST's efficiency

For GDCF system, the old version and PDST yielded 2.42 and 0.77 kg CO_2eq/kg of ECM and 2.38 and 0.76 kg CO_2eq/kg of FPCM, respectively. Both sets of values are deemed valid in the context of the Greek case study, with the PDST aligning more closely with literature ranges for similar farming systems.

For the PDCF, the old version and the PDST generated 3.5 and 2.7 kg CO_2-eq/kg of ECM and 3.44 and 2.65 kg CO_2eq/kg of FPCM, respectively. Excluding crop-related GHG emissions, livestock emissions were 1.16 and 0.88 kg CO_2eq/kg of ECM and 1.14 and 0.87 CO_2eq/kg of FPCM, respectively. Although the results for the PDCF were higher than for the GDCF, they also fall within the range of literature results, with the PDST again yielding results closer to the literature findings for similar systems.

Various studies highlighted emission values for non-pasture scenarios, aligning with this study's context. For instance, a Danish study (Kristensen et al., 2011) reported emissions ranging from 0.97 to 1.56 kg CO_2eq/kg ECM for conventional farms (with 0-23% pasture), while on-farm emissions excluding fossil fuels ranged from 0.73 to 1.03 kg CO_2-eq/kg ECM. Similarly, a non-grazing farm in Quebec, Canada (Mc Geough et al., 2012), found on-farm GHG emissions of 0.92 kg CO_2eq/kg FPCM, with direct livestock-related emissions (enteric CH_4, manure CH_4, manure N_2O) totalling 0.59 kg CO_2eq/kg FPCM. In another LCA study encompassing Danish, German, and Italian farms (Guerci et al., 2013), non-grazing farms exhibited emissions ranging from 1.11 to 1.91 kg CO_2eq/kg ECM, with livestock-related emissions ranging from 0.89 to 1.64 kg CO_2eq/kg ECM. Additionally, Hagemann et al. (2011) found that a forage-based farm in Germany emitted 1.19 kg CO_2eq/kg ECM, with livestock-related emissions totalling 0.833 kg CO_2eq/kg ECM.

Overall, a range of GHG emissions for non-grazing farms, spanning from 0.59 to 2.35 kg CO_2eq/kg ECM is provided in the available literature.

3.4. Future improvements

Instead of relying on the already available mean values for each agro-ecological zone, the PDST could be further customized by incorporating specific climate, livestock, feeding, manure management, housing, crop, and fertilizer data from individual countries. This approach would enhance the quality of the results of the PDST and the relevance to local conditions. In an updated version of the PDST, an advisory module could be integrated, providing targeted emission mitigation options related to cattle housing and manure management. While the tool currently uses extensive parameters and functions for managing diverse data, the trajectory for decision support tools is trending towards simplification without sacrificing reliability (Rotz, 2018). Consequently, the PDST's future development should prioritize a user-friendly interface to enhance its appeal and facilitate broader adoption.

4. Conclusions

This study examines the development and validation of a prototype decision support tool (PDST) for on-farm GHG emissions' assessment, based on the latest version of the FarmAC model and integrating real data from two dairy cattle farms in different countries (Poland and Greece). The PDST incorporates parameters such as emission factors and climate data and the latest emissions estimation methodologies. The input data were reviewed and adjusted to align with the producers' reported production levels and ensure balanced cattle growth. The estimated GHG emission values of both case studies agreed with findings from existing literature for similar farming systems. The PDST exhibited in general lower emission values than its predecessor for both farms due to modifications in the estimation methods of GHG emissions from manure management and enteric fermentation and the use of updated climate data and adjusted livestock and feed parameters. The agreement of the derived GHG emission results with the international literature and the fact that their deviation from the previous version of the tool is explainable suggest that the PDST is valid for estimating gaseous emissions at the level of the dairy cattle farm, enhancing its practical application for stakeholders in

Poland and Greece.

References

ASAE. 2005. Manure Production and Characteristics American Society of Agricultural Engineers.

CEDA. 2023. CRU CY4.05: Climatic Research Unit Year-by-Year Variation of Selected Climate Variables by Country Version 4.05 (Jan. 1901 - Dec. 2020); Available online: https://catalogue.ceda.ac.uk/uuid/7a5529a8758041eb83b9c32f8461e50d (accessed on 10 December 2023)

EMEP/EEA. 2023. Air Pollutant Emission Inventory Guidebook 2023. Technical Guidance to Prepare National Emission Inventories

Gislon, G.; Bava, L.; Colombini, S.; Zucali, M.; Crovetto, G.M.; Sandrucci, A. 2020. Looking for High-Production and Sustainable Diets for Lactating Cows: A Survey in Italy. J Dairy Sci, 103, 4863–4873, doi:10.3168/jds.2019-17177

Guerci, M., Knudsen, M.T., Bava, L., Zucali, M., Schönbach, P., Kristensen, T. Parameters. 2013. Affecting the Environmental Impact of a Range of Dairy Farming Systems in Denmark, Germany and Italy. Journal of Clean Production, 54, 133–141. doi:10.1016/j.jclepro.2013.04.035.

Hagemann, M., Hemme, T., Ndambi, A., Alqaisi, O., Sultana, M.N. 2011. Benchmarking of Greenhouse Gas Emissions of Bovine Milk Production Systems for 38 Countries. Animal Feed Science Technology, 166–167, 46–58, doi:10.1016/j.anifeedsci.2011.04.002.

Hörtenhuber, S.J.; Seiringer, M.; Theurl, M.C.; Größbacher, V.; Piringer, G.; Kral, I.; Zollitsch, W.J. 2022. Implementing an Appropriate Metric for the Assessment of Greenhouse Gas Emissions from Livestock Production: A National Case Study. Animal, 16(10). doi:10.1016/j.animal.2022.100638

Feedtables. 2023. Available online: https://www.feedtables.com (accessed on 10 December 2023).

Feedipedia. 2023. Available online: https://www.feedipedia.org/ (accessed on 10 December 2023).

Forster, P., T. Storelvmo, K. Armour, W. Collins, J. L. Dufresne, D. Frame, D. J. Lunt, T. Mauritsen, M. D. Palmer, M. Watanabe, M. Wild, H. Zhang. 2021. The Earth's Energy Budget, Climate Feedbacks, and Climate Sensitivity. In: Climate Change 2021: The Physical Science Basis. Contribution of Working Group I to the Sixth Assessment Report of the Intergovernmental Panel on Climate Change [Masson-Delmotte, V., P. Zhai, A. Pirani, S. L. Connors, C. Péan, S. Berger, N. Caud, Y. Chen, L. Goldfarb, M. I. Gomis, M. Huang, K. Leitzell, E. Lonnoy, J.B.R. Matthews, T. K. Maycock, T. Waterfield, O. Yelekçi, R. Yu and B. Zhou (eds.)]. Cambridge University Press. In Press.

IDF. 2015. A Common Carbon Footprint Approach for Dairy. The IDF Guide to Standard Life Cycle Assessment Methodology for the Dairy Sector. Bulletin of the International Dairy Federation 479/2015.

IPCC. 2019. N2O Emissions from Managed Soils, and CO_2 Emissions From Lime and Urea Application. 2019 Refinement to the 2006 IPCC Guidelines for National Greenhouse Gas Inventories, 1–48.

Kipling, R.P., Bannink, A., Bartley, D.J., Blanco-Penedo, I., Faverdin, P., Graux, A.-I., Hutchings, N.J., Kyriazakis, I., Macleod, M., Østergaard, S., et al. 2021. Short Communication: Identifying Key Parameters for Modelling the Impacts of Livestock Health Conditions on Greenhouse Gas Emissions. Animal, 15(1), 100023, doi:10.1016/j.animal.2020.100023.

Kristensen, T., Mogensen, L., Knudsen, M.T., Hermansen, J.E. 2011.Effect of Production System and Farming Strategy on Greenhouse Gas Emissions from Commercial Dairy Farms in a Life Cycle Approach. Livestock Science, 140, 136–148. doi:10.1016/j.livsci.2011.03.002.

Mc Geough, E.J., Little, S.M., Janzen, H.H., McAllister, T.A., McGinn, S.M., Beauchemin, K.A. 2012. Life-Cycle Assessment of Greenhouse Gas Emissions from Dairy Production in Eastern Canada: A Case Study. Journal of Dairy Science, 95, 5164–5175. doi:10.3168/jds.2011-5229.

Rose, D.C., Parker, C., Fodey, J., Park, C., Sutherland, W.J., Dicks, L. V. 2018. Involving Stakeholders in Agricultural Decision Support Systems: Improving User-Centred Design. International Journal of Agricultural Management, 6(3-4), 80–89, doi:10.5836/ijam/2017-06-80

Rotz, C.A. 2018. Modeling Greenhouse Gas Emissions from Dairy Farms. Journal of Dairy Science, 101(7), 6675–6690. doi:10.3168/jds.2017-13272 .

UNECE. 2015. United Nations Economic Commission for Europe Framework Code for Good Agricultural Practice for Reducing Ammonia Emissions.

D4AgEcol Platform: A web platform to promote the use of digital tools and technologies in agroecology

Evangelos Anastasiou[a,*], Panagiotis Stamatelopoulos[a], Pothitos Kotsiomitis[a], Spyros Fountas[a], Friederike Schwierz[b], Andreas Meyer-Aurich[b]

[a] Department of Natural Resources Management & Agricultural Engineering, Agricultural University of Athens, Iera Odos 75, Athens 11855, Greece

[b] Leibniz Institute for Agricultural Engineering and Bioeconomy (ATB), Max-Eyth-Allee 100, 14469 Potsdam, Germany

* Corresponding author. Email: evangelos_anastasiou@aua.gr

Abstract

Agroecology is an important approach to address modern challenges in agriculture, such as climate change, soil degradation, and food insecurity. Digitalisation can support agroecology by enabling farmers to work more precisely, efficiently, and sustainably. Digital technologies can help farmers to collect and analyze data on soil health, weather patterns, and crop yields, which can inform decision-making and improve resource management. However, it is important to align digitalisation and agroecology to ensure that it supports a transformation agenda towards sustainable and equitable food systems. D4AgEcol, a Horizon Europe funded research project, aims to provide knowledge for the transition to agroecological farming by identifying appropriate digital tools and technologies. To facilitate its aim, a platform in the form of a web application was developed in the scope of the D4AgEcol project. Through D4AgEcol project's web platform, agricultural stakeholders can derive information related to the use of digital tools and technologies in the context of agroecology from research articles, research projects and commercial products. In these categories, the visitors of the D4AgEcol platform can find useful information on the farming systems that can be used, characteristics, and the social, economic and environmental impacts they have on the various farming sectors. More than 500 records belonging to the aforementioned categories can be found on the platform which were identified through extensive search and screening in relevant online databases as well as on commercial websites. The D4AgEcol platform will contribute to the farming sector by enhancing the knowledge of farmers and other stakeholders on the ways that digital tools and technologies can be utilized in the context of agroecology to promote increased agricultural productivity, improved resource efficiency, increased environmental protection, and mitigation of climate change impacts. Ultimately, the D4AgEcol platform aims to contribute to the adoption of more resilient and sustainable agricultural practices by farmers and other agricultural stakeholders.

Keywords: agroecology, smart farming technologies, digitalisation, web platform, Horizon Europe project

1. Introduction

Agroecology is an integrative approach that applies ecological concepts and principles to the design and management of sustainable agricultural systems. It emphasizes the dynamics between biophysical and socioeconomic processes and components of agroecosystems. The importance of agroecology lies in its potential to deliver sustainable food production, enhance biodiversity, recycle nutrients, improve soil fertility, and sustain the livelihoods of billions of people worldwide, particularly smallholder farmers. The complexity of interactions in agroecological systems demands comprehensive management strategies that consider the multifunctional aspects of agriculture, integrating crop production, animal husbandry, and forest conservation (Ewert et al., 2023).

The burgeoning need for digital tools in agroecology arises from the necessity to navigate and optimize these multifaceted systems efficiently. Digital technologies in agriculture have revolutionized the way farmers monitor crop health, manage pest outbreaks, and utilize inputs such as water and fertilizers judiciously, reducing waste and environmental footprint. The deployment of digital tools such as terrestrial robots, Unmanned Aerials Vehicles (UAVs), Farm Management Information Systems (FMIS), Internet of Things (IoT) systems, multispectral cameras have provided a digital backbone for precision agriculture practices, enabling real-time data collection and analysis for decision-making. These systems have contributed significantly to enhancing the efficiency of crop production through improved monitoring and targeting of inputs (Burns et al., 2022). Accordingly, in livestock farming, digital tools are critical in

monitoring animal health and welfare, optimizing feeding strategies, and ensuring efficient resource utilization. Technologies such as automated feeders, health monitoring wearables, and data management systems can lead to improved animal health outcomes and productivity while reducing labor requirements and environmental impacts (Gómez et al., 2021).

Thus, the adoption of digital tools across these diverse farming systems is essential for advancing agroecology. They provide the necessary data and models to inform sustainable practice and policy, foster resilience in food systems, and ultimately contribute to the health of the planet and its inhabitants. By harnessing the power of digital tools, agroecology can evolve to meet the global challenges of food security, environmental sustainability, and climate change adaptation (Ajena et al., 2022).

By giving farmers access to a multitude of tools and information that can improve their production, efficiency, and sustainability, web-based knowledge platforms hold the potential to completely transform the agriculture industry. The platforms can increase market accessibility, strengthen agricultural extension services, empower farmers, encourage environmental sustainability, and build their capability (Ong et al., 2024; Lagos-Ortiz et al., 2020).

In this context, the EU-funded D4AgEcol project will show the potential of digitalisation as an enabler for agroecological farming systems in Europe. One of the main outputs of the project was the production of the D4AgEcol platform to increase awareness among agricultural stakeholders about digital tools that can be utilized in agroecology. Thus, the main objective of this study is to present the specification and characteristics of the D4AgEcol platform, which will include existing and emerging digital tools that are used in crop and livestock farming and can be used for the purposes of agroecology.

2. Materials and Methods

The work consisted of three steps: (i) collection of data; (ii) data screening and aggregation; and (iii) platform implementation.

2.1. Collection of data

Three different sources were utilized for the collection of digital tools, namely research articles, research projects and commercial products. Specifically, relevant digital tools were identified through research articles that were retrieved through the Web of Science database (https://www.webofscience.com/wos/woscc/advanced-search). For this purpose, a query was placed to the search engine to identify relevant digital tools that can contribute to agroecology. The query consisted of digital tools identified in review articles, FAO's ten elements of agroecology, and the farming systems that were under study (open agriculture, livestock farming, and agro-forestry).

A similar approach was also followed for the mapping of the research projects. More specifically, the CORDIS search engine (https://cordis.europa.eu/search/en) was used to identify finished relevant Horizon 2020 projects due to the fact that they are well documented in the database compared to research projects from previous programmes.

To map the commercial solutions that can be used in agroecology, data from web search and relevant databases, such as smartAKIS and 4D4F, were utilized during June 2023.

2.2. Data screening and aggregation

After the data collection process, the research articles and projects were mapped by utilizing the Preferred Reporting Items for Systematic Reviews and Meta-Analyses (PRISMA) methodology. PRISMA is an evidence-based minimum set of items for reporting in systematic reviews and meta-analyses (Moher et al., 2010). Thus, the final number of suitable articles and projects that were evaluated in depth for this study were 305 and 90, respectively. These were added to the initial 107 solutions that were identified from web search and relevant databases. The selected digital tools were classified accordingly to address the topics of the project (digitalization, farming systems, agroecology). The categorization of the research articles was based on various review articles that addressed relevant topics (Akhigbe et al., 2021; Balafoutis et al., 2017; Gómez et al., 2021; Ramil Brick et al., 2022). Additionally, the digital tools were assessed in terms of their technology readiness level to existing (TRL8-9) and emerging (TRL5-7). The detailed classification is presented in **Error! Reference source not found.**1.

Table 1. Classification of the digital tools under the different topics.

Classes	**Options**	**Classes**	**Options**
Farming System	Agriculture Livestock Farming Agro-forestry	Platform	Satellite UAV UGV Crewed Ground Vehicles Stationary Wearable Mobile Ground Crewed Aerial Vehicles
Farming Type	Arable Crops Vegetable Crops Orchard Crops Vineyards Ruminants Poultry Pigs	Sensors	Hyperspectral Multispectral Thermal RGB/RGB-D LIDAR Weather Station RFID/Eid Rumen Bolus Accelerometer Load Cell Sound Sensor Flow Meter Temperature Sensor Weight Sensor Soil Sensor Dendrometer Stem Water Potential Sensor NIRS Smart Collar Smart Trap Synthetic Aperture Radar GNSS Soil Electrical Conductivity ensor Canopy Sensor Fluorescence Nitrate Sensor Water Quality Sensor Ground Penetratitng Radar Soil Cutting Resistance ensor Electronic Plate Meter Smart Feeder Force Plate Moocal Device pH Sensor Leg Sensor Milk Meter Milk Sensor
Farming System Type	Conventional Organic Integrated Management	Software	Software FMIS DSS Social Platform Digital Marketplace
Operation Type	Land Preparation Irrigation Fertilization Pest Control Weeding Harvest Monitoring Marketing	Technology Readiness Level	Existing (TRL8-9) Emerging (TRL5-7)

Classes	Options	Classes	Options
	Breeding Feeding Animal Health care Dairy production Egg production Meat Production		
Application Type	Guidance/Steering Recording/Monitoring/Mapping Reacting/VRA/control Information/Knowledge sharing		

2.3. Platform implementation

Based on the information collected from the research articles, the research projects, the commercial products and the collected impact, a relational database was designed to be used for the development of the online platform.

The MariaDB (10.3.39-MariaDB-0ubuntu0.20.04.2 - https://mariadb.org/) database management system was used for the storage of the related data, while PHP (version 8.3 - https://www.php.net/) programming language and specifically the Laravel framework (version 11 - https://laravel.com/) was used for the development of the backend of the platform. To better facilitate the data collection process, initially, the relevant datasets were processed in an online excel sheet that was later migrated/seeded into the designed database.

Early in the development process a set of wireframes of the platform were developed to depict how the user interface shall function. To better understand the user needs and design effective and valuable wireframes, other similar and successful platforms from relevant research projects were identified and analyzed (e.g., Fairshare, Smart-AKIS). Through this process, useful characteristics were identified that could be an asset to the D4AgEcol platform. Additionally, the visual identity of the project as implemented by the official website was considered and accounted for during the user interface design.

The user interface of the online platform was developed using the ReactJS framework (https://react.dev/). React is one of the most popular frontend JavaScript frameworks, suitable for creating modern and interactive web applications. It is highly supported by all major web browsers (i.e. Firefox, Chrome, Edge) and its especially known for its rendering and code reuse capabilities.

3. Results and Discussion

3.1. Data screening and aggregation

In total, 304 research articles, 90 research projects and 107 commercial products were identified to refer to digital tools that can be applied in agroecology. These digital tools can be applied in various sectors (agriculture, livestock farming and agro-forestry) to address specific needs in various operations (e.g., weeding, spraying, fertilization, irrigation). Moreover, these digital tools may refer to terrestrial or aerial robots, smart implements, FMIS, online tools, multispectral and thermal cameras, market places and other covering different needs.

As it is presented in Figure 1, most of the digital tools that were included in the database are related to agriculture (91.7% from research articles, 86.7% from research projects and 72.9%) while digital tools related to livestock farming and agro-forestry presented significant lower percentages.

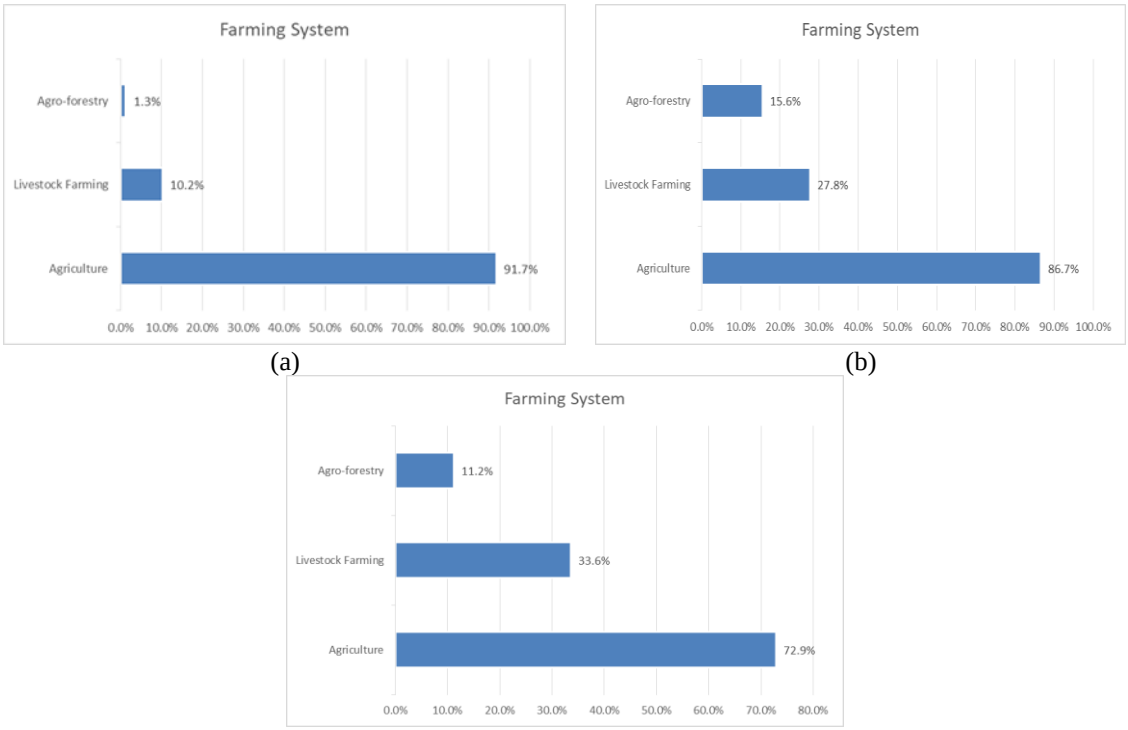

Figure 2. Digital tools percentages per farming system for (a) research articles; (b) research projects; and (c) commercial products

3.2. Platform implementation

The Entity Relationship Diagram (ERD) of the designed database is illustrated in Figure 2. This diagram visually presents all of the main entities and the relationships among them, indicating the cardinalities and constraints that govern the interactions between different entities. In the scope of the D4AgEcol platform the main entities include the users, the research projects, the commercial products and the research articles, where, the relationships consist of tables/properties such as platforms, farming types, application types and more.

Figure 2. D4AgEcol platform Entity Relationship Diagram (ERD).

Wireframes of the platform were developed to depict the user interface of the platform by analysing other similar platforms from other research projects (e.g., Fairshare, Smart-AKIS) to identify useful characteristics that could be used in the development of the D4AgEcol platform. Then, the wireframes were presented to the consortium for fine-tuning. Specifically, the wireframes included the landing page, the catalog and the profile card (Figure 3).

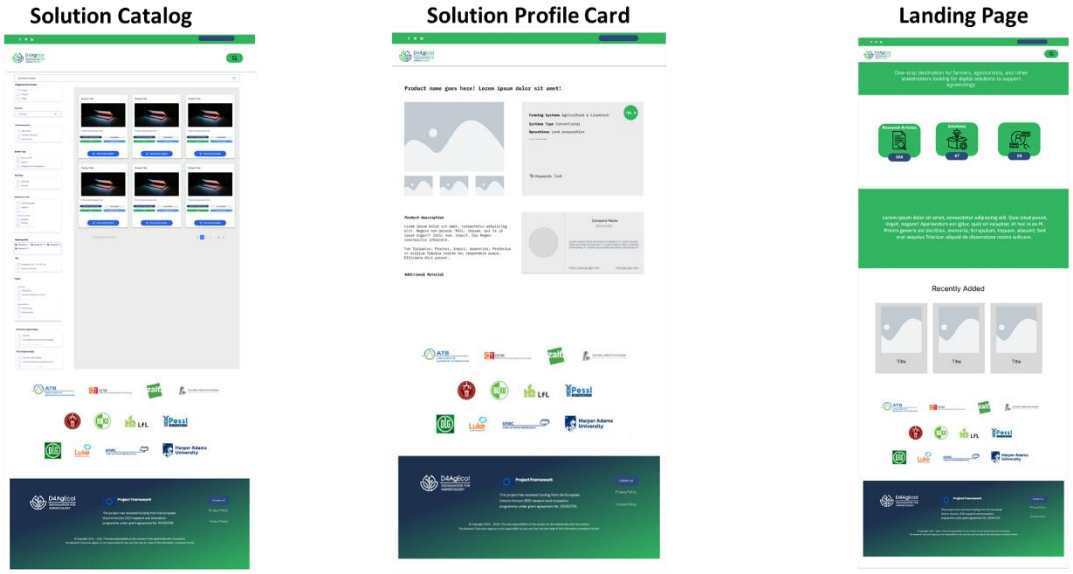

Figure 3. Wireframes of the D4AgEcol Platform.

Based on the aforementioned information, the user interface of the platform was developed using the ReactJS framework. The landing page, the catalogue and the profile card pages of the D4AgEcol platform are presented below (Figure 4). A dedicated menu item will be placed to the projects official website, navigating visitors to the D4AgEcol platform (https://d4agecol.eu).

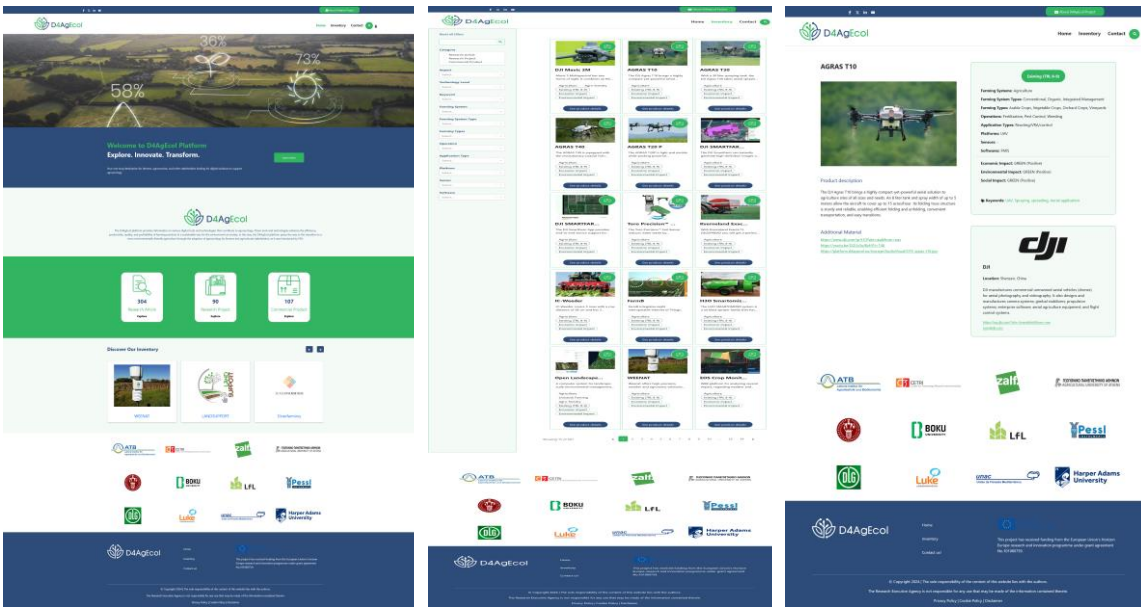

(a) (b) (c)

Figure 4. (a) The lading page; (b) the catalogues and (c) the profile card of the D4AgEcol Platform.

Additionally, D4AgEcol users are able to register with the online platform and submit information (research publications, research projects, and commercial items) on digital tools for agroecology. There are multiple tiers of users, each with varied access permissions. Specifically, admin users have full access to the platform's records and are able to monitor and publish them, as well as assign records for review. The reviewers are able to upload, review, and publish material, whilst the other users are able to post information that then can be allocated to reviewers by admin users (Figure 5).

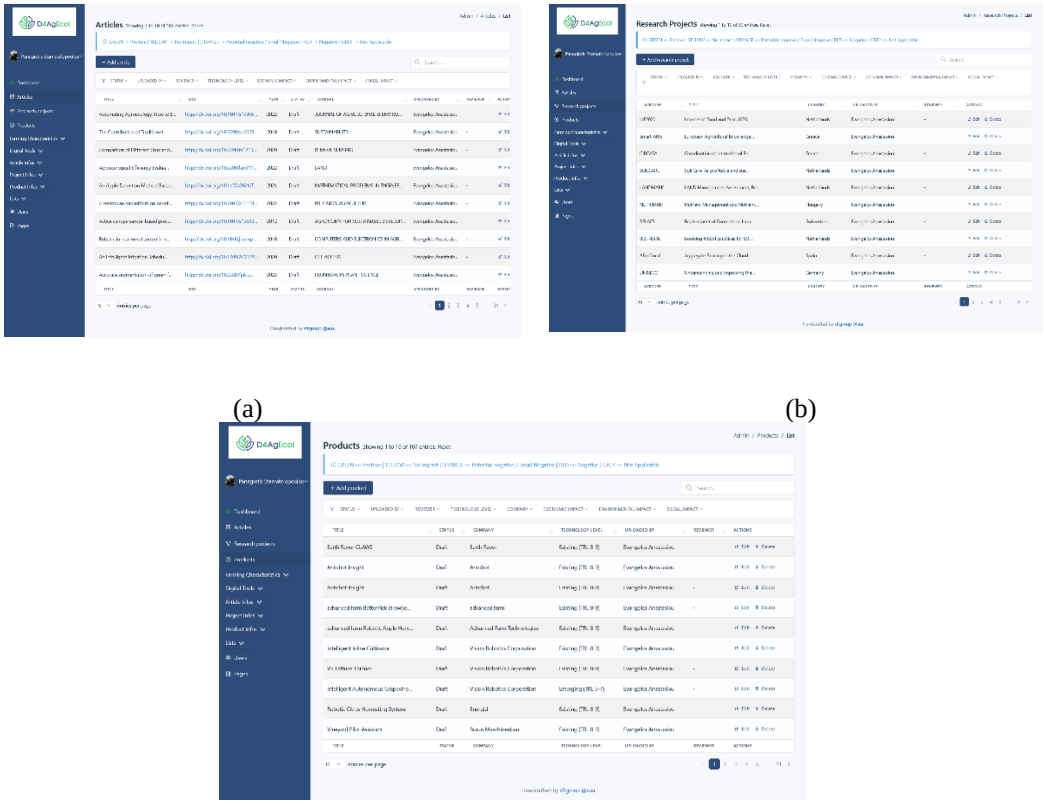

(a) (b)

(c)

Figure 5. Pages for uploading information for (a) research articles; (b) research projects and (c) commercial products.

4. Conclusions

The D4AgEcol platform is a useful tool for agricultural stakeholders to help in the collection of information on digital tools that could be used for the purposes of agroecology. The platform is "self-sustainable" because its increased awareness of its presence among key stakeholders would result in additional inputs. Through this first solid foundation and implementation of a methodology to collect valid innovative and useful records on information of digital tools, the platform is effective for its overarching goal. The D4AgEcol platform is used jointly with other communication and dissemination tools and activities to increase awareness among agricultural and non-agricultural stakeholders about the benefits of digital tools in agroecology.

Acknowledgements

This research has received funding from the European Union's Horizon Europe research and innovation programme under grant agreement No.101060759, D4AgEcol – Digitalisation for Agroecology and co-funded by UK Research and Innovation (UKRI Reference No.10037994).

References

Ajena, F., Bossard, N., Clément, C., Hibeck, A., Tiselli, E., Oehen, B., 2022. Agroecology & Digitalisation: traps and opportunities to transform the food system. IFOAM Organics Europe, Brussels, Belgium.

Akhigbe, B. I., Munir, K., Akinade, O., Akanbi, L., Oyedele, L. O., 2021. IoT Technologies for Livestock Management: A Review of Present Status, Opportunities, and Future Trends. Big Data and Cognitive Computing. 5(1), 10. https://doi.org/10.3390/bdcc5010010

Balafoutis, A. T., Beck, B., Fountas, S., Tsiropoulos, Z., Vangeyte, J., van der Wal, T., Soto-Embodas, I., Gómez-Barbero, M., Pedersen, S. M., 2017. Smart Farming Technologies – Description, Taxonomy and Economic Impact. In S. M. Pedersen & K. M. Lind (Eds.), Precision Agriculture: Technology and Economic Perspectives. Springer International Publishing. 21–77. https://doi.org/10.1007/978-3-319-68715-5_2

Burns, S. A., Dittmer, K. M., Shelton, S. W., Wollenberg, E. K., 2022. *Exemplary features of digital tools for agroecology: A global review.* Cali (Colombia): ATDT. 7 p. https://hdl.handle.net/10568/126016

Ewert, F., Baatz, R., Finger, R., 2023. Agroecology for a Sustainable Agriculture and Food System: From Local Solutions to Large-Scale Adoption. Annual Review of Resource Economics, 15, 351–381. https://doi.org/10.1146/annurev-resource-102422-090105

Gómez, Y., Stygar, A. H., Boumans, I. J. M. M., Bokkers, E. A. M., Pedersen, L. J., Niemi, J. K., Pastell, M., Manteca, X., Llonch, P., 2021. A Systematic Review on Validated Precision Livestock Farming Technologies for Pig Production and Its Potential to Assess Animal Welfare. Frontiers in Veterinary Science. 8, 660565. https://doi.org/10.3389/fvets.2021.660565

Lagos-Ortiz, K., Salas-Zárate, M. D. P., Paredes-Valverde, M. A., García-Díaz, J. A., Valencia-Garcia, R., 2020. AgriEnt: A knowledge-based web platform for managing insect pests of field crops. Applied Sciences. 10(3), 1040.

Ong, R. J., Sudin, S., Raof, R. A. A., Choong, K. Y., Al-Hadi, A. A., Yacob, Y., Nasir, S. N. B. M. (2024, February). Dynamic web-based knowledge management system (KMS) in small scale agriculture. In *AIP Conference Proceedings*. Perlis, Malaysia. AIP Publishing. Eds. N. F. Zakaria, M. F. Ahmad, M. N. Norizan, M. R. Zakaria, Q.W. Oung and H. L. Lee. 2898 (1), 030013. https://doi.org/10.1063/5.0196279

Ramil Brick, E. S., Holland, J., Anagnostou, D. E., Brown, K., Desmulliez, M. P. Y., 2022. A review of agroforestry, precision agriculture, and precision livestock farming—The case for a data-driven agroforestry strategy. Frontiers in Sensors. 3, 998928. https://doi.org/10.3389/fsens.2022.998928

LIFE AgrOassis - Regenerative approaches for building climate change resilience into EU agricultural regions prone to desertification

C. Cavalaris[1], P. Maletsika[1], G. Nanos[1], A. Kyparissis[1], C. Karamoutis[1], V. Giouvanis[1], P. Dalias[2], S. Stylianou[2], G. Theofanous[3], F. Filippou[4], A. Christodoulou[5], D. Sarris[6], A. Stelikou[6], A. Miliotou[6], I.N. Vogiatzakis[7], S. Zotos[7], P. Manolaki[7], E. Tzirkalli[7], Ch. Kalaitzidis[8], P. Champas[9], P. Paradisiotis[10], V. Perakis[11], A. Markinos[12], K. Kiourtsis[12], A. Yiordamli[13] and K. Orountiotis[13]

1. University of Thessaly, Dp. of Agriculture, Crop Production & Rural Environment. Fytokou str 38446 Volos Greece.

2. Ministry of Agriculture, Rural Development, and the Environment of Cyprus, Agricultural Research Institute, Department of Natural Resources and Environment, P.O. Box 22016, Nicosia 1516, Cyprus.

3. Ministry of Agriculture, Rural Development & Environment. Cyprus – Dp. of Agriculture Amfipoleos 6, 2025 Strovolos Nicosia,

4. Ministry of Agriculture, Rural Development, and the Environment of Cyprus – Department of Environment, Amfipoleos 6, 2025 Strovolos Nicosia,

5. Ministry of Agriculture, Rural Development, and the Environment of Cyprus – Department of Forests, Amfipoleos 6, 2025 Strovolos Nicosia,

6. KES Research Center Limited. Grevenon 2, Nicosia 1055, Cyprus.

7. Open University of Cyprus, Faculty of Pure & Applied Sciences, 89 Yiannou Kranidioti Avenue, 2231 Latsia, Nicosia, Cyprus.

8. Mediterranean Agronomic Institute of Chania. Alsylio Agrokipio - Makedonias 1, Chania 73100, Greece.

9. Union of Cypriot Farmers, Androcleous 4, Nicosia 1060, Cyprus

10. Paradisiotis Ltd. Spyros Kyprianou Str., 3rd Industrial Zone, Ypsonas 4012, Cyprus

11. Municipality of Sitia, P. Vartholomeou 9, Sitia 72300 Greece

12. Land Reclamation Organization of Tavropos. Iroon Politechneiou 16, Karditsa 431 00, Greece.

13. Laona Foundation. SW Corner of Koumandarias and Agiou Andrea Street, Limassol 3036, Cyprus.

* Corresponding author. Email: chkaval@uth.gr

Abstract

The current work presents the main concept and preliminary actions from the LIFE AgrOassis project. The project proposes nature-based solutions and circular economy approaches for combating desertification within degraded agroecosystems of Cyprus and Greece (Thessaly and Crete). Co-funded by the European Union LIFE program, LIFE AgrOassis project started in 2022 and will continue until 2026. The main land management interventions focus on changing soil management by promoting minimum tillage, no-tillage, mulching and compost application as well as introducing hedgerow structures on the most vulnerable parts of the fields. Through the above soil management interventions, the project aims to revert soil degradation and upgrade soil quality by improving the soil structure, preventing soil erosion, enriching soil carbon, preserving soil water, enhancing soil fertility, and promoting soil biodiversity. Combined with the hedgerow's beneficial impacts on microclimate, windborne erosion, and local biodiversity, the interventions are expected to support the ecosystem services within the prone to desertification farmlands. On the other hand, the fixation of CO_2 into soil carbon pools, the CO_2 sequestration into woody tissues on the hedgerows, along with the avoidance of carbon losses from uncontrolled green waste disposal and the reduction of GHGs emissions through fossil fuel savings from minimum and no-tillage are expected to contribute towards climate change mitigation. Finally, the use of compost is expected to promote the circular economy concept within the agro-sector community. Through the exploitation of a multi partner, multi actor approach, the LIFE AgrOassis project aims to mobilize the primary food production sector towards close-to-market solutions on sustainable solutions and seeks to identify and remove obstacles related to inappropriate governance and policies, that obstruct the implementation of the EU's Green Deal Agenda.

Keywords: Conservation agriculture, no-tillage, mulching, hedgerows, compost.

1. Land desertification in Cyprus and Greece

Agriculture is highly exposed to climate change, as farming activities directly depend on climatic conditions. The IPCC projections for the Mediterranean basin are alarming, particularly for the Eastern Mediterranean and the Middle East, and show increased temperature, decreased annual rainfall, increased

drought risk and high heat stress. The result will be decreased crop yields and decreased land availability for crop cultivation (Giannakopoulos 2009; Lelieveld et al 2016). The projected increased periods of drought will act as the limiting factor for agroecosystems and farming practices. Drought reduces plant productivity, biodiversity and soil cover making drylands vulnerable to soil erosion and land degradation.

Intensive agricultural practices like frequent and deep soil tillage can accelerate land degradation through several processes like soil erosion, compaction, losses in soil organic matter (SOM) and other. As a result, soil quality and productivity is deteriorating and the landscape and biodiversity can be seriously damaged as the desertification accelerates. Agricultural soils in Cyprus and Greece have generally low SOM, poor soil structure and small water infiltration rates. They are therefore highly vulnerable to wind/water erosion and prone to desertification.

One of the most important quality indicators for desertification is the low soil organic matter (SOM) of degraded fields, and actions to combat desertification and degradation of agricultural soils often aim to increase SOM level. Increasing the SOM in agricultural fields, directly increases their water storage capacity, creates a healthy habitat for beneficial soil bacteria and other biodiversity, captures carbon and makes the soils more resilient for withstanding climate change. The predominant land management practices however in cereals and olive groves include both extensive and intensive tillage to combat weeds, a practice which increases the loss of SOM, accelerates erosion and degrades the soil structure and quality. Furthermore, cereal farmers in Cyprus attempt to maximize straw production for use as animal feed by strip mowing the crop during harvesting. Thus, very little plant residue is left on the field to promote mulching, soil protection and carbon enriching. More worthy, farmers in Cyprus practice tillage after the cereal harvest (or in Olive groves many times during the year) so the ground remains exposed during the greatest part of the dry season permitting the acceleration of the desertification processes. On bare ground temperatures higher than 55 ^{o}C may occur in lowlands of Cyprus during the driest part of the year (Hadjimitsis et al. 2013), which further reduces soil moisture, soil microorganism activity and nutrient recycling; a process that urgently needs to be reversed for combating desertification.

2. The LIFE AgrOassis approach

The LIFE AgrOassis project targets on nature-based solutions that handle the problem of desertification and create conditions that will reverse the process by helping agricultural systems to become adapted to the new climate regime. The project focuses both on seasonal and permanent crops at the two countries. Seasonal crops include mainly cereals but other crops like legumes, maize and cotton are expected to be exploited in the frame of the regular regional rotations. The targeted permanent crop is olives.

Treatments and techniques to halt and reverse the process of land degradation and desertification relay on protecting topsoil. For example, if the ground in summer remains covered by plant residue it may significantly reduce topsoil temperature (e.g. up to 15^{o}C) and increase soil moisture (by ca. 20%; as measured by Christofi 2020 in Cyprus). Plant shade can have the similar effect, while plant roots and mulching can secure soil from wind and runoff erosion. Plants adapted to drought can even reverse the progress of desertification by increasing SOM, providing additional benefits by supporting the conservation of biodiversity and re-stabilising lost ecosystem services for the agroecosystem, by improving water retention and enhancing carbon sequestration.

2.1. Conservational tillage practices

Conservation tillage practices including minimum tillage, no-tillage and mulching eliminate soil organic carbon losses and promote soil carbon sequestration. According to Gonzalez-Sanchez et al. (2018) the application of conservation agriculture practices in Cyprus and Greece has the potential to increase soil carbon by 0.81 tons per ha and year. Conservation agriculture includes no-tillage as a core element, but other studies in Greece and Spain has also shown the even reduced tillage can provide comparable benefits (at least 60% of no-till) by preventing carbon losses from the soil and improving SOM, especially under the Mediterranean conditions (Gemtos et al., 2002. Garcia et al., 2015, Goula et al., 2020). Considering that the project will focus primarily on poor soils with a baseline carbon content lower than 14g/kg for arable farms and less than 23g/kg in orchards, an increase in SOM at the end of the project by 30% is reasonably anticipated. Furthermore, an improvement in summer topsoil water holding capacity by 30% is also expected from retaining the mulch. This will also cause a decrease in soil surface temperature by 15-20^{o}C due to

ground shading (Hadjimitsis et al. 2013). Additionally, the no-tilling or conservation tilling techniques will also secure better ground structure and prevent erosion, enhance the soil organic carbon, rainfall infiltration and soil moisture, to produce an increase by 30% in microbial and invertebrate biodiversity. LIFE AgrOassis capitalizes on the long-time experience of University of Thessaly in Conservation Agriculture systems and the special equipment for no-tillage planting owned by the Laboratory of Farm Mechanization to provide the initiatives for a wider adoption in Thessaly and the opportunities for the dissemination of the knowledge in Cyprus (Figure 1).

Figure 1. No-tillage sowing of winter wheat in pilot farms in Thessaly on Nov. 2023.

2.2. Hedgerow installation

Hedgerow installation in degraded agricultural land is expected to slow down or even halt soil erosion processes especially on steep farmlands by providing a physical obstacle to water runoff and facilitating infiltration of rainwater and ground aquifer recharging. Through dead plant biomass and stabilisation of field soil an increase in SOM is also anticipated in the neighbouring area. In addition, a greater amount of carbon will be sequestered from the atmosphere and stored in the woody biomass assisting that way to climate change mitigation. Local shading is expected to reduce ground temperature during summer and retain soil moisture. The altered condition will provide refugia for biodiversity and assist with natural pest control and pollination.

LIFE AgrOassis capitalize on the lessons learnt from past and ongoing agro-ecosystem restoration attempts in Cyprus (e.g. Life Rizoelia 2017; Blackgold 2021) to overcome high levels of plant establishment failure. Novel ecological engineering techniques are employed combining the specialized production in nurseries using planting tubes that permit deep root development of stress adapted plant species that can act as ecological facilitators (Figure 2). These are combined with soil bio-stimulants and stress alleviating products (water retaining minerals e.g. attapulgite), while supported in the field by the ecological traits of nitrogen fixing soil covering plants. Such innovative techniques, methods and approaches are designed to assist the survival of shrubs and trees under harsh conditions and are expected to improve plants resistance to abiotic stresses, increase nutrient/moisture acquisition and thus facilitate productivity (Figure 3).

The plant species are selected by four key criteria. They are plants that: (a) act as ecological facilitators (i.e. plants that prepare the area for other plants to become established), (b) offer fire resistance, (c) provide an extra opportunity to improve the farmers income from fruits and other tradable products (e.g. *Ceratonia siliqua, Morus nigra, Lavandula officinalis* and other) and (d) set the stage for farmers to become engaged in carbon farming.

Figure 2. Plant nursery for hedgerow seedlings at the premises of MARE-DF in Cyprus. Plants are prepared with the special protocol.

Figure 3. Hedgerow installation on Dec. 23 in Cyprus

2.3. Composting

The application of compost into degraded soils can considerably accelerate the increase in SOM (Daoyuan Wang et. al. 2022). At the same time its production and application permit carbon from organic waste to be captured before it is emitted back into the atmosphere. However, this practice is not common in Cyprus and Greece and rarely is linked with the agricultural sector, despite the abundance of organic waste from pruning or other practices (e.g. municipal and industrial wastes). Although there is no specific data available, municipal green waste on Cyprus is conservatively estimated at 20.000 tonnes. The kick-starting compost production actions of the project in Cyprus is expected to further demonstrate the special tools to improve soil conditions and combat desertification. A low cost, special machine for compost turning were constructed for the purposes of the project and is operating at the premises of ARI (Figure 4).

Figure 4. Composting of green waste prunings at the premises of MARE-ARI in Cyprus.

3. Aims and objectives.

LIFE AgrOassis aim through a wide range of actions and initiatives to reduce the negative impacts of desertification and assist the adaptation to climate change for Cyprus and Greece, the two most southeasterly countries in EU. Both are exposed severely to desertification risks and the preformed actions are expected to leverage the adaptation of resilient agriculture schemes in the agri-food sector. In particular, the main objectives of the project aim to:

- Intergrade a total of 500 ha of arable crops and orchards, prone to desertification in Cyprus (350ha) and Greece (100ha in Thessaly and 50 ha in Crete) into a resilient management system utilizing mulching, minimum tillage and no-tillage practices. Specifically for Thessaly, 85ha will be converted to minimum tillage and 15ha into a no-tillage system.
- Install 30 km of hedgerows with different plant species in Cyprus and 3 km in Thessaly and Crete. A total of 6.000 trees and 12.000 shrubs are scheduled to be planted in burnt and/or degraded agricultural land in Cyprus and another 600 trees and 1200 shrubs in Thessaly and Crete by the end of the project. Another 1000 ha of neighbouring farmland is expected to become benefited from the hedgerows in terms of microclimate change, biodiversity improvement and protection from windborne soil erosion,
- Produce totally 2600 m^3 of compost obtained from shredded green/garden and chicken waste at two partners premises in Cyprus and spread the material at 10 ha per year on farmers' selected fields to substitute the mineral fertilizers.
- Identify and remove obstacles related to inappropriate governance and policies, that obstruct the implementation of the EU's Green Deal Agenda and the aim to reach climate neutrality by 2050. The project will provide additional remote sensing means to government and authorities to monitor land cover and discriminate mulching techniques from abandoned fields.
- Promote educational activities in both countries for at least 800 farmers, students and stakeholders on how to effectively combat desertification and how this can be turned into profit (Figure 5).
- Mobilize the agricultural sector in Cyprus towards a circular economy market scheme by kick-starting compost production through the creation of two pilot facilities, one based on municipal waste and the other on pruning from fire-affected plant biomass and chicken manure.
- Shift farmer attitude from compliance to performance by rewarding farmers for managing and storing carbon in the soil, for improving soil nutrients availability, for reducing emissions and increasing soil water retention.
- Engage at least 2.000 farmers, stakeholders and policy makers, in the three project areas and disseminate to over 45.000 directly interested recipients (farmers/consultants/academics) the

progress and outcome of LIFE AgrOassis.

- Provide the foundation for large scale replication of such successful technical and policy related solutions and promote conservation agriculture adaptation by integrating related objectives into agricultural policies with a catalytic role not only in Cyprus and Greece, but also in other EU regions prone to desertification.

Figure 5. Farmers enrolment campaign in Cyprus (Nikosia) and Greece (Thessaly) during 2023.

4. Impact monitoring and reporting

The impacts of the scheduled actions will be registered through systematic records, measurements, and monitoring.

- The changes in soil quality will be identified by measurements in SOM, water permeability and soil water content, soil temperature, soil ground cover, dry bulk density, penetration resistance, water-stable aggregates and soil microbial activity.
- Hedgerow installation will be qualified by monitoring the plant survival and growth with vegetation indices obtained with drones.
- Effects on crop yields (grain /straw) will be estimated by harvesting separately each field and weighting the total production. In the case of availability of harvesters with yield monitors, yield maps will be produced. Grain quality parameters like protein content, hectoliter weight, yellow index etc will also be recorded.
- The economic impacts will be assessed through detailed registration of all the farm inputs by delivering predefined questionnaires to the farmers and collecting the yield results after each year harvest.
- The environmental impacts will be assessed by calculating the carbon fixation into the soil and the carbon sequestration into the woody biomass of the hedgerows. Emission reductions from energy and fertilizers conservations will be also quantified. MRV tools (Measuring, Reporting and Verifying) like the CoolFarmTool will be utilized for that scope. And the impacts will be expressed into CO_2 equivalents.
- Impact on Ecosystem Services will be assessed by applying a standard methodology for monitoring key species for biodiversity. The monitoring will cover the conservational tillage fields at a distance of at least 500m away from the established hedgerows to document their effect on mobile animal taxa (insects, reptiles, and birds).
- Socio economic impact will be estimated by assessing key indicators as economic performance, market uptake, replication/transfer, jobs created, expected revenues, awareness rising and behavioural change.

5. Project consortium

The LIFE AgrOassis project brings together a complementary and high-quality consortium in terms of expertise and actors engaged in agriculture in Greece and Cyprus from all sectors (private, public, academia, NGOs). Each organization is assigned discrete and prescribed roles in the consortium that help achieve the overall objectives. The Ministry of Agriculture, Rural Development and Environment of Cyprus (MARE) participates in the project with its Research Institute and three of its departments namely that of Agriculture,

Environment and Forests.

- The **Agricultural Research Institute (MARE-ARI**) conducts research on plant and animal production problems in Cyprus. MARE-ARI is the co-ordinator of the project and also leads the work package for sustainable production of the compost and its application on degraded soils.
- The **Department of Agriculture (MARE-DA)** implements the legislative and regulatory acquis which falls within its competence for fulfilment of Cyprus' obligations to the EU. Its role to the project is to suggest to the farmers new applicable measures in order to adapt to climate change and reduce the effects from it and to contribute to the science policy dialogue.
- The **Department of Environment (MARE-DE**) is the coordinating body for Cyprus government programmes for the protection of the environment. It is assigned to assist on the impact monitoring and evaluation and contribute to the science policy dialogue.
- The **Department of Forests (MARE-DF)** manages the state forest land and implements national forest legislation and policy in Cyprus. It leads resilient hedgerow installation in Cyprus.
- The **Open University of Cyprus (OUC)** is a public institution in Cyprus that leads the corresponding actions for biodiversity monitoring as well as the monitoring of the project's impact on biodiversity changes.
- The **Mediterranean Agronomic Institute of Chania (MAICh)** is a constituent Institute of the International Centre of Advanced Mediterranean Agronomic Studies (CIHEAM). The role of MAICh will be mainly in the education dissemination activities regarding the project outcomes.
- The **Department of Agriculture, Crop Production & Rural Environment (UTH-DACPRE)** of **University of Thessaly** has a long-term experience with conservational practices in agriculture. It will lead the replication activities of conservational tillage and hedgerow installation in Greece.
- The **KES Research Centre (KESRC)** is a non-profit research organization that conduct independently fundamental and industrial research and disseminates the results through teaching and publications. It has a core role to the project by organizing the preparatory actions, scheduling the project implementation plan and assisting on the education and dissemination activities.
- The **Union of Cypriot farmers (EKA)** is a farmer association consisting of more than 6000 members. The role of the association is to encourage uptake and implement the project best practices and assist in policy formation.
- The **Paradisiotis Ltd (PRD)** is one of the largest companies in the field of poultry grower and trader of poultry, meat, fish, feed, etc. in Cyprus. The partner will participate in the compost production.
- The **TOEV Tavropos (TOEV**) is a local organization with more than 8000 members in Karditsa Thessaly with main objective the management and improvement of the irrigation facilities. The main role of the partner is to enable its members to implement the conservation tillage and hedgerow actions in Thessaly.
- The **Municipality of Sitia (MoS)** manages the Sitia Geopark, and among its actions is the protection of the environment. The role of MoS will be mainly in replicating in olive orchards in Crete the mulching and hedgerow actions carried out in Cyprus
- The **Laona Foundation (Laona)** is a non-profit organization which supports the Laona agrotourism initiative. It has been assigned the project management and the support of the dissemination and communication actions.

Besides the individual roles, the project establishes an efficient intercommunication plan to assist the effective collaboration among the partners and facilitate the performance of the multidisciplinary roles.

6. Ambitions

By its end, the LIFE AgrOassis aims to have laid the foundation for four close-to-market solutions through:

1. Sustainable Soil Management Practices that permit cutting costs, carbon farming and higher

yields

2. Specialized production of stress adapted plants in nurseries that permit marketing new types of resilient plant seedlings
3. Resilient hedgerow installation that permits carbon farming and promote ecosystem services
4. Sustainable production of compost that permits marketing substitutes for conventional fertilizers and promotes carbon farming

Acknowledgements

The AgrOassis project is funded by the EU LIFE program LIFE21-CCA-CY-LIFE AgrOassis 101074744

References

BlackGold. 2021. Final Report of WP4 Sustainable Carob Tree Cropping Systems. Carobs, the black gold of Cyprus: Science meets Industry. BlackGold INTEGRATED/0916/0019 is co-financed by the European Regional Development Fund and the Republic of Cyprus through the Research Promotion Foundation.

Christofi E. 2019. Evaluation of abiotic soil properties for the establishment of a novel carob intercropping system. Dept of Biological Sciences, University of Cyprus, Nicosia, Diploma Thesis.

Daoyuan Wang, Jonathan Y. Lin, Jordan M. Sayre, Radomir Schmidt, Steven J. Fonte, Jorge L.M. Rodrigues, Kate M. Scow, 2022. Compost amendment maintains soil structure and carbon storage by increasing available carbon and microbial biomass in agricultural soil – A six-year field study, Geoderma, Volume 427, 2022, 116117, https://doi.org/10.1016/j.geoderma.2022.116117.

Garcia-Franco, N., Albaladejo, J., Almagro, M., Martínez-Mena, M. 2015. Beneficial effects of reduced tillage and green manure on soil aggregation and stabilization of organic carbon in a Mediterranean agroecosystem. Soil Tillage Res. 2015, 153, 66–75, https://doi:10.1016/j.still.2015.05.010.

Gemtos T.A., Cavalaris C., Demis Vl, Pateras D. and Tsidari Chr. 2002. Effect of changing tillage practices after four years of continuous reduced tillage. ASAE Annual International Meeting / CIGR World Congress. July 2002, Chicago Paper No 021135.

Giannakopoulos, C., Le Sager, P., Bindi, M., Moriondo, M., Kostopoulou, E., & Goodess, C. M. 2009. Climatic changes and associated impacts in the Mediterranean resulting from a 2 C global warming. Global and Planetary Change, 68(3), 209-224 https://doi.org/10.1016/j.gloplacha.2009.06.001.

González-Sánchez E., Moreno-García M., Kassam A., Holgado-Cabrera A.,Triviño-Tarradas P., Carbonell-Bojollo R., Pisante M., Veroz-González O., Basch G. 2018. Conservation Agriculture: Making Climate Change Mitigation and Adaptation Real in Europe. European Conservation Agriculture Federation (ECAF). www.ecaf.org

Goula I.M., Gougoulias N., Cavalaris C., Gemtos, Th, Pateras D., Chouliaras, N. 2020. Effect of crop rotations and soil tillage to soil organic matter and nutrients availability. Interciencia Journal 2020 4(1)

Hadjimitsis D.G., Retalis A., Michaelides S., Tymvios F., Paronis D., Themistocleous K., Agapiou A. 2013. Satellite and Ground Measurements for Studying the Urban Heat Island Effect in Cyprus, Chapter 1 In: Hadjimitsis DG. (Eds.), Remote Sensing of Environment - Integrated Approaches, InTech. https://doi.org/10.5772/39313

Lelieveld, J., Proestos, Y., Hadjinicolaou, P., Tanarhte, M., Tyrlis, E., & Zittis, G. 2016. Strongly increasing heat extremes in the Middle East and North Africa (MENA) in the 21st century. Climatic Change, 137(1), 245-260. https://doi.org/10.1007/s10584-016-1665-6

LIFE Rizoelia. 2017. LIFE12 NAT/CY/000758, http://www.liferizoelia.eu

Harmonising agroecology and digitalisation for sustainable European agriculture

Andreas Meyer-Aurich[a*], Friederike Schwierz[a], Alma Moroder[b], Jochen Kantelhardt[c], Karl Reimand[c], Søren Marcus Pedersen[d], Andrea Landi[d], Karl Behrendt[e], Elias Maritan[e], Andreas Gabriel[f], Spyros Fountas[g], Evangelos Anastasiou[g]

[a]Technology Assessment Department, Leibniz Institute for Agricultural Engineering and Bioeconomy (e.V.) (ATB), Potsdam, Germany

[b] Land Use and Governance, Leibniz Centre for Agricultural Landscape Research (ZALF), Müncheberg, Germany

[c]Institute of Agricultural and Forestry Economics, BOKU University of Natural Resources and Life Sciences, Vienna, Austria

[d]Department of Food and Resource Economics, University of Copenhagen, Copenhagen, Denmark

[e]Food, Land & Agribusiness Management Department, Harper Adams University, Newport, United Kingdom

[f] Institute for Agricultural Engineering and Animal Husbandry ,·Bavarian State Research Center for Agriculture, Ruhstorf a. d. Rott, Germany

[g]Department of Natural Resources Management & Agricultural Engineering, Agricultural University of Athens, Athens, Greece

* Corresponding author. Email: ameyer-aurich@atb-potsdam.de

Abstract

In response to pressing challenges faced by European agriculture such as biodiversity loss, pollution reduction, climate change, and the urgency to adapt to market dynamics amid ageing rural populations and labour shortages, there is a need to explore the transformative potential of digital tools and technology in fostering more sustainable agriculture.

Within the framework of the EU and UKRI funded Horizon Europe Coordination and Support Action, *Digitalisation for Agroecology* (D4AgEcol), a consortium comprising twelve partners from eight European countries, is actively investigating the potentials, barriers, and pathways for utilising digitalisation to enhance European agriculture, particularly through the lens of agroecology.

The ongoing project employs Digital Tool Scoping Workshops to engage farmers and stakeholders in the analysis of technologies such as virtual fencing, robots in arable farming, weed detection tools, and livestock health sensors. The workshops include an analysis of the compatibility of the selected technologies with the concept of agroecology, as well as the adoption potential among target groups of farmers. To date, these workshops, conducted in the UK, Denmark, Germany, Finland and Greece have involved more than 100 participants, including farmers, advisors, researchers, technology specialists, and other stakeholders.

Preliminary results from the workshops reveal promising opportunities for the analysed technologies, yet underscore challenges related to profitability and compliance with the agroecology concept. These include potential impacts on agroecological principles, in ways perhaps not planned during the development of the assessed digital tools. The consortium acknowledges the need for further analysis and stakeholder engagement across participating countries and aims to develop a roadmap that paves the way for the harmonious integration of agroecology and digitalisation in European agriculture.

Keywords: Multi-actor approach, policy roadmaps, adoption, digital tool scoping workshop, co-creation

1. Introduction

The transition towards sustainable agriculture in compliance with the concept of agroecology is one of the major challenges of European agriculture. Digitalisation can be a key enabler for achieving sustainable agricultural and food systems in Europe. However, there is limited available knowledge about how digital tools and technologies can facilitate this process. The concept of agroecology is currently dominating the discourse on the future of sustainable agriculture. While agroecology has been regarded as an area of scientific inquiry in the past, it is now also seen as a movement or a policy framework which shall address current problems in agriculture (Wezel et al., 2009). The Food and Agriculture Organisation of the United Nations (FAO, 2018) published a set of 10 elements of agroecology to guide the transformation to large-scale sustainable agriculture. These elements are being widely adopted and accepted by many stakeholders worldwide.

Digital tools and technologies can help address specific challenges in agriculture, which also enable agroecology and more sustainable farming (Rozenstein et al., 2024). For example, Spykman et al. (2023) highlighted how small robots can assist organic farmers in managing labour shortages for weed control in sugar beet cultivation. Additionally, the incorporation of robots into arable farming can yield environmental and social benefits (Spykman et al., 2021). In animal husbandry, digital tools and technologies are being widely used to monitor animal health (van Erp-van der Kooij and Rutter, 2020). For example, automated milking systems contribute to higher labour productivity and improved animal welfare (Cogato et al. 2021).

However, the adoption of technologies alone will not contribute to agroecology *per-se*, but rather, it needs a tailored framing by actors and stakeholders to develop agriculture towards agroecology (Tataridas and Freitas, 2024). Thus, there is a need to assess the potential impact of new digital tools and technologies on agroecology, which helps navigate the transition towards agroecology. In order to support this task the EU and UKRI funded Coordination and Support Action, "Digitalisation for Agroecology (D4AgEcol)" is investigating the potentials, barriers, and pathways for utilising digitalisation to enable agroecology in Europe. The consortium of eight European countries has coordinated Digital Tool Scoping Workshops to engage farmers and stakeholders in the analysis of technologies like virtual fencing, robots in arable farming, weed detection tools, and animal health sensors. Furthermore, roadmaps to guide action in science, policy, and the society are being developed (Landi et al., 2023).

2. Materials and Methods

In order to contribute information for actors and stakeholders on digital tools and technologies, the consortium has developed an online platformproviding an overview of available digital technologies which can contribute to agroecology. Furthermore, D4AgEcol developed a framework to simultaneously investigate the impact of digital tools and technologies on agroecology and their adoption by farmers (Figure 1). The framework, referred to as Digital Tool Scoping Workshops (DTSW), consists of structured analyses of specific technologies in collaboration with farmers, stakeholder and experts on digitalisation and agroecology. Where appropriate, this is supported through the preliminary analysis of the impacts of the digital technology on economic and environmental outcomes (e.g. Maritan et al. 2023, Maritan et al. 2024a, Maritan et a. 2024b). The consortium has identified 10 technologies (e.g., robot applications, sensors in animal husbandry, site-specific fertilizer application and prognostic models/decision support tools), which are being investigated within the DTSW framework. At the time of writing, most of the workshops have been completed.

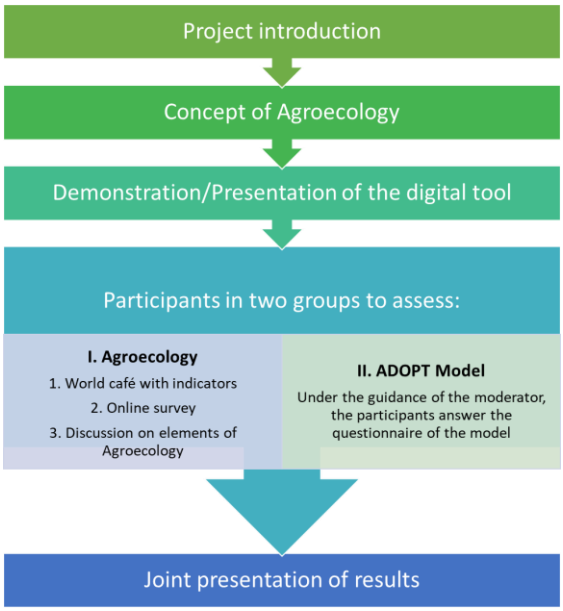

Figure 1 Digital Tool Scoping Workshop framework: Multi-actor approach designed to assess the agroecological implications of a specific digital technology simultaneously to the quantification of the potential peak adoption and time to peak adoption of the technology in a specific region.

The analysis of the potential impact of the technologies are investigated in a world-cafe format based on indicators developed by the D4AgEcol consortium (Moroder et al., 2024). In parallel, a group of farmers analyse the adoption potential of the innovation based on expected financial capacities of the farmers and their specific attitudes following the ADOPT procedure (Kuehne et al. 2017). At the end of the DTSW, the results of the two groups are exchanged to enable the co-design of outcomes in a joint session.

3. Results and Discussion

Preliminary results of the DTSWs showed that the potential of digital tools and technologies to enable agroecology substantially depends on the technology under investigation. For example, mechanical weeding robots can support the viability of organic farming systems, especially where there is limited availability of workers for manual weed control. However, the analysis of a specific weeding robot (e.g., FD20) showed that this technology possesses some drawbacks that limit its adoption potential. For example, high costs and low operating speeds appear to hamper the adoption of weeding robots in arable systems (Maritan et al., 2023). Furthermore, among other factors, a low degree of trialability and high complexity in handling the technology hamper its adoption. For a sound understanding of the impacts of this technology on agroecology, the available knowledge is too limited to confidently understand its impact on the complex aspects of agroecology. Similar insights have also been discovered with other technologies. In general, when digital technologies are targeted to sustainable but rarely used practices such as crop robots suited for strip intercropping, the result is a double innovation that further demotivates adoption of agroecologically desirable digital tools. In other words, the process of agroecological digitalisation should start from technically unchallenging and more widespread tools and practices. Specific downsides of technologies have to be kept in focus to ensure the potential positive effects of digital tools and technologies are realised.

4. Conclusions

Digital tools and technologies can make a contribution to agroecology. However, available knowledge of the effects of specific tools and technologies on agroecology is limited, This in turn makes it difficult to steer the development of agroecological practices within European agriculture. The DTSWs have illustrated the potentials and downsides of a limited range of selected technologies. There is currently wide scope for producing more evidence for the complex interactions between different farming systems, digital tools and agroecological principles. Building on the experience matured during the DTSWs, the D4AgEcol consortium will further interact with stakeholders and policymakers to identify key barriers to the widespread adoption of agroecological farming in Europe.

Acknowledgements

This research has received funding from the European Union's Horizon Europe research and innovation programme under grant agreement No.101060759, D4AgEcol – Digitalisation for Agroecology and co-funded by UK Research and Innovation (UKRI Reference No.10037994).

References

Cogato, A., M. Brščić, H., Guo, F., Marinello, F and A. Pezzuolo. 2021. Challenges and Tendencies of Automatic Milking Systems (AMS): A 20-Years Systematic Review of Literature and Patents. Animals. 2021; 11(2):356. https://doi.org/10.3390/ani11020356

FAO (2018). The 10 elements of Agroecology: Guiding the transition to sustainable food and agricultural systems. FAO, Rome, Italy. p 15. https://openknowledge.fao.org/handle/20.500.14283/i9037en

Kuehne G., Llewellyn R., Pannell D., Wilkinson R., Dolling P., Ouzman J., Ewing M., 2017. Predicting farmer uptake of new agricultural practices: A tool for research, extension and policy, *Agricultural Systems* 156:115-125. https://doi.org/10.1016/j.agsy.2017.06.007

Landi, A., Anastasiou, E., Aviziotis, I., Behrendt, K., Borchard, N., Kantelhardt, J., Pedersen, S.M., Pesonen, L., Reimand, K., Santos Silva, C., Schwierz, F., Meyer-Aurich, A. (2023) Digitalisation for Agroecology: Agenda for an inclusive policy roadmap. In: K. Behrendt, D. Paparas, A. Mumbi, N. Hill, and J. Lowenberg-DeBoer (eds.) *Proceedings of the 6th Symposium on Agri-Tech Economics for Sustainable Futures*. Global Institute for Agri-Tech Economics, Food, Land & Agribusiness Management Department, Harper Adams University. HAU Publications, Newport, United Kingdom, 18-19 September 2023, pp 41-46.

Maritan, E., Behrendt, K. and Lowenberg-DeBoer, J., 2024a. A preliminary economic and environmental analysis of virtual fencing for intensive lowland grazing. *The 98th Annual Conference of The Agricultural Economics Society*, University of Edinburgh, UK, 18th - 20th March 2024.

Maritan, E., Hoffmann, G., Schwierz, F., Rutter, M., Meyer-Aurich, A., Lowenberg-DeBoer, J., Behrendt, K., 2024b. An economic analysis of bolus-sensor technology for precision dairy cattle management. *AgEng2024 International Conference of EurAgEng*, 1-4 July 2024, p 9.

Maritan, E., Lowenberg-DeBoer, J., Behrendt, K., 2023. A multi-objective optimisation analysis of autonomous mechanical weeding in arable farming. In: K. Behrendt, D. Paparas, A. Mumbi, N. Hill, and J. Lowenberg-DeBoer (eds.) *Proceedings of the 6th Symposium on Agri-Tech Economics for Sustainable Futures*. Global Institute for Agri-Tech Economics, Food, Land & Agribusiness Management Department, Harper Adams University. HAU Publications, Newport, United Kingdom, 18-19 September 2023, pp 147-151.

Moroder, A., Bellingrath-Kimura, S., Reimand, K., Kantelhardt, J. and A. Meyer-Aurich, 2024. Assessing the contribution of digital technologies to agroecological principles in the European context. In *Referate der 44. GIL-Jahrestagung*. Stuttgart-Hohenheim, Feb 27.-28. Bonn: GI. Eds. C. Hoffmann, A. Stein, E. Gallmann, J. Dörr, C. Krupitzer and F. Floto, 347-352.

Rozenstein, O.; Alchanati, V.; Behrendt, K.; Bonfil, D.J.; Cohen, Y.; Eshel, G.; Harari, A.; Harris, W.E.; Klapp, I.; Laor, Y.; Linker, R.; Paz-Kagan, T.; Peets, S.; Rutter, S.M.; Salzer, Y.; Lowenberg-DeBoer, J. (2024). Data-Driven Agriculture and Sustainable Farming: Friends or Foes? *Precision Agriculture*. 25:520-531. https://doi.org/10.1007/s11119-023-10061-5

Spykman, O., A. Gabriel, M. Ptacek, and M. Gandorfer, 2021. Farmers' Perspectives on Field Crop Robots – Evidence from Bavaria, Germany. Computers and Electronics in Agriculture 186 (2021/07/01/ 2021): 106176.

Spykman, O., A. Roßmadl, J. Pfrombeck, S. Kopfinger and A. Busboom. 2023. Wirtschaftlichkeitsbewertung eines Feldroboters auf Basis erster Erfahrungen im Praxiseinsatz. In *Referate der 43. GIL-Jahrestagung*. Osnabrück, Feb 13.-14. Bonn: GI. Eds. C. Hoffmann, A. Stein,A. Ruckelshausen, H. Müller, T. Steckel and H. Floto, 255-265.

Tataridas, A. and H. Freitas. 2009. The path forward: integrating agroecology into global policy frameworks. Agroecology and Sustainable Food Systems, 1-10.

van Erp-van der Kooij, E. and Rutter, S.M. 2020. Using precision farming to improve animal welfare. *CAB* Reviews, https://doi:10.1079/PAVSNNR202015051.

Wezel, A., S. Bellon, T. Doré, C. Francis, D. Vallod and C. David. 2009. Agroecology as a science, a movement and a practice. A review. Agronomy for Sustainable Development 29, 503-515.

Mechanical termination of cover crops - Corn cultivation for less erosion and less herbicide use

Markus Demmel*, Hans Kirchmeier
Bavarian State Research Center for Agriculture, Institute for Agricultural Engineering and Animal Husbandry
* Corresponding author. Email: markus.demmel@lfl.bayern.de

Abstract

Soil erosion control requires the soil to be covered with plant residues / organic material (>30% soil cover) and therefore no-till, min-till or mulch-till in combination with cover crops are necessary. Typically, no-till, min-till and mulch-till with or without cover crops require the use of a non-selective herbicide (e.g.: Glyphosate) before planting corn to reach good germination and perfect plant growth. The European Green Deal and the Farm-to-Fork strategy require a reduction of pesticide resp. herbicide use as well as a maximal control of erosion. To solve this conflict of goals a project was conducted to investigate the possibilities and limits of different measures to mechanically terminate cover crops to reduce the use of herbicides as well as ensures high erosion control.

Field trials on two locations have been conducted over four years. Three factors and their combinations have been investigated: The factors were catch crop / cover crop (4 variants), methods of termination (3 variants), and herbicide strategy (3 variants). All 36 factor combinations have been repeated 4 times and randomised at each location. Corn germination, soil coverage, weed coverage, plant height, and corn yield have been measured and statistically analysed.

The investigations showed that there are measures and options to reduce the use of herbicides and optimize erosion control at the same time without significantly reducing the yield. This includes the cultivation of winter cover crops, which offer better erosion control in spring and the use of a knife roller / roller crimper or mulching mower to terminate them. The study has shown that good field emergence and yields can be achieved without seedbed preparation and without the use of a non-selective herbicide. Shallow seedbed preparation (mulch-tillage) increased corn yields significantly but also reduced erosion control clearly.

Therefore, the recommendation is to establish dense and lush (hardy) cover crops, even if there is only a small risk of erosion, but also to be able to reduce herbicide use. In dry years or dry regions, it can be difficult to establish optimal cover crop stocks. They must be free of weeds and volunteer grains, that terminating with a roller crimper or mulching mower and reduced herbicide use brings the desired success.

Keywords: Corn production, erosion control, herbicide reduction, conservation tillage.

1. Introduction

In Bavaria and many other Western European Regions, alongside winter wheat, maize is a main crop and is grown in almost all locations. However, in addition to its many advantages, maize has one decisive disadvantage. Because it is sown late in the spring and the rows do not close until June, it is particularly exposed to erosion during the heavy rain and critical thunderstorm periods in late spring and early summer. To prevent soil erosion in row crops, an optimal soil structure and a soil cover of >30% organic material is required. These conditions can usually only be achieved with mulch tillage with gentle or completely without seedbed preparation ("direct sowing"). To control the old weeds, either a non-selective herbicide is applied and/or mechanical tillage is carried out before sowing. In the context of further EU efforts to reduce the use of chemical pesticides and against the background of the controversial discussion about the further authorisation of the active ingredient glyphosate, alternative strategies are required to control old weeds especially in mulch tillage (preferably completely without seedbed preparation).

2. Materials and Methods

The Bavarian State Research Centre for Agriculture conducted research into such alternatives in a project from 2019-2022 funded by the Bavarian State Ministry of Food, Agriculture, Forestry and Tourism.

Following a comprehensive preliminary trial, promising variants were selected and compared with standard methods. The factors "catch crop / cover crop" (freezing mixture, winter turnip rape, winter peas and winter incarnate clover + winter vetches), "cover crop treatment" (knife roller / roller crimper, mulcher, mulcher + power harrow) and "herbicide strategy" (untreated/control, maize herbicide, non-selective herbicide + maize herbicide) were investigated in a comprehensive, randomised large plot trial (plot size 30 m x 3 m) at 2 locations with 144 plots each.

Table 1. Factors of the field trials 2019-2022.

Factor	Variants	Abbreviation
Catch crop / Cover crop	GeoVital MS100 A (freezing mixture)	MSA
	Winter turnip rape seed	RUE
	Winter peas	EFB
	Winter incarnate clover + winter vetches	TAR
Treatment / Tillage	Knife roller / Roller crimper	MW
	Mulcher	MU
	Mulcher + power harrow	KE
Herbicide strategy	Control (without any herbicide)	UK
	Non-selective herbicide + maize herbicide	GLY
	Maize herbicide	SH

The selected catch crops / cover crops were sown after the cereal harvest on two dates (GeoVital MS100A and winter turnip rapeseed in early August; winter peas and winter incarnate clover + winter vetches in late August). In the spring before maize sowing, these were terminated (knife roller, mulcher) and then either the maize was sown directly without tillage (with well-equipped precision seed drills suitable for mulch sowing) or, in one variant, the soil was tilled beforehand with a power harrow after mulching (Figure 1). In the variant “non-selective herbicide + maize herbicide), the respective catch crop was treated before the maize was sown with a non-selective herbicide. The individual herbicide application took place after field emergence. During the entire vegetation period, various parameters were recorded, and assessments carried out. Finally, a plot of grain maize was harvested (core threshing) with yield and moisture determination.

Figure 1. left: Knife roller / roller crimper in winter peas, middle: Mulcher in winter turnip rape, right: Power harrow after mulcher in Geo Vital MS 100A.

3. Results and Discussion

In the following, the results are broken down into the 3 factors described above (table 1). Figure 2 (Factor ‘Cover crop / catch crop’), for example, shows the degree of soil cover broken down by the 4 individual catch crops. Each bar contains all values of the respective plots with this one catch crop, regardless of whether with or without weed control and regardless of whether with knife roller, mulcher or mulcher + power harrow. The same applies to the two other factors ‘treatment’ (Figure 3) and ‘herbicide strategy’ (Figure 4).

3.1. Soil cover with organic material

The first parameter determined after maize sowing was the degree of soil cover with the catch crop / cover crop mulch. Here there were some clear differences with regard to the catch crop. The degree of soil cover

was significantly lowest at around 42% after the freezing catch crop / cover crop (Figure 2).

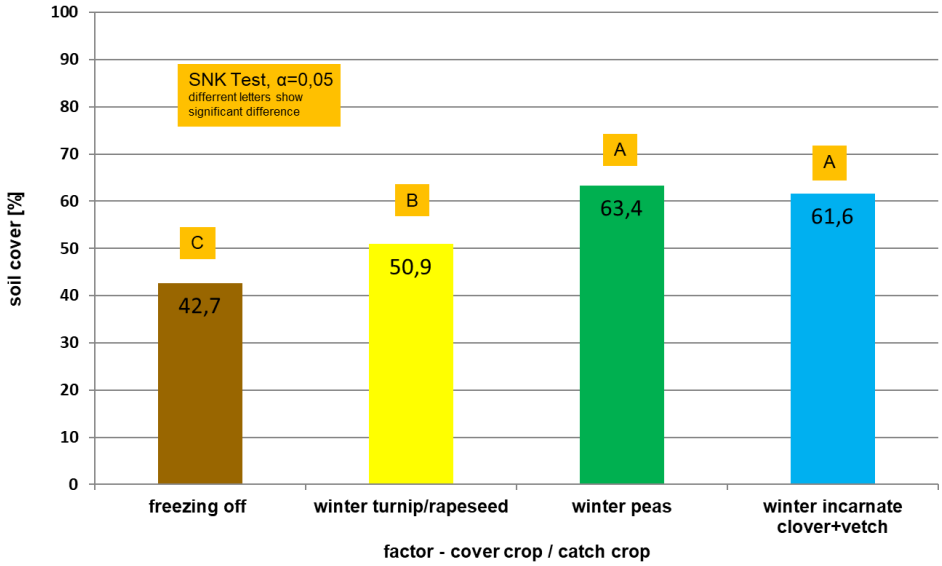

Figure 2. Soil cover with organic material after corn planting depending on cover crop / catch crop.

It was slightly higher for the turnips, which began to grow again in early spring and were able to provide slightly more material than the dead MS 100 A at the time of flowering. At a good 63% and 61% respectively, the value was 10% higher for the two legumes, which also continue to grow in spring (albeit much later than the turnips) and only really take off from May onwards. This increase (the wait until flowering) had to be paid for by sowing maize around 3 - 4 weeks later than the two legumes. Due to the somewhat later sowing of the two legumes in October as a catch crop, the crop failure rate was generally lower, but the erosion protection in autumn and winter was also significantly lower than with the turnips and MS 100 A.

The tillage factor (Figure. 3) before maize sowing also had an enormous effect on the degree of soil cover in some cases. Compared to cultivation with the roller crimper / knife roller (69%) or the mulcher (65%), the average degree of soil cover after using the power harrow was only just under 30%.

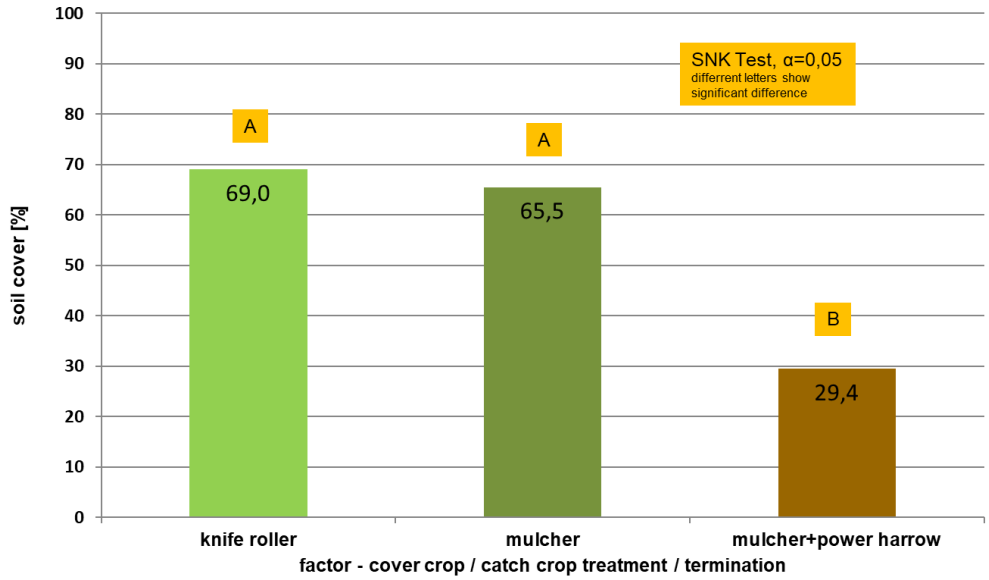

Figure 3. Soil cover with organic material after corn planting depending on treatment.

The crop protection factor also had an effect on the degree of soil cover (Figure 4). The use of a non-selective herbicide (e.g.: Glyphosate) on the catch crops reduced the degree of coverage by around 10% points to an average of 48% for all glyphosate plots. The (early) application stops the growth of the catch crops, causing the material to die and become brittle.

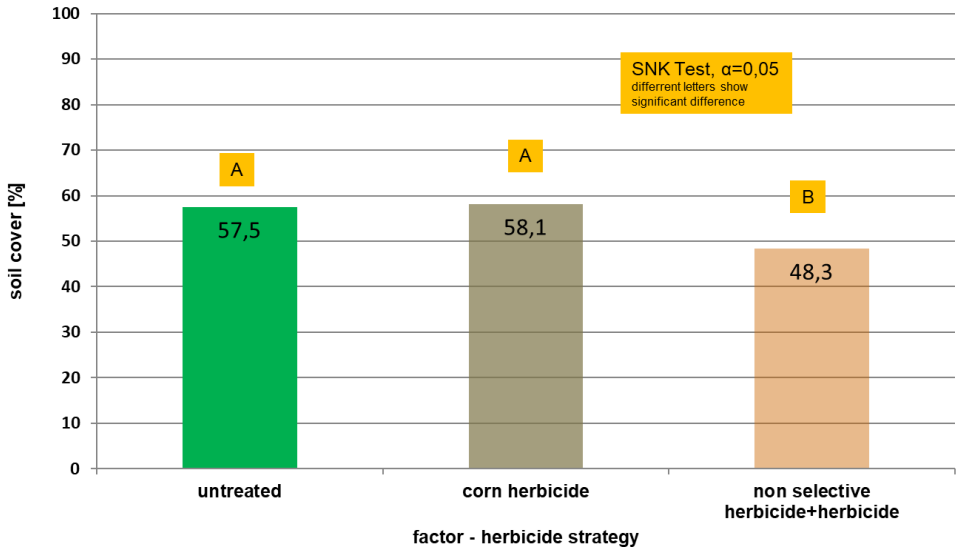

Figure 4. Soil cover with organic material after corn planting depending on herbicide strategy.

In addition, Figure 5 shows the soil cover of selected factor combinations to illustrate the interaction of cover crop / catch crop, the treatment or way of termination and the herbicide strategy.

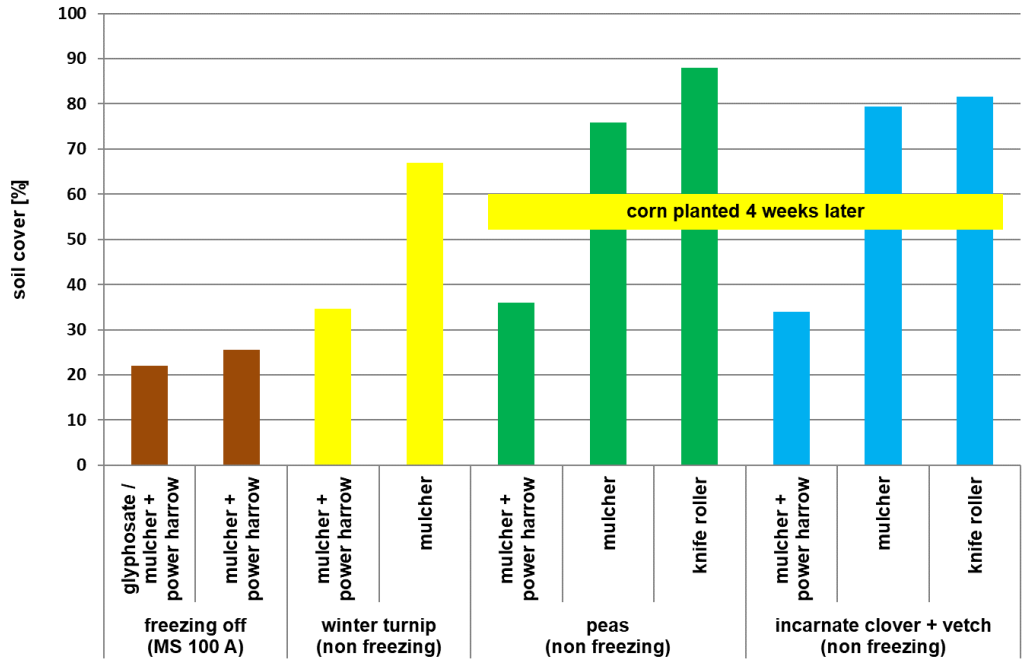

Figure 5. Soil cover of selected factor combinations.

3.2. Field emergence

There were slight differences in field emergence for the cover crop / catch crop factor. Turnip rape showed a significantly positive result. This may be due to the fact that the turnips were easier to cultivate than the lush and tough legumes. In addition, they showed better volunteer grain suppression, which also had a positive effect on cultivation and thus field emergence. There was no difference in field emergence between the maize after the knife roller and mulcher, but the maize field emergence after the roundabout harrow was around 10% points better. The use of herbicides also improved field emergence by around 10%, as this obviously reduced or eliminated weed competition on the maize. Results for selected factor combinations are shown in Figure 6.

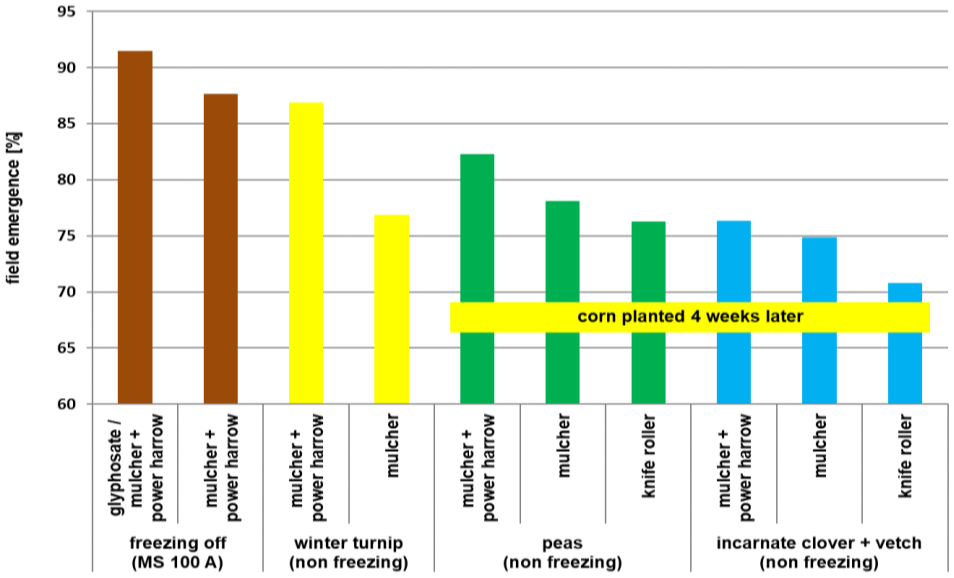

Figure 6. Field emergence of selected factor combinations.

3.3. Weed suppression and residual weed

The good soil cover of the two legumes also had a positive effect on weed suppression (measured in the residual weed cover after the herbicide treatments). At around 20% for the legumes, this was significantly lower than for the turnips (29%) and the MS 100 A (38%) (Figure 7).

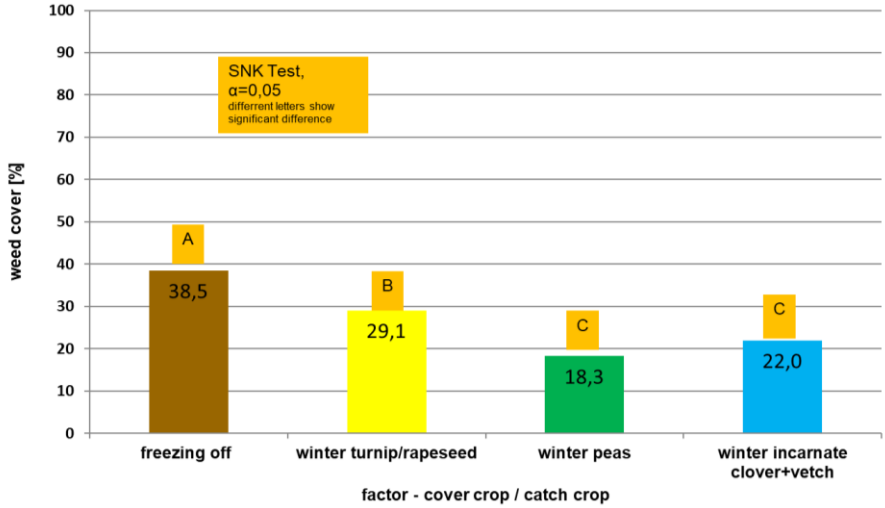

Figure 7. Weed suppression and residual weeds depending on cover crop / catch crops.

The cultivation of the catch crops and in particular the soil cultivation with the power harrow also had an influence on weed suppression and residual weed cover (Figure 8).

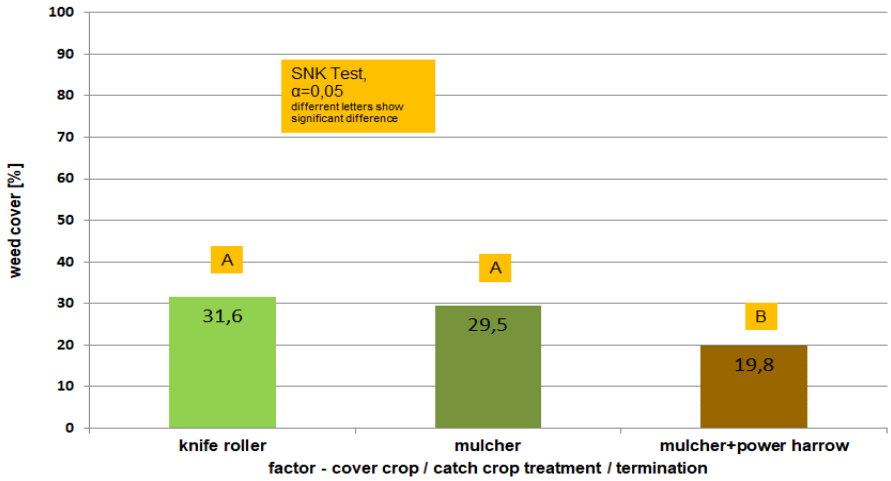

Figure 8. Weed suppression and residual weeds depending on treatment / tillage.

While the effect on catch crops, volunteer cereals and old weeds was limited in terms of destruction or resprouting by the knife roller (but also largely by the mulcher), the power harrow was able to achieve good effects here. The mulcher was at least able to kill off the flowering peas and turnips when working at a shallow depth. Without soil intervention (mulcher, knife roller), the maize herbicide applied often hit the robust 'old weed' and the effect was correspondingly moderate (as can be seen from a residual weed coverage of approx. 30%). After cultivation with the power harrow, it was mainly newly germinating weed (in the cotyledon stadium) against which the maize herbicide was more successful (residual weed coverage approx. 20%). Broken down according to the herbicide factor, the following picture emerged (Figure 9).

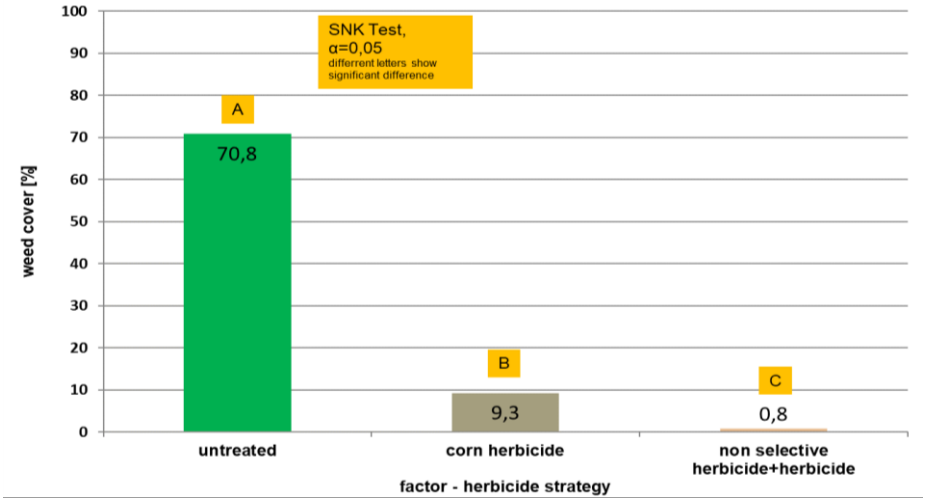

Figure 9. Weed suppression and residual weeds depending on herbicide strategy.

When a non-selective herbicide (e.g.: glyphosate) was applied to the catch crops, the residual weed coverage in maize was only 0.8% on average. The non-selective herbicide was able to eliminate not only the overwintering catch crop, but also the old weeds and volunteer cereals (even without tillage). Newly germinating weeds in maize were thus well controlled. Without it, weed coverage increased to 9.3% in the pure post-emergence variant. In the untreated maize control plots, an average of 70.8% of the soil was covered with weeds (volunteer cereals, living catch crop). Results for selected factor combinations are shown in Figure 10.

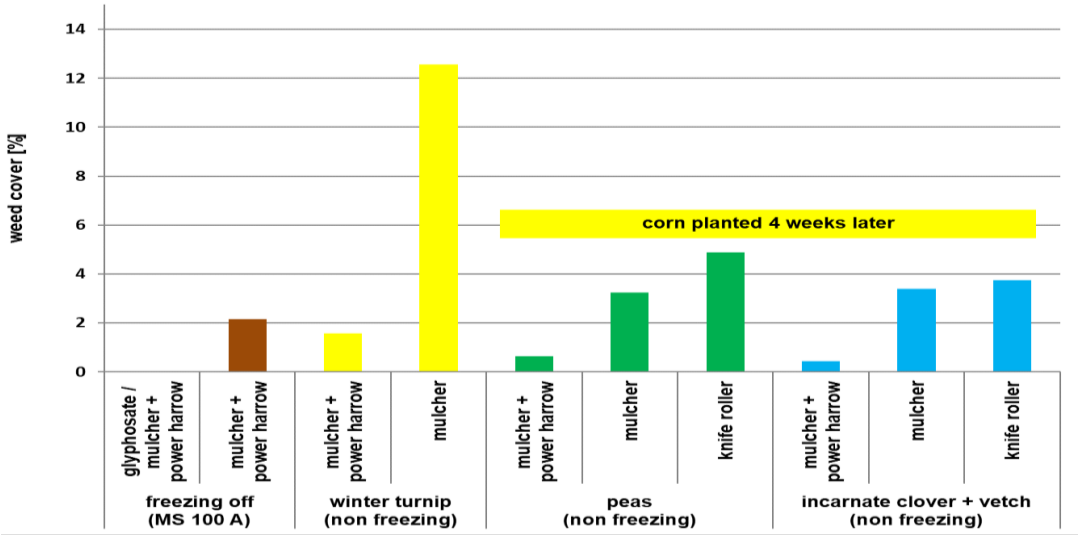

Figure 10. Weed suppression and residual weeds of selected factor combinations.

3.4. Grain maize yield

In addition to the expected results, there was also a surprise in terms of grain maize yield. For example, the yield after the catch crops peas (9.7 Mg/ha on average across all varieties) was significantly highest, although the maize could only be sown delayed in mid to late May. Due to the generally warmer temperatures in May, the late-sown maize was able to germinate very quickly and grow without interruption (usually no more cold phase). The early-sown maize after the turnip rape (8.9 Mg/ha) and the MS 100 A (8.3 Mg/ha) was significantly lower in yield on average. The very good yielding varieties (power harrow + herbicide and/or glyphosate) of MS 100 A could not raise the average of all plots as much, as the untreated controls in particular were very poor. This can be explained by the high degree of weed cover in or with the freezing catch crop. The knife roller and mulcher also had hardly any reducing influence on the weed occurrence and thus also on the yield. The soil loosening and warming effect explains why the average yield of all variants was around 1.5 Mg/ha higher with the powere harrow. The influence of herbicide use on yield was also clearly significant. In the untreated plots, the yield averaged a good 7.0 Mg/ha, with herbicide a good 9.4 Mg/ha and with additional glyphosate in the catch crop a good 10.1 Mg/ha. Results for selected factor combinations are shown in Figure 11.

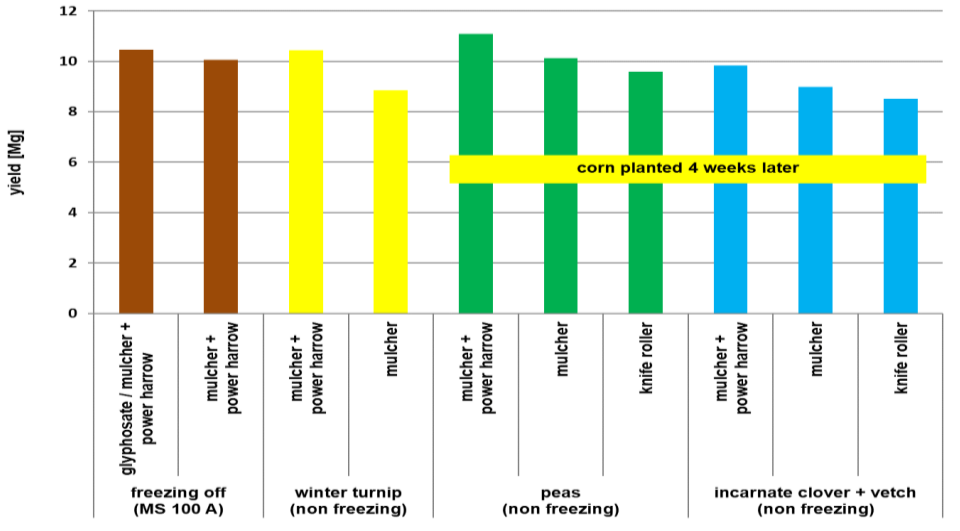

Figure 11. Corn yield of selected factor combinations.

4. Conclusions

The results have shown that there are many ways to reduce the use of pesticides and at the same time optimise erosion control without jeopardising yields too much. These include the cultivation of non-freezing catch crops, which can offer significantly more erosion protection and good weed suppression in spring thanks to a denser mulch layer.

The starting point, even before the maize is planted, is the selection of a suitable catch crop / cover crop. There were already clear differences in the growth in autumn. While the two earlier sown and faster growing catch crops already formed a dense stand in autumn, the later sown crops (e.g.: winter peas and winter incarnate clover + winter vetches) did not grow properly until (late) spring, but then formed better (later!) erosion protection. The additional and later tillage for sowing (at the beginning of October) resulted in less volunteer cereals.

Tillage before maize sowing also had an influence on the degree of soil cover. Although the mulcher shredded the material much more than the knife roller, the differences in the degree of soil cover were small. In contrast, the additional use of the power harrow significantly reduced the value. As the non-selective herbicide also had a clearly negative influence on the ground cover, it is not advisable to use it on an already poor catch crop. This is because, on the one hand, the non-selective herbicide immediately stops the growth of the catch crop and there is less emergence for maize sowing. On the other hand, treated plants - the subsequent mulch material - degrade more quickly and crumble more easily during cultivation. The time of treatment should therefore be as close as possible to maize sowing. Another contradiction can arise here with non-overwintering catch crops, some of which are heavily interspersed with volunteer cereals that can only be controlled by (intensive) tillage or a non-selective herbicide.

The results thus emphasise the importance of a well-growing, lush catch crop that is as free of weeds and volunteer cereals as possible and the associated dense mulch cover. The use of a non-selective herbicide would allow a reduction or omission of tillage, as volunteer cereals, weeds and further growing catch crops are reliably terminated. For direct sowing or mulch sowing, the omission of glyphosate means that an important component will be missing, which in many cases will be replaced by increased tillage. The study has again shown that good field emergence and yields can be achieved with tillage. However, erosion protection decreases very quickly. The recommendation is therefore to use dense and lush (winter-hardy) catch crops, especially where there is a risk of erosion, but also to reduce the use of crop protection products. In dry years or regions, it can be quite difficult to establish optimal catch crop stands. These must be as free of weeds and volunteer cereals as possible so that (reduced) cultivation with a knife roller or mulcher can bring the desired success. Only with shallow and less intensive tillage are soil cover rates of over 30% possible with very good catch crop stands.

Acknowledgements

The research project was financially supported by the Bavarian State Ministry of Food, Agriculture, Forestry and Tourism (A/17/10). The authors would particularly like to thank the staff of the Bavarian State Farm Achselschwang and the farmers Mayerhofer Parschalling and Diewald Kettenham for their dedicated and active support.

References

Ashford, D. L., D. W. Reeves, 2003. Use of a mechanical roller-crimper as an alternative kill method for cover crops. American Journal of Alternative Agriculture. Vol.18, No. 1, 37-45.

Laflen, J.M., M. Amemya, E.A. Hinz, 1981. Measuring crop residue cover. Soil and water conservation. Vol. 36, 341 - 343.

Bayerische Landesanstalt für Landwirtschaft, 2017. Zwischenfruchtanbau zum Erosions- und Gewässerschutz. LfL Information, 5. Auflage.

Boessl, F.-J. 2020. Winterruebsen als Lebendmulch. LOP, No. 6, 40-43.

N.N., 2014. Direkt in die Zwischenfrucht saen. LOP. 2012, No. 6; 4-13.

FiBL, 2024. Direktsaat von Mais im Biolandbau. Report.

Bayerische Landesanstalt für Landwirtschaft, 2024. Anwendungsbestimmungen gegen Abschwemmung. https://www.lfl.bayern.de/ips/recht/102762/index.php

Effect of solar panels on fruit quality for photovoltaic greenhouses

Pablo González-Planells [a *], Coral Ortiz [a], Francisco Rovira-Más [a], Elena Chaveli-López [c], Carmina Reig [c], Víctor Añón [b]

[a] Agricultural Robotics Laboratory, Universitat Politècnica de València, Valencia, Spain

[b] INDEREN, Ingeniería y Desarrollos Renovables, Valencia, Spain

[c] Mediterranean Agroforestry Research Institute, Universitat Politècnica de València, Valencia, Spain

* Corresponding author: pabgonpl@upvnet.upv.es

Abstract

Agricultural photovoltaic systems (APV) integrate crop production with energy production from photovoltaic technology. However, the effect of reducing solar radiation on fruit quality under the panels is still uncertain. This study investigates the impact of solar panels on fruit quality in an experimental agrivoltaic greenhouse located in Spain. The experimental design incorporates two high-value crops, dragon fruit and fig crop, under different support configurations, with three varieties of dragon fruit and one of figs. The fruits were harvested at their commercial harvesting stage, weighed, colour-evaluated, and analysed for mechanical firmness and soluble solid content. The results for dragon fruit showed a significant effect of the variety and significant lower sugar content and R-B colour components for fruits collected from the areas without solar panels. These outcomes suggest a potentially advantageous impact of solar panel coverage on dragon fruit quality. On the other hand, the results for fig crop showed that high-density coverage of solar panels significantly reduced fruit weight and productivity, whereas half-density coverage in a chessboard pattern resulted in a moderate reduction of weight without altering sugar content but reducing firmness. These results are promising for efficiently combining solar panels and agricultural production in greenhouses.

Keywords: Agrivoltaic, Dragon Fruit, ultra-intensive fig tree, circularity production, photovoltaic technology, data-driven agriculture.

1. Introduction

The agrivoltaic, or agricultural photovoltaic systems (APV), concept was early mentioned by Goetsberger and Zastrow (1982). However, after a period of declining interest over the past three decades, attention towards APV reignited in the early 21st century. This renewed interest was stimulated by advances in technology and cost-effectiveness of photovoltaic (PV) systems, resulting in a significant global increase in APV applications and research (Magarelli et al., 2024; Trommsdoff et al., 2022; UNEF, 2023). APV represents a promising solution for reducing the current reliance on energy-importing nations and mitigating the impacts of climate change, as well as promoting social cohesion by energetic communities in rural areas (UNEF, 2023). These systems offer solutions for promoting renewable energy and enhancing the sustainability of food production. Chalgynbayeva et al. (2023) propose APV as a means to alleviate drought stress on crops, thereby reducing water requirements and environmental strain while increasing food output.

According to Dupraz et al. (2011), there exist two types of APV systems. The first type involves splitting the land area into two parts, one devoted to food production and the other to PV production (ground-mounted PV). This type of separated production may be considered the dominant scheme till 2011 (Dupraz et al., 2011; Kuemmel et al., 1998). The second type combines photovoltaic parks and food production on the same land unit to enhance their integration. Photovoltaic panels can be configured in three different setups (Ali & Victoria, 2023). The first configuration is the **optimal tilted PV system**, where PVs are fixed at some angle (commonly 20º-30º) for the optimisation of solar radiation. The second is the **horizontal single-axis tracking PV system**, which can help the crops in physiologically sensible moments, such as flowering or sprouting (Ali & Victoria, 2023; Magarelli et al., 2024), as well as enhance electricity production since the panels track the azimuth angle to obtain the maximum solar radiation. The third configuration is the **vertical bifacial PV system**, where the panels are vertically set on a north-south orientation, leaving some sides oriented to the west and others to the east. Additionally, PV systems can vary in their density (Dupraz et al., 2011). **Half-density PV** feature a spatial distribution of panels to optimise solar radiation while minimising PV energy

loss yielding about 36 W/m^2, whereas **Full-density PV** optimise the panel spacing for an energy production of about 72 W/m^2. According to Trommsdoff et al. (2022), the investment cost depends on the APV configuration, with substructure, surface preparation, and installation being the main capital expenditures compared to ground traditional solar parks.

The shade generated in PV parks influences crop yield (Dupraz et al., 2011; Marrou et al., 2013; Trommsdoff et al., 2022). In particular, yield reduction depends on the type of crop, as some crops have more requirements in sunlight than others, such as C4 plants (Ali & Victoria, 2023; UNEF, 2023). APV offers a significant potential for high-value crops (vineyards, tree crops or horticulture). However, it can result in biomass reduction for apple orchards, and yield reductions in general (Juillon et al., 2022). A decrease in photoassimilates produces a limitation in fruit size, and thus important economic losses. However, not all plants behave similarly under shading conditions, so each case should be studied for each specific situation (Trommsdoff et al., 2022). On the other hand, some advantages have been related to APV systems. Shading reduces the hydric stress, leading to lower irrigation requirements and more favourable tree water status. In addition, PV structures protect the crop from hail, freezing damage, solar damage and fruit cracking due to rain (Ali & Victoria, 2023; Ramos-Fuentes et al., 2023; Trommsdoff et al., 2022; UNEF, 2023).

Fruit quality assessment is crucial to respond to market and consumer demands. Firmness, soluble solid content (SSC), acidity, and colour are the main postharvest parameters that generally determine fruit quality (Pereira et al., 2017). Fruits can be sorted according to quality through postharvest parameters and market requirements. There are limited results regarding the impact of PV shading on fruit quality within APV systems (Magarelli et al., 2024). Following Trommsdoff et al. (2022), viticulture can take advantage of PV-shading in arid and high-irradiance countries, since high solar radiation in vineyards provokes an increase of sugar content in grapes, resulting in a high alcohol content. However, in the case of apple orchards, PV shading produced a reduction in fruit size (Juillion et al., 2022). The objective of this article is to study the impact of three configurations of solar panels on dragon fruit and figs, with the purpose of confirming the suitability of APV for these two high-value crops.

2. Materials and Methods

An experimental APV greenhouse located in Valencia, Spain (39º 22’ 31.1’’; -0º 30’ 58.0’’), was divided into two sections with dragon fruit and fig crops. The dragon fruit section comprises three different varieties (*Nevada*, *Purple*, and *Thai*) randomly planted in four rows (Table 1), under alternating rows of solar panels mounted in the ceiling according to Figure 1. The plants were planted in the greenhouse in February 2023, when they were one year old. The plant spacing is 0.6 m between plants and variable between rows according to Fig. 1. Dragon fruit branches were supported by a trellised structure built with metallic shafts and wires. Dragon fruits must be manually pollinated with a specific tool by pollen of a different variety to avoid self-pollination (cross-pollination). This task is essential for maintaining high-quality fruits and proper yield production.

Table 1. Number of plants in each row per variety (Fig. 1).

Row	V. Purple	V. Thai	V. Nevada	APV	**Total Plants**
1	7	5	10	Under PV	23
2	6	7	7	Under PV	20
3	7	6	6	Under PV	20
4	6	5	3	Open	14
Total Plants	26	23	26		77

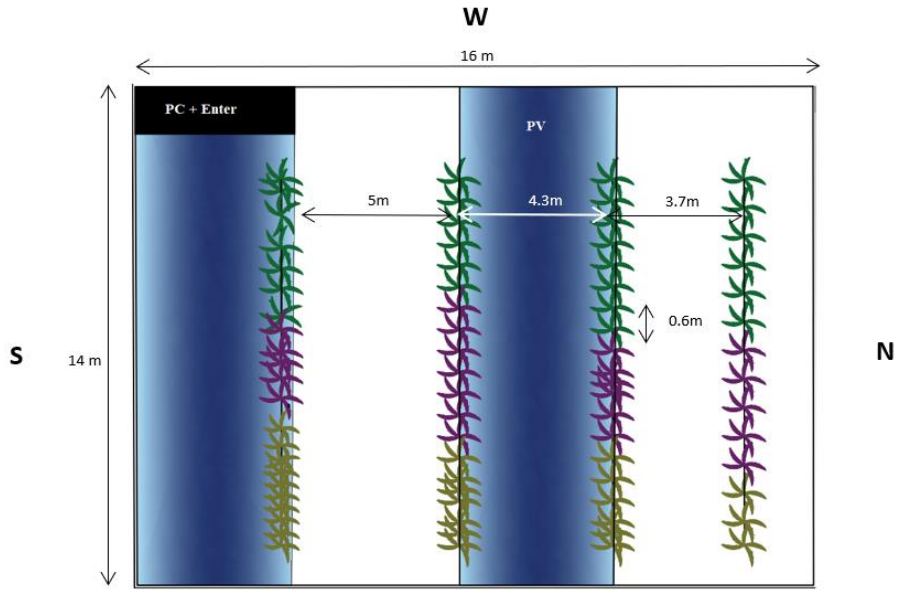

Figure 1. Dragon Fruit setup: open and (blue) full-density PV area; green plants correspond to *Purple* variety, magenta plants are *Thai* variety, and yellow plants are *Nevada* variety.

In the trellised intensive **fig crop**, only variety *B. Turkey* was planted in February 2023 (Table 2), with 100 % coverage of solar panels (Full-Density), 50 % coverage (Half-Density), and no solar panels (Control), distributed according to Figure 2. The plants were arranged in nine rows (23 plants per row), with a separation of 0.4 m between plants and 2-2.5 m between rows (Figure 2). The crop was pruned with three main branches per plant to ensure the proper production of figs in the 2023 season.

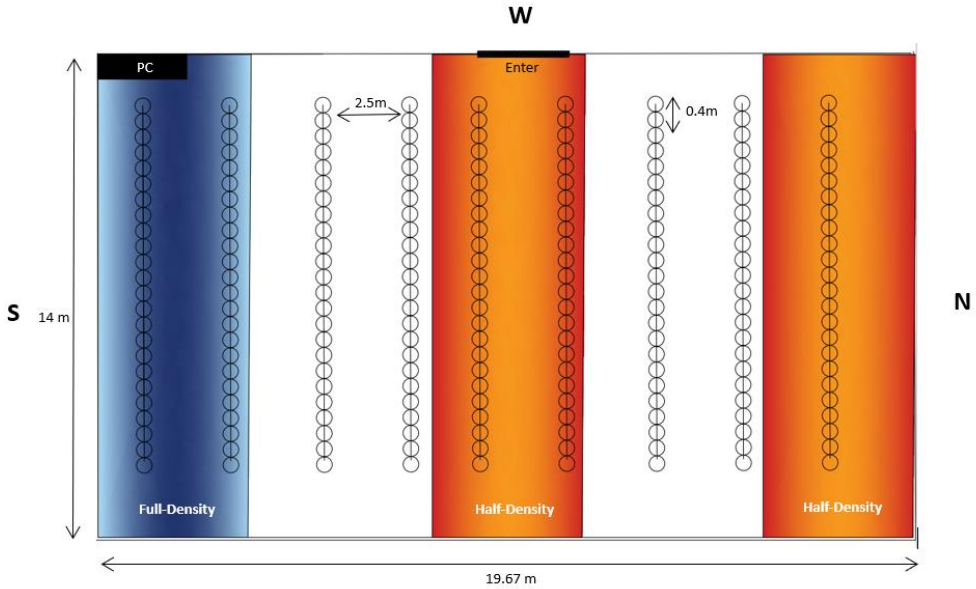

Figure 2. Intensive fig production: half-density PV (orange) and full-density PV (blue).

Table 2. Number of plants per row and row spacing. *: Control with PV partially influenced by FD

Row Number	Fig plants	APV	Row spacing (cm)
1	23	Full-Density	130
2	23	Full-Density	250
3	23	PV-influenced*	270
4	23	PV-influenced*	250
5	23	Half-Density	200
6	23	Half-Density	250
7	23	Control	260
8	23	Control	250
9	23	Half-Density	250
			250
Total Plants	207		

Drip irrigation with common fertilisers in the water (fertigation) was used according to local recommendations for both crops. The fruits were harvested according to their commercial ripeness stage. After harvesting, the fruits were carried to the laboratory for postharvest quality analysis. All the dragon fruits collected in the experimental greenhouse were tested, as well as a sample of 235 figs, for weight, colour, destructive mechanical firmness, and soluble solid content. Weight was measured using a digital balance (Mettler Toledo AL104, Im Langacher, Greifensee, Switzerland). Mechanical fruit firmness was measured with a universal stress-strain machine (IBTH 2730, Ibertest, Madrid, Spain), keeping a speed of 1.7 ms^{-1} at three points of the equatorial area, using a 0.008 m probe for flesh firmness and a 0.001 mm rod for skin firmness, making three repetitions per test and fruit. Fruit soluble solid content was determined with a digital refractometer (Atago PAL-3; Atago Co., Tokyo, Japan). For measuring colour in dragon fruit, an image analysis prototype (www.Greenvision.com) was used to assess fruit external R, G and B colour components. Fruit diameters were also measured for fig crops.

3. Results and Discussion

3.1. Dragon Fruit

A two-way ANOVA analysis was developed to study the effect of variety and row on the measured variables. For the weight, both factors significantly affected the size of the fruits (Figure 3), which was significantly higher for the Thai variety. Row 1 (under full panel coverage) produced fruits with significantly lower sizes (average 295.3 g compared to 365 g for the other rows). In terms of production, it was larger for rows 2 and 3, which experienced partial shading from PV panels, unlike row 1 (highest shading from panels) and row 4 (control), which were adversely affected by either excessive shading or exposure to sunlight. For the skin and flesh mechanical firmness, however, both factors significantly affected the firmness of the fruits (Figure 4), which was significantly lower for the Thai variety. Row number 1 (completely covered by solar panels) yielded fruits with significantly lower firmness. Only the variety had a significant effect on sugar content, as fruits from the Thai variety showed a higher sugar content, as plotted in Figure 5. The colour analysis showed that the red component was affected by the variety and the row. Fruits from row 4 without any panel coverage had a significant decrease in red component. This result (Figure 6) shows the capability of solar panels to effectively reduce the solar radiation in sensitive crops, such as dragon fruits.

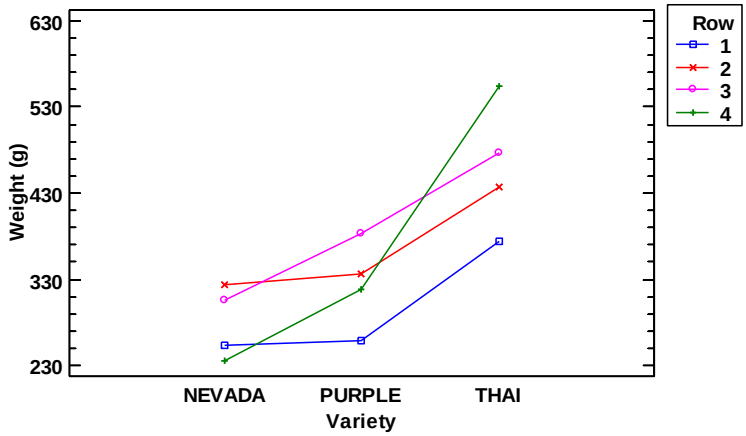

Figure 3. Interaction analysis on weight (g) (two-way ANOVA) for variety and row.

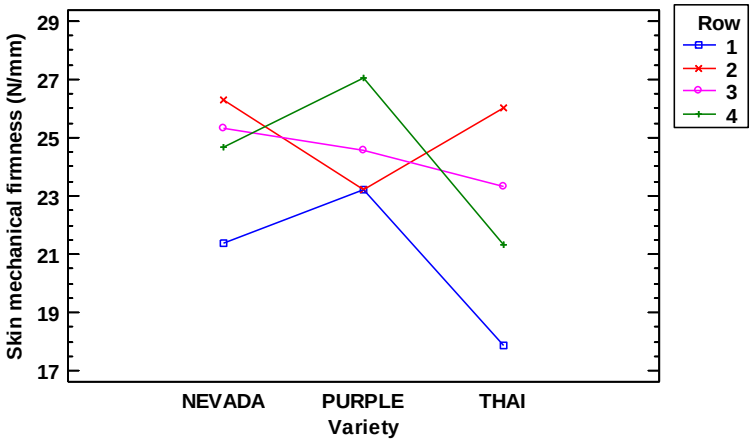

Figure 4. Interaction analysis of the effect of variety and row on skin mechanical firmness (N/mm).

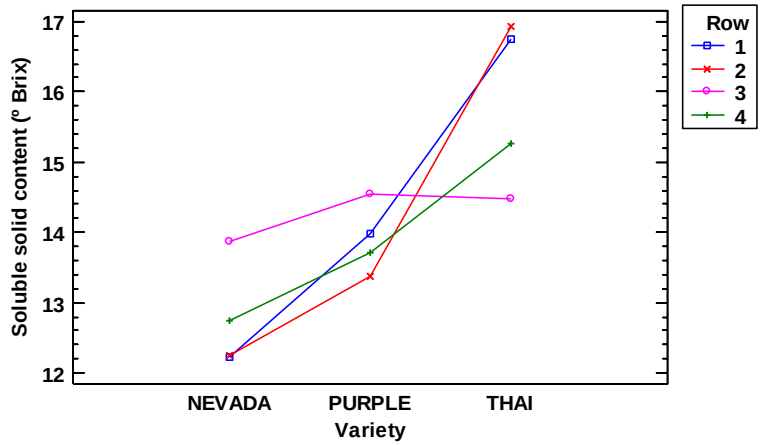

Figure 5. Interaction analysis of the effect of variety and row on soluble solid content (° Brix).

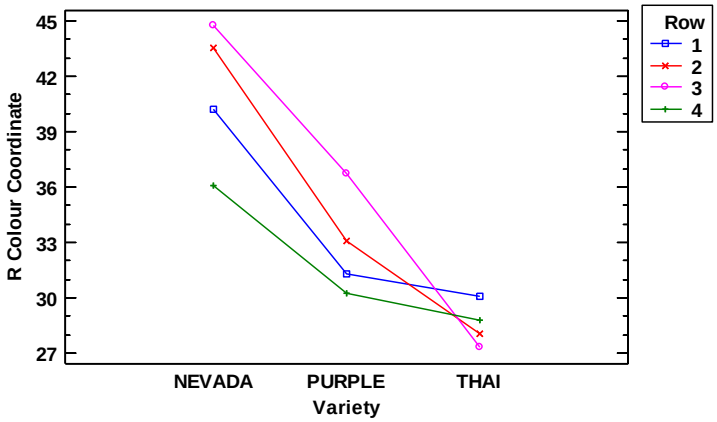

Figure 6. Interaction analysis of the effect of variety and row on red colour component.

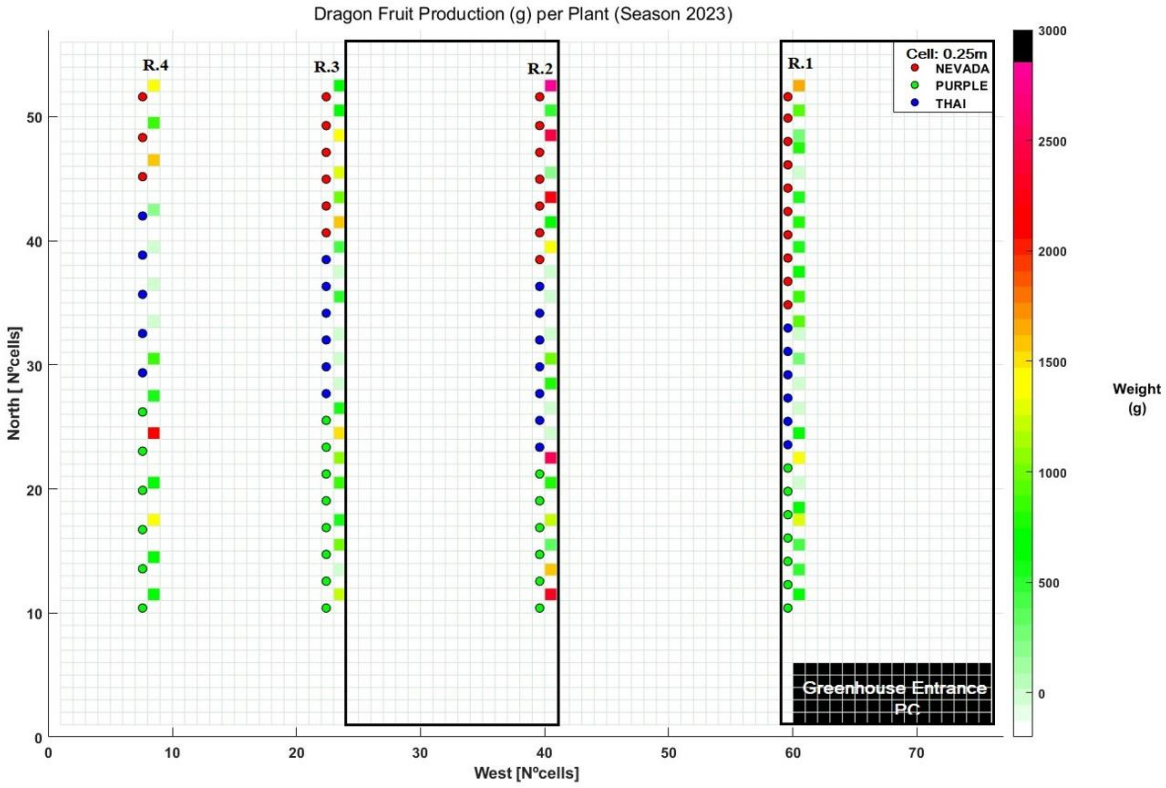

Figure 7. Crop productivity map of dragon fruit (weight of fruit per plant) in 2023 season.

The yield map of Figure 7 evidences that row 1, which experienced a major shading, and row 4, which is fully open, exhibit lower fruit production compared to rows 2 and 3. This pattern suggests that shading from PV installations influences fruit yield by reducing fruit weight. Conversely, the absence of PV panels in row 4 also correlates with lower fruit production due to a less optimised growth environment when compared to rows 2 and 3, which benefit from an intermediate balance of shade and sunlight.

3.2. Fig Crop

The fig fruits produced under the full-density (FD) coverage area had significantly lower weight, production and size, as indicate in Figure 9. The FD setup even affected neighbouring rows 3 and 4, initially set as open-air control, because of cast shade (Fig. 9). In order to account for such influence, the statistical

analysis considered the two control sections (open air) separately, resulting in four independent production areas: FD, HD, Control, and PV-influenced, where the latter represents open-air rows influenced by neighbouring full-coverage section. With this division of rows, there were statistical differences among the control and half-density categories as represented in Figure 8. Fig trees, having high solar radiation requirements, reduced productivity even under partial shading.

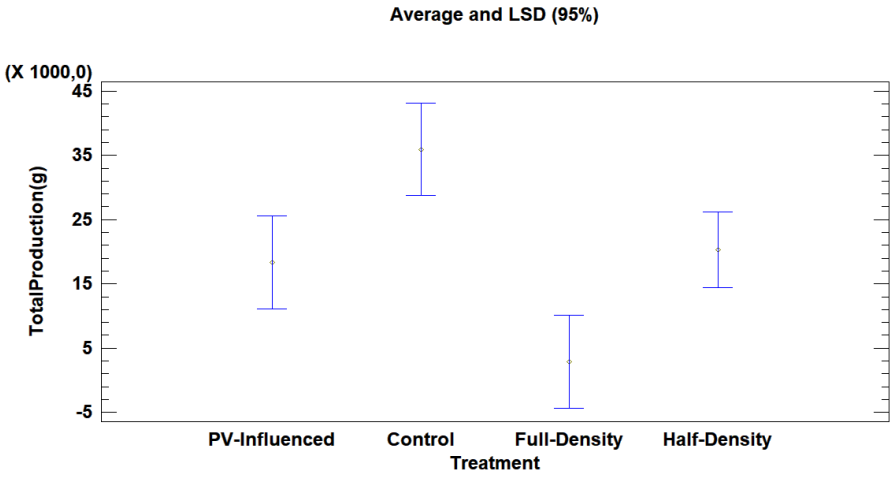

Figure 8. Average and LSD (95 %) total production (g) in the figs greenhouse.

The analysis of fig production per treatment revealed the highest yield for the control section, followed by half-density and PV-influenced with similar outcomes, being full-density significantly lower, and therefore unviable. As shown in Figure 9, productivity increases from row 1 to row 7. The first rows, having significant shading (FD), experienced a drastic reduction in productivity. Despite being uncovered, rows 3 and 4 did not achieve the high degree of productivity reached by rows 7 and 8, also uncovered, due to their proximity to the full-covered area (FD). Rows 5, 6, and 9 set under a semi-covered panel distribution in a chessboard arrangement (HD) yielded intermediate productivity levels, whereas fully uncovered rows 7 and 8 (control) had the highest productivity, as represented in Figure 9, with row 7 receiving the highest radiation and thus reaching the best productivity. In number of fruits, however, rows 7 and 8 did not show statistical differences. Related to fruit firmness and sugar content, no significant effect was found. The colour analysis of figs showed confusing results related to Cielab coordinates. This fact could be due to the difficulty in selecting the appropriate number of representative measuring points compared to the procedure followed with dragon fruits.

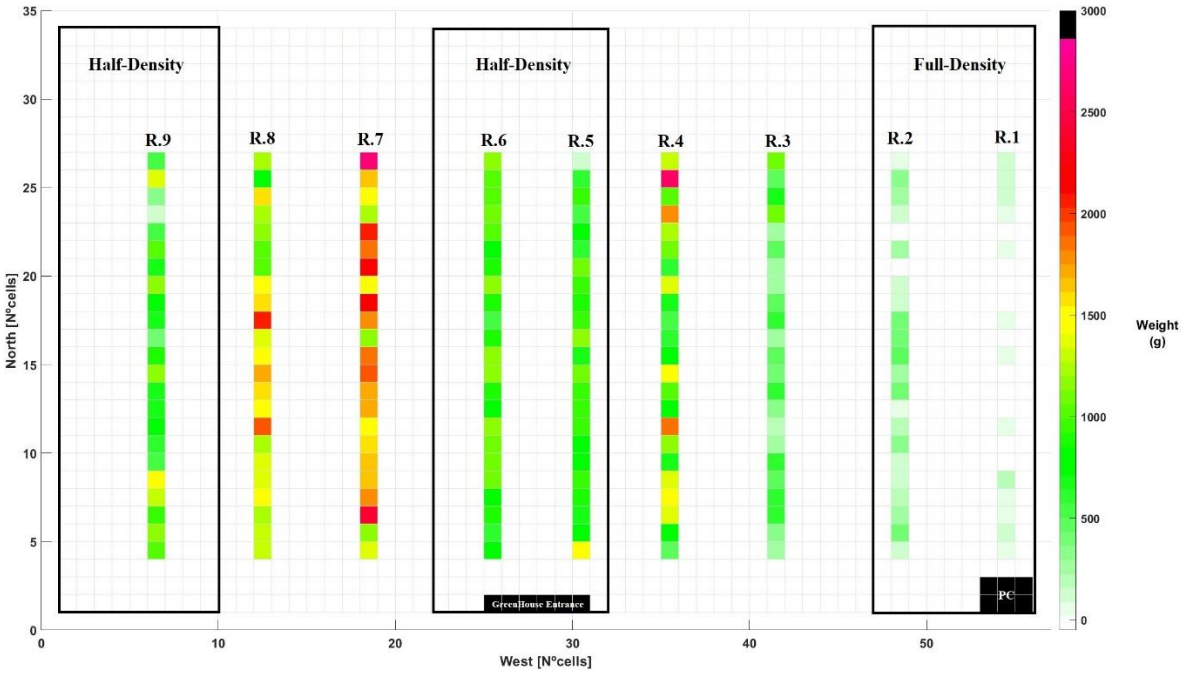

Figure 9. Yield map of fig productivity (weight of fruit per plant) for 2023 season (0.45 m per cell).

4. Conclusions

The findings of these preliminary study on the impact of solar panel shading on two distinct crops, dragon fruit and figs, showed the potential of agrivoltaic system for certain crops in particular. In relation to dragon fruit, the presence of full-density solar panels had a significant impact on the crop, resulting in reduced fruit size, production and weight. However, the absence of coverage also reduced the red colour component of fruits, a crucial market-quality attribute in dragon fruit. In fig crops, half-density solar panels showed a moderate reduction of fruit size when compared to the major reduction observed under full-density solar panels, demonstrating that production under half-density arrangements could be profitable as long as the loss in fig yield is counterweighted by the production of electricity by the half-density panel arrangement. Overall, both crops offered a promising alternative for a shared use of agricultural land in the context of a regenerative agriculture.

Acknowledgements

This study has been funded by the following Valencian Regional Government (Agencia Valenciana de Innovacion) projects: *Recolección inteligente y automatizada de cultivos de alta valor en invernaderos sostenibles* (DRAGONBOT) (INNEST/2023/106) and *Integración de sistemas agronómicos y fotovoltaicos para la producción inteligente de cultivos mediterráneos y subtropicales* (SMART AGRIVOLTAICA) (INNEST/2022/115). Additionally, we would like to thank José Martínez (MIPITAYA, Puzol, Spain) for technical support in the cultivation of dragon fruits.

References

Ali Khan Niazi, K., & Victoria, M. (2023). Comparative analysis of photovoltaic configurations for agrivoltaic systems in Europe. Progress in Photovoltaics: Research and Applications, 31(11), 1101-1113.; 1-13. doi:10.1002/pip.3727

Chalgynbayeva, A., Gabnai, Z., Lengyel, P., Pestisha, A., & Bai, A. (2023). Worldwide research trends in agrivoltaic systems—a bibliometric review. Energies, 16(2), 611.https://doi.org/10.3390/en16020611

Darling, S. B., & You, F. (2013). The case for organic photovoltaics. Rsc Advances, 3(39), 17633–17648.

Dupraz, C., Marrou, H., Talbot, G., Dufour, L., Nogier, A., & Ferard, Y. (2011). Combining solar photovoltaic panels and food crops for optimising land use: Towards new agrivoltaic schemes. Renewable energy, 36(10), 2725-2732.

Friman-Peretz, M., Ozer, S., Geoola, F., Magadley, E., Yehia, I., Levi, A., ... & Teitel, M. (2020). Microclimate and crop performance in a tunnel greenhouse shaded by organic photovoltaic modules–comparison with conventional shaded and unshaded tunnels. Biosystems Engineering, 197, 12-31.

Goetzberger, A., & Zastrow, A. (1982). On the coexistence of solar-energy conversion and plant cultivation. International Journal of Solar Energy, 1(1), 55-69. Available from: https://www.tandfonline.com/doi/abs/10.1080/01425918208909875

Juillion, P., Lopez, G., Fumey, D., Lesniak, V., Génard, M., & Vercambre, G. (2022). Shading apple trees with an agrivoltaic system: Impact on water relations, leaf morphophysiological characteristics and yield determinants. Scientia Horticulturae, 306, 111434.

Kuemmel, B., Langer, V., Magid, J., De Neergaard, A., & Porter, J. R. (1998). Energetic, economic and ecological balances of a combined food and energy system. Biomass and bioenergy, 15(4-5), 407-416.

Larson, B. Transforming energy. Organic Photovoltaic Solar Cells. Consulted by National Renewable Energy Laboratory (NREL). Available from: (https://www.nrel.gov/pv/organic-photovoltaic-solar-cells.html#:~:text=OPV%20is%20a%20rapidly%20emerging,roll%20manufacturing%20using%20solution%20processing. [Last accessed: 30/03/2024])

Trommsdorff, M., Simon, G. S., & Keinath, T. (2022). Agrivoltaics: Opportunities for Agriculture and the Energy Transition. Fraunhofer Institute for Solar Energy Systems ISE. (Available from: www.ise.fraunhofer.de [Last accessed: 21/03/24])

Unión Española Fotovoltaica [UNEF] (2023) Sinergia entre la actividad agropecuaria y la fotovoltaica: Promoviendo la Bioagrovoltaica.

Magarelli, A., Mazzeo, A., & Ferrara, G. (2024). Fruit Crop Species with Agrivoltaic Systems: A Critical Review. Agronomy, 14(4), 722.

Marrou, H., Wéry, J., Dufour, L., & Dupraz, C. (2013). Productivity and radiation use efficiency of lettuces grown in the partial shade of photovoltaic panels. European Journal of Agronomy, 44, 54-66.

Pereira, C., Sánchez, M. J. S., Gragera, F. P., González, A. M., Rivera, M. C. V., & Corrales, M. L. (2017). Evaluation of agronomic and fruit quality traits of fig tree varieties (Ficus carica L.) grown in Mediterranean conditions. Spanish Journal of Agricultural Research, 15(3), 16.

Ramos-Fuentes, I. A., Elamri, Y., Cheviron, B., Dejean, C., Belaud, G., & Fumey, D. (2023). Effects of shade and deficit irrigation on maize growth and development in fixed and dynamic AgriVoltaic systems. Agricultural Water Management, 280, 108187.

Yang, F., Zhang, Y., Hao, Y., Cui, Y., Wang, W., Ji, T., ... & Wei, B. (2015). Visibly transparent organic photovoltaic with improved transparency and absorption based on tandem photonic crystal for greenhouse application. Applied optics, 54(34), 10232–10239.

Zisisa, C., Pechlivani, E. M., Tsimikli, S., Mekeridis, E., Laskarakis, A., & Logothetidis, S. (2019). Organic photovoltaics on greenhouse rooftops: effects on plant growth. Materials Today: Proceedings, 19, 65-72.

Technologies for monitoring pig and broiler welfare at the slaughterhouse – tracing back to farm, loading, transport and slaughter

Jarissa Maselyne [a,*], Slađana Blažević [b], Sandra Stojanović [b], Christian Manteuffel [c], Kristina Maschat [d], Konstantinos Perakis [e], Thomas Banhazi [f], Nicolas Galtier [g], Pol Llonch [h], Bas Rodenburg [i], Martijn Bouwknegt [j] , Ronald Klont [j], Bart de Ruiter [j], Josep Reixach [k], Pauline Créach [l], Nemanja Kajari [m], Joanna Marchewka [n], Petra Thobe [o], Carsten Cruse [p], Jan Schulte-Landwehr [p], Christoph Bonk [p], Juliette Zamparini [q], Jorinde Mulder [q], Shanida Mullatahiri [a], Kenny van Langeveld [a], Noémie Van Noten [a], Anneleen Watteyn [a], Frank Tuyttens [a], Anneleen De Visscher [a]

[a] ILVO (Flanders Research Institute for Agriculture, Fisheries and Food), Merelbeke, Belgium

[b] Center for Innovation and Business Development, BioSense Institute, University of Novi Sad, Serbia

[c] Research Institute for Farm Animal Biology (FBN), Dummerstorf, Germany

[d] Center of Animal Nutrition and Welfare, University of Veterinary Medicine Vienna, Austria

[e] UBITECH, Athens, Greece

[f] InnoTech Vision, Tjele, Denmark

[g] Wel2be, Rennes, France

[h] School of Veterinary Science, Autonomous University of Barcelona (UAB), Barcelona, Spain

[i] Faculty of Veterinary Medicine, Utrecht University, The Netherlands

[j] Vion Food, Boxtel, The Netherlands

[k] Selección Batallé, Riudarenes, Spain

[l] ITAVI, Paris, France

[m] Carnex DOO, Vrbas, Serbia

[n] Institute of Genetics and Animal Biotechnology, Polish Academy of Sciences, Magdalenka, Jastrzębiec, Poland

[o] Thuenen Institute of Farm Economics, Germany

[p] CLK GmbH, Altenberge, Germany

[q] Plukon Food Group, Wezep, The Netherlands

* Corresponding author. Email: jarissa.maselyne@ilvo.vlaanderen.be

Abstract

The aWISH project (HEurope, grant nr. 101060818) aims to perform large-scale automated monitoring of animal-based indicators at slaughterhouses in order to obtain information about animal welfare on farm, during transport and at slaughter of broilers and grower-finisher pigs. The project is centred around six European pilots where technologies are developed, tested and validated. Each pilot consists of a slaughterhouse, in cooperation with a local research partner, associated farms and various technology providers. The pig pilots are located in Austria, the Netherlands, Serbia and Spain, while the broiler pilots are situated in France and Poland. Different technologies have been selected to measure a range of welfare indicators for pigs (ear lesions, skin lesions, tail length, tail lesions, blood parameters, stress vocalisation, tear staining, stunning effectiveness, environmental parameters, body weight, lung lesions, liver lesions, food consumption, meat quality) and broilers (hock burn, footpad lesions, catching damage, back scratches, stress vocalisations, activity, stunning effectiveness, environmental parameters, on-farm welfare assessment). These technologies are installed mainly in the slaughterhouse, but some are also installed on-farm, in the transport truck or obtained via human observations supported by digital tools (for ex. smartphone applications). They include mostly vision and sound-based systems with a technology readiness level (TRL) from 2 to 9. The data collected in the pilots will be used to provide feedback to farmers, transporters, catching teams (for broilers) and slaughterhouses. A data platform and online user interface have been developed for this purpose that will allow a clear view of individual indicator levels as well as the aggregate welfare scores per stage of production (on-farm, depopulation, transportation, slaughter). The data will also be further used in the aWISH project to document animal welfare improvements, to investigate the socio-economic and environmental impact of welfare-improving initiatives and to create best practice guides. This project will therefore make a significant contribution to the objective assessment of welfare of pigs and broilers across Europe and potentially world-wide.

Keywords: animal welfare, automation, precision livestock farming, slaughterhouse

1. Introduction

Despite many initiatives by the livestock sector, research organisations and welfare legislation, it still remains a challenge to reconcile the societal and moral demand for high animal welfare (AW) with other aspects of sustainable livestock production. Still today, 82% of Europeans think that farm animals should be better protected than they are currently (European Commission, 2015). Broiler and pig productions are the main concern of EU citizens (Martelli, 2009), but these livestock sectors are also the main meat-producing industries in the EU and worldwide. Considerable AW problems persist during all stages of production (on farm, loading & transport, unloading & slaughter) for both pigs and broilers, to the extent that the social acceptance of these industries is being questioned by an increasingly large number of citizens. The welfare of farm animals is regulated by EU legislation on farm, during transport and at slaughter. However, in addition to these regulations, which contain mainly resource-based measures, AW can also be measured through animal-based indicators that assess the outcomes of management impact on the animals themselves, regardless of the conditions in which they are kept (EFSA, 2012). Animal-based measures are now recognised as a better and more direct methodology to assess AW when compared to resource-based measures (Whay et al., 2005). This has resulted in the development of novel outcome-based welfare assessment protocols, pioneered by the Welfare Quality® protocol first (Blokhuis et al., 2010) or AWIN® later (Wickens, 2015), to mention the most notorious ones. An instrument is needed for monitoring livestock welfare in an objective and practical way. The Welfare Quality® and other protocols, like AWIN® do this to a certain extent, but it is very labour-intensive and does not assess each phase in the production chain.

To evaluate a large number of animals, slaughterhouses are suitable places to carry out these assessments, as the animals are brought in from various farms, which allows for high labour efficiency (Knage-Rasmussen et al., 2015; Van Staaveren et al., 2017). In addition, biosecurity is better guaranteed in this way. However, monitoring at the slaughterhouse has the limit of being retrospective, so AW improvements are no longer possible for this slaughter batch, but for the next batch. Pigs and broilers have frequent rotation of batches however, so feedback can be given frequently. According to Grandin (2017), there are two categories of animal welfare indicators (AWI) that can be assessed at a slaughterhouse: 1) acute or traumatic conditions that recently occurred and are associated with loading or transport, such as bruises, dead animals, fresh injuries, non-ambulatory animals, and 2) long-term chronic conditions which were present before animals were loaded for transport, such as lameness, shoulder sores in pigs, breast blisters on chickens, neglected injuries, necrotic prolapses. Each slaughterhouse has a system for quality control, including AW, for which the AW officers employed by the slaughterhouses are responsible. Furthermore, controls to verify compliance with legislation is carried out by official veterinarians (Berg, 2013). They inspect the animals at all slaughter stages: at unloading (e.g. fit-for-slaughter assessment), at lairage and at the stunning area (where stunning effectiveness is assessed), followed by the bleeding procedures. However, systematic, reliable and adequate monitoring of outcome-indicators of all animals by humans is almost impossible without slowing down the line speed. Limited or biased sampling, observer differences and subjective judgements hamper the use of such human-based assessments for motivating actors to take corrective actions or for justifying premium prices or access to quality labels (Giammarino et al., 2021; Maegher, 2009). These limitations can now be overcome by the rapid developments in technology and artificial intelligence (AI).

Many Precision Livestock Farming (PLF) technologies are commercially available in pigs (Gómez et al., 2021), such as load cells to measure body weight and feed intake, flowmeters to measure water intake, cameras to register animal behavior and activity, microphones to detect animal sounds like coughs. In broilers, not a lot of technologies are yet commercialized, only to monitor weight, activity and distribution of birds. Most of those techniques, however, were mainly developed for monitoring the production characteristics of the animals during rearing (Rowe et al., 2019). However, the monitoring of AW during depopulation, transport and pre-slaughter phase is of great importance. Unfortunately, such monitoring technologies are only scarce in scientific literature. Souza et al. (2018) studied the potential use of carcass condemnation data of broiler chicken slaughterhouses as indicators in an AW monitoring program. In a German slaughterhouse, a monitoring system consisting of five cameras was implemented successfully for the AWI ear and tail lesions in fattening pigs (Blömke et al., 2020). Video cameras also exist to monitor unloading, handling, and stunning (Grandin, 2017). In addition to the technical development, precise descriptions of AWI, their threshold values and how they relate to the welfare of animals are essential. New technologies and algorithms ought to be validated before they are launched on the market (Gómez et al., 2021) and lots of them remain at the proof of concept stage. Validation entails checking the system performance by quantifying the prediction accuracy, sensitivity and specificity relative to the gold (or silver)

standard using data other than the training dataset (Wieringa, 2014).

Different stakeholders, such as producers, consumers, retail, governmental bodies and scientists, state that AW is important, but they vary in the extent to which economic considerations align with AW concerns. Overall, stakeholders agree that a sustainable monitoring system is needed (Bracke et al., 2005). Therefore, the aWISH project was initiated to develop validated and automated monitoring systems, with a complete platform of data-analyses, benchmarking per production type and direct feedback to the actors involved, supported by the entire sectors. Thus, the main objective of the aWISH project is to develop and offer the capacity to evaluate and improve the welfare of meat-producing livestock throughout Europe via automated monitoring of animal-based welfare indicators at the slaughterhouse in order to give feedback and advice on best practices to those responsible for the various stages of production (farmer, catching team, transporter, slaughterhouse). This approach will be developed and evaluated in close collaboration with all actors involved, from primary producers up to policy makers and citizens.

2. Materials and Methods

2.1. Project methodology

The Horizon Europe aWISH project (grant nr. 101060818) has started on 1st of November 2022, and will last four years. The project consortium consists of 28 partners from 11 European countries. This project aims to build the capacity to improve farm AW at large scale as effectively and efficiently as possible. This aspiration is reflected in the focus on broiler and pig production, and in the methodological approach of the whole project. Figure 1 depicts the key concept of aWISH with the following main components:

(1) AWI Catalogue: AWI measured with automated technologies at slaughterhouses (SH), routine and existing data sources will be collated and published in an AWI Catalogue;

(2) aWISH Data Platform and feedback tool: a centralized data platform that generates feedback and benchmarking visualisations for the various actors in the production chain will be created;

(3) Integrated AW assessment: a spontaneous intervention study will evaluate the impact of the entire feedback loop on AW; risk and success factors will be identified at farm, chain, regional and national level.

(4) Best Practice Guides (BPGs): guidelines for best practices will be created to improve AW, incl. results of impact assessment on environmental and socio-economic level of these best practices;

(5) Supporting mechanisms: stakeholder engagement will be initiated incl. expert panel, lean multi-actor approach and piloting activities, and a multi-dimensional impact assessment of proposed BPs (AW, socio-economic and environmental assessment).

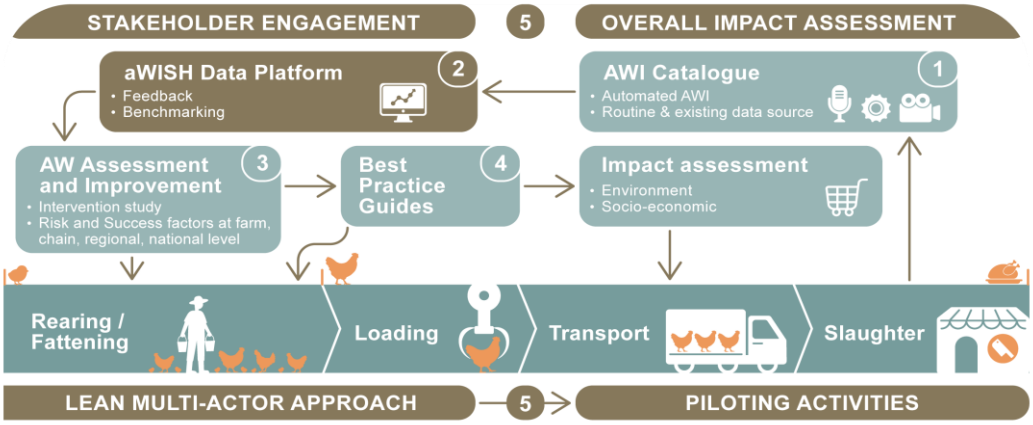

Figure 1. Key concepts in the aWISH project.

2.2. Pilots

Besides these key concepts, the core of the project is formed by six pilots across Europe, that consist of multi-disciplinary teams with a SH in the lead and a local scientific partner as co-lead. Furthermore, the teams include technology providers, researchers, and end-users incl. integrators, meat processors, and their supplying farmers and transporters. These pilots develop and test the novel AW monitoring technologies, test the aWISH feedback loop (use the aWISH data platform and activate actors in their supplying chain) and collect data and insights for the aWISH results.

The six pilots implemented within the aWISH project represent various regions of the European Union (EU), including both Member States and Associated Countries (Table 1, Figure 2). Four first phase pilots were engaged in technology data collection activities within the first year of the project. The second phase pilots will finalize installation of the new technologies towards the end of the 2nd year. The primary aim of the second phase pilots is to expand the scope of piloting efforts and geographical reach of developed aWISH solutions. This phase will ameliorate validating technologies and data collection procedures while integrating innovative technologies into the process. The broiler pilots will be each other's validation site.

Table 1. List of animals, leading companies and location of each aWISH pilot.

Pilot [1]	Species	Lead	Scientific lead	Location
Pilot 1	Pigs	Vion Food	Utrecht University	The Netherlands (NL)
Pilot 2	Pigs	Selección Batallé	Autonomous University of Barcelona	Spain (ES)
Pilot 3	Broilers	Plukon Food Group	ITAVI	France (FR)
Pilot 4	Broilers	Plukon Food Group	Institute of Genetics and Animal Biotechnology	Poland (PL)
Pilot 5	Pigs	Großfurtner	University of Veterinary Medicine Vienna	Austria (AT)
Pilot 6	Pigs	Carnex DOO	BioSense Institute	Serbia (RS)

[1]Four 1st phase pilots (Pilot 1-4) were engaged in technology data collection activities within the first year of the project. The 2nd phase pilots (Pilot 5-6) will finish installation of the new technologies towards the end of the second year.

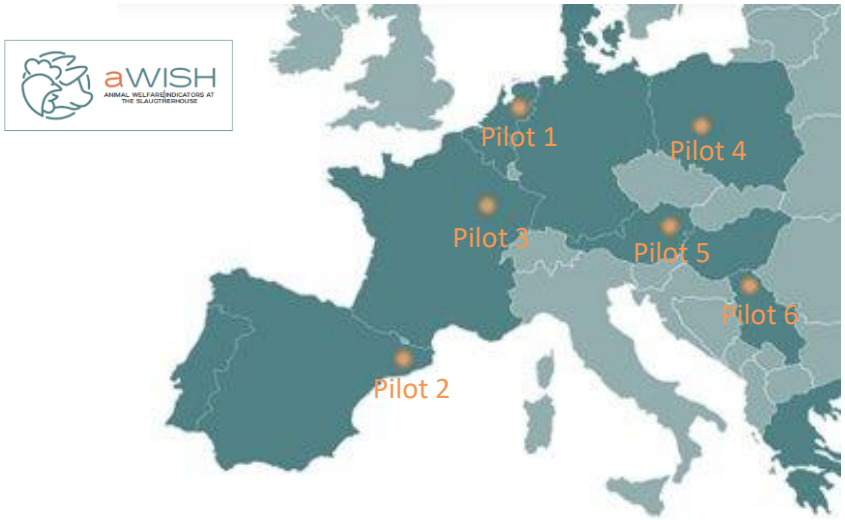

Figure 2. Map of the aWISH pilot locations.

2.3. Technologies used to measure AWI

Technologies that will be developed by the project partners include:

(1) Novel technologies with interesting potential (TRL 2-3) for the measurement of AWI, incl. tear staining, lung and liver lesions monitoring, loin bruises and long-term stress levels for pigs, and stunning effectiveness and scratches on the back for broilers.

(2) Technologies with a proof of concept validated in experimental conditions (TRL ≥4). Often these technologies build upon previous developments (sometimes from other fields or other species), but have not yet been validated in operational environment.

(3) Already significantly developed technological solutions (TRL ≥7). These technologies are already used and sufficiently developed, and will be used as a data source in the project.

In addition, some of the pilot sites have already installed other technologies or are in the process of developing other technologies at the SH, or on farms or trucks delivering livestock to the SH.

2.4. Data platform

Data collected from the pilots' production chains (automated technologies in SH, relevant existing data, routinely collected data, regional data sources, on-farm/transport sensors, etc.) will be stored in the secure storage of the aWISH data platform that will enable linking all relevant AW data. This will feed the research and development activities in the project. Moreover, a web-portal will be developed for the operators in the production chain, so that they can receive automatic and immediate feedback of the collected AWI that relate to their part of the production chain via a user-friendly graphical user interface (GUI). The feedback will provide early warning, longitudinal company trends and benchmarking.

3. Results and Discussion

3.1. Pilot status and installed technologies

The project has currently implemented 18 novel installations in the four 1st phase pilots and 1 novel installation in pilot 5, as shown in Table 2. For the 2nd phase pilots, pilot 5 and 6, more installations will be done in a later stage of the project. The status of the technologies at the start of the project was TRL 2-8 (mean 3.7), which was after 18 months of the project already increased to TRL 2-9 (mean 5.3). Most novel installations are in the SH, at various areas covering both the live animals and the stunning, bleeding and processing areas.

In addition to these systems installed during the aWISH project, also data of eight existing systems will be used. These measure the following additional parameters:

- Pig behavior inside the pen, barn climate, feeding behaviour (pig farm)
- Overall welfare evaluation, barn climate and performances (broiler farm)
- CO_2, temperature, humidity (truck)
- Pig behaviour and handling at unloading (SH)
- Tail length of pig (SH)
- pH and meat quality (SH)
- Back fat and muscle depth across the carcass (SH)
- Back fat and muscle depth locally (SH)

In total, a large number of welfare indicators for pigs (ear lesions, skin lesions, tail length, tail lesions, blood parameters, stress vocalisation, tear staining, stunning effectiveness, environmental parameters, body weight, lung lesions, liver lesions, food consumption, meat quality) and broilers (hock burn, footpad lesions, catching damage, back scratches, stress vocalisations, activity, stunning effectiveness, environmental parameters, on-farm welfare assessment) is being collected.

Table 2. Current technology installations performed, incl. current TRL levels.

Pilot	Tech. Provider	Technology name	Location	What is measured/ monitored	TRL
1	CLK GmbH	PigInspector	SH (after bleeding area)	Ear lesions, tail lesions, tail length and skin lesions on the back	4-9
1	FBN	STREMODO	SH (lairage)	Stress vocalizations	4
1	FBN	IGFBPs	SH (bleeding area)	Stress level in exsanguination blood	3
2	Wel2be	Stunning effectiveness for pigs	SH (bleeding area)	Corneal reflex assessment – stunning effectiveness	5
2	Wel2be	Tear staining sensor	SH (after bleeding area)	Surface of tear staining	2
2	Innotech Vision	Lesion Detect (lungs/ liver)	SH (viscera remove area)	Pulmonary and liver health monitoring	2
2	Innotech Vision	Enviro Detect	Farm	Barn climate monitoring	6-7
2	Innotech Vision	Weight Detect	Farm	Weight predicting via camera	6-7
3	CLK	ChickenCheck Footpad	SH (after cutting of feet)	Footpad lesions	9
3	CLK	ChickenCheck Hockburn	SH (after plucking)	Hockburns	9
3	Wel2be	Stunning effectiveness for broilers	SH (after stunning)	Movement of broilers after stunning – stunning effectiveness	2
3	ITAVI	EBENE®	Farm	On-farm overall welfare assessment	9
3	ITAVI	Environmental monitoring	Transport	Heat stress detection	5
3	ITAVI	EBroilerTrack image	Farm	Individual broiler activity on farm	5
3	ITAVI	EBroilerTrack sound	SH (lairage)	Vocalization related to stress in the lairage area	5
4	CLK	ChickenCheck Footpad	SH (after cutting of feet)	Footpad lesions	9
4	CLK	ChickenCheck Hockburn	SH (after plucking)	Hockburns	9
4	CLK	ChickenCheck CatchDamage	SH (after plucking)	Catch damage on wings, breast, legs; scratches on the back	2-4
4	ITAVI	EBENE®	Farm	On-farm overall welfare assessment	9
5	CLK	PigInspector	SH (after bleeding area)	Ear lesions, tail lesions, tail length and skin lesions on the back	4-9

3.2. Insights

Key insights encountered during pilot implementation so far are:

- Monitoring the most critical aspects of AWI within SHs was predominantly manual, indicating a substantial technical gap in automation.
- Small SHs face significant challenges due to the individual nature of their infrastructure, hindering the seamless integration of technologies, particularly in digitizing routine processes.

- The reliability of obtained results hinges on proper validation procedures, which requires allocating sufficient resources for algorithm development and validation.
- Clear and detailed upfront discussions and agreements significantly reduce ambiguities and misunderstandings throughout project or process execution.
- Effective awareness campaigns on AW assessment at SHs are crucial for progress, but the sensitivity of the topic elicits diverse reactions.

3.3. Data platform status

For the data platform, the requirements and architecture has been defined. The dataset type, size, frequency and specifics of the different technologies and other data sources have been analysed. Different user roles were set-up, with different access rules for production chain stakeholders, technical partners, researchers and external parties. Besides the different data platform component interactions, also a demo version of the data platform and web-app was made available to the aWISH partners and further defined through questionnaires and workshops. Figure 3 shows one of the mock-ups of the web app.

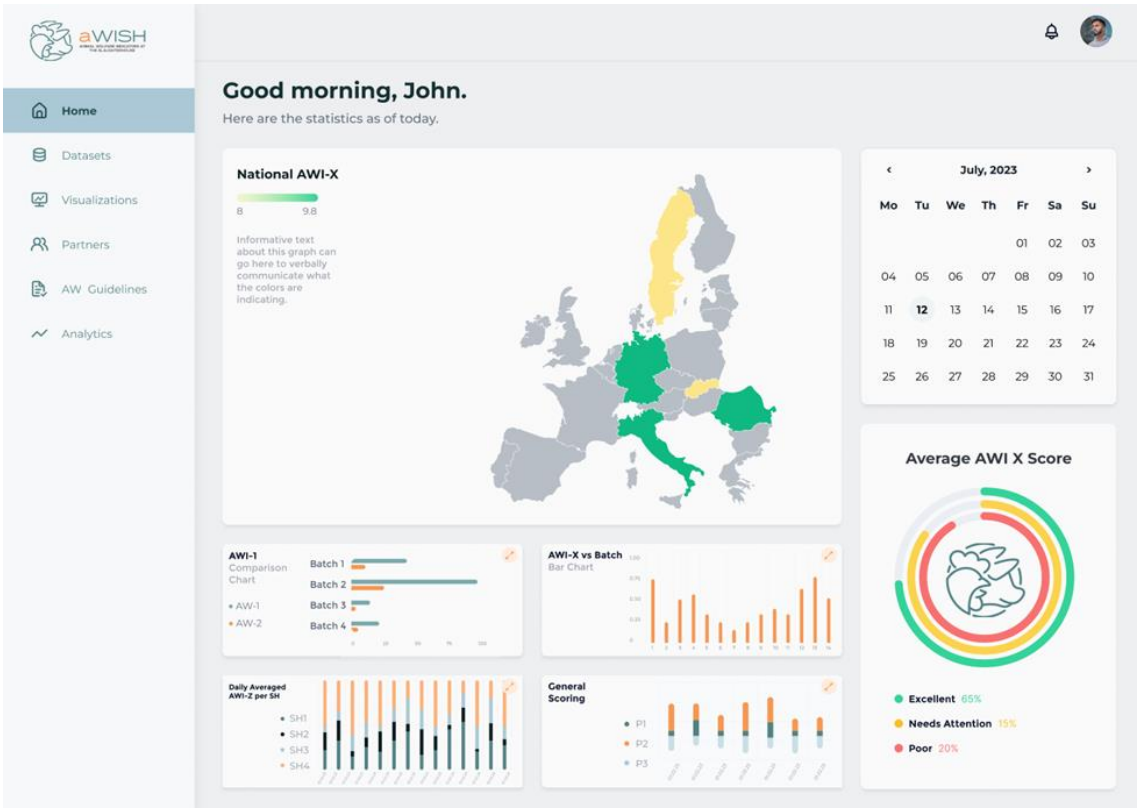

Figure 3. The envisaged aWISH web application home page (demo mock-up).

3.4. Future work

Future work will focus on the increased and standardized data collection from each of the systems installed at the pilots, as well as validation work for several of these systems in collaboration between the technology providers and researchers. The collected and validated data will then become available for the aWISH feedback loop through the data platform. Every pilot will have farmers, catching teams and transporters that will test the feedback loop using their own data. These same chain actors will also deliver data for the spontaneous intervention study to assess animal welfare improvements. Alongside, a socio-economic and environmental impact assessment will be done and the best practice guides will be developed. For the multi-actor approach of the project, the aWISH expert panel will deliver further input for the project in order to deliver a maximum impact for industry, policy makers and society by large.

4. Conclusions

The aWISH project has started with installing technologies (19 novel installations) of various technology readiness levels (TRL 2-9) in order to monitor the welfare of broiler chickens and growing-finishing pigs via animal-based welfare indicators. These installations are spread throughout Europe, in six pilots. Most of the technologies measure animal welfare indicators on the live animals or carcasses in various areas of the slaughterhouses, but some also rely on on-farm measurements. In some transportation trucks, existing sensors are being used. Besides these installations, the first steps are made in the development of a data platform and graphical user interface through a web-app that will be used by farmers, catching teams, transporters and slaughterhouses to get individualized data and advice on best practices for improved animal welfare.

Acknowledgements

Funded by the European Union (project "Animal Welfare Indicators at the Slaughterhouse - aWISH", Horizon Europe under grant agreement ID: 101060818). Views and opinions expressed are however those of the author(s) only and do not necessarily reflect those of the European Union. Neither the European Union nor the granting authority can be held responsible for them. We would like to thank the aWISH consortium, expert panel and stakeholder advisory board members for their valuable contributions.

References

Berg, C., 2013. Monitoring animal welfare at slaughterhouses. In: Sustainable Agriculture. Baltic University Press. Chapter 48, pp 349-351.

Blömke, L., Volkmann, N., Kemper, N., 2020. Evaluation of an automated assessment system for ear and tail lesions as animal welfare indicators in pigs at slaughter. Meat science, 159, 107934. https://doi.org/10.1016/j.meatsci.2019.107934

Bracke, M. B. M., Greef, K. D., Hopster, H., 2005. Qualitative stakeholder analysis for the development of sustainable monitoring systems for farm animal welfare. Journal of Agricultural and Environmental Ethics, 18, 27-56.

EFSA, 2012. Statement on the use of animal-based measures to assess the welfare of animals. The EFSA Journal 10, 2767. https://doi.org/10.2903/j.efsa.2012.2767

European Commission, 2015. Directorate-General for Health and Food Safety, Attitudes of Europeans towards animal welfare – Report, https://data.europa.eu/doi/10.2875/884639

Giammarino, M., Mattiello, S., Battini, M., Quatto, P., Battaglini, L. M., Vieira, A. C. L., Stilwell, G., Renna, M., 2021. Evaluation of Inter-Observer Reliability of Animal Welfare Indicators: Which Is the Best Index to Use? Animals. 2021; 11(5):1445. https://doi.org/10.3390/ani1105144 5

Gómez, Y., Stygar, A. H., Boumans, I. J. M. M., Bokkers, E. A. M., Pedersen, L. J., Niemi, J. K., Pastell, M., Manteca, X., & Llonch, P., 2021. A Systematic Review on Validated Precision Livestock Farming Technologies for Pig Production and Its Potential to Assess Animal Welfare. Frontiers in veterinary science, 8, 660565. https://doi.org/10.3389/fvets.2021.660565

Grandin, T., 2017 On-farm conditions that compromise animal welfare that can be monitored at the slaughter plant. Meat Science 132: 52–58. https://doi.org/10.1016/j.meatsci.2017.05.004

Knage-Rasmussen, K. M., Rousing, T., Sørensen, J. T., Houe, H., 2015. Assessing animal welfare in sow herds using data on meat inspection, medication and mortality. Animal, 9(3), 509-515. doi:10.1017/S1751731114002705

Martelli, G., 2009. Consumers' perception of farm animal welfare: an Italian and European perspective. Italian Journal of Animal Science, 8(sup1), 31–41. https://doi.org/10.4081/ijas.2009.s1.31

Meagher, R. K. (2009). Observer ratings: Validity and value as a tool for animal welfare research. Applied Animal Behaviour Science, 119(1-2), 1-14. https://doi.org/10.1016/j.applanim.2009.02.026

Rowe, E., Dawkins, M. S., & Gebhardt-Henrich, S. G., 2019. A systematic review of precision livestock farming in the poultry sector: Is technology focussed on improving bird welfare?. Animals, 9(9), 614. https://doi.org/10.3390/ani9090614

Souza, A. P. O., Taconeli, C. A., Plugge, N. F., Molento, C. F. M., 2018. Broiler chicken meat inspection data in Brazil: a first glimpse into an animal welfare approach. Brazilian Journal of Poultry Science 20(3). https://doi.org/10.1590/1806-9061-2017-0706

Van Staaveren, N., Doyle, B., Manzanilla, E. G., Calderón Díaz, J. A., Hanlon, A., Boyle, L. A., 2017. Validation of carcass lesions as indicators for on-farm health and welfare of pigs. Journal of Animal Science, 95(4), 1528-1536. https://doi.org/10.2527/jas.2016.1180

Whay, H. R., Main, D. C. J., Green, L. E., Webster, A. J. F., 2003. Animal-based measures for the assessment of welfare state of dairy cattle, pigs and laying hens: consensus of expert opinion. Animal Welfare 12(2): 205-217. doi:10.1017/S0962728600025641

Wickens, S., 2015. AWIN welfare assessment protocols: donkeys, goats, horses, sheep and turkeys. Animal Welfare, 24(3), 357–358. doi:10.1017/S0962728600006990

Wieringa, R. (2014). Empirical research methods for technology validation: Scaling up to practice. Journal of systems and software, 95, 19-31. https://doi.org/10.1016/j.jss.2013.11.1097

Interaction of agroecosystems and aquaculture through engineering: experiences with small-scale tilapia farms, aquaponics and agroecological systems in South Mexico

Francisco Javier Martínez-Cordero [a,*] and Laura Patricia Silva-Ledezma [a]

[a] Laboratory of Aquaculture Economics and Foresight, Research Center for Food and Development CIAD,A.C México

* Corresponding author. Email: cordero@ciad.mx

Abstract

For high-poverty households of rural areas in the South Pacific Mexico, agroecological systems integrated with small-scale aquaculture provide not only food for own consumption but the possibilities of generating an extra income by selling excess production. These production systems face similar problems related to water scarcity and droughts as bigger-scale farms, but the consequences are bigger due to their vulnerability. In this paper we report results of incorporating aquaponics in rural, small-scale agroecological systems in order to reduce vulnerability as an adaptation strategy to Climate Change. Engineering allows achieving a reduced-cost system, operating an integrated production model that is easy to learn and respects traditions and cultural habits of farmers. For example, the aquaponics ´plant or vegetable (or group of them) to be reared, are decided by the own farmers according to their needs and traditions, reusing available material and in some cases incorporating models of rain-water collection. In general they are low-technique, very practical from the engineering point of view.

Complementing this innovative, small-scale rural production model, in the marketing chain the agroecological, tilapia and aquaponics products are directly offered by the farmers to their final clients (usually in short-chain or last-mile markets) using digitalization and the platform AUAKAN. The impacts of these systems in multilevel poverty were evaluated (at farmers households' level), proving the benefits of incorporating these models.

Keywords: Agroecological systems, aquaponics, rural farming, poverty

1. Introduction

In Mexico, tilapia is the second most produced species in aquaculture, and almost 60% of tilapia farming operations are micro farms with earth ponds, circular plastic tanks, or floating cages, with annual productions lower than 0.5 ton/year (Martínez-Cordero et al., 2021). The characteristics of these farms are in accordance with the FAO description of AREL in Latin America (Flores Nava, 2013) which include (i) self-employment, full time in aquaculture or complemented with other jobs; (ii) limited access to key production inputs; and (iii) low household income that may not be sufficient to maintain food security. Specifically in the southern Pacific region of Mexico, it has been documented that micro and small-scale tilapia farms contribute to poverty reduction. However, the income of tank and pond farmers is lower compared to that of floating cage farmers.(Martinez-Cordero and Sanchez-Zazueta, 2022).

Integrated agriculture-aquaculture (IAA) is a good example of successful agroecology. Even when agroecology does not target a specific aquaculture model, for aquaculture systems, transition towards agroecology allows to bring solutions to some of the constraints that current production models are facing (Halwart et al., 2019). For aquaponic farming, the aquaponic principle which combines aquaculture and plant production saving resources, is applied (Baganz et al., 2021). The incorporation of aquaponic farming in micro tilapia farms in México represents an opportunity to develop an agroecology system from an aquaculture one. Several models of aquaponic farming have been proposed going from large commercial to micro sustenance systems, from high technology to low technology systems, and from intensive to semi-intensive production systems. From aquaculture transition to agroecology, one of the food system change levels proposed by Gliessman,(2016) is the system redesign which can be done through, participatory, and change-oriented research and action.

2. Materials and Methods

A participatory action intervention was performed to implement semi-intensive aquaponic systems on micro tilapia farms. Identification of interested micro tilapia producers into aquaponic systems was done via the aquatic health committees of Guerrero and Oaxaca states (COSAEG and COSIA, respectively). The interested tilapia farmers were invited to participate in a workshop where the aquaponic system, its principles and component's function were explained by a member of the research group. Posteriorly, they identified local available materials that can be used to implement the each one of the aquaponic system components. The producers with interest in implementing a semi-intensive aquaponic system in its farm provide information regarding the tank size, culture density, cycle length, initial and final weight. With the information received a basic semi-intensive aquaponic model was proposed. The aquaponic model was designed to work as semi-intesive system in wich initially, fish management will be maintained as usual and adjustments were done to fit the model within the specific farm context. The model was sent to the interested producers, and they provide feedback to conclude with a final model that was developed for each farm trough participatory design.

System implementation was carried out by the farmers with technical support using a combination of their own resources and some material provided by the research group. Technical capacitation on aquaponics was also provided onsite and virtually for system management, plant fertilization and pest prevention.

3. Results and Discussion

Three producers began the implementation of the aquaponic system in different zones of Oaxaca state, each one according to their context (Figure 1).

Figure 1. Installation and capacitation of aquaponic systems with local and reused materials on micro tilapia farms of Oaxaca distributed in the regions a) Papaloapan, b) Mixteca and c) Istmo.

The design and implementation of the aquaponic systems through participatory co-design and action allowed to have a better understanding an accounting of the unique circumstances of farmers and the local system that needs to be changed (Lacombe et al., 2018). This facilitates the utilization of locally available, cost-free, or reused materials, such as discarded fiberglass containers in the Papaloapan region, 'laja' rocks in the Mixteca, and sandy soil in the Istmo. This understanding will assist farmers in comprehending the functioning of their own cropping system and in future redesign efforts (Toffolini et al., 2017).

Regarding plant production, based on their context, the producers ask for specific plants for culturing in the aquaponic system. A common characteristic among the producers' requests for aquaponic plants was their preference for those with high local demand but low supply, often resulting in high prices or scarcity. In the case of the Papaloapan region, producers ask for aromatic herbs used in the region for cooking. According to the tilapia producers, these plants are grown in some home gardens within the community. Nevertheless, the market needs to be supplied by external sellers. In the Mixteca and Istmo region the producers were interested primarily into lettuce production; the principal reason is that in both communities the lettuce supply is low. In the case of the farm located in the Mixteca, there are restaurants where the lettuce is consumed, and it is common to travel 45 km to the nearest market to supply it. In the community where the Istmo farm is located, an external seller supplies lettuce only once a week, and the demand is not satisfied. In the three cases, the sharing of knowledge, specifically the producers' knowledge related to markets and institutions, was essential for the co-creation of the new agroecology system (FAO, 2024).

As an example, description of the aquaponic system in the Istmo region is presented. The farm has three plastic tanks for tilapia culture, one of which (4 m diameter) was linked to the aquaponic system. The system components are the tilapia tank (28 m^3), one Mechanical filter for solids removal (200 L), one bacterial biofilter (200 L), three hydroponic beds (3m^2) and a reservoir for water recirculation (450 L) (Figure 2).

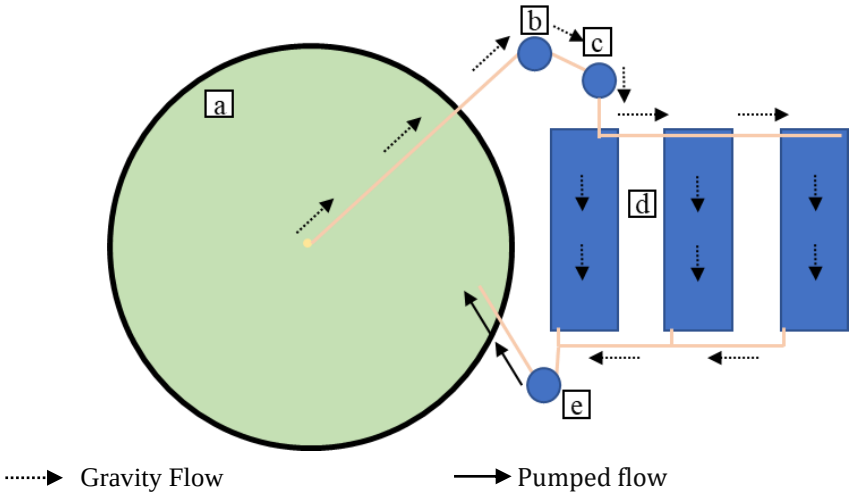

Figure 2. Diagram of the aquaponic model proposed by the research group. a) Fish tank, b) Mechanical filter, c) Second mechanical filter and biological filter, d) Hydroponic beds, e) Reservoir.

The construction of the system was carried out by the tilapia producers with assistance of the research group. The producers use two 200L recycled plastic barrels as solid filter and biofilter, volcanic rock as media for bacteria fixation, plumbing material bought close to the farm community, local sandy soil for the hydroponic beds structure, plastic liner for the impermeabilization of the hydroponic bed, a solar pump for water recirculation (provided by COSIA) and water tank as reservoir. To protect the hydroponic beds and plants a shade net house was constructed using local material (Figure 3).

Figure 3. Aquaponic system implemented through co-design and participatory action in the state of Oaxaca, México.

The implemented system will enable the production of 45 – 56 lettuces every week, with the producers' plans to increase aquaponic lettuce production as their expertise in aquaponics grows.

Commercialization and Socioeconomic Impacts

In two complementary topics of the research project, technology and innovation is also transferred to the small-scale producers for the commercialization of their products. A joint digitalization-omnichannel approach was constructed with the small farmers, developing a portfolio of contents to reach their final consumers, in usually short-chain or last-mile markets. The work was based on identifying local uses of digitalization and cellular phones, in order to be more efficient, tanking into account that in many of these rural areas, connectivity is a challenge.

Although the approach has raised interest among farmers and consumers, we recognize that its successful implementation requires a sustained presence of both supply and demand agents in the omnichannel. Since these small farmers depend on different economic activities for the household income -where aquaculture and aquaponics are only two of the possible activities-, assigning time to this digital/omnichannel approach must be based on a clearly-perceived benefit in terms of income.

Finally, the socioeconomic impacts of these multiple elements of engineering, technology and innovation transfer at the small scale enterprise (SME) were evaluated. It is already documented (Martínez Cordero and Sánchez, 2022) that the small-scale tilapia project has a positive impact on multi-level poverty in rural areas. In a continuation of this research, we will test whether this positive impact is increased when other production activities like aquaponics or agroecology are incorporated, whose set-up require adaptation of engineering models usually developed for bigger scales. At the territory and mainly for this SMEs, this joint development of production activities means the continuation of traditional production -many times cultural-inherited- and resilience of both farmers and their communities.

4. Conclusions

The project is focused on technology and innovation transfer to small-scale tilapia aquaculturists in the south Pacific States of Mexico. Aquaponics, digitalization/omnichannel, added-value to tilapia, were the main activities for this approach. From the engineering point of view, designing a cost-effective tilapia/aquaponics/agroecological system is a challenge since at this scale of producers, every farm has different characteristics, and the production model has to be designed accordingly.

Acknowledgements

This project is funded by the National Council of Humanities, Science and Technology (CONAHCYT) in Mexico, grant 317100 of the PRONACES Soberanía Alimentaria. The first author is the technical responsible of the project. It is linked to ongoing work in Mexico by the National Laboratory CONAHCYT Tilapia Mexico Network (Laboratorio Nacional CONAHCYT Red Tilapia México).

References

Baganz, G.F.M., Junge, R., Portella, M.C., Goddek, S., Keesman, K.J., Baganz, D., Staaks, G., Shaw, C., Lohrberg, F., Kloas, W., 2021. The aquaponic principle — It is all about coupling. Rev Aquac 1–13. https://doi.org/10.1111/raq.12596

Flores Nava, A., 2013. Diagnóstico de la Acuicultura de Recursos Limitados (AREL) y de la Acuicultura de la Micro y Pequeña Empresa (AMYPE) en América Latina. FAO.

Gliessman, S., 2016. Transforming food systems with agroecology. Agroecology and Sustainable Food Systems. https://doi.org/10.1080/21683565.2015.1130765

Halwart, M., Dabbadie, L., Beveridge, B., 2019. Agroecology in aquaculture. FAO Aquaculture Newsletter .

Lacombe, C., Couix, N., Hazard, L., 2018. Designing agroecological farming systems with farmers: A review. Agric Syst. https://doi.org/10.1016/j.agsy.2018.06.014

Martínez-Cordero, F.J., Delgadillo Tiburcio, S., Sánchez-Zazueta, E., Cai, J., 2021. TILAPIA AQUACULTURE IN MEXICO: ASSESSMENT WITH A FOCUS ON SOCIAL AND ECONOMIC PERFORMANCE. FAO Fisheries and Aquaculture Circular No. 1219. FAO , Rome.

Martinez-Cordero, F.J., Sanchez-Zazueta, E., 2022. Poverty and vulnerability assessment of tilapia farmers in the southwestern States of Oaxaca, Guerrero, and Chiapas in Mexico. Aquaculture Economics and Management 26, 36–56. https://doi.org/10.1080/13657305.2021.1896604

Bacillus subtilis and Burkholderia seminalis in promoting the growth of Solanum lycopersicum L.

Henrique F. E. de Oliveira[a,*], Thiago Dias Silva[a], Priscila Jane Romano Goncalves Selari[a], Wesley Rangel de Melo[a], Jhon Lennon Bezerra da Silva[a], Marcio Mesquita[b], Marcus Vinicius da Silva[c]

[a] Cerrado Irrigation Graduate Program, Goiano Federal Institute, Ceres, Goiás, Brazil

[b]Faculty of Agronomy, University of Goiás (UFG), Goiânia, Goiás, Brazil

[c] Department of Agricultural Engineering, Federal Rural University of Pernambuco (UFRPE), Recife, Pernambuco, Brazil,

* Corresponding author. Email: henrique.fonseca@ifgoiano.edu.br

Abstract

The use of microorganisms has proven to be a promising technique in agriculture, providing greater efficiency in the use of water and nutrients by crops. The study focused on the use of microorganisms *Bacillus subtilis* (strain ATCC 23858) and *Burkholderia seminalis* (strain TC3.4.2R3) and the evaluation of the effects of inoculation on the growth of cherry tomato (Solanum lycopersicum var. cerasiforme) in a protected environment. Adopted a randomized block design (DBC) with three treatments: i) Bacillus subtilis ATCC 23858, ii) Burkholderia seminalis TC3.4.2R3, and iii) without inoculation (SI). Eight blocks were used in the experiment. Morphometric parameters were measured at 15 and 30 days after sowing (DAS). Parameters evaluated included germination rate, emergency germination speed, water content foliar, and morphometric analyses. At 15 DAS Burkholderia seminalis showed higher germination rates compared to the non-inoculated treatment and Bacillus subtilis resulted in greater plant and root height compared to the non-inoculated treatment. At 30 DAS Bacillus subtilis and Burkholderia seminalis inoculations led to statistically significant differences in emergence speed index (IVE), fresh mass (MFPA), dry mass (MSPA), and root length (CR). Inoculation with *Bacillus subtilis* and *Burkholderia seminalis* demonstrated the potential to promote plant growth, increase productivity, and improve the quality of fruits. The study suggests that these bioinoculants can be used in sustainable agricultural management.

Keywords: bioinoculant, BPCP, solanaceae, Tomato, main component analysis.

1. Introduction

Growers have been pursuing sustainability by employing biological inputs to control pests and diseases while promoting plant growth. Therefore, the use of bioinputs has gained prominence, as they act as bioinsecticides or biofertilizers, promoting plant health and development and ensuring higher crop productivity (Khatoon et al., 2020; Basu et al., 2021) and fruit quality (Rouphael and Colla, 2018). The use of plant growth-promoting bacteria (PGPB) stands out, as they can mitigate impacts caused by biotic and abiotic stressors (Alcantara and Porto, 2019).

Tomato belongs to the Solanaceae family and is one of the most consumed and popular vegetables worldwide (Cardoso et al., 2018). Due to its widespread cultivation, especially in protected environments (Silva et al., 2023), crop management strategies focus on minimizing the impacts of pathogens, pests, and/or abiotic stressors such as water deficit and salinity. The use of inoculants in tomato production aims to increase crop productivity, fruit resistance, antioxidant activity, and the concentration of secondary metabolites (Zulfiqar et al., 2020).

Among the bacteria used to produce commercial inoculants based on PGPB, the genus Bacillus stands out, composed of rod-shaped, spore-forming bacteria, members of the Firmicutes phylum, especially the non-pathogenic species Bacillus subtilis, commonly found in soils. The efficacy among strains can vary significantly; therefore, although there are commercial inoculants of Bacillus subtilis, the ATCC 23858 strain has not yet been tested for this purpose. Some bacteria live inside plants and colonize the interior of the host plant without causing diseases, referred to as endophytic, such as the species Burkholderia seminalis. This species associates with different plants such as Arabidopsis, Chinese cabbage, Chinese amaranth, lettuce, rice, sugarcane, maize, and onion, promoting plant growth and production (Araújo et al., 2016; Hwang et al., 2021). The Burkholderia seminalis TC3.4.2R3 strain, isolated endophytically from sugarcane roots and associated with promoting plant growth, is recognized for its ability to produce bioactive molecules to control the development of the phytopathogenic fungus Fusarium oxysporum and the bacterium Burkholderia gladioli (Araújo et al., 2016; Araújo et al., 2017).

The objective of this study was to evaluate the impact of microbial inoculation with Bacillus subtilis

strain ATCC 23858 and Burkholderia seminalis strain TC3.4.2R3 on cherry tomato in a protected environment and examine the influence on plant growth parameters compared to the non-inoculation treatment. Additionally, we discuss the potential of microbial inoculation as a sustainable and efficient technique for crop management in protected environments.

2. Materials and Methods

2.1. Experimental site

The experiment was conducted from April and October 2022 in a greenhouse located in the experimental area of the Goiano Federal Institute of Education, Science and Technology (IF Goiano – Campus Ceres), located in Ceres, Goiás, Brazil (15°21'02" S latitude, 49°35'55" W longitude, and 564 m of altitude). The region's climate was classified as Aw (tropical savannah climate with dry winter characteristics) according to the Köppen-Geiger classification (Peel et al., 2007).

The temperature and relative humidity inside the greenhouse were recorded using a weather station (Vantage Pro 2; Davis; Hayward, CA, USA). The recorded minimum and maximum air temperatures were 8.8 and 38.6°C, respectively, and the relative humidity ranged from 41.4 to 85.6%. The average temperature and relative humidity values throughout the study were 23.4 °C and 62.4%, respectively.

2.2. In vitro germination of tomato seeds

For the germination test, a randomized block design was adopted, with three treatments, consisting of inoculation with i) Bacillus subtilis ATCC 23858, ii) Burkholderia seminalis TC3.4.2R3, and iii) a control non-inoculation (NI), across eight blocks.

The inoculum was standardized to an optical density of 1.0 at 600 nm in a spectrophotometer (Double Beam UV-Visible model GTA-101; Global Analyzer, Calgary, Canada) to achieve a final concentration of 109 Colony Forming Units (CFU) mL^{-1}.

The cherry tomato seeds were microbiolized with the bacterial suspensions for 20 minutes, at a ratio of 1 mL of bioinoculant per g of seed, in a laminar fume hood. For the non-inoculation treatment, the seeds were soaked in sterile nutrient broth under the same conditions.

Fifty seeds per block were evaluated, totaling 400 seeds per treatment. The seeds were moistened on sterile blotting paper at a 1:2.5 ratio (w/v) - one gram of blotting paper to 2.5 mL of sterile distilled water. The moistened blotting paper was placed in Gerbox germination boxes, which were incubated at 25 ºC for 14 days in a B.O.D. incubator without a photoperiod (Brazil, 2009). The germination rate was determined at the end of the incubation period (number of normal seedlings x 100) / 50).

2.3. Greenhouse cultivation

A randomized block design was adopted, with three treatments, consisting of inoculation with i) Bacillus subtilis ATCC 23858, ii) Burkholderia seminalis TC3.4.2R3, and iii) a control non-inoculation (NI), with eight blocks. Each experimental plot consisted of eight plants.

The spacing used was 0.7 m between plants, 0.7 m between rows, and 1 m between double rows, equivalent to a population of 20,408 plants per hectare. Cherry tomato seeds were disinfected and microbiolized. After that, sowing was carried out in expanded polystyrene trays with 128 cells (Isoeste, Castanhal, PA, Brazil). The trays contained substrate (Topstrato HA; Genfértil, Provaso, Industrial, and Commercial of Organic Fertilizers, Mogi Mirim, São Paulo, Brazil), composed of pine bark and peat, vermiculite, NPK Fertilizer (fraction 14.16.18), potassium nitrate, and simple superphosphate (fertilizer obtained by adding acids to rocks, containing 18% phosphorus, 16% calcium and 10% sulfur).

At 15 days after sowing (DAS), the emergence speed index (Popinigis, 1985) and morphometric analyses of the seedlings were determined. Other seedlings were replanted into 200 cm^3 containers filled with the same substrate. Here, reinoculation was performed by drenching the base of the plant with 5 mL of a bacterial suspension (109 CFU ml^{-1}). The treatment non-inoculation received 5 mL of sterile nutrient broth.

After transplanting, the plants were reinoculated by drenching the base with 10 mL of bacterial suspension (109 CFU mL^{-1}). New inoculations were carried out every two weeks until 120 DAT. The treatment non-inoculation received sterile nutrient broth under the same conditions.

Before transplanting, the moisture of the substrates contained in the pots was raised to the pot capacity (0.37 m^3 m^{-3}) (Casaroli and De Jong Van Lier, 2008; Agbna et al., 2017; Oliveira et al., 2021) and daily

irrigations replenished the water volume necessary to return to this parameter.

A drip irrigation system was used, using self-compensating button-type drippers featuring a flow rate of 2 L h^{-1}. Irrigation was controlled by an automated system described by Campos et al. (2021), which collected and processed data from soil moisture sensors (10HS; METER Group, Pullman, WA, USA). The sensors underwent specific calibration for the substrate, according to the methodology described by Cobos and Chambers (2010).

An automated system took sensor readings every 30 minutes, and when the volumetric water content of the substrate dropped below the threshold (0.37 m^3 m^{-3}), the irrigation system automatically activated the solenoid valves (HVF-100; Rain Bird, Azuza, CA, USA), which remained open for 60 seconds, which applied a water volume of 33 mL, equivalent to an irrigation depth of 0.60 mm.

2.4. Experimental analyses

The morphometric analyses were conducted at 15 and 30 DAS (days after sowing), assessing plant height, stem diameter, and length of root with the help of a digital caliper (King Tools, Pompéia, SP, Brazil). At 30 DAS, the number of leaves and root volume were also evaluated using the graduated cylinder method (Basso, 1999).

The biomass production analysis was carried out at 15 and 30 DAS, determining the shoot fresh weight and root fresh weight, shoot dry weight, and root dry weight. The fresh weight was kept in a forced air circulation oven for 72 hours at 65 °C.

The relative growth rate (RGR) was determined according to Magalhães (1985), using Equation (1).

$$RGR = \ln (RDW30 + SDW30) - \ln (RDW15 + SDW15)) / (T30 - T15) \quad (1)$$

where ln = natural logarithm; T15 = time of biometric analysis in seedlings (15 days); T30 = time of biometric analysis in saplings (30 days); SDW15 = shoot dry weight (SDW) at 15 DAS; SDW30 = shoot dry weight (SDW) at 30 DAS; RDW15 = root dry weight (RDW) at 15 DAS; RDW30 = root dry weight (RDW) at 30 DAS.

Six leaf discs of 6 mm diameter each were used to determine the relative water content. After their initial weighing, the leaf discs were soaked in distilled water and stored in a refrigerator for 6 hours. They were then weighed again to determine the turgid weight and placed in a forced-air circulation oven at 80 °C for 24 hours to determine the dry weight. The leaf water content (LWC) was determined according to Equation (2) by Smart and Bingham (1974):

$$LWC = ((FM - DM) / (TM - DM)) \times 100 \quad (2)$$

where LWC = leaf water content (%); FM = Fresh weight of leaf discs (mg); DM = Dry weight of leaf discs (mg); TM = Turgid mass of leaf discs (mg).

The data were tabulated and analyzed with the Shapiro-Wilk test for normality of data (5%) to verify homoscedasticity followed by the analysis of variance (ANOVA) with the F test. Significant variables were compared using Tukey's test for mean comparison at the 5% and 1% significance levels. All analyses were performed using R Statistical software (version R 3.3.0+ for Windows; R Core Team, 2023).

3. Results

3.1. Tomato seed germination in vitro

Inoculation was significant for the germination test ($P < 0.05$) (Table 1). Seeds inoculated with Burkholderia seminalis TC3.4.2R3 showed higher germination rates ($P < 0.05$), at 72.5%, followed by seeds inoculated with Bacillus subtilis ATCC 23858 at 67.5%, and the non-inoculation treatment at 61.0% (Table 1).

Table 1. Cherry tomato germination rate after microbiolization.

Microbiolization	**Germination (%)**
Non-inoculation	61.0 ± 10.09 b
Bacillus subtilis	67.5 ± 7.01 ab
Burkholderia seminalis	7.5 ± 7.91 a
S.V.	**p-*value***
Microbiolization	0.0433*
C.V. (%)	12.23

*Significant at the 5% level using the Tukey test; **Significant at the 1% Tukey test level; nsNot significant; S.V.: source of variation; C.V. (%): coefficient of variation.

3.2. Greenhouse cultivation

Inoculation was significant for the emergence speed index (P < 0.01) (Table 2). Seeds inoculated with Bacillus subtilis ATCC 23858 and Burkholderia seminalis TC3.4.2R3 showed higher emergence speed indices, 6.77 and 6.54, respectively (P < 0.01), not statistically different from each other, but differing from the non-inoculation treatment (3.61), demonstrating that inoculation promotes tomato growth by accelerating seedling emergence.

Table 2. Emergence speed index of cherry tomatoes after microbiolization.

Microbiolization	**Emergence Speed Index**
Non-inoculation	3.61 ± 0.66 b
Bacillus subtilis	6.77 ± 1.24 a
Burkholderia seminalis	6.54 ± 1.03 a
S.V.	**p-*value***
Microbiolization	0.0042**
C.V. (%)	18.35

*Significant at the 5% level using the Tukey test; **Significant at the 1% Tukey test level; nsNot significant; S.V.: source of variation; C.V. (%): coefficient of variation.

Seedlings from microbiolized seeds produced more dry weight and had greater root length at 15 DAS (P<0.01) (Table 3).

Table 3. Stem diameter, plant height, shoot fresh weight, shoot dry weight, length radicle, root fresh weight and root dry weight of seedlings at 15 DAS.

Microbiolization	**Stem Diameter**	**Plant Height**	**Shoot Fresh Weight**	**Shoot Dry Weight**
	mm		mg	
Non-inoculation	0.67 ± 0.14 a	20.65 ± 4.65 a	10.69 ± 1.32 a	1.65 ± 0.29 a
Bacillus subtilis	0.78 ± 0.08 a	21.37 ± 2.60 a	10.91 ± 1.21 a	1.80 ± 0.49 a
Burkholderia seminalis	0.81 ± 0.29 a	22.04 ± 3.96 a	10.37 ± 1.62 a	1.73 ± 0.29 a
S.V.	***p-values***			
Microbiolization	0.4033ns	0.7567ns	0.7805ns	0.7381ns
C.V. (%)	27.32	17.28	14.46	21.77
Microbiolization	**Length Radicle**		**Root Fresh Weight**	**Root Dry Weight**
	mm		mg	
Non-inoculation	25.31 ± 7.02 c		6.43 ± 1.33 a	0.60 ± 0.20 b
Bacillus subtilis	57.77 ± 4.62 a		13.10 ± 1.825 a	1.02 ± 0.13 a
Burkholderia seminalis	39.19 ± 9.09 b		8.70 ± 1.52 a	0.72 ± 0.29 b
S.V.	***p-values***			
Microbiolization	<0.001**		0.4298ns	<0.001**
C.V. (%)	17.00		106.92	21.03

*Significant at the 5% level using the Tukey test; **Significant at the 1% Tukey test level; nsNot significant; S.V.: source of variation; C.V. (%): coefficient of variation.

As observed in Table 3, seedlings from seeds inoculated with Bacillus subtilis ATCC 23858 showed 1.02 mg of root dry weight, which was 70% higher than the non-inoculation treatment (0.60 mg). Additionally, a greater root length was observed (57.57 mm), being 1.47 times higher than the treatment inoculated with Burkholderia seminalis TC3.4.2R3 (39.19 mm) and 2.28 times higher than the non-inoculation treatment (25.31 mm) (Figure 4). Inoculation with Burkholderia seminalis TC3.4.2R3 compared to the non-inoculation treatment increased root length by 1.55 times.

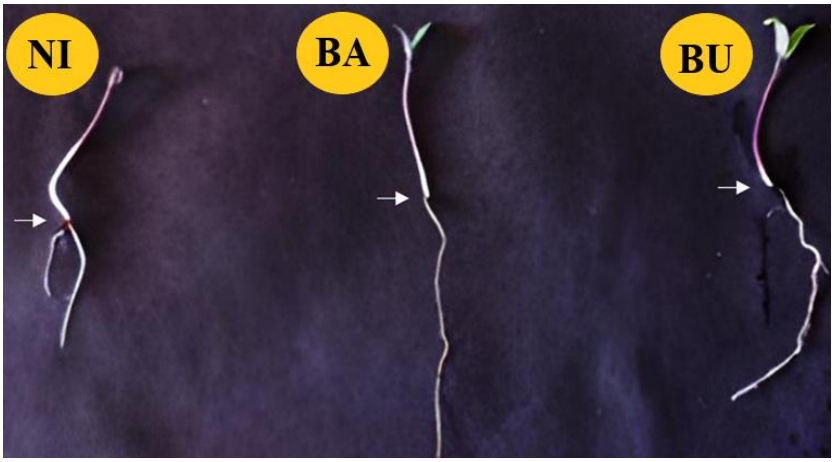

Figure 1. Radicle length of cherry tomato seedlings, non-inoculation (NI), inoculated with *Bacillus subtilis* ATCC 23858 (BA) and *Burkholderia seminalis* TC3.4.2R3 (BU).

At 30 DAS, inoculation with Bacillus subtilis ATCC 23858 and Burkholderia seminalis TC3.4.2R3 resulted in higher dry and fresh shoot and root mass and longer root length (Table 4). Root volume at 30 DAS was not affected by inoculation with Bacillus subtilis ATCC 23858 and Burkholderia seminalis TC3.4.2R3. The plant height of those inoculated with Bacillus subtilis ATCC 23858 was higher than that of plants inoculated with Burkholderia seminalis TC3.4.2R3 and non-inoculation plants.

Table 4. Stem diameter, plant height, root length, root volume, number of leaves, shoot fresh weight, root fresh weight, shoot dry weight and root dry weight of the plants at 30 DAS.

Microbiolization	**Stem Diameter**	**Plant Height**	**Root Length**	**Root Volume**	**Number of Leaves**
		mm		cm^3	
Non-inoculation	3.47 ± 0.68 a	18.06 ± 2.85 b	9.16 ± 2.81 b	1.63 ± 0.74 a	4.11 ± 0.64 a
Bacillus subtilis	3.62 ± 0.22 a	19.99 ± 3.28 a	18.84 ± 4.17 a	2.38 ± 0.38 a	3.89 ± 0.53 ab
Burkholderia seminalis	3.17 ± 0.34 b	16.10 ± 2.89 c	14.38 ± 2.54 a	2.25 ± 0.71 a	3.73 ± 0.76 b
S.V.			***p*-values**		
Microbiolization	<0.001**	<0.001**	<0.001**	0.1832^{ns}	<0.001**
C.V. (%)	10.94	17.90	24.17	39.37	16.82
Microbiolization	**Shoot Fresh Weight**	**Root Fresh Weight**	**Shoot Dry Weight**	**Root Dry Weight**	
			g		
Non-inoculation	2.07 ± 0.91 b	0.52 ± 0.40 b	0.13 ± 0.08 b	0.03 ± 0.03 b	
Bacillus subtilis	4.67 ± 1.28 a	1.49 ± 0.53 a	0.45 ± 0.12 a	0.10 ± 0.04 a	
Burkholderia seminalis	4.03 ± 0.55 a	1.38 ± 1.01 ab	0.33 ± 0.11 a	0.07 ± 0.04 ab	
S.V.			***p*-values**		
Microbiolization	<0.001**	0.0358*	<0.001**	0.0077**	
C.V. (%)	26.93	64.17	42.89	54.73	

**Significant at the 1% Tukey test level; ^{ns}Not significant; S.V.: source of variation; C.V. (%): coefficient of variation.

As observed in Table 4, Bacillus subtilis ATCC 23858 exhibited a root length of 18.84 cm, which was 1.31 times higher than the Burkholderia seminalis TC3.4.2R3-inoculated treatment (14.38 cm) and 2.05 times higher than the non-inoculation treatment (9.16 cm) (Figure 2). Inoculation with Burkholderia seminalis TC3.4.2R3 compared to the non-inoculation treatment increased root length by 1.57 times.

Figure 2. Roots of tomato seedlings in the treatments non-inoculation (NI), inoculated with Burkholderia seminalis TC3.4.2R3 (BU), and Bacillus subtilis ATCC 23858 (BA).

4. Discussion

4.1. Seed germination of tomato in vitro

Inoculation with Burkholderia seminalis TC3.4.2R3 and Bacillus subtilis ATCC 23858 promoted an increase in cherry tomato germination rate. Seed germination depends on embryo viability and dormancy breakage from environmental conditions (Luna-Martínez et al., 2013). Plant growth-promoting bacteria can influence dormancy breakage, as the reduction in ethylene levels due to the activity of ACC deaminase enzyme from bacteria present in the seed increases germination, along with the production of indole-3-acetic acid, which stimulates cell division to promote embryo growth (Glick et al., 2007; Jalili et al., 2009). Seed germination is also directly related to the production of abscisic acid, ethylene, gibberellins, auxins, and cytokinins (Miransari and Smith, 2014). These compounds are produced by bacteria of the genus Bacillus (Wagi and Ahmed, 2019).

4.2. Greenhouse cultivation

The emergence speed index of seeds inoculated with Bacillus subtilis and Burkholderia seminalis demonstrates that inoculation promotes tomato growth, accelerating seedling emergence compared to the non-inoculation treatment.

Different authors have demonstrated that seed microbiolization enables an increase in seed vigor and, consequently, seedling vigor, as well as accelerates seedling emergence, due to the production of phytohormones (e.g., auxins, gibberellins, and cytokinins) (Ibanhes Neto et al., 2021; Junges et al., 2016).

The initial growth of cherry tomatoes was increased by inoculation with Bacillus subtilis ATCC 23858 and Burkholderia seminalis TC3.4.2R3. The use of these bacteria in cherry tomato production resulted in significant increases in fresh and dry plant mass and root length, demonstrating the potential of using PGPB under the study conditions.

Inoculation of seeds with the microorganisms promoted the growth of seedlings with longer root length and increased dry weight production ($P<0.01$), as observed in Table 3. Cendales et al. (2017) found that the Bacillus subtilis GIBI 200 strain promotes the growth of tomato seedlings at 37 days old, leading to significant increases in stem and root length and fresh weight ($p<0.05$). The results are similar to those described by other authors who have also demonstrated Bacillus strain inoculation positive effect on tomato plant growth (Lagunas-Lagunas et al., 2001; Luna Martinez et al., 2013).

Inoculation of plant growth-promoting microorganisms, especially from the genus Bacillus and Burkholderia, aids in seed germination, promoting radicle growth, inducing the formation of root hairs, increasing the number of lateral and adventitious roots (Romagna et al., 2019), enlarging root volume and surface area (Tallapragada et al., 2015), enhancing plant height, and increasing fresh and dry weight production of both root and shoot (Tripti et al., 2017; Kumar et al., 2020).

Inoculation with Bacillus subtilis ATCC 23858 or Burkholderia seminalis TC3.4.2R3 promotes increased growth rate with higher biomass accumulation in the initial phase of cherry tomato (Figure 6), highlighting that the use of biostimulants in seeds can enhance germination and emergence, as well as

promote greater vigor and plant growth. However, the mechanisms involved in these stages and their interaction with the plant (genome, enzymatic activity, among others) still need to be identified (Silva et al., 2021).

5. Conclusions

The study demonstrates the promising impact of inoculation with Bacillus subtilis strain ATCC 23858 and Burkholderia seminalis strain TC3.4.2R3 on cherry tomato plants in a protected environment. The results indicate that Burkholderia seminalis positively influences the germination rate, while Bacillus subtilis contributes to increased plant height and root mass. Overall, the findings underscore the potential benefits of employing specific Bacillus subtilis and Burkholderia seminalis strains in cultivating cherry tomatoes in protected environments. This approach promotes plant growth, and emphasizes sustainable and efficient crop management through using microorganisms in agriculture. The study encourages further exploration and adoption of microbial inoculation techniques as a viable strategy for enhancing agricultural practices and achieving more resource-efficient and sustainable crop production.

Acknowledgements

This work was supported by the National Council for Scientific and Technological Development (CNPq) through Call CNPq/MCTI/FNDCT nº 18/2021 (Grant number 407465/2021-9) and nº 10/2023 (Grant number 420296/2023-9) and Goiano Federal Institute - Call nº 19 of July 9, 202. The authors extend their heartfelt appreciation to the Foundation for Research Support of Goiás State (FAPEG) through Call 11/2024 and for the master's assistantship (grant no. 202110267000503) provided to the first author.

References

Alcantara, H.P., Porto, F.G.M., 2019. Influência de fertilizante foliar com aminoácidos na cultura do jiló. Brazilian Journal of Development, 5:6, 5554–5563.

Araújo, F.D.S., Araújo, W.L., Eberlin, M.N., 2017. Potential of Burkholderia seminalis TC3.4.2R3 as Biocontrol Agent Against Fusarium oxysporum Evaluated by Mass Spectrometry Imaging. Journal of The American Society for Mass Spectrometry, 28:5, 901–907. https://doi.org/10.1007/s13361-017-1610-6.

Araújo, W.L., Creason, A.L., Mano, E.T., Camargo-Neves, A.A., Minami, S.N., Chang, J. H., Loper, J.E., 2016. Genome sequencing and transposon mutagenesis of Burkholderia seminalis TC3.4.2R3 identify genes contributing to suppression of orchid necrosis caused by B. gladioli. Molecular Plant-Microbe Interactions, 29:6, 435-446. https://doi.org/10.1094/MPMI-02-16-0047-R

Basso, S.M.S., 1999. Caracterização morfológica e fixação biológica de nitrogênio de espécies de Adesmia DC. E Lotus L. 1999. 268 f. Tese (Doutorado em Zootecnia) – Universidade Federal do Rio Grande do Sul, Porto Alegre.

Basu, A., Prasad, P., Das, S.N., Kalam, S., Sayyed, R.Z., Reddy, M.S., El Enshasy, H., 2021. Plant growth promoting rhizobacteria (PGPR) as green bioinoculants: recent developments, constraints, and prospects. Sustainability, 13, 1140. https://doi.org/10.3390/su13031140

Brasil., 2009. Ministério da Agricultura, Pecuária e Abastecimento. Secretaria de Defesa Agropecuária. Regras para análise de sementes.

Campos, H.M., Oliveira, H.F.E., Mesquita, M., Castro, L.E.V., Ferrarezi, R.S., 2021. Low-cost open-source platform for irrigation automation. Computers and Electronics in Agriculture, 190. https://doi.org/10.1016/j.compag.2021.106481

Cardoso, F.B. Martinez, H.E.P., Silva, D.J.H.D., Milagres, C.D.C., Barbosa, J.G., 2018. Yield and quality of tomato grown in a hydroponic system, with different planting densities and number of bunches per plant. Pesquisa Agropecuária Tropical, 48, 340-349. https://doi.org/10.1590/1983-40632018v4852611

Casaroli, D., De Jong van Lier, Q., 2008. Critérios para determinação da capacidade de vaso. Revista Brasileira de Ciências do Solo, 32, 59–66. https://doi.org/10.1590/S0100-06832008000100007

Cendales, T.C., Rodríguez-González, C.A., Villota-Cuásquer, C.P., Tapasco-Alzate, O.A., Hernández-Rodríguez, A., 2017. Bacillus effect on the germination and growth of tomato seedlings (Solanum lycopersicum L). Acta Biológica Colombiana, 22:1, 37-44. https://doi.org/10.15446/abc.v22n1.57375

Cobos, D.R., Chambers, C., 2010. Calibrating ECH2O soil moisture sensors. Application note, Decagon Devices Inc.: Pullman, WA, USA, 2010. Disponível em:

<http://www.decagon.com/assets/Uploads/13393-04-CalibratingECH2OSoilMoistureProbes.pd>. Acesso em: 19 de abril de 2022.

Glick, B.R., Cheng, Z., Czarny, J., Duan, J., 2007. Promotion of plant growth by ACC deaminase-producing soil bacteria. European Journal of Plant Pathology, 329-339. https://doi.org/10.1080/07352680701572966

Hwang, H.H., Chien, P.R., Huang, F.C., Hung, S.H., Kuo, C.H., Deng, W.L., Huang, C.C., 2021. A plant endophytic bacterium, Burkholderia seminalis strain 869T2, promotes plant growth in Arabidopsis, pak choi, Chinese amaranth, lettuces, and other vegetables. Microorganisms, 9:8. https://doi.org/10.3390/microorganisms9081703

Ibanhes Neto, H.F., Silva, A.C.D., Sumida, C.H., Gouveia, M.D.S., Pellizzaro, V., Takahashi, L.S.A., 2021. Physiological potential of green bean seeds treated with Bacillus subtilis. Journal of Seed Science, 43, 1–12. https://doi.org/10.1590/2317-1545v43248603

Khatoon, Z., Huang, S., Rafique, M., Fakhar, A., Kamran, M.A., Santoyo, G., 2020. Unlocking the potential of plant growth-promoting rhizobacteria on soil health and the sustainability of agricultural systems. Journal of Environmental Management, 273, 111-118. https://doi.org/10.1016/j.jenvman.2020.111118

Kumar, P., Aeron, A., Shaw, N., Singh, A., Bajpai, V.K., Pant, S., Dubey, R.C., 2020. Seed bio-priming with tri-species consortia of phosphate solubilizing rhizobacteria (PSR) and its effect on plant growth promotion. Heliyon, 6:12. https://doi.org/10.1016/j.heliyon.2020.e05701

Lagunas-Lagunas, J., Zavaleta, E., Osada, S., Aranda, S., Luna, I., Vaquera, H., 2001. Bacillus firmus como agente de controle biológico de Phytophthora capsici Leo. en jitomate (Lycopersicon esculentum Mill.). Revista Mexicana de Fitopatología, 19:1, 57-65.

Luna-Martínez, L., Martínez Peniche, R.A., Hernández Iturriaga, M., Arvizu Medrano, S.M., Pacheco Aguilar, J.R., 2013. Caracterización de rizobacterias aisladas de tomate y su efecto en el crecimiento de tomate y pimiento. Revista Fitotecnia Mexicana, 36:1, 63-69. https://doi.org/10.35196/rfm.2013.1.63

Miransari, M., Smith, D.L., 2014. Plant hormones and seed germination. Environmental and Experimental Botany, 99, 110-121. https://doi.org/10.1016/j.envexpbot.2013.11.005

Peel, M.C., Finlayson, B.L., McMahon, T.A., 2007. Updated world map of the Köppen-Geiger climate classification. Hydrology and earth system sciences, 11:5, 1633-1644. https://doi.org/10.5194/hess-11-1633-2007

R Core Team., 2023. R: A Language and Environment for Statistical Computing. Vienna, Austria: R Foundation for Statistical Computing. https://www.R-project.org/.

Romagna, I.S., Junges, E., Karsburg, P., Pinto, S.D.Q., 2019. Bioestimulantes em sementes de olerícolas submetidos a testes de germinação e vigor. Scientia Plena, 15:10. https://doi.org/10.14808/sci.plena.2019.100201

Rouphael, Y., Colla, G., 2018. Synergistic biostimulatory action: Designing the next generation of plant biostimulants for sustainable agriculture. Frontiers in Plant Science, 9. https://doi.org/10.3389/fpls.2018.01655

Silva, M.B.P., Silva, V.N., Vieira, L.C., 2021. Biopriming of sweet pepper and tomato seeds with Ascophyllum nodosum. Revista Facultad Nacional de Agronomia Medellin, 74:1, 9423–9430. https://doi.org/10.15446/rfnam.v74n1.88240

Silva, P.C., Ferreira, A.F.A., Araújo, E.S., Bessa Neto, J.V., Costa, A.R., Fernandes, L.S., Martins, A.A.S., Cândido, R.S., Jardim, A.M.R.F., Pandorfi, H., Silva, M.V., 2023. Cherry Tomato Crop Management Under Irrigation Levels: Morphometric Characteristics and Their Relationship with Fruit Production and Quality. Gesunde Pflanzen 75, 1277–1288. https://doi.org/10.1007/s10343-022-00770-8

Tallapragada, P., Dikshit, R., Seshagiri, S., 2015. Isolation and optimization of IAA producing Burkholderia seminalis and its effect on seedlings of tomato. Songklanakarin Journal of Science & Technology, 37:5. ISSN: 01253395.

Tripti, A., Kumar, Z., Usmani, V., Anshumali, K., 2017. Biochar and flyash inoculated with plant growth promoting rhizobacteria act as potential biofertilizer for luxuriant growth and yield of tomato plant. Journal of Environmental Management, 190, 20-27. https://doi.org/10.1016/j.jenvman.2016.11.060

Wagi, S., Ahmed, A., 2019. Green production of AgNPs and their phytostimulatory impact. Green Processing and Synthesis, 8, 885–894. https://doi.org/10.1515/gps-2019-0059

Zulfiqar, F., Akram, N.A., Ashraf, M., 2020. Osmoprotection in plants under abiotic stresses: new insights into a classical phenomenon. Planta, 251:3. https://doi.org/10.1007/s00425-019-03293-1

Indoor vertical greening for regulating building microclimate

Fabiana Convertino [a,*], Evelia Schettini [a], Giuliano Vox [a]

[a] Department of Soil, Plant and Food Sciences, University of Bari, Bari, Italy

* Corresponding author. Email: fabiana.convertino@uniba.it

Abstract

The integration of vegetation in buildings can increase the environmental sustainability of urban contexts as well as produce other relevant unquantifiable effects. Vegetation can be applied both on the exterior side of the buildings' envelope and inside, in different ways and layouts. Green façades are a specific kind of vertical greening for buildings consisting of plants covering vertical walls of buildings. The presence of vegetation on the envelope positively affects the building's thermal and acoustic performance, air quality, aesthetics, with relevant consequences in terms of energy and cost savings and human well-being. Until now, research has focused mainly on vertical greening systems applied to the exterior side of the buildings, but indoor applications deserve attention as well. This is the reason behind the present research: assessing the physical functioning of an indoor green façade. To this end, an experimental prototype of an indoor greening system was designed and realized to be monitored, at the University of Bari. The prototype consists of a sealed chamber, with evergreen plants, properly equipped with sensors for collecting air, soil and plant parameters, needed for studying the system functioning. The database created with the collected data enables investigations of the green façade behaviour and effects. A better understanding of this green technology, allowing for informed design and knowledge of induced effects, can promote the spread of indoor green façades.

Keywords: Urban agriculture, Green façade, Evapotranspiration, Canopy temperature, Heat transfer.

1. Introduction

The uncontrolled urban sprawl is resulting in various undesired problems worldwide. The main can be considered the lack of green spaces, the environmental pollution and the intense energy and resources consumption. The scarcity of natural elements has recently been particularly emphasised by researchers as an element linking the problems of urban contexts and, at the same time, nature-based solutions have been identified as the key to achieving ecological goals (Al-Kayiem et al., 2020). This consideration has been behind the promotion of studies and the implementation of different types of green infrastructures (GIs). As cities do not offer many horizontal free areas for the introduction of green elements, the vertical surfaces of buildings have increasingly been considered for the implementation of GIs in the form of vertical greenery systems (VGSs). VGSs mainly relate to green walls (GWs), realized according to two main technical solutions, the living walls (LWs) and the green façades (GFs) (Blanco and Convertino, 2023; Irga et al., 2023; Pérez et al., 2011). LWs and GFs each have their own engineering specifications, relating to construction system, plant types and maintenance methods. Available research demonstrated that VGSs provide numerous advantages in terms of increased sustainability to the whole environment and specifically to the urban context. These include mitigation of the urban heat island effect, increased energy efficiency, noise reduction, improved air quality and aesthetics.

While VGSs applied on the external side of the building's envelope have been more investigated, applied and have attracted more attention, the indoor VGSs (iVGSs) applications are more recent and still need to be studied in depth (Ghazalli et al., 2019). The integration of vegetation inside buildings deserves particular attention due to the potential benefits this can provide and also considering that people spend, on average, more than 80% of their time indoors (Klepeis et al., 2001; Wang et al., 2016). Indoor living environments must have specific microclimatic conditions and quality characteristics, often lacking. Buildings rooms are often polluted due to the presence of huge quantity of synthetic materials inside, as well as the constructive materials themselves, as natural materials are increasingly being replaced by artificial ones. This often leads to the presence of hazardous gases indoors. The dreariness and greyness of many living and working environments are other aspects to be considered.

With reference to these issues and the requirements that indoor environments must have, iVGSs can make valuable contributions to improving the quality of indoor environments. Vegetation can contribute to regulating air humidity and temperature inside (De Lucia et al., 2021; Fernández-Cañero et al., 2012;

Kazemi et al., 2020; Shao et al., 2021). Noise can be reduced too (Davis et al., 2017; Scamoni et al., 2022). Plants inside buildings can be a phytoremediation solution for reducing the concentration of CO_2, volatile organic compounds, particulate matter, and dust levels, by filtering, absorbing and retaining particles (Pettit et al., 2017; Shao et al., 2021; Suárez-Cáceres and Pérez-Urrestarazu, 2021). Relevant aspects are also those related to the enhanced aesthetics and, in turn, to the increased psychological and biological comfort of the indoor environments (Han et al., 2022). Even electronic equipment can benefit from presence of plants, in particular from the dust reduction and the limitation of its accumulation on components and clogging of air intakes. Improved quality of buildings rooms leads to increased comfort conditions for the occupants in terms of health, well-being, and productivity. Visual and physical contact with vegetation can reduce stress and increase resistance to illness. The presence of plants can improve recovery of patients in hospital rooms (Dijkstra et al., 2008). At school and in working environments, the greenery can improve morale, productivity, and limit absenteeism (Gray, 2018; Mangone et al., 2017; Pichlhöfer et al., 2021). Overall, a greener environment is a more user-friendly environment (Ghazalli et al., 2018).

Regarding constructive technologies, similarly to external VGSs, iVGSs can have different configurations, as LWs, consisting of modular cultivated panels, or GFs, with climbing or cascading plants grown in pots. A specific classification for iVGSs, mainly related to their phytoremediation function, is that distinguishing between passive and active systems, the latter also referred to as breathing walls (Abdo and Huynh, 2021; Irga et al., 2018; Soreanu et al., 2013). In passive systems, realized mainly as potted plant systems, biofiltration occurs by the simple diffusion of polluted air through the green component. In the breathing walls, having mainly the LW configuration, mechanical ventilation is used to force air passing through substrate, planting bed, rhizosphere, and foliage, being purified and providing natural cooling. Compared to passive systems, active iVGS are more focused on increasing indoor thermal comfort and improving air quality, thus reducing the building energy demand for air conditioning and treating. Active systems can also be combined with heating, ventilation and air conditioning (HVAC) equipment to increase the efficiency in providing comfortable thermal environment and air quality (Meng et al., 2022). An important aspect to consider in the realization of iVGSs is the radiation. It frequently happens that these green systems are placed in areas of the building where they provide a greater aesthetic impact, such as corridors or conference rooms, but that do not guarantee adequate solar radiation for the plants. Consequently, iVGSs are often provided with artificial lighting to maintain plant health and activity and lighting systems have to be properly selected taking into account the intensity and quality of radiation provided (Dominici et al., 2021; Kaltsidi et al., 2020). The functioning of the iVGS depends on the plant species as well. Thus, the plant selection should take into account indoor parameters as temperature, humidity, radiation, but also water, nutrient and medium and often indoor conditions are less favourable than outdoor conditions for plants. The installation method and the location are other driving factors in the plant selection (Wang et al., 2016). Several plants, with different characteristics, have been tested showing different induced effects in terms of thermal regulation and specific pollutants removed (Bandehali et al., 2021; Irga et al., 2018; Pettit et al., 2017; Pichlhöfer et al., 2021; Wang et al., 2016).

Based on the above considerations, it is clear that iVGSs represent a great opportunity for improving physical and non-physical aspects of the indoor living environments. To obtain the maximum quantifiable benefits from iVGSs application, their physical functioning has to be known in depth. This can allow their informed design and realization and promote their integration in buildings as well. This research aims at studying the behaviour and the induced effects of an iVGS, in the form of a potted GF, in a real scale application. The paper reports the first step of this experimental study and relates to the initial designing and assembling phases. An active system inserted into a sealed chamber is described. This prototype, properly integrated with sensors, will allow the physical data recording and monitoring and the collected data will help investigating the system functioning. Aim of the research is studying plants behaviour in relation with environmental conditions also using sensors for plants status monitoring. Results will be used to build a model describing the system functioning as an air conditioning system. The experimental set up is not unmodifiable, but it could be also provided with other sensors to analyse further relevant parameters. Having data on a long-term and real scale iVGS application will contribute to enrich the knowledge of iVGSs and promote their spread into new and existing buildings.

2. System design

The experimental prototype of iVGS was designed to be realized at the Department of Soil, Plant and

Food Sciences (Di.S.S.P.A.) of the University of Bari, Italy. The system was thought to be placed at the end of a corridor, on the first floor of the oldest part of the department building, overlooked by offices and laboratories. The corridor is 2.40 m wide and has the axis northeast-southwest oriented. In addition to three large windows on one long side, on the short side facing southwest where the prototype will be placed, the corridor is provided with a large glass door that makes the area of the system position well lit.

The first step in the experimentation was the design of the system. The construction characteristics, plant species and equipment to be implemented were carefully studied. The system components were bought, and the assembling phase is ongoing.

2.1. Constructive characteristics

Based on the objective of the test, i.e. analysing the heat and gas exchanges taking place in the system, it was decided to design a closed system. The designed prototype consists of a sealed chamber, having a rectangular plan, with dimensions of 2.00 m x 0.60 m and 2.00 m high (Figure 1).

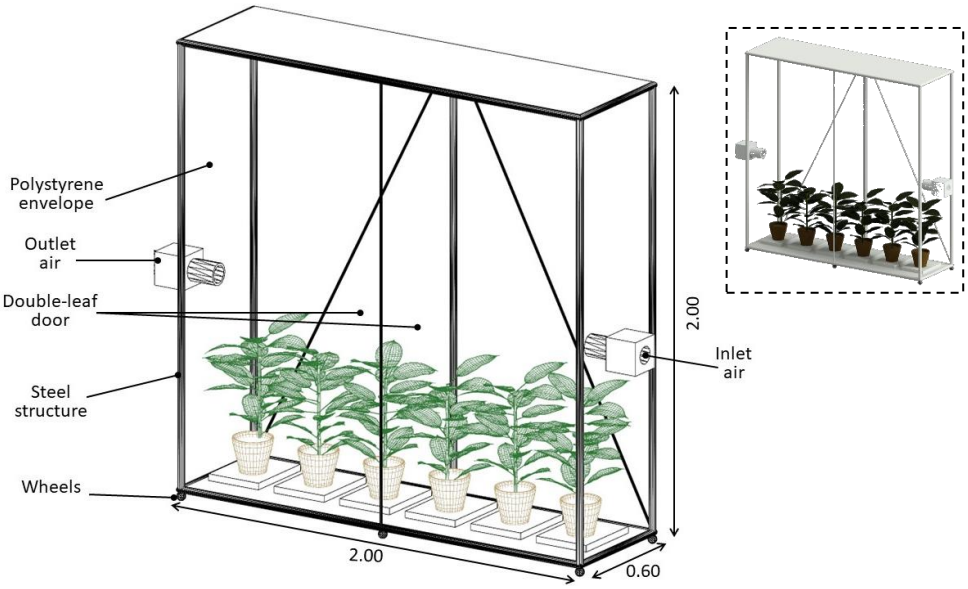

Figure 1. 3D views of the designed prototype.

The prototype was designed with a light steel structure. The envelope was thought to be made of opaque steel plates as for the inferior and superior horizontal parts.

The lateral envelope was designed in smooth transparent polystyrene sheets having thickness of 2.5 mm. The radiometric characteristics of the polystyrene sheets were evaluated at the laboratory of Di.S.S.P.A. at the University of Bari to assess its suitability for the test purpose. The sheets spectral direct transmissivity in the solar wavelength range (200−2500 nm) was measured by a double beam UV-VIS-NIR spectrophotometer (Lambda 950, Perkin Elmer Instruments, Norwalk, CT, USA). Measurements were performed in steps of 10 nm using radiation with a direct perpendicular incidence. The spectral total and diffuse transmissivity and reflectivity were measured through an integrating sphere (diameter 100 mm) used as receiver of the spectrophotometer, with a double beam comparative method. The spectral transmissivity and reflectivity in the longwave infrared (LWIR) range (2500−25000 nm) were measured by a FT-IR spectrophotometer (1760 X, Perkin Elmer Instruments, Norwalk, CT, USA) in steps of 4 cm^{-1}. The spectral transmissivity was measured using radiation with a direct perpendicular incidence; reflectivity was measured at near normal incidence (10°). Five samples (40 mm x 40 mm) were used to perform transmissivity and reflectivity measurements both in the solar and in the LWIR range. The radiometric coefficients in the solar wavelength range (200−2500 nm) and in the PAR range (400−700 nm) were calculated as the weighted average value of the spectral transmissivity using the spectral distribution of the solar radiation at ground level as a weighting function (Vox et al., 2005). The transmissivity coefficients in

the LWIR range were calculated as average values of the spectral transmissivity in the wavelength range from 7500 nm to 12500 nm. The polystyrene sheets showed total solar transmissivity and reflectivity equal to 85.6% and 9.9% respectively, and a LWIR emissivity of 94.2%.

The access to the inside of the chamber, necessary to manage plants and equipment, is allowed through double-leaf door on one long side of the prototype. The chamber was perfectly sealed at joints and provided with wheels at the vertical supports and under the door leaves to ease prototype movement and door opening.

The two lateral short sides of the prototype were designed having two holes, one each, in the middle of the polystyrene sheets. These holes are needed to let air in and out of the chamber and to control airflow parameters. Through interposed aluminium tubes these holes connect the chamber to two white polystyrene boxes, one on each side, having holes on the opposite sides and specifically designed and equipped to measure inlet and outlet air temperature, relative humidity, speed, and direction. The box placed at the air inlet side is also provided with a fan to push air into the chamber and enable air exchange cycles.

2.2. Vegetation

The green component of the system is made of plants. Ornamental evergreen plants suitable for indoor environments were selected and specifically plants of *Syngonium podophyllum*. These plants have decorative foliage that develops aerial roots and leaves, lobed in shape, that become especially large as they grow. As the plants age, they become climbing and drooping, with stems that can reach up to two meters in length, so these are particularly suited to the purpose of indoor GF. The optimal mean temperature to grow these plants is in the range 18–20 °C, while they do not tolerate temperature lower than 13 °C. Thus, in the Mediterranean climate context of the experimental test, these plants can be cultivated only indoor. Moreover, *Syngonium* plants need radiation, but not direct solar radiation, and air exchanges, but not cold air currents. These characteristics also make this species particularly suited to the study purpose and were taken into account in the prototype design as well. As for irrigation, these plants need moist soil and abundant watering especially in spring and summer. Therefore, an automated irrigation system will be designed and implemented as well.

The *Syngonium* plants of 20 cm were bought in mid-September 2023 and transplanted in bigger pots on 26 September (Figure 2). Since then, the plants have been watered manually and periodically fertilized with a NPK 7-5-5 fertiliser solution with boron, copper, iron, manganese, and zinc.

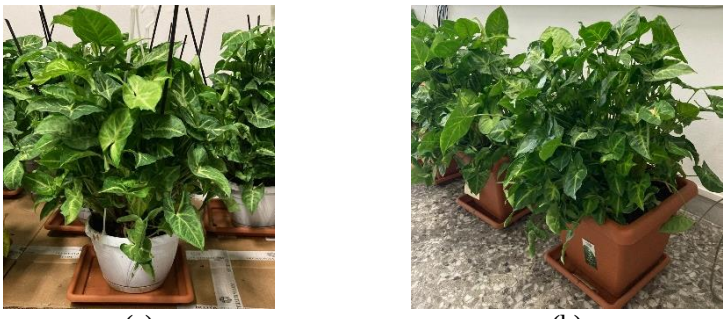

(a) (b)

Figure 2. *Syngonium* plant before (a) and after transplanting (b).

2.3. Equipment

The system design also concerned several sensors to allow the system parameters recording and monitoring. Recorded data are useful to assess the physical behaviour of the green system.

The recording equipment is made of a data logger (CR1000, Campbell, Logan, USA) and sensors for parameters detection. The following sensors were selected to be included in the experimental set up: HygroClip-S3 sensors (Rotronic, Zurich, Switzerland) to measure air temperature and relative humidity; Apogee SI 400 radiometers (Logan, UT, USA) for canopy temperature; a pyranometer PIR02 (Geoves s.n.c., Conegliano, Italy) to measure solar radiation in the wavelength range 0.3–3 mm; ultrasonic anemometers (ATMOS 22, METER Group, Inc., Pullman, WA, USA) for measuring air velocity and

direction; ECH2O 10HS sensors (METER Group, Inc., Pullman, WA, USA) for detecting soil volumetric water content; load cells (Scaime, Juvigny, France) placed under two plants pots to measure plants evapotranspiration rate through the pot-plant system weight variation (Figure 3). The parameters measurement frequence is 60 s; data are averaged and recorded by the data logger every 15 min. The equipment has been tested and its final layout, showing sensor types and positions, is reported in Figure 4.

By assembling all the components, the structure, the plants and the equipment, the starting configuration of the experimental prototype was realized (Figure 5), with the possibility of further development and refinement.

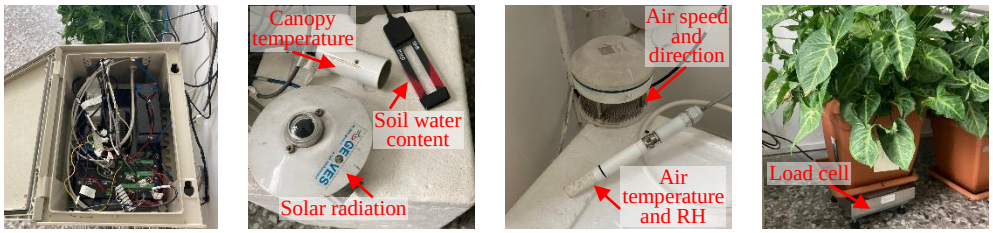

(a) (b) (c) (d)

Figure 3. Set up equipment: datalogger (a), sensors for measuring solar radiation, canopy temperature and soil water content (b), air temperature and relative humidity and air speed and direction (c), load cell under the plant pot (d).

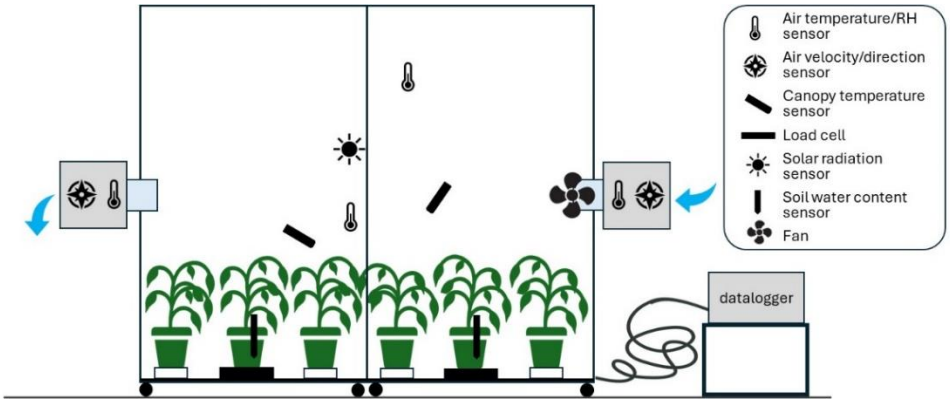

Figure 4. Equipment layout.

Figure 5. Views of the realized prototype.

3. Conclusions

Given that, nowadays, most people live in urban context and that the greatest part of their time is passed inside buildings, providing comfortable indoor living environments is imperative. Greenery systems integrated within buildings areas can be a proper valid solution to achieve this aim. Specific applications are the indoor vertical greenery systems, able to provide physical and non-physical benefits to the buildings occupants.

This study is the first step of a research on an indoor vertical greenery. It refers to the design of an active green façade to be realized as a sealed chamber in a building corridor of the University of Bari. The constructive characteristics of the system were carefully defined. The plant species, an evergreen ornamental one, was selected and several plants have been grown in pots. The equipment, needed to make the system work and to measure and monitor the main physical parameters was designed as well. Once fully assembled, this system will allow the investigation of its physical behaviour and the collection of several data. The obtained database will be precious for analysing the occurring heat and gaseous exchanges, building a model describing the indoor greenery system functioning, thus allowing their better comprehension. Moreover, the designed system could be integrated with other sensors for detecting other important parameters and extending the study. The enhanced knowledge this research aims to providing about the indoor greenery systems will make their design and application more informed and optimized. Ultimately, this could give an important input to the spread of such green technology.

Acknowledgements

This study was carried out within the Agritech National Research Center and received funding from the European Union Next-GenerationEU (PIANO NAZIONALE DI RIPRESA E RESILIENZA (PNRR) – MISSIONE 4 COMPONENTE 2, INVESTIMENTO 1.4 – D.D. 1032 17/06/2022, CN00000022). This manuscript reflects only the authors' views and opinions, neither the European Union nor the European Commission can be considered responsible for them.

References

Abdo, P., Huynh, B.P., 2021. An experimental investigation of green wall bio-filter towards air temperature and humidity variation. J. Build. Eng. 39, 102244. https://doi.org/10.1016/j.jobe.2021.102244

Al-Kayiem, H.H., Koh, K., Riyadi, T.W.B., Effendy, M., 2020. A comparative review on greenery ecosystems and their impacts on sustainability of building environment. Sustain. 12, 1–26. https://doi.org/10.3390/su12208529

Bandehali, S., Miri, T., Onyeaka, H., Kumar, P., 2021. Current state of indoor air phytoremediation using potted plants and green walls. Atmosphere (Basel). 12, 473. https://doi.org/10.3390/atmos12040473

Blanco, I., Convertino, F., 2023. Thermal performance of green façades: research trends analysis using a science mapping approach. Sustainability 15, 9981. https://doi.org/10.3390/su15139981

Davis, M.J.M., Tenpierik, M.J., Ramírez, F.R., Erez, M.E.P., 2017. More than just a Green Facade: The sound absorption properties of a vertical garden with and without plants. Build. Environ. 116, 64–72. https://doi.org/10.1016/j.buildenv.2017.01.010

De Lucia, M., Treves, A., Comino, E., 2021. Rice husk and thermal comfort: Design and evaluation of indoor modular green walls. Dev. Built Environ. 6, 100043. https://doi.org/10.1016/j.dibe.2021.100043

Dijkstra, K., Pieterse, M.E., Pruyn, A., 2008. Stress-reducing effects of indoor plants in the built healthcare environment: The mediating role of perceived attractiveness. Prev. Med. (Baltim). 47, 279–283. https://doi.org/10.1016/j.ypmed.2008.01.013

Dominici, L., Fleck, R., Gill, R.L., Pettit, T.J., Irga, P.J., Comino, E., Torpy, F.R., 2021. Analysis of lighting conditions of indoor living walls: Effects on CO2 removal. J. Build. Eng. 44, 102961. https://doi.org/10.1016/j.jobe.2021.102961

Fernández-Cañero, R., Pérez Urrestarazu, L., Salas, A.F., 2012. Assessment of the cooling potential of an indoor living wall using different substrates in a warm climate. Indoor Built Environ. 21, 642–650. https://doi.org/10.1177/1420326X11420457

Ghazalli, A.J., Brack, C., Bai, X., Said, I., 2019. Physical and Non-Physical Benefits of Vertical Greenery Systems: A Review. J. Urban Technol. 26, 53–78. https://doi.org/10.1080/10630732.2019.1637694

Ghazalli, A.J., Brack, C., Bai, X., Said, I., 2018. Alterations in use of space, air quality, temperature and

humidity by the presence of vertical greenery system in a building corridor. Urban For. Urban Green. 32, 177–184. https://doi.org/10.1016/j.ufug.2018.04.015

Gray, T., 2018. Retrofitting biophilic design elements into office site sheds: does 'going green' enhance the well-being and productivity of workers?, in: Landscape Architecture - The Sense of Places, Models and Applications. InTech. https://doi.org/10.5772/intechopen.71890

Han, K.T., Ruan, L.W., Liao, L.S., 2022. Effects of indoor plants on human functions: a systematic review with meta-analyses. Int. J. Environ. Res. Public Health 19, 7454. https://doi.org/10.3390/ijerph19127454

Irga, P.J., Pettit, T.J., Torpy, F.R., 2018. The phytoremediation of indoor air pollution: a review on the technology development from the potted plant through to functional green wall biofilters. Rev. Environ. Sci. Bio/Technology 17, 395–415. https://doi.org/10.1007/s11157-018-9465-2

Irga, P.J., Torpy, F.R., Griffin, D., Wilkinson, S.J., 2023. Vertical greening systems: a perspective on existing technologies and new design recommendation. Sustainability 15, 6014. https://doi.org/10.3390/su15076014

Kaltsidi, M.P., Fernández-Cañero, R., Pérez-Urrestarazu, L., 2020. Assessment of different LED lighting systems for indoor living walls. Sci. Hortic. (Amsterdam). 272, 109522. https://doi.org/10.1016/j.scienta.2020.109522

Kazemi, F., Rabbani, M., Jozay, M., 2020. Investigating the plant and air-quality performances of an internal green wall system under hydroponic conditions. J. Environ. Manage. 275, 111230. https://doi.org/10.1016/j.jenvman.2020.111230

Klepeis, N.E., Nelson, W.C., Ott, W.R., Robinson, J.P., Tsang, A.M., Switzer, P., Behar, J. V., Hern, S.C., Engelmann, W.H., 2001. The National Human Activity Pattern Survey (NHAPS): a resource for assessing exposure to environmental pollutants. J. Expo. Anal. Environ. Epidemiol. 11, 231–252. https://doi.org/10.1038/sj.jea.7500165

Mangone, G., Capaldi, C.A., Van Allen, Z.M., Luscuere, P.G., 2017. Bringing nature to work: Preferences and perceptions of constructed indoor and natural outdoor workspaces. Urban For. Urban Green. 23, 1–12. https://doi.org/10.1016/j.ufug.2017.02.009

Meng, X., Yan, L., Liu, F., 2022. A new method to improve indoor environment: Combining the living wall with air-conditioning. Build. Environ. 216, 108981. https://doi.org/10.1016/j.buildenv.2022.108981

Pérez, G., Rincón, L., Vila, A., González, J.M., Cabeza, L.F., 2011. Green vertical systems for buildings as passive systems for energy savings. Appl. Energy 88, 4854–4859. https://doi.org/10.1016/j.apenergy.2011.06.032

Pettit, T., Irga, P.J., Abdo, P., Torpy, F.R., 2017. Do the plants in functional green walls contribute to their ability to filter particulate matter? Build. Environ. 125, 299–307. https://doi.org/10.1016/j.buildenv.2017.09.004

Pichlhöfer, A., Sesto, E., Hollands, J., Korjenic, A., 2021. Health-related benefits of different indoor plant species in a school setting. Sustainability 13, 9566. https://doi.org/10.3390/su13179566

Scamoni, F., Scrosati, C., Depalma, M., Barozzi, B., 2022. Experimental evaluations of acoustic properties and long-term analysis of a novel indoor living wall. J. Build. Eng. 47, 103890. https://doi.org/10.1016/j.jobe.2021.103890

Shao, Y., Li, J., Zhou, Z., Zhang, F., Cui, Y., 2021. The impact of indoor living wall system on air quality: A comparative monitoring test in building corridors. Sustainability 13, 7884. https://doi.org/10.3390/su13147884

Soreanu, G., Dixon, M., Darlington, A., 2013. Botanical biofiltration of indoor gaseous pollutants - A mini-review. Chem. Eng. J. 229, 585–594. https://doi.org/10.1016/j.cej.2013.06.074

Suárez-Cáceres, G.P., Pérez-Urrestarazu, L., 2021. Removal of volatile organic compounds by means of a felt-based living wall using different plant species. Sustainability 13, 6393. https://doi.org/10.3390/su13116393

Vox, G., Schettini, E., Scarascia-Mugnozza, G., 2005. Radiometric properties of biodegradable films for horticultural protected cultivation, in: Acta Horticulturae. International Society for Horticultural Science, pp. 575–582. https://doi.org/10.17660/ActaHortic.2005.691.69

Wang, C., Er, S.-S., Abdul-Rahman, H., 2016. Indoor vertical greenery system in urban tropics. Indoor Built Environ. 25, 340–356. https://doi.org/10.1177/1420326X14550508

Usage of artificial lighting to promote seed germination for microgreen production

Christos Vatistas [a,*], Dafni D. Avgoustaki [a], and Thomas Bartzanas [a]

[a] Department of Natural Resources and Agricultural Engineering, Agricultural University of Athens, Iera Odos 75, Athens 118 55, Greece.

* Corresponding author. Email vatistasx@aua.gr

Abstract

Growing vegetables in controlled environmental agriculture (CEA) systems has contributed significantly in recent years to increasing local production within urban areas, providing consumers with fresh vegetables. The use of artificial lighting during cultivation in these systems promotes plant growth by providing them with the required daily amount of photosynthetic photon flux density (PPFD) and at the same time enables precise planning of the harvest time from the moment of sowing. One category of cultivation in CEA systems is that of microgreens, where seedlings are consumed just a few days after sprouting. Cultivation takes place on shelves, utilizing artificial lighting to provide the necessary energy to the seedlings. The purpose of this experiment was to investigate whether lighting facilitates faster germination of cabbage and arugula seeds, and if any specific spectrum has a better effect on them. The seeds were placed under 9 different light spectra for photoperiods of 4, 8 and 16 hours daily. The spectra studied were in the range of UV, blue, green, orange, red, farred, combination of blue-red, combination of blue-red-farred and a full spectrum cool-white LED. The results of the experiments showed that lighting has a positive effect in terms of time and the percentage of seeds that germinate, compared to their germination in the dark. The seedlings grown had different morphological characteristics under different spectra and a different amount of biomass was produced under the different lighting treatments. Production can be increased by using combinations of lighting during cultivation. An initial exposure of seeds to the spectrum with the highest germination rates increases the number of produced seedlings, while exposure to the lighting spectrum that produced the most biomass subsequently increases the quantity of the final yield.

Keywords: microgreens, seeds, control-environmental agriculture, lighting, germination

1. Introduction

The cultivation of plants in closed and controlled environments has seen significant growth in recent years. This method primarily employs hydroponic systems and vertical farming on shelves, which maximizes production per unit area. By consistently providing optimal environmental conditions, these systems enhance production by promoting faster plant growth and allowing for denser planting within the same space (Rajan et al., 2019). Microgreens are a relatively new specialty crop that is gaining momentum in the global market (Lanoue et al., 2022). They are tender seedlings, mostly derived from vegetable seeds, and are harvested once the cotyledons have fully developed, usually before the first true leaves appear (Zhang et al., 2021). As a result, their cultivation period ranges from about 7 days to three weeks. Due to their short shelf life post-harvest, local cultivation near consumption points is the most effective strategy (Cowden et al., 2023). The ever-increasing demand and high market value have made microgreen cultivation very attractive to producers. Microgreens are primarily used to enhance the nutritional value and flavor of food. Several studies have shown that microgreens contain high concentrations of antioxidant compounds, such as polyphenols, carotenoids, and ascorbic acid (Lerner et al., 2024; Shibaeva et al., 2022; Maru et al., 2024).

Key factors for enhancing microgreen production include seed germination, robust seedling growth, and the appropriate quality and quantity of lighting. Cultivation mainly uses LED lamps, with either a full spectrum or a targeted spectrum, depending on the specific needs of each crop (Toscano et al., 2021). Within the broad spectrum of solar radiation, the range that plants use for growth falls between 400-700 nm and is known as Photosynthetically Active Radiation (PAR). However, wavelengths outside this range can also influence plant growth and seed germination (Rengasamy et al., 2022). Plants have evolved mechanisms to detect light's quality, quantity, duration, and direction. These mechanisms, known as photoreceptors, are proteins that include cryptochromes, phytochromes, and phototropins. These photoreceptors regulate various genes and their responses to different light spectra (Wong et al., 2020).

Similarly, seeds receive the stimulus of light and germination is promoted in smaller seeds before they penetrate deep into the soil, or germination is avoided if they are in a place where the required light conditions are not met (Bu et al., 2017). Light is one of the most important factors for seed germination as it initiates stimulation by breaking the dormancy period and activating the seed germination process (Foschi et al., 2022). Some seeds germinate in the dark, others need a certain amount of light, while others germinate equally well in both darkness and light (Vatistas et al., 2024; Bu et al., 2017).

Enhanced microgreen production relies on healthy seeds with high germination rates. The aim of this study is to investigate whether different light spectra influence seed germination rates and if faster germination can be achieved with a specific spectrum or lighting treatment. The species studied were cabbage and arugula seeds, which are widely cultivated microgreens. The objective is to find better lighting management practices to increase overall production yield.

2. Material and Methods

2.1. Seedling growth for germination comparison

The studied leafy greens were cabbage (*Brassica oleracea var. capitate*) and arugula (*Eruca vesicaria ssp. sativa*), and their growth took place in a growth chamber with controllable conditions. The temperature inside the growth chamber varied between 19-21 ^{o}C during the day and 16-18 ^{o}C during the night. Twenty seeds from each plant were placed in small square plastic containers (12x12x5 cm) and absorbent paper saturated with water was used as a substrate. The relative humidity in the growth area varied between 80% and 90% and was maintained at these levels by using a transparent film to cover the containers.

2.2. Photoperiods and different spectra

An initial sowing was conducted under dark conditions to compare its effect on seed germination. The experiments were conducted with photoperiods of 4, 8, and 16 hours, and using 9 different light spectra. The studied spectra were 1) UV (peak 364nm), 2) blue (peak 448nm), 3) green (peak 516nm), 4) orange (peak 594nm), 5) red (peak 630), 6) farred (peak 729nm), 7) combination of blue and red, 8) combination of blue-red-farred and 9) cool-white LED. Each light treatment had duration of 7 days (168 hours). The intensity of each spectrum was measured in photosynthetic photon flux density (PPFD) units using a spectroradiometer (UPRTEK PG200N). The peak point of each spectrum was measured also with the spectroradiometer. PPFD units was equal to 30 μmol/m^2/s for each spectra, except UV which was equal to 0,29 μmol/m^2/s.

Table 1. Abbreviations of experiments.

	Spectra								
Photoperiod	**UV**	**Blue**	**Green**	**Orange**	**Red**	**Farred**	**Blue-Red**	**Blue-Red-Farred**	**Cool-White**
4 hours	4hUV	4hB	4hG	4hOr	4hR	4hFR	4hBR	4hBRFR	4hCW
8 hours	8hUV	8hB	8hG	8hOr	8hR	8hFR	8hBR	8hBRFR	8hCW
16 hours	16hUV	16hB	16hG	16hOr	16hR	16hFR	16hBR	16hBRFR	16hCW

2.3. Microgreens production

Microgreens were cultivated in plastic containers with holes at the bottom, placed above another plastic container to collect irrigation water. The soil used as a substrate consisted of composed of peat, plant residues, and organic fertilizer. For both plants studied, a quantity of 0.85 grams of seeds was used per container. The cultivation of microgreens was carried out using three different methods for each plant. In the first case, seeds were placed in darkness for 3 days and

then exposed to artificial lighting with a blue-red-far-red spectrum for 16 hours photoperiod, for both plants. In the second case, they were directly placed under the aforementioned lighting treatment. This lighting combination was chosen because it produced seedlings with the highest dry:fress weight (DW:FW) biomass ratio, for both plants. In the third case, for cabbage, seeds were placed under blue spectrum lighting for 5 days and for 16 hours photoperiod and then under 16 hours of blue-red-far-red spectrum, while for arugula, the initial lighting was 8 hours under green spectrum for 5 days also. The selection of the initial lighting treatment was based on the treatment that gave the highest final percentage of germination and root development in a shorter period of time. The intensity of the growth spectrum was 120 μmol/m^2/s. The overall cultivation of microgreens lasted 12 days from seeding to harvest.

2.4. Measurements and Analysis

The initial measurements involved recording the number of seeds that developed roots and the time it took after sowing to grow the first observed root. Next, the number of seeds that developed shoots was recorded. At the end of each treatment the developed shoots and leaves were collected and weighed in order to measure their fresh biomass. The fresh biomass was placed in a drying oven for 24 hours at 80 ºC, and then the dry biomass was weighed. Finally, the ratio of dry to fresh biomass was calculated. This procedure was carried out both for the seedlings grown during the comparison of different spectra, and for the microgreens grown in the next stage of the experiment.

The weighing for each treatment was conducted based on the biomass produced by the seeds that successfully developed a shoot. Therefore, the mass diagrams generated represent the total biomass produced per container and per 20 seeds. Descriptive analysis was employed for the comparison of the produced biomasses, utilizing the SPSS statistical package.

3. Results and Discussion

The germination percentages for cabbage seeds under each lighting treatment, as well as in dark conditions, are presented in Table 2. Additionally, Table 2 presents the percentages of seeds that developed a shoot by the end of the treatment period (168 hours), as well as the time required for the first root development to be observed under each lighting condition.

Table 2. Percentages of root-shoot development and first root appearance, for all lighting treatments of cabbage.

	4 hours			8 hours			16 hours		
	Root (%)	**Shoot (%)**	**1st root (h)**	**Root (%)**	**Shoot (%)**	**1st root (h)**	**Root (%)**	**Shoot (%)**	**1st root (h)**
Dark				10	5	96			
UV	30	25	72	55	45	72	10	10	72
Blue	10	10	96	25	25	72	55	55	72
Green	25	25	96	45	15	48	25	20	96
Orange	35	30	72	25	10	72	40	40	72
Red	10	5	72	30	15	96	35	30	72
Farred	25	25	48	30	15	96	15	10	72
BR	20	15	72	45	20	72	25	25	72
BRFR	35	35	72	20	20	72	15	5	120
CoolWhite	15	10	72	50	35	72	25	25	72

As shown in Table 2, the lowest germination percentage observed was 10%. This resulted from the treatment in dark conditions, with the Blue and Red spectrum at 4 hours of photoperiod, and at 16 hours for the UV spectrum. The highest rates were observed in the treatments 8hUV and 16hB, equal to 55%. At 4 hours of photoperiod, the germination percentages ranged from 10% (Blue, Red) to 35% (Orange, BRFR). At 8 hours photoperiod ranges from 20% (BRFR) to 55% (UV) and at 16 hours from 10% (UV) to 55% (Blue). The percentages of seeds that managed to develop a shoot ranged from 5% (Red) to 35% (BRFR) for the 4-hour photoperiod, from 10% (Orange) to 45% (UV)

for the 8-hour photoperiod, and from 10% (UV) to 55% (Blue) for the 16-hour photoperiod. The dark treatment also gave a low rate of shoot development, as expected from the low germination rate obtained, equal to 5%. Regarding root development time, the shortest duration was observed in the 4hFR and 8hGr treatments, at 48 hours, while the most delayed root development occurred at 120 hours in the 16hBRFR treatment.

The results indicate that lighting yields significantly better results compared to dark conditions for cabbage seeds. Among the studied photoperiods, Orange and BRFR lighting were more efficient for short photoperiods, UV for medium durations, while blue lighting demonstrates greater efficiency for longer photoperiods.

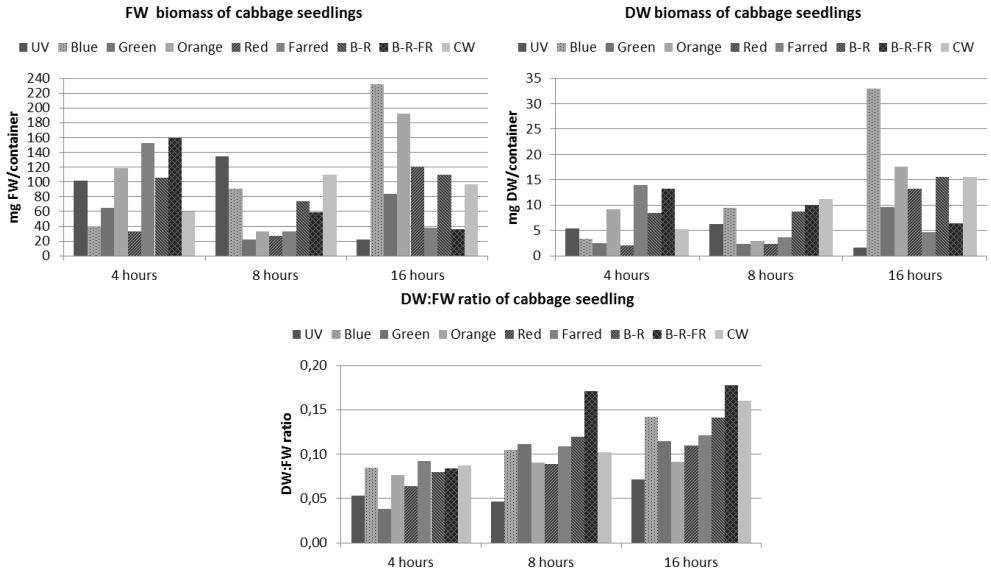

Figure 1. Fresh weight (FW), dry weight (DW) and ratio of fresh weight to dry weigh (FW:DW) of seedlings biomass produced from each lighting treatment of cabbage seeds. Biomass corresponds to the total produced by those of the 20 seeds that developed a shoot in each treatment.

As can be seen from the diagrams in Figure 1, the values in the produced biomasses of cabbage seedlings exhibit several differences both between the spectra and between the different exposures of the seedlings to the same lighting spectrum. The highest fresh biomass was produced in the 16hB treatment, measuring 232.1 mg, which also had the highest percentage of developed seedlings. In contrast, the lowest amount of fresh biomass was produced in the 16hUV treatment, measuring 22.4 mg.

Seedlings grown under low photoperiods exhibited increased shoot length, suggesting the occurrence of scotomorphogenesis, where seedlings elongate to reach light. Consequently, the lowest ratio of dry to fresh biomass was observed in almost all spectra for the 4-hour photoperiod. With increasing photoperiod, the length of the developed seedlings decreased by almost half compared to those exposed to 4 hours of light. The DW:FW biomass ratios were higher in longer photoperiods, indicating an increase in dry biomass and, consequently, an increase in biochemical reactions within the plant. Specifically, the highest dry biomass was produced in the 16hB treatment, measuring 33 mg, followed by the 16hOr treatment, which produced 17.6 mg. High values were also observed with the B-R and Cool White spectra, each yielding 15.5 mg of dry biomass under the 16-hour photoperiod. The lowest dry biomass production was observed in the 16hUV treatment, measuring 1.6 mg, with only 10% developed shoots.

Dry-to-fresh biomass ratios ranged from 0.05 for the 4hG treatment to 0.18 for the 16hBRFR treatment. High ratios were also observed for the 8hBRFR treatment at 0.17, the 16hCW treatment at 0.16, and the 16hBR and 16hB treatments, both at 0.14.

Table 3. Percentages of root-shoot development and first root appearance, for all lighting treatments of arugula.

	4 hours			**8 hours**			**16 hours**		
	Root (%)	**Shoot (%)**	**1st root (h)**	**Root (%)**	**Shoot (%)**	**1st root (h)**	**Root (%)**	**Shoot (%)**	**1st root (h)**
Dark				65	55	48			

UV	65	65	24	70	60	24	75	60	24
Blue	70	70	24	75	25	24	70	50	24
Green	75	75	24	90	75	24	70	70	24
Orange	75	65	24	65	50	24	75	65	24
Red	70	65	24	85	70	24	65	55	24
Farred	75	70	24	60	50	24	85	80	24
BR	65	65	24	70	70	24	75	55	24
BRFR	70	70	24	75	75	24	60	60	24
CoolWhite	85	65	24	70	60	24	50	25	24

As Table 3 indicates, the lowest percentage of arugula seed germination was observed in the 16hCW treatment, at 50%. Next lower percentage was for the same photoperiod and the BRFR spectrum, and for 8hFR treatment, equal to 60%. In all other treatments, germination percentages ranged from 65% to 90%. Specifically, at the 4-hour photoperiod, the percentages were 65% (UV, BR), the lowest, and 85% (Cool White), the highest. In the 8-hour photoperiod, the percentages ranged from 60% (Farred) to 90% (Green), which is the highest percent of all treatments, while at 16 hours they ranged from 50% (CoolWhite) to 85% (Far Red). Corresponding percentages of shoot growth ranged from 65% (UV, Orange, Red, BR, Cool White)), for most of the 4-hour photoperiod lighting spectra, to 75% (Green). In the 8-hour photoperiod, the 4hB treatment presented a fairly low percentage, equal to 25%, while for the rest of the spectrum, the percentages ranged from 50% (Orange, Farred) to 75% (Green, BRFR). Also, for the 16-hour photoperiod and Cool White lighting, a low percentage equal to 25% was observed, while for the rest of the spectrum, the percentages ranged from 50% (Blue) to 80% (Far Red). The corresponding figure for growth in the dark was 55%. For all the lighting treatments studied, the first root development was observed within the first 24 hours, while in the dark, root development was observed after 48 hours.

Based on the germination results, lighting significantly enhances the speed of root growth compared to darkness. Overall, germination rates are high in most of lighting treatments. Specifically, Green spectrum for 8 hours proves to be the most efficient, while Cool White spectrum performs optimally under shorter photoperiods (4 hours). Additionally, Farred spectrum shows increasing efficiency with longer photoperiods, reaching peak effectiveness at 16 hours.

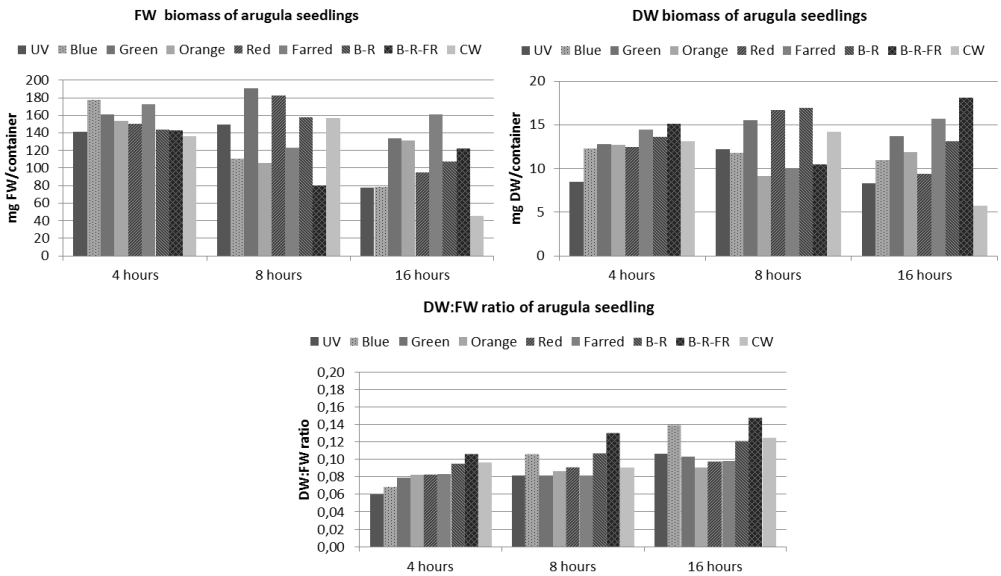

Figure 2. Fresh weight (FW), dry weight (DW) and ratio of fresh weight to dry weigh (FW:DW) of seedlings biomass produced from each lighting treatment of arugula seeds. Biomass corresponds to the total produced by those of the 20 seeds that developed a shoot in each treatment.

Arugula seedlings, similar to cabbage seedlings, developed longer shoots under low photoperiods and shorter shoots under a 16-hour photoperiod. The lowest value of fresh biomass was observed in the 16hCW treatment, measuring 45.7

mg, which also had the lowest dry biomass at 5.7 mg. The highest fresh biomass was produced in the 8hG treatment, measuring 190.5 mg, which also had the highest percentage of germination. The highest production of dry biomass occurred in the 16hBRFR treatment, measuring 18.12 mg, and this treatment also exhibited the highest ratio of dry to fresh biomass at 0.15. High values of dry biomass were also observed in treatments 8hR, at 16.66 mg, and 8hBR, at 16.94 mg. The remaining dry biomass values, apart from those mentioned above, ranged from 8.3 mg (16hUV) to 15.68 mg (16hFR). The highest DW:FW biomass ratios were observed for all spectra at the 16-hour photoperiod, ranging from 0.09 (Green spectrum) to 0.15 (BRFR spectrum).

Table 4. Produced microgreen biomasses of cabbage and arugula for the three investigated methods.

	Cabbage			Arugula		
	FW (mg)	**DW(mg)**	**DW:FW**	**FW (g)**	**DW(g)**	**DW:FW**
1st method	1455	139	0.096	9.75	1.2	0.123
2nd method	1615	148	0.092	9.74	1.26	0.129
3rd method	2189	173	0.079	10.93	1.46	0.134

1st method is the same for both cabbage and arugula: 3 days in darkness followed by 9 days in 16hBRFR treatment.
2nd method is the same for both cabbage and arugula: 16hBRFR treatment from the beginning and for 12 days.
3rd method: for cabbage was 5 days in 16hB treatment followed by 7 days in 16hBRFR treatment and for arugula was 5 days in 8hG treatment followed by 16hBRFR treatment.

Table 4 presents the values for cabbage and arugula microgreens grown using three different methods. For cabbage, the first method with initial exposure to darkness, yielded the least fresh and dry biomass, while the third method, with initial exposure to lighting spectrum with the highest percentage of germination, resulted in the highest production of both fresh and dry biomass. The fresh biomass produced in the third method was 50.44% higher than that of the first method and 35.54% higher than that of the second method. The corresponding percentages for the dry biomass produced were 24.46% and 16.9% respectively. The ratio of DW:FW biomass for the third method was the lowest observed among the three, equal to 0.079.

In the case of arugula, the third method also yielded higher results compared to the other two, with the highest ratio of DW:FW biomass, equal to 0.134. The produced fresh biomass measured 10.93 g, which was 12.1% higher than that of the first method and 12.21% higher than that of the second method. Similarly, the dry biomass was 1.46 g, representing a 21.7% increase compared to the first method and a 15.9% increase compared to the second method.

4. Conclusions

According to the results of the present study, initiating lighting from the beginning of sowing has positive effects on the seed germination for both cabbage and arugula. By using an appropriate spectrum and photoperiod, an increase in the germination rate can be achieved, as well as a reduction in the germination time of the seeds. Specifically, the treatment involving a 16-hour photoperiod with a blue spectrum demonstrated higher results for cabbage, with root and shoot growth reaching 55%. As for arugula, optimal results were observed in the treatment with an 8-hour photoperiod using a green light spectrum, resulting in root development in 90% of the seeds and shoot development in 75%.

After germination, the biomass of the seedlings is significantly influenced by the quality of the lighting they are exposed to. The combination of Blue-Red and Farred spectra, along with a 16-hour photoperiod, resulted in the highest dry-to-fresh biomass ratios for both plants studied. Pre-treating seeds with suitable lighting can significantly increase the percentage of seedlings that develop, while subsequent exposure to appropriate lighting can notably enhance final production. According to the results, different seeds respond differently to light spectra and photoperiods, highlighting the need for tailored and individualized treatments for each species.

References

Bu, H., Ge, W., Zhou, X., Qi, W., Liu, K., Xu, D., ... & Du, G., 2017. The effect of light and seed mass on seed germination of common herbaceous species from the eastern Qinghai-Tibet Plateau. Plant species biology, 32(4), pp.263-269.
https://doi.org/10.1111/1442-1984.12147.

Cowden, R.J., Markussen, B., Ghaley, B.B. & Henriksen, C.B., 2024. The Effects of Light Spectrum and Intensity, Seeding Density, and Fertilization on Biomass, Morphology, and Resource Use Efficiency in Three Species of Brassicaceae Microgreens. Plants, 13(1), p.124.
https://doi.org/10.3390/plants13010124.

Foschi, M.L., Juan, M., Pascual, B., Pascual-Seva, N, 2022. Influence of lighting and laser irradiation on the germination of caper seeds. Agriculture 12 (10), 1612.
https://doi.org/10.3390/agriculture12101612.

Lanoue, J., St. Louis, S., Little, C. & Hao, X., 2022. Continuous lighting can improve yield and reduce energy costs while increasing or maintaining nutritional contents of microgreens. Frontiers in Plant Science, 13, p.983222.
https://doi.org/10.3389/fpls.2022.983222.

Lerner, B. L., Strassburger, A. S., & Schäfer, G. (2024). Cultivation of arugula microgreens: seed densities and electrical conductivity of nutrient solution in two growing seasons. Bragantia, 83, e20230183.
https://doi.org/10.1590/1678-4499.20230183.

Maru, R.N., Wesonga, J., Okazawa, H., Kavoo, A., Neondo, J.O., Mazibuko, D.M., ... & Orsini, F., 2024. Evaluation of Growth, Yield and Bioactive Compounds of Ethiopian Kale (Brassica carinata A. Braun) Microgreens under Different LED Light Spectra and Substrates. Horticulturae, 10(5), p.436. https://doi.org/10.3390/horticulturae10050436.

Rajan, P., Lada, R.R. & MacDonald, M.T., 2019. Advancement in indoor vertical farming for microgreen production. American Journal of Plant Sciences, 10(08), p.1397.
https://doi.org/10.4236/ajps.2019.108100.

Rengasamy, N., Othman, R.Y., Che, H.S. & Harikrishna, J.A., 2022. Beyond the PAR spectra: impact of light quality on the germination, flowering, and metabolite content of Stevia rebaudiana (Bertoni). Journal of the Science of Food and Agriculture, 102(1), pp.299-311.
https://doi.org/10.1002/jsfa.11359.

Shibaeva, T.G., Sherudilo, E.G., Rubaeva, A.A. & Titov, A.F., 2022. Continuous LED lighting enhances yield and nutritional value of four genotypes of Brassicaceae microgreens. Plants, 11(2), p.176.
https://doi.org/10.3390/plants11020176.

Toscano, S., Cavallaro, V., Ferrante, A., Romano, D. & Patané, C., 2021. Effects of different light spectra on final biomass production and nutritional quality of two microgreens. Plants, 10(8), p.1584.
https://doi.org/10.3390/plants10081584.

Vatistas, C., Avgoustaki, D.D., Monedas, G. & Bartzanas, T., 2024. The effect of different light wavelengths on the germination of lettuce, cabbage, spinach and arugula seeds in a controlled environment chamber. Scientia Horticulturae, 331, p.113118.
https://doi.org/10.1016/j.scienta.2024.113118.

Wong, C.E., Teo, Z.W.N., Shen, L. & Yu, H., 2020. Seeing the lights for leafy greens in indoor vertical farming. Trends in Food Science & Technology, 106, pp.48-63.
https://doi.org/10.1016/j.tifs.2020.09.031.

Zhang, Y., Xiao, Z., Ager, E., Kong, L. & Tan, L., 2021. Nutritional quality and health benefits of microgreens, a crop of modern agriculture. Journal of Future Foods, 1(1), pp.58-66.
https://doi.org/10.1016/j.jfutfo.2021.07.001.

Effect of foliar application of silicon on the cultivation of mini watermelon cv. Sugar Baby in mitigating the effects of water deficit

Marcio Mesquita [a,*], Viviane Correira dos Santos [a], Rafael Battisti [a], Rilner Alves Flores [a], Moemy Gomes de Moraes [a], Henrique Fonseca Elias de Oliveira [b]

[a] Graduate Program in Agronomy, Federal University of Goiás, Goiânia, Brazil

[b] Cerrado Irrigation Graduate Program, Goiano Federal Institute, Ceres, Brazil

* Corresponding author. Email: marcio.mesquita@ufg.br

Abstract

The Plants in ambient conditions are subject to dealing with biotic and abiotic stresses. Water deficit, being an abiotic stress, causes changes in plants that make them respond in several ways, such as reduced growth, leaf senescence and lower fruit growth rate, production of Reactive Oxygen Species (ROS), caused by a deficiency in the dissipation of energy due to impaired photosynthesis. The application of silicon becomes an alternative to mitigate the effects of this stress on plants, being deposited in the cell wall, providing rigidity, and increasing the plant's defense enzymes. The study aimed to understand the morphological, physical, and post-harvest responses of mini watermelon according to different soil humidity associated with the foliar application of silicon. The study was conducted in a greenhouse using the mini watermelon *cv. Sugar Baby*. The experimental design was in randomized blocks, in a 3x2 factorial scheme, with three water tensions in the soil (-35 kPa without water deficit, -50 kPa moderate water deficit, and -65 KPa severe water deficit) and two doses of foliar Si (0 and 1.5 g L^{-1}), with four repetitions. The variables plant length, stem diameter and shoot dry mass, root dry mass, total soluble carbohydrates, proline, gas exchange, and post-harvest analyses were analyzed. There was a significant difference for the variables ($p>0.05$), but there was no interaction between tension and Si. Proline levels were not statistically significant. The water deficit promoted shorter plant length, aerial part dry mass, root dry mass and Si provided greater stem diameter. For biochemical variables, water deficit caused a higher carbohydrate content in the leaf and lower gas exchange rates. Si influenced skin thickness and average fruit weight. Thus, SI proves to be a strategy for cultivating mini watermelon in conditions of deficient water application.

Keywords: sustainability, irrigation management, efficient use of water, plant nutrition, micronutrient

1. Introduction

Plants under environmental conditions are subject to dealing with biotic and abiotic stresses. Water deficit, being a possible abiotic stress, causes changes in plants that make them respond in several ways (SELEIMAN, et al., 2021). At a visual level, reduced growth, leaf senescence, and lower fruit growth rate (VOLSCHENK, 2021). And at the molecular level, where the plant produces Reactive Oxygen Species (ROS), caused by a deficiency in energy dissipation due to impaired photosynthesis (MILLER et al., 2010). Blum (2011) says that water deficit occurs when the water supply is less than the crop's demand. To mitigate the effects of water deficit on plants, an alternative is the use of silicon (Si), which, associated with water stress, provides a lower rate of transpiration, but at levels that do not affect cellular metabolism and rather help with the efficiency of water use. water through the plant (MAJUMDAR and PRAKASH, 2020). In addition to structural benefits such as deposition in the cell wall, providing rigidity, Si acts in conjunction with the antioxidant system, contributing to its increase and protecting the plant from oxidative stress (SHI et al., 2016).

The benefits of Si have been highlighted over the years, and despite not being considered essential, it has been recognized as a relevant nutrient for several crops, playing an important role in adverse situations that the plant may experience, such as biotic and abiotic stresses, which trigger morphological and physiological changes. Furthermore, another benefit is that nutrition with silicon can reduce the use of fungicides and pesticides (KOVÁCS et al., 2022). Epstein (1994) already said that Si is an anomalous element, due to its non-essentiality, however, when available to the plant, it presents advantages for it.

Watermelon *cv. Sugar Baby* (*Citrullus lanatus*) is a vegetable-fruit belonging to the cucurbitaceae family, which requires a large amount of water during its cycle. In the initial stages with 2 to 3 true leaves and when the first flowers and fruits appear, it consumes around 170ml and 250ml of water per day, respectively in each phase (KHURRAMOVNA and OGLI, 2022). This vegetable-fruit is grown mainly in semi-arid regions around the world. Counting on the help of irrigation during times of greater water deficiency, its production is sustained (MELO et al., 2020). Thus, aiming to reduce the amount of water used and thinking about the scenario of water variations, this research aimed to understand the morphological, physical, and post-harvest responses of mini watermelon according to different soil humidity associated with the foliar application of silicon.

2. Materials and Methods

The research was conducted in two cycles cultivating the watermelon cv. *Sugar Baby (Citrullus lanatus)* in a greenhouse located at (16º59'61"23 S e 49º27'99"06 W). The experimental unit consisted of cultivation in 3-liter pots, filled with soil samples with the following attributes: fertility;; pH= 5.3, P (Mehl)= 1.5 mg dm^{-3} , H + Al= 1.9 cmolc dm^{-3}, K= 77 mg dm^{-3}, Ca= 280 mg dm^{-3}, Mg= 60.75 mg dm^{-3}, matter organic: 1.2 , and cation exchange capacity (CEC)= 4.0 cmolc dm^{-3}; and physical composition of 43% sand, 15% de silt and 42% clay. After homogenizing the soil, sowing took place directly in the pots and the water deficit began when the plants reached the 3rd definitive leaf.

The experiment was designed in randomized blocks with treatments arranged in a 3 x 2 factorial scheme, corresponding to three water tensions in the soil: -35, -50 and -65 kPa and presence or absence of Si applied to the leaves: 0.0 (control) and 1.5 g L^{-1}. Irrigation was carried out by drip, starting when the soil water potential reached -35, -50 and -65 kPa and ending when the potential reached -15, -25 and -35 kPa respectively. Being maintained throughout the crop cycle.

Biometric analyzes were carried out based on the standardization of plants at the vegetative stage (30 Days After Emergence). Plant height was measured from the base of the plant to the apex of the main stem, using a tape measure, and the diameter of the stem was measured at the base of the plant using a manual caliper (BEZERRA, 2017). Other parameters such as dry mass of the aerial part (stem and leaves) and dry mass of the root were measured by collecting 3 plants from each plot, drying them in an oven at 65º C until constant mass (CAMPAGNOL et al., 2012).

The post-harvest analyzes carried out were number of fruits per plant (NFP); average fruit weight (AFW); shell thickness (ST); pulp thickness (PT); fruit length (FL) and diameter (FD), hydrogen potential (Ph) and Soluble Solids (BRIXº). The NFP was obtained by adding the number of fruits in each plot divided by the number of plants in the plot. The AFW was measured by weighing all the fruits individually on a digital scale, which were then added together and divided by the number of fruits harvested, Ribeiro (2015). The thickness of the peel comprises the region that goes from the epidermis to the transition zone of pulp color (white-red) and was measured with a manual caliper, as well as the thickness of the pulp from the transition zone (white-red) to the center of the fruit (SILVA, et al., 2017). The length and diameter were measured with a manual caliper, including measurements from the peduncle to the apex of the fruit and the middle part of the fruit (SILVA, 2014). pH was measured following the Adolfo Lutz Institute methodology (1985). While Brixº was measured from watermelon juice in a digital refractometer (NRB-01, Next Instrumentos).

The data were subjected to Tukey mean test analysis at 5% probability using the AgroEstat® statistical software.

3. Results and Discussion

Tables 1 and 2 present the results of the analysis of variance for the variables plant length, stem diameter, shoot dry mass (SDM) and root dry mass (RDM), respectively, for the first and second cycle. Table 3 presents the results of post-harvest analyses.

Tabela 1. ANOVA summary of the biometric variables of the first cycle, that is, plant length (m), stem diameter (mm), Shoot Dry Mass (SDM) and Root Dry Mass (MSR).

Treatment	Biometric Analyzes			
	Plant Lenght (m)	Stem Diameter (mm)	DM (g)	RDM (g)
Water tension in the soil (kPa)				
-35	2.32^{a}	6.16^{a}	73.91^{a}	3.97^{a}
-50	1.99^{b}	5.86^{a}	68.67^{a}	2.92^{b}
-65	2.00^{b}	5.86^{a}	38.98^{b}	1.41^{c}
F	6.94**	1.33^{ns}	44.23**	38.41**
Doses of Si (g L^{-1})				
0.0	1.86^{b}	5.73^{a}	56.45^{b}	2.48^{b}
1.5	2.35^{a}	6.19^{b}	64.59^{a}	3.06^{a}
F	33.96**	6.98*	6.20*	6.00**
Interaction kPa x Si				
F	1.43^{ns}	2.28^{ns}	3,49^{ns}	0.26^{ns}
Overall Average	2.10	5.96	60.52	2.77
CV	9.7	7.12	13.23	21.17

(*) Significant at 5% by F test; (**) significant at 1% by F test; (ns) not significant at 5% by F test. Values followed by different lowercase letters in the same column differ significantly at 0.05.

No significant effect was observed in the interaction of soil water tension and Si application on all biometric variables in both cultivation cycles. Length, shoot dry mass and root dry mass showed significant effects in the first cycle for water tension and Si demonstrated effects on all biometric parameters. In the second cycle, the analysis indicated significant effects of voltage variation on all biometric parameters, while the presence of silicon (Si) did not

demonstrate any influence on these effects. It is observed that the growth in length was directly proportional to water availability. Furthermore, there was a significant increase in plant length when Si was applied, resulting in a percentage increase of 27.71% compared to plants without silicon. However, in the second cycle, only tension was shown to influence the length of the plants, with the highest tensions (-35kPa and -50 kPa) being responsible for the greatest lengths.

Tabela 2. ANOVA summary of the biometric variables of the first cycle, that is, plant length (m), stem diameter (mm), Shoot Dry Mass (SDM) and Root Dry Mass (MSR).

Treatment	Biometric Analyzes			
	Plant Lenght (m)	Stem Diameter (mm)	DM (g)	RDM (g)
Water tension in the soil (kPa)				
-35	1.44^{a}	5.85^{a}	54.39^{a}	1.20^{a}
-50	1.29^{a}	5.47^{a}	51.35^{a}	1.00
-65	0.95^{b}	4.18^{b}	27.11^{b}	0.81
F	11.50**	47.08**	38.81**	5.41*
Doses of Si (g L $^{-1}$)				
0.0	1.14^{a}	5.02^{a}	41.51^{a}	1.04^{a}
1.5	1.31^{a}	5.31^{a}	47.06^{a}	0.97^{a}
F	4.21^{ns}	3.59^{ns}	4.01^{ns}	0.54^{ns}
Interaction kPa x Si				
F	0.11^{ns}	1.09^{ns}	0.72^{ns}	1,60
Overall Average	1.22	5.17	44.29	1,00
CV	17.03	6.95	15.32	23,64^{ns}

(*) Significant at 5% by F test; (**) significant at 1% by F test; (ns) not significant at 5% by F test. Values followed by different lowercase letters in the same column differ significantly at 0.05.

For stem diameter, the significant effect was expressed in the treatment with Si application, in the first cycle, obtaining an increase of 8.02% in relation to the treatment without Si application. In the second cycle, the variable that affected the increase in diameter was tension, with the -65 kPa tension being the one that resulted in the smallest diameter of the stem. That is, the presence of Si in the second cycle, possibly due to the accumulation of phytoliths along the cell wall, reduced the effect of water deficit. This fact was evidenced by Yan et al. (2021) and Lux et al., (2020) who confirmed the deposition of Si throughout the endodermis of the rice root, consequently the water deficit led to the accumulation of Si in the endodermis and cell wall as a response to the stress suffered by the plant.

The dry weight of the shoot was influenced by tension, showing that the increase in water deficit resulted in a reduction in the dry weight of the shoot. Plants with the application of silicon (Si) had a significant increase of 14.40% in dry weight, compared to plants without Si, in the first cycle. Si treatments were shown to significantly attenuate the reduction in MSPA and MSR loss in response to the increase in water deficit. Corroborating Wang et al. (2015), in cucumber plants, where they found a higher proportion of root: shoot in plants that had Si applied, also suggesting that the greater water absorption was due to the addition of Si. Souri et al. (2021) reports studies carried out in which they believe that the greater turgor of cells is due to the binding of Si to hemicelluloses in plant cell walls. This fact explains the high correlation of these variables where the plant changes its root structures to absorb a greater amount of water (STROCK et al., 2020). For the variable root dry mass, the different water potentials differed from each other, with the highest and lowest root values, respectively, at a tension of -35 kPa and the lowest value at a tension of -65kPa. The Si dose provided an increase in root dry weight. However, for the second cycle, as occurred with MSPA, the dry mass of the root was influenced only by water tension, obtaining lower dry mass at the tension of -65kPa.

Average fruit weight reduced significantly in response to the deficit, compared to the control treatment (-35 kPa). The same happened for the Si dose, where the dose influenced the average weight, increasing the value at a dose of 1.5 g L^{-1}. For the average values of shell thickness, there was an interaction between tension and Si dose. The availability of water provided a higher value of shell thickness at a tension of -65 kPa with Si application, but the deficit treatment was equivalent to the treatment control. As for pulp thickness, only the different tensions had an influence, presenting significantly higher values for the control treatment (-35 kPa), however, statistically both the moderate tension and the deficit tension presented similar results, showing an equality in these treatments. The tension with the greatest deficit (-65 kPa) did not show a significant difference when compared to the moderate tension of -50 kPa for the evaluations of fruit diameter and length. The control treatment (-35 kPa) showed a higher value of fruit length and diameter.

Tabela 3. ANOVA summary of the postharvest parameters, number of fruits per plant (NFP), average fruit weight (AFW), shell thickness (ST); pulp thickness (PT); fruit length (FL) and diameter (FD), hydrogen potential (Ph) and Soluble Solids (BRIXº) and e texture (Text).

Treatment	Postharvest Parameters								
	NFP	PMF	EC	EP	CF	DF	pH	Brixº	Text
Water tension in the soil (kPa)									
-35	2.25^{a}	0.40^{a}	6.20^{a}	41.08^{a}	94.50^{a}	99.67^{a}	6.88^{a}	6.81^{a}	12.14^{a}
-50	2.25^{a}	0.21^{b}	4.45^{b}	31.84^{b}	69.58^{b}	76.09^{b}	6.56^{ab}	6.20^{a}	9.87^{a}
-65	2.12^{a}	0.15^{c}	5.62^{ab}	30.09^{b}	68.67^{b}	77.92^{b}	6.33^{b}	4.96^{b}	10.92^{a}
F	0.05^{ns}	82.79**	4.77*	9.27**	53.92**	21.18**	5.37*	19.39**	2.99^{ns}
Doses of Si (g L -1)									
0.0	2.33^{a}	0.23^{b}	4.80^{b}	33.83^{a}	76.27^{a}	84.02^{a}	6.55^{a}	6.06^{a}	11.17^{a}
1.5	2.08^{a}	0.28^{a}	6.04^{a}	35.38^{a}	78.89^{a}	85.10^{a}	6.53^{a}	5.92^{a}	10.78^{a}
F	0.41^{ns}	10.85**	6.80*	0.53^{ns}	1.29^{ns}	0.11^{ns}	0.88^{ns}	0.34^{ns}	0.25^{ns}
Interaction kPa x Si									
F	0.14^{ns}	0.03^{ns}	5.26*	0.16^{ns}	1.74^{ns}	0.19^{ns}	0.25^{ns}	3.37 ^{ns}	0.08^{ns}
Overall Average	2.20	0.25	5.42	34.60	77.58	84.56	6.59	5.99	10.98
CV (%)	43.42	15.70	18.47	13.07	7.27	9.53	4.41	8.74	16.91

(*) Significant at 5% by F test; (**) significant at 1% by F test; (ns) not significant at 5% by F test. Values followed by different lowercase letters in the same column differ significantly at 0.05.

Average fruit weight reduced significantly in response to the deficit, compared to the control treatment (-35 kPa). The same happened for the Si dose, where the dose influenced the average weight, increasing the value at a dose of 1.5 g L^{-1}. For the average values of shell thickness, there was an interaction between tension and Si dose. The availability of water provided a higher value of shell thickness at a tension of -65 kPa with Si application, but the deficit treatment was equivalent to the treatment control. As for pulp thickness, only the different tensions had an influence, presenting significantly higher values for the control treatment (-35 kPa), however, statistically both the moderate tension and the deficit tension presented similar results, showing an equality in these treatments. The tension with the greatest deficit (-65 kPa) did not show a significant difference when compared to the moderate tension of -50 kPa for the evaluations of fruit diameter and length. The control treatment (-35 kPa) showed a higher value of fruit length and diameter.

Si applied via foliar was accumulated in greater quantities in the control treatment, but its effects were widely expressed in the deficit treatments. The deficit reduced the accumulation of this element in the aerial part of the plants, but treatments containing Si were shown to attenuate the effects of water deficit. Si influenced PMF and EC, these factors were probably affected by the addition of phytoliths, as was the case with the increase in stem diameter. Kovács et al. (2022) states that accumulation occurs beyond the primary cortex of the root, in the epidermis of the leaf, but also in the pericarp of the fruit. Mitani et al. (2011) also confirmed the accumulation of this element in the skin of pumpkin fruits, indicating better post-harvest quality.

4. Conclusions

The water tension in the soil affects plant development and the quality of watermelon cv. Sugar Baby (Citrullus lanatus) fruits.

The application of silicon promotes beneficial effects due to lack of water during cultivation.

Acknowledgements

To the National Council for Scientific and Technological Development for the first author's productivity grant, Process 312854/2023-4.

References

Bezerra, J. D., 2017. Crescimento, fisiologia e produção da melancieira sob irrigação com águas salinas e adubação orgânica. DS Thesis, Universidade Federal University of Paraíba, Brazil.

Blum, A., 2011. Plant Water Relations, Plant Stress and Plant Production. In: Plant Breeding for Water-Limited Environments. Springer, New York, NY.

Campgnol, R.; Mello, S. C.; Barbosa, J. C., 2012. Vertical growth of mini watermelon according to the training height and plant density. Horticultura Brasileira, 30, 726-732. https://doi.org/10.1590/S0102-05362012000400027.

Epstein, E., 1994. The anomaly of silicon in plant biology. Proceedings of the National Academy of Sciences of the United States of America, 91, 11-17.

Khurramovna, S. S. & Ogli, Z. K. G., 2022. The reaction of watermelon *(CITRULLUS LANATUS (THUNB.) MATSUM. ET NAKAI*.) to environmental factors. Spectrum Journal of Innovation, Reforms and Development, 3, 99-102. https://sjird.journalspark.org/index.php/sjird/article/view/28.

Kovács, S.; Kutasy, E.; Csajbók, J., 2022. The multiple role of silicon nutrition in alleviating environmental stresses in sustainable crop production. Plants, 11 (9), 1223. https://doi.org/10.3390/plants11091223.

Lux, A; Lukacová, Z.; Vaculík, M.; Švubová, R.; Kohanová, J.; Soukup, M.; Martinka, M.; Bokor, B., 2020. Silicification of Root Tissues, Plants, 9 (1), 111. https://doi.org/10.3390/plants9010111.

Majumdar S., Prakash N. B., 2020. An Overview on the Potential of Silicon in Promoting Defence Against Biotic and Abiotic Stresses in Sugarcane. Journal of Soil Science and Plant Nutrition, 20,1969–1998. https://doi.org/10.1007/s42729-020-00269-z.

Melo, T. K.; Espinola Sobrinho, J.; Medeiros, J. F.; Figueiredo, V. B.; Silva, J. S.; Sá, F. V. S., 2020. Impacts of climate change scenarios in the Brazilian semiarid region os watermelon cultivars. Revista Caatinga, 3 (33), 794-802. https://doi.org/10.1590/1983-21252020v33n323rc.

Miller, G.; Suzuki, N.; Ciftci-Yilmaz, S.; Mittler, R. 2010. Reactive oxygen species homeostasis and signalling during drought and salinity stresses. Plant, Cell & Environment, 33 (4), 453-467. https://doi.org/10.1111/j.1365-3040.2009.02041.x.

Mitani, N.; Yamaji, N.; Ago, Y.; Iwasaki, K.; Ma, J. F., 2011. Isolation and functional characterization of an influx silicon transporter in two pumpkins cultivars contrasting in silicon accumulation. The Plant Journal, 66, 231–240. https://doi.org/10.1111/j.1365-313X.2011.04483.x.

Ribeiro, I. A., 2015. Características produtivas e de tolerância ao déficit hídrico de genótipos de melancia forrageira. 61 f. Ms Thesis, Federal University of Vale do São Francisco, Petrolina, Brazil.

Shi, P.; Manivannan, A.; Soundararajan, P.; Munner, S.; Ko, C. H.; Jeong, B. R., 2016. Silicon Mitigates Salinity Stress by Regulating the Physiology, Antioxidant Enzyme Activities, and Protein Expression in Capsicum annuum 'Bugwang'. BioMed Research International, 2016, 14. https://doi.org/10.1155/2016/3076357.

Seleiman, M.F.; Al-Suhaibani, N.; Ali, N.; Akmal, M.; Alotaibi, M.; Refay, Y.; Dindaroglu, T.; Abdul-Wajid, H.H.; Battaglia, M.L., 2021. Drought Stress Impacts on Plants and Different Approaches to Alleviate Its Adverse Effects. Plants , 10 (2), 259. https://doi.org/10.3390/plants10020259.

Silva, E. S.; Carmo, I. L. G. S.; Monteiro Neto, J. L. L.; Medeiros, R. D.; Menezes, P. H. S.; Rodriguez, C. A., 2017. Características agronômicas de cultivares de melancia nas condições do cerrado de Roraima, Brasil. Scientia Agropecuaria, 8 (3), 193-201. https://doi.org/10.17268/sci.agropecu.2017.03.02.

Souri, Z.; Khanna, K.; Karimi, N.; Ahmad, P., 2021. Silicon and Plants: Current Knowledge and Future Prospects. Journal of Plant Growth Regulation, 40, 906-925. https://doi.org/10.1007/s00344-020-10172-7.

Strock, C. F.; Burridge, J. D.; Niemiec, M. D.; Brown, K. M.; Lynch, J. P., 2020. Root metaxylem and architecture phenotypes integrate to regulate water use under drought stress. Plant, Cell & Environment, 44 (1), 49-67. https://doi.org/10.1111/pce.13875.

Volschenk, T., 2021. Effect of water deficits on pomegranate tree performance and fruit quality – A review. Agricultural Water Management, 246. https://doi.org/10.1016/j.agwat.2020.106499.

Yan, G.; Fan, X.; Zheng, W.; Gao, Z.; Yin, C.; Li, T.; Liang, Y., 2021. Silicon alleviates salt stress-induced potassium deficiency by promoting potassium uptake and translocation in rice (Oryza sativa L.). Journal of Plant Physiology, 258, 153379. https://doi.org/10.1016/j.jplph.2021.153379.

Wang, Z.; Yang, Y.; Yadav, V.; Zhao, W.; He, Y.; Zhang, X.; Wei, C., 2022. Drought-induced proline is mainly synthesized in leaves and transported to roots in watermelon under water deficit. Horticultural Plant Journal, 8 (5), 1-12. https://doi.org/10.1016/j.hpj.2022.06.009.

Effects of bedding material on performance, welfare and ammonia emissions of broiler chickens

Shutong Dong [a,*], Jan van Harn [a], Kris De Baere [b], Ine Kempen [b], Albert Winkel [a]

In cooperation with **Anne-Jo Smits [c], Jan Workamp [c]**

[a] Wageningen Livestock Research, Wageningen, The Netherlands

[b] Proefbedrijf Pluimveehouderij (Experimental Poultry Centre), Province of Antwerp, Geel, Belgium

[c] Poultry Expertise Centre, Aeres, Barneveld, the Netherlands

* Corresponding author. Email: shutong.dong@wur.nl

Abstract

Peat is a bedding material regularly used in Dutch broiler farms. It has a relatively low pH due to humid compounds/acids produced by soil bacteria under low oxygen levels, which may potentially reduce ammonia emissions. A study was conducted in experimental broiler houses with fast-growing broilers (Ross 308) to determine the potential of peat bedding in reducing ammonia emissions in broiler production compared with wood shavings, the mixture of wood shavings and peat, and straw pellets bedding, with attention to litter characteristics, animal production and animal welfare (footpad lesions and hock dermatitis). Measurements were done with 42,800 broilers during two rounds from September 2022 to February 2023. Results showed that peat had an ammonia emission of 12.81 (g animal place^{-1} year^{-1}), which was significantly ($P < 0.001$) higher than wood shaving (4.75 g animal place^{-1} year^{-1}). The bedding material had no influence on the production performance (body weight, growth rate, feed conversion ratio, mortality) of broilers and the final litter composition (total N, ammonium N, P, K, ash, dry matter content, pH). However, broilers kept on peat bedding had fewer footpad lesions and hock dermatitis than broilers kept on wood shavings. It can be concluded that peat as a bedding material cannot reduce ammonia emissions from broiler houses compared with wood shavings, probably due to the drier and more friable litter, but it can improve animal welfare.

Keywords: Broiler, peat, wood shaving, ammonia emission

1. Introduction

In Europe, various materials are used as bedding in broiler houses and wood shaving is one of the most common materials. Since the poultry industry constantly seeks methods to enhance animal welfare, peat is regularly used as bedding materials in the Netherlands in recent years since it can reduce the incidence of footpad lesions (Kaukonen et al., 2017). As the need to reduce ammonia emissions in broiler husbandry grows, the idea arose that peat as a litter material could potentially reduce ammonia emissions from broiler houses. Peat has a relatively low pH of 3.5 to 4.2 due to humid compounds/acids produced by soil bacteria under low oxygen levels (Agroveen, 2022a; 2002b). This can shift the ammonia–ammonium) equilibrium towards ammonium, which is non-volatile, potentially reducing the evaporation of ammonia from the bedding material and thus the ammonia emission from the broiler house. It is also claimed that peat has a higher absorbent capacity of water, brings a lower incidence of footpad lesions and a better indoor air quality compared with wood shavings (Agroveen, 2022a; 2002b). A study was conducted to determine the potential of peat bedding in reducing ammonia emissions, compared with wood shavings, straw pellets and a combination of wood shavings and peat. Furthermore, the effects of bedding materials on personal dust (PM_{10}) exposure, technical performance of the broilers, footpad lesions, hock dermatitis, litter quality and composition were studied.

2. Materials and Methods

2.1. General design

The study was conducted in two experimental broiler barns (barn ABCD and barn E) of the Experimental Poultry Centre in Geel, Belgium from September 2022 to February 2023. A total number of 42,800 day-old fast-growing broilers (Ross 308) were housed with a density of 20.4 animals/m^2 for 40 days for two

production rounds. Four types of bedding materials were applied across the rooms (randomly assigned): wood shavings (WS, control, 1.0 kg/m^2), peat (PE, 1.5 kg/m^2), straw pellets (SP, 1.5 kg/m^2), the mixture of wood shavings and peat (WS+PE, 0.5 kg/m^2 + 0.75 kg/m^2).

Barn ABCD consists of 4 mechanically ventilated rooms (A, B, C and D) of 300 m^2 (length 18.75 m, width 16 m). Each room is divided into 4 pens of 75 m^2, separated by fences. Barn E comprises 8 mechanically ventilated rooms (E1 to E8). Each room covers 112.5 m^2 (length 18.75 m, width 6 m) and is divided into 2 pens of 56.25 m^2, separated by fences.

In barn ABCD, only peat and wood shavings were compared (2 rooms * 2 rounds = 4 replicates per bedding material). In barn E, all four beddings were compared (2 rooms * 2 rounds = 4 replicates per litter type). Therefore, wood shavings and peat were replicated 8 times in total, while straw pellets and the mixture of wood shavings and peat were replicated 4 times. Aerial, litter, and animal variables were measured by different methods throughout the production rounds on multiple days (summary in Table 1).

Table 1. Variables and measurement methods.

Variable	Measurement method	Unit	Days (0-40)[1]
Emission			
NH_3	Wet chemical method; Dräger Polytron P8100 sensor; FTIR[6] analyser (Gasmet CX4000)	ppm	Continuously[2] 25, 31 (1st round); 11, 18, 25, 34 (2nd round)[3]
CO_2	Lung method; Vaisala GMP252 (0-5000 ppm) sensor; FTIR analyser (Gasmet CX4000)	ppm	Continuously[4] 25, 31 (1st round); 11, 18, 25, 34 (2nd round)[5]
Personal PM_{10} exposure	DustTrak™ II Aerosol Monitor	mg m^{-3}	21, 25, 28, 32, 35 (1st round); 11, 18, 22, 25, 34, 36 (2nd round)
Environmental condition			
Temperature	Vaisala HMP60 sensor for barn ABCD; Fancom temperature sensor standard for barn E	ºC	Continuously
Relative humidity	Vaisala HMP60 sensor for barn ABCD; Fancom RV sensor RHM.2 / RHO.2 for barn E	%	Continuously
Ventilation rate	Fan-wheel anemometers (Fancom ATM35 and ATM80), CO_2 mass balance method	m^3 h^{-1}	Continuously
Bird performance			
Mortality (MRT)	Visual inspection, counting	%	Daily
Body weight	Automatic weighing device	g	Daily
Average end body weight (weighing of all birds delivered to slaughterhouse, BW)	Manual weighing	g	40
Total body weight growth (BWG)	Calculation	g	40
Average daily feed consumption (ADFC)	Feed weighing system	kg d^{-1} room^{-1}	Daily
Average daily water consumption (ADWC)	Water meter	L d^{-1} room^{-1}	Daily
Water:feed ratio (WFR)	Calculation	-	-
Daily body weight growth rate (dBWG)	Calculation	g d^{-1}	-
Feed conversion ratio (FCR)	Calculation	-	-
Footpad lesions	Visual observation, scoring	Score	31, 39 (1st round); 32, 39 (2nd round)
Hock dermatitis	Visual observation, scoring	Score	31, 39 (1st round); 32, 39 (2nd round)
Litter characteristic			
Dry matter (DM) content	Oven-drying, weighing	g kg^{-1}	Weekly
Total nitrogen content	NEN-7434	g kg^{-1}	40
Ammoniacal content	NEN-7438	g kg^{-1}	40

P content	NEN-7435	g kg^{-1}	40
K content	NEN-7436	g kg^{-1}	40
Ash content	NEN-7432	-	40
pH	pH meter	-	Weekly
Thickness	Meter	cm	Weekly
Floor and litter temperature	Infrared thermometer	°C	Weekly
Friability	Visual observation, scoring	Score	6, 13, 20, 27, 34, 38 (1st cycle); 14, 21, 28, 35, 39 (2nd round)
Wetness	Visual observation, scoring	Score	6, 13, 20, 27, 34, 38 (1st cycle); 14, 21, 28, 35, 39 (2nd round)

[1] Days: Numbers refer to measurement days for two production rounds, otherwise: measurement frequency.

[2] This frequency applies to the Dräger Polytron P8100 sensor and the FTIR Gasmet CX4000 analyser.

[3] Measurement days apply for the wet chemical method.

[4] This frequency applies to the Vaisala GMP252 (0-5000 ppm) sensor; and FTIR Gasmet CX4000 analyser.

[5] Measurement days apply for the lung method.

[6] Fourier Transform Infrared Spectroscopy (FTIR)

2.2. Animals and management

In barn ABCD, 6,120 one-day-old broilers (Ross 308, as hatched) were placed per room (24,480 in total, 1,530 broilers per pen) and in rooms of barn E, 2,300 were placed (18,400 in total, 1,150 broilers per pen). The broilers originated from a parent stock of 48 (round 1) and 42 (round 2) weeks of age and were obtained from a commercial hatchery (Belgabroed, Merksplas, Belgium). Broilers were delivered to the slaughterhouse at 40 days of age, at a live weight of approximately 2.6 to 2.8 kg. Broilers had *ad libitum* access to feed and drinking water. Thinning was done on day 33 (estimated body weight around 2.1 kg, male/female were taken randomly) by taking out 1,280 (20.9%) broilers from each room of barn ABCD, 560 (24.3%) from each room of barn E for round 1, and 1,280 (20.9%) from each room of barn ABCD and 576 (25.0%) from each room of barn E for round 2.

All the rooms were pre-heated to 32 °C three days before the broilers arrived to ensure sufficient dryness of the bedding materials (around 85%), especially for peat. Ambient temperature was gradually reduced from 34 °C upon arrival to 20 °C until 40 d. The minimum ventilation rate was set at 1.5 m^3 h^{-1} per kg live weight on day 0 and gradually decreased to 0.7 m^3 h^{-1} per kg live weight on day 20, until the end of the trials. The ventilation rates increased automatically by a climate computer based on the expected weight development and climate inside. When a production round ended, litter was removed and barns were cleaned (wet) and disinfected.

2.3. Measurements of variables

2.3.1. Ammonia and carbon dioxide concentration

The ammonia concentration was measured using three methods: wet chemical method (background, room E3 and E4), Dräger sensor (all rooms in barn ABCD, room E3 and E4) and FTIR sensor (background, room E1 – E8). Dräger and FTIR measurements were calibrated by the wet chemical method for emission calculation.

Carbon dioxide concentrations were measured by: lung method (background, room E3 and E4), Vaisala sensor (all rooms in barn ABCD, room E3 and E4) and FTIR sensor (room E1 – E8). Vaisala and FTIR measurements were calibrated by the lung method for ventilation rate calculation.

2.3.2. Litter characteristics

Litter quality in each room was assessed by a panel of two persons. Friability and wetness were scored visually based on a 1 - 10 point scale (van Harn et al., 2017).

Litter samples were taken every week (100 g litter per sample for day 0, 6/7, 13/14 and 250 g for day 20/21, 27/28, 34, 38/39). Three samples per pen (near drinking line, feeding line and in-between) were taken in 8 out of 16 pens in barn ABCD and 16 pens in barn E (24+48=72 samples per measurement day). Samples were dried in an oven at 105 °C for 24 h to determine the dry matter content of the litter (weighed before and after oven-drying).

At the end of this study, representative samples of the litter were taken. In contrast to the weekly dry matter samples, the 6 - 8 samples per room were pooled into one representative sample per (climate) room (= treatment). These pooled samples were frozen (-20 °C) and transported to the lab for analysis.

2.3.3. Footpad lesions and hock dermatitis

Occurrence and severity of footpad lesions and hock dermatitis were determined before thinning and slaughter by an experienced assessor according to the Welfare Quality (WQ) assessment protocol for poultry (Welfare Quality®, 2009). Footpad dermatitis and hock dermatitis were scored on a scale from 0 (no lesions) to 4 (severe lesions on the foot or hock). 40 animals (20 males/20 females) per pen (in total 24 pens, 8 pens from barn ABCD and 16 pens from barn E) were randomly chosen for assessment.

2.4. Data processing and statistical analysis

The ventilation rates in barn E were determined directly by fan-wheel anemometers and the ventilation rates in barn ABCD were calculated by the CO_2 mass balance method (CIGR, 2002).

The ammonia emission rate *E* (g per animal place per year) was calculated by the following equation:

$$E = ([NH_3]_{outlet} - [NH_3]_{inlet}) * \beta * V' * \frac{24\ hours}{1\ day} * \frac{365\ days}{1\ year} * \frac{1g}{1000mg} * 0.82 \quad (1)$$

where:

- $[NH_3]_{outlet}$ = NH_3 concentration at the outlet of the barn (ppm)
- $[NH_3]_{inlet}$ = NH_3 concentration at the inlet of the barn (ppm)
- β = coefficient of conversion from ppm to mg m^{-3} for NH_3 gas at a certain temperature
- *V*' = ventilation rate (m^3 h^{-1} per animal place)
- 0.82 (40/49) = vacancy factor

The experimental unit was each room. All measurements were considered statistically independent. The statistical analysis were performed using R (version 4.3.2; R Core Team, 2021) and Genstat (VSN, 2022). Bedding material types were identified as the main effect and the barn types as the random effect. The normality of the data was checked with the Shapiro-Wilk test. When the data was normally distributed, unbalanced one-way ANOVA was performed. In case of a significant effect, the Bonferroni post-hoc test was used to determine the significant differences between groups. When the data was not normally distributed (non-parametric data), the data was converted to a logarithmic scale. All differences were declared statistically significant at a *P*-value < 0.05. Results are reported as least square means and standard error MEAN ± SE.

3. Results and discussion

3.1. Litter quality and litter composition

Figure 1 presents the friability and wetness of the litter. Peat had significantly higher friability scores than wood shavings on day 20-21, indicating more friable litter (better litter quality). On day 34-35, peat and straw pellets had higher friability scores than wood shavings. From day 27-28 and on, 70% - 90% of the litter was caked. Moreover, the litter was wet and could be pressed into ball shapes. No interactions between barns and bedding materials were found.

Table 2 shows the average litter DM content, litter pH, litter thickness, litter and floor temperature. Peat and the mixture of wood shavings and peat litter had a higher DM on day 6-7 compared with day 0, because fresh peat has relatively higher moisture and the room temperature caused the moisture to evaporate and the litter to dry. After that, all groups had a similar trend with no significant effects observed. The DM remained 75% to 80% from day 6-7 to day 13-14 and then dropped drastically to 55% on day 20-21. After that, it slightly decreased until the end of the round to around 50%. The litter thickness increased as the broilers aged and the excreta accumulated. The litter layer in barn E was thicker than in barn ABCD. The litter pH increased from day 6-7 until day 20-21 (from 5 to 7) and then decreased until the end of the trial (5.5). The litter and floor temperature increased from day 13-14 (26 °C) to day 27-28 (28 °C) and then decreased until day 38-39

(27 °C). The rooms in barn ABCD had higher floor and litter temperatures than the rooms in barn E.

Table 3 shows the litter composition on day 40. Bedding materials did not have any significant effects on litter composition. The litter pH in barn E was higher than in barn ABCD. No interactions between barns and bedding materials were found.

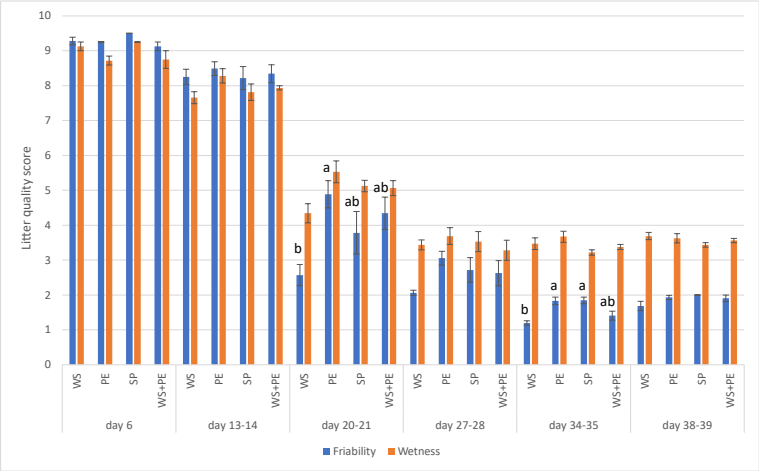

Figure 1. Average scores of friability and wetness on different days

Table 2. Average DM, pH, thickness, litter and floor temperature.

Variable	Barn ABCD	Barn E	WS	PE	SP	WS+PE	*P*-value (bedding)	*P*-value (barn)	*P*-value (bedding*barn)
DM content	61.47% ± 1.72%	61.22% ± 1.28%	59.78% ± 1.81%	62.11% ± 1.81%	62.93% ± 2.43%	61.66% ± 2.43%	0.715	0.746	0.976
pH	5.85 ± 0.11	6.15 ± 0.08	5.96 ± 0.12	6.03 ± 0.12	6.48 ± 0.16	6.16 ± 0.16	0.028	0.182	0.396
Thickness	3.13 ± 0.24^{b}	3.97 ± 0.18^{a}	3.53 ± 0.25	3.79 ± 0.25	4.18 ± 0.33	3.96 ± 0.33	0.243	0.021	0.865
Temperature (°C)	27.19 ± 0.21^{a}	26.55 ± 0.16^{b}	26.52 ± 0.23	26.97 ± 0.23	26.56 ± 0.30	26.62 ± 0.30	0.571	0.030	0.136
Floor temperature (°C)	27.45 ± 0.25^{a}	26.69 ± 0.19^{b}	26.75 ± 0.26	27.12 ± 0.26	26.78 ± 0.35	26.65 ± 0.35	0.596	0.032	0.301

$^{a-b}$ Values between barns and beddings with different superscripts have significant differences (P<0.05).

Table 3. Average litter composition.

Variable	Barn ABCD (n=8)	Barn E (n=16)	WS (n=8)	PE (n=8)	SP (n=4)	WS+PE (n=4)	*P*-value (bedding)	*P*-value (barn)	*P*-value (bedding*barn)
Total-N (g/kg)	24.08 ± 0.55	22.89 ± 0.41	22.98 ± 0.58	23.25 ± 0.58	23.28 ± 0.78	23.54 ± 0.78	0.669	0.135	0.263
Ammonium-N (g/kg)	2.36 ± 0.12	2.48 ± 0.09	2.23 ± 0.13	2.68 ± 0.13	2.28 ± 0.17	2.58 ± 0.17	0.052	0.507	0.574
P-content (g/kg)	2.81 ± 0.10	2.89 ± 0.07	2.83 ± 0.11	2.90 ± 0.11	2.86 ± 0.14	2.91 ± 0.14	0.903	0.521	0.598
K-content (g/kg)	12.98 ± 0.28	13.08 ± 0.21	12.79 ± 0.30	13.31 ± 0.30	13.10 ± 0.40	13.07 ± 0.40	0.548	0.783	0.602
Dry matter content (g/kg)	488.7 ± 11.16	488.5 ± 8.32	482.6 ± 11.76	488.8 ± 11.76	493.9 ± 15.78	500.2 ± 15.78	0.745	0.892	0.361
Ash content	60.73 ± 2.04	60.93 ± 1.52	60.38 ± 2.15	60.16 ± 2.15	61.25 ± 2.88	64.17 ± 2.88	0.700	0.800	0.329
pH	5.05 ± 0.04^{b}	5.19 ± 0.03^{a}	5.10 ± 0.04	5.21 ± 0.04	5.16 ± 0.06	5.20 ± 0.06	0.218	0.011	0.663

[a-b] Values between barns and beddings with different superscripts have significant differences (P<0.05).

3.2. Personal dust (PM_{10}) exposure

Figure 2 shows the personal exposure to PM_{10} and Table 4 shows the average personal PM_{10} exposure over the measured moments. The PM_{10} concentrations went up from day 10 (around 0.5 mg/m^3) until day 24-25 (around 1.1 mg/m^3) and then dropped slightly (around 0.9 mg/m^3). This could be caused by the poor litter quality (less friable litter) in the late days of the period and therefore less (fine) dust (see section 3.1). Significant differences were observed only on day 10, where peat (0.751 mg/m^3) caused higher PM_{10} exposure than wood shavings (0.317 mg/m^3). The average PM_{10} concentrations (Table 4) were below the values of common Dutch broiler barns (1.931 mg/m^3, Winkel et al., 2015). The PM_{10} concentrations in rooms with peat (0.996 mg/m^3) and straw pellets (1.017 mg/m^3) were 32% and 35% higher respectively than in rooms with wood shaving (0.753 mg/m^3). No interactions between barns and bedding materials were found.

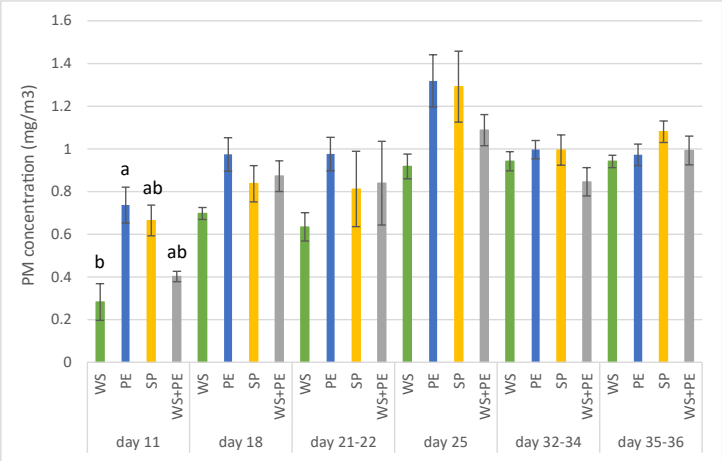

Figure 2. PM_{10} concentration (mg m^{-3}). Standard errors were presented in the error bars.

Table 4. Average PM_{10} concentration (mg m^{-3}).

Variable	Barn ABCD (n=44)	Barn E (n=88)	WS (n=44)	PE (n=44)	SP (n=22)	WS+PE (n=22)	*P*-value (bedding)	*P*-value (barn)	*P*-value (bedding *barn)
PM_{10} concentration (mg m^{-3})	0.920 ± 0.053	0.881 ± 0.032	0.753 ± 0.043^{b}	0.996 ± 0.043^{a}	1.017 ± 0.085^{a}	0.863 ± 0.085^{ab}	<0.001	0.965	0.693

[a-b] Values between barns and beddings with different superscripts have significant differences (P<0.05).

3.3. Ammonia emission

Figure 3 (left) shows the linear regression fit for the NH_3 concentrations measured by the wet chemical method (reference), FTIR (y_1, in blue) and Dräger (y_2, in red) sensors. Dräger had a better estimate of the ammonia concentration (y = 0.27 + **1.01*x**, R^2 = 94.9%) than FTIR (y = 0.04 + **0.91*x**, R^2 = 95.6%). One data point in round 1 was discarded because condensation was observed in the tubes of the wet chemical method, which led to an unrealistic lower ammonia concentration (outlier). It is important to mention that noticeable differences were observed in a few replicates (max/min values = from 1 to 10) of the wet chemical method. Figure 3 (right) shows the linear regression fit for ammonia concentration (ppm) measured by FTIR (x) and Dräger (y). The two-tailed paired *t*-test showed there are significant differences between the two methods (P < 0.001). Periodical recalibrations are essential for both Dräger and FTIR sensors.

Table 5 shows the average ammonia concentration and emission rate per barn and bedding material. On average, barn ABCD had a similar ammonia concentration to barn E. No interactions between barns and bedding materials were found. Peat had an ammonia emission rate of 12.81 g per year per animal place, which was 2.7 times as high as wood shavings (4.75 g per year per animal place). Both barns ABCD and

barn E have a category between E 5.15 and E 5.100 (E 5 Diercategorie Vleeskuikens, n.d.). However, the ammonia emission rates were significantly lower than the emission factors: 21 and 68 g per year per animal place for E 5.15 and E 5.100, respectively (E 5 Diercategorie Vleeskuikens, n.d.). This could be related to the poor litter quality and the low dry matter content (see section 3.1). From day 27-28 and on, more than 70% of the litter was caked and the wet litter could be pressed ball-shaped due to the high moisture. It was demonstrated that the crust formed on the top litter layer and a low litter friability (caked litter) can slow down ammonia volatilization (Brink et al., 2022). It was found that the ammonia formation from the litter decreases when the dry matter content is higher than 80% or lower than 60% (Groot Koerkamp et al., 2000), which could also explain why such low amounts of ammonia were observed. Additionally, peat has a rather high moisture content, and it tends to keep the moisture it absorbs. Therefore, the preheating should be carried out thoroughly.

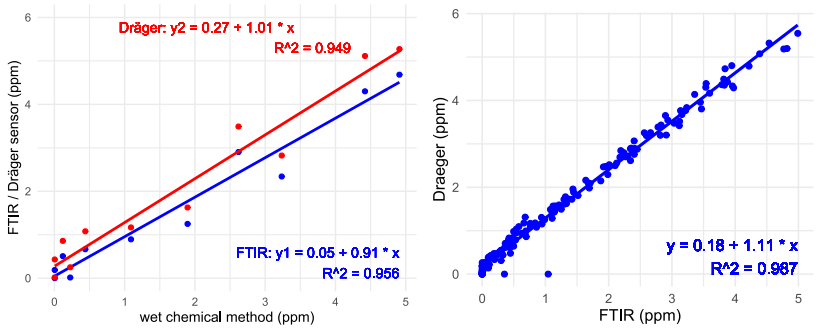

Figure 3. Left: Linear regression fit for the NH_3 concentrations (ppm) measured by the wet chemical method (x), FTIR (y_1, in blue), Dräger (y_2, in red). Right: Linear regression fit for ammonia concentration (ppm) measured by FTIR (x) and Dräger (y).

Table 5. Ammonia concentrations and emissions.

Variable	Barn ABCD (n=8)	Barn E (n=16)	WS (n=8)	PE (n=8)	SP (n=4)	WS+PE (n=4)	*P*-value (bedding)	*P*-value (barn)	*P*-value (bedding *barn)
Ventilation rate (m^3 h^{-1} $animal^{-1}$)	1.231 ± 0.111	1.267 ± 0.082	1.234 ± 0.117	1.272 ± 0.117	1.294 ± 0.157	1.253 ± 0.157	0.991	0.831	0.881
Ammonia concentration (ppm)	1.693 ± 0.154	1.302 ± 0.115	0.969 ± 0.162^{b}	1.829 ± 0.162^{a}	1.486 ± 0.217^{ab}	1.318 ± 0.217^{ab}	0.005	0.058	0.547
Ammonia emission rate (g animal $place^{-1}$ $year^{-1}$)	9.095 ± 1.119	8.875 ± 0.834	4.748 ± 1.179^{b}	12.811 ± 1.179^{a}	9.947 ± 1.582^{ab}	8.814 ± 1.582^{ab}	<0.001	0.768	0.646

$^{a-b}$ Values between barns and beddings with different superscripts have significant differences (P<0.05).

3.4. Zootechnical performance

Table 6 shows the average zootechnical performance over the two production rounds. The bedding materials did not affect the overall zootechnical performance of broilers from 0 - 40 days. The broilers in barn ABCD had lower average daily water consumption and water:food ratio than broilers in barn E. No interactions between barns and bedding materials were found.

Table 6. Average zootechnical performance.

Treatment	ADFC	ADWC	WFR	BW	BWG	dBWG	FCR	MRT
Barn ABCD (n=8)	95.4 ± 0.7	164.0 ± 1.2^{b}	1.72 ± 0.01^{b}	2521 ± 15	2476 ± 15	61.9 ± 0.4	1.541 ± 0.012	2.2 ± 0.5
Barn E (n=16)	94.7 ± 0.5	168.5 ± 0.9^{a}	1.78 ± 0.01^{a}	2524 ± 11	2481 ± 11	62.0 ± 0.3	1.527 ± 0.009	3.1 ± 0.3
WS (n=8)	95.2 ± 0.8	166.2 ± 1.3	1.75 ± 0.01	2529 ± 160	2486 ± 16	62.2 ± 0.4	1.532 ± 0.013	2.4 ± 0.5

PE (n=8)	94.7 ± 0.8	167.2 ± 1.3	1.77 ± 0.01	2521 ± 16	2476 ± 16	61.9 ± 0.4	1.530 ± 0.013	2.6 ± 0.5
SP (n=4)	93.8 ± 1.0	167.1 ± 1.7	1.78 ± 0.01	2500 ± 21	2457 ± 21	61.4 ± 0.5	1.527 ± 0.017	4.3 ± 0.7
WS+PE (n=4)	95.7 ± 1.0	171.6 ± 1.7	1.79 ± 0.01	2537 ± 21	2492 ± 21	62.3 ± 0.5	1.536 ± 0.017	3.5 ± 0.7
P-value (bedding)	0.559	0.250	0.169	0.572	0.586	0.586	0.982	0.110
P-value (barn)	0.482	0.005	<0.001	0.747	0.714	0.714	0.377	0.485
P-value (bedding*barn)	0.537	0.888	0.475	0.400	0.424	0.424	0.980	0.878

[a-b] Values between barns and beddings with different superscripts have significant differences ($P<0.05$).

3.5. Footpad lesions and hock dermatitis

Figure 4 presents the average percentage per footpad lesion score class (left) and per hock dermatitis score class on day 31-32 and day 39 of age. The incidence and severity of footpad lesions and hock dermatitis increased as the broilers aged. Severe footpad lesions occurred more often when the broilers reached slaughter age. On day 31-32 and day 39, broilers kept on wood shavings had a higher incidence and severity of footpad lesions than broilers kept on peat. On day 39, broilers reared on wood shavings had a higher incidence and severity of hock dermatitis than broilers kept on straw pellets. Overall, broilers reared on wood shavings had the worst animal welfare. On day 39, more hock dermatitis was observed in barn ABCD than in barn E. No interactions between barns and bedding materials were found.

Figure 4. Average percentage of footpad lesion (left) and hock dermatitis (right) scores on day 31-32 and day 39.

4. Conclusions

From this study, it can be concluded that:

- The ammonia emission rate of broilers kept on peat litter was significantly higher than broilers kept on wood shavings (12.81 and 4.75 g per year per animal place, respectively).
- Peat (0.996 mg/m^3) and straw pellets (1.017 mg/m^3) caused higher personal bound PM_{10} concentrations than wood shavings (0.753 mg/m^3).
- Peat bedding was more friable compared with wood shavings on day 20-21 and day 34-35 (better litter quality).
- Bedding materials did not influence the overall litter DM content, litter pH, litter layer thickness, litter and floor temperature, final litter composition (total N, ammonium N, P, K, DM, ash, pH) and the zootechnical performance of broilers.
- For animal welfare, peat had a lower incidence and severity of footpad lesions compared with wood shavings on day 31-32. Bedding types did not influence the incidence and severity of hock dermatitis. On day 39, peat, straw pellets and the mixture had less incidence and severity of footpad lesions than wood shavings. Straw pellets reduced the incidence and severity of hock dermatitis compared with wood shavings.

5. References

Agroveen, 2022a. Turfstrooisel als bodembedekking voor pluimvee. Agroveen, Uden, the Netherlands. https://agroveen.nl/pluimvee/

Agroveen, 2022b. De unieke waarde van Turfstrooisel. Agroveen, Uden, the Netherlands. URL: https://agroveen.nl/turfstrooisel/

Brink, M., Janssens, G., Demeyer, P., Bagci, Ö., & Delezie, E. (2022). Ammonia concentrations, litter quality, performance and some welfare parameters of broilers kept on different bedding materials. British Poultry Science, 63(6), 768–778. https://doi.org/10.1080/00071668.2022.2106775

CIGR. 2002. 4th Report of Working Group on Climatization of animal houses. Heat and moisture production at animal and house levels (eds. Pedersen, S.; K. Sällvik).

E 5 diercategorie vleeskuikens. (n.d.). Kenniscentrum InfoMil. https://www.infomil.nl/onderwerpen/landbouw/emissiearme-stalsystemen/emissiefactoren-per/map-staltypen/5-diercategorie/

Groot Koerkamp, P.W.G., Middelkoop, J.H. van en Evers, E. (2000). Ammoniakemissie vleeskuikenstallen toegenomen. De Pluimveehouderij, 30(21), 10–11. http://library.wur.nl/WebQuery/wurpubs/312922

Kaukonen, E., Norring, M., & Valros, A. (2017). Evaluating the effects of bedding materials and elevated platforms on contact dermatitis and plumage cleanliness of commercial broilers and on litter condition in broiler houses. British Poultry Science, 58(5), 480–489. https://doi.org/10.1080/00071668.2017.1340588

Van Harn, J., Dijkslag, M., & Van Krimpen, M. (2017). Effect of low protein diets supplemented with free amino acids on growth performance, slaughter yield, litter quality, and footpad lesions of male broilers. Poultry Science, 98(10), 4868–4877. https://doi.org/10.3382/ps/pez229

Welfare Quality® (2009). Welfare Quality® assessment protocol for poultry (broilers, laying hens). Welfare Quality® Consortium, Lelystad, Netherlands.

Winkel, A., Mosquera, J., Koerkamp, P. G., Ogink, N., & Aarnink, A. (2015). Emissions of particulate matter from animal houses in the Netherlands. Atmospheric Environment, 111, 202–212. https://doi.org/10.1016/j.atmosenv.2015.03.047

Analysis of wall pressures and discharge rates in corrugated steel silos with centric and eccentric hoppers by discrete element models

Ana Grande-Gutiérrez*, José-María Fuentes, Eutiquio Gallego, Francisco Ayuga

[a] BIPREE Research Group, Universidad Politécnica de Madrid, Madrid, Spain

* Corresponding author. Email: ana.grandeguti@upm.es

Abstract

Corrugated steel silos are widely used to store all types of agricultural and industrial materials due to their excellent structural performance and resistance to buckling. Occasionally, commercial silos are designed with an eccentric hopper to facilitate the handling or flow of bulk solids stored during the discharge process. However, the eccentricity of the hopper can cause an asymmetry in the normal pressure distribution around the silo walls during discharge. This study investigates the normal and tangential forces on the walls of a corrugated steel silo to store biomass wood pellets with centred and off-centre hoppers by performing simulations with EDEM 2022.3 software, based on the Discrete Element Method (DEM). A model silo with corrugated steel walls, a square cross section (0.75 m in height and 0.45 m width and length) and two different bottom configurations (a pyramidal hopper with a centred outlet and a 100% eccentric hopper) was used to validate the numerical models. Depth and wavelength of corrugations were 13 mm and 75 mm, respectively. Cylindrical wood pine pellets of 6 mm diameter and average length of 14.7 mm (±6 mm) were used as granular material to fill the silo. The walls pressures and the discharge rate during the emptying operation were investigated in this study. The DEM results during discharge indicate that when the hopper was eccentric, the pressure on the far side of the eccentric discharge location was higher than on the nearest side. The DEM simulations, properly validated, can also be used to explore the effects of geometrical parameters, such as the corrugation dimensions, wall friction coefficient or particle size, amongst others, on pressures and material flow pattern.

Keywords: Silo, Discrete Element Method, DEM, Corrugated wall, Eccentric discharge.

1. Introduction

Steel silos are a widely used storage solution in agricultural facilities or food industries to store granular materials such as cereals, animal feed, fertilisers, or biomass, among others. The use of solid biomass (firewood, wood chips, sawdust, shavings, briquettes, or pellets, among some other options) for energy production has grown significantly in recent years, as part of a global strategy to reduce dependence on fossil fuels (Pradhan et al., 2018). In this context, the use of wood pellets as biofuel is rapidly increasing worldwide, reaching a global production of more than 46 million tons in 2022 (Geelen et al., 2023).

The use of corrugated steel sheets by silo manufacturers (Figure 1) is a common technical choice, given the higher bending stiffness and buckling resistance offered by this solution compared with a smooth steel sheet of a similar thickness (Wiącek et al., 2021).

Figure 1. Corrugated silos in a livestock farm.

However, the geometry of the corrugation determines the existing friction between the stored material and the silo walls, thus conditioning the pressures exerted, as well as the discharge rate and the flow of the particles during silo emptying. The European standard EN 1991-4 (CEN, 2006), based on previous experimental studies, proposes an empirical formula to evaluate the effective coefficient of friction between the stored material and the corrugated wall by a weighted average of the tangent of the angle of internal friction of the stored granular material ($\tan \phi_i$) and the coefficient of friction of the stored solid against a smooth steel surface (μ_w). The influence of both factors depends on a geometric parameter called 'wall contact factor' (a_w), which depends on the geometry of the wall sheeting profile, although a general value of 0.2 is recommended for sinusoidal walls regardless of the geometry. However, such a simplification does not consider influencing parameters such as the relationship between the size of the particles and the height of the corrugation, whose detailed influence on the friction mechanism requires further studies (Gallego et al., 2019; Grabowski et al., 2021).

The presence of hoppers in silos also determines the flow of granular particles and the value of the pressures exerted by the stored material against the walls during discharge (Vidal et al., 2006). Commercial silos are occasionally designed with an eccentric hopper, which leads to an asymmetry in the pressures generated, with possible local buckling effects (Sadowski and Rotter, 2011).

The Discrete Element Method (DEM) has been successfully used to simulate the flow of disaggregated solids inside silos and to determine the forces exerted by the particles against the walls in the filling and emptying processes (Goda et al., 2005; González-Montellano et al., 2012; Kobyłka and Molenda, 2014; Ramírez-Gómez, 2020). The aim of this work is to exploit the advantages offered by the discrete element method for the analysis of corrugated sheet walls in centred and off-centred hopper silos. Using Altair EDEM 2022 software, a silo with corrugated sheet walls and two different hopper configurations (centred and eccentric) containing wood pellets has been modelled to compare the pressures exerted by the stored material, the effective friction against the walls, and the discharge rates produced in both cases. To validate the numerical models, an experimental silo instrumented with load cells at different positions was also build.

2. Materials and Methods

EDEM 2022.3 software, based on the discrete element method (DEM), was used to develop the numerical simulations. The Hertz-Mindlin contact model, with viscous damping and slip in the tangential direction of the contact, was used to simulate the forces occurring during the physical collision between the particles or between the particles and the silo walls. The wood pellets were randomly generated at the top of the silo at a constant rate of 1.5 kg/s until they fill the entire volume of the silo, which required approximately 260,000 particles and a total mass of 107.8 kg of material. It was verified that the total kinetic energy of the system at the end of the filling phase was less than 10^{-8} J, to ensure the static condition of the particles before starting the discharge. Time integration was carried out by using the Euler method, adopting a time step of $1.3 \cdot 10^{-5}$ s (i.e., 20% of the Rayleigh time step) to guarantee the robustness of the calculations and to avoid large fluctuations in the results of the subsequent calculation steps. The time interval used to save data was 0.2 s to reduce the size of the files generated. Pine wood pellets were simulated using the multi-spheres method. Five different types of particles were used, matching the particle size distribution measured experimentally (Figure 2).

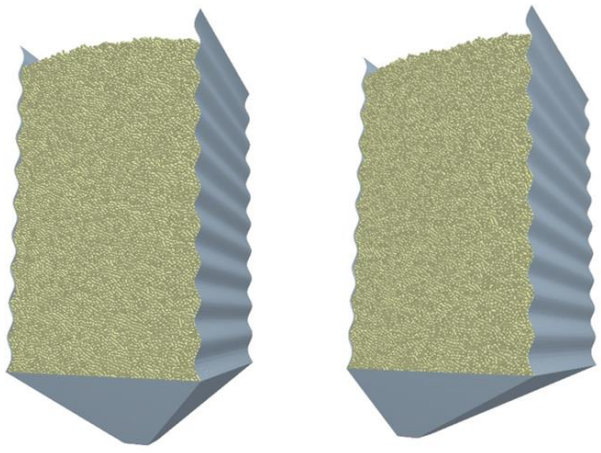

Figure 2. Discrete element model of the silo. Left: centred hopper silo, and right 100% eccentric hopper silo.

The mechanical properties of the materials and the particle-particle and particle-wall interaction properties required for the DEM simulations are shown in Table 1.

Table 1. Properties of the materials used in DEM simulations.

Mechanical properties of materials			
Material	Solids density (kg/m^3)	Young's modulus (MPa)	Poisson's ratio
Wood pellets	1100	7330	0.4
Galvanised steel walls	7850	210000	0.3
Polymethylmethacrylate walls (PMMA)	1190	3150	0.4
Interaction properties contemplated in the models			
Materials interacting	Coefficient of restitution	Coefficient of static friction	Coefficient of rolling friction
particle-to-particle	0.62	0.4	0.02
particle-to-wall (steel sheet)	0.5	0.26	0.01
particle-wall (PMMA)	0.67	0.4	0.01

An experimental prototype of a square-section silo with the same dimensions as the one used in the computational research was used to validate the numerical results (Figure 3). The side walls of the silo prototype were made from a commercial galvanised corrugated steel sheet profile, with a corrugation depth of 13 mm and wavelength of 75 mm, and its front and rear walls were manufactured from transparent polymethyl methacrylate (PMMA) to visualise the flow of the bulk material during emptying. The experimental silo is equipped with beam-type sensors to monitor the weight of the stored bulk material and the forces exerted by it against the walls. Two different bottom configurations were used for silo discharge: (i) a pyramidal hopper with a centric outlet and (ii) an oblique hopper with an eccentricity of 100%, with a 60 x 60 mm^2 square section outlet in both cases.

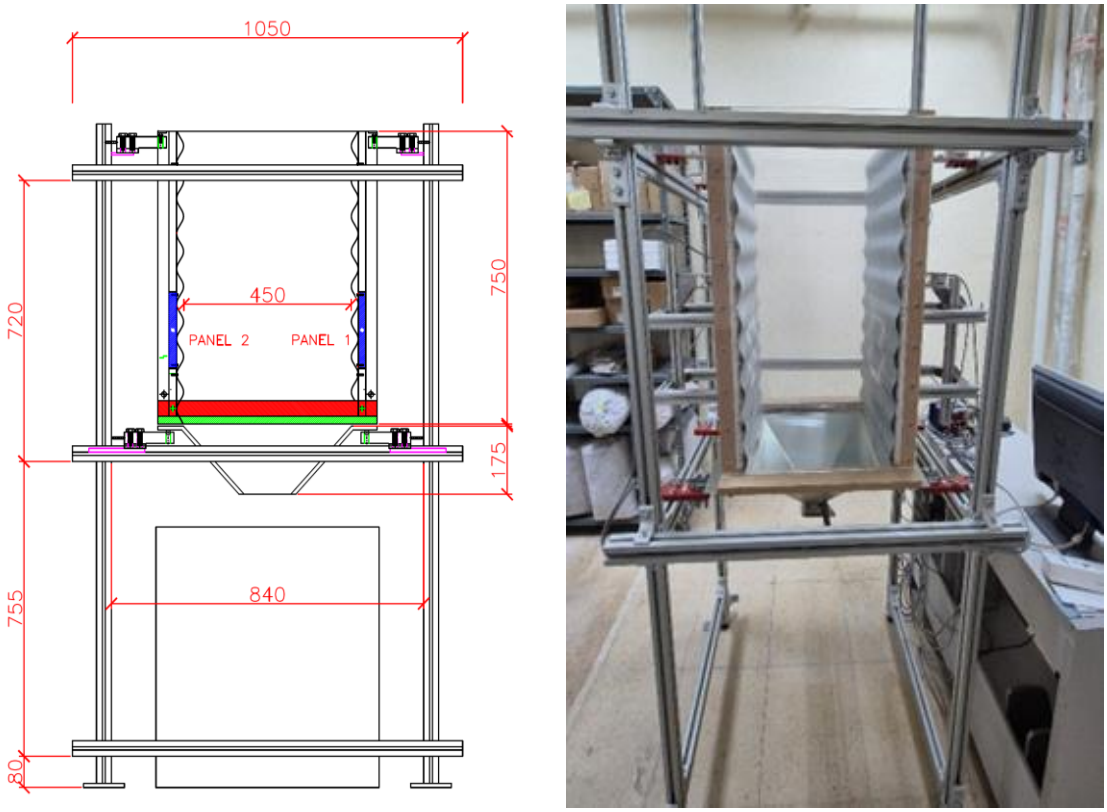

Figure 3. Experimental silo used to validate the numerical models.

The granular material used in the experimental assays was cylindrically shaped pine wood pellets 6mm in diameter (±0.1 mm) and variable length (14.7 mm ±6 mm), having experimentally determined physical and mechanical properties as shown in Table 2 (Gallego et al., 2020).

Table 2. Mechanical properties of biomass pellets used in this research.

Parameter	Value
Bulk solid density [kg/m^3]	680
Angle of repose [º]	40.5
Angle of internal friction [º]	39.5
Coefficient of friction (with a smooth steel sheet)	0.3
Moisture [%]	6.5
Modulus of elasticity [MPa]	21.3
Poisson's ratio	0.13

Seven repetitions of each test were carried out to guarantee the repeatability of the experimental assays and to be able to perform a statistical analysis of the results.

3. Results and Discussion

3.1. Experimental validation of the numerical models

The aim of the experimental validation process was to determine whether the DEM models were able to reliably predict the bulk solid density of the stored material at the end of the filling phase and the discharge rate obtained in the laboratory tests. Table 3 shows a comparison of the values of the different parameters obtained in the simulations and in the experimental tests conducted. As can be seen, the differences for the bulk density of the stored material (1%) and the average mass flow rate during discharge (3.4-8.7%) are minor, indicating a reasonably good fit between the numerical models and the experimental tests.

Table 3. Mean values of different parameters obtained in computer simulations versus experimental tests.

Parameter	Centred hopper			Eccentric hopper (100%)		
	DEM	Exp. tests	Diff.	DEM	Exp. Tests	Diff.
Bulk solid density (kg/m^3) at the end of the filling stage	687	680	1.0%	687	680	1.0%
Total time required for discharge (s)	225	217	3.7%	174	188	7.4%
Average mass flow rate during discharge (kg/s)	0.477	0.494	3.4%	0.620	0.571	8.7%

Table 4 shows the evolution of the experimental and numerical values of the mass flow rate at different intervals of the total discharge time (T). The experimentally measured and computer-calculated values are quite close for the different time intervals, with both the numerical models and the experimental tests showing a certain reduction in the discharge rate as the emptying process progressed.

Table 4. Evolution of the mean flow rates (kg/s) at different intervals of the complete discharge process.

Discharge interval	Centric hopper		Eccentric hopper (100%)	
	DEM	Experimental tests	DEM	Experimental tests
0 T - 0.25 T	0.495	0.518	0.621	0.609
0.25 T - 0.50 T	0.486	0.505	0.626	0.592
0.5 T - 0.75 T	0.468	0.480	0.622	0.586
0.75 – 1.0 T	0.460	0.470	0.614	0.476

3.2. Pressures on the silo walls, effective wall friction coefficients, and discharge rates predicted by the Discrete Element Models

Figure 4 shows the pressures exerted by the wood pellets on the corrugated walls on two 15x15 cm^2 panels located at a height of 25 cm above the transition of the vertical section of the silo with the hopper. In

the case of a silo with an eccentric hopper, panel 1 is the one located on the wall closest to the hopper outlet, and panel 2 is the one furthest away from it.

As can be seen, in the centred hopper silo, the normal and tangential pressure curves are similar for both walls, while in the case of the eccentric hopper silo, significant differences exist between both walls during the emptying of the silo. In that case, higher pressures were recorded on the wall that is most distant from the outlet than on the wall that is closest to the outlet. This may be explained by the lower mobility of the granular material on the opposite side to the hopper outlet.

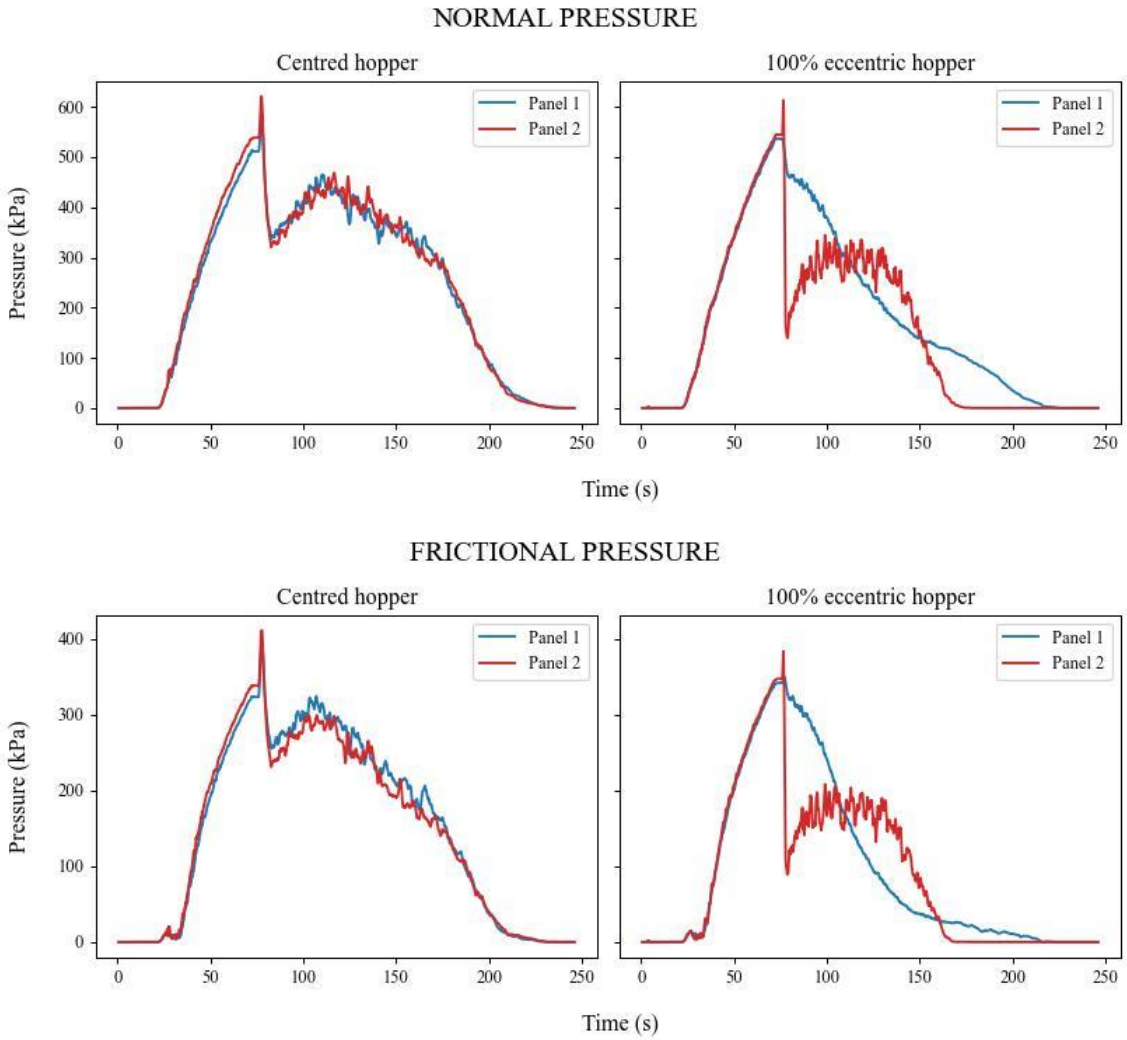

Figure 4. Pressures exerted by the wood pellets on the corrugated sheet metal walls of the model silo.

Figure 5 shows the evolution of the effective wall friction coefficients (μ_{eff}) at positions 1 and 2 during filling and discharge for both simulated silos. As can be seen, the curves corresponding to the effective wall friction coefficient during filling are very similar in all cases. However, differences are found during emptying. In the centred hopper silo, the two corrugated walls (1 and 2) show a similar behaviour, with higher values of μ_{eff} than those recorded during filling for the same height of stored material. Meanwhile, in the case of the eccentric hopper silo, differences were found in the behaviour of the wall closest to and most distant from the outlet. In the most distant wall, the μ_{eff} values were very similar to those recorded during filling and slightly lower than those obtained in the centred hopper silo. However, on the wall closest to the outlet, there is a significant drop in the effective wall friction coefficient. Maximum values were obtained in any case when the silo was completely full of granular material (h=H).

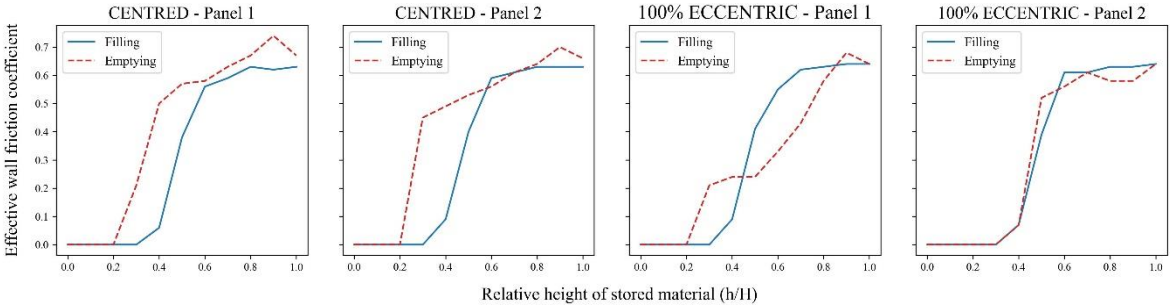

Figure 5. Effective wall friction coefficients

Figure 6 shows the evolution of the discharge rate or the mass flow index (MIF) for both bottom configurations studied. As can be seen, the registered discharge rate value was quite stable throughout the entire emptying process in both cases, with a slight decrease as the discharge progresses (Table 4). The discharge rate took higher values in the silo with an eccentric hopper compared to the centred hopper silo (0.620 vs. 0.477 kg/s), which also resulted in a faster emptying (174 vs. 225 s). This behaviour was also noticed in the experimental tests.

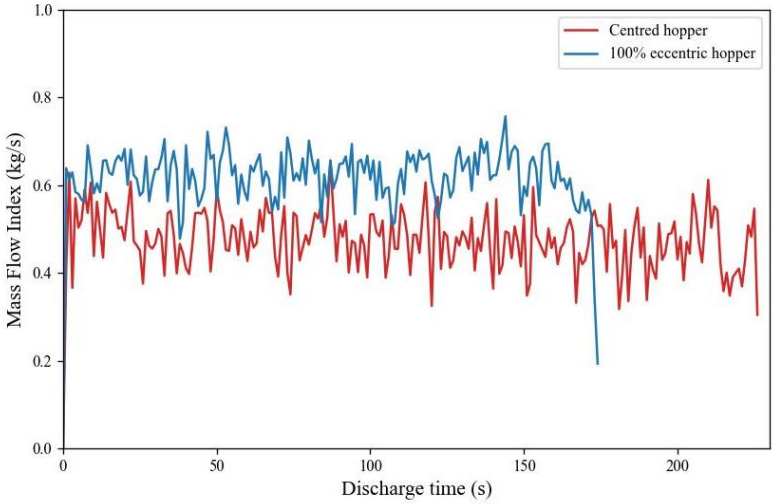

Figure 6. Discharge rate on the silo predicted by the DEM models.

4. Conclusions

In the present work, discrete element models have been developed to analyse the pressures, effective wall friction coefficients and the discharge rates in two similar corrugated steel silos with a centred and an eccentric hopper, containing wood pellets. The main conclusions derived from the research are the following:

• DEM models have been validated through experimental tests in a silo prototype of similar dimensions based on the density of the stored material at the end of the filling phase and the average mass flow rate during the discharge, obtaining a reasonably good fit, with differences of less than 1 and 8.7 %, respectively.

• The presence of an eccentric outlet hopper affects the normal and tangential pressures recorded on the walls of the silo during emptying, resulting in an increase in the wall most distant from the outlet and a reduction in the opposite wall, compared to the case of the centred hopper silo.

• The effective wall friction coefficients predicted by the DEM models for the discharge differ depending on whether the silo has a centred or an eccentric hopper. In the second case, a reduction in effective friction was observed on both walls, especially on the wall most distant from the outlet.

• The presence of an eccentric hopper affects the discharge rate, producing an increase in the mass flow rate of around 30%. The higher mass flow rate also means a shorter emptying time (174 vs. 225 s.) in that case.

Acknowledgements

This research was funded by the Spanish Agencia Estatal de Investigación via the research project '*Study of the structural behavior of corrugated wall silos using Discrete Element Models (SILODEM)*' (grant number PID2019-107051GB-I00/AEI/10.13039/501100011033). The authors gratefully acknowledge the Universidad Politécnica de Madrid (www.upm.es) for providing computing resources on Magerit Supercomputer and the staff of the Construction and Geotechnical Laboratory of the ETSIAAB (J.L. Alejandre, S. Abril, and J. Dorado) for their help to carry out the experimental tests.

References

CEN. 2006. EN 1991-4. Eurocode 1 - Actions on structures. Part 4: Silos and tanks (1st ed.). Brussels: European Committee for Standardization (CEN).

Gallego, E., J.M. Fuentes, A. Ruiz, G. Hernández-Rodrigo, P. Aguado, F. Ayuga. 2020. Determination of mechanical properties for wood pellets used in DEM simulations. International Agrophysics. 34(4), 485-494. https://doi.org/10.31545/intagr/130634

Gallego, E., J.M. Fuentes, J. Wiącek, J.R Villar, F. Ayuga. 2019. DEM analysis of the flow and friction of spherical particles in steel silos with corrugated walls. Powder Technology. 355, 425-437. https://doi.org/10.1016/j.powtec.2019.07.072.

Geelen, J., M. Karampinis, J.M. Jossart. 2023. Bioenergy Europe. Statistical Report Pellets. Brussels: Bioenergy Europe. 113 p.

Goda, T.J., F. Ebert. 2005. Three-dimensional discrete element simulations in hoppers and silos. Powder Technology. 158(1-3), 58–68. https://doi.org/10.1016/j.powtec.2005.04.019

González-Montellano, C., E. Gallego, A. Ramírez-Gómez, F. Ayuga. 2012. Three-dimensional discrete element models for simulating the filling and emptying of silos: Analysis of numerical results. Computers & Chemical Engineering. 2012, 40, 22- 32. https://doi.org/10.1016/j.compchemeng.2012.02.007

Grabowski, A., M. Nitka, J. Tejchman, 2021. Micro-modelling of shear localization during quasi-static confined granular flow in silos using DEM. Computers and Geotechnics. 134, 104-108. https://doi.org/10.1016/j.compgeo.2021.104108.

Kobyłka, R., Molenda, M. DEM simulations of loads on obstruction attached to the wall of a model grain silo and of flow disturbance around the obstruction. Powder Technology. 2014, 256: 210–221. https://doi.org/10.1016/j.powtec.2014.02.030

Pradhan, P., S.M. Mahajani, A. Arora. 2018. Production and utilization of fuel pellets from biomass: A review. Fuel Processing Technology. 181, 215–232. https://doi.org/10.1016/j.fuproc.2018.09.021.

Ramírez-Gómez, Á. (2020). The discrete element method in silo/bin research. Recent advances and future trends. Particulate Science and Technology, 38(2), 210–227. https://doi.org/10.1080/02726351.2018.1536093

Sadowski, A.J., J.M. Rotter. 2011. Steel silos with different aspect ratios: II—behaviour under eccentric discharge. Journal of Constructional Steel Research, 67(10), 1545-1553. https://doi.org/10.1016/j.jcsr.2011.03.028

Vidal, P., A. Couto, F. Ayuga, M. Guaita. 2006. Influence of Hopper Eccentricity on Discharge of Cylindrical Mass Flow Silos with Rigid Walls. Journal of Engineering Mechanics. 132 (9). 1026-1033. https://doi.org/10.1061/(ASCE)0733-9399(2006)132:9(1026)

Wiącek J., E. Gallego, P. Parafiniuk, R. Kobyłka, M. Bańda, J. Horabik, M. Molenda. 2021. Experimental analysis of wheat-wall friction and grain flow in a steel silo with corrugated walls. Biosystems Engineering. 209, 216-231. https://doi.org/10.1016/j.biosystemseng.2021.07.003.

Optimization of poultry house ventilation system using computational fluid dynamics

Timothy Denen Akpenpuun[a]*, Sunday John Oluwaseun[a], Oyindamola Oluwadamilola Toye[a]

[a]Department of Agricultural and Biosystems Engineering, University of Ilorin, Ilorin 240003, Nigeria.

* Corresponding author. Email: akpenpuun.td@unilorin.edu.ng

ABSTRACT

Effective ventilation is crucial for the well-being and productivity of poultry in response to the growing global demand for poultry products. Properly designed and managed ventilation systems aid to remove contaminants and maintain uniform environmental conditions, benefiting both animals and workers in poultry houses. Computational fluid dynamics (CFD) modeling has become an essential tool in designing and evaluating ventilation systems, offering control over influencing factors and cost-effective solutions to address indoor environmental challenges in poultry housing. Through CFD simulations, airflow patterns within the poultry house will be analyzed to pinpoint areas for potential enhancement. A detailed 3D model of the poultry house and ventilation system is created within the CFD software with various simulation scenarios which are defined, considering different parameters like air inlet and outlet locations, fan settings, and environmental conditions. The process iterates until an optimal configuration is achieved, ensuring improved indoor air quality and enhanced poultry well-being and productivity. The simulation results indicated a moderately even temperature distribution but uneven air velocity in the baseline poultry house due to natural ventilation. Other results present the mass fraction distribution of ammonia (NH_3), humidity, and carbon dioxide (CO_2) for both systems and variations in air velocity and ammonia concentration in the baseline system. The analysis and comparison of the baseline and optimised poultry house ventilation systems reveal significant improvements with the optimised system.

Keywords: ventilation, computational fluid dynamics (CFD), simulation, poultry

1. Introduction

Effective ventilation systems play a pivotal role in creating a healthier and more productive environment for both animals and human occupants by addressing indoor air quality issues. Studies, such as those by Cao et al. (2023), emphasize the importance of ventilation in preventing respiratory issues and other health problems in poultry. Ensuring uniform indoor environmental conditions through proper airflow distribution helps remove humidity, particulate matter, and gases, fostering a healthier environment. Also, Glatz et al. (2013) highlight that inadequate ventilation can lead to a buildup of harmful gases like ammonia and carbon dioxide, negatively affecting bird health and productivity. Studies like those by Lewis and Both (2022) support the idea that uniform airflow can mitigate risks associated with temperature hotspots and pollutant concentrations in poultry houses. People widely acknowledge the importance of ensuring uniform indoor environmental conditions in livestock housing. Proper airflow distribution facilitates the removal of humidity, particulate matter, and gases, thereby fostering a healthier and more productive environment for both animals and human occupants. Moreover, airflow patterns decisively influence the uniformity of key indoor environmental parameters such as temperature, contaminant levels, and humidity. Scientific literature, including the work by Lewus and Both (2022), has reported that uniform airflow can mitigate the risks associated with hotspots of high temperature or pollutant concentration, which can otherwise lead to stress and reduced productivity in poultry.

The adoption of computational fluid dynamics (CFD) in agricultural engineering has facilitated the modeling of airflow fields and the prediction of ventilation system performance, enabling comprehensive design and evaluation processes. In CFD simulations, precise control over influencing factors provides information about how airflow changes in the computational domain while keeping costs and time to a minimum (Van Wagenberg et al., 2004). By visualizing and optimizing ventilation systems, researchers and engineers can ensure uniform air distribution, manage heat loads effectively, and maintain optimal humidity levels. Natural ventilation is a primary method to control humidity, temperature, and carbon dioxide concentration inside enclosures such as greenhouses and poultry houses (Lee and Short, 2000). Natural ventilation is the most effective among passive cooling techniques in lowering high air temperatures inside greenhouses (Rasheed et al., 2019). The main advantage of CFD lies not only in the prediction of the ventilation rate but also of the airflow pattern, temperature, and humidity distribution inside an enclosure (Choi et al., 2023). Experimental studies have pointed out the impact of vent configurations on airflow patterns, particularly when natural ventilation is the main source of air exchange between an enclosure and the external environment.

The present study aims to leverage CFD simulation techniques to optimized ventilation poultry housing, focusing on enhancing air quality, reducing energy consumption, and optimizing system performance for maximum efficiency and effectiveness. A computational fluid dynamics (CFD) program (FLUENT 19.0, ANSYS, New York, NY, USA) was used to analyze temperature and humidity distribution within the simulated poultry house. The study aims to enhance productivity and welfare in poultry farming operations, contributing to more sustainable agricultural practices. We expect the findings to provide practical solutions for real-world implementation, aiding poultry farmers in maintaining healthier flocks and achieving better economic outcomes.

2. Materials and Methods

The experimental poultry house comprises a four-walled structure constructed with 22 mm concrete block walls, featuring dimensions of 1.9 m in width and 2.9 m in length, resulting in a total area of 5.51 m², complemented by a flat roof design. For this study, a single case scenario was selected and meticulously modelled to examine fan and air inlet configurations. The model incorporates two air inlet vents positioned at the front of the poultry building to facilitate natural air intake. To facilitate air ventilation within the building, two fans with diameters of 3.9 m and an airflow rate of 28,000 m³/h are strategically placed at the rear section of the structure. External air ingress occurs through intake vents measuring 0.26 m x 0.26 m, driven by the negative pressure generated by the installed fans.

The experimental location is characterized by a tropical wet and dry or savanna climate classification. It experiences an annual temperature range between 22.39 ºC and 33.54 ºC, with January registering the lowest average temperature of 20.7 ºC and February recording the highest average temperature of 38.54 ºC. Figure 1 presents a schematic diagram illustrating the layout of the poultry house, while Figure 2 provides detailed information regarding the building's geometry and dimensions of fans and air inlet vents. These architectural and climatic considerations are crucial for understanding the environmental dynamics within the poultry house and informing the experimental design for optimizing ventilation strategies.

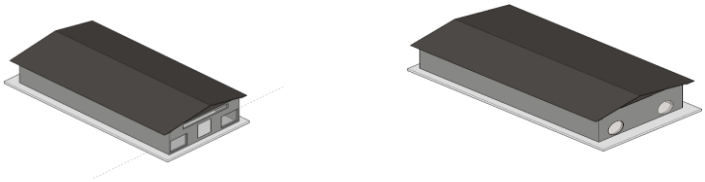

Figure 1. Schematic drawing of the poultry house

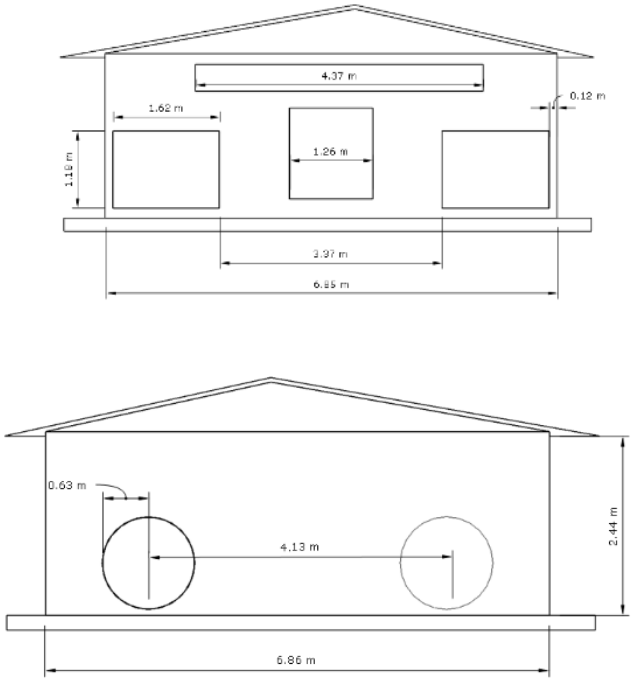

Figure 2. Poultry house geometry and dimensions.

2.1 Data collection and analysis

The study employed a typology of poultry houses commonly found in Nigeria, which mirrors the prevailing construction practices in tropical and subtropical regions favouring natural ventilation systems. Specifically, the poultry house dimensions were 1.9 m in width, 2.9 m in length, and a ceiling height of 3.0 m, with walls measuring 0.20 m in thickness. This structure housed broilers at a high density, aged approximately 39 days (close to the slaughter age).

The simulation utilized input parameters specifying a maximum fluid velocity of 1.5 m/s upon entry into the poultry shed, at a temperature of 25 °C. For the simulation, boundary conditions were meticulously defined for the birds, air inlets, and exhaust fans. The walls, doors, and floors of the poultry house were assigned no-slip and adiabatic (heat flux

= 0) conditions to accurately model heat transfer dynamics. Furthermore, the chickens were represented as spherical entities with a constant heat flux, providing a realistic approximation of heat generation within the poultry environment. These comprehensive input parameters and boundary conditions ensure the fidelity and accuracy of the simulation, enabling a detailed examination of airflow and thermal dynamics within the poultry house (Pawar *et al.*, 2007). According to Reece *et al.* (1969), the heat produced by poultry birds grown in a litter housing is 40% sensible and 60% latent as shown in Eqs (2) and (3).

Total heat production by a single broiler can be derived using Eq (1).

$$THP = \frac{M \times HPR}{A} \quad (1)$$

THP = Total heat production, W/m^2; M = metabolic rate of the broiler (in watts or joules per unit time); HPR = heat production rate (joules per unit time per unit weight); A = weight of the broiler (in kilograms).

The heat flux leaving the birds can then be derived using Eqs (4) and (5).

$$Q_{sensible} = 0.40 \times Q_{total} \quad (2)$$

$$Q_{latent} = 0.40 \times Q_{total} \quad (3)$$

$$\text{Heat flux} = THP \times Q_{sensible} \quad (4)$$

$$\text{Heat flux} = THP \times Q_{latent} \quad (5)$$

The total moisture produced by all the birds in a poultry house, in terms of per volume air is derived by Eq. (6).

$$\text{Total moisture } (kgH_2O/m^3) = \frac{\text{moisture produced}(kgH_2O)}{\text{house volume}(m^3)} \quad (6)$$

Total water consumption by a total of 100 birds in the poultry house is 20 liters per day and the poultry house moisture content is 30%, the moisture produced(kgH_2O) by the birds is derived by

$$\text{Moisture produced}(kgH_2O) = \frac{\text{Total water consumption (litres)}}{\text{Poultry house moisture content}} \quad (7)$$

Inlets were specified at the two-side walls and a rear end facing the exhaust fan of the poultry house. These inlets were given constant velocity boundary conditions and constant air temperature based on the scenario adopted for the simulation process. Outlets were specified where the air leaves the poultry house, which was stationed at the opposite wall facing the rear end inlet air opening. The two outlet fans were represented by setting the gauge pressure above the ambient pressure to simulated a difference in pressure based on the size of the fan selected and temperature equal to ambient temperature. Relative humidity of the air coming through the inlets was set at a constant condition of 60% for all simulations, a reasonable approximation of average afternoon humidity in Kwara state region during the dry season.

2.3 CFD simulation setup

The mass, momentum, and energy conservation equations employed in the CFD simulation are illustrated in equations 5-7 (Fluent, 2008)

$$\frac{\delta \rho}{\delta t} + \nabla \cdot (\rho \vec{v}) = S_m \quad 3.10$$

$$\frac{\partial}{\partial t} + (\rho \vec{v}) + \nabla . (\rho \vec{v} \vec{v}) = -\nabla P + \nabla . (\overline{\tau}) + \rho \vec{g} + \vec{F} \quad 3.11$$

$$\frac{\partial}{\partial t} + (\rho E) + \nabla . (\vec{v}(\rho E + P)) = \nabla (k_{eff} \nabla \mathrm{T} - (x + a)^n = \sum h_j j_j + (\overline{\tau}_{eff} \vec{V})) + S_h \quad 3.12$$

Where, ρ is density (kg m^{-3}), v is velocity (ms^{-1}), P is constant pressure (Pa), τ is stress tensor (Pa), g is gravitational acceleration (ms^{-2}), F is external force vector (Nm^{-3}), S_m is mass source (kgm^{-3}), K_{eff} is heat transmission coefficient, j_j is component of diffusion flux (kgm^{-2} s^{-1}), and S_h is total entropy (J K^{-1}).

For various configurations of input vents combined with exhaust fans in the poultry house, the airflow pattern and ventilation rate were examined using a computational fluid dynamics (CFD) program (V.19, Fluent, ANSYS - Fluent Inc.). Autodesk Revit Pro version 2018 software was used for this study's first pre-processing stage to create 3D models of poultry houses. Additionally, meshing was done in the ANSYS mesh component. ANSYS Fluent version 19 R3 was used to execute simulations in the second step for numerous instances. Finally, (ANSYS 2019 R3) software implemented post-processing of the simulation results (Rasheed *et al.*, 2019). Figure 3 is showing the flowchart of simulation procedure.

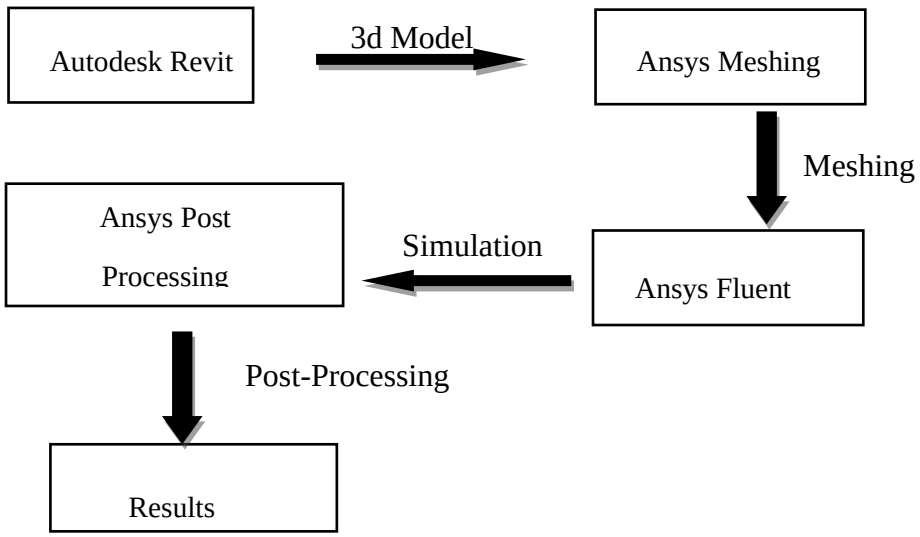

Figure 3. Flowchart of simulation procedure.

2.4 Simulation parameters

The meshing of the computational domain of the studied internal environment is shown in Table 1 contains a list of the meshing properties and information on the boundary conditions and material properties that were employed in the simulations.

Table 1. Simulation parameters.

Mesh Properties		**Cell Zone and Boundary conditions**		
Properties	**Value**	**Parameter**	**Unit**	**Value**
Type of mesh	Hybrid	Inlet velocity	m/s	constant
Number of meshes	10,318	Inlet temperature	^{o}C	constant
Size function	Curvature	outlet temperature	^{o}C	constant
Curvature normal angle	100	Air Density	$kg{\cdot}m^{-3}$	0.000293
Element size	0.015m	outlet pressure	Pa	0.275
Relevance	25	Relative Humidity	%	60
		Specific heat	$Jkg^{-1}K^{-1}$	1006

Four scenarios were tested to evaluate the influence of varying inlet velocities and ambient temperatures on the environment within the poultry house. These scenarios involved two different inlet velocities and three different ambient temperatures as shown in Table 2. The inlet velocity conditions were determined based on typical values observed from field measurements, while the selected temperatures were representative of those commonly experienced during the dry season in the Kwara state region. This comprehensive approach allowed for a thorough examination of how different inlet velocities and outdoor temperatures affect the poultry house environment.

Table 2. Inlet conditions.

Scenario	**Inlet temperature (°C)**	**Inlet air velocity (m/s)**
1	29	1.5
2	28.5	3.0
3	28.8	1.5
4	30	3.0
5	27	1.5
6	27.7	3.0

In the simulation, a pressure-based solver was employed to model the airflow dynamics within the poultry house. Turbulent airflow conditions, typical in ventilating flows, were assumed based on previous research findings (Norton *et al.*, 2010). The boundary conditions were established to account for the mass fraction of moisture generated within the poultry house and the influx of water vapour from external sources. For further clarity, a summary of the solution methods employed in the simulation is provided in Table 3. This approach ensures a comprehensive understanding of the airflow and moisture dynamics within the poultry house environment.

Table 3. Solution methods.

Solution method	Setting
Pressure-velocity coupling	SIMPLE
Gradient	Least squares cell based
Pressure	Second order upwind
Momentum	Second order upwind
Turbulent kinetic energy	Second order upwind
Turbulent dissipation rate	Second order upwind
H_2O	Second order upwind
Energy	Second order upwind

3. Results and Discussion

3.1. Analysis of baseline ventilation system

The temperature, velocity and humidity values as observed in both the conventional and optimised case was indicated based on the plane of reference which is most suitable for the positioning of the birds in the poultry at a given point in time at the same time the Local conditions at 5 crucial points within the poultry house were also evaluated for temperature, air velocity and relative humidity. The conditions of the poultry house based on a plane of reference and the six points of reference are illustrated in Table 4 and 5.

The temperature, velocity, and humidity values observed in both the test case and the optimised scenario were compared, considering the ideal positioning of the birds within the poultry. Additionally, local conditions at five key points within the poultry house were assessed for temperature, air velocity, and relative humidity. The simulation outcomes presented in Table 5 provide valuable insights into the thermal distribution within the poultry house, revealing a moderately homogeneous temperature profile in the simulated result. However, the velocity distribution exhibited non-uniformity, and this situation can be attributed to the inherent variability associated with natural ventilation in the baseline system. It was observed that the average temperature within the poultry house under optimised ventilation was 28.8 °C, and the average humidity was 50%. This temperature falls within the range of 27 to 36.2 °C reported by Furlan *et al.* (2000), Cangar *et al.* (2008), and Nääs *et al.* (2010) Furlan et al. (2000), Cangar et al. (2008), and Nääs et al. (2010) for a poultry house housing 42-day-old birds. This condition is recommended for birds in the age range of 42-61 days to eliminate the risk of heat stress, as the temperature of birds generally varies with changes in the air temperature of the environment (Zmrhal *et al.*, 2023). In terms of air velocity, the ventilation set up for the baseline systems shows an uneven velocity distribution across the poultry house due to the fact that the baseline ventilation system adopts a natural mode of poultry house ventilation.

Table 4. Simulation results for baseline ventilation system.

Cases 1	Velocity Magnitude (m/s)	Ammonia Concentration (%)	CO_2 Concentration (%)	Temperature (ºC)	Relative Humidity (%)	Vapour Pressure Deficit (mmHg)
Point a	0.9	0.5	3.1	29.6	70	12.5
Point b	0.92	0.4	11	29.2	40	24.1
Point c	0.6	2.1	4.7	28.8	60	16
Point d	1.55	2.67	9	28.3	56	17
Point e	1.6	3.2	8	28	60	15.1

Table 5. Simulation results for optimised ventilation system.

Cases 2	Velocity Magnitude (m/s)	Ammonia Concentration (%)	CO_2 Concentration (%)	Temperature (ºC)	Relative Humidity (%)	Vapour Pressure Deficit (mmHg)
Point a	1.3	0.5	1.4	29	71	12
Point b	1.5	3.3	7.0	29.2	47	21.05
Point c	1.6	3.8	4.2	29	40	24.1

Point d	3.9	2.3	4.2	28.9	45	22.1
Point e	4	2.5	4.2	28	47	19.8

The simulated results presented in Table 5 provide insights into optimised ventilation system of the poultry house under Case 1 conditions. The maximum and minimum temperatures recorded across the ground plane of the poultry house showcase the temperature distribution pattern. Notably, the temperature distribution appears relatively uniform, with minimal variation observed across different locations. Figures 4, 5 and 6 offer visualizations of the internal temperature dynamics and NH_3, H_2O mass fraction distribution and CO_2 mass fraction distributions within the baseline system, respectively. Figures 7, 8 and 9 show the NH_3 mass fraction and air velocity distribution, temperature distribution and H_2O mass fraction and CO_2 mass fraction for optimised ventilation system. The velocity distribution chart Figure 5 shows that the air velocity is more consistent when an exhaust fan is utilized, leading to lower concentrations of ammonia towards the outlet opening. Simmons *et al.* (2003), conducted a similar study showing that an increased wind speed between 0.25 m/s and 3m/s favoured the growth and development in older birds. The study examines the correlation among relative humidity, vapour pressure deficit, and temperature in relation to the optimised ventilation system. Findings reveal that the relative humidity levels in the poultry area remain consistently stable with the optimised ventilation system, contrasting with fluctuations observed in the baseline ventilation system. In a review done by Oloyo (2018), it was reported that internal temperature above 26.7 °C combined with high relative humidity adversely affected the feed efficiency, feathering, pigmentation, and weight gain of chicken. These findings contribute to the scientific understanding of poultry house ventilation dynamics and underscore the importance of optimizing ventilation strategies to enhance air quality and animal welfare.

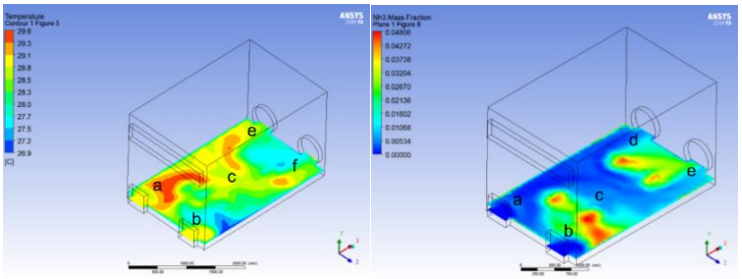

Figure 4. Internal temperature and NH_3 mass fraction for baseline ventilation system

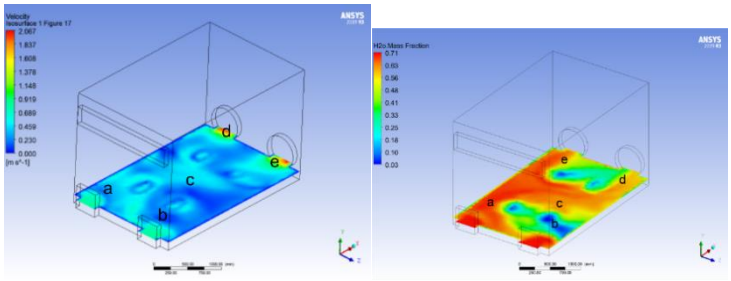

Figure 5. Air velocity and H_2O mass fraction for baseline ventilation system

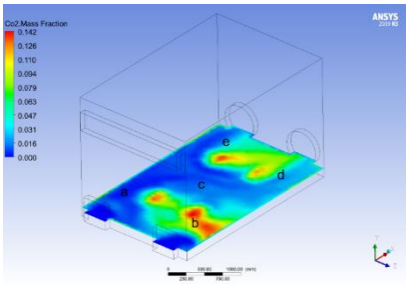

Figure 6. CO_2 mass fraction for baseline ventilation system

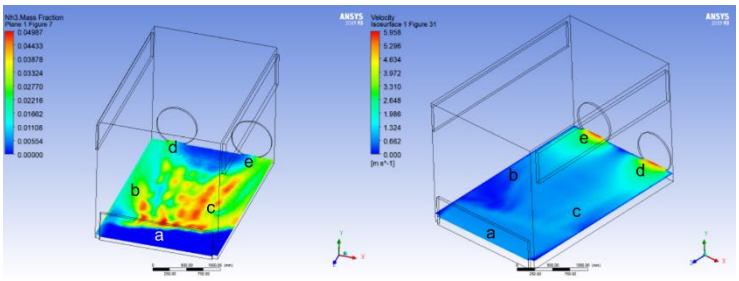

Figure 7. NH_3 mass fraction and air velocity distribution for optimised ventilation system

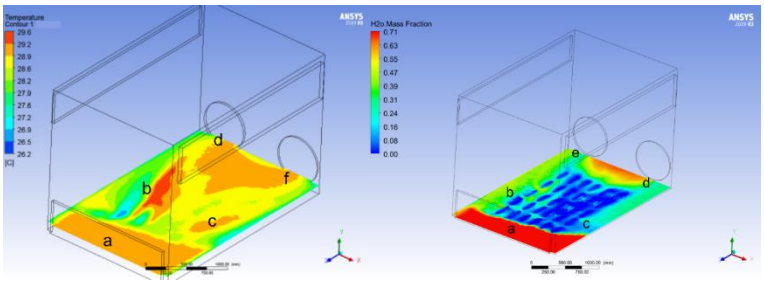

Figure 8. Temperature distribution and H_2O mass fraction for optimised ventilation system.

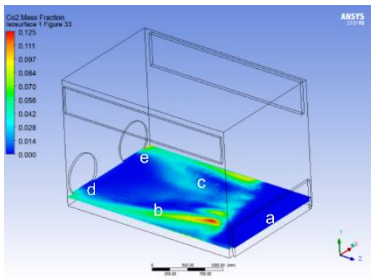

Figure 9. CO_2 mass fraction for optimised ventilation system.

3.2. Comparison of baseline and optimised systems

Figures 10 and 11 show the velocity distribution, Ammonia (NH_3) and CO_2 concentration for baseline and simulated ventilation systems, respectively. Figures 12 and 13 show the relative humidity and vapour pressure deficit vs temperature for baseline and simulated ventilation systems, respectively. The scenario in the baseline system indicates the absence of a pressure differential where an exhaust fan is not utilized to expel the air from the poultry house. Figure 12 illustrates the relationship between relative humidity, vapour pressure deficit, and temperature for the baseline ventilation system. It shows that as the temperature increases, the relative humidity decreases, resulting in a lower vapour pressure deficit. This trend suggests that higher temperatures correspond to lower relative humidity levels in the poultry house.

Figure 10. Velocity distribution, Ammonia and CO_2 concentration chart for baseline ventilation system.

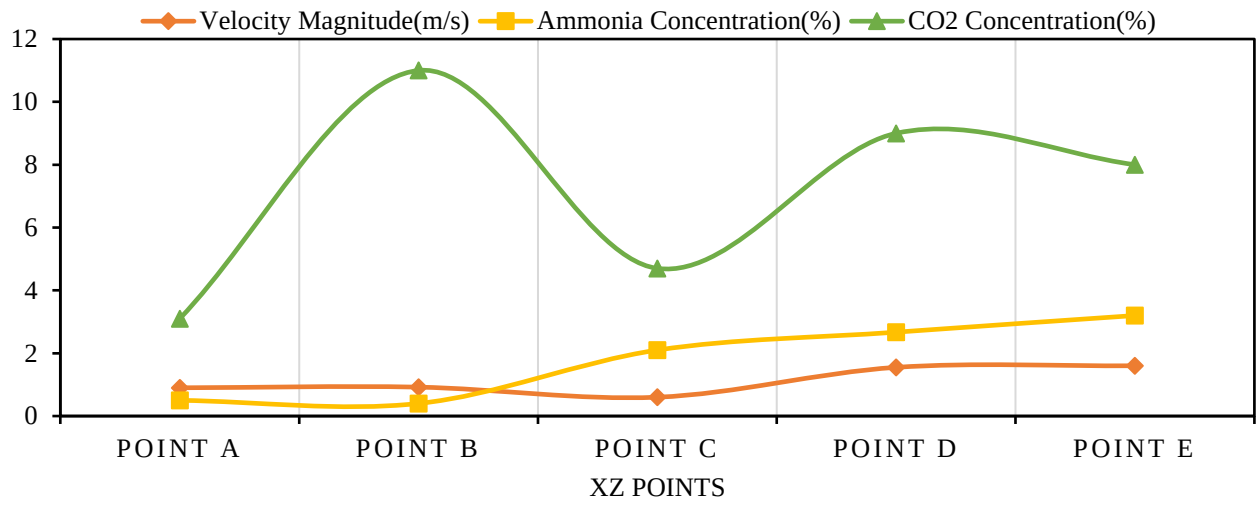

Figure 11 illustrates the velocity distribution within the poultry house under the optimised ventilation system, offering insights into air velocity, ammonia concentration, and CO_2 concentration. The chart reveals a more consistent air velocity profile when utilizing an exhaust fan, with the velocity gradient increasing towards the outlet points of the house. Notably, higher concentrations of ammonia were observed at points b and c, corresponding to areas where birds are typically present. However, concentrations gradually decreased towards the outlet opening where the exhaust fan was positioned, indicating effective ventilation and pollutant removal. This observation underscores the significance of optimizing ventilation strategies to maintain optimal air quality and environmental conditions within the poultry house.

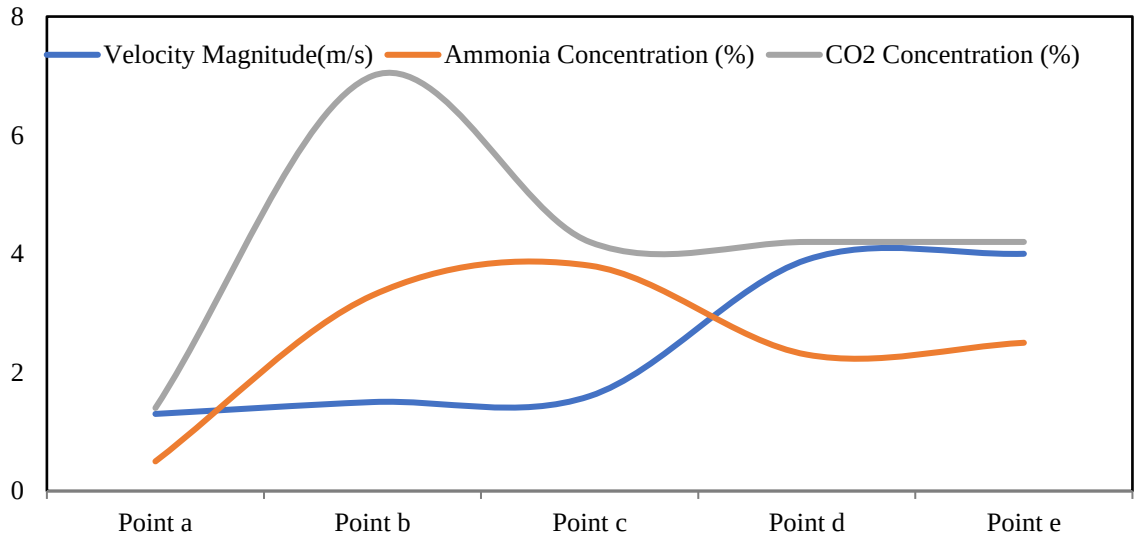

Figure 11. Velocity distribution, Ammonia and CO_2 concentration chart for optimised ventilation system.

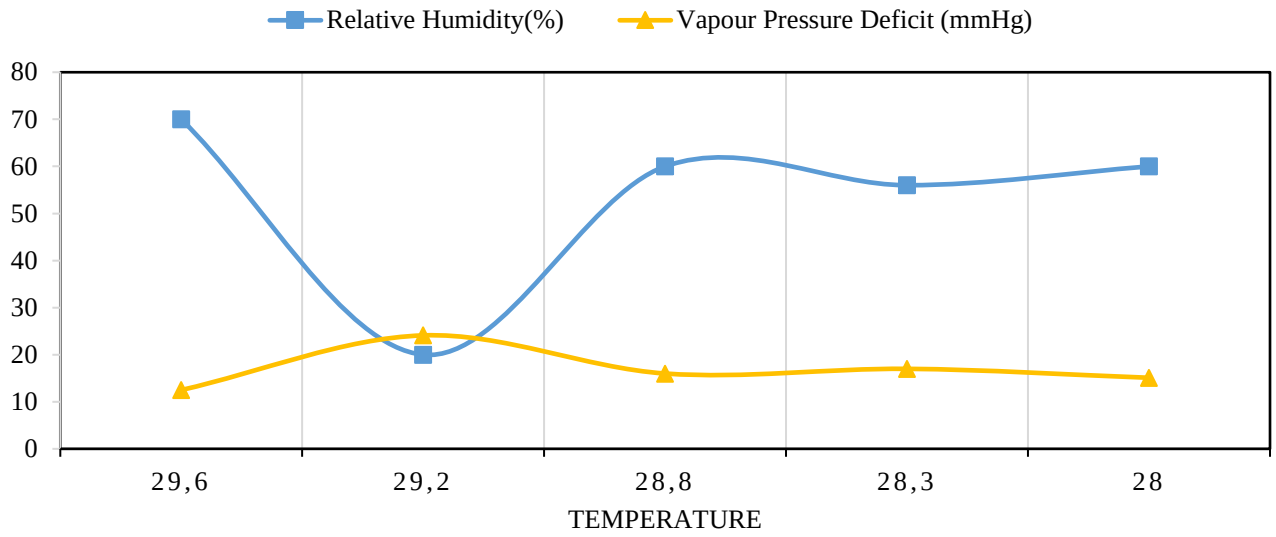

Figure 12. Relative humidity and vapour pressure deficit vs temperature chart for baseline ventilation system.

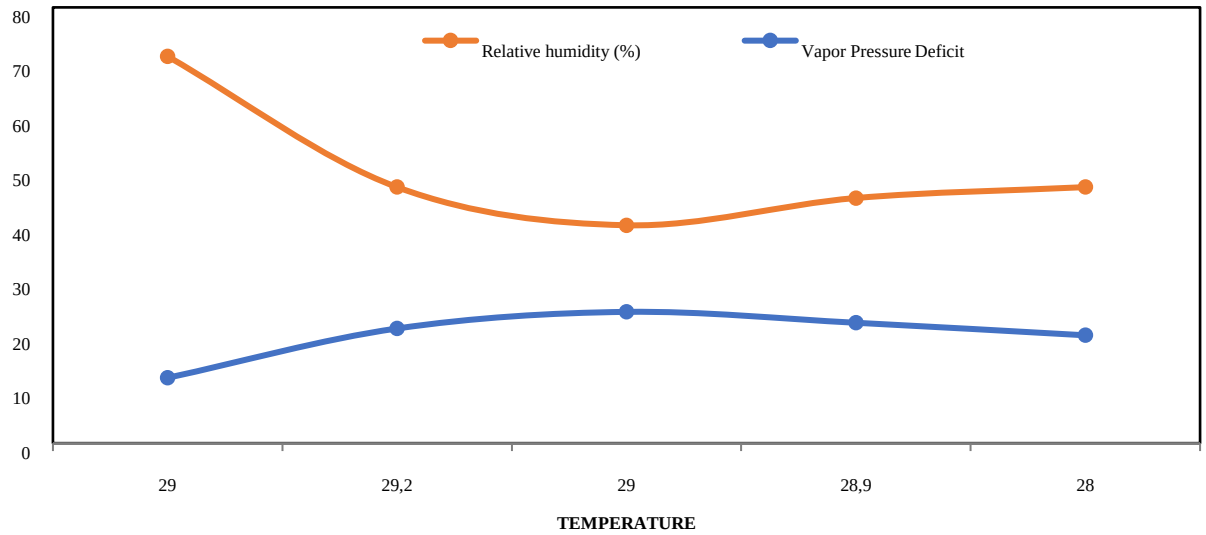

Figure 13. Relative humidity and Vapour pressure deficit vs temperature chart for optimised ventilation system.

4. Conclusion

Following a comprehensive analysis and comparison of the baseline and optimised ventilation systems, it is evident that the optimised system markedly enhances the overall conditions within the poultry house. While the baseline ventilation system exhibits a reasonably uniform temperature distribution, the velocity distribution is notably uneven owing to the inherent variability associated with natural ventilation mechanisms. In contrast, the optimised ventilation system yields a more consistent air velocity profile. This observation underscores the efficacy of incorporating an exhaust fan in the optimised system, which facilitates the creation of a pressure differential, thereby enhancing air circulation throughout the poultry house.

Moreover, the concentration of ammonia, which tends to be highest in areas frequented by birds, exhibits a gradual decrease towards the outlet opening where the exhaust fan is strategically positioned in the optimised system. This signifies the optimised system's efficacy in mitigating airborne contaminants, such as ammonia, thereby fostering improved air quality for the poultry inhabitants. Regarding relative humidity, the baseline system demonstrates a decline in humidity levels with increasing temperature, resulting in a lower vapour pressure deficit. In contrast, the

optimised ventilation system manifests a more balanced relationship between relative humidity, vapour pressure deficit, and temperature, indicative of its capacity to sustain a stable and comfortable environment within the poultry house.

Acknowledgements

We extend our heartfelt appreciation to Eniola David for his invaluable contribution to the success of this paper and acceptance for the conference.

REFERENCES

Cangar, Ö.; Aerts, J.-M.; Buyse, J., and Berckmans, D. J. P. s. (2008). Quantification of the spatial distribution of surface temperatures of broilers. 87(12), 2493-2499.

Cao, M.; Yi, Q.; Wang, K.; Li, J., and Wang, X. (2023). Predicting Ventilation Rate in a Naturally Ventilated Dairy Barn in Wind-Forced Conditions Using Machine Learning Techniques. 13(4), 837.

Choi, Y. B., Kim, J. G., Cho, J. H., Lee, S. Y., Park, S. J., Decano-Valentin, C., Jeong, D. Y., & Lee, I. B. (2023). Estimation of ventilation rate in a piglet house considering ventilation system characteristics. Biosystems Engineering, 227, 1–18. https://doi.org/10.1016/j.biosystemseng.2023.01.008

Fluent. (2008). Fluent user's guide. Fluent Inc., ver 6.3.26. Lebanon, N.H., USA.

Furlan, R.; Macari, M.; Secato, E.; Guerreiro, J., and Malheiros, E. J. J. o. A. P. R. (2000). Air velocity and exposure time to ventilation affect body surface and rectal temperature of broiler chickens. 9(1), 1-5.

Glatz, P.; Pym, R. J. P. D. R., and FAO: Rome, I. (2013). Poultry housing and management in developing countries. 24-28.

Lewus, D. C., and Both, A. J. (2022). Using Computational Fluid Dynamics to Evaluate High Tunnel Roof Vent Designs. 4(3), 719-732.

Nääs, I. d. A.; Romanini, C. E. B.; Neves, D. P.; Nascimento, G. R. d., and Vercellino, R. d. A. J. S. A. (2010). Broiler surface temperature distribution of 42 day old chickens. 67, 497-502.

Norton, T.; Grant, J.; Fallon, R.; Sun, D.-W. J. C., and Agriculture, E. i. (2010). Improving the representation of thermal boundary conditions of livestock during CFD modelling of the indoor environment. 73(1), 17-36.

Oloyo, A. J. P. S. J. (2018). The use of housing system in the management of heat stress in poultry production in hot and humid climate: A review. 6(1), 1-9.

S. R. Pawar, J. M. Cimbala, E. F. Wheeler, & D. V. Lindberg. (2007). Analysis of Poultry House Ventilation Using Computational Fluid Dynamics. Transactions of the ASABE, 50(4), 1373–1382. https://doi.org/10.13031/2013.23626

Rasheed, A., Lee, J. W., Kim, H. T., & Lee, H. W. (2019). Efficiency of Different Roof Vent Designs on Natural Ventilation of Single-Span Plastic Greenhouse. Protected Horticulture and Plant Factory, 28(3), 225–233. https://doi.org/10.12791/ksbec.2019.28.3.225

Reece, F.; Deaton, J., and Bouchillon, C. J. P. S. (1969). Heat and Moisture Production of Broilers: 1. Summer Conditions. 48(4), 1297-1303.

Simmons, J.; Lott, B., and Miles, D. J. P. s. (2003). The effects of high-air velocity on broiler performance. 82(2), 232-234.

Van Wagenberg, A.; Bjerg, B., and Bot, G. A. J. A. E. I. C. J. (2004). Measurements and simulation of climatic conditions in the animal occupied zone in a door ventilated room for piglets.

Zmrhal, V.; Svoradova, A.; Venusova, E., and Slama, P. (2023). The Influence of Heat Stress on Chicken Immune System and Mitigation of Negative Impacts by Baicalin and Baicalein. Animals, 13(16), 2564.

Effect of installing organic photovoltaic panels on the environmental performance of greenhouse tomato in Greece

Andreas Giakoumatos [a,*], Vasileios Anestis [a], Thomas Bartzanas [a], Nikolaos Katsoulas [b]

[a] Laboratory of Farm Structures, Department of Natural Resources Development and Agricultural Engineering, Agricultural University of Athens, Athens, Greece

[b] Laboratory of Agricultural Constructions and Environmental Control, Department of Agriculture Crop Production and Rural Environment, University of Thessaly, Volos, Greece

* Corresponding author. Email: vanestis@aua.gr

Abstract

The objective of this study was to assess the potential environmental benefits of installing Organic Photovoltaic (OPV) panels on the roof of a 200m^2 plastic greenhouse for tomato production in Greece while using different types of roofs. The study employs a cradle-to-greenhouse gate approach, with 1 kg of fresh tomatoes at the greenhouse gate as the functional unit and a temporal boundary of 1 year. Comparative assessments were conducted to estimate the environmental performance of the greenhouse tomato supply chain after the installation of OPV panels. The results were compared to the respective performance before the installation of OPV panels. Four systems were defined: B-OPV, which represents the situation before the installation of OPV, and A-OPV-PR, A-OPV-AR, and A-OPV-GR, which represent the situation after the installation of OPV on a pitched roof, arched roof, and gothic roof greenhouse, respectively. Various environmental impact categories were addressed, using indicators in accordance with the EU – Environmental Footprint method. The highest weighted environmental impact category indicators (EICI) regarding the total environmental score were GWP-100 (Climate change), ADP-fossil (Abiotic resource depletion - fossil fuels), and PE_{FE} (Freshwater Eutrophication). An inversely proportional relationship was observed between the electricity produced from the OPVs and the value of the EICI for these EICIs. This indicates that the higher the electricity production of the OPVs, the lower the values of the EICIs per kg of fresh tomato at the greenhouse gate. The A-OPV-PR and B-OPV systems showed the largest difference in environmental impact, with potential average variations of 15% for GWP-100, 73% for PE_{FE}, and 14% for ADP-fossils over a 25-year period. Additionally, installing OPV panels on the greenhouse roof improved the overall environmental performance of the tomato supply chain and most environmental impact indicators. Furthermore, the type of greenhouse roof was found to affect the amount of electricity generated by the OPV panels that can be fed back into the grid, thereby potentially affecting the overall annual environmental performance per kilogram of greenhouse tomatoes. These results demonstrate the potential for on-farm installation of OPV panels to decrease the environmental impact of fresh horticultural products.

Keywords: Organic Photovoltaic Panels, Environmental Performance, LCA, Greenhouse tomato supply chains, Greece

1. Introduction

In the pursuit of sustainable agricultural practices, the integration of renewable energy sources in greenhouse operations has gathered significant attention. Organic Photovoltaics (OPVs) present a promising solution for reducing the environmental impact of energy consumption in greenhouse farming (Zimmermann et al., 2012). However, the potential environmental benefits of OPVs must be carefully evaluated, particularly concerning their installation and operational effects on the supply chain of agricultural products (Zimmermann et al., 2012).

A critical aspect of this assessment is the use of OPVs for energy production within a net metering framework. This grid-connected system allows the greenhouse to utilize energy generated by OPVs (La Notte et al., 2020). The energy produced by OPVs is used primarily for greenhouse processes needs, and the extra energy is injected into the national electrical grid. When locally produced energy is insufficient to cover greenhouse needs, energy is imported from the grid. This netting process over a specific period provides a clear picture of the balance between the energy produced and consumed, highlighting the potential for renewable energy sources to reduce the environmental footprint of greenhouse operations.

Assessing the environmental impact of energy production and consumption in greenhouse farming is particularly pertinent in regions where the national grid relies heavily on fossil fuels, such as crude oil and natural gas, which contribute significantly to greenhouse gas emissions. In Greece, for instance, the dependence of public network electricity on these energy sources underscores the importance of exploring renewable alternatives such as OPVs to reduce the environmental burden of greenhouse

products' supply chains. In contrast, in countries such as France, where a notable fraction of public network electricity is derived from renewable sources, a different environmental profile for greenhouse energy consumption can be detected (Koch and Salou, 2022).

Life Cycle Assessment (LCA) is a comprehensive analytical tool used to evaluate the environmental impacts associated with all stages of a product's life cycle, from raw material extraction through production, use, and disposal (Wolf et al., 2010). This methodology provides a systematic framework for assessing the environmental performance of products and processes by considering a wide range of impact categories, such as greenhouse gas emissions, energy consumption, water use, and waste generation. By examining each phase of the life cycle, LCA enables the identification of critical areas where improvements can be made to reduce the overall environmental footprint. Through detailed quantification and analysis, LCA could help stakeholders make decisions that promote environmental sustainability and resource use efficiency in agricultural supply chains (Alhashim et al., 2021). In the context of agricultural operations, such as greenhouse tomato production, LCA could be particularly valuable for comparing their environmental profile due to different energy sources, including the integration of renewable technologies such as Organic Photovoltaics (OPVs) (Tsang et al., 2016).

This study focuses on assessing the potential environmental benefit of incorporating OPVs into a tomato greenhouse, using key environmental impact category indicators (EICIs) estimated per kilogram of tomatoes produced. It aims to use an LCA approach to compare the potential environmental performance of a greenhouse tomato supply chain utilizing electricity from OPV panels installed on the greenhouse roof versus the conventional method of consuming electricity imported from the national grid. By examining these potential environmental performances, the present study seeks to examine the potential environmental benefits and of integrating OPVs in greenhouse structures.

2. Materials and Methods

2.1. System definition

For this assessment, a typical plastic greenhouse of 200m^2 was used (width: 8m, length: 25m, and gutter height: 3.2m, roof height: 4.9m) and three types of roofs were examined: i) a pitched roof, ii) an arched roof, and iii) a gothic roof. This greenhouse was considered to operate in Central Greece and was oriented in a north–south position (Baxevanou et al., 2023). In each case, covering the greenhouse roof with OPVs (max. 50% of the roof surface) did not negatively affect the growth of the tomato crop (Baxevanou et al., 2020).

The B-OPV reference system (Table 1) includes the greenhouse tomato supply chain using the default Agribalyse dataset (Koch and Salou, 2022) as the basis, considering the Greek low-voltage electricity grid mix. The A-OPV systems include the greenhouse tomato supply chain with the OPV units installed on the greenhouse roof, for three different types of roofs (Table 1), considering:

a) the necessary OPV units to cover 50% of the roof's surface;
b) the avoided energy from the Greek low-voltage electrical grid mix;
c) the energy produced from the OPV units, according to the considered roof area covered by the OPV units (108.3 m^2).

Table 1. The scenarios examined in this study.

B-OPV system	A-OPV systems
No OPVs	OPVs Pitched Roof (A-OPV-PR)
	OPVs Arched Roof (A-OPV-AR)
	OPVs Gothic Roof (A-OPV-GR)

The A-OPV system models were run for a 25-year period, using already available data for the OPV energy production, aiming to compare the environmental performance of the A-OPV systems with the respective of the B-OPV system. The system boundaries were defined as 'cradle-to-greenhouse gate', while the functional unit as '1 kg of harvested tomato at the greenhouse gate'.

Life cycle impact assessment was conducted using environmental impact category indicators (EICIs), characterization, normalization and weighting factors in accordance with the Environmental Footprint v.3.1 methodology (Andreasi Bassi et al., 2023; Fazio et al., 2018).

2.2. Development of the greenhouse tomato life cycle model

The life cycle inventory and life cycle impact assessment stages were performed using SimaPro v.9.6.0.1 PhD (PRe-Consultants, 2023). The development of the greenhouse tomato system's life cycle model was based on a suitable life cycle inventory dataset, the conventional greenhouse for tomato growth of the Agribalyse database (Koch and Salou, 2022), covering 10,000m^2. In line with the defined system boundaries of the present study, this dataset includes the following material and energy inputs: (1) equipment for irrigation, fertilization, pest and pathogen control, heating, and harvesting; (2) the greenhouse structure and mobile machinery and (3) young plants (nursery), fertilizers (mineral and organic), growing media, active substances, water for irrigation, fuels, and energy, as well as transport to the farm. Emission outputs were further included: direct gas emissions due to fuel combustion, tire abrasion, and direct emissions from the greenhouse (emissions to air, water and soil). The temporal border is one year of tomato production.

In the databases currently available in SimaPro, there is insufficient data for modeling OPVs' supply chains. Specifically, OPV is a complicated technology, and there is insufficient data on the bill of materials (BoM) for OPV production processes, rendering the development of a representative dataset for OPVs by directly using available SimaPro background data, impossible. Therefore, the environmental analysis was carried out with additional assumptions regarding OPV's BoM, as the BoM used in the study is based on the existing literature (Tsang et al., 2016).

Different energy results are produced by OPVs in all different types of greenhouses (various A-OPV systems). These produced electricity values were used in the compilation of the A-OPV datasets. In the cases that annual electricity production exceeded the annual electricity needs, the amount equal to the electricity needs of the greenhouse tomato production was considered as an avoided input from the national grid. In the same cases, the produced energy was further considered as a product output of the greenhouse tomato production system.

Since the total electricity produced by the OPVs was assessed as a product output there were two outputs in total in the A-OPV system, electricity in kWh and fresh tomato in kg. An economic allocation approach based on the potential annual income from sold fresh tomato and sold electricity was used to determine the environmental load associated with each of these two product outflows. Since it was out of the scope of this study to assess price fluctuations for fresh tomato and electricity, a constant price throughout the years was considered for both these A-OPV system outflows.

3. Results and Discussion

The electricity needed to operate the 200 m^2 plastic greenhouse both in the B-OPV and A-OPV systems was 1,417.17 kWh/year. It was found that the produced energy from the OPVs on an annual basis exceeded this necessary electricity amount for all three types of greenhouses and all 25 years of assessment. Thus, in the A-OPV systems (for all 25 years), this amount of electricity was considered as an avoided input. As a result, there was no electricity input from the national grid (contrary to the B-OPV system), and the associated environmental load was not only neglected but an environmental benefit was estimated. On the other hand, the total electricity produced by the OPV panels (A-OPV systems) was considered as a product output from the greenhouse tomato production and the total environmental load was economically allocated to both the fresh tomato and electricity product outflows.

The potential estimates (25-year averages) of the environmental impact category indicators (per kg of fresh tomato at the greenhouse gate) for all B-OPV and A-OPV systems are presented in **Table 2**.

Table 2. Potential values for the Environmental Impact Category Indicators of the B-OPV (average annual) and A-OPV (average annual, 25-year) systems.

Environmental Impact Category Indicator	Units (per kg of fresh tomato at the greenhouse gate)	A-OPV systems			B-OPV system
		A-OPV-PR	A-OPV-AR	A-OPV-GR	
Accumulated Exceedance ($AE_{AC\text{-}T\&FW}$)	mol H+ eq	0.003	0.003	0.003	0.004
Global Warming Potential – 100 years (GWP-100)	kg CO_2 eq	1.451	1.460	1.471	1.707
Comparative Toxic Unit for ecosystems ($CTUe_{FWET}$)	CTUe	3.994	4.019	4.049	2.042

Disease Incidence due to kg of PM2.5 emitted ($DI_{PM2.5}$)	disease inc.	3.38 ×E-08	3.40 ×E-08	3.43 ×E-08	3.87× E-08
Nitrogen equivalents (NE_{ME})	kg N eq	0.002	0.002	0.002	0.002
Phosphorus equivalents (PE_{FE})	kg P eq	1.61 ×E-04	1.62 ×E-04	1.63 ×E-04	0.001
Accumulated Exceedance (AE_{TE})	mol N eq	0.008	0.008	0.008	0.009
Comparative Toxic Unit for human, cancer ($CTUh_C$)	CTUh	2.63 ×E-10	2.65 ×E-10	2.66 ×E-10	1.98 ×E-10
Comparative Toxic Unit for human, non-cancer ($CTUh_{NC}$)	CTUh	3.09 ×E-09	3.11 ×E-09	3.14 ×E-09	7.10 ×E-10
Ionizing Radiation Potential (IRP)	kBq U-235 eq	0.036	0.036	0.036	0.040
Soil Quality Index (SQI)	Pt	0.115	0.116	0.117	0.134
Ozone Depletion Potential (ODP)	kg CFC-11 eq	2.49 ×E-07	2.51 ×E-07	2.52 ×E-07	2.81 ×E-07
Photochemical Ozone Creation Potential (POCP)	kg NMVOC eq	0.002	0.002	0.002	0.002
Abiotic resource depletion – fossil fuels (ADP-fossil)	MJ	21.877	22.016	22.177	25.557
Abiotic resource depletion (ADP – ultimate reserve, ADP-UR)	kg Sb eq	1.81 ×E-05	1.82 ×E-05	1.84 ×E-05	3.45 ×E-06
m^3 of water equivalents deprived (WED)	m^3 depriv.	0.846	0.851	0.858	0.939

Error! Reference source not found. presents the % differences between the B-OPV and the three A-OPV systems for the most affected impact category indicators. The highest negative difference (**meaning that A-OPV values are increased compared to B-OPV**) was for the ADP-UR which was more than 4 times higher in the A-OPV systems than in the B-OPV system, followed by the differences for the CTU_{hNC} and the $CTUe_{FWET}$ indicators. On the other hand, the larger positive differences were observed for PE_{FE} (73%), $AE_{AC\text{-}T\&FW}$ (30%), GWP-100 (14%), POCP (14%), ADP-fossil (14%) and SQI (13%). The rest of the environmental impact category indicators also show potential, lower positive differences between the A-OPV and B-OPV systems.

Table 3. Differences (percentage) between A-OPV and B-OPV systems (D = EICIB-OPV – EICIA-OPV).

Environmental Impact Category Indicator	A-OPV-PR	A-OPV-AR	A-OPV-GR
ADP-UR	-425%	-428%	-432%
$CTUh_{NC}$	-336%	-339%	-342%
$CTUe_{FWET}$	-96%	-97%	-98%
$CTUh_C$	-33%	-34%	-35%
PE_{FE}	73%	73%	73%
$AE_{AC\text{-}T\&FW}$	30%	29%	29%
GWP-100	15%	14%	14%
POCP	15%	14%	14%
ADP-fossil	14%	14%	13%
SQI	14%	13%	13%
$DI_{PM2.5}$	13%	12%	11%
NE_{ME}	12%	12%	11%
AE_{TE}	12%	11%	10%
ODP	11%	11%	10%

IRP	10%	9%	9%
WED	10%	9%	9%

The B-OPV system is generally associated with higher or similar EICI values than the A-OPV systems (**Error! Reference source not found.**). This implies a potential improvement of the environmental performance of the greenhouse tomato production system when installing OPV panels and that the contribution that the unit process for producing the OPV panels is not important to the total indicator estimates (expressed per kg of tomato at the greenhouse gate).

The OPV material has a significant influence on the EICIs connected to negative differences between the B-OPV and A-OPV systems. $CTUe_{FWET,}$ $CTUh_{NC,}$ and ADP-UR are the most negatively influenced EICIs. These results can be explained in the case of the first two EICIs due to the indium tin oxide (ITO) material existing in the PET Lamination of the OPV which potentially increasingly affects the total hydrogen sulfite emissions. In the case of ADP-UR, the most important material flows that lead to an increase in this EICI is mainly silver (60% of total ADP-UR) which was used as an OPV construction material as well as indium tin oxide (ITO) 20% of total ADP-UR).

The total weighted environmental score (Table 4) based on all environmental impact category indicators was higher for the B-OPV system than the A-OPV systems. The impact categories with higher relative importance for the total environmental performance were climate change, resource use (fossil fuels), freshwater eutrophication, and water use (Table 4).

Table 4. Relative importance of the various environmental impact category indicators for the total environmental load of the B-OPV and A-OPV systems.

		B-OPV	**A-OPV-PR**	**A-OPV-AR**	**A-OPV-GR**
	Unit	**Total**	**Total**	**Total**	**Total**
Total (100%)	µPt	144.41	116.81	117.55	118.41
GWP-100	%	39.09	34.64	34.64	34.64
ADP-fossil	%	26.86	23.97	23.97	23.97
PE_{FE}	%	8.62	2.41	2.41	2.41
WED	%	5.72	5.37	5.37	5.37
$DI_{PM2.5}$	%	4.78	4.36	4.36	4.36
$AE_{AC\text{-}T\&FW}$	%	4.02	2.95	2.95	2.95
ADP-UR	%	3.36	18.39	18.39	18.39
NE_{ME}	%	2.50	2.29	2.29	2.29
POCP	%	1.93	1.71	1.71	1.71
AE_{TE}	%	1.60	1.47	1.47	1.47
$CTUh_{C}$	%	0.57	1.16	1.16	1.16
IRP	%	0.39	0.36	0.36	0.36
ODP	%	0.28	0.26	0.26	0.26
$CTUe_{FWET}$	%	0.20	0.28	0.28	0.28
$CTUh_{NC}$	%	0.08	0.38	0.38	0.38
SQI	%	0.01	0.01	0.01	0.01

According to the weighted results, the relative importance of $CTUe_{FWET,}$ $CTUh_{NC,}$ and ADP-UR to the total environmental score is lower than other indicators such as GWP-100, ADP-fossil, PE_{FE} and WED, resulting in a decrease in the total weighted environmental score per kg of fresh tomato at the greenhouse gate for the A-OPV systems.

The electricity produced by OPV panels (as well as the avoided electricity input from the national grid) seems to be connected to a benefit for most of the environmental impact category indicators (GWP-100, SQI, ADP-fossil, WED, $AE_{AC\text{-}T\&FW}$, $DI_{PM2.5}$, NE_{ME}, PE_{FE}, $AE_{TE,}$ POCP, IRP, ODP). The avoidance of using electricity from the national grid and the reduction in the environmental burden allocation percentage to the fresh tomato product (when injecting renewable electricity back into the national grid as a product) result in a potentially positive effect on the environmental performance of greenhouse tomato production.

The highest effect of installing OPV panels can be observed for the GWP-100 (kg CO_2-eq/kg fresh tomato at the greenhouse gate), the ADP-fossil (MJ/kg fresh tomato at the greenhouse gate) indicators, and PE_{FE} (kg P/kg fresh tomato at the greenhouse gate). For these indicators, the difference between the three A-OPV systems as well as between the A-OPV and the B-OPV systems ranges between 13% for the ADP-fossil and 73% for the PE_{FE}. The largest difference can be observed between the A-OPV-PR system and the B-OPV system where the potential differences for the 25-year average values of GWP-100, $PE_{FE,}$ and ADP-fossils are 15%,73%, and 14% respectively.

4. Conclusions

The installation of OPV panels has an aggregate positive effect on the total environmental performance of the greenhouse tomato supply chain and on the values of most of the environmental impact category indicators. This is achieved by assuming that the total amount of the produced electricity by the OPV panels returns to the grid (as an additional product of the greenhouse production process) and that an amount of electricity equal to the electricity needs of the tomato production in the greenhouse is avoided. Moreover, the additional environmental load that is imported to the system due to the OPV panels' supply chain was too low to counteract the positive effect of their installation and use. These results are highly dependent on the modelled environmental load per kWh of electricity in the national grid. Moreover, the type of greenhouse was found to affect the amount of produced electricity by the OPV panels that can be returned to the grid and therefore potentially influences the total environmental performance per kg of greenhouse tomato. The Pitched roof greenhouse (A-OPV-PR system) was associated with the highest electricity production by OPV panels and consequently linked to the highest potential differences in the environmental performance (total and per separate indicator) from the B-OPV system.

Finally, although the assumptions made influence the size of the point estimates for the environmental performance results, the installation of OPV panels on the roof of a greenhouse producing tomato seems to have a positive effect (i.e. focusing on the existence of differences) on the environmental performance of the associated fresh tomato supply chain.

Nevertheless, as OPV panels constitute an emerging technology, further research would be necessary on the assessment of the environmental impacts of horticulture products' supply chains in which OPV panels are used, using the LCA approach. More detailed Bills of Materials for OPV panels would need to be developed for LCA model development of such horticulture products' supply chain systems and more detailed LCAs (e.g. from a primary data collection point of view) would be a prerequisite for higher quality estimates of the potential benefit of using OPV panels in different types of greenhouses and horticulture products.

References

Alhashim, R, Raveendranpillai D, Aavudai, A. 2021. "Environmental Impact Assessment of Agricultural Production Using LCA: A Review" Climate 9, no. 11: 164. https://doi.org/10.3390/cli9110164.

Andreasi Bassi, S., Biganzoli, F., Ferrara, N., Amadei, A., Valente, A., Sala, S., Ardente, F. 2023. Updated characterisation and normalisation factors for the Environmental Footprint 3.1 method, EUR 31414 EN, Publications Office of the European Union, Luxembourg, ISBN 978-92-76-99069-7, doi:10.2760/798894, JRC130796.

Baxevanou, C., Fidaros, D., Katsoulas, N., Mekeridis, E., Varlamis, C., Zachariadis, A., Logothetidis, S. 2020. Simulation of radiation and crop activity in a greenhouse covered with semitransparent organic photovoltaics. *Applied Sciences (Switzerland)*, *10*(7). https://doi.org/10.3390/app10072550.

Baxevanou, C., Fidaros, D., Papaioannou, C., Katsoulas, N. 2023. Design and Optimization of a Hybrid Solar–Wind Power Generation System for Greenhouses. *Horticulturae*, *9*(2). https://doi.org/10.3390/horticulturae9020181.

Fazio, S., Castellani, V., Sala, S., Schau, EM., Secchi, M., Zampori, L., Diaconu, E. 2018. Supporting information to the characterisation factors of recommended EF Life Cycle Impact Assessment methods, version 2, from ILCD to EF 3.0, EUR 29600 EN, European Commission, Ispra, ISBN 978-92-79-98584-3, doi:10.2760/002447, JRC114822.

Koch P., Salou T. 2022. AGRIBALYSE®: Methodology, Agricultural stage – Version 3.1. – Initial version v1.0 ; 2014. Ed ADEME. Angers. France. 312 p.

La Notte, L., Giordano, L., Calabrò, E., Bedini, R., Colla, G., Puglisi, G., Reale, A. 2020. Hybrid and organic photovoltaics for greenhouse applications. *Applied Energy*, *278*, 115582. https://doi.org/https://doi.org/10.1016/j.apenergy.2020.115582.

Pre-Consultants. 2023. SimaPro 9. https://simapro.com/

Tsang, M. P., Sonnemann, G. W., Bassani, D. M. 2016 Life-cycle assessment of cradle-to-grave opportunities and environmental impacts of organic photovoltaic solar panels compared to conventional technologies. *Solar Energy Materials and Solar Cells*, *156*, 37–48. https://doi.org/10.1016/j.solmat.2016.04.024.

Wolf, M.-A., Chomkhamsri, K., Brandao, M., Pant, R., Ardente, F., Pennington, D., Manfredi, S., De, C. C., Goralczyk, M. 2010. *International Reference Life Cycle Data System (ILCD) Handbook-general guide for life cycle assessment-detailed guidance*.

Zimmermann, Y. S., Schäffer, A., Hugi, C., Fent, K., Corvini, P. F. X., Lenz, M. 2012. Organic photovoltaics: Potential fate and effects in the environment. In *Environment International* (Vol. 49, pp. 128–140). Elsevier Ltd. https://doi.org/10.1016/j.envint.2012.08.015

Wind loads on two insect-proof tunnel nethouses: Full-scale and CFD analysis

Anastasios Giannoulis [a,*], Antonis Mistriotis [a], Demetres Briassoulis [a]

[a] Department of Agricultural Engineering, Agricultural University, Athens, Greece

* Corresponding author. Email: agian@aua.gr

Abstract

Insect-proof nethouses can provide efficient protection against harmful insects and environmental hazards, and microclimate regulation in favor of protected cultivation. In this study, a full-scale experiment and CFD simulations were employed to estimate the wind pressures exerted on two neighboring low-rise insect-proof nethouses. Moreover, the airflow pattern windward, leeward, and inside the nethouses was analyzed. Two different types of novel insect-proof nets were used as covering materials: The 3353BT Biorete AirPlus 50 mesh that allowed for improved ventilation rates; and the OptiNet 50 mesh that provided optical exclusion of pests. Anemometers installed windward, leeward, and inside the insect-proof nethouses measured wind velocities at different locations. Specially designed pressure differential sensors were used to measure the wind loads at the nethouses' windward and leeward sides. The full-scale experiment was simulated through a 3D numerical model. The net coverings were simulated as porous domains of porosity and aerodynamic coefficients previously measured by wind tunnel experiments. Velocities were less retarded inside the AirPlus nethouse (Full-scale: 46%, CFD: 57%), than for the denser mesh OptiNet nethouse (Full-scale: 63%, CFD: 67%). Lower wind loads were recorded for the windward side of the enhanced ventilation technology AirPlus insect-proof net (Full-scale: C_P = 0.39, CFD: C_P = 0.46) as compared to the OptiNet net (Full-scale: C_P = 0.48, CFD: C_P = 0.54). On the contrary, at the leeward sides of the nethouses, increased wind loads were measured for the AirPlus nethouse (Full-scale: C_P = -0.28, CFD: C_P = -0.24) as compared to the OptiNet nethouse (Full-scale: C_P = -0.24, CFD: C_P = -0.23). The field experiment and numerical results were in good agreement. The numerical model was further utilized to visualize the 3D airflow pattern and the pressure distribution on the nethouses.

1. Keywords: field experiment, CFD, wind pressure, airflow pattern, **insect-proof**Introduction

The use of greenhouses as crop protection systems during summer is not possible due to high temperatures. For this reason, many vegetables are grown in unprotected open-field cultivations. However, this type of cultivation is susceptible to extreme climatic conditions and enemy insects. Over the last decade, the use of agricultural nets as means of protection and the construction of nethouses has significantly expanded. They offer protection from environmental hazards, such as hail and wind, while they moderately regulate the internal microclimate through natural ventilation, allowing for the production of improved quality and quantity and reduced irrigation and insecticide inputs.

Insect-proof nets or exclusion nets have denser mesh structures as compared to the other types of agricultural nets imposing higher resistance to the impinging airflow leading to decreased ventilation rates (Mahmood et al., 2018). As a result, increased temperature and humidity levels may develop at the nethouse interior. For this reason, net manufactures introduced innovative types of agricultural nets, such as nets with increased ventilation rates and optical exclusion nets (through additives that interfere with specific visible and UV spectrum ranges) (Giannoulis et al., 2021).

The aerodynamic behaviour of the agricultural nets can be estimated through wind tunnel experiments (Castellano et al., 2016). The interaction of the airflow with the nethouse cladding is critical since it affects several parameters such as heat, water vapour, and CO_2 exchange (Tanny et al., 2003), the interior airflow velocities (Mistriotis & Castellano, 2012) and the wind forces on the nethouse (Robertson et al., 2002). Several publications have pointed out that it is more accurate to relate the air velocity reduction caused by net-covered structures to the aerodynamic coefficients of the net than its porosity ratio (Mistriotis and Castellano, 2012). The air velocity reduction inside nethouses reported in various publications ranged between 0.2 and 0.91. This wide range was attributed to the fact that several parameters could affect the air velocity values inside a nethouse such as the net aerodynamic characteristics, the presence of vegetation, the height and density of vegetation, the locations of the anemometers, and the terrain roughness parameter z_o (Tanny, 2013)

Nethouses are lightweight structures as compared to greenhouses. They are subjected to reduced wind

loads because of their permeable character. Studies regarding wind pressures on nethouses are scarce, since the standard pressure measuring equipment is not applicable (Briassoulis et al, 2010, Giannoulis et al, 2015). Wind loads on nethouses have only been estimated through numerical analysis (CFD) (Mistriotis et al., 2012, Teitel et al., 2022) but not through full-scale or wind tunnel experimental work. Especially for wind tunnels, creating scaled nethouse models appears to be further problematic. The small-sized net fibres are impossible to be scaled down to smaller dimensions. Robertson et al., 2002 measured wind pressures on an arched and a flat roof nethouses in a large wind tunnel (scaling 1:2).

The objective of this research work was the estimation of the wind loads on two neighboring low-rise tunnel nethouses on the field and through numerical simulations. The nethouses were covered by two different novel insect-proof nets. For the field experiment, wind loads were recorded through a special configuration that allowed for the measurement of the pressure difference that occurs at the net covering. The airflow pattern windward, leeward, and inside the insect-proof nethouses was also evaluated both through field measurements and CFD analysis, in order to contribute to the limited published data regarding the airflow velocities inside and around nethouse structures. The validated 3D numerical model allowed for further analysis of the detailed airflow pattern and the pressure distribution on the nethouses.

2. Materials and Methods

2.1. Full-scale experiment

Each nethouse was a low-rise semi-cylindrical steel frame structure (tunnel) with a ridge height of 2 m, span width of 4 m, and length equal to 8 m (Figure 1, middle). Two different insect-proof nets were employed as covering materials. The OptiNet 50 mesh (Ginegar Plastic Products Ltd., Israel, OptiNet for the rest of the document) and the 3353BT Biorete 50 Mesh AirPlus (Arrigoni, Italy; AirPlus for the rest of the document). The OptiNet was installed at the northern nethouse structure (OptiNet Nethouse for the rest of the document), while the southern nethouse was covered with the AirPlus insect-proof net (AirPlus Nethouse for the rest of the document) (Figure 1, middle). The nethouses were parallel to each other. They were oriented almost perpendicular to the N-S direction, with a small deviation of 4° to the NNE-SSW direction. The nets were fixed through specially designed clips on the frame.

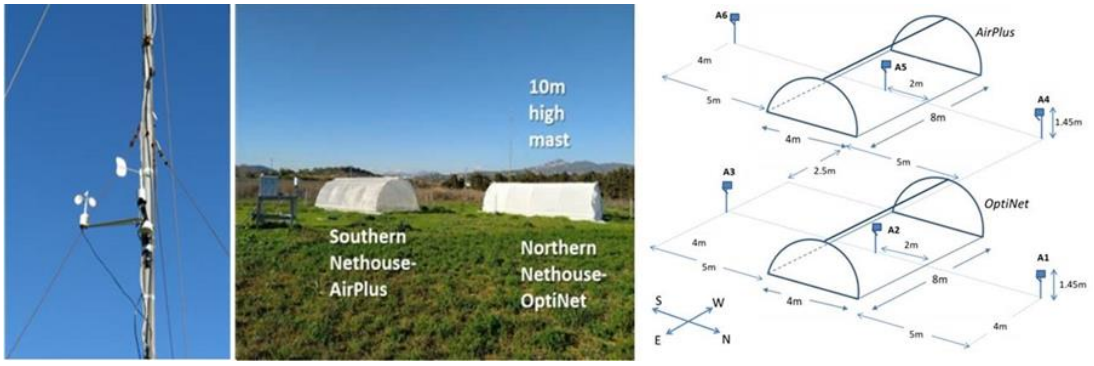

Figure 1. The anemometer and the wind vane at 4m high (left); the full-scale nethouse structures (middle); mapping of the locations of the rotary cup anemometers (right)

Eight (8) rotary cup anemometers (Vector Instruments, A100K, accuracy: 0.1 m s^{-1}) were used for the estimation of the airflow at discrete points windward, leeward, and inside the nethouses. Two of them were located on a 10 m high mast at 10 m and 4 m (M10 and M4 correspondingly, Figure 1, left and middle). The remaining six anemometers (A1-A6) were located along the centerline of each nethouse (three anemometers at each nethouse, Figure 1, right). The anemometers inside the nethouses were located at the mid-point of the interior area of the structure, while the outside anemometers were placed 5 m away from the nethouses sides. All were at a height of 1.45 m. The anemometer on the mast at 10 m height served as the reference anemometer. The rest of the anemometers were correlated to it. Wind velocity data were recorded and

analysed only for the South wind direction, which was perpendicular to the sides of the nethouses. A potentiometer wind vane was set at 4 m high to constantly monitor the wind direction (Vector Instruments, W200P, accuracy: ±2º). The anemometers on the 10 m high mast (M10 and M4) were also used for the accurate estimation of the terrain roughness parameter z_o through the logarithmic wind profile.

The total wind pressure on an agricultural net is the static pressure difference between its windward and leeward sides. For this reason, pressure differential sensors were mounted on specially designed setups (Figure 2, left). The pressure differential sensors were housed in waterproof plastic boxes used for electrical applications so that they are protected from external conditions.

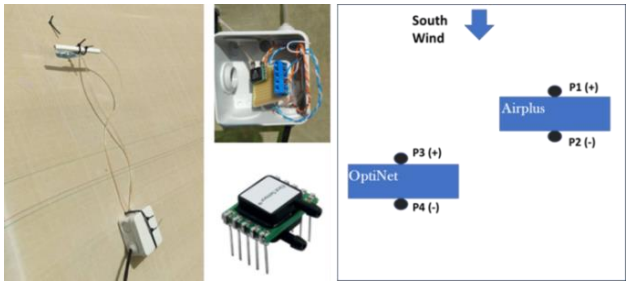

Figure 2. Configuration and installation of the pressure differential sensors (left); Waterproof box for housing the circuit board with the differential pressure sensor mounted and the LDES100B pressure differential sensor (middle); Graphical representation of the locations of the pressure differential sensors at the field (right)

The pressure differential sensors (First Sensor AG, LDES100B, Germany) were mounted and wired on a circuit board. The pressure difference was measured as the pressure difference at the two nozzles on the sensor (Figure 2, middle). Two thin elastic tubes originated from each nozzle. One was placed outside the nethouse and the other at its interior at the same height. Both tubes were placed inside secondary rigid plastic tubes so that their open end would constantly be perpendicular to the airflow that passed through the agricultural net (bleed flow). The sensor was bilinear (could measure both positive and negative pressure differences) and the measurements could range between -100 Pa to 100 Pa. Its accuracy was equal to ± 0.4 % of reading and could be operational for temperatures between -20 ºC to 80 ºC and relative humidity up to 97 %.

Four similar devices measuring net pressure were installed at each side of the two nethouses (two sensors for each nethouse, P1, P2 for the AirPlus nethouse; P3, P4, for the OptiNet nethouse, (Figure 2, right) at their mid-length (4 m) and at a height equal to 1.5 m from the ground. The waterproof boxes were secured on the net covering 0.3 m below the tubes so that they would not disturb the incoming flow (Figure 2, left). The elastic tubes were installed so that at the nethouses windward and leeward side the pressure would correspondingly be positive (overpressure, (+)) and negative (suction, (-)) (Figure 2, right).

Net pressure coefficients (C_P) were estimated by Eq. 1, where: ΔP (Pa) was the the measured air pressure drop at the insect-proof net coverings, ρ was the air density (equal to 1.2 kg m^{-3}), V_{ref} was the velocity of the wind at the reference height of the structure (equal to the nethouses ridge height, 2 m). The wind velocity at the reference height could be calculated from the logarithmic wind profile.

$$C_P = \frac{\Delta P}{\frac{1}{2}\rho V_{ref}^2} \qquad (1)$$

2.2. CFD model

A numerical model has been employed in order to represent the full-scale experiments. A 3D model was created in order to simulate the interaction of the wind with the two insect-proof nethouses. The nethouses were assumed to be enclosed by a parallelepiped wind tunnel domain (field domain). The model wind tunnel size was 200m, 15m and 100m along the x, y and z directions respectively. The nethouses were accurately modelled based on their geometrical characteristics and their configuration at the experimental field.

The finite volume mesh consisted of both 3D tetrahedral and hexahedral elements. The hexahedral elements were used for the nethouses interior domains, while for the remaining domains (insect-proof nets,

wind tunnel) the mesh was formed by tetrahedral elements (Figure 3). This combination was preferred because the mesh could be easier formulated, refinement was improved and better quality results and faster convergence could be achieved.

Three mesh refinement layers were used (Figure 3, right) for the numerical simulation. Mesh structure was finer close to the studied structures, in order to accurately simulate the interaction of the impinging wind with the insect-proof nethouses. The 3D mesh consisted of 14.5 million elements and 3.3 million nodes. Further mesh refinement did not affect significantly the results.

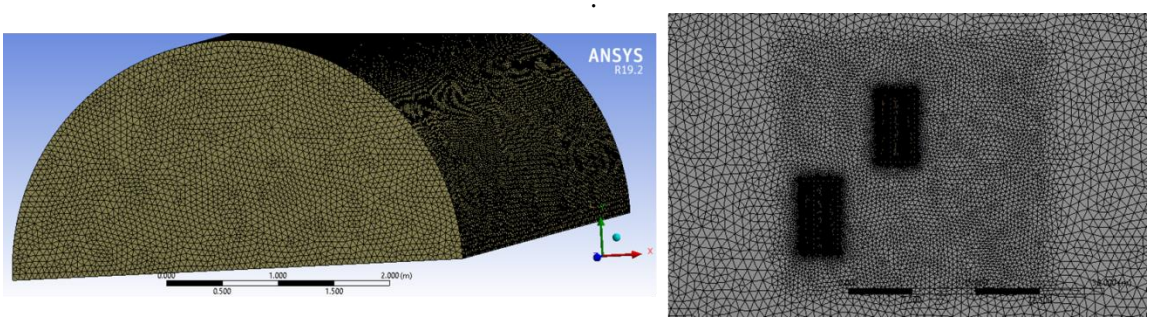

Figure 3. The insect-proof net domain mesh (left); Three different mesh layers (right)

Permeable materials (insect-proof nets) were numerically simulated using the Forchheimer's equation (Lage, 1998). The pressure drop across a porous material of thickness Δx (m) is expressed by the following equation:

$$\Delta P = \alpha V^2 + \beta V \qquad (2)$$

The parameters α (kg m^{-3}) and β (kg m^{-2} s^{-1}) in Eq. (2) are the aerodynamic coefficients which are representative for each porous material. They are also known as the linear (β, multiplied to V) and the quadratic (α, multiplied to V2) aerodynamic coefficients. The basic aerodynamic characteristics of the insect-proof nets, namely the porosity and the aerodynamic coefficients are shown in Table 1 as measured at Giannoulis et al., 2021. These values served as input for the setup of the domains that represented the net coverings (thickness: Δx = 0.05 m) at the numerical model.

Table 1. Aerodynamic characteristics of the installed insect-proof nets

		Laboratory Results		*Numerical Model Input*	
Net (name)	*Porosity (%)*	*α (kg m^{-3})*	*β (kg m^{-2} s^{-1})*	*a/Δx (kg m^{-4})*	*β/Δx(kg m^{-3} s^{-1})*
AirPlus	53.4	1.220	1.586	24.40	31.72
OptiNet	38.7	2.591	2.010	51.82	40.20

The standard *k-ε* turbulence model was selected. The wind velocity profile was set to be logarithmic at the inlet of the wind tunnel, where the velocity V_z of the wind at a height *z* is given by Eq. 4.

$$V_z = \frac{u_*}{K} ln\left(\frac{z}{z_0}\right) \qquad (4)$$

$$k = \frac{u_*^2}{\sqrt{C_\mu}} \qquad \varepsilon = \frac{u_*^2}{K(z+z_0)} \qquad (5)$$

Where z (m) is the height, V_z (m s^{-1}) the velocity at height z, u_* (m s^{-1}) the friction velocity, z_o (m) the terrain roughness and K is the von Karman constant (=0.41). Inlet boundary conditions should also provide profiles for the turbulent characteristics of the wind, namely the turbulent kinetic energy k (m^2 s^{-2}) and the

dissipation of the turbulent kinetic energy ε (m s^{-2}) (Eq. 5). Inlet velocities up to 7 m s^{-1} (at 10 m height) where examined through the numerical model. At the lower wall it was assumed that wall boundary conditions existed. At the outlet of the wind tunnel the pressure was set to zero to simulate the open wind tunnel end. Finally, the upper and side walls of the wind tunnel were set as frictionless barriers (free slip condition), so only the vertical wind velocity component was set equal to zero. The residuals target was set at 10^{-5}. Convergence at 10^{-6} was also tested but the results were insignificantly affected.

3. Results and Discussion

3.1. Airflow Pattern

Figure 4 (left) presents the correlation of the data between the anemometers M10 and M4 mounted at the 10 m high mast. Using Eq. 4 the terrain roughness parameter z_o was calculated equal to 0.07 m.

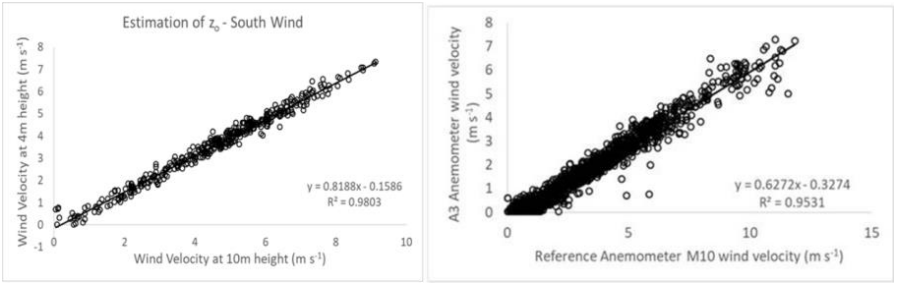

Figure 4. Correlation of the M10 and M4 anemometers for the estimation of z_o (left); correlation of the ground anemometer A3 and M10 (right)

Velocity ratios of the A1-A6 ground level anemometers with the 10 m high reference anemometer M10 for the full-scale experiment are given in Table 2. Wind velocity ratios were similar, as expected, for the windward anemometers of the nethouses (A6/M10=0.61, A3/M10=0.63 (Figure 4, right)). The wind velocity ratios decreased at the interior of both nethouses as the wind passed through the insect-proof net claddings (A5/M10 = 0.33, A2/M10 = 0.23). The wind velocity reduction was more significant for the OptiNet (anemometer A2 - 63% air velocity reduction) than for the AirPlus (anemometer A5 - 46% air velocity reduction) because of the latter's increased ventilation rates.

Table 2. Wind velocity ratios comparison between the full-scale data and the numerical simulation

SOUTH WIND	**Wind Velocity Ratios**					
Correlated anemometers	$\frac{A6}{M10}$	$\frac{A5}{M10}$	$\frac{A4}{M10}$	$\frac{A3}{M10}$	$\frac{A2}{M10}$	$\frac{A1}{M10}$
Full Scale	0.61	0.33	0.22	0.63	0.23	0.24
Numerical Model	0.63	0.27	0.21	0.67	0.22	0.17

Table 2 also provides the corresponding wind velocity ratios from the numerical analysis. Results appear to be in very good agreement for all cases, providing air velocity reduction equal to 57% (AirPlus Nethouse) and 67% (OptiNet nethouse).

The validated model allowed for further analysis of the airflow vector field. Figure 5 presents 3D numerical results regarding the velocity vectors around the insect-proof nethouses at an X-Z plane and an X-Y plane for the windward (AirPlus) and the leeward (OptiNet) nethouse. The air impinges on both nethouses, passes through the interior, and exits from their leeward net-covered sides. The wind velocity appears to drop right after it exits the nethouses (blue-colored vectors) and recovers afterwards tending to reach the initial (undisturbed) velocity. On the other hand, the wind that does not penetrate the nethouses accelerates at the nethouses sides and roof (Figure 5, left and middle, orange/red colored vectors).

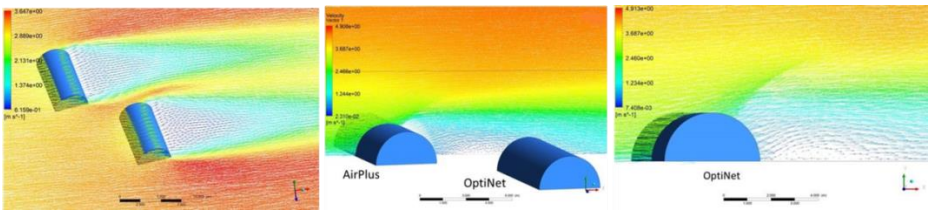

Figure 5. The airflow pattern at a: X-Z plane (left); X-Y plane for the windward nethouse (middle); X-Y plane for the leeward nethouse (right)

However, at the X-Y plane airflow pattern, leeward of the OptiNet nethouse (Figure 5, right) a small recirculation is formed, which is an indication of increased turbulence. This can be initially attributed to the less aerodynamic behavior of the OptiNet insect-proof net as compared to the AirPlus net. Further analyzing the 3D airflow pattern, it appears that a significant portion of the airflow that impinges on the nethouses becomes bleed flow (passes through), and the remaining airflow shifts towards the ridge and the sides of the nethouse structures. The airflow from the ridge, the sides, and the nethouse interior meet at the leeward of structure and compose the airflow presented in Figure 5. The wind impinges on the OptiNet nethouse after it has already interacted with the AirPlus nethouse (windward nethouse). Additionally, the wind velocity increases at certain locations (in between the two nethouses). For these reasons, the wind around the OptiNet nethouse becomes more complex.

3.2. Wind Pressure

Figure 6 presents the relationship between the pressure differential sensors measurements and the wind velocity at 10 m high for both the field experiment and the CFD model. For the field experiment, very high wind velocities due to wind gusts were not considered. The regression lines given in the graphs of Figure 6 are represented by quadratic equations as expected since the pressure (P) / velocity (V) relationship is quadratic ($P \sim V^2$). In all cases, the regression lines showed zero pressures for zero velocities, confirming that the pressure differential sensors were calibrated and configured properly.

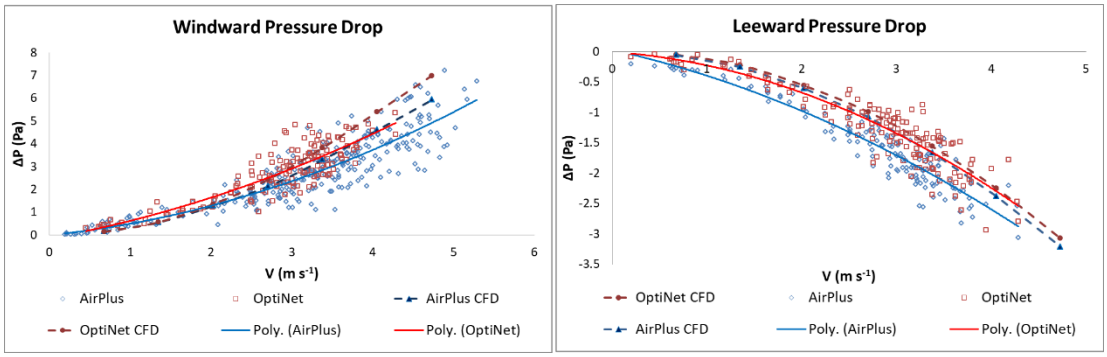

Figure 6. Full-scale and numerical results for the windward and leeward pressure drop at the nethouses

For the windward pressure sensors of the field experiment, the quadratic regression lines show that wind loads were calculated to be higher for the OptiNet nethouse (red continuous line) as compared to the AirPlus nethouse (blue continuous line). This was also the case for the numerical simulation results (OptiNet: red discontinuous lines; AirPlus: blue discontinuous lines). This confirms that the wind loading was higher for the less porous OptiNet nethouse, as expected. However, as shown in Figure 6, the regression lines for the leeward nethouses' sides showed that wind loading was higher for the AirPlus nethouse (in agreement with the measured air velocity ratio). Comparison between the experimental and the numerical results for the air pressure drop was very good, as shown in Figure 6, further validating the numerical model.

Analysis of the experimental data showed that the C_P measurements converged toward a constant value at velocities higher than 3.5 m s^{-1} at the reference height (2 m). For this reason, the proposed design C_P values

were calculated as averages over the set of air velocities at reference height that exceed this threshold. For the numerical model the C_P was also estimated for similar range of velocities at 2 m height. Both analyses results appear in Table 3. As expected, windward average C_P values were positive (inward), while the corresponding leeward values were negative (outward). The windward average C_P was higher for the OptiNet nethouse (Full scale: C_P = 0.48; CFD: 0.54) than the AirPlus nethouse value (Full scale: C_P = 0.39; CFD: 0.46) because of its denser mesh imposing higher air pressure drop and thus a higher average C_P value. At the leaward side, the average C_P value was higher for the AirPlus nethouse (Full scale: C_P = -0.28; CFD: -0.24) than the OptiNet nethouse (Full scale: C_P = -0.24; CFD: -0.23). This can be explained by the lower indoor air velocity, observed in the OptiNet nethouse, which results in a lower net pressure coefficient at the leeward side of the nethouse. Average C_p results between the experiment and the CFD simulation were also in good agreement.

Table 3. Average net pressure coefficients C_P.

	Average C_P	
Analysis	Windward	Leeward
	AirPlus Nethouse	
Full-scale	0.39 ± 0.09	-0.28 ± 0.04
Numerical	0.46 ± 0.02	-0.24 ± 0.00
	OptiNet Nethouse	
Full-scale	0.48 ± 0.07	-0.24 ± 0.04
Numerical	0.54 ± 0.03	-0.23 ± 0.00

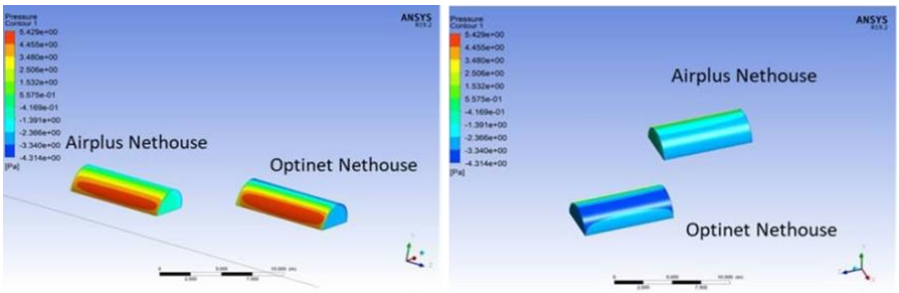

Figure 7. Wind pressure contours windward (left) and leeward (right) of the nethouses

Figure 7 presents the pressure distribution on the windward and leeward sides of the nethouses. The wind pressure was higher at the lower part of the windward side of the nethouses, while it became smaller close to their ridge. Because of the nethouses semi-circular geometry, the air that impinges close to the ridge was mostly directed above the nethouses. For the OptiNet nethouse the highest wind pressure contour (red coloured) expanded at a larger area and conforming the previous average C_p results.

For the entire leeward side of the AirPlus nethouse the wind pressure was higher and constant (light blue contours). For the OptiNet nethouse the wind pressure varies from the lower to the upper leeward side (light blue, higher negative pressure; dark blue contours, lower negative pressure). This was also a proof of higher negative pressures at the leeward side of the AirPlus nethouse as compared to the OptiNet nethouse leeward pressures.

4. Conclusions

A full-scale experiment and numerical simulations were carried out regarding two small low-rise neighbouring insect-proof nethouses. The nethouses were covered by innovative agricultural nets as cladding materials, namely an enhanced ventilation technology (AirPlus) and an optical exclusion insect-proof net (OptiNet). The ventilation efficiency and the wind pressures on these structures were studied. Specifically, the indoor air velocity dropped to 63 % (full-scale) and 67 % (CFD) of the wind velocity at the same height

(1.45 m above the ground) for the denser OptiNet insect-proof net, while for the AirPlus net the corresponding decrease was equal to 46 % (full scale) and 57 % (CFD). Nevertheless, the net coverings allowed for wind velocity reduction at the nethouses interior that confirmed their protective character against potential cultivation damages from strong winds.

The increased ventilation (low aerodynamic coefficients) of AirPlus net allowed for decreased wind pressures at the AirPlus nethouse windward side as compared to the OptiNet nethouse. The OptiNet insect-proof net has a mesh structure and aerodynamic behaviour similar to typical insect-proof nets. Its manufacturing novelty is based on the incorporated insect disorienting additives. This means that instead of a 50-mesh net (such as the one used here), a 40-mesh net could be used, since less enemy insects would reach the nethouse. Using a 40-mesh OptiNet insect-proof net is the next step of this experimental work. On the other hand, leeward pressures where smaller for the OptiNet nethouse due to the decreased velocities to its interior. These results are critical and should be taken into account for the design of nethouses using this type of cladding materials.

A good agreement was observed between experimental and numerical results regarding the wind velocities and pressures around the nethouse structures, validating the numerical model. Further 3D numerical analysis showed that the interaction of the incoming wind with two insect-proof nethouses close to each other exhibited complex airflow pattern, especially leeward of the OptiNet nethouse where an eddy was formed. The 3D pressure distribution on the windward and leeward sides of the nethouses was also indicative of the average C_p results.

The innovative pressure differential sensors used in the current experiment could be further used for the estimation of wind loads on large nethouse structures. The net pressure coefficients, measured in the present study, could be used for design purposes of similar tunnel-type nethouses.

Acknowledgements

This research was implemented within the framework of the research project «Integrated design methodology for innovative insect-proof nethouse systems for high-value horticultural production in Greece -SmartNethouse» (code:865) supported by the Hellenic Foundation of Research and Innovation (HFRI) of the General Secretariat of Research and Technology (GSRT).

References

Anti-insect (polysack) nets, Ginegar, (2021).

Biorete ® Air Plus insect screen, Arrigoni, (2018).

Briassoulis, D., Mistriotis, A., & Giannoulis, A., (2010). Wind forces on porous elevated panels. *Journal of Wind Engineering and Industrial Aerodynamics, 98, 919-928.*

Castellano, S., Scarace, G., De Pascalis, L., Lippolis, M., & Scarascia-Mugnozza, G. (2016). Experimental results on air permeability of agricultural nets. *Journal of Agricultural Engineering, 542, 134-141*.

Giannoulis, A., Briassoulis, D., & Mistriotis, A., (2015). Design and analysis of the response of elastically supported wind-break panels of two different permeabilities under wind load. *Biosystems Engineering, 129, 57-69.*

Giannoulis, A., Briassoulis, D., Papardaki, N. G., & Mistriotis, A., (2021). Evaluation of insect-proof agricultural nets with enhanced functionality. *Biosystems Engineering, 208, 98-112.*

Lage, J.L. (1998). The Fundamental Theory of Flow through Permeable Media from Darcy to Turbulence, in Transport Phenomena in Porous Media, 1-31, edited by D.B. Ingham & I. Pop, Pergamon Press, Oxford.

Mahmood, A., Hu, Y., Tanny, J., & Asante, E. A. (2018). Effects of shading and insect-proof screens on crop microclimate and production: A review of recent advances. *Scientia Horticulturae, 241, 241-251*.

Mistriotis, A., & Castellano, S., (2012). Airflow through net covered tunnel structures at high wind speeds. *Biosystems Engineering, 113, 308-317.*

Tanny, J., Cohen, S., & Teitel, M. (2003). Screenhouse microclimate and ventilation: an experimental study. *Biosystems Engineering, 84, 331-341.*

Tanny, J., Haijun, L., & Cohen, S. (2013). Airflow characteristics, energy balance and eddy covariance measurements in a banana screenhouse. *Agricultural and Forest Meteorology, 1-2, 105-118.*

Teitel, M., Ozer. S., & Mendelovich, V. (2022). Airflow temperature and humidity patterns in a screenhouse with flat insect-proof screen roofand impermeable walls – Computational fluid dynamics (CFD) results. *Biosystems Engineering, 214, 165-176.*

Microclimate conditions in two insect-proof tunnel nethouses with tomato cultivation: Full-scale and CFD analysis

Anastasios Giannoulis [a,*], Antonis Mistriotis [a], Demetres Briassoulis [a]

[a] Department of Agricultural Engineering, Agricultural University, Athens, Greece

* Corresponding author. Email: agian@aua.gr

Abstract

Nethouses can be considered as intermediate low-cost technology for protected crops between greenhouse and open-field cultivation. The inherent properties of the net cladding allow them to provide passively controlled conditions by modifying the exchange rates of mass, and radiation between the crop and the environment. Insect-proof nets have lower porosity as compared to the other types of nets and may impose decreased ventilation rates, and thus, increased temperatures and relative humidity (RH) inside the nethouse.

A field experiment of two single-span small-sized tunnel nethouses with tomato cultivation, each with a different insect-proof net covering (OptiNet 50 mesh, porosity: 53.4%; Biorete 50 Mesh AirPlus, porosity: 38.7%) was carried out. The 50 mesh Airplus net allowed for increased ventilation through its thinner-thread configuration. Temperature and RH levels at the interior of the insect-proof tunnel nethouses were recorded through full-scale experiments. Results were compared to the field temperature and RH values. A CFD model representing the field experiment was also employed for the estimation of the microclimatic parameters.

Results showed that for high wind velocities the temperatures inside the nethouses were almost equal to the ambient temperatures (convection becomes dominant). For low wind velocities, the highest average daytime temperature increased by 1.1^{o}C for the nethouse covered with the denser mesh OptiNet 50 mesh net and equal to 0.9^{o}C for the 50 mesh Airplus net covered nethouse. RH measurements were similar to the ambient RH values. The highest daytime average RH difference was equal to 2% for the nethouse with the OptiNet 50 mesh net, while most of the indoor RH recordings differed from the ambient ones by less than 1%. CFD results were in good agreement with the full-scale measurements. In addition, a detailed CFD analysis of the distribution of the temperature and the RH in the interior of the nethouses is presented.

Keywords: field experiment, CFD, temperature, relative humidity, tomato plants

1. Introduction

The use of agricultural nets as a means of protection steadily expanded over the last decade. One of their most common applications is their use as covering materials for nethouses. Nethouses are lightweight, low-cost structures that use two types of agricultural nets as cladding materials, namely shading and insect-proof nets. They can be an alternative to the summer open-field cultivations which are prone to significant damage due to excessive solar radiation, strong winds, and enemy insects. Nethouses offer regulation of their interior climate through their naturally ventilated permeable cladding. They decrease the incoming solar regulation and/or prohibit even the smallest insects from entering the protected cultivation area. They also exhibit an environmentally friendly character, since the requirements for irrigation and insecticide inputs significantly decrease compared to greenhouses or open-field cultivations.

Increased temperatures and RH at the interior of the insect-proof nethouses have been reported to be a significant disadvantage, especially during the summer period caused by low ventilation levels (Tanny et al., 2003). The mesh of insect-proof nets is denser in comparison to other commercial types of agricultural nets reducing the exchange of air mass of the structure with the environment (Mahmood et al., 2018). As a result, increased levels of temperature and humidity may develop at the nethouse interior. Lately, net manufacturing companies introduced innovative types of nets in order to alleviate such issues (Giannoulis et al., 2021).

The objective of this research work was the estimation of the temperature and RH levels at the interior of two neighboring low-rise tunnel nethouses on the field. A 3D numerical model representing the field experiment was also employed for this reason. The nethouses were covered by two different novel insect-proof nets. The nethouses and the environment temperatures and RH values were compared so that the efficiency of the nethouses regarding their microclimate would be investigated. After the validation of the 3D numerical model, the 3D distribution of temperatures and RH at the nethouses' interior was examined.

2. Materials and Methods

2.1. Full-scale experiment

The nethouses were low-rise tunnel-type structure structures. Their ridge was at a height of 2 m, their span width was 4 m, and their length was equal to 8 m (Figure 1, middle). Two different insect-proof nets were used as covering materials. The OptiNet 50 mesh (Ginegar Plastic Products Ltd., Israel, OptiNet for the rest of the document) and the 3353BT Biorete 50 Mesh AirPlus (Arrigoni, Italy; AirPlus for the rest of the document). The OptiNet was installed at the northern nethouse structure (OptiNet Nethouse for the rest of the document), while the southern nethouse was covered with the AirPlus insect-proof net (AirPlus Nethouse for the rest of the document) (Figure 1, middle). The nethouses were parallel to each other with an almost perpendicular orientation to the N-S direction (small deviation of 4^o to the NNE-SSW).

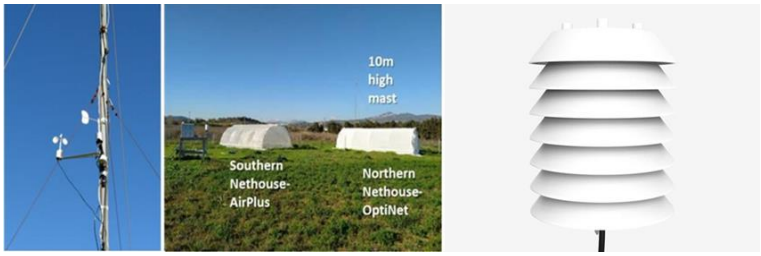

Figure 1. The anemometer and the wind vane at 4m high (left); the full-scale nethouse structures (middle); The temperature and relative humidity sensor ATMOS 14 (right)

Two (2) rotary cup anemometers (Vector Instruments, A100K, accuracy: 0.1 m s^{-1}) were located on a 10 m high mast at 10 m and 4 m (M10 and M4 correspondingly, Figure 1, left). Wind velocity data were recorded and analysed only for the South wind direction, which was perpendicular to the sides of the nethouses. A potentiometer wind vane was set at 4 m high to constantly monitor the wind direction (Vector Instruments, W200P, accuracy: ±2^o). The anemometers on the 10 m high mast (M10 and M4) were used for the accurate estimation of the terrain roughness parameter z_o through the logarithmic wind profile (Eq. 4).

Temperature and RH values were monitored by special sensors (Meter Group, Inc., ATMOS 14, accuracy: RH ±2%, temperature ±0.2^{o}C, Figure 1, right). Three sensors were used. All were at a height of 1.45 m. Two of them were inside each of the nethouse structures and one monitored the field temperature and RH. The temperature and RH data recorded at the interior of the nethouses were compared to the measurements of the outside probe for the nethouses with tomato cultivation. Recordings were averages of five (5) 1-min measurements.

The solar radiation (W m^{-2}) was measured with two full spectrum range pyranometers (Kipp & Zonen, CMP6b, accuracy: <4 %). One was installed in turns at the interior of the two nethouse structures, while the second was located outside in order to measure the total incoming solar radiation. Monitoring the ambient and the nethouses' interior solar radiation allowed for estimating the net shading factor of the structure.

2.2. CFD model

The nethouses were assumed to be enclosed by a 3D parallelepiped wind tunnel domain (field domain). The model wind tunnel size was 340 m, 15 m, and 100 m along the x, y, and z directions respectively (Figure 1, left). The nethouses were accurately modelled based on their actual geometrical characteristics and their configuration at the experimental field. The tomato plants inside the nethouses were simulated as continuous porous volumes (porous domains). They were 1.6 m high, 0.4 m thick, and 7.6 m long (Figure 1, right). Two more domain (volume) types existed, namely the insect-proof net and the nethouse interior domains.

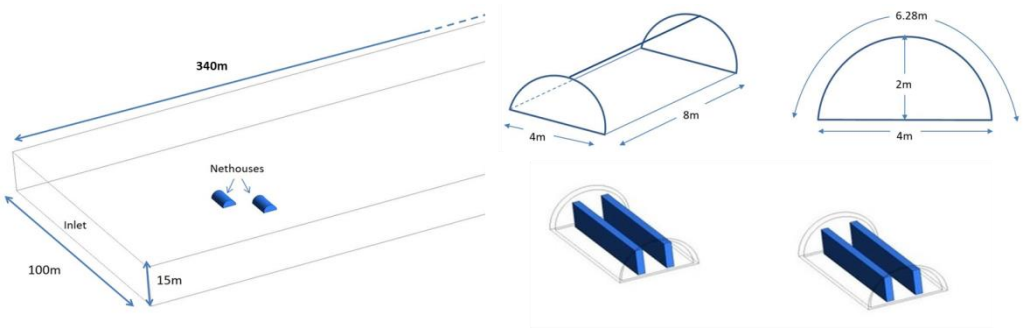

Figure 2. The field domain (left); the nethouses geometrical characteristics and the tomato plants domains inside the nethouses (right)

The finite volume mesh consisted of both 3D tetrahedral and hexahedral elements. The hexahedral elements were used for the insect-proof nets and the tomato plants domains, while for the remaining domains (nethouses interior, wind tunnel) the mesh was formed by tetrahedral elements (Figure 3). This combination was preferred because the mesh could be easier formulated and faster convergence could be achieved. The mesh structure was finer close to the studied structures in order to accurately simulate the airflow, the temperature, and RH values. The 3D mesh consisted of 2.9 million elements and 0.6 million nodes. Further mesh refinement had an insignificant impact on the results.

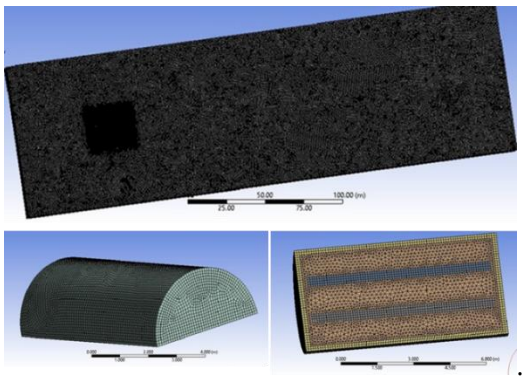

Figure 3. The field domain mesh (up); the insect-proof net and tomato plants mesh (down)

Table 1. Aerodynamic characteristics of the installed insect-proof nets

		Laboratory Results		*Numerical Model Input*	
Net (name)	*Porosity (%)*	*α (kg m^{-3})*	*β (kg m^{-2} s^{-1})*	*a/Δx (kg m^{-4})*	*β/Δx(kg m^{-3} s^{-1})*
AirPlus	53.4	1.220	1.586	6.10	7.93
OptiNet	38.7	2.591	2.010	12.96	10.05

Permeable materials (insect-proof nets) were numerically simulated using the Forchheimer's equation (Lage, 1998). The pressure drop across a porous material of thickness Δx (m) is expressed by Eq. 1:

$$\Delta P = \alpha V^2 + \beta V \qquad (1)$$

The parameters α (kg m^{-3}) and β (kg m^{-2} s^{-1}) in Eq. (1) are the aerodynamic coefficients, representative for porous materials. The porosity and the aerodynamic coefficients are shown in Table 1 as measured at

Giannoulis et al., 2021. These values served as input for the setup of the domains that represented the net coverings (thickness: Δx = 0.2 m) at the numerical model.

The tomato plants also acted as a momentum sinks, similarly to the net cladding. They were simulated using Eq. (2) where C_d was the Drag Coefficient of the tomato plants and LAD was their Leaf Area Density:

$$\frac{\Delta P}{\Delta x} = -\rho C_d LAD\, V^2 \ , \quad a = -\rho C_d LAD \qquad (2)$$

From values reported in the literature regarding full grown tomato plants, it was chosen that: C_d = 0.28 and LAD = 2.26 (Teitel et al., 2022). This way the quadratic aerodynamic coefficient α (kg m^{-3}), similar to the Forchheimer Equation could be calculated equal to α=0.76.

Water vapor and heat exchange between the tomato plants and the ambient air were also modeled. Part of the total incoming solar radiation would be absorbed or reflected by the insect-proof nets based on their shading factor, which was calculated by the pyranometers' data (radiation absorbed to total incoming radiation, equal to: 11.1 %, Airplus nethouse; 39.9 %, Optinet nethouse). The numerical model simulated the conditions for a day with low wind velocities, increased temperatures, and low RH (average wind velocity at 10 m height: 1.8 m s^{-1}, average daytime temperature of 35.16ºC, and RH =30 %), where the average daytime incoming solar radiation was measured to be equal to 700 Wm^{-2}. From this value and the measured shading factors the heat flux from the net cladding (set as source) to the nethouse interior could be estimated (Table 2). The insect-proof nets were set as the single heat source of the nethouses' interior in the numerical model.

The heat provided by the net to the nethouse interior would result in the sensible heat inside the nethouses (H_{sens}), the latent heat absorbed by the tomato plants (H_{lat}), and the heat absorbed by the soil (H_{soil}). The energy balance is given by Eq. 4:

$$H_{net} = H_{sens} + H_{lat} + H_{soil} \qquad (4)$$

Table 2. Numerical model inputs for the aerodynamic coefficients and heat sources/sinks for the net covering, the tomato plants canopy and the soil.

	Nets		***Canopy***			***Soil***
Nethouse	*Heat source (Wm^{-2})*	*Shading Factor (%)*	*α (kg m^{-3}) for tomato plants*	*H_{lat} (Wm^{-2})*	*Water Vapor production rate (kg $m^{-2}s^{-1}$)x 10^{-6}*	*H_{soil} (Wm^{-2})*
AirPlus	622.3	11.1	0.76	-41.8	6.32	-6
OptiNet	420.7	39.9	0.76	-41.8	6.32	-6

The soil surface was modeled as a heat sink, the tomato plants canopy also acted as a heat sink and a water vapor source due to its transpiration. Based on literature data (Teitel et al., 2022) these values are given in Table 2 which summarizes all the sources/sinks and the quadratic aerodynamic coefficients that were used as input for the numerical simulation setup.

The standard *k-ε* turbulence model was selected. The wind velocity profile was set to be logarithmic at the inlet of the wind tunnel (1.8 m s^{-1} at 10 m height), where the velocity V_z of the wind at a height *z* is given by Eq. 4.

$$V_z = \frac{u_*}{K} ln\left(\frac{z}{z_0}\right) \qquad (4)$$

$$k = \frac{u_*^2}{\sqrt{C_\mu}} \qquad \varepsilon = \frac{u_*^2}{K(z+z_0)} \qquad (5)$$

Where z (m) is the height, V_z (m s^{-1}) the velocity at height z, u_* (m s^{-1}) the friction velocity, z_o (m) the

terrain roughness and K is the von Karman constant (=0.41). Inlet temperature and RH were set equal to 35.16ºC and 30 %, respectively. Gravitational forces were taken into account and the Boussinesq model was applied. Inlet boundary conditions should also provide profiles for the turbulent characteristics of the wind (Eq. 5). At the lower wall it was assumed that wall boundary conditions existed. At the outlet of the wind tunnel, the pressure was set to zero to simulate the open wind tunnel end. Finally, the upper and side walls of the wind tunnel were set as frictionless barriers (free slip condition), so only the vertical wind velocity component was set equal to zero. The residuals' target was set at 10^{-5}.

3. Results and Discussion

3.1. Daytime Field Temperatures

Selected data recorded for a 12-day period (8 to 20 August 2021) are presented, for the tomato cultivation at its full growth. For this period of the year, the sun rises at 6:40 am and sets at approximately 8:20 pm. For this study, the daytime was assumed the time-span from 07:00 am to 8:00 pm.

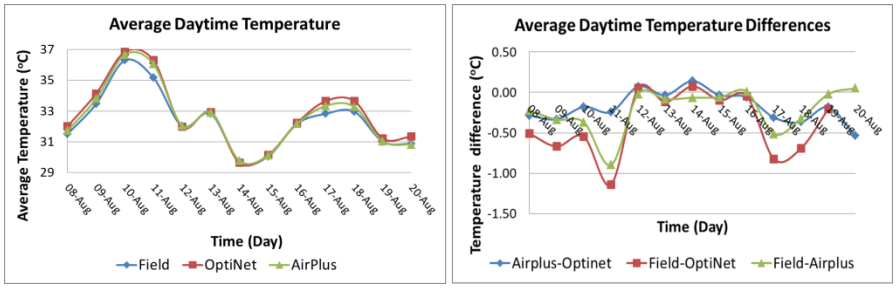

Figure 4. Daytime average temperature variation outside and inside the nethouses (left); daytime average temperature difference variation between the nethouses and the outside temperature (right).

Figure 4 presents the average daytime temperature and temperature difference variations. Higher average temperatures were observed at the interior of the Optinet nethouse (highest: 36.85ºC, 10th of August). Average temperature differences were estimated to be insignificant between the nethouses and the field (less than 0.5ºC) except for specific days and mostly between the Optinet nethouse and the field temperatures (highest: 1.1ºC, 11th of August). The average temperature differences between the two nethouses were also small, around 0.5ºC. For the differences between the field and the Airplus nethouse average temperature recordings did not exceed the value of 0.5ºC except for the 11th of August when this value was equal to 0.9ºC.

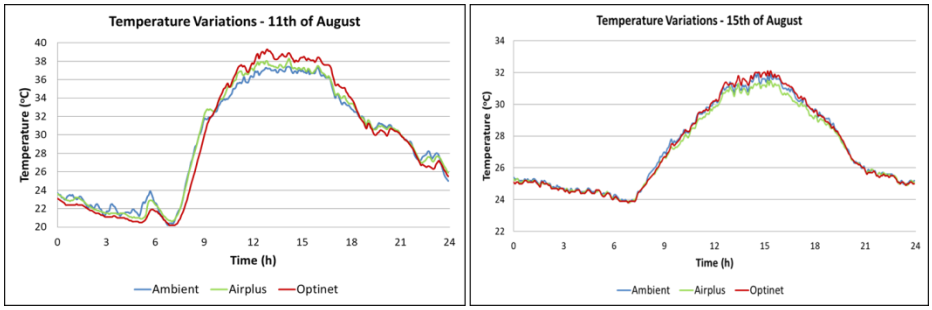

Figure 5. Daily temperature variation: 11th of August (left); 15th of August (right)

The average daytime temperatures graphs in Figure 4 appear to be very similar for the 12th to the 16th of August, while for 8th to 11th of August, the average temperatures inside the nethouses (mostly for the OptiNet nethouse) were higher. For high wind velocities the average daytime temperatures at both nethouses are similar to the field average temperatures, since the airflow convection becomes dominant and the air mass flow from the environment to the small-sized nethouses is constant and rapid. For lower wind velocities, air convection is less significant and temperatures show an increase, especially at the interior of the Optinet nethouse. The Airplus nethouse with an enhanced ventilation technology cladding (AirPlus net) allows for

higher ventilation rates even for low values of wind velocity.

The 11th of August was a day of high temperatures (average field temperature: 35.16ºC) and low wind velocities (average wind velocity at 10m high: 1.8 m s^{-1}) while the 15th of August was a day of –at that time of year- regular temperatures (average field temperature: 30ºC) and high wind velocities (average wind velocity at 10m high: 7.48 m s^{-1}).

As presented in Figure 5 the daytime temperatures during the 11th of August were increased for both the OptiNet and the Airplus nethouse. Higher temperature differences with the field were recorded for the Optinet nethouse (highest value: 2.1ºC). For the Airplus nethouse the maximum temperature difference was equal to 1.7 ºC.

On the other hand, for the high wind velocity 15th of August maximum temperature differences between the field and the nethouses were very small, namely 0.6ºC for the Optinet nethouse and 0.5ºC for the Airplus nethouse.

3.2. Daytime Field Relative Humidity

Figure 6 presents the average daytime RH and average daytime RH difference variations for the 12-day period of measurements. Average daytime RH graphs are similar for both nethouses and the field. Average daytime RH differences showed a maximum difference of 2% between the Optinet nethouse and the field on the 8th of August, while for all the other days this value did not exceed 1%.

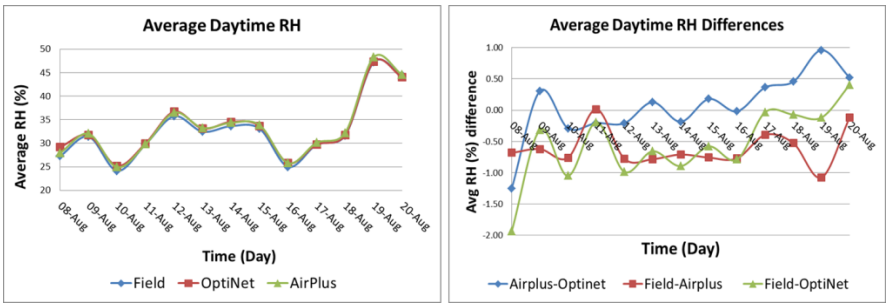

Figure 6. Daytime average RH variation outside and inside the nethouses (left); daytime average temperature difference variation between the nethouses and the outside temperature (right).

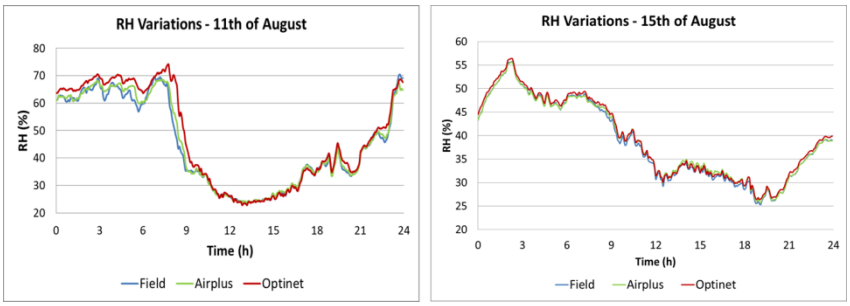

Figure 7. Daily RH variation: 11th of August (left); 15th of August (right)

Figure 7 presents the RH (%) variation for the nethouses and the field for the 11th and the 15th of August, in order to compare different environmental conditions (low and high wind velocities, respectively). Both the AirPlus and the OptiNet nethouses RH (%) measurements were similar to the field RH (%) for the daytime with maximum RH differences of the nethouses interior and the environment less than 2%.

For the 11th of August, the unexpected abrupt increase of the RH (%) that occurred mostly for the Optinet nethouse in the morning around 7.00 a.m. to 8.00 a.m. was because of the irrigation system that was programmed to work in the early morning hours (around 6 a.m.) and this means that the RH (%) values would increase inside the nethouses at this time. After 9 a.m. all RH (%) values became similar (Figure 7).

3.3. Numerical Model Results

The numerical model represented a hot day (11th of August) of average field daytime temperature equal to 35.16 ºC and RH of 30 %.

Table 3. Temperature (ºC) and RH (%) values for the nethouses interior for the field experiment and the numerical model at the center of the nethouses.

	Field Experiment		*Numerical Model*	
Case	*Temperature (ºC)*	*RH (%)*	*Temperature (ºC)*	*RH (%)*
AirPlus Nethouse	36.06	29.80	36.39	30.20
OptiNet Nethouse	36.30	29.80	36.11	30.15
Field	35.16	30.00	35.16	30.00

Table 3 presents the temperatures and the RH (%) values at the centre of the nethouses for the experimental field measurements and the results from the numerical model. A very good agreement can be observed. Temperatures inside the nethouses are almost similar, as for the field measurements, since the high shading factor of the OptiNet nethouse compensates for the lower ventilation rates as compared to the AirPlus nethouse. The numerical model was further used to evaluate the temperature and RH (%) distribution inside the nethouses.

Figure 8 presents isothermal contours in the insect-proof nethouses mid-height (1 m). Temperatures increased as the wind moved further inside the nethouses (as velocity decreased). For the AirPlus nethouse the area behind the second row of tomato plants R2 (R1: plants row 1; R2: plants row 2) temperatures reached values between the range of 37.7 – 39.6ºC. Similarly, inside the Optinet nethouse and behind the R2 plant row for that case, temperatures also increased (37.2 – 38.8ºC). However, these values did concern a large area inside the nethouse.

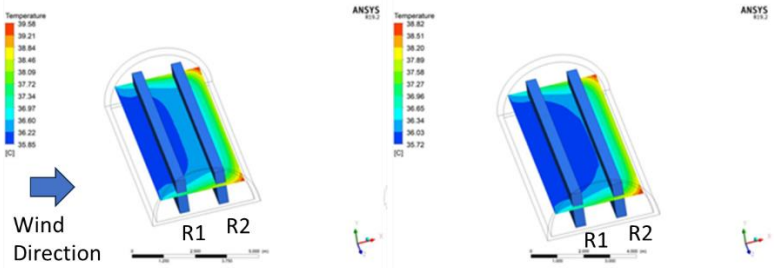

Figure 8. Temperature distribution at mid-height of the insect-proof nethouses. Airplus nethouse (left); Optinet nethouse (right)

Figure 20 presents the RH (%) distribution inside the insect-proof nethouses at mid-height (1 m). The values are given in kg kg-1 from which the RH (%) was calculated. The RH (%) values increased after the R1 and the R2 plants rows inside both the nethouses. For the Airplus nethouse, behind the second plants row R2 values ranged between 30.25 - 30.35%. For the corresponding area inside the Optinet nethouse the RH (%) values were between 30.35 – 30.43%. However, these differences are very small and not important.

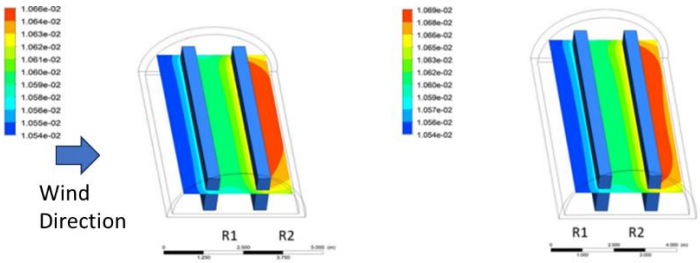

Figure 9. RH (%) distribution at mid-height of the insect-proof nethouses. Airplus (left); Optinet (right)

4. Conclusions

A full-scale experiment and numerical simulations were carried out regarding two small low-rise neighbouring insect-proof nethouses with tomato cultivation. The nethouses were using innovative agricultural nets as cladding materials, namely an enhanced ventilation technology (AirPlus) and an optical exclusion insect-proof net (OptiNet).

The two types of insect-proof nethouses did not exhibit increased temperature and RH values in their interior proving that the used nets can be effective as covering materials for nethouses structures offering a favourable microclimate for the protected cultivation. For the AirPlus nethouse, its enhanced natural ventilation rates led to increased air mass exchange with the environment and consequently temperatures and RH values were close to the ambient ones. On the other hand, the denser mesh OptiNet nethouse that imposed higher resistance to the incoming air prevented high values of temperature in its interior because of its increased shading factor (39.9 %). The small dimensions of the two insect-proof nethouses allowed for the quick airflow exchange between the structures and the field and the small number of tomato plants at the nethouses interior did not significantly contribute to the RH (%) levels.

Experimental and numerical results were in good agreement, validating the numerical model. Further 3D numerical analysis showed that the temperature increased behind the second row of tomato plants, but for a small area. For the RH (%) distribution, an insignificant increase was also detected at the same location. The numerical model simulated the field experiment accurately, proving that it can be a useful tool for such analyses. For larger nethouses with a significant number of plants rows, a 3D numerical analysis could reveal problematic areas of high temperatures and/or RH (%) values.

Acknowledgements

This research was implemented within the framework of the research project «Integrated design methodology for innovative insect-proof nethouse systems for high-value horticultural production in Greece -SmartNethouse» (code:865) supported by the Hellenic Foundation of Research and Innovation (HFRI) of the General Secretariat of Research and Technology (GSRT).

References

Anti-insect (polysack) nets, Ginegar, (2021).

Biorete ® Air Plus insect screen, Arrigoni, (2018).

Giannoulis, A., Briassoulis, D., Papardaki, N. G., & Mistriotis, A., (2021). Evaluation of insect-proof agricultural nets with enhanced functionality. *Biosystems Engineering, 208, 98-112.*

Lage, J.L. (1998). The Fundamental Theory of Flow through Permeable Media from Darcy to Turbulence, in Transport Phenomena in Porous Media, 1-31, edited by D.B. Ingham & I. Pop, Pergamon Press, Oxford.

Mahmood, A., Hu, Y., Tanny, J., & Asante, E. A. (2018). Effects of shading and insect-proof screens on crop microclimate and production: A review of recent advances. *Scientia Horticulturae, 241, 241-251.*

Tanny, J., Cohen, S., & Teitel, M. (2003). Screenhouse microclimate and ventilation: an experimental study. *Biosystems Engineering, 84, 331-341.*

Teitel, M., Ozer. S., & Mendelovich, V. (2022). Airflow temperature and humidity patterns in a screenhouse with flat insect-proof screen roof and impermeable walls – Computational fluid dynamics (CFD) results. *Biosystems Engineering, 214, 165-176.*

Reducing ambient temperature to reduce NH_3, N_2O and CH_4 emissions from a fattening piggery

Guingand Nadine [a*], Rousselière Yvonnick [a], Thomas Johan [a]

[a] Ifip institut du porc, Pacé, France

*Corresponding author: nadine.guingand@ifip.asso.fr

Abstract

In France, most buildings that house growing-finishing pigs are operated in a dynamic mode with a set-temperature of 22-24°C throughout the fattening period. In contrast, certain northern European countries use a set-temperature of 18°C with the stated aim of maintaining zootechnical performance and reducing ammonia emissions from these buildings. The aim of this experiment was to study the influence of ambient temperature on zootechnical and gaseous emissions by keeping temperatures cooler (16, 18 and 22°C) throughout the fattening period of pigs. Performance of these of pigs were compared to those kept in a conventional room with a set-temperature of 22°C. Pigs were weighted at the entry, the day of the food transition and the day before departure for the slaughterhouse. The quantity of feed distributed to pigs per treatment were weighted daily. NH_3, N_2O and CH_4 concentrations were semi-continuously measured by using a photoacoustic multi-gas monitor (Innova 1512). At the same time, the ventilation rate was continuously monitored. Data validation was achieved by applying the mass balance method for nitrogen and carbon including the calculation of inputs (piglet carcases, feed intake) and outputs (fattening pig carcases, slurry composition, gaseous emissions). Pig performance and environmental parameters (gaseous emissions and slurry volume and composition) of the reference room were validated to be representative of commercial breeding units. Afterwards, the comparison with the other rooms was done. Zootechnical performance did not differ between the rooms at the lower set-temperatures and the reference room. However, the rooms at 16, 18 and 22°C emitted 42 %, 36 % and 39 % less ammonia, respectively, than the reference room and 57 %, 53 % and 27 % less methane, respectively. In contrast, no effect on nitrous oxide emissions was observed. Reducing of ambient temperature could be one way to investigate how existing buildings can decrease their environmental impacts.

Keywords: Temperature, pig, housing, gaseous emission

1. Introduction

In most pig farms in France, buildings housing growing-finishing pigs are operated in a dynamic mode with a set-temperature of 22-24°C throughout the fattening period. The aim of this ventilation strategy is to maintain an ambient temperature that is appropriate to animal comfort and lead to optimal performance in terms of growth gain, feed conversion and carcass quality. A multitude of studies (Rinaldo and Le Dividich, 1991, Faure *et al.*, 2012, Quiniou *et al.*, 1997, Quiniou *et al.*, 2000) have been conducted to investigate the impact of ambient temperature on the performance of fattening pigs. Conversely, other countries such as Denmark and the Netherlands apply set-temperatures of around 18°C with the aim of maintaining zootechnical performance and above all, reducing ammonia emissions from the building concerned. This difference in ventilation management has been of concern to us for many years, particularly when combined with a change in the floor type, such as the introduction of partially slatted floor (Guingand *et al.*, 2010).

France's commitments at the European level to reduce ammonia emissions (-15% by 2030 compared to 2005 levels) and the desire to reduce the exposure of pigs and workers bring the need to explore new reduction pathways, adaptable to existing buildings, to the forefront of research and development priorities. Indeed, with a stock of buildings over 20 years old (Bertin and Ramonet, 2016) managed by a population of farm managers with an average age of 49 years in 2020 (Roguet, 2023), the proposed reduction solutions must be adaptable to existing building configurations without requiring costly major structural modifications. In the conventional system, widely applied in France, slurry is stored in the pit beneath the animals during the whole fattening period. The production of ammonia mainly results from the degradation of urea present in the urine by urease, an enzyme produced by microorganisms present in the feces. This process is sensitive to temperature and pH (Buscher *et al.*, 1997). Indeed, the increase of temperature influences the NH3-NH4+ dissociation coefficient promote diffusion and favors the activation of bacteria activity responsible of urea decomposition until inactivation temperature (Degré *et al.*, 2001). Thus, modifying the management of building ventilation by reducing the set temperature could represent a way to reduction ammonia concentration inside buildings and its emission to the atmosphere.

The aim of this study is to determine the influence of low ambient temperatures – under the thermoneutrality – on pig performance and on NH_3, N_2O and CH_4 emissions.

2. Material and methods

2.1. Design of the rooms

To study the influence of temperature on air quality without neglecting its influence on zootechnical performance, Ifip built a temperature-controlled unit called Climatotec at its experimental station in Romillé (35). This unit consists of two identical rooms with precise and independent ambient temperature control. The unit allows for the application of constant temperatures ranging from 15 to 30°C per room, thanks to a temperature-controlled block comprising a heater, a heat pump, and a heat dissipator/collector (Guingand et al., 2024). Each room can house twenty animals raised on fully slatted floor with effluent storage in a pre-pit for the entire fattening period. The air inlet – cold for this study – is through the attic and then through a Flud'R (Rose), while the extraction is low, under the slats. For this study, three different set-temperatures were applied: 16, 18, and 22°C. Due to the unit's configuration, the temperature comparison was conducted in two steps: the first comparing the two lowest set temperatures in the Climatotec unit (referred to as room T16 and room T18), and the second comparing the effect of maintaining a temperature at 22°C in the Climatotec unit (referred to as room T22) with a control room operated in parallel in the Ifip Pilot unit with a set temperature of 22°C (referred to as room REF22). This room, with air intake through a ceiling diffuser and low extraction, houses a total of 54 pigs raised on fully slatted floor with effluent storage in a pre-pit for the entire fattening period. The configuration and ventilation management of this room are considered representative of field conditions. The study was conducted between July 2022 and May 2023.

2.2. Pig management

The management of the pigs was identical in both type of rooms (Climatotec and control room). At the start of fattening, the animals were grouped by weight and sex to ensure an identical average weight per pen within and between rooms and a sex ratio of 1 per pen. The animals were fed ad libitum with a two-phase diet consisting of a growing feed (16% Crude Protein) provided until pigs reach approximately 65 kg and a finishing feed (14.5% Crude Protein) provided until slaughter. Water was supplied by a bowl-type drinker in each pen. The slurry produced by the pigs was stored in a pre-pit for the entire fattening period. Pigs from all rooms implicated in the study were sent to slaughter at the same time to facilitate the completion of the mass balance.

2.3. Measurements and recording

Measurements carried out in the Climatotec unit were identical to those carried out in the control room. Individual weighing of the animals was performed at the start of fattening, at each feed change, and on the day before slaughter. Feed distributed per pen was daily weighed and refusals were weighed at the time of feed change and at slaughter. Water consumption for each pen was recorded once a week. The slurry depth at various points in each pen was measured every 15 days, permitting the calculation of slurry production kinetics and volume produced per pig. A slurry sample was taken at each feed change and immediately after the animal departure for slaughterhouse. Slurry samples were taken from various points in the pen, pooled, and manually homogenized to create an average sample. Effluent analysis included pH, dry matter (DM), total nitrogen (Kjeldahl), ammoniacal nitrogen (NH_3-N), and total carbon (Ct). At the slaughterhouse, carcasses were weighed, lean meat content was measured by using Image Meater.

Regarding the environment, ventilation percentages were recorded using the ventilation control unit in each room of the Climatotec unit; recordings were made every 15 minutes throughout the pigs' presence. These percentages were then converted into ventilation rates in $m^3.h^{-1}$ using ventilation equations established per batch and per room at the pig entry; ventilation rates were measured in percentage increments to establish the relationship between percentage and ventilation rate based on the air speed in the extraction duct. Ambient temperatures were recorded every 15 minutes during the animals' presence using sensors (EasyLog MOTE-TH, Lascar, UK) positioned in the center of the room. Similarly, sensors (EasyLog Wifi-T, Lascar, UK) placed in watertight containers were installed on the slurry surface and at the bottom of the pre-pit, recording slurry temperature per room every 15 minutes.

Ammonia (NH_3), nitrous oxide (N_2O), and methane (CH_4) concentrations were measured in the ambient air using an infrared photoacoustic analyzer (Innova 1512, Lumasens Technologies A/S, Denmark) coupled with a 6-way sampler (Innova 1409, Lumasens Technologies A/S, Denmark). Measurements were taken in the ambient air

every 3 minutes throughout the animals' presence. Gas emissions were then calculated by multiplying the average hourly concentrations (in mg/m^3) of each gas by the average hourly ventilation rate (in m^3/h) and expressed in kg of N or C per pig place per year.

For feed conversion ratio, slurry volume, water consumption, statistical analysis was limited to calculating mean and standard deviation due to an insufficient number of values per category.

3. Results and discussion

3.1. Ambiance

For the trial comparing T16 to T18, the average ambient temperatures were 16.5±1.1°C and 18.1±0.8°C respectively for T16 and T18. The cold temperature targets have thus been achieved.

For the trial comparing T22 to REF22, the average ambient temperatures were 23.2±1.9°C and 26.3±1.4°C respectively for T22 and REF22. The average temperature in room C22 was higher than the imposed set temperature of 22°C but remained significantly lower than the average temperature in room T22, with a difference of 3°C. During this period, the average outdoor temperature was 19.8 ± 6.8°C, making it more challenging to achieve the 22°C target in the Climatotec unit. With high outdoor temperatures, it becomes more difficult to lower the ambient temperature despite increasing the air exchange rate, which explains why the average temperature in room T22 was much higher than the set value of 22°C.

3.2. Pig performance

Pig performance calculated up to slaughter are presented in Table 1. The duration of pig's presence per batch varies between 81 to 85 days.

For the trial 1 – T16 vs T18 – no significant difference was observed in the weight of pigs during growing and finishing phases. Although the slaughter weight of pigs exposed to 16°C was lower than that of exposed to 18°C, the difference was not significant. During the growing phase, the ADG of pigs exposed to 16°C was lower than that of pigs exposed to 18°C with a significant difference. Nevertheless, for the whole fattening period, there was no significant difference. Concerning FCR, data were not statistically analysed due to insufficient data, but the difference between rooms was very small, around 0.1. For the lean meat content and the added value per carcass, no significant difference was observed between T16 and T18.

Table 1: Pig performance per trial

Trial	1			2		
Room	T16	T18	RSD	T22	REF22	RSD
Initial LW, kg	30.3±2.2^a	30.5±2.5^a	2.3	35.6±3.0^a	37.4±3.6^a	3.5
Final LW, kg	105.6±12.2^a	111.7±8.3^a	4.0	122.3±8.1^a	122.3±7.8^a	5.7
ADG growing p., g.d^{-1}	924±86^b	985±83^a	84	950±71^a	993±90^a	85
ADG finishing p., g.d^{-1}	990±149^a	1 020±142^a	141	1 069±112^a	981±135^b	130
Overall ADG, g.d^{-1}	956±142^a	1 002±94^a	117	1 001±77^a	987±84^a	82
FCR growing p. kg.kg^{-1}	2.35±0.05	2.18±0.02	-	2.35±0.02	2.38±0.4	-
FCR finishing p. kg.kg^{-1}	2.69±0.08	3.09±0.07	-	2.60±0.01	2.76±0.3	-
Overall FCR, kg.kg^{-1}	2.52±0.07	2.64±0.04	-	2.48±0.01	2.56±0.3	-
Lean meat content, %	60.7±2.1^a	60.7±2.0^a	2.1	60.5±1.9^a	60.8±1.9^a	1.9
Added value, €/kg	0.13±0.06^a	0.16±0.07^a	0.06	0.16±0.05^a	0.16±0.05^a	0.05

LW: Live weight; ADG: average daily gain; FCR: feed conversion ratio; TMP: muscle content rate; Growing P.: growing phase, corresponds to the period between the pig's entry and the time they reach approximatively 65kg. Finishing P.: finishing phase, corresponds to the period after the growing phase and until the departure to the slaughterhouse. (a,b) : values followed by a different letter are statistically different – P<0.05

For the trial 2 – T22 vs REF22 – no significant difference was observed in weight, ADG, FCR, lean meat content and added value per carcass.

According to Le Dividich *et al.*, (1987), cold temperatures do not have significant effect on the total fat mass of pig carcass but rather on its distribution, with an increase in the weight and thickness of back fat while the weight of the leaf fat decreases.

3.3. Gaseous emissions

Gaseous emissions are given in Table2.

Regarding ammonia, the pigs in room REF22 emitted 2.87 ± 0.36 kg N_NH_3/place/year during the fattening period. These emission values are consistent with those obtained under identical conditions at the experimental station in Romillé (Guingand and Courboulay, 2019) and with those reported in the literature (Philippe *et al*., 2011; Santonia *et al*., 2017), which suggest values between 2.5 and 3.0 kg per place per year. The pigs in rooms T16, T18, and T22 emitted 1.67 ± 0.30, 1.84 ± 0.40, and 2.04 ± 0.30 kg N_NH_3/place/year, respectively, during the fattening period, which corresponds to 42%, 36%, and 29% less than the pigs in room REF22. In our study, the lower the temperature, the greater the reduction in ammonia emissions. There is limited literature on the impact of cold temperatures on ammonia emissions. According to Ocepek and Andersen (2022), the ammonia concentration in the environment increases as soon as the ambient temperature exceeds 20°C. Tabase *et al.* (2018) studied the impact of three set-point temperature levels (21, 23, and 25°C) on ammonia emission from "simulated" pigs on fully slatted floors with under-slat air entry and over-floor extraction; a system diametrically opposed to our study setup and to the majority of French farms. In this study, ammonia emission is influenced by the temperature of the incoming air rather than the set-point temperature. In Pouliot *et al.* (2011), the three ventilation scenarios studied start at temperatures between 21 and 22°C at the beginning of fattening, reaching 20°C for the control scenario, 17.2°C for the intermediate scenario, and 14.4°C for the "cold" scenario. The lack of effect of the "cold" treatment on ammonia emissions is explained by the author as a compensation between the increase in airflow rate for the "cold" scenario, raising ammonia concentrations, and the increase in temperatures for the control scenario, raising ammonia emissions. In our study, airflow rates are equivalent between the rooms in the thermoregulated unit, with the reduction in ambient temperature ensured by cooling the incoming air (Guingand *et al.*, 2024).

Table 2: Gaseous emissions per ambient temperature

Room	T16	T18	T22	REF22	RSD
N_NH_3 emission, kg/place[1]/year	1.67±0.3[b]	1.84±0.40[b]	2.04±0.30[b]	2.84±0.36[a]	0.32
N_N_2O emission, kg/place/year	0.24±0.03[a]	0.22±0.02[a]	0.20±0.04[a]	0.23±0.02[a]	0.02
C_CH_4 emission, kg/place/year	1.66±0.15[c]	1.60±0.14[c]	2.50±0.23[b]	3.42±0.16[a]	0.14

[1] the calculation per place is based on 3 rotations per finishing pig place per year - (a,b) : values followed by a different letter are statistically different – P<0.05

Regarding nitrous oxide, pigs in room REF22 emitted 0.23 ± 0.02 kg N_N_2O/place/year during the fattening period. This value is consistent with those reported by various authors (Philippe *et al.*, 2015; IPCC, 2019), who cite values between 0.10 and 0.25 kg N_N_2O per place per year. The emissions measured in rooms T16, T18, and T22 are very close to those measured in room REF22, ranging from 0.20 to 0.24 kg N_N_2O per place per year. In our study, temperature does not seem to affect nitrous oxide emissions. In the literature, the effect of temperature on nitrous oxide production from slurry is only documented for high temperatures (>50°C), which could inhibit the bacteria involved in the nitrification-denitrification process (Kebreab *et al.*, 2006).

Regarding methane, room REF22 emitted 3.42 ± 0.16 kg/place/year during the fattening period. This emission level is consistent with previous publications (Philippe *et al*., 2011; IPCC, 2019), which report values between 2 and 4 kg per place per year. The emissions measured in rooms T16, T18, and T22 were respectively 51%, 53%, and 27% lower compared to REF22. In relation with our study, the "cold" scenario in Pouliot *et al.* (2011) led to a reduction in methane emissions, with a 42% decrease compared to the "hot" scenario, where the setpoint temperatures were very close to those in our room REF22. In both our study and Pouliot *et al.* (2011), the cold ambient temperature reduced the activity of methanogenic bacteria in the slurry, bacteria that are particularly sensitive to the temperature of their environment (Dabert *et al.*, 2015).

Reducing the temperature to levels below thermoneutrality (T16 and T18) limits the volatilization and degradation processes, resulting in lower ammonia and methane emissions compared to room REF22. Maintaining the temperature at 22°C in room t22 throughout the day prevents the increase of temperature observed in room REF22, particularly in the afternoon, which promotes ammonia volatilization and its evacuation from the room due to the increased ventilation level.

3.4. Water consumption

The average water consumption of pigs in room REF22 was 8.1 ± 2.6 l per pig per day (Table 3). This consumption level is consistent with the 7.0 ± 1.7 l per pig per day reported by Massabie *et al*. (2014) for fattening pigs. The water consumption of pigs in rooms T16, T18, and T22 was significantly lower than that of pigs in room REF22 ($P<0.05$). These results confirm those of Pouliot *et al*. (2011) obtained with the "cold" scenario (setpoint temperatures decreasing from 21.1 to 14.4°C), with average consumptions of 4.36 l per pig per day.

Table 3: Water consumption, volume and temperature of slurry in relation with ambient temperature

Room	T16	T18	T22	REF22
Water consumption, l/p/d	4.2±0.7[a]	4.8±1.2[a]	5.7±1.4[a]	8.1±2.6[b]
Slurry volume, l/p	396	406	491	540
Ambient temperature, °C	16.5±1.1	18.1±0.8	23.2±1.9	26.3±1.4
Slurry temperature – surface, °C	14.9±2.5	15.8±2.7	22.1±1.8	26.2±1.0
Slurry temperature – pit bottom, °C	14.4±2.4	15.1±2.5	21.1±1.5	23.6±1.1

Regarding the volume of effluents, the animals in REF22 produced 540 l of slurry during the fattening period, which is close to the value of 480 l per finishing pig proposed by Levasseur (2013). The pigs kept T16 and T18 produced 25% less slurry than those kept in REF22. This low effluent production is related to the lower water consumption of the animals reported previously.

The temperature of the slurry was measured at two heights: at the bottom of the pit and at the surface. For all rooms, the temperature difference between the two heights is very small. The slurry temperature at the pit bottom is always lower than the ambient temperature—measured at 1.8 m above the slatted floor in the center of the room—by 2.1°C for T16 and T22 and 3.0°C for T18. This difference is likely related to the configuration of the sensors, which are protected in a rigid plastic box, creating an insulating shield around the sensor. The lower insulation at the pit bottom also likely contributes to the reduction in slurry temperature.

4. Conclusions

In our study, the zootechnical performances (slaughter weight, ADG, FCR, lean meat content) of animals exposed to cold temperatures below thermoneutrality were not significantly affected. Regarding environmental performance, continuous exposure to cold temperatures during fattening leads to a reduction in ammonia and methane emissions, water consumption by animals, and the volume of slurry produced per pig. No effect was observed on nitrous oxide emissions.

This study was conducted in a thermoregulated unit where ambient temperatures stayed very close to the setpoint temperatures imposed. Transposing these findings to actual farming conditions will likely not achieve to the same levels of reduction at equivalent setpoint temperatures. Indeed, the differences between setpoint temperature and ambient temperature can vary considerably, particularly during warm periods. Further trials under conventional ventilation conditions, where temperatures fluctuate more than in our thermoregulated unit, will be needed to validate the effectiveness of this practice. Although the reduction in greenhouse gas emissions may be less pronounced than in this study, lowering the setpoint temperature to around 18°C could prove to be a beneficial practice for reducing the environmental impact of pig farming. However, it will require careful control of airflow to avoid high air speeds on the pigs, which could significantly compromise their health and zootechnical performance.

Acknowledgments

The authors would like to thank ADEME (APR Cortea – Temporalis – 1962C0014) and PNDAR for their financial support.

References

Bertin C., Ramonet Y., 2015. Etat des lieux des bâtiments d'élevage de porcs en Bretagne chez les naisseurs-engraisseurs en 2015. Journées Rech. Porcine, 48, 1-7.

Buscher W., Jungbluth T., Hartung E., 1997. Modeling emissions. In *Ammonia and odour control from animal production facilities*. Vinkeloord, The Netherlands, October 6-10, 15-22.

Dabert P., Beline F., Lendormi T., 2015. Projet Promethis. Optimisation de la méthanisation des lisiers porcins à basse température. Aspects microbiologiques. Rapport final. Irstea. 90 pp.

Degré A., Verhève D., Debouche C., 2001. Emissions gazeuses en élevage porcin et modes de réduction: revue bibliographique. Biotechnol. Agron. Soc. Environ. 5 ,3, 135-143.

Faure J., Lefaucheur L., Kouba M., Lebret B., 2012. Croissance du porc à une température d'élevage basse: effets sur les performances et la composition corporelle. Journées Rech. Porcine 44, 281-282.

Guingand N., Quiniou N., Courboulay V., 2010. Comparison of ammonia and greenhouse gas emission from fattening pigs kept either on partially slatted floor in cold conditions or on fully slatted floor in thermoneutral conditions. In *International Symposium on Air Quality and Manure Management for Agriculture*. 13-16 September. Dallas, Texas. ASABE Publication Number: 711P0510cd.

Guingand N., Courboulay V., 2019. Effet du fractionnement des apports d'eau dans la technique du lisier flottant pour réduire les émissions d'ammoniac et d'odeurs en engraissement. Journées Rech. Porcine, 51, 181-186.

Guingand N., Rousselière Y., Thomas J., Colin A., 2024. Conception d'un module thermorégulé pour l'étude de l'influence des températures sur les performances zootechniques et environnementales de porcs à l'engraissement. Journées Rech. Porcine 56, 419-420.

IPCC, 2019. Refinement to the 2006 IPCC guidelines for national greenhouse gas inventories. Chapter 10. Emissions from livestock and manure management. 209 pp.

Kebreab E., Clark K., Wagner-Riddle C., France J., 2006. Methane and nitrous oxide emissions from Canadian animal agriculture: a review. Canadian J. Anim. Sci. 86,2, 135-158. doi: 10.4141/a05-010.

Le Dividich J., Noblet J., Bikawa T., 1987. Effect of environmental temperature and dietary energy concentration on the performance and carcass characteristics of growing-finishing swine fed to equal rate of gain. Livest. Prod. Sci. 17, 235-246.

Levasseur P., 2013. Production et capacités de stockage des lisiers de porc. TechPorc 10, 12-14.

Masssabie P., Roy H., Boulesstreau-Boulay A.H., Dubois A., 2014. La consommation d'eau en élevage de porcs – Des leviers pour réduire la consommation d'eau en élevage de porcs. Editions Ifip. 16 pp

Ocepek M., Andersen I.L., 2022. The effects of pen size and design, bedding, rooting material and ambient factors on pen and pig cleanliness and air quality in fattening pig houses. Animals, 12,12, 1580. https://doi.org/10.3390/ani12121580.

Philippe F.X., Cabaraux J.F., Nicks B., 2011. Ammonia emission from pig houses: influencing factors and mitigations techniques. Agriculture, Ecosystems and Environment 141, 245-260.

Philippe F.X., Laitat M., Wavreille J., Nicks B., Cabaraux J.F., 2015. Effects of high-fibre diet on ammonia and greenhouse gas emissions from gestating sows and fattening pigs. Atmos. Env. 109, 197-204.

Pouliot F., Dufour V., Belzile M., Feddes J., Lemay S., Morin M., Godbout S., 2011. Impacts de différentes stratégies de contrôle de la température ambiante en engraissement sur les performances zootechnique, les émissions gazeuses et la consommation d'énergie. Journées Rech. Porcine, 53, 193-197.

Quiniou N., Noblet J., Le Dividich J., Dubois S., Labroue F., 1997. Influence de l'abaissement de la température ambiante et du poids vif sur le comportement alimentaire des porcs en croissance élevés en groupe. Journées Rech. Porcine 29, 135-140.

Quiniou N., Renaudeau D., Collin A., Noblet J., 2000. Effets de l'exposition au chaud sur les caractéristiques de la prise alimentaire du porc à différents stades physiologiques. Inra Prod.Anim. 13,4,233-245.

Rinaldo D., Le Dividich J., 1991. Influence de la température ambiante sur les performances de croissance du porc. Inrae Productions Animales 4, 1, 57-65.

Roguet C., 2023. Evolution, diversité et typologie des exploitations porcines en France : enseignement du recensement agricole de 2020, comparaison aux recensements de 2010 et 2000. Journées Rech. Porcine, 55, 1-6.

Santonia G.G., Georgitzikis K., Scalet B.M., Montobbio P., Roudier S., Delgado L., 2017. Best Available Techique (BAT) Reference Document for the Intensive Rearing of Poultry or Pigs. EUR 28674 EN. doi: 10.2760/020485

Tabase R.K., Millet S., Brusselman E., Ampe B., Sonck B., Demeyer P.., 2018. Effect of ventilation settings on ammonia emission in an experimental pig house equipped with artificial pigs. Biosystems Engineering 176, 125-139 https://doi.org/10.1016/j.biosystemseng.2018.10.010.

RES4LIVE – Progress on pilot systems for energy smart livestock farming towards zero fossil fuel consumption

Dimitrios Tyris [a,*], Thomas Amon [b,c], Lukas Wannasek [b], Christian Ammon [b], Stefano Benni [d], Francesco Tinti [e], Jarissa Maselyne [f], Manon Everaert [f,g], Petros Demissie Tegenaw [f], Steven Lecompte [g], Olivier Marchand [h], Thomas Bartzanas [a], Dimitrios Manolakos [a]

[a] Department of Natural Resources Management and Agricultural Engineering, Agricultural University of Athens, Athens, Greece

[b] Leibniz Institute for Agricultural Engineering and Bioeconomy e.V., Department of Engineering for Livestock Management, Potsdam, Germany

[c] Institute of Animal Hygiene and Environmental Health, Department of Veterinary Medicine, Freie Universität Berlin, Berlin, Germany

[d] Department of Agricultural and Food Sciences, University of Bologna, Bologna, Italy

[e] Department of Civil, Chemical, Environmental, and Materials Engineering, University of Bologna, Bologna, Italy

[f] Technology and Food Science Unit, Flanders Research Institute for Agriculture, Fisheries and Food (ILVO), Merelbeke, Belgium

[g] Department of Electromechanical, Systems and Metal Engineering, Ghent University, Ghent, Belgium

[h] CRMT SAS, Lyon, France

* Corresponding author. Email: dtyris@aua.gr

Abstract

The utilization of fossil fuels in agriculture has elevated its status as a significant contributor to Greenhouse Gas (GHG) emissions, thereby impacting global climate change and posing a potential threat to food security. A major contributor to these emissions is intensive livestock farming, a highly energy-consuming sub-sector heavily dependent on fossil fuels. This practice requires a diverse range of energy sources, including electricity and thermal energy for heating and cooling indoor livestock facilities, equipment operation, lighting, and ventilation. The H2020 RES4LIVE project aims to eliminate fossil fuel consumption in certain areas of industrial livestock farming by introducing cost-effective Renewable Energy Sources (RES) technologies, enhancing thermal comfort for animals. The project showcases and evaluates various innovative RES technologies on four European pilot farms with swine (Belgium and Italy), dairy cattle (Germany), and laying hens (Greece). The present study elaborates on the design and installation process of the most distinctive parts of integrated systems (PV/PVT, heat pump, geothermal energy storage, biogas upgrading and biomethane tractor) in the four pilot farms and provides performance results obtained after the first months of their operation. The results add to the existing knowledge on incorporating RES into livestock systems and provide valuable perspectives on the adaptability of the studied systems for use in commercial facilities.

Keywords: Renewable Energy Sources, Intensive livestock farming, Livestock farming de-fossilization, Climate resilience.

1. Introduction

During the last decade, it has become apparent that fossil fuel use in the agricultural domain has negative effects, rendering it a major source of greenhouse gas (GHG) emissions, exacerbating global climate change and risking food security (Dubois et al., 2017; FAO, 2019). The intensive livestock sector remains heavily reliant on fossil fuels, accounting for a substantial portion of energy demand in agriculture (Peyraud and Macleod, 2020). According to recent data, agriculture accounts for 10.3% of the EU's GHG emissions, with the livestock sector alone accounting for around 70% of all GHG emissions (European Court of Auditors, 2021). Direct, i.e., on-farm, energy use accounts for 3.2% of the EU's total energy consumption (Eurostat, 2021). Energy consumption in intensive livestock farming is multifaceted, encompassing both electricity and thermal energy needs, depending on the structures used, the agroclimatic conditions, and the types of livestock used. These requirements range from maintaining optimal environmental conditions within livestock buildings (such as heating, cooling, and ventilation) (Costantino et al., 2016) to powering equipment (e.g., milking process, manure management) (Shine et al., 2020; Loyon, 2018) lighting, and transportation (e.g., tractors). Recognizing these challenges, there has been a growing emphasis on transitioning towards more sustainable practices and reducing dependence on fossil fuels in livestock production. National and EU policy is increasingly focused on improving environmental sustainability and animal welfare of

livestock production. To achieve the goals set out in the Green Deal and the Farm to Fork strategy (EU Commission, 2019; 2020), livestock rearing, and production will need to transform in the coming decades. Advancements in Renewable Energy Sources (RES) technologies, coupled with declining costs and improved reliability, have created new opportunities to embrace renewable energy production (Paris et al., 2022). Established technologies, such as solar photovoltaic (PV) panels, and biomass/ biogas systems are among the RES technologies increasingly adopted by farmers to meet their energy needs (Majeed et al., 2023), while more ascending ones, such as Thermal-Photovoltaics (PVT), heat pumps (HP), are attracting interest. The H2020 RES4LIVE project contributes to the effort of fossil fuel-free agriculture by developing and assessing the performance of innovative RES systems for the livestock sector in four European pilot farms. In the following sections, the main parts of the completed systems, as well as their first performance results, are presented.

2. Pilot Farms and Integrated Renewable Energy Sources (RES) Systems

Towards the imperative for de-fossilized livestock farming, within the framework of RES4LIVE, the design, installation, testing, and monitoring of different integrated RES systems is realized. The integrated systems have been specifically designed to fit the needs of each pilot farm, aiming at an optimal combination of adapted and commercial Renewable Energy Sources (RES) solutions. The developed units are fine-tuned by a smart control system, to achieve minimisation of fossil fuels-based energy, while enhancing the welfare of hosted animals. In the following sections, the design and installation process of the most distinctive parts of integrated systems in the four pilot farms are presented, alongside the performance results obtained after the first months of their operation.

2.1. EV ILVO swine farm in Belgium – PVT and Multi-Source Heat Pumps

The farm “Varkenscampus” is managed by EV ILVO, UGENT, and HoGent for research and educational purposes alongside normal commercial production. It is a farrow-to-finish pig farm hosting at any moment sows, piglets, and fattening pigs. The RES4LIVE installations include:

i. an 8.4 kWp PVT system accompanied by a Solar Station (see below), connected to the short-term thermal energy storage (TES) tank
ii. two multi-source HPs, high - and low-temperature
iii. a smart control system for the RES systems and the ventilation in one fattening pig room, as well as environmental sensors and energy meters

Figure 1. The PVT system (left) and HPs (right) at EV ILVO farm.

The PVT system and HPs (Figure 1) provide heat and power to the entire facility. The developed two multi-source, modular HPs substitute a 60 kW gas condensing boiler. They can provide heating at different temperature levels, and cooling. The low-temperature (25kW) will provide floor heating (42°C), while the high-temperature (40kW) will provide air heating and domestic hot water (60°C). The HPs are coupled with the PVT system through a short-term TES tank to enhance their Coefficient of Performance (COP). Furthermore, in the case that solar energy will not suffice to cover the required thermal load at the evaporator, a dry cooler will also be available. The high-temperature HP will also make it possible to cool in the fattening pigs’ compartments and nursery. Therefore, cold water will go through the twin tubes of the air heating system.

The developed solar pumping circuit, or “Solar Central”, is a standardised group of components that operate and run the PVT system in an optimized way to deliver heat and electricity to the required

integration point. The solar thermal circuit delivers the heat down from the PVT collectors to the solar station, which is coupled with the heat storage, or fitted with a heat exchanger, depending on the case. In all RES4LIVE interventions including PVT systems, the developed solar central concept is incorporated.

2.2. GOLINELLI swine farm in Italy – PVT, BTES, and Multi-Source Heat Pump

The second pilot farm is the commercial pig farm GOLINELLI located in the Modena province, Italy. The farm consists of a farrowing barn, a nursery barn, a gestation barn, and a hog barn with a gestation sector. The interventions include (Figure 2):

i. a 7.68 kW_{el}, 25 kW_{th} PVT system accompanied with a solar station
ii. a Borehole Thermal Energy Storage (BTES) system, storing the excess heat from the PVT system
iii. a multi-source, medium-temperature HP of 35 kW
iv. environmental sensors and energy meters

Figure 2. The PVT system (left), BTES system (middle), and HP (right) at GOLINELLI farm.

The HP unit was designed to substitute a 34 kW LPG boiler providing hot water to the space heating system of the nursery barn. The PVT collectors are connected to the solar central which is the main operational pumping unit with the control system to operate the PVTs. The Solar Central is connected to the BTES system to store the heat produced over an extended period. This way, heat is flowing from the PVTs to the HPs through the BTES system, while the ambient heat is exploited through an air dry cooler. The HP is a multi-source one, selecting between ground and air heat by activating and deactivating the fans. To achieve increased COPs, the source selection between ground and air is based on the comparison between the geothermal fluid return temperature T_g and the two temperature thresholds decided by the user, T_a and T_b, in the following manner:

- $T_g > T_a$ - Operates as a Ground-source HP. The two fans are deactivated, and the geothermal pump is active
- $T_b < T_g < T_a$ - Operates as a Dual-source HP. The fans are activated and the whole system is active
- $T_g < T_b$ - Operates as an Air-source HP. The geothermal pump is deactivated, while the fans remain active

2.3. AUA laying hens farm in Greece – PV and Heat Pump

The experimental poultry farm for egg production has been established on the Agricultural University of Athens (AUA) campus and occupies an area of 90 m^2, hosting approximately 400 animals at least. It is further divided into two separate equally sized rooms, pullets' and a laying hens' house. Both pullets and hens are raised in a 3-tier colony cage production system. Hens are housed in enriched cages. The RES4LIVE system (Figure 3) includes:

i. a 10 kW HP, for heating, cooling, and dehumidification
ii. a 9 kWp standard PV system, on the rooftop of a nearby building
iii. smart control and new LED systems

Figure 3. The PV system (left) and HP (right) at AUA farm.

Before the project's interventions, the facility relied mainly on forced ventilation to remove the thermal loads, applied with direct drive fans in both rooms, while the pullets' house used to be heated only by infrared heating lamps. The goal of the project's main interventions is twofold; first, they aim at enhancing the thermal comfort of the hosted animals by regulating the indoor air quality, temperature, and relative humidity with the use of HP. Keeping the temperature and relative humidity, ideally, in the thermo-neutral zone, or thermal comfort zone, is determining for animal welfare and increased production. Second, to minimize the electricity consumption from the electricity grid.

2.4. LVAT dairy farm in Germany – Bio-CNG Plant and Retrofitted Biomethane Tractor

The Educational and Experimental Centre for Animal Breeding and Husbandry (LVAT) is located in Groß Kreutz, in Brandenburg, Germany. The farm includes three barns for milk production, with an overall number of 445 cows and calves. The produced manure feeds an existing biogas plant of 1000 Nm^3 per day capacity, combined heat, and power (CHP) generation. Within RES4LIVE, the following RES interventions are demonstrated (Figure 4):

i. a biogas to biomethane upgrading unit, equipped with a fuel-filling station,
ii. a diesel farm tractor retrofitted for biomethane use
iii. an innovative PVT system for decentralized heat and electrical power generation, coupled with a Solar Station and an existing milk cooling system
iv. a smart system for barn climate control based on ventilation tubes, using pre-cooled air for evaporative cooling
v. a smart management and control system to efficiently control heat and electricity consumption

Figure 4. The Bio-CNG plant and filling station (left) and the biomethane tractor at the LVAT farm.

The new, small-scale (5 $Nm^3\ h^{-1}$ biomethane) technological setup with a hollow fiber membrane in the very low-pressure range (7-8 bar) and a hybrid compression was set up. In a one-stage membrane separation process, methane (CH4) is extracted from raw biogas. Using a closed cycle concept, this process ensures that only methane is produced and compressed as BioCNG (Compressed Natural Gas) for use as fuel. All CO_2-containing gas from the membrane separation process is fed back into the raw biogas storage. Moreover, the unit incorporated a Bio-CNG filling station characterized by a simplified and compact design in terms of the compression process.

One of the farm's diesel tractors was also modified for BioCNG use. Its engine, with a nominal power of 59 kW, was converted from diesel to biomethane to provide the same torque and power after the conversion and handle the same duty cycle, mainly for food mixing and delivery. Multiple aspects were considered, including the thermal stress of the engine to keep with the reliability of the diesel engine, the reduction of the exhaust emissions, the compactness of the gas tank system, containing 26 kg of biomethane, and the design-to-cost objective of the modification, aiming at reusing the maximum number of the diesel parts.

3. RES Systems' Performance Results and Discussion

The installation and commissioning of the RES systems were followed by a period of monitoring and fine-tuning. The sections below present the preliminary performance results of the main systems at each pilot farm. The availability of logged data in each case was influenced by the managerial schedules of the respective farms.

3.1. EV ILVO RES Systems Performance

After a series of tests, the high-temperature HP effectively maintains the setpoint of 60°C, providing sanitary hot water and air heating. The low-temperature HP, with a setpoint temperature of 42°C, is connected only to the underfloor heating system used for piglets. The utilization of two HPs appears to be beneficial to the efficiency of the system, as compared to the original installation. Before the project, a natural gas boiler provided water at 70°C for all subsystems, and afterwards, it was cooled down to 42°C for the underfloor heating, losing valuable heat in the process.

When the temperature of the TES tank is above 37°C, the HPs operate as water-to-water, until the temperature drops below 17°C. Below this point, the dry cooler serves as a heat source for the HPs using either one or two fans, depending on the heat demand, thus operating as air-to-water. The PVTs' heating circuit operates only when solar irradiance is higher than 200 W/m² for longer than 60 seconds, providing the TES tank with heat. The HPs' water temperature variation alongside the outdoor temperature and irradiance between 07 and 28/05/2024 are shown in Figure 5.

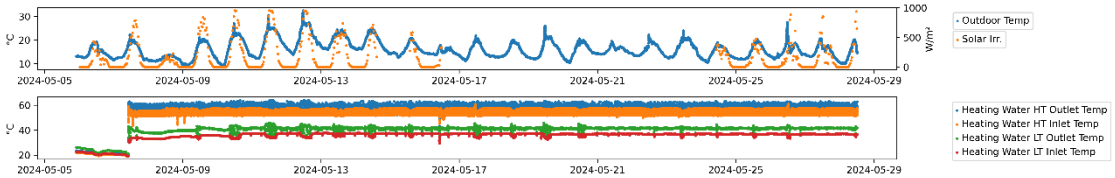

Figure 5. Environmental conditions and HPs' water temperature variation at EV ILVO farm, between 07/05 and 28/05/2024.

During the most recent tests that took place between 07/05 and 28/05/2024, the overall system performed as intended. The HPs operated longer as water-to-water compared to previous test periods, as solar irradiance was increased during May. The power consumption and heating capacity of both HPs are presented in Figure 6 below.

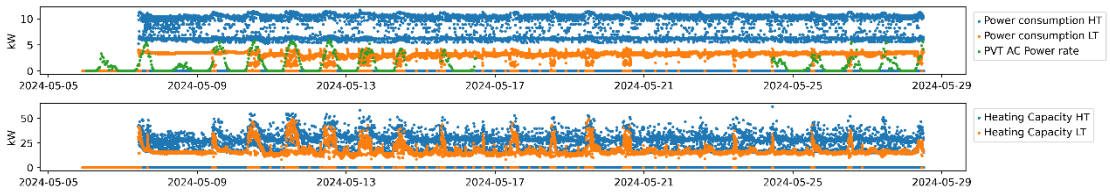

Figure 6. Power consumption and heating capacity of the high- and low-temperature HPs at the EV ILVO farm, between 07/05 and 28/05/2024.

The low-temperature HP appears to be slightly oversized, operating at a lower compressor capacity, which negatively influences the part load ratio of the HP. The high-temperature HP, though continuously going into ON/OFF mode, performs well. During this testing phase, the system operated for 85% in the air-water and 15% in the water-water mode, respectively. During the air-water mode, the average COP of the high-temperature is estimated at 2.95, while for the low-temperature HP, the

COP is 4.87. During water-water operation, the high- and low-temperature HPs use considerably less electricity, increasing their COPs to 9.85 and 4.10, respectively. The solar electricity was being logged from the 7th of May but stopped on the 14th. During these seven days, the PVTs contributed 0.25 MWh or 18% electricity, entailing about 18% of the electricity demand of the HPs (1.37 MWh).

3.2. GOLINELLI RES Systems Performance

To analyse the performance of the PVT-HP-BTES system at GOLINELLI farm, a representative period, between the 10th and 25th of April 2024 was chosen. Between the 10th and 17th, where the average temperature and irradiance were higher than usual (above 20°C and 300 W m^{-2}, respectively), the PVT and the solar central station both were activated, and solar heat was injected into the BTES system. From the 17th to the 25th, the weather temperature dropped abruptly, with the presence of precipitation, and reduced irradiance. The average weather temperature reduced to 11°C, with low peaks down to 2.5°C during the night. During this period, high variability of weather temperature occurred (Figure 7). In these conditions, the hallway of the piglets' building started to drop its ambient temperature and the HP was automatically activated to provide the necessary comfort, by extracting the heat from the borehole heat exchangers (BHE) of the BTES and, working in hybrid mode, from the ambient air. The two consecutive periods are representative then of the sequence injection-extraction of the PVT-BTES-HP system.

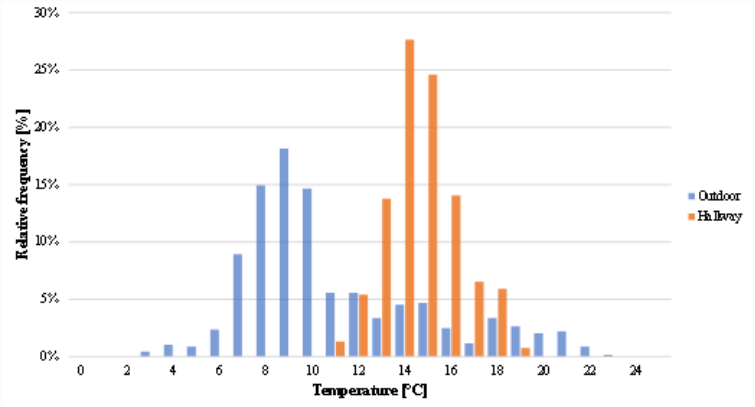

Figure 7. Frequency distribution of outdoor/indoor temperature between 17/04 and 24/04/2024 in GOLINELLI farm.

From the monitoring system, it was possible to record the values from various sensor temperatures on the PVT and the BTES circuit. The calculated stored energy was around 2160 MJ, equal to 600 kWh. The HP extracts energy from the BTES to cover the needs of the hallway of the piglets' building. At the moment, the HP works only in heating mode, but it is designed for cooling as well. For most of the testing period, the HP was able to keep the temperature of the hallway very close to the desired setpoint temperature, being activated for 17.4% of the total time. The measured temperature data in the hallway are present in Figure 7 as well. The heating fluid temperature and the cumulative energy provided are presented in Figure 8.

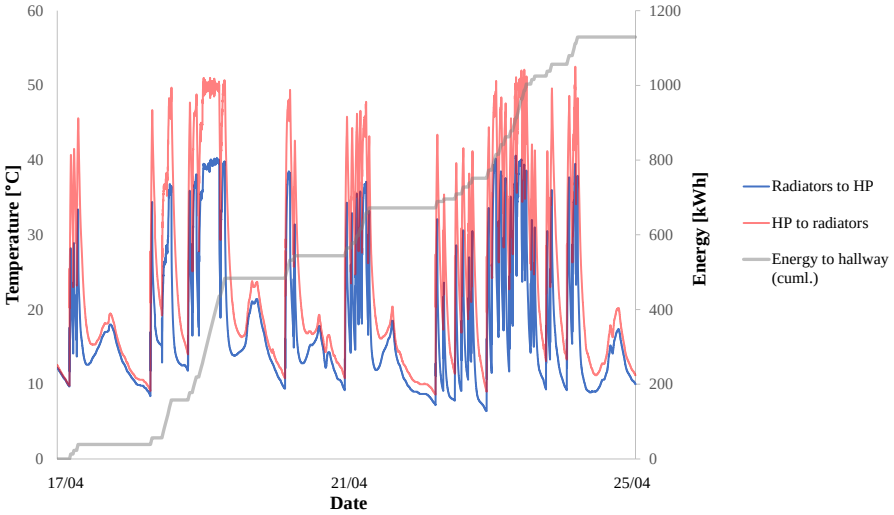

Figure 8. Energy provided to the hallway by the HP in the period 17/04 and 25/04/2024 (grey), and related inlet and outlet temperatures (blue and red).

The total energy provided by the HP to the building was around 1200 kWh, and the electric energy used was around 300 kWh. The total heat provided during the Ground mode was about 670 kWh (approx. 75%), while the remaining 230 kWh were extracted during the Hybrid Mode (approx. 25%). The Hybrid mode was necessary mostly during the night when temperatures were lower. The Air mode was not activated during this testing period. In conclusion, the average COPs for each mode of the HP for the period between 17 and 25/04/2024 is presented in Table 1.

Table 1. Average COP of the HP in the reference period 17/04 and 25/04/2024.

HP mode	Average COP
Ground	4.67
Air	(not activated during this period)
Hybrid	3.50
Overall	4.34

3.3. AUA RES Systems Performance

Though the installations were completed earlier, the integrated RES system in the AUA poultry farm became fully operational in May 2023 when a new laying hen batch arrived. The data analysed during two characteristic periods, summer and winter, are presented and discussed next. In both, only the laying hens' room was operational, with the HP operating in one mode each time, cooling, and heating, respectively. In Table 2, the total amount of energy consumed by the facility as well as that produced by the PVs, and the Seasonal COP (SCOP) of the HP, are presented for both periods.

Table 2. Energy and HP performance-related data for the AUA pilot farm.

Period (mode)	Total electricity used (kWh)	Total electricity produced (kWh)	Self-sufficiency (%)	Seasonal COP
Summer (cooling)	4,031.23	908.50	22.54	2.42
Winter (heating)	2,389.52	482.71	20.20	3.65

Indicative figures are presented for the period between 30/07 and 09/08/2023. Despite the summer of 2023 being one of the warmest of the last years in Greece, the HP regulated the indoor temperature effectively (Figure 9). The profile for power consumption and PV power production for an indicative period in summer (23-25/07/2024) are presented in Figure 10 below.

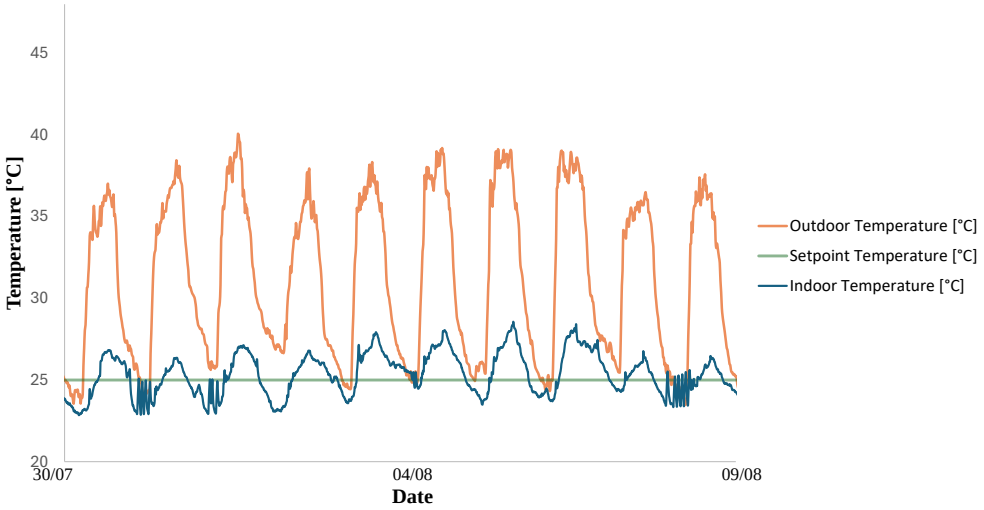

Figure 9. Indoor temperature regulation by the AUA pilot farm HP between 30/07 and 09/08/2023.

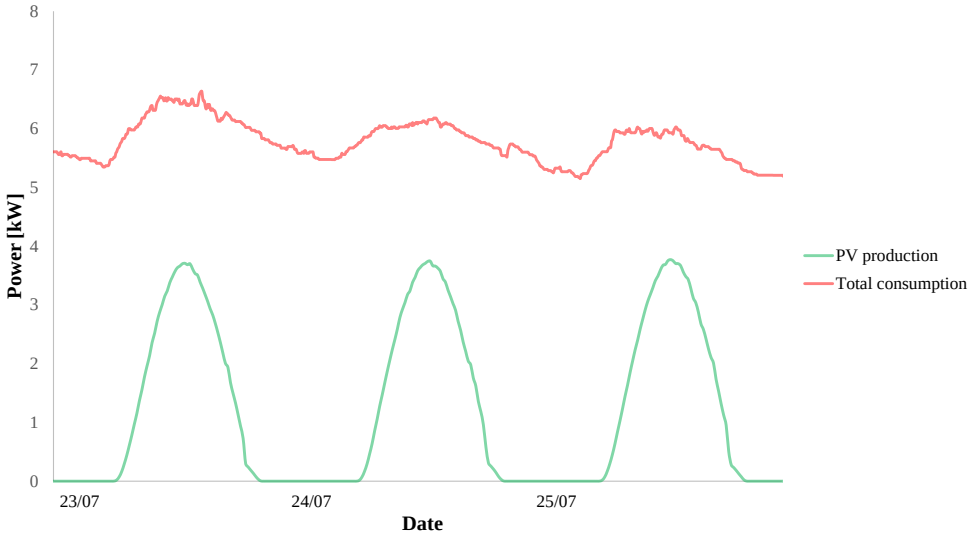

Figure 10. Power consumption and PV power production profile of the AUA pilot farm for an indicative period in summer (23-25/07/2023).

3.4. LVAT RES Systems Performance

The commissioning of the BioCNG plant at LVAT took place between 19/07 and 21/07/2023, and the data collection began. The first data evaluation was based on 20-second intervals, but up to 4-second intervals are possible and were used for technical optimization of the system. In Figure 11 graphs represent the first data acquired, while Table 3 illustrates the main performance indicators of the plant.

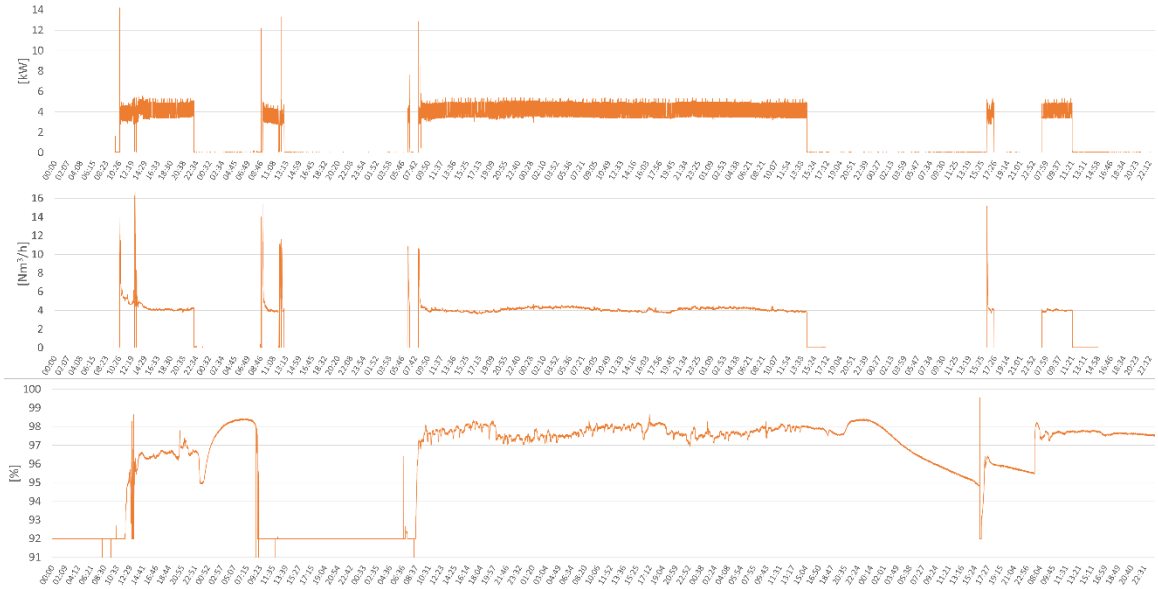

Figure 11. BioCNG plant power consumption (top), BioCNG flow rate (middle), and CH4 concentration of BioCNG (bottom) at the LVAT pilot farm.

Table 3. Key performance indicators from the data monitoring of the LVAT biogas upgrading pilot plant.

Performance indicator	Average
Specific energy consumption [kWh_{el} Nm^{-3} BioCNG]	0,94
Separation pressure hollow fiber membrane [bar]	7,83
Separation temperature hollow fiber membrane [°C]	57,44
Methane concentration [%]	96,75
Start-up time until BioCNG production [min]	26,78

Initially, a two-week testing period took place, using the biomethane tractor mainly for transport operations. Indicative data of the tractor speed are presented in Figure 12.

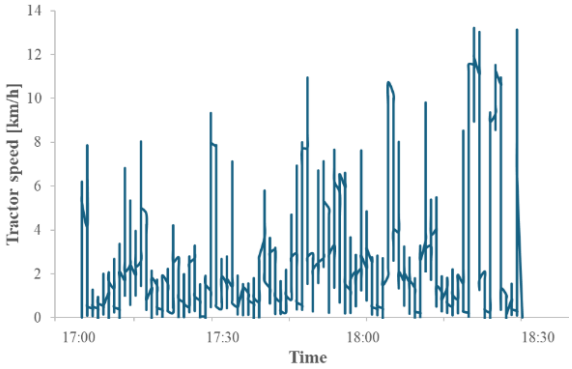

Figure 12. Tractor speed during the first tests at LVAT premises.

After analysing the data of this period, the biomethane tractor presented an average fuel consumption of approximately 4.5 kg BioCNG per hour of operation, or 15.75 kg BioCNG daily, for approximately 3.5 hours of operation.

4. Conclusions

The results obtained during the first months of the RES systems operation largely appear satisfactory. Of course, further experimentation and finetuning are in progress to optimize their performance on-farm. The installed RES technologies are further monitored in each pilot farm to draw

solid techno-economic figures for their overall performance. Each integrated system is assessed in terms of technical, environmental, and economic performance, as well as social acceptance. The next steps of the project concern the communication of the outcome that this ongoing work will bring. Their dissemination will concern – besides the scientific community – relevant stakeholders involved in livestock farming, and intensive agriculture in general, with the aim to add to the existing knowledge on incorporating RES into livestock systems and provide valuable perspectives on the adaptability of the studied systems for use in commercial facilities.

Acknowledgements

RES4LIVE Project has received funding from the European Union's Horizon 2020 Research and Innovation Programme under Grant Agreement No. 101000785.

References

Costantino, A., E. Fabrizio, A. Biglia, P. Cornale, L. Battaglini. 2016. Energy Use for Climate Control of Animal Houses: The State of the Art in Europe. Energy Procedia 101 (September): 184–91. https://doi.org/10.1016/j.egypro.2016.11.024.

Dubois, O., A. Flammini, A. Kojakovic, I. Maltsoglou, M. Puri, L. Rincon, and FAO, 2017. Energy Access. Food and Agriculture.The World Bank, Washington DC, USA.

EU Commission. 2019. The European Green Deal. https://doi.org/10.34625/issn.2183-2705(35)2024.ic-03.

EU Commission. 2020. Farm to Fork Strategy. https://ec.europa.eu/food/sites/food/files/safety/docs/f2f_action-plan_2020_strategy-info_en.pdf.

European Court of Auditors. 2021. Special Report 16/2021: Common Agricultural Policy (CAP) and Climate, 1–65.

Eurostat. 2021. "Agriculture & Forestry Energy Consumption Stable in 2021." 2021.

FAO. 2019. The State of Food and Agriculture 2019. Moving Forward on Food Loss and Waste Reduction. Routledge Handbook of Religion and Ecology, Rome, Italy.

Loyon, Laurence. 2018. Overview of Animal Manure Management for Beef, Pig, and Poultry Farms in France. Frontiers in Sustainable Food Systems 2 (July): 1–10. https://doi.org/10.3389/fsufs.2018.00036.

Majeed, Y., M.U. Khan, M. Waseem, U. Zahid, F. Mahmood, F. Majeed, M. Sultan, and A. Raza. 2023. "Renewable Energy as an Alternative Source for Energy Management in Agriculture." Energy Reports 10: 344–59. https://doi.org/10.1016/j.egyr.2023.06.032.

Paris, B., F. Vandorou, D. Tyris, A.T. Balafoutis, K. Vaiopoulos, G. Kyriakarakos, D. Manolakos, and G. Papadakis. 2022. Energy Use in the EU Livestock Sector: A Review Recommending Energy Efficiency Measures and Renewable Energy Sources Adoption. Applied Sciences (Switzerland) 12 (4). https://doi.org/https://doi.org/10.3390/app12042142.

Peyraud, J., and M. Macleod. 2020. Future of EU Livestock: How to Contribute to a Sustainable Agricultural Sector. Brussels.

Shine, P., J. Upton, P. Sefeedpari, and M.D. Murphy. 2020. Energy Consumption on Dairy Farms: A Review of Monitoring, Prediction Modelling, and Analyses. Energies 13 (5): 1–25. https://doi.org/10.3390/en13051288.

Source segregation in dairy housing effectively separates organic matter and nutrients and facilitates acidification for ammonia emission reduction

J. El Mahdi[a]*, P. W. G. Groot Koerkamp,[a] J. Deru,[c] J. W. De Vries[a,b]

[a] Agricultural Biosystems Engineering, Department of Plant Sciences, Wageningen University and Research, P.O. Box 16, 6700 AA Wageningen, the Netherlands

[b] Applied Research Centre, VHL University of Applied Sciences, P.O. Box 9001, 6880 GB, Velp, Netherlands

[c] Louis Bolk Instituut, Kosterijland 3-5, Bunnik, AJ 3981, The Netherlands

*Jihane.elmahdi@wur.nl

Abstract

Source segregation (SS) of faeces and urine in the animal house is a strategy to reduce emissions and improve nutrient management, but its performance in dairy housing is unknown. This study aims at exploring the separation efficiencies of nutrients and organic matter (OM) of a novel SS floor in dairy housing and to explore its effect on nutrient losses in the animal house. In addition, the study aims to explore pH dynamics of urine after? acidification as a potential alternative to traditional slurry acidification, because urine is hypothesized to require less acid and a lower frequency of acidification. For this, faeces and urine were collected in two time points from the novel floor and slurry from a traditional slatted floor, both at an experimental dairy farm in the Netherlands. The chemical composition of each fraction was analysed and served to calculate the separation efficiency (SE(x)) for selected compounds: (dry matter (DM), organic matter (OM), total nitrogen (TN), total ammoniacal nitrogen (TAN), total phosphorus (TP), and water soluble phosphorus (SP)). For the acidification test, a titration curve was drawn using 5M sulfuric acid to determine the amount of acid needed to reach pH 5.5, then the pH of the acidified urine was monitored for 30 days. The results from this pilot system showed that on average 88% of DM, 94% of OM, 95% of TP, 97% of SP, 67% of TN and 24% of TAN accumulated in the faeces. Further, the SS system had higher N content in the excreta, calculated by mass balance, than the slurry system during the first collection and a lower one during the second collection. The reasons for this remain unclear and need further investigation. In the acidification test, urine required 1.7 ml sulfuric acid kg^{-1} to reach a pH of 5.5, which was lower than the range reported for slurry (2.8 to 5.7 ml kg^{-1}). In addition, the urine maintained the 5.5 pH (5.4 ± 0.3) for the totality of the test with a single acidification. Finally, faeces and urine were also collected from the same SS floor in four practical farms and the results showed similar SE(x) for DM, OM and TP, but different ones for TN and TAN. Further investigations are needed to understand the variations in N separation and emissions under practical circumstances. We concluded that the novel SS system can effectively separate OM and P as compared to post-separation of slurry, which additionally requires more energy and inputs. Further, SS can improve targeted reduction of ammonia emissions by acidifying urine instead of slurry because less acid is required and foaming is limited. Further investigations are, however, needed to understand the implications of the segregation on emissions in-house and during management further down-stream.

Keywords: Source segregation, dairy housing, separation efficiency, nitrogen losses, urine acidification.

1. Introduction

Growth of intensive livestock production has led to manure surpluses in areas where more manure is produced than can be legally applied to the field, e.g. in western Europe (CBS, 2021; Yan et al., 2017). In the Netherlands, dairy manure, mainly in the form of slurry which is the mixture of urine and faeces after excretion, has the largest surplus at farm level although dairy farms have the most land to apply it (Yan et al., 2017). This manure surplus raises environmental concerns as manure storage and application to land are a main source of greenhouse gas (GHG) and nitrogen (N) emissions and nutrient leaching. Many regulations are in place to limit these emissions such as the European nitrate directive, phosphate application ceilings, and obligations for farmers to process and export their excess manure (Schröder et al., 2007; Yan et al., 2017). Consequently, various treatment systems to process manure, often slurry, have been developed.

A common first step in slurry treatment is separation into a liquid and solid fraction. This allows more practicability in processing and transport, partly separates and concentrates N and phosphorus (P) and helps reduce GHG emissions from slurry storage (Møller et al., 2002; Fangueiro et al., 2008; Kaparaju et al., 2008; Hjorth et al., 2011; Zhang et al., 2022). Separation can be achieved by mechanical and chemical technologies such as screw pressing, centrifugation, and flocculation, all having their specific (dis)advantages (Hjorth et al., 2011; Zhang et al., 2022). For example, centrifugation results in up to 86% separation efficiency of dry matter (DM), which is the highest compared to other techniques, often <50% DM separation efficiency. Pre-treatments before centrifugation, such as flocculation or coagulation, results in up to 90% P separation efficiency which is the highest as compared to other techniques typically resulting in around 60% P separation efficiency (Hjorth et al., 2011; Zhang et al., 2022). High separation efficiencies, however, often require high inputs of energy and/ or additives (Møller and Sommer, 2000). As an alternative to separation of slurry, source segregation (SS) of urine and faeces directly after excretion can be considered. Source segregation is achieved through systems under the flooring, e.g. V-shaped scrapers and conveyor belts (Aarnink & Ogink, 2007; Koger et al., 2014; Vu et al., 2016), by systems on the flooring, e.g. grooved and permeable floors (Swierstra et al., 2001, Deru et al., 2023) or by systems under the animals' tail, e.g. the cow toilet (Galama et al., 2020). With such SS systems, no slurry is created at forehand and thus less contamination of urine with organic matter (OM) takes place and minimal energy and/ or chemicals are required. Minimal OM contamination can have advantages on the practice of acidification in the animal house, typically used on slurry to reduce NH_3 emissions. This is because urine could have much less buffering capacity than slurry and thus requires less acid and less acid additions. In addition, N and P can easily be kept separate in the fractions, because P is mainly present in the faeces thus easing treatment and handling downstream. Separation of N and P is specifically important because mixed forms of animal manure, such as slurry, have unbalanced N/P ratios compared to crop demand and their application can thus lead to P over application, potentially causing P losses to the environment (Knowlton et al., 2004).

Source segregation systems and their separation efficiencies are well described for pig houses but less in dairy houses. The separation efficiency of SS systems in pig housing were found to be over 90% for DM, OM, and P (Von Bernuth et al., 2005; Vu et al., 2016). In a study by Vu et al. (2016), a V-shaped belt under the slatted floor had 92% DM, 96% OM, and 97% P in the faeces which was higher than other solid-liquid separation techniques for slurry. Moreover, SS reduced NH_3 emission up to 49% compared to conventional housing systems with slurry (Lachance et al., 2005; Stewart et al., 2004; Panetta et al., 2005; Von Bernuth et al., 2005; Vu et al., 2016). In dairy housing, however, little is known about the performance of SS systems. A study by Swierstra et al 2001 evaluated a grooved floor that drained urine into the pit and scraped faeces to a separate outside storage (Swierstra et al., 2001). This grooved floor reduced NH_3 emissions by 46%, but its separation efficiency was not investigated. Other SS systems are currently available for dairy housing in The Netherlands, such as permeable floors and the cow toilet. These systems are being tested at Dairy campus in the Netherlands and further developed by the respective companies. However, little is known about their separation efficiencies and potential to limit nutrient losses. In this research, we focus on the permeable floor system as it currently receives the most interest in practice.

The objective of this study is to investigate the separation efficiency of OM, DM and nutrients (N and P) at two different time points of a pilot permeable SS floor in a dairy house, and unveil its potential N losses reduction compared to a conventional slurry system. In addition, we aimed to provide first results of the dynamics of segregated urine acidification, including the amount of acid required and pH stability. Finally, we aimed to check the separation efficiency of this SS floor in practical farms.

2. Materials and Methods

2.1. Collection of slurry and segregated manure fractions

2.1.1. Pilot separation system

Samples of slurry and dairy manure fractions were collected on the 29th of March 2021 and 18th of January 2022 to account for possible seasonal differences in separation efficiency. Samples were taken from the SS floor and from the traditional slurry pit at Dairy Campus (Leeuwarden, Netherlands).

The selected SS floor in our study was a commercial system (Zeraflex) made with adjacent tiles of a synthetic and permeable material allowing urine to drain to an underneath pit while keeping the faeces on top. The system was equipped with an automated scraper that moved the faeces out of the barn to an outside covered storage. The traditional slurry pit and the SS floor were in the same experimental unit with the same number of cows, floor area and feeding regime. The feeding ration consisted of grass silage, silage maize, barley meal and soy meal in addition to pelleted concentrates.

Slurry and segregated urine were taken from the storage pit under the animal house using a cylinder slid through the floor slats. The cylinder was used to mix the urine and take the samples at ten representative points in the pit. The ten subsamples were mixed to a homogeneous sample from which again three subsamples were taken for chemical analysis.

The segregated faeces were collected from the temporary storage which was emptied daily. From the collected faeces, we took three subsamples for chemical analysis. All samples were stored at 2°C for two weeks on average before analysis.

2.1.2. Practical farms

Samples of source segregated faeces and urine were taken from four practical farms in different parts of The Netherlands. The four farms had a permeable floor system originating from the same commercial supplier of the pilot system (Zeraflex). The details of each farm, including location, farming system, cows breed and farm number are in Table 1. The urine samples were taken from the pit while the faeces were taken from over the floor while they were being scraped outside.

Table 1: Details of the practical farms with permeable floor source segregation systems.

Farm number	Location	Farming system	Cow breed	Number of cows
1	Maasland, South Holland	Organic	Holstein-Friesian	67
2	Leidschendam, South Holland	Organic	Mix (mainly Holstein-Friesian)	50
3	Hoogland, Utrecht	Conventional	Holstein-Friesian	105
4	Easterwierrum, Friesland	Organic	Holstein-Friesian	90

2.2. Acidification of urine

An acidification test was conducted with the pilot scale collected urine. To determine the amount of acid needed to reduce the pH of urine from 9.0 to 5.5, a titration curve was drawn by gradually adding 10µl of 5M sulfuric acid to 5 g urine. This was replicated five times. The 5M acid solution was prepared by diluting concentrated 18M sulfuric acid (98%). When the amount of acid was determined, four replicates of 1kg of urine were acidified to 5.5 pH and stored at 10 °Cfor 40 days, where the pH was monitored every day for the first week and once a week for the remaining time of the test.

2.3. Analytical methods

Chemical analysis of dry matter (DM), ash, total nitrogen (TN), total ammoniacal nitrogen (TAN), total phosphorous (TP), water soluble phosphorus (SP), total potassium (K), and pH was done according to standard methods (APHA, 1995) in the local laboratory at Wageningen Livestock Research. Organic matter content (OM) is defined here as the difference between DM and ash. Organic nitrogen is defined here as the difference between TN and TAN.

2.4. Calculations

a) Separation efficiency

To evaluate the separation efficiency, we calculated the SE(x), which is the percentage of a compound (x)

accumulated in the solid fraction (SS faeces) using the following formulas:

$$SE(x) \text{ in } \% = (Ms(x)) / (Ms(x)+Ml(x)) \times 100 \quad \text{(Hjorth et al., 2011; Vu et al., 2016)} \quad \text{Eq. (1)}$$

$$Ms(x) \text{ in g} = Cs(x) \times 0.6 \text{ kg} \quad \text{Eq. (2)}$$

$$Ml(x) \text{ in g} = Cl(x) \times 0.4 \text{ kg} \quad \text{Eq. (3)}$$

Where Ms(x) is the mass of a compound x in the solid fraction in grams and Ml(x) is the mass of a compound x in the liquid in grams. Cs(x) is the concentration of compound x in the solid in g/ kg while Cl(x) is the concentration of compound x in the liquid in g/kg. According to Dairy campus, the mass separation is estimated to yield 0.6 kg faeces (taken as solid fraction) and 0.4 kg urine (taken as liquid fraction) for 1 kg of excreta (Galama, 2021a). The same estimation was used for the practical farms.

b) Mass balance calculations and nutrient losses

The mass balance for 1 kg of excreta of a selected compounds in the SS system was calculated and compared to the slurry system. Based on this comparison, we were able to see if N-losses between systems differed or not. This N loss gives a proxy for N emissions that were not directly measured in this study, but by Dairy Campus themselves. The mass balance for compounds in SS fractions was calculated by adding up Ms(x) and Ml(x) to Mss (Eq. 4):

$$Mss(x) \text{ in g} = Ms(x) + Ml(x) \quad \text{Eq. (4)}$$

2.5. Statistical analysis

All differences between systems and compounds were statistically tested based on a general linear model performed in SPSS 28 (IBM Corp, 2021). The independence of variables and normality of residual observations were checked prior to fitting the models. When significant differences were obtained, the equality of variance between groups was checked using Levene's test. For multiple comparisons of means, Tukey B test was used when the variances were found equal, while Dunnett's T3 test was used when the variances were found non-equal.

3. Results and Discussion

3.1. Chemical composition

Table 2 summarizes the average contents of DM, OM and nutrients of SS Faeces, SS urine and slurry for all measurement times. The composition of slurry was in accordance with ranges found in literature (Prado et al, 2022). For most of the chemical characteristics the SS faeces and SS urine were significantly different from slurry meaning that the separation floor created clearly distinct fractions.

The average DM content of the SS faeces and SS urine was 13.2% and 2.8%, respectively, which is in line with the composition range of faeces and urine collected separately and directly after excretion from dairy cows (typically between 13.2 and 18.6% for faeces and between 3.5 and 5.3% for urine) (Tomlinson et al., 1996; van Vliet et al., 2007; Vicente et al., 2021). This alignment with literature was also valid for total ammoniacal nitrogen (TAN) (typically between 0.3 and 0.8 g kg^{-1} for faeces and between 1.3 and 5.2 g kg^{-1} for urine) and total P (TP) concentrations (typically between 1.0 and 1.5 g kg^{-1} for faeces and between 0.1 and 0.2 g kg^{-1} for urine). On average we found 0.6 g kg^{-1} TAN and 1.0g kg^{-1} TP in the SS faeces and 2.8 g kg^{-1} TAN and 0.1 g kg^{-1} TP in the SS urine. The TN content was 4.2 g kg^{-1} for the SS faeces and 3.2 g kg^{-1} for SS urine, which are in the range reported for TN content in dairy faeces typically between 4.1 and 5.2 g kg^{-1}, but not that of urine being typically between 5.2 and 10.2 g kg^{-1}. The much lower TN content found for SS urine could be caused by losses through ammonia volatilization as we sampled from the pit where urine accumulated for a long period. Indications of results from the experiments at Dairy Campus indeed showed high NH_3 losses experimental unit (Galama, 2021b). Therefore, for most parameters, SS Faeces and SS urine were in the same range as the isolated dairy faeces and urine meaning that the separation floor in the study effectively separated urine from faeces.

Table 2: Chemical composition of the segregated faeces and urine and slurry from the pilot flooring systems of Dairy Campus. The results represent the mean of two collection periods ± standard deviation (n= 2).

	DM (%)	OM g/kg	Total-N g/kg	TAN g/kg	Total-P g/kg	SP mg/l	Total-K g/kg	pH
Slurry	11.5^{b}±0.6	91.8^{b}±4.6	5.0^{a}±0.2	2.2^{b}±0	0.8^{b}±0.1	15^{a}±4	4.5^{b}±0.0	7.2^{b}±0
SS Faeces	13.2^{a}±0.9	110.6^{a}±6.4	4.2^{b}±0.6	0.6^{c}±0.1	1.0^{a}±0.2	45^{a}±20	2.5^{c}±0.5	6.7^{c}±0.2
SS urine	2.8^{c}±0.2	9.8^{c}±0.5	3.2^{c}±0.7	2.8^{a}±0.8	0.1^{c}±0.1	2^{b}±2	6.7^{a}±0.7	8.5^{a}±0.8

SS source segregation, DM: dry matter, OM: organic matter, TAN: total ammoniacal N, SP: water soluble phosphorus. Different subscripts per column indicate significant different means P<0.05.

3.2. Separation efficiencies

The separation efficiencies (SE(x)) calculated per collection period and as average are presented in Table 3. The results show that on average the SE(x) was 88, 94, 67, 24, 95 and 97% for DM, OM, TN, TAN, TP and SP respectively. When comparing between the two collection periods, the SE(x) varied significantly for TN, TAN, TP and SP.

3.2.1. Dry matter

The SE(DM) showed that 88% of DM accumulated in the faeces, with no significant difference between the two collection periods. This was higher than the DM separation efficiency of slurry separation methods typically reaching up to 75% (Hjorth et al, 2011; Zhang et al, 2022). Compared to the conveyor belt SS systems in pig housing, our SE(DM) was similar to the 88% found by Aarnink and Ogink (2007), but lower than the 92% found by Vu et al. (2016).

3.2.2 Organic matter

The SE(OM) was on average 94% and showed no significant differences between collection periods. This is also higher than the SE(OM) achieved with solid-liquid separation of slurry, which is typically not higher than 62% (Zhang et al, 2022). As compared to other SS systems, our results were similar to Vu et al., (2016) who found a 96% SE(OM) with the conveyor belt in pig housing.

3.2.3 Total nitrogen

The SE(TN) showed that on average 67% of TN accumulated in the SS Faeces. When comparing between collection periods, SE(TN) varied significantly and ranged from 65 to 68%. The SE(TN) from both periods, however, is higher than the separation efficiencies obtained with solid-liquid separation, where centrifugation following flocculation was reported to have the highest separation efficiency of 60% (Hjorth et al., 2011; Zhang et al., 2022). For other SS systems, Aarnink and Ogink, (2007) and Vu et al., (2016) showed a SE(TN) of 66% in pig housing being in the same range of our results.

3.2.4 Total ammoniacal nitrogen

SE(TAN) showed significant differences between sampling periods, ranging from 18 to 29% and with an average of 24%. Although variations, the SE(TAN) stayed in the same range obtained with solid-liquid separation of slurry typically between 16 and 23% (Hjorth et al., 2011; Zhang et al., 2022). Further, SE(TAN) separation in our study was lower than that obtained with conveyor belt SS of pig manure (35 to 38%) (Aarnink and Ogink, 2007; Vu et al., 2016), which means that more TAN was kept in SS urine in our study.

3.2.5 Total P and water soluble phosphorus

SE(TP) was on average 95% and varied significantly from 92 to 98% between collection periods. Nevertheless, the SE(TP) of both periods were similar to the highest separation efficiencies obtained with solid-liquid separation of slurry, which is around 95%, but which requires significantly more chemical inputs (Hjorth et al. 2011; Zhang et al. 2022). Other SS systems even showed SE(TP)'s of more than 95% (Von Bernuth et al., 2005; Aarnink and Ogink, 2007; Vu et al., 2016).

Water soluble phosphorus (SP) is an important component of TP as it is correlated with P runoff and leaching from soils amended with animal manures (Chapuis-Lardy et al., 2003; Kang et al., 2011). Our results showed SE(SP) significantly differed between the two periods ranging from 94 to 99%, meaning that very little SP is present in urine.

Summing up, our SE(x) results show that SS had high separation efficiencies for DM, OM, N and P. The separation efficiencies significantly varied between the two collection periods but were always higher than those achieved with solid-liquid separation of slurry. Moreover, the studied SS system showed high separation efficiencies for all compounds whereas solid-liquid separation techniques in literature show high separation efficiencies only for a limited number of compounds. Hence, using SS to segregate faeces and urine at source is a more effective strategy to separate nutrients and OM than separation after slurry formation. Vu et al., (2016) also reported a similar conclusion for a SS system in pig housing.

Table 3: The separation efficiencies of the source segregation floor for two sampling moments. The results represent mean ± standard deviation (n= 2).

	DM	OM	Total-N	TAN	Total-P	SP
	%	%	%	%	%	%
March	87 ^{ns}±0	94 ^{ns}±0	65 *±1	18 *±1	98 *±0	99 *±0
January	88 ±0	94 ±0	68 ±0	29 ±2	92 ±0	94 ±2
Average	88±1	94±0	67±2	24±8	95±4	97±4

DM: dry matter, OM: organic matter, TAN: total ammoniacal N, SP: water soluble phosphorus.
** indicates means are significantly different ?and ns indicates that means not significantly different (P<0.05).*

3.3. Mass balances and potential nutrient losses

Mass balances were estimated for the SS floor and the slurry system and are presented in Table 4. The results show that on average there were no significant differences between the nutrient contents of slurry and the SS system. However, the different collection periods showed few trends of mass balance variations between SS and slurry.

In the March collection, there was a significant 1.3 g (3%) higher TN in the SS system compared to slurry meaning there were less losses of TN in the SS system as compared to the slurry system. SS is expected to limit contact between urease and urea and contact time with free air, and thus reduce NH_3 emissions, which might be the reason for lower N losses (Vaddella et al., 2010). In the same period, TAN of both systems was comparable. Although the slurry system had lower TN, its TAN content might have been compensated with more mineralization of N than SS system, through for example anaerobic carbon decomposition to CH_4 (Möller et al., 2012). TP was statistically not different for SS and slurry systems.

In January, TP was again not significantly different between slurry and the SS system. TAN, however, was significantly lower in SS, contrarily to March observations. At the same time, SE(TAN) was the highest in January (Table 2), meaning there was higher TAN left in the SS faeces after segregation.

Summing up, our findings from this section suggest that SS has a potential to reduce N losses from dairy manure in the barn at high separation efficiencies (above 90% SE(OM) and 65% SE(TN)) looking at March results as an example. We also depict from this study that the SS system can increase N losses, most likely from the urine, but no cause-effect relationship could be made.

*Table 4: Estimated mass balances of N and P for the slurry compared to source segregation (SS) system. Results are displayed as mean± standard deviation (n=3 samples per period), and represent the mass of the compounds in 1 kg of slurry/ SS fractions. The statistical comparisons shown are between slurry and SS within each period. * represent significant differences and ns non-significant differences (p<0.05, n=3).*

	March		January		Average	
	Slurry	SS	Slurry	SS	Slurry	SS
Total-N g	43.3 *±0.3	44.6 ±02	43.4 *±0.1	38.6 ±0.1	43.4 ^{ns}±0.1	42.3±3.3
TAN g	17.9 ^{ns}±0.3	17.7±0.2	19.7 *±0.1	14.6 ±0.5	18.8 ^{ns}±1.3	16.2±2.2
Total-P g	7.1 ^{ns}±0.0	7.2±0.1	6.7 ^{ns}±0.0	6.6±0.1	6.9 ^{ns}±0.1	6.9±0.4

TAN: total ammoniacal N.

3.4. Urine acidification test

The titration curve established for urine acidification and the development of the pH of the acidified urine during the 40 days test are shown in Figure 1. The results show that the urine required 31 µl of 5M sulfuric acid per 5 g to go from pH 9 to 5.5, which is equivalent to 1.7 ml 18M sulfuric acid (98%) per kg. This is lower than the 2.8 to 5.7 ml kg^{-1} found for slurry acidification with sulfuric acid (Sørensen, P., Eriksen, 2009; Regueiro et al., 2016; and Overmeyer et al., 2021), although slurry is characterised by a lower initial pH than urine. In addition, the results show that pH of the acidified urine remained fairly stable in the 5.5-5.1 range during the test. This is also different from the behaviour of slurry acidified with sulfuric acid to pH 5.5, where pH increases quickly to reach 6.5 at around 30 days after acidification (Regueiro et al., 2016; Overmeyer et al., 2021). Urine requiring less acid and maintaining a low pH as opposed to slurry was linked to its lower buffering capacity. Slurry is known to have a high buffering capacity because of its content of carbonates, phosphates and volatile fatty acids (Sommer and Husted, 1995; Regueiro et al., 2016). Urine has very low content of carbon and phosphorus.

The results thus show that source segregation followed by urine acidification could facilitate the practice of acidification, which intended to reduce NH_3 emissions during storage in the animal house and after application to the field. Acidifying urine instead of slurry can reduce the required amount of acid and limit other constraints that

come with the higher buffering capacity of slurry such as foaming (Fangueiro et al., 2015). This is because we have not observed notable foaming when acidifying with 5M sulfuric acid and very limited foaming when acidifying with 18M sulfuric acid. However, further testing with urine collected from practical farms having different N and OM separation efficiencies is needed to substantiate these results.

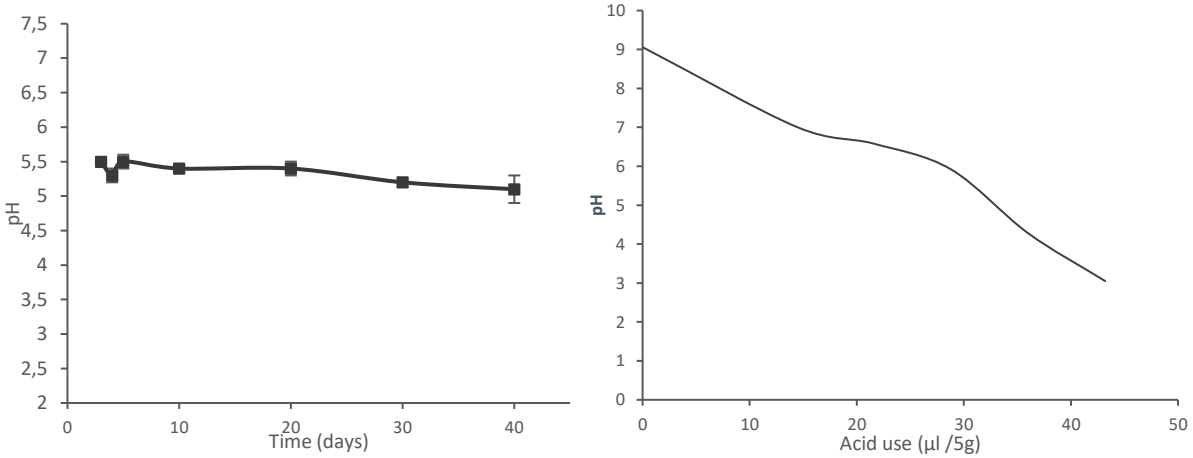

Figure 1: Development of the pH of acidified urine with sulfuric acid (on the left) and the titration curve of urine acidification (on the right). Error bars represent standard deviation (n=5).

3.5. Separation efficiency of SS systems at practical farms

The contents of DM, OM, TN, TAN, TP and K of the segregated faeces and urine collected from four practical farms are shown in Table 5. The SE(X) of the different compounds are also shown in Table 5. The results show that the contents of all compounds in the faeces and urine varied between farms which can be related to variations in feeding and management between farms. However, the ranges found for DM (10.6-16.7% for faeces, 1.2-2.3% for urine) and TP (1.7-2.9 g kg^{-1} for faeces and 0.0 to 0.3 g kg^{-1} for urine) are within the bounds of literature for dairy faeces and urine (Tomlinson et al., 1996; van Vliet et al., 2007; Vicente et al., 2021). The SE(X) results also showed some variation between farms. The SE(DM) ranged from 89% to 93%, which overlaps with the 88% found in the pilot study. Similarly, the SE(OM) range was 92% to 97% overlapping with the 94% found in the pilot test. The SE(TP) was also in the high range similarly to what we found in the pilot test, with 91 to 97% of TP in the faeces. The S(TN) and S(TAN) results, however, showed larger differences between farms and deviations from the separation efficiency results in the pilot test. The SE(TN) ranged from 74% to 81%, which is higher than the 67% found in the pilot test. The reason for the higher SE(TN) in the practical farms seems to be the low TN content of urine, which was as low as 1.5 g kg^{-1} in two of the farms. The SE(TAN) in three out of the four farms ranged from 31% to 56%, which was also higher than that found in the pilot test (14% to 29%). This difference can also be related to the TAN content of urine being consistently low in the farms as compared to in the pilot test (1.7±0.8 g kg^{-1} as compared to 2.8±0.8 g kg^{-1}). The low urine N content can be linked to a lower N intake of the cows in the practical farms, as three out of four are organic farms, or to lower N excretion because of different cow breeds. However, lower N in urine can also indicate substantial N losses, which can occur through NH_3 emissions.

The results thus showed that SS systems in dairy housing can effectively separate DM, OM and TP also in practice and achieve separation efficiencies higher than those of sloid-liquid separation of slurry. However, it appears that N separation is a critical aspect of these systems as they show considerable variation and possibly lead to high N losses. Future research needs to focus on understanding the factors influencing N separation and losses with SS systems and research additional measures to reduce these losses, such as acidification or air scrubbing in the pit.

Table 5: Chemical characteristics of source segregated faeces and urine collected from four farms in The Netherlands and the separation efficiencies (SE) of the corresponding source segregation floor. The results are based on one collection per farm.

Farm		DM	OM	Total-N	TAN	Total-P
		%	g/kg	g/kg	g/kg	g/kg
1	SS Faeces	11.8	92	3.5	0.8	2.1
	SS Urine	1.6	8	1.5	1.1	0.3
	SE	92%	95%	78%	52%	91%
2	SS Faeces	10.6	90	2.8	0.1	1.7
	SS Urine	1.2	5.0	1.1	0.9	0.1
	SE	93%	96%	78%	14%	98%
3	SS Faeces	12.6	103	4.1	0.5	2.1
	SS Urine	2.3	13	2.1	1.7	0.1
	SE	89%	92%	74%	31%	97%
4	SS Faeces	16.7	121	4.4	1.0	2.6
	SS Urine	1.8	6	1.5	1.2	0.1
	SE	93%	97%	81%	56%	97%

**SE: separation efficiency, DM: dry matter, OM : organic matter, TAN: total ammoniacal nitrogen.*

3.6. Conclusions and future prospects

This study revealed that source segregation in dairy housing can effectively separate DM, OM, TN, TAN and TP by up to 88%, 94%, 67%, 24% and 95%, respectively, without intensive use of energy and chemical inputs traditionally used to separate slurry. While these results sourced from a pilot SS system, we also found similar trends of high separation efficiencies with SS systems installed in four practical farms, particularly for DM, OM and TP. For TN and TAN however, the trends showed variations between farms and from the pilot study, and understanding these variations require further investigations including measuring N emissions in the animal house. Moreover, the SS faeces and SS urine obtained can be more adapted to the downstream manure processing. With the high separation of OM achieved, SS faeces can substitute slurry in anaerobic digestion and thus reduce digester size and transport costs (EL Mahdi et al., 2024). The SS faeces are also low in TAN which is an inhibitor of the anaerobic digestion process above certain thresholds (Labatut et al., 2014; Kang et al., 2021). Vu et al., (2016) reported that digesting the solids from a SS system can increase economic feasibility of mono-digestion of pig manure. A similar investigation on SS dairy excreta is the objective of our future work. In addition, SS urine can be applied to land to provide readily available N for crops combined to an NH_3 emission reduction treatment like acidification. Acidification of the SS urine was found to require less acid and to be more stable than acidification of slurry.

Another potential benefit of SS is the reduction of emissions and nutrient losses. Previous studies reported SS to reduce N losses by limiting ammonia emissions in both pig and dairy houses (Swierstra et al., 2001; Lachance et al., 2005; Stewart et al., 2004; Panetta et al., 2005; Von Bernuth et al., 2005; Vu et al., 2016). In this study, we did not directly measure N losses, but based on the slurry, SS faeces and SS urine compositions, we estimated the mass balances and derived the potential losses. Our results showed varying effects in the different collection periods where N losses were either increased or decreased with the SS system compared to slurry. Further investigations are needed to understand the factors that might affect the nutrient balances, like floor material, management aspects and contamination of the urine in the pit. This information can then be used to identify critical aspects to achieve the desired separation and nutrient loss reduction effects. Further investigations are also needed to depict and understand trade-offs of urine acidification, as it was suspected to increase N_2O emissions and solubilisation of phosphorus in urine to measure emissions from the segregated fractions downstream.

Funding

The research leading to these results has received funding from the European Union's Horizon 2020 research and innovation programme under the Marie Sklodowska-Curie grant agreement No. 860127 (FertiCycle project).

Acknowledgements

The authors acknowledge Geert Kupers from Wageningen livestock research for supporting with analytical methods, and Herman De Boer from Dairy Campus for facilitating the collection of manure material and providing information. We would also like to acknowledge Joachim Deru from the Louis Bolk Institute and Debby Van Rotterdam from the Nutrient Management Institute for providing the practical farms data collected as part of the *Gescheiden met waarde* project.

References

Aarnink, A. J. A., & Ogink, N. W. M. (2007). Environmental impact of daily removal of pig manure with a conveyer belt system. In International Symposium on Air Quality and Waste Management for Agriculture, 6-19 September 2007, Broomfield, Colorado, USA.

APHA (American Public Health Association). (1995). Standard methods for the examination of water and wastewater (19th ed.) Washington, DC, USA.

Braam, C.R., J.J.M.H. Ketelars, and M.C.J. Smits. 1997. Effects of floor design and floor cleaning on ammonia emission from cubicle houses for dairy cows. Neth. J. Agric. Sci. 45:49–64.

CBS, PBL, RIVM, WUR (2021). Manure surpluses in agriculture, 1970-2019 (indicator 0096, version 20, 8 April 2021). www.environmentaldata.nl. Statistics Netherlands (CBS), The Hague; PBL Netherlands Environmental Assessment Agency, The Hague; RIVM National Institute for Public Health and the Environment, Bilthoven; and Wageningen University and Research, Wageningen.

Von Bernuth, R. D., Hill, J. D., Henderson, E., Godbout, S., Hamel, D., & Pouliot, F. (2005). Efficacy of a liquid/solid isolation system for swine manure. Transactions of the ASAE, 48(4), 1537-1546.Dai, X., Karring, H. 2014. A determination and comparison of urease activity in faeces and fresh manure from pig and cattle in relation to ammonia production and pH changes. *PLoS One*, **9**(11), e110402.

Deru J., Van Rotterdam D., EL Mahdi J., De Stigter J., Beek J. (2023) Ammoniak- en broeikasgasemissies van gescheiden mestfractie in een incubatie-experiment. Wageningen, Netherlands: Louis Bolk Instituut, 2023-01 LbD.

EL Mahdi, J., Nyang'au, J.O., De Vries, J.W., van Eekert, M.H.A., Koerkamp, P.G., Møller, H.B. 2024. Biomethane yield of novel source segregated dairy excreta under different anaerobic digestion systems. Environmental Technology & Innovation, 103684.

Fangueiro, D., Coutinho, J., Chadwick, D., Moreira, N., Trindade, H. 2008. Effect of Cattle Slurry Separation on Greenhouse Gas and Ammonia Emissions during Storage. *Journal of Environmental Quality*, **37**(6), 2322-2331.

Galama P.J., Ouweltjes W., Endres M.I., et al. (2020) Symposium review: Future of housing for dairy cattle. Journal of Dairy Science 103: 5759-5772.

Galama P.J. (2021a) Wisselende effecten bij mestscheiden aan de bron. Retrieved January 30, 2023, from https://www.wur.nl/nl/nieuws/wisselende-effecten-bij-mestscheiden-aan-de-bron.htm.

Galama P.J (2021b) Doorlaatbare tegelvloer in bedrijfsverband. Retrieved January 30, 2023, from https://www.wur.nl/nl/nieuws/doorlaatbare-tegelvloer-in-bedrijfsverband.htm.

Hjorth, M., Christensen, K.V., Christensen, M.L., Sommer, S.G. 2011. Solid–Liquid Separation of Animal Slurry in Theory and Practice. in: *Sustainable Agriculture Volume 2*, (Eds.) E. Lichtfouse, M. Hamelin, M. Navarrete, P. Debaeke, Springer Netherlands. Dordrecht, pp. 953-986.

Yan, J., De Buisonjé, F.E., Melse, R.W. 2017. Livestock Manure Treatment Technology of the Netherlands and Situation of China. Wageningen Livestock Research, Wageningen, Report 1048.

Kang, J., Amoozegar, A., Hesterberg, D., Osmond, D.L. 2011. Phosphorus leaching in a sandy soil as affected by organic and inorganic fertilizer sources. *Geoderma*, **161**(3), 194-201.

Kaparaju, P.L.N., Rintala, J.A. 2008. Effects of solid–liquid separation on recovering residual methane and nitrogen from digested dairy cow manure. *Bioresource Technology*, **99**(1), 120-127.

Knowlton K.F., Radcliffe J.S., Novak C.L., et al. 2004. Animal management to reduce phosphorus losses to the environment. J Anim Sci 82 E-Suppl: E173-195.

Koger J.B., O'Brien B.K., Burnette R.P., et al. 2014. Manure belts for harvesting urine and faeces separately and improving air quality in swine facilities. Livestock Science 162: 214-222.

Lachance, I., Jr, Godbout, S., Lemay, S. P., & Larouche, F. P. J. P. (2005). Separation of Pig Manure Under Slats: to Reduce Releases in the Environment! Paper presented at the ASAE Annual International Meeting, St. Joseph, MI.

Møller, H.B., Lund, I. and Sommer, S.G. 2000. Solid–liquid separation of livestock slurry: efficiency and cost. Bioresource Technology 74: 223-229.

Møller, H.B., Sommer, S.G., Ahring, B.K. 2002. Separation efficiency and particle size distribution in relation to manure type and storage conditions. Bioresource Technology, 85(2), 189-196.

Möller, K. and Müller, T. (2012), Effects of anaerobic digestion on digestate nutrient availability and crop growth: A review. Eng. Life Sci., 12: 242-257.

Labatut R.A., Angenent L.T. and Scott N.R. (2014) Conventional mesophilic vs. thermophilic anaerobic digestion: a trade-off between performance and stability? Water Res 53: 249-258.

Overmeyer, V., Kube, A., Clemens, J., Büscher, W., Trimborn, M. 2021. One-Time Acidification of Slurry: What Is the Most Effective Acid and Treatment Strategy? Agronomy, 11(7), 1319.

Panetta, D.M., Powers, W.J., Lorimor, J.C. 2005. Management Strategy Impacts on Ammonia Volatilization from Swine Manure. *Journal of Environmental Quality*, **34**(3), 1119-1130.

Prado, J., Ribeiro, H., Alvarenga, P., Fangueiro, D. 2022. A step towards the production of manure-based fertilizers: Disclosing the effects of animal species and slurry treatment on their nutrients content and availability. *Journal of Cleaner Production*, **337**, 130369.

Regueiro, I., Coutinho, J., Fangueiro, D. 2016. Alternatives to sulfuric acid for slurry acidification: impact on slurry composition and ammonia emissions during storage. Journal of Cleaner Production, 131, 296-307.

Schröder, J.J., Aarts, H.F.M., van Middelkoop, J.C., Schils, R.L.M., Velthof, G.L., Fraters, B., Willems, W.J. 2007. Permissible manure and fertilizer use in dairy farming systems on sandy soils in The Netherlands to comply with the Nitrates Directive target. *European Journal of Agronomy*, **27**(1), 102-114.

Sommer, S.G., Husted, S. 1995. The chemical buffer system in raw and digested animal slurry. The Journal of Agricultural Science, 124(1), 45-53.

Sørensen, P., Eriksen, J. 2009. Effects of slurry acidification with sulphuric acid combined with aeration on the turnover and plant availability of nitrogen. Agriculture, Ecosystems & Environment, 131(3), 240-246.

Stewart, K.J., Lemay, S.P., Barber, E.M., Laguë, C., Crowe, T. 2004. Experimental Manure Handling Systems for Reducing Airborne Contamination of Fecal Origin, Paper presented at the ASAE Annual International Meeting. St. Joseph, MI.

Swierstra, D., R. Braam, C., C. Smits, M. 2001. Grooved Floor System for Cattle Housing: Ammonia Emission Reduction and Good Slip Resistance. *Applied Engineering in Agriculture*, **17**(1), 85-90.

Tomlinson, A. P., Powers, W. J., Van Horn, H. H., Nordstedt, R. A., Wilcox, C. J. 1996. Dietary Protein Effects on Nitrogen Excretion and Manure Characteristics of Lactating Cows. *Transactions of the ASAE*, **39**(4), 1441-1448.

Vaddella, V.K., Ndegwa, P.M., Joo, H.S., Ullman, J.L. 2010. Impact of Separating Dairy Cattle Excretions on Ammonia Emissions. *Journal of Environmental Quality*, **39**(5), 1807-1812.

Van Vliet, P.C.J., Reijs, J.W., Bloem, J., Dijkstra, J., de Goede, R.G.M. 2007. Effects of Cow Diet on the Microbial Community and Organic Matter and Nitrogen Content of Faeces. *Journal of Dairy Science*, **90**(11), 5146-5158.

Vicente, F., Elouadaf, D., Sánchez-Vera, A., Soldado, A., De La Torre-Santos, S., Martínez-Fernández, A. 2021. The Dairy Cow Slurry Composition Used as Organic Fertilizer Is Influenced by the Level and Origin of the Dietary Protein. *Anima*ls, 11(10), 2812.

Vu, P. T., Melse, R. W., Zeeman, G., & Groot Koerkamp, P. W. G. 2016. Composition and biogas yield of a novel source segregation system for pig excreta. Biosystems Engineering, 145, 29-38.
Whitehead, D.C., Raistrick, N. 1993. Nitrogen in the excreta of dairy cattle: changes during short-term storage. The Journal of Agricultural Science, 121(1), 73-81.
Zhang, X., Liu, C., Liao, W., Wang, S., Zhang, W., Xie, J., Gao, Z. 2022. Separation efficiency of different solid-liquid separation technologies for slurry and gas emissions of liquid and solid fractions: A meta-analysis. Journal of Environmental Management, 310, 114777.

Performance evaluation of different pumps and pumpsets for agricultural application

Arthur L. Fajardo[a*], Charleen Grace V. Deniega[b], Fatima Joy J. Raytana-Aying[c], Marie Jehosa B. Reyes[c], Jerson Jose T. Menguito[c], Yaminah Mochica M. Pinca[c]

[a] Agribiosystems Machinery and Power Engineering Division, University of the Philippines Los Baños, Los Baños, Philippines

[b] Sorsogon State University, Sorsogon City, Philippines

[c] Agricultural Machinery Testing and Evaluation Center, University of the Philippines Los Baños, Los Baños, Philippines

* Corresponding author. Email: alfajardo@up.edu.ph

Abstract

The Philippine government has identified agricultural mechanization as a strategy for addressing national food security challenges. Performance evaluation of pumps and pumpsets serves as a guide for government agencies and private institutions deciding on units to buy, distribute, and install on the farms. This study aimed to evaluate the performance of agricultural pumps and pumpsets. Performance data of centrifugal pumps and pumpsets tested by the Agricultural Machinery Testing and Evaluation Center (AMTEC) from 1989 to 2022, based on Philippine Agricultural Engineering Standards (PAES) 115:2000, were used in the study. The selected sizes for both pump and pumpset include 50×50 mm, 75×75 mm, and 100×100 mm. Only engine-powered units were selected for the pumpsets. The performance of the agricultural pumps was evaluated using four (4) schemes. Scheme 1 was patterned from Resurreccion et al. (2008) while Schemes 2, 3, and 4 were a modified version. In Schemes 3 and 4, the performance data were adjusted using pump affinity law. Results showed that most pumps are within the minimum requirements (6 points and above) under Scheme 1. All non-self-priming 100×100 mm pumps passed the minimum requirements for Scheme 1. On the other hand, using Schemes 2 and 4, most 50×50 mm pumps were below the minimum requirements. Most 50×50 mm pumpsets were below performance for all the rating schemes except for the close-coupled, self-priming, air-cooled diesel and gasoline types under Scheme 2. Most 75×75 mm non-self-priming, water-cooled diesel, V-belt and pulley transmission pumpsets passed the rating for all evaluation schemes. Most 100×100 mm non-self-priming, water-cooled diesel, V-belt and pulley transmission pumpsets passed the rating for all evaluation schemes. With the modified scheme, putting weight on the efficiency (pump or system) has an impact on the performance evaluation of pumps and pumpsets. Appropriate tools (i.e., statistical) or systems should be utilized to determine the optimum weight assignment for the evaluation scheme.

Keywords: agricultural mechanization, agricultural machinery testing, centrifugal pumps and pumpsets

1. Introduction

The Agricultural and Fisheries Mechanization (AFMech) Law of 2013 and the 2019 Rice Competitiveness Enhancement Fund (RCEF) program of the Philippines both aim to attain food security and increase farmer's income through agricultural mechanization. RCEF allocates a PhP 5-billion annual budget for agricultural mechanization from 2019 to 2024. The goal of the RCEF mechanization program is to improve farmer's yield, income, and competitiveness in the global market through access to appropriate agricultural machinery from land preparation to postharvest operation. One of the machinery types distributed by this program is the irrigation pump.

Centrifugal pump is a type of pump with impellers rotating inside a closed casing that draws water into the pump through a central inlet opening and forces water out through a discharge outlet at the periphery of the housing using centrifugal force. A centrifugal pumpset is a pump directly- or indirectly- coupled to a prime mover, either with an engine or electric motor. An engine pumpset could be powered by a diesel (either water-cooled or air-cooled) or a gasoline engine (air-cooled). The common types of power transmission systems for engine-powered pumpsets include close-coupled, direct-coupled, and belt-and-pulley transmission. In the Philippines, centrifugal pumps and pumpset are tested in accordance with PAES 115:2000 (Agricultural Machinery – Centrifugal, Mixed Flow, and Axial Flow Water Pumps – Method of

Test). The test is conducted by operating the pump at the manufacturer's recommended pump speed.

A performance rating system was developed as a guiding tool in the appropriate selection of agricultural pumps (Resurreccion et al., 2008). The performance evaluation of different bare pumps and pumpsets serves as a guide for government agencies and private institutions in deciding the pumpset and bare pump to buy, distribute, and install on farms. The main objective of this study is to evaluate and compare the performance of bare pumps and pumpsets based on different parameter weighting.

2. Materials and Methods

The performance data of pumps and pumpsets tested in AMTEC from 1989 to 2022 were collected, processed, and evaluated. The sizes selected only include 50×50mm, 75×75mm, and 100×100mm for both pumps and pumpsets. For the pumpsets, only the engine-powered units were considered. These selection criteria were based on the common sizes and prime mover used for shallow tubewells (STW) and low-lift pumps (LLP) in the Philippines.

The pumps were then grouped based on the priming method (non-self-priming and self-priming) for each pump size. On the other hand, the pumpsets were grouped by priming method (non-self-priming and self-priming), engine type (diesel engine and gasoline engine), and power transmission type (close-coupled and belt-and-pulley transmission). Direct transmission pumpsets were grouped under the close-coupled transmission category.

The performance rating scheme (Scheme 1) adopted from the study of Resurreccion et al. (2008) was used to evaluate the centrifugal pumps (Table 1) and pumpsets (Table 2). The performance data of pumps and pumpsets tested were evaluated using the following parameters for Scheme 1: discharge-to-input power ratio, suction lift, maximum efficiency, and input speed. Parameters were rated on a scale of 2 to 10, with 2 representing the lowest rating and 10 the highest. The final rating points were computed by dividing the total rating points by the number of parameters used. If the pump or pump set receives a final rating point of 6 or higher, it satisfies the minimum requirements for performance, whereas a score of 4 or less does not. Regardless of whether the pump met the minimum requirements based on PAES 115, it should be noted that the parameters used have equal weights for determining the final rating.

Table 1. Criteria for the performance rating of centrifugal pumps (Resurreccion et al., 2008).

Parameter	Minimum Requirement	Range of Values	Equivalent Points
Discharge-Input Power Ratio	0.75	1.30 and above	10
		1.00-1.29	8
		0.75-0.99	6
		0.50-0.74	4
		Below 0.50	2
Pump Efficiency, %			
Self-priming	50.00%	60.00 and higher	10
		55.00 to 59.99	8
		50.00 to 54.99	6
		45.00 to 49.99	4
		Below 45.00	2
Non-self-priming	55.00%	65.00 and higher	10
		60.00 to 64.99	8
		55.00 to 59.99	6
		50.00 to 54.99	4
		Below 50.00	2
Total Suction Lift, m	8.0	9.0 and higher	10
		8.5 to lower 9.0	8
		8.0 to lower 8.5	6
		7.5 to lower 8.0	4
		7.5 and lower	2
Input Speed, rpm	1800-2400	1800-2400	10
		2400-3000	8
		1500-1800	6

		3000 and above	4
		Below 1500	2

Table 2. Criteria for the performance rating of centrifugal pumpsets (Resurreccion et al., 2008).

Parameter	Minimum Requirement	Range of Values	Equivalent Points
Discharge-Input Power Ratio	0.75	1.30 and above	10
		1.00-1.29	8
		0.75-0.99	6
		0.50-0.74	4
		Below 0.50	2
System Efficiency, %	10.0%	14.0 and above	10
		12.0-13.9	8
		10.0-11.9	6
		8.0-9.9	4
		Below 8.0	2
Total Suction Lift, m	8.0	9.0 and higher	10
		8.5 to lower 9.0	8
		8.0 to lower 8.5	6
		7.5 to lower 8.0	4
		7.5 and lower	2
Input Speed, rpm	1800-2400	1800-2400	10
		2400-3000	8
		1500-1800	6
		3000 and above	4
		Below 1500	2

A modification of the evaluation scheme by Resurreccion et al. (2008) was performed for this study (Scheme 2). The modified weight distribution is as follows for Scheme 2: pump/system efficiency – 40%, input speed – 30%, and suction lift – 30%. A higher weight for pump and system efficiency was considered since it is the most important performance parameter. Then, the discharge-to-input power ratio was not included since it is almost the same with efficiency except for the inclusion of the total head. Also, the equivalent points for the input speed were modified. Lower pump speed was given higher points since local farmers tend to set the engine throttle to near the lowest speed (near idling speed). Moreover, setting the pump to a higher shaft speed will also increase its power requirement thereby increasing its fuel consumption. Different shaft speed requirement was set for self-priming and non-self-priming pumps and pumpsets under Scheme 2 (Table 3). This was based on observations from pump test data that the common pump shaft speed for non-self-priming types is 1500-1800 rpm and 2000-2200 rpm for self-priming types. However, it was also observed that the pumps and pumpsets were tested at different shaft speeds (Fajardo et al., 2023). With this, it was proposed to evaluate the bare pump and pumpset performance using the common shaft speed.

Table 3. Criteria for the input speed (rpm) of centrifugal pumps and pumpsets under Scheme 2.

Priming Method	Minimum Requirement	Range of Values	Equivalent Points
Self-priming	1800-2400	1800-2400	10
		2400-3000	8
		1500-1800	4
		3000-up	6
		Below 1500	2
Non-self-priming	1500-1800	1800-2400	8
		2400-3000	6
		1500-1800	10
		3000-up	4
		Below 1500	2

Performance parameters were adjusted using the pump affinity laws. Pump affinity laws state that for the same impeller diameter, if the pump speed is changed, the flow rate is directly proportional to the speed, whereas the head is directly proportional to the square of the speed. As with diameter change, the brake horsepower is proportional to the cube of the impeller speed (Karassik et al., 2008). For the bare pumps, the discharge, head, input power, and pump efficiency were recomputed at 2000rpm shaft speed. Whereas for centrifugal pumpsets, the discharge, head, fuel consumption, and system efficiency were re-computed at 2000rpm for units with V-belt and pulley transmission and 3600rpm for units with close-coupled transmission. Fuel consumption was recomputed using the input power-shaft speed relationship (proportional to the cube).

After the recomputations, performance was evaluated using the original scheme of Resurreccion et al. (2008), excluding the input speed (Scheme 3). Also, another modified version (Scheme 4) was applied using the following weight distribution: pump/system efficiency – 60% and suction lift – 40%.

Therefore, four (4) evaluation schemes were used in the study: a) Scheme 1 – based on Resurreccion et al. (2008); b) Scheme 2 – a modified scheme by Resurreccion et al. (2008) with adjusted input speed scores and higher weight for pump or system efficiency; c) Scheme 3 – adjusted shaft speed to 2000 or 3600rpm, then applied the scheme based from Resurreccion et al. (2008) excluding input speed; and d) Scheme 4 – adjusted shaft speed to 2000 or 3600rpm, then applied modified scheme by Resurreccion et al. (2008) excluding input speed and higher weight given for pump or system efficiency.

3. Results and Discussion

3.1. Bare Pumps

The performance data of pumps and pumpsets tested by the AMTEC in the University of the Philippines Los Baños from 1989 to 2022 were gathered. Data from a total of 341 bare pumps were sorted by size (50×50 mm, 75×75 mm, and 100×100 mm) and priming method (non-self-priming and self-priming). A total of 49 bare pump units have a size of 50×50 mm which include 31 self-priming units and 18 non-self-priming units. Then, there were 114 units of 75×75 mm bare pumps. Of the 114 75×75 mm bare pumps, 50 units were self-priming and 64 units were non-self-priming. The remaining 178 units are 100×100 mm bare pumps, which included 72 self-priming units and 106 non-self-priming units.

Table 4 presents the performance of the different sizes of bare pumps tested. Pump efficiency and discharge capacity increase with pump size, though the pump efficiencies of 75×75 mm and 100×100 mm bare pumps have relatively slight differences for each type.

Table 4. Total head and discharge capacity at maximum pump efficiency of the different bare pump sizes tested at AMTEC.

Pump Size	Priming Method	Maximum Pump Efficiency, %	Total Head, m	Discharge Capacity, L/s
50×50 mm	Non-self-priming	52.99	16.40	7.78
	Self-priming	39.11	15.91	5.37
75×75 mm	Non-self-priming	61.05	16.62	15.78
	Self-priming	45.14	15.48	10.82
100×100 mm	Non-self-priming	62.21	14.39	25.54
	Self-priming	47.24	15.90	16.66

Source: Fajardo et al., 2023

3.2. Performance Evaluation Scheme Analysis of Bare Pumps

Four (4) parameters were used for the performance evaluation scheme: discharge-input ratio, pump efficiency (%), total suction lift (m), and input speed (rpm). Most pumps are within the minimum requirements (6 points and above) under Scheme 1 as presented in Table 5. All non-self-priming 100×100 mm pumps passed the minimum requirements for Scheme 1. On the other hand, using Schemes 2 and 4, most 50×50mm pumps were below the minimum requirements (less than 6 points). Moreover, most of the self-priming pumps have the highest decline in number after using Schemes 2, 3, and 4. The reduction of the number of units that passed the minimum requirements using Schemes 2 and 4 shows that the pump efficiency

has a greater impact on the evaluation scheme.

Table 5. Number of units of different bare pump sizes that passed the performance evaluation scheme.

Pump Size	Priming Method	Scheme 1	Scheme 2	Scheme 3	Scheme 4
50×50 mm	Non-self-priming (18)	16	9	13	6
	Self-priming (31)	28	5	17	3
75×75 mm	Non-self-priming (64)	60	45	59	35
	Self-priming (50)	48	15	35	9
100×100 mm	Non-self-priming (106)	106	87	100	75
	Self-priming (72)	71	29	41	5

3.3. Centrifugal Pumpsets

Tables 6 to 8 present the performance of the 50×50 mm, 75×75 mm, and 100×100 mm centrifugal pumpsets at maximum system efficiency, respectively. Results showed that, in general, the pumpsets' system efficiency is relatively higher for the non-self-priming units than the self-priming type (same with bare pump efficiency). Considering engine type, the system efficiency is relatively higher for diesel engine-powered pumpsets than those powered by gasoline engines. Also, the system efficiency of the pumpsets was observed to be relatively higher for units driven by water-cooled engines than air-cooled engines.

Table 6. Performance of the AMTEC-tested 50×50 mm centrifugal pumpsets at maximum system efficiency.

Type	Maximum System Efficiency, %	Fuel Consumption, L/h	Total Head, m	Discharge Capacity, L/s	Range of Engine Rated Power, kW
Close-coupled Non-self-priming, Water-cooled diesel engine	10.70	1.48	28.50	6.19	3.73 – 5.97
Self-priming, Air-cooled diesel engine	10.18	0.94	16.86	5.89	2.24-5.22
Self-priming, Gasoline engine	7.97	1.30	16.63	5.70	2.24 -5.22
V-belt and pulley Non-self-priming, Water-cooled diesel engine	11.28	1.76	30.09	6.73	5.10 – 5.27
Self-priming, Water-cooled diesel engine	8.45	1.48	23.63	5.92	5.10 – 6.18

Source: Fajardo et al., 2023

Table 7. Performance of the AMTEC-tested 75×75 mm centrifugal pumpsets at maximum system efficiency.

Type	Maximum System Efficiency, %	Fuel Consumption, L/h	Total Head, m	Discharge Capacity, L/s	Range of Engine Rated Power, kW
Close-coupled Non-self-priming, Air-cooled	18.99	1.34	15.60	17.30	4.80

diesel engine					
Non-self-priming, Water-cooled diesel engine	14.95	1.80	13.78	17.05	3.73 – 5.22
Self-priming, Air-cooled diesel engine	11.47	1.33	16.12	9.84	2.80 – 8.96
Self-priming, Water-cooled diesel engine	8.36	0.84	10.7	7.07	5.10
Self-priming, Gasoline engine	10.01	1.56	15.63	9.97	2.83 – 5.60
V-belt and pulley					
Non-self-priming, Air-cooled diesel engine	15.25	1.26	14.09	13.85	4.90 – 9.00
Non-self-priming, Water-cooled diesel engine	13.87	1.81	19.19	13.33	4.48 – 7.09
Self-priming, Air-cooled diesel engine	10.08	1.72	16.18	11.27	4.90 – 7.46
Self-priming, Water-cooled diesel engine	11.79	1.49	15.00	12.30	5.12 – 7.09

Source: Fajardo et al., 2023

Table 8. Performance of the AMTEC-tested 100×100 mm centrifugal pumpsets at maximum system efficiency.

Type	Maximum System Efficiency, %	Fuel Consumption, L/h	Total Head, m	Discharge Capacity, L/s	Range of Engine Rated Power, kW
Close-coupled					
Non-self-priming, Water-cooled diesel engine	17.49	1.32	12.79	18.77	3.73 – 5.97
Self-priming, Air-cooled diesel engine	11.99	1.48	14.83	12.87	4.00-7.50
Self-priming, Gasoline engine	8.44	2.46	16	11.55	5.20 – 5.60
V-belt and pulley					
Non-self-priming, Air-cooled diesel engine	11.90	2.41	13.24	20.61	6.62 – 9.00
Non-self-priming, Water-cooled diesel engine	13.38	2.08	14.06	20.75	5.10 – 8.96

Self-priming, Air-cooled diesel engine	9.51	2.14	14.40	14.94	7.30 – 7.46
Self-priming, Water-cooled diesel engine	10.62	2.59	16.53	15.25	5.10 – 10.30

Source: Fajardo et al., 2023

3.4. Performance Evaluation Scheme Analysis of Centrifugal Pumpsets

As presented in Table 9, most 50×50 mm pumpsets were below performance for all the rating schemes except for the close-coupled, self-priming, air-cooled diesel engine-powered units and gasoline engine-powered units under Scheme 2. Moreover, it could be observed that for all schemes, no changes were observed for the non-self-priming, water-cooled diesel engine-powered pumpsets with V-belt and pulley transmission systems. In comparison to the 50×50 mm self-priming bare pumps, the number of units increased from Scheme 1 to Scheme 2 for self-priming close-coupled pumpsets. One reason for this is that the input speed did affect the overall rating of the 50×50mm self-priming closed-coupled pumpsets.

Table 9. The number of 50×50 mm centrifugal pumpsets that passed under the different performance schemes.

Type	Scheme 1	Scheme 2	Scheme 3	Scheme 4
Close-coupled (111)				
Non-self-priming, Water-cooled diesel engine (2)	1	1	0	0
Self-priming, Air-cooled diesel engine (22)	3	16	9	9
Self-priming, Gasoline engine (87)	8	56	21	8
V-belt and pulley (10)				
Non-self-priming, Water-cooled diesel engine (4)	3	3	3	3
Self-priming, Water-cooled diesel engine (6)	0	1	0	0

Table 10 presents that most non-self-priming, water-cooled diesel engine-powered pumpsets with V-belt and pulley transmission systems passed the rating for all evaluation schemes. On the contrary, for all evaluation schemes, most of the close-coupled, self-priming pumpsets did not pass the rating. It could also be observed that a relatively higher number of units passed the evaluation for Schemes 3 and 4 for the self-priming close-coupled gasoline engine-powered pumpsets. Increasing the pump shaft speed for the 75×75 mm self-priming pumpsets affected its performance.

Table 10. The number of 75×75 mm centrifugal pumpsets that passed under the different performance schemes.

Type	Scheme 1	Scheme 2	Scheme 3	Scheme 4
Close-coupled (106)				
Non-self-priming, Air-cooled diesel engine (1)	1	1	1	1
Non-self-priming, Water-cooled diesel engine (5)	4	4	4	4
Self-priming, Air-cooled diesel engine (32)	9	8	13	12
Self-priming, Water-cooled diesel engine (1)	0	0	0	0
Self-priming, Gasoline engine (68)	12	12	29	24
V-belt and pulley (50)				
Non-self-priming, Air-cooled diesel engine (2)	1	1	1	1
Non-self-priming, Water-cooled diesel engine (27)	23	18	15	15
Self-priming, Air-cooled diesel engine (2)	1	1	1	1
Self-priming, Water-cooled diesel engine (19)	14	8	7	6

In Table 11, it could be observed that most non-self-priming, water-cooled diesel engine-powered pumpsets with V-belt and pulley transmission systems passed the rating for all evaluation schemes. Also, for the close-coupled, self-priming, air-cooled diesel engine-powered pumpsets, the number of units that passed the rating increases with Schemes 2 and 3. For all sizes of pumpsets, the modified evaluation (Schemes 2 to

4) showed the impact of pumpset efficiency in the performance evaluation. On the other hand, a relatively higher number of units passed the evaluation for Schemes 3 and 4 for the self-priming, closed-coupled, air-cooled diesel engine-powered pumpsets. Similar to the observation with the 75×75 mm pumpsets, increasing the pump shaft speed for the 100×100 mm self-priming pumpsets also affected its performance.

Table 11. The number of 100×100 mm centrifugal pumpsets that passed under the different performance schemes.

Type	Scheme 1	Scheme 2	Scheme 3	Scheme 4
Close-coupled (30)				
Non-self-priming, Water-cooled diesel engine (5)	2	2	3	3
Self-priming, Air-cooled diesel engine (23)	8	6	13	13
Self-priming, Gasoline engine (2)	0	0	0	0
V-belt and pulley (177)				
Non-self-priming, Air-cooled diesel engine (7)	4	5	4	4
Non-self-priming, Water-cooled diesel engine (90)	69	73	57	57
Self-priming, Air-cooled diesel engine (8)	4	3	2	2
Self-priming, Water-cooled diesel engine (72)	58	34	28	26

4. Summary and Conclusions

Agricultural pumps and pumpsets tested in the Agricultural Machinery Testing Evaluation Center (AMTEC) from 1989 to 2022 were the focus of the study. Testing data of the centrifugal pumpsets and bare pumps were subjected to four (4) performance evaluation schemes based on the study of Resurreccion et al. (2008). Pump and system efficiency, as well as adjustments in the pump shaft speed, affected the performance evaluation in the selection of centrifugal pumps and pumpsets.

5. Recommendations

To further improve the results of this study, analysis of the pumps and pumpsets performance can be done in terms of assigning weights on specific parameters using statistical tools such as the Analytic Hierarchy Process (AHP) or Multi-Criteria Decision Analysis (MCDA). This is to determine the ideal (or optimum) weight distribution to better guide stakeholders in the selection of pumps and pumpsets. Further, it is also recommended to use the performance of pumps and pumpsets using a common pump shaft speed for evaluation.

References

Fajardo, A.L., C.G.V. Deniega, F.J.J. Raytana, M.J.B. Reyes, J.J.T. Menguito, Y.M.M. Pinca. 2023. Performance of Different Pumps and Pump Sets for Agricultural Applications Tested by the Agricultural Machinery Testing and Evaluation Center, Philippines. Philippine Journal of Agricultural and Biosystems Engineering, 19-2: 3-15.

Karassik, I.J., J.P. Messina, P. Cooper, C. Charles. 2008. Pump Handbook. 4th Edition, The McGraw-Hill Companies, Inc., New York.

PAES 114:2000 Agricultural Machinery – Centrifugal Pump – Specifications

PAES 115:2000 Agricultural Machinery – Centrifugal, Mixed Flow, and Axial Flow Water Pumps – Methods of Test

Republic Act No. 10601: An Act Promoting Agricultural and Fisheries Mechanization Development in the Country. https://www.officialgazette.gov.ph/2013/06/05/republic-act-no-10601/

Resurreccion, A.N., R.E. Eusebio, D.C. Aranguren, R.P. Santiago, D.C. Suministrado, 2008. AMTEC performance rating system: a guiding tool in the appropriate selection of agricultural machinery. Philippine Agricultural Mechanization Journal, 15 (1), 14-35.

Rice Competitiveness Enhancement Fund (RCEF). Agricultural Training Institute | Home of the Philippine e-Extension. (2020, August 6). https://ati.da.gov.ph/ati-main/PROGRAMS/RCEF

Development of an inline injection and mixing system for sensor-guided variable-rate sprayers

Heping Zhu*, Zhihong Zhang, Yue Shen, Hongyoung Jeon
USDA-ARS Application Technology Research Unit, Wooster, Ohio, USA.
* Corresponding author. Email: heping.zhu@usda.gov

Abstract

The laser-guided intelligent spray technology has been rapidly adopted by specialty crop growers to significantly reduce pesticide waste, increase production profitability, and safeguard the environment. However, improvements are needed to eliminate the tank mixture leftover waste which is a common problem for all variable-rate sprayers. An inline injection and mixing system was developed as an attachment to the laser-guided variable-rate orchard sprayer. Major components of the system consisted of a chemical metering pump, a water pump, a two-stage static mixer, a premixing tank, a buffer tank, an electric shut-off valve, a chemical container assembly, electronic control boards, a graphical user interface, and an embedded computer with a touch screen unit. Liquid level sensors were mounted in all tanks and the chemical container to control the liquid discharge process and prevent overflows. The graphical user interface with visual operation functions was designed for operators to communicate with the system and monitor the operation status shown on the touch screen. During spray applications, the system performed with loops in dispensing, mixing, and transferring desired amounts of water and chemical concentrates automatically to maintain spray mixtures with a constant concentration for variable-rate nozzles to discharge. The system could be rinsed automatically when the spray application task was completed. Test results demonstrated that the simulated pesticide and water could be accurately delivered into the injection line and could be mixed well in the buffer tank before the spray mixture was discharged to the nozzles. The inline injection and mixing system would be a potential technique to further reduce pesticide waste and improve environmental stewardship for both conventional and new precision variable-rate sprayers.

Keywords: Precision application, Laser-guided sprayer, Pesticide disposal, Environment protection, Automation

1. Introduction

Structure and density of horticultural crops in fields generally are not as uniform as traditional row crops such as corn and soybeans. The use of conventional constant-rate sprayers to apply pesticides to protect horticultural crops has caused tremendous amount of pesticide waste and environment contamination. To solve these problems, a laser-guided air-assisted precision spray technology was developed to automatically adjust spray rates that match the crop structure and density for precision delivery of agrochemicals in real time (Chen et al., 2012; Shen et al., 2017). This technology is designed as a retrofit attachment for new, used and autonomous sprayers commonly used in orchards, vineyards and nurseries. With the attachment, growers can use their existing sprayers rather than buying new sprayers to achieve precision applications. Sprayers retrofitted with the intelligent spray control system detect crops with tens of thousands of laser beams and then spray the body of crops but not the empty spaces in the field. During a growing season, the sprayers can reduce pesticide use between 30% and 85% and reduce spray drift by up to 90% (Chen et al., 2013a, 2013b; Zhu et al., 2017; Boatwright et al., 2020; Chen et al., 2021; Fessle et al., 2021; Fessler et al., 2023; Wodzicki, et al., 2023). Smart Apply Inc (Indianapolis, Indiana, USA) commercialized the technology with the trade name "SmartApply® – Intelligent Spray Control System™" in 2019, and John Deere acquired Smart Apply in 2023 to strengthen the production capability and service (https://www.deere.com/en/news/all-news/john-deere-acquires-smart-apply/). Many growers in the USA and other countries have been using this reliable and profitable technology to protect their crops and safeguard the environment. Crops include apples, citrus, grapes, berries, cherries, pecans, almonds, hops, nurseries and many others (https://smartapply.com/).

However, all variable-rate sprayers equipped with sensor control systems encounter the same problem as the conventional constant-rate sprayers to dispose excess tank mixtures after spray tasks (Shen and Zhu, 2015). For variable-rate orchard sprayers, the required volume of tank mixture to be applied varies with plant size, shape, foliage density and growth stage as well as plant density in the field. For variable-rate boom sprayers to apply herbicides, the amount of sprays varies with weed population in the field but weed densities are usually unknown. Thus, it is difficult for applicators to prepare the exact amount of tank mixtures needed before they go to the field to spray crops or weeds. The problem may not be obvious for large orchard fields requiring multiple tank refills because applicators usually have an accurate estimation on the amount of tank mixture for the last tank refill after they have multiple refills of full tanks to spray majority of the field. However, for small orchard operations which require less than a full tank of mixture to complete the task, excessive tank mixture leftover is usually inevitable. This leftover problem can be serious especially for large boom sprayers to apply variable-rate herbicides.

Therefore, real-time in-line injection systems are needed for variable-rate sprayers, regardless they are used for orchards or row crops, to solve the problems such as pesticide exposure, tank mixture leftover and rinsed water disposal associated with conventional spray applications (Shen and Zhu, 2015; Zhang et al., 2019).

To eliminate the tank mixture leftover problem for conventional constant-rate sprayers, direct in-line injection systems to discharge concentrated pesticide formulations directly into the carrier stream or nozzles have been investigated and improved over past several decades (Reichard and Ladd, 1983; Marchant and Frost, 1989; Way et al., 1990; Sudduth et al., 1995; Zhu et al., 1998; Womac et al., 2002; Downey et al., 2006; Vondricka and Lammers, 2009). However, these conventional in-line injection systems cannot be used for variable-rate sprayers because of their unsolved problems associated with the long lag time, inconsistent mixture uniformity and inaccurate dispense of very low chemical flow rates (Shen and Zhu, 2015). Also, spray outputs from variable-rate sprayers can be suddenly changed from zero to full capacity due to instant changes in plant canopy structures and plant presence or absence status. To maintain a constant chemical concentration in the spray mixture to be discharged from every nozzle in the variable-rate mode, it would require chemical pumps to dispense chemicals into carrier lines with widely variable ranges instantaneously to respond the sudden changes of the spray outputs. However, there are no such available metering pumps or valves capable of responding such sudden changes precisely.

Therefore, the objectives of this research were to: (1) design, build and test an automatic in-line injection and mixing system for variable-rate spray applications; (2) validate the system accuracy in providing uniform tank mixtures at desired mixture concentrations.

2. Materials and Methods

2.1. Design of in-line injection and mixing system

Figure 1 shows the schematic diagram of the developed in-line injection and mixing system integrated in a variable-rate sprayer (Zhang et al., 2020a). Major components of the system were a 16-L premixing tank, an electric shut-off valve, a 16-L buffer tank, a water pump, a chemical tank assembly, a chemical metering unit, a microprocessor-controlled unit, a two-stage static mixer, and a corrosion-resistant rectangular enclosure. The chemical metering unit and the microprocessor-controlled unit were stored in the corrosion-resistant enclosure. A metal frame was fabricated to mount these components and was attached to the sprayer.

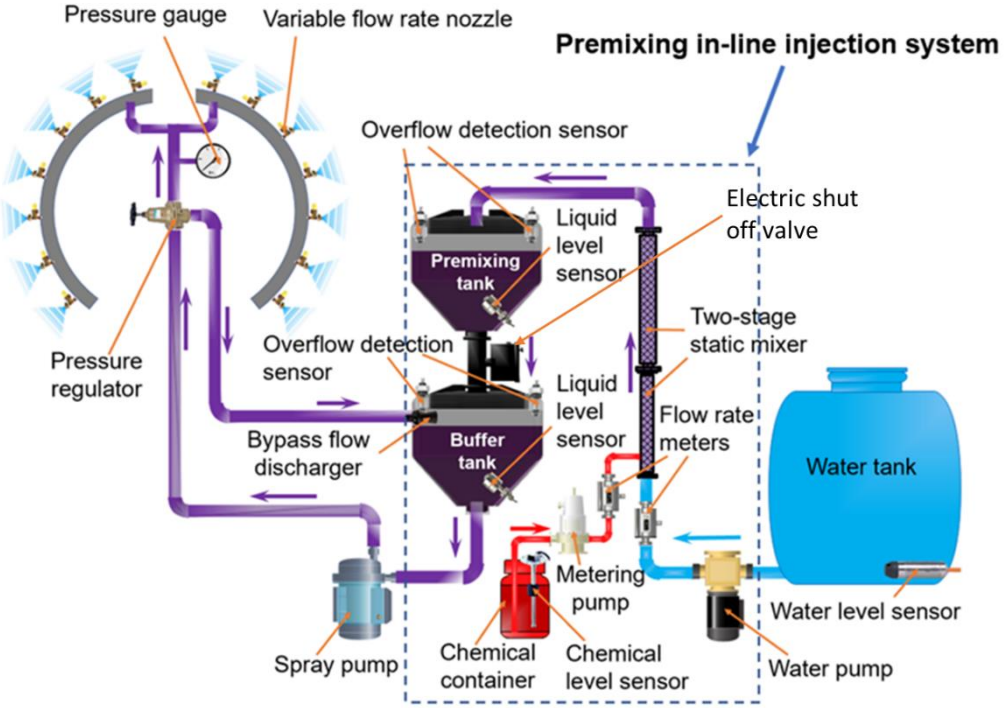

Figure 1. Schematic diagram of the in-line injection and mixing system integrated into a sensor-guided variable-rate sprayer.

A 5-chamber diaphragm pump was used as the water pump to discharge water as the pesticide carrier from the water tank to the injection point. The pump was powered with the 12 VDC tractor battery and had the capacity of 26.5 L min^{-1} at 414 kPa pressure. A water level sensor was mounted at the bottom of the water tank to estimate

the amount of remaining water in the tank. The sensor measured the water level and the amount of remaining water in the tank. In addition, there were two flow sensors mounted diagonally near the top of each premixing tank and buffer tank to detect overflows. When the liquid level in the premixing or buffer tank reached the overflow detection sensors, the water and metering pumps would be automatically turned off, and the electric shut-off valve would be closed.

The chemical metering unit was an integration of a ceramic piston metering pump with a precision electronic controller. This unit was used to dispense desired amounts of chemical concentrates from the chemical container to injection point near the two-stage mixer. The metering pump was able to discharge liquid at variable rates ranging from 5 to 635 mL min^{-1} by synchronizing the piston rotation speeds and stem motor pulses (Shen and Zhu, 2015). The synchronization was manipulated by the microprocessor-controlled unit.

The chemical container assembly consisted of a 2-L chemical container, a magnetic stirrer, a stainless-steel chemical level sensor, refilling bottles and a storage box. The magnetic stirrer was used to agitate the chemical concentrates with adjustable speeds. The chemical container sat on the stirrer and a 35 mm long and 9 mm diameter magnetic bar was placed at the bottom inside the container. Besides the chemical container, there were eight bottles in the storage box for refilling the chemical container with additional chemical concentrates as needed. The chemical level sensor was mounted on the container lid to measure the chemical concentrate level in the chemical container at 20% resolution. The sensor shaft end was 5-cm above the bottom of the chemical container. This 5-cm clearance was used to remind operators to refill the chemical container and also prevent the metering pump from running dry.

Premixing and buffer tanks were two 16-L capacity rectangular-funnel reservoirs. The premixing tank was mounted above the buffer tank. The electric shut-off valve was mounted between the two tanks for the spray mixture transfer. The valve was operated by an electric motor with a rotational speed of 25 rpm, and it could be fully opened or closed within 0.6 s for quick liquid transfer. Two stainless steel liquid level sensors were mounted in premixing and buffer tanks separately. One sensor was located at the bottom of the premixing tank to detect whether this tank was nearly empty. This sensor was also used to trigger both water pump and metering pump to start discharging water and dispensing chemical concentrates to refill the premixing tank. The other sensor was located at the bottom of the buffer tank and was used to activate the electric shut-off valve to ensure sufficient spray mixture in the buffer tank.

A motionless embedded computer with a touch screen was used as the main processor for the in-line injection and mixing system. The microprocessor-controlled unit mainly consisted of an Arduino circuit board, which was placed adjacent to the metering-dispensing unit inside the corrosion-resistant enclosure. Computer programs were written with Visual C++ and were installed in the embedded computer to manipulate the microprocessor-controlled unit. A graphical user interface was also designed for operators to manage the system operations and view the operation status through the touch screen. Serial commands from the embedded computer to the Arduino board included: turning on or off the mixing process, setting the chemical concentration in percentage, starting or stopping the metering pump and water pump, activating the electric shut-off valve, performing the auto-rinse function, preventing the overflow, and terminating the system operation. Similarly, the serial communications between the Arduino board and the embedded computer interface included status of mixing process, metering pump operation, water pump operation, electric shut-off valve activation, chemical concentration calculation, mixture levels in premixing and buffer tanks, auto-rinse function, overflow prevention in premixing and buffer tanks, water level in the water tank, and chemical concentrate level in the chemical container.

With the computer programs and the graphical user interface, the system was performed with six steps in loops automatically after the operator provided the desired chemical concentration during spray applications: (1) dispensing desired amounts of water and chemical concentrates into the static mixer based on mixture concentration input; (2) mixing water and chemical concentrates in the static mixer while flowing into the premixing tank; (3) transferring the mixture from the premixing tank to the buffer tank through the electric shut-off valve for further agitation and for discharge from the spray pump to variable flow-rate nozzles; (4) repeating steps (1) and (2) when the premixing tank nearly empty; (5) repeating step (3) when the buffer tank neared empty; (6) rinsing the system lines with the tank water when the spray application task was completed. In addition, liquid levels in the chemical container, water tank, premixing tank and buffer tank were also shown on the screen for visual observation. Operators could manually start or stop the system operation.

A ‘Zero leftover’ function was designed and displayed on the user interface to dispose small amounts of leftovers in the premixing and buffer tanks before spray tasks were completed. When the spray task was nearly completed, the operator could turn off the automatic mode and turn on the ‘Zero leftover’ function. When the function was enabled, the system would automatically turn on the electric shutoff valve to transfer the remaining mixture in the premixing tank to the buffer tank, and continued to spray the same field until the buffer tank was empty.

The in-line injection and mixing system was attached on a laser-guided variable-rate intelligent orchard sprayer for experiments (fig. 2). The sprayer mainly consisted of a 200-L spray tank, a diaphragm pump, a 0.6-m

diameter axial fan, 14 hollow cone nozzles coupled with 14 pulse width modulation (PWM) solenoid valves, a high-speed 2-D laser scanning sensor, an automatic flow controller and an embedded computer with a touch screen. To perform variable rate functions to match variable canopy architectures, a specially designed laser-guided variable-rate spray control system (Liu et al., 2014) was integrated in the sprayer. With the integration, the sprayer could be operated with either automatic variable-rate mode or manual constant-rate mode as needed. The 200-L spray tank was used as the water tank for the in-line injection and mixing system. Flow rates of the 14 nozzles were independently manipulated with the 14 PWM valves by tree presence, canopy volume and shape and sprayer travel speed in real-time.

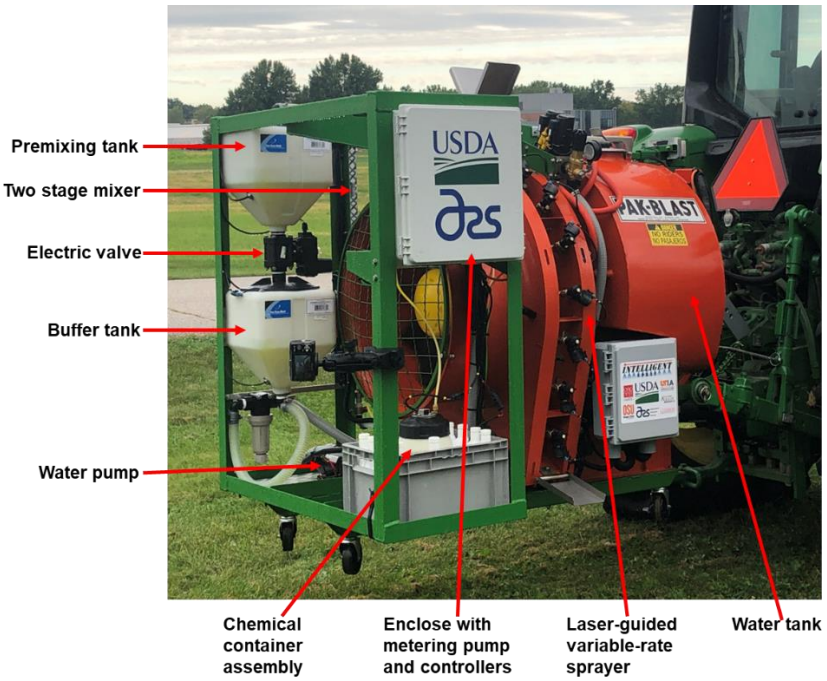

Figure 2. The in-line injection and mixing system attached to a laser-guided variable-rate orchard sprayer for tests.

2.2. System accuracy validation

A platform using the IO-Link technology was designed to validate the accuracy of dispensing desired amounts of water and chemical concentrates into the system. A magnetic-inductive flow meter with the measurement range of 5 to 3000 mL min^{-1} and resolution of 1 mL min^{-1} was used to measure chemical concentrates dispensed from the metering pump. Another magnetic-inductive flow meter with the measurement range of 0.2 to 100 L min^{-1} and resolution of 0.1 L min^{-1} was used to measure the amount of water discharged from the water pump.

The two flow meters were connected to an IO-Link master which was then connected to the embedded computer by using a RJ45 connection cable. The IO-Link was used to display instantaneous flow rates in real-time and totalized flows after each test run.

The concept of the in-line injection and mixing system was validated through previous laboratory tests (Shen and Zhu, 2015; Zhang et al., 2019). Previous validations included the system accuracy for dispensing simulated pesticides to achieve uniform spray mixtures. Due to the fact that the metering pump in the new system remained the same as the previous system (Zhang et al., 2019) while the other major components including computer-controlled programs for the metering pump and the entire system operation process, the static mixer design and the chemical concentrate container assembly were modified and new liquid level detections and controls were added, the accuracy of the chemical concentrates dispensed to the mixing line and the mixture uniformity in the buffer tank must be evaluated again after the new system was attached to the orchard sprayer.

Because the capacity of the premixing tank was 16 L, the desired volume of water discharged through the water pump was assigned as 10 L for the spray mixture preparation in each operational loop. Experiments were conducted to evaluate the metering pump accuracy to dispense desired amounts of chemical concentrates, the water pump accuracy to discharge 10 L of water, and uniformity of the spray mixture in the buffer tank. To avoid the engineering laboratory was contaminated by toxic pesticides, distilled water mixed with a fluorescence tracer Brilliant Sulfaflavine (BSF) was used as the simulated pesticide concentrate for the experiments. For these tests, the mixture concentration was defined as the ratio between the volume of the simulated pesticide dispensed from

the metering pump and the volume of water discharged from the water pump.

For the chemical metering accuracy evaluation, desired mixture concentrations used for the tests were 0.1%, 0.5%, 1.0%, 1.5%, 2.0%, 2.5%, and 3.0%, and they were inputted into the embedded computer through the user interface shown on the touch screen. Corresponding to these desired concentrations, desired volumes of the simulated pesticide dispensed by the metering pump were 10, 50, 100, 150, 200, 250 and 300 mL, respectively.

For the mixture uniformity evaluation, the test was designed with four mixture concentrations (0.5%, 1.0%, 1.5%, and 2.0%). Based on preliminary trials, to achieve a fluorescent intensity that fell within the linear range of the fluorometer, the concentration of BSF in the simulated pesticide concentrates was selected as 2.0 g L^{-1}. With this test design, the final BSF concentrations in spray mixtures in the buffer tank were assumed to be 10, 20, 30 and 40 mg L^{-1} for the concentrations of 0.5%, 1.0%, 1.5%, and 2.0%, respectively.

Spray mixture samples were collected from the outlet of the buffer tank with thirty 120-mL glass bottles in a sequence at 3 s intervals. It took about 90 s to complete the collection of 30 samples for each mixture concentration. After the collection, each sample was transferred to a 4-mL square cuvette for fluorescence intensity analyses. The BSF tracer concentration as a function of fluorescence intensity was calibrated before the experiments. Measured BSF tracer concentrations in the buffer tank were determined with the linear calibration equation,

$$y = (9.47\times10\text{-}4)\,x + 1.80, \quad R^2 = 0.982 \qquad (1)$$

Where y is the BSF tracer concentration (mg L^{-1}), and x is the solution fluorescence intensity (unitless) measured with the fluorometer ($16.7 < x < 4.2\times105$).

3. Results and Discussion

3.1. System accuracy

The mean measured amounts of the simulated pesticide dispensed from the metering pump agreed well with the desired amounts across the desired concentrations ranging from 0.1% to 3.0% (table 1). For example, the maximum relative error between measured and desired amounts of the simulated pesticide was 6.33% which occurred at the 2.0% desired concentration. Similarly, the measured amounts of water discharged to the injection line were also very close to the desired amount of 10 L. Consequently, measured concentrations of the spray mixture agreed well with the desired concentrations over the range from 0.1% to 3.0% (table 1).

Table 1. Mean measured amounts of simulated pesticide dispensed from the chemical container by the metering pump and water discharged from the water tank by the water pump for desired concentrations of 0.1%, 0.5%, 1.0%, 1.5%, 2.0%, 2.5%, and 3.0%. Standard deviations for the mean measured amounts are presented following the symbol '±'.

Desired Concentration	Amount of Simulated Pesticide (mL)		Relative error	Amount of Water (L)		Relative error	Actual Concentration
(%)	Desired	Measured	(%)	Desired	Measured	(%)	(%)
0.1	10	9.67±1.15	3.3	10	10.42±0.19	4.2	0.09±0.01
0.5	50	52.33±0.58	4.66	10	10.57±0.33	5.7	0.50±0.01
1.0	100	103.33±0.58	3.33	10	10.58±0.15	5.8	0.98±0.02
1.5	150	152.33±0.58	1.55	10	10.54±0.15	5.4	1.45±0.03
2.0	200	212.67±0.58	6.33	10	10.49±0.35	4.9	2.03±0.06
2.5	250	265.33±2.08	6.13	10	10.52±0.11	5.2	2.52±0.01
3.0	300	318.33±0.58	6.11	10	10.56±0.04	5.6	3.01±0.02

3.2. Mixture uniformity

Measured BSF concentrations also agreed well with the desired concentrations of 0.5%, 1.0%, 1.5% and 2.0% (fig. 3). Variations in the measured concentrations were very small over the 90 s sampling duration (fig. 3a). For desired concentrations of 0.5%, 1.0%, 1.5% and 2.0%, the average measured concentrations were 0.48%, 0.99%, 1.43%, and 1.97% with coefficients of variations of 0.92%, 1.53%, 1.26%, and 1.16%, respectively (fig. 3b). Relative errors were 3.89%, 1.22%, 4.70%, and 1.26% between measured and desired concentrations. Thus, these tests demonstrated that the in-line injection and mixing system was able to provide consistent mixture uniformity ready for the downstream variable flow-rate spray nozzles to discharge.

The in-line injection and mixing system attached to the variable-rate sprayer was preliminarily tested in a nursery field (fig. 4). As expected, the system performed automatic loops of mixing and refilling water and chemical concentrates in premixing and buffer tanks when the sprayer discharged variable-rate spray outputs to match tree presence, canopy characteristics and travel speeds. Details on validations of the spray system performance under laboratory conditions could also be found in previous publications by Zhang et al. (2020b, 2021).

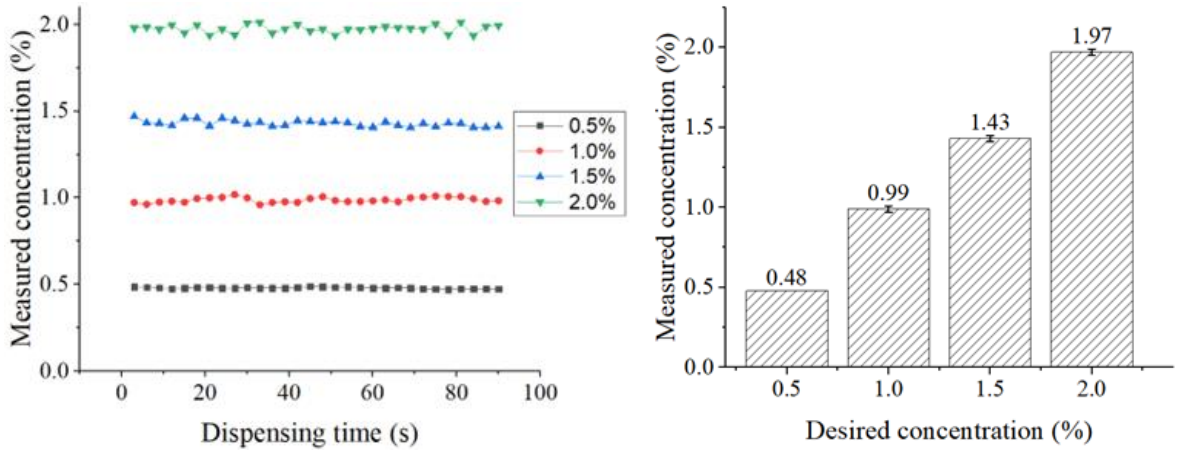

(a) Measured concentrations over time (b) Measured and desired concentrations

Figure 3. Measured concentrations (%) of the simulated pesticide concentrate in spray mixtures collected from the buffer tank for the desired concentrations of 0.5%, 1.0%, 1.5% and 2.0%.

Figure 4. The in-line injection and mixing system attached to a laser-guided variable-rate orchard sprayer for field tests.

4. Conclusions

Hardware and software of the in-line injection and mixing system were designed and assembled as an attachment to a laser-guided variable-rate orchard sprayer. A graphical user interface was integrated into the system for operators to manage and view the operation process on the touch screen.

Following functions could be achieved with this newly designed in-line injection and mixing system: detecting individual components separately before spray operations to ensure they were functional; setting mixture concentrations with step increase or decrease of 0.1% in real-time; using the virtual level gauge to indicate liquid levels in the chemical container, water tank, premixing tank, and buffer tank, to help operators monitor the system operation process; using the protection sensors to prevent premixing and buffer tanks from overflow; rinsing premixing and buffer tanks, chemical lines automatically after spray applications.

Laboratory experiments illustrated that the simulated pesticide and water could be accurately dispensed into the injection line according to the concentration inputs and could be well mixed in the buffer tank. For spray mixtures containing 0.5 to 2.0% simulated pesticide, the in-line injection and mixing system provided consistent mixture uniformity, and relative errors between measured and desired concentrations were below 4.7%, and coefficients of variations were below 1.53%.

Future investigations will include comprehensive validations of the accuracy, repeatability and reliability of the laser-guided variable-rate sprayer equipped with the in-line injection and mixing system to apply chemical

concentrates with different physical properties and solubilities under field conditions.

Acknowledgements

Mention of company or trade names is for description only and does not imply endorsement by the USDA. The USDA is an equal opportunity provider and employer. The authors acknowledge invaluable technical assistance from Adam Clark, Barry Nudd, and Andy Doklovic.

References

Boatwright, H., H. Zhu, A. Clark, G. Schnabel, 2020. Evaluation of the Intelligent Sprayer System in peach production. Plant Disease. 104 (12), 3207-3212. https://doi.org/10.1094/PDIS-04-20-0696-RE.

Chen, Y., H.E. Ozkan, H. Zhu, R.C. Derksen, C.R. Krause, 2013a. Spray deposition inside tree canopies from a newly developed variable-rate air-assisted sprayer. Transactions of the ASABE. 56(6), 1263-1272.

Chen, L., H. Zhu, L. Horst, M. Wallhead, M. Reding, A. Fulcher, 2021. Management of pest insects and plant diseases in fruit and nursery production with laser-guided variable-rate sprayers. HortScience. 56(1), 94–100.

Chen, Y., H. Zhu, H.E. Ozkan, R.C. Derksen, C.R. Krause, 2013b. Spray drift and off-target loss reductions with a precision air-assisted sprayer. Transactions of the ASABE. 56(6), 1273-1281.

Fessler, L., A. Fulcher, L. Schneider, W.C. Wright, H. Zhu, 2021. Reducing the nursery pesticide footprint with laser-guided, variable-rate spray application technology. HortScience. 56(12),1572-1584.

Fessler, L., X. Sun, W.C. Wright, H. Zhu, A. Fulcher, 2023. Intelligent, variable-rate spray technology reduces total pesticide output while controlling foliar disease of Shumard oak. Journal of Environmental Horticulture. 41(3), 109-120.

Liu, H., H. Zhu, Y. Shen, Y. Chen, H.E. Ozkan, 2014. Development of digital flow control system for multi-channel variable-rate sprayers. Transactions of the ASABE. 57(1), 273-281.

Downey, D., T.G. Crowe, D.K. Giles, D.C. Slaughter, 2006. Direct nozzle injection of pesticide concentrate into continuous flow for intermittent spray applications. Transaction of ASAE. 49(4), 865-873.

Marchant, J.A., A.R. Frost, 1989. Concentrate dispensing device. UK Patent Application PA 8906165.9.

Reichard, D.L., T.L. Ladd, 1983. Pesticide injection and transfer system for field sprayers. Transaction of ASAE. 26(3), 683-686.

Shen, Y., H. Zhu, 2015. Embedded computer-controlled premixing inline injection system for air-assisted variable-rate sprayers. Transactions of the ASABE. 58(1), 39-46. https://doi.org/10.13031/trans.58.11037.

Shen, Y., H. Zhu, H. Liu, Y. Chen, E. Ozkan, 2017. Development of a laser-guided, embedded-computer-controlled, air-assisted precision sprayer. Transactions of the ASABE. 60(6), 1827-1838.

Sudduth, K.A., S.C. Borgelt, J. Hou, 1995. Performance of a chemical injection sprayer system. Applied Eng. in Agric. 11(3), 343-348.

Vondricka, J., P.S. Lammers, 2009. Evaluation of a carrier control valve for a direct nozzle injection system. Biosystems Engineering. 103, 43-48.

Way, T.R., L.L. Bashford, K. Von Bargen, R.D. Grisso, 1990. Peristaltic pump accuracy in metering herbicides. Applied Eng. in Agric. 6(3), 273-276.

Wodzicki, L.M., L.V. Madden, E.Y. Long, H. Zhu, M.L. Ivey, 2023. Evaluation of a laser-guided intelligent sprayer for disease and insect management on grapes. American Journal of Enology and Viticulture. Article 0740024. DOI: 10.5344/ajev.2023.2301.

Womac, A.R. D.L. Valcore, R.A.II. Maynard, 2002. Variable-concentration direct injection from fixed-ratio diluent-driven pumps. Transaction of ASAE. 45(6), 1721-1728.

Zhang, Z., H. Zhu, H. Guler, Y. Shen, 2019. Improved premixing in-line injection system for variable-rate orchard sprayers with Arduino platform. Computers and Electronics in Agriculture. 162(1), 389-396. https://doi.org/10.1016/j.compag.2019.04.023.

Zhang, Z., H. Zhu, C. Hu, 2020a. Hardware and software design for premixing in-line injection system attached on variable-rate orchard sprayers. Transactions of the ASABE. 63(4), 823-831. https://doi.org/10.13031/trans.13730.

Zhang, Z., H. Zhu, R. Salcedo, Z. Wei, 2020b. Assessment of chemical concentration accuracy and mixture uniformity of premixing in-line injection system. Computers and Electronics in Agriculture. 176: Article 105670. https://doi.org/10.1016/j.compag.2020.105670.

Zhang, Z., H. Zhu, Z. Wei, R. Salcedo, 2021. Chemical concentration and spatial uniformity of a premixing in-line injection system attached to a variable-rate orchard sprayer. Transactions of the ASABE. 64(6), 1977-1987. https://doi.org/10.13031/trans.14113.

Zhu, H., H. Ozkan, D.R. Fox, R.D. Brazee, R.C. Derksen, 1998. Mixture uniformity in supply lines and spray patterns of a laboratory injection sprayer. Applied Engineering in Agriculture. 14(3), 223-230.

Zhu, H., R. Rosetta, M.E. Reding, R.H. Zondag, C.M. Ranger, L. Canas, A. Fulcher, R.C. Derksen, E.H. Ozkan, C.R. Krause, 2017. Validation of a laser-guided variable-rate sprayer for managing insects in ornamental nurseries. Transactions of the ASABE. 60, 337-345. https://doi.org/10.13031/trans.12020.

Preliminary evaluation of a knapsack sprayer prototype that combines electrostatic technology and hydraulic spraying

Alba Vigo-Morancho[a,*], María Videgain[a,b], Mariano Vidal[a], Antonio Boné[a], F. Javier García-Ramos[a,b]

[a] Escuela Politécnica Superior, University of Zaragoza, Ctra. Cuarte s/n, 22071 Huesca, Spain.

[b] Instituto Agroalimentario de Aragón – IA2 (CITA-University of Zaragoza), EPS, University of Zaragoza, Ctra. Cuarte s/n, 22071 Huesca, Spain.

* Corresponding author email: albavm@unizar.es

Abstract

Electrostatic technology based is an advancement that, despite having been studied decades ago, has not yet been widely incorporated in terms of agriculture spray applications. Regarding Pesticide Application Equipment (PAEs), particularly focusing on small knapsack sprayers, it should not be dismissed that their utilization remains high in many countries. However, the lack of regulation and control of these sprayers makes it difficult to track their acquisition and usage. Therefore, pesticide application research and improvement efforts must encompass this category of PAEs.

The objective of this study was to conduct a preliminary evaluation of an electrostatic knapsack sprayer prototype designed to operate at 1 kV and equipped with a hydraulic nozzle that provides a range of droplet size values of Dv50 from 136 µm to 386 µm in the pressure range between 2 and 6 bar. In this sense, two sprayer configurations associated with connected or disconnected electrostatic system (ES or NES, respectively) were tested. Horizontal and vertical liquid distribution, as well as qualitative evaluation of deposition using water-sensitive papers, were carried out under laboratory conditions. Results showed no differences between ES and NES in terms of flow rate (L min^{-1}) provided by the nozzle at any pressure. The total accumulated volume when evaluating the vertical distribution profile with NES was higher than with ES and this difference decreased at greater distances of application. However, percentage values of coverage, both on the side facing the nozzle and on the opposite side, were significantly higher when using ES, with increments of up to 20 % compared to NES in some cases. The results obtained suggest that this technology could be a feasible option for enhancing treatment efficacy and integrating it into this type of equipment. Therefore, further experiments in terms of quantitative deposition and crop trials will be conducted to support these findings.

Keywords: Crop protection, charged droplets, pesticide, coverage.

1. Introduction

The continuous advancement of technology has been enhancing plant protection product application equipment for decades, allowing for a wide range of machinery that can adapt to the diverse types of crops and planting frameworks seen today. This is particularly evident with intensive crops, specifically those where the product is applied to a three-dimensional. In such cases, it is crucial to emphasize the amount of product that reaches the vegetation to minimize losses due to drift, runoff, or the product falling to the ground before reaching the crop due to gravity (Doruchowski *et al.*, 2009; Gil *et al.*, 2007; Llorens *et al.*, 2010; Salcedo *et al.*, 2020).

Advancements made have enabled precise adjustments in the amount of product needed, based on various factors such as the forward speed of the equipment and the characteristics of the vegetation. To further optimize spraying, electrostatic technology can be applied; this exposes the droplets at the nozzle outlet to an electric field, typically charging them negatively. As the droplets approach the crop, they are attracted to the positively charged leaves (Law, 2001). This technology has been applied in various industries such as disinfection, painting, etc. (Appah *et al.*, 2019). Although some manufacturers have included this technology in large-scale agricultural sprayers, there are few studies or commercialized knapsack sprayers, similar to traditional ones, that incorporate this technology in a compact and easy to use manner. Actually, this category of PAEs, whose acquisition tracking is difficult due to the lack of purchase control or inspection, are still used today, both in greenhouse plantations (Li *et al.*, 2018), where the difficulty of accessing crop rows makes operator applied spraying the norm, and also in larger plantations, such as vineyards, where some spot applications are still carried out using handheld sprayers.

One of the concepts referenced in the study of spray performance or efficiency when discussing this technology is the Charge-to-Mass Ratio (CMR), associated with the charge generated on the droplets at the

nozzle outlet. This parameter, expressed in mC kg^{-1}, has been evaluated in relation to other application parameters considered influential on the effectiveness of electrostatic technology. Some studies have shown that the CMR is affected by factors such as droplet size (Pascuzzi and Cerruto, 2015); application distance (Patel *et al.*, 2017; Zhao *et al.*, 2008); intrinsic characteristics of the electrode, such as its geometry (Mamidi *et al.*, 2013; Patel *et al.*, 2016), material (Patel *et al.*, 2013); applied voltage (Laryea and No, 2003), and even the viscosity or nature of the sprayed product (Maski and Durairaj, 2010).

Some authors have defined certain CMR values where efficient spraying with electrostatic technology has been observed, such as the pneumatic nozzle evaluated in the study by Pascuzzi & Cerruto, where CMR values of 10 mC kg^{-1} resulted in significant higher coverage for small droplets provided by a pneumatic nozzle (Pascuzzi and Cerruto, 2015). However, there is still work to be done, overall when studying equipment equipped with hydraulic nozzles, where the efficiency of coverage associated with charging the droplets and the CMR values associated with larger droplet sizes have not been thoroughly evaluated.

In this context, the present work aims to conduct a preliminary analysis of an electrostatic backpack sprayer equipped with a hydraulic nozzle, with the objective of evaluating its performance in terms of coverage. This includes preliminary analyses of droplet size characterization, spray distribution, and charge analysis of the droplets at the nozzle exit.

2. Materials and Methods

2.1. Spray Application Equipment

The knapsack sprayer (Tecnostatic, Zaragoza, Spain) is a commercial electric unit equipped with a 12V diaphragm pump and a pressure regulator fitted on the lance that allows adjusting the flow rate through the nozzle between 2 bar and 6 bar of pressure. Additionally, the equipment includes a charge induction system in the nozzle, operating at a voltage of 1 kV, which is controlled by a switch located next to the pressure regulator.

2.2. Nozzle characterisation

2.2.1. Droplet size and liquid distribution

To understand the nature of the spray, droplet size characterization tests were conducted for each combination of pressure (2 bar, 4 bar, and 6 bar) and electrostatic system configuration (connected 'ES' or disconnected 'NES'). The droplet size distribution was determined using the Insitec® T laser diffraction system (Malvern Panalytical, United Kingdom). From the cumulative volume function, the percentiles Dv10, Dv50, and Dv90 were obtained. Thus, 50% of the atomized liquid is contained in droplets smaller than Dv50, representing the median droplet size. Additionally, Dv10 and Dv90 provide a measure of the distribution width, described by the value of “relative span” or Span. According to Amaya and Bayat (2023), this dimensionless number is given by Eq (1), and indicates whether the distribution spread is narrow or wide.

$$Span = \frac{Dv_{90} - Dv_{10}}{Dv_{50}} \quad (1)$$

The nozzle flow rate was determined for all pressure settings following the methodology described in ISO 5682-2:1997 (ISO, 1997). Finally, product distribution tests were conducted to obtain both the horizontal spray pattern and the vertical distribution profile, as well as to evaluate the effect of the electrostatic system on these parameters.

The horizontal distribution profile was evaluated at 50 cm for all pressure settings provided by the device (from 1 bar to 6 bar, in 1 bar increments) and for the two electrostatic system configurations (ES or NES). The vertical profile was assessed by positioning the sprayer lance facing a vertical patternator (AAMS-Salvarani, Maldegem, Belgium), which collected the amount of product every 20 cm in height. The sprayer was placed at distances of 20 cm, 35 cm, 50 cm, and 65 cm. This profile was obtained for both electrostatic system configurations (ES and NES) and for 5 working pressures (2 bar, 3 bar, 4 bar, 5 bar, and 6 bar).

2.2.2.Droplet size Charge-to-mass ratio (CMR)

The CMR has traditionally been measured using a Faraday cage system, described in several methodologies (Law and Cooper, 1987; Marchant and Green, 1982). However, in this case, small current values did not allow to measure the charge at a great distance from the outlet. For this reason, accurate measurements were recorded by employing a metal conical device that encompassed the entire nozzle outlet flow and that was connected to a digital multimeter, which measured the current (µA) for each working pressure, i.e., based on the flow rate provided by the nozzle. Considering the flow rate data in L min^{-1} and amperage in C s^{-1}, the CMR value (mC kg^{-1}) was obtained for each configuration.

2.3. Coverage trials

A qualitative study of deposition was conducted by analysing the coverage percentage for each combination of equipment working conditions: 2 electrostatic system configurations (ES or NES), 3 working pressures (2 bar, 4 bar, and 6 bar), and 3 application distances (20 cm, 35 cm, and 50 cm). For this purpose, water sensitive papers measuring 26 x 76 mm were placed along a vertical post, with 9 water sensitive papers at known heights located at both the side facing the spray (side A) and the underside/opposite side to the lance (side B), as detailed in Figure 1.

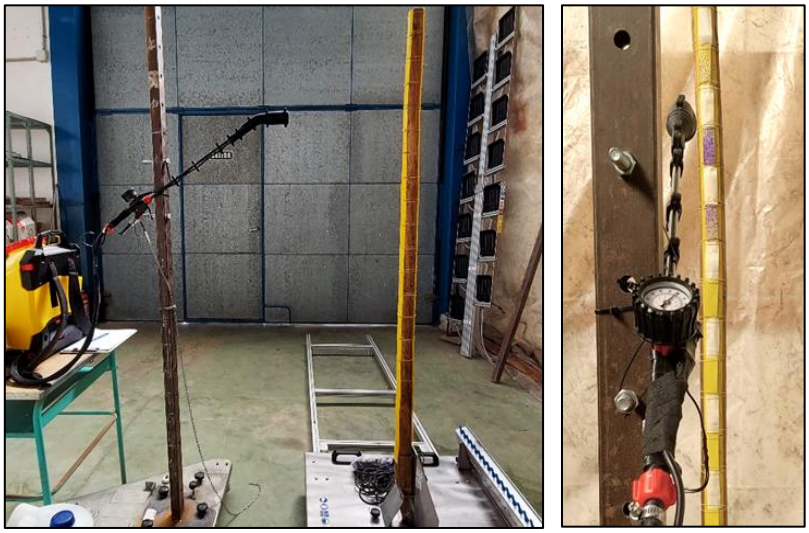

Figure 1. Knapsack sprayer setting with respect to the vertical post (left) and water sensitive locations on the side A of the post (right).

The vertical post was placed on a device mounted on 2 rails that allowed the movement in the plane perpendicular to the lance at a speed of 0.20 m s^{-1}, ensuring identical working conditions between repetitions. Three repetitions were performed for each factor configuration, resulting in a matrix of 972 coverage data points. Water sensitive papers were processed using ImageJ software. The results were statistically analysed using IBM SPSS Statisticsv.26 software package (IBM Corp., Armonk, NY, USA), to establish differences in coverage percentage associated with pressure (droplet size), distance, or application height.

3. Results and Discussion

3.1. Nozzle Characterisation

The nominal flow rate of the nozzle ranged from 0.32 L min^{-1} at the lowest pressure (2 bar) to 0.50 L min^{-1} at the highest pressure (6 bar). On the other hand, no significant effect of the electrostatic system connection on droplet size was observed at any of the studied pressures, so the values presented below are relative to the electrostatic system being connected. At 2 bar pressure, a Dv50 of 386 µm was obtained, indicating a spray of coarse droplets with a relative span of 1.66. As the pressure increased, the droplet size decreased, as expected in pressure spraying equipment, with a Dv50 value of 173 µm at 4 bar pressure, and a span of 1.74. Finally, the finest droplet size was observed at 6 bar pressure, with a Dv50 value of 136 µm

and a span of 2.02.

The horizontal distribution profile, obtained by facing the nozzle toward a horizontal test bench that collected the sprayed liquid volume in 5 cm segments, showed a pattern associated with a hollow cone nozzle type. Additionally, no significant differences were observed in the total collected volume ($p<0.05$) based on the ES or NES configuration.

Regarding the vertical distribution profile, in all configurations, the total accumulated volume was higher in the NES configuration compared to the ES configuration, but this difference was not significant ($p>0.05$) and decreased at greater application distances. This could possibly be due to the presence of a slight backflow of charged droplets attracted to the spray lance itself. Furthermore, beyond an application distance of 30 cm, the recovered volume decreased for all studied pressures ($p<0.001$). Regarding the liquid distribution by height, it was observed that turning off the electrostatic system resulted in a drop of droplets to the lower heights of the patternator, highlighting the attraction force of the structure itself on droplet distribution in the ES configuration.

Figure 2 shows how the droplet size, represented through the Dv50 parameter, decreased as the working pressure increased. Furthermore, same Figure also shows the droplet charge variation at each pressure configuration, represented by the Charge-to-Mass Ratio (CMR). An inverse relationship between these two variables was observed, with results that align with those of other authors who evaluated the influence of these parameters on deposition in electrostatic pesticide application (Patel *et al.*, 2017; Zhao *et al.*, 2008).

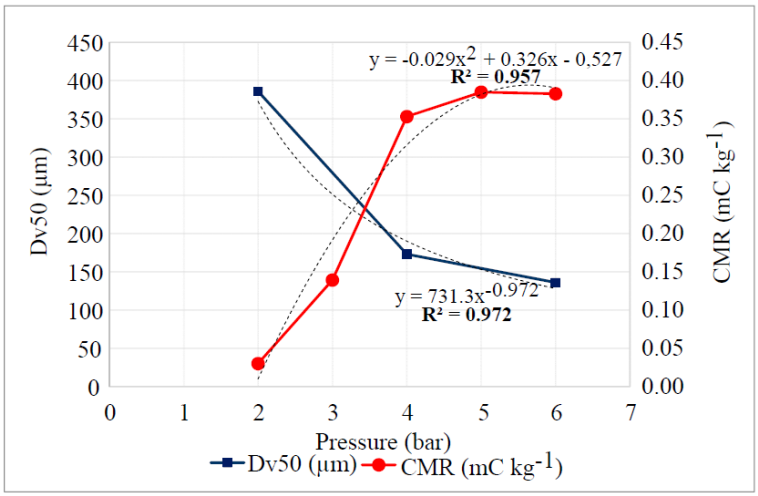

Figure 2. Dv50 values (in µm, blue line) and CMR (in mC kg^{-1}, red line) as a function of pressure (bar).

CMR was found to range from 0.03 mC kg^{-1} to 0.38 mC kg^{-1}. It increased exponentially as the droplet size decreased, up to 4 bar pressure, where the curve began to flatten, reaching its maximum at 5 bar and remaining constant at 6 bar despite the continued decrease in droplet size.

3.2. Coverage

Coverage results from water sensitive papers analysis for each configuration, pressure, distance, and height are shown in Figure 3.

A clear effect of the electrostatic system effectiveness on the covered surface was observed. With the system disconnected, the product did not reach the underside of the post in any case. Furthermore, there was an effect of application distance and working pressure on the percentage of coverage. At closer distances (20 and 35 cm), the percentage of coverage on the underside reached up to 60% for those located at heights associated with the surroundings of the lance position. Focusing on the effect of working pressure on the percentage of coverage, the electrostatic effect was hardly noticeable at the lowest pressure (2 bar); on average, the percentage of the covered surface increased by only 1% when the electrostatic system was switched on. However, it increased considerably with higher pressure, reaching a maximum of 22% at a distance of 35 cm and a pressure of 6 bar.

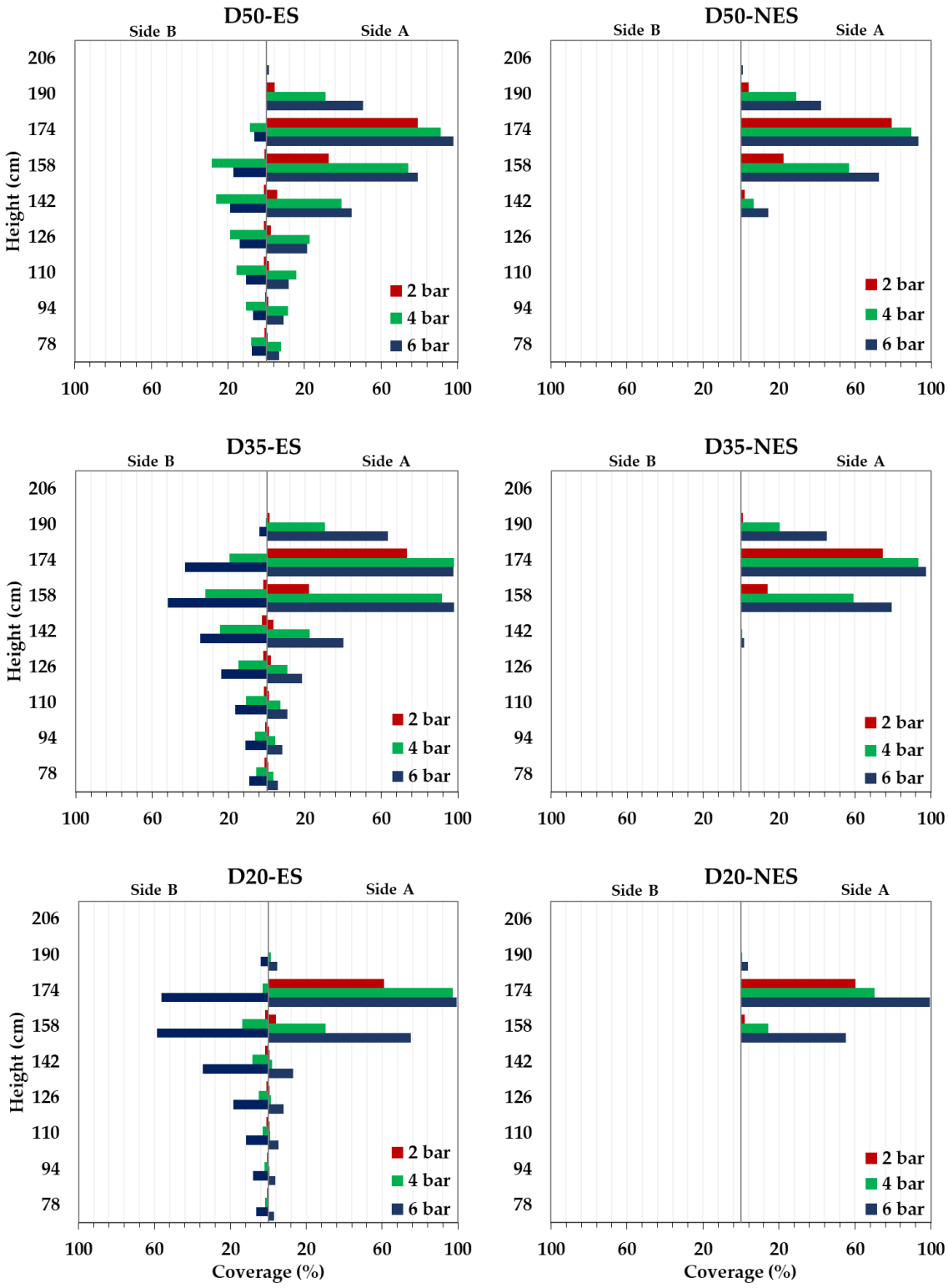

Figure 3. Coverage results (%) obtained in laboratory at 3 distances (20 cm, 35 cm and 50 cm), 3 pressures (2 bar, 4 bar and 5 bar) and 2 electrostatic configurations (connected, ES vs. disconnected, NES).

The highest values were observed on side B at distances of 20 cm and 35 cm when operating at 6 bar. However, at a distance of 50 cm, the highest coverage values on side B were recorded at 4 bar rather than the highest pressure. These results align with those obtained in the vertical distribution profile, where, at a distance of 50 cm and ES configuration, the accumulated volume was higher at 4 bar than at 6 bar. This suggests that Dv50 values lower than 170 µm could result in excessive dispersion of the small charged

droplets, potentially leading to difficulties in reaching the underside of leaves due to adhesion to other regions before reaching the crop.

These results partially agree with those obtained by some authors, such as Laryea and No (2003), who achieved a considerable improvement in deposition using a hydraulic nozzle with similar droplet sizes and a charge-to-mass ratio of 0.27 mC kg^{-1}. However, it should be noted that they applied a voltage of 4.0 kV, which is considerably higher than that evaluated in the present study, and they also used air assistance in their equipment. Similarly, more recent studies have reported higher deposition values on both the adaxial and abaxial surfaces of leaves when applying a charge to the droplet distribution (Gan-Mor *et al.*, 2014; Maski and Durairaj, 2010; Sánchez-Hermosilla *et al.*, 2022). It should be considered that the reviewed literature provides a more comprehensive analysis of the application of electrostatic technology in air-assisted or pneumatic equipment, which generates small droplets and higher CMR values.

4. Conclusions

Electrostatic technology, implemented in an electric knapsack sprayer equipped with a hydraulic nozzle was tested in laboratory conditions in terms of flow rate, droplet size, distribution profiles, charge-to-mass ratio, and qualitative assessment of coverage. Based on these initial findings, it can be concluded that this technology offers a viable solution for basic handheld applications without air assistance, demonstrating a significant enhancement in coverage compared to conventional methods, particularly on the underside of treated areas. Consequently, its integration could be contemplated in a wider range of equipment, such as hydraulic boom sprayers, commonly used in extensive crops.

Further experimentation is necessary, particularly focusing on quantitative deposition, encompassing both controlled laboratory settings and real crop applications. This will enable a comprehensive evaluation of the technology's ability to penetrate the canopy effectively and optimize its performance in practical agricultural scenarios.

Acknowledgements

The authors would like to thank the company Euro Denker S.L. for their collaboration in the development of this research.

References

Amaya, K. and Bayat, A. (2023). Determining effects of induction electrode geometry on charging efficiency of droplets in pesticide electrostatic spraying applications. *Smart Agricultural Technology, 4*, 100190. doi:https://doi.org/10.1016/j.atech.2023.100190

Appah, S., Wang, P., Ou, M., Gong, C. and Jia, W. (2019). Review of electrostatic system parameters, charged droplets characteristics and substrate impact behavior from pesticides spraying. *International Journal of Agricultural and Biological Engineering, 12*(2), 1-9. doi:10.25165/j.ijabe.20191202.4673

Doruchowski, G., Balsari, P. and Van De Zande, J. (2009). *Development of a crop adapted spray application system for sustainable plant protection in fruit growing*. Paper presented at the International Symposium on Application of Precision Agriculture for Fruits and Vegetables 824.

Gan-Mor, S., Ronen, B. and Ohaliav, K. (2014). The effect of air velocity and proximity on the charging of sprays from conventional hydraulic nozzles. *Biosystems engineering, 121*, 200-208. doi:http://dx.doi.org/10.1016/j.biosystemseng.2014.03.004

Gil, E., Escolà, A., Rosell, J., Planas, S. and Val, L. (2007). Variable rate application of plant protection products in vineyard using ultrasonic sensors. *Crop Protection, 26*(8), 1287-1297.

ISO. (1997). Equipment for Crop Protection - Spraying Equipment - Part 2: Test Methods for Hydraulic Sprayers. ISO 5682-2:1997. International Organization for Standardization Publications, Geneva. Available from: http://www.iso.org/iso/home/store/catalogue_tc/catalogue_detail.htm?csnumber=25409 In.

Laryea, G. N. and No, S.-Y. (2003). Development of electrostatic pressure-swirl nozzle for agricultural applications. *Journal of electrostatics, 57*(2), 129-142.

Law, S. E. (2001). Agricultural electrostatic spray application: a review of significant research and development during the 20th century. *Journal of electrostatics, 51*, 25-42. doi:10.1016/S0304-3886(01)00040-7

Law, S. E. and Cooper, S. C. (1987). Induction charging characteristics of conductivity enhanced vegetable-oil sprays. *Transactions of the ASAE, 30*(1), 75-0079.

Li, Y., Li, Y., Pan, X., Li, Q. X., Chen, R., Li, X., Pan, C. and Song, J. (2018). Comparison of a new air‐assisted sprayer and two conventional sprayers in terms of deposition, loss to the soil and residue of azoxystrobin and tebuconazole applied to sunlit greenhouse tomato and field cucumber. *Pest Management Science, 74*(2), 448-455.

Llorens, J., Gil, E., Llop, J. and Escolà, A. (2010). Variable rate dosing in precision viticulture: Use of electronic devices to improve application efficiency. *Crop Protection, 29*(3), 239-248. doi:10.1016/j.cropro.2009.12.022

Mamidi, V. R., Ghanshyam, C., Kumar, P. M. and Kapur, P. (2013). Electrostatic hand pressure knapsack spray system with enhanced performance for small scale farms. *Journal of electrostatics, 71*(4), 785-790. doi:http://dx.doi.org/10.1016/j.elstat.2013.01.011

Marchant, J. and Green, R. (1982). An electrostatic charging system for hydraulic spray nozzles. *Journal of Agricultural Engineering Research, 27*(4), 309-319.

Maski, D. and Durairaj, D. (2010). Effects of charging voltage, application speed, target height, and orientation upon charged spray deposition on leaf abaxial and adaxial surfaces. *Crop Protection, 29*(2), 134-141. doi:10.1016/j.cropro.2009.10.006

Pascuzzi, S. and Cerruto, E. (2015). Spray deposition in "tendone" vineyards when using a pneumatic electrostatic sprayer. *Crop Protection, 68*, 1-11. doi:https://doi.org/10.1016/j.cropro.2014.11.006

Patel, M. K., Ghanshyam, C. and Kapur, P. (2013). Characterization of electrode material for electrostatic spray charging: Theoretical and engineering practices. *Journal of electrostatics, 71*(1), 55-60.

Patel, M. K., Kundu, M., Sahoo, H. K. and Nayak, M. K. (2016). Enhanced performance of an air-assisted electrostatic nozzle: Role of electrode material and its dimensional considerations in spray charging. *Engineering in Agriculture, Environment and Food, 9*(4), 332-338.

Patel, M. K., Praveen, B., Sahoo, H. K., Patel, B., Kumar, A., Singh, M., Nayak, M. K. and Rajan, P. (2017). An advance air-induced air-assisted electrostatic nozzle with enhanced performance. *Computers and Electronics in Agriculture, 135*, 280-288. doi:https://doi.org/10.1016/j.compag.2017.02.010

Salcedo, R., Zhu, H., Zhang, Z., Wei, Z., Chen, L., Ozkan, E. and Falchieri, D. (2020). Foliar deposition and coverage on young apple trees with PWM-controlled spray systems. *Computers and Electronics in Agriculture, 178*, 105794.

Sánchez-Hermosilla, J., Pérez-Alonso, J., Martínez-Carricondo, P., Carvajal-Ramírez, F. and Agüera-Vega, F. (2022). Evaluation of Electrostatic Spraying Equipment in a Greenhouse Pepper Crop. *Horticulturae, 8*(6), 541. doi:doi.org/10.3390/horticulturae8060541

Zhao, S., Castle, G. and Adamiak, K. (2008). Factors affecting deposition in electrostatic pesticide spraying. *Journal of electrostatics, 66*(11-12), 594-601. doi:10.1016/j.elstat.2008.06.009

Assessing the adaptive capability of an intelligent recycling tunnel sprayer system to vine canopy size

Ramón Salcedo [a,*], Nehad El Aissaoui [a], Bernat Martí [a], Bernat Salas [a], Jordi Biscamps [a], Jordi Llop [a], Francisco García-Ruiz [a], Emilio Gil [a]

[a] Department of Agri-Food Engineering and Biotechnology, Technical University of Catalonia, Castelldefels, Spain

* Corresponding author. Email: ramon.salcedo@upc.edu

Abstract

Air-assisted recycling tunnel sprayers for trellised vineyard's PPP applications incorporate panels, enabling the recovery of the majority of the sprayed liquid fraction that remains unretained by the leaves during the process. In this study, a new tunnel sprayer has been developed with an automatic variable-rate application (VRA) control unit. This system is able to execute previously generated prescription maps based on remote sensors (such as satellites) and Decision Support System for vineyards (Dosaviña®). Furthermore, there is also the option to include ultrasonic sensors to identify canopy size, increasing the accuracy of the application rate. Currently, regardless of the VRA spray mode selected, a third option is being considered to adapt the separation between recovery panels depending on the width of the vine canopies along the row. To verify the operability of the prototype, numerous tests were done concerning the effect of air, the capacity to recover the flow from the panels and the losses to the ground. First, the effect on air stream patterns between panels was studied. The air velocities at different positions were recorded between panels. Then, the flow rate recovery capacity was checked, for different distances between panels and air flow rates, including the presence of canopies. These tests were carried out under laboratory conditions and with the sprayer in static mode. The last part was performed in an experimental vineyard plot. The operating capacity of the ultrasonic sensors to carry out a variable application was assessed, as well as the effectiveness of the panel design to reduce losses to the ground. The tests were conducted using Petri dishes as collectors to evaluate both direct losses under the canopies and ground deposits outside the plot. The prototype was compared with a conventional multi-row sprayer without panels. The tests demonstrated the ability to adapt the application rate, reducing losses outside the plantation, although more tests are still necessary.

Keywords: Precision application, Recovery panels, Airflow analysis, Adaptive control, Ultrasonic sensors.

1. Introduction

The application of Plant Protection Products (PPP) remains one of the major challenges in agriculture, particularly in the cultivation of 3D crops, such as fruit orchards and vineyards. In the context of viticulture, this issue is of significant importance within the European Union, which stands as the world's largest producer of grapes and wine (EPRS, 2023). Given the socioeconomic relevance, farmers are highly motivated to ensure that the final product reaches consumers with the highest possible quality, maintaining productivity levels without the presence of agrochemical residues. Consequently, Variable-Rate Application (VRA) systems are gaining increasing interest among growers (Gil et al., 2023).

VRA sprayers involves variably applying the amount of product needed for each area of the target plantation based on its vegetative characteristics, primarily the size and density of the foliage. This method optimizes the amount of PPP used, maintaining efficacy against pests and diseases, while reducing losses and saving resources. Currently, there are two main ways to work with a VRA system: using onboard proximal sensors that characterize canopy structure in real-time (Salas et al., 2024), or through prescription maps generated from aerial images collected by drones and/or satellites (Garcia-Ruiz et al., 2023). In these cases, Decision Support Systems (DSS), such as Dosaviña® for vineyards (Gil et al., 2019), based in the Leaf Wall Area (LWA) method, help refine these prescription maps. The first method can be much more precise, whereas the second tends to be less expensive with reasonable field resolution.

To encourage farmers to adopt these technologies sooner (Warneke et al., 2021), VRA systems are being developed that can be integrated into existing commercial sprayers (Salcedo et al., 2020). In the case of viticulture, it would be beneficial to integrate an intelligent device into a multi-row sprayer with recovery panels. These sprayers can operate on two rows simultaneously and have a hydraulic circuit that

recovers the sprayed liquid that does not deposit on the leaves, theoretically reducing losses even further compared to a conventional sprayer. By incorporating VRA technology, this application could become even more efficient. In this regard, the SENSORECUFIT-F2 (AEI-010500-2022b-213) Spanish project, funded by the Spanish Ministry of Science, is currently investigating this by means of a vineyard sprayer.

The obvious first step is to assess the properties of the recycling tunnel spraying system in order to understand the influence of the design on the spray application quality. In this regard, the objective of this research work was to characterize the sprayer's performance in terms of fan currents and flow rate recovery, as well as to evaluate its capacity to detect vegetation and reduce ground losses during an application using ultrasonic sensors.

2. Materials and Methods

2.1. Spray mode

The VRA system was integrated into a multi-row sprayer SH-R1000-1A Saher (Saher, Barcelona, Spain) with recovery panels. This sprayer was designed to treat two rows of vines simultaneously (Figure 1). It was equipped with side panels that capture and recover the sprayed liquid that does not adhere to the leaves or grapes, reducing liquid losses and increasing application efficiency. There were four side panels, grouped in pairs of two on each side of the sprayer. The sprayer featured a pneumatic circuit with five pistons to deploy the panels (upwards, downwards, and to open between themselves). Each panel had an internal vertical downpipe through which the nozzles and air stream were distributed. Each downpipe presented six nozzles spaced 20 cm apart. The air was generated by a dual intake turbine with two-speed positions at the gearbox. The arrangement of the downpipes on opposite ended of each panel pair, with the downpipe on the panel adjacent to the sprayer placed at the farthest end from the tractor, and the reverse configuration for the other panel. This design pretended to maximize the efficiency in the application by forming an air circulation pattern to promote a recirculation around the canopy. These panels were foldable for easy transport and storage.

Figure 1. General schematic view of the experimental tunnel sprayer (left) and use of recovery panels during a spray application (right).

The sprayer included a hydraulic system to regulate pressure and spray volume, as well as advanced technology such as sensors and electronic controllers to optimize the use of PPP. This sprayer managed the application rate by regulating the working pressure through a WAATIC electronic controller (Waatic S.L., Barcelona, Spain), which was connected to an integrated GNSS receiver and an automatic section controller. Originally, this VRA sprayer was designed to operate based on maps obtained via UAV or satellites. However, it also offered the option to spray in real-time, incorporating 10 ultrasonic sensors, 5 on each side of the sprayer, aligned vertically on the same metal structure and spaced 20 cm apart for optimal canopy characterization. The unit control was capable of operating in both VRA modes. In the case of the ultrasonic sensors, it was continuously monitoring the measurements collected. The data from the ultrasonic sensors was converted into vegetation volume using the Tree Row Volume (TRV) method, which, through a conversion factor (Gil and Escolà, 2009), was transformed into application rate (L ha^{-1}). For the case of using maps, the external support of the Dosaviña® DSS could be utilized to determine the spray volume for each different level of vigour.

2.2. Experimental site

The experimental layouts were performed at the facilities of the Agropolis center, which belongs to the Polytechnic University of Catalonia (UPC). This is place where the Agricultural Mechanization research team has a laboratory and an experimental vineyard plot. It is located in Viladecans in Barcelona (Spain).

2.3. Characterization trials under lab conditions

2.3.1. Air behaviour

The airflow rates from the downpipes were measured. For this, a hot-wire anemometer (Handle model; Testo, S.A., Barcelona, Spain) was placed at the centre of each air outlet opening of all the downpipes of the sprayer. The anemometer was oriented following the direction of the main current. Data was recorded at every individual outlet, until the values stabilized within a defined range. Air velocities were obtained for each of the four panels, by combining the two fan speeds, with the PTO at 480 rev min^{-1}, as recommended by the sprayer's manufacturer. There were two replications per measurement. The flow rate was calculated based on the area through which the air exited to the exterior.

Additionally, a 3D ultrasonic anemometer (3D WindMaster 1590-PK-020 model; Gill Instruments Ltd., Hampshire, United Kingdom) was used to acquire the instantaneous air flow velocities in the three spatial directions between the panels. The velocities were measured on one side of the machine, with the sprayer in a stationary position. The two fan speeds were tested again. Air velocities were recorded in three different planes, subdivided into six heights and two depths, inspired on the methodology exposed by Salcedo et al. (2021). For each point, velocities were recorded for 60 s at a frequency of 10 Hz.

2.3.2. Flow rate recovery

The capacity of the sprayer's hydraulic system to recover the flow rate emitted by the nozzles between two panels was estimated. On the left side of the machine, the flow rate returning to the tank from the recovery panels was measured using a precision scale. The hose from the left side pump to the tank was redirected to an individual container, which was filled for 60 s and then weighed to determine the flow rate (L min^{-1}). Four scenarios were tested: 1) panels completely closed; 2) panels separated by 60 cm; 3) panels separated by 100 cm with an artificial vine in the middle with a width of 40 cm; 4) and panels separated by 140 cm with two artificial canopies together in the middle of 40 cm-width each.

The tests were conducted supposing a theoretical application rate of 250 L ha^{-1}, assuming a width of 2.8 m and a forward speed of 5.5 km h^{-1}, which are typical values in the Penedés area (Barcelona, Spain). The corresponding operating pressure was 550 kPa, and 24 nozzles (6 per downpipe) were used, according to the recommendation provided by Dosaviña®. The nozzles were hollow cone TR-01 nozzles (Lechler GmbH, Metzingen, Germany). The test was conducted in a static setup of the sprayer. The panels were positioned 40 cm above the ground, and only water was used. For each test, both fan speed positions, as in the air assays, were combined. The same side than the air velocities test was selected.

2.4. Ground losses during a field application

The prototype was compared in field conditions with a conventional constant-rate IRIS multi-row sprayer (Ilemo-Hardi, SAU, Lleida, Spain), with the VRA spray mode disconnected. It was intended to evaluate the panels design to reduce ground losses. For the reference spray system, it was capable to treat two rows at the same time too, with four vertical booms also and six nozzles per downpipe. Half of the plot was treated with the conventional sprayer, while the other part was sprayed with the prototype. The forward speed was 5.5 km h^{-1} and the spacing rows was 3.0 m. According to the characteristics of the canopies, Best Management Practices (BMP) were applied, and only three TR-015 hollow cone nozzles per downpipe were used on each sprayer. The theoretical application rate was 200 L ha^{-1} for both sprayers, recommended by Dosaviña®, and operating at a spray pressure of 700 kPa. On both sprayers the low gear of the fan gearbox was chosen considering the BMP. Although the prototype was working with a constant application rate, the ultrasonic sensors were operating monitoring the dimensions of the canopies in real time. The prototype was operating with a constant application rate, the ultrasonic sensors were monitoring the dimensions of the canopy in real-time, monitoring the changes with a resolution at 10 L ha^{-1} application rate estimated intervals. The idea was to determine if they were capable of identifying vegetative

differences within the plot and if they estimated application rates similar to those estimated with the DSS Dosaviña®.

Each of the two treated halves was further divided into two sides (right and left). On each side, in the central zone of the vine rows, there were four rows of Petri dishes used as collectors to sample the losses to the ground. Each row was spaced 1.0 m apart. Within each row, there were eight Petri dishes. Four of these were positioned directly beneath the canopies, corresponding to the four outermost rows of vines on each side of the plot. The other four dishes were placed at distances of 2.5, 3.5, 5.5, and 9.5 m from the last vines row. The tracer used was Tartrazine at a theoretical concentration of 3 g L^{-1}. Meteorological data were monitored with a portable weather station (Campbell Scientific Inc., Logan, UT) that included a 2D sonic anemometer and a digital temperature and relative humidity sensor. Wind speeds never exceeded 3.0 m s^{-1}, in accordance with Spanish regulations for PPP applications (BOE, 2012).

3. Results

3.1. Airflow behaviour

Variations in the air velocity vectors between panels were found for the two positions of the fan gearbox, showcasing shifts in both direction and magnitude. Particularly noticeable was the increasingly erratic behaviour observed as the height above ground level increased. This variability manifested in vectors diverging in opposite directions, indicative of complex airflow patterns. The observed changes in air direction pointed out the formation of air vortices between panels. The higher the fan speed, the more evident this phenomenon was. Moreover, notable disparities in airflow rates were observed between the use of short and long gear settings, underscoring again the impact of fan gearbox speed on these critical parameters.

3.2. Liquid recovery

Recovery capacity of sprayed liquid varied from 100% with the panels closed to approximately 18% when the panels were further apart, with the vegetation in the middle, for both fan speeds. For the separation of 60 and 100 cm, respectively, there was a noticeable difference between short and high-speed position. Generally, the low fan speed showed higher water recovery. The combination of distance and additional fan speed decreased liquid recovery compared to simpler conditions (panels closed). The bigger the fan speed, the less effective the recovery capacity. The higher fan speeds and complex airflow patterns between panels, including vortices, could be affecting the efficiency of liquid recovery

3.3. Ground losses

The results of losses to the ground were disparate. On the one hand, in terms of direct losses to the ground within the plot, the conventional sprayer produced fewer losses than the prototype. The mean ground deposition was 2.5 μg cm^{-2} with the prototype, while with the reference application it was 3.2 μg cm^{-2}. This increase could be explained by the design of the panels, which concentrates the air currents in the form of an eddy. It could favour the sprayed droplets to precipitate in greater amounts to the ground. On the other hand, the Hardi sprayer applied from a single downpipe and the droplets could travel beyond the canopy, without the presence of the wide panel. In fact, the collectors outside the plot exposed lower losses with the prototype, with a mean deposition of 0.05 μg cm^{-2}, compared to the reference sprayer, with a mean deposition close to 0.3 μg cm^{-2}. It was probably due to the effect of the panels on the air, although there could be other reasons such as the spray profile of the nozzles.

Additionally, the ultrasonic sensors were able to detect differences in canopy dimensions. However, the recommended average application volumes were lower than those estimated by Dosaviña (20-55 L ha-1). The explanation likely lies in the calculation algorithm used by the control unit. Therefore, it is necessary to review the agronomic parameters used by the intelligent system, as such a low application rate would not be viable.

4. Conclusions

The fan settings influenced on the air stream between panels, generating even vortices, and probably diminishing the recovery flow rate capacity. The better recovery values were achieved with low fan speeds, but at certain distance and/or dimensions of the canopy this effect is neglected. Increased separation and higher fan speeds reduce recovery rates with more intensity. During a field application, the prototype sprayer leads to higher ground losses within the plot, maybe due to concentrated eddy currents. However, it performs better in reducing losses outside the plot compared to the conventional sprayer. Finally, the sensors were able to characterize the vegetation but the proposed application rates showed that it is necessary to continue adjusting the prototype algorithms. This work highlights the importance of characterizing the effect of air fan on the VRA sprayers, as well as continuing to further investigate this prototype.

Acknowledgements

The SENSORECUFIT-F2 project (AEI-010500-2022b-213) was funded by the Spanish Ministry of Science and Universities. The authors would also like to thank AgriArgo Ibérica, Ilemo Hardi and Lechler GmbH for their collaboration.

References

BOE (Boletín Oficial del Estado). 2012. Real Decreto 1311/2012, de 14 de septiembre por el que se establece el marco de actuacion para conseguir un uso sostenible de los productos fitosanitarios. BOE N 223, 65127–65171 de 15 de septiembre, 2012.

European Parliamentary Research Service. 2023. The EU wine sector. PE 751.399. Available at: https://www.europarl.europa.eu/RegData/etudes/BRIE/2023/751399/EPRS_BRI(2023)751399_EN.pdf

Garcia-Ruiz, F., J. Campos, J. Llop, E. Gil. 2023. Assessment of map based variable rate strategies for copper reduction in hedge vineyards. Computers and Electronics in Agriculture, 207, 107753. https://doi.org/10.1016/j.compag.2023.107753

Gil, E., A. Escolà. 2009. Design of a decision support method to determine volume rate for vineyard spraying. Applied Engineering in Agriculture, 25(2), 145-151. https://doi.org/10.13031/2013.26323

Gil, E., J. Campos, P. Ortega, J. Llop, A. Gras, E. Armengol, R. Salcedo, M. Gallart. 2019. DOSAVIÑA: Tool to calculate the optimal volume rate and pesticide amount in vineyard spray applications based on a modified leaf wall area method. Computers and Electronics in Agriculture, 160, 117-130. https://doi.org/10.1016/j.compag.2019.03.018

Gil, E., J. Campos, R. Salcedo, F. García-Ruiz. 2023. Variable Rate Application in fruit orchards and vineyards in Europe: canopy characterization and system improvement. In *2023 ASABE Annual International Meeting*. Omaha, Nebraska (USA), July 9-12. Published by the American Society of Agricultural and Biological Engineers, St. Joseph, Michigan. Ed. Sudhagar Mani. https://doi.org/10.13031/aim.202301130

Salas, B., R. Salcedo, F. Garcia-Ruiz, E. Gil. 2024. Design, implementation and validation of a sensor-based precise airblast sprayer to improve pesticide applications in orchards. Precision Agriculture, 25(2), 865-888. https://doi.org/10.1007/s11119-023-10097-7

Salcedo, R., H. Zhu, Z. Zhang, Z. Wei, L. Chen, E. Ozkan, D. Falchieri. 2020. Foliar deposition and coverage on young apple trees with PWM-controlled spray systems. Computers and Electronics in Agriculture, 178, 105794. https://doi.org/10.1016/j.compag.2020.105794

Salcedo, R., A. Fonte, M. Grella, C. Garcerá, P. Chueca. 2021. Blade pitch and air-outlet width effects on the airflow generated by an airblast sprayer with wireless remote-controlled axial fan. Computers and Electronics in Agriculture, 190, 106428. https://doi.org/10.1016/j.compag.2021.106428

Warneke, B. W., H. Zhu, J. W. Pscheidt, L. L. Nackley. 2021. Canopy spray application technology in specialty crops: A slowly evolving landscape. Pest Management Science, 77(5), 2157-2164. https://doi.org/10.1002/ps.6167

Evaluation of agrochemical aerial distribution from UAS on a vineyard

Alberto Sassu[a], Vasilis Psiroukis[b], Francesco Bettucci[c], Luca Ghiani[d], Spyros Fountas[b], and Filippo Gambella[a,e*]

[a]Department of Agricultural Sciences, University of Sassari, Sassari, Italy

[b]Laboratory of Agricultural Engineering, Department of Natural Resources Management & Agricultural Engineering, School of Environment and Agricultural Engineering, Agricultural University of Athens, Athens, Greece

[c]Department of Land Environment Agriculture and Forestry, University of Padova, Legnaro, Italy

[d]Departement of Biomedical sciences, University of Sassari, Sassari, Italy

[e]Interdepartmental Center IA - INNOVATIVE AGRICULTURE, Surigheddu, Alghero, Italy.

* Corresponding author. Email: gambella@uniss.it

Abstract

Addressing the challenge of replacing airplane and helicopter Plant protection products (PPPs) spraying characterized by distribution inaccuracies, product overdoses, and losses, Unmanned Aerial Spraying Systems (UASSs) emerge as a transformative solution with unique capabilities such as navigating complex terrains and executing low-altitude flights. This study explores the impact of UASS flight height, speed, and position on vineyard spraying coverage, canopy penetration, and off-target dispersion employing Water Sensitive Papers and a MATLAB image analysis script. The investigation revealed the optimal performance of the UASS operating at a 2 m height while flying over the inter-row (IR), minimizing off-target and ground dispersion. The IR flight configuration with strategically positioned nozzles above the canopy facilitated canopy penetration, reaching lower sections, and reducing off-target dispersion. The performance exhibited sensitivity to changes in flight speed, where faster rotation aided canopy opening and droplet penetration. The positive relationship between higher speed and improved efficiency underscores the significance of speed optimization in achieving optimal flight outcomes. The positioning of the flight significantly impacted the deposition of droplets on the target, off-target, and ground, leading to an increased coverage area in over-row (OR) treatments with higher flight heights. In IR treatments, a lower flight height was associated with reduced product dispersion, resulting in greater coverage area and penetration rate. Flight position and speed correlate closely, as higher speed and propeller rotation induce increased downward flow. OR treatments exhibit heightened influence in lower positions, facilitating ground and side-row waste. The droplet analysis method presented in this study showed potential in refining UASS spraying strategies in vineyards and open to further research to comprehensively assess the aerial PPP distribution effectiveness and environmental impact in agriculture. These investigations are crucial for the responsible implementation of this technology, particularly in regions where aerial treatments lack regulatory approval.

Keywords: Unmanned Aerial System spraying, Aerial spraying, PPP, Precision Viticulture, WSP analysis.

1. Introduction

With the escalating global demand for food and the significant impact of biotic factors on annual yield losses (FAO 2017), plant protection products (PPP) persist in safeguarding crops from insects, pests, and fungi (Lykogianni et al. 2021). PPP distribution is a high-risk operation, resulting in residues in food, water bodies, and non-target organisms, which poses substantial risks with profound implications for consumer safety and the environment (Akpan et al. 2023). Commonly distributed through spraying systems implemented on board of terrestrial vehicles, PPP application is a challenging operation in terms of time, labour, and health risks for operators. As farmers predominantly favour traditional ground spraying methods, evaluating application efficiency becomes crucial to minimize human and environmental hazards (V. Dhananjayan et al. 2020; Kestur et al. 2020).

Airplane and helicopter aerial spraying are considered an economical and fast method for PPP spraying, prone to poor distribution accuracy (Quantick 1979), high product overdose and losses, and not suitable for small-scale farms requiring large areas for take-off and landing (Baio et al. 2019). Addressing these concerns has stimulated policy initiatives, legislative regulations, and a growing demand for environmentally friendly management methods, leading the European Parliament to prohibit aerial PPP distribution in Union countries

(European Parliament 2009) except in specific limited situations where conventional operations are not feasible.

In recent years, multi-rotor Unmanned Aerial Spraying Systems (UASSs) have gained attention due to their ability to follow complex patterns, fly at low altitudes, adapt to hilly terrain, take off and land vertically, perform low-volume and site-specific PPP applications, limit operator's health risks with a low operational cost, preserving the crops and soil's structure form physical damage (Qin et al. 2016). Pump pressure, flight height and speed, payload capacity, weather conditions, flight range, and environmental dispersion (drift effect and ground leaking) are the aspects to consider that may affect the treatment's results (H. Chen et al. 2021).

Vineyards, exposed to several recurring diseases at certain times of the year and in specific climatic conditions and growth phases, require timely and successful treatments (Pertot et al. 2017). Despite being a viable alternative to conventional application methods, the application of UASS in vineyards is not yet well investigated. As a relatively new technology, evaluating their effectiveness and spraying configuration is essential to understand when and how to implement UASS in agricultural PPP distribution scenarios and to compare them to terrestrial machinery performances.

The initial hypothesis of the manuscript suggests that UASS can effectively and safely perform PPP spraying on the rows of a vineyard, given the appropriate environmental conditions and flight settings. Specifically, this research aims to verify and characterize the uniformity and dispersion of UASS distribution by testing different combinations of flight parameters over a vineyard. The spraying performance, assessed with Water Sensitive Papers (WSPs) placed inside the canopy and on the ground along the inter-row, was obtained using a MATLAB code, able to extrapolate WSPs' covered area on target and off-target rows and the penetration rate through the canopy.

2. Materials and Methods

2.1. Study area

The experimental field was a Savatiano variety (*Vitis* Vinifera L.) 480 m^2 vineyard located in Spata, Greece (228285.983 East – 4208689.259 North; WGS84 – UTM 35 N, EPSG: 32635) at 123 m above the sea level, 20 km East from Athens. The grapevines, planted with a 1.5 m × 2 m spacing with an NW-SE rows' orientation, were trained as Vertical Shoot Position (VSP). The survey area was a small flat plot far from the field borders of the experimental vineyard owned by the Agricultural University of Athens. Experiments took place on 21, 22, 28 June, and 13 July 2022 (BBCH 77). The weather conditions faced during the experiments were optimal for UASS operations: sunny days, clear sky, and wind absence.

2.2. UASS platform

The UASS Agras T16 (DJI Technology Co., Ltd, Shenzhen, China) was used for the trials. Equipped with a spraying system with a 16 L thank, eight nozzles (XR11001VS, Teejet Technologies, Glendale Heights, Illinois, USA), an RTK navigation system, a DBF imaging Radar, and FPV camera, the Agras T16 weights 18.5 kg excluding the battery and an empty thank, with a hovering time varying from 18 minutes to 10 minutes depending on the take-off weight, the wind speed, and the flight's settings. The air-injection flat fan nozzles were chosen to perform water spray distribution over the rows, because of their better deposition performance, uniformity, and reduced drift than hollow cone ones (C. Wang et al. 2021).

2.3. Experimental design

The experiment employed a factorial design involving flight height Above Ground Level (AGL) (H), flying speed (S), and the UASS over-row (OR) and inter-row (IR) overflight positions with two levels per factor, for a total of eight treatments repeated three times. The UASS flew OR and IR at 2 m and 2.5 m AGL at 1 m s^{-1} and 1.5 m s^{-1} (Table 1). The OR treatments' target was the row the UASS was flying over, with the two adjacent rows used to evaluate the off-target dispersion, for a total of three rows. Instead, the IR flights had as target the two rows surrounding the inter-row area overflown by the UASS, with the two external rows used to evaluate the off-target dispersion, for a total of four rows. Figure 1 reports the two flying paths with the sampling points' position consisting of WSPs (7.6 cm x 2.6 cm; 19.86 cm^2, Syngenta

Crop Protection AG, Basel, Switzerland) located along three deposition lines spaced 20 m from each other to collect droplets. Test area boundaries were marked visibly in the field using a red tape. A 20 m preparation zone was defined to allow the UASS to reach the aimed speed and pump distribution pressure before entering the test zone.

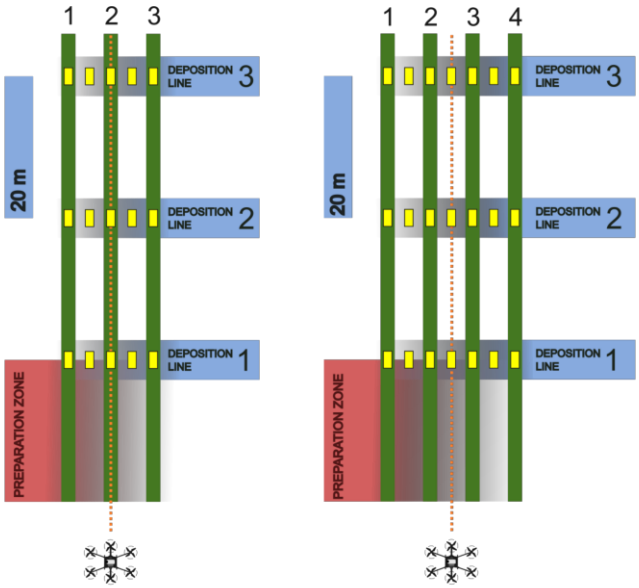

Figure 1. A graphical representation obtained using the SVG software Inkscape 1.2.2. (Software Freedom Conservancy) of OR (left) and IR (right) treatments seen from above.

Table 1. The eight treatments included in the experiment and the respective factors' values.

Treatment	Factors	Values
A	H1-S1-OR	2.5 m -1 m s^{-1} - over row
B	H1-S2-OR	2.5 m - 1.5 m s^{-1} - over row
C	H2-S1-OR	2.0 m -1 m s^{-1} - over row
D	H2-S2-OR	2.0 m - 1.5 m s^{-1} - over row
E	H1-S1-IR	2.5 m -1 m s^{-1} - inter row
F	H1-S2-IR	2.5 m - 1.5 m s^{-1} - inter row
G	H2-S1-IR	2.0 m -1 m s^{-1} - inter row
H	H2-S2-IR	2.0 m - 1.5 m s^{-1} - inter row

For each row's sampling point three WSPs were hooked to the trellis at 0.3 m, 0.6 m, and 1 m AGL to measure the PPP penetration inside the canopy. Four WSPs for the OR treatments and six WSPs for the IR treatments for each deposition line, were placed on the ground in the inter-rows (2 WSPs per inter-row) over wooden dedicated supports to evaluate the off-target PPP ground deposition. All the WSPs were manually positioned by the operators using latex gloves to prevent stains on the WSPs, sensitive to water and humidity.

The treatments were performed with a wind speed lower than 3 m/s direction N, NW, parallel to the rows, with a 1.3 l min^{-1} to 1.8 l min^{-1} average pump flow velocity values. Weather conditions were monitored by a weather station located Sud east at the border of the field 15 m off the flight path, close to the piloting zone, at 1.5 m AGL. The weather requirements (suggested by the ISO 23117-1:2023) necessary to perform the aerial distribution were an ambient dry temperature between 10 °C and 35 °C, a relative humidity under 70%, and a mean wind speed under 2.0 m s^{-1}.

2.4. Automatic droplets detector development

The first step to perform the automatic droplets detection was scanning the WSPs with 1200 dpi maximum resolution office scanner (Epson L3250). All the WSPs hooked to the trellis system belonging to the same deposition line, were scanned in the same image (9 WSPs for OR and 12 for IR operations). The same

procedure was applied to the WSPs located on the ground support (4 for OR and 6 for IR operations). The WSPs used for the test were then analyzed through a MATLAB R2021b code. Further details about the automatic droplet detector development are described in (Ghiani et al. 2020). WSP's droplets covered area (cm^2) was used to evaluate the UASS distribution performance.

2.5. Statistical analysis for spray performance evaluation

Spray features and UASS performance were evaluated using the MATLAB-based WSPs analysis and then processed using Python (Python Software Foundation) scripts through Pandas, Statsmodel, and Matplotlib packages, respectively for data frame manipulation, statistical analysis, and plotting. The statistical analysis was prompted by the works of Biglia et al. (2022); S. Chen et al. (2020); Sarri et al. (2019); C. Wang et al. (2021, 2022). The covered area was plotted for each sampling height (high, medium, and low) by averaging the three repetitions (corresponding to each deposition line) of each treatment and separating the target and off-target rows results. The same procedure was applied to the ground samples by averaging all the WSPs results of the same treatment. A three-way analysis of variance (ANOVA) test was performed to detect the effect of flight speed, flight height, and UAS flight position factors and their combination on each of the three variables, differentiating target rows, off-target rows, and ground loss. The significance of statistical computations for ANOVA and Tukey test was considered for $P<0.05$ unless otherwise stated. Data distribution and homoscedasticity were respectively tested through Shapiro-Wilk and Levene's test. If the ANOVA performed on the fitted model showed a significant factors effect, the Tukey's test for multiple comparisons was performed to compare mean values of parameters between treatments, and results showed inside the respective bar plots.

To characterize droplets Penetration Rate (PR) at each collection point (representing the efficiency of the treatment to reach the lower part of the row where the protection products are more needed), the ratio of the lower WSP's droplets covered area (CA_{low}) to the sum of the upper (CA_{up}) and mid (CA_{mid}) WSPs' droplets covered area was used, as explained by the equation 1 (C. Wang et al. 2022):

$$PR = \frac{CA_{low}}{CA_{up}+CA_{mid}} \times 100\% \quad (1)$$

3. Results

The results are presented in two main sections reporting respectively the distribution of target and off-target rows droplet deposition for the covered area at each height position of the WSPs, and the PR results through the canopy.

3.1. Covered area

Covered area results (Figure 2) tent to decrease from the higher to the lower canopy section, with treatments A and B gaining the largest covered area. Treatment H got a similar result in the lower position, impacting on the PR. The higher covered area in treatments A and B could be related to the position of the UASS perpendicular to the row and the higher flight altitude AGL, which led a larger volume of product to reach the upper-mid part of the canopy. Treatments C and D, instead, due to the lower flight altitude and the location of the nozzles perpendicular to the inter-rows, gained a lower covered area, leading a conspicuous volume of product to hit the off-target rows. In fact, despite the UASS frame was positioned over the target row, due to the large diameter of the UASS and the derived location of the nozzles over the inter-rows, treatments C and D flight settings caused a lower covered area on the target row compared to A and B. Treatment H results at low sampling height (Figure 1c) could derive from the combined action of flight height and speed. The first one helped reduce the off-target dispersion (larger in treatments E and F, specifically at low positions), while the second one, thanks to the higher spinning rotation of the propellers, caused a bigger canopy opening, allowing the droplets to reach the lower position. It is essential to emphasize the importance of finding the proper flight setting that allows a homogeneous distribution of product throughout the canopy height, with a specific focus on the mid-low parts, known to be the main canopy's infection sites, which require more than others to be treated and limiting an over-coverage of the highest part. The results obtained in the IR treatments (E, F, G, and H) could be attributed to the same reason described above, where, this time, the UASS propellers, and consequentially the nozzles located below, were positioned over the two target

rows. This condition provoked a generally smaller covered area on the two target rows at the three sampling heights, a large covering at the lower sampling height (probably derived by the action of the propellers that opened the canopy), and a lower dispersion on off-target rows compared to low flight height over-row treatments (C and D). These differences were also emphasized by the longer distance of the off-target rows from the UASS in IR treatments compared to the OR ones and the different generated turbulence between the rows.

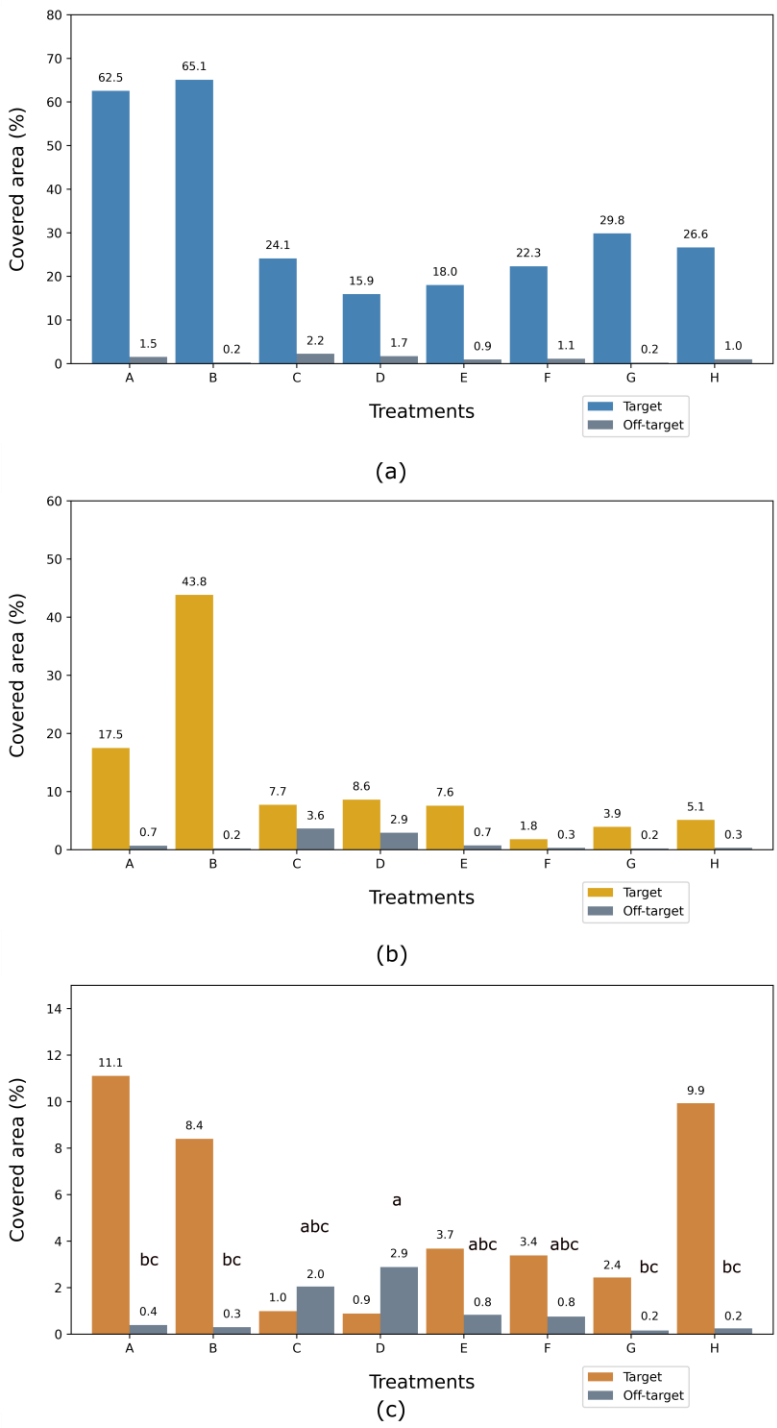

Figure 2. The bar charts containing the mean covered area results and Tukey's test group division for target and off-target rows divided for each treatment at high (a), medium (b), and low (c) WSPs heights.

According to the three-way ANOVA (Table 2), the factors flight height and UASS flight position had a significant influence on the area covered in the upper part of the canopy, also showing a significant interaction effect. The two factors probably caused treatments A and B to get a larger WSPs' covered area, specifically at the higher sampling position. Since flying speed was not considered a significant predictor of the covered area, spraying operations could be performed at a higher speed to cover larger surfaces in less time.

Table 2. Covered area 3-way ANOVA results divided by high, medium, and low WSP's canopy height for target and off-target rows.

	Target rows p-value			Off-target rows p-value		
Factors	H	M	L	H	M	L
UASS height	0.042*	0.137	0.333	0.444	0.058	0.024*
UASS speed	0.889	0.444	0.727	0.594	0.563	0.551
UASS position	0.044*	0.057	0.877	0.153	0.034	0.009**
UASS height : UASS speed	0.581	0.531	0.413	0.449	0.918	0.389
UASS height : UASS position	0.005**	0.141	0.082	0.088	0.026*	0.000***
UASS speed : UASS position	0.837	0.287	0.430	0.106	0.743	0.562
UASS height : UASS speed : UASS position	0.922	0.278	0.680	0.933	0.755	0.544

* = p-value < 0.05
** = p-value < 0.01
*** = p-value < 0.001

The 3-ways ANOVA table also suggested that the two mentioned factors, singularly and combined, influenced the off-target results at the lowest off-target sampling position. As shown in Figure 1c, the treatments C, D, E, and F reported a higher off-target dispersion. For the OR treatments (C and D), this effect was probably caused by the position of the nozzles on the two inter-rows alongside the target row, which helped disperse the product on the inter-rows and the lower part of the off-target rows. The E and F treatments provoked a smaller off-target dispersion probably because of the different nozzles' position on the target rows (perpendicular to them) and the greater distance from the off-target rows. The higher position of treatments E and F compared to G and H probably provoked a drift effect due to the wind effect, which pushed the droplets far from the monitored off-target rows.

Averaged ground dispersion results reported in Figure 3a showed a general difference between OR treatments, characterized by a higher covered area (most of all treatment B), and IR ones. Such a result suggests a better performance for IR treatments, which showed a lower ground dispersion of product, especially for treatments E and F, and a higher one for treatments G and H. This behaviour could be related to the higher flight performed in treatments E and F, which involved an increased droplets' exposition to the wind action (especially the smaller ones), which influenced distribution results and provoked value fluctuation.

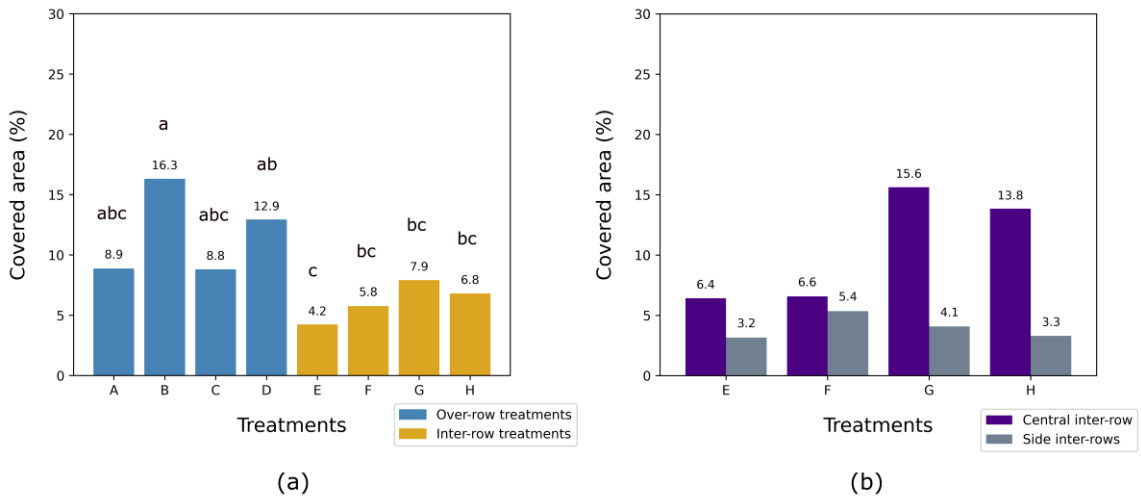

Figure 3. Covered area results with Tukey's test grouping divided by treatments for ground WSPs (a) and a specific focus on IR treatments' ground dispersion (b), larger in central inter-row of treatments G and H.

The three-way ANOVA shows how the speed and UASS flight position (singularly and combined) influenced the ground results (Table 3). As described above, the position of the nozzles over the target rows in the IR flying treatments helped reach good covering results and limit the quantity of product that reached the ground, differently from the other treatments, characterized by the nozzles spraying perpendicular to the inter-row. The flight speed and the consequent higher propellers' speed rotation could have provoked an increased downward flow that pushed the droplets onto the ground, as described by Wen et al. (2019), visible in treatments B and D. In the OR treatments, the treated inter-rows were only two, where the UASS sprayed identically through each nozzle positioned above. Differently, in IR flights, the sprayed inter-rows were three: a central inter-row sprayed by both UASS's side nozzles and two side inter-rows, respectively sprayed from half part of the nozzles. While treatments E and F showed almost homogeneous results throughout the inter-rows, treatments G and H showed higher coverage percentages on the central inter-row. Such result determines the influence of the flight height on the downward direction of the droplets in IR flights, limiting the wind effect on the spray jet, protected by the target rows and how, in general, the central row receives an increased volume of PPP.

Table 3. Covered area 3-way ANOVA results for ground WSPs.

Factors	p-value
UASS height	0.524
UASS speed	0.035*
UASS position	5.76-06***
UASS height : UASS speed	0.206
UASS height : UASS position	0.081
UASS speed : UASS position	0.018*
UASS height : UASS speed : UASS position	0.882

* = p-value < 0.05
** = p-value < 0.01
*** = p-value < 0.001

3.2. Penetration rate

The PR is highly connected to the covered area variable, as shown in Formula 2. For this reason, high PR was obtained because of the ratio between lower sampling points results characterized by an expanded covered area value and a small high and mid-sampling points sum.

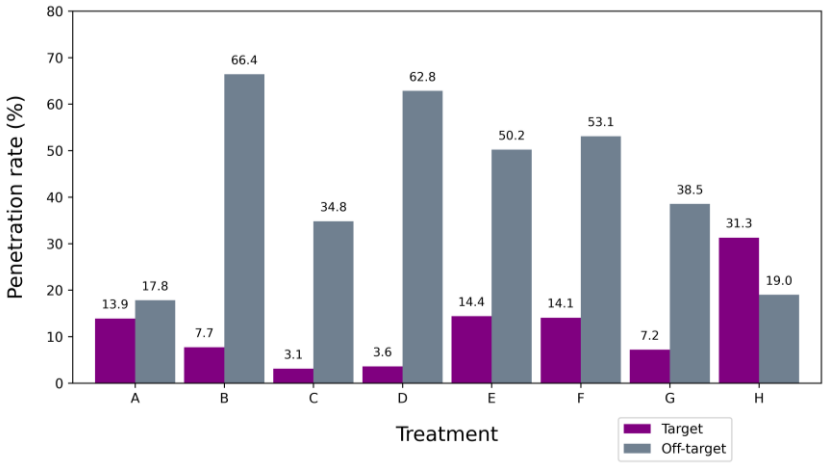

Figure 4. The mean PR results bar chart for target and off-target rows divided by treatments.

For instance, even if treatment B showed an increased coverage in all three sampling heights, it showed a lower PR compared to treatment H, which instead gained a reduced coverage in the higher parts of the canopy and a large coverage in the lower parts. The same interpretation could be transferred to off-target results, which showed reduced PR than target rows. It is essential to stress that the mid-low part of the canopy is the one that, more than others, requires adequate PPP coverage, and for this reason, treatments with higher PR are preferred. Also, for off-target rows, WSPs in lower positions were hit more than the higher ones but,

if visually inspected, the results derived from almost empty WSPs, meaning that few droplets reached the off-target rows' lower part and even less in the upper parts, with a crucial product saving.

No significant results were found in PR ANOVA table.

4. Discussion

Flight position was the factor that, more than others, influenced the covered area results for target, off-target, and ground WSPs. The treatments that gained a higher covered area were treatments A, B, and H. The first two showed an apparent homogeneous distribution of the canopy but the upper WSPs were over-covered, a sign of a less efficient application than that achieved by the H-treatment. This behaviour was in agreement with the experiments of Wen et al. (2019), where lower altitude flights with a speed of around 2 m s^{-1} were also identified as optimal for increased foliage coverage and drift reduction. Off-target rows showed similar results for these three treatments, while ground WSPs revealed a larger dispersion of PPP for OR treatments.

Even if the ANOVA tables mainly showed a significant impact of flight position and height on the high and mid-levels, it confirms the importance of the position of the UASS to limit spray over-dosage on leaves and how flight height also played a crucial role in OR treatments, causing a higher coverage where the UASS flew higher (treatments A and B), and also in IR treatments where a lower height helped increasing the spray coverage through the canopy height. Flight position and height appeared strictly connected because in OR treatments the bigger height helped improve the covered area of treatments A and B, while in IR flight position, the lower height helped reduce the dispersion of product and increase the covered area and the PR (as in treatment H). As a result of the nadiral nozzles' position over the row, the turbulence effect generated by the propellers helped to open the canopy to facilitate the PPP penetration, specifically for treatment H, where the rotary speed of the propellers was higher (Martinez-Guanter et al. 2020).

As described above, although with a reduced results impact, also flight position and speed were strictly connected. The flight speed and the consequent higher propellers' speed rotation could have provoked an increased downward flow. For OR treatments, the higher speed pushed the droplets on the ground (Biglia et al. 2022), increasing the dispersion (this effect is most visible in treatments B and D), while IR flights generated an efficient product penetration inside the canopy.

All treatments showed similar results in terms of product dispersion, but OR treatments C and D showed an increased influence in the lower positions, probably due to the lower flight height and position, which, more than other treatments, facilitated ground and side-row waste. In addition, the higher flight altitude of treatments A and B could have provoked droplets to drift further over the sampled rows, providing only a partial representation of the total dispersion.

It is essential to highlight that the treatments that reached a higher PR are preferable (A, B, and H) since most current PPP treatments applied to grapevine have the lower part of the canopy, where the grapes are located, as a target. Based on the results, treatment H seems to be the most appropriate one since it provided good PR results, it did not provoke an over-dosage effect in the upper part of the canopy, the ground dispersion is lower than treatments A and B, and it allows to treat two rows simultaneously and at higher speed, with crucial performance benefits.

These findings must be traced back to the specific diameter of the UASS (which in the presented trials helped reach both rows simultaneously in IR treatments), the number, model, position, and angle orientation of the nozzles under the propellers, generally used for herbaceous crops in this configuration. Specific nozzles for UASS arboreal operation, with a smaller spray angle, differently oriented would have taken to probably different and better results. In the same way, the vineyard's plant spacing along and between the rows would have affected the results.

Further studies are required in vineyard UASS application to analyse the effect of speed on spraying performance and to learn what is the limit over which the downward movement that improves droplet penetration ends and their dispersion begins. Turbulences represented the unknown factor that could have influenced the results. Appropriate sensors should be placed inside and outside the canopy and on the inter-row to evaluate the effect on the droplets' penetration and dispersion. Strictly correlated with the turbulence is the shape and configuration of the UASS. It is essential to define what is the most appropriate configuration (size, diameter, number of propellers and their orientation, etc.) to gain the best performances (C. Wang et al. 2022) in viticultural scenario. As with every application scenario, UASS PPP application should benefit from specific nozzles designed to reduce product dispersion and modulate droplet spectra depending on the chosen protection product and the environmental requirements. Since the experiments were conducted only

on one (OR treatments) and two target rows (IR treatments), it is crucial to evaluate the spray coverage derived from treating an extended surface and give better details about the overlapping results of parallel applications along the rows.

Further research is needed to provide the necessary guidelines for aerial distribution by UASS, to limit the dispersion of pesticides (according to ISO 22866), to evaluate the economic benefit and to boost the aerial spraying sector in agriculture, which is restricted to specific situations where terrestrial treatments are not feasible. These restrictions, mostly limited to the European Union, have repercussions on technological progress and the implementation of this technology in specific scenarios that could benefit from this approach, such as viticulture traditionally located in Europe, and limit the research development.

5. Conclusions

The work showed the flight position, height, and speed factors effect on PPP aerial distribution from UAS on vineyards, and how the obtained results were influenced by the UASS model and the vineyard characteristics. 2.0 m height inter-row flight position showed the best performance, with the lowest off-target and ground dispersion, demonstrating how flying over the inter-row, with nozzles right above the canopy, represents the best setting to facilitate droplets penetration inside the canopy, reaching the lowest parts, generally more affected from disease, and reduce off-target dispersion. Flight speed did not significantly affect the performance, apart the cases where a faster propeller rotation helped open the canopy and facilitate the droplet penetration. This result represents an essential logistic information, enabling the performance of shorter flight missions and increasing the general efficiency of the system. The droplet analysis procedure showed high potential and it could help boost the UAS spraying scenarios in vineyards. Further research is required to evaluate the aerial PPP distribution from UASs effectiveness and assess the environmental impact in agricultural scenarios. This knowledge is essential to boost the implementation of such technologies, specifically in those countries where aerial treatments are not still allowed.

Acknowledgements

The authors would like to express their gratitude to the management personnel of the experimental vineyard of the Agricultural University of Athens for their assistance in conducting the field trials.

References

Akpan, G. E., Ndukwu, M. C., Etim, P. J., Ekop, I. E., I. E. Udoh, 2023. Food Safety and Agrochemicals: Risk Assessment and Food Security Implications. In M. C. Ogwu & S. Chibueze Izah (Eds.), One Health Implications of Agrochemicals and their Sustainable Alternatives (Vol. 34, pp. 301–333). Singapore: Springer Nature Singapore. https://doi.org/10.1007/978-981-99-3439-3_11

Baio, F. H. R., Antuniassi, U. R., Castilho, B. R., Teodoro, P. E., E. E. D. Silva, 2019. Factors affecting aerial spray drift in the Brazilian Cerrado. PLOS ONE, 14(2), e0212289. https://doi.org/10.1371/journal.pone.0212289

Biglia, A., Grella, M., Bloise, N., Comba, L., Mozzanini, E., Sopegno, A., et al., 2022. UAV-spray application in vineyards: Flight modes and spray system adjustment effects on canopy deposit, coverage, and off-target losses. Science of The Total Environment, 845, 157292. https://doi.org/10.1016/j.scitotenv.2022.157292

Chen, S., Lan, Y., Zhou, Z., Ouyang, F., Wang, G., Huang, X., et al., 2020. Effect of Droplet Size Parameters on Droplet Deposition and Drift of Aerial Spraying by Using Plant Protection UAV. Agronomy, 10(2), 195. https://doi.org/10.3390/agronomy10020195

Chen, H., Lan, Y., K Fritz, B., Clint Hoffmann, W., S.1. Liu, 2021. Review of agricultural spraying technologies for plant protection using unmanned aerial vehicle (UAV). International Journal of Agricultural and Biological Engineering, 14(1), 38–49. https://doi.org/10.25165/j.ijabe.20211401.5714

Dhananjayan, V., Jayakumar, S., B. Ravichandran, 2020. Conventional Methods of Pesticide Application in Agricultural Field and Fate of the Pesticides in the Environment and Human Health. In R. K. R., S. Thomas, T. Volova, & J. K. (Eds.), Controlled Release of Pesticides for Sustainable Agriculture (pp. 1–39). Cham: Springer International Publishing. https://doi.org/10.1007/978-3-030-23396-9_1

European Parliament, C. of the E. (2009). Directive 2009/128/EC of the European Parliament and Of the Council of 21 October 2009 establishing a framework for Community action to achieve the sustainable use of pesticides (Text with EEA relevance). Official Journal of the European Union, 1–16.

FAO. (2017). The future of food and agriculture: trends and challenges. Rome: Food and Agriculture Organization of the United Nations.

Ghiani, L., Sassu, A., Piccirilli, D., Marcialis, G. L., F. Gambella, 2020. Development of a Matlab Code for the Evaluation of Spray Distribution with Water-Sensitive Paper. In A. Coppola, G. C. Di Renzo, G. Altieri, & P. D'Antonio (Eds.), Innovative Biosystems Engineering for Sustainable Agriculture, Forestry and Food Production (Vol. 67, pp. 845–853). Cham: Springer International Publishing. https://doi.org/10.1007/978-3-030-39299-4_91

Kestur, R., Omkar, S. N., & Subhash, S. (2020). Unmanned Aerial System Technologies for Pesticide Spraying. In A. K. Chakravarthy (Ed.), Innovative Pest Management Approaches for the 21st Century (pp. 47–60). Singapore: Springer Singapore. https://doi.org/10.1007/978-981-15-0794-6_3

Lykogianni, M., Bempelou, E., Karamaouna, F., K. A. Aliferis, 2021. Do pesticides promote or hinder sustainability in agriculture? The challenge of sustainable use of pesticides in modern agriculture. Science of The Total Environment, 795, 148625. https://doi.org/10.1016/j.scitotenv.2021.148625

Martinez-Guanter, J., Agüera, P., Agüera, J., M. Pérez-Ruiz, 2020. Spray and economics assessment of a UAV-based ultra-low-volume application in olive and citrus orchards. Precision Agriculture, 21(1), 226–243. https://doi.org/10.1007/s11119-019-09665-7

Pertot, I., Caffi, T., Rossi, V., Mugnai, L., Hoffmann, C., M. S. Grando, 2017. A critical review of plant protection tools for reducing pesticide use on grapevine and new perspectives for the implementation of IPM in viticulture. Crop Protection, 97, 70–84. https://doi.org/10.1016/j.cropro.2016.11.025

Qin, W.-C., Qiu, B.-J., Xue, X.-Y., Chen, C., Xu, Z.-F., Q.-Q. Zhou, 2016. Droplet deposition and control effect of insecticides sprayed with an unmanned aerial vehicle against plant hoppers. Crop Protection, 85, 79–88. https://doi.org/10.1016/j.cropro.2016.03.018

Quantick, H. R. (1979). Safety aspects of the aerial application of pesticides. The Aeronautical Journal, 83(821), 175–182. https://doi.org/10.1017/S0001924000095749

Sarri, D., Martelloni, L., Rimediotti, M., Lisci, R., Lombardo, S., M. Vieri, 2019. Testing a multi-rotor unmanned aerial vehicle for spray application in high slope terraced vineyard. Journal of Agricultural Engineering, 50(1), 38–47. https://doi.org/10.4081/jae.2019.853

Wang, C., Herbst, A., Zeng, A., Wongsuk, S., Qiao, B., Qi, P., et al., 2021. Assessment of spray deposition, drift and mass balance from unmanned aerial vehicle sprayer using an artificial vineyard. Science of The Total Environment, 777, 146181. https://doi.org/10.1016/j.scitotenv.2021.146181

Wang, C., Liu, Y., Zhang, Z., Han, L., Li, Y., Zhang, H., et al., 2022. Spray performance evaluation of a six-rotor unmanned aerial vehicle sprayer for pesticide application using an orchard operation mode in apple orchards. Pest Management Science, 78(6), 2449–2466. https://doi.org/10.1002/ps.6875

Wen, S., Han, J., Ning, Z., Lan, Y., Yin, X., Zhang, J., Y. Ge, 2019. Numerical analysis and validation of spray distributions disturbed by quad-rotor drone wake at different flight speeds. Computers and Electronics in Agriculture, 166, 105036. https://doi.org/10.1016/j.compag.2019.105036

Insertion of carbon-rich exogenous materials with bio-stimulants into subsoil for promoting maize growth

Dewen Qiao[a], Ajit Borundia[a], Cristina Cruz[b], Abdul Mounem Mouazen[a]*

[a] Department of Environment, Ghent University, Coupure Links, 9000, Gent, Belgium

[b] Centre for Ecology, Evolution, and Environmental Changes (cE3c) & CHANGE—Global Change and Sustainability Institute, Faculty of Sciences, University of Lisbon, Lisbon, Portugal

*Corresponding author. Email: Abdul.Mouazen@UGent.be

Abstract

Recent research suggests that soil microorganisms (fungi and bacterial) might be an important component of the soil organic carbon (SOC) pool, in addition to facilitating carbon sequestration by providing biophysical protection. The present study evaluated the influences of inserting available carbon-rich exogenous material with and without microorganisms incorporation in enhancing carbon capture within top-to-subsoil depth (down to 60 cm) in order to improve soil health and productivity, and consequently maize growth. The materials (including two carbon-rich exogenous materials, i.e., liquid digestate and humic acid, plus with three microorganisms, i.e., bacteria, mycorrhizal fungi as well as Trichoderma) were injected into the soil down to 60 cm depth using a novel drilling machine 45 days after maize seeding in two fields. The results showed that the combined application of humic acid and mycorrhizal fungi (HM) led to the highest NDVI (0.79 ± 0.07) and chlorophyll content (4.47 ± 0.93) among other treatments. The treatment of the liquid digestate incorporating mycorrhizal fungi (LM) presented the highest corn cob mass (0.30 ± 0.04 kg) and total plant mass (0.68 ± 0.16 kg). Therefore, it is recommended to apply humic acid as well as mycorrhizal fungi in the subsoil, as a means of increasing the growth of maize and indirectly promoting the photosynthesis process, thus helping mitigate the CO_2 to the atmosphere.

Key words: soil organic carbon, exogenous material, greenhouse gas, subsoil, maize growth

1. Introduction

The constantly increasing world population has been pressuring the cropland to produce more grains. The results were more land reclamation and overuse of agriculture land, along with extensive application of inorganic fertilizers and pesticides. Consequently, nearly 1.12 ±0.25 Pg C has been emitted to the atmosphere annually by the land use change (Houghton et al., 2012), which appears to be one of the main drivers of global climate change, causing most frequent and dramatic natural disasters. While the overuse of cropland and abuse of inorganic fertilizer have depleted essential soil nutrients particularly phosphorus (P), potassium (K) and micronutrients, crucially, they have also resulted in a gradual decrease in soil organic matter (SOM) content in the soil. The application of inorganic fertilizers certainly has resulted in a yield increase, however, which is also highly related to soil, caused water and air pollution (Komakech et al., 2015). But what is most worrisome for farmers is the affordability of fertilizers, provoked by the high energy prices.

To replenish SOM and other nutrient deficits caused by crop removal, in fact, farmers have been using organic fertilizers to maintain soil fertility since early times. Some studies (D'Hose et al., 2020; Han et al., 2020; Wang et al., 2021) have shown that the application of organic fertilizers can be an efficient agricultural management approach for promoting the productivity of cropland, particularly for improving the stability and sustainability of the crop production. For example, the addition of OM through organic amendments not only provides nutrients but also improves soil aggregation and stimulates microbial diversity and activity (Ferreras et al., 2006). With a study aims at investigating the effects of humic acids (HA) on growth improvement in rice plants, de Castro (de Castro et al., 2021) found that HA caused an increase in photosynthetic efficiency carbohydrates and total biomass. This may be down to the strong cation adsorption and exchange capacities, which can effectively improve soil structure and SOM, and promote crop growth. Soils are complex systems often limited by factors like the impact of rhizosphere beneficial microbes on plant nutrient use and SOC sequestration. Recent studies have found that SOC is mainly derived from roots and rhizomicroorganism interactions (Cheng et al., 2014; Holden and Treseder, 2013). Arbuscular mycorrhizal fungi (AMF) was found to be the most effective microbial symbioses for improving the growth and yield through

enhancing the photosynthetic rate and the availability and translocation of various nutrients (Gao et al., 2020). Therefore, exploring the addition of organic amendments with beneficial microorganisms would be meaningful to help improve the crop yield and even bring the ancillary benefits of increasing SOC. This will be of special interest if these material are applied to subsoils that suffer not only from soil compaction, but poor structure and OM, and consequently minimal microbial activity with negative effects of soil health.

However, most researches (Page-Dumroese et al., 2018; Wang et al., 2014) on these organic amendments have focused on their effects on soil physical, chemical as well as biological properties, and there are few studies on the adaptive characteristics and response of maize to soil amendment with microorganisms application, needless to say applying them to subsoil. Therefore, identifying the soil amendment and microorganisms that can facilitate maize growth through facilitating nutrients availability and microbial activity, and quantifying their influences on soil quality is key to sustainable soil management. This research aims at evaluation of the influences of inserting humic acid and liquid digestate with and without microorganisms incorporation on enhancing maize growth within top-to-sub-soil depth (down to 60 cm) in order to improve soil health and productivity. To ascertain the efficacy of these treatments in promoting maize growth, several vital metrics were carefully selected for evaluation. These included height, perimeter, total mass, corn mass as well as leaf parameters such as chlorophyll content, NDVI, LAI, et al, as they play a crucial role in influencing and reflecting crop growth.

2. Materials and Methods

2.1. Soils

In current study, an out-door pot experiment was conducted in the northwestern region of Belgium. The pot experiments was carried out at Beervelde (51°04'25.0"N 3°53'57.9"E), located about 12 km northeast of Gent, Belgium (Fig. 1). The study area is a relatively flat region with an average slope of 1%. It has a marine west coast climate. The annual rainfall of the area is about 858.8 mm and the mean monthly sunshine hours are 1618. Maize, potato as well as barley are the three main crops in local area, and most of the maize are used as silage for dairy cattle. The main soil textures in the study area is sand and loamy sand, which accounts for more than 50% of the total area (Zomlot et al., 2015). The basic physical and chemical properties of the study site soil are listed in Table 1.

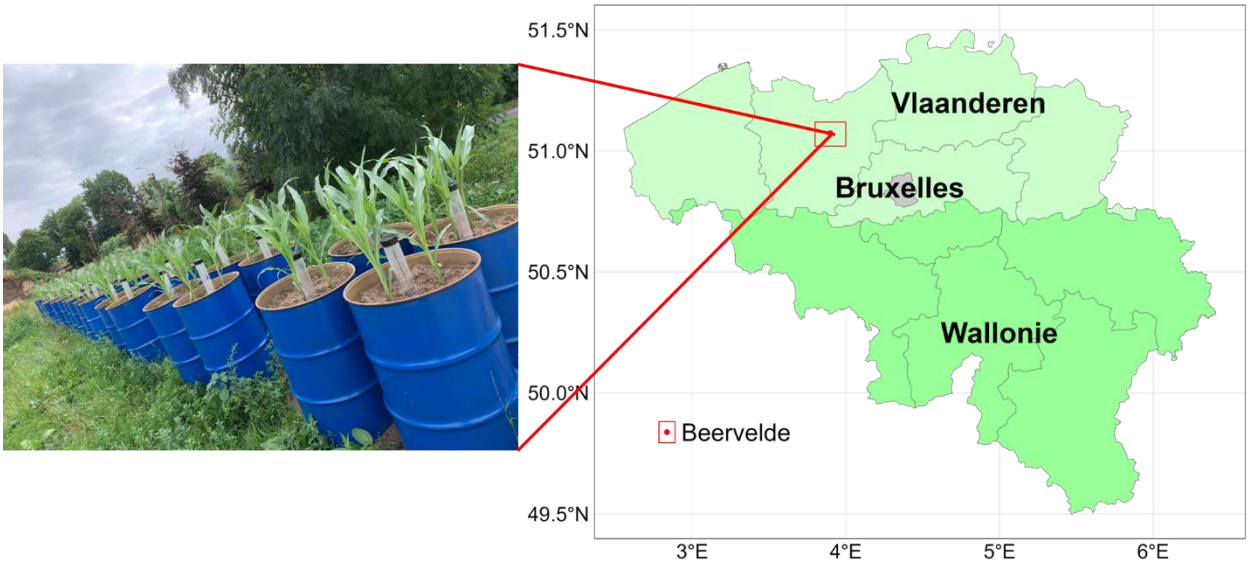

Fig. 1. Location map of research place (Beervelde) nearby Ghent, Belgium and the pot experiment.

Table 1. Basic properties of the soil used in the pot experiment.

Parameter	Potassium	phosphorus	total sulfur	sodium	magnesium	calcium	Soil type	total carbon	total organic carbon	pH-KCl (ISO)
unit			(mg/100 g)					(%)	(%)	
soil	15	24	17	1.1	9	60	15	1.29	1.14	4.6

2.2. Organic amendments and bio-stimulants

The liquid digestate (Table 2) were directly taken from the digester of a farm, which made from a combination of manure, energy crops, vegetable or animal waste. The biogas (primarily CH_4 and CO_2) emitted from anaerobic digestion are used for electricity generation. The humic acid is a standard product sold as a fertilizer (Humifirst WG) (Tradecorp, Belgium). Mycorrhizal fungi (Mycoshell Dripper) and Bacterial (Kiplant AllGrip) were provided by Asfertglobal (Asfertglobal, Portugal). Trichoderma (Trianum-P) was obtained from Koppert (Koppert, Belgium).

Table 2 The basic properties of liquid digestate and humic acid.

Parameter	dry matter (g/1000 g)	organic matter (g/100 0g)	Total nitrogen (mg/100 g)	P (P_2O_5)(g/1000 g)	C/N ratio
Liquid digestate	75	53	4.9	1.32	6.4

2.3. Pot experiments

The pots are made of iron with a diameter of 56 cm and a height of 85 cm (Fig. 1). To better facilitate the subsequent experimental operation and avoid the accumulation of rainwater in the pots, several holes were drilled at the bottom of the pots. For each pot, the soil filling processes were carried out with three steps (e.g., by adding three layers), the bottom layer and middle layer were compacted to simulate the real situation in the field, while the top layer was naturally filled. A hole of 64 mm diameter were drilled in the middle of each pot using a ring knife to set up transparent tube to visualize and measure crop roots. Lastly, 10 maize (Zea Mays) seeds were evenly planted in each pot, the maize seeds (P8685) are from Pioneer(Pioneer, USA). During the third growing stage, 7 maize plants were removed and only 3 were maintained. All the pots received the same amount of chemical fertilizers according to local standard. The chemical N, P and K fertilizers used were urea, calcium superphosphate and potassium sulphate, respectively. Besides, 3 holes were drilled when crops are at 5-10 cm height to inject biomaterials and microorganisms. A total of 12 treatments were applied in a completely randomized block design with four replications. The treatments are as follow: 1. Blank control (CK, no materials and bio-stimulants but seeds). 2. Liquid digestate (L). 3. Humus (H). 4. Trichoderma (T). 5. Bacterial (B). 6. Mycorrhizal fungi (M). 7. Liquid digestate + Trichoderma (LT). 8. Liquid digestate + Bacterial (LB). 9. Liquid digestate + Mycorrhizal fungi (LM). 10. Humus + Trichoderma (HT). 11. Humus + Bacterial (HB). 12. Humus + Mycorrhizal fungi (HM).

2.4. plant growth measurements

12 weeks after seeding, plants were harvested to record the observations. The height of each plant was determined by measuring this parameter from the soil's surface to the top of the plant. Subsequently, the average height of the three plants was calculated as the plant height for each pot. The perimeter of the maize stem was measured by a flexible rule. The weight of the fresh maize as well as the cob were recorded using top loading balance. Sampling and measuring of maize leaf parameters were performed at the silking growing stage. A Crop Circle Phenom canopy sensor (Holland Scientific, Lincoln, NE, USA) was used to measure the chlorophyll content and normalized difference vegetation index (NDVI) of the three fully grown leaves at the top of maize plants.

2.5. Data analysis

The collected data on various leaf and crop parameters were statistically analyzed using one-way analysis of variance (ANOVA) in MS Excel. Differences among the treatments were assessed at a 5% significance level using the one-sample t-test. Figures were created with R studio. Principal component analysis (PCA) was applied to evaluate how much of the variance of the data can be interpreted by the measured variables in order to unveil the effects of organic amendments and microorganism on maize growth. To improve the quality and accuracy, the data was standardized to eliminate bias due to scale differences before PCA analysis. PCA was implemented via stats(Team and Worldwide, 2002) packages in R.

3. Results and Discussion

3.1. Plant growth

The data concerning plant growth (total mass, stem perimeter and plant height) under different treatments are presented in Fig. 2. Overall, all treatments of organic amendments with microorganisms increased the total mass of maize and the stem perimeter, compared with CK treatment, although this trend was most obvious from perimeter. The highest total mass of maize was observed in the soil amended with LM (0.68 ± 0.16 kg), while HM had a similar effect. The control group had the lowest total mass (0.55 ± 0.08 kg). The treatment response pattern for stem perimeter was LM > LB > HT > HM > LT > HB, and treatments that included both organic materials and microorganisms showed significantly greater promotion compared to those with single additives (Fig. 2b). Especially, the LM and HM treatments significantly increased ($p < 0.05$) the stem perimeter by 24.66% and 21.57%, respectively, compared with CK treatment. It is worth mentioning that maize height did not show a consistent trend with stem perimeter or total mass. CK resulted in the highest height (238.41 ± 27.46 cm), followed by L (228.67 ± 16.74 cm) and LB (225.39 ± 12.56 cm).

Generally, with respect to total mass and stem perimeter, treatments that included liquid digestate performed much better than those with humic acid. This may be attributed to the richness of labile organic compounds and additional nitrogen present in the liquid digestate, which can be readily available in the soil, thus promoting plant growth within a short period (Kirchmann and Lundvall, 1993; Slepetiene et al., 2023), while humic acid is much more stable, as it formed during long-term decomposition of biomass residues. However, the advantages of improving soil properties (Nardi et al., 2002), plant growth (Ampong et al., 2022), especially soil carbon sequestration (Spaccini et al., 2002) in the long run have been proved. Among the three types of microorganisms, mycorrhizal fungi had the greatest effect plan growth, followed by Trichoderma, while bacteria showed the least promotion. This may be down to single-celled organisms of Bacteria, which need a film of water to survive, while fungi are multi-celled organisms that grow rapidly and can extend great lengths in the soil. This allows fungi to bridge gaps in the soil and transport nutrients easily over relatively long distances back to the plants (Allen, 2007).

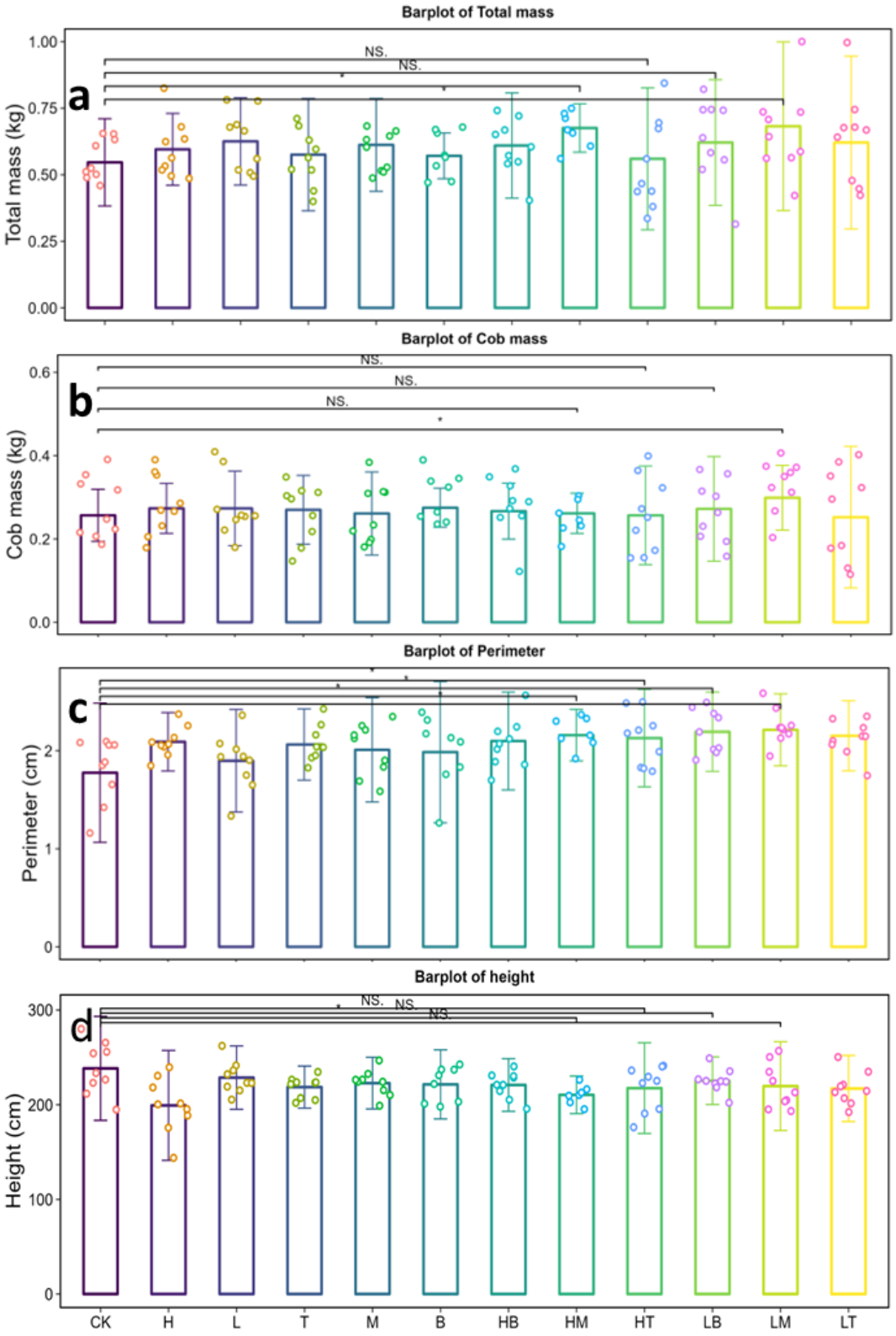

Fig. 2. Effect of amendments on (a) maize total mass (kg), (b) cob mass (kg), (c) stem perimeter (cm), and (d) plant height (cm). Bars show values of means from three replicates and contain the ± standard deviation of means (n = 3).

In each panel, bars marked with *, ** and *** indicating significance at $p < 0.05$, $p < 0.01$ and $p < 0.001$, respectively. The treatments are as follow: 1. Blank control (CK, no materials and bio-stimulants but seeds). 2. Liquid digestate (L). 3. Humus (H). 4. Trichoderma (T). 5. Bacterial (B). 6. Mycorrhizal fungi (M). 7. Liquid digestate + Trichoderma (LT). 8. Liquid digestate + Bacterial (LB). 9. Liquid digestate + Mycorrhizal fungi (LM). 10. Humus + Trichoderma (HT). 11. Humus + Bacterial (HB). 12. Humus + Mycorrhizal fungi (HM).

3.2. Photosynthetic parameters

A positive effect of several treatments were also been observed on the photosynthesis in maize leaves (Fig. 3). Plants subjected to HM, HT, LB, LM, treatments displayed significantly improved chlorophyll content and NDVI and subsequently exhibited an increase in net photosynthesis. Specifically, the LM and HM treatments significantly increased ($p < 0.05$) the chlorophyll content by 26.28% and 9.28%, respectively, compared with the M treatment. And M treatment significantly improved the chlorophyll content and NDVI by 69.99% and 15.58%, respectively, compared with CK treatment. Whereas the treatments with bacteria did not show eminent increase in chlorophyll content. Pearson's correlation coefficients (r) between chlorophyll content and total mass is 0.54, which was probably due to the important role of chlorophyll in photosynthesis that generate energy for plant organ development. Many studies indicate that the application of humic acid can positively increase the leaf chlorophyll concentration by improving uptake of macro and micronutrients (Rose et al., 2014; Sible et al., 2021). For instance, in a pot experiment, Chen et al. 2022) reported that humic acid modulates growth and photosynthesis of maize under drought conditions, resulting in a 19.7% increase in maize yield compared to the control treatment. This was attributed to the high cation exchange capacity of humic acid, leading to maxim nutrient uptake by maize.

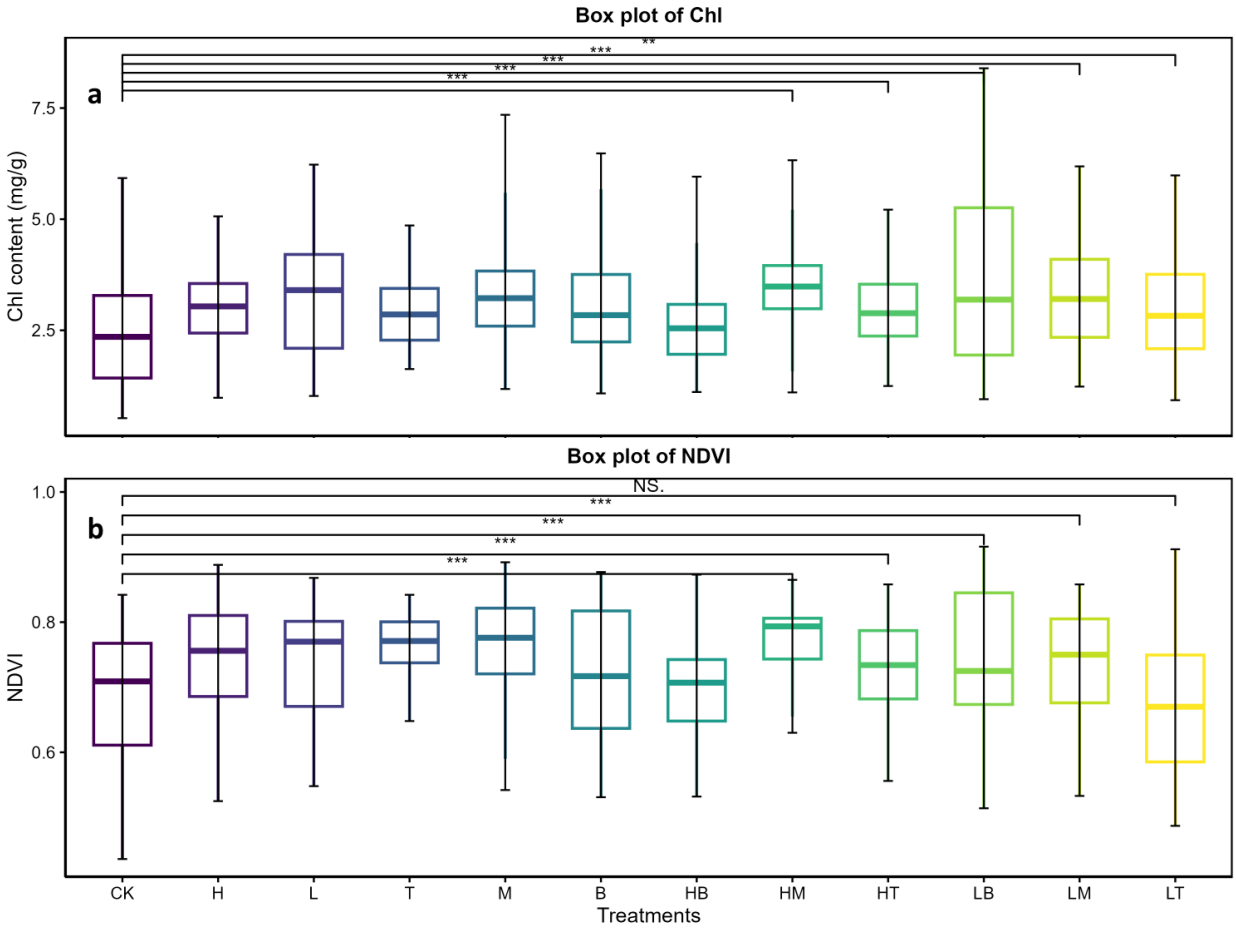

Fig. 3. Effect of amendments on a) chlorophyl content (mg/g), b) normalized difference vegetation index (NDVI). Boxes show values of means from three replicates and contain the ± standard deviation of means (n = 3). In each panel, bars marked with *, ** and *** indicating significance at $p < 0.05$, $p < 0.01$ and $p < 0.001$, respectively. The treatments are as follow: 1. Blank control (CK, no materials and bio-stimulants but seeds). 2. Liquid digestate (L). 3. Humus (H). 4. Trichoderma (T). 5. Bacterial (B). 6. Mycorrhizal fungi (M). 7. Liquid digestate + Trichoderma (LT). 8. Liquid digestate + Bacterial (LB). 9. Liquid digestate + Mycorrhizal fungi (LM). 10. Humus + Trichoderma (HT). 11. Humus + Bacterial (HB). 12. Humus + Mycorrhizal fungi (HM).

3.3. Relationships among maize growth and leaf parameters

To investigate the overall relationship between key parameters such as corn growth and chlorophyll content under different treatments, this study conducted PCA and correlation analysis. The first two principal components explained 69.9% of the total variance, 47.2% of the variance was explained by the principle component 1 (Fig. 4), which was positively correlated with chlorophyl content as well as three leaf indexes (e.g., NDVI, leave area index [LAI], and normalized difference red edge index [NDRE]). Principal component 2 explained 22.7% of the variance of the data (Fig. 4), and total mass of the maize positively correlated with the mass of the cob as well as stem perimeter. All variables were negatively correlated with the height of the plant.

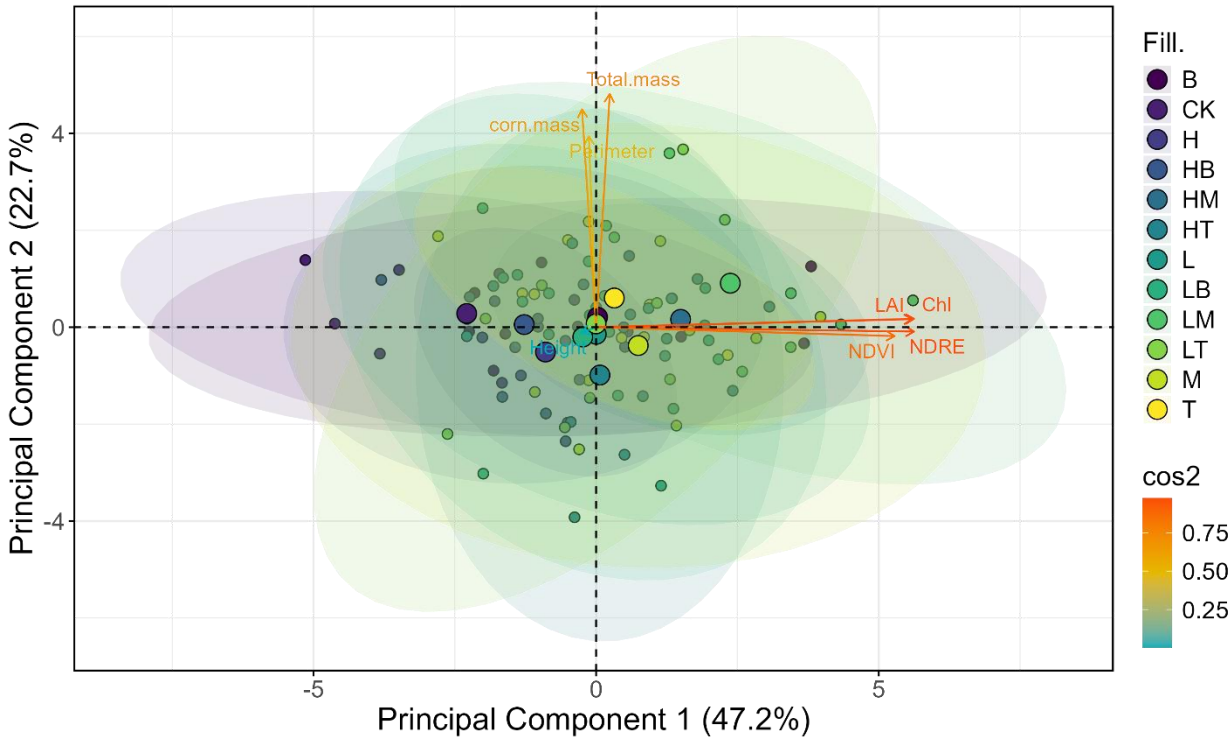

Fig. 4. Principal component analysis (PCA) of plant growth and leaf parameters. Cos2 represents the quality of variations in the PCA, and a higher value of cos2 indicates a larger contribution of variation to the principal component. The treatments are as follow: 1. Blank control (CK, no materials and bio-stimulants but seeds). 2. Liquid digestate (L). 3. Humus (H). 4. Trichoderma (T). 5. Bacterial (B). 6. Mycorrhizal fungi (M). 7. Liquid digestate + Trichoderma (LT). 8. Liquid digestate + Bacterial (LB). 9. Liquid digestate + Mycorrhizal fungi (LM). 10. Humus + Trichoderma (HT). 11. Humus + Bacterial (HB). 12. Humus + Mycorrhizal fungi (HM).

4. Conclusions

Based on the observed results, it can be concluded that the addition of liquid digestate, humic acid, microorganisms, and their combinations significantly improved the height, stem perimeter, and total mass of maize. An increase in chlorophyll content in the leaves was also observed. In particular, Liquid digestate + Mycorrhizal fungi (LM) and Humus + Mycorrhizal fungi (HM) treatments showed the highest promotion of maize growth. Overall, due to the easily decomposable materials in liquid digestate, it had more immediate and positive effects on maize growth compared to humic acid in the short term. However, for improving the carbon content in the soil, humic acid would be a more suitable option and further studies on changes in soil properties are useful and necessary.

Acknowledgements

Authors acknowledge the financial support received from the Research Foundation - Flanders (FWO)for Odysseus I SiTeMan Project (Nr. G0F9216N). Further acknowledgment goes to China Scholarship Council (CSC) for Dewen Qiao (File No. 202307650032).

References

Allen, M.F., 2007. Mycorrhizal fungi: highways for water and nutrients in arid soils. Vadose Zone Journal 6(2), 291-297. https://doi.org/10.2136/vzj2006.0068

Ampong, K., Thilakaranthna, M.S., Gorim, L.Y., 2022. Understanding the role of humic acids on crop performance and soil health. Frontiers in Agronomy 4, 848621. https://doi.org/10.3389/fagro.2022.848621

Chen, Q., Qu, Z., Ma, G., Wang, W., Dai, J., Zhang, M., Wei, Z., Liu, Z., 2022. Humic acid modulates growth, photosynthesis, hormone and osmolytes system of maize under drought conditions. Agricultural Water Management 263, 107447. https://doi.org/10.1016/j.agwat.2021.107447

Cheng, W., Parton, W.J., Gonzalez-Meler, M.A., Phillips, R., Asao, S., McNickle, G.G., Brzostek, E., Jastrow, J.D., 2014. Synthesis and modeling perspectives of rhizosphere priming. New Phytologist 201(1), 31-44. https://doi.org/10.1111/nph.12440

D'Hose, T., Debode, J., De Tender, C., Ruysschaert, G., Vandecasteele, B., 2020. Has compost with biochar applied during the process added value over biochar or compost for increasing soil quality in an arable cropping system? Applied Soil Ecology 156, 103706. https://doi.org/10.1016/j.apsoil.2020.103706

de Castro, T.A.v.T., Berbara, R.L.L., Tavares, O.C.H., da Graca Mello, D.F., Pereira, E.G., de Souza, C.d.C.B., Espinosa, L.M., García, A.C., 2021. Humic acids induce a eustress state via photosynthesis and nitrogen metabolism leading to a root growth improvement in rice plants. Plant Physiology and Biochemistry 162, 171-184. https://doi.org/10.1016/j.plaphy.2021.02.043

Ferreras, L., Gomez, E., Toresani, S., Firpo, I., Rotondo, R., 2006. Effect of organic amendments on some physical, chemical and biological properties in a horticultural soil. Bioresource technology 97(4), 635-640. https://doi.org/10.1016/j.biortech.2005.03.018

Gao, C., El-Sawah, A.M., Ali, D.F.I., Alhaj Hamoud, Y., Shaghaleh, H., Sheteiwy, M.S., 2020. The integration of bio and organic fertilizers improve plant growth, grain yield, quality and metabolism of hybrid maize (Zea mays L.). Agronomy 10(3), 319. https://doi.org/10.3390/agronomy10030319

Han, X., Hu, C., Chen, Y., Qiao, Y., Liu, D., Fan, J., Li, S., Zhang, Z., 2020. Crop yield stability and sustainability in a rice-wheat cropping system based on 34-year field experiment. European Journal of Agronomy 113, 125965. https://doi.org/10.1016/j.eja.2019.125965

Holden, S.R., Treseder, K.K., 2013. A meta-analysis of soil microbial biomass responses to forest disturbances. Frontiers in microbiology 4, 163. https://doi.org/10.3389/fmicb.2013.00163

Houghton, R.A., House, J.I., Pongratz, J., Van Der Werf, G.R., Defries, R.S., Hansen, M.C., Le Quéré, C., Ramankutty, N., 2012. Carbon emissions from land use and land-cover change. Biogeosciences 9(12), 5125-5142. https://doi.org/10.5194/bg-9-5125-2012

Kirchmann, H., Lundvall, A., 1993. Relationship between N immobilization and volatile fatty acids in soil after application of pig and cattle slurry. Biology and fertility of soils 15, 161-164. https://doi.org/10.1007/BF00361605

Komakech, A.J., Sundberg, C., Jönsson, H., Vinnerås, B., 2015. Life cycle assessment of biodegradable waste treatment systems for sub-Saharan African cities. Resources, Conservation and Recycling 99, 100-110. https://doi.org/10.1016/j.resconrec.2015.03.006

Nardi, S., Pizzeghello, D., Muscolo, A., Vianello, A., 2002. Physiological effects of humic substances on higher plants. Soil Biology and Biochemistry 34(11), 1527-1536. https://doi.org/10.1016/S0038-0717(02)00174-8

Page-Dumroese, D.S., Ott, M.R., Strawn, D.G., Tirocke, J.M., 2018. Using organic amendments to restore soil physical and chemical properties of a mine site in northeastern Oregon, USA. Applied engineering in agriculture 34(1), 43-55. https://doi.org/10.2136/vzj2006.0068

Rose, M.T., Patti, A.F., Little, K.R., Brown, A.L., Jackson, W.R., Cavagnaro, T.R., 2014. A meta-analysis and review of plant-growth response to humic substances: practical implications for agriculture. Advances in agronomy 124, 37-89. https://doi.org/10.1016/B978-0-12-800138-7.00002-4

Sible, C.N., Seebauer, J.R., Below, F.E., 2021. Plant biostimulants: A categorical review, their implications for row crop production, and relation to soil health indicators. Agronomy 11(7), 1297. https://doi.org/10.3390/agronomy11071297

Slepetiene, A., Ceseviciene, J., Amaleviciute-Volunge, K., Mankeviciene, A., Parasotas, I., Skersiene, A., Jurgutis, L., Volungevicius, J., Veteikis, D., Mockeviciene, I., 2023. Solid and liquid phases of anaerobic digestate for sustainable use of agricultural soil. Sustainability 15(2), 1345. https://doi.org/10.3390/su15021345

Spaccini, R., Piccolo, A., Conte, P., Haberhauer, G., Gerzabek, M., 2002. Increased soil organic carbon sequestration through hydrophobic protection by humic substances. Soil Biology and Biochemistry 34(12), 1839-1851. https://doi.org/10.1016/S0038-0717(02)00197-9

Team, R.C., Worldwide, C., 2002. The R stats package. R Foundation for Statistical Computing

Wang, L., Sun, X., Li, S., Zhang, T., Zhang, W., Zhai, P., 2014. Application of organic amendments to a coastal saline soil in North China: Effects on soil physical and chemical properties and tree growth. PloS one 9(2), e89185. https://doi.org/10.1371/journal.pone.0089185

Wang, X., Wang, J., Wang, J., 2021. Seasonality of soil respiration under gypsum and straw amendments in an arid saline-alkali soil. Journal of Environmental Management 277, 111494. https://doi.org/10.1016/j.jenvman.2020.111494

Zomlot, Z., Verbeiren, B., Huysmans, M., Batelaan, O., 2015. Spatial distribution of groundwater recharge and base flow: Assessment of controlling factors. Journal of Hydrology: Regional Studies 4, 349-368. https://doi.org/10.1016/j.ejrh.2015.07.005

The bulbous bow shape adaptability for the soil ripper tool

Egidijus Katinas [a,*], Regita Bendikienė [a], Vytenis Jankauskas [b], Antanas Čiuplys[a]

[a] Kaunas University of Technology, K. Donelaičio st. 73, LT-44249 Kaunas, Lithuania

[b] Vytautas Magnus University, K. Donelaičio st. 58, LT-44248 Kaunas, Lithuania

* Corresponding author. Email: egidijus.katinas@ktu.lt

Abstract

Soil processing in agriculture requires high energy because of soil resistance, like the ship's motion in water. The ship's bulbous bow reduces fuel consumption by 12-15%. It protrudes water likewise to the ripper in the soil. The unique three types (delta, oval and nabla) of bulbous bow elements are designed for the soil ripper. The designed elements are simulated using the discrete element method. Prototypes are printed 3D printed to verify the simulation values and measure draught force in the sand bin. The simulation results showed at most 2% higher values than the laboratory measurements. Compared to the original soil ripper element, the draught force values have the highest increase of 2.8% of the nabla shaped bulbous bow soil ripper element. Other samples showed lower differences. Based on the obtained results, the bulbous bow-shaped element is promising, especially for wear analysis. The original soil ripper tool has a similar rounding of the lower part as the bulbous bow element.

Keywords: soil ripper, bulbous bow, DEM, draught force, sand bin.

1. Introduction

The European Union's common agricultural policy supports no-tillage technology, mainly covering the field with 30-100% crop residue. Organic residues cover the soil surface to reduce soil erosion and moisture losses by evaporation(Achankeng & Cornelis, 2023). This soil processing technology (no-tillage) helps to improve carbon sequestration in agricultural soils (Guyomard et al., 2020). But at the same time, the no-tillage process requires special machines to properly prepare and ensure good seedbed preparation for the sowing process. The soil ripper is used as a soil opener to loosen the soil. The tool's shape or position has a high impact on energy consumption (Liu et al., 2023; Sun et al., 2018). As agricultural equipment works under high abrasion conditions, the machine elements must have a wear resistance property. There are two options to increase the longevity of agricultural machine elements: use hardfacings to protect the most wearable parts or optimize the shape of agricultural machine elements. The second option helps to save energy and greenhouse gas emissions. The proper design, new coatings, materials, and technology for machine wear protection can reduce energy losses by 40% in long-term conditions (Holmberg & Erdemir, 2017). This is a significant value for a greenhouse gas emission and climate change.

The previous soil ripper wear analysis (Katinas et al., 2019) gave an idea to improve the design of the soil ripper element. The worn ripper element, which works at the 0.2 m working depth, is round at the bottom (Figure 1). If the soil resistance removes the tool's edges, it is possible to design a soil ripper element that does not have sharp edges and corners on the main contact surface with the soil. The ships have similar motion in water as the agricultural tools in the soil. The vessel has a bulbous bow element in the front of the body. The bulbous bow is a water-protruding element (bulb) in the front of the ship to modify the water flow around the hull (Szelangiewicz et al., 2021). It is a solution to improve ships' economic efficiency, reduce total resistance and increase stability. The properly optimised bulb resulting the reduction of total resistance by 12-15% and increased fuel economy for the same amount or improves hydrodynamic and plow-in phenomena (Gia Tran et al., 2021; Song Zhang et al., 2022).

Given the similarities between the bulbous bow and soil ripper movement, the ship's bulbous bow design could potentially be adopted in agriculture.

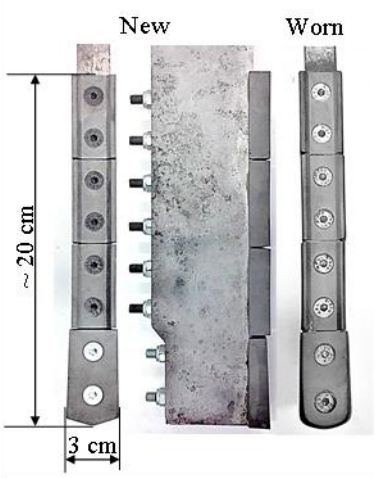

Figure 1. Soil ripper with wear resistant hard facings: new and worn (208 km wear track).

The design of the bulbous bow for the soil ripper tool inspired by the experience and benefits of the marine industry. There are three types of ship's bulbs, discussed by the authors(Hoyle, 1985; Kracht, 1978) (Figure 2):

- Delta type bulb (Δ) or the shape of the drop sectional area where the mass centre is below the vertical axis middle point.
- Oval type bulb (O) has the mass centre in the middle of the vertical axis.
- Nabla type bulb (∇) has an upside-down shape of the drop, but the mass centre is above the vertical axis middle point.

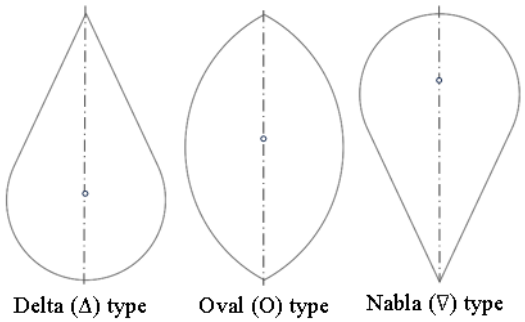

Figure 2. Ship bulb types provided by Kracht's (Kracht, 1978).

The ship industry's practise gives a promising prediction that bulbous bow shape element in soil processing will show reasonable results. The prototyping process of the bulbous bow element for the soil ripper will take time, expenses, and materials because of the design element validation in the field. To shorten the testing period, the discrete element method (DEM) will be used to test the designed element virtually. The DEM is a specific method developed to simulate granular material (Cundall & Strack, 1979). It is beneficial for agricultural simulation processes such as ploughing, soil disturbance, seeding, grain threshing, fertilizing, wear prediction, etc. processes (Barr et al., 2018; Chen et al., 2022; Liu et al., 2023; Wang et al., 2020; Shilin Zhang et al., 2023; Zhao et al., 2021). Virtual testing improves the design stage of agricultural machine elements, but it is mandatory to verify simulation results, which can be done in a sand-filled bin. During the experiment, the draught force is measured to evaluate the resistance force of the tool. (Ucgul et al., 2017). This study aims to design, simulate, and experimentally validate the bulbous bow for a soil ripper tool. The draught force evaluation in a sand bin with a designed and 3D printed bulbous bow elements and DEM simulation enables us to compare results and find the most suitable shape to continue research.

2. Materials and Methods

The experimental setup is carried out in three stages: design of the bulbs for the soil ripper according to Figure 2; soil ripper processing in the sand bin by DEM model; draught force measurement of soil ripper

with 3D printed bulb.

2.1. Soil ripper and bulbous bow types

The soil ripper type is selected based on previous research (Katinas et al., 2019) (Figure 1). According to Kracht's bulb types in Figure 2, bulbous bow elements are designed and created for the soil ripper. The delta, oval and nabla type elements (Figure 3) replace an original shape element. The delta and nabla-type elements have the same shape; the difference is that they are rotated around the vertical axis by 180°.

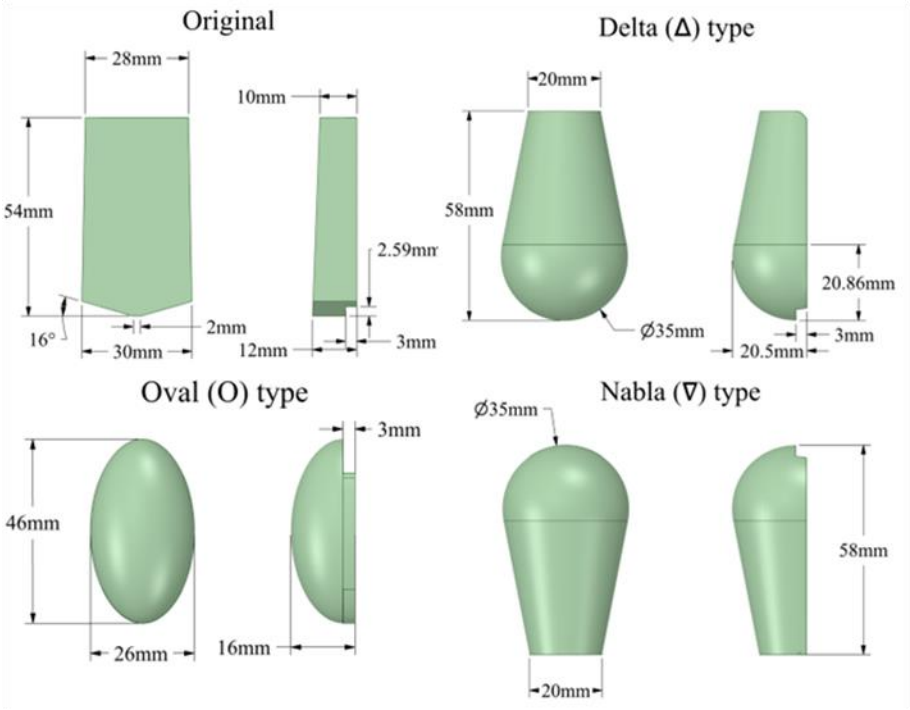

Figure 3.Original and designed bulbous bow types for the soil ripper.

The designed elements were tested in the laboratory sand bin to reduce the testing time and material (steel) consumption. 3D printing technology shortens the production process compared to the production of steel samples. The real-size bulbous bow elements were printed using an ABS+ filament. The working depth of the soil ripper in the field is about 20 cm, but it is reduced to 10 cm for laboratory tests in the sandbox and DEM model as it helps to decrease the amount of sand and computational time because of the lower number of sand particles in the model.

2.2. DEM model

The DEM simulation used ANSYS Rocky software (ANSYS, Inc., U.S.). The soil bin (0.5×1.5×0.25 m) was filled with a sphere particle size of 0.005 m (total number of the sand particles 817,558) (Figure 4Figure 3). The working depth of the tool is – 0.1 m, and the velocity of the geometry is – 0.1 $m \cdot s^{-2}$. The simulation time was 11 s, and the data retention was 0.01 s, the total computation time was approx. 6 hours.

The simulation physics, material properties and material interaction parameters used for simulation are given in

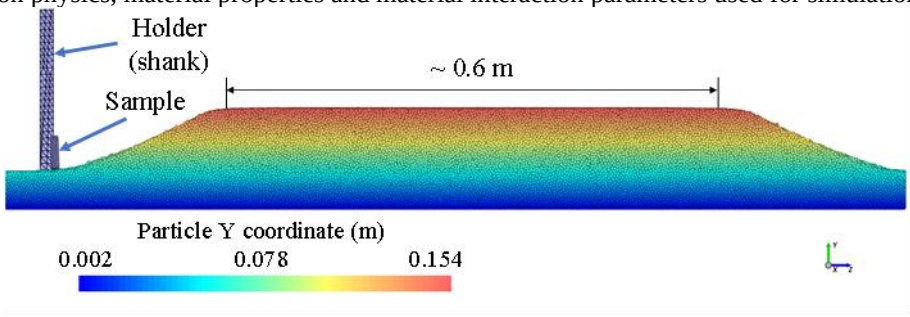

Figure 4. The sand bin prepared for simulation.

Table 1 (Kuře et al., 2021). The bulbous bow elements (sample) were meshed by the ANSYS Workbench platform, where the nonlinear mechanical physics preferences were selected for meshing with a 3 mm mesh element size, while the holder element size was increased to 10 mm.

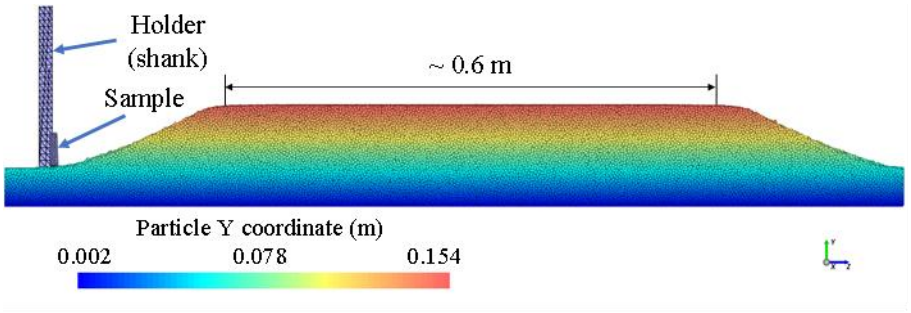

Figure 4. The sand bin prepared for simulation.

Table 1. DEM parameters used in the simulation (Kuře et al., 2021).

Simulation physics:		
Normal force	Hysteretic linear spring	
Tangential force	Linear spring coulomb limit	
Gravity ($m \cdot s^{-2}$)	9.81	
Sand properties:		
Bulk density ($kg \cdot m^{-3}$)	1533	
Particle size (m)	0.005	
Poisson's ratio	0.3	
Young Modulus (MPa)	1.7	
Rolling resistance	0.14	
Restitution coefficient	0.3	
Material interaction properties:	*Sand-sand*	*Sand-geometry*
Static friction	0.7	0.4
Dynamic friction	0.6	0.3
Tangential stiffness ratio	1	1
Restitution coefficient	0.3	0.3

2.3. Draught force measurement

The draught force measurement in the sand bin test was made according to the description of the Kure (Kuře et al., 2021) work. The sand bin dimensions, soil ripper working depth, and movement velocity are the same as those used for a DEM model Figure 3. The silica sand fraction (0.1-0.3 mm) was used to fill a bin. The force sensor measures the draught force required to move the soil ripper with a sample (bulbous bow shape element) in the sand (Figure 4). The maximal measured force of the sensor is 2kN. The measurement was repeated three times to get statistically proven data. The bulbous bow elements were positioned to the square pipe (holder) to ensure a working depth of 0.1 m.

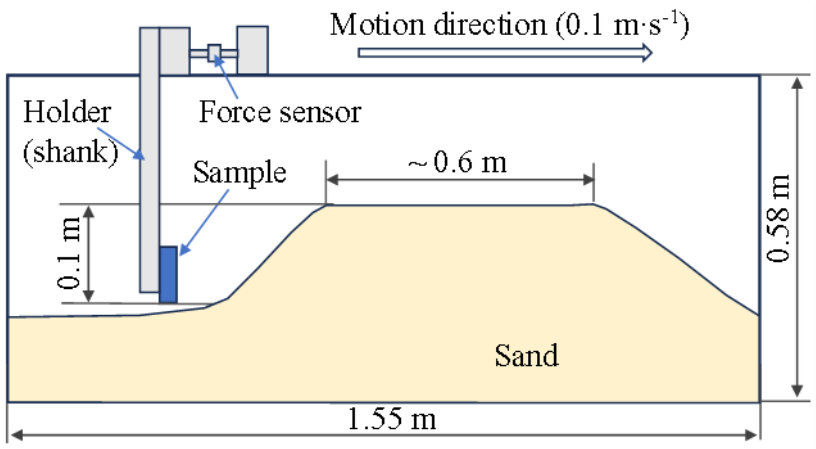

Figure 5. Draught force measurement in a sand bin.

3. Results and Discussion

The main evaluation criterion of designed soil ripper bulbous bows is draught force. Figure 6 shows measurement values in the sand bin and DEM model results. The draught force values are reaching their peak in the middle of the distance because of the sand pile shape. The model has more data points because the force values were measured ten times more frequently than in the case of the sand bin test. The formed pile of sand in a bin is not smooth throughout the whole length of the bin. This is a reason why draught force values fluctuate. The ripper motion starts at 0 N because there is no contact with sand. When the ripper begins to move, the force increases to the maximum value (40-50 N); after the distance of 0.7 m, it stops in the sand. The model and measured draught force values in sand are in correct arrangement.

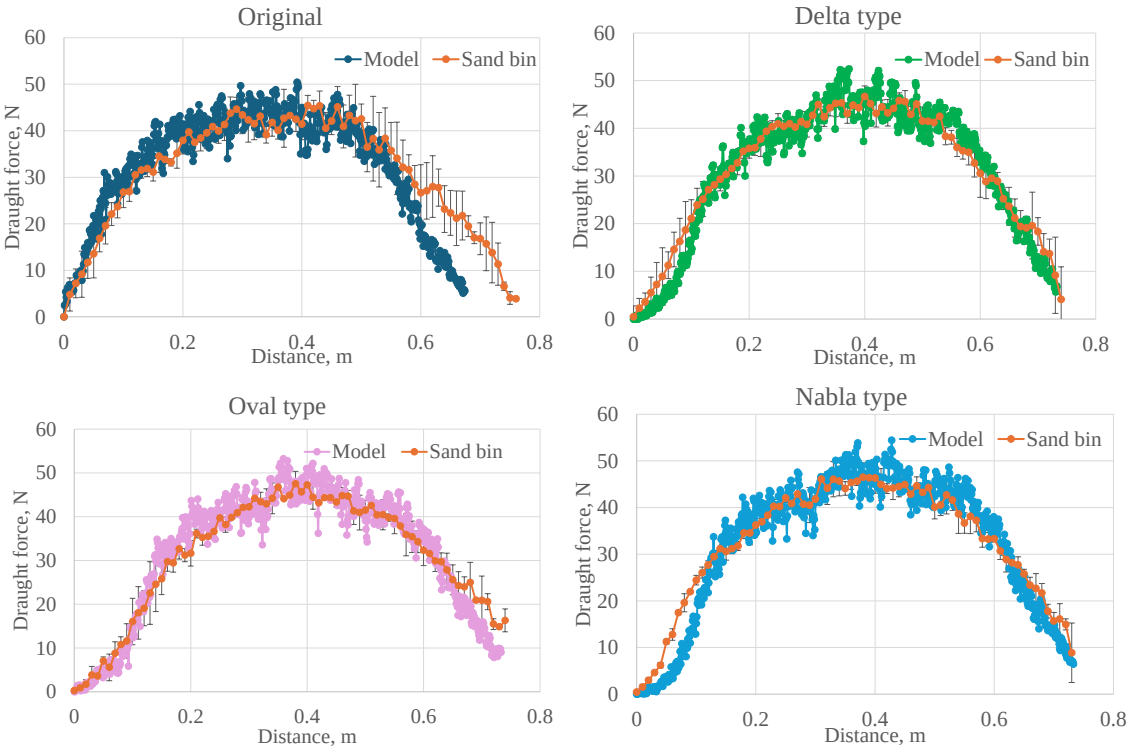

Figure 6. Draught force results of modelled and measured in a sand bin test of original, delta, oval and nabla elements.

A better comparison of the draught force of designed shape tools can be seen if the average force values are estimated at 0.2-0.5 m (Figure 6). This distance interval helps to compare maximal values during the sand

processing in the bin. The average draught force values at the distance of 0.2-0.5 m are given in Table 2. The lowest measured draught force value in a laboratory sand bin is a ripper with an original shape tool, which creates an average force of 41.85 N resistance. The designed delta, oval and nabla-shaped bulbous bow showed higher draught force values than the original shape: delta – by 1.7%, oval – by 2.3%, and nabla has the highest draught force measured in the sand bin – 2.8%. The standard deviation values show that the draught force values have slight differences for the designed tools compared to the original tool.

Table 2. Average values of draught force at 0.2-0.5 m distance measured in a sand bin and model.

Shape	*Sand bin*	*Model*
Original	41.85±2.16 N	42.04±3.27 N
Delta	42.57±2.01 N	42.82±4.12 N
Oval	42.83±2.51 N	43.66±4.06 N
Nabla	43.07±2.13 N	43.94±4.03 N

The laboratory test in a sand bin showed lower draught force values compared to the model results obtained from the DEM. The highest difference, 2%, appeared in the nabla shape tool model compared to the measurement in a sand bin. The rest of the model results of bulbous bow elements showed lower differences compared to the laboratory measurement (sand bin): 0.5% (original), 0.6% (delta) and 1.9% (oval). The model results show high standard deviation values (Table 2) because of high fluctuation at the entire maximal force evaluation at a specific distance (0.2-0.5 m) (Figure 6). The draught force oscillation appeared because of the geometry mesh and particle sizes. However, the sand fraction size (0.1-0.3 mm) used in the sand bin is much smaller than the model particle size (5 mm). Larger model particle size optimises computational time while the force results remain close to the laboratory measurement values. The particle size is not the only factor that influences the model results. The model parameters sensitivity analysis is discussed in previous literature (Katinas et al., 2021; Kuře et al., 2021).

The difference of draught force measurement in sand bin can be influenced by the layer height during the 3D printing process. The 0.2 mm layer height was set for the printing of samples. Figure 7shows the 3D-printed, delta-shaped soil ripper tool. The layered structure appeared on the sample surface after the printing process. The Figure 7b shows the contact variation during the sand processing in a bin. The sand particle size varied from 0.1-0.3 mm, while the printed layer height was 0.2 mm. The ideal way is for a larger fraction sand particles to have a particle-geometry contact region (Figure 7, in yellow).

Nevertheless, the smaller sand particles (0.1-0.2 mm) can be placed in the corners of the geometry where particles hide geometry, and the primary interaction appears for the particle-particle contact region (Figure 7, in green). From the DEM parameters setting

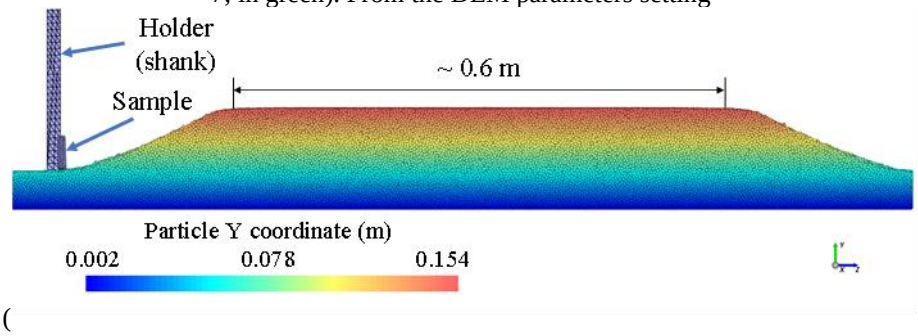

(

Figure 4. The sand bin prepared for simulation.

Table 1), we can see that the interaction of particle-geometry and particle-particle has different static and dynamic friction. The prevailing particle-particle interaction can change the draught force values because static and dynamic friction coefficients are lower than particle-geometry interaction.

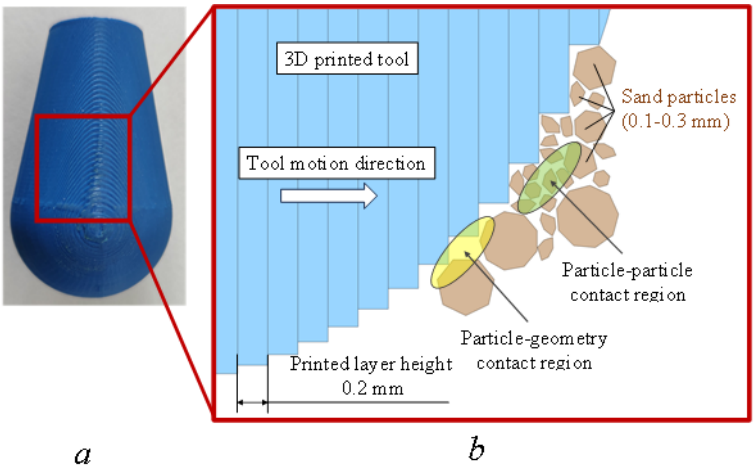

Figure 7. Sand particles and geometry contact scheme of the 3D printed delta shape tool.

4. Future plan

One of the most valuable factors during soil processing is tool longevity. If the tool can process many hectares without replacing, the machine's downtime and material consumption will be reduced. Simultaneously, the critical raw material (tungsten) will be consumed less. The designed delta, oval and nabla shape soil ripper elements show slightly higher draught force results than the original shape element. As previously mentioned, a factor of the tool's longevity, the bulbous bow design shape tool must be analysed as a wearable element to predict its longevity. The original tool shape is round at the bottom of the soil ripper after 208 km of wear track. This tendency suggests that wear analysis must be done with delta, oval and nabla shape tools to predict an abrasive wear resistance.

5. Conclusions

The ship's bulbous bow shape element was adapted to the soil ripper tool. The delta, oval, and nabla-shaped soil ripper elements were designed and tested virtually using the discrete element method. The draught force measurement in a laboratory sand bin was used to evaluate the advantages of the newly created elements. The increase in draught force is only 1.7-2.8% for newly designed delta, oval, and nabla shape elements compared to the original shape element. The model and laboratory experiment measurements differ by up to 2%. The adopted bulbous elements can be used in soil processing machines because the draught force consumption results do not show huge differences. However, agricultural machines work in highly abrasive conditions where material loss plays an important role. The designed bulbous bow shape elements must be tested under abrasive wear conditions to verify the shape's effectiveness for abrasive wear resistance.

Funding

This project has received funding from the Research Council of Lithuania (LMTLT), agreement No S-PD-24-31.

Acknowledgements

The authors are especially grateful for Czech University of Life Sciences Prague, Faculty of Engineering for cooperation.

References

Achankeng, E., & Cornelis, W. (2023). Conservation tillage effects on European crop yields: A meta-analysis. *Field Crops Research*, *298*, 108967. https://doi.org/10.1016/j.fcr.2023.108967

Barr, J. B., Ucgul, M., Desbiolles, J. M. A., & Fielke, J. M. (2018). Simulating the effect of rake angle on narrow opener performance with the discrete element method. *Biosystems Engineering*, *171*, 1–15. https://doi.org/10.1016/j.biosystemseng.2018.04.013

Chen, Z., Wassgren, C., & Ambrose, R. P. K. (2022). Development and validation of a DEM model for

predicting impact damage of maize kernels. *Biosystems Engineering*, *224*, 16–33. https://doi.org/10.1016/j.biosystemseng.2022.09.012

Cundall, P. A., & Strack, O. D. L. (1979). A discrete numerical model for granular assemblies. *Geeotechnique*, *29*(1), 47–65. https://doi.org/10.1680/geot.1979.29.1.47

Gia Tran, T., Van Huynh, C., & Cheol Kim, H. (2021). Optimal design method of bulbous bow for fishing vessels. *International Journal of Naval Architecture and Ocean Engineering*, *13*, 858–876. https://doi.org/10.1016/j.ijnaoe.2021.10.006

Guyomard, H., Bureau, J., Chatellier, V., Detang-Dessendre, C., Dupraz, P., Jacquet, F., Reboud, X., Requillart, V., Soler, L., & Tysebaert, M. (2020). *Research for AGRI Committee - The Green Deal and the CAP: policy implications to adapt farming practices and to preserve the EU's natural resources*.

Holmberg, K., & Erdemir, A. (2017). Influence of tribology on global energy consumption, costs and emissions. In *Friction* (Vol. 5, Issue 3, pp. 263–284). https://doi.org/10.1007/s40544-017-0183-5

Hoyle, J. W. (1985). *Optimization of bow-bulb for resistance and seakeeping characteristics*. https://apps.dtic.mil/sti/tr/pdf/ADA158831.pdf

Katinas, E., Chotěborský, R., Linda, M., & Jankauskas, V. (2019). Wear modelling of soil ripper tine in sand and sandy clay by discrete element method. *Biosystems Engineering*, *188*, 305–319. https://doi.org/10.1016/j.biosystemseng.2019.10.022

Katinas, E., Chotěborský, R., Linda, M., & Kuře, J. (2021). Sensitivity analysis of the influence of particle dynamic friction, rolling resistance and volume/shear work ratio on wear loss and friction force using DEM model of dry sand rubber wheel test. *Tribology International*, *156*, 106853. https://doi.org/10.1016/j.triboint.2021.106853

Kracht, A. (1978). Design of bulbous bows. *SNAME Transactions*, *86*, 197–217.

Kuře, J., Linda, M., Chotěborský, R., Černilová, B., & Hromasová, M. (2021). DEM modelling of tillage tools in sand and verification of draft forces in the soil box. *Agronomy Research*, *19*(4), 1813–1822. https://doi.org/10.15159/AR.21.147

Liu, L., Wang, X., Zhang, X., Zhong, X., Wei, Z., Geng, Y., Cheng, X., Zhao, K., & Bai, M. (2023). Determination and verification of parameters for the discrete element modelling of single disc covering of flexible straw with soil. *Biosystems Engineering*, *233*, 151–167. https://doi.org/10.1016/J.BIOSYSTEMSENG.2023.08.001

Sun, J., Wang, Y., Ma, Y., Tong, J., & Zhang, Z. (2018). DEM simulation of bionic subsoilers (tillage depth >40 cm) with drag reduction and lower soil disturbance characteristics. *Advances in Engineering Software*, *119*, 30–37. https://doi.org/10.1016/j.advengsoft.2018.02.001

Szelangiewicz, T., Abramowski, T., Żelazny, K., & Sugalski, K. (2021). Reduction of Resistance, Fuel Consumption and GHG Emission of a Small Fishing Vessel by Adding a Bulbous Bow. *Energies 2021, Vol. 14, Page 1837*, *14*(7), 1837. https://doi.org/10.3390/EN14071837

Ucgul, M., Saunders, C., & Fielke, J. M. (2017). Discrete element modelling of tillage forces and soil movement of a one-third scale mouldboard plough. *Biosystems Engineering*, *155*, 44–54. https://doi.org/10.1016/j.biosystemseng.2016.12.002

Wang, Q., Mao, H., & Li, Q. (2020). Modelling and simulation of the grain threshing process based on the discrete element method. *Computers and Electronics in Agriculture*, *178*, 105790. https://doi.org/10.1016/j.compag.2020.105790

Zhang, Shilin, Zhao, H., Wang, X., Dong, J., Zhao, P., Yang, F., Chen, X., Liu, F., & Huang, Y. (2023). Discrete element modeling and shear properties of the maize stubble-soil complex. *Computers and Electronics in Agriculture*, *204*, 107519. https://doi.org/10.1016/J.COMPAG.2022.107519

Zhang, Song, Liu, J., Li, S., Yasukawa, H., & Wu, Q. (2022). Impact of bow shapes on hydrodynamic derivatives due to drifting conditions. *Ocean Engineering*, *245*, 110347. https://doi.org/10.1016/J.OCEANENG.2021.110347

Zhao, H., Huang, Y., Liu, Z., Liu, W., & Zheng, Z. (2021). Applications of Discrete Element Method in the Research of Agricultural Machinery: A Review. *Agriculture 2021, Vol. 11, Page 425*, *11*(5), 425. https://doi.org/10.3390/AGRICULTURE11050425

Development of a numerical rating system for the selection of agricultural and fisheries machinery in the Philippines

Rossana Marie C. Amongo[1*], Ralph Kristoffer B. Gallegos,[3]
Adrian A. Borja[4], Arthur L. Fajardo [1], Arsenio N. Resurreccion[2]
Adrian Daniel L. Pantano[5], Julius John Paul A. Cunan[5]
*Corresponding Author: rcamongo@up.edu.ph

[1]Professor, [2]Professor Emeritus,
[3]Assoociate Professor, [4]Assistant Professor [5]Research Associate
Institute of Agricultural and Biosystems Engineering
College of Engineering and Agro-Industrial Technology
University of the Philippines Los Baños, College, Los Baños, Laguna
*Corresponding Author: rcamongo@up.edu.ph

ABSTRACT

The purposive acquisition and distribution of Agricultural and Fisheries Machinery (AFM) by the Philippine government has improved the level of agricultural mechanization of the country over the years. However, the lack of unified protocols and limited considerations in selecting the best machine has resulted in machinery mismatches, leading to over-utilized, under-utilized, or not utilized AFM in the agricultural production and postproduction systems. This study addresses the knowledge gaps by developing a decision tool for the selection of AFMTs using a numerical system that presents the overall machine rating. The Multiple Criteria Decision Making (MCDA) approach was used to establish the numerical rating system. Three major factors, namely performance-based, manufacturer-based, and end-user-based factors were considered. Specific criteria for each factor were identified. Analytical Hierarchy Process (AHP) and Rank Sum (RS) method were used to determine the weights of the factors and their respective criteria. Six target machines were considered in this study, namely, 2-wheel tractors, 4-wheel tractors, small engines, threshers, combine harvesters, and pump sets. The rating scales were established using 20-year test data from the Agricultural Machinery Testing and Evaluation Center (AMTEC) for the performance-based criteria, while results of the field surveys conducted were used to identify the manufacturer and end-user-based criteria. Data analyses and consultations reveal that the three identified major factors influenced the holistic performance of the machine/technology which should be considered in the machinery distribution program of the government. The results of this study can aid in the planning and formulation of policies by the government for the selection of the best machine to specific end-users' needs. This will also aid in the efficient use of resources that would help uplift the lives of Filipino farmers.

Keywords: Agricultural and Fisheries Machinery, Numerical Rating Scale, Multiple Criteria Decision Making, Analytical Hierarchy Process, Rank Sum Method.

1. INTRODUCTION

The global landscape has always oriented itself towards food security especially in local communities through the Sustainable Development Goals (SDGs). In the Philippines and most tropical countries, agriculture serves as the main source of income in the rural sector, with rice crop with largest production (Mataia et al., 2018). Other crops such as corn, coffee, and cacao serve as other sources of income for farmers (Takeshima, 2017). Throughout the years, the Philippine government has already initiated efforts on upscaling rice production with its intensive mechanization program for the organized farmers. Mechanizing the agricultural sector gave them access to technologies that will improve their productivity by increasing their farms' mechanization index (Lantin, 2016). Since the last decade, these efforts have already distributed 39,393 and 100 units of SPIS from 2011-2019 for the rice and corn program on all regions in the Philippines, majority of which are centered with rice (NAFIAT, 2021). These mechanization efforts were spearheaded by the Philippine government through the Department of Agriculture- Bureau of Agricultural and Fisheries Engineering (DA-BAFE) whose main responsibility is to oversee the distribution of the machines with regards to its technical specifications and fitting the correct machine to the needs of the farmers (Bautista et al., 2017). On the other hand, the Philippine Council for Agriculture and Fisheries (DA-PCAF) is also involved in mechanizing the agricultural sector by providing policy recommendations for the improvement of the government distribution program.

While these efforts have significantly increase rice farmers' productivity over the years, there have been reports of machine mismatches that were distributed. DA-PCAF reported in 2018 that two out of ten machines that were distributed were under-utilized, or not utilized at all. The sources of mismatching of the machines are said to be categorized into three main factors, Technical, Environmental, and Socio-economic factors. Environmental factors deal with the terrain of the farm to which the machine is being used, while Socio-economic factors are those that are concerned with financial security amongst the end-users like monetary allowances for repairs and other after-sales services (Van den Berg et al., 2007). Technical factors; however, has only considered machine specifications in recent evaluations of AFMs. In the knowledge of many, this factor only deals with how much power a machine can give to the farm.

Studies centered machine selection already exist in literature over the recent years. In the Philippines, Resurreccion et al. (2008) first recommended a rating system based on different machine performance parameters to select the best machine among alternatives. However, this study considers only the performance test data of the machines, and not the perspective of other machine usability factors such as the provisions of after-sales services, or the level of acceptability of the machines by the farmers. It is in this light that this study is conducted to establish a numerical rating system for the selection of AFMs which considers not only the performance of machines, but also the perspective of the other players and conditions in the distribution system.

2. MATERIALS AND METHODS

This study is divided into two main components, namely the evaluation of the status of historical machine performance test results from AMTEC, and development of a numerical rating system, The selection of machines should not only consider machine performance which would not suffice the efficient usage of these machines given that economic and cultural practices which also play a part in determining if a certain machine is effective to be deployed in a specific area. With this, three main dimensions were considered in the development of such protocols, namely performance-based factors, manufacturer-based factors, and the end-user-based factors. The process flow is shown in **Error! Reference s ource not found.** while the three main factors considered in this study is shown in **Error! Reference source not found.**.

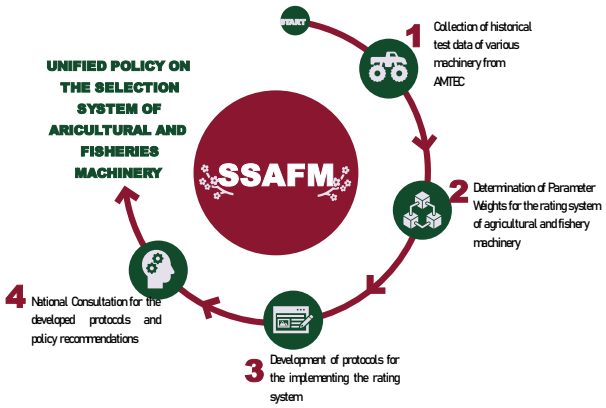

Figure 1. General Methodology of the Study.

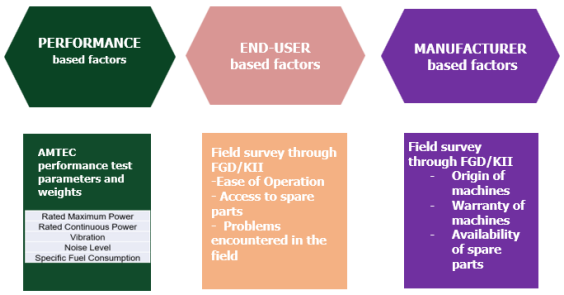

Figure 2. Three main factors identified for the selection of Agricultural and Fisheries Machinery.

2.1 Status of machinery testing, evaluation, and selection in the Philippines

Six target machines were identified in this study, namely 2-wheel tractors, 4-wheel tractors, small engines, threshers, combine harvesters, and pump sets. The performance test data of each machine from year 2000 to present were obtained from AMTEC for analysis which served as the foundation for the establishment of the numerical rating system. Field surveys were conducted to determine the status of the distributed machines, as well as the identification of the criteria for each of the three factors. The study identified three key sectors in the conduct of the survey namely the Farmer Cooperative beneficiaries of the machine distribution programs, DA RFO officials who evaluates and monitors the distributed machines, as well as manufacturers, suppliers and distributors who supply and deliver machines to the beneficiaries through government biddings. The status and gaps of the machine distribution program were holistically identified which set a strong support for the development of the necessary machine selection protocols.

2.2 Selection of Project Survey Sites

Four regions were selected as study sites based on the following considerations:

a. Rice production area (in ha)
b. Presence of agricultural machinery manufacturers, suppliers, and distributors based on AMTEC database,
c. Number of active Farmer Cooperatives (FO) according to the latest database of the Regional Field Offices (RFOs) ; and,
d. Number of Agricultural and Fisheries Machines (AFMs) received from the government.

Regions II, V, VI, XIII, and NCR were selected as project sites (Figure 3) to have a regional cluster representation for the North Luzon cluster, South Luzon cluster, Visayas cluster, and the Mindanao cluster. Provincial locations of the RFOs were visited for the actual survey, namely Tuguegarao City in Cagayan (Region II), Naga City in Camarines Sur (Region V), Iloilo City (Region VI), and Butuan City in Agusan Del Norte (Region XIII). Focus Group-Discussions (FGD) with the DA RFO key officials, while Key Informant Interview (KII) were done for the identified FOs and manufacturers. Three farmer cooperatives with different service areas were selected. Key officials for each farmer cooperative, including the operator of the machines were invited for the conduct of the on-site FGD. For manufacturers/suppliers/ distributors, a sampling plan was developed to identify these private respondents based on the database provided by AMTEC on the accredited machine manufacturers, suppliers, and distributors.

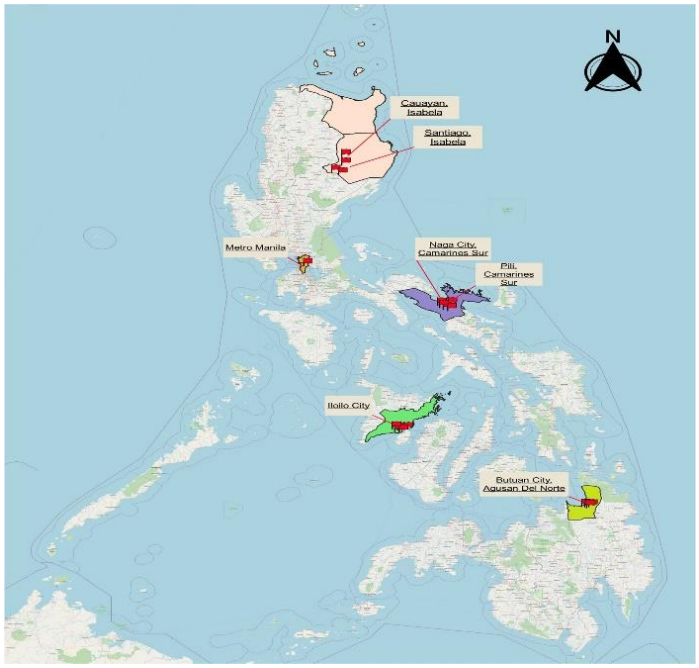

Figure 3 The project sites.

2.3 Development of Survey Instruments

Three types of survey instruments (RFOs, FOs and Manufacturers) were devised with a printed, and online versions. FOs and machine operators were interviewed using the printed questionnaire For some manufacturers, suppliers, and distributors that opted to participate in the survey through virtual platform, a version of the questionnaire was made in Google Sheets, which also served as data backup of the results of the project field survey that was accomplished using the printed questionnaires. A database of the survey responses was also created to analyze the results. The survey instrument contains the following parts:

2.3.1 For all respondents (FOs, DA-RFO Key Officials, and Manufacturers/ Suppliers/Dealers)

a. **Demographic Information**: Contains basic details of both the interviewer and respondent, including the name of the respondent, affiliation, contact details including the date and time of the survey.
b. **Machines acquired/Distributed/received**: this section determined the machines distributed by DA-RFOs and received by the FOs and manufactured/supplied machinery by the manufacturers/ suppliers/dealers in relation to the six identified (AFMs). Included in this part are the machine specifications such as the brand, model, power rating, and machine supplier.

2.3.2 For Farmer Cooperative Respondents Only

a. **Ease on Operation:** Ease of operation for each machine included:
   i. **Maneuverability, Control, Balance:** For all machines except for the pump/pumpsets; this refers to the ease in which the operator can operate/drive the machine without disrupting its assigned path in the field nor cause any discomfort to the operator and cause any damages to the machine.
   ii. **Ease of Refueling:** This is the number of times the engine was refilled with fuel assuming that the tank is originally full, and the machine has been used for a productive 10-hour operation.
   iii. **Ease of cranking/starting**: This section is included only in the questionnaires for small engines and pump sets; this refers to the easiness of starting the machine. For this project, this is measured by the number of tries for the operator to fully start the engine.
b. **Ease of access to spare parts**: This is the longest possible time for the FOs to acquire spare parts for each of the machines. The longest time of acquisition means either that the specific part is not available in their city proper or needed to be shipped from Manila or outside the country. The respondents were also asked which parts were mostly replaced and the nearest suppliers. Also included in this section are the common problems that the operators face with the machines that they have received and are operating.
c. **Ease of access for after-sales services**: Along with the access to spare parts, the FO respondents were also asked about the process in which they seek after-sales service. The coverage of these after-sales service provisions includes, but is not limited to access for on-site repair, checkups, and access to service caravans. The questions for this section revolve on the time for the farmer to reach the after-sales services that they require, starting from the initial contact with the supplier to the success of the repair of the machine.
d. **Coordination with DA RFO**: This includes the response time of the RFOs regarding machine registration, after-sales services, and coordination with the supplier/s of the distributed machines.

2.3.3 For DA RFO Official Respondents only

a. **Concerns of the FO recipients**: RFO officials were asked to reiterate the common concerns of FOs regarding the machines received. The concerns include but were not limited to access to spare parts, access to after-sales services, and concerns regarding the suppliers of the distributed machines. **For Manufacturers/Suppliers/Dealers.**
b. **Turnover rate**: This is the number of units that were manufactured (for manufacturers) or sold (for suppliers and distributors) per year.
c. **Ratio of government to private clients**: This is the overall percentage of manufacturers' clients acquired through government biddings or private sector- clients. Additional questions were also asked regarding the process in which the manufacturers participate in bidding (if applicable), or the number of private clients they have served for the recent year, including the months when most clients request machines.
d. **Warranty**: As a main component of machine sales, the duration of warranty was asked for each machine that they deal with, including the specific coverage, part replacements, labor/services provided, check-ups, and other forms of services. Specific questions for each warranty component were also included such as the types of parts that are only included in the warranties, or the requirements that must be accomplished by the clients for their machine to be eligible for warranty-covered labor.

e. **Response time for access to spare parts**: This is the time it takes for the manufacturers/suppliers to respond to the needs of their clients regarding parts replacement.
f. **Response time for access to after-sales services**: This is the time to respond to after sales services given that the supplier has on-call mechanics (their number of available mechanics was also asked in the questionnaire) and the time it takes for a mechanic to reach their farthest client for hands-on machine repair. In case the manufacturer/supplier has multiple service centers, the farthest region in which they can offer their services was also asked.

2.4 Survey Sites

With the volume of production and presence of NAMDAC accredited agricultural and fisheries machinery manufacturers as bases for selection, Regions II, V, VI, and XIII were considered as the project survey sites. As seen in Table 1, the volume of production of palay in 2022 for Regions II, V, VI, and XII was 2,928,165.70 MT, 1,329,004.41 MT, 2,321,593.72 MT, and 520,181.03 MT , respectively. Regions II, V, VI, and XIII had 8, 2, 5, and 1 NAMDAC-accredited AFM manufacturers, respectively. The team conducted a face-to-face courtesy meeting and FGD/KII with the DA-RFOs, Manufacturers and FOs in Regions II, V, VI, and XIII using the formulated survey instruments. The actual survey intends to verify the parameters to be used for the unified selection system of the agricultural and fisheries machinery. A total of 88 participants attended the courtesy meeting and FGD/KII, wherein 27 participants were from FOs, 17 participants from DA-RFOs, and 44 participants from Agricultural Machinery Manufacturers. NCR was also included in the survey since most of the large manufacturers/dealers/suppliers of agricultural machinery are located (Table 1).

Table 1. Survey respondents from the four regions with the addition of NCR manufacturers.

Region	Volume of Production (MT) (2022)	Area Harvested (Has) (2022)	NAMDAC Accredited Manufacturer in the area	End Users/ Farmer Coop	Regional Field Office	Manufacturers
REGION II (Cagayan Valley)	2,928,165.70	621,995.30	8	8	3	6
REGION V (Bicol Region)	1,329,004.41	348,848.02	2	7	4	7
REGION VI (Western Visayas)	2,321,593.72	681,300.26	5	6	4	14
REGION XIII (CARAGA)	520,181.03	159,519.02	1	6	6	6
NCR				-	-	11
TOTAL				27	17	44

2.5 Establishment of a numerical rating system

The Multiple Criteria Decision Making (MCDA) approach was used to establish the numerical rating system. The criteria for each of the three factors were identified. For performance-based factors, the criteria for each target machine were identified using the historical performance test data from AMTEC. For the manufacturer and end-user-based factors, their respective criteria were identified using the project field surveys in the study regions, as well as consultative meetings with manufacturers, DA RFO officials, and members of selected FOs. With the presence of historical test data for the performance-based factors, statistical analysis was used to determine the minimum acceptable value for each of the criteria, which serves as baseline for the rating system. A specific range of values for each criterion was then identified corresponding to a certain rating. The weighted sum of the criteria for the three factors were integrated to get the overall machine selection rating. The criteria weights per factor for each machine considered was determined using the weighing by ranking method while the weights of the three factors, namely the performance, manufacturer, and end-user-based factors were determined using the Analytical Hierarchy Process (AHP) The general framework for the establishment of the numerical rating system is shown in Figure 4. Using the individual rating scores from the three factors, the overall machine selection rating is determined by obtaining the weighted sum of the scores.

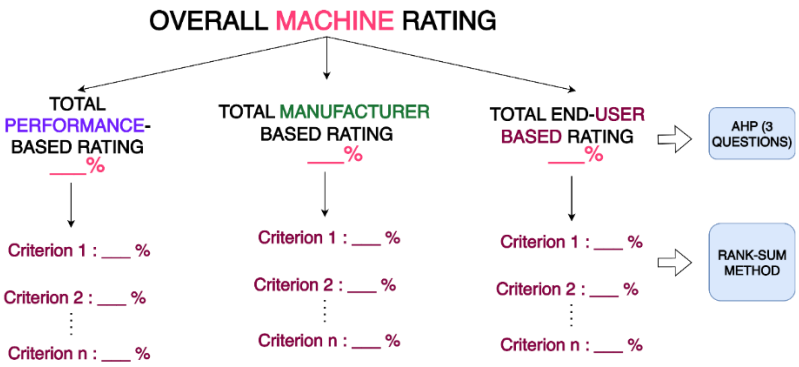

Figure 4. Framework for the establishment of the numerical rating system

3. RESULTS AND DISCUSSION

3.1 Survey Results from the Department of Agriculture Regional Field Offices (DA-RFOs)

There were 4 selected regions (Region II, V.VI and XIII) where the RFOs, Manufacturers', Farmer Organizations and other stakeholders were interviewed to gather primary data on the selection scheme for the agricultural machinery distribution program of the government. In Region II, all six identified machines were distributed by RFO II. The highest number of machines distributed were the 4-wheel tractors in which a large portion was supplied by Kubota, a well-known manufacturer of various agricultural machines with numerous service centers across the Philippines. RFO II also revealed that other brands of combine harvesters, threshers, and 2-wheel tractors were also present supplied by ACT, which is a local manufacturer for two-wheel tractors. Based on the survey results from DA RFO II officials, the common problems reported by the FO recipients were the inappropriateness of the machines received. Some of the machines that were distributed to the farmers are not suitable to their corresponding farm because of the type of soil in the area or concerns that the machine parts needed for repair are not readily available from the nearest city.

The FGD with the officials from RFO V shows that most of the distributed machines to the farmers in the regions were 2-wheel and 4-wheel tractors supplied by local manufacturers and distributed by private institutions. Common concerns that were raised to RFO V from farmers was the lack of service center that could accommodate some parts especially belts that are specific to a certain brand only. Given that there are not many manufacturers present in the region, the supply of machines largely depends on private suppliers and distributors. This means that the lack of spare parts would become a problem for the farmers once the existing service centers run out of pertinent parts.

In the focus group discussion conducted with the officials of DA-RFO VI it shows that all six identified machineries were procured by the region in the last 5 years. The FGD also showed that the region conducted needs assessments before procuring the AFMs. Among Only thresher and pump/pump sets were reported by the recipients with problems. According to the recipients, these two machineries were heavy making hauling the machines difficult.

The discussion between the UPLB, DA-PCAF, and DA RFO XIII teams mainly centered on the review of the appropriateness protocols involved in the distribution program to FO recipients. These protocols include the extent of the needs assessment conducted on the prospective FOs to get a better insight of the machines needed by the famers. The conduct of trainings directed to the operators of the cooperatives on basic repair and maintenance of the machines were also identified to lessen the services of a custom-hired mechanic, which also attributes to their expenses.

3.2 Numerical Rating System

The rating system implemented in this study is the 5-point Likert scale, in which scores of 1 to 5 with Table 2 as guide. Having this kind of system can be easily understood by the general stakeholders which makes the results of this study more comprehensible. Moreover, this scoring system is advantageous especially for representing the manufacturer and end-user-based criteria because the Likert scale is a psychometric measure of a person's range of acceptance for a certain aspect (Bernstein, 2005). With the addition of intermediate scales (scores of 2, 3, and 4), the central tendency bias of the respondents towards one decision is significantly reduced (Jebb et al., 2021). Hence, the qualitative measures on after-sales provision and ease of operation for farmers can be quantified with the assignment

of a numerical score on the 5-point Likert scale. Though the Likert scale has multiple ranges, the 5-point scale was adopted with the basis on the results of Clark and Watson (2019) stating that a five-to-seven-point Likert scale generates higher mean scores compared to the highest score possible and having a significant statistical difference as compared with the 10-point Likert scale.

Table 2. Guide in assessing AFM selection using the established numerical rating system.

Rating Score	Interpretation
1	Minimum acceptable value is met but is not considered as competitive for machine selection
2	Falls above the minimum acceptable value but is still considered unsatisfactory for machine selection
3	Values are within the average for the specified criterion for machine selection
4	Satisfactory values which are above average and is considered favorable for machine selection
5	Values possess the highest preference for a specific criterion and is considered as most favorable for machine selection

For the performance-based factor, the historical AMTEC test data were the primary bases for selection of the criteria. Notably, some were chosen from consultative activities with mechanization experts. These performance-based criteria represent the machine parameters that have the greatest impact on field operation as validated by the FOs. The specifications of the prime mover, as well as machine characteristics such as efficiencies, and the provision of safety features were identified as major concerns. It was also found out that accessibility to after-sales services constitute one of the most concerns of the FOs. The survey instrument contains information on the frequency of machine breakdown while in operation which is closely related to the accessibility of spare parts and after-sales services such as on-site machine repair.

Aside from the standards from the Philippine Agricultural Engineering Standards (PAES), manufacturer provisions for warranty duration and coverage, as well as service reach and repair service area were also identified as manufacturer-based criteria. Included in the survey activity were the acceptance of the farmers on the target machines that they have received for farm operation. The results revealed that ease of operation (maneuverability, control, and balance), ease of refueling for a maximized productive operation, and ease of spare parts and services acquisition comprise the end-user-based criteria as these parameters are farmer-specific indicators on how well the machine fits for farm operation. The identified criteria for performance, manufacturer, and end-user-based factors are summarized from Tables 3 to 5.

Table 3. Identified performance criteria and sub-criteria for the target machines.

SMALL ENGINES	
TECHNICAL PARAMETER	**UNIT OF MEASURE**
1. Percent of Rated Maximum Power at Varying Load	Percent
2. Percent Continuous Power at Rated Speed	Percent
3. Specific Fuel Consumption	mL kW-h^{-1}
4. Noise Level	db(A)
5. Vibration	g
6. Volume of Fuel Tank Per Max Engine Power in Name Plate	mL kW^{-1}
HAND TRACTORS	
TECHNICAL PARAMETER	**UNIT OF MEASURE**
1. PRIME MOVER:	
a. Percent Continuous Power at Varying Load	Percent
b. Specific Fuel Consumption	mL kW-h^{-1}
c. Volume of Fuel Tank Per Max Engine Power in Name Plate	mL kW^{-1}
2. POWER TRANSMISSION:	
Overall Transmission Efficiency (Percent Continuous Power of the Engine X Belt Efficiency X **Peak Transmission Efficiency**)	Percent

3. IMPLEMENT: (2-bottom disc plow)	
a. Forward Speed During Field Operation	kph
b. Percent Wheel Slippage	Percent
c. Field Capacity Per Max Engine Power in Name Plate	Ha h-kW^{-1}
4. SYSTEM:	
Safety Features (e.g., belt cover, mud guard, light, emergency stop, etc)	
FOUR-WHEEL TRACTORS	
TECHNICAL PARAMETER	**UNIT OF MEASURE**
1. PRIME MOVER:	
a. Power Output Efficiency (Max and Continuous)	%
b. Specific Fuel Consumption	mL kW-h^{-1}
c. Noise	Db(A)
d. Volume of Fuel Tank Per Max Engine Power in Name Plate	mL kW^{-1}
2. POWER TRANSMISSION:	
a. Overall Power Transmission Efficiency to PTO	Percent
b. Overall Power Transmission Efficiency to Hydraulic System	Percent
3. IMPLEMENT (Plow and Rototiller)	
a. Forward Speed during field operation	kph
b. Percent Wheel Slippage	Percent
c. Field Capacity Per Max Engine Power in Name Plater	Ha h-kW^{-1}
4. SYSTEM:	
Safety Features (e.g., canopy, lights, horn, etc)	
THRESHERS	
TECHNICAL PARAMETER	**UNIT OF MEASURE**
1. PRIME MOVER:	
a. Percent Continuous Power at Varying Load	Percent
b. Specific Fuel Consumption	mL kW-h^{-1}
c. Volume of Fuel Tank Per Max Engine Power in Name Plate	mL kW^{-1}
2. POWER TRANSMISSION:	
Overall Transmission Efficiency (Percent Continuous Power of the Engine X Belt Efficiency X Peak Transmission Efficiency)	Percent
3. MACHINE:	
a. Threshing Capacity Per Max Engine Power in Name Plate	kg h- kW^{-1}
b. Threshing Efficiency	Percent
c. Threshing Loss	Percent
d. Purity	Percent
e. Broken Grains	Percent
f. Cracked Grains	Percent
4. SYSTEM:	
Safety Features (e.g., belt guard, length of feeding chute, emergency stop	
COMBINE HARVESTERS	
TECHNICAL PARAMETER	**UNIT OF MEASURE**

1. PRIME MOVER:	
a. Percent Continuous Power at Varying Load	Percent
b. Specific Fuel Consumption	L kW-h^{-1}
c. Volume of Fuel Tank Per Max Engine Power in Name Plate	mL kW^{-1}
2. POWER TRANSMISSION:	
Overall Transmission Efficiency (Percent Continuous Power of the Engine X Belt Efficiency X Peak Transmission Efficiency)	Percent
3. MACHINE:	
a. Threshing Capacity Per Max Engine Power in Name Plate	kg h-kW^{-1}
b. Field Efficiency	Percent
c. Total machine loss	Percent
d. Purity	Percent
e. Broken Grains	Percent
f. Cracked Grains	Percent
4. SYSTEM:	
Safety Features (e.g., belt guard, length of feeding chute, emergency stop	
PUMPSETS	
TECHNICAL PARAMETER	**UNIT OF MEASURE**
1. Maximum discharge capacity per input power	L s-kW^{-1}
2. Maximum pump efficiency	Percent
3. Total head per input power	m kW^{-1}

Table 4. Identified end-user-based criteria and sub-criteria for the target machines.

TECHNICAL PARAMETER	**UNIT OF MEASURE**
1. EASE OF OPERATION:	
a. Maneuverability, Comfort, and Balance	
b. Between field transfer	
c. Ease of Refueling	Number per 8 h operation
2. RECORD OF BREAKDOWN:	
a. Frequency of Prime Mover Breakdown	Number (1-3-5 yrs. record)
b. Frequency of Transmission Breakdown	Number (1-3-5 yrs. record)
c. Frequency of Implement/Machine Breakdown	Number (1-3-5 yrs. record)
3. AFTER-SALES SERVICE:	
a. Call Response Time	h
b. Service Time (e.g., change oil/filter, replacement of consumable parts, adjustments, etc)	h
c. Repair Time (e.g., engine over hauling, replacement of major transmission and implement/machine parts, etc)	h

Table 5. Identified manufacturer-based criteria and sub-criteria for the target machines.

TECHNICAL PARAMETER	UNIT OF MEASURE
1. Number of Service Centers:	
a. Company-owned Service Centers	Number
b. Accredited Service Centers	Number
2. Description of a Typical Service Center (Random Selection):	
a. Service Area	m^2
b. Stock Room Area	m^2
c. Admin and Reception Area	m^2
d. Number of Consumable Spare Parts on stock	Number
e. Number of Major Spare Parts on stock	Number
f. Number of Technicians	Number
g. Number of Sets of Basic Repair Tools	Number
h. Number of Service Vehicles	Number

For the data dependent performance-based criteria, the values for each rating were determined based on their normal distribution curve, in which the Mean and the Standard Deviation (MSD) was used to identify the minimum acceptable values. The intervals of which were determined based on the maximum or minimum value of each data sets. With the consideration of the MSD, this numerical rating scheme would take into consideration all the test data for the machines that were tested by AMTEC from year 2000, which gives a more accurate description on the ideal range of values for each performance criteria. The use of MSD simply serves as tools on where to draw the threshold line which is considered as the minimum acceptable value. For the manufacturer and end-user-based criteria, the similar Likert scale used in the field survey was used in the rating system, since the survey instrument is already designed to assign a numerical rating on the level of ease of the farmer for their field operation. The established numerical rating scale done in this study is summarized from Tables 6 to 11.

Table 6. Established rating scales for the evaluation of 2-wheel tractors.

PEAK TRANSMISSION EFFICIENCY (%)		FIELD CAPACITY (ha h^{-1})	
Rating	**Range**	**Rating**	**Range**
1	77 and below	1	0.09 and below
2	78-81	2	0.1-0.3
3	82-85	3	0.31-0.5
4	86-89	4	0.51-0.7
5	90 and above	5	0.71 and above
TRAVEL SPEED (kph)		**SAFETY FEATURES (# of provisions)**	
Rating	**Range**	**Rating**	**Range**
1	2 and below	1	Provision of 1 safety feature
2	2.1-4	2	Provision of 2-3 safety features
3	4.1-5.3	3	Provision of 4-5 safety features
4	5.4-7	4	Provision of 6-7 safety features
5	7.1 and above	5	Provision of 8 safety features

Table 7. Established rating scales for the evaluation of 4-wheel tractors.

SPECIFIC FUEL CONSUMPTION (g kW-h^{-1})	
Rating	**Range**
1	218 and above
2	219-208

3	207-198
4	197-188
5	187 and below

OVERALL, POWER TRANSMISSION EFFICIENCY TO PTO (%)		SAFETY FEATURES (# of provisions)	
Rating	**Range**	**Rating**	**Range**
1	80 and below	1	Provision of 1 safety feature
2	81-85	2	Provision of 2 safety features
3	86-90	3	Provision of 3 safety features
4	91-95	4	Provision of 4 safety features
5	96 above	5	Provision of 5 safety features

Table 8. Established rating scales for the evaluation of small engines.

PERCENT OF RATED MAXIMUM POWER AT VARYING LOAD (%)		SPECIFIC FUEL CONSUMPTION (g kW-h^{-1})	
Rating	**Range**	**Rating**	**Range**
1	80 and below	1	787 and above
2	81-85	2	786-636
3	86-89	3	635-486
4	90-93	4	485-336
5	94 and above	5	335 and below
NOISE LEVEL (dB)		**VOLUME OF FUEL TANK PER MAXIMUM ENGINE POWER (L kW^{-1})**	
Rating	**Range**	**Rating**	**Range**
1	96 and above	1	0.44 and below
2	95-91	2	0.45-0.69
3	90-85	3	0.7-0.94
4	84-79	4	0.95-1.2
5	78 and below	5	1.21 and above

Table 9. Established rating scales for the evaluation of threshers.

SPECIFIC FUEL CONSUMPTION (L kW-h^{-1})		Volume of Fuel Tank Per Max Engine Power (L kW^{-1})	
Rating	**Range**	**Rating**	**Range**
1	1.36 and above	1	0.32 and above
2	1.35-1	2	0.31-0.25
3	0.99-0.75	3	0.24-0.18
4	0.74-0.45	4	0.17-0.11
5	0.44 and below	5	0.1 and below
Threshing Capacity Per Max Engine Power (kg kW-h^{-1})		**Cracked grains (%)**	
Rating	**Range**	**Rating**	**Range**
1	144 and below	1	7 and above
2	145-244	2	6.9-5
3	245-344	3	4.9-3
4	345-444	4	2.9-1.6
5	445 and above	5	1.59 and below
Threshing Efficiency (%)		**Threshing loss (%)**	
Rating	**Range**	**Rating**	**Range**

1	99.1-99.3	1	2.2 and above
2	99.4-99.5	2	2.1-1.6
3	99.6-99.7	3	1.5-1.1
4	99.8-99.9	4	1-0.56
5	100	5	0.55 and below
Purity (%)		**Broken grains (%)**	
Rating	**Range**	**Rating**	**Range**
1	94 and below	1	0.86 and above
2	94.1-95	2	0.85-0.65
3	95.1-96	3	0.64-0.43
4	96.1-97	4	0.42-0.21
5	97.1 and above	5	0.2 and below

SAFETY FEATURES (# of provisions)	
Rating	**Range**
1	Provision of 1 safety feature
2	Provision of 2 safety features
3	Provision of 3 safety features
4	Provision of 4 safety features
5	Provision of 5 safety features

Table 10. Established rating scales for the evaluation of combine harvesters.

SPECIFIC FUEL CONSUMPTION (L kW-h^{-1})		**Field Efficiency (%)**	
Rating	**Range**	**Rating**	**Range**
1	0.2 and above	1	62 and below
2	0.19-0.14	2	63-71
3	0.13-0.1	3	72-80
4	0.09-0.06	4	81-88
5	0.05 and below	5	89 and above
Threshing Capacity Per Max Engine Power (kg kW-h^{-1})		**Threshing loss (%)**	
Rating	**Range**	**Rating**	**Range**
1	43 and below	1	1.83 and above
2	44-83	2	1.82-1.4
3	85-124	3	1.39-0.96
4	125-165	4	0.95-0.52
5	166 and above	5	0.51 and below
Purity (%)		**Threshing loss (%)**	
Rating	**Range**	**Rating**	**Range**
1	92 and below	1	1.65 and above
2	93-94	2	1.64-1.1
3	95-96	3	1.09-0.57
4	97-98	4	0.56-0.03
5	99-100	5	0.02 below
Broken grains (%)		**Cracked grains (%)**	
Rating	**Range**	**Rating**	**Range**
1	0.97 and above	1	8 and above
2	0.96-0.73	2	7.9-6.2

3	0.72-0.49	3	6.1-4.2
4	0.48-0.24	4	4.1-2.1
5	0.23 and below	5	2 and below

SAFETY FEATURES (# of provisions)	
Rating	**Range**
1	Provision of 1 safety feature
2	Provision of 2 safety features
3	Provision of 3 safety features
4	Provision of 4 safety features
5	Provision of 5 safety features

Table 11. Established rating scales for the evaluation of pumpsets.

MAXIMUM DISCHARGE CAPACITY PER INPUT POWER, (L s-kW^{-1})		**MAXIMUM PUMP EFFICIENCY (%)**	
Rating	**Range**	**Rating**	**Range**
1	18 and below	1	10 and below
2	19-34	2	10-19
3	35-50	3	20-28
4	51-66	4	29-36
5	67 and above	5	37 and above

TOTAL HEAD PER INPUT POWER (%)	
Rating	**Range**
1	8 and below
2	9-14
3	15-20
4	21-26
5	27 and above

For the manufacturer-based factors, the scale revolves around their respective response time in which they can accommodate the replacement of spare parts requested by their clients, as well as the time it takes for their on-site mechanic to reach the farthest client for in-field machine repair. This is apart from their warranty in which coverage duration comprise the rating scales. It was revealed that manufacturers who have multiple service centers spread across different regions provided better services for their clients, as compared to some that requires the farmers to bring the machine to their service centers for repairs. The numerical rating system ensures that the manufacturers who have better service reach and quick response time would be favored over the ones that are not responsive to their clients.

The end-user-based criteria takes into consideration how the farmers react with the machines that they received in terms of daily operation. Having the advantage of the bipolar scaling of the Likert system in which respondents can have different levels of perception on agreement and disagreement towards an issue, the perception of the farmer towards different machine usage aspects such as the ease of operation and the number of times they need to refuel their machines for daily operation is quantified with the assignment of scores for each criterion. Since the overall machine selection rating depends on the ratings for the varying scores for the different performance, manufacturer, and end-user-based criteria can provide a more holistic description on which machine is to be selected amongst alternatives as this rating system is not solely dependent on performance factors only.

3. CONCLUSION

This study was conducted to establish a more holistic approach on selecting the Agricultural and Fisheries Machinery (AFM) by means of a numerical rating system. An overall machine selection rating is obtained from three factors namely: the performance, manufacturer, and the end-user-based factors. The respective criteria for these factors were identified

through the analysis of historical performance test data from AMTEC, as well as the conduct of project field surveys in four identified representative regions. Results revealed that the use of a 5-point Likert scale is an effective approach to evaluate the manufacturer and end-user-based criteria because it allows the respondents to quantifiably assess the range of acceptance towards the contents of the survey instruments which were the primary basis of the identifying the criteria for each factor. For performance-based factors, the use of the MSD was found to be effective in determining the range of values corresponding to each rating since it considers the normal distribution curve of the historical data. The developed rating system can be used by relevant agencies and policy makers in improving the protocols on selecting AFMs which can be a mediator for better machine allocations for farmers to achieve food security.

4. ACKNOWLEDGEMENT

The UPLB-DA-PCAF team would like to express their gratitude towards the following agencies and companies for their support on the completion of the study:

DA- RFO II	Topline Reaper Republic & Agricultural Machineries	Iloilo New Agri-Industrial Marketing and General Services, Inc.
DA-RFO V	GRJC Agri Industrial Machineries	Jorque Trading & Manufacturing Corp
DA-RFO VI	Liam Alexander Agri Machineries	KARAGA Farmers shop
DA-RFO XIII	ECA Agri Machineries	Ely Welding Shop
ACT Corporation	Isabela EBC Builders Const., Inc.	Iritec Intl. Co. Ltd.
ADA Manufacturing Corporation	Kolbi Tropics Agro Industries, Inc	Leadstech Corporation
Agricom Machineries & Const. Corp.	AIMS Agriventures, Inc.	Deutsche Motorgate Inc.
All Certified Equipment Trading Corp.	REEM Agri Trading	Harbest Agribusiness Corporation
Central Isabela Agri Manufacturing Corp.	Agricom Visayas Inc	Kubota Philippines, Inc.
Equity Machineries Inc	NEOPHIL	Columbian Autocar Corporation
Isabela General Enterprise	Noly Hontarciego Metal Craft	Yanmar Philippines Corporation
3R Metal Craft	Solanda Enterprises	Fit Corea Trading Phils, Inc
K Four Enterprises		Brixton Construction

5. REFERENCES

Bautista, E. G., Kim, J., Kim, Y., & Panganiban, M. E. (2017). Farmer's Perception on Farm mechanization and Land reformation in the Philippines. *Journal of the Korean Society of International Agricultue*, *29*(3), 242–250. https://doi.org/10.12719/KSIA.2017.29.3.242

Bernstein, I. H. (2005). Likert Scale Analysis. *Encyclopedia of Social Measurement*, 497–504. https://doi.org/10.1016/B0-12-369398-5/00104-3

Clark, L. A., & Watson, D. (2019). Constructing validity: New developments in creating objective measuring instruments. *Psychological Assessment*, *31*(12), 1412–1427. https://doi.org/10.1037/pas0000626

Jebb, A. T., Ng, V., & Tay, L. (2021). A Review of Key Likert Scale Development Advances: 1995–2019. *Frontiers in Psychology*, *12*. https://doi.org/10.3389/fpsyg.2021.637547

Lantin, R. M. (2016). Agricultural mechanization in the Philippines, Part I: Brief history. *AMA, Agricultural Mechanization in Asia, Africa and Latin America*, *47*, 80–86.

Mataia, A., Beltran, J., Manalili, R., Catudan, B., Francisco, N., & Flores, A. (2018). *Rice value chain analysis in the PhiliPPines*.

Resurreccion, A., Eusebio, R., Aranguren, D., Santiago, R., & Suministrado, D. (2008). AMTEC performance rating system: a guiding tool in the appropriate selection of agricultural machinery. *Philippine Agricultural Mechanization Journal*, *15*(1), 14–35.

Takeshima, H. (2017). Custom-hired tractor services and returns to scale in smallholder agriculture: a production function approach. *Agricultural Economics*, *48*(3), 363–372. https://doi.org/10.1111/agec.12339

van den Berg, M. M., Hengsdijk, H., Wolf, J., van Ittersum, M. K., Guanghuo, W., & Roetter, R. P. (2007). The impact of increasing farm size and mechanization on rural income and rice production in Zhejiang province, China. *Agricultural Systems*, *94*(3), 841–850. https://doi.org/10.1016/J.AGSY.2006.11.010

Tracing pistachio nuts' origin and irrigation practices through hyperspectral imaging

Raquel Martínez-Peña[a], Salvador Castillo-Gironés[b], Sara Álvarez[c]* and Sergio Vélez[d]

[a] Woody Crops Department, Regional Institute of Agri-Food and Forestry Research and Development of Castilla-La Mancha (IRIAF), Agroenvironmental Research Center "El Chaparrillo", CM412 Ctra.Porzuna km.4, 13005 Ciudad Real, Spain.

[b] Agroenineering department, Valencian Institute for Agricultural Research (IVIA), CV-315, km 10.7, 46113 Moncada, Valencia, Spain.

[c] Instituto Tecnológico Agrario de Castilla y León (ITACyL), Ctra. Burgos km 119, 47071 Valladolid, Spain.

[d] Group Agrivoltaics, Fraunhofer Institute for Solar Energy Systems ISE, 79110 Freiburg, Germany.

* Corresponding author. Email: alvmarsa@itacyl.es

Abstract

The commercialisation of pistachio nuts often faces issues of adulteration or misrepresentation concerning their cultivation practices and geographical origins. In this investigative study, we harnessed the capabilities of Hyperspectral Imaging (HSI) employing a SPECIM IQ camera to discern the irrigation treatments and geographical variations in pistachio nuts harvested from two distinct orchards in Spain, namely "La Seca" and "La Moraleja". Two experimental plots were designated as control and high irrigation within each orchard. Hyperspectral data, covering the spectral range of 400-1000 nm, were meticulously captured and analyzed to unravel the contrasts in water management practices and their implications on pistachios' commercial quality and yield.

The ensuing image analysis encompassed a broad spectrum of parameters, including water supplied and yield, and assessing percentage distribution among split, non-split, and blank nuts. Additionally, the origin and commercial calibre were evaluated to gauge the commercial viability of the yield. Three different Machine Learning (ML) models were used: Partial Least Squares-Discriminant Analysis (PLS-DA), Support Vector Machine (SVM) and XGBoost, which robust models were conceived. The results show that pistachio origin and water treatment predictions showed high accuracy with F1 scores of 0.99 and 0.92, respectively, and a combined prediction achieving 0.97, indicating the significant impact of location and irrigation. In contrast, other predictions like yield were strong (R2 score of 0.88), but shell split and calibre predictions were less accurate, highlighting the potential of advanced modelling to enhance pistachio quality predictability.

Our analysis accentuates the profound potential of HSI, especially when deployed with a SPECIM IQ camera, in delineating the irrigation treatment and tracing the geographical origin of pistachio nuts. This endeavour paves the way for ensuring authenticity and commercial quality in the pistachio trade. It augments our understanding of the interplay between irrigation practices and nut commercial quality, fostering a sustainable and informed agricultural paradigm.

Keywords: Commercial Quality, Machine learning, *Pistacia vera*, Post-harvest, Traceability.

1. Introduction

Pistachio trees, originating from southern Central Asia, have spread globally, reaching regions such as modern-day Syria around 2000 years ago (Mir-Makhamad *et al.,* 2022). Pistachio nuts are renowned for their unique flavour and are celebrated for their high protein, dietary fibre, and essential vitamins and minerals (Mandalari *et al.,* 2021). As significant crops in global agriculture, pistachios are in high demand. In 2022, Iran led in harvested area with 497,484 hectares, followed by Turkey (408,709 hectares) and the United States (173,207 hectares) (FAO, 2024). However, production quantities were highest in the United States (400,070 tons), with Turkey and Iran producing 241,669 tons and 239,289 tons, respectively. Despite market instability and import competition, Spain has seen increased interest in pistachio cultivation and rising consumption (CBI, 2020). The pistachio industry faces challenges such as adulteration, mislabelling, and the diverse

impacts of irrigation practices on yield and quality. These issues necessitate robust, non-invasive techniques to trace the geographical origin and determine irrigation treatments. Spectroscopy, which analyses material interactions with electromagnetic radiation, offers a solution by examining light spectra. This technique, used to evaluate fruit quality (Lin & Ying, 2009), leaf water content (Rodríguez-Pérez, 2017), and disease assessment (Vélez *et al.*, 2024; Xie *et al.*, 2017), has been applied in the agri-food sector. Hyperspectral Imaging (HSI), combining imaging systems and spectroscopic instruments to provide spatially resolved spectral data, has gained popularity in this field (Wu *et al.*, 2022).

Unlike traditional spectrometers, HSI captures spectral profiles across areas, offering comprehensive characterization of absorption and reflection bands linked to objects and their conditions (Khan *et al.*, 2022). HSI has proven feasible for disease detection, classification, grading, and chemical attribute detection in various agricultural products (B. Wang *et al.*, 2023). By capturing and analysing images across a broad spectrum of wavelengths, HSI systematically detects nuances in grains, fruits, vegetables, and meats (Zhu *et al.*, 2020). Over the past two decades, HSI has shown promise in measuring quality and protecting horticultural and agricultural products, evolving from remote sensing, computer vision, and point spectroscopy to provide superior defect and contamination detection (Sethy *et al.*, 2022). These spectral signatures are crucial for acquiring agricultural information and detecting quality attributes of products like pistachio nuts (C. Wang *et al.*, 2021). The post-harvest phase, critical for biosecurity, diagnostics, and quality assessment, significantly impacts commercial value and consumer acceptance (Palumbo *et al.*, 2022). HSI contains hundreds of spectral bands, unlike RGB images with three colour channels. Despite the complexity of analysing this data, its potential is undeniable, with new techniques continually evolving (L. Wang & Zhao, 2016). Machine Learning (ML) has enhanced HSI applications for non-destructive, real-time food quality and safety assessments, from sorting to sales (Kang *et al.*, 2022). Integrating HSI with ML has revolutionized non-destructive testing in agriculture and food quality assessment. ML has enabled precise pistachio mass estimation (Saglam & Cetin, 2022), damage detection in mango using NIR hyperspectral images (Vélez Rivera *et al.*, 2014), accurate prediction of apple quality parameters (Çetin *et al.*, 2022), and mango ripeness estimation via field hyperspectral imaging and ML (Gutiérrez *et al.*, 2019). These advances highlight the significant impact of HSI and ML in improving food quality, agri-food production, and safety inspection.

This study explores HSI technology and ML's potential to differentiate between irrigation treatments and the geographical origins of pistachios from two Spanish orchards. Using Python, Scikit libraries, and ML models like PLS-DA, SVM, and XGBoost, the study hypothesizes that irrigation methods and locations significantly affect pistachio yield and commercial quality. HSI images were used to build models for classifying pistachios based on origin and irrigation treatments, enhancing their traceability and authenticity.

2. Materials and Methods

In 2022, a study was conducted in two pistachio orchards in Valladolid, Castilla y León, Spain. These orchards, named "Moraleja de las Panaderas" (M) and "La Seca" (S), hosted pistachio plants from the *Pistacia vera* cv. Kerman variety. These 7-year-old (Moraleja) and 15-year-old (La Seca) plants were grafted onto UCB rootstock, a *P. atlantica* × *P. integerrima* hybrid, and planted in a 7 × 6 m triangular pattern to maximise sunlight and resource use. The male cultivar used was cv. Peter. Standard agricultural practices, including agrochemical applications, were followed to ensure optimal yield. Two irrigation treatments were applied: a high irrigation treatment (H) delivering 50% more water than the control (C). In "La Seca", irrigation from January to October used a computer-controlled drip system, providing 2,750 $m^3\ ha^{-1}$ for the control (SC) and 4,660 $m^3\ ha^{-1}$ for the high irrigation treatment (SH). In "Moraleja", irrigation from May to October provided 844 $m^3\ ha^{-1}$ for the control (MC) and 1,161 $m^3\ ha^{-1}$ for the high treatment (MH). This systematic variation aimed to study the effects of different irrigation levels on pistachio growth and productivity.

By October 2022, twenty trees (five per treatment and location) were harvested. Agronomic and commercial quality metrics were assessed, including yield (kg per tree) and nut size (number per ounce). In addition, percentages of open husk (Split), closed husk (Non-Split) and empty nuts (Blank) were determined from representative subsamples of twenty-five nuts per tree.

Hyperspectral imagery was captured using the SPECIM IQ camera, equipped with a VNIR CMOS sensor, offering a 400-1000 nm spectral range. The camera, controlled via Specim's software, stored data on SD cards and operated on a 5200 mAh Li-Ion battery. This setup facilitated capturing high-quality images under optimal conditions (temperatures between +5°C and +40°C, and up to 95% non-condensing humidity). The collected pistachios were obtained from three bunches per tree across different orientations and heights. Due to tree age differences, some height samples were unobtainable from the Moraleja site. After processing, peeling and drying, a total of 158 images (2,818 pistachio nuts) were captured.

Python 3.9 was used for image processing and model creation alongside libraries like *Pandas, Numpy, Scikit-learn*, and *Scikit-image*. The reflectance of the images was corrected using white and dark references, and Scikit-image's Otsu's binarisation removed the background. The spectra were scatter-corrected using standard normal variate (SNV) before analysis. Hyperspectral data analysis involved extracting the mean spectra of each pistachio and using Machine Learning (ML) models to predict various parameters. The models employed were Partial Least Squares Discriminant Analysis (PLS-DA), Support Vector Machine (SVM), and Extreme Gradient Boosting (XGBoost), trained on an Intel i9 processor with 16 GB of RAM and an NVIDIA GeForce RTX 3070Ti GPU. Model evaluation used metrics like F1 scores, confusion matrices, R^2, Mean Absolute Error (MAE), and Mean Squared Error (MSE). The dataset was split into training (70%) and validation (30%) sets. Scikit-learn's RandomizedsearchCV optimized model parameters using 10-fold cross-validation to achieve high accuracy and low Root Mean Squared Error (RMSE).

3. Results

Origin

The study found notable spectral differences between the two locations, particularly in the Near-Infrared (NIR) region around 970 nm, associated with water content (Büning-Pfaue, 2003). More pronounced differences were observed at wavelengths 675 nm (chlorophyll) and 450 nm (carotenoids) (Wellburn, 1994), especially in the "La Seca" location. The predictive models reflected these spectral variations, with all achieving F1 scores above 94%. The PLS and SVM models performed similarly overall (both with an F1 score of 0.99). However, SVM excelled in predicting "La Seca" pistachios, while PLS was better for "Moraleja" pistachios (Table 1).

Irrigation Treatment

The study also identified spectral differences based on irrigation treatments, especially in the NIR region at 970 nm, linked to water content, and at 480 nm, related to carotenoids. These differences were more noticeable in the "La Seca" location. The predictions reflected these spectral variations with high F1 scores. XGBoost had the lowest performance (F1 score of 0.72), while PLS achieved the highest F1 score of 0.92 (Table 1).

Origin and Irrigation Treatment

Combining origin and irrigation treatment for predictions provided better results than mixing different locations, which could lead to poorer outcomes. Table 1 shows significant differences across the entire wavelength range for the four origin and irrigation treatment combinations. This approach improved classification accuracy, obtaining higher F1 scores. SVM produced the highest F1 score of 0.97, while XGBoost had the lowest at 0.87 (Table 1).

Table 1. Prediction results of the pistachio origin and irrigation treatment models and their interaction classification.

Origin

PLS F1 = 0.99				**XGBoost** F1 = 0.94				**SVM** F1 = 0.99			
		Predicted				Predicted				Predicted	
		La Seca	Moraleja			La Seca	Moraleja			La Seca	Moraleja
Real	La Seca	412	3	Real	La Seca	391	24	Real	La Seca	415	0
	Moraleja	5	428		Moraleja	22	409		Moraleja	7	424

Irrigation treatment

PLS F1 = 0.92				**XGBoost** F1 = 0.72				**SVM** F1 = 0.77			
Class		Predicted		Class		Predicted		Class		Predicted	
		High	Control			High	Control			High	Control
Real	High	259	59	Real	High	170	148	Real	High	254	64
	Control	9	519		Control	93	435		Control	128	400

Origin and irrigation treatment

PLS F1 = 0.95						**XGBoost** F1 = 0.87						**SVM** F1 = 0.97					
Class		Predicted				Class		Predicted				Class		Predicted			
		MH	SH	MC	SC			MH	SH	MC	SC			MH	SH	MC	SC
Real	MH	121	0	0	0	Real	MH	90	17	7	7	Real	MH	120	0	1	0
	SH	0	310	0	0		SH	1	296	9	4		SH	0	308	2	0
	MC	0	2	166	29		MC	1	9	161	26		MC	0	0	189	8
	SC	0	0	10	208		SC	2	5	23	188		SC	0	0	15	203

MH, Moraleja High; **SH,** La Seca High; **MC,** Moraleja High; **SC,** La Seca control

Yield and commercial quality traits predictions.

In pistachio production, yield, split, non-split, blank, and calibre are critical quality factors. PLSR, XGBoost, and SVM regression models were tested to predict these parameters. Accurate yield prediction, crucial for economic planning, showed high R^2 scores of 0.89 for PLS, 0.88 for SVM, and 0.38 for XGBoost. For split pistachios, SVM performed best with an R^2 of 0.58, while PLS and XGBoost had R^2 values of 0.56 and 0.37, respectively. Non-split predictions were lower, with PLS achieving the highest R^2 of 0.37. PLS excelled with an R^2 of 0.71 for blanks, compared to XGBoost's 0.48. Lastly, SVM predicted calibre most accurately with an R^2 of 0.57 (Table 2).

Table 2. Prediction results of the regression models for pistachio yield, split, non-split, blank and calibre.

Model	Yield	**R²**	**MAE**	**MSE**	Calibre	**R²**	**MAE**	**MSE**
PLS		0.89	0.72	0.81		0.54	0.71	0.75
XGBOOST		0.38	1.84	4.57		0.45	0.90	1.21
SVM		0.88	0.72	0.89		0.57	0.63	0.70

Model	Split	**R²**	**MAE**	**MSE**	Non-Split	**R²**	**MAE**	**MSE**	Blank	**R²**	**MAE**	**MSE**
PLS		0.56	6.74	74.15		0.37	5.30	55.53		0.71	5.11	49.56
XGBOOST		0.37	8.96	104.33		0.23	6.13	68.10		0.48	6.92	90.69
SVM		0.58	6.28	70.98		0.27	4.97	64.26		0.67	4.94	57.23

MAE, Mean Absolute Error**; MSE,** Mean Squared Error.

4. Discussion

This study investigates the use of non-invasive techniques, specifically HSI in the 400-1000 nm range, to predict the geographic origin of pistachios and evaluate the impact of different irrigation practices. The research also aims to predict key quality and yield metrics of pistachios. Models using Partial Least Squares (PLS), Support Vector Machine (SVM), and Extreme Gradient Boosting (XGBoost), performed excellently distinguishing pistachios from the La Seca and Moraleja locations, achieving F1 scores above 94%. PLS and SVM models achieved an F1 score of 0.99 for water content and colour pigments, demonstrating precise differentiation based on these spectral characteristics. In predicting geographic origin, the models were inspired by previous research using deep learning techniques, which have also achieved high accuracy in classifying pistachio types (Singh *et al.,* 2022). For instance, the EfficientNet-B3 model successfully identified Iranian pistachio cultivars with an average precision, recall, and F1 score of around 96.7% (Soleimnipour *et al.,* 2022). This demonstrates the strong capability of machine learning models to ensure the traceability and authenticity of agricultural products.

The study also explored the effects of irrigation treatment on pistachio spectral signatures, revealing significant differences, particularly at the 970 nm peak in the Near-Infrared (NIR) region, which is linked to water content (Büning-Pfaue, 2003). The best F1 score for distinguishing between different irrigation treatments was 0.92 with the PLS model. Differences at the 675 nm and 450 nm bands associated with chlorophyll and carotenoids were also noted (Walsh *et al.,* 2020; Wellburn, 1994). Combining geographic origin and irrigation treatment variables improved classification performance, achieving higher F1 scores. The SVM model reached an F1 score of 0.97, demonstrating its effectiveness in this combined approach. Similar results were found in predicting the origin of *Zanthoxylum bungeanum* Maxim with a 97% accuracy (Ke *et al.,* 2020) or in *Jatropha curcas* L. seeds (Gao *et al.,* 2013) with a 94% correct classification. This highlights the subtle impact of both geographical origin and irrigation practices on the spectral signatures of pistachios.

Regression models developed in the study showed high R^2 scores for predicting yield and commercial quality factors. The yield prediction achieved an R^2 of 0.88 with the SVM model, while the prediction of blank quality reached an R^2 of 0.71 with the PLS model. As previous research (Caporaso *et al.,* 2018; Elmasry *et al.,* 2012; Torres-Rodríguez *et al.,* 2022; B. Wang *et al.,* 2023), these models effectively forecast essential agricultural metrics, offering valuable tools for optimizing pistachio production. However, modelling the split and non-split conditions of pistachios proved challenging, with lower R^2 scores highlighting the difficulties in using spectral data for these specific quality attributes.

The study underscores the potential of combining HSI with machine learning in agricultural science, particularly for identifying the unique characteristics of pistachios based on their geographic origin, irrigation methods, and quality markers. Despite challenges in classifying certain features accurately, the findings lay a foundation for future research into the spectral analysis of various pistachio varieties. Integrating these insights with precision agriculture technologies could significantly improve agricultural productivity and management. Advancements in HSI technology, such as its application through drone technology, offer promising avenues for optimizing water usage, enhancing crop quality, and promoting sustainable management practices in pistachio orchards. These developments could lead to more efficient and sustainable

pistachio production, benefiting increased efficiency, improved productivity, and reduced environmental impact.

5. Conclusions

This study demonstrates the effectiveness of Hyperspectral Imaging (HSI) and Machine Learning (ML) in accurately identifying the geographic origin of pistachios and assessing the impact of irrigation practices on their spectral properties. By using advanced models like Partial Least Squares (PLS), Support Vector Machine (SVM), and Extreme Gradient Boosting (XGBoost), high F1 scores above 94% were achieved, particularly in distinguishing pistachios from La Seca and Moraleja. PLS and SVM models excelled with F1 scores of 0.99 in evaluating water content and colour pigments, underscoring HSI's potential in precision agriculture. The study also highlighted distinct spectral signatures from different irrigation treatments, especially the NIR region's notable peak at 970 nm. The PLS model stood out with an F1 score of 0.92, illustrating HSI's role in improving sustainable agricultural resource management. Regression models showed promising results, with an R^2 score of 0.88 for yield predictions using SVM and 0.71 for blank predictions with PLS. Despite challenges in predicting shell split and calibre, the study confirms HSI as a precise tool for identifying pistachio characteristics and forecasting commercial quality and yield, marking a significant advancement in optimizing pistachio production.

Acknowledgements

This work was supported by:

- Project CDTI (IDI-20200822) and by MCIN/AEI/10.13039/501100011033 and European Union «NextGenerationEU»//PRTR, grant number RYC2021-033890. Co-financed by FEADER funds and Junta de Castilla y León (Spain).
- COST Action CA21142 titled "Fruit tree Crop REsponses to Water deficit and decision support Systems applications (FruitCREWS)", https://www.cost.eu/actions/CA21142/.
- Salvador Castillo-Gironés thanks INIA for the FPI-INIA grant number. PRE2020–094491, partially supported by European Union FSE funds.
- Dr. Sergio Vélez's contract has been supported by the Iberdrola Foundation and the European Commission under the Marie Skłodowska-Curie Actions (MSCA)—E4F, part of the Horizon 2020 program (Grant Agreement No 101034297, https://doi.org/10.3030/101034297).

References

1. Büning-Pfaue, H. (2003). Analysis of water in food by near infrared spectroscopy. *Food Chemistry*, *82*(1), 107–115. https://doi.org/10.1016/S0308-8146(02)00583-6
2. Caporaso, N., Whitworth, M. B., & Fisk, I. D. (2018). Near-Infrared spectroscopy and hyperspectral imaging for non-destructive quality assessment of cereal grains. *Applied Spectroscopy Reviews*, *53*(8), 667–687. https://doi.org/10.1080/05704928.2018.1425214
3. CBI - Centre for the Promotion of Imports from developing countries. (2020). *The European market potential for pistachios*. Ministry of Foreign Affairs of the Netherlands. https://www.cbi.eu/market-information/processed-fruit-vegetables-edible-nuts/pistachios/market-entry
4. Çetin, N., Karaman, K., Kavuncuoğlu, E., Yıldırım, B., & Jahanbakhshi, A. (2022). Using hyperspectral imaging technology and machine learning algorithms for assessing internal quality parameters of apple fruits. *Chemometrics and Intelligent Laboratory Systems*, *230*, 104650. https://doi.org/10.1016/j.chemolab.2022.104650
5. Elmasry, G., Kamruzzaman, M., Sun, D.-W., & Allen, P. (2012). Principles and Applications of Hyperspectral Imaging in Quality Evaluation of Agro-Food Products: A Review. *Critical Reviews in Food Science and Nutrition*, *52*(11), 999–1023. https://doi.org/10.1080/10408398.2010.543495
6. FAO. (2024). *FAOSTAT Database*. https://www.fao.org/faostat/en/#data/QCL
7. Gao, J., Li, X., Zhu, F., & He, Y. (2013). Application of hyperspectral imaging technology to discriminate different geographical origins of Jatropha curcas L. seeds. *Computers and Electronics in Agriculture*, *99*, 186–193. https://doi.org/10.1016/j.compag.2013.09.011

8. Gutiérrez, S., Wendel, A., & Underwood, J. (2019). Spectral filter design based on in-field hyperspectral imaging and machine learning for mango ripeness estimation. *Computers and Electronics in Agriculture*, *164*, 104890. https://doi.org/10.1016/j.compag.2019.104890

9. Kang, Z., Zhao, Y., Chen, L., Guo, Y., Mu, Q., & Wang, S. (2022). Advances in Machine Learning and Hyperspectral Imaging in the Food Supply Chain. *Food Engineering Reviews*, *14*(4), 596–616. https://doi.org/10.1007/s12393-022-09322-2

10. Ke, J., Rao, L., Zhou, L., Chen, X., & Zhang, Z. (2020). Non-destructive determination of volatile oil and moisture content and discrimination of geographical origins of Zanthoxylum bungeanum Maxim. By hyperspectral imaging. *Infrared Physics & Technology*, *105*, 103185. https://doi.org/10.1016/j.infrared.2020.103185

11. Khan, A., Vibhute, A. D., Mali, S., & Patil, C. H. (2022). A systematic review on hyperspectral imaging technology with a machine and deep learning methodology for agricultural applications. *Ecological Informatics*, *69*, 101678. https://doi.org/10.1016/j.ecoinf.2022.101678

12. Lin, H., & Ying, Y. (2009). Theory and application of near infrared spectroscopy in assessment of fruit quality: A review. *Sensing and Instrumentation for Food Quality and Safety*, *3*(2), 130–141. https://doi.org/10.1007/s11694-009-9079-z

13. Mandalari, G., Barreca, D., Gervasi, T., Roussell, M. A., Klein, B., Feeney, M. J., & Carughi, A. (2021). Pistachio Nuts (Pistacia vera L.): Production, Nutrients, Bioactives and Novel Health Effects. *Plants*, *11*(1), 18. https://doi.org/10.3390/plants11010018

14. Mir-Makhamad, B., Bjørn, R., Stark, S., & Spengler, R. (2022). Pistachio (Pistacia vera L.) Domestication and Dispersal Out of Central Asia. *Agronomy*, *12*(8), 1758. https://doi.org/10.3390/agronomy12081758

15. Ozkan, I. A., Koklu, M., & Saraçoğlu, R. (2021). Classification of Pistachio Species Using Improved K-NN Classifier. *Progress in Nutrition*, *23*(2), e2021044. https://doi.org/10.23751/pn.v23i2.9686

16. Palumbo, M., Attolico, G., Capozzi, V., Cozzolino, R., Corvino, A., De Chiara, M. L. V., Pace, B., Pelosi, S., Ricci, I., Romaniello, R., & Cefola, M. (2022). Emerging Post-harvest Technologies to Enhance the Shelf-Life of Fruit and Vegetables: An Overview. *Foods*, *11*(23), 3925. https://doi.org/10.3390/foods11233925

17. Rodríguez-Pérez, J. R. (2017). Leaf water content estimation by functional linear regression of field spectroscopy data. *J. R.*, 11.

18. Saglam, C., & Cetin, N. (2022). Prediction of Pistachio (Pistacia vera L.) Mass Based on Shape and Size Attributes by Using Machine Learning Algorithms. *Food Analytical Methods*, *15*(3), 739–750. https://doi.org/10.1007/s12161-021-02154-6

19. Sethy, P. K., Pandey, C., Sahu, Y. K., & Behera, S. K. (2022). Hyperspectral imagery applications for precision agriculture—A systemic survey. *Multimedia Tools and Applications*, *81*(2), 3005–3038. https://doi.org/10.1007/s11042-021-11729-8

20. Singh, D., Taspinar, Y. S., Kursun, R., Cinar, I., Koklu, M., Ozkan, I. A., & Lee, H.-N. (2022). Classification and Analysis of Pistachio Species with Pre-Trained Deep Learning Models. *Electronics*, *11*(7), 981. https://doi.org/10.3390/electronics11070981

21. Torres-Rodríguez, I., Sánchez, M.-T., Entrenas, J.-A., Vega-Castellote, M., Garrido-Varo, A., & Pérez-Marín, D. (2022). Hyperspectral Imaging for the Detection of Bitter Almonds in Sweet Almond Batches. *Applied Sciences*, *12*(10), 4842. https://doi.org/10.3390/app12104842

22. Vélez Rivera, N., Gómez-Sanchis, J., Chanona-Pérez, J., Carrasco, J. J., Millán-Giraldo, M., Lorente, D., Cubero, S., & Blasco, J. (2014). Early detection of mechanical damage in mango using NIR hyperspectral images and machine learning. *Biosystems Engineering*, *122*, 91–98. https://doi.org/10.1016/j.biosystemseng.2014.03.009

23. Vélez, S., Barajas, E., Rubio, J. A., Pereira-Obaya, D., & Rodríguez-Pérez, J. R. (2024). Field-Deployed Spectroscopy from 350 to 2500 nm: A Promising Technique for Early Identification of Powdery Mildew Disease (Erysiphe necator) in Vineyards. *Agronomy*, *14*(3), 634. https://doi.org/10.3390/agronomy14030634

24. Walsh, K. B., Blasco, J., Zude-Sasse, M., & Sun, X. (2020). Visible-NIR' point' spectroscopy in post-harvest fruit and vegetable assessment: The science behind three decades of commercial use. *Post-harvest Biology and Technology*, *168*, 111246. https://doi.org/10.1016/j.postharvbio.2020.111246

25. Wang, B., Sun, J., Xia, L., Liu, J., Wang, Z., Li, P., Guo, Y., & Sun, X. (2023). The Applications of Hyperspectral Imaging Technology for Agricultural Products Quality Analysis: A Review. *Food Reviews International*, *39*(2), 1043–1062. https://doi.org/10.1080/87559129.2021.1929297

26. Wang, C., Liu, B., Liu, L., Zhu, Y., Hou, J., Liu, P., & Li, X. (2021). A review of deep learning used in the hyperspectral image analysis for agriculture. *Artificial Intelligence Review*, *54*(7), 5205–5253. https://doi.org/10.1007/s10462-021-10018-y

27. Wang, L., & Zhao, C. (2016). *Hyperspectral Image Processing*. Springer Berlin Heidelberg. https://doi.org/10.1007/978-3-662-47456-3

28. Wellburn, A. R. (1994). The Spectral Determination of Chlorophylls a and b, as well as Total Carotenoids, Using Various Solvents with Spectrophotometers of Different Resolution. *Journal of Plant Physiology*, *144*(3), 307–313. https://doi.org/10.1016/S0176-1617(11)81192-2

29. Wu, Y., Xu, Z., Yang, W., Ning, Z., & Dong, H. (2022). Review on the Application of Hyperspectral Imaging Technology of the Exposed Cortex in Cerebral Surgery. *Frontiers in Bioengineering and Biotechnology*, *10*, 906728. https://doi.org/10.3389/fbioe.2022.906728

30. Xie, C., Yang, C., & He, Y. (2017). Hyperspectral imaging for classification of healthy and gray mold diseased tomato leaves with different infection severities. *Computers and Electronics in Agriculture*, *135*, 154–162. https://doi.org/10.1016/j.compag.2016.12.015

31. Zhu, M., Huang, D., Hu, X., Tong, W., Han, B., Tian, J., & Luo, H. (2020). Application of hyperspectral technology in detection of agricultural products and food: A Review. *Food Science & Nutrition*, *8*(10), 5206–5214. https://doi.org/10.1002/fsn3.1852

The aquaphotomic approach in the discrimination of the metabolic condition of dairy cows

Simone Giovinazzo [a], Laura Marinoni [b], Tiziana M.P. Cattaneo [b], Carlo Bisaglia [a], Massimo Brambilla [a*]

[a] Research Centre for Engineering and Agro-Food Processing, Council for Agricultural Research and Economics (CREA), Via Milano, 43 – 24047, Treviglio (BG), Italy
[b] Research Centre for Engineering and Agro-Food Processing, Council for Agricultural Research and Economics (CREA), Via G. Venezian, 26 – 20133, Milano, Italy
* Corresponding author. Email: massimo.brambilla@crea.gov.it

Abstract

Modern dairy farming has intensified considerably, and its production model has led to an increase in milk production per cow; however, it has also been associated with an elevated incidence of nutrition-related metabolic disorders, such as ketosis. This condition frequently goes undetected by farmers because it is often not severe enough to show symptoms, but it still impacts animal welfare and productivity. Hence, the significant challenge lies in the timely detection by the farmers.

In-line milk monitoring systems based on NIR spectroscopy offer insights into cows' metabolic conditions resulting from milk composition analysis. However, such instruments may struggle distinguishing between ketotic and healthy animals, especially during subclinical metabolic conditions. In contrast, aquaphotomics can constitute an innovative approach to detect subtle biochemical changes at the onset of the disease. This discipline considers the molecular spectrum of water as a biomarker to point out any biological system's behaviour and functionality. Such a chemometric approach leverages water's ubiquitous presence as a mirror that reflects any system perturbation, representing a promising avenue for enhancing the sustainability of modern dairy production.

A study was conducted on 621 milk spectra from three Italian dairy farms. Milk samples underwent NIR spectroscopy analysis, and the collected data underwent processing using the open-source software Gnu Octave. The developed script enabled the identification of the most significant absorption wavelengths of water for distinguishing between healthy and ketotic cows using multivariate spectral analysis and chemometrics methods (e.g. Quadratic Discriminant Analysis - QDA, and Partial Least Square Regression Analysis - PLSR). Preliminary results from the QDA, utilising only three water wavelengths, showed a 77.7% accuracy rate classification. Meanwhile, the PLSR analysis suggests that there is a significant opportunity for improvement. The aim is to expand the number of samples and farms to create a more robust mathematical model to increase classification accuracy.

Keywords: Livestock Production, Subclinical Ketosis, Diagnostic Methods, Data Processing, Programming Language

1 Introduction

The agri-food supply chain is undergoing a transformation towards increased sustainability: it is necessary to produce more while using fewer resources to meet the growing and changing global population's food demands. In particular, the dairy industry has experienced a significant intensification in its production model in recent years, with global production of cow's milk reaching more than 757 million tons in 2022 (CLAL, 2024). Despite a reduction in the livestock heritage of dairy cattle in highly developed countries such as North America, Europe and Oceania, there has been a notable increase in the average annual milk production per cow, primarily driven by North America. There, milk production per cow reached 10.6 million tonnes in 2022, reflecting a 25% increase compared to the production recorded in 2000 (FAO, 2023). The reasons behind this intensification can be attributed to advancements in technology within the dairy cattle industry through automation, robotics, big data, sensors, artificial intelligence, and significant scientific breakthroughs in genetics (Neethirajan, 2020).

The production scenarios foresee a steady expected increase in the coming years, with annual milk yields potentially doubling in the next 50 years (Britt et al., 2018). However, such a drive for increasingly high-performance production conditions may affect the economic, social, and environmental sustainability of livestock farming, particularly in the case that the welfare and health of the animals are not prioritised. It is a pressing concern that affects both farmers and consumers. A significant aspect arising from the intensification of agricultural practices is the heightened occurrence of metabolic disorders in dairy cattle, such as ketosis. Ketosis is a metabolic disease characterised by elevated levels of ketone bodies in the bloodstream, resulting from alterations in carbohydrate and fatty acid metabolism (Deniz et al., 2020). However, beyond the clinically evident form, dairy cattle may experience a subclinical manifestation of the

disease: this hidden form of ketosis silently compromises animal welfare, productivity, and reproductive performance, exacerbating the economic and sustainability issues faced by the dairy industry (Guliński, 2021).

Conventional veterinary diagnostic methods and sensoristic technologies based on NIR spectroscopy for real-time monitoring of milk composition may have limitations in the early detection of ketosis, following their inability to directly assess metabolic changes at the molecular level, especially during the subclinical phase of the disease. In this context, aquaphotomics emerges as a promising approach to overcome these limitations (Tsenkova, 2005). This scientific discipline focuses on the molecular interactions between water and other constituents, offering a deeper understanding of the status, behaviour, and functionality of a biological system. In particular, the three-dimensional molecular network of hydrogen bonds within water is considerably influenced by the chemical content and the biological and physical conditions of the system. This dynamic equilibrium leads to conformational changes in water molecules, which alters the absorption pattern of water in its near-infrared spectrum, acting as a molecular mirror of matter and energy reflecting the intricate characteristics of a system (Muncan and Tsenkova, 2019). Veterinary diagnostic studies conducted using aquaphotomics for the early identification of mastitis in dairy cattle demonstrate the potential of water as a biomarker responsive to the perturbations induced by the onset of the disease. During the initial stages this metabolic state, the concentration of many analytes varies, resulting in subtle changes that may not be visible when analysing the spectra of those compounds alone. Water amplifies these signals, enhancing their discernibility and facilitating more comprehensive monitoring of the animal's physio-pathological state (Tsenkova and Muncan, 2021). As with spectroscopic analysis methods, chemometrics and pattern classification methods are essential tools in aquaphotomics (Tsenkova et al., 2018).

This study aims to assess the effectiveness of a mathematical model developed in the Gnu Octave programming language for determining the metabolic state of dairy cattle using the spectral pattern of water as a biomarker. This approach proposes innovative monitoring of animals' metabolic performance for the early detection of ketosis in intensive farming.

2 Materials and Methods

2.1 Milk samples

The experimental activity involved three dairy farms located in the Lombardy region (Italy), all equipped with an automated milking system incorporating AfiLab ™ (S.A.E. Afikim, Afikim, Israel) (Leitner et al., 2012), a device for real-time analysis of the qualitative and quantitative characteristics of the milk produced. This NIR device provides accurate information on the fat, protein, lactose concentration, somatic cell counts or electric conductivity for each cow, allowing rigorous daily monitoring of animals. In particular, the fat-protein ratio represents a valuable indicator parameter for a preliminary assessment of the cow's health status: if it is higher than 1.4, it indicates the possibility of subclinical ketosis (Guliński, 2021).

The sampling took place for two years to ensure the representation of different production conditions and cow populations. Each milk sample underwent analysis for its fat-protein ratio, and if higher than 1.4, this was classified as "Ketotic", based on the established criteria. Following the collection and labelling, samples were stored frozen at -18°C until the day before NIR analysis when they were thawed. The samples were then preheated to 40°C in a water bath before being measured with a portable NIR spectrophotometer.

2.2 NIR analysis

NIR spectra were collected in reflectance mode with the MicroNIR ™ OnSite-W (VIAVI Srl, Italy), within the 908 nm to 1676 nm wavelength range (50 scans; 125 reading points). For each sample, spectra were acquired in triplicate, including pure water spectra as control. Before the analysis, the instrument underwent calibration for the black, in the air, and for the white, using the provided standard.

The spectral data obtained were then processed to verify the suitability of the water molecular system in determining the metabolic state of dairy cattle and, in particular, to discriminate between healthy and ketotic cattle.

2.3 Data Processing

The GNU Octave software language program (version 8.4.0 https://www.gnu.org/software/octave/) was used to realise a script for a chemometric model to identify the class of belonging of a given milk sample based on the chemical characteristics of its near-infrared spectrum. The code enables the execution of multivariate spectral analysis and the application of chemometric models to NIR spectra of milk to extract the spectral pattern of water absorption related to the onset of ketosis. Spectral data elaborations included:

- Spectral subtraction of the average spectrum of pure water to isolate the specific spectral characteristics of all the components contained in the milk.
- The second derivative Savitzky-Golay smoothing (second-order polynomial fit, 21 points), to improve the spectral resolution, bringing to evidence information partially obscured by background noise.
- Multiplicative Scatter Correction and Normalisation to reduce the physical variability between samples caused by the scattering of incident light.
- Aquagrams graphic representation to visualise and interpret the interactions between water molecules and other analytes.
- Principal Component Analysis (PCA) to investigate the variables most involved in the differentiation of samples and to uncover complex relationships between spectral variables.
- Quadratic Discriminant Analysis (QDA) to maximise the separation between classes in the spectral data.
- Partial Least Squares Regression (PLSR) to establish quantitative relationships between spectral data and the variable of interest (i.e. the fat-protein ratio).

The identification of the most representative wavelengths for the aquagrams construction was carried out by subtracting the average value of the two normalised matrices obtained from *ketotic* and *healthy* groups of samples. The common wavelengths between the two groups for which the normalised absorbances differed the most were then selected.

PCA was carried out using a limited portion of the spectrum, with wavelengths between 1310 and 1589 nm, aligning with the intervals defined by the Water Matrix Coordinates (WAMACS) (Tsenkova, 2009). This range corresponds to the absorption coordinates of the water matrix, with specific molecular conformation and distinctive spectral properties, as Vitalis et al. (2023) pointed out. These bands typically exhibit activation in response to any perturbations of the system. From the analysis of the loadings on the three principal components, it was possible to identify the top ten water wavelengths most involved in the differentiation between the two classes.

QDA was performed to identify the combination of three water wavelengths (among those resulting from the PCA) and the lactation number of the animals, that maximises the separation of the two groups of samples. The dataset was split into a calibration set, containing 60% of the observations chosen randomly, and a validation set, with the remaining 40%. For each set, confusion matrices were constructed to evaluate the performance of the classification models, and to verify its ability to distinguish between the two categories of samples.

PLSR was employed to establish a predictive model relating the fat-protein ratio of the milk samples to the selected water wavelengths in the interval between 1310 and 1589 nm. The model performance was assessed using metrics such as coefficient of determination (R^2), root mean square error (RMSE), per cent bias (PBIAS), root mean square residual (RSR) and correlation index (r) on both the calibration and validation datasets (Moriasi et al., 2007).

3 Results and Discussion

A total of 207 milk samples were collected from the farms participating in the study. Among these, 146 samples were from “Agricultural Society Della Bona Faustino” (Gambara, BS, Italy), 45 from “Agricultural Society Brocajoli Dr Massimo Luigi” (Marcaria, MN, Italy) and 16 from “Agricultural Society Our Dream’s Farm Colombo Matteo” (Brignano Gera d’Adda, BG, Italy). For each sample, three spectra were obtained, resulting in a total of 621 spectra, with 54 classified into the ketotic group (prevalence 8.7%). The observed incidence of ketosis is lower compared to reported Italian literature data, which suggests a prevalence of 23% (Bellato et al., 2023).

Figure 1 shows the raw spectra of the milk samples collected from the three farms, with the pure water spectra as control.

The raw milk spectra in the NIR region revealed the presence of specific absorption peaks at 970, 1190, and 1450 nm, associated with water absorption bands and indicative of the molecular vibration modes of water molecules present in milk samples. For the purposes of the multivariate spectral analysis, preprocessing methods were therefore applied to enhance the quality of the data. These steps included Spectral Subtraction (Fig. 2a), Second derivative Savitzky-Golay Smoothing (Fig. 2b), Multiplicative Scatter Correction and Normalisation (Fig. 2c).

The visualisation of the role of water in discriminating the metabolic conditions of dairy cattle has required the construction of aquagrams, which are graphical representations of water absorbance spectral patterns reporting the normalised absorbance within the WAMACS. The absorption bands detected in the normalised spectra are: 1323, 1329, 1335, 1391, 1397, 1404, 1410, 1515, 1521 and 1527 nm. These wavelengths correspond to a specific structural characterisation of water molecules. In particular, 1323, 1329 and 1335 nm are water bands indicating the presence of water molecules bound to protons, forming small clusters: a possible explanation is that the onset of ketosis alters the acid-base balance of the organism because acetone, acetoacetate and beta-hydroxybutyrate, the main ketone bodies released in the blood, are weak acids. The 1391 nm band is associated with trapped water, which are molecules with

limited mobility following the formation of a three-dimensional network of water hydrogen bonds that restrict their movement: also, in this case, this could be related to water trapped within the solvation shells. The 1397, 1404 and 1410 nm are bands correlated with free water molecules without hydrogen bonds or trapped water: during ketosis, there is a significant mobilisation of lipids, which are non-polar compounds that do not interact with water, thus increasing the fraction of free water in the system. The 1515 nm corresponds to water strongly bound: the presence of ketone bodies facilitates strong hydrogen bonding with water molecules due to the presence of carbonyl functional groups (C=O) and hydroxyl groups (OH), which can act as donors or hydrogen bond acceptors. Similarly, 1521 and 1527 nm correspond to hydrogen-bonded hydroxyl groups: the propensity of ketone bodies to form hydrogen bonds with water could explain the activation of these wavelengths during ketosis.

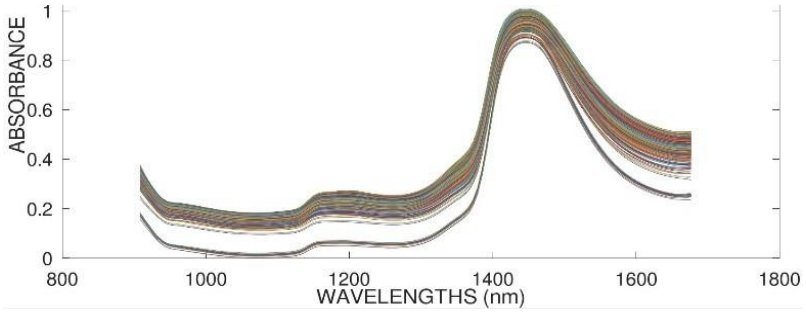

Figure 1 Raw milk spectra, where each colour represents a NIR acquisition. Observations with lower absorbance values correspond to water pure spectra.

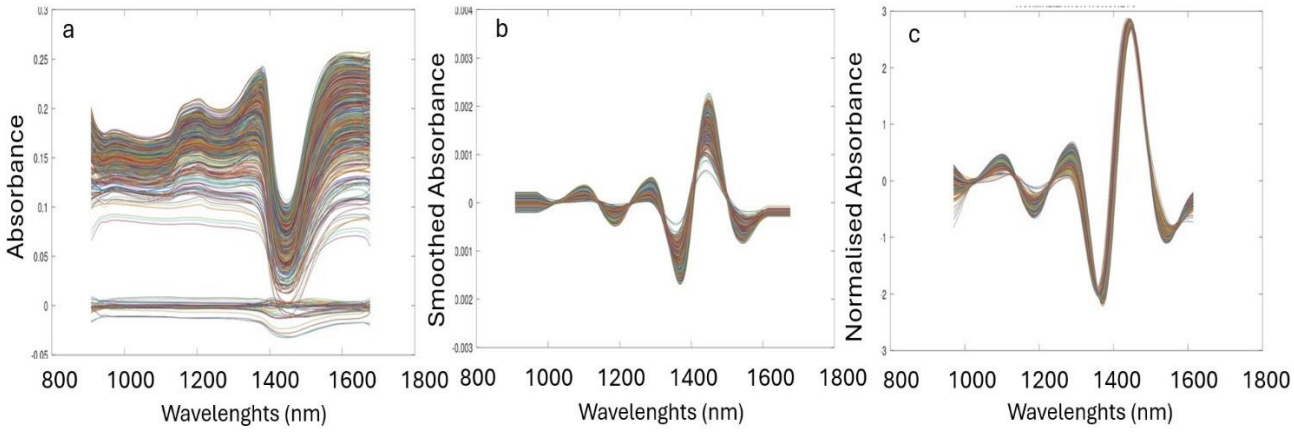

Figure 2 Spectral preprocessing methods; spectral subtraction of the average spectrum of pure water (a), second derivative Savitzky-Golay smoothing (b) and normalisation of samples (c).

Figure 3 reports the aquagrams resulting from the samples of the three farms analysed, highlighting differences among ketosis and healthy conditions.

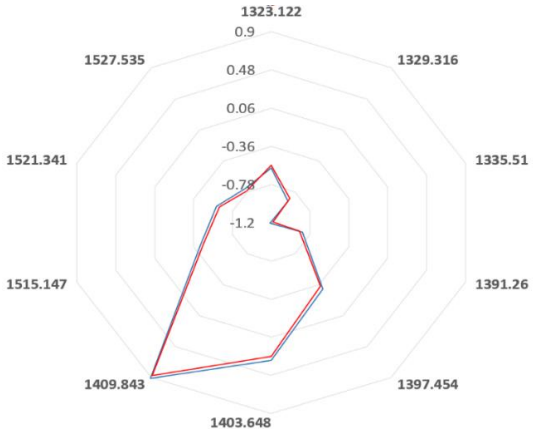

Figure 3 Aquagrams of milk samples from the three dairy farms. Red line for animals with the ketosis condition and blue line for healthy cattle.

The PCA was conducted utilising three principal components. The score plot (Fig. 4a) using PC1 (81.8% of cumulative explained variance) vs. PC2 (94.8% of cumulative explained variance) vs. PC3 (99.4% of cumulative explained variance) revealed that ketotic samples tend to separate primarily along the second and third principal components, although this separation is not as pronounced. The loading plot (Fig. 4b) indicates that this separation is mainly attributed to 10 specific wavelengths: 1323, 1329, 1335, 1404, 1410, 1416, 1422, 1497, 1503 and 1509 nm.

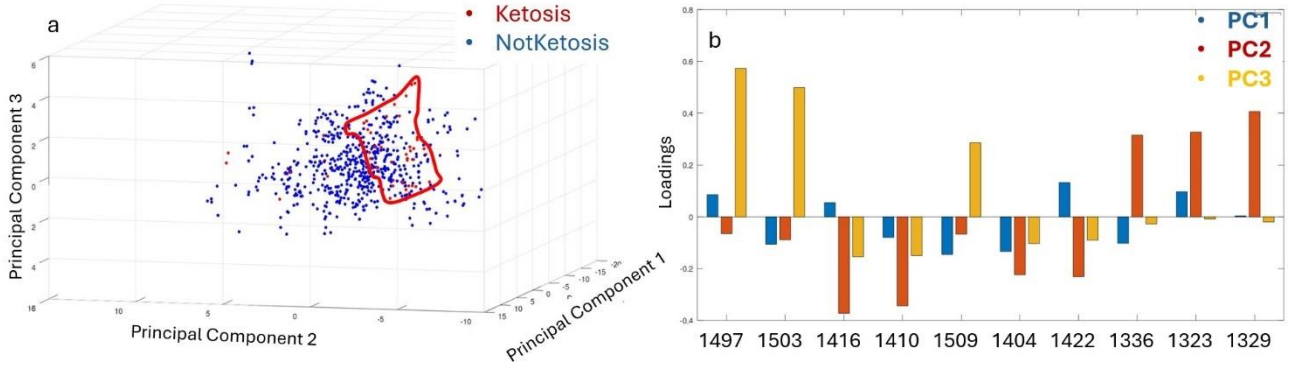

Figure 4 Score (a) and Loading (b) plots of milk samples from the three dairy farms. Red dots for animals with the ketosis condition and blue dots for healthy cattle. The majority of ketotic samples identified by PCA are enclosed within the red line.

The 10 water absorption bands extracted from PCA nearly overlapping with those identified during the construction of the aquagram. Despite the lack of clear differentiation evident in both the aquagram and PCA score plot between the two sample classes, this overlap emphasises the importance of these wavelengths in distinguishing between healthy and ketotic cattle. Table 1 summarises the structural characterisation and the assignment of water absorption bands found to be activated during the preliminary processing of the spectra and with the execution of PCA.

Table 1 Coordinates of the molecular matrix of water with their spectroscopic and structural characterisation (Tsenkova, 2009; Kojić et al., 2014; Vitalis et al., 2023).

Wavelengths (nm)	Assignation
1323-1329-1335	Free OH in small proton hydrates $H^+(H_2O)_5$, $H^+(H_2O)_2$
1391-1397	Trapped water and H_2O symmetric stretch in proton hydrate $H+(H_2O)_4$
1404-1410-1416	Free water molecules without hydrogen bonds (S0) and free OH^- or trapped water
1422	Water hydration, H-OH and O-O bond
1497	Water molecules with four hydrogen bonds (S4)
1503-1509-1515	ν1, ν2 and strongly bound water
1521-1527	Hydrogen-bonded hydroxyl groups, the first overtone of hydrogen-bonded O-H stretching and bending fundamental

The QDA was implemented on the calibration set of the three dairy farms participating in the study (32 milk spectra from ketotic group, 340 from healthy group). The code developed with GNU Octave randomly selects samples for splitting between calibration and validation sets for each run. Overall, the accuracy achieved is high indicating the adequacy of the mathematical model built on the theoretical principles of aquaphotomics. However, the results obtained underscore also the limitations of the QDA model, which is not immune to misclassifications. Specifically, the presence of a significant number of non-ketotic samples erroneously classified as ketotic (22.9%) suggests a similar response of the water bands utilised in the model to both samples' classes. While the use of only three water bands highlights the model's robustness, it also indicates challenges for broader practical applications, such as in a milking parlour setting. Expanding the spectral range by incorporating additional wavelengths could potentially address this limitation, offering improved discrimination between ketotic and non-ketotic samples, reducing in this way the need for extensive verification and analysis by the farmer.

Excellent results were also achieved for the validation set (22 milk spectra from ketotic group, 227 from healthy group), using the combination of wavelengths defined by the calibration set. The results of QDA are summarised in Table 2.

Table 2 Confusion matrices for the calibration and for the validation sets

Calibration Set	Ketosis	Not Ketosis	**Validation Set**	Ketosis	Not Ketosis
Ketosis	27	78	Ketosis	18	55
Not Ketosis	5	262	Not Ketosis	4	172
Total	32	340	Total	22	227
Correctly Classified	27	262	Correctly Classified	18	172
Total Accuracy	77.69%		Total Accuracy	76.31%	
Ketosis Accuracy	84.38%		Ketosis Accuracy	81.82%	
Not Ketosis Accuracy	77.06%		Not Ketosis Accuracy	75.77%	

The PLSR model was finally developed to predict the fat-protein ratio from the absorbance measured for each wavelength defined by the Water Matrix Coordinates interval. Considering 15 components, the predictive model was applied using the same calibration and validation sets utilised with the QDA. Figure 5 shows the scatter plot of the model, applied to the calibration (a) and to the validation (b) sets, with the resulting metrics obtained.

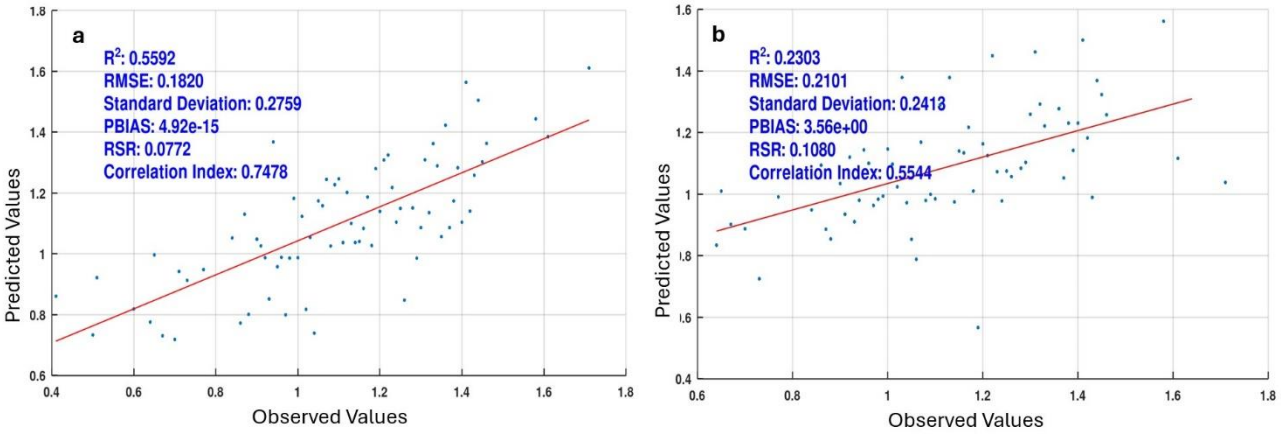

Figure 5 Scatter Plot of the PLSR on the calibration (a) and validation (b) sets. In the legend the resulting metrics, including R^2, RMSE, Standard Deviation, PBIAS, RSR and the correlation index.

The resulting metrics suggested that the PLSR model, utilising wavelengths based on water matrix coordinates, has achieved satisfactory performance in predicting the fat-protein ratio for the calibration set. In particular, the coefficient of determination exceeds 0.5, indicating the ability of the model to describe a significant portion of the variation in the observed data. Moreover, the RMSE value is lower than the observed values' standard deviation, suggesting that the model's predictions exhibit a higher precision compared to the inherent variability present in the observed data. The PBIAS is close to zero, so the tendency to overestimate or underestimate the observed values is minimal, while the low RSR values suggest that the model's predictions are precise compared to the variability in the observed values. The correlation index, in addition, indicate a strong linear relationship between the predicted and observed values, further supporting the reliability of the PLSR model in predicting the fat-protein ratio for the analysed samples. However, in the validation set, results are not as satisfactory as in the calibration set especially regarding the values of R^2 and the correlation index.

4 Conclusions

The script code developed for discriminating between a healthy and diseased system, even in the subclinical phase of ketosis, could be preliminary for the realisation of an innovative sensor tool for real-time and non-invasive monitoring of milk's qualitative and quantitative characteristics in the milking parlour. The aim is to assist farmers in monitoring the health status of individual animals, facilitating timely health treatment. Nevertheless, data processing is still in early

stages: the aim is to expand the sample size for analysis and the number of farms to create a more robust mathematical model capable of accurately classifying samples based on their characteristic spectra.

The aquaphotomics approach was suitable for studying dairy cattle's metabolic conditions, as demonstrated by the results obtained from PCA, QDA, and PLSR. However, there is a need for future studies focusing on analysing samples from each farm separately, allowing for the independent examination of both ketotic and non-ketotic samples within each farm to verify any potential improvement in accuracy.

Acknowledgements

The authors acknowledge the Department of Economics, Engineering, Society and Business Organization (DEIM) in cooperation with the Department of Agriculture and Forestry Sciences (DAFNE) of the University of Tuscia for this work carried out as part of the PhD in Engineering for Energy and Environment – Biosystems and Environment.
Acknowledgements are also extended to *"Agricultural Society Della Bona Faustino", "Agricultural Society Brocajoli Dr Massimo Luigi"* and *"Agricultural Society Our Dream' S Farm Colombo Matteo"* for their cooperation and support in the realisation of this study.

References

Bellato, A., A. Tondo, L. Dellepiane, A. Dondo, A. Mannelli, S. Bergagna, 2023. Estimates of dairy herd health indicators of mastitis, ketosis, inter-calving interval, and fresh cow replacement in the Piedmont region, Italy. Preventive Veterinary Medicine. 212, 105834. https://doi.org/10.1016/j.prevetmed.2022.105834

Britt, J.H., R.A. Cushman, C.D. Dechow, H. Dobson, P. Humblot, M.F. Hutjens, G.A. Jones, P.S. Ruegg, I.M. Sheldon, J.S. Stevenson, 2018. Invited review: Learning from the future—A vision for dairy farms and cows in 2067. Journal of Dairy Science. 101(5), 3722–3741. https://doi.org/10.3168/JDS.2017-14025

CLAL, 2024. World: Milk production and population. https://www.clal.it/en/?section=produzioni_popolazione_world

Deniz, A., K. Aksoy, M. Metin, 2020. Transition period and subclinical ketosis in dairy cattle: Association with milk production, metabolic and reproductive disorders and economic aspects. Medycyna Weterynaryjna. 76(9), 495–502. https://doi.org/10.21521/MW.6427

Food and Agriculture Organization of the United Nations – with major processing by Our World in Data, 2023. Milk yield per animal. https://ourworldindata.org/grapher/milk-yields-per-animal

Guliński, P., 2021. Ketone bodies – causes and effects of their increased presence in cows' body fluids: A review. Veterinary World. 14(6), 1492. https://doi.org/10.14202/VETWORLD.2021.1492-1503

Kojić, D., R. Tsenkova, K. Tomobe, K. Yasuoka, M. Yasui, 2014. Water confined in the local field of ions. ChemPhysChem. 15 (18):4077-4086. doi:10.1002/cphc.201402381

Leitner, G., U. Merin, L. Lemberskiy-Kuzin, D. Bezman, G. Katz, 2012. Realtime visual/near-infrared analysis of milk-clotting parameters for industrial applications. Animal. 6, 1170-1177. https://doi.org/10.1017/S175173111100245X

Moriasi, D.N., J.G. Arnold, M.W. Van Liew, R.L. Bingner, R.D. Harmel, T.L. Veith, 2007. Model Evaluation Guidelines for Systematic Quantification of Accuracy in Watershed Simulations. Transactions of the ASABE. 50(3), 885–900. https://doi.org/10.13031/2013.23153

Muncan, J., R. Tsenkova, 2019. Aquaphotomics—From Innovative Knowledge to Integrative Platform in Science and Technology. Molecules. 24, 2742. https://doi.org/10.3390/molecules24152742

Neethirajan, S., 2020. The role of sensors, big data and machine learning in modern animal farming. Sensing and Bio-Sensing Research. 29, 100367. https://doi.org/10.1016/J.SBSR.2020.100367

Tsenkova, R., 2005. Visible-Near Infrared perturbation spectroscopy: Water in Action Seen as Great Source of Information. In *Proceedings of the 12th International Conference on Near-infrared Spectroscopy.* Auckland, New Zealand, April 9–15. 514–519.

Tsenkova, R., 2009. Introduction aquaphotomics: Dynamic spectroscopy of aqueous and biological systems describes peculiarities of water. Journal of Near Infrared Spectroscopy. Vol. 17, Issue 6, pp. 303–314. https://doi.org/10.1255/jnirs.869

Tsenkova, R., J.S. Muncan, B. Pollner, Z. Kovacs, 2018. Essentials of aquaphotomics and its chemometrics approaches. Frontiers in Chemistry. 6(AUG). https://doi.org/10.3389/fchem.2018.00363

Tsenkova, R., J.S. Muncan, 2021. Aquaphotomics for Bio-diagnostics in Dairy. Applications of Near-Infrared Spectroscopy. Springer Nature Singapore. 328 p.

Vitalis, F., J.S. Muncan, S. Anantawittayanon, Z. Kovacs, R. Tsenkova, 2023. Aquaphotomics Monitoring of Lettuce Freshness during Cold Storage. Foods. 12(2). https://doi.org/10.3390/foods12020258

Multispectral Imaging (MSI) application for food safety and quality evaluation: A mini review

Marianna I. Kotzabasaki[a*], Dimitris Giannopoulos[a], Chrysanthos Maraveas[a] and Thomas Bartzanas[a]

[a]Farm Structures Lab., Department of Natural Resources and Agricultural Engineering, Agricultural University of Athens, 11855 Athens, Greece

* Corresponding author. Email: mariannakotz@aua.gr

Abstract

Food producers must ensure the quality of their products at all stages of production. Food contamination can occur at several stages of the processing chain, posing a health risk. Control is necessary to assure quality. Many use machine vision for this task, but only a few employs multispectral cameras. Multispectral imaging (MSI) is a non-destructive sensing technique that can be used to evaluate the quality and safety of food products. It involves capturing images of food products at different optical wavelengths, which can reveal information about the chemical composition, structure, and other properties of the food. This technique can be used to detect defects, such as bruises or insect damage, in fruits and vegetables. It can also be used to identify contaminants, such as bacteria or foreign objects, in food products. Multispectral imaging has the potential to improve food safety and quality by providing more accurate and efficient methods for inspection and quality control. This review paper explores the principles, applications, challenges, and future perspectives of multispectral imaging in the context of food safety and quality assessment, proposing potential avenues for future research and development. Through a comprehensive examination of multispectral imaging applications, this review underscores its significance in advancing food safety and quality evaluation practices, while also highlighting the need for continued innovation and exploration in this rapidly evolving field.

Keywords: Multispectral imaging (MSI), Non-destructive, Imaging, Spectroscopy, Food quality & safety

1. Introduction

Food safety and quality assurance are paramount concerns for food producers worldwide, necessitating rigorous measures to mitigate risks associated with contamination throughout the production process. Contamination incidents can occur at various stages of the food processing chain, posing significant health hazards and economic consequences. To uphold stringent quality standards and ensure consumer well-being, effective control mechanisms are imperative (Gemeda et al., 2023).

While traditional approaches to quality control often rely on visual inspection or machine vision systems, recent advancements in sensing technology have introduced novel methods for enhancing inspection accuracy and efficiency (Ali et al., 2021). One such technology gaining traction in the food industry is multispectral imaging, offering a non-destructive means of assessing food quality and safety (Liu et al., 2023).

Multispectral imaging (MSI) involves the acquisition of images across multiple wavelengths of light, providing valuable insights into the chemical composition, structural integrity, and other intrinsic characteristics of food products (Patel et al., 2024). This technique enables the detection of defects such as bruises or insect damage in fruits and vegetables, as well as the identification of contaminants like bacteria or foreign objects in food matrices.

(Ropodi et al., 2017) emphasized the potential of MSI as a non-invasive rapid method for monitoring the quality, safety, and authenticity of foods, particularly meat products. The study highlighted the importance of hyperspectral and multispectral imaging in ensuring food quality standards. In a study by (Fan & Su, 2022), the authors explored the applications of fluorescence spectroscopy, RGB, and multispectral imaging for quality determinations of white meat products, demonstrating the effectiveness of these analytical methods for non-destructive quality assessment. Additionally, Wang et al. (2018) provided an overview of emerging spectroscopic and spectral imaging techniques for the rapid detection of microorganisms in food,

highlighting the potential of MSI in ensuring food safety. In another study researchers explored the potential of imaging spectroscopy, including MSI, for determining the quality parameters of potatoes and sweet potatoes, highlighting the non-destructive classification capabilities of this technology (Su & Xue, 2021).

In light of these developments, this review paper aims to explore the principles, applications, challenges, and future perspectives of MSI in the context of food safety and quality evaluation. By synthesizing existing literature and highlighting emerging trends, this review underscores the significance of MSI in advancing food safety and quality assurance practices, showcasing its potential as a valuable tool for ensuring the integrity of food products.

2. Multispectral imaging technology (MSI)

MSI technology (**Figure 1**) involves capturing images across multiple wavelengths of light, providing insights into the chemical composition, structural integrity, and other intrinsic characteristics of food products (Giannoni et al, 2018). Unlike traditional imaging methods, which capture images in a single wavelength, multispectral imaging offers a more comprehensive understanding of food properties by analyzing data from various wavelengths within the electromagnetic spectrum (Tang et al., 2022).

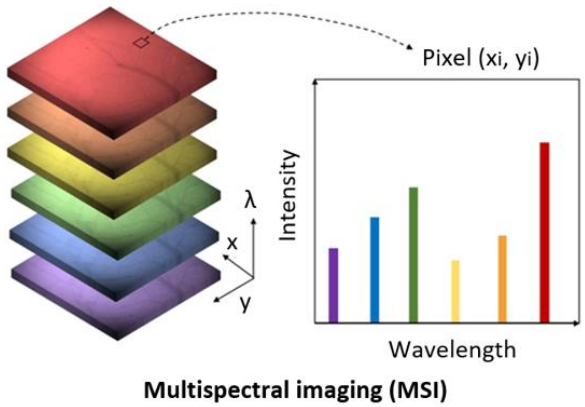

Figure 1. Multispectral imaging (MSI) is optical spectroscopy imaging technique. Discrete and discontinuous portions of the spectral range are considered (Giannoni et al., 2018).

This technique facilitates the detection of defects such as bruises or insect damage in fruits and vegetables, as well as the identification of contaminants like bacteria or foreign objects in food matrices (Wang et al., 2018). By analyzing the spectral signatures of food samples, MSI can reveal subtle differences indicative of quality attributes or potential safety hazards (Liu et al., 2023).

In the realm of food evaluation, MSI offers several advantages over traditional methods. One key advantage is the non-destructive and rapid assessment of food quality and safety, enabling repeated measurements without compromising food integrity. This makes this method suitable for real-time quality control and inspection applications in the food industry, where rapid and accurate assessment of product quality is essential. By analyzing the spectral signatures of food items, MSI can detect defects, assess ripeness, and identify contaminants without altering the physical properties of the samples (ElMasry et al., 2019). This capability is particularly valuable in postharvest applications, such as evaluating chilling injury in mangoes, where MSI has been successfully employed (Hu et al., 2020).

The key components of multispectral imaging systems used in food industry applications typically include sensors capable of capturing images at multiple wavelengths, data processing units for spectral analysis, and software for image interpretation and feature extraction (**Figure 2**) (ElMasry et al., 2019). These systems are designed to acquire spatio-spectral data across a wide range of the electromagnetic spectrum, allowing for detailed characterization of food products (ElMasry et al., 2019). Additionally, advancements in MSI technology have facilitated its integration with other techniques like chemometric analysis and artificial intelligence (AI), enhancing its utility in food quality control and seed science research (ElMasry et al., 2019).

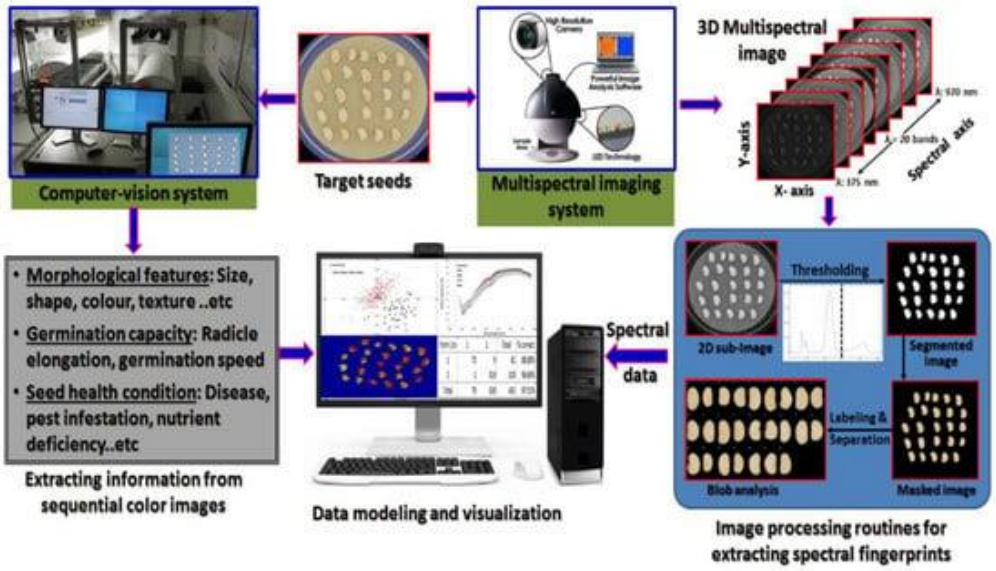

Figure 2. Schematic representation of a computer-aided image analysis system for seed quality evaluation based on computer-vision and multispectral imaging techniques (ElMasry et al., 2019).

In summary, MSI technology offers a powerful tool for non-destructive evaluation of food quality and safety, providing valuable insights into product characteristics and enabling timely detection of defects or contaminants. Its versatility, coupled with ongoing technological advancements, holds significant promise for revolutionizing food inspection and quality assurance practices in the food industry.

3. Applications of MSI technology in Food Safety

3.1 The role of MSI in detecting microbial contamination in food products

The role of MSI in detecting microbial contamination in food products is crucial for ensuring food safety and quality. This technology has emerged as a powerful tool in the food industry for detecting various types of contaminants, including microbial, chemical, and physical impurities (Soni et al., 2022). MSI allows for nondestructive and robust detection of foreign particles in food, aiding in the identification of microbial contaminants that can pose serious health risks to consumers (Mantilla et al., 2017).

Microbial contamination in food products is a significant concern due to its potential to cause foodborne illnesses and spoilage. Detecting microorganisms at low levels of contamination and identifying biofilm growth spots are crucial for maintaining food safety standards (Lorenzo et al., 2020). Biofilm formation, a common challenge in the food industry, can lead to food contamination incidents, emphasizing the importance of effective detection and prevention strategies (Dehkordi et al., 2023).

Efficient process controls and robust food safety management systems are essential for reducing microbial contamination and enhancing food security (El-Khishin et al., 2017). Microbial contamination typically occurs at various stages, from production to consumption, highlighting the need for preventive measures and early detection methods in the food industry (Gholami-Shabani et al., 2023). The presence of microbial contaminants in food products can result in foodborne diseases and spoilage, underscoring the importance of stringent quality control measures (Bintsis, 2018).

In conclusion, the integration of MSI technologies, plays a crucial role in detecting microbial contamination in food products. By leveraging advanced imaging techniques and effective management practices, the food industry can enhance food safety, minimize contamination risks, and safeguard consumer health.

3.2 The role of MSI in identifying physical contaminants (foreign objects or defects) in food items

The utilization of MSI in the food industry is crucial for identifying physical contaminants in food items, ensuring food safety and quality control. MSI technology is increasingly used to detect and classify physical contaminants in food products by capturing images at various wavelengths across the electromagnetic spectrum. This enables the differentiation of materials based on their spectral signatures, facilitating the identification of foreign objects or defects that may compromise the safety and quality of food items (Nguyen et al., 2021).

X-ray inspection systems are commonly used in the food industry to detect physical contaminants in packaged food products, thereby maintaining a high level of food safety for consumers (Nguyen et al., 2021). Furthermore, the development of handheld multispectral fluorescence imaging systems has provided a means to detect and disinfect surface contamination, addressing concerns related to food safety and contamination for food distributors, restaurant owners, and caterers (Sueker et al., 2021).

Physical contaminants can enter the food supply chain through various channels, such as equipment breakdowns, incorrect handling practices, or foreign items in raw materials. Detecting and mitigating physical hazards in food processing require risk assessment and preventive strategies to uphold the safety of food products and prevent potential health risks to consumers (Onyeaka, 2023).

In summary, the application of MSI technology in the food industry is essential for identifying physical contaminants in food items, thereby enhancing food safety, quality control, and consumer protection. Through the implementation of advanced imaging techniques and preventive measures, the food industry can effectively detect and mitigate physical hazards, ensuring the delivery of safe and high-quality food products to consumers.

3.3 Case studies of MSI used for food safety purposes

3.3.1 Detection of Contaminants in Meat Products

The objective of the study of Ye et al. (2016) was to evaluate the effectiveness of MSI in detecting contaminants in meat products. Researchers utilized MSI to capture images of chicken meat samples at various wavelengths, analyzing the spectral data to identify contaminants such as bacterial pathogens and foreign objects. The findings demonstrated that MSI could accurately detect contaminants in chicken meat products, distinguishing between safe and contaminated areas based on their spectral signatures. This method proved to be faster and more reliable than traditional microbiological testing methods.

3.3.2 Quality Assessment of Fruits and Vegetables

The objective of the study of Lorente et al. (2012) was to assess the quality of fruits and vegetables using MSI. Researchers employed MSI to capture images of apples and tomatoes at different wavelengths, analyzing the spectral data to detect defects such as bruises, ripeness levels, and insect damage. The findings demonstrated that MSI was effective in identifying various quality attributes of the fruits and vegetables, detecting bruises and assessing ripeness levels, thereby providing a non-destructive method for real-time quality assessment.

3.3.3 Detection of Mycotoxins in Grains

The objective of the study of Shi et al. (2020) was to detect mycotoxins in grains using MSI. Researchers imaged grain samples at various wavelengths with MSI and processed the spectral data to identify the presence of mycotoxins, which are harmful fungal metabolites. The findings demonstrated that MSI successfully detected mycotoxins in the grain samples, providing a rapid and non-destructive method for mycotoxin screening and improving the efficiency of detection compared to traditional chemical analyses.

3.3.4 Monitoring Fish Freshness

The objective of the study of Cheng et al. (2014) was to monitor the freshness of fish using MSI. Researchers used MSI to capture images of fish samples over different storage periods, analyzing the spectral data to monitor changes in freshness. The findings demonstrated that MSI effectively tracked the freshness of the fish, identifying spectral changes associated with spoilage, and provided a non-destructive and rapid assessment tool for determining fish quality during storage.

3.3.5 Detecting Adulteration in Dairy Products

The objective of the study of Munir et al. (2018) was to detect adulteration in dairy products using MSI. Researchers imaged milk samples containing various adulterants (e.g., water, urea, starch) with MSI and analyzed the spectral data to identify and quantify the adulterants. The findings demonstrated that MSI accurately detected and quantified the adulterants in milk samples, providing a non-destructive and efficient method for ensuring the purity and safety of dairy products.

Overall, these case studies and examples illustrate the diverse applications of MSI in enhancing food safety and quality assessment across a range of food products, from meat and dairy to fruits, vegetables, grains, and seafood. The successful utilization of multispectral imaging in these contexts underscores its importance in safeguarding food quality and ensuring consumer protection.

4. Applications of MSI technology in Food Quality Evaluation

4.1 Use of MSI technology for assessing various quality parameters in food products, such as color, texture, and ripeness

MSI is a versatile and powerful tool for assessing various quality parameters in food products, such as color, texture, and ripeness. By providing detailed and accurate information through non-destructive means, MSI enhances the ability to ensure food safety and quality, ultimately benefiting both producers and consumers.

Color is a primary quality attribute influencing consumer preference and perception of freshness in food products. MSI can measure color more accurately than conventional imaging by analyzing specific wavelengths associated with the food's color characteristics. MSI captures images at multiple spectral bands across the visible spectrum. Each band provides specific information about the reflectance or absorbance of light at that wavelength. For example, in apples, MSI can detect slight variations in color that indicate ripeness or the presence of bruises. By analyzing reflectance data, it is possible to create detailed color maps that highlight even subtle color differences not visible to the human eye (Lorente et al., 2012).

Texture is another vital quality parameter that impacts the sensory experience of food products. MSI can assess texture by analyzing the surface and subsurface properties of food items. MSI captures images at different wavelengths that penetrate the food surface to varying depths. This allows for the detection of structural differences beneath the surface. For instance, in meat products, MSI can differentiate between tender and tough regions by analyzing the scattering properties of light. Changes in the microstructure due to factors like fat content and muscle fiber orientation can be detected, providing insights into the texture (s (Kamruzzaman et al., 2012).

Ripeness significantly affects the taste, texture, and overall quality of fruits and vegetables. MSI can assess ripeness by detecting biochemical changes that occur during the ripening process. MSI captures images across various wavelengths, including those outside the visible spectrum (near-infrared and short-wave infrared), which can provide information on the internal chemical composition. For example, in tomatoes, MSI can detect changes in chlorophyll and carotenoid levels, which are indicative of ripening stages. By analyzing these spectral signatures, it is possible to classify fruits according to their ripeness level accurately (Lorente et al., 2012).

4.2 Use of MSI technology for Grading and Sorting Food Items Based on Quality Attributes

MSI has become an invaluable tool in the food industry, particularly for grading and sorting food items based on various predefined quality attributes. The ability to non-destructively assess multiple quality parameters simultaneously makes MSI highly effective for ensuring food quality and safety.

MSI systems can be integrated into automated sorting lines, enabling real-time assessment and sorting of food products. Automated systems equipped with MSI can rapidly process large volumes of food items, increasing efficiency and consistency in grading and sorting. These systems provide objective, quantitative data that enhances the accuracy of grading and sorting processes. The ability to detect subtle variations in quality attributes ensures that only products meeting stringent standards reach the market.

In Kim et al. (2014) study, MSI was used to sort citrus fruits based on quality attributes. Images of citrus fruits were captured at various wavelengths. The spectral data were analyzed to classify the fruits into different grades based on predefined quality criteria. The MSI-based sorting system effectively differentiated between high-quality fruits and those with defects or suboptimal ripeness, improving the overall quality of the sorted batches (Kim et al., 2014).

In conclusion, MSI offers a versatile and efficient approach for grading and sorting food items based on quality attributes such as color, texture, and ripeness. The technology's non-destructive nature, real-time capabilities, and ability to provide detailed spectral information make it a valuable tool for quality assessment in the food industry.

5. Challenges and Future Perspectives

MSI technology, while offering considerable advancements in food safety and quality evaluation, encounters several limitations and challenges that need to be addressed for broader and more effective implementation. One primary challenge is the high cost of MSI systems. Advanced multispectral cameras and associated equipment can be expensive, making it difficult for small to medium-sized food producers to afford them. Additionally, the operational complexity of MSI systems requires specialized training and expertise, which can increase operational costs and limit accessibility. The technology generates large volumes of data, necessitating robust storage solutions and significant computational power for effective data processing and analysis. Developing and refining the complex algorithms needed for accurate data interpretation is resource-intensive and technically demanding, presenting a significant barrier to widespread adoption.

Another significant challenge is the calibration and standardization of MSI systems. Accurate calibration is essential for obtaining consistent and reliable spectral data, but this process can be affected by variations in lighting conditions, sensor sensitivity, and environmental factors. Without standardized protocols for MSI application in food quality assessment, there can be inconsistencies in data interpretation and application across different contexts. Furthermore, MSI is primarily effective for surface-level analysis, which limits its ability to detect internal defects or contaminants that are not visible on the surface of food products. Environmental conditions such as lighting, temperature, and humidity can also impact MSI performance, complicating its use in field conditions. Addressing these challenges requires continuous technological advancements, the development of cost-effective solutions, improved calibration techniques, and the establishment of industry-wide standards. These efforts will enhance the reliability, accessibility, and overall effectiveness of MSI in food safety and quality evaluation.

The future of multispectral imaging (MSI) in food analysis promises exciting advancements that can significantly enhance its capabilities and applications. One potential development is the miniaturization and cost reduction of MSI systems. Advances in sensor technology and manufacturing processes are likely to make MSI equipment more affordable and accessible, even for small and medium-sized food producers. Portable and handheld MSI devices could become more prevalent, enabling on-the-spot quality assessments in various settings, from farms to supermarkets. These portable systems could be integrated with mobile devices, allowing for real-time data processing and analysis through advanced applications.

Another promising area is the integration of MSI with other emerging technologies, such as artificial intelligence (AI) and machine learning. AI can enhance the interpretation of MSI data by automating the detection and classification of defects, contaminants, and quality attributes in food products. Machine learning algorithms can be trained on extensive datasets to improve the accuracy and speed of MSI analyses, making the technology more efficient and reliable. Additionally, combining MSI with other imaging modalities, such as hyperspectral imaging or X-ray imaging, can provide a more comprehensive assessment

of food quality and safety. These hybrid systems can leverage the strengths of each technology to offer detailed information on both surface and internal properties of food items.

Furthermore, advancements in data analysis and computational techniques will play a crucial role in the future of MSI. The development of more sophisticated algorithms and software tools can improve the processing of large volumes of MSI data, enhancing the precision and usability of the results. Cloud-based platforms for MSI data storage and analysis can facilitate collaborative research and the sharing of datasets, accelerating innovation and the development of new applications. Improved calibration methods and the establishment of standardized protocols will ensure consistency and comparability across different MSI systems and applications.

Lastly, the expansion of MSI applications to new areas of food safety and quality assessment is anticipated. For instance, MSI could be used to monitor the freshness and shelf-life of perishable products, detect food fraud and adulteration, and assess nutritional content more accurately. Research into new spectral indices and imaging techniques will continue to uncover novel applications and improve the sensitivity and specificity of MSI for various food quality parameters. As the technology evolves, MSI is expected to become an integral part of the food industry's efforts to ensure high standards of safety and quality, ultimately benefiting both producers and consumers.

6. Conclusions

This review highlights the significant potential of MSI in enhancing food safety and quality control. MSI technology, which involves capturing images at different wavelengths, allows for the non-destructive assessment of food products, providing detailed information about their chemical composition, structure, and properties. MSI can detect surface-level defects, contaminants, and quality attributes such as color, texture, and ripeness. Despite its high cost and operational complexity, advancements in sensor technology, data processing, and machine learning integration are making MSI more accessible and efficient. The review emphasizes the need for standardized calibration protocols and improved environmental robustness to ensure consistent and reliable results. By combining MSI with other imaging modalities and focusing on specific food products, the technology's applicability and accuracy can be further enhanced. Addressing these challenges and exploring future developments will significantly improve the effectiveness of MSI in the food industry, leading to better food safety and quality assurance practices.

MSI plays a pivotal role in advancing food safety and quality evaluation practices by providing a sophisticated, non-destructive method for assessing various attributes of food products. The technology's ability to capture detailed images at multiple wavelengths enables the detection of subtle changes in color, texture, and chemical composition, which are often indicative of quality and safety issues. MSI can identify surface defects, such as bruises or insect damage in fruits and vegetables and detect contaminants like bacteria and foreign objects that are not easily visible to the naked eye. This level of detailed analysis is critical for ensuring that food products meet safety standards and quality expectations.

Moreover, MSI enhances the efficiency and accuracy of food quality control processes. By integrating with advanced data processing and machine learning algorithms, MSI systems can automate the inspection and sorting of food items based on precise quality criteria. This reduces the reliance on manual inspection, which can be time-consuming and prone to error, and increases the throughput of food processing lines. The real-time capabilities of MSI allow for continuous monitoring and immediate detection of issues, enabling prompt corrective actions that prevent contaminated or substandard products from reaching consumers.

The adoption of MSI also supports compliance with stringent food safety regulations and helps build consumer trust by ensuring high standards of quality control. As technology continues to evolve, MSI is expected to become even more accessible and versatile, further solidifying its role as an essential tool in the food industry. By addressing current challenges and leveraging future advancements, MSI will significantly contribute to safer, higher-quality food products, benefiting producers, regulators, and consumers alike.

To fully realize the benefits of MSI, continued research and innovation are imperative. We must focus on reducing costs, enhancing data processing capabilities, establishing standardized protocols, and improving the robustness and applicability of MSI systems. By investing in these areas and fostering collaboration between industry, academia, and regulatory bodies, we can overcome current limitations and unlock new possibilities for MSI technology. Let us commit to advancing this critical field, ensuring that the food industry can consistently deliver safe, high-quality products to consumers worldwide.

Acknowledgements

"The MI4SaferFOOD project has indirectly received funding from the European Union's Horizon Europe research and innovation action programme, via the FOODITY – Open Call #1 issued and executed under the FOODITY project (Grant Agreement no. 101086105)."

References

Ali, M. M., Hashim, N., & Abd Aziz, S. et al. (2021). Quality inspection of food and agricultural products using artificial intelligence. *Advances in Agricultural and Food Research Journal*, *2*(2), a0000237. https://doi.org/10.36877/aafrj.a0000237

Bintsis, T. (2018). Microbial pollution and food safety. *AIMS Microbiology*, *4*(3), 377-396. https://doi.org/10.3934/microbiol.2018.3.377

Cheng, J.-H., & Sun, D.-W. (2014). Hyperspectral imaging as an effective tool for quality analysis and control of fish and other seafoods: Current research and potential applications. *Trends in Food Science & Technology*, *37*(2), 78-91. https://doi.org/10.1016/j.tifs.2014.03.006

Dehkordi, P., Moshtaghi, H., & Abbasvali, M. (2023). Effects of magnesium oxide and copper oxide nanoparticles on biofilm formation of Escherichia coli and Listeria monocytogenes. *Nanotechnology*, *34*(15), 155102. https://doi.org/10.1088/1361-6528/acab6f

El-Khishin, M., Gooneratne, R., & Hussain, M. (2017). Microbial safety of foods in the supply chain and food security. *Advances in Food Technology and Nutritional Sciences - Open Journal*, *3*(1), 22-32. https://doi.org/10.17140/aftnsoj-3-141

ElMasry, G., Mandour, N. S., Al-Rejaie, S. S., Belin, É., & Rousseau, D. (2019). Recent applications of multispectral imaging in seed phenotyping and quality monitoring—An overview. *Sensors*, *19*(5), 1090. https://doi.org/10.3390/s19051090

Fan, K., & Su, W. (2022). Applications of fluorescence spectroscopy, RGB- and multispectral imaging for quality determinations of white meat: A review. *Biosensors*, *12*(2), 76. https://doi.org/10.3390/bios12020076

Gemeda, F., et al. (2023). Review on food safety, quality assurance and control. *IAR Journal of Agricultural Science and Food Research*, *3*(2), 1-9.

Giannoni, L., Lange, F., & Tachtsidis, I. (2018). Hyperspectral imaging solutions for brain tissue metabolic and hemodynamic monitoring: Past, current and future developments. *Journal of Optics*, *20*(4), 044009.

Gholami-Shabani, M., Shams-Ghahfarokhi, M., & Razzaghi-Abyaneh, M. (2023). Food microbiology: Application of microorganisms in food industry. https://doi.org/10.5772/intechopen.109729

Hashim, N., Onwude, D. I., & Osman, M. S. (2018). Evaluation of chilling injury in mangoes using multispectral imaging. *Journal of Food Science*, *83*(5), 1271-1279. https://doi.org/10.1111/1750-3841.14127

Kamruzzaman, M., Elmasry, G., Sun, D. W., & Allen, P. (2012). Prediction of some quality attributes of lamb meat using near-infrared hyperspectral imaging and multivariate analysis. *Analytica Chimica Acta*, *714*, 57–67. https://doi.org/10.1016/j.aca.2011.11.037

Kim, D. G., Burks, T. F., Ritenour, M. A., & Qin, J. (2014). Citrus black spot detection using hyperspectral imaging. *International Journal of Agricultural and Biological Engineering*, *7*(6), 20–27. https://doi.org/10.25165/IJABE.V7I6.1143

Liu, Y., & Huang, X. (2023). Application of multispectral imaging technology in food quality and safety inspection. *International Journal of Food Science and Agriculture*, *7*(3), 396-400. https://doi.org/10.26855/ijfsa.2023.09.009

Lorente, D., Aleixos, N., Gómez-Sanchis, J., Cubero, S., García-Navarrete, O. L., & Blasco, J. (2012). Recent advances and applications of hyperspectral imaging for fruit and vegetable quality assessment. *Food and Bioprocess Technology*, *5*(4), 1121-1142. https://doi.org/10.1007/s11947-011-0725-1

Lorenzo, F., Sanz-Puig, M., Bertó, R., & Orihuel, E. (2020). Assessment of performance of two rapid methods for on-site control of microbial and biofilm contamination. *Applied Sciences*, *10*(3), 744. https://doi.org/10.3390/app10030744

Ma, F., Yuan, M., & Kozak, I. (2023). Multispectral imaging: Review of current applications. *Survey of*

Ophthalmology, *68*(5), 889-904. https://doi.org/10.1016/j.survophthal.2023.06.004

Mantilla, R., Jara, R., & Yimer, W. (2017). Evaluation of biological contaminants in foods by hyperspectral imaging: A review. *International Journal of Food Properties*, 1-34. https://doi.org/10.1080/10942912.2017.1338729

Munir, M. T., Wilson, D. I., Yu, W., & Young, B. R. (2018). An evaluation of hyperspectral imaging for characterising milk powders. *Journal of Food Engineering*, *221*, 1-10. https://doi.org/10.1016/j.jfoodeng.2017.10.001

Nguyen, J., Rodesch, P., Richtsmeier, D., Iniewski, K., & Bazalova-Carter, M. (2021). Optimization of a CZT photon counting detector for contaminant detection. *Journal of Instrumentation*, *16*(11), P11015. https://doi.org/10.1088/1748-0221/16/11/p11015

Onyeaka, H. (2023). Mitigating physical hazards in food processing: Risk assessment and preventive strategies. *Food Science & Nutrition*, *11*(12), 7515-7522. https://doi.org/10.1002/fsn3.3727

Patel, D., Bhise, S., & Kapdi, S. S. et al. (2024). Non-destructive hyperspectral imaging technology to assess the quality and safety of food: A review. *Food Production, Processing and Nutrition*, *6*, 69. https://doi.org/10.1186/s43014-024-00246-4

Ropodi, A., Panagou, E. Z., & Nychas, G. E. (2017). Multispectral imaging (MSI): A promising method for the detection of minced beef adulteration with horsemeat. *Food Control*, *73*, 57-63. https://doi.org/10.1016/j.foodcont.2016.05.048

Shi, Y., Liu, W., Zhao, P., Liu, C., & Zheng, L. (2020). Rapid and nondestructive determination of deoxynivalenol (DON) content in wheat using multispectral imaging (MSI) technology with chemometric methods. *Analytical Methods*, *12*(26), 3390-3396. https://doi.org/10.1039/D0AY00859A

Soni, A., Dixit, Y., Reis, M., & Brightwell, G. (2022). Hyperspectral imaging and machine learning in food microbiology: Developments and challenges in detection of bacterial, fungal, and viral contaminants. *Comprehensive Reviews in Food Science and Food Safety*, *21*(4), 3717-3745. https://doi.org/10.1111/1541-4337.12983

Sueker, M., Stromsodt, K., Gorji, H., Vasefi, F., Khan, N., Schmit, T., ... & Tavakolian, K. (2021). Handheld multispectral fluorescence imaging system to detect and disinfect surface contamination. *Sensors*, *21*(21), 7222. https://doi.org/10.3390/s21217222

Su, W., & Sun, D. (2018). Multispectral imaging for plant food quality analysis and visualization. *Comprehensive Reviews in Food Science and Food Safety*, *17*(1), 220-239. https://doi.org/10.1111/1541-4337.12317

Su, W., & Xue, H. (2021). Imaging spectroscopy and machine learning for intelligent determination of potato and sweet potato quality. *Foods*, *10*(9), 2146. https://doi.org/10.3390/foods10092146

Tang, T., Zhang, M., & Mujumdar, A. S. (2022). Intelligent detection for fresh-cut fruit and vegetable processing: Imaging technology. *Comprehensive Reviews in Food Science and Food Safety*, *21*(6), 5171-5198. https://doi.org/10.1111/1541-4337.13039

Wang, K., Pu, H., & Sun, D. (2018). Emerging spectroscopic and spectral imaging techniques for the rapid detection of microorganisms: An overview. *Comprehensive Reviews in Food Science and Food Safety*, *17*(2), 256-273. https://doi.org/10.1111/1541-4337.12323

Ye, X., Iino, K., & Zhang, S. (2016). Monitoring of bacterial contamination on chicken meat surface using a novel narrowband spectral index derived from hyperspectral imagery data. *Meat Science*, *122*, 25-31. https://doi.org/10.1016/j.meatsci.2016.07.015

Strategies to reduce mechanical harvesting costs in traditional olive orchards

Arlindo Almeida [a, *], Anabela Fernandes-Silva [b]

[a] Centro de Investigação de Montanha (CIMO), Instituto Politécnico de Bragança, Campus de Santa Apolónia, 5300-253 Bragança, Portugal

[b] Centre for Research and Technology of Agro-Environment and Biological Sciences; University of Trás-os-Montes e Alto Douro, Quinta dos Prados, 5000-801 Vila Real, Portugal

* Corresponding author. Email: acfa@ipb.pt

Abstract

Olive harvesting mechanization is adopted in different types of olive orchards: traditional, intensive, in hedgerows.

In Mediterranean basin, traditional olive orchards have an important economic value. In this type of olive orchards planting densities are 100 to 240 trees per hectare, and over 30 years old.

In these olive orchards, the most used mechanical harvesting system is based on a trunk shaker to detach fruits, and an inverted umbrella to collect them.

With this harvesting system it is usual to collect 70% to 90% of the production.

The olives that remain in the tree is a problem. To solve it, farmers adopt manual harvesting as a complementary task.

This procedure increases the cost of harvesting with the addition of labour and reduces the mechanical harvesting system work rate (trees hour^{-1}).

It is important to understand if this complementary manual harvesting is advantageous or not.

In field tests carried out in the Northeast of Portugal on traditional olive orchards with "Cobrançosa" and "Verdeal Transmontana", cultivars, two different procedures were compared: (I) mechanical harvest performance complemented by manual harvesting; (II) mechanical harvest performance without the addition of manual work.

In both procedures were evaluated: a) work rate (trees hour^{-1}); b) production harvested; b) associated costs; c) harvest efficiency considering it as the percentage of fruits collected in relation to total production.

To evaluate work rate system, a methodology based on measurement of each elementary operation time (in minutes) was adopted.

Costs was computed under international standards for agricultural machinery management.

The reduction in work rate and the increase in harvesting costs with complementary harvesting may be balanced by the increase in production that is harvested in this way. However, this does not seem to be the case, given the results presented.

Complementary manual harvesting may be a solution, but an evaluation of other agronomic and mechanical solutions is recommended.

Keywords: olive orchard; mechanization; trunk shaker; costs; labour.

1. Introduction

The mechanical harvesting system mostly adopted in traditional olive orchards in the Northeast of Portugal consists on a trunk shaker to detach olives and an inverted umbrella to collect fruits, both mounted on the front loader of four-wheel drive tractors of 70 kW to 95 kW.

In these olive orchards planting densities range from 100 to 240 trees per hectare, and are over 30 years old.

With this harvesting system, the entire production is not removed from the olive trees.

It is usual to harvest 70% to 90% of the olives (Sola-Guirado et al, 2018). Harvesting 80% to 85% of production is already a reasonable objective (Castro-Garcia et al, 2012).

It is important to improve the mechanical harvesting efficiency, considering it as the percentage of fruits removed in relation to total production (Ferguson 2006), (Ravetti et al 2014), in order to obtain a better net return for farmers.

Harvest efficiency is one of the most important factors to consider on mechanical harvesting olives for olive oil (Ferguson 2006).

To avoid this loss of production, farmers usually adopt traditional manual harvesting methods to remove the olives that remain on the tree, after the trunk shaker work.

This procedure improves harvesting cost: (I) by the increase in labour and (II) by the reduction of mechanical harvesting system work rate (trees $hour^{-1}$). This reduction in work rate is a consequence of the time required for manual harvesting.

It is important to assess if olives manual removal remaining on the tree after the trunk shaker work has a compensatory cost.

With this objective field tests were carried in the Northeast of Portugal on traditional olive orchards with "Cobrançosa" and "Verdeal Transmontana" cultivars, to evaluate the work rate (trees ha^{-1}) of this harvesting system, through the measurement of each elementary operation time.

In these field tests harvest system performance was compared: (I) without supplementary manual harvesting; (II) with the addition of manual harvesting and in this case evaluated the increase in production harvested.

In both procedures were evaluated: a) work rate (trees $hour^{-1}$); b) production harvested; b) associated costs; c) harvest efficiency considering it as the percentage of fruits collected in relation to total production.

The results can contribute to a better decision-making by farmers.

2. Materials and Methods

Field tests took place in Portugal - Trás-os-Montes region from 2018 to 2020 in irrigated olive orchards with the cultivars "Cobrançosa" and "Verdeal Transmontana", with 200 trees per hectare, spaced 7 m x 7 m (Figure 1).

Figure 1. Olive orchard example used in field trials

Tests were carried out in four different olive orchards (L1; L2; L3 and L4). L1 and L2 in 2018 (L1A and L2A) and 2019 (L1B and L2B). In 2020, the tests were carried out in olive groves L3 and L4.

Olive orchards L1, L2 and L4 are "Cobrançosa" cultivar. L3 olive orchard is "Verdeal Transmontana" cultivar.

In L1 olive orchard there were 3 replications in randomized blocks in each of the years considered (2018 and 2019). In L2 olive orchard there were 2 replications in randomized blocks in each of the years considered (2018 and 2019). In L3 olive orchard there were 3 replications in randomized blocks (in 2020). In L4 olive orchard there were 2 replications in randomized blocks (in 2020).

The harvesting system is based on a trunk shaker to detach the olives and an inverted umbrella to collect them. The inverted umbrella can temporarily store 200 to 250 kg of olives in a collecting tray. Under the inverted umbrella a door can be hydraulically opened to allow unload the olives.

Four-wheel drive tractors of 70 to 95 kW were used.

To assess harvesting system work rate, the following elementary operation time were measured in

minutes:

Tvib – average trunk shaking time;

Tvar – average additional manual harvesting time;

TvibVar – average trunk shaking time and complementary manual harvesting simultaneously;

Tdesloc – average time to move the tractor with trunk shaker from one tree to the next;

Tlimpfolhas – average time for cleaning leaves accumulated on the inverted umbrella;

Tdesclinha – average tractor travel time, from one headland to the other. Farmer's option due to the slope of the olive orchard greater than 10%. Traveling in reverse from the higher level headland to the lower level headland;

Tdesc – average time to discharge the inverted umbrella;

Na – number of trees between inverted umbrella discharges.

Work rate harvesting system (trees hour^{-1}) was computed by the following equation Eq (1):

$$Ct = \frac{3600}{Tvib+Tvar+TvibVar+Tdesloc+Tlimpfolhas+Tdesclinha+\frac{Tdesc}{Na}} \quad (1)$$

In each field test not all of the elementary operation referred in the equation were used. In cases where any of the elementary operation was not recorded, it was not considered in the equation.

In each of the olive orchard, per replication, the quantity of olives harvested was evaluated.

In order to evaluate harvest efficiency, in olive orchards L1, L2 and L4, the amount of olives that remained in the tree after shaking was evaluated. This assessment was carried out by randomly choosing 1 tree in every 10. In cases where additional manual harvesting was used, this procedure was interrupted in the trees selected for this assessment.

In order to estimate the cost kg^{-1} of mechanical harvesting without manual complementary harvesting and with manual complementary harvesting after and during mechanical shaking, the following assumptions were adopted:

Cost hour^{-1} of trunk shaker, inverted umbrella and operator = € 75.

Labour cost for additional harvesting (1 operator) = € 6.25 hour^{-1}.

Figure 2 shows the complementary manual harvesting procedure.

Figure 2. Complementary manual harvesting procedure

In 2018, replications of three of the olive orchards, L1 (L1AR1; L1AR2; L1AR3), L2 (L2AR1; L2AR2) and in 2020 in L3 (L3R1; L3R2) the harvest was carried out with complementary manual harvesting. In 2019, replications of four of the olive orchards, L1 (L1BR1; L1BR2; L1BR3), L2 (L2BR1; L2BR2) and in 2020 in L3 (L3BR3) and L4 (L4R1; L4R2) the harvest was carried out without additional manual harvesting.

3. Results

Tables 1 and 2 show the results obtained in olive orchards where harvest was carried out using complementary manual harvesting.

Table 3 shows results obtained in olive orchards where harvest was carried out without additional manual harvesting.

Table 1. Olive orchards with manual complementary harvesting: total production and per tree; measured and estimated work rate without manual harvesting and harvest time per tree. In the "work rate" and "minutes per tree" columns, the maximum and minimum values are marked in bold.

Orchard	Total production (kg)	kg tree^{-1}	Work rate (tree hour^{-1})	Minutes tree^{-1}	Estimated work rate without manual harvesting (trees hour^{-1})
L1AR1	1511	30.2	33.10	1.81	52.41
L1AR2	1215	21.7	**37.94**	**1.58**	50.68
L1AR3	2143	33.5	34.36	1.75	46.34
L2AR1	905	18.1	15.22	3.94	20.70
L2AR2	638	10.6	22.72	2.64	29.22
L3R1	920	17.4	14.27	4.20	17.55
L3R2	750	14.2	**10.96**	**5.47**	13.63
Average		20.81	24.08	3.06	32.93

Table 2. Olive orchards with manual complementary harvesting: production by manual harvesting, harvesting efficiency, costs kg^{-1} of total harvested production, estimated costs kg^{-1} without complementary manual harvesting and costs kg^{-1} of production harvested by complementary manual harvesting. In columns 2, 3 and 6, the maximum and minimum values are marked in bold.

Orchard	Production by manual harvesting (kg)	Harvesting efficiency (%)	Costs kg^{-1} of total harvested production, (€)	Estimated costs kg^{-1} without manual harvesting (€)	Costs kg^{-1} of production harvested by manual harvesting (€)
L1AR1	82.5	94.5	0.07	0.05	0.52
L1AR2	**58.24**	95.2	0.07	0.07	**0.07**
L1AR3	65.92	**96.9**	0.06	0.05	0.45
L2AR1	**130**	85.6	0.17	0.14	0.66
L2AR2	100.8	**84.2**	0.23	0.22	**0.76**
Average		91.28	0.12	0.11	0.49

Table 3. Olive orchards without complementary harvesting: total production and production per tree, harvesting efficiency, work rate, harvesting time per tree and costs kg^{-1} of harvested production. In columns 4, 5 and 6, the maximum and minimum values are marked in bold.

Orchard	Production harvested (kg)	kg tree^{-1}	Harvesting efficiency (%)	Work rate (tree hour^{-1})	Minutes tree^{-1}	Cost kg^{-1} harvested production (€)
L1BR1	910	19	94.0	47.38	1.27	0.08
L1BR2	720	13	96.9	49.76	1.21	0.12
L1BR3	890	15	**100**	**68.34**	**0.88**	0.07
L2BR1	1184	24	**100**	42.39	1.42	0.07
L2BR2	2994	49	**100**	32.84	1.83	0.05
L3R3	584	17.7	**100**	**24.57**	**2.44**	0.08
L4R1	703	20.7	**91.1**	63.46	0.95	0.05
L4R2	725	17.7	95.0	67.12	0.89	0.06
Average		2.01	97.13	49.48	1.36	0.07

As it is not possible to present for all the olive orchards in which field tests were carried out the values of the elementary working times that allowed to compute working rate and its relative importance, was taken the

option to present these results for two representative olive orchards, one in which additional manual harvesting was used (Figure 3) and another in which this option was not taken (Figure 4).

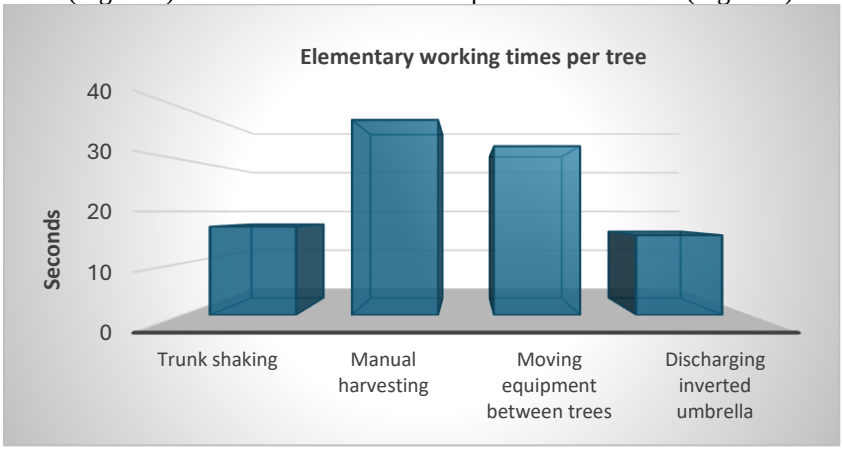

Figure 3. Olive orchard L1AR1 with additional manual harvesting - elementary working time per tree.

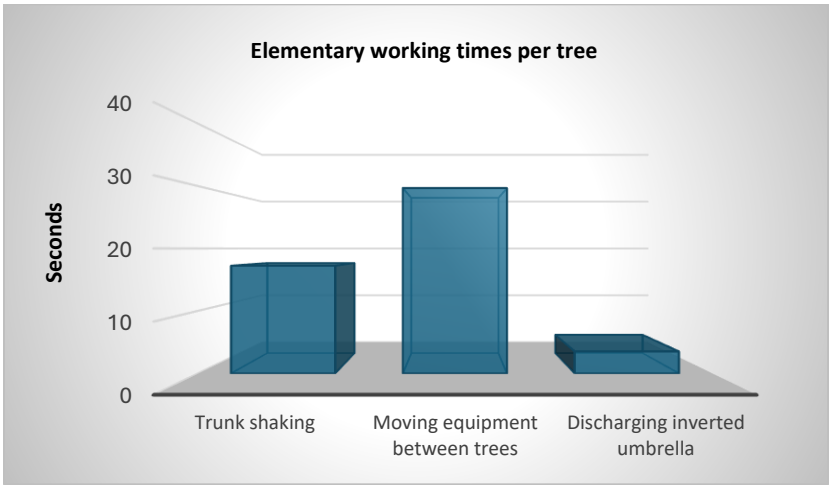

Figure 4. Olive orchard L4R2 without additional manual harvesting - harvesting elementary working time per tree.

4. Discussion

Results presented in tables 1 to 3 show important differences between the performance of the harvesting system when there is use of complementary manual harvesting and when there is no use of complementary manual harvesting.

Work rate with complementary harvesting (Table 1) varies from 10.96 trees h^{-1} to 37.94 trees h^{-1}. Without additional harvesting (Table 3), work rate varies from 24.57 trees h^{-1} to 68.34 trees h^{-1}.

These results show a work rate reduction when supplementary harvesting is used. The same can be seen in the time spent per tree (Table 1), which ranges from 1.58 minutes $tree^{-1}$ to 5.47 minutes $tree^{-1}$ using complementary harvesting and from 0.88 minutes $tree^{-1}$ to 2.44 minutes $tree^{-1}$ without complementary harvesting (Table 3).

Based on values presented in the fifth column of Table 2, it is assumed that a reduction in the cost kg^{-1} of harvest would be possible if there were no use of additional manual harvesting.

The cost of production harvested mechanically with complementary manual harvesting (Table 2) is on average €0.12 kg^{-1}. The cost of production harvested mechanically without manual harvesting is on average €0.07 kg^{-1} (Table 3).

The reduction in work rate and the increase in harvesting costs with complementary harvesting can be balanced by the increase in production harvested in this way. However, this does not seem to be the case,

given the results presented in the second and sixth columns of Table 2. It can be seen that the increase in harvested production varies from 130 kg in an olive grove with a total production of 905 kg, to an increase in harvested production from 58.24 kg in an olive grove with a total production of 1,215 kg. Labour costs to obtain this increase in harvest range from €0.07 kg^{-1} to €0.76 kg^{-1} with an average value of €0.49 kg^{-1} (Table 2).

It will be worth reflecting on these costs for additional manual harvesting. The results obtained show that the increase in harvest is reduced and the price per kg of this increase in harvested production is much higher than the commercial value of the olives.

Harvest efficiency results show that in the olive orchards where complementary manual harvesting was used (Table 2), the values varied from 84.2% to 96.9%, with an average of 91.28%. In olive orchards where no additional manual harvesting was used (Table 3), values ranged from 91.1% to 100%, with an average of 97.13%.

These harvest efficiency values are above 85%, a value that is referred to by (Castro-Garcia et al, 2012) as an objective for harvesting systems based on trunk shakers. For (Farinelli et al 2012), harvesting efficiency of 85% is considered the breakeven point for mechanical harvesting of olives with a trunk shaker, meaning that 15% or less of the total production remaining on the tree, losing it, is worthwhile compared to the cost reduction that the harvesting system provides.

Figure 3 show the substantial value that the elementary time for manual harvesting has in the set of elementary working times, followed by the elementary time for moving equipment between trees.

Figures 3 and 4 show the importance that time for moving equipment between trees has for work rate. All measures that reduce this value, such as good trafficability conditions of the equipment within the olive orchard and the use of mechanical devices that allow easy and quick coupling of the shaker to the tree, contribute to improving the work rate of this harvesting system.

5. Conclusions

Mechanical olive harvesting systems based on trunk shakers do not detach all production.

The majority of farmers who use this type of harvesting equipment, to harvest the entire production opt for complementary manual harvesting with the consequent increase in labour.

Before making the most appropriate decision, it is worth checking the cost/benefit ratio of this solution.

Mechanization brings considerable benefits, such as significantly reducing the time required for the operation, which allows harvesting a larger area of olive orchards in the time period considered optimal. With effective operation management, this increase in work rate reduces the time required and harvesting costs, despite not harvesting the entire production. The references cited in previous points indicate that with a harvesting efficiency of 85% the breakeven point is reached, that is, it is economically worthwhile to lose some production that remains on the tree.

With these harvest efficiency values (>85%), the use of complementary manual harvesting results in an unnecessary increase in costs, without obtaining a compensatory increase in harvested production.

This is what the results obtained in this work show. In the field tests carried out, (Table 2) for an average harvesting efficiency of 91.28%, the olives harvested by complementary harvesting had an average cost of €0.49 kg^{-1}, much higher than their value.

Being harvesting efficiency less than 85%, it is necessary to adopt solutions that can include complementary harvesting, or others such as agronomic solutions, or such as better mechanical solutions, which increase harvest efficiency.

A set of agronomic factors are known that affect harvest efficiency, such as canopy shape and density, pruning, orchard density and cultivar (Ferguson et al, 2010).

The shape and density of the canopy can affect the efficiency of mechanical harvesting, impairing the performance of the trunk shaker, by reducing the capacity to transmit vibration energy to the fruiting zone (Martin, 1994).

The density of the canopy can affect mechanical harvesting (Tombesi et al, 2002), as it makes difficult the visibility for the operator and jeopardize the equipment performance by limiting access for the shaker clamp to the most convenient area of the trunk.

Proper pruning should provide enough space under the canopy to facilitate shaker access to the trunk and efficiently transmit vibration to the fruiting zone. Suitable olive orchard density for trunk shakers is between 150 to 400 trees per hectare (Ferguson et al, 2010).

Among the factors linked to the cultivar, fruit removal force (FRF), fruit weight (P) and the relationship between them are important for harvest efficiency (Tombesi 1990; Ferguson 2006, Farinelli et al 2012). To know FRF/P ratio that can be used as an indicator of good harvesting efficiency is an important objective that remains to be carried out. In addition to the cultivar, it depends on the agro-ecological region in which the olive grove is located.

The choice of mechanical equipment is another factor that affects harvesting efficiency. For Ferguson (2006), the vibration pattern must be characterized by a short amplitude, less than 2.5 cm and a high frequency, above 2500 cycles minute^{-1}.

Before making the decision to use complementary harvesting, it is important to assess if it is really need, for instance, what harvesting efficiency is expected. With the values obtained in the field tests presented, it may have led to an increase in harvesting costs, without the corresponding return.

Being expected a harvesting efficiency lower than the reference values, complementary manual harvesting can be a solution, but an evaluation of the other agronomic and mechanical solutions mentioned is recommended.

Acknowledgements

For the financial support: to the European Agricultural Fund for Rural Development (EAFRD) and the Portuguese Government within the scope of Action 1.1 “Operational Groups” integrated in measure 1. “Innovation” of PDR 2020 – Mainland Rural Development Program PDR2020-101-032185 Olive and Olive Oil Operational Group (SustainOlive), and national funds through FCT/MCTES (PIDDAC): CIMO, UIDB/00690/2020 (DOI: 10.54499/UIDB/00690/2020) and UIDP/00690/2020 (DOI: 10.54499/UIDP/00690/2020); and SusTEC, LA/P/0007/2020 (DOI: 10.54499/LA/P/0007/2020).
To the farmers whose collaboration and availability made possible to carry out the field tests.

References

Castro-García, S., Blanco Roldán, G.L., Jiménez-Jiménez, F., Gil-Ribes, J.A., Ferguson, L., Glozer, K., Krueger, W.H., Fichtner, E.J., Burns, J.K., Miles, J.A. and Rosa, U.A. (2012). Preparing Spain and California table olive industries for mechanical harvesting. Acta Hortic. 965, 29-40 DOI: 10.17660/ActaHortic.2012.965.1 https://doi.org/10.17660/ActaHortic.2012.965.1

Farinelli, D., Tombesi, S., Famiani, F. and Tombesi, A. (2012). The fruit detachment force/fruit weight ratio can be used to predict the harvesting yield and the efficiency of trunk shakers on mechanically harvested olives. Acta Hortic. 965, 61-64 DOI: 10.17660/ActaHortic.2012.965.5 https://doi.org/10.17660/ActaHortic.2012.965.5

Ferguson, L., (2006). Trends in Olive Harvesting in Trends in Olive Fruit Handling Previous to its Industrial Transformation. Grasas y Aceites, 57 (1): 9-15. DOI: https://doi.org/10.3989/gya.2006.v57.i1.17

Ferguson, L., U.A. Rosa, S. Castro-Garcia, S.M. Lee, J.X. Guinard, J. Burns, W.H. Krueger, N.V. O'Connell, and K. Glozer. "Mechanical Harvesting of California Table and Oil Olives." *Advances in Horticultural Science* 24, no. 1 (2010): 53-63. Accessed July 15, 2021. http://www.jstor.org/stable/42882754.

Martin, George. C. (1994). Mechanical olive harvest: use of fruit loosening agents. Acta Hortic. 356, 284-291 DOI: 10.17660/ActaHortic.1994.356.60 https://doi.org/10.17660/ActaHortic.1994.356.60

Ravetti, L.M. (2014). Technology for improving the efficiency of mechanical harvesting in modern olive growing. Acta Hortic. 1057, 221-229 DOI: 10.17660/ActaHortic.2014.1057.26 https://doi.org/10.17660/ActaHortic.2014.1057.26

Sola-Guirado, R.R., Castillo-Ruiz, F.J., Blanco-Roldán, G.L., Castro-García, S., Colmenero, J.T. and Gil-Ribes, J.A. (2018). Mecaolivar outcomes: testing newly developed harvesters in traditional and intensive olive orchards. Acta Hortic. 1199, 321-326 DOI: 10.17660/ActaHortic.2018.1199.50 https://doi.org/10.17660/ActaHortic.2018.1199.50

Tombesi, A. (1990). Physiological and mechanical advances in olive harvesting. Acta Hortic. 286, 399-412 DOI: 10.17660/ActaHortic.1990.286.83 https://doi.org/10.17660/ActaHortic.1990.286.83

Tombesi, A., Boco, M., Pilli, M. and Farinelli, D. (2002). Influence of canopy density on efficiency of trunk shaker on olive mechanical harvesting. Acta Hortic. 586, 291-294 DOI: 10.17660/ActaHortic.2002.586.56 https://doi.org/10.17660/ActaHortic.2002.586.56

Comparing the impact of different work phases on operator and driver exposure to whole-body vibration during olive harvesting activities

Gianluca Coltrinari[a], Massimo Cecchini[a,*], Danilo Monarca[a]

[a] Department of Agriculture and Forest Sciences, University of Tuscia, Viterbo, Italy

* Corresponding author. Email: cecchini@unitus.it

Abstract

During olive harvesting activities, special machines are used that expose drivers to Whole-Body Vibration (WBV). This issue is significant because machines drivers are subjected to mechanical stresses that can lead to serious health problems. Italian legislative decree 81/2008 requires that the assessment of the risk of exposure to WBV is based on the evaluation of daily exposure *A(8)*, expressed as equivalent continuous acceleration over an eight-hour period. The vibratory stress is caused by the tractor engine and the movements of the mechanical arm installed at the rear for olive harvesting. The objective of this work is to compare the influence of different work phases on the operator's and driver's exposure to WBV during olive harvesting activities. An experimental campaign was conducted in a farm in central Italy under the same boundary conditions. Whole-body vibration (WBV) measurements, according to ISO 2631, were performed on two different vehicles during the olive harvest: a New Holland TD5105 tractor and a New Holland TN55D. During the experimental campaign, signals from front and rear and vertical accelerations were acquired at the driver's seat using a tri-axial accelerometer in both vehicles. In order to characterize the actual exposure of the workers, field measurements were conducted under real working conditions for the drivers of both machines (tractor and olive harvester). The data obtained show that the highest WBV values were recorded with the olive harvester in an upright position for both tractors; the mechanical movement of the arm influences the accelerations because it generates high stresses at maximum extension compared to the source signal produced by the tractor engine. Furthermore, the data were compared to highlight the differences between the operator of the mechanical arm and the tractor driver. The same computing process was applied to compare the values obtained in the measurement campaign with those established by Italian legislative decree 81/2008.

Keywords: tractor, farm, whole body vibration, human health, driver.

1. Introduction

Whole-body vibrations (WBV) are a physical agent for workers using tractors in agricultural activities (Kumar et al., 1999; Scarlett et al., 2007). The scientific literature points out that an operator in contact with a vibration source for a prolonged period may have problems with his or her health (Bovenzi and Betta, 1994; Bovenzi and Hulshof, 1998), (Ahmadi, 2013; Boshuizen et al., 1990 a). In fact, prolonged exposure to vibration can generate over the long-term problems of different kinds (Lings and Leboeuf-Yde, 2000) (Boshuizen et al., 1990 b), such as musculoskeletal disorders, spinal problems (human nervous system problems and spinal damage (Kumar et al., 1999). This issue affects drivers of different types of vehicles such as trucks, cars, buses and even tractors (Cutini et al., 2019). Numerous studies that have been carried out in the field of agriculture, point out that tractors are a very significant source of vibration for the drivers (Cutini et al, 2017; Cvetanovic and Zlatkovic, 2013; Futatsuka et al., 1998; Langer et al., 2015; Sorainen et al., 1998). European studies show that every year there are many workers who have health problems due to exposure to vibration (Kabir et al., 2017; Khaksar et al., 2013).

On this issue, a physical agents' directive has been issued that establishes minimum requirements for the health protection of workers exposed to WBV. A key parameter for exposure assessment is the actual working time affecting the worker, and the standard value of 8 hours is defined and, with reference to this parameter, the limit values of 0.5 m/s^2 (action value) and 1.0 m/s^2 (exposure limit) are defined. There are numerous factors that influence whole-body exposure, such as ground conditions (Oncescu et al., 2022), type of tires (Deboli et al., 2008), speed vehicle, wear degree (Cecchini et al., 2021), suspension (Kim et al., 2018) anthropometric characteristics of the driver and the seat (Abouel-seoud, 2019; Deboli et al., 2017; Melemez et al., 2013). Fundamental turns out to be the process of defining the typical day of the worker driving the tractor on a farm in order to be able to determine the actual exposure dose for the driver. During the activities performed the different phases may lead to different exposure is precisely why a daily exposure dose assessment is established. In particular, the latter can be a valuable tool in order to be able to reduce the dose

of exposure at the same time an improper functioning of the seat can lead to a worsening of the situation with an enlargement of the vibratory signal. Suspension and tires can also greatly influence the stress on the tractor driver's body. Some researchers have pointed out that proper suspension selection can lead to a dampening of the vibration signal reaching the driver. In agriculture, the soil plays a key role as it leads the medium to significant stresses along all directions according to the standard *x*, *y* and *z* reference system. Especially because the vehicle is advancing over terrain that in most cases is uneven and therefore causes considerable stresses (Oncescu et al., 2022).

2. Materials and Methods

A measurement campaign was carried out on a farm in Viterbo, central Italy. The activity involved measuring the vibrations induced on an operator during olive harvesting. To perform this operation, a mechanical arm is connected to rear part the vehicle; it is connected to the tractor engine by a cardan joint. The operator stands on a seat on the rear of the tractor, and he can move the mechanical arm that acts on the trees to drop olives. This system consists of a special component consisting of several plastic rods that shake the tree, causing olives to fall but without damaging the branch. This mechanical device is movable and can be uncoupled from the tractor so that it can be used on more than one farm tractor.

Figure 1. Triaxial accelerometer fixed on the seat and PC connected to analyse the signal.

Measurements were realized with a triaxial accelerometer attached to the operator's seat according to the directions established by the standard reference system (ISO 2631-1, 1997). It was fixed on the seat using scotch tape, which made it integral to the vehicle and avoided displacement of the instrument on the seat. The system requires there to be two seats: one for the tractor driver and the other one destinated to the worker that moving the mechanical arm, as shown in the figures. The measurements were all repeated under the same boundary conditions in the farm field. Table 1 report the instrument characteristics (Fig. 1).

In order to be able to highlight the influence of the source on the operator's whole-body exposure, two different tractors were tested, and the characteristics are reported in Table 2.

Table 1. Characteristics of instruments.

Model	Sensivity	Position
Triaxial accelerometer SEN027-PCB	X axis:10.52 mV/(m/s^2) Yaxis:10.55 mV/(m/s^2) Z axis:10.58 mV/(m/s^2)	Driving seat of the truck in the position which corresponds to the driver's sacroiliac joints (his buttocks)

Table 2. Characteristics of tractors.

Tractor Model	Engine Power [kW]	Mass [ton]
New Holland TD5.105	79	3,74
New Holland TN55D	36	2,7

Fig. 2 and 3 show the two tractor models used in the experimental campaign and the mechanical olive harvesting arm: this is a device that is mounted on both vehicles.

Figure 2. First tractor for the measurement campaign: New Holland TD5.105.

Figure 3. Second tractor for the measurement campaign: New Holland TN55D.

The campaign consisted of the following steps: firstly, vibration measurement for the operator on the tractor with the minimum engine rotation speed (rpm) in order to be able to characterize the source signal. Subsequently the measurements were carried out with three different configurations of the mechanical arm: the first with maximum extension relative to the tractor; a second closer to the tractor; and the last with the arm in an intermediate position (Fig. 4 and 5). The vehicles employed in the experimental campaign can carry out the tasks described below. The weather conditions were always the same and there was no wind. before using the mechanical arm on the rear of the tractor, stability was checked using the stabilizers.

Figure 4. Different mechanical arm configurations on the tractor.

Figure 5. Activities with the mechanical arm for olive harvesting.

Operators of the tractor were instructed to perform their normal duties during the data collection period in order to replace the real conditions. The percentage of time spent in each work phase was defined on the basis of the driver's interview. In the field tests, WBV exposure were measured according to the standard procedure of the ISO 2631-1 (1997) guidelines. The duration of measurements was kept sufficiently long to ensure reasonable signal precision and to ensure that the vibration is typical of the exposures of the drivers for the specific tasks. The acquisition time was of 3 minutes for each specific task. According to ISO 2631-1 (1997) guidelines the signal was acquired in a three-axis coordinate system to consider the entry points of vibration in worker's body: the x-axis to measure vibration in the anterior posterior direction, the y-axis in the medial lateral direction, and the z-axis in the vertical direction. The guidelines are applicable to the vibration in the frequency range from 0.5 Hz to 80 Hz, transmitted to the body as a whole through the seat pad. As described above, the Italian Decree-Law 81/2008 establishes that the evaluation of the daily exposure *A(8)*, expressed as the equivalent continuous root mean square (r.m.s.) acceleration over an height hour period, allows the evaluation of the risk to whole-body vibration. It is calculated as the highest (r.m.s.) value of the frequency-weighted accelerations, determined on the three orthogonal axes following the expression:

$$a_{w,max} = max\ (K_x\ a_{wx},\ K_y\ a_{wy},\ K_z\ a_{wz}) \quad (1)$$

where K_x = 1.4, K_y = 1.4, K_z = 1 and $a_{w,max}$ is the maximum value among $1.4 \cdot a_{w,x}$, $1.4\ a_{w,y}$ and $1 \cdot a_{w,z}$ for a seated or standing worker.

The frequency-weighted root mean square acceleration was calculated using the following expression:

$$A(8) = a_w \sqrt{\frac{T_{esp}}{8}} \quad (2)$$

where:

A(8) is the daily dose expressed as [m/s^2];

T_{esp} is the exposure time expressed as [hour];

a_w is the equivalent continuous r.m.s acceleration also expressed as [m/s^2].

3. Results

The following graphs (Fig. 6, 7 and 8) highlights the trend of solicitation for the measurement realized on the tractors with the different processing configurations for olive harvesting. Each line represents the trend of the signal acquired with the instrument. The green line shows the signal along *z*-axis, the red line for *y*-axis and finally the blue line is the signal of *x*-axis. The graph shows the acceleration values (m/s^2) on *y*-axis and the time expressed in terms of seconds (s) on *x*-axis. Only the most significant graphs of the measurement campaign have been reported.

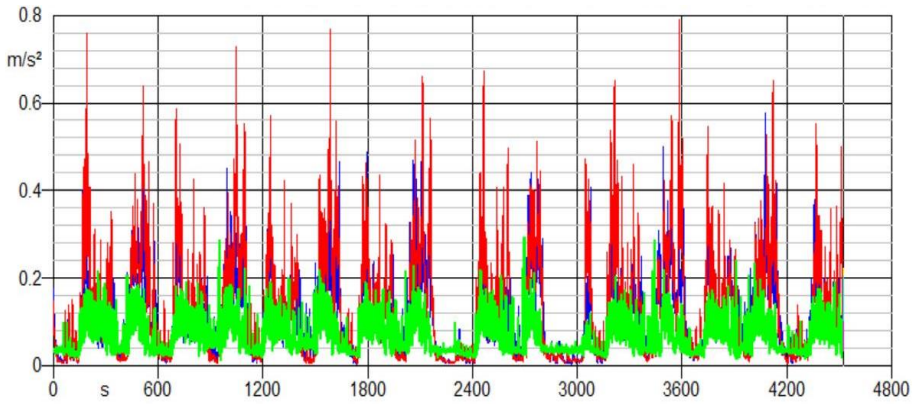

Figure 6. Time history of accelerations of the driver for New Holland TN55D.

.

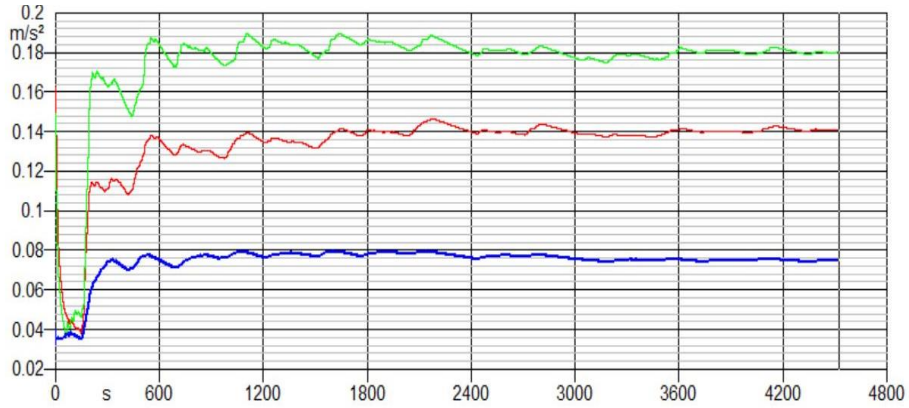

Figure 7. Trend of the a_w values for the driver of the tractor New Holland TD5.105.

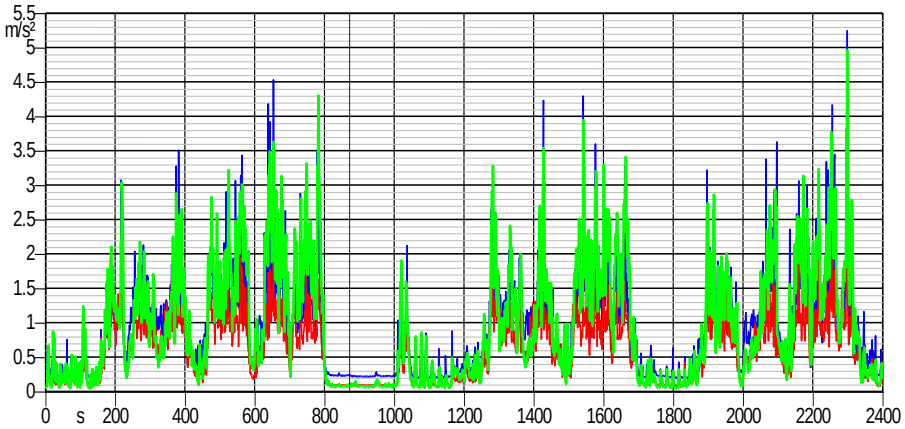

Figure 8. Time history of accelerations for the operator on New Holland TD5.105.

The previous graphs represent the trend of the measurements carried out under all the conditions described above. The following graph (Fig. 9) represents the course of the frequency spectra expressed in terms of Hertz on the *x*-axis while the *y*-axis represents the acceleration values. The box at the top right in figure 9 represents the analysis that was carried out. For each sequence, acceleration values along all three reference axes were analysed simultaneously. This is because the signal analysis software provides a value for each frequency expressed in terms of third octaves.

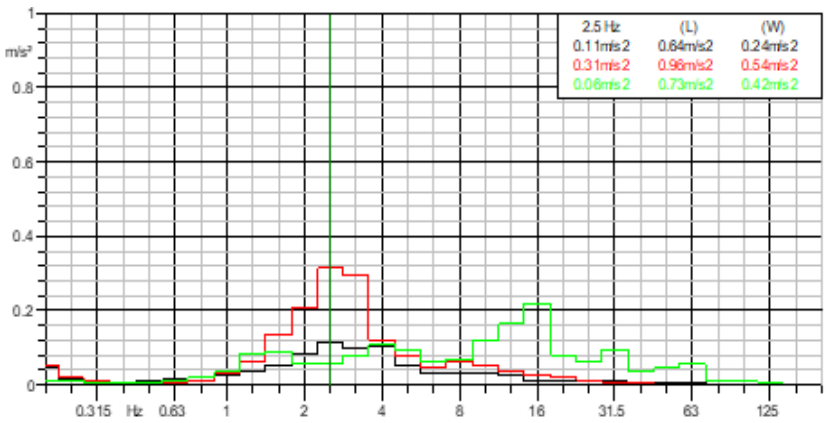

Figure 9. Time history of accelerations for the driver.

Results show that in all of three directions and at different operations maximum amplitude of WBV energy which was transmitted to operator's body through driver's seat take place at low frequencies (less than 30 Hz). Tables 3, 4, 5 and 6 show the results obtained in terms of acceleration and frequency spectrum for the driver and for the operator. The results have been separated for each mechanical arm configuration; near to tractor (Pos.1), intermediate position (Pos.2) and maximum elongation (Pos.3). The table also shows the dominant frequency for each measurement and the respective calculation value of the parameter *A(8)*.

Table 3. Data obtained for driver on tractor TD5.105.

	Tractor driver TD5.105		
	Pos.1	Pos.2	Pos.3
Frequency-weighted r.m.s. accelerations (m/s^2)	a_{wx}=0.03 a_{wy}=0.10 a_{wz}=0.3	a_{wx}=0.05 a_{wy}=0.10 a_{wz}=0.60	a_{wx}=0.03 a_{wy}=0.02 a_{wz}=0.04
Dominant frequencies (Hz)	DF_x = 8 DF_y =12.5 DF_z = 6	DF_x =2.5 DF_y =6.4 DF_z =8	DF_x = 12.5 DF_y =16 DF_z =4
Estimated daily exposure (8 h)	0.36	0.83	0.32

Table 4. Data obtained for harvesting arm operator on tractor TD5.105.

	Harvesting arm operator TD5.105		
	Pos.1	Pos.2	Pos.3
Frequency-weighted r.m.s. accelerations (m/s^2)	a_{wx}=0.32 a_{wy}=0.33 a_{wz}=0.17	a_{wx}=0.26 a_{wy}=0.51 a_{wz}=1.x26	a_{wx}=0.32 a_{wy}=0.42 a_{wz}=1.52
Dominant frequencies (Hz)	DF_x =2 DF_y =8 DF_z =12	DF_x = 6.4 DF_y = DF_z = 16	DF_x =16 DF_y = 12.5 DF_z = 1.3
Estimated daily exposure (8 h)	1.34	1.06	1.19

Table 5. Data obtained for driver on tractor TN55D.

	Tractor driver TN55D		
	Pos.1	Pos.2	Pos.3
Frequency-weighted r.m.s. accelerations (m/s^2)	a_{wx}=0.03 a_{wy}=0.10 a_{wz}=0.30	a_{wx}=0.05 a_{wy}=0.10 a_{wz}=0.60	a_{wx}=0.03 a_{wy}=0.01 a_{wz}=0.04
Dominant frequencies (Hz)	DF_x =4 DF_y =8 DF_z =1.5	DF_x =8 DF_y =12 DF_z =16.5	DF_x = 12 DF_y =6 DF_z =1.5
Estimated daily exposure (8 h)	0.24	0.44	0.28

Table 6. Data obtained for harvesting arm operator on tractor TN55D.

	Harvesting arm operator TN55D		
	Pos.1	Pos.2	Pos.3
Frequency-weighted r.m.s. accelerations (m/s^2)	a_{wx}=0.35 a_{wy}=0.19 a_{wz}=0.44	a_{wx}=0.08 a_{wy}=0.10 a_{wz}=0.20	a_{wx}=0.10 a_{wy}=0.20 a_{wz}=0.05
Dominant frequencies (Hz)	DF_x =8 DF_y =16 DF_z =4	DF_x =4 DF_y = 1.6 DF_z =20	DF_x =16 DF_y =8 DF_z =1.5
Estimated daily exposure (8 h)	0.52	0.43	0.50

4. Conclusions

This study consists of measurement and analysis of WBV on two different tractors during olive harvesting activities. Particularly the aim of this paper is highlighting the influence of the employing of a mechanical arm fixed on the rear of the vehicle on the WBV exposure for the operator and the driver. Vibration transmitted through tractor seat surface to human body were considered such as the vibration source signal. For the aim to better analysis of the amount of transmitted vibration energy to driver and operator's body, WBV at different frequencies and in all three directions (*x*, *y* and *z*) were considered.

The results clearly show that it is the operator who manoeuvres the harvesting arm who is most exposed to vibrations in mechanized olive harvesting operations, while the tractor driver is always exposed to lower levels.

Although theoretically to decrease the WBV energy at lower frequencies and consequently the value of the *A(8)* parameter, the best way would be to define a position close to the olive tree so as to reduce the lever arms of the inertia forces, the results measurements do not always confirm this.

One key aspect remain the limitation of the operator's working time with the farm tractor to the allowable exposure time, which ensures that the exposure limit is observed. The relatively small number of individual tractor/operation with mechanical arm combinations investigated may give an important contribute to the study of the WBV exposure but it doesn't permit to define a unique solution in order to define the correlation between activities and WBV effects. Others detailed studies in the similar boundary conditions are certainly necessary with aim to find the influence of the mechanical arm position on the vibration signal.

References

Abouel-seoud, S. A. H., 2019. Control of driver whole-body vibration ride comfort in agricultural tractor. Agricultural Engineering International: CIGR Journal. 21(2), 40-51.

Ahmadi, I. 2013. Health hazard assessment of tractor driver whole-body vibration utilizing the ISO 2631 standard. Agriculturae Conspectus Scientificus. 78(1), 71-78.

Boshuizen, H. C., C. T. Hulshof, P. M. Bongers, 1990. Long-term sick leave and disability pensioning

due to back disorders of tractor drivers exposed to whole-body vibration. International archives of occupational and environmental health. 62, 117-122.

Boshuizen, H. C., P. M. Bongers, C. T. Hulshof,1990. Self-reported back pain in tractor drivers exposed to whole-body vibration. International archives of occupational and environmental health. 62, 109-115.

Bovenzi, M., A. Betta, 1994. Low-back disorders in agricultural tractor drivers exposed to whole-body vibration and postural stress. Applied ergonomics. 25(4), 231-241.

Bovenzi, M., C. T. J. Hulshof, 1998. An updated review of epidemiologic studies on the relationship between exposure to whole-body vibration and low back pain. J. Sound Vib, United States. 215(4), 595–611.

Cecchini M., F. Piccioni, S. Ferri, G. Coltrinari, L. Bianchini, A. Colantoni, 2021. Preliminary investigation on systems for the preventive diagnosis of faults on agricultural operating machines. Sensors. 21(4), 1547.

Cutini, M., M. Brambilla, C. Bisaglia, 2017. Whole-body vibration in farming: Background document for creating a simplified procedure to determine agricultural tractor vibration comfort. Agriculture. 7(10), 84.

Cutini, M., M. Brambilla, C. Bisaglia, 2019. Assessment of a ride comfort number for agricultural tractors: A simplified approach. Biosystems Engineering. 185, 35-44.

Cvetanovic, B., D. Zlatkovic, 2013. Evaluation of whole-body vibration risk in agricultural tractor drivers. Bulgarian journal of agricultural science. 19(5), 1155-1160.

Deboli, R., A. Calvo, C. Preti, G. Paletto, 2008. Whole Body Vibration (WBV) transmitted to the operator by tractors equipped with radial tires. In Innovation Technology to Empower Safety, Health and Welfare in Agriculture and Agro-food Systems.

Deboli, R., A. Calvo, C. Preti, 2017. Whole-body vibration: Measurement of horizontal and vertical transmissibility of an agricultural tractor seat. International journal of industrial ergonomics. 58, 69-78.

Futatsuka, M., S. Maeda, T. Inaoka, M. Nagano, M. Shono, T. Miyakita, 1998. Whole-body vibration and health effects in the agricultural machinery drivers. Industrial health. 36(2), 127-132.

International Organization for Standardization, ISO 2631-1, Mechanical Vibration and skock - Evaluation of human exposure to whole-body vibration, Part 1: General requirements, 1997.

Kabir, M. S. N., S. O. Chung, Y. J. Kim, N. S. Sung, S. J. Hong, 2017. Measurement and evaluation of whole body vibration of agricultural tractor operator. International Journal of Agricultural and Biological Engineering. 10(1), 248-255.

Khaksar, Z., H. Ahmadi, S. S. Mohtasebi, 2013. Whole body vibration analysis of tractor operators using power spectral density. Journal of Mechanical Engineering and Technology. 1(1), 6-12.

Kim, J. H., J.T. Dennerlein, P. W. Johnson, 2018. The effect of a multi-axis suspension on whole body vibration exposures and physical stress in the neck and low back in agricultural tractor applications. Applied ergonomics. 68, 80-89.

Kumar, A., M. Varghese, D. Mohan, P. Mahajan, P. Gulati, S. Kale, 1999. Effect of whole-body vibration on the low back: a study of tractor-driving farmers in north India. Spine. 24(23), 2506.

Langer, T. H., M. K. Ebbesen, A. Kordestani, 2015. Experimental analysis of occupational whole-body vibration exposure of agricultural tractor with large square baler. International journal of industrial ergonomics. 47, 79-83.

Lings, S., C. Leboeuf-Yde, 2000. Whole-body vibration and low back pain: a systematic, critical review of the epidemiological literature 1992–1999. Int. Arch. Occup. Environ. Health, Germany. 73(5), 290–297.

Melemez, K., M. Tunay, T. Emir, 2013. The role of seat suspension in whole-body vibration affecting skidding tractor operators. J. Food Agric. Environ. 11, 1211-1215.

Oncescu, A. T., C. Persu, I. Dumitru, D. Prunoiu, L. Grigorie, D. Tarnita, 2022. Influence Of The Road Type On The Whole Body Vibrations Transmitted To The Driver Of An Electric Tractor. Acta Technica Napocensis-Series: Applied Mathematics, Mechanics, And Engineering. 65(2s).

Scarlett, A. J., J. S. Price, R. M. Stayner, 2007. Whole-body vibration: Evaluation of emission and exposure levels arising from agricultural tractors. Journal of terramechanics. 44(1), 65-73.

Sorainen, E., J. Penttinen, M. Kallio, E. Rytkönen, K. Taattola, 1998. Whole-body vibration of tractor drivers during harrowing. American Industrial Hygiene Association Journal. 59(9), 642-644.

Automatic feed pushing in dairy barns: Considerations of TMR leftovers particle size

Andrea Lazzari [a,b], Simone Giovinazzo [b], Massimo Brambilla [b*], Francesco Maria Tangorra [c], Aldo Calcante [c], Carlo Bisaglia [a]

[a] Research Centre Animal Production and Aquaculture, Council for Agricultural Research and Economics (CREA), Via Antonio Lombardo, 11, 26900 Lodi (LO), Italy
[b] Research Centre for Engineering and Agro-Food Processing, Council for Agricultural Research and Economics (CREA), Via Milano, 43 – 24047, Treviglio (BG), Italy
[c] Department of Agricultural and Environmental Sciences-Production Territory Agroenergy, Università Degli Studi di Milano, Via Celoria 2, 20133 Milan, Italy.
* Corresponding author. Email: massimo.brambilla@crea.gov.it

Abstract

Dairy cows are typically fed a total mixed ration (TMR), which includes a blend of forage, cereals, by-products, supplements, vitamins, and mineral salts tailored to each farm's specific needs. Providing a quality ration is crucial for the production cycle, but optimizing feed bunk management is equally important to maximize TMR's nutritional benefits. Consistent feeding times, high-quality components, and frequent replenishment of the TMR near the feeding bunk ensure cows have a regular, high-quality diet 24 hours a day, every day of the week. The study involves monitoring the TMR leftovers from four dairy farms and one fattening bull farm in Northern Italy. These farms utilized automatic feeding systems (AFS) and mixing wagons for TMR processing, while leftover feed pushing occurred both manually (twice a day) and automatically using a rotary drum feed pusher and AFS. TMR leftover samples, collected just before the administering of fresh feed, underwent particle size analysis using a Penn State Particle Separator with screens of 19, 8, and 1.18 mm and a bottom pan. Data processing has pointed out that leftover particle size composition varies depending on feed-pushing techniques. The pushing-up action of the AFS results in a leftover particle size like the operator-based one and contains a high percentage of particles higher than 8 mm. On the other hand, pushing back the feed with a drum feed pusher results in leftover particle size with a high percentage of long fibres in the 19 mm and 8 mm screens, which results from the animal sorting activity against longer particles. These results indicate that the way feed is pushed back to the feeding trough affects the innate feed-sorting behaviour of the animals, interacting with the other factors resulting from the housing characteristics.

Keywords: TMR quality, Penn State Particle Separator, Animal welfare, Automatic Feeding System

1. Introduction

Total Mixed Ration (TMR), as we know it today, did not exist before the 1950s; the first study about it appeared in 1966. The introduction of TMR has brought several advantages to the farmer, such as i) increasing milk production, ii) reducing animal sorting between forage and concentrates, iii) providing a balanced diet and iv) the possibility of mechanising the operation of TMR feeding (Schingoethe, 2017).

The hotspot for providing cows with a good TMR foresees high-quality feed, a good preparation practice, and, finally, managing the feeding bunk appropriately. TMR mechanisation is based on trailed mixer wagons or self-propelled loading mixer wagons; nowadays automation is catching on very fast in cow farming.

The scientific literature provides many studies on evaluating the TMR quality, mainly using the Penn State Particle Separator (PSPS). The PSPS is an instrument composed of three sieves (19 mm, 8 mm, 4 or 1.18 mm) and a bottom pan. Placing a sample of TMR on the top of the sieving structure, followed by applying a constant shake, results in information on the homogeneity of the ration (Heinrichs and Jones, 2022).

Moallem and Lifshitz (2020) compared using trailed and self-propelled mixing wagons to prepare TMR. The self-propelled wagon has more intensive chopping action than the trailer wagon, as the resulting TMR contained 2.9 % fewer long particles (>19 mm) and 3.3% more short particles (< 8 mm). Dairy cows' milk yields reflect such a difference in TMR homogeneity. Another study compares five typologies of mixing wagons: four trailed wagons and one self-propelled one. The self-propelled mixing wagon has achieved the best results, meeting the PSPS requirements; the other technologies have very large differences in results (Kowalik et al., 2018). Unfortunately, to our best knowledge, there isn't literature on the effect of TMR particle size on automatic feeding systems (AFS).

Good management of the feeding bunk is crucial to avoid the natural feed sorting behaviour of cows against long particles of TMR. This behaviour influences the TMR intake and reduces the nutritional supply across the day. When cows sort out the long forage, they end up consuming more concentrated feed, which can lead to changes in their milk composition and a decrease in pH levels (Miller-Cushon and DeVries, 2017). As well as chemical alterations, the activity

of sorting takes the availability of TMR away from cows making it necessary to push it back to the feed bunk (Barrett and Dahl, 2014). Such action is usually done more than 4 times a day manually or with the use of machinery, mechanical or automated (Romano et al., 2023).

Mechanical feed pushing machines operated by an operator may be trailed or self-propelled and outfitted with a reel of rakes or brushes. However, manual pushing of the feed only happens when operators are not occupied with other farming tasks and does not occur more than four times a day, commonly. The innovative technology is the automatic feed pushing performed by an Automatic Feed Pusher (AFP) or AFS (the latter when not distributing the ration).

AFPs play a crucial role in ensuring the availability of TMR in the feed bunk. Thanks to their automatic action, they can carry out this activity multiple times a day, providing numerous benefits to both cattle and farmers. (Barrett and Dahl, 2014). The agricultural feed pushers (AFPs) available on the market are all electrically powered and can be divided into two main categories: automatic guided and self-propelled feed pushers. The automatic guided feed pushers follow a track that provides them with energy and direction, while the self-propelled feed pushers follow a path determined by various technical solutions such as a sequence of magnetic strips placed within the paving material, proximal sensors, or lidar scanning of the environment. When automated, the feed-pushing activity can occur up to twelve times daily using AFPs and AFSs.

This study aims to evaluate the feed-sorting activity of cows with an evaluation of TMR leftovers given by PSPS instrument under different conditions of TMR distribution and following management of feeding through.

2. Materials and Methods

Between October 2021 and November 2022, TMR leftover sampling occurred on four dairy farms and one fattening bull farm in Northern Italy (Figure 1). TMR samples were collected before the distribution of fresh feed along the feeding bunk. The TMR leftovers underwent particle size analysis using the Penn State Particle Separator (PSPS) method (Heinrichs and Jones, 2022).

Figure 1. Farm localisation in northern Italy. Placemarks (from A to E) provide indication for farming sites' positions.

2.1 Description of the sampling sites' operativity

A brief description of the farms is hereafter reported based on the kind of feed-pushing activity:

- Automatic feeding system: two out of five cattle farms operated an automatic feeding system. *Farm "A"* (400 lactating cows) and *Farm "B"* (1100 fattening bulls) both operated a self-propelled and self-loading automatic feeding system (Vector, Lely, Maassluis, The Netherlands) with two 2 m^3 wagons with a vertical auger that provide for TMR preparation and distribution. Here, the system provides for leftovers pushing back because, when not delivering the feed, the AFS wagons act as drum-pushing systems.
- Operator based feed-pushing: occurred in two farms. *Farm "C"* hosts 1,300 lactating cows and uses three 24, 27 and 32 m^3 self-propelled cutter mixing wagons (Rover Jumbo Up 24, Italmix srl, Ghedi, BS, Italy; SelfLine 500+ and Selfline 100+, Siloking, Tittmoning, Germany) with vertical augers to prepare and distribute the TMR. For leftovers management, one operator runs a self-propelled feed pusher with 5 hydraulically controlled rotating

reels equipped with brushes (Motobrush, Storti S.p.A., Belfiore, VR, Italy). *Farm "D"* hosts 250 lactating cows. Here, TMR preparation and distribution occurs running a trailed 20 m^3 cutter mixing wagon with horizontal augers (Samurai5, Seko Industries Srl, Curtarolo, PD, Italy) while to push the feed back into the feedbunk, the operator runs a small tractor with a front-mounted rubber-coated metal mould.

- Automatic drum feed pushing: *Farm "E"*, hosting 300 lactating cows, operates an automatic drum feed pushing machine. In this site, TMR preparation and administration occurs running one self-propelled 20 m^3 cutter mixing wagon with a vertical auger (Dobermann SW 220 evo, Storti S.p.A., Belfiore, VR, Italy). TMR leftovers are then pushed back thanks to one automatic self-moving drum-pushing system (Ranger 2, Boumatic, Madison, WI, USA).

Farms operating mixing wagons fed the TMR twice daily, typically between 5:00 and 6:00 AM and 4:00 and 5:00 PM. In contrast, farms with AFS continuously fed TMR throughout the day, with frequencies up to twelve distributions. Figure 2 represents the different typologies of mechanical and automatic pushing utilized in the analysis. The loading sequence for farms using mixing wagons was long-stemmed hay requiring extended processing, grains or premixes, pre-processed forages (e.g. silages), minerals and vitamins, and finally, water and other liquid ingredients. Farmers relied on their experience to assess the mixing-chopping time required (when asked about it, their mixing-chopping times ranged between 10 and 12 minutes).

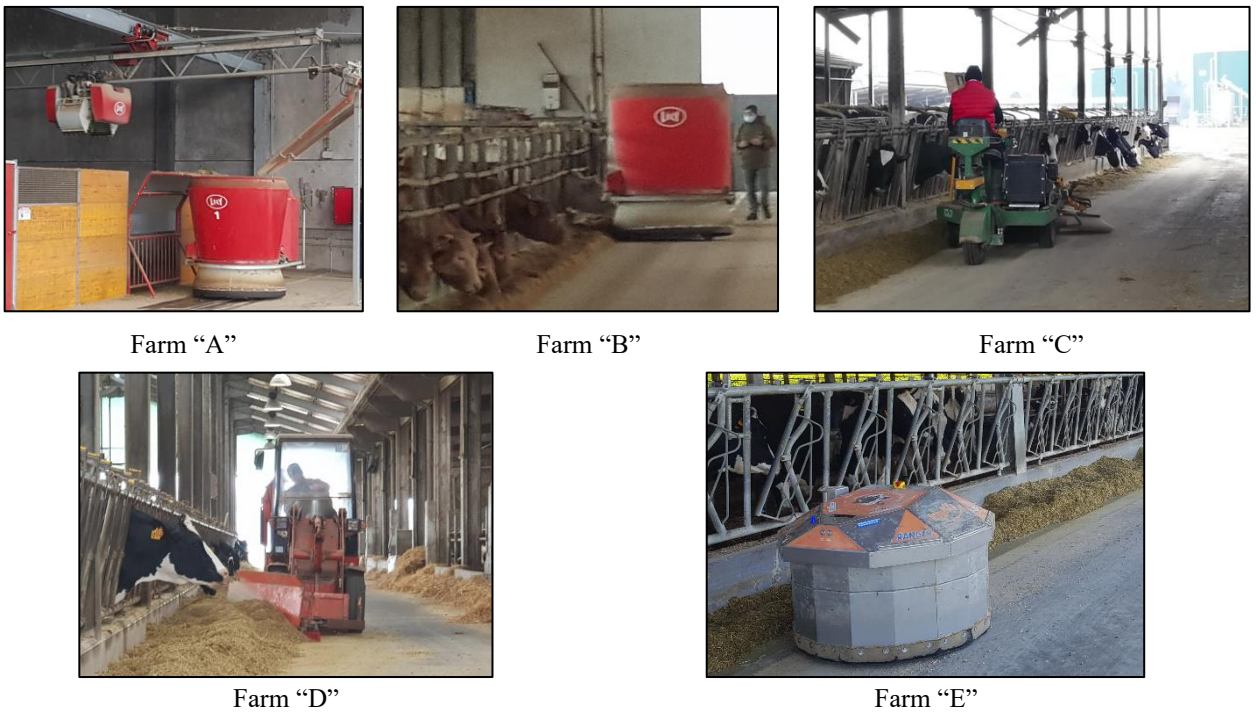

Farm "A" Farm "B" Farm "C"

Farm "D" Farm "E"

Figure 2. The feed-pushing machinery in the five farms under analysis: automatic feeding systems (Farm A, B), operator-based feed pushing (Farm C, D), automatic drum feed pushing (Farm E).

2.2 TMR leftovers sampling and analysis

The dry matter content and particle size distribution of fresh TMR in each farm were evaluated by sampling five representative TMR samples (500g each) immediately before fresh TMR delivery along the feed bunks every 5 meters. For each sample, a subsample of approximately 300g underwent particle size analysis on-site using a Penn State Particle Separator with screens of 19mm, 8mm, and 1.18 mm, following the manual shaking procedure outlined by Heinrichs (2013) to determine the particle size of the administered TMR. Particle size distribution (%) resulted from equation 1:

$$P_{i,j} = \frac{W_{i,j}}{\Sigma_{i=1}^{4} W_{i,j}} x\ 100 \qquad (1)$$

where Pi,j is the percentage weight of the particles that each separator screen retained and Wi,j is the amount of TMR fraction that the 19, 8, and 1.18 mm screens (i = 1, 2, and 3) and the bottom pan (i = 4) intercepted for each jth sampling site along the feed bunk (j = 1, 2, 3, 4 and 5).

2.3 Data processing

The data was analysed using Minitab 17 statistical software (Minitab Inc., 2010). First, the Levene test ($p < 0.05$) was used to check the equality of variances within the dataset, and the Kolmogorov-Smirnov test was used to assess the normality distribution of the data. Then, an analysis of variance (ANOVA) was conducted using the generalised linear model (GLM) multivariate procedure, followed by the Tukey post-hoc test ($p < 0.05$). The fixed factors considered in the study were the farms, PSPS screens (19, 8, and 1.18 mm, bottom pan, labelled S_1 to S_4), and the feed-pushing technology used. The dependent variable in the study was the weight percentage of TMR leftover sample that each separator screen retained (S_i).

3. Results and Discussion

Figure 3 reports the results of the GLM processing on the weight percentage distribution of the TMR leftovers particles. The processing pointed out that the farm was not a significant factor. However, the interaction between the PSPS screens and TMR feed pushing technology was significant. When pushing back the sorted TMR with the AFS and the conventional operator-based feed pushing machines, the 8 mm screen intercepted the highest quantity of particles. In contrast, using the automatic drum feed pusher resulted in the highest quantity of particles retained by the 19 mm screen, meaning that somehow the used machinery has an effect on the ration eaten by the animals (the pushing-up action of the AFS results in a leftover particle size like the operator-based one and contains a high percentage of particles higher than 8 mm, which provide evidence for increased feed sorting when using automatic feed pushers).

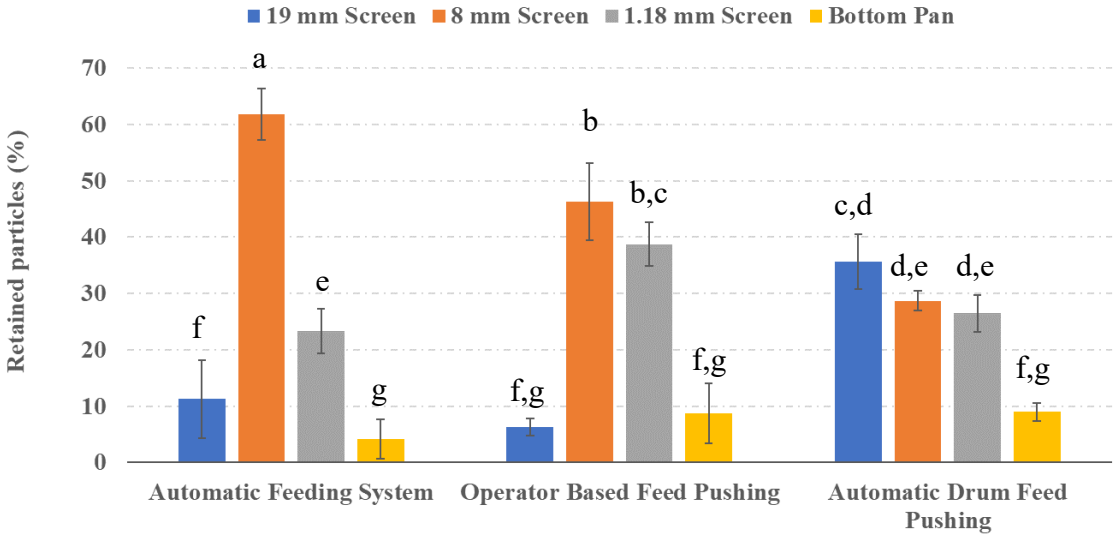

Figure 3. Weight per cent distribution of the TMR leftovers particles retained by the PSPS screens at varying TMR feed pushing technology. The means not sharing a letter differ significantly ($p<0.05$).

These results are in line with the study by DeVries et al. (2005) who found that increasing the feed delivery frequency reduced the feed-sorting activity of cows, especially when the ration was provided one to two times a day; no significant effects were restored when the TMR was delivered two to four times a day. Additionally, such findings partly agree with Endres and Espejo (2010). Their work, based on studying the feed delivery frequency of 50 herds in Minnesota, even though not directly addressing the feed sorting activity of cows, pointed out that feeding management practices could result in changes in TMR particle size over time (NDF content) and therefore implementing management changes (e.g., increasing feeding frequency to twice daily) could increase TMR consistency in time and, therefore, reduce the feed sorting activity of the animals. The same results were obtained by Sova et al. (2013) who pointed out a decrease in feed sorting in a twice-day TMR delivery compared to one a day.

Based on our current understanding, there is a need for studies that specifically examine how TMR pushing practices, such as conventional operator-based feed approach and automatic feed pushers, impact the feed sorting behaviour of cattle. Leonardi and Armentano (2007) observed that feeding groups of cows in a free-stall barn leads to a significant tendency to sort the feed, which is more pronounced than in cows individually fed in a tie-stall barn. As a result, there is still a need to refine specific feeding strategies involving TMR distribution and approach.

In the studied farm sites, operating an AFS resulted in small amounts of leftovers as animals tended to finish all the feed they were provided with. Therefore, the frequent TMR distribution rate (12 distributions daily in both the farms) allowed them to have fresh feed available many times during the day reducing their propensity to sorting, which explains the small per cent particle retention of the 19 mm screen. The same result occurred when pushing feed four times daily

as an operator-based farming task: in this case, the intervals between distributions were relatively long, so animals had fewer opportunities to selectively consume specific components of the ration. Feed sorting activity was not observed because the tendency of cows, in this case, was to consume the entire provided ration.

Concerning the particle size analysis of TMR leftovers resulting from using an automated drum feed pusher, the high percentage of long fibres retained by the 19 mm and 8 mm screens, results from the animal sorting activity against longer particles. In this farm, the sampling of the leftovers occurred early in the morning, just before the TMR administration and therefore the resulting particle size composition reflected accounts for the number of feed rapprochements that the machine had carried out. Despite this, the animal feed sorting against long fibres was considerable as if animals were not stimulated enough in consuming it. DeVries et al. (2003) and Oberschätzl-Kopp et al. (2016) observed that, albeit frequent feed push-ups with automatic machinery provide continuous access to feed deliveries, they do not have the same stimulating effect on feeding activity provoked by the delivery of fresh feed. It should be considered that such a reduced stimulating effect may represent a potential threat for the animals: their high-sorting activity influences the amount of physically effective NDF (peNDF), important for chewing activity, with a diminution of ruminal pH and impairment of liver health variables (Kröger et al., 2019).

4. Conclusions

The findings underscore the importance of considering the type of TMR feed-pushing technology used, as it can have a significant impact on the particle size distribution of leftovers, which, in turn, reflects the natural feed-sorting behavior of the animals.

Both the AFS and operator-based feed-pushing tasks produced similar results, with a small amount of TMR available in the feeding bunk at the time of sampling, indicating that the cows consumed all the TMR provided. However, when an automatic drum feed pusher with a thrust action that does not mix the TMR leftovers is used, a high proportion of long particles are discarded by the animals, suggesting that the sorting activity continues throughout the day.

To gain a better understanding of feed sorting throughout the day, future studies need to focus on the specific interaction between cattle and the machinery used.

Acknowledgements

The authors acknowledge the Regione Lombardia, Italy, for funding the research within the EIP-AGRI Operational Group project of the European Agricultural Fund for Rural Development (2014-2020).

Acknowledgements are also extended to the Department of Economics, Engineering, Society and Business Organization (DEIM) in cooperation with the Department of Agriculture and Forestry Sciences (DAFNE) of the University of Tuscia for this work carried out as part of the PhD in “Engineering for Energy and Environment – Biosystems and Environment”.

References

Barrett, K., B. Dahl, 2014. Automated feed pushers. Dairy BusinessEAST Pro-Dairy. 23–25. https://ecommons.cornell.edu/bitstream/handle/1813/37339/23.pdf?sequence=2

DeVries, T.J., M.A.G. von Keyserlingk, K.A. Beauchemin, 2003. Short Communication: Diurnal Feeding Pattern of Lactating Dairy Cows. Journal of Dairy Science. 86(12), 4079–4082. https://doi.org/10.3168/jds.S0022-0302(03)74020-X

DeVries, T.J., M.A.G. von Keyserlingk, K.A. Beauchemin, 2005. Frequency of Feed Delivery Affects the Behavior of Lactating Dairy Cows. Journal of Dairy Science. 88(10), 3553–3562. https://doi.org/10.3168/jds.S0022-0302(05)73040-X

Endres, M.I., L.A. Espejo, 2010. Feeding management and characteristics of rations for high-producing dairy cows in freestall herds. Journal of Dairy Science. 93(2), 822–829. https://doi.org/10.3168/jds.2008-2007

Heinrichs, J., C.M. Jones, 2022. Penn State Particle Separator. https://extension.psu.edu/penn-state-particle-separator

Kowalik, I., Z. Grześ, P. Rybacki, T. Michalski, 2018. A Comparison of Quality of Work of the Feed Mixer Wagons With Vertical and Horizonthal Mixing Systems. Journal of Research and Applications in Agricultural Engineering. 63(2), 124–128. https://bibliotekanauki.pl/articles/334937

Kröger, I., E. Humer, V. Neubauer, N. Reisinger, Q. Zebeli, 2019. Feeding Diets Moderate in Physically Effective Fibre Alters Eating and Feed Sorting Patterns without Improving Ruminal pH, but Impaired Liver Health in Dairy Cows. Animals. 9(4), 128. https://doi.org/10.3390/ani9040128

Leonardi, C., L.E. Armentano, 2007. Short communication: Feed selection by dairy cows fed individually in a tie-stall or as a group in a free-stall barn. Journal of Dairy Science. 90(5), 2386–2389. https://doi.org/10.3168/jds.2006-537

Miller-Cushon, E.K., T.J. DeVries, 2017. Feed sorting in dairy cattle: Causes, consequences, and management. Journal of Dairy Science. 100(5), 4172–4183. https://doi.org/10.3168/jds.2016-11983

Minitab Inc., 2010. Minitab 17 Statistical Software [computer program]. https://www.minitab.com

Moallem, U., L. Lifshitz, 2020. Accuracy and homogeneity of total mixed rations processed through trailer mixer or self-propelled mixer, and effects on the yields of high-yielding dairy cows. Animal Feed Science and Technology. 270, 114708. https://doi.org/10.1016/j.anifeedsci.2020.114708

Oberschätzl-Kopp, R., B. Haidn, R. Peis, K. Reiter, H. Bernhardt, 2016. Untersuchungen zum Verhalten von Milchkühen bei automatischer Fütterung in einem AMS-Betrieb (Studies on dairy cow behaviour with automatic feeding in a herd milked by an AMS). Landtechnik. 71(2), 55–65. https://doi.org/10.15150/lt.2016.3122

Romano, E., M. Brambilla, M. Cutini, S. Giovinazzo, A. Lazzari, A. Calcante, F.M. Tangorra, P. Rossi, A. Motta, C. Bisaglia, A. Bragaglio, 2023. Increased Cattle Feeding Precision from Automatic Feeding Systems: Considerations on Technology Spread and Farm Level Perceived Advantages in Italy. Animals. 13(21), 3382. https://doi.org/10.3390/ani13213382

Schingoethe, D.J. 2017. A 100-Year Review: Total mixed ration feeding of dairy cows. Journal of Dairy Science. 100(12), 10143–10150. https://doi.org/10.3168/jds.2017-12967

Sova, A.D., S.J. LeBlanc, B.W. McBride, T.J. DeVries, 2013. Associations between herd-level feeding management practices, feed sorting, and milk production in freestall dairy farms. Journal of Dairy Science. 96(7), 4759–4770. https://doi.org/10.3168/jds.2013-6679

Harvesting date influence on multi-trunk traditional olive productivity in next years

Francisco J. Soto-Torres[a], Gregorio L. Blanco-Roldán[a], Sergio Peña-Valero[a, b], Francisco J. Castillo-Ruiz[a].

[a] Departamento de Ingeniería Rural, Construcciones Civiles y Proyectos de Ingeniería, G. I. AGR-126 Mecanización y Tecnología Rural, E.T.S. de Ingeniería Agronómica y de Montes, Universidad de Córdoba, Campus de Rabanales, Edificio Leonardo Da Vinci, E-14071 Córdoba, España.

[b] Construcciones Mecánicas Alcay S. L. Calle Barbastro sn., E-22310, Castejón del Puente (Huesca).

* Corresponding author. Email: castillo-ruiz@uco.es

Abstract

Olive (Olea europaea L.) was mainly distributed within the Mediterranean basin, being Spain the main producer with 2.77 million hectares. Modern olive orchards require high technology control systems to optimize agronomical behavior, and mechanized processes to keep costs under control. Harvesting requires the highest amount of labor hours for both, machines and workforce, thus, optimize harvesting date and resources required was highly important in areas in which olive supposes a monoculture. The aim of this research was to determine if harvesting date influence next year production of fruit or olive oil. For this purpose, production data of several orchards from two different farmers located in Jaén Province, southeastern Spain, were gathered. All data was obtained from multi-trunk traditional olive orchards, which have the highest requirements in terms of labor and machine work to be harvested. Harvesting date was considered as the date in which fruit was delivered to the olive mill. Dates were transformed into day of the year (DOY) and modified DOY which zero value was considered as 1st November. Harvesting dates for fruit harvested from the soil were not considered because it did not affect next year production. Fruit, oil and oil yield were analyzed to determine if olive productivity was affected by previous harvesting dates. Optimal harvesting data will help to plan labor and machine resources to maximize obtained olive oil in terms of quantity and quality. Harvesting date influence on olive oil quality was already demonstrated, but the present research provided new evidence to encourage farmers from some areas of southern Spain to came early harvesting.

Keywords: time of harvest, olive yield, on year yield, off year yield, delay costs.

1. Introduction

The olive tree (Olea europea L.) is a fundamental crop in the Mediterranean area, especially in Spain, the world's largest producer and exporter of olive oil (IOC, 2021). It extends for 3,800 km from east to west in the Mediterranean basin and has a great adaptation to the Mediterranean climate, being resistant to drought and frost (Arenas-Castro et al., 2020). In addition to its expanse, the olive tree has a great historical and cultural importance influencing economic and social aspects (Ojeda-Rivera et al., 2018). In Spain, olive groves cover 2.78 million hectares, a quarter of the world's woody crop area (ESYRCE, 2023) Andalusia is the region with the largest olive grove area globally, with 1,638,320 hectares in 2021, representing 60.1% of the national area, 32.8% of the EU area and 14.2% worldwide. Most of the Andalusian olive grove is destined to olive oil production, while a small part is dedicated to table olive production (CAPDR, 2023).

Although the olive grove is the most common permanent crop in the world. its expansion continues. especially between 30º and 45º latitude in both hemispheres (Oteros, 2014; Hernández, 2018). Despite this, most of the world's olive oil production remains concentrated in the Mediterranean basin, with the European Union as the main producer. As for the area of traditional mechanizable and intensive olive groves in Spain, according to AEMO 2023, they are 1,106,632 ha and 713,163 ha respectively. Most of the traditional olive grove is characterized by having several rootstocks, wide plantation frames and densities from 100 to 150 trees ha^{-1}, with variable yields depending on the cultivation system and water availability.

High density olive orchard used to be single trunk trained with 200 to 800 trees ha^{-1}, while super high density hedgerow orchards were planted at 800 to 2,500 trees ha^{-1} (generally with irrigation and high unit productions). Field observation has shown that extending the distances between trees and rows improves sunshine and solar radiation capture, increasing the fat yield in olives and reducing crop management costs (Todolivo. n.d.).

In contrast, traditional olive groves are gradually losing importance, from about 600,000 hectares in 2001 to about 420,000 hectares at present, being replaced by higher density types of olive groves (CAPDR, 2002). The high cultivation costs of traditional olive groves make them less competitive than the new intensive and super high-density orchards, which benefit from mechanization to optimize production (CAPDR, 2023).

Olive oil production costs varied from 1.49 to 10.03 € kg^{-1} olive oil in general oscillating from 4.48 to 6.98 € kg^{-1} for traditional olive orchard suitable for mechanization, considering effects of inflation and drought (AEMO, 2023). Other source reported different costs for non-mechanized rainfed olive orchards it is around 3-4.5 € kg^{-1} and 1.5-2 € kg^{-1} of oil for high-density irrigated olive orchards (CAPDR, 2023). Overall production costs have increased significantly between the 2012/13 and 2021/22 seasons, with harvesting being the most important expense, highlighting the importance of mechanization for farm profitability (AEMO, 2023).

Detailed knowledge of the agronomic and technological characteristics of olive varieties is crucial to predict their performance in different growing areas and to optimize the profitability of new plantations (Barranco et al., 2005). In new high-density olive plantations, planting density and irrigation can bring forward the entry into production, seeking to maximize profitability (Todolivo. n.d.). Olive trees have a marked tendency to alternate between productive and non-productive years (Sola-Guirado et al., 2017). Olive orchard production is strongly influenced by several factors related to its management. The proper selection of varieties adapted to the local climate and soil together with soil management practices such as fertilization, irrigation, and pruning, are critical for success in obtaining productive olive trees. The implementation of sustainable cultivation techniques and integrated pest and disease management are essential to improve long-term productivity (Fernández Escobar et al., 2013).

Climate change is bringing in advace the optimal harvest time of olive trees by several weeks (Lorite et al., 2018; Benloch-González et al., 2019). This situation could motivate growers to bring forward harvesting, as they currently only perceive improvements in oil quality, although they face difficulties due to higher fruit holding strength (Dag et al., 2011; Castillo-Ruiz et al., 2018). In a context of below average olive oil yields, optimizing production is essential to mitigate current high prices (Castillo-Ruiz, 2023). Fat yield over wet matter, which usually increases during fruit ripening, is crucial for the producer (Lavee and Wodner. 1991, 2004; Salvador et al., 2001). Another important factor for profitability is harvesting, which represents up to 40 % of costs per hectare in traditional systems (AEMO, 2023). In addition to profitability, the quality of the olive oil obtained is also a key factor; a healthy and minimally damaged product is fundamental to obtain high quality oil (García. 1994; Garcia et al., 1996; Garcia and Yousfi, 2006; Fregapane and Salvador, 2013). However, too early harvesting can produce oils with excessive concentrations of polyphenols, resulting organoleptically unacceptable.

Harvesting technology significantly affects both oil quality and associated costs (Saglam et al., 2014) although all available harvesting technologies make possible to detach the fruit with different vibration patterns (Sola-Guirado et al., 2014). It is important to start harvesting when all the oil is formed in the fruit to obtain maximum quality (García-Ortiz Civantos, 2003). Harvesting is not only costly, but also crucial for annual production and oil quality (Rallo, 2009). Harvesting criteria should consider both efficiency and oil quality (López-Villalta, 1996). In addition, olives damaged during harvesting can deteriorate rapidly, negatively affecting oil quality (Garcia and Yousfi, 2006).

2. Materials and Methods

Olive harvesting data from two different olive growers were collected from different harvesting seasons. These data included harvested fruit per harvesting date, olive oil yield and plot. These data were gathered and classified to be analyzed. All plots were in two different locations of southeast Spain which olive mill

was located in N 38°19'53.65" O 3°15'26.06" and N 37°32'38.94" O 3°56'24.29"

The data collection process for the study involves obtaining olive harvest data from several seasons. Farmer 1 data were extracted from the website of olive mill "Ntra. Sra. del Pilar", based in Villacarrillo (Jaén, Spain), selecting information from the 2020/2021 season to the most recent 2023/2024 season. Farmer 2 data were obtained from olive mill "San José", based in Castillo de Locubín (Jaén, Spain). Gathered data include several important values for the study:

Date: Indicates the day on which the entry of fruit in the mill was recorded, which coincided with harvesting data to ensure olive oil quality.
Origin: Information that distinguishes whether the olive comes from the ground or directly from the tree.
Fruit weight: Quantity of olives harvested on the specified date.
Oil yield: Percentage of oil contained per kg of olives.
Plot: Identification of the specific location from which the olives were harvested.

Once these data are collected, they are organized in a first daily database. The database consists of 10 variables (Table 1).

Table 1. Example of the daily database.

Date	DOY	DOY modified	Fruit weight (kg)	Oil yield	Oil weight (kg)	Origin	Plot	Season	Farmer
03/12/2011	337	32	846	20.75	175.54	1	1	1112	2
20/01/18	20	80	607	31.54	191.44	1	7	1718	2
12/01/2022	12	72	16,940	24.73	4,189.26	1	18	2122	1
…	…	…	…	…	…	…	…	…	…

Date: Corresponds to the day of entry of the olive.

DOY (Day of the Year): Indicates the day of the year on which the olives were harvested. It is calculated from the date of entry and it could varied from 1 (1st of January) to 365 or 366 (31st of December) (1).

DOY= Number of days elapsed from the beginning of the year to the given date (1).

Modified DOY: The DOY value is adjusted to consider November 1 as the first day of the year in the study. This calculation assumes that harvesting always start after 1st of November, and then, DOY for harvesting dates varied from a lower to a higher number (2).

If DOY > 305 modified DOY = DOY-305 (2)

If DOY < 305 modified DOY = DOY+60 (2)

Fruit weight: Quantity of olives harvested on the corresponding date.

Oil yield: Percentage of weight of olive oil obtained per unit of weight of fruit.

Oil weight: Quantity of oil obtained from the olives harvested (3).

$$\boldsymbol{Oil\ weight} = \frac{\boldsymbol{Kg\ olives} * \boldsymbol{Yield}}{\mathbf{100}} \qquad (\mathbf{3})$$

Origin: A number is used to indicate whether the olive comes from the tree (1) or from the ground (2).

Plot: Identification of the plot from which the fruit was harvested, classified by correlative numbers.

Season: Indicates the season to which the olive entry belongs. It will be expressed using a four-digit format, for example, the season 1112 will correspond to 2011-2012 and so on with each one.

Farmer: Identification of the farmer from whom the data was collected.

A second database will be created with annualized data (Table 2) per plot calculated from the daily database. The variables related to fruit or oil production are calculated as the sum for each plot divided by the area of each plot, while the DOY and mean yield variables are calculated as weighted averages (4 and 5). It is important to indicate that we include the average DOY for each year, and the DOY of the previous year, in order to calculate the harvest date influences the amount of crop harvested the following year.

$$\boldsymbol{Yearly\ oil\ yield} = \frac{\sum_{i=1}^{n}(\boldsymbol{Fruit\ production_i} * \boldsymbol{Oil\ yield_i})}{\sum_{i=1}^{n}(\boldsymbol{Fruit\ production_i})} \qquad (\mathbf{4})$$

$$\boldsymbol{Modified\ DOY} = \frac{\sum_{i=1}^{n}(\boldsymbol{Fruit\ production_i} * \boldsymbol{Modified\ DOY_i})}{\sum_{i=1}^{n}(\boldsymbol{Fruit\ production_i})} \qquad (\mathbf{5})$$

Table 2. Example of an annualized database.

Plot	Season	Fruit weight (kg)	Fruit production (kg ha^{-1})	Yearly oil yield (%)	Oil production (kg ha^{-1})	DOY mod	Previous DOY
1	1213	1.236.74	624.62	17.01	125.74	42.72	69.67
5	1819	5.462	6206.82	22.90	1.421.36	90.7	85.65
13	2324	253.615	6549.97	18.59		41.47	40.96
…	…	…	…	…	…	…	…

For statistical analysis, the SPSS software (Armonk. NY: IBM Corp.) was used.

3. Results and Discussion

First, the average data of fruit and oil production as well as the previous weighted average DOY by season and plot are obtained. A first step is to visualize the data by season for fruit production, olive oil and harvest date (Table 3). There are seasons for which data are missing because they were not available from the farmers.

Table 3. Results of fruit production, olive oil and harvest date for the different plots and seasons analysed.

Season	11/12			12/13			13/14		
Plot	**Fruit production (kg ha^{-1})**	**Oil production (kg ha^{-1})**	**Previous DOY**	**Fruit production (kg ha^{-1})**	**Oil production (kg ha^{-1})**	**Previous DOY**	**Fruit production (kg ha^{-1})**	**Oil production (kg ha^{-1})**	**Previous DOY**
1	6422.2	1528.5		624.6	125.7	69.7	5281.3	1183.0	42.7
2	5988.4	1291.7		965.2	225.2	60.7	2502.7	540.1	48.7
3	10294.4	2102.1		1151.5	228.7	34.3	10432.9	1872.7	33.0
4	11328.4	2821.9		3672.0	915.4	70.8	7037.3	1696.0	56.4
5	3647.7	764.6		727.0	149.9	78.4	3479.5	634.3	80.5
6	6925.9	1604.7		4903.4	1170.0	72.6	1374.1	357.8	56.7
7	8130.7	1941.6		3827.3	944.2	85.3	2624.5	640.9	68.2
8	7027.0	2017.5		5785.0	1246.7	102.0			
9	6321.2	1271.2		469.8		42.9	6068.6	1489.2	60.0
10	6161.0	1394.8		1144.3		63.2	8037.2	1748.1	60.0
11									

12	1260.8	396.6		542.4	135.1	109.4			
		14/15			**15/16**			**16/17**	
1							5020.2	1152.1	
2							4429.5	1080.3	
3							10471.9	2091.2	
4							7585.3	2069.3	
5							5811.4	1203.0	
6							11124.1	2487.4	
7							9444.0	2182.5	
8							5260.1	1323.5	
9	1415.3		43.7	4616.9		120.4	4665.3	931.3	32.0
10	2096.0		85.5	4272.4		56.0	7278.6	1408.1	39.2
11									
12							1335.1	362.2	
		17/18			**18/19**			**20/21**	
1	277.3	50.5	80.1	7211.6	1580.1	67.4			
2	2864.3	711.5	60.6	4542.0	1075.1	52.9			
3	8541.1	1737.3	50.0	13225.1	2064.4	36.4			
4	5954.9	1551.3	59.6	8668.6	2126.4	59.7			
5	2253.4	529.6	126.5	6206.8	1421.4	85.6			
6	6572.4	1614.8	68.2	11291.4	2343.0	89.7			
7	2616.2	672.4	81.7	11495.9	2638.3	75.9			
8	4638.5	1147.6	106.6	9756.8	2243.1	102.3			
9									
10									
11	2011.6	455.6		5327.2	1162.9	66.9			
12				843.5	178.2				
13							9428.7	1827.3	
14							10811.7	2160.2	
15							7905.0	2215.0	
16							6426.2	1788.4	
17							10473.1	2368.0	
18							11674.4	2582.4	
		21/22			**22/23**			**23/24**	
1	4986.9	848.3		.0	.0	60.6	49.0	9.6	.0
2	5449.1	1010.3		1371.4	297.1	32.0	230.4	45.7	52.8
3	7735.9	1303.5		14311.7	2636.2	17.5	3095.2	444.8	48.0
4	10287.3	2420.6		1643.1	458.9	48.8	421.6	89.5	41.3
5	6184.2	955.5		1171.6	152.9	81.1	84.1	17.0	78.3
6	10244.8	2226.2		1256.9	290.5	73.1	606.9	130.4	56.7
7	9124.5	1876.0		527.0	99.0	74.6	414.9	94.1	74.0
8	6853.0	1500.1		962.8	179.2	88.2	675.7	136.7	83.0
9									
10									
11	7530.9	1247.1		2271.4	382.1	71.1	1307.5	249.9	64.2
12									
13	8252.8	1789.2	39.5	3091.4	676.4	41.0	6550.0	1217.6	41.5
14	8461.3	1772.6	40.2	4723.4	971.6	42.3	7491.7	1401.0	35.1
15	9649.7	2248.4	90.8	1400.0	338.9	58.6	9781.7	1829.2	66.6
16	8941.1	2288.9	90.2	3433.1	850.7	76.0	8697.7	1937.0	87.5
17	8299.2	2000.1	82.7	5040.1	1202.6	54.2	4965.9	1075.6	71.6
18	11178.4	2882.9	55.3	6282.8	1279.2	80.3	11702.8	2419.0	33.2

Fruit and olive oil production did not significantly correlate with harvesting date in the previous year while there was a significant correlation between harvesting date in the current and the previous year (Table 4). This fact indicated that the farmers used to harvest their plots in a very similar order between years, which could also interact with the hypothesis of fruit or oil production was correlated with harvesting date in the previous year.

(Table 4). Correlation for all plots and seasons with data between fruit production, olive oil and harvest date of the previous year which is always represented as DOY modified.

Variable 1	Variable 2	Correlación Pearson	Sig.
Fruit production (kg ha^{-1})	**Harvesting date previous year**	-0.100	0.381
Oil production (kg ha^{-1})	**Harvesting date previous year**	-0.046	0.701
Harvesting date in the current year	**Harvesting date previous year**	0.362	0.001

The hypothesis of this research was not validated, this may be due to different causes such as the fact that early harvesting of the same plots always distorts the data. The results may also be influenced by climate change and the drought that has severely affected olive production in the last two seasons (2022/23 and 2023/24), considering that drought affect olive photosynthetic activity, generates oxidative stress and imbalance in plant nutrition (Brito et al., 2019). Furthermore, climate change has come early several weeks optimal olive harvesting date (Lorite et al., 2018 and Benloch-González et al., 2019) which could lead to different requirements to keep high olive oil quality, mainly in harvesting machinery effective field capacity, which should be increased to avoid fruit falling to soil reducing olive oil quality and hindering harvesting.

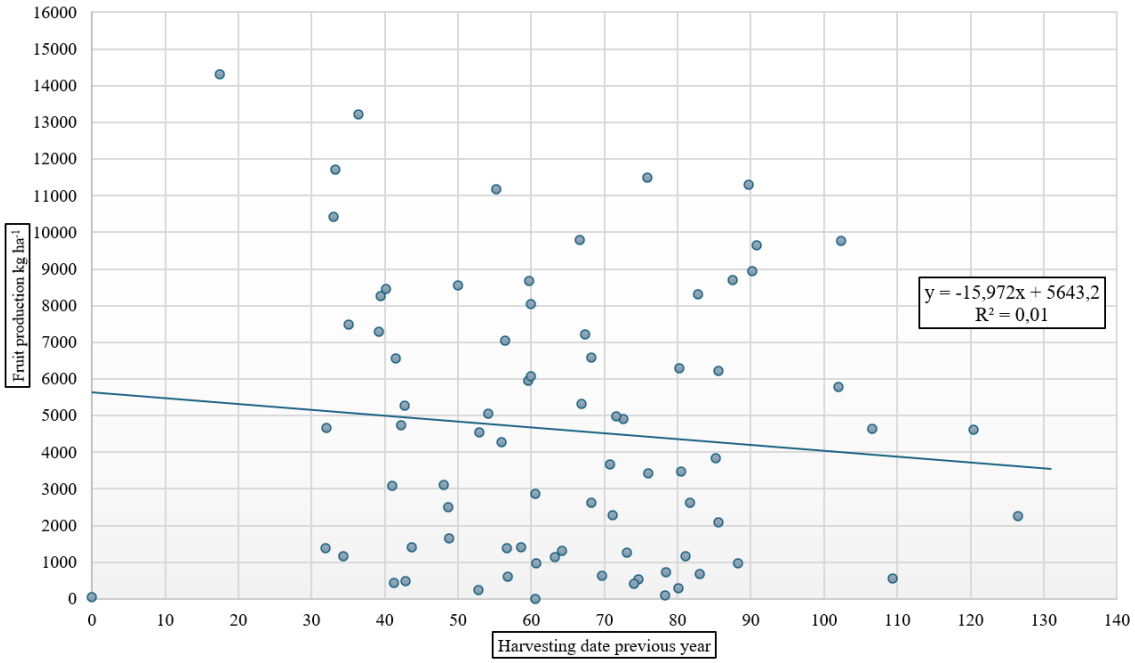

Figure 1: Regression between fruit production (kg ha^{-1}) and harvest date of previous season.

4. Conclusions

No significant relationship between fruit or oil production and the harvest date of the previous year was found with the data analysed, although this fact was considered true by many farmers and technicians. These findings imply that, under the conditions and data set analysed, there is insufficient evidence to establish significant relationships between fruit and oil production and harvesting date in the previous year. It is possible that other factors not considered in this analysis may influence the variables studied, or that a larger sample size or a different study design may be required to find significant relationships. The absence of this relationship could be due to interactions with other variables such as plot production potential, climate conditions, farmer practices or even interactions between these variables. Further research was needed to clarify these points.

References

AEMO, 2023. Asociación Española de Municipios del Olivo. Aproximación a los costes del cultivo del olivo. https://www.aemo.es/slides/slide/estudio-aemo-de-costes-cultivo-olivo-2023-266/download
Arenas-Castro, S., Gonçalves, J. F., Moreno, M., Villar, R. 2020. Projected climate changes are expected to decrease the suitability and production of olive varieties in southern Spain. Science of The Total Environment, 709, 136161.
Barranco D, Trujillo I and Rallo L. 2005 Elaiografía hispánica, in Variedades de olivo en España, ed. by Barranco D, Caballero JM, Del Río C, Martín A, Tous J and Trujillo I. Junta de Andalucía, MAPA and Mundi Prensa, Madrid, pp. 46–231.
Benlloch-González, M., Sánchez-Lucas, R., Bejaoui, M. A., Benlloch, M., Fernández-Escobar, R. 2019. Global warming effects on yield and fruit maturation of olive trees growing under field conditions. Scientia horticulturae, 249, 162-167.Brito, C., Dinis, L. T., Moutinho-Pereira, J., & Correia, C. M. 2019. Drought stress effects and olive tree acclimation under a changing climate. Plants, 8(7), 232.
Castillo-Ruiz, F. J., Tombesi, S., & Farinelli, D. 2018. Olive fruit detachment force against pulling and torsional stress. Spanish Journal of Agricultural Research, 16(1), e0202-e0202.
Castillo-Ruiz. 2023. ¿Me están robando al comprar aceite de oliva? Último acceso: 05/02/2024. Disponible en: https://ellibre.es/me-estan-robando-al-comprar-aceite-de-oliva/
CAPDR, 2023. Consejería de Agricultura, Pesca, Agua y Desarrollo Rural. Junta de Andalucía. Primera estrategia andaluza para el sector del olivar 2023-2027.
Dag, A., Kerem, Z., Yogev, N., Zipori, I., Lavee, S., Ben-David, E. 2011. Influence of time of harvest and maturity index on olive oil yield and quality. Scientia Horticulturae, 127(3), 358-366.
ESYRCE. 2023. Encuesta sobre superficies y rendimientos de cultivos. Ministerio de Agricultura, Pesca y Alimentación. Disponible en: https://www.mapa.gob.es/es/estadistica/temas/estadisticas-agrarias/agricultura/esyrce/
ESPINOLA LOZANO, F. 1996 Cambios tecnológicos en la extracción del aceite de oliva virgen. Alimentación, equipos y Tecnología 51-56.
Fernández Escobar, R., & Guerrero, M. 2013. Olive Growing (Vol. 2). Mundi-Prensa Libros.
Fregapane, G.; Salvador, M.D. Production of superior quality extra virgin olive oil modulating the content and profile of its minor components. Food Research International 2013, 54, 1907- 1914.
Garcia-Ortíz Civantos, C. La recolección de la aceituna y su influencia en la calidad del aceite. January 2003. Instituto de investigación y formación agraria y pesquera.
García, J.M., Gutiérrez, F., Castellano, J.M., Perdiguero, S., Morilla, A., Albi, M.A., 1996. Storage of Olives destined for oil extraction. Acta Horticulturae, 368, 673-681.
García, J.M., Gutiérrez, F., Barrera, M.J., Albi, M.A., 1996. Storage of Mill Olives on an Industrial Scale. Journal of Agricultural and Food Chemistry, 44, 590–593.
García, J.M., Yousfi, K., 2006. The postharvest of mill olives. Grasas y Aceites, 57, 16-24.
Hernández, J. V. 2018. La olivicultura internacional. Agricultura: Revista agropecuaria y ganadera, (1022), 42-45.
COI, 2021. International Olive Council. Organización intergubernamental en el mundo que congrega a las partes interesadas en la producción y el consumo tanto de aceite de oliva como de aceitunas de

mesa. Disponible en: https://www.internationaloliveoil.org/what-we-do/economic-affairs-promotionunit
Lavee, S., Wodner, M., 1991. Factors affecting the nature of oil accumulation in fruit of olive. J. Hort. Sci., 66, pp. 583-591.
Lavee, S., Wodner, M.,2004. The effect of yield, harvest time and fruit size on the oil content in fruits of irrigated olive trees (Olea europaea), cvs Barnea and Manzanillo. Sci. Hort., 99 (3–4), pp. 267-277.
Lorite, I.J.; Gabaldón-Leal, C.; Ruiz-Ramos, M.; Belaj, A.; de la Rosa, R.; León, L.; Santos, C., 2018. Evaluation of olive response and adaptation strategies to climate change under semi-arid conditions. Agricultural Water Management, 204, 247–261.
L. Rallo., 2009. Iberian olive growing in a time of change. Chronica Hort., 49, pp. 15-17
M.D. Salvador, F. Aranda, G. Fregapane., 2001. Influence of fruit ripening on Cornicabra virgin olive oil quality. A study of four successive crop seasons. Food Chem., 73, pp. 45-53.
Ojeda-Rivera, J. F., Andreu-Lara, C., Infante-Amate, J., 2018. Razones y recelos de un reconocimiento patrimonial: los paisajes del olivar andaluz. Boletín De La Asociación De Geógrafos Españoles, (79).
Oteros, J., 2014. Modelización del ciclo fenológico reproductor del olivo (Olea europaea L.) (Doctoral dissertation). Universidad de Córdoba. España.
Sola-Guirado, R. R., Castro-García, S., Blanco-Roldán, G. L., Jiménez-Jiménez, F., Castillo-Ruiz, F. J., & Gil-Ribes, J. A., 2014. Traditional olive tree response to oil olive harvesting technologies. Biosystems Engineering, 118, 186-193.
Sola-Guirado, R. R., Castillo-Ruiz, F. J., Jiménez-Jiménez, F., Blanco-Roldan, G. L., Castro-Garcia, S., Gil-Ribes, J. A., 2017. Olive actual “on year” yield forecast tool based on the tree canopy geometry using UAS imagery. Sensors, 17(8), 1743.
Saglam C., Tuna Y.T., Gecgel U., Atar E.S., 2014. Effects of olive harvesting methods on oil quality. APCBEE Procedia, 8: 334–342.
Todolivo. s.f. Disponible en: https://www.todolivo.com/olivar-en-seto/los-nuevos-marcos-de-plantacion/

Hitched two sides windrowing and chipping prototype development for olive pruning management in an only tractor wipe

Sergio Peña-Valero[a, b], Francisco J. Castillo-Ruiz[a], Francisco J. Soto-Torres[a], Gregorio L. Blanco-Roldán[a].

[a] Departamento de Ingeniería Rural, Construcciones Civiles y Proyectos de Ingeniería, G. I. AGR-126 Mecanización y Tecnología Rural, E.T.S. de Ingeniería Agronómica y de Montes, Universidad de Córdoba, Campus de Rabanales, Edificio Leonardo Da Vinci, E-14014 Córdoba, España.

[b] Serrat Trituradoras®. Construcciones Mecánicas Alcay S. L. Ctra. N-240, km 149,3, E-22310, Castejón del Puente (Huesca).

* Corresponding author. Email: castillo-ruiz@uco.es

Abstract

Pruning is essential to keep olive (Olea europaea L.) in adequate conditions for both keep high olive production capacity, and adapt canopy volume, and shape to different harvesting systems. On this matter, there are different olive categories which could be simplified to three: Traditional olive orchards; high density olive orchards adapted to trunk shaker harvesting; and hedgerow orchards adapted to straddle canopy shakers. All these olive orchards require pruning, windrowing, and chipping or shredding operations to keep olive orchards in adequate condition. Currently, the most common practices were pruning using handheld chainsaws, windrowing manually, or using tractor hitched rotary vertical shaft windrowers, and tractor hitched auto feed shredders. All these operations were performed in different wipes which makes the orchard not available for other operations between pruning and chipping. The objective of this research was to develop a tractor hitched windrowing and chipping prototype for olive pruning management in an only tractor wipe to improve orchard availability and attempt to reduce pruning management costs. The prototype was developed, tested, and redesigned to achieve an adequate windrowing efficiency. The prototype consisted of two side windrowers, bottom and upper feeders, vertical and horizontal rollers as compression system, and disk blade mounted chipper. The rollers of the compression system included an automatic adjustment system that regulated rotary speed which made possible to adapt the fed amount of pruning to chip according to tractor engine load. This feature made possible to avoid chipper block or tractor overload when idle time was reduced as much as possible depending on available pruning amount. The prototype was designed to be adapted to all olive orchard categories except those which rows spacing were under 5 m. Furthermore, once the pruning residues were chipped, it is possible to lend them to cover soil or harvest them through a vacuum system to use as biomass. Final prototype theoretical weight and dimensions were 4,500 kg and 4.9 x 2.2 x 3.32 m (width, height, and length). These features made the prototype heavier and wider than conventional shredders which varied from 1000 to 2500 kg, and 1,5 to 2,4 m. However, these features reduced labour requirements up to 81,8 % respect to manual windrowing and subsequent shredding.

Keywords: shredding, chopping, soil cover, biomass harvesting, pruning residues.

1. Introduction

Olive is one of the most important woody crops in the world having 11.6 Mha distributed in 66 different countries (Vilar, 2023). Spain is the largest olive grower in the world with 2,8 Mha of which 88 % were olives for oil and 69 % were rainfed (ESYRCE, 2023). Olive growing required different essential labours such as weeding, fertilizing, spraying, pruning, and harvesting, of these labours at least weeding, pruning, and harvesting should be carried out annually to keep the crop in adequate condition. The risk of abandonment affects a great olive orchards surface, mainly of those plots non suitable for mechanization, which was estimated in 5,5 Mha in the world (ASOLITE, 2021).

Pruning was a key labour for olives, but it produced an important amount of pruning residues which can varied from 10 to 60 kg tree^{-1} (700 to 4,800 kg ha^{-1}) in a multi trunk traditional olive orchard (Castillo-Ruiz et al., 2017). To manage this volume of residues, they could be burnt which is highly inadvisable except in case of risk of *Verticilium dahliae* or other pathogens spreading (Michalopoulos et al., 2020). Other optionse were left chipped residues on the soil as a mulching protection, organic matter addition and to increase soil

moisture (Taguas et al., 2021) or harvested for energetic purposes, although a minimum amount of residues is required to be economically feasible having into account that this material has around 12,2 MJ/kg Lower Heating Value (LHV) (Kougioumtzis et al., 2022) depending on the moisture.

Currently, available hand labour is scarce in Spain (Banco de España, 2024), as take place in many other countries, especially for agriculture purposes. This fact led farmers to mechanize all labours as much as possible to reduce hand labour requirements and to improve productivity and competitiveness. In this context, a Pre-Commercial Procurement project (European Commission, n.d.) was developed by University of Cordoba within Serrat mulchers participated to develop an olive pruning residues windrower, chipper, and harvester. This prototype could perform the three tasks in an only wipe to reduce hand and tractor labour requirements and to make easier olive pruning residues management shorting the time in which the orchard is not available from pruning to chipping.

The prototype should be suitable for work at least in traditional and high-density olive orchards (BASF, n.d.) Firstly, traditional olive orchards used to be around 100 trees ha^{-1} sometimes irregular spacing and multi-trunk trained. Secondly, high-density olive orchards were between 200 and 800 trees ha^{-1} single trunk trained vase-shaped to facilitate harvesting with trunk shakers that could include a reverse umbrella as a catching frame. Finally, super high-density olive orchards used to be planted at 800 to 2.500 trees ha^{-1} setting a hedge to be mechanically harvested using straddle canopy shakers, and sometimes they are also mechanically pruned which used to provide much smaller residues than traditional or high-density olive trees.

The objective of this research was to develop a machine that could windrow and chip or shred olive pruning residues in an only wipe. This machine could leave the chipped residues on the soil or alternatively could harvest them.

2. Materials and Methods

The first step was to define the requirements that should be achieved by the prototype, which was included in the technical request by the University of Córdoba which previously gathered data from farmers, agricultural machinery builders and other actors in the olive sector. Additionally, 12 deliverables schedule was also defined along 44 months to establish a time development for the project to avoid delays that could affect the result. The process was competitive with 3 main phases: Exploratory phase or market inquiring, Initial 3D designs, and prototype development, building and testing. Along these phases, up to 6 different machinery developers participated, although finally, only 2 of them built a final prototype.

The prototype should accomplish different requirements that were initially defined according to marketing inquiring phase:

- The prototype should windrow pruning residues before chip or shred them. It was desirable that the prototype could chip or shred trunks up to 70 mm diameter.
- The prototype could distribute the chipped residues in a homogenous way in the soil or alternatively it could harvest pruning residues for energetic purposes. In both cases, chipped residues should be as small as required for used and to avoid the development of pests, which meant that pruning residues length should be under 30 mm.
- Pruning residues should be previously removed from under the trees canopy manually or by other machines. Once the residues were between the tree rows, the prototype should windrow them with high efficiency.
- To make possible to achieve the windrow objective in traditional, high-density, and even super high density olive orchards, the windrow width should be adjustable from 4 or 5 m to 2 or 3 m. Windrowing devices should be adjustable in terms of width, angle and windrowing capacity.
- Fuel consumption reduction of 15 % respect to conventional windrowers and chippers or shredders considering the two operations.
- Smooth peak values for torque and power requirements of the machine respect to conventional chippers or shredders improving the performance of the tractor engine.
- Improvement of the effective field capacity of the current around 20 % regarding current windrowers and chippers or shredders and including manual windrowing as a conventional practice.
- Windrowing and chipping cost should be under conventional mechanical or manual windrowing and mechanical chipping or shredding.

3. Results and Discussion

Prototype requirements were adapted to a wide range of working conditions, which made necessary to design and build several adjustable systems in the prototype with using the latest available technology in hydraulic systems. For instance, to control chipper feeding, the compression rollers should regulate their rotary speed according to tractor engine load. Furthermore, to work at different rows spacing, the windrowers could tilt to change prototype working width adapting the windrowers to the soil geometry. Selected windrowers were twin basket rake type with a horizontal axis. Moreover, windrowers could move in two main directions, vertically, and horizontally, to adapt to different soil plot conditions. Working width could be adjustable from 2 to 4.8 m in working conditions (Figure 1), although for transport, machine width could be reduced up to 1.5 m (Figure 2).

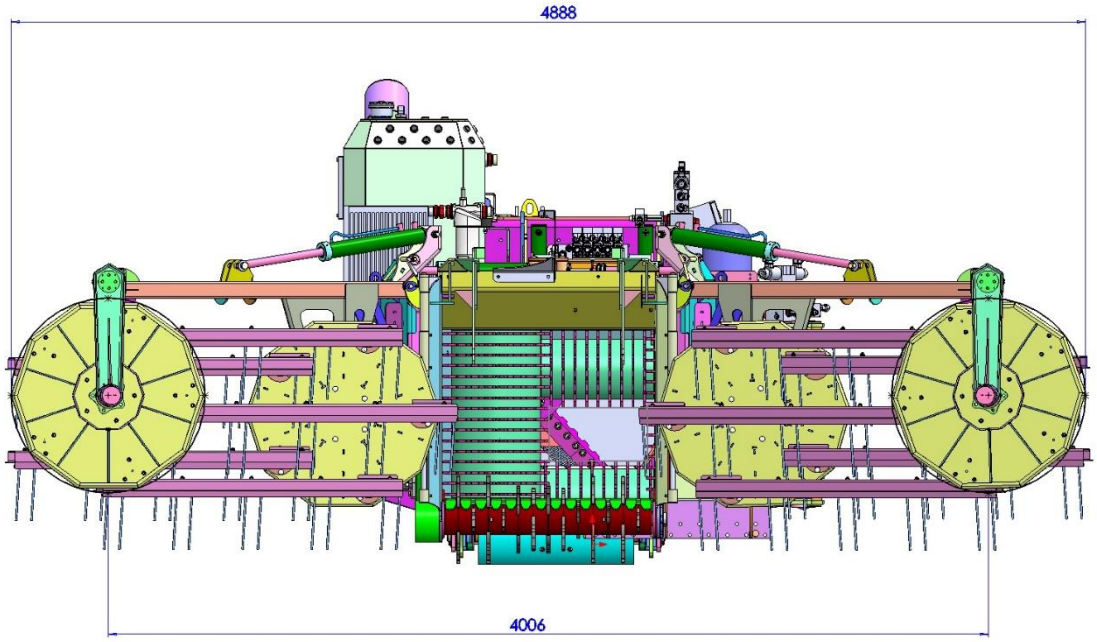

Figure 1. Prototype design with maximum working width.

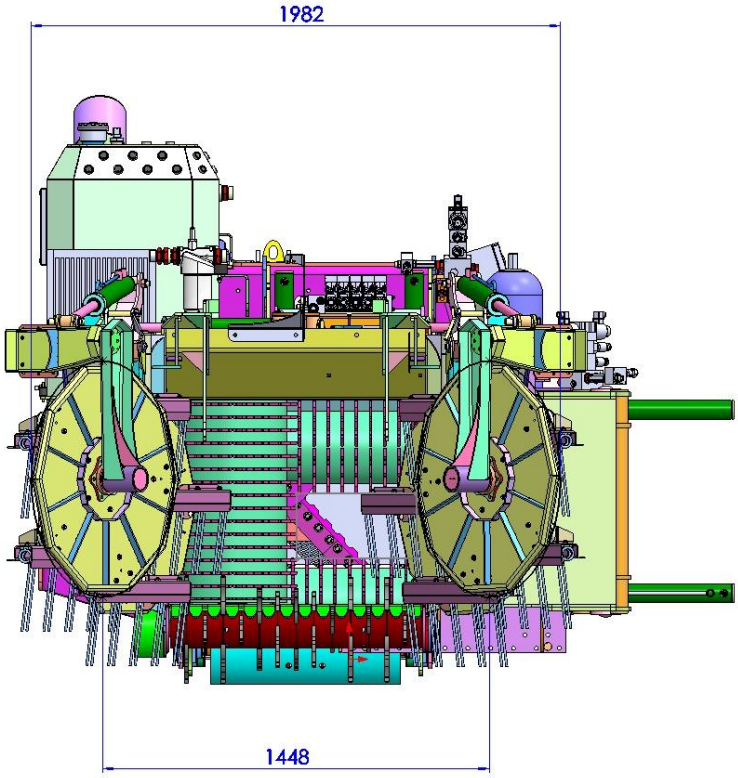

Figure 2. Prototype design with folded windrowers at transport position.

After windrowing, the pruning residues were move up from the soil by a horizontal feeder at the bottom of the prototype to the compression system. To avoid the pruning residues to pass over the prototype, an upper feeder with auto-adjustable height was included, which also helped to compact residues previously to pass to the next step.

Due to pruning residues high volume in relation to weight, they should be compacted previously to chip them. Moreover, this prototype presented a worse situation compared to manual windrowing, considering that pruning residues fell in a disorderly way which may affect the movement of these residues from feeding to chipping. For this reason, a compression system was included, to increase prototype working capacity by reducing the pruning residues bulk density. In this sense, previous studies have shown that pruning bulk density could also varied depending on pruning residues size (Castillo-Ruiz et al., 2021) and spatial variability of pruning residues amount depends on canopy volume, tree projected area (Rodriguez-Lizana et al., 2023), pruning system and intensity (Castillo-Ruiz et al., 2017). The compression system was divided into two steps, the first step was composed of two vertical rollers which could adjust the distance between them according to the resistance of the compressed material. Afterwards, the second step was composed of two horizontal rollers. All rollers include a rotation system moved by a hydraulic engine and each pair of rollers include a compression system composed of hydraulic cylinders.

The compression system worked as an automatic adjustment of the prototype, considering that the rollers could rotate quickly or slowly depending on the chipping system load. The higher the chipping system load, the slower the rollers rotation up to stop the rollers if the chipping load was excessive for the tractor power. Furthermore, the rollers could rotate in the opposite direction to help the prototype to discharge pruning residues in case of chipping system blockage. These features made possible to avoid chipper block or tractor overload when idle time was reduced as much as possible depending on available pruning amount making possible tractor restart if necessary.

After pruning residues compression, the prototype performed the material chipping by four blades mounted on a rotating disk which moves around an imaginary horizontal axis that was situated along the pruning residues feeding and compression path. The disk was the only prototype system that was directly moved by the power take-off from the tractor to ensure that the total tractor engine power could be transmitted

to the chipping system. The rest of the systems were moved hydraulically which made possible to adjust, control an automatize several tasks having much more versatile prototype.

After chipping, the material was conducted to a fan which propelled it from the rear part of the tractor to a front loader basket hitched to a front loader system through a 300 mm diameter pipe to avoid blockages. This pipe could be detached from the chipper or from the front loader basket to distribute the chipping material as a mulching in the soil.

The prototype was designed to be adapted to all olive orchard categories except those which rows spacing were under 5 m. Furthermore, once the pruning residues were chipped, it is possible to lend them to cover soil or harvest them through the fan system to use as biomass. Final prototype theoretical weight and dimensions were 4,500 kg and 4.9 x 2.2 x 3.32 m (width, height, and length). These features made the prototype heavier and wider than conventional shredders which varied from 1000 to 2500 kg, and 1,5 to 2,4 m. However, these features reduced labour required to windrow olive pruning for the prototype which was one of the previous requirements, but made necessary to use tractors with high three-point hitch lifting capacity.

The prototype was monitored by a modem device that sent data to a host control platform in order to analyse working time (Figure 3). During in field tests, the prototype provided high windrowing and chipping efficiency between 87 and 91 % while effective field capacity varied from 0.54 to 0.63 ha h^{-1} considering the windrowing, chipping and harvesting biomass process and including unloading of chipped material when the front loader basket was full (Figure 4). The main improvement of this prototype respect to manual or mechanical windrowing and subsequent shredding was the reduction of tractor wipes, from two or more in the conventional way, to one wipe with the prototype. If pruning residues were managed with manual windrowing and subsequent shredding with auto feed shredders, effective field capacity will be around 0.1 ha h^{-1} and $worker^{-1}$ for windrowing 1 to 2 ha h^{-1}. However, if pruning residues were managed with mechanical windrowing, effective field capacity for mechanical equipment will be of 1 to 2 ha h^{-1} plus a highly variable on foot working requirements of 1 to 5 h ha^{-1}. In the worst case, the prototype had the same effective field capacity than the conventional way of pruning management, while in the best case, this prototype could save up to 9 h ha^{-1} of working time.

Figure 3. Recorded data on the host control platform during one day of in-field tests.

Figure 4. The prototype windrowing, chipping and harvesting olive biomass during field tests.

The prototype harvest between 1.8 and 8.2 t h^{-1} of fresh biomass, which was a really high rate considering that the machine perform 3 tasks (windrowing, chipping and harvesting) in an only wipe Other shredder and biomass harvester, without windrowing in all cases, achieve an effective material capacity between 2.7 to 4.7 t h^{-1} while other harvesters working in olives achieve an effective material capacity between 3 and 9 t h^{-1} (Spinelli and Picchi, 2010). However, self-propelled forage harvester with a purpose-built coppice header achieves higher productivity which varied from 10 to 78 t h^{-1} harvesting hybrid poplar and excluding headland activities (Eisenbies et al., 2017). At this point, it should be noted that effective material capacity strongly depends on biomass amount. For this reason, further research is needed to compare effective material capacity in the same working conditions.

4. Conclusions

It is possible to windrow, chip and harvest olive pruning residues in an only wipe, but this complexity implies that the machine will be heavier and bigger than conventional windrowers or shredders, which lead to use tractors with high lifting capacity at the three-point hitch. Moreover, it is highly complex to design, build and test such a complex machine, which requires high technical level. It should be noted that this prototype was focused on the reduction of hand labour mainly for manual windrowing, considering that there are very few commercial windrowers that are feasible for olive residues windrowing in a reliable way. In this sense, results show that the designed prototype could save up to 9 h ha of working time which supposes 81,8 % of the working time required for conventional way of managing pruning residues by manual windrowing and shredding. In the worst case, the prototype required the same working time than conventional management using mechanical windrowing and shredding when mechanical windrowing provided high efficiency. However, effective material capacity will depend on available amount of biomass, which along with high benefits provided by biomass mulching could make olive biomass harvesting only in a very few cases.

Acknowledgements

Authors thank public pre-commercial procurement agreement Innolivar[1] from Spanish Ministry of

Science, Innovation and Universities along with Spanish Olive Oil Interprofessional Organization (https://www.aceitesdeolivadeespana.com/) support. Furthermore, authors want to acknowledge Construcciones mecánicas Alcay S.L. / Serrat trituradoras (https://www.serrat.es/), specially to José Serrat, Pedro Serrat, and Raúl Serrat by their collaboration.

[1]Public procurement of innovative solutions specifically pre-commercial procurement Innolivar according to the agreement signed by before Ministry of Economy, Industry and Competitiveness (current Ministry of Science, Innovation and Universities) and University of Cordoba co-funded by ERDF funds (80 %) within multiregional operational program of Spain 2014-2020.

References

ASOLITE, 2021. La olivicultura internacional y su incidencia sobre la salud, economía, sociedad, sostenibilidad, y biodiversidad. El caso particular del cultivo tradicional. https://drive.google.com/file/d/18q_kpzJPT_w5FcLnqNvz-D9SIa8ITs0g/view

Banco de España, 2024. El mercado de trabajo español: evolución reciente y retos de futuro. https://www.bde.es/f/webbe/GAP/Secciones/SalaPrensa/IntervencionesPublicas/Gobernador/Arc/Fic/IIPP-2024-02-15-hdc-es-or.pdf

BASF, n.d. El olivar en España: Tradicional, intensivo y superintensivo. https://www.agro.basf.es/es/Camposcopio/Secciones/Protecci%C3%B3n-y-sanidad/olivar-en-espana/

Castillo-Ruiz, F. J., Colmenero-Martinez, J. T., Bayano-Tejero, S., Gonzalez-Sanchez, E. J., Lara, F. M., Blanco-Roldán, G. L. 2021. Methodology for olive pruning windrow assessment using 3D time-of-flight camera. Agronomy, *11*(6), 1209.

Castillo-Ruiz, F. J., Sola-Guirado, R. R., Castro-Garcia, S., Gonzalez-Sanchez, E. J., Colmenero-Martinez, J. T., Blanco-Roldán, G. L. 2017. Pruning systems to adapt traditional olive orchards to new integral harvesters. Scientia Horticulturae, *220*, 122-129.

Eisenbies, M. H., Volk, T. A., Espinoza, J., Gantz, C., Himes, A., Posselius, J., Shuren, R., Stanton, B., Summers, B. 2017. Biomass, spacing and planting design influence cut-and-chip harvesting in hybrid poplar. Biomass and Bioenergy, 106, 182-190.

ESYRCE, 2023. Encuesta sobre Superficies y Rendimientos de Cultivos. https://www.mapa.gob.es/es/estadistica/temas/estadisticas-agrarias/agricultura/esyrce/default.aspx

European Commission, n.d. Pre-Commercial Procurement. https://research-and-innovation.ec.europa.eu/strategy/support-policy-making/shaping-eu-research-and-innovation-policy/new-european-innovation-agenda/innovation-procurement/pre-commercial-procurement_en#:~:text=suppliers%20for%20PCP%3F-,What%20is%20Pre%2DCommercial%20Procurement%3F,and%20associated%20staff%20working%20document%20.

Kougioumtzis, M. A., Karampinis, E., Grammelis, P., Kakaras, E. 2022. Integrated harvesting and biomass haulage of olive tree prunings. Evaluation of a two year harvesting campaign in central Greece and fuel characterization of the prunings collected. Biomass and Bioenergy, *165*, 106572.

Michalopoulos, G., Kasapi, K. A., Koubouris, G., Psarras, G., Arampatzis, G., Hatzigiannakis, E., Kavvadias, V., Xiloyannis, C., Montanaro, G., Malliaraki, S., Angelaki, A., Manolaraki, C., Giakoumaki, G., Reppas, S., Kourgialas, N., Kokkinos, G. 2020. Adaptation of Mediterranean olive groves to climate change through sustainable cultivation practices. *Climate,* 8(4), 54.

Rodríguez-Lizana, A., Ramos, A., Pereira, M. J., Soares, A., Ribeiro, M. C. 2023. Assessment of the spatial variability and uncertainty of shreddable pruning biomass in an olive grove based on canopy volume and tree projected area. Agronomy, 13(7), 1697.

Spinelli, R., Picchi, G. 2010. Industrial harvesting of olive tree pruning residue for energy biomass. Bioresource Technology, 101(2), 730-735.

Taguas, E. V., Marín-Moreno, V., Díez, C. M., Mateos, L., Barranco, D., Mesas-Carrascosa, F. J., Perez, R., García-Ferrer, A., Quero, J. L. 2021. Opportunities of super high-density olive orchard to improve soil quality: Management guidelines for application of pruning residues. Journal of Environmental Management, 293, 112785.

Vilar, J. 2023. Al olivo se le empieza a quedar pequeño el planeta. https://www.juanvilar.com/al-olivo-se-le-empieza-a-quedar-pequeno-el-planeta/

Development of an oyster mushroom (Pleurotus spp.) substrate compactor-bagger

Jordan L. Abad[a*], Helen F. Gavino[b], Romeo B. Gavino[b], and Melba M. Denson[b]

[a]Department of Science and Technology Regional Office 1, La Union, Philippines
[b]Department of Agricultural and Biosystems Engineering, College of Engineering, Central Luzon State University, Science City of Munoz, Nueva Ecija, Philippines
*Corresponding author: Email: abad_jordanzoe71@yahoo.com

Abstract

The low supply of mushrooms in the Philippines evident to 90% importation is ironic to the abundant biomass resource the country could offer. The low biomass utilization rate affected by the lack of appropriate technologies also applies to the low productivity in the bagging of substrate in the mushroom industry using manual labor with a capacity of 25 bags/hr. These problems enthuse the study to design, fabricate, and evaluate a mushroom substrate compactor-bagger adaptable to local practices and mushroom production technologies in the country. The 1432mm x 741mm x 2040mm (l x w x h) 140kg machine was designed using 152 x 305mm, 0.02 mil polypropylene plastic bags with a compaction height of 203mm and 95mm diameter. A weight of 750 grams of substrate per bag was determined as a setting using the CLSU formulation (70-30 RS-S) and BSU (80-15-5 S-RB-L) formulation. Performance evaluation of the machine using the two formulations was tested with different loading weights of 10kg, 15kg, and 20kg per batch. It was evaluated using simple CRD and means were compared using an LSD test. Results of the study revealed that CLSU formulation at 15kg loading gained 71.67% bagging efficiency, 70.78% filling efficiency, 204 bags/hr bagging capacity, and an average of 740.90 grams/bag. Using BSU formulation, the machine loaded with 20kg produced the highest bagging and compacting efficiencies of 88% and 83.48%. It had a capacity of 307 bags/hr with an average of 759 grams/bag. The average weight per bag was within the acceptable weight of 750 ±50 grams. The cost analysis of the machine for a year of operation at six hours per day, three times a week with a custom rate of PhP1.5/bag could generate an income of PhP96,736.00-PhP191,749.00 per year and a payback period of 0.30-0.60 years for the BSU and CLSU formulations, respectively. With the developed machine, there would be increased biomass waste utilization, more production of oyster mushroom at lower cost and hence, more benefits to the farmers and the mushroom industry.

Key Words: biomass utilization, compactor-bagger, oyster mushroom, substrate formulation

1. Introduction

According to economic analysts, mushrooms are seen as another significant crop of the country due to its growing local demand (Philippine News Agency, 2010). Being an agricultural country with well-endowed livestock and forestry products and cultivates major crops like rice, coconut, and sugarcane, the state can generate substantial amount of residues favorable for the production of mushrooms. However, the Philippine mushroom industry set its lowest production volume of 355 metric tons (MT) in 2009 and worsened since 1995 (Chang et al., 2014) as almost 90% of the mushroom consumed was imported from different countries of South East Asia (Business Diary Ph, 2015).

The lack of appropriate research for mushroom mechanization facing the country's small-scale and or village-level mushroom industry could be observed in the bagging of substrate materials where manual labor is employed and described to be labor-intensive (De la Torre, 2010). As Oei (2005) explained it, more people are needed to do the filling of bags than in other operations before bagging. Mechanization technology suited for the scale of production in the bagging or filling of substrate bags and other related operations could encourage the use of available biomass resource and could further boost the mushroom industry towards self-sufficiency of mushroom supply in the country.

With these problems of low mushroom supply and the potentials of untapped biomass resource in the country, a need for efficient and cost-effective biomass utilization technologies and equipment compared to existing production technologies could be seen to encourage the cultivation of mushroom. Thus, the study aimed to develop an oyster mushroom (*Pleurotus* spp.) substrate compactor-bagger using locally available materials and fabrication technologies. The specific objectives of the study include the establishment of the optimum weight of substrate in bags; to design a substrate bagger adaptable to existing technologies of mushroom production in the Philippines; to fabricate the machine using local manufacturing technologies; to evaluate the operating performance of the machine in terms of capacity, efficiency, and uniformity in weight of substrate bags; and, to perform cost analysis in using the machine.

With the study, bagging of the mushroom substrate would be made easier resulting in higher output in terms of mushroom substrate in bags. The creation of the machine could also lead to increasing biomass resource utilization which was not given too much attention. It would also provide opportunity to the local machinery industry as this machine could be added to the list of machines that could be fabricated locally, thereby may also increase the income of local machinery shops. Thus, the study would help improve the production of the mushroom substrate and the mushroom itself creating a more profitable farmer but also in the utilization of biomass resource for food production and profit creation.

2. Materials and Methods

The study was set to design, fabricate, and evaluate a machine mechanizing the compacting and bagging of mushroom fruiting bags using two of the most commonly used formulation, the (a) 70 parts rice straw and 30 parts sawdust or CLSU Technology and (b) 80-15-5 parts of sawdust-rice bran-lime or BSU Technology.

The study started with the gathering of benchmark data to support the claim of mechanizing the bagging of the mushroom substrate. The data gathered in the form of a survey questionnaire was conducted related to the existing technologies in the country on bag cultivation. Data gathered like the dimension of polypropylene plastic (PP) bag, the capacity of laborer and weight of substrate served as basis or design considerations for the fabrication of the machine.

2.1 Establishment of optimum weight of substrate in bags.

To standardize the weight of the substrate bagged by the machine, the establishment of the optimum weight of substrate in bags was conducted. It was used in the conceptualization of some settings for the fabrication of the machine. The planting spawn weighs 40 grams per bag placed in 102mm x 152mm PP bags plugged with cotton through a PVC neck. It was sterilized in an autoclave for one and a half hour at 120 degrees Celsius, 21psi.

Formulation of the substrate follows CLSU technology and BSU technology. The substrate was manually bagged using 152mm x 305mm PP bags with 0.02 mil thickness. The bags were approximately uniform in volume since height was maintained at 203mm while diameter at 95mm. It was inoculated with the prepared spawn and was incubated in a dark room. It was then transferred to the fruiting area after full ramification.

Data gathered include the number of days for full mycelial ramification, yield per bag, and flushing interval. Meanwhile, the statistical analysis used was (2x3) factorial by Completely Randomized Design. Factor A of the study included the types of substrate mixture: (F1) 70% Rice Straw and 30% sawdust; and (F2) 80% sawdust, 15% rice bran, 5% lime while Factor B was the different weight per substrate bag: (A) 500 grams, (B) 750 grams, and (C) 1000 grams compacted in the same volume (95mm diameter x 203mm height). \

2.2 Design of the mushroom substrate compactor-bagger

The machine had the following components: the flywheel and compactor assembly, the conveyor-hopper assembly, the rotating disc assembly, the mechanism to rotate the rotating disc assembly, the frame assembly and the power transmission system. The hopper was designed to accommodate 32-35kg of substrate per batch. The volume of the hopper was determined using Eq (1) using density of uncompacted substrate for BSU formulation of 347kg/m^3 and CLSU formulation with 320kg/m^3

$$V_h = \frac{W_1}{\rho} \quad (1)$$

where V_h is volume of hopper, m^3, W_1 is weight of substrate per batch, kg, and $\boldsymbol{\rho}$ is density of substrate, kg/m^3

The design of the spiral conveyor was based from Henderson and Perry (1955) for screw conveyors. The diameter of the shaft was calculated using Eq (2) where the density of sawdust was used and the diameter of the spiral conveyor.

$$C_T = (D^2\text{-}d^2)/36.6)\ x\ P\ x\ V \quad (2)$$

where C_T is theoretical capacity (x 60%), ft^3/hr., D is spiral diameter, in, d is shaft diameter, in, P is pitch diameter, in (usually equals to D) and V is speed of shaft, rpm

The size of the PP bags dictated that the diameter of the compression chamber was 95mm and the height was 295mm lower than the computed value of 305mm to facilitate easier mounting of PP bag wherein the remaining gap would be augmented by using the adjustable stopper depending on the type of substrate. After the dimensions and sizes of components were calculated, a final design plan was drawn using SolidWorks software.

2.3 Fabrication and assembly of the machine

Local technologies and skills of manufacturing industry in the country was utilized in the fabrication using mainly the instruments found in a local fabricating shop. Some of the equipment used were: welding machine, grinding machine, drilling machine, oxy-acetylene gas, and cutting disc. The assembled components were set to their proper timing before conducting the preliminary test.

2.4 Machine testing and evaluation

After the machine was fabricated, initial testing was conducted to validate the timing and functions of all components. The study was laid out in Completely Randomized Design, ANOVA was used to evaluate the effects of different weights per batch in the machine using two formulations. Since the two formulations used differed in physical property especially the bulk density of uncompacted materials, a separate evaluation of the machine using the two substrates was conducted. There were three varying weight per batch per kind of formulation. With this, there were three replications per treatment for each of the two formulations.

The methods of preparation for the substrate materials in the testing for the machine were similar with the preparation of a substrate in the establishment of optimum weight per substrate bag. Data gathered during the evaluation include productive time, unproductive time, total bagging time, number of bags within the acceptable limit, total number of bags produced, and total weight of loaded inputs or substrate.

The bagging capacity of the machine was determined using the Eq (3)

$$C = \frac{B_{in}}{T} \quad (3)$$

where C is bagging capacity, bags/h, B_{in} is number of bags produced within the limit, and T total bagging time

The bagging and filling efficiencies of the machine were calculated using Eq (4) and (5)

$$Eff_B = \frac{B_{in}}{B_T} x\ 100 \quad (4)$$

$$Eff_F = \frac{W_{in}}{W_T} x\ 100 \quad (5)$$

where Eff_b is bagging efficiency, B_{in} is number of bags produced within the limits, B_T is total number of bags produced, W_{in} total weight of bags within the limit, and W_T is the total weight of load input

2.5 Cost analysis

To evaluate the cost of using the machine, the following equations by Hunt (2001) as presented in Table 1 were used.

Table 1. Formula used for the simple cost analysis of the study.

Particulars	Formula	
Salvage value, (10% IC)	SV =	10% IC
Depreciation, PhP/yr	D =	(IC-SV)/n
Interest on Investment, PhP/yr	I =	((IC+SV)/2) i
Fixed Cost, PhP/yr	Fc =	D+I+TIS
Variable Cost, PhP/yr	Vc =	C_p+C_l+RM+C_{lub}
Total bagging cost, PhP/yr	Tc =	Fc+Vc
Bagging Cost, PhP/bag	B_c =	Vc/C*T
Breakeven point, bag/yr	BEP =	Fc/Cr-B_c
Net Income per year, PhP/yr	NI =	C*T*Cr-Tc
Payback Period, yr	PBP =	IC/IN

where *Fc* is annual fixed cost, PhP/yr., *D* is depreciation, PhP/yr., *I* is interest on investment, PhP/yr., *TIS* is tax, insurance and shelter, PhP/yr., *Vc* is variable cost, PhP/yr., *Lu* is lubricant cost, PhP/yr., *Cp* is fuel cost, PhP/yr., *RM* is repair and maintenance cost, PhP/yr., *Cl* is labor cost, PhP/yr., *Tc* is annual cost, PhP/yr., *C* is bagging capacity, bags/hr., *Vc* is variable cost, PhP/yr., *Bc* is Bagging Cost, PhP/bag, *Cu* is cost of using the machine, PhP/bag, *T* is annual operating time, hrs./yr., *Cr* is custom rate, PhP/bag, *BEP* is break-even point is the number of bags that the machine would properly compact and bag to recover the capital investment, and *PBP* is payback period is the time it takes to recover the investment cost.

To conduct the cost analysis of using the machine, assumptions were laid to facilitate computation. Six hours were allotted for the total operating hours per day of the machine, considering 8-hr operation for the laborer. The labor cost per laborer is PhP300.00/day at 6hr/day.

Assuming that in a community with several mushroom and fruiting bag producers, 3 days/week was allotted for custom hiring at PhP1.50/ bag. The custom rate is 75% of the manual bagging cost of PhP2.00 considering the cost of manual bagging for 25 bags/hour. If the machine is used for a year, it would operate for 156 days or 939 hours. Considering that the machine uses 0.368kW of motor at 7.13 pesos per kilowatt hour rate, the cost per hour of operation is PhP2.64.

3. Results and Discussion

3.1 Optimum weight of substrates

For the average mycelial ramification, the analysis of variance revealed significant difference between the formulation, weight of substrate, and their interactions. The comparison of means revealed that the 500g weight per bag with 26 days of full ramification vary significantly to that of the 750g and 1000g bags with 31 days and 40.6 days. The mean ramification of 27.33 days for CLSU formulation varied significantly to the 37.73 days of BSU formulation. For the interaction of the factors, Table 2 shows that the least ramification days was recorded in CLSU formulation at 500g/bag with 20 days only while highest at 41.20 days in 1000g/bag BSU formulation. The simple effects vary significantly with each other except to that of BSU at 750g and CLSU at 1000g with 40 days ramification period.

Table 2. Mycelial ramification (days) per formulation as affected by different weight of substrate.

Formulation	Weight, g			Mean
	A-500g	B-750g	C-1000g	

CLSU	20 ^{z}	22 ^{y}	40.00^{w}	27.33^{b}
BSU	32 ^{x}	40 ^{w}	41.20^{v}	37.73^{a}
Mean	26^{l}	31^{k}	40.60^{j}	32.53

*Means with the same letter are not significantly different

The results revealed that the higher the weight of substrate in bags the longer it would take for the mycelial run for both substrate formulations. This result is supported by a similar study on the mycelial run for *Pleurotus florida* by Mondal et. al (2010) which resulted in lesser time for colonization in rice straw-based substrate than the traditional substrate of sawdust.

The results of the analysis of variance of the average yield per bag as affected by substrate formulation and weight per bag show significant difference between the weight per bag and interaction while no significant difference in formulation. The comparison among means as affected by weight per bag presented in Table 3 would show that the 750g produced the average yield per bag of 130.25g and was significantly different to the 113.65g/bag of the 500g substrate bag and the 76.75g yield of the 1000g. For the interactions, yield for both formulations at 500g and 750g did not differ significantly with each other but differ significantly to that of the 1000g/bag.

Table 3. Yield (g) per formulation as affected by different weight of substrate.

Formulation	Weight, g			Mean
	A-500g	B-750g	C-1000g	
CLSU	109.21^{v}	133.50^{v}	73.40^{w}	105.37
BSU	118.10^{v}	127.00^{v}	80.10^{w}	108.40
MEAN	113.65^{k}	130.25^{j}	76.75^{l}	106.89

*Means with the same letter are not significantly different

The result in yield was similar to the results of Zireva et al. (2007) on oyster mushroom yield using tray method of cultivation whereby from 2kg to 10kg per tray, 6kg was seen to be favorable for growing. The results emphasized that the decrease in yield below the optimum weight was attributable to earlier depletion of nutrients due to limited substrate quantity while increasing the substrate quality did not increase in mushroom production but only a waste of resources.

The comparison among means in Table 4 shows that the flushing interval means of BSU formulation with 11.40 days significantly differed to CLSU with 18.07 days flushing interval. For the weight of bags, 750g per bag resulted to lowest flushing interval of 8.75 significantly different to the 14 days of 500g and 21.45 days of the 1000g. The interaction effects of the two factors were seen to be significantly different with each other where CLSU at 750g with 8 days flushing interval differ significantly to all other treatment combinations except with BSU at 750g with 9.50 days. The BSU formulation at 750g also did not vary significantly to BSU at 500g with 11.10 days but differed to other treatment combinations. Meanwhile, BSU formulation at 500g and 1000g did not differ significantly with each other but differed from the rest of the treatment combinations.

Table 4. Flushing interval (days) per formulation group as affected by different levels of weight.

FORMULATION	WEIGHT			MEAN
	A-500g	B-750g	C-1000g	
CLSU	16.90 ^{w}	8.00 ^{z}	29.30 ^{v}	18.07^{a}
BSU	11.10 ^{xy}	9.50 ^{yz}	13.60 ^{x}	11.40^{b}
MEAN	14.00^{k}	8.75^{l}	21.45^{j}	14.71

*Means with the same letter are not significantly different

Based on the results of the statistical analysis conducted, both formulations were affected by the different weight levels of substrate in bags. In selecting what type of formulation would be more favorable than the other, CLSU formulation revealed better results in terms of mycelial ramification (days) and flushing interval (days) than BSU mixture but had no difference in yield for two flushing periods.

For the weight of substrate used in both formulations, although the 500g substrate recorded the least ramification span for both formulations, 750g had favorable results in terms of yield and flushing intervals. During the study, it was also observed that the 500g substrate formulation was difficult to manage as they were easily disintegrated and substrate materials would shrink with the use of the hanging method if hanged one after the other. Meanwhile, the heaviest weight recorded the highest span of ramification in days, lowest yields and the highest flushing intervals. The recommended setting of 750 grams for both formulations has been seen to prove the not too tight not too loose recommendation of various authors and books on mushroom cultivation.

3.2 Description and operation of the machine

The major components of the machine were the following: the four-cylinder rotating disc assembly, the molder or compaction chamber assembly, the piston compressor assembly, spiral-conveyor and hopper assembly, push-to-rotate

lever assembly, the frame assembly, and the power transmission system as shown in Figure 1. These components were fabricated and assembled to form an operational compactor-bagger machine.

Figure 1. The mushroom bagger-compactor

The machine was made of locally available materials and was fabricated using local manufacturing technologies. It was powered using a 0.367kW electric motor and was equipped with wheels for mobility in the mushroom house. The machine was operated by three persons with a specified task. One who supervised the level of the substrate in the feeding hopper, the other in putting the PP bag in the molder, and the last person in charge of the exit of the substrate bags or the collector of the compacted and bagged substrate.

3.3 Performance characteristics of the machine using CLSU formulation

The machine was evaluated in terms of bagging efficiency, filling efficiency, and bagging capacity. The average bagging efficiency of the machine as affected by different weights per batch using the CLSU formulation is presented in Table 5. Analysis of variance for the bagging efficiency revealed that the means of bagging efficiency as affected by the weight per batch differ significantly from each other at 5% level of significance.

Comparison among means using Least Significant Difference (LSD) at 5% level of significance shown in Table 5 revealed that weight per batch of 15kg with the highest bagging efficiency varies significantly with the 10kg and 20kg weight per batch.

Table 5. Bagging efficiency (%) as affected by different weight per batch.

Weight per batch, kg	Replicate			Mean
	I	II	III	
10	46.15	38.46	53.85	46.15 [b]
15	75.00	75.00	65.00	71.67 [a]
20	2.63	17.65	21.88	14.05 [c]

*Means with the same letter are not significantly different

It is also noted that using the weight per batch type, the machine produced acceptable weight per bag ranging from 708.13 to 740.90g/bag and with an average of 725.42g/bag when using the CLSU formulation. On the filling efficiency of the machine as affected by weight per batch using CLSU formulation, analysis of variance showed that there was a significant difference in the mean effects of weight per batch in the filling efficiency of the machine at 5% level of significance.

Comparison among means presented in Table 6 revealed that weight per batch of 15kg with 70.78% vary significantly with the 10kg and 20kg weight per batch. The lowest recorded filling efficiency is at 20kg weight per batch with only 16.75%.

Table 6. Filling efficiency (%) as affected by different weight per batch.

Weight per batch, kg	Replicate			Mean
	I	II	III	

10	42.40	35.6	49.40	42.47 [b]
15	73.60	74.13	64.60	70.78 [a]
20	3.75	21.60	24.91	16.75 [c]

*Means with the same letter are not significantly different

The summary of the machine's bagging capacity as affected by different weight per batch is presented in Table 7. The analysis of variance of the bagging capacity affected by the weight per batch at 5% level of significance revealed no significant difference between means at 15kg and 10kg weight per batch but varied significantly with 20kg weight per batch.

Table 7. Bagging capacity (bags/hr) as affected by different weights per batch.

Weight per batch, kg	Replicate			Mean
	I	II	III	
10	171.43	130.43	201.6	167.82 [a]
15	214.29	215.14	180	203.14 [a]
20	8.18	53.33	64.62	42.04 [b]

Means with the same letter are not significantly different

3.4 Performance characteristics of the machine using BSU formulation

The average bagging efficiency of the machine as affected by weight per batch and BSU formulation is presented in Table 8. The highest bagging efficiency was computed in the 20kg weight per batch with 88% decreasing as the weight per batch decrease with 15kg at 84.21% and 10kg at 83.33%. Analysis of variance shows that the weight per batch had no significant effect on the bagging efficiency of the machine when using the BSU formulation at 5% level of significance.

Table 8. Bagging efficiency (%) at different weight per batch.

	Replicate			
Weight per batch, kg	I	II	III	Mean
10kg	83.33	83.33	93.33	83.33
15kg	84.21	84.21	84.21	84.21
20kg	88.00	88.00	88.00	88.00

Also, the bagged substrate using the BSU formulation resulted to uniform weight per bag of substrate within the acceptable limit with an average of 755.25g/bag close to the 750g/bag. Meanwhile, the results of the analysis of variance for filling efficiency revealed that the treatment means varied significantly with each other. Comparison among means using LSD as presented in Table 9 shows that the three weights per batch differed significantly with each other with 20kg as the highest filling efficiency of 83.48%.

Table 9. Average filling efficiency (%) as affected by different weight per batch.

Weight Per Batch, Kg	Replicate			Mean
	I	II	III	
10	75.90	75.90	75.80	75.87[c]
15	79.60	79.60	80.20	79.80[b]
20	84.00	83.35	83.10	83.48[a]

*Means with the same letter are not significantly different

Based on Table 10, the bagging capacity as affected by weight per batch in the BSU formulation recorded 306.59~ 307 bags/hr when using the 20kg weight per batch. It was followed by the 15kg weight per batch of 302.11 bags/hr and 10kg with 292 bags/hr. Results of the analysis of variance revealed significant difference in the mean bagging capacity as affected by weight per batch. A comparison of means presented in Table 10 shows that the bagging capacity in 20kg and 15kg weight per batch did not vary significantly but differed significantly from the 10kg weight per batch.

Table 10. Average bagging capacity (bags/hr) as affected by different weights per batch

Weights per batch, kg	Replicate			Mean
	I	II	III	
10	300.00	288.00	288.00	292.00[b]
15	303.16	300.00	303.16	302.11[a]

20	306.98	304.62	308.17	306.59[a]

*Means with the same letter are not significantly different

Other observations during the evaluation of the machine include the elimination of PP bag breakage which was observed in the manual bagging of substrates. This could be attributed to the controlled force of compaction as compared to manual labor with varying forces exerted during bagging.

3.5 Cost of Using the Machine for the two types of formulation

To determine whether the machine was cost-effective in bagging substrates, a simple cost analysis was conducted. The analysis used the highest capacity recorded for both formulations as a result of evaluating the performance of the machine using the treatments. For the CLSU formulation, 204 bags/hour were used as the bagging capacity as it showed significant results based on the findings of the study while 307 bags/hour when using the BSU formulation.

The machine was assumed to be operational thrice a week with a total of 156 days/year or 939 hours per year total operating time for every six-hour per day operation. There were three operators for the machine with PhP300.00 per laborer as labor cost. The custom rate of PhP1.5/bag was based on the 75% cost per bag for manual bagging with PhP2.00/bag pegged at PhP300.00 per day at 6-hour per day. It was used since there was no existing bagger in the locality. While the calculated values are presented in Table 11.

Table 11 shows that the total bagging cost per year in using the machine is PhP190,731.92 with labor as the main contributor with PhP140,785.71 for the three operators for a year. The bagging cost for the CLSU formulation resulted to 0.995~1.00 peso per bag while 0.66 pesos per bag for BSU formulation. The difference is due to the higher capacity of the later contributing to a higher net income per year with a total of PhP191,749.00. Meanwhile, the net income for CLSU formulation is PhP96,736.00.

The computed breakeven point for the CLSU formulation is 32,997 bags per year with a projected payback period of 0.60 years of machine operation for the investment to be recovered. When using the BSU formulation, 0.304 years is the payback period of the machine considering the assumptions. The breakeven point for bags per year is calculated at 22,119 bags/year using the custom rate of PhP1.50/bag.

Table 11. Comparison of cost analysis results for the two substrate formulations.

PARTICULARS	CLSU	BSU
	Specifics	
Salvage value, (10% IC)	5,825.70	5,825.70
Depreciation, PhP/yr	10,486.26	10,486.26
Interest on Investment, PhP/yr	6,728.68	6,728.68
Taxes, Insurance and Shelter, PhP/yr (5% IC)	2,912.85	2,912.85
Fixed Cost, PhP/yr	20,127.79	20,127.79
Variable Cost, PhP/hr	181.77	181.77
Total bagging cost, PhP/yr	190,731.92	190,731.92
Bagging Cost, PhP/bag	0.995	0.66
Breakeven point, bag/yr	32,997.00	22,119.00
Net Income per year, PhP/yr	96,736.00	191,749.00
Payback Period, yr	0.60	0.304

The cost curve of using the two formulations in the machine is shown in Figure 2. The figure shows that the area covered by the net income of the BSU formulation in using the machine is greater than that of the CLSU formulation and that the custom rate is higher than the cost of producing per bag for the two formulations.

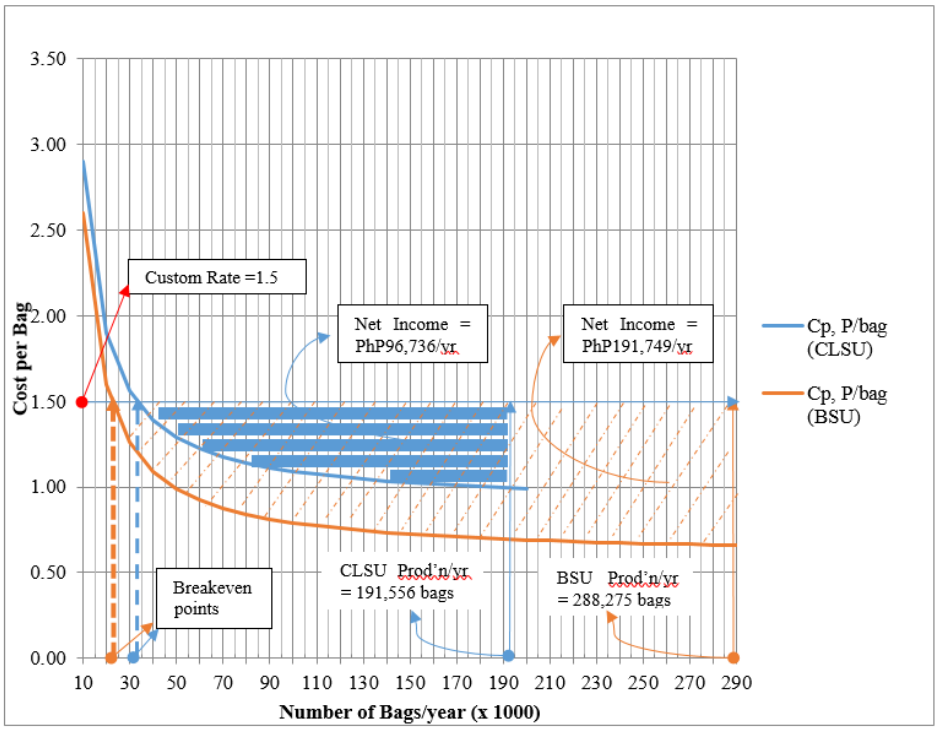

Figure 2. The cost curve of the machine using the two formulations.

Acknowledgements

The support of DOST, the Department of Agricultural and Biosystems Engineering of the College of Engineering through the project leader of the CLSU-DOST-ERDT Program Dr. Ireneo C. Agulto, and the the Central Luzon State University- Center for Tropical Mushroom Research and Development (CLSU-CTMRD) with its project leader- Dr. Sofronio Kalaw, and the Benguet State University -Mushroom Project is highly recognized in this paper.

References

Philippine News Agency. (2010). Raise mushroom; DOST urges farmers. Retrieved from www.balita.ph: http://balita.ph/2010/07/06/raise-mushroom-dost-urges-farmers/ (Chang et al., 2014)

Business Diary Ph (2015, January 31). DA puts up P8 million Mushroom Technology Center in Tarlac to boost production, substitute mushroom import from Taiwan. Retrieved from Make Money – Business Diary Ph.: http://businessdiary.com.ph/

De la Torre, E. (2010). Strengthening the Capabilities of climate change risk management and Disaster Preparedness in Selected Provinces of the Philippines (Bicol Region). FAO, DA.

Oei, P. (2005). Small-scale mushroom. Digigrafi, Wageningen, The Netherlands: Agromisa Foundation and CTA.

Henderson, S. Milton., Perry, R. L. (1955). Agricultural process engineering. New York: Wiley.

Hunt, D. O. (2001). Farm Power and Machinery Management. Iowa State University Pres. Ames, Iowa. 10th Edition. Reissued 2008 by Waveland Press Inc.

Mondal, S., Rehana, J., Norman, M., and Adhikary, S. (2010). Comparative study on growth and yield performance of oyster mushroom on differerent substrates. journal of Bangladesh Agriculture University.

Zireva, D.T., M. Fanadzo and Mashingaidze, A.B. (2007). Effect of Substrate Quantity and Shelf Position on Yield of Oyster Mushroom (Pleurotus sajor caju). Pakistan Journal of Biological Sciences, 10: 3458-3461.

Terrain aware monoplotting for ortho UAV images

Ufuk Can Bicici [a,*], Peter Riegler-Nurscher [a]

[a] Josephinum Research, Wieselburg, Austria

* Corresponding author. Email: ufuk.bicici@josephinum.at

Abstract

Aerial photography using affordable UAVs is an invaluable tool for monitoring crop growth, soil changes, pest invasion, and plant diseases. These images typically undergo photogrammetry algorithms, such as rectification and bundle adjustment, before further processing. Obtaining overlapping images for structure-from-motion algorithms is not always feasible due to time or cost limitations. The Monoplotting technique can be used for georeferencing, involving Ground Control Points (GCP) and a Digital Elevation Map. Alternatively, UAV sensor readings (GPS coordinates, barometer altitude, and camera metadata) can facilitate Monoplotting without GCPs. We introduce a Terrain Aware Monoplotting framework for generating georeferenced 2D images compatible with GIS tools like QGIS. Unlike methods relying solely on UAV sensor readings, our approach leverages terrain properties. Our first algorithm uses ray tracing to calculate terrain intersection points of rays from the camera through image pixels. A least-squares approach fits a plane parallel to the xz-plane to minimize geometric error, allowing a direct affine transformation from image to geographical coordinates. Our second algorithm generates a warped image in the image space, considering perspective constraints such as foreshortening due to terrain altitude differences. Ray tracing identifies camera ray and terrain intersection points, fitting a minimum rotated rectangle to their 2D geographic coordinates. This rectangle serves as the image canvas, where real-world terrain coordinates for each pixel are calculated. Rays are shot back toward the camera center, and bilinear interpolation calculates color values, filling the canvas with a perspectively correct projection of the mapped area. The resulting image can be georeferenced with a basic affine transformation. Visual and measurement results of our algorithms are provided.

Keywords: Monoplotting, UAV, Ray Tracing, GIS

1. Introduction

The advent of unmanned aerial vehicles (UAVs) has significantly transformed agricultural monitoring, offering a new dimension of precision and efficiency. UAVs provide high-resolution, real-time imagery of vast agricultural fields, enabling farmers and researchers to gain critical insights into various aspects of crop production, soil conditions, pest infestations, and plant diseases. This technology facilitates timely interventions and enhances the overall management of agricultural practices, contributing to increased productivity and sustainability. One of the primary methods for processing UAV imagery in agriculture is photogrammetry. This technique involves capturing multiple overlapping images and employing algorithms to stitch them together into a comprehensive and accurate 3D model of the terrain. Photogrammetry encompasses several key processes, including image rectification, point matching, camera calibration, and bundle adjustment. These steps result in unified and georeferenced images that are essential for detailed analysis and decision-making (Linder, 2009, Ghosh 2005).

Despite its advantages, photogrammetry requires a significant amount of overlapping imagery, which can be challenging to obtain due to time, cost, and environmental constraints. In such cases, Monoplotting offers a viable alternative. Monoplotting is a technique that georeferences single images using known ground control points (GCPs) and a digital elevation model (DEM) (Makarovič, 1973). This method can also leverage UAV sensor data, such as GPS coordinates, barometric altitude, and camera metadata, to achieve accurate georeferencing without extensive overlapping images.

The application of Monoplotting in agricultural fields provides a practical solution when traditional photogrammetry is not feasible. By utilizing terrain properties and UAV sensor data, Monoplotting can generate georeferenced 2D images that are compatible with geographic information system (GIS) tools like QGIS (Moyroud, 2018). This approach allows for the creation of accurate maps and imagery under suboptimal conditions, offering significant benefits for agricultural monitoring and management. Classical applications of Monoplotting employ terrestrial oblique photography, however, this is usually an under-utilized approach due to the difficulty of extracting geospatial data from single images (Bozzini et al. 2011). (Bozzini et al. 2011) developed a user-friendly Monoplotting tool, the "WSL Monoplotting Tool", that requires mapping of key points in an oblique image with their actual geospatial coordinates. Using camera collinearity equations that are employed in Photogrammetry applications (Ghosh 2005) and using the image – real-world coordinate mappings, this tool calibrates the camera, by finding the actual camera extrinsic parameters like the camera position, orientation, and intrinsic parameters like the focal length. The application uses a Digital Elevation Map (DEM) for this purpose. It is used for mapping historical landscapes, reconstructing past natural events, and monitoring current environmental processes. (Gabellieri, Watkins 2019) assesses the WSL Monoplotting Tool for georeferencing and vectorizing historical landscape photographs to measure land-use changes over time. They first digitize historical photographs and georeferenced them using technical maps and Digital Terrain Maps (DTMs). Control points were identified to align photographs accurately with geographic coordinates, allowing for the creation of vectorized maps that illustrate historical land-use patterns and changes.

(Bayr, 2021) controls the accuracy of the geospatial data obtained through monoplotting of historical landscape photographs. In this study, again the WSL Monoplotting tool has been utilized. The study uses oblique landscape photographs from Norway, georeferenced with the WSL-MPT using control points and DTMs of different resolutions (1m and 10m). The accuracy of spatial data is assessed by comparing the georeferenced points and polygons against corresponding features on aerial photographs. The paper concludes that the WSL Monoplotting Tool is effective for extracting accurate geospatial data from historical landscape photographs, facilitating the study of long-term landscape changes. In a similar study, (Altmann et al. 2023) explore long-term landscape changes in a lateral moraine section of the Gepatsch glacier in the Ötztal Alps, Austria. Using a combination of historical terrestrial oblique photographs and aerial photos, the study quantifies morphodynamic and land-cover changes from 1890 to 2020. The paper demonstrates the effectiveness of the WSL Monoplotting Tool in quantifying long-term landscape changes using historical photographs. It provides a comprehensive analysis of the morphodynamic and land-cover changes over 130 years, offering significant contributions to the understanding of glacial and paraglacial processes. (Crouzy et al. 2015) employs monoplotting to georeference terrestrial photographs for identifying avalanche detachment zones. This technique integrates digital elevation models (DEMs) and control points with the photographs to accurately map two-dimensional image data to three-dimensional coordinates. Monoplotting ensures precise spatial data, which is crucial for calibrating the stochastic model used for avalanche prediction, thereby enhancing the accuracy and reliability of the study's avalanche analysis. It turns out that Monoplotting is a common tool to use in avalanche prediction analysis. (Mitterer et al. 2016) also utilizes monoplotting to georeference terrestrial photographs of avalanche releases, transforming oblique photos into accurately georeferenced polygons. This process provides detailed spatial data on avalanche areas, lengths, and slope angles, which is crucial for validating and refining snow cover models like SNOWPACK. The precise georeferenced data obtained through monoplotting enhances the accuracy of wet-snow avalanche predictions and improves the understanding of avalanche dynamics.

One of the issues that hinders the widespread usage of the Monoplotting technique is the manual mapping of image key points to the actual world coordinates (Bozzini et al. 2011). (Golparvar, Wang 2021) proposes a study that aims to facilitate this otherwise tedious step. The paper introduces an AI-supported semi-automatic monoplotting framework designed to georeference oblique visual data from sources like drones and smartphones. This new method automates key point detection using ORB and improves camera parameter estimation with regularized gradient-based optimization, significantly reducing the need for manual input. The framework's effectiveness is demonstrated through numerical experiments, showing its potential for large-scale and real-time geospatial data processing, enhancing the accessibility and scalability of monoplotting for various applications.

As can be seen in the literature, the use of Monoplotting is mainly limited to the assessment of historical landscape changes, glacier analysis, and avalanche prediction applications. It is also apparent that such methods generally use oblique photos of the landscape obtained at different points in time. The usage of aerial, orthogonal UAV images is uncommon in the Monoplotting literature. Also, the domain of agricultural usage is missing.

In our paper, we explore the potential of Monoplotting techniques for UAV-based agricultural monitoring. We present a Terrain Aware Monoplotting framework designed to enhance the accuracy of georeferenced images by incorporating terrain properties into the process. In difference to the other methods in the literature, we do not depend on the use of manually paired images and world points, known as Ground Control Points (GCPs) for camera calibration. We use the assumption of the near orthogonality of the UAV images and camera metadata for a simple mathematical camera model. To georeference the UAV images, our framework includes two algorithms that employ efficient ray tracing and least-squares optimization to minimize geometric errors and produce perspectively correct projections. The resulting images can be seamlessly integrated into GIS tools, facilitating comprehensive analysis and informed agricultural decision-making. We have also developed supporting image processing algorithms that coherently spatially cluster large sets of images, collected by UAVs to produce georeferenced images that have manageable sizes for storage and efficient viewing in GIS tools.

2. Materials and Methods

In this work, we present a Terrain Aware Monoplotting framework designed to generate georeferenced 2D images that are compatible with GIS tools like QGIS. Unlike simple methods that rely solely on UAV sensor readings for georeferencing, our approach utilizes terrain properties. Our first algorithm uses efficient ray tracing to determine where camera rays intersect the terrain through image pixels. By applying a least-squares method, we fit a plane parallel to the xz-plane to minimize geometric errors between the plane and the terrain intersection points, creating a horizontal mathematical approximation of the terrain surface. This enables a direct affine transformation from image coordinates to geographical coordinates. We call this method *Horizontal Fitting.* Our second algorithm, called *Warped Fitting*, creates a warped image in the image space while adhering to perspective constraints like foreshortening due to terrain altitude differences. Utilizing ray tracing, it determines where camera rays intersect with the terrain and fits a minimum rotated rectangle to their 2D geographic coordinates. This rectangle serves as the image canvas, from which real-world terrain coordinates for each pixel are calculated. Rays are then projected back to the camera center from these coordinates, intersecting with the sensor plane, to indicate sampling locations in the original image. Bilinear interpolation calculates color values, filling the canvas with a perspectively correct projection of the mapped area. The resulting image can be georeferenced with a basic affine transformation. In this section, we will give more details on both algorithms.

2.1. Horizontal Fitting

Horizontal fitting treats the problem of georeferencing a planar image as a horizontal approximation problem. Georeferenced images contain an affine transformation that converts the pixel in the image space to real-world space, such that each pixel's width and height consist of horizontal and vertical components. (Esri, 2015) defines the following affine transformation:

$$\begin{bmatrix} x' \\ y' \end{bmatrix} = \begin{bmatrix} A & B & C \\ D & E & F \end{bmatrix} \begin{bmatrix} x \\ y \\ 1 \end{bmatrix}$$

Where A is the dimension of a pixel in map units in the x direction, B and D are rotation terms, C and F are translation terms (representing the x and y coordinates of the upper left pixel's center), and E is the negative dimension of a pixel in map units in the y direction (since in image coordinates, the y dimension increases downwards). This transformation is global, applying uniformly to all image pixels and allowing only for rotation, translation, and scaling of the original pixel coordinates. It does not permit individual pixel-wise transformations to convey perspective-warping effects caused by the terrain surface.

One way to address this issue is to include terrain surface information with a horizontal approximation. Using the pinhole camera model, each pixel in the image plane is formed by shooting a ray from the center of the camera, passing through a pixel center, and intersecting with the terrain. In this model, the terrain is represented by a Digital Elevation Model (DEM). Imagining a hypothetical horizontal approximation plane π that represents the georeferenced image in real-world coordinates, the image rays would also intersect this plane. π is assumed to be strictly parallel to the xz-plane due to the restrictions imposed by the affine transformation. Each of the rays can be represented as $r_i(t) = c + td_i$, where the ray that passes through the i^{th} image pixel also passes through c, the camera center, and follows the direction vector d_i Each ray intersects the elevation model at points q_i and the horizontal approximation plane at points $p_i(t) = c + td_i$. The setting is displayed in Figure 1.

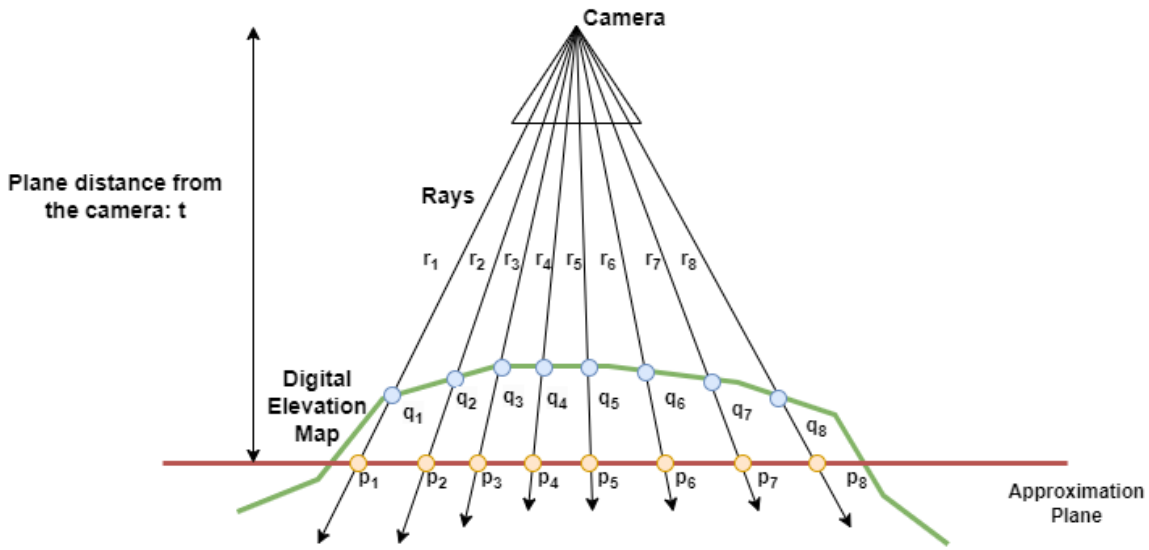

Figure 1. The geometrical setting for the Horizontal Fitting approach.

In this formulation, the best horizontal approximation to the terrain surface is assumed to be the scalar parameter t that minimizes the total distance between q_i and $p_i(t)$ for every image pixel i. Mathematically, it can be represented with the following squared distance:

$$L(t) = \sum_{i=1}^{N} \left|\left|q_i - p_i(t)\right|\right|_2 = \sum_{i=1}^{N} \left|\left|q_i - c - td_i\right|\right|_2$$

This least squares problem can solved analytically by taking the derivative of $L(t)$ with respect to t, setting it equal to zero:

$$\frac{dL}{dt} = \sum_{i=1}^{N} \sum_{j=1}^{3} -2d_{ij}\left(q_{ij} - c_j - td_{ij}\right) = 0$$

Solving for t then yields:

$$\boldsymbol{t} = \frac{\sum_{i=1}^{N}\sum_{j=1}^{3} d_{ij}q_{ij} - \sum_{i=1}^{N}\sum_{j=1}^{3} d_{ij}c_j}{\sum_{i=1}^{N}\sum_{j=1}^{3} d_{ij}^2}$$

In both calculations, j runs over x, y, and z coordinates. Setting t in that way leads to the optimal distance of the horizontal approximation plane from the camera, in a way the discrepancy between the terrain surface and the horizontal approximation is minimized. The affine transformation between the image and horizontal

approximation planes still needs to be calculated. For this, a few steps are required. In the first step, image pixel dimensions are scaled to be equal to the real-world dimensions. We build the following scaling matrix for this operation:

$$S = \begin{bmatrix} \frac{S_w t}{P_w f} & 0 & 0 \\ 0 & -\frac{S_h t}{P_h f} & 0 \\ 0 & 0 & 1 \end{bmatrix}$$

Here, S_w is the sensor width in real-world units (meters), t is the calculated optimal horizontal altitude, P_w is the sensor width in pixels, f is the focal length of the camera, S_h is the sensor height in real-world units (meters) and P_h is the sensor height in pixels. The minus sign in the y-axis handles that in image coordinates, y increases while moving downwards. In the second step, we translate the image center to the world origin:

$$T_1 = \begin{bmatrix} 1 & 0 & -\frac{S_w t}{2f} \\ 0 & 1 & \frac{S_h t}{2f} \\ 0 & 0 & 1 \end{bmatrix}$$

The third step includes the rotation of the image according to the compass heading θ. To handle negative headings, we define the angle $\phi = I[\theta > 0]360 - \theta$, where $I[.]$ is the indicator function that outputs 1 in case of true conditions and 0 in case of false conditions:

$$R = \begin{bmatrix} \cos\phi & -\sin\phi & 0 \\ \sin\phi & \cos\phi & 0 \\ 0 & 0 & 1 \end{bmatrix}$$

The final step translates the image to the actual geographical coordinates of the UAV (usually longitude, and latitude):

$$T_2 = \begin{bmatrix} 1 & 0 & X \\ 0 & 1 & Y \\ 0 & 0 & 1 \end{bmatrix}$$

The compound transformation from the image coordinates to the world coordinates is then given as:

$$\begin{bmatrix} x_{world} \\ y_{world} \\ 1 \end{bmatrix} = T_2 R T_1 S \begin{bmatrix} x_{pixel} \\ y_{pixel} \\ 1 \end{bmatrix}$$

2.2. Warped Fitting

We saw in Horizontal Fitting that an affine transformation alone is not sufficient to reflect the pixel-wise perspective distortion. To account for each pixel's perspective distortion, one needs to compute the actual 3D positions of every pixel in the georeferenced image, considering the Digital Elevation Model, and then project rays towards the camera center. The points where rays from the ground intersect the image plane will constitute the locations where the actual color for that ground point should be calculated. By transforming these intersection points into image-space coordinates, one can use techniques like bilinear interpolation to calculate ground colors. It is also possible that the rays intersect the image plane outside of the image rectangle. Such points lie outside of the camera frustum and will be assigned a value of 0 in the alpha channel to render them transparently in GIS applications. The algorithm first starts with ray tracing of each pixel, starting from the camera point, going through the center of every image pixel, using the same approach as in the horizontal fitting. The intersection points with the terrain is calculated by utilizing the Digital Elevation

Map (DEM) afterward. In our implementation, we use the QuadTree algorithm for efficient ray-terrain intersection comparisons.

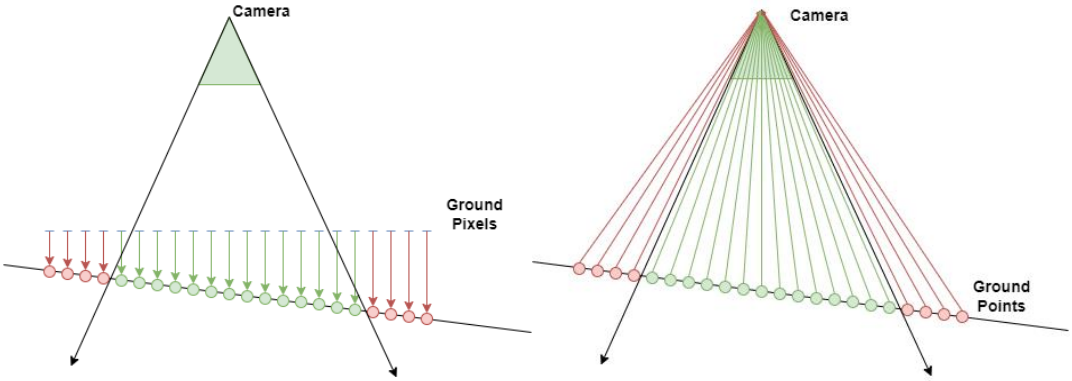

Figure 2. The geometrical setting for the Warped Fitting approach. Red pixels receive no color (will become transparent) where green ones will receive bilinearly interpolated colors from the UAV image.

After the intersection points on the terrain are determined, the tightest bounding rectangle around these points is calculated. The 2D tightest bounding rectangle is divided into pixels with a predetermined pixel count. These pixels are called Ground Pixels since they will contain the perspective-aware colors for the underlying terrain surface. From the centers of these pixels, their corresponding Ground Points are calculated. These ground points contain the same real-world coordinates as ground pixels, however their height value is equal to the surface of the DEM. Finally, from these ground points, rays are shot towards the camera center. These rays intersect the camera plane at various points; if these points belong inside the actual image boundaries, the ground pixel color is calculated by bilinear interpolation. Otherwise, no color is calculated. The calculated colors will constitute the perspective-aware monoplotting image. This process is called *Warped Fitting* and is described in Figure 2. The final step involves the calculation of an affine transformation matrix from the image coordinates to ground coordinates. Only considering x and y coordinates, we easily determine this transformation by solving the following system of linear equations:

$$\begin{bmatrix} x_{image}^{0} & y_{image}^{0} & 1 & 0 & 0 & 0 \\ 0 & 0 & 0 & x_{image}^{0} & y_{image}^{0} & 1 \\ . & . & . & . & . & . \\ . & . & . & . & . & . \\ . & . & . & . & . & . \\ x_{image}^{N-1} & y_{image}^{N-1} & 1 & 0 & 0 & 0 \\ 0 & 0 & 0 & x_{image}^{N-1} & y_{image}^{N-1} & 1 \end{bmatrix} \begin{bmatrix} A \\ B \\ C \\ D \\ E \\ F \end{bmatrix} = \begin{bmatrix} x_{world}^{0} \\ y_{world}^{0} \\ . \\ . \\ . \\ x_{world}^{N-1} \\ y_{world}^{N-1} \end{bmatrix}$$

With the solution of this system, the perspective-warped images can be used as monoplotting results in GIS applications.

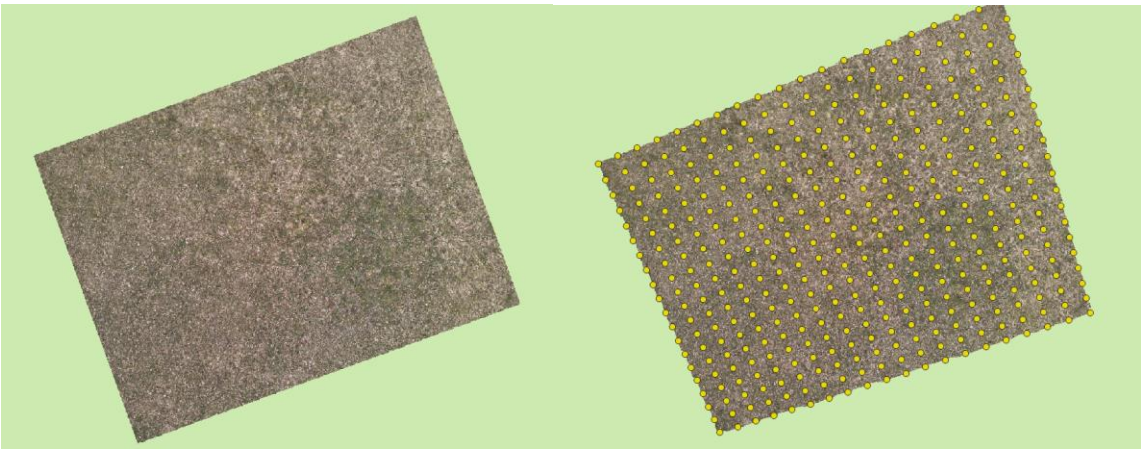

Figure 3. The warping effect of the Warped Fitting Method. Yellow points are camera ray – terrain intersection points; projected to 2D coordinates.

3. Results and Discussion

To evaluate the effectiveness of our algorithms, we applied them to a custom UAV flight on a field, with markers placed on the ground. The UAV maintained a constant barometric altitude of 12 meters relative to its starting point. We obtain images with a resolution of 4000x3000. We captured overlapping images throughout the flight to later generate a reference image using OpenDroneMap software, allowing us to compare the deviation of both methods from the ground truth. We used five markers, and during the flight, collected a total of 325 images. We manually selected the images that contained markers and measured the distance from their corresponding ground truth locations in the OpenDroneMap image. We selected 30 random samples for each algorithm, measuring deviations from the ground truth image using QGIS software. The DEM used for the evaluation method is the 1-meter resolution Austrian Height Map (Bev 2024), The results were as follows:

Table 1. Deviation of the Horizontal Fitting and Warped Fitting Methods from a Ground Truth Photogrammetry application.

Method	Mean Error (meters)	Std. Dev. Error (meters)
Horizontal Fitting	2.82	1.19
Warped Fitting	2.41	0.92

On average, the Warped Fitting method produced slightly better estimations of the actual marker locations, with a lower standard deviation. However, the Warped Fitting method involves ray tracing from the fitted locations back to the camera, resulting in a heavy computational load. In contrast, the Horizontal Fitting method uses a linear approximation for Monoplotting, making it much more efficient in terms of computation.

4. Conclusions

To efficiently render orthogonal images from UAV flights, we developed two different Monoplotting algorithms that do not require image overlapping like advanced photogrammetry methods or Ground Control Points (GCPs). Our only assumption is that the UAV photos are taken in a near-orthogonal manner. The first method, Horizontal Fitting, uses a horizontal approximation to the Digital Elevation Map (DEM) surface with a least squares approach. The second method, Warped Fitting, casts rays from the camera's ray-terrain intersection points back to the image plane and uses bilinear sampling to gather color values from corresponding locations. We tested both methods in a custom UAV flight with markers to measure their

deviation from a photogrammetry application obtained from OpenDroneMap software. The results showed that Warped Fitting slightly produced better results, but it required longer processing time compared to Horizontal Fitting.

References

Altmann, M., Ramskogler, K., Mikolka-Flöry, S., Pfeiffer, M., Haas, F., Heckmann, T., ... & Becht, M. 2023. Quantitative Long-Term Monitoring (1890–2020) of Morphodynamic and Land-Cover Changes of a LIA Lateral Moraine Section. Geosciences, 13(4), 95.

Bayr, U. 2021. Quantifying historical landscape change with repeat photography: an accuracy assessment of geospatial data obtained through monoplotting. International Journal of Geographical Information Science, 35(10), 2026-2046.

Bev, 2024 https://data.bev.gv.at/geonetwork/srv/metadata/9a4e3e4f-2cd5-4f73-af51-384beb9331d0 (Accessed 29.05.2024)

Bozzini, C., Conedera, M., & Krebs, P. 2011, September. A new tool for obtaining cartographic georeferenced data from single oblique photos. In *Proceedings of the XXIIIrd International CIPA Symposium*, Prague, Czech Republic (Vol. 1216, p. 6).

Crouzy, B., Forclaz, R., Sovilla, B., Corripio, J., & Perona, P. 2015. Quantifying snowfall and avalanche release synchronization: A case study. Journal of Geophysical Research: Earth Surface, 120(2), 183-199.

Esri, 2015, https://support.esri.com/en-us/knowledge-base/what-is-the-format-of-the-world-file-used-for-georefere-000002860 (Accessed 23.05.2024)

Gabellieri, N., & Watkins, C. 2019. Measuring long-term landscape change using historical photographs and the WSL Monoplotting Tool. Landscape History, 40(1), 93-109.

Ghosh, S.K. 2005. *Fundamentals of computational photogrammetry*, New Delhi, Concept Publishing Company, 2005.

Golparvar, B., & Wang, R. Q. 2021. AI-Supported framework of semi-automatic monoplotting for monocular oblique visual data analysis. arXiv preprint arXiv:2111.14021.

Linder, W. 2009. *Digital photogrammetry (Vol. 1)*. Berlin/Heidelberg, Germany: Springer.

Makarovič, B, 1973. Digital monoplotters, The ITC journal, 4, 583-600.

Mitterer, C., Heilig, A., Schmid, L., van Herwijnen, A., Eisen, O., & Schweizer, J. 2016, October. Comparison of measured and modelled snow cover liquid water content to improve local wet-snow avalanche prediction. In *International Snow Science Workshop Proceedings* (Vol. 5).

Moyroud, N., & Portet, F. 2018. Introduction to QGIS. QGIS and generic tools, 1, 1-17.

Investigation of production of grapevine seedlings inoculated with AMF and grown using organic compost with wine lees under water stress conditions

Pinelopi Baltzoi [a, *], Ioannis Tsirogiannis [a], Georgios Patakioutas[a], Olga Kostoula[b], Vasileios Papantzikos[a], Eleni Lampraki[a]

[a] Department of Agriculture, University of Ioannina, Arta, Greece

[b] Department of Biological Applications and Technology, University of Ioannina, Ioannina, Greece

* Corresponding author. Email: pinelbalt@uoi.gr

Abstract

The need for drought tolerant and well adapted to environmental stresses grapevine seedlings is essential for a successful establishment in the vineyard. Nursery plants hardening can be enhanced by arbuscular mycorrhizal fungi (AMF) symbiosis. The scope of the experiment was to evaluate an organic compost that included untreated wine lees used to grow grapevine nursery plants of "Debina" wine variety and to test the production of AMF-inoculated grapevine plants under limited water conditions aiming to produce robust grapevine seedlings.

The experimental treatments included two deficit irrigation treatments and inoculated plants with two types of mycorrhizal inoculums. The applied irrigation water amount was set at 90% of ET_c (moderate stress) and at 75% of ET_c (substantial stress). Plant growth parameters were measured, and the relative growth rate (RGR) was computed. Plants mycorrhizal colonization was detected by histological examination. Leaves total chlorophyll content, total phenolics and proline content were measured as stress indicators. Also the Water Footprint (WF) at whole plant basis was computed. The compost did not inhibit plant growth. Mychorrhiza colonization was not affected by the untreated wine lees neither by the applied deficit irrigation. Inoculated plants irrigated at 90% ET_c, showed higher shoot, leaves and roots dry weight, total biomass and relative growth rate, compared to no-inoculated plants. Plants inoculated with a single fungus inoculum under water stress, showed higher phenolic content in comparison to no-inoculated plants. Deficit irrigation did not affect the chlorophyl content of leaves neither the proline content. Plants irrigated at 75% ET_c resulted in a lower WF. The practical value of the research is the evaluation of usage of wine lees as composting material and the successful production of grapevine saplings with high potential to thrive under water stress conditions.

Keywords: Debina seedlings; Arbuscular mycorrhizal fungi; water stress; water footprint

1. Introduction

Grapevine (*Vitis vinifera* L.) cultivation and winemaking is an important agricultural activity in Greece. According to FAO for 2022 in Greece the harvested area of grapes was 84.260 ha (FAOSTAT, 2024). Vineyards in Greece are found in many regions from mainland to islands where wines with special characteristics are produced. The Hellenic Statistical Authority states that total vineyards in Greece in 2021 was 1.029.349 acres from which the 62,5% were wine vineyards (Maniatis, 2023).

Grapevine seedlings production in Greece is a dynamic agricultural sector. Nurseries play an important role in the production of high-quality grapevine seedlings as well as in the preservation and propagation of local and traditional grape varieties. The increase of grapevine cultivation has led to an increase of need for grapevine seedlings production which reveals the need for guidelines regarding viability of the vineyard (Ronga, et al., 2019). Given the fact that recent climatic change has affected grapevine cultivation, grapevine nurseries should produce plants that are resilient to new climatic conditions for vineyards to adapt to new weather conditions and traditional varieties should also be preserved well-adapted to environmental stresses (Paraskevopoulou, et al., 2022). Especially for Greek vineyards that their majority are located at semiarid areas, like islands and hills, the production of drought tolerant grapevine seedlings is essential for a successful establishment of the vineyard.

Peat is the most widely used material as growing medium for grapevine seedlings in nurseries. At the same time, peat is a non-renewable resource which must be protected from depletion. In this framework, organic composts could be used instead of peat as an alternative growing media in nurseries (Ronga, et al., 2019). Wineries produce large quantities of organic wastes like grape pomace, grape seeds and stems and

wine lees. These organic residues can be recycled and valorized through composting and can be used as a nutritious growing media for plants. However, little information is available regarding the composting method of wine lees and the effect of the produced organic soil amendment to grapevines (Pinto, et al., 2021)

The use of grapevine crop residues as compost materials is a common practice in sustainable viticulture. The Common Agricultural Policy (CAP) encourages the sustainable use of compost in agriculture and through the recently introduced Eco-schemes, promotes the composting of grapevine pruning residues and the general use of organic composts (Ministry of Rural Development and Food, 2023). Furthermore, the EU Soil Strategy for 2030 encourages the recycling of agricultural residues (European Commission, 2021). Since the direct disposal of wine lees can be harmful for the soil and the underground water, the use of wine lees as compost component can be an alternative solution instead of discharging the lees at the environment. The addition of wine lees at composting material can improve the nutrient content of the organic compost and improve the composting C/N ratio (Moldes et al., 2008) while the composting process appeared to reduce the total phenolic content of the compost material with initial ratio C/N of 10/1 (Lampraki, et al., 2023).

Water footprint (WF) is an environmental indicator that can be calculated as the water volume consumed and polluted per unit of product. In the framework of sustainable viticulture WF is used as a tool for efficient water management (Mekonnen & Hoekstra, 2011). It is consisted of three components, the WF_{green}, which accounts for the usage of precipitation water, the WF_{blue}, which is the applied irrigation water and the WF_{grey}, which is the amount of fresh water that is needed to assimilate the pollutants of the water and restore it to specific quality standards (Mekonnen & Hoekstra, 2011).

'Debina' is a Greek white wine grape variety which is mainly cultivated at the region of Epirus where it represents the 55,8% of the wine vineyards. The total area of 'Debina' wine grape in Greece is 171.76 ha, of which 136.26 are found at the municipality of Zitsa (Western Greece, Epirus) (OPEKEPE, 2022). It produces dry, sparkling dry and sparkling semi-sweet wines with the EU Protected Designation of Origin (PDO) (Tsiraki & Savvaidis, 2022).

Grapevine is a drought tolerant plant, and this attribute varies with the rootstock of the plant. Grapevines have been found to form symbiotic mychorrhizas with arbuscular mycorrhizal fungi (AMF). This formation, among other benefits, favors the growth of the vines and the quality of the berries through enhanced nutrient uptake, while increases the durability of grapes to water stress condition (Torres et al., 2021). The symbiosis with AMF can benefit nursery plants too. It has been found that the inoculation of saplings with AMF at the greenhouse, can enhance their rootstock resistance to pathogens after their transplanting to the vineyards (Moukarzel, et al., 2022). Regarding the effect of compost addition to AMF colonization, it has been observed that it depends on the mycorrhiza species. *Glomus intraradices* and *Glomus mossaea* have been found to increase the roots colonization with the organic compost addition (Cavagnaro, 2015).

The scope of the experiment was to evaluate the usage of an organic compost with untreated wine lees to grapevine nursery plants and to test the production of AMF-inoculated grapevine plants under limited water conditions for the purpose of having grapevine seedlings well-adapted to water scarcity. The wine lees was used without any treatment for removing phenolic compounds. Seedlings were irrigated at different fractions of ET_c and chlorophyll content, proline concentration and total phenolics of leaves were determined.

2. Materials and Methods

The experiment was conducted in a glasshouse of the Department of Agriculture of the University of Ioannina, cited at the University campus of Arta, Epirus, northwest Greece (Tsirogiannis, et al, 2010). The saplings of Vitis vinifera var. 'Dedina' were grafted onto 110R rootstocks. The indoor glasshouse relative humidity and temperature were continuously monitored with a microclimate sensor - Passive Radiation Shield (ATMOS-l4 w, Meter Group, Inc.). The indoor solar radiation (W/m^2) was recorded every 30 min with a pyranometer (PYR Solar Radiation Sensor, Meter Group, Inc.). During the experimental period the average air temperature ranged from 35,7°C το 24,9°C and the relative humidity ranged from 65,1% to 61,5%.

2.1. Compost production

The composting process took place in compost bins with self-aeration. The materials used were grapevine crop residues, vine shoots and leaves from plants Vitis vinifera var. 'Dedina' and wine lees from red grapes. The portion of the added wine lees was 10% and it was in untreated form while the initial compost ratio C/N

was 30/1 (Yin Quan Wang & Schuchardt, 2010). According to a preliminary experiment that was carried out in 2021, it was observed that the addition of small amounts of untreated wine lees in compost material does not negatively affect the growth of Debina grapevine saplings, while the composting process appeared to reduce the total phenolic content of the compost material with initial ratio C/N of 10/1 (Lampraki, et al., 2023).

2.2. Irrigation and substrate water content

Irrigation was performed through a micro irrigation system using 8 L h^{-1} drippers. of. The applied water amount was determined according to the actual water needs by calculating the crop evapotranspiration ET_c which was calculated by weighing periodically representative (same) pots from each treatment. During the experimental period the ET_c calculation was made five times. Because plants were growing very fast, more frequent measurements would probably provide more accurate results.. Irrigation was provided as a percentage of actual water needs.. During the experimental period two deficit irrigation treatments were applied. The irrigation water amount was applied at 90% of ET_c as a moderate water stress -IRR1 and at 75% of ET_c as a substantial water stress – IRR2. The initial goal was the 100% and 75% of ET_c, but this was not achieved. The moisture of the growing substrate for selected pots of all treatments was monitored daily with a portable soil moisture sensor (model SM150T, Delta-T Devices, UK). Measurement was made daily at the same time in the morning at depth of 0-6 cm. As a result of the applied water stress practice the substrate moisture remained under the theoretically estimated container capacity (Savvas and Gruda, 2018) for a long period.

2.3. Plant inoculation with mycorrhizal fungi and colonization detection

Two different commercial inoculums (AMF1, AMF2) were applied to inoculate with mycorrhizal fungi the plants in pots. The first inoculum AMF1 (one mycorrhizal species) was the commercial inoculum OZOR (Bioplanet, Italy) containing 500 reproduction fungal particles (spores and hyphae g^{-1}). The second inoculum AMF2 (a combination of two mycorrhizal species) was the commercial inoculum ATTRIVA MICROGRANULE (Hello Nature International Srl, Italy), containing two natural strains (50 fungal spores g-1) belonging to two Glomus species (Italpollina S.p.A strains), 25 spores g^{-1} of *Glomus intraradices* and 25 spores g^{-1} of *Funneliformis mosseae*. Plants were inoculated three times by watering with 200 ml of fungal suspension. The pot substrate mixtures had not been sterilized before the transplanting.

Mycorrhizal colonization was made from root samples randomly selected, 45, 90 and 120 days post 1st plants' inoculation. Root clearing and staining was accomplished using modifications on (Giovannetti et al., 2001) protocol. The mycorrhizal colonization of plants root has been verified based on the presence of key fungal features in root specimens (Brundrett M., 2004).

2.4. Pot experimental design

The pot experiment with grapevine saplings was conducted from June to October 2022 (140 days). Two years old saplings of 'Debina' cultivar (*Vitis vinifera* L.) were planted in 10 L pots with a mixture of peat and perlite 1:1 and 30% of the produced organic compost. Saplings were at the same growth stage and similar shape and had a central stem with average height of 65 cm. The thirty-six (36) pots were placed in a completely randomized design on the greenhouse benches. Six experimental treatments were designed which included two regulated deficit irrigation treatments (IRR1 and IRR2) for inoculated plants with two types of mycorrhizal inoculums (AMF1 and AMF2) and for no-inoculated plants.

The following treatments of irrigation at 90% ETc (moderate water stress) were implemented:

1. Plants with peat, perlite, organic compost – not inoculated (IRR1)
2. Plants with peat, perlite, organic compost inoculated with AMF1 (AMF1_IRR1)
3. Plants with peat, perlite, organic compost inoculated with AMF2 (AMF2_IRR1)

and the corresponding treatments of irrigation at 75% ETc (substantial water stress)

4. Plants with peat, perlite, and organic compost– not inoculated (IRR2)
5. Plants with peat, perlite, organic compost inoculated with AMF1 (AMF1_IRR2)
6. Plants with peat, perlite, organic compost inoculated with AMF2 (AMF2_IRR2)

2.5. Plant development

Plant growth parameters were measured during and at end of the experimental period. The height of the central stem was measured from above the graft union to the top. The length of all the lateral shoots was measured from the base to the top. The growth of the central stem and the lateral shoots were summed to the total plant height. The increase rate was calculated among the first and the last aggregate measurement of the central stem and the lateral shoots. The diameter of the central stem at the 6 cm of the graft union was measured and the increase rate between the beginning and the end of the experiment was calculated. Also, the number of the leaves and the number of the internodes was counted and the increase rate among the first and the last measurement was calculated. Plant biomass was estimated for two plants per treatment at the end of the experiment. Also, the Relative Growth Rate (RGR) of the plants was calculated (Cambrollé et al., 2013). The total leaf area was estimated at the end of the experiment by using the ImageJ software (Schroeder et al., 2020).

2.6. Total Chlorophyll, phenolic content, and proline content

Total chlorophyll content was measured during the experimental period as a stress indicator. Measurements were made with the portable leaf chlorophyll meter SPAD-502 in the morning of fully sunshine days. For the correlation of SPAD readings, leaf chlorophyll concentration was determined in mg/cm^2 through leaf extraction with acetone and the chlorophyll extract was measured in the spectrophotometer at two wavelengths, 661 nm and 644 nm (Uddling et al., 2007).

Total phenolics were measured as a physiological indicator that can be affected from abiotic stress. Measurements were made three times during the experiment at the beginning (Day 25), middle (Day 70) and near the end (Day 114). Phenolic content was extracted and measured as described by Folin-Ciocalteu method according to (Katalinić, et al., 2009) protocol.

Proline content was measured three times during the experiment at the beginning (Day 25), middle (Day 70) and near the end (Day 114). Proline was extracted and measured as described by (Bates et al., 1973) protocol with slight modifications.

2.7. Water footprint computation

The water footprint (WF) for all treatments of grapevine plants was computed according to WFN method (Hoekstra et al., 2011) where the WF results from the sum of $_{WFgreen}$, WF_{blue} and WF_{grey} and is computed using the following equation (1):

$$WFtotal = WFgreen + WFblue + WFgrey \quad (1)$$

Since the WF is expressed as water volume per yield, yield was each item of vine plant (Fotia et al., 2022). Given the fact that the grapevine plants were kept in a glasshouse and there was no rain, the WF_{green} is zero. The WF_{blue} is represented from the amount of the irrigation water applied which was a percentage of their actual water needs and is equal to crop water used. Since the plants were irrigated at two different water deficit levels, 90% ET_c and 75% ET_c, using adequate water flow, there was no water leaching during the experiment and thus the WF_{grey} is assumed to be zero.

2.8. Statistical analysis

Statistical analyses were performed with SPSS software (SPSS 20.0, IBM Corp., Armonk, NY, USA). The analysis of Variance (ANOVA) was applied, and means were compared by LSD test at the 5% level.

3. Results and Discussion

3.1. Mychorrhiza colonization confirmation

45 days after the 1st inoculation with AMF1 AMF2, all inoculated plants, regardless treatment, were found colonized by the mycorrhizal fungi. Control plants found negative for mycorrhizal colonization. Mycorrhizal fungi formed vesicular-arbuscular mycorrhizae (VA) in cortex cells in rather limited sites of plants' root. 90 days post 1st inoculation, *G. intraradices* alone (AMF1) or in combination with *F. mosseae* (AMF2) and

regardless treatment developed hyphal network, arbuscules and vesicles and/or spores in the cortex cells of plants' roots. 120 days post 1st inoculation both mycorrhizal fungi and regardless treatment formed a well-developed intra and inter-radical hyphal network, arbuscules and vesicles/spores in high extent of the root. The results ensure the establishment of the mycorrhizal symbiosis (early stages) for both species and regardless treatment, 45 days post 1st inoculation. Previous reports also have shown that *Funneliformis mosseae* and *Rhizophagus intraradices* form a vesicular-arbuscular mycorrhizae (VA) in cortex cells of grapevines, frequently after 2-4 months after first inoculation of host plants (Eftekhari et al., 2010; Torres et al., 2021).

It appeared that mychorrhiza colonization was not affected by the organic compost with untreated wine lees which encourages the usage of mycorrhiza inoculums after the addition of organic compost. Also, the applied deficit irrigation practices did not affect the mycorrhiza presence after inoculation which is in accordance with (Torres et al., 2021) where the implemented water amount did not affect the colonization.

3.2. Plant development

The substantial water stress of 75% ET_c did not affect the growth rates of shoot length, number of leaves and inter nodes and stem diameter, in comparison to the moderate water stress situation of 90% ET_c and neither affected the plants leaf area at the end of the experiment. The increase rates of the inoculated plants did not differ significantly from non-inoculated plants. This finding has been observed in other studies too where the inoculation of vine plants does not affect the growth of the plants (Holland et al., 2019).

Differences were detected at shoot, leaves and roots dry weights of the plants. In particular, the AMF1_IRR1 and AMF2 _IRR1 treatments showed the highest shoot dry weight with significant difference from others, which indicates the positive effect of mycorrhizal fungi under moderate water stress level (Ye et al., 2022). The shoot dry weight seems to be affected negatively from the substantial water stress status of 75% ET_c and the mycorrhizal inoculation did not manage to alleviate this negative effect.

The inoculation with the two fungi inoculum (AMF2) significantly increased the dry weight of the leaves under moderate water stress status. The same positive effect with significant difference was detected with the single fungus inoculum (AMF1). The substantial water stress status reduces the leaves dry weight among inoculated plants with significant difference between AMF2 treatments. As for the root development, the highest root dry weight was produced from AMF1 treatment under moderate water stress status, with significant difference from non-inoculated plants under the same irrigation level. The highest plant biomass with significant differences from other treatments was performed from the inoculated plants under moderate water stress level. The substantial water stress to inoculated plants resulted to reduction of plant biomass with no significant differences of the non-inoculated plants. This finding is in accordance with the fact that one of the restricted factors for the mycorrhizal development is the water deficit.

Table 1. Dry weights at the end of the experiment

Treatment	Shoot dry weight (g)	Leaves dry weight (g)	Root dry weight (g)	Plant biomass (g)	RGR (%)
IRR1	18,6 ab	20,5 a	56,8 a	95,9 a	1,14 a
IRR2	15,1 a	28 b	49,9 a	93 a	1,12 a
AMF1_IRR1	21,9 b	33,6 b	67,3 b	122,7 b	1,32 b
AMF1_IRR2	15,7 a	24,7 ab	56,9 ab	97,36 a	1,16 a
AMF2_IRR1	20,7 b	35,3 c	60,6 ab	116,59 b	1,28 b
AMF2_IRR2	14,6 a	23,3 ab	52,3 a	90,31 a	1,10 a

The observed increase in dry weights of shoots, leaves, roots, and total biomass at inoculated plants under greenhouse conditions are in accordance with the findings of other studies were the inoculation with *Glomus intraradices* enhanced the plant growth (dry weight) of grapevine saplings in Richter 110 rootstock in comparison to no-inoculated plants at a greenhouse cultivation (Popescu, 2016). The beneficial effect of mycorrhizal inoculation on saplings growth has been confirmed from other studies too (Eftekhari et al., 2010).

Regarding the RGR, the inoculated plants under moderate water stress had the highest RGR with

significant difference from other treatments which indicates the positive effect of inoculation. The presence of mycorrhiza did not manage to alleviate the negative effects of the substantial water stress to RGR %.

3.3. Leaf total phenol content

Some researchers point out that leaves total phenolic content reduces under various abiotic stresses (Krol et al., 2014) or it can increase (Weidner, et al., 2009b) while other represent leaf phenolics as a physiological plant indicator that is increased when plant is under abiotic stress condition (Weidner et al., 2009a), (Petridis et al., 2012). On day 114, at AMF2 treatment, the 75% ET_c water stress caused reduction of the leaf's phenolic compounds with a statistically significant difference among them which is in line with the fact that water stress can decrease the content of phenolic compounds at leaves (Krol et al., 2014). The AMF1 inoculation treatments, on day 114, have statistically significant higher phenolic content from other treatments which is in accordance with Eftekhari et al. (2010) where leaves of inoculated plants presented increased phenolic compounds.

3.4. Leaf proline and chlorophyl content

Proline is an organic compound that under water stress condition can accumulate in plants as an osmoticum and helps plants to preserve their photosynthetic activity. Some researchers support that under water stress AM fungi increases proline concentration in plants (Ye et al., 2023) while others found that with AMF plants have lower proline concentration (Valentine et al., 2006).
Leaves proline content did not differ significantly among treatments, either at the midterm or near the end of the experimental period. From this it can be concluded that AMF did not have the time to act protectively for the plants by increasing proline concentration.

Various studies support that AMF inoculation enhances chlorophyl content of leaves through alleviation of the adverse effects of water stress (Ye et al., 2022) or indirectly through the increase of specific nutrients (Moukarzel et al., 2022). At our study, the water deficit practice did not affect the chlorophyl concentration. This is in line with the findings by Giorgi et al. (2019). Despite the findings form other studies, in our case the mycorrhizal inoculation did not affect the chlorophyl concentration of leaves. This finding is in accordance with leaves proline concentration where no differences among treatments were detected and this can reinforce the possibility that AMF did not act supportively to the plants probably due to little time from their establishment.

3.5. Water Footprint

The amount of irrigation water applied for the irrigation water amount was applied at 90% of ET_c - substantial water stress -IRR I and at 75% of ET_c – moderate water stress – IRR2 was 88,01 L/pot for the IIR1 treatments and 73,31 L/pot for the IRR2 treatments. The WF per treatment was estimated at the end of the experiment as the amount of irrigation water in L that was applied to each plant. Plants irrigated at the 75% of ET_c had lower total WF per plant.

Table 2. The water footprint of grapevine seedlings per irrigation treatment

	CWU_{blue} (L/plant)	CWU_{total} (L/plant)	WF_{blue} (L/plant)	WF_{total} (L/plant)
IRR1 treatments	88,01	88,01	88,01	88,01
IRR2 treatments	73,31	73,31	73,31	73,31

4. Conclusions

The usage of organic compost with untreated wine lees did not inhibit plant growth. Inoculated plants irrigated at 90% ET_c, showed highest shoot, leaves and roots dry weight, highest total biomass and RGR% compared to no-inoculated plants. The presence of AMF at 75% ET_c irrigated plants did not increase the plants growth parameters. Plants inoculated with the single fungus inoculum AMF1 under both water stress levels, had higher phenolic content in comparison to no-inoculated plants. Water deficit irrigation did not affect the chlorophyl content of leaves neither the proline content. Regarding the water management, plants

irrigated at 75% ET_c had lower water footprint.

The above findings reveal that the inoculation of grapevine saplings with AMF improves water use efficiency of plants under deficit irrigation practice. The combination of mycorrhizal inoculation and reduced irrigation at glasshouse, can be used as a water saving practice. Further research is needed to optimize the water use efficiency of grapevine saplings.

Acknowledgements

The work is co-financed by the European Union (European Regional Development Fund) and National Resources, under the operational program "Competitiveness, Entrepreneurship and Innovation (EPAnEK)", "NSRF 2014 - 2020",Call 111: "Support for Regional Excellence (project: MIS 5047215).

References

Bates, L., Waldren, R., & Teare, I. 1973. Rapid determination of free proline for water stress studies. Plant Soil (39), 205-207.

Brundrett, M. (2004). Diversity and classification of mycorrhizal associations. Biol Rev.(78), 473-495.

Cavagnaro, T. R. (2015). Advances in Agronomy (Vol. 129). Elsevier Inc. http://dx.doi.org/10.1016/bs.agron.2014.09.005

Eftekhari, M., Alizadeh, M., Mashayekhi, K., Asghari, H., & Kamkar, B. (2010). Integration of Arbuscular Mycorrhizal Fungi to Grape Vine (Vitis vinifera L.) in Nursery Stage. Journal of Advanced Laboratory Research in Biology, 1(2).

European Commission. (2021, October 15/10/2023). EUR-Lex Access to European Union law. Retrieved 2023. https://eur-lex.europa.eu/legal-content/EN/TXT/?uri=CELEX%3A52021DC0699

FAOSTAT. (2024, February 14). https://fenix.fao.org/faostat/internal/en/#data/QCL

Fotia, K., Nanos, G., & Barouchas, P. (2022). Growth Development, Physiological Status and Water Footprint Assessment of Nursery Young Olive Trees (Olea europaea L. 'Konservolea') Irrigated with Urban Treated Wastewater. Resources, 11(40). https://doi.org/10.3390/resources11050040

Giorgi, E. G., Sadras, V. O., Keller, M., & Perez, P. (2019). Interactive effects of high temperature and water deficit on Malbec grapevines. Australian Journal of Grape and Wine Research, 25(3), 345-356. https://doi.org/10.1111/ajgw.12398

Giovannetti, M., Fortuna, P., Citernesi, A., Morini, S., & Nuti, M. (2001). The occurrence of anastomosis formation and nuclear exchange in intact arbuscular mycorrhizal networks. New Phytol.(151), 717-724.

Hoekstra, A., Chapagain, A., Aldaya, M., & Mekonnen, M. (2011). The Water Footprint Assessment Manual. London, UK: Earthscan.

Holland, T., Bowen, P., Kokkoris, V., Urbez-Torres, J., & Hart, M. (2019). Does Inoculation with Arbuscular Mycorrhizal Fungi Reduce Trunk Disease in Grapevine Rootstocks? Horticulturae(5). https://doi.org/10.3390/horticulturae5030061

Katalinić, V., Generalić, I., Skroza, D., Ljubenkov, I., Teskera, A., Konta, A., & Boban, M. (2009). Insight in the phenolic composition and antioxidative properties of Vitis vinifera leaves extracts. Croat. J. Food Sci. Technol., 7-15.

Krol, A., Amarowicz, R., & Weidner, S. (2014). Changes in the composition of phenolic compounds and antioxidant properties of grapevine roots and leaves (Vitis vinifera L.) under continuous of long-term drought stress. Acta Physiol Plant(36), 1491–1499. https://doi.org/10.1007/s11738-014-1526-8

Lampraki, E., Baltzoi, P., Patakioutas, G., Tsirogiannis, I., Mantzos, Hela D., Malamos N. and Gizas G. (2023). Properties of organic compost from vineyard pruning residues and wine lees and evaluation when used in substrates for grapevine saplings under various irrigation treatments. Angers - France: 31st International Horticultural Congress.

Mekonnen, M., & Hoekstra, A. (2011). National Water Footprint Accounts: the Green, Blue and Grey Water Footprint of Production and Consumption, Value of Water Research Report Series No. UNESCO-IHE, Delft, the Netherlands.

Ministry of Rural Development and Food. (2023). Ανάκτηση October 15/10/2023, 2023, από https://www.minagric.gr/2013-04-05-10-13-09/ministry-example/diavoylefsi-i-kap-meta-to-2020-list/12311-kap2023-2027-130122

Moldes, A. B., Vazquez, M., Domınguez, J. M., Dıaz-Fierros, F., & Barral, M. T. (2008). Negative effect of discharging vinification lees on soils. Bioresource Technology (99), σσ. 5991–5996. https://doi.org/10.1016/j.biortech.2007.10.004

Moukarzel, R., Ridgway, H., Waller, L., Guerin Laguette, A., Cripps Guazzone, N., & Jones, E. (2022). Soil Arbuscular Mycorrhizal Fungal Communities Differentially Affect Growth and Nutrient Uptake by Grapevine Rootstocks. Microbial Ecology (86), σσ. 1035-1049. https://doi.org/10.1007/s00248-022-02160-z

Paraskevopoulou, A. T., Pappous, E., Biniari, K., Bertsouklis, K. F., Daskalakis, I., & Perdikis, D. (2022). Enhancing the Rural Landscape Character: The Low Frequency of Inter-Row Wildflower Meadow Harvest Positively Affects Biodiversity While Maintaining Grape Quantitative and Qualitative Traits in a 'Sultanina' Vineyard in Greece. Agronomy, 12(550). https://doi.org/10.3390/agronomy12030550

Petridis, A., Therios, I., Samouris, G., Koundouras, S., & Giannakoula, A. (2012). Effect of water deficit on leaf phenolic composition, gas exchange, oxidative damage and antioxidant activity of four Greek olive (Olea europaea L.) cultivars. Plant Physiol. Biochem.(60), 1-11.

Pinto, R., Brito, L., Gonçalves, F., Mourão, I., Torres, L., & Coutinho, J. (2021). Recycling wastes from Douro wine industry by composting. Acta Hortic. ISHS(1305). https://doi.org/10.17660/ActaHortic.2021.1305.39

Popescu, G. C. (2016). ARBUSCULAR MYCORRHIZAL FUNGI - AN ESSENTIAL TOOL TO SUSTAINABLE VINEYARD DEVELOPMENT: A REVIEW. Current Trends in Natural Sciences, 5(11).

Ronga, D., Francia, E., Allesina, G., Pedrazzi, S., Zaccardelli, M., Pane, C., . . . Bignami, C. (2019). Valorization of Vineyard By-Products to Obtain Composted Digestate and Biochar Suitable for Nursery Grapevine (Vitis vinifera L.) Production. Agronomy, 9(420). https://doi.org/10.3390/agronomy9080420

Savvas Dimitrios and Gruda S. Nazim. 2018. Application of soilless culture technologies in the modern greenhouse industry – A review. European Journal of Horticultural Science 83(5):280-293. https://doi.org/10.17660/eJHS.2018/83.5.2

Schroeder Alexandra B., Ellen T. A. Dobson, Curtis T. Rueden, Pavel Tomancak, Florian Jug, Kevin W. Eliceiri. 2020. The ImageJ ecosystem: Open-source software for image visualization, processing, and analysis. https://doi.org/10.1002/pro.3993

Torres, N., Yu, R., & Kurtural, S. K. (2021). Arbuscular Mycrorrhizal Fungi Inoculation and Applied Water Amounts Modulate the Response of Young Grapevines to Mild Water Stress in a Hyper-Arid Season. Front. Plant Sci.(11:622209). https://doi.org/10.3389/fpls.2020.622209

Torres, N., Yu, R., Martínez-Lüscher, J., Kostaki, E., & Kurtural, S. (2021). Effects of Irrigation at Different Fractions of Crop Evapotranspiration on Water Productivity and Flavonoid Composition of Cabernet Sauvignon Grapevine. Front. Plant Sci.(12:712622). https://doi.org/10.3389/fpls.2021.712622

Tsiraki, M. I., & Savvaidis, I. N. (2022). Quality study of PDO (Protected Designation of Origin) Greek white wines of the grape variety 'Debina'. Notulae Botanicae Horti Agrobotanici Cluj-Napoca, 50(3). https://doi.org/10.15835/nbha50312823

Tsirogiannis, I., Katsoulas, N., & Kittas , C. (2010, February). Effect of Irrigation Scheduling on Gerbera Flower Yield and Quality. HORTSCIENCE, pp. 265-270.

Uddling, J., Gelang-Alfredsson, J., & Piikki, K. (2007). Evaluating the relationship between leaf chlorophyll concentration and SPAD-502 chlorophyll meter readings. Photosynth Res(91), 37-46. https://doi.org/10.1007/s11120-006-9077-5

Valentine, A., Mortimer, P., Lintnaar, M., & Borgo, R. (2006). Drought responses of arbuscular mycorrhizal grapevines. SYMBIOSIS(41), σσ. 127-133.

Weidner, S., Karolak, M., Karamac, M., Kosinska, A., & Amarowicz, R. (2009a). Phenolic compounds and properties of antioxidants in grapevine roots (Vitis vinifera) under drought stress followed by regeneration. Acta Soc Bot Pol, 97–103.

Weidner, S., Kordala , E., Brosowska-Arendt, W., Karamac, M., Amarowicz , R., & Kosin´ska, A. (2009b). Phenolic compounds and properties of antioxidants in grapevine roots followed by recovery. Acta Soc Bot Pol (78), 279-286

Ye, Q., Wang, H., & Li, H. (2022). Arbuscular Mycorrhizal Fungi Improve Growth, Photosynthetic Activity, and Chlorophyll Fluorescence of Vitis vinifera L. cv Ecolly under Drought Stress. Agronomy, 12(1263). https://doi.org/10.3390/agronomy12071563

Ye, Q., Wang, H., & Li, H. (2023). Arbuscular Mycorrhizal Fungi Enhance Drought Stress Tolerance by Regulating Osmotic Balance, the Antioxidant System, and the Expression of Drought-Responsive Genes in Vitis vinifera L. Australian Journal of Grape and Wine Research. https://doi.org/10.1155/2023/7208341

Training needs analysis for intergrating bioeconomy approaches into the EU's agricultural sector

Dimitris Michas [a, *], Athanasios Balafoutis [a], Bas Paris[a], Ioannis Thermos[a], Duarte Pimentel[b], Carlota Silva[b]

[a] CERTH/IBO Centre for Research and Technology, Institute for Bio-Economy and Agri-Technology (IBO), Athens, Hellas

[b] Terinov Science and Technology Park, Angra do Heroísmo, Portugal

* Corresponding author. Email: d.michas@certh.gr

Abstract

This paper presents the result of a Training Needs Analysis (TNA) conducted with both training providers and learners across four partner EU countries (Greece, Italy, Portugal, and Sweden). These results are based on a survey with 196 respondents. Based on multiple presented data points and sources we reach three main conclusions. Education and training in bioeconomy reflects megatrends associated with the green transition in terms of generating hybrid and emerging knowledge subfields, often embedded in traditional scientific disciplines such as farming or forestry that require a fast adaptation to new and promising professional profiles. Moreover, our results also reflect digitalization megatrends. Specifically, education and teaching institutions are still biased towards in-person teaching methods, while learners show a significant preference for blended or online learning methods, especially among those with higher qualifications (agronomists, consultants, and policymakers). Importantly, significant trends in bioeconomy education and training were also detected. For instance, due to its novelty, bioeconomy education and training is becoming more relevant across the European Union, but developments are not homogeneous. Importantly, secondary education programs and VET supply seem to be slowly adapting to the demand for competencies and skills in this sector.

Finally, we highlight that according to the learners involved in our training needs analysis it is vital to disseminate comprehensive curricula in the bioeconomy sector, targeting technical, but also digital, entrepreneurial, soft, and transversal skills to address current professional requirements. Based on our conclusions, we offer some recommendations which may improve the quality and effectiveness of programs, in this field. Our recommendations cover issues such as curricula content, skills update of teachers and trainers, human-centred approaches to training design or appropriate use of digitalization.

Keywords: Bioeconomy; education; training; training needs analysis; HEI; VET.

1. Introduction

Bioeconomy is the production, utilization, conservation, and regeneration of biological resources, including related knowledge, science, technology, and innovation, to provide sustainable solutions (information, products, processes, and services) within and across all economic sectors and enable a transformation to a sustainable economy (Kalnbalkite et al., 2022). Bioeconomy corresponds to a complex, hybrid subfield of knowledge, stemming from the inputs of several scientific fields. It is also a sector strongly informed by the major driving forces of current societies and economies. The dual transition, namely the green transition and digitalization, are among these drivers that help shape the bioeconomy's present and future.

The European bioeconomy is one of the EU's largest and most important sectors, encompassing agriculture, forestry, fisheries, food, bioenergy, and bio-based products. It has an annual turnover of around 2 trillion euros and employs around 18 million people. The first EU bioeconomy strategy, 'Innovating for Sustainable Growth: A Bioeconomy in Europe,' was adopted in 2012 and took action through existing policies in various sectors (Common Agriculture Policy, Common Fishery Policy). The main goals of this strategy were:

- Ensure food and nutrition security.
- Manage our natural resources sustainably.
- Reduce dependence on non-renewable, unsustainable resources.

- Mitigate and adapt to climate change.
- Create jobs across Europe.

Considerable gaps exist in our understanding of the existing practices around bioeconomy-related training and education. This can partly be explained by the relative newness of the bioeconomy as a concept (Kalnbalkite et al., 2022), but also because multiple educational practices and approaches that are conceptually within the bioeconomy are not explicitly labeled as such. A range of previous projects and studies have investigated bioeconomy education programs and approaches (BRANCHES - Boosting Rural Bioeconomy Networks). However, a critical review of training methods and approaches across higher education (HE) and vocational education and training (VET) is lacking. This is especially relevant as previous studies have highlighted that education, training, and knowledge development in bioeconomy sectors vary widely across Europe. According to the European Commission, there is a particular lack of training on bioeconomy for small enterprises and at low levels (Hakovirta & Lucia, 2019; Pubule et al., 2020; Watkinson et al., 2011; Ciriminna et al., 2021). Various recent publications investigate bioeconomy-related education and programs. Pubule et al. (2020) analyze 10 master's programs in bioeconomy and highlight the interdisciplinary nature of the approaches used. Kalnbalkite et al. (2021) look more widely at education for the bioeconomy. Ruxandra et al. (2018) investigate the role of universities in developing human capital for a sustainable bioeconomy. Masiero et al. (2020) explores bioeconomy-related perceptions among 1400 students in 29 universities. Less recently, Watkinson et al. (2011) conducted a review of advanced bioenergy education and training in Europe, and Ray et al. (2016) highlighted the importance of linking bioeconomy development with education in developing countries, emphasizing the potential of e-learning courses.

In recent years, numerous platforms have emerged to support education processes by hosting and sharing relevant bioeconomy knowledge. These include the Rural Bioeconomy Portal, the European Bioeconomy Network, the European Bioeconomy Library, the Bio-based Industry Consortium's (BIC) bioeconomy platform, the European Bioeconomy University, the European Bioeconomy Alliance, and the Circular Bioeconomy Alliance. These platforms, which sometimes overlap, generally support bioeconomy knowledge and information sharing, stakeholder collaboration, policy development, and provide tools and support for relevant stakeholders.

In this study, we present the results of a Training Needs Analysis (TNA) conducted with both training providers and learners across the four partner countries of the RELIEF consortium (Greece, Italy, Portugal, and Sweden). This survey included 196 respondents and offers multiple insights that can be triangulated with the information collected in the previous three sections resulting from desk research. We organize the main findings according to the concepts of megatrends, trends, and weak signals. These concepts are time- and data-driven and, therefore, help to establish a prospective analysis of education and training programs in the bioeconomy sector.

2. Methodology

In the RELIEF project, an analysis was conducted of the current education and training provisions at the vocational education and training (VET) and higher education levels in the field of bioeconomy within the farming sector across EU countries. This task involved an online desk research approach comprising two main steps. Firstly, utilizing a pre-organized course form developed and provided by some project partners (TERINOV, CESIE, and OTC), the consortium gathered relevant information related to bioeconomy course provision in the field of agriculture across European Union countries. This process expanded to include detailed information from training provisions available across EU countries that do not formally integrate into the project's consortium. The main criterion for inclusion in this mapping was that the training offer must be currently active and/or accepting new learners. Subsequently, data was extracted directly from higher education institutions and VET providers' curricula available on the institutional websites of each organization and from publicly available databases from official bodies responsible for accrediting training provisions (e.g., Direção-Geral do Ensino Superior and Direção-Geral da Educação, Portugal). Figure 2 depicts full education and training

programs as well as programs with curricular units on bioeconomy across the EU by country, as identified through the mapping procedure.

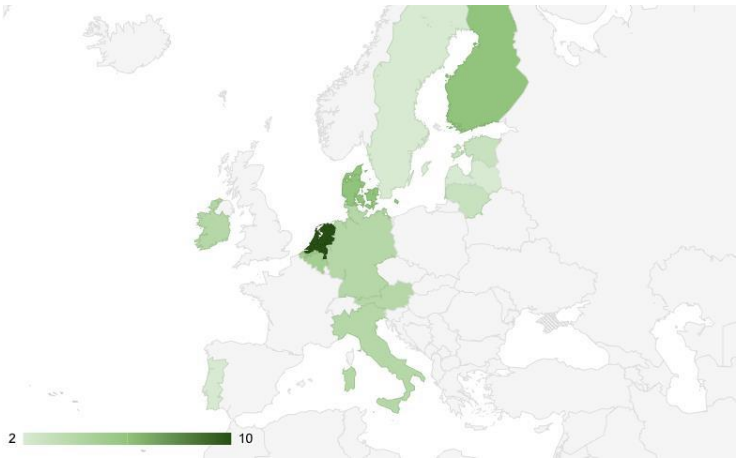

Figure 1. Training Curricula on bioeconomy by EU country

The Training Needs Analysis (TNA) approach followed the principle of multiple informants to better understand the learning needs in the bioeconomy and, therefore, to target commonalities and differences among different stakeholders. Potential participants from higher education institutions and VET providers were identified and contacted to participate in the study directly by the partners of the consortium. Potential learners, including farmers, agronomists, consultants, and policymakers, were identified and contacted with the invaluable help of local, regional, and national farmers' associations, universities, and government bodies, who kindly shared the questionnaires with their stakeholders. A total of 95 questionnaires for higher education institutions and VET providers and 230 questionnaires for potential learners were sent out via email but also made available in paper-and-pencil format. The questionnaires were filled in between October 20, 2022, and May 12, 2023. To conduct a comprehensive TNA, the RELIEF consortium developed two questionnaires. The first questionnaire targeted training providers. The first part of this questionnaire aimed to characterize the training providers in terms of active training fields associated with the bioeconomy sector, institutional typology (VET provider, professional training, higher education, or other), and degrees awarded (if any). This part of the questionnaire also included a depiction of learning courses/programs offered by training providers, covering elements such as training types, duration, learning methods, or fees. In the second part of the questionnaire, participants were asked about the opportunities and challenges of their training packages, including strengths and weaknesses, elements of effective training, or non-technical skills covered. The questionnaire also comprised some open-ended questions regarding expected training updates, improvements, or partnerships for program implementation. The second questionnaire focused on learners. Learners covered by this questionnaire were farmers or farming companies, agronomists, farming consultants, and policymakers. In many ways, this questionnaire mirrored the questionnaire for training providers to ensure comparability. The first part of the instrument covered personal information about the learners in terms of the highest educational qualification achieved, duration of the latest qualification, number of curricular units associated with bioeconomy attended, and professional identity (e.g., agronomist, farmer, etc.). The second part focused specifically on farmers' perceptions and expectations regarding bioeconomy learning needs. This section of the questionnaire included questions about the level of interest in learning more about the sector, preferred learning language, or preferred learning methods. This section also encompassed a series of questions using a 5-point Likert scale (from 1 "not at all" to 5 "extremely important") to rate the relevance of promoting different entrepreneurial (e.g., creativity), digital (e.g., digital content creation), and transversal skills (e.g., self-efficacy). The third part of the questionnaire aimed specifically at agronomists, farming consultants, or policymakers, covering largely the same questions and items rated using the 5-point Likert scale. Both the second and third sections of the questionnaire for learners included some open-ended questions.

2.1. Data Analysis

The results from the questionnaires for training providers and learners were categorized into three parts: (a) description of training supply by training providers; (b) learners' qualifications; and (c) learning needs. We conducted a descriptive statistical analysis using primarily two approaches. For characterization questions, we depicted response frequencies and percentages. For Likert scale questions aimed at learners, we presented mean values. The results are presented in graphical displays in the results section.

3. Results

The survey targeting training providers commenced by identifying the fields of education related to the bioeconomy sector offered by the institutions represented by these participants. The consortium identified a total of 55 training curricula on bioeconomy or including curricular units on bioeconomy subjects in the farming sector across 13 countries. The distribution of curricular programs included in the RELIEF database ranged from 2 in Portugal and Sweden to 10 in The Netherlands. Importantly, of the 55 education and training curricula added to our database, 48 (87.2%) were delivered by public universities. The results show that training offers were more often made available in the agriculture field (25.2%; n = 26), followed by forestry (23.3%; n = 24), environment and sustainability (13.6%; n = 14), biorefineries and green chemistry (13.6%; n = 10), and renewable energies (13.6%; n = 10). Notably, a portion of the training providers indicated that they did not provide training in any of the proposed areas of the survey (11.7%; n = 12).

Regarding the educational levels offered by the VET providers, VET equivalent to different certification degrees (EQF 3 to 5) (55.1%; n = 27) was the most frequently offered education level according to the institutions involved, followed by a mix of education levels (26.5%; n = 13), tertiary education (16.3%; n = 8), and other (2.0%; n = 1). Most of the VET providers' courses offer more than 5 UCs (credit units) on bioeconomy (71.1%; n = 32), followed by those providing 1 UC (13.3%; n = 6), 2 UCs (6.7%; n = 3), and 5 UCs (2.2%; n = 1). Some training providers did not provide any answer to this question (6.7%; n = 3).

Regarding the main aims of the current bioeconomy-related courses, Goal 8 "other" (27.2%; n = 22) was the most selected one by the participants, followed by Goal 5 "Methodologies for environmental impact assessment" (24.7%; n = 20), Goal 6 "Necessary skills to deal with the biomass to energy chain" (22.2%; n = 18), Goal 7 "Necessary skills to deal with the biorefinery and Green Chemistry topics" (6.2%; n = 5), Goal 3 "Knowledge on bioeconomy strategies" (6.2%; n = 5), Goal 2 "Systematic approach to conduct economic analysis to evaluate costs and benefits" (6.2%; n = 5), Goal 4 "Knowledge on biomass markets" (4.9%; n = 4), and Goal 1 "To provide the key concepts in microeconomics" (2.5%; n = 2). According to the surveyed training providers, bioeconomy-related training most often lasted for 2 years (40.4%; n = 19), followed by training courses with a duration of 3 years (27.7%; n = 13). Short-term training courses were less common, whether they lasted less than 3 months (17.0%; n = 8), 4 to 6 months (8.5%; n = 4), or finally 7 to 12 months (6.4%; n = 3).

The primary teaching language of the current bioeconomy-related courses, bioeconomy-related courses are more often delivered in English (29.8%; n = 14), followed by a similar share of courses provided in Greek and Portuguese languages (both 21.3%; n = 10). Courses in this area provided only in Italian (14.9%; n = 7), and Swedish (12.8%; n = 6) were less common. The most common methodological approach to training in the bioeconomy-related training courses, according to the participants, is in-person training (59.6%; n = 31), followed by the blended method (28.8%; n = 15), online (9.6%; n = 5), and other (1.9%; n = 1). Overall, tuition fees were implemented by half of the training providers (50.0%; n = 23). Among these, tuition fees ranged considerably from being less than 1000€ (17.8%; n = 8) to more than 6000€ (11.1%; n = 4), with some falling between 1000€-3000€ and 3000€-6000€ (both 8.9%; n = 4). It is important to note here, nevertheless, that tuition variability certainly overlaps with the variety of training opportunities provided by the surveyed training institutions, according to the results displayed in Figure 6. It is also important to note that most of the training providers did not provide any answer to this question (53.3%; n = 24).

According to the training providers the key conclusions form the TNA where the following**:**
Agriculture and forestry account for almost 50% of the training areas offered by VET providers. Interestingly, emerging areas associated with the green transition already account for almost 39.8% of all bioeconomy related training.
• VET is the predominant training approach to bioeconomy.
• In most cases, bioeconomy is nonetheless a relevant dimension of the training curricula. More than 70% of the training providers indicated that they offered at least 5 curricular units related to the sector.
• The goals associated with the provided bioeconomy training opportunities cover multiple targets, showing that the approach followed by the training providers inquired by the RELIEF project acknowledges the hybrid nature of the sector.
• Bioeconomy training is mostly provided as part of long-term curricula (lasting for 2 or 3 years). Short-term training is therefore less recurrent, raising the question of how much specialization is offered in the sector.
• Almost a third of bioeconomy training is provided in English.
• Blended and online forms of training already account for almost 40% of the training delivered by the training providers enrolled in our survey.

Learners' qualifications and learning need**.**

The data analyzed in the following subsection refer to the Training Needs Analysis (TNA) conducted by the consortium with learners. According to the survey, the participants were very diverse regarding their educational background. The most common qualification among the participants was a bachelor's degree (22.5%; n = 34), followed by a high school diploma (21.2%; n = 32), a master's degree (20.5%; n = 31), a high school dropout (7.9%; n = 12), other (6.6%; n = 10), a doctoral degree (5.3%; n = 8), a summer course (4.6%; n = 7), a post-graduate course (4.0%; n = 6), VET (2.0%; n = 3). Eight learners did not provide any answer to this question (5.3%; n = 8). The graduation years ranged from 1976 to 2023.

Unsurprisingly, given the distribution by level of qualification, the duration of the latest qualification, course, or degree attained by the learners was long-term, whether it was more than 3 years (43%; n = 65), 3 years (19.2%; n = 29), or 2 years (12.6%; n = 19). However, some of them were enrolled in 7-12 months (4.0%; n = 6), less than 3 months (2.6%; n = 4), or 4-6 months courses (0.7%; n = 1). Importantly, 24 of the learners did not answer this question (53.3%; n = 24). Additionally, regarding the number of curricular units/disciplines related to bioeconomy, most learners reported 0 UC's (credit units) (68.4%; n = 104), followed by 1 UC (5.9%; n = 9), 2 UC's (4.6%; n = 7), 3 UC's (3.9%; n = 5), more than 5 UC's (2.6%; n = 4), and 4 UC's (0.7%; n = 4). Some learners did not provide any answer to this question (13.2%; n = 20). One of the learners considered this question not to be applicable (NA - 0.7%; n = 1).

The participants clearly stated a preference for agriculture as the most interesting area for promoting further bioeconomy training, irrespective of being farmers (25.4%; n = 71) or having another professional background (agronomists/farmer's consultants/policy makers) (11.1%; n = 31). Training expectations associated with Environment and Sustainability (agronomists/farmer's consultants/policy makers - 10.4%; n = 29; farmers - 9.3%; n = 26) came second, followed by renewable energies, widely mentioned by farmers (8.9%; n = 25) and agronomists/farmer's consultants/policy makers (7.9%; n = 22). Bioenergy (e.g., energy crops, forestry use for energy, biofuels, etc.) also captured some attention among the respondents, although with different distributions among agronomists/farmer's consultants/policy makers' answers (6.4%; n = 18) and farmers (4.6%; n = 13). Bioeconomy was equally selected by both groups (5.0%; n = 14); Forestry was selected mostly by farmers (3.9%; n = 11) compared to agronomists/farmer's consultants/policy makers' (1.4%; n = 4). The option "other areas" was selected only by one farmer (0.4%; n = 1), while only one learner (i.e., agronomists/farmer's consultants/policy makers) answered "Biorefineries, Green Chemistry" (0.4%; n = 1).

Based on the outcomes of the survey, the preferred teaching language for training differs depending on the country of the learner. Importantly, English is not the top preference for both farmers (8.0%; n = 13) and agronomists/farmer's consultants/policy makers (4.3%; n = 7). In general, both groups show a preference for their native languages as the most wanted teaching language for training. As for the methods, the online method covers a great number of preferences in total. This was particularly true among agronomists/farmer's consultants/policy makers (25.1%; n = 52) who more often preferred the online method when compared to

farmers (14.5%; n = 30). The blended method (in-person/online) comes next and is preferred in almost even numbers by agronomists/farmer's consultants/policy makers (17.4%; n = 36) and farmers (15.5%; n = 32). Farmers showed more interest in learning in person (17.9%; n = 37) than agronomists/farmer's consultants/policy makers (9.7%; n = 20). Regarding the willingness to pay for the courses, most farmers are not willing to pay tuition fees for bioeconomy-related training (43.7%; n = 66), similar to agronomists/farmer's consultants/policy makers (21.9%; n = 33). A group of farmers (20.5%; n = 31) were available to pay tuition fees, with a few more agronomists/farmer's consultants/policy makers choosing this option as well (21.9%; n = 20). "Circular economy standards and assessment method" was the most often chosen option by both groups, especially by farmers (24.7%; n = 59), compared to agronomists/farmer's consultants/policy makers (17.6%; n = 42). "Energy management and conservation" came next among farmers (21.8%; n = 52) and agronomists/farmer's consultants/policy makers (7.9%; n = 19). Lastly, "sustainable waste management" (waste classification and environmental impact, supply chain management and the 5Rs - Reduce, Reuse, Refurbish, Repair, and Recycle) was chosen by farmers (19.7%; n = 47) and agronomists/farmer's consultants/policy makers (8.4%; n = 20).

The final questions of the RELIEF survey for learners focused on the importance of different sets of skills to undertake bioeconomy activities. The selected skills are inspired by DigitComp and the EntreComp competences frameworks presented in section 3 of this report. Our inquiries are, thus, aligned with the EU skills framework for digitalization and entrepreneurship. Mean results for the different items are presented: the adopted Likert scale ranges from 1 (not at all) to 5 (extremely important). In general, both farmers and agronomists, consultants, and policymakers give great importance to digital skills, with mean values above 4, contrary to information and data literacy and to communication and collaboration, with mean values below 1. It is also relevant to stress that mean values are similar across the two groups in each of the different digital competences/skills assessed.

Overall, the pattern of mean results for both learners' groups found for entrepreneurial and soft skills is similar to the one found for digital competences and skills. Indeed, both farmers and agronomists, consultants, and policymakers display considerably high values for all the proposed entrepreneurial and soft skills that might be relevant for the bioeconomy sector. There are, however, a few differences. For instance, farmers tend to give less importance, on average, to creativity, valuing ideas, ethical and sustainable thinking or self-awareness and self-efficacy compared to agronomists, consultants, and policymakers. The reverse trend can be observed regarding financial and economic resources. Again, as it happened with the digital and with the entrepreneurial and soft competences as skills, both farmers and agronomists, consultants, and policymakers had strong average perceptions, above level 4, about the relevance of transversal skills for undertaking bioeconomy activities.

The RELIEF consortium also wanted to understand which were the strengths and weaknesses of the bioeconomy training programs. Therefore, the final part of the survey was dedicated to these two points, covering a wide range of factors which can constitute both pros and cons to implement educational and training programs in this emerging sector.

Summarizing the results provided by the respondents regarding the strengths of the bioeconomy training programs: the most often selected strength among farmers (8.1%; fi = 21) and agronomists/farmer's consultants/policy makers (6.6%; fi = 17) was applicability to real life/working environments and contexts. Importantly, the most selected option was other, especially among farmers (20.1%; fi = 52) but also with a relevant number of answers among agronomists/farmer's consultants/policy makers (7.7%; fi = 20). Unfortunately, only rarely did the participants specify which other strengths they had in mind.

One important trend emerging is that farmers more often identify weaknesses compared to agronomists, consultants, and policymakers. That mismatch is clear regarding factors such as applicability to real life/working environments' contexts - farmers (12.4%; fi = 55); agronomists/farmer's consultants/policy makers (4.8%; fi = 21), followed by weak connection with industries and the business sector - farmers (11.5%; fi = 51); agronomists/farmer's consultants/policy makers (7.9%; fi = 35), lack of available tools (e.g., access to labs and software) - farmers (11.3%; fi = 50); agronomists/farmer's consultants/policy makers

(6.3%; fi = 28) - or not well-defined scope - farmers (11.1%; fi = 49); agronomists/farmer's consultants/policy makers (5.7%; fi = 25).

Finally, the key conclusions stemming from the TNA for the learners are the following:

- The number of curricular units dedicated to bioeconomy is often low.
- The fact that farming is the main area of bioeconomy training indicates the need for training associated with practical knowledge (short-term training, upskilling/reskilling, VET).
- Programs delivered in English language are not a priority among learners, whether they are farmers or agronomists/consultants/policymakers.
- Learners are somewhat open to the use of digitalization – although that seems to be more the case with agronomists, consultants, and policymakers.
- The perceived importance of almost all digital skills is very high.
- High importance is given to all sets of skills beyond the technical skills, namely those covered by the DigiComp and the EntreComp frameworks. Still, it is relevant to underline that some skills related to direct management of these activities - funding - are more important, on average, for farmers.
- Weaknesses of training packages are very often selected by farmers.

4. Discussion

Our discussion will integrate three key elements. Firstly, we will specifically analyze the results provided by RELIEF's critical review, incorporating the identification of professional areas, mapping of education and training opportunities, and assessment of training needs in the bioeconomy area as reported by both training providers and learners. Secondly, by triangulating data and informants, we aim to highlight the most significant findings emerging from our diverse sources of information. Lastly, considering the prospective nature of this report, we will further elucidate these findings by interpreting them through the lens of future-oriented concepts such as megatrends, trends, and weak signals.

Megatrends

Megatrends represent significant shifts in society, policy, markets, and education and training, driven by environmental, social, and technological factors. These overarching trends have the potential to produce profound societal impacts on a global or continental scale. Examples of megatrends relevant to the aims of RELIEF include the green transition, digitalization, and globalization. Megatrends often interact with each other, creating synergies that lead to major innovations and societal transformations.

Trends

Trends are clear-cut developments in society, economy, or technology supported by credible sources and statistics. Unlike megatrends, trends may have more localized impacts and can vary in their scope and intensity within different territories. Trends are typically identified through longitudinal studies or expert analysis of recent developments within specific fields. Examples of current trends include the growth of sustainable consumption and the rise of populism in Western countries.

Weak Signals

Weak signals refer to unusual or unexpected issues that may have significant implications for future changes in organizations, societies, or environments. Identifying and analyzing weak signals is crucial for anticipating future developments and relevant prospects for bioeconomy education and training. Incorporating weak signals into scenario planning allows for a deeper exploration of potential future scenarios and their impact on education and training initiatives in the bioeconomy sector.

4.1 Bioeconomy education and training and megatrends

Several findings from the RELIEF project align well with key megatrends, particularly the green transition and digitalization. The green transition signifies a shift towards sustainable economic growth, reducing reliance on fossil fuels and promoting circular economy practices. In the European Union, this transition is driven by initiatives like the European Green Deal, which aims for net-zero greenhouse gas emissions by 2050 and sustainable economic growth.

Two aspects of bioeconomy education and training identified in our research are closely linked to the green transition megatrend. Firstly, these programs are designed to address unsustainable production models that compromise environmental and social sustainability. Our analysis, including critical reviews, mapping of educational programs, and Training Needs Assessment (TNA), indicates a strong focus on environmental sustainability goals within bioeconomy education and training. For instance, Vocational Education and Training (VET) providers prioritize methodologies for environmental impact assessment over purely economic considerations.

Secondly, our data suggests that bioeconomy education and training are adapting to the complexity of sustainability challenges posed by the green transition. The bioeconomy sector faces multifaceted or "wicked" problems, requiring innovative and interdisciplinary approaches to address them effectively. Our findings indicate that education and training programs in this field are evolving to meet these challenges, incorporating diverse perspectives and methodologies to tackle complex environmental and economic issues.

In summary, the alignment between bioeconomy education and training and megatrends like the green transition underscores the importance of sustainability and innovation in shaping the future of education and training in the bioeconomy sector.
Two additional findings from the RELIEF project align with another significant megatrend: digitalization. Digitalization refers to the sociotechnical process of applying digitizing technologies to broader social and institutional contexts, involving the conversion of analogue signals into digital form.

Firstly, a notable discrepancy emerged between the predominant teaching methodologies reported by learners in our Training Needs Assessment (TNA) and those identified in our mapping of existing education and training programs by providers. While most programs in our database were delivered in person according to providers, learners expressed a stronger preference for online or blended teaching methods. Interestingly, farmers showed the least preference for teaching methods other than in-person instruction. This discrepancy may reflect the shift towards digitalized education, especially following the COVID-19 pandemic, which has become more prevalent in lifelong learning contexts. However, it's important to note that our mapping and survey primarily focused on higher education programs, where in-person teaching remains the standard. Thus, this contradiction requires careful consideration.

Secondly, learners with higher professional qualifications, such as agronomists, consultants, and policymakers, displayed greater openness to digital alternatives in bioeconomy education and training compared to farmers. This inclination can be attributed to their increased exposure to digital tools in their daily work routines. Leveraging digital tools for online learning may be an effective means to reach farmers, particularly in remote areas with limited training resources. However, challenges related to digital literacy and connectivity, especially in rural areas, must be addressed. These challenges contribute to digital inequalities, which are pertinent issues in the field of bioeconomy education and training.

Furthermore, the RELIEF survey highlighted the importance of digital skills and competencies among learners, as evidenced by high average ratings for digital skills items inspired by the DigiComp framework. However, lower mean values for data literacy warrant attention. It's crucial to recognize that perceived digital literacy often exceeds actual digital literacy, emphasizing the need to improve digital literacy across EU countries. When designing educational programs, both delivery methods and digital skills development should be carefully considered.

Moreover, the perception that collaboration is not inherent in the development of digital skills, particularly among farmers, requires nuanced interpretation. Qualitative studies suggest that farmers utilize digital skills

and tools for collaboration, especially in rural areas where official support may be lacking. Therefore, this finding may not universally apply or may vary across different contexts.

In summary, addressing digital inequalities and integrating digital literacy into educational programs are essential steps in leveraging digitalization for effective bioeconomy education and training. Additionally, recognizing the collaborative potential of digital skills among diverse learner groups is crucial for fostering innovation and knowledge exchange in the bioeconomy sector.
Globalization refers to the spread of trans planetary connections between people, increasingly extending to sup aterritorial realms. It signifies how the world has become more interconnected and interdependent through trade and technology exchanges (Scholte, 2008). Communication is a crucial aspect of globalization, as it facilitates exchanges between individuals and organizations on a global scale. The use of a common, standardized language is essential for enabling interactions across different geographic locations, cultures, and societal groups.

English has emerged as a symbol of international communication, particularly in the education and training sector. The RELIEF project investigated the extent to which education and training in the bioeconomy domain is becoming more international by adopting English as the primary teaching language. Our findings reveal nuanced trends that may initially appear contradictory.

Our mapping of training programs indicates that nearly three-quarters of the programs in our database are delivered in English. However, data from our Training Needs Assessment (TNA), gathered from both training providers and learners, suggests a lower proportion of programs delivered in English and a preference for native languages among learners. It's important to note that our mapping predominantly covered advanced courses, such as master's programs.

The prevalence of international programs taught in English is on the rise across Europe, spanning various knowledge domains, including bioeconomy and related fields. However, our TNA also captured a significant portion of individuals without tertiary education who may not be proficient in international languages. For these individuals, accessing learning environments in their native languages is particularly relevant and impactful.

4.2 Bioeconomy education and training trends

As previously mentioned, trends are emerging social, economic, or technological developments supported by multiple data points and sources. In the realm of education and training in the bioeconomy sector, trends primarily reflect promising or relevant developments in the supply and demand nexus of training. One prominent trend evident from the various data sources utilized by the RELIEF project, particularly from our critical review, is the increasing significance of bioeconomy in curricula across Europe. This trend is corroborated by training providers surveyed, with over 70% indicating the inclusion of at least five curricular units related to the bioeconomy sector. However, the dissemination of bioeconomy education and training programs is uneven and not yet fully independent as a training field.

Our Training Needs Assessment (TNA) also reveals that agriculture and forestry comprise nearly half of the bioeconomy-related training opportunities offered by providers. Notably, emerging areas associated with the green transition are gaining prominence in bioeconomy training. Both farmers and agronomists, consultants, and policymakers recognize the importance of integrating bioeconomy into traditional knowledge fields like farming and new, hybrid curricula driven by megatrends such as the green transition. However, a significant proportion of learners noted the absence of bioeconomy topics in the programs they attended, particularly those enrolled in Vocational Education and Training (VET) courses.

From a supply and demand perspective, the field of education and training in bioeconomy is undergoing a transitional phase marked by unbalanced and somewhat contradictory developments. While bioeconomy is increasingly relevant in advanced training, the basics of bioeconomy appear less prioritized in VET programs. The lack of VET programs or curricular units dedicated to bioeconomy is evident in our critical review and mapping efforts.

Another trend associated with this transitional process is the limited access to bioeconomy curricula for VET learners. VET is considered crucial for enhancing educational attainment across all knowledge areas, as emphasized by strategic policies like the European Skills Agenda. However, the scarcity of intermediate-level professionals equipped with practical skills hinders progress in sectors vital to regional economies, particularly in rural areas.

Addressing the gap in bioeconomy training supply within the VET sector is a trend that needs to be addressed in the future. Additionally, our research highlights the importance of a comprehensive set of competencies and skills for success in the bioeconomy sector. Learners recognize the significance of skills beyond technical expertise, aligning with frameworks such as EntreComp and DigiComp. Notably, farmers exhibit a greater inclination toward developing managerial skills, such as funding, reflecting the daily challenges they face in managing their farms and balancing profitability with sustainable production practices.

4.3 Bioeconomy education and training weak signals

Weak signals are current anomalies or peculiarities that can help anticipate future changes. Throughout our research efforts, the RELIEF project has identified some weak signals associated with bioeconomy education and training. While further research is needed, these weak signals could serve as starting points for innovation and the future dissemination of bioeconomy educational programs.

One weak signal we have detected relates to the duration of curricula. Bioeconomy training is primarily offered as part of long-term curricula lasting 2 or 3 years. Consequently, short-term training opportunities are less common, raising questions about the level of specialization offered and required in the sector. However, given the anticipated increase in the need for upskilling/reskilling due to technological advancements, the prevalence of lifelong learning paradigms, and the European ambitions outlined in the European Green Deal, we anticipate that short-term training opportunities will become more frequent.

The assessment of weaknesses, particularly those identified by farmers, has caught our attention as a potential weak signal. Farmers have shown keen interest in highlighting several gaps in bioeconomy education and training packages. This indicates an imbalance between the importance placed on advanced training and the lack of short-term, problem-solving oriented courses for professionals, as discussed in the previous subsection. We interpret this as farmers representing a target group that will become increasingly relevant in the bioeconomy sector in the future, a development that has not been adequately addressed thus far.

Additionally, it is essential to consider that a significant portion of learners showed little to no motivation to pay tuition for training in bioeconomy. This weak signal from the data is crucial for authorities considering expanding knowledge in this field. If prioritized, the allocation of public resources must be carefully considered to ensure that on-the-ground professionals, particularly farmers, are adequately enrolled in educational packages.

5.Conclusion

The depiction of bioeconomy education and training across the European Union evokes the image of someone in adolescence, experiencing a period of transition filled with both opportunities and uncertainties.

Undoubtedly, the bioeconomy is an emerging sector. Over recent years, there has been a notable increase in knowledge production, professional occupations, and associated training packages, as highlighted by our critical review and identification of professional pathways. Our mapping and TNA of bioeconomy educational and training programs further indicate a growing relevance of learning opportunities in this sector. These developments are influenced by megatrends, particularly the green transition, which has led to the emergence of hybrid bioeconomy training packages or curricular units integrated into traditional scientific disciplines like farming or forestry. These programs aim to adapt to the evolving demands of the green transition and its associated professional profiles.

Digitalization is another significant driver of bioeconomy development. Learners are increasingly drawn to online and blended teaching environments, although educational institutions still predominantly favor in-person teaching methods. This shift towards online learning is especially pronounced among individuals with higher qualifications, such as agronomists, consultants, and policymakers.

Moreover, the RELIEF project has identified notable trends in bioeconomy education and training. While the sector is gaining relevance across the EU, developments are not uniform across countries and educational levels. Secondary education programs and vocational education and training (VET) opportunities related to the bioeconomy remain limited. However, there is a gradual adaptation of education and training offerings to meet the demand for practical competencies and skills in this field.

It is crucial to emphasize the importance placed by learners in our TNA on disseminating comprehensive curricula in the bioeconomy sector. These curricula should encompass technical as well as digital, entrepreneurial, soft, and transversal skills to address current professional requirements.

In conclusion, our report underscores the need to balance sustainability principles with the management requirements of training programs in the bioeconomy field. It advocates for continuous professional development and updating of trainers and teachers, thoughtful digitalization of learning programs to mitigate digital inequalities, particularly among farmers, and the expansion of VET curricula associated with bioeconomy activities to facilitate integrated training pathways from secondary education to advanced tertiary education.

References

A European Green Deal | European Commission. (n.d.). Retrieved October 18, 2022, from https://ec.europa.eu/info/strategy/priorities-2019-2024/european-green-deal_en

Bejinaru, R., Hapenciuc, C. V, Condratov, I., & Stanciu, P. (2018). *Perspectives of Bioeconomy: The Role of Intellectual Capital and of Knowledge Management THE UNIVERSITY ROLE IN DEVELOPING THE HUMAN CAPITAL FOR A SUSTAINABLE BIOECONOMY*. *20*(49). https://doi.org/10.24818/EA/2018/49/583

Bettencourt, L., Simões, F., Fernandes, B., & Fonseca, J. (2023). Designing vocational training policies in an outermost European region: Highlights from a participatory process. *European Educational Research Journal*. https://doi.org/10.1177/14749041231157445

BRANCHES - Boosting Rural Bioeconomy Networks BRANCHES. (n.d.). Retrieved May 29, 2024, from https://www.branchesproject.eu/

Buchanan, J., Anderson, P., & Power, G. (2017). *Skill ecosystems*. 444–465. https://doi.org/10.1093/OXFORDHB/9780199655366.001.0001/OXFORDHB-9780199655366-E-21

Ciriminna, R., Albanese, L., Meneguzzo, F., & Pagliaro, M. (2021). Educating the managers of the bioeconomy. *Authorea Preprints*. https://doi.org/10.22541/AU.164004623.37302520/V1

Fields Database | erasmus-fields. (n.d.). Retrieved May 29, 2024, from https://www.erasmus-fields.eu/database/

Hakovirta, M., & Lucia, L. (2019). Informal STEM education will accelerate the bioeconomy. *Nature Biotechnology*, *37*(1), 103–104. https://doi.org/10.1038/NBT.4331

Hiltunen, E. (2008). The future sign and its three dimensions. *Futures*, *40*(3), 247–260. https://doi.org/10.1016/J.FUTURES.2007.08.021

Kalnbalkite, A., Pubule, J., & Blumberga, D. (2022). Education for Advancing the Implementation of the Green Deal Goals for Bioeconomy. *Environmental and Climate Technologies*, *26*(1), 75–83. https://doi.org/10.2478/RTUECT-2022-0007

Masiero, M., Secco, L., Pettenella, D., Da Re, R., Bernö, H., Carreira, A., Dobrovolsky, A., Giertlieova, B., Giurca, A., Holmgren, S., Mark-Herbert, C., Navrátilová, L., Pü, H., Ranacher, L., Salvalaggio, A., Sergent, A., Sopanen, J., Stelzer, C., Stetter, T., … Wallin, I. (n.d.). SOCIAL DIMENSIONS OF A FOREST-BASED BIOECONOMY Bioeconomy perception by future stakeholders: Hearing from European forestry students. *Ambio*, *49*. https://doi.org/10.1007/s13280-020-01376-y

Megatrends, Trends and Change Drivers: Understanding the Larger Picture and Path-dependencies — Futures Platform. (n.d.). Retrieved May 29, 2024, from https://www.futuresplatform.com/blog/megatrends-trends-and-change-drivers-the-larger-picture-and-path-dependencies

Pubule, J., Blumberga, A., Rozakis, S., Vecina, A., Kalnbalkite, A., & Blumberga, D. (2020). Education for advancing the implementation of the bioeconomy goals: An analysis of MASTER study programmes in bioeconomy. *Environmental and Climate Technologies*, *24*(2), 149–159. https://doi.org/10.2478/RTUECT-2020-0062

Ray, S., Srivastava, S., Diwakar, S., Nair, B., & özdemir, V. (2016). Delivering on the promise of bioeconomy in the developing world: Link it with social innovation and education. *Biomarker Discovery in the Developing World: Dissecting the Pipeline for Meeting the Challenges*, 73–81. https://doi.org/10.1007/978-81-322-2837-0_6

Scholte, J. A. (2008). Defining Globalisation. *World Economy*, *31*(11), 1471–1502. https://doi.org/10.1111/J.1467-9701.2007.01019.X

Susanna, L. K., & Tuomas, K. (2022). How Farmers Conceive and Cope with Megatrends: The Case of Finnish Dairy Farmers. *Sustainability 2022, Vol. 14, Page 2265*, *14*(4), 2265. https://doi.org/10.3390/SU14042265

Tilson, D., Lyytinen, K., & Sørensen, C. (2010). Digital infrastructures: The missing IS research agenda. *Information Systems Research*, *21*(4), 748–759. https://doi.org/10.1287/ISRE.1100.0318

Unay-Gailhard, İ., & Simões, F. (2022). Becoming a Young Farmer in the Digital Age—An Island Perspective*. *Rural Sociology*, *87*(1), 144–185. https://doi.org/10.1111/RUSO.12400

Watkinson, I. I., Bridgwater, A. V, & Luxmore, C. (2011). *Advanced education and training in bioenergy in Europe*. https://doi.org/10.1016/j.biombioe.2011.06.038

Zheng, Y., & Walsham, G. (2021). Inequality of what? An intersectional approach to digital inequality under Covid-19. *Information and Organization*, *31*(1), 100341. https://doi.org/10.1016/J.INFOANDORG.2021.100341

Advancing circular nitrient flows through the development of biofertilizers: P2GreeN project perspective

Athanasios Balafoutis [a, *], Bas Paris [a], Dimitris Michas [a], Michalis Moraitis [a], Ioannis Thermos [a]

[a] CERTH/IBO Centre for Research and Technology, Institute for Bio-Economy and Agri-Technology (IBO), Athens, Hellas*

Corresponding author. Email: d.michas@certh.gr

Abstract

This perspective paper provides an overview of the current research results and expected outputs of the Horizon Europe P2GreeN project which pilots four innovative technology and implementation systems in Germany, Sweden and Spain that capture and turn human sanitary waste into safe bio-based fertilizers for agricultural production. This paper presents the current status of the implementation of these technologies in the pilot regions and the first results of the field trials of the project. Initial results document the process of setting up each pilot region and indicate that the bio-based fertilizers produced are safe for agricultural production and in line with the production efficiency as compared to conventional chemical fertilizers. A policy and governance analysis for the implementation and scaling of these technologies in the pilot regions and the EU is also presented.

In parallel the project explores the potential of implementing and scaling these systems to other areas in the EU with a particular focus on Italy, Greece, Hungary and France. In this regard the project undertakes a number of feasibility studies evaluating the potential of each system in specific cases. Initial results document the cases to be explored in each follower region for the final feasibility studies. The paper also presents the results of expert consultations from focus groups and workshops. Results from the focus groups indicate broad support amongst experts for the implementation of these types of technologies and fertilizers emphasizing their potential in various regions, despite challenges such as implementation costs. Various social considerations centered around acceptance and quality were also highlighted. While there is a need for the development of a supportive policy framework at both EU and national levels.

Keywords: circular nutrient flows, farm to fork, air and water pollution control, fertilizer, wastewater management

1. Introduction

Nutrient losses in the environment are a major threat to the functioning of terrestrial and aquatic ecosystems. Nitrogen (N) and phosphorus (P) flows are considered the most critical, as high N & P loads are associated with problems such as groundwater pollution, eutrophication of aquifers and loss of biodiversity (too much to lose). The agri-food sector plays a key role here as it is significantly contributing to N & P pollution on the one hand but at the same time the agricultural production in Europe depends on mineral fertilisers, with an estimated consumption of approximately 11 million tonnes N & P per year (*Eurostat*,). Current mainstream production methods for N & P fertiliser are not sustainable. Mineral N fertilisers (the most used nutrient in the EU in terms of volume) result from energy-intensive industrial processes that are heavily dependent on fossil fuels (for energy use and as a feedstock) and are a major source of industrial and agricultural emissions in the EU. Mineral P fertilizers are sourced outside of the EU and often mined under precarious and unsustainable conditions (Vermeulen et al., 2012). Furthermore, the supplies of N & P are not guaranteed due to increased costs and limited supplies. Higher energy prices impact on N fertilizer production and the world's P reserves may be exhausted at the end of the 21st century if today's fertilization practices continue. Together, these factors challenge the EU's food security. Moreover, nutrient losses of N & P include diffuse emissions from agriculture and point emissions from wastewater treatment plants (WWTPs.) (Desmit et al., 2018). The intensive use of fertilizers in agricultural production is a major factor for N & P pollution. High nutrient concentrations are also found in human sanitary waste streams from where they are ultimately released to rivers and coastal zones, including effluxes from WWTPs. Nutrient removal in WWTPs is very energy intensive and also in modern WWTPs not all N can be removed from wastewater.

The removed N is ultimately ending up in the atmosphere as molecular nitrogen (N2) and to a lower share (~ 1%) as the very potent greenhouse gas nitrous oxide (N2O). For P, only 34% of WWTP inputs are recycled by spreading sewage sludge on agricultural fields. The use of sewage sludge for fertilization, however, is connected to problems such as micro pollutants, which are rarely removed by WWTPs (Gianico et al., 2021).

2. P2GreeN's novel concept

P2GreeN's goal is to develop the nutrient cycle between urban settings with high levels of nutrients in wastewater (blue infrastructure) and rural areas with a high demand of nutrients for agricultural production (green infrastructure). Various innovative and safe approaches have been developed to efficiently recover nutrients from human excreta. However, these have yet to be scaled up to fulfil their true potential. About 3.1 Tg (i.e. 109 kg) N and 0.6 Tg P are excreted every year by the EU's population, corresponding to 30% and 55% of the amount of mineral fertilisers applied on agricultural fields in the EU. P2GreeN addresses this potential and will transform nutrient streams on a regional level to close N & P cycles from sanitation (via new bio-based fertilisers) to agricultural production (from waste to farm to fork). To facilitate systemic change, co-creation strategies including the participation of all relevant stakeholders,(Larsen et al., 2013) as well as harmonised governance frameworks that foster innovations will be key to P2GreeN. Collaborative innovation networks of technology provider, industry, farmers, scientific communities, public administration and citizens will help maximise the value of knowledge production, circulation and use of the project's transformative approaches. The involvement of local municipalities and regional governments as well as the interaction with policy makers on the national and EU level will also be a key part of P2GreeN.

P2GreeN's envisaged transformation (Fig. 1) will (i) reduce municipal waste streams, thereby helping to achieve the 2030 targets of the EU's Zero Pollution Action Plan, the Urban Waste Water Treatment Directive (UWWTD) and Sewage Sludge Directive (SSD); (ii) increase self-sufficiency of P in the EU; (iii) save water resources ; (iv) reduce harmful production practices of mineral fertilisers; (v) reduce nutrient losses of N & P; (vi) enable tailored fertilisers, reducing nutrient loss further; (vii) minimise cropland expansion through optimal fertiliser use increasing yield on the existing agricultural area17; (viii) open new market potentials for bio-based fertilisers, and (ix) simultaneously enable micropollutants such as pharmaceutical residues or hormones to be more easily removed. Overall, the circular systems will help to increase sustainability and resilience of the agri-food system and will contribute to the EU objectives on reducing nutrient losses by 50% until 2050.

Figure 1. P2GreeN's envisaged transformation to circular nutrient streams in Europe.

To achieve its objectives, P2GreeN will draw upon innovative technological approaches to efficiently recover nutrients from human excreta close to source and will further develop these approaches in 3 pilot regions towards multi-sectoral circular governance solutions where discarded N & P from urban sanitary systems become a valuable resource. This will be done through the implementation of 4 different "waste-recycling technologies for the agri-food value chain by reusing sanitary waste as bio-based fertilisers, thus closing N & P nutrient cycles between rural and urban environments.

2.1. Methodology

The P2GreeN Concept is built upon a holistic and circular multi-sectoral systems approach encompassing the upscaling of innovative technologies, the development of circular business models, the engagement of stakeholders along the entire value chain, the mobilisation of policymakers and the creation of adequate governance models that will enable the envisaged nutrient system transformation. The concept will be validated and demonstrated in P2GreeN's 3 pilot regions and upscaled to 4 follower regions in year 3 of the project. The application of recycling fertilisers in P2GreeN will be based on the nutrient demand of each crop, considering the aim of the Farm to Fork strategy to restrict fertiliser use to a sustainable level, and following existing regional guidelines. This includes determining the nutrient content of soils prior to fertilisation, calculation of plant N and P demand according to local soil conditions and climate and limiting surplus fertilisation as far as possible. If the composition of recycling fertilisers does not allow to supply crops with all nutrients in the needed amounts (without supplying one nutrient in excess), single nutrients will be added in the form of mineral fertilisers. Up-to-date and efficient fertilisation practices will be used to reduce pollution by N and P leaching as well as gaseous N emissions:

- Urea fertilisers used for barley cultivation in the Swedish pilot region will be incorporated into soil during sowing to limit N losses from ammonia emissions and leaching. Further measures such as the use of nitrification inhibitors to reduce nitrate leaching and nitrous oxide emissions will be considered as well.
- N and P fertilisation in the German pilot region will be done according to the German Fertilising Ordinance, which already sets strict limits to reduce nutrient pollution, and following recommendations from DIN-SPEC 91421. The faecal composts produced will be applied to agricultural fields (rye, buckwheat) prior to sowing according to the existing recommendations for compost fertilisers (max. 510 kg N/ha in 3 years). To fully cover crop N demands, supplemental fertilisation will be done with urine-based fertiliser using state-of-the-art application techniques (i.e. by umbilical injector). In case the P demand is already covered by the faecal compost, the application of urine-based fertiliser will be restricted to avoid excess P fertilisation. The addition of biochar and clay minerals during the composting process contributes to the reduction of N and P leaching and nitrous oxide emissions through the formation of stable organic-mineral complexes. In addition, nutrients bound to it are released slowly in the course of cultivation so that they can be efficiently taken up by the plants.
- The Spanish pilot will demonstrate a nutrient monitoring tool integrated in the MBR-based RichWater reclamation system. This technological solution will be designed to perform an adequate nutrient balance that takes into account nutrients contained in the effluent of the MBR (i.e. reclaimed water). According to existing literature (1), farmers disregard nutrients in reclaimed water leading to negative environmental impacts and economic losses. Thus, fertilisation and irrigation (fertigation) will be performed according to the crop demand. An experimental test site will be arranged with sub-tropical crops (e.g. avocado and mango trees) in the region of La Axarquia to get on site data. Online nutrient analysis together with the mixing station and soil sensors will allow to adjust the composition of the nutrient solution depending on input nutrient concentrations contained in the reclaimed water and momentary crop needs, according to the growth stage and soil and weather conditions. Thus, the optimal number of fertilisers will be used maximising crop management efficiency and minimising environmental risks.

3. Results and Discussion

3.1 Pilot Regions

The pilot regions in Sweden, Germany, and Spain were chosen because they face similar pressures from nitrogen and phosphorus flows, such as poor chemical and ecological status of water bodies. They also represent different framework conditions along a north-south trajectory, reflecting the heterogeneity of EU regions. Gotland (Sweden) and Malaga (Spain) are comparable in terms of tourism pressure and water scarcity, despite being exposed to very different climates. Lower Saxony (Germany) is vulnerable to fundamental dietary changes due to its large-scale meat industry, which is dependent on international market trends.

These pilot regions exhibit distinct urban-rural interdependencies and territorial scales. They all include urban settlements where nutrients from human excreta are fed into central wastewater treatment systems but are not yet effectively recovered. Surrounding these urban areas are rural regions with intensive agricultural production, which necessitates the use of fertilizers. All three pilot regions are located less than 160 km from coastal zones with high nutrient loads and associated problems such as eutrophication.

Local initiatives in these regions have developed distinct strategies and technological approaches to address the issues caused by linear nutrient flows and to create new value chains based on the efficient and decentralized recycling of nutrients from human excreta. P2GreeN aims to build on these initiatives and their innovative solutions to mainstream circular nutrient flows into the European agri-food system and transfer these newly created value chains to other EU regions. Each regional system offers a suitable solution for circular nutrient flows, building on successfully evaluated technologies and local value chains. However, these technological set-ups are limited by the current governance framework. The immature governance framework inhibits investments in business scale-up and larger value chain innovations. Therefore, further developing this framework will be a key focus of the project.

Gotland region, Sweden

The Swedish pilot region of Gotland features a urine-drying system provided by Sanitation360. This portable, off-grid system processes urine on-site in the toilets. It has been optimized and deployed at various locations on Gotland using the existing network and maintenance contracts of mobile toilet provider Touch Down. Key locations include public toilets in the city of Visby and nearby facilities.

In the Swedish Pilot, urine serves as a valuable resource collected, processed, and utilized to cultivate barley, subsequently brewed into beer. The technology for producing solid urine fertilizer originated from the Swedish University of Agricultural Sciences (SLU), with Sanitation360 (S360), a spin-off from SLU, established in 2019 to further develop this innovation. In a bid to bolster urine collection efforts and foster a closed-loop system, Touch Down (TD), a local toilet rental company, and Gotlands Bryggeri, a local beer brewer, have partnered to form a circular value chain.

Under the P2GreeN initiative, the goal is to collect 150 m3 of urine by project completion to refine into a dry fertilizer compatible with conventional farming equipment. Present operations are concentrated in Gotland, Uppsala, and Malmö. Over the next three years, expansion plans involve scaling up urine collection efforts to encompass additional regions in Sweden and neighboring countries like Norway. Collection sources encompass both rural and urban areas, inclusive of public and private buildings, contingent on the installation infrastructure.

A key aspect of the project entails the development of methods for removing pharmaceuticals and other toxic substances from urine, ensuring the provision of a quality-assured fertilizer. Consequently, tailoring the urine fertilizer to meet the specific needs of farmers represents a significant focus of the endeavor.

In 2023, subcontracted farmers used the pelletized recycling fertilizers in field trials (covering 3-6 hectares) with barley on Gotland. These trials demonstrated a highly effective fertility impact on the crops. The local brewery Gotland Bryggeri is currently validating the suitability of barley grown with urine-based fertilizer for beer production. Within the project timeline, they aim to produce commercially available beer, thereby closing the value chain.

The island of Gotland is situated amidst a "dead zone" within the Baltic Sea, a consequence of eutrophication and rising temperatures. In Sweden, over 15,000 tons of nitrogen are discharged annually into the aquatic system by small and municipal wastewater treatment plants, accounting for approximately 30% of total anthropogenic nitrogen emissions. To address this issue, HELCOM's Baltic Sea Action Plan aims to reduce nutrient inputs from wastewater. Gotland faces challenges with old and partially non-functional decentralized sewage treatment plants, exacerbated by high seasonal peaks of nutrient loads from tourism. These discharges impact both groundwater and surface water, necessitating new solutions to enhance nitrogen and phosphorus retention.

Support from Science Park Gotland, local NGOs, and government organizations will facilitate source separation and urine drying expansion in Visby, with the technology provided by SLU and S360. The dried urine powder will be delivered to local farmers for barley cultivation, with the harvested product used by GB for beer production in Visby. This initiative creates a new value chain bridging the urban area of Visby with the surrounding rural area, thereby reducing nitrogen and phosphorus loads in wastewater and mitigating pollution in the coastal zone of Gotland.

Field trials conducted by SLU will assess the impact of bio-based urine fertilizer on barley yield, quality, and agro-ecological parameters. Additionally, stakeholders' perceptions and attitudes towards new sanitation systems and technologies will be evaluated to understand the socio-technical system. The knowledge gained from the Gotland region will be instrumental in developing a blueprint for remote areas with high tourism activity.

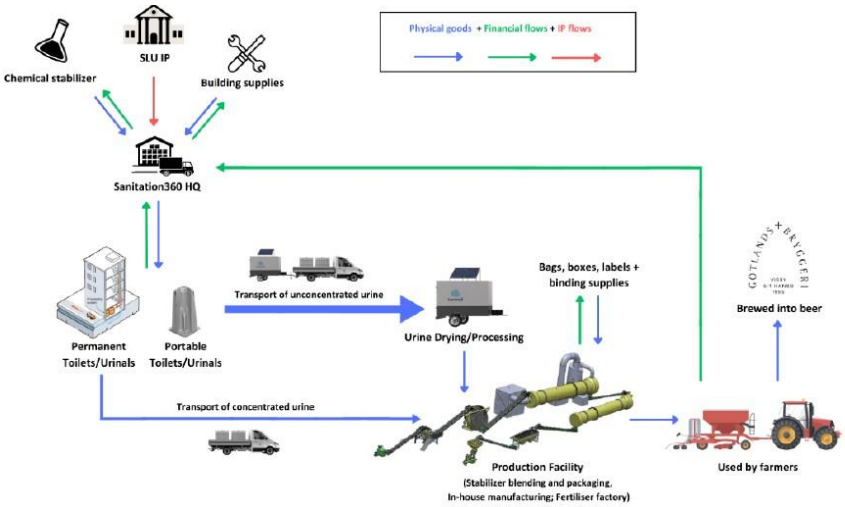

Figure 2. Gotland pilot region, value chain scheme

La Axarquaia region, Spain

In the Spanish pilot region of La Axarquia, Bioazul has installed a water reclamation plant to treat and transform municipal wastewater from the wastewater treatment plant of Algarrobo into nutrient-optimized irrigation water for customized agricultural application. TROPS is currently applying the treated water to avocado and mango plots (120 trees total) in an optimized way, supported by a Smart Fertigation Tool, a technology under development by AgriSmart Data. This tool focuses on the smart addition of nutrients tailored to the specific nutritional demands of the crops. This approach adds significant value for producers by promoting the reuse of wastewater resources for crop fertigation.

The Axarquía region encompasses a group of municipalities in the province of Malaga, located in Southern Spain, and stands as the primary producer of subtropical crops in Europe. It features a blend of rural areas with robust agricultural activity in the interior and densely populated coastal zones that experience a high influx of tourists, especially during the summer months. However, the region grapples with water scarcity issues, characterized by groundwater overexploitation, depleted water reservoirs, and the looming threat of desertification. Wastewater from various sources, alongside significant nitrogen and phosphorus runoff from agricultural activities, directly flows into the Mediterranean Sea, leading to eutrophication along the coastal zones. Approximately 40% of river waters face potential non-compliance with the European Union's Water Framework Directive (WFD).

The circular value chain in the Axarquía pilot region initiates with the collection of sewage from Algarrobo municipality and neighboring areas. This wastewater is then conveyed to the Algarrobo Municipal Wastewater Treatment Plant (WWTP) managed by AXARAGUA, receiving an average influent of 2,150 m3/day (equivalent to 12,247 population equivalents) and with a maximum capacity of 24,000 population equivalents. AXARAGUA, a public company formed by the "Association of Municipalities of the Costa del Sol-Axarquía," oversees not only Algarrobo but also wastewater treatment in Vélez-Málaga, Rincón de la

Victoria, Torrox, and Benamocarra municipalities. Upon entry into the WWTP, raw wastewater undergoes primary and secondary filtration, sedimentation, and flocculation processes to meet the optimal treatment standards stipulated by European Directive 91/271/EEC. Following secondary treatment, the treated effluent is discharged into the sea through an underwater outfall. Notably, due to the absence of a denitrification process, the nitrogen discharge from the Algarrobo WWTP into the Mediterranean Sea is relatively high, totaling 28.8 tN/year.
BIOAZUL oversees the operation of the Water Reclamation Plant as the coordinator of the pilot region.
Within the P2GreeN project, the irrigation system will be enhanced with a nutrient monitoring tool to optimize fertilization practices and prevent over-fertilization of crops irrigated with reclaimed water, thereby advancing its Technology Readiness Level (TRL) from 6 to 8. A decision support system will be collaboratively developed with ASD, a provider of smart irrigation tools. Field trials will be conducted in partnership with local avocado and mango farmers from the TROPS producer association, with agroecological and agronomic impacts monitored by the water research center, CET (WP2). The formulation of regional governance mechanisms will involve close collaboration with local public authorities (AXA, Algarrobo municipality, Malaga province).

Wastewater reclamation efforts address the region's vulnerability to droughts while yielding ecological benefits by reducing the demand for mineral fertilizers and curbing nitrogen, phosphorus, and micropollutant emissions into water bodies, thereby aligning with the objectives of the WFD. This approach holds promise for widespread adoption not only in southern Spain and the Mediterranean region but also in other water-stressed areas across Europe. In the P2GreeN project, facilitating the transferability of this approach involves defining financial considerations related to water reclamation, ensuring compliance with EU Regulation 2020/741 on wastewater reclamation, devising a risk management plan, and formulating a strategic roadmap for expanding reclaimed water usage while fostering societal acceptance.
In this context, the Smart Fertigation Tool will serve as a comprehensive solution for monitoring the crucial nutrients and elements in the soil that significantly influence crop development. It facilitates the integration of sensors and transducers embedded in the soil, which gather data on various parameters. Moreover, the tool enables automated management of irrigation and fertilization processes based on real-time data from the plant roots. It will also incorporate information from water sensors installed in the deposit tank containing reclaimed water.

Furthermore, the tool features remote control capabilities to regulate fertilizer dosage and water source mixture automatically, leveraging an integrated Decision Support System (DSS). By analyzing data, the Smart Fertigation Tool can determine whether additional nutrients are required in the reclaimed water, allowing for the incorporation of mineral fertilizers. Additionally, it can assess the necessity of diluting the nutrient-rich effluent with local water sources, primarily groundwater. This intelligent fertigation approach helps prevent excessive nutrient application, thereby reducing the risk of polluting leachates entering water bodies, including nitrogen (N) and phosphorus (P) emissions into surface and groundwater.

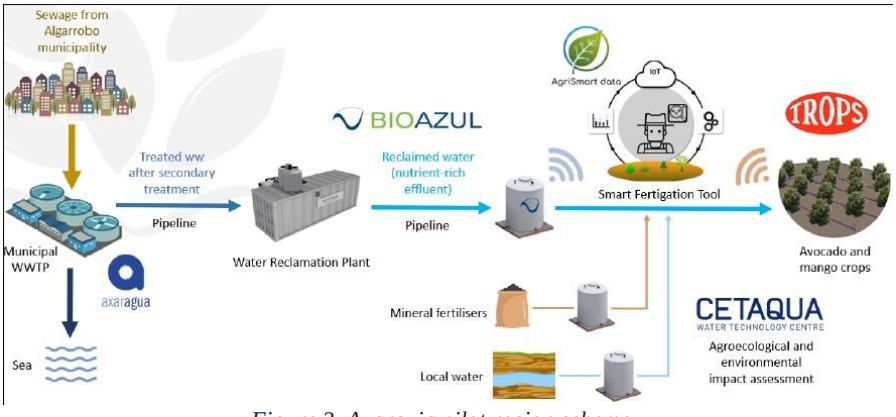

Figure 3. Axarquia pilot region scheme

Hamburg- Hanover region, Germany

The German pilot region of Hamburg-Hannover includes the housing cooperative ecovillage hannover, which plans to install commercially available ceramic urine-diverting flush toilets for 230 residents. They aim to collect approximately 100 m³ of urine per year in cooperation with Goldeimer. The urine will be processed at the ecovillage in a central facility using the urine treatment system provided by VunaNexus, which will also handle necessary adjustments, operation, and maintenance of the system. The resulting Aurin® fertilizer will be marketed by VunaNexus.

These areas face significant nitrogen (N) and phosphorus (P) pollution in water bodies due to intensive agriculture in rural zones and effluents from urban wastewater treatment plants (WWTPs). The river basins of the Elbe and Weser, as well as the coastal areas of the North Sea, are particularly affected, with approximately 90% of water bodies classified as being in moderate to poor ecological and chemical condition. Mitigation measures are necessary to comply with the OSPAR agreement and reduce pollution in the North-East Atlantic. Additionally, groundwater quality is compromised, with nitrate levels exceeding 50 mg N/L due to agricultural runoff. WWTPs remain significant contributors to N and P emissions into aquatic environments, with high energy consumption associated with N and P removal processes.

Two pilot cases have been identified in the region. The first case involves the housing cooperative EVH in Hanover, which plans to construct a new city district with 500 dwellings. These dwellings will be equipped with urine-separating flush toilets, allowing for the adsorption of micropollutants and the recovery of nutrients from human excreta. A treatment plant for collected urine will be established and operated at the EVH site by the Swiss technology provider VN, aiming to scale up their Aurin® technology from TRL 6 to TRL 8.

The second pilot case focuses on the establishment of a faecal composting plant in Ollsen, south of Hamburg. GE is active in collecting dry toilet contents and separating urine from various sources in the region. A new composting plant for dry toilet contents will be implemented at the Vagtshoff farm (VH) in Ollsen, using an automated container-based approach developed by Finizio and IGZ. The resulting faecal compost will be applied in field trials at VH to improve soil health and reduce nutrient leaching. Additionally, Aurin® fertilizer produced at EVH will be added as needed to meet crop nitrogen demand. The agronomic and agro-ecological effects of using faecal composts and urine-based fertilizers will be monitored by IGZ.

Overall, the P2GreeN solutions in Lower Saxony will benefit from the lighthouse effect of EVH and the extensive network of GE with other sustainable sanitation initiatives, facilitating the scaling up of these innovative approaches. During the 2023 season, Goldeimer collected dry toilet contents from festivals, allotment gardens, and off-grid nature tourism destinations. A thermophilic container-based composting plant for faeces is being set up, further automating the technology developed by Goldeimer's network partner Finizio. This facility will be operated by Goldeimer on the Vagtshoff farm in Lower Saxony near Hamburg. The Vagtshoff farmers provide industrial waste heat and biochar for the composting facility, as well as agricultural land (6 hectares) for fertilizer application.

Figure 4.Hamburg-Hanover pilot region scheme

3.2 Policy

Despite Sweden's pioneering efforts in developing resource recovery sanitation solutions since the 1990s, the adoption rates of these systems have remained stagnant for decades (Bengtsson & Tillman, 2004; Söderholm et al., 2023). The reasons for this stagnation are multifaceted, including expanded sanitary regulations, a lack of acceptance and awareness of alternative solutions, and the highly centralized nature of the Swedish sanitation system, which presents a significant technological lock-in barrier (Söderholm et al., 2023). Moreover, the governance framework introduces uncertainty for source separation systems due to the absence of explicit definitions for urine, sludge, and wastewater in regulations, complicating their classification. Source-separated fractions, including urine, do not align neatly with existing regulations such as the water and wastewater provision regulation (SFS 2006:412), the sludge regulation (SNFS 1994:2), or the waste management regulations (SFS 1998:808, SFS 1998:899, and SFS 1998:944). Specifically, the regulation governing the use of plant nutrients in agriculture (SJVFS 2004:62), although explicitly addressing sludge, does not mention human urine (M. Ahlström, personal communication, November 17th, 2023).

In practice, urine is permitted for use in conventional farming in Sweden, allowing S360 to market the urine fertilizer to conventional farmers, who can then legally sell their produce. However, there's a historical aspect to this permission: prior to Sweden's accession to the EU in 1994, urine was also allowed in organic farming. EU membership obligated Sweden to adhere to the EU's regulations for organic farming, which do not permit urine as a fertilizer. In Sweden, another prevalent certification for sustainable farming is KRAV, which could potentially accommodate urine as a fertilizer. However, to become KRAV certified, a farmer in Sweden must first obtain EU organic certification.

As for the Germany pilot region, the primary entry barriers for P2GreeN products revolve around legal compliance and ensuring their safety. Additionally, in the process of transitioning from waste to a qualified resource fit for production, various barriers exist across different sectors and laws. While yellow water collected from sources with less than 50,000 population equivalents appears suitable for nitrogen (N) and phosphorus (P) recycling as sewage sludge under the CMC regulation, the same cannot be said for contents from dry toilets. Dry toilet contents face hurdles stemming from municipal statutes based on the Water Household Act (WHG §55/56), the Circular Economy Act (BioAbfV §3), and the Fertilizer Act (DüMV Annex II, Table 7). Moreover, there is a lack of guidance for the waste classification of sanitary waste from dry toilets (91/689/EEC; AVV), which contradicts the waste hierarchy principle of Prevention, Reuse, Recycle, Recover, Dispose, as outlined in the federal Circular Economy Act (KrWG §6). The source separation and local treatment of yellow water have not yet been authorized for the Ecovillage Hannover. As a result of these delays, the engineering of the decentralized wastewater system for EVH has been put on hold. However, there have been multiple insights into the Water Household Act and its subordinate rules concerning yellow water. In Germany, the overall technological and legislative approach to sanitary waste strictly encompasses it as wastewater. The updated sewage sludge regulation AbfKlärV 2017, along with its governance framework, is directing stakeholders towards the mono-incineration of sewage sludge, aiming for phosphorus reclamation from ashes. However, this approach compromises the soil-regenerating and nitrogen (N) potentials of sanitary waste.

With the recent implementation of Regulation (EU) 2020/741 of the European Parliament and the Council dated 25th May 2020 on minimum requirements for water reuse, a unified European legal framework now exists for all member states. This regulation sets out provisions for the utilization of reclaimed water in agriculture, imposing stringent requirements on water quality and monitoring. However, while this regulation will be directly applicable in each national context, there are numerous existing regulations within the Spanish and Andalusian frameworks that require updating. The implementation of this regulation offers guidance and assurance to farmers and consumers by establishing high water quality standards to adhere to. However, meeting other new obligations, such as the submission of a Risk Management Plan, presents challenges. Addressing this challenge is a key focus within P2GreeN, as one of our governance solutions includes the preparation of a Risk Mitigation Plan for the Axarquía pilot. A revision of the current Spanish regulation on water reuse (i.e., Royal Decree 1620/2007) is imperative to align with the provisions of Regulation (EU) 2020/741. Additionally, procedures for granting licenses to users of reclaimed water must be adapted to the new situation by the regional government of Andalusia and water basin authorities, which hold the authority for licensing water reuse permits. National and regional actors must collaborate to conduct a comprehensive revision of the existing legal framework.

3.3 Follower regions

Greece

As part of the project, Greece is one of the four follower regions. The Greek follower region, under the leadership of CERTH, will be divided into three distinct case studies. These studies will evaluate the implementation of various technologies in different contexts to ascertain their feasibility and potential impact.

The first case study will be conducted in **T.O.E.V Tavropou,** where organizations oversee extensive land improvement works, particularly irrigation projects. The focus here will be on assessing the barriers to implementing BioAzul's RichWater technology, which involves irrigating and fertilizing nearby agricultural fields with treated municipal wastewater.

The second case study will take place at the **Agricultural University of Athens**. Research will be conducted in a renovated three-story building to evaluate the implementation of Vuna Nexus technology in existing toilet systems. The objective is to utilize the resulting fertilizer in the university's agricultural fields.

For the third feasibility study, a partnership will be established with a **toilet renting company** that services festivals in the city of Athens. The aim is to demonstrate the implementation of sustainable toilet technologies and establish a twinning relationship between the pilot region and a following region. This twinning initiative is intended to facilitate the scaling up of the technology's impact.
Each of these case studies will provide valuable insights into the challenges and opportunities associated with the adoption of sustainable technologies in Greece, contributing to the broader objectives of the project.

Italy

In Italy, the highway station provider Chef Express is considering implementing urine separation and collection in their toilets to produce fertilizer using VN's treatment system. This innovative approach would enable the creation of urine-based liquid fertilizer, which could then be marketed in small bottles directly at the service stations. Additionally, the Finagricola agricultural cooperative in Campania is exploring the possibility of using BioA's RichWater technology to irrigate and fertilize crops with treated wastewater sourced from the municipality of Battipaglia. However, they are also open to the idea of utilizing fertilizer produced from source-separated urine. This demonstrates a growing interest in sustainable agricultural practices and the utilization of alternative resources within the Italian agricultural sector.

Hungary

In Hungary, the feasibility study aims to thoroughly analyze how P2GreeN's solutions can be effectively implemented within the Eastern European context. This study will also identify potential partners who can contribute to forming a Hungarian follower region. The key components of the feasibility study include:

(i) Analysis of national and regional policies and regulations: This will involve a comprehensive examination of existing policies and regulations related to water management, wastewater treatment, and agricultural practices in Hungary.

(ii) Identification of relevant institutional/governance framework and funding pathways: This aspect of the study will focus on identifying the key institutions, stakeholders, and governance structures involved in water and agriculture sectors in Hungary. Additionally, potential funding sources and pathways for implementing P2GreeN solutions will be explored.

(iii) Analysis of technical, economic, and social aspects relevant for implementation: This will entail assessing the technical feasibility, economic viability, and social acceptance of implementing P2GreeN solutions in Hungary. Factors such as technological adaptability, cost-effectiveness, and societal attitudes towards sustainable water management practices will be evaluated.

The study aims to identify three suitable sites for replicating different technological approaches from the pilot regions and initiate the transfer of project results at the conclusion of the P2GreeN project. This process will facilitate the dissemination and adoption of innovative water reuse and resource recovery solutions in Hungary, contributing to sustainable development in the region.

France

In this follower region the City of Paris has already started the transition in the block of buildings in Saint-Vincent-de-Paul. More specifically, the building of Chaufferie has already started the process of implementing a storage of collection and recycling of urine. The work began in 2021 and should be completed in 2027. The wastewater transport networks, and that for urine, were built in 2021/2022. The buildings of the different lots will be built gradually from 2024. The urine treatment plant should be built in 2025. The case study of this follower region is going to work as a preliminary stage and as reference point to the development of the feasibility studies in the other follower regions. City of Paris will give the opportunity to the P2GreeN partners to extract important results on social-economic level.

4. Conclusions

P2GreeN's has already completed the first year successfully extracting important results both in the pilot regions and the follower regions. The feasibility studies have already started in all the four follower regions with the help of the interested stakeholders.

References

Desmit, X., Thieu, V., Billen, G., Campuzano, F., Dulière, V., Garnier, J., Lassaletta, L., Ménesguen, A., Neves, R., Pinto, L., Silvestre, M., Sobrinho, J. L., & Lacroix, G. (2018). Reducing marine eutrophication may require a paradigmatic change. *Science of The Total Environment*, *635*, 1444–1466. https://doi.org/10.1016/J.SCITOTENV.2018.04.181

Gianico, A., Braguglia, C. M., Gallipoli, A., Montecchio, D., & Mininni, G. (2021). *Land Application of Biosolids in Europe: Possibilities, Con-Straints and Future Perspectives*. https://doi.org/10.3390/w13010103

Home - Eurostat. (n.d.).

Larsen, T. A., Udert, K. M., & Lienert, J. (2013). Source Separation and Decentralization for Wastewater Management. *Source Separation and Decentralization for Wastewater Management*. https://doi.org/10.2166/9781780401072

Vermeulen, S. J., Campbell, B. M., & Ingram, J. S. I. (2012). Climate change and food systems. *Annual Review of Environment and Resources*, *37*(Volume 37, 2012), 195–222. https://doi.org/10.1146/ANNUREV-ENVIRON-020411-130608/CITE/REFWORKS

A critical review of the EU bioeconomy: Current status and the transition to a circular bioeconomy

Bas Paris [a] [b], Dimitris Michas [b], Athanasios T. Balafoutis [b], George Papadakis [a]

[a] Department of Natural Resources and Agricultural Engineering, Agricultural University of Athens, 75 Iera Odos str., 11855, Athens, Greece

[b] Institute of Bio-Economy & Agro-Technology, Centre of Research & Technology Hellas, Dimarchou Georgiadou 118, 38333, Volos, Greece

* Corresponding author. Email: *(bparis@certh.gr)

Abstract

This study presents a critical review of the current status of the European Bioeconomy, containing all the main 5 themes (agriculture, water systems, forestry, bioenergy, biomaterials) as well as the existing bioeconomy national strategies, trends. Across the EU the largest consumption of the biomass is food and feed, followed by energy and biomaterials. The EU economy is transforming from an economy based on linear economic models to circular economic models, this transformation is still at its early stages and will require the transformation of existing production systems and value chains as well as the creation of new innovative value chains. In recent years EU policy has become very supportive of the development of a sustainable EU bioeconomy and the updated EU bioeconomy strategy operates in parallel to multiple other policy initiatives such as the new CAP, Green Deal, Farm to Fork strategy and the Circular economy action plan. In the short term, the further development of national strategies dedicated to the bioeconomy will strengthen the policy environment. In addition, the development of the bioeconomy has a crucial environmental dimension and current policy is supportive of efforts that support and strengthen environmental services and biodiversity.

Keywords: circular bioeconomy, biobased solutions, biomass flows

1. Introduction

Over the past decades, the concept of the bioeconomy has emerged as a central pillar in the EU policy discourse, aiming to harness the potential of biological resources to drive economic growth, enhance environmental sustainability, and foster rural prosperity. Within this framework, the bioeconomy, encompasses the food and agriculture, forestry, water based, biomaterial and biorefinery and bioenergy sectors, has garnered increasing attention as a key driver of regional development and innovation.

Simultaneously, As the EU moves to achieve its ambitious sustainability goals outlined in the European Green Deal and the Circular Economy Action Plan, there is growing recognition of the need to transition from a linear to a circular model of economic production and consumption. The concept of the circular bioeconomy, which emphasizes the regeneration and reuse of biological resources, presents a compelling vision for achieving this transition while addressing pressing environmental challenges such as climate change, biodiversity loss, and resource depletion.

The current EU bioeconomy continues to rely on non-renewable materials and fossil-based raw energy, such as nitrogen fertilizers, organic chemicals and polymers which are predominantly derived from petroleum and gas. For the EU to meet its medium and long term goals it is clear that on the one hand the bioeconomy needs to transition towards more circular production and consumption patterns whilst also expand to become a major supplier of renewable materials.

Against this backdrop, this article critically reviews the current status of the EU rural bioeconomy and explores the challenges and opportunities associated with its transition to a circular bioeconomy. By synthesizing existing literature, policy documents, and empirical evidence, we aim to provide a comprehensive understanding of the key dimensions shaping the rural bioeconomy landscape in the EU and the pathways towards a more sustainable and resilient future.

Specifically, this review seeks to address the following questions:

- What is the current state of the EU rural bioeconomy in terms of its structure, performance, and contribution to regional development and sustainability?
- What are the key drivers, enablers, and barriers influencing the transition from a linear to a circular

bioeconomy in rural areas?

- What are the policy implications and governance challenges associated with promoting a circular bioeconomy agenda in the EU rural context?
- What are the emerging trends, innovations, and best practices that offer potential solutions to accelerate the transition towards a circular bioeconomy in rural areas?

By critically examining these questions, we aim to shed light on the opportunities and constraints facing the EU rural bioeconomy and to offer insights for policymakers, practitioners, and researchers engaged in shaping the future trajectory of rural development and sustainability within the EU and beyond.

There are a variety of relevant bioeconomy related publications to the current status of the bioeconomy published by Eurostat (*Home - Eurostat*, n.d.) These publications focus on the different material flows that exist in the EU, giving the opportunity to develop a database for all the available information that all the Member States can extract every year. Using this, the JRC has developed a Sankey Biomass tool that depicts biomass flows according to bioeconomy sector from supply to use (Gurria et al., 2017) . Other studies, take a different approach, Hamelin et al (2019) investigates the residual biomass potential in the EU finding that around 8500 PJ y^{-1} residual biomass is available, equivalent to the combined primary energy consumption of Italy and Belgium (Hamelin et al., 2019). Popp et al. (2021) investigate biomass supply and demand in the EU highlighting the complex interrelations between the demand of biobased products and land use and also advocating for a transformation towards the production of biobased chemicals (Popp et al., 2021). This highlights the complexity of dealing with biobased value chains and encompassing them under one term. While, Antar et al (Antar et al., 2021) provide a global overview of biomass production and utilization (Antar et al., 2021). A number of studies have been conducted that investigate the development of the bioeconomy on a national level. Hayek et al. (Hájek et al., 2021) for the Czech Republic, Wozniak and Twardowski (Woźniak & Twardowski, 2018) and Szarka et al. (Szarka et al., 2021) in Germany, Ahlqvist and Sirvio (Ahlqvist & Sirviö, 2019) in Finland.

2. Materials and Methods

2.1 Conceptual framework

2.1.1 The bioeconomy

The concept of the bioeconomy encompasses various definitions and approaches, ranging from broad to specific interpretations. The European Commission defines it as the utilization of renewable biological resources from both land and sea, including crops, forests, fish, animals, and micro-organisms, to generate food, materials, and energy. Further elaboration provided in the EU Bioeconomy Strategy expands this to encompass all systems reliant on biological resources, such as biomass, animals, plants, and organisms, along with their associated functions and principles. This includes not only land and marine ecosystems but also primary production sectors like agriculture, forestry, fisheries, and aquaculture, as well as all economic and industrial sectors utilizing biological resources to produce food, feed, biobased products, energy, and services.

Based on this definition, the bioeconomy can be conceptually divided into five main themes, aligned with the EU bioeconomy strategy:

- Food and agriculture systems, which cover the entire value chains involved in farming and the production of food and biological feedstocks across the EU's 10.5 million farms.
- Forestry and natural habitats systems, which serve as sources of environmental public goods, raw materials, and services, encompassing the management and utilization of the EU's 182 million hectares of forests.
- Water systems, which include all aquatic environments and related economic activities such as fisheries, aquaculture, and aquatic biomass production.
- Bioenergy, referring to energy derived from organic sources, representing the largest renewable energy source in the EU, accounting for 12% of total energy demand.

- Biomaterials and bio-based products, which are produced from renewable biological feedstocks and include both conventional products like timber and textiles, as well as advanced products like bio-plastics and pharmaceuticals produced in biorefineries.

2.1.2 The circular bioeconomy

Simply put the circular bioeconomy refers to applying and integrating circular economy principles into the bioeconomy. Key concepts include use of waste residues as productive inputs into other processes. Resource efficiency Cascading use of biomass (Stegmann, Londo and Junginger, 2020). A circular bioeconomy is also interpreted as an idea to stimulate the economic growth of developed economies that combines the 'what' (circular economy) with a feasible, viable 'how' (bioeconomy)(Giampietro, 2019). Alternatively, a circular bioeconomy is simply interpreted as a more efficient resource management of bio-based renewable resources by integrating circular economy principles into the bioeconomy (D'Amato, Veijonaho and Toppinen, 2020). It is also a framework for an economic model which aims to create economic, natural, and social capital based on three core principles:

- Design out of waste and pollution.
- Keep products and materials in use and carbon products in the loop.
- Regenerate natural systems.

2.1.3 Biobased solutions

Bio-based solutions are innovative technologies, processes and/or end-products based on circularity that produce or utilise biomass sustainably as compared to mainstream technologies or processes that produce non-innovative end products or utilise biomass without significant innovations or sustainable outputs. An adopter must either produce an innovative/sustainable biobased end-product or use a sustainable technology or sustainable process during the production of a biobased product**.**

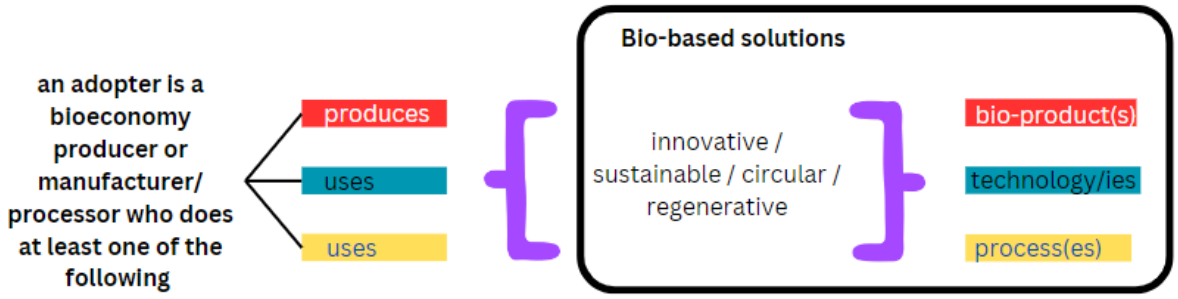

Figure 1. Authors' interpretation of bio-based solutions

In particular, for the production of raw biomass/feedstocks we consider sustainable practices and technologies to be biobased solutions. For the processing of biomass/feedstocks we consider sustainable technologies, processes and end products to be biobased solutions. This distinction exists as in the production of biobased feedstocks it is generally the process and technologies used in the producing of the feedstock that determines its level of sustainability/circularity. While for processed and finished products it's a combination of efficient production systems (efficient technologies and processes) and the production of a sustainable bio end-product that distinguishes it from mainstream/traditional processing practices.

2.2 Data sources, Search strategy, Data collection, Selection process

The process of selecting studies involved several meticulous steps. Initially direct consultations were held with bioeconomy experts from: research organizations, associations and extension services, industry SMEs, innovation brokers and NGOs, in order to identify key topics bioeconomy topics relevant for our review as well as initial data. This approach was chosen since the bioeconomy concept is relatively new yet broad, as such the inputs of a diversity of experts helped us identify key bioeconomy topics. Research organizations that were included: the Institut fur ZukunftsEnergie Stoffstromsysteme (IZES), the University of Aarhus (AU), the Institute for Soil Science & Plant Production (IUNG), Vytauto Didziojo Universitetas (VDU), Latvijas Lauksaimniecibas Universitate (LLU), University of Coimbra (UC), and University of Ljubliana (UL). Relevant associations/extension services included: DELPHY, AVEBIOM, Centro da

Biomassa para a Energia (CBE), Associazione Italiana Energie Agroforestali (AIEL), Asociata Green Energy (GEA). Industry SMEs included NaturePlast (NP) and AlgEn (ALGEN). Innovation borkers and NGOs included: Valorial, Green Growth Platform (GGP), Food Scale Hub (FSH) and InCommOn (ICO).

Afterwards, potentially relevant studies were pinpointed by conducting keyword searches on SCOPUS and Google Scholar. Keywords used in these searches included 'bioeconomy' and key concepts topics that were deemed relevant to the review. These keywords included: 'biomass flows', 'biobased value chains', bioeconomy policy, 'biorefining' and 'bioeconomy learning' as well as specific keyword searches related to each of the 5 main bioeconomy themes summarized in the conceptual framework.

Identified studies and papers were screened and evaluated based firstly on relevance and reliability, particularly focusing on journal articles sourced from reputable publications and peer-reviewed journals. These selected studies were chosen due to their focus on the bioeconomy and one of the identified themes. Information from these studies was systematically extracted, organized, and categorized based on various aspects relevant to the bioeconomy themes.

2.3 Limitations

There are a number of key limitations associated with the present review. Conceptually, the bioeconomy is a general term which can be extended to include any economic processes thing including biological material and processes. In effect, in its current interpretation by the European Commission and key actors it combines results from a number of large sectors, that were previously considered separate, including food and agriculture, water systems, bioenergy, biomaterials.

Moreover as the bioeconomy, and in particular the circular bioeconomy, is a relatively new concept there are relatively few publications that focus specifically on the bioeconomy. In effect, these limitations are conceptual. In our view, these limitations are acceptable, for a general review as the present review but in the future it is clear that the bioeconomy concept, its boundaries and terms needs to become more specific. These are also addressed in our discussion section.

3. Results and Discussion

3.1 Current status

3.1.1 Key figures: Employment and Value Added

Overall, based on the latest data from the JRC around 17.42 million people are employed in the EU Bioeconomy, representing around 9% of the entire EU workforce. Around 50% of these are employed in agriculture, 26.4% in food beverage and tobacco production, 7.6% in wood products and furniture, 4.5% in bio-based textiles, 3.6 in paper production, 3% in forestry, 2.7% in biobased chemicals, plastics and rubber, 0.9% in fishing and agriculture, 0.1% in bio-based electricity and 0.1% in liquid biofuels (Figure 2).

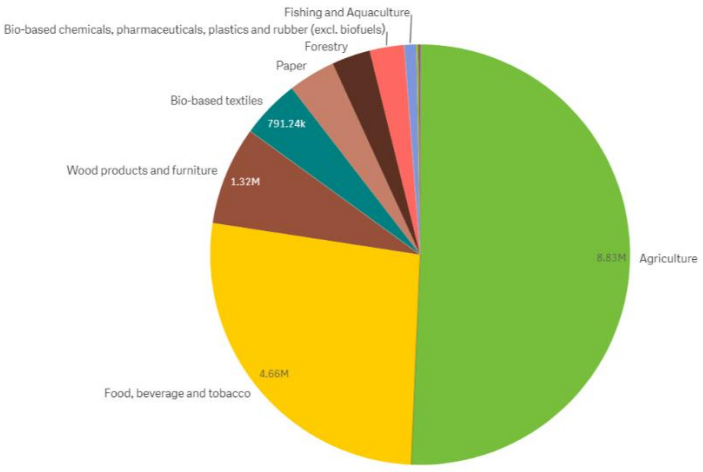

Figure 2.Employment by bioeconomy sector in EU27 (2019) (number of people employed). (JRC, 2022)

The number of people employed in the bioeconomy sector as a whole has been steadily decreasing from 20.15 million people in 2008 to 17.42 in 2019. The largest decreases are observed in the agricultural and textile sectors. By contrast large increases are observed, from a low base, in biobased electricity and biofuels sectors, and to a lesser extent in the biobased-chemicals sector (Figure 3).

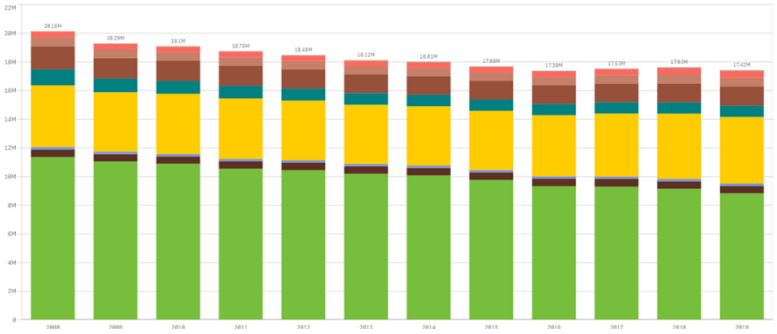

Figure 3. Development of the number of people employed in selected sectors (EU27, 2008-2019). (JRC, 2022)

The entire EU Bioeconomy has an annual turnover of around €2.2 trillion with an added value of 657 billion euros. The food, beverage and tobacco sector accounts for 36.2%, followed by agriculture at 29.4%, biobased chemicals, plastics and rubber at 9.8%, wood products and furniture at 7.6%, paper at 7.3%, bio-based textiles at 3.9%, forestry at 3.8%, fishing and aquaculture at 0.9%, bio-based electricity at 0.8% and liquid biofuels at 0.5% (Figure 4).

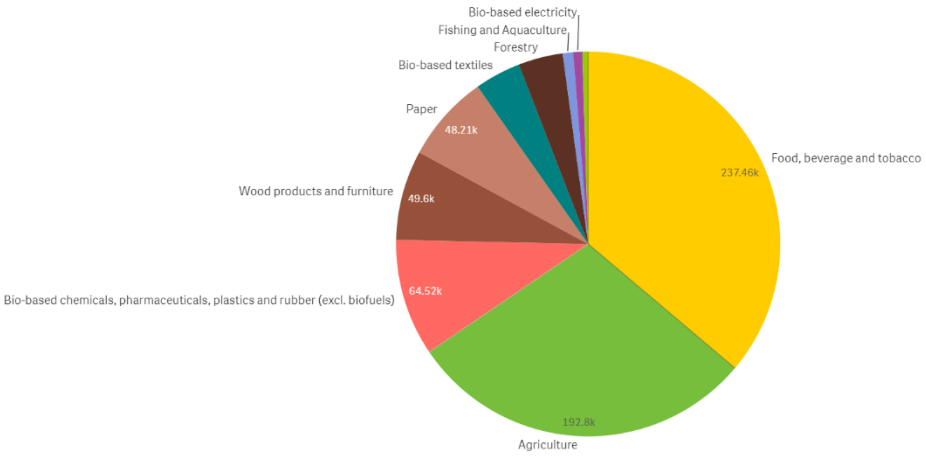

Figure 4. Value added by sector in EU27 (2019) (million €) Source: (JRC, 2022).

In contrast to the trends in employment all sectors have experience gains in the total valued added by the bioeconomy increasing from 515 billion euros in 2008 to 657 billion euros in 2018. In particular the liquid biofuels and biobased electricity sectors have seen rapid growth over a 100%. This contrast between a decrease in employment but increase in value added suggests considerable improvements in productivity in the bioeconomy in recent years.

3.1.2 Biomass flows

The following section provides an overview of the biomass flows according to the 5 bioeconomy themes; these flows are particularly useful in providing an overview of biomass supply, processing and

consumption. There is considerable variation in the types and geographic availability of biomass across the EU, the main biomass supply types originate from the following sources, including: forests (thinning, logging residues), by- products of the wood industry, energy crops, agricultural by-products, biomass from waste streams, by- products from agro-food industry, aquatics biomass. The EC's JRC produces regular overviews in their EU Biomass Flows tool, more detailed data is available there (Gurria *et al.*, 2017).

Overall, the total production of biomass in the EU consisted of around 1.1 billion tons of dry matter of which 95% is produced locally and 5% imported. Agriculture is the biggest supply sector (65% dry matter). The level of contribution in this biomass flow differs according to the country and their potentials for example countries like Greece, Malta, Hungary and Cyprus have a number 0f 90% because of the agricultural and field areas but on the other hand Finland has only 13% because instead of agricultural areas the country is covered by forests, and this is the reason why the forestry contribution numbers 87%. On the other hand, the fishery sector is not so well developed and numbers less than 1% where the agriculture and forestry sectors play the most important role. Although the agriculture and forestry sector an in high levels, Europe faces a problem with the unused and abandoned areas which represent about 15.8% of the total land use in EU 28.

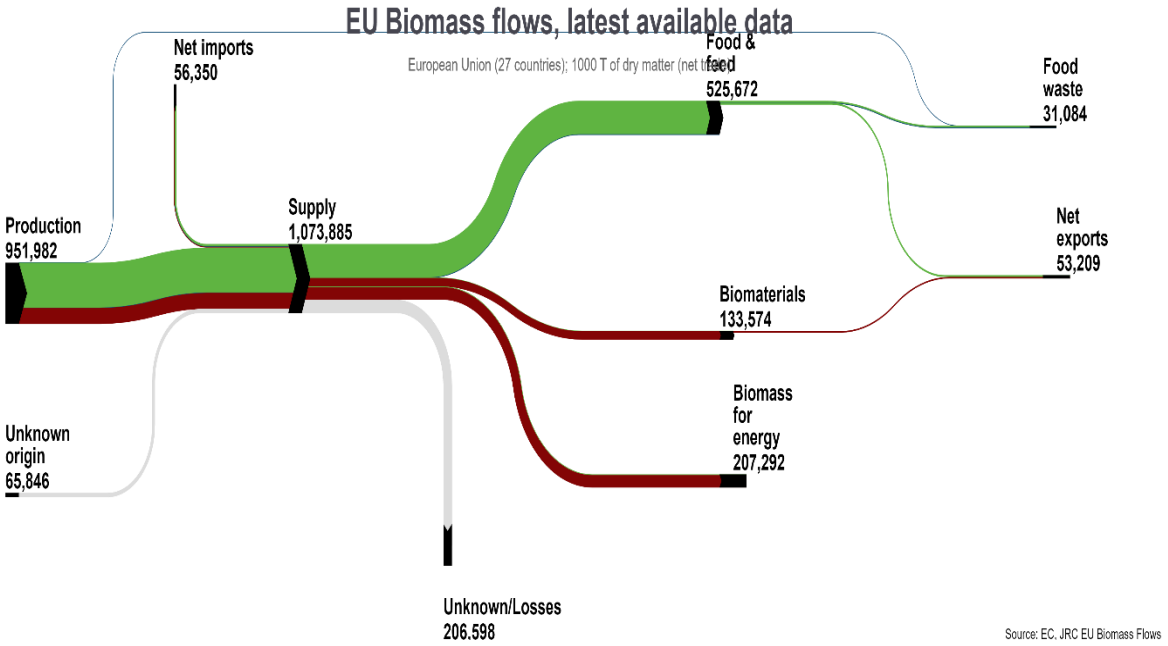

Figure 5. Biomass flows in Europe. Source: (Gurria et al., 2017a)

3.1.3 Bioeconomy related Policies

The first EU Bioeconomy strategy was launched in 2012, "Innovating for sustainable growth – A bioeconomy for Europe" (European Commission, 2012) with a main goal to accelerate the deployment of a sustainable bioeconomy and to transform the EU's approach to the production, consumption, processing, storage, recycling, and disposal of biological resources. The latest EU Bioeconomy strategy was updated in 2018 and in 2022 a report was released that asses the progress made in the implementation of the Bioeconomy strategy (European Commission, 2022a).

Bioeconomy policies take a cross-sectoral perspective to improve policy coherence, identify and resolve trade-offs like land and biomass demand. These policies are designed around 3 sustainability dimensions. According to the latest EU Bioeconomy Strategy Progress Report (EU Bioeconomy Strategy Progress Report, n.d.), there are actions on track to enhance the main objectives of Bioeconomy strategy. Increasing

number of national and regional bioeconomy strategies promoting cross-sectoral cooperation and sustainability principles and invest in bioeconomy innovations. The EU bioeconomy strategy enables a green transition covering all the 3 dimensions of sustainability (environment, society, economy)

- Environmental sustainability: By optimizing the use of biological resource from land and sea, the bioeconomy maximizes co-benefits. Production of biomass, mitigating the climate change and enhancing the biodiversity are some factors that safeguard and benefit the ecosystem services.
- Economic sustainability: Bioeconomy policies boost sustainable innovation and create solutions for sustainable food and bio-based products, bio-based and bioderived chemicals, advanced biofuels, and the bioenergy for the future.
- Societal sustainability: Bioeconomy policies enables a green transition developing sustainable business models based on the principles of diligence, and by promoting sustainable trade and social fairness in Europe.

The updated Bioeconomy strategy builds upon and stresses the continued importance of the goals of the 2012 bioeconomy strategy to ensure food and nutrition security; manage natural resources sustainably; reduce dependence on non-renewable, unsustainable resources; and limit and adapt to climate change; strengthen European competitiveness and create jobs. The associated bioeconomy action plan outlines 14 actions to accelerate the development of the EU Bioeconomy including:

- "Strengthen and scale up the biobased sectors, unlock investments and markets.
    - mobilize stakeholders in developing and deploying sustainable biobased solutions.
    - launch a €100 million circular bioeconomy thematic investment platform.
    - analyze enablers and bottlenecks for the deployment of biobased innovations.
    - Promote and develop standards.
    - facilitate the deployment of new sustainable biorefineries.
    - develop substitutes to fossil-based materials that are biobased, recyclable and marine biodegradable.
- Deploy local bioeconomies rapidly across the whole of Europe.
    - launch a strategic deployment agenda for sustainable food and farming systems, forestry and biobased products.
    - launch pilot actions for the deployment of bioeconomies in rural, coastal and urban areas.
    - support regions and EU countries to develop bioeconomy strategies.
    - promote education, training and skills across the bioeconomy.
- Understand the ecological boundaries of the bioeconomy.
    - enhance knowledge on biodiversity and ecosystems.
    - monitor progress towards a sustainable bioeconomy.
    - promote good practices to operate the bioeconomy within safe ecological limits.
    - enhance the benefits of biodiversity in primary production." (European Commission, 2018a)

The 2022 EU Bioeconomy Strategy Progress Report highlights a number of key important trends in the development of the EU Bioeconomy. These include that national bioeconomy strategies are developing across Europe, the main use of biomass continues to be for food and feed while biomass sourced from wood is increasingly utilized, important innovations are happening across the EU bioeconomy, in particular in food and bio-based industries, that research and innovation results have shown considerable promise and should continue to be strengthened (European Commission, 2022b).

One of the main actions highlighted in the 2018 updated strategy was the necessity to develop detailed national policies, enabling countries and regions to design transition pathways according to their specific challenges and opportunities benefiting a non-prescriptive integrated and systemic framework ('EU Bioeconomy Strategy Progress Report', no date) supporting the development of strong societies, a resilient environment and sustainable economy.

Currently, multiple EU members have already developed multiple strategies, while others have strategies under development. Finland, France, Italy, Poland, Spain, and Sweden have developed an intense, regional strategic actions to deploy bioeconomy. Additionally, there are 15 countries having at least one region with bioeconomy relevant strategy in regional level (Austria, Belgium, Croatia, Czechia, Denmark, Germany, Greece, Hungary, Ireland, Latvia, Lithuania, Netherlands, Portugal, Romania, and Slovakia). In these countries the number of regional strategies vary between 1 and 17. A few member states have yet to develop their national strategies (Bulgaria, Cyprus, Estonia, Luxemburg, Malta, Slovenia).

The following map (Figure 6) illustrates the members' states according to the status of their strategies. Other have already developed strategies, other are under development but some others have strategies related to bioeconomy. Austria, Germany, Denmark, Latvia, Netherlands, France, Portugal, Spain, Finland, Ireland, and Italy are some of the members that have a developed strategy for bioeconomy having it updated lately. In addition, some others like Greece have national strategies for energy, climate, agriculture referring to bioeconomy.

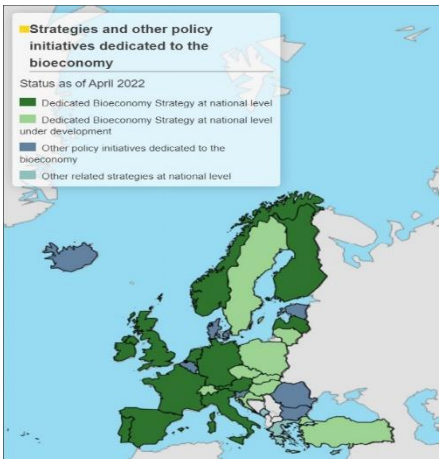

Figure 6. EU Bioeconomy strategies. Source: (Bioeconomy Strategy | Knowledge for Policy)

3.2 Discussion

This report provides an overview of the current bioeconomy status in the EU and the transition to a circular bioeconomy. On the one hand overall employment is decreasing while the overall value of the bioeconomy is increasing. The decrease in employment can be attributed to a number of trends, there is a notable decline in the agricultural sector which is driven by demographic changes and a consolidation of farm holdings. On the other hand, large increases in employment are observed in the bioenergy sector and the biomaterials and bioindustry sectors (JRC and Novo-Institute, 2022). These trends are expected to continue as the transition towards a more circular European economy is heavily dependent on the replacement of fossil energy and fossil-based products.

Regarding biomass flows, the JRC provides detailed overviews of biomass flows within countries, per sector and for the EU as a whole (JRC, 2022). The continued update and effective dissemination of this knowledge, across all main primary and secondary sectors, is crucial for our understanding of the development of the bioeconomy. It is clear that current biomass flows are dominated by agricultural production for supply and food and feed for use/consumption. It is unlikely that the importance of the food and agricultural sector will diminish, but it is clear that for a sustainable transition and to achieve EU climate goals, both supply and use in other sectors that replace fossil fuels and fossil-based products will need to expand rapidly.

In this sense, there are important considerations around the availability of sufficient biomass supply. On the one hand feedstocks that do not compete with land for food and feed need to continue to be developed.

Multiple studies have shown for instance that Perennial biomass crops (PBC) are a crucial feedstock for the development of biomass supply that is not in competition for land used for food production. (Choi *et al.*, 2019). Other sources such as algal feedstocks have been shown to also have considerable potential. On the other hand, biomass supply can be improved by increases in the efficiency of biomass production but also the reuse of bio-waste into productive sectors. Improvements in productive efficiency output for biomass grown on land currently under production is a complex issue with important environmental considerations. In the past considerable production efficiency improvements have been achieved through the increased application of synthetic fertilisers and pesticides in combination with fossil energy. It is now well documented that increased production efficiencies will need to be combined with decreases in synthetic and fertiliser use as well as fossil fuels and that this will require a transformation of the production of EU biomass supply. Alternative approaches that can support such a transition include practices based on conservation agriculture or agroforestry (Paris *et al.*, 2022).

The EU is often considered as a leader in the recovery and reuse of biowaste. Despite this and considerable policy efforts considerable amounts of bio-waste are not or under-utilised. Numerous studies have indicated that the effective use of this bio-waste could provide large amounts of sustainable feedstocks for the wider EU bioeconomy (EEA, 2020). The total potential capture of biowaste per kilogram per person per year in the EU is 222, while currently only 77kg is collected (Favoino, Giavini and Rupp, 2020a). The development of effective value chains that collect and process this waste into functional raw materials is especially important for certain agricultural wastes and urban-bio waste. For instance, large amounts of bio-waste from urban areas are currently landfilled in the EU, the development of effective biowaste optimisation processes are required (Favoino, Giavini and Rupp, 2020b). In particular, Fava et al. (2015) highlight that there are also many opportunities' for integrating biowaste feedstocks into biorefineries (Fava *et al.*, 2015).

One of the key goals of the Updated EU bioeconomy strategy is to 'strengthen and scale-up the bio-based sectors' (European Commission, 2018b). The overview presented in this report indicates that the development of a circular bioeconomy is still in its relatively infant stages but that important initiatives towards circularity exist throughout the biobased economy. In this sense, small scale biobased solutions, which have the potential to scale rapidly are crucial to the transformation of the EU economy. This report clearly documents a large number of small-scale biobased solutions and initiatives relevant to the circular transition and in order to accelerate their impact these need to be supported through relevant policy mechanisms and continued access to significant research and innovation funding.

The production of bioenergy in the EU has experienced a transformation in the past decade currently accounting for the majority of renewable energy produced. This has happened in tandem with considerable developments in feedstock supply and conversion methods. Mandley et al (2020) investigate the potential of bioenergy development in the EU until 2050 highlighting that despite large uncertainties EU biomass production has the potential to facilitate future bioenergy demand while also experiencing large increases in the import of biomass (Mandley *et al.*, 2020).

There are a number of important niche sectors that have the potential to considerably scale in the future. The development of biobased industries and biorefineries supported by biobased innovation processes are a key priority for the EC. The 2022 EU blue economy report highlights the importance of preserving and enhancing the natural capital of water bodies in the EU while also the importance of the 'blue biotechnology' sector as one of the key emerging sectors within water systems. Particularly promising is the development of the algae sector as well as related biorefineries, offshore aquaculture, the use of fish by-products and cellular mariculture and cell-based seafood (European Comission, 2022). The 2021 EU Forest Strategy for 2030 highlights the importance of supporting the socio-economic functions of forest while enhancing the forest based bio-economy within sustainable boundaries, key to this is the development of sustainable raw wood biomass supply, the sustainable use of wood products in particular for bioenergy, promoting the non-wood bioeconomy and services for instance through eco-tourism, whilst simultaneously protecting, restoring and enlarging EU forests ensuring climate resilience and biodiversity (European Commission, 2021).

This study identifies a number of key areas for future research including more detailed overviews of the bioeconomy for all EU member states; an in-depth analyses of specific bio-based value chains; the relationship between economy, society and the environment; the relationship between the bioeconomy, other sectors and the circular economy; indicators that measure the impact and potentials of the bioeconomy and its sectors are being developed and need to be strengthened further; and future research providing projections and scenario analyses on the future state of the bioeconomy in the medium and long-term. In addition, the conceptual understanding of the bioeconomy by relevant stakeholders appears limited, for instance, at times the terms bioeconomy and bio-based economy as well as biorefineries and bio-based industries appear mislabelled. Important steps are being made by the EC to correct this and continued policy efforts need to be implemented through for instance the development of unified national bioeconomy strategies for all member states. Furthermore, on a geographical and regional level, it is clear that the bioeconomy plays a crucial role in economies across the EU but that recent developments are unequal. For instance, the development of biorefineries is more prevalent in north western Europe. More research into these geographical variations and research that distinguishes the linear bioeconomy with a circular bioeconomy and how its value chains differ are needed.

4. Conclusions

This study provides a review of the current status of the European Bioeconomy, containing all the main 5 themes (agriculture, water systems, forestry, bioenergy, biomaterials), as well as the existing bioeconomy national strategies, trends and opportunities that exist in the EU together with successful small-scale biobased solutions.

The information presented in this report illustrates the diversity and complexity of the EU bioeconomy. There are a number of important trends occurring in the EU bioeconomy: overall employment in the bioeconomy is decreasing while the overall value of the bioeconomy is increasing. Certain sectors, including the bioenergy and biomaterials sectors that are still relatively small as compared to their fossil-based equivalents, are experiencing rapid growth, these sectors are expected to continue to grow rapidly in the medium and long-term supporting sustainable transitions across the economy.

The EU economy is transforming from an economy based on linear economic models to circular economic models however, this transformation is still at its early stages and will require the transformation of existing production systems and value chains as well as the creation of new innovative value chains.

In recent years EU policy has become very supportive of the development of a sustainable EU bioeconomy and the updated EU bioeconomy strategy operates in parallel to multiple other policy initiatives such as the new CAP, Green Deal, Farm to Fork strategy and circular economy action plan. In the short term, the further development of national strategies dedicated to the bioeconomy will strengthen the policy environment. In addition, the development of the bioeconomy has a crucial environmental dimension and current policy is supportive of efforts that support and strengthen environmental services and biodiversity.

References

Ahlqvist, T., & Sirviö, H. (2019). Contradictions of Spatial Governance: Bioeconomy and the Management of State Space in Finland. Antipode, 51(2), 395–418. https://doi.org/10.1111/ANTI.12498

Antar, M., Lyu, D., Nazari, M., Shah, A., Zhou, X., & Smith, D. L. (2021). Biomass for a sustainable bioeconomy: An overview of world biomass production and utilization. Renewable and Sustainable Energy Reviews, 139, 110691. https://doi.org/10.1016/J.RSER.2020.110691

Choi, H.S. *et al.* (2019) 'Potential trade-offs of employing perennial biomass crops for the bioeconomy in the EU by 2050: Impacts on agricultural markets in the EU and the world', *GCB Bioenergy*, 11(3), pp. 483–504. Available at: https://doi.org/10.1111/GCBB.12596.

D'Amato, D., Veijonaho, S. and Toppinen, A. (2020) 'Towards sustainability? Forest-based circular bioeconomy business models in Finnish SMEs', *Forest Policy and Economics*, 110, p. 101848. Available at: https://doi.org/10.1016/J.FORPOL.2018.12.004.

EEA (2020) *Bio-waste in Europe — turning challenges into opportunities*. Luxembourg.

'EU Bioeconomy Strategy Progress Report' (no date). Available at: https://doi.org/10.2777/29289.

European Comission (2022) *Blue Economy Report 2022*, *European Union*. Brussels: European Commission.

European Commission (2012) *Innovating for sustainable growth*. Available at: https://op.europa.eu/en/publication-detail/-/publication/1f0d8515-8dc0-4435-ba53-9570e47dbd51 (Accessed: 20 February 2023).

European Commission (2018a) *A sustainable Bioeconomy for Europe: strengthening the connection between economy, society and the environment*. Available at: https://doi.org/10.2777/478385.

European Commission (2021) *Communication from the commission to the european parliament, the council, the european economic and social committee and the committee of the regions: New EU forest strategy for 2030*. Brussels.

European Commission (2022a) 'EU Bioeconomy Strategy Progress Report European Bioeconomy policy: stocktaking and future developments'.

Fava, F. *et al.* (2015) 'Biowaste biorefinery in Europe: opportunities and research & development needs', *New Biotechnology*, 32(1), pp. 100–108. Available at: https://doi.org/10.1016/J.NBT.2013.11.003.

Favoino, E., Giavini, M. and Rupp, M. (2020a) *Communication from the commission to the european parliament, the council, the european economic and social committee and the committee of the regions: New EU forest strategy for 2030*. Brussels.

Giampietro, M. (2019) 'Methodological and Ideological Options On the Circular Bioeconomy and Decoupling: Implications for Sustainable Growth'. Available at: https://doi.org/10.1016/j.ecolecon.2019.05.001.

Gurria, P. *et al.* (2017) *Biomass flows in the European Union: The Sankey biomass diagram-towards a cross-set integration of biomass*, *European Commission Joint Research Centre: Seville, Spain*. Available at: https://doi.org/10.2760/352412.

Hájek, M., Holecová, M., Smolová, H., Jeřábek, L., & Frébort, I. (2021). Current state and future directions of bioeconomy in the Czech Republic. New Biotechnology, 61, 1–8. https://doi.org/10.1016/J.NBT.2020.09.006

Hamelin, L., Borzęcka, M., Kozak, M., & Pudełko, R. (2019). A spatial approach to bioeconomy: Quantifying the residual biomass potential in the EU-27. Renewable and Sustainable Energy Reviews, 100, 127–142. https://doi.org/10.1016/J.RSER.2018.10.017

JRC (2022) *Biomass flows, data from the BIOMASS project, European Commission – Joint Research Centre.* Available at: https://datam.jrc.ec.europa.eu/datam/mashup/BIOMASS_FLOWS/index.html (Accessed: 20 February 2023).

JRC and Novo-Institute (2022) *Jobs and Wealth in the EU Bioeconomy: (Biomass producing and converting sectors)*. Available at: https://datam.jrc.ec.europa.eu/datam/mashup/BIOECONOMICS/ (Accessed: 20 February 2023).

Mandley, S.J. *et al.* (2020) 'EU bioenergy development to 2050', *Renewable and Sustainable Energy Reviews*, 127, p. 109858. Available at: https://doi.org/10.1016/J.RSER.2020.109858.

Paris, B. *et al.* (2022) 'Energy use in open-field agriculture in the EU: A critical review recommending energy efficiency measures and renewable energy sources adoption', *Renewable and Sustainable Energy Reviews*, 158, p. 112098. Available at: https://doi.org/10.1016/J.RSER.2022.112098.

Popp, J., Kovács, S., Oláh, J., Divéki, Z., & Balázs, E. (2021). Bioeconomy: Biomass and biomass-based energy supply and demand. New Biotechnology, 60, 76–84. https://doi.org/10.1016/J.NBT.2020.10.004

Stegmann, P., Londo, M. and Junginger, M. (2020) 'The circular bioeconomy: Its elements and role in European bioeconomy clusters', *Resources, Conservation and Recycling: X*, 6. Available at: https://doi.org/10.1016/J.RCRX.2019.100029.

Szarka, N., Haufe, H., Lange, N., Schier, F., Weimar, H., Banse, M., Sturm, V., Dammer, L., Piotrowski, S., & Thrän, D. (2021). Biomass flow in bioeconomy: Overview for Germany. Renewable and Sustainable Energy Reviews, 150, 111449. https://doi.org/10.1016/J.RSER.2021.111449

Woźniak, E., & Twardowski, T. (2018). The bioeconomy in Poland within the context of the European Union. New Biotechnology, 40, 96–102. https://doi.org/10.1016/J.NBT.2017.06.003

Effects of assistance of high-frequency dielectric heating on vacuum freeze drying characteristics of all biomass wet-extruded plate

Hana Tsuneoka, Ken-ichiro Suehara, Hiroshi Nonaka, Atsushi Hashimoto *

Graduate School of Bioresources, Mie University, Tsu, Japan

* Corresponding author. Email: hasimoto@bio.mie-u.ac.jp

Abstract

To reduce drying time for biomass wet-extruded plates while minimizing deformation, we aim to develop a vacuum freeze drying method enhanced by high-frequency dielectric heating. Cylindrical plates made from wood powders were prepared as samples and subjected to drying experiments using a lab-scale vacuum chamber equipped with a high-frequency dielectric heating system. Combining high-frequency heating with vacuum freeze drying accelerated the drying rate, particularly in the latter half of the process, while only raising the sample temperature by a few degrees. The effect of high-frequency heating on accelerating drying was more pronounced with higher irradiation power, leading to a reduction in drying time by several tens of percent. Additionally, near-infrared spectroscopic imaging, visible imaging, and material strength measurements were conducted to evaluate the chemical, morphological, and mechanical characteristics of the samples after drying. No significant differences were observed except for the near-infrared absorption band of water at 1940 nm. Samples dried under irradiation at 25 W exhibited significant shrinkage and deformation, resulting in weaker material strength compared to those dried under other conditions. These results suggest that high-frequency dielectric irradiation at 20 W is optimal for this combined drying method. In conclusion, by integrating high-frequency dielectric heating with vacuum freeze drying of biomass wet-extruded materials made from wood powder, drying time can be significantly reduced while preserving chemical quality and preventing significant deformation of the sample after drying.

Keywords: wood powder, drying characteristics, near-infrared spectroscopic imaging, shape analysis.

1. Introduction

Japan Clean Ocean Materials Alliance (CLOMA), a platform dedicated to accelerating solutions for marine plastic litter, has been established to promote the 3Rs of plastics, as well as the development and use of biodegradable plastics and paper products in Japan (Japan Clean Ocean Materials Alliance, 2019). While paper, a cellulosic material, is guaranteed to be metabolized within the Earth's purification capacity, it is not a sufficient substitute for plastic products. It lacks the versatility of plastics, being unable to be injection- or extrusion-molded. Moreover, it is crucial to utilize biomass resources holistically, without favoring cellulose over other components. Responding to this need, Nonaka et al. have promoted research and development of "all-biomass molded products" by enhancing the plasticity and shape retention of biomass powder through the use of a water-soluble cellulose derivative as an auxiliary agent, rather than combining it with plastic. This approach involves wet extrusion molding (Kawamura et al., 2018; Matsuoka and Nonaka, 2020, Nonaka, 2023). However, deformation and shrinkage during drying after molding pose significant challenges in the production process, making a drying method that minimizes deformation while reducing drying time highly desirable. This study focuses on a vacuum freeze drying (VFD) method combined with high-frequency dielectric (HFD) heating for shortening the drying time while minimizing deformation.

2. Materials and Methods

2.1. Drying samples

The mixture of wood powders, hydroxypropyl methylcellulose (HPMC) and deionized water was extruded into a sheet. The cylindrical plates (ϕ47 mm x h4.3 mm) were cut from the sheet. The plates were frozen in a freezer at 253 K overnight and used as the drying samples.

2.2. Drying experimental apparatus

Drying experiments were performed in a Lab-scale vacuum chamber (Espec Co., Ltd., Osaka, Japan) equipped with a high frequency dielectric heating system. A scheme of the drying equipment is presented in Figure 2. The upper ⑦ and lower ⑧ electrode plates are equipped in the vacuum chamber ①. The output power of the high frequency dielectric heating is automatically adjusted to a set point by the matching box ⑨ during freeze-drying. A vacuum pump was used for maintaining the vacuum in the chamber. The data of the pressure, high frequency traveling wave power and high frequency reflection wave power are recorded using the data logger ⑭.

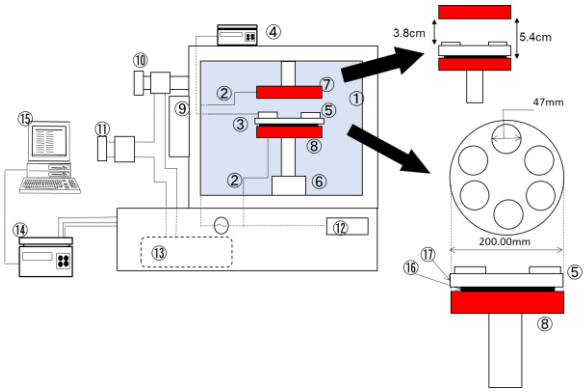

① Vacuum chamber, ② HFD introduction part, ③ Optical fiber, ④ Thermometer, ⑤ Drying samples, ⑥ Thermal and electrical insulator, ⑦ Upper electrode, ⑧ Lower electrode, ⑨ Matching box, ⑩ Vacuum exhaust valve, ⑪ Piping leak valve, ⑫ HFD power source (13.56 MHz), ⑬Oil-sealed rotary vacuum pump, ⑭ Data logger (Pressure, HFD power), ⑮ PC, ⑯Teflon°,R O-ring, ⑰ Teflon°,R plate

Figure 1. Schematic diagram of high frequency dielectric heating with freeze-dryer.

2.3. Drying experiments

Six frozen biomass samples were put on the Teflon® plate (82× 82× 10.5 mm) kept in a freezer set at 253 K overnight. to avoid the heat transfer from the lower electrode to the samples. After the pressure was reduced to 100 Pa, and the samples were irradiated with high-frequency waves (0 to 25 W). The moisture content of the samples was measured by sampling over time. Near-infrared (NIR) spectroscopic imaging and shape measurements were performed to characterize the samples after drying.

2.4. Measurements of dried sample characteristics

2.4.1.NIR spectroscopic image measurement

The NIR spectroscopic image acquisition was performed using a hyper spectral imaging system (Compovision, Sumitomo Electric Industries, Ltd., Osaka, Japan) equipped with a halogen lamp as the light source was used, and the diffuse reflectance spectrum at each pixel on the sample was collected in the range from1000 to 2350 nm.

2.4.2.Size and shape

The diameter (D), thickness (h) and apparent thickness (h_{app}) of the sample plate were measured using a caliper. Using these values the volume and shape characteristics were obtained.

3. Results and Discussion

3.1. Drying characteristics

The influences of the HFD power on the combined vacuum freeze drying characteristics of the frozen biomass plates were experimentally studied. Figure 2 shows the influences of the HFD power on the time

courses of the normalized moisture content (ω/ω_0) relative to the initial one (ω_0 [kg-H_2O/kg-dry material) of the frozen biomass plate. The temporal change in the normalized moisture content could be fitted by a two-stage exponential functions as follows (Hashimoto et al., 2018).

$$\omega/\omega_0 = \exp(-k_1 t) \quad (1)$$

$$\omega/\omega_0 = \{(\omega/\omega_0)_c - 1\} + \exp\{-k_2(t - t_c)\} \quad (2)$$

Here, ω: moisture content based on dry weight [kg-H_2O/kg-dry material], t: drying time [h], k: drying rate constant [h^{-1}], and the subscripts 1 and 2 refer to the first and second stages of the drying process. The subscripts 0 and c are the initial value and the critical value at the first and second stages of drying, respectively.

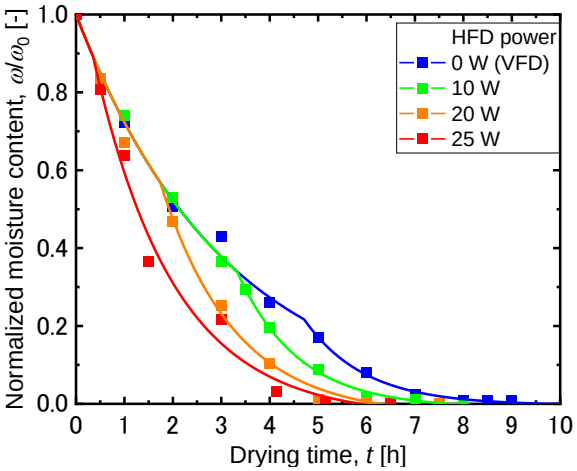

Figure 2. Influence of HFD power on time courses of normalized moisture content.

The time at which the normalized moisture content is 0,001 (1/1000 of the initial moisture content) is then defined as the drying time (t_d). The drying time t_d was 9.76 h at 0 W (vacuum freeze-drying), 7.7 h at 10 W, 6.3 h at 20 W, and 5.9 h at 25 W, respectively. The drying time could be shortened under all conditions by using HFD heating in combination, and the shortening rate was 21% from 0 W to 10 W, 36% from 0 W to 20 W, and 40% from 0 W to 25 W, respectively, with the shortening rate increasing with the increase in HFD power. It was also found that the higher the HFD power, the earlier the start time of the second stage. Therefore, the combination of HFD heating with vacuum freeze-drying of the biomass material could reduce in drying time.

For press forming after heating and drying, the time (t_{20}) required for the moisture content to decrease to lower than about 20% of the wet basis moisture content and the reduction of the drying time using the combination of HFD heating at that time were calculated using the above fitting parameters. The calculated drying times t_{20} were respectively 4.0 h at 10 W, 3.3 h at 20 W, and 2.7 h at 25 W by combining HFD heating. The drying time reduction rate was almost the same as that for t_d. These results experimentally indicate that the combination of HFD heating can shorten the drying time and that increasing the HFD power can further improve the drying time reduction effect. These results mean that the power consumption required for drying can be reduced by several tens of percent along with the reduction in drying time.

Using the above fitting parameters, the intersection points $(t_c, (\omega/\omega_0)_c)$ of the curve fitting curve in the first and second drying stages were obtained. The intersection time t_c and normalized moisture content $(\omega/\omega_0)_c$ respectively became shorter and higher as the HFD power increased. Additionally, the drying rate coefficient k_2 for the second stage became smaller as the HFD power increased. These results suggest that heating could be very effective in the early stages of drying.

3.2. Material characteristics after dryings

Since the effectiveness of HFD heating combination of VFD of all biomass wet-extruded plate, we studied the influences of HFD heating on the dried products. The NIR image analysis and size and shape change measurements were performed respectively as the chemical and physical properties.

3.2.1.NIR spectroscopic image characteristics

Figure 3 shows the examples of the second derivative spectrum of absorbance in the NIR region of the biomass plate after drying. The characteristic absorption peak bands were observed around 1210, 1350, 1460, 1580, 1710, 1810, 1940 and 2080 nm mainly relating to C-H stretching (cellulose), C-H stretching and deformation (hemicellulose), O-H stretching (water and cellulose), C-H stretching vibration (hemicellulose), water and lignin, O-H stretching and C-H deformation (cellulose), respectively.

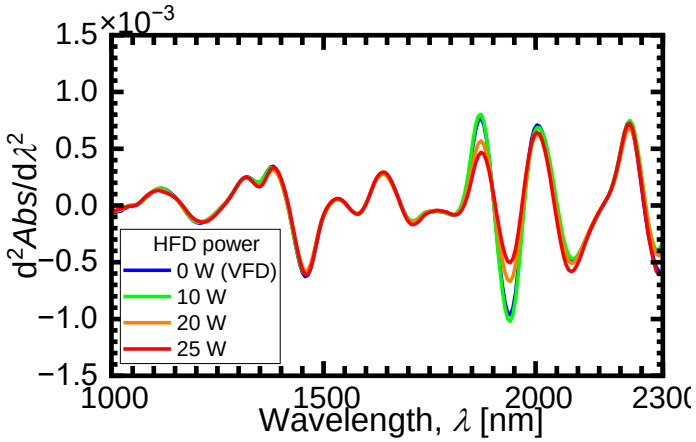

Figure 3. Examples of NIR reflectance spectra of sample plates after drying.

By focusing on these absorption bands, the NIR absorption images were generated, and the absorption intensity differences were compared between the images of the samples after VFD and combined drying. The examples of the images were indicated in Figure 4. No significant differences were observed in the absorption intensity distribution between the cases with and without HFD heating. However, the differences were observed only for the images generated using the spectral information at 1940 nm, where the strongest water absorption band is observed. This suggests that the samples after combined drying at 20 and 25 W of HFD power were drier than the control samples without HFD heating (0 W). In addition, the absorption intensity distribution was almost uniform in all images, and the distribution of components in the dried samples was also almost uniform. It was then considered that influences of the combined use of HFD heating could be chemically negligible.

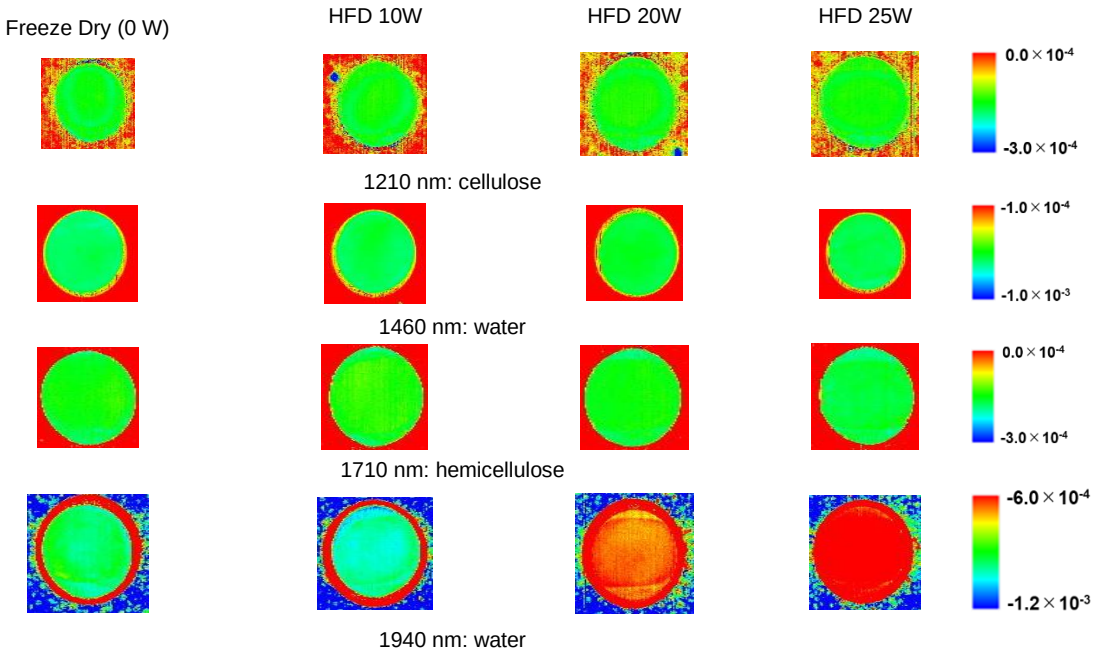

Figure 4. Examples of NIR spectroscopic images of sample plates after drying.

3.2.2. Size and shape characteristics

The shrinkage and deformation of the dried samples were investigated. Figure 5(a) shows changes in the volume ratio before and after drying, and the volume was calculated using the above measurement values. The influences of the HFD power on the volume ratio could be experimentally negligible and depended on the moisture contents. The vertical axis of the Figure 5(b) is the changes in the ratio of h_{app} to D before and after drying and means the shape changes. The deformation for the sample during VFD (0 W) increased as the dry basis moisture content decreased. and the shape could be maintained until the dry basis moisture content value below 0.2 kg-H_2O/kg-dry material for the HFD power conditions of 10 and 20 W. However, in the case of the HFD power of 25 W, the ratio was larger than that samples dried under the other conditions in the region of the dry basis moisture content lower than 0.5 kg-H_2O/kg-dry material. This is thought to be due to the rapid decrease in the moisture content.

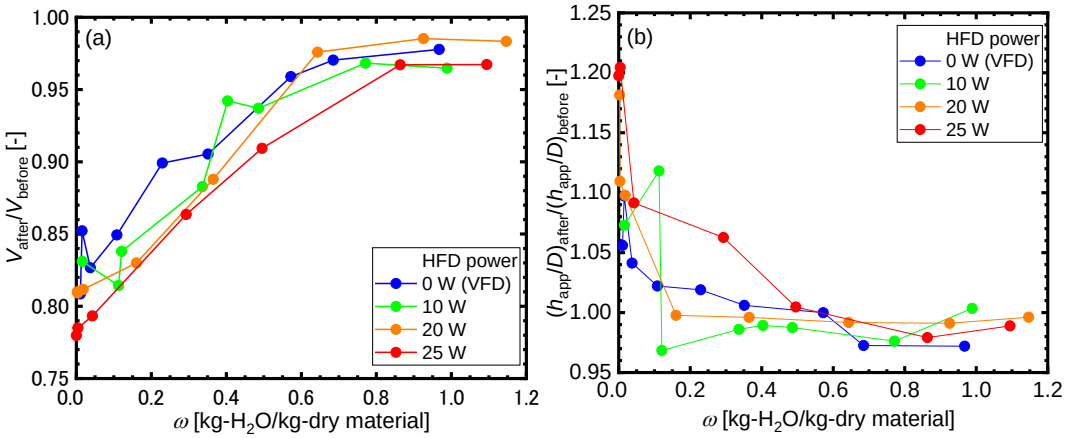

Figure 5. Influences of HFD power on size and shape changes during drying. (a) volume ratio before and after drying, (b) ratio of h_{app} to D before and after drying.

4. Conclusions

To shorten the drying time of wet-extruded wood flour compacts while suppressing deformation caused by drying, HFD heating was combined with the VFD method. NIR imaging results showed that the combined use of HFD heating had no significant effect on the chemical properties and uniformly dried the samples. Furthermore, it was confirmed that drying time could be shortened by using HFD heating and increasing the HFD power, and this behavior was quantitatively demonstrated. Compared to VFD alone (HFD power of 0 W), no significant changes in shape or shrinkage were observed after drying at HFD powers of 10 and 20 W. The shrinkage behavior was primarily influenced by the decrease in moisture content and not by the presence or absence of HFD heating. However, the sample dried under 25 W of HFD power exhibited different shrinkage behavior compared to the others. In conclusion, the VFD method combined with HFD heating successfully reduced drying time by several tens of percent without compromising the chemical and morphological characteristics of the samples after drying. Considering the characterization of the dried samples, the optimal HFD power under the experimental conditions of this study was determined to be 20 W.

Acknowledgements

We would like to thank the financial support for this research by the Environmental Restoration and Conservation Agency (JPMEERF20221C03).

References

Japan Clean Ocean Materials Alliance, 2019. Alliance creates new innovation. https://cloma.net/english/.

Hashimoto, A., K. Suehara, T. Kameoka, and K. Kawamura, 2018. Effects of assistance of high frequency dielectric and infrared heating on vacuum freeze drying characteristics of food model. In *Proceedings of 21st International Drying Symposium*. Valencia, Spain. September 11-14, 2018. Valencia, Spain: Universitat Politècnica de València. Ed. J.A. Cárcel. 795-802. http://dx.doi.org/10.4995/ids2018.2018.7461.

Kawamura, K., T. Abera, and H. Nonaka, 2018. Extrusion molding of cellulosic fibers using cellulose derivative. Japan TAPPI Journal. 72 (3) 321-327. https://dx.doi.org/10.2524/jtappij.72.321.

Matsuoka, T., and H. Nonaka, 2020. Wet extrusion of wood powder using a cellulose derivative. Japan TAPPI Journal. 74(5) 516-524. https://dx.doi.org/10.2524/jtappij.74.516.

Nonaka, H, 2023. Extrusion molding of biomass powder with cellulose derivatives. Glycoforum. 2023 26 (6), A22. https://dx.doi.org/10.32285/glycoforum.26A22.

Composting off-gas as alternative source of carbon dioxide for spirulina cultivation – a preliminary study

Kelechi E. Anyaoha[a,1], Felix Krujatz[b], Isla Hodgkinson[a], Roman Maletz[a], Christina Dornack[a]*

[a] Technische Universität Dresden, Chair of Waste Management and Circular Economy, Pirna, Germany

[b] TU Chemnitz, Chair of Automatic Control and System Dynamics, Chemnitz and Biotopa gGmbH, Center for Applied Aquaculture & Bioeconomy, Radeberg, Germany

*Corresponding author. Email: christina.dornack@tu-dresden.de

Abstract

Climate change increases drought, erosion, glacial melt, and flooding, and reduces groundwater reserves, and soil fertility among other global challenges. Avoidance, reduction, and sequestration of greenhouse gas emissions are measures to mitigate climate change. Sequestration of emissions from biological processes such as composting contributes to negative emissions. This study investigated the dynamics of carbon dioxide (CO_2) evolution from a passive composting system and compared composting off-gas and air as CO_2 sources on Spirulina biomass productivity. Three plastic bag composting reactors were used to compost food waste and sawdust (5:1 mixing ratio) in a 'staged' composting process. The gas produced is pumped from one reactor to the next to increase the CO_2 concentration in the off-gas. Three samples were used in a composting cycle for a total retention time of 21 days. Four treatments consisting of air (AirA and AirB) and off-gas (ofgA and ofgB) as sources of CO_2 were used in the spirulina cultivation. AirB and ofgB received additional air and CO_2, respectively. A different composting experiment was used in Spirulina cultivation and the percentage of CO_2 used in the Spirulina experiment ranged from 2.93 to 4.87 %. The result of the composting experiment shows that the concentration of CO_2 in the off-gas was between 2.93 and 8.47 % throughout the duration of the experiment. The results of the Spirulina experiment showed the maximum biomass productivity of 20.7, 19.5, 16.9 and 14.0 mg/L/day for ofgB, ofgA, AirB and AirA, respectively. The study demonstrated the possibility of increasing the CO_2 concentration of composting off-gas using a novel staged composting system and its importance as a carbon source for Spirulina cultivation.

Keywords: Composting, off-gas, spirulina, carbon sequestration, negative emissions.

1. Introduction

Climate change has been linked to changes in drought and flood regimes precipitation patterns, groundwater reserves, erosion, glacial melt and soil fertility, low agricultural incomes, reduced infrastructural lifespan, social insecurity, mortality, and acute hospital visits (Anyaoha et al., 2024). While carbon dioxide (CO_2) emissions from biomass are carbon neutral, any effort to capture them will result in negative emissions. One process through which biomass or bio-waste emits greenhouse gases including CO_2 and methane is composting. While CO_2 is the main GHG emitted through composting off-gas, the others (methane and nitrous oxide) are influenced by the process parameters of composting. Composting takes place either in the open (Luskar et al., 2022) or closed systems (Soto-Herranz et al., 2021). While the closed systems allow better control over some parameters such as airflow and temperature, the generated off-gas is released directly into the atmosphere.

There are ongoing efforts to reduce GHG emissions from composting directed towards factors such as composting different substrates (Komilis & Ham, 2006) and aeration (Qasim et al., 2018). Qasim et al. (2018) used airflow rates of 0.25, 0.50 and 0.75 L/min/kg Organic Matter (OM) to investigate variations in temperature, ammonia and carbon dioxide emissions, pH, electrical conductivity, organic matter and the seed germination index during mixture of chicken manure, sawdust and wood shavings composting. The report showed that more CO_2 emissions occurred at the earlier stage of the composting process for all airflow rates, while the 0.75 L/min/kg OM treatment resulted in the highest variation. On the other hand, Komilis & Ham (2006) demonstrated CO_2 emissions of 150, 220 and 370 g CO_2–C for individually composted mixed paper waste, yard waste and food waste, respectively. The report showed a large variation in CO_2 emissions from different substrates. A total of CH_4 and N_2O ranging from 0.084 to 7.82 gCO_2-eq./kg are emitted by composting different combinations of organic materials (Lv et al., 2018; Chen et al., 2019; Raza et al., 2021) while Chen et al. (2019) reported up to 358.2 gCO_2-eq/kg Dry Matter (DM) CH_4 emission. Most composting reports have shown varying levels of CH_4 and NO_2 emissions.

The capture or sequestration of CO_2 remains a visible option for climate change mitigation in the bio-waste management sector. Therefore, the use of photosynthetic organisms offers an opportunity for the sequestration of CO_2 from composting. Spirulina (Arthrospira platensis) are photosynthetic cyanobacteria that use CO_2 and carbonate for biomass production and contribute to efforts to reduce GHG emissions and climate change. Spirulina adaptation in alkaline environments eliminates competing species in the growth culture (Phang et al., 2000).

There is limited research in harnessing and sequestering CO_2 from composting off-gas using photosynthetic microorganisms (Abid et al., 2017; Lu et al., 2019). Interestingly, these two reports did not actively influence the concentration of CO_2 in the off-gas. A key factor in the effective use of CO_2 from composting off-gas is the concentration of CO_2 in the off-gas relative to other gases, including oxygen, methane and N_2O. This explains the advantage of the expensive commercial source of 100 % CO_2. To increase the effectiveness of CO_2 sequestration from composting off-gas, it is necessary to rethink the composting process to increase CO_2 the concentration in the off-gas. It is reported that the O_2 concentration should be 10 % or more to avoid metabolic activity inhibition (Zeng et al., 2018). However, the rate of microbial activity decreases as the organic matter is degraded and consequently less O_2 is required for metabolic activity as composting processes. As CO_2 concentration increases, that of O_2 reduces. To the authors knowledge, there is limited literature report on this subject. Therefore, the research aims at harnessing CO_2 from a novel closed composting system for Spirulina cultivation. The specific objectives are (1) to investigate the dynamics of CO_2 evolution from a passive composting system and (2) to compare the Spirulina dry weight, biomass productivity and specific growth fed with composting off-gas and air.

2. Materials and Methods

2.1. Organic waste characteristics and culture medium

The food waste (84.07 % moisture content) was collected from a restaurant in Pirna (Saxony, Germany), and consisted of a mixture of food preparation waste and unsold food. The sawdust was obtained from Pollmeier Massivholz GmbH & Co.KG (Creuzburg) and of beech wood chips. The sawdust was used as delivered. In the first composting experiments, 800 g of food waste and sawdust mixture was used. The mixture was first homogenised and stored at -20 ºC. Before use, each sample was thawed for up to 24 hours in the autumn period. In the second composting experiment, used for Spirulina cultivation, 1000 g of food waste-sawdust mixture was used for each sample. The mixing ratio of food waste and sawdust was estimated to be 5:1 using an assumed carbon/nitrogen (C/N) ratio of 30.

Spirulina, which was grown in a commercial photobioreactor under 24-hour light was sourced from PUEVIT GmbH (Dresden, Germany). Modified KG medium ($NaNO_3$ – 1.0 g/L, K_2HPO_4 – 0.5 g/L, K_2SO_4 – 0.5 g/L, NaCl – 0.5 g/L, $MgSO_4 \cdot 7H_2O$ – 0.2 g/L, $CaCl \cdot 2H_2O$ – 0.04 g/L and Hutners trace elements – 0.1 mL/L) without $NaHCO_3$ was used as the nutrient source for the experiment. Prepared KG nutrient medium (200 mL) in ultra-sterilised water (200 mL) was poured into clean 2 litre borosilicate glass bottles and then a concentrated suspension of microalgae (200 mL at 1.15 optical density) was added to make up 600 mL volume. The initial pH of the culture was 9.78 at 24.5ºC.

2.2. Composting experiment and Spirulina platensis cultivation

The composting experiment consisted of three vacuum bags (made of polyethylene and measuring 100 x 80 cm in size) used as reactors, and another for the off-gas storage in the second experiment. In the system, each sample is composted for a total of 21 days. During the loading period of the first experiment, which took place between September and October 2023, sample 1 is placed in reactor 1 with a total air volume of 0.188 m^3/kg DM supplied using an electronic air pump (Dirk Rossman GmbH, Germany) as inlet pump through an 8 mm internal diameter silicon hose for 3 minutes at 13.5 L/min with a flow meter (LZQ-7 Flow Meter 2-20LPM Acrylic Air Oxygen Flow Meter). The produced off-gas was evacuated for one minute and fresh air was introduced every three hours. After seven days, sample 2 was introduced and placed in reactor 2. Reactor 2 was connected to the inlet pump as described above, while another pump was connected between reactor 2 and reactor 1, which evacuated the off-gas in reactor 2 for one minute every three hours and it became feed gas of reactor 1. After a further seven days, sample 3 was introduced into reactor 3, completing the loading period. Reactor 3 replaced reactor 2 above, another pump was introduced between them, which

evacuates the off-gas of reactor 3 for one minute every three hours and it became the feed gas of reactor 2. After a further three hours, the off-gas in reactor 2 was evacuated as feed gas for reactor 1. Finally, after a further three hours the off-gas in reactor 1 was evacuated or stored in the air bag for use as a CO_2 source for spirulina cultivation during the second experiment. In summary, after the evacuation of reactor 1, the off-gas from reactor 2 was pumped into reactor 1, followed by the off-gas in reactor 3 to reactor 2 and finally fresh air to reactor 3. This was done every three hours for the duration of the experiment. The pumps were controlled by a mechanical timer (Masterclear – Wermelskirchen, Germany). After 21 days, sample 1 is removed and the composted waste allowed to cure, sample 2 is moved to reactor 1, sample 3 is moved to reactor 2 while fresh sample (sample 4) was introduced into reactor 3. This is repeated every seven days to ensure a continuous system. The connections between the three reactors and air bag are shown in Figure 1. The second composting experiment took place between November and December 2023, using 1000 g of each sample and adjusting the total volume of air accordingly. The thermometer was placed in the centre of the composting matrix for each sample.

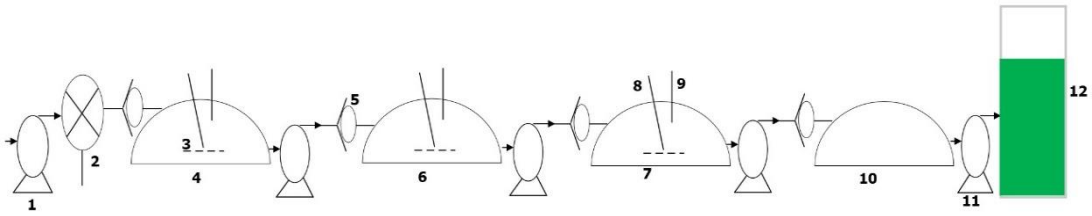

Figure 1. The sketch of the composting reactors and photobioreactor. 1 – air pump; 2- rotameter; 3 – perforated grate for biomass; 4 – reactor 1; 5 - one-way valve; 6 and 7 – composting reactors, 8 - thermometer inserted inside the composting matrix, 9 – off-gas sampling point, 10 – off-gas storage, 11 – aquatic pump connected with a sparger, 12 – photobioreactor.

Spirulina cultivation was carried out using borosilicate glass bottles (Simax) as photobioreactors (600 mL working volume) placed in a heated water bath set at 34°C (FEDOUR 25 W Mini Aquarium Heating Rod) for seven days. Three LED bulbs (Philips warm white 2700K – 806 lumens each) mounted 20 cm from the top of the photobioreactors were used to provide 1 hour 30 minutes of illumination and 30 minutes of darkness between 14:00 and 07:30 throughout the experiment. Similar studies have reported a 24-hour photoperiod for Spirulina cultivation (Jung et al., 2023). The experiment was conducted by replacing the carbon source (Na_2CO_3/$NaHCO_3$) in the nutrient solution with CO_2 in air (0.04 % v/v) for treatments AirA and AirB and composting off-gas (between 2.93 and 4.87 % CO_2 recorded) for treatments OfgA and OfgB. AirB and OfgB were additionally injected with air and off-gas every three hours for two minutes, respectively. An aquarium air pump (FEDOUR 3 W Quiet Aquarium Air Pump) was used to inject the air and off-gas in the mixture through a porous stone sparger placed on the bottom of the photobioreactors at 0.24 vvm for 3 minutes at 02:00, 07:00, 11:00, 16:00, and 21:00 hours throughout the trial while the additional sparging lasted for 2 minute only every 3 hours. Mechanical timer was used to control the LED bulbs and air pumps.

2.3 Analytical methods and Measurements

Culture samples obtained on the first day of the experiments were filtered using a Sartorius membrane filter (Göttingen, Germany) and filter paper (Whatman, GF/F) pre-dried in an oven at temperature of 60°C for 24 hours. The biomass and the filter paper were then dried overnight at a temperature of 60°C. The difference in weight was used to estimate the initial dry weight of biomass. Similarly, the optical density of the cultures was measured using a Thermo Scientific™ GENESYS™150 UV-Vis spectrophotometer at 750 nm. The corresponding optical density and dry weight values were used for the standard growth curve (equation 1). The optical density of each culture (5 mL) was measured daily and used for subsequent calculation of dry weight using equation 1. Cultures received 5 mL nutrient solution after each sampling. The pH and temperature of the culture were measured daily using a pH meter (WTW pH 323). The maximum biomass productivity and specific growth were calculated using equations 2 and 3, respectively.

$$\mathbf{y = 0.8428x + 0.0643} \qquad \mathbf{R^2 = 0.9611} \tag{1}$$

where y and x are biomass concentration (g L^{-1}) and OD_{750}, respectively.

$$\boldsymbol{P = \frac{X_t - X_0}{t_t - t_0}} \tag{2}$$

where p is maximum biomass productivity, mg/L/day, X_t and X_o are maximum concentration at time t_t and initial biomass concentration at time t_o, respectively.

$$\mu_{max} = \frac{In(X_t - X_0)}{t_t - t_0} \tag{3}$$

where μ_{max} is specific growth rate, per day.

The composition of the off-gas in the reactors and air-bag were measured using Dräger X-am 8000 gas analyser (Germany). Room and sample temperatures were measured using a digital and an analogue thermometers, respectively.

Statistics

Analyses were performed in replicates and means with standard deviation were reported using EXCEL (Microsoft Office Enterprise, 2016) where applicable. The analysis of variance (ANOVA) was performed using R 4.3.2 software.

3. Results and Discussion

3.1. Variation of substrate temperature

The composting operation occurred within the temperature range for mesophilic micro-organisms (25-55ºC) (Wang et al., 2022). Temperature variation allows the survival of the different mesophilic, moderate thermophilic, and hyperthermophilic microorganisms. Due to the low ambient temperature in autumn, it took at least 12 hours for the temperature of the substrates to change, which marks the start of the composting process. In Table 1, the temperature of samples 1, 2 and 3 varied between 22 to 35ºC, 22 to 31ºC and 26 to 30ºC, respectively. There was a rapid increase in temperature at the beginning of the composting process for each of the samples. Higher temperatures indicate high biological activity and degradation. The mesophilic temperature range recorded was due to the low temperatures in the autumn period and because the reactors were not insulated. Similarly, the novelty of the composting system means that the water vapour released by substrate decomposition remains in the reactor, contributing to a low temperature. Most of the heat produced was lost. However, this did not stop the decomposition of the organic materials. For example, the substrate temperature of sample 1 was above 25ºC in the first 13 days of composting, which is within the minimum temperature for mesophilic microorganisms (Wang et al., 2022). Similar results were observed for the first six days of samples 2 and 3, indicating higher microbial activity at the earlier stages of the composting operation. While there were consistently higher substrate temperatures than ambient, the differences decreased as composting progressed. The maximum temperature reached was 35ºC in sample 1 during the first two days.

Table 1. Temperature readings and Compositions of the off-gas from composting experiment

Sample/parameter	Substrate Temperature (ºC)	Room Temperature (ºC)	CO_2 (%)	Oxygen (%)
		Day 1		
Sample 1	30.00±0.00	27.30±0.00	2.00±0.00	18.60±0.00
		Day 2		
Sample 1	35.00±0.00	25.78±1.30	6.77±4.40	13.90±2.38

		Day 3		
Sample 1	27.00±1.41	24.25±2.05	2.90±0.14	18.35±0.07
		Day 4		
Sample 1	27.33±2.52	25.07±2.18	2.97±0.31	18.47±0.41
		Day 5		
Sample 1	27.00±4.24	24.95±3.18	3.15±0.21	17.85±0.21
		Day 6		
Sample 1	27.00±0.00	24.60±0.00	3.10±0.00	18.00±0.00
		Day 7		
Sample 1	29.00±0.00	28.30±00	0.70±0.00	19.70±0.00
Sample 2	31.00±0.00		2.80±0.00	18.50±0.00
		Day 8		
Sample 1	27.00±1.41	24.55±0.78	4.37±0.31	17.23±0.29
Sample 2	29.50±2.12		5.30±0.99	16.55±1.06
		Day 9		
Sample 1	27.00±0.00	25.27±0.47	4.00±0.42	16.60±0.71
Sample 2	28.33±0.58		3.70±0.35	17.23±0.75
		Day 10		
Sample 1	23.67±1.53	22.13±2.00	2.77±0.40	18.17±0.51
Sample 2	25.33±0.58		2.43±0.32	18.73±0.39
		Day 11		
Sample 1	23.25±0.50	22.53±0.56	7.73±0.49	12.20±0.29
Sample 2	24.00±0.82		7.13±1.04	14.20±0.81
Sample 3	30.00±0.00		5.9±0.35	15.55±0.31
		Day 12		
Sample 1	23.00±0.00	22.35±0.07	7.35±0.35	13.75±0.21
Sample 2	23.00±0.00		5.70±0.14	15.55±0.07
Sample 3	28.50±0.71		4.35±0.07	16.90±0.00
		Day 13		
Sample 1	22.20±0.42	21.30±1.07	5.50±1.32	15.48±1.40
Sample 2	22.00±0.00		4.73±0.27	16.30±0.41
Sample 3	27.33±0.58		3.80±0.26	17.20±0.26
		Day 14		
Sample 1	22.00±0.00	20.75±0.86	6.65±0.42	13.47±0.62
Sample 2	22.00±0.00		4.10±0.28	16.90±0.28
Sample 3	26.75±0.96		3.25±0.06	17.78±0.10
		Day 15		
Sample 1	24.00±2.83	23.30±3.11	6.02±0.86	14.52±1.30
Sample 2	27.00±4.36		3.50±0.20	17.6±0.26
Sample 3	27.67±2.08		2.90±0.26	18.23±0.38

3.2. Gaseous emissions and Spirulina platensis cultivation

In the biological process, oxygen and carbon in the biomass were reduced to carbon dioxide after the injection of ambient air into the reactor. A decrease in oxygen concentration and an increase in CO_2 are

indications of the composting process or biological activity. This is reflected in the observed changes shown in Table 1. The concentration of CO_2 ranged between of 0.7-7.73 % while that O_2 is 12.2-19.7 % for sample 1. The CO_2 concentration ranges for samples 2 and 3 are 2.4-7.13 % and 2.9-5.9 %, respectively. It should be noted that the highest CO_2 recorded for sample 1 occurred after the loading period, with fresh air entering only through sample 3. No methane was recorded during the entire sampling period, which is a clear indication of the system's contribution in GHG emissions reduction. sample 1 recorded the highest CO_2 and temperature during the same period before the introduction of sample 2.

The final off-gas from the composting experiment conducted between November and December 2023 was collected in a bag and the composition was sampled daily and used for Spirulina cultivation. The results are shown in Table 2. The highest CO_2 concentration in the bag was 4.87 % with a corresponding O_2 content of 16.4 %. The lower temperature of the approaching winter may have played a significant role in the relatively lower concentration of CO_2 due to low microbial activity compared to the results in Table 1.

Table 2. Composition of the off-gas in the air-bag.

Parameter/Day	Carbon dioxide (%volume)	Oxygen (%volume)	Hydrogen (%volume)
Day 1	4.0±0.00	16.4±0.00	0.06±0.00
Day 2	4.3±0.06	17.0±0.00	0.05±0.01
Day 3	4.1±0.15	16.9±0.00	0.08±0.00
Day 4	4.4±0.1	16.5±0.00	0.08±0.00
Day 5	3.9±0.06	17.4±0.12	0.07±0.01
Day 6	4.5±0.00	16.7±0.00	0.04±0.02
Day 7	4.9±0.06	16.4±0.00	0.03±0.01
Day 8	4.3±0.00	16.9±0.06	n/a
Day 9	3.2±0.06	18.0±0.00	0.03±0.00
Day 10	3.7±0.06	17.3±0.00	0.13±0.01
Day 11	2.9±0.06	18.1±0.00	0.06±0.00
Day 12	3.7±0.00	17.6±0.06	0.06±0.00

3.3. Characteristic of the spirulina

Spirulina is known to thrive in an alkaline environment typically pH of 9.5 – 10.5 (Jiménez et al., 2003). Another advantage of this pH range is the prevention of contamination by phototrophic microorganisms. However, the process of Spirulina cultivation reduces the alkalinity of the environment by dissolving CO_2, which tends to decrease H+ and carbonic anhydrase (Chen et al., 2020; Aditya et al., 2023). An active increase in CO_2 injection reduces the pH of the culture medium, resulting in the inhibition of Spirulina growth. In this study, the pH of treatments AirA and AirB remained within the recommended range, with the lowest values of 9.55 and 9.28 recorded on the last day, respectively. Further sparging of AirB increased CO_2 available in the medium, resulting in reduced pH as observed in Figure 2. However, this means more CO_2 available in the medium for photosynthesis, resulting in higher Spirulina biomass productivity (16.9 and 14.0 mg/L/day) and specific growth (0.108 and 0.088 per day) compared to AirA. A similar improvement was observed for the biomass concentration (dry weight) of AirB compared to that of AirA. After seven days, AirB recorded 220 mg/L dry weight (DW) compared to 209 mg/L DW of AirA (Figure 3). Figure 2 shows the temperature of the culture as measured by the pH metre. Except for the first day, the temperatures were maintained within the temperature range for Spirulina (25 – 35^{o}C), ensuring the optimal environment for growth of the organism.

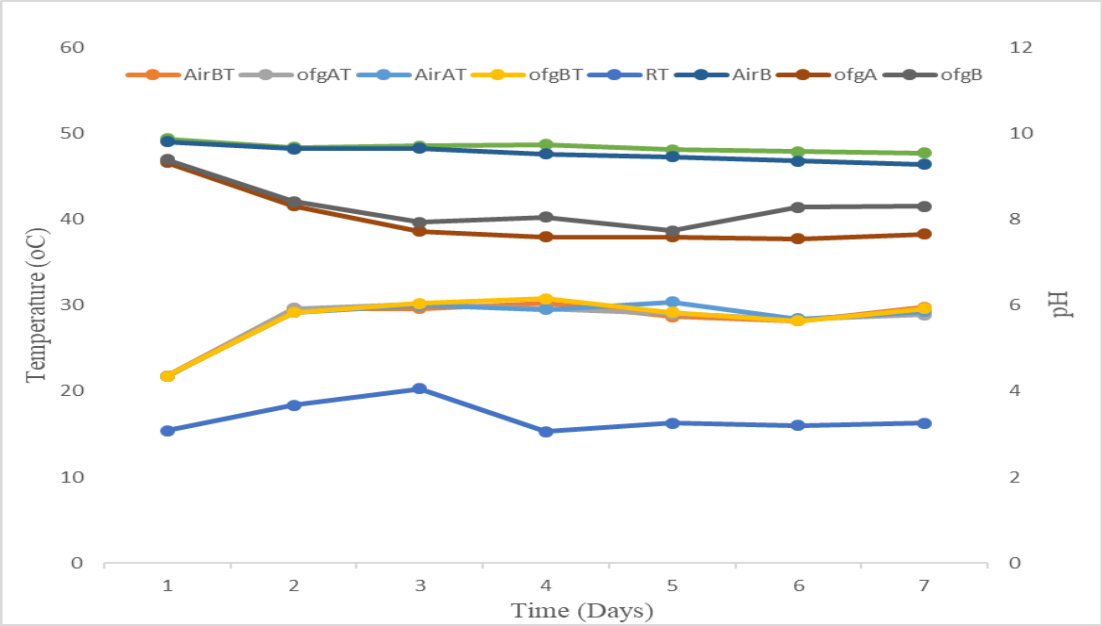

Figure 2. pH of the four treatments and temperature of the cultures during pH measurement. pH and temperature of treatment fed with off-gas (ofgA and ofgAT), off-gas with sparging (ofgB and ofgBT), air (AirA and AirAT), air with sparging (AirB and AirBT), respectively. RT is room temperature.

On the other hand, ofgB had the highest biomass productivity of 20.7 mg/L/day and specific growth of 0.126 per day. This was as a result of increased CO_2 injection and sparging. The biomass productivity and specific growth of ofgA were 19.5 mg/L/day and 0.114 per day, respectively. While both ofgA and ofgB received the same amount of CO_2 from the air bag, resulting in a decrease in the pH of the cultures when compared to AirA and AirB, the additional sparging of ofgB increased its alkalinity more than that of ofgA and as well balanced the culture solution for optimal conditions. Notably, ofgA had a higher biomass dry weight in the first two days than ofgB. ofgB showed a sharp increase in pH in the last few days. Figure 3 shows the increase in the dry weight from day 1 to day 7 of the measurement; cultures that receiving off-gas CO_2 showed higher concentrations. At the end of the experiment, ofgB recorded 243 mg/L dry weight (DW) compared to 242 mg/L DW for ofgA (Figure 3). This clearly demonstrates the benefits of combining composting with Spirulina cultivation. Despite the improvements due to the off-gas, no significant difference in dry weight was observed between all the treatments.

Results from other studies are presented in Table 3 and compared with this study. The maximum specific growth in this study is lower than in the others. Many factors may be responsible for this, including the difference in photobioreactor type. For example, De Morais & Costa (2007) compared flask and vertical photobioreactor in their experiment and recorded higher maximum specific growth with the vertical photobioreactor.

Table 3. Comparisons of maximum specific growth with other literature reports

Parameter	(De Morais & Costa, 2007)				(Lu et al., 2019)		(Phang et al., 2000)		This study
CO_2 conc. (%)	0.04	6	12	18					2.93-4.87 %
(μ_{max}) per day	0.24	0.18	0.19	0.16	0.49	0.51	0.62	0.57	0.126
Culture media	Zarrouk medium without bicarbonate				Zarrouk's medium		Kosaric Medium	Digested sago effluent	KG medium
Number of days	20				12		16		7

μ_{max} - maximum specific growth

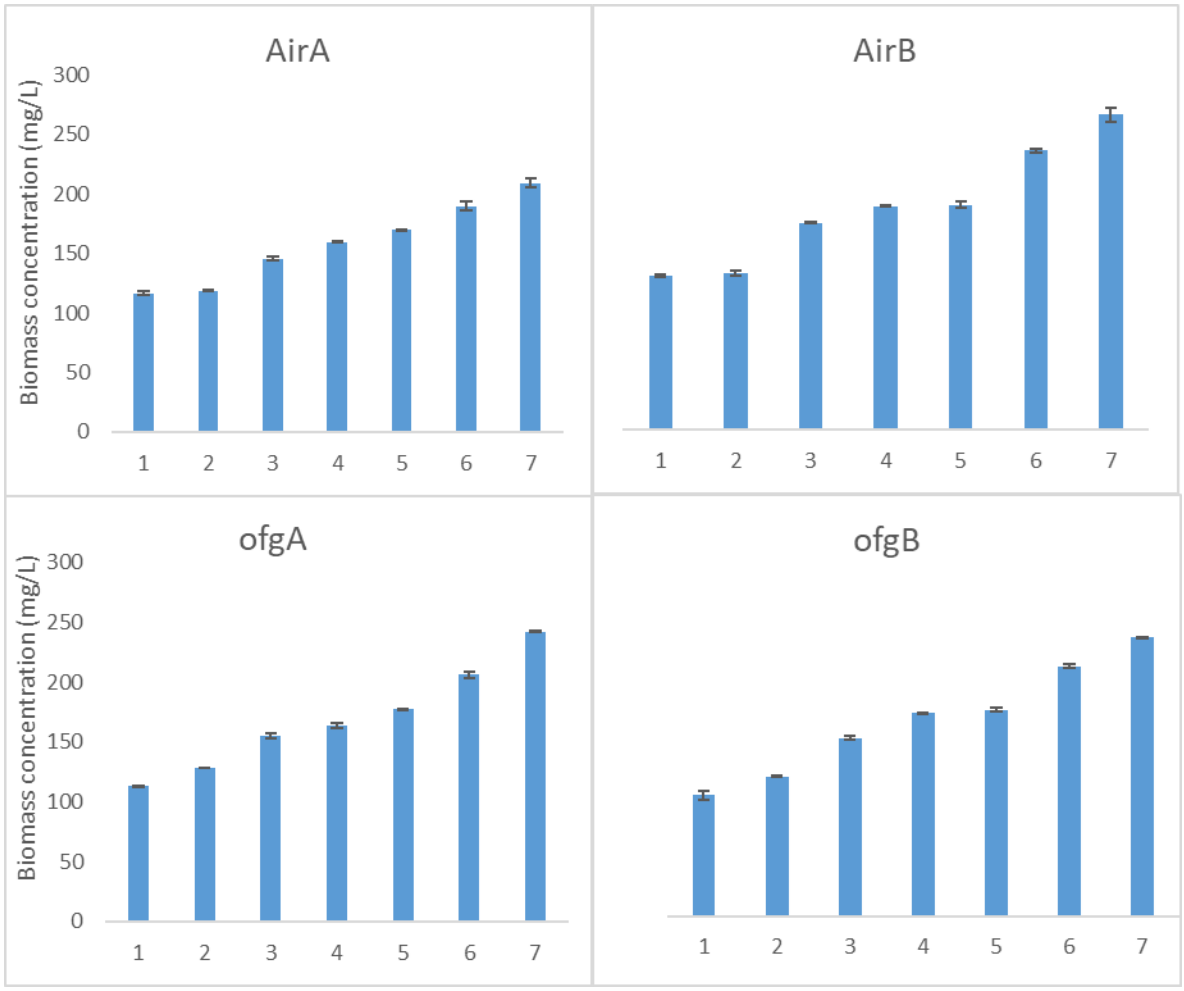

Figure 3. The biomass concentration of the culture for the 7 days of growth.

4. Conclusions

This study investigated the dynamics of CO_2 evolution from a passive composting system and compared the dry weight, biomass productivity and specific growth of Spirulina fed with composting off-gas and air. Through a novel 'staged composting', the CO_2 concentration of off-gas collected in an air bag increased to up to 4.87 %. A maximum of 7.73 % CO_2 and no methane was also detected in a composting reactor. By replacing CO_2 from the air with that from the composting off-gas, the study showed an increase of up to 32 % in biomass productivity and 30 % in specific growth compared to reference experiments. These results demonstrated the importance of composting in providing a cheap source of CO_2 in spirulina cultivation. Furthermore, the study demonstrated the possibility of increasing the CO_2 concentration of composting off-gas using a novel staged composting system. However, while the combination of composting and Spirulina cultivation in this study demonstrated innovation, further work is needed to optimise the composting process and increase the rate of conversion of CO_2 to biomass using spirulina. Other parameters such as light intensity and CO_2 concentration need to be optimised to ensure a pH balance, which is a limiting factor with increased CO_2 supply in the Spirulina culture. Despite this limitation, this study contributes to existing the literature on harnessing CO_2 for biomass production and provides new insights in organic matter composting through the staged process.

Funding information

Funded by the Deutsche Forschungsgemeinschaft (DFG, German Research Foundation) – Projektnummer 498389300.

References

Abid, A., Saidane, F., Hamdi, M. 2017. Feasibility of carbon dioxide sequestration by Spongiochloris sp microalgae during petroleum wastewater treatment in airlift bioreactor. Bioresource Technology, 234, 297–302. https://doi.org/10.1016/j.biortech.2017.03.041.

Aditya, L., Vu, H. P., Hasan, A., Mahlia, T. M. I., Silitonga, A. S. 2023. Role of culture solution pH in balancing CO_2 input and light intensity for maximising microalgae growth rate. Chemosphere, 343, 140255. https://doi.org/10.1016/j.chemosphere.2023.140255.

Anyaoha, K. E., Krujatz, F., Hodgkinson, I., Maletz, R., Dornack, C. 2024. Microalgae contribution in enhancing the circular economy drive of biochemical conversion systems – A review. Carbon Resources Conversion, 7(2), 100203. https://doi.org/10.1016/j.crcon.2023.10.003.

Čeh, B., Luskar, L., Hladnik, A., Trošt, Ž., Polanšek, J., Naglič, B. 2022. The Quantity and Composition of Leachate from Hop Plant Biomass during Composting Process. Applied Sciences (Switzerland), 12(5). https://doi.org/10.3390/app12052375.

Chen, J., Hou, D., Pang, W., Nowar, E. E., Tomberlin, J. K., Hu, R., Chen, H., Xie, J., Zhang, J., Yu, Z., Li, Q. 2019. Effect of moisture content on greenhouse gas and NH3 emissions from pig manure converted by black soldier fly. Science of the Total Environment, 697, 133840. https://doi.org/10.1016/j.scitotenv.2019.133840.

Chen, Y., Xu, C., Vaidyanathan, S. 2020. Influence of gas management on biochemical conversion of CO_2 by microalgae for biofuel production. Applied Energy, 261, 114420. https://doi.org/10.1016/j.apenergy.2019.114420.

De Morais, M. G., Costa, J. A. V. 2007. Carbon dioxide fixation by Chlorella kessleri, C. vulgaris, Scenedesmus obliquus and Spirulina sp. cultivated in flasks and vertical tubular photobioreactors. Biotechnology Letters, 29(9), 1349–1352. https://doi.org/10.1007/s10529-007-9394-6.

Jiménez, C., Cossío, B. R., Niell, F. X. 2003. Relationship between physicochemical variables and productivity in open ponds for the production of Spirulina: A predictive model of algal yield. Aquaculture, 221(1–4), 331–345. https://doi.org/10.1016/S0044-8486(03)00123-6.

Jung, C. G. H., Nghinaunye, T., Waldeck, P., Braune, S., Petrick, I., Küpper, J. H., Jung, F. 2023. Decarbonization of Arthrospira platensis production by using atmospheric CO_2 as an exclusive carbon source: proof of principle. International Journal of Environmental Science and Technology. https://doi.org/10.1007/s13762-023-05215-x.

Komilis, D. P., Ham, R. K. 2006. Carbon dioxide and ammonia emissions during composting of mixed paper, yard waste and food waste. Waste Management, 26(1), 62–70. https://doi.org/10.1016/j.wasman.2004.12.020.

Lu, W., Alam, M. A., Luo, W., Asmatulu, E. 2019. Integrating Spirulina platensis cultivation and aerobic composting exhaust for carbon mitigation and biomass production. Bioresource Technology, 271(September 2018), 59–65. https://doi.org/10.1016/j.biortech.2018.09.082.

Luskar, L., Polanšek, J., Hladnik, A., Čeh, B. 2022. On-Farm Composting of Hop Plant Green Waste—Chemical and Biological Value of Compost. Applied Sciences (Switzerland), 12(9). https://doi.org/10.3390/app12094190.

Lv, B., Zhang, D., Cui, Y., Yin, F. 2018. Effects of C/N ratio and earthworms on greenhouse gas emissions during vermicomposting of sewage sludge. Bioresource Technology, 268(June), 408–414. https://doi.org/10.1016/j.biortech.2018.08.004.

Phang, S. M., Miah, M. S., Yeoh, B. G., Hashim, M. A. 2000. Spirulina cultivation in digested sago starch factory wastewater. Journal of Applied Phycology, 12(3–5), 395–400. https://doi.org/10.1023/a:1008157731731.

Qasim, W., Lee, M. H., Moon, B. E., Okyere, F. G., Khan, F., Nafees, M., Kim, H. T. 2018. Composting of chicken manure with a mixture of sawdust and wood shavings under forced aeration in a closed reactor system. International Journal of Recycling of Organic Waste in Agriculture, 7(3), 261–267. https://doi.org/10.1007/s40093-018-0212-z.

Raza, S. T., Tang, J. L., Ali, Z., Yao, Z., Bah, H., Iqbal, H., Ren, X. 2021. Ammonia volatilization and greenhouse gases emissions during vermicomposting with animal manures and biochar to enhance sustainability. International Journal of Environmental Research and Public Health, 18(1), 1–18. https://doi.org/10.3390/ijerph18010178.

Soto-Herranz, M., Sánchez-Báscones, M., Antolín-Rodríguez, J. M., Martín-Ramos, P. 2021. Reduction of ammonia emissions from laying hen manure in a closed composting process using gas-permeable membrane technology. Agronomy, 11(12). https://doi.org/10.3390/agronomy11122384.

Wang, Z., Wu, D., Lin, Y., Wang, X. 2022. Role of Temperature in Sludge Composting and Hyperthermophilic Systems: a Review. Bioenergy Research, 15(2), 962–976. https://doi.org/10.1007/s12155-021-10281-5.

Zeng, J., Yin, H., Shen, X., Liu, N., Ge, J., Han, L., Huang, G. 2018. Effect of aeration interval on oxygen consumption and GHG emission during pig manure composting. Bioresource Technology, 250, 214–220. https://doi.org/10.1016/j.biortech.2017.11.010.

Oenotrace – A data-driven approach to trace sustainable practices in wine-growing

Marco Bignardi [a,*], Andreas Heiß [a], Nikos Tsoulias [a], Dimitrios Argyropoulos [b], Dimitrios T. Davarakis [b], Marco Moriondo [c], Davide Cammarano [d], Cristina Balaceanu[e], George Suciu [e], Dimitrios S. Paraforos [a].

[a] Department of Agricultural Engineering, Hochschule Geisenheim University, Geisenheim, Germany.

[b] Agriculture and Food Science Centre, University College Dublin, Belfield, Ireland.

[c] National Research Council – Bio-Economy Institute, Florence, Italy.

[d] Department of Agroecology, Aarhus University, Tjele, Denmark.

[e] R&D Department, BEIA Consult International, Bucharest, Romania.

* Corresponding author. Email: Marco.Bignardi@hs-gm.de

Abstract

The wine-making industry plays a significant role in the agri-food sector and there has been an increasing emphasis on assessing its environmental impact. However, the estimation of emissions from field operations may lead to inaccurate analysis due to the lack of site-specific data. It is essential to examine the factors contributing to the environmental impact of grapevine cultivation, particularly due to its vulnerability to climate change while holding significant potential to mitigate it by acting as a C sink. The European project Oenotrace aims to establish a data-based infrastructure for tracing sustainable practices in grapevine growing. A major challenge within the project is to quantify the environmental impact of grapevine cultivation comprehensively. Therefore, novel sustainability metrics shall be used within the wine-making sector and to communicate with customers. Initially, the prevailing aspects contributing to the environmental impact have been identified in two different territories, Italy and Germany. An experimental sensor-based data acquisition architecture has been designed to estimate the CO_2 balance from anthropogenic and natural origins. The system leverages a carbon balance model to estimate the net CO_2 emission of the agroecosystem coupled with data from various sensors. A machine telemetry module allows for monitoring machine-related emissions during field operations. A further IoT-architecture was designed to transfer this approach to a commercial winery in Germany. This architecture encompasses the entire value chain to transfer the vineyard-related sustainability metrics to the customers. A thorough mapping of the state of the use case winery highlighted significant technical challenges. These will be overcome by means of IoT technology and a data platform, which will serve as a pivotal point for automated data aggregation and management, as well as the involvement of stakeholders. These first results propose a starting point for developing precise data-driven environmental impact analysis approaches for future viticulture.

Keywords: Grapevine cultivation, Sustainability assessment, Agro-environmental modelling, IoT system

1. Introduction

In the last decades, climate change has been identified as one of the most important threats to mankind because of its detrimental effects on politics, economics and society. Agriculture can be negatively affected by this phenomenon because of its fundamental changes in weather conditions, which can affect negatively crop growth (Droulia and Charalampopoulos, 2022). Meanwhile, the agricultural sector is responsible for about 30 % of the global anthropogenic emissions (both direct and indirect) contributing to climate change (Lal, 2021). Among the different sectors, the viticulture industry has undergone a profound transformation, spurred by a growing recognition of the urgent need for sustainability (Jackson, 2008). What was once primarily a pursuit of quality and yield has evolved into a complex balancing act between ecological stewardship, economic viability, and social responsibility (Pretty, 2008). Thus, the environmental impact of vine cultivation, being one of the most diffused crop worldwide, has received increasing importance throughout the wine-making industry. Specifically, the assessment of the wine-making carbon footprint has drawn enhanced attention because of its contribution to global warming (Navarro et al., 2017), while having the potential to mitigate its effects, by acting like a carbon sink (Tezza et al., 2019; Schultz H., 2022).

Since the 2000s, efforts to assess and mitigate the environmental impact of grape cultivation have evolved significantly, with Life Cycle Assessment (LCA) methodologies playing a pivotal role (Falcone et al., 2016). LCA can provide a comprehensive framework for evaluating the environmental performance of viticultural systems across all stages of production, from vineyard establishment to wine distribution focusing primarily on quantifying the environmental impacts associated with vineyard inputs, such as water, energy, fertilizers, and pesticides (Happonen et al., 2021). However, as the field has matured, the researchers have increasingly recognized the importance of considering A broader system boundaries and accounting for indirect impacts (Rouault et al., 2020). In viticulture, LCA involves a multi-step process defining the system boundaries, collecting data on grape production inputs and outputs, using a life cycle inventory model to measure environmental flows associated with each stage of the grape growing process and the results are analyzed and interpreted to identify opportunities for improving the environmental performance (Volanti et al., 2021).

Moreover, recent advancements in environmental monitoring techniques have facilitated more precise assessments of agriculture environmental impact (Zaks and Kucharik, 2011). For example, eddy covariance methods, originally developed for atmospheric research, have been adapted for use in vineyard ecosystems to measure carbon dioxide (CO_2) exchange between the canopy and the atmosphere (Baldocchi et al., 2001). By continuously monitoring fluxes of CO_2, these techniques provide valuable data for quantifying the carbon sequestration potential of vineyards and identifying opportunities for emissions reduction (Callesen et al., 2022). Eddy covariance systems consist of gas analyzers and a sonic anemometer mounted on towers in vineyards to measure carbon dioxide exchange between the vine canopy and the atmosphere. Therefore, monitoring CO_2fluxes over time allows for the evaluation of management strategies to reduce emissions and understanding the level of carbon sequestration in vineyard soils (Ibrom et al., 2007).

Nevertheless, the two abovementioned methodologies while giving fundamental insights about the environmental impact of production value chain at different magnitudes, they also face some drawbacks for high-resolution analysis. Specifically, LCAs rely on databases encompassing data acquired at the regional or national level when primary data is not available and the Eddie Covariance system is used to analyse the agro-ecological emissions fluxes at the whole field, accounting for the entire agro-ecosystem (Chiriacò et al., 2019).

To overcome such limitations, in this paper, a novel IoT architecture designed to quantify the CO_2 emissions produced during grapevine cultivation and to transfer this information to the bottle is depicted. The architecture leverages an array of sensors and agronomical models to account for anthropological and biological gas emissions following a Precision Agriculture approach aimed at assessing the variability of carbon emissions up to the plant level. The aim is to create an infrastructure for addressing the environmental impacts of grape cultivation at higher spatial resolution, based on field-specific data and to provide information to the different actors playing in the wine value chain, from the farmer to consumers and other stakeholders.

2. System description

At first, the wine-making value chain of the Rhein Valley has been explored to identify the different actors and production steps involved in the wine making to understand the technical boundaries of the sector in Germany. The resulted information flow is illustrated in Figure 1. Subsequently, tree main areas have been detected where the establishment IoT architecture would be required for carrying out the sustainability assessment: (i) Empirical assessment of gas fluxes during the cultivation phase; (ii) Emissions data transfer through the winery stage; and (iii) Data collection in a cloud platform.

To achieve this, the first step was to identify the stakeholders, which directly contribute to the production value chain. To achieve that, a state winery with variegate production cycles has been identified as use case. A collaboration with a winegrower association has been established to explore the intricate dynamics between farmers needs and law regulations. The potential consumer response has been assessed based on the expertise of the consortium as a whole and the results of a literature review.

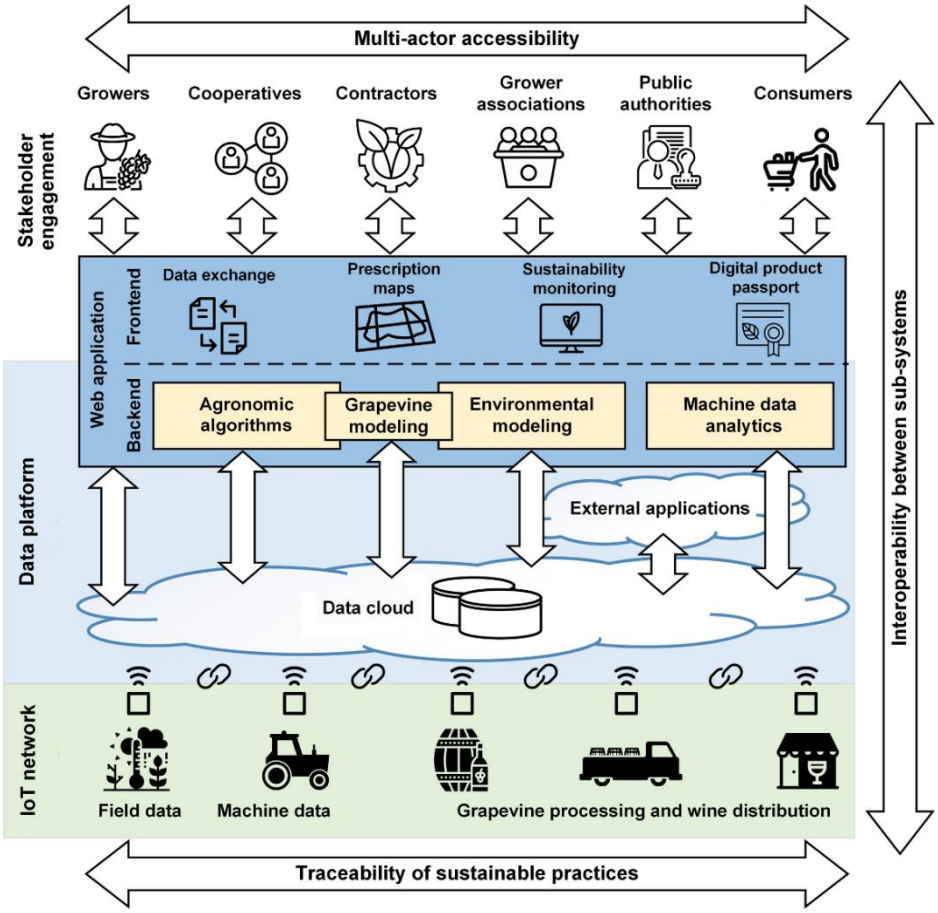

Figure 1. Conceptual structure of the IoT architecture boundaries and involved stakeholders.

2.1. Field empirical data

The acquisition of the carbon emissions in the field from human operations and within the agro-ecosystem are assessed using data acquired by different sensors, which are utilised as inputs in an agro-environmental model in order to process and quantify CO_2 emissions. . A scheme of the different type of data required is illustrated below (Figure 2). The agro-environmental model integrates the GRASSVISTOCK model (Bellini et al., 2023), which simulates the daily accumulation of biomass and carbon fluxes in grasslands, with the Roth C module (Coleman and Jenkinson, 1996), used for estimating organic carbon turnover and soil respiration. The model is trained with empirical data retrieved from field trials during the growing season in two different vineyards located in Rüdesheim am Rhein, Germany (49° 59' 20.70" N, 7° 55' 58.29" E) of approximately 1 ha, and another located Castelnuovo Berardenga, Italy (43° 22' 59.83" N, 11° 29' 14.81" E) of 4 ha. The field trials follow a data acquisition protocol.

This protocol considers various factors, such as plant physiological parameters, weather data, and soil data, to determine the carbon balance of the vineyard ecosystem, considering the above-ground biomass of both vines and weeds. Initially, the vineyard is divided into a minimum of three sub-parcels based on the vigour of vines, allowing for a comprehensive characterization of the plant diversity within the field. The data acquisition protocol includes the following parameters for measurements on one hectare:

- Weather data: A weather station equipped with sensors for measuring precipitation, air temperature, and humidity is used to acquire daily microclimate data.
- Soil data: Four soil probes are used to monitor the daily soil moisture at 10, 30, and 50 cm, while in parallel soil texture measurements are used to estimate the plant water availability.
- Vines: On a monthly basis, the geometrical parameters of the canopy (e.g. height, leaf area and shoot length), are measured using a light detection and range (LiDAR) laser scanner, an RGB and

hyperspectral cameras. Whereas canopy light interception is determined by means of ceptometers. Additionally, the harvested grapes' °Brix, fresh and dry weight are recorded. To ensure the accuracy of these measurements, a destructive validation analysis is required, which involves counting the bud-to-shoots ratio, manually weighing and measuring the shoots, and leaf defoliation.

- Inter-row weeds: The presence of weeds in the inter-row of a vineyard can significantly impact the carbon balance of the entire ecosystem. To monitor this, the height of the weeds is obtained for each row, considering the various species present. Ceptometers are utilised to evaluate the extent of ground cover by the weeds. To validate the data, one sub-sample per homogeneous sub-parcel undergoes analysis of its dry weight.
- Upscaling data: In order to acquire meaningful information at larger scale, as vigour variability, spectral indices measurements (e.g. NDVI) is carried out at least three times during the growing season.
- Machine data: a machine telemetry module is utilised to monitor machine-related emissions during field operations. The module, known as the EXAtrek T2 module (EXA Computing GmbH, Hamm, Germany), is an established telemetry device that connect to the ISO/CAN bus system of the tractor. It is capable of monitoring and recording machinery usage and calculating operational costs of agricultural machines and implements, as well as fuel consumption. Moreover, the module provides an estimation of CO_2 emissions produced by the machinery based on the executed operations. This data will be integrated into the agro-environmental module to account for machine emissions throughout the year as part of the cultivation carbon balance.

As shown in Figure 2, data from the various sensors is sent to a custom online platform. This platform stores the algorithm for the abovementioned model and machine-related emissions estimation. It also stores the resulting information and generates a QR code for the specific field data to be printed on the corresponding wine bottle, allowing it to be shared with the different parties involved in the wine production process.

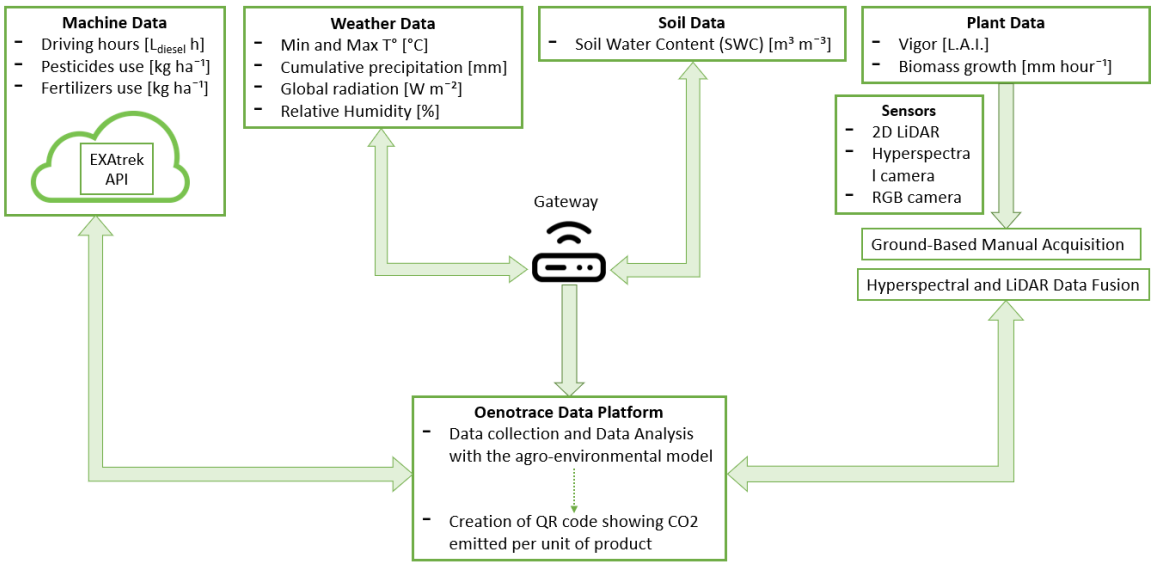

Figure 2. Schematic representation of the different type of data for the in-field emission assessment.

2.2. Grape emission traceability

The proposed architectural plan has been expanded to incorporate the inclusion of a commercial winery. This addition aims to assess its suitability and to evaluate the impact of grape harvesting and transportation on the processing facilities in a real-world commercial environment. The state-owned winery Kloster Eberbach was selected as the initial point to establish a concrete data flow for the development of an IoT system. The resulting architecture is illustrated in Figure 3. The previously developed system is employed to

assess the actual growing conditions in an experimental field and validate them in the commercial vineyard case study. Furthermore, the first analysed product will adhere to the one-vineyard-one-bottle approach, where a wine label is created with grapes from a single vineyard. As a first step, this simplifies the data acquisition process while being representative of a commonly employed technique in the Rhine Valley wine-making region.

In the initial phases, the transportation of grapes from the fields to the processing facility is a pivotal process for ensuring product traceability. A potential solution lies in the utilisation of the data platform in conjunction with the EXAtrek tracking device, which holds significant promise in addressing these challenges. Specifically, the telemetry device's capacity to monitor machinery movements facilitates the tracing of the origin of harvested batches. Furthermore, the integration of the latest online interface with the project's data platform via API facilitate the automated management of this information.

The use of software tools is prevalent in managing various processes; however, there is significant diversity as four different types of software are utilised for specific tasks. This diversity is evident in the vineyard, where distinct tools are employed for documentation and task management. Furthermore, separate software applications are utilised for grape reception at the cellar and winemaking. Additionally, the winery encounters challenges in meeting legal documentation required by the regulative administration, such as the "Herbstbuch", necessitating manual extraction of information related to yield, harvest data, and grape must quality. This analysis underlined the lack of a certain degree in the interoperability between the management tools. Leading to loss of information (Figure 3 "Winemaking") and impeding the possibility of data collection automation.

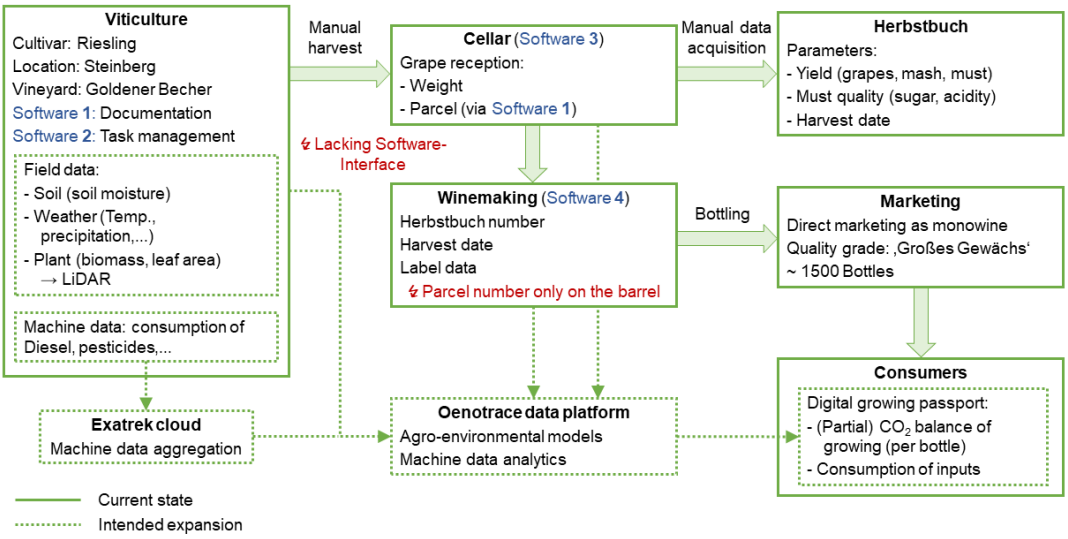

Figure 3. Schematic of the commercial winery value chain with specification of the different subsystems.

2.3. Data platform

All data is aggregated and stored on a data cloud. The steps along the value chain can be verified using blockchain technologies. On a central web application, data analysis and information provision take place. Its backend contains the acquired data of the analysed production cycle, integrating the machine data analytics as well as the agro-environmental model for calculating the sustainability indicators. These provide information about the CO_2 footprint at the field and winery level. Another important aspect of the data platform layer is the link to external web resources providing open data related to weather, as well as the connection to external applications of associated partners using their APIs.

In the platform frontend, the accessibility to information is tailored to provide the necessary data for other subsystems management or the value chain actors. There are possibilities for data exchange to provide additional field data from hyperspectral imagery and LiDAR laser scanning of the grapevines, which is mainly processed in the ecosystem model. Additionally, using the sustainability indicators, the frontend provides means for grower associations and public authorities to evaluate the sustainability of different

production realities. A digital product passport is provided as a mean to communicate to consumers the sustainability indicators related to the specific bottle of wine they purchase., offering easily understandable, yet fact-based and quantified information.

Interoperability between the different layers, as well as future scalability and adaptability, is ensured by the development of suitable APIs and the adoption of current standardized data exchange models for managing information from different domains. This includes support for standardized and open data formats such as XML, JSON, PHP, and HTML protocol.

3. Discussion

As described above, the wine value chain has been divided in the focal parts contributing negatively to CO_2 emission. Subsequently, two principal phases have been described, indicating the necessity to apply different systems because of their intrinsic distinct characteristics, the field management and the transformation facility. In the first, the main contributors to the gas emissions have been identified in the agricultural machinery usage and the plants' respiration. On one hand, the machinery emissions can be estimated with relative ease, on the other hand the contribution of plants can be complex due to their dual role in emitting and immobilizing the atmospheric CO_2. Therefore, among other the devices, various optical sensors are implemented to estimate the plants' biomass growth. This is considered an important aspect because of the contribution of the biomass to the soil carbon balance. The soil is considered as a factor into the carbon balance model by using the agro-environmental data as a proxy for its contribution in the vineyard system.

The second phase for the sustainable practice's traceability is the transformation stage from grape transportation to the bottle. During this phase examination various challenges have been encountered.

For example, most high-quality wines are more suitable for a traceability solution like Oenotrace, because they are bottled directly by producers. This allows them to oversee the entire value chain up to the bottle, where sustainability information is communicated using methods such as QR codes on the label. On the contrary, utilising only one commercial case study cannot be fully representative of the complex variability in the different business models pursued from all the wineries, especially when comparing different countries. This limitation is overcome by the focus of the project on the assessment of sustainable practices, which could be performed by the methodology proposed. In this context, a fundamental aspect is the scalability of the methodology leveraging open-access data on broader surfaces, like satellite imagery, to facilitate its adoption at wide scale.

Furthermore, a discrepancy has been found between consumer demands as reported by experts and findings from literature. While literature indicates that customer behaviour is a key driver in implementing sustainable production practices (Dangelico and Vocalelli, 2017), and that consumers increasingly demand sustainable wine and are willing to pay premium prices for environmentally friendly production (Baiano, 2021), experts observed a gap between consumers' expressed desire for sustainability and their actual purchasing behaviour, with a tendency to choose cheaper products. Therefore, both literature and expert feedback agree that information needs to be easily understandable, considering the brief time consumers spend acquiring such information while shopping.

In the context of data stewardship, a significant outcome was the recognition of growers' heightened sensitivity towards data privacy. While the industry generally embraces novel data-driven business models, it necessitates a discernible value proposition. Notably, it is crucial that the sustainability monitoring envisioned in Oenotrace does not devolve into a form of digital surveillance. Therefore, it should not be employed for direct comparisons among wineries, given the substantial variability in their operational contexts, but should focus on the comparison between different cultivation management.

4. Conclusions

Oenotrace aims to apply interoperability techniques by means of precision viticulture technologies in order to enhance the sustainability of the wine value chain. This architecture provides new metrics for customers to improve their consciousness regarding environmental sustainability of wine production while supporting a fair product value for farmers' economical sustainability. The capability of the technology is not limited only to the wine industry but has the potential to be adapted to other food value chains, particularly those associated with specialty crops such as olive oil and fruit juices, without excluding its use on arable

farming. This would be possible considering and adapting the system to the intrinsic variability of each production reality. Simultaneously, this approach presents an opportunity for IT companies to offer new services based on the principals for automated traceability digital infrastructure. For instance, growers could receive immediate feedback on the financial impact of implementing Precision Agriculture practices. Which still is a deterring question in novel technologies adoption. In this regard, it is crucial to ensure an appropriate level of anonymity to preserve growers' privacy. Furthermore, public authorities and professionals of the sector could gain objective insights into the sustainability of growing practices to guide their decisions.

Acknowledgements

The project Oenotrace is part of the ERA-NET Cofund ICT-AGRI-FOOD, with funding provided by national sources [BLE] and co-funding by the European Union's Horizon 2022 research and innovation program, Grant Agreement number 862665.

References

Baiano, A., 2021. An overview on sustainability in the wine production chain. Beverages 7, 15. https://doi.org/10.3390/BEVERAGES7010015

Baldocchi, D., Falge, E., Gu, L., Olson, R., Hollinger, D., Running, S., Anthoni, P., Bernhofer, C., Davis, K., Evans, R., Fuentes, J., Goldstein, A., Katul, G., Law, B., Lee, X., Malhi, Y., Meyers, T., Munger, W., Oechel, W., U, K.T.P., Pilegaard, K., Schmid, H.P., Valentini, R., Verma, S., Vesala, T., Wilson, K., Wofsy, S., 2001. FLUXNET: A New Tool to Study the Temporal and Spatial Variability of Ecosystem-Scale Carbon Dioxide, Water Vapor, and Energy Flux Densities. Bulletin of the American Meteorological Society 82, 2415–2434. https://doi.org/10.1175/1520-0477(2001)082<2415:FANTTS>2.3.CO;2

Bellini, E., Moriondo, M., Dibari, C., Bindi, M., Staglianò, N., Cremonese, E., Filippa, G., Galvagno, M., Argenti, G., 2023. VISTOCK: A simplified model for simulating grassland systems. Eur. J. Agron. 142. https://doi.org/10.1016/j.eja.2022.126647

Callesen, T.O., Gonzalez, C.V., Bastos Campos, F., Zanotelli, D., Tagliavini, M., Montagnani, L., 2022. Gross and net primary productivity in a vineyard assessed by eddy covariance and biometric measurements. Acta Hortic. 423–430. https://doi.org/10.17660/ActaHortic.2022.1355.54

Chiriacò, M.V., Belli, C., Chiti, T., Trotta, C., Sabbatini, S., 2019. The potential carbon neutrality of sustainable viticulture showed through a comprehensive assessment of the greenhouse gas (GHG) budget of wine production. Journal of Cleaner Production 225, 435–450. https://doi.org/10.1016/j.jclepro.2019.03.192

Coleman, K., Jenkinson, D.S., 1996. RothC-26.3 - A Model for the turnover of carbon in soil, in: Powlson, D.S., Smith, P., Smith, J.U. (Eds.), Evaluation of Soil Organic Matter Models. Springer, Berlin, Heidelberg, pp. 237–246. https://doi.org/10.1007/978-3-642-61094-3_17

Danese, P., Mocellin, R., Romano, P., 2021. Designing blockchain systems to prevent counterfeiting in wine supply chains: a multiple-case study. Int. J. Oper. Prod. Manag. 41, 1–33. https://doi.org/10.1108/IJOPM-12-2019-0781

Dangelico, R.M., Vocalelli, D., 2017. "Green Marketing": An analysis of definitions, strategy steps, and tools through a systematic review of the literature. J. Clean. Prod. 165, 1263–1279. https://doi.org/10.1016/j.jclepro.2017.07.184

Droulia, F., Charalampopoulos, I., 2022. A Review on the Observed Climate Change in Europe and Its Impacts on Viticulture. Atmosphere 13, 837. https://doi.org/10.3390/atmos13050837

Falcone, G., De Luca, A.I., Stillitano, T., Strano, A., Romeo, G., Gulisano, G., 2016. Assessment of Environmental and Economic Impacts of Vine-Growing Combining Life Cycle Assessment, Life Cycle Costing and Multicriterial Analysis. Sustainability 8, 793. https://doi.org/10.3390/su8080793

Happonen, A., Morales García, A.S., García-Alcaraz, J., Aryanfar, Y., Díaz-Reza, J., Blanco, J., 2021. Life Cycle Assessment in The Wine Industry – A Bibliometric Analysis.

Ibrom, A., Dellwik, E., Flyvbjerg, H., Jensen, N.O., Pilegaard, K., 2007. Strong low-pass filtering effects on water vapour flux measurements with closed-path eddy correlation systems. Agricultural and Forest Meteorology 147, 140–156. https://doi.org/10.1016/j.agrformet.2007.07.007

Jackson, R.S., 2008. Wine science: principles and applications. Academic press.

Laca, A., Gancedo, S., Laca, A., Díaz, M., 2021. Assessment of the environmental impacts associated with vineyards and winemaking. A case study in mountain areas. Environ. Sci. Pollut. Res. 28, 1204–1223. https://doi.org/10.1007/s11356-020-10567-9

Lal, R., 2021. Climate change and agriculture, in: Climate Change. Elsevier, pp. 661–686. https://doi.org/10.1016/B978-0-12-821575-3.00031-1

Litskas, V., Mandoulaki, A., Vogiatzakis, I.N., Tzortzakis, N., Stavrinides, M., 2020. Sustainable Viticulture: First Determination of the Environmental Footprint of Grapes. Sustainability 12, 8812. https://doi.org/10.3390/su12218812

Makrygiannis, K., 2019. EY blockchain platform supports Blockchain Wine Pte. Ltd. to launch TATTOO Wine marketplace across Asia Pacific. https://www.ey.com/en_gl/news/2019/11/ey-blockchain-platform-supports-blockchain-wine-pte-ltd-to-launch-tattoo-wine-marketplace-across-asia-pacific (accessed 27.03.2024).

Navarro, A., Puig, R., Kılıç, E., Penavayre, S., Fullana-i-Palmer, P., 2017. Eco-innovation and benchmarking of carbon footprint data for vineyards and wineries in Spain and France. Journal of Cleaner Production 142, 1661–1671

Pretty, J., 2008. Agricultural sustainability: concepts, principles and evidence. Phil. Trans. R. Soc. B 363, 447–465. https://doi.org/10.1098/rstb.2007.2163

Rouault, A., Perrin, A., Renaud-Gentié, C., Julien, S., Jourjon, F., 2020. Using LCA in a participatory eco-design approach in agriculture: the example of vineyard management. Int J Life Cycle Assess 25, 1368–1383. https://doi.org/10.1007/s11367-019-01684-w

Schultz, H., 2022. Soil, vine, climate change; the challenge of predicting soil carbon changes and greenhouse gas emissions in vineyards and is the 4 per 1000 goal realistic? This article is published in cooperation with Terclim 2022 (XIVth International Terroir Congress and 2nd ClimWine Symposium), 3-8 July 2022, Bordeaux, France. OENO One 56, 251–263.

https://doi.org/10.20870/oeno-one.2022.56.2.5447

Tezza, L., Vendrame, N., Pitacco, A., 2019. Disentangling the carbon budget of a vineyard: The role of soil management. Agriculture, Ecosystems & Environment 272, 52–62. https://doi.org/10.1016/j.agee.2018.11.002

Zaks, D.P.M., Kucharik, C.J., 2011. Data and monitoring needs for a more ecological agriculture. Environ. Res. Lett. 6, 014017.

https://doi.org/10.1088/1748-9326/6/1/014017

Volanti, M., Martínez, C., Cespi, D., Lopez-Baeza, E., Vassura, I., Passarini, F., 2021. Environmental sustainability assessment of organic vineyard practices from a life cycle perspective. International Journal of Environmental Science and Technology 19. https://doi.org/10.1007/s13762-021-03688-2

Evaluation of water and nutrients use efficiency in a cucumber-melon cascade hydroponic system

Nikolaos Katsoulas*, Ioannis Naounoulis, Sofia Faliagka, Efi Levizou

University of Thessaly, Dept. of Agriculture Crop Production and Rural Env., Fytokou Str, 38446, Volos, Greece

* Corresponding author. Email: email: nkatsoul@uth.gr

Abstract

Minimising water and fertiliser consumption is of high importance for the sustainability of greenhouse cultivation in the Mediterranean. Cascade soilless systems, have the ability to increase the water and nutrients use efficiency, while significantly reducing the water and nutrients leaching into the environment. In this study, a cascade cropping system in which the drainages from a hydroponic cucumber crop were recycled to irrigate a hydroponic melon crop was evaluated. The results showed that the recycled nutrient solution did not affect the yield of the melon plants compared to those irrigated with a standard nutrient solution. Additionally, the leaching of nitrates and phosphates into the environment was decreased by 75% and 86%, respectively. Finally, the implementation of the cascade system, increase by 22% the water use efficiency compared to the cucumber monoculture system.

Keywords: drainage management; water recirculation; fertilisers use efficiency; water productivity; greenhouse.

1. Introduction

The high productivity of greenhouse crops is related to high resource consumption. The soilless cultivations where they are growing in a substrate, are aver-irrigated (25-40%) in order to avoid salt accumulation in the rhizosphere. In closed hydroponic systems, the drained nutrient solution is collected and reused, maximising the water and nutrient use efficiency while significantly reducing the environmental impact of agriculture (Thomson et al., 2007; Massa et al., 2020). However, the use of low-quality irrigation water prevents the application of a totally closed hydroponic system (Katsoulas and Voogt, 2014). Consequently, after a certain number of recycles, it becomes necessary to remove the drainage nutrient solution to prevent the high concentration of toxic ions in the rhizosphere (Carmassi et al., 2005; Massa et al., 2010). As a result, many growers in the Mediterranean region act their systems as open hydroponic systems polluting the groundwater, due to the leaching of nitrate and phosphate ions.

A sustainable approach is the recycling and reusing of the drainage nutrient solution, to meet the needs of a secondary crop with higher salinity tolerance through a cascade hydroponic system. In these systems, the drainage of a primary (donor) crop, is collected and reused for the irrigation of a secondary (receiver) crop, which is more resistant to salinity (Karatsivou et al., 2023). While the drainage solution is reused, it becomes progressively more saline, but the concentration of nutrients such as nitrate and phosphate ions significantly decrease (Muñoz et al., 2010). A cascade hydroponic system is based on the idea of the circular economy, where according to the EU (EU 2008), resources remain within the system for the purpose of reuse and reducing waste in the environment. Additionally, a cascade hydroponic system is compatible and economically sustainable for lower-tech hydroponic installations, which are predominant in the Mediterranean region (Elvanidi et al., 2020).

Some preliminary studies were conducted on soil-grown cultivations such as in California's San Joaquin Valley. The system was developed to reuse high-conductivity drainage irrigation water on plants with moderate sensitivity to salinity as well as on halophytes (Grieve and Suarez, 1997; Shannon et al., 2000). However, there were difficulties concerning its technical application. In experiments conducted by Muñoz et al. (2010), the drainage solution from a hydroponic tomato crop was used to irrigate a soil-grown tomato crop. The adoption of this system resulted in a 21% reduction in the environmental footprint of the secondary crop.

More recent studies, focuses on the strategy of reusing drainage solution in crops with progressively increasing salt tolerance and lower input requirements. One of the main issues is finding alternative cultivated species that remain productive under high salinity conditions (Grieve and Suarez, 1997). Additionally, the heterogeneity of crops within a system may necessitate greater technical specialisation in system management (Massa et al., 2020). Moreover, the ratio of the cultivated area of primary to secondary crops

required by each system is one of the key factors in selecting the appropriate "pairing" of species to be cultivated. The economic performance of the secondary crop can significantly limit the income of producers, as the cultivation of lower input-demanding crops often results in reduced yield per unit area. Therefore, further investigation is necessary to find suitable combinations and develop profitable cascade cropping systems.

Aim of this study was to evaluate the sustainability and the performance of a cascade hydroponic cultivation system, in which the drainages from a cucumber (donor) crop were collected and reused to meet the needs of a melon (receiver) crop. The findings of this research are expected to significantly contribute to the advancement of cascade cultivation systems, while simultaneously providing solutions for minimising water and fertiliser requirements in the agricultural sector.

2. Materials and Methods

2.1. Experimental Design

The experiment was conducted at the greenhouse park of the Laboratory of Agricultural Constructions and Environmental Control, of the Department of Agriculture Crop Production and Rural Environment at the University of Thessaly, in the area of Velestino (39° 22', 22° 44', 85 m).

The transplanting of the primary cucumber crop (*Cucumis sativus* cv. Columbia) took place on March 15, 2023, in two compartments of a gothic-type greenhouse with a polyethylene roof covering, each with a total area of 240 m². Each compartment consisted of 6 hydroponic channels, each 20 m in length. The roof of each compartment was equipped with a continuous opening for ventilation, and the cooling system consisted of a wet pad and a fan. The plants were received in rock wool cubes (Grodan, Netherlands) (7.5x7.5 cm) and placed in perlite bags (Hydroperl, NORDIA AGRO, Athens, Greece), with a total volume of 33 L. The planting density was 1.08 plants m^{-2}. The primary crop was fertigated with a nutrient solution for cucumber crops in open systems (Savvas, 2011). The climate was automated controlled via a climate computer (Sercom, Netherlands). The irrigation system was activated through an automation system (Argos Electronics, Athens, Greece).

The secondary crop was developed in a modified simple arched greenhouse, with a total ground area of 160 m² and a cultivated area of 86 m². Eight hydroponic channels, each 12.5 m long, were installed inside the greenhouse. A fog system (Air Petri, Lucca, Italy) was used for greenhouse cooling, while climate and irrigation were automatically controlled (Argos Electronics, Athens, Greece). Transplanting took place on April 10, 2023, and the cultivation period lasted a total of 101 days. The melon seedlings (*Cucumis melo* cv. Masada) were received in rock wool cubes (Grodan, Netherlands) (7.5x7.5 cm) and placed in perlite bags of 33 L (Geoflor, Athens). The planting density was set at 2.25 plants m^{-2}. The experimental design included two treatments: the "control" treatment, where the melon crop was irrigated with a standard hydroponic solution for melon crops in open systems according to Savvas (2011), and the "cascade" treatment, where the melon plants were irrigated with 100% drainage nutrient solution from the cucumber crop, after pH adjustment.

To evaluate the system's performance, a series of measurements were conducted concerning the total water uptake, nitrogen leaching, and water use efficiency. These measurements were carried out on a weekly basis, allowing for monitoring the system's progress.

2.2. Statistical Analysis

The comparison of mean values was performed using One Way ANOVA at a 95% confidence level ($p \leq 0.05$) with the statistical package SPSS (Statistical Package for Social Sciences, IBM, Armonk, NY, USA). Additionally, the Least Significant Difference (LSD) method was used at a 5% significance level.

3. Results and Discussion

3.1. Water Consumption

A necessary condition for the proper design and implementation of a cascade cropping system is the proper ratio of cultivated area in order for the volume of the drainage nutrient solution from the primary crop to meet the water consumption needs of the secondary crop.

The total volume of the irrigation and drainage nutrient solution in the primary crop was 331.5 L m^{-2} and 136.2 L m^{-2}, respectively. For the irrigation of the secondary crop cascade during the cultivation period, a total of 385.8 L m^{-2} of the drainage solution of the primary crop was used, with a leaching fraction of 24%. The nutrient solution absorption in the cascade treatment did not differ from that in the control. According to the aforementioned values, the drainages from 1 m^2 of the primary cucumber crop were sufficient to meet the irrigation needs of 0.35 m^2 of the secondary melon crop. The ratio of cultivated area between the primary and secondary crops was, therefore, 3:1. More specifically, 1 m^2 of the cascade system studied was composed of 0.74 m^2 of the primary crop and 0.26 m^2 of the secondary crop. Additionally, the drainage nutrient solution that was ultimately discharged into the environment amounted to 9.6% of the initial irrigation solution volume of the primary crop, contrary to the 40% of the single cucumber crop (Table 1). Few studies have evaluated the ratio of the cultivated area between primary and secondary crops. García-Caparrós et al. (2018), reported a 1:4 ratio in a rosemary crop when irrigated with 100% drainage from a hydroponic melon crop. Incrocci et al. (2003) used the discharged solution from a semi-closed tomato cultivation system to irrigate a more salt-tolerant tomato crop. Their conclusions indicated that the discharged solution was sufficient to meet 50% of the secondary crop's water needs. However, contrary to the present study, Neocleous and Savvas (2016), in a hydroponic melon cultivation, observed that the crop consumed significantly less water when a slight increase in EC was recorded.

Table 1. Cumulative nutrient solution irrigation and drainage (L m^{-2}) during the cultivation period

	Irrigation	Drainage
Primary Crop (cucumber)	331.5	136.2
Secondary crop control (melon)	401.7	109.9
Secondary crop cascade (melon)	385.8	90.2
Cascade system (cucumber+melon)	245.4	23.6

3.2. Water Use Efficiency

Water use efficiency (WUE) was calculated as the total fruit production (kg m^{-2}) in relation to the total water consumption (m^3 m^{-2}). The results indicated a significant increase of the WUE when the cascade system was implemented. More specifically, the application of the cascade system increased the WUE by 22.1 and 131.8% compared to the cucumber and melon monoculture system, respectively (Table 2).

Similar results were also presented by Muñoz et al. (2017) where the reuse of drainages from a soilless tomato crop did not affect the WUE of a soil-based tomato crop. In case the cascade cropping system is considered as a single system and the drainage solution used for the irrigation of the secondary crop is not considered as a separate input to the system, then the WUE of the secondary crop increases significantly (Elvanidi et al., 2020).

Table 2. Water use efficiency (kg m^{-3}) (± S.E.) of the primary, secondary crop control, secondary crop cascade, and cascade system. Different letters indicate the statistically significant differences ($p<0.05$)

	WUE
Primary Crop (cucumber)	46.7±1.5 ^{b}
Secondary crop control (melon)	24.6±1.4 ^{c}
Secondary crop cascade (melon)	26.4±3.2 ^{c}
Cascade system (cucumber+melon)	57.1±1.3 ^{a}

3.3. Total nitrate and phosphate leaching into the environment

The total leaching of N and P into the environment throughout the cultivation period, for both the primary and secondary crops as well as the combined cascade cropping system, are shown in Table 3. The total nitrate

drainage from the control and the cascade melon treatment presented similar results. The higher values recorded in the control treatment were a result of the higher drainage volume. Considering the two crops as a combined system, a significant reduction in nitrate leaching into the environment was observed. Specifically, from 1 m² of the primary crop resulted in an 70% reduction in nitrate ion leaching into the environment compared to the amount that would have been released without the implementation of the cascade cropping system. A significant reduction was also observed in the total phosphate discharge. As shown in Table 3, the total phosphate leaching from the cascade treatment was 50% lower than that of the control. Notably, the reduction was even more significant with the cascade cropping system where phosphate leaching from 1 m² of the primary crop decreased by 80%. This system effectively absorbs significant amounts of key macronutrients responsible for groundwater pollution.

Table 3. Mean total nitrogen and phosphorus leaching (g m^{-2}) (±S.E.) of the primary, secondary crop control, secondary crop cascade, and cascade system. Different letters indicate the statistically significant differences ($p<0.05$)

	Nitrogen leaching	Phosphorus leaching
Primary Crop (cucumber)	18.4±0.1 ^{c}	2.8±0.1 ^{c}
Secondary crop control (melon)	22.4±1.6 ^{a}	4.0±0.2 ^{a}
Secondary crop cascade (melon)	20.9±0.2 ^{b}	2.1±0.1 ^{b}
Cascade system (cucumber+melon)	5.44±0.1 ^{d}	0.6±0.1 ^{d}

The results of related studies conclude that the implementation of a cascade cropping system significantly reduces environmental impacts (Incorci et al., 2003; Muñoz et al., 2010; García-Caparrós et al., 2015; Elvanidi et al., 2020). García-Caparrós et al. (2018) emphasised that the application of a cascade cropping system resulted in water savings and nitrate removal, which is a significant advantage in arid and semi-arid regions, such as the Mediterranean.

3.4. Crop Yield

To assess of the productivity of a cascade cropping system, the evaluation of the yield of the secondary crop in considered necessary. In this study, the fruit harvest for both treatments began on the 71st day of the experiment and lasted for 32 days. As shown in Figure 4, the total cumulative yield did not differ between treatments. Specifically, at the last harvest, the total yield for both treatments was 9.8 kg m^{-2} and 9.7 kg m^{-2} for the control and the cascade treatment, respectively.

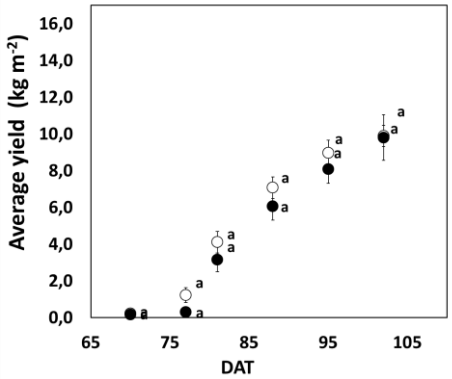

Figure 4. Cumulative yield (±S.E.) of the secondary crop (kg m^{-2}). Empty dots indicate the control treatment; filled dots indicate cascade treatment.

Melon is characterised as a moderately sensitive to salinity crop, as opposed to cucumber crops that are in general more susceptible to salinity (Savvas, 2011). Bar-Yosef (2008) reported that an increase in EC in the root zone from 2.1 to 4.6 dS m^{-1} in a closed hydroponic melon cultivation system reduced yield by 19.6%. The adverse effects of high EC in the root environment of melon plants can be mitigated by using grafting techniques (Colla et al., 2006). Indeed, the results of this study are consistent with those of Romero et al. (1997), where grafted melon plants did not show a reduction in yield even when exposed to an EC of 4.6 dS m^{-1}. Similar studies have recorded a decrease in the yield of the secondary crop with the application of a coupled system (García-Caparrós et al., 2018, Elvanidi et al., 2020, Avdouli et al., 2021, Karatsivou et al.,

2023). In experiments where the secondary crop was grown in soil (Muñoz et al., 2010; Muñoz et al., 2017), there was no significant decrease in yield, making it a sustainable solution for waste management.

4. Conclusions

The combination of primary and secondary crops is the main factor for the sustainability of a cascade cropping system. The composition of the drainage solution from the primary crop should meet the nutrient needs of the secondary crop. The reusing of cucumber drainages to meet the needs of a soilless melon crop proves to be a sustainable combination. The reuse of the drainage solution did not negatively affect the yield of the melon crop. At the same time, significant amounts of major pollutants were removed, making the final discharged solution safer for the environment. The simplicity of implementing the system and the lack of need for specialised knowledge for its application make it an ideal solution for addressing the environmental impacts caused by greenhouse production.

Acknowledgements

This work is part of the ECONUTRI project funded by the European Union's Horizon 2020 Research and Innovation Program under the Horizon Europe Grant agreement: 101081858

References

Avdouli, D., Max, J. F., Katsoulas, N., & Levizou, E. (2021). Basil as Secondary Crop in Cascade Hydroponics: Exploring Salinity Tolerance Limits in Terms of Growth, Amino Acid Profile, and nutrient composition. Horticulturae,7(8),203. https://doi.org/10.3390/horticulturae7080203

Carmassi, G., Incrocci, L., Maggini, R., Malorgio, F., Tognoni, F., & Pardossi, A. (2005). Modeling salinity build-up in recirculating nutrient solution culture. Journal of Plant Nutrition, 28(3). https://doi.org/10.1081/PLN-200049163

Colla, G., Rouphael, Y., Cardarelli, M., Massa, D., Salerno, A., & Rea, E. (2006). Yield, fruit quality and mineral composition of grafted melon plants grown under saline conditions. Journal of Horticultural Science and Biotechnology, 81(1). https://doi.org/10.1080/14620316.2006.11512041

Djurović, N., Ćosić, M., Stričević, R., Savić, S., & Domazet, M. (2016). Effect of irrigation regime and application of kaolin on yield, quality and water use efficiency of tomato. Scientia Horticulturae, 201. https://doi.org/10.1016/j.scienta.2016.02.017

García-Caparrós, P., Llanderal, A., Maksimovic, I., & Lao, M. T. (2018). Cascade cropping system with horticultural and ornamental plants under greenhouse conditions. Water (Switzerland), 10(2). https://doi.org/10.3390/w10020125

Elvanidi, A., Benitez Reascos, C. M., Gourzoulidou, E., Kunze, A., Max, J. F., & Katsoulas, N. (2020). Implementation of the Circular Economy Concept in Greenhouse Hydroponics for Ultimate Use of Water and Nutrients. Horticulturae, 6(4), 83. https://doi.org/10.3390/horticulturae6040083

Granados, M. R., Thompson, R. B., Fernández, M. D., Martínez-Gaitán, C., & Gallardo, M. (2013). Prescriptive-corrective nitrogen and irrigation management of fertigated and drip-irrigated vegetable crops using modeling and monitoring approaches. Agricultural Water Management, 119. https://doi.org/10.1016/j.agwat.2012.12.014

Karatsivou, E., Elvanidi, A., Faliagka, S., Naounoulis, I., & Katsoulas, N. (2023). Performance Evaluation of a Cascade Cropping System. Horticulturae, 9(7), 802. https://doi.org/10.3390/horticulturae9070802

Katsoulas, N., & Voogt, W. (2014). Recent trends in salinity control for soilless growing systems management. Acta Horticulturae, 1034. https://doi.org/10.17660/ActaHortic.2014.1034.53

Massa, D., Magán, J. J., Montesano, F. F., & Tzortzakis, N. (2020). Minimizing water and nutrient losses from soilless cropping in southern Europe. In Agricultural Water Management (Vol. 241). Elsevier B.V. https://doi.org/10.1016/j.agwat.2020.106395

Muñoz, P., Paranjpe, A., Montero, J. I., & Antón, A. (2010, August). Cascade crops: An alternative solution for increasing sustainability of greenhouse tomato crops in Mediterranean zone. In XXVIII International Horticultural Congress on Science and Horticulture for People (IHC2010): International Symposium on 927 (pp. 801-805).

Muñoz, P., Flores, J. S., Antón, A., & Montero, J. I. (2017). Combination of greenhouse and open-field crop fertigation can increase sustainability of horticultural crops in the Mediterranean region. Acta Horticulturae, 1170. https://doi.org/10.17660/ActaHortic.2017.1170.78

Neocleous, D., & Savvas, D. (2015). Effect of different macronutrient cation ratios on macronutrient and water uptake by melon (Cucumis melo) grown in recirculating nutrient solution. Journal of Plant Nutrition and Soil Science, 178(2). https://doi.org/10.1002/jpln.201400288

Neocleous, D., & Savvas, D. (2016). NaCl accumulation and macronutrient uptake by a melon crop in a closed hydroponic system in relation to water uptake. Agricultural Water Management, 165. https://doi.org/10.1016/j.agwat.2015.11.013

Rhoades, J. D. (1989). Intercepting, isolating and reusing drainage waters for irrigation to conserve water and protect water quality. Agricultural Water Management, 16(1–2). https://doi.org/10.1016/0378-3774(89)90039-5

Romero, L., Belakbir, A., Ragala, L., & Ruiz, J. M. (1997). Response of plant yield and leaf pigments to saline conditions: Effectiveness of different rootstocks in melon plants (cucumis melo l.). Soil Science and Plant Nutrition, 43(4). https://doi.org/10.1080/00380768.1997.10414652

Rufí-Salís, M., Parada, F., Arcas-Pilz, V., Petit-Boix, A., Villalba, G., & Gabarrell, X. (2020). Closed-Loop Crop Cascade to Optimize Nutrient Flows and Grow Low-Impact Vegetables in Cities. Frontiers in Plant Science, 11. https://doi.org/10.3389/fpls.2020.596550

Sonneveld, C., & Voogt, W. (2009). Nutrient Management in Substrate Systems. In Plant Nutrition of Greenhouse Crops. https://doi.org/10.1007/978-90-481-2532-6_13

Thompson, R. B., Gallardo, M., Valdez, L. C., & Fernández, M. D. (2007). Using plant water status to define threshold values for irrigation management of vegetable crops using soil moisture sensors. Agricultural Water Management, 88(1–3). https://doi.org/10.1016/j.agwat.2006.10.007

Assessing the liquid-phase from hydrothermal liquefaction (HTL) of distilled biomass of *Lavandula x intermedia* for novel herbicide development

Gonzalo Ortiz de Elguea-Culebras [a,*], Jaime Carrasco[a], Tamara Ferrando-Beneyto[a], Enrique Melero-Bravo[a], Antti Haapala [b,c], Aitor Barbero-López[b]

[a] Agri-food and Forestry Regional Research and Development Centre (IRIAF), Agroforestry Research Centre of Albaladejito (CIAF), Carretera Toledo-Cuenca km 174, Cuenca 16194, Spain

[b] Department of Chemistry, University of Eastern Finland, P.O. Box 111, Joensuu 80101, Finland

[c] FSCN Research Centre, Mid Sweden University, SE-85170 Sundsvall, Sweden

* Corresponding author. Email: gonzaloo@jccm.es

Abstract

Lavandin (*Lavandula x intermedia*) is an aromatic species widely cultivated for its essential oil (EO), leading to many commercial applications. However, since its EO yield is typically within the range of 1-5%, the vast majority of the plant material arises as residual biomass, comprising more than 95% of the raw vegetal material. This underscores the importance of exploring comprehensive biomass utilization and strategies to minimize waste generation. Hydrothermal liquefaction (HTL) has emerged as leading technique for residual biomass conversion, using reactors operating under standardized conditions. This process generates different fractions, including a solid (known as hydrochar) a liquid and a gas phase, with rich chemistry. The liquid fractions may hold promising applications in the development of green alternative phytosanitary products for agriculture. Hydrochar has previously demonstrated notable efficacy as an agronomic soil improver; whereas along this study demonstrated promising potential as a natural and low-toxicity herbicide for the liquid phase, showing anti-germinative effects on test model seeds, including *Lactuca sativa* and *Lolium perenne*. Results showed full inhibitory effects at concentrations exceeding 5-10% (v/v). These findings may lead to the development of novel plant-based phytosanitary treatments derived from residual sources, aligning with the principles of the circular bioeconomy as outlined in the UN's 2030 Agenda. Harnessing lavandin biomass in this manner not only minimizes waste release but also promotes sustainable agricultural and environmental practices.

Keywords: circular bioeconomy, hydrothermal liquefaction (HTL), *Lavandula x intermedia*, residual biomass valorization, zero-waste generation.

1. Introduction

Lavandin (*Lavandula x intermedia*) is as a hybrid species resultant by the crossing between lavender (*L. angustifolia* Mill.) and spike lavender (*L. latifolia* Medik.), with its development primarily focused towards the increase of essential oil (EO) yields. Traditionally associated with regions such as French Provence, its cultivation has spread globally, experiencing a notable expansion in countries belonging to the Mediterranean basin. Despite lavandin possesses a distinct chemical composition to lavender (renowned for its use in high-value perfumes), its production generates significant demand in many industrial sectors, especially as a versatile flavouring agent. Specifically in Spain, lavandin cultivation has shown a substantial increase, from 1,600 hectares in 2009 to a notable 7,200 hectares by 2021, predominating the varieties 'Super' and 'Grosso' (Ortiz de Elguea-Culebras et al., 2024). Consequently, an emerging culture has prospered in certain Spanish regions, such as *La Alcarria* in central Spain, where annual festivals and concerts attract many national and international tourists. These events also include different gastronomic experiences around the cultivation of lavandin, along with the development of plant-based products such as ice creams, soaps, aromatic liqueurs, etc.

Essential oils are generally extracted through distillation processes, which may involve hydro-distillation in stills or Clevenger-type apparatus, especially for home-scale production. However, on a larger industrial scale, steam distillation emerges as the predominant technique to efficiently extract these vegetable oils. Considering that extraction yields rarely exceed 5% (Kara and Baydar, 2013; Kara and Üniversitesi, 2012; Périno-Issartier et al., 2013; Pokajewicz et al., 2023), this causes the release of more than 95% of an undervalued plant biomass that is accumulated in the distillery's facilities, thus requiring an appropriate

management. Despite being traditionally used as a source of thermal energy by burning it in the boilers of the distillers, many of them currently use more efficient alternative sources of energy production.

Considering that distilled plants of lavandin still retain different non-volatile metabolites with significant biological potential, subsequent extracts can find applications across diverse industrial sectors. For example, Ortiz de Elguea-Culebras (2017) extensively advocated for their utilization in the development of agrochemicals. This author demonstrated the efficacy of using lavandin ethanolic extracts as biocontrol agents, unveiling their (1) repellent capabilities against model phytophagous insects such as *Leptinotarsa decemlienata, Spodoptera littoralis, Myzus persicae* or *Rhopalosiphum padi*; (2) for its phytotoxic effects on test seeds such as *Lactuca sativa* and *Lolium perenne*; along with (3) antifungal properties against *Aspergillus flavus*, a common phytopathogen in numerous crops. Although this approach offers a promising alternative for utilizing agroforestry waste and increasing the overall profitability of its cultivation, a non-extractable fraction remains, primarily composed of lignocellulosic material. Therefore, it is essential to valorise this fraction to achieve zero-waste generation, aligning with the bioeconomy principles of the UN's 2030 Agenda.

Alternatively, the hydrothermal liquefaction (HTL) is becoming a leading technique for biomass decomposition, using reactors under rigorously controlled conditions. This process covers temperature ranges from 250 °C to 450 °C and pressures exceeding 100 bar. The thermal process generates a wide range of fractions, covering a solid (hydrochar), liquid (water soluble phase and bio-oil) and gas phase (Castello et al., 2018; Toor et al., 2011), standing out for its rich chemistry. The published results anticipate promising properties for the development of phytosanitary eco-products with potential for application in agroforestry. For instance, Barbero-López et al., (2024) demonstrated the potential of the hydrothermal liquids as a low ecotoxicity antifungal agent against wood-decaying fungi.

This study assesses the potential phytotoxic effects of the aqueous phase derived from the hydrothermal liquefaction (HTL) of distilled lavandin biomass. The objective of the research is to explore the viability of the development of plant herbicides from agro-industrial residues, through comprehensive valorization of the solid waste generated after EO extraction of cultivated lavandin.

2. Materials and Methods

2.1. Vegetal material collection

Vegetal samples of *Lavandula x intermedia* Super and Grosso were harvested in 2022 during the flowering season by Vallejondo Esencial SL (Villares del Saz, Cuenca). Following harvest, essential oils were extracted through steam distillation using an industrial distillery. Subsequently, the distilled biomass was dried and then provided to the Department of Chemistry of the University of Eastern Finland for further processing.

2.2. Hydrothermal liquefaction (HTL) process

The HTL process was executed according to the following procedure: Initially, a mixture comprising 20% dry distilled biomass of *L. x intermedia* Super or Grosso and 80% water was prepared and introduced into the HTL reactor. Subsequently, a pressure of 10 bars of nitrogen was introduced into the atmosphere within the HTL reactor. The temperature was set at 300°C and maintained for 90 minutes, while ensuring continuous stirring to facilitate optimal reaction kinetics and product yield. The mixture was then cooled down in the reactor overnight. After the reaction, the two remaining fractions were mechanically separated: the solid (or hydrochar) from the liquid aqueous phase, with the latter subsequently stored in a refrigerator at 5°C. Previous to biological evaluation, the liquid fraction was decanted and filtered using a 0.45 µg syringe filter.

2.3. Phytotoxic evaluation of the aqueous phase

The potential herbicidal capacities of the aqueous phase produced from the hydrothermal liquefaction (HTL) process of *L. x intermedia* were evaluated by conducting assays with model seeds of *Lactuca sativa* L. var. Carrascoy (dicotyledonous) and *Lolium perenne* L. var. certified (2n) (monocotyledonous) obtained from Semillas Fitó (Spain). The experiment involved 2.5 cm diameter paper filters introduced in quadruplicate in 12-well plates, with 10 seeds each (*L. perenne* were prehydrated for 24 hours). Subsequently,

700 µl of each sample, prepared in concentrations ranging from 0-100% (v/v) in H_2O were added to the wells. The plates were then sealed in plastic bags and incubated at 22°C with a photoperiod of 16:8 (L:D). Germination rates were recorded every 24 hours for 7 days for *L. sativa* and 10 days for *L. perenne*. Finally, 25 random seedlings were collected and the lengths of roots (*L. sativa*) or roots and leaves (*L. perenne*) were measured using the Image J software.

3. Results and Discussion

The germination inhibition percentages (%GI) for *L. sativa* and *L. perenne* seeds, following the assessment of the HTL aqueous phase of lavandin Super and Grosso, are presented in Tables 1 and 2, respectively.

Table 1 Germination (%) of *L. sativa* seeds in the presence of Lavandin Super and Grosso HTLs.

Concentration (% HTL/H_2O)	1 day		4 days		7 days	
	Super	**Grosso**	**Super**	**Grosso**	**Super**	**Grosso**
100.00	0.00±0.0	0.00±0.0	0.00±0.0	0.00±0.0	0.00±0.0	0.00±0.0
50.00	0.00±0.0	0.00±0.0	0.00±0.0	0.00±0.0	0.00±0.0	0.00±0.0
25.00	0.00±0.0	0.00±0.0	0.00±0.0	0.00±0.0	0.00±0.0	0.00±0.0
12.50	0.00±0.0	0.00±0.0	0.00±0.0	0.00±0.0	0.00±0.0	0.00±0.0
6.25	0.00±0.0	0.00±0.0	0.00±0.0	0.00±0.0	0.00±0.0	0.00±0.0
3.13	0.00±0.0	0.00±0.0	77.50±9.6	65.00±12.9	100.00±0.0	100.00±0.0
1.56	0.00±0.0	0.00±0.0	65.00±26.5	90.00±8.2	100.00±0.0	100.00±0.0
0.78	2.50±5.0	0.00±0.0	87.50±9.6	97.50±5.0	100.00±0.0	100.00±0.0
Control	95.00±10.0		95.00±10.0		100.00±0.0	

Table 2 Germination (%) of *L. perenne* seeds in the presence of Lavandin Super and Grosso HTLs.

Concentration (% HTL/H_2O)	3 days		6 days		10 days	
	Super	**Grosso**	**Super**	**Grosso**	**Super**	**Grosso**
100.00	0.00±0.0	0.00±0.0	0.00±0.0	0.00±0.0	0.00±0.0	0.00±0.0
50.00	0.00±0.0	0.00±0.0	0.00±0.0	0.00±0.0	0.00±0.0	0.00±0.0
25.00	0.00±0.0	0.00±0.0	0.00±0.0	0.00±0.0	0.00±0.0	0.00±0.0
12.50	0.00±0.0	0.00±0.0	0.00±0.0	0.00±0.0	0.00±0.0	0.00±0.0
6.25	7.50±9.6	2.50±5.0	47.50±9.6	10.00±20.0	97.50±5.0	82.50±12.6
3.13	40.00±8.2	50.00±28.3	77.50±17.1	95.00±5.8	87.50±9.6	100.00±0.0
1.56	72.50±9.6	70.00±0.0	92.50±9.6	100.00±0.0	100.00±0.0	100.00±0.0
0.78	70.00±28.3	70.00±20.0	90.00±8.2	87.50±18.9	100.00±0.0	97.50±5.0
Control	85.00±12.9		95.00±5.8		100.00±0.0	

Full inhibition was observed at concentrations near to 10% in the tested model seeds. *L. sativa* seeds were more sensitive to the presence of HTLs, showing significant inhibition at concentrations below 3%, with both HTLs from lavandin Super and Grosso exhibiting similar effects. Although seeds exposed to lower HTL concentrations eventually achieved complete germination by the end of the experiment (7 days for *L. sativa* and 10 days for *L. perenne*), strong inhibition was noted during the initial 2 days. However, this inhibitory effect decreased after 3 days, with over 50% of seeds germinating after 4 days for all assayed concentrations.

Additionally, root growth for *L. sativa* and both leaf and root growth for *L. perenne* were measured to assess the growth inhibition potential of distilled lavandin HTLs. The results are exposed in Figures 1 and 2 for *L. sativa* and *L. perenne*, respectively.

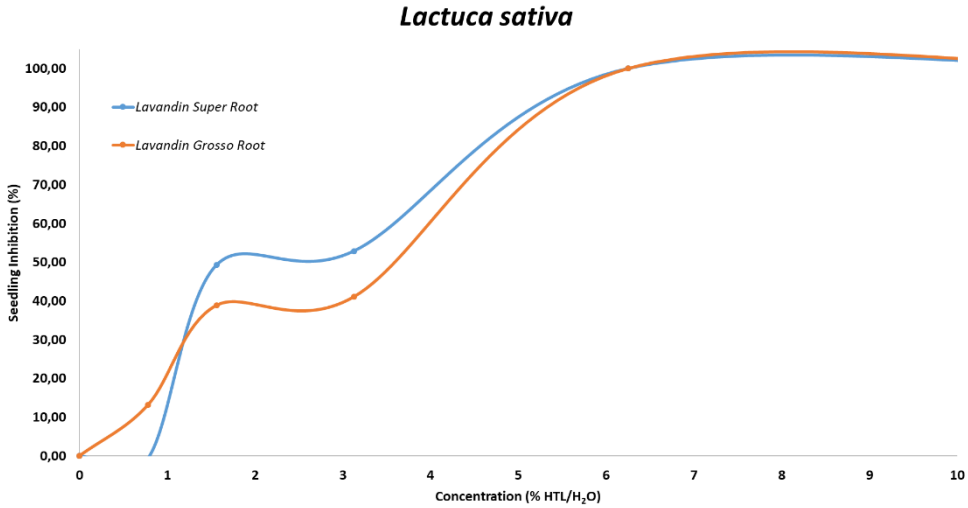

Fig. 1 Growth inhibition (%) capacities of lavandin Super and Grosso HTLs on *L. sativa* roots after 7 days.

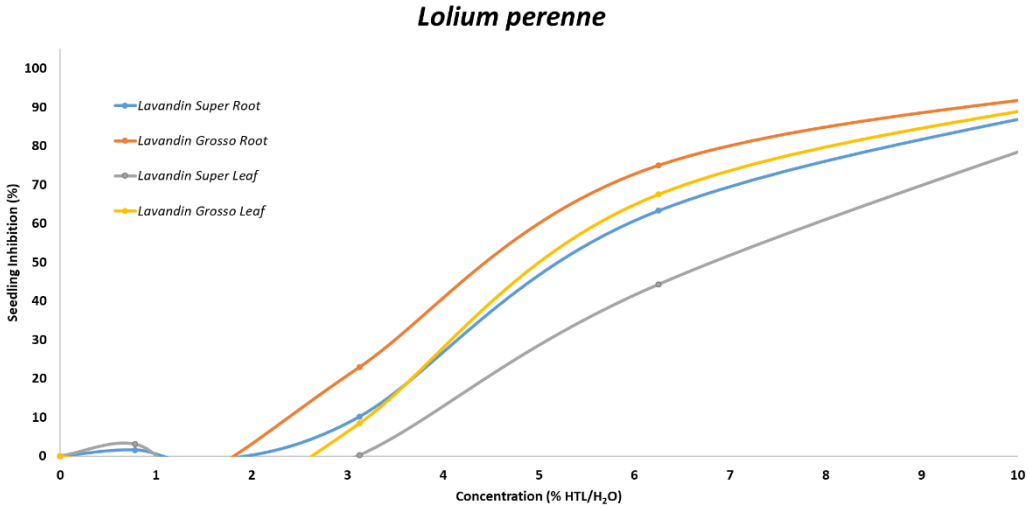

Fig. 2 Growth inhibition (%) capacities of lavandin Super and Grosso HTLs on *L. perenne* roots after 10 days.

HTLs exhibited similar growth inhibition profiles with an IC_{50} (concentration that inhibits 50% of plant growth) of 3% and a minimum inhibitory concentration (MIC) around 6% for *L. sativa*. For *L. perenne*, low inhibitory effects were observed at concentrations below 2%. However, inhibition potential increased thereafter, with an IC_{50} value ranging between 6-7%, whereas the MIC was determined to be over 12%. Among the samples, the HTL of lavandin Super showed moderately higher inhibition effects on *L. sativa* roots, whereas that of lavandin Grosso was more effective against the roots and leaves of *L. perenne* seedlings.

Previously, Barbero-López et al. (2024) showed antifungal potential for the HTL liquid fraction derived from spent mushroom substrates of *Pleurotus ostreatus* and *Agaricus bisporus* in wood preservation, with lower ecotoxicity than the commercial wood preservatives used in industry. Similarly, complete fungal inhibition was also observed in concentration near to 10%. Chemical characterization of this HTL liquid was conducted via NMR, revealing the presence of main organic radicals such as ketones (being the main

responsible for plant protecting against pathogens and hervibores), alcohols and aliphatic hydrocarbons. This suggests the necessity for evaluating the chemical composition of the HTL liquid of distilled lavandin to elucidate the components responsible for its phytotoxicity (work currently in progress).

4. Conclusions

This study shows the potential of HTL technology to process distilled lavandin biomass, producing an aqueous phase with potent phytotoxic effects. This presents promising applications for weed control in various sectors such as agriculture, photovoltaic parks, gardening, etc. In particular, low concentrations of HTL demonstrated substantial inhibition capabilities in the model seeds tested, with phytotoxic effects ranging from moderate to high. These findings imply that additional evaluations could contribute to the development of an effective herbicide, along with optimal agricultural management practices for specific applications. Consequently, additional tests should be performed at the greenhouse or field scale to validate and determine appropriate HTL concentrations for practical use. Despite this being a preliminary study on the valorisation of an underestimated agroindustrial by-product, it is crucial to identify the chemical compounds responsible for these effects to optimize the operating conditions of the HTL reactors and obtain fractions enriched with phytotoxic components. Furthermore, it is also essential to evaluate the possible ecotoxic effects on sensitive flora and fauna. This research aligns with the principles of a circular economy by transforming waste products into valuable agricultural inputs, thereby reducing waste and promoting sustainable practices. The integration of HTL technology in the management of lavandin by-products contributes to waste reduction, provides an environmentally friendly solution for weed control, improves the value of a traditional crop in many Mediterranean countries and shows potential to improve the general sustainability of agricultural and horticultural practices.

Acknowledgements

GOdEC thanks the Regional Institute of Castilla-La Mancha for Agri-Food and Forestry Research and Development (IRIAF) for its financing contract, TFB and EMB thank the Government of Castilla-La Mancha for the BIOALLIFUNGI Project [grant number 16-Q1300422A-PA-01] and ABL acknowledges the support by the Niemi foundation [grant number 2022007]. JC is the recipient of a Ramon y Cajal contract [RYC2021-032796-I], funded by MCIN/AEI/10.13039/ 501100011033 and the European Union "NextGenerationEU"/PRTR». We also thank to Vallejondo Esencial SL for providing the vegetal material and Amparo Calvo Martínez, María Vicenta García and David Prieto for technical and analytical support.

References

Barbero-López, A., López-Gómez, Y.M., Carrasco, J., Jokinen, N., Lappalainen, R., Akkanen, J., Mola-Yudego, B., Haapala, A., 2024. Characterization and antifungal properties against wood decaying fungi of hydrothermal liquefaction liquids from spent mushroom substrate and tomato residues. Biomass and Bioenergy 181. https://doi.org/10.1016/j.biombioe.2023.107035

Castello, D., Pedersen, T.H., Rosendahl, L.A., 2018. Continuous hydrothermal liquefaction of biomass: A critical review. Energies 11. https://doi.org/10.3390/en11113165

Kara, N., Baydar, H., 2013. Influence of distillation time and fractions on essential oil content and composition of lavandin (Lavandula × intermedia Emeric ex Lois). Res. Crop. 14, 1128–1134.

Kara, N., Üniversitesi, T.C.S.D., 2012. Essential oil contents and composition of lavenders and lavandins cultivated in Turkey. Res. Crop. 13, 675–681.

Ortiz de Elguea-Culebras, G., 2017. Biological activities of essential oils and related by-products from the industrial distillation of Hyssopus officinalis L., Lavandula x intermedia Emeric ex Loisel var. super and Santolina chamaecyparissus L.: Applications on cheese industry and bioplagu. University of Castilla-La Mancha.

Ortiz de Elguea-Culebras, G., Herraiz-Peñalver, D., Prieto-Blanco, D., Cerro-Ibáñez, N., Sánchez-Vioque, R., Navarro-Rocha, J., Pérez-Magariño, S., Herrero, B., Melero-Bravo, E., 2024. Essential oils of lavandin (Lavandula x intermedia Emeric ex Loisel.) of Spain: a case study on clones ´Grosso´ and ´Super´. J. Appl. Res. Med. Aromat. Plants In Press. https://doi.org/10.1016/j.jarmap.2024.100550

Périno-Issartier, S., Ginies, C., Cravotto, G., Chemat, F., 2013. A comparison of essential oils obtained from lavandin via different extraction processes: Ultrasound, microwave, turbohydrodistillation, steam and hydrodistillation. J. Chromatogr. A 1305, 41–47. https://doi.org/10.1016/j.chroma.2013.07.024

Pokajewicz, K., Czarniecka-Wiera, M., Krajewska, A., Maciejczyk, E., Wieczorek, P.P., 2023. Lavandula × intermedia—A bastard lavender or a plant of many values? Part I. Biology and chemical composition of lavandin. Molecules 28. https://doi.org/10.3390/molecules28072943

Toor, S.S., Rosendahl, L., Rudolf, A., 2011. Hydrothermal liquefaction of biomass: A review of subcritical water technologies. Energy 36, 2328–2342. https://doi.org/10.1016/j.energy.2011.03.013

Energy management system for charging autonomous viticultural robotic vehicles with photovoltaic stations in a microgrid topology

Vasilis Arapostathis [a*], Christos-Spyridon Karavas [a], Athanasios T. Balafoutis [a,b], George Papadakis [a]

[a] Department Natural Resources and Agricultural Engineering, Agricultural University of Athens, Athens, Greece

[b] Institute for Bio-economy & Agri-technology, Centre of Research & Technology Hellas, Volos, Greece

* Corresponding author. Email: varapostathis@aua.gr

Abstract

In recent years, there has been an increase in the use of robotic applications in agriculture, such as Unmanned Aerial Vehicles (UAVs) and Unmanned Ground Vehicles (UGVs), which are used for monitoring crops. Their use can enhance productivity and profitability for the producer while also providing workplace safety. However, even commercially available UAVs and UGVs for agricultural use often operate as autonomous solutions rather than part of a combined system where the two types of vehicles collaborate. The main drawback of electrically powered UAVs and UGVs is their limited operational time due to the restricted storage capacity of electrical energy. This issue is exacerbated in agriculture due to difficulties in accessing charging points, as these vehicles often operate in areas remote from the local power grid. A possible solution is the adoption of microgrids, small-scale local energy systems that can operate independently from the grid and are designed to provide reliability, resilience, and incorporate renewable energy sources.

Purpose of this research involves the design and development of an Energy Management System (EMS) for the operation of an autonomous precision viticulture system based on the activities of electrically powered UAVs and UGVs. These vehicles charge at small-scale photovoltaic charging stations in a microgrid topology. The EMS is responsible for determining the charging power of each vehicle's battery using Fuzzy Cognitive Maps, without violating the operational constraints of the microgrid. The EMS takes into consideration the State-Of-Charge of the vehicles' batteries, the State-Of-Charge of the microgrid's batteries, and the energy generated by the photovoltaic panels. The proposed EMS ensures smooth operation in the charging process of the electric vehicles and strengthens the microgrid's autonomy by covering the system's energy needs in the most efficient way.

Keywords: Energy Management System, Electric Vehicles, Photovoltaic charging stations in Microgrid, Variable Charging, Fuzzy Cognitive Maps

1. Introduction

The continuous increase in population demands the expansion of agricultural production, which is jeopardized by many challenges such as climate change, labor shortages, and productivity performance costs (EU, 2017). In recent years, the use of Smart Agriculture Technologies is rapidly increasing and appears to be a reliable solution for the above challenges (EPRS, 2016). Smart Agriculture Technologies include Farm Management Information Systems (FMIS), precision agriculture systems (PA), agricultural automation, and robotic applications that increase yield, improve product quality, make the use of inputs rational and efficient, reduce energy consumption and protect soil and water resources (EPRS, 2016; Zheng et al., 2011; Fountas et al., 2005).

While Smart Agriculture Technologies related to FMIS, PA methods, and automation have been commercially developed, only a few cases of robotic systems are at a commercial level (Shamshiri et al., 2018; Pedersen et al., 2006). Nevertheless, robotics is showing significant progress, with autonomous Unmanned Aerial Vehicles (UAV) and Unmanned Ground Vehicles (UGV) gradually incorporating advanced technological equipment for crop monitoring and the application of agricultural practices. Their use can increase productivity, profitability, work safety, and environmental sustainability (Bac et al., 2014).

However, even the commercially available UAVs and UGVs for agricultural use, function as standalone solutions and not as a combined system where the two kind of robots assist each other. There is research regarding the interconnection of ground and aerial means (Vu et al., 2018; Salah et al., 2017; Hood et al., 2017), but it has not yet resulted in commercial solutions for combined use and control in the field.

Such systems could find multiple agricultural applications, but ideally in high-value crops that, due to their specialized requirements (e.g., high final product quality), and the high income they provide to the

producer, allow their initial adoption. An example of such a crop is wine grapes, which require continuous monitoring and extensive agricultural practices during their cultivation (Nuske et al., 2014).

Regarding the powering of autonomous vehicles, electrification is now the optimal solution for all types of UAVs and UGVs (with few exceptions), as they benefit from zero emissions (Ma et al., 2012), high engine efficiency, up to 90-92% (Jorgensen, 2008), their contribution to the integration of renewable energy sources into the energy system (Richardson 2013), lower operating costs compared to fossil/liquid fuels (Thomas, 2009), and charging during the night, which can smooth the operating cycle of power plants and reduce their additional startups (Clement-Nyns et al., 2010). The main disadvantage of electric UAVs and UGVs is the reduced operational range due to limited energy storage, which is exacerbated in agriculture due to limited access to a charging source as they often operate in areas remote from the local power grid. One potential solution is to adopt microgrids, which are small-scale local energy systems capable of operating independently from the main grid, integrating renewable energy sources.

The purpose of this research is to design and develop an Energy Management System (EMS) for operating an autonomous precision viticulture system utilizing electrically powered UAVs and UGVs. These vehicles are charged at small-scale photovoltaic stations within a microgrid topology. The EMS uses Fuzzy Cognitive Maps to determine the charging power for each vehicle's battery while ensuring the operational constraints of the microgrid are not violated.

2. Materials and Methods

2.1. System Topology

In Fig. 1, the microgrid with all of its components is presented. Microgrid consists of: a) a renewable energy production source: photovoltaic charging station with an array of typical monocrystalline silicon panels, b) a storage system: deep discharge solar lead-acid battery bank, c) electrically powered UAVs and UGVs, as energy consumption units.

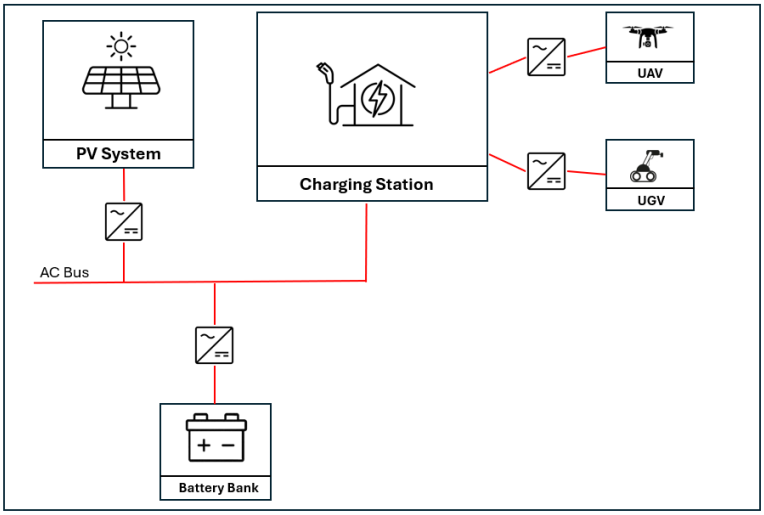

Figure 1: Proposed system topology

2.2. Fuzzy Cognitive Maps

Kosko (1986) developed a Fuzzy Cognitive Map (FCM) based on the fuzzy logic introduced by Zadeh (1965). Since then, numerous researchers have applied FCMs in various fields. FCM is a soft computing method that can be used to recognize, describe, and model complex systems (Stylios et al., 2004; Zhang et al., 1989). It serves as a general term for a set of methods that helps decision-makers obtain a graphical depiction of a person's perception in relation to a particular discussion or problem, making it easy to understand and providing valuable insights into the structure of information (Langfield-Smith, 1992; Spicer,

1998). FCM represents a network of elements and relationships of a complex phenomenon as a graph or map, offering a qualitative model that illustrates how a system operates (Avdeeva et al., 2018; Bakhtavar et al., 2019). Rather than predicting numerical values, the FCM method demonstrates the behavior of the system based on the relationships between concepts and the initial state of those concepts (Rezaee et al., 2017).

In Fig. 2, a typical FCM example can be seen. In this context, Ci represents nodes or concepts connected by weighted arcs (Papageorgiou et al., 2017; Salmeron et al., 2016). Each relationship between the concepts Ci and Cj has a weight Wij (the weight between the i-th and j-th nodes), which can be positive, negative, or neutral (indicating that there is no relationship between the two concepts) (Coban et al., 2017). Based on Kosko's FCM (1986), the relationship between concepts has transformed from states {0,1} or {−1,0,1} to a range of states represented by a number in the interval [0,1] or [−1,1], or by fuzzy linguistic terms (Salmeron et al., 2019).

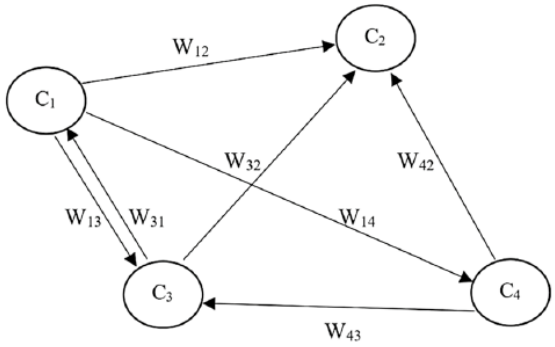

Figure 2: A typical Fuzzy Cognitive Maps example

After creating the map, mathematical formulas are used for modeling. To find the values of a node, the values of other nodes connected to it must be determined through Eq. (1) (Bakhatavar et al., 2021).

$$A_i^{k+1} = f\left(A_i^k + \sum_{j=1, j\neq i}^{n} W_{ij}A_j^k\right) \quad (1)$$

where A_i^{k+1} is the value of concept Ci in iteration, A_i^k is the value of concept Ci in iteration and $f\ (x)$ is the activation function.

In literature, there are four activation functions, the sigmoid, the hyperbolic, the step and the threshold function. The most used activation function is the sigmoid (Bueno et al., 2009), which was also used in this study. The sigmoid activation function can be seen in Eq. (2).

$$\mathrm{f(x)} = \frac{1}{1+e^{-\lambda x}} \quad (2)$$

where λ, is the parameter that describes the steepness of the curve. When λ is large, the transition between 0 and 1 becomes steeper, when k is small, the transition is more gradual. The parameter λ usually take the value 1, as it provides good results (Karavas et al., 2015).

2.3. FCM control of the microgrid

The simulation of the microgrid system was conducted using the MATLAB platform. All components of the system were designed and simulated in MATLAB. The analysis and data were processed on a per-minute basis, reflecting the dynamic nature of the environment. Each component may change its actions every minute, depending on the gathered data and the behavior of the other components.

In Fig. 3, the logical diagram for the control of the microgrid is presented. The EV operates in the field until it reaches the minimum discharge threshold, which is recommended by the manufacturer to minimize battery degradation. Upon reaching this threshold, the EV moves to the photovoltaic station to recharge. At the station, the EV charges at a variable percentage of its maximum nominal charging power, depending on the state of various components within the system.

The Variable Charging algorithm considers the EV's State-of-Charge (SOC), the battery bank's SOC, and

the power produced by the photovoltaic (PV) panels to determine the charging power for the EV every minute. The PV power production is calculated based on solar radiation and air temperature data from a meteorological station. The EV charges with the calculated power, and the Energy Management System (EMS) checks if the SOC has reached 100%. If the EV is not fully charged, the EMS recalculates the charging power and continues charging until the SOC reaches 100%. Once fully charged, the EV is ready to be deployed back to the field. The EMS checks the EV's SOC every hour between 10:00 and 17:00 and deploys the EV back to the field if it is fully charged. This time period is chosen because UGVs and UAVs monitor crops during the daytime to gather valuable data on plant health.

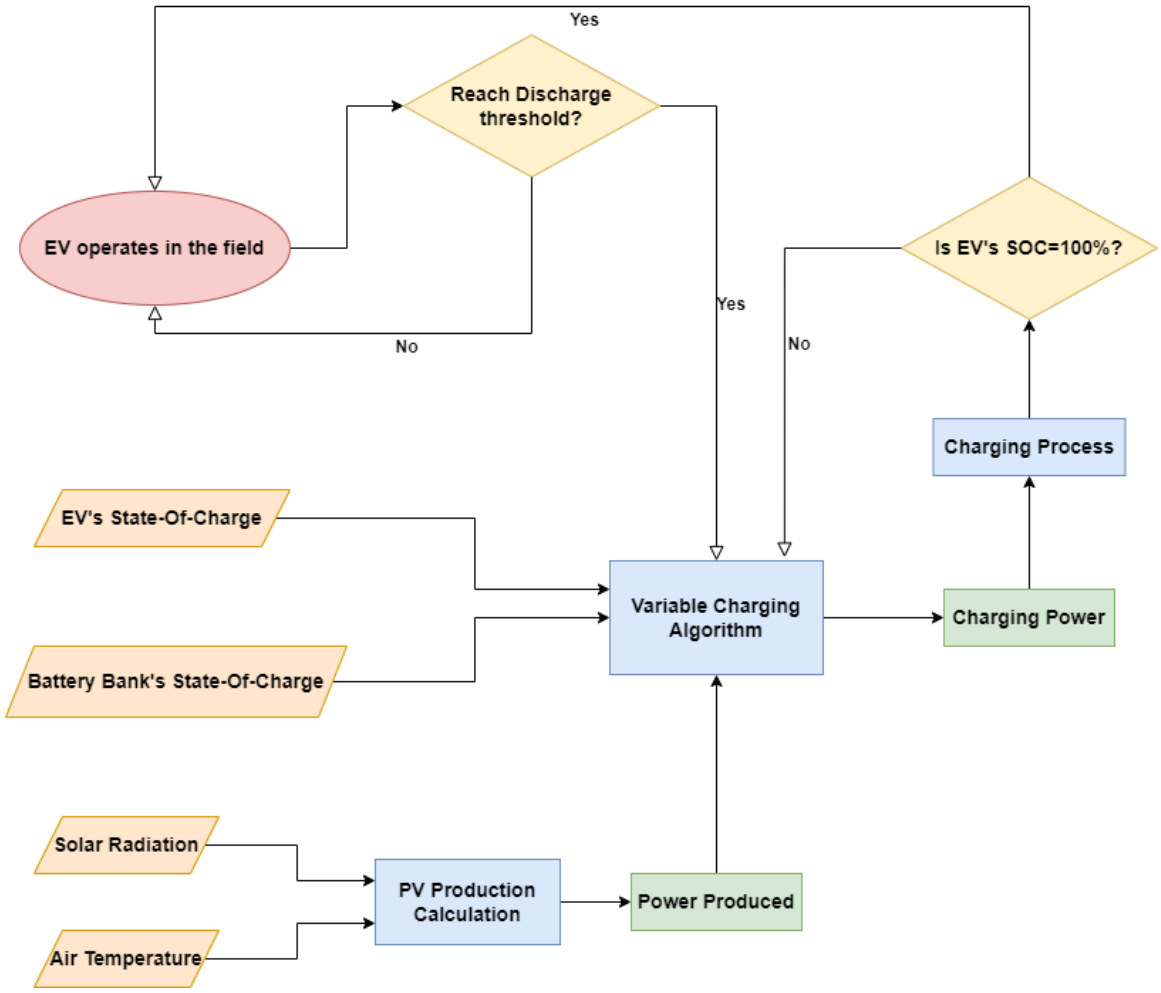

Figure 3:The proposed Energy Management System

2.4. Scenarios

In the current study, the system includes typical monocrystalline PV modules of 400 Wp, a battery bank of 1000 Wh, and the “Anafi” UAV manufactured by Parrot. The “Anafi” drone has a maximum power consumption of 52 W and a battery capacity of 20.52 Wh. A fleet of 10 “Anafi” UAVs operates within the system, with a total maximum power consumption of 520 W, considering that all drones are operating and charging together. Experiments were conducted to determine the UAV's discharge rate during operation, which was essential for designing the drone’s behavior. Meteorological data, collected at 15-minute intervals, were processed through linear interpolation to match the EMS's per-minute analysis. The simulations cover a two-day period and it is considered that the fleet must operate twice per day. Initial SOC for both the batteries and the drones is 100%. The EMS-controlled microgrid was compared with a typical microgrid to determine which system provides better results.

3. Results and Discussion

Fig. 4 presents the power generated by the PV, indicated by the green color, and the charging power, indicated by the red color, as was calculated by the proposed EMS. Fig. 5 presents the EV's SOC, indicated by the red color, and the battery bank's SOC, indicated by the green color. As can be seen in Fig. 5, the fleet go to operate in the field at 10.00 and their SOC starts decreasing. They operate for 14 minutes until they reach their minimum discharging threshold (35%) and they go to charge. They start charging at 10.15 with power of 436 W, as it has been calculated by the EMS (Fig. 4). At 10.15, PV produces 81 W (Fig. 4), so the battery bank provides the remaining 355W and as a result the batteries' SOC starts decreasing (Fig. 5). In the next minutes, the EMS keeps calculating and charging the EVs with a decreasing rate (Fig. 4) because of the FCM control, the system provides lower power as EV's SOC is increasing and system's batteries' SOC is decreasing in order to ensure its smooth operation. At 11.00, EVs are still not fully charged, so EMS keeps them at the charging point (Fig. 5). At 11.30 the EVs reach 100% and the energy that the PV produces is directed to the system's batteries, charging them (Fig. 5). At 12.00, EMS sends the UAVs back to the field. The batteries of the system keep charging until 12.15, when the UAVs return to charge and the batteries need to provide energy in order to cover the load. After the two days span, the system's batteries are at 81% SOC.

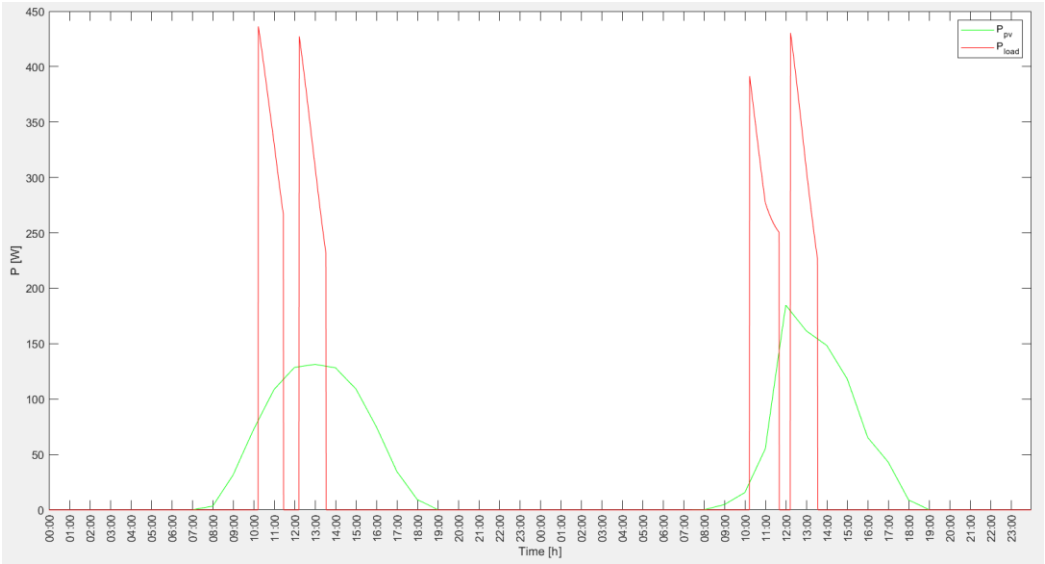

Figure 4:Power generated by the PV (green colour) and charging power calculated by the EMS (red colour)

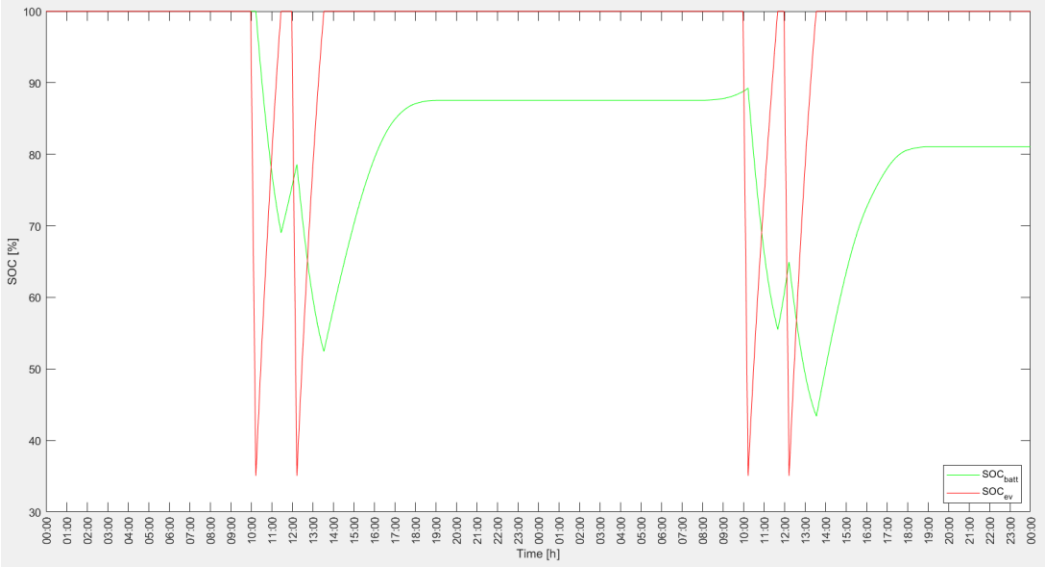

Figure 5:EV's SOC (red colour) and battery bank's SOC (green colour) utilizing the FCM EMS

Fig. 6 presents the power generated by the PV, indicated by the green color, and the power demand, indicated by the red color, in a typical microgrid. Fig. 7 presents the EV's SOC, indicated by the red color, and the battery bank's SOC, indicated by the green color in a typical microgrid. As can be seen in Fig. 6, without the proposed EMS, the power demand is always at its maximum value, i.e. 520 W. Although, in the first charging process, at 10.15, the system is able to cover the demand, in the second charging process, at 12.15, it falls short and the system's batteries reach the lowest allowed limit at 20%. While the system manages to charge the UAVs with support from the PV, the batteries only charge up to 60% by the end of the day. As a result, it is even more challenging for the system to meet the high demand on the second day. During both charging processes, the batteries struggle to provide adequate power due to their insufficient charge. After the two days span, the system's batteries are at 66% SOC.

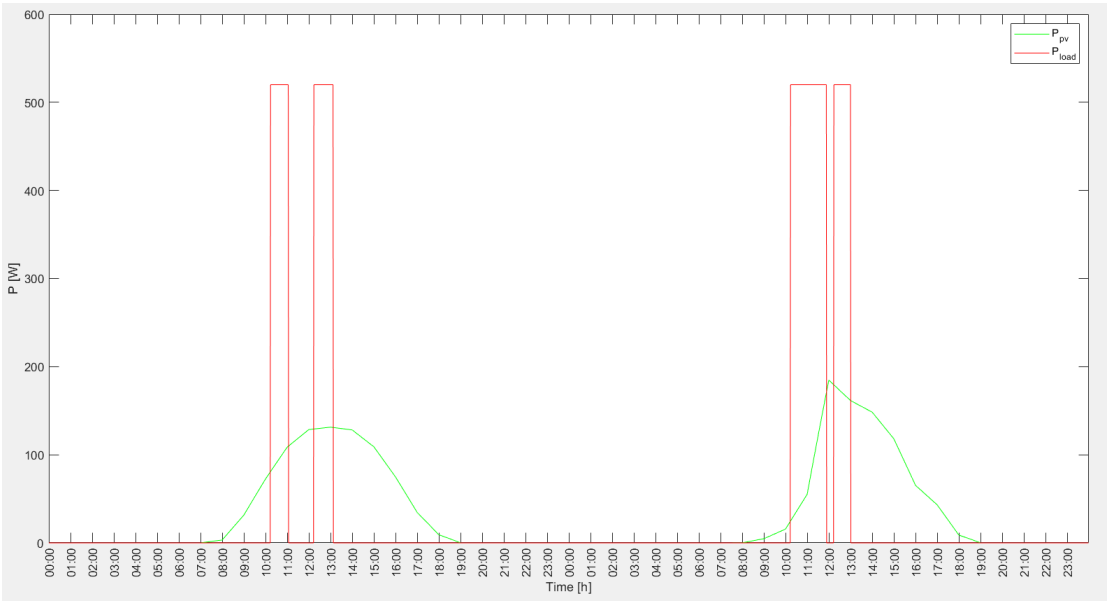

Figure 6: Power generated by the PV (green colour) and power demand (red colour) in a typical microgrid

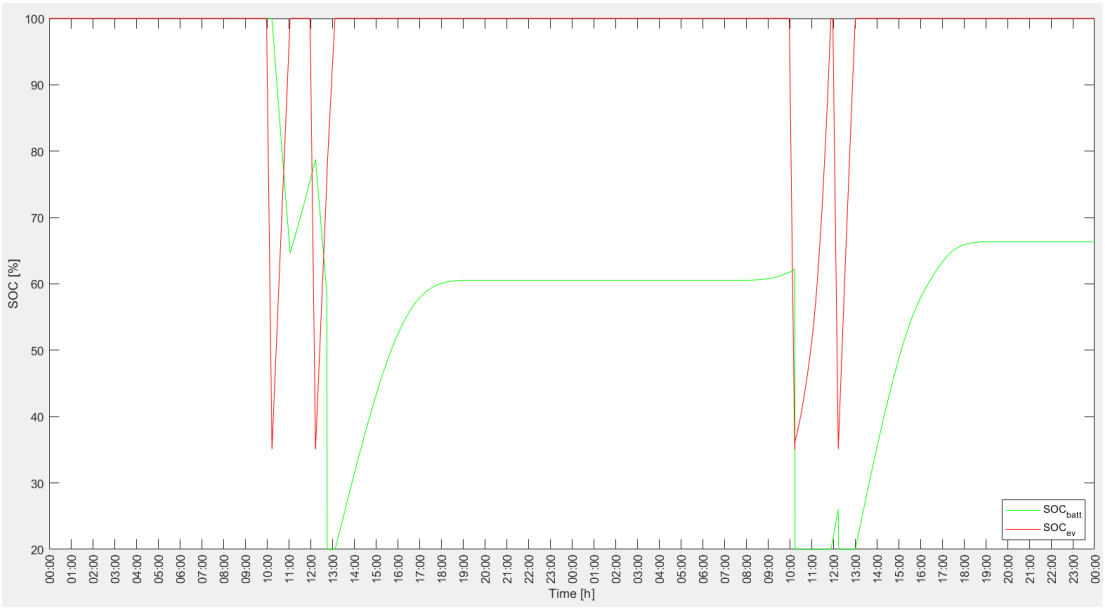

Figure 7: EV's SOC (red colour) and battery bank's SOC (green colour) in a typical microgrid

As shown in Fig.7, the typical microgrid system fails to cover the energy demands, experiencing three battery disruptions totaling almost four hours across four charging processes and by the end of the second day, the battery SOC is at 66%. On the contrary, the EMS-controlled microgrid meets the energy demands

with no disruptions and ends the second day with an 81% SOC (Fig. 5). The proposed EMS seems to respect the operational constraints of the microgrid, ensure smooth operation during the charging process of the EVs and strengthen the microgrid's autonomy by covering the systems needs with an efficient way.

4. Conclusions

The integration of robotic applications, such as Unmanned Aerial Vehicles (UAVs) and Unmanned Ground Vehicles (UGVs), in agriculture has demonstrated significant potential in enhancing productivity, profitability, and workplace safety. However, the limited operational time of these electrically powered vehicles, due to restricted energy storage capacity and difficulties accessing charging points, poses a challenge. This research addresses this challenge by proposing a microgrid system with an Energy Management System (EMS) for the efficient operation of autonomous precision viticulture using UAVs and UGVs charged at photovoltaic stations.

The EMS, utilizing Fuzzy Cognitive Maps, dynamically determines the optimal charging power for the vehicles based on real-time data, including the State-of-Charge (SOC) of the vehicles' batteries, the microgrid's battery bank, and the power generated by photovoltaic panels. The proposed system was compared to a typical microgrid without EMS, and the results indicate a significant improvement in energy management and system performance. The EMS-controlled microgrid effectively manages the charging process, ensuring smooth operation and avoiding battery disruptions, as evidenced by maintaining an 81% SOC after two days of operation. In contrast, the typical microgrid experiences multiple battery disruptions and struggles to meet energy demands, ending with a lower SOC of 66%. The EMS respects the operational constraints of the microgrid, ensuring that energy demands are met efficiently, thereby enhancing the microgrid's autonomy and reliability.

The EMS-controlled microgrid demonstrates greater autonomy, resulting in shorter idle periods for the EVs and allowing them to complete tasks more quickly. If the system reaches its minimum energy limits, the EVs remain idle until sufficient energy is available for charging. This efficient energy management enables the EMS-controlled microgrid to complete operations in significantly fewer days compared to a typical microgrid.

Overall, the proposed EMS demonstrates its capability to optimize the charging process of electric vehicles within a microgrid, ensuring continuous operation and strengthening the system's autonomy. In the lon This approach not only addresses the energy storage limitations but also promotes the use of renewable energy sources, contributing to sustainable agricultural practices.

Acknowledgements

The proposed system is being developed in the context of the Greek national program "AGROSYS" (https://www.agrosys-project.gr) funded by the General Secretariat of Research and Innovation (GSRI) through the National Recovery and Resilience Plan (Greece 2.0).

References

Avdeeva, Z.,K., Kovriga, S.,V., 2018. On governance decision support in the area of political stability using cognitive maps. IFACPapersOnLine 51(30):498–503

Bakhtavar E., Yousefi S., Jafarpour A., 2019. Evaluation of shaft locations in underground mines: fuzzy multi objective optimization by ratio analysis with fuzzy cognitive map weights. J South Afr Inst Min Metall 119(10):855–864

Bakhtavar, E., Valipour, M., Yousefi, S., Sadiq, R., Hewage, K., 2021. Fuzzy cognitive maps in systems risk analysis: a comprehensive review. Complex & Intelligent Systems, 7, pp.621-637.

Bac, C.W., Van Henten, E.J., Hemming, J. and Edan, Y., 2014. Harvesting robots for high-value crops: State-of-the-art review and challenges ahead. Journal of field robotics, 31(6), pp.888-911.

Bueno S., Salmeron J.L., 2009. Benchmarking main activation functions in fuzzy cognitive maps. Exp Syst Appl;36:5221–9.

Clement-Nyns, K., Haesen, E. and Driesen, J., 2009. The impact of charging plug-in hybrid electric vehicles on a residential distribution grid. IEEE Transactions on power systems, 25(1), pp.371-380.

Çoban V., Onar S.Ç. 2017. Modeling renewable energy usage with hesitant Fuzzy cognitive map. Complex Intel Syst 3:155–166.

European Parliamentary Research Service, 2016. Precision agriculture and the future of farming in Europe. www.europarl.europa.eu/RegData/etudes/STUD/2016/581892/EPRS_STU(2016)581892_EN.pdf

European Union Agriculture Overview, 2017. https://europa.eu/european-union/topics/agriculture_en

Fountas, S., Aggelopoulou, K. and Gemtos, T.A., 2015. Precision agriculture: Crop management for improved productivity and reduced environmental impact or improved sustainability. *Supply chain management for sustainable food networks*, pp.41-65.

Hood, S., Benson, K., Hamod, P., Madison, D., O'Kane, J.M. and Rekleitis, I., 2017, June. Bird's eye view: Cooperative exploration by UGV and UAV. In *2017 International Conference on Unmanned Aircraft Systems (ICUAS)* (pp. 247-255). IEEE.

Jorgensen, K., 2008. Technologies for electric, hybrid and hydrogen vehicles: Electricity from renewable energy sources in transport. Utilities Policy, 16(2), pp.72-79.

Karavas, C.S., Kyriakarakos, G., Arvanitis, K.G. and Papadakis, G., 2015. A multi-agent decentralized energy management system based on distributed intelligence for the design and control of autonomous polygeneration microgrids. Energy Conversion and Management, 103, pp.166-179.

Kosko, B., 1986. Fuzzy cognitive maps. Int J Man Mach Stud, 24(1):65–75

Langfield-Smith K., 1992. Exploring the need for a shared cognitive map. J Manage Stud 29(3):349–368

Ma, H., Balthasar, F., Tait, N., Riera-Palou, X. and Harrison, A., 2012. A new comparison between the life cycle greenhouse gas emissions of battery electric vehicles and internal combustion vehicles. Energy policy, 44, pp.160-173.

Nuske, S., Gupta, K., Narasimhan, S. and Singh, S., 2014. Modeling and calibrating visual yield estimates in vineyards. In *Field and service robotics: Results of the 8th international conference* (pp. 343-356). Springer Berlin Heidelberg.

Papageorgiou, E.,I., Hatwágner, M.,F., Buruzs, A., Kóczy, L.,T., (2017) A concept reduction approach for fuzzy cognitive map models in decision making and management. Neurocomputing 232:16–33

Pedersen, S.M., Fountas, S., Have, H. and Blackmore, B.S., 2006. Agricultural robots—system analysis and economic feasibility. Precision agriculture, 7, pp.295-308.

Rezaee, M.J., Yousefi, S., Babaei, M., 2017. Multi-stage cognitive map for failures assessment of production processes: an extension in structure and algorithm. Neurocomputing 232:69–82

Richardson, D.B., 2013. Electric vehicles and the electric grid: A review of modeling approaches, Impacts, and renewable energy integration. Renewable and Sustainable Energy Reviews, 19, pp.247-254.

Salah, K. and Chen, X., 2017. Cooperative Robotic Systems in Agriculture. In *Robotics and Mechatronics for Agriculture* (pp. 131-156). CRC Press.

Salmeron, J.L., Froelich, W., 2016. Dynamic optimization of fuzzy cognitive maps for time series forecasting. Knowl Based Syst 105(1):29–37.

Salmeron, J.L., Palos-Sanchez, P.R., 2019. Uncertainty propagation in fuzzy grey cognitive maps with Hebbian-like learning algorithms. IEEE Trans Cybern 49(1):211–220

Shamshiri, R., Weltzien, C., Hameed, I.A., J Yule, I., E Grift, T., Balasundram, S.K., Pitonakova, L., Ahmad, D. and Chowdhary, G., 2018. Research and development in agricultural robotics: A perspective of digital farming.

Spicer, D.P., 1998. Linking mental models and cognitive maps as an aid to organisational learning. Career Dev Int 3(3):125–132

Stylios, C.D., Groumpos, P.P., 2004. Modeling complex systems using fuzzy cognitive maps. IEEE Trans Syst Man Cybern Part A Syst Hum 34(1):155–162

Thomas, C.S., 2009. Transportation options in a carbon-constrained world: Hybrids, plug-in hybrids, biofuels, fuel cell electric vehicles, and battery electric vehicles. International Journal of hydrogen energy, 34(23), pp.9279-9296.

Vu, Q., Raković, M., Delic, V. and Ronzhin, A., 2018. Trends in development of UAV-UGV cooperation approaches in precision agriculture. In *Interactive Collaborative Robotics: Third International Conference*, ICR 2018, Leipzig, Germany, September 18–22, 2018, Proceedings 3 (pp. 213-221). Springer International Publishing.

Zadeh, L.A., 1965. Fuzzy sets. Inform Control 8(3):338–353

Zhang, W.R., Chen, S.S., Bezdek, J.C., 1989. Pool2: A generic system for cognitive map development and decision analysis. IEEE Trans Syst Man Cybern 19(1):31–39

Zheng, L., Li, M., Wu, C., Ye, H., Ji, R., Deng, X., Che, Y., Fu, C. and Guo, W., 2011. Development of a smart mobile farming service system. Mathematical and computer modelling, 54(3-4), pp.1194-1203.

Empirical determination of the compression behaviour of miscanthus round bales

Bargen-Herzog Niklas [a,*], Knapp Johannes [a], Prof. Dr.-Ing. Geimer Marcus [a]

[a] Institute of Mobile Machines, Karlsruhe Institute of Technology, Karlsruhe, Germany

* Email: niklas.bargen-herzog@kit.edu

Abstract

Miscanthus x giganteus (miscanthus) is a renewable raw material and a climate-friendly alternative to fossil fuels. However, to utilise the energy crop economically, technical prerequisites are required to cultivate, harvest and transport miscanthus in large quantities. As there is little knowledge about the material behaviour of miscanthus, tests were carried out on miscanthus round bales. The test results provide information about the compression behaviour of miscanthus and thus form the basis for optimising large-scale processing of miscanthus.

During the tests, conventional round bales of miscanthus were compressed in a customised pressing box by a descending hydraulic pressing plunger. In each of five test series, a round bale of miscanthus was first compressed up to a pressure of 4 MPa and then up to a pressure of 8.5 MPa.

The pressure increases approximately linearly to the density of the bale at the beginning of the pressing process. The linear increase in force is transitioning into a nonlinear compaction behaviour as soon as the bale has reached the density of the previous maximum compaction. The measuring points of all test series in this range can be described by a single trend line, which can be approximated by a quadratic function.

When the plunger is lifted, the bale is relieved and its density decreases. The decompression of the bale corresponds to the linear curves that describe the compression behaviour at the start of the subsequent pressing process.

In summary, three key characteristics of the pressing process were identified from the pressing tests: The initial linear increase of the pressing force, the subsequent quadratic progression and the relaxation behaviour. The approximated curves for describing these findings describe the measurement results with a normalised absolute deviation of 8.8 % and make it possible to describe the pressing process schematically.

Keywords: Bioenergy, Renewable raw material, Miscanthus, Material properties, Compression tests

1. Introduction

One of the biggest challenges of our time is to move materials management towards circularity. This requires the development of bioeconomic value chains. Miscanthus, a perennial plant that originally comes from the East Asian region and occurs in different species, represents a potential raw material for such a value chain (Greef and Deuter, 1993). The genotype Miscanthus x giganteus (Greef and Deuter, 1993) was brought to Denmark by Aksel Olsen in the 1930s and cultivated there for the first time in Europe (Linde-Laursen, 1993). It has been observed that the plant has good adaptability and is suitable for the climatic conditions in Europe and North America (Linde-Laursen, 1993). This makes miscanthus one of the few C4 grasses that occur naturally in temperate climates (Lewandowski et al., 2000). C4 grasses are characterised by the property that they have a special photosynthetic pathway. Compared to C3 grasses, they have the advantage that they have higher efficiencies in terms of radiation, water and nitrogen consumption (Long, 1983). Due to these properties, miscanthus is predestined for the production of sustainable electricity, heat and synthetic fuel.

Even though there is great global potential for miscanthus as a raw material, it has not yet been possible to utilise this economically due to a lack of technology and machinery. One of the biggest challenges on the way to highly scalable utilisation of miscanthus currently lies in the compression of the material. For example, conventional baling presses used to harvest miscanthus achieve densities of 150 to 250 kg m^{-3}. In order to make the transport of miscanthus economical, significantly higher densities should be achieved.

This requires the development of new pressing processes. However, there is little knowledge about the material behaviour of miscanthus. Kaack and Schwarz (2001) have investigated the mechanical properties of miscanthus as a function of various influencing factors. Initial findings on the compression behaviour of miscanthus can be found in the research of Miao et al. (2015). It was shown that there is a non-linear relationship between the contact pressure and the density.

The pressing tests presented in this article are intended to provide further information about the compression of miscanthus, especially miscanthus round bales. The aim is to demonstrate the relationship between the contact pressure and the density by means of a schematic diagram. The results of the tests should form the basis for designing new baling processes.

2. Materials and Methods

2.1. Analysed miscanthus round bales

The material analysed is Miscanthus x giganteus, which was grown in southern Germany. The material was harvested in spring 2022 and wound into round bales using a conventional baler. Subsequently, the round bales were stored for about a year. At the time of the trials, the bales had a moisture content of approx. 11%. During the trials, five round bales were analysed, which differed in size and weight according to Table 1.

Table 1. Characterization of the examined miscanthus bales.

Bale no.	Volume in m^3	Mass in kg	Density in kg m^{-3}
1	0.178	28.3	159
2	0.181	28.8	159
3	0.257	46.2	180
4	0.236	41.3	175
5	0.126	25.1	200

The mechanical properties of the individual miscanthus stems were randomly sampled. The values measured were within the ranges determined by Kaack and Schwarz (2001) as part of a large-scale field study for Miscanthus stems. According to them, miscanthus stems consist of 8 to 13 internodes, each of which is 120 to 260 mm long and 7 to 12 mm in diameter. Both the length and the diameter of the internodes tend to decrease with increasing height. In total, the miscanthus stems reach a length of 1.6 to 2.4 m. (Kaack and Schwarz, 2001)

The trend that the values decrease with increasing height of the internodes and nodes also applies to the moment of inertia, the modulus of elasticity and the bending stiffness. In addition, there are differences between the material properties of the nodes and the internodes, with the nodes having a higher modulus of elasticity but a lower bending stiffness than the corresponding internodes. The modulus of elasticity of miscanthus ranges from approx. 2 GPa at the highest internode to approx. 8 GPa at a node near the ground. The flexural rigidity assumes values in the range between approx. 0.5 and 5 N m^2, the moment of inertia ranges from 10,000 to 65,000 m^4. (Kaack and Schwarz, 2001; Kaack et al., 2003)

2.2. Experimental setup and test procedure

A Wagner P800 hydraulic press and a customised pressing box were used to press the miscanthus round bales. The schematic structure of the test stand is presented in Figure 1. The pressing system has a nominal force of 8 MN and a stroke of 830 mm. The internal dimensions of the pressing box are 776 mm wide and 596 mm deep, and it is open at the top so that the pressing stamp can enter from above.

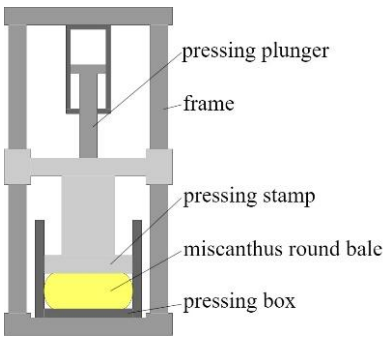

Figure 1. Experimental setup.

The pressing tests involve five test series, in each of which a different miscanthus round bale was analysed. Each test series consists of two consecutive compressions. In the first compression, the pressure is increased to approx. 4 MPa, in the second compression to approx. 8.5 MPa. Between the pressings, the pressing plunger is moved upwards to relieve the pressure on the bale. During the pressing processes, the path travelled by the plunger and the pressing force applied are recorded. From the position of the plunger and the dimensions of the pressing box, the volume and thus the density of the miscanthus bale can be determined at any time. The contact pressure is calculated from the pressing force and the area of the pressing stamp.

2.3. Evaluation methods

To derive a characteristic scheme for the pressing process, functional equations are required to approximate the recorded measuring points. These functional equations are optimised and evaluated using the following key indicators.

The mean absolute error (MAE) is regarded as an easy-to-interpret key indicator. It represents the mean value of the difference between the predicted value y' and the measured value y for a number of n measuring points (Eq. (1)). By dividing the MAE by the mean value of the measured values $\bar{y}$, the normalised mean absolute error (NMAE) can be determined (Eq. (2)).

$$MAE = \frac{1}{n}\sum_{k=1}^{n}|y' - y| \quad (1)$$

$$NMAE = \frac{MAE}{\bar{y}} \quad (2)$$

Similarly, the mean square error (MSE) is defined as the average of the squared differences between the predicted value y' and the measured value y of n measurement points (Eq. (3)). In addition to the distance between the predicted and measured values, the MSE also takes into account the scatter of the predicted values. It is therefore well suited for evaluating the quality of an approximation.

$$MSE = \frac{1}{n}\sum_{k=1}^{n}(y' - y)^2 \quad (3)$$

3. Results and Discussion

3.1. Observations

The pressure-density curves determined for the five test series are shown in Figure 2. During the first pressing processes of the five test series, the pressure initially increases approximately linearly to the density. From a certain density, in the range between 250 and 300 kg m^{-3}, the relationship between the pressure and density changes to a non-linear one. The contact pressure increases to approx. 4 MPa until the first pressing process is completed. The plunger then moved upwards to relieve the pressure on the bale. It was not technically possible to record the pressure during the relaxation process. However, it was observed that the density of the bale was noticeably reduced by the relaxation.

An approximately linear relationship between contact pressure and density can also be recognised at the start of the second pressing processes. The linearity is given until the density is reached up to which the miscanthus bale was compressed during the first pressing process. During the subsequent compression, the contact pressure increases non-linearly to the density. Again, the contact pressure is increased up to a fixed value, in this case approx. 8.5 MPa. In contrast to the first pressing process, the maximum contact pressure is maintained for a few seconds during the second pressing. The bale is compressed even further while the contact pressure remains the same. However, compression is much slower and eventually comes to a standstill. Relieving the pressure on the bale leads to its relaxation again.

The consideration of all determined pressure-density curves shows that the gradient of the linear curves at the beginning of a pressing process is approximately the same. Only the second pressing process of the fifth test series represents a recognisable outlier, in which the gradient is significantly smaller. For this reason, this pressing process was not taken into account for the further analysis of the linear curves.

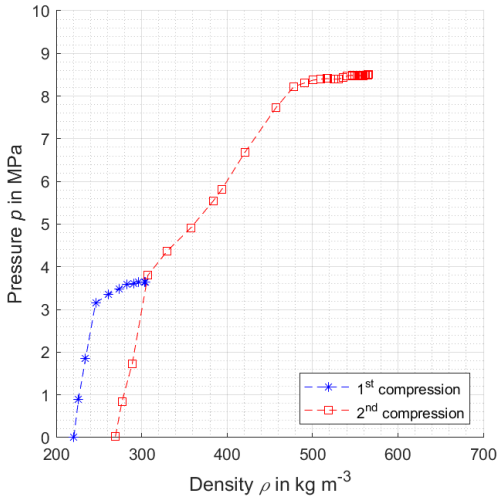

(a) 1st test series

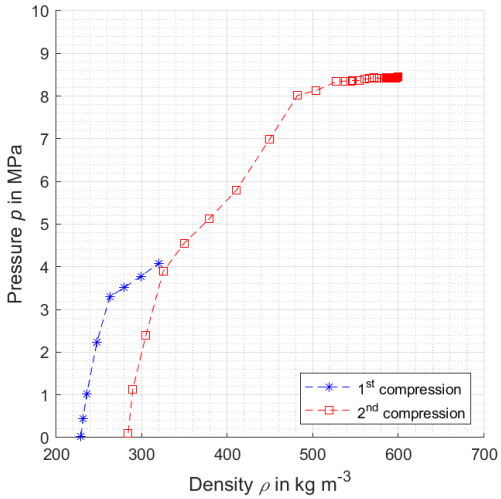

(b) 2nd test series

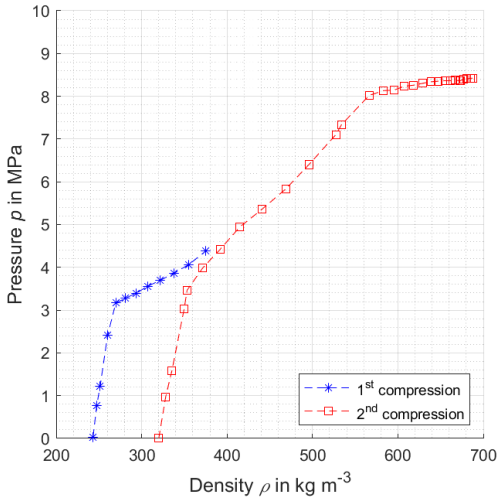

(c) 3rd test series

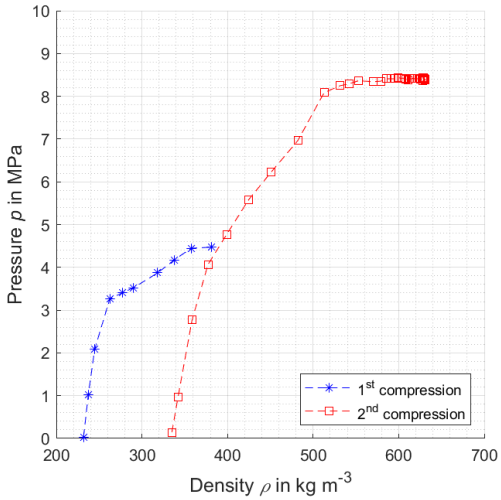

(d) 4th test series

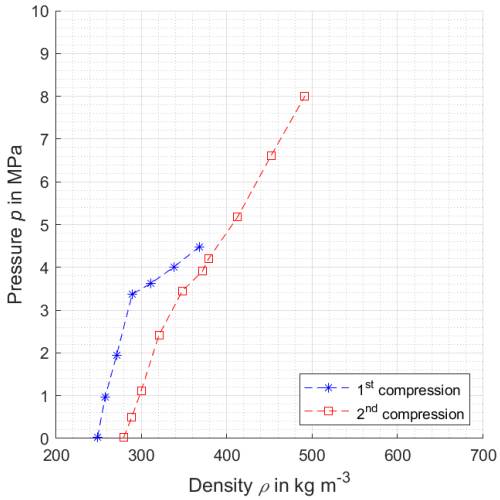

(e) 5th test series

Figure 2. Visualisation of the measuring points of the five test series.

3.2. Interpretation

According to the observations described, the pressing processes can be divided into four areas: a linear area at the start of a pressing process, a non-linear area during further compaction, the post-compaction when the maximum contact pressure is maintained and the relaxation. The post-compaction was not investigated further, as it is primarily highly dynamic pressing processes that are of interest.

To further analyse the initially linear and subsequently non-linear relationship between contact pressure and density, the measuring points of all tests were divided according to their affiliation to the two areas, see Figure 3.

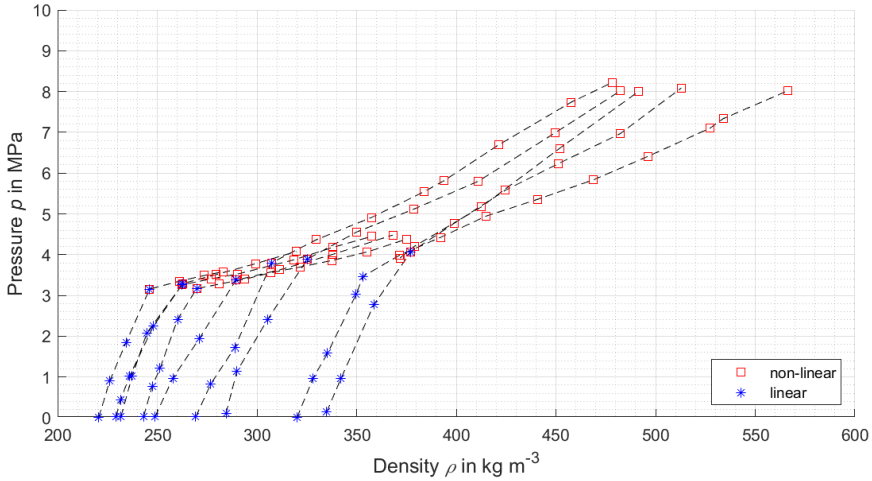

Figure 3. Allocation of measuring points into linear and non-linear behaviour.

3.2.1. Linear material behaviour

For the linear progressions of the i pressing processes, the assumption was made that they can be described by the set of functions $p_i(\rho)$. In the corresponding linear equation Eq. (4), the gradient m is the same for all pressing processes, while the Y-intercepts c_i differ.

$$p_i(\rho) = m \cdot \rho + c_i \quad (4)$$

An optimisation was carried out using the MSE to identify the common gradient m and the Y-intercepts c_i. The parameters determined are listed in Table 2. Figure 4 contains the visualisation of the linear equations with the corresponding measurement points. The quality of the linear approximation can be indicated by the evaluation indices shown in Table 3.

Table 2. Parameters for linear approximations.

	i	m	c_i
1st test series, 1st compression	1		-20.87
1st test series, 2nd compression	2		-25.94
2nd test series, 1st compression	3		-21.88
2nd test series, 2nd compression	4		-27.16
3rd test series, 1st compression	5	0.0964	-23.00
3rd test series, 2nd compression	6		-30.71
4th test series, 1st compression	7		-21.93
4th test series, 2nd compression	8		-32.07
5th test series, 1st compression	9		-24.14

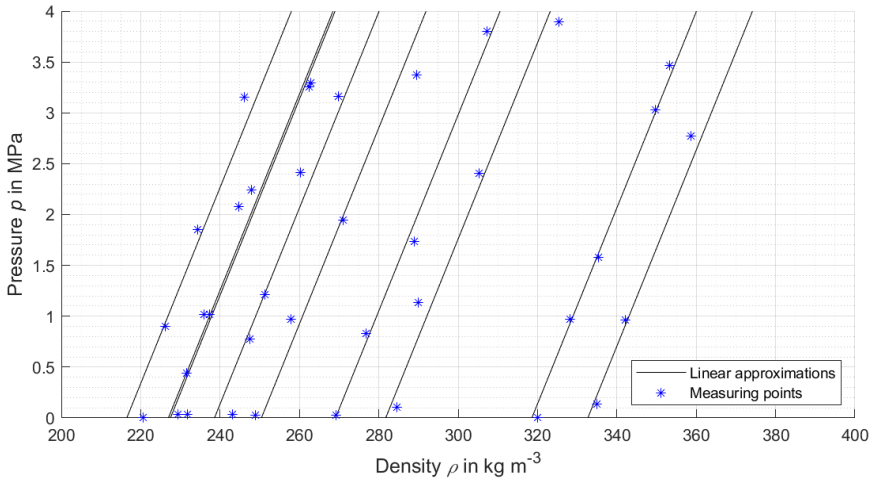

Figure 4. Linear approximations of measuring points.

Table 3. Evaluation of the approximations of the measuring points using the MAE and MSE.

	MAE in MPa	NMAE in %	MSE in MPa^2
Measuring points of linear area			
Linear set of functions	0.173	10.5	0.046
Measuring points of non-linear area			
Quadratic function	0.413	8.4	0.289
Exponential function	0.409	8.3	0.304
Power function	0.418	8.5	0.301
All measuring points			
Linear set of functions + quadratic function	0.257	8.8	0.356

3.2.2.Non-linear material behaviour

Three different approaches were investigated to approximate the measuring points in the area with non-linear behaviour: a quadratic function, an exponential function and a power function (Eq. (5-7)). The function parameters a, b, c were determined by optimisation using the MSE and can be obtained from Table 4.

$$\mathrm{p}(\rho) = a \cdot \rho^2 + b \cdot \rho + \mathrm{c} \quad (5)$$

$$\mathrm{p}(\rho) = a \cdot e^{b \cdot \rho} \quad (6)$$

$$\mathrm{p}(\rho) = a \cdot \rho^b \quad (7)$$

The quality of the approximations using the three different approaches differs only slightly according to the key indicators listed in Table 3. Even though the MAE is smallest with the exponential approach, the quadratic approach proves to be the most promising due to the lowest MSE. Figure 5 shows the measuring points associated with the non-linear range and the determined quadratic approximation.

Table 4. Parameters for non-linear approximations.

	a	b	c
Quadratic function	0.000018992	0.002928	1.040
Exponential function	1.338	0.00338	-
Power function	0.002266	1.2941	-

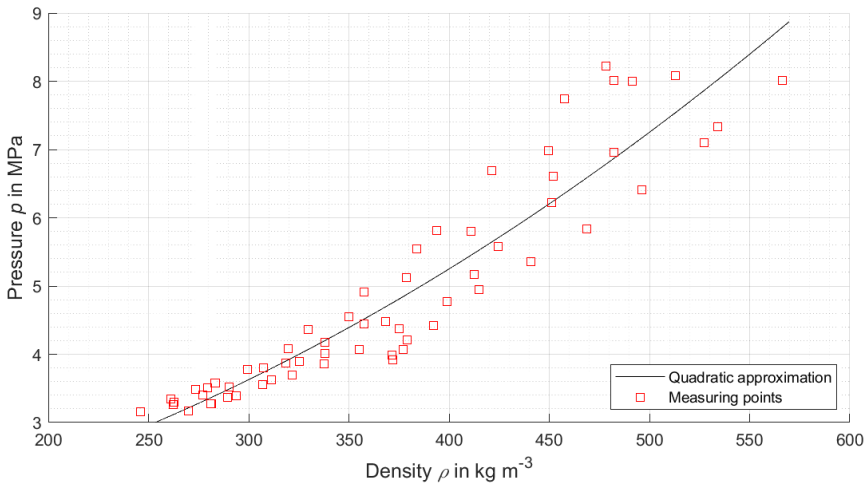

Figure 5. Quadratic approximation of measuring points.

3.2.3. Relaxation behaviour

It was observed that the bale relaxes, i.e. that the density of the bale decreases as soon as the contact pressure also decreases. However, no measurement data could be generated when the pressing stamp was raised. Therefore, the observations of the subsequent pressing process are used in order to make statements about the relaxation behaviour of the bale.

It is assumed that the pressure required to retain the bale at a certain density during the relaxation process corresponds to the pressure required to compress the bale to this density in the subsequent compression process. Taking this assumption into account, the linear relationship found between pressure and density can also be applied to the decompression.

4. Conclusions

The pressing tests carried out allow the conclusion that the pressing process can be divided into 2 sub-processes with different behaviour. Firstly, the increase in contact pressure over the density can be described using a linear approximation. The linear relationship exists until the density is reached up to which the material was compressed in a previous pressing operation. From then on, the compression behaviour is non-linear and can be approximated using a quadratic function. The approximations found can be used to reproduce the measuring points of the five test series with a MAE of 0.257 MPa. In relation to the mean value of the measuring points, this corresponds to a percentage deviation of 8.8 %.

If the contact pressure is reduced after pressing, the density decreases again. Assuming that the relaxation corresponds to the start of the subsequent pressing process, the linear approximation found is also valid for the relaxation process.

These findings can be summarised in a schematic diagram, see Figure 6. The diagram also contains the course of an exemplary pressing process and is intended to show how the pattern can be used as a basis for the design of compression processes for miscanthus. In the exemplary case, a bale with an initial density of 250 kg m^{-3} is compressed up to a contact pressure of 6.6 MPa. The bale thus reaches a density of 470 kg m^{-3} in the compression box. After the bale has been relaxed, it finally has a density of 400 kg m^{-3}.

Further material tests with miscanthus are planned to confirm the relationships found. In particular, the evaluation of the different approaches for describing the non-linear material behaviour and the process of relaxation requires further measurement data.

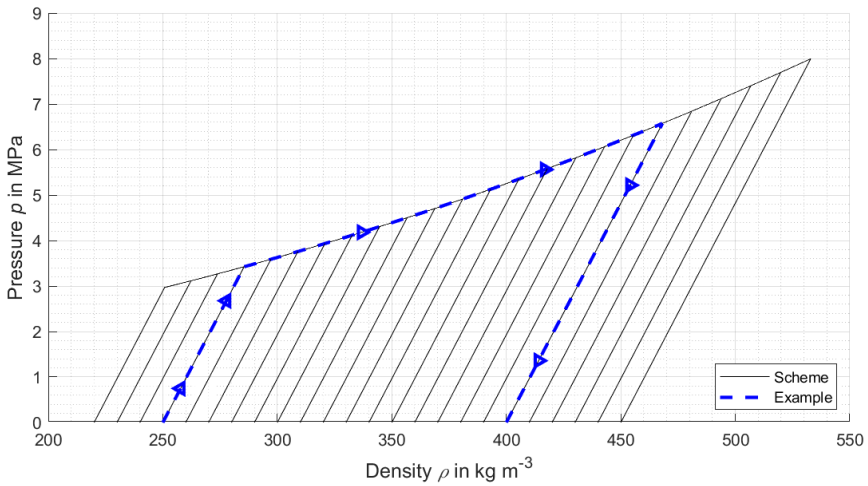

Figure 6. Scheme for the compression of miscanthus round bales including an example.

Acknowledgements

The research was carried out as part of a research project funded by the Ministry of Economics, Labour and Tourism of Baden-Württemberg.

Baden-Württemberg
MINISTERIUM FÜR WIRTSCHAFT, ARBEIT UND TOURISMUS

References

Greef, J.M, M. Deuter, 1993. Syntaxonomy of Miscanthus x giganteus. Angewandte Botanik. 67, 87-90. 0066-1759.

Kaack, K., K.-U. Schwarz, 2001. Morphological and mechanical properties of Miscanthus in relation to harvesting, lodging, and growth conditions. Industrial Crops and Products. 14 (2), 145-154. https://doi.org/10.1016/S0926-6690(01)00078-4

Kaack, K., K.-U. Schwarz, P.E. Brander, 2003. Variation in morphology, anatomy and chemistry of stems of Miscanthus genotypes differing in mechanical. Industrial Crops and Products. 17 (2), 131-142. https://doi.org/10.1016/S0926-6690(02)00093-6

Lewandowski, I., J.C. Clifton-Brown, J.M.O. Scurlock, W. Huisman, 2000. Miscanthus: European experience with a novel energy crop. Biomass and Bioenergy. 19 (4), 209-227. https://doi.org/10.1016/S0961-9534(00)00032-5

Linde-Laursen, I., 1993. Cytogenetic Analysis of Miscanthus‘Giganteus’, an Interspecific Hybrid. Hereditas. 119 (3), 297-300. https://doi.org/10.1111/j.1601-5223.1993.00297.x

Long, S.P., 1983. C_4 photosynthesis at low temperatures. Plant, Cell and Environment. 6 (4), 345-363. https://doi.org/10.1111/1365-3040.ep11612141

Miao, Z., J.W. Philips, T.E. Grift, S.K. Mathanker, 2015. Measurement of Mechanical Compressive Properties and Densification Energy Requirement of Miscanthus × giganteus and Switchgrass. BioEnergy Research. 8 (1), 152-164. https://doi.org/10.1007/s12155-014-9495-8

Thermal and electrical performance evaluation of a hybrid solar system for a livestock farm in Belgium

Petros Demissie Tegenaw [a, *], Manon Everaert [a, b], Iván P. Acosta-Pazmiño[c], Alexander Loris[c], Steven Lecompte[b], Jarissa Maselyne[a]

[a] ILVO (Flanders Research Institute for Agriculture, Fisheries and Food), Merelbeke, Belgium

[b] UGent (Ghent University), Ghent, Belgium

[c] MG Sustainable Engineering AB, Stationsgatan 23, Uppsala, Sweden

* Corresponding author. Email: petrosdemissie.tegenaw@ilvo.vlaanderen.be

Abstract

On-farm energy use for livestock farming is a major contributor to CO_2 emissions. The integration of renewable energy sources (RES) is an important step to mitigate these emissions. RES4LIVE is an EU Horizon 2020 project focused on reducing fossil fuel usage in livestock farms. During the project, a hybrid solar thermal system was installed on a typical pig farm under Belgian weather conditions. This hybrid system converts solar radiation into both electrical and thermal energy. The electrical energy is directly used by the barn's feeding pumps and ventilation system, whereas the thermal energy is stored in an 800 liter buffer tank used as a heat source for a 60 kW heat pump installation. The hybrid solar system consists of 24 photovoltaic thermal (PVT) flat plate collectors installed in four groups of six panels with a total aperture area of 45.12 m². The PVT system has an installed electrical and thermal capacity of 8.4 $kW_{electrical}$ and 28.8 $kW_{thermal}$. The heat transfer fluid (HTF) consists of 35 % propylene glycol and its flow in the system is dynamically controlled by a modular solar central control unit. The electrical and thermal performance parameters of the system are recorded every minute, including the temperature of the HTF, its flow rate and the incoming solar radiation. The data collected from the hybrid solar system is continuously being analyzed to evaluate thermal and electrical performance. During an average summer day of 2023, the HTF has gained a maximum temperature rise of about 30 °C relative to the ambient temperature. From July to February, the hybrid solar system generated approximately 4.5 MWh of thermal energy. During the five months from October to February, it produced around 2.3 MWh of electrical energy. In December 2023, the system recorded the lowest thermal and electrical energy production, corresponding with the month's lowest solar insolation. The analysis also showed that both thermal and electrical energy generated varied primarily based on the amount of insolation. The performance evaluation has shown the capability of such hybrid solar system to reduce carbon emissions and effectively replace fossil fuel consumption in the livestock sector in real working conditions.

Keywords: livestock, pig farm, renewable energy, hybrid solar thermal, photovoltaic thermal panels.

1. Introduction

Livestock farming represents a significant challenge in the context of climate change mitigation efforts, primarily due to its substantial carbon footprint stemming from energy consumption, waste production, and land use change (Steinfeld et al., 2006). Among various mitigation strategies, the integration of renewable energy sources (RES) into agricultural operations has garnered attention for its potential to reduce greenhouse gas emissions while ensuring sustainable production (Thornton, 2010).

The RES4LIVE project, supported by the EU's Horizon 2020 program (grant agreement nr. 101000785), exemplifies this approach by focusing on the implementation of renewable energy technologies in livestock farms to diminish reliance on fossil fuels . This initiative aligns with broader European efforts to transition towards a low-carbon economy and mitigate climate change impacts across sectors, including agriculture (European Commission, 2018). Solar energy, in particular, holds promise for on-farm energy generation due to its abundance and scalability. Solar photovoltaic (PV) systems have been increasingly adopted in agricultural settings worldwide, offering opportunities for decentralized electricity production and reduced operational costs. However, the intermittent nature of solar PV necessitates complementary technologies to ensure reliable energy supply, especially in settings with high energy demands such as livestock farming operations (Jäger-Waldau, 2007).

Hybrid solar thermal systems, which combine photovoltaic and thermal energy conversion technologies, present a compelling solution to address this challenge. By simultaneously generating electricity and heat from solar radiation, these systems offer enhanced energy yields and greater flexibility in meeting diverse on-farm energy needs. The integration of solar thermal technology in agriculture has been explored in various studies, highlighting its potential to improve energy efficiency and reduce greenhouse gas emissions in farming operations (Sakhare et al., 2022). Additionally, advancements in hybrid solar systems have demonstrated their applicability across different climatic conditions, with notable success in temperate regions such as Europe (Hussain et al., 2016).

The installation of a hybrid solar thermal system on a typical pig farm, as described in the RES4LIVE project, represents a novel application of this technology in the livestock sector. By leveraging both electrical and thermal energy outputs, the system addresses the multifaceted energy demands of modern farming practices while contributing to carbon emission reductions. The main objective of this study is to quantify the thermal and electrical performance of the hybrid solar system based on real life measured data.

2. Materials and Methods

The study is performed on a pig farm located in Melle (Flanders, Belgium). The farm is managed by ILVO, UGENT and HoGent for research and educational purposes alongside commercial production. It is a farrow-to-finish pig farm, housing around 105 sows, 600 piglets and 750 fattening pigs. The total building area is around 2,500 m². It is constructed out of concrete with polypropylene insulation panels dividing the compartments and partially slatted concrete floors above the manure pits. Heating is provided by a 60 kW gas boiler with a yearly fossil gas consumption of 220 MWh. Additionally heating is provided by heat lamps and a diesel powered heat cannon. The heating system is steered based on ambient temperature measurements at the animal compartments and on the stage of production. Table **1** shows heat demand (in terms of temperature) and the existing heating system with the respective production stage.

Table **1 Heat demand in the ILVO pig farm**

Production stage	Heating demand	Heating system
New-born piglets	35 - 37 °C	Floor heating (boiler) and heat lamps
Weaned piglets	28 °C at the start and reducing to 25 °C	heating of incoming air (boiler) and floor heating (boiler)
Fattening pigs	20 - 25 °C	Gas cannon heating of incoming air
Sows	18 - 23 °C	no need for extra heating

Two modular heat pumps of 25 and 40 kW were installed to provide heating at different temperature levels. Besides, 24 PVT collectors were installed as described in Section 2.1.1.

2.1. Solar thermal system description

Figure 1 (A) shows a simplified schematic overview of the installed renewable energy technologies that makeup the solar-thermal system. The main components are 24 hybrid solar panels on the roof (Figure 1 C), a solar control system (Figure 1 B), two modular heat pumps of 30 kW each, and 800 liter thermal energy storage tank.

The heat transfer fluid is 35 % glycol solution heated up in the solar hybrid panels and stores the energy in the thermal storage tank. The two modular heat pumps – a high and a medium temperature heat pump - raise the temperature of water that will be circulating in the domestic hot water, air heaters and floor heater circuits of the pig farm. The thermal energy stored in the tank will be a source for the heat pumps with the aim to increase the COP. On the other hand electricity is not stored but either directly used or injected into the electricity grid.

2.1.1. Hybrid solar collector panels

The hybrid solar collector panels used in ILVO pig farm are Abora aH72SK panels (Abora, Zaragoza, Spain). They are flat plate PVT thermal collectors with Mono-crystalline. This model is capable of generating a peak electrical power of 350 W with a module rated efficiency of 17.8 % and 1200 W of thermal

power. The hybrid solar collector system consists of 24 collectors installed as four groups of six panels, resulting in a total aperture area of 45.12 m² on the roof of the pig farm. The PVT system has an installed electrical and thermal capacity of 8.4 $kW_{electrical}$ and 28.8 $kW_{thermal}$, respectively. The PVTs are connected to an inverter (FIMER, Millano, Italy) on the farm for electricity supply directly to the farm.

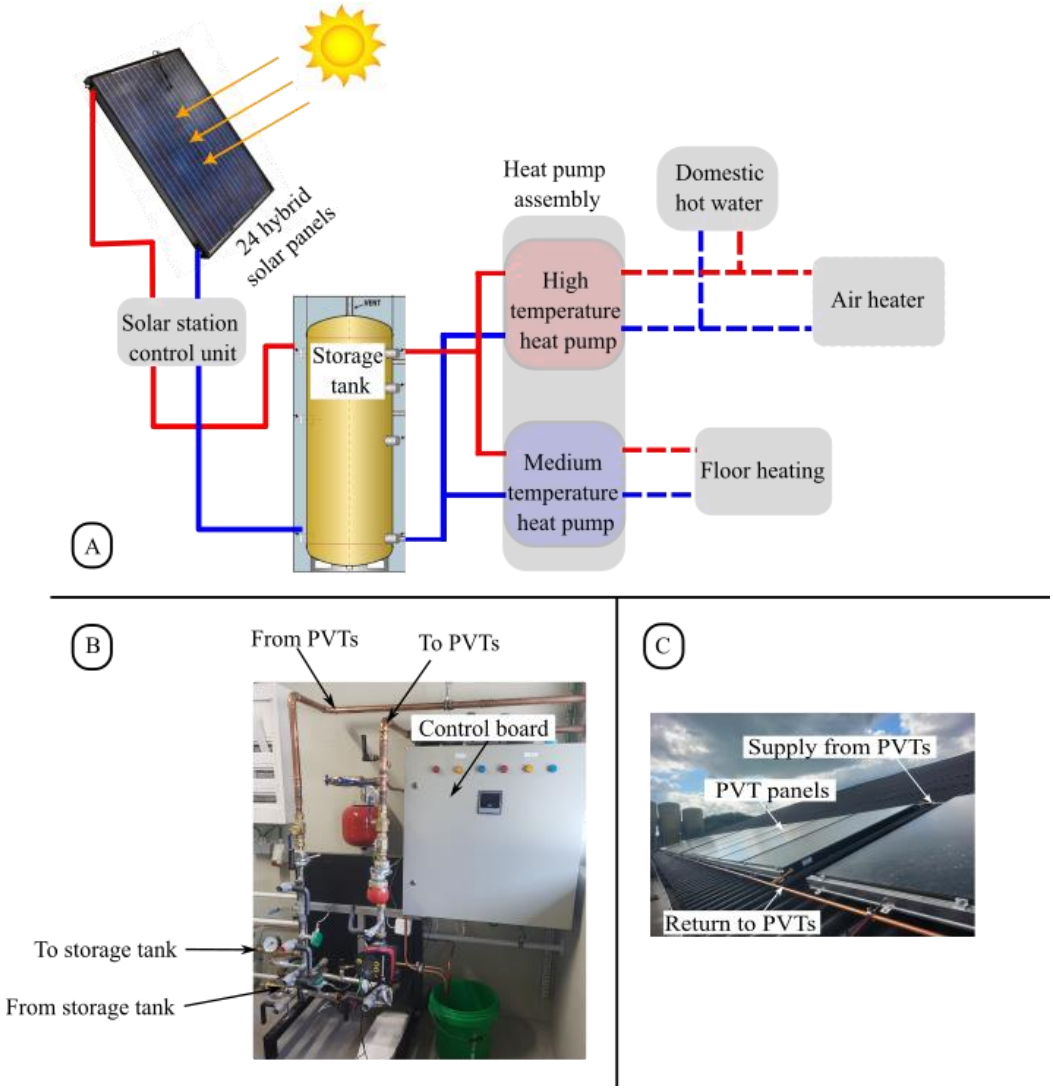

Figure 1 A) Schematic overview of the installed solar-thermal system, B) picture of the installed solar control system and C) picture of the installed hybrid solar panels on the roof of the pig farm at ILVO. Where: the red and blue lines represent supply and return pipe lines, respectively. The solid lines show passage lines for the 35 % glycol solution whereas the dotted lines indicate water pipes.

2.1.2. Solar station unit and central controller description (MG)

The solar station is the main pumping system to transfer heat from the solar thermal collectors to the end user. The solar station used was designed by MG Sustainable Engineering AB (Sweden) with the goal to standardise solar stations for mid-size PVT applications such as in livestock farms. It was manufactured by KEterm AB in Sweden. The pump transfers heat from the solar field to the solar station heat exchanger; and an intermediate circuit transfers heat from the heat exchanger to the storage tank through another pump. Heat stored in the storage tank is used by the heat pumps to deliver the final heat to the farm.

The control system used is a RESOL MX solar controller with a RESOL DL2 datalogger which communicates data in real time to a server. The control algorithm was developed by MG Sustainable

engineering. The controller activates the solar circuit pump as soon as the solar collectors are hotter than the tank, or if solar irradiance is above a threshold (>200 W/m^2 for 60 seconds. There are two heat flow meters; one for the heat delivered from the solar collectors to the solar station and one for the heat delivered to the tank. The pumps are not operated on variable speed and the flow rate in the solar circuit is ca. 30 l/min.

2.2. Data processing

Solar energy increases the temperature of HTF and the amount of heat transferred (Q) in kilowatts (kW) to the HTF can then be calculated using the equation given below.

$$Q = \dot{m} C_p \Delta T$$

Where $\dot{m}[kg/s]$ is the mass flow rate of the HTF, $C_p[\frac{\text{J}}{\text{kg K}}]$ is the specific heat capacity of the HTF at constant pressure, and ΔT $[K]$ is the temperature difference between the hot and cold sides of the hybrid solar collector. Note that, the value of C_p of propylene glycol, which is the heat transfer fluid, is estimated using the weighted average method considering 65% water and 35% propylene glycol from **Table 2**.

Table 2. Physical properties of the heat transfer fluid 65 % water and 35 % propylene glycol (Murali et al., 2024).

	Water	Propylene glycol
Specific heat capacity, C_p $\left[\frac{J}{kgK}\right]$	4186	2200
Density, ρ at 25 ℃ $\left[\frac{kg}{m^3}\right]$	1000	1110

3. Results and Discussion

3.1. Solar irradiance levels

Figure 2 shows the solar irradiance data from July 2023 to February 2024 as a carpet plot. In four months July, August, September and October more than 1000 W/m² insolation was recorded. The maximum solar irradiance recorded was 350 W/m² in December 2023.

3.2. Hybrid solar system performance analysis

3.2.1. Thermal performance analysis

Figure 3 shows the daily amount of thermal energy produced by the hybrid solar system during the measurement period from August 2023 to February 2024. The solar irradiance values integrated over time for each day are also shown as blue bars in Figure 3. There were days when the daily thermal energy production was higher than 100 kWh in the months of August (early August) and September (early September). On the contrary, negligible heat generation is recorded in the months of December 2023 and January 2024. The produced thermal energy is as expected directly correlated the respective solar insolation data. Higher solar insolation corresponds with the higher thermal energy produced and conversely, low thermal energy output corresponds to low insolation. During the month of August 2023, the thermal energy production was nearly consistent, except for some days at the end of the month which were cloudy.

Figure 4 shows the monthly average amount of thermal energy produced by the hybrid solar system during the measurement period from August 2023 to February 2024 with the corresponding solar radiation. The produced thermal energy trend is correlated the respective solar radiation. The heat energy production reached its peak during the midday hours when the irradiance was highest. In the summer the days are longer and hence the thermal energy production is also longer. There are momentary dips in heat production around midday during winter, these are due to the circulation of relatively warm heat transfer fluid to the colder PVT panels.

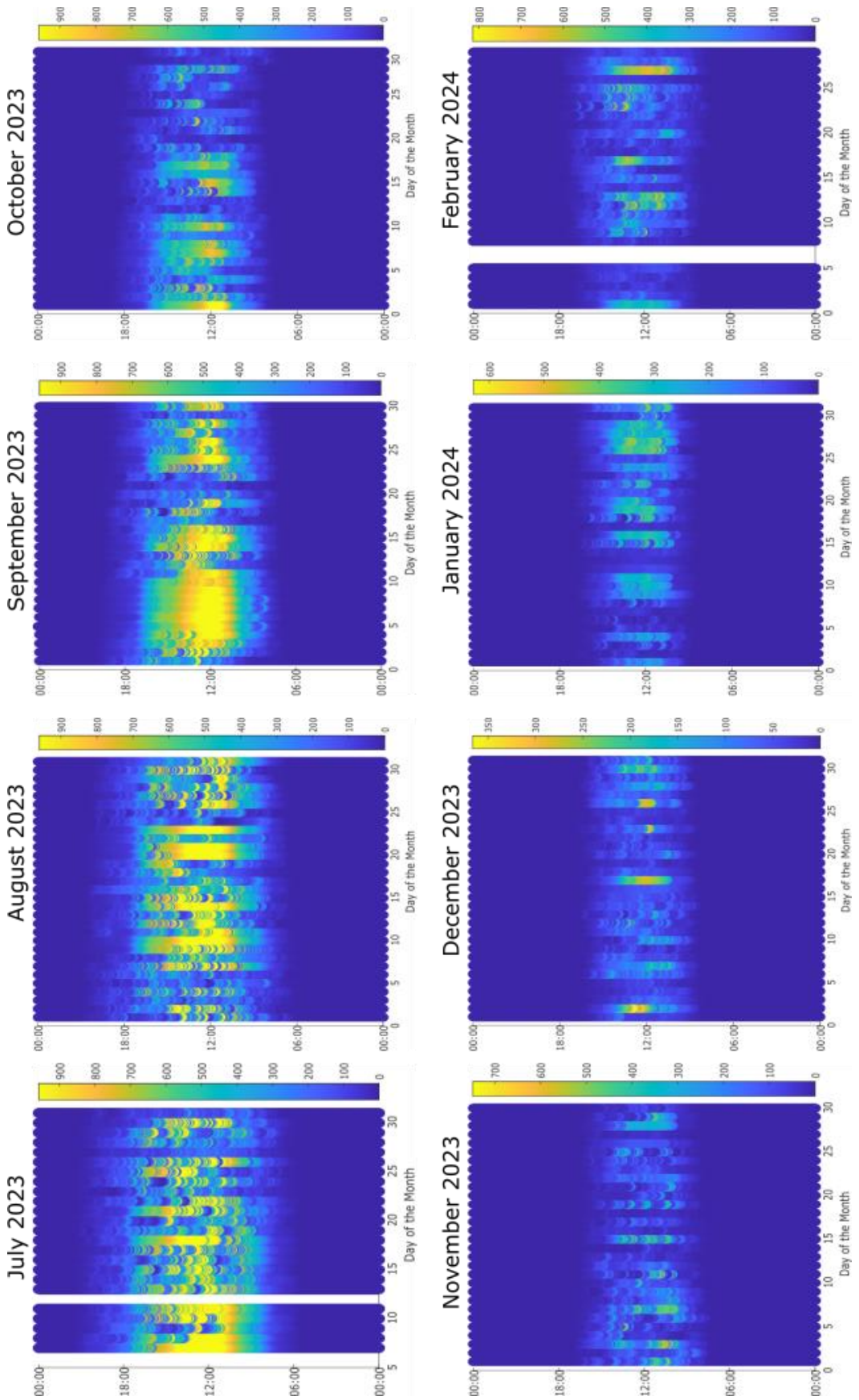

Figure 2. Solar Irradiance levels (W/m²) during the months of July 2023 to February 2024

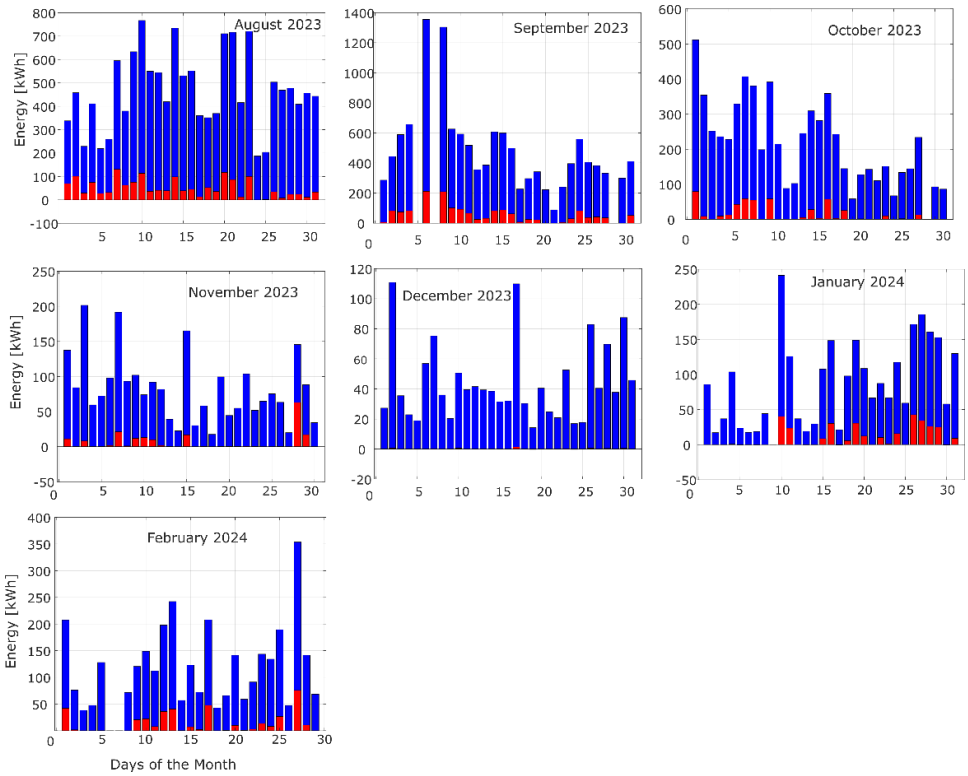

Figure 3 Daily thermal energy production (red bars) and insolation (blue bars) during the months of August to December 2023 and January and February of 2024.

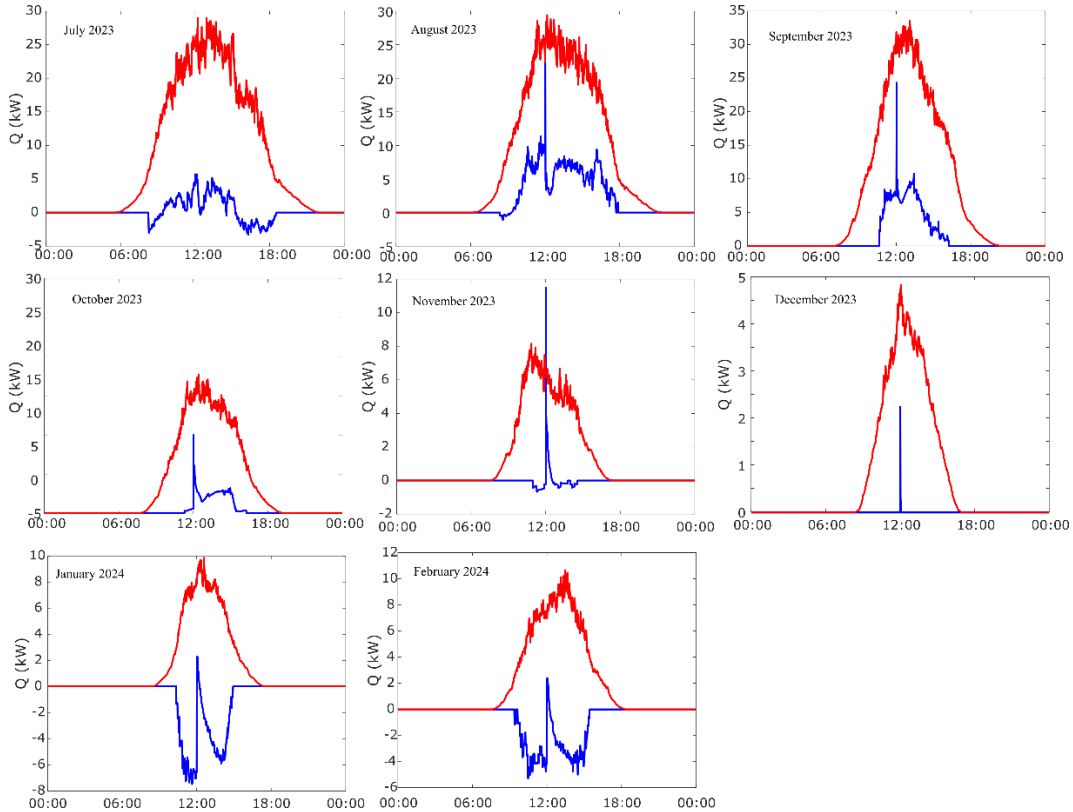

Figure 4 Average monthly heat energy generated (Blue) and solar radiation collected (Red) in kW during hours of a day,.

3.2.2.Electrical performance analysis

Figure 5 shows the daily amount of electrical energy produced by the hybrid solar system during the measurement period from October 2023 to February 2024. There were days when the daily electrical energy production was not recorded as the integrated system was on performance tests. Likewise the heat energy production the electrical energy production of the hybrid solar system is in varying in relation to the solar insolation.

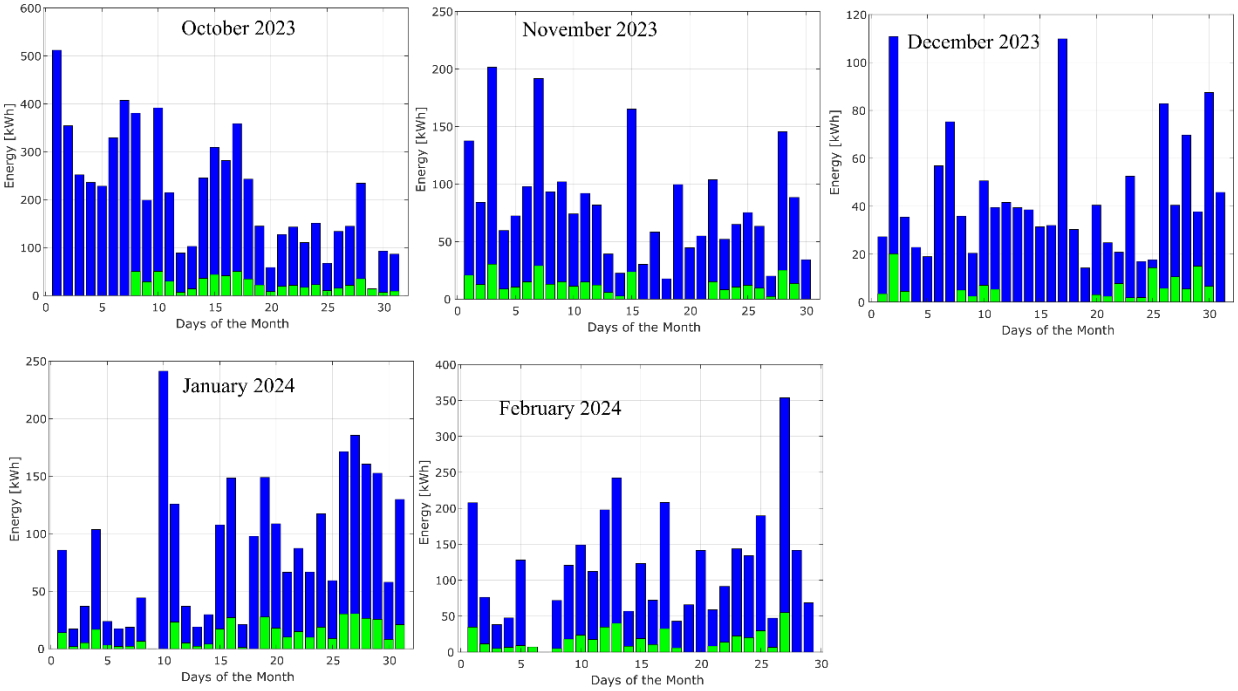

Figure 5 Daily electrical energy production (green bars) and insolation (blue bars) during the months of October 2023 and February of 2024

3.2.3. Electrical and thermal performance combined

Table 3 summarizes amount of average thermal and electrical energy produced by the hybrid solar system during the measurement period from August 2023 to February 2024 per day. During the seven consecutive months around 4.5 MWh thermal energy was generated by the hybrid solar system. In the five consecutive months from October to February around 2.3 MWh electrical energy was produced by the installed hybrid solar system. The month of December 2023 has days with the lowest thermal and electrical energy production that corresponds with its lowest solar isolation.

Table 3 Daily average thermal and electrical energy generated in each of the measurement months with respect to the solar isolation.

Month	Daily average Thermal energy generated [kWh]	Daily average Electrical energy generated [kWh]	Daily average Insolation [kWh]
August	51	-	465
September	52	-	434
October	16	25	213
November	6	14	82
December	0	7	44
January	10	14	87
February	13	19	115

4. Conclusions

A hybrid solar system comprising 24 collectors was installed at the ILVO pig farm. The system is being monitored based on the temperature and flow rate of the heat transfer fluid (HTF), as well as radiation and ambient temperature. Commissioned in mid-July 2023, the system's performance has been analysed over the following seven months.

From July to February, the hybrid solar system generated approximately 4.5 MWh of thermal energy. During the five months from October to February, it produced around 2.3 MWh of electrical energy. In December 2023, the system recorded the lowest thermal and electrical energy production, corresponding with the month's lowest solar insolation. The analysis also showed that both thermal and electrical energy generated varied primarily based on the amount of insolation. The performance evaluation has shown the capability of such hybrid solar system to reduce carbon emissions and effectively replace fossil fuel consumption in the livestock sector in real working conditions.

Acknowledgements

Funded by the European Union (project "Energy Smart Livestock Farming towards Zero Fossil Fuel Consumption - RES4LIVE", Horizon Europe under grant agreement ID: 101000785). Views and opinions expressed are however those of the author(s) only and do not necessarily reflect those of the European Union. Neither the European Union nor the granting authority can be held responsible for them. We thank the ILVO technicians and consortium partners that helped to achieve the installations and results.

References

EU Horizon 2020. (n.d.). *Horizon 2020 - The EU Framework Programme for Research and Innovation*.

European Commission. (2018). *A Clean Planet for all: A European strategic long-term vision for a prosperous, modern, competitive and climate neutral economy.* .

Hussain, C. M. I., Norton, B., & Duffy, A. (2016). Technological assessment of different solar-biomass systems for hybrid power generation in Europe. *Renewable and Sustainable Energy Reviews*, *68*. https://doi.org/10.1016/j.rser.2016.08.016

Jäger-Waldau, A. (2007). Photovoltaics and renewable energies in Europe. *Renewable and Sustainable Energy Reviews*, *11*, 1414–1437. https://doi.org/10.1016/j.rser.2005.11.001

Murali, D., Acosta-Pazmiño, I. P., Loris, A., García, A. C., Benni, S., Tinti, F., & Gomes, J. (2024). Experimental assessment of a solar photovoltaic-thermal system in a livestock farm in Italy. *Solar Energy Advances*, *4*, 100051. https://doi.org/10.1016/J.SEJA.2024.100051

Sakhare, K. P., Kiran, Balsoriya, H., & Kesari, J. P. (2022). Opportunities for solar thermal systems across dairy, agricultural, hotel & automobile industries. *Materials Today: Proceedings*, *56*, 3656–3668. https://doi.org/https://doi.org/10.1016/j.matpr.2021.12.353

Steinfeld, H., Gerber, P. J., Wassenaar, T., Castel, V., Rosales, M., & De haan, C. (2006). Livestock's Long Shadow: Environmental Issues and Options. In *Food and Agriculture Organization of the United Nations* (Vol. 24).

Thornton, P. K. (2010). Livestock production: recent trends, future prospects. *Philosophical Transactions of the Royal Society B: Biological Sciences*, *365*(1554), 2853–2867. https://doi.org/10.1098/rstb.2010.0134

Assessing the environmental benefits of switching to renewable energy sources in cheese production: A case study from Western Macedonia, Greece

S. Konstantinidi[a], A. Vatsanidou[a], V. Anestis[b]

[a]*Department Agricultural Development, Agri-Food & Management of Natural Resources, National and Kapodistrian University of Athens, 34400, Psachna, Evia, Greece*
[b]*Laboratory of Farm Structures, Department of Natural resources and Agricultural Engineering, Agricultural University of Athens, 11855, Athens, Greece*

Abstract

This study presents an environmental Life Cycle Analysis (LCA) of the PDO 'Kasseri – kefali' cheese which was produced in a dairy industry in Western Macedonia, Greece. The main objective was to evaluate the environmental benefits of installing photovoltaic panels to supply the energy needs of the production process at the dairy. The Environmental Footprint 3.1 method was used to align with the PEFCR guidelines and standardize the environmental impact assessment. A comparative approach was followed, considering two scenarios: cheese production with the current reliance on the conventional energy grid versus a theoretical scenario, where the dairy's energy needs are met exclusively by the installed photovoltaic solar panels. The comparison was made for 1 kg of packaged and ready-to-supply 'Kaseri Kefali PDO' cheese, at the gate of the dairy unit. The study revealed that switching to photovoltaic energy resulted in a 6.2% reduction of the carbon footprint (CF) of the cheese for the entire cradle-to-dairy-unit supply chain. Specifically, the study focused on energy inputs, and found a 41% reduction in the CF associated solely with energy inputs, highlighting the potentially critical role of renewable energy sources, particularly solar energy, in enhancing the environmental profile of the Greek cheese production industry.

Keywords: Life Cycle Assessment, Carbon Footprint, Green Energy, PEFCR, Cheese Production, Greece

1. Introduction

Sustainability is vital to maintain the well-being of current and future generations. It plays a crucial role in ensuring environmental, social, and economic balance and longevity in all sectors, including the food industry. The adoption of environmentally sustainable practices in the food industry is increasingly recognized as critical for several reasons. Firstly, food production and processing contribute significantly to greenhouse gas (GHG) emissions (Canellada et al. 2018; Breen, Upton, and Murphy 2020; Ghinea and Leahu 2023) and embracing sustainable practices can greatly reduce their carbon footprint (CF) and help mitigate climate change. Moreover, responsible practices aid in preserving resources such as water, energy, and raw materials, which is essential to maintain ecosystems and ensure their availability for future generations. Additionally, there is a growing emphasis on social responsibility. Consumers are increasingly concerned about the environmental impact of their dietary choices, leading to a demand for products produced in an ethical and sustainable way. It is therefore imperative to embrace environmentally sustainable practices in the food industry to ensure a balance between environmental and social concerns.

In the agri-food sector, energy consumption, water utilization, and environmental impact are emerging issues to be addressed in response to climate change. The use of fossil energy in agricultural processes exacerbates climate change through both on-farm emissions from fuel combustion and off-farm emissions from the production and transport of agricultural inputs. The efficient use of fossil resources and increased adoption of renewable energies are essential for developing more sustainable agro-food production systems (Murgia et al. 2013). The Greek energy sector's greenhouse gas (GHG) emissions accounted for 69.17% of the country's total GHG emissions in 2021 (Ministry of Environment and Energy 2023). These emissions have decreased by approximately 33.02% compared to 1990 levels, mainly due to the integration of natural gas and renewable energy sources (RES) into the electricity production system. Conducting Life Cycle Assessment (LCA) studies that focus on the integration of RES in the food industry can provide useful insights into the potential environmental benefits associated with such initiatives. Notably, the EU promotes RES across all sectors and industries. The Commission's proposal to increase the target in the Renewable Energy Directive to 45% by 2030 underscores the commitment to integrating RES in industries and sectors that currently rely on conventional resources (European Comission 2022).

This study focuses on conducting an environmental LCA of the PDO 'Kasseri – kefali' cheese in Western Macedonia, Greece primarily aiming to evaluate the potential environmental benefit of integrating photovoltaic panels within the dairy unit to meet the energy requirements for the production. The study underscores the

opportunities and benefits associated with utilizing solar energy and intends to provide valuable insights into the environmental sustainability of cheese production.

2. Materials and Methods

The functional unit (FU) of this study was defined as "the production of 1 kg of PDO 'Kasseri – kefali' cheese, packaged, at the gate of the dairy unit". This choice aligns with the Product Environmental Footprint Category Rules (PEFCR) guidelines for dairy products and the proposed approach for environmental burden allocation (European Dairy Association 2018). The system boundaries (Fig. 1) included milk inputs, production process ingredients (such as rennet, salt, etc.), packaging materials, cleaning agents, electricity, natural gas and water. In addition, transport activities from the suppliers to the dairy industry, involving the transport of raw milk, ingredients of the production process, cleaning agents, packaging materials and all the other transport processes in the supply chains of the inputs to the dairy industry, were included within the system boundaries.

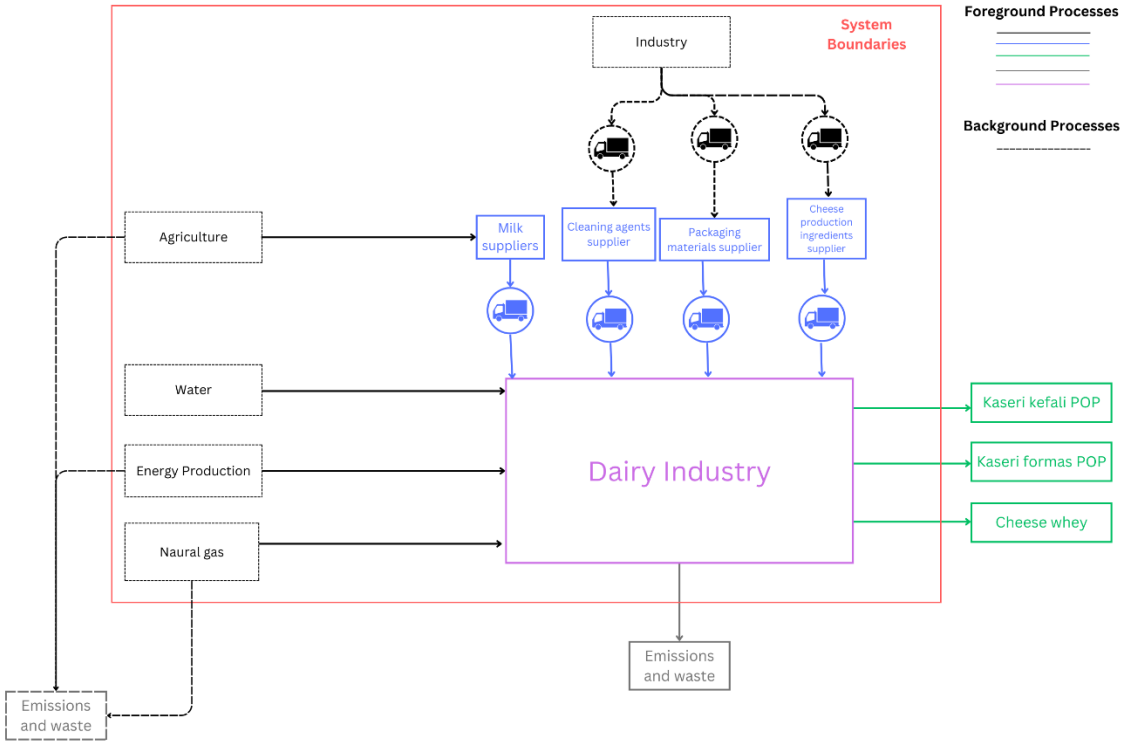

Figure 1. The study's system boundaries (cradle-to-dairy-unit-gate).

In this study, the Environmental Footprint 3.1 method was used (European Commission. Joint Research Centre. 2020). This method offers many advantages, especially when aligned with the guidelines provided by the PEFCR rules (European Dairy Association, 2018). By following this method, a standardized approach for assessing the environmental footprint was ensured. Compliance with the PEFCR guidelines ensures transparency in the assessment process and enhances the reliability of the findings.

The dairy unit, located in Grevena, has an important production capacity for North Greece, focusing on producing a variety of dairy products. It produces eleven different dairy products, with Kasseri cheese being the primary product at 14 tons per year, followed by Goat cheese and Graviera, each at 5 tons per year. Additionally, the unit produces several other products in smaller quantities. To ensure accurate allocation of the total energy, fuel, post-processing and other process inputs to the different dairy products, the PEFCR rules were followed. The PEFCR guidelines recommend allocation based on the dry weight or dry matter content of the products under study and their by-products. Due to this allocation approach, the more concentrated products, such as Kasseri cheese, received a greater proportion of the impact of processing, given the greater amount of raw milk required to produce them (Table 1).

Table 1. Annual production volumes and dry matter content of the dairy unit's products.

Product	Annual Production, kg	Dry Matter Content, %	Allocation, %
Feta	24500	47	29.2

Goat Cheese	5500	47	6.5
Yogurt	2400	18	1.1
Anevato	6000	47	7.1
Graviera	4000	56	5.7
Aged Graviera	1400	56	2.0
Kasseri. Formas	2080	55	2.9
Kasseri. Kefali	12925	55	18.0
Kefalotyri	12925	56	18.3
Mpazios	240	56	0.3
Cheese whey for Gkiza production	25500	7	4.5

The LCA followed a comparative approach, by modelling two production systems. The first system represented the actual operating state of the supply chain ending at the dairy unit (AOS), describing the existing operations of the dairy facility, while the second system illustrated a theoretical operation state (TOS), assuming that all energy inputs were provided by solar panels, which were installed in the dairy facility. In the TOS scenario, electricity from the network was avoided, as it was the energy input that was saved in comparison to the AOS system. Since the production process of Kasseri cheese gives three products, “Kasseri Kefali PDO”, “Kasseri Forma PDO” and “Cheese Whey”, the inputs were again allocated according to the dry matter content of these products. The inputs and products of the production process of Kasseri for both AOS and TOS systems are summarized in Table 2.

Table 2. Inputs and products of the AOS and TOS systems.

Products	Unit	AOS	TOS
Kasseri Kefali PDO	kg	13294.29	13294.29
Kasseri Formas PDO	kg	2218.67	2218.67
Cheese Whey	kg	112537.5	112537.5
Avoided Products			
Electricity	kWh	-	12158.47
Inputs from Nature			
Water	m^3	1000	1000
Land Use	m^2a	561.385	561.385
Materials			
Goat & Sheep Milk	kg	245886.6	245886.6
Transport of sheep and goat milk by articulated lorry, <7.5 tonnes	tkm	1967.09	1967.09
Acidic Detergents	kg	41.82	41.82
Alkaline Detergents	kg	209.11	209.11
Transport of detergents by articulated lorry, <7.5 tonnes	tkm	20.07	20.07
Rennet	kg	16.72	16.72
Salt	kg	2500	2500
Transport of process ingredients by articulated lorry, <7.5 tonnes	tkm	1000	1000
Conventional Energy Consumption	kWh	12158.47	0
Monocrystalline Solar Panels	m^2	0	48
Natural Gas	kg	5080.51	5080.51
Packaging Film	m^2	380.2	380.2
Plastic bags	m^2	608.32	608.32
Paper Labels	m^2	116.17	116.17
Transport of packaging materials by articulated lorry, <7.5 tonnes	tkm	9.41	9.41
Private Car Use	km	180	180
Carton Boxes	kg	1915.76	1915.76
Transport of carton boxes	tkm	344.8	344.8

The data used to model the systems were primarily sourced directly from the dairy unit. The primary data collection included detailed foreground data, such as the types and quantities of products produced, along with their dry matter content. The specific collected data points encompassed land use, water use, and materials use. Data on electricity inputs, packaging materials, transport activities to and from the dairy unit, waste management practices, and building infrastructure were also collected. In cases where primary data were not available, alternative sources were employed to supplement the missing information. Specifically, data on the dry matter content of the whey and the quantity of whey produced during the cheese-making process were sourced from the PEFCR guidelines (European Dairy Association 2018). To model the background system, processes that are consistent with the PEF methodology (European Comission 2019) were exclusively used.

To model the TOS scenario, it was necessary to calculate the total number of solar panels needed to power the dairy unit all year round. It was essential that the calculations are based on real data. Therefore, the solar panels used in the scenario were sources from a reputable PV panel supplier and the modeling was carried out using the specific characteristics of their panels (The Green Watt 2023). The scenario assumed that the panels used are monocrystalline and data used in the calculation included their wattage, their solar output, the peak sun hours of the area and the number of operation days for the dairy unit. All data mentioned were collected from the solar panel's supplier documentations. The annual energy production of the panels was considered enough to supply the needs of the unit and the available space within the unit's facilities was considered sufficient to accommodate the calculated number of solar panels.

3. Results

3.1. Impact Assessment

The results of this study were presented for nine impact categories as suggested by the PEFCR guidelines (European Dairy Association 2018). These categories provided a comprehensive view of the environmental impacts associated with the production of PDO 'Kasseri – kefali' cheese. The results were expressed as percentages of potential improvement or deterioration when transitioning from the current AOS to the TOS. Those were calculated following the eq. (1):

$$Percentage\ of\ improvement\ or\ deterioration_i, \% = \frac{Impact\ Score\ TOS_i - Impact\ Score\ AOS_i}{Impact\ Score\ AOS_i} * 100 \quad (1)$$

The transition to photovoltaic energy showed improvements in almost all the impact categories studied per kg of cheese at the dairy unit's gate, as shown in Figure 2. The most significant improvement was noticed in the resource use, fossils and climate change impact categories, where the impacts were reduced by 17.0% and 6.2% respectively, when transitioning from the AOS to the TOS.

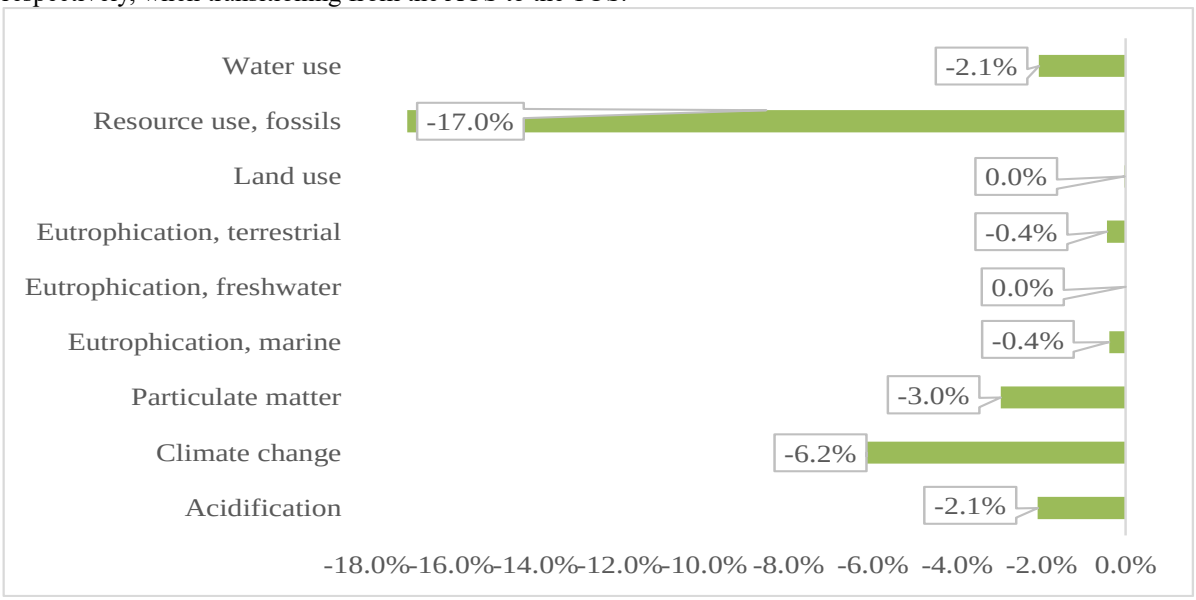

Figure 2. Impact Assessment Results: Percentages of improvement or deterioration after transitioning from AOS to TOS.

3.2. Process Contribution

The CF of the "production of 1 kg of one kilogram of PDO 'Kasseri – kefali' cheese" was predominantly (>90%) attributed to the raw sheep and goat milk input. For the "Resources Use, fossils" impact category, more than 68% of the total impact was associated with the cheese production process. A comprehensive figure that illustrates the contribution analysis for climate change and resource use is presented below (Fig. 3). Figure 3 illustrates the contributions of six groups of processes to two environmental impact categories: climate change and resource use, fossils, for TOS and AOS scenarios. For the climate change impact category, the milk inputs, were the dominant contributor, accounting for 91% and 97% of the total impact in AOS and TOS, respectively. In the resource use fossils category, the processes associated with milk remained the primary contributor, with 68% and 82% in AOS and TOS, respectively. The energy and fuels process groups (which included the natural gas consumption in the dairy) also showed a significant contribution to this impact category, with 7.5% in AOS which dropped to 1.1% in TOS. For both impact categories analyzed, the contribution of the rest of the process groups was less than 1%.

Given the study's focus on assessing the benefits of transitioning the dairy's energy supply to renewable sources, a contribution analysis to the above impact categories, focusing solely on the energy-related inputs of the AOS and TOS systems, was also of interest (Fig. 4). Figure 4 reveals the significant improvement associated with the energy shift towards green energy sources to cover the industry's energy needs. The CF resulting from energy-related inputs was reduced by 41%, a reduction entirely attributed to the shift from conventional to green energy. A similar observation could be made for the "resource use, fossils" impact category where the category indicator drops by 30% when switching from the AOS to the TOS scenario.

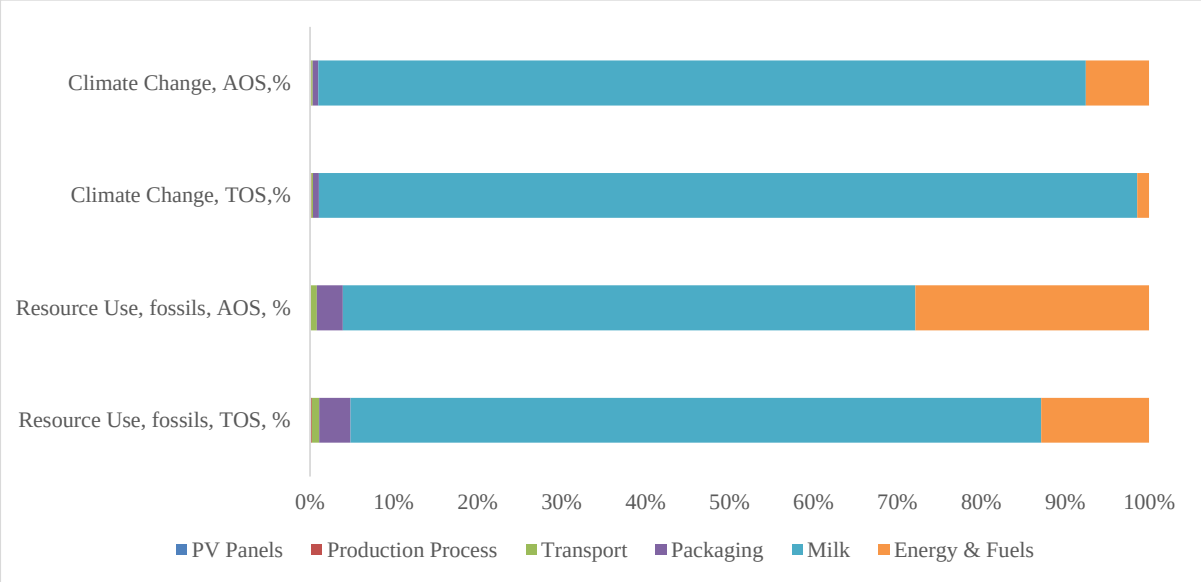

Figure 3. Contribution Analysis for "Climate change" and "Resource Use", fossils impact categories

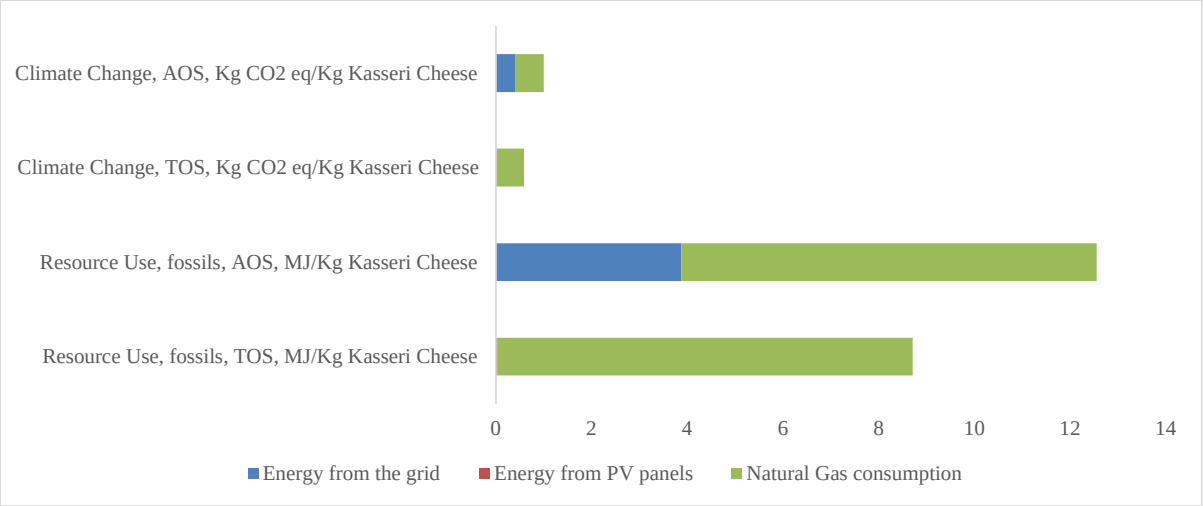

Figure 4. Carbon footprint and Resource use, fossils contribution analysis, isolating the energy and fuels processes

4. Discussion

This study demonstrates the benefits of a dairy industry's transition to renewable energy sources, with a focus on solar energy. Studies on the environmental and CF of dairy products highlight the environmental benefits of decoupling from conventional energy sources.

Canellada et al. (2018) investigated the environmental footprint of cheese production in southern Europe, in particular of the Spanish "Franxon" and "Casin" cheeses. They concluded that milk production and land use change were the largest contributors to the environmental footprint, with milk production accounting for more than 75% of climate change impacts. Energy consumption accounted for about 10% of this environmental impact. The results of the present study align with their findings, as milk production was also the main contributor in the present analysis, with more than 90% contribution, followed by energy consumption, which accounted for 7% of the CF.

Murgia et al. (2013) analyzed the energy needs and CO_2 emissions of dairy farms. They identified cooling and milk processing as the most energy-intensive processes. For the production of 1 kg of milk, CO_2 emissions were 0.085 kg CO_2 eq. The integration of photovoltaic panels on dairy farms reduced the CF by 0.023 kg CO_2 eq, which corresponds to a 27% reduction. In addition, these systems can exceed energy needs during the summer, allowing farms to sell surplus energy to the grid. The present study's outcomes showed a 6.2% improvement in the CF per kg of Kasseri cheese associated with the integration of solar panels in the dairy unit. Nevertheless, it has to be considered that one of the assumptions of the present study was that the solar panels produce only the necessary electrical energy for running the dairy unit, explaining the lower CF improvement in comparison to Murgia et al. (2013), while it cannot be neglected that the functional unit in our study is different.

Similarly, the present study reveals the benefits of the transition from conventional to green energy. The shift to solar energy has a notable effect on decreasing the supply chain system's GHG emissions as well as its dependency on fossil fuels. By integrating renewable energy systems, dairy farms can potentially lower their CF and achieve improved environmental performance. The comparative analysis between the actual and the theoretical operating scenario highlights that the cheese production process, primarily driven by milk production, was the major contributor to both climate change and resource use impacts. However, with the incorporation of green energy, there was a notable, potential reduction in these impacts, demonstrating the advantages of renewable energy adoption.

5. Conclusions

The present study explores the environmental benefits per kg of PDO 'Kasseri-kefali' cheese of transitioning a dairy unit's energy supply from conventional to renewable resources. Comparing the current operation state with a theoretical scenario powered solely by integrated solar panels showed potential sustainability improvements.

The CF reduction from this transition is notable, particularly when focusing on energy and fuel inputs. Specifically, the study found a 41% improvement in the CF and a 30% reduction in fossil fuel use, changes that are solely associated with the energy inputs in the unit. This improvement was attributed to the utilization of solar energy and the dairy plant's decoupling from the conventional energy grid, underscoring the critical role that energy consumption plays in the dairy's operations.

Our study supports the transition to green energy, demonstrating notable improvements in both the CF and resource use, underscoring the potential of such practices to enhance the environmental performance of cheese production in Greece.

References

Breen, M., J. Upton, and M.D. Murphy. 2020. “Photovoltaic Systems on Dairy Farms: Financial and Renewable Multi-Objective Optimization (FARMOO) Analysis.” *Applied Energy* 278 (November):115534. https://doi.org/10.1016/j.apenergy.2020.115534.

Canellada, Fernando, Amanda Laca, Adriana Laca, and Mario Díaz. 2018. “Environmental Impact of Cheese Production: A Case Study of a Small-Scale Factory in Southern Europe and Global Overview of Carbon Footprint.” *Science of The Total Environment* 635 (September):167–77. https://doi.org/10.1016/j.scitotenv.2018.04.045.

European Comission. 2019. “JRC Annual Report.”

———. 2022. “Directive (EU) 2023/2413 of the European Parliament and of the Council of 18 October 2023 Amending Directive (EU) 2018/2001, Regulation (EU) 2018/1999 and Directive 98/70/EC as Regards the Promotion of Energy from Renewable Sources, and Repealing Council Directive (EU) 2015/652.” http://data.europa.eu/eli/dir/2023/2413/oj.

European Commission. Joint Research Centre. 2020. *Guide for EF Compliant Data Sets.* LU: Publications Office. https://data.europa.eu/doi/10.2760/537292.

European Dairy Association. 2018. “Product Environmental Footprint Category Rules for Dairy Products.” https://eda.euromilk.org/uploads/media/PEFCR-DairyProducts_2018-04-25_V1.pdf.

Ghinea, Cristina, and Ana Leahu. 2023. “Life Cycle Assessment of Sheep Cheese Production in a Small Dairy Factory from Romanian Rural Area.” *Environmental Science and Pollution Research* 30 (3): 6986–7004. https://doi.org/10.1007/s11356-022-22644-2.

Ministry of Environment and Energy. 2023. “Climate Change Emissions Inventory.”

Murgia, Lelia, Giuseppe Todde, Maria Caria, and Antonio Pazzona. 2013. “A Partial Life Cycle Assessment Approach to Evaluate the Energy Intensity and Related Greenhouse Gas Emission in Dairy Farms.” *Journal of Agricultural Engineering* 44 (2s). https://doi.org/10.4081/jae.2013.279.

The Green Watt. 2023. “How to Calculate Solar Panel Output? (+ kWh Calculator). How to Calculate Solar Panel Output? (+ kWh Calculator).” 2023. thegreenwatt.com.

Compact Bio-CNG farm filling fuel production from anaerobic digestion: Hollow fibre permeation and hybrid compression for technically and economically feasible small scale biofuel production

Lukas Wannasek[a*], Dimitris Tyris [b], Josef Hoeckner[c], Detlef May [d], Christian Ammon[a], Barbara Amon[a], Olivier Marchand[e], Dimitris Manolakos[b], Thomas Amon[a]

[a] Leibniz Institute of Agricultural Engineering and Bio-economy e.V. – ATB, Max-Eyth Allee 100, 14469 Potsdam, Germany

[b] Agricultural University of Athens, Iera Odos 75, 11855 Athina , Greece

[c] BioG GmbH, Weilbolden 18, 4972 Utzenaich, Austria

[d] Lehr- und Versuchsanstalt für Tierzucht und Tierhaltung e.V. – LVAT, Neue Ch. 6, 14550 Kreutz (Havel), Germany

[e] CRMT SAS, 3 Chemin de la Brocardière, 69570 DARDILLY, France

[*] Corresponding author. Email: Lukas.wannasek@gmx.at

Abstract

As several studies have shown, agricultural residues can produce the total fuel requirement for the agricultural sector as non-fossil fuels. Challenges that could be solved largely with the realized pilot plant within this study were the economic feasibility of very small Bio-CNG production plants from 10m^3 raw biogas/h and the achievement of fuel quality >97% CH_4.

The study shows the results from the operation of the two pilot plants (i) the one with 10 m^3/h of raw biogas at the Leibniz Innovation Farm for Sustainable Bioeconomy near Potsdam, Germany, and (ii) the other with 35 m^3/h of raw biogas in Utzenaich, Austria. The pilot plant in Potsdam has operated since January 2024 and supplies the farm's fuel for CNG-powered tractors. The study describes the measured key performance indicators of the two pilot plants, such as bio-CNG quality, specific energy consumption, and manufacturing costs of market-ready plants. Taking into account current market prices for raw biogas and electricity as well as investment costs for the Bio-CNG plant, total costs for Bio-CNG production (@>250bar) of 1.51€/kg Bio-CNG for the 35 m^3/h plant, and 2.25€/kg Bio-CNG for the 10 m^3/h plant could be determined. The energy consumption was determined at ~1 kWh per Nm^3 of biomethane (purified and highly compressed) in pilot operation. With the results from the monitoring of the two realized pilot plants, the study also determines the expected unit costs per plant as well as specific costs of €/kg Bio-CNG fuel for further plant sizes of 65 m^3/h and 100 m^3/h raw biogas. The expected cost degression is seen between the system sizes. The development of the small-scale micro-Bio-CNG farm filling station is proving to be technically and economically feasible based on pilot plant data.

Keywords: biomethane, Livestock farming, de-fossilization, membrane separation, anaerobic digestion

1. Introduction

Biomethane production from biogas (derived from manure) can be either upgraded to electricity and heat in Combined Heat and Power plants (CHP) or to fuel for farm tractors. One of the main barriers to producing own fuel on the farm from biogas is the economic feasibility on a very small scale. A promising biogas to biomethane upgrading technology that could be applied in the project is based on membranes separation. The membrane-based biogas upgrading technology achieves biomethane production of 98% clean CH_4 with limited slip (< 0.1%), using a variety of biogas compositions and qualities. The aim is to further optimise the series of processes, focusing on the pre-treatment, to reduce the energy consumption of the integrated system by about 5%, and enable its wide use in livestock farms. Further aim of the pilot and demo plant here is to create a possibility for the processing of biogas to Bio-CNG on small biogas plants in the smallest farm filling standard through technical further developments. For this purpose, the current status of biogas production at the pilot-farm LVAT (Leibniz Innovation Farm for Sustainable Bioeconomy) was surveyed, and literature and market research were carried out for the smallest Bio-CNG product. Since there were hardly any economically viable systems on such a small scale (10 Nm³ h^{-1} biogas) on the market, a new technological setup with a hollow fiber membrane in the low-pressure range (8 bar) and 2 in 1 hybrid compression was set up. With the new concept, the decarbonization of a company's or livestock farms own vehicle fleet should be able to take place in an efficient and economical way using micro-Bio-CNG production from Biogas.

Fuel production from biogas is predestined for energy use in agriculture and forestry in order to protect the climate, strengthen regional value chains, and establish bioeconomy cycles by switching from fossil fuels to sustainable and domestic biofuels.

Especially for agricultural livestock farms, off-grid biogas upgrading with small upgrading plants (10 and 35 $Nm^3\ h^{-1}$ biogas) and on-farm biomethane use as fuel for tractor propulsion is an interesting solution. Typical for such farms is a seasonally strongly fluctuating fuel demand, so that a timely and continuous biomethane supply in the course of the year is usually not given and, in addition, different energy sources (heat, electricity, and fuel) are needed simultaneously on a daily basis. Therefore, a concept with coupled biomethane and electricity production is aimed for.

However, there is still little operational experience and data on the technical and economic feasibility of such plant concepts. For the economic viability of micro-treatment plants, technically simplified plant concepts must be developed that achieve low specific investment costs and at the same time guarantee the required safety requirements. In addition to the lower specific investment costs, further revenues from greenhouse gas avoidance costs are to be achieved.

The research and development project H2020 RES4LIVE aims at a coupled biomethane and electricity production with integrated micro upgrading plants for biogas for internal biomethane use. There is a need for optimization due to the overlapping of the demand for the energy sources over time. Conventional diesel engines are also to be retrofitted to run on gas, especially for in-plant mobile drives, to reduce costs and expand the range of applications for the existing demand. The aim is to record the technical parameters of the operation of micro biogas upgrading plants, the retrofitting of existing diesel engines for gas operation with optimization of the operation (load response and emissions), primarily for internal applications, and the determination of the economic efficiency and greenhouse gas avoidance potential.

2. Materials and Methods

The present study is carried out as part of the Horizon project RES4LIVE (Grant Agreement No. 101000785), which in general will adapt and test promising RES technologies in energy-intensive livestock farming for greatly reducing the fossil energy that is the main source to covering the energy demand. Dedicated, optimal designs combined with energy efficiency and other solutions are proposed, demonstrated in 4 pilot farms, and evaluated technically, economically, environmentally, and socially. The overall objective is to provide advanced and cost-effective technologies to the livestock sector that ensure the sustainability of the farms' operation, and the superior thermal comfort of the animals for increased productivity with minimum climate change impact. The strategic objective of RES4LIVE is to develop and bring into the market integrated, cost-effective, and case-sensitive RES solutions towards achieving fossil-free livestock farming.

2.1. Novelty of micro-Bio-CNG plant

The Bio-CNG farm filling station developed in this project is characterized by its very simplified and compact design in terms of compression. By integrating the biogas to biomethane processing in the existing biogas CHP process, a 1-stage (single membrane) process can be used for CH_4 concentration instead of a multi-stage membrane process. As a result, there are no direct emissions at the Biomethane-, and further compressed to Bio-CNG plant. Through further development with the integration of a hybrid compressor, the processes of membrane gas permeation [>95% CH_4 biogas] and CNG production by means of high compression can be managed with just one electric motor and compressor block. Among other things, hybrid compression makes a significant contribution to reducing maintenance costs, reducing investment costs, and reducing operating (energy) costs. The high compression up to 250 bar takes place by means of piston compressor stages 2 and 3, whereby the CH_4 separation process after piston stage 1 is integrated directly into the piston compression without pressure loss.

The membrane separation process was specially designed in the low-pressure range at 7-8 bar through simulation to create better integration into hybrid compression and to maintain the energy saving effect. For further cost savings and to prevent the formation of explosion zones in closed rooms, the Bio-CNG farm filling station and processing was constructed entirely in an open-frame design on a 20ft frame. For summer/winter operation, all system components are thermally insulated and zones at risk of frost are permanently protected against frost. The heat-insulated zones of the system, which are not at risk of frost, are

also preheated by means of heating for a shorter start-up operation. The system is operated stop-and-go and has a 250 bar intermediate storage to be able to optimize the production times of the system and to reduce the refuelling time to a minimum.

The farm filling station for Bio-CNG with direct production of biomethane from biogas on-site represents a strictly non-public operation compared to conventional systems. Complex parts like electronically controlled odorization for example can therefore be dispensed with.

Due to the processing of biogas with the property as a combustible gas and the potential possibility of the formation of explosive gas mixtures in the presence of oxygen, a large part of the plant must be equipped with ATEX-compliant (components for flammable gases manufactured according to the explosion protection directive) machines and devices. Only the control unit and the cooling water set are not designed according to ATEX directives and are located on the compact open frame 20ft system frame (all in one) at a corresponding distance from the designated Ex (ATEX) zones.

2.2. Design concept of the pilot plants

The system design is based on the basic principle of the most simplified possible technical operation due to the very strong need for downscaling for the realization of such small systems. In order to operate the farm filling station in the simplified 1-stage system, a maximum of 20% of the total raw gas flow of the biogas plant is used, so that the OFF-GAS, which contains a lot of CO_2, from the biogas processing only dilutes the raw gas for the combined heat and power plant to the permissible extent. In contrast to larger commercial systems, the present concept deliberately designed a completely ventilated system in an open-frame design instead of the conventional closed design.

The input streams into the plant represent water-saturated raw biogas with ~52% CH_4 content and electrical energy. The output streams of the plant are Bio-CNG, OFF-GAS with > 80% CO_2 content and H_2O condensate from cooling and dehumidification of the raw biogas.

Due to the open-frame design, all system components are directly exposed to the ambient temperatures. To protect the system parts against frost in winter and to ensure sufficient temperature for start-up operation, all system parts are thermally insulated and equipped with accompanying heating and accompanying temperature control throughout. Due to the direct electrical heating and preheating under the thermal insulation instead of inside the housing to be tempered, a very low heat requirement and thus low operating costs are expected. Due to the heat generated during compression, no heating or temperature control is necessary during operation. Since the system runs in stop-and-go mode and can be out of operation for days and hours, the system is divided into areas to be protected against frost and areas to be preheated to prevent unnecessary energy inputs with regard to energy efficiency. Areas to be protected against frost are kept permanently at >3C° when the system is at a standstill, with areas to be preheated being automatically temperature-controlled up to 20 minutes before the system starts.

The biogas is purified from ~52% CH_4 to >95% CH_4 using a 4-inch hollow fiber membrane made by EVONIK. The quality of the product gas is influenced by temperature, flow rate, and pressure. The control parameters mentioned, above all flow and pressure, are adjusted to the desired gas quality using a CH_4 quick measurement (CH_4% = controlled variable).

An additional outdoor temperature-compensated filling prevents the storage tank and vehicles from being overfilled in summer/winter operation. In contrast to commercial filling stations, where the temperature-compensated filling is regulated directly in the vehicle, the temperature-compensated filling is already carried out for cost reasons by switching off the storage tank filling depending on the outside temperature.

2.3. Hybrid 2 in 1 compressor design

The re-design of the piston compressor for the processing and high compression of the raw biogas to Bio-CNG to a hybrid compressor plays an important role in the feasibility of the farm filling station in terms of investment cost reduction and energy consumption. As shown in Figure 1, the 1st stage of the compressor block acts to compress the raw gas which is taken from the 1st cylinder for processing. The compressor stages 2 and 3 only compress the processed biomethane to CNG. A significant change is the reduction of the gas volume flow of 10 $Nm^3\ h^{-1}$ in the 1st stage to about 4 $Nm^3\ h^{-1}$ in the 2nd and 3rd stages.

For this purpose, a constructive change was made to reduce the volume of the 2nd and 3rd cylinder stage in order to ensure compression without damage to the compressor and with the corresponding efficiency despite the gas volume reduction within the 3-stage compression process.

After the gas has been removed from the 1st stage [Figure 1], the remaining cleaned gas volume flow of around 4 $Nm^3\ h^{-1}$ is fed back to the structurally smaller 2nd compression stage for high compression. The pressure from the 1st stage was increased in hybrid compression to up to 8 bar compared to conventional compression to be able to create sufficient raw biogas processing. The design pressure of the membrane was selected with the comparatively low pressure of 8 bar for hollow fiber membranes to have a further safety and control margin.

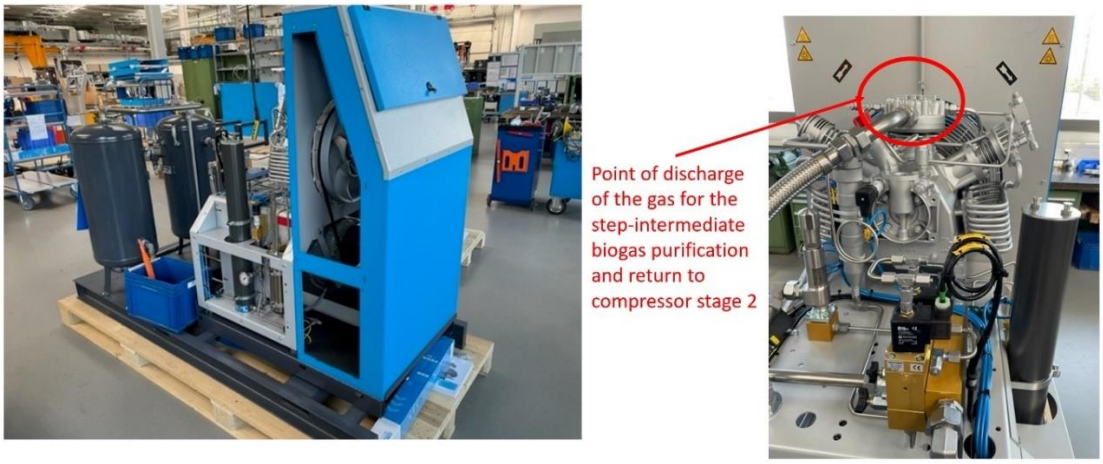

Figure 1 Hybrid 2 in 1 compressor

2.4. Technical characteristics of micro-Bio-CNG 10 $Nm^3\ h^{-1}$ raw biogas plant

As shown in Figure 2, the micro-Bio-CNG plant operates as a fully closed cycle process, with the exception of the Bio-CNG CH_4 fuel discharged. The raw biogas is sucked from the gas storage tank of the biogas plant into the farm filling station at about 35 C° and 3 mbar in a water-saturated state. In the system, a small ATEX side channel compressor with $250W_{el.}$ ensures that the raw biogas is sucked in from the biogas storage tank and is available at around 100 mbar on the input side of the 3-stage piston compressor. There is an automatic condensate drain and an iron pellet filter for desulfurization in the intake line in front of the side channel compressor. Starting at 100 mbar, the desulfurized raw biogas is brought to a pressure of around 8 bar in the 1st compressor stage.

The 10 $Nm^3\ h^{-1}$ raw biogas are now within the compression process dewatered with the pressure of 8 bar from the 1st compression stage, oil separated, NH_3 separated, and fine particles separated. Finally, 4 of the 10 $Nm^3\ h^{-1}$ are concentrated to a CH_4 content of around 97%. The remaining 4 $Nm^3\ h^{-1}$ are highly compressed to CNG with the same compressor. The off-gas flow with CO_2 and CH_4 is completely recycled back into the biogas storage. The dilution of the raw biogas with regard to the CH_4 content (by separating 97% CH_4 gas from the biogas storage) may only be carried out sufficiently up to the permissible level for the existing CHP.

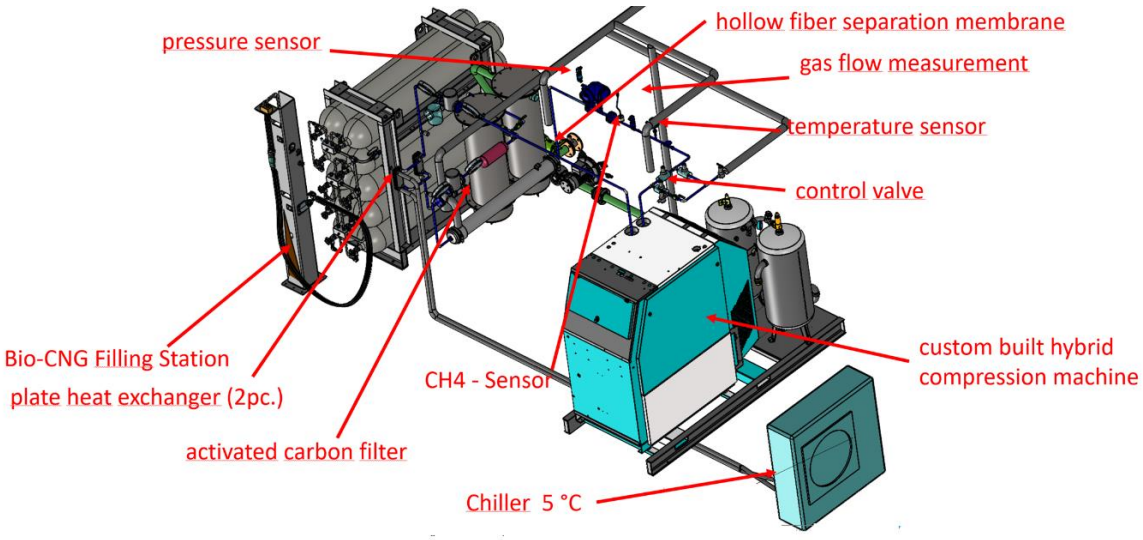

Figure 2 Construction of the micro-Bio-CNG plant

3. Results and Discussion

The pilot operation of the 10 $Nm^3\ h^{-1}$ raw biogas plant started with first trials in 07/2023. The results from the data monitoring of the 10 m^3 $Nm^3\ h^{-1}$ raw biogas plant, as well as the 35 $Nm^3\ h^{-1}$ raw biogas plant launched a few months later, show promising findings in terms of stable process technology and economics. With a look at the figures for the use of bio-CNG as fuel in tractors known from the literature, the potential that micro-Bio-CNG plants of this type hide for the de-fossilization of agriculture becomes clear. Literature data shows that the manure from a single cow can be used to plow the equivalent of 6-8 hectares per year.

The pilot plant showed soon after the start of trial operations that the initially risky hybrid compression technology shows consistently stable technical operating conditions and that the compression of different gas volumes in the 3 compression stages actually works. The only few technical faults were rectified just a few days after the pilot plant was first started up at the LVAT pilot-farm (Leibniz Innovation Farm for Sustainable Bioeconomy). The official approval process for the approval of a micro-bio-CNG plant of this type in the Brandenburg area of Germany proved to be very complicated. This barrier must be significantly reduced for future plants in cooperation with politics and the authorities.

3.1. Key performance indicators of the 10 $Nm^3\ h^{-1}$ raw biogas pilot plant

As shown in table 1, from the logged data of the 10 $Nm^3\ h^{-1}$ raw biogas system over a period of more than half a year (winter/summer operation), a specific energy consumption of 0.94 kWh_{el}/Nm^3 Bio-CNG (±0.15) was recorded. This energy consumption covers the energy requirement for the separation of CO_2 from the biogas and thus the purification of biomethane, as well as the compression of the biomethane to 250 bar to Bio-CNG. Assuming an energy content of 10.5 kWh_{el} per Nm^3 of bio-CNG, this results in an energy consumption of 9.0% as a proportion of the fuel. The average separation pressure in the hollow fiber membrane and the average membrane inlet temperature in the measured data are 7.38 bar (±0.47) and 57.44 °C (±2.49). The measured pressure in the hollow fiber membrane for gas separation is a comparatively low value for membrane separation.

Table 1 Key performance indicators from the data monitoring of the pilot plant 10 Nm³ h⁻¹ raw biogas upgrading and Bio-CNG farm filling station at LVAT pilot-farm within H2020 project Res4Live

key indicator	x̄	SD	n
specific energy consumption [kWh_{el}/Nm^3 BioCNG]	0,94	0,15	14896
separation pressure hollow fiber membrane [bar]	7,83	0,47	18771
separation temperature hollow fiber membrane [°C]	57,44	2,49	18771
methane concentration [%]	96,75	1,28	29771
start-up time until BioCNG production OK [min]	26,78	5,49	9

The average methane concentration achieved in the data measured in the 1-stage membrane process is 96.75 %. It should be noted that this is far sufficient for refueling CNG vehicles, as the CH_4 concentration for use in the gas engine is allowed to be lower compared to the requirement in this point for gas grid injection. The average time from starting the pilot plant with raw biogas after a longer standstill to reaching the necessary bio-CNG methane concentration (>95%) is 26.78 minutes. It was observed that this time was slightly higher in the colder season than in the warmer months. In the months of January and February, for example, the average time to achieve the same gas quality was over 30 minutes. Nevertheless, these values of around half an hour represent acceptable values for practical operation, as the system only restarts once a day in normal operation and completely fills the empty gas storage cylinders.

3.2. Economic data of 10 and 35 Nm^3 h^{-1} raw biogas pilot plants

In order to estimate the economic efficiency of the micro-Bio-CNG plants, a total cost calculation was made on the basis of the measured data for the 10 and 35 Nm^3 h^{-1} raw biogas pilot plant, assuming costs for the raw biogas of €0.5/kgCH_4, electricity costs of €0.2/kWh_{el}, and a depreciation period of 10 years.

Taking into account the energy consumption measured at the pilot plants, the total costs are €2.25/kg Bio-CNG for the 10 Nm^3 h^{-1} raw biogas plant and €1.51/kg Bio-CNG for the 35 Nm^3 h^{-1} raw biogas plant. The degression in the total costs per fuel unit is almost entirely due to the depreciation caused by the investment. The calculated costs therefore already represent an economic business case for very small Bio-CNG plants such as those examined here. The remuneration of greenhouse gas quotas, which may be obtained in the future for the production and utilization of biofuel, would significantly improve the economic feasibility even further.

4. Conclusions

A technically simplified micro-Bio-CNG technology was developed for the on-farm own processing of biogas into biomethane. The biomethane is to be used as a fuel to drive tractors. As a further consequence, systems of this type can contribute to the reduction of the consumption of fossil fuels, if they are used across the board. The decentralized use of such technology can quickly pay off, especially with rising energy prices and rising costs for transporting energy sources. The total cost calculation based on the determined values of both plants shows that an economic operation for such a micro-Bio-CNG plant is feasible. Another source of income for farmers who pursue the Bio-CNG fuel production will be the revenue from greenhouse gas quotas in the future. Based on the project results, the on-farm Bio-CNG production thus represents a promising

possibility for the de-fossilization of the entire agricultural economy.

Acknowledgements

This Project has received funding from the European Union's Horizon 2020 Research and Innovation Program under Grant Agreement No. 101000785.

References

[1-6] The references used are available for inspection at the corresponding author.

Modelling of energy usage on dairy farms using ANN
"Case study in Canterbury province, New Zealand"

Majeed Safa, Hafiz Muhammad Abrar Ilyas
Department of Land Management and Systems, Lincoln University, New Zealand

Abstract

This study was conducted over 35,300 hectares of pastoral (PDFs) and barn (BDFs) dairy farming systems in Canterbury. Total energy consumption on these dairy farms was estimated at 5295 MJ/ha. On average, fertilizer and electricity were the most used energy sources, accounting for approximately 30% and 35% of the total energy consumption, respectively. The energy consumption for milk production in pastoral (PDFs) and barn (BDFs) dairy farming systems was estimated at 50,538 MJ/ha and 55,833 MJ/ha, respectively.

Several direct and indirect factors were identified in this study to create a Multi-Layered Perception (MLP) artificial neural network (NN) model to predict energy use in milk production, achieving an R-square value of 0.91. The final model can predict energy consumption based on farm conditions (number of cows), farmers' social considerations (farmer's age), and energy inputs (electricity).

Keywords: Modelling, Energy Consumption, Neural Networks dairy farming, New Zealand

1. Introduction

Energy is a crucial element in modern agriculture. Without it, farming would be impossible, as modern agriculture heavily depends on energy use and fossil resources. Energy consumption in agriculture has been rising due to the limited supply of arable land, a growing population, technological advancements, and the desire for higher living standards (Hatirli et al., 2006; Kizilaslan, 2008; Safa and Samarasinghe, 2011; Manaloor and Sen, 2009).

Unlike other sectors, energy use in agriculture has received very little attention from scientists in various countries. This lack of scientific focus is primarily due to data shortages and a lower level of multidisciplinary work, causing researchers to overlook this area. However, energy consumption in agricultural production has been increasing more rapidly than in many other sectors. It is evident that energy use in modern agriculture has increased. However, the growth rate of production has been even higher, resulting in lower energy use per unit than in the past (Singh, 2023; Sauerbeck, 2001).

Some studies show that there is a positive relationship between energy usage and productivity. To minimize greenhouse gas (GHG) emissions, it is essential to reduce farm energy inputs (fossil fuels, fertilizers, etc.). This goal can be achieved in two ways: either by substantially increasing energy efficiency, where the same output is produced with less energy input, or by using more sustainable energy sources such as solar, wind, biomass, etc.. (Singh et al., 2004; Karkacier and Gokalp Goktolga, 2005; Outlaw et al., 2005; Hatirli et al., 2006; Karkacier et al., 2006; Baruah and Bora, 2008; Smil, 2008). Also, there is a significant relationship between energy output and weather, price, yield, and technology (Ozkan et al., 2004). Some energy sources in the agriculture sector are classified under other sectors. For instance, fuel consumption for farm operations might be categorized under the transport sector, and indirect energy sources like fertilizers, seeds, and agrichemicals might be estimated in the industrial sector. As a result, official national statistics often do not accurately reflect energy use in agriculture, and they pay very little attention to energy consumption within the agriculture sector. (Pellizzi, 1992). New Zealand is one of the countries with the highest energy input per unit (in agriculture) in the world (Safa and Samarasinghe, 2011; Conforti and Giampietro, 1997). Furthermore, rising global fuel prices have a greater impact on New Zealand farming compared to other countries, especially in terms of shipping.

Energy modeling is a compelling subject for engineers and scientists interested in energy production, consumption, and environmental impacts (Tester, 2005; Al-Ghandoor et al., 2009). In the field of energy, a wide range of models have been utilized, from geological models for researching natural resources to models for predicting future energy demand (Tester, 2005). Neural networks are capable of modeling complex nonlinear systems in a flexible and adaptive manner. As a result, they are increasingly being used to solve various problems in science and engineering (Jebaraj and Iniyan, 2006).

The advantages of using NN models include their simplicity of application and the robustness of their results. NNs have evolved into a powerful approach capable of approximating any nonlinear input-output mapping function with high accuracy through iterative processes. They possess several attractive

properties for modeling complex production systems, such as universal function approximation capability, resilience to noisy or missing data, accommodation of multiple nonlinear variables with unknown interactions, and strong generalization ability (Hagan et al., 2002; Samarasinghe, 2007).

n most studies, a feed-forward Multi-Layered Perceptron (MLP) paradigm, consisting of one or more input layers, hidden layers, and an output layer trained via backpropagation (BP), is used. Due to its well-documented ability to model any function, MLP trained with BP is chosen to develop models for apparatus, processes, and product prediction (Safa and Samarasinghe, 2011). During the processing of inputs by the network, each neuron in the first layer (hidden layer) computes the weighted inputs using a transfer function to generate its output. These transfer functions can be linear or nonlinear and include options like Logistic, Hyperbolic-tangent, Gaussian, and Sine functions. The specific transfer function used determines the output. This output is then transmitted to neurons in the next layer via weighted connections, where they complete their outputs by processing the sum of weighted inputs through their respective transfer functions. In the case of the output layer, the neuron's output represents the predicted output (Safa and Samarasinghe, 2011).

Various methods of error estimation have been proposed, with Mean Square Error (MSE) over all training patterns being the most commonly used indicator. MSE is particularly valuable for comparing different models as it demonstrates the network's ability to predict the correct output. Mathematically, MSE can be expressed as:

$$MSE = \frac{1}{2N}\sum_{i}^{N}(t_i - z_i)^2 \quad (1)$$

where ti and zi are the actual and the predicted output for the ith training pattern, and N is the total number of training patterns (Samarasinghe, 2007). Root mean square error (RMSE) is another error estimation, which shows the error in the units of actual and predicted data.

It's generally more effective to tackle problems with the minimum number of variables. When dealing with a significantly high number of variables, especially with a limited number of samples, data reduction becomes advantageous. Additionally, when some input variables are correlated with each other, a problem known as multicollinearity arises. Correlation among inputs diminishes the likelihood of finding a unique solution (Samarasinghe, 2007). The most commonly used method for data reduction and removal of multicollinearity is Principal Component Analysis (PCA). PCA is a valuable technique for selecting the most important uncorrelated variables. It operates by utilizing the mean, variance, and covariance of each input variable to construct a covariance matrix (COV) (Samarasinghe, 2007). This matrix is then transformed to derive independent components, which are linear combinations of the original inputs. The resulting components allow for the selection of either individual uncorrelated variables or the use of independent components as inputs to the model.

2. Methodology

The study was conducted on pastoral (PDFs) and barn (BDFs) dairy systems in Canterbury, New Zealand, a significant dairy region comprising 10% of dairy herds and 16% of dairying land in the country (DairyNZ, 2019). Carbon footprints, in the form of CO2 emissions associated with energy consumption, were measured in this study, excluding CO2 emissions from agricultural soils.

Energy consumption in this context refers to the energy utilized in milk production that leaves the farm. Data collection involved three main sources: questionnaires, literature reviews, and field measurements. The energy inputs considered in this study encompass those involved in on-farm production systems prior to post-harvest processes. Natural energy sources such as radiation, wind, and rain were not included in the analysis.

The analysis of energy consumption on dairy farms focused on both direct and indirect energy sources, which include human labor, fuel, fertilizers, pesticides, machinery, and seeds. Total energy input (E) was calculated as the sum of input factors (Ai) multiplied by the appropriate energy conversion coefficient for each factor (Ci), expressed by the formula:

$$E = \Sigma(Ai\ Ci) \quad (2)$$

Various energy conversion coefficients are used to convert farm inputs and outputs into energy equivalents. Table 1 presents the energy equivalents of different inputs as reported in important references. Discrepancies among these coefficients arise from differences in technology, estimation methods, and other factors, some of which are significant.

Table 1. Energy equivalents of different inputs and outputs

Inputs items	Unit	Energy Coefficients (MJ unit^{-1})	References
Direct Energy Inputs			
Diesel	litres	45	MED (2012)
Petrol	litres	42	MED (2012)
Electricity	kWh	8	MED (2012)
Human Labour	hours	1.96	Mani, Kumar, Panwar, and Kant (2007)
Indirect Energy Inputs			
Fertilizers			
Nitrogen (N)	kg	64.1	Wheeler (2018)
Phosphorous (P)	kg	28.4	Wheeler (2018)
Potassium (K)	kg	17.8	Wheeler (2018)
Sulphur (S)	kg	3.24	Wheeler (2018)
Feed Supplement			
Grass Silage	t DM	1781	Wheeler (2018)
Maize/Cereal Silage	t DM	1564	Wheeler (2018)
Hay	t DM	1329	Wheeler (2018)
Grains	t DM	3905	Wheeler (2018)
Concentrates	t DM	1800	Wheeler (2018)
Machinery & Equipment			
Tractors	kg	160	Wells (2001)
Utes	kg	160	Wells (2001)
2-Wheeler Motorbikes	kg	160	Wells (2001)

* For different varieties, different equivalents were used

In this study, careful investigation and selection of energy conversion coefficients were conducted. Apart from direct and indirect energy inputs, various other factors, including technical, social, geographical, and financial aspects, could indirectly influence energy consumption. Approximately 60 factors were examined, such as farmers' social status, age of equipment, power of machinery, paddock numbers and sizes, and yield, to design a model predicting energy consumption in milk production. Incorporating these indirect factors into energy prediction could potentially minimize energy consumption at minimal cost and without significantly impacting farmers' income.

Identifying suitable variables is crucial in model creation. Extracting all relevant input variables was straightforward, with farmers having a clear understanding of them. Following data processing and input reduction, three variables were selected: Number of cows, farmer’s age, and electricity consumption (KWh). These variables were chosen based on their lack of correlation and were determined using Principle Component Analysis (PCA). For instance, significant correlations were observed between the number of cows and farm size, as well as between nitrogen consumption and electricity consumption, leading to the removal of nitrogen consumption and farm area from the input variable list.

Neural networks (NNs) proved effective in describing the influence of energy sources, agricultural operations, and indirect factors on energy consumption in milk production. The study utilized a sample size of 55 farms, with 40 farms randomly selected for training initially, and the remaining 15 farms used for validation.

After several trials using Peltarion Synapse software, a MLP neural network with two hidden layers was chosen. This MLP network structure involves a series of independent neural networks after the input layer, each performing subtasks trained separately with different examples from the sample, with their outputs summed in the output layer. This structure equips the network to simultaneously utilize different

model functions for the data.

The Quick Prop learning method was employed due to its efficiency in error reduction and model optimization. Quick Prop utilizes the second derivative of error to adjust weights, regulating the update for weights in each iteration.

$$w_{m+1} = w_m + \Delta w_m$$

$$\Delta w_m = \frac{d_m}{d_{m-1} - d_m} \Delta w_{m-1}$$

$$d_m = \sum_{n-1}^{N} \left[\frac{\partial E}{\partial w_m} \right]_n$$

where Δwm is the current weight increment, dm is the average derivative of the error with respect to the weight for the current epoch m; and ∂E/∂wm is the current error gradient for a particular input vector (Samarasinghe, 2007).

Preliminary trials revealed that networks with two hidden layers produced superior results compared to those with only one hidden layer. Various functions were tested, and for the final model, the hyperbolic tangent (tanh) function was chosen for the first hidden layer, while the logistic function was employed for the second hidden layer.

It's worth noting that numerous combinations of layers and neurons, as well as different functions, structures, and learning methods, were explored to identify the optimal model with minimal iterations. The number of neurons was optimized using a genetic algorithm program.

3. Results

3.1 Energy Consumption

On average, energy consumption on dairy farms in Canterbury was approximately 5295 MJ/ha. To provide a clearer understanding, the energy consumption was analyzed separately for pastoral and barn dairy farming systems (Table 2).

Table 2. Energy Consumption of Pastoral & Barn Dairy Farming Systems (MJ/ha)

	Pastoral				Barn			
Items	**Avg**	**SD**	**Min**	**Max**	**Avg**	**SD**	**Min**	**Max**
Direct Energy Inputs								
Diesel	1824	778	436	4124	5099	4776	1570	15750
Petrol	687	379	113	1752	1178	458	900	2198
Electricity	17917	14626	3312	78954	19447	11206	10095	34020
Labour	86	21	46	141	114	30	55	150
Indirect Energy Inputs								
Fertilizer	15128	4139	3579	19064	9206	5071	0	16244
Feed Supplements	6937	4338	0	16124	12515	2035	10580	16655
Machinery	7959	2546	1031	15680	8274	2252	3688	10559
Total Energy Use	50538	16598	18539	108750	55833	11494	40737	69872
Output								
Milk	60571	17480	32693	94141	64121	18447	44894	96710

3.2 The Model Results

As previously mentioned, after evaluating different learning algorithms, neuron activation functions, and network structures, a MLP network with two hidden layers was developed, as illustrated in Figure 1. In the final model, the Quick Prop learning method outperformed other gradient descent methods. The hyperbolic tangent (tanh) function was selected for the first hidden layer, while the logistic function was used for the second hidden layer. The number of neurons in each layer was optimized using a genetic algorithm.

As depicted in Figure 1, the MLP network with two hidden layers had the best results with minimum

margin of error. The genetic algorithm optimized the number of neurons of each layer to 63 in the first hidden layer and 17 in the second hidden layer. The results of second hidden layer was transferred to the output layer to produce the final output, which is the energy consumption.

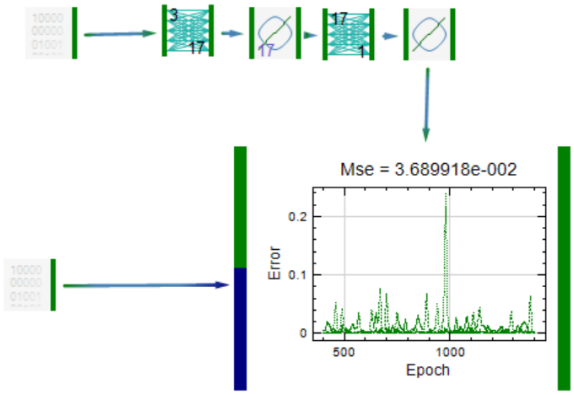

Figure 1. Structure of MLP network and number of neurons in each layer

After 2250 iterations, the neural network (NN) model achieved optimal results with a scaled mean squared error (MSE) of 3.7 E-2 (inputs and outputs were scaled between -1 and +1 for the neural network model). The actual root mean squared error (RMSE) of the final NN model was estimated to be 2130 MJ/ha and 2340 MJ/ha for the training and validation data, the lowest RMSE among the various NN models examined in this study.

As shown in Figures 2 and 3, the NN model's energy consumption estimates accounted for 95% and 96% of the actual variability in energy consumption for the training and validation data, respectively. The correlation between observed and predicted energy consumption was very high, with an R^2 of 0.90 and r of 0.93 for the training data. These figures indicate a higher correlation compared to the multiple linear regression model.

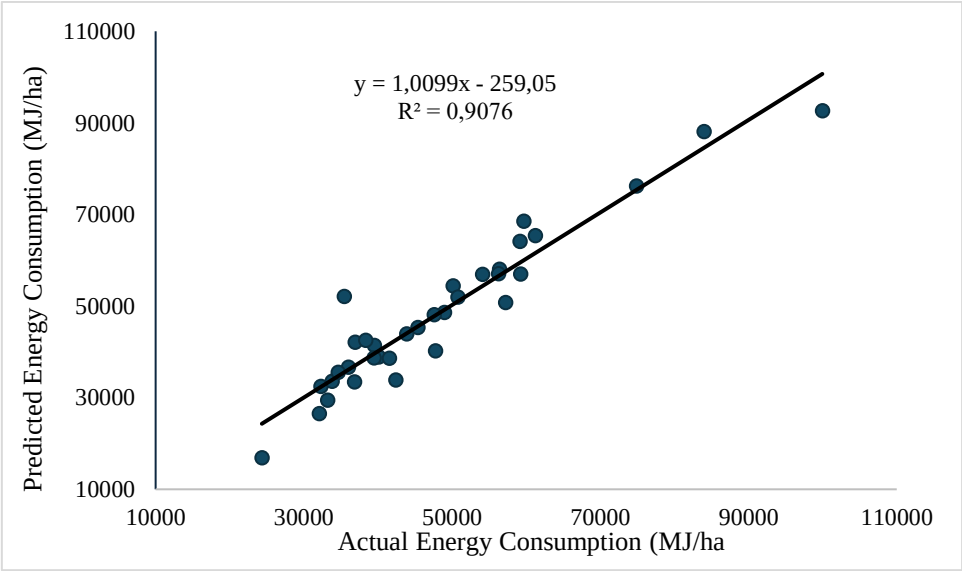

Figure 2.Relationships between the observed and NN model predicted energy consumption (Training data)

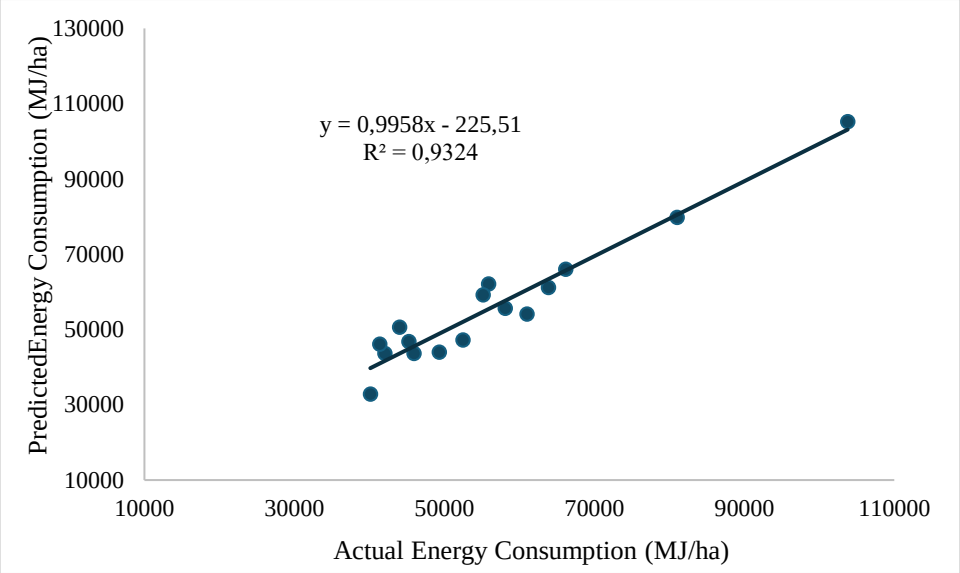

Figure 1. Relationships between the actual and the NN model predicted energy consumption (Validation data)

In agricultural production, numerous uncontrolled factors can influence energy consumption on farms, making the results of this study particularly valuable. The final model can predict energy use in milk production with an acceptably small error. It is important to note that some variables in the final model are fixed and represent farming conditions, such as farmer education, which indirectly affects energy consumption. Therefore, future studies should explore the detailed relationships between input variables and energy consumption in agricultural production.

The NN model can estimate energy use per hectare in milk production and facilitate easy comparisons of energy use across farms. Farmers can utilize the model to identify factors with the greatest potential to reduce energy use on their farms. Additionally, decision-makers and scientists can estimate energy use in different regions of Canterbury and investigate the effects of various energy inputs on energy consumption in milk production.

4. Conclusion

neural network (NN) model was developed based on a MLP neural network with two hidden layers. It can predict energy consumption based on farm conditions (number of cows), social factors (farmers' age), and energy inputs (electricity consumption). In agricultural studies, where numerous uncontrolled factors can influence outcomes, achieving small error margins is remarkable.

The results of this study demonstrate the NN model's ability to predict energy consumption on dairy farms using heterogeneous data. Incorporating diverse variables, such as farm conditions and social factors, enhances the capacity of decision-makers to address the problem from various perspectives. Given the findings, the most significant areas for improving overall modeling and conserving energy are:

- Investigating energy consumption on dairy farms can enhance our understanding of technological advancements and the improvement of farmers' skills, as well as how these factors have contributed to changes in energy efficiency.
- Developing an NN model to estimate energy use in milk solid production, which is crucial for comparing different farming systems.
- Applying the same methodology to develop models predicting fuel consumption, CO2 emissions, and various agricultural outputs, including milk. The existing database can support these investigations. Modeling fuel consumption, CO2 emissions, and energy consumption based on social and technical parameters can drive advancements in agriculture and modeling.

References

Al-Ghandoor, A., Jaber, J.O., Al-Hinti, I., Mansour, I.M., 2009. Residential past and future energy consumption: Potential savings and environmental impact. Renewable and Sustainable Energy Reviews 13, 1262-1274.
Baruah, D.C., Bora, G.C., 2008. Energy demand forecast for mechanized agriculture in rural India. Energy Policy 36, 2628-2636.
Colwell, J.D., 1994. Estimating fertilizer requirements : a quantitative approach. CAB International, Wallingford.
Conforti, P., Giampietro, M., 1997. Fossil energy use in agriculture: an international comparison. Agriculture, Ecosystems & Environment 65, 231-243.
DairyNZ. Zero Carbon Bill; DairyNZ Limited: Hamilton, New Zealand, 2019
Fang, Q., Hanna, M.A., Haque, E., Spillman, C.K., 2000. Neural Network Modeling Of Energy Requirments, For Size Reduction Of Wheat. ASAE 43(4): 947-952.
Hagan, M., Demuth, H., Beale, M., 2002. Neural network design. Boston, USA: PWS Publishing Company.
Hatirli, S.A., Ozkan, B., Fert, C., 2006. Energy inputs and crop yield relationship in greenhouse tomato production. Renewable Energy 31, 427-438.
Jebaraj, S., Iniyan, S., 2006. A review of energy models. Renewable and Sustainable Energy Reviews 10, 281-311.
Karkacier, O., Gokalp Goktolga, Z., 2005. Input-output analysis of energy use in agriculture. Energy Conversion and Management 46, 1513-1521.
Karkacier, O., Gokalp Goktolga, Z., Cicek, A., 2006. A regression analysis of the effect of energy use in agriculture. Energy Policy 34, 3796-3800.
Kizilaslan, H., 2008. Input-output energy analysis of cherries production in Tokat Province of Turkey. Applied Energy In Press, Corrected Proof.
Lackner, M. Energy Efficiency: Comparison of Different Systems and Technologies. In Handbook of Climate Change Mitigation and Adaptation; Springer: New York, NY, USA, 2017; pp. 1309–1384.
Manaloor, V., Sen, C., 2009. Energy Input Use and CO2 Emissions in the Major Wheat Growing Regions of India. International Association of Agricultural Economists Conference,, Beijing, China.
Mani, I.; Kumar, P.; Panwar, J.; Kant, K. Variation in energy consumption in production of wheat–maize with varying altitudes in hilly regions of Himachal Pradesh, India. Energy 2007, 32, 2336–2339.
MED. *Energy Data File 2011*; Ministry of Economic Development: Wellington, New Zealand, 2012
Nguyen, M.L., Haynes, R.J., Goh, K.M., 1995. Nutrient budgets and status in three pairs of conventional and alternative mixed cropping farms in Canterbury, New Zealand. Agriculture, Ecosystems & Environment 52, 149-162.
Outlaw, J.L., Collins, K.J., Duffield, J.A., 2005. Agriculture as a producer and consumer of energy. Wallingford, Oxfordshire, UK ; Cambridge, MA, USA CABI Pub.,.
Ozkan, B., Akcaoz, H., Fert, C., 2004. Energy input-output analysis in Turkish agriculture. Renewable Energy 29, 39-51.
Pellizzi, G., 1992. Use of energy and labour in Italian agriculture. Journal of Agricultural Engineering Research 52, 111-119.
Safa M. and Samarasinghe S. Determination and modelling of energy consumption in wheat production using neural networks: “A case study in Canterbury province, New Zealand”. Energy, 36(8): 5140-5147, 2011.
Samarasinghe, S., 2007. Neural networks for applied sciences and engineering : from fundamentals to complex pattern recognition. Auerbach, Boca Raton, FL.
Sauerbeck, D.R., 2001. CO2 emissions and C sequestration by agriculture – perspectives and limitations Nutrient Cycling in Agroecosystems 60, 253-266.
Singh, P., Singh, G., Gupta, A., Singh Sodhi, G., 2023. Data envelopment analysis based energy optimization for improving energy efficiency in wheat established following rice residue management in rice-wheat cropping system, Energy 283.
Singh, H., Mishra, D., Nahar, N.M., 2004. Energy use pattern in production agriculture of a typical village in arid zone--Part III. Energy Conversion and Management 45, 2453-2472.
Smil, V., 2008. Energy in nature and society : general energetics of complex systems. The MIT Press, Cambridge, Mass.
Sözen, A., 2009. Future projection of the energy dependency of Turkey using artificial neural network. Energy Policy 37, 4827-4833.
Tester, J.W., 2005. Sustainable energy : choosing among options. MIT Press, Cambridge, Mass.

Wheeler. OVERSEER Technical Manual: Carbon Dioxide, Emboided and Other Gaseous Emissions; AgResearch Ltd.: Hamilton, New Zealand, 2018
Wells, C. Total energy indicators of agricultural sustainability: Dairy farming case study. In *Technical Paper 2001/13*; MAF: Wellington, New Zealand, 2001; Volume 13.

Fuel consumption prediction based on GNSS recordings of agricultural machinery

Ying Chen[a,b,*], Liwei Pan[a,b], Xiaoqiang Zhang[a,b], Xiang Luo[a,b], and Caicong Wu[a,b]

[a]College of Information and Electrical Engineering, China Agricultural University, Beijing, China

[b]Key Laboratory of Agricultural Machinery Monitoring and Big Data Application, Ministry of Agriculture and Rural Affairs, Beijing, China

* Corresponding author. Email: chenying@cau.edu.eu

Abstract

With the rapid advancement of agricultural mechanization, fuel consumption in tractors has witnessed an increase, leading to a high production cost. Both tractor selection by operators and tractor optimization by manufactures requires a method to evaluate fuel consumption in practical operation scenarios. In this paper, we propose a novel approach which can automatically predict the fuel flow rate of tractors. Specifically, the approach predicts the fuel flow rate at each point in GNSS (Global Navigation Satellite System) recordings. We initially constructed a fuel consumption dataset containing GNSS recordings collected from 30 tractors. Besides GNSS information, the recordings also contain the engine information and fuel flow rate of these tractors operating from May 2023 and June 2023. Then, we characterize each point with two engine parameters (torque and engine speed) and two motion parameters (driving speed and acceleration), and these parameters serve as the input to a model to predict the fuel flow at that point, where the prediction model has been developed using a machine learning method, Light Gradient Boosting Machine (LGBM). Finally, experiments have been made on the dataset, where, the GNSS recordings of 27 tractors and 3 tractors serve as the training data and test data, respectively. Experimental results demonstrate that the proposed method achieved state-of-the-art performances in predicting fuel flow rate with a R^2 value of 0.946, and motion parameters can significantly improve the robustness of fuel consumption prediction models. The outcomes of this study are crucial for managing fuel consumption in agricultural machinery operations and further advancing agricultural modernization, holding significant application prospects in the field of agricultural mechanization.

Keywords: fuel consumption, prediction model, engine information, GNSS information.

1. Introduction

Fuel consumption evaluation plays an important role in aiding operators in tractor selection and assisting manufactures in power efficiency optimization. Tractors, the power sources for various implements and agricultural machinery, have been widely used in agriculture (Lee et al., 2016). The analysis showed that fuel is the most demanded component in the operation of tractors, followed by machinery depreciation and labor (Romanelli and Milan, 2012). Although measurements of fuel consumption are normally conducted under steady-state conditions, fuel consumption is actually dependent on practical operation performed by tractors. Therefore, the evaluation of fuel consumption should be conducted under practical operation scenarios, where the practical operation scenarios refer to the ones in which various operations made by different tractors.

The literature survey has revealed various fuel consumption modelling methods proposed for tractors during their field operations. Most of the methods examined the factors involving fuel consumption, including engine condition (Grisso et al., 2004), operation mode (Moinfar et al., 2020; Siddique, 2023), field configuration (Janulevičius et al., 2019), soil texture (Battiato et al., 2019), tractor specification (Md-Tahir et al., 2021) and implement specification (Damanauskas et al., 2019; Al-Sager et al., 2024). To evaluate the methods experimentally, well-designed experiments were performed on several tractors. However, in such experiments, only some field operations and factors are considered and examined. So, the fuel consumption of tractors in practical operation scenarios has not been investigated yet.

In order to evaluate the practical fuel consumption of tractors, a fuel consumption predication method was proposed, which automatically predicts fuel flow rate based on engine conditions and motion characteristics of tractors. Firstly, a fuel consumption dataset was constructed, which contained GNSS (Global Navigation Satellite System) recordings collected from 30 tractors with a specific model. Such recordings were recorded from May 2023 to June 2023 and distributed across eight provinces in China, representing the practical operation scenarios of tractors. Then, each point in the GNSS recordings was represented by a vector consisting four parameters extracted from GNSS recordings: two engine parameters

(torque and engine speed), and two motion parameters (driving speed and acceleration). Next, a model was developed using a tradition machine learning method, Light Gradient Boosting Machine (LGBM) (Ke et al., 2017), which is input with the four parameters of a point and output the fuel flow rate at that point. Finally, the method was validated in the fuel consumption dataset.

To our best knowledge, it is the first attempt to construct a fuel consumption dataset involving a number of tractors operating in various regions, reflecting the practical fuel consumption of tractors. Then, a fuel consumption model was developed using a machine learning method and engine information augmented with motion characteristics.

2. Materials and Methods

2.1. Datasets

The experiment in this paper was conducted on a fuel consumption dataset about WH1804, a tractor model produced by Jiangsu World Agricultural Machinery Co., Ltd. Firstly, 30 tractors were randomly selected from all tractors with WH1804 Model in the Precision Agriculture Application Project Data Service Platform, which receives the GNSS recordings of agricultural machinery from multiple agricultural machinery manufacturers in China (Wu et al., 2023). Then, for each tractor, its data recorded between May 2023 and June 2023 were retrieved from the platform. In order provide clean input data, existing data preprocessing (Chen et al., 2021) was applied on the dataset, which includes smoothing noise points and removing duplicated points.

An example of GNSS recordings is shown in Table 1, whose recording updated frequency is 5s. For each record (i.e., a point or a sample), there are seven recorded parameters: longitude (WGS84), latitude (WGS84), timestamp (YYYY:MM:DD-hh:mm:ss), speed (m/s), torque percentage (instantaneous torque/nominal torque, %), engine speed (rpm), and fuel flow rate (L/h). The first four parameters are provided by GNSS receivers with a collection accuracy of 5 meters (CEP), and the latter three parameters are collected by other sensors installed on the tractors. In the experiments, the recorded fuel flow rate parameter serves as ground-truth values.

To demonstrate scenarios in which our data were collected, the GNSS recording of each tractor was split into daily trajectories, where a daily trajectory refers to a set of points recorded in the same day. There are totally 361 daily trajectories in our dataset. Then, a field-road trajectory segmentation system (Chen et al., 2021) was used to segment each trajectory into field segments and road segments. Table 2 lists the data statistics, showing that the dataset has more than 1 billion of points, and contains 863 field segments and 593 segments. Moreover, the trajectories are distributed across eight provinces in China, as shown in Fig. 1. The statistics indicates that our dataset can reflect the practical operations of tractors.

Table 1. An example of GNSS recordings

Longitude	Latitude	Timestamp	Speed	Torque percentage	Engine speed	Fuel flow rate
116.374255	29.951972	20230525085016	5	38	2709	19.1
116.374191	29.951945	20230525085021	5	41	2704	19.55
…	…	…	…	…	…	
117.782574	37.469909	20230614054437	6	23	1788	6.25

Table 2. Data statistics

Total Points	Field Points / Percentage	Road Points / Percentage
1,523,954	1,376,873/90%	147,081/10%
Total Segments	Field Segments/ Percentage	Road Segments/ Percentage
1,456	863/59%	593/41%

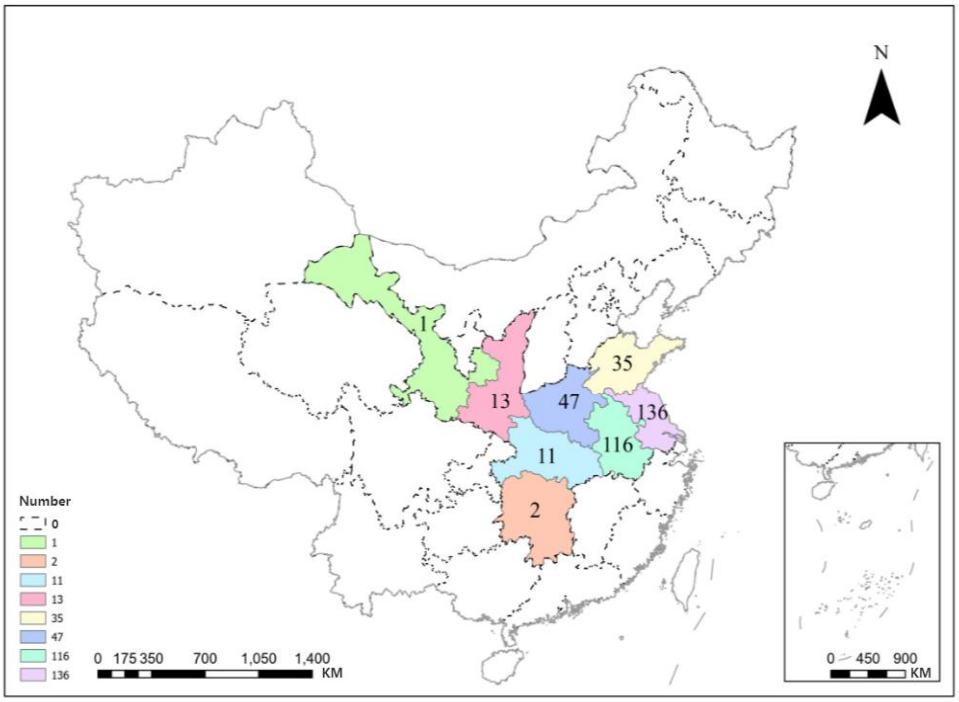

Fig. 1. The regional distribution of the fuel consumption dataset. Legend: the number of trajectories located in the province of China.

2.2. Methods

Our fuel consumption predication method consists of two steps: input feature extraction and model development. The input feature extraction provides model input data based on the daily trajectories, and the model development trains and evaluates a fuel consumption predication model.

2.2.1. Input Feature Extraction

As previous studies on tractors (Grisso et al., 2004; Almaliki et al., 2016) have pointed out instant engine conditions play a crucial role in the fuel consumption, two parameters (torque and engine speed) were selected to represent the instant engine conditions. Besides, there are other factors affecting fuel consumption, such as operative setting and conditions (Bietresato et al., 2015). In this paper, we consider that instant motion characteristics can somewhat reflect such factors. So, another two parameters (driving speed and acceleration) were selected to represent the instant motion characteristics of tractors.

To gain deeper insights into the engine conditions and motion characteristics of tractors, each trajectory point was transformed into a four-dimensional vector, including torque, engine speed, driving speed and acceleration. The former three parameters (torque, engine speed, and driving speed) are the ones recorded in GNSS recordings, and driving acceleration is a parameter derived from driving speed with the calculation used in Poteko et al. (2021).

2.2.2. Model Development

Learning Method: As fuel consumption predication is a complex problem, recent studies have used various machine learning methods to develop predication models (Rahimi-Ajdadi and Abbaspour-Gilandeh, 2011; Almaliki et al., 2016). In this paper, LightGBM (Light Gradient Boosting Machine), an efficient gradient boosting framework based on decision tree algorithms, was used. It is designed to handle large-scale training data (e.g., billions of points in Table 2) quickly, and provide highly accurate predictive capabilities, making it particularly suitable for tasks requiring high performance and calculation speed.

Model Training and Test: The 30 tractors in the dataset was divided into 90% and 10% for model training and test, respectively. For training (or test) tractors, all trajectories of these tractors serve as training

(test) data. Eventually, there are 312 and 49 trajectories in the training and test data, respectively. Moreover, the tractor division needs to ensure that the ratio of the point number in the training data and test data is about 9:1.

Then, the training data were used to train a LightGBM model, and the test data were fed to the model to obtain their predicted values. As the fuel consumption predication is a regression problem, similar to the previous work (Sayin et al., 2007), three performance metrics, R^2 (determination coefficient), RMSE (root mean squared error), and MAE (mean absolute error), were used to evaluate model performances.

3. Results and Discussion

In this section, the experiments were designed to examine the following two questions:

1) Whether it is possible to predict the fuel consumption of tractors using only the engine and parameters?

2) Which of these parameters are more important?

Table 3. Average performances of models with different input parameter combinations (EngSpd: Engine speed; DrivSpd: Driving speed; DrivAcc: Driving acceleration)

	Point-based Average			Trajectory-based Average		
Parameters	R^2	**RMSE**	**MAE**	R^2	**RMSE**	**MAE**
Torque	0.653	3.428	2.800	0.494	3.706	2.989
EngSpd	0.729	3.027	2.036	0.652	3.129	2.128
DrivSpd	0.047	5.677	4.659	-0.162	5.820	4.779
DrivAcc	0.000	5.817	4.799	-0.140	5.797	4.810
Torque+EngSpd	0.912	1.720	1.132	0.858	1.921	1.236
Torque+EngSpd+DrivSpd	0.940	1.425	0.966	0.932	1.401	0.956
Torque+EngSpd+DrivSpd+DrivAcc	0.946	1.348	0.951	0.938	1.328	0.940

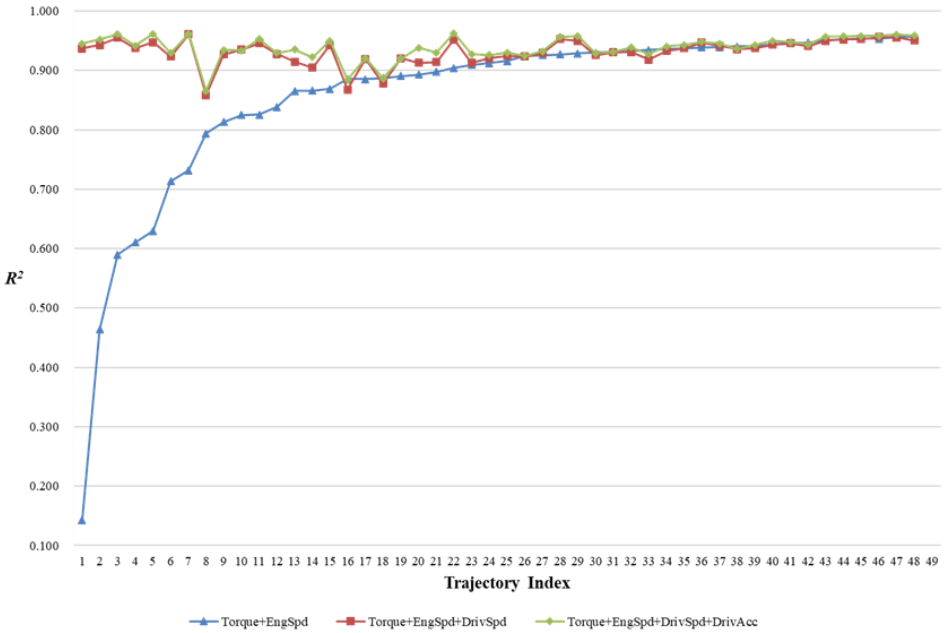

Fig. 2. The point-based average performance for each trajectory in the test data.

3.1.Experimental Settings

Baselines: In order to examine the importance of input parameters (torque, engine speed, driving speed and acceleration), several input parameter combinations were manually selected. For each input parameter combination, a fuel consumption prediction model was trained and tested using the way in Sec. 2.2.2.

Implementation Details: LightGBM was implemented with Scikit-learn (a Python-based machine learning library, Pedregosa et al., 2011). Moreover, as LightGBM is supervised machine learning methods, training data were used to learn its parameter values.

3.2.Comparisons and Discussion

In order to examine model accuracy and robustness, two ways to calculate the average performance on the test data were designed, point-based average performance and trajectory-based average performance, as shown in Table 3. The former is the average of performances of all points in the test data. The latter is the average of performances of all trajectories in the test data, calculated as follows: for each trajectory, its point-based average performance was calculated (e.g., the performances shown in Fig. 2), and then, the final performance was the mean of these average performances.

Overall performance: The accuracy of our fuel consumption predication model is examined, as shown in Tables 3 (Row: Torque+EngSpd+ DrivSpd+ DrivAcc; Column: Point-based Average). It was observed that our model can predict the fuel consumption quite well, yielding a high R^2 of 0.946, a low RMSE of 1.348 L/h, and a low MAE of 0.951 L/h. This indicates the effectiveness of our proposed method.

Parameter Importance: The accuracy of models with different input parameter combinations is examined, as shown in Table 3 (Column: Point-based Average). It was found that the engine conditions (torque and engine speed) were crucial factors determining fuel consumption, achieving a R^2 of 0.912, a RMSE of 1.720 L/h, and a MAE of 1.132 L/h. This observation is consistent with previous studies on fuel consumption modelling (Rahimi-Ajdadi and Abbaspour-Gilandeh, 2011). Furthermore, when the motion characteristics were incorporated, the model performances were increased slightly (from 0.94 to 0.946 in R^2 values), indicating motion characteristics are marginally helpful for fuel consumption prediction.

Model Robustness: The robustness of models with different input parameter combinations is examined. Fig. 2 shows the point-based average performances of different models on each trajectory, and Table 3 (Column: Trajectory-based Average) lists the trajectory-based average performances of different models on all trajectories.

In Fig. 2, the performance of the Torque+EngSpd model varies much on different trajectories. This indicates the fuel consumption predication cannot rely merely on engine conditions, particularly in practical operation scenarios. In contrast, the two models augmented with motion parameters (Torque+EngSpd+DrivSpd and Torque+EngSpd+DrivSpd+DrivAcc) perform stable on all trajectories. This indicates motion characteristics are much helpful to improve the robustness of fuel consumption predication models.

In Table 3, the two average performances (point-based and trajectory-based) are much different for the same model. For example, R^2 values of the Torque+EngSpd model are 0.912 and 0.858 for the two average performances, respectively. This indicates the robustness of such a model is limited. In contrast, the Torque+EngSpd+DrivSpd+DrivAcc model achieves similar performances on both point-based and trajectory-based average performances (0.946 vs. 0.938). This validates the contribution of the motion characteristics to model robustness.

4. Conclusions

In this paper, we proposed a novel fuel consumption predication method that estimates the fuel flow rate of tractors in practical operation scenarios. In order to evaluate practical fuel consumption of tractors, a fuel consumption dataset was constructed, which contains 361 daily trajectories collected from 30 tractors operating in various regions. Then, a fuel consumption predication model was developed using LightGBM plus four parameters: torque and engine speed (reflecting engine conditions), and driving speed and acceleration (reflecting motion characteristics). The experiments on the fuel consumption dataset shown that our method outperformed the methods on only engine conditions in terms of model accuracy and robustness. Our in-depth experimental analyses demonstrate the potential of motion characteristics in predicate fuel

consumption.

Our future studies will focus on two directions: constructing a fuel consumption dataset containing more types of agricultural machinery, such as harvesters, sowers, and so on, and developing a powerful fuel consumption predication method that can handle various trajectories recorded from different agricultural machinery. We believe that such directions can further understand the fuel consumption of agricultural machinery in practical operation scenarios.

Acknowledgements

The research was financially supported by National Precision Agriculture Application Project (Grant/Contract number: JZNYYY001).

References

Al-Sager, S. M., Almady, S. S., Marey, S. A., Al-Hamed, S. A., & Aboukarima, A. M. (2024). Prediction of Specific Fuel Consumption of a Tractor during the Tillage Process Using an Artificial Neural Network Method. Agronomy, 14(3), 492.

Almaliki, S.A., Alimardani, R., & Omid, M. (2016). Artificial Neural Network Based Modeling of Tractor Performance at Different Field Conditions. Agricultural Engineering International: The CIGR Journal, 18, 262-274.

Battiato, A., & Diserens, E. (2019). Influence of Soil on the Traction Performance of a 65 kW MFWD Tractor. Journal of Agricultural Science, 11(17), 11.

Bietresato, M., Calcante, A., & Mazzetto, F. (2015). A neural network approach for indirectly estimating farm tractors engine performances. Fuel, 143, 144-154.

Chen, Y., Zhang, X., Wu, C., & Li, G. (2021). Field-road trajectory segmentation for agricultural machinery based on direction distribution. Computers and Electronics in Agriculture, 186, 106180.

Damanauskas, V., Velykis, A., & Satkus, A. (2019). Efficiency of disc harrow adjustment for stubble tillage quality and fuel consumption. Soil and Tillage Research, 194, 104311.

Grisso, R. D., Kocher, M. F., & Vaughan, D. H. (2004). Predicting tractor fuel consumption. Applied Engineering in Agriculture, 20(5), 553-561.

Janulevičius, A., Šarauskis, E., Čiplienė, A., & Juostas, A. (2019). Estimation of farm tractor performance as a function of time efficiency during ploughing in fields of different sizes. Biosystems engineering, 179, 80-93.

Ke, G., Meng, Q., Finley, T., Wang, T., Chen, W., Ma, W., ... & Liu, T. Y. (2017). Lightgbm: A highly efficient gradient boosting decision tree. Advances in neural information processing systems, 30.

Lee, J. W., Kim, J. S., & Kim, K. U. (2016). Computer simulations to maximise fuel efficiency and work performance of agricultural tractors in rotovating and ploughing operations. Biosystems engineering, 142, 1-11.

Md-Tahir, H., Zhang, J., Xia, J., Zhou, Y., Zhou, H., Du, J., ... & Mamona, H. (2021). Experimental investigation of traction power transfer indices of farm-tractors for efficient energy utilization in soil tillage and cultivation operations. Agronomy, 11(1), 168.

Moinfar, A., Shahgholi, G., Gilandeh, Y. A., & Gundoshmian, T. M. (2020). The effect of the tractor driving system on its performance and fuel consumption. Energy, 202, 117803.

Poteko, J., Eder, D., & Noack, P. O. (2021). Identifying operation modes of agricultural vehicles based on GNSS measurements. Computers and Electronics in Agriculture, 185, 106105.

Pedregosa, F., Varoquaux, G., Gramfort, A., Michel, V., Thirion, B., Grisel, O., ... & Duchesnay, É. (2011). Scikit-learn: Machine learning in Python. the Journal of machine Learning research, 12, 2825-2830.

Rahimi-Ajdadi, F., & Abbaspour-Gilandeh, Y. (2011). Artificial neural network and stepwise multiple range regression methods for prediction of tractor fuel consumption. Measurement, 44(10), 2104-2111.

Romanelli, T. L., & Milan, M. (2012). Machinery management as an environmental tool-material embodiment in agriculture. Agricultural Engineering International: CIGR Journal, 14(1), 63-73.

Sayin, C., Ertunc, H. M., Hosoz, M., Kilicaslan, I., & Canakci, M. (2007). Performance and exhaust emissions of a gasoline engine using artificial neural network. Applied thermal engineering, 27(1), 46-54.

Siddique, M. A. A., Baek, S. Y., Baek, S. M., Jeon, H. H., Lee, J. H., Son, M. A., ... & Lim, R. G. (2023). The Selection of an Energy-Saving Engine Mode Based on the Power Delivery and Fuel Consumption of a 95 kW Tractor during Rotary Tillage. Agriculture, 13(7), 1376.

Wu, C., Li, D., Zhang, X., Pan, J., Quan, L., Yang, L., Yang, W., Ma, Q., Su, C., Zhai, W. (2023). China's agricultural machinery operation big data system. Computers and Electronics in Agriculture, 205, 107594.

A greenhouse plants' heating system based on low temperature long wave radiation emission[1]

George Papadakis [a,*]

[a] Department of Natural Resources and Agricultural Engineering, Agricultural University of Athens, Athens, Greece

* Corresponding author. Email: gpap@aua.gr

Abstract

The present paper regards an invention of a radiant heating system comprising low temperature radiant heating assemblies (the heated screens) suitable to maintain the greenhouse plants (and not the greenhouse air) at a desired optimum temperature. Heat is provided to a movable screen (a curtain that when deployed encloses the plants) and subsequently the screen provides the necessary heat to the plants by long wave radiation. The temperature of the heated screen is kept a few degrees Celsius higher than the temperature required by the plants. Calculations have shown that temperatures of the heated screen such as slightly above the optimum plant temperature above the required plant temperature, are adequate to maintain the plants at the required temperature at very low air temperatures outside the greenhouse, while achieving high energy saving relative to conventional greenhouse (air) heating systems. Renewable energy can be used to heat the screen.

Keywords: greenhouse, low temperature radiant heating system, plants' heating.

1. Introduction and State of the Art

Greenhouse cultivation is evolving rapidly in recent years because depending on the equipment used and their technological level, crop production can be 10-20 times higher per unit area than the outdoor one, (Shamim Ahamed et al. 2019). A controlled environment provides conditions for optimal plant growth and production throughout the year, resulting in higher productivity and products of higher quality, (Kaushık et al. 2011). However, to achieve optimum plants' growth conditions, even at mild winter climate, greenhouses must be equipped with a heating system. The thermal losses of the greenhouse due to its thin walls and light construction are estimated to be 6-12 times greater than those of an ordinary urban building of equal volume and heating constitutes one of the major costs for modern high technology greenhouses even for the Mediterranean countries, (De Pascale and Maggio 2004). To reduce energy consumption, some straightforward measures can be applied, such as double-glazing insulation, use of different types of covering materials on the roof and side walls (such as glass panes with modified optical properties, polyethylene plastic sheets with reduced transparency to long wave radiation, double inflated polyethylene plastic sheets), use of insulating materials on the North facing side walls, implementation of passive (i.e., unheated) curtains usually called "thermal screens", (Papadakis et al. 2000, Gupta and Chandra 2002, Kittas et al. 2003, Sethi and Sharma 2008, Teitel et al. 2009, Hemming et al. 2017).

Although these methods do result in energy saving, they do not question the traditional concept of heating the entire greenhouse (air, structure, and cover) and then letting the plants gain energy from it which results in high energy consumption. Today, most conventional greenhouse heating systems are based either on circulation of hot water through a piping system (expensive) or on direct use of air heaters (less expensive), i.e., forced air heating. The design and operational objective of conventional heating systems is to maintain the air temperature inside the greenhouse at values optimal for plant growth, neglecting the fact that the target object are the plants themselves and not the air. Heat is supplied to the greenhouse air to maintain the air at a temperature a little higher than the value opted for the plants so that to keep them within a physiologically defined temperature range for optimal growth termed as physiologically optimum temperature range.

Temperature considerably influences plant growth and development during the various stages of growth, i.e., seed germination, vegetative phase, reproductive phase, and ripening phase. The optimum temperature of a plant species changes as the plant grows from a seedling to a mature plant. In horticultural practice it is well known today the ranges of optimum temperatures for most of the greenhouse grown crops, (Ramin Shamshiri et al. 2018, Stanghellini et al. 2019, Hochmuth 2018, https://burea-uinsurance.com/en/the-

[1] Patent pending. International Publication Number WO 2023/094843 A1, International Publication Date 01 June 2023. Title, A GREENHOUSE PLANTS' HEATING SYSTEM. Inventor PAPADAKIS Georgios.

temperature-in-the-greenhouse-for-cucumbers).

It is also important to note that plants do not have any internal temperature regulation mechanism such as mammals and their temperature depend on their instantaneous energy and mass balance and since (most) plants do not store heat, the heating system must provide the necessary heat in order to compensate for their long wave radiation and convection losses considering that the mass transfer (plant's transpiration) is very small during the night, (Papadakis et al. 1994).

The above-mentioned conventional heating systems dominate the greenhouse commercial practice even though as early as in the 70's, more efficient options had been proposed, e.g. Itagi and Takahashi 1978. It has been proven that long wave radiant heating with radiant tubes (commercially known as "infrared radiant heaters"), can be more efficient than the widely spread forced air or hot pipes heating systems, (Kavga et al. 2009, Kavga et al. 2015). Long wave radiant heating is based on the radiative heat transfer mechanism rather than the convective one as the case of the forced air system. Experimental and simulation results show that (high temperature) radiant heating can efficiently supply heat to cover the plants' heat losses, while the greenhouse air temperature during the night remains several degrees lower than the actual plant temperature, (Kavga et al. 2009, Kavga et al. 2015). Such results have shown a significant potential for energy saving over other conventional heating systems. Though, such greenhouse radiant heating has also many disadvantages. The cost of the initial system is high and supplying heat to tall greenhouse crops is relatively difficult because radiation cannot reach the lower plant leaves since the very hot radiant tubes (temperature range 500 ºC to 2000 ºC) should be kept at a safe distance from the plants, while there are also fire risks. Such systems do not distribute the heat uniformly to the plants since the radiant heat is produced by linear sources in which the temperature is not uniform along their length. Such systems typically provide for reflective insulating panels which, are unsatisfactory since the plants need uniform heat.

Radiant heating systems have been used to heat greenhouses. Such systems provide an indirect source of heat and generally have heating elements which can be suitably positioned inside a greenhouse. Radiant heating systems typically employ metallic energy-emitting tubular conduits mounted overhead of an area to be heated. Such systems usually include a burner which fires a heated effluent into the conduit, an opaque reflector mounted over the conduit, and an exhaust system to expel the effluent and products of combustion outside the greenhouse. One such radiant heater system is disclosed in the patent US 3399833 A.

A characteristic of these radiant heating systems is the wide variance in the amount of thermal energy emitted from the hot conduit over its working length. While the temperature inside the metallic conduit immediately adjacent the burner may reach levels more than 1150 K the temperature inside the conduit at the exhaust end, depending on length, may be as low as 350 K. This results in an uneven emission of thermal energy over the length of the conduit. Unless the spacing of the tube from the area being heated is varied, there are correspondingly uneven temperatures in the area being heated by the system. This is especially true with low overhead mounted systems in high heat loss structures, such as greenhouses.

One attempt to more evenly distribute the thermal energy radiated by the metallic conduit is disclosed in patent US 4319125 A. It employs a dispersing reflector adjacent to the relatively hot initial portion of the metallic conduit and a parabolic or concentrating reflector adjacent to the colder end portion of the conduit to compensate for the varying intensity of thermal energy radiated over the length of the conduit. While the shaped reflector may provide some measure of improvement in the distribution of the thermal energy throughout the area serviced by the heater system, the opaque conduit and reflector obstruct sun radiation entering the greenhouse and produce a shadow which adversely affects the growth of plants thereunder.

In another attempt, (patent KR 2010 0110659), the greenhouse is to be heated by large diameter metal ducts (e.g., from aluminium) located inside the greenhouse, bearing holes that supply hot air. This system however does not provide radiant heat to the plants, but it heats the air of the greenhouse through a heat exchanger and then that hot air is distributed inside the greenhouse through the holes along the metallic ducts.

Another heating system is disclosed in patent CN 212 851 983 U, where flat heating elements are presented for supplying heat to the greenhouse. Hot water is circulated inside the heating elements which in turn is supplied to the greenhouse. However not many details are provided such as to where the heating elements are placed inside the greenhouse, what are their dimensions, what is the hot water temperatures or the temperature of the surface of the heating element.

In patent CN 206 042 941 U, a heating system is disclosed regarding a nursery for seeds' germination or keep young seedlings in the nursery at an appropriate temperature environment. The seeds' bed or the pots located at the nursery bed are heated through a heating wire mesh positioned between two film layers.

Electrical energy is provided to the wire which is heated and subsequently the heat is provided to the substrate of the nursery to keep it at a desired temperature. The nursery bed is covered on its top by a cover layer made of a plastic material which can be rolled to cover the seedbed or unrolled so that to uncover the seedbed. This cover layer is not heated by any means and therefore the heat produced by the wire mesh is provided to the seeds' bed or the seedlings' pots by conduction that is, no radiant heating is involved in this heating system. In patent WO 92/22196 A1 a radiant heating system for greenhouse is disclosed that uses plastic tubes of large diameter, permanently fixed under the greenhouse roof, where hot air of 200 ºF (~93.3 ºC) is circulated through a heat exchanger.

The main drawbacks of the prior art heating systems to heat greenhouses using either conventional or radiant heating systems are the high energy consumption required to heat all the volume of the greenhouse (including the inside air, the greenhouse frame, and the covering material), the high temperature (greater than 90 ºC and up to about 2000 ºC) and uneven temperature distribution, and the significant heat loses due to the high temperature differences between inside and outside of the greenhouse.

2. Description of the Invention, Results and Discussion

The present invention as depicted in Figure 1, provides for the heating of the plants inside a greenhouse structure (10) in an easily assembled, substantially uniform, radiant heating system including a heat generating assembly (1), a heated air transport, distribution, and recirculation ducts' network (4, 5), heated screen units between the greenhouse trusses (16) which is the radiant heating assemblies, generally composed of horizontal (2) and vertical (3) parts. It is essential that the screen units, both the horizontal and the vertical ones, when deployed they fully enclose the plantation of the greenhouse. Generally, the heat generating air distribution and recirculation assembly (1) produces a low temperature heated air effluent through an incorporated heat exchanger and the heated air is then distributed and recirculated via an incorporated blower, and the recirculation ducts' network (4, 5) to the several heated screen units/modules, horizontal (2) and vertical (3) ones (Fig. 1).

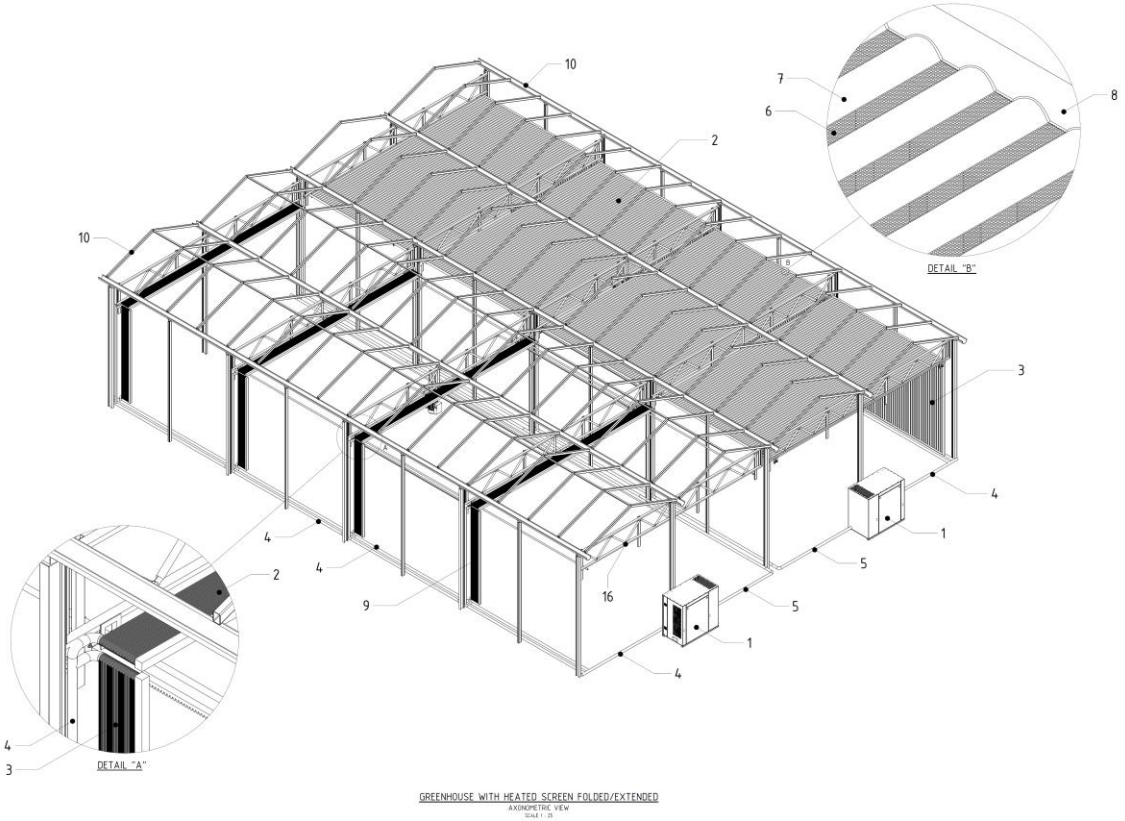

Figure 1. A schematic representation of a greenhouse equipped with a movable heated plastic screen (Detail A), heated through warm air recirculation in channels (Detail B).

The present invention provides a radiant heating system comprising low temperature radiant heating assemblies (heated screen units or screen units) of simple and inexpensive construction which deliver controlled and uniform low temperature heating so that to maintain the greenhouse plants (and not necessarily the greenhouse air) at a physiologically required temperature range for optimum growth of a specific plant species which is well known to the skilled to the art.

The disclosed system provides the necessary heat primarily to the screen itself (and not to the greenhouse air) and subsequently the screen will provide the necessary heat to the plants by long wave radiation, while part of the heat supplied to the screen will be (inevitably) supplied to the greenhouse air by convection. The temperature of the heated screen units is kept a few degrees Celsius higher than the optimum temperature required by the plants for their optimum growth. It is emphasised that the intended system is to provide heat by long wave radiation to the plants themselves and not to heat the greenhouse air. This fact and the low temperature of the heated screen ensure the high energy efficiency of the present invention over the prior art.

In some embodiments, the heated screen units are installed inside the greenhouse, horizontally under the roof and vertically near the inside side of the vertical walls so that to fully enclose the plants when the heating system is in operation and the system will operate approximately from sunset to sunrise during the cold periods of the year. This concept of heating is based on the proven fact that the temperature of the plants in the greenhouse under radiant heating is kept some degrees higher than the greenhouse air because the plants' convection losses to the colder greenhouse air are compensated by the received radiant heat, (Kavga et al. 2009, Kavga et al. 2015).

In some embodiments the heated screen units are manufactured from impermeable to air polymer (plastic) materials (such as polyethylene) and as the screen units are heated by heated air, they include air flow channels for its heating. Low temperature heated air (in a range of few degrees above the optimum plant growth temperature is supplied to the air flow channels of the screen units through suitably connected plastic (rigid or non-rigid) air ducts that run along the greenhouse length and width and distribute uniformly the heated air to the screen units.

In some embodiments the heated air is supplied to the screen units flow channels by one or more blowers which recirculate the air of the flow channels through a heat exchanger where the air is heated to the desired temperature by a burner/furnace where the heat is produced by means of any kind of solid, liquid, gaseous fossil fuel combustion or renewable fuel combustion (such as biofuels) or by an electrical heat pump or the air is heated by an electrically heated element such as an electrical resistance.

An industrial electronic controller will manage the operation of the burner/furnace, heat exchanger, and blower with the associated motorized air dampers, to produce air of appropriate temperature to be re-circulated in the flow channels of the screen units. By controlling the air temperature in the air flow channels, the temperature of the screen is regulated and in turn adjust the radiant heat required by the plants to attain their optimum temperature. The temperature of the screen and the plants is identified, recorded, and controlled in real time using suitable temperature sensors located at suitable places on the screen and the leaves of the plants or contactless sensors that read the temperatures of the screen surface and of the leaves of the plants, e.g., by Infra-Red (IR) radiation thermometers.

In the case of a heated screen with air flow channels the parts of the screen between the air flow channels (i.e. outside the area of the flow channels), may be perforated so that to allow the greenhouse air and moisture to move through, from the one side of the screen to the other, that is from the space that encloses the plants (which will have a higher humidity due to the plants' transpiration) to the space between the screen unit and the greenhouse cover (which will have a lower humidity).

In other embodiments an alternative type of heated screen is used which is made of a textile (fabric) material that is heated by electricity, via incorporated resistive wires or other electricity conductive material configured to produce heat upon the application of electricity. Electricity may be provided to the resistive wires (or conductive material) of the screen units by any source, such as the electricity grid, a renewable energy system (e.g., wind generator, photovoltaic system), or an electricity storage system such as batteries. In the case of the heated screen units made of a textile (fabric) material, an industrial electronic controller regulates in real time the voltage and current supplied from the electricity source to the resistive wires of the screen units via the wiring network so that to regulate the temperature of the resistive wires (or other type of electrical conductors) and subsequently regulate the temperature of the screen using temperature sensors located at suitable locations on the screen and the plants (or other type of contactless temperature sensors).

In the case where the heated screen units are made of textile with embedded resistive wires (or other electricity conductive material configured to produce heat upon the application of electricity), the textile weaving is sparse enough so that to allow the greenhouse air and moisture to move through, (for the same purpose and similarly to the heated screen with the embedded air flow channels).

It was found to be essential for high energy savings, the screen unit surface facing to the cover at the roof and side walls of the greenhouse, is aluminized so that to provide a low emissivity and high reflectivity to long wave radiation and reduce radiation emission from that screen surface, while the side of the screen facing the plants will have high emissivity (as most of polymer plastic materials physically have) to intensify radiant heat emission towards the plants. Such differentiation in the emissivity values on the one and the other side of the heated screen will ensure that the heat released by radiation from the screen will be directed primarily to the plants while small amounts of radiative heat will be lost towards the cover. This is important to allow to heat the plants with radiant heat with the heated screen having only a few degrees above their optimum temperature. The prior art teaches away because the aluminized surface of the passive, unheated thermal screens facing the plants is of low emissivity (and high reflectivity) to long wave radiation to reflect the radiant heat of the plants backwards.

Given the fact that no experimental (or simulation) data exist in the literature for the proposed radiant heating system, a model was developed and executed (see details in the published patent application, Papadakis, 2023) to obtain answers to critical questions about the radiant heating system configuration and operation. With the use of the model, it was possible to answer critical questions regarding the proposed radiant heating system, by answering as well as selecting appropriate parameters used in greenhouses:

1. What the temperature of the screen should be so that the crop (e.g., a tomato plantation) to be maintained at a desired temperature of 13 ^{o}C during a cold night (e.g., at sub-freezing air temperature outside the greenhouse enclosure)?
2. What the air temperature inside the greenhouse would then be?
3. How and in what form heat should be supplied to the screen to maintain it at the required temperature (with no other heating system in the greenhouse)?
4. What heat quantity would be required for heating the screen at the desired temperature level?

For executing the mathematical model appropriate values for several parameters were selected from the literature (Gupta and Chandra 2002, Papadakis et al. 1992, Wanga et al. 2017), (see notation in Table 1). Input values to the model are listed in Table 2. The results in Table 3 show that under the assumed cold winter weather conditions, the heated screen can fully supply the required heat, so that the plants to be maintained at the desired temperature conditions while the screen itself is being kept at a temperature of merely less than 2 ^{o}C above the desired temperature for the plants (Table 3). It is also seen in Table 3 that the cover temperature (θ_c) remains at low temperature, lower than the outside temperature as expected because the cover is cooled down to a temperature below that of the outside air, due its intense long wave radiation emission (heat losses) to the sky, especially at clear skies (the sky becomes a radiation sink). The air temperature (θ_a) inside the greenhouse is found to be lower than the plants' temperature (see Table 3), as expected.

An attempt is made to compare the cost of heating the screen to the required temperature either by burning oil or by grid electricity. Calculations are summarised in Table 4 where it is seen that to heat the screen by hot air produced by burning oil may be more economic than using electricity, but this is highly depended on the electricity unit price, the oil price and the efficiency of the equipment used in the one or the other case.

An attempt is also made to estimate the required electrical energy for heating the screen with photovoltaics (PV) integrated in the glass roof of a glasshouse. Assuming a local solar photovoltaic (PV) energy production potential of 1200 kWh/kW$_p$ and that commercially available greenhouse "solar glass" panes (https://www.britesolar.com/solar-glass) of an area of about 2 m^2 of nominal PV power 115 W$_p$ (57.5 W$_p$/m^2) are used for the greenhouse covering, then the greenhouse roof PV can produce 57.5 W$_p$/m^2 x 1200 kWh/kW$_p$ = 69 kWh/m^2 year. Assuming that the screen heating needs at extremely cold conditions will be about 60 W/m^2 for a continuous period of 5 hours per day for 6 months a year (see Table 3), then the screen heating needs will be 60 W/m^2 x 5 h x 30 days x 6 months = 54 kWh/m^2 year. Therefore, the PV production outweighs the heating needs of the screen, and the grower would heat the greenhouse for free and will also receive additional income by selling the surplus PV kWh to the grid.

Table 1. Symbols and parameters used in the model

$h_{c.i}$ convection coefficient at the inside of the cover	ε_p emissivity of the plants
h_p convection coefficient (plants' leaves - inside air)	$\varepsilon_{s.c}$ emissivity of the side of the screen facing the greenhouse cover
$h_{c.o}$ convection coefficient at the outside of the cover	$\varepsilon_{s.p}$ emissivity of the side of the screen facing the plants
h_s convection coefficient between screen and air (uniform at all sides of the screen horizontal & vertical)	ε_c emissivity of the cover (assumed having same values on the outside and the inside sides)
A_p area of the plants' leaves (one side)	$F_{s.c}$ radiation shape factor between screen and cover
A_s area of the screen (horizontal part plus the vertical part parallel to the greenhouse walls)	$F_{s.p}$ radiation shape factor between screen and plants
A_c area of the cover (roof and side walls)	$F_{p.s}$ radiation shape factor between plants and screen

Table 2. Inputs to the model (see symbol explanation in Table 1), (Gupta and Chandra 2002, Papadakis et al. 1992, Wanga et al. 2017)

$h_{c.i}$ =1.5x10^{-3} kW/m^2 ^{o}C	$h_{c.o}$ =4.5x10^{-3} kW/m^2 ^{o}C	$F_{s.c}$ =0.196	$F_{s.p}$ =1.660	$\varepsilon_{s.p}$ =0.9	ε_p =0.95	A_s=1400 m^2	LAI=3
h_s =2.5x10^{-3} kW/m^2 ^{o}C	h_p =1.0x10^{-3} kW/m^2 ^{o}C	$F_{p.s}$ =0.775	ε_c =0.9	$\varepsilon_{s.c}$ =0.1	A_g=1000 m^2	A_c=1525 m^2	A_p=3000 m^2

Table 3. Model results (with desired plants' temperature θ_p set equal to 13 ^{o}C and inputs as in Table 1)

Outside air temperature θ_o (^{o}C)	-10	-8	-6	−4	−2	0	2	4	6	8
Greenhouse cover temperature θ_c (^{o}C)	-9.8	-8.2	-6.6	−5.1	−3.5	−1.9	-0.3	1.3	2.9	4.5
Greenhouse inside air temperature θ_a (^{o}C)	10.2	10.4	10.5	10.8	10.9	11.2	11.4	11.6	11.8	11.9
Heated screen temperature θ_s (^{o}C)	14.3	14.2	14.2	14.1	13.9	13.9	13.8	13.7	13.6	13.5
Heated Screen power required, Q (kW)	61	57	53	49	45	40	36	32	27	23
Heated Screen energy required for 5 hours heating, E_s (kWh)	308	287	266	246	225	203	182	161	139	117
Conventional (forced hot air system) power required, (kW)	175	160	145	130	114	99	84	69	53	38
Conventional heat energy (forced hot air), required for t=5 hours heating, E_c (kWh)	877	801	724	648	572	496	419	343	267	191
Energy saving achieved by the Heated Screen (%), (E_c - E_s)/ E_c x 100	64.9	64.2	63.2	62.1	60.7	58.9	56.6	53.2	47.9	38.4

Table 4. Operating costs per day (€ spent for 5 hours heating based on the input values to the model of Table 2 and the Q values of Table 3)

Outside air temperature θ_o (^{o}C)	-10	-8	-6	−4	−2	0	2	4	6	8
Heated Screen using oil for heat production (€)*	30	28	26	24	22	20	18	16	14	12
Conventional (forced hot air system) using oil for heat production (€)*	87	80	72	64	57	49	42	34	26	19
Heated Screen using grid electricity for heat production (€)**	46	43	40	36	33	30	27	24	21	17

* Oil cost: 1 €/10.12 kWh (1 €/L, the calorific value of 1 L of oil is 10.12 kWh)

** Electricity cost: 0.15 €/kWh

3. Conclusions

The invented radiant heating system is the sole heating system in the greenhouse. It is not a supplementary energy saving system such as the commercially available passive (unheated) so called "thermal screen" system.

The invented radiant heating system requires the heated screen to be at low temperature (just a few degrees Celsius above the required plants' temperature) contrary to the existing commercially available high temperature radiant heating systems (in the order of several tens or hundreds of degrees Celsius).

The objective of the invented radiant heating system is to provide heat to the plants (direct heating of the plants) and not heat the greenhouse air. Existing conventional greenhouse heating systems (such as those based on circulation of hot water in steel pipes or on direct use of air heaters) heat the greenhouse air which in turn provides the heat to the plants by convection which is a major reason of low heating efficiency and high energy consumption.

The low operating temperature of the invented system allows for using inexpensive plastic materials for the heated screen, such as low-density polyethylene, while other proposed radiant heating systems requiring higher temperatures cannot not use a cheap material such as polyethylene (because of its low melting point).

Essential prerequisites of the invented radiant heating system to achieve high energy savings compared to the prior art are, (1) when deployed, it fully encloses the plantation so that the radiated heat from the screen is effectively receipted from the plants while the radiated heat from the plants cannot escape to the cold greenhouse cover, (2) the heated screen side facing the cover has a very low emissivity (e.g. lower than 0.2) while the heated screen side facing the plants has a very high emissivity.

The invented heated screen requires significantly less amount of energy to keep the plants at the required temperature and can save energy up to 60% in comparison to conventional heating systems.

PV can be incorporated in the greenhouse roof so that the produced energy to be used (indirectly) to heat the screen, that is the PV energy will be sold to the grid to offset the consumed electricity from the grid (e.g. net-metering). In this way the grower can heat the greenhouse for free and get additional income from selling the PV electricity production to the grid.

References

CN 206 042 941 U (ZHENGZHOU VEGETABLE RES INST) 29 March 2017

CN 212 851 983 U (HANGZHOU TIANBANG AGRICULTURAL FACILITIES CO LTD) 2 April 2021

De Pascale, S., & Maggio, A. Sustainable protected cultivation at Mediterranean climate, perspectives and challenges. Acta Horticulturae, (2004), 691, 29-42.

Gupta M J & Chandra P, Effect of greenhouse design parameters on conservation of energy for greenhouse environmental control. Energy, Vol 27, (2002), 777-794.

Hemming S., Baeza E., Mohammadkhani V. & van Breugel B., Energy saving screen materials, Wageningen University & Research, Report GTB-1431, (2017), pp 92.

Hochmuth G. J. Production of Greenhouse Tomatoes - Florida Greenhouse Vegetable Production Handbook, Vol 3. This document is HS788, one of a series of the Horticultural Sciences Department, UF/IFAS Extension. Original publication date December 1990. Revised January 2012. Reviewed November 2018. Visit the EDIS website at https://edis.ifas.ufl.edu for the currently supported version of this publication. https://edis.ifas.ufl.edu/pdf/CV/CV266/CV266-4429807.pdf (Accessed May 2024).

https://www.britesolar.com/solar-glass (accessed May 2024).

Itagi T., & Takahashi, M. Studies on the practical use of infrared heater in greenhouse. Kanagawa Hort. Exp. Station Bill, (1978), 25, 45-5.

Kaushık, G., & Chel, A. Renewable energy for sustainable agriculture. Agron. Sustain. Development, (2011), 31(1), 91-118.

Kavga A., Konstas T., Panidis I., T. Assessment of infrared heating benefits in a production greenhouse. Applied Engineering in Agriculture, (2015), Vol. 31(1): 143-151.

Kavga A., Panidis T., Bontozoglou V., & Pantelakis S. Infrared heating of greenhouses revisited: an experimental and modeling study. Transactions of the ASABE, (2009), vol. 52, no. 6, pp. 2055–2065.

Kittas C., Katsoulas N., Baille A. Influence of an aluminized thermal screen on greenhouse microclimate and canopy energy balance, Transactions of the American Society of Agricultural Engineers (2003), 46(6), 1653-1663.

KR 2010 0110659 A (KIM HONG GEUN [KR]) 13 October 2010

Md. Shamim Ahamed, H. Guo, K. Tanino. Energy saving techniques for reducing the heating cost of conventional greenhouses. Biosystems Engineering, (2019), 178, 9-33.

Papadakis G, Briassoulis D, Scarascia Mugnozza G, Vox G, Feuilloley P, Stoffers JA. Radiometric and thermal properties of, and testing methods for, greenhouse covering materials. Journal of Agriculture Engineering Research, (2000), 77(1): 7-38.

Papadakis G. Patent application, International Publication Number WO 2023/094843 A1, International Publication Date 01 June 2023. Title, A GREENHOUSE PLANTS' HEATING SYSTEM.

Papadakis G., Frangoudakis A., Kyritsis S. Experimental investigation and modelling of heat and mass transfer between a tomato crop and the greenhouse environment. Journal of Agricultural Engineering Research, (1994), 57, pp 217-227.

Papadakis G., Frangoudakis A., Kyritsis S. Mixed, forced and free convection heat transfer at the greenhouse cover. Journal of Agricultural Engineering Research, (1992), 51 pp 191-205.

Ramin Shamshiri R., Jones J.W, Thorp K.R., Desa A., Che Man H., and Taheri S. Review of optimum temperature, humidity, and vapour pressure deficit for microclimate evaluation and control in greenhouse cultivation of tomato: a review. International Agrophysics, 2018, 32, 287-302.

Sethi, V. P., & Sharma S. K. Survey and evaluation of heating technologies for worldwide agricultural greenhouse applications. Solar energy, 82, no. 9 (2008): 832-859.

Stanghellini C., van 't Ooster B. and Heuvelink Ep. Greenhouse horticulture. Technology for optimal crop production. Wageningen Academic Publishers, The Netherlands, 2019, ISBN: 978-90-8686-329-7, doi: 10.3920/978-908686879-7.

Teitel M., Barak M., Antler A., Effect of cyclic heating and a thermal screen on the nocturnal heat loss and microclimate of a greenhouse. Biosystems Engineering, 102, (2009): 162-170.

The temperature in the greenhouse for cucumbers. https://burea-uinsurance.com/en/the-temperature-in-the-greenhouse-for-cucumbers/. (Accessed May 2024).

US 3399833 A (COMBUSTION RESEARCH CORP) 3/9/1968

US 4319125 A (SOLARONICS INC) 9/3/1982

Wanga H., Sánchez-Molinaa J.A., Li M., Berenguel M., Yang X.T., Bienvenido J.F. Leaf area index estimation for a greenhouse transpiration model using external climate conditions based on genetics algorithms, back-propagation neural networks and nonlinear autoregressive exogenous models. Agricultural Water Management, 183 (2017) 107–115.

WO 92/22196 A1 (COMBUSTION RES CORP [US]) 23 December 1992

Renewable sources and energy retrofitting solutions for microclimatic control in pig barns

Stefano Benni [a*], Carlos A. Perez Garcia [a], Marco Bovo [a], Alberto Barbaresi [a], Francesco Tinti [b], Patrizia Tassinari [a], Daniele Torreggiani [a]

[a] Department of Agricultural and Food Science, University of Bologna, 40127 Bologna (BO), Italy

[b] Department of Civil, Chemical, Environmental and Materials Engineering, University of Bologna, 40131 Bologna (BO), Italy

* Corresponding author. Email: stefano.benni@unibo.it

Abstract

Livestock farming is a key and energy-intensive sector of agriculture, significantly contributing to greenhouse gas (GHG) emissions. To mitigate this, the scientific community is exploring retrofitting approaches for existing farms, focusing on innovative Renewable Energy Sources (RES)-based equipment. In swine farming, maintaining optimal environmental conditions in nursery barns is crucial for weaner health and growth, but it is challenging in old facilities with poor insulation. Typically, achieving proper microclimatic control requires energy-intensive HVAC systems reliant on fossil fuels, contributing to significant GHG emissions.

This research aims to develop sustainable heating systems and energy retrofitting for livestock barns as alternatives to fossil-fuel-based systems. The study focuses on a pilot swine farm in northern Italy, housing 500 sows and 2500 weaners. It involves designing and testing an integrated RES system, including a photovoltaic-thermal plant, geothermal heat storage unit, and a modular heat pump. The retrofitting addressed the challenges of a poorly performing hog barn in winter and summer by designing and installing an energy-efficient solution with smart opening and ventilation systems. A sophisticated control system was developed to monitor energy usage and environmental conditions.

The results show that a customized combination of RES can be effectively implemented in specific livestock farms, utilizing available renewable resources. Energy retrofitting improved the thermo-hygrometric conditions of existing pig barns, reducing the farm's energy demand. Monitoring outdoor and indoor environmental parameters was crucial for collecting data, evaluating system effectiveness, and enabling remote control of the equipment. This study demonstrates that integrated RES systems and targeted retrofitting can significantly enhance the sustainability and efficiency of livestock farming.

Keywords: Pig barn, Geothermal storage, Animal welfare, Energy efficiency, Smart monitoring.

1. Introduction

Swine farming, like many intensive livestock farming activities, demands meticulous control of environmental conditions to ensure the health and optimal growth of weaners. The nursery barn environment is crucial in mitigating stress factors that can affect the animals' well-being and productivity. Temperature and humidity are two key parameters that require careful management throughout the year, especially during periods with extreme weather. Research has consistently shown the profound impact of environmental conditions on swine health and performance. Rearing pigs involves various stages, each with different thermo-neutral zone limits, influenced by factors such as air velocity, floor type, building insulation, relative humidity, and air composition. Despite advancements in genetics and nutrition, the boundaries of the thermo-neutral zone are mostly based on outdated research, requiring new studies to address the changing needs of recent genotypes. The scientific literature highlights the importance of maintaining optimal temperature and humidity levels to prevent heat stress in pigs, which can lead to reduced feed intake, impaired growth, and increased susceptibility to diseases (Niu, Zhong, and Hu 2024). Similarly, inadequate temperature regulation during cold seasons can compromise piglet health and increase mortality rates, necessitating proper heating in pig barns (Costantino 2023).

Addressing these challenges requires a holistic approach, integrating innovative infrastructure design, advanced ventilation systems, and precision management practices. Heating, ventilation, and air conditioning (HVAC) systems are indispensable tools for controlling the environmental parameters in swine barns.

However, traditional systems often rely on fossil fuels for energy, leading to significant greenhouse gas (GHG) emissions. This has raised concerns about the sustainability of intensive swine production systems, particularly in light of the growing emphasis on reducing carbon footprints across intensive animal productions (Tyris et al. 2022). Efforts to address the environmental impact of HVAC systems in swine farming have spurred research into alternative technologies and management strategies (Shin et al. 2024). For instance, advancements in energy-efficient heating systems, such as radiant heating and heat recovery ventilation, offer promising solutions for reducing energy consumption and mitigating GHG emissions (Deeken et al. 2023). Additionally, integrating renewable energy sources, such as solar panels or geothermal heat exchangers, for microclimatic control can further reduce reliance on fossil fuels and enhance sustainability (Tinti et al. 2023). Optimizing the design and operation of HVAC systems through computational modelling and advanced control algorithms can maximize energy efficiency while maintaining optimal environmental conditions for pig welfare. Research in this area has demonstrated significant potential for reducing energy consumption and GHG emissions without compromising animal performance (Mun et al. 2022). The control of environmental conditions in swine nursery barns is thus crucial for ensuring the health and productivity of weaners.

The intersection of sustainability and animal welfare goals in livestock farming necessitates the development of renewable energy systems capable of meeting the energy demands of farm buildings while ensuring optimal conditions for animal health and productivity. Achieving this balance requires not only the availability of renewable energy but also the implementation of smart monitoring and actuation systems to effectively manage energy production and usage in real time. The intermittent nature of renewable energy sources presents challenges in matching energy supply with demand, particularly in agricultural settings where energy requirements fluctuate based on factors such as weather conditions and animal metabolism. To address this issue, smart monitoring and actuation systems are essential for dynamically adjusting energy production and usage in response to real-time demand.

The application of smart technologies as a sustainable strategy in swine farming has also been analysed in literature (Mahfuz et al. 2022), identifying three stages of development in smart livestock farming. The first generation focused on animal monitoring; the second on environment control, health management, and big data and AI; and the third on energy management and automation of farming. By harnessing renewable energy sources and optimizing energy management in real-time, farmers can reduce their environmental footprint while ensuring optimal conditions for animal health and productivity.

This research focuses on devising sustainable heating systems and energy retrofitting for livestock barns, as alternatives to existing fossil-fuel-based systems, with reference to the pilot case of the nursery barn of a farrow-to-nursery swine farm. We designed and tested a Renewable Energy Source (RES) system incorporating a borehole thermal energy storage (BTES) and photovoltaic thermal (PVT) collectors, integrated with a Dual-Source Heat Pump (DSHP). The retrofitting issue was addressed by analyzing the case of a hog barn poorly performing both in winter and in summer: an energy efficient solution based on smart opening and ventilation systems was designed, installed and tested in the pilot farm. A smart control system was developed and installed to monitor RES production, energy uses and the environmental conditions outdoor and in the various sectors of the barn. The data collected were processed to define the optimal settings of the integrated plant for energy production and efficiency.

2. Materials and Methods

The pilot case presented in this research is a swine farm located in Modena province (northern Italy), rearing 500 sows and 2500 weaners. The experimental study focused on the nursery barn, and the hog barn. The former is made of ten rooms for weaners and a technical room, all accessible from a hallway placed along the western side of the building. This corridor also represents a filter zone for pre-treatment of the clean air conveyed inside the nursery rooms, as it has windows both on the outer wall and in the separation wall of the weaners' rooms. Air pre-treatment is carried out by managing the opening of the outer windows and through a heating system consisting in four finned pipes placed all along the hallway, beside the outer windows. Each room can host up to 240 weaners, while additional pigs can be reared in temporary shelters outside the southern façade. Every room is equipped with five thermal lamps of 1.8 kW each and a chimney with extraction fan. The thermal lamps, the windows on the corridor and the fans of the nursery rooms are controlled on the basis of temperature, which is monitored through sensors in every room. Minimum setpoint temperature is 28°C for one-month old piglets, weighting around 8 kg, and decreases down to 24°C for

weaners of about 3 months weighting 25-30 kg. Extraction fans work at 5% of maximum power below the minimum temperature, and the working rate linearly increases with temperature up to 100% at 32°C. The minimum temperature in the hallway is set by the farmer at 15°C at the windows height, as this temperature is suitable to properly balance hair exchange and heating in the weaners' rooms.

The hog barn has area of 663 m^2 to rear 400 sows and it can be heated by an LPG boiler of 115 kW, while ventilation is achieved through an extraction fan and windows' opening.

A smart monitoring and control system was developed and installed to monitor environmental variables and automate the integrated RES plant. Data has been collected since May 2021. The system comprises a gateway, weather station powered through PV, monitoring nodes for gases and environmental conditions in different areas, including the hallway and two rooms of the nursery barn. Further sensor nodes monitor all the relevant parameters of the DSHP, including the temperature of cooling and heating water at inlet and outlet, power consumption, heating capacity and the source used (air, BTES, or both). The RES4LIVE gateway, powered by a Raspberry Pi 4 model B with 4gb RAM, 128gb SSD, and 32gb microSD for initialization, is cost-effective and efficient.

2.1. RES system for the nursery barn

The RES system was designed to replace a 34 kW LPG boiler used to pre-heat the air in the hallway of the building, so that the inlet airflows into the nursery room, driven by extraction fans, have adequate temperature during the cold season. Specifically, the integrated system is composed of photovoltaic thermal collectors (PVT), a dual-source heat pump (DSHP), and a borehole thermal energy storage (BTES). The heating load provided by the geothermal heat pump can rise the temperature of the radiant pipes up to 55°C, i.e. the operating temperature targeted with the previous fossil-based plant. The fundamental system architecture incorporates a dual-source heat pump featuring not only an air-cooled evaporator but also a heat exchanger for transferring heat with a water/glycol blend sourced from a sequence of PVT collectors connected to boreholes. The PVT system is controlled through RESOL VBus, a communication protocol allowing various devices to connect and exchange data, since May 2023 (Murali et al. 2024). The primary novelty of the system resides in its capability for hybrid operation, enabling simultaneous utilization of both ground-sourced and air-sourced heat, resulting in increased heating capacity and COP efficiency.

2.2. Retrofitting of the hog barn

Two tests of thermal conductance of the perimeter walls of the building were carried out in 2021, specifically one in the warm season and one in the cold season through a wireless heat flux meter Thermozig. The analysis of the physical properties of the building pointed out that the roof was already properly insulated, thanks to the layer of double insulated corrugated sheet, which can provide a thermal transmittance assessed 0,18 W/m^2K. The test of the thermal transmittance of the boundary walls of the building, performed by means of heat flux meter during the cold season, showed that the thermal transmittance is around 0.3 W/m^2K, that represents a satisfactory value for the energy performance of the building (**Error! Reference source not found.**). The test and the analyses of the building led to the conclusion that the most critical parts in terms of performance of the building envelope are the windows. In fact, the two longitudinal walls were equipped with a total of 34 windows of 2.8 m x 0.8 m, with steel single-layer frames and 4 mm thick glass surfaces. These features resulted in a thermal transmittance assessed 5.9 W/m^2K. Moreover, the operational system is totally manual, so that it is not possible to control the opening of the windows in a way that can limit heat losses and, more importantly, there is no way to minimize the thermal dispersions.

Therefore, the retrofitting solution finally designed did not include insulation layer for the walls, as they showed adequate transmittance without particular requirement of further reduction. The retrofitting was totally focused on the replacement of the existing windows with a high performing system, with much lower thermal transmittance, equipped with automation devices suitable to control the opening in a way that minimizes heat loss while assuring proper air exchange.

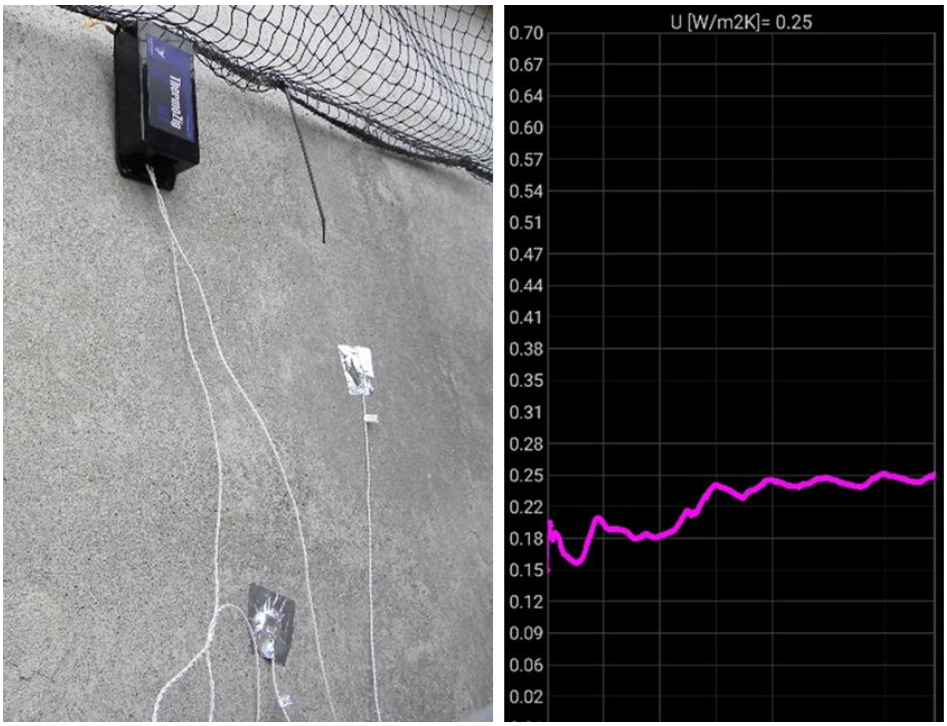

Figure 1. Test to assess the thermal conductance of the exterior wall of the hog barn.

The new windows are composed of a perimeter frame in tubular stainless steel, frame and upper counterframe in stainless steel, with transparent infill in 16mm thick double chamber alveolar polycarbonate. This solution can assure a thermal transmittance of 2 W/m^{2}K, i.e. around one third of the previous. situation

Moreover, the system includes six gearmotors with limit switch for the mechanical opening, environmental sensors and actuators for the automatic openings based on temperature and air quality parameters.

3. Results and Discussion

3.1. Performances of the integrated RES system

Based on the results of hydro-geological analyses, the potential for underground thermal storage was quantified, heat dispersion due to groundwater movement was assessed, and the BTES behaviour was modelled under different operational scenarios. A depth of 30-meter was deemed the most efficient solution for the thermal loads of the weaners' nursery building and, on such basis, 8 BHEs of this depth were drilled for the BTES field as the result of system dimensioning (Tinti et al. 2023). To create a Thermal Core (TC) at the centre of the BTES system for optimal thermal storage, hybrid connections were employed among the BHEs in series/parallel configurations. Heat is thus injected from the TC to the boundaries during heat storage, resulting in higher temperature rise compared to different configurations. During the exploitation phase, heat is extracted first from the boundaries and then from the TC. The BTES field, designed to meet, consists of 4x2 BHEs arranged in a rectangular configuration, spaced 3 meters apart in the North-South direction and 2 meters apart in the East-West direction to optimize land use in the farmyard. The average temperature measured in a 30m borehole in March 2023, before BTES installation, was 15.9°C; the average temperature in 30m boreholes measured on 10 Sep 2023, i.e. at the end of the heat injection season, was 20.5°C. Therefore, the increase in TC temperature due to solar heat injection from May to August 2023 was 4.6°C, i.e. corresponding to the best scenario expected.

The integrated heating system of the nursery barn was analysed on the basis of the temperature and humidity data recorded in the period 17-24 April 2024. In this week, outside temperature proved significantly low, with 9.2°C as average and 2.9°C as minimum value, thus calling for heating almost continuously the hallway through the DSHP. The temperature in the hallway was then kept above the setpoint of 15°C (with

a tolerance interval of 0.5°C) for the period considered, with the temperature in the finned pipes reaching over 50°C in several periods. The two monitored rooms, indicated in Figure 1, hosted weaners until 17 April and room 1 also from 24 April. However, other rooms in the building hosted weaners also in the period 18-23 April, that is why the hallway was continuously kept heated during the entire period. The heating system developed proved effective also for the control of humidity conditions in cold season, as it is witnessed by the THI trends in the weaners' rooms (**Error! Reference source not found.**), that is substantially kept below the alert threshold of 75.

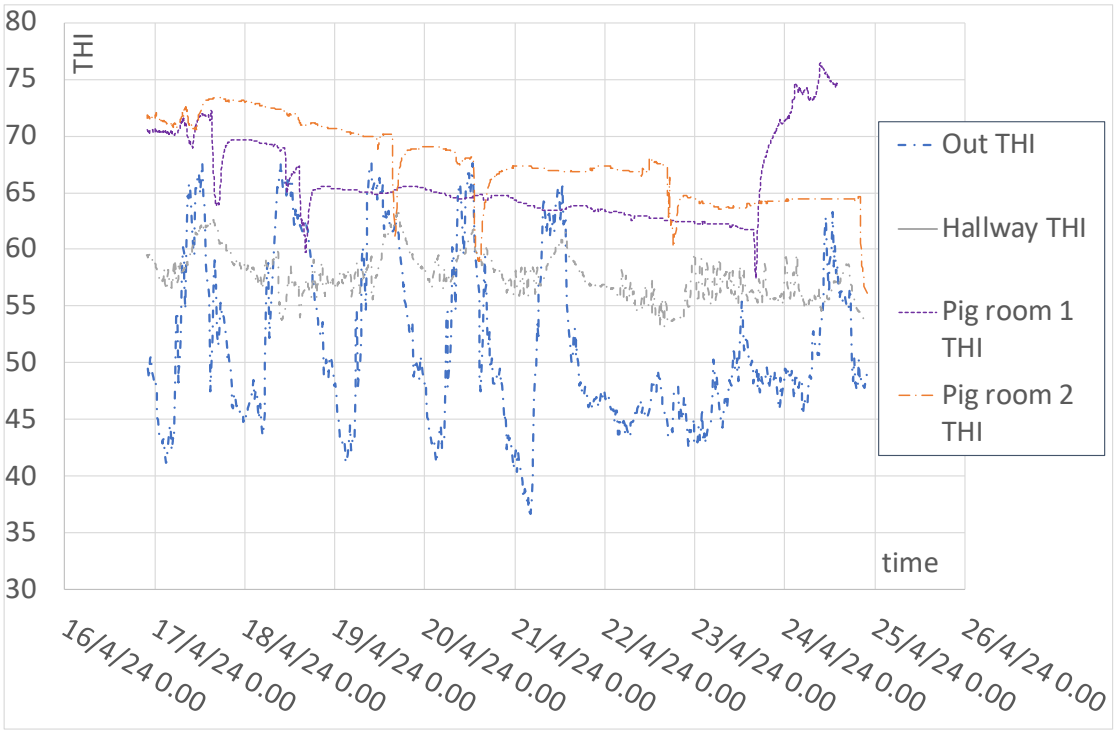

Figure 2. THI measured in the monitored indoor spaces of the nursery barn and outside.

The geothermal source was always used during the working time of the heating system and the circulation through the BHEs produced a temperature increase up to 9.1 K in the cold side of the DSHP. The average temperature difference between the flows from and to BTES during the period analysed, i.e. the effect of the heat extraction was 3.0 K, corresponding to an average thermal power of 15.3 kW. The exploitation of the geothermal storage thus allowed to achieve high efficiency in the DSHP, as it is shown by the ratio of the heating capacity and the electric power used, reported in Figure 4. The resulting coefficient of performance (COP) is represented as well in the same diagram with hourly intervals, and the average COP in the studied period was 4.34. The COP of the DSHP when operating only in geo-source mode increased to 4.67.

3.2. Performances of building retrofitting

The retrofitting action carried out on the hog barn resulted in a significant improvement of the thermal performances of the building. In particular, the effect was measured in the warm season, by comparting temperature and humidity data recorded inside the barn before and after the retrofitting, under the same utilization conditions. Figure 3 shows the reduction of the indoor temperature with reference to outdoor climatic conditions and in particular the difference between indoor and outdoor temperature was in general significantly lower after the intervention.

Then we considered relative humidity as well, so we computed the benefit in terms of THI. Specifically in August 2022, before retrofitting, the average difference between indoor THI and outdoor THI (computed at 30 min interval rate) was +1.94. Subsequently the retrofitting, such difference was -2.38. Therefore, the capacity of reduction of indoor THI was on average 4.32.

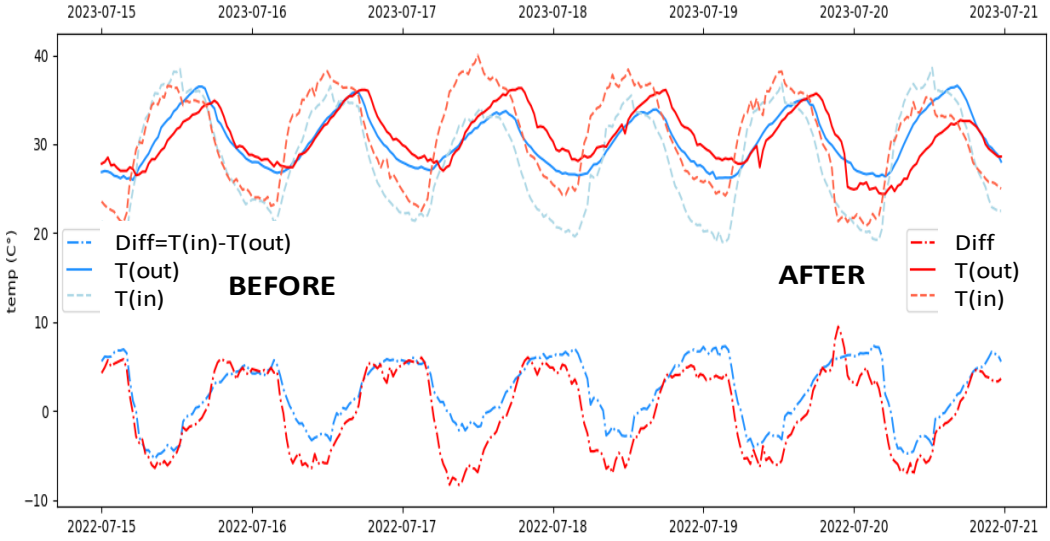

Figure 3. THI measured in the monitored indoor spaces of the nursery barn and outside.

4. Conclusions

The experimental study carried out demonstrated that a carefully planned mix of RES components can be seamlessly integrated into an automated heating system to meet the farm needs. By harnessing solar energy and utilizing thermal energy storage, coupled with the efficiency of a DSHP, the system effectively managed indoor temperatures without reliance on fossil sources. Future developments aim to extend this approach to other farm building typologies, such as farrowing barns, and to integrate solar and geothermal energy resources also to regulate temperature and humidity in warmer climatic conditions.

Monitoring outdoor and indoor environmental parameters was crucial for collecting data, evaluating system effectiveness, and enabling remote control of the equipment. Data collection prove fundamental for the correct definition of technical solutions in the design of retrofitting interventions, to increase the energy efficiency of existing livestock barns. This study thus demonstrates that integrated RES systems and targeted retrofitting can significantly enhance the sustainability livestock farming.

Ongoing research and innovation in this field will continue to refine and optimize these integrated systems, utilizing advancements in renewable energy technology to improve farm operations, enhance environmental stewardship, and promote animal welfare. The successful deployment of such solutions establishes a promising example for the wider adoption of renewable energy systems in agriculture, moving towards a more sustainable and resilient future for livestock production.

Acknowledgements

This research was funded by the European Commission, within the Horizon 2020 program for the Innovation Action project RES4LIVE "Energy Smart Livestock Farming towards Zero Fossil Fuel Consumption", running in the period 2020-2024, Grant agreement ID: 101000785, DOI 10.3030/101000785.

References

Costantino, Andrea. 2023. "Development, Validation, and Application of Building Energy Simulation Models for Livestock Houses: A Systematic Review." *Agriculture* 13(12). doi: 10.3390/agriculture13122280.

Deeken, H. F., A. Lengling, M. S. Krommweh, and W. Büscher. 2023. "Improvement of Piglet Rearing's Energy Efficiency and Sustainability Using Air-to-Air Heat Exchangers—A Two-Year Case Study." *Energies* 16(4). doi: 10.3390/en16041799.

Mahfuz, Shad, Hong-Seok Mun, Muhammad Ammar Dilawar, and Chul-Ju Yang. 2022. "Applications of Smart Technology as a Sustainable Strategy in Modern Swine Farming." *Sustainability* 14(5). doi: 10.3390/su14052607.

Mun, Hong-Seok, Muhammad Ammar Dilawar, Shad Mahfuz, Keiven Mark B. Ampode, Veasna Chem, Young-Hwa Kim, Jong-Pil Moon, and Chul-Ju Yang. 2022. “Effects of a Combined Geothermal and Solar Heating System as a Renewable Energy Source in a Pig House and Estimation of Energy Consumption Using Artificial Intelligence-Based Prediction Model.” *Animals* 12(20). doi: 10.3390/ani12202860.

Murali, Damu, Iván P. Acosta-Pazmiño, Alexander Loris, Abel Climente García, Stefano Benni, Francesco Tinti, and João Gomes. 2024. “Experimental Assessment of a Solar Photovoltaic-Thermal System in a Livestock Farm in Italy.” *Solar Energy Advances* 4:100051. doi: https://doi.org/10.1016/j.seja.2024.100051.

Niu, Kunyu, Jianing Zhong, and Xiangdong Hu. 2024. “Impacts of Climate Change-Induced Heat Stress on Pig Productivity in China.” *Science of The Total Environment* 908:168215. doi: https://doi.org/10.1016/j.scitotenv.2023.168215.

Shin, Hakjong, Sang-yeon Lee, Jun-gyu Kim, Dae-Heon Park, Seng-Kyoun Jo, and Younghoon Kwak. 2024. “Applicability Evaluation of a Temperature Humidity Index-Controlled Ventilation System in Livestock Using a Building Energy Simulation Model.” *Case Studies in Thermal Engineering* 57:104335. doi: https://doi.org/10.1016/j.csite.2024.104335.

Tinti, F., P. Tassinari, D. Rapti, and S. Benni. 2023. “Development of a Pilot Borehole Storage System of Solar Thermal Energy: Modeling, Design, and Installation.” *Sustainability (Switzerland)* 15(9). doi: 10.3390/su15097432.

Tyris, D., D. Manolakos, T. Bartzanas, S. Benni, T. Amon, J. Maselyne, S. Lecompte, P. Grammelis, A. Balafoutis, G. Zhang, P. Bakalis, S. Kalogridis, O. Marchand, H. Hoes, and J. Gomes. 2022. “RES4LIVE – Energy Smart Livestock Farming towards Zero Fossil Fuel Consumption.” *VDI Berichte* 2022(2406):493–98. doi: 10.51202/9783181024065-493.

Wood vinegar: A renewable product for a sustainable agriculture

Carolina Fabbri [a*], Lorenzo Pezzola [a], Valerio Magalotti [a], Roberto Mussi [a]

[a] YANMAR R&D EUROPE, Florence, Italy
* Corresponding author. Email: carolina_fabbri@yanmar.com

Abstract

Wood vinegar is a promising product for pest insect control in agriculture, deriving from pyrogasification process of woody material. Yanmar R&D Europe developed a prototype gasifier using farm agricultural prunings to produce energy, heat, biochar and wood vinegar. Olive Fruit Fly Bactrocera oleae which impact the quantity and quality olive production, is considered one of the most serious olive pests in Italy and in the world. The present study assessed the repellent efficacy of wood vinegar from agricultural prunings against olive fly attack under open field conditions at 0.5 and 1% v/v concentrations over two growing seasons. The tests were conducted in two olive farms, located one on the inland and the other on the coast side of Tuscany. The data were analyzed and compared with Control (no treated) and commercial wood vinegar application. The results showed that Yanmar R&D wood vinegar and commercial provided olive fly repellence at both dosages, significantly higher than Control. Wood vinegar from agricultural prunings can help farmers protect crops from insect pest and find a functional use of agricultural prunings in the field. In a "circular economy" perspective, this would allow obtaining useful products at low cost.

Keywords: wood vinegar; olive fly; repellence activity

1. Introduction

The gasification of wood waste is considered nowadays an interesting source of energy and heat production. Indeed, the conversion of biomass into high-value products used instead of fossil fuels is necessary in the fight against climate change, to provide renewable products that meet the world increasing energy demand (Narnaware et al., 2022). The gasification process involves a gaseous phase known as syngas (energy and heat), a liquid phase comprising bio-oils (wood vinegar), and a solid fraction (biochar).

Until some time ago, wood vinegar and biochar were considered waste, but in recent years, studies have shown their validity for use in agroecosystems (Ouattara et al., 2023; Tibor et al, 2022; European Commission, 2020).

Biochar is a vegetable charcoal, used in agriculture as a soil improver, and among its characteristics stand out its ability to remediate soils, increase soil water retention, and raise soil pH (Liao et al., 2019).

Wood vinegar, instead, is a product derived from the condensation process of combustion gases and it is a compound rich in numerous organic molecules, such as polyphenols, acetic acid, and tannins, which are usually found into wood. Wood vinegar is available in the market as plant stimulant. However, it is currently being studied in laboratory and field trials to assess its efficacy as insect repellent, antimicrobial, herbicidal agent, and more (Chalermsan et al., 2009; Becagli et al., 2021; Iacomino et al., 2024). In fact, wood vinegar produced through various processes (temperature, pressure, etc.) and derived from different raw materials (forest wood, straw, etc.) exhibit various biochemical compositions, consequently yielding diversified results in terms of active properties.

In particular, as regard anti-insect activity, Dewi et al., (2020) tested the application of wood vinegar in a laboratory experiment against whitefly attacks on mulberry plants, observing a repellent effect at doses of 2.5%. Salim et al. (2021) reported that wood vinegar exhibited anti-mold properties in both sesenduk (Endospermum spp.) and jelutong (Dyera costulata) hardwood species as a result of treating the wood with wood vinegar derived from the pyrolysis of quercus wood. Alias et al., (2019) conducted a test against fruit flies, indicating that pure bamboo vinegar (100% v/v) exhibits insecticidal properties equivalent to a commercial insecticide. Othman et al., (2023) tested wood vinegar made from 100% mangrove trees against Rice Weevil under storing conditions showing lethal conditions at 77.62 ppm concentration.

Olive Fruit Fly Bractocera oleae (olive fly) represents the key pest of olives cultivated in the Mediterranean environment. The insect attack has been reported to create a damage up to15% of the olive crop, although,

pesticide treatments are applied every year to control the fly population, causing environmental pollution. The damage caused by the olive fly results in: a) decrease in yield and quality of fruit and lowering quality of olive oil. b) use of high-cost chemicals and application machinery that increase production cost. c) use of toxic chemicals with consequence for the environmental protection (Basilios et al., 2002). The use of organic solutions for containing this dipteran could have a significant impact from an economic, environmental, and social sustainability perspective.

Yanmar R&D Europe (based in Florence), the research centre of Yanmar company, has developed a prototype gasifier capable of utilizing agricultural woody pruning waste to produce energy, heat, biochar and wood vinegar. The project's idea is to create circular economy within the farm, where all gasification products can be reused in the same farm management. In the Mediterranean area, key crops for rural economy are mainly vineyards and olive trees. The use of pruning waste from these plants is even more interesting given the new Common Agricultural Policy directive banning agricultural pruning burning (EU, 2022). In fact, the unmanaged pruning could otherwise be abandoned in the fields, causing inconvenience to farmers and also, can serve as a source of disease inoculum, spreading more easily in the field.

The project's idea is therefore to find a “circular solution” where the use of olive pruning can be a source of wood vinegar production, which is then reused by the farmer as a remedy against olive fly infestation. This could represent a resilient system where residues are no longer waste but a solution. The purpose of this first trial was to test wood vinegar from agricultural prunings against the olive fly attack in Tuscany and determine the effect, appropriate methods and doses of application.

2. Materials and Methods

2.1. Wood vinegar

Wood vinegar (WV) used in this study was prepared starting from agricultural woody prunings pelletized. WV was the results of condensed vapours resulting from an experimental gasification process by Yanmar R&D Europe. The gasifier uses wood waste from agricultural production to produce energy, heat, biochar and wood vinegar. Condensable volatile compounds from reactor are reformed in the catalytic filter, after that are condensed and collected in tanks and kept for a certain period at room temperature inside containers. Then, the wood distillate is ready to be used providing the necessary chemical analysis compliancy.

2.2. Field test

WV was tested on field trials as repellent against olive fly during two olive growing seasons: 2022 and 2023. In 2022 it was applied in two farms: one near Grosseto (on the coast) cultivating Maurino cultivar (A1) and the other in the hinterland near Florence, cultivating Frantoio cultivars (A2) (Figure 1). In the first year, the product was applied in both farms and two doses of Yanmar derived Wood Vinegar (WVY) (0.5 %v/v and 1% v/v) were tested over approximately 60 plants each farm. Over the two years, a portion of the plot was left untreated and used as Control. The second year, only one dose of WVY was tested (0.5 % v/v) in A2 farm, and a treatment with commercial WV (WVC) derived from chestnut tannin extract was performed. The product was applied, from olive kernel hardening (July) to harvesting (October), via spray mode using an atomizer barrel on the entire canopy, with an around 14-day interval from the hardening phase of the kernel to harvest (Table 1). WVY was derived by pelletized agricultural woody prunings derived by an experimental gasifier under R&D located in Florence.

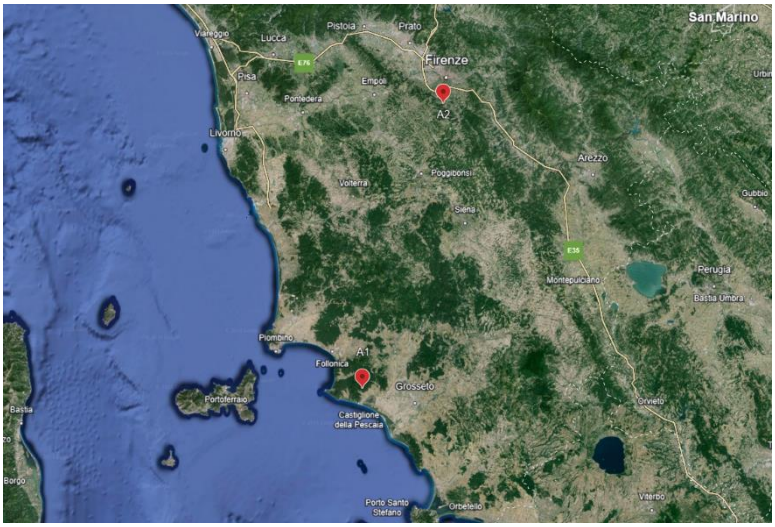

Figure 1. Location of experimental farms in Tuscany region.

Wood vinegar: application time	
2022	18/07/2022
	02/08/2022
	22/08/2022
	05/09/2022
	14/09/2022
	22/09/2022
	03/10/2022
2023	19/07/2023
	06/08/2023
	21/08/2023
	01/09/2023

Table 1. Application time of wood vinegar during the growing season 2022 and 2023 in olive orchards.

2.3 Monitoring schedule

In the plots, chromotropic attracting traps for olive fly were placed on sample olive trees and periodically the number of flies trapped were monitored: one trap for each treated plot and one for each control plot were placed and substituted every month with new traps. Additionally, 50 olives were periodically sampled in the plots, collected randomly in the field, placed in bags, and monitored using a magnifying lens to observe the infestation % (presence of eggs/pupae or larvae) (Table 2).

Inland	**Coast**	**Inland**
2022	**2022**	**2023**
18-Jul	29-Jul	11-Aug
02-Aug	05-Aug	25-Aug
22-Aug	12-Aug	31-Aug

05-Sep	26-Aug	06-Sep
14-Sep	02-Sep	13-Sep
22-Sep	09-Sep	21-Sep
03-Oct	16-Sep	28-Sep
10-Oct	23-Sep	05-Oct

Table 2. Monitoring time of traps and collection of olives to detect attack.

2.4 Statistical analysis

For the statistical analyses, R software (R 4.0.3) was used in the RStudio environment. Statistical analysis of mean olive flies captured, and olive infested was then calculated by using a one-way analysis of variance, one-way ANOVA with Duncan test procedure as post hoc test. The data were considered significant at p= 0.005.

3. Results and Discussion

The efficiency of WV application both from Yanmar R&D and commercial, during the olive growth season, were evaluated in 2022 and 2023, based on the availability of farmers. The test was performed to test the repellent effect against olive flies and the % attack of olives in open field conditions.
The average number of olive flies trapped have been reported in Figure 2. In both years Control showed the highest number of olive flies captured in comparison to WVY and WVC. In 2022, the application of WVY in central and cost Tuscany areas showed similar results both for 0.5% v/v and 1% v/v concentration. Due to this result, in 2023 the experiment was replicated using only 0.5% v/v WVY and making a comparison with WVC at same dosage (rate suggested by the product label). Also, in this case the results were similar, showing not statistical difference in number of trapped olive flies. However, the results have been influenced by the low presence of olive fly population during the experimental years, especially during 2022, in those specific geographic areas.

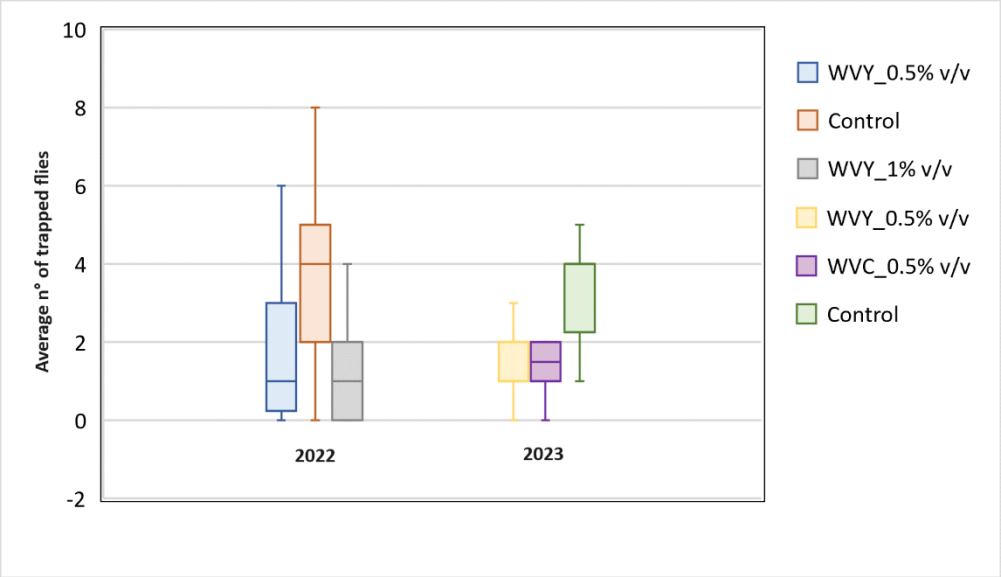

Figure 2. Average number of trapped olive flies during the season 2022 and 2023 for each treatment. WVY (wood vinegar Yanmar); WVC (wood vinegar commercial); Control (no treatment).

The fruit infestation was lower in 2022 (Figure 3), showing similar results for WVY and WVC. The

highest number of larvae/pupae were detected for Control, statistically different from the other treatments. No statistical difference was found as regard sterile puncture for the three treatments. In 2023 (Figure 4) the results were similar for WVY and WVC, showing no statistical difference for both number larvae/pupae and sterile puncture. On the contrary, Control was statistically different in comparison to WVY and WVC, but only as regard the % of larvae/pupae infestation.

Considering the need of integrated solutions for olive fly control, WV could be an interesting product with a repellence and oviposition deterrence effect. However, higher WV dosage (1% v/v) did not show higher repellent effect that lower rate (0.5% v/v). For that reason, it is auspicial a lower application rate of the product for an economic advantage. As regard sterile puncture presence, we can say that having the same number of sterile punctures does not pose a significant issue in controlling the dipteran. It would be interesting to test the presence of organic components in WVY, causing not only repellent effects but also larvicidal or ovicidal effects. In this contest, Akkus et al., 2022 reported that the type of wood used in the wood vinegar, the type of chemicals presents, and the concentration applied usually influence the larval mortality of insects. Liscia et al., 2013 reported that olive fly is influenced by number of volatile compounds influencing the olfactory sensitivity of dictera.

The use of an organic, locally sourced product, produced within a circular economy framework in the same company, could have a significant impact on agricultural businesses for controlling pathogenic insects. The excessive use of insecticides has negative impacts from both an economic and environmental perspective, increasing dependence on synthetic chemical products.

The use of wood vinegar in this case has shown repellent and fly attack characteristics similar to the tested commercial product. For this reason, the farmer who decides to invest in the gasifier could have a product similar to the commercial one, which on the market costs around 20 euros per litre.

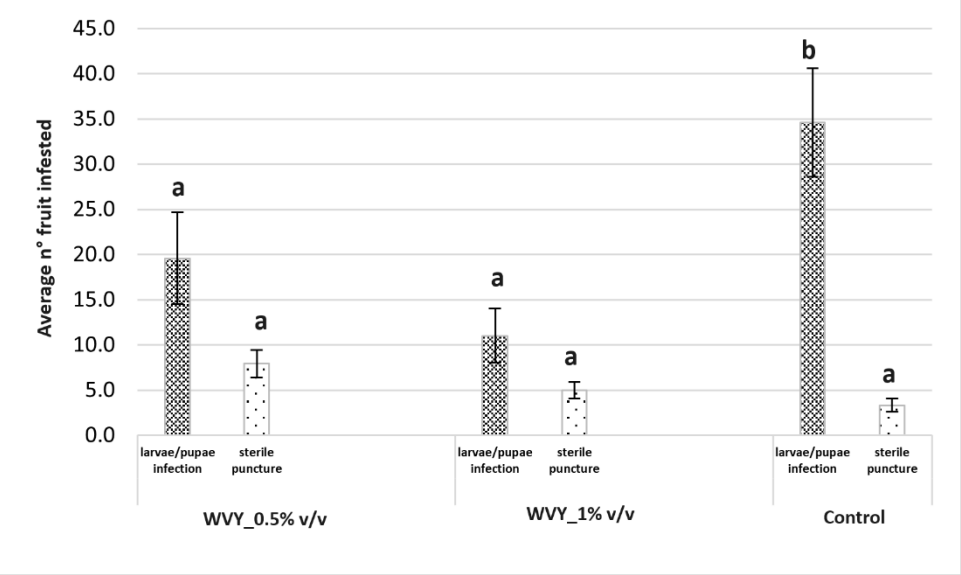

Figure 3. Average number of olives attacked by olive fly (presence of larvae/pupae and sterile puncture) during the season 2022 for each treatment. WVY (wood vinegar Yanmar); WVC (wood vinegar commercial); Control (no treatment).

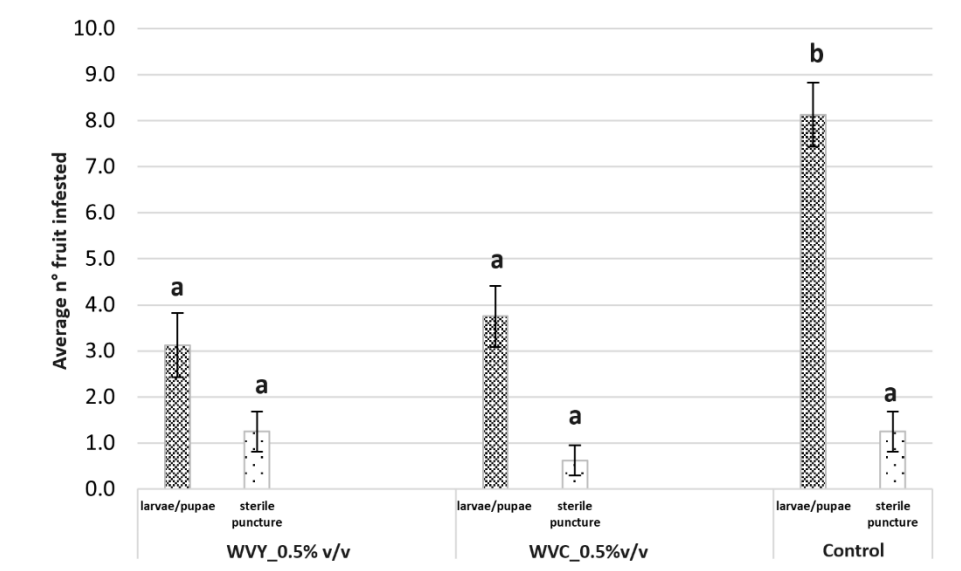

Figure 4. Average number of olives attacked by olive fly (presence of larvae/pupae and sterile puncture) during the season 2023 for each treatment. WVY (wood vinegar Yanmar); WVC (wood vinegar commercial); Control (no treatment).

4. Conclusions

In conclusion, the aim of the test was to study the effect of wood vinegar from agricultural prunings for olive fly control. Further research could pay attention on the specific compounds effect of wood vinegar, finding the active principle and optimal application rate functional for specific agricultural applications. Our study underscores the notable biological activity of wood vinegar against olive flies applied at 0.5 and 1 % v.v. The results of repellence activity were similar as regard both dosages, but significantly lower that Control. The effect of wood vinegar from different crop prunings as repellent for other pest insects should be tested. The results of this study introduce a way to bring circular economy solutions in a farm producing prunings: from wastes to helpful products for the farms. The possibility to use natural-based insecticides such as wood vinegar as a potential agent in olive fly attack control could bring environmental, economic and social sustainability to the agricultural sector.

References

Alias, N.Z., Abdullah, S., Shaari, S.S., Junik, J.J., Kamal, M.L., Masdar, N.D., 2020. The Potential of Bamboo Vinegar (Gigantochloa albociliata) as Insecticide. In: *Alias, N., Yusof, R. (eds) Charting the Sustainable Future of ASEAN in Science and Technology*. Springer, Singapore. https://doi.org/10.1007/978-981-15-3434-8_7

Becagli, M.; Santin, M.; Cardelli, R. Co-Application of Wood Distillate and Biochar Improves Soil Quality and Plant Growth in Basil (Ocimum Basilicum)#. J. Plant Nutr. Soil Sci. 2022, 185, 120–131. https://doi.org/10.1002/jpln.202100239

Chalermsan, Y., Peerapan, S., 2009. Wood vinegar: by-product from rural charcoal kiln and its role in plant protection. Asian Journal of Food and Agro-Industry. 2, S89-S195.

Dewi, R., Hastiti, N., Nuraeni, Y., 2020. Utilization of wood vinegar as plant based insecticide in mulberry (Morus sp). IOP Conf. Ser.: Mater. Sci. Eng. 935(1):012027. https://doi.org/10.1088/1757-899X/935/1/012027

European Commission. COMMISSION IMPLEMENTING REGULATION (EU) 2019/2164 of 17 December 2019. Official J. Europ. Union (2020) L328/61, 18.12.2019. Available at: https://eur-lex.europa.eu/legal-content/EN/TXT/?uri=CELEX%3A32019R2164

EU 2022. COMMON AGRICULTURAL POLICY FOR 2023-2027 28 CAP STRATEGIC PLANS AT A GLANCE. https://agriculture.ec.europa.eu/system/files/2022-12/csp-at-a-glance-eu-countries_en.pdf

Iacomino, G., Idbella, M., Staropoli, A., Nanni, B., Bertoli, T., Vinale, F., Bonanomi, G., 2024. Exploring the Potential of Wood Vinegar: Chemical Composition and Biological Effects on Crops and Pests. Agronomy. 14(1), 114. https://doi.org/10.3390/agronomy14010114

Liao, W., Thomas, S.C., 2019. Biochar particle size and post-pyrolysis mechanical processing affect soil pH, water retention capacity, and plant performance. Soil Systems. 3(1), 14. https://doi.org/10.3390/soilsystems3010014

Mazomenos, B.E., Pantazi-Mazomenou, A., Stefanou, D., 2002. Attract and kill of the olive fruit fly Bactrocera oleae in Greece as a part of an integrated control system. IOBC wprs Bulletin. 25(9), 137-146.

Narnaware, Sunil L., Panwar, N.L. 2022. Biomass gasification for climate change mitigation and policy framework in India: A review. Bioresource Technology Reports. 17:100892. https://doi.org/10.1016/j.biteb.2021.100892

Othman, N., Elias, N. H., Zainalabidin, N., 2023. Wood Vinegar as an Alternative Insecticide in Controlling Rice Weevil, Sitophylus oryzae (Coleoptera: Curculionidae). Advances in Agricultural and Food Research Journal, 4(1). https://doi.org/10.36877/aafrj.a0000315

Ouattara, H. A. A., Niamké, F. B., Yao, J. C., Amusant, N., Garnier, B.m, 2023. Wood vinegars: Production processes, properties, and valorization. Forest Products Journal. 73(3), 239-249. https://doi.org/10.13073/FPJ-D-23-00021

Salim, S., Yi, L.Y., Ashaari, Z., Choi, Y.S., Kim, G.H., 2021. Crude wood vinegar as a potential anti-mould chemical for sesendok and jelutong. In: *International Conference on The Future Wood Science and Technology Education* (FWSTE2021), Putra, Malaysia.

Sebestyen Tihamer Tibor, Carlos A. Grande, 2022. Industrial production of activated carbon using circular bioeconomy principles: Case study from a Romanian company. Cleaner Engineering and Technology. Volume 7, 100443, ISSN 2666-7908. https://doi.org/10.1016/j.clet.2022.100443.

Energy management in agriculture - potential for farmers and the region

Heinz Bernhardt [a,*], Jörn Stumpenhausen [b], Christoph Bader [a,b], Martin Höhendinger [a,b]

[a] Technical University of Munich, School of Life Sciences, Agricultural Systems Engineering, Freising, Germany

[b] University of Applied Sciences Weihenstephan-Triesdorf, Freising, Germany

* Corresponding author. Email: heinz.bernhardt@tum.de

Abstract

Effective energy management in dairy cowsheds is crucial for the sustainability and profitability of farms. The principles and effects of the CowEnergy concept will be presented here. It aims to make optimum use of energy resources in the dairy barn while minimizing the environmental impact. The structure and the experience gained in practical projects will be presented.

CowEnergy is divided into several areas. A central pillar of CowEnergy is the use of renewable energy sources on the farm. By installing photovoltaic systems on the barn roofs, recycling liquid manure and feed residues into biogas and integrating wind turbines on the farm premises, a large proportion of the energy required can be generated on site. This not only reduces dependence on external energy suppliers, but also helps to reduce greenhouse gas emissions.

In addition to generating electricity from renewable sources, the CowEnergy concept is supported by intelligent energy management in the barn. Energy consumption is optimized through the use of energy-efficient lighting and ventilation systems as well as modern milking and feeding technologies. The use of electric drives for farm vehicles such as wheel loaders or self-propelled feed mixers makes it possible to dispense with combustion fuels here too. Automated processes and sensor technologies help to analyze and adjust energy requirements in order to avoid overcapacity and use resources efficiently.

A storage system for the energy is also necessary to balance out the fluctuations in the generation of renewable energy systems. This can take various forms. In dairy farming, for example, ice water cooling for the milk is an option. For biogas, it can be an oversized gas storage tank. Electrical energy from PV systems can be stored in vehicle batteries or external batteries. In the future, hydrogen may also be available.

Another important aspect of CowEnergy is the regional energy supply. This involves the exchange of energy peaks and troughs in the region. This offers, for example, the possibility of centralized energy storage or the exchange of available energy between different users. This not only strengthens the regional economy, but also promotes independence from fossil fuels and helps to protect the environment. One current problem in Germany is the legal situation in energy trading.

By integrating regional and renewable energy sources and optimizing energy consumption, it not only increases the profitability of farms, but also makes an important contribution to environmental protection.

Keywords: energy management, dairy cows, renewable energy, regional grid.

1. Introduction

The social debate about the future direction of our energy supply can be observed worldwide. Many aspects such as sustainability, CO2 neutrality, regionality and general compatibility with the UN's 17 Sustainable Development Goals (SDGs) play a role here. The aim of this study is to show the possibilities for dairy farms to generate, store and use energy. Energy encompasses a wide variety of energy sectors, such as electrical energy, thermal energy, chemical energy and mechanical energy.

The immediate aim of farmers is to reduce their energy costs or to build up another economic mainstay through energy trading. Another goal is to integrate into regional and social energy management. This ranges from the stabilization of regional energy grids, to community electricity management, to emergency power supply and control centers in the event of a disaster.

The focus here is on the situation in Germany. However, the general concept is transferable to many other countries.

2. Materials and Methods

An energy management system (EMS) was set up on a dairy farm to analyse the potentials. This system

is able to regulate the energy production on the farm and the energy consumption in the barn and in the external grid. On the farm, the EMS records energy generation via photovoltaics, biogas, wind and geothermal energy; at the same time, it records energy consumption in the barn via milking robots, cleaning robots, the battery of the feed mixer, cow brush and slurry pump, and the various storage options such as biogas storage, battery storage and ice water storage serve as a balancing system.

3. Results and Discussion

The analysis of dairy farms reveals a significant potential for sustainable energy production, indicating a promising future for the integration of renewable energy systems in agricultural operations. One of the primary methods for harnessing this potential is through the utilization of biogas. By processing manure and other organic materials in biogas plants, dairy farms can generate approximately 8.3 kWh of electrical energy per cow per day. This method not only provides a reliable source of electricity but also produces considerable amounts of thermal energy as a byproduct, which can be utilized for heating purposes within the farm, enhancing overall energy efficiency.

In addition to biogas, photovoltaic (PV) systems present another viable option for dairy farms. The installation of PV panels on available roof space can significantly contribute to the farm's energy needs. Depending on the roof's location and orientation, it is possible to achieve about 0.2 kWp of nominal capacity per square meter. This form of solar energy harnessing is particularly advantageous due to the relatively large roof areas typically available on dairy farms, allowing for substantial energy generation.

Wind energy also holds considerable promise for dairy farms situated in suitable locations. Modern wind turbines are highly efficient and can generate an impressive average of 15 million kWh of electricity per year. The integration of wind turbines can be particularly effective in areas with consistent wind patterns, providing a steady and robust source of renewable energy.

Moreover, dairy farms can explore the use of combined heat and power (CHP) plants that utilize biomass, such as wood chips. These CHP systems are capable of producing both electricity and heat from a single fuel source, thereby maximizing energy efficiency and reducing reliance on external energy supplies. Additionally, geothermal energy, particularly when harnessed from beneath the barn area, can provide a consistent and sustainable source of heating.

Small-scale energy production methods also offer valuable opportunities for dairy farms. For instance, the utilization of waste heat from barn air or milk can be an efficient way to reclaim energy that would otherwise be lost. This approach not only improves the overall energy balance of the farm but also contributes to environmental sustainability by reducing waste.

When the energy production capabilities of a dairy farm are compared with its energy consumption—typically around 640 kWh per cow per year—it becomes apparent that the farm has the potential to generate significantly more energy than it consumes. This energy surplus remains viable even as dairy farms advance towards greater automation, incorporating technologies such as milking robots, feeding robots, cleaning robots, and other electrically operated machinery. These innovations, while increasing the farm's energy demand, do not offset the substantial energy production achieved through renewable sources.

One of the primary challenges encountered by dairy farms revolves around the asynchronous nature of energy production and consumption. This misalignment underscores the necessity for robust energy storage capabilities. Among the array of potential solutions, options such as storing biogas for subsequent utilization, converting biogas into methane for prolonged storage, deploying battery systems, or leveraging hydrogen storage technologies emerge as prominent contenders. Tailoring solutions to the specific requirements of dairy operations, energy storage in the form of ice for milk cooling emerges as particularly pertinent.

Further expanding the scope to encompass agricultural settings, additional avenues for energy storage present themselves. These may include heat retention in manure through the integration of heat exchangers, the implementation of flywheel storage mechanisms, or the utilization of sand batteries. Such diversified approaches to energy storage not only address the immediate challenges posed by energy intermittency but also contribute to fostering resilience and sustainability within dairy and broader agricultural operations.

The Energy Management System (EMS) plays a pivotal role in orchestrating and regulating both energy generation and consumption. Beyond its intrinsic function of internal energy management within individual systems, the EMS serves as a crucial intermediary interfacing with regional energy grids. This dual

functionality enables it to synchronize internal energy demand and supply dynamics with those prevailing externally.

Notably, the EMS facilitates targeted external communication, a necessity particularly evident in the context of Germany's energy landscape. Here, renewable energy harnessed from biomass, solar, and wind sources is often integrated into the energy grid with minimal regulatory oversight. Consequently, the onus falls upon energy supply entities to manage grid energy levels. Presently, this entails resorting to measures such as disconnecting energy-generating facilities from the grid, primarily during periods of peak production, to mitigate the risk of grid overloading.

By leveraging the capabilities of the EMS, surplus energy can be strategically injected into the regional grid at opportune junctures. Armed with insights into internal energy consumption patterns, the EMS can dynamically adjust the energy consumption profiles of its constituents to cater to heightened regional demand, thereby augmenting energy availability in a timely manner. Conversely, in scenarios characterized by grid overload, the EMS serves as a conduit for temporary storage of excess energy within its storage infrastructure, thereby fostering grid stability.

Furthermore, the EMS is engineered with autonomous startup functionality, a feature of significant relevance, especially in agricultural contexts. Given the perennial presence of farmers within agricultural settings, the EMS can be initiated and monitored autonomously by a farmer, contributing decisively to grid restoration efforts in the aftermath of power outages. This aspect assumes heightened significance when envisioning the widespread deployment of EMS across agricultural landscapes. Such a deployment model would engender a proliferation of decentralized EMS units across the region, collectively bolstering the resilience and restorative capacities of regional energy grids.

However, notwithstanding the potential benefits, operationalizing these capabilities vis-à-vis established energy supply entities poses formidable challenges. The successful integration of EMS technologies necessitates a paradigm shift characterized by enhanced collaboration, networking, and adaptability on the part of major energy corporations. Addressing these complexities is indispensable to unlocking the full spectrum of benefits offered by EMS technologies in the realm of energy management and grid resilience.

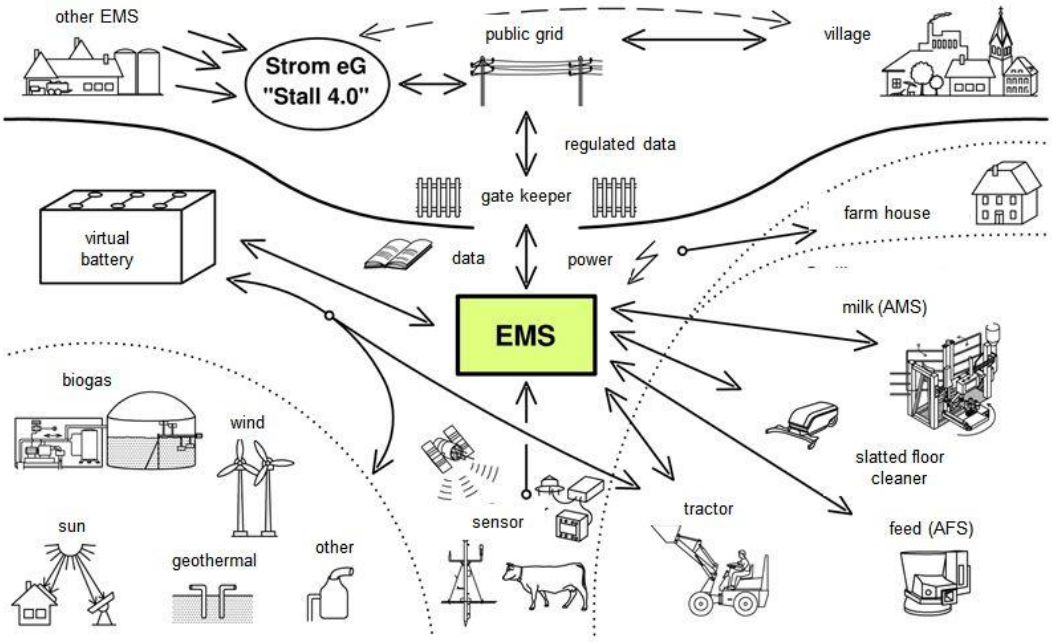

Figure 1. Energy Management System (EMS)

However, an energy management system (EMS) also presents numerous opportunities for the region. As elucidated earlier, the heightened regionalization of electricity grids engenders improved security and

heightened stability. Moreover, residential dwellings and small-scale enterprises can seamlessly integrate into this burgeoning system.

Presently, a discernible trend is emerging whereby homeowners are embracing the installation of autonomous energy storage systems to harness their self-generated power. Through the establishment of a shared energy network, the potential for energy storage within dairy farms comes to the fore. The stored electricity could subsequently be reclaimed and autonomously utilized during evening hours. Notably, the substantial cost advantage of employing the dairy farm's expansive energy storage facility over individual, diminutive storage units is evident. Additionally, the communal battery storage facility on dairy farms boasts a heightened level of resilience against overheating and fire hazards. This stems from its customary placement within a segregated structure on the farm premises, rendering it more accessible for cooling measures by firefighting personnel. In contrast, residential abodes often house their energy storage units in basements, thus elevating the risk of consequential damage in case of overheating incidents.

Moreover, enterprises endowed with in-house energy generation capacities can seamlessly integrate into the production and demand framework. This facilitates the judicious management of peak loads among diverse stakeholders. Given the distinct load profiles characteristic of businesses vis-à-vis dairy farms, the resultant variance simplifies the task of system equilibrium.

Beyond these conventional applications, the EMS presents an array of possibilities in the event of calamitous occurrences such as floods. Leveraging the inherent autonomy conferred by the EMS, dairy farms, endowed with expansive infrastructure including large-scale tractors, paved areas, and ample fuel reserves, emerge as pivotal emergency response sites. Often, the establishment of a rescue site necessitates only minimal additional investments in radio technology, thus streamlining the process of fortifying emergency preparedness within the region.

However, the realization of these options afforded by the energy management system (EMS) currently faces significant challenges. Regulatory frameworks governing energy marketing and grid infrastructure in Germany pose formidable barriers to progress. One such impediment lies in the requirement for grid usage fees when electricity traverses between two points via the "public" grid, even if these points are mere meters apart. This imposition of dual grid usage fees often renders collaborative energy storage initiatives economically unviable. A potential solution could entail the implementation of a flat-rate grid usage fee within a 50km radius, allowing for unlimited transfers of the same electricity within the grid and thereby fostering innovation in shared energy storage endeavors.

Moreover, existing practices empower grid operators to directly curtail the operation of larger energy installations, such as photovoltaic or biogas facilities, during periods of grid congestion. Consequently, the opportunity for self-consumption dissipates. A more optimal approach would involve implementing shutdown mechanisms at the point of grid injection, thereby preserving the feasibility of self-consumption.

In essence, effecting a seamless energy transition necessitates enhanced networking and flexibility on the part of major energy corporations. By fostering greater collaboration and innovation, these entities can spearhead initiatives to navigate regulatory constraints and propel the realization of societal aspirations for sustainable energy transitions. Central to this endeavor is the imperative of directly engaging and empowering the populace, ensuring that they derive tangible benefits from such transformative initiatives.

4. Conclusions

This observation underscores the substantial capacity of dairy farms for energy generation, thereby positioning them as pivotal contributors to the enduring stability of energy networks, notably within rural locales. Moreover, this potential empowers dairy farms to catalyse the inception of innovative energy paradigms.

Acknowledgements

The project was supported by funds of the Federal Ministry of Food and Agriculture (BMEL) based on a decision of the Parliament of the Federal Republic of Germany via the Federal Office for Agriculture and Food (BLE) under the innovation support programme.

References

Höhendinger, M.; Krieg, H.-J.; Dietrich, R.; Rauscher, S.; Stumpenhausen, J.; Bernhardt, H. Impacts of Divergent Moving Drives on Energy Efficiency and Performance of Various AMS in Operative Conditions. Agriculture 2021, 11, 806. doi: 10.3390/agriculture11090806

Ilyas, H.M.A.; Safa, M.; Bailey, A.; Rauf, S.; Khan, A. Energy Efficiency Outlook of New Zealand Dairy Farming Systems: An Application of Data Envelopment Analysis (DEA) Approach. Energies 2020, 13, 251. doi: 10.3390/en13010251

Theunissen, T.C., Bernhardt, H.: Revenue increase for German dairy farmers through cross-value chain energy management, 2022 ASABE Annual International Meeting 2200711. doi: 10.13031/aim.202200711

Shine, P., Upton, J., Murphy, M.: The development of a national-level energy assessment tool for the dairy industry, 2022 ASABE Annual International Meeting 2200539. doi: 10.13031/aim.202200539

Neser, St., Neiber, J.: Energieverbrauch im Milchviehbetrieb-Effizienz und Einsparpotential, 2014 LfL Bayern,https://www.lfl.bayern.de/mam/cms07/publikationen/daten/informationen/energieverbrauch_im_milchviehstall_065687.pdf

Energy use and indoor climate in livestock buildings for pigs in North America and Europe - A literature review

Therese Malm [a,*], Knut-Håkan Jeppsson [a], Dennis Johansson [b], Vahid M. Nik [b], Jenny Yngvesson [a], Marie-Claude Dubois [a, b]

[a] Department of Biosystems and Technology, Swedish University of Agricultural Sciences (SLU), Alnarp, Sweden

[b] Department of Building and Environmental Technology, Lund University (LTH), Lund, Sweden

* Corresponding author. Email: therese.malm@slu.se

Abstract

Climate change can raise average temperatures and humidity and induce more frequent and stronger extreme weather events. This intensifies the need for studies on indoor climate and energy use in livestock buildings as it will affect animal welfare and farmers' economy in terms of production, energy demand and needed investments. The aim of this review was to identify knowledge gaps and the need for further research about energy use and indoor climate of livestock buildings for pigs, including passive and active adaptation measures. In total 29 articles were reviewed, published during 2000-2023, from Europe and North America.

One key finding was that the studies conducted had different aims and approaches regarding the scope and presentation of results. The energy use data were presented using various definitions and units with total energy use for a specific category and number of pigs and a given period being the most common. However, when housing area and pig data were provided, key figures on energy use could have been calculated to enable benchmarking. Indoor climate conditions were also reported in different ways, ranging from detailed information on temperature and humidity to no information on indoor climate conditions at all.

Our review revealed that the variety of scopes, periods and types of results make it difficult to compare or generalise research findings with different production systems. Studies are needed on energy performance related to building and housing systems, outdoor climate conditions, and fulfilment of indoor climate requirements for good animal welfare, expressed in well-defined key figures. Furthermore, more research is needed to understand the effect of climate change and the potential of adaptation measures, to improve energy-efficiency, cost-effectiveness, indoor climate, and animal welfare in buildings for pigs.

Keywords: climate change, heat stress, adaptation measures**,** building envelope, animal welfare

1. Introduction

Pig farming faces two significant challenges due to climate change. The first revolves around the imperative challenge to reduce greenhouse gas (GHG) emissions stemming from production processes, including feed choice, manure management and housing considerations (Hörtenhuber et al. 2020). The second challenge pertains to the anticipated thermal comfort problems due to warmer and more humid climates (Renaudeau & Dourmad 2022). Most pigs raised for pork production reside in confined buildings, meaning limited space and no outdoor access (Lassaletta et al. 2019). This implies that housing and indoor climate are key factors of animal welfare. Additionally, it is imperative to develop energy-efficient and innovative cooling strategies that maintain an acceptable indoor climate, while mitigating GHG emissions.

Indoor climate requirements in pig buildings vary depending on the pigs' size and age, as well as on national legislation. In a cold environment, the pigs need a higher energy intake and huddle to keep their core temperature constant. In a warmer environment, the lying behaviour changes as they lie more individually, increasing respiration rate and water intake, while feed intake diminishes (Huynh et al. 2005). Pigs possess only very few sweat glands and, therefore cannot sweat to regulate their body temperature and their natural behaviour is to wallow in mud to increase the evaporative heat loss from their skin (Bracke 2011). In confined buildings, the pigs have no possibility of wallowing in mud; thus, they are forced to wallow in their own faeces and urine. Additionally, when heat stressed, the pigs want to lie in the coldest place in the pen, often the slatted dunging area, and they use the lying area for excretion, which will be fouled (Aarnink et al. 2006). This is primarily a welfare issue, as pigs are naturally clean animals, but this behavior is a result of their need to avoid hyperthermia (Bracke 2011). Additionally, this leads to production problems since it is unhygienic and may lead to diseases and antimicrobial resistance (Schmithausen et al. 2018). The failure to maintain suitable indoor climate severely affects the pigs' welfare, including their health. They will also have a reduced

growth (Larsen et al. 2018; Gourdine et al. 2021), which negatively affects production outcomes (Renaudeau & Dourmad 2022).

Heating and ventilation are common measures to maintain the indoor climate within acceptable limits. Ventilation serves the purpose of reducing the content of moisture and airborne pollutants as well as heat from in indoor air by replacing it with fresh outdoor air (Abel & Elmroth 2007). During warm periods, increased ventilation through larger openings or higher airflow rates are common measures to reduce indoor temperatures. Two additional frequently used cooling strategies are evaporative cooling and increased air velocity in the animal zone to create a cooling air movement (Pexas et al. 2021). Evaporative cooling methods, such as cooling pads and fogging, utilize water to reduce the air temperature through evaporation. However, these methods increase the relative humidity in the air (Pertagnol et al. 2013), while increased air velocity on the pig poses risks for undesirable draughts (Jeppsson et al. 2021).

Energy use data for pig buildings is limited (Costantino et al. 2016). The building's energy balance depends on outdoor climate, transmission losses through the building envelope, solar radiation, heat storage in building materials, and internal heat loads, such as dissipation from equipment and occupants (Abel & Elmroth 2007). The heat dissipation from the pigs varies according to their size, activity and surrounding temperatures (Gourdine et al. 2021).

With the anticipated warmer outdoor climates, it is reasonable to expect difficulties in ventilating excess heat. Additional adaptation measures are thus required to reduce indoor temperatures. These measures must be energy-efficient and cost-effective to maintain production and economic profitability, while also mitigating GHG emissions caused by pig farming. This review aims to evaluate applied methods and identify possible gaps in information to obtain a first understanding of energy use and indoor climate in livestock buildings for pigs considering present and future climates.

2. Method

2.1. Data collection

This literature review examines energy use and indoor climate in livestock buildings for pigs, encompassing both passive and active adaptation measures. A keyword search was conducted in Scopus on January 13, 2023 (Table 1). The search included all journal and conference published in the period between January 1, 2000 and January 13, 2023. Additionally, a supplementary search was conducted in Scopus on January 4, 2024, for articles published between January 14 and December 31, 2023. The search encompassed the following regions:

- North America (the US and Canada)
- The EU (Austria, Belgium, Bulgaria, Czech Republic, Croatia, Cypress, Denmark, Estonia, Finland, France, Germany, Greece, Hungary, Ireland, Italy, Lithuania, Latvia, Luxembourg, Malta, Netherlands, Poland, Portugal, Rumania, Slovakia, Slovenia, Serbia, Spain, Sweden)
- Iceland, Liechtenstein, Monaco, Norway, Switzerland, United Kingdom
- Unspecified countries (in Scopus)

Table 1: Keyword search in Scopus, each subject was combined with AND.

Subject	Keywords
Energy efficiency	energ* OR resource* OR {environmental impact} OR efficien*
Indoor climate	thermal OR {internal climate} OR {indoor climate} OR air OR microclimate OR {micro climate} OR overheat* OR temperature OR humid* OR heat OR cold OR airflow OR {stay zone} OR {animal zone} OR {production zone}
Pig	pig OR pigs OR swine* OR hog OR sow OR sows OR hogs OR piglet* OR gilt* OR pork
Building	building* OR hous* OR pigsty OR pigsties OR {pig stable} OR farm* OR barn OR premis*
Adaptation measures	passive OR active OR cool* OR adapt* OR measur* OR ventil* OR heat* OR design OR concept* OR model*

Articles identified through the keyword search were manually screened for inclusion or exclusion based on the content following the process outlined in Figure 1.

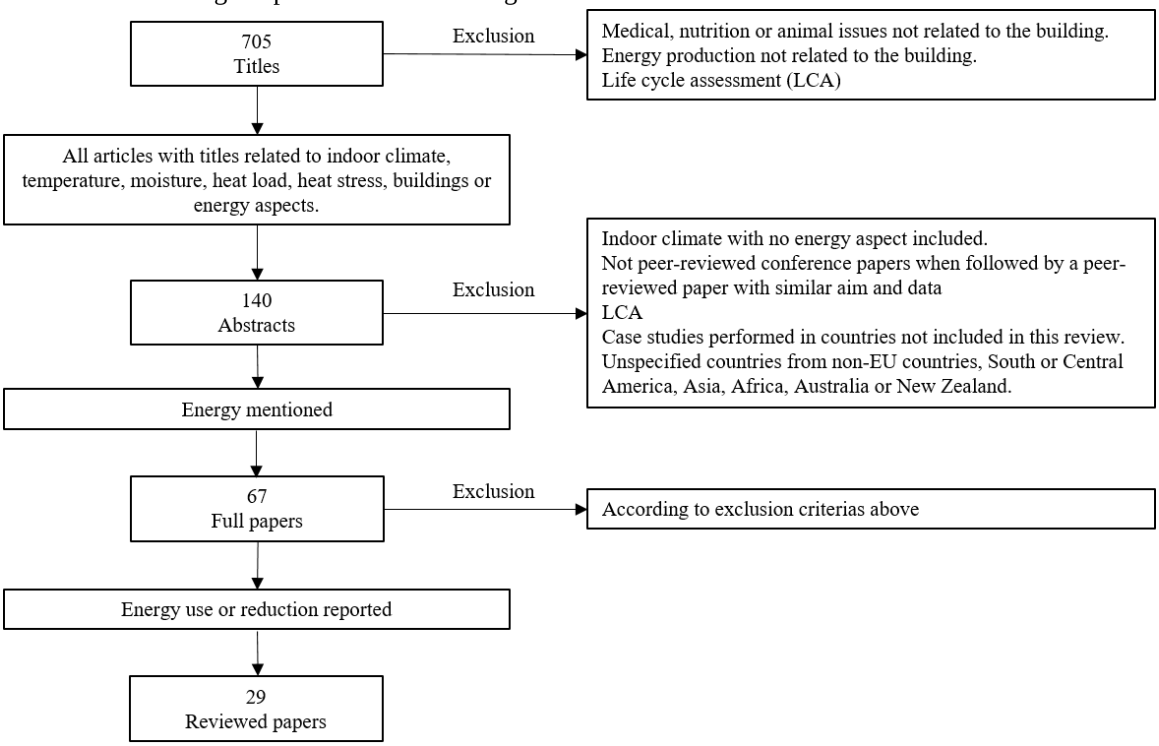

Figure 1**:** Principles for inclusion and exclusion in the review on energy use and indoor climate in pig buildings.

The reviewed articles were screened regarding information on outdoor and indoor climate conditions, building envelope properties, equipment and adaptations, pig data, as well as energy use. The relevant information was extracted according to the guidelines in Table 2 and we evaluated how this information was incorporated into the article. The extracted data was then saved in a standardised form.

Table 2. Extracted data from reviewed papers.

Subject	Extracted data
Reviewed article	Author(s), publication year, title, country
Equipment and adaptations	Maximum and minimum ventilation, heating type, operation time, cooling or heating adaptations
Energy use, outcome per period	Outcome and period
Outdoor climate conditions	Outcome and period
Indoor climate conditions	Outcome and period
Building Envelope	Materials or U-values for external walls, roof or ceiling, and floor
Pig, density and heat load	Housing area, number of pigs, weight, heat dissipation from pigs

2.2. Reviewed research

Studies on energy use have been published during the entire search period and the number of publications increased notably in 2013 with one to three studies published annually until the end of 2023. We have categorised the results on energy use into three subsections - measured, modelled and reported data. Articles presenting modelled data that also incorporated measurements as a validation tool for the model are not included in the measured data subsection. Reported data concern studies based on data from farmers or previous studies. Notably, two articles, one from the US (Hanna et al. 2016) and one from Belgium (Everaert et al. 2023) are evaluated twice as they include data on both measured and reported energy use. In total, 17 studies are based on measured data, 11 on modelled data, and three on reported data. The review encompasses studies from ten countries with first authors from the US and Italy being the primary contributors to these

articles (Table 3).

Table 3. Reviewed articles on energy use of livestock buildings for pigs in 2000 through 2023 in part of Europe and in North America. The table indicates whether energy use data is presented as measured, modelled or reported data. One study each in the United States and Belgium is included twice as they assess both measured and reported data.

Reviewed Article, measured data	Country	Reviewed Article, modelled data	Country
(Deeken et al. 2023)	BE	(Costantino et al. 2022)	IT
(Everaert et al. 2023)	BE	(Faes et al. 2021)	BE
(Fernandez et al. 2020)	ES	(Panagakis & Axaopoulos 2019)	GR
(Lane et al. 2020)	US	(Xie et al. 2019)	US
(Licharz et al. 2020)	DE	(Jackson et al. 2018)	UK
(Bilardo et al. 2019)	IT	(Fabrizio et al. 2014)	IT
(Alberti et al. 2018)	IT	(Jacobson et al. 2011)	US
(Sharpe et al. 2018)	US	(Valino et al. 2010)	UK
(Shah et al. 2017)	US	(Panagakis & Axaopoulos 2004)	GR
(Hanna et al. 2016)	US	(Lambert et al. 2001)	CA
(Ilsters et al. 2015)	LV	(Turnpenny et al. 2001)	UK
(Krommweh et al. 2014)	DE		
(Love et al. 2014)	US		
(Johnston et al. 2013)	US	Reviewed Article, reported data	Country
(Pertagnol et al. 2013)	DE	(Deeken et al. 2023)	BE
(Godbout et al. 2004)	CA	(Costantino et al. 2016)	IT
(Riva et al. 2000)	IT	(Hanna et al. 2016)	US

3. Results and Discussion

In this section, we have summarised the types of implemented adaptation measures found in the reviewed articles, followed by a compilation of employed units and terms for energy use. In the subsection on measured, modelled, and reported data, we highlight the importance of understanding building and production types, as well as indoor and outdoor climate conditions, for accurately interpreting energy use. Additionally, we discuss how modeling and simulations contribute to knowledge in this area.

3.1. Adaptation measures

Different adaptation measures such as heat pumps (HP) and heat exchangers (HE) sourced from the ground or the air were used for either the heating, cooling season, or both (Deeken et al. 2023; Licharz et al. 2020; Alberti et al. 2018; Jackson et al. 2018; Shah et al. 2017; Ilsters et al. 2015; Pertagnol et al. 2013; Jacobsen et al. 2011; Riva et al. 2000). For the warm season, increased ventilation was the most common measure for cooling, sometimes combined with evaporative cooling. In colder climates, mobile or permanently installed, heat sources were usually implemented, and preheating of inlet are through a solar wall or channel has been studied (Godbout et al. 2004; Love et al. 2014).

Some studies showed that adaptation measures were not as effective as anticipated. For instance, Riva et al. (2000) found that energy use was reduced with a heat pump (HP) during the heating season compared to a boiler heating system. However, during the cooling season, the HP solution required more energy but resulted in fewer variations in ambient temperature. Another example is a study by Krommweh et al. (2014) involving a ground-based HE that inadvertently reheated precooled air during summer. The HE precooled the supply air in a ground pipe and distributed it to the uninsulated attic through vertical shafts. However, the air was reheated due to high surrounding temperatures during transportation from the ground to the attic. Subsequently, the air was supplied to the pigs from the attic via ceiling openings. Despite this, the system preheated and precooled the supply air, showing potential for reducing energy demand. However, the system was not deemed suitable for GFP, as it supplied too much heat. Additionally, one study found that pressure drops in the ventilation system could increase energy use due to warm prolonged fan operation (Pertagnol et al., 2013). These results highlight the importance of designing adaptation measures tailored to specific buildings and sites for optimising energy efficiency.

3.2. Energy use and indoor climate

3.2.1. Energy use definitions

Four ways of expressing energy use were identified in this review: energy consumption (EC), energy balance (EB), energy demand (ED), and energy saving potential (ESP). Energy consumption was the predominant method used to express energy use for measured data, followed by energy balance and energy demand. Energy demand was most commonly employed for modelled data, followed by energy consumption. Finally, for reported data, energy consumption was the sole method utilised to express energy use.

Applying standardised definitions of energy concepts simplifies the communication of energy use results. Typically, 'energy consumption' refers to measured energy obtained through installed energy meters or the amount of fuel used, aligning with the defined actual measured energy use according to the European ISO standard for energy performance (EN ISO 52000-1:2017). Within this standard, 'energy demand' is utilised to calculate a building´s energy performance under typical condition adjusted for typical outdoor climate conditions and building use. Energy demand may also factor in peak load calculations for building design in summer and winter scenarios. In studies employing an 'energy balance' approach, both energy losses and gains are accounted for, providing a comprehensive overview of a building's energy flows over a given moment or specific period. When evaluating the 'energy saving potential', a clearly defined reference value is crucial for comparative analysis within the study, as the potential energy savings of an adaptation measure vary depending on climate and building design.

The standard (EN ISO 52000-1:2017) is primarily designed for assessing the energy performance of buildings for human occupancy. While certain aspects of the standard, such as definitions, boundaries, and primary energy calculations, may be applicable to the agricultural sector, adjustments tailored to the specific use of agricultural buildings are necessary.

3.2.2. Units for energy use

To benchmark energy use across different sites, production stages, and climate zones, it is crucial to standardise the presentation of energy data. Energy use is reported in ten different units (Table 4). However, some studies reported more than one unit (Deeken et al. 2023; Bilardo et al. 2019; Costantino et al. 2016). The most common units were total kWh or MJ per studied period, followed by total kWh per production cycle. The diversity of units and covered periods makes it challenging to generalise research findings or draw any conclusions for this body of research. Presenting energy data as key figures, such as kWh per fattening pig, per pig space, or per kilogram of meat, would offer the opportunity for comparison (Deeken et al. 2023; Everaert et al. 2023; Fernandez et al. 2020; Sharpe et al. 2018; Costantino et al. 2016; Hanna et al. 2016; Jacobson et al. 2011; Turnpenny et al. 2001). Additionally, it is crucial to include information on outdoor and indoor climate conditions, as well as production data such as building type, pig sizes, and density, to facilitate benchmarking.

Table 4: Reported units and expression used for energy use or power need in reviewed papers.

Reported units	EC	ED	EB	ESP
Total kWh or MJ for evaluated period	7	2	3	3
kWh pig day $^{-1}$	1			
Total kWh per cycle or month	4			1
kWh pig space	3			
kWh pig	2		1	
kWh m^{-2} cycle $^{-1}$	1			
KWh m^{-2} year $^{-1}$	1			
kWh or MJ kg meat	2	1		
kWh weight unit	1			
W m^{-2}		1	1	
% savings				1

EC: Energy consumption, ED: Energy demand, EB: Energy balance, ESP: Energy saving potential

3.3. Measured energy use data

Energy use and indoor climate conditions result from current outdoor air conditions, building properties, the capacity of potential heating, ventilation and cooling equipment as well as internal heat loads (Abel & Elmroth 2007). In this subsection, we summarise and discuss the findings, focusing on how outdoor and indoor climate conditions, building properties, and pig production data are reported in articles based on measured energy use data.

Most of the studies include at least one year of energy measurements, followed by studies focusing on limited periods during the cold season. Annual reviews provide a more comprehensive view of energy use for heating and cooling, accounting for seasonal differences in a region. However, energy use during a specific period is influenced by outdoor climate conditions. Outdoor conditions were reported to varying extents in the studies, including average temperature or humidity per month or cycle (Fernandez et al. 2020; Ilster et al. 2015; Godbout et al. 2004; Riva et al. 2000). One study supplemented this information with minimum and maximum temperatures within the evaluated period (Deeken et al. 2023). Other studies include frequent temperature measurements, taken either per minute or averaged per hour, throughout part or all of the studied period (Licharz et al. 2020; Alberti et al. 2018; Krommweh et al. 2014; Love et al. 2014; Bilardo et al. 2019). However, six studies did not report any outdoor climate data at all (Everaert et al. 2023; Sharpe et al. 2018; Shah et al. 2017; Hanna et al. 2016; Johnston et al. 2013; Pertagnol et al. 2013). Given that the energy needs are dependent on outdoor climate conditions, data covering the entire studied period are valuable for interpreting energy use result in any study.

To achieve an acceptable level of animal welfare, indoor temperatures should be kept within the thermal neutral zone (Gourdine et al. 2021). The building and its equipment establish the framework for the energy use and indoor climate while management practices determine how heating and ventilation actually operate, thereby affecting energy use (Hanna et al. 2016). Climate control and variation in set point temperatures are possible tools for improving indoor climate while reducing energy demand (Johnston et al. 2013).

Information on indoor climate conditions was reported to varying extents in six cases, sometimes covering the entire period and other times only a limited part of the studied period. The findings were presented consistently with outdoor climate conditions in some studies (Fernandez et al. 2020; Licharz et al. 2020; Alberti et al. 2018; Krommweh et al. 2014; Riva et al. 2000). One study focused on temperatures related to heat stress and temperature- humidity index (THI) (Bilardo et al. 2019). In a few studies, the preheating or precooling capacity of the supply air temperature was evaluated (Deeken et al. 2023; Shah et al. 2017; Love et al. 2014; Pertagnol et al. 2013; Godbout et el. 2004), and one study examined the possibility of gaining heat to the indoor premises through HE from manure (Ilsters et al. 2015). Finally, five studies did not present any information on prevailing indoor climate conditions during the studied period (Everaert et al. 2023; Lane et al. 2020; Sharpe et al. 2018; Hanna et al. 2016). Just as outdoor climate conditions are important, information about indoor climate conditions is crucial for evaluating and enabling comparisons of results on energy use.

Information on the building envelope, including materials or transmission losses, is reported in two out of the 17 reviewed articles. Measured data are obtained from existing pig buildings, potentially resulting in a lack of information on aspects such as insulation level. Nevertheless, studies have concluded that insulated building envelopes and mechanical ventilation are essential for maintaining an acceptable indoor climate in confined buildings, especially considering the anticipated warmer climate (Hörtenhuber et al. 2020).

Most of the studies provided data on housing area, pig weight, and quantity, offering opportunities to present results in key figures, such as energy performance per pig space, per fattening pig, per kilogram of meat, or per square meter.

3.4. Modelled energy use data

In this section, we review studies with modeled data and discuss the use of models. In some cases, the studies aimed to develop or evaluate the accuracy of a model rather than presenting results on energy use or indoor climate. Like studies with measured energy use data, the extent of relevant reported data varies among the studies, and this variability is not further discussed.

Models were developed as part of the study in eight of the articles, while three studies utilised commercial software programs specifically developed for energy and heat balance simulations, namely Staldvent (Jacobsen et al. 2011) and EnergyPlus (Jackson et al 2018; Fabrizio et al. 2014). All studies considered energy

(heat) balance, reporting energy demand or consumption for a specific period. When calculating the heat balance for a building to predict expected indoor temperatures (Jackson et al. 2017; Vitt et al. 2017; Anthony et al., 2014), it should also possible to incorporate energy balance calculations.

Transmission losses through the building envelope were typically considered but not always reported. Axaopoulos et al. (2017), have emphasized the significance of optimal insulation levels in various climates. In a few studies, the insulation level is discussed, and one study demonstrated the effect of insulation level and thermal mass on energy use and indoor climate (Jackson et al. 2018). However, the influence of possible floor insulation was rarely included and not discussed in the studies. With underfloor heating, heat losses are expected if there is no underlying insulation, but heat loss might have a positive effect in the warm season due to heat conduction from the pigs when the floor is cooler than the pigs. Further research on the effects of ground insulation and the efficiency of underfloor heating or cooling is motivated.

The studies demonstrate that through modelling, it is not only possible to evaluate energy performance or indoor climate, but also to assess the effects of building materials, supply air temperature, building geometry, solar radiation, future climate scenarios, and more. Costantino et al. (2022) highlighted the need for applying energy engineering principles to modelling within the agricultural sector. However, Fabrizio et al. (2014) emphasized that the heat load from animals and manure varies with indoor temperature and humidity, complicating the accuracy of simulation results.

3.5. Reported energy use data

Three articles presented reported data, all focusing on energy consumption (Deeken et al. 2023; Costantino et al. 2016; Hanna et al. 2016). None of these articles included information on pig density or heat dissipation, nor did they provide details on indoor and outdoor climate conditions corresponding to the reported energy consumption. Sufficient reported data allows the application of statistical methods to assess energy use. However, information on climate zones and pig production type - such as sows, weaned pigs, or fattening pigs - is essential for result comparison, given the varying heating and cooling demands.

4. Conclusions

This review was conducted using a keyword search in Scopus focusing on energy use and indoor climate of livestock buildings for pigs, including passive and active adaptation measures. Based on the review of 29 articles, the following knowledge gaps and need for further research have been identified:

- Variations in scope and prerequisites make comparing studies and generalising results on energy use difficult. Relevant key figures are essential for facilitating comparison of energy performance, and the energy standard EN ISO52000-1:2017 may be used as a common platform. However, further research is needed to explore how energy use can be adjusted for outdoor climate and production factors such as indoor climate, sustained production, and animal welfare, to enhance feasibility of comparing the energy performance of livestock buildings.
- Studies about the effect on energy use and indoor climate of building properties such as thermal mass, heat transmission, and building orientation are scarce. Further research on passive energy saving strategies is desirable.
- Computer modelling is a promising method for incorporating and evaluating the performance of livestock buildings in terms of energy use and indoor climate over extended periods.

Overall, this review suggests that research in this field is still in its infancy or scarce and a more methodical and standardised way of presenting research findings is desirable to provide guidance on how to design energy-efficient and thermally comfortable buildings for pigs in current and future climates.

Acknowledgements

We thank the Swedish Energy Agency for funding this study, which is part of a PhD-project entitled "Improving energy-efficiency and indoor climate of livestock buildings through passive and active adaptation measures".

References

Aarnink, A.J.A., Schrama, J.W., Heetkamp, M.J.W., Stefanowska, J. & Huynh, T.T.T. (2006). Temperature and body weight affect fouling of pig pens. Journal of Animal Science, 84 (8), 2224–2231. https://doi.org/10.2527/jas.2005-521

Abel and Elmroth (2007). Buildings and Energy - a systematic approach. T6:2007. FORMAS, 2007, ISBN: 978-91-540-5997-3.

Alberti, L., Antelmi, M., Angelotti, A. & Formentin, G. (2018). Geothermal heat pumps for sustainable farm climatization and field irrigation. Agricultural Water Management, 195, 187–200. https://doi.org/10.1016/j.agwat.2017.10.009

Anthony, T.R., Altmaier, R., Park, J.H. & Peters, T.M. (2014). Modeled effectiveness of ventilation with contaminant control devices on indoor air quality in a swine farrowing facility. Journal of Occupational and Environmental Hygiene, 11 (7), 434–449. https://doi.org/10.1080/15459624.2013.875186

Axaopoulos, P., Panagakis, P. & Axaopoulos, I. (2017). OPTIMIZATION OF EXTERIOR WALL AND ROOF INSULATION THICKNESS OF A GROWING-FINISHING PIGGERY BUILDING. TRANSACTIONS OF THE ASABE, 60 (2), 489–495. https://doi.org/10.13031/trans.12009

Bilardo, M., Comba, L., Cornale, P., Costantino, A. & Fabrizio, E. (2019). Relation between energy use and indoor thermal environment in animal husbandry: A case study. 2019. EDP Sciences. https://doi.org/10.1051/e3sconf/201911101042

Bracke, M.B.M. (2011). Review of wallowing in pigs: Description of the behaviour and its motivational basis. Applied Animal Behaviour Science, 132 (1–2), 1–13. https://doi.org/10.1016/j.applanim.2011.01.002

Costantino, A., Comba, L., Cornale, P. & Fabrizio, E. (2022). Energy impact of climate control in pig farming: Dynamic simulation and experimental validation. APPLIED ENERGY, 309. https://doi.org/10.1016/j.apenergy.2021.118457

Costantino, A., Fabrizio, E., Biglia, A., Cornale, P. & Battaglini, L. (2016). Energy Use for Climate Control of Animal Houses: The State of the Art in Europe. 2016. 184–191. Elsevier Ltd. https://doi.org/10.1016/j.egypro.2016.11.024

Costantino, A., Fabrizio, E. & Calvet, S. (2021). The role of climate control in monogastric animal farming: The effects on animal welfare, air emissions, productivity, health, and energy use. Applied Sciences (Switzerland), 11 (20). https://doi.org/10.3390/app11209549

Deeken, H.F., Lengling, A., Krommweh, M.S. & Büscher, W. (2023). Improvement of Piglet Rearing's Energy Efficiency and Sustainability Using Air-to-Air Heat Exchangers—A Two-Year Case Study. Energies, 16 (4). https://doi.org/10.3390/en16041799

Everaert, M., Faes, W., Maselyne, J. & Lecompte, S. (2023). Economical and ecological optimization of renewable energy solutions for thermal demands of livestock barns. Proceedings of 36th International Conference on Efficiency, Cost, Optimization, Simulation and Environmental Impact of Energy Systems, ECOS 2023, 2023. 1530–1541. https://doi.org/10.52202/069564-0139

European ISO standard (2017) Energy performance of buildings – Overarching EPB assessment – Part 1: General framework and procedures" (EN ISO 52000-1:2017)

Fabrizio, E., Airoldo, G. & Chiabrando, R (2014) Li et al. (eds), Proceedings of the 8th International Symposium on Heating, Ventilation, and air conditioning. Lecture notes in Electrical engineering 263, DOI: 10.1007/978-3-642-39578-9_1, Springer-Verlag Berlin Heidelberg 2014

Fabrizio, E., Airoldi, G. & Chiabrando, R. (2014). Study of the environmental control of sow farrowing rooms by means of dynamic simulation. 11. https://doi.org/10.1007/978-3-642-39578-9_1

Faes, W., Maselyne, J., De Paepe, M. & Lecompte, S. (2021). Modelling the energetic performance of a pig stable. Proceedings of ECOS 2021 - 34th International Conference on Efficency, Cost, Optimization, Simulation and Environmental Impact of Energy Systems, 2021. 910–915. https://www.scopus.com/inward/record.uri?eid=2-s2.0-85134402520&partnerID=40&md5=0bf3073d611d8b8c2598fe4ae57ad3cf

Fernandez, M.D., Losada, E., Ortega, J.A., Arango, T., Ginzo-Villamayor, M.J., Besteiro, R., Lamosa, S., Barrasa, M. & Rodriguez, M.R. (2020). Energy, production and environmental characteristics of a

conventional weaned piglet farm in North West Spain. Agronomy, 10 (6). https://doi.org/10.3390/agronomy10060902

Godbout, S., Pouliot, F., Lachance, I., Guimont, H., Leblanc, R., Pelletier, F. & Hamelin, L. (2004). Feasibility and energy recovery of a solar wall in pig nursery. 2004. 5679–5693. https://www.scopus.com/inward/record.uri?eid=2-s2.0-30044439309&partnerID=40&md5=366e9bff612af1a1b90b405237112e58

Gourdine, J.-L., Rauw, W.M., Gilbert, H. & Poullet, N. (2021). The Genetics of Thermoregulation in Pigs: A Review. Frontiers in Veterinary Science, 8. https://doi.org/10.3389/fvets.2021.770480

Hanna, H.M., Harmon, J.D. & Schweitzer, D.D. (2016). Energy use for field operations, crop drying and swine housing on university farms. Applied Engineering in Agriculture, 32 (6), 769–781. https://doi.org/10.13031/aea.32.11720

Huynh, T.T.T., Aarnink, A.J.A., Gerrits, W.J.J., Heetkamp, M.J.H., Canh, T.T., Spoolder, H.A.M., Kemp, B. & Verstegen, M.W.A. (2005). Thermal behaviour of growing pigs in response to high temperature and humidity. Applied Animal Behaviour Science, 91 (1–2), 1–16. https://doi.org/10.1016/j.applanim.2004.10.020

Hörtenhuber, S.J., Schauberger, G., Mikovits, C., Schönhart, M., Baumgartner, J., Niebuhr, K., Piringer, M., Anders, I., Andre, K., Hennig-Pauka, I. & Zollitsch, W. (2020). The effect of climate change-induced temperature increase on performance and environmental impact of intensive pig production systems. Sustainability (Switzerland), 12 (22), 1–17. https://doi.org/10.3390/su12229442

Ilsters, A., Ziemelis, I. & Putans, H. (2015). Efficiency of heat recovery from pigsty manure. 2015. 94–99. Latvia University of Agriculture. https://www.scopus.com/inward/record.uri?eid=2-s2.0-84937393836&partnerID=40&md5=70e0cc7c4b5554dba272d8a3e5cd6eee

Jackson, P., Guy, J., Edwards, S.A., Sturm, B. & Bull, S. (2017). Application of dynamic thermal engineering principles to improve the efficiency of resource use in UK pork production chains. Energy and Buildings, 139, 53–62. https://doi.org/10.1016/j.enbuild.2016.12.090

Jackson, P., Guy, J.H., Sturm, B., Bull, S. & Edwards, S.A. (2018). An innovative concept building design incorporating passive technology to improve resource efficiency and welfare of finishing pigs. Biosystems Engineering, 174, 190–203. https://doi.org/10.1016/j.biosystemseng.2018.07.008

Jacobson, L.D., Schmidt, D.R. & Koehler, R. (2011). Reducing the environmental footprint of pig finishing barns., 2011. 4450–4464. American Society of Agricultural and Biological Engineers. https://www.scopus.com/inward/record.uri?eid=2-s2.0-81255158355&partnerID=40&md5=83d9172579ab8a3ee0f66e5643e1a03f

Jeppsson, K.-H., Olsson, A.-C. & Nasirahmadi, A. (2021a). Cooling growing/finishing pigs with showers in the slatted area: Effect on animal occupation area, pen fouling and ammonia emission. Livestock Science, 243. https://doi.org/10.1016/j.livsci.2020.104377

Jeppsson, K.-H., Olsson, A.-C. & Nasirahmadi, A. (2021b). Increased air velocity in the lying area improves pen hygiene and reduces ammonia emissions from houses with partly slatted pens for growing/finishing pigs. Livestock Science, 251. https://doi.org/10.1016/j.livsci.2021.104607

Johnston, L.J., Brumm, M.C., Moeller, S.J., Pohl, S., Shannon, M.C. & Thaler, R.C. (2013). Effects of reduced nocturnal temperature on pig performance and energy consumption in swine nursery rooms. Journal of Animal Science, 91 (7), 3429–3435. https://doi.org/10.2527/jas.2012-5824

Krommweh, M.S., Rösmann, P. & Büscher, W. (2014). Investigation of heating and cooling potential of a modular housing system for fattening pigs with integrated geothermal heat exchanger. Biosystems Engineering, 121, 118–129. https://doi.org/10.1016/j.biosystemseng.2014.02.008

Lambert, M., Lemay, S.P., Barber, E.M., Crowe, T.G. & Chénard, L. (2001). Humidity control for swine buildings in cold climate - Part I: Modelling of three control strategies. Canadian Biosystems Engineering / Le Genie des biosystems au Canada, 43, 529–536

Lammers, P.J., Kenealy, M.D., Kliebenstein, J.B., Harmon, J.D., Helmers, M.J. & Honeyman, M.S. (2012). Energy use in pig production: An examination of current Iowa systems. JOURNAL OF ANIMAL SCIENCE, 90 (3), 1056–1068. https://doi.org/10.2527/jas.2010-3782

Lane, K.J., Johnson, A.K., Stilwill, C.E.J., Karriker, L.A., Harmon, J.D. & Stalder, K.J. (2020). Comparison of heat lamps and heat mats in the farrowing house: Effect on piglet production, energy use, and piglet and sow behavior through live observation. Journal of Swine Health and Production, 28 (4), 205–212

Larsen, M.L.V., Bertelsen, M. & Pedersen, L.J. (2018). Review: Factors affecting fouling in conventional pens for slaughter pigs. Animal, 12 (2), 322–328. https://doi.org/10.1017/S1751731117001586

Lassaletta, L., Estellés, F., Beusen, A.H.W., Bouwman, L., Calvet, S., van Grinsven, H.J.M., Doelman, J.C., Stehfest, E., Uwizeye, A. & Westhoek, H. (2019). Future global pig production systems according to the Shared Socioeconomic Pathways. Science of the Total Environment, 665, 739–751. https://doi.org/10.1016/j.scitotenv.2019.02.079

Licharz, H., Rösmann, P., Krommweh, M.S., Mostafa, E. & Büscher, W. (2020). Energy efficiency of a heat pump system: Case study in two pig houses. Energies, 13 (3). https://doi.org/10.3390/en13030662

Love, C.D., Shah, S.B., Grimes, J.L. & Willits, D.W. (2014). Transpired solar collector duct for tempering air in North Carolina turkey brooder barn and swine nursery. Solar Energy, 102, 308–317. https://doi.org/10.1016/j.solener.2013.11.028

Panagakis, P. & Axaopoulos, P. (2004). Comparison of two modeling methods for the prediction of degree-hours and heat-stress likelihood in a swine building. TRANSACTIONS OF THE ASAE, 47 (2), 585–590

Panagakis, P. & Axaopoulos, P. (2019). Comparison of heating and cooling loads in a controlled environment growing-finishing piggery under different climatic conditions., 2019. American Institute of Physics Inc. https://doi.org/10.1063/1.5138515

Pertagnol, J., Gallmann, E., Pflanz, W. & Jungbluth, T. (2013). Efficiency of resources of different cooling systems for fattening pigs. Landtechnik, 68 (5), 353–358

Pexas, G., Mackenzie, S.G., Jeppsson, K.-H., Olsson, A.-C., Wallace, M. & Kyriazakis, I. (2021). Environmental and economic consequences of pig-cooling strategies implemented in a European pig-fattening unit. Journal of Cleaner Production, 290. https://doi.org/10.1016/j.jclepro.2021.125784

Renaudeau, D. & Dourmad, J.Y. (2022). Review: Future consequences of climate change for European Union pig production. Animal, 16. https://doi.org/10.1016/j.animal.2021.100372

Riva, G., Pedretti, E.F. & Fabbri, C. (2000). Utilization of a heat pump in pig breeding for energy saving and climate and ammonia control. Journal of Agricultural and Engineering Research, 77 (4), 449–455. https://doi.org/10.1006/jaer.2000.0624

Schmithausen, R.M., Schulze-Geisthoevel, S.V., Heinemann, C., Bierbaum, G., Exner, M., Petersen, B. & Steinhoff-Wagner, J. (2018). Reservoirs and transmission pathways of resistant indicator bacteria in the Biotope pig stable and along the food chain: A review froma One Health Perspective. Sustainability (Switzerland), 10 (11). https://doi.org/10.3390/su10113967

Shah, S.B., Lentz, Z.A., Van Heugten, E., Currin, R.D., Jr. & Singletary, I. (2017). Tempering ventilation air in a swine finishing barn with a low-cost earth-to-water heat exchanger. Journal of Renewable and Sustainable Energy, 9 (2). https://doi.org/10.1063/1.4979359

Sharpe, K.T., Reese, M.H., Buchanan, E.S., Tallaksen, J.E., Janni, K.A. & Johnston, L.J. (2018). Electrical and thermal energy consumption in midwest commercial swine facilities. Applied Engineering in Agriculture, 34 (5), 857–864. https://doi.org/10.13031/aea.12771

Swedish standard (2014). Farm buildings – ventilation and heating requirements in animal buildings. SS 951050:2014. Swedish standards institutes.

Tabase, R.K., Van Linden, V., Bagci, O., De Paepe, M., Aarnink, A.J.A. & Demeyer, P. (2020). CFD simulation of airflows and ammonia emissions in a pig compartment with underfloor air distribution system: Model validation at different ventilation rates. COMPUTERS AND ELECTRONICS IN AGRICULTURE, 171. https://doi.org/10.1016/j.compag.2020.105297

Turnpenny, J.R., Parsons, D.J., Armstrong, A.C., Clark, J.A., Cooper, K. & Matthews, A.M. (2001). Integrated models of livestock systems for climate change studies. 2. Intensive systems. Global Change Biology, 7 (2), 163–170. https://doi.org/10.1046/j.1365-2486.2001.00401.x

Valino, V., Perdigones, A., Iglesias, A. & Garcia, J.L. (2010). Effect of temperature increase on cooling systems in livestock farms. CLIMATE RESEARCH, 44 (1), 107–114. https://doi.org/10.3354/cr00915

Vitt, R., Weber, L., Zollitsch, W., Hörtenhuber, S.J., Baumgartner, J., Niebuhr, K., Piringer, M., Anders, I., Andre, K., Hennig-Pauka, I., Schönhart, M. & Schauberger, G. (2017). Modelled performance of energy saving air treatment devices to mitigate heat stress for confined livestock buildings in Central Europe. Biosystems Engineering, 164, 85–97. https://doi.org/10.1016/j.biosystemseng.2017.09.013

Xie, Q., Ni, J.-Q., Bao, J. & Su, Z. (2019). A thermal environmental model for indoor air temperature prediction and energy consumption in pig building. Building and Environment, 161. https://doi.org/10.1016/j.buildenv.2019.106238

Dragon fruit quality assessment using a grading machine prototype based on image analysis

Pablo González-Planells [a], Coral Ortiz [a,*], Francisco Rovira-Más [a], Vicente Alegre [b]

[a] Rural and Agrifood Engineering Department, Universitat Politècnica de València, Valencia, Spain

[b] Greenvision (GreenVision - Quality Sorting Systems), Benifayó Valencia, Spain

* Corresponding author. cortiz@dmta.upv.es

Abstract

Dragon fruit or pitahaya is a tropical product which demand has recently increased Europe. The Mediterranean are of Valencia (Spain) is obtaining promising results for pitahaya production. The dragon fruit quality is crucial to assure and increase consumers acceptance of this new and high price product. Size, colour and sugar content are important parameters to define fruit quality. Nowadays, the assessment of fruit quality is addressed at the packing houses using image analysis sorting machines. In the present study the objective was to assess product quality using a prototype image analysis device. In the experiment 177 dragon fruits (144 from the variety Nevada y 33 from the variety Purple) were measured non-destructively with the image analysis system. Whole fruit external RGB colour coordinates, maximum and minimum diameters, external estimated perimeter and estimated area were measured, two repetitions were developed per fruit. After the non-destructive image analysis, weight (g), destructive mechanical firmness (N/mm) with and without skin, soluble solid content (° Brix) and titratable acidity were measured. Besides, internal flesh colour parameters were also measured after cutting the fruit in two halves. Promising results were found, a multiple regression analysis could explain sugar content and weight based on the image analysis parameters (R^2 of 95.33 % and 89.25 % for weight in Nevada y Purple; 52.40 % and 87.95 % for soluble solid content in Nevada y Purple, respectively). These preliminary results, suggest the possibility of assessing dragon fruit quality using image analysis during grading.

.

Keywords: pitahaya, sorting machine, fruit attributes.

1. Introduction

Dragon fruit, also known as pitaya or pitahaya, is a tropical fruit with exotic appearance, vibrant colours, and nutritional benefits (Ortiz et al., 2020). As the demand for dragon fruit continues to rise in global markets, ensuring and maintaining the quality of this tropical fruit becomes paramount. Considering this product is becoming more popular in Europe and other regions, dragon fruit quality measurement plays a crucial role in meeting the expectations of new consumers. In dragon fruit the most important quality attributes are colour, sugar content and firmness (Ho et al., 2021).

Advancements in non-destructive testing methods, such as spectroscopy and imaging technologies, offer promising perspectives for evaluating dragon fruit quality and assuring a high-quality product for the consumers (Patil et al., 2021).

Spectroscopic tools, including near-infrared (NIR) and hyperspectral imaging, enable researchers to analyse the internal composition of pitaya, measuring attributes such as sugar content, acidity, and moisture levels (da Silva et al., 2023). These non-destructive techniques offer a rapid and efficient means of quality assessment, facilitating real-time monitoring at different stages of the post-harvest process.

The objective of the present study was to assess sugar content and weight of Purple and Nevada dragon fruits using external colour and image analysis parameters.

2. Materials and Methods

In the experiment, 177 dragon fruits (144 from the variety Nevada y 33 from the variety Purple) were measured non-destructively with the image analysis grading prototype, Figure 1.

Figure 1. Image analysis grading prototype.

A digital colorimeter (CR410. Chroma meter, Konica Minolta sensing) was used to obtain L, a and b colour coordinates From the grading prototype es), whole fruit external RGB colour coordinates, maximum and minimum diameters, external estimated perimeter, and estimated area were measured, Figure 2. Two repetitions were developed per fruit. After the non-destructive image measurements were finished, weight, whole and pulp fruit firmness, soluble solid content and titratable acidity were tested. Besides, internal flesh colour parameters were also measured after cutting the fruit in two halves. Weight was measured using a digital balance (Mettler Toledo AL104 electronic balance, Im Langacher 44, 8606 Greifensee, Switzerland). Firmness was measured using a universal stress strain machine (Ibertest, model IBTH 2730, www.ibertest.es (accessed May 2024), with a constant speed of 1.67 ms^{-1}. The firmness of each fruit was measured at three points of the equatorial area by using an 0.008 m probe, with (whole fruit firmness) and without peel (fruit flesh firmness). Three repetitions were carried out per test and fruit. The dragon fruits were juiced individually using a blender, and the filtered liquid was used to measure chemical parameters. Soluble solid content was determined with a digital refractometer (Atago model PAL-3; Atago Co., Tokyo, Japan). The statistical analysis was performed with a commercially available software package (Statgraphics Centurion 18 Software, version 18.1.13 (Statgraphics Technologies, Inc., The Plains, VA, USA)).

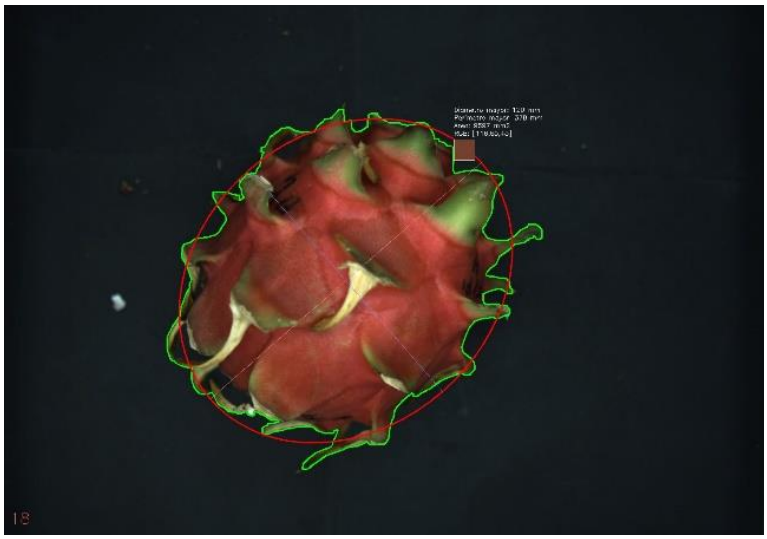

Figure 2. Example of the parameters extracted from the image analysis grading prototype, RGB colour coordinates, maximum and minimum diameters, external estimated perimeter, and estimated area, es).

3. Results and Discussion

A multiple forward step by step regression analysis was developed to assess soluble solid content (° Brix) according to the external colour variables, Figures 3 and 4. The external colour parameters could explain soluble solid content based on the image analysis parameters (R^2 of 52.40 % and 87.95 % in Nevada y Purple respectively).

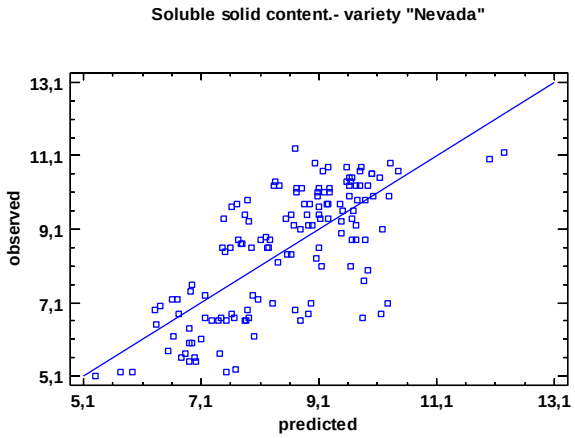

Figure 2. Observed and predicted soluble solid content (° Brix) from the multiple regression analysis based on the external colour parameters, variety Nevada.

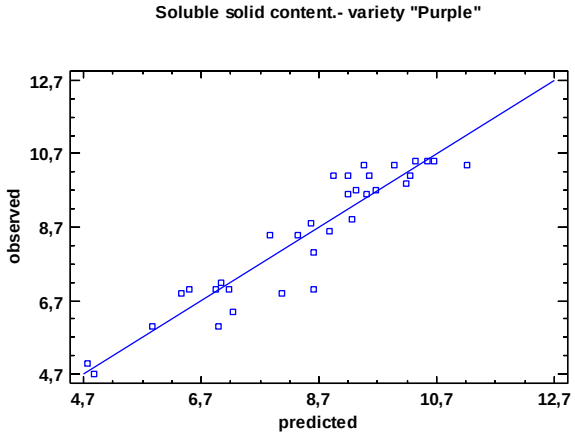

Figure 4. Observed and predicted soluble solid content (° Brix) from the multiple regression analysis based on the external colour parameters, variety Purple.

$$SS\ (°Brix) = 6.8730 + 0.0007A\ (mm^2) + 0.0016P\ (mm) + 0.0743D(mm) + 0.0710d\ (mm) + 0.4043B + 0.2660G$$

Where:

S= Soluble solid content (°Brix)

A= Image analysis area (mm^2)

P= Image analysis perimeter (mm)

D= Image analysis maximum diameter (mm)

d= Image analysis minimum diameter (mm)
B= B colour from RGB image analysis colour coordinates
G= G colour from RGB image analysis colour coordinates

A multiple forward step by step regression analysis was developed to assess and weight (g) according to the external colour variables, Figures 5 and 6. The external colour parameters could explain weight based on the image analysis parameters (R2 of 95.33 % and 89.25 % in Nevada y Purple respectively).

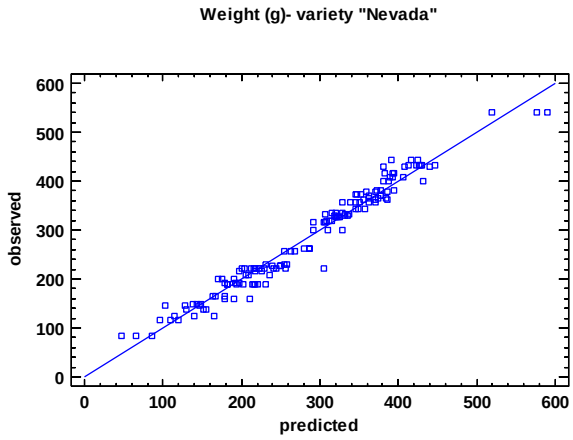

Figure 5. Observed and predicted weight (g) from the multiple regression analysis based on the external colour parameters, variety Nevada.

$$W\ (g) = 214.7410 + 0.0480A(mm^2) + 0.1044P\ (mm) + 0.3313D(mm) + 0.4043B + 0.2660G + 0.6771B$$

Where:
W= Weight (g)
A= Image analysis area (mm^2)
P= Image analysis perimeter (mm)
D= Image analysis maximum diameter (mm)
B= B colour from RGB image analysis colour coordinates
G= G colour from RGB image analysis colour coordinates
R= R colour from RGB image analysis colour coordinates

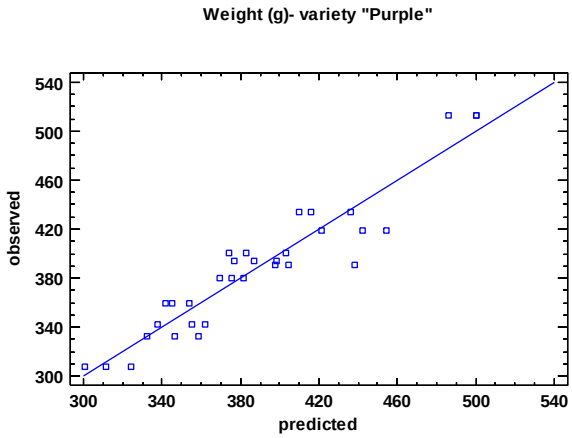

Figure 6. Observed and predicted weight (g) from the multiple regression analysis based on the external colour parameters, variety Purple.

$$W\ (g) = 312.9870 + 0.0925A(mm^2) + 3.3458D(mm) + 4.1652d\ (mm) + 6.0328B + 4.0477G$$

Where:
W= Weight (g)
A= Image analysis area (mm^2)
D= Image analysis maximum diameter (mm)
d= Image analysis minimum diameter (mm)
B= B colour from RGB image analysis colour coordinates
G= G colour from RGB image analysis colour coordinates

These results showed the relation between the image analysis variables, related to shape and size and eternal colour, and the quality parameters weight and sugar content. Besides, a good relation was found between the external parameters and the crucial internal attribute, sugar content for Purple variety (with R^2 of 89.25 %). Further analysis should be developed in order to explore the possibility of predicting sugar content in dragon fruit based on image analysis external parameters or classifying the fruit according to sugar content in different quality categories based on external variables.

4. Conclusions

These preliminary results, suggest the possibility of assessing dragon fruit quality using image analysis during grading. Sugar content and weight could be assessed using image analysis parameters (RGB colour parameters and size parameters).

Acknowledgements

This study has been funded by the Valencian Regional Government (Agencia Valenciana de la Innovacion) projects: Recolección inteligente y automatizada de cultivos de alta valor en invernaderos sostenibles (DRAGONBOT) (INNEST/2023/106) and Integración de sistemas agronómicos y fotovoltaicos para la producción inteligente de cultivos mediterráneos y subtropicales (SMART AGRIVOLTAICA) (INNEST/2022/115).

References

da Silva Ferreira, M. V., de Moraes, I. A., Passos, R. V. L., Barbin, D. F., & Barbosa Jr, J. L. (2023). Determination of pitaya quality using portable NIR spectroscopy and innovative low-cost electronic nose. Scientia Horticulturae, 310, 111784.

Ho, P. L., Tran, D. T., Hertog, M. L., & Nicolaï, B. M. (2021). Effect of controlled atmosphere storage on the quality attributes and volatile organic compounds profile of dragon fruit (Hylocereus undatus). Postharvest Biology and Technology, 173, 111406.

Ortiz, T. A., & Takahashi, L. S. A. (2020). Pitaya fruit quality (Hylocereus undatus [Haworth] Britton & Rose) according to physiological maturity. A review. Revista Colombiana de Ciencias Hortícolas, 14(1), 63-75.

Patil, P. U., Lande, S. B., Nagalkar, V. J., Nikam, S. B., & Wakchaure, G. C. (2021). Grading and sorting technique of dragon fruits using machine learning algorithms. Journal of Agriculture and Food Research, 4, 100118.

The effects of combined hot-air, microwave and infrared drying on color and β-carotene content of sweet potatoes

Khuthadzo Mugodo [a,*], Tilahun Seyoum Workneh [b], Naushad Emmambux [c], Sunette Laurie [d]

[a,b] Agricultural Engineering discipline, University of KwaZulu-Natal, Pietermaritzburg, South Africa

[b]Department of Consumer and Food Science, University of Pretoria, Pretoria, South Africa

[A]gricultural Research Council-Vegetables, Industrial and Medicinal Plants, Pretoria, South Africa

* Corresponding author. Email: mugodok@ukzn.ac.za

Abstract

The purpose of this study was to evaluate the effects of a combination of drying techniques on the quality of sweet potatoes (SP). To ensure consistency, the study implemented a Randomized Complete Block (RCBD) experiment design. This design comprised three blocks of experiments labelled as cultivar, drying methods, and pre-drying treatment factors. The drying techniques that were investigated were convective hot-air drying (CH), infrared drying (IR), and microwave drying (MW), both individually and in combination under preset conditions. The SP cultivars were orange-fleshed (Bophelo) and two cream-fleshed varieties (Blesbok and Ndou), with blanching as the pre-drying treatment technique. Results showed that the drying time was significantly ($p \leq 0.05$) affected by the drying method, whereas SP variety and blanching did not have a significant ($p > 0.05$) impact on this parameter. Furthermore, the CH+MW+IR method dried the SP more rapidly than the CH, CH+IR, and CH+MW methods. Additionally, it was evident that the product quality was significantly impacted by a reduction in the drying time of up to 15 minutes. The Blesbok and Ndou SP varieties did not contain a detectable amount of β-carotene, while the highest of β-carotene concentration was found in fresh Bophelo (225 μg. g^{-1}). The CH+MW+IR method retained 67% of the β-carotene in Bophelo and preserved a fresh-like color in the samples. In summary, this investigation determined that the utilization of combined drying methods, blanching pre-drying treatment and SP variety was effective in preserving the color and β-carotene content of SP. The total color change (ΔE) was lower for the combined CH+MW+IR drying method, with the order of ΔE being CH+MW+IR< CH+IR < CH+MW< CH.

Keywords: sweet potatoes, combined drying, β-carotene, color

1. Introduction

With a global production of 86 million tons, sweet potato (*Ipomoea batatas L.*) is a significant commodity, with Africa accounting for 15.7% of the production (FAO, 2024). Therefore, it is designated as a food security crop in the Sub-Saharan Africa region (SSA) (Motsa et al., 2015; Sapakhova et al., 2023). Consequently, the developing countries of SSA, including South Africa, have developed an interest in expanding the forms in which it is supplied through value addition, because SP is a natural source of vital micro-nutrients, including vitamin A. Laurie et al. (2022) stated that the primary benefit of SP is the reduction of vitamin A deficiency, through the use of vitamin A biofortified varieties. In order to satisfy the 2039 Agenda of the Sustainable Development Goals (SDG's) of the United Nations (Laurie et al., 2023). The potential of SP varieties, such as orange fleshed sweet potato (OFSP), which are natural sources of vitamin A, and contribute to the resolution of the persistent vitamin A deficiency (VAD), have not been investigated at large in countries like South Africa (Laurie et al., 2018; Sebben et al., 2017). The vulnerable populations, such as pregnant women and children under the age of five, continue to depend on the costly vitamin A injection to address VAD (Govender et al., 2021).

Research conducted in Africa has demonstrated that OFSP contains provitamin A (β-carotene) that can satisfy the daily nutritional needs of the most vulnerable groups (Gurmu et al., 2014; Laurie et al., 2018; Sebben et al., 2017). Historically, the use of SP to supplement traditional crops and in food fortification is conducted on a limited scale. However, agro-processing has significant potential to expand the range and forms in which SP is available to consumers, including shelf-stable flours. To accomplish this, it is necessary to investigate the primary process of flour production, which is drying. Previous research has demonstrated that the conventional drying techniques consume relatively high amount of energy and require relatively lengthy periods to dry produce to a safe storage moisture content. As a result, it is imperative to determine

the most appropriate drying methods for SP, especially for the heat and light-sensitive OFSP varieties. This is in light of the fact that numerous research studies have demonstrated that the quality of SP is adversely affected by the conventional drying methods, such as convective hot-air drying. Therefore, in recent years research has been directed towards the development of innovative solutions that can lead to reduced drying time and energy consumption, and enhanced product quality. For instance, Haruna et al. (2018) discovered that that the prevalent convective hot-air dry technique can result in β-carotene losses of up to 73.9%. Additional research has demonstrated that the retention of β-carotene is contingent upon the drying conditions of convective hot-air drying, including the drying temperature. The degree of oxidation of β-carotene is higher at relatively high drying temperatures of 80 °C, which has been observed to result in β-carotene losses of up to 54.1%. Microwave drying has been discovered to yield relatively high losses of β-carotene (64%), despite its relatively reduced energy consumption (Motevali et al., 2011). Although freeze drying preserved the entire content β-carotene content, it is relatively expensive and requires a prolonged drying time (Yang et al., 2010). The other disadvantages of using conventional techniques, such as convective hot-air and infrared drying, include an elevated total colour change (ΔE), which suggests enzymatic browning (Onwude et al., 2018; Thi Lan Khanh et al., 2018).

The individual use of microwave, infrared and convective hot-air drying has been discovered to have shortcomings in research studies. Including the minimal retention of physico-chemical properties of color and β-carotene. As well as novel drying techniques, such as combined infrared and convective hot-air (Onwude et al., 2019) and microwave and convective hot- air drying (An et al., 2024). The use of pre-drying treatments has been one of the solutions to preserve these properties, by increasing the drying rates (Sun et al., 2022). There are no studies that evaluated the effect of pre-drying techniques and combined drying methods, despite extensive work being done to improve the cultivar psychochemical properties of South African-based SP varieties. Therefore, this investigation assessed the impact of combined drying methods on pre-treated orange fleshed and cream-fleshed sweet potato varieties.

2. Materials and Methods

2.1. Plant material

Fresh sweet potato cultivars Bophelo, Ndou, and Blesbok with an average initial moisture content of 79.51±2% (w.b.) were obtained from the Agricultural Research Council-Industrial and Medicinal Plants, Pretoria, SA. The samples were hand washed and dipped in 1% sodium hypochlorite for 10 minutes and sliced into 0.3 mm slices using a vegetable slicing machine (Hengxing Kitchen Equipment Co.Ltd, China). The samples were subsequently divided into batches and were blanched at 60-80 °C for 10 minutes, and a clean cloth was used to remove the surface water before drying. The dried samples were stored in a freezer at -20 °C until the analysis of color and β-carotene.

2.2. Experimental drying methods

Drying experiments were conducted in a hybrid dryer that facilitated the drying of SP using convective hot air (CH), microwave (MW) and infrared (IR) drying technologies, both individually and in combination as illustrated in Figure 1. Throughout the drying process, the following four stages were implemented: (i) convective hot air drying (CH), (ii) CH combined with MW (CH+MW), (iii) CH combined with IR (CH+IR), and (iv) CH combined with MW and IR (CH+MW+IR). During the CH, the relative humidity (RH) and drying air temperature was measured by a sensor that was embedded inside the dryer. The values were 20±2% and 72±2 ℃, respectively. MW drying was conducted at a set power of 100 W, and the drying temperature and RH were measured at 78±2 ℃ and 12±2%, respectively. IR drying was set at a power of 240 W, and the drying air temperature and RH were measured at 84±2 ℃ and 8±2%, respectively. The airflow was parallel to the samples and was measured at the air outlet using an anemometer (average air velocity =0.32 ± 0.02 m. s^{-1}). During the drying process, the instantaneous moisture content was determined using the equation described by (Mugodo & Workneh, 2021). The initial moisture content was determined by drying the SP samples for 48 h at 105 ℃, following the standard drying method [method 950.46 B(a)] (AOAC, 2002). The moisture content during drying was determined by weighing the samples at 15-minute intervals during the drying process until a safe storage moisture content of 10±2% was achieved. The dried samples were milled into flour using a handheld food grinder before quality analysis experiments.

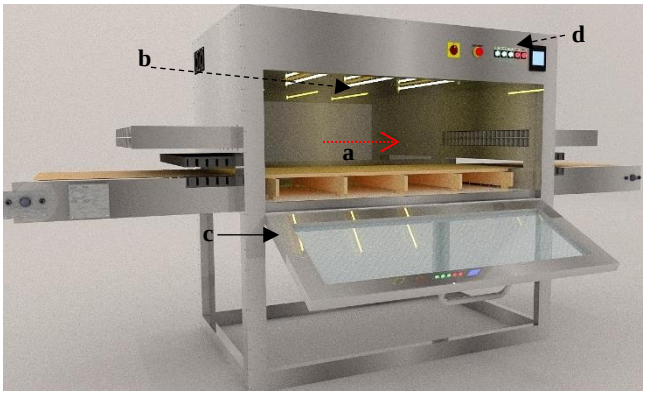

Figure 1. A schematic diagram of the hybrid dryer that illustrated (a) direction of air flow from inlet to outlet, (b) the position of infrared bulbs, (c) dryer door, and (d) the control panel and indicator lighting.

2.3. Measuring the color changes

Surface color measurements of dried and fresh SP samples were performed using a handheld chromameter (Konica Minolta, Japan), as shown in Figure 1. Black and white standardization tiles were used to calibrate the instrument, which was set to view the average standard. The glass cup of the chromameter was covered prior to taking the readings and three readings were taken on each side of the samples to obtain an average L^* value (lightness), a^* value (redness) and b^* value (yellowness). L^* measures the lightness ranging from black (zero) to white (100), a^* measures the red (+) and green colors and b^* measures the yellow (+), and blue (−) colors. The total color change (ΔE) was calculated using Equation 1 (Mugodo & Workneh, 2021).

$$\Delta E = \sqrt{\left(L^*_{dried} - L^*_{fresh}\right)^2 + \left(a^*_{dried} - a^*_{fresh}\right)^2 + (b^*_{dried} - b^*_{fresh})^2} \quad (1)$$

2.4 Measuring the β-carotene content and retention

Magnetic stirring was used to extract 2 g of SP flour in a small beaker, using 10 ml tetrahydrofuran (THF) for 30 minutes. The mixture was centrifuged at 3000 rpm for 10 minutes and the supernatant was set aside. The extraction was repeated until the residue of the flour was colorless and each time a fresh 10 ml THF aliquot was used. A rotary evaporator was used to evaporate the THF to dryness and the crude carotenes were re-dissolved in 10 ml toluene. A 0.45 µm PTFE membrane was used to filter the carotene extract in toluene into amber vials for chromatography. A Prominence UFLC (Shimadzu, Tokyo, Japan) was used to conduct chromatographic analysis of the β-carotene content. This was equipped with a DGU-20A3 Prominence degasser, SIL-20A Prominence auto-sampler, SPD-M20A Prominence diode array detector, and CTO-10AS VP Shimadzu column oven. The UV/Vis spectra of carotenoids were recorded between 200 and 600 nm, with detection of β-carotene at 450 nm. To separate the carotenoids a C18 Waters Nova-Pak carotenoid column (300 x 3.9 mm, 4 µm particle size) was used at 30 ˚C on a by isocratic elution, this was done with acetonitrile (58%). A mobile phase of HPLC grade methanol (35%) and THF (7%) was then added at a flow rate of 1.0 ml.min^{-1} for 30 minutes. A standard β-carotene curve was used to determine the β-carotene content. The β-carotene content and retention were determined using Equations 2 and 3, where C is the β-carotene content (µg.g^{-1}), that was obtained from the calibration curve, V is the final volume (ml) and W is the sample weight (g) (Ruttarattanamongkol et al., 2016). β_i is the β-carotene content of fresh SP and β_t is the β-carotene content of dried SP (Suvarnakuta et al., 2005).

$$\beta - carotene\ content = \frac{CV}{W} \quad (2)$$

$$\beta - carotene\ retention = \frac{\beta_t}{\beta_i} \times 100 \quad (3)$$

3. Results and Discussion

3.1 Drying time

SP was dried from an average initial moisture content of 79±1.95% w.b. to an average moisture content of 10±1.89% w.b. The findings indicated that the drying time was not influenced by the type of SP variety or blanching. Additionally, the drying durations of SP were compared in this study using a variety of drying techniques, including (i) CH, (ii) CH+IR+MW, (iii) CH+IR, and (iv) CH+MW. The results indicated that the drying time varied substantially ($p \leq 0.05$) among the drying combinations. The SP dried 60 minutes slower in CH than with the CH+IR+MW combination. Additionally, CH+IR+MW was more rapid than the CH+IR and CH+MW drying. SP samples were dried 30 and 15 minutes quicker by CH+IR+MW than CH+IR and CH+MW, respectively. The extended drying time observed in CH, may be attributed to the lower drying rates. Abbaspour-Gilandeh et al. (2021) and Marzuki et al. (2021) observed comparable results when drying green pepper, hawthorn fruit and purple-fleshed SP, respectively. This investigation determined that the microwave drying process enhances moisture transport by increasing moisture diffusivity (Łechtańska et al., 2015). Furthermore, it is a more rapid process that entails volumetric heating of the product, which primarily heats mainly water and facilitates mass and heat transfer processes (Marzuki et al., 2021; Schweinberger et al., 2020). This is due to the direct supply of energy to the surface of the sample, it results in rapid heating. In comparison to convective hot-air drying, which was research has demonstrated that in this study, infrared drying can reduce the drying time by 46% (Nowak & Lewicki, 2004). Previous studies has demonstrated that CH+IR and CH+MW can reduce drying time by up to 88% and 146%, respectively (Abbaspour-Gilandeh et al., 2021). The molecular vibration of the inner surface layer of the SP is enhanced by volumetric heating that is generated by the combined effect of CH, IR and MW within the product. This accelerates the rate of moisture migration across the SP sample surface. According to Onwude et al. (2018) the removal of moisture from the surface is contingent upon the utilization of convective air assistance in conduction with other drying methods. Therefore, the drying time is significantly reduced by the CH+IR+MW combination.

Table 1. The typical drying time of blanched and unblanched (control) SP that was dried using combined techniques

Drying method	Pre-drying treatment	Drying time (h)
CH	Blanched	2
CH+MW	Blanched	1
CH+IR	Blanched	1.3
CH+MW+IR	Blanched	1.5
CH	Control	2
CH+MW	Control	1
CH+IR	Control	1.3
CH+MW+IR	Control	1.5

3.2 Colour changes

In comparison to the other varieties, Bophelo exhibited the highest total color change (ΔE), of up to 30.3, as indicated in Table 2. The ΔE values of unblanched (control) SP were high, with a range of 12.9 to 33.9. For the blanched samples the order of increase in ΔE was as follows: CH+IR+MW< CH+MW < CH+IR < CH. This indicates that SP samples that were dried in CH experienced the highest total color change. The Maillard reaction, carotenoid degradation, non-enzymatic browning are the primary causes of color change during drying. These processes are influenced by extended drying periods, such as those observed in CH. In addition, this study was unable to reach the same conclusion, despite the fact that previous research suggested that pre-treated samples experience less color changes (Lagnika et al., 2019). In contrast to the prevailing belief, numerous studies have demonstrated that blanching is linked to a reduction in drying rates, which leads to extended drying periods. (Chinenye et al., 2022; Xiao et al., 2009).

Table 2. The total change in colour of SP dried by combined drying techniques

Drying method	ΔE		
	Bophelo	Blesbok	Ndou
Blanched			
CH	30.29	17.75	8.82
CH+MW	8.60	20.40	6.88
CH+IR	20.71	17.98	12.90
CH+MW+IR	12.476	4.32	9.74
Control			
CH	19.17	29.18	20.39
CH+MW	20.73	29.50	33.88
CH+IR	16.21	17.78	22.42
CH+MW+IR	12.90	23.86	29.44

3.3 Changes in β-carotene

β-carotene was not detected in the Ndou and Blesbok varieties. The β-carotene concentration of fresh (raw) Bophelo was the highest at 225 $\mu g.g^{-1}$. Table 3 illustrates the variations in β-carotene that occurred during the drying process. In comparison to the fresh samples, all the drying techniques employed resulted in a substantial decrease in β-carotene levels, with the control samples exhibiting the most significant losses. The β-carotene content was reduced by approximately 50% when samples were dried in CH+MW, CH+IR, and CH. β-carotene is a reactive compound due to its unsaturated structure (Zhao et al., 2016). Consequently, it is susceptible to degradation, which can be induced by oxygen exposure, which results in β-carotene degradation. In addition, the degradation of β-carotene has been detected to be induced by enzymatic activity and light (photo-oxidation). This is further stimulated by extended drying periods and elevated drying temperatures (Falade & Solademi, 2010). The β-carotene content is significantly reduced as a result of the significant increase in oxidation that occurs as dehydration temperatures exceeding 55 ℃ (Pénicaud et al., 2011).Furthermore, it was observed that the highest β-carotene retention was observed when CH+MW+IR was used, compared to the use of drying techniques alone (YAN et al., 2013). This could have been caused by the reduced drying time. Blanched samples in CH+MW+IR retained β-carotene better (67%) during the drying process, compared to the control. After drying SP with a vacuum belt drying Xu et al. (2013) observed a comparable trend, with a 69.9% retention of β-carotene retention. In addition, the absence of pre-drying treatment leads to a decrease in the chemical concentration of the samples following the drying process (Workneh et al., 2014). In contrast to the results of the study, blanching is a preferred pre-drying treatment over chemicals such as citric acid and metabisulfite, and it has been demonstrated to enhance the β-carotene content of SP (Nicanuru et al., 2015).

Table 3. Concentration and % retention of β-carotene in the Bophelo variety

Drying method	β-carotene content ($\mu g.g^{-1}$)	% Retention of β-carotene
Fresh SP	225	
CH-blanched	145	64.4
CH+MW-blanched	100	44.4
CH+IR- blanched	145	64.4
CH+IR+MW-blanched	112	49.8
CH-control	151	67.1
CH+MW-control	100	44.4
CH+IR-control	150	66.7
CH+MW+IR-control	110	48.9

4 Conclusions

Research on convective hot-air drying and its combination with infrared and microwave drying has shown that the drying time of CH is reduced, the natural colour is preserved, and approximately 67% of β-carotene is retained in blanched orange sweet potato samples when CH+MW+IR is used. The Bophelo cultivar exhibits the highest levels of β-carotene and the highest sensitivity to colour loss as a consequence of hot-air (CH) and light (IR). Consequently, the preservation of product quality is considerably enhanced by a reduction in the drying time, by as much as 15 minutes. In order to ascertain the technical efficacy of combined drying methods, additional research is required to examine their energy consumption. Additionally, it is imperative to conduct additional research on alternative pre-drying treatments, including ultrasound-assisted methods, to retain β-carotene, given the ineffectiveness of blanching in reducing the drying time. This will be advantageous, as the subsequent processing of the material into flour and value-added products may lead to an additional reduction in β-carotene. The blanching factors of SP can also be further investigated to determine the optimal conditions, which may further enhance the drying process. This includes the blanching time and temperature. Furthermore, the study did not definitely demonstrate a correlation between β-carotene and colour as a quality parameter when blanching was considered. Therefore, it is advised that additional research be conducted to identify the quality parameters that are significant and the variations that occur, as this may result in improved β-carotene retention in SP varieties.

Acknowledgements

The authors acknowledge the National Research Foundation (NRF) for providing financial support for conducting this research and the Department of Science and Innovation (DSI)-National Research foundation (NRF) Centre of Excellence in Food Security.

References

Abbaspour-Gilandeh, Y., Kaveh, M., Fatemi, H., & Aziz, M. (2021). Combined Hot Air, Microwave, and Infrared Drying of Hawthorn Fruit: Effects of Ultrasonic Pretreatment on Drying Time, Energy, Qualitative, and Bioactive Compounds' Properties. *Foods*, *10*(5), 1006. https://www.mdpi.com/2304-8158/10/5/1006

An, N.-n., Sun, W., Li, D., Wang, L.-j., & Wang, Y. (2024). Effect of microwave-assisted hot air drying on drying kinetics, water migration, dielectric properties, and microstructure of corn. *Food chemistry*, *455*, 139913. https://doi.org/https://doi.org/10.1016/j.foodchem.2024.139913

AOAC. (2002). *Official Methods of Analysis*. Association of Official Analytical Chemists.

Chinenye, N. M., Onyenwigwe, D. I., Abam, F., Lamrani, B., Simo-Tagne, M., Bekkioui, N., Bennamoun, L., & Said, Z. (2022). Influence of hot water blanching and saline immersion period on the thermal effusivity and the drying kinetics of hybrid solar drying of sweet potato chips. *Solar Energy*, *240*, 176-192.

Falade, K. O., & Solademi, O. J. (2010). Modelling of air drying of fresh and blanched sweet potato slices. *International journal of food science & technology*, *45*(2), 278-288.

FAO. (2024). *Production quantities of sweet potatoes by country* FAOSTAT. https://www.fao.org/contact-us/terms/db-terms-of-use/en/

Govender, L., Pillay, K., Siwela, M., Modi, A. T., & Mabhaudhi, T. (2021). Assessment of the Nutritional Status of Four Selected Rural Communities in KwaZulu-Natal, South Africa. *Nutrients*, *13*(9). https://doi.org/10.3390/nu13092920

Gurmu, F., Hussein, S., & Laing, M. (2014). The potential of orange-fleshed sweet potato to prevent vitamin A deficiency in Africa. *Int J Vitam Nutr Res*, *84*(1-2), 65-78. https://doi.org/10.1024/0300-9831/a000194

Haruna, S., Adejumo, B., Chinma, C., Akanya, H., & Okolo, C. (2018). The influence of drying temperature on selected properties of flour produced from orange fleshed sweet potato tubers. *International Journal of Engineering Research & Technology*, *7*(07), 338-341.

Lagnika, C., Jiang, N., Song, J., Li, D., Liu, C., Huang, J., Wei, Q., & Zhang, M. (2019). Effects of pretreatments on properties of microwave-vacuum drying of sweet potato slices. *Drying Technology*, *37*(15), 1901-1914. https://doi.org/10.1080/07373937.2018.1543702

Laurie, S., Mulabisana, J., Sutherland, R., Sivakumar, D., Pofu, K., Mphela, W., Truter, M., Plooy, I., Araya, N., Araya, H. T., Nyathi, M., Kistnasamy, A., Cloete, M., Nkosi, B., Shimelis, H., Laing, M., Malebane, M., & Bairu, M. (2023). Seventy years of sweetpotato (Ipomoea batatas L. (LAM)) research in South Africa. *Crop Science*, *64*. https://doi.org/10.1002/csc2.21097

Laurie, S. M., Bairu, M. W., & Laurie, R. N. (2022). Analysis of the Nutritional Composition and Drought Tolerance Traits of Sweet Potato: Selection Criteria for Breeding Lines. *Plants*, *11*(14), 1804.

Laurie, S. M., Faber, M., & Claasen, N. (2018). Incorporating orange-fleshed sweet potato into the food system as a strategy for improved nutrition: The context of South Africa. *Food Research International*, *104*, 77-85. https://doi.org/https://doi.org/10.1016/j.foodres.2017.09.016

Łechtańska, J., Szadzińska, J., & Kowalski, S. (2015). Microwave-and infrared-assisted convective drying of green pepper: Quality and energy considerations. *Chemical Engineering and Processing: Process Intensification*, *98*, 155-164.

Marzuki, S. U., Pranoto, Y., Khumsap, T., & Nguyen, L. T. (2021). Effect of blanching pretreatment and microwave-vacuum drying on drying kinetics and physicochemical properties of purple-fleshed sweet potato. *Journal of Food Science and Technology*, *58*, 2884-2895.

Motevali, A., Minaei, S., & Khoshtagaza, M. H. (2011). Evaluation of energy consumption in different drying methods. *Energy Conversion and Management*, *52*(2), 1192-1199. https://doi.org/https://doi.org/10.1016/j.enconman.2010.09.014

Motsa, N. M., Modi, A. T., & Mabhaudhi, T. (2015). Sweet potato (Ipomoea batatas L.) as a drought tolerant and food security crop. *South African Journal of Science*, *111*(11/12), 8. https://doi.org/10.17159/sajs.2015/20140252

Mugodo, K., & Workneh, T. S. (2021). The kinetics of thin-layer drying and modelling for mango slices and the influence of differing hot-air drying methods on quality. *Heliyon*, *7*(6).

Nicanuru, C., Laswai, H., & Sila, D. (2015). Effect of sun-drying on nutrient content of orange fleshed sweet potato tubers in Tanzania. *Sky Journal of Food Science*, *4*(7), 91-101.

Nowak, D., & Lewicki, P. P. (2004). Infrared drying of apple slices. *Innovative Food Science & Emerging Technologies*, *5*(3), 353-360. https://doi.org/https://doi.org/10.1016/j.ifset.2004.03.003

Onwude, D. I., Hashim, N., Abdan, K., Janius, R., & Chen, G. (2018). Investigating the influence of novel drying methods on sweet potato (Ipomoea batatas L.): Kinetics, energy consumption, color, and microstructure. *Journal of Food Process Engineering*, *41*(4), e12686. https://doi.org/https://doi.org/10.1111/jfpe.12686

Onwude, D. I., Hashim, N., Abdan, K., Janius, R., & Chen, G. (2019). The effectiveness of combined infrared and hot-air drying strategies for sweet potato. *Journal of Food Engineering*, *241*, 75-87. https://doi.org/https://doi.org/10.1016/j.jfoodeng.2018.08.008

Pénicaud, C., Achir, N., Dhuique-Mayer, C., Dornier, M., & Bohuon, P. (2011). Degradation of β-carotene during fruit and vegetable processing or storage: Reaction mechanisms and kinetic aspects: A review. *Fruits*, *66*(6), 417-440.

Ruttarattanamongkol, K., Chittrakorn, S., Weerawatanakorn, M., & Dangpium, N. (2016). Effect of drying conditions on properties, pigments and antioxidant activity retentions of pretreated orange and purple-fleshed sweet potato flours. *Journal of Food Science and Technology*, *53*(4), 1811-1822. https://doi.org/10.1007/s13197-015-2086-7

Sapakhova, Z., Raissova, N., Daurov, D., Zhapar, K., Daurova, A., Zhigailov, A., Zhambakin, K., & Shamekova, M. (2023). Sweet Potato as a Key Crop for Food Security under the Conditions of Global Climate Change: A Review. *Plants*, *12*(13), 2516. https://www.mdpi.com/2223-7747/12/13/2516

Schweinberger, C. M., Sebben, J. A., Schultz, P. H., Trierweiler, J. O., & Trierweiler, L. F. (2020). Study of three drying methods in production of nutritious flours from the fermentation slurry of orange‐fleshed sweet potato. *Journal of Food Processing and Preservation*, *44*(9), e14658.

Sebben, J. A., Trierweiler, L. F., & Trierweiler, J. O. (2017). Orange‐fleshed sweet potato flour obtained by drying in microwave and hot air. *Journal of Food Processing and Preservation*, *41*(1), e12744.

Sun, Q., Song, X., Arun S, M., Zhang, L., Yu, X., Zhou, C., Tang, Y., & Yagoub, A. E. A. (2022). Effects of blanching drying methods on the structure and physicochemical properties of starch in sweet potato slices. *Food Hydrocolloids*, *127*, 107543. https://doi.org/https://doi.org/10.1016/j.foodhyd.2022.107543

Suvarnakuta, P., Devahastin, S., & Mujumdar, A. S. (2005). Drying kinetics and β‐carotene degradation in carrot undergoing different drying processes. *Journal of Food Science*, *70*(8), s520-s526.

Thi Lan Khanh, P., Chittrakorn, S., Rutnakornpituk, B., Phan Tai, H., & Ruttarattanamongkol, K. (2018). Processing effects on anthocyanins, phenolic acids, antioxidant activity, and physical characteristics of Vietnamese purple‐fleshed sweet potato flours. *Journal of Food Processing and Preservation*, *42*(9), e13722.

Workneh, T. S., Zinash, A., & Woldetsadik, K. (2014). Blanching, salting and sun drying of different pumpkin fruit slices. *J Food Sci Technol*, *51*(11), 3114-3123. https://doi.org/10.1007/s13197-012-0835-4

Xiao, H.-W., Lin, H., Yao, X.-D., Du, Z.-L., Lou, Z., & Gao, Z.-j. (2009). Effects of different pretreatments on drying kinetics and quality of sweet potato bars undergoing air impingement drying. *International Journal of Food Engineering*, *5*(5).

Xu, S., Pegg, R. B., & Kerr, W. L. (2013). Sensory and Physicochemical Properties of Sweet Potato Chips Made by Vacuum-Belt Drying. *Journal of Food Process Engineering*, *36*(3), 353-363. https://doi.org/10.1111/jfpe.12002

YAN, W. Q., Zhang, M., HUANG, L. L., Mujumdar, A. S., & Tang, J. (2013). Influence of microwave drying method on the characteristics of the sweet potato dices. *Journal of Food Processing and Preservation*, *37*(5), 662-669.

Yang, J., Chen, J.-f., Zhao, Y.-y., & Mao, L.-c. (2010). Effects of Drying Processes on the Antioxidant Properties in Sweet Potatoes. *Agricultural Sciences in China*, *9*(10), 1522-1529. https://doi.org/https://doi.org/10.1016/S1671-2927(09)60246-7

Zhao, D., Wang, Y., Zhu, Y., & Ni, Y. (2016). Effect of carbonic maceration pre-treatment on the drying behavior and physicochemical compositions of sweet potato dried with intermittent or continuous microwave. *Drying Technology*, *34*(13), 1604-1612.

Authentication of cattle finishing diets (conventional vs. vegetable by-products) using near-infrared spectroscopy

Sara León-Ecay [a, *], Ainara López-Maestresalas [a], Irantzu Goenaga [a,b], José Antonio Mendizabal [a], Kizkitza Insausti [a]

[a] IS-FOOD, Universidad Pública de Navarra, 31006 Pamplona, Spain

[b] Tratamiento Subproductos Agroalimentarios, 31320 Milagro, Spain

* Corresponding author. Email: sara.leon@unavarra.es

Abstract

This study explored the potential of a portable near-infrared (NIR) spectrophotometer (1200 – 2200 nm; 2-nm bandwidth) to discriminate meat and carcasses from cattle fed two different diets: a control of 90% barley and 10% straw (C, n = 12) and, a ration including 37.5% of vegetable by-products (VBPR, n = 11). At 24 h postmortem spectra were collected on the exterior surface of the left carcass, first, between the 5th and 6th ribs, and afterwards, on the 12th and 13th ribs. After fabrication and 7 d of aging, spectral data was acquired from the intact steaks while keeping muscle integrity. When spectra were collected from the carcasses, partial least squares-discriminant analysis (PLS-DA) correctly classified (%CC) >66.67% in both Train and cross-validation (CV) whereas radial basis function-support vector machine (RBF-SVM) discriminated 100 – 83.33% in Train and CV, respectively, using the full spectrum. Reducing the initial matrix (λ=501) by interval-PLS (iPLS) led into a >75% of well-sorted carcasses by finishing diet while RBF-SVM increased the %CC up to >83.33%. Using both discriminant approaches, carcasses were authenticated with a subtle improvement over intact meat (>90% vs. >75% in Train and >80% vs. >65% in CV for C and VBPR, respectively). Variable importance in projection (VIP) scores showed how variables >1592 nm had higher weight in the discrimination process. The results achieved showed the potential of NIR technology as a sustainable, fast and chemical-free tool to assist the integration of the meat industry into the digital age of connectivity and digitization.

Keywords: beef, feeding diet, chemometrics, machine learning

1. Introduction

European strategies such as Farm to Fork promote the acceleration towards a sustainable food production model, including new input sources able to enhance the circularity of the economic system. Focusing on the agri-food sector, there are scenarios in which circular economy procedures can be integrated. For instance, Santos et al. (2022) estimated that 22% of the total food losses and wastes along the supply chain are associated to vegetable by-products (VBPR). During postharvest and storage, 54% of the vegetable waste is produced, while 46% occurs downstream from processing, distribution, and consumption (Espinosa-Alonso et al., 2020). Among the potential uses of these low-economical-value by-products is ruminant feed, since rumen microbes have the unique capacity to digest fiber (Mirzaei-Aghsaghali and Maheri-Sis, 2008). Thus, the production of nutrient-dense food (meat, milk and, eggs) for human consumption by circular economy techniques contributes to the reduction of food/feed competition (Salami et al., 2019).

The need for traceability and transparency from primary production to final consumption, leads to fight against food fraud/crime; and therefore, facilitate consumers to recognize the added value products at the time of purchase. To date, techniques as gas chromatography (GC), high performance liquid chromatography (HPLC), or DNA-based methods have been widely applied for food authentication (Alikord et al., 2018). Consequently, the shift to novel feeds requires a rapid tool capable of authenticating the finishing diets supplied to cattle in a non-destructive, chemical-free and sustainable way. Near infrared spectroscopy (NIRS) stands out in the agri-food sector as a tool able to speed up decision-making and reduce the costs associated to quality control processes. Therefore, the aim of the study was to discriminate cattle finishing diets, either vegetable by-products-based (VBPR) or concentrate-based diets (C), from both the carcasses at the abattoir (*on-line*) and intact meat in the laboratory (*at-line*).

2. Materials and Methods

2.1. Experimental design: animals and diets

In this study, twenty-three entire young Pirenaica bulls were reared under the Protected Geographical Indication (PGI) "Ternera de Navarra" in compliance with the European Directive 2010/63/EU (EEC, 2010). Twelve animals were used as control, and they were supplied a 90% barley and 10% straw diet (C, conventional diet), whereas eleven were provided a diet composed by 53.08% concentrated feed, 37.4% of vegetable by-products, 5.45% beet pulp and 4.07% straw, as previously described in Goenaga et al. (2023). After 139.73 ± 18.54 d on feed, and in conformity with the PGI guidelines (from 6 to 13 mo of age), the animals were transported 19 km to an EU-commercial abattoir. They were stunned with a captive bolt and slaughtered and dressed under the specifications set forth in Directive 93/119/1993/EEC (EEC, 1993). From each carcass, a steak (25 mm-thick ± 0.2 mm) was collected from the *longissimus lumborum* (LL, striploin) and aged for 7 d at 5 ºC and 80% of relative humidity.

2.2. Spectral data capture and processing

Spectral data were collected from both (a) carcasses in the abattoir 24 h postmortem and (b) intact meat after 7 d of aging. In both scenarios, the near-infrared (NIR) data were collected using a portable Luminar 5030 NIR spectrophotometer in the 1200 – 2200 nm range with a bandwidth of 2-nm. In the coolers, a total of 20 reflectance spectra were recorded on the surface of the left carcass, 10 spectra being between the 5th and 6th ribs, and the remaining 10 entries on the 12th and 13th ribs. At the laboratory, ten replicates per steak were obtained from the intact meat. Subsequently, spectra were visually observed for outliers and the average was calculated.

The spectral matrixes were then imported into the PLS_Toolbox 9.3 software under MATLAB R2023b for analysis. Prior to chemometric modelling, several pre-processing techniques were applied to diminish the effect of environmental conditions during acquisition that could alter data quality. Multiplicative Scatter Correction (MSC), 1st derivative (1stder), Standard Normal Variate (SNV), Smoothing (SM) and, Mean Center (MC) were tested either individually or in combination with other pre-treatments to enhance their effectiveness (Zeaiter and Rutledge, 2009). Partial Least Squares-Discriminant Analysis (PLS-DA) and Radial Basis Function-Support Vector Machines (RBF-SVM) machine learning algorithms were used for carcass and meat discrimination by diet. The basis of the chemometric algorithms have been widely detailed, for instance, by Ballabio and Consonni (2013) and Yue et al. (2003). Indeed, to reduce data dimensionality, variable selection was performed by interval-PLS (iPLS), where a number of intervals with size between 10 and 20 were automatically selected in 2-nm increments.

3. Results and Discussion

Figure 1 shows the raw mean reflectance profile of the (a) carcasses and (b) striploin according to the diet provided to the young bulls. As it can be observed, the spectral signature was similar between carcasses and intact meat, however, at some precise points the magnitude of the reflectance varied. Focusing on the carcass profile (Fig. 1a), four prominent valleys were observed in 1422; 1505; 1718; 1944 nm and four peaks in 1482; 1684; 1812; 2090 nm. However, the animals from the two diets were almost indistinguishable until 1684 nm, from where carcasses coming from VBPR animals reflected more light than C animals. In fact, intact meat (Fig. 1b) sheared the <1684 nm spectral region with the carcasses, despite from this point the fingerprint was not as smooth. In this scenario, three highlighted valleys can be observed at 1422; 1502; 1927 nm whereas three peaks can be identified at 1479; 1671 and 1744 nm. Oppositely to cattle carcasses, intact meat from C animals reflected a larger amount of light compared to meat from VBPR animals.

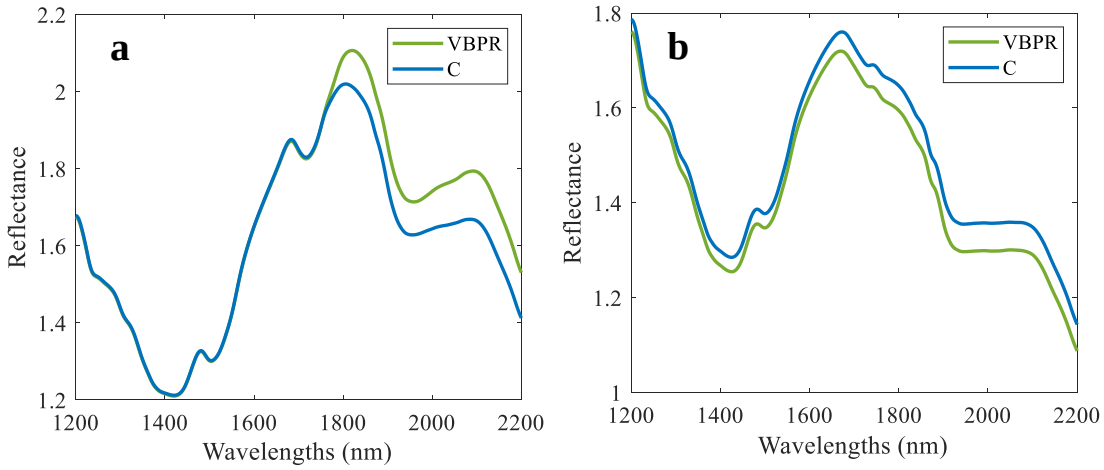

Figure 1. Raw mean reflectance profile in the 1,200 – 2,200 nm spectral range for: (a) carcass, (b) intact meat.

Table 1 gathers the best results to authenticate the nature of the diet supplied to cattle by both PLS-DA and RBF-SVM. When the spectra were collected directly on animal carcasses, PLS-DA correctly classified 90.91% and 66.67% of C and VBPR samples, respectively, in both Train and CV using the full NIR region. When RBF-SVM was performed for the full spectrum, the correctly classified percentage of carcasses from C-fed cattle was slightly increased up to 100% and 91.67% in Train and CV, respectively, although the %CC for VBPR-fed animals was 100% in Train and modestly inferior in CV (83.33%). Lower discriminative rates were achieved when analysing the spectra from intact meat. For instance, by PLS-DA the correctly classified percentage in Train was 70 – 72.73% while in cross-validation was reduced to 60.00 – 60.64% for meat coming from barley and vegetable by-products-fed cattle.

Table 1.Partial least squares-discriminant and radial basis function-support vector machine results for carcass and intact meat by feeding diet.

					$\%CC_{Train}$			$\%CC_{CV}$		
	Model	Pre-processing	Spectra included	LV	Barley	Vegetable by-products	Overall	Barley	Vegetable by-products	Overall
Carcass	PLS-DA									
		MSC	Full (λ = 501)	3	90.91	66.67	78.79	90.91	66.67	78.79
		1st der+SNV+MC	iPLS14 (λ = 28)	4	81.82	75.00	78.41	81.82	75.00	78.41
	RBF-SVM									
		Raw data	Full (λ = 501)		100	100	100.00	91.67	83.33	87.50
		1st der+SNV+MC	iPLS14 (λ = 28)		90.91	91.67	**91.29**	90.91	83.33	**87.12**
Intact meat	PLS-DA									
		SM+MC	Full (λ = 501)	4	70.00	72.73	71.37	60.00	60.64	60.32
		MSC	iPLS18 (λ = 72)	6	90.00	75.00	82.50	90.00	66.67	78.34
	RBF-SVM									
		1st der+SNV+MC	Full (λ = 501)		91.67	100	95.84	66.67	72.72	69.70
		1st der+SNV+MC	iPLS16 (λ = 48)		75.00	90.91	**82.96**	66.67	90.91	**78.79**

CC, Correctly classified; CV, Cross-validation; LV, Latent variable; PLS-DA, Partial Least Squares-Discriminant Analysis; RBF-SVM, Radial Basis Function-Support Vector Machines; MSC, Mean scatter correction; 1st der, First derivative; SNV, Standard normal variate; MC, Mean center; SM, Smoothing; λ, Wavelength; iPLS-*: interval partial least squares (*: interval size). Values in bold correspond to the best results obtained in terms of highest %CC in both Train and CV.

However, the speed of food processing lines requires accurate and fast control to streamline decision making. Therefore, the wavelengths that have the strongest weight in the model have been specified and modelled to compare the performance. When downsizing the initial spectral matrix (λ = 501) by the iPLS reduction method, the number of bands involved in the modelling procedure was substantially decreased. For instance, by iPLS14 only 28 wavelengths were considered whereas iPLS16 and iPLS18 took into

consideration 48 and 72 wavelengths, respectively. In this sense, cattle carcasses were discriminated by PLS-DA with an overall accuracy of 78.79% in Train and cross-validation with the full spectrum whereas when using the reduced matrix, the average percentage in Train and CV was maintained in 78.41%. Nevertheless, the iPLS reduction method performed better when applying RBF-SVM compared to PLS-DA, as the %CC reached 91.29 and 87.12% of well-sorted animals in Train and CV by a model involving 1stder+SNV+MC as pre-processing. In this sense, intact meat was better classified with the reduced matrix compared to the full spectrum when considering average rates between Train and CV. By PLS-DA, 71.37 and 60.32% of the carcasses were correctly discriminated involving 501 wavelengths whereas when reducing the matrix to 72 variables, 82.5 and 78.34% of the animals were well-sorted. On the opposite hand, by RBF-SVM, 95.84 and 69.70% of the cattle carcasses were faultless classified, in average, with 501 bands whereas with 48 variables an 82.96% and 78.79% in Train and CV was achieved, respectively. The best results were obtained by the models built under reduced matrix conditions; therefore, the hypothesis that variable selection identified the subset of variables that conduct to the minimum possible errors for discriminating samples was satisfied (Xiaobo et al., 2010).

Figure 2 represents the variable importance in projection (VIP) for carcass (Fig. 2a) and intact meat (Fig. 2b) through PLS-DA for the models built with the full NIR spectrum. Thus, the variables with greater weight in the discriminant procedure (VIP ≥ 1) could be identified. There were some spectral regions that surpassed the threshold of 1 for both types of samples. Concisely, bands over 1644, 1708, 1900 and 2100 nm have been noted as key for classifying carcasses and meat from cattle fed different diets. In those regions, mainly C-H combinations and 1st overtone together with O-H and N-H bonds vibration could be captured (Osborne, 2000). However, as previously studied by León-Ecay et al. (2024) no differences were found in the reference measurement results (i.e., intramuscular fat, protein, instrumental texture by Warner Bratzler Share Force, soluble collagen and meat color traits: *L**, *a**, *b**, Chroma and Hue) when analysing the meat of the animals fed C and VBPR-based diets. In this sense, the lipid profile (i.e., hydrocarbon bonds) influenced the classification approach as meat from VBPR-fed cattle had higher content of PUFA individual fatty acids compared to C-fed meat samples. Moreover, the influence of water absorption in fresh meat is of such importance, even though O-H absorption was different among both types of carcasses and intact meat (1,790 nm). However, other studies of similar nature, as the one carried out by Barragán et al. (2021), discriminated intact meat from barley, blend and corn-fed cattle with a well classified samples rate of 57, 46 and 48% in cross validation for each feeding system, respectively. Focusing on carcass discrimination, Zamora-Rojas et al. (2012) achieved similar sorting performances (overall accuracy of 87.07% and 83.63% in Train and Test, respectively) when classifying Iberian pig carcasses raised under three feeding regimes (“Acorn”, “Recebo” and “Feed”).with a micro-electro-mechanical system spectrometer (1,600–2,400 nm).

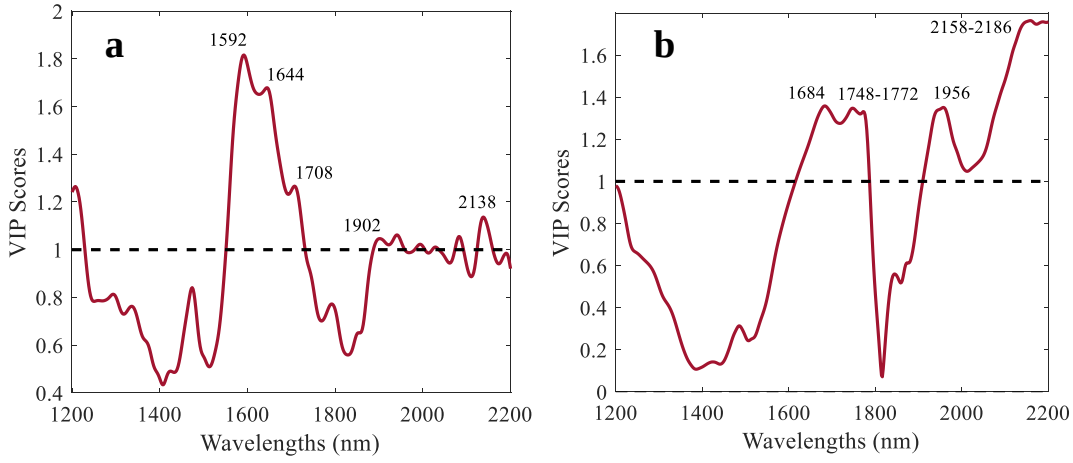

Figure 2. Variable importance in projection for the PLS-DA models built with the full spectrum: (a) MSC, 3 LV for carcass discrimination, (b) SM+MC, 4 LV for intact meat.

4. Conclusions

Suppling animals with novel feeds during their fattening period require a distinctive mark. To ensure the authentication of this local and sustainable beef product, the potential of portable NIRS, both in a commercial

abattoir environment and at laboratory scale, was demonstrated to discriminate cattle carcasses and intact meat according to the finishing diet (C vs. VBPR-based). Variable selection together with the RBF-SVM algorithm showed potential to correctly sort both cattle carcasses and intact meat. The attained results showed the promising application of NIR spectroscopy as a sustainable, fast and chemical-free tool to assist the integration of the meat industry into the digital age of connectivity and digitization.

Acknowledgements

This research has been founded by the Government of Navarra and the European Regional Development Fund via project BEEF+ "Carne saludable a través de la economía circular" (0011-1365-2020-000288), by Universidad Pública de Navarra through a PhD scholarship UPNA-2022 (Res.2178/2022) and, an Industrial PhD 2020 scholarship from the Government of Navarra (0011-1408-2020-000009).

References

Ballabio, D., Consonni, V., 2013. Classification tools in chemistry. Part 1: Linear models. PLS-DA. Analytical Methods, 5 (16), 3790. https://doi.org/10.1039/c3ay40582f

Barragán, W., Aalhus, J. L., Penner, G., Dugan, M. E. R., Juárez, M., López-Campos, Ó., Vahmani, P., Segura, J., Angulo, J., Prieto, N., 2021. Authentication of barley-finished beef using visible and near infrared spectroscopy (Vis-NIRS) and different discrimination approaches. Meat Science, 172, 108342. https://doi.org/10.1016/j.meatsci.2020.108342

EEC. (1993). *Council Directive 93/119/EC of 22 December 1993 on the protection of animals at the time of slaughter or killing*.

EEC. (2010). *Directive 2010/63/EU of the European Parliament and of the Council of 22 September 2010 on the protection of animals used for scientific purposes*.

Espinosa-Alonso, L. G., Valdez-Morales, M., Aparicio-Fernandez, X., Medina-Godoy, S., Guevara-Lara, F., 2020. Vegetable By-products. In R. Campos-Vega, B. D. Oomah, H. A. Vergara-Castañeda (Eds.), *Food Wastes and By-products* (1st ed., pp. 223–266). Wiley. https://doi.org/10.1002/9781119534167.ch8

Goenaga, I., García-Rodríguez, A., Goiri, I., León-Ecay, S., De Las Heras, J., Aldai, N., Insausti, K., 2023. Vegetable By-Products as Alternative and Sustainable Raw Materials for Ruminant Feeding: Nutritive Evaluation and Their Inclusion in a Novel Ration for Calf Fattening. Animals, 13 (8), 1391. https://doi.org/10.3390/ani13081391

León-Ecay, S., Insausti, K., Arazuri, S., Goenaga, I., López-Maestresalas, A., 2024. Combination of spectral and textural features of hyperspectral imaging for the authentication of the diet supplied to fattening cattle. Food Control, 159, 110284. https://doi.org/10.1016/j.foodcont.2024.110284

Mirzaei-Aghsaghali, A., Maheri-Sis, N. (2008). Nutritive value of some agro-industrial by-products for ruminants - A review. 3 (2), 40–46.

Osborne, B. G. (2000). Near-Infrared Spectroscopy in Food Analysis. In R. A. Meyers (Ed.), Encyclopedia of Analytical Chemistry (p. a1018). John Wiley & Sons, Ltd. https://doi.org/10.1002/9780470027318.a1018

Salami, S. A., Luciano, G., O'Grady, M. N., Biondi, L., Newbold, C. J., Kerry, J. P., Priolo, A., 2019. Sustainability of feeding plant by-products: A review of the implications for ruminant meat production. Animal Feed Science and Technology, 251, 37–55. https://doi.org/10.1016/j.anifeedsci.2019.02.006

Santos, D., Lopes Da Silva, J. A., Pintado, M., 2022. Fruit and vegetable by-products' flours as ingredients: A review on production process, health benefits and technological functionalities. LWT, 154, 112707. https://doi.org/10.1016/j.lwt.2021.112707

Xiaobo, Z., Jiewen, Z., Povey, M. J. W., Holmes, M., Hanpin, M., 2010. Variables selection methods in near-infrared spectroscopy. Analytica Chimica Acta, 667(1–2), 14–32. https://doi.org/10.1016/j.aca.2010.03.048

Yue, S., Li, P., Hao, P., 2003. SVM classification:Its contents and challenges. Applied Mathematics-A Journal of Chinese Universities, 18 (3), 332–342. https://doi.org/10.1007/s11766-003-0059-5

Zamora-Rojas, E., Pérez-Marín, D., De Pedro-Sanz, E., Guerrero-Ginel, J. E., Garrido-Varo, A., 2012. In-situ Iberian pig carcass classification using a micro-electro-mechanical system (MEMS)-based near infrared (NIR) spectrometer. Meat Science, 90 (3), 636–642. https://doi.org/10.1016/j.meatsci.2011.10.006

Zeaiter, M., Rutledge, D. (2009). Preprocessing Methods. In Comprehensive Chemometrics (pp. 121–231). Elsevier. https://doi.org/10.1016/B978-044452701-1.00074-0

Developing a plant for processing PGI 'Cipolla Rossa di Tropea Calabria' spring onions using compressed air

Matteo Sbaglia[a], Lorenzo M. Abenavoli[a], Bruno Bernardi[a,*]

[a]Dipartimento di Agraria, Università Mediterranea di Reggio Calabria, Reggio Calabria, Italy

* Corresponding author. Email: bruno.bernardi@unirc.it

Abstract

One of the best-known Italian products is 'Cipolla Rossa di Tropea Calabria PGI', which refers to the Allium cepa L. onion, limited to the local ecotypes of Tondo Piatta (early), Mezza Campana (medium) and Allungata (late). A mark identifying red onion bulbs in spring onion, fresh onion and onion for preserving that meet the conditions and requirements of this specification, following Regulation (EC) No 510/2006. Depending on the stage and type of product being processed, the mechanical plant plays a key role in the processing chain. In post-harvest operation, plants based on large quantities of water are widely used for processing spring onions, allowing them to be washed, rooted, and peeled simultaneously. They generally consist of cutting, peeling, and cleaning equipment. Two pairs of shearing blades usually carry out both root and leaf-cutting. Peeling is carried out by 2 pairs of rotating rollers, usually of the brush type, and during the peeling phase, washing is also carried out through a series of special sprayers. However, a problem with this type of system is that the water stagnating in the cut onions tends to spoil them, reducing their shelf life. A processing line that uses compressed air to clean the onions was developed to solve this problem. A processing line that uses compressed air to clean the onions was developed to solve this problem. This research reports on the functional structure of the realised plant.

Keywords: design, mechanical engineering, simulation, shelf life, water saving

1. Introduction

Certified with the Protected Geographical Indication (PGI) label since 2008, Tropea red onions have a supply chain of 20,000 tons of certified production, 20% of which is intended for processing, for a consumption volume of 60 million euros. Production extends over 2,000 hectares of land along the coast between Nicotera and Fiumefreddo Bruzio, in Cosenza, Catanzaro, and Vibo Valentia provinces, where these onions have been cultivated for 4,000 years (E.C. 284/2008). Among the produce types, spring onions are the first to be harvested before the bulb is fully formed (Bernardi et al., 2013). Sowing takes place from August onwards, whereas transplanting takes place from October to March depending on the ecotype. After harvest, the fresh product is mechanically sorted to prepare it for packaging. The spring onion bulbs then undergo removal of the dirty outer layer of soil and trimming of the tails with cuts ranging from 30 to 60 cm. Subsequently, the bulbs are grouped into bundles of 1.5–6 kg each and placed in boxes or crates, before being sent to the market. Therefore, the packaging of the product is crucial. Although weighing is now automated using specific machinery, various operations such as washing, peeling, and cutting are performed manually (requiring considerable manpower) or by using machines which are non-specific equipment and do not guarantee the appropriate processing of the product, resulting in large quantities of waste. Bernardi et al. (2024) discussed the operation of a spring-onion-processing plant (Figure 1) among the various commercial solutions adopted. Once collected, the spring onions are placed on a conveyor belt and lightly pre-washed before being sent to a washing tunnel. Here, the tails are cut off by using two pairs of opposing blades, and then, the tunics are partially removed by employing the alternating movement of two pairs of rollers. The first pair is equipped with brushes, whereas the second pair is made of rubber. Both have perpendicular and alternating movements with respect to the direction in which the product moves. Poonam et al. (2022) developed a peeler consisting of an aluminium drum mounted on a rotating disc. The onions were first cut and then washed for 10 min; subsequently, they were air-dried for 1–2 min to remove excess water and then placed in the peeler. This type of system still requires a large number of workers to obtain the final product. Moreover, the use of water in large amounts increases the risk of rotting because when water penetrates the tail of the spring onions, it alters the product and reduces its shelf life. To address this problem, a novel processing line that uses compressed air to clean the onions was developed. It was equipped with a single-blade cutting system with an adjustable position and a nebulisation system that prolongs the maintenance of freshness until consumption, while reducing the risk from exposure to large quantities of water.

Figure 1. Commercial onion-processing plant

2. Materials and Methods

2.1. Structure of the system

A system was designed to address the aforementioned problems, and its schematic view is shown in Figure 2. It includes a conveyor-belt-based handling system, capable of continuously transporting the spring onions towards a compressed-air cleaning system to remove tunics and soil. This is followed by a cutting and washing system that uses the nebulisation technique.

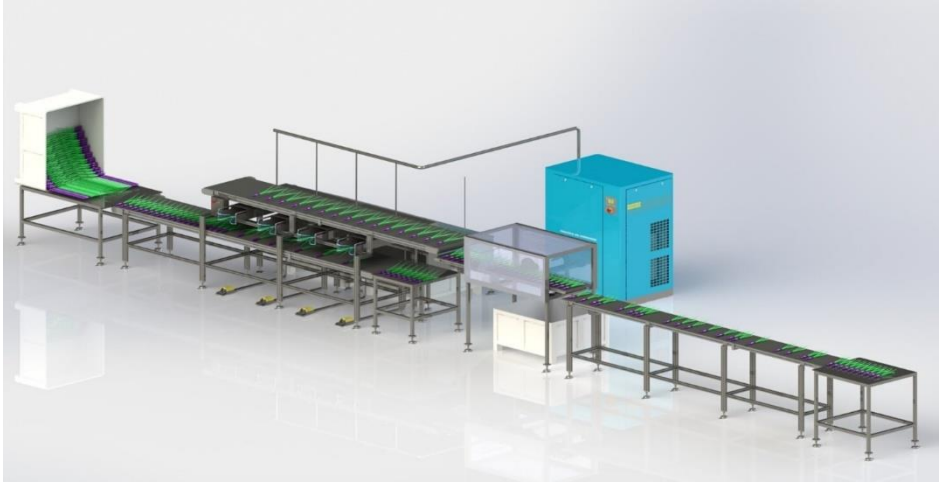

Figure 2. 3D drawing of the processing plant

The processing cycle (Figure 3) begins with the unloading of the boxes arriving from the collection site to the transport line, comprising smooth rubber conveyor belts (A), by means of a special tipper. Therefore, the spring onions arrive well-aligned at the cleaning stations, which operate with compressed air. The pneumatic system (B) consists of a compressed air production unit with a minimum output of 7000 Nl min^{-1} and a steel compressor outlet pipe with a minimum diameter of DN32. The inlet pipe of the compressed air management valve is made of steel with a minimum diameter of DN15. The 3/2 NC monostable pneumatic pedal valves have a progressive flow with a maximum flow of 1200 Nl min^{-1} at 6 bar; the air flow can be managed through these valves depending on the requirements. These values were obtained by considering

two main factors, namely, pressure drop and air losses, based on the following equation:

$$D = \sqrt{\frac{4 \cdot p_a \cdot L}{\pi \cdot p_u \cdot v_{eff}}} \; [m] \tag{1}$$

where:
D= initial diameter
p_a= suction pressure
p_u= compressor output pressure
v_{eff}= effective air velocity

The effective air velocity is expressed as follows:

$$v(eff) = \frac{p_a}{p_u} \cdot \frac{T_c}{T_a} \cdot \frac{Q}{\frac{\pi \cdot D^2}{4}} \; [m\, s^{-1}] \tag{2}$$

where:
Q= air flow rate
T_c= temperature of compressed air
T_a= room temperature

Subsequently, the distributed pressure drops at the individual straight sections were calculated using the following equation:

$$\Delta P = \lambda \cdot \rho \cdot \frac{v^2 L}{2D} \; [Pa] \tag{3}$$

where:
ΔP= drop in pressure [Pa]
λ= coefficient of friction of air movement
ρ= compressed air density [kg m^{-3}]
v= flow velocity
D= internal pipe diameter [m]
L= pipe length [m]

Simplified experimental equations are often used in research. In this study, the following equation was applied:

$$\Delta P = 1.6 \cdot 10^8 \cdot \frac{Q^{1.85} L}{d^5 p} [Pa] \tag{4}$$

where:
ΔP= drop in pressure [Pa]
Q= air flow rate [$m^3\, s^{-1}$]
d= internal pipe diameter [mm]
L= pipe length [m]
p= compressed air pressure [bar]

The cleaning block with pneumatic nozzles (Figure 4) comprises four semi-rigid tubes (Exair model 9268) that can be positioned by the operator; the spring onion to be processed is placed between the tubes. At the ends of the tubes, nozzles with a minimum blowing force of 360 g are located at a distance of 300 mm (Exair model 1011SS). Owing to their particular shape, the nozzles create a cone that drags in the air present in the atmosphere and amplifies the flow that reaches the spring onions. The number and arrangement of the nozzles ensure that the airflow cones act over the entire surface of the spring onions. Finally, varying the position of

the nozzles widens or narrows the area in which the spring onions can be cleaned.

At this stage, the spring onions are picked manually by the operators and positioned corresponding to the pneumatic nozzles activated by the foot pedal. Here, the cleaning residue is dragged by the air flow through a secondary duct into a special container positioned on the side (C) to prevent it from spreading. The operators then place the clean spring onions, that is, free of husks and soil, on a second conveyor belt (D), which takes them to the next stage of cutting and washing (E).

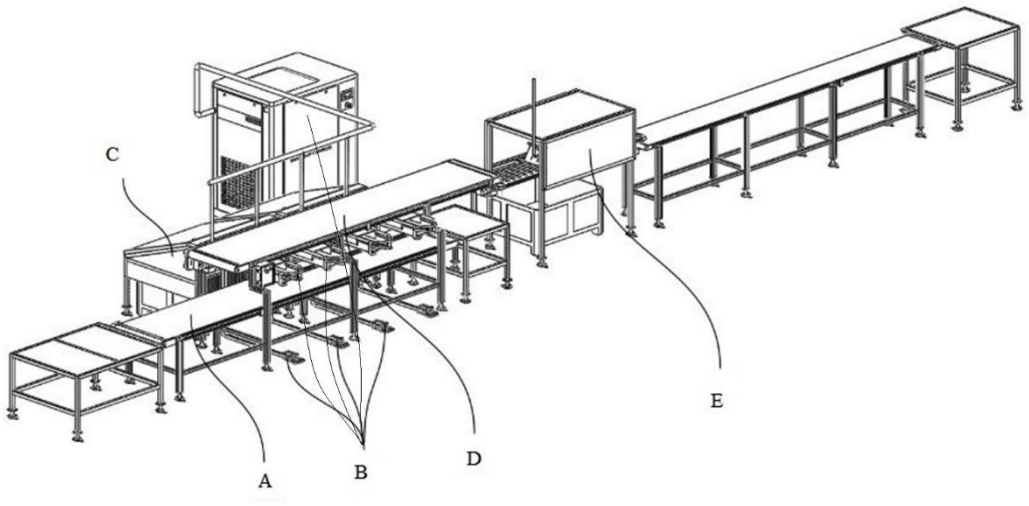

Figure 3: Processing flow. A) Conveyor belt; B) pneumatic pedal drive; C) container for collecting processing waste; D) second conveyor belt; E) cutting, washing, and drying block

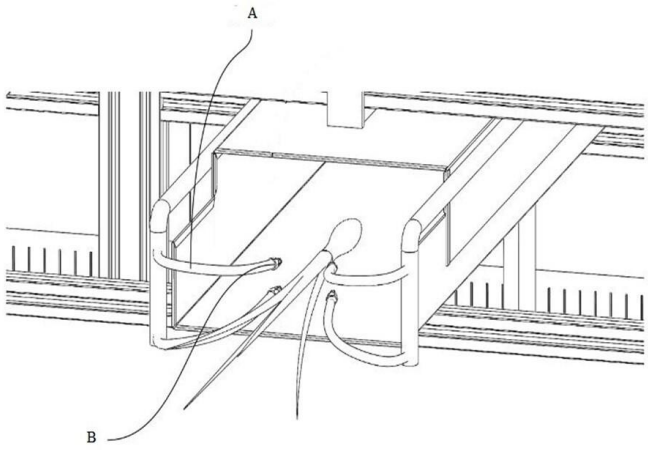

Figure 4. Pneumatic cleaning station. A) Semi-rigid hoses; B) nozzles

For the subsequent cutting and washing phases, the spring onions are moved along the second conveyor belt towards a processing block (E) that is not accessible to operators for safety reasons. The block consists of a 40 × 40 mm tubular structure and plexiglass panels. Inside this block, to maintain the freshness of the product but prevent water from entering the tails, the spring onions are humidified using nozzles having a

flow rate of 1 L min^{-1} at 2 bar (Lechler series 490.403) and placed at the top with respect to the forward movement. Then, to meet production specifications, the spring onion tails are cut by using a single-tooth blade with an adjustable position (Figure 5).

Figure 5. Cutting blade

Made from stainless steel, the cutting blade has a diameter of 300 mm and a rotation speed of 200–250 rpm and is coupled to a conveyor belt with adjustable feed speed. The precise number of revolutions combined with a suitable feed speed can help to exploit the onion's inertia for a clean decisive cut. Another technical solution is adopted to make the cutting system adjustable and versatile depending on the dimensional characteristics of the product. This solution involves manual adjustment of the height of the cutting blade with a groove system to manage the effect of the contact of the rotating blade on the tail (Figure 6).

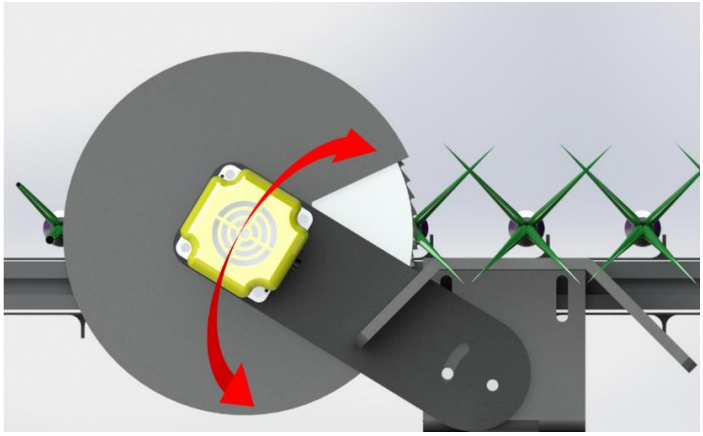

Figure 6. Blade height adjustment device

The final part of the processing line consists of an additional conveyor belt that allows operators to manually refine the product and send it to the subsequent weighing and packaging stages. These operations are then performed independent of the prototype system by using other machines already present in the facility.

3. Conclusions

As the market demand for PGI-labelled Tropea red onions is high, the lack of specialised machinery for processing these onions in the post-harvest phase should be addressed. A prototype machine, which is currently under construction, is proposed herein as a practical solution for increasing the productivity of the spring onion supply chain. The proposed machine prevents the rapid rotting of onions because it can eliminate the use of large amounts of water, which can become stagnant in the tails of the onions. Thus, the use of compressed air can extend the shelf life of the product by a few days, thereby opening up new and interesting economic prospects for operators in the sector.

Acknowledgements

This paper has been funded by "Fondo Europeo Agricolo per lo Sviluppo Rurale: l'Europa investe nelle zone rurali. PSR Calabria 2014-2020 Reg. UE n. 1305/2013 – DDG n. 3601/2018 Misura 16 Intervento 16.02.01 Progetto "Eccellenza Rossa" CUP J22C22000460005.

References

Commission Regulation (EC) No 284/2008 of 27 March 2008 registering certain names in the Register of protected designations of origin and protected geographical indications (Lingot du Nord (PGI), Cipolla Rossa di Tropea Calabria (PGI), Marrone di Roccadaspide (PGI))

Bernardi, B., Zimbalatti, G., Proto, A.R., Benalia, S., Fazari, A., Callea, P., 2013. Mechanical grading in PGI Tropea red onion post harvest operations. Journal of Agricultural Engineering, 44 (e63), 317-322, http://dx.doi.org/10.4081/jae.2013.s2.e63

Bernardi, B., Messina, G, Cilea, I., Neri, A., Sbaglia, M., Abenavoli, L.M.M., Zimbalatti, G., 2024. Assessment of Mechanical Damage to Tropea Red Onion PGI during Processing. In *Networks, Markets & People: Communities, Institutions and Enterprises towards post-humanism epistemologies and AI challenges*. Reggio Calabria, Italy, May 22-24. Lecture Notes in Networks and Systems (In Press)

Poonam, Manisha Verma, Raja Ram Bunker and Subhita Kumawat (2022). Post-Harvest Management in Onion: Deserve Concern. Biological Forum – An International Journal, 14(4a): 608-612

Effect of maltogenic-amylase and tamarind paste mixture on the nutritional composition of bread

Musliu Olushola Sunmonu [a]*, Mayowa Saheed Sanusi[a], AbdulKareem Bamidele Bello[a], Aishat Teni Ahman[a], Islamiyat Dolapo Jimoh[a], Omoniyi Akinnusi Friday[a]

[a]Department of Food Engineering, University of Ilorin, Ilorin, Nigeria.

*Corresponding Author: Sunmonu.mo@unilorin.edu.ng

Abstract

The incorporation of blends of maltogenic-amylase and tamarind paste in dough could serve a possible potential for improving bread quality. This study aimed to evaluate the effect of varying proportions of maltogenic-amylase and tamarind paste on the nutritional quality of bread. The proximate composition, minerals (calcium, magnesium, potassium and phosphorus), vitamin C and total phenolic content were determined using standard procedures. Maltogenic amylase and tamarind paste at varying proportions were interacted using a central composite design of response surface methodology while Pareto plot was used to identify the most significant factor. The moisture content of the bread ranged from 26.83 to 34.58%, fat (2.29 – 3.49%), fibre (0.42-0.64%), ash (2.47-3.53%), protein (12.02-18.56%) and carbohydrate (45.24 – 50.13%). The calcium content ranged from 135.63 to 164.25 mg/100g, magnesium (112.38 – 128.42 mg/100g), potassium (210.22 – 228.55 mg/100g), phosphorus (60.15 – 75.25 mg/100g). The total phenolic content of the bread ranged from 120.64 – 145.18 mg GAE/g and Vitamin C from 11.56 to 16.55 mg/100g. The linear effect of maltogenic-amylase exerted a more significant influence on the nutritional composition of the bread compared to tamarind paste. The findings from this study underscore the potential for optimizing bread quality through the strategic incorporation of maltogenic-amylase and tamarind paste.

Keywords: Bread, Maltogenic amylase, Tamarind, Nutritional composition

1. Introduction

Bread is a staple food in human diet with its consumption dating back to the ancient Egypt (Carocho *et al*., 2020). Bread is consumed throughout the world in various form and shape with average consumption of 70 kg per year capita (Gębski *et al*., 2019; Carocho *et al*., 2020). It is a fermented confectionary product made mostly from raw materials including wheat flour, water, yeast, and salt and processes such as mixing, kneading, proofing, shaping, and baking. Bread can be produced from varieties of cereals namely maize, rice, barley, sorghum, millet, oats, rye and others, however the most widely accepted cereal for bread is wheat. Due to several complex reaction that occur during the storage of bread which is referred to staling and the short shelf life of bread, researchers has investigated several ways of improving bread quality and extending the shelf life of bread. Chemicals used in the production of bread are known to pose several health risk, such as potassium bromate may cause some forms of cancer (Kornbrust *et al.,* 2012) and azodicarbonamide can causes allergic reactions (Arts and Kimberly, 2017). The incorporation of enzyme such as maltogenic-amylase and tamarind paste as an alternative to the chemical compound employed in the production of bread may improve the quality and extend the shelf life.

The use of enzymes in commercial applications has increased in recent years as consumers demand bakery products with more natural sounding ingredients. Maltogenic amylase is an enzyme mainly produced by alpha amylase and belonging to the member of the glycoside hydrolase family 13. It is a primary enzyme responsible for starch degradation and widely used to extending the shelf life of baked product, improves its elasticity, and preserves its flavor without affecting dough processing (Liu *et al*., 2023). According to Korompokis *et al*. (2021), maltogenic-amylase liberates maltose from the non-reducing ends of starch polymers and thereby results in a significant shortening of the outer amylopectin side chains which, consequently, are less prone to retrograde during storage of baked product.

Tamarind (*Tamarindus indica*) is an arboreal fruit which belongs to the family leguminosae. It is a podded fruit which contains pulp, seed, fiber and shell. According to Joshi *et al*. (2023), tamarind tree is a multifunctional tree whose all parts are valuable either medicinally or nutritionally. A tamarind fruit contains 55% pulp, 34% seeds, 11% shell and fiber (Muzaffar and Kumar, 2017). The tamarind pulp is highly regarded as a good source of B-vitamins, high in

phenolic content and mineral which include potassium, calcium, phosphorus, magnesium and sodium while the seed is rich in protein, amino acid and some major sugar such 20% pentose, 17-35% mannose and 11-80% glucose (Banu, 2018; Nagar *et al.,* 2022). Several research have been done on the improvement of bread quality and extending the shelf life as reported by (Zhang *et al.,* 2019; Bender and Schönlechner, 2020; Parenti *et al.,* 2020; Fratelli *et al.,* 2021; Goel *et al.,* 2021). However, literature is sparse on effect of maltogenic-amylase and tamarind paste mixture on the nutritional composition of bread. Therefore, this study aims to evaluate the effect of varying proportions of maltogenic-amylase and tamarind paste mixture on the nutritional quality of bread.

2. Materials and Methods

2.1 Materials

Wheat flour and maltogenic amylase used for this study was obtained from Flour mill of Nigeria and a chemical laboratory, respectively in Lagos, Nigeria. While the sugar and salt were obtained from Dangote Company, Lagos, Nigeria. Other ingredient for bread baking such as oil, instant dry yeast and margarine were obtained from a confectionaries store in Ilorin, Nigeria. Tamarind fruit was purchased from a local market in Ilorin, Nigeria.

2.2 Methods

2.2.1 Tamarind paste production

The tamarind paste was prepared by soaking tamarind pulp in water for 45 minutes to soften the pod. And then gently mashing the softened pulp with mortar and pestle to release paste from the fibers and seeds. The paste was then strained through a sieve to remove fibers and seeds. The straining was done in batches. The strained paste was cooked for 75 minutes over medium heat to evaporate the water and thicken it to the desired consistency. The paste was then leave to cool after which it was packaged and stored in a refrigerating condition. Figure 1 shows the flowchart involved in the production of tamarind paste.

2.2.2 Response surface experimental design

Central composite design of Response Surface Methodology was used to study the effect of maltogenic-amylase and tamarind paste mixture on the nutritional composition of bread using Design Expert version 13, UK. Table 1 shows the experimental outline for the interaction of maltogenic-amylase and tamarind paste mixture on the nutritional composition of bread.

Table 1: Experimental outline for the effect of maltogenic-amylase and tamarind paste mixture on the nutritional composition of bread

Samples	Tamarind Paste (g)	Maltogenic-amylase (g)
A	0	0
B	100	0
C	0	15
D	100	15
E	0	7.5
F	100	7.5
G	50	0
H	50	15
I	50	7.5

2.2.3 Production of Bread

The dough for the tamarind and enzyme mixture bread were prepared by weighing the dry ingredients; 1500g of wheat flour, 250g of sugar, 20g of yeast, 25g of salt and alpha-amylase (as indicated in the experimental design) and weighing of the wet ingredients; 50g of margarine, 25g of oil, 784g of water and tamarind paste (as indicated in the experimental design). The dry ingredients was mixed with the wet ingredients until a dough was formed. The dough was kneaded by

locally fabricated kneading machine to develop the gluten. The dough was shaped into portions and placed in greased pans. The pans were covered with aluminium foil before they were placed in the proofer. The dough was proofed for 1 hour at a temperature of 35°c before it was baked in a rotary oven for one and half hour at a temperature of 130°c. The bread were checked at intervals for doneness after which they were brought out of the oven and allowed to cool and packaged in a transparent nylon. Bread dough for the control sample batch was produced using a similar approach but with exception of tamarind paste and enzyme. Bread dough was prepared for nine different batches; Sample A is the control sample without tamarind or enzyme; Sample B contains 100g of tamarind and no enzyme; Sample C contains no tamarind and 15g of enzyme; Sample D contains 100g of tamarind and 15g of enzyme; Sample E contains no tamarind and 7.5g of enzyme; Sample F contains 100g of tamarind and 7.5g of enzyme; Sample G contains 50g of tamarind and no enzyme; Sample H contains 50g of tamarind and 15 of enzyme, Sample I contains 50g of tamarind and 7.5g of enzyme.

2.2.4 Proximate composition analysis

Proximate composition analysis (Moisture content, crude fat, fiber, ash, protein and carbohydrate) was performed on the bread samples using the standard method of Association of Analytical Chemists (AOAC, 2010).

2.2.5 Mineral composition

For the mineral analysis of the bread four minerals were analyzed namely calcium, magnesium, phosphorus, and potassium. Atomic Absorption Spectroscopy (AAS) was used to determine the concentration of the specific minerals in the bread by measuring the absorption of light at characteristic wavelengths.

2.2.6 Determination of Vitamin C

Chemically, vitamin C was measured using a 2,6-dichlorophenolindophenol solution titration technique. 5 g of the material was pulverized for each test in a mortar and pestle along with some acid-washed sand and 10% TCA solution. After filtering the extract, the leftover material was thoroughly cleaned with a TCA solution until it was colorless. 100 mL of the total volume was created. Three conical flasks each held 10 mL of the solution, which was titrated with indophenol solution until a pink color emerged. The results were then used to calculate vitamin C (Shitanda *et al.*, 2006).

2.2.7 Determination of Total Phenol Content (TPC)

Phenolic compounds' content was determined in triplicate by the Folin-Ciocalteu spectrophotometric method, described by Singleton & Rossi (1965), with some modifications. A 0.5 mL aliquot from each extract was added to 2.5 mL Folin-Ciocalteu's reagent solution (0.2 M) (Alphatec, USA). The solution was left to rest for 5 min before being added with 2 mL of 7.5% p/v sodium carbonate (Impex, Brazil). The resulting color absorbance was measured at 760 nm in a UV-Vis spectrophotometer after 15 min reaction time at 40 ºC. To obtain the phenolic compounds' concentration data, a calibration curve was constructed using different concentrations of gallic acid (10 to 70 mg·L-1). Total phenolic compounds' content was expressed in mg of gallic acid equivalents per L of sample (EAG·L-1 of sample).

2.2.8 Statistical Analysis

All the experiments were conducted in three replications in a completely randomized design. The data was analysed by analysis of variance using Statistical Package for the social sciences (SPSS version 22). Mean were significantly different and is separated by the least significant difference. Significance is accepted at $p<0.05$.

3 Results and Discussion

3.1 Effect of maltogenic-amylase and tamarind paste mixture on proximate composition of bread

Moisture content is important composition of food that helps in establishing proper storage conditions. The percentage moisture content ranged from 26.83% - 35.21% (Figure 1). All values are significantly different at $p<0.05$. Sample C (0g of tamarind paste and 15g of enzyme) had the lowest moisture content (26.3%) while sample G (50g of tamarind paste and 0g of enzyme) had the highest moisture content (35.21%). The decrease in moisture content of sample C may be attributed to the incorporation of maltogenic-amylase which breaks down complex carbohydrates into simpler sugars which absorb more water during dough formation. This result aligns with the findings of Ahmad *et al*. (2014), who also reported a decrease in moisture content of baked product with the incorporation of enzyme as a means of improving the texture and extending the shelf life of the products.

Figure 1 shows that the percentage fat content ranges between 2.29% and 3.49%. All values are significantly different at $p<0.05$. The minimum fat content was observed in sample E (0g tamarind paste and 7.5g enzyme) while the maximum fat content was observed in sample H (50g tamarind paste and 15g enzyme). The increase in fat content of sample H may be attributed to the reaction between tamarind and enzyme. This could be as a result of the enzymatic

action on fats, which can lead to fat modification or breakdown. This result corroborates with the findings of Uthai and Chetyakamin, (2020), who reported that the fat content of products can be improved through enrichment with tamarind.

The fibre content ranged from 0.42% - 0.64% as depicted in Figure 1. All values are significantly different at $p<0.05$. Sample B (100g of tamarind paste and 0g of enzyme) had the lowest fibre content while sample H (50g of tamarind paste and 15g of enzyme) had the highest fibre content of all bread samples. The increase in fiber content may be attributed to the presence of dietary fiber naturally occurring in tamarind paste, as well as the enzymatic action of maltogenic amylase potentially breaking down starches into resistant starches, which act as dietary fiber in the final product. Similar result was reported by Dahiya *et al*. (2020), who stated that the fibre content of baked products can be improve by incorporation of enzyme as a means of enriching the bread.

Ash content refers to the inorganic residue that remains after burning of the organic matter in a food sample. Figure 1 shows that the effect of the additives on the ash content of the bread ranged from 2.47% - 3.53%. All values are significantly different at $p<0.05$. Sample B (100g of tamarind paste and 0g of enzyme) had the lowest ash content while sample H (50g of tamarind paste and 15g of enzyme) had the highest ash content. The decrease in the ash content of sample B compare to sample H may be attributed to the combine effect of the tamarind paste and maltogenic amylase, however it has been reported that tamarind contains a high proportion of minerals which can be converted to ash content during baking. Therefore, this result contradicts the findings of Peluola-Adeyemi *et al*. (2021), who reported that increase in ash content of sample with high minerals will increase the ash content of the food sample.

Protein cotains amino acids which are beneficial for the daily body functioning. Figure 1 indicated that the percentage protein content ranges between 12.02% and 18.56%. All values are significantly different at $p<0.05$. Sample B (100g of tamarind paste and 0g of enzyme) had the lowest protein content while sample H (50g of tamarind paste and 15g of enzyme) had the highest protein content of all bread samples. The observed decrease in protein content of sample B could potentially be due to the higher tamarind paste content, tamarind contain proteases which break down proteins. An increase in tamarind content could lead to increased protease activity leading to decrease in the overall protein of sample B. This result contradicts the findings of Tangariya and Srivastava, (2022), who reported that the protein content of a baked product can be increased with the incorporation of tamarind.

Carbohydrate provides major source of energy in the human diet. The percentage carbohydrate content ranged from 45.24% - 50.13% in Figure 1. All values are significantly different at $p<0.05$. The sample with the highest carbohydrate content was sample A which is the control (0g of tamarind paste and 0g of enzyme) while the bread sample with the lowest carbohydrate content was sample G (50g of tamarind paste and 0g of enzyme). The decrease in the carbohydrate content of sample G may be attribute to the reaction of tamarind leading to the production of sugar and fibre, however since bread is a carbohydrate-rich itself due to it flour content leading to high carbohydrate content for sample C. Similar result was reported by Uthai and Chetyakamin, (2020), who observed a similar trend, suggesting that minor components in the flour might be more noticeably affected by tamarind addition compared to major components like carbohydrates. Since wheat flour boasts a significantly higher carbohydrate content than tamarind, the overall impact of tamarind on the final bread's carbohydrate content might be minimal. As illustrated in Figure 2a, 2b, 2c, 2d, 2e and 2f it shows that the several interactions are significant at $p<0.05$, however linear interaction of enzyme has the highest significant for percentage moisture, fibre, ash, protein while quadratic interaction of enzyme has the highest significant for percentage fat and carbohydrates.

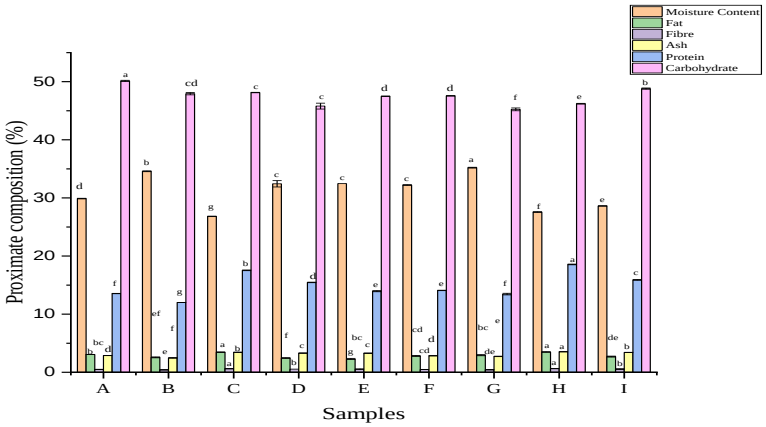

Figure 1: effect of maltogenic-amylase and tamarind paste mixture on proximate composition of bread.
Mean values and superscripts with dissimilar letters along the same column are significantly different at p <0.05
Sample A is the control (without tamarind paste or enzyme), Sample B containing 100g of tamarind paste and 0g of enzyme, Sample C containing 0g of tamarind paste and 15g of enzyme, Sample D containing 100g of tamarind paste and 15g of enzyme, Sample E containing 0g of tamarind paste and 7.5g of enzyme, Sample F containing 100g of tamarind paste and 7.5g of enzyme, Sample G containing 50g of tamarind paste and 0g of enzyme, Sample H containing 50g of tamarind paste and 15g of enzyme, Sample I containing 50g of tamarind paste and 7.5g of enzyme.

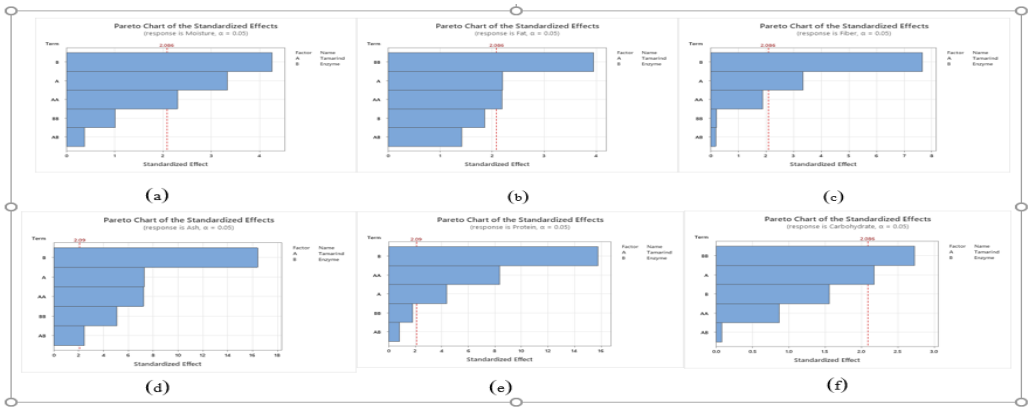

Figure 2: Pareto chart for the effect of maltogenic-amylase and tamarind paste mixture on the proximate composition of bread (a) Moisture (b) Fat (c) Fibre (d) Ash (e) Crude protein (f) Carbohydrate.

3.7. Effect of maltogenic-amylase and tamarind paste mixture on minerals content of bread

The calcium content of the bread ranges between 135.63 to 164.25 mg/100g as shown in Figure 3. All values are significantly different at $p < 0.05$. The highest calcium content was attained at sample H, 50g tamarind paste and 15g enzyme while the least calcium content was attained at sample B, 100g tamarind paste and 0g of enzyme. The increase in calcium content could be attributed to the incorporation of calcium-rich compounds from the maltogenic amylase and the lower dilution effect of tamarind paste, allowing for a higher concentration of calcium per gram of dough. The magnesium content of the bread ranges between 112.38 to 128.42 mg/100g as shown in Figure 3. The highest magnesium content was attained at sample H, 50g tamarind paste and 15g enzyme while the least magnesium content was attained at sample B, 100g tamarind paste and 0g of enzyme. All values are significantly different at $p<0.05$. The increase in magnesium content may be attributed to the effect of maltogenic amylase, which could enhance the bioavailability of magnesium, leading to a higher concentration of magnesium per unit weight of the bread. The potassium content of the bread ranges between 210.22 to 228.55 mg/100g as shown in Figure 3. All values are significantly different at $p< 0.05$. The highest potassium content was attained at sample H, 50g tamarind paste and 15g enzyme while the least potassium content was attained at sample B, 100g tamarind paste and 0g of enzyme. The decrease in potassium content of sample B may be attributed to a dilution effect which result in lower concentration of potassium while the increase in sample H could be attributed to the presence of maltogenic amylase, which might enhance potassium bioavailability through enzymatic processesThe phosphorus content of the bread ranges between 60.15 and 75.25 mg/100g as shown in Figure 3. All values are significantly different at $p< 0.05$. The highest phosphorus content was attained at sample H, 50g tamarind paste and 15g enzyme while the least phosphorus content was attained at sample B, 100g tamarind paste and 0g of enzyme. The increase in phosphorus contain may be attributed to the combine effect of tamarind and enzyme, tamarind contains phosphorus in minute quantity and enzymes helps to break down phytic acid which may lead to slight increase in bioavailability of phosphorus therefore increasing the overall phosphorus content of the bread. Figure 4 shows that linear interaction of enzyme has the most significant influence on percentage minerals of bread. This result corroborates with the findings of Dahiya *et al*. (2020), that maltogenic amylase can serve as a means of improving the available minerals in bread making. Also, the study contradicts the findings of Uthai and Chetyakamin, (2020), who reported that the incorporation of tamarind will significantly increase the minerals content of the food.

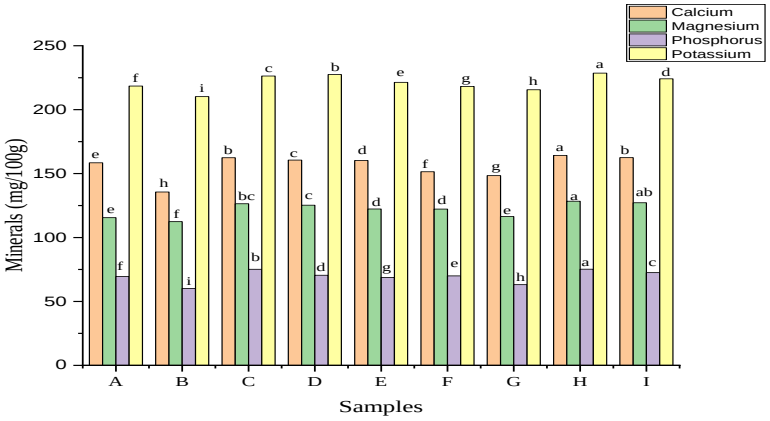

Figure 3: effect of maltogenic-amylase and tamarind paste mixture on minerals content of bread

Mean values and superscripts with dissimilar letters along the same column are significantly different at $p<0.05$.

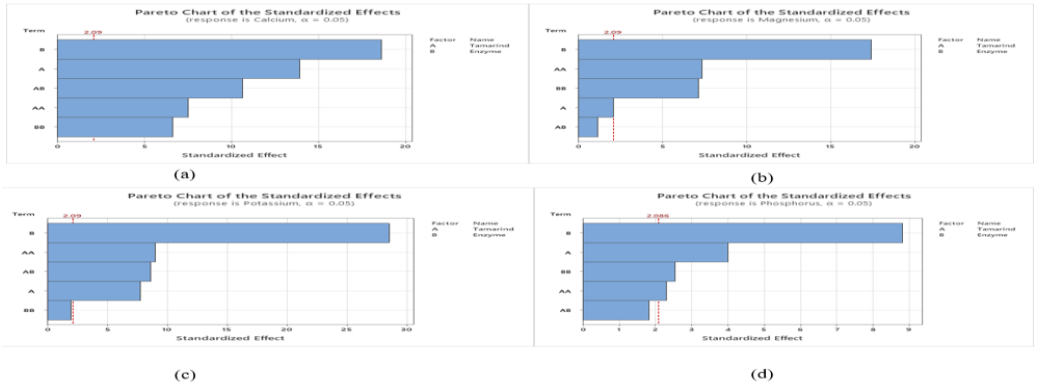

Figure 4: Pareto chart for the effect of maltogenic-amylase and tamarind paste mixture on the mineral content of bread (a) calcium (b) magnesium (c) potassium (d) phosphorus

3.8. Effect of maltogenic-amylase and tamarind paste mixture on vitamin C content of bread

The vitamin C content of the bread ranged between 11.56±0.03 and 16.55±0.04 mg/100g Table 2. All values are significant different at $p<0.05$. The high vitamin C content of the bread was obtained in sample H produced from 50 g of tamarind and 15 g of alpha amylase while the least was obtained in sample A which is the control sample with no tamarind or alpha amylase. It was observed that enrichment of the bread will increase it vitamin C content. As depicted in Figure 3a, the linear interaction of enzyme, quadratic interaction of tamarind and interaction of tamarind and enzyme has significant effect on the vitamin C content of the bread. The linear interaction of enzyme was observed to have the highest significant effect on the vitamin C content of the sample. The increase in the vitamin C content may be as a result of the synergistic effect of the tamarind and enzyme, which may enhance the preservation and bioavailability of vitamin C through reduced oxidative degradation and improved enzymatic activity during processing. Also, natural antioxidant properties of tamarind may contribute to vitamin C content in an enriched sample. This result corroborate with the findings of Kowalczewski *et al*. (2021) that enzymes can break down complex molecules into simpler forms, potentially increasing the availability of nutrients like vitamin C. Also, Binou *et al*. (2021) reported that the enrichment of product with tamarind contribute to the increment in the vitamin C content.

3.9. Effect of maltogenic-amylase and tamarind paste mixture on moisture content of bread

The measurement of total phenol content in food product is crucial as it serve as an indicator of their potential health benefit, with foods boasting high total phenol content generally regarded as more nutritious and beneficial for consumer well-being. The total phenol content of the bread under the effect of maltogenic-amylase and tamarind paste mixture ranged from 120.64±0.02 to 145.18±0.11 (Table 2).

Table 2: Effect of maltogenic-amylase and tamarind paste mixture on vitamin C and total phenol content of bread.

Samples	Vitamin C (mg/100g)	TPC (mg GAE/g)
A	11.56±0.03^{i}	141.12±0.10^{c}
B	12.04±0.02^{h}	120.64±0.02^{h}
C	15.23±0.02^{b}	142.33±0.44^{b}
D	13.53±0.04^{d}	140.21±0.22^{d}
E	12.49±0.03^{f}	138.31±0.21^{e}
F	12.60±0.02^{e}	135.45±0.28^{f}
G	12.12±0.01^{g}	130.27±0.26^{g}
H	16.55±0.04^{a}	145.18±0.11^{a}
I	14.25±0.02^{c}	142.56±0.03^{b}

Means with the same superscript along the column and row do not differ significantly according to DMRT at $p \leq 0.05$

The highest total phenol content was found at sample H produced from 50 g of tamarind and 15 g of alpha amylase while the lowest was found at sample B produced from 100 g of tamarind only. The linear effect of enzyme had the most impactful effect on the total phenol content (Figure 3b) and this could be attributed to the synergistic effect of enzyme activity which facilitate the release of phenolic compounds from tamarind, leading to higher phenol extraction. Also, the linear interaction of enzyme, linear interaction of tamarind, quadratic interaction of tamarind, quadratic interaction of enzyme and interaction of tamarind and enzyme. All values are significant at $p<0.05$ on the total phenol content of the bread. This result align with the findings of Drakula *et al*. (2021) that the antioxidant capacity of the product melanoidins increased due to the enrichment with tamarind and enzyme, which can be partially attributed to the bound phenolics.

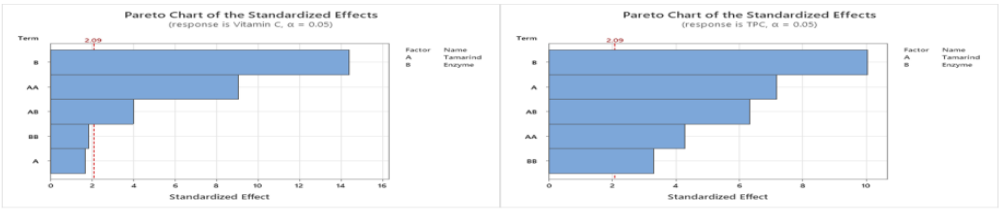

(a) (b)

Figure 3: Pareto chart for the effect of maltogenic-amylase and tamarind paste mixture on the Vitamin C and TPC of bread.

4. Conclusions

This research investigated the effect of maltogenic-amylase and tamarind paste mixture on the nutritional composition of bread. The findings reveal variations in proximate composition (moisture, fat, fiber, ash, protein, and carbohydrate) ranging from 26.83% to 35.21%, 2.29% to 3.49%, 0.42% to 0.64%, 2.47% to 3.53%, 12.02% to 18.56%, and 45.24% to 50.13%, respectively. The study identified an optimal combination of 50g tamarind paste and 7.5g enzyme for most favorable effects on the bread's nutritional content. While the best outcome for total phenol content ranged from 120 to 146 mg GAE/g, and vitamin C content ranged from 11.56 to 16.55 mg/100g. Moreover, the mineral composition varied across samples, with sample H (50g tamarind paste and 15g enzyme) demonstrating the highest mineral content, including calcium (135.63 to 164.25 mg/100g), magnesium (112.38 to 128.42 mg/100g), phosphorus (60.15 to 75.25 mg/100g), potassium (210.22 to 228.55 mg/100g, while maintaining acceptable levels of other nutrients. Conclusively, this research demonstrates that incorporating a maltogenic-amylase and tamarind paste mixture can influence the nutritional profile of bread. For a well-rounded nutritional profile with increased fiber, minerals, vitamin C, and phenols, a combination of 50g tamarind paste and 15g enzyme appears to be most favorable.

References

Ahmad, Z., Butt, M. S., Ahmed, A., Riaz, M., Sabir, S. M., Farooq, U. and Rehman, F. U. (2014). Effect of Aspergillus niger xylanase on dough characteristics and bread quality attributes. *Journal of food science and technology*, *51*, 2445-2453.

Arts, J. and Kimber, I. (2017). Azodicarbonamide (ADCA): A reconsideration of classification as a respiratory sensitiser. *Regulatory Toxicology and Pharmacology* 89, 268-278.

Association of Offcial Analytical Chemist AOAC, *Offcial methods of Analysis of Association of Offcial Analytical Chemists International*, 18th edn. (Published by AOAC International, Gaithersburg, 2010)

Banu, M. S. (2018). Chemistry of tamarind. *Tamarind Science and Technology*, 33 -40.
Bender, D., & Schönlechner, R. (2020). Innovative approaches towards improved gluten-free bread properties. *Journal of Cereal Science*, *91*, 102904.
Binou, P., Yanni, A. E., Stergiou, A., Karavasilis, K., Konstantopoulos, P., Perrea, D. & Karathanos, V. T. (2021). Enrichment of bread with beta-glucans or resistant starch induces similar glucose, insulin and appetite hormone responses in healthy adults. *European journal of nutrition*, *60*, 455-464.
Boshra, V. and Tajul, A.Y. (2013). Tropical fruits: A new frontier in the bakery industry. International Journal of Medical Sciences and Biotechnology, 1, 51-60
Carocho, M., Morales, P., Ciudad-Mulero, M., Fernandez-Ruiz, V., Ferreira, E., Heleno, S., ... & Ferreira, I. C. (2020). Comparison of different bread types: Chemical and physical parameters. *Food chemistry*, *310*, 125954.
Dahiya, S., Bajaj, B. K., Kumar, A., Tiwari, S. K., & Singh, B. (2020). A review on biotechnological potential of multifarious enzymes in bread making. *Process Biochemistry*, *99*, 290-306.
Drakula, S., Novotni, D., Mustač, N. Č., Voučko, B., Krpan, M., Hruškar, M., & Ćurić, D. (2021). Alteration of phenolics and antioxidant capacity of gluten-free bread by yellow pea flour addition and sourdough fermentation. *Food Bioscience*, *44*, 101424.
Fratelli, C., Santos, F. G., Muniz, D. G., Habu, S., Braga, A. R. C., & Capriles, V. D. (2021). Psyllium improves the quality and shelf life of gluten-free bread. *Foods*, *10*(5), 954.
Gębski, J., Jezewska-Zychowicz, M., Szlachciuk, J., & Sosicka- Gębski, M. (2019). Impact of nutritional claims on consumer preferences for bread with varied fibre and salt content. *Food Quality and Preference*, 76, 91-99.
Goel, S., Singh, M., Grewal, S., Razzaq, A., & Wani, S. H. (2021). Wheat proteins: a valuable resources to improve nutritional value of bread. *Frontiers in Sustainable Food Systems*, *5*, 769681.
Joshi, A. V., Urmila, A., Swapnil, G., and Shahrukh, S. (2023). Review on Tamarindusindica. *Journal of Pharmacognosy and Phytochemistry*, *12*(1), 303-308.
Kornbrust, B. A., Forman, T. and Matveeva, I. (2012). Woodhead Publishing. Applications of enzymes in bread making. In Bread making, 470-498.
Korompokis, K., Deleu, L. J., De Brier, N., & Delcour, J. A. (2021). Investigation of starch functionality and digestibility in white wheat bread produced from a recipe containing added maltogenic amylase or amylomaltase. *Food Chemistry*, *362*, 130203.
Kowalczewski, P. Ł., Gumienna, M., Rybicka, I., Górna, B., Sarbak, P., Dziedzic, K., & Kmiecik, D. (2021). Nutritional value and biological activity of gluten-free bread enriched with cricket powder. *Molecules*, *26*(4), 1184.
Liu, P., Ma, L., Duan, W., Gao, W., Fang, Y., Guo, L., ... & Cui, B. (2023). Maltogenic amylase: Its structure, molecular modification, and effects on starch and starch-based products. *Carbohydrate Polymers*, 121183.
Muzaffar, K., and Kumar, P. (2017). Tamarind-a mini review. *MOJ Food Processing & Technology*, *5*(3), 296-297.
Nagar, C. K., Dash, S. K., and Rayaguru, K. (2022). Tamarind seed: Composition, applications, and value addition: A comprehensive review. *Journal of Food Processing and Preservation*, *46*(10), e16872.
Parenti, O., Guerrini, L., Cavallini, B., Baldi, F., & Zanoni, B. (2020). Breadmaking with an old wholewheat flour: Optimization of ingredients to improve bread quality. *LWT*, *121*, 108980.
Peluola-Adeyemi, O., Abdus-Salaam, R., B., Obi, T. E. and Toyiemedo, N. C. (2021). *Quality Evaluation of Bread Produced from Wheat Flour using Avocado (Perseaamericana) Paste as Substitute, Journal.* Food. Stability 4 (1): 1-12.
Shitanda, D., and Wanjala, N. V. (2006). Effect of different drying methods on the quality of jute (Corchorusolitorius L.). *Drying Technology*, *24*(1), 95-98.
Singh, S., Mishra, D. S. and Singh, A. K. (2021). Tamarind (Tamarindus indica L.). *Tropical Fruit Crops Theory to Practical*, 610-631.
Tangariya, P., & Srivastava, S. (2022). Comparison of functional properties of tamarind kernel powder with whole wheat flour, lentil powder and evaluation of sensory and nutritional quality of tamarind kernel powder incorporated cookies. *The Pharma Innovation Journal. SP-11 (3)*, 18-22.
Uthai, N., & Chetyakamin, L. (2020). Effect of partial substitution of wheat flour with tamarind seed flour on physical, chemical, antioxidant and sensory properties of noodles. *African Journal of Food, Agriculture, Nutrition and Development*, *20*(4), 16063-16084.
Zhang, L., Li, Z., Qiao, Y., Zhang, Y., Zheng, W., Zhao, Y. & Cui, Z. (2019). Improvement of the quality and shelf life of wheat bread by a maltohexaose producing α-amylase. *Journal of cereal science*, *87*, 165-171.

Acceptance of cutting-edge technologies in viticulture: A students' perspective

Tetiana Pavlenko[a,*], Eva Gößwein[b,c], Dimitrios S. Paraforos[d], Megan K. Bartlett[e], Spyros Fountas[f], Jacob Kambuta[g], Francesco Marinello[h], George Papadopoulos[f], Leo Pichon[i], Bruno Tisseyre[i], Magnus Liebherr[b,c]

[a]Institute of Agricultural Engineering, University of Hohenheim, Garbernstr. 9, 70599, Stuttgart, Germany

[b]Chair of General Psychology: Cognition, Faculty of Computer Science, University of Duisburg-Essen, Forsthausweg 2, 47057 Duisburg, Germany

[c]Chair of Mechatronics, Faculty of Engineering, University of Duisburg-Essen, Forsthausweg 2, 47057 Duisburg, Germany

[d]Department of Agricultural Engineering, Hochschule Geisenheim University, Von-Lade-Str.1, 65366, Geisenheim, Germany

[e]Department of Viticulture and Enology, University of California, 595 Hilgard Ln, Davis, CA 95616, United States

[f]Department of Natural Resources Management and Agricultural Engineering, Agricultural University of Athens, Iera Odos 75, Athens 118 55, Greece

[g]Department of Land Management and Systems, Faculty of Agribusiness and Commerce, Poplars Building 007, PO Box 85084, Lincoln University, Lincoln 7647, Christchurch, New Zealand

[h]Department of Land, Environment, Agriculture and Forestry, University of Padova, Viale dell'Università 16, 35020 Legnaro, Italy

[i]ITAP, Univ.Montpellier, Institut Agro, INRAE, 2 Place P. Viala, 34060, Montpellier, France

*Corresponding author. Email: tetiana_pavlenko@uni-hohenheim.de

Abstract

A major push in technology development has brought a host of innovations for precision farming (PF). Sensors, information technologies, and site-specific applications are designed to make farming easier and deliver environmental and economic benefits. Acceptance of these new technologies is a key factor in their implementation. However, despite their rapid proliferation, farmers' reluctance to accept them is leading to low adoption rates. This is particularly true in traditional sectors such as viticulture.

Therefore, this study aims to understand the status of digital technology acceptance in viticulture. To investigate the current attitudes and visions of potential future farmers and/or future advisors, an online questionnaire was developed and distributed to students involved in viticulture studies. Germany, France, Italy, USA, New Zealand and Greece participated. A total of 95 complete responses were collected, of which 16 were excluded from further analysis due to a perceived lack of conscientiousness.

Four variables were used to measure their correlation with acceptance of PF technologies: climate change perceptions, technology commitment, adaptability, and trust in technology. All variables showed a significant correlation with the acceptance of PF technologies, with climate change perception, technology commitment, and adaptability demonstrating moderate correlations, while trust exhibited a weak correlation. According to the multiple regression analysis, four predictors explained 34.7% of the variance. Future steps may consider increasing sample size and involving other stakeholder groups such as farmers and/or researchers to confirm these results.

Keywords: precision viticulture, adaptability, technology acceptance, trust, technology commitment

1. Introduction

Precision farming (PF) has become more and more the center of interest in viticulture in recent years. Precision viticulture (PV) can play a crucial role in making on-farm management decisions and adapting the standard cultivation techniques based on the vineyard variability that exists within the field (Ammoniaci et al., 2021). Despite a wide range of available technologies and increasing research in the area of digital farming, the number of publications on PV is only 5% of the number of publications on PF (Ferro and Catania, 2023). This highlights the need to intensify efforts in order to strengthen knowledge dissemination as well as technology acceptance among different groups of stakeholders.

Tardaguila et al. (2021) provided a review of existing technologies in viticulture that might be used by wine growers in order to improve the efficiency of agricultural production systems and produce quality wines in economically viable and environmentally friendly ways. Usage of available technologies in winemaking requires fast and reliable data analysis and interpretation that creates a challenge of proper management at a winery level. To overcome the challenges that exist and reach a successful implementation of digital solutions, a collaborative approach between the value chain stakeholders is vital. Next to the challenges of the interoperability between systems and costs of investments, another significant challenge is connected to the lack of innovative mindset among industry stakeholders and resistance to change (Bastard and Chaillet, 2023).

Technology acceptance is pivotal for usage behavior as it profoundly impacts the readiness of individuals or organizations to embrace and incorporate new technological solutions into their workflows or daily practices. Various theories have been proposed to provide diverse insights into the adoption process, encompassing factors such as perceived usefulness, perceived ease of use, social influences, and individual characteristics. Among the most prominent theories are the Technology Acceptance Model (Davis, 1989), the Unified Theory of Acceptance and Use of Technology (Venkatesh et al., 2003), and the Diffusion of Innovations theory (Rogers Everett, 2003). Several studies explored the

influence of behavioral factors on adoption processes. Toma et al. (2018) investigated factors that influenced technology adoption in Scottish crop farming. The findings confirmed that among others, the perceived usefulness of information sources had an impact on technological adoption. In their study, Aubert et al. (2012) also focused on individual perceptions as drivers of PF technology adoption in Canada. As a result, they concluded that for a farmer to adopt a PF technology, a perception of usefulness and ease of use should be present. Venkatesh et al. (2003) described performance expectancy as a degree to which the user believed in the usefulness of using technology to reach gains in job performance. Based on the results, this variable appeared to be a determinant of the intention to use a technology. In the realm of PF, Mohr and Kühl (2021) proposed a modified model based on the Technology Acceptance Model and the theory of planned behavior (Ajzen, 1991) to explore the behavioral factors shaping the acceptance of artificial intelligence in agriculture. Building upon their study, our work endeavors to enhance the understanding of the factors influencing human perception of Cutting-Edge Technologies in Viticulture. Within the present exploratory study, we focus on aspects of technology commitment, adaptability, trust, and climate change perception to understand their impact on individuals' acceptance of PF technologies.

Technology commitment refers to the degree of dedication or attachment an individual has toward using technology. From the field of autonomous driving, we know that individuals who are highly committed to technology are more likely to embrace new tools and innovations, contributing positively to technology acceptance (Rainieri et al. 2023, Wicki et al. 2019). Adaptability measures an individual's ability to adjust to new situations and environments. In the context of PF technologies, adaptability reflects how easily individuals can adapt their practices to incorporate new digital tools and techniques (VandenBos 2015, van Dam and Meulders 2021). High levels of adaptability suggest a greater openness to change, which can facilitate the acceptance and integration of new technologies into existing practices. Trust in technologies refers to the belief or confidence that individuals have in the reliability, effectiveness, and safety of technologies (Gefen et al., 2003). Trust plays a crucial role in technology acceptance as individuals are more likely to adopt and use technologies that they perceive as trustworthy (Gößwein and Liebherr, under review). Climate change perception encompasses individuals' beliefs about the reality of climate change, the causes of climate change, and the consequences of climate change (Poortinga et al. 2019, van Valkengoed et al. 2021). In the context of PF technologies, we propose that climate change perception can influence technology acceptance by shaping individuals' perceptions of the relevance and importance of these technologies in addressing climate-related challenges.

This work goes beyond the already known classical Technology Acceptance Model putting the focus on the exploration of additional variables and their correlation with the acceptance of PF technologies. In addition to that, the novelty of this paper is also supported by the fact that the students enrolled in viticulture studies participated.

2. Methods

An online survey using the tool LimeSurvey was sent out to six institutions, where viticulture can be studied. The institutions were based in Greece, France, Italy, the United States of America (USA), New Zealand and Germany. The survey was available in both German and English languages and required approximately 15 minutes to complete. It included sections for demographic data, a brief explanation of PF, participants' indication of prior PF usage, and the questionnaires. Data collection was open for four months, from January 2024 until the end of April 2024. A total of 95 complete responses were collected, of which 16 were excluded from further analysis because of an alleged lack of conscientiousness as these participants gave a wrong answer to an attention check item. We used Jamovi software version 2.0.0.0 to analyze the data.

2.1. Measures

Technology Commitment

A short scale for technology commitment by Neyer et al. (2012) was implemented. The variable was found to correlate with technology usage behavior and technical experiences and is supposed to deliver a personality-psychological perspective on the matter of technology acceptance (Neyer et al., 2012). The scale was used in its validated form consisting of twelve items rated on a five-point Likert scale, e.g., *"I am very curious about new technical developments"*. The validity of the scale within our sample was good ($\alpha = .723$).

Adaptability

To assess adaptability, we used a validated scale (van Dam and Meulders, 2021) consisting of ten items rated on a five-point Likert scale. With this measurement, an overarching factor is captured referring to the individual tendency to handle new situations resiliently and with an open mind. It showed good validity in our sample ($\alpha = .802$).

Trust in Precision Farming

We measured technology trust via the trust in automation subscale (Körber, 2019), which consists of two items rated on a five-point Likert scale. In the instruction of the scale PF as a reference system was specified and explained*: "Precision Farming involves the use of new and emerging technologies, including sensors, to collect information and*

data on various parameters of the vines and the terroir that affect vines' growth.". Thereby, even participants with little or no practical experience in handling PF were able to rate their alleged trust in the technology. In our sample, the scale showed good validity (α = .737).

Climate Change Perception

A single-item scale was implemented to investigate participant's perceptions of climate change (van Valkengoed et al., 2021). It consists of five items, which each refer to one of the subdimensions of the long scale: reality, causes, valence of consequences, spatial-, and temporal distance of consequences. The items are rated on a seven-point Likert scale and the scale showed good validity within our sample (α = .752).

Acceptance of Precision Farming Technologies

We measured the acceptance of PF technologies using two items derived from prior research (Mohr and Kühl, 2021): *"I think that my interest in precision farming will increase until 2030"* and *"I think that I will never use precision farming."*. Responses were collected on a six-point Likert scale and ratings of the second item were reversed. Utilizing these items offered the advantage of capturing students' future acceptance of PF, without being hindered by their current limited experience with these technologies. Cronbach's alpha of the implemented scale was acceptable in our sample (α = .676).

3. Results

3.1. Participants

The final sample consisted of 79 individuals (28 women, 51 men), aged between 20 and 60 years (M = 26.38, SD = 7.57). The participants were mainly based in Italy (30 responses), Germany (19 responses), and Greece (17 responses). The majority of participants were students, with 27.8% pursuing a bachelor's degree and 43.0% pursuing a master's degree. Additionally, 35.4% of our sample reported current usage of PF technology, accounting for 28 participants.

3.2. Descriptive statistics and intercorrelations

Table 1 provides a summary of participant characteristics for the key variables examined in this study.

Table 1. Descriptive Statistics.

	M	*SD*	*min*	*max*
Climate Change Perception	5.94	0.942	3.40	7.00
Technology Commitment	3.51	0.516	2.25	4.75
Adaptability	3.45	0.611	1.90	5.00
Trust in Technology	3.56	0.794	1.00	5.00
Acceptance PF Systems	5.33	0.891	1.50	6.00

Note: *M* = Mean; *SD* = Standard deviation

Table 2. Correlation Matrix.

	Climate Change Perception	Technology Commitment	Adaptability	Trust in Technology	Acceptance PF Systems
Climate Change Perception	-				
Technology Commitment	r = .254* p = .024	-			
Adaptability	r = .297** p = .008	r = .290** p = .010	-		
Trust in Technology	r = .138 p = .224	r = .116 p = .311	r = .384*** p < .001	-	
Acceptance PF Systems	r = .428*** p < .001	r = .429*** p < .001	r = .369*** p < .001	r = .283* p = .012	-

Note: * p < .05, ** p < .01, *** p < .001, presented are values of Pearson's r and their significances.

Within Table 2 the intercorrelations between the variables are described. Correlations were analyzed using Pearson's r, where values of $r \geq .10$ indicate a weak, $r \geq .30$ indicate a moderate, and $r \geq .50$ indicate a strong correlation (Cohen,

1988). All variables show a significant correlation with the acceptance of PF technologies. Moderate correlations are found with climate change perception, technology commitment, and adaptability. A weak correlation was identified between acceptance of PF systems and trust in PF.

3.3. Multiple Regression Analysis: Predictors of PF Acceptance

To further explore the acceptance of PF technologies, multiple regression analysis was used to test if the personality variables technology commitment and adaptability, trust in the systems, or climate change perception are significant predictors of this variable. Results of the regression indicated that these four predictors explained 34.7% of the variance (R^2=.347, F(4,74)=9.82, p < .001). It was found that technology commitment significantly predicted acceptance of PF technology (β=.298, p=.004), as did climate change perception (β=.290, p=.005). Adaptability (β=.136, p=.213) and technology trust (β=.156, p=.130) did not turn out to be significant predictors.

4. Discussion

In the present study, our primary objective was to explore the factors influencing the acceptance of PF systems in viticulture, focusing on climate change perception, technology commitment, adaptability, and trust in technology. We found significant relationships between the acceptance of PF systems and all variables considered. However, the regression analysis revealed that only climate change perception and technology commitment were significant predictors of PF system acceptance.

Our findings highlight the significant role of climate change perception in predicting the adoption of PF technology in viticulture, indicating that winegrowers who recognize and are concerned about climate change are more likely to adopt PF technologies. This aligns well with previous research across related fields, which has consistently demonstrated the importance of climate change awareness in driving technology adoption (Lorencová et al. 2019, Li et al. 2022). So far, only a few considered climate change awareness as an antecedent within technology acceptance models (Nguyen and Drakou, 2021). Although Mohr and Kühl (2021) introduced a relatively comprehensive modification of the Technology Acceptance Model in order to explain the acceptance of AI systems in agriculture, they did not consider any aspect of climate change perception. Further evidence from previous studies indicates that climate change perception is shaped by multiple factors, such as age, gender, and sociodemographics (Lorencová et al. 2019, Li et al. 2022). Interestingly, studies identified that direct experiences with climate change may not be particularly effective in shaping awareness. This ineffectiveness may be due to individuals' attribution styles and adaptability, which influence how they perceive and respond to climate-related events (Xia et al., 2022). Findings so far underscore the critical need for proactive education initiatives aimed at increasing awareness of climate change. Our study focused on young students, a demographic group that is crucial in shaping future attitudes and actions toward environmental issues. Similarly, Filho et al. (2021) concentrated on university students and stressed the rising significance of climate change knowledge among future professionals. They highlighted the growing demand for professionals equipped with training in environmental sustainability across various academic fields, emphasizing the necessity for curricular innovation.

Consistent with prior research across various fields, such as autonomous driving and robotics (Bernotat and Eyssel 2017, Lidynia et al. 2022), we found that general technology commitment emerged as a significant predictor for the acceptance of PF technology. To ensure users remain committed to technology, maintaining its effectiveness is crucial. Research by Wang and Datta (2009) demonstrated that people were more likely to feel loyal to the technology if it performed well and met their expectations over time. Consequently, higher satisfaction with the use of technology induces effect-based commitment in the longer term. This could serve as an important motivator for technology producers and advisors to support the effectiveness of their products and maintain users' technology commitment at a higher level. At the same time, a high level of post-adoption technology commitment poses additional challenges for competitors to persuade users to switch to alternatives.

In contrast to previous studies on technology acceptance, we did not find adaptability and technology trust to be significant predictors of PF acceptance. This could be explained by the fact that the students were not yet fully involved in farming or had insufficient experience of working with the PF technologies. However, the situation may be reversed in the future. For instance, Nicholas-Davies et al. (2021) found that adaptation was dominated by intergenerational change. This included transferable skills being brought onto the farm as additional drivers. The finding of trust being not a significant predictor was rather unexpected as trust is usually considered to be an important factor. For example, Pavlou (2003), using two samples consisting of students and online consumers, showed that trust was the most influential predictor of the intention to use Internet technology for e-commerce operations. Similarly, Jakku et al. (2019), after conducting several interviews with grain farmers, concluded that trust was one of the central factors meditating perceptions about smart farming technologies and big data in agriculture. To sum up, the present results, along with previous findings, highlight the need for further exploration of the influence of trust on the acceptance of PF. Including a larger sample of students, as well as other stakeholders such as farmers and/or researchers, could lead to a higher percentage of respondents who have more practical experience with PF technologies. As a result, it could increase the power of a trust predictor and serve as a basis to show the need to adjust study curricula in favour of building an initial trusting attitude towards PF technologies. Properly organised and timely education of the younger generations can be a good start for forming a more positive perception of PF technologies and their faster implementation in agricultural

enterprises in the future. For example, Cabiddu et al. (2022) investigated how users experienced interaction with AI-based algorithms over time. The study showed a transition from initial trust to trust over time. After becoming familiar with the algorithm-based work, users tended to trust the technology more and perceive the system-like qualities of the algorithms. In the beginning, the technology was perceived by the users as a human counterpart. Thus, trust depended on the integrity of the algorithm, which included fairness, transparency, autonomy, and accountability. Therefore, improved educational processes can help build initial trust among students, reduce the probability of seeing technologies as a danger, and accelerate the perception of technologies by farmers.

5. Conclusion

This paper provides an initial basis for understanding students' intentions to adopt PV technologies. This was done by analysing the correlations between climate change perceptions, technology commitment, adaptability, and trust in technology with technology acceptance. Future steps for this research may include: i) widening the sample by including more students as well as increasing the number of participating educational institutions; ii) including other stakeholder groups such as researchers/teachers and/or farmers; iii) analysing the correlation between the availability of practical experience in the use of PF technologies and the intention to use these technologies; iv) investigating the differences in responses between participating countries and/or different stakeholder groups.

References

Ajzen, I., 1991. The theory of planned behavior. Organ. Behav. Hum. Decis. Process. 50, 179–211. https://doi.org/10.1016/0749-5978(91)90020-T

Ammoniaci, M., Kartsiotis, S.P., Perria, R., Storchi, P., 2021. State of the art of monitoring technologies and data processing for precision viticulture. Agric. 11, 1–21. https://doi.org/10.3390/agriculture11030201

Aubert, B.A., Schroeder, A., Grimaudo, J., 2012. IT as enabler of sustainable farming: An empirical analysis of farmers' adoption decision of precision agriculture technology. Decis. Support Syst. 54, 510–520. https://doi.org/10.1016/j.dss.2012.07.002

Bastard, A., Chaillet, A., 2023. Digitalization from vine to wine: Successes and remaining challenges - A review. BIO Web Conf. 68, 1–11. https://doi.org/10.1051/bioconf/20236801034

Bernotat, J., Eyssel, F., 2017. A robot at home - How affect, technology commitment, and personality traits influence user experience in an intelligent robotics apartment. RO-MAN 2017 - 26th IEEE Int. Symp. Robot Hum. Interact. Commun. 2017-Janua, 641–646. https://doi.org/10.1109/ROMAN.2017.8172370

Cabiddu, F., Moi, L., Patriotta, G., Allen, D.G., 2022. Why do users trust algorithms? A review and conceptualization of initial trust and trust over time. Eur. Manag. J. 40, 685–706. https://doi.org/10.1016/j.emj.2022.06.001

Cohen, J., 1988. Set Correlation and Contingency Tables. Appl. Psychol. Meas. 12, 425–434. https://doi.org/10.1177/014662168801200410

Davis, F.D., 1989. Perceived usefulness, perceived ease of use, and user acceptance of information technology. MIS Q. Manag. Inf. Syst. 13, 319–339. https://doi.org/10.2307/249008

Ferro, M.V., Catania, P., 2023. Technologies and Innovative Methods for Precision Viticulture: A Comprehensive Review. Horticulturae 9. https://doi.org/10.3390/horticulturae9030399

Filho, W.L., Sima, M., Sharifi, A., Luetz, J.M., Salvia, A.L., Mifsud, M., 2021. Handling climate change education at universities : an overview. Environ. Sci. Eur 33, 1-19. https://doi.org/10.1186/s12302-021-00552-5

Gefen, D., Karahanna, E., Straub, D.W., 2003. Inexperience and experience with online stores: The importance of TAM and trust. IEEE Trans. Eng. Manag. 50, 307–321. https://doi.org/10.1109/TEM.2003.817277

Gößwein, E., Liebherr, M., n.d. Embracing Change in the Modern Working Environment: Exploring Trust, Experimentation, and Adaptability in the Acceptance of New Technologies [Manuscript under review]. SAGE Open.

Jakku, E., Taylor, B., Fleming, A., Mason, C., Fielke, S., Sounness, C., Thorburn, P., 2019. "If they don't tell us what they do with it, why would we trust them?" Trust, transparency and benefit-sharing in Smart Farming. NJAS - Wageningen J. Life Sci. 90–91, 100285. https://doi.org/10.1016/j.njas.2018.11.002

Körber, M., 2019. Theoretical considerations and development of a questionnaire to measure trust in automation. Adv. Intell. Syst. Comput. 823, 13–30. https://doi.org/10.1007/978-3-319-96074-6_2

Li, X., Cao, Z., Shi, X., 2022. How do farmer's disaster experiences influence their climate change perception and

adaptation? Clim. Dev. 14, 523–536. https://doi.org/10.1080/17565529.2021.1949572

Lidynia, C., Luca Liehner, G., Ziefle, M., 2022. Paving the Way to Autonomy – Influencing Factors for the Acceptance of Autonomously Operating Transportation Services in Rural Germany. Hum. Factors Transp. 60, 261–271. https://doi.org/10.54941/ahfe1002456

Lorencová, E.K., Loučková, B., Vačkářů, D., 2019. Perception of climate change risk and adaptation in the Czech Republic. Climate 7, 4–16. https://doi.org/10.3390/cli7050061

Mohr, S., Kühl, R., 2021. Acceptance of artificial intelligence in German agriculture: an application of the technology acceptance model and the theory of planned behavior. Precis. Agric. 22, 1816–1844. https://doi.org/10.1007/s11119-021-09814-x

Neyer, F.J., Felber, J., Gebhardt, C., 2012. Entwicklung und Validierung einer Kurzskala zur Erfassung von Technikbereitschaft. Diagnostica 58, 87–99. https://doi.org/10.1026/0012-1924/a000067

Nguyen, N., Drakou, E.G., 2021. Farmers intention to adopt sustainable agriculture hinges on climate awareness: The case of Vietnamese coffee. J. Clean. Prod. 303, 126828. https://doi.org/10.1016/j.jclepro.2021.126828

Nicholas-Davies, P., Fowler, S., Midmore, P., Coopmans, I., Draganova, M., Petitt, A., Senni, S., 2021. Evidence of resilience capacity in farmers' narratives: Accounts of robustness, adaptability and transformability across five different European farming systems. J. Rural Stud. 88, 388–399. https://doi.org/10.1016/j.jrurstud.2021.07.027

Pavlou, P.A., 2003. Consumer acceptance of electronic commerce: Integrating trust and risk with the technology acceptance model. Int. J. Electron. Commer. 7, 101–134. https://doi.org/10.1080/10864415.2003.11044275

Poortinga, W., Whitmarsh, L., Steg, L., Böhm, G., Fisher, S., 2019. Climate change perceptions and their individual-level determinants: A cross-European analysis. Glob. Environ. Chang. 55, 25–35. https://doi.org/10.1016/j.gloenvcha.2019.01.007

Rainieri, G., Buizza, C., Ghilardi, A., 2023. The psychological, human factors and socio-technical contribution: A systematic review towards range anxiety of battery electric vehicles' drivers. Transp. Res. Part F Traffic Psychol. Behav. 99, 52–70. https://doi.org/10.1016/j.trf.2023.10.001

Rogers Everett, M., 2003. *Diffusion of Innovations* (5th ed.). New York: The Free Press. 576 p.

Tardaguila, J., Stoll, M., Gutiérrez, S., Proffitt, T., Diago, M.P., 2021. Smart applications and digital technologies in viticulture: A review. Smart Agric. Technol. 1, 100005. https://doi.org/10.1016/J.ATECH.2021.100005

Toma, L., Barnes, A.P., Sutherland, L.A., Thomson, S., Burnett, F., Mathews, K., 2018. Impact of information transfer on farmers' uptake of innovative crop technologies: a structural equation model applied to survey data. J. Technol. Transf. 43, 864–881. https://doi.org/10.1007/s10961-016-9520-5

van Dam, K., Meulders, M., 2021. The Adaptability Scale: Development, internal consistency, and initial validity evidence. Eur. J. Psychol. Assess. 37, 123–134. https://doi.org/10.1027/1015-5759/a000591

van Valkengoed, A.M., Steg, L., Perlaviciute, G., 2021. Development and validation of a climate change perceptions scale. J. Environ. Psychol. 76. https://doi.org/10.1016/j.jenvp.2021.101652

VandenBos, G.R., (Ed.). 2015. *APA dictionary of psychology* (2nd ed.). American Psychological Association. 1221 p. https://doi.org/doi.org/10.1037/14646-000

Venkatesh, V., Morris, M.G., Davis, G.B., Davis, F.D., 2003. User Acceptance of Information: Towar a Unified View. MIS Q. 27, 425–478.

Wang, Y.K., Datta, P., 2009. A technology commitment model of post-adoption behavior. Inf. Resour. Manag. J. 22, 1–22. https://doi.org/10.4018/irmj.2009061901

Wicki, M., Guidon, S., Becker, F., Axhausen, K., Bernauer, T., 2019. How technology commitment affects mode choice for a self-driving shuttle service. Res. Transp. Bus. Manag. 32, 100458. https://doi.org/10.1016/j.rtbm.2020.100458

Xia, Z., Ye, J., Zhou, Y., Howe, P.D., Xu, M., Tan, X., Tian, X., Zhang, C., 2022. A meta-analysis of the relationship between climate change experience and climate change perception. Environ. Res. Commun. 4, 105005. https://doi.org/10.1088/2515-7620/ac9bd9

Growing together: Enhancing skill and cultivating sustainable winegrowing communities

Manuel Pérez-Ruiz [a,*], Abdul Mouazen [b], Anastasios Michailidis [c], Daniele Sarri [d]

[a] Department of Aerospace Engineering and Fluid Mechanical, University of Sevilla, Sevilla, Spain

[b] Department of Environment, University of Ghent, Ghent, Belgium

[c] Department of Agricultural Economics, School of Agriculture, Aristotle University of Thessaloniki, Thessaloniki, Greece

[b] Department of Agriculture, Food, Environmental and Forestry, University of Florence, Florence, Italy

* Corresponding author. Email: manuelperez@us.es

Abstract

Today's agricultural machinery, e.g., tractors, planters, harvesters, and sprayers, are far from what our parents used. Thanks to advances in sensors, telemetry, precision technologies, and cloud-based data management, data collection has become simpler, allowing us to transform this data into valuable information and insights. This necessitates a shift in the education and training approach for stakeholders within the agricultural sector. The VTSkill project was born to be highly useful and broad-reaching in the viticulture sector of Mediterranean Europe. This initiative brings together four higher education institutions (HEI), three vocational education and training (VET) institutions, and seven labour market actors. The consortium aims to foster the adoption of environmentally, socially, and economically responsible practices within the viticulture industry. Sustainable Precision Viticulture (SPV) merges the principles of precision agriculture with those of organic farming, facilitating the intelligent utilization of technology in harmony with preserving an agricultural ecosystem. This project aims to develop an innovative, transnational curriculum tailored to viticulture studies. It is designed to equip HEI students, consultants, managers, technicians, and farmers with a comprehensive set of skills in digitalization, sustainability, and resilience, specifically tailored to the nuances of SPV. This process will begin by identifying the key digital, ecological, and resilience/entrepreneurial competencies lacking in the viticulture industry. The research will employ natural language processing (NLP) and data mining techniques and will be validated through interactive research with farmers. Following this, partners will design a new SPV curriculum tailored to the needs of HEIs and VET centres. The training courses will use a micro-credentials approach, be tested in partner organizations, and involve HEI learners, VET learners, farmers/workers, and consultants. Finally, partners will design and test the VTskills e-demofarm, a new model of demo-farm that features three primary components: formative (delivering challenge-based learning educational experiences), informative (referring to events and EU-funding opportunities that might benefit farmers), and demonstrative (virtualizing good practices already carried out by farmers). By implementing effective and efficient communication strategies, the project enhances visibility and engages with over 20,000 European stakeholders, fostering new skills and creating synergies for sustainable precision viticulture.

Keywords: precision viticulture, education, competencies, e-demofarm, resilience

1. Introduction

Focusing on Europe, particularly within the Mediterranean ring, Italy, France, Spain, and Greece collectively account for about half of Europe's annual wine production, which in 2023 was estimated at 150 million hectoliters (OIV, 2023). These statistics are impressive, yet it's crucial to acknowledge a consistent decline in vineyard area and production volume each year, largely attributed to significantly low harvest volumes in these major EU countries. As has been observed over the past 40 years, climate change is profoundly altering the foundations of traditional viticulture practices and technologies (Santos et al., 2020).

The wine industry is deeply ingrained in European culture, making substantial contributions to socio-economic, environmental, and societal realms: vineyards not only beautify the landscape but also employ millions of Europeans, supporting the backbone of rural communities and maintaining a lifestyle quintessential to European culture (CEEV, 2023). This sector primarily consists of numerous small and medium-sized enterprises (SMEs). It is significantly more atomized than other food and beverage industries, leading to its highly fragmented nature (Naigeon et al., 2023). In this setting, ample entrepreneurial opportunities are yet to be harnessed throughout the agricultural process and by auxiliary agents, leveraging

advanced technologies to create scalable projects with significant social and economic impacts. Additionally, viticulture demands specialized knowledge and skills and encompasses a variety of agricultural practices, including soil management, pest and disease control, pruning, and harvesting. Consequently, viticulture is a critical area for research and innovation within the agricultural sector. Technological advancements and research in viticulture can significantly enhance wine production's quality, sustainability, efficiency, and profitability (Gutiérrez et al., 2021).

Adding to the points discussed, we must consider that a more discerning consumer base and the global supply chain increasingly demand more sustainable wines. In this context, initiatives and projects like the one outlined in this study are starting to make much more sense. VTskills aims to promote adopting environmentally, socially, and economically sustainable practices in viticulture to align with the objectives of the Green Deal, the Common Agricultural Policy (CAP), the Farm to Fork strategy, and Biodiversity strategies.

To drive innovation in the wine sector, it is crucial to prioritize digitization, embrace the principles of the circular economy, and develop and implement innovative business models. These elements, which VTskills identifies as digital, green and resilience skills, are paramount for viticulture farmers and workers, as they enable the effective and sustainable management of activities within the industry. By integrating digital technologies, adopting sustainable practices, and creating new business approaches, the wine sector can enhance its competitive edge while ensuring long-term environmental and economic sustainability. Green skills drive digital expertise towards sustainable management, ensuring the efficient use of resources and adopting environmentally friendly practices. At the same time, resilience skills encourage entrepreneurial and intrapreneurial initiative, cultivating innovative attitudes and corporate social responsibility. This latter set of skills makes profitable green achievements through the practical application of digital skills.

The transition to digital technologies is a significant constraint, requiring adjustments in the economic structure of farms and the competencies and technology introduction capacity (Kane, 2019). Technological advancement allows for collecting and analysing vast amounts of data, providing deeper insights and more informed decision-making in environmental sustainability. Despite these benefits, the limited acceptance of smart farming presents significant challenges, largely due to a lack of awareness about their advantages compared to traditional methods (Vecchio et al., 2020) and difficulties in managing extensive and complex technology and data. Precision Agriculture (PA) offers a solution by integrating information and production to boost efficiency, productivity, and long-term profitability while minimizing environmental impacts.

The project targets various actors involved with the viticulture sector, such as students and winegrowers, with a particular emphasis on small and medium enterprises (SMEs) and consulting entities that can support companies in the industry. Offering appropriate training to enhance skills and promote lifelong learning seems necessary. The VTskills project aims to develop transnational sector-wide curricula that connect higher education (HE), vocational education and training (VET) systems, and enterprises. VTskills seeks to facilitate effective transnational cooperation, align education with labour market demands, and create new opportunities in line with the European Skills Agenda.

The project promotes the concept of Sustainable Precision Viticulture (SPV), which integrates organic farming with PA for sustainable agricultural practices and aims to create a new green professional profile, an “SVP specialist” who will possess green, digital, and resilience/entrepreneurial skills. Thanks to a three-year collaboration with project partners, we expect to create synergies among all the actors involved in the viticulture ecosystem and give them access to re- and up-skilling opportunities providing the SPV key competencies.

2. Materials and Methods

The project started in January 2024 and is scheduled to finish in December 2026 for 36 months.

2.1. Partnership

The VTskills consortium brings together 14 partners from different geographical locations (Spain, Italy, Greece, France and Belgium) and organizational backgrounds, such as universities, VET providers, sectoral associations, innovation and technology companies, public administrations and European vineyards companies as shown in Figure 1.

Figure 1. Logos of the 14 European partners collaborating within the VTskills project, including 4 Higher Education Institutions (HEIs), 3 vocational education and training (VET) providers, and 7 labour market actors.

The partnership's composition underscores the project's transnational dimension, the collaboration among various professional groups, and the potential for VTskills results to be applied in other agricultural sectors.

2.2. Project Plan

VTskills (https://www.vtskills.eu/) is divided into 6 work packages (WPs), each further into several tasks. While WP1 and WP6 are active throughout the project's duration, the other WPs have specific durations, as they depend on one another. The work plan scheme is illustrated in Figure 2.

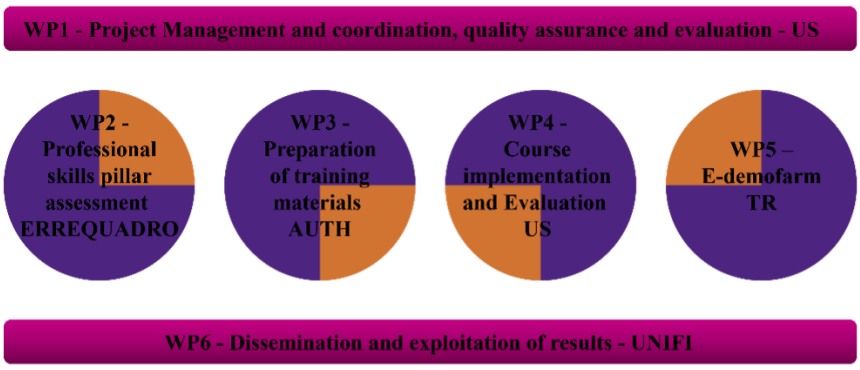

Figure 2. VTskills Work Plan, including the number and name of the Work Packages, along with their respective leadership.

WP1 aims to ensure efficient and effective project management and control of all activities. It also focuses on maintaining high-quality project results in line with EU publication standards and evaluating (both internally and externally) the validity of project planning and implementation.

WP6 aims to promote the project, its goals, and the partnership to ensure sustainability and engagement. This entails involving stakeholders from the beginning of the project, seeking their input to improve results, and disseminating the results to potential multiplier agents. A key focus is national and EU integration across sectors and countries.

The initial phase of the VTskills project (WP2) involves identifying SPV's main competencies, which are categorized into three groups: digital, green, and resilience skills, and developing new professional profiles associated with these competencies. This process will begin with a data-mining analysis of various sources, followed by an evaluation through surveys and the collection of best practices.

Secondly, the consortium in WP3 will develop the material for the e-learning modules. The skills and job profiles resulting from WP2 will form the cornerstone for building the VTskills training course to fill the identified knowledge and skills gaps. The training path will be open to all actors in EU countries' viticulture and enology, including students, agronomists, enologists, consultants, VET, researchers, organic farms, and farms adopted by PA or PV. However, the project's long-term objective is to create knowledge and training content that can be applied to other fields, thereby boosting innovation in the broader agricultural sector.

In WP4, to create conditions for access to re-skilling and up-skilling opportunities will be created. The consortium will conduct pilot tests of the VTskills e-learning courses in higher education institutions (HEI) and vocational education and training (VET) centres, leading to micro-credentials in the viticulture sector grounded in a challenge-based learning approach. Based on the data collected, the project will evaluate and improve the training materials and prepare a handbook on replicating the VTskills courses.

In the final stage, VTskills will establish a virtual hub called "VTskills e-demo farm" under WP5 to provide viticulture stakeholders access to innovative training and information. The goal is to strengthen regional ecosystems and disseminate SPV knowledge. The VTskills e-demo farm will offer demonstrative, formative, and informative services, including interactive tools and simulations. These resources allow users to experiment with various vineyard management techniques and observe crop quality and yield changes. This approach encourages collaboration and knowledge sharing among different actors, facilitating the exchange of ideas for more sustainable and efficient practices.

3. Results and Discussion

Although VTskills has only been running for five months, despite its planned three-year duration, significant progress is already underway. While few tangible results have been achieved yet, activities have begun for WP 1, 2, and 6.

Through the tasks established in WP1 to ensure the overall monitoring and management of project activities, partnerships have created comprehensive project and risk management tools. For WP6, the Dissemination Plan has been shared with all partners to ensure a cohesive project visibility and outreach approach. Several activities have been initiated to promote the project, including creating a dedicated website and establishing a presence on social media platforms.

Work Package 2 (WP2) has achieved more concrete results, which commenced at the beginning of the VTskills project and is scheduled for completion by the ninth month of the first year. Supported by identifying technology and drivers of change, the consortium has successfully produced two valuable documents: “Set of Skills for SPV Farmers/Workers” and “SVP Job Profiles.” The “Set of Skills for SPV Farmers/Workers” outlines the necessary competencies in green, digital, and resilience/entrepreneurial skills required for Sustainable Precision Viticulture. Meanwhile, the “SVP Job Profiles” document details this sector's specific roles and responsibilities, providing a comprehensive overview of the job market dynamics. At the project's current stage, these documents are set to undergo a thorough multi-stakeholder analysis to ensure the robustness and validity of these results.

This step is crucial for establishing a solid foundation for the subsequent phases of the VTskills project, where the consortium will develop training content as e-learning modules for HEIs and VET providers. The goal is to create a well-informed, skilled workforce capable of advancing sustainable precision viticulture practices. The training material based on SPV and the VTskills’ e-learning course for HEIs and VETs will be the outcomes produced in WP3 and WP4. These WPs will span most of the project's duration from the tenth to the thirty-fifth month. A significant emphasis will be placed on determining which of the two e-learning courses (one for HEIs and one for VETs) best meets the needs of professionals within the viticulture industry.

Additionally, the partnership will draft a comprehensive Handbook. This document will detail all the recommended steps for replicating the e-learning courses, providing a valuable resource for other institutions and organizations interested in implementing similar training programs. The last outcome will be the creation and implementation of the e-demo farm, the tool through which the VTskills project will present its output and promote initiatives that boost the innovation of the viticulture sector.

The expected and desired impacts will be achieved at socioeconomic, environmental, employment and scientific levels:

1. Encouraging entrepreneurial and innovative HEIs and VETs by enhancing their training offerings with new teaching and learning tools and methodologies (VTskills approach);
2. Addressing the skills gap caused by the current digital transformation, steering towards sustainable practices in viticulture;
3. Reducing the carbon footprint of agricultural activities through precise training that raises awareness and improves the ability of the project's target groups to respond to climate change and implement more efficient resource use;
4. Establishing a regional ecosystem of diverse demonstrators to build professional and academic networks focused on SPV.

4. Conclusions

The VTskills project is structured to ensure efficient management and high-quality results. WP1, dedicated to project management, emphasizes maintaining standards in line with EU publication requirements and involves internal and external evaluations of the project's planning and implementation processes. This comprehensive approach ensures that all activities are effectively controlled and meet the desired quality benchmarks.

The project focuses on identifying and developing key competencies in the viticulture sector, mainly digital, green, and resilience skills. WP2 initiates this process through data mining and evaluation, while WP3 and WP4 build on these findings by creating e-learning modules and conducting pilot tests in educational institutions. The training materials and courses are designed to fill identified knowledge gaps and offer reskilling and upskilling opportunities, ultimately aiming to boost innovation in the broader agricultural sector.

WP6 aims to promote the project's goals and ensure sustainability by involving stakeholders from the outset and disseminating results to potential multiplier agents. Creating the VTskills e-demo farm under WP5 further supports this goal by providing a virtual hub for training and information dissemination. This hub facilitates collaboration, knowledge sharing, and the adoption of sustainable practices among viticulture stakeholders, thereby strengthening regional ecosystems and enhancing the project's overall impact.

Acknowledgements

The authors would like to express their gratitude to the VTskills project established within the ERASMUS+ EU Programme. Project identifier: 101139985

References

Comité Européen des Entreprises Vins. (2023). Wine Market Report. Retrieved from http://www.ceev.eu/wine-market-report

Gutiérrez S., Hernández I., Ceballos S., Barrio I., Díez-Navajas A.M., Tardaguila J. 2021. Deep learning for the differentiation of downy mildew and spider mite in grapevine under field conditions. Computers and Electronics in Agriculture, Volume 182, 2021, 105991, ISSN 0168-1699, https://doi.org/10.1016/j.compag.2021.105991.

International Organisation of Vine and Wine (OIV). 2023. State of the World Vine and Wine Sector in 2023.

Kane, G. 2019. The technology fallacy: people are the real key to digital transformation. Research-Technology Management, 62(6), 44-49.

Naigeon N., Picardat S. and Auguste P., 2023. DATA for decision-making in viticulture in the face of climate change: Looking beyond production issues. BIO Web Conf. 68 01040.

https://doi.org/10.1051/bioconf/20236801040

Santos J.A., Fraga H., Malheiro A.C., Moutinho-Pereira J., Dinis L., Correia C., et al. 2020. A review of the potential climate change impacts and adaptation options for european viticulture. Applied Sciences, vol. 10, no. 9.

Vecchio, Y., Agnusdei, G.P., Miglietta, P.P., Capitanio, F. 2020. Adoption of precision farming tools: The case of Italian farmers. Int. J. Environ. Res. Public Health, 17, 869.

Irrigation and population dynamics in depopulated rural environments: Causes, implications, and sustainable solutions

M. T. Gómez-Villarino[1], D. Pereira[1], A. I. García[1], A. Sánchez de Medina[1], E. Ayuga-Téllez[1], M. Hidalgo[2], J. M. García-Asensio[2], F. Ayuga[1]

[1] BIPREE Research Group, Universidad Politécnica de Madrid, Spain

[2] Grupo TRAGSA-SEPI, Spain

* Corresponding author. Email: francisco.ayuga@upm.es

Abstract

The demographic evolution of Spain in recent years reveals an undesirable depopulated rural environment with internal imbalances and severe population decline. While various factors contribute to depopulation, such as aging, low birth rates, masculinization, and infrastructure deficiencies, a fundamental cause is the low profitability of agricultural operations, given that it is the main source of income for the population in these areas. This low profitability is linked to the Spanish agricultural structure, where 76% of the nearly 17 million hectares of cultivation are dedicated to rainfed agriculture, and only 24% to irrigation, in a country with a severe hydric deficit. Demographic analysis over the past decade indicates that provinces with a lower proportion of irrigated crops experience greater population loss, while those with higher proportions maintain or increase their population. Therefore, the work hypothesis states that the transformation into irrigation can be the key to establishing and increasing the population in depopulated rural areas, highlighting the importance of guaranteeing the sustainability of irrigation to improve its contribution to population fixation. Study objectives include establishing a scientific model for rural development in depopulated areas, analysing elements of population fixation and growth, and exploring interdependence in irrigation sustainability and resilience. The systematic methodology involves comprehensive data collection on depopulated areas, focusing on the "España Vaciada," and irrigation interventions using GIS tools. Subsequently, demographic data collection will address economic, social, and environmental factors influencing population evolution in rural areas. The next phase involves selecting demographic study areas, identifying those representatives of the issue, and highlighting model areas with successful population fixation through irrigation. The development of a survey, crucial in these areas, will be carried out simultaneously with the creation of an initial systems dynamics model, which will evolve into a definitive model after survey processing and statistical analysis of the results. The conclusions summarize findings to provide a solid foundation for decision-making and implementing measures to promote irrigation sustainability and population fixation in rural areas.

Keywords: sustainable irrigation, depopulated areas, rural demography, GIS, systems dynamics model

1. Introduction

The study conducted within the framework of the Observatory of Irrigation Sustainability (Spanish Agency) aims to scientifically establish the relationship between the benefits of implementing irrigation systems in depopulated areas and the stabilization and increase of the population (Silvestre & Clar, 2010). It also examines how population growth contributes to the sustainability of irrigation practices. The study is based on a hypothesis formulated from ethical principles, which guide the objectives and scientific methodology employed to test the hypothesis. The ethical foundations include the responsible and rational use of nature, the equal dignity and rights of all humans, and the balance between individual freedom and the common good, reflecting principles from international declarations and academic works (Steffen, W. et al., 2015).

This research aligns with international and European legislation and goals, such as the Sustainable Development Goals (SDGs), particularly Goal 6, which emphasizes efficient water use and community involvement in water management. It recognizes that despite the dominance of rain-fed agriculture, irrigation is essential for meeting future food demands, as highlighted in reports by the UN and various legislative frameworks. In Spain, significant policies like the National Irrigation Plan and emergency measures for water conservation underscore the importance of irrigation for agricultural productivity and rural population stabilization (Garcia-Asensio & Ayuga, 2017).

Spain's demographic evolution in recent years shows an undesirable concentration and territorial polarization, with two extremes: congested large cities and depopulated rural areas with significant internal imbalances and severe population decline (Figure 1).

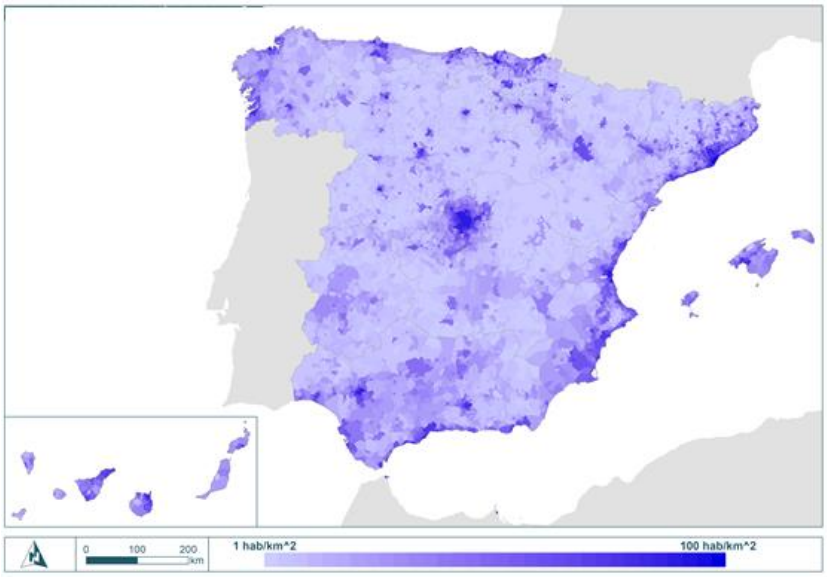

Figure 1. Population Density Distribution in 2021.

According to the National Institute of Statistics (INE) 2021 data (INE, 2021), 64% of the national territory has a population density of less than 25 inhabitants per km², housing only 6% of the total Spanish population. In contrast, 80% of the population is concentrated in urban areas, which cover just 20% of the territory. Moreover, municipalities with a density below 12.5 inhabitants per km², considered sparsely populated by the EU, occupy approximately 49% of the territory, where only 2.7% of the population lives. Areas with extreme depopulation risk, with a density of 8 inhabitants per km² or less, comprise 38% of the national territory and just 1.7% of the population.

The term "España Vaciada" (Emptied Spain) describes rural municipalities, primarily in regions like Castilla-La Mancha, Castilla y León, Aragón, Extremadura, Galicia, and Asturias, where a pronounced decline is evident. This situation worsens in disadvantaged areas, such as mountainous regions (40% of Spanish territory) and areas with challenging climatic conditions or low primary productivity potential (39% of the territory). Despite this, some rural municipalities with low or very low population densities are experiencing demographic revival through economic diversification, signalling a "rural renaissance". This depopulation is driven by high aging, low birth rates, masculinization, a technological gap with urban areas, reduced public services, and infrastructure deficits, particularly in agriculture, where 76% of nearly 17 million hectares of cultivated land is rainfed, and only 24% is irrigated. The demographic and irrigation data analysis between 2011 and 2021 indicates that provinces with significant population loss often have a lower proportion of irrigated land (Figure 2).

Derived from the outlined ethical principles and background, the initial hypotheses of this study are as follows:

- The transformation into irrigated land is a valuable tool for stabilizing and increasing the population in depopulated rural areas.
- Ensuring the sustainability of irrigation enhances its effectiveness in stabilizing the population.

The objectives derived from these hypotheses are:

- To establish a scientific model that incorporates irrigation activities for rural development in depopulated areas.
- To analyze the elements that contribute to population stabilization and growth.
- To explore the interdependence between the sustainability and resilience of irrigation systems.

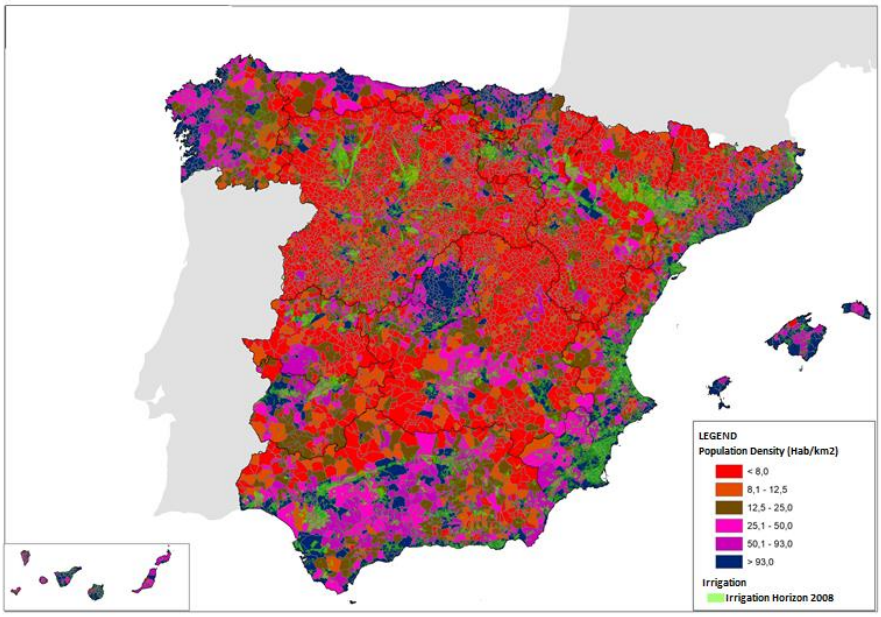

Figure 2. Map of Population Density in the Municipalities of Spain and Distribution of Irrigation Systems Horizon 2008

2. Materials and Methods

The methodology is divided into four key stages. Firstly, a comprehensive compilation of information on depopulated areas in Spain was carried out, as well as interventions in irrigation systems. This compilation was conducted using Geographic Information Systems (GIS).

Subsequently, information was gathered on demographic evolution based on various economic, social, and environmental factors, as well as scientific studies applying system dynamics to this evolution in rural areas and to the establishment and sustainability of irrigation systems. This literature review provides a solid theoretical framework for the study.

Based on this information, the selection of demographic study areas and model areas representing best practices was carried out. A survey was developed and distributed throughout Spain, with a special focus on the selected areas.

Simultaneously, a systems dynamic model of the relationship system between population and agriculture was developed, considering both direct and indirect employment generated by the activity (Pluchinotta et al, 2018). This model encompasses various productive modalities, including irrigation, allowing for the assessment of the effects on rural population of different change scenarios that may arise.

This method enables the derivation of conclusions and recommendations, providing a solid basis for the formulation of policies and strategies in the field of rural development and risk management.

2.1. Study areas

The strategic selection of study areas aims to shed light on the impact of irrigation on population and local socioeconomic development. Criteria such as demographic data analysis, consideration of agricultural diversity, and inclusion of successful cases guide the selection process. By focusing on agricultural regions as the unit of analysis, the study ensures a comprehensive understanding of irrigation's effects, accounting for factors like agricultural homogeneity, geographical context, and regional decision-making dynamics. The chosen regions, including Esla-Campos, Monegros, Bajo Aragón, Campos de Liria, Campo de Cartagena, Don Benito, and La Loma, represent diverse geographical and socio-economic contexts, providing valuable insights applicable to broader agricultural policy formulation.

The selected regions (Figure 3) offer a diverse yet representative sample to explore the intricate relationship between irrigation and population dynamics. Each region, characterized by unique demographic challenges and agricultural practices, presents an opportunity to identify patterns and learn from successful

cases. By analyzing factors such as labor intensity, profit margins, and local decision-making processes, the study aims to provide actionable insights for policymakers and stakeholders seeking to promote sustainable development in rural areas. Through a comprehensive examination of these regions, the study seeks to contribute to a nuanced understanding of the role of irrigation in shaping local economies and communities.

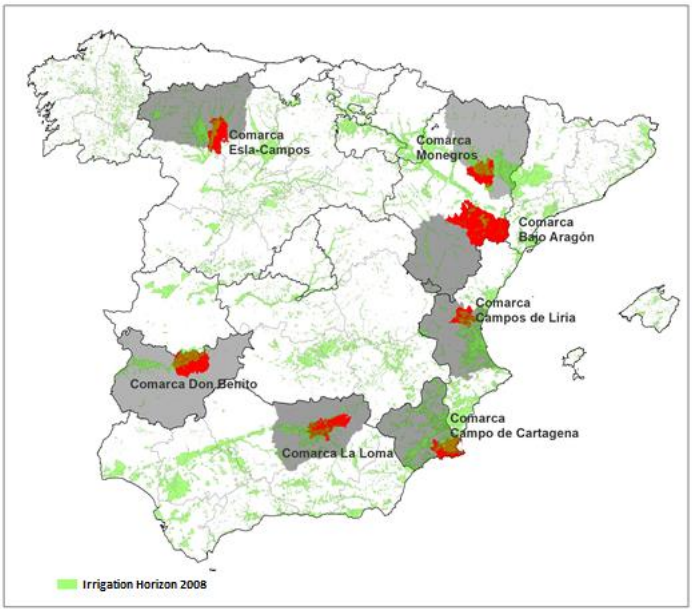

Figure 3. Study areas

2.2. Survey design

The methodology for designing the survey relied on the expert judgment-based decision-making method, utilizing group dynamics extensively (Colectivo IOÉ, 2015). A rigorous process was followed to identify experts, considering criteria such as their experience in the field, reputation in the community, availability and motivation to participate, as well as impartiality and personal qualities (Escobar-Pérez & Martínez, 2008). A natural focus group consisting of 10 individuals meeting these criteria was formed and used to gather relevant information on social cognitions related to the study (Skjong & Wentworth, 2001). Survey results were analyzed using descriptive statistics, employing tests like the Kolmogorov-Smirnov test to assess goodness of fit, the $\chi 2$ test to check the independence of categorical variables, and the Mann-Whitney W test to contrast central values (Ayuga-Téllez et al., 2013). Additionally, group comparison methods such as the Scheffe method or the Duncan method were applied to identify potential significant differences between them (Milliken & Johnson, 2009; Skjong & Wentworth, 2001). These statistical techniques ensured a rigorous evaluation of the results and provided a solid foundation for data interpretation.

2.3. Conceptual Formulation of the dynamic model

A dynamic model of the relationship system between population and agriculture has been designed, considering both direct and indirect employment generated by the activity. The model encompasses various productive modalities, including irrigation, allowing for the evaluation of the effects on the rural population of different scenarios of change. This design relies on identifying and analyzing all potential sources of statistical information that can feed into the system and establish statistical relationships between the different processes that comprise the model. The existence of different sources of information, each with its own characteristics and biases, allows for their incorporation into the model through sensitivity analyses, enabling the management of uncertainty levels associated with it.

The model estimates direct and indirect employment through an analysis organized into five different modules (Figure 4):

- Surface Module: Analyses the number, area, and characteristics of farms. It allows incorporating

existing trends in land use changes, farm structure, and crop changes into the model.

- Direct Employment Module: Calculates employment generated on the farm, distinguishing between cultivation systems, dimensions, and logically differentiating between rainfed and irrigated land.
- Indirect Employment Module: Designed based on farm expenses related to crop cultivation, machinery rental and maintenance, and energy consumption.
- Product Transformation Module: Estimates employment generated by locally performed industrial transformation processes.
- Family Module: Analyses the population effects of the working population on other population groups (non-active population) based on family statistics. It considers minors, the elderly, family members engaged in family tasks (including caregiving).

The general approach of the model, described below, is summarized in the Figure 5, where each module is represented by a color code: Green: Surface module, Blue: Direct employment module, Red: Indirect employment module, Yellow: Employment in the food industry module, Gray: Family module.

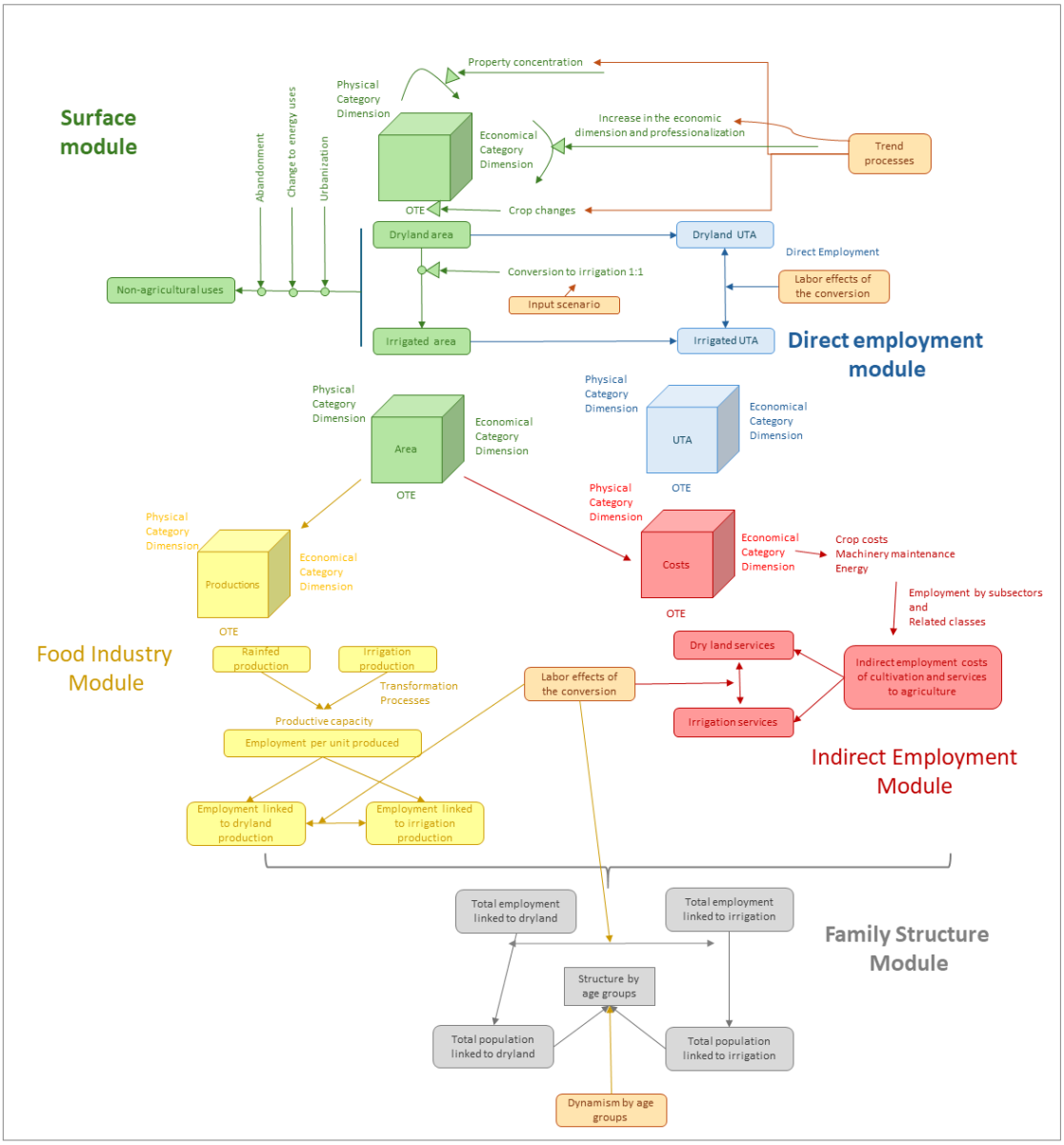

Figure 4. According to the type of agricultural exploitation of the respondents' municipality

In addition to its conceptual design, the model is being incorporated into specific system dynamics software. For this purpose, the STELLA®, program has been chosen, which allows for the inclusion of all the relationships described in the preceding pages. Moreover, it enables sensitivity analysis, which makes it possible to identify which elements of the model produce the greatest changes and where it is most important to complement tools for statistical analysis of official data with other sources of information, such as specific surveys or fieldwork, which could illustrate future lines of work. It also allows for the analysis of the effect of the statistical variability expected to be found in the identified relationships.

3. Results and Discussion

For the survey design two meetings were held, one to discuss a questionnaire proposal presented by the group moderator, with a consensual outcome agreed upon by all members. The second meeting was held to discuss some minor modifications to the questionnaire, issues that arose after its application to a pilot group of 50 participants, mainly irrigation cooperative managers. The result is a questionnaire consisting of 45 questions, with 12 aimed at characterizing the population, 28 focusing on their attitudes toward rural life conditions, and 5 regarding the improvement in life brought about by irrigated crops.

The survey is structured into two main parts: one directed at population in irrigated areas and another at population in rainfed areas, with some common questions at the beginning. The first section gathers basic demographic data, such as age, gender, education level, and employment status. It also explores satisfaction with rural life and the necessary conditions to remain in these areas.

Subsequently, depending on whether the participant lives in an irrigated or rainfed area, they are directed to specific questions. For irrigated areas, perceptions about the importance of these crops for the local economy, population retention, and improvement of services and employment are explored. For rainfed areas, questions are asked about the potential implementation of irrigated crops and their effects.

In both sections, the impact of various factors on rural-to-urban migration is assessed. The sequential and thematic structure of the survey allows for the collection of detailed and relevant information to understand the needs and preferences of rural communities.

The survey was implemented using the Google tool and the link was emailed to the mayors of 2,000 town councils in sparsely populated areas, requesting its dissemination to more residents of the town.

The survey respondents' characteristics are representative of the population, with gender and age well represented. With over 1000 responses obtained, the statistical reliability of the results is ensured. The data obtained mostly correspond to municipalities with low population. The sample is fairly balanced in most aspects, except for the composition of education levels, where the number of responses from individuals with no education or primary education is lower than the rest.

Regarding the dynamic model of the relationship system between population and agriculture, the application of the model was made on the selected areas and validated with the official real data. First results have shown that the accuracy improve significantly when applied to larger areas. Initially, provinces were used for the analysis, but this caused distortions in the results, leading to the selection of regions with similar climatic characteristics, based primarily on average precipitation. Despite these adjustments, representativity problems persist, especially in less common production systems. Additionally, technical-economic orientations (OTE) do not adequately differentiate between rainfed and irrigated systems, which affects the combination of agricultural and livestock activities.

To address these challenges, it was decided to analyze farms with pure characteristics of the production system. The dominant crop types were studied on farms with more than 80% in that type, and the minority types on farms with more than 50%. When there is sufficient representativity, the method reflects cost savings due to economies of scale well. However, smaller farms distort the model due to low representativity and high dispersion of labor data.

The model improved by grouping the smaller classes into those dominated by larger farms, thus correcting the deviations. However, this correction is not applicable to all types of production systems, especially in crops like citrus or intensive horticultural crops, where the distortion in small farms is lower.

The differences between rainfed and irrigated farms vary between 6% and 10% in crops with equivalence between the two and are greater in those without equivalents. At the regional level, the results reflect official employment data well, although there is dispersion at the municipal level since the model is based on typical farms and might not fully adjust to reality. The farm cost data are also adequately reflected, although the

transformation data show greater discrepancies.

4. Conclusions

From the survey results, it is concluded that the improvement in services, including internet access, is considered essential for retaining rural population and preventing migration, even more so than increasing job opportunities. Satisfaction with life in rural areas is high, and the perception of the importance of irrigation and improving rural living conditions is also high and shared by individuals living in municipalities with and without irrigation. The majority opinion is that the implementation of irrigated crops improves economic and social conditions and job opportunities; it promotes the increase and/or improvement of services (healthcare, education, commercial), and would help in retaining the population.

The system dynamics model demonstrates good representational capacity and significant improvement by adjusting the analysis zones and grouping farms, although it still faces challenges in representativity and accuracy at the local level and in certain production systems. It is necessary to deepen the discrimination of industry types and their relationship with industrial land, on the one hand, and the productive differences between rainfed and irrigated systems, on the other. When data is entered into the model, changes in farm structure (towards concentration) and land use have a greater impact than the differences between rainfed and irrigated systems. However, there are fewer losses in irrigated areas, which are more stable from a labor perspective. The project will continue by improving this SD model and making simulations for the future in different scenarios.

Acknowledgements

The authors are grateful to the Spanish Ministry of Agriculture through the Observatory of Irrigation Sustainability for funding the research and collaborating in all aspects. We also thank FENACORE (the Federation of Spanish Irrigation Cooperatives) for their support in adjusting and disseminating the survey.

References

Ayuga-Téllez, E., González García C., Martín Fernández S., Martínez Falero, E., 2013. Estadística: Guía Práctica y Ejercicios. Fundación Conde del Valle de Salazar (FUCOVASA), Madrid, España. 377pp

Colectivo IOÉ, 2010 "¿Para qué sirve el grupo de discusión? Una revisión crítica del uso de técnicas grupales en los estudios sobre migraciones." EMPIRIA. Revista de Metodología de Ciencias Sociales, vol. 19, p. 73-99. https://doi.org/10.5944/empiria.19.2010.2015

Escobar-Pérez, J., Martínez, A., 2022. Validez de contenido y juicio de expertos: Una aproximación a su utilización. Avances en Medición, vol. 6, p. 27-36, January 2008. Disponible en: Avances en medición (unam.mx) Visto en: Dec. 7

García-Asensio, J. M., & Ayuga, F. 2017. Irrigation engineering in Spain and how it has changed the country's landscape. European countryside, 9 (1), 211-229.

INE. 2021. Instituto Nacional de Estadística. Censos de Población y viviendas 2021. Proyecto Técnico. Madrid: https://www.ine.es/censos2021/censos2021_proyecto.pdf

Milliken, G. A., & Johnson, D. E., 2009. Analysis of messy data, volume I: Designed Experiments, Second Edition. Chapman and Hall/CRC. Nueva York, USA. 674 pp

Pluchinotta, I., Pagano, A., Giordano, R., & Tsoukiàs, A. (2018). A system dynamics model for supporting decision-makers in irrigation water management. Journal of environmental management, 223, 815-824.

Steffen, W. et al., 2015. Planetary boundaries: Guiding human development on a changing planet. Science 347,1259855

Silvestre, J., & Clar, E. (2010). The demographic impact of irrigation projects: A comparison of two case studies of the Ebro basin, Spain, 1900–2001. Journal of Historical Geography, 36(3), 315-326.

Skjong, R. & Wentworth, H. B., 2001. "Expert Judgment and Risk Perception." In Proc. The Eleventh International Offshore and Polar Engineering Conference, ' 05

PROFESSIONAL CONGRESS ORGANIZER

convin
www.convin.gr

MEMBER OF

IAPCO ACCREDITED

ICCA Member

YOUR *FLEX*STABILITY PARTNER!!